به نام خدا

مرکز دانلود رایگان
مهندسی متالورژی و مواد

---

www.Iran-mavad.com

ASM Handbook®

Volume 13B
Corrosion: Materials

Prepared under the direction of the
ASM International Handbook Committee

Stephen D. Cramer and Bernard S. Covino, Jr., Volume Editors

Charles Moosbrugger, Project Editor
Bonnie R. Sanders, Manager of Production
Madrid Tramble, Senior Production Coordinator
Gayle J. Anton, Editorial Assistant
Jill Kinson, Production Editor
Pattie Pace, Production Coordinator
Kathryn Muldoon, Production Assistant
Scott D. Henry, Senior Product Manager

Editorial Assistance
Elizabeth Marquard
Heather Lampman
Marc Schaefer
Beverly Musgrove
Cindy Karcher
Kathy Dragolich

Materials Park, Ohio 44073-0002
www.asminternational.org

First printing, November 2005

This book is a collective effort involving hundreds of technical specialists. It brings together a wealth of information from worldwide sources to help scientists, engineers, and technicians solve current and long-range problems.

Great care is taken in the compilation and production of this Volume, but it should be made clear that NO WARRANTIES, EXPRESS OR IMPLIED, INCLUDING, WITHOUT LIMITATION, WARRANTIES OF MERCHANTABILITY OR FITNESS FOR A PARTICULAR PURPOSE, ARE GIVEN IN CONNECTION WITH THIS PUBLICATION. Although this information is believed to be accurate by ASM, ASM cannot guarantee that favorable results will be obtained from the use of this publication alone. This publication is intended for use by persons having technical skill, at their sole discretion and risk. Since the conditions of product or material use are outside of ASM's control, ASM assumes no liability or obligation in connection with any use of this information. No claim of any kind, whether as to products or information in this publication, and whether or not based on negligence, shall be greater in amount than the purchase price of this product or publication in respect of which damages are claimed. THE REMEDY HEREBY PROVIDED SHALL BE THE EXCLUSIVE AND SOLE REMEDY OF BUYER, AND IN NO EVENT SHALL EITHER PARTY BE LIABLE FOR SPECIAL, INDIRECT OR CONSEQUENTIAL DAMAGES WHETHER OR NOT CAUSED BY OR RESULTING FROM THE NEGLIGENCE OF SUCH PARTY. As with any material, evaluation of the material under end-use conditions prior to specification is essential. Therefore, specific testing under actual conditions is recommended.

Nothing contained in this book shall be construed as a grant of any right of manufacture, sale, use, or reproduction, in connection with any method, process, apparatus, product, composition, or system, whether or not covered by letters patent, copyright, or trademark, and nothing contained in this book shall be construed as a defense against any alleged infringement of letters patent, copyright, or trademark, or as a defense against liability for such infringement.

Comments, criticisms, and suggestions are invited, and should be forwarded to ASM International.

Library of Congress Cataloging-in-Publication Data

ASM International

ASM Handbook
Includes bibliographical references and indexes
Contents: v.1. Properties and selection—irons, steels, and high-performance alloys—v.2. Properties and selection—nonferrous alloys and special-purpose materials—[etc.]—v.21. Composites

1. Metals—Handbooks, manuals, etc. 2. Metal-work—Handbooks, manuals, etc. I. ASM International. Handbook Committee. II. Metals Handbook.
TA459.M43 1990 620.1′6 90-115
SAN: 204-7586

ISBN: 0-87170-707-1

ASM International®
Materials Park, OH 44073-0002
www.asminternational.org

Printed in the United States of America

Multiple copy reprints of individual articles are available from Technical Department, ASM International.

Foreword

Enhancing the life of structures and engineered materials, while protecting the environment and public safety, is one of the paramount technological challenges for our nation and the world. Corrosion-related problems span a wide spectrum of materials and systems that impact our daily lives, such as aging aircraft, high-rise structures, railroads, automobiles, ships, pipelines, and many others. According to a study conducted in 1998, the total direct and indirect cost of corrosion to the United States alone exceeds $550 billion per year. While major technological advances have been made during the last three decades, numerous new innovations need to be made in the coming years. ASM International is pleased to publish *ASM Handbook,* Volume 13B, *Corrosion: Materials,* the second book in a three-volume revision of the landmark 1987 *Metals Handbook,* 9th Edition, on corrosion. The information from the 1987 Volume has been revised, updated, and expanded to address the needs of the members of ASM International and the technical community for current and comprehensive information on the physical, chemical, and electrochemical reactions between specific materials and environments. Since the time the 1987 *Corrosion* volume was published, knowledge of materials and corrosion has grown, which aids the material selection process. Engineered systems have grown in complexity, however, making the effects of subtle changes in material performance more significant.

ASM International continues to be indebted to the Editors, Stephen D. Cramer and Bernard S. Covino, Jr., who had the vision and the drive to undertake the huge effort of updating and revising the 1987 *Corrosion* volume. *ASM Handbook,* Volume 13A, *Corrosion: Fundamentals, Testing, and Protection,* published in 2003, is the cornerstone of their effort. The project will be completed with the publication of *ASM Handbook,* Volume 13C, *Corrosion: Environments and Industries,* in 2006. The Editors have brought together experts from across the globe making this an international effort. Contributors to the corrosion Volumes represent Australia, Belgium, Canada, Crete, Finland, France, Germany, India, Italy, Japan, Korea, Mexico, Poland, South Africa, Sweden, Switzerland, and the United Kingdom, as well as the United States. The review, revisions, and technical oversight of the Editors have added greatly to this body of knowledge.

We thank the authors and reviewers of the 1987 *Corrosion* volume, which at the time was the largest, most comprehensive volume on a single topic ever published by ASM. This new edition builds upon that groundbreaking project. Thanks also go to the members of the ASM Handbook Committee for their oversight and involvement, and to the ASM editorial and production staff for their tireless efforts.

We are especially grateful to the over 120 authors and reviewers listed in the next several pages. Their willingness to invest their time and effort and to share their knowledge and experience by writing, rewriting, and reviewing articles has made this Handbook an outstanding source of information.

Bhakta B. Rath
President
ASM International

Stanley C. Theobald
Managing Director
ASM International

Policy on Units of Measure

By a resolution of its Board of Trustees, ASM International has adopted the practice of publishing data in both metric and customary U.S. units of measure. In preparing this Handbook, the editors have attempted to present data in metric units based primarily on Système International d'Unités (SI), with secondary mention of the corresponding values in customary U.S. units. The decision to use SI as the primary system of units was based on the aforementioned resolution of the Board of Trustees and the widespread use of metric units throughout the world.

For the most part, numerical engineering data in the text and in tables are presented in SI-based units with the customary U.S. equivalents in parentheses (text) or adjoining columns (tables). For example, pressure, stress, and strength are shown both in SI units, which are pascals (Pa) with a suitable prefix, and in customary U.S. units, which are pounds per square inch (psi). To save space, large values of psi have been converted to kips per square inch (ksi), where 1 ksi = 1000 psi. The metric tonne ($kg \times 10^3$) has sometimes been shown in megagrams (Mg). Some strictly scientific data are presented in SI units only.

To clarify some illustrations, only one set of units is presented on artwork. References in the accompanying text to data in the illustrations are presented in both SI-based and customary U.S. units. On graphs and charts, grids corresponding to SI-based units usually appear along the left and bottom edges. Where appropriate, corresponding customary U.S. units appear along the top and right edges.

Data pertaining to a specification published by a specification-writing group may be given in only the units used in that specification or in dual units, depending on the nature of the data. For example, the typical yield strength of steel sheet made to a specification written in customary U.S. units would be presented in dual units, but the sheet thickness specified in that specification might be presented only in inches.

Data obtained according to standardized test methods for which the standard recommends a particular system of units are presented in the units of that system. Wherever feasible, equivalent units are also presented. Some statistical data may also be presented in only the original units used in the analysis.

Conversions and rounding have been done in accordance with IEEE/ASTM SI-10, with attention given to the number of significant digits in the original data. For example, an annealing temperature of 1570 °F contains three significant digits. In this case, the equivalent temperature would be given as 855 °C; the exact conversion to 854.44 °C would not be appropriate. For an invariant physical phenomenon that occurs at a precise temperature (such as the melting of pure silver), it would be appropriate to report the temperature as 961.93 °C or 1763.5 °F. In some instances (especially in tables and data compilations), temperature values in °C and °F are alternatives rather than conversions.

The policy of units of measure in this Handbook contains several exceptions to strict conformance to IEEE/ASTM SI-10; in each instance, the exception has been made in an effort to improve the clarity of the Handbook. The most notable exception is the use of g/cm^3 rather than kg/m^3 as the unit of measure for density (mass per unit volume).

SI practice requires that only one virgule (diagonal) appear in units formed by combination of several basic units. Therefore, all of the units preceding the virgule are in the numerator and all units following the virgule are in the denominator of the expression; no parentheses are required to prevent ambiguity.

Preface

Corrosion, while silent and often subtle, is probably the most significant cause of degradation of society's structures. Over the past 100 years, efforts have been made to estimate the cost of corrosion to the economies of various countries. These efforts have been updated to 2004 in this Handbook, and extrapolated to the global economy to provide an estimate of the global cost of corrosion (Ref 1). With a 2004 global Gross Domestic Product (GDP) of about $50 trillion United States dollars (USD), the direct cost of corrosion was estimated to be $990 billion (USD) annually, or 2.0 percent of the world GDP (Ref 1). The direct cost is that experienced by owners and operators of manufactured equipment and systems and of other man-made objects (Ref 2). The indirect cost of corrosion, representing costs assumed by the end user and the overall economy (Ref 2), was estimated to be $940 billion (USD) annually (Ref 1). On this basis, the 2004 total cost of corrosion to the global economy was estimated to be about $1.9 trillion (USD) annually, or 3.8 percent of the world GDP. The largest contribution to this cost comes from the United States at 31 percent, with other major contributions being: Japan—6 percent, Russia—6 percent, Germany—5 percent, and the UK, Australia, and Belgium—1 percent.

ASM Handbook Volume 13B, *Corrosion: Materials,* is the second volume in a three-volume update, revision, and expansion of *Corrosion* published in 1987 as Volume 13 of the ninth edition *Metals Handbook*. The first volume—*ASM Handbook* Volume 13A, *Corrosion: Fundamentals, Testing, and Protection*—was published in 2003. Volume 13C, *Corrosion: Environments and Industries,* will be published in 2006. The purpose of these three volumes is to present the current state of knowledge of corrosion, efforts to mitigate corrosion's effects on society's structures and economies, and some perspective on future trends in corrosion prevention and mitigation. Metals remain the primary materials focus of the Handbook, but nonmetallic materials occupy a more prominent position, reflecting their wide and effective use to solve problems of corrosion and their frequent use with metals in complex engineering systems. Wet (or aqueous) corrosion remains the primary environmental focus, but dry (or gaseous) corrosion is also addressed, reflecting the increased use of elevated or high temperature operations in engineering systems, particularly energy-related systems where corrosion and oxidation are important considerations.

As with Volume 13A, Volume 13B recognizes the diverse range of materials, environments, and industries affected by corrosion, the global reach of corrosion practice, and the levels of technical activity and cooperation required to produce cost-effective, safe, and environmentally-sound solutions to materials problems in chemically aggressive environments. As we worked on this project, we marveled at the spread of corrosion technology into many engineering technologies and fields of human activity. This occurred because the pioneers of corrosion technology from the early to mid-20th century, and the organizations they helped create, were able to effectively communicate and disseminate their knowledge to an ever widening audience through educational, training, and outreach activities. One quarter of the articles in Volume 13B did not appear in the 1987 Handbook. Authors from eight countries contributed to Volume 13B. The references for each article are augmented by Selected References to provide access to a wealth of additional information on corrosion.

Volume 13B is organized into three major sections addressing the materials used in society's structures and their performance over time. These sections recognize that materials are chemicals and respond to the laws of chemistry and physics, that with sufficient knowledge corrosion is predictable, and therefore, within the constraints of design and operating conditions, corrosion can be minimized to provide economic, environmental, and safety benefits.

The first Section, "Corrosion of Ferrous Metals," examines the corrosion performance of wrought carbon steels, wrought low alloy steels, weathering steels, metallic-coated steels, organic-coated steels, cast irons, cast carbon and low alloy steels, wrought stainless steels, and cast stainless steels. These materials include a wide spectrum of end-use products utilizing steel's desirable characteristics of lightness, high strength and stiffness, adaptability, ease of prefabrication and mass production, dimensional stability, durability, abrasion resistance, uniform quality, noncombustibility, and ability to be recycled. In today's worldwide market, cost comes into play in the material selection process only after the user's functional requirements, particularly durability, are met. Expectations for low maintenance and long life, crucial for a favorable life cycle cost evaluation, require that long-term durability, including corrosion performance, can be substantiated through prior experience and test data.

The second Section, "Corrosion of Nonferrous Metals and Specialty Products," addresses the corrosion performance of metals and alloys made from aluminum, beryllium, cobalt, copper, hafnium, lead, magnesium, nickel, niobium, precious metals, tantalum, tin, titanium, uranium, zinc, zirconium, and specialty products including brazed and soldered joints, thermal spray coatings, electroplated hard chromium, clad metals, powder metallurgy materials, amorphous metals, intermetallics, carbides, and metal matrix composites. Numerous nonferrous alloys have extremely desirable physical and mechanical properties and have much higher resistance to corrosion and oxidation than steels and stainless steels. The most widely used nonferrous materials are those based on aluminum, copper, nickel, and titanium. Powder metallurgy materials, amorphous metals, intermetallics, cemented carbides, and metal matrix composites are defined less by their compositions than by their microstructures, which provide physical, mechanical, and corrosion and oxidation resistance unlike those of the traditionally processed metals and alloys. In most structures designed to resist corrosion, joints represent the greatest challenge. Coatings and claddings protect vulnerable substrate materials by resisting the impact of corrosive or oxidizing media or by acting as sacrificial anodes.

The third Section, "Environmental Performance of Nonmetallic Materials," addresses the performance of refractories, ceramics, concrete, protective coatings, rubber linings, elastomers, and thermosetting resins and resin matrix composites in aggressive environments. A significant number of engineering materials applications are fulfilled by nonmetallic materials. While nonmetallic materials are extensively used in engineering systems, they can degrade is with time, sometimes with catastrophic effect. The goal of this section is to indicate the chemical resistance of a variety of commonly used nonmetallic materials and provide further references for those seeking more in-depth information on their environmental performance. In this regard, testing for chemical and mechanical compatibility is usually warranted before nonmetallic materials are placed into a specific service.

The Handbook concludes with the estimate of the "Global Cost of Corrosion" noted at the beginning of this Preface and a "Gallery of Corrosion Damage." Using earlier cost studies as a basis, the 2004 total cost of corrosion to the global economy, including both direct and indirect costs,

was estimated to be about $1.9 trillion (USD) annually, or 3.8 percent of the world GDP. The "Gallery of Corrosion Damage" contains color photographs of corrosion damage to complement the many black and white examples that accompany individual articles in the three volume series. The Gallery was assembled from photographs taken by experts in their practice of corrosion control and prevention in industrial environments. The photographs illustrate forms of corrosion and how they appear on inspection in specific environments, with a brief analysis of the corrosion problem and discussion of how the problem was corrected.

Supporting material at the back of the handbook includes a variety of useful information. A "Periodic Table of the Elements" provides fundamental information on the elements and gives their organization by group using three conventions: Chemical Abstract Service (CAS), International Union of Pure and Applied Chemistry (IUPAC)-1970, and IUPAC-1988. A concise description of "Crystal Structure" is given. "Density of Metals and Alloys" gives values for a wide range of metals and alloys. "Reference Electrodes" provides data on the commonly used reference electrodes and "Overpotential" distinguishes overpotential and overvoltage. The "Electrochemical Series" from the CRC Handbook is reproduced giving standard reduction potentials for a lengthy array of elements. A "Galvanic Series of Metals and Alloys in Seawater" shows materials by their potential with respect to the saturated calomel electrode (SCE) reference electrode. The "Compatibility Guide" serves as a reference to metal couples in various environments. A "Corrosion Rate Conversion" includes conversions in both nomograph and tabular form. The "Metric Conversion Guide" gives conversion factors for common units and includes SI prefixes. "Abbreviations and Symbols" provides a key to common acronyms, abbreviations, and symbols used in the Handbook.

Many individuals contributed to Volume 13B. In particular we wish to recognize the efforts of the following individuals who provided leadership in organizing subsections of the Handbook (listed in alphabetical order):

Chairperson	Subsection title
Rajan Bhaskaran	Global Cost of Corrosion
Arthur Cohen	Corrosion of Copper and Copper Alloys
Bernard Covino, Jr.	Corrosion of Specialty Products
Stephen Cramer	Corrosion of Carbon and Alloy Steels, Corrosion of Low Melting Metals and Alloys
Paul Crook	Corrosion of Cobalt and Cobalt-Base Alloys, Corrosion of Nickel-Base Alloys
Peter Elliott	Gallery of Corrosion Damage
John F. Grubb	Corrosion of Stainless Steels
Gil Kaufman	Corrosion of Aluminum and Aluminum Alloys
Barbara Shaw	Corrosion of Magnesium and Magnesium-Base Alloys
David C. Silverman	Environmental Performance of Non-Metallic Materials
Richard Sutherlin	Corrosion of Reactive and Refractory Metals and Alloys
Gregory Zhang	Corrosion of Zinc and Zinc Alloys

These knowledgeable and dedicated individuals generously devoted considerable time to the preparation of the Handbook. They were joined in this effort by more than 70 authors who contributed their expertise and creativity in a collaboration to write and revise the articles in the Handbook, and by the many reviewers of these articles. These volunteers built on the contributions of earlier Handbook authors and reviewers who provided the solid foundation on which the present Handbook rests.

For articles revised from the 1987 edition, the contribution of the previous author is acknowledged at the end of the article. This location in no way diminishes their contribution or our gratitude. Those authors responsible for the current revision are named after the title. The variation in the amount of revision is broad. The many completely new articles presented no challenge for attribution, but assigning fair credit for revised articles was more problematic. The choice of presenting authors' names without comment or with the qualifier "Revised by" is solely the responsibility of the ASM staff.

We thank ASM International and the ASM staff for the skilled support and valued expertise in the production of this Handbook. In particular, we thank Charles Moosbrugger, Gayle Anton, and Scott Henry for their encouragement, tactful diplomacy, and many helpful discussions. We are most grateful to the Albany Research Center, U.S. Department of Energy, for the support and flexibility in our assignments that enabled us to participate in this project. In particular, we thank Jeffrey A. Hawk and Cynthia A. Powell for their gracious and generous encouragement throughout the project.

Stephen D. Cramer
Bernard S. Covino, Jr.,
U.S. Department of Energy
Albany Research Center

REFERENCES

1. R. Bhaskaran, N. Palaniswamy, N.S. Rengaswamy, and M. Jayachandran, "Global Cost of Corrosion—A Historical Review," in *Corrosion: Materials,* ASM Handbook 13B, ASM International, Materials Park OH, 2005
2. Gerhardus H. Koch, Michiel P.H. Brongers, Neil G. Thompson, Y. Paul Virmani, and Joe H. Payer, *Corrosion Cost and Preventive Strategies in the United States,* FHWA-RD-01-156, Federal Highway Administration, U.S. Department of Transportation, Washington D.C., March 2002

Officers and Trustees of ASM International (2004–2005)

Bhakta B. Rath
President and Trustee
U.S. Naval Research Laboratory
Reza Abbaschian
Vice President and Trustee
University of Florida
Robert C. Tucker, Jr.
Immediate Past President and Trustee
The Tucker Group LLC
Paul L. Huber
Treasurer
Seco/Warwick Corporation
Stanley C. Theobald
Secretary and Managing Director
ASM International

Trustees

Rodney R. Boyer
Boeing Commercial Airplane Group
Dianne Chong
The Boeing Company
Roger J. Fabian
Bodycote Thermal Processing
William E. Frazier
Naval Air Systems Command
Richard L. Kennedy
Allvac
Frederick J. Lisy
Orbital Research Incorporated
Frederick Edward Schmidt
Engineering Systems Incorporated
Richard D. Sisson, Jr.
Worcester Polytechnic Institute
Lawrence C. Wagner
Texas Instruments

Members of the ASM Handbook Committee (2004–2005)

Jeffrey A. Hawk
(Chair 2005–; Member 1997–)
U.S. Department of Energy
Larry D. Hanke (1994–)
(Vice Chair 2005–; Member 1994–)
Materials Evaluation and Engineering Inc.
David E. Alman (2002–)
U.S. Department of Energy
Tim Cheek (2004–)
International Truck & Engine Corporation
Lichun Leigh Chen (2002–)
Engineered Materials Solutions
Craig V. Darragh (1989–)
The Timken Company
Henry E. Fairman (1993–)
Cincinnati Metallurgical Consultants
Michael A. Hollis (2003–)
Delphi Corporation
Dennis D. Huffman (1982–)
The Timken Company (retired)
Kent L. Johnson (1999–)
Engineering Systems Inc.
Ann Kelly (2004–)
Los Alamos National Laboratory
Donald R. Lesuer (1999–)
Lawrence Livermore National Laboratory
Huimin Liu (1999–)
Ford Motor Company
Alan T. Male (2003–)
University of Kentucky
William L. Mankins (1989–)
Metallurgical Services Inc.
Toby Padfield (2004–)
ZF Sachs Automotive of America
Srikanth Raghunathan (1999–)
Nanomat Inc.
Karl P. Staudhammer (1997–)
Los Alamos National Laboratory
Kenneth B. Tator (1991–)
KTA-Tator Inc.
George F. Vander Voort (1997–)
Buehler Ltd.

Previous Chairs of the ASM Handbook Committee

R.J. Austin
(1992–1994) (Member 1984–1985)
L.B. Case
(1931–1933) (Member 1927–1933)
T.D. Cooper
(1984–1986) (Member 1981–1986)
C.V. Darragh
(1999–2002) (Member 1989–)
E.O. Dixon
(1952–1954) (Member 1947–1955)
R.L. Dowdell
(1938–1939) (Member 1935–1939)
Henry E. Fairman
(2002–2004) (Member 1993–)
M.M. Gauthier
(1997–1998) (Member 1990–2000)
J.P. Gill
(1937) (Member 1934–1937)
J.D. Graham
(1966–1968) (Member 1961–1970)
J.F. Harper
(1923–1926) (Member 1923–1926)
C.H. Herty, Jr.
(1934–1936) (Member 1930–1936)
D.D. Huffman
(1986–1990) (Member 1982–)
J.B. Johnson
(1948–1951) (Member 1944–1951)
L.J. Korb
(1983) (Member 1978–1983)
R.W.E. Leiter
(1962–1963) (Member 1955–1958, 1960–1964)
G.V. Luerssen
(1943–1947) (Member 1942–1947)
G.N. Maniar
(1979–1980) (Member 1974–1980)
W.L. Mankins
(1994–1997) (Member 1989–)
J.L. McCall
(1982) (Member 1977–1982)
W.J. Merten
(1927–1930) (Member 1923–1933)
D.L. Olson
(1990–1992) (Member 1982–1988, 1989–1992)
N.E. Promisel
(1955–1961) (Member 1954–1963)
G.J. Shubat
(1973–1975) (Member 1966–1975)
W.A. Stadtler
(1969–1972) (Member 1962–1972)
R. Ward
(1976–1978) (Member 1972–1978)
M.G.H. Wells
(1981) (Member 1976–1981)
D.J. Wright
(1964–1965) (Member 1959–1967)

Authors and Contributors

Safaa J. Alhassan
International Lead Zinc Research Organization, Inc.

Jim Alexander
Consultant

Robert Baboian
RB Corrosion Service

Brian Baker
Special Metals Corporation

James P. Bennett
U.S. Department of Energy, Albany Research Center

R. Bhaskaran
Central Electrochemical Research Institute

Malcolm Blair
Steel Founders' Society of America

Arthur Cohen
Arthur Cohen & Associates

Terry W. Cowley
DuPont

Paul Crook
Haynes International, Inc.

Jim Crum
Special Metals Corporation

P.K. Datta
Advanced Materials Research Institute, Northumbria University

Terry DeBold
Carpenter Technology Corporation

Larry DeLashmit
Polycorp, Ltd.

Christopher Dellacorte
NASA Glenn Research Center

Manish Dighe
Hi TecMetal Group

H.L. Du
Advanced Materials Research Institute, Northumbria University

Peter Elliott
Corrosion & Materials Consultancy, Inc.

F.B. Fletcher
Mittal Steel USA

Lee Flower
Haynes International, Inc.

Dennis S. Fox
NASA Glenn Research Center

James D. Fritz
TMR Stainless

Ronald A. Graham
ATI Wah Chang, Allegheny Technologies

John F. Grubb
ATI-Allegheny Ludlum

Robert J. Hanrahan, Jr.
Los Alamos National Laboratory

Warren J. Haws
Brush Wellman, Inc.

L.H. Hihara
The University of Hawaii at Manoa

D.R. Holmes
ATI Wah Chang, Allegheny Technologies

Nathan S. Jacobson
NASA Glenn Research Center

M. Jayachandran
H.H. The Rajah's College

Allen R. Jones
Atotech

G. Kaufman
Kaufman Associates, Ltd.

Pradip Khaladkar
DuPont

Dwaine Klarstrom
Haynes International, Inc.

Toshiaki Kodama
Nakabohtec Corrosion Protection Co., Ltd.

Kyei-Sing Kwong
U.S. Department of Energy, Albany Research Center

Jay W. Larson
American Iron and Steel Institute

Kang N. Lee
Cleveland State University

Jennifer A. Lillard
Los Alamos National Laboratory

Ashley Lucente
University of Virginia

Steve Matthews
Haynes International

Tapio Mäntylä
Tampere University of Technology

Sabrina Meck
Haynes International, Inc.

Bert Moniz
DuPont

Raymond W. Monroe
Steel Founders' Society of America

Thomas G. Oakwood
Consultant

Elizabeth J. Opila
NASA Glenn Research Center

George Oprea
University of British Columbia

N. Palaniswamy
Central Electrochemical Research Institute

William C. Panarese
Portland Cement Association

Raul Rebak
Lawrence Livermore Laboratory

N.S. Rengaswamy
Central Electrochemical Research Institute

Michel Rigaud
CIREP, École Polytecnique Montreal

Mark Rowe
Haynes International, Inc.

Ronald W. Schutz
RMI Titanium Company

John R. Scully
University of Virginia

C. Ramadeva Shasty
International Steel Group, Inc.

Barbara A. Shaw
Pennsylvania State University

David C. Silverman
Argentum Solutions, Inc.

James L. Smialek
NASA Glenn Research Center

Gaylord D. Smith
Special Metals Corporation

Thomas C. Spence
Flowserve Corporation

Krishna Srivastava
Haynes International, Inc.

Bill Stahl
DuPont Performance Elastomers

Richard C. Sutherlin
ATI Wah Chang, Allegheny Technologies

Hiroyuki Tanabe
Dai Nippon Toryo Company

Kenneth B. Tator
KTA-Tator, Inc.

Tommy Taylor
DuPont Performance Elastomers

Mikko Uusitalo
Metso Powdermet Oy

Stephen M. Winder
U.K. Software Services

Ryan C. Wolfe
Pennsylvania State University

Jim Wu
Deloro Stellite, Inc.

Te-Lin Yau
Te-Lin Yau Consultancy

X. Gregory Zhang
Teck Cominco Metals Ltd.

Reviewers

Robert L. Bratton
Nuclear Materials Disposition and Engineering

Juan Bustillos
Dow Chemical

Gary Carinci
TMR Stainless

Tim Cheek
International Truck & Engine Corporation

L. Chen
Engineered Materials Solutions

Desmond C. Cook
Old Dominion University

Larry Craigie
American Composites Manufacturers Association

Craig Darragh
The Timken Company

Subodh Das

Kenneth deSouza
Dofasco, Inc.

John B. Dion
BAE Systems

David Dombrowski
Los Alamos National Laboratory

Richard W. Drisko

John DuPont
Lehigh University

Henry E. Fairman
Cincinnati Metallurgical Consultants

Robert Filipek
AGH University of Science and Technology

John J. Goetz
Thielsch Engineering

Jeffrey A. Hawk
U.S. Department of Energy Albany Research Center

M. Swyn Hocking
Imperial College London

Merv Howells
Honeywell

Dennis Huffman
The Timken Company

Russell H. Jones
U.S. Department of Energy
Pacific Northwest National Laboratory

Don Kelley
Dow Chemical

Don Kim

Dale Kingseed

David Kolman
U.S. Department of Energy
Los Alamos National Laboratory

Roger A. LaBoube
University of Missouri-Rolla

Lionel Lemay
National Ready-Mixed Concrete Association

William LeVan
Cast Iron Soil Pipe Institute

Scott Lillard
U.S. Department of Energy
Los Alamos National Laboratory

Graham McCartney
University of Nottingham

Karthik H. Obla
National Ready-Mixed Concrete Association

Toby V. Padfield
ZF Sachs Automotive of America

Steven J. Pawel
U.S. Department of Energy
Oak Ridge National Laboratory

G. Louis Powell
Y-12 National Security Complex

Raul Rebak
U.S. Department of Energy
Lawrence Livermore National Laboratory

Michael Renner
Bayer Technology Services GmbH

Elwin L. Rooy
Elwin L. Rooy and Associates

B.J. Sanders
BJS and Associates

Mark Schilling

William L. Silence

Donald Snyder
Atotech R&D Worldwide

David L. Sponseller
OMNI Metals Laboratory, Inc.

Karl P. Staudhammer
U.S. Department of Energy
Los Alamos National Laboratory

Oscar Tavares
Lafarge North America Inc.

Michael E. Tavary
Dow Chemical

John Tundermann

Elma van der Lingen
MINTEK

David J. Willis
BlueScope Steel

Roger Wildt
RW Consulting Group

Gregory Zhang
Teck Cominco

Contents

ASM International is the society for materials engineers and scientists, a worldwide network dedicated to advancing industry, technology, and applications of metals and materials.

ASM International, Materials Park, Ohio, USA
www.asminternational.org

Publication title	Product code
ASM Handbook, Volume 13B, Corrosion: Materials	06508G

To order products from ASM International:

Online Visit www.asminternational.org/bookstore

Telephone 1-800-336-5152 (US) or 1-440-338-5151 (Outside US)

Fax 1-440-338-4634

Mail Customer Service, ASM International
9639 Kinsman Rd, Materials Park, Ohio 44073, USA

Email CustomerService@asminternational.org

In Europe American Technical Publishers Ltd.
27-29 Knowl Piece, Wilbury Way, Hitchin Hertfordshire SG4 0SX, United Kingdom
Telephone: 01462 437933 (account holders), 01462 431525 (credit card)
www.ameritech.co.uk

In Japan Neutrino Inc.
Takahashi Bldg., 44-3 Fuda 1-chome, Chofu-Shi, Tokyo 182 Japan
Telephone: 81 (0) 424 84 5550

ASM Handbook, Volume 13B: Corrosion: Materials
S.D. Cramer, B.S. Covino, Jr., editors, p3-4
DOI: 10.1361/asmhba0003804

Introduction to Corrosion of Ferrous Metals

Jay W. Larson, American Iron and Steel Institute

DURABILITY IS A KEY FACTOR to the designers, manufacturers, and users of products made from ferrous metals, such as iron and steel. In the presence of moisture, ferrous metals are susceptible to corrosion. Therefore, care must be taken to shield these ferrous metals from moisture, protect them from corrosion in other ways, or make an allowance in the design for the eventual corrosion.

Industry Overview

Ferrous metals, by definition, are metals that contain primarily iron and may have small amounts of other elements added to give desired properties. Iron is found in nature as iron ore, most of which is iron oxide. Metallic iron is produced by removal of oxygen from iron oxide. The most common process is to first reduce the ore in a blast furnace to an impure iron containing a high percentage of carbon, known as pig iron, which is further refined into steel by means of a basic oxygen furnace to reduce the carbon content to the appropriate level. Worldwide in 2003, 67% of steel was produced by this integrated process, and 33% came from remelting scrap steel in electric arc furnaces (Ref 1).

Worldwide production of steel products has increased from under 200 million metric tonnes in 1950 to over 1 billion metric tonnes in 2004. Iron and steel products are produced throughout the world; however, 90% of world production is concentrated in twenty countries. The steel industry is undergoing significant consolidation and restructuring; nevertheless, the industry remains highly fragmented, with the largest producer representing less than 5% of the global market. The industry is characterized by relatively large imbalances between production and consumption in many regions. The former USSR is the most dramatic example of this, producing 11.2% of the world supply yet consuming only 3.7%. On the other hand, North America imports approximately 20 to 25% of the steel it consumes. Therefore, the impact of imports and trade policies has become a key industry driver (Ref 1).

In North America, groundbreaking labor/management agreements have facilitated industry consolidation. Broadened job scopes and streamlining of management personnel have produced dramatic operational efficiencies and increased worker involvement. Swiftly changing customer demands and expanding global competition have triggered a sweeping transformation and modernization of the North American steel industry. Today, the North American steel industry is in the world's top tier of productivity, environmental responsibility, competitiveness, and product quality. Labor productivity has more than tripled since the early 1980s, going from an average of 10.1 man-hours per finished ton to an average of 3 man-hours per finished ton in 2004. Many North American plants are producing a ton of finished steel in less than 1 man-hour (Ref 2).

Steel Products and Characteristics

Steel products include hot rolled shapes, bars, rods, wire, hot and cold rolled sheet and strip, plates, tin mill products, metallic-coated sheet, steel tubes, castings, and forgings. These steel products, in turn, are used in most industries, including construction, automotive, industrial equipment, energy, shipping, containers, appliances, agriculture, fasteners, and furniture.

The end-use products cover a wide spectrum, such as railway track, concrete reinforcing bars, structural framing, machinery, pipelines, conduit, storage tanks, building and bridge structures, guard rail, culverts, roofing and siding, deck, doors, and food containers. Steel is selected for these varied uses in varied environments because it offers many desirable characteristics, including lightness, high strength and stiffness, adaptability, ease of prefabrication and mass production, dimensional stability (nonshrinking and noncreeping at ambient temperatures), durability (termite-proof, rot-proof), abrasion resistance, availability, uniform quality, and noncombustibility. Further, because most ferrous metals are magnetic, they are very easy to separate from the waste stream. This important property allows steel to be the most recycled material, which is done for economic as well as environmental reasons. This combination of factors often results in steel being the most cost-effective solution, either on a first cost or life-cycle cost basis.

However, cost only comes into play in the materials selection process after the customer's functional requirements, including durability, have been met. This requirement may be explicit, in the form of a specification or regulation, or subjective. Expectations for low maintenance and long life, crucial for a favorable life-cycle cost evaluation, require that claims about long-term durability can be substantiated through previous experience or test data.

Role of Corrosion

In the presence of moisture, iron combines with atmospheric oxygen or dissolved oxygen to form a hydrated iron oxide, commonly called rust. The oxide is a solid that retains the same general form as the metal from which it is formed but is porous and somewhat bulkier and relatively weak and brittle. Corrosion is undesirable because of its adverse effect on strength, serviceability, and aesthetics. For the same chemical analysis and heat treatment, corrosion resistance is not generally dependent on whether the steel is cast or is subject to further forging or rolling.

Methods that are used to prevent or control the rusting of ferrous materials that are detailed in this section include:

- Alloying so that the iron will be chemically resistant to corrosion, resulting in materials such as stainless steel sheet, alloy castings, and weathering steels
- Coating with a material that will react with the corroding substances more readily than the iron does and thus, while being consumed, protects the steel, such as hot dip galvanized or aluminum-zinc-coated sheet
- Covering with an impermeable surface coating so that air and water cannot reach the iron, such as organic coating systems and tin plating

It is important to determine the suitability of the aforementioned methods for the end-use application. Cathodic protection is often the most economic approach to protection of underground and underwater steel structures. This topic is addressed in the article "Cathodic Protection" in *ASM Handbook,* Volume 13A, 2003.

Corrosion resistance can be an important consideration in the design of products and the selection of materials. Naturally, customer specifications or regulations must be met. However, providing increased life expectancy, assuring lower maintenance costs or claims, and increasing consumer confidence can provide a competitive advantage and increased market share. Growth areas for ferrous materials include the use of stainless steels for food manufacturing and storage equipment, weathering steel (nickel alloy) plate for bridge girders, and Galvalume* (aluminum-zinc alloy) sheet for low-slope structural standing seam roofing.

The long-term durability of properly design and protected steel products has led to significant growth opportunities for steel, including prepainted, metallic-coated sheet steel for high-slope architectural and residential roofing, and galvanized steel framing for light commercial, industrial, and residential framing. Increased durability also allows steel to defend against competitive threats of other materials in established markets, such as canned foods and automotive.

REFERENCES

1. *2004 Edition World Steel in Figures,* International Iron and Steel Institute, 2004
2. "Fact Sheet—The New Steel Industry," American Iron and Steel Institute, 2004

*Galvalume is a registered trademark of BIEC International or its licensed producers.

ASM Handbook, Volume 13B: Corrosion: Materials
S.D. Cramer, B.S. Covino, Jr., editors, p5-10
DOI: 10.1361/asmhba0003805

Corrosion of Wrought Carbon Steels

Toshiaki Kodama, Nakabohtec Corrosion Protection Co., Ltd.

CARBON STEEL is the most widely used engineering material, so the cost of dealing with corrosion of carbon steels is a significant portion of the total cost of corrosion. The latest report describes the annual total cost of metallic corrosion in the United States and the preventive strategies for optimal corrosion management (Ref 1). The total direct cost of corrosion is estimated at $276 billion per year, which is 3.1% of the 1998 U.S. gross domestic product. This report is summarized in the article "Direct Cost of Corrosion in the United States" in *ASM Handbook,* Volume 13A, 2003. This cost was determined by analyzing 26 industrial sectors in which corrosion is known to exist and by extrapolating the results for a nationwide estimate. In Japan, the cost of corrosion was estimated in 1997 by three methods. One of them, the Hoar method, estimated for 1997 that the cost was 5258 billion yen (40.5 billion U.S. dollars), which was equivalent to 1.02% of the gross national product of Japan. The estimated total was doubled when indirect cost was taken into consideration (Ref 2).

Corrosion control methods are classified as materials modification, isolation of steels from aggressive environments, and environmental mitigation, including cathodic protection (CP). Carbon or mild steels are, by their nature, of limited alloy content, usually less than 2% by weight for the total of all additions. Unfortunately, these levels of addition do not generally produce any remarkable changes in general corrosion behavior. The first category of corrosion control (alloying or structural modification) is therefore generally not effective for carbon steels. However, weathering steels, which contain small additions of copper, chromium, nickel, and/or phosphorus, do produce significant reductions in the atmospheric corrosion rate in certain environments. See the article "Corrosion of Weathering Steels" in this Volume. At the levels present in low-alloy steels, the usual impurities have no significant effect on corrosion rate in neutral waters, concrete, or soils.

The isolation of metals from the corrosive environment is the most commonly applied technique for the protection of carbon steels. Isolation methods include painting, coating, and lining. Surveys have revealed that most of the cost for the protection of metallic materials is for paintings and metallic coatings. The corrosion loss survey in Japan showed that among corrosion preventive measures in industries, 58 and 26% of the total cost are directed to painting and other surface treatments, respectively, while expenditure for corrosion-resistant materials such as stainless steels is 11% of the total.

The third category, environmental mitigation, includes inhibitor addition, deaeration of water, and CP, of which the economic impact is rather small (approximately 2%). Its effectiveness, however, is pronounced when it is employed in conjunction with coatings, as in the cathodic protection of polymer-coated pipelines.

Atmospheric Corrosion

The atmospheric corrosion of carbon steel is understood by considering the electrochemical process that occurs in aqueous media. If carbon steel is placed in a completely dry atmosphere in ambient temperature, oxide film growth is so small that corrosion rate would be virtually negligible. Ideally, a clean metal surface is free from a water layer below the dewpoint. However, in actual conditions, water condensation occurs even below the dewpoint because of the deposition of saline aerosols to the metal surface or by the deposition of solid particles such as dust, soil, and corrosion products. Magnesium chloride ($MgCl_2$) in seawater is a prime factor for water film formation because of its deliquescent nature. The relative humidity (RH) in equilibrium with solid $MgCl_2$ is 33%, meaning that a metal surface contaminated with saline aerosols becomes wet at 33% RH. Owing to capillary condensation, wetting also occurs at a RH below the dewpoint in the presence of deposited solid substance. Atmospheric corrosion of metals proceeds under a water film through aqueous electrochemical process, even in an apparently dry atmosphere. Thus, by International Organization for Standardization (ISO) 9223 (Ref 3), the definition of time of wetness (TOW) is given as time in hours per year (h/yr) when RH > 80% and the temperature, T, > 0 °C (32 °F).

Corrosion Film Formation and Breakdown. The corrosion of iron in the atmosphere proceeds by the formation of hydrated oxides. The formation of oxyhydroxides is the principal anodic process of rusting:

$$Fe + 2H_2O \rightarrow FeOOH + 3H^+ + 3e^- (anodic)$$

The group of ferric oxyhydroxides includes α-FeOOH (goethite), β-FeOOH (akaganeite), and γ-FeOOH (lepidocrocite). Among the three types of FeOOH, goethite is the most stable and is the main constituent of rust in atmospheric corrosion. Lepidocrocite is also prevalent but is transformed to more stable goethite during long exposure. β-FeOOH occurs only in chloride-laden marine and coastal environments (Ref 4–6). Additionally, amorphous ferric products $Fe(OH)_3$ and γ-Fe_2O_3 are observed.

The cathodic process involved with rusting is almost exclusively the reduction of oxygen:

$$O_2 + 2H_2O + 4e^- \rightarrow 4OH^-$$

The ferric oxyhydroxides are stable in dry atmospheres. They are, however, readily reduced to a mixed ferric/ferrous state, most notably to ferrous ion (Fe^{2+}) and magnetite (Fe_3O_4), by an electrochemical reaction in which ferric hydroxides act as an oxidant and the anodic reaction is oxidation of iron to Fe_3O_4. To make the situation worse, the reduced ferrous ion is more soluble in water than the ferric ions. The readiness of oxides (including oxyhydroxides) to form the more soluble ferrous ions is the principal reason for poor protectiveness and easy spallation of iron rust. This cycle of redox reaction in rust is known as the Evans cycle (Ref 7–9).

Atmospheric Factors. Because there is a substantial variation in the corrosion rates of carbon steels at different atmospheric-test locations, it is only logical to ask which factors contribute to these differences. Although the prediction of corrosivity is still not precise, it appears that TOW or RH, temperature, the levels of chloride deposition, and the presence of atmospheric pollutants such as SO_x, NO_x, and H^+ (acid rain) are important factors. In ISO 9224 (Ref 10), the corrosivity of atmosphere is ranked (C1 to C5 in the order of severity), which is described in Table 1.

Time of Wetness. Because atmospheric corrosion is an electrochemical process, the presence of an electrolyte is required. This should not be taken to mean that the steel surface must

be soaked in water; a very thin adsorbed film of water is all that is required. During an actual exposure, the metal spends some portion of the time awash with water because of rain or splashing and a portion of the time covered with a thin adsorbed water film. Dewing, the state in which a metal surface is covered with a thin water film, is more pronounced in the case when the metal surface is contaminated with the deposit of saline particles. Because TOW is defined as the time (h/yr) the RH is greater than 80% at an air temperature higher than 0 °C (32 °F), it can be calculated directly from monitored data of the temperature and RH.

Sulfur dioxide (SO_2) resulting from the combustion of fossil fuel is the most aggressive pollutant to metallic corrosion. In major developed countries, both total emission and pollutant concentration have decreased drastically, although in developing countries where coal is the major source of energy, the decrease is less remarkable. A summary of air quality change in the United States is reported by its Environmental Protection Agency (EPA) and is shown in Table 2. Average SO_2 ambient concentrations have decreased 54% from 1983 to 2002 and 39% over the more recent 10 year period of 1993 to 2002, while SO_2 emissions decreased 33 and 31%, respectively. Nitrogen compounds, in the form of NO_x, also tend to accelerate atmospheric attack. Statistics by the EPA showed slower improvement of NO_x compared with SO_x. The average pollutant concentration level in 2002 in the United States is 0.01 ppm for SO_x and 0.02 ppm for NO_x. In actual atmospheric corrosion data analysis, NO_x attracts less attention because NO_x influences corrosion less. In countries where coal is the major power source, SO_x in the atmosphere is still the key factor affecting atmospheric corrosion, although the highest corrosion is segregated in industrial areas (Ref 11).

Table 1 ISO corrosivity categories from first year exposure data

	Corrosion rate		
Corrosivity category	$g/m^2 \cdot yr$	mm/yr	mils/yr
C1	0–10	0–1.3	0–51.2
C2	10–200	1.3–25	51.2–985
C3	200–400	25–50	985–1970
C4	400–650	50–80	1970–3150
C5	650–1500	80–200	3150–7880

Source: Ref 10

Table 2 Changes in air quality and total emission in the United States

Pollutant	1983–2002	1993–2002
Change in air quality, %		
NO_x	−21	−11
SO_x	−54	−39
Change in emissions, %		
NO_x	−15	−12
SO_x	−33	−31

Negative numbers indicate improvement. Source: Ref 11

Atmospheric salinity distinctly accelerates atmospheric corrosion of steels. The deposited saline particle enhances surface electrolyte formation, owing to the deliquescence of $MgCl_2$. In marine and coastal areas, metal surfaces become and remain wet even when the RH is low. Figure 1 shows the relationship between the chloride deposition rate onto the steel surface and the corrosion rate of carbon steel (Ref 12). At an active anode front, chloride forms ferrous chloride complexes, which tend to be unstable (soluble), resulting in further stimulation of corrosive attack. The ferrous chloride is oxidized to ferric hydroxide (rust) on contact with air. By this process, chloride ions are released and again supply the active anode front. Figure 2 shows the morphological change of rust as a function of chloride pickup (Ref 13). With increasing chloride contamination in rust, flaky and large-grained rusts are formed, resulting in the spallation of rust and the acceleration of the corrosion rate.

In ISO 9226, TOW, SO_2 level (P), and airborne salinity (S) are defined as the most influential factors in atmospheric corrosion, allowing the corrosivity categories of Table 1 to be estimated (Ref 14). The TOW is classified to five levels, T1 to T5 (Table 3), and SO_2 and salinity are each divided into four classes of P0 to P3 and S0 to S3, respectively (Table 4). The corrosivity category, ranging from C1 to C5, is assessed by

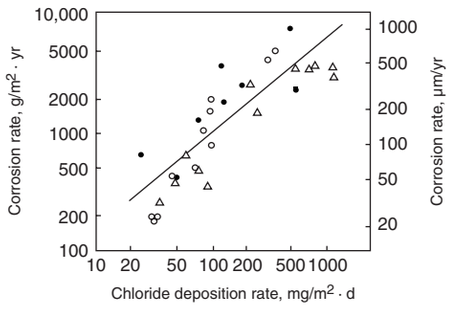

Fig. 1 Influence of chloride deposition on the corrosion rate of steel. Test data from three sources. Source: Ref 12

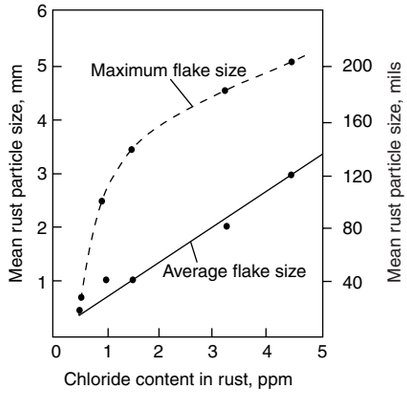

Fig. 2 Dependence of rust particle flake size on the chloride content in the rust. Source: Ref 13

the T, P, and S classifications, and the estimation is listed in Table 5.

Another factor to consider is the effect of microclimates. In large steel structures, local temperature differences create local wet and dry cycles. In atmospheric exposure tests of uncoated steels, local attack is influenced by the exposure direction (skyward or groundward) and the rinsing of deposited salts by rain (open-air or sheltered conditions). In a coastal environment, higher corrosion rates are observed on the groundward surface and in the sheltered condition, where there is a smaller chance for rinsing of salt deposits by rain.

Effects of Alloying Additions. Because carbon steels are, by definition, not highly alloyed, it is not surprising that most grades do not exhibit large differences in atmospheric corrosion rate. Nevertheless, alloying can make changes in the atmospheric corrosion rate of carbon steel (Fig. 3). The elements generally found to be most beneficial in this regard are copper, nickel, silicon, chromium, and phosphorus. Commercial products of steels alloyed with the aforementioned elements are weathering steels (Ref 16, 17). Although phosphorus is beneficial from the point of corrosion, phosphorus-bearing weathering steels are not common because of the deteriorated weldability. In the initial stage of atmospheric exposure, those containing beneficial elements show no distinct difference from ordinary carbon steels until the corrosion rate decreases to a level of several micrometers per year. These elements are effective because a more compact and less permeable rust is formed. Mechanisms for the improved protectiveness are thought to be refinement of rust grain size, a trend to amorphous ferric hydroxide, and selective ion

Table 3 ISO wetness classification

	Time of wetness	
Wetness class	h/yr	%
T1	< 10	< 0.1
T2	10–250	0.1–3
T3	250–2600	3–30
T4	2600–5200	30–60
T5	> 5200	> 60

Source: Ref 14

Table 4 ISO sulfur dioxide and chloride classification

Class	Deposition rate, $mg/m^2 \cdot d$	Concentration, mg/m^3
Sulfur dioxide(a)		
P0	< 10	< 12
P1	10–35	12–40
P2	36–80	41–90
P3	81–200	91–250
Chloride(b)		
S0	< 3	...
S1	3–60	...
S2	61–300	...
S3	> 300	...

(a) Sulfation plate measurement. (b) Chloride candle measurement

permeation through rust. Weathering steels appear most effective in an industrial atmosphere rich in SO_2 but less effective in salt-laden marine and coastal environments.

Kinetics of Atmospheric Corrosion. The rate of atmospheric corrosion of steels is not constant with time but usually decreases as the length of exposure increases. This fact indicates the difficulty in using most of the published atmospheric-corrosion data in any quantitative way. Much of the published data consists of weight loss due to corrosion averaged over the time of exposure. Such corrosion rate calculations are misleading, especially when the exposure time is short, because the long-term rate of attack can be considerably lower.

The atmospheric corrosion rate law is most commonly expressed in the form (Ref 18, 19):

$$\Delta W = Kt^n \qquad \text{(Eq 1)}$$

where ΔW is the loss in mass or thickness of metal due to corrosion, expressed in milligrams or millimeters, and t is the exposure time in years. K is an empirical constant indicating the loss in the first year, and n is another empirical constant representing the protectiveness of corrosion products on metal. Because the values of K and n depend on the exposure site, environmental factors, and the alloying composition, a great deal of work must be done before Eq 1 can be used in real applications. If the rust layer is not protective, a linear rate law ($n = 1$) applies, although it is rare in atmospheric corrosion. The case of $n = 1/2$ is often encountered in high-temperature oxidation, suggesting that the corrosion rate is determined by mass transport through the corrosion product. Actually, cases of $n < 1/2$ exist in mild atmospheres. Compared with carbon steels, weathering steels show very low n-values—normally, a value less than $1/2$.

Equation 1 can be useful in estimating long-term corrosion behavior from as little as 2 years of data (Ref 18), although 3 to 4 years of data provide better extrapolations. Most importantly, Eq 1 points out that it is impossible to describe the extent or rate of corrosion under atmospheric conditions with a single parameter. When the results of a several-year exposure test are condensed to a single value, such as the average loss per year or the total loss for the exposure period, one cannot estimate the values of the kinetic parameters governing the system. Without the values of these parameters, the extrapolation of the results to longer exposure periods is quite unreliable. When good estimates for the kinetic parameters are available, extrapolations to 7 or 8 year performance from 1 and 2 year data have been found to agree within 5% of the observed performance (Ref 18). In the salt-laden atmosphere of a coastal region, a break away from Eq 1 occurs, even for weathering steels; in this case, flaky rusts are formed due to the aggressive nature of the chloride ion.

Table 5 ISO corrosivity category estimation by environmental factors

Chloride classification(b)	T1			T2			T3			T4			T5		
	S0–S1	S2	S3	S0–S1	S2	S3	S0–S1	S2	S3	S0–S1	S2	S3	S0–S1	S2	S3
P0, P1	C1	C1	C1–C2	C1	C2	C3–C4	C2–C3	C3–C4	C4	C3	C4	C5	C3–C4	C5	C5
P2	C1	C1	C1–C2	C1–C2	C2–C3	C3–C4	C3–C4	C3–C4	C4–C5	C4	C4	C5	C4–C5	C5	C5
P3	C1–C2	C1–C2	C2	C2	C3	C4	C4	C4–C5	C5	C5	C5	C5	C5	C5	C5

Definition of corrosivity categories C1 to C5 is given in Table 1. See Table 3 for wetness classifications T1–T5. See Table 4 for SO_2 classifications S0–S3.

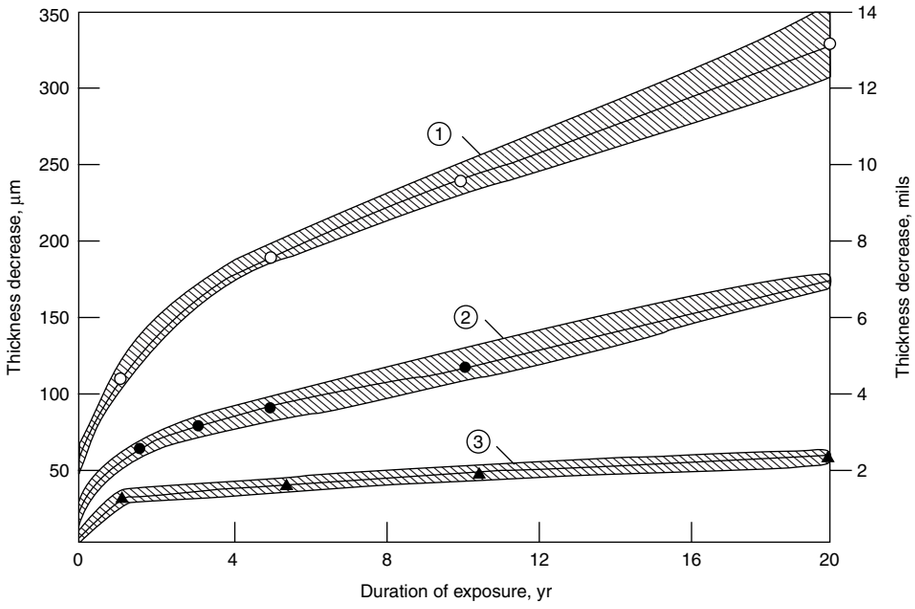

Fig. 3 Corrosion of steels exposed to an industrial atmosphere. Curve 1, unalloyed; curve 2, copper alloyed; curve 3, weathering steel. Source: Ref 15

Aqueous Corrosion

Compared with nonferrous metals, such as copper and zinc, the corrosion behavior of carbon steel is less sensitive to water quality. This is due to the fact that anodic products on carbon steels are not protective, and therefore, corrosion rate is controlled by the cathodic process, that is, the supply of dissolved oxygen.

Freshwater Corrosion. In stagnant water, cathodic current for dissolved oxygen (DO) is 10 $\mu A/cm^2$ under saturated conditions in water at ordinary temperature. Because corrosion is an electrochemical process, the anodic current or corrosion rate of iron is equivalent to DO reduction. The corresponding corrosion rate for iron is approximately 0.1 mm/yr (3.9 mils/yr). The classical data by Whitman are still valid as a first-order approximation. In the pH range of 4 to 10, the corrosion rate for carbon steel is constant in soft waters (Fig. 4). Below pH 4, corrosion is accelerated due to hydrogen evolution as a cathodic reaction. Above pH 10, corrosion is suppressed owing to passivation, the formation of a very thin, invisible oxide film on the steel surface (Ref 22, 23). In waters containing high bicarbonate and chloride ions, the corrosion rate is maximized at a pH of approximately 8.0, which is due to the increased pitting tendency with increased pH and decreased buffer capacity in carbonate equilibria (Fig. 5).

The determining nature of the cathodic rate is shown in Fig. 6, where the effect of corrosion rate as a function of flow velocity and salt concentration is given. Curve 1 is for distilled water with 10 ppm chloride ion added (Ref 22, 23), and curve 2 is the result obtained for Tokyo city water with electrical conductivity of 250 μS/cm (Ref 24). In freshwaters, the corrosion rate

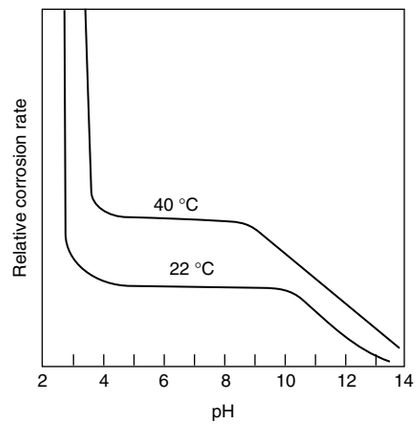

Fig. 4 Effect of pH and temperature on the corrosion rate of carbon steel in soft water. Source: Ref 21

increases with increasing flow velocity to a critical value, above which steel is passivated due to a sufficient supply of oxygen for stable oxide film to be created. With increasing salt concentration, passivation is less liable to occur.

In hard water that contains high calcium (Ca^{2+}) and bicarbonate (HCO_3^-) ions, calcium carbonate ($CaCO_3$) film may be used for corrosion protection if its formation is properly controlled. For the prediction of calcareous film formation, the Langelier index analysis is used (Ref 20, 25), in which ionic equilibrium of $CaCO_3$ deposition is expressed as a function of Ca^{2+}, HCO_3^- concentrations, pH, ionic strength, and temperature. In freshwater of normal pH range, bicarbonate ion is predominant among carbonates. Increases dissolved Ca^{2+} and HCO_3^-, which favors $CaCO_3$ deposition (scaling tendency). An increase in pH accelerates the dissociation of bicarbonate to carbonate (CO_3^{2-}), resulting in the enhancement of the activity of CO_3^{2-}. The solubility of $CaCO_3$ is decreased with increasing temperature, indicating that $CaCO_3$ deposits on high-temperature zones, such as heat-exchanger surfaces, may lead to overheating in the system. Corrosion and excessive scaling are conflicting phenomena; thus, water treatment mitigation is necessary to avoid both.

Most alloying does not cause differences in the corrosion rate of carbon steel in freshwater. Such elements as copper, which is beneficial for atmospheric corrosion, do not improve freshwater corrosion resistance, because compact adherent film is not established under fully wet conditions without a dry cycle. For the protection of steel pipes for plumbing, galvanizing is the most common method. However, in the last two decades, steel pipes with polymer lining are replacing galvanized piping.

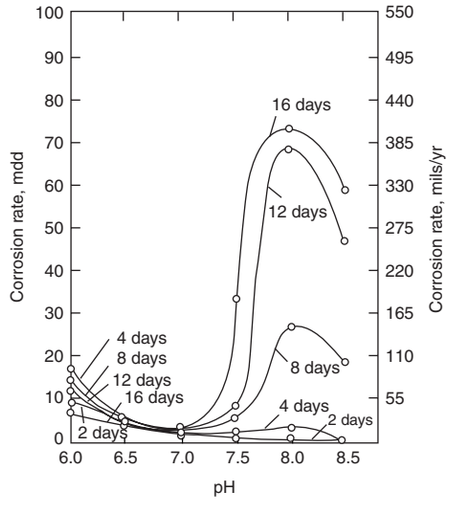

Fig. 5 Corrosion rate (mdd, milligrams per square decimeter per day) as a function of pH in hard water containing high bicarbonate ion. Pitting tendency is increased at pH values higher than 7.5. Source: Ref 22 and 23

Seawater Corrosion. Chlorinity of seawater is loosely defined as the total amount (in kilograms) of halide ions (mostly chloride) dissolved in 1 kg (2.2 lb) of seawater. Salinity is the corresponding total amount of salts dissolved in seawater and is expressed as:

$$\text{Salinity} = 1.80655 \times \text{Chlorinity}$$

Although there exist small variations in salinity, the proportions of major constituents of seawater do not change. Surprisingly, the pH of surface seawater globally is quite constant, at approximately 8.2. The corrosion rates of carbon steel specimens completely immersed in seawater do not appear to depend on the geographical location of the test site; therefore, by inference, the mean temperature does not appear to play an important role directly. Because the corrosion rate in seawater is controlled by the diffusion of DO, it is of the same level as freshwater (approximately 0.1 mm/yr, or 4 mils/yr) but is dependent on the flow velocity. Water temperature does affect the amount of DO available.

The corrosion rates on steel piling surfaces normally vary vertically by zone. The profile for steel sheet piling, averaged for several harbor installations, is shown in Fig. 7 (Ref 26). In general, the maximum reduction in metal thickness occurs in the splash zone immediately above the mean high-water level. A significant loss usually occurs a short way below mean low water in the continuously submerged zone. With the exception of those few cases where scour is a factor, the least affected zone is usually found below the mudline, with higher losses at the water-mudline interface. Another low-loss area exists in the tidal zone approximately halfway between mean high-water and mean low-water levels. The minimum corrosion within the tidal zone and the secondary peak just below the tidal zone are due to differential aeration (Ref 27). The continuously submerged zones of steel structures can be efficiently protected by means of CP.

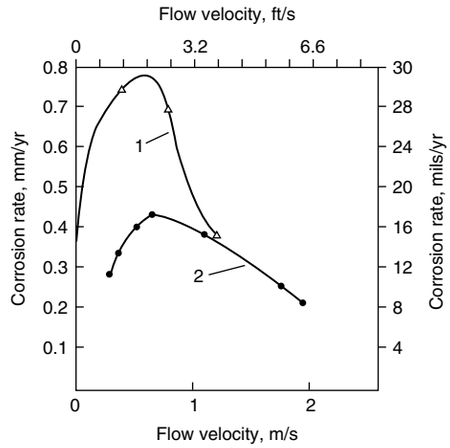

Fig. 6 Corrosion rate of carbon steel as a function of flow velocity in freshwater. Curve 1, distilled water with 10 ppm chloride; duration, 14 d. Curve 2, Tokyo city water; duration, 67 d. Source: Ref 24

High electric conductance of seawater favors the use of CP. Calcareous films grow on cathodically polarized surface, because seawater is slightly oversaturated with $CaCO_3$. On the cathode surface, pH is increased, favoring the deposition of $CaCO_3$. While the initial cathodic current required for steel in stagnant seawater is 150 mA/m^2 (14 mA/ft^2), it can drop to 30 mA/m^2 (3 mA/ft^2), owing to the protective nature of calcareous film. The protection of steel in the tidal and splash zones is more difficult but can be attained by various types of coatings and coverings consisting of polymers, metals, and mortar.

In actual marine exposures, periods of rapid flow from tidal motion may not be effective, because the slack periods at reversal may allow marine organisms to attach themselves to the metal surface. If these organisms can survive the subsequent high flow, then a growth on the exposed surface can develop. This effectively reduces the velocity of seawater at the metal-water interface so that bulk flow rates are no longer rate-determining.

Soil Corrosion

The behavior of carbon steel in soil depends primarily on the nature of the soil and certain other environmental factors, such as the availability of moisture and oxygen. These factors affect the corrosion rate of carbon steel. The evaluation of soil aggressivity was first proposed by the National Bureau of Standards (now the National Institute of Standards and Technology) (Ref 28), then Deutsche Industrie-Normen (DIN) (Ref 29, 30) and American National Standards Institute/American Water Works Association (ANSI/AWWA) (Ref 31). Factors that influence aggressivity are soil type, resistivity, water content, pH, buffer capacity, sulfides, neutral salts, sulfates, groundwater, horizontal homogeneity, vertical homogeneity, and electrode potential.

The water content, together with the oxygen and carbon dioxide contents, are major corrosion-determining factors. The supply of oxygen is comparatively large above the groundwater table but is considerably less below it and is influenced by the type of soil. It is high in sand but low in clay. The different aeration characteristics may lead to significant corrosion problems due to the creation of oxygen concentration cells.

The pH value of soil is determined by the carbonic acid/bicarbonate ratio, minerals, organic acids, and by industrial wastes or acid rain. In the normal pH range of 5 to 8, factors other than pH have greater influence on the corrosion of steel.

Resistivity of soil is the most frequently used parameter for determining its aggressiveness. Resistivity also influences the localized nature of corrosion. The risk of localized corrosion (pitting) is high if the soil resistivity is lower than 1000 Ω·cm. The low resistivity favors the ability of macrocell current to flow between portions

exposed to different electrolytes and different levels of aeration. The redox potential in the soil becomes nobler with the increase of oxygen concentration in the soil. Similarly, a difference in pH generates a macrocell. Steel in contact with a strong alkali, such as concrete, becomes passivated, leading to the ennoblement of the electrode potential. It is the difference in redox potential that can lead to the macrocorrosion cell.

Rating values are given in DIN 50929-3 for the aforementioned twelve items of soil quality (Ref 29, 30). By summing the rating numbers, the soil aggressivity, the tendency for macrocell corrosion, and other factors are evaluated. Similarly, ANSI/AWWA gives a point system for predicting soil corrosivity, which is shown in Table 6 (Ref 31).

The corrosion rate in soil is expressed as:

$$W = at^m \qquad \text{(Eq 2)}$$

where W is either the average mass loss or maximum pit depth, t is time of exposure, and a and m are constants that depend on the specific soil corrosion situation. Equation 2 is of the same form as Eq 1 for atmospheric corrosion.

Sulfate-reducing bacteria (such as *Desulfovibrio desulfuricans*), which occur under anaerobic conditions such as in deep soil layers, catalyze the reduction of sulfate (SO_4^{2-})ion to sulfide (S^{2-}), forming iron sulfide as a corrosion product. Anaerobic bacterial corrosion is more serious when it is combined with a differential aeration cell, in which the anaerobic zone works as a local anode.

Steel structures buried in the ground, such as pipelines, provide a better electrical conductor than the soil for stray return currents from electric rail systems, electrical grounding equipment, and CP systems on nearby pipes. Accelerating corrosion occurs at the point where the current leaves the pipe to the earth.

Corrosion in Concrete

The environment provided by good-quality concrete to steel reinforcement is one of high alkalinity due to the presence of the hydroxides of sodium, potassium, and calcium produced during the hydration reactions. Sound concrete gives a pH value higher than 13.0. In such an environment, steel is protected by passive oxide films. The standard ASTM C 876-91 gives electrochemical means of predicting corrosion of reinforcing steel in concrete (Ref 32). The criteria for corrosion are given as follows when the electrode potential of the reinforcing steel (E) is measured in volts referenced to the copper/copper sulfate electrode (V_{CSE}):

- If $E > -0.2$ V_{CSE}, there is a 90% probability of no steel corrosion.
- If -0.2 $V_{CSE} > E > -0.35$ V_{CSE}, corrosion activity is uncertain.
- If $E < -0.35$ V_{CSE}, corrosion occurs with 90% probability.

It should be noted that the protection is achieved only when the electrode potential is higher than a critical value, which contrasts the case of protection of steel in seawater or soil where protection is attained at potentials below a critical value. This reflects the passive nature of the uncorroded steel surface in concrete. Corrosion starts on the reinforcement if the passive film is removed or depassivated by the reduced alkalinity of its surroundings or by the attack of chloride ions. The former is caused by the neutralization action of mortar by carbon dioxide in air, by which calcium hydroxide in concrete is transformed into calcium carbonate. The depth of carbonation in a structure can be established by the use of a phenolphthalein indicator on the freshly exposed material.

Another type of deterioration of concrete is caused by alkali aggregate reaction, where free alkali oxides, namely sodium and potassium oxide, in concrete react with reactive silica or carbonates in aggregates to form alkali silicates

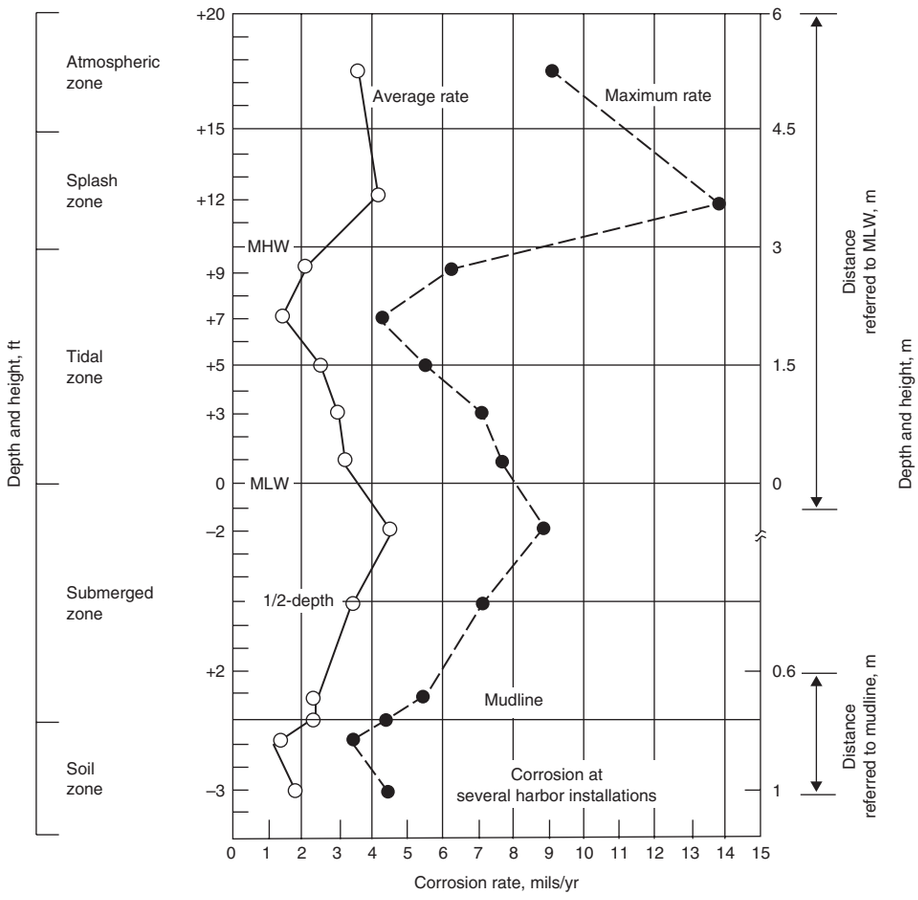

Fig. 7 Corrosion rate profile of steel sheet piling as a function of height. MLW, mean low water. MHW, mean high water. Source: Ref 26

Table 6 American National Standards Institute/American Water Works Association point system for predicting soil corrosivity

When the point total of a soil in the following scale is equal to or higher than 10, corrosion protective measures, such as cathodic protection, are recommended for cast iron alloys.

Soil parameter	Points
Resistivity, Ω·cm	
<700	10
700–1000	8
1000–1200	5
1200–1500	2
1500–2000	1
>2000	0
pH	
0–2	5
2–4	3
4–6.5	0
6.5–7.5	0
7.5–8.5	0
>8.5	3
Redox potential, mV	
>100	0
50–100	3.5
0–50	4
<0	5
Sulfides	
Positive	3.5
Trace	2
Negative	0
Moisture	
Poor drainage, continuously wet	2
Fair drainage, generally moist	1
Good drainage, generally dry	0

that absorb moisture, resulting in volume expansion and crack formation in concrete. Current practices to mitigate the detrimental effects of alkali-silica reactivity include the use of nonreactive aggregates, reducing the alkali content of the concrete by using low-alkali cement where available, and by using supplementary cementing materials or blended cements proven by testing to control the reaction. Supplementary cementing materials include fly ash; ground, granulated blast furnace slag; silica fume; and natural pozzolans. See the article " Environmental Performance of Concrete" in this Volume.

Chloride ions may enter the set concrete from external sources, such as seawater or deicing salt. The concentration of chloride ions required to initiate and maintain corrosion depends on the alkalinity. It has been shown that there is an almost linear relationship between hydroxyl ion concentration and the respective threshold level of the chloride. Depassivation by chloride starts as the result of breakdown of the film, similar to the pitting corrosion on stainless steels. Although chloride attack starts at potentials higher than a critical value, the electrochemical potential drops in the propagation stage of corrosion, which leads to the reduced potential (E) in corrode zones. This, in turn, can result in staining of the concrete by rust and spalling of the cover due to the volume increase associated with the conversion of iron to iron hydroxide.

Surprisingly, the steel in mortar is free from corrosion when the concrete structure is fully submerged in seawater. Complete deaeration is achieved in secluded seawater in mortar after the lapse of time, because diffusion of oxygen is sufficiently low under an unstirred condition. For marine concrete structures, corrosion is the most severe in the splash zone and the atmospheric zone.

The permeability of concrete is important in determining the extent to which aggressive external substances can attack the steel. A thick concrete cover of low permeability is likely to prevent chloride ions from an external source from reaching the steel and causing depassivation. Where an adequate depth of cover is difficult to achieve, additional protection may be required for the embedded steel. The steel reinforcement itself may be protected by a metallic coating, such as galvanizing, epoxy resin, or stainless steel cladding. In extreme circumstances of marine environments, the addition of a calcium nitrite inhibitor to concrete is recommended. The most secure method of protection is CP, although there still exist difficulties in the installation of suitable insoluble anodes.

Boiler Service

Corrosion in steel boilers is a special case of aqueous corrosion that involves elevated temperatures. Corrosion control is attained most often by means of water treatment. In modern boiler systems, DO is first removed mechanically and then by chemically scavenging the remainder. The mechanical degasification is typically carried out with vacuum degasifiers that reduce oxygen levels to less than 0.5 to 1.0 mg/L or with deaerating heaters that reduce oxygen concentration to the range of 0.005 to 0.010 mg/L. Even this small amount of oxygen is corrosive at boiler system temperatures and pressures. Removal of the last traces of oxygen is accomplished by treating the water with a reducing agent that serves as an oxygen scavenger. Hydrazine and sodium sulfite are widely used oxygen scavengers. In closed-loop systems, the initial oxygen supply of the water is rapidly consumed in the early stages of film formation, so that corrosion rates are usually not a problem. In non-closed-loop systems, deaeration is usually adequate for eliminating general corrosion problems.

Of more concern in boiler systems is the occurrence of pitting. In pitting corrosion, both DO and carbon dioxide (CO_2) promote attack. Deaeration is useful in stopping the oxygen attack, but CO_2 pitting is more effectively handled by maintaining an alkaline pH in the water. Surface deposits of corrosion products, mill scale, or even oil films have occasionally been implicated in the pitting attack of boilers. Another major source of corrosion in the condensate return piping is the presence of carbonic acid in the condensate. Natural and softened water contains quantities of HCO_3^- that tends to decompose into CO_2 gas at elevated temperature. Liberated CO_2 then dissolves in condensate to form carbonic acid in the pipes and metallic equipment, resulting in carbonic acid corrosion. The carbonic acid corrosion can be avoided by deionizing the supply water or by adding vapor-phase inhibitors.

REFERENCES

1. "Corrosion Cost and Preventive Strategies in the United States," FHWA-RD-01-156, supplement to *Mater. Perform,* Vol 3, July 2002
2. Survey of Corrosion Cost in Japan, *Zairyo-to-Kankyo (Corros. Eng.),* Vol 50, 2001, p 490
3. "Corrosion of Metals and Alloys—Corrosivity of Atmospheres—Classification," ISO 9223 : 1992, International Organization for Standardization
4. T. Misawa, *Corros. Sci.,* Vol 13, 1972, p 648
5. K. Hashimoto and T. Misawa, *Corros. Sci.,* Vol 13, 1982, p 229
6. P. Refait and J.M.R. Genin, *Corros. Sci.,* Vol 33, 1993, p 797
7. U.R. Evans, *Nature,* Vol 206, 1968, p 980
8. I. Suzuki, Y. Hisamatsu, and N. Masuko, *J. Electrochem. Soc.,* Vol 127, 1980, p 2211
9. M. Stratmann, K. Bohnenkamp, and T. Ramchandran, *Corros. Sci.,* Vol 27, 1987, p 905
10. "Corrosion of Metals and Alloys—Corrosivity of Atmospheres—Guiding Values for the Corrosivity Categories," ISO 9224: 1992, International Organization for Standardization
11. "National Air Quality and Emissions Trends Report, 2003 Special Studies Edition," U.S. Environmental Protection Agency, 2003
12. S. Feliu, M. Morcillo, and B. Chico, *Corrosion,* Vol 55, 1999 p 883
13. A. Raman, *Degradation of Metals in Atmosphere,* STP 965, ASTM, 988, p 16
14. "Corrosion of Metals and Alloys—Corrosivity of Atmospheres—Determination of Corrosion Rate of Standard Specimens for the Evaluation of Corrosivity," ISO 9226: 1992, International Organization for Standardization
15. G. Becker, D. Dhingra, and C. Thoma, *Arch. Eisenhüttenwes.,* Vol 40 (No. 4), 1969, p 341
16. C.P. Larrabee and S.K. Coburn, *Proc. First Int. Cong. on Metallic Corrosion,* Butterworths, 1961, p 276
17. H.E. Townsend, *Corrosion,* Vol 57, 2001, p 497
18. R.A. Legault and A.C. Preban, Kinetics of the Atmospheric Corrosion of Low-Alloy Steels in an Industrial Environment, *Corrosion,* Vol 31, 1975, p 117
19. R.A. Legault and V.P. Pearson, *Kinetics of Atmospheric Corrosion of Galvanized Steel,* STP 646, ASTM
20. W.F. Langelier, *J. Am. Water Works Assoc.,* Vol 38, 1946, p 169
21. S.G. Whitman, L. Long, and H. Ywang, *Ind. Eng. Chem.,* Vol 18,1926, p 363
22. T.E. Larson and R.V. Skold, *Corrosion,* Vol 14, 1958, p 285
23. V. Skold and T.E. Larson, *Corrosion,* Vol 13, 1957, p 139t
24. T. Fujii, T. Kodama, and H. Baba, *Boshku Gijutsu (Corros. Eng.),* Vol 31, 1982, p 637
25. S.T. Powell, H.E. Bacon, and J.R. Hull, *Ind. Eng. Chem.,* Vol 37, 1945, p 842
26. W.E. Edwards, Marine Corrosion: Its Cause and Care, *Proceedings of the Eighth Annual Appalachian Underground Corrosion Short Course,* Technical Bulletin 69, 1963, p 486
27. H.A. Humble, *Corrosion,* Vol 5, 1988, p 171
28. M. Romanoff, "Underground Corrosion," Circular 579, National Bureau of Standards, 1957
29. "Corrosion of Metals," DIN 50929-3, Deutsche Industrie-Normen, 1985
30. W. Baeckmann and W. Schwenk, *Handbuch des KathodisherKorrosion Schultes,* Vol 55, Verlag, Chemie GmbH, 1971 (in German)
31. "American National Standard for Polyethylene Encasement for Ductile-Iron Pipe Systems," ANSI/AWWA C-105/A21.5-99, American National Standards Institute/ American Water Works Association, 1972
32. "Standard Test Method for Half-Cell Potentials of Uncoated Reinforcing Steel in Concrete," C 876-91, *Annual Book of ASTM Standards,* ASTM, 1999

ASM Handbook, Volume 13B: Corrosion: Materials
S.D. Cramer, B.S. Covino, Jr., editors, p11-27
DOI: 10.1361/asmhba0003806

Corrosion of Wrought Low-Alloy Steels

Revised by Thomas G. Oakwood, Consultant

LOW-ALLOY STEELS comprise a category of ferrous materials that exhibit mechanical properties superior to those of ordinary carbon steels as the result of additions of such alloying elements as chromium, nickel, and molybdenum. Total alloy content of low-alloy steels can range from 0.5 to 1% and up to levels just below that of stainless steels. For many low-alloy steels, the primary function of the alloying elements is to increase hardenability in order to optimize mechanical properties and toughness after heat treatment. In some cases, however, alloying additions are used to reduce environmental degradation under certain specified service conditions.

Low-alloy steels are used in a broad spectrum of applications. In some cases, corrosion resistance is a major factor in alloy selection; in other applications, it is only a minor consideration. The information available on the corrosion resistance of low-alloy steels is end-use oriented and often addresses rather specialized types of corrosion. As a result, this article emphasizes those applications where corrosion resistance is either a major factor in steel selection or where available data have shown that variations in alloy content or steel processing affect resistance to corrosion.

For many applications, steels with a relatively low alloy content are used. Such steels include those designated by ASTM International and the Society of Automotive Engineers (SAE) as standard alloy steels and modifications of these grades. In addition, potential standard (PS) grades, formerly SAE PS and EX (experimental) grades, are applicable, along with high-strength low-alloy and structural alloy steels. Small additions of some alloying elements will enhance corrosion resistance in moderately corrosive environments. In severe environments, however, the corrosion resistance of this group of steels is often no better than that of carbon steel (see the article "Corrosion of Wrought Carbon Steels" in this Volume).

Other applications require more highly alloyed steels that, in addition to achieving the necessary mechanical properties, provide increased resistance to specific types of corrosion in certain environments. In this group of steels, corrosion resistance is an important factor in alloy design (see the article "Corrosion of Wrought Stainless Steels" in this Volume).

An extensive collection of data on low-alloy steel products, which encompasses compositions, mechanical and physical properties, applications, and service characteristics, can be found in *Properties and Selection: Irons, Steels, and High-Performance Alloys,* Volume 1 of *ASM Handbook,* 1990. Information on the metallographic preparation and microstructural interpretation of alloy steels is available in *Metallography and Microstructures,* Volume 9 of *ASM Handbook,* 1985. Finally, fracture characteristics of alloy steels are reviewed in *Fractography,* Volume 12 of *ASM Handbook,* 1987.

Corrosive Environments Encountered in the Use of Alloy Steels

Atmospheric corrosion is a factor in many applications of low-alloy steels. It is the principal form of corrosion of concern in the automotive, off-highway equipment, machinery, construction, and aerospace industries. The atmospheric corrosion resistance of various alloy steels, as well as the role of various alloying elements, depends on the severity of the environment in rural, industrial, urban, and marine applications. Some industries that use low-alloy steels present certain specific corrosion problems. These include the production, refining, and distribution of oil and gas; energy conversion systems involving the combustion of fossil fuels; the chemical-process industries; and certain marine applications.

During the drilling and primary production of oil and gas, low-alloy steels are exposed to crude oil and gas formations containing varying amounts of hydrogen sulfide (H_2S), carbon dioxide (CO_2), water, and chloride compounds. High pressures and temperatures are also encountered in some cases. Refining operations subject low-alloy steels to environments containing both hydrogen and hydrocarbons. Transmission and distribution of oil and gas expose pipelines and piping systems to environments containing varying amounts of many of the constituents mentioned previously.

In energy conversion systems, contaminants in coal, oil, and natural gas result in the accelerated attack of low-alloy steels at elevated temperatures. In steam-generating electric power plants, corrosion due to impurities in boiler feedwater and in high-pressure high-temperature steam needs to be addressed.

Low-alloy steels used in the construction of chemical-processing plants are subject to corrosion from a wide variety of environments. Compounds of chlorine, sulfur, ammonia (NH_3), and acids and alkalis are typical.

Finally, low-alloy steels are often used in marine environments involving direct contact with seawater. Applications include ship construction and offshore drilling structures and equipment.

Atmospheric Corrosion Resistance of Low-Alloy Steels

The atmospheric corrosion resistance of low-alloy steels is a function of the specific environment and steel composition. The effects of various alloying elements on corrosion resistance and data on specific low-alloy steel grades provide a guide for the selection of a low-alloy steel based on overall alloy content.

Table 1 lists some of the results of a study of 270 high-strength low-alloy steels (Ref 1). Experimental heats of steel involving systematic combinations of chromium, copper, nickel, silicon, and phosphorus were tested to determine their individual and joint contributions to corrosion resistance. These data were developed over 15.5 years in three environments: industrial (Kearny, NJ), semirural (South Bend, PA), and marine (Kure Beach, NC). The data show that the long-term atmospheric corrosion of carbon steel can be reduced with a small addition of copper. Additions of nickel are also effective, and chromium in sufficient amounts is helpful if copper is present. The maximum

resistance to corrosion was obtained in this study when alloy contents were raised to their highest levels.

Figure 1 summarizes some of the results from industrial environments (Ref 1). The carbon steel corrosion rate became constant after approximately 5 years. The corrosion rate of the copper steel leveled off to a constant value after approximately 3 years, and the high-strength low-alloy steel, which uses several alloy elements, exhibited a constant rate after approximately 2 years. Eventually, corrosion of the high-strength low-alloy steel virtually ceased. Table 2 compares the corrosion behavior of carbon steel, a copper steel, and ASTM types A242, A588, A514, and A517 low-alloy steels in a variety of environments (Ref 1). It is evident that the low-alloy steels exhibit significantly better performance than either carbon steel or the structural copper steel.

Although these data provide good estimates of average corrosion behavior, it is important to note that corrosion rates can increase significantly in severe environments. Table 3 lists corrosion rates for several steels exposed to various atmospheres in chemical plants (Ref 2). Comparison of these data with the industrial atmosphere data shown in Table 2 illustrates the significant increase in corrosion rate associated with severe environments. Table 3 also demonstrates the effectiveness of increased alloy content on corrosion resistance.

Protective coatings provide significant additional protection from atmospheric corrosion. Well-cleaned, primed, and painted steel can give good service in many applications (see the article

Table 1 Effect of composition on 15.5 year atmospheric corrosion of high-strength low-alloy steels

Selected alloying elements, %					Average reduction in thickness					
					Industrial(a)		Semirural(b)		Moderate marine(c)	
Cu	Ni	Cr	Si	P	μm	mils	μm	mils	μm	mils
0.01	...	...	...	...	731	28.8	312	12.3	1320	52
0.04	...	...	...	...	224	8.8	201	7.9	363	14.3
0.24	...	...	...	...	155	6.1	163	6.4	284	11.2
0.008	1	...	...	...	155	6.1	132	5.2	244	9.6
0.2	1	...	...	...	112	4.4	117	4.6	203	8.0
0.01	...	0.61	...	...	1060	41.7	419	16.5	401(d)	15.8(d)
0.2	...	0.63	...	...	117	4.6	145	5.7	229	9.0(d)
0.1	...	1.3	...	...	419	16.5	287	11.3	465	18.3(d)
0.22	...	1.3	...	...	89	3.5	114	4.5	...	...
0.012	...	...	0.22	...	373	14.7	257	10.1	546	21.5
0.22	...	...	0.20	...	152	6.0	155	6.1	251	9.9
0.02	...	...	...	0.06	198	7.8	175	6.9	358	14.1
0.21	...	...	...	0.06	124	4.9	130	5.1	231	9.1
0.01	1	0.62	0.26	0.08	86	3.4	89	3.5	130	5.1
0.2	1	0.61	0.17	0.1	58	2.3	71	2.8	102	4.0

(a) Kearny, NJ. (b) South Bend, PA. (c) Kure Beach, NC, approx. 250 m (800 ft) from ocean. (d) Estimated. Source: Ref 1

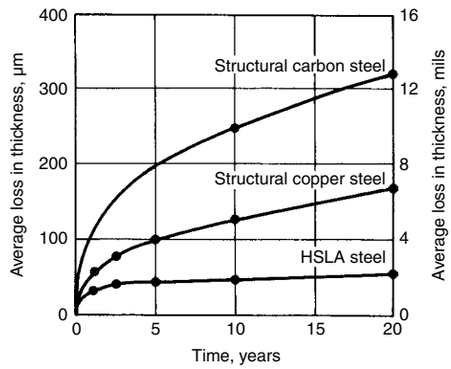

Fig. 1 Atmospheric corrosion versus time in a semi-industrial or industrial environment. HSLA, high-strength low-alloy. Source: Ref 1

Table 2 Corrosion of structural steels in various environments

Type of atmosphere	Time, years	Average reduction in thickness											
		Structural carbon steel		Structural copper steel		UNS K11510(a)		UNS K11430(b)		UNS K11630(c)		UNS K11576(d)	
		μm	mils	μm	mils	μm	mils	μm	mils	μm	mils	μm	mils
Industrial (Newark, NJ)	3.5	84	3.3	66	2.6	33	1.3	46	1.8	36	1.4	56	2.2
	7.5	104	4.1	81	3.2	38	1.5	53	2.1	43	1.7	...	...
	15.5	135	5.3	102	4.0	46	1.8	...	...	53	2.1	...	...
Semiindustrial (Monroeville, PA)	1.5	56	2.2	43	1.7	28	1.1	36	1.4	30	1.2	41	1.6
	3.5	94	3.7	64	2.5	30	1.2	53	2.1	36	1.4	61	2.4
	7.5	130	5.1	81	3.2	36	1.4	61	2.4	43	1.7	...	...
	15.5	185	7.3	119	4.7	46	1.8	...	...	46	1.8	...	...
Semiindustrial (South Bend, PA)	1.5	46	1.8	36	1.4	25	1.0	33	1.3	25	1.0	38	1.5
	3.5	74	2.9	56	2.2	33	1.3	48	1.9	38	1.5	61	2.4
	7.5	117	4.6	81	3.2	46	1.8	69	2.7	48	1.9	...	...
	15.5	178	7.0	122	4.8	56	2.2	...	...	64	2.5	...	...
Rural (Potter County, PA)	2.5	...	...	33	1.3	20	0.8	30	1.2	...	...	...	...
	3.5	51	2.0	43	1.7	28	1.1	36	1.4	30	1.2	46	1.8
	7.5	76	3.0	64	2.5	33	1.3	38	1.5	38	1.5	...	...
	15.5	119	4.7	97	3.8	36	1.4	...	...	51	2.0	...	...
Moderate marine (Kure Beach, NC, 250 m or 800 ft. from ocean)	0.5	23	0.9	20	0.8	15	0.6	20	0.8	18	0.7	25	1.0
	1.5	58	2.3	48	1.9	28	1.1	43	1.7	30	1.2	43	1.7
	3.5	124	4.9	84	3.3	46	1.8	64	2.5	48	1.9	56	2.2
	7.5	142	5.6	114	4.5	64	2.5	94	3.7	74	2.9	...	...
Severe marine (Kure Beach. NC, 25 m or 80 ft. from ocean)	0.5	183	7.2	109	4.3	56	2.2	97	3.8	28	1.1	18	0.7
	2.0	914	36.0	483	19.0	84	3.3	310	12.2	...	...	53	2.1
	3.5	1448	57.0	965	38.0	...	...	729	28.7	99	3.9	99	3.9
	5.0	...	(e)	...	(e)	493	19.4	986	38.8	127	5.0	...	...

(a) ASTM A242 (type 1). (b) ASTM A588 (grade A). (c) ASTM A514 (type B) and A517 (grade B). (d) ASTM A514 (type F) and A517 (grade F). (e) Specimen corroded completely away. Source: Ref 1

"Organic Coatings and Linings" in *ASM Handbook,* Volume 13A, 2003).

Galvanizing is used to provide protection under conditions in which the corrosive environment is severe. The zinc coating is anodic and corrodes preferentially; this protects exposed steel surfaces existing at cut edges or other areas where breaks in the coating are found. Corrosion resistance increases with coating thickness. In mild environments, galvanized steels can be used with no further treatment. In more severe environments, galvanized steels can be painted. In some cases, a prior treatment is used to provide a zinc phosphate conversion coating over the zinc coating to improve paint adherence. Information on zinc-base coatings can be found in the articles " Continuous Hot Dip Coatings," "Batch Process Hot Dip Galvanizing," and "Zinc-Rich Coatings" in *ASM Handbook,* Volume 13A, 2003.

Finally, electroplating, usually with chromium, can be used where decorative requirements must be met in addition to atmospheric corrosion resistance. See the article "Electroplated Coatings" in *ASM Handbook,* Volume 13A, 2003.

Corrosion of Low-Alloy Steels in Specific End-Use Environments

As with carbon steels, low-alloy steels are used in a wide variety of industrial applications. This section reviews four major industries that rely heavily on alloy steel products: oil and gas production, energy conversion systems, marine applications, and chemical processing.

Oil and Gas Production

Drilling and Primary Production. A variety of corrosion forms and mechanisms are encountered in the drilling and primary production of oil and gas. Most importantly, these include hydrogen-induced cracking, sulfide stress cracking (SSC), along with general corrosion, pitting corrosion, and corrosion fatigue.

In relatively shallow wells, lower-strength carbon or carbon-manganese steels can be employed in many of the components. Oil and gas deposits are often such that corrosion is limited to weight loss corrosion, which can be effectively controlled by chemical inhibition. For deep wells, however, high-strength low-alloy steels are usually required. Furthermore, very hostile environments are often encountered—high H_2S levels ranging from 28 to 46% concentration, temperatures to 200 °C (390 °F), along with pressures to 140 MPa (20 ksi). Also, H_2S is often found in combination with chloride-containing brines and CO_2, adding to the harshness of the environment.

Although chemical inhibition is used even in deep wells to control weight loss corrosion, the presence of H_2S can still result in the embrittlement of high-strength steels. The SSC phenomenon (Fig. 2) depends on H_2S concentration, acidity, salt concentrations, and temperature. Figures 3 and 4 illustrate typical SSC data for alloy steels used in oil field tubular components (Ref 3). The data shown are for high-strength steels now designated by the American Petroleum Institute in API Spec 5CT/ISO 11960 (Ref 4). Certain proprietary grades are also included.

As temperatures increase, some higher-strength steels can be used, and resistance to SSC can be maintained. However, higher-strength steels are generally more susceptible to SSC than lower-strength steels.

Sulfide stress cracking resistance is influenced by steel microstructure, which in turn depends on steel composition and heat treatment. It has been observed that a tempered martensitic structure provides better SSC resistance than other microstructures. Figure 5 illustrates this for a molybdenum-niobium modified SAE 4135 steel (compositions of the steels discussed in Fig. 5 to 7 are given in Table 4) (Ref 5). The data in Fig. 5(a) were developed by using simple beam specimens strained in three-point bending for

Table 3 Corrosion losses for high-strength low-alloy (HSLA) steels and carbon steel exposed to various atmospheres in chemical plants

			Average reduction in thickness					
			Carbon steel		A242 type 1 HSLA steel		A588 grade A HSLA steel	
Type of plant	Atmospheric constituents	Exposure period, months	µm	mils	µm	mils	µm	mils
Elastomers	Chlorine and sulfur compounds	6	33	1.3	20	0.8	23	0.9
		16	81	3.2	46	1.8	46	1.8
		24	122	4.8	51	2.0	48	1.9
Chlor-alkali	Moisture, lime, and soda ash	6	69	2.7	30	1.2	33	1.3
		12	119	4.7	43	1.7	46	1.8
		24	211	8.3	53	2.1	48	1.9
Chlor-alkali	Moisture, chlorides, and lime	6	104	4.1	61	2.4	69	2.7
		12	244	9.6	81	3.2	99	3.9
		24	478	18.8	145	5.7	188	7.4
Sulfur	Chlorides, sulfur, and sulfur compounds	6	394	15.5	188	7.4	239	9.4
		12	660	26.0	277	10.9	470	18.5
		24	1100	43.3	518	20.4	823	32.4
Petrochemical	Chlorides, hydrogen sulfide, and sulfur dioxide	6	51	2.0	23	0.9	30	1.2
		12	76	3.0	30	1.2	41	1.6
		24	86	3.4	30	1.2	48	1.9
Sulfuric acid	Sulfuric acid fumes	6	84	3.3	46	1.8	48	1.9
		12	114	4.5	53	2.1	56	2.2
		24	226	8.9	76	3.0	84	3.3
Chlorinated hydrocarbons	Chlorine compounds	6	137	5.4	46	1.8	46	1.8
		12	272	10.7	56	2.2	56	2.2
		24	1120	44.1	104	4.1	117	4.6
Petrochemical	Ammonia and ammonium acetate fumes	6	38	1.5	25	1.0	28	1.1
		12	58	2.3	33	1.3	48	1.9
		24	86	3.4	43	1.7	74	2.9
Detergent	Alkalis and organic compounds	6	20	0.8	15	0.6	15	0.6
		12	33	1.3	20	0.8	20	0.8
		24	48	1.9	23	0.9	25	1.0
Detergent	Sulfur compounds	6	30	1.2	15	0.6	23	0.9
		12	53	2.1	23	0.9	30	1.2
		24	81	3.2	23	0.9	30	1.2
Alkylation	Moisture, chlorides	8	460	18.1	292	11.5	297	11.7
		12	668	26.3	432	17.0	409	16.1
		36	1468	57.8	1016	40.0	1016	40.0
Hydrochloric acid	Chlorine, hydrochloric acid fumes	6	312	12.3	147	5.8	180	7.1
		12	640	25.2	345	13.6	396	15.6
		24	1265	49.8	640	25.2	803	31.6

Source: Ref 2

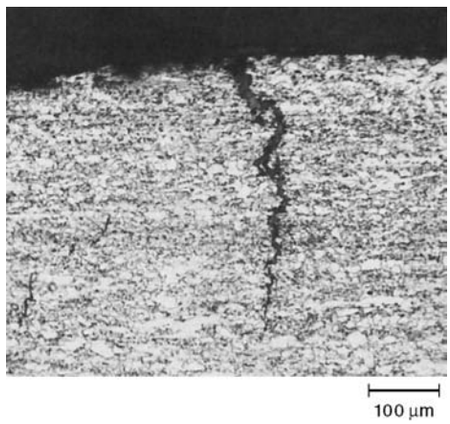

Fig. 2 Sulfide stress corrosion cracking in a low-alloy steel. Original magnification 100×

measuring a critical stress, S_c, and the data in Fig. 5(b) were obtained by testing double-cantilever beam specimens to determine a threshold stress intensity, K_{ISSC}. Thus, it is important to select an alloy steel that has sufficient hardenability to achieve 100% martensite for a given application.

Furthermore, proper tempering of martensite is essential in order to maximize SSC resistance. Figure 6 illustrates the effects of tempering temperature on SSC behavior (Ref 5). It is evident that higher tempering temperatures improve SSC performance. The presence of untempered martensite, however, is extremely detrimental to SSC resistance. This is illustrated in Fig. 7, which shows the effect of tempering above the Ac_1 temperature for molybdenum-niobium modified 4130 steels containing two levels of silicon (Ac_1 is the temperature at which martensite begins to transform to austenite) (Ref 5). Water quenching from above the Ac_1 temperature results in austenite transforming back to untempered martensite, with a subsequent loss in SSC resistance. It has also been found that the development of a fine prior-austenite grain size and the use of accelerated cooling rates after tempering improve SSC resistance. The necessity for adequate hardenability is quite evident when considering low-alloy steels for heavy section wellhead components. Figure 8 shows how the SSC resistance of conventional steels used in wellhead equipment can be improved through modifications in composition, which increase hardenability (Ref 6).

With the advent of enhanced oil recovery techniques, additional corrosion problems must be considered. Carbon dioxide injection is one method of displacing crude oil from a formation for increased recovery. This method involves development of CO_2 source wells, that is, those having large quantities of CO_2-containing gas. The gas from these wells is processed, transported to the production reservoir, and injected. Corrosion in source wells and in production wells results from the highly acidic environment created when CO_2 and water are present. The presence of chlorides, H_2S, and elevated temperature adds to the aggressiveness of the environment.

Figure 9 illustrates the complexities of corrosion in CO_2 environments (Ref 7). In Fig. 9(a), the effects of increasing CO_2 concentration on weight loss corrosion at 65 °C (150 °F) are shown. The lower-alloy steels show a slight increase in corrosion rate with increasing CO_2 concentration, but the higher-alloy materials show little or no dependence on CO_2 level. As chromium content increases, corrosion resistance improves at a given CO_2 level. At a temperature of 175 °C (350 °F), however, the corrosion resistance of the lower-alloy steels improves, but that of the higher-alloy steels remains the same or decreases (Fig. 9b). With the addition of significant amounts of chloride at 65 °C (150 °F), some of the higher-alloyed steels begin to show an increase in corrosion rate with increasing CO_2 level (Fig. 9c). An increase in chloride concentration, along with an increase in temperature, results in a significant increase in the corrosion rate of the more highly alloyed steels (Fig. 9d). Finally, if H_2S is present in CO_2-brine environments, Table 5 indicates that the corrosion rate of lower-alloy steels can be expected to increase (Ref 7).

The corrosion rates of various low-alloy steels in CO_2-brine-H_2S environments vary considerably with the specific environment encountered. As a result, control of the environment through chemical inhibition becomes an important tool, along with proper alloy selection, in reducing corrosion failures.

Petroleum Refining/Hydrocarbon Processing. A principal concern in petroleum refining and hydrocarbon processing is the problem of the interaction of hydrogen with the low-alloy steels used in these applications. Prolonged exposure to hydrogen, particularly at elevated temperatures, results in loss of ductility and premature failure. Figure 10 shows the delayed-failure characteristics of SAE 4340 steel resulting from cathodic charging of hydrogen (Ref 8). At higher tensile strengths, the effects of hydrogen become more severe.

The phenomenon often encountered in actual service is hydrogen attack. This involves the chemical reaction of hydrogen with metal carbides at elevated temperatures to form methane (CH_4). Because CH_4 cannot diffuse out of steel, an accumulation occurs, and this causes fissuring and blistering. The combined action of decarburization and fissuring results in loss of strength and ductility. The empirical

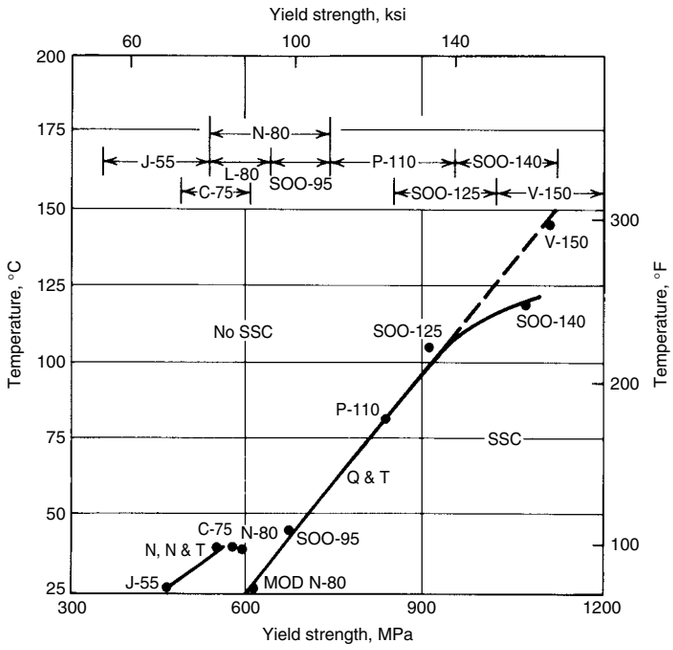

Fig. 3 Effect of temperature on sulfide stress cracking (SSC) of high-strength steels identified by American Petroleum Institute and proprietary designations. N, normalized; N & T, normalized and tempered; Q & T, quenched and tempered. Source: Ref 3

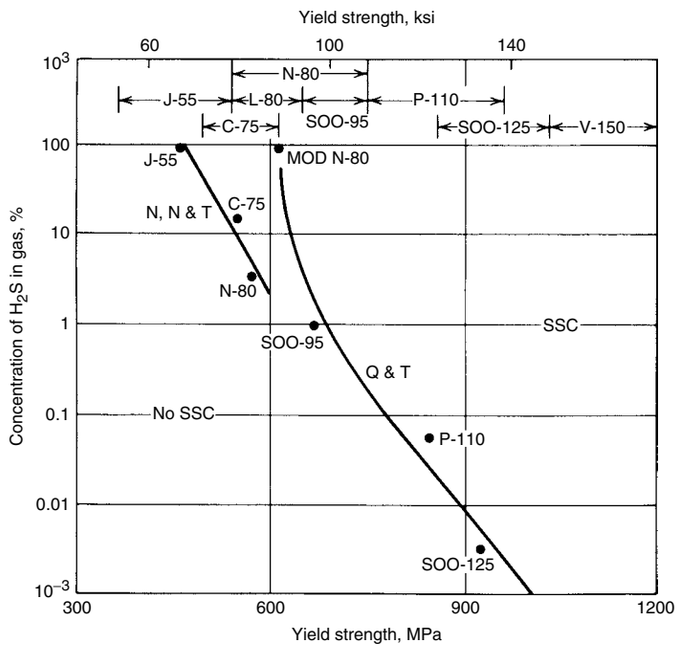

Fig. 4 Effect of H_2S concentration on sulfide stress cracking (SSC) of high-strength steels identified by American Petroleum Institute and proprietary designations. See Fig. 3 for definitions. Source: Ref 3

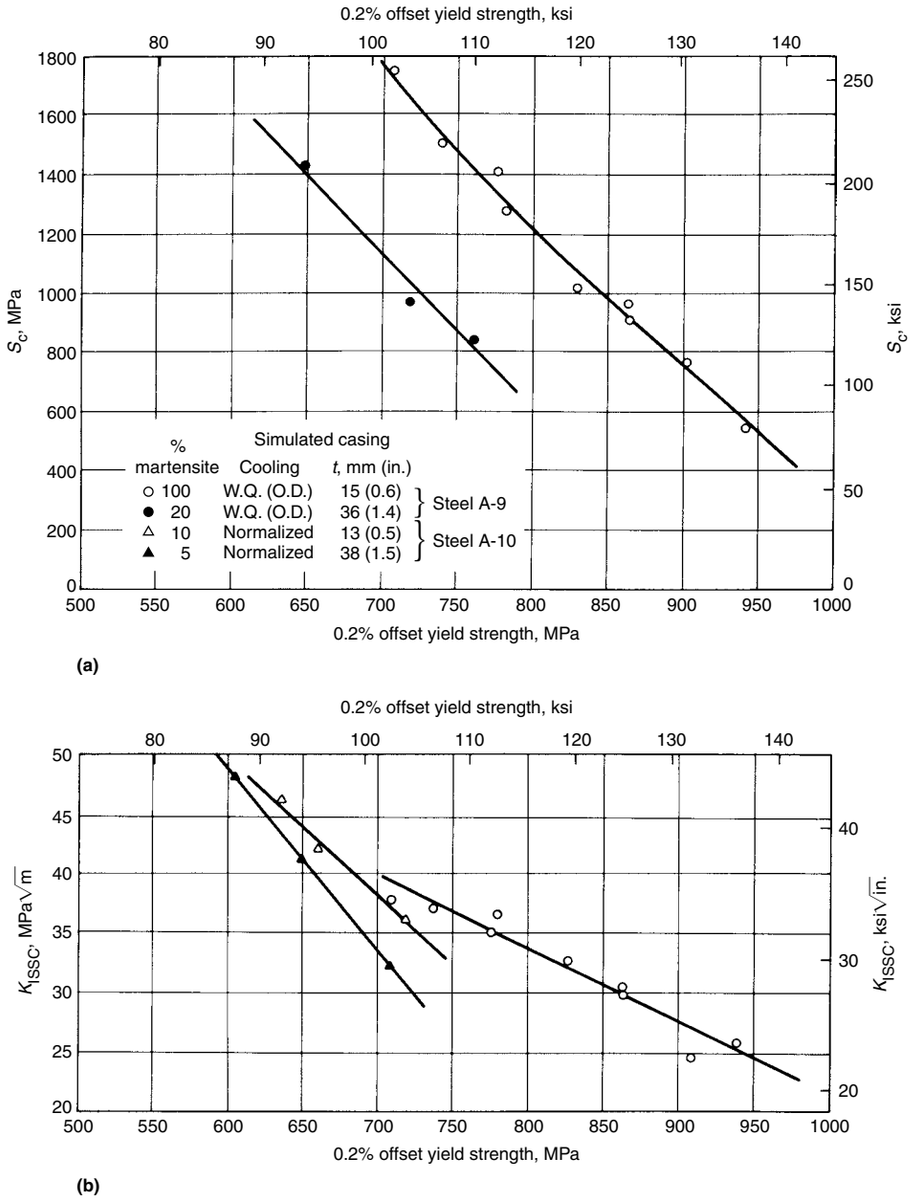

Fig. 5 Effect of yield strength on the critical stress, S_c, and sulfide fracture toughness, K_{ISSC}, of molybdenum-niobium modified 4135 steel cooled from the austenitizing temperature at different rates to produce a wide range of martensite contents and then tempered. W.Q. (O.D.), externally water quenched. (a) Bent-beam test. (b) Double-cantilever beam test (without salt). See Table 4 for steel compositions. Source: Ref 5

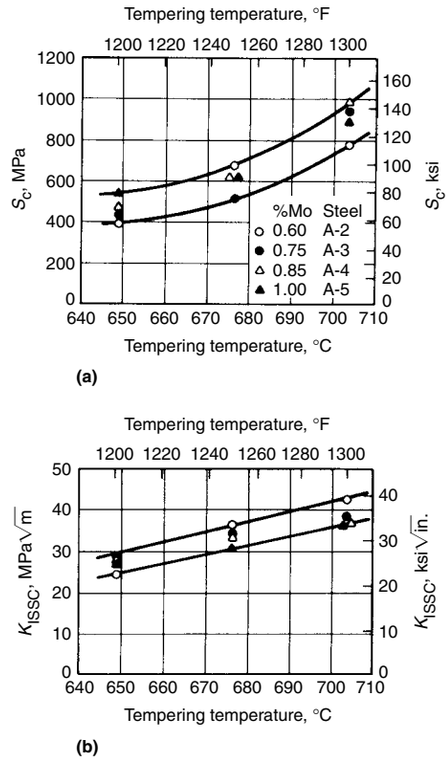

Fig. 6 Effect of temperature of a 1 h temper on the critical stress, S_c, and sulfide fracture toughness, K_{ISSC}, of molybdenum-niobium modified 4130 steels. (a) Bent-beam test. (b) Double-cantilever beam test. See Table 4 for steel compositions. Source: Ref 5

Table 4 Chemical compositions of the molybdenum-niobium modified 4130/4135 test steels discussed in Fig. 5 to 7

	Composition, wt%									
Steel code	C	Mn	Si	Cr	Mo	Nb	P	S	Al	N, ppm
A-2	0.34	0.74	0.39	1.06	0.60	0.035	0.030	0.022	0.12	208
A-3	0.31	0.73	0.39	1.05	0.75	0.036	0.034	0.021	0.16	166
A-4	0.32	0.74	0.39	1.04	0.85	0.035	0.027	0.026	0.16	138
A-5	0.32	0.74	0.40	1.05	0.98	0.036	0.027	0.025	0.17	148
A-9	0.34	0.68	0.38	1.00	0.75	0.034	0.025	0.027	ND	260
A-10	0.36	0.68	0.29	1.03	0.74	0.033	0.017	0.014	0.078	151
A-14	0.27	0.69	0.21	1.04	0.72	0.033	0.018	0.017	0.051	170
A-15	0.33	0.23	0.71	1.04	0.73	0.031	0.018	0.015	0.047	180

ND, not determined. Source: Ref 5

limits on the use of low-alloy steels commonly used in a hydrogen environment are shown in Fig. 11.

Oil and Gas Transmission. The transmission of oil and gas involves consideration of the corrosion problems associated with linepipe steels. In addition to carbon steels, high-strength low-alloy steels are often used in pipeline service. Atmospheric corrosion needs to be considered for exposed pipelines, and the corrosive actions of various soil formations must be addressed for underground pipelines. A summary of an extensive study of the corrosion encountered by various low-alloy steels in several different types of soils is presented in Fig. 12(a) and (b). It is evident that factors such as soil pH, resistivity, degree of aeration, and level of acidity have more bearing on the severity of corrosion encountered than the alloy content of the steel. In some cases, increasing alloy content has a beneficial effect, but in other cases, it does not. In general, the use of protective coatings and cathodic protection offers the best means of reducing the level of corrosive attack.

Linepipe steels can be susceptible to a specialized form of hydrogen damage when H_2S is present in oil and gas. This type of

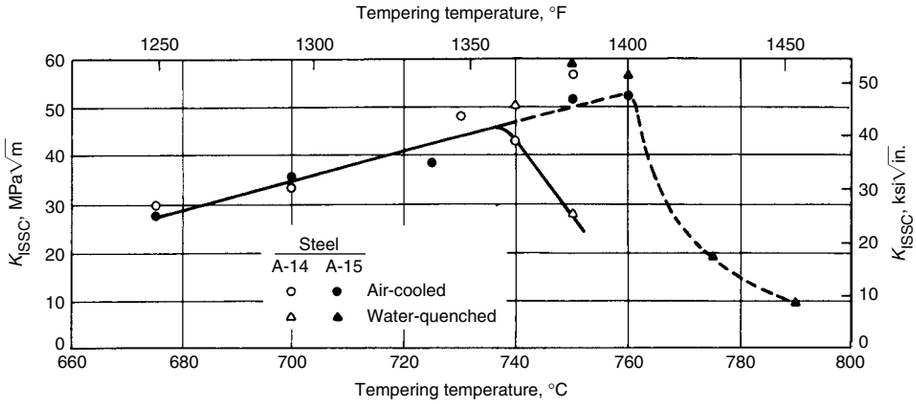

Fig. 7 Effect of tempering temperature on sulfide fracture toughness, K_{ISSC}, of molybdenum-niobium modified 4130 steels A-14 and A-15. See Table 4 for steel compositions. Source: Ref 5

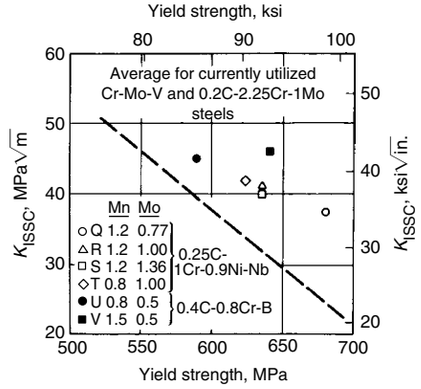

Fig. 8 Effects of molybdenum and manganese content on the sulfide stress cracking resistance of Mn-Ni-Cr-Mo-Nb and Mn-Cr-Mo-B steels. Open symbols are 400 mm (16 in.) section thickness; closed symbols are 250 mm (10 in.). Source: Ref 6

embrittlement, known as hydrogen-induced cracking (HIC), results from the accumulation of hydrogen at internal surfaces within the steel. Interfaces at nonmetallic inclusions and at microstructure constituents that differ significantly from the surrounding matrix are possible locations for accumulation. Martensite islands in a ferrite-pearlite matrix would be typical. Microcracks that form at these interfaces grow in a stepwise fashion toward the surface of the pipe, with the result being failure (Fig. 13).

Very few failures due to HIC have been reported. However, they can be catastrophic, and considerable investigative work has been done to understand the nature of the problem and to develop preventive measures. Hydrogen-induced cracking can usually be prevented by control of the environment—for example, dehydration to remove water and through chemical inhibition. A number of metallurgical factors have also been identified that influence resistance to HIC and offer a means of reducing the susceptibility of linepipe steels to this form of embrittlement.

Two factors that influence the susceptibility of linepipe steels to HIC are steel cleanliness and degree of alloying element segregation. This might be expected, because the degree of steel cleanliness affects the volume fraction of nonmetallic inclusions present and therefore the number of interfaces available for the accumulation of hydrogen. Segregation of alloying elements can lead to the formation of low-temperature austenite decomposition products, thus providing additional sites for hydrogen accumulation.

Hydrogen-induced cracking has been found to be associated with manganese sulfide inclusions that have become elongated during hot rolling. Elongated silicate inclusions also provide interfaces for hydrogen accumulation. Laboratory tests have shown that reduction in the sulfur level of a linepipe steel reduces susceptibility to HIC. Reducing the sulfur content to

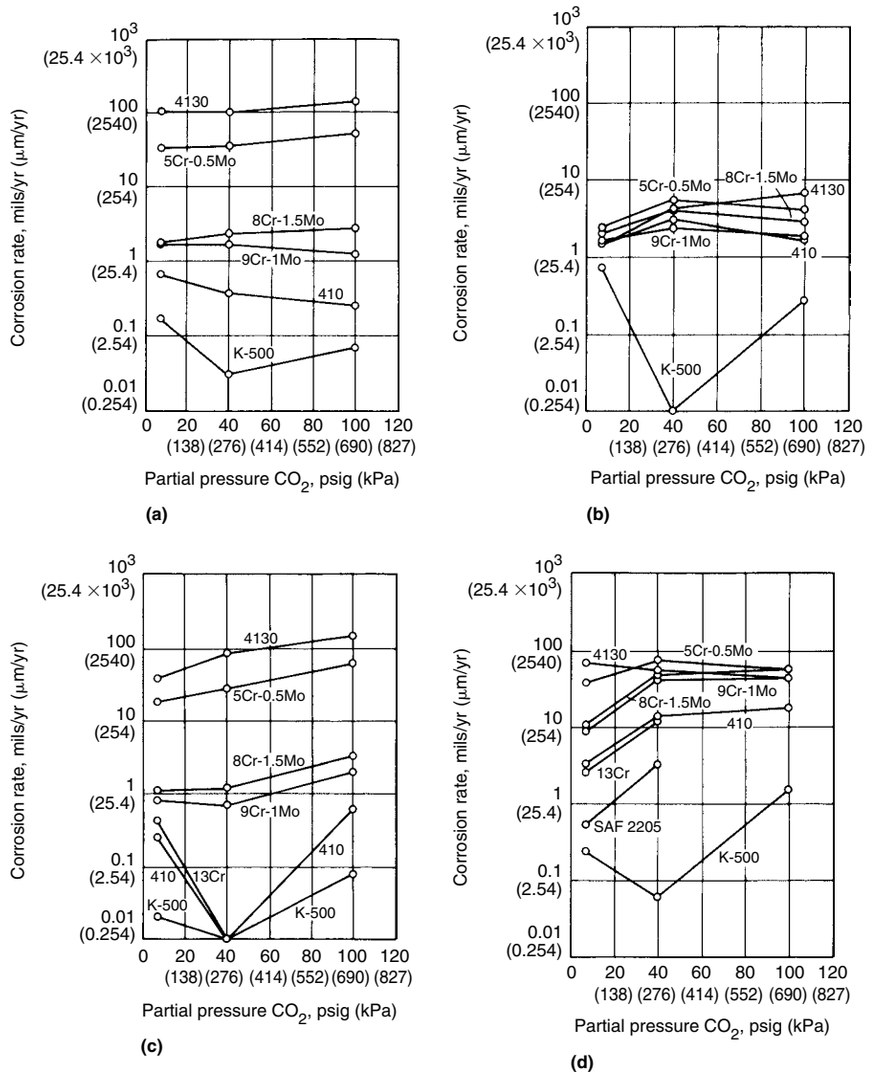

Fig. 9 Effect of partial pressure of CO_2 on the corrosion rates of various alloy steels. (a) 0% chlorides at 65 °C (150 °F). (b) 0% chlorides at 175 °C (350 °F). (c) 15.2% chlorides at 65 °C (150 °F). (d) 15.2% chlorides at 175 °C (350 °F). Source: Ref 7

levels of 0.002% or less can result in a significant improvement in resistance to HIC. It has also been observed that resistance to HIC can be improved through the use of sulfide shape control techniques. Calcium or rare-earth metals are added to the steel to form calcium or rare-earth sulfides. These inclusions are not plastic at hot working temperatures and therefore do not elongate during hot rolling.

The effects of various alloying elements on resistance to HIC are uncertain and somewhat controversial. The alloying element that has received the most attention is copper. Laboratory results have shown that copper can significantly reduce susceptibility to HIC. Apparently, the benefits of copper are realized only in environments with a pH of 4.5 and above. At pH levels less than this, copper has no effect on resistance to HIC. See the article "Hydrogen Damage" in *ASM Handbook,* Volume 13A, 2003.

Energy Conversion Systems

Fossil fuel power systems have corrosion problems associated with the combustion of fossil fuels, such as oil, gas, and coal, as well as with energy conversion that may involve steam boilers and steam or gas turbines and associated equipment. These systems are addressed elsewhere in this Volume.

Combustion of fossil fuels can result in so-called fire-side corrosion, which is an elevated-temperature attack on metal surfaces stemming from the products of combustion. There are three general areas where external corrosion problems occur: the water wall or boiler tubes near the firing zone, the high-temperature superheater and reheater tubes, and the ductwork that handles the combustion flue gases.

Corrosion on water wall, superheater, or reheater tubes results from fuel ash deposits at higher temperatures. In these situations, the corrosive nature of fossil fuels varies considerably with the chemical composition of the fuel. It should be noted that many fuels are not especially corrosive. However, coals containing significant levels of sulfur and alkali metals are particularly damaging, as are oils that contain alkali metals, sulfur, and vanadium. These constituents have been identified as principal sources of corrosive attack in a number of studies involving the analysis of fuel ash deposits on boiler and superheater tubes.

Corrosion of the ductwork is a low-temperature attack that results mainly from acid condensation. Prevention of this corrosion depends primarily on maintaining flue gas temperatures and metal surface temperatures above acid dewpoints. In the case of coal combustion, corrosive attack results from complex chemical reactions involving sulfur and alkali metals (sodium and potassium) to form

Table 5 Corrosion rate data for alloys exposed to seawater solutions at 175 °C (350 °F) with and without H_2S

	Corrosion rates			
	1.93% Cl^-, 690 kPa (100 psig) CO_2, no H_2S		1.92% Cl^-, 690 kPa (100 psig) CO_2, 0.1% H_2S	
Material	μm/yr	mils/yr	μm/yr	mils/yr
AISI 4130	890	35	2565	101
5Cr-1.5 Mo	330	13	1016	40
Type 410	36	1.4	30	1.2
13% Cr	...	...	25	1.0
Monel K-500	3	0.12	43	1.7

Source: Ref 7

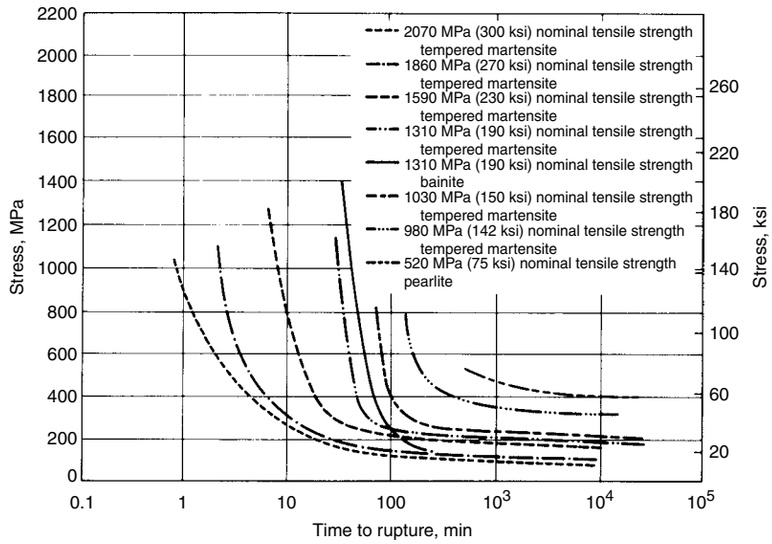

Fig. 10 Delayed-failure characteristics of unnotched specimens of SAE 4340 steel during cathodic charging with hydrogen under standardized conditions. Electrolyte: 4% H_2SO_4 in water. Poison: 5 drops/liter of cathodic poison composed of 2 g phosphorus dissolved in 40 mL CS_2. Current density: 1.2 mA/cm^2 (8 mA/in.^{2}). Source: Ref 8

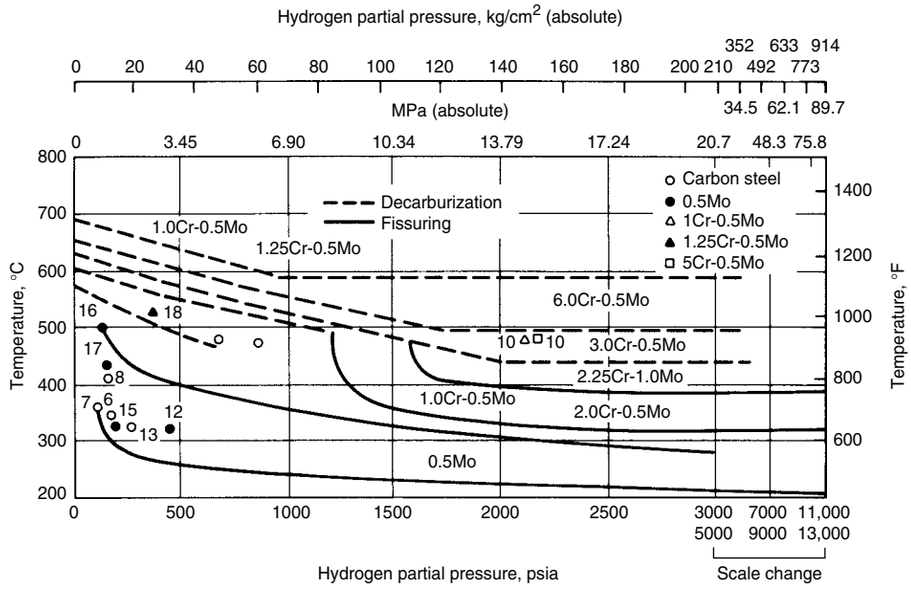

Fig. 11 Nelson curves defining safe upper limits for steels in hydrogen service. Source: Ref 8

alkali sulfates. These alkali sulfates, along with sulfur trioxide (SO_3), react with the protective iron oxide. This reaction breaks down the iron oxide and forms a complex alkali iron sulfate. At temperatures of 425 to 480 °C (800 to 900 °F), this deposit can spall from the surface, exposing fresh iron for further attack. Such would be the case with water wall tubing. As temperatures increase to levels encountered by superheater or reheater tubing—for example, 565 to 705 °C (1050 to 1300 °F)—the complex sulfate created by combustion becomes liquid and attacks the tubing directly. Figure 14 compares the corrosion behavior of two alloy steels and an austenitic stainless steel in this higher temperature range (Ref 9). The data were developed in a laboratory simulation that created the complex alkali iron sulfates. Corrosion rates increase with temperature until the sulfates become unstable, leading to a decrease in corrosion rate. Figure 15 illustrates weight loss data obtained from corrosion probes that were fabricated from various alloy steels and installed in a coal-fired steam boiler system (Ref 10). It is evident from both Fig. 14 and 15 that, although they can be used in these environments, alloy steels do not perform as well as stainless steels.

Several courses of action are taken to prevent fire-side corrosion in coal-fired facilities. At the lower temperature encountered by water wall tubing, procedures are implemented to avoid spalling of combustion deposits. These procedures involve controlling fuel flow and combustion conditions to avoid impingement by particulate matter on critical metal surfaces. At higher temperatures, where liquid-phase attack can occur, protective shields have been used to maintain metal surfaces at temperatures above the corrosive range. The use of coal blending to counteract the corrosive nature of a given coal offers an additional means of corrosion prevention. Also, studies have shown that certain additives to coal are effective in reducing corrosion rates. Success has been achieved with kaolin, diatomaceous earth, and magnesium oxide or other alkaline earth oxides. These additives prevent the formation of complex alkali iron sulfates by forming stable compounds with one or more of their components. The lower-alloy chromium-molybdenum steels have limited corrosion resistance to highly aggressive coals. Although some improvement can be achieved by using 9Cr-1Mo steels, such as ASTM A213 grade T-9, maximum corrosion resistance requires the use of stainless steels.

In oil-fired boilers, the principal source of corrosion comes from a fluxing action of molten sodium-vanadium complexes with the protective oxide scale formed on metal surfaces. Although this can occur at lower temperatures if the correct ratio of sodium to vanadium is present, this form of corrosion generally takes place at temperatures above 595 °C (1100 °F). Superheater and reheater tube corrosion rates of as

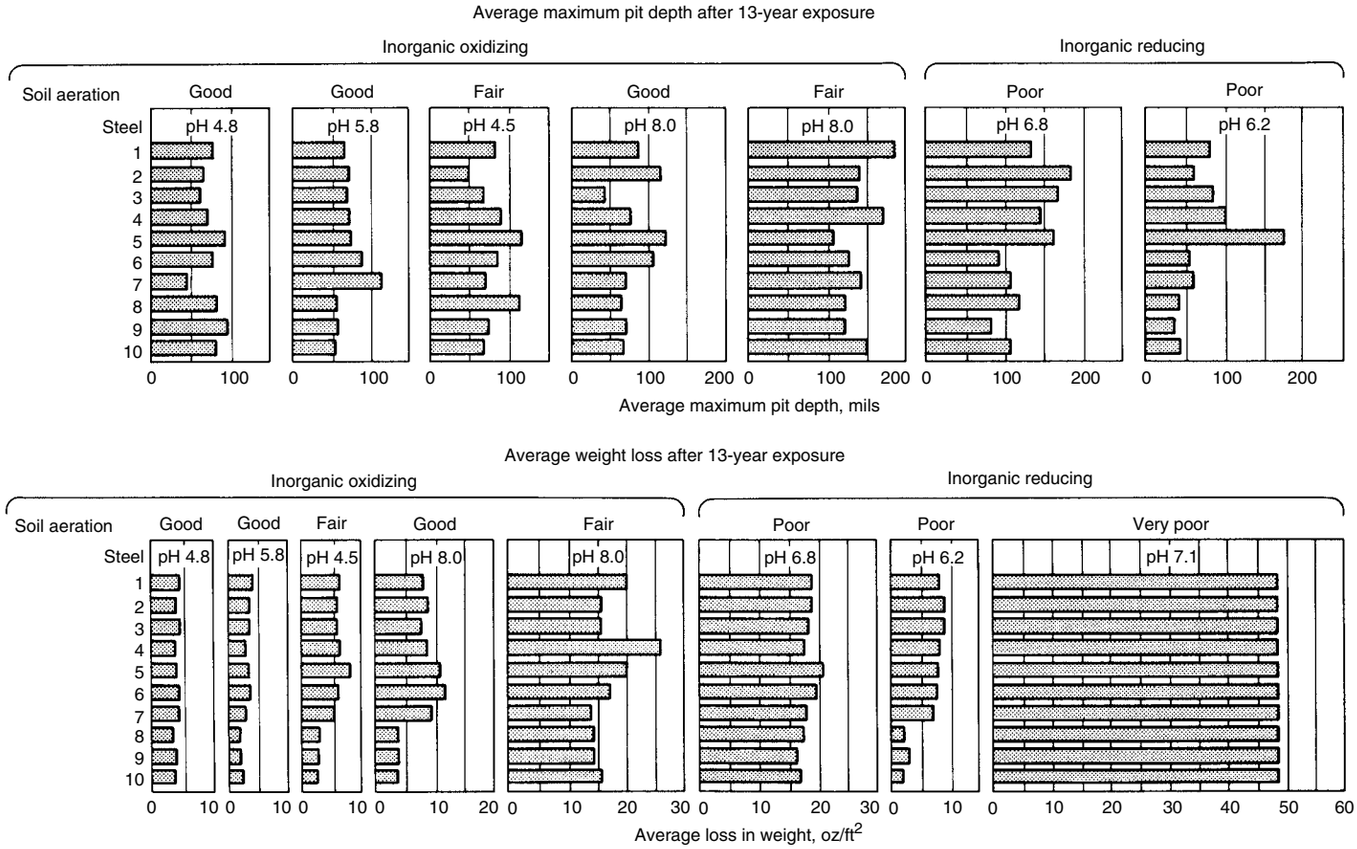

Element	Compositions, for steel numbers 1	2	3	4	5	6	7	8	9	10
Chromium	0.049	0.02	0.02	…	…	1.02	2.01	5.02	4.67	5.76
Nickel	0.034	0.15	0.14	0.52	1.96	0.22	0.07	0.09	0.09	0.17
Copper	0.052	0.45	0.54	0.95	1.01	0.428	0.004	0.008	0.004	0.004
Molybdenum	…	0.07	0.13	…	…	…	0.57	…	0.51	0.43

Fig. 12(a) Effect of composition on corrosion of low-alloy ferrous materials in various disturbed (backfilled) soils. Environmental data are given in Fig. 12(b).

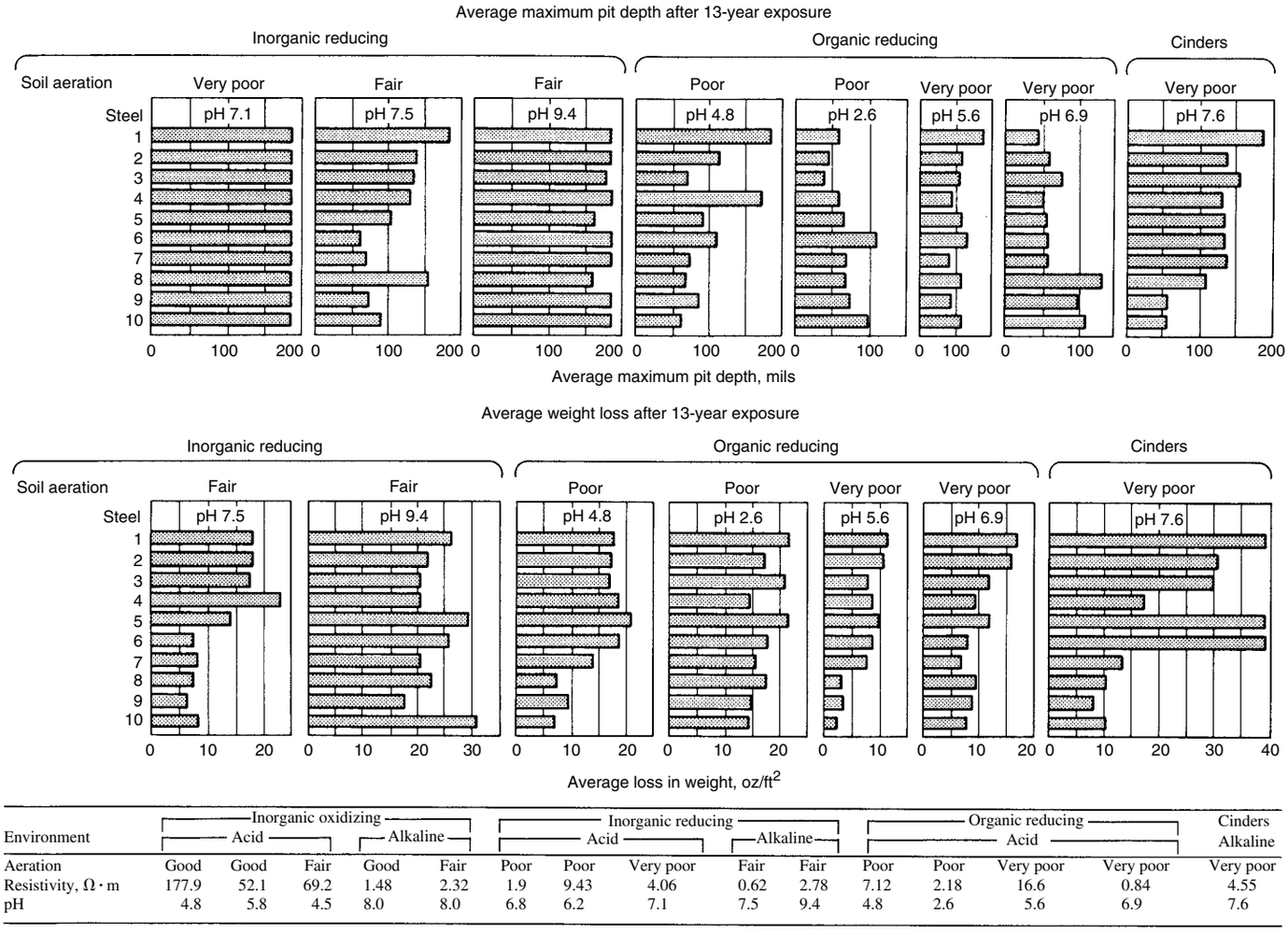

Environment	Inorganic oxidizing					Inorganic reducing					Organic reducing				Cinders
	Acid			Alkaline		Acid			Alkaline		Acid				Alkaline
Aeration	Good	Good	Fair	Good	Fair	Poor	Poor	Very poor	Fair	Fair	Poor	Poor	Very poor	Very poor	Very poor
Resistivity, Ω · m	177.9	52.1	69.2	1.48	2.32	1.9	9.43	4.06	0.62	2.78	7.12	2.18	16.6	0.84	4.55
pH	4.8	5.8	4.5	8.0	8.0	6.8	6.2	7.1	7.5	9.4	4.8	2.6	5.6	6.9	7.6

Fig. 12(b) Effect of composition on corrosion of low-alloy ferrous materials in various disturbed (backfilled) soils. Compositions are given in Fig. 12(a).

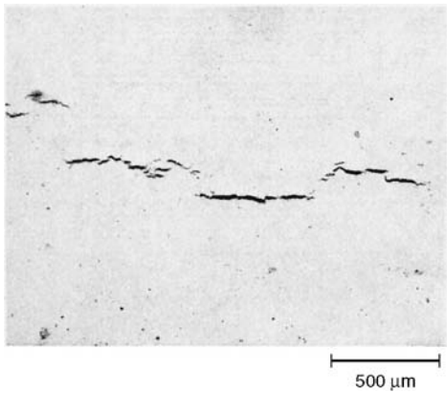

Fig. 13 Hydrogen-induced cracking in a linepipe steel. Original magnification 30×

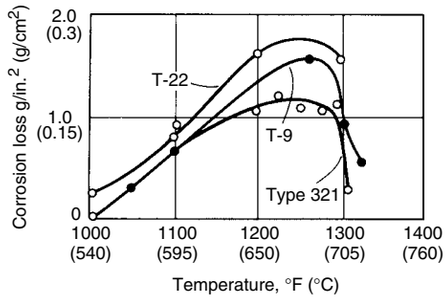

Fig. 14 Effect of alloying on corrosion rate of T-9 (UNS S50400; 8.0-10.0Cr, 0.90-1.10Mo), T-22 (UNS K21590; 1.9-2.6Cr, 0.87-1.13Mo), and type 321 (UNS S32100; 17-19Cr, 9-12Ni) steels. Source: Ref 9

much as 0.75 mm/yr (30 mils/yr) have been observed in field measurements.

An effective method of preventing oil ash corrosion is to remove vanadium, alkali metals, and sulfur chemically from the fuel. However, this approach can be costly. Certain magnesium and calcium compounds have been found to be effective in reducing corrosion rates. These compounds form high-melting-point complexes with oil ash constituents. In terms of low-alloy steel selection, it has been found that the 9Cr-1Mo alloys exhibit excellent corrosion resistance to oil ash corrosion. In addition, modifications of these alloys with additional molybdenum and/or vanadium provide high corrosion resistance and increased strength. Thus, for this application, low-alloy steels are available at a lower cost than stainless steels.

Steam-water-side corrosion is another major problem encountered in fossil fuel power plants. In most cases, contaminant deposition reduces equipment efficiency and induces corrosion by a variety of mechanisms and is implicated in a variety of boiler tube failure mechanisms that are most common in water walls and economizers, which are often constructed from low-chromium ferritic steel such as ASTM A213 grade T-11.

Water-side deposits often begin as accumulations of corrosion products transported to

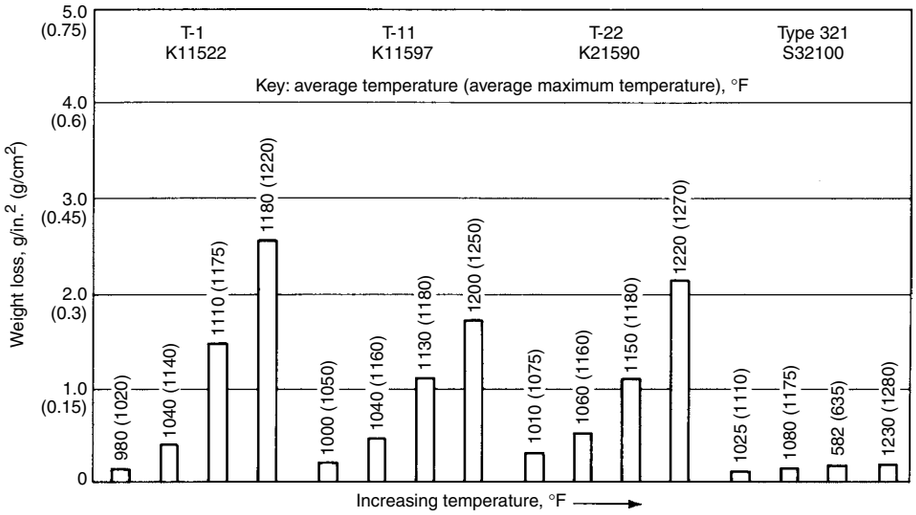

Fig. 15 Weight loss versus temperature data for corrosion probes made of alloy steels (T-1, T-11, T-22) and type 321 stainless steel. Source: Ref 10

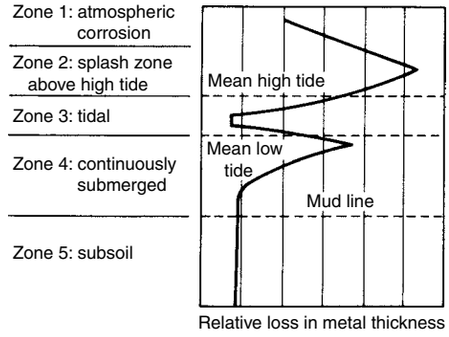

Fig. 16 Corrosion profile of steel piling after 5 years of exposure in seawater at Kure Beach, NC. Source: Ref 11

the boiler from other parts of the system. The corrosion product deposit is porous, unlike the protective magnetite (Fe_3O_4) film. This porous deposit serves as a trap for corrosive impurities, such as caustic, chlorides, and acid sulfates.

Low-alloy steel boiler tube failures in steam-containing tubing have also almost exclusively been the result of contaminant entrainment within the steam. Chlorides, sulfates, and caustic are the most common contaminants. However, the growth of Fe_3O_4 on the inside tube surface can also be a secondary contributor to tube failure. If its rate of growth is excessive, this will act as a thermal barrier and cause the tube wall temperature to rise, sometimes above the point at which excessive creep damage will result in an overheating failure. Additional information is available in the articles about corrosion in the fossil and alternative fuel industries in this Volume.

Nuclear Power Systems. High-strength chromium-molybdenum and nickel-chromium-molybdenum low-alloy steels are also used in components for commercial light water reactors. For example, most modern light water reactor steam turbine rotors in the United States are made from 3.5NiCrMoV steel in conformance with the requirements of ASTM A471 (class 1 through 6). A serious concern associated with steam turbine materials is that of stress-corrosion cracking (SCC), which has occurred in quenched-and-tempered and normalized-and-tempered low-alloy steels with a wide range of grain sizes.

Wet steam erosion-corrosion of nuclear plant piping represents another serious problem that can lead to costly power outages and repairs. The most widely used material for U.S. nuclear plant wet steam piping has been carbon steel, which has shown a susceptibility to erosion-corrosion. With alloying additions of chromium, copper, and molybdenum, however, erosion-corrosion resistance can be significantly improved. In comparison to ordinary carbon steel, erosion-corrosion rates can be reduced by three times with carbon-molybdenum steel and more than ten times with chromium-molybdenum steels. Field experience has shown that 1.25Cr, 0.5Mo, and 2.25Cr-1Mo steels are virtually immune to erosion-corrosion in nuclear power plant applications.

Nuclear Waste Disposal. The disposal of high-level nuclear waste in deep underground repositories requires the development of waste packages that will keep the radioisotopes contained. A number of low-alloy steels are being considered around the world for the structural members of waste packages.

Marine Applications

Carbon and low-alloy steels are used for submerged or partly submerged structures—both in harbors for sea walls and piers, for example, and offshore for oil drilling platforms.

Marine structures exhibit five separate zones that are susceptible to corrosion at different rates, depending primarily on elevation above the tidal zone or depth of immersion in seawater. These zones are described as follows and are identified in Fig. 16, which also shows the usual relative corrosion rate associated with each zone:

- *Atmospheric zone:* The portion of the elevated structure subject to a marine atmosphere, including sea mist and high relative humidity, but without significant wetting by splash from waves

Table 6 Corrosion factors for carbon and alloy steel immersed in seawater

Factor in seawater	Effect on iron and steel
Chloride ion	Highly corrosive to ferrous metals. Carbon steel and common ferrous metals cannot be passivated (sea salt is approx. 55% chloride).
Electrical conductivity	High conductivity makes it possible for anodes and cathodes to operate over long distances: thus, corrosion possibilities are increased, and the total attack may be much greater than that for the same structure in freshwater.
Oxygen	Steel corrosion is cathodically controlled for the most part. Oxygen, by depolarizing the cathode, facilitates the attack: thus a high oxygen content increases corrosivity.
Velocity	Corrosion rate is increased, especially in turbulent flow. Moving seawater may destroy rust barrier and provide more oxygen. Impingement attack tends to promote rapid penetration. Cavitation damage exposes the fresh steel surface to further corrosion.
Temperature	Increasing ambient temperature tends to accelerate attack. Heated seawater may deposit protective scale or lose its oxygen: either or both actions tend to reduce attack.
Biofouling	Hard-shell animal fouling tends to reduce attack by restricting access of oxygen. Bacteria can take part in corrosion reaction in some cases.
Stress	Cyclic stress sometimes accelerates failure of a corroding steel member. Tensile stresses near yield also promote failure in special situations.
Pollution	Sulfides, which are normally present in polluted seawater, greatly accelerate attack on steel. However, the low oxygen content of polluted waters could favor reduced corrosion.
Silt and suspended sediment	Erosion of the steel surface by suspended matter in the flowing seawater greatly increases the tendency toward corrosion.
Film formation	A coating of rust or of rust and mineral scale (calcium and magnesium salts) will interfere with the diffusion of oxygen to the cathode surface, thus slowing the attack.

Source: Ref 11

- *Splash zone:* The portion above the level of mean high tide that is subject to wetting by large droplets of seawater
- *Tidal zone:* The portion of the structure between mean high tide and mean low tide; it is alternately immersed in seawater and exposed to a marine atmosphere
- *Submerged zone:* The portion of the structure from approximately 0.3 to 1 m (1 to 3 ft) below mean low tide down to the mud line
- *Subsoil zone:* The portion below the mud line, where the structure has been driven into the ocean bottom

The effects of each of these zones on the corrosion behavior of low-alloy steels are given here and in more detail in the articles about corrosion in marine environments in this Volume. A summary of some of the more influential variables is presented in Table 6.

Atmospheric-Zone Corrosion. Low-alloy steels demonstrate greatly improved resistance to marine atmospheres compared to the resistance of carbon steels. Early studies indicated that copper-bearing steels had improved

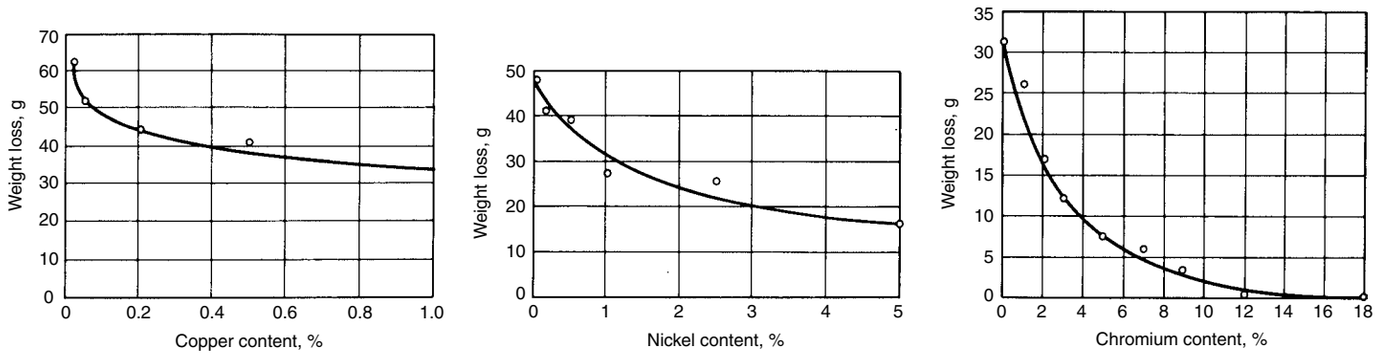

Fig. 17 Effect of alloying additions on the corrosion of steel in a marine atmosphere at Kure Beach, NC (90-month exposure). (a) Effect of copper (100×150 mm, or 4×6 in., specimen). (b) Effect of nickel (100×150 mm, or 4×6 in., specimen). (c) Effect of chromium (75×150 mm, or 3×6 in., specimen). Source: Ref 14

Table 7 Corrosion of low-alloy steels in a marine atmosphere

Data collected over 15.5 years at 250 m (800 ft) lot, Kure Beach, NC

Group	Description	Composition, %									Approximate total alloy content, %	Weight loss(a), mg/dm^2
		C	Mn	Si	S	P	Ni	Cu	Cr	Mo		
I	High-purity iron plus copper	0.020	0.020	0.003	0.03	0.006	0.05	0.020	...	...	...	...
		0.020	0.023	0.002	0.03	0.005	0.05	0.053	...	...	0.1	43
		0.02	0.07	0.01	0.03	0.003	0.18	0.10	...	...	0.4	29.8
II	Low-phosphorus steel plus copper	0.040	0.39	0.005	0.02	0.007	0.004	1.03	0.06	...	1.5	17.3
III	High-phosphorus steel plus copper	0.09	0.43	0.005	0.03	0.058	0.24	0.36	0.06	...	1.2	16.9
		0.095	0.41	0.007	0.05	0.104	0.002	0.51	0.02	...	1.0	16.5
IV	High-manganese and -silicon steels plus copper	0.17	0.67	0.23	0.03	0.012	0.05	0.29	0.14	...	1.4	16.6
V	Copper steel plus chromium and silicon	0.072	0.27	0.83	0.02	0.140	0.03	0.46	1.19	...	2.9	6.3
VI	Copper steel plus molybdenum	0.17	0.89	0.05	0.03	0.075	0.16	0.47	...	0.28	1.9	11.8
VII	Nickel steel	0.16	0.57	0.020	0.02	0.015	2.20	0.24	...	...	3.0	9.4
		0.19	0.53	0.009	0.02	0.016	3.23	0.07	...	...	3.9	9.2
		0.17	0.58	0.26	0.01	0.007	4.98	0.09	...	...	5.9	6.1
		0.13	0.23	0.07	0.01	0.007	4.99	0.03	0.05	...	5.4	7.5
VIII	Nickel steel plus chromium	0.13	0.45	0.23	0.03	0.017	1.18	0.04	0.65	0.01	2.6	10.5
IX	Nickel steel plus molybdenum	0.16	0.53	0.25	0.01	0.013	1.84	0.03	0.09	0.24	3.0	9.8
X	Nickel steel plus chromium and molybdenum	0.10	0.59	0.49	0.01	0.013	1.02	0.09	1.01	0.21	3.4	6.5
		0.08	0.57	0.33	0.01	0.015	1.34	0.19	0.74	0.25	3.4	7.6
XI	Nickel-copper steel	0.12	0.57	0.17	0.02	0.01	1.00	1.05	...	...	2.8	10.6
		0.09	0.48	1.00	0.03	0.055	1.14	1.06	...	...	3.8	5.6
		0.11	0.43	0.18	0.02	0.012	1.52	1.09	...	...	3.2	10.0
XII	Nickel-copper steel plus chromium	0.11	0.65	0.13	0.02	0.086	0.29	0.57	0.66	...	2.4	10.5
		0.11	0.75	0.23	0.04	0.020	0.65	0.53	0.74	...	2.9	9.3
		0.08	0.37	0.29	0.03	0.089	0.47	0.39	0.75	...	2.4	9.1
XIII	Nickel-copper steel plus molybdenum	0.03	0.16	0.01	0.03	0.009	0.29	0.53	...	0.08	1.1	18.2
		0.13	0.45	0.066	0.02	0.073	0.73	0.573	...	0.087	2.0	11.2

(a) A weight loss of 10 mg/dm^2/15.5 years = 0.32 mil/yr. Source: Ref 13

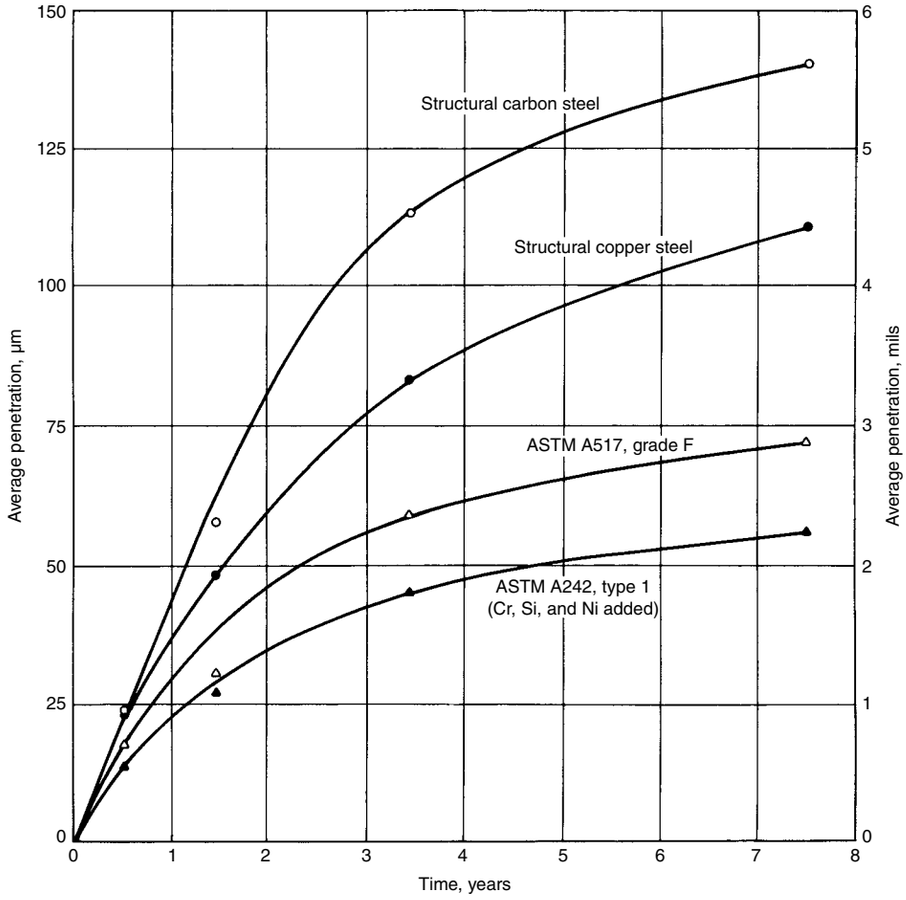

Fig. 18 Comparative corrosion performance of constructional steels exposed to moderate marine atmosphere at Kure Beach, NC. Source: Ref 19

endurance in industrial atmospheres (Ref 11). It was later found that copper-bearing steels also perform better than plain carbon steels at ocean sites (Ref 12).

A number of marine corrosion studies have evaluated the benefits of copper, nickel, chromium, and phosphorus additions to steel (Ref 1, 13–18). The benefit derived from the addition of copper to steel exposed to an industrial atmosphere has been attributed to the relatively insoluble basic sulfates from the SO_2 in the polluted air, which slowly develop a fine-grain, tightly adherent protective rust film (Ref 11). Additions of nickel, chromium, silicon, and phosphorus also promote relatively insoluble corrosion products (Ref 13). Chlorine, as chlorides, has a deleterious effect on the protective rust layer on low-alloy steels, and the manner in which protective rust coats form in marine atmospheres is less understood than in the case of the industrial atmosphere. However, tests have shown that alloying additions do provide enhanced corrosion resistance in marine atmospheres. The effects of individual additions of copper, nickel, and chromium are shown in Fig. 17.

Tests performed at a 240 m (800 ft) lot at Kure Beach, NC, for 15.5 years indicated a corrosion rate of 7.6 µm (0.3 mil/yr) or less for copper-bearing and low-alloy steels (Ref 13). Table 7 identifies the compositions of the steels used in these tests and gives the weight losses determined. A wide range of compositions gave improved corrosion resistance. A comparison of marine atmosphere corrosion of plain carbon steel, a copper-bearing steel, and two low-alloy steels is shown in Fig. 18. Data for a series of low-alloy steels with total alloy additions up to 3.5% are shown in Fig. 19.

Splash- and Tidal-Zone Corrosion. Low-alloy steel undergoes decidedly less corrosion at the splash zone (zone 2, Fig. 16) than carbon steel (Ref 11) does. Some experimental results comparing carbon and low-alloy steel 6 m (20 ft) specimens after 5 years of exposure to splash, seawater, and mud zones are presented in Table 8. At the 0.45 and 0.75 m (1.5 and 2.5 ft) levels, the loss in thickness for the carbon steel was three to six times higher than that for the low-alloy steels. A graphical comparison of the 5 year results for a plain carbon and an Fe-0.54Ni-0.5Cu-0.12P low-alloy steel is shown in Fig. 20. Other experiences with low-alloy steels, especially in exposures in which the wave action is vigorous, also indicate that they have considerable merit for splash-zone service (Ref 11).

Submerged Zone. Low-alloy steels exhibit corrosion rates in the range of approximately 65 to 125 µm/yr (2.5 to 5 mils/yr) when fully immersed in seawater (Ref 11). As such, low-alloy steels offer no particular advantage over carbon steel in applications involving submergence in the ocean. Examples of corrosion rates for plain carbon steel and low-alloy steels after 8 and 16 years in the Pacific Ocean near the Panama Canal are given in Table 9. The inferior corrosion performance of low-alloy steels in seawater is due to the fact that the conditions in the atmosphere that lead to the formation of the protective rust films do not operate in the submerged condition.

Low-alloy steels also develop deeper pits in seawater than carbon steels do. This is demonstrated by the 8 year results from the Panama-Pacific exposures given in Table 10. The total penetration calculated from the weight loss (column 1) is compared with the average of the 20 deepest pits (column 2) and with the deepest pit (column 3). Assuming that the average of the 20 deepest pits is a more significant criterion than the deepest pit, this average pitting value can be compared with the weight loss penetration. The ratio of these two values for low-carbon steel at the 4.25 m (14 ft) depth is 2.6. The range for the low-alloy steels, some of which have higher weight loss penetrations to start with, is 1.6 to 3.7. At the mean tide level, the factor is lower, as is the pit depth for many of the steels involved in the comparison.

For a given required strength, a designer may be tempted to specify a thinner wall for a low-alloy steel than a plain carbon steel. In a seawater application, because the corrosion rate is higher, corrosion failure would be more rapid. Thus, from a design standpoint, the corrosion allowance for a low-alloy steel should be greater than that for a low-carbon steel. However, low-alloy steels, have good strength characteristics, and if protective coatings were applied, these steels could be used to advantage. Cathodic protection must be applied with care for high-strength low-alloy steels, because some tend to be more susceptible to hydrogen damage than carbon steel (Ref 21).

Burial Zone. Bottom conditions vary, but local attack is sometimes observed just above the mud zone or in the bottom mud itself (Ref 11). As in the soil, bottom mud is often aggressive to steel because of the presence of sulfate-reducing bacteria. For steel structures standing in the mud, the anodic and cathodic sites may be a considerable distance apart, and their locations may shift somewhat with time.

Galvanic corrosion in seawater is a matter of concern because the corroding medium has a fairly high conductivity. Service conditions can

differ considerably because of solution composition, solute concentration, agitation, aeration, temperature, and purity of the metals, as well as corrosion product formation and biological growth, each of which can result in a different galvanic series.

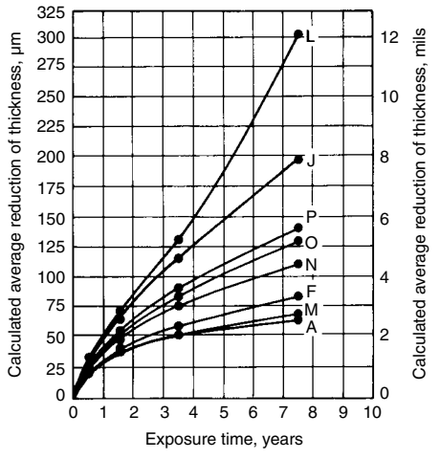

Steel	Composition, % C	Mn	P	S	Si	Cu	Ni	Cr
A(a)	0.09	0.24	0.15	0.024	0.80	0.43	0.05	1.1
M(a)	0.06	0.48	0.11	0.030	0.54	0.41	0.51	1.0
F(a)	0.05	0.36	0.05	0.016	0.008	1.1	2.0	0.01
N(a)	0.11	0.55	0.08	0.026	0.06	0.55	0.28	0.31
O(a)	0.16	1.4	0.013	0.021	0.18	0.30	0.50	0.03
P(a)	0.23	1.5	0.018	0.021	0.19	0.29	0.04	0.08
J(b)	0.19	0.52	0.008	0.039	0.01	0.29	0.05	0.05
L(b)	0.16	0.42	0.013	0.021	0.01	0.02	0.02	0.01

(a) High-strength low-alloy steels. (b) Structural carbon and structural copper steels

Fig. 19 Effect of exposure time on corrosion of steels in marine atmosphere at Kure Beach, NC. Source: Ref 17

In a structural joint, the ratio of the areas of two dissimilar metals has enormous influence on the corrosion rate of one of the members of the joint—the one that is more anodic in the galvanic series. The greater the ratio of the cathode to the anode, the greater the corrosion rate. A surprisingly small difference in solution potential can often result in a significant difference in corrosion rate. Tests were conducted in which carbon steel was coupled to itself and to ASTM A242 (type 1) high-strength low-alloy steel and type 410 stainless steel and in which ASTM A242 (type 1) high-strength low-alloy steel was coupled to itself and to type 410 stainless steel. The results of these tests after 6 months of immersion in seawater are given in Table 11. Coupling carbon steel to stainless steel in an anode-to-cathode ratio of 1 to 8 can result in an approximately eightfold greater corrosion loss for the carbon steel. Also important to design engineers is the significant increase in corrosion that occurs when carbon steel is coupled to high-strength low-alloy steel, despite the fact that their solution (galvanic) potentials are practically the same. An example of a carbon steel/alloy steel galvanic couple is shown in Fig. 21.

Ship and Submarine Applications. The selection of low-alloy steels for ship and submarine hulls, structures, and deck railings is based on toughness, ductility, and weldability rather than corrosion performance. Protection from corrosion is generally supplied by coatings and cathodic protection. Compositions of high-strength low-alloy steels used for ship and

Table 8 Average decrease in thickness of 6 m (20 ft) specimens after 5 year exposure to splash, seawater, and mud zones at Harbor Island, NC

Average distance from top		Decrease in thickness: Sheet steel piling		0.54Ni-0.52Cu-0.12P		0.55Ni-0.22Cu-0.17P		0.54Ni-0.20Cu-0.11P		0.55Ni-0.20Cu-0.14P		0.28Ni-0.20Cu-0.14P		0.28Ni-0.22Cu-0.17P	
m	ft	μm	mils	μm	mils	μm	mils	μm	mils	μm	mils	μm	mils	μm	mils
0.15	0.5(a)	229	9	279	11	305	12	229	9	610	24	229	9	254	10
0.46	1.5	2210	87	330	13	406	16	762	30	457	18	533	21	533	21
0.76	2.5	2490	98	432	17	660	26	1372	54	762	30	1143	45	1854	73
Approximate high-tide line															
1.1	3.5	1219	48	102	4	229	9	229	9	178	7	152	6	559	22
1.4	4.5	25	1	25	1	51	2	25	1	51	2	25	1	51	2
1.7	5.5	51	2	25	1	51	2	51	2	178	7	76	3	51	2
2.0	6.5	356	14	940	37	864	34	1041	41	737	29	711	28	610	24
Approximate low-tide line															
2.3	7.5	1422	56	1321	52	1321	52	1626	64	1346	53	1067	42	1168	46
2.6	8.5	1143	45	1041	41	1118	44	1245	49	1067	42	965	38	864	34
2.9	9.5	1321	52	965	38	1041	41	1245	49	1245	49	1092	43	813	32
3.2	10.5	1346	53	1219	48	1016	40	1245	49	1067	42	1041	41	813	32
3.5	11.5	1143	45	991	39	890	35	1245	49	1067	42	940	37	813	32
3.8	12.5	1168	46	940	37	965	38	1168	46	813	32	890	35	838	33
Approximate ground line															
4.1	13.5	1143	45	330	13	610	24	940	37	279	11	305	12	457	18
4.4	14.5	736	29	152	6	610	24	610	24	152	6	178	7	432	17
4.7	15.5	533	21	127	5	127	5	356	14	127	5	152	6	457	18
5.0	16.5	559	22	254	10	330	13	279	11	178	7	381	15	711	28
5.3	17.5	762	30	457	18	559	22	254	10	305	12	711	28	787	31
5.6	18.5	762	30	305	12	381	15	254	10	559	22	635	25	864	34
5.9	19.5	686	27	381	15	610	24	432	17	991	39	965	38	787	31

Note: Approximate mean high ride 0.6 to 0.9 m (2 to 3 ft) from tops of specimens: approximate mean low tide about 1.8 m (6 ft) from tops of specimens. (a) Unrealistic values because of partial protection from top supporting member. Source: Ref 18

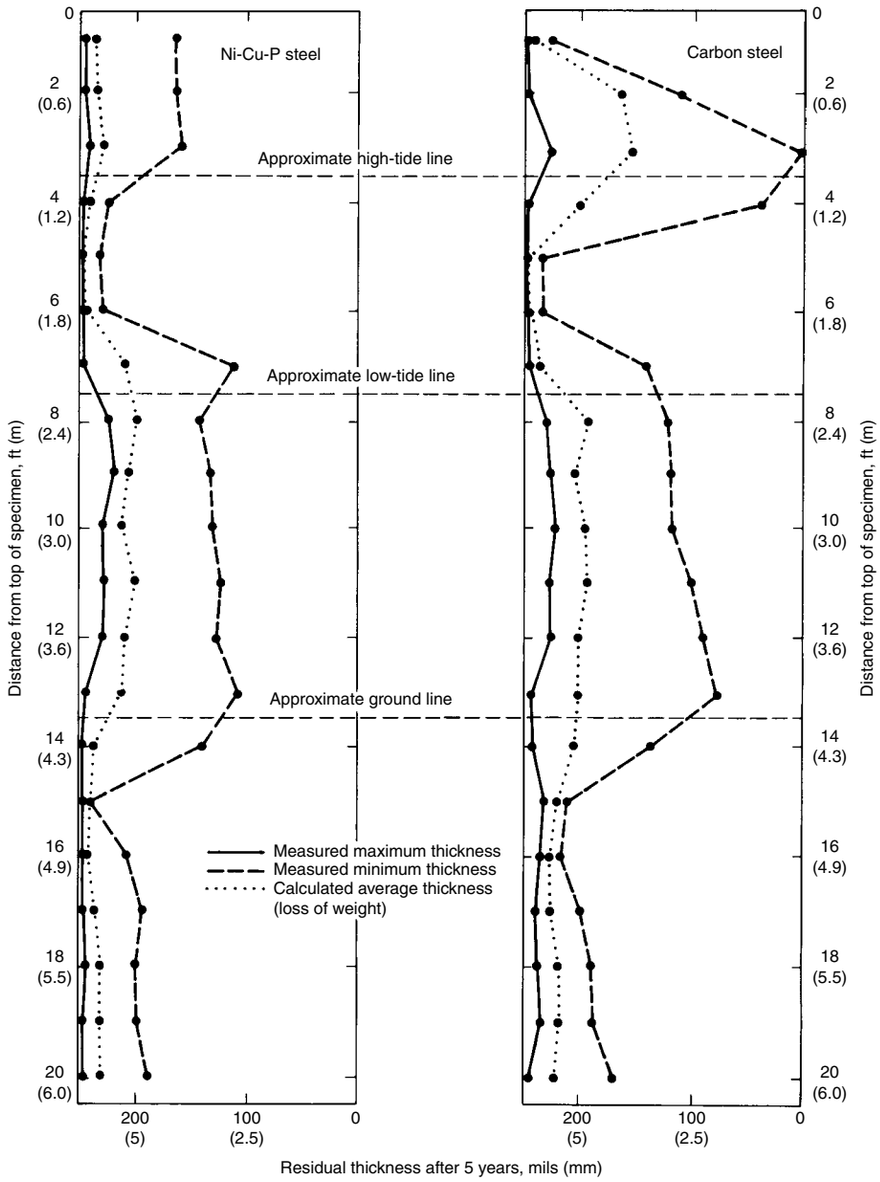

Fig. 20 Comparison of corrosion results for two steels in marine environments. Source: Ref 18

submarine structural applications are given in Table 12. Of the compositions given, the corrosion resistance of ASTM A710 in both flowing and still seawater has been characterized (Ref 22). These results are given in Fig. 22(a) and (b), where ASTM A710 is compared with several other high-strength steels as well as with carbon steel. The conclusion drawn from this study is that ASTM A710 exhibits corrosion resistance comparable to other high-strength and carbon steels.

Chemical-Processing Industry

Many factors, such as temperature, pressure, and velocity of the process stream, influence corrosion in the chemical-processing industry. Minute amounts of contaminants can result in large increases in corrosion rates. The use of low-alloy steels in such environments is generally limited to static or low-velocity applications, such as storage tanks or low-velocity piping. Applications for bare steel are particularly limited. More often, some form of protection is used both to protect the steel equipment and to maintain the purity of the product. Organic linings are commonly used for this purpose; the use of cathodic and anodic protection is also becoming more common. Some applications for alloy steels in the chemical-processing industry are listed as follows.

Sulfuric Acid. Steel tanks are used to store sulfuric acid at ambient temperatures at all concentrations to 100%. Corrosion can rapidly become catastrophic at these concentrations and at temperatures above 25 °C (75 °F). When product purity is of concern, anodic protection can be used to limit iron contamination over long storage periods (see the article "Anodic Protection" in *ASM Handbook,* Volume 13A, 2003). The addition of 0.1 to 0.5% Cu to steels used for sulfuric acid storage has been shown to reduce corrosion rates in acid concentrations to approximately 55%, but this beneficial effect has not been

Table 9 Composition of structural steels and their corrosion rates immersed 4.25 m (14 ft) deep in the Pacific Ocean near the Panama Canal Zone

		Composition, %									Corrosion rate			
											8 years		16 years	
Steel	Type	C	Mn	P	S	Si	Cr	Ni	Cu	Mo	μm/yr	mils/yr	μm/yr	mils/yr
A	Unalloyed low carbon	0.24	0.48	0.040	0.027	0.008	0.03	0.051	0.080	...	74	2.9	69	2.7
D	Copper bearing	0.22	0.44	0.019	0.033	0.009	Trace	0.14	0.35	...	76	3.0	...	...
E	Nickel (2%)	0.20	0.54	0.012	0.023	0.18	0.15	1.94	0.63	...	97	3.8	69	2.7
F	Nickel (5%)	0.13	0.49	0.010	0.014	0.16	0.10	5.51	0.062	...	91	3.6	69	2.7
G	Chromium (3%)	0.08	0.44	0.010	0.017	0.13	3.16	0.16	0.11	0.02	147	5.8	97	3.8
H	Chromium (5%)	0.08	0.41	0.020	0.019	0.20	5.06	0.11	0.062	0.52	109	4.3	89	3.5
I	Low alloy (Cu-Ni)	0.08	0.47	0.007	0.026	0.060	None	1.54	0.87	...	76	3.0	69	2.7
J	Low alloy (Cu-Cr-Si)	0.15	0.45	0.113	0.026	0.47	0.68	0.49	0.42	...	135	5.3	122	4.8
K	Low alloy (Cu-Ni-Mn-Mo)	0.078	0.75	0.058	0.022	0.04	Trace	0.72	0.61	0.13	69	2.7	64	2.5
L	Low alloy (Cr-Ni-Mn)	0.13	0.60	0.089	0.021	0.15	0.55	0.30	0.61	0.059	140	5.5	127	5.0

Source: Ref 20

Table 10 Corrosion penetration of alloy steels immersed in the Pacific Ocean near the Panama Canal Zone after 8 years

See Table 9 for compositions

		Penetration												
		Mean tide(a)							4.25 m (14 ft) below surface(a)					
		1		2		3			1		2		3	
Steel	Type	µm	mils	µm	mils	µm	mils	Ratio(b)	µm	mils	µm	mils	µm	mils	Ratio(b)
A	Low carbon	589	23.2	1016	40	1651	65	1.7	648	25.5	1676	66	2184	86	2.6
D	Copper bearing	615	24.2	1143	45	1600	63	1.9	704	27.7	1600	63	2743	108	2.3
E	Nickel (2%)	582	22.9	991	39	1270	50	1.7	805	31.7	2388	94	4547	179	3.0
F	Nickel (5%)	508	20.0	991	39	1905	75	2.0	813	32.0	2972	117	5436	214	3.7
G	Chromium (3%)	653	25.7	2082	82	2362	93	3.2	1029	40.5	1651	65	1981	78	1.6
H	Chromium (5%)	622	24.5	2235	88	2515	99	3.6	813	32.0	1600	63	2286	90	2.0
I	Low alloy (Cu-Ni)	1008	39.7	1778	70	3404	134	1.8	671	26.4	2083	82	3861	152	3.2
J	Low alloy (Cu-Cr-Si)	536	21.1	1194	47	1372	54	2.2	1097	43.2	2032	80	4445	175	1.8
K	Low alloy (Cu-Ni-Mn-Mo)	630	24.8	1016	40	2388	94	1.6	648	25.5	1422	56	3531	139	2.2
L	Low alloy (Cr-Ni-Mn)	521	20.5	991	39	1270	50	1.9	1115	43.9	2464	97	6579	259(c)	2.2

(a) 1, calculated from weight loss; 2, average of 20 deepest pits; 3, deepest pit. (b) Ratio of average of 20 deepest pits to weight loss penetration. The higher the number the greater is the pitting tendency in relation to the corrosion rate. (c) Completely perforated. Source: Ref: 20

Table 11 Corrosion of members of couples in seawater after 6 months

		Weight loss ($mg/m^2/d$) for area ratio(a) of					
		1:1		8:1		1:8	
Specimen 1	Couple specimen 2	1	2	1	2	1	2
Carbon steel	Carbon steel	5.5	. . .	. . .	. . .	. . .	. . .
Carbon steel	ASTM A242(b)	8.2	2	6.7	2.7	17	3.2
Carbon steel	Type 410 stainless steel	13	0.03	7.0	. . .	47	0.04
ASTM A242(b)	ASTM A242(b)	4.5	. . .	. . .	. . .	. . .	. . .
ASTM A242(b)	Type 410 stainless steel	9.5	0.03	6.2	0.04	35	0.02

(a) Area of specimen 1 to area of specimen 2. (b) Type 1, containing chromium, silicon, copper, nickel, and phosphorus. Source: Ref 14

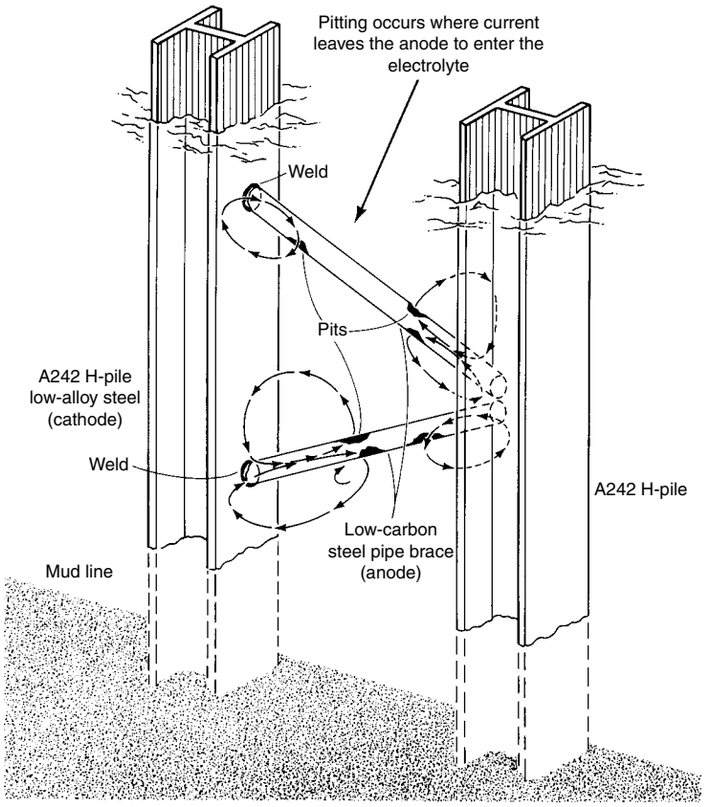

Fig. 21 Example of a carbon steel/alloy steel galvanic couple. Source: Ref 21

observed at concentrations greater than 60% (Ref 23).

Organic Acids. Low-alloy steel can be used for ambient-temperature storage of some high-molecular-weight organic acids, but steel is attacked rapidly by formic, acetic, and propionic acids.

Alkalis. Bare steel storage tanks are used for sodium hydroxide at concentrations to 50% and at temperatures to approximately 65 °C (150 °F). Where iron contamination of the product is of concern, spray-applied neoprene latex or phenolic-epoxy linings are used.

Anhydrous Ammonia. Low-alloy steel storage tanks have been used for many years for ammonia storage. Stress-corrosion cracking has been the primary corrosion problem in these vessels. It has been shown in several investigations that high stresses and oxygen (air) contamination are the primary causes of such cracking and that the addition of 0.1 to 0.2% H_2O inhibits SCC in alloy steel storage vessels (Ref 24–29).

Chlorine. Steel is used to handle dry chlorine, and corrosion rates are generally low. Ignition can be a problem, however, and the recommended maximum service temperature in this application is 150 °C (300 °F) (Ref 30). Steel is also used to handle refrigerated liquid chlorine, but care must be taken at potential leak sites. Chlorine from small leaks can be trapped beneath ice formed on the equipment; this will form corrosive wet chlorine gas. More information on corrosion by these and other specific chemical environments is contained in articles in this Volume.

ACKNOWLEDGMENT

This article is based on Thomas Oakwood, "Corrosion of Alloy Steels," *Corrosion,* Volume 13, *ASM Handbook*, ASM International, 1987.

Table 12 High-strength alloy steels used for ship and submarine structural applications

Steel	Composition, %									
	C	Mn	S	P	Si	Ni	Cr	Mo	Cu	Other (max)
HY-80	0.12–0.18	0.10–0.40	0.020(max)	0.020(max)	0.15–0.35	2.00–3.25	1.0–1.80	0.20–0.60	0.25	0.02Ti, 0.03V, 0.025Al, 0.025Sb, 0.030Sn
HY-100	0.12–0.18	0.10–0.40	0.020(max)	0.020(max)	0.15–0.35	2.25–3.50	1.0–1.80	0.20–0.60	0.25	0.02Ti, 0.03V, 0.025Al, 0.025Sb, 0.030Sn
HY-130	0.12(max)	0.60–0.90	0.015(max)	0.010(max)	0.15–0.35	4.75–5.25	0.4–0.7	0.30–0.65	0.25	0.02Ti, 0.05–0.10V
HY-180	0.12–0.15	0.30(max)	0.30(max)	0.010(max)	...	10.0	2.0	1.0	...	
ASTM A 710 grade A(a)	0.035	0.44	0.015	0.010	0.28	0.89	0.68	0.21	1.16	0.045NB

(a) Typical value. Data supplied by David Taylor. A Naval Ship Research and Development Center

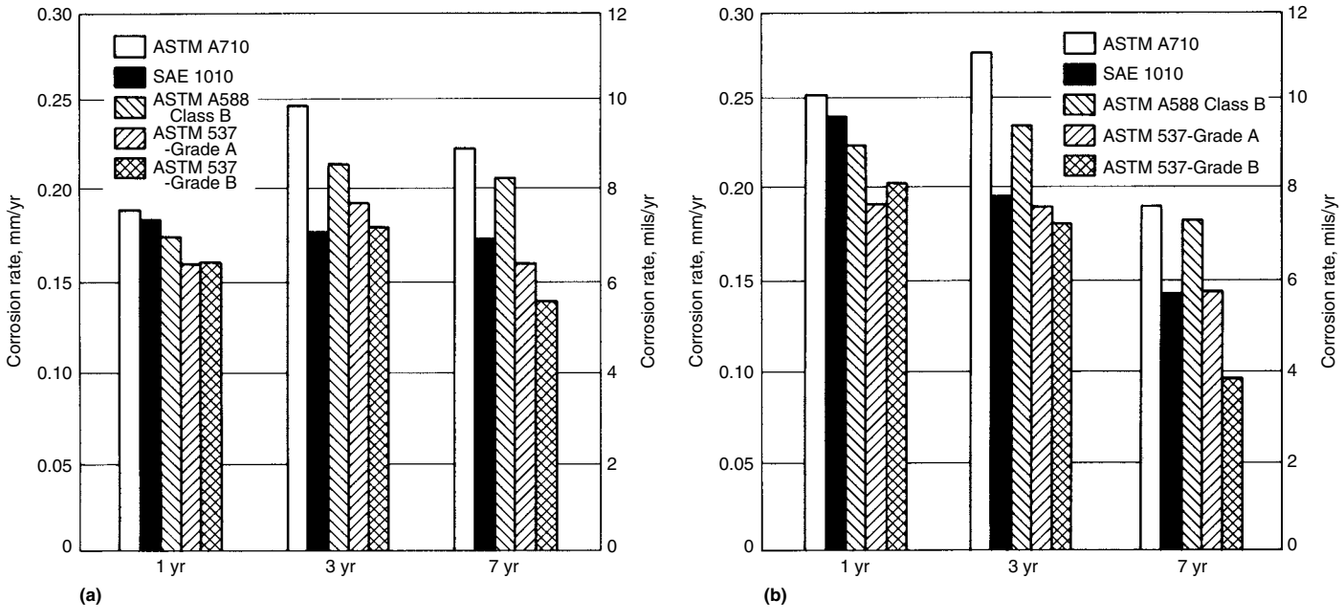

Fig. 22 Corrosion results for ASTM A710 and other steels exposed to (a) low-velocity (0.5 m/s, or 1.6 ft/s) seawater and (b) quiet (still) seawater. Source: Ref 22

REFERENCES

1. C.P. Larrabee and S.K. Coburn, The Atmospheric Corrosion of Steels as Influenced by Changes in Chemical Composition, *Metallic Corrosion—First International Congress on Corrosion,* Butterworths, 1962, p 276–284
2. R.T. Jones, Carbon and Alloy Steel, *Process Industries Corrosion,* National Association of Corrosion Engineers, 1986
3. R.D. Kane and W.K. Boyd, Materials Technology for Oil and Gas Production, *Alloys for the Eighties,* Climax Molybdenum Company, p 225–233
4. "Specification for Casing and Tubing, Petroleum and Natural Gas Industries—Steel Pipe Used as Casing or Tubing for Wells," API Spec 5CT/ISO 11960, 7th ed., American Petroleum Institute, 2001
5. D.L. Sponseller, R. Garber, and J.A. Straatmann, Effect of Microstructure on Sulfide-Stress-Cracking Resistance of High-Strength Casing Steels, *MiCon '82: Optimization of Processing, Properties, and Service Performance through Microstructural Control,* STP 792, American Society for Testing and Materials, 1983, p 172–204
6. R. Garber, T. Wada, F.B. Fletcher, and T.B. Cox, *J. Mater. Energy Syst.,* Vol 7 (No. 2), 1985, p 91
7. J.R. Bryant and C.B. Chitwood, Paper 58, presented at Corrosion/83, National Association of Corrosion Engineers, 1983
8. G.R. Prescott, Material Problems in the Hydrocarbon Processing Industries, *Alloys for the Eighties,* Climax Molybdenum Company, p 303–315
9. *Corrosion Problems in Coal Fired Boiler Superheater and Reheater Tubes—Fireside Corrosion,* Publication CS1653, Electric Power Research Institute, 1980
10. A.L. Plumley, J.A. Burnett, and V. Vaidya, paper presented at CIM 21st Annual Conference of Metallurgists, 1982
11. D.M. Buck, The Influence of Very Low Percentages of Copper in Retarding the Corrosion of Steel, *Proceedings ASTM,* Vol 19, American Society for Testing and Materials, 1919, p 224
12. M. Schumacher, Ed., *Seawater Corrosion Handbook,* Noyes Data Corporation, 1979
13. H.R. Copson, Long-Time Atmospheric Corrosion Tests on Low Alloy Steels, *ASTM Proceedings,* Vol 60, American Society for Testing and Materials, 1960, p 650–665
14. F.L. LaQue, Corrosion Testing, *ASTM Proceedings,* Vol 51, American Society for Testing and Materials, 1951, p 495–582
15. C.P. Larrabee, Steel Has Low Corrosion Rate During Long Seawater Exposure, *Mater. Prot.,* Vol 1 (No. 12), 1962, p 95–96
16. C.P. Larrabee, Corrosion of Steels in Marine Atmospheres and in Seawater, *Trans. Electrochem. Soc.,* Vol 87, 1945, p 161–182
17. C.P. Larrabee, Corrosion Resistance of High Strength Low-Alloy Steels as

Influenced by Composition and Environment, *Corrosion,* Vol 9 (No. 8), 1953, p 259–271
18. C.P. Larrabee, Corrosion Resistant Experimental Steels for Marine Applications, *Corrosion,* Vol 14 (No. 11), 1958, p 501t–504t
19. R.J. Schmitt and E.H. Phelps, Corrosion Performance of Constructional Steels in Marine Applications, *J. Met.,* March 1970
20. C.R. Southwell and A.L. Alexander, "Corrosion of Structural Ferrous Metals in Tropical Environments—Sixteen Year's Exposure to Sea and Fresh Water," Paper 14, Preprint, NACE Conference (Cleveland, OH), National Association of Corrosion Engineers, 1968
21. H.S. Preiser, Cathodic Protection, *Handbook of Corrosion Protection for Steel Pile Structures in Marine Environments,* American Iron and Steel Institute, 1981, p 67–100
22. D.G. Melton and D.G. Tipton, *Corrosion Behavior of A710 Grade A Steel in Marine Environments,* LaQue Center for Corrosion Technology Inc., Wrightsville Beach, NC, June 1983
23. H. Endo and S. Morioka, "Dissolution Phenomenon of Copper-Containing Steels in Aqueous Sulfuric Acid Solutions of Various Concentrations," paper presented at the third symposium, Japanese Metal Association, April 1938
24. A.W. Loginow and E.H. Phelps, *Corrosion,* Vol 18 (No. 8), 1962, p 299–309
25. D.C. Deegan and B.E. Wilde, *Corrosion,* Vol 29 (No. 8), 1973, p 310–315
26. D.C. Deegan, B.E. Wilde, and R.W. Staehle, *Corrosion,* Vol 32 (No. 4), 1976, p 139–142
27. T. Kawamoto, T. Kenjo, and Y. Imasaka, *IHI Eng. Rev.,* Vol 10 (No. 4), 1977, p 17–25
28. F.F. Lyle and R.T. Hill, "SCC Susceptibility of High-Strength Steels in Liquid Ammonia at Low Temperatures," Paper 225, presented at Corrosion/78, National Association of Corrosion Engineers, 1978
29. K. Farrow, J. Hutchings, and G. Sanderson, *Br. Corros. J.,* Vol 16 (No. 1), 1981, p 11–19
30. W.Z. Friend and B.B. Knapp, *Trans. AIChE,* Section A, 25 Feb 1943, p 731

SELECTED REFERENCES

- H.G. Byers, *Corrosion Control in Petroleum Production,* TPC 5, 2nd ed., National Association of Corrosion Engineers, 1999
- "Corrosion Control in the Chemical Process Industries," MTI Publication 45, 1994
- B. Craig and D. Anderson, Ed., *Handbook of Corrosion Data,* 2nd ed., ASM International, 1994
- J.R. Davis, Ed., *Carbon and Alloy Steels,* ASM Specialty Handbook, ASM International, 1996
- Forms of Corrosion—Recognition and Prevention, *NACE Handbook 1,* Vol 1 and 2, National Association of Corrosion Engineers, 1997
- L. Garverick, Ed., *Corrosion in the Petrochemical Industry,* ASM International, 1994
- T.E. Graedel and C. Leygraf, *Atmospheric Corrosion,* Wiley-VCH, 2000
- "Materials Resistant to Sulfide Stress Cracking in Corrosive Petroleum Refining Environments," MR0103–2003, National Association of Corrosion Engineers, 2003
- "Petroleum and Natural Gas Industries—Materials for Use in H_2S-Containing Environments in Oil and Gas Production," MR0175/ISO15156, National Association of Corrosion Engineers, 2003.
- K.M. Pruett, Chemical Resistance Guide for Metals and Alloys, Compass Publications, 1995

ASM Handbook, Volume 13B: Corrosion: Materials
S.D. Cramer, B.S. Covino, Jr., editors, p28-34
DOI: 10.1361/asmhba0003807

Corrosion of Weathering Steels

Revised by F.B. Fletcher, Mittal Steel USA

WEATHERING STEELS contain deliberate additions of alloying elements intended to increase the atmospheric corrosion resistance of steel. Their invention inadvertently created the classification of high-strength low-alloy (HSLA) steels. The most recent weathering steels for bridges and other structural applications are the high-performance steels. The essential feature of all these weathering steels is the development of a hard, dense, tightly adherent, protective rust coating on the steel when it is exposed to the atmosphere, permitting them to be used outdoors with or without paint. The rust imparts a pleasing dark surface to weathering steels, and, compared to unalloyed plain carbon steels, weathering steels have significantly reduced corrosion rates in the atmosphere.

Copper-Bearing Steels

Weathering steels are direct descendents of the copper-bearing steels that came into use early in the 20th century. Steels of that time were made exclusively from iron ore that contained less than approximately 0.02% Cu. It was first reported (Ref 1) in 1900 that when exposed to the weather, some copper-containing irons and steels corroded more slowly than others. By 1911, two U.S. steel producers were marketing copper-bearing steels for improved resistance to corrosion in the atmosphere. After a decade of studying this behavior by exposing samples at three different geographic locations in the United States, Buck reported (Ref 2) in 1913 that a small amount of copper (0.03% Cu) in the steel lowered its corrosion rate significantly. These results stimulated more extensive atmospheric corrosion studies in the United States, Germany, and the United Kingdom. Specific data varied considerably, but by 1919, a consensus had developed that copper-bearing steels with more than 0.15% Cu provided a 50% improvement in service life of steel. On this basis, the Pennsylvania Railroad adopted copper-bearing steel for all sheet steel to be used in cars (Ref 3).

High-Strength Low-Alloy Steels

Additional outdoor studies were initiated in the 1920s by steel companies and by technical committees made up of particularly motivated engineers. It was quickly recognized that in addition to copper, adding small quantities of other alloying elements provided greater atmospheric corrosion resistance and also enhanced the strength of the steel. In 1933, United States Steel introduced COR-TEN (high corrosion resistance and high tensile strength) steel, which was quickly followed by competing proprietary steels from other steel producers. Thus were born the HSLA steels. In addition to copper, these steels generally contained elevated levels of phosphorus, silicon, and manganese, all of which were considered to have beneficial effects on atmospheric corrosion resistance.

The first commercial HSLA steels in the United States were used by the railroad industry for coal hopper cars in the unpainted condition. When steel specification ASTM A 242 (Ref 4) was established by ASTM specification in 1941, it encompassed steels with a range of chemical composition and minimum yield points from 290 to 345 MPa (42 to 50 ksi) and with corrosion resistance equal to or greater than copper-bearing steels (twice that of copper-free plain carbon steels) in most environments. The specification ASTM A 242 continues to be used by producers and purchasers of weathering steels in North America and elsewhere for materials up to and including 100 mm (4 in.) thickness. When the heavier (thicker) structural grades of HSLA steels became available, they were described and specified by ASTM A 588 (Ref 5). Weathering steels used in North American bridges are currently covered by ASTM A 709 (Ref 6). Table 1 shows the compositional requirements for these commonly specified weathering steels.

Atmospheric Corrosion Testing

The performance of weathering steel compositions can be quantified through the exposure of test panels in various atmospheres (Ref 7). The standard method for measuring corrosion rates for comparative purposes is to boldly expose accurately measured and weighed 100 by 150 mm (4 by 6 in.) panels on test racks at an inclination of 30° from the horizontal facing south. After prescribed periods of time—for example, one, two, four, eight, and sixteen years—duplicate or triplicate panels are removed to the laboratory. The oxide (rust) surface is stripped off by mechanical or chemical means (Ref 8), and the weight (mass) loss of the coupon is measured. The mass loss value is

Table 1 Specified compositions for several important weathering steels

ASTM designation		Composition, wt%										
Specification	Grade	C	Mn	P	S	Si	Cu	Ni	Cr	Mo	V	Other
A 242	Type 1	0.15	1.00	0.15	0.05	...	0.20(a)	...	...	...	...	...
A 588	B	0.20	0.75–1.35	0.04	0.05	0.15–0.50	0.20–0.40	0.50	0.40–0.70	...	0.01–0.10	...
A 709	50W	0.23	1.35	0.04	0.05	0.15–0.50	0.20–0.40	0.50	0.40–0.70	...	0.01–0.10	...
A 709	HPS 50W and HPS 70W(b)	0.11	1.10–1.35	0.020	0.006	0.30–0.50	0.25–0.40	0.25–0.40	0.45–0.70	0.02–0.08	0.04–0.08	0.010–0.040 Al; 0.015 N
A 709	HPS 100W(b)	0.08	0.95–1.50	0.015	0.006	0.15–0.35	0.90–1.20	0.65–0.90	0.40–0.65	0.40–0.65	0.04–0.08	0.01–0.03 Nb; 0.020–0.050 Al; 0.015 N

See the relevant specification for complete details. Single values are maximum unless noted. (a) Minimum. (b) HPS, high-performance steel

converted to a thickness loss per exposed specimen surface, which is the conventional dependent variable of the test. In addition to measuring the corrosion behavior of alloys, atmospheric corrosion tests permit a comparison of the aggressiveness of the environment in particular geographic locations. It was common in the 20th century to conduct atmospheric corrosion studies at locations intended to be representative of rural, industrial, and marine conditions. However, the implementation of environmental legislation in the latter decades of the century caused some long-standing industrial test sites to become less aggressive, while acid rain caused some rural test sites to become more aggressive. Thus, comparisons of atmospheric corrosion behavior is a dynamic experimental challenge, and the test dates as well as location should be considered when analyzing data.

In 1962, the results of an extensive 15.5 year study were published (Ref 9) in which some 270 different steels had been exposed in three atmospheres. The sites were at Kearny, NJ (industrial); South Bend, PA (semirural); and Kure Beach, NC (moderate marine; 250 m, or 800 ft, from the ocean). These data formed a basis for quantifying the effects of copper, nickel, chromium, silicon, and phosphorus on weathering steel performance. Table 2 lists the thickness reduction of 18 representative compositions in which the different levels of copper are combined with one or more other alloying elements to show their respective influences on corrosion in the industrial and marine sites.

Estimating Atmospheric Corrosion Behavior of Weathering Steels

The formation of a protective rust film results in deceleration, but not cessation, of corrosion. Mass loss and thickness reduction due to atmospheric corrosion of steel can be represented by an equation of the form $W = Kt^n$, where W is the mass loss (or thickness reduction) of metal due to corrosion, t is the exposure time in years, and K and n are empirical constants.

Consensus standards have been developed to estimate the atmospheric corrosion behavior of weathering steels (Ref 7). Two methods are recognized:

- Perform short-term exposure tests and extrapolate the thickness loss results to the service life of interest, using regression analysis to determine the empirical constants in the predictive equation given previously.
- Calculate a corrosion index based on the steel composition.

Currently, two corrosion indexes are in use. One older index (Ref 10) was developed from the 270-steel database described in Ref 9, and the newer index (Ref 11) was established from a database of 275 steels exposed, starting in 1934, for times up to 16 years in industrial Bethlehem, PA; 227 steels exposed in more rural Columbus, OH; and 248 steels exposed in industrial Pittsburgh, PA. The two indexes are based on entirely different empirical approaches, although they share the characteristic that pure iron has an index value of 0. The higher the value of either index, the greater the predicted corrosion resistance. The maximum possible value for the newer index is 10.0.

The corrosion index can be used as a defining criterion for weathering steels. A minimum corrosion index value of 6.0 (calculated by the older approach) has been established by some steel specifications as the threshold for a steel to have weathering characteristics. For the newer index, a value of 5.4 is a reasonable value for such a threshold value. Figure 1 is a histogram of calculated corrosion indexes for 3461 weathering steel heats produced by three different North American steel mills in the early years of the 21st century. The alloying levels used in modern weathering steels are capable of providing excellent atmospheric corrosion resistance, as predicted by their corrosion indexes.

Table 2 Average reduction in thickness of steel specimens after 15.5 year exposure in different atmospheres

	Composition, wt%					Thickness reduction			
						Kearny, NJ (industrial)		Kure Beach, NC, 250 m (800 ft) lot (moderate marine)	
Specimen	Cu	Ni	Cr	Si	P	µm	mils	µm	mils
1	0.012	...	...	...	...	731	28.8	1321	52.0
2	0.04	...	...	...	...	223	8.8	363	14.3
3	0.24	...	...	...	...	155	6.1	284	11.2
4	0.008	1	...	...	...	155	6.1	244	9.6
5	0.2	1	...	...	...	112	4.4	203	8.0
6	0.01	...	0.61	...	...	1059	41.7	401	15.8
7	0.22	...	0.63	...	...	117	4.6	229	9.0
8	0.01	...	...	0.22	...	373	14.7	546	21.5
9	0.22	...	...	0.20	...	152	6.0	251	9.9
10	0.02	...	...	...	0.06	198	7.8	358	14.1
11	0.21	...	...	...	0.06	124	4.9	231	9.1
12	...	1	1.2	0.5	0.12	66	2.6	99	3.9
13	0.21	...	1.2	0.62	0.11	48	1.9	84	3.3
14	0.2	1	...	0.16	0.11	84	3.3	145	5.7
15	0.18	1	1.3	...	0.09	48	1.9	97	3.8
16	0.22	1	1.3	0.46	...	48	1.9	94	3.7
17	0.21	1	1.2	0.48	0.06	48	1.9	84	3.3
18	0.21	1	1.2	0.18	0.10	48	1.9	97	3.8

Source: Ref 9

Mechanism of Corrosion Resistance of Weathering Steels

The atmospheric corrosion of iron and steels is a function of the following factors: composition of the steel; environmental conditions; characteristics of the existing rust layers, especially porosity; cyclic wetting and drying periods; and contamination by particulates. This article highlights some generalities about corrosion mechanisms; References 12 and 13 provide more thorough treatments. Also see the article "Atmospheric Corrosion" in *ASM Handbook,* Volume 13A, 2003.

Many studies over the years have attempted to quantify the effects of various alloying elements on atmospheric corrosion resistance. One such study (Ref 9) found that five elements, phosphorus, silicon, chromium, copper, and nickel, had a measurable effect (Table 2). Reference 11 concluded that in addition to these, carbon, molybdenum, and tin are beneficial to atmospheric corrosion resistance; sulfur is detrimental; and vanadium, manganese, and aluminum have no significant effect. While it is appealing to believe that individual alloying elements have a consistent and predictable effect on weathering of steel, the multifaceted nature of atmospheric corrosion makes it impossible to quantify elemental effects except in general terms.

Microclimatic conditions can lead to significantly different corrosion resistance. For example, the corrosion rate (loss of thickness) of the downward-facing surface is generally faster than the skyward-facing surface of the same corrosion coupon. In one study (Ref 14), the skyward surface that was washed by the rain and warmed by the wind and sun contributed 37% to

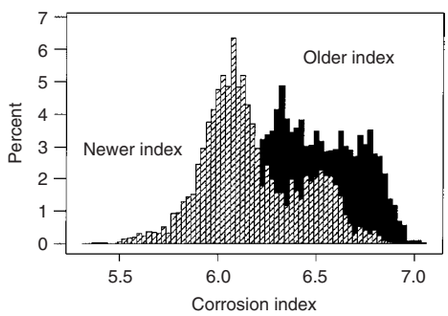

Fig. 1 Histogram of calculated corrosion indexes of weathering steel heats from the early 21st century

the weight loss, while the groundward-facing surface that was never washed by the rain nor dried as much by the sun contributed 63% to the weight loss. The sheltered surface had a coarse granular oxide film. The loosely attached initial oxide film tended to retain dampness and to promote additional corrosion. This finding supports the idea that the density and morphology of the rust have a controlling effect on the corrosion process.

Rust is a mixture of iron compounds that develop in the presence of water. Approximately 20 different compounds—iron oxides and oxy-hydroxides—have been reported in rusts, although a single rust sample usually contains only a few compounds. Corrosion products most commonly observed in weathering steel rust are:

Name	Formula
Magnetite	Fe_3O_4
Hematite	α-Fe_2O_3
Maghemite	γ-Fe_2O_3
Goethite	α-FeO(OH)
Lepidocrocite	γ-FeO(OH)
Akaganeite	β-FeO(OH)

A complete description of weathering steel corrosion products consists of the relative amounts of these iron compounds as well as the distribution of crystal sizes and their arrangement in layers, if any.

When weathering steel is manufactured, the surface becomes entirely oxidized, because a free iron surface develops an oxide scale in a matter of milliseconds at usual finish hot rolling temperatures. The resulting mill scale is typically 10 to 20 μm (0.4 to 0.8 mil) thick. The mill scale is predominantly wustite (FeO) and magnetite (Fe_3O_4) with some quantity of hematite (α-Fe_2O_3). However, wustite is thermodynamically unstable at room temperature and quickly reacts with oxygen in the atmosphere to form maghemite and more magnetite. When water is present, lepidocrocite [γ-FeO(OH)] also forms. The relative amounts and the crystal size distribution of these compounds depend on the kinetics of the chemical reactions, which, in turn, depend principally on the environmental conditions but also on the steel composition.

The first rust to form is porous and poorly adherent, especially on iron. When water is sorbed onto the surface and penetrates this porous rust, the underlying iron dissolves, and Fe^{2+} and/or Fe^{3+} ions become available to precipitate on drying as a stable oxide or hydroxide corrosion product. Lepidocrocite [γ-FeO(OH)] and goethite [α-FeO(OH)] are the crystalline forms most often observed during the early stages of weathering steel corrosion. These oxyhyroxides exhibit crystal size distributions that depend to some degree on the steel composition. Carbon steel rust contains relatively less goethite and relatively more lepidocrocite than a similarly exposed weathering steel. When it is fully developed, the protective patina on weathering steels may be 75 to 80% goethite, with an average crystal size less than 15 nm. This nanophase (previously referred to as amorphous) iron oxyhydroxide carbon steel rust contrasts with rust on carbon steel that contains less goethite, and this goethite is coarser (50 to 100 nm).

Over a period of years, the rust on low-alloy weathering steels changes; the amount of goethite increases, while the relative amount of lepidocrocite diminishes. Weathering steel develops multiple layers of rust on the surface. The inner layers are mostly dense nanophase goethite, and this provides the relative resistance to further oxidation of the underlying steel (Ref 15).

The necessary condition for steel oxidation is delivery of oxygen to the underlying steel. Oxygen diffusion can occur when the oxide/hydroxide rust layer is porous, as, for example, when there are cracks in the rust that penetrate to the steel. Thus, the structural integrity of the existing rust layer plays an important role in the overall corrosion process. The nanophase goethite provides for an excellent adherent rust that resists cracking and thereby protects the steel beneath from contact with gaseous oxygen.

Corrosion Behavior under Different Exposure Conditions

If goethite formation is inhibited by excessive times of wetness or the presence of high concentrations of chlorides, weathering steel does not develop a protective rust, and its corrosion rate is similar to that of carbon steel.

The key diurnal or periodic process to the development of the hydroxide species on the steel is the drying of a moistened surface. If drying does not occur frequently enough, the hydroxide species that forms on the surface is predominantly maghemite; goethite precipitation and formation does not occur. Thus, when weathering steel is located where it experiences excessive time of wetness, such as protracted and frequent periods of rainfall, fog, or persistent mist, it will rust similarly to carbon steel. This behavior has long been recognized, and the use of bare, unpainted weathering steel when the yearly average time of wetness exceeds 60% is not recommended (Ref 16).

Another environment that is contraindicated for weathering steel is when the chloride level exceeds 0.5 mg/100 cm^2 · day (Ref 15). High chloride level in the rust causes the formation of akaganeite [β-FeO(OH)] in preference to goethite. Thus, when akaganeite is found in the rust of a weathering steel, it is common that the atmospheric corrosion behavior of the steel is inferior. Figure 2 shows the surface removal due to corrosion of an ASTM A 588 grade B weathering steel measured at two inland sites and two sites close to the seashore. Salt deposits on the weathering steel at the seaside locations caused significantly higher corrosion rates. Heavy use of road salt on highways and beneath bridges can make it impossible for weathering steel to develop the protective oxide layer, and under this situation, weathering steel structures corrode similarly to carbon steel.

High sulfide and sulfate contents also negate the effectiveness of weathering steels. In areas of severe air pollution due to sulfate, for example, deposits on the weathering steel create localized areas of high acidity that may dissolve the protective oxide.

Under conditions of long-term immersion in freshwater or seawater, the corrosion rate of weathering steel is the same as that for carbon steel. Similarly, burial in soil having varying moisture levels will result in behavior similar to that of carbon steel. In both of these environments, the lack of a drying cycle inhibits the formation of the protective oxide film. The implication, then, is to avoid features in any structure, such as pockets, that can retain water for lengthy periods and to paint any portion of a structure that will be in the soil subject to rain and snow drainage. The ideal exposure conditions for weathering steel are those in which the surface is washed frequently to remove contaminants and the sun is present to dry the surface.

Case Histories and Design Considerations

Based on the mechanism of atmospheric corrosion resistance of weathering steel, working rules for creating the protective oxide film have evolved. The following case histories illustrate both the violations of these rules and suggestions on how to avoid certain maintenance problems that may be encountered with weathering steels.

Example 1: Assessing the Influence of Location. The Gulf Coast and other seashore locations, where onshore breezes are common, experience considerable penetration of salt air. Thus, weathering steel structures experience a

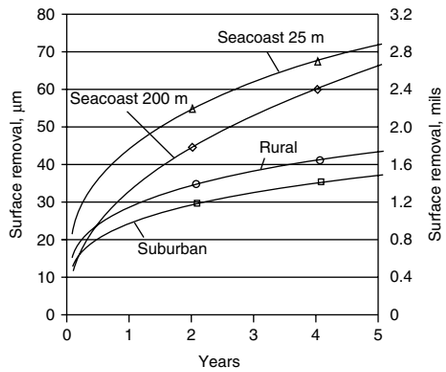

Fig. 2 Surface removal due to corrosion of ASTM A 588 grade B weathering steel at two inland sites and two sites close to the seashore. Salt deposits on the weathering steel at the seaside locations caused significantly higher corrosion rates.

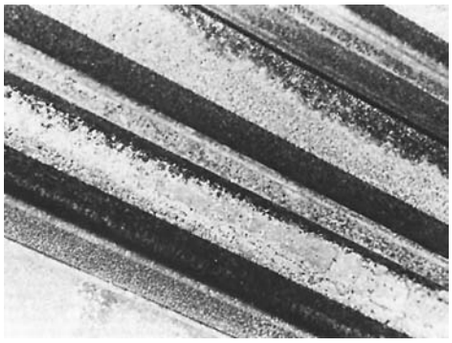

Fig. 3 View of loosely attached rust scale that formed among nested angles in a utility storage yard

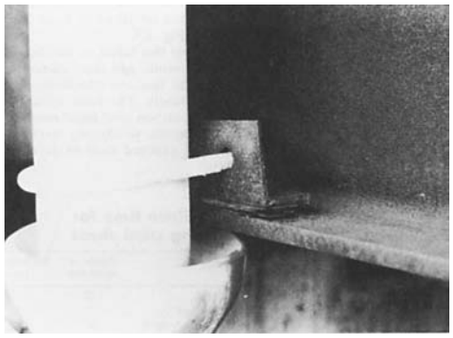

Fig. 4 Results of mixing carbon steel angle in a weathering steel structure

buildup of a salt residue that can inhibit formation of the protective oxide film. The resulting atmospheric corrosion rates are significantly higher than at inshore locations. To assess the conditions at a particular location, one can expose a small test rack for 18 to 24 months with panels of weathering steel and plain carbon steel. Care must be taken that the plain carbon steel is obtained from the same mill source as the potential structural steel, because many modern electric furnace steel mills produce plain carbon steels with high residual alloy contents that may unintentionally impart weathering characteristics. If the test panel of plain carbon steel comes from such a mill, a misleading conclusion may be drawn from the test results. Two or three removals for weight loss determination will indicate whether a protective oxide is forming on the weathering steel. If proximity to the ocean is a question, then exposure of a chloride candle, either at ground level or preferably at an elevation comparable to the height of the structure, should be made, and the monthly chloride determinations should be performed for at least 12 months in order to assess the influence of the seasons.

Example 2: Storage and Stacking of Weathering Steels. When girders, H-beams, and formed weathering steel components such as angles and channels are stored in the open by fabricators or contractors, the steel should be stored face down rather than nested face up. This reduces the possibility of retaining water between the nested members. The steel should be stored with one end elevated to facilitate drainage, although draping with a cover cloth is preferred. When angles or channels are nested so that they can retain water, a loose voluminous rust scale develops, as seen in Fig. 3. If it develops, such scale can be readily removed by hammering, brushing, or with a power-driven wire wheel.

Before heavy girders and columns are erected, they should be inspected by hammering to ensure that a laminated sheet of rust has not formed during the storage period. If this inspection is not performed, the rusted slab may begin to delaminate once in place, and this will raise questions as to whether the steel was truly of the weathering composition.

Example 3: Galvanic Corrosion Problems. Care must be exercised to prevent the mixing of carbon steel with a weathering steel stock. If a weathering steel component is missing, the erection crews may substitute a carbon steel member. This may go unnoticed for several years and then result in excessive deterioration, such as that shown in Fig. 4.

One of the more vivid examples of galvanically coupled metals is the use of the hanger pin detail, shown in Fig. 5, to facilitate girder movement during expansion and contraction. In this case, a bronze washer is part of the assembly. When such a device is used in the snow-belt states, it can create a strong galvanic cell with the steel when deicing salt solution drains from the deck through the expansion joint and through the crevice created by the connection. The outcome can be excessive corrosion of the steel, with the resulting rust formation freezing and therefore immobilizing the joint. The resulting corrosion is evident in Fig. 6.

Example 4: Packout Rust Formation, Bolting, and Sealing. One of the major differences between a galvanized steel bolted structure and a weathered structure is the inability of the latter to tolerate loose joints from a corrosion aspect. For a galvanized structure, moisture draining between a loose gusset plate and structural angle because of a loose bolt will cause little or no corrosion harm. In contrast, such retained drainage can initiate corrosion and rust formation in weathering steel joints. Such rust buildup can pry apart the joint. This condition, called packout, is seen in Fig. 7.

To minimize the possibility of packout formation, it is necessary to seal a joint effectively by an appropriate distribution of bolts in a properly designed and installed joint. This reduces any tendency toward wicking action through capillary openings. The working guidelines for bolting deal with the establishment of bolt spacing and bolt-to-edge distances to provide adequate joint stiffness in order to avoid distortion due to packout corrosion products. Briefly, the pitch (spacing on a line of fasteners adjacent to a free edge of plates or shapes in

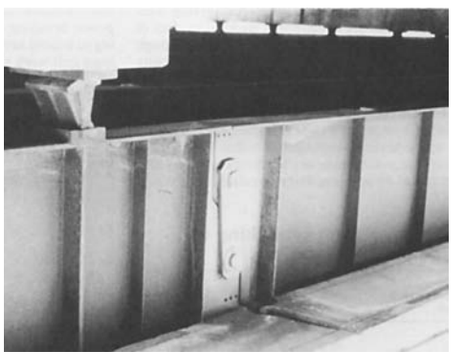

Fig. 5 Typical hanger pin assembly with bronze washer

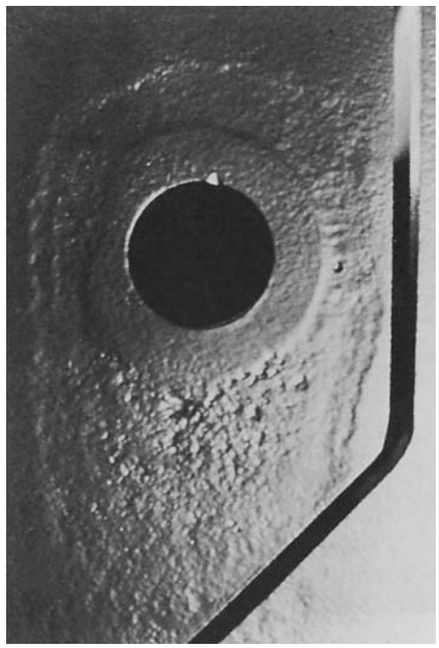

Fig. 6 View of blast-cleaned assembly showing effects of corrosion due to crevice attack and galvanic activity

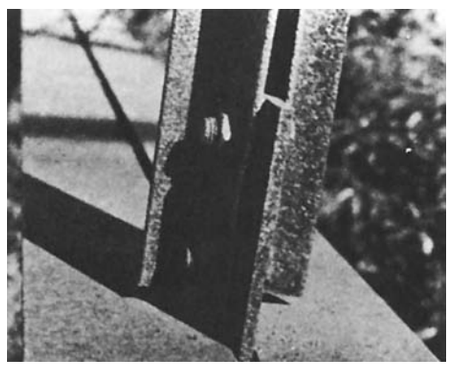

Fig. 7 Distortion caused by packout rust formation because excessive spacing between bolts permitted entry of moisture into joint

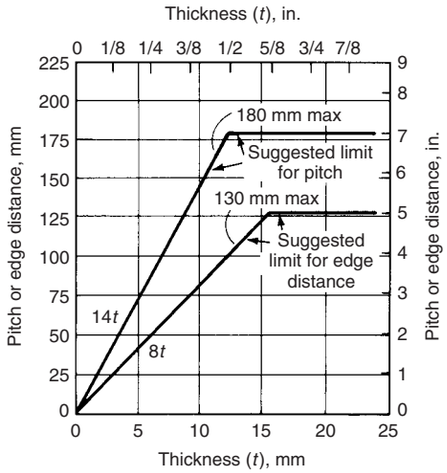

Fig. 8 Suggested spacing limits for joints in bolted weathering steel structures

contact with one another) should not exceed the smaller of 14 times the thickness of the thinnest part, or 180 mm (7 in.). The distance from the center of any bolt to the nearest free edge of plates or shapes in contact with one another should not exceed the smaller of 8 times the thickness of the thinnest part, or 130 mm (5 in.). These factors are illustrated in Fig. 8. At times, it is appropriate to apply a caulk or sealant to the edges to ensure an effective means for preventing the entry of moisture (Fig. 9).

Example 5: Protection of Buried Members. When columns are located on concrete footers below grade, they must be installed in a coated condition. If not, moisture wicking upward from beneath the concrete pad can create a condition of lamellar corrosion above grade (Fig. 10). To avoid this, the surface is prepared by blast cleaning or power brushing, and a coal tar epoxy coating is applied to extend several inches above grade. Arranging a grill work and drainage system is a desirable means of drawing off rainwater drainage and melted snow.

Example 6: Contact with Fire-Retardant Wood Panels. A condition is often encountered in which a weathering steel curtain wall is placed over plywood panels that are treated with preservatives or fire retardants. Because most fire-retardant compositions consist of inorganic salts capable of being leached from the panels if they become wet through entry of water or through high relative humidities, it is necessary to insert a vapor barrier such as polyethylene. Alternatively, the interior face of the steel must be painted with a system capable of resisting the presence of water and the resulting salt leachate.

The major cause of failure of weathering steel curtain walls is inside-out corrosion due to the intrusion of moisture. A primary reason is that the quality of the interior protective coating is inadequate for resisting the destructive effects of long-term or frequent contact with liquid water rather than moisture vapor. Another cause is the failure of certain types of foamed-in-place

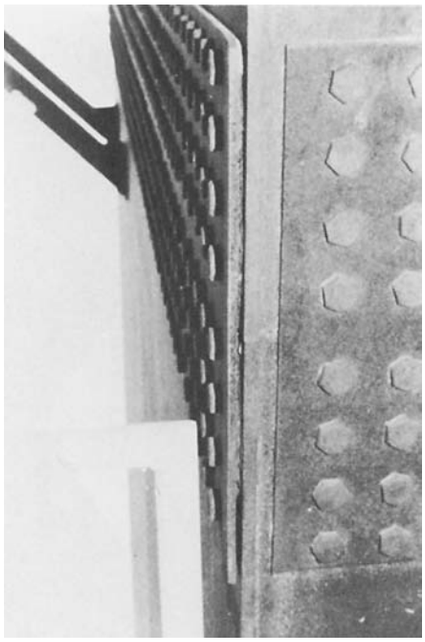

Fig. 9 Gusset plate that should be strip caulked to prevent entry of moisture. Note the possibility for wicking action.

insulation to adhere completely over the entire interior surface of the curtain wall.

Example 7: Painted Weathering Steels. Experience has demonstrated that paint, regardless of composition, will adhere better and give longer service when applied to an appropriately prepared weathering steel surface as compared to a carbon steel surface. This was demonstrated by

Fig. 10 Formation of lamellar rust due to moisture wicking upward from beneath concrete pad. The buried portion must be painted.

exposing ten different paint systems over blast-cleaned panels of COR-TEN steel and carbon steel in the 25 m (80 ft) lot at Kure Beach, NC, for 15 years (Fig. 11). The paint systems that failed on the (from left to right) fourth, seventh, and tenth carbon steel panels continued to function effectively on the weathering steel panels. The paint system that failed on the sixth carbon steel panel reached its true service life on the weathering steel panel; this permitted the exposed steel to develop its protective oxide film to resist further environmental degradation. In addition, it can be seen that the integrity of the paint, regardless of its composition, is retained on all but the sixth and seventh weathering steel panels. From this test and other similar exposure tests, it is conservatively suggested that paint life over a weathering steel surface can be doubled.

Example 8: Steel Thickness for Curtain Walls. Experience has demonstrated that if there is a desire to use a weathering steel as a

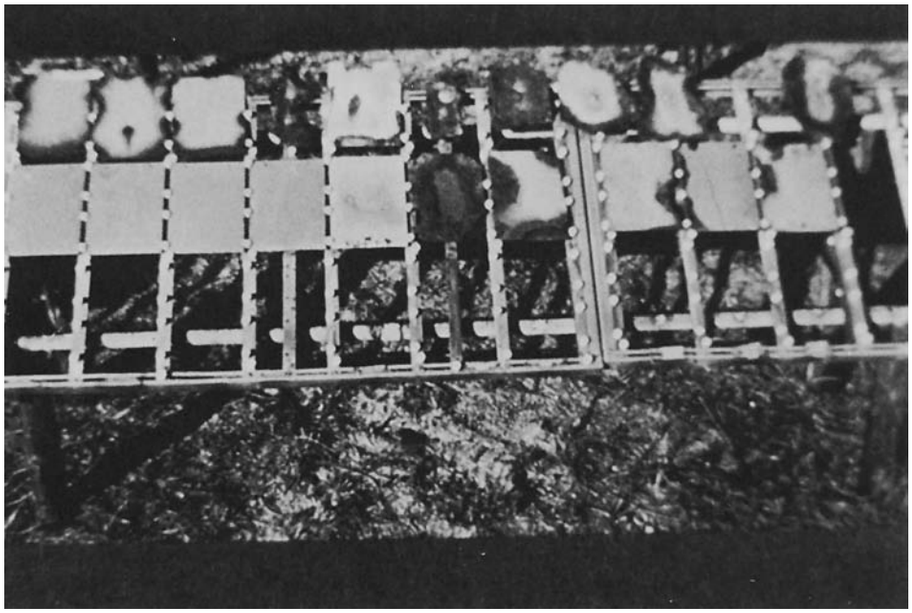

Fig. 11 Exposure test of ten paint systems applied to carbon steel panels (top) and weathering steel panels 25 m (80 ft) from ocean after 15 years. Courtesy of the LaQue Center for Corrosion Technology

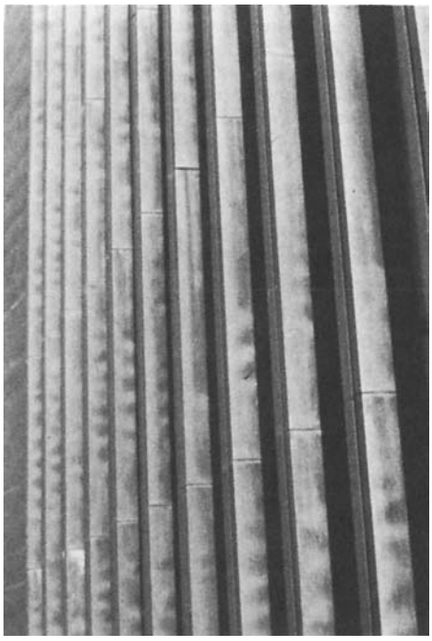

Fig. 12 Clad columns with less than 18-gage cover, resulting in oil canning

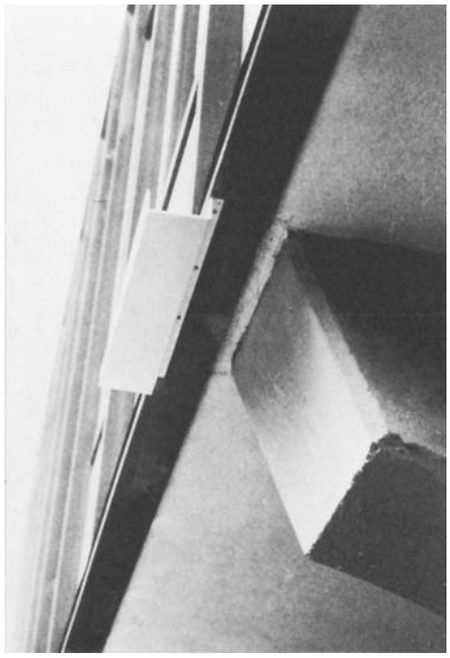

Fig. 13 Protection offered by anodized aluminum channel to retain and divert dew condensate drippage

Fig. 14 Use of stiff rubberized sheeting beneath beam to divert drainage beyond stone wall

curtain wall, the minimum thickness specified should be 18 gage (1.2141 mm, or 0.0478 in.). Thinner sections result in oil canning, which leads to irregular weathering, as noted in Fig. 12.

Example 9: Removing or Avoiding Stains. Staining can result when water-soluble iron oxides in the rust drain down the sides of a structure under the effect of condensed dew or rain. The iron-containing water may dry on window panes or in the surface pores of concrete columns and sidewalks. These deposits can be removed from windows with household abrasives. Such stains can be removed from concrete using typical building supplier products. These concrete stain removers are generally acidic in nature and eliminate the stain by removing an extremely thin layer of concrete.

Effective design with weathering steel demands that steps be taken to contain or divert water drainage off the weathering steel components. To avoid staining of building entrance walks, one designer installed an anodized aluminum channel to divert drainage (Fig. 13). Another installed a firm plastic sheet beneath a structural member to act as a deflector to protect lower walls (Fig. 14). Where horizontal and vertical structural members project beyond lower members, condensate drippage can be retained through the use of shrubbery beds.

Example 10: Protection of Tower Legs and Lighting Standards. A very important form of protection for transmission tower legs and lighting standards at ground level is to maintain a clean area free of grass, bushes, and field crops. Plant life tends to maintain a damp environment for long periods and interfere with the development of the protective oxide film. They are especially damaging when covering bolts and nuts at the base of these towers around concrete footers; the bolts and nuts in these areas can lose section and weaken in just a few years.

Summary of Case Histories and Design Considerations. Weathering steels, used within the limitations noted previously, are useful structural materials. Depending on environmental conditions, they can be used unpainted or painted. In the painted condition, weathering steels contribute synergistically to extending the service life of the protective coating and therefore reduce maintenance costs.

The primary limitations involve frequent and long-term contact with water caused by the inadvertent creation of pockets and crevices that trap and retain moisture. Another limitation is that found on bridge structures in which insufficient attention is paid to preventing attack of the below-deck structural members by deicing salt solution leaking through poorly maintained expansion joint devices.

Like any below-ground carbon steel structure, the weathering steels require a protective coating, as they do when constantly immersed in freshwater or seawater. The protective oxide coating can develop only under conditions of alternate wetting and drying that occur in normal day and night exposure.

To avoid the staining that results from the drainage of moisture that contains particles of rust, one must resort to the techniques of retention and diversion. Finally, care must be taken to protect field installations at ground level from the destructive effects of damp shrubbery, grass, and field crops. Clear space is necessary so that the structure can maintain a dry state, except for the usual periods of rain and snow.

ACKNOWLEDGMENT

This article is adapted from S.K. Coburn and Yong-Wu Kim, Weathering Steels, *Corrosion,* Vol 13, *ASM Handbook,* ASM International, 1987.

REFERENCES

1. F.H. Williams, Influence of Copper in Retarding Corrosion of Soft Steel and Wrought Iron, *Proc. Eng. Soc. West. Pennsylvania,* Vol 16, 1900, p 231–233; *Iron Age,* Vol 66, 1900, p 16
2. D.M. Buck, Influence of Very Low Percentages of Copper in Retarding the Corrosion of Steel, *Proceedings of the American Society for Testing Materials,* Vol 19 (Part II), 1919, p 224–237
3. M.E. McDonnell, The Rust-Proofing of Materials, *Mech. Eng.,* Vol 47, 1925, p 875–880
4. "High-Strength Low-Alloy Structural Steel," A 242/A 242M, *Annual Book of ASTM Standards,* Vol 01.04, ASTM International, 2005
5. "High-Strength Low-Alloy Structural Steel with 50 ksi (345 MPa) Minimum Yield Point to 4 in. (100 mm) Thick," A 588/A 588M, *Annual Book of ASTM Standards,* Vol 01.04, ASTM International, 2005
6. "Standard Specification for Structural Steel for Bridges," A 709/A 709M, *Annual Book of ASTM Standards,* Vol 01.04, ASTM International, 2005
7. "Standard Guide for Estimating the Atmospheric Corrosion Resistance of Low-Alloy Steel," G 101, American Society for Testing and Materials, *Annual Book of ASTM Standards,* Vol. 03.02, ASTM International, 2005
8. "Standard Practice for Preparing, Cleaning, and Evaluating Corrosion Test Specimens,"

G 1, American Society for Testing and Materials, *Annual Book of ASTM Standards*, Vol. 03.02, ASTM International, 2005
9. C.P. Larrabee and S.K. Coburn, The Atmospheric Corrosion of Steels as Influenced by Changes in Chemical Composition, *Proceedings of the First International Congress on Metallic Corrosion,* Butterworths, 1962, p 276–285
10. R.A. Legault and H.P. Leckie, *Effect of Alloy Composition on the Atmospheric Corrosion Behavior of Steel Based on a Statistical Analysis of the Larrabee-Coburn Data Set,* STP 558, American Society for Testing and Materials, 1974, p 334–347
11. H.E. Townsend, Estimating the Atmospheric Corrosion Resistance of Weathering Steels, *Outdoor Atmospheric Corrosion,* STP 1421, American Society for Testing and Materials, 2002
12. T.E. Graedel and R.P. Frankenthal, Corrosion Mechanisms for Iron and Low Alloy Steels Exposed to the Atmosphere, *J. Electrochem. Soc.,* Vol 137 (No. 8), Aug 1990, p 2385–2394
13. D.C. Cook, Application of Mössbauer Spectroscopy to the Study of Corrosion, *Hyperfine Interact.,* Vol 153, 2004, p 61–82
14. C.P. Larrabee, The Effect of Specimen Position on Atmospheric Corrosion Testing on Steel, *Trans. Electrochem. Soc.,* 1945, p 297
15. D.C. Cook, S.J. Oh, and H.E. Townsend, "The Protective Layer Formed on Steels after Long-Term Atmospheric Exposure," Paper 343, Corrosion 98, NACE International, 1998
16. "Uncoated Weathering Steel in Structures," Technical Advisory T4140.22, U.S. Department of Transportation, Federal Highway Administration, Oct 3, 1989

SELECTED REFERENCES

- P. Albrecht, Corrosion Control of Weathering Steel Bridges, *Corrosion Forms and Control for Infrastructure,* STP 1137, American Society for Testing and Materials, 1992, p 108–125
- P. Albrecht, S.K. Coburn, F.M. Wattar, G. Tinklenberg, and W.P. Gallagher, "Guidelines for the Use of Weathering Steel in Bridges," NCHRP Report 314, Transportation Research Board, National Research Council, Washington, D.C., 1989
- P. Albrecht and T.T. Hall, Atmospheric Resistance of Structural Steels, *J. Mater. Civil Eng.,* Vol 15 (No. 1), 2003, p 2–24
- D.C. Cook, Application of Mössbauer Spectroscopy to the Study of Corrosion, *Hyperfine Interact.,* Vol 153, 2004, p 61–82
- R.H. McCuen and P. Albrecht, A Re-Analysis of Thickness Loss Data for Weathering Steel, *J. Mater. Civil Eng.,* Vol 16 (No. 3), May/June 2004, p 237–246
- T. Misawa, Corrosion Science of Iron and Weathering-Steel Rusting, *Corros. Eng.,* Vol 37, 1988, p 441–446
- S. Oesch, The Effect of SO_2, NO_2, NO and O_3 on the Corrosion of Unalloyed Carbon Steel and Weathering Steel—The Results of Laboratory Exposures, *Corros. Sci.,* Vol 38 (No. 8), 1996, p 1357–1368
- S.J. Oh, D.C. Cook, and H.E. Townsend, Study of the Protective Layer Formed on Steels, *Hyperfine Interact.,* C3, 1998, p 84–87
- A. Raman, A. Razvan, B. Kuban, K.A. Clement, and W.E. Graves, Characteristics of the Rust from Weathering Steels in Louisiana Bridge Spans, *Corrosion,* Vol 42 (No. 8), 1986, p 447–455
- H.E. Townsend, Atmospheric Corrosion Performance of Quenched-and-Tempered, High-Strength Weathering Steel, *Corrosion,* Vol 56 (No. 9), 2000, p 883–886
- J.H. Wang, F.I. Wei, and H.C. Shih, Assessing Performance of Painted Carbon and Weathering Steels in an Industrial Atmosphere, *Corrosion,* Vol 53 (No. 3), 1997, p 206–215
- M. Yamashita, T. Misawa, H.E. Townsend, and D.C. Cook, Quantitative Analysis of Ultra-Fine Goethite in Rust Layer on Steel Using Mössbauer and X-Ray Diffraction Spectroscopy, *J. Jpn. Inst. Met.,* Vol 64 (No. 1), 2000, p 77–78

ASM Handbook, Volume 13B: Corrosion: Materials
S.D. Cramer, B.S. Covino, Jr., editors, p35-39
DOI: 10.1361/asmhba0003808

Corrosion of Metallic Coated Steels

Revised by C. Ramadeva Shastry, Metal Steel USA

THE MAIN REASON TO APPLY A METALLIC COATING to a steel substrate is corrosion protection. Most metallic coatings are applied either by hot dipping in a molten bath of metal or by electroplating in an aqueous electrolyte. To a lesser extent, coatings are also applied by such methods as metal spraying, cementing, and metal cladding. Coating processes are reviewed in "Electroplated Coating," "Continuous Hot Dip Coatings," "Batch Process Hot Dip Galvanizing," and "Thermal Spray Coatings" in *ASM Handbook,* Vol 13A.

From the standpoint of corrosion protection of iron and steel, metallic coatings can be classified into two types—noble coatings and sacrificial coatings. Noble coatings such as lead, copper, or silver are noble in the galvanic series with respect to steel. For noble coatings, at areas with surface defects or porosity, the galvanic current accelerates attack of the base steel and eventually undermines the coating. Sacrificial coatings, such as zinc or cadmium, are anodic (more active) to steel. For sacrificial coatings at uncoated areas (pores), the direction of galvanic current through the electrolyte is from coating to the base steel; as a result, the base steel is cathodically protected. In general, the thicker the coating, the longer the duration of cathodic protection. This article will emphasize hot-dipped zinc, aluminum, zinc-aluminum alloy and aluminum-zinc alloy coatings, which are summarized in Table 1. More detailed information is provided in the articles "Thermal Spray Coatings for Corrosion Protection in Atmospheric Aqueous Environments," "Corrosion of Clad Metals," and "Corrosion of Zinc and Zinc Alloys" in this Volume, and in "Continuous Hot-Dip Coatings for Steel" in *ASM Handbook,* Vol 5, *Surface Engineering*.

Zinc-Base Coatings

Types. Zinc-coated steels are generally produced by either hot dipping or electroplating. The main difference between these two types of zinc coatings is in their coating structure. The hot-dip galvanized coatings consist of a layer of zinc-iron or iron-aluminum-zinc intermetallics at the steel/zinc coating interface (Ref 1, 2). The type of intermetallics formed depends on the aluminum content of the zinc melt, which is generally in the 0.1 to 0.3% range (by weight) in most commercial operations. An alloy layer consisting of one or more zinc-iron intermetallics forms when the melt aluminum is between 0.10 and 0.15%. Possible zinc-iron intermetallics that may occur in the alloy layer are shown in Fig. 1.

A typical microstructure of a hot-dipped zinc coating produced from a low-aluminum melt (0.1–0.15% Al) is shown in Fig. 2. For galvanized sheet steel with better coating adhesion and good coating-forming properties, the thickness of the zinc-iron intermetallic layers should be less than 20% of the total coating thickness. The growth of the zinc-iron intermetallic layer is determined by the aluminum level in the zinc melt. In coatings produced from melts containing more than 0.15% Al, the formation of zinc-iron intermetallics is usually fully suppressed, and a zinc-containing iron-aluminum intermetallic forms at the steel/zinc interface instead. This layer is generally very thin, less than about 0.3 μm (120 μin.), and not resolvable under a light microscope. A typical microstructure of a galvanized coating produced from a high-aluminum melt (Al ≥ 0.15%) is shown in Fig. 3.

The appearance of the coating is also affected by the composition of the zinc melt. Coatings produced from melts containing 0.07 to 0.15%

Table 1 Metallic coatings for sheet steel

			Coating, 1 side			
Process	Coating type	Composition, %	Weight, g/m^2	Thickness, μm	Characteristics	Typical applications
Electrolytic	Zinc	Pure Zn	20–100	3–14	Sacrificial coating, good corrosion resistance	Autobody panels, appliance housings
	Zinc-iron	11–20 Fe	30–50	4–7	Good corrosion resistance, excellent spot weldability and paintability	Autobody panels
	Zinc-nickel	9–13 Ni	20–50	3–7	Superior corrosion protection with thin coatings	Autobody panels
Hot-dip	Zinc	Zn(a)	42–550	6–78	Sacrificial coating, good corrosion resistance	Automotive, metal building, construction, and appliances
	Zinc-iron (galvanneal)	7–14 Fe	30–90	4–13	Good corrosion resistance, excellent spot weldability and paintability	Autobody panels, floor pans, wheel house liners, rails, and cross-members
	Zinc-aluminum	4–7 Al	45–350	6–48	Superior corrosion resistance and paintability similar to zinc	Metal building roofing and siding, fence posts, appliances, and automotive
	Aluminum-zinc	Zinc-55Al-1.6Si	75–80	20–24	Excellent outdoor corrosion resistance	Metal building roofing and siding, culverts, appliances, and automotive
	Aluminum, type I	5–11 Si	35–60	12–20	Good formability and resistance to high temperatures	Metal building, appliance and automotive exhaust parts
	Aluminum, type II	0.5Si-2.5Fe	100–150	30–48	Excellent resistance to atmospheric corrosion	Metal building and construction
	Terne	Pb-Sn	40–170	3–15	Barrier protection	Automotive fuel tanks, radiator parts, tubing

(a) Commercially pure

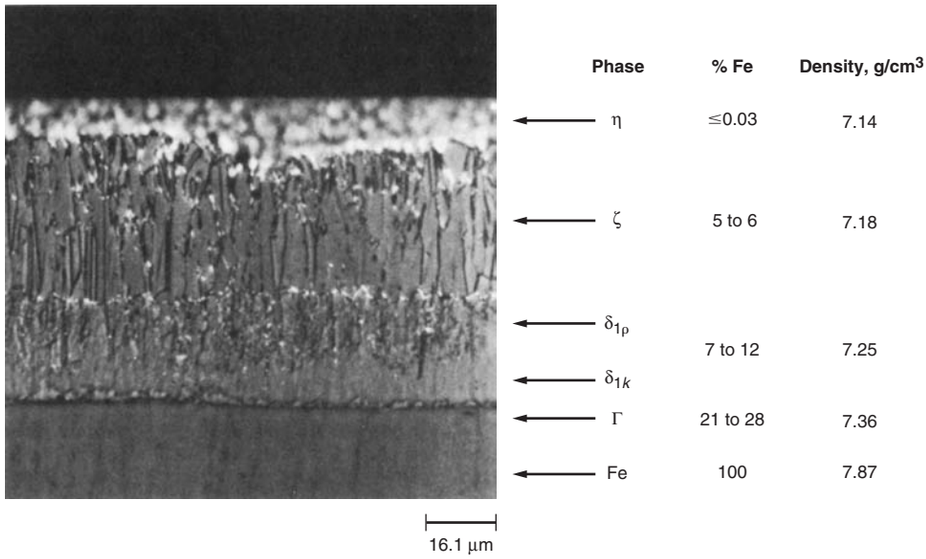

Fig. 1 Typical coating microstructure for prolonged immersion of carbon steel in prime western zinc at 450 °C (842 °F)

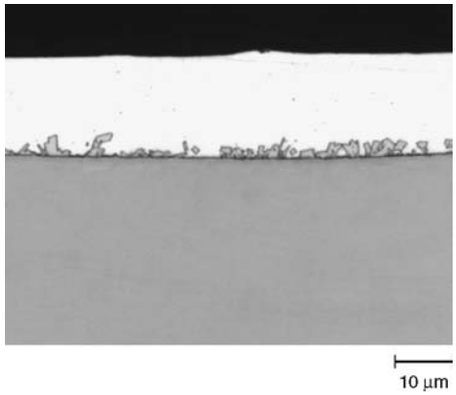

Fig. 2 Typical microstructure of hot-dip galvanized coatings produced from a low aluminum (0.10–0.15% Al) melt. Courtesy of Phil Fekula, Metal Steel USA.

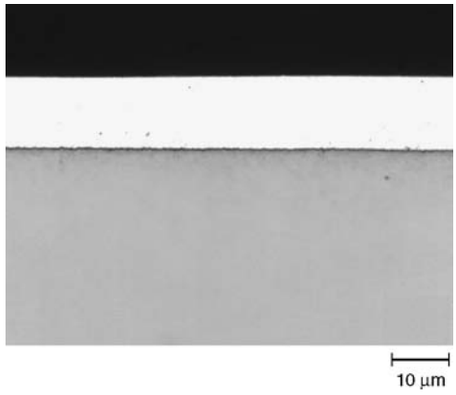

Fig. 3 Typical microstructure of hot-dip galvanized coatings produced from a high aluminum (>0.15% Al) melt. Courtesy of Phil Fekula, Metal Steel USA.

Pb or 0.02 to 0.15% Sb in addition to Al have a spangled appearance. Coatings produced from baths free of lead or antimony have a smooth and spangle-free surface.

Electrogalvanized steels display a smooth, uniform, and spangle-free coating and do not have an intermetallic layer. Electrogalvanized steels, and zinc-iron alloy (galvanneal) coated steels produced by thermally alloying hot-dipped zinc with iron from the base steel, are generally used in painted automotive applications. Currently, almost all hot-dip galvanized sheet steel in the United States is produced by continuous process. The two commercial processes used are the Sendzimir process and the Cook-Norteman process.

In the Sendzimir process, the steel strip is heated in a high-temperature furnace consisting of an oxidizing atmosphere to remove organic oils and surface contaminants, followed by heating in a reducing furnace with a hydrogen-rich atmosphere to reduce the surface oxide layer and to anneal the steel substrate. The discharge end of the reducing furnace is below the surface of the zinc bath; this allows the continuous sheet to enter the bath without passing through a contaminating atmosphere. Precise control of the oxidizing and reducing temperature is critical in developing and maintaining the cleanliness of the steel surface.

In recent years, the Sendzimir (hot) process has been significantly modified to improve product quality and appearance for critical applications. The modifications include a multistage cleaning section to achieve a high degree of surface cleanliness before the strip enters the annealing furnace; elimination of the oxidizing atmosphere and the addition of a radiant-heat annealing furnace with a leaner hydrogen-nitrogen reducing atmosphere (5–10% H_2); and vertical furnace design for a more compact operation and reduced likelihood of strip damage in the furnace. Reference 3 provides an excellent review of recent advances in the hot zinc-coating process.

In the Cook-Norteman process, an in-line furnace is not used. The sheet is chemically cleaned by alkaline degreasing and acid pickling. After cleaning, the sheet is coated with a film of zinc ammonium chloride, dried, and preheated to less than 260 °C (500 °F) before entering the galvanizing bath.

Aqueous Corrosion of Galvanized Steel. Zinc is an amphoteric metal that corrodes in acid and alkaline solutions. The hydrogen ion concentration in water and aqueous solutions has a significant effect on the corrosion rate of zinc. This effect is shown in Fig. 4, which plots the average overall corrosion rate versus the hydrogen ion concentration expressed in terms of pH value (Ref 4). In the pH range of 6 to 12.5, a protective film is formed on the zinc surface, and the zinc corrodes very slowly. At pH values below 4 and above 12.5, the major form of attack on zinc is hydrogen evolution, and zinc corrodes very rapidly. The pH values for natural water and mildly alkaline, soap-bearing water are within the safe range and will not corrode zinc coatings. The corrosion rate is higher in soft water than in hard water because the latter often forms a protective film. In hard water the corrosion rate of pure zinc by weight loss is 110 g/m^2/yr (0.36 oz/ft^2/yr), or by thickness loss, 15.4 μm/yr (0.61 mil/yr). In distilled water the losses are 986 g/m^2/yr (3.22 oz/ft^2/yr) or 138 μm/yr (5.44 mil/yr). It has been observed that in aerated hot water, the polarity between the zinc coating and the base steel is reversed at 60 °C (140 °F) and higher (Ref 5). In this case, zinc becomes a noble coating instead of a sacrificial coating and induces pitting of the bare steel. In seawater, zinc coatings corrode at approximately 181 g/m^2/yr (0.59 oz/ft^2/yr) or 1 mil/yr (25.4 μm/yr).

Atmospheric Corrosion of Galvanized Steel. The corrosion rate of zinc coatings exposed to the outdoors depends on such factors as the frequency and duration of moisture contact, the rate of drying, and the extent of industrial pollution. In general, the corrosion rate of zinc coatings in a rural atmosphere is very low. Seacoast atmospheres are less corrosive to zinc coating than industrial atmospheres.

A large-scale long-term test program was conducted on galvanized steel wire (both hot-dipped and electroplated) by ASTM (Ref 6). Carbon steel wires with different coating weights were exposed at several testing sites, which at that time were catagoized as Pittsburgh, PA (severe industrial); Sandy Hook, NH (marine); Bridgeport, CT (industrial); State College, PA (rural); Lafayette, IN (rural); Ithaca, NY (rural); and Ames, IA (rural). After fifteen years of exposure at these sites, the average corrosion rates of the zinc coatings were obtained by dividing the loss of coating weight (oz/ft^2) by the

number of years of exposure before the first rust was observed. These rates are summarized in Table 2. The service life of the zinc coating appears to be in direct proportion to the weight of the coating. The corrosion rate can range from 12 g/m^2/yr (0.04 oz/ft^2/yr) in a rural atmosphere, to 104 g/m^2/yr (0.34 oz/ft^2/yr) in a severe industrial atmosphere. The gage of the wire or the type of zinc coating (either hot-dipped or electro-deposited) within the test limits seems to have had no effect on the corrosion rate of the zinc coating.

In 1969, the atmospheric-corrosion behavior of hot-dip galvanized steel sheet was evaluated at three testing sites: a semi-industrial test site (Porter County, IN), a severe industrial test site (East Chicago, IN), and a marine test site (Kure Beach, NC) (Ref 7). The galvanized steel used was 0.81 mm (0.032 in.) thick with an average coating weight of 168 g/m^2 (0.55 oz/ft^2). All test panels were 100 by 150 mm (4×6 in.) in size. Two panels were made into one sandwich-type test specimen for exposure, so that the corrosion rate on the skyward and groundward side of each specimen could be evaluated independently. All specimens were exposed inclined 30° from the horizontal. Forty sandwich type test specimens were placed at each of the three test sites. Specimens were removed at the conclusion of the exposure period of 6 months, 1, 2, 3, 4, and 5 years. The standard ASTM recommended practice G 1 was used in preparing, cleaning, and evaluating the specimens (Ref 8). The average weight loss data obtained from the skyward panels of each specimen were fitted to the equation:

$$W = kt^n \qquad \text{(Eq 1)}$$

where W is weight loss of metal due to corrosion, t is exposure time in years, and n and k are empirical constants.

Predictions of corrosion rates using Eq 1 are shown in Fig. 5. The correlation coefficients (R^2) shown demonstrate the high-quality fit of each curve in Fig. 5. These curves can be used to predict the service life of galvanized steel for a given coating thickness, or determine the thickness required for a desired design life.

Intergranular Corrosion of Galvanized Steel. It has been known since 1923 that zinc die casting alloys are susceptible to intergranular attack in an air-water environment (Ref 9). The adverse effect of intergranular corrosion of hot-dip galvanized steel was first observed in 1963 and was investigated at Inland Steel Company in 1972 (Ref 10). The observed effect associated with intergranular corrosion was termed "delayed adhesion failure." Delayed adhesion failure is a deterioration in coating adhesion due to selective corrosion at grain boundaries. It was found that the small amount of lead normally added to commercial galvanizing spelters was a critical factor in the susceptibility of the zinc coating to intergranular attack. By using lead-free zinc spelter (<0.01% Pb), the damaging effect of intergranular corrosion was essentially eliminated.

For the continuous hot-dip galvanizing process, the main reason for adding 0.07 to 0.15% Pb to zinc spelter was to produce a spangled coating and to lower the surface tension of the zinc bath in order to provide the necessary fluid properties to produce a ripple-free coating. It was found that by adding antimony to the zinc spelter, beneficial effects similar to those obtained by adding lead could be achieved without causing intergranular corrosion. For galvanized coatings produced by an electroplating process, no intergranular corrosion has been observed.

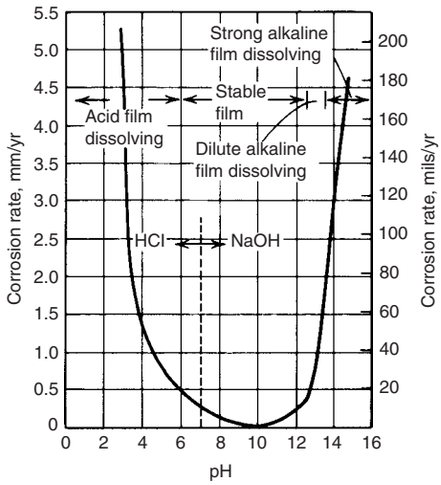

Fig. 4 Effect of pH value on the corrosion of zinc

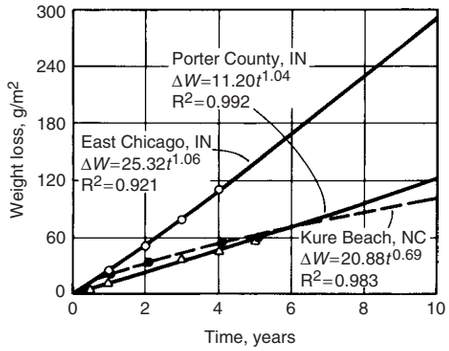

Fig. 5 Predictive equations for galvanized steel, based on 5 years of exposure

Table 2 Atmospheric-corrosion rates of zinc-coated wire

Test site	Type of atmosphere	Average corrosion rate			
		g/m^2/yr	oz/ft^2/yr	mil/yr	μm/yr
Pittsburgh, PA	Severe industrial	104	0.34	0.58	14.7
Sandy Hook, NJ	Marine (a)	40	0.13	0.22	5.6
Bridgepoint, CT	Industrial	40	0.13	0.22	5.6
State College, PA	Rural	18	0.06	0.10	2.5
Lafayette, IN	Rural	21	0.07	0.12	3.0
Ithaca, NY	Rural	18	0.06	0.10	2.5
Ames, IA	Rural	12	0.04	0.07	1.7

(a) 275 m, or 900 ft, from ocean. Source: Ref 6

Aluminum-Base Coatings

Types. Aluminum coatings on steel are primarily produced by spraying or hot dipping. Spray coatings are mainly applied to structural steel by using a wire-type gun. Pure aluminum or aluminum alloy wires are continually melted in the oxygen-fuel gas flame and atomized by a compressed air blast that carries the melted metal particles to the prepared surface, where they agglomerate to form a coating. The coating thickness is in the range of 0.08 to 0.2 mm (3 to 8 mils). Coatings are commonly sealed with organic lacquers or paints to delay the formation of visible surface rust.

Aluminum coatings on sheet steel are primarily produced by a continuous hot-dip process (the Sendzimir process). Molten baths of aluminum for hot dipping usually contain silicon in the range of 7 to 11% to retard the growth of a brittle iron-aluminum intermetallic layer. This alloy, which is one of the most fluid and easily cast aluminum alloys, forms a coating with a much thinner and more uniform alloy layer. This coated product, which has relatively good coating adhesion and forming properties, was commercially introduced in 1940; it is now identified as type I aluminized steel. A typical type I coating bath contains 9% Si, 87.5% Al, and 3.5% Fe.

Type II aluminized steel, with a coating consisting mainly of pure aluminum, was commercially produced in 1954. This coating could withstand mild forming, such as corrugating and roll forming. A typical type II coating bath contains 97.5% Al, 2% Fe, and 0.5% Si.

Aqueous Corrosion of Aluminized Steels. In aqueous environments, pure aluminum or aluminum-silicon alloy coatings exhibit good general corrosive resistance. The coatings become passive in a pH range between 4 and 9 and corrode rapidly in acid or alkali solutions. These coatings tend to pit in environments containing chloride ions (Ref 11), particularly at crevice or stagnant areas where passivity breaks down through the action of a differential aeration cell.

In soft water, aluminum coatings exhibit a potential that is positive to steel; therefore, they act like a noble coating. In seawater or in

aqueous environments containing Cl^- or SO_4^{2-}, the potential of aluminum coatings becomes active, and the polarity of aluminum-iron couples may reverse. Under these conditions, the aluminum coating is sacrificial and cathodically protects steel.

Atmospheric Corrosion of Aluminized Steel. The atmospheric-corrosion resistance of aluminum coatings is generally related to that of solid aluminum of the same thickness. The protection of steel by aluminum coating depends partly on cathodic protection and partly on the inert barrier layer of oxide film that forms on the metal surface. For thermally sprayed aluminum coatings, initial corrosion may produce slight superficial rust staining through pores in the coating. Subsequently, insoluble aluminum corrosion products block the pores and retard further corrosion of the coating.

When type I aluminized steel is exposed to the atmosphere, pitting corrosion can occur because of the difference in electrochemical potential between the silicon-rich phase and the aluminum matrix. The resulting corrosion product causes a red-brown blush discoloration on the metal surface (Ref 12). The corrosion product retards any further corrosion reaction. Type I panels have been exposed to a mild industrial atmosphere for over 40 years with no evidence of base metal corrosion.

For type II aluminum coating, the alloy layer is much thicker than that of the type I coating. Because of the protective nature of the oxide film formed on the coating surface, type II aluminum coatings have shown much better atmospheric-corrosion resistance than type I coatings.

In 1969, type I and type II aluminized steels were evaluated at three atmospheric-testing sites (Ref 7). The weight loss data obtained from the skyward panels of each specimen were fitted to Eq 1, which has been used for hot-dipped zinc coatings. The results of this curve fitting, together with k and n values obtained for type I and type II aluminum coatings, are shown in Fig. 6 and 7 for all three test sites. Table 3 provides a summary of the predicted weight loss for type I and type II aluminized steel in comparison with hot-dip zinc coatings based on 5-year exposure data. As indicated in Table 3, the atmospheric-corrosion rate of aluminum coating (type I or type II) is equivalent to only 10 to 40% of the corrosion rate of zinc coating, depending on the type of atmosphere.

Zinc-Aluminum Alloy Coatings

Zinc-aluminum alloy coatings are produced by the Sendzimir (hot) process. Zinc alloy coatings containing 4 to 7% aluminum are commercially produced under the tradenames Galfan and Superzinc. In addition to about 5% aluminum, Galfan contains about 0.05% mischmetal, a mixture of the rare earth elements lanthanum and cerium. Mischmetal additions are made to the alloy melt to improve the wetability of the bath and reduce the incidence of uncoated spots in the coating. Superzinc is similar to Galfan in composition, except that about 0.20% magnesium replaces the mischmetal in the coating. Galfan is used mostly in the unpainted condition, whereas Superzinc is intended for use in the painted condition.

Because the zinc-aluminum alloy composition is similar to the zinc-aluminum eutectic, the alloy coating has a eutectic structure containing scattered islands of primary zinc. An Fe-Al-Zn intermetallic is present at the alloy coating/steel interface (Ref 14). However, because this intermetallic layer is only about 1 μm (0.04 mil) thick, it is not normally detected by a light microscope. The zinc-aluminum melt does not contain lead; as a result, the alloy coatings are free of spangle and superior in cracking resistance to spangled galvanized coatings.

The 4 to 7% aluminum alloy coatings have better corrosion resistance than pure zinc coatings in a severe marine environment. However, as indicated in Table 4, performance of the 4 to 7% aluminum alloy coatings in moderate marine, rural, and industrial environments is about the same as that of pure zinc coatings (Ref 15, 16).

Aluminum-Zinc Alloy Coatings

Since the early 1970s, sheet steel coated with a 55% aluminum-zinc alloy has been produced commercially under a variety of trade names, including Galvalume (BIEC International), Zincalume (Australia and New Zealand), Aluzinc (Luxemberg), Zalutite (U.K.), Zintro-Alum (Mexico), Algafort (Spain), Zincalit (Italy), Cincalum (Argentina), and Zn-Alum (Chile). The 55% aluminum-zinc alloy coated sheet is produced using the Sendzimir process. The actual coating composition is about 55% aluminum, 1.6% silicon, and 43.4% zinc. Processing is similar to hot-dip galvanizing, except that the bath temperature is higher, nearly 593 °C (1100 °F). The coating microstructure is rather complex, consisting of aluminum-rich dendrites separated by zinc-rich interdendritic regions. A thin Fe-Al-Zn intermetallic layer is present at the steel surface. The intermetallic layer is separated from the alloy overlay by a thin silicon-rich layer. Silicon is also present in the microstructure

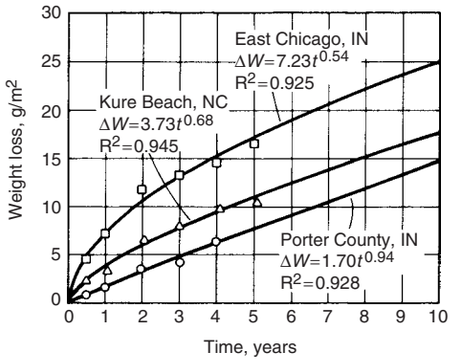

Fig. 6 Predictive equations for type I aluminized steel, based on 5 years of exposure

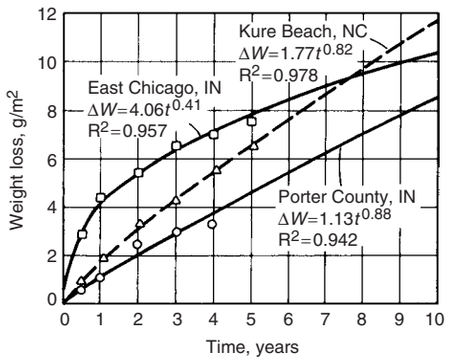

Fig. 7 Predictive equations for type II aluminized steel, based on 5 years of exposure

Table 3 Predicted weight loss (using Eq 1) after 10 year atmospheric exposure of hot-dip galvanized steel and type I and type II aluminized steel based on 5 year exposure data

	Ten year corrosion loss								
	Hot-dip galvanized			Type I aluminized			Type II aluminized		
Test site	g/m²	mils	μm	g/m²	mils	μm	g/m²	mils	μm
Porter County, IN (semi-industrial)	121.6	0.68	17.2	14.7	0.19	4.9	8.5	0.10	2.6
East Chicago, IN (semi-industrial)	290.1	1.61	41.0	25.2	0.33	8.4	10.5	0.13	3.3
Kure Beach, NC (240 m, 800 ft, lot—marine)	103.3	0.57	14.6	17.8	0.23	5.9	11.6	0.14	3.6

Coating thicknesses calculated from densities in g/m³ as follows (Ref 13): zinc, 7.07; Aluminum type I, 3.017; Aluminum type II, 3.21. Source: Ref 7

Table 4 Durability of coated sheet steels

	Years to first rust			
Environment	Zn	Zn-4%Al	Zn-7%Al	55%Al-Zn
Severe marine 24 m (80 ft) Kure Beach, NC	4	9	9	15
Moderate marine 240 m (800 ft) Kure Beach, NC	16	15	14	>30
Rural Saylorsburg, PA	14	14	14	>30
Industrial Bethlehem, PA	10	10	9	>30

Source: Ref 15, 16

as needlelike particles in the interdendritic regions.

The 55% aluminum-zinc coating combines some of the best features of both galvanized and aluminum-coated steels. The aluminum-rich dendrites constitute about 80% of the coating volume and provide excellent long-term atmospheric-corrosion resistance similar to aluminum. At the same time, the zinc-rich interdendritic regions provide sacrificial protection to steel similar to that of zinc. Most of the corrosion of the alloy coating takes place in the zinc-rich intermetallic regions. As these regions corrode, zinc-corrosion products plug up the resulting interdendritic interstices, creating a barrier against further corrosion. As a result, the corrosion rate of the alloy coating diminishes with time. On the basis of thickness, the 55% aluminum-zinc alloy has at least two to four times the resistance to atmospheric corrosion of a galvanized coating (see Table 4). In most environments, the 55% aluminum-zinc coating provides adequate galvanic protection against cut edges of the sheet one millimeter or less in thickness (Ref 16). Cut-edge protection is also provided by type II aluminum coatings in moderate marine environments, but not in the rural and industrial environments where aluminum is passive and a barrier coating. The corrosion resistance of the 55% aluminum-zinc alloy is enhanced by refining the dendritic structure through accelerated cooling after coating.

ACKNOWLEDGMENTS

This article was adapted from Harvie H. Lee, "Metallic Coated Steels," in *Corrosion,* Vol 13, *ASM Handbook,* ASM International, 1987, p 526–530.

Galfan is a tradename of ILZRO and Superzinc is a tradename of Nissan Steel Corporation.

REFERENCES

1. R.P. Krepski, "The Influence of Bath Alloy Additions in Hot-Dip Galvanizing," St. Joe Minerals Corporation, 1980
2. V. Furdanowicz and C. Ramadeva Shastry, *Met. Trans.,* Vol 30A, Dec 1999, p 3031
3. V. Jagannathan, *JOM,* Vol 45 (No. 8), Aug 1993, p 48
4. B. Roetheli, G. Cox, and W. Littreal, *Met. Alloys,* Vol 3, 1932, p 73
5. G. Schikorr, *Trans. Electrochem. Soc.,* Vol 76, 1939, p 247
6. A.P. Jahn, Atmospheric Corrosion of Steel Wires, in *ASTM Proceedings,* Vol 52, American Society for Testing and Materials, 1952, p 987
7. R.A. Legault and V.P. Pearson, "The Atmospheric Corrosion of Galvanized and Aluminized Steel," Research Report, Inland Steel Company, 1980
8. "Standard Practice for Preparing, Cleaning, and Evaluating Corrosion Test Specimens," G 1, *Annual Book of ASTM Standards,* Vol 03.02, American Society for Testing and Materials
9. H.F. Brauer and W.M. Peirce, The Effect of Impurities on the Oxidation and Swelling of Zinc-Aluminum Alloys, *Trans. Am. Inst. Min. Metall. Eng.,* Vol 60, 1923, p 796
10. H.H. Lee, Galvanized Steel with Improved Resistance to Intergranular Corrosion, *Proc. Galvanized Committee,* Vol 69, 1977, p 17
11. H.H. Uhlig, *Corrosion and Corrosion Control,* John Wiley & Sons, 1971, p 335
12. J.H. Rigo, *Corrosion,* Vol 17 (No. 5), 1961, p 245
13. ASTM A 641, Standard Specification for Zinc-Coated (Galvanized) Steel Wire. 1993 *Annual Book of ASTM Standards,* Vol 01.06, *Coated Steel Products,* ASTM Philadelphia, 1993
14. L.A. Rocha and M.A. Barbosa, *Corrosion,* Vol 47 (No. 7), July 1991, p 536–541
15. J.J. Friel and H.E. Townsend, Corrosion Resistance of Zinc and Zinc Aluminium Alloys, *Sheet Metal Industries,* Vol 60 (No. 9), 1984, 506–507
16. H.E. Townsend and A.R. Borzillo, *Mater. Perform*. Vol. 35 (No. 4), April 1996, p 30–36

SELECTED REFERENCES

- *8th International Rolling Conference and International Symposium on Zinc-Coated Steels, 44th Mechanical Working and Steel Processing Conference Proceedings,* Iron & Steel Society, Warrendale, PA, 2004
- *Galvatech '95 Conference Proceedings: The Use and Manufacture of Zinc and Zinc Alloy Coated Sheet Steel Products into the 21st Century,* September 17–21, 1995, Chicago, The Iron and Steel Society, 1995, Warrendale, PA
- The Physical Metallurgy of Zinc Coated Steel, *Proceedings of TMS International Conference, San Francisco, CA,* February 27–March 3, 1994, A.R. Marder, Ed., TMS, Warrendale, PA 1993
- *Proceedings of Fourth International Conference on Zinc and Zinc Alloy Coated Steel Sheet, Galvatech '98,* September 20–23, 1998, Chiba, Japan, The Iron and Steel Society of Japan, Tokyo, 1998
- *Proceedings of Fifth International Conference on Zinc and Zinc Alloy Coated Steel Sheet, Galvatech 2001,* June 26–28, 2001, Brussels, Belgium, M. Lamberights, Ed., Verlag Stahleisen GmBH, Dusseldorf, 2001
- *Proceedings of Galvatech '04, the International Conference on Zinc and Zinc Alloy Coated Sheet Steels,* April 4–7, 2004, Chicago, IL, Association for Iron & Steel Technology, Warrendale, PA, 2004
- *Proceedings of International Conference on Zinc and Zinc Alloy Coated Steel Sheet, Galvatech '89,* September 5–7, 1989, Tokyo, Japan, The Iron and Steel Society of Japan, Tokyo, 1989
- *Proceedings of Second International Conference on Zinc and Zinc Alloy Coated Steel Sheet, Galvatech '92,* September 8–10, 1992, Amsterdam, Verlag Stahleisen mBH, Dusseldorf, 1992
- Zinc-Based Coating Systems: Metallurgy and Performance, *Proceedings of TMS International Conference,* G. Krauss and D.K. Matlock, Ed., TMS, Warrendale, PA, 1990
- Zinc-Based Steel Coating Systems: Production and Performance, *Proceedings of TMS International Symposium,* February 1–19, 1998, San Antonio, TX, TMS, Warrendale, PA, 1998

ASM Handbook, Volume 13B: Corrosion: Materials
S.D. Cramer, B.S. Covino, Jr., editors, p40-42
DOI: 10.1361/asmhba0003809

Corrosion of Organic Coated Steels

Revised by Hiroyuki Tanabe, Dai Nippon Toryo Company

PAINT is applied to a steel product for one or both of the following reasons: enhancement of the esthetic value of the product or preservation of structural or functional integrity. The latter goal is the focus of this article. The advantage of corrosion protection is discussed as it applies to steel structures and prepainted steel.

Recently, new functions, such as a NO_x purification coating material using titanium dioxide photocatalyst, have been added to coatings (Ref 1). In order to preserve global environments, increasing numbers of environmentally friendly coatings, such as waterborne paints with remarkably reduced volatile organic compounds, have been developed and used.

The paint systems generally used to protect steel structures and steel sheet from corrosion, and how they deter corrosion, are described in this article. In addition, related standards on corrosion protection of steel structures are discussed, as are the prepainting process, the primary differences between prepaint formulations, the essential considerations about part design, and the selection criteria for the appropriate paint system. More detailed information on organic coating materials can be found in the articles "Organic Coatings and Linings" and "Paint Systems" in *ASM Handbook,* Volume 13A, 2003, and in the article "Painting" in *Surface Engineering,* Volume 5, *ASM Handbook,* 1994.

How Paint Films Deter Corrosion

In the presence of water and oxygen, iron corrodes to form oxides and hydroxides. The corrosion rate is accelerated when electrolytic solutes, such as chloride or sulfate salts of alkali metals, are present. Temperature also increases the corrosion rate, so the service life of a part can be increased by decreasing the service temperature. However, because little can usually be done to change service temperature, the exclusion of one or more of the principal reactants (oxygen, water, or electrolytes) from the steel surface is the primary means for deterring corrosion. The purpose of a paint film is to exclude the reactants.

There are primarily three methods of protecting steels from corrosion using paints: barrier coatings, passivation of the steel surface, and galvanic protection. In barrier protection, the paint film retards the diffusion of water, oxygen, or salts to the steel substrate. In 1952, the permeability of water and oxygen through the paint film was reported to be rapid and more than that required to support corrosion of uncoated steel (Ref 2). From further tests, it was felt that the permeability of the coating and the diffusion of moisture do not have the effect on the protective properties that may have been anticipated (Ref 3). However, by 1978 it was reported that film permeability of oxygen was less than that required to support corrosion of uncoated steel (Ref 4). Thus, remarkable progress was made in coatings technology during that period, and the limited permeation of oxygen provides a means for controlling corrosion of coated steel. The important contribution of the coating is to increase the electrolytic resistance, thereby lowering the corrosion rate (Ref 5). In addition, flake-shaped pigment particles can increase the path length that a reactant must traverse before reaching the substrate, which increases the effectiveness of the barrier film. Some aluminum and stainless steel pigments protect in this fashion.

With passivation of the steel, the reactivity of the steel surface can be decreased when the paint film contains anticorrosive pigments such as phosphate salts, chromate salts, and lead oxide.

Paints can also be formulated with zinc pigments for both barrier and galvanic protection (Ref 6). The zinc loading must be sufficiently high for interparticle contact, a condition that requires the critical pigment volume to be exceeded. The pigment particles are not completely wetted by the paint vehicle. Although some galvanic protection is afforded, most of the protection is provided by the barrier formed by zinc corrosion products. Zinc-rich primer is a typical component of a heavy-duty coatings system.

Corrosion Protection of Steel Structures by Organic Coatings

All features that are important in achieving adequate corrosion protection must be considered when using paints. The ISO 12944 (Ref 7) consists of eight parts that provide useful information on the following paint application topics: introduction (part 1), classification of environment (part 2), design consideration (part 3), type of surfaces and surface preparation (part 4), protective paint systems (part 5), laboratory performance test methods (part 6), execution and supervision of paint work (part 7), development of specifications for new work and maintenance (part 8). The classification of the environment into the categories described in ISO 12944 part 2 consists of five levels of atmospheric corrosivity and three categories for water and soil. Determining the category of the service environment is an important consideration when selecting a paint system.

Design of Steel Structures for Coating

Design of steel structures to be coated is an important consideration to avoid premature corrosion failures (Ref 7). The shape of a structure influences its susceptibility to corrosion damage. Basic design criteria for corrosion protection are:

- *Accessibility:* The steel component should be designed to be accessible for the purpose of applying, inspecting, and maintaining the protective paint system. Narrow spaces between structural elements should be avoided. Space must accommodate the surface preparation and painting equipment.
- *Treatment of gaps:* Narrow gaps, blind crevices, and lap joints are potential points for corrosion attack arising from retention of moisture and dirt, including any abrasive used for surface preparation.
- *Surface configurations:* Surface configurations that trap water and foreign matter should be avoided.
- *Edges:* Round edges are desirable in order to apply the protective coating uniformly and to attain adequate coating thickness on the edges.
- *Surface preparation:* Surface preparation is necessary to ensure removal of oxides, grease and oil, and foreign matter to obtain a surface that permits satisfactory paint adhesion to the steel.

Table 1 Brief history of organic coating systems for bridges in Japan

Year of construction	Name of bridge	Coating system
Before 1960	All bridges	Oil-type anticorrosion paint
1961	Wakato Ohashi Bridge	Shop primer Oil-type anticorrosive paint (in fabrication) Alkyd paint (on site)
1970	Sakai Suidou Ohashi Bridge	Zinc-rich primer Chlorinated rubber paint
1971	Kanmon Ohashi Bridge	Zinc metal spray Phenol MIO paint(a) Chlorinated rubber paint
1974	Minato Ohashi Bridge	Oil-type anticorrosion paint Phenol MIO paint Chlorinated rubber
1983	Innoshima Ohashi Bridge	Zinc-rich paint Epoxy paint Polyurethane paint
1985	Ohnaruto Hashi Bridge	Zinc-rich paint Epoxy paint Polyurethane paint
1988	Seto Ohashi Bridge	Zinc-rich paint Epoxy paint Polyurethane paint
1995	Akashi Ohashi Bridge	Zinc-rich paint Epoxy paint Fluoropolymer paint

(a) MIO, micaceous iron oxide formulated

Paint Systems for Bridges

Paints have a long history as coating systems for steel bridges and have been widely studied. Many large bridges have been constructed in corrosive environments such as bays, rivers, and coastlines. Protective coating systems for bridges in Japan have changed with time and are shown in Table 1.

In 1961, a shop primer and an oil-based anticorrosive paint with alkyd topcoat were used on the Wakato Ohashi Bridge and were the main bridge paint system of the 1960 s. Different coatings systems were used in the case of long bridges constructed over the sea. For example, the coatings system on the Kanmon Ohashi Bridge (constructed in 1971) was a phenol zinc-chromate paint, phenol micaceous iron oxide formulated interval-free paint, and chlorinated rubber top coat on a zinc metal spray coating. A new technical standard on corrosion protection of the Honshuu Shikoku Bridge was drafted in 1974. The protective coating system consisted of zinc-rich primer, epoxy intermediate coat, and polyurethane topcoat and has been used on many bridges since then. Bridges are also expected to be attractive in addition to their anticorrosive performance. Fluoropolymer (Ref 8, 9) topcoat has excellent weatherability and has been used instead of polyurethane topcoat. The fluoropolymer topcoat has an important role not only from the point of view of esthetic value but also durability. Other coating systems are also used, depending on environmental criteria and desired service life.

Present and future trends for steel structure coatings systems involve three main social requirements: environmental preservation, harmonization between esthetic value and environmental considerations, and reducing application costs. A number of weathering steel bridges have been constructed without any coating application. However, the advantage of coatings systems must be considered not only from the point of view of corrosion damage but also esthetic values. See the article "Corrosion of Weathering Steels" in this Volume.

Prepaint Processing

Much of painted steel used today is prepainted in coil form (coil coated) before shipment to fabricators. Modern, high-speed paint lines can apply a variety of organic coatings on bare steel and metallic-coated steel strip. After uncoiling, the first step in the prepaint process is to clean the steel strip with an alkaline detergent. The steel strip is then brushed with an abrasive roll to remove mill oils and grime and to reduce the level of an amorphous form of surface carbon indigenous to steel strip processing. Cleaning is usually more effective on flat strip than on a formed part.

Next, the strip is rinsed and pretreated to improve paint adhesion and corrosion protection. A prepaint treatment may consist of a phosphate coating or an organic pretreatment known as a wash primer or etching primer. Following the prepaint processing, paint is applied and then cured in an oven. Depending on the paint formulation and the paint line, the dwell time in the oven is generally between 20 and 50 s. A second coat may be applied and cured.

Differences between Prepaint and Postpaint

In formulating a paint designed for prepaint application, the paint must be flexible to endure the strains induced in subsequent forming operations. It must not craze on bending, a condition that would compromise corrosion resistance. In addition, the bend radii in the forming stages are often more severe than for the final part.

The coating must also withstand the abrasive forces of handling and forming. For a given coating type, the harder the coating, the more abrasion resistant the coating will be. Unfortunately, flexibility and hardness are inversely related; that is, the more flexible the coating, the softer the coating.

Flexibility and hardness are also considerations for the end use of postpainted parts, while the ability to withstand forming and handling are additional factors of concern in the formulation of paint designed for prepainting steel strip.

The final dried paint thickness, or dry-film thickness, on prepainted steel strip is usually no more than 0.025 mm (1 mil); plastisols and organosols are the major exceptions. The prepaint dry-film thickness is much less than the typical dry-film thickness on postpainted parts. Moreover, because of the method of application, the film is more evenly distributed and results in significantly fewer areas of low dry-film thickness and in the elimination of many of the appearance defects observed on finished postpainted parts. The formulations for prepaints are engineered to account for the lower dry-film thickness.

The film thickness is more variable on postpainted parts, with some areas receiving little paint because of the shape of the part. Film thickness in excess of that specified must be avoided as well, because this can lead to premature degradation caused by entrapped solvents or cracking in addition to surface imperfections.

Part Design Consideration in Coated Steel Sheet

When designing a part to be fabricated from prepainted steel, the maximum bend radius, the forming equipment, and the joining method must be considered. As mentioned earlier, the maximum bend radius during fabrication may be smaller than that specified for the final part because of springback. The design radius should be as generous as the structural and decorative criteria will allow. In considering part shape, avoidance of catchment areas, where possible, will decrease failures due to corrosion. The forming equipment should be well maintained to avoid marring the surface. Where possible, roll foaming is preferable to stamping. In cases where hard finishes in conjunction with tight radii (high flexibility) are required, prepainted strip can be warm formed. In warm forming, the paint is heated to or above its glass transition temperature range. At these temperatures, the paint is softer and more flexible, thus allowing tighter radii to be achieved during forming. After cooling, the paint becomes harder and more abrasion resistant.

Lastly, the part may require joining. Welding and mechanical fastening can damage the paint film. Therefore, it is necessary to touch up the scars to restore corrosion resistance. Adhesive bonding eliminates the need for touchup of damaged areas. Taking these factors into account, prepainted steel has been successfully fabricated into finished or semifinished (requiring postfinish coatings application) parts in many automotive, appliance, and office furniture manufacturing plants. Prepainted parts have been produced on production lines designed for their use as well as on existing lines, sometimes with no modification to the line.

Table 2 Relative rankings of various coatings in different performance categories

Category key: A, hardness; B, flexibility; C, humidity resistance; D, corrosion resistance to industrial atmospheres; E, salt spray; F, exterior durability, pigmented film; G, exterior durability, clear film; H, paint cure temperature, in°C (°F); I. cost guide. Ratings key: 1, excellent; 2, good; 3, fair; 4, poor; H, high cost; M, moderate cost; L, low cost

Type	A	B	C	D	E	F	G	H	I
Silicone acrylic	1	3	2	2	2	2	1	232 (450)	H
Thermoset acrylic	2	2	1	2	1	2	2	221 (430)	M
Amine-alkyd	2	3	2	2	3	2	3	170 (340)	L
Silicone alkyd	2	3	2	2	2	1	2	216 (420)	H
Vinyl-alkyd	2	2	1	2	2	3	3	170 (340)	M
Straight epoxy	1	2	1	1	1	4	4	204 (400)	H
Epoxy-ester	2	2	1	2	1	4	4	204 (400)	M
Organosol	2	1	1	1	1	2	3	177 (350)	L
Plastisol	3	1	1	1	1	2	3	177 (350)	L
Polyester (oil-free)	1	2	1	2	1	2	3	204 (400)	M
Silicone polyester	2	2	1	2	1	1	2	232 (450)	H
Poly-vinyl fluoride	2	1	1	1	1	1	1	232 (450)	H
Poly-vinyl idene fluoride	2	1	1	1	1	1	1	232 (450)	H
Solution vinyl	2	1	1	2	1	2	3	150 (300)	M

Selection Guideline

As an aid to understanding the coatings evaluation process, Table 2 compares various common coatings in several categories of performance. Changes in pigmentation and resin source for the vehicle can influence the rating. Table 2 is merely a guideline to the performance of these coatings. Comments from technical personnel should be sought before making any decision on paint selection.

The lettered columns in Table 2 are self-explanatory, with the exception of those involving exterior durability and salt spray. Exterior durability is the resistance to weathering, particularly the resistance to ultraviolet light. Ultraviolet light causes some coatings to chalk. For some coatings, proper pigmentation will prevent these phenomena, and this can be determined by comparing the columns for pigmented (F) and clear (G) films.

Salt spray (E) is not a predictor of service life, and coatings cannot be compared for end use on this basis. However, salt spray does detect coating defects and can be put to good use for detecting induced flaws by comparing results for flat panels with coating defects induced, for example, by forming or abrasion.

The first step in the paint system evaluation for a specific application is selection of a steel mill and/or paint company that is willing and able to help evaluate the needs of the final product. These needs can be categorized as either preservice or service. The preservice conditions involve forming, handling, and joining. The service conditions are those to which the customer exposes the product: humidity, temperature, corrosive agents, sunlight, and abrasion. Of course, preservice conditions can affect the service life of the final product, and these effects should be evaluated.

The next step in paint system evaluation is test program experimental design. Where possible, the test program compares candidate materials to the current products. Evaluation in actual service conditions is often not possible because of time limitations, and accelerated and laboratory tests are needed. From these results, acceptable candidates are identified and included in the next level of tests. A set of suitable steel parts is identified for testing the candidate paint systems. After the parts are tested, they are inspected to determine whether coatings damage occurred and whether corrosion resistance was compromised. In general, one material will not be superior in all aspects. Therefore, the desirable properties must be prioritized.

Advantages of Prepainted Steels

Although the aforementioned evaluation sequence may seem formidable, many manufacturers have found the use of prepainted steel to be productive and economical. The use of prepainted steel reduces or eliminates the problem of waste treatment of emissions from paint lines. The postpainting line is often the slow step in the production process, and using prepainted steel increases output. Although the material cost of prepainted steel is higher than the bare steel, the final part cost is lower because of increased productivity and the reduction of other costs, such as emission control. Although prepainted steel cannot replace postpainted steel in every application, prepainted steel has demonstrated its productive and economic advantages.

ACKNOWLEDGMENT

This article has been adapted from the article by James H. Bryson, Organic Coated Steels, *Corrosion,* Vol 13, *ASM Handbook,* ASM International, 1987, p. 528–530.

REFERENCES

1. N. Ishida, T. Fujii, and S. Emi, The 13th Asian-Pacific Corrosion Control Conference, Japan Society of Corrosion Engineering, 2003
2. J.E.O. Mayne, *Research*, Vol 6, 1952, p 278
3. K.A. Chandler and D.A. Bayliss, *Corrosion Protection of Steel Structures,* Elsevier, 1985, p 84
4. W. Funke, *Ind. Eng. Chem., Prod. Res. Dev.*, Vol 17, 1978, p 50
5. C.C. Maitland and J.E.O. Mayne, *Off. Digest*, Vol 34, 1962, p 972
6. H. Tanabe, T. Shinohara, and Y. Sato, *Boshoku Gijutsu (Corros. Eng.)*, Vol 29, 1980, p 290–296
7. "Paints and Varnishes—Corrosion Protection of Steel Structures by Protective Paint Systems," ISO 12944, International Organization for Standardization, 1998
8. M. Nagai, H. Matuno, H. Tanabe, and M. Kano, Proceedings of the Symposium on Advances in Corrosion Protection by Organic Coatings, Corrosion and Protection Centre, University of Manchester Institute of Science and Technology, 1944
9. S. Munekata, *Prog. Org. Coatings*, Vol 16, 1988, p 113–134

SELECTED REFERENCES

- Y. Sato, *Bousei Boushoku Tosou Gijutu (Protective Coating Technology)*, Kougaku Tosho, 1981
- D. Scantlebury, Proceedings of the Advances in Corrosion Protection by Organic Coatings, Corrosion and Protection Centre, University of Manchester Institute of Science and Technology, 1993
- L. M. Smith, *Generic Coating Types,* SSPC: The Society for Protective Coatings, 1996

ASM Handbook, Volume 13B: Corrosion: Materials
S.D. Cramer, B.S. Covino, Jr., editors, p43-50
DOI: 10.1361/asmhba0003810

Corrosion of Cast Irons

Revised by Thomas C. Spence, Flowserve Corporation

CAST IRON is a generic term that identifies a large family of ferrous alloys. Cast irons are primarily alloys of iron that contain more than 2% carbon and 1% or more silicon. Low raw material costs and relative ease of manufacture make cast irons the least expensive of the engineering metals. Cast irons can be cast into intricate shapes because of their excellent fluidity and relatively low melting points and can be alloyed for improvement of corrosion resistance and strength. With proper alloying, the corrosion resistance of cast irons can equal that of stainless steels and nickel-base alloys in many services.

Because of the excellent properties obtainable with these low-cost engineering materials, cast irons find wide application in environments that demand good corrosion resistance, such as in water, soils, acids, alkalis, saline solutions, organic compounds, sulfur compounds, and liquid metals.

Basic Metallurgy of Cast Irons

The metallurgy of cast irons is similar to that of steels except that sufficient silicon is present to necessitate use of the iron-silicon-carbon ternary phase diagram rather than the simple iron-carbon binary diagram. Figure 1 shows a section of the iron-iron carbide-silicon ternary diagram at 2% Si. The eutectic and eutectoid points in the iron-silicon-carbon diagram are both affected by the introduction of silicon into the system. In the 1 to 3% Si levels normally found in cast irons, eutectic carbon levels are related to silicon levels as follows:

$$\%C + {}^1/_3(\%Si) = 4.3 \qquad \text{(Eq 1)}$$

where %C is the eutectic carbon level, and %Si is the silicon level in the cast iron. The metallurgy of cast iron can occur in the metastable iron-iron carbide system, the stable iron-graphite system, or both. This causes structures of cast irons to be more complex than those of steel and more susceptible to processing conditions.

An appreciable portion of carbon in cast irons separates during solidification and appears as a separate carbon-rich constituent (e.g., graphite, iron carbides) in the microstructure. The level of silicon in the cast iron has a strong effect on the manner in which the carbon segregates in the microstructure. Higher silicon levels favor the formation of graphite, but lower silicon levels favor the formation of iron carbides. The form and shape in which the carbon occurs determine the type of cast iron (Table 1).

The structure of the metal matrix around the carbon-rich constituent establishes the class of iron within each type of iron. As in steel, the five basic matrix structures occur in cast iron: ferrite, pearlite, bainite, martensite, and austenite.

Ferrite is generally a soft constituent, but it can be solid solution hardened by silicon. When silicon levels are below 3%, the ferrite matrix is readily machined but exhibits poor wear resistance. Above 14% Si, the ferritic matrix becomes very hard and wear resistant but is essentially nonmachinable. The low carbon content of the ferrite phase makes hardening difficult. Ferrite can be observed in cast irons on solidification but is generally present as the result of special annealing heat treatments. High silicon levels promote the formation of ferritic matrices in the as-cast condition.

Pearlite consists of alternate layers of ferrite and iron carbide (Fe_3C, or cementite). It is very strong and tough. The hardness, strength, machinability, and wear resistance of pearlitic matrices vary with the fineness of its laminations. The carbon content of pearlite is variable and depends on the composition of the iron and its cooling rate.

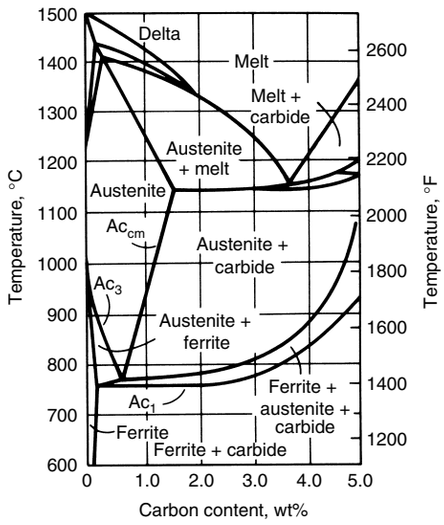

Fig. 1 Section of the iron-iron carbide-silicon ternary phase diagram at 2% Si

Bainite is an acicular structure in cast irons that can be obtained by heat treating, alloying, or combinations of these. Bainitic structures provide very high strength at a machinable hardness.

Martensitic structures are produced by alloying, heat treating, or a combination of these practices. Martensitic microstructures are the hardest, most wear-resistant structures obtainable in cast irons. Molybdenum, nickel, manganese, and chromium can be used to produce martensitic or bainitic structures. Silicon has a negative effect on martensite formation, because it promotes the formation of pearlite or ferrite.

Austenitic structures are typically found in the Ni-Resist cast irons and the austempered ductile irons. Austenite is a face-centered cubic atomic structure created primarily by alloying with austenite-forming elements such as nickel. Austenite is generally the softest and more corrosion-resistant matrix structure. However, the carbon-enriched austenite of austempered ductile iron has higher hardness and other unique characteristics over conventional ductile irons (Ref 1).

Influence of Alloying

Alloying elements can play a dominant role in the susceptibility of cast irons to corrosion attack. The alloying elements generally used to enhance the corrosion resistance of cast irons

Table 1 Summary of cast iron classification based on carbon form and shape

Type of cast iron	Carbon form and shape
White cast iron	Iron carbide compound
Malleable cast iron	Irregularly shaped nodules of graphite
Gray cast iron	Graphite flakes
Ductile cast iron	Spherical graphite nodules
Compacted graphite cast iron	Short, fat, interconnected flakes (intermediate between ductile and gray cast iron)

include silicon, nickel, chromium, copper, and molybdenum. Other alloying elements, such as vanadium and titanium, are sometimes used, but not to the extent of the first five elements mentioned.

Silicon is the most important alloying element used to improve the corrosion resistance of cast irons. Silicon is generally not considered an alloying element in cast irons until levels exceed 3%. Silicon levels between 3 and 14% offer some increase in corrosion resistance to the alloy, but above approximately 14% Si, the corrosion resistance of the cast iron increases dramatically. Silicon levels up to 17% have been used to enhance the corrosion resistance of the alloy further, but silicon levels over 16% make the alloy extremely brittle and difficult to manufacture. Even at 14% Si, the strength and ductility of the material is low, and special design and manufacturing parameters are required to produce and use these alloys.

Alloying with silicon promotes the formation of strongly adherent surface films in cast irons. Considerable time may be required to establish these films fully on the castings. Consequently, in some services, corrosion rates may be relatively high for the first few hours or even days of exposure, then may decline to extremely low steady-state rates for the rest of the time the parts are exposed to the corrosive environment (Fig. 2).

Nickel is used to enhance the corrosion resistance of cast irons in a number of applications. Nickel increases corrosion resistance by the formation of protective oxide films on the surface of the castings. Up to 4% Ni is added in combination with chromium to improve both strength and corrosion resistance in cast iron alloys. The enhanced hardness and corrosion resistance obtained is particularly important for improving the erosion-corrosion resistance of the material. Nickel additions enhance the resistance of cast irons to corrosion by reducing acids and alkalis. Nickel additions of 12% or greater are necessary to optimize the corrosion resistance of cast irons. The Ni-Resist group are high-nickel alloys (13.5 to 36% Ni) having high resistance to wear, heat, and corrosion. Nickel is not as common an alloying addition as either silicon or chromium for enhancing the corrosion resistance in cast irons. It is much more important as a strengthening and hardening addition.

Chromium is frequently added alone and in combination with nickel and/or silicon to increase the corrosion resistance of cast irons. As with nickel, small additions of chromium are used to refine graphite and matrix microstructures. These refinements enhance the corrosion resistance of cast irons in seawater and weak acids. Chromium additions of 15 to 35% improve the corrosion resistance of cast irons to oxidizing acids, such as nitric acid (HNO_3). Chromium increases the corrosion resistance of cast iron by the formation of protective oxides on the surface of castings. The oxides formed will resist oxidizing acids but will be of little benefit under reducing conditions. High-chromium additions, similar to higher-silicon additions, reduce the ductility of cast irons.

Copper is added to cast irons in special cases. Copper additions of 0.25 to 1% increase the resistance of cast iron to dilute acetic (CH_3COOH), sulfuric (H_2SO_4), and hydrochloric (HCl) acids as well as acid mine water. Small additions of copper are also made to cast irons to enhance atmospheric-corrosion resistance. Additions of up to 10% are made to some high-nickel-chromium cast irons to increase corrosion resistance. The exact mechanism by which copper improves the corrosion resistance of cast irons is not known.

Molybdenum. Although an important use of molybdenum in cast irons is to increase strength and structural uniformity, it is also used to enhance corrosion resistance, particularly in high-silicon cast irons. Molybdenum is particularly useful in hydrochloric acid (HCl). As little as 1% Mo is helpful in some high-silicon irons, but for optimal corrosion resistance, 3 to 4% Mo is added.

Other Alloying Additions. In general, other alloying additions to cast irons have a minimal effect on corrosion resistance. Vanadium and titanium enhance the graphite morphology and matrix structure and impart slightly increased corrosion resistance to cast irons. Few other additions are made to cast irons that have any significant effect on corrosion resistance.

Influence of Microstructure

Although the graphite shape and the amount of massive carbides present are critical to mechanical properties, these structural variables do not have a strong effect on corrosion resistance. Flake graphite structures may trap corrosion products and retard corrosion slightly in some applications. Under unusual circumstances, graphite may act cathodically with regard to the metal matrix and accelerate attack.

While the structure of the matrix has a slight influence on corrosion resistance, the effect is small compared to that of matrix composition. In gray irons, ferrite structures are generally the least corrosion-resistant, and graphite flakes exhibit the greatest corrosion resistance. Pearlite and cementite show intermediate corrosion resistance, while an austenitic structure imparts higher corrosion resistance.

Shrinkage or porosity can degrade the corrosion resistance of cast iron parts by acting as natural crevices. The presence of porosity permits the corrosive medium to enter the body of the casting and can provide continuous leakage paths for corrosives in pressure-containing components.

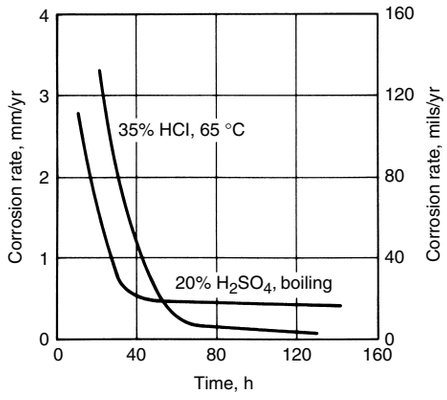

Fig. 2 Corrosion rates of high-silicon cast irons as a function of time and corrosive media

Commercially Available Cast Irons

Based on corrosion resistance, cast irons can be grouped into the following five classes.

Unalloyed gray, ductile, malleable, and white cast irons represent the first and largest class. All of these materials contain carbon and silicon of 3% or less and no deliberate additions of nickel, chromium, copper, or molybdenum. As a group, these materials exhibit a corrosion resistance that equals or slightly exceeds that of unalloyed steels, but they show the highest rate of attack among the classes of cast irons. These materials are available in a wide variety of configurations and alloys. Major ASTM standards that cover these materials are listed in Table 2.

Low- and moderately alloyed cast irons constitute the second major class. These irons contain the iron and silicon of unalloyed cast irons plus up to several percent of nickel, copper, chromium, or molybdenum. As a group, these materials exhibit two to three times the service life of unalloyed cast irons. Austempered ductile iron (ADI) is the newest group of alloys in this

Table 2 ASTM standards that include unalloyed cast irons

Standard	Materials/products covered
A 47	Ferritic malleable iron castings
A 48	Gray iron castings
A 74	Cast iron soil pipe and fittings
A 126	Gray iron castings for valves, flanges, and pipe fittings
A 159	Automotive gray iron castings
A 197	Cupola malleable iron
A 220	Pearlitic malleable iron castings
A 278	Gray iron castings for pressure-containing parts for temperatures up to 345 °C (650 °F)
A 319	Gray iron castings for elevated temperatures for nonpressure-containing parts
A 395	Ferritic ductile iron pressure-retaining castings for use at elevated temperatures
A 476	Ductile iron-castings for paper mill dryer rolls
A 536	Ductile iron castings
A 602	Automotive malleable iron castings
A 716	Ductile iron culvert pipe
A 746	Ductile iron gravity sewer pipe
A 823	Statically cast permanent mold gray iron castings
A 842	Compacted graphite iron castings
A 874	Ferritic ductile iron castings suitable for low-temperature service

category, and they have some unique properties. The ADI delivers twice the strength of conventional ductile irons for a given level of elongation. In addition, ADI offers exceptional wear and fatigue resistance (Ref 1). Major ASTM standards that cover these materials are listed in Table 3.

High-nickel austenitic cast irons represent a third major class of cast irons for corrosion service. These materials contain large percentages of nickel and copper and are fairly resistant to such acids as concentrated sulfuric (H_2SO_4) and phosphoric (H_3PO_4) acids at slightly elevated temperatures, hydrochloric acid at room temperature, and organic acids such as acetic (CH_3COOH), oleic, and stearic. When nickel levels exceed 18%, austenitic cast irons are nearly immune to alkali or caustics, although stress corrosion can occur. High-nickel cast irons can be nodularized to yield ductile irons. Major ASTM standards that cover these materials are listed in Table 4.

High-chromium cast irons are the fourth class of corrosion-resistant cast irons. These materials are basically white cast irons alloyed with 12 to 35% Cr. Other alloying elements may also be added to improve resistance to specific environments. When chromium levels exceed 20%, high-chromium cast irons exhibit good resistance to oxidizing acids, particularly nitric acid (HNO_3). High-chromium irons are not resistant to reducing acids. They are used in saline solutions, organic acids, phosphate mining, marine, and industrial atmospheres. These materials display excellent resistance to abrasion, and, with proper alloying additions, they can also resist combinations of abrasives and liquids, including some dilute acid solutions. High-chromium cast irons are covered in ASTM A 532. In addition, many proprietary alloys not covered by national standards are produced for special applications, such as wear components in mining operations or slurry pumps.

High-silicon cast irons are the fifth class of corrosion-resistant cast irons. The principal alloying element is 12 to 18% Si, with more than 14.2% Si needed to develop excellent corrosion resistance. Chromium and molybdenum are also used in combination with silicon to develop corrosion resistance to specific environments. High-silicon cast irons represent the most universally corrosion-resistant alloys available at moderate cost. When silicon levels exceed 14.2%, high-silicon cast irons exhibit excellent resistance to H_2SO_4, HNO_3, HCl, CH_3COOH, and most other mineral and organic acids and corrosives. These materials display good resistance in oxidizing and reducing environments and are not appreciably affected by concentration or temperature. Exceptions to universal resistance are hydrofluoric acid (HF), fluoride salts, sulfurous acid (H_2SO_3), sulfite compounds, strong alkalis, and alternating acid-alkali conditions. High-silicon cast irons are defined in ASTM A 518 and A 861.

Forms of Corrosion

Cast irons exhibit the same general forms of corrosion as other metals and alloys:

- Uniform or general attack
- Galvanic or two-metal corrosion
- Crevice corrosion
- Pitting
- Intergranular corrosion
- Selective leaching (graphitic corrosion)
- Erosion-corrosion
- Stress corrosion
- Corrosion fatigue
- Fretting corrosion
- Microbiological

Graphitic Corrosion. A form of corrosion unique to cast irons is a selective leaching attack commonly referred to as graphitic corrosion or graphitization. Graphitic corrosion is observed in gray cast irons in relatively mild environments in which selective leaching of iron leaves a brittle graphite network. Selective leaching of the iron takes place because the graphite is cathodic to the iron, and the gray cast iron structure establishes an excellent galvanic cell. While graphitic corrosion of gray cast iron is considered a form of selecting leaching, its mechanism on a microstructural level is similar to galvanic corrosion. This form of corrosion generally occurs only when corrosion rates are low. If the metal corrodes more rapidly, the entire surface, including the graphite, is removed, and more or less uniform corrosion occurs. Graphitic corrosion can cause significant problems because, although no dimensional changes occur, the cast iron loses its strength and metallic properties. Thus, without detection, potentially dangerous situations may develop in pressure-containing applications. Graphitic corrosion is observed only in gray cast irons. In both nodular and malleable cast iron, the lack of graphite flakes provides a more favorable anode/cathode ratio and no network to hold the corrosion products together. By maximizing the area of the anodic component while decreasing the area of the cathodic constituent, the potential for galvanic (graphitic) corrosion has been reduced. Because graphitization is so common with cast iron and it compromises the structural integrity of the metal, instrumentation using eddy-current measurements has recently been developed to detect and measure it (Ref 2).

Fretting corrosion is commonly observed when vibration or slight relative motion occurs between parts under load. The relative resistance of cast iron to this form of attack is influenced by such variables as lubrication, hardness variations between materials, the presence of gaskets, and coatings. Table 5 compares the relative fretting resistance of cast iron under different combinations of these variables.

Pitting and Crevice Corrosion. The presence of chlorides and crevices or other shielded areas presents conditions that are favorable to the pitting and crevice corrosion of cast iron. Pitting has been reported in such environments as dilute alkylaryl sulfonates, antimony trichloride ($SbCl_3$), and calm seawater. Alloying can influence the resistance of cast irons to pitting and crevice corrosion. For example, in calm seawater, nickel additions reduce the susceptibility

Table 3 ASTM standards that include low-alloyed cast iron materials

Standard	Materials/products covered
A 159	Automotive gray iron castings
A 319	Gray iron castings for elevated temperatures for nonpressure-containing parts
A 532	Abrasion-resistant cast irons
A 897	Austempered ductile iron castings

Note: Because most cast iron standards make chemical composition subordinate to mechanical properties, many of the standards listed in Table 2 may also be used to purchase low-alloyed cast iron materials.

Table 4 ASTM standards that include high-nickel austenitic cast iron materials

Standard	Materials/products covered
A 436	Austenitic gray iron castings
A 439	Austenitic ductile iron castings
A 571	Austenitic ductile iron castings for pressure-containing parts suitable for low-temperature service

Table 5 Relative fretting resistance of cast iron

Poor	Average	Good
Aluminum on cast iron	Cast iron on cast iron	Cast iron on cast iron with phosphate coating
Magnesium on cast iron	Copper on cast iron	Cast iron on cast iron with coating of rubber cement
Cast iron on chrome plate	Brass on cast iron	Cast iron on cast iron with coating of tungsten sulfide
Laminated plastic on cast iron	Zinc on cast iron	Cast iron on cast iron with rubber gasket
Bakelite on cast iron	Cast iron on silver plate	Cast iron on cast iron with Molykote lubricant
Cast iron on tin plate	Cast iron on copper plate	Cast iron on stainless with Molykoke lubricant
Cast iron on cast iron with coating of shellac	Cast iron on amalgamated copper plate	
	Cast iron on cast iron with rough surface	

Source: Ref 3

of cast irons to pitting attack. High-silicon cast irons with chromium and/or molybdenum offer enhanced resistance to pitting and crevice corrosion. Although microstructural variations probably exert some influence on susceptibility to crevice corrosion and pitting, there are few reports of this relationship.

Intergranular attack is relatively rare in cast irons. In stainless steels, in which this type of attack is most commonly observed, intergranular attack is related to chromium depletion adjacent to grain boundaries. Because only the high-chromium cast irons depend on chromium to form passive films for resistance to corrosion attack, few instances of intergranular attack related to chromium depletion have been reported. The only reference to intergranular attack in cast irons involves ammonium nitrate (NH_4NO_3), in which unalloyed cast irons are reported to be intergranularly attacked. Because this form of selective attack is relatively rare in cast irons, no significant references to the influence of either structure or chemistry on intergranular attack have been reported.

Erosion-Corrosion. Fluid flow by itself or in combination with solid particles can cause erosion-corrosion attack in cast irons. Two methods are known to enhance the erosion-corrosion resistance of cast irons. First, the hardness of the cast irons can be increased through solid-solution hardening or phase-transformation-induced hardness increases. For example, 14.5% Si additions to cast irons cause substantial solid-solution hardening of the ferritic matrix. In such environments as the sulfate liquors encountered in the pulp and paper industry, this hardness increase enables high-silicon iron equipment to be successfully used, while lower-hardness unalloyed cast irons fail rapidly by severe erosion-corrosion. Use of martensitic or white cast irons can also improve the erosion-corrosion resistance of cast irons as a result of hardness increases.

Second, better inherent corrosion resistance can also be used to increase the erosion-corrosion resistance of cast irons. Austenitic nickel cast irons can have hardnesses similar to unalloyed cast irons but may exhibit better erosion resistance because of the improved inherent corrosion resistance of nickel-alloyed irons compared to unalloyed irons. Microstructure can also affect erosion-corrosion resistance slightly. Gray cast irons generally show better resistance than steels under erosion-corrosion conditions. This improvement is related to the presence of the graphite network in the gray cast iron. Iron is corroded from the gray iron matrix as in steel, but the graphite network that is not corroded traps corrosion products; this layer of corrosion products and graphite offers additional protection against erosion-corrosion attack.

Flow-induced corrosion stemming from fluid velocity alone is another type of erosion-corrosion for steels and cast irons. In certain services where unalloyed or low-alloyed cast irons are used, their corrosion resistance is due to the formation of a thick, poorly adherent corrosion product rather than the usual passive oxide layer associated with the more common corrosion-resistant alloys. Examples of such situations are concentrated sulfuric or hydrofluoric acids. In these services, the cast irons develop, respectively, a thick iron sulfate film or iron-fluoride film, and at low velocities these films remain intact and provide protection. However, at velocities greater than a couple feet per second, these films are washed away, allowing further corrosion of the cast irons.

Microbiologically induced corrosion (MIC) is the corrosion of metals resulting from the activity of a variety of living microorganisms, which, as a result of their growth or metabolism, either produce corrosive wastes or participate directly in electrochemical reactions on the metal surfaces. This phenomenon is often associated with biofouling and corrosion of buried structures. Soils containing sulfate concentrations support conditions where MIC of cast iron pipe can occur. An Australian study estimates that 50% of all failures of buried metal were due to microbiological causes (Ref 4). Prevention is difficult, but cathodic protection and the use of protective coatings can be beneficial (Ref 5).

Stress-corrosion cracking (SCC) is observed in cast irons under certain combinations of environment and stress. Because stress is necessary to initiate SCC and because design factors often limit stresses in castings to relatively low levels, SCC is not observed as often in cast irons as in other more highly stressed components. However, under certain conditions, SCC can be a serious problem. Because unalloyed cast irons are generally similar to ordinary steels in resistance to corrosion, the same environments that cause SCC in steels will likely cause problems in cast irons. Environments that may cause SCC in unalloyed cast irons include these solutions (Ref 6):

- Sodium hydroxide (NaOH)
- Sodium hydroxide-sodium silicate (NaOH-Na_2SiO_2)
- Calcium nitrate ($Ca(NO_3)_2$)
- Ammonium nitrate (NH_4NO_3)
- Sodium nitrate ($NaNO_3$)
- Mercuric nitrate ($Hg(NO_3)_2$)
- Mixed acids (H_2SO_4-HNO_3)
- Hydrogen cyanide (HCN)
- Seawater
- Acidic hydrogen sulfide (H_2S)
- Molten sodium-lead alloys
- Acid chloride
- Oleum (fuming H_2SO_4)

Graphite morphology can play an important role in SCC resistance in certain environments. In oleum, flake graphite structures present special problems. Acid tends to penetrate along graphite flakes and corrodes the iron matrix. The corrosion products formed build up internal pressure and eventually crack the iron. This problem is found in both gray cast irons and high-silicon cast irons, which have flake graphite morphologies. It is not seen in ductile cast irons that have nodular graphite shapes.

Resistance to Corrosive Environments

No single grade of cast iron will resist all corrosive environments. However, a cast iron can be identified that will resist most of the corrosives commonly used in industrial environments. Cast irons suitable for the more common corrosive environments are discussed as follows.

Sulfuric Acid. Unalloyed, low-alloyed, and high-nickel austenitic as well as high-silicon cast irons are used in H_2SO_4 applications. Use of unalloyed and low-alloyed cast iron is limited to low-velocity, low-temperature concentrated (>70%) H_2SO_4 service. Unalloyed cast iron is rarely used in dilute or intermediate concentrations, because corrosion rates are substantial. In concentrated H_2SO_4, as well as other acids, ductile iron is generally considered superior to gray iron, and ferritic matrix irons are superior to pearlitic matrix irons. In hot, concentrated acids, graphitization of the gray iron can occur. In oleum, unalloyed gray iron will corrode at very low rates. However, acid will penetrate along the graphite flakes, and the corrosion product that forms can build up sufficient pressure to split the iron. Interconnecting graphite is believed to be necessary to cause this form of cracking; therefore, ductile and malleable irons are generally acceptable for oleum service. Some potential for galvanic corrosion between cast iron and steel has been reported in 100% H_2SO_4.

High-nickel austenitic cast irons exhibit acceptable corrosion resistance in room-temperature and slightly elevated-temperature H_2SO_4 service. As shown in Fig. 3, their performance is adequate over the entire range of

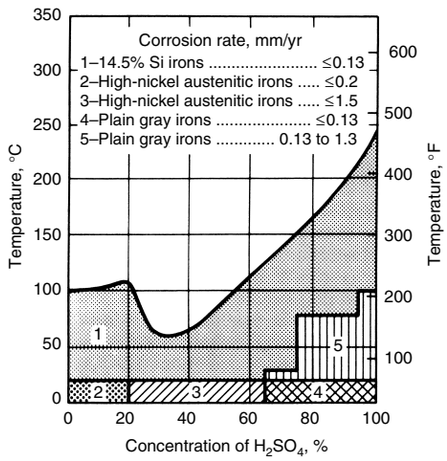

Fig. 3 Corrosion of high-nickel austenitic cast iron in H_2SO_4 as a function of acid concentration and temperature. Source: Ref 6

H_2SO_4 concentrations, but they are a second choice compared to high-silicon cast irons.

High-silicon cast irons are the best choice among the cast irons and perhaps among the commonly available engineering material for resistance to H_2SO_4. This material has good corrosion resistance to the entire H_2SO_4 concentration range at temperatures to boiling (Fig. 4). Rapid attack occurs at concentrations over 100% and in service containing free sulfur trioxide (SO_3). High-silicon cast irons are relatively slow to passivate in H_2SO_4 service. Corrosion rates are relatively high for the first 24 to 48 h of exposure and then decrease to very low steady-state rates (Fig. 2).

Nitric Acid. All types of cast iron, except high-nickel austenitic iron, find some applications in HNO_3. The use of unalloyed cast iron in HNO_3 is limited to low-temperature, low-velocity concentrated acid service. Even in this service, caution must be exercised to avoid dilution of acid because the unalloyed and low-alloyed cast irons both corrode very rapidly in dilute or intermediate concentrations at any temperature. High-nickel austenitic cast irons exhibit essentially the same resistance as unalloyed cast iron to HNO_3 but cannot be economically justified for this service.

High-chromium cast irons with chromium contents over 20% give excellent resistance to HNO_3, particularly in dilute concentrations (Fig. 5). High-temperature boiling solutions attack these grades of cast iron.

High-silicon cast irons also offer excellent resistance to HNO_3. Resistance is exhibited over essentially all concentration and temperature ranges, with the exception of dilute, hot acids (Fig. 6). High-silicon cast iron equipment has been used for many years in the manufacture and handling of HNO_3 mixed with other chemicals, such as H_2SO_4, sulfates, and nitrates. Contamination of HNO_3 with HF, such as might be experienced in pickling solutions, may accelerate attack of the high-silicon iron to unacceptable levels.

Hydrochloric Acid. Use of cast irons is relatively limited in HCl. Unalloyed cast iron is unsuitable for any HCl service. Rapid corrosion occurs at a pH of 5 or lower, particularly if appreciable velocity is involved. Aeration or oxidizing conditions, such as the presence of metallic salts, result in rapid destructive attack of unalloyed cast irons, even in very dilute HCl solutions.

High-nickel austenitic cast irons offer some resistance to all HCl concentrations at room temperature or below. High-chromium cast irons are not suitable for HCl services.

High-silicon cast irons offer the best resistance to HCl of any cast iron. When alloyed with 4 to 5% Cr, high-silicon cast iron is suitable for all concentrations of HCl at temperatures up to 28 °C (80 °F). When high-silicon cast iron is alloyed with chromium, molybdenum, and higher silicon levels, the temperature for use can be increased (Fig. 7). In concentrations up to 20%, ferric ions (Fe^{3+}) or other oxidizing agents inhibit corrosion attack on high-silicon cast iron alloyed with chromium. At over 20% acid concentration, oxidizers accelerate attack on the alloy. As in H_2SO_4, corrosion rates of high-silicon cast iron are initially high in the first 24 to 48 h of exposure then decrease to very low steady-state rates (Fig. 2).

Phosphoric Acid. All cast irons find some application in H_3PO_4service, but the presence of contaminants must be carefully evaluated before selecting a material. Unalloyed cast iron finds little use in H_3PO_4, with the exception of concentrated acids. Even in concentrated acids, use may be severely limited by the presence of fluorides, chlorides, or H_2SO_4.

High-nickel cast irons find some application in H_3PO_4 at and slightly above room temperature. These cast irons can be used over the entire H_3PO_4 concentration range. Impurities in the acid may greatly restrict the applicability of this grade of cast iron.

High-chromium cast irons exhibit generally low rates of attack in H_3PO_4 up to 60% concentration and are commonly used in the phosphate mining industry where abrasion resistance is needed. High-silicon cast irons show good-to-excellent resistance at all concentrations and temperatures for pure acid. The presence of fluoride ions (F^-) in H_3PO_4 makes the high-silicon irons unacceptable for use.

Organic acids and compounds are generally not as corrosive as mineral acids. Consequently, cast irons find many applications in handling these materials. Unalloyed cast iron can be used to handle concentrated acetic acid, CH_3COOH, and fatty acids but will be attacked by more dilute solutions. Unalloyed cast irons are used to handle methyl, ethyl, butyl, and amyl alcohols. If the alcohols are contaminated with water and air, discoloration of the alcohols may occur. Unalloyed cast irons can also be used to handle glycerine, although slight discoloration of the glycerine may result.

Austenitic nickel cast irons exhibit adequate resistance to CH_3COOH, oleic acid, and stearic acid. High-chromium cast irons are adequate for CH_3COOH but will be more severely corroded by formic acid (HCOOH). High-chromium cast irons are excellent for lactic and citric acid solutions.

High-silicon cast irons show excellent resistance to most organic acids, including HCOOH and oxalic acid, in all temperature and concentration ranges. High-silicon cast irons also exhibit excellent resistance to alcohols and glycerine.

Alkali solutions require material selections that are distinctly different from those of acid solutions. Alkalis include sodium

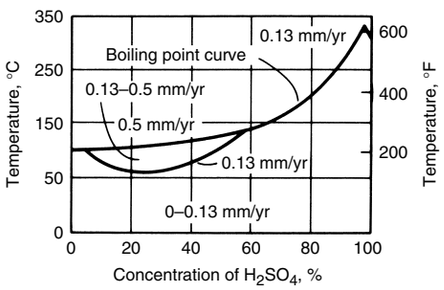

Fig. 4 Corrosion of high-silicon cast iron in H_2SO_4 as a function of acid concentration and temperature

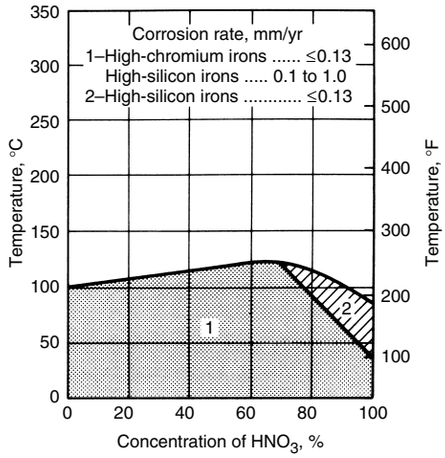

Fig. 5 Corrosion of high-chromium cast iron in HNO_3 as a function of acid concentration and temperature. Source: Ref 6

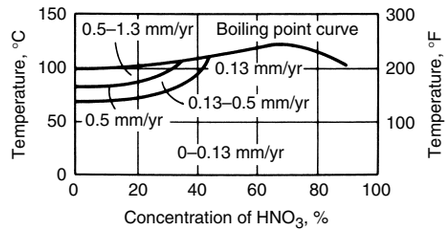

Fig. 6 Corrosion of high-silicon cast iron in HNO_3 as a function of acid concentration and temperature

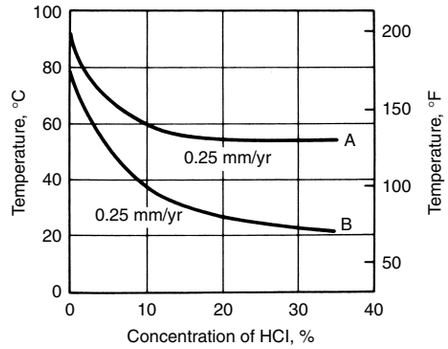

Fig. 7 Isocorrosion diagram for two high-silicon cast irons in HCl. A, Fe-14.3Si-4Cr-0.5Mo; B, Fe-16Si-4Cr-3Mo

hydroxide (NaOH), potassium hydroxide (KOH), sodium silicate (Na_2SiO_3), and similar chemicals that contain sodium, potassium, or lithium.

Unalloyed cast irons exhibit generally good resistance to alkalis—approximately equivalent to that of steel. These unalloyed cast irons are not attacked by dilute alkalis at any temperature. Hot alkalis at concentrations exceeding 30% attack unalloyed iron. Temperatures should not exceed 80 °C (175 °F) for concentrations up to 70% if corrosion rates of less than 0.25 mm/yr (10 mils/yr) are desired. Ductile and gray iron exhibit approximately equal resistance to alkalis. However, ductile cast iron is susceptible to cracking in highly alkaline solutions, but gray cast iron is not. Alloying with 3 to 5% Ni substantially improves the resistance of cast irons to alkalis. High-nickel austenitic cast irons offer even better resistance to alkalis than unalloyed or low-nickel cast irons.

High-silicon cast irons show good resistance to relatively dilute solutions of NaOH at moderate temperatures but should not be applied for more concentrated conditions at elevated temperatures. High-silicon cast irons are usually economical over unalloyed and nickel cast irons in alkali solutions only when other corrosives are involved for which the lesser alloys are unsuitable. High-chromium cast irons have inferior resistance to alkali solutions and are generally not recommended for alkali services.

Atmospheric corrosion is basically of interest only for unalloyed and low-alloy cast irons. Atmospheric corrosion rates are determined by the relative humidity and the presence of various gases and solid particles in the air. In high humidity, sulfur dioxide (SO_2) or similar compounds found in many industrialized areas and chlorides found in marine atmospheres increase the rate of atmospheric attack on cast irons.

Cast irons typically exhibit very low corrosion rates in industrial atmospheres—generally under 0.13 mm/yr (5 mils/yr)—and the cast irons are usually found to corrode at lower rates than steel structures in the same environment. White cast irons show the lowest rate of atmospheric corrosion of the unalloyed cast irons. Pearlitic cast irons are generally more resistant that ferritic cast irons to atmospheric corrosion.

In marine atmospheres, unalloyed cast irons also exhibit relatively low rates of corrosion. Low alloy additions are sometimes made to improve corrosion resistance further. Higher alloy additions are even more beneficial but are rarely warranted. Gray cast iron offers some added resistance over ductile cast iron in marine atmospheres.

Corrosion in Soils. Cast iron use in soils, as in atmospheric corrosion, is basically limited to unalloyed and low-alloyed cast irons. Corrosion in soils is a function of soil porosity, drainage, and dissolved constituents in the soil. Irregular soil contact can cause pitting, and poor drainage increases corrosion rates substantially above the rates in well-drained soils.

Neither metal-matrix nor graphite morphology has an important influence on the corrosion of cast irons in soils. Some alloying additions are made to improve the resistance of cast irons to attack in soils. For example, 3% Ni additions to cast iron are made to reduce initial attack in cast irons in poorly drained soils. Alloyed cast irons would exhibit better resistance than unalloyed or low-alloyed cast irons but are rarely needed for soil applications, because unalloyed cast irons generally have long service lives, particularly if coatings and cathodic protection are used. Anodes placed in soils for impressed current cathodic protection are frequently constructed from high-silicon cast iron. The high-silicon cast iron is not needed to resist the basic soil environment but rather to extend service life when subjected to the high electrical current discharge rates commonly used in cathodic protective anodes.

Several thousands of miles of cast iron pipe have been buried underground for decades, handling water distribution and collection for hundreds of municipalities. Much of this pipe is reaching the end of its useful life. Fortunately, technologies have been developed to line cast iron pipe in situ with polymer linings such as polyurethane or cement mortar (Ref 7, 8). These cure-in-place systems provide an economical alternative to open trench replacement, and the old cast iron pipe can still provide many years of structural integrity for the polymer or cement liners.

Corrosion in Water. Unalloyed and low-alloyed cast irons are the primary cast irons used in water service. The corrosion resistance of unalloyed cast iron in water is determined by its ability to form protective scales. In hard water, corrosion rates are generally low because of the formation of calcium carbonate ($CaCO_3$) scales on the surface of the iron. In softened or deionized water, the protective scales cannot be fully developed, and some corrosion will occur.

In industrial waste waters, corrosion rates are primarily a function of the contaminants present. Acid pH waters increase corrosion, but alkaline pH waters lower rates. Chlorides increase the corrosion rates of unalloyed cast irons, although the influence of chlorides is small at a neutral pH.

Seawater presents some special problems for cast irons. Gray cast iron may experience graphitic corrosion in calm seawater. It will also be galvanically active, that is, anodic, in contact with most stainless steels, copper-nickel alloys, titanium, and chrome-molybdenum nickel-base alloys. Because these materials are frequently used in seawater structures, this potential for galvanic corrosion must be considered. In calm seawater, the corrosion resistance of cast iron is not greatly affected by the presence of crevices. However, intermittent exposure to seawater is very corrosive to unalloyed cast irons.

Use of high-alloy cast irons in water is relatively limited. High-nickel austenitic cast irons are used to increase the resistance of cast iron components to pitting in calm seawater. Chromium containing high-silicon cast iron is used to produce anodes for the anodic protection systems used in seawater and brackish water.

Corrosion in Saline Solutions. The presence of salts in water can have dramatic effects on the selection of suitable grades of cast iron. Unalloyed cast irons exhibit very low corrosion rates in such salts as cyanides, silicates, carbonates, and sulfides, which hydrolyze to form alkaline solutions. However, in salts such as ferric chloride ($FeCl_3$), cupric chloride ($CuCl_2$), stannic salts, and mercuric salts, which hydrolyze to form acid solutions, unalloyed cast irons experience much higher rates. In salts that form dilute acid solutions, high-nickel cast irons are acceptable. More acidic and oxidizing salts, such as $FeCl_3$, usually necessitate the use of high-silicon cast irons.

Chlorides and sulfates of alkali metals yield neutral solutions, and unalloyed cast iron experiences very low corrosion rates in these solutions. More highly alloyed cast irons also exhibit low rates but cannot be economically justified for this application.

Unalloyed cast irons are suitable for oxidizing salts, such as chromates, nitrates, nitrites, and permanganates, when the pH is neutral or alkaline. However, if the pH is less than 7, corrosion rates can increase substantially. At a lower pH with oxidizing salts, high-silicon cast iron is an excellent material selection.

Ammonium salts are generally corrosive to unalloyed iron. High-nickel, high-chromium, and high-silicon cast irons provide good resistance to these salts.

Other Environments. Unalloyed cast iron is used as a melting crucible for such low-melting metals as lead, zinc, cadmium, magnesium, and aluminum. Resistance to molten metals is summarized in Table 6. Ceramic coatings and washes are sometimes used to inhibit molten metal attack on cast irons.

Cast iron can also be used in hydrogen chloride and chloride gases. In dry hydrogen chloride, unalloyed cast iron is suitable to 205 °C (400 °F), while in dry chlorine, unalloyed cast iron is suitable to 175 °C (350 °F). If moisture is present, unalloyed cast iron is unacceptable in HCl and Cl_2 at any temperature.

Coatings

Four general categories of coatings are used on cast irons to enhance corrosion resistance: metallic, organic, conversion, and enamel coatings. Coatings on cast irons are generally used to enhance the corrosion resistance of unalloyed and low-alloy cast irons and to lessen the requirements for cathodic protection. High-alloy cast irons such as Ni-Resist or white irons are rarely coated.

Metallic coatings are used to enhance the corrosion resistance of cast irons. These coatings may either be sacrificial metal coatings, such as zinc, or barrier metal coatings, such as

nickel-phosphorus. From a corrosion standpoint, these two classes of coatings have important differences. Sacrificial coatings are anodic when compared to iron, and the coatings corrode preferentially to protect the cast iron substrate. Small cracks and porosity in the coatings have a minimal overall effect on the performance of the coatings. Barrier coatings are cathodic compared to iron, and the coatings can protect the cast iron substrate only when porosity or cracks are not present. If there are defects in the coatings, the service environment will attack the cast iron substrate at these imperfections, and the galvanic couple set up between the relatively inert coating and the casting may accelerate attack on the cast iron.

Metallic coatings may be applied to cast irons by electroplating, hot dipping, flame or thermal spraying, diffusion coating, or hard facing. Table 7 lists the metals that can be applied by these techniques.

Zinc is one of the most widely used coatings on cast irons. Although zinc is anodic to iron, its corrosion rate is very low, and it provides relatively long-term protection for the cast iron substrate. A small amount of zinc will protect a large area of cast iron. Zinc coatings provide optimal protection in rural and arid areas.

Other metal coatings are also commonly used on cast irons. Cadmium provides atmospheric protection similar to that of zinc. Tin coatings are frequently used to improve the corrosion resistance of equipment intended for food handling, and aluminum coatings protect against corrosive environments containing sulfur fumes, organic acids, salts, and compounds of nitrate-phosphate chemicals. Lead and lead-tin coating are primarily applied to enhance the corrosion resistance of iron castings to H_2SO_3 and H_2SO_4. Nickel-phosphorus diffusion coatings offer corrosion resistance approaching that obtainable with stainless steel.

Organic coatings can be applied to cast irons to provide short-term or long-term corrosion resistance. Short-term rust preventatives include oil, solvent-petroleum-based inhibitors and film formers dissolved in petroleum solvents, emulsified-petroleum-based coatings modified to form a stable emulsion in water, and wax.

For longer-term protection and resistance to more corrosive environments, rubber-based coatings, bituminous paints, asphaltic compounds, or thermoset and thermoplastic coatings can be applied. Rubber-based coatings include chlorinated rubber neoprene, and Hypalon (DuPont Dow Elastomers). These coatings are noted for their mechanical properties and corrosion resistance but not for their decorative appearance. Bituminous paints have very low water permeability and provide high resistance to cast iron castings exposed to water. Use of bituminous paints is limited to applications that require good resistance to water, weak acids, alkalis, and salts. Asphaltic compounds are used to increase the resistance of cast irons to alkalis, sewage, acids, and continued exposure to tap water. Their application range is similar to that of bituminous paints. Cast irons are also lined with thermoset and thermoplastics, such as epoxy and polyethylene, to resist attack by fluids.

Fluorocarbon coatings offer superior corrosion resistance except in abrasive services. Fluorocarbon coatings applied to cast irons include such materials as polytetrafluoroethylene (PTFE), perfluoroalkoxy resins (PFA), polyvinyldene fluoride (PVDF), ethylene chlorotrifluoroethylene (ECTFE), ethylene tetrafluoroethylene (ETFE), and fluorinated ethylene polypropylene (FEP). Fully fluorinated fluorocarbon coatings resist deterioration in most common industrial services and can be used to 205 °C (400 °F), whereas partially fluorinated coatings are limited to approximately 150 °C (300 °F). Cast iron lined with fluorocarbon polymers can be very competitive with stainless, nickel-base, and even titanium and zirconium materials in terms of range of services covered and product cost.

Conversion coatings are produced when the metal on the surface of the cast iron reacts with another element or compound to produce an iron-containing compound. Common conversion coatings include phosphate coatings, oxide coatings, and chromate coatings. Phosphate coatings enhance the resistance of cast iron to corrosion in sheltered atmospheric exposure. If the surface of the casting is oxidized and black iron oxide or magnetite is formed, the corrosion resistance of the iron can be enhanced, particularly if the oxide layer is impregnated with oil or wax. Chromate coatings are formed by immersing the iron castings in an aqueous solution of chromic acid (H_2CrO_4) or chromium salts. Chromate coatings are sometimes used as a supplement to cadmium plating in order to prevent the formation of powdery corrosion products. The overall benefits of conversion coatings are small with regard to atmospheric corrosion.

Enamel Coatings. In the enamel coating of cast irons, glass frits are melted on the surface and form a hard, tenacious bond to the cast iron substrate. Good resistance to all acids except HF can be obtained with the proper selection and application of the enamel coating. Alkaline-resistant coatings can also be applied, but they offer only marginal improvement in the resistance to alkalis.

Proper design and application are essential for developing enhanced corrosion resistance on cast irons with enamel coatings. Any cracks, spalling, or other coating imperfections may permit rapid attack of the underlying cast iron.

Selection of Cast Irons

Cast irons provide excellent resistance to a wide range of corrosion environments when properly matched with that service environment. The basic parameters to consider before selecting cast irons for corrosion services include:

- Concentration of solution components in weight percent

Table 6 Resistance of gray cast iron to liquid metals at 300 and 600 °C (570 and 1110 °F)

Liquid metal	Liquid metal melting point, °C	Resistance of gray cast iron(a)	
		300 °C (570 °F)	600 °C (1110 °F)
Mercury	−38.8	Unknown	Unknown
Sodium, potassium, and mixtures	−12.3 to 97.9	Limited	Poor
Gallium	29.8	Unknown	Unknown
Bismuth-lead-tin	97	Good	Unknown
Bismuth-lead	125	Unknown	Unknown
Tin	321.9	Limited	Poor
Bismuth	271.3	Unknown	Unknown
Lead	327	Good at 327 °C (621 °F)	Unknown
Indium	156.4	Unknown	Unknown
Lithium	186	Unknown	Unknown
Thallium	303	Unknown	Unknown
Cadmium	321	Good at 321 °C (610 °F)	Good
Zinc	419.5		Poor
Antimony	630.5		Poor at 630.5 °C (1167 °F)
Magnesium	651		Good at 651 °C (1204 °F)
Aluminum	660		Poor at 660 °C (1220 °F)

(a) Good, considered for long-time use. <0.025 mm/yr (<1.0 mil/yr); Limited, short-time use only, 0.025–0.25 mm/yr (1.0–10 mils/yr); Poor, no structural possibilities, >0.25 mm/yr (>10 mils/yr); Unknown, no data for these temperatures. Source: Ref 9

Table 7 Summary of metallic coating techniques to enhance corrosion resistance of cast irons

Coating technique	Metals/alloys applied
Electroplating	Cadmium, chromium, copper, lead, nickel, zinc, tin, tin-nickel, brass, bronze
Hot dipped	Zinc, tin, lead, lead-tin, aluminum
Hard facing	Cobalt-base alloys, nickel-base alloys, metal carbides, high-chromium ferrous alloys, high-manganese ferrous alloys, high-chromium and nickel ferrous alloys
Flame spraying	Zinc, aluminum, lead, iron, bronze, copper, nickel, ceramics, cermets
Diffusion coating	Aluminum, chromium, nickel-phosphorus, zinc, nitrogen, carbon

- Dissolved contaminants, even at parts per million levels
- pH of solution
- Solution temperature, potential temperature extremes, and rate of change of temperature
- Degree of solution aeration
- Percent and type of solids suspended in the solution
- Duty cycle, continuous or intermittent operation or exposure
- Potential for upset conditions, for example, temperature and concentration excursions
- Unusual conditions, such as high solution velocity or vacuum
- Materials present in the system and the potential for galvanic corrosion

Although it is advisable to consider each of the parameters before ultimate selection of a cast iron, the information needed to properly assess all variables of importance is often lacking. In such cases, introduction of test coupons of the candidate materials into the process stream should be considered before extensive purchases of equipment are made. If neither test coupons nor complete service data are viable alternatives, consultation with a reputable manufacturer of the equipment or the cast iron, with a history of applications in the area of interest, should be considered.

ACKNOWLEDGMENT

This article is adapted from "Corrosion of Cast Irons", by Donald R. Stickle, Flowserve Corporation, *Corrosion*, Volume 13, *ASM Handbook*, ASM International, 1987, p 566–572.

REFERENCES

1. J.R. Keough, Austempered Ductile Iron, Section IV, *Ductile Iron Data,* The Ductile Iron Society, 1998 (available on website)
2. Development of a Cast Iron Graphitization Measurement Device, *NYGAS Technol. Briefs,* Issue 99-690-1, Jan 1999
3. J.R. McDowell, in *Symposium on Fretting Corrosion,* STP 144, American Society for Testing and Materials, 1952, p 24
4. P. Ferguson and D. Nicholas, *Corros. Australas.,* April 1984, p 12
5. S.L. Chawla and R.K. Gupta, *Materials Selection for Corrosion Control,* ASM International 1993, p 56–59
6. E.C. Miller, *Liquid Metals Handbook,* 2nd ed., Government Printing Office, 1952, p 144
7. New Lining System Upgrades Boston Gas Distribution System, *Pipeline Gas J.,* April 1995, p 24–29
8. B.B. Hall, Rehabilitation of 1940's Water Mains, *Am. Water Works Assoc.,* Vol 91 (No. 12), 1999, p 91–94
9. R.I. Higgins, Corrosion of Cast Iron, *J. Res.,* Feb 1956, p 165–177

SELECTED REFERENCES

- S.A. Bradford, *CASTI Practical Handbook of Corrosion Control in Soils,* co-published by CASTI and ASTM, 2000
- "Corrosion Control of Ductile and Cast Iron Pipe," 37254, NACE, 2001
- *Corrosion Data Survey,* 6th ed., National Association of Corrosion Engineers, 1985
- J.R. Davis, Ed., *ASM Specialty Handbook: Cast Irons,* ASM International, 1996
- M.G. Fontana, *Corrosion Engineering,* 3rd ed., McGraw-Hill, 1986
- "High Silicon Iron Alloys for Corrosion Services," Bulletin A/2, Flowserve Corporation, Aug 1998
- *Properties and Selection: Irons, Steels, and High-Performance Alloys,* Vol 1, *ASM Handbook,* ASM International, 1990
- M. Szeliga, *Corrosion of Ductile Iron Piping,* NACE, 1995
- C.F. Walton, Ed., *The Gray Iron Castings Handbook,* A.L. Garber, 1957
- C.F. Walton, Ed., *Gray and Ductile Iron Castings Handbook,* R.R. Donnelley & Sons, 1971

ASM Handbook, Volume 13B: Corrosion: Materials
S.D. Cramer, B.S. Covino, Jr., editors, p51-53
DOI: 10.1361/asmhba0003811

Corrosion of Cast Carbon and Low-Alloy Steels

Revised by Raymond W. Monroe, Steel Founders' Society of America

STEEL CASTING COMPOSITIONS are generally divided into the categories of carbon and low-alloy, corrosion-resistant, or heat-resistant, depending on alloy content and intended service. Castings are classified as corrosion resistant if they are capable of sustained operation when exposed to attack by corrosive agents at service temperatures normally below 315 °C (600 °F).

Carbon and low-alloy steels, the subject of this article, are considered resistant only to very mild corrosives, while the various high-alloy grades are applicable for varying situations from mild to severe services, depending on the particular conditions involved. For design and materials selection, the specific rate of corrosion may not be as important as the predictability and confidence in predicting a rate of corrosion.

It can be misleading to list the comparative corrosion rates of different alloys exposed to the same corroding medium. In this article, no attempt is made to recommend alloys for specific applications, and the data supplied should be used only as a general guideline. Alloy casting users will find it helpful to consult materials and corrosion specialists when selecting alloys for a particular application. The factors that must be considered in materials selection include:

- The principal corrosive agents and their concentrations
- Known or suspected impurities, including abrasive materials and their concentration
- Average operating temperature, including variations even if experienced only for short periods
- Presence (or absence) of dissolved oxygen or other gases in solution
- Continuous or intermittent operation
- Fluid velocity

Each of these can have a significant effect on the service life of cast equipment, and such detailed information must be provided to make the appropriate materials selection. Many rapid failures are traceable to these details being overlooked—often when the information was available.

Selection of the most economical alloy can be made by the judicious use of corrosion data. However, discretion and caution are suggested in evaluating the relative corrosion rates of various steels because of uncertainties in the results from controlled laboratory tests and simulated service condition tests, as well as anomalies in the intended environment. The best information is obtained from equipment used under actual operating conditions.

Cast carbon and low-alloy steel and wrought steel of similar composition and heat treatment exhibit approximately the same corrosion resistance in the same environments. More detailed information in the articles "Corrosion of Wrought Carbon Steels" and "Corrosion of Wrought Low-Alloy Steels" in this Volume is applicable to cast alloys. Plain carbon steel and some of the low-alloy steels do not ordinarily resist drastic corrosive conditions, although there are some exceptions, such as concentrated sulfuric acid (H_2SO_4).

Atmospheric Corrosion

Unless shielded by a protective coating, iron and steel corrode in the presence of water and oxygen; therefore, steel will corrode when it is exposed to moist air. The rate at which corrosion proceeds in the atmosphere depends on the corroding medium, the conditions of the particular location in which the material is in use, and the steps that have been taken to prevent corrosion. The rate of corrosion also depends on the character of the steel as determined by its chemical composition and heat treatment. To increase the corrosion resistance of steel significantly, amounts of alloying elements are increased. Small amounts of copper and nickel slightly improve the resistance of steel to atmospheric attack, but appreciably larger amounts of other elements, such as chromium and nickel, improve corrosion resistance significantly.

The rate of corrosion of a material in an environment can generally be estimated with confidence only from long-term tests. A 15 year research program compared the corrosion resistance of nine cast steels in marine and industrial atmospheres. Table 1 shows the compositions of the cast steels tested. The cast steel specimens exposed were 13 mm ($^1/_2$ in.) thick, 100 by 150 mm (4 by 6 in.) panels with beveled edges. The surfaces of half the specimens were machined. Specimens of each composition and surface condition were divided into three groups. One group was exposed to an industrial atmosphere at East Chicago, IN, and the other two groups were exposed to marine atmospheres 24 and 240 m (80 and 800 ft) from the ocean at Kure Beach, NC. The weight losses of the specimens

Table 1 Compositions of cast steels tested in atmospheric corrosion

	Composition(a),%										
Cast steel	Ni	Cu	Mn	Cr	V	C	Mo	P	S	Si	Other
Carbon, grade A	0.10	0.13	0.61	0.21	0.03	0.14	trace	0.016	0.026	0.41	
Nickel-chromium-molybdenum	0.56	0.13	0.80	0.60	0.04	0.26	0.15			0.44	
1Ni-1.7Mn	1.08	0.08	1.70	0.08	0.04	0.27		0.02	0.023	0.42	
2% Ni	2.26	0.12	0.77	0.19	0.03	0.17	trace	0.017	0.021	0.65	
Carbon, grade B	0.03	0.03	0.65	0.10	0.04	0.25		0.011	0.021	0.51	
1% Cu	0.04	0.94	0.87	0.11	0.07	0.28				0.42	
1.36Mn-0.09V	0.01	0.15	1.36	0.08	0.09	0.37		0.031	0.038	0.34	
1.42% Mn	0.01	0.13	1.42	0.16	0.04	0.37		0.027	0.022	0.38	
1.5Mn-0.05Ti	0.01	0.11	1.48	0.04	0.03	0.33		0.016	0.025	0.40	0.05 Ti

(a) All compositions contain balance of iron. Source: Ref 1

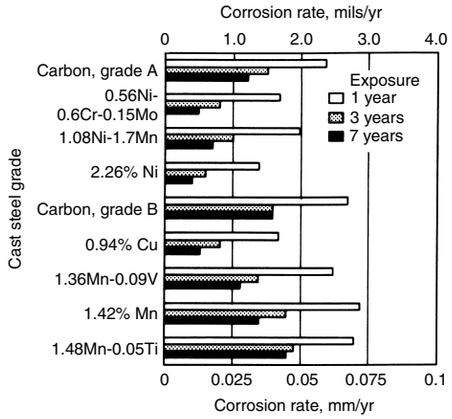

Fig. 1 Corrosion rates of various cast steels in a marine atmosphere. Nonmachined specimens were exposed 24 m (80 ft) from the ocean at Kure Beach, NC. Source: Ref 1

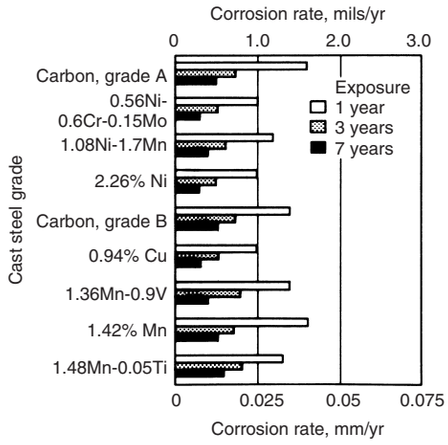

Fig. 2 Corrosion rates of various cast steels exposed at the 240 m (800 ft) site at Kure Beach, NC. Specimens were not machined. Source: Ref 1

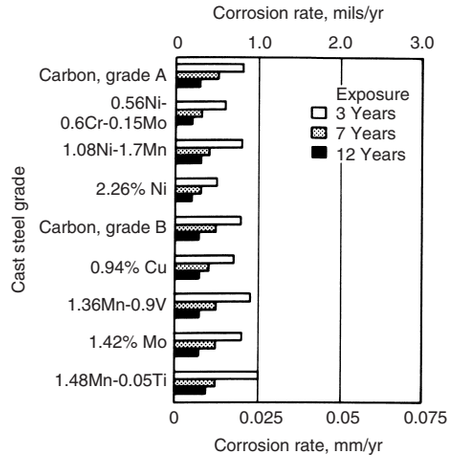

Fig. 3 Corrosion rates for cast steels in an industrial atmosphere. Nonmachined specimens were exposed at East Chicago, IN. Source: Ref 1

during exposure were converted to corrosion rates in terms of millimeters (mils) per year. The results of this research are shown in Fig. 1 to 4. These are uniform corrosion rates that do not apply to localized corrosion modes, such as crevice corrosion, pitting, or local galvanic coupling.

Figure 5 shows the results of another portion of this project. Corrosion rates for a 3 year exposure of various cast steels, wrought steels, and malleable iron in both atmospheres are compared. The following conclusions can be drawn from these tests:

- The condition of the specimen surface has no significant effect on the corrosion resistance of cast steels. Unmachined surfaces with the casting skin intact have corrosion rates similar to those of machined surfaces, regardless of the atmospheric environment.
- The highest corrosion rate occurs in the marine atmosphere 24 m (80 ft) from the ocean, with lower but similar corrosion rates occurring in the industrial atmosphere and the marine atmosphere 240 m (800 ft) from the ocean.
- The corrosion rate of cast steel decreases as a function of time, because corrosion products (scale and rust coating) build up and act as a protective coating on the cast steel surface. However, the corrosion rate of the most resistant cast steel (2% Ni) is always less than that of lesser corrosion-resistant cast steels.
- Cast steels with small amounts of copper or chromium, or slightly larger amounts of nickel, have corrosion resistance superior to that of cast carbon steel with manganese as an alloying element, when exposed to the atmospheres (Ref 1).
- Increasing the nickel and the chromium contents of cast steel increases the corrosion resistance in all three of the atmospheric environments.

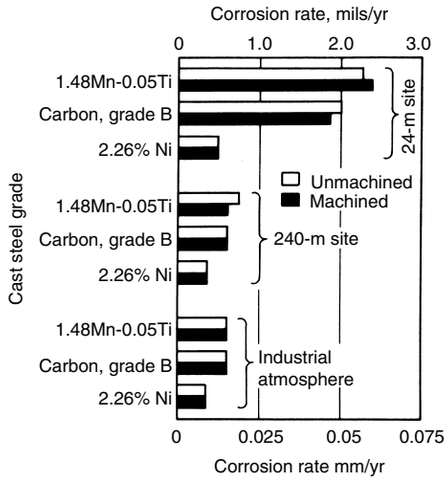

Fig. 4 Corrosion rates of machined and nonmachined specimens of cast steels after 7 years in three environments. The effect of surface finish on corrosion rates is negligible. Source: Ref 1

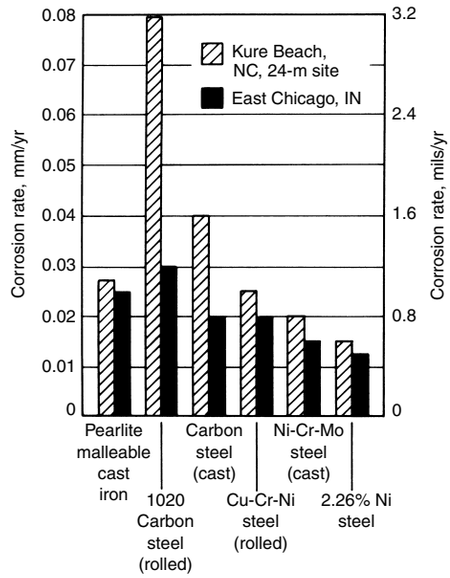

Fig. 5 Comparison of corrosion rates of cast steels, malleable cast iron, and wrought steel after 3 years of exposure in two atmospheres. Source: Ref 1

Table 2 Corrosion of cast carbon and alloy steels in steam at 650 °C (1200 °F) for 570 h

	Composition, %				Average penetration rate	
Type of steel	C	Cr	Ni	Mo	mm/yr	mils/yr
Carbon	0.24				0.3	12
	0.25				0.28	11
Carbon-molybdenum	0.21			0.49	0.3	12
	0.20			0.49	0.25	10
Nickel-chromium-molybdenum	0.35	0.64	2.13	0.26	0.25	10
	0.28	0.73	2.25	0.26	0.25	10
5Cr-molybdenum	0.22	5.07		0.47	0.1	4
	0.27	5.49		0.43	0.1	4
7Cr-molybdenum(a)	0.11	7.33		0.59	0.05	2
9Cr-1.5Mo	0.23	9.09		1.56	0.025	1

(a) Not a cast steel. Source: Ref 1

Table 3 Petroleum corrosion resistance of cast steels

1000 h test in petroleum vapor under 780 N (175 lb) of pressure at 345 °C (650 °F)

	Weight loss	
Type of material	mg/cm^2	mg/in.^{2}
Cast carbon steel	3040	196
Cast steel, 2Ni-0.75Cr	2370	153
Seamless tubing, 5% Cr	1540	99.2
Cast steel, 5Cr-1W	950	61.5
Cast steel, 5Cr-0.5Mo	730	47
Cast steel, 12% Cr	6.4	100
Stainless steel. 18Cr-8Ni	2.1	30

Source: Ref 1

Table 4 Corrosion of cast steels in waters

		Corrosion factor(a)		
Corrosive medium	Exposure time, months	Fe-0.29C-0.69Mn-0.44Si	Fe-0.32C-0.66Mn-1.12Cr	Fe-0.11C-0.41Mn-3.58Cr
Tap water	2	100	85	58
	6	100	73	61
Seawater	2	100	60	26
	6	100	80	40
Alternate immersion	2	100	93	30
and drying	6	100	109	25
Hot water	1	100	100	64
0.05% H_2SO_4	2	100	71	68
	6	100	89	102
0.50% H_2SO_4	2	100	223	61

(a) Corrosion factor is the ratio of average penetration rate of the alloy in question to Fe-0.29C-0.69Mn-0.44Si steel. Source: Ref 1

Table 5 Corrosion of cast chromium and carbon steels in mineral acids

	Weight loss in 5 h					
	5% H_2SO_4		5% HCl		5% HNO_3	
Steel	mg/cm^2	mg/in.^{2}	mg/cm^2	mg/in.^{2}	mg/cm^2	mg/in.^{2}
Carbon steel, 0.31% C	2.7	17.42	2.1	13.55	80.79	521.1
Chromium steel, 0.30C-2.42Cr	4.9	31.6	5.41	34.9	47.36	305.5

Source: Ref 1

All cast steels have greater corrosion resistance than malleable iron in industrial atmospheres and are superior or equivalent to the wrought steels in this environment. The corrosion rate in the marine atmosphere depends primarily on the alloy content. The cast carbon steel is much superior to the AISI 1020 wrought steel but is slightly inferior to malleable iron (Ref 2).

Other Environments

Several low- and high-alloy cast steels have been studied regarding their corrosion resistance to high-temperature steam. Test specimens 150 mm (6 in.) in length and 13 mm ($1/2$ in.) in diameter were machined from test coupons and then exposed to steam at 650 °C (1200 °F) for 570 h. The steel compositions and test results are given in Table 2. Table 3 shows the resistance of cast steels to petroleum corrosion, and Tables 4 and 5 supply similar data relating to water and acid attack. These data show the value of higher chromium content for improved corrosion resistance.

ACKNOWLEDGMENT

This article has been adapted from Raymond Monroe and Steven Pawel, Corrosion of Cast Steels, *Corrosion,* Volume 13, *ASM Handbook,* ASM International, 1987.

REFERENCES

1. C.W. Briggs, Ed., *Steel Casting Handbook,* 4th ed., Steel Founders' Society of America, 1970, 662–667
2. C.W. Briggs, "Atmospheric Corrosion of Carbon and Low Alloy Cast Steels," ASTM Corrosion Symposium, 1967

ASM Handbook, Volume 13B: Corrosion: Materials
S.D. Cramer, B.S. Covino, Jr., editors, p54-77
DOI: 10.1361/asmhba0003812

Corrosion of Wrought Stainless Steels

Revised by John F. Grubb, ATI-Allegheny Ludlum
Terry DeBold, Carpenter Technology Corporation
James D. Fritz, TMR Stainless

STAINLESS STEELS are iron-base alloys containing at least 10.5% Cr. With increasing chromium content and the presence or absence of some ten to fifteen other elements, stainless steels can provide an extraordinary range of corrosion resistance. Various grades have been used for many years in environments as mild as open air in architectural applications and as severe as the chemically active product streams in the chemical processing industries. Stainless steels are categorized in five distinct families according to their crystal structure and strengthening mechanism. Each family exhibits its own general characteristics in terms of mechanical properties and corrosion resistance. Within each family, there is a range of grades that varies in composition, corrosion resistance, and cost.

Stainless steels are susceptible to several forms of localized corrosive attack. The avoidance of such localized corrosion is the focus of most of the effort involved in selecting stainless steels. Furthermore, the corrosion performance of stainless steels can be strongly affected by practices of design, fabrication, surface conditioning, and maintenance.

The selection of a grade of stainless steel for a particular application involves the consideration of many factors but always begins with corrosion resistance. It is first necessary to characterize the probable service environment. It is not enough to consider only the design conditions. It is also necessary to consider the reasonably anticipated excursions or upsets in service conditions. The suitability of various grades can be estimated from laboratory tests or from documentation of field experience in comparable environments. Once the grades with adequate corrosion resistance have been identified, it is then appropriate to consider mechanical properties, ease of fabrication, the types and degree of risk present in the application, the availability of the necessary product forms, and cost.

Identification Systems for Stainless Steels

Grades of stainless steel are most commonly designated in one or more of the following ways: the American Iron and Steel Institute (AISI) numbering system, the Unified Numbering System (UNS), and proprietary designations. The AISI ceased issuing designations for new stainless steels several decades ago. These designations have persisted in ASTM and similar standards where they are now called common names or types. Other designations have been established by the national standards organizations of various major industrialized countries. These systems are generally similar to those of the United States, but there can be significant differences that must be taken into account when designing under these codes or using materials from these areas. Outside North America, the Deutsche Industrie-Normen (DIN) system, which has been adopted by Euronorm, is commonly used for identifying stainless steels. For example, the designations X5CrNi18-10 or 1.4301 identify an alloy similar to type 304 stainless steel. A cross-index such as *Stahlschlussel (Key to Steel)* (Ref 1) or *Worldwide Guide to Equivalent Irons and Steels* (Ref 2) should be consulted.

The AISI System. The most common designations are those based on AISI, which recognized grades as standard compositions on the basis of meeting criteria of total production and number of sources. Most of these grades have a three-digit designation in the 200, 300, or 400 series, and some have a one- or two-letter suffix that indicates a particular modification of the composition. There is a general association of the various microstructural families of grades with particular parts of the numbering series, but there are several significant exceptions to the system. Table 1 lists the AISI grades and their chemical analyses. Some proprietary designations are similar in structure to the AISI system but are not standard grades. Also, commercial offerings of the standard grades may use the AISI number with some additional prefix or suffix to indicate the producer or a particular modification of the grade for a certain type of application.

The UNS system was introduced in the 1970s to provide a systematic and encyclopedic listing of metal alloys, including the stainless steels. Although not perfect, the UNS numbering system has been successful in maintaining a degree of order during a period when many new grades were introduced. Most stainless steels—those having more than 50% Fe—have a UNS number that consists of the letter "S" followed by five digits. Some older alloys with less than 50% Fe had been classified as nickel-base alloys and assigned UNS N08*xxx* designations. To conform to international standards, all new stainless alloys having more iron than any other single element are being designated as stainless steels and assigned UNS S*xxxxx* designations. For the AISI grades, the first three digits of the UNS usually correspond to an AISI number. The basic AISI grades have 00 as the last two digits, while the modifications of the most basic grades show some other two digits. There are some significant exceptions in the UNS system, just as there are in the AISI system.

These designations are not normally a sufficient basis for specifying a stainless steel. To purchase a particular grade and product form, it is advisable to consult a comprehensive specification. The ASTM International specifications, for example, are the most commonly used in North America. These specifications usually define compositional limits; minimum mechanical properties; production, processing, and testing requirements; and, in some cases, particular corrosion performance requirements. Other standard specifications, such as those of ASME, NACE International, the American Petroleum Institute (API), TAPPI, or those of individual companies, may apply to certain types of equipment.

Proprietary Designations. In addition to the standard grades, there are well over 100 special grades that represent modifications, extensions, or refinements of the basic grades. In the early 1970s, the introduction of new stainless steel refining practices, most commonly argon-oxygen decarburization (AOD), greatly facilitated the production of stainless steels. In addition to permitting the use of lower-cost forms of alloy element additions, AOD also allows precise control of individual elements. This process also makes possible the economical removal of interstitial and tramp elements that are detrimental to corrosion resistance, mechanical properties, and processing.

Table 1 Compositions of standard grades of stainless steels

UNS designation	Type	Composition(a); wt%								
		C	Mn	P	S	Si	Cr	Ni	Mo	Others
Austenitic grades										
S20100	201	0.15	5.5–7.5	0.060	0.030	1.00	16.0–18.0	3.5–5.5	...	0.25N
S20200	202	0.15	7.5–10.0	0.060	0.030	1.00	17.0–19.0	4.0–6.0	...	0.25N
S30100	301	0.15	2.00	0.045	0.030	1.00	16.0–18.0	6.0–8.0	...	0.10N
S30200	302	0.15	2.00	0.045	0.030	0.75	17.0–19.0	8.0–10.0	...	0.10N
S30215	302B	0.15	2.00	0.045	0.030	2.00–3.00	17.0–19.0	8.0–10.0	...	0.10N
S30300	303	0.15	2.00	0.20	0.15 min	1.00	17.0–19.0	8.0–10.0	0.60	...
S30323	303Se	0.15	2.00	0.20	0.06	1.00	17.0–19.0	8.0–10.0	...	0.15Se min
S30400	304	0.08	2.00	0.045	0.030	0.75	18.0–20.0	8.0–10.5	...	0.10N
S30403	304L	0.030	2.00	0.045	0.030	0.75	18.0–20.0	8.0–12.0	...	0.10N
S30409	304H	0.04–0.10	2.00	0.045	0.030	0.75	18.0–20.0	8.0–10.5	...	...
S30451	304N	0.08	2.00	0.045	0.030	0.75	18.0–20.0	8.0–10.5	...	0.10–0.16N
S30500	305	0.12	2.00	0.045	0.030	0.75	17.0–19.0	10.5–13.0	...	...
S30800	308	0.08	2.00	0.045	0.030	0.75	19.0–21.0	10.0–12.0	...	...
S30900	309	0.20	2.00	0.045	0.030	1.00	22.0–24.0	12.0–15.0	...	...
S30908	309S	0.08	2.00	0.045	0.030	0.75	22.0–24.0	12.0–15.0	...	...
S31000	310	0.25	2.00	0.045	0.03	1.50	24.00–26.00	19.00–22.00	...	...
S31008	310S	0.08	2.00	0.045	0.030	1.50	24.0–26.0	19.0–22.0	...	...
S31400	314	0.25	2.00	0.045	0.030	1.50–3.00	23.0–26.0	19.0–22.0	...	...
S31600	316	0.08	2.00	0.045	0.030	0.75	16.0–18.0	10.0–14.0	2.00–3.00	0.10N
S31603	316L	0.030	2.00	0.045	0.030	0.75	16.0–18.0	10.0–14.0	2.00–3.00	0.10N
S31651	316N	0.08	2.00	0.045	0.030	0.75	16.0–18.0	10.0–14.0	2.00–3.00	0.10–0.16N
S31700	317	0.08	2.00	0.045	0.030	0.75	18.0–20.0	11.0–15.0	3.0–4.0	0.10N
S31703	317L	0.030	2.00	0.045	0.030	0.75	18.0–20.0	11.0–15.0	3.0–4.0	0.10N
S32100	321	0.08	2.00	0.045	0.030	0.75	17.0–19.0	9.0–12.0	...	TC: 5(C + N) min
N08330	330	0.08	2.00	0.030	0.030	0.75–1.50	17.0–20.0	34.0–37.0	...	...
S34700	347	0.08	2.00	0.045	0.030	0.75	17.0–19.0	9.0–13.0	...	Nb: 10 × C min
S34800	348	0.08	2.00	0.045	0.030	0.75	17.0–19.0	9.0–13.0	...	Nb: 10 × C min
S38400	384	0.08	2.00	0.045	0.030	1.00	15.0–17.0	17.0–19.0	...	...
Ferritic grades										
S40500	405	0.08	1.00	0.040	0.030	1.00	11.5–14.5	0.60	...	0.10–0.30Al
S41008	410S	0.08	1.00	0.040	0.030	1.00	11.5–13.5	0.60	...	...
S42900	429	0.12	1.00	0.040	0.030	1.00	14.0–16.0	...	...	...
S43000	430	0.12	1.00	0.040	0.030	1.00	16.0–18.0	0.75	...	...
S43020	430F	0.12	1.25	0.06	0.15 min	1.00	16.0–18.0	0.75	0.60	...
S43023	430FSe	0.12	1.25	0.06	0.06	1.00	16.0–18.0	0.75	...	0.15Se min
S43400	434	0.12	1.00	0.040	0.030	1.00	16.0–18.0	...	0.75–1.25	...
S43600	436	0.12	1.00	0.040	0.030	1.00	16.0–18.0	...	0.75–1.25	Nb: 5×C–0.80
S43035	439	0.030	1.00	0.040	0.030	1.00	17.0–19.0	0.50	...	4(C + N) + 0.20 ≤Ti ≤1.10
S44200	442	0.20	1.00	0.040	0.040	1.00	18.0–23.0	0.60	...	...
S44400	444	0.025	1.00	0.040	0.030	1.00	17.5–19.5	1.00	1.75–2.50	4(C + N) + 0.20 ≤Ti + Nb≤0.80
S44600	446	0.20	1.50	0.040	0.030	1.00	23.0–27.0	0.75	...	0.25N
Martensitic grades										
S40300	403	0.15	1.00	0.040	0.030	0.50	11.5–13.0	0.60	...	...
S41000	410	0.08–0.15	1.00	0.040	0.030	1.00	11.5–13.5	0.75	...	...
S41400	414	0.15	1.00	0.040	0.030	1.00	11.5–13.5	1.25–2.50	...	...
S41600	416	0.15	1.25	0.060	0.15 min	1.00	12.0–14.0	...	0.60	...
S41623	416Se	0.15	1.25	0.060	0.060	1.00	12.0–14.0	...	...	0.15Se min
S42000	420	0.15 min	1.00	0.040	0.030	1.00	12.0–14.0	0.75	0.50	...
S42020	420F	0.15 min	1.25	0.060	0.15 min	1.00	12.0–14.0	0.50	0.60	0.60Cu
S42200	422	0.20–0.25	1.00	0.025	0.025	0.50	11.0–12.5	0.50–1.00	0.90–1.25	0.20–0.30V, 0.90–1.25W
S43100	431	0.20	1.00	0.040	0.030	1.00	15.0–17.0	1.25–2.50	...	...
S44002	440A	0.60–0.75	1.00	0.040	0.030	1.00	16.0–18.0	...	0.75	...
S44003	440B	0.75–0.95	1.00	0.040	0.030	1.00	16.0–18.0	...	0.75	...
S44004	440C	0.95–1.20	1.00	0.040	0.030	1.00	16.0–18.0	...	0.75	...
Precipitation-hardening grades										
S17400	630	0.07	1.00	0.040	0.030	1.00	15.0–17.5	3.00–5.00	...	3.00–5.00Cu, 0.15–0.45Nb
S17700	631	0.09	1.00	0.040	0.030	1.00	16.0–18.0	6.50–7.75	...	0.75–1.50Al
S15700	632	0.09	1.00	0.040	0.030	1.00	14.0–16.0	6.5–7.7	2.00–3.00	0.75–1.50Al
S35000	633	0.07–0.11	0.50–1.25	0.040	0.030	0.50	16.0–17.0	4.00–5.00	2.50–3.25	0.07–0.13N
S35500	634	0.10–0.15	0.50–1.25	0.040	0.030	0.50	15.0–16.0	4.00–5.00	2.50–3.25	0.07–0.13N
S66286	660	0.08	2.00	0.040	0.030	1.00	13.5–16.0	24.0–27.0	1.00–1.50	1.90–2.35Ti, 0.35Al, 0.10–0.50V, 0.001–0.010B

(a) Maximum unless otherwise indicated; all compositions include balance of iron

Because of these capabilities, stainless steel producers have greatly extended the range of stainless steel grades. Very few of these grades were accepted as AISI standards, but all were assigned UNS numbers when they were introduced into ASTM standards. Table 2 provides a representative sampling of these grades across the range of alloy content and corrosion resistance. Some of the grades are identified by common trade names or trade marks in order to facilitate understanding and to enhance the usefulness of this discussion. This listing is not intended to be exhaustive, and the omission of a grade does not indicate its disqualification from consideration.

Families of Stainless Steels

There are five major families of stainless steels, as defined by crystallographic structure.

Table 2 Compositions of some proprietary and nonstandard stainless steels

UNS designation	Common name	Composition(a), wt%								
		C	Mn	P	S	Si	Cr	Ni	Mo	Others
Austenitic grades										
S20430	204Cu	0.15	6.5–9.0	0.06	0.03	1.00	15.5–17.5	1.50–3.00	...	2.00–4.00 Cu, 0.05–0.25N
S20910	Nitronic 50 (22-13-5)	0.06	4.0–6.0	0.040	0.030	0.75	20.5–23.5	11.5–13.5	1.50–3.00	0.1–0.3Nb, 0.2–0.4N, 0.1–0.3V
S21900	Nitronic 40 (21-6-9)	0.08	8.0–10.0	0.06	0.03	1.00	19.0–21.50	5.5–7.5	...	0.15–0.40N
S24100	18Cr-2Ni-12Mn	0.15	11.0–14.0	0.060	0.03	1.00	16.50–19.50	0.5–2.50	...	0.2–0.45N
S30345	303Al Modified	0.15	2.00	0.050	0.11–0.16	1.00	17.00–19.00	8.00–10.00	0.40–0.60	0.60–1.00Al
	303BV(b)	0.11	1.75	0.03	0.14	0.35	17.75	9.00	0.50	0.75Al
	302HQ-FM	0.06	2.00	0.04	0.14	1.00	16.00–19.00	9.00–11.00	...	1.3–2.4Cu
S30431	302HQ-FM	0.06	2.00	0.04	0.14	1.00	16.00–19.00	9.00–11.00	...	1.3–2.4Cu
S30430	302HQ	0.10	2.00	0.045	0.03	1.00	17.00–19.00	8.00–10.00	...	3.0–4.0Cu
S30453	304LN	0.030	2.00	0.045	0.030	0.75	18.0–20.0	8.0–12.0	...	0.10–0.16N
S31653	316LN	0.030	2.00	0.045	0.030	0.75	16.0–18.0	10.0–14.0	2.00–3.00	0.10–0.16N
S31753	317LN	0.030	2.00	0.045	0.030	0.75	18.0–20.0	11.0–15.0	3.0–4.0	0.10–0.22N
S31725	317LM	0.030	2.00	0.045	0.030	0.75	18.0–20.0	13.0–17.0	4.0–5.0	0.20N
S31726	317LMN	0.030	2.00	0.045	0.03	0.75	18.0–20.0	13.0–17.0	4.0–5.0	0.10–0.20N
N08904	904L	0.020	2.00	0.045	0.035	1.00	19.0–23.0	23.0–28.0	4.0–5.0	0.10N, 1.0–2.0Cu
N08700	JS700	0.04	2.00	0.040	0.030	1.00	19.0–23.0	24.0–26.0	4.3–5.0	0.5Cu, Nb: (8×C) − 1.00
	JS777	0.025	1.70	0.03	0.03	0.50	19.00–23.00	24.0–26.0	4.00–5.00	2.10Cu, 0.25Nb
N08020	20Cb-3	0.07	2.00	0.045	0.035	1.00	19.0–21.0	32.0–38.0	2.00–3.00	3.0–4.0Cu, Nb: (8×C) − 1.00
N08028	Alloy 28	0.030	2.50	0.030	0.030	1.00	26.0–28.0	29.5–32.5	3.0–4.0	0.6–1.4Cu
N08367	AL-6XN	0.030	2.00	0.040	0.030	1.00	20.0–22.0	23.5–25.5	6.0–7.0	0.18–0.25N, 0.75Cu
S31254	254SMO	0.020	1.00	0.030	0.010	0.80	19.5–20.5	17.5–18.5	6.0–6.5	0.50–1.00Cu, 0.18–0.22N
N08926	25-6MO, 1926hMo	0.020	2.00	0.030	0.010	0.50	19.0–21.0	24.0–26.0	6.0–7.0	0.5–1.5Cu, 0.15–0.25N
S32654	654SMO	0.020	2.0–4.0	0.03	0.005	0.50	24.0–25.0	21.0–23.0	7.00–8.00	0.45–0.55N, 0.30–0.60Cu
Ferritic grades										
S40910	409	0.030	1.00	0.040	0.020	1.00	10.50–11.75	0.50	...	Ti: 6×(C + N)–0.50, N 0.030, Cb 0.17
S40920	409	0.030	1.00	0.040	0.020	1.00	10.50–11.75	0.50	...	Ti: 0.15–0.50, N 0.030, Cb 0.10
S40930	409	0.030	1.00	0.040	0.020	1.00	10.50–11.75	0.50	...	Ti 0.05 min, N 0.030 (Ti + Cb): 0.08 + 8(C + N) min, 0.75 max
S44627	E-Brite	0.010	0.40	0.020	0.020	0.40	25.0–27.0	0.50	0.75–1.50	0.05–0.2Nb, 0.2Cu, 0.015N
S44660	Sea-Cure	0.030	1.00	0.040	0.030	1.00	25.0–28.0	1.0–3.5	3.0–4.0	0.040N, Nb + Ti: 6(C + N)
S44735	AL-29-4C	0.030	1.00	0.040	0.030	1.00	28.0–30.0	1.00	3.6–4.2	0.045N, Nb + Ti: 6(C + N)
S44800	AL-29-4-2	0.010	0.30	0.025	0.020	0.20	28.0–30.0	2.00–2.50	3.5–4.2	0.15Cu, 0.020N, C + N: 0.025 max
Duplex grades										
S31200	44LN	0.030	2.00	0.045	0.030	1.00	24.0–26.0	5.5–6.5	1.20–2.00	0.14–0.20N
S31260	DP-3	0.030	1.00	0.030	0.030	0.75	24.0–26.0	5.5–7.5	2.5–3.5	0.20–0.80Cu, 0.10–0.30N, 0.10–0.50W
S31500	3RE60	0.030	1.20–2.00	0.030	0.030	1.40–2.00	18.0–19.0	4.30–5.20	2.50–3.00	...
S31803	2205	0.030	2.00	0.030	0.020	1.00	21.0–23.0	4.5–6.5	2.5–3.5	0.08–02N
S32001	19D	0.030	4.0–6.0	0.040	0.030	1.0	19.5–21.5	1.0–3.0	0.60	1.0Cu, 0.05–0.17 N
S32003	AL 2003	0.030	2.0	0.030	0.020	1.0	19.5–22.5	3.0–4.0	1.50–2.0	0.14–0.20 N
S32101	2101	0.040	4.0–6.0	0.030	0.030	1.0	21.0–22.0	1.35–1.70	0.10–0.80	0.10–0.80 Cu, 0.20–0.25 N
S32205	2205	0.030	2.00	0.030	0.020	1.00	21.0–23.0	4.5–6.5	2.5–3.5	0.014–0.2N
S32304	2304	0.030	2.50	0.040	0.030	1.0	21.5–24.5	3.0–5.5	0.05–0.60	0.05–0.60Cu, 0.05–0.20N
S32550	Ferralium 255	0.04	1.50	0.040	0.030	1.00	24.0–27.0	4.5–6.5	2.9–3.9	1.50–2.50Cu, 0.10–0.25N
S32750	SAF 2507	0.030	1.20	0.035	0.020	0.80	24.0–26.0	6.0–8.0	3.0–5.0	0.24–0.32N
S32760	Zeron 100	0.030	1.00	0.030	0.010	1.00	24.0–26.0	6.0–8.0	3.0–4.0	0.50–1.00Cu, 0.50–1.00W, 0.20–0.30N
S32950	7Mo-Plus	0.030	2.00	0.035	0.010	0.60	26.0–29.0	3.5–5.2	1.00–2.50	0.15–0.35N
Martensitic grades										
S41040	XM-30	0.18	1.00	0.040	0.030	1.00	11.5–13.0	...	...	0.05–0.30Nb
S41610	XM-6	0.15	1.50–2.50	0.06	0.15 min	1.00	12.0–14.0	...	0.60	...
Precipitation-hardenable grades										
S13800	PH13-8Mo, XM-13	0.05	0.20	0.01	0.008	0.10	12.25–13.25	7.50–8.50	2.00–2.50	0.90–1.35Al, 0.01N
S15500	15-5PH, XM-12	0.07	1.00	0.04	0.03	1.00	14.00–15.50	3.50–5.50	...	2.50–4.50Cu, 0.15–0.45Nb
S45000	Custom 450	0.05	1.00	0.03	0.03	1.00	14.00–16.00	5.00–7.00	0.5–1.00	1.25–1.75Cu, Nb: 8×C min
S45500	Custom 455	0.05	0.50	0.04	0.03	0.50	11.00–12.50	7.50–9.50	0.50	0.1–0.5Nb, 1.50–2.50Cu, 0.8–1.40Ti
S46500	Custom 465	0.02	0.25	0.015	0.01	0.25	11.00–12.50	10.75–11.25	0.75–1.25	0.01N, 1.50–1.80Ti

(a) Maximum unless otherwise indicated; all compositions contain balance of iron. (b) Nominal composition

Each family is distinct with regard to its typical mechanical properties. Furthermore, each family tends to share a common nature in terms of resistance/susceptibility to particular forms of corrosion. However, within each family, it is possible to have a substantial range of composition. Therefore, each family is applicable to a broad range of corrosion environments.

Ferritic Stainless Steels. The simplest stainless steels contain only iron and chromium. Chromium is a ferrite stabilizer; therefore, the stability of the ferritic structure increases with chromium content. Ferrite has a body-centered cubic crystal structure, and it is characterized as magnetic and relatively high in yield strength but low in ductility and work hardenability. Ferrite shows an extremely low solubility for such interstitial elements as carbon and nitrogen. The ferritic grades exhibit a transition from ductile to brittle behavior over a rather narrow temperature range. At higher carbon and nitrogen contents, especially with higher chromium levels, this ductile-to-brittle transition can occur above ambient temperature. This possibility severely limited the use of ferritic grades before the use of AOD. The ferritic family was then limited to

type 446 for oxidation-resistant applications and to types 430 and 434 for such corrosion applications as automotive trim. The fact that these grades were readily sensitized to intergranular corrosion as a result of welding or thermal exposure further limited their use.

With AOD, it was possible to reduce the levels of carbon and nitrogen significantly. The activity of carbon and nitrogen could further be reduced by the use of stabilizers, which are highly reactive elements, such as titanium and niobium, that precipitate the remaining interstitials. Second-generation ferritic stainless steels include type 444 and the more highly alloyed ferritic grades shown in Table 2. With control of interstitial elements, it is possible to produce grades with unusually high chromium and molybdenum contents. At these low effective carbon levels, these grades are tougher and more weldable than the first generation of ferritic stainless steels. Nevertheless, their limited toughness generally restricts use of these grades to sheet or thin-wall tubulars.

Ferritic stainless steels are highly resistant, and in some cases immune, to chloride stress-corrosion cracking (SCC). These grades are frequently considered for thermal transfer applications.

Enhanced formability and oxidation resistance are responsible for the extraordinary development of the lowest-alloyed grade of the ferritics, type 409. This grade, developed for automotive muffler and catalytic converter service, has gained in technical sophistication. It is increasingly used in automotive exhaust systems and in other moderately severe atmospheric-exposure applications.

Austenitic Stainless Steels. The detrimental effects of carbon and nitrogen in ferrite can be overcome by changing the crystal structure to austenite, a face-centered cubic crystal structure. This change is accomplished by adding austenite stabilizers—most commonly nickel but also manganese and nitrogen. Austenite is characterized as nonmagnetic, and it is usually relatively low in yield strength with high ductility, rapid work-hardening rates, and excellent toughness. These desirable mechanical properties, combined with ease of fabrication, have made the austenitic grades, especially types 304 and 304L, the most common of the stainless grades. Processing difficulties tend to limit increases in chromium content; therefore, improved corrosion resistance is usually obtained by adding molybdenum. The use of nitrogen as an intentional alloy addition stabilizes the austenite phase, particularly with regard to the precipitation of intermetallic compounds. With the addition of nitrogen, it is possible to produce austenitic grades with up to 7% Mo for improved corrosion resistance in chloride environments. Other special grades include the high-chromium grades for high-temperature applications and the high-nickel grades for inorganic acid environments.

The austenitic stainless steels can be sensitized to intergranular corrosion by welding or by longer-term thermal exposure. These thermal exposures lead to the precipitation of chromium carbides in grain boundaries and to the depletion of chromium adjacent to these carbides. Sensitization can be greatly delayed or prevented by the use of lower-carbon L-grades ($<0.03\%$ C) or stabilized grades, such as types 321 and 347, which include additions of carbide-stabilizing elements (titanium and niobium, respectively).

The common austenitic grades, types 304 and 316, are especially susceptible to chloride SCC. All austenitic stainless steels exhibit some degree of susceptibility, but several of the high-nickel, high-molybdenum grades are satisfactory with respect to stress-corrosion attack in most engineering applications.

Martensitic Stainless Steels. With lower chromium levels and relatively high carbon levels, it is possible to obtain austenite at elevated temperatures and then, with moderate cooling, to transform this austenite to martensite, which has a body-centered tetragonal structure. Just as with plain carbon and low-alloy steels, this strong, brittle martensite can be tempered to favorable combinations of high strength and adequate toughness. Because of the ferrite-stabilizing character of chromium, the total chromium content, and thus the corrosion resistance, of the martensitic grades is somewhat limited. In recent years, nitrogen, nickel, and molybdenum additions at somewhat lower carbon levels have produced martensitic stainless steels of improved toughness and corrosion resistance.

The duplex stainless steels can be thought of as chromium-molybdenum ferritic stainless steels to which sufficient austenite stabilizers have been added to produce steels in which a balance of ferrite and austenite is present at room temperature. Such grades can have the high chromium and molybdenum responsible for the excellent corrosion resistance of ferritic stainless steels as well as the favorable mechanical properties of austenitic stainless steels. In fact, the duplex grades with approximately equal amounts of ferrite and austenite have excellent toughness, and their strength exceeds either phase present singly.

First-generation duplex grades, such as type 329, achieved this phase balance primarily by nickel additions. These early duplex grades have superior properties in the annealed condition, but segregation of chromium and molybdenum between the two phases as re-formed after welding often significantly reduced corrosion resistance. The addition of nitrogen to the second generation of duplex grades restores the phase balance more rapidly and minimizes chromium and molybdenum segregation without annealing. The newer duplex grades, such as type 2205 stainless steel, combine high strength, good toughness, high corrosion resistance, good resistance to chloride SCC, and good production economy in the heavier product forms. Higher molybdenum-content duplex alloys, such as SAF 2507 and Zeron 100 (UNS S32750 and S32760, respectively), have been developed for seawater service. Recently, several lower-molybdenum, nitrogen-enhanced duplex stainless steels have been introduced. They offer the same high resistance to chloride SCC along with improved weldability and economy in less aggressive environments.

The precipitation-hardening stainless steels are chromium-nickel grades that can be hardened by an aging treatment at a moderately elevated temperature. These grades may have austenitic, semiaustenitic, or martensitic crystal structures. Semiaustenitic structures are transformed from a readily formable austenite to martensite by a high-temperature austenite-conditioning treatment. Some grades use cold work to facilitate transformation. The strengthening effect is achieved by adding such elements as copper and aluminum, which form strengthening precipitates during aging. In the solution-annealed condition, these grades have properties similar to those of the austenitic grades and are therefore readily formed. Hardening is achieved after fabrication within a relatively short time at 480 to 620 °C (900 to 1150 °F). The precipitation-hardened grades must not be subjected to further exposure to temperatures near or above the precipitation aging temperature by welding or environment, because the strengthening can be lost by overaging of the precipitates. The precipitation-hardened grades have corrosion resistance generally comparable to that of the chromium-nickel grades of similar chromium and molybdenum contents.

Mechanism of Corrosion Resistance

The mechanism of corrosion protection for stainless steels differs from that for carbon steels, alloy steels, and most other metals. In these other cases, the formation of a barrier of true oxide separates the metal from the surrounding atmosphere. The degree of protection afforded by such an oxide is a function of the thickness of the oxide layer, its continuity, its coherence and adhesion to the metal, and the diffusivities of oxygen and metal in the oxide. In high-temperature oxidation, stainless steels use a generally similar model for corrosion protection. However, at low temperatures, stainless steels do not form a layer of true oxide. Instead, a passive film is formed. One mechanism that has been suggested is the formation of a film of hydrated oxide, but there is not total agreement on the nature of the oxide complex on the metal surface. However, the oxide film must be continuous, nonporous, insoluble, and self-healing if broken in the presence of oxygen.

Passivity exists under certain conditions for particular environments. The range of conditions over which passivity can be maintained depends on the precise environment and on the family and composition of the stainless steel. When conditions are favorable for maintaining passivity, stainless steels exhibit extremely low corrosion rates. If passivity is destroyed under conditions that do not permit restoration of the passive film,

then stainless steel will corrode much like a carbon or low-alloy steel.

The presence of oxygen is essential to the corrosion resistance of a stainless steel. The corrosion resistance of stainless steel is at its maximum when the steel is boldly exposed and the surface is maintained free of deposits by a flowing bulk environment. Covering a portion of the surface—for example, by biofouling, painting, or installing a gasket—produces an oxygen-depleted region under the covered region. The oxygen-depleted region is anodic relative to the well-aerated boldly exposed surface, and a higher level of alloy content in the stainless steel is required to prevent corrosion.

With appropriate grade selection, stainless steel will perform for very long times with minimal corrosion, but an inadequate grade can corrode and perforate more rapidly than a plain carbon steel will fail by uniform corrosion. Selection of the appropriate grade of stainless steel is then a balancing of the desire to minimize cost and the risk of corrosion damage by excursions of environmental conditions during operation or downtime.

Confusion exists regarding the meaning of the term *passivation,* which is used to describe a chemical treatment used to optimize the corrosion resistance of a stainless steel. It is not necessary to chemically treat a stainless steel to obtain the passive film; the film forms spontaneously in the presence of oxygen. Most frequently, the function of passivation is to remove free iron and other surface contamination. For example, in the steel mill, the stainless steel may be pickled in an acid solution, often a mixture of nitric and hydrofluoric acids ($HNO_3 + HF$), to remove oxides formed in heat treatment. Once the surface is cleaned and the bulk composition of the stainless steel is exposed to air, the passive film forms immediately.

Effects of Composition

Chromium is the one element essential in forming the passive film. Other elements can influence the effectiveness of chromium in forming or maintaining the film, but no other element can, by itself, create the properties of stainless steel. The film is first observed at approximately 10% Cr, but it is rather weak at this composition and affords only mild atmospheric protection. Increasing the chromium content to 17 to 20%, as typical of the austenitic stainless steels, or to 26 to 29%, as possible in the newer ferritic stainless steels, greatly increases the stability of the passive film. However, higher chromium may adversely affect mechanical properties, fabricability, weldability, or suitability for applications involving certain thermal exposures. Therefore, it is often more efficient to improve corrosion resistance by altering the content of other elements, with or without some increase in chromium.

Nickel, in sufficient quantities, will stabilize the austenitic structure; this greatly enhances mechanical properties and fabrication characteristics. Nickel is effective in promoting repassivation, especially in reducing environments. Nickel is particularly useful in resisting corrosion in mineral acids. Increasing nickel content to approximately 8 to 10% decreases resistance to SCC, but further increases begin to restore SCC resistance. Resistance to SCC in most service environments is achieved at approximately 20 to 30% Ni. In the ferritic grades, in which the nickel addition is less than that required to destabilize the ferrite phase, there are still substantial effects. In this range, nickel increases yield strength, toughness, and resistance to reducing acids, but it makes the ferritic grades susceptible to SCC, especially in concentrated magnesium chloride ($MgCl_2$) solutions.

Manganese in moderate quantities and in association with nickel additions will perform many of the functions attributed to nickel. Very high manganese steels have some unusual and useful mechanical properties, such as resistance to galling. Manganese interacts with sulfur in stainless steels to form manganese sulfides. The morphology and composition of these sulfides can have substantial effects on corrosion resistance, especially pitting resistance. Manganese also increases the solubility of nitrogen in stainless steels, especially in the melt.

Molybdenum in combination with chromium is very effective in terms of stabilizing the passive film in the presence of chlorides. Molybdenum is especially effective in increasing resistance to the initiation of pitting and crevice corrosion. Molybdenum may decrease corrosion resistance in highly oxidizing environments such as strong nitric acid.

Carbon is useful to the extent that it permits hardenability by heat treatment, which is the basis of the martensitic grades, and that it provides strength in the high-temperature applications of stainless steels. In all other applications, carbon is detrimental to corrosion resistance through its reaction with chromium. In the ferritic grades, carbon is also extremely detrimental to toughness.

Nitrogen is beneficial to austenitic stainless steels in that it enhances pitting resistance, retards the formation of the chromium-molybdenum sigma (σ) phase, and strengthens the steel. Nitrogen is essential in the newer duplex grades for increasing the austenite content, diminishing chromium and molybdenum segregation, and for raising the corrosion resistance of the austenitic phase. Nitrogen is highly detrimental to the mechanical properties of the ferritic grades and must be treated as comparable to carbon when a stabilizing element is added to the steel.

Pitting resistance equivalent (PRE) is a calculated parameter used to estimate expected resistance to localized corrosion by chlorides. It is calculated from composition using the empirical formula:

$$\text{PRE} = \text{Cr} + 3.3 \cdot \text{Mo}$$

where chromium and molybdenum are the respective concentrations of these elements in the alloy expressed in percentages by weight. For austenitic and duplex stainless steels, where nitrogen also confers resistance to localized corrosion, the pitting resistance equivalent with nitrogen (PREN) is generally preferred. There is some disagreement about the exact coefficient for nitrogen in the PREN calculation, and popular equations range from:

$$\text{PREN} = \text{Cr} + 3.3 \cdot \text{Mo} + 16 \cdot \text{N}, \text{ to}$$

$$\text{PREN} = \text{Cr} + 3.3 \cdot \text{Mo} + 30 \cdot \text{N}$$

The numerical value of the PREN is approximately equal to the critical crevice temperature (°C) in natural seawater or in ferric chloride solutions.

Effects of Processing, Design, Fabrication, and External Treatments

Corrosion failures in stainless steels can often be prevented by suitable changes in design or process parameters and by use of the proper fabrication technique or treatment. The solution to a corrosion problem is not always to upgrade the stainless steel. It is very important to establish the types of corrosion that may occur in a given service environment, and if failure does occur, it also is important to establish the type of corrosion that caused the failure in order that the proper preventative measures can be implemented.

Heat Treatment

Improper heat treatment can produce deleterious changes in the microstructure of stainless steels. The most troublesome problems are carbide precipitation (sensitization) and precipitation of various intermetallic phases, such as sigma (σ), chi (χ), and Laves.

Sensitization, or carbide precipitation at grain boundaries, can occur when austenitic stainless steels are heated for a period of time in the range of approximately 425 to 870 °C (800 to 1600 °F). Time at temperature will determine the amount of carbide precipitation. When the chromium carbides precipitate in grain boundaries, the area immediately adjacent is depleted of chromium. When the precipitation is relatively continuous, the depletion renders the stainless steel susceptible to intergranular corrosion, which is the dissolution of the low-chromium layer or envelope surrounding each grain. Sensitization also lowers resistance to other forms of corrosion, such as pitting, crevice corrosion, and SCC. In some cases, sensitization can be caused by precipitation of chromium nitrides.

Time-temperature-sensitization curves are available that provide guidance for avoiding sensitization and illustrate the effect of carbon content on this phenomenon (Fig. 1). The curves

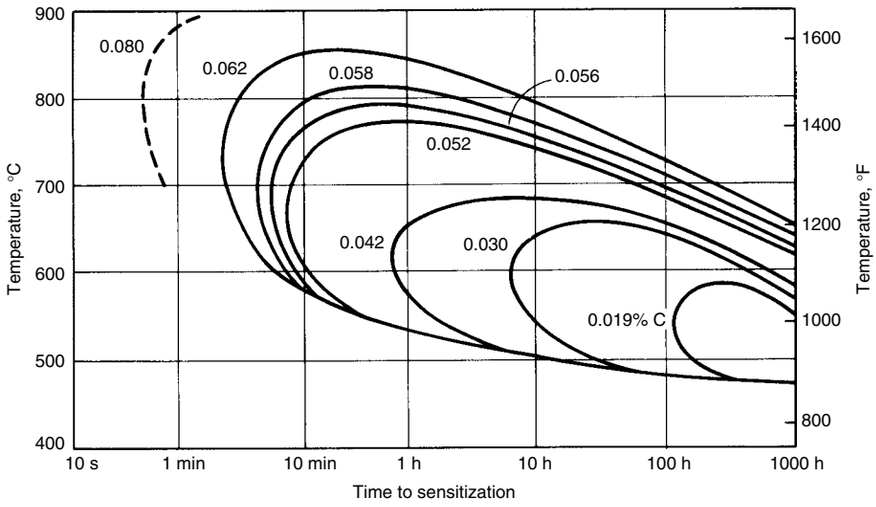

Fig. 1 Time-temperature-sensitization curves for type 304 stainless steel in a mixture of $CuSO_4$ and H_2SO_4 containing free copper. Curves show the times required for carbide precipitation in steels with various carbon contents. Carbides precipitate in the areas to the right of the various carbon content curves.

shown in Fig. 1 indicate that a type 304 stainless steel with 0.062% C would have to cool below 595 °C (1100 °F) within approximately 5 min to avoid sensitization, but a type 304L with 0.030% C could take approximately 20 h to cool below 480 °C (900 °F) without becoming sensitized. These curves are general guidelines and should be verified before they are applied to various types of stainless steels.

Another method of avoiding sensitization is to use stabilized steels. Such stainless steels contain titanium and/or niobium. These elements have an affinity for carbon and form carbides readily; this allows the chromium to remain in solution even for long exposures to temperatures in the sensitizing range. Typically, type 304L can avoid sensitization during the relatively brief exposure of welding, but it will be sensitized by long exposures.

Annealing is the only way to correct a sensitized stainless steel. Because different stainless steels require different temperatures, times, and quenching procedures, the user should contact the material supplier for such information. A number of tests can detect sensitization resulting from carbide precipitation in austenitic and ferritic stainless steels. The most widely used tests are described in ASTM standards A 262 and A 763 (Ref 3, 4). More detailed information on sensitization of stainless steels can be found in the article "Metallurgically Influenced Corrosion" in *ASM Handbook,* Volume 13A, 2003.

Precipitation of Intermetallic Phases. Sigma-phase precipitation and precipitation of other intermetallic phases also increase susceptibility to corrosion. Sigma phase is a chromium-molybdenum-rich phase that can render stainless steels susceptible to intergranular corrosion, pitting, and crevice corrosion. It generally occurs in higher-alloyed stainless steels (high-chromium, high-molybdenum stainless steels). Sigma phase can occur at a temperature range between 540 and 900 °C (1000 and 1650 °F). Like sensitization, it can be corrected by solution annealing. Precipitation of intermetallic phase in stainless steels is also covered in detail in the article "Metallurgically Influenced Corrosion" in *ASM Handbook,* Volume 13A, 2003.

Cleaning Procedures. Any heat treatment of stainless steel should be preceded and followed by cleaning. Steel should be cleaned before heat treating to remove any foreign material that may be incorporated into the surface during the high-temperature exposure. Carbonaceous materials on the surface could result in an increase in the carbon content on the surface, causing carbide precipitation. Salts could cause excessive intergranular oxidation. Therefore, the stainless steel must be clean before it is heat treated.

After heat treatment, unless an inert atmosphere was used during the process, the stainless steel surface will be covered with an oxide film. Such films are not very corrosion resistant and must be removed to allow the stainless steel to form its passive film and provide the corrosion resistance for which it was designed. Because the oxides are typically chromium-rich, their formation can create a surface chromium-depleted layer. This layer must also be removed to restore the full corrosion resistance inherent in the alloy. There are numerous cleaning methods that may be used before and after heat treating. Excellent guidance is found in ASTM A 380 and ASTM A 967 (Ref. 5, 6).

Welding

The main problems encountered in welding stainless steels are the same as those seen in heat treatment. The heat of welding (portions of the base metal adjacent to the weld may be heated to 430 to 870 °C, or 800 to 1600 °F) can cause sensitization and formation of intermetallic phases, thus increasing the susceptibility of stainless steel weldments to intergranular corrosion, pitting, crevice corrosion, and SCC. These phenomena often occur in the heat-affected zone of the weld. Sensitization and intermetallic phase precipitation can be corrected by solution annealing after welding. Alternatively, low-carbon or stabilized grades may be used.

Austenitic stainless steels with less than 0.08% C are resistant to sensitization in many environments when welded by single-pass procedures. Multiple-pass welds, frequently required for plate welding, are more likely to sensitize the stainless steels and may necessitate the use of low-carbon or stabilized grades. Where stress-relief annealing is required, usually when stainless steels are welded to plain carbon or low-alloy steels, use of low-carbon or stabilized grades is generally necessary. Because sensitization occurs more rapidly in ferritic stainless steels, stabilized or extralow interstitial grades of ferritic stainless steels should be selected for welded applications. Ferritic stainless steels may also be affected by the related high-temperature embrittlement phenomenon.

Another problem in high heat input welds is grain growth, particularly in ferritic stainless steels. Excessive grain growth can increase susceptibility to intergranular attack and reduce toughness. Thus, when welding most stainless steels, it is wise to limit weld heat input as much as possible. More detailed information on welding of stainless steels and the problems encountered can be found in the article "Corrosion of Stainless Steel Weldments" in *ASM Handbook,* Volume 13A, 2003.

Cleaning Procedure. Before any welding begins, all materials, chill bars, clamps, hold-down bars, work tables, electrodes, and wire, as well as the stainless steel, must be cleaned of all foreign matter. Moisture can cause porosity in the weld that would reduce corrosion resistance. Organic materials, such as grease, paint, and oils, may result in carbide precipitation. Copper contamination may cause cracking. Other shop dirt can cause weld porosity and poor welds in general. Information on cleaning is available in Ref 5.

Weld design and procedure are very important in producing a sound corrosion-resistant weld. Good fit and minimal out-of-position welding will minimize crevices and slag entrapment. The design should not place welds in critical flow areas. When attaching such devices as low-alloy steel support and ladders on the outside of a stainless steel tank, a stainless steel intermediate pad should be used. In general, high-molybdenum stainless steels with higher alloy content than type 316 should be welded with weld metal richer in chromium, nickel, and molybdenum than the base metal. If such high-molybdenum alloys are welded autogenously (i.e., without filler metal), they should be post-weld solution annealed if maximum corrosion resistance is needed. Every attempt should be made to minimize weld spatter.

After welding, all weld spatter, slag, and oxides should be removed by brushing, blasting, grinding, or chipping. All finishing equipment must be free of iron contamination. It is advisable to follow the mechanical cleaning and finishing with a chemical cleaning. Such a cleaning will remove any foreign particles that may have been embedded in the surface during mechanical cleaning without attacking the weldment. Procedures for such cleaning and descaling are given in Ref 5 and in *Surface Engineering,* Volume 5 of *ASM Handbook,* 1994. More information on welding of stainless steels is available in *Welding, Brazing, and Soldering,* Volume 6 of *ASM Handbook,* 1993.

Surface Condition

To ensure satisfactory service life, the surface condition of stainless steels must be given careful attention. Smooth surfaces, as well as freedom from surface imperfections, blemishes, and traces of scale and other foreign material, reduce the probability of corrosion. In general, a smooth, highly polished, reflective surface has greater resistance to corrosion. Rough surfaces are more likely to catch dust, salts, and moisture, which tend to initiate localized corrosive attack.

Oil and grease can be removed by using hydrocarbon solvents or alkaline cleaners, but these cleaners must be removed before heat treatment. Hydrochloric acid (HCl) formed from residual amounts of chlorinated solvents, which may be used for degreasing, has caused severe attack of stainless steels. Surface contamination may be caused by machining, shearing, and drawing operations. Small particles of metal from tools become embedded in the steel surface and, unless removed, may promote localized corrosion. These particles are best removed by the passivation treatments described subsequently.

Shotblasting or sandblasting should be avoided unless iron-free silica is used; metal shot, in particular, will contaminate the stainless steel surface. If shotblasting or shot peening with metal grit is unavoidable, the parts must be cleaned after blasting or peening by immersing them in an HNO_3 solution, as noted previously.

Passivation Techniques

During handling and processing operations, such as machining, forming, tumbling, and lapping, particles of iron, tool steel, or shop dirt may be embedded in or smeared on the surfaces of stainless steel components. These contaminants may reduce the effectiveness of the natural oxide (passive) film that forms on stainless steels exposed to oxygen at low temperatures (the formation of these passive films is discussed in the section "Mechanism of Corrosion Resistance" in this article). If allowed to remain, these particles may corrode and produce rustlike spots on the stainless steel that can reduce the resistance to localized chloride attack. To prevent this condition, semifinished or finished parts are given a passivation treatment. This treatment consists of cleaning and then immersing stainless steel parts in a solution of HNO_3 or of HNO_3 plus oxidizing salts. The treatment dissolves the embedded or smeared iron, restores the original corrosion-resistant surface, and maximizes the inherent corrosion resistance of the stainless steel.

Cleaning. Each workpiece to be passivated must be cleaned thoroughly to remove grease, coolant, or other shop debris (Ref 7). A worker will sometimes eliminate the cleaning step based on the reasoning that the cleaning and passivation of a grease-laden part will occur simultaneously by immersing it in an HNO_3 bath. This assumption is mistaken. The grease will react with the HNO_3 to form gas bubbles, which collect on the surface of the workpiece and interfere with passivation. Also, contamination of the passivating solution (particularly with high levels of chlorides) can cause flash attack, which results in a gray or black appearance and deterioration of the surface.

To avoid such problems, each part should be wiped clean of any large machining chips or other debris. More tenacious deposits should be removed by brushing with a stainless steel wire brush, grinding, polishing with an iron-free abrasive, or sandblasting. Tools and materials used for these processes should be clean and used only for stainless steels. Machining, forming, or grinding oils must be removed in order for passivation to be effective. Cleaning should begin with solvent cleaning, which may be followed by alkaline soak cleaning and thorough water rinsing. Optimal results are obtained in passivation when the parts to be treated are as clean as they would have to be for plating. When large parts or bulky vessels are to be cleaned, it may be necessary to apply cleaning liquids by means of pressure spray; exterior surfaces may be cleaned by immersion or swabbing.

Passivating. After cleaning, the workpiece can be immersed in the passivating acid bath. As shown in Table 3, the composition of the acid bath depends on the grade of stainless steel. The 300-series stainless steels can be passivated in 20 vol% HNO_3. A sodium dichromate ($Na_2Cr_2O_7{\cdot}2H_2O$) addition or an increased concentration of HNO_3 is used for less corrosion-resistant stainless steels to reduce the potential for flash attack. In response to environmental concerns with the use of chromates, citric-acid-based and electrochemical passivation treatments (Ref 6) have been developed. Conventional passivation in nitric acid for several material classes is described in Table 3.

The procedure suggested for passivating free-machining stainless steels is somewhat different from that used for non-free-machining grades (Ref 7). This is because sulfides of sulfur-bearing free-machining grades, which are totally or partially removed during passivation, create microscopic discontinuities in the surface of the machined part. Even normally efficient water rinses can leave residual acid trapped in these discontinuities after passivation. This acid can then attack the surface of the part unless it is neutralized or removed. For this reason, a special passivation process, referred to as the alkaline-acid-alkaline method, is suggested for free-machining grades.

The following steps should be followed when passivating free-machining stainless steels with the alkaline-acid-alkaline technique:

- After degreasing, soak the parts for 30 min in 5 wt% sodium hydroxide (NaOH) at 70 to 80 °C (160 to 180 °F)
- Water rinse
- Immerse the part for 30 min in 20 vol% HNO_3 plus 22 g/L (3 oz/gal) $Na_2Cr_2O_7{\cdot}2H_2O$ at 50 to 60 °C (120 to 140 °F)
- Water rinse
- Immerse for 30 min in 5 wt% NaOH at 70 to 80 °C (160 to 180 °F)
- Water rinse and dry

Passivation in citric acid follows the same general principles as that in nitric acid, as seen in Table 4.

Testing is often performed to evaluate the passivated surface. For example, 400-series, precipitation-hardening, and free-machining stainless steels are often tested in a cabinet capable of maintaining the sample moist in 100% humidity at 35 °C (95 °F) for 24 h. Material that is properly passivated will be virtually free of rust, although light staining may occur (Ref 7). Austenitic 300-series grades can be evaluated using a technique given in ASTM A 380 (Ref 5). This test consists of swabbing the part with a copper sulfate ($CuSO_4{\cdot}5H_2O$)/sulfuric acid (H_2SO_4) solution; wetness should be maintained for 6 min (Ref 7). Free iron, if present, plates out the copper from the solution, and the surface develops a copper cast or color. Precautions for this procedure and details on additional tests for detecting the presence of iron on passivated surfaces are outlined in Ref 5 and 7. Information on passivation treatments for corrosion-resistant steels is also available in ASTM A 967 (Ref 6).

Design

Corrosion can often be avoided by suitable changes in design without changing the type of steel. The factors to be considered include joint

Table 3 Passivating solutions for stainless steels (non-free-machining grades)

Grade	Passivation treatment
Austenitic 300-series grades Grades with ≥17% Cr (except 440 series)	20 vol% HNO_3 at 50–60 °C (120–140 °F) for 30 min
Straight chromium grades (12–14% Cr)	20 vol% HNO_3 plus 22 g/L (3 oz/gal) $Na_2Cr_2O_7{\cdot}2H_2O$ at 50–60 °C (120–140 °F) for 30 min; or
High-carbon/high-chromium grades (440 series)	
Precipitation-hardening grades	50 vol% HNO_3 at 50–60 °C (120–140 °F) for 30 min

Source: Ref 7

Table 4 Passivation with citric or nitric acids

			10 wt% citric acid passivated 30 min as below				Percent nitric acid passivated 30 min at 50 °C/ 60 °C (120 °F/140 °F)	
Stainless family	Example stainless steels	% Cr	°C	°F	pH(a)	Process(b)	Volume %(c)	Process(b)
Austenitic	Type 304/304L Type 316/316L Custom Flo 302HQ Type 305 Nitrogen strengthened	15.0–23.5	65	150	...	1	20%	1
Martensitic-PH	Custom 630 (17Cr-4Ni) Custom 450 Custom 455 Custom 465 15Cr-5Ni	11.0 17.5	65	150	...	1	20% + $Na_2Cr_2O_7$	1
Ferritic	Type 430	≥16	65	150	...	1	20% + $Na_2Cr_2O_7$	1
Ferritic	Type 409Cb	<12	80–90	180–200	...	2	20% + $Na_2Cr_2O_7$ Use care: low Cr	
Martensitic	Type 410 Type 420 TrimRite	≤15	50–55	120–130	...	2	20% + $Na_2Cr_2O_7$	1
Austenitic-FM	Type 303	17–19	65	150	...	2	20% + $Na_2Cr_2O_7$	2
Ferritic-FM	Types 430F and 430FR	≥16	NA(d)	NA	NA	NA	20% + $Na_2Cr_2O_7$	2
Ferritic-FM	Chrome Core 18-FM	≥16	40	100	...	2	NA	NA
Ferritic-FM	Type 409Cb-FM	≤13	45	110	5	2	20% + $Na_2Cr_2O_7$ Use care: low Cr	2
Martensitic–FM	Type 416	≤13	45	110	5	2	Preferred vs. citric 20% + $Na_2Cr_2O_7$	2

Note: pH, precipitation hardenable. FM, free machining.

(a) pH adjusted with sodium hydroxide. (b) Process 1: Clean/degrease, water rinse, passivate as indicated, water rinse, and dry. Process 2: Clean degrease in 5 wt% NaOH at 71–82 °C (160–180 °F) for 30 min, water rinse, passivate as indicated, water rinse, neutralize in 5 wt% NaOH at 71–82 °C (160–180 °F) for 30 min, water rinse, and dry. (c) Na2Cr2O_7 means add 22 g/L (3 oz/gal) of sodium dichromate to the 20% nitric acid. An alternative to this mixture is 50% nitric acid without sodium dichromate. (d) Not applicable. Source: Ref 8

design, surface continuity, and concentration of stress. Designs that tend to concentrate corrosive media in a small area should be avoided. For example, tank inlets should be designed such that concentrated solutions are mixed and diluted as they are introduced (Fig. 2). Otherwise, localized pockets of concentrated solutions can cause excessive corrosion.

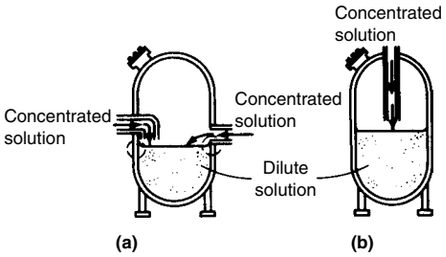

Fig. 2 Poor (a) and good (b) designs for vessels used for mixing concentrated and dilute solutions. Poor design causes concentration and uneven mixing of incoming chemicals along the vessel wall (circled areas). Good design allows concentrated solutions to mix away from vessel walls.

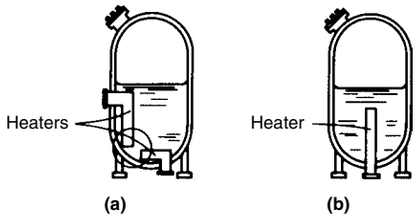

Fig. 3 Poor (a) and good (b) designs for heating of solutions. Poor design creates hot spots (circled area) that may induce boiling under the heater at the bottom of the vessel or may cause deposits to form between heaters and vessel walls. Good design avoids hot spots and pockets in which small volumes of liquid can become trapped between the heater and the vessel wall.

Poor design of heaters can create similar problems, such as those that cause hot spots and thus accelerate corrosion. Heaters should be centrally located (Fig. 3). If a tank is to be heated externally, heaters should be distributed over as large a surface area as possible, and circulation of the corrosive medium should be encouraged, if possible.

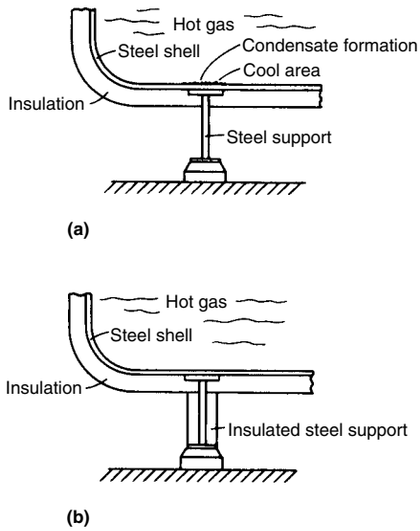

Fig. 4 Design to reduce localized cooling. In the poor design (a), the uninsulated steel support radiates heat, which causes a cool area on the steel shell. In (b), the steel support is insulated to minimize temperature decrease at the base of the shell.

Hot gases that are not corrosive to stainless steel may form corrosive condensates on the cold portions of a poorly insulated unit. Proper design or insulation can prevent such localized cooling (Fig. 4). Conversely, vapors from noncorrosive liquids may cause attack; exhausts and overflows should be designed to prevent hot vapor pockets (Fig. 5). In general, the open ends of inlets, outlets, and tubes in heat exchangers should be flush with tank walls or tubesheets to avoid buildup of harmful corrodents, sludges, and deposits (Fig. 6). This is also true of tank bottom and drainage designs (Fig. 7).

Tanks and tank supports should be designed to prevent or minimize corrosion due to spills and

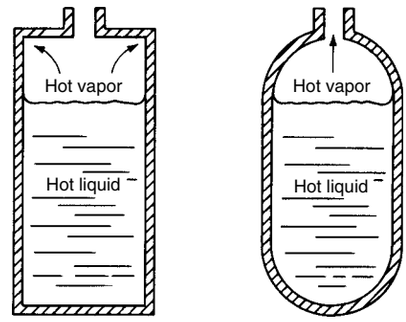

Fig. 5 Poor (a) and good (b) designs for vessels holding both liquid and vapor phases. Sharp corners and protruding outlet end in (a) allow hot gases to become trapped in the vapor space. This is avoided in (b) by using rounded corners and mounting the vessel outlet pipe flush.

overflows (Fig. 8). A tank support structure may not be as corrosion resistant as the tank itself, but it is a very important part of the unit and should not be made vulnerable to spilled corrodents.

Designs that increase turbulence or result in excessive flow rates should be avoided where erosion-corrosion may be a problem (Fig. 9). Gaskets in flanges should fit properly, intrusions in a flow stream should be avoided, and elbows should be given a generous radius. Finally, crevices should be avoided. Where crevices cannot be avoided, they should be sealed by welding, soldering, or the use of caulking compounds or sealants. Additional information is available in the article "Designing to Minimize Corrosion" in *ASM Handbook,* Volume 13A, 2003.

Forms of Corrosion of Stainless Steels

The various forms of corrosive attack are briefly discussed in this section. Detailed information on each of these forms of corrosion is available in the Section "Forms of Corrosion" in *ASM Handbook,* Volume 13A, 2003.

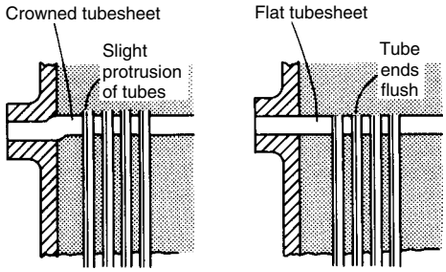

Fig. 6 Poor (a) and good (b) designs for tube/tubesheet assemblies. Crowned tubesheet and protruding tubes in (a) allow buildup of corrosive deposits; in (b), tubesheet is flat and tubes are mounted flush.

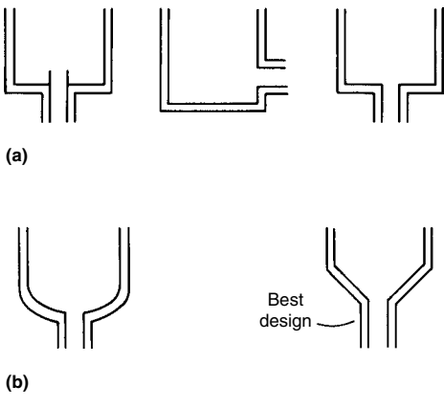

Fig. 7 Examples of poor (a) and good (b) designs for drainage, corners, and other dead spaces in vessels. Sharp corners and protruding outlet pipes in (a) can cause buildup of corrosive deposits and crevice corrosion; these design features are avoided in (b).

General (uniform) corrosion of a stainless steel suggests an environment capable of stripping the passive film from the surface and preventing repassivation. Such an occurrence could indicate an error in grade selection. An example of such an error is the exposure of a lower-chromium ferritic stainless steel to a moderate concentration of hot sulfuric acid (H_2SO_4).

Galvanic corrosion results when two dissimilar metals are in electrical contact in a corrosive medium. As a highly corrosion-resistant metal, stainless steel can act as a cathode when in contact with a less noble metal, such as steel. The corrosion of steel parts—for example, steel bolts in a stainless steel construction—can be a significant problem. However, the effect can be used in a beneficial way for protecting critical stainless steel components within a larger steel construction. In the case of stainless steel connected to a more noble metal, consideration must be given to the active-passive condition of the stainless steel. If the stainless steel is passive in the environment, galvanic interaction with a more noble metal is unlikely to produce significant corrosion. If the stainless steel is active or only marginally passive, galvanic interaction with a more noble metal will probably produce sustained rapid corrosion of the stainless steel without repassivation. The most important aspect of galvanic interaction for stainless steels is the necessity of selecting fasteners and weldments of adequate corrosion resistance relative to the bulk material, which is likely to have a much larger exposed area.

Pitting is a localized attack that can produce penetration of a stainless steel with almost negligible weight loss to the total structure. Pitting is associated with a local discontinuity of the passive film. It can be a mechanical imperfection, such as an inclusion or surface damage, or it can be a local chemical breakdown of the film. Chloride is the most common agent for initiation of pitting. Other halides, notably bromide, are also pitting agents. Once a pit is formed, it in effect becomes a crevice; the local chemical environment is substantially more aggressive than the bulk environment. This explains why very high flow rates over a stainless steel surface tend to reduce pitting corrosion; the high flow rate prevents the concentration of corrosive species in the pit. The stability of the passive film with respect to resistance to pitting initiation is controlled primarily by chromium and molybdenum. Minor alloying elements can also have an important effect by influencing the amount and type of inclusions (for example, sulfides) in the steel that can act as pitting sites.

Pitting initiation can also be influenced by surface condition, including the presence of deposits, and by temperature. For a particular environment, a grade of stainless steel may be characterized by a single temperature, or a very narrow range of temperatures, above which pitting will initiate and below which pitting will not initiate. This is the critical pitting temperature (CPT). It is therefore possible to select a grade that will not be subject to pitting attack if the chemical environment and temperature do not exceed the critical levels. If the range of operating conditions can be accurately characterized, a meaningful laboratory evaluation is possible. Formation of deposits in service can reduce the pitting temperature.

Although chloride is known to be the primary agent of pitting attack, it is not possible to establish a single critical chloride limit for each grade. The corrosivity of a particular concentration of chloride solution can be profoundly affected by the presence or absence of various other chemical species that may accelerate or inhibit corrosion. Chloride concentration may increase where evaporation or deposits occur. Because of the nature of pitting attack—rapid penetration with little total weight loss—it is rare that any significant amount of pitting will be acceptable in practical applications.

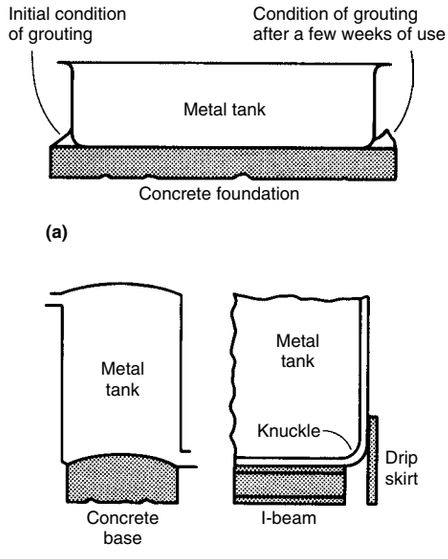

Fig. 8 Design for preventing external corrosion from spills and overflows. (a) Poor design. (b) Good designs

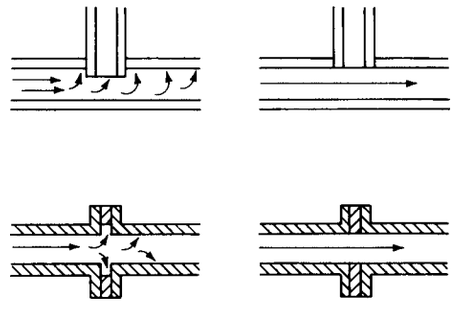

Fig. 9 Designs for preventing excessive turbulence. (a) Poor designs (both top and bottom). (b) Good designs (both top and bottom)

Crevice corrosion can be considered a severe form of pitting. Any crevice, whether the result of a metal-to-metal joint, a gasket, fouling, or deposits, tends to restrict oxygen access, concentrate the chloride ion, and reduce the pH, resulting in attack. In practice, it is extremely difficult to prevent all crevices, but every effort should be made to do so. Higher-chromium, and especially higher-molybdenum, grades are more resistant to crevice attack. Just as there is a CPT for a particular environment, there is also a critical crevice temperature (CCT). This temperature is specific to the geometry and nature of the crevice and to the precise corrosion environment for each grade. The CCT can be useful in selecting an adequately resistant grade for particular applications.

Intergranular corrosion is a preferential attack at the grain boundaries of a stainless steel. It is generally the result of sensitization. This condition occurs when a thermal cycle leads to grain-boundary precipitation of a carbide, nitride, or intermetallic phase without providing sufficient time for chromium diffusion to fill the locally depleted region. A grain-boundary precipitate is not the point of attack; instead, the low-chromium region adjacent to the precipitate is susceptible.

Sensitization is not necessarily detrimental unless the grade is to be used in an environment capable of attacking the region. For example, elevated-temperature applications for stainless steel can operate with sensitized steel, but concern for intergranular attack must be given to possible corrosion during downtime when condensation might provide a corrosive medium. Because chromium provides corrosion resistance, sensitization also increases the susceptibility of chromium-depleted regions to other forms of corrosion, such as pitting, crevice corrosion, and SCC. The thermal exposures required to sensitize steel can be relatively brief, as in welding, or can be very long, as in high-temperature service.

Stress-corrosion cracking is a corrosion mechanism in which the combination of a susceptible alloy, sustained tensile stress, and a particular environment leads to cracking of the metal. Stainless steels are particularly susceptible to SCC in chloride environments; temperature and the presence of oxygen tend to aggravate chloride SCC of stainless steels. Most ferritic and duplex stainless steels are either immune or highly resistant to SCC. All austenitic grades, especially types 304 and 316, are susceptible to some degree. The highly alloyed austenitic grades are resistant to boiling sodium chloride (NaCl) solutions, but crack readily in $MgCl_2$ solutions. Although some localized pitting or crevice corrosion probably precedes SCC, the amount of pitting or crevice attack may be so small as to be undetectable. Stress corrosion is difficult to detect while in progress, even when pervasive, and can lead to rapid catastrophic failures of pressurized equipment.

It is difficult to alleviate the environmental conditions that lead to SCC. The level of chlorides required to produce SCC is very low. In operation, there can be evaporative concentration or a concentration in the surface film on a heat-rejecting surface. Temperature is often a process parameter, as in the case of a heat exchanger. Tensile stress is one parameter that might be controlled. However, the residual stresses associated with fabrication, welding, or thermal cycling, rather than design stresses, are often responsible for SCC, and even stress-relieving heat treatments do not completely eliminate these residual stresses.

Erosion-Corrosion. Corrosion of a metal or alloy can be accelerated when there is an abrasive removal of the protective oxide layer. This form of attack is especially significant when the thickness of the oxide layer is an important factor in determining corrosion resistance. In the case of a stainless steel, erosion of the passive film can lead to some acceleration of attack.

Oxidation. Because of their high chromium contents, stainless steels tend to be very resistant to oxidation. Important factors to be considered in the selection of stainless steels for high-temperature service are the stability of the composition and microstructure of the grade upon thermal exposure and the adherence of the oxide scale upon thermal cycling. Because many of the stainless steels used for high temperatures are austenitic grades with relatively high nickel contents, it is also necessary to be alert to the possibility of sulfidation attack.

Corrosion in Specific Environments

Selection of a suitable stainless steel for a specific environment requires consideration of several criteria. The first is corrosion resistance. Alloys are available that provide resistance to mild atmospheres (for example, type 430) or to many food-processing environments (for example, type 304 stainless). Chemicals and more severe corrodents require type 316 or a more highly alloyed material, such as 20Cb-3 alloy or one of the 6 Mo stainless steels. Factors that affect the corrosivity of an environment include the concentration of chemical species, pH, aeration, flow rate (velocity), impurities (such as chlorides), and temperature, including effects from heat transfer.

The second criterion is mechanical properties, or strength. High-strength materials often sacrifice resistance to some form of corrosion, particularly SCC.

Third, fabrication must be considered, including such factors as the ability of the steel to be machined, welded, or formed. Resistance of the fabricated article to the environment must be considered—for example, the ability of the material to resist attack in crevices that cannot be avoided in the design.

Fourth, total cost must be estimated, including initial alloy price, installed cost, and the effective life expectancy of the finished product. Finally, consideration must be given to product availability.

This section discusses the corrosivity of various environments for stainless steels.

Atmospheric Corrosion

The atmospheric contaminants most often responsible for the rusting of structural stainless steels are chlorides and metallic iron dust. Chloride contamination may originate from the calcium chloride ($CaCl_2$) used to make concrete or from exposure in marine or industrial locations. Iron contamination may occur during fabrication or erection of the structure. Contamination should be minimized, if possible.

The corrosivity of different atmospheric exposures can vary greatly and can dictate application of different grades of stainless steel. Rural atmospheres, uncontaminated by industrial fumes or coastal salt, are extremely mild in terms of corrosivity for stainless steel, even in areas of high humidity. Industrial or marine environments can be considerably more severe.

Table 5 demonstrates that resistance to staining can depend on the specific exposure. For example, several 300-series stainless steels showed no rust during long-term exposures in New York City. On the other hand, staining was observed after much shorter exposures at Niagara Falls in a severe industrial-chemical environment near plants producing chlorine or hydrogen chloride (HCl).

Table 5 Atmospheric corrosion of austenitic stainless steels at two industrial sites

	New York City (industrial)		Niagara Falls (industrial-chemical)	
Type(a)	Exposure time, years	Specimen surface evaluation	Exposure time, years	Specimen surface evaluation
302	5	Free from rust stains	$<2/3$	Rust stains
302	26	Free from rust stains	...	...
304	26	Free from rust stains	<1	Rust stains
304	...	...	6	Covered with rust spots and pitted
347	26	Free from rust stains	...	...
316	23	Free from rust stains	$<2/3$	Slight stains
316	...	...	6	Slight rust spots, slightly pitted
317	...	...	$<2/3$	Slight stains
317	...	...	6	Slight stains
310	...	...	<1	Rust stains
310	...	...	6	Rust spots; pitted

(a) Solution-annealed sheet, 1.6 mm ($1/16$ in.) thick

Although marine environments can be severe, stainless steels often provide good resistance. Table 6 compares AISI 300-series stainless steels after a 15 year exposure to a marine atmosphere 240 m (800 ft) from the ocean at Kure Beach, NC. Materials containing molybdenum exhibited only extremely slight rust stain, and all grades were easily cleaned to reveal a bright surface. Type 304 stainless steel may provide satisfactory resistance in many marine applications, but more highly alloyed grades are often selected when the stainless steel is sheltered from washing by the weather and is not cleaned regularly.

Type 302 and 304 stainless steels have had many successful architectural applications. Type 430 stainless steel has been used in many locations, but there have been problems. For example, type 430 stainless steel rusted in sheltered areas after only a few months exposure in an industrial environment. The type 430 stainless steel was replaced by type 302, which provided satisfactory service. In more aggressive environments, such as marine or severely contaminated atmospheres, type 316 stainless steel is especially useful.

The surface finish can influence the corrosion resistance of stainless steel exposed to the atmosphere. Smooth surface finishes tend to hold less contaminants and are more readily washed by precipitation, resulting in improved corrosion resistance. The improvement in corrosion resistance is typically observed when the surface roughness (R_a) is 0.5 μm (20 μin.) or smoother.

Stress-corrosion cracking is generally not a concern when austenitic or ferritic stainless steels are used in atmospheric exposures. Several austenitic stainless steels were exposed to a marine atmosphere at Kure Beach, NC. Annealed and quarter-hard wrought AISI types 201, 301, 302, 304, and 316 stainless steels were not susceptible to SCC. In the as-welded condition, only type 301 stainless steel experienced failure. Following sensitization at 650 °C (1200 °F) for 1.5 h and furnace cooling, failures were obtained only for materials with carbon contents of 0.043% or more (Ref 10).

Stress-corrosion cracking must be considered when quench-hardened martensitic stainless steels or precipitation-hardening grades are used in marine environments or in industrial locations where chlorides are present. Several hardenable stainless grades were exposed as U-bends 24 m (80 ft) from the ocean at Kure Beach, NC. Most samples were cut longitudinally, and two alloys received different heat treatments to produce different hardness or strength levels. The results of the study (Table 7) indicated that Custom 450 stainless and stainless alloy 355 resisted cracking. Stainless alloy 355 failed in this type of test when fully hardened; resistance was imparted by the 540 °C (1000 °F) temper. Precipitation-hardenable grades are expected to exhibit improved corrosion resistance when higher aging temperatures (lower strengths) are used.

Resistance to SCC is of particular interest in the selection of high-strength stainless steels for fastener applications. Cracking of high-strength fasteners is possible and often results from hydrogen generation due to corrosion or contact with a less noble material, such as aluminum. Resistance to SCC can be improved by optimizing the heat treatment, as noted previously.

Fasteners for atmospheric exposure have been fabricated from a wide variety of alloys. Type 430 and unhardened type 410 stainless steels have been used when moderate corrosion resistance is required in a lower-strength material. Better-than-average corrosion resistance has been obtained by using 305 and 302HQ stainless steels when lower strength is acceptable.

Table 6 Corrosion of AISI 300-series stainless steels in a marine atmosphere

Based on 15 year exposures 240 m (800 ft) from the ocean at Kure Beach, NC

	Average corrosion rate		Average depth of pits		
AISI type	mm/yr	mils/yr	mm	mils	Appearance(a)
301	$<2.5\times10^{-5}$	<0.001	0.04	1.6	Light rust and rust stain on 20% of surface
302	$<2.5\times10^{-5}$	<0.001	0.03	1.2	Spotted with rust stain on 10% of surface
304	$<2.5\times10^{-5}$	<0.001	0.028	1.1	Spotted with slight rust stain on 15% of surface
321	$<2.5\times10^{-5}$	<0.001	0.067	2.6	Spotted with slight rust stain on 15% of surface
347	$<2.5\times10^{-5}$	<0.001	0.086	3.4	Spotted with moderate rust stain on 20% of surface
316	$<2.5\times10^{-5}$	<0.001	0.025	1.0	Extremely slight rust stain on 15% of surface
317	$<2.5\times10^{-5}$	<0.001	0.028	1.1	Extremely slight rust stain on 20% of surface
308	$<2.5\times10^{-5}$	<0.001	0.04	1.6	Spotted by rust stain on 25% of surface
309	$<2.5\times10^{-5}$	<0.001	0.028	1.1	Spotted by slight rust stain on 25% of surface
310	$<2.5\times10^{-5}$	<0.001	0.01	0.4	Spotted by slight rust stain on 20% of surface

(a) All stains easily removed to reveal bright surface. Source: Ref 9

Table 7 Stress-corrosion cracking of U-bend test specimens 24 m (80 ft) from the ocean at Kure Beach, NC

Alloy	Final heat treatment	Hardness, HRC	Specimen orientation	Time to failure of each specimen(a), days
Custom 450	Aged at 480 °C (900 °F)	42	Transverse	NF, NF, NF, NF, NF
Type 410	Tempered at 260 °C (500 °F)	45	Longitudinal	379, 379, 471
	Tempered at 550 °C (1025 °F)	35	Longitudinal	4, 4
Alloy 355	Tempered at 540 °C (1000 °F)	38	Longitudinal	NF, NF, NF
15Cr-7Ni-Mo	Aged at 510 °C (950 °F)	49	Longitudinal	1, 1, 1
17Cr-4Ni	Aged at 480 °C (900 °F)	42	Longitudinal	93, 129, NF
	Aged at 620 °C (1150 °F)	32	Longitudinal	93, 129, NF
14Cr-6Ni	Aged at 480 °C (900 °F)	39	Longitudinal	93, 872, NF

(a) NF, no failure in over 4400 days for Custom 450 and 1290 days for the other materials. Source: Ref 11

Corrosion in Waters

Waters may vary from extremely pure to chemically treated water to highly concentrated chloride solutions, such as brackish water or seawater, further concentrated by recycling. This chloride content poses the danger of pitting or crevice attack of stainless steels. When the application involves moderately increased temperatures, even as low as 50 °C (120 °F), and particularly when there is heat transfer into the chloride-containing medium, there is the possibility of SCC. It is useful to consider water with two general levels of chloride content: freshwater, which can have chloride levels up to approximately 600 ppm, and seawater, which encompasses brackish and severely contaminated waters. The corrosivity of a particular level of chloride can be strongly affected by the other chemical constituents present, making the water either more or less corrosive.

Under some circumstances, SCC of stainless steels can occur at room temperature. This has been a particular problem for indoor swimming pools, where condensation of hypochlorous acid vapors, in association with zinc, iron, or aluminum chlorides, has led to catastrophic failures (Ref. 12).

Permanganate ion (MnO_4^-) has been related to pitting of type 304 stainless steel. The presence of sulfur compounds and oxygen or other oxidizing agents can affect the corrosion of copper and copper alloys but does not have very significant effects on stainless steels at ambient or slightly elevated temperatures.

Freshwater. Type 304 and 316 alloys are the standard stainless steels specified for natural, raw, and potable freshwaters. In freshwater, type 304 stainless steel has provided excellent service for such items as valve parts, weirs, fasteners, and pump shafts in water and wastewater treatment plants. Custom 450 stainless steel has been used as shafts for large butterfly valves in potable water. The higher strength of a precipitation-hardenable stainless steel permits reduced shaft diameter and increased flow. Type 201 stainless steel has seen service in revetment mats to reduce shoreline erosion in freshwater. Type 316 stainless steel has been used as wire for microstrainers in tertiary sewage treatment and is suggested for waters containing minor amounts

of chloride. Based on laboratory trials and service experience, the recommended maximum chloride levels for the 304/304L and 316/316L alloys in water systems at ambient to near-ambient temperatures are 200 and 1000 ppm, respectively. The increased pitting and crevice corrosion resistance of grades such as 317LMN, 904L, and 2205 will increase this maximum chloride level to the 5000 ppm range. When water environments are too demanding for standard grades, high-performance stainless steels with higher PREN values and improved chloride SCC resistance are good alternatives. Figures 10 and 11 show the pitting and crevice thresholds of various austenitic stainless steels as a function of temperature and chloride concentration. Stress-corrosion cracking of types 304 and 316 can occur in neutral aqueous chloride solutions when temperatures exceed approximately 50 °C (120 °F).

Oxidizers such as chlorine will raise the corrosion potential, making pitting and crevice corrosion more likely. Investigations with chlorinated freshwater have shown that the 304/304L steels are susceptible to crevice attack with chlorination levels in the 3 to 5 ppm range (Ref 14). Alloys with higher PREN values will provide better resistance.

In the presence of higher-than-usual water manganese levels, the 304 and 316L steels have failed in waters that are thought to be non-corrosive, based on their chloride content and temperature. When manganese contamination is present in the water, MnO_2 deposits can form, which will promote pitting failures. Soluble Mn(II) can be oxidized to MnO_2 by biological processes or chemically by oxidizing biocides such as chlorine, peroxide, or ozone. When the biological or chemical conversion processes are present in an environment, the level of manganese required for this effect is exceedingly small, less than 1 ppm. When the creation of manganic ion occurs by these reactions, the standard grades such as 304 and 316 may not be resistant to pitting in the resulting environment even if the chloride content is below 200 or 1000 ppm, respectively. Selecting alloys with higher chloride pitting resistance can solve the problem of manganese-induced corrosion. High-performance stainless steels, such as 6% Mo super-austenitic stainless, and highly alloyed ferritic grades, such as S44660 and AL 29-4C alloys, have successfully replaced standard stainless grades in high-manganese waters.

There are circumstances where microbial activity can influence the corrosion process. This often involves microbes that metabolize sulfur compounds, producing a localized environment containing hydrogen sulfide at lower pH. In some cases, the presence of microbial activity will produce localized corrosion on standard stainless steel grades. This form of attack is called microbiologically influenced corrosion (MIC) and most frequently occurs on welds and heat-affected zones in stagnant or slowly moving waters. There have been few, if any, reports of MIC failures with high-alloyed grades such as 2205 and the 6% Mo stainless steels. The important factor in avoiding MIC appears to be the increased corrosion resistance that is provided by stainless steels with relatively high PREN values (PREN > 35).

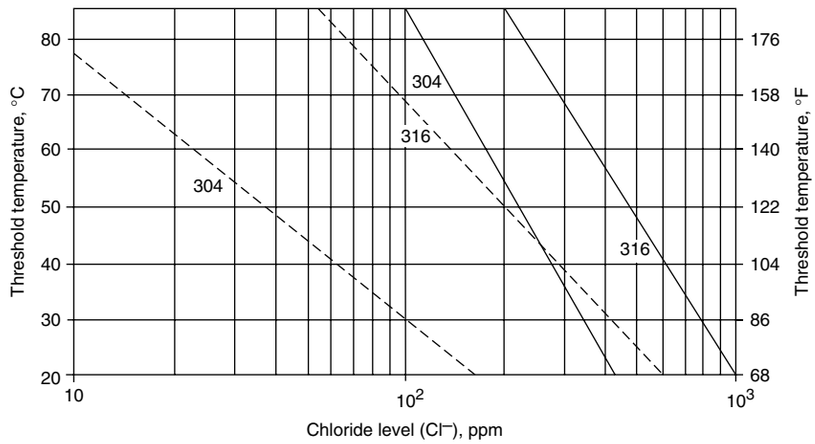

Fig. 10 Risk of pitting (solid line) and crevice corrosion (dashed line) of standard grades of stainless steel in oxygen-saturated waters with varying chloride levels. Source: Ref 13

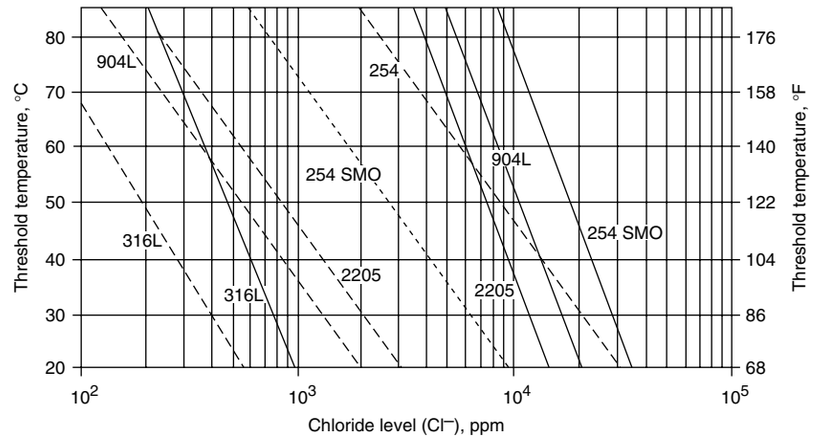

Fig. 11 Risk of pitting (solid line) and crevice corrosion (dashed line) of higher-alloyed stainless steels in oxygen-saturated waters with varying chloride levels. Dotted line is a plate heat exchanger. Source: Ref 13

Seawater is a very corrosive environment for many materials. The high chloride content of seawater, coupled with the susceptibility of many stainless steels to chloride-induced localized corrosion, is especially challenging for stainless steels. Lower-alloyed stainless steels, such as 304, 316, and 317, do not have sufficient corrosion resistance for long-time exposures to seawater. It was not until the introduction of stainless steels with PREN of 40 or greater that truly seawater-resistant stainless steels became available. Testing has shown that stainless steels require a critical crevice corrosion temperature (CCT) measured with an ASTM G 48 (Ref 15) ferric chloride crevice test of approximately 35 °C (95 °F) or higher to resist seawater exposure (Ref 16). This is demonstrated in the plot shown in Fig. 12.

Stainless steels are more likely to be attacked in low-velocity seawater. In quiescent natural seawaters, stainless steels will develop noble potentials due to the formation and influence of a microbial slime layer. The noble potentials, typically in the range of 300 to 350 mV (saturated calomel electrode, or SCE), increase the risk of pitting and crevice corrosion. Hence, living seawater is more aggressive than sterile solutions such as synthetic seawater and laboratory NaCl solutions where this ennoblement is absent. The biofilm catalyzes the oxygen reduction reaction, which is the predominant cathodic reaction in water exposures. Because of this, localized corrosion is more likely to initiate, and the rate of localized corrosion attack in seawater will be higher in the presence of an intact biofilm.

Stainless steels also are more likely to be attacked at crevices resulting from equipment design or attachment of barnacles. Type 304 and 316 stainless steels suffer deep pitting if the seawater flow rate decreases below approximately 1.5 m/s (5 ft/s) because of the effects of biofouling. However, in one study, type 316 stainless steel provided satisfactory service as

tubing in the heat recovery section of a desalination test plant with relatively high flow rates (Ref 17).

The choice of stainless steel for seawater service can depend on whether or not stagnant conditions can be minimized or eliminated. For example, boat shafting of 17Cr-4Ni stainless steel has been used for trawlers where stagnant exposure and the associated pitting would not be expected to be a problem. When seagoing vessels are expected to lie idle for extended periods of time, more resistant boat shaft materials, such as 22Cr-13Ni-5Mn stainless steel, are considered. Boat shafts with intermediate corrosion resistance are provided by 18Cr-2Ni-12Mn and high-nitrogen type 304 (type 304HN) stainless steels.

The most severe exposure conditions are often used in seawater test programs. The crevice corrosion performance of various stainless steels and nickel-base alloys in filtered seawater at 30 °C (85 °F) is given in Table 8. Samples were prepared with plastic multiple-crevice washers, each containing 20 plateaus or crevices. The panels were exposed for at least 30 days in filtered seawater flowing at a velocity of less than 0.1 m/s (<0.33 ft/s).

The results given in Table 8 show the number of sides that experienced crevice attack and the maximum attack depth at any crevice for that alloy. A crevice corrosion index (CCI) was calculated by multiplying the maximum attack depth times the number of sides attacked. This provided a ranking system that accounts for both initiation and growth of attack. Lower values of the CCI imply improved resistance.

Attack in the previously mentioned test does not mean that materials with high CCIs cannot be used in seawater. For example, 22Cr-13Ni-5Mn stainless steel with a CCI of 20 has proved to be a highly resistant boat shaft alloy. Some of the more resistant materials in the aforementioned tests have been used for utility condenser tubing. These include AL-29-4C, 254SMO, Sea-Cure, and AL-6XN alloys.

The possibility of galvanic corrosion must be considered if stainless steel is to be used in contact with other metals in seawater. Figure 13 provides corrosion potentials in flowing seawater for several materials. Preferably, only those materials that exhibit closely related electrode potentials should be coupled to avoid attack of the less noble material. Galvanic differences have been used to advantage in the cathodic protection of stainless steel in seawater. Many examples of the successful use of the common grades of stainless steel (e.g., type 316) in seawater may be a result of inadvertent galvanic protection from adjacent carbon steel and so on. Crevice corrosion and pitting of austenitic type 302 and 316 stainless steels have been prevented by cathodic protection, but type 410 and 430 stainless steels develop hydrogen blisters at current densities below those required for complete protection. Superferritic stainless steels, which do not require cathodic protection themselves, have been damaged by hydrogen embrittlement caused by cathodic protection applied to protect other nonstainless components (Ref. 20).

Other factors that should be noted when applying stainless steels in seawater include the effects of high velocity, aeration, and temperature. Stainless steels generally show excellent resistance to high velocities, impingement attack, and cavitation in seawater. The corrosivity of natural seawater is often greatest at the ambient local temperature, presumably because the indigenous microbes are most active at these temperatures. Heating of the water will kill the biofilm and stop catalytic activity. Increasing the temperature from ambient to approximately 50 °C (120 °F) often reduces attack of stainless steels (Ref 21). Further temperature increases can result in increased corrosion, such as SCC.

In many applications, seawater is chlorinated to avoid fouling problems. Chlorine and hypochlorite are oxidants, that also polarize the surface of the stainless steel to more noble potentials. Chlorination of seawater can produce potentials in the 500 to 600 mV SCE range. Consequently, chlorination can substantially increase the risk of localized attack. Because the chlorine will kill the biofilm, there is no catalysis of the oxygen reaction. Therefore, corrosion attack in seawater may be increased or decreased by chlorination. The probability of corrosive attack increases with chlorine concentration and temperature. The chlorine level required to prevent microbial activity on a stainless steel surface has been reported to be 0.1 to 0.2 ppm (Ref 22, 23) If intermittent chlorination is used, a residual level of 1 ppm of chlorine for 30 min per day seems to be sufficient to stop the microbial activity (Ref 24).

The performance of duplex stainless steels immersed in natural and in chlorinated seawater is summarized in Tables 9 and 10. The results of pipe loop testing of various stainless steels in seawater at two chlorination levels are shown in Table 11.

The seawater test results show the superduplex alloys such as UNS S32750 and S32760 are similar to the 6% Mo superaustenitic alloys in seawater exposures. Based on practical experience, the offshore industry tends to restrict the use of both superduplex and superaustenitic steels to 30 to 35 °C (85 to 95 °F) and 1 ppm residual chlorine (Ref 16).

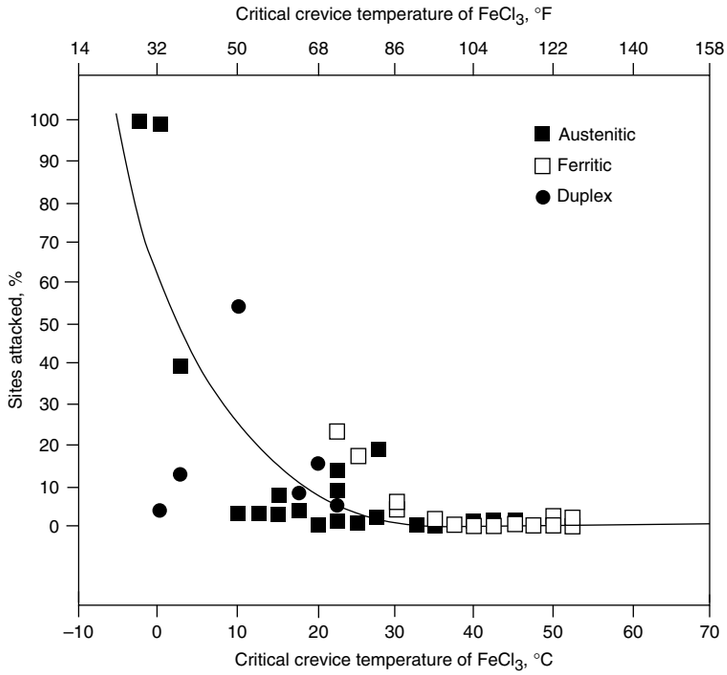

Fig. 12 Crevice corrosion sites attacked in seawater exposure at 35 °C (95 °F) for various stainless steels having different ferric chloride critical crevice temperatures. Source: Ref 16

Corrosion in Chemical Environments

Selection of stainless steels for service in chemicals requires consideration of all forms of corrosion, along with impurity levels and degree of aeration. When an alloy with sufficient general corrosion resistance has been selected, care must be taken to ensure that the material will not fail by pitting or SCC due to chloride contamination. Aeration may be an important factor in corrosion, particularly in cases of borderline passivity. If dissimilar-metal contact or stray currents occur, the possibility of galvanic attack or hydrogen embrittlement must be considered.

Alloy selection also depends on fabrication and operation details. If a material is to be used in

the as-welded or stress-relieved condition, it must resist intergranular attack in service after these thermal treatments. In chloride environments, the possibility of crevice corrosion must be considered when crevices are present because of equipment design or the formation of adherent deposits. Higher flow rates may prevent the formation of deposits but in extreme cases may also cause accelerated attack due to erosion or cavitation. Increased operating temperatures generally increase corrosion. In heat-transfer applications, higher metal wall temperatures result in higher corrosion rates than expected from the lower temperature of the bulk solution. These and other items may require consideration in the selection of stainless steels, yet suitable materials continue to be chosen for a wide variety of chemical plant applications (see the articles about corrosion in the chemical processing industry in this Volume).

Some generalizations can be made regarding the performance of various categories of stainless steels in certain types of chemical environments. These observations relate to the compositions of the grades. For example, the presence of nickel and copper in some austenitic grades greatly enhances resistance to H_2SO_4 compared to the resistance of the ferritic grades. However, combinations of chemicals that are encountered in practice can be either more or less corrosive than might be expected from the corrosivity of the individual components. Testing in actual or simulated environments is always recommended as the best procedure for selecting a stainless steel grade. Additional information describing service experience is available from alloy suppliers.

Mineral Acids. The resistance of stainless steel to acids depends on the hydrogen ion (H^+) concentration, presence of halides, and the oxidizing capacity of the acid, along with such material variables as chromium content, nickel content, carbon content, and heat treatment (Ref 26). For example, annealed stainless steel resists strong nitric acid (HNO_3) in spite of the low pH of the acid, because HNO_3 is highly oxidizing and forms a passive film due to the chromium content of the alloy. On the other hand, stainless steels are rapidly attacked by strong HCl because a passive film is not easily created or maintained in this environment. Even in strong HNO_3, stainless steels can be rapidly attacked if they contain sufficient carbon and are sensitized. The presence of oxidizing species, such as ferric salts, results in reduced general corrosion in some acids but can cause accelerated pitting attack if chloride ions (Cl^-) are present.

Nitric Acid. As noted previously, stainless steels have broad applicability in HNO_3 primarily because of their chromium content. Most AISI 300-series stainless steels exhibit good or excellent resistance in the annealed condition in concentrations from 0 to 65% up to the boiling point. Fig. 14 illustrates the good resistance of type 304 stainless steel, particularly when compared with the lower-chromium type 410 stainless steel. More severe environments at elevated temperatures require alloys with higher chromium. In HNO_3 cooler-condensers, such stainless alloys as 7-Mo Plus (UNS S32950) and 2RE10 (UNS S31002) are candidates for service. In very concentrated (greater than 90%) nitric acid, silicon-bearing alloys such as A610 or A611 (UNS S30600 and S30601, respectively) exhibit enhanced resistance.

Sulfuric Acid. Stainless steels can approach the borderline between activity and passivity in sulfuric acid. Conventional ferritic grades, such

Table 8 Crevice corrosion ranking of alloys evaluated for 30 days in filtered seawater at 30 °C (85 °F)

Rank	Alloy	UNS designation	Composition, (wt%) Cr	Ni	Mo	Mn	Cu	Other	Number of sides (S) attacked	Maximum depth (D) of attack mm	in.	CCI(a) (S×D)	PREN(b)
1	Hastelloy C-276	N10276	15.5	54.7	15.5	0.5	0.1	3.8 W	0	0.00	0.00	0.00	66.7
	Inconel 625	N06625	22.3	61.0	8.5	0.1	...	3.6 Nb	0	0.00	0.00	0.00	50.4
	AL 29-4	S44700	29.6	0.1	4.0	...	...	...	0	0.00	0.00	0.00	42.8
	AL 29-4-2	S44800	29.5	2.2	4.0	...	...	...	0	0.00	0.00	0.00	42.7
	AL 29-4C	S44735	28.8	0.8	3.8	0.2	...	0.6 Ti	0	0.00	0.00	0.00	41.3
	Monit	...	25.3	4.1	3.8	0.4	0.4	...	0	0.00	0.00	0.00	37.8
2	Sea-Cure	S44660	25.6	2.1	2.9	0.2	...	0.5 Ti	1	0.05	0.002	0.05	35.2
3	Ferralium 255	S32550	26.2	5.6	3.2	0.8	1.8	0.19 N	2	0.08	0.003	0.16	36.8
4	Hastelloy G-3	N06985	22.8	43.7	7.0	0.8	1.8	3.5 Co	1	0.21	0.008	0.21	45.9
5	Haynes 20 Mod	...	21.6	25.5	5.0	0.9	...	0.5 Co	2	0.46	0.018	0.92	38.1
6	26-1S	S44626	25.0	0.2	1.0	0.2	...	1.1 Ti	4	0.30	0.012	1.2	28.3
7	20Mo-6	N08026	23.9	33.4	5.6	0.4	3.3	...	3	0.53	0.020	1.6	42.4
8	E-Brite	S44627	25.9	0.1	1.0	...	...	0.1 Nb	4	0.46	0.018	1.8	29.2
9	AL-4X	...	20.2	24.4	4.4	1.4	1.5	...	4	0.50	0.019	2.0	34.7
10	AL-6X	N08366	20.4	24.6	6.4	1.4	...	...	4	0.62	0.024	2.5	41.5
11	254SMO	S31254	20.0	17.9	6.1	0.5	0.8	0.2 N	5	0.51	0.020	2.6	46.1
12	Hastelloy G	N06007	22.2	46.8	5.8	1.5	1.9	3.5 Co	4	0.87	0.034	3.5	41.3
13	904L	N08904	20.5	24.7	4.7	1.5	1.6	...	5	0.74	0.029	3.7	36.0
14	AISI 216	S21600	20.0	6.0	2.5	8.0	...	0.35 N	6	0.64	0.025	3.8	38.8
15	254SFER	...	29.4	22.2	2.1	1.7	0.1	0.15 N	5	0.90	0.035	4.5	40.8
16	254SLX	N08904	19.9	25.0	4.7	1.6	1.7	0.04 N	6	0.92	0.036	5.5	36.6
17	Rex 734	S31675	21.3	9.4	2.7	3.8	...	0.42 N	6	1.00	0.039	6.0	42.8
18	Type 317 LM	S31725	19.5	14.5	4.1	1.3	0.2	0.06 N	6	1.07	0.042	6.4	34.8
19	Nitronic 50	S20910	21.1	13.7	2.3	4.8	...	0.26 N	6	1.10	0.043	6.6	36.5
20	JS 700	N08700	20.7	25.2	4.4	1.6	0.2	0.26 Nb	5	2.00	0.079	10	35.2
21	Type 316	S31600	17.5	10.7	2.4	1.6	0.3	...	6	1.93	0.076	12	25.4
22	20 Cb-3	N08020	19.4	33.2	2.2	0.4	3.2	0.51 Nb	5	3.10	0.122	16	26.7
23	JS 777	N08777	20.8	25.6	4.5	1.4	2.2	0.24 Nb	6	2.90	0.114	17	35.7
24	44 LN	S31200	25.0	5.9	1.5	1.8	0.1	0.2 N	6	3.35	0.132	20	36.0
Perforated													
	34 LN	...	16.8	13.8	4.2	1.6	...	0.14 N	6	1.04	0.041	6.2	34.9
	AISI 444	S44400	18.9	0.1	2.0	0.4	...	0.4 Nb	6	1.21	0.048	7.3	25.5
	Type 329	S32900	27.0	4.2	1.4	0.3	0.1	...	6	1.29	0.051	7.7	31.6
Attack outside crevice areas													
	AISI 439	S43035	17.7	0.3	...	0.3	...	0.4 Ti	6	0.72	0.028	4.3	17.7
	AISI 317L +	S31725	18.3	15.8	4.2	1.5	0.2	0.16 Co	6	1.09	0.043	6.5	32.2
	AISI 317L	S31703	18.9	12.2	3.6	1.7	...	0.06 N	6	1.92	0.076	12	32.6
	Incoloy 825	N08825	22.0	44.0	2.7	0.4	1.7	0.7 Ti	6	2.42	0.095	15	30.9

(a) CCI, crevice corrosion index. (b) PREN, pitting resistance equivalent with nitrogen. Source: Ref 18

as type 430, have limited use in H_2SO_4, but the newer ferritic grades containing higher chromium and molybdenum (for example, 28% Cr and 4% Mo) with additions of at least 0.25% Ni have shown good resistance in boiling 10% H_2SO_4 (Ref 28), but corrode rapidly when acid concentration is increased.

The conventional austenitic grades exhibit good resistance in very dilute or highly concentrated H_2SO_4 at slightly elevated temperatures. Acid of intermediate concentration is more aggressive, and conventional grades have very limited utility. Resistance of several stainless steels in up to approximately 50% H_2SO_4 is shown in Fig. 15. Aeration or the addition of other oxidizing species can significantly reduce the attack of stainless steels in H_2SO_4. This occurs because the more oxidizing environment is better able to maintain the chromium-rich passive oxide film.

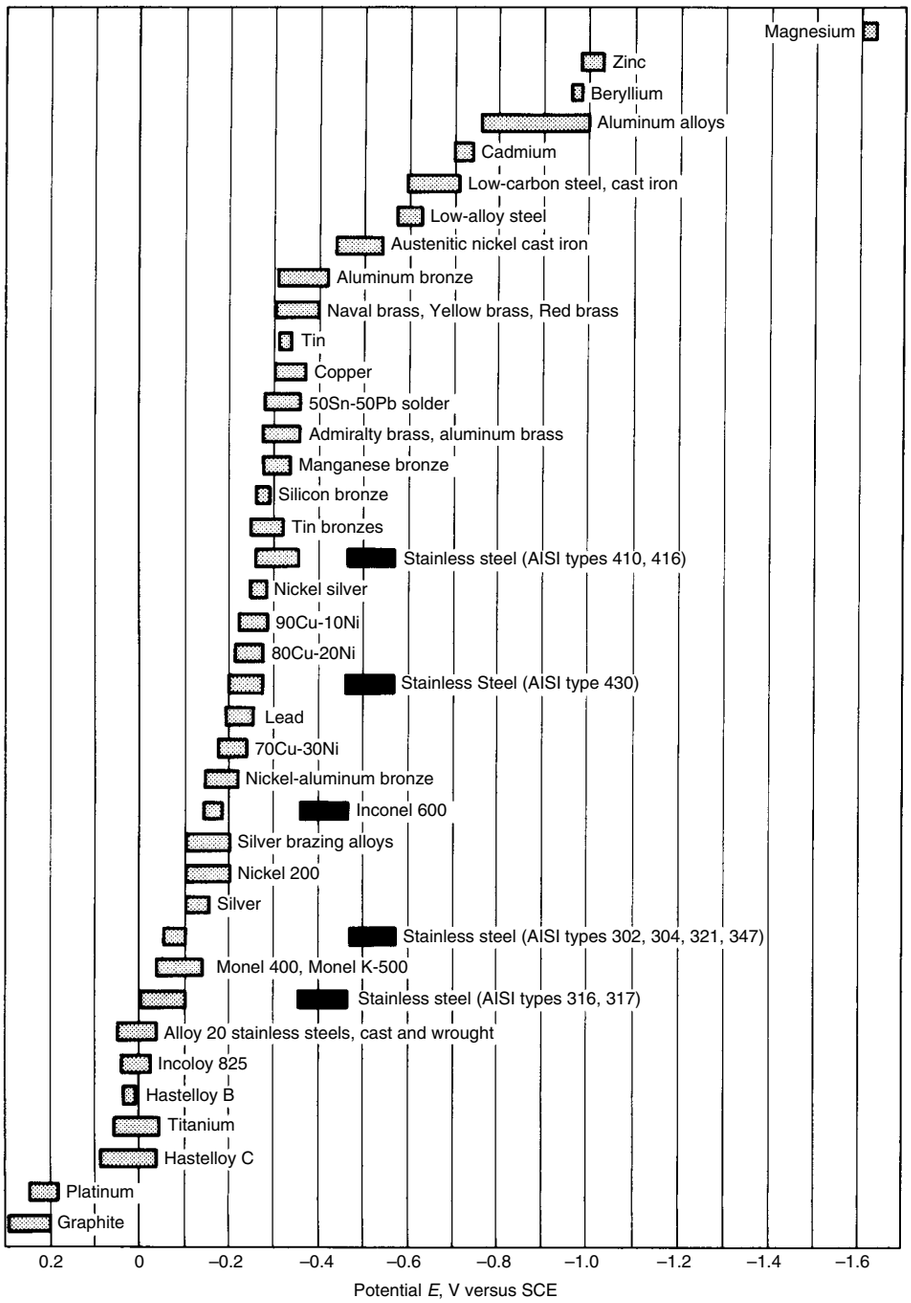

Fig. 13 Corrosion potentials of various metals and alloys in flowing seawater at 10 to 25 °C (50 to 80 °F). Flow rate was 2.5 to 4 m/s (8 to 13 ft/s); alloys are listed in order of the potential versus saturated calomel electrode (SCE) that they exhibited. Those metals and alloys indicated by a black bar may become active and exhibit a potential near – 0.5 V versus SCE in low velocity or poorly aerated water and in shielded areas. Source: Ref 19

Improved resistance to H_2SO_4 has been obtained by using austenitic grades containing high levels of nickel and copper, such as 20Cb-3 stainless steel. In addition to reducing general corrosion, the increased nickel provides resistance to SCC. Because of its resistance to these forms of corrosion, 20Cb-3 stainless steel has been used for valve springs in H_2SO_4 service. See Ref 29 for more information.

Phosphoric Acid. Conventional straight-chromium stainless steels have very limited general corrosion resistance in phosphoric acid (H_3PO_4) and exhibit lower rates only in very dilute or more highly concentrated solutions. Conventional austenitic stainless steels provide useful general corrosion resistance over the full range of concentrations up to approximately 65 °C (150 °F); use at temperatures up to the boiling point is possible for acid concentrations up to approximately 40%.

In commercial applications, however, wet-process H_3PO_4 environments include impurities derived from the phosphate rock, such as chlorides, fluorides, and H_2SO_4. These three impurities accelerate corrosion, particularly pitting or crevice corrosion in the presence of the halogens. Higher-alloyed materials than the conventional austenitic stainless steels are required to resist wet-process H_3PO_4. Candidate materials include alloy 904L, JS700, alloy 28, 20Cb-3, 20Mo-4, and 6% Mo stainless steels.

Hydrochloric Acid. Stainless steels are generally not used for HCl service, except perhaps for very dilute solutions at room temperature. Stainless steels can be susceptible to accelerated general corrosion, SCC, and pitting in HCl environments. See Ref 30 for more information.

Sulfurous Acid. Although sulfurous acid (H_2SO_3) is a reducing agent, several stainless steels have provided satisfactory service in H_2SO_3 environments. Conventional austenitic stainless steels have been used in sulfite digesters, and type 316, type 317, 20Cb-3, and cast Alloy Casting Institute alloys CF-8M and CN-7M stainless steels have seen service in wet sulfur dioxide (SO_2) and H_2SO_3 environments. Cast stainless steels are discussed in the article "Corrosion of Cast Stainless Steels" in this Volume. Service life is improved by eliminating crevices, including those from settling of suspended solids, or by using molybdenum-containing grades. In some environments, SCC is also a possibility.

Organic acids and compounds are generally less aggressive than mineral acids because they do not ionize as completely, but they can be corrosive to stainless steels, especially when impurities are present. The presence of oxidizing agents in the absence of chlorides can reduce corrosion rates.

Acetic Acid. Corrosion rates for several stainless steels in acetic acid are listed in Table 12. Resistance to pure acetic acid has been obtained by using type 316 and 316L stainless steels over all concentrations up to the boiling point. Type 304 stainless steel may be considered in all concentrations below

approximately 90% at temperatures up to the boiling point. Impurities present in the manufacture of acetic acid, such as acetaldehyde, formic acid, chlorides, and propionic acid, are expected to increase the attack of stainless steels. Chlorides may cause pitting or SCC. See Ref 32 for more information.

Formic acid is one of the more aggressive organic acids, and corrosion rates can be higher in the condensing vapor than in the liquid. Type 304 stainless steel has been used at moderate temperatures. However, type 316 stainless steel or higher alloys, such as 20Cb-3, are often preferred, and high-alloy ferritic stainless steels containing 26% Cr and 1% Mo or 29% Cr and 4% Mo also show some promise.

Other Organic Acids. The corrosivity of propionic and acrylic acids at a given temperature is generally similar to that of acetic acid. Impurities are important and may strongly affect the corrosion rate. In citric and tartaric acids, type 304 stainless steel has been used for moderate temperatures, and type 316 has been suggested for all concentrations up to the boiling point.

Organic Halides. Most dry organic halides do not attack stainless steels, but the presence of water allows halide acids to form and can cause pitting or SCC. Therefore, care should be exercised when using stainless steels in organic halides to ensure that water is excluded.

Other Organic Compounds. Type 304 stainless steel has generally been satisfactory in aldehydes, in cellulose acetate at lower temperatures, and in fatty acids up to approximately 150 °C (300 °F). At higher temperatures, these chemicals require type 316 or 317. Type 316 stainless steel is also used in amines, phthalic anhydride, tar, and urea service.

Stainless steels have been used in the plastic and synthetic fiber industries. Type 420 and 440C stainless steels have been used as plastic mold steels. More resistant materials, such as Custom 450, have been used for extruding polyvinyl chloride (PVC) pipe. Spinnerettes, pack parts, and metering pumps of Custom 450 and Custom 455 stainless steels have been used in the synthetic fiber industry to produce nylon, rayon, and polyesters.

Alkalis. All stainless steels resist general corrosion by all concentrations of sodium hydroxide (NaOH) up to approximately 65 °C (150 °F). Type 304 and 316 stainless steels exhibit low rates of general corrosion in boiling NaOH up to nearly 20% concentration. Stress-corrosion cracking of these grades can occur at approximately 100 °C (212 °F). Good resistance to general corrosion and SCC in 50% NaOH at 135 °C (275 °F) is provided by E-Brite and 7-Mo stainless steels (Ref 33). In ammonia (NH_3) and ammonium hydroxide (NH_4OH), stainless

Table 11 Results of testing in parallel 50 mm (2 in.) pipe loops in chlorinated seawater, 30 °C (85 °F), 85 days

	Number attacked of 12			
	Chlorination, ppm			
	0.5		1.5	
Alloy	Flanges	Welds	Flanges	Welds
2205	7	0	6	0
255	3	6	2	7
2507	0	1	4	1
S32760	0	2	3	0
254SMO	0	0	3	0
AL-6XN	1	0	2	0

Source: Ref 25

Table 9 Corrosion of duplex stainless steels in natural seawater

Test temperature		Exposure time, months	Specimen type	Alloy(a)			
°C	°F			255	2507	S32760	254SMO
Ambient		24	Crevice	o	...	...	o
Ambient		3	Crevice	o	o	o	...
30	85	6	Crevice	o	...	...	...
35	95	3	Crevice	...	o	...	o
35	95	3	Welded	...	o	...	...
30	85	3	Crevice	...	...	o/o	o/o
40	105	3	Crevice	...	...	o/p	o/p
70	160	3	Crevice	...	...	o/p	o/p
Ambient		1	Crevice	cc	...	o	o
40	105	6	Crevice	...	...	o	...
60	140	6	Crevice	...	...	cc	...
Ambient		3	Crevice	...	cc	o	cc

(a) o, no corrosion; p, pitting corrosion; cc, crevice corrosion. Source: Ref 25

Table 10 Corrosion of duplex stainless steels in chlorinated seawater

	Test temperature		Exposure time, months		Alloy(a)			
$[Cl_2]$, ppm	°C	°F		Specimen type	255	2507	S32760	254SMO
2	35	95	3	Crevice	...	o	...	o
2	35	95	3	Welded	...	o	...	...
2	45	115	3	Crevice	...	cc	...	cc
2	45	115	3	Welded	...	o	...	...
1	30	85	5	Butt welded tubes	...	o	...	o
1	40	105	5	Butt welded tubes	...	o	...	o
1	Ambient		1	Crevice	cc	...	o	o
10	45	115	3	Crevice	...	cc	...	cc
2	55	130	3	Crevice	...	cc	...	cc
2	55	130	3	Welded	...	p	...	...
(b)	55	130	3	Crevice	...	cc	...	...
(b)	55	130	3	Welded	...	p	...	...
1.5	30	85	3	Crevice	...	...	o/o	...
1.5	40	105	3	Crevice	...	...	o/p	...
1.5	70	160	3	Crevice	...	...	o/p	...
3.0	30	85	3	Crevice	...	...	cc/p	...
3.0	40	105	3	Crevice	...	...	cc/p	...
3.0	70	160	3	Crevice	...	...	cc/o	...

(a) o, no corrosion; p, pitting corrosion; cc, crevice corrosion. (b) Intermittent chlorination (2 ppm, 1 h/d) for 1 mo. followed by continuous chlorination (2 ppm) for 2 mo. Source: Ref 25

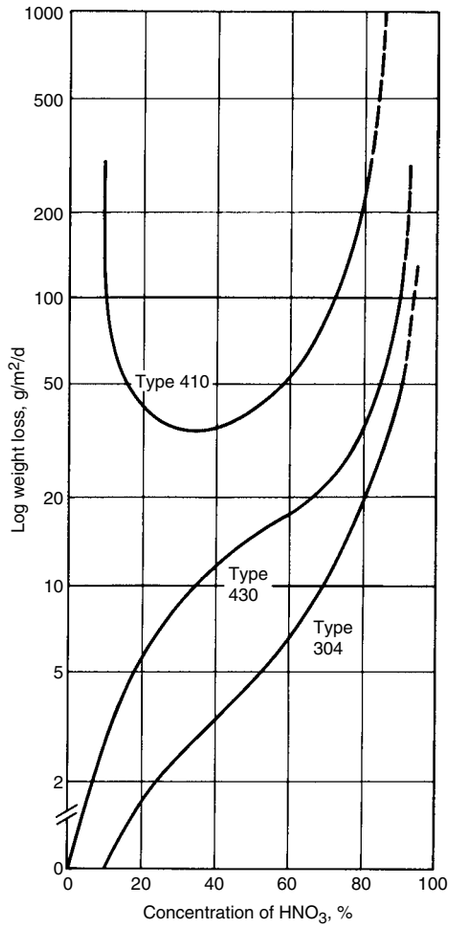

Fig. 14 Corrosion rates of various stainless steels in boiling HNO_3. Source: Ref 27

steels have shown good resistance at all concentrations up to the boiling point.

Salts. Stainless steels are highly resistant to most neutral or alkaline nonhalide salts. In some cases, type 316 is preferred for its resistance to pitting, but even the higher-molybdenum type 317 stainless steel is readily attacked by sodium sulfide (Na_2S) solutions.

Halogen salts are more corrosive to stainless steels because of the ability of the halide ions to penetrate the passive film and cause pitting. Pitting is promoted in aerated or mildly acidic oxidizing solutions. Chlorides are generally more aggressive than the other halides in their ability to cause pitting.

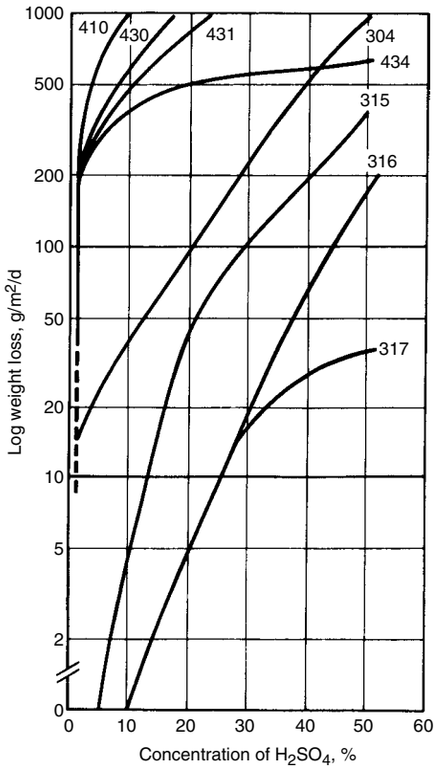

Fig. 15 Corrosion rates of various stainless steels in underaerated H_2SO_4 at 20 °C (68 °F). Source: Ref 27

Table 12 Corrosion of austenitic stainless steels in boiling glacial acetic acid

Data are from averaged results of 11, 12, and 21 day field tests.

	Corrosion rate	
AISI type	mm/yr	mils/yr
304	0.46	18
321	1.19	47
347	1.04	41
308	1.35	53
310	0.99	39
316	0.015	0.6

Source: Ref 31

Gases. At lower temperatures, most austenitic stainless steels resist chlorine or fluorine gas if the gas is completely dry. The presence of even small amounts of moisture results in accelerated attack, especially pitting and possibly SCC.

Oxidation. At elevated temperatures, stainless steels resist oxidation primarily because of their chromium content. Increased nickel minimizes spalling when temperature cycling occurs. Table 13 lists generally accepted maximum safe service temperatures for wrought stainless steels. Maximum temperatures for intermittent service are lower for the austenitic stainless steels but are higher for most of the martensitic and ferritic stainless steels listed.

Contamination of the air with water and CO_2 often increases corrosion at elevated temperatures. Increased attack can also occur because of sulfidation as a result of SO_2, H_2S, or sulfur vapor.

Carburization of stainless steels can occur in carbon monoxide (CO), methane (CH_4), and other hydrocarbons. Carburization can also occur when stainless steels contaminated with oil or grease are annealed without sufficient oxygen to burn off the carbon. This can occur during vacuum or inert gas annealing as well as open air annealing of oily parts with shapes that restrict air access. Chromium, silicon, and nickel are useful in combating carburization.

Nitriding can occur in dissociated NH_3 at high temperatures. Resistance to nitriding depends on alloy composition as well as NH_3 concentration, temperature, and pressure. Stainless steels are readily attacked in pure NH_3 at approximately 540 °C (1000 °F).

Liquid Metals. The 18-8 stainless steels are highly resistant to liquid sodium or sodium-potassium alloys. Mass transfer is not expected up to 540 °C (1000 °F) and remains at moderately low levels up to 870 °C (1600 °F). Accelerated attack of stainless steels in liquid sodium occurs with oxygen contamination, with a noticeable effect occurring at approximately 0.02% oxygen by weight (Ref 26).

Exposure to molten lead under dynamic conditions often results in mass transfer in common stainless alloy systems. Particularly severe corrosion can occur in strongly oxidizing conditions. Stainless steels are generally attacked by molten aluminum, zinc, antimony, bismuth, cadmium, and tin.

Table 13 Generally accepted maximum service temperatures in air for stainless steels

	Maximum service temperature			
	Intermittent service		Continuous service	
Type	°C	°F	°C	°F
Austenitic grades				
201	815	1500	845	1550
202	815	1500	845	1550
301	840	1545	900	1650
302	870	1600	925	1700
304	870	1600	925	1700
308	925	1700	980	1795
309	980	1795	1095	2000
310	1035	1895	1150	2100
316	870	1600	925	1700
317	870	1600	925	1700
321	870	1600	925	1700
330	1035	1895	1150	2100
347	870	1600	925	1700
Ferritic grades				
405	815	1500	705	1300
406	815	1500	1035	1895
430	870	1600	815	1500
442	1035	1895	980	1795
446	1175	2145	1095	2000
Martensitic grades				
410	815	1500	705	1300
416	760	1400	675	1250
420	735	1355	620	1150
440	815	1500	760	1400

Source: Ref 34

Corrosion in Various Applications

Every industry features a variety of applications encompassing a range of corrosion environments. This section characterizes the experience of each industry according to the corrosion problems most frequently encountered and suggests appropriate grade selections. Many applications for stainless steels, particularly those involving heat exchangers, can be analyzed in terms of a process side and a water side. The process side is usually a specific chemical combination that has its own requirements for a stainless steel grade. The water side is common in many applications.

Food and Beverage Industry. Stainless steels have been relied on in these applications because of the lack of corrosion products that could contaminate the process environment and because of the superior cleanability of the stainless steels. The corrosion environment often involves moderately to highly concentrated chlorides on the process side, often mixed with significant concentrations of organic acids. The water side can range from steam heating to brine cooling. Purity and sanitation standards require excellent resistance to pitting and crevice corrosion.

Foods such as vegetables represent milder environments and can generally be handled by using type 304 stainless steel. Sauces and pickle liquors, however, are more aggressive and can pit even type 316 stainless steel. For improved pitting resistance, alloys such as 22Cr-13Ni-5Mn, 904L, 20Mo-4, 254SMO, AL-6XN, and SeaCure stainless steels should be considered.

At elevated temperatures, materials must be selected for resistance to pitting and SCC in the presence of chlorides. Stress corrosion must be avoided in heat-transfer applications, such as steam jacketing for cooking or processing vessels or in heat exchangers. Cracking may occur from the process or water side or may initiate outside the unit under chloride-containing insulation. Brewery applications of austenitic

stainless steels have been generally successful except for a number of cases of SCC of high-temperature water lines. The use of ferritic, duplex, or higher-alloyed austenitic stainless steels can be an appropriate remedy for the SCC.

Stainless steel equipment should be cleaned frequently to prolong its service life. The equipment should be flushed with freshwater, scrubbed with a nylon brush and detergent, and then rinsed. On the other hand, consideration should be given to the effect of very aggressive cleaning procedures on the stainless steels, such as in the chemical sterilization of commercial dishwashers. In some cases, it may be necessary to select a more highly alloyed stainless steel grade to deal with these brief exposures to highly aggressive environments.

Conventional stainless steel grades provide satisfactory service in many food and beverage applications. Type 304 stainless steel is widely used in the dairy industry, and type 316 finds application as piping and tubing in breweries. These grades, along with type 444 and Custom 450 stainless steels, have been used for chains to transfer food through processing equipment. Machined parts for beverage-dispensing equipment have been fabricated from type 304, 304L, 316, 316L, 303Al Modified, 302HQ-FM, and 303BV stainless steels. When the free-machining grades are used, it is important to passivate and rinse properly before service in order to optimize corrosion resistance.

Food-handling equipment should be designed without crevices in which food can become lodged. In more corrosive food products, extra-low-carbon stainless steels should be used when possible. Improved results have been obtained when equipment is finished with a 2B (general-purpose cold-rolled) finish rather than No. 4 (general-purpose polished) finish. Alternatively, an electropolished surface may be considered.

Pharmaceutical Industry. The production and handling of drugs and other medical applications require exceedingly high standards for preserving the sterility and purity of process streams. Process environments can include complex organic compounds, strong acids, chloride solutions comparable to seawater, and elevated processing temperatures. Higher-alloy grades, such as type 316 or higher, may be necessary instead of type 304 in order to prevent even superficial corrosion. Electropolishing may be desirable in order to reduce or prevent adherent deposits and the possibility of under-deposit corrosion. Superior cleanability and ease of inspection make stainless steel the preferred material.

The 18-8 stainless grades have been used for a wide variety of applications from pill punches to operating tables. However, care is required in selecting stainless steels for pharmaceutical applications because small amounts of contamination can be objectionable. For example, stainless steel has been used to process vitamin C, but copper must be eliminated because copper in aqueous solutions accelerates the decomposition of vitamin C. Also, stainless is not used to handle vitamin B_6 hydrochloride, even though corrosion rates may be low, because trace amounts of iron are objectionable.

The effects of temperature and chloride concentration must be considered. At ambient temperature, chloride pitting of 18Cr-8Ni stainless steel may occur, but SCC is unlikely. At approximately 50 °C (120 °F) or above, SCC of austenitic grades must be considered. Duplex alloys, such as 7-Mo Plus, alloy 2205, Ferralium 255, and 2507, possess improved resistance to SCC in elevated-temperature chloride environments. Ferritic grades with lower nickel content, such as 18Cr-2Mo stainless steel, provide another means of avoiding chloride SCC.

Stainless steels have also found application as orthopedic implants. Material is required that is capable of moderately high strength and resistance to wear and fretting corrosion, along with pitting and crevice attack. Vacuum-melted type 316 stainless steel has been used for temporary internal fixation devices, such as bone plates, screws, pins, and suture wire. Higher purity improves electropolishing, and increased chromium (17 to 19%) improves corrosion resistance.

In permanent implants, such as artificial joints, very high strength and resistance to wear, fatigue, and corrosion are essential. Cobalt-, zirconium-, or titanium-base alloys are used for these applications.

Oil and Gas Industry. Stainless steels were not frequently used in oil and gas production until the tapping of sour reservoirs (those containing hydrogen sulfide, H_2S) and the use of enhanced recovery systems in the mid-1970s. Sour environments can result in sulfide stress cracking (SSC) of susceptible materials. This phenomenon generally occurs at ambient or slightly elevated temperatures; it is difficult to establish an accurate temperature maximum for all alloys. Factors affecting SSC resistance include material variables, pH, H_2S concentration, total pressure, maximum tensile stress, temperature, and time. A description of some of these factors, along with information on materials that have demonstrated resistance to SSC, is available in Ref 35.

The resistance of stainless steels to SSC improves with reduced hardness. Conventional materials, such as type 410, 430, and 304 stainless steels, exhibit acceptable resistance at hardnesses below 22 HRC. Specialized grades, such as 22Cr-13Ni-5Mn, Custom 450, 20Mo-4, and some duplex stainless steels, have demonstrated resistance at higher hardnesses. Duplex alloy 2205 has been used for its strength and corrosion resistance as gathering lines for CO_2 gas before gas cleaning. Custom 450 and 22Cr-13Ni-5Mn stainless steels have seen service as valve parts. Other grades used in these environments include 254SMO and AL-6XN alloys for chloride resistance and alloy 28 for sulfide resistance.

In addition to the lower-temperature SSC, resistance to cracking in high-temperature environments is required in many oil field applications. Most stainless steels, including austenitic and duplex grades, are known to be susceptible to elevated-temperature cracking, probably by a mechanism similar to chloride SCC. Failure appears to be accelerated by H_2S and other sulfur compounds. Increased susceptibility is noted in material of higher yield strength, for example, because of the high residual tensile stresses imparted by some cold-working operations.

The previous discussion is pertinent to the production phase of a well. However, drilling takes place in an environment of drilling mud, which usually consists of water, clay, weighting materials, and an inhibitor (frequently an oxygen scavenger). Chlorides are also present when drilling through salt formations. Austenitic stainless steels containing nitrogen have found use in this environment as nonmagnetic drill collars, as weight for the drill bit, and as housings for measurement-while-drilling (MWD) and logging-while-drilling (LWD) instruments. Nonmagnetic materials are required for operation of these instruments, which are used to locate the drill bit in directional-drilling operations and to compile various data for formation evaluation. Nonstandard stainless steels used as drill collars or MWD/LWD components include 15-15LC Modified, 15-15HS, AG-17HS, Datalloy 2, P 530, P 530 HS, P 550, P 580, P 750, SMF 166, SMF 2000, NMS 100, NMS 140, DNM 110, and RM 118.

In refinery applications, the raw crude contains such impurities as sulfur, water, salts, organic acids, and organic nitrogen compounds. These and other corrosives and their products must be considered in providing stainless steels for the various refinery steps.

Raw crude is separated into materials from petroleum gas to various oils by fractional distillation. These materials are then treated to remove impurities, such as CO_2, NH_3, and H_2S, and to optimize product quality. Refinery applications of stainless steels often involve heat exchangers. Duplex and ferritic grades have been used in this application for their improved SCC resistance. Type 430 and type 444 stainless steel exchanger tubing has been used for resisting hydrogen, chlorides, and sulfur and nitrogen compounds in oil refinery streams.

Power Industry. Stainless steels are used in the power industry for generator components, feedwater heaters, boiler applications, heat exchangers, condenser tubing, flue gas desulfurization (FGD) systems, and nuclear power applications.

Generator blades and vanes have been fabricated of modified 12% Cr stainless steel, such as ASTM types 615 (UNS S41800) and 616 (UNS S42200). In some equipment, Custom 450 has replaced AISI type 410 and ASTM type 616 stainless steels.

Heat Exchangers. Stainless steels have been widely used in tubing for surface condensers and feedwater heaters. Both of these are shell and tube heat exchangers that condense steam from the turbine on the shell side. In these heat

exchangers, the severity of the corrosion increases with higher temperatures and pressures. Stainless steels resist failure by erosion and do not suffer SCC in NH_3 (from decomposition of boiler feedwater additives), as do some nonferrous materials.

Stainless steel must be chosen to resist chloride pitting. The amount of chloride that can be tolerated is expected to be higher with higher pH and cleaner stainless steel surfaces, that is, the absence of deposits. For example, type 304 stainless steel may resist pitting in chloride levels of 1000 ppm or higher in the absence of fouling, crevices, or stagnant conditions. The presence of one or more of these conditions can allow chlorides to concentrate at the metal surface and initiate pits. This may reduce the chloride limit for resistance to pitting of type 304 to approximately 200 ppm. Several high-performance stainless steels have been used to resist chloride pitting in brackish water or seawater. High-performance austenitic grades have been useful in feedwater heaters, although duplex stainless steels may also be considered because of their high strength. Ferritic stainless steels have proved to be economically competitive in exchangers and condensers. High-performance austenitic and ferritic grades have been satisfactory for seawater-cooled units. These grades include AL-29-4C, Usinor 290 Mo, Sea-Cure, AL-6XN, and 254SMO stainless steels.

Compatibility of materials and good installation practice are required. Tubes of such materials as those listed previously have been installed in tubesheets fabricated of alloy 904L, 20Mo-4, AL-6XN, and 254SMO stainless steels. Crevice corrosion can occur when some tube materials are rolled into type 316 stainless steel tubesheets (Ref 37). Appropriate levels of cathodic protection have been identified (Ref 38).

Flue Gas Desulfurization. A wide variety of alloys have been used in scrubbers, which are located between the boiler and smokestack of fossil fuel powder plants to treat effluent gases and to remove SO_2 and other pollutants. Typically, fly ash is removed, and the gas travels through an inlet gas duct, followed by the quencher section. Next, SO_2 is removed in the absorber section, most often using either a lime or limestone system. A mist eliminator is employed to remove suspended droplets, and the gas proceeds to the treated-gas duct, reheater section, and the stack.

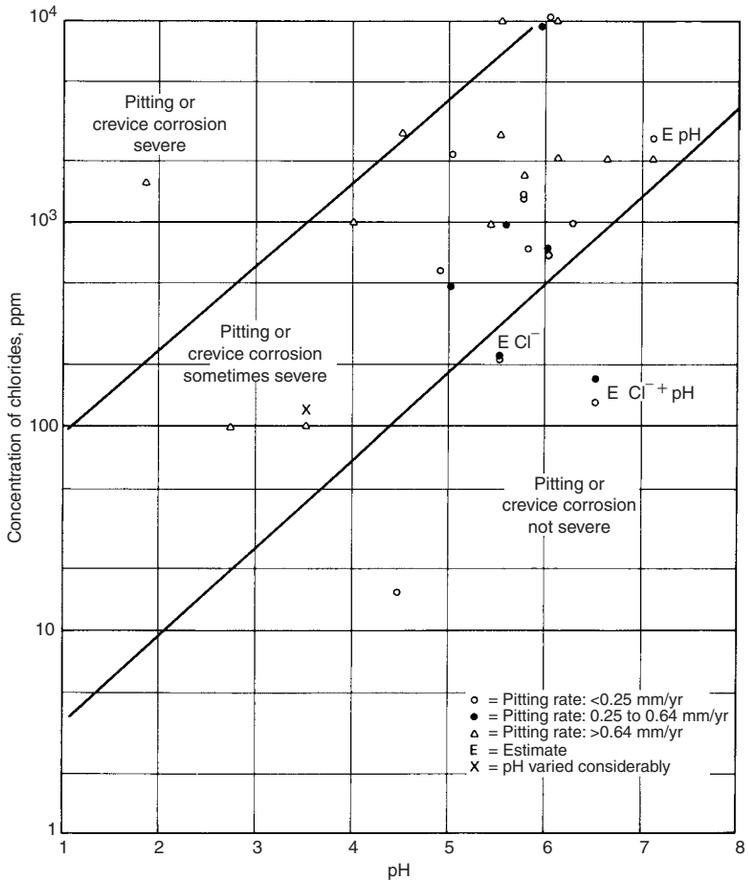

Fig. 16 Pitting of type 316L stainless steel in flue gas desulfurization scrubber environment. Solid lines indicate zones of differing severity of corrosion; because the zones are not clearly defined, the lines cannot be precisely drawn. Source: Ref 39

Two important items for consideration in selecting stainless steels for resistance to pitting in scrubber environments are pH and chloride level. Stainless steels are more resistant to higher pH and lower chloride levels, as shown in Fig. 16 for type 316L stainless steel. Environments that cause pitting or crevice attack of type 316 stainless steel can be handled by using higher-alloy materials, for example, those with increased molybdenum and chromium.

Some of the materials being considered and specified for varying chloride levels are given in Ref 40. Other materials can also provide good resistance, as evidenced by the results given in Table 14 for samples exposed to several scrubber environments. The maximum depth of localized corrosion and pit density is given for the stainless steels tested. Exposure at the quencher spray header (above slurry) was more severe than expected, probably because of wet-dry concentration effects. Severe attack also occurred in the outlet duct. Samples in this area were exposed to high chlorides, high temperatures, and low pH during the 39 days on bypass operation.

Nuclear Power Applications. Type 304 stainless steel piping has been used in boiling-water nuclear reactor power plants. The operating temperatures of these reactors are approximately 290 °C (550 °F), and a wide range of conditions can be present during startup, operation, and shutdown. Because these pipes are joined by welding, there is a possibility of sensitization. This can result in intergranular SCC in chloride-free high-temperature water that contains small amounts of oxygen, for example, 0.2 to 8 ppm. Nondestructive electrochemical tests have been used to evaluate weldments for this service (Ref 42).

Type 304 stainless steel with additions of boron (approximately 1%) has been used to construct spent-fuel storage units, dry storage casks, and transportation casks. The high boron level provides neutron-absorbing properties. More information on nuclear applications is available in the articles about corrosion in the nuclear power industry in this Volume.

Pulp and Paper Industry. In the kraft process, paper is produced by digesting wood chips with a mixture of Na_2S and NaOH (white liquor). The product is transferred to the brown stock washers to remove the liquor (black liquor) from the brown pulp. After screening, the pulp may go directly to the paper mill to produce unbleached paper or may be directed first to the bleach plant to produce white paper.

The digester vapors are condensed, and the condensate is pumped to the brown stock washers. The black liquor from these washers is concentrated and burned with sodium sulfate (Na_2SO_4) to recover sodium carbonate (Na_2CO_3) and Na_2S. After dissolution in water, this green liquor is treated with calcium hydroxide ($Ca(OH)_2$) to produce NaOH to replenish the white liquor. Pulp bleaching involves treating with various chemicals, including chlorine (Cl_2), chlorine dioxide (ClO_2), sodium hypochlorite

Table 14 Pitting of stainless steel spool test specimens in a flue gas desulfurization system

The slurry contained 7000 ppm dissolved Cl^-; test duration was 6 months, with 39 days on bypass

Spool location(a)	pH	Maximum temperature °C	Maximum temperature °F	Maximum chloride concentration, ppm	Maximum pit depth, mm (mils), and pit density: Type 304	Type 316L	Type 317L	Type 317LM	Incoloy 825	JS700	JS777	904L	20Mo-6
Wet/dry line at inlet duct	1–2(b)	60–170	140–335	7000(b)	>1.24 (>49) Profuse	>0.91 (>36) Profuse	0.53 (21) Sparse	0.53 (21) Sparse	0.74 (29) Profuse	0.33 (13) Sparse	0.33 (13) Profuse	0.43 (17) Sparse	(c)
Quencher sump (submerged; 1.8 m, or 6 ft, level)	4.4	60	140	7000	>1.19 (>47) Sparse	>0.91 (>36) Sparse	0.28 (11)	0.1 (4) Single	<0.02 (<1)	nil	nil	nil	nil
Quencher sump (submerged; 3.4 m, or 11 ft, level)	4.4	60	140	7000	>1.2 (>48) Profuse	>0.9 (>36) Sparse	<0.03 (<1)	0.05 (2)	0.25 (10)	nil	nil	nil	nil
Quencher spray header, above slurry	4.4	60	140	100	>1.19 (>47) Profuse	0.58 (23) Profuse	0.61 (24) Profuse	0.46 (18) Profuse	0.66 (26) Profuse	0.33 (13) Sparse	0.61 (24) Profuse	0.25 (10) Sparse	0.15 (6) Sparse
Absorber, spray area	6.2	60	140	100	0.58 (23) Sparse	0.10 (4)	nil	nil	nil	nil	nil	nil	nil
Outlet duct	2–4(d)	55	130(d)	100(d)	>1.19 (>47) Profuse	>0.91 (>36) Profuse	0.58 (23) Profuse	0.58 (23) Profuse	0.48 (19) Profuse	0.18 (7) Single	0.51 (20) Profuse	0.53 (21) Profuse	0.36 (14) IG etch
	1.5(e)	170	335(e)	82,000(e)									

(a) Slurry contained 7000 ppm dissolved Cl^-. Deposits in the quencher, inlet duct, absorber, and outlet ducting contained 3000–4000 ppm Cl^- and 800–1900 ppm F^-. (b) Present as halide gases. (c) Not tested. (d) During operation. (e) During bypass. Bypass condition gas stream contained SO_2, SO_3, HCl, HF, and condensate. Source: Ref 41

(NaClO), calcium hypochlorite ($Ca(ClO)_2$), hydrogen peroxide (H_2O_2), caustic soda (NaOH), quicklime ($Ca(OH)_2$), ozone (O_3), or oxygen (O_2).

The sulfite process uses a liquor in the digester that is different from that used in the kraft process. This liquor contains free SO_2 dissolved in water, along with SO_2 as a bisulfite. The compositions of the specific liquors differ, and the pH can range from 1 for an acid process to 10 for alkaline cooking. Sulfur dioxide for the cooking liquor is produced by burning elemental sulfur, cooling rapidly, absorbing the SO_2 in a weak alkaline solution, and fortifying the raw acid.

Various alloys are selected for the wide range of corrosion conditions encountered in pulp and paper mills. Paper mill headboxes are typically fabricated from type 316L stainless steel plate with superior surface finish and are sometimes electropolished to prevent scaling, which may affect pulp flow. The blades used to remove paper from the drums have been fabricated from type 410 and 420 stainless steels and from cold-reduced 22Cr-13Ni-5Mn stainless steel.

Duplex stainless steels have been selected for construction of digesters, and so on. The duplex alloys provide resistance both to the chlorides that cause SCC in austenitic stainless steels and to the caustic that causes SCC of low-alloy steels.

Evaporators and reheaters must deal with corrosive liquors and must minimize scaling to provide optimal heat transfer. Type 304 stainless steel ferrite-free welded tubing has been used in kraft black liquor evaporators. Cleaning is often performed with HCl, which attacks ferrite. In the sulfite process, type 316 (2.75% Mo) and type 317 stainless steels have been used in black liquor evaporators. Digester liquor heaters in the kraft and sulfite processes have used duplex stainless for resistance to caustic or chloride SCC.

Bleach plants have used type 316 and 317 stainless steels and have upgraded to austenitic grades containing 4.5 and 6% Mo in problem locations. Tightening of environmental regulations has generally increased temperature, chloride level, and acidity in the plant, and this requires grades of stainless steel that are more highly alloyed than those used in the past. Tall oil units have shifted from type 316 and 317 stainless steels to such alloys as 904L or 20Mo-4 stainless steels, and most recently, to 254SMO and AL-6XN stainless steels.

Tests including higher-alloyed materials have been coordinated by the Metals Subcommittee of the TAPPI Corrosion and Materials Engineering Committee. Racks of test samples, which included crevices at polytetrafluoroethylene (PTFE) spacers, were submerged in the vat below the washer in the C (chlorination), D (chlorine dioxide), and H (hypochlorite) stages of several paper mills. The sum of the maximum attack depth on all samples for each alloy—at crevices and remote from crevices—is shown in Fig. 17. It should be noted that the vertical axes are different in Fig. 17(a), (b), and (c). Additional information on corrosion in this industry is available in the articles about corrosion in the pulp and paper industry in this Volume.

Transportation Industry. Stainless steels are used in a wide range of components in transportation that are both functional and decorative. Bright automobile parts, such as trim, fasteners, wheel covers, mirror mounts, and windshield wiper arms, have generally been fabricated from 17Cr or 18Cr-8Ni stainless steel or similar grades. Example alloys include type 430, 434, 304, and 305 stainless steels. Type 302HQ-FM remains a candidate for such applications as wheel nuts, and Custom 455 stainless has been used as wheel lock nuts. Use of type 301 stainless steel for wheel covers has diminished with the weight reduction programs of the automotive industry.

Stainless steels also serve many nondecorative functions in automotive design. Small-diameter shafts of type 416 and, occasionally, type 303 stainless steels have been used in connection with power equipment, such as windows, door locks, and antennas. Solenoid grades, such as type 430FR stainless steels, have also found application. Type 409 stainless steel has been used for mufflers and catalytic converters for many years, but it is now being employed throughout the exhaust system. Because weld decay was observed in some lots of type 409, three new compositions (UNS S40910, S40920, and S40930)—all of which bear the type 409 designation—have been created. All are more highly stabilized than the original type 409 stainless and exhibit improved weld corrosion resistance. Increased exhaust system temperatures and increased expectations about appearance have created a demand for exhaust system materials having more corrosion resistance than type 409. These newer materials include types 439, 441, and 444 ferritic stainless steels and aluminum-coated type 409 stainless steel. The articles about corrosion in the land transportation industries in this Volume contain detailed information on corrosion in the automotive environment.

In railroad cars, external and structural stainless steels provide durability, low-cost maintenance, and superior safety through crashworthiness. Type 201 stainless steel, especially in lightly temper-rolled conditions such as 1/4 hard, has found extensive use in both freight hopper and passenger railcars. The fire resistance of stainless steel is a significant safety advantage. Modified type 409 (3CR12) stainless steel is used in railroad hopper cars and as structural components in buses. Types 430 and 304 are used for

exposed functional parts on buses. Type 304 stainless steel has provided economical performance in truck trailers. For tank trucks, type 304 has been the most frequently used stainless steel, but type 316 and higher-alloyed grades have been used where appropriate to carry more corrosive chemicals safely over the highways. The high strength and corrosion resistance of duplex stainless steels make them particularly attractive for such uses.

Stainless steels are used for seagoing chemical tankers, with types 304, 316, 317, and alloy 2205 being selected according to the corrosivity of the cargoes being carried. Conscientious adherence to cleaning procedures between cargo changeovers has allowed these grades to give many years of service with a great variety of corrosive cargoes.

In aerospace, quench-hardenable and precipitation-hardenable stainless steels have been used in varying applications. Heat treatments are chosen to optimize fracture toughness and resistance to SCC. Stainless steel grades 17-7PH, 15-7PH, 15-5PH, 17-4PH, and PH13-8Mo have been used in structural parts, and A286, 17-7PH, and PH13-8Mo stainless steels have served as fasteners. Parts in cooler sections of the engine have been fabricated from type 410 or A286 stainless steel. Custom 455, 17-4PH, 17-7PH, and 15-5PH stainless steels have been used in the space shuttle program (see the articles about corrosion in the air transportation industry in this Volume).

Architectural Applications. Typically, type 430 or 304 has been used in architectural applications. In bold exposure, these grades are generally satisfactory; however, in marine and industrially contaminated atmospheres, type 316 is often suggested and has performed well.

The surface finish can impact the corrosion performance of stainless steel, particularly in environments where aggressive contaminants, such as chlorides, can collect on the stainless steel surface. Specific examples would be 304 and 316 stainless steel exposed at coastal locations or areas close to highways that receive deicing salts during the winter. Smoother exterior surfaces are more readily washed by natural rainfall and retain less dirt and debris; therefore, they generally provide better corrosion resistance than rougher finishes (Ref. 44). The benefit of a smooth surface is most apparent with finishes that have a surface roughness value of R_a 0.5 μm (20 μin.) or less (Ref 45). The European standard EN 10088 recommends a surface roughness of R_a 0.5 μm (20 μin.) or less for polished surfaces that will be exposed to high levels of particulate, corrosive pollution, and/or salt exposure and in applications where regular maintenance is unlikely. Use of higher-alloy products may be required in situations where cleaning is difficult and especially if salt spray can accumulate.

In all applications, but particularly in these cases where appearance is important, it is

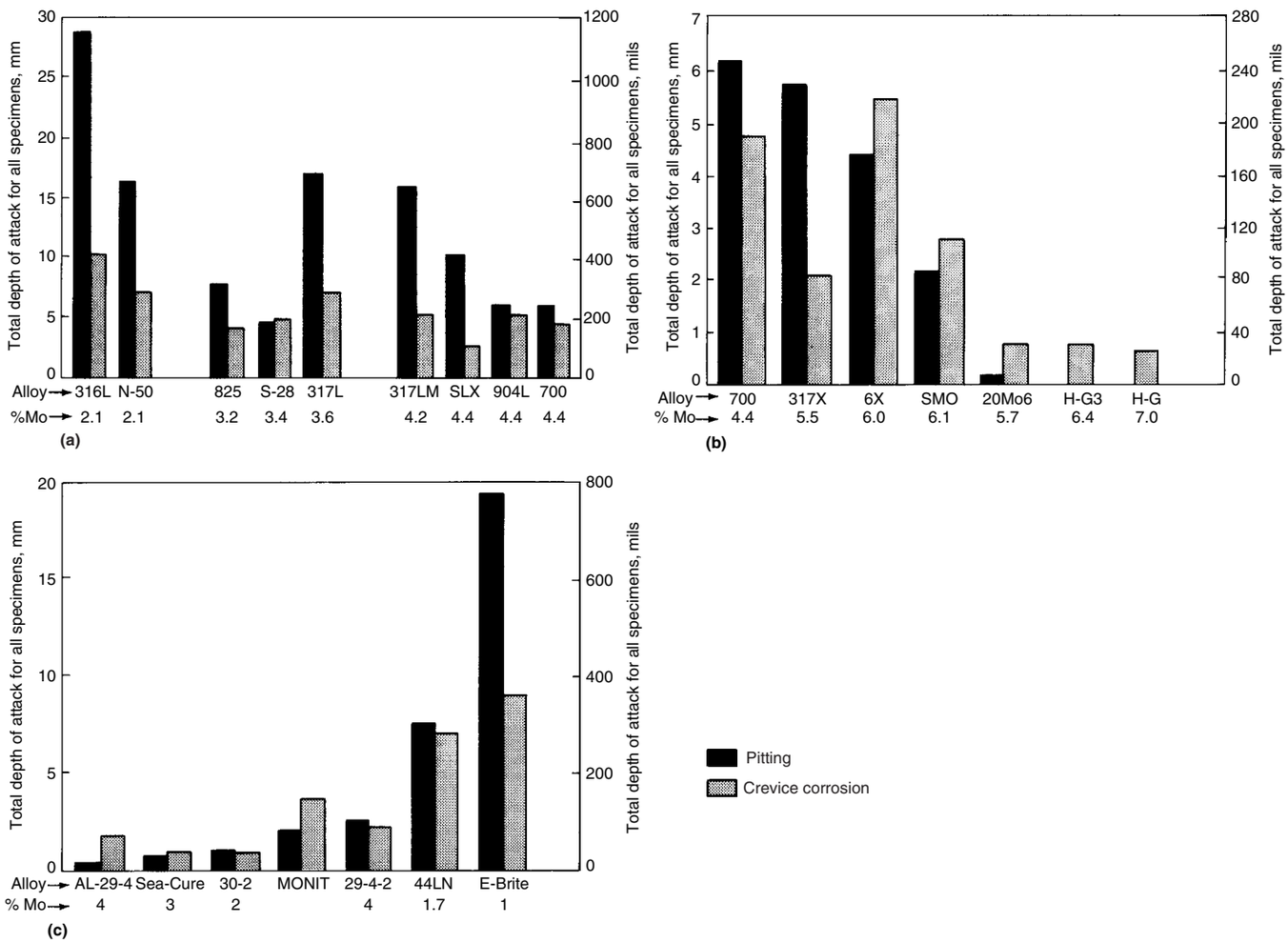

Fig. 17 Resistance of stainless steels to localized corrosion in a paper mill bleach plant environment. Total depth of attack has been divided by 4 because there were four crevice sites per specimen. (a) Austenitic stainless steels containing 2.1 to 4.4% Mo. (b) Austenitic stainless steels containing 4.4 to 7.0% Mo. (c) Ferritic and duplex stainless steels. Source: Ref 43

essential that any chemical cleaning solutions be thoroughly rinsed from the metal.

Corrosion Testing

The physical and financial risks involved in selecting stainless steels for particular applications can be reduced through corrosion tests. However, care must be taken when selecting a corrosion test. The test must relate to the type of corrosion possible in the application. The steel should be tested in the metallurgical condition and stress state in which it will be applied. In some environments, the surface quality can affect corrosion resistance. The test conditions should be representative of the operating conditions and all reasonably anticipated excursions of operating conditions.

Corrosion tests vary in their degree of simulation of operation in terms of the design of the specimen and the selection of medium and test conditions. Standard tests use specimens of a defined nature and geometry exposed in precisely defined media and conditions. Standard tests can confirm that a particular lot of steel conforms to the level of performance expected of a standard grade. Standard tests can also rank the performance of standard and proprietary grades.

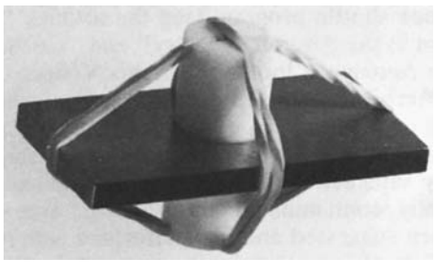

Fig. 18 Assembled crevice corrosion test specimen. Source: Ref 47

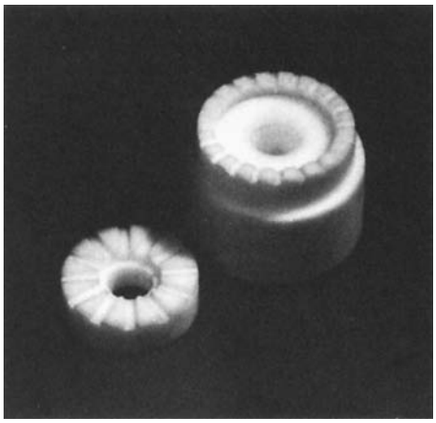

Fig. 19 Multiple-crevice cylinders for use in crevice corrosion testing. Source: Ref 47

The relevance of test results to performance in particular applications increases as the specimen is made to resemble more closely the final fabricated structure—for example, bent, welded, stressed, or creviced. Galvanic contact between dissimilar metals may also be necessary to provide relevant data if such contact occurs in the fabricated structure. Relevance also increases as the test medium and conditions more closely approach the most severe operating conditions. One example is velocity, which can accelerate attack versus static conditions. However, many types of failures occur only after extended exposures to operating cycles. Therefore, there is often an effort to accelerate testing by increasing the severity of one or more environmental factors, such as temperature, concentration, aeration, and pH. Care must be taken that the altered conditions do not give spurious results. For example, an excessive temperature may either introduce a new failure mode or prevent a failure mode relevant to the actual application. The effects of minor constituents or impurities on corrosion are of special concern in simulated testing.

Pitting and crevice corrosion are readily tested in the laboratory by using small coupons and controlled-temperature conditions. Procedures for such tests using 6% $FeCl_3$ (10% $FeCl_3 \cdot 6H_2O$) and acidified 6% $FeCl_3$ are described in ASTM G 48 (Ref 15). The coupon may be evaluated in terms of weight loss, pit depth, pit density, and appearance. Several suggestions for methods of pitting evaluation are given in ASTM G 46 (Ref 46). The G 48 specification also describes the construction of a crevice corrosion coupon and includes practices for conducting critical pitting and critical crevice corrosion temperatures (Fig. 18). It is possible to determine a temperature below which pitting or

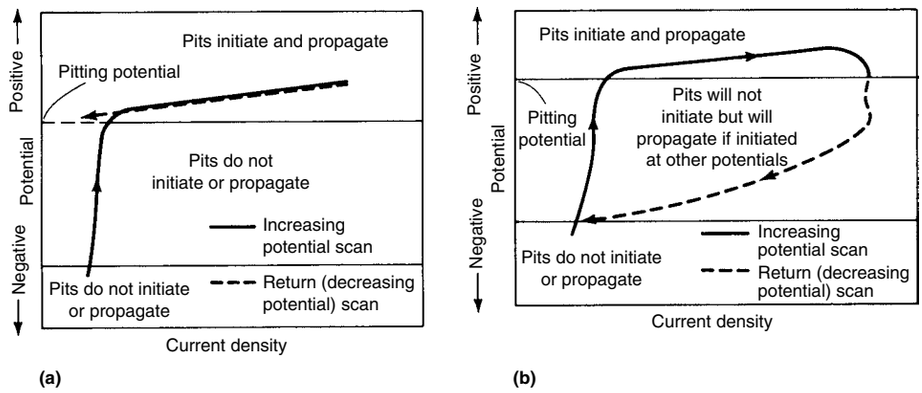

Fig. 20 Schematics showing how electrochemical tests can indicate the susceptibility to pitting of a material in a given environment. (a) Specimen has good resistance to pitting. (b) Specimen has poor resistance to pitting. In both cases, attack occurs at the highest potentials. Source: Ref 47

Table 15 ASTM standard tests for susceptibility to intergranular corrosion in stainless alloys

ASTM standard	Test media	Test duration	Applicable alloys
A 262-A	Oxalic acid etch	Etch test	Screening for selected alloys in other A 262 practices
A 262-B	$Fe_2(SO_4)_3$-H_2SO_4	120 h	UNS S30400, S30403, S31600, S31603, S31700, S31703, S32100, S34700, J92500, J92600, J92800, J92900, J92999, J93000
A 262-C	HNO_3 (Huey test)	240 h(a)	Same as A 262-B(b)
A 262-E	Cu-$CuSO_4$-16%H_2SO_4	24 h(c)	UNS S20100, S20200, S30100, S30400, S30403, S30409, S31600, S31603, S31609, S31700, S31703, S32100, S34700
A 262-F	Cu-$CuSO_4$-50%H_2SO_4	120 h	UNS J92800, J92900
G 28-A	$Fe_2(SO_4)_3$-H_2SO_4 (similar to A 262-B)	24 or 120 h(d)	UNS N10276, N06455, N06007, N06200, N06686, N06985, N08020, N06600, N06625, N08800, N08825, N06022, N06030, N06059, N08367
G 28-B	$H_2SO_4 + HCl + FeCl_3 + CuCl_2$	24 h	UNS N10276, N06022, N06059, N06200, N06686
A 763-W	Oxalic acid etch (similar to A 262-A)	Etch test	UNS S44400, S44626, S44660, S43035, XM27
A 763-X	$Fe_2(SO_4)_3$-H_2SO_4 (similar to A 262-B)	24, 72, or 120 h(d)	UNS S43000, S44600, S44700, S44800, XM27
A 763-Y	Cu-$CuSO_4$-50%H_2SO_4 (similar to A 262-F)	96 or 120 h(d)	UNS S44600, S44626, S44660, S44735, S44700, S44800, XM27
A 763-Z	Cu-$CuSO_4$-16%H_2SO_4 (same as A 262-E)	24 h	UNS S43000, S43400, S43600, S44400, S43035

(a) Shorter duration permitted in some cases. (b) The nitric acid test has also been applied less frequently to other austenitic, ferritic, and martensitic grades. (c) Typically 24 h. (d) Duration depends on alloy. Source: Ref 47

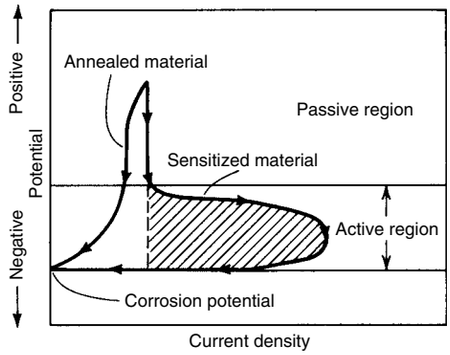

Fig. 21 Schematic showing the use of the electrochemical potentiostatic reactivation test to evaluate sensitization. The specimen is first polarized up to a passive potential at which the metal resists corrosion. Potential is then swept back through the active region, where corrosion may occur. Source: Ref 47

Table 16 Stress-corrosion cracking resistance of stainless steels

	Stress-corrosion cracking test(a)		
Grade	Boiling 42% $MgCl_2$	Wick test	Boiling 25% NaCl
304	F(b)	F	F
316	F	F	F
317	F	[P(c) or F](d)	(P or F)
317LM	F	(P or F)	(P or F)
Alloy 904L	F	(P or F)	(P or F)
AL-6XN	F	P	P
254SMO	F	P	P
20Mo-6	F	P	P
409	P	P	P
439	P	P	P
444	P	P	P
E-Brite	P	P	P
Sea-Cure	F	P	P
Monit	F	P	P
AL 29-4	P	P	P
AL 29-4-2	F	P	P
AL 29-4C	P	P	P
3RE60	F	NT(e)	NT
2205	F	NT	(P or F)(f)
Ferralium	F	NT	(P or F)(f)

(a) U-bend tests, stressed beyond yielding. (b) Fails, cracking observed. (c) Passes, no cracking observed. (d) Susceptibility of grade to SCC determined by variation of composition within specified range. (e) Not tested (f) Susceptibility of grade to SCC determined by variation of thermal history. Source: Ref 48

crevice corrosion are not initiated for a particular material and test environment. The critical pitting temperature (CPT) and the critical crevice temperature (CCT) can provide useful rankings of stainless steels. For the CCT or CPT to be directly applicable in design, it is necessary to determine that the test medium and conditions relate to the most severe conditions to be encountered in service.

Figure 19 shows two examples of frequently used types of multiple-crevice assembly. The presence of many separate crevices helps to deal with the statistical nature of corrosion initiation. The severity of the crevices can be regulated by means of a standard crevice design and the use of a selected torque in its application.

An electrochemical technique has been developed for determining the CPT of a stainless steel. This method has better sensitivity than immersion tests and has the advantage of shorter test times. The procedure for measuring the electrochemical CPT is outlined in ASTM G 150.

Laboratory media do not necessarily have the same response of corrosivity as a function of temperature as do engineering environments. For example, the ASTM G 48 solution is thought to be roughly comparable to seawater at ambient temperatures. However, the corrosivity of $FeCl_3$ increases steadily with temperature. The response of seawater to increasing temperature is quite complex, relating to such factors as concentration of oxygen and biological activity. Also, the various families of stainless steels will be internally consistent but will differ from one another in response to a particular medium.

Pitting and crevice corrosion may also be evaluated by electrochemical techniques. When immersed in a particular medium, a metal coupon will assume a potential that can be measured relative to a standard reference electrode. It is then possible to impress a potential on the coupon and observe the corrosion as measured by the resulting current. Various techniques of scanning the potential range provide extremely useful data on corrosion resistance. Figure 20 demonstrates a simplified view of how these tests may indicate the pitting corrosion resistance for various materials and media.

The nature of intergranular sensitization has been discussed earlier in this article. There are many corrosion tests for detecting susceptibility to preferential attack at the grain boundaries. The appropriate media and test conditions vary widely for the different families of stainless steels. Table 15 summarizes the ASTM tests for intergranular sensitization. Figure 21 shows that electrochemical techniques may also be used, as in the single-loop electrochemical potentiostatic reactivation test.

Stress-corrosion cracking covers all types of corrosion involving the combined action of tensile stress and corrodent. Important variables include the level of stress, the presence of oxygen, the concentration of corrodent, temperature, and the conditions of heat transfer. It is important to recognize the type of corrodent likely to produce cracking in a particular family of steel. For example, austenitic stainless steels are susceptible to chloride SCC (Table 16). Martensitic and ferritic grades are susceptible to cracking related to hydrogen embrittlement.

It is important to realize that corrosion tests are designed to single out one particular corrosion mechanism. Therefore, determining the suitability of a stainless steel for a particular application will usually require consideration of more than one type of test. No single chemical or electrochemical test has been shown to be an all-purpose measure of corrosion resistance. More information on corrosion testing is available in the Section "Corrosion Testing and Evaluation" in *ASM Handbook,* Volume 13A, 2003.

ACKNOWLEDGMENT

This article is adapted from the article "Corrosion of Stainless Steels" by Ralph M. Davison, Terry DeBold, and Mark J. Johnson that appeared in *Corrosion,* Volume 13, *ASM Handbook,* 1987.

REFERENCES

1. C.W. Wegst, *Stahlschlussel (Key to Steel),* 20th ed., Verlag Stahlschlüssel, 2004
2. W.C. Mack, *Worldwide Guide to Equivalent Irons and Steels,* 4th ed., ASM International, 2000
3. "Standard Practices for Detecting Susceptibility to Intergranular Corrosion Attack in Austenitic Stainless Steels," A 262, *Annual Book of ASTM Standards,* American Society for Testing and Materials
4. "Standard Practices for Detecting Susceptibility to Intergranular Attack in Ferritic Stainless Steels," A 763, *Annual Book of ASTM Standards,* American Society for Testing and Materials
5. "Standard Recommended Practice for Cleaning and Descaling Stainless Steel Parts, Equipment, and Systems," A 380, *Annual Book of ASTM Standards,* American Society for Testing and Materials
6. "Chemical Passivation Treatments for Stainless Steel Parts," A 967, *Annual Book of ASTM Standards,* American Society for Testing and Materials
7. T. DeBold, Passivating Stainless Steel Parts, as published in *Mach. Tool Blue Book,* Nov 1986, copyright Carpenter Technology Corp.
8. T.A. DeBold and J.W. Martin, How to Passivate Stainless Steel Parts, as published in *Mod. Mach. Shop,* Oct 2003, copyright Carpenter Technology Corp.
9. *Corrosion Resistance of the Austenitic Chromium-Nickel Stainless Steels in Atmospheric Environments,* The International Nickel Company, Inc., 1963
10. K.L. Money and W.W. Kirk, Stress Corrosion Cracking Behavior of Wrought Fe-Cr-Ni Alloys in Marine Atmosphere, *Mater. Perform.,* Vol 17, July 1978, p 28–36
11. M. Henthorne. T.A. DeBold, and R.J. Yinger, "Custom 450—A New High Strength Stainless Steel," Paper 53, presented at Corrosion/72, National Association of Corrosion Engineers, 1972
12. J.W. Oldfield and B. Todd, Ambient-Temperature Stress-Corrosion Cracking of Austenitic Stainless Steel in Swimming Pools, *Mater. Perform.,* Dec 1990
13. "High Alloyed Austenitic Stainless Steel," Information 212801GB, AvestaPolarit, March 2002
14. R.E. Avery, S. Lamb, C.A. Powell, and A.H. Tuthill, "Stainless Steel for Potable Water Treatment Plants," NiDI Technical

Series 10 087, Nickel Development Institute, 1999
15. "Standard Test Methods for Pitting and Crevice Corrosion Resistance of Stainless Steels and Related Alloys by the Use of Ferric Chloride Solution," G 48, *Annual Book of ASTM Standards,* American Society for Testing and Materials
16. C.W. Kovach and J.D. Redmond, "Correlation Between the Critical Crevice Temperature, PRE-Number, and Long-Term Crevice Corrosion Data for Stainless Steels," Paper 267, presented at Corrosion/93, National Association of Corrosion Engineers, 1993
17. *The Role of Stainless Steels in Desalination,* American Iron and Steel Institute, 1974
18. A.P. Bond and H.J. Dundas, *Mater. Perform.,* Vol 23 (No. 7), July 1984, p 39
19. A.H. Tuthill and C.M. Schillmoller, *Guidelines for Selection of Marine Materials,* The International Nickel Company, Inc., 1971
20. J.F. Grubb and J.R. Maurer, "Use of Cathodic Protection with Superferritic Stainless Steels in Seawater," Paper 28, presented at Corrosion/84, 2–6 April 1984 (New Orleans, LA), National Association of Corrosion Engineers
21. R.M. Kain, "Crevice Corrosion Resistance of Austenitic Stainless Steels in Ambient and Elevated Temperature Seawater," Paper 230, presented at Corrosion/79, National Association of Corrosion Engineers, 1979
22. R. Gunderson et al., "The Effect of Sodium Hypochlorite on Bacteria Activity and the Electrochemical Properties of Stainless Steel in Seawater," U.K. Corrosion/88, Institute of Corrosion, Leighton Buzzard, UK, Oct 1988, p 125
23. R. Gunderson et al., "The Effect of Sodium Hypochlorite on Bacteria Activity and the Electrochemical Properties of Stainless Steel in Seawater," Paper 108, presented at Corrosion/89, National Association of Corrosion Engineers, 1989
24. H. Haselmair, *Mater. Perform.,* Vol 31 (No. 6), 1992, p 60
25. B. Wallen, "Corrosion of Duplex Stainless Steels in Seawater," ACOM 1–1998, Avesta Sheffield AB, 1998
26. F.L. LaQue and H.R. Copson, Ed., *Corrosion Resistance of Metals and Alloys,* Reinhold, 1963, p 375–445
27. J.E. Truman, in *Corrosion: Metal/Environment Reactions,* Vol 1, L.L. Shreir, Ed., Newness-Butterworths, 1976, p 352
28. M.A. Streicher, Development of Pitting Resistant Fe-Cr-Mo Alloys, *Corrosion,* Vol 30, 1974, p 77–91
29. C.P. Dillon and W. Pollock, Ed, *MS-1 Materials Selector for Hazardous Chemicals, Volume 1: Concentrated Sulfuric Acid and Oleum,* MTI, 1997
30. *MS-3 Materials Selector for Hazardous Chemicals, Volume 3: Hydrochloric Acid, Hydrogen Chloride and Chlorine,* MTI, 1999
31. H.O. Teeple, Corrosion by Some Organic Acids and Related Compounds, *Corrosion,* Vol 8, Jan 1952, p 14–28
32. C.P. Dillon and W. Pollock, Ed., *MS-2 Materials Selector for Hazardous Chemicals, Volume 2: Formic, Acetic and Other Organic Acids,* MTI, 1997
33. T.A. DeBold, J.W. Martin, and J.C. Tverberg, Duplex Stainless Offers Strength and Corrosion Resistance, *Duplex Stainless Steels,* R.A. Lula, Ed., American Society for Metals, 1983, p 169–189
34. L.A. Morris, in *Handbook of Stainless Steels,* D. Peckner and I.M. Bernstein, Ed., McGraw-Hill, 1977, p 17–1
35. "Petroleum and Natural Gas Industries—Materials for Use in H_2S-Containing Environments in Oil and Gas Production—Part 3: Cracking-Resistant CRAS (Corrosion Resistant Alloys) and Other Alloys," MR0175/ISO 15156-3, NACE International
36. "Materials Resistant to Sulfide Stress Cracking in Corrosive Petroleum Refining Environments," MR0103–2003, National Association of Corrosion Engineers
37. J.R. Kearns, M.J. Johnson, and J.F. Grubb, "Accelerated Corrosion in Dissimilar Metal Crevices," Paper 228, presented at Corrosion/86, National Association of Corrosion Engineers, 1986
38. L.S. Redmerski, J.J. Eckenrod, and K.E. Pinnow, "Cathodic Protection of Seawater-Cooled Power Plant Condensers Operating with High Performance Ferritic Stainless Steel Tubing," Paper 208, presented at Corrosion/85, National Association of Corrosion Engineers, 1985
39. E.C. Hoxie and G.W. Tuffnell, A Summary of INCO Corrosion Tests in Power Plant Flue Gas Scrubbing Processes, *Resolving Corrosion Problems in Air Pollution Control Equipment,* National Association of Corrosion Engineers, 1976
40. J.D. Harrington and W.L. Mathay, *Nickel Stainless Steels and High-Nickel Alloys for Flue Gas Desulfurization Systems,* Nickel Development Institute, 1990
41. G.T. Paul and R.W. Ross, Jr., "Corrosion Performance in FGD Systems at Laramie River and Dallman Stations," Paper 194, presented at Corrosion/83, National Association of Corrosion Engineers, 1983
42. A.P. Majidi and M.A. Streicher, "Four Non-Destructive Electrochemical Tests for Detecting Sensitization in Type 304 and 304L Stainless Steels," Paper 62, presented at Corrosion/85, National Association of Corrosion Engineers, 1985
43. A.H. Tuthill, Resistance of Highly Alloyed Materials and Titanium to Localized Corrosion in Bleach Plant Environments, *Mater. Perform.,* Vol 24, Sept 1985, p 43–49
44. *Stainless Steels in Architecture, Building and Construction—Guidelines for Corrosion Prevention,* NiDI Reference Book Series 11 024, Nickel Development Institute, 2001
45. "Architect's Guide to Stainless Steel," Publication SCI-P-179, The Steel Construction Institute, Berkshire, England, 1997
46. "Standard Recommended Practice for Examination and Evaluation of Pitting Corrosion," G 46, *Annual Book of ASTM Standards,* American Society for Testing and Materials
47. T.A. DeBold, Which Corrosion Test for Stainless Steels, *Mater. Eng*., Vol 2 (No. 1), July 1980
48. R.M. Davison et al., *A Review of Worldwide Developments in Stainless Steels in Specialty Steels and Hard Materials,* Pergamon Press, 1983, p 67–85

SELECTED REFERENCES

- S. Lamb, Ed., *CASTI Handbook of Stainless Steels and Nickel Alloys,* 2nd ed., Codes and Standards Training, Inc., 2002
- R.W. Revie, Ed., *Uhlig's Corrosion Handbook,* 2nd ed., John Wiley & Sons, 2000
- A.J. Sedriks, *Corrosion of Stainless Steels, Corrosion Monograph Series,* 2nd ed., Wiley-Interscience, 1996

ASM Handbook, Volume 13B: Corrosion: Materials
S.D. Cramer, B.S. Covino, Jr., editors, p78-87
DOI: 10.1361/asmhba0003813

Corrosion of Cast Stainless Steels

Revised by Malcolm Blair, Steel Founders' Society of America

CAST STAINLESS STEELS are usually specified on the basis of composition by using the alloy designation system established by the Alloy Casting Institute (ACI). The ACI designations, such as CF-8M, have been adopted by ASTM International and are preferred for cast alloys over the designations originated by the American Iron and Steel Institute (AISI) for similar wrought steels.

The first letter of the ACI designation indicates whether the alloy is intended primarily for liquid corrosion service (C) or heat-resistant service (H). The second letter denotes the nominal chromium-nickel type, as shown in Fig. 1. As the nickel content increases, the second letter in the ACI designation increases from A to Z. The numerals following the two letters refer to the maximum carbon content (percent × 100) of the alloy. If additional alloying elements are included, they can be denoted by the addition of one or more letters after the maximum carbon content. Thus, the designation CF-8M refers to an alloy for corrosion-resistant service (C) of the 19Cr-9Ni (F) type, with a maximum carbon content of 0.08% and containing molybdenum (M).Corrosion-resistant cast stainless steels are also often classified on the basis of microstructure. The classifications are not completely independent, and a classification by composition often involves microstructural distinctions. Cast corrosion- and heat-resistant alloy compositions are listed in Table 1.

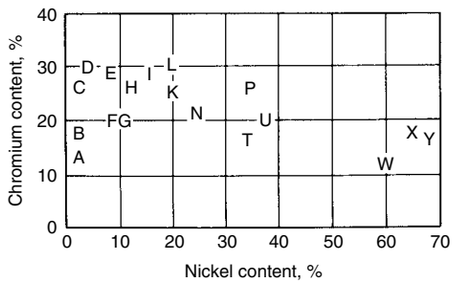

Fig. 1 Chromium and nickel contents in ACI standard grades of heat- and corrosion-resistant castings. See text for details. Source: Ref 1

Composition and Microstructure

The principal alloying element in the high-alloy family is usually chromium, which, through the formation of protective oxide films, results in the corrosion protection or stainless behavior. For most purposes, stainless behavior requires at least 12% Cr. Corrosion resistance further improves with additions of chromium to at least the 30% level. As indicated in Table 1, significant amounts of nickel and lesser amounts of molybdenum and other elements are often added to the iron-chromium matrix.

Although chromium is a ferrite and martensite promoter, nickel is an austenite promoter. By varying the amounts and ratios of these two elements (or their equivalents), almost any desired combination of microstructure, strength, or other property can be achieved. Varying the temperature, time at temperature, and cooling rate of the heat treatment also controls the desired results.

It is useful to think of the compositions of high-alloy steels in terms of the balance between austenite promoters and ferrite promoters. This balance is shown in the widely used Schaeffler diagrams (Fig. 2). It should be noted that the Schaeffler diagram is used for welding and that the phases shown are those that persist after cooling to room temperature at rates consistent with fabrication (Ref 1, 2). The Schoefer diagram (Fig. 3) gives an indication of the amount of ferrite that may be expected based on the composition of the alloy in question. An ASTM standard provides note on the Schoefer diagram and methods for estimating ferrite content (Ref 3).

The empirical correlations shown in Fig. 2 can be understood from the following. The field designated as martensite encompasses such alloys as CA-15, CA-6NM, and even CB-7Cu. These alloys contain 12 to 17% Cr, with adequate nickel, molybdenum, and carbon to promote high hardenability, that is, the ability to transform completely to martensite when cooled at even the moderate rates associated with the air cooling of heavy sections. High alloys have low thermal conductivities and cool slowly. To obtain the desired properties, a full heat treatment is required after casting; that is, the casting is austenitized by heating to 870 to 980 °C (1600 to 1800 °F), cooled to room temperature to produce the hard martensite, and then tempered at 595 to 760 °C (1100 to 1400 °F) until the desired combination of strength, toughness, ductility, and resistance to corrosion or stress corrosion is obtained (Ref 1, 2).

Increasing the nickel equivalent (moving vertically in Fig. 2) eventually results in an alloy that is fully austenitic, such as CC-20, CH-20, CK-20, or CN-7M. These alloys are extremely ductile, tough, and corrosion resistant. On the other hand, the yield and tensile strength may be relatively low for the fully austenitic alloys. Being fully austenitic, they are nonmagnetic. Heat treatment consists of a single step: water quenching from a relatively high temperature at which carbides have been taken into solution. Solution treatment may also homogenize the structure, but because no transformation occurs, there can be no grain refinement. The solutionizing step and rapid cooling ensure maximum resistance to corrosion. Temperatures between 1040 and 1205 °C (1900 and 2200 °F) are usually required (Ref 1, 2).

Adding chromium to the lean alloys (proceeding horizontally in Fig. 2) stabilizes the δ-ferrite that forms when the casting solidifies. Examples are CB-30 and CC-50. With high chromium content, these alloys have relatively good resistance to corrosion, particularly in sulfur-bearing atmospheres. However, being single-phase, consisting only of ferrite, they are nonhardenable, have moderate-to-low strength, and are often used as-cast or after only a simple solution heat treatment. Ferritic alloys also have relatively poor impact resistance (toughness) (Ref 1, 2).

Between the fields designated M, A, and F in Fig. 2 are regions indicating the possibility of two or more phases in the alloys. Commercially, the most important of these alloys are the ones in which austenite and ferrite coexist, such as CF-3, CF-8, CF-3M, CF-8M, CG-8M, and CE-30. These alloys usually contain 3 to 30% ferrite in a matrix of austenite. Predicting and controlling ferrite content is vital to the successful application of these materials. Alloys that contain both ferrite and austenite offer superior strength, weldability, and corrosion resistance compared to alloys that contain only austenite. Strength, for

Table 1 Compositions of Alloy Casting Institute (ACI) heat- and corrosion-resistant casting alloys

ACI designation	UNS No.	Wrought alloy type(a)	Composition (balance iron)(b), %							
			C	Mn	Si	P	S	Cr	Ni	Other elements
CA-15	J91150	410	0.15	1.00	1.50	0.04	0.04	11.5–14.0	1.00	0.5Mo(c)
CA-15M	J91151	...	0.15	1.00	0.65	0.04	0.04	11.50–14.0	1.00	0.15–1.00Mo
CA-40	J91153	420	0.20–0.40	1.00	1.50	0.04	0.04	11.5–14.0	1.00	0.5Mo(c)
CA-6NM	J91540	...	0.06	1.00	1.00	0.04	0.03	11.5–14.0	3.5–4.5	0.4–1.0Mo
CA-6N	J91650	...	0.06	0.50	1.00	0.02	0.02	10.5–12.0	6.0–8.0	...
CB-30	J91803	431	0.30	1.00	1.50	0.04	0.04	18.0–21.0	2.00	...
CB-7Cu-1	...	...	0.07	0.70	1.00	0.035	0.03	14.0–15.5	4.5–5.5	0.15–0.35Nb, 0.05N, 2.5–3.2Cu
CB-7Cu-2	...	...	0.07	0.70	1.00	0.035	0.03	14.0–15.5	4.5–5.5	0.15–0.35Nb, 0.05N, 2.5–3.2Cu
CC-50	J92615	446	0.50	1.00	1.50	0.04	0.04	26.0–30.0	4.00	...
CD-4MCu	...	...	0.04	1.00	1.00	0.04	0.04	24.5–26.5	4.75–6.00	1.75–2.25Mo, 2.75–3.25Cu
CE-30	J93423	...	0.30	1.50	2.00	0.04	0.04	26.0–30.0	8.0–11.0	...
CF-3	J92500	304L	0.03	1.50	2.00	0.04	0.04	17.0–21.0	8.0–21.0	...
CF-8	J92600	304	0.08	1.50	2.00	0.04	0.04	18.0–21.0	8.0–11.0	...
CF-20	J92602	302	0.20	1.50	2.00	0.04	0.04	18.0–21.0	8.0–11.0	...
CF-3M	J92800	316L	0.03	1.50	1.50	0.04	0.04	17.0–21.0	9.0–13.0	2.0–3.0Mo
CF-8M	J92900	316	0.08	1.50	2.00	0.04	0.04	18.0–21.0	9.0–12.0	2.0–3.0Mo
CF-8C	J92710	347	0.08	1.50	2.00	0.04	0.04	18.0–21.0	9.0–12.0	3 × C min, 1.0 max Nb
CF-16F	J92701	303	0.16	1.50	2.00	0.17	0.04	18.0–21.0	9.0–12.0	1.5Mo, 0.2–0.35Se
CG-12	J93001	...	0.12	1.50	2.00	0.04	0.04	20.0–23.0	10.0–13.0	...
CG-8M	...	317	0.08	1.50	1.50	0.04	0.04	18.0–21.0	9.0–13.0	3.0–4.0Mo
CH-20	J93402	309	0.20	1.50	2.00	0.04	0.04	22.0–26.0	12.0–15.0	...
CK-20	J94202	310	0.20	2.00	2.00	0.04	0.04	23.0–27.0	19.0–22.0	...
CN-7M	N08007	...	0.07	1.50	1.50	0.04	0.04	19.0–22.0	27.5–30.5	2.0–3.0Mo, 3.0–4.0Cu
CN-7MS	...	...	0.07	1.00	2.50–3.50	0.04	0.03	18.0–20.0	22.0–25.0	2.0–3.0Mo, 1.5–2.0Cu
CW-12M	N30002	...	0.12	1.00	1.50	0.04	0.03	15.5–20.0	bal	7.5Fe
CY-40	N06040	...	0.40	1.50	3.00	0.03	0.03	14.0–17.0	bal	11.0Fe
CZ-100	N02100	...	1.00	1.50	2.00	0.03	0.03	...	bal	3.0Fe, 1.25Cu
N-12M	...	...	0.12	1.00	1.00	0.04	0.03	1.0	bal	0.26–0.33Mo, 0.60V, 2.50Co, 6.0Fe
M-35	...	...	0.35	1.50	2.00	0.03	0.03	...	bal	28–33Cu, 3.5Fe
HA	...	...	0.20	0.35–0.65	1.00	0.04	0.04	8.0–10.0	...	0.90–1.20Mo
HC	J92605	446	0.50	1.00	2.00	0.04	0.04	26.0–30.0	4.00	0.5Mo(c)
HD	J93005	327	0.50	1.50	2.00	0.04	0.04	26.0–30.0	4.0–7.0	0.5Mo(c)
HE	J93403	...	0.20–0.50	2.00	2.00	0.04	0.04	26.0–30.0	8.0–11.0	0.5Mo(c)
HF	J92603	302B	0.20–0.40	2.00	2.00	0.04	0.04	18.0–23.0	8.0–12.0	0.5Mo(c)
HH	J93503	309	0.20–0.50	2.00	2.00	0.04	0.04	24.0–28.0	11.0–14.0	0.5Mo(c), 0.2N
HI	J94003	...	0.20–0.50	2.00	2.00	0.04	0.04	26.0–30.0	14.0–18.0	0.5Mo(c)
HK	J94224	310	0.20–0.60	2.00	2.00	0.04	0.04	24.0–28.0	18.0–22.0	0.5Mo(c)
HL	J94604	...	0.20–0.60	2.00	2.00	0.04	0.04	28.0–32.0	18.0–22.0	0.5Mo(c)
HN	J94213	...	0.20–0.50	2.00	2.00	0.04	0.04	19.0–23.0	23.0–27.0	0.5Mo(c)
HP	...	...	0.35–0.75	2.00	2.50	0.04	0.04	24.0–28.0	33.0–37.0	0.5Mo(c)
HP-50WZ	...	...	0.45–0.55	2.00	2.00	0.04	0.04	24.0–28.0	33.0–37.0	4.0–6.0W, 0.2–1.0Zr
HT	J94605	330	0.35–0.75	2.00	2.50	0.04	0.04	15.0–19.0	33.0–37.0	0.5Mo(c)
HU	N08004	...	0.35–0.75	2.00	2.50	0.04	0.04	17.0–21.0	37.0–41.0	0.5Mo(c)
HW	N08001	...	0.35–0.75	2.00	2.50	0.04	0.04	10.0–14.0	58.0–62.0	0.5Mo(c)
HX	N06006	...	0.35–0.75	2.00	2.50	0.04	0.04	15.0–19.0	64.0–68.0	0.5Mo(c)

(a) Cast alloy chemical composition ranges are not the same as the wrought composition ranges; buyers should use cast alloy designations for proper identification of castings. (b) Maximum, unless range is given. (c) Molybdenum not intentionally added

example, increases directly with ferrite content. Achieving specified minimums may necessitate controlling the ferrite within narrow bands. Figure 3 and Schoefer's equations are used for this purpose. These duplex alloys should be solution heat treated and rapidly cooled before use to ensure maximum resistance to corrosion (Ref 1, 2).

The presence of ferrite is not beneficial for every application. Ferrite tends to reduce toughness, although this is not of great concern, given the extremely high toughness of the austenite matrix. However, in applications that require exposure to elevated temperatures, usually 315 °C (600 °F) and higher, the metallurgical changes associated with the ferrite can be severe and detrimental. In the low end of this temperature range, the observed reductions in toughness have been attributed to carbide precipitation or reactions associated with 475 °C (885 °F) embrittlement. The 475 °C (885 °F) embrittlement is caused by precipitation of an intermetallic phase with a composition of approximately 80Cr-20Fe. The name derives from the fact that this embrittlement is most severe and rapid when it occurs at approximately 475 °C (885 °F). At 540 °C (1000 °F) and above, the ferrite phase may transform to a complex Fe-Cr-Ni-Mo intermetallic compound known as sigma (σ) phase, which reduces toughness, corrosion resistance, and creep ductility. The extent of the reduction increases with time and temperature to approximately 815 °C (1500 °F) and may persist to 925 °C (1700 °F). In extreme cases, Charpy V-notch energy at room temperature may be reduced 95% from its initial value (Ref 1, 2). It has been demonstrated that the impact properties of duplex stainless steels in the solution heat treated condition, in the cast and wrought form, are comparable (Fig. 4). More information on the metallography and microstructures of these alloys is available in the article "Metallography and Microstructures of Stainless Steels and Maraging Steels" in *Metallography and Microstructures,* Volume 9 of *ASM Handbook,* 2004.

Corrosion Behavior of H-Type Alloys

The ACI heat-resistant (H-type) alloys must be able to withstand temperatures exceeding 1095 °C (2000 °F) in the most severe high-temperature service. Chromium content is

important to the corrosion behavior of these alloys. Chromium imparts resistance to oxidation and sulfidation at high temperatures by forming a passive oxide film. Heat-resistant casting alloys must also have good resistance to carburization. More information on the corrosion of metals and alloys in high-temperature gases is available in the article "Introduction to Fundamentals of Corrosion in Gases" in *ASM Handbook,* Volume 13A, 2003.

Oxidation. Resistance to oxidation increases directly with chromium content (Fig. 5). For the most severe service at temperatures above 1095 °C (2000 °F), 25% or more chromium is required. Additions of nickel, silicon, manganese, and aluminum promote the formation of relatively impermeable oxide films that retard further scaling. Thermal cycling is extremely damaging to oxidation resistance, because it leads to breaking, cracking, or spalling of the protective oxide film. The best performance is obtained with austenitic alloys containing 40 to 50% combined nickel and chromium. Figure 6 shows the behavior of the H-type grades.

Sulfidation environments are becoming increasingly important. Petroleum processing, coal conversion, utility and chemical applications, and waste incineration have heightened the need for alloys resistant to sulfidation attack in relatively weak oxidizing or reducing environments. Fortunately, high chromium and silicon contents increase resistance to sulfur-bearing environments. On the other hand, nickel has been found to be detrimental to the most aggressive gases. The problem is attributable to the formation of low-melting nickel-sulfur eutectics. These produce highly destructive liquid phases at temperatures even below 815 °C (1500 °F). Once formed, the liquid may run onto adjacent surfaces and rapidly corrode other metals. The behavior of H-type grades in sulfidizing environments is represented in Fig. 7.

Carburization. High alloys are often used in nonoxidizing atmospheres in which carbon diffusion into metal surfaces is possible. Depending on chromium content, temperature, and carburizing potential, the surface may become extremely rich in chromium carbides,

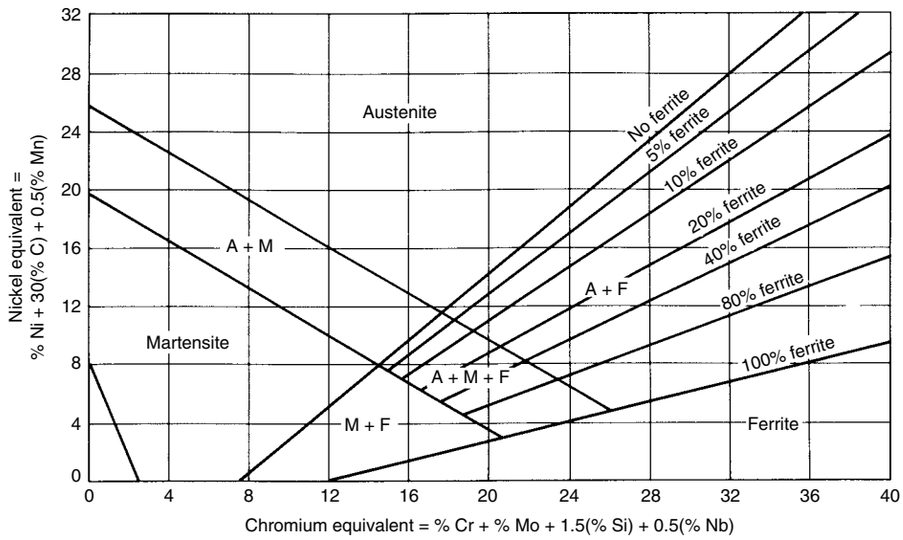

Fig. 2 Schaeffler diagram showing the amount of ferrite and austenite present in weldments as a function of chromium and nickel equivalents. Source: Ref 1

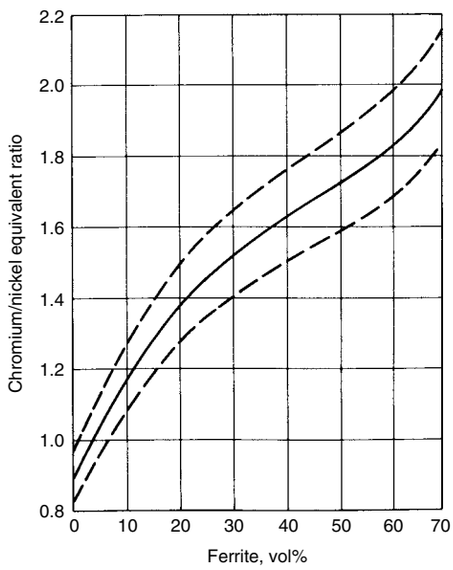

Fig. 3 Schoefer diagram for estimating the average ferrite content in austenitic iron-chromium-nickel alloy castings. Source: Ref 1

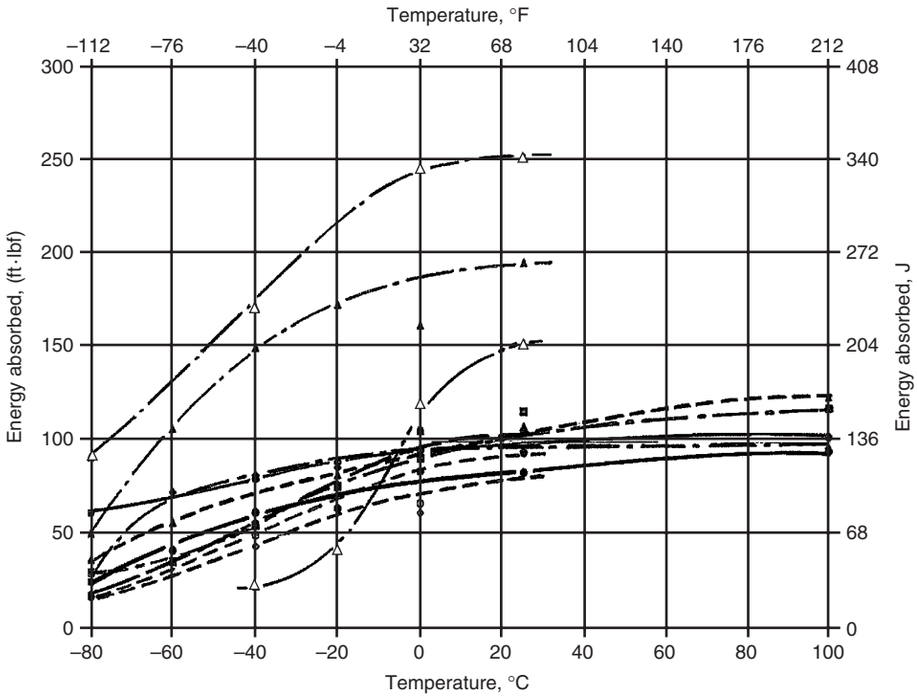

Fig. 4 Toughness of solution-annealed duplex stainless steel castings (closed symbols) and companion wrought alloys (open symbols) as a function of test temperature. Source: Ref 4

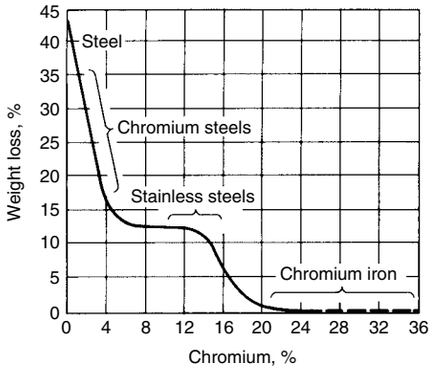

Fig. 5 Effect of chromium on oxidation resistance of cast steels. Specimens (13 mm, or 0.5 in., cubes) were exposed for 48 h at 1000 °C (1830 °F). Source: Ref 2

rendering it hard and possibly susceptible to cracking. Silicon and nickel are thought to be beneficial and enhance resistance to carburization (Ref 5).

Corrosion Behavior of C-Type Alloys

The ACI C-type stainless steels must resist corrosion in the various environments in which they regularly serve. The influence of the metallurgy of these materials on general corrosion, intergranular corrosion, localized corrosion, corrosion fatigue, and stress corrosion are discussed.

General Corrosion of Martensitic Alloys. The martensitic grades include CA-15, CA-15M, CA-6NM, CA-6NM-B, CA-40, CB-7Cu-1, and CB-7Cu-2. These alloys are generally used in applications requiring high strength and modest corrosion resistance.

Alloy CA-15 typically exhibits a microstructure of martensite and ferrite. This alloy contains the minimum amount of chromium to be considered a stainless steel (11 to 14% Cr) and as such may not be used in aggressive environments. It does, however, exhibit good atmospheric corrosion resistance, and it resists staining by many organic environments. Alloy CA-15M may contain slightly more molybdenum than CA-15 (up to 1% Mo) and therefore may have improved general corrosion resistance in relatively mild environments. Alloy CA-6NM is similar to CA-15M except that it contains more nickel and molybdenum, which improves its general corrosion resistance. Alloy CA-6NM-B is a lower-carbon version of this alloy. The lower strength level promotes resistance to sulfide stress cracking. Alloy CA-40 is a higher-strength version of CA-15, and it also exhibits excellent atmospheric-corrosion resistance after a normalize and temper heat treatment. Microstructurally, the CB-7Cu alloys usually consist of mixed martensite and ferrite, and because of the increased chromium and nickel levels compared to the other martensitic alloys, they offer improved corrosion resistance to seawater and some mild acids. These alloys also have good atmospheric-corrosion resistance. The CB-7Cu alloys are hardenable and offer the possibility of increased strength and improved corrosion resistance among the martensitic alloys.

General Corrosion of Ferritic Alloys. Alloys CB-30 and CC-50 are higher-carbon and higher-chromium alloys than the CA alloys previously mentioned. Each alloy is predominantly ferritic, although a small amount of martensite may be found in CB-30. Alloy CB-30 contains 18 to 21% Cr and is used in chemical-processing and oil-refining applications. The chromium content is sufficient to have good corrosion resistance to many acids, including nitric acid (HNO_3) (Fig. 8). Alloy CC-50 contains substantially more chromium (26 to 30%) and offers

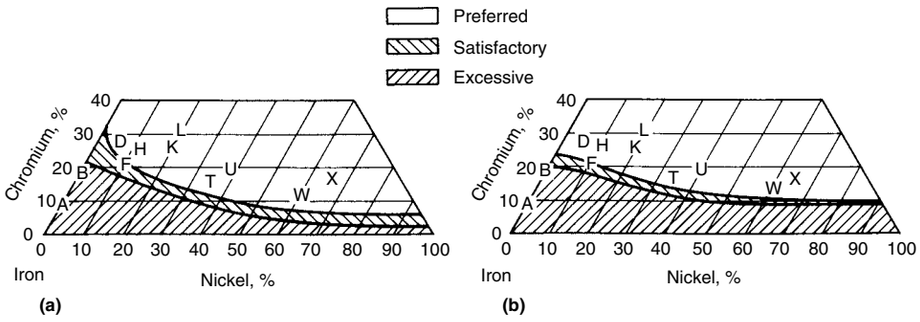

Fig. 6 Corrosion behavior of ACI H-type (heat-resistant) alloy castings in (a) air and in (b) oxidizing flue gases containing 5 grains of sulfur per 2.8 m^3 (100 ft^3) of gas. Source: Ref 2

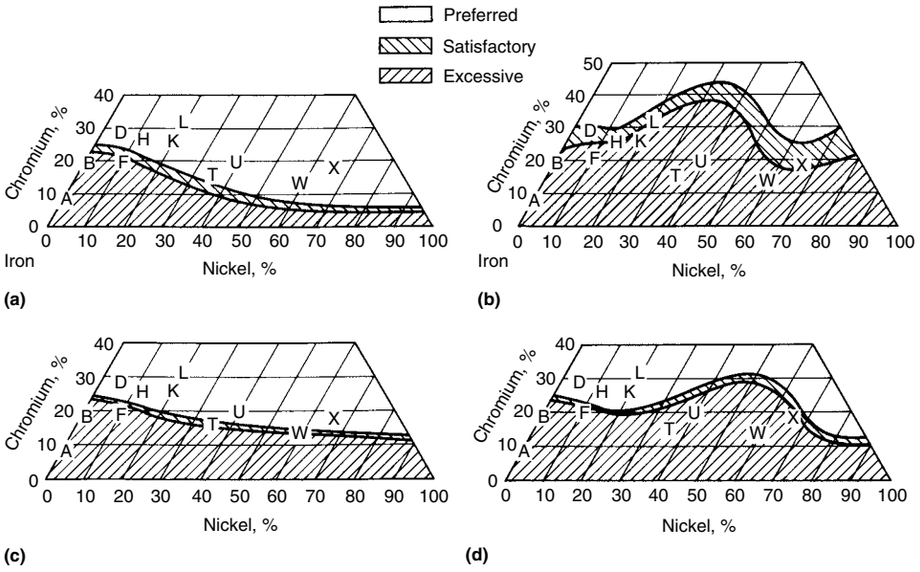

Fig. 7 Corrosion behavior of ACI H-type alloys in 100 h tests at 980 °C (1800 °F) in reducing sulfur-bearing gases. (a) Gas contained 5 grains of sulfur per 2.8 m^3 (100 ft^3) of gas. (b) Gas contained 300 grains of sulfur per 2.8 m^3 (100 ft^3) of gas. (c) Gas contained 100 grains of sulfur per 2.8 m^3 (100 ft^3) of gas; test at constant temperature. (d) Same sulfur content as gas in (c), but cooled to 150 °C (300 °F) each 12 h

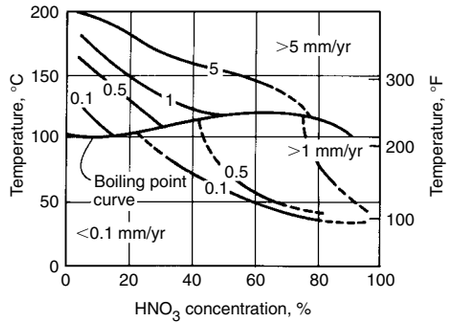

Fig. 8 Isocorrosion diagram for ACI CB-30 in HNO_3. Castings were annealed at 790 °C (1450 °F), furnace cooled to 540 °C (1000 °F), and then air cooled to room temperature.

relatively high resistance to localized corrosion and high resistance to many acids, including dilute H_2SO_4 and such oxidizing acids as HNO_3.

General Corrosion of Austenitic and Duplex Alloys. Alloy CF-8 typically contains approximately 19% Cr and 9% Ni and is essentially equivalent to type 304 wrought alloys. Alloy CF-8 may be fully austenitic, but it more commonly contains some residual ferrite (3 to 30%) in an austenite matrix. In the solution-treated condition, this alloy has excellent resistance to a wide variety of acids. It is particularly resistant to highly oxidizing acids, such as boiling HNO_3. Figure 9 shows isocorrosion diagrams for CF-8 in HNO_3, phosphoric acid (H_3PO_4), and sodium hydroxide (NaOH). The duplex nature of the microstructure of this alloy imparts additional resistance to stress-corrosion cracking (SCC) compared to its wholly austenitic counterparts. Alloy CF-3 is a reduced-carbon version of CF-8 with essentially identical corrosion resistance, except that CF-3 is much less susceptible to sensitization (Fig. 10). For applications in which the corrosion resistance of the weld heat-affected zone (HAZ) may be critical, CF-3 is chosen.

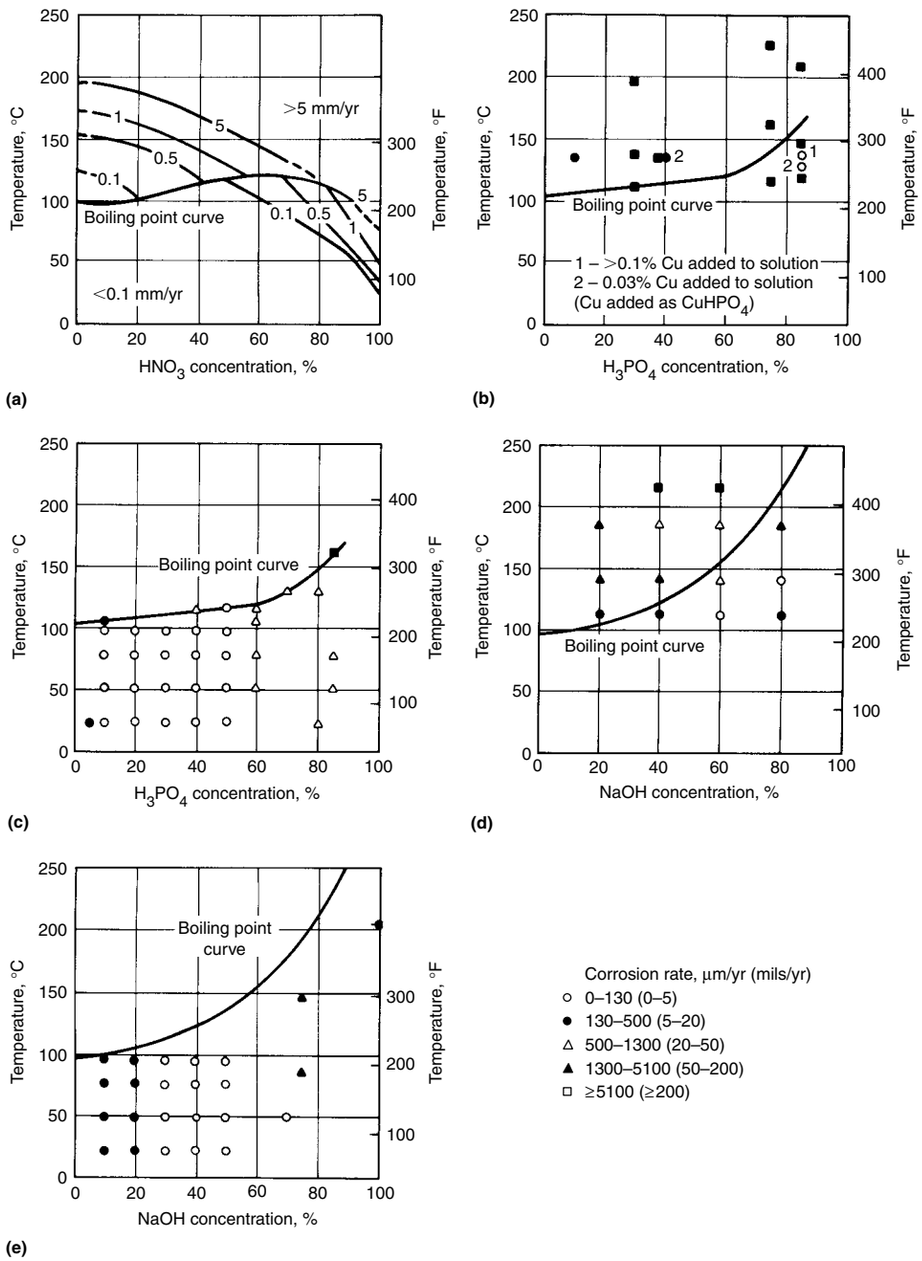

Fig. 9 Isocorrosion diagrams for ACI CF-8 in (a) HNO_3, (b and c) H_3PO_4, and (d and e) NaOH solutions. (b) and (d) Tests performed in a closed container at equilibrium pressure. (c) and (e) Tested at atmospheric pressure

Alloys CF-8A and CF-3A contain more ferrite than their CF-8 and CF-3 counterparts. Because the higher ferrite content is achieved by increasing the chromium/nickel equivalent ratio, the CF-8A and CF-3A alloys may have slightly higher chromium or slightly lower nickel contents than the low-ferrite equivalents. In general, the corrosion resistance is very similar, but the strength increases with ferrite content. Because of the high ferrite content, service should be restricted to temperatures below 400 °C (750 °F) due to the possibility of severe embrittlement. Alloy CF-8C is the niobium-stabilized grade of the CF-8 alloy class. This alloy contains small amounts of niobium, which tend to form carbides preferentially over chromium carbides and improve intergranular corrosion resistance in applications involving relatively high service temperatures. The development of niobium carbides is achieved through a heat treatment at 870 to 900 °C (1600 to 1650 °F); this is often referred to as a stabilizing heat treatment.

Alloys CF-8M, CF-3M, CF-8MA, and CF-3MA are 2 to 3% Mo-bearing versions of the CF-8 and CF-3 alloys. The addition of molybdenum increases resistance to corrosion by seawater and improves resistance to many chloride-bearing environments. The presence of molybdenum also improves crevice corrosion and pitting resistance, compared to the CF-8 and CF-3 alloys. Molybdenum-bearing alloys are generally not as resistant to highly oxidizing environments when phases rich in molybdenum are formed (this is particularly true for boiling HNO_3), but for weakly oxidizing environments and reducing environments, molybdenum-bearing alloys are generally superior.

Alloy CF-16F is a selenium-bearing free-machining grade of cast stainless steel. Because CF-16F nominally contains 19% Cr and 10% Ni, it has adequate corrosion resistance to a wide range of corrodents, but the large number of selenide inclusions makes surface deterioration and pitting definite possibilities.

Alloy CF-20 is a fully austenitic, relatively high-strength corrosion-resistant alloy. The 19% Cr content provides resistance to many types of oxidizing acids, but the high carbon

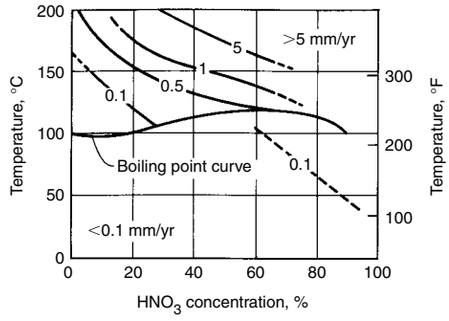

Fig. 10 Isocorrosion diagram for solution-treated quenched and sensitized ACI CF-3 in HNO_3

content makes it imperative that this alloy be used in the solution-treated condition for environments known to cause intergranular corrosion.

Alloy CE-30 is a nominally 27Cr-9Ni alloy that typically contains 10 to 20% ferrite in an austenite matrix. The high carbon and ferrite contents provide relatively high strength. The high chromium content and duplex structure act to minimize corrosion resulting from the formation of chromium carbides in the microstructure. This particular alloy is known for good resistance to sulfurous acid and sulfuric acid, and it is extensively used in the pulp and paper industry.

Alloy CG-8M is slightly more highly alloyed than the CF-8M alloys, with the primary addition being increased molybdenum (3 to 4%). The increased amount of molybdenum provides superior corrosion resistance to halide-bearing media and reducing acids, particularly H_2SO_3 and H_2SO_4 solutions. The high molybdenum content, however, renders CG-8M generally unsuitable in highly oxidizing environments.

Alloy CD-4MCu is the most highly alloyed material in this group, with a composition of Fe-26Cr-5Ni-2Mo-3Cu. The chromium/nickel equivalent ratio for this alloy is quite high, and a microstructure containing approximately equal amounts of ferrite and austenite is common. The low carbon content and high chromium content render the alloy relatively immune to intergranular corrosion. High chromium and molybdenum provide a high degree of localized corrosion resistance (crevices and pitting), and the duplex microstructure provides SCC resistance in many environments. This alloy can be precipitation hardened to provide strength and is also relatively resistant to abrasion and erosion-corrosion. Figures 11 and 12 show isocorrosion diagrams for CD-4MCu in HNO_3 and H_2SO_4, respectively. CD-4MCu does not require control of the nitrogen content, which can lead to excessive levels of ferrite that reduce the toughness of the material. The control of nitrogen within the range specified for CD-4MCuN eliminates this problem. The ASME Pressure Vessel Code recognized this fact and has replaced CD-4MCu with CD-4MCuN.

The results of a series of corrosion tests on CD-4MCuN, CD-3MN, CE-3MN, and CD-3MWCuN are shown in Table 2. The ASTM A 923 test detects the presence of detrimental intermetallic phases. The weight loss is associated with local depletion. The critical pitting temperature indicates the minimum temperature that pitting occurs. Grades CE-3MN and CD-3MWCuN are known as superduplex stainless steels. A method of ranking the pitting resistance of duplex stainless steels has been developed. It is an empirical measure and is known as the pitting resistance number (PREN). The PREN is based on the composition of the alloy, and for super duplex stainless steels, the PREN should not be less than 40:

$$\text{PREN} = \%\times\text{Cr} + 3.3\times\%\text{Mo} + 16\times\%\text{N}$$

Table 2 shows the improved pitting resistance of these alloys.

Fully Austenitic Alloys. Alloys CH-10 and CH-20 are fully austenitic and contain 22 to 26% Cr and 12 to 15% Ni. The high chromium content minimizes the tendency toward the formation of chromium-depleted zones during heat treatment in the sensitizing temperature range. These alloys are often used for handling paper pulp solutions and are known for good resistance to dilute H_2SO_4 and HNO_3.

Alloy CK-20 contains 23 to 27% Cr and 19 to 22% Ni and is less susceptible than CH-20 to intergranular corrosion attack in many acids after brief exposures to the chromium carbide formation temperature range. Alloy CK-20 possesses good corrosion resistance to many acids and, because of its fully austenitic structure, can be used at relatively high temperature.

Alloy CN-7M, with a nominal composition of Fe-29Ni-20Cr-2.5Mo-3.5Cu, exhibits excellent corrosion resistance in a wide variety of environments and is often used for H_2SO_4 service. Figure 13 shows isocorrosion diagrams for CN-7M in H_2SO_4, HNO_3, H_3PO_4, and NaOH. Relatively high resistance to intergranular corrosion and SCC make this alloy attractive for very many applications. Although relatively highly alloyed, the fully austenitic structure of CN-7M may lead to SCC susceptibility for some environments and stress states.

Intergranular Corrosion of Austenitic and Duplex Alloys. The optimal corrosion resistance for these alloys is developed by solution treatment. Depending on the specific alloy in question, temperatures between 1040 and 1205 °C (1900 and 2200 °F) are required to ensure complete solution of all carbides and other high-alloy phases, such as σ and χ, that sometimes form in highly alloyed stainless steels. Alloys containing relatively high total alloy content, particularly high molybdenum content, often require the higher solution treatment temperature. Water quenching from the temperature range of 1040 to 1205 °C (1900 to 2200 °F) normally completes the solution treatment.

Failure to solution treat a particular alloy or an improper solution treatment may seriously compromise the observed corrosion resistance in service. Inadvertent or unavoidable heat treatment in the temperature range of 480 to 820 °C (900 to 1500 °F), such as caused by welding, may destroy the intergranular corrosion resistance of the alloy. When austenitic or duplex (ferrite in austenite matrix) stainless steels are heated in or cooled slowly through this temperature range, chromium-rich carbides form at grain boundaries in austenitic alloys and at ferrite/austenite interfaces in duplex alloys. These carbides deplete the surrounding matrix of chromium, thus diminishing the local corrosion resistance of the alloy. An alloy in this condition of reduced corrosion resistance due to the formation of chromium carbides is said to be sensitized. In small amounts, these carbides may lead to localized pitting in the alloy, but if the chromium-depleted zones are interconnected throughout the alloy or HAZ of a weld, the alloy may disintegrate intergranularly in some environments.

If solution treatment of the alloy after casting and/or welding is impractical or impossible, the

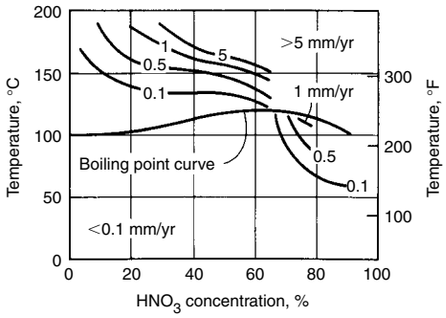

Fig. 11 Isocorrosion diagram for ACI CD-4MCu in HNO_3. The material was solution treated at 1120 °C (2050 °F) and water quenched.

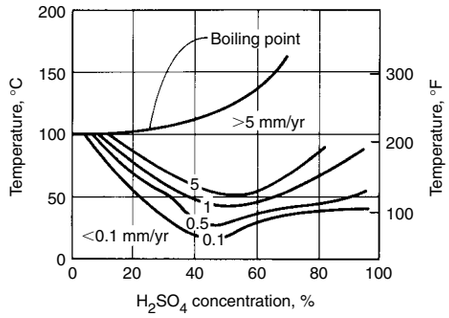

Fig. 12 Isocorrosion diagram for ACI CD-4MCu in H_2SO_4. The material was solution annealed at 1120 °C (2050 °F) and water quenched.

Table 2 Duplex stainless steel corrosion test results

		A 923C(b)		G 48(c)
Grade(a)	Heat	Corrosion rate, mdd(d)	CPT, °C	CPT, °C
CD-4MCuN	1	0.00	35	35
	2	0.00	40	40
	3	3.45	30	30
	4	2.87	35	35
CD-3MN	1	0.73	40	40
	2	2.19	25	35
	3	0.00	50	50
	4	0.00	45	45
	4(e)	2.12	50	50
CE-3MN	1	2.64	65	65
	2	0.00	50	50
	3	0.00	65	65
	3(e)	0.00	50	50
CD-3MWCuN	1	0.00	65	65
	2	0.00	70	70
	3	0.67	55	55

(a) ASTM A 890, solution annealed. (b) ASTM A 923 method C ferric chloride corrosion test. (c) ASTM G 48 method C critical pitting temperature (CPT) test, 6% $FeCl_3$, 24 h. (d) Corrosion rate calculated from weight loss; mdd is mg/dm^2/day. Maximum acceptable corrosion rate is 10 mdd; all specimens passed. (e) Centrifugally cast specimens

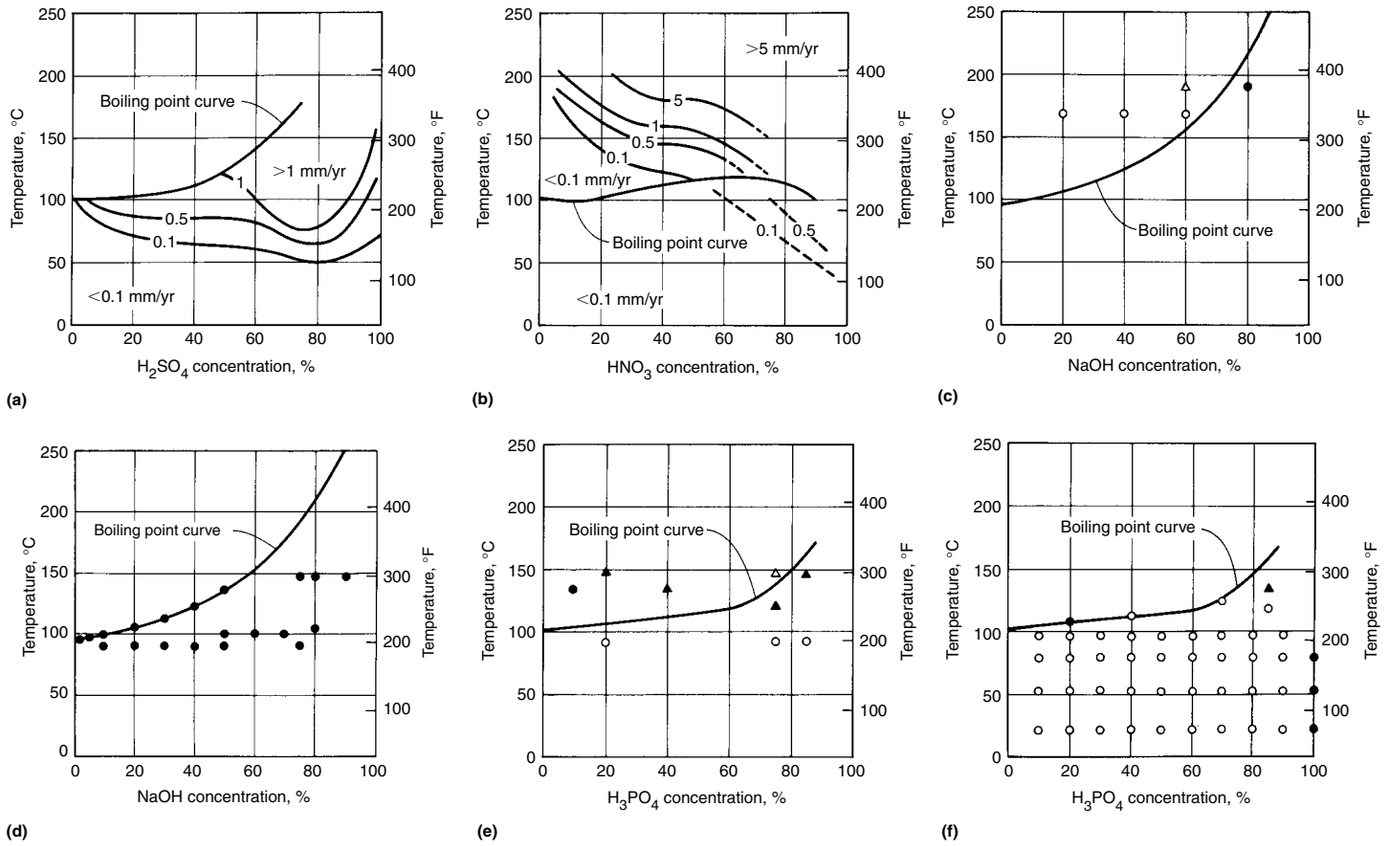

Fig. 13 Isocorrosion diagrams for solution-annealed and quenched ACI CN-7M in H_2SO_4, HNO_3, NaOH, and H_3PO_4. (a), (b), (d), and (f) Tested at atmospheric pressure. (c) and (e) Tested at equilibrium pressure in a closed container. See Fig. 9 for legend.

metallurgist has techniques to minimize potential intergranular corrosion problems. These include stabilizing of carbides by the addition of niobium, as described earlier, by cathodic protection, or by reducing the carbon content. The low-carbon grades CF-3 and CF-3M are commonly used as a solution to the sensitization incurred during welding. The low carbon content (0.03% C maximum) of these alloys precludes the formation of an extensive number of chromium carbides. In addition, these alloys normally contain 3 to 30% ferrite in an austenitic matrix. By virtue of rapid carbide precipitation kinetics at ferrite/austenite interfaces compared to austenite/austenite interfaces, carbide precipitation is confined to ferrite/austenite boundaries in alloys containing a minimum of approximately 3 to 5% ferrite (Ref 6, 7). If the ferrite network is discontinuous in the austenite matrix (depending on the amount, size, and distribution of ferrite pools), then extensive intergranular corrosion will not be a problem in most of the environments to which these alloys would be subjected.

An example of attack at the ferrite/austenite boundaries is shown in Fig. 14. These low-carbon alloys need not sacrifice significant strength compared to their high-carbon counterparts, because nitrogen may be added to increase strength. However, a large amount of nitrogen will begin to reduce the ferrite content, which will cancel some of the strength gained by interstitial hardening. Appropriate adjustment of the chromium/nickel equivalent ratio is beneficial in such cases. Fortunately, nitrogen is also beneficial to the corrosion resistance of austenitic and duplex stainless steels (Ref 8). Nitrogen seems to retard sensitization and improve the resistance to pitting and crevice corrosion of many stainless steels (Ref 9).

The standard practices of ASTM A 262 (Ref 10) are commonly implemented to predict and measure the susceptibility of austenitic and duplex stainless steels to intergranular corrosion. Table 3 indicates some representative results for CF-type alloys as tested according to practices A, B, and C of Ref 10 as well as two electrochemical tests described in Ref 11and 12. Table 4 lists the compositions of the alloys investigated. The data indicate the superior resistance of the low-carbon alloys to intergranular corrosion. It also indicates that for highly oxidizing environments (represented here by A 262C-boiling HNO_3), the CF-3 and CF-3M alloys are equivalent in the solution-treated condition, but that subsequent heat treatment causes the corrosion resistance of the CF-3M alloys to deteriorate rapidly for service in oxidizing environments (Ref 14). In addition, the

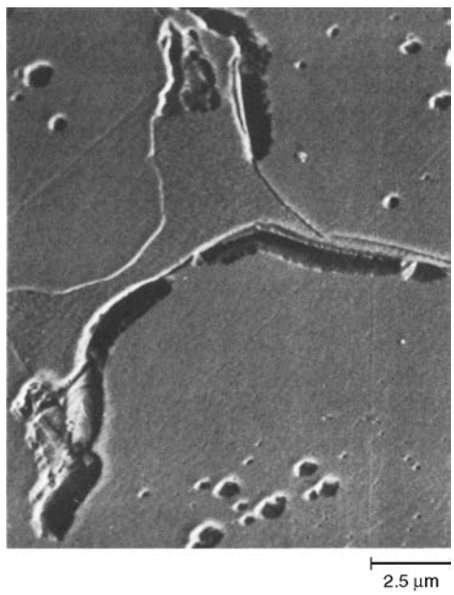

Fig. 14 Ferrite/austenite grain-boundary ditching in as-cast ACI CF-8. The specimen, which contained 3% ferrite, was electrochemical potentiokinetic reactivation tested. SEM micrograph. Original magnification 4550×. Source: Ref 7

Table 3 Intergranular corrosion test results for Alloy Casting Institute casting alloys

Metallurgical condition	Test(a)	Alloy(b)/Test results(c)											
		CF-8 (4)	CF-8 (11)	CF-8 (20)	CF-8M (5)	CF-8M (11)	CF-8M (20)	CF-3 (2)	CF-3 (5)	CF-3 (8)	CF-3M (5)	CF-3M (9)	CF-3M (16)
Solution treated	A 262A	P	P	P	P	P	P	P	P	P	P	P	P
	A 262B	P	P	P	P	P	P	P	P	P	P	P	P
	A 262C	P	P	P	P	P	P	P	P	P	P	P	P
	EPR	P	P	P	P	P	P	P*	P*	P*	P	P	P
	JEPR	P	P	P	P	P	P	P	P	P	P	P	P
Simulated weld repair	A 262A	X	X	X	X	X	X	P	P	P	P	P	P
	A 262B	X	X	X	X	X	X	P	P	P	P	P	P
	A 262C	X	X	X	X	X	X	P	P	P	P	P	P
	EPR	X	X	X	P	P	P	P*	P*	P*	P	P	P
	JEPR	X	X	X	P	P	P	P	P	P	P	P	P
Solution treated, held 1 h at 650 °C (1200 °F)	A 262A	X	X	X	X	X	X	X	X	X	X	X	X
	A 262B	X	X	X	X	X	X	P	P	P	P	P	P
	A 262C	X	X	X	X	X	X	P	P	P	X	X	X
	EPR	X	X	X	X	X	X	X/P*	X/P*	X/P*	X/P	P	P
	JEPR	X	X	X	P	X	X	P	P	P	P	P	P
As-cast	A 262A	X	X	X	X	X	X	X	X	X	X	X	X
	A 262B	X	X	X	X	X	X	P	P	P	P	X	P
	A 262C	X	X	X	X	X	X	P**	P**	P**	X	X	X
	EPR	X	X	X	X	X	X	X/P*	X/P*	X/P*	X/P	X/P	P
	JEPR	X	X	X	X	X	X	X/P	P	P	P	P	P

(a) See Ref 10 for details of ASTM A 262 practices. EPR, electrochemical potentiokinetic reactivation test: see Ref 10 for details. JEPR, Japanese electrochemical potentiokinetic reactivation test: see Ref 11 for details. (b) Parenthetical value is the percentage of ferrite. See Table 4 for alloy compositions. (c) P, pass; X, fail based on the following criteria: A 262A ditching < 10% = pass; A 262B, penetration rate < 0.64 mm/yr (25 mils/yr) = pass; A 262C, penetration rate < 0.46 mm/yr (18 mils/yr) and not increasing = pass; EPR, peak current density < 100 μA/cm^2 (645 μA/in.^{2}) = pass; JEPR, ratio < 1% = pass: P*, pass, but matrix pitting complicates test results. X/P, near pass. X/P*, likely pass; small EPR indication complicated by matrix pitting p**, pass; actual heat treatment 4 h at 650 °C (1200 °F) after solution treatment rather than as-cast. Source: Ref 7, 13, 14

degree of chromium depletion necessary to cause susceptibility to intergranular corrosion appears to increase in the presence of molybdenum (Ref 7). The passive film stability imparted by molybdenum may offset the loss of solid-solution chromium for mild degrees of sensitization.

Intergranular Corrosion of Ferritic and Martensitic Alloys. Ferritic alloys may also be sensitized by the formation of extensive chromium carbide networks, but because of the high bulk chromium content and rapid diffusion rates of chromium in ferrite, the formation of carbides can be tolerated if the alloy has been slowly cooled from a solutionizing temperature of 780 to 900 °C (1435 to 1650 °F). The slow cooling allows replenishment of the chromium adjacent to carbides. Martensitic alloys normally do not contain sufficient bulk chromium to be used in applications in which intergranular corrosion is likely to be of concern. Typical chromium contents for martensitic alloys may be as low as 11 to 12%.

Pitting and Crevice Corrosion. Austenitic and martensitic alloys display a tendency toward localized corrosion in some environments. The conditions conducive to this behavior may be any situation in areas where flow is restricted and an oxygen concentration cell may be established. Duplex alloys have been found to be less susceptible. Localized corrosion is particularly acute in environments containing chloride ion (Cl^-) and in acidic solutions.

Increasing the alloy content improves resistance to localized corrosion, as indicated by the PREN increase. Molybdenum has long been recognized as effective in reducing localized corrosion, although it is not a total solution.

Table 4 Composition of alloys tested in Table 3

Material	Ferrite number(a)	Composition, %								
		C	Mn	Si	P	S	Cr	Ni	Mo	N
CF-8 LO	4	0.058	0.60	1.52	0.012	0.013	18.53	9.98	0.02	0.02
CF-8 INT	11	0.086	0.84	1.10	0.031	0.012	19.90	8.73	0.50	0.02
CF-8 HI	20	0.066	0.79	1.25	0.031	0.011	20.81	8.85	0.45	0.02
CF-8M LO	5	0.063	0.94	1.21	0.011	0.014	18.26	11.17	2.28	0.02
CF-8M INT	11	0.083	1.20	1.20	0.030	0.013	19.78	9.53	2.21	0.02
CF-8M HI	20	0.071	1.19	1.16	0.030	0.011	19.92	9.40	1.95	0.02
CF-3 LO	2	0.016	0.98	1.12	0.010	0.008	17.36	10.10	0.10	0.04
CF-3 INT	5	0.023	0.68	1.24	0.011	0.009	19.35	10.27	0.10	0.06
CF-3 HI	8	0.015	0.67	1.09	0.013	0.006	19.82	8.73	0.10	0.04
CF-3M LO	5	0.027	0.96	0.85	0.011	0.010	17.55	12.00	2.18	0.04
CF-3M INT	9	0.027	1.04	1.02	0.009	0.009	18.78	10.79	2.12	0.03
CF-3M HI	16	0.022	0.94	1.14	0.012	0.007	19.85	10.08	2.26	0.02

(a) This value is the percentage of ferrite.

Excellent results have been obtained with CG-8M, but the CF-3M or CN-7M alloys are readily attacked. Nitrogen is also effective at retarding localized corrosion.

A technique for comparing resistance to localized corrosion is to ascertain the critical crevice temperature (CCT). This involves determining the maximum temperature at which no crevice attack occurs during a 24 h testing period in standardized (or service-specific) environments. Tests have been conducted on a number of cast stainless alloys; the results are given in Table 5. Although the CCT has been shown to correlate well with tests in aerated seawater (Ref 19), it must not be used as the maximum operating temperature in seawater or other chloride-containing media, because it is simply a comparative tool regarding relative resistance. The ferric chloride ($FeCl_3$) test environment is a very severe, highly

Table 5 Critical crevice temperatures (CCTs) for several common cast and wrought alloys

Alloy	Structure	CCT		Ref
		°C	°F	
Wrought AISI type 317L	Austenitic	2	35	15
Cast CF-3M	90% austenite, 10% ferrite	2	35	16
Cast CN-7M	Austenitic	−1.1	30	16
Cast CF-8M	90% austenite, 10% ferrite	−2.5	28	17
Wrought AISI type 316L	Austenitic	−2.5	28	18
Wrought AISI type 316	Austenitic	−3	27	15

Note: See text and Ref 16 for information on CCTs.

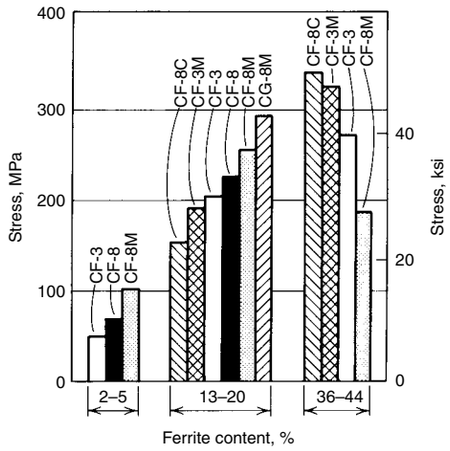

Fig. 15 Stress required to produce stress-corrosion cracking in several ACI alloys with varying amounts of ferrite

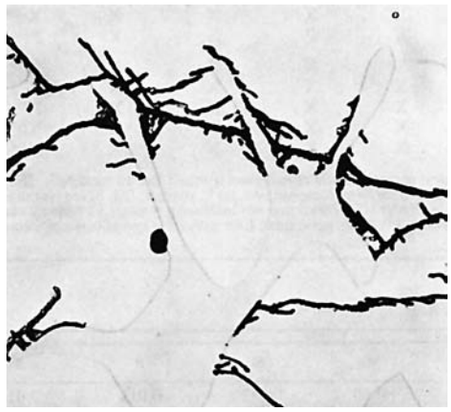

Fig. 16 Ferrite pools blocking the propagation of stress-corrosion cracks in a cast stainless steel

oxidizing environment containing approximately 39,000 ppm Cl^- at a pH of approximately 1.4. Therefore, the $FeCl_3$ CCT is lower than that normally found in aerated seawater (Ref 19), which contains approximately 20,000 ppm Cl^- with a pH of approximately 7.5 to 8.0.

Corrosion fatigue is one of the most destructive and unpredictable corrosion-related failure mechanisms. The behavior is highly specific to the environment and alloy, and the extent of the interaction between corrosion and mechanical damage is not easy to quantify. The martensitic materials are degraded the most in both absolute and relative terms. For example, if left to corrode freely in seawater, they have very little resistance to corrosion fatigue. This is remarkable in view of their very high strength and fatigue resistance in air.

Cathodic protection is a method of reducing corrosion; however, because martensitic stainless steels are susceptible to hydrogen embrittlement, cathodic protection must be carefully applied. Too large a protective potential will lead to catastrophic hydrogen stress cracking.

Austenitic materials are also severely degraded in corrosion fatigue strength under conditions conducive to pitting, such as in seawater. However, they are easily cathodically protected without fear of hydrogen embrittlement and perform well in freshwaters. The corrosion fatigue behavior of duplex alloys in chloride environments is less than that obtained for austenitic stainless steels (Ref 20).

Stress-corrosion cracking of cast stainless steels has been investigated for only a limited number of environments, heat treatments, and test conditions. From the limited information available, the following generalizations apply.

As the composition is adjusted to provide increasingly greater amounts of ferrite in an austenitic matrix, SCC resistance seems to improve. This trend continues to a certain level, apparently near 50% ferrite (Fig. 15, 16). Lower nickel contents tend to improve SCC resistance in cast duplex alloys, possibly because of its effect on ferrite content (Ref 21). The mere presence of the ferrite phase, which is generally much more resistant to SCC than austenite, forces the crack to expend more energy traveling around rather than through ferrite. This slows propagation significantly, discouraging SCC. At low and medium stress levels, the ferrite tends to block the propagation of stress-corrosion cracks. This may be due to a change in composition and/or crystal structure across the austenite/ferrite boundary (Fig. 16). As the stress level increases, crack propagation may change from austenite/ferrite boundaries to transgranular propagation (Ref 21, 22). Finally, reducing the carbon content of cast stainless alloys—thus reducing the susceptibility to sensitization—improves SCC resistance. This is also true for wrought alloys (Ref 21, 23–25).

ACKNOWLEDGMENT

This article was adapted from Corrosion of Cast Steels by Raymond W. Monroe and Steven J. Pawel in *Corrosion,* Volume 13, *ASM Handbook,* 1987, p 573–582.

REFERENCES

1. M. Prager, Cast High Alloy Metallurgy, *Steel Casting Metallurgy,* J. Svoboda, Ed., Steel Founders' Society of America, 1984, p 221–245
2. C.E. Bates and L.T. Tillery, *Atlas of Cast Corrosion-Resistant Alloy Microstructures,* Steel Founders' Society of America, 1985
3. "Standard Practice for Steel Casting, Austenitic Alloy, Estimating Ferrite Content Thereof," A 800, ASTM International
4. C. Lundin et al., Corrosion, Toughness, Weldability and Metallurgical Evaluation of Cast Duplex Stainless Steels, *Proceedings of Duplex America 2000 Conference on Duplex Stainless Steels,* Stainless Steel World, p 449–460
5. D.B. Roach, "Carburization of Cast Heat Resistant Alloys," ACI progress report, Project A-80, Alloy Casting Institute
6. T.M. Devine, Mechanism of Intergranular Corrosion and Pitting Corrosion of Austenitic and Duplex 308 Stainless Steel, *J. Electrochem. Soc.,* Vol 126 (No. 3), 1979, p 374
7. E.E. Stansbury, C.D. Lundin, and S.J. Pawel, Sensitization Behavior of Cast Stainless Steels Subjected to Simulated Weld Repair, *Proceedings of the 38th SFSA Technical and Operating Conference,* Steel Founders' Society of America, 1983, p 223
8. S.J. Pawel, Literature Review on the Role of Nitrogen in Austenitic Steels, *Steel Founders' Res. J.,* Issue 5, 1st Quarter, 1984
9. S.J. Pawel, E.E. Stansbury, and C.D. Lundin, Role of Nitrogen in the Pitting of Cast Duplex CF-Type Stainless Steels, *Corrosion,* Vol 45 (No. 2), 1989, p 125–133
10. "Standard Practices for Detecting Susceptibility to Intergranular Attack in Austenitic Stainless Steels," A 262, *Annual Book of ASTM Standards,* American Society for Testing and Materials
11. W.L. Clarke, R.L. Cowan, and W.L. Walker, Comparative Methods for Measuring Degree of Sensitization in Stainless Steel, *Intergranular Corrosion of Stainless Alloys,* STP 656, R.F. Steigerwald, Ed., American Society for Testing and Materials, 1978, p 99
12. M. Akashi et al., Evaluation of IGSCC Susceptibility of Austenitic Stainless Steels Using Electrochemical Methods, *Boshoku Gijutsu (Corros. Eng.),* Vol 29, 1980, p 163 (BTSITS trans.)
13. S.J. Pawel, "The Sensitization Behavior of Cast Stainless Steels Subjected to Weld Repair," MS thesis, University of Tennessee, June 1983
14. S.J. Pawel, E.E. Stansbury, and C.D. Lundin, Evaluation of Post Weld Repair Requirements for CF3 and CF3M Alloys—Exposure to Boiling Nitric Acid, *First International Steel Foundry Congress Proceedings,* Steel Founders' Society of America, 1985, p 45
15. J.R. Maurer and J.R. Kearns, "Enhancing the Properties of a 6% Molybdenum Austenitic Alloy with Nitrogen," Paper 172, presented at Corrosion/85, National Association of Corrosion Engineers, 1985
16. J.A. Larson, 1984 SCRATA Exchange Lecture: New Developments in High Alloy Cast Steels, *Proceedings of the 39th SFSA T & O Conference,* Steel Founders' Society of America, 1984, p 229–239
17. A. Poznansky and P.J. Grobner, "Highly Alloyed Duplex Stainless Steels," Paper 8410-026, presented at the International

Conference on New Developments in Stainless Steel Technology, (Detroit, MI), American Society for Metals, Sept 1984
18. A.P. Bond and H.J. Dundas, "Resistance of Stainless Steels to Crevice Corrosion in Seawater," Paper 26, presented at Corrosion/84, National Association of Corrosion Engineers, 1984
19. A. Garner, Crevice Corrosion of Stainless Steels in Seawater: Correlation of Field Data with Laboratory Ferric Chloride Tests, *Corrosion,* Vol 37 (No. 3), March 1981, p 178–184
20. L. Coudreuse and J. Charles, Fatigue and Corrosion—Fatigue Behavior of Duplex Stainless Steels, *Sixth World Duplex Conference,* 17–20 Oct 2000 (Venice, Italy), Italian Metallurgical Association, p 629–630
21. S. Shimodaira et al., Mechanisms of Transgranular Stress Corrosion Cracking of Duplex and Ferrite Stainless Steels, *Stress Corrosion Cracking and Hydrogen Embrittlement in Iron Base Alloys,* NACE Reference Book 5, National Association of Corrosion Engineers, 1977
22. P.L. Andresen and D.J. Duquette, The Effect of Cl^- Concentration and Applied Potential on the SCC Behavior of Type 304 Stainless Steel in Deaerated High Temperature Water, *Corrosion,* Vol 36 (No. 2), 1980, p 85–93
23. J.N. Kass et al., Stress Corrosion Cracking of Welded Type 304 and 304L Stainless Steel under Cyclic Loading, *Corrosion,* Vol 36 (No. 6), 1980, p 299–305
24. J.N. Kass et al., Comparative Stress Corrosion Behavior of Welded Austenitic Stainless Steel Pipe in High Temperature High Purity Oxygenated Water, *Corrosion,* Vol 36 (No. 12), 1980, p 686–698
25. G. Cragnolino et al., Stress Corrosion Cracking of Sensitized Type 304 Stainless Steel in Sulfate and Chloride Solutions at 250 and 100C, *Corrosion,* Vol 37 (No. 6), 1981, p 312–319

ASM Handbook, Volume 13B: Corrosion: Materials
S.D. Cramer, B.S. Covino, Jr., editors, p93-94
DOI: 10.1361/asmhba0003814

Introduction to Corrosion of Nonferrous Metals and Specialty Products

Paul Crook, Haynes International, Inc.

NONFERROUS METALS AND ALLOYS are widely used to resist corrosion. At one end of the spectrum, they are used for water piping and food preparation. At the other end, they are vital to the operation of many chemical plants dealing with aggressive acids and alkalis. There are two reasons why nonferrous materials are preferred over steels and stainless steels for many applications. First, numerous nonferrous metals and alloys have extremely desirable physical and mechanical properties, for example, high strength-to-weight ratios or high thermal and electrical conductivities. Second, many of the nonferrous metals and alloys possess much higher resistance to corrosion than the steels and stainless steels. In this Section, materials based on the following elements are discussed: aluminum, beryllium, cobalt, copper, gold, hafnium, iridium, lead, magnesium, nickel, niobium (columbium), osmium, palladium, platinum, rhodium, ruthenium, silver, tantalum, tin, titanium, uranium, zinc, and zirconium. Also covered in this section are several specialty nonferrous products that cannot easily be categorized by elemental base. These include electroplated hard chromium, thermal spray coatings, clad metals, powder metallurgy materials, amorphous metals, intermetallics, cemented carbides, metal-matrix composites, and joints.

Copper

The most widely used nonferrous materials are those based on aluminum, copper, nickel, and titanium. Copper has the distinction of being the first metal used by man in significant quantities. The name *copper* is an anglicized version of the Latin name for Cyprus, an early source of the metal. Since the dawn of civilization, copper has been the primary material for water systems. Indeed, it has been estimated that, in the last 40 years, approximately 5.3 million miles of copper plumbing tube have been installed in buildings in the United States alone. The success of copper in this application is due not only to the fact that it is resistant to corrosion in various types of water but also that it is biostatic, meaning bacteria will not grow on its surface.

Building construction is the largest end-use market for copper and its alloys, accounting for approximately 46% of total U.S. consumption. Other important uses are electrical and electronic products (23%), which make use of the high electrical conductivity of copper; consumer products (11%); transportation (10%); and industrial machinery and equipment (10%). There are many alloys of copper, notably the brasses and bronzes. The main reason for alloying copper is to provide materials of higher strength with the corrosion characteristics of copper. Zinc, tin, and nickel are the most commonly used alloying additions in copper. The bronzes are particularly useful as bearing materials, because they are very resistant to sliding wear.

Nickel

The second of the widely used nonferrous metals to be discovered was nickel, in 1751. Its name has a rather negative connotation; it derives from a German word meaning devil and was given this name because German miners in the Middle Ages found that it interfered with the smelting of copper. Despite this inauspicious start, nickel has become a vital engineering element, with much of its success due to the need for corrosion-resistant materials.

Nickel occurs in nature in the form of oxides, sulfides, and silicates. It is mined in many countries and on all continents. Approximately 1 million tonnes of nickel are produced per annum throughout the world. This compares with over 10 million tonnes for copper. Of the nickel consumed (this includes a significant quantity of recycled material), 65% is used in the manufacture of stainless steels, 12% in nickel alloys, 10% in other steels, 8% in electroplating, and 5% for other products, including chemicals.

Many of the nickel alloys designed to resist aqueous corrosion possess higher resistance to hydrochloric acid and chloride-induced phenomena (pitting, crevice attack, and stress-corrosion cracking) than the stainless steels. Nickel alloys are also among the few metallic materials capable of withstanding warm hydrofluoric acid. Commercially pure nickel is particularly resistant to caustic soda. On the high-temperature side, strong nickel alloys are available to resist oxidation, carburization, metal dusting, and sulfidizing-oxidizing conditions.

Titanium

Despite being the ninth most abundant element in the crust of the Earth, titanium (named after Titan, a giant in Greek mythology) was not discovered until 1791. Even more surprising, methods of producing the pure metal were not available until 1910. In fact, the metal did not become widely available to industry until 1946, when a commercial process for reducing titanium tetrachloride with magnesium was developed.

There are five classifications of titanium and its alloys. Those in groups 1, 2, and 3 exhibit predominantly hexagonal close-packed (alpha) structures and are used largely for nonaerospace applications, where resistance to aqueous corrosion is the primary requirement. The group 5 materials, which exhibit body-centered cubic (beta) structures, and the alpha-beta group 4 materials can be heat treated to provide very high strength-to-weight ratios; as a result, they are used extensively in the compressor sections of aircraft gas turbines. In fact, titanium alloy components constitute 20 to 30% of the dry weight of modern jet engines. The group 1 materials are the commercially pure grades of titanium. Their resistance to aqueous corrosion derives from their ability to form extremely protective oxide films in the presence of oxygen. The group 2 materials contain small quantities of either palladium or ruthenium, which have a powerful, positive influence on corrosion resistance. The group 3 materials are more highly alloyed but maintain their predominantly alpha microstructures. They possess higher strengths than the group 1 and 2 materials, thus making them attractive for applications where moderate

strength, light weight, and corrosion resistance are required.

Titanium and its alloys are part of a larger family of materials known as the reactive metals. All of these reactive metals, notably titanium, zirconium, niobium, and tantalum, benefit from highly protective oxide films. As a result, their corrosion rates are extremely low in many environments.

Aluminum

Aluminum is the third most abundant element in the Earth's crust. It is surprising, therefore, that its existence was not established until 1808, and that it was considered a precious metal until 1886, when the Hall-Héroult process of production was invented. Since then, its use has grown to the point where, today, more aluminum is produced than all other nonferrous metals combined. Aluminum, or aluminium as it is also known, was derived from the Latin (*alumen*) for a naturally occurring compound containing the metal. It was first given the name alumium, but this was soon altered to aluminum. The alternative name aluminium was suggested in the mid-1800s by the International Union of Pure and Applied Chemists to bring the name into line with those of other elements (ending in "ium") being discovered at the time.

Obviously, the main attribute of aluminum and its alloys is their low density. Like titanium, aluminum and its alloys are protected from many potentially corrosive environments by oxide films that form readily on freshly exposed surfaces. The chief markets for aluminum and its alloys are transportation, packaging (particularly of food and beverages), construction, and electrical. In the field of transportation, aluminum has been critical to the growth of air travel. It is also the material of choice for trailer trucks for road haulage, buses, and modern passenger rail cars (carriages).

While aluminum and its alloys possess only moderate corrosion resistance relative to copper, nickel, and titanium (and their alloys), this is a key attribute in the packaging industry. The aluminum oxide films that form on aluminum and its alloys are stable in the pH range of 4.5 to 8.5. Foods and beverages outside this range are typically packaged in polymer-coated aluminum containers.

There are two types of wrought aluminum alloy: those that can be heat treated to increase their strengths, and those that cannot. The wrought alloys are also categorized according to the principal alloying elements, using a four-digit system. For example, the 1*xxx* series includes the commercially pure compositions, and the 2*xxx* series contains copper as the primary alloying element. Of the seven main series, those designated 2*xxx*, 6*xxx*, and 7*xxx* can be strengthened by heat treatment. The remainder are not heat treatable but can be strengthened by work hardening.

Specialty Products

Turning to specialty nonferrous products, the use of electroplated hard chromium for corrosion protection and decoration is well known. Chromium derives its resistance to corrosive environments from passive oxide films, which heal rapidly in air if scratched. Decorative chromium coatings are generally less than 1.2 μm (0.05 mil) thick, while coatings thicker than this are used to resist both corrosion and wear. In this Section, the reader learns of the preplating and postplating treatments required to ensure optimal performance.

Two types of thermal spray coating are used for the protection of steels in aqueous environments. First, metals and alloys less noble than steel (notably zinc and aluminum) can be sprayed onto steels to provide cathodic protection (the coatings become sacrificial anodes). In such cases, coating porosity is acceptable, and low-cost/rapid-deposition spray processes can be used. Second, dense coatings of metals and alloys with much higher corrosion resistance than steel (notably titanium and nickel-base) can be used, provided they are dense enough to prevent corrosive media from reaching the steels. One of the largest uses of dense thermal spray coatings is in the protection of gas turbine engine components from high-temperature oxidation.

There are parallels between thermal spray coating and cladding, a process by which metallic materials are bonded to one another prior to component fabrication. Common methods of attachment include roll bonding, extrusion bonding, and explosion bonding. All of these methods induce the breakdown of existing oxide films, followed by intimate metal-to-metal contact. Like thermal spray coatings, clad materials are selected to either resist the corrosive media or to act as sacrificial anodes.

In most structures designed to resist corrosion, joints represent the greatest challenge, whether they are welded, soldered, or brazed. For most wrought corrosion-resistant alloys, there are matching weld filler metals. However, weldments are generally less corrosion resistant, due to elemental segregation. Also, weld heat-affected zones in wrought alloy structures may be prone to preferential attack, if the heat of welding induces microstructural changes. In this Section, there is a separate article on the corrosion of soldered and brazed joints. The greatest concern with soldering, which is commonly used to join copper and aluminum alloys, is removal of the flux, which can interfere with protective oxide films. Brazing presents an even greater challenge, because elements with high diffusivity (from the braze material) can alter the microstructures, hence corrosion resistance, of adjacent bulk materials. Also, an understanding of the effects of the brazing heat treatment on the material(s) to be joined is critical if problems are to be avoided.

Powder metallurgy materials, amorphous metals, intermetallics, cemented carbides, and metal-matrix composites are defined less by their compositions than by their microstructures, which provide physical, mechanical, and corrosion characteristics unlike those of the traditionally processed metals and alloys. In this Section, the reader gains an understanding of the progress with these exciting technologies and learns of their applicability under corrosive conditions.

ASM Handbook, Volume 13B: Corrosion: Materials
S.D. Cramer, B.S. Covino, Jr., editors, p95-124
DOI: 10.1361/asmhba0003815

Corrosion of Aluminum and Aluminum Alloys

Revised by J.G. Kaufman, The Aluminum Association (Retired)

ALUMINUM, as indicated by its position in the electromotive force series, is a thermodynamically reactive metal; among structural metals, only beryllium and magnesium are more reactive. Aluminum owes its excellent corrosion resistance and its use as one of the primary metals of commerce to the barrier oxide film that is bonded strongly to its surface and that, if damaged, re-forms immediately in most environments. On a surface freshly abraded and then exposed to air, the barrier oxide film is only 1 nm (0.04 μin.) thick but is highly effective in protecting the aluminum from corrosion.

The oxide film that develops in normal atmospheres grows to thicknesses much greater than 1 nm (0.04 μin.) and is composed of two layers (Ref 1). The inner oxide next to the metal is a compact amorphous barrier layer whose thickness is determined solely by the temperature of the environment. At any given temperature, the limiting barrier thickness is the same in oxygen, dry air, or moist air. Covering the barrier layer is a thicker, more permeable outer layer of hydrated oxide. Most of the interpretation of aluminum corrosion processes has been developed in terms of the chemical properties of these oxide layers.

The film growth can be visualized as the result of a dynamic equilibrium between opposing forces—those tending to form the compact barrier layer and those tending to break it down. If the destructive forces are absent, as in dry air, the natural film will consist only of the barrier layer and will form rapidly to the limiting thickness. If the destructive forces are too strong, the oxide will be hydrated faster than it is formed, and little barrier will remain. Between these extremes, where the opposing forces reach a reasonable balance, relatively thick (20 to 200 nm, or 0.8 to 8 μin.) natural films are formed (Ref 2).

The conditions for thermodynamic stability of the oxide film are expressed by the Pourbaix (potential versus pH) diagram shown in Fig. 1. As shown by this diagram, aluminum is passive (is protected by its oxide film) in the pH range of approximately 4 to 8.5. The limits of this range, however, vary somewhat with temperature, with the specific form of oxide film present, and with the presence of substances that can form soluble complexes or insoluble salts with aluminum. The relative inertness in the passive range is further illustrated in Fig. 2, which gives results of weight loss measurements for alloy 3004-H14 specimens exposed in water and in salt solutions at various pH values.

Beyond the limits of the passive range, aluminum corrodes in aqueous solutions because its oxides are soluble in many acids and bases, yielding Al^{3+} ions in the former and AlO_2^- (aluminate) ions in the latter. There are, however, instances when corrosion does not occur outside the passive range, for example, when the oxide film is not soluble or when the film is maintained by the oxidizing nature of the solution (Ref 4).

Pitting Corrosion

Corrosion of aluminum in the passive range is localized, usually manifested by random formation of pits. The pitting-potential principle establishes the conditions under which metals in the passive state are subject to corrosion by pitting (Ref 5–7). Simply stated, pitting potential, E_p, is that potential in a particular solution above which pits will initiate and below which they will not. See the article "Pitting Corrosion" in *ASM Handbook,* Volume 13A, 2003.

Four laboratory procedures have been developed to measure E_p—one based on fixed current and the other three on controlled potential (Ref 8). The most widely used is controlled potential, in which the potential of a specimen, usually immersed in a deaerated electrolyte of interest, is made more positive and the resulting current density from the specimen measured. The potential at which the current density increases sharply and remains high is called the oxide breakdown potential, E_{br}. With polished specimens in many electrolytes, E_{br} is a close approximation of E_p, and the two are used interchangeably.

An example is shown in Fig. 3. A specimen of aluminum alloy 1100 (99.0% Al) was immersed in a neutral deaerated sodium chloride (NaCl) solution, and the relationship between anode potential and current density was plotted (solid

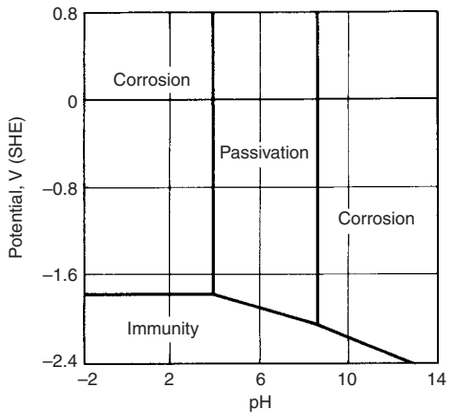

Fig. 1 Pourbaix diagram for aluminum with an $Al_2O_3 \cdot 3H_2O$ film at 25 °C (75 °F). Potential values are for the standard hydrogen electrode (SHE) scale. Source: Ref 3

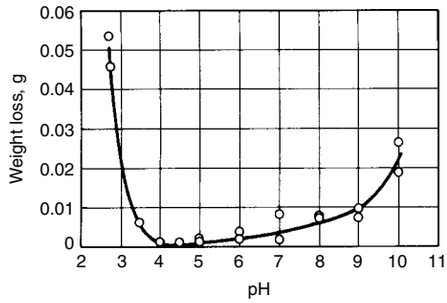

Fig. 2 Weight loss of alloy 3004-H14 exposed 1 week in distilled water and in solutions of various pH values. Specimens were 1.6 × 13 × 75 mm (0.06 × 0.5 × 3 in.). The pH values of solutions were adjusted with HCl and NaOH. Test temperature was 60 °C (140 °F).

line, Fig. 3). At potentials more active (anodic) than E_p, where the oxide layer can maintain its integrity, anodic polarization occurs readily, and corrosion is slow and uniform. Above E_p, anodic polarization is difficult, and the current density sharply increases. The oxide ruptures at random weak points in the barrier layer and cannot repair itself, and localized corrosion develops at these points.

Potential-current relationships for various cathodic reactions are indicated by the dashed lines in Fig. 3. Only when the cathodic reaction is sufficient to polarize the metal to its pitting potential will significant current flow and pitting corrosion start.

For aluminum, pitting corrosion is most commonly produced by halide ions, of which chloride (Cl^-) is the most frequently encountered in service. The effect of chloride ion concentration on the pitting potential of aluminum 1199 (99.99+%Al) is shown in Fig. 4. Pitting of aluminum in halide solutions open to the air occurs because, in the presence of oxygen, the metal is readily polarized to its pitting potential. In the absence of dissolved oxygen or other cathodic reactant, aluminum will not corrode by pitting because it is not polarized to its pitting potential. Generally, aluminum does not develop pitting in aerated solutions of most nonhalide salts, because its pitting potential in these solutions is considerably more noble (cathodic) than in halide solutions, and it is not polarized to these potentials in normal service (Ref 7).

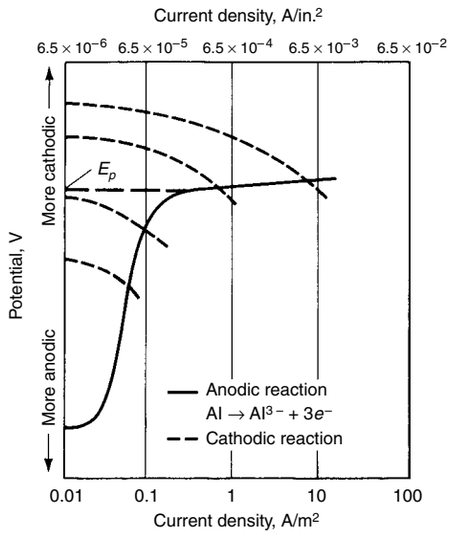

Fig. 3 Anodic-polarization curve for aluminum alloy 1100. Specimens were immersed in neutral deaerated NaCl solution free of cathodic reactant. Pitting develops only at potentials more cathodic than the pitting potential, E_p. The intersection of the anodic curve for aluminum (solid line) with a curve for the applicable cathodic reaction (one of the representative dashed lines) determines the potential to which the aluminum is polarized, either by cathodic reaction on the aluminum itself or on another metal electrically connected to it. The potential to which the aluminum is polarized by a specific cathode reaction determines corrosion current density and corrosion rate

Pitting potentials for selected aluminum alloys in several electrolytes are reported in Ref 8. Examples of application of pitting-potential analysis to particular corrosion problems are given in Ref 9 and 10.

Solution Potentials

Because of the electrochemical nature of most corrosion processes, relationships among solution potentials of different aluminum alloys, as well as between potentials of aluminum alloys and those of other metals, are of considerable importance. Furthermore, the solution-potential relationships among the microstructural constituents of a particular alloy significantly affect its corrosion behavior. Compositions of

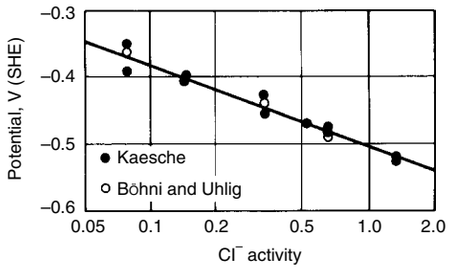

Fig. 4 Effect of chloride-ion activity on pitting potential of aluminum 1199 in NaCl solutions. SHE, standard hydrogen electrode. Source: Ref 5, 6

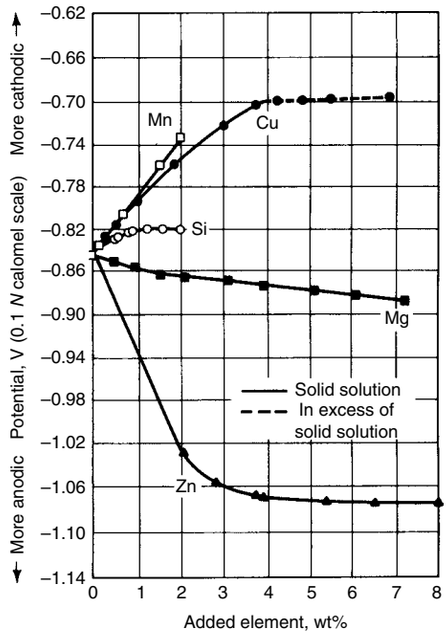

Fig. 5 Effects of principal alloying elements on the electrolytic-solution potential of aluminum. Potentials are for solution-treated and quenched high-purity binary alloys in a solution of 53 g/L NaCl plus 3 g/L H_2O_2 at 25 °C (75 °F)

solid solutions and additional phases, as well as amounts and spatial distributions of the additional phases, may affect both the type and extent of corrosion.

The solution potential is the electrode potential where half-cell reaction involves only the metal electrode and its ion. The solution potential of an aluminum alloy is primarily determined by the composition of the aluminum-rich solid solution, which constitutes the predominant volume fraction and area fraction of the alloy microstructure (Ref 11). Solution potential is not affected significantly by second-phase particles of microscopic size, but because these particles frequently have solution potentials differing from that of the solid-solution matrix in which they occur, localized galvanic cells may be formed between them and the matrix.

The effects of principal alloying elements on solution potential of high-purity aluminum are shown in Fig. 5. For each element, the significant changes that occur do so within the range in which the element is completely in solid solution. Further addition of the same element, which forms a second phase, causes little additional change in solution potential.

Most commercial aluminum alloys contain additions of more than one of these elements; effects of multiple elements in solid solution on solution potential are approximately additive. The amounts retained in solid solution, particularly for more highly alloyed compositions, depend highly on fabrication and thermal processing so that heat treatment and other processing variables influence the final electrode potential of the product. Tables 1 to 4, present representative solution potentials of commercial aluminum alloys and of several other metals and alloys.

The data in Tables 1 to 5, and those represented in Fig. 5, were collected using the method current at the time. The corrosion potential was measured in 53 g NaCl+3 g/L H_2O_2 with a 0.1 *N* calomel electrode. The method of measuring the corrosion potentials of aluminum alloys has been standardized in ASTM G 69 (Ref 12). A solution of 58.5±1 g of NaCl plus 9±1 mL of 30% H_2O_2 per liter of solution and a saturated calomel electrode are used. A 25 °C (77 °F) solution satisfies both methods. Appendix X1 of the G 69 standard suggests that to a good approximation, values measured under the earlier method may be converted to those measured by the G 69 practice by adding 0.092 V. The values in these tables are converted by this method, but because the earlier data were reported with a precision to 0.01 V, 0.09 V has been added. These values are approximate, but what is significant is the relative value of these potentials.

The amounts of second phases present in aluminum and aluminum alloy products vary from nearly zero in those of aluminum 1199 and some others that also are nearly pure solid solutions to over 20% in hypereutectic aluminum-silicon casting alloys, such as 392.0 and 393.0. These phases are generally intermetallic

compounds of binary, ternary, or higher-order compositions, although some elements in excess of their solid solubility are present as elemental phases. Electrode potentials of some of the simpler second-phase constituents have been measured and are presented in Table 5.

Table 1 Solution potentials of non-heat-treatable commercial wrought aluminum alloys

Values are the same for all tempers of each alloy.

Alloy	Potential(a), V
1060	−0.75
1100	−0.74
3003	−0.74
3004	−0.75
5050	−0.75
5052	−0.76
5154	−0.77
5454	−0.77
5056	−0.78
5456	−0.78
5182	−0.78
5083	−0.78
5086	−0.76
7072	−0.87

(a) With reference to a saturated calomel electrode, values calculated from data measured in 53 g/L (6 oz/gal) NaCl plus 3 g/L (0.3 oz/gal) H_2O_2 at 25 °C (77 °F), using a 0.1 *N* calomel electrode. Original data from Alcoa Laboratories.

Table 2 Solution potentials of heat treatable commercial wrought aluminum alloys

Alloy	Temper	Potential(a), V
2014	T4	−0.60(b)
	T6	−0.69
2219	T3	−0.55(b)
	T4	−0.55(b)
	T6	−0.71
	T8	−0.73
2024	T3	−0.60(b)
	T4	−0.60(b)
	T6	−0.72
	T8	−0.73
2036	T4	−0.63
2090	T8E41	−0.74
6009	T4	−0.71
6010	T4	−0.70
6151	T6	−0.74
6351	T5	−0.74
6061	T4	−0.71
	T6	−0.74
6063	T5	−0.74
	T6	−0.74
7005	T6	−0.85
7021	T6	−0.90
7029	T6	−0.76
7049	T73	−0.75(c)
	T76	−0.75(c)
7050	T73	−0.75(c)
	T76	−0.75(c)
7075	T6	−0.74(c)
	T73	−0.75(c)
	T76	−0.75(c)
7175 and 7475	T6	−0.74(c)
	T73	−0.75(c)
	T76	−0.75(c)
7178	T6	−0.74(c)

(a) With reference to a saturated calomel electrode, values calculated from data measured in 53 g/L (6 oz/gal) NaCl plus 3 g/L (0.3 oz/gal) H_2O_2 at 25 °C (77 °F), using a 0.1 *N* calomel electrode. Original data from Alcoa Laboratories. (b) Varies ±0.01 V with quenching rate. (c) Varies ±0.02 V with quenching rate

Solution-potential measurements are useful for the investigation of heat treating, quenching, and aging practices and are applied principally to alloys containing copper, magnesium, or zinc. In aluminum-copper and aluminum-copper-magnesium (2*xxx*) alloys, potential measurements can determine the effectiveness of solution heat treatment by measuring the amount of copper in solid solution. Also, by measuring the potentials of grain boundaries and grain bodies separately, the difference in potential responsible for intergranular corrosion, exfoliation, and stress-corrosion cracking (SCC) can be quantified. Solution-potential measurements of alloys containing copper also show the progress of artificial aging as increased amounts of precipitates are formed and the matrix is depleted of copper.

Potential measurements are valuable with zinc-containing (7*xxx*) alloys for evaluating the effectiveness of the solution heat treatment, for following the aging process, and for differentiating among the various artificially aged tempers. These factors can affect corrosion behavior. In the magnesium-containing (5*xxx*) alloys, potential measurements can detect low-temperature precipitation and are useful in qualitatively evaluating stress-corrosion behavior. Potential measurements can also be used to follow the diffusion of zinc or copper in alclad products, thus determining whether the sacrificial cladding can continue to protect the core alloy (Ref 13).

Table 3 Solution potentials of cast aluminum alloys

Alloy	Temper	Type of mold(a)	Potential(b), V
208.0	F	S	−0.68
238.0	F	P	−0.65
295.0	T4	S or P	−0.61
	T6	S or P	−0.62
	T62	S or P	−0.64
296.0	T4	S or P	−0.62
308.0	F	P	−0.66
319.0	F	S	−0.72
	F	P	−0.67
355.0	T4	S or P	−0.69
	T6	S or P	−0.70
356.0	T6	S or P	−0.73
443.0	F	S	−0.74
	F	P	−0.73
514.0	F	S	−0.78
520.0	T4	S or P	−0.80
710.0	F	S	−0.90

(a) S, sand; P. permanent (b) With reference to a saturated calomel electrode, values calculated from data measured in 53 g/L (6 oz/gal) NaCl plus 3 g/L (0.3 oz/gal) H_2O_2 at 25 °C (77 °F), using a 0.1 *N* calomel electrode. Original data from Alcoa Laboratories.

Table 4 Solution potentials of some nonaluminum base metals

Metal	Potential(a), V
Magnesium	−1.65
Zinc	−1.01
Cadmium	−0.73
Mild carbon steel	−0.49
Lead	−0.46
Tin	−0.40
Copper	−0.11
Bismuth	−0.09
Stainless steel(b)	−0.01
Silver	+0.01
Nickel	−0.02
Chromium	−0.31 to +0.21

(a) With reference to a saturated calomel electrode, values calculated from data measured in 53 g/L (6 oz/gal) NaCl plus 3 g/L (0.3 oz/gal) H_2O_2 at 25 °C (77 °F), using a 0.1 *N* calomel electrode. Original data from Alcoa Laboratories. (b) Series 300, type 430

Table 5 Solution potentials of some second-phase constituents in aluminum alloys

Phase	Potential(a), V
Si	−0.17
Al_3Ni	−0.43
Al_3Fe	−0.47
Al_2Cu	−0.64
Al_6Mn	−0.76
Al_8Mg_5	−1.15

(a) With reference to a saturated calomel electrode, values calculated from data measured in 53 g/L (6 oz/gal) NaCl plus 3 g/L (0.3 oz/gal) H_2O_2 at 25 °C (77 °F), using a 0.1 *N* calomel electrode. Original data from Alcoa Laboratories

Effects of Composition and Microstructure on Corrosion

1*xxx* Wrought Alloys. Wrought aluminum alloys of the 1*xxx* series conform to composition specifications that set maximum individual, combined, and total contents for several elements present as natural impurities in the smelter-grade or refined aluminum used to produce these products. Alloys 1100, 1120, and 1150 differ somewhat from the others in this series by having minimum and maximum specified copper contents. Corrosion resistance of all 1*xxx* compositions is very high, but under many conditions, it decreases slightly with increasing alloy content. Iron, silicon, and copper are the elements present in the largest percentages. The copper and part of the silicon are typically in solid solution. The second-phase particles present contain either iron or iron and silicon—Al_6Fe, Al_3Fe, and $Al_{12}Fe_3Si_2$ (Ref 14). The specific phase present or the relative amounts when more than one are present depend on the ratio of iron to silicon and on thermal history. The microstructural particles of these phases are cathodic to the aluminum solid solution, and exposed surfaces of these particles are covered by an oxide film thinner than that covering exposed areas of the solid solution (Ref 15). Corrosion may be initiated earlier and progress more rapidly in the aluminum solid solution immediately surrounding the particles. The number and/or size of such corrosion sites is proportional to the volume fraction of the second-phase particles.

Not all impurity elements are detrimental to corrosion resistance of 1*xxx*-series aluminum alloys, and detrimental elements may reduce the resistance of some types of alloys but have

Table 6 Relative ratings of resistance to general corrosion and to stress-corrosion cracking (SCC) of wrought aluminum alloys

Alloy	Temper	Resistance to corrosion	
		General(a)	SCC(b)
1060	All	A	A
1100	All	A	A
1350	All	A	A
2011	T3, T4, T451	D(c)	D
	T8	D	B
2014	O	...	...
	T3, T4, T451	D(c)	C
	T6, T651, T6510, T6511	D	C
2017	T4, T451	D(c)	C
2018	T61	...	...
2024	O	...	...
	T4, T3, T351, T3510, T3511, T361	D(c)	C
	T6, T861, T81, T851, T8510, T8511	D	B
	T72	...	...
2025	T6	D	C
2036	T4	C	...
2117	T4	C	A
2218	T61, T72	D	C
2219	O	...	...
	T31, T351, T3510, T3511, T37	D(c)	C
	T81, T851, T8510, T8511, T87	D	B
2618	T61	D	C
3003	All	A	A
3004	All	A	A
3105	All	A	A
4032	T6	C	B
5005	All	A	A
5050	All	A	A
5052	All	A	A
5056	O, H11, H12, H32, H14, H34	A(d)	B(d)
	H18, H38	A(d)	C(d)
	H192, H392	B(d)	D(d)
5083	All	A(d)	B(d)
5086	O, H32, H116	A(d)	A(d)
	H34, H36, H38, H111	A(d)	A(d)
5154	All	A(d)	A(d)
5182	All	A	A
5252	All	A	A
5254	All	A(d)	A(d)
5454	All	A	A
5456	All	A(d)	B(d)
5457	O	A	A
5652	All	A	A
5657	All	A	A
5754	All	A	A
6005	All	A	A
6009	All	A	A
6111	All	A	A
6022	All	A	A
6053	O	A	A
	T6, T61	...	...
6061	O	B	A
	T4, T451, T4510, T4511	B	B
	T6, T651, T652, T6510, T6511	B	A
6063	All	A	A
6066	O	C	A
	T4, T4510, T4511, T6, T6510, T6511	C	B
6070	T4, T4511, T6	B	B
6101	T6, T63, T61, T64	A	A
6151	T6, T652	...	...
6201	T81	A	A
6262	T6, T651, T6510, T6511, T9	B	A
6463	All	A	A
7001	O	C(c)	C
7005	T5	C	C
7075	T6, T651, T652, T6510, T6511	C(c)	C
	T73, T7351	C	B
7116	T5	C	C
7129	T5	C	C
7178	T6, T651, T6510, T6511	C(c)	C

(a) Ratings are relative and in decreasing order of merit, based on exposure to NaCl solution by intermittent spraying or immersion. Alloys with A and B ratings can be used in industrial and seacoast atmospheres without protection. Alloys with C, D, and E ratings generally should be protected, at least on faying surfaces. (b) SCC ratings are based on service experience and on laboratory tests of specimens exposed to alternate immersion in 3.5% NaCl solution. A, no known instance of failure in service or in laboratory tests; B, no known instance of failure in service; limited failures in laboratory tests of short-transverse specimens; C, service failures when sustained tension stress acts in short-transverse direction relative to grain structure; limited failures in laboratory tests of long-transverse specimens; D, limited service failures when sustained stress acts in longitudinal or long-transverse direction relative to grain structure. (c) In relatively thick sections, the rating would be E. (d) This rating may be different for material held at elevated temperatures for long periods.

no adverse effects in others. Therefore, specification limitations established for impurity elements are often based on maintaining consistent and predictable levels of corrosion resistance in various applications rather than on their effects in any specific application.

2*xxx* wrought alloys and 2*xx.x* casting alloys, in which copper is the major alloying element, are less resistant to corrosion than alloys of other series, which contain much lower amounts of copper. Alloys of this type were the first heat treatable high-strength aluminum-base materials and have been used for more than 75 years in structural applications, particularly in aircraft and aerospace applications (Ref 16). Much of the thin sheet made of these alloys is produced as an alclad composite, but thicker sheet and other products for many applications require no protective cladding.

Electrochemical effects on corrosion can be stronger in these alloys than in alloys of many other types because of two factors: greater

Table 7a Relative ratings of resistance to general corrosion and to stress-corrosion cracking (SCC) of aluminum sand casting alloys

Alloy	Temper	Resistance to corrosion	
		General(a)	SCC(b)
Sand castings			
208.0	F	B	B
224.0	T7	C	B
240.0	F	D	C
242.0	All	D	C
A242.0	T75	D	C
249.0	T7	C	B
295.0	All	C	C
319.0	F, T5	C	B
	T6	C	C
355.0	All	C	A
C355.0	T6	C	A
356.0	T6, T7, T71, T51	B	A
A356.0	T6	B	A
443.0	F	B	A
512.0	F	A	A
513.0	F	A	A
514.0	F	A	A
520.0	T4	A	C
535.0	F	A	A
B535.0	F	A	A
705.0	T5	B	B
707.0	T5	B	C
710.0	T5	B	B
712.0	T5	B	C
713.0	T5	B	B
771.0	T6	C	C
850.0	T5	C	B
851.0	T5	C	B
852.0	T5	C	B

(a) Relative ratings of general corrosion resistance are in decreasing order of merit, based on exposures to NaCl solution by intermittent spray or immersion. (b) Relative ratings of resistance to SCC are based on service experience and on laboratory tests of specimens exposed lo alternate immersion in 3.5% NaCl solution. A, no known instance of failure in service when properly manufactured; B, failure not anticipated in service from residual stresses or from design and assembly stresses below approximately 45% of the minimum guaranteed yield strength given in applicable specifications; C, failures have occurred in service with either this specific alloy/temper combination or with alloy/temper combinations of this type; designers should be aware of the potential SCC problem that exists when these alloys and tempers are used under adverse conditions.

change in electrode potential with variations in amount of copper in solid solution (Fig. 5) and, under some conditions, the presence of non-uniformities in solid-solution concentration. Note the test method described in the caption. However, that general resistance to corrosion decreases with increasing copper content is not primarily attributable to these solid-solution or second-phase solution-potential relationships, but to galvanic cells created by formation of minute copper particles or films deposited on the alloy surface as a result of corrosion. As corrosion progresses, copper ions, which initially go into solution, replate onto the alloy to form metallic copper cathodes. The reduction of copper ions and the increased efficiency of O_2 and H^+ reduction reactions in the presence of copper increase the corrosion rate.

These alloys are invariably solution heat treated and are used in either the naturally aged or the precipitation heat treated temper. Development of these tempers using good heat treating practice can minimize electrochemical effects on corrosion resistance. The rate of quenching and the temperature and time of artificial aging can both affect the corrosion resistance of the final product.

2*xxx* Wrought Alloys Containing Lithium. Lithium additions decrease the density and increase the elastic modulus of aluminum alloys, making aluminum-lithium alloys good candidates for replacing the existing high-strength alloys, primarily in aerospace applications.

One of the first commercial aluminum alloys containing lithium was 2020. This alloy in the T6 temper was introduced in 1957 as a structural alloy with good strength properties up to 175 °C (350 °F). It has a modulus 8% higher and a density 3% lower than alloy 7075-T6 but was rarely used in aircraft because of its relatively low fracture toughness. It was used in the thrust structure of the Saturn S-II, the second stage of the Saturn V launch vehicle (Ref 17). Alloy 2020 is no longer commercially available.

Two other lithium-bearing alloys are 2090 and 8090. Alloy 2090, in T8-type tempers, has a higher resistance to exfoliation than that of 7075-T6, and the resistance to SCC is comparable (Ref 18). Alloy 8090 was designed by various producers to meet other combinations of mechanical-property goals (Ref 19).

Although lithium is highly reactive, addition of up to 3% Li to aluminum shifts the pitting potential of the solid solution only slightly in the anodic direction in 3.5% NaCl solution (Ref 20). In an extensive corrosion investigation of several binary and ternary aluminum-lithium alloys, modifications to the microstructure that promote formation of the δ phase (AlLi) were found to reduce the corrosion resistance of the alloy in 3.5% NaCl solution (Ref 21). It was concluded that an understanding of the nucleation and growth of the δ phase is central to an understanding of the corrosion behavior of these alloys.

3*xxx* Wrought Alloys. Wrought alloys of the 3*xxx* series (aluminum-manganese and aluminum-manganese-magnesium) have very high resistance to corrosion. The manganese is present in the aluminum solid solution, in submicroscopic particles of precipitate, and in larger particles of $Al_6(Mn,Fe)$ or $Al_{12}(Mn,Fe)_3Si$ phases, both of which have solution potentials almost the same as that of the solid-solution matrix (Ref 22). Such alloys are widely used for cooking and food-processing equipment, chemical equipment, and various architectural products requiring high resistance to corrosion.

4*xxx* Wrought Alloys and 3*xx.x* and 4*xx.x* Casting Alloys. Elemental silicon is present as second-phase constituent particles in wrought alloys of the 4*xxx* series, in brazing and welding alloys, and in casting alloys of the 3*xx.x* and 4*xx.x* series. Silicon is cathodic to the aluminum solid-solution matrix by several hundred millivolts and accounts for a considerable volume fraction of most of the silicon-containing alloys. However, the effects of silicon on the corrosion resistance of these alloys are minimal because of low corrosion current density resulting from the fact that the silicon particles are highly polarized.

Corrosion resistance of 3*xx.x* casting alloys is strongly affected by copper content, which can be as high as 5% in some compositions, and by impurity levels. Modifications of certain basic alloys have more restrictive limits on impurities, which benefit corrosion resistance and mechanical properties.

5*xxx* Wrought Alloys and 5*xx.x* Casting Alloys. Wrought alloys of the 5*xxx* series (Al-Mg-Mn, Al-Mg-Cr, and Al-Mg-Mn-Cr) and casting alloys of the 5*xx.x* series (aluminum-magnesium) have high resistance to corrosion, and this accounts in part for their use in a wide variety of building products and chemical-processing and food-handling equipment, as well as marine applications involving exposure to seawater (Ref 23).

Alloys in which magnesium is present in amounts that remain in solid solution, or is partially precipitated as Al_8Mg_5 particles dispersed uniformly throughout the matrix, are generally as resistant to corrosion as commercially pure aluminum and are more resistant to saltwater and some alkaline solutions, such as those of sodium carbonate and amines. Wrought alloys containing approximately 3% or more magnesium under conditions that lead to an almost continuous intergranular Al_8Mg_5 precipitate, with very little precipitate within the grains, may be susceptible to exfoliation or SCC (Ref 24). Tempers have been developed for these higher-magnesium wrought alloys to produce microstructures having extensive Al_8Mg_5 precipitate within the grains, thus eliminating such susceptibility.

In the 5*xxx* alloys that contain chromium, this element is present as a submicroscopic precipitate, $Al_{12}Mg_2Cr$. Manganese in these alloys

Table 7b Relative ratings of resistance to general corrosion and to stress-corrosion cracking (SCC) of aluminum permanent mold, die casting, and rotor metal alloys

		Resistance to corrosion	
Alloy	Temper	General(a)	SCC(b)
Permanent mold casting			
242.0	T571, T61	D	C
308.0	F	C	B
319.0	F	C	B
	T6	C	C
332.0	T5	C	B
336.0	T551, T65	C	B
354.0	T61, T62	C	A
355.0	All	C	A
C355.0	T61	C	A
356.0	All	B	A
A356.0	T61	B	A
F356.0	All	B	A
A357.0	T61	B	A
358.0	T6	B	A
359.0	All	B	A
B443.0	F	B	A
A444.0	T4	B	A
513.0	F	A	A
705.0	T5	B	B
707.0	T5	B	C
711.0	T5	B	A
713.0	T5	B	B
850.0	T5	C	B
851.0	T5	C	B
852.0	T5	C	B
Die castings			
360.0	F	C	A
A360.0	F	C	A
364.0	F	C	A
380.0	F	E	A
A380.0	F	E	A
383.0	F	E	A
384.0	F	E	A
390.0	F	E	A
392.0	F	E	A
413.0	F	C	A
A413.0	F	C	A
C443.0	F	B	A
518.0	F	A	A
Rotor metal(c)			
100.1	...	A	A
150.1	...	A	A
170.1	...	A	A

(a) Relative ratings of general corrosion resistance are in decreasing order of merit, based on exposures to NaCl solution by intermittent spray or immersion. (b) Relative ratings of resistance to SCC are based on service experience and on laboratory tests of specimens exposed to alternate immersion in 3.5% NaCl solution. A, no known instance of failure in service when properly manufactured; B, failure not anticipated in service from residual stresses or from design and assembly stresses below approximately 45% of the minimum guaranteed yield strength given in applicable specifications; C, failures have occurred in service with either this specific alloy/temper combination or with alloy/temper combinations of this type; designers should be aware of the potential SCC problem that exists when these alloys and tempers are used under adverse conditions. (c) For electric motor rotors

Table 8 Combinations of aluminum alloys used in some alclad products

Core alloy	Cladding alloy
2014	6003 or 6053
2024	1230
2219	7072
3003	7072
3004	7072 or 7013
6061	7072
7075	7072, 7008, or 7011
7178	7072

is in the form of $Al_6(Mn,Fe)$, both submicroscopic and larger particles. Such precipitates and particles do not adversely affect corrosion resistance of these alloys.

6*xxx* Wrought Alloys. Moderately high strength and very good resistance to corrosion make the heat treatable wrought alloys of the 6*xxx* series (Al-Mg-Si) highly suitable in various structural, building, marine, machinery, and process-equipment applications. The Mg_2Si phase, which is the basis for precipitation hardening, is unique in that it is an ionic compound and is not only anodic to aluminum but also reactive in acidic solutions. However, either in solid solution or as submicroscopic precipitate, Mg_2Si has a negligible effect on electrode potential. Because these alloys are normally used in the heat treated condition, no detrimental effects result from the major alloying elements or from the supplementary boron, chromium, manganese, titanium, or zirconium, which are added in some cases to control grain structure. Copper additions, which augment strength in many of these alloys, are limited to small amounts to minimize effects on corrosion resistance. In general, the level of resistance decreases somewhat with increasing copper content.

When the magnesium and silicon contents in a 6*xxx* alloy are balanced (in proportion to form only Mg_2Si), corrosion by intergranular penetration is slight in most commercial environments (Ref 25). If the alloy contains silicon beyond that needed to form Mg_2Si or contains a high level of cathodic impurities, susceptibility to intergranular corrosion increases (Ref 26).

7*xxx* wrought alloys and 7*xx.x* casting alloys contain major additions of zinc, along with magnesium or magnesium plus copper in combinations that develop various levels of strength. Those containing copper have the highest strengths and have been used as constructional materials, primarily in aircraft applications, for more than 40 years. The copper-free alloys of the series have many desirable characteristics: moderate-to-high strength; excellent toughness; and good workability, formability, and weldability. Use of these copper-free alloys has increased in recent years and now includes automotive applications (such as bumpers), structural members and armor plate for military vehicles, and components of other transportation equipment.

The 7*xxx* wrought and 7*xx.x* casting alloys, because of their zinc contents, are anodic to 1*xxx* wrought aluminums and to other aluminum alloys. They are among the aluminum alloys most susceptible to SCC. However, SCC can be avoided by proper alloy and temper selection and by observing appropriate design, assembly, and application precautions (Ref 27). Stress-corrosion cracking of aluminum alloys

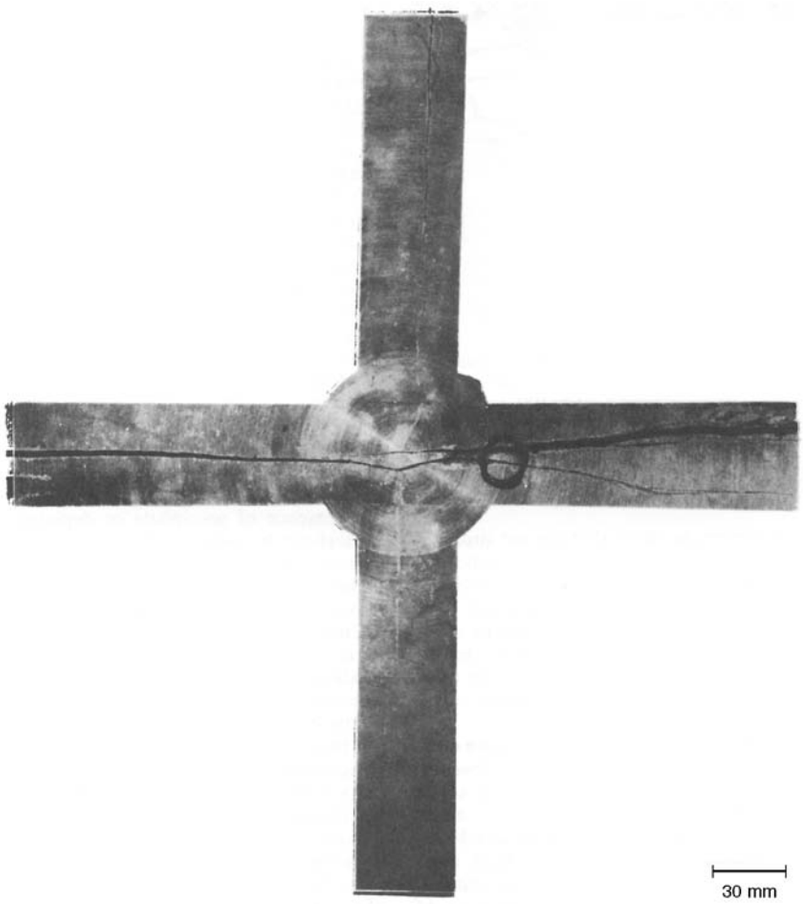

Fig. 6 Section through cruciform weldment of alloy 5083-H131 plate cracked by mercury. Attack was initiated by applying a few drops of mercury chloride ($HgCl_2$) solution and zinc amalgam to the sectioned surface at the circled area (right of center). Original magnification is 0.33×

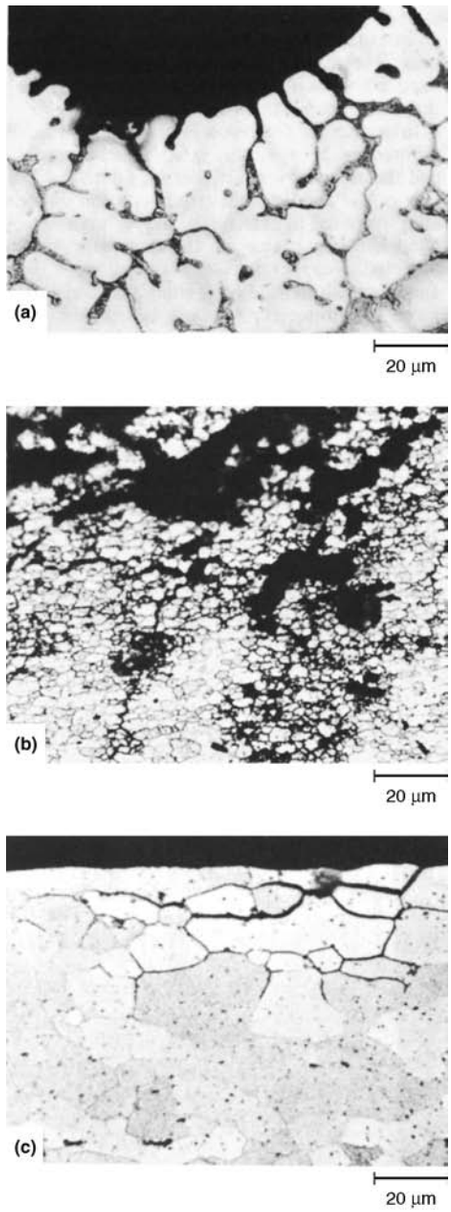

Fig. 7 Various types of intergranular corrosion. (a) Interdendritic corrosion in a cast structure. (b) Interfragmentary corrosion in a wrought, unrecrystallized structure. (c) Intergranular corrosion in a recrystallized wrought structure. All etched with Keller's reagent. Original magnification is 500×

is discussed in greater detail in a subsequent section in this article.

Resistance to general corrosion of the copper-free wrought 7*xxx* alloys is good, approaching that of the wrought 3*xxx,* 5*xxx,* and 6*xxx* alloys (Ref 28). The copper-containing alloys of the 7*xxx* series, such as 7049, 7050, 7075, and 7178, have lower resistance to general corrosion than those of the same series that do not contain copper. All 7*xxx* alloys are more resistant to general corrosion than 2*xxx* alloys but less resistant than wrought alloys of other groups.

Although the copper in both wrought and cast alloys of the Al-Zn-Mg-Cu type reduces resistance to general corrosion, it is beneficial from the standpoint of resistance to SCC. Copper allows these alloys to be precipitated at higher temperatures without excessive loss in strength and thus makes possible the development of T73 tempers, which couple high strength with excellent resistance to SCC (Ref 29).

Composites. Aluminum alloys reinforced with silicon carbide (Ref 30), graphite (Ref 31), beryllium, or boron (Ref 32) show promise as metal-matrix composites for lightweight structural applications with increased modulus and strength and are potentially well suited to aerospace and military needs. The corrosion behavior of composites is governed by galvanic action between the aluminum matrix and the reinforcing material. When both are exposed to an aggressive environment, corrosion of the aluminum is accelerated. Silicon carbide, graphite, and boron are cathodic to aluminum and do not polarize easily. The electrical potential of beryllium is very close to aluminum in seawater. See the article "Corrosion of Beryllium and Aluminum-Beryllium Composites" in this Volume for more information about the aluminum-beryllium composites.

For a useful service life, the silicon carbide, graphite, and boron composites need some form of corrosion protection. Aluminum thermal spraying has been reported as a successful protection method for discontinuous silicon carbide/aluminum composites; for continuous graphite/aluminum or silicon carbide/aluminum, sulfuric acid (H_2SO_4) anodizing has provided protection, as have organic coatings or ion vapor deposited aluminum (Ref 33).

Effects of Additional Alloying Elements. In addition to the major elements that define the various alloy systems discussed previously, commercial aluminum alloys may contain other elements that provide special characteristics. Lead and bismuth are added to alloys 2011 and 6262 to improve chip breakage and other machining characteristics. Nickel is added to wrought alloys 2018, 2218, and 2618, which were developed for elevated-temperature service, and to certain 3*xx.x* cast alloys used for pistons, cylinder blocks, and other engine parts subjected to high temperatures. Cast aluminum bearing alloys of the 850.0 group contain tin. In all cases, these alloying additions introduce constituent phases that are cathodic to the matrix and decrease resistance to corrosion in aqueous saline media. However, these alloys are often used in environments in which they are not subject to corrosion.

Corrosion Ratings of Alloys and Tempers

Simplified ratings of resistance to general corrosion and to SCC for wrought and cast aluminum alloys are presented in Tables 6 and 7(a) and (b). These ratings may be useful in evaluating and comparing alloy/temper combinations for corrosion service (more detailed ratings of resistance to SCC for high-strength wrought aluminum alloys are given in Table 9 and in Ref 34).

Galvanic Corrosion and Protection

The calculated potential values versus the saturated calomel electrode (SCE) in Tables 1 to 4 form a galvanic series for aluminum alloys and other metals. The galvanic relationships indicated by these values have wide applicability because of the similarity of the electrochemical behavior of these metals in the NaCl solution to that in marine and other saline environments. This galvanic series, however, is not necessarily valid in nonsaline solutions. For example, aluminum is anodic to zinc in an aqueous 1 *M* sodium chromate (Na_2CrO_4) solution and cathodic to iron in an aqueous 1 *M* sodium sulfate (Na_2SO_4) solution.

Under most environmental conditions frequently encountered in service, aluminum and its alloys are the anodes in galvanic cells with most other metals, protecting them by corroding sacrificially. Only magnesium and zinc are more anodic. Sacrificial corrosion of aluminum or cadmium is slight when these two metals are coupled in a galvanic cell, because of the small difference in electrode potential between them.

Contact of aluminum with more cathodic metals should be avoided in any environment in which aluminum by itself is subject to pitting corrosion. Where such contact is necessary,

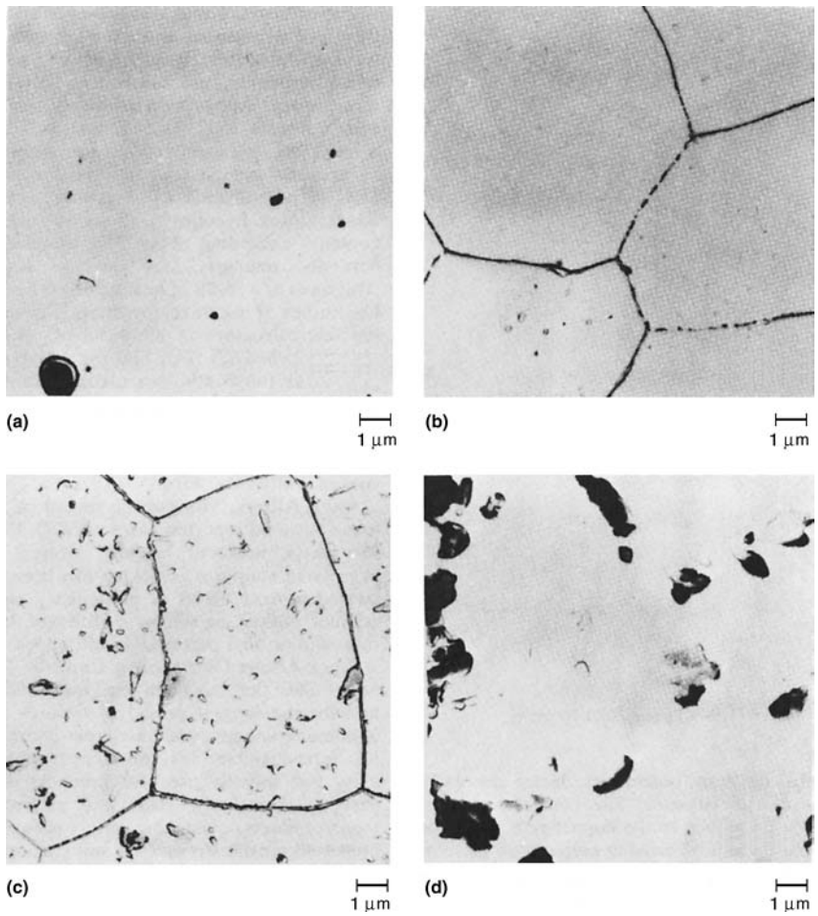

Fig. 8 Microstructures of alloy 5356-H12 after treatment to produce varying degrees of susceptibility to stress-corrosion cracking. (a) Cold rolled 20%; highly resistant. (b) Cold rolled 20%, then heated 1 year at 100 °C (212 °F); highly susceptible. (c) Cold rolled 20%, then heated 1 year at 150 °C (300 °F); slightly susceptible. (d) Cold rolled 20%, then heated 1 year at 205 °C (400 °F); highly resistant

protective measures should be implemented to minimize sacrificial corrosion of the aluminum. In such an environment, aluminum is already polarized to its pitting potential, and the additional potential imposed by contact with the more cathodic metal greatly increases the corrosion current. In many environments, aluminum can be used in contact with chromium or stainless steels with only slight acceleration of corrosion; chromium and stainless steels are easily polarized cathodically in mild environments, so that the corrosion current is small despite the large differences in the open-circuit potentials between these metals and aluminum.

To minimize corrosion of aluminum wherever contact with more cathodic metals cannot be avoided, the ratio of the exposed surface area of the aluminum to that of the more cathodic metal should be as high as possible to minimize the current density at the aluminum and therefore the rate of corrosion. The area ratio may be increased by painting the cathodic metal or both metals, but painting only the aluminum is not effective and may even accelerate corrosion. Corrosion of aluminum in contact with more cathodic metals is much less severe in solutions of most nonhalide salts, in which aluminum alone normally is not polarized to its pitting potential, than in solutions of halide salts, in which it is. As shown in Fig. 3, increases in potential, as long as the value does not reach the pitting potential, have small effects on current density.

Galvanic current between aluminum and another metal also can be reduced by removing oxidizing agents from the electrolyte. Thus, the corrosion rate of aluminum coupled to copper in seawater is greatly reduced wherever the seawater is deaerated. In closed multimetallic systems, the corrosion rate of aluminum, although initially high, decreases to a low value whenever the cathodic reactant is depleted. Galvanic current is also low in solutions having high electrical resistivity, such as high-purity water, but some semiconductors, such as graphite and magnetite, are cathodic to aluminum, and when in contact with them, aluminum corrodes sacrificially.

In alclad products, the difference in solution potential between the core alloy and the cladding alloy provides cathodic protection to the core (Ref 35). These products, primarily sheet and tube, consist of a core clad on one or both surfaces with a metallurgically bonded layer of an alloy that is anodic to the core alloy. The thickness of the cladding layer is usually less than 10% of the overall thickness of the product.

Cladding alloys are generally of the non-heat-treatable type, although heat treatable alloys are sometimes used for higher strength. For mechanical-design calculations, such sacrificial claddings are treated as corrosion allowances and are not normally included in the determination of the strength of an alclad product.

Composition relationships of core and cladding alloys are generally designed so that the cladding is 80 to 100 mV anodic to the core. Table 8 lists several core alloy/cladding alloy combinations for common alclad products. Because of the cathodic protection provided by the cladding, corrosion progresses only to the core/cladding interface, then spreads laterally. This is highly effective in eliminating perforation of thin-wall products.

Surface Treatments. A process that produces an effect similar to that of conventional sacrificial cladding is called diffusion cladding. Aluminum products can be clad using this process, regardless of their shape (Ref 36). The process involves two steps: first, a thin film of zinc is deposited on the aluminum surface by chemical displacement from an alkaline zincate solution, then the zinc is diffused into the aluminum to produce a zone of zinc-enriched alloy that is anodic to the underlying aluminum. It was found that 3003 aluminum with a correctly balanced zinc diffusion treatment exhibited uniform corrosion and that the depth of corrosion was restricted to approximately one-half the thickness of the diffusion zone (Ref 37). These results suggest that a zinc diffusion treatment may be as effective as conventional alcladding for the prevention of localized pitting.

Another way to simulate alcladding is to apply a coating of an anodic alloy to an aluminum surface by thermal spray techniques, such as flame or plasma spray. These coatings act in the same way as the cladding layer on an alclad product and corrode sacrificially to protect the core alloy (Ref 38, 39).

Cathodic Protection. In some applications, aluminum alloy parts, assemblies, structures, and

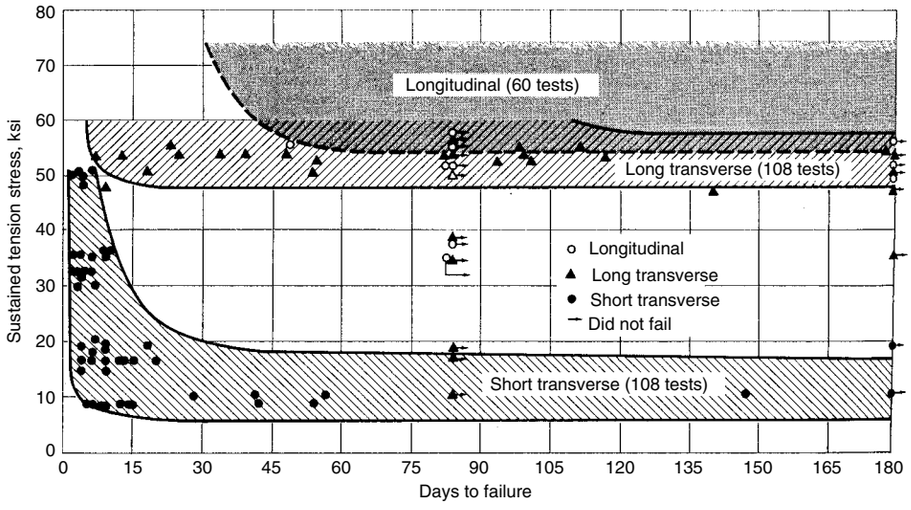

Fig. 9 The relative resistance to stress-corrosion cracking of 7075-T6 plate is influenced by direction of stressing. Samples are alternately immersed in 3.5% NaCl. Plate thickness, 6.4 to 76 mm (0.25 to 3 in.). Source: Ref 63

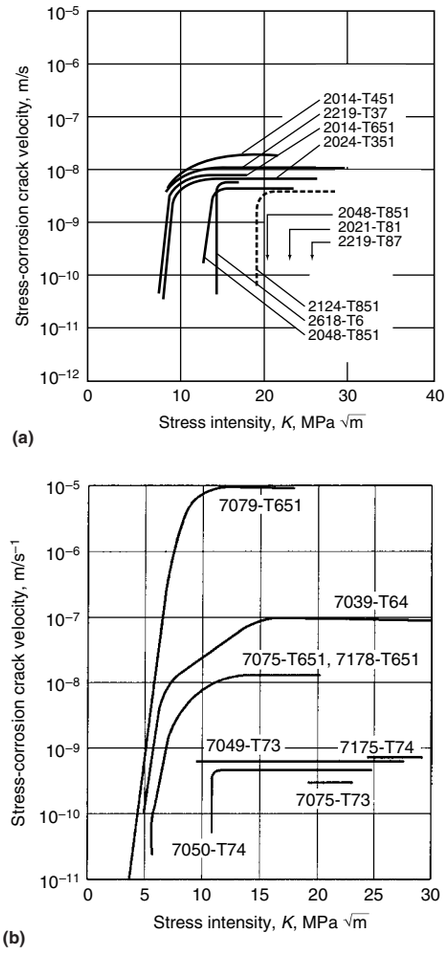

Fig. 10 (a) Crack propagation rates in stress-corrosion tests using precracked thick, double-cantilever beam specimens of high-strength 2*xxx*-series aluminum alloy plate, TL (SL) orientation. Specimens were wet twice a day with an aqueous solution of 3.5% NaCl, 23 °C (73 °F). (b) Crack propagation rates in stress-corrosion tests using precracked specimens of 7*xxx*-series aluminum alloys; 25 mm (1 in.) thick, double-cantilever beam, short-transverse orientation of die forging, long-transverse orientation of hand forgings and plate. Specimens were subject to alternate immersion tests, 3.5% NaCl solution, 23 °C (73 °F). Source: Ref 66

pipelines are cathodically protected by anodes either made of more anodic metals or made anodic by using impressed potentials. In either case, because the usual cathodic reaction produces hydroxyl ions, the current on these alloys should not be high enough to make the solution sufficiently alkaline to cause significant corrosion (Ref 40).

The criterion for cathodic protection of aluminum in soils and waters has been published by NACE International (Ref 41). The suggested practice is to shift the potential at least −0.15 V but not beyond the value of −1.20 V, as measured against a saturated copper sulfate ($Cu/CuSO_4$) reference electrode. In some soils, potentials as low as −1.4 V have been encountered without appreciable cathodic corrosion (Ref 42). Essentially the same criterion is followed in Eastern Europe (Ref 43).

Several examples of cathodic protection of aluminum equipment in chemical plants, as well as a preference for sacrificial anodes of zinc or aluminum-zinc alloy, are discussed in Ref 44. Such protection is most successful in electrolytes in the pH range of 4 to 8.5—the so-called neutral range. The cathodic protection of aluminum structures is reviewed in Ref 45, which supports general experience that cathodic protection is effective in preventing or greatly reducing several types of corrosion attack.

Buried aluminum pipelines are usually protected by sacrificial anodes—zinc for coated lines and magnesium for uncoated lines. It is generally accepted that coatings such as extruded polyethylene or a tape wrap should be applied to aluminum pipes for underground service. Because of the effectiveness and longevity of sacrificial anode systems and the need to avoid overprotection, impressed current (rectifier) systems generally are not used to protect aluminum pipelines.

The cathodic protection of aluminum alloys in seawater has been extensively studied (Ref 46,

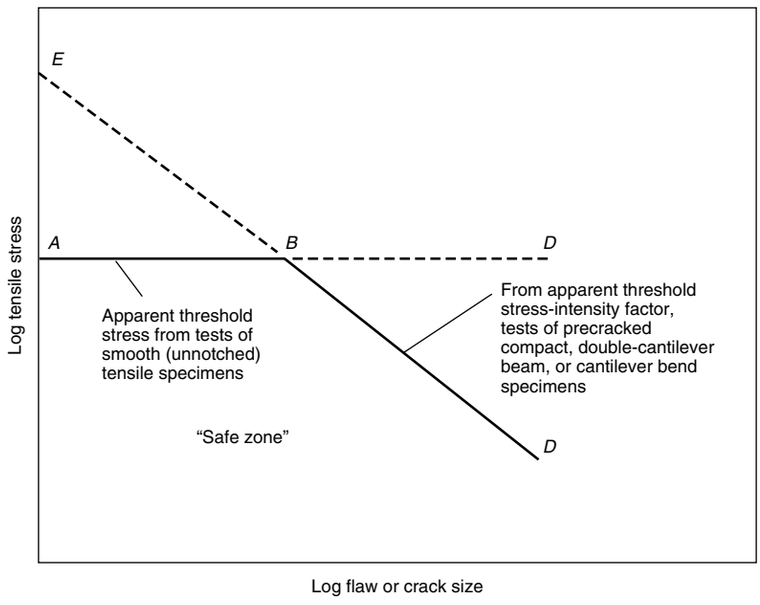

Fig. 11 Stress-corrosion safe-zone plot. Apparent threshold stress is maximum stress at which tensile specimens do not fail by stress-corrosion cracking when stressed in environment of interest. Apparent threshold stress-intensity factor is maximum stress intensity at which no significant stress-corrosion crack growth takes place in precracked fracture specimens, environment of interest

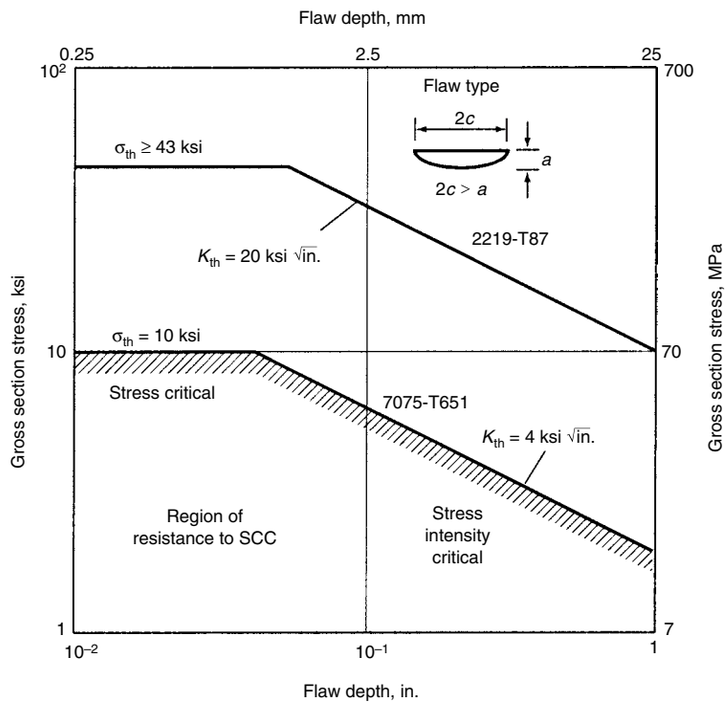

Fig. 12 Composite stress/stress intensity for stress-corrosion cracking (SCC) threshold safe-zone plot for two aluminum alloys exposed in a salt-dichromate-acetate solution. σ_{th} is threshold of applied tensile stress for SCC in smooth specimens. K_{th} is threshold of applied stress intensity for SCC in notched or precracked specimens

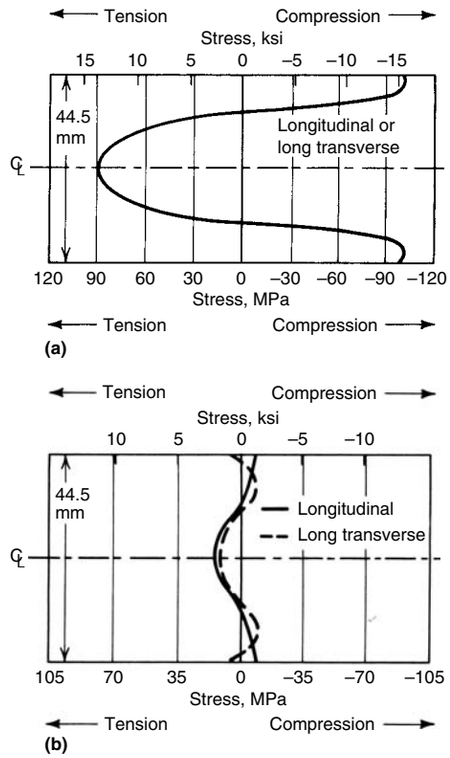

Fig. 13 Comparison of residual stresses in a thick, constant cross-section 7075-T6 aluminum alloy plate before and after stress relief. (a) High residual stresses in the solution-treated and quenched alloy. (b) Reduction in stresses after stretching 2%. Source: Ref 68

47). Sacrificial anodes were found to be effective in reducing surface pitting and crevice corrosion without causing cathodic attack.

Deposition Corrosion

In designing aluminum and aluminum alloys for satisfactory corrosion resistance, it is important to keep in mind that ions of several metals have reduction potentials that are more cathodic than the solution potential of aluminum and therefore can be reduced to metallic form by aluminum. For each chemical equivalent of so-called heavy-metal ions reduced, a chemical equivalent of aluminum is oxidized. Reduction of only a small amount of these ions can lead to severe localized corrosion of aluminum, because the metal reduced from them plates onto the aluminum and sets up galvanic cells. The more important heavy metals are copper, lead, mercury, nickel, and tin. The effects of these metals on aluminum are of greatest concern in acidic solutions; in alkaline solutions, they have much lower solubilities and therefore much less severe effects.

Copper is the heavy metal most commonly encountered in applications of aluminum. A copper-ion concentration of 0.02 to 0.05 ppm in neutral or acidic solutions is generally considered to be the threshold value for initiation of pitting on aluminum. A specific value for the copper-ion threshold is normally not proposed, because the pitting tendency also depends on the aluminum alloy; the pH of the water; concentrations of other ions in the water, particularly bicarbonate HCO_3^-, chloride (Cl^-), and calcium (Ca^{2+}); and on whether the pits that develop are open or occluded (Ref 48). Copper contamination of solutions in contact with aluminum should be minimized or avoided. As discussed previously, the relatively low corrosion resistance of aluminum-copper alloys results from reduction of copper ions present in the corrosion product of the alloy.

Ferric (Fe^{3+}) ion can be reduced by aluminum but does not form a metallic deposit. This ion is rarely encountered in service because it reacts preferentially with oxygen and water to form insoluble oxides and hydroxides, except in acidic solutions outside the passive range of aluminum. On the other hand, at room temperature, the most anodic aluminum alloys (those with a corrosion potential approaching −1.0 V versus the SCE) can reduce ferrous (Fe^{2+}) ions to metallic iron and produce a metallic deposit on the surface of the aluminum. The presence of (Fe^{2+}) ion also tends to be rare in service; it exists only in deaerated solutions or in other solutions free of oxidizing agents (Ref 49).

Mercury amalgamates with aluminum with difficulty, because the natural oxide film on aluminum prevents metal-to-metal contact. However, after the two metals have been brought together, if the oxide film is broken by mechanical or chemical action, amalgamation occurs immediately, and in the presence of moisture, corrosion of the aluminum proceeds rapidly (Ref 50). Aluminum in contact with a solution of a mercury salt forms metallic mercury, which then readily amalgamates the aluminum. Of all the heavy metals, mercury can cause the most corrosion damage to aluminum (Ref 51). The effect can be severe when stress is present. For example, attack by mercury and zinc amalgam combined with residual stresses from welding caused cracking of the weldment (Fig. 6). The corrosive action of mercury can be serious with or without stress, because amalgamation, once initiated, continues to propagate unless the mercury can be removed. If an aluminum surface has become contaminated with mercury, the mercury can be removed by treatment with 70% nitric acid (HNO_3) or by evaporation in steam or hot air (Ref 52). It is difficult to determine the safe level of mercury that can be tolerated on aluminum. In solutions, concentrations exceeding a few parts per billion should be viewed with suspicion; in atmospheres, any amount exceeding that allowed by Environmental Protection Agency (EPA) regulations is suspect.

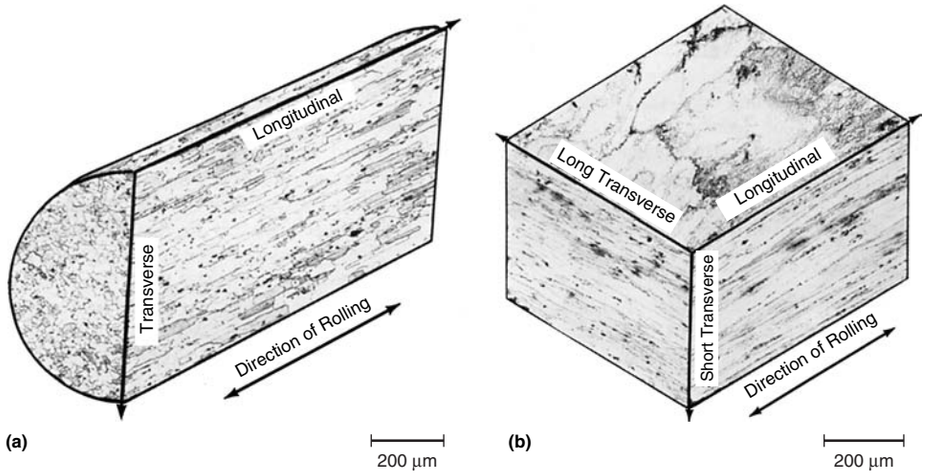

Fig. 14 Composite micrograph showing grain structure of alloy 7075-T6. (a) Rolled rod, 25.4 mm (1 in.) diam. Original 50×. (b) Plate, 38 mm (1.5 in.) thick. Original 55×. Both Keller's etch. Source: Ref 63

Intergranular Corrosion

Intergranular (intercrystalline) corrosion is selective attack of grain boundaries or closely adjacent regions without appreciable attack of the grains themselves. Intergranular corrosion is a generic term that includes several variations associated with different metallic structures and thermomechanical treatments (Fig. 7).

Intergranular corrosion is caused by potential differences between the grain-boundary region and the adjacent grain bodies (Ref 53). The location of the anodic path varies with the different alloy systems. In 2*xxx*-series alloys, it is a narrow band on either side of the boundary that is depleted in copper; in 5*xxx*-series alloys, it is the anodic constituent Mg_2Al_3 when that constituent forms a continuous path along a grain boundary; in copper-free 7*xxx*-series alloys, it is generally considered to be the anodic zinc- and magnesium-bearing constituents on the grain boundary; and in the copper-bearing 7*xxx*-series alloys, it appears to be the copper-depleted bands along the grain boundaries (Ref 54, 55). The 6*xxx*-series alloys generally resist this type of corrosion, although slight intergranular attack has been observed in aggressive environments. The electrochemical mechanism for intergranular corrosion proposed by E.H. Dix has been verified (Ref 56) and related to the pitting potentials of aluminum (Ref 57).

Because intergranular corrosion is involved in SCC of aluminum alloys, it is often presumed to be more deleterious than pitting or general corrosion. However, in alloys that are not susceptible to SCC—for example, the 6*xxx*-series alloys—intergranular corrosion is usually no more severe than pitting corrosion, tends to decrease with time, and, for equal depth of corrosion, its effect on strength is no greater than that of pitting corrosion, although fatigue cracks may be more likely to initiate at areas of intergranular corrosion than at random pits.

Evaluation of intergranular attack is more complex than evaluation of pitting. Visual observations are generally not reliable. For 5*xxx*-series alloys, a weight loss method has been accepted by ASTM International (Ref 58). Electrochemical techniques provide some evidence of the susceptibility of a particular alloy or microstructure to intergranular corrosion, but such techniques should be accompanied by a metallographic examination of carefully prepared sections.

Stress-Corrosion Cracking

Only aluminum alloys that contain appreciable amounts of soluble alloying elements, primarily copper, magnesium, silicon, and zinc, are susceptible to SCC. For most commercial alloys, tempers have been developed that provide a high degree of immunity to SCC in most environments.

The electrochemical theory of stress corrosion, which was developed in approximately 1940, describes certain conditions required for SCC of aluminum alloys (Ref 53, 59, 60). Generally, the combination of a corrosive environment such as saltwater with surface tensile stress in a susceptible alloy and microstructure is required. Further research showed inadequacies in this theory, and the complex interactions among factors that lead to SCC of aluminum alloys are not yet fully understood (Ref 61). However, there is general agreement that for aluminum the electrochemical factor predominates, and the electrochemical theory continues to be the basis for developing aluminum alloys and tempers resistant to SCC (Ref 62).

Stress-corrosion cracking in aluminum alloys is characteristically intergranular. According to the electrochemical theory, this requires a condition along grain boundaries that makes them anodic to the rest of the microstructure so that corrosion propagates selectively along them. Such a condition is produced by localized decomposition of solid solution, with a high degree of continuity of decomposition products, along the grain boundaries. The most anodic regions may be either the boundaries themselves (most commonly, the precipitate formed in them) or regions adjoining the boundaries that have been depleted of solute.

In 2*xxx* alloys, the solute-depleted regions are the most anodic; in 5*xxx* alloys, it is the Mg_2Al_3 precipitate along the boundaries. The most anodic grain-boundary regions in other alloys have not been identified with certainty. Strong evidence for the presence of anodic regions, and of the electrochemical nature of their corrosion in aqueous solutions, is provided by the fact that SCC can be greatly retarded, if not eliminated, by cathodic protection (Ref 60).

Figure 8 shows four different microstructures in an alloy containing 5% Mg. These microstructures represent degrees of susceptibility to SCC, ranging from high susceptibility to high resistance, depending on heat treatment. The treatments that provide high resistance to cracking are those that produce microstructures either free of precipitate along grain boundaries (Fig. 8a) or with precipitate distributed as uniformly as possible within grains (Fig. 8d).

Table 9 Relative stress-corrosion cracking ratings for wrought products of high-strength aluminum alloys

Resistance ratings are as follows: A, very high; B, high; C, intermediate; D, low. See text for more detailed explanation of these ratings

Alloy and temper(a)	Test direction(b)	Rolled plate	Rod and bar(c)	Extruded shapes	Forgings	Alloy and temper(a)	Test direction(b)	Rolled plate	Rod and bar(c)	Extruded shapes	Forgings
2011-T3, -T4	L	(d)	B	(d)	(d)	7149-T73	L	(d)	(d)	A	A
	LT	(d)	D	(d)	(d)		LT	(d)	(d)	A	A
	ST	(d)	D	(d)	(d)		ST	(d)	(d)	B	A
2011-T8	L	(d)	A	(d)	(d)	7050-T74	L	A	(d)	A	A
	LT	(d)	A	(d)	(d)		LT	A	(d)	A	A
	ST	(d)	A	(d)	(d)		ST	B	(d)	B	B
2014-T6	L	A	A	A	B	7050-T76	L	A	A	A	(d)
	LT	B(e)	D	B(e)	B(e)		LT	A	B	A	(d)
	ST	D	D	D	D		ST	C	B	C	(d)
2024-T3, -T4	L	A	A	A	(d)	7075-T6	L	A	A	A	A
	LT	B(e)	D	B(e)	(d)		LT	B(e)	D	B(e)	B(e)
	ST	D	D	D	(d)		ST	D	D	D	D
2024-T6	L	(d)	A	(d)	A	7075-T73	L	A	A	A	A
	LT	(d)	B	(d)	A(e)		LT	A	A	A	A
	ST	(d)	B	(d)	D		ST	A	A	A	A
2024-T8	L	A	A	A	A	7075-T74	L	(d)	(d)	(d)	A
	LT	A	A	A	A		LT	(d)	(d)	(d)	A
	ST	B	A	B	C		ST	(d)	(d)	(d)	B
2048-T851	L	A	(d)	(d)	(d)	7075-T76	L	A	(d)	A	(d)
	LT	A	(d)	(d)	(d)		LT	A	(d)	A	(d)
	ST	B	(d)	(d)	(d)		ST	C	(d)	C	(d)
2124-T851	L	A	(d)	(d)	(d)	7175-T736	L	(d)	(d)	(d)	A
	LT	A	(d)	(d)	(d)		LT	(d)	(d)	(d)	A
	ST	B	(d)	(d)	(d)		ST	(d)	(d)	(d)	B
2219-T3, -T37	L	A	(d)	A	(d)	7475-T6	L	A	(d)	(d)	(d)
	LT	B	(d)	B	(d)		LT	B(e)	(d)	(d)	(d)
	ST	D	(d)	D	(d)		ST	D	(d)	(d)	(d)
2219-T6, -T8	L	A	A	A	A	7475-T73	L	A	(d)	(d)	(d)
	LT	A	A	A	A		LT	A	(d)	(d)	(d)
	ST	A	A	A	A		ST	A	(d)	(d)	(d)
6061-T6	L	A	A	A	A	7475-T76	L	A	(d)	(d)	(d)
	LT	A	A	A	A		LT	A	(d)	(d)	(d)
	ST	A	A	A	A		ST	C	(d)	(d)	(d)
7005-T53, -T63	L	(d)	(d)	A	A	7178-T6	L	A	(d)	A	(d)
	LT	(d)	(d)	A(e)	A(e)		LT	B(e)	(d)	B(e)	(d)
	ST	(d)	(d)	D	D		ST	D	(d)	D	(d)
7039-T63, -T64	L	A	(d)	A	(d)	7178-T76	L	A	(d)	A	(d)
	LT	A(e)	(d)	A(e)	(d)		LT	A	(d)	A	(d)
	ST	D	(d)	D	(d)		ST	C	(d)	C	(d)
7049-T73	L	A	(d)	A	A	7079-T6	L	A	(d)	A	A
	LT	A	(d)	A	A		LT	B(e)	(d)	B(e)	B(e)
	ST	A	(d)	B	A		ST	D	(d)	D	D
7049-T76	L	(d)	(d)	A	(d)						
	LT	(d)	(d)	A	(d)						
	ST	(d)	(d)	C	(d)						

(a) Ratings apply to standard mill products in the types of tempers indicated and also in T*x*5*x* and T*x*5*xx* (stress-relieved) tempers and may be invalidated in some cases by use of nonstandard thermal treatments, or mechanical deformation at room temperature by the user. (b) Test direction refers to orientation of direction in which stress is applied relative to the directional grain structure typical of wrought alloys, which for extrusions and forgings may not be predictable on the basis of the cross-sectional shape of the product: L, longitudinal; LT, long-transverse; ST, short-transverse. (c) Sections with width-to-thickness ratios equal to or less than two, for which there is no distinction between LT and ST properties. (d) Rating not established because product not offered commercially. (e) Rating is one class lower for thicker sections: extrusions. 25 mm (1 in.) and thicker; plate and forgings. 38 mm (1.5 in.) and thicker

In the latter case, corrosion along boundaries is minimized because the presence of precipitate or depleted regions throughout the microstructure increases the ratio of the total area of anodic regions to that of cathodic ones, thereby reducing the corrosion current on each anodic region. For alloys requiring microstructural control to avoid susceptibility, resistance is obtained by using treatments that produce precipitate throughout the microstructure, because precipitate always forms first along boundaries, and its formation there usually cannot be prevented.

According to electrochemical theory, susceptibility to intergranular corrosion is a prerequisite for susceptibility to SCC, and treatment of aluminum alloys to improve resistance to SCC also improves their resistance to intergranular corrosion. For most alloys, however, optimal levels of resistance to these two types of failure require different treatments, and resistance to intergranular corrosion is not a reliable indication of resistance to SCC.

In many cases, susceptibility to SCC of an aluminum alloy cannot be predicted reliably by examining its microstructure. Many observations have been made of the progressive changes in dislocation network, precipitation pattern, and other microstructural features that occur as an alloy is treated to improve its resistance to SCC, but these changes have not been correlated quantitatively with susceptibility.

The phenomenology of SCC and the mechanisms of crack propagation are discussed in "Stress-Corrosion Cracking" *ASM Handbook,* Volume 13A, 2003.

Effect of Stress. Whether or not SCC develops in a susceptible aluminum alloy product depends on the magnitude, direction, and duration of tensile stress acting at the surface. The effects of the factors have been established most commonly by means of accelerated laboratory tests; results of one set of such tests are reflected in the shaded bands in Fig. 9. Despite introduction of fracture-mechanics techniques capable of determining crack growth rates, such tests continue to be the basic tools used in evaluating resistance of aluminum alloys to SCC. See the article "Evaluating Stress-Corrosion Cracking" in *ASM Handbook,* Volume 13A, 2003.

These tests suggest a minimum (threshold) stress that is required for cracking to develop. Although empirical in nature, the threshold value provides a valid measure of the relative susceptibilities of aluminum alloys to SCC under the specific conditions of a particular test or environment. Also, for some alloy/temper combinations, results of accelerated laboratory tests reliably predict stress-corrosion performance in service; for example, results of an 84 day alternate immersion test of alloy 7075 and alloy 7178 products correlated well with performance of these products in a seacoast environment.

Effect of Stress-Intensity Factor

As noted previously, certain 2*xxx* and 7*xxx* aluminum alloys, when subjected to stresses in the short-transverse (through-the-thickness) direction of thick plate, forgings, and extrusions, are subject to intergranular SCC (Ref 64). While this phenomenon has long been studied with tensile loading of smooth specimen subjected to exposure in potentially troublesome environments, it also can be examined in fracture-mechanics terms of the rate of crack growth, *da/dt*, as a function of the applied stress-intensity factor, K_I (Ref 65).

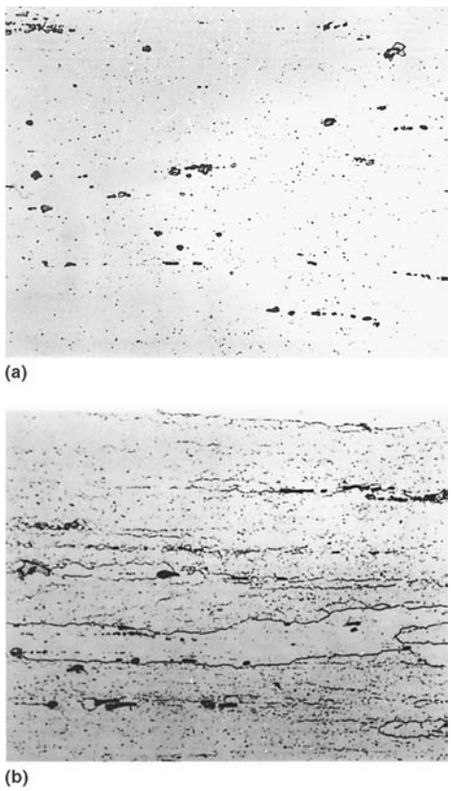

Fig. 15 Microstructures of alloy 5083-O plate stretched 1%. (a) As-stretched. (b) After heating 40 days at 120 °C (250 °F)

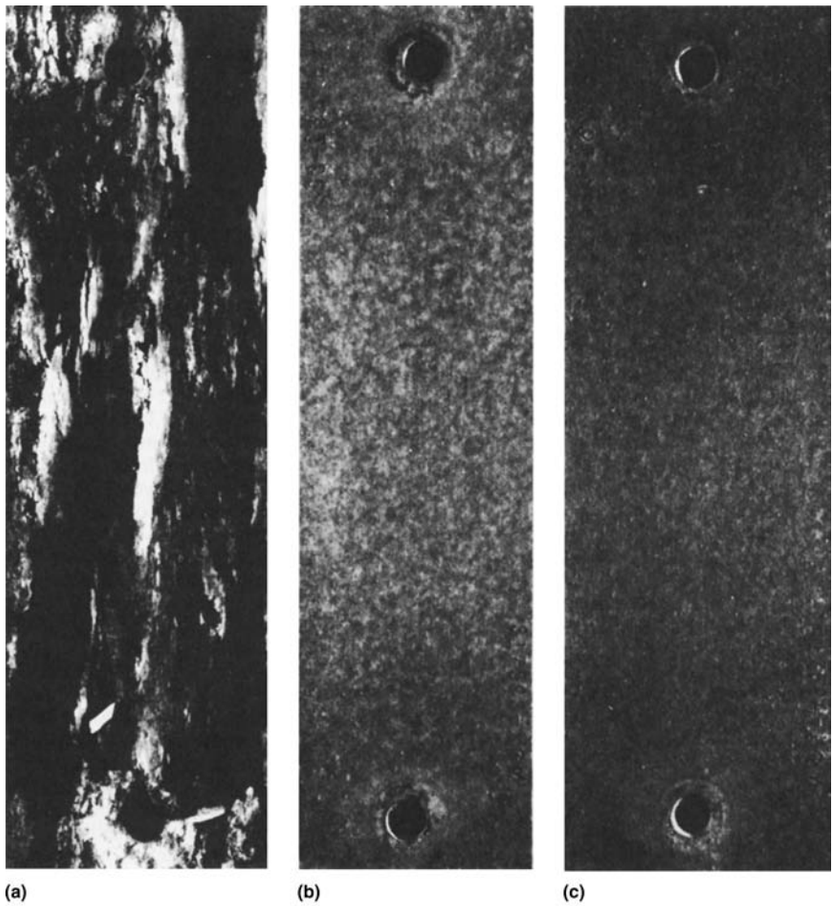

Fig. 16 Effect of temper on exfoliation resistance of an alloy 7075 extrusion exposed in a seacoast environment. Specimens were exposed for 4 years. (a) Specimen in the T6510 temper that developed exfoliation after only 5 months. (b) and (c) Specimens in the T76510 and T73510 tempers that were unaffected after 4 years

Representative data of this type are shown in Fig. 10 for several aluminum alloys (Ref 64). Such presentations are similar to those for fatigue and creep crack growth, except that a more pronounced upper limit to the rate of crack growth is apparent; at stress intensities beyond the bend in the curve, crack growth continues but at a rate no longer greatly dependent on the instantaneous applied stress intensity.

Once again, it should be assumed when designing with these alloys under short-transverse stresses that the largest crack that cannot be detected reliably may be present in the stress field; the crack growth rate data can be used to determine how rapidly that crack may grow to the critical size indicated by the fracture toughness tests. Thus, presentation of SCC growth data, like fatigue and creep crack growth data, provides a means of estimating life expectancy of structures potentially susceptible to such phenomena.

For non-fracture-mechanicians, there is a particularly useful way of dealing with design against SCC growth that combines the results of conventional smooth-specimen and precracked-specimen SCC testing, as illustrated in Fig. 11 (Ref 64, 67). It has been the experience of investigators in stress-corrosion testing of smooth tensile specimens that there are thresholds of applied stress below which SCC growth and failure are not likely to occur. Combining such results with the safe stress-flaw size results from fracture-mechanics types of SCC tests leads to the dual treatment in Fig. 11. On the left side of the chart in Fig. 11, where flaw size is quite small, SCC growth is governed by stress, and levels above line *A-B* are to be avoided. On the right side of the chart, for larger flaw sizes, SCC growth is governed by stress-intensity factor, and stresses above line *D-B* are to be avoided. Representative presentations of this type for aluminum alloys 2219-T87 and 7075-T651 are presented in Fig. 12.

Despite the direct application of this fracture-mechanics approach to design analyses, it is not widely used, simply because the usual practice is to select alloys and tempers that will avoid the possibility of SCC completely.

Stress Relieving. Residual stresses are induced in aluminum alloy products when they are solution heat treated and quenched. Figure 13(a) shows the typical distribution and magnitude of residual stresses in thick high-strength material of constant cross section. Quenching places the surfaces in compression and the center in tension. If the compressive surface stresses are not disturbed by subsequent fabrication practices, the surface has an enhanced resistance to SCC because a sustained tensile stress is necessary to initiate and propagate this type of corrosion. On the other hand, one of the most common practices associated with SCC problems is machining into the residual high tensile stress areas of material that has not been stress relieved. If the exposed tensile stresses are in a transverse direction or have a transverse component and if a susceptible alloy or temper is involved, the probability of SCC is present (Ref 68).

Aluminum products of constant cross section are stress relieved effectively and economically by mechanical stretching (such as T651 or T7X51) or compression (T652 or T7352). The stretching operation must be done after quenching and, for most alloys, before artificial aging. Note the low magnitude of residual stresses after stretching in Fig. 13(b) as compared to the as-quenched material in Fig. 13(a). Aluminum Association, ASTM International, and federal specifications for rolled and extruded products provide for stress relieving by stretching on the order of 1 to 3%.

Thus, the use of the stress-relieved temper for heat treated mill products will minimize SCC problems related to quenching stresses. The stress-relieved temper for most alloys is identified by the designation T*x*5*x* or T*x*5*xx* after the alloy number, for example, 2024-T351 or 7075-T6511 (Ref 69).

Effects of Grain Structure and Stress Direction. Many wrought aluminum alloy products have highly directional grain structures (Fig. 14). Such products are highly anisotropic with respect to resistance to SCC (Fig. 9). Resistance, which is measured by magnitude of tensile stress required to cause cracking, is highest when the stress is applied in the longitudinal direction, lowest in the short-transverse direction, and intermediate in other directions. These differences are most noticeable in the more susceptible tempers but are usually much lower in tempers produced by extended precipitation treatments, such as T6 and T8 tempers for 2*xxx* alloys and T73, T736, and T76 tempers for 7*xxx* alloys.

Thus, direction and magnitude of stresses anticipated under conditions of assembly and service may govern alloy and temper selection. For products of thin section, applied in ways that induce little or no tensile stress in the short-transverse direction, resistance of 2*xxx* alloys in T3 or T4 tempers or of 7*xxx* alloys in T6 tempers may suffice. Resistance in the short-transverse direction usually controls application of products that are of thick section or are machined or applied in ways that result in sustained tensile stresses in the short-transverse direction. More resistant tempers are preferred in these cases.

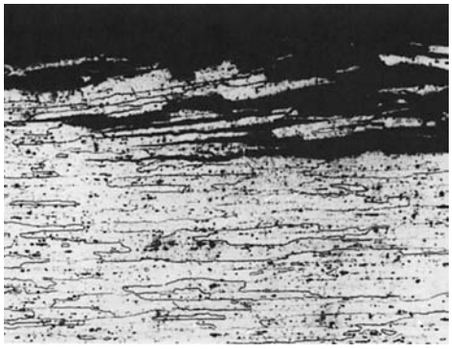

Fig. 17 Exfoliation corrosion in an alloy 7178-T651 plate exposed to a seacoast environment. Cross section of the plate shows how exfoliation develops by corrosion along boundaries of thin, elongated grains

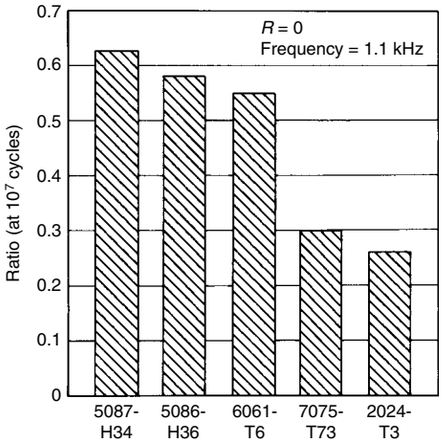

Fig. 18 Ratio of axial-stress fatigue strength of aluminum alloy sheet in 3% NaCl solution to that in air. Specimens were 1.6 mm (0.064 in.) thick

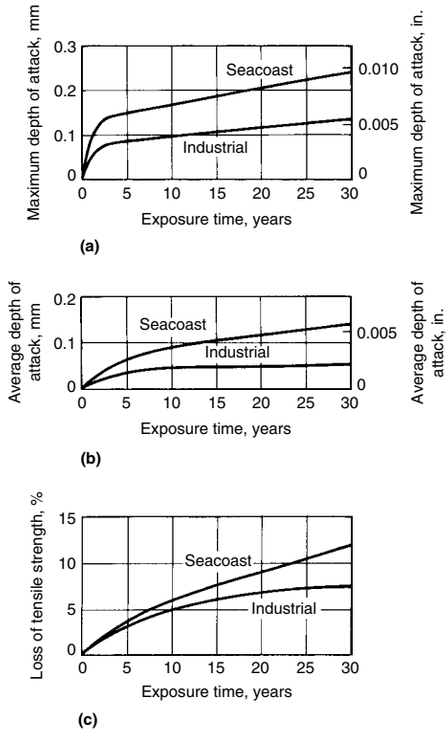

Fig. 19 Depth of corrosion and loss of tensile strength for alloys 1100, 3003, and 3004 (shown in graphs a, b, and c, respectively). Data are given for the average performance of the three alloys, all in the H14 temper. Seacoast exposure was at a severe location (Pt. Judith, RI); industrial exposure was at New Kensington, PA. Tensile strengths were computed using original cross-sectional areas, and loss in strength is expressed as a percentage of original tensile strength

Effects of Environment. Research indicates that water or water vapor is the key environmental factor required to produce SCC in aluminum alloys. Halide ions have the greatest effects in accelerating attack. Chloride is the most important halide ion because it is a natural constituent of marine environments and is present in other environments as a contaminant. Because it accelerates SCC, Cl^- is the principal component of environments used in laboratory tests to determine susceptibility of aluminum alloys to this type of attack. In general, susceptibility is greater in neutral solutions than in alkaline solutions and is greater still in acidic solutions.

Stress-Corrosion Ratings. A system of ratings of resistance to SCC for high-strength aluminum alloy products has been developed by a joint task group of ASTM International and the Aluminum Association to assist alloy and temper selection and has been incorporated into Ref 34. Definitions of these ratings, which range from A (highest resistance) to D (lowest resistance), are as follows:

Rating	Definition
A: Very high	No record of service problems; SCC not anticipated in general applications
B: High	No record of service problems; SCC not anticipated at stresses of the magnitude caused by solution heat treatment. Precautions must be taken to avoid high sustained tensile stresses (exceeding 50% of the minimum specified yield strength) produced by any combination of sources, including heat treatment, straightening, forming, fit-up, and sustained service loading.
C: Intermediate	Stress-corrosion cracking not anticipated if total sustained tensile stress is maintained below 25% of minimum specified yield strength. This rating is designated for the short-transverse direction in products used primarily for high resistance to exfoliation corrosion in relatively thin structures, where appreciable stresses in the short-transverse direction are unlikely.
D: Low	Failure due to SCC is anticipated in any application involving sustained tensile stress in the designated test direction. This rating is currently designated only for the short-transverse direction in certain products.

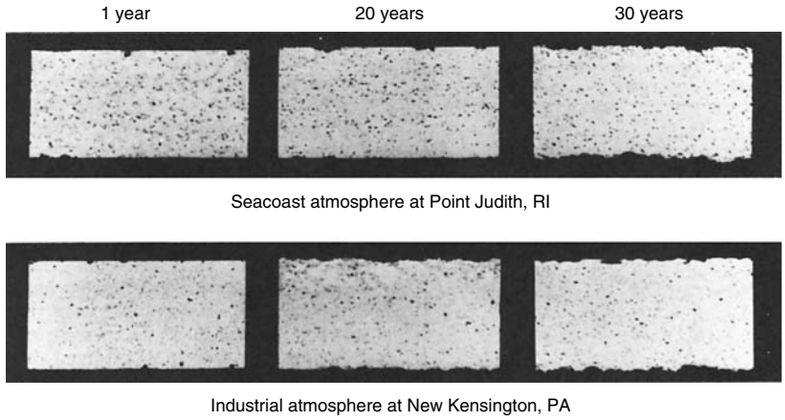

Fig. 20 Sectioned specimens cut from 1.6 mm (0.064 in.) thick alloy 3003-H14 panels after exposure in two environments

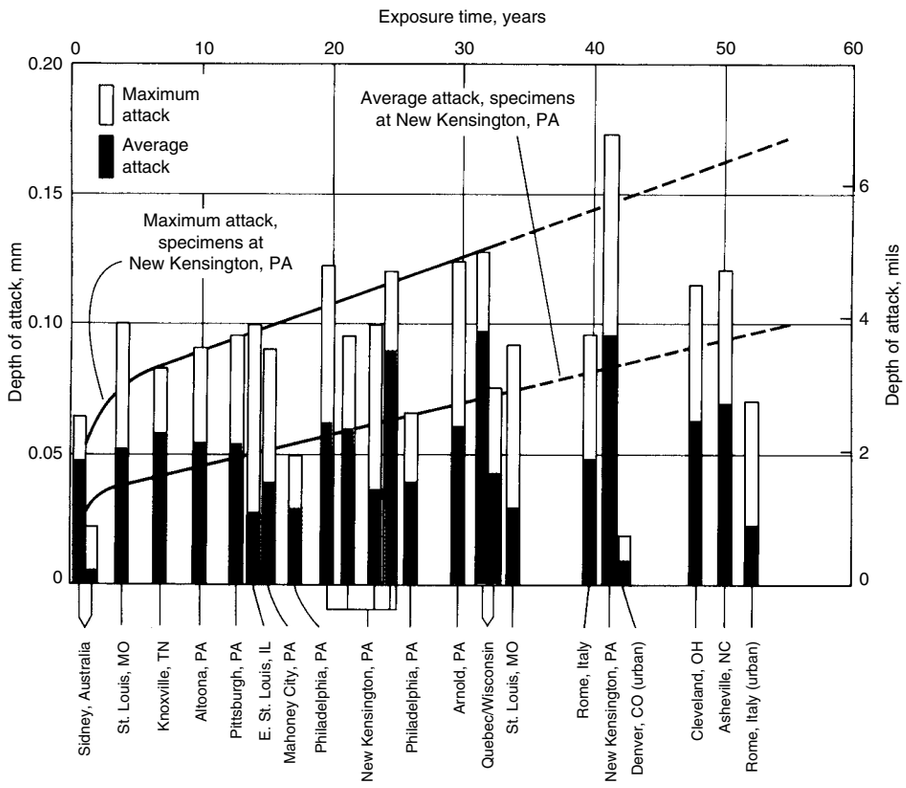

Fig. 21 Correlation of weathering data for specimens of alloys 1100, 3003, and 3004 (all in H14 temper) exposed to industrial atmosphere (curves) with service experience with aluminum alloys in various locations (bars)

These stress levels are not to be interpreted as threshold stresses and are not recommended for design. Documents such as MMPDS (previously MIL-HDBK-5), MIL-STD-1568, NASC SD-24, and MSFC-SPEC-522A should be consulted for design recommendations.

The relative ratings of resistance to SCC for high-strength wrought aluminum alloys are presented in Table 9. These ratings, assigned primarily by alloy and temper, also distinguish among test directions and product types.

2*xxx* Alloys. Thick-section products of 2*xxx* alloys in the naturally aged T3 and T4 tempers have low ratings of resistance to SCC in the short-transverse direction. Ratings of such products in other directions are higher, as are ratings of thin-section products in all directions. These differences are related to the effects of quenching rate (largely determined by section thickness) on the amount of precipitation that occurs during quenching. If 2*xxx* alloys in T3 and T4 tempers are heated for short periods in the temperature range used for artificial aging, selective precipitation along grain or subgrain boundaries may further impair their resistance.

Longer heating, as specified for T6 and T8 tempers, produces more general precipitation and significant improvements in resistance to SCC. Precipitates are formed within grains at a greater number of nucleation sites during treatment to T8 tempers. These tempers require stretching, or cold working by other means, after quenching from the solution heat treatment temperature and before artificial aging. These tempers provide the highest resistance to SCC and the highest strength in the 2*xxx* alloy.

Some studies on Al-Cu-Li alloys indicate that these alloys have their highest resistance to SCC at or near peak-aged tempers (Ref 70–72). Underaging of these alloys (for example, 2090) is detrimental; overaging decreases resistance

only slightly. The susceptibility of the underaged microstructure has been attributed to the precipitation of an intermetallic constituent, Al_2CuLi, on grain boundaries during the early stages of artificial aging. This constituent is believed to be anodic to the copper-rich matrix of an underaged alloy, causing preferential dissolution and SCC. As aging time increases, copper-bearing precipitates form in the interior of the grains, thus increasing the anode-cathode area ratio in the microstructure to a more favorable value that avoids selective grain-boundary attack. Similar studies of stress-corrosion behavior are being conducted on Al-Li-Cu-Mg alloys (for example, 8090) (Ref 73).

5*xxx* alloys are not considered heat treatable and do not develop their strength through heat treatment. However, these alloys are processed to H3 tempers, which require a final thermal stabilizing treatment to eliminate age softening, or to H2 tempers, which require a final partial annealing. The H116 or H117 tempers are also used for high-magnesium 5*xxx* alloys and involve special temperature control during fabrication to achieve a microstructural pattern of precipitate that increases the resistance of the alloy to intergranular corrosion and SCC. The alloys of the 5*xxx* series span a wide range of magnesium contents, and the tempers that are standard for each alloy are primarily established by the magnesium content and the desirability of microstructures highly resistant to SCC and other forms of corrosion.

Although 5*xxx* alloys are not heat treatable, they develop good strength through solution hardening by the magnesium retained in solid solution, dispersion hardening by precipitates, and strain-hardening effects. Because the solid solutions in the higher-magnesium alloys are more highly supersaturated, the excess magnesium tends to precipitate out as Mg_2Al_3, which is anodic to the matrix. Precipitation of this phase with high selectivity along grain boundaries, accompanied by little or no precipitation within grains, may result in susceptibility to SCC.

The probability that a susceptible microstructure will develop in a 5*xxx* alloy depends on magnesium content, grain structure, amount of strain hardening, and subsequent time/temperature history. Alloys with relatively low magnesium contents, such as 5052 and 5454 (2.5 and 2.75% Mg, respectively), are only mildly supersaturated; consequently, their resistance to SCC is not affected by exposure to elevated temperatures. In contrast, alloys with magnesium contents exceeding approximately 3%, when in strain-hardened tempers, may develop susceptible structures as a result of heating or even after very long times at room temperature. For example, the microstructure of alloy 5083-O (4.5% Mg) plate stretched 1% (Fig. 15a) is relatively free of precipitate (no continuous second-phase paths), and the material is not susceptible to SCC. Prolonged heating below the solvus, however, produces continuous precipitate, which results in susceptibility (Fig. 15b).

6*xxx* Alloys. The service record of 6*xxx* alloys shows no reported cases of SCC. In laboratory tests, however, at high stresses and in aggressive solutions, cracking has been demonstrated in 6*xxx* alloys of particularly high alloy content, containing silicon in excess of the Mg_2Si ratio and/or high percentages of copper.

7*xxx* Alloys Containing Copper. The 7*xxx*-series alloy that has been used most extensively and for the longest period of time is 7075, an Al-Zn-Mg-Cu-Cr alloy. Introduced in 1943, this aircraft construction alloy was initially used for products with thin sections, principally sheet and extrusions. In these products, quenching rate is normally very high, and tensile stresses are not encountered in the short-transverse direction; thus, SCC is not a problem for material in the highest-strength (T6) tempers. When 7075 was used in products of greater size and thickness, however, it became apparent that such products heat treated to T6 tempers were often unsatisfactory. Parts that were extensively machined from large forgings, extrusions, or plate were frequently subjected to continuous stresses, arising from interference misfit during assembly or from service loading, that were tensile at exposed surfaces and aligned in unfavorable orientations. Under such conditions, SCC was encountered in service with significant frequency.

This problem resulted in the introduction (in approximately 1960) of the T73 tempers for thick-section 7075 products. The precipitation treatment used to develop these tempers requires two-stage artificial aging, the second stage of which is done at a higher temperature than that used to produce T6 tempers. During the preliminary stage, a fine high-density precipitation dispersion is nucleated, producing high strength. The second stage is then used to develop resistance to SCC and exfoliation. Extensive accelerated and environmental testing has demonstrated that 7075-T73 resists SCC even when stresses are oriented in the least favorable direction, at stress levels of at least 300 MPa (44 ksi). Under similar conditions, the maximum stress at which 7075-T6 resists cracking is approximately 50 MPa (7 ksi). The excellent test results for 7075-T73 have been confirmed by extensive service experience in various applications.

The additional aging treatment required to produce 7075 in T73 tempers, which have high resistance to SCC, reduces strength to levels below those of 7075 in T6 tempers. Alloy 7175, a variant of 7075, was developed for forgings. In the T74 temper, 7175 has strength nearly comparable to that of 7075-T6 and has better resistance to SCC. Other newer alloys—such as 7049 and 7475, which are used in the T73

Table 10 Weathering data for 0.89 mm (0.035 in.) thick aluminum alloy sheet after 20 year exposure (ASTM International program started in 1931)

Alloy and temper	Corrosion rate		Average depth of attack		Maximum depth of attack		Change in tensile strength, %
	nm/yr	μin./yr	μm	mils	μm	mils	
Phoenix, AZ (desert)							
1100-H14	76	3.0	8	0.3	18	0.7	0
2017-T3	76	3.0	23	0.9	51	2.0	0
2017-T3, alclad	13	0.5	10	0.4	23	0.9	0
3003-H14	13	0.5	5	0.2	10	0.4	0
6051-T4	13	0.5	28	1.1	74	2.9	0
State College, PA (rural)							
1100-H14	76	3.0	36	1.4	89	3.5	−3
2017-T3	102	4.0	25	1.0	81	3.2	−2
2017-T3, alclad	76	3.0	10	0.4	25	1.0	0
3003-H14	89	3.5	23	0.9	56	2.2	−3
6051-T4	76	3.0	23	0.9	96	3.8	0
Sandy Hook, NJ (seacoast)							
1100-H14	279	11.0	96	3.8	231	9.1	−3
2017-T3	...	...	43	1.7	132	5.2	−10
2017-T3, alclad	...	...	23	0.9	33	1.3	...
3003-H14	356	14.0	36	1.4	84	3.3	...
6051-T4	343	13.5	58	2.3	137	5.4	−9
La Jolla, CA (seacoast)							
1100-H14	584	23.0	102	4.0	356	14.0	−8
2017-T3	2260	89.0	147	5.8	515	20.3	−20
2017-T3, aclad	584	23.0	33	1.3	74	2.9	0
3003-H14	610	24.0	107	4.2	259	10.2	−7
6051-T4	775	30.5	84	3.3	307	12.1	−20
New York, NY (industrial)							
1100-H14	749	29.5	89	3.5	213	8.4	−7
2017-T3	1260	49.6	51	2.0	180	7.1	−7
2017-T3, alclad	762	30.0	28	1.1	36	1.4	0
3003-H14	965	38.0	51	2.0	163	6.4	−8
6051-T4	914	36.0	74	2.9	170	6.7	−12

Source: Ref 94

temper, and 7050, which is used in the T74 temper—couple high strength with very high resistance and improved fracture toughness.

The T76 tempers, which also require two-stage artificial aging and which are intermediate to the T6 and T73 tempers in both strength and resistance to SCC, are developed in copper-containing 7*xxx* alloys for certain products. Comparative ratings of resistance for various products of all these alloys, as well as for products of 7178, are given in Table 9.

The microstructural differences among the T6, T73, and T76 tempers of these alloys are differences in size and type of precipitate, which changes from predominantly Guinier-Preston zones in T6 tempers to η′, the metastable transition form of η ($MgZn_2$), in T73 and T76 tempers. None of these differences can be detected by optical metallography. In fact, even the resolutions possible in transmission electron microscopy are insufficient for determining whether the precipitation reaction has been adequate to ensure the expected level of resistance to SCC. For quality assurance, copper-containing 7*xxx* alloys in T73 and T76 tempers are required to have specified minimum values of electrical conductivity and, in some cases, tensile yield strengths that fall within specified ranges. The validity of these properties as measures of resistance to SCC is based on many correlation studies involving these measurements, laboratory and field stress-corrosion tests, and service experience.

Copper-Free 7*xxx* Alloys. Wrought alloys of the 7*xxx* series that do not contain copper are of considerable interest because of their good resistance to general corrosion, moderate-to-high strength, and good fracture toughness and formability. Alloys 7004 and 7005 have been used in extruded form and, to a lesser extent, in sheet form for structural applications. More recently introduced compositions, including 7016, 7021, 7029, and 7146, have been used in automobile bumpers formed from extrusions or sheet.

As a group, copper-free 7*xxx* alloys are less resistant to SCC than other types of aluminum alloys when tensile stresses are developed in the short-transverse direction at exposed surfaces. Resistance in other directions may be good, particularly if the product has an unrecrystallized microstructure and has been properly heat treated. Products with recrystallized grain structures are generally more susceptible to cracking as a result of stresses induced by forming or mechanical damage after heat treatment. When cold forming is required, subsequent solution heat treatment or precipitation heat treatment is recommended. Applications of these alloys must be carefully engineered, and consultation among designers, application engineers, and product producers or suppliers is advised in all cases.

Casting Alloys. The resistance of most aluminum casting alloys to SCC is sufficiently high that cracking rarely occurs in service. The microstructures of these alloys are usually nearly isotropic; consequently, resistance to SCC is unaffected by orientation of tensile stresses.

Relative ratings of cast alloys, based primarily on accelerated laboratory tests, are listed in Tables 7(a) and (b). It has been indicated by accelerated and natural-environment testing and verified by service experience that alloys of the aluminum-silicon 4*xx.x* series, 3*xx.x* alloys containing only silicon and magnesium as alloying additions, and 5*xx.x* alloys with magnesium contents of 8% or lower have virtually no susceptibility to SCC. Alloys of the 3*xx.x* group that contain copper are rated as less resistant, although the numbers of castings of these alloys that have failed by SCC have not been significant.

Significant SCC of aluminum alloy castings in service has occurred only in the higher-strength aluminum-copper 2*xx.x* alloys and Al-Zn-Mg 7*xx.x* alloys, and also in the aluminum-magnesium alloy 520.0 in the T4 temper. For such alloys, factors that require careful consideration include casting design, assembly and service stresses, and anticipated environment exposure.

Specifications and Tests. Several aluminum alloy product specifications require defined levels of performance with respect to resistance to SCC. Standard tests used to measure such performance are described in the methods standards and are referenced in materials specifications. Among these are tests for evaluating resistance to SCC of 2*xxx* alloys and of 7*xxx* alloys that contain copper by alternate immersion in 3.5% NaCl solution (Ref 74, 75). Lot acceptance criteria for products of 7*xxx* copper-containing alloys in T76, T73, and T736 tempers are based on combined requirements for tensile strength and electrical conductivity.

Table 11 Weathering data for 1.27 mm (0.05 in.) thick aluminum alloy sheet after 7 year exposure (ASTM International program started in 1958)

Average values from Kure Beach, NC, and Newark, NJ

Alloy and temper	Corrosion rate(a)		Maximum depth of attack in 7 years		Average depth of attack in 7 years		Change in tensile strength in 7 years, %
	nm/yr	μin./yr	μm	mils	μm	mils	
Non-heat-treatable alloys							
1100-H14	345	13.6	70	2.6	29	1.1	0
1135-H14	321	12.6	83	3.3	37	1.5	–0.4
1188-H14	250	9.8	121	4.8	46	1.8	0
1199-H18	205	8.1	96	3.8	57	2.2	–3.9
3003-H14	295	11.6	86	3.4	52	2.0	–1.1
3004-H34	414	16.3	119	4.7	44	1.7	–1.1
4043-H14	335	13.2	105	4.1	34	1.3	–2.8
5005-H34	373	14.7	76	3.0	27	1.1	–0.9
5050-H34	349	13.7	107	4.2	58	2.3	–0.5
5052-H34	362	14.3	62	2.4	43	1.7	–0.8
5154-H34	326	12.8	91	3.6	65	2.6	–0.9
5454-O	348	13.7	95	3.7	41	1.6	–1.5
5454-H34	342	13.5	105	4.1	30	1.2	–0.5
5456-O	381	15.0	104	4.1	37	1.5	–0.4
3357-H34	292	11.5	138	5.4	102	4.0	–0.4
5083-O	469	18.5	102	4.0	52	2.0	–1.8
5083-H34	375	14.8	88	3.5	56	2.2	–2.2
5086-H34	436	17.2	105	4.1	76	3.0	–1.9
Heat treatable alloys							
2014-T6	644	25.4	77	3.0	50	2.0	–1.7
2024-T3	1022	40.2	76	3.0	67	2.6	–2.0
2024-T81	725	28.5	97	3.8	76	3.0	–6.0
2024-T86	806	31.7	77	3.0	58	2.3	–6.2
6061-T4	378	14.9	57	2.2	38	1.5	–0.4
6061-T6	422	16.6	98	3.9	42	1.7	–0.7
7075-T6	688	27.1	119	4.7	71	2.8	–1.7
7079-T6	635	25.0	65	2.6	37	1.5	–0.5
Alclad alloys—heat treatable and non-heat treatable							
2014-T6	358	14.1	43	1.7	28	1.1	0
2024-T3	264	10.4	46	1.8	27	1.1	0
3003-H14	345	13.6	128	5.0	117	4.6	0
5155-H34	345	13.6	53	2.1	35	1.4	0
6061-T6	356	14.0	98	3.9	25	1.0	–0.7
7075-T6	502	19.8	53	2.1	41	1.6	–0.1
7079-T6	324	12.8	72	2.8	36	1.4	0

(a) Based on weight change. Source: Ref 93

Exfoliation Corrosion

In certain tempers, wrought products of aluminum alloys are subject to corrosion by exfoliation, which is sometimes described as lamellar, layer, or stratified corrosion. In this

type of corrosion, attack proceeds along selective subsurface paths parallel to the surface. As shown in Fig. 16(a), layers of uncorroded metal between the selective paths are split apart and pushed above the original surface by the voluminous corrosion product formed along the paths of attack. Because it can be detected readily at an early stage and is restricted in depth, exfoliation does not cause unexpected structural failure, as does SCC.

Exfoliation occurs predominantly in products that have markedly directional structures in which highly elongated grains form platelets that are thin relative to their length and width (Fig. 17). Susceptibility to this type of corrosion may result from the presence of aligned intergranular or subgrain-boundary precipitates or from aligned strata that differ slightly in composition. The intensity of exfoliation increases in slightly acidic environments or when the aluminum is coupled to a cathodic dissimilar metal. Exfoliation is not accelerated by stress and does not lead to SCC.

Alloys most susceptible to exfoliation are the heat treatable 2*xxx* and 7*xxx* alloys and certain cold-worked 5*xxx* alloys, such as 5456-H321 boat hull plates. Exfoliation problems with 5*xxx* alloys led to the development of special boat hull plate tempers, H116 and H117, for alloys 5083, 5086, and 5456. In these alloys, exfoliation is primarily caused by unfavorable distribution of precipitate. The processing to eliminate this form of attack promotes either more uniform precipitation within grains or a more advanced stage of precipitation. Thus, increases in the precipitation heat treating time or temperature are as effective in reducing susceptibility to exfoliation as they are in reducing susceptibility to SCC.

During long-duration or high-temperature precipitation treatments, maximum resistance to exfoliation is usually achieved sooner than maximum resistance to SCC. Thus, precipitation treatments used to produce T76 tempers in 7*xxx* alloys, which use times and temperatures intermediate to those of T6 and T73 treatments, provide excellent resistance to exfoliation (Fig. 16b) but only intermediate resistance to SCC. The T73 tempers provide the highest resistance to both types of corrosion (Fig. 16c) but at a sacrifice in strength compared to T76 tempers.

Among the standard tests for evaluating resistance to exfoliation of 2*xxx*, 5*xxx*, and 7*xxx* alloys are those that require total immersion in aggressive acidified solutions of mixed salts or exposure to cyclic, acidified salt spray tests. Such tests are described in Ref 76 for 5*xxx* alloys and in Ref 77 and 78 for 2*xxx* and 7*xxx* alloys. Acceptability of aluminum-magnesium alloys 5083, 5086, and 5456 is based on a comparison of the microstructure disclosed by etching in a defined manner with a reference microstructure that is predominantly free from a continuous grain-boundary network of Al_8Mg_5 precipitate particles (Ref 79). Material containing such precipitate in amounts exceeding that shown by the reference standard is unacceptable unless it can be demonstrated by testing (Ref 76) that the material has acceptable resistance to exfoliation. References 80 to 84 compare the performance in these accelerated test methods to those in outdoor atmospheres.

Corrosion Fatigue

Fatigue strengths of aluminum alloys are lower in such corrosive environments as seawater and other salt solutions than in air, especially when evaluated by low-stress long-duration tests (Ref 85, 86). As shown in Fig. 18, such corrosive environments produce smaller reductions in fatigue strength in the more corrosion-resistant alloys, such as the 5*xxx* and 6*xxx* series, than in the less resistant alloys, such as the 2*xxx* and 7*xxx* series.

Like SCC of aluminum alloys, corrosion fatigue requires the presence of water. In contrast to SCC, however, corrosion fatigue is not appreciably affected by test direction, because the fracture that results from this type of attack is predominantly transgranular.

Table 12a Change in tensile strength for wrought aluminum alloys during various atmospheric exposures (ASTM International program)

Exposed as 102 × 203 mm (4 × 8 in.) panels. Calculated from average tensile strength of several specimens (usually four)

	Change in strength, %, during exposure of indicated length at														
	State College, PA					New York, NY					Kure Beach, NC				
Alloy and temper	6 mo	1 yr	3 yr	5 yr	10 yr	6 mo	1 yr	3 yr	5 yr	10 yr	6 mo	1 yr	3 yr	5 yr	10 yr
1.62 mm (0.064 in.) sheet															
2024-T3	8	1	2	0	1	2	–8	–7	–11(a)	–11(a)	6	–3	–4	–6	–4
3003-H14	6	0	2	0	1	4	–4	–5	–8	–6	5	0	–2	–4	0
3004-H34	6	–1	0	0	1	7	–2	–5	–5	–7	6	2	–2	–2	–1
5050-H34	6	0	–1	0	–1	4	–2	–1	–8	–4	5	–1	–1	–1	–2
5052-H34	9	0	–1	–1	0	. . .	–1	–6(a)	–5(a)	–7(a)	6	0	–2	–3(a)	–1
6061-T6	5	–2	–2	–3	0	. . .	–3	–7	–8	–11	4	–1	–1	–1	–4
7075-T6	5	–1	–3	0	–1	3	–1	–5	–6(a)	–8(a)	4	–2	–2	–4	–4
1.62 mm (0.064 in.) alclad sheet															
2014-T6	5	–1	–1	–2	2	4	1	–2	–4	–4	–2(a)	–1	–1	–4	–2
2024-T3	7	–1	1	1	0	8	–2	–1	–3	–3	6	1	0	0	–1
7075-T6	6	0	6	–2	–2	5	1	–2	–5	–5	6	2	2	–1	0
6.35 mm (0.25 in.) plate															
2014-T4	–3	0	0	0	0	–5	0	–2	–1	–4	–4	1	0	0	–12
2014-T6	0	–1	0	0	1	0	–2	–1	–1	–1	–2	–2	–1	–1	–1
6061-T6	–4	0	–2	–1	–5	7	–1	–2	4	3	–4	–1	0	–1	–8
6.35 mm (0.25 in.) alclad plate															
2014-T6	0	–1	0	1	–1	0	0	1	–1	–2	–1	0	0	0	0
2024-T3	0	0	0	–1	1	0	–2	–2	–2	–2	2	0	1	2	1
7075-T6	0	0	0	0	0	0	1	–1	0	1	0	1	0	0	–11(a)
6.35 mm (0.25 in.) extruded bar															
2014-T4	2	3	1	–1	–4	1	1	0	1	–2	0	0	–1	–1	–13
2014-T6	–1	0	0	–1	0	–1	1	–2	–1	–2	–1	2	–1	–2	–1
6061-T6	0	0	0	–1	7	–2	–1	0	–3	–3	–1	–1	–2	–1	6
6063-T5	1	–1	–1	–1	1	1	–1	–2	9	11	–1	8	3	6	2
7075-T6	–1	–1	–3	–2	–3	–1	–2	–2	–1	–4	–2	–1	0	1	–2

(a) Average tensile strength values were below required minimum. Source: Ref 95

Table 12b Change in tensile strength for wrought aluminum alloys during various atmospheric exposures (ASTM International program)

Exposed as 102 × 203 mm (4 × 8 in.) panels. Calculated from average tensile strength of several specimens (usually four)

	Change in strength, %, during exposure of indicated length at									
	Point Reves, CA					Freeport, TX				
Alloy and temper	6 mo	1 yr	3 yr	5 yr	10 yr	6 mo	1 yr	3 yr	5 yr	10 yr
1.62 mm (0.064 in.) sheet										
2024-T3	...	–13(a)	–19(a)	–19(a)	–23(a)	3	–2	–9(a)	–8	–13(a)
3003-H14	...	1	–3	–1	–4	3	0	–5	1	–4
3004-H34	...	–3	–1	–1	1	5	–1	–4	0	–2
5050-H34	...	2	–1	0	–2	5	0	–4	0	–3
5052-H34	...	–1	–2	0	–1	4	–1	–7(a)	0	–1
6061-T6	...	–3	–4	–5	–5	1	–3	–4	–1	–3
7075-T6	...	–3	–4	–4	–11(a)	1	–1	–5	–3	–8(a)
1.62 mm (0.064 in.) alclad sheet										
2014-T6	...	–3	–1	–4	–4	3	–1	–3	–3	–2
2024-T3	...	–1	–1	–1	–3	6	–1	–2	0	–3
7075-T6	...	3	–2	–3	–6	5	4	–1	–1	–2
6.35 mm (0.25 in.) plate										
2014-T4	...	–1	–3	–6	–5	1	...	–2	–1	–22(a)
2014-T6	...	–13(a)	–4	–8(a)	–8(a)	0	...	–2	0	–2
6061-T6	...	1	0	2	0	–4	0	–2	0	–2
6.35 mm (0.25 in.) alclad plate										
2014-T6	...	0	–1	0	–1	–1	2	–1	0	–2
2024-T3	...	2	0	–1	1	1	0	–1	0	0
7075-T6	...	1	–1	0	–1	0	2	–1	1	0
6.35 mm (0.25 in.) extruded bar										
2014-T4	...	3	–6	–3	–8	1	3	–2	2	–5
2014-T6	...	...	–4	–3	–7	1	1	–1	–2	–3
6061-T6	...	–1	–1	–1	...	0	0	–2	–1	–2
6053-T5	...	3	3	3	7	11	2	0	8	–1
7075-T6	...	–3	–3	–4	0	0	0	–1	–1	–4

(a) Average tensile strength values were below required minimum. Source: Ref 95

Erosion-Corrosion

In noncorrosive environments, such as high-purity water, the stronger aluminum alloys have the greatest resistance to erosion-corrosion, because resistance is controlled almost entirely by the mechanical components of the system. In a corrosive environment, such as seawater, the corrosion component becomes the controlling factor; thus, resistance may be greater for the more corrosion-resistant alloys even though they are lower in strength. Corrosion inhibitors and cathodic protection have been used to minimize erosion-corrosion, impingement, and cavitation on aluminum alloys (Ref 87).

Atmospheric Corrosion

Most aluminum alloys have excellent resistance to atmospheric corrosion (often called weathering), and in many outdoor applications, such alloys do not require shelter, protective coatings, or maintenance. Aluminum alloy products that have no external protection and therefore depend critically on this property include electrical conductors, outdoor lighting poles, ladders, and bridge railings. Such products often retain a bright metallic appearance for many years, but their surfaces may become dull, gray, or even black as a result of pollutant accumulation. Corrosion of most aluminum alloys by weathering is restricted to mild surface roughening by shallow pitting, with no general thinning. However, such attack is more severe for alloys with higher copper contents, and such

Table 13a Change in tensile strength for cast aluminum alloys during various atmospheric exposures (ASTM International program)

Exposed as separately cast tensile specimens. Calculated from average tensile strength of several specimens (usually six)

	Change in strength, %, during exposure of indicated length at														
	State College, PA					New York, NY					Kure Beach, NC				
Alloy and temper	6 mo	1 yr	3 yr	5 yr	10 yr	6 mo	1 yr	3 yr	5 yr	10 yr	6 mo	1 yr	3 yr	5 yr	10 yr
Sand castings															
208.0-F	–1	–2	–2	–1	–2	–1	–4	–4	–3	0	–2	–5	–7	–6	–4
295.0-T6	1	–3	–2	–4	–2	–2	–6	–6	–5	–5	–7	–9	–9	–10	–9
319.0-T6	0	–1	–3	0	–3	1	–2	–6	–8	–5	–1	–5	–7	–6	–4
355.0-T6	0	1	–2	1	–3	1	0	–3	–1	–3	2	2	0	–1	–3
356.0-T6	1	–1	0	–1	–1	1	–1	–2	–2	–3	1	–1	0	–2	–2
443.0-F	3	0	–2	–2	–2	0	3	–2	–4	–3	–2	0	0	–1	–2
520.0-T4	1	–5	–4	–6	...	2	–1	–1	–2	...	–2	–2	–5	–6	...
705.0-T5	1	–2	–6	–4	–1	0	0	–4	–3	–10	1	–2	–3	–3	–4
707.0-T5	1	–2	–1	–3	0	2	1	–5	–9	–15	2	–3	–9	–13	–18
710.0-T5	2	–2	–2	–1	–5	1	–3	–3	–2	–1	2	–1	–1	–2	–1
712.0-T5	0	–8	–3	–2	–7	0	–2	–4	–5	–2	–4	–3	–8	–2	–8
713.0-T5	1	3	–2	1	–1	–3	–4	–1	–1	–5	–5	–3	–8	–1	–3
Permanent mold castings															
319.0-T61	1	–2	–1	–2	–2	1	–3	0	–4	–4	–5	–3	–4	–7	–5
355.0-T6	3	0	7	2	–4	1	–2	8	–2	–7	2	–7	5	–1	–5
443.0-F	3	0	–1	–1	–2	1	–3	–1	1	0	–1	0	–6	2	0
705.0-T5	–1	–2	–3	–5	–3	–2	0	–2	–3	–7	–3	–3	–5	–9	–5
707.0-T5	2	–2	–3	–3	–4	0	–2	–1	–4	–7	1	–2	–4	–7	–12
711.0-T5	–8	–11	–7	–6	–8	2	–4	–5	–2	–6	–2	–6	–6	–6	–11
713.0-T5	–2	–2	0	–1	–2	–1	–11	–2	–7	–2	–11	–12	–6	–4	–1

Source: Ref 95

alloys are seldom used in outdoor applications without protection.

Corrosivity of the atmosphere to metals varies greatly from one geographic location to another, depending on such weather factors as wind direction, precipitation and temperature changes, amount and type of urban and industrial pollutants, and proximity to natural bodies of water. Service life may also be affected by the design of the structure if weather conditions cause repeated moisture condensation in unsealed crevices or in channels with no provision for drainage. Laboratory exposure tests, such as salt spray, total-immersion, and alternate-immersion tests, provide useful comparative information but have limited value for predicting actual service performance and sometimes exaggerate differences among alloys that are negligible under atmospheric conditions (Ref 88). Consequently, extensive long-term evaluations of the effects of exposure in different industrial, chemical, seacoast, tropical, and rural environments have been made (Ref 89–92).

Data collected in these programs include measurements of maximum and mean depth of attack, weight loss, and changes in tensile properties. Because of the localized nature of the prevalent pitting corrosion, which leaves some (in many cases, most) of the original surface intact even after many years of weathering, weight loss or calculated average dimensional change based on weight loss may have limited significance. Changes in tensile strength, which reflect the effects of size, number, distribution, and acuity of pits, are generally most significant from a structural standpoint, while depth-of-attack determinations provide realistic measures of penetration rate.

Table 13b Change in tensile strength for cast aluminum alloys during various atmospheric exposures (ASTM International program)

Exposed as separately cast tensile specimens. Calculated from average tensile strength of several specimens (usually six)

	Change in strength, %, during exposure of indicated length at									
	Point Reyes, CA					Freeport, TX				
Alloy and temper	6 mo	1 yr	3 yr	5 yr	10 yr	6 mo	1 yr	3 yr	5 yr	10 yr
Sand castings										
208.0-F	...	–11	–13	–11	–10	–4	–5	–5	–9	–6
295.0-T6	...	–13	–15	–17	–16	–2	–9	–10	–10	–12
319.0-T6	...	–9	–14	–11	–10	–2	–1	–7	–6	–4
355.0-T6	...	–4	–8	–7	–10	1	–1	–4	–3	–7
356.0-T6	...	0	–1	–2	–5	2	–3	0	–3	–4
443.0-F	...	–7	–10	–10	–10	0	–1	–2	–4	–6
520.0-T4	1	–3	–6	–7	...	1	–4	–7	–11	...
705.0-T5	...	3	–8	–6	–4	6	3	–5	–4	–8
707.0-T5	...	–5	–8	–7	–9	–1	–5	–15	–16	–32(a)
710.0-T5	...	–1	–3	–4	–3	4	–1	–1	0	–2
712.0-T5	...	–7	–7	–8	–14	1	–7	–6	–9	–9
713.0-T5	...	–3	–6	0	–3	–4	–6	–7	–6	–9
Permanent mold castings										
319.0-T61	...	–7	–15(a)	–14(a)	–16(a)	0	–7	–4	–5	–5
355.0-T6	...	–6	–2	–8	–13	4	–4	5	–2	–7
443.0-F	...	–7	–11	–8	–10	0	–1	–3	–2	–2
705.0-T5	...	–5	–6	–3	–4	–3	–5	–5	–8	–14
707.0-T5	...	–3	–2	–2	–9	1	–3	–6	–10	–24(a)
711.0-T5	...	–5	–9	–6	–9	1	–4	–3	–1	–8
713.0-T5	...	–9	–6	–4	–9	–6	–9	–2	0	–6

(a) Average tensile strength values were below required minimum. Source: Ref 95

Table 14 Atmospheric corrosion rates for aluminum and other nonferrous metals at several exposure sites

		Depth of metal removed per side(a), in μm/yr, during exposure of indicated length for specimens of							
		Aluminum(b)		Copper(c)		Lead(d)		Zinc(e)	
Location	Type of atmosphere	10 yr	20 yr	10 yr	20 yr	10 yr	20 yr	10 yr	20 yr
Phoenix, AZ	Desert	0.000	0.076	0.13	0.13	0.23	0.10	0.25	0.18
State College, PA	Rural	0.025	0.076	0.58	0.43	0.48	0.30	1.07	1.07
Key West, FL	Seacoast	0.10	...	0.51	0.56	0.56	...	0.53	0.66
Sandy Hook, NJ	Seacoast	0.20	0.28	0.66	...	...	...	1.40	...
La Jolla, CA	Seacoast	0.71	0.63	1.32	1.27	0.41	0.53	1.73	1.73
New York, NY	Industrial	0.78	0.74	1.19	1.37	0.43	0.38	4.8	5.6
Altoona, PA	Industrial	0.63	...	1.17	1.40	0.69	...	4.8	6.9

(a) Calculated from weight loss, assuming uniform attack, for 0.89 mm (0.035 in.) thick panels. (b) Aluminum 1100-H14. (c) Tough pitch copper (99.9% Cu). (d) Commercial lead (99.92% Pb). (e) Prime western zinc (98.9% Zn). Source: Ref 98

Effect of Exposure Time. A very important characteristic of weathering of aluminum and of corrosion of aluminum under many other environmental conditions is that corrosion rate decreases with time to a relatively low, steady-state rate (Ref 89). This deceleration of corrosion (Fig. 19–21) occurs regardless of alloy composition, type of environment, or the parameter by which the corrosion is measured. However, loss in tensile strength, which is influenced somewhat by pit acuity and distribution but is basically a result of loss of effective cross section, decelerates more gradually than depth of attack (Fig. 19).

The decrease in rate of penetration of corrosion is dramatic. In general, rate of attack at discrete locations, which is initially approximately 0.1 mm/yr (4 mils/yr), decreases to much lower and nearly constant rates within a period of approximately 6 months to 2 years. For the deepest pits, the maximum rate after approximately 2 years does not exceed approximately 0.003 mm/yr (0.11 mil/yr) for severe seacoast locations and may be as low as 0.0008 mm/yr (0.03 mil/yr) in rural or arid climates. The dramatic deceleration in penetration is illustrated by the specimen cross sections shown in Fig. 20 and by the depth-of-attack curves shown in Fig. 21, both of which are from the same 30 year test program (Ref 93). Also shown in Fig. 21 are results (shown as vertical bars) from other test programs in which various articles made of aluminum alloys were continuously exposed for various periods and in different locations, many of which are less severe than the relatively aggressive industrial environment of New Kensington, PA.

Data for Wrought Alloys. Several major test programs have been conducted under the supervision of ASTM International to investigate the weathering of aluminum alloy sheet. The first program, started in 1931, was limited in the variety of alloys tested but included desert, rural, seacoast, and industrial exposures. Data obtained after 20 years of exposure are listed in Table 10. Corrosion rates were calculated from cumulative weight loss after 20 years, and average and maximum depths of attack were measured microscopically. In aggressive (seacoast and industrial) environments, the bare (nonalclad) heat treated alloys—2017-T3 and, to a lesser extent, 6051-T4—exhibited more severe corrosion and greater resulting loss in tensile strength than the non-heat-treatable alloys. Alclad 2017-T3, although as severely corroded as the non-heat-treatable materials, did not show measurable loss in strength; in fact, some specimens of this alloy were 2 to 3% higher in strength after 20 years because of long-term natural aging.

Data from a comprehensive program initiated in 1958 were compiled from examinations and tests performed after 7 years of exposure (Ref 93). Thirty-four combinations of alloy and temper in the form of 1.27 mm (0.050 in.) thick sheet were exposed at four sites—two seacoast, one industrial, and one rural; Table 11

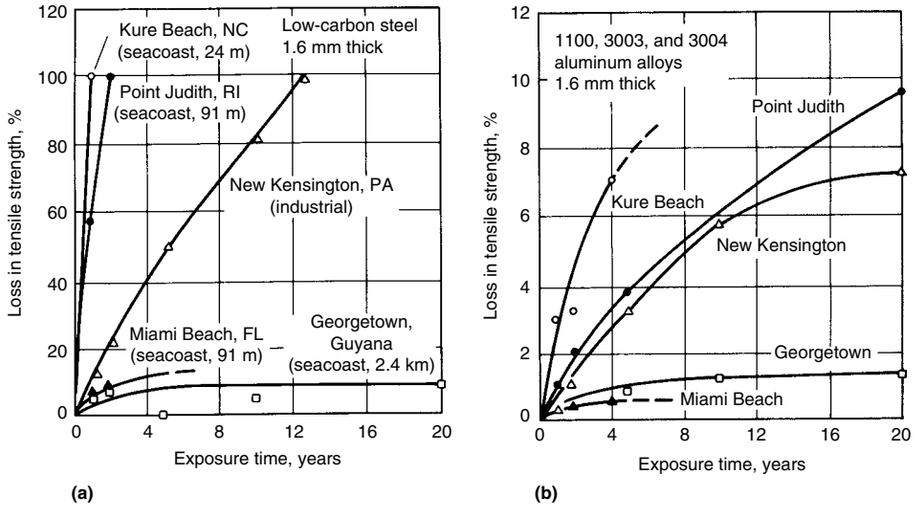

Fig. 22 Tensile-strength losses for (a) low-carbon steel and (b) representative non-heat-treatable aluminum alloys at several atmospheric exposure sites. Strength losses of the aluminum alloys are less than one-tenth that of the low-carbon steel

lists average values of measurements reported at two of the more aggressive sites. In another ASTM International program, 10 years of weathering produced the changes in tensile strength reported in Table 12.

Data from these and other weathering programs (Ref 96, 97) demonstrate that differences in resistance to weathering among non-heat-treatable alloys are not great, that alclad products retain their strength well because corrosion penetration is confined to the cladding layer, and that corrosion and resulting strength loss tend to be greater for bare (nonalclad) heat treatable 2*xxx*- and 7*xxx*-series alloys.

Data for Casting Alloys. The testing program that was the source of the strength change data for wrought alloys given in Tables 9(a) and (b) also provided weathering data for casting alloys exposed for the same period of time and at the same sites. Specimens were separately sand-cast and permanent mold-cast tensile bars, each with a reduced section 12.7 mm (0.5 in.) in diameter. Strength change data for these alloys are summarized in Table 13. Alloys with relatively high copper contents, such as 295.0-T6, 208.0-F, 319.0-T6, and 319.0-T61, showed the greatest losses. Alloys of the zinc-containing 7*xx.x* series generally exhibited larger strength losses than alloys having low zinc or copper contents. In all cases, as for wrought materials, severity of corrosion varied widely, depending on environmental conditions.

Comparison with Other Metals. Other metals were exposed to the same weathering environments over the same time periods used to evaluate corrosion of aluminum alloys. Comparative corrosion rates (average loss in thickness per side calculated from weight losses measured after exposures of 10 and 20 years) are listed in Table 14 for aluminum, copper, lead, and zinc panels. Figure 22 compares losses in tensile strengths at several weathering sites for unprotected low-carbon steel (0.09C, 0.07Cu) and for aluminum alloys.

Filiform Corrosion

Filiform corrosion, sometimes termed worm-track corrosion, occurs on aluminum when it is coated with an organic coating and exposed to warm, humid atmospheres. The corrosion appears as threadlike filaments that initiate at defects in the organic coating, are activated by chlorides, and grow along the metal/coating interface at rates to 1 mm/d (0.04 in./d). The moving end of the filament is called the head, and the remainder of the track is called the tail. It is not clear why this type of corrosion forms tracks instead of circular spots of increasing diameter.

Filiform corrosion occurs only in the atmosphere, and relative humidity is the single most important factor. This type of attack is rare on aluminum below approximately 55% relative humidity or above 95%. In natural atmospheres, it occurs most readily on aluminum at relative humidities between 85 and 95%. Although temperature and the thickness of the organic coating are minor factors, elevating the temperature increases the rate of filament growth if the relative humidity stays within the critical range.

The presence of oxygen is fundamental because it supplies the primary reactant for the cathodic reaction. Essentially, filiform corrosion is a type of oxygen concentration cell in which the anodic area is the head of the filament and the cathode is the area surrounding it, including the tail (Ref 99).

Considerable acidity is generated at the leading edge of the head. Measurements of pH as low as 1.5 to 2.5 have been reported, with the electrolyte in the head containing large concentrations of chloride (Ref 100). Such acidic solutions can be highly corrosive to aluminum alloys if the filament head should stop moving.

Phosphate coatings or chromium-containing conversion coatings applied to the metal surface before the organic coating are widely used to protect against filiform corrosion, but they are not completely successful. Perfect coatings, the absence of chlorides, or relative humidity below 30 to 40% would also be beneficial, but these conditions are not likely to be encountered outside the laboratory.

Corrosion in Waters

High-Purity Water. Suitability of the more corrosion-resistant aluminum alloys for use with high-purity water at room temperature is well established by both laboratory testing and service experience (Ref 101). The slight reaction with the water that occurs initially ceases almost completely within a few days after development of a protective oxide film of equilibrium thickness. After this conditioning period, the amount of metal dissolved by the water becomes negligible.

Corrosion resistance of aluminum alloys in high-purity water is not significantly decreased by dissolved carbon dioxide or oxygen in the water or, in most cases, by the various chemicals added to high-purity water in the steam power industry to provide the required compatibility with steel. These additives include ammonia and neutralizing amines for pH adjustment to control carbon dioxide, hydrazine and sodium sulfate to control oxygen, and filming amines (long-chain polar compounds) to produce nonwettable surfaces. Somewhat surprisingly, the effects of alloying elements on corrosion resistance of aluminum alloys in high-purity water at elevated temperatures are opposite to their effects at room temperature; elements (including impurities) that decrease resistance at room temperature improve it at elevated temperatures.

At 200 °C (390 °F), high-purity aluminum of sheet thickness disintegrates completely within a few days of reaction with high-purity water to form aluminum oxide. In contrast, Al-Ni-Fe alloys have the best elevated-temperature resistance to high-purity water of all aluminum metals; for example, alloy X8001 (1.0Ni-0.5Fe) has good resistance at temperatures as high as 315 °C (600 °F) (Ref 102).

Natural Waters. Aluminum alloys of the 1*xxx,* 3*xxx,* 5*xxx,* and 6*xxx* series are resistant to corrosion by many natural waters (Ref 103–105). The more important factors controlling the corrosivity of natural waters to aluminum include water temperature, pH, and conductivity; availability of cathodic reactant; presence or absence of heavy metals; and the corrosion potentials and pitting potentials of the specific alloys. Various correlations of the corrosivity of natural waters to aluminum have been attempted (Ref 106), but none predicts the corrosivity of all natural waters reliably.

Seawater. Service experience with 1*xxx*, 3*xxx*, 5*xxx*, and 6*xxx* wrought aluminum alloys in marine applications, including structures, pipeline, boats, and ships, demonstrates their good resistance and long life under conditions of partial, intermittent, or total immersion. Casting alloys of the 356.0 and 514.0 types also show high resistance to seawater corrosion, and these alloys are used widely for fittings, housings, and other marine parts.

Among the wrought alloys, those of the 5*xxx* series are most resistant and most widely used because of their favorable strength and good weldability. Alloys of the 3*xxx* series are also highly resistant and are suitable where their strength range is adequate. With the 3*xxx*- and 5*xxx*-series alloys, thinning by uniform corrosion is negligible, and the rate of corrosion based on weight loss does not exceed approximately 5 μm/yr (0.2 mil/yr), which is generally less than 5% of the rate for unprotected low-carbon steel in seawater. Corrosion is mainly of the pitting or crevice type, characterized by deceleration of penetration with time from rates of 3 to 6 μm/yr (0.1 to 0.2 mil/yr) in the first year to average rates over a 10 year period of 0.8 to 1.5 μm/yr (0.03 to 0.06 mil/yr).

The Al-Mg-Si 6*xxx* alloys are somewhat less resistant; although no general thinning occurs, weight loss may be two to three times that for

Table 15 Average weight loss and maximum depth of pitting for aluminum alloy plate specimens after immersion in seawater

Specimens were 6.35 × 305 × 305 mm (0.250 × 12 × 12 in.) and weighed approximately 1.6 kg (3.5 lb).

Test series	Alloy and temper	Harbor Island, NC(a)				Halifax, NS				Esquimalt, BC(a)			
		1 yr	2 yr	5 yr	10 yr	1 yr	2 yr	5 yr	10 yr	1 yr	2 yr	5 yr	10 yr
Weight loss, g													
1	1100-H14	4.4	5.4	10.3	11.1	1.9	3.5	5.3	12.7	0.0	2.4	1.3	2.3
	3003-H14	4.1	6.4	9.3	11.2	0.0	3.3	4.6	7.5	0.0	0.0	3.0	2.2
	5052-H34	4.5	6.5	9.0	14.9	2.8	3.3	...	14.2	1.7	0.0	0.0	0.6
	6051-T4	3.7	4.9	9.9	12.3	0.0	0.7	3.5	8.0	1.9	7.8	19.0	14.6
	6051-T6	4.4	5.7	10.3	13.1	2.1	5.5	6.1	19.5	22.5	13.8	19.9	27.3
	6061-T4	4.8	6.6	12.4	18.6	4.4	6.0	8.0	15.6	0.9	2.3	28.2	62.0
	6061-T6	5.5	7.7	14.0	21.5	4.3	7.3	12.7	22.8	6.7	7.1	11.1	44.3
	7072...	...	...	...	10.2	...	...	...	15.9	...	...	...	3.1
	7075-T6	...	...	...	149.0	...	...	...	242.6	...	...	...	246.5
2	5083	2.5	3.7	...	7.3	2.8	0.0	6.1	8.5	1.3	1.9	2.7	3.3
	5083	4.7	3.4	5.7	8.1	2.6	3.2	5.2	7.5	15.3	16.3	36.3	31.1
	5056	3.7	4.7	6.0	9.2	2.5	3.3	5.7	10.4	10.7	16.5	19.5	28.9
	5056	4.5	5.2	...	16.7	4.0	4.1	5.5	11.1	7.0	6.0	11.0	11.4
	6051-T4	3.9	4.2	12.1	9.1	3.6	3.1	5.5	9.2	9.1	18.8	15.3	51.0
	6051-T6	4.1	4.5	7.7	10.6	5.3	4.1	8.4	18.6	17.2	23.3	30.6	33.5
	6053-T6	4.1	4.5	6.6	9.7	3.0	3.3	5.6	14.8	15.7	25.1	19.3	25.8
	6061-T4	7.6	13.4	29.4	51.6	9.8	11.2	33.2	48.5	12.3	26.8	48.7	48.0
	6061-T6	5.5	6.5	15.4	34.2	10.0	9.4	19.1	54.1	7.3	7.0	21.3	18.6
	Al-7 Mg	4.1	4.1	6.5	9.4	2.4	2.4	4.6	8.0	1.6	2.9	2.1	3.3
	Low-carbon steel(b)	219.0	294.0	471.3	979.8	208.0	292.6	761.1	1450.0	277.0	455.4	1012.4	2240.8
3	5154	2.8	5.2	6.0	...	2.4	2.6	3.8	...	1.4	2.1	2.6	...
	5083	3.5	4.6	6.0	...	2.0	2.8	3.6	...	0.2	2.2	2.8	...
	6053-T6	3.8	6.6	25.9	...	19.3	29.2	4.7	...	45.6	80.4	86.0	...
	7075-T6	60.4	49.3	74.8	...	44.8	66.1	116.0	...	50.9	71.3	153.5	...
	3003. alclad	4.3	12.0	...	...	1.6	2.3	...	...	...	1.9	...	...
	6061, alclad	4.3	3.9	5.7	...	8.4	3.3	6.5	...	20.8	15.8	34.3	...
	7075, alclad	4.4	5.2	6.1	...	2.8	3.6	6.8	...	8.5	14.5	16.6	...
Maximum depth of pitting, mils													
1	1100-H14	0	0	40	40	17	32	0	32	30	26	15	30
	3003-H14	0	0	13	21	13	15	21	22	5	20	0	20
	5052-H34	0	0	0	0	5	20	6	12	16	6	0	5
	6051-T4	0	0	5	0	0	10	0	62	10	65	51	37
	6051-T6	2	0	5	0	19	56	15	64	70	60	181	238
	6061-T4	0	13	2	14	12	18	21	33	15	50	20	50
	6061-T6	36	24	60	95	36	43	43	54	30	25	80	116
	7072	...	...	...	56	...	...	...	150	...	...	...	26
	7075-T6	...	...	...	66	...	...	...	(c)	...	...	...	(c)
2	5083	12	9	6	0	3	0	12	7	13	5	0	6
	5083	16	13	6	10	4	23	16	22	29	38	47	55
	5056	7	10	7	5	3	0	12	15	20	39	34	35
	5056	10	10	5	28	0	0	10	24	20	1	0	11
	6051-T4	16	4	7	15	3	0	9	35	25	47	109	170
	6051-T6	11	17	9	15	5	8	25	60	55	34	184	200
	6053-T6	30	15	14	58	28	34	66	95	93	126	165	105
	6061-T4	67	100	144	130	50	67	90	122	60	100	125	125
	6061-T6	15	27	36	40	38	47	58	67	35	48	60	55
	Al-7 Mg	12	7	8	8	3	0	12	14	8	12	0	7
3	5154	12	9	5	...	0	12	15	...	0	0	3	...
	5083	22	1	7	...	0	11	7	...	0	0	5	...
	6053-T6	28	150	186	...	93	91	34	...	81	118	118	...
	7075-T6	25	25	25	...	18	17	(d)	...	15	11	(d)	...
	3003, alclad	0	12	...	...	0	13	...	...	...	13	...	...
	6061, alclad	10	10	9	...	9	11	9	...	11	13	9	...
	7075, alclad	10	15	13	...	13	14	12	...	12	14	15	...

(a) Harbor Island is near Wilmington, NC; Esquimalt is near Victoria, BC. (b) Original weight approximately 4.8 kg (10.6 lb). (c) Plate was perforated. (d) Could not determine because no original surface left. Source: Ref 2

5*xxx* alloys. The more severe corrosion is reflected in larger and more numerous pits.

Alloys of the 2*xxx* and 7*xxx* series, which contain copper, are considerably less resistant to seawater than 3*xxx,* 5*xxx,* and 6*xxx* alloys and are generally not used unprotected. Protective measures, such as use of alclad products and coating by metal spraying or by painting, provide satisfactory service in certain situations.

Aluminum boats operating in saltwater require antifouling paint systems, because aluminum and its alloys do not inhibit growth of marine organisms. Aluminum is impervious to worms and borers, and the acids exuded from marine organisms are not corrosive to aluminum; but the accumulation of biofouling on the bottom of the boat impairs performance. Aluminum boats operating in both salt- and freshwater, which alleviates fouling problems, have been able to leave underwater hull areas unpainted (Ref 107).

To make antifouling paint systems adhere properly to aluminum, careful surface preparation of the metal is necessary. A thorough precleaning and either a conversion coating or a washcoat primer are required, followed by a corrosion-inhibiting primer and a topcoat. The antifouling paint is applied to the topcoat. Primers containing red lead should not be used, because this substance may cause galvanic corrosion of the aluminum. For the same reason, copper-containing antifouling paints should not be used on aluminum hulls. The preferred antifouling paints for aluminum are those containing organic tin compounds.

The literature on corrosion testing of aluminum alloys in seawater is extensive. Summaries of information are provided in Ref 108 and 109 and in most of the selected references. Table 15 lists results of 10 year immersion testing of various alloys in the form of rolled plate exposed in three locations. The relationships among the types of alloys that have been discussed and a comparison with unprotected low-carbon steel are apparent. Similar data for extruded products of several 6*xxx* alloys and one 5*xxx* alloy are given in Table 16. Direct comparison of the data in Tables 15 and 16 is provided in Table 17, in which corrosion is expressed in terms of average weight loss, and in Fig. 23, which illustrates the deceleration of corrosion rate with time that is characteristic of aluminum alloys. Data on corrosion rates, maximum and average depth of pitting, and changes in tensile strength compiled during 10 year tidal and full-immersion exposure of seven 5*xxx* alloys and superpurity aluminum 1199 are summarized in Table 18. Full immersion generally resulted in more extensive corrosion than tidal exposure, although the reverse relationship has also been observed. Tensile-strength losses were 5% or less, and yield-strength losses were less than 5% in the panels completely immersed and generally lower in those exposed to tidal immersion.

The data in Table 19 illustrate the corrosion resistance of aluminum alloy plates, with and without riveted or welded joints, in flowing seawater. All assemblies and panels underwent only moderate pitting and retained most of their original strength.

The corrosion behavior of aluminum alloys in deep seawater, judging from tests at a depth of 1.6 km (1 mile), is generally the same as at the surface except that the rate of pit penetration may be higher and the effect of crevices somewhat greater (Ref 111). The corrosivity of unpolluted full-strength seawater depends on several factors: dissolved oxygen content; pH, temperature, and velocity of the water flow; and the presence or absence of heavy-metal ions, particularly copper (Ref 48). The corrosion rate tends to be increased by decreasing temperature, pH, and flow velocity and by increasing dissolved oxygen (Ref 48, 112–114). The higher corrosion rate in deep water is not caused by low dissolved oxygen, as stated in the older literature, but is caused by the combination of low pH and low temperature.

Surface-water conditions at various tropical locations are benign to aluminum alloys because of their high temperature, high pH, and the virtual absence of heavy-metal contamination (Ref 115–117). A variety of aluminum alloys in the form of heat-exchanger tubing have been tested for up to 3 years in surface water off Keahole Point, HI, with no significant pitting or crevice corrosion (Ref 115).

Experience with seawater desalination units has demonstrated the high degree of resistance of aluminum alloys to deaerated seawater at temperatures to 120 °C (250 °F). For example, an 11,355 L/day (3000 gal/day) multiflash aluminum unit at the Office of Saline Water Materials Test Center at Freeport, TX, operated at 99% efficiency and with minimal corrosion for more than 3 years under process conditions selected to match those of a commercial installation. Such experience has shown, however, that galvanic attack of aluminum alloys in contact with dissimilar metals is more

Table 16 Average weight loss and maximum depth of pitting for aluminum alloy extruded specimens after immersion in seawater

Specimens were 6.35 mm (0.250 in.) thick, 0.170 m^2 (1.83 ft^2) in area, and weighed approximately 1.2 kg (2.6 lb).

		Harbor Island, NC(a)				Halifax, NS				Esquimalt, BC(a)			
Test series	**Alloy and temper**	**1 yr**	**2 yr**	**5 yr**	**10 yr**	**1 yr**	**2 yr**	**5 yr**	**10 yr**	**1 yr**	**2 yr**	**5 yr**	**10 yr**
Weight loss, g													
1	6051-T4	2.9	0.0	8.0	8.2	7.8	1.5	4.5	6.3	2.8	0.0	...	...
	6051-T6	6.2	0.0	...	14.6	9.0	10.5	12.8	23.4	15.4	40.7	29.7	83.0
	6061-T4	4.7	10.9	...	7.4	0.0	0.4	4.3	7.4	0.2	10.0	29.8	38.3
	6061-T6	3.0	6.9	8.1	16.4	3.8	5.0	7.1	15.5	15.5	14.1	25.2	59.2
2	5056	3.2	2.7	6.3	9.9	6.3	2.8	4.2	6.2	5.0	1.9	3.6	4.8
	6051-T4	3.0	3.4	6.5	8.0	13.1	9.2	7.8	12.0	16.0	16.7	18.0	35.4
	6051-T6	4.9	11.1	5.7	9.4	19.9	...	23.0	78.9	23.0	30.2	41.3	122.8
	6053-T6	3.3	4.9	6.9	10.6	2.6	3.0	4.5	8.9	4.5	43.5	35.3	99.9
3	5056	2.0	5.2	5.1	...	1.3	1.3	2.1	...	3.5	9.4	2.4	...
	6063-T5	2.6	3.3	6.5	...	2.4	3.5	4.9	...	6.6	13.4	13.1	...
	6053-T6	2.8	3.0	5.3	...	25.7	12.0	30.6	...	43.5	29.9	77.1	...
Maximum depth of pitting, mils													
1	6051-T4	0	0	27	20	27	27	14	32	35	23	65	72
	6051-T6	70	40	46	67	52	68	125	(b)	70	(b)	160	(b)
	6061-T4	23	23	27	12	25	20	12	32	33	45	56	70
	6061-T6	13	13	10	15	15	9	14	27	20	30	46	45
2	5056	13	7	35	32	60	0	16	41	30	17	99	50
	6051-T4	57	5	20	15	34	65	30	74	66	65	90	115
	6051-T6	58	>100	34	45	100	...	84	(b)	64	85	107	>200(c)
	6053-T6	13	25	93	46	0	0	7	34	80	110	175	210
3	5056	28	68	17	...	0	3	15	...	37	72	63	...
	6063-T5	42	35	45	...	27	25	30	...	70	66	136	...
	6053-T6	28	1	20	...	185	90	(b)	...	178	(b)	(b)	...

(a) Harbor Island is near Wilmington. NC; Esquimalt is near Victoria. BC. (b) Plate was perforated. (c) In thick web of angle. Source: Ref 2

severe at elevated temperatures than at room temperature.

Corrosion in Soils

Soils differ widely in mineral content, texture and permeability, moisture, pH and aeration, presence of organic matter and microorganisms, and electrical resistivity. Because of these variations, the corrosion performance of buried aluminum varies considerably, and a clear understanding of its behavior has depended on the accumulation of many field corrosion tests and actual case histories over an extended period of time (Ref 2, 118, 119).

Corrosion of the copper-containing 2*xxx*- and 7*xxx*-series alloys in moist low-resistivity soils, measured by weight loss and pitting depth, is several times greater than corrosion of the more resistant 1*xxx*-, 3*xxx*-, 5*xxx*-, and 6*xxx*-series alloys, and applications of the copper-bearing alloys for buried service is limited accordingly. Use of cathodic protection or alclad products effectively reduces corrosion or limits penetration.

Aluminum alloys 3003, 6061, and 6063 are most frequently used for surface and underground pipelines for irrigation, petroleum, and mining applications. Most early installations used uncoated pipe (Ref 120). Hundreds of miles of pipe were installed, ranging in wall thickness from 1.5 to 19 mm (0.06 to 0.75 in.). Some of these have been in service for over 40 years. When used, coatings are usually bituminous products or tape wraps. Unprotected sections exhibited corrosion attack ranging from almost none to deep pitting. Cathodically protected sections of some of the same pipes in corrosive soil showed either no attack or only mild etching. Cathodic protection of buried aluminum was standardized in 1963 (Ref 41). In addition to pipelines, extensive experience was gained with aluminum culverts in various soils (Ref 121).

Soil resistivity provides a useful guideline to soil corrosivity; corrosion problems are usually limited to soils having resistivities less than 1500 Ω · cm (Ref 122). Experience has shown that soils, at least to the depth normally used to bury pipelines, are noncorrosive to aluminum over large areas of North America. However, noncorrosive soils can be rendered corrosive if they become contaminated with certain substances, such as cinders, and variability of soils along a long pipeline can lead to galvanic corrosion of portions of the line.

Techniques for installing buried aluminum pipelines have improved, including better joining methods and the ability to plow in long lengths of pipe directly from coils. A high-energy joining technique has replaced conventional field welding (Ref 122). The technique does not require filler metal and is sufficiently rapid that it does not produce heat-affected zones in the metal.

Table 17 Average weight loss (mg/m^2) for aluminum alloys in seawater (from Tables 12 and 13)

	Harbor Island, NC				Halifax, NS				Esquimalt, BC			
Test series	**1 yr**	**2 yr**	**5 yr**	**10 yr**	**1 yr**	**2 yr**	**5 yr**	**10 yr**	**1 yr**	**2 yr**	**5 yr**	**10 yr**
Series 1: plate(a)												
1100, 3003, 5052	22	32	49	64	9	18	26	60	3	4	7	9
6051, 6061	24	32	60	85	12	25	39	85	41	40	101	191
Series 1: extrusions(b)												
6051, 6061	25	26	47	68	30	26	42	78	50	95	166	354
Series 2: plate(a)												
Al-Mg	20	22	32	52	15	13	28	47	37	39	74	81
Al-Mg-Si	26	34	75	119	55	54	75	149	64	111	140	183
Series 2: extrusions(b)												
Al-Mg	19	19	38	62	25	16	21	37	18	11	15	26
Al-Mg-Si	22	38	38	41	70	24	70	196	85	177	185	506

(a) Plate surface area 0.193 m^2 (2.08 ft^2). (b) Extrusion surface area. 0.170 m^2 (1.83 ft^2). Source: Ref 2

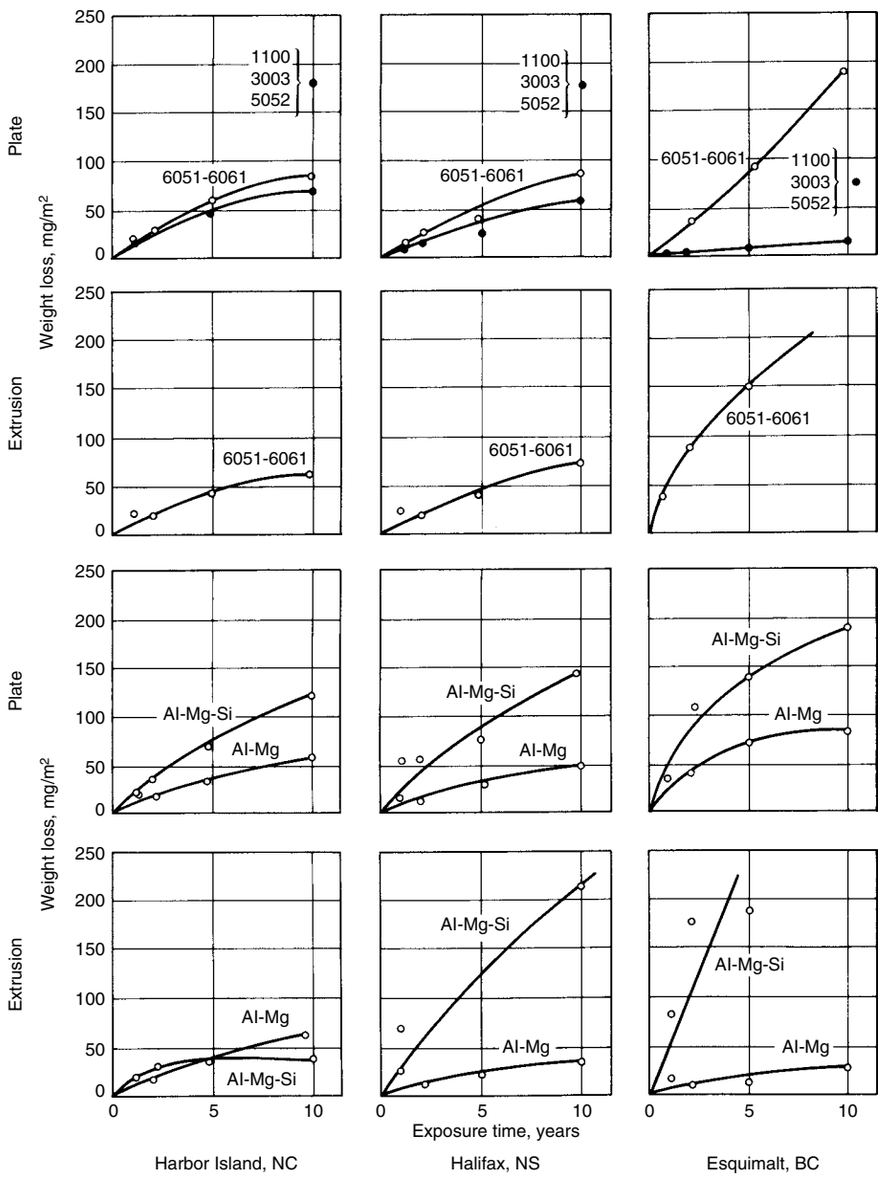

Fig. 23 Weight loss as a function of exposure time for three aluminum alloys in seawater

Table 18 Summary of data from 10 year seawater exposures at Wrightsville Beach, NC

Alloy and temper	Mg, %	Thickness		Corrosion rate based on weight change		Maximum depth of attack in 10 years		Average depth of attack in 10 years		Change in tensile strength in 10 years, %
		mm	in.	μm/yr	mil/yr	mm	mil	mm	mil	
Half-tide exposure										
1199	...	1.27	0.050	0.91	0.036	0.99	0.039	0.07	0.003	0
5154-H38	3.5	1.27	0.050	0.94	0.037	0.50	0.020	0.13	0.005	–2.1
5454-H34	2.7	6.35	0.250	1.04	0.041	0.39	0.015	0.07	0.003	–0.7
5457-H34	1.0	1.02	0.040	0.91	0.036	0.56	0.022	0.03	0.001	–4.2
5456-O	5.1	6.17	0.243	0.36	0.014	1.74	0.069	0.32	0.013	–0.4
5456-H321	5.1	6.17	0.243	1.29	0.051	1.83	0.072	0.34	0.013	–4.5
5083-O	4.5	6.35	0.250	0.91	0.036	0.97	0.038	0.31	0.012	0
5086-O	4.0	2.03	0.080	0.89	0.035	0.69	0.027	0.06	0.002	–2.7
Full-immersion exposure										
1199	...	1.27	0.050	1.55	0.061	...	...	...	...	0
5154-H38	3.5	1.27	0.050	1.40	0.055	...	...	...	...	–5.1
5454-H34	2.7	6.35	0.250	1.50	0.059	0.51	0.020	0.10	0.004	–0.5
5457-H34	1.0	1.02	0.040	1.42	0.056	...	...	...	...	–5.2
5456-O	5.1	6.17	0.243	2.95	0.116	3.33	0.131	1.01	0.040	–3.0
5456-H321	5.1	6.17	0.243	1.62	0.064	1.12	0.044	0.31	0.012	–1.1
5083-O	4.5	6.35	0.250	1.50	0.059	0.61	0.024	0.03	0.001	0
5086-O	4.0	2.03	0.080	1.45	0.057	...	...	...	...	–3.7

Source: Ref 110

Table 19 Corrosion resistance of aluminum alloy plate, with and without joints, partially immersed in flowing seawater at Kure Beach, NC

Alloy and temper	Type of joint	Exposure period, years	Maximum depth of attack, mils			Change in tensile strength due to corrosion(a), %
			Plate		Rivet or weld	
			Outside surface	Faying surface		
Continuously immersed						
6053-T6	Riveted(b)	6	1.4	3.0	8.4	0
6061-T6	Riveted(c)	1	1.4	2.8	2.8	0
6053-T6	Welded(d)	2	5.0	...	4.2	...
6061-T6	Welded(d)	1	5.0	...	9.8	...
6061-T4	None	3	2.1	...	...	2
6061-T6	None	3	1.4	...	...	1
2024-T4 alclad(e)	None	5	4.2	...	...	0
3004-H14 alclad(f)	None	5	1.4	...	...	−5
520.0-T4(g)	None	3	4.2	...	...	−4
Not immersed (atmospheric exposure)						
6053-T6	Riveted(d)	6	5.6	5.6	11.7	−1
6061-T6	Riveted(e)	1	5.6	2.1	8.5	0
6053-T6	Welded(f)	2	3.3	...	9.8	...
6061-T6	Welded(f)	1	7.0	...	9.8	...
6061-T4	None	3	2.1	...	...	1
6061-T6	None	3	4.2	...	...	1
2024-T4 alclad(e)	None	5	8.4	...	...	0
3003-H14 alclad(f)	None	5	7.0	...	...	−5
520.0-T4(g)	None	3	1.4	...	...	4

(a) Results of testing 6.4 mm (0.25 in.) thick ASTM International tensile specimens cut from indicated location in test plate (generally, two specimens were cut from each test plate and the results were averaged). (b) 6053-T6 rivets. (c) 6061-T43 rivets. (d) 4043 filler metal. (e) Average thickness of cladding on each surface, 297 μm (11.7 mils). (f) Average thickness of cladding on each surface. 307 μm (12.1 mils). (g) Sand cast. Source: Ref 4

It was concluded from early field experience that buried aluminum pipelines should be coated, because the risk of pitting could not be eliminated, even in high-resistivity soils. In addition, and in keeping with similar requirements for buried steel lines, buried aluminum lines should be cathodically protected. The current density requirement for protecting aluminum is roughly 10% of that required for similarly coated steel. Because of the risk of alkaline corrosion, applied cathodic voltages should not be more negative than −1.20 V versus the saturated $Cu/CuSO_4$ electrode.

Resistance of Anodized Aluminum

Anodizing is an electrolytic oxidation process that produces on an aluminum surface an integral coating of amorphous aluminum oxide that is much thicker than the natural barrier layer. The anodic coatings used for decoration and/or protection of aluminum have a thin, nonporous barrier-type layer adjacent to the metal interface and a porous outer layer that can be sealed by hydrothermal treatment in water or in a metal salt solution to increase its protective value. The entire coating adheres tightly to the aluminum substrate, resists abrasion, and, when adequate in thickness, provides greatly improved protection against weathering and other corrosive conditions (Ref 123).

For outdoor applications of aluminum parts, a coating thickness of 5 to 7.6 μm (0.2 to 0.3 mil) is normally specified for bright automotive trim and 17 to 30 μm (0.7 to 1.2 mils) for architectural product finishes. Dichromate sealing affords added protection in severe saline environments. Because coatings can be attacked and stained by alkaline building materials (such as mortar, cement, and plaster), a clear, nonyellowing lacquer is often applied to anodized aluminum architectural parts to protect the finish during construction. An added advantage of lacquer coatings is that they minimize soil accumulation during service.

In general, chemical resistance of anodic coatings is greatest in approximately neutral solutions, but such coatings are usually serviceable and protective if the pH is between 4 and 8.5. More acidic and more alkaline solutions attack anodic coatings.

Under atmospheric weathering, the number of pits developed in the base metal decreases exponentially with increasing coating thickness (Fig. 24). The pits may form at minute discontinuities or voids in the coating, some of which result from large second-phase particles in the microstructure. The pit density was determined by dissolving the anodic coating in a stripping solution that does not attack the metal substrate. After the 8½ year exposure, the pits were of pin-point size and had penetrated less

than 50 μm (2.0 mils). Specimens with coatings at least 22 μm (0.9 mil) thick were practically free of pitting.

Weathering of anodic coatings involves relatively uniform erosion of the coating by windborne solid particles, rainfall, and some chemical reaction with pollutants. The available information indicates that such erosion occurs at a reasonably constant rate, which averaged 0.33 μm/yr (0.013 mil/yr) for several alloys exposed to an industrial atmosphere for 18 years (Fig. 25).

A 3 year seacoast exposure of specimens of several alloys with 23 μm (0.9 mil) thick sulfuric acid coatings caused no visible pitting except in several alloys of the 7*xxx* series and in a 2*xxx* alloy (Table 20). Alloys that exhibited pitting where not protected any more effectively by 51 μm (2 mils) thick coatings. This confirms a general observation that optimal protection against atmospheric corrosion is achieved in the coating thickness range of 18 to 30 μm (0.7 to 1.2 mils) and that thicker coatings provide little additional protection.

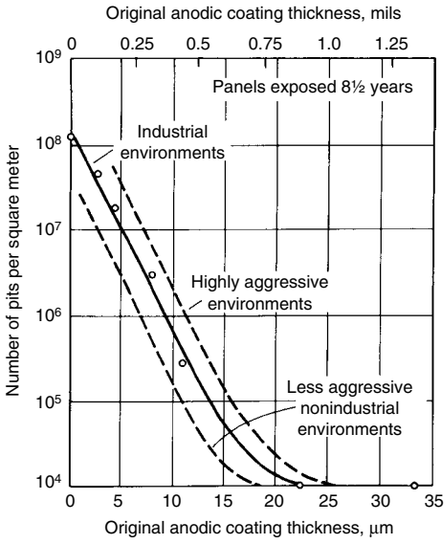

Fig. 24 Number of corrosion pits in anodized aluminum 1100 as a function of coating thickness. Source: Ref 124

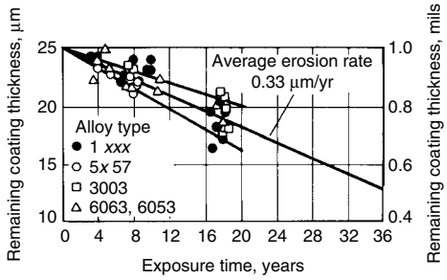

Fig. 25 Weathering data for anodically coated aluminum in an industrial atmosphere

Anodized aluminum exterior automotive parts, such as bright trim and bumpers, exhibit good resistance to deicing salts and other ingredients of road splash despite the limited thickness applied to maintain brightness and image clarity. Development of a hazy coating appearance is considered more of a problem than pitting during service in these applications. The hazy appearance results from scattering of light from a coating surface that has been microroughened as a result of inadequate sealing or use of excessively harsh alkaline cleaners.

Anodic coatings, unless used as part of a protective system that includes such other measures as shot peening or painting, are not reliable for protection against SCC of susceptible alloys. Data obtained with short-transverse direction specimens from plate of alloy 7075-T651 and other susceptible alloys show that the anodic coating may retard, have no effect, or even accelerate SCC, depending on the level of stress and, to some extent, on whether or not the stress was present before anodizing. High stresses applied after anodizing crack the coating. The effects of several applied protective measures on lifetimes of specimens in industrial and seacoast environments under relatively high elastic strain are shown in Fig. 26, in which the relatively small protective value of anodic coatings is apparent (Ref 125).

Effects of Nonmetallic Building Materials

Many nonmetallic building materials that contact aluminum during and after construction, either intentionally or accidentally, have been evaluated to determine their corrosive effects (Ref 126). Many of these materials that contain calcium or magnesium hydroxides are alkaline and, when wet, may cause overall surface attack of bare aluminum. This early reaction produces protective films of limited solubility that resist further corrosion. Such materials cause only superficial or mild surface attack, most of which occurs during initial stages of exposure.

Drainage from freshly applied concrete, plaster, mortar, or stucco is highly alkaline and causes slight attack and discoloration. This is most likely to occur during or shortly after construction, and leaching by subsequent rains, as well as conversion to carbonates, reduces the alkalinity and further attack. Staining can be effectively prevented by organic coatings.

Some insulating materials that are porous and absorbent may cause corrosion when wet. If more cathodic metals, such as steel or copper alloys, are electrically coupled with the aluminum through these materials, galvanic attack may occur. Protective paint films on the cathodic metal, moisture barriers, or chemical inhibition are required for optimal performance under these conditions.

Concrete, plaster, mortar, and cements also cause superficial etching of aluminum, most of which occurs during the curing period. The surface attack involves dissolution of the natural oxide film and some of the metal, but a new film is formed that prevents further corrosion. Coupling with more cathodic metals has little effect on aluminum embedded in these materials, except in those that contain certain curing or antifreeze additives.

When partly embedded in concrete, some metals undergo accelerated corrosion where the metal intersects the exposed surface of the concrete. This effect is usually not important for aluminum, but special consideration must be given to protection of faying surfaces or crevices between the aluminum and the concrete, which may entrap environmental contaminants. For example, highway railings and streetlight standards and stanchions are usually coated with a

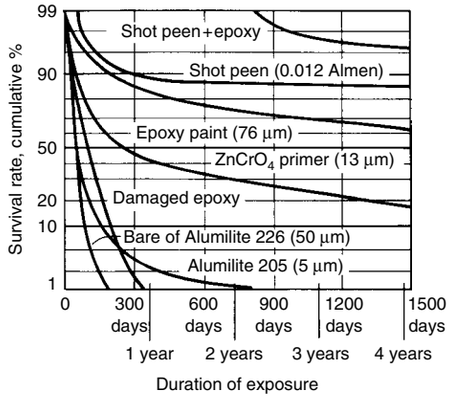

Fig. 26 Relative effectiveness of various protective systems in preventing stress-corrosion cracking of susceptible aluminum alloys. Combined data for highly elastically strained specimens of alloys 2014-T651 and 7079-T651 exposed at Pt. Judith, RI; Comfort, TX; and New Kensington, PA

Table 20 Results of 3 year seacoast exposure testing of anodized aluminum alloys

Alloy and temper	Results
Sheet	
1100	No visible pitting
2024-T3, alclad	Edge pitting only
5456-H343	No visible pitting
5086-H34	No visible pitting
6061-T6	No visible pitting
7039-T6	No visible pitting
7075-T6	Edge pitting only
7075-F, alclad	Edge pitting only
7079-T6	Edge pitting only
Extrusions	
6351-T6	No visible pitting
6061-T6	No visible pitting
6063-T5	No visible pitting
6070-T6	No visible pitting
7039-T6	Scattered small pits

Note: H_2SO_4 anodic coatings 23 μm (0.9 mil) thick, sealed in boiling water on test panel 100 × 150 mm (4 × 6 in.) cut from sheet and extrusions

sealing compound where they are fastened to concrete in order to prevent entry of salt-laden road splash into crevices.

Contact with Foods, Pharmaceuticals, and Chemicals

The widespread use of aluminum in processing, handling, and packaging of foods, beverages, and pharmaceutical and chemical products is based on economic factors and the excellent compatibility of aluminum with many of these products (Ref 127). In addition to high corrosion resistance in contact with such products, many of these applications depend on the nontoxicity of aluminum and its salts, as well as its freedom from catalytic effects that cause product discoloration. Aluminum for packaging foods, beverages, and pharmaceutical products accounts for approximately 20% of the aluminum marketed in the United States (Ref 128). The largest amount is used in beverage cans, and a smaller amount for foods. These cans generally have both internal and external organic coatings, primarily for decoration and for protection of product taste.

Large quantities of aluminum foil, either uncoated or with plastic coatings, are used in flexible packages. Coated foil is also used with fiber board in construction of rigid containers. The foil in such rigid containers, because of its extreme thinness, must be coated; only the slightest corrosion can be tolerated, and perforation must not occur even during long periods of storage. Packaging foils are produced from unalloyed aluminum corresponding to composition limits for aluminum 1230. Sheet for beverage can bodies is generally alloy 3004, food can bodies alloys 5352 or 5050, and can ends alloy 5182. These alloys have high corrosion resistance and are not normally subject to corrosion problems in such applications.

Aluminum alloy household cooking utensils, usually made of alloy 1100 or 3003, have been used for many years. These utensils, as well as commercial food-processing equipment, do not require protective coatings; however, ceramic coatings are often applied to the exteriors of cooking utensils for aesthetic reasons, and polymeric coatings to the food-contacting surfaces for nonsticking characteristics. Alloys used in commercial food processing include alloy 3003, 5*xxx* alloys, and casting alloys 444.0 and 514.0.

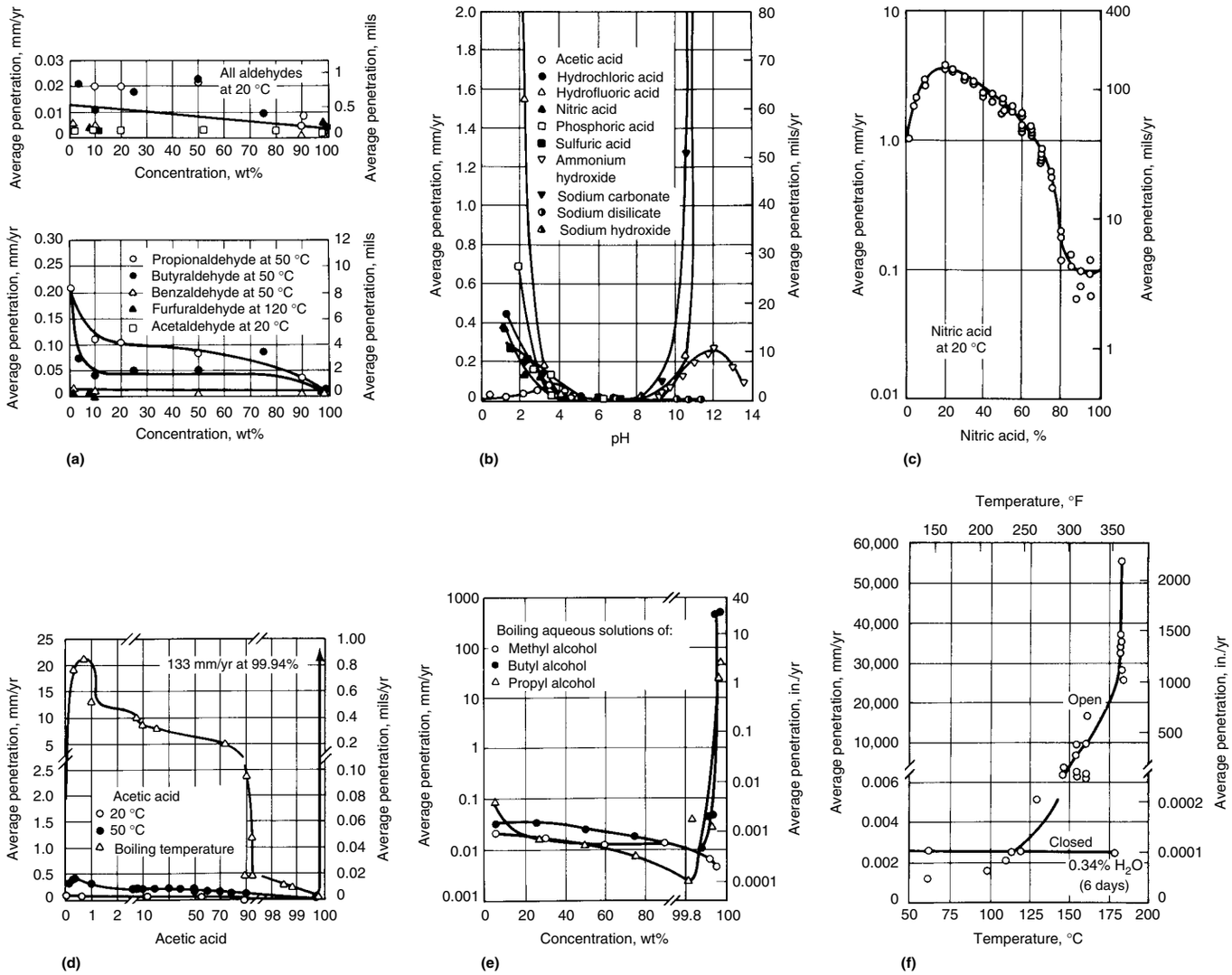

Fig. 27 Corrosion of aluminum 1100-H14 in various chemical solutions. Average penetration calculated from weight loss data in short-term tests. (a) Effect of concentration of aqueous solutions of several aldehydes. Rates of attack indicate that aluminum should be satisfactory for handling all these solutions. (b) Effect of pH. The concentration of all the solutions ranged from 0.00001 to 0.1 *N*, except acetic acid (0.00001 to 17.4 *N*), ammonium hydroxide (NH_4OH) (0.00001 to 15 *N*), and sodium disilicate ($Na_2Si_2O_5$) (0.00001 to 1 *N*). (c) Effect of concentration of HNO_3 solutions at room temperature. (d) Effect of concentration and temperature of acetic acid. (e) Effect of concentration of boiling aqueous solutions of three alcohols. (f) Effect of temperature of phenol. Rapid reaction above 120 °C (250 °F) can be stopped by small additions of steam or water

Unsatisfactory performance is sometimes caused by use of improper cleaners. Some alkaline cleaners cause excessive corrosion and should not be used unless they are inhibited effectively.

Aluminum alloys are used in processing, handling, and packaging a wide variety of chemical products (Ref 129, 130). Aluminum alloys are compatible with dry salts of most inorganic chemicals. Factors controlling compatibility of aluminum alloys with aqueous solutions have been discussed in earlier sections in this article. Within their passive pH range (approximately 4 to 9), aluminum alloys resist corrosion by solutions of most inorganic chemicals, but they are subject to pitting in aerated solutions, particularly halide solutions, in which they are polarized to their pitting potentials.

Figure 27 illustrates the corrosion behavior of aluminum in several acids and bases. Aluminum alloys are not suitable for handling mineral acids, with the exception of HNO_3 in concentrations above 82 wt% and H_2SO_4 from 98 to 100 wt%. Aluminum alloys resist most alcohols; however, some alcohols may cause corrosion when extremely dry and at elevated temperatures (Fig. 27d). The same characteristics are associated with phenol (Fig. 27f). Aldehydes have little or no action on aluminum (Fig. 27e). Under most conditions, particularly at room temperature, aluminum alloys resist halogenated organic compounds, but under some conditions, they may react rapidly or violently with some of these chemicals. If water is present, these chemicals may hydrolyze to yield mineral acids that destroy the protective oxide film of aluminum. Such corrosion by mineral acids may in turn promote further reaction with the chemicals themselves, because the aluminum halides formed by this corrosion are catalysts for some such reactions. To ensure safety, service conditions should be ascertained before aluminum alloys are used with these chemicals, and the most stringent precautions should be exercised before they are used in finely divided form.

Reactivity of aluminum alloys with halogenated organic chemicals is inversely related to the chemical stability of these reagents. Thus, they are most resistant to chemicals containing fluorine and are decreasingly resistant to those containing chlorine, bromine, and iodine. Aluminum alloys resist highly polymerized halogenated chemicals, reflecting the high degree of stability of these chemicals.

Resistance of aluminum and its alloys to many foods and chemicals, representing practically all classifications, has been established in laboratory tests and, in many cases, by service experience. Data are readily available from handbooks, proprietary literature, and trade association publications. Reference 131 is especially useful.

Much of the data from laboratory tests are for chemicals of high purity. Caution should be exercised in using these data to predict performance of aluminum alloys with commercial grades of chemicals. Corrosion of aluminum alloys by inorganic chemicals is frequently caused by such impurities as copper, lead, mercury, and nickel, and corrosion by organic chemicals often results from the presence of other organic chemicals. The combined effect of impurities may exceed the sum of their individual effects.

Care of Aluminum

Handling and Storage. Because of the excellent corrosion resistance of aluminum alloys, users occasionally do not employ good practice in the handling and storage of these alloys. This can result in water stains or pitting. Methods to avoid these unsightly surface effects are described in the article "Surface Engineering of Aluminum and Aluminum Alloys" in *Surface Engineering,* Volume 5 of *ASM Handbook,* 1994.

Water stain is superficial corrosion that occurs when sheets of bare metal are stacked or nested in the presence of moisture. The source of moisture may be condensation from the atmosphere that forms on the edges of the stack and is drawn between the sheets by capillary action. Aluminum should not be stored at temperatures or under atmospheric conditions conducive to condensation. When such conditions cannot be avoided, the metal sheets or parts should be separated and coated with oil or a suitable corrosion inhibitor. Once formed, water stain can be removed by either mechanical or chemical means, but the original surface brightness may be altered.

Outdoor storage of aluminum, even under a tarpaulin, is generally not desirable for long periods of time; this varies with the alloy, the end product, and the local environment. Moisture can collect on the surface, sometimes at relative humidities below the dewpoint, because of the hygroscopic nature of the dust or particles that deposit on the metal from the atmosphere. The resulting staining or localized pitting, although of little structural consequence in the 1*xxx*, 3*xxx*, 4*xxx*, 5*xxx*, and 6*xxx* alloys, is undesirable if the aluminum will be used for an end product for which surface finish is critical. The 2*xxx* and 7*xxx* bare alloys are susceptible to intergranular attack under these conditions, and for these alloys, use of strippable coatings, protective wrappers, papers, or inhibited organic films is advisable when adverse conditions cannot be avoided.

Mechanical damage can be easily avoided by good housekeeping practices, proper equipment, and proper protection during transportation. When transporting flat sheets or plates, the aluminum should be oiled or interleaved with approved paper to prevent traffic marks, where fretting action at points of contact causes surface abrasion. Practices to avoid these defects are described in Ref 132.

Cleaning and Deactivation of Corrosion. For many applications, minor surface corrosion is of little consequence, and no cleaning is necessary. Where corrosion occurs that is detrimental to strength or appearance if allowed to continue, aluminum can be cleaned by a number of methods (Ref 132). Removal of corrosion products can be followed by deoxidizing or brightening cleaners, if desired. Specifications for all cleaners should state that they are suitable for aluminum. For architectural aluminum products, aggressive or heavy-duty cleaners should be avoided in favor of more frequent use of mild cleaners. Other preventive and maintenance procedures are discussed in Ref 133.

ACKNOWLEDGMENT

This is a revision of the article Corrosion of Aluminum and Aluminum Alloys by E.H. Hollingsworth and H.Y. Hunsicker of the Aluminum Company of America, *Corrosion,* Volume 13, *ASM Handbook,* 1987, p 582–609.

REFERENCES

1. M.S. Hunter and P. Fowle, Naturally and Thermally Formed Oxide Films on Aluminum, *J. Electrochem. Soc.,* Vol 103, 1956, p 482
2. H.P. Godard, W.B. Jepson, M.R. Bothwell, and R.L. Kane, *The Corrosion of Light Metals,* John Wiley & Sons, 1967
3. M. Pourbaix, *Atlas of Electrochemical Equilibria in Aqueous Solutions,* Pergamon Press, 1966, p 171
4. J.E. Hatch, Ed., *Aluminum: Properties and Physical Metallurgy,* American Society for Metals, 1984, p 242
5. H. Kaesche, Investigation of Uniform Dissolution and Pitting of Aluminum Electrodes, *Werkst. Korros.,* Vol 14, 1963, p 557
6. H. Bohni and H.H. Uhlig, Environmental Factors Affecting the Critical Pitting Potential of Aluminum, *J. Electrochem. Soc.,* Vol 116, 1969, p 906
7. J.R. Galvele, S.M. de Micheli, I.L. Muller, S.B. DeWexler, and I.L. Alanis, Critical Potentials for Localized Corrosion of Aluminum Alloys, *Localized Corrosion,* B.F. Brown, J. Kruger, A. Agrawal, and R.W. Staehle, Ed., National Association of Corrosion Engineers, 1974, p 580
8. I.L. Muller and J.R. Galvele, Pitting Potentials of High Purity Binary Aluminum Alloys—Part I: Al-Cu Alloys, *Corros, Sci.,* Vol 17, 1977, p 179; Part II: Al-Mg and Al-Zn Alloys, *Corros. Sci.,* Vol 17, 1977, p 995
9. R.L. Horst and G.C. English, Corrosion Evaluation of Aluminum Easy-Open Ends on Tinplate Cans, *Mater. Perform.,* Vol 16 (No. 3), 1977, p 23
10. R.A. Bonewitz and E.D. Verink, Jr., Correlation Between Long Term Testing of Aluminum Alloys for Desalination and Electrochemical Methods of Evaluation, *Mater. Perform.,* Vol 14, 1975, p 16

11. R.H. Brown, W.L. Fink, and M.S. Hunter, Measurement of Irreversible Potentials as a Metallurgical Research Tool, *Trans. AIME,* Vol 143, 1941, p 115
12. "Standard Practice for Measurement of Corrosion Potentials of Aluminum Alloys," G 69, *Annual Book of ASTM Standards,* Vol 03.02, American Society for Testing and Materials
13. M.S. Hunter, A.M. Montgomery, and G.W. Wilcox, Microstructure of Alloys and Products, *Aluminum,* Vol 1, K.R. Van Horn, Ed., American Society for Metals, 1967, p 77
14. J.E. Hatch, Ed., *Aluminum: Properties and Physical Metallurgy,* American Society for Metals, 1984, p 60
15. R.B. Mears and R.H. Brown, Causes of Corrosion Currents, *Ind. Eng. Chem.,* Vol 33, 1941, p 1001
16. J.D. Edwards et al., *The Aluminum Industry: Aluminum Products and Their Fabrication,* McGraw-Hill, 1930, p 13
17. C.L. Burton, L.W. Mayer, and E.H. Spuhler, Aircraft and Aerospace Applications, *Aluminum,* Vol II, K.R. Van Horn, Ed., American Society for Metals, 1967
18. P.E. Bretz and R.R. Sawtell, 'Alithilite' Alloys: Progress, Products and Properties, *Proceedings of the Third Aluminum-Lithium Conference,* The Institute of Metals, 1986, p 47
19. C.J. Peel, B. Evans, and D. McDarmaid, Current Status of U.K. Lightweight Lithium-Containing Aluminum Alloys, *Proceedings of the Third Aluminum-Lithium Conference,* 1986, p 26
20. H.F. DeJong and J.H.M. Martens, Investigation of the Pitting Potential of Rapidly Solidified Aluminum-Lithium Alloys, *Aluminum,* Vol 61 (No. 6), 1985, p 416
21. P. Niskanen, T.H. Sanders, Jr., J.G. Rinker, and M. Marek, Corrosion of Aluminum Alloys Containing Lithium, *Corros. Sci.,* Vol 22 (No. 4), 1982, p 283
22. M. Zamin, The Role of Mn in the Corrosion Behavior of Al-Mn Alloys, *Corrosion,* Vol 37, 1981, p 627
23. L.F. Mondolfo, *Aluminum Alloys: Structure and Properties,* Butterworths, 1976, p 812
24. E.H. Dix, W.A. Anderson, and M.B. Shumaker, "Development of Wrought Aluminum-Magnesium Alloys," Technical Paper 14, Alcoa Research Laboratories, 1958
25. H.P. Godard, W.B. Jepson, M.R. Bothwell, and R.L. Kane, *The Corrosion of Light Metals,* John Wiley & Sons, 1967, p 72
26. J. Zahavi and J. Yahalom, Exfoliation Corrosion of AlMgSi Alloys in Water, *J. Electrochem. Soc.,* Vol 129 (No. 6), 1982, p 1181
27. D.O. Sprowls and E.H. Spuhler, "Avoiding Stress-Corrosion Cracking in High Strength Aluminum Alloy Structures," Green Letter, Alcoa, Jan 1982
28. L.F. Mondolfo, *Aluminum Alloys: Structure and Properties,* Butterworths, 1976, p 851
29. P.L. Mehr, E.H. Spuhler, and L.W. Mayer, "Alcoa Alloy 7075-T73," Green Letter, Revision 1, Alcoa, Sept 1971
30. S.V. Nair, J.K. Tien, and R.C. Bates, SiC-Reinforced Aluminum Metal Matrix Composites, *Int. Met. Rev.,* Vol 30 (No. 6), 1985, p 275
31. D.M. Aylor, R.J. Ferrara, and R.M. Kain, Marine Corrosion and Protection for Graphite/Aluminum Metal Matrix Composites, *Mater. Perform.,* Vol 23 (No. 7), 1984, p 32
32. S.L. Fohlman, Corrosion and Electrochemical Behavior of Boron/Aluminum Composites, *Corrosion,* Vol 34 (No. 5), 1978, p 156
33. D.M. Aylor and P.J. Moran, "An Investigation of Corrosion Properties and Protection for Graphite/Aluminum and Silicon Carbide/Aluminum Metal Matrix Composites," Paper 202, presented at Corrosion/86, National Association of Corrosion Engineers, 1986
34. "Classification of Resistance to Stress-Corrosion Cracking of High-Strength Aluminum Alloys," G 64, *Annual Book of ASTM Standards,* Vol 03.02, American Society for Testing and Materials
35. R.H. Brown, Aluminum Alloy Laminates: Alclad and Clad Aluminum Alloy Products, *Composite Engineering Laminates,* A.G.H. Dietz, Ed., M.I.T. Press, 1969
36. M.R. Bothwell, New Technique Enhances Corrosion Resistance of Aluminum, *Met. Prog.,* Vol 87, March 1985, p 81
37. H. Ikeda, Protection Against Pitting Corrosion of 3003 Aluminum Alloy by Zinc Diffusion Treatment, *Aluminum,* Vol 58 (No. 8), 1982, p 467
38. D.J. Scott, Aluminum Sprayed Coatings—Their Use for the Protection of Al Alloys and Steel, *Trans. IMF,* Vol 49, 1971, p 111
39. V.E. Carter and H.S. Campbell, Protecting Strong Aluminum Alloys Against Stress-Corrosion with Sprayed Metal Coatings, *Br. Corros. J.,* Vol 4, 1969, p 15
40. W.J. Schwerdtfeger, Effects of Cathodic Protection on the Corrosion of an Aluminum Alloy, *J. Res. Natl. Bur. Stand.,* Vol 68C (No. 4), 1964, p 283
41. Recommended Practice for Cathodic Protection of Aluminum Pipe Buried in Soil or Immersed in Water, *Mater. Prot.,* Vol 2 (No. 10), 1963, p 106
42. F.W. Hewes, Investigation of Maximum and Minimum Criteria for the Cathodic Protection of Aluminum in Soil, *Oil Week,* Vol 16 (No. 24–28), Aug-Sept 1965
43. M. Cerny, Present State of Knowledge About Cathodic Protection of Aluminum, *Prot. Met.,* Vol 11 (No. 6), 1975, p 645
44. R.B. Mears and H.J. Fahrney, Cathodic Protection of Aluminum Equipment, *Trans. AIChE,* Vol 37 (No. 6), 1941, p 911
45. B. Sandberg and A. Bairamov, "Cathodic Protection of Aluminum Structures," Report 1985:2, Swedish Corrosion Institute, 1985
46. T.J. Lennox, M.H. Peterson, and R.E. Groover, "Corrosion of Aluminum Alloys by Antifouling Paint Toxicants and Effects of Cathodic Protection," Paper 16, presented at NACE Conference (Cleveland, OH), National Association of Corrosion Engineers, 1968
47. R.E. Groover, T.J. Lennox, and M.H. Peterson, Cathodic Protection of 19 Aluminum Alloys Exposed to Seawater—Corrosion Behavior, *Mater. Prot.,* Vol 8 (No. 11), 1969, p 25
48. S.C. Dexter, Localized Corrosion of Aluminum Alloys for OTEC Heat Exchangers, *J. Ocean Sci. Eng.,* Vol 8 (No. 1), 1981, p 109
49. E.H. Cook and F.L. McGeary, Electrodeposition of Iron from Aqueous Solutions onto an Aluminum Alloy, *Corrosion,* Vol 20 (No. 4), 1964, p 111t
50. J.D. Edwards, F.C. Frary, and Z. Jeffries, *The Aluminum Industry: Aluminum Products and Their Fabrication,* McGraw-Hill, 1930
51. M.H. Brown, W.W. Binger, and R.H. Brown, Mercury and Its Compounds: A Corrosion Hazard, *Corrosion,* Vol 8 (No. 5), 1952, p 155
52. R.C. Plumb, M.H. Brown, and J.E. Lewis, A Radiochemical Tracer Investigation of the Role of Mercury in the Corrosion of Aluminum, *Corrosion,* Vol 11 (No. 6), 1956, p 277t
53. E.H. Dix, Acceleration of the Rate of Corrosion by High Constant Stresses, *Trans. AIME,* Vol 137, 1940, p 11
54. W.L. Fink and L.A. Willey, Quenching of 75S Aluminum Alloy, *Met. Technol.,* Vol 14 (No. 8), 1947, p 5
55. M.S. Hunter, G.R. Frank, and D.L. Robinson, in *Proceedings of Conference: Fundamental Aspects of Stress-Corrosion Cracking,* R.W. Staehle, Ed., National Association of Corrosion Engineers, 1969, p 497
56. H. Kaesche, Pitting Corrosion of Aluminum and Intergranular Corrosion of Aluminum Alloys, *Localized Corrosion,* B.F. Brown, J. Kruger, and R.W. Staehle, Ed., National Association of Corrosion Engineers, 1974, p 516
57. J.R. Galvele and S.M. de Micheli, Mechanism of Intergranular Corrosion of Al-Cu Alloys, *Corros. Sci.,* Vol 10, 1970, p 795
58. "Standard Practice for Determining the Susceptibility to Intergranular Corrosion of 5*xxx* Series Aluminum Alloys by Weight Loss After Exposure to Nitric Acid (NAWLT Test)," G 67, *Annual Book of ASTM Standards,* Vol 03.02,

American Society for Testing and Materials
59. R.B. Mears, R.H. Brown, and E.H. Dix, Jr., A Generalized Theory of the Stress-Corrosion Cracking of Alloys, *Symposium on Stress-Corrosion Cracking of Metals,* American Society for Testing and Materials and American Institute of Mining and Metallurgical Engineers, 1945, p 323
60. D.O. Sprowls and R.H. Brown, Stress-Corrosion Mechanisms for Aluminum Alloys, *Fundamental Aspects of Stress-Corrosion Cracking,* R.W. Staehle, A.J. Forty, and D. VanRooyen, Ed., National Association of Corrosion Engineers, 1969, p 466
61. M.O. Speidel, Hydrogen Embrittlement of Aluminum Alloys, *Hydrogen in Metals,* L.M. Bernstein and A.W. Thompson, Ed., American Society for Metals, 1974, p 249
62. V.A. Marichev, The Mechanism of Crack Growth in Stress Corrosion Cracking of Aluminum Alloys, *Werkst. Korros.,* Vol 34, 1983, p 300
63. D.O. Sprowls and R.H. Brown, What Every Engineer Should Know About Stress Corrosion of Aluminum, *Met. Prog.,* Vol 81 (No. 4), April 1962, p 79–85
64. R.J. Bucci, G. Nordmark, and E.A. Starke, Jr., Selecting Aluminum Alloys to Resist Failure by Fracture Mechanisms, *Fatigue and Fracture,* Vol 19, *ASM Handbook,* ASM International, 1996, p 771–812
65. J.G. Kaufman, *Fracture Resistance of Aluminum Alloys: Notch Toughness, Tear Resistance, and Fracture Toughness,* ASM International, 2001
66. M.O. Speidel, *Met. Trans.,* Vol 6A, 1975, p 631
67. J.G. Kaufman, G.T. Sha, R.F. Kohm, and R.J. Bucci, *Notch-Yield Ratio as a Quality Control Index for Plane Strain Fracture Toughness,* STP 601, ASTM, July 1976, p 169–190
68. E.H. Spuhler and C.L. Burton, "Avoiding Stress-Corrosion Cracking in High Strength Aluminum Alloy Structures," Green Letter, Alcoa, 1970
69. *Aluminum Standards and Data,* The Aluminum Association, 2003
70. J.G. Rinker, M. Marek, and T.H. Sanders, Jr., Microstructure, Toughness and SCC Behavior of 2020, *Aluminum-Lithium Alloys,* T.H. Sanders, Jr. and E.A. Starke, Jr., Ed., American Institute of Mining, Metallurgical, and Petroleum Engineers, 1983, p 597
71. A.K. Vasudevan, P.R. Ziman, S.C. Jha, and T.H. Sanders, Jr., Stress-Corrosion Resistance of Al-Cu-Li-Zr Alloys, *Aluminum-Lithium Alloys,* Vol III, C. Baker, P.J. Gregson, S.J. Harris, and C.J. Peel, Ed., The Institute of Metals, 1986, p 303
72. E.L. Colvin, S.J. Murtha, and R.K. Wyss, The Effect of Aging Time on the Stress-Corrosion Cracking Resistance of 2090-T8E41, *Proceedings of the International Conference on Aluminum Alloys,* 15–20 June 1986 (Charlottesville, VA)
73. N.J.H. Holroyd, A. Gray, G.M. Scamans, and R. Herman, Environment-Sensitive Fracture of Al-Li-Cu-Mg Alloys, *Aluminum-Lithium Alloys,* Vol III, C. Baker, P.J. Gregson, S.J. Harris, and C.J. Peel, Ed., The Institute of Metals, 1986, p 310
74. "Standard Recommended Practice of Alternate Immersion Stress Corrosion Testing in 3.5% Sodium Chloride Solution," G 44, *Annual Book of ASTM Standards,* Vol 03.02, American Society for Testing and Materials
75. "Standard Recommended Practice for Determining Susceptibility to Stress-Corrosion Cracking of High-Strength Aluminum Alloy Products," G 47, *Annual Book of ASTM Standards,* Vol 03.02, American Society for Testing and Materials
76. "Standard Test Method for Visual Assessment of Exfoliation Corrosion Susceptibility of 5*xxx* Series Aluminum Alloys (ASSET Test)," G 66, *Annual Book of ASTM Standards,* Vol 03.02, American Society for Testing and Materials
77. "Standard Test Method for Exfoliation Corrosion Susceptibility in 2*xxx* and 7*xxx* Series Aluminum Alloys (EXCO Test)," G 34, *Annual Book of ASTM Standards,* Vol 03.02, American Society for Testing and Materials
78. "Standard Practice for Modified Salt Spray (Fog) Testing," G 85, *Annual Book of ASTM Standards,* Vol 03.02, American Society for Testing and Materials
79. "Standard Specification for Aluminum and Aluminum-Alloy Sheet and Plate," B 209, *Annual Book of ASTM Standards,* Vol 02.02, American Society for Testing and Materials
80. "Exfoliation Corrosion Testing of Aluminum Alloys 5086 and 5456," Technical Report T1, Aluminum Association, circa 1972
81. D.O. Sprowls, J.D. Walsh, and M.B. Shumaker, Simplified Exfoliation Testing of Aluminum Alloys, *Localized Corrosion—Cause of Metal Failure,* STP 516, American Society for Testing and Materials, 1972, p 38
82. T.J. Summerson, "Aluminum Association Task Group on Exfoliation and Stress-Corrosion Cracking of Aluminum Alloys for Boat Stock," Interim Report, *Proceedings of the Tri-Service Conference on Corrosion of Military Equipment,* Technical Report AFML-TR-75–42, Vol II, 1972, p 193
83. S.J. Ketcham and P.W. Jeffrey, Exfoliation Corrosion Testing of 7178 and 7075 Aluminum Alloys, *Localized Corrosion—Cause of Metal Failure,* STP 516, American Society for Testing and Materials, 1972, p 273
84. B.W. Lifka and D.O. Sprowls, Relationship of Accelerated Test Methods for Exfoliation Resistance in 7*xxx* Series Alloys with Exposure to a Seacoast Atmosphere, *Corrosion in Natural Environments,* STP 558, American Society for Testing and Materials, 1974, p 306
85. O.F. Devereux, A.J. McEvily, and R.W. Staehle, Ed., *Corrosion Fatigue: Chemistry, Mechanics, and Microstructure, Part VII, Aluminum Alloys,* National Association of Corrosion Engineers, 1972, p 451
86. H.L. Craig, T.W. Hooker, and D.W. Hoeppner, Ed., *Corrosion Fatigue Technology,* STP 642, American Society for Testing and Materials, 1978, p 51
87. J.E. Hatch, Ed., *Aluminum: Properties and Physical Metallurgy,* American Society for Metals, 1984
88. S.J. Ketcham and E.J. Jankowsky, Developing an Accelerated Test: Problems and Pitfalls, *Laboratory Corrosion Tests and Standards,* STP 866, G.S. Haynes and R. Babioan, Ed., American Society for Testing and Materials, 1985, p 14
89. G. Sowinski and D.O. Sprowls, Weathering of Aluminum Alloys, *Atmospheric Corrosion,* W.H. Ailor, Ed., John Wiley & Sons, 1982, p 297
90. M.A. Pelensky, J.J. Jaworski, and A. Galliccio, Corrosion Investigations at Panama Canal Zone, *Atmospheric Factors Affecting the Corrosion of Engineering Materials,* STP 646, S.K. Coburn, Ed., American Society for Testing and Materials, 1976, p 58
91. C.J. Walton, D.O. Sprowls, and J.A. Nock, Jr., Resistance of Aluminum Alloys to Weathering, *Corrosion,* Vol 9 (No. 10), 1953, p 345
92. W.W. Binger, R.H. Wagner, and R.H. Brown, Resistance of Aluminum Alloys to Chemically Contaminated Atmospheres, *Corrosion,* Vol 9 (No. 12), 1953, p 440
93. F.L. McGeary, E.T. Englehart, and P.J. Ging, Weathering of Aluminum, *Mater. Prot.,* Vol 6 (No. 6), 1967, p 33
94. C.J. Walton and W. King, Resistance of Aluminum-Base Alloys to 20-Year Atmospheric Exposure, in *STP 174,* American Society for Testing and Materials, 1956, p 21
95. S.M. Brandt and L.H. Adams, Atmospheric Exposure of Light Metals, in *STP 435,* American Society for Testing and Materials, 1968, p 95
96. W.K. Boyd and F.W. Fink, "Corrosion of Metals in the Atmosphere," Report MCIC-74-33, Battelle Memorial Institute, 1974
97. S.C. Byrne and A.C. Miller, Effect of Atmospheric Pollutant Gases on the Formation of Corrosive Condensate on Aluminum, *Atmospheric Corrosion of Metals,* STP 767, S.W. Dean, Jr. and E.C. Rhea, Ed., American Society for Testing and Materials, 1982, p 395

98. F. Mattsen and S. Lindgren, Hard-Rolled Aluminum Alloys, *Metal Corrosion in the Atmosphere,* STP 435, American Society for Testing and Materials, 1968, p 240
99. T.P Hoar, Discussion on Filiform Corrosion, *Chem. Ind.,* Nov 1952, p 1126
100. W.H. Slaybaugh, W. DeJager, S.E. Hoover, and L.L. Hutchinson, Filiform Corrosion of Aluminum, *J. Paint Technol.,* Vol 44 (No. 556), 1972, p 76
101. W.W. Binger and C.M. Marstiller, Aluminum Alloys for Handling High Purity Water, *Corrosion,* Vol 13 (No. 9), 1957
102. J.E. Draley and W.E. Ruther, Aqueous Corrosion of Aluminum, Part 2—Methods of Protection Above 200 °C, *Corrosion,* Vol 12 (No. 10), 1965, p 480t
103. D.W. Sawyer and R.H Brown, Resistance of Aluminum Alloys to Fresh Waters, *Corrosion,* Vol 3 (No. 9), 1947, p 443
104. H.P. Godard, The Corrosion Behavior of Aluminum in Natural Waters, *Can. J. Chem. Eng.,* Vol 38, 1960, p 167
105. W.H. Ailor, Jr., A Review of Aluminum Corrosion in Tap Water, *J. Hydronautics,* Vol 3 (No. 3), 1969, p 105
106. B.R. Pathak and H.P. Godard, Equations for Predicting the Corrosivities of Natural Fresh Waters to Aluminum, *Nature,* Vol 218 (No. 5144), June 1968, p 893
107. W.A. Prey, N.W. Smith, and C.L. Wood, Jr., Marine Applications, *Aluminum,* Vol II, K.R. Van Horn, Ed., American Society for Metals, 1967, p 389
108. K.G. Compton, Seawater Tests, *Handbook on Corrosion Testing and Evaluation,* W.H. Ailor, Ed., John Wiley & Sons, 1971, p 507
109. J.A. Beavers, G.N. Koch, and W.E. Berry "Corrosion of Metals in Marine Environments," Report MCIC-86-50, Battelle, 1986
110. W.H. Ailor, Jr., Ten-Year Seawater Tests on Aluminum, *Corrosion in Natural Environments,* STP 558, American Society for Testing and Materials, 1974, p 117
111. F.M. Reinhart, "Corrosion of Metals and Alloys in the Deep Ocean," Report R834, U.S. Naval Engineering Laboratory, 1976
112. S.C. Dexter, Effect of Variations in Seawater upon the Corrosion of Aluminum, *Corrosion,* Vol 36 (No. 8), 1980, p 423
113. H.T. Rowland and S.C. Dexter, Effects of the Seawater Carbon Dioxide System on the Corrosion of Aluminum, *Corrosion,* Vol 36 (No. 9), 1980, p 458
114. S.C. Dexter, K.E. Lucas, J. Mihm, and W.E. Rigby, "Effect of Water Chemistry and Velocity of Flow on Corrosion of Aluminum," Paper 64, presented at Corrosion/83 (Anaheim, CA), National Association of Corrosion Engineers, 1983
115. J. Larsen-Basse and S.H. Zaida, Corrosion of Some Aluminum Alloys in Tropical Surface and Deep Ocean Seawater, *Proceedings of the International Congress on Metallic Corrosion,* Vol 4, June 1984, p 511
116. R.S.C. Munier and H.L. Craig, "Ocean Thermal Energy Conversion (OTEC) Biofouling and Corrosion Experiment (1977), St. Croix, U.S. Virgin Is., Part II, Corrosion Studies," Report PNL-2739, Pacific Northwest Laboratory, Feb 1978
117. D.S. Sasscer, T.O. Morgan, R. Ernst, T.J. Summerson, and R.C. Scott, "Open Ocean Corrosion Test of Candidate Aluminum Materials for Seawater Heat Exchangers," Paper 67, presented at Corrosion/83 (Anaheim, CA), National Association of Corrosion Engineers, 1983
118. M. Romanoff, "Underground Corrosion," NBS 579, National Bureau of Standards, 1957
119. D.O. Sprowls and M.E. Carlisle, Resistance of Aluminum Alloys to Underground Corrosion, *Corrosion,* Vol 17, 1961, p 125t
120. T.E. Wright, New Trends in Buried Aluminum Pipelines, *Mater. Perform.,* Vol 15 (No. 9), 1976, p 26
121. J.A. Apostolos and F.A. Myhres, "Cooperative Field Survey of Aluminum Culverts," Report FHWA/CA/TL80-12, California Department of Transportation, 1980
122. T.E. Wright, The Corrosion Behavior of Aluminum Pipe, *Mater. Perform.,* Vol 22 (No. 12), 1983, p 9
123. W.C. Cochran, Anodizing, *Aluminum: Fabrication and Finishing,* Vol III, K.R. Van Horn, Ed., American Society for Metals, 1967, p 641
124. W.C. Cochran and D.O. Sprowls, "Anodic Coatings for Aluminum," Paper presented at Conference on Corrosion Control by Coatings, Lehigh University, Nov 1978
125. D.O. Sprowls et al., "Investigation of the Stress-Corrosion Cracking of High Strength Aluminum Alloys," Final Report, Contract NAS-8-5340 for the period of May 1963 to Oct 1966, Accession No. NASA CR88110, National Technical Information Center, 1967
126. C.J. Walton, F.L. McGeary, and E.T. Englehart, The Compatibility of Aluminum with Alkaline Building Products, *Corrosion,* Vol 13, 1957, p 807t
127. *Aluminum in the Chemical and Food Industries,* The British Aluminum Company, Norfolk House, 1959
128. *Aluminum Statistical Review for 2003,* The Aluminum Association, 2003
129. E.H. Cook, R.L. Horst, and W.W. Binger, Corrosion Studies of Aluminum in Chemical Process Operations, *Corrosion,* Vol 17 (No. 1), 1961, p 97
130. R.L. Horst, Structures and Equipment for the Chemical, Food, Drug, Beverage and Atomic Industries, *Aluminum: Design and Application,* Vol II, K.R. Van Horn, Ed., American Society for Metals, 1967, p 259
131. *Guidelines for the Use of Aluminum with Food and Chemicals,* The Aluminum Association, April 1994
132. *Care of Aluminum,* The Aluminum Association, 2002
133. E.T. Englehart, Cleaning and Maintenance of Surfaces, *Aluminum,* Vol III, K.R. Van Horn, Ed., American Society for Metals, 1967, p 757

SELECTED REFERENCES

- D.G. Altopohl, *Aluminum: Technology, Applications, and Environment,* 6th ed., TMS, 1999
- J.R. Davis, Ed., *Corrosion of Aluminum and Aluminum Alloys,* ASM International, 1999
- J.D. Edwards, F.C. Frary, and Z. Jeffries, *The Aluminum Industry: Aluminum Products and Their Fabrication,* McGraw-Hill, 1930
- U.R. Evans, *The Corrosion and Oxidation of Metals: Scientific Principles and Practical Applications,* E. Arnold, 1960
- H.P. Godard, W.B. Jepson, M.R. Bothwell, and R.L. Kane, *The Corrosion of Light Metals,* John Wiley & Sons, 1967
- *Guidelines for the Use of Aluminum with Foods and Chemicals,* Aluminum Association, Inc., April 1994
- J.E. Hatch, Ed., *Aluminum: Properties and Physical Metallurgy,* American Society for Metals, 1984
- J.G. Kaufman, *Introduction to Aluminum Alloys and Tempers,* ASM International, 2000
- J.G. Kaufman and E.L. Rooy, *Aluminum Alloy Castings: Properties, Processes, and Applications,* ASM International, 2004
- F.L. LaQue and H.R. Copson, *Corrosion Resistance of Metals and Alloys,* 2nd ed., Reinhold, 1963
- L.F. Mondolfo, *Aluminum Alloys: Structure and Properties,* Butterworths, 1976
- L.L. Shrier, *Corrosion,* Vol I and II, 2nd ed., Newnes-Butterworths, 1976
- H.H. Uhlig, Ed., *Corrosion Handbook,* 2nd ed., John Wiley & Sons, 2000
- K.R. Van Horn, Ed., *Aluminum,* Vol I, II, and III, American Society for Metals, 1967

ASM Handbook, Volume 13B: Corrosion: Materials
S.D. Cramer, B.S. Covino, Jr., editors, p125-163
DOI: 10.1361/asmhba0003816

Corrosion of Copper and Copper Alloys

Revised by Arthur Cohen, Arthur Cohen & Associates

COPPER AND COPPER ALLOYS are widely used in many environments and applications because of their excellent corrosion resistance, which is coupled with combinations of other desirable properties, such as superior electrical and thermal conductivity, ease of fabricating and joining, wide range of attainable mechanical properties, and resistance to biofouling. Copper corrodes at negligible rates in unpolluted air, water, and deaerated nonoxidizing acids. Examples of the corrosion resistance of copper alloys are artifacts that have been found in nearly pristine condition after having been buried in the earth for thousands of years, and copper roofing in rural atmospheres has been found to corrode at rates of less than 0.4 mm (15 mils) in 200 years. Copper alloys resist many saline solutions, alkaline solutions, and organic chemicals. However, copper is susceptible to more rapid attack in oxidizing acids, oxidizing heavy-metal salts, sulfur, ammonia (NH_3), and some sulfur and NH_3 compounds. Resistance to acid solution depends mainly on the severity of oxidizing conditions in the solution. Reaction of copper with sulfur and sulfides to form copper sulfide (CuS or Cu_2S) usually precludes the use of copper and copper alloys in environments known to contain certain sulfur species.

Copper and copper alloys provide superior service in many applications:

- Architectural components requiring resistance to atmospheric exposure, such as roofing, hardware, building fronts, grillework, handrails, lock bodies, doorknobs, and kick plates
- Freshwater supply lines and plumbing fittings requiring resistance to corrosion by various types of waters and soils
- Freshwater and seawater marine applications—supply lines, shafting, valve stems, and marine hardware
- Heat exchangers and condensers in marine service, steam power plants, and chemical process applications, as well as liquid-to-gas or gas-to-gas heat exchangers in which either process stream may contain a corrosive contaminant
- Industrial and chemical plant process equipment involving exposure to a wide variety of organic and inorganic chemicals
- Electrical wire and cable, hardware, and connectors; printed circuit boards; and electronic applications that require demanding combinations of electrical, thermal, and mechanical properties, such as semiconductor packages, lead frames, and connectors
- Industrial products such as molds and bearings

Copper and its alloys are unique among the corrosion-resistant alloys in that they do not form a truly passive corrosion product film. In aqueous environments at ambient temperatures, the corrosion product predominantly responsible for protection is cuprous oxide (Cu_2O). This Cu_2O film is adherent and follows parabolic growth kinetics. Cuprous oxide is a *p*-type semiconductor formed by the electrochemical processes:

$$4Cu + 2H_2O \rightarrow 2Cu_2O + 4H^+ + 4e^- \quad \text{(anode)} \qquad \text{(Eq 1)}$$

and

$$O_2 + 2H_2O + 4e^- \rightarrow 4(OH)^- \quad \text{(cathode)} \qquad \text{(Eq 2)}$$

with the net reaction: $4Cu + O_2 \rightarrow 2Cu_2O$.

For the corrosion reaction to proceed, copper ions and electrons must migrate through the Cu_2O film. Consequently, reducing the ionic or electronic conductivity of the film by doping with divalent or trivalent cations should improve corrosion resistance. In practice, alloying additions of aluminum, zinc, tin, iron, and nickel are used to dope the corrosion product films, and they generally reduce corrosion rates significantly.

Effects of Alloy Composition

Copper alloys are traditionally classified under the groupings listed in Table 1. The Unified Numbering System (UNS) numbers are administered by the Copper Development Association. Similar compositionally based designation systems are used internationally.

Coppers and high-copper alloys have similar corrosion resistance. They have excellent resistance to seawater corrosion and biofouling but are susceptible to erosion-corrosion at high water velocities. The high-copper alloys with beryllium, cadmium, and chromium are used in applications that require enhanced mechanical performance, often at slightly elevated temperature, with good thermal or electrical conductivity. Processing for increased strength in the high-copper alloys generally improves their resistance to erosion-corrosion. A number of alloys in this category have been developed for electronic applications—such as contact clips, springs, and lead frames—that require specific mechanical properties, relatively high electrical conductivity, and atmospheric-corrosion resistance.

Copper-Beryllium Alloys. These alloys (C17000, C17200, and C17500) are essentially immune to cracking in sodium, potassium, magnesium, and mixed chloride salt solutions. They show no loss of ductility or strength under severe hydrogen-charging conditions. Superior corrosion resistance and high hardness has led to their long successful service as undersea components, mold materials for plastic component manufacture, and instrument housings for oil and gas well drilling.

Brasses. The most widely used group of copper alloys is the brasses, which are copper-zinc alloys. The resistance of brasses to corrosion by aqueous solutions does not change markedly as long as the zinc content does not exceed 15%; above 15% Zn, dezincification (dealloying) may occur. Selective removal of zinc leaves a relatively porous and weak layer of copper. Dezincification may be either plug-type (Fig. 1) or layer-type (Fig. 2).

By contrast, the resistance to pitting is almost total when the zinc content exceeds 15%. The brasses that resist pitting are severely degraded by dezincification, however, causing them to lose much of their strength, as illustrated in Fig. 3.

Quiescent or slowly moving saline solutions, brackish water, and mildly acidic solutions are environments that often lead to the dezincification of unmodified brasses. Susceptibility to stress-corrosion cracking (SCC) is significantly affected by zinc content; alloys that contain more zinc are more susceptible. Resistance to SCC increases substantially as zinc content decreases

Table 1 Classification of copper alloys

Generic name	UNS numbers	Composition
Wrought alloys		
Coppers	C10100–C15815	Most >99% Cu
High-copper alloys	C16200–C19900	>96% Cu
Brasses	C21000–C28000	Cu-Zn
Leaded brasses	C31200–C38500	Cu-Zn-Pb
Tin brasses	C40400–C48600	Cu-Zn-Sn-Pb
Phosphor bronzes	C50100–C52400	Cu-Sn-P
Leaded phosphor bronzes	C53400–C54400	Cu-Sn-Pb-P
Copper-phosphorus and copper-silver-phosphorus brazing filler metal	C55180–C55285	Cu-P-Ag
Thermal spray wire	C56000	Cu-Zn-Ag
Aluminum bronzes	C60800–C64210	Cu-Al-Ni-Fe-Si-Sn
Silicon bronzes	C64700–C66100	Cu-Si-Sn
Other copper-zinc alloys	C66200–C69710	. . .
Copper-nickels	C70100–C72420	Cu-Ni-Fe
Copper-nickel-tin, spinodal alloy	C72500–C72950	Cu-Ni-Sn
Nickel silvers	C73500–C79830	Cu-Ni-Zn
Cast alloys		
Coppers	C80100–C81200	>99% Cu
High-copper alloys	C81400–C82800	>94% Cu
Red and leaded red brasses	C83300–C84800	Cu-Zn-Sn-Pb (75–89% Cu)
Yellow and leaded yellow brasses	C85200–C85800	Cu-Zn-Sn-Pb (57–74% Cu)
Manganese and leaded manganese bronzes	C86100–C86800	Cu-Zn-Mn-Fe-Pb
Silicon bronzes, silicon brasses	C87300–C87800	Cu-Zn-Si
Copper-bismuth and copper-bismuth-selenium	C89320–C89940	Cu-Zn-Sn-Bi (64–91% Cu)
Tin bronzes and leaded tin bronzes	C90200–C94500	Cu-Sn-Zn-Pb
Nickel-tin bronzes	C94700–C94900	Cu-Ni-Sn-Zn-Pb
Aluminum bronzes	C95200–C95900	Cu-Al-Fe-Ni
Copper-nickels	C96200–C96950	Cu-Ni-Fe
Nickel silvers	C97300–C97800	Cu-Ni-Zn-Pb-Sn
Leaded coppers	C98200–C98840	Cu-Pb
Miscellaneous alloys	C99300–C99750	. . .

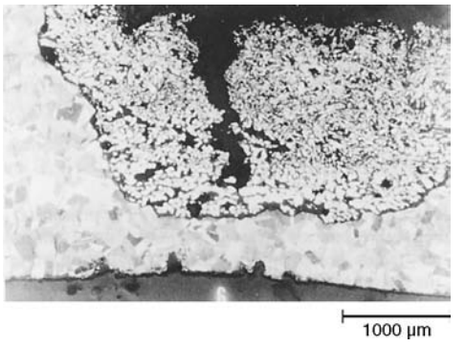

Fig. 1 Plug-type dezincification cross section in a yellow brass (C26000, cartridge brass) tube. Original magnification 15×. Source: Used with permission of ASTM International

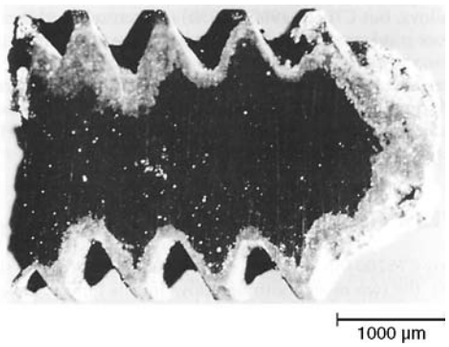

Fig. 2 Layer-type dezincification cross section in yellow brass (C26000, cartridge brass) threaded fastener. Original magnification 15×. Source: Used with permission of ASTM International

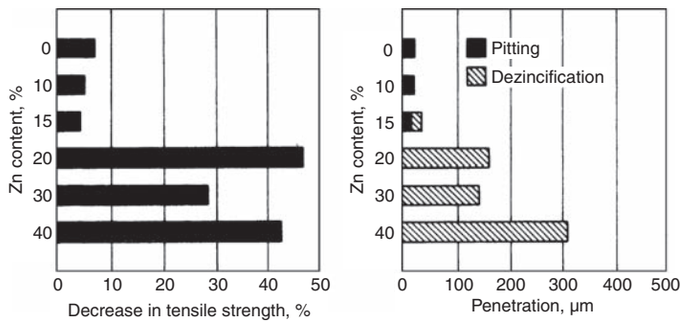

Fig. 3 Effect of zinc content on corrosion of brasses. Brass strip, 0.8 mm (0.032 in.) thick, was immersed for 60 days in 0.01 M NH_4Cl solution at 45 °C (113 °F).

from 15 to 0%. Stress-corrosion cracking is practically unknown in commercially pure copper.

Elements such as lead, tellurium, beryllium, chromium, phosphorus, and manganese have little or no effect on the corrosion resistance of coppers and binary copper-zinc alloys. These elements are added to enhance such mechanical properties as machinability, strength, and hardness.

Tin Brasses. Tin additions significantly increase the corrosion resistance of some brasses, especially dezincification. Examples of this effect are two tin-bearing brasses: uninhibited admiralty metal (no active UNS number) and uninhibited naval brass (C46400). Uninhibited admiralty metal was once widely used to make heat-exchanger tubes but has largely been replaced by inhibited grades of admiralty metal (C44300, C44400, and C44500), which have even greater resistance to dealloying. Admiralty metal is a variation of cartridge brass (C26000) that is produced by adding approximately 1% Sn to the basic 70Cu-30Zn composition. Similarly, naval brass is the alloy resulting from the addition of 0.75% Sn to the basic 60Cu-40Zn composition of Muntz metal (C28000).

Cast tin brasses for marine use are also modified by the addition of tin, lead, and, sometimes, nickel. The cast marine brasses are used for plumbing in seawater piping systems and in deck hardware, for which they are subsequently chrome plated.

Aluminum Brass. Aluminum oxide (Al_2O_3) is an important constituent of the corrosion film on brass that contains a few percent aluminum in addition to copper and zinc. This markedly increases the resistance to impingement attack in turbulent high-velocity saline water. For example, the arsenical aluminum brass C68700 (76Cu-22Zn-2Al) is frequently used for marine condensers and heat exchangers in which impingement attack is likely to pose a serious problem. Aluminum brasses are susceptible to dezincification unless they are inhibited, which is usually done by adding 0.02 to 0.10% As.

Inhibited Alloys. Addition of phosphorus, arsenic, or antimony (typically 0.02 to 0.10%) to admiralty metal, naval brass, or aluminum brass effectively produces high resistance to dezincification. Inhibited alloys have been extensively used for such components as condenser tubes, which must accumulate years of continuous service between shutdowns for repair or replacement.

Phosphor Bronzes. Addition of tin and phosphorus to copper produces good resistance to flowing seawater and to most nonoxidizing acids except hydrochloric (HCl). Alloys containing 8 to 10% Sn have high resistance to impingement attack. Phosphor bronzes are much less susceptible to SCC than brasses and are similar to copper in resistance to sulfur attack. Tin bronzes—alloys of copper and tin—tend to be used primarily in the cast form, in which they are modified by further alloy additions of lead, zinc, and nickel. Uses include pumps, valves,

gears, and bushings. Wrought tin bronzes are known as phosphor bronzes and find use in high-strength wire applications, such as wire rope. This group of alloys has fair resistance to impingement and good resistance to biofouling.

Copper-Nickels. Alloy C71500 (Cu-30Ni) has the best general resistance to aqueous corrosion of all the commercially important copper alloys, but C70600 (Cu-10Ni) is often selected because it offers good resistance at lower cost. Both of these alloys, although well suited to applications in the chemical industry, have been most extensively used for condenser tubes and heat-exchanger tubes in recirculating steam systems. They are superior to coppers and to other copper alloys in resisting acid solutions and are highly resistant to SCC and impingement corrosion.

Nickel Silvers. The two most common nickel silvers are C75200 (65Cu-18Ni-17Zn) and C77000 (55Cu-18Ni-27Zn) and are so named because of their luster, rather than silver content. They have good resistance to corrosion in both fresh and saltwaters. Primarily because their relatively high nickel contents inhibit dezincification, C75200 and C77000 are usually much more resistant to corrosion in saline solutions than brasses of similar copper content.

Copper-Silicon Alloys. These alloys generally have the same corrosion resistance as copper, but they have higher mechanical properties and superior weldability. These alloys appear to be much more resistant to SCC than the common brasses. Silicon bronzes are susceptible to embrittlement by high-pressure steam and should be tested for suitability in the service environment before being specified for components to be used at elevated temperature.

Aluminum Bronzes. These alloys, containing 5 to 12% Al, have excellent resistance to impingement corrosion and high-temperature oxidation. Aluminum bronzes are used for beater bars and for blades in wood pulp machines because of their ability to withstand mechanical abrasion and chemical attack by sulfite solutions.

In most practical commercial applications, the corrosion characteristics of aluminum bronzes are primarily related to aluminum content. Alloys with up to 8% Al normally have completely face-centered cubic α structures and good resistance to corrosion attack. As aluminum content increases above 8%, α-β duplex structures appear. The β phase is a high-temperature phase retained at room temperature on fast cooling from 565 °C (1050 °F) or above. Slow cooling, which allows long exposure at temperatures from 320 to 565 °C (610 to 1050 °F), tends to decompose the β phase into a brittle $\alpha + \gamma_2$ eutectoid having either a lamellar or a nodular structure. The β phase is less resistant to corrosion than the α phase, and eutectoid structures are even more susceptible to attack.

Depending on specific environmental conditions, β phase or eutectoid structure in aluminum bronze can be selectively attacked by a mechanism similar to the dezincification of brasses. Proper quench-and-temper treatment of duplex alloys, such as C62400 and C95400, produces a tempered β structure with reprecipitated acicular α crystals, a combination that is often superior in corrosion resistance to the normal annealed structures.

Iron-rich particles are distributed as small round or rosette particles throughout the structures of aluminum bronzes containing more than approximately 0.5% Fe. These particles sometimes impart a rusty tinge to the surface but have no known effect on corrosion rates (Fig. 4).

Nickel-aluminum bronzes are more complex in structure with the introduction of the κ phase. Nickel appears to alter the corrosion characteristics of the β phase to provide greater resistance to dealloying and cavitation-erosion in most liquids. For C63200 and perhaps C95800, quench-and-temper treatments may yield even greater resistance to dealloying. Alloy C95700, a high-manganese (11 to 14% Mn) cast aluminum bronze, is somewhat inferior in corrosion resistance to C95500 and C95800, which are lower in manganese and slightly higher in aluminum.

Aluminum bronzes are generally suitable for service in nonoxidizing mineral acids, such as phosphoric (H_3PO_4), sulfuric (H_2SO_4), and HCl; organic acids, such as acetic (CH_3COOH) or oxalic; neutral saline solutions, such as sodium chloride (NaCl) or potassium chloride (KCl); alkalis, such as sodium hydroxide (NaOH), potassium hydroxide (KOH), and anhydrous ammonium hydroxide (NH_4OH); and various natural waters, including sea, brackish, and potable waters. Environments to be avoided include nitric acid (HNO_3); some metallic salts, such as ferric chloride ($FeCl_3$) and chromic acid (H_2CrO_4); moist, chlorinated hydrocarbons; and moist HN_3. Aeration can result in accelerated corrosion in many media that appear to be compatible.

Exposure under high tensile stress to moist NH_3 can result in SCC. In certain environments, corrosion can lower the fatigue limit to 25 to 50% of the normal atmospheric value.

Cast Copper-Bismuth and Copper-Bismuth-Selenium Alloys. Cast alloys C89320 to C89940 substitute bismuth and bismuth-selenium for lead to facilitate machinability and pressure tightness in fluid-carrying applications. Lead is intentionally not added to these alloys, to minimize the amount that may leach in potable water systems and in other applications, such as dairy product processing.

Types of Attack

Coppers and copper alloys are susceptible to several forms of corrosion, depending primarily on environmental conditions. Table 2 lists the identifying characteristics of the forms or mechanisms of corrosion that commonly attack copper metals, as well as the most effective means of combating each. When studying a particular form of corrosion or a particular environment, take note of the Selected References at the end of this article, which are grouped by form and environment.

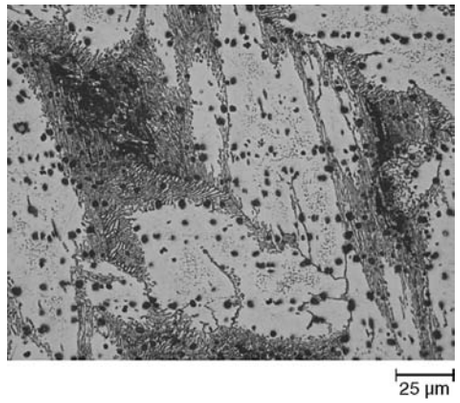

Fig. 4 Cast aluminum bronze (Cu-10Al-5Mo-5Fe), annealed and furnace cooled. Alpha needles in a pearlitic matrix of kappa and alpha. The small points are rosettes and rods of kappa, a quarterly phase of CuAlNiFe. Acid etched in ferric chloride. Original magnification 400×. Courtesy of Frauke Hogue, Hogue Metallography

Uniform Corrosion

Uniform corrosion is the slowest and most predictable form of attack. Weight loss data can be used to estimate penetration rates accurately for a given environment. Uniform corrosion of copper alloys results from prolonged contact with environments in which the corrosion rate is very low, such as fresh, brackish, and saltwaters; many types of soil; neutral, alkaline, and acid salt solutions; organic acids; and sugar juices. Other substances that cause uniform thinning at a faster rate include oxidizing acids, sulfur-bearing compounds, NH_3, and cyanides. Additional information on this form of attack is available in the articles "Evaluating Uniform Corrosion," "Aqueous Corrosion," and "Atmospheric Corrosion" in *ASM Handbook*, Volume 13A, 2003.

Galvanic Corrosion

Galvanic corrosion occurs when materials with differing surface electrical potentials are in electrical contact with each other in a conductive electrolytic solution. A potential difference can occur between dissimilar metals, between different areas of the same alloy, or between a metal and a conductive nonmetal. The corrosion of the more electronegative member of the couple (the anode) is enhanced, and the more electropositive member (the cathode) is partly or completely protected. Copper metals are cathodic to most other common structural metals, such as steel and aluminum. When steel or aluminum is in contact with a copper metal, the corrosion rate of the steel or aluminum increases but that of the copper metal decreases. The common grades of stainless steel exhibit variable behavior; that is,

Table 2 Guide to corrosion of copper alloys

Form of attack	Characteristics	Preventive measures
General thinning	Uniform metal removal	Select proper alloy for environmental conditions based on weight loss data.
Galvanic corrosion	Corrosion preferentially near a more cathodic metal	Avoid electrically coupling dissimilar metals; maintain optimal ratio of anode to cathode area; maintain optimal concentration of oxidizing constituent in corroding medium.
Pitting	Localized pits, tubercles; water line pitting; crevice corrosion, pitting under foreign objects or dirt	Alloy selection; design to avoid crevices; keep metal clean.
Impingement Erosion-corrosion Cavitation	Erosion attack from turbulent flow plus dissolved gases, generally as lines of pits in direction of fluid flow	Design for streamlined flow; keep velocity low; remove gases from liquid phase; use erosion-resistant alloy.
Fretting	Chafing or galling, often occurring during shipment	Lubricate contacting surfaces; interleave sheets of paper between sheets of metal; decrease load on bearing surfaces.
Intergranular corrosion	Corrosion along grain boundaries without visible signs of cracking	Select proper alloy for environmental conditions based on metallographic examination of corrosion specimens.
Dealloying	Preferential dissolution of zinc or nickel, resulting in a layer of sponge copper	Select proper alloy for environmental conditions based on metallographic examination of corrosion specimens.
Corrosion fatigue	Several transgranular cracks	Select proper alloy based on fatigue tests in service environment; reduce mean or alternating stress.
Stress-corrosion cracking	Cracking, usually intergranular but sometimes transgranular, that is often fairly rapid	Select proper alloy based on stress-corrosion tests; reduce applied or residual stress; remove mercury compounds or NH_3 from environment.

copper metals may be anodic or cathodic to the stainless steel, depending on conditions of exposure. Copper metals usually corrode preferentially when coupled with high-nickel alloys, titanium, or graphite. Additional information, including the galvanic series of metals in seawater, is available in the article "Galvanic Corrosion" in *ASM Handbook*, Volume 13A, 2003.

Corrosion potentials of copper metals generally range from −0.2 to −0.4 V when measured against a saturated calomel electrode; the potential of pure copper is approximately −0.3 V. Alloying additions of zinc or aluminum move the potential toward the anodic (more electronegative) end of the range; additions of tin or nickel move the potential toward the cathodic (less electronegative) end. Galvanic corrosion between two copper metals is seldom a significant problem, because the potential difference is so small.

The metals that are in proximity in a galvanic series can be coupled to each other without significant galvanic damage. However, the larger the difference in galvanic potential between metals, the greater the corrosion damage to the anodic metal. Accelerated damage due to galvanic effects is usually greatest near the junction, where the electrochemical current density is the highest.

The ratio of the surface areas affects the galvanic corrosion damage. An unfavorable area ratio exists when the cathodic area is large relative to the anodic area. The corrosion rate of the small anodic area may be several hundred times greater than if the anodic and cathodic areas were equal in size. Conversely, when a large anodic area is coupled to a small cathodic area, current density and damage due to galvanic corrosion are much less. For example, copper rivets fastening steel plates together would survive in seawater, but steel rivets used to fasten copper plates would be completely destroyed during the same period.

Pitting

Pitting is sometimes general over the entire copper surface, giving the metal an irregular and roughened appearance. In other cases, pits are concentrated in specific areas and are of various sizes and shapes. Detailed information on this form of attack is available in the article "Pitting Corrosion" in *ASM Handbook*, Volume 13A, 2003.

Localized pitting can be more damaging because the function of the part can be compromised by reduction of load-carrying capacity due to increased stress concentration at the pits. If the part is designed to contain a fluid under pressure, a single throughhole will jeopardize the function.

Pitting is usually associated with a breakdown in the protective film on metals, such as aluminum and stainless steel. Because copper alloys do not have a true protective film, pitting is not a prime corrosion mechanism; however, because of metallurgical and environmental factors, the corroded surface does show a tendency toward nonuniformity. The occurrence of pitting is somewhat random regarding the specific location of a pit on the surface as well as whether it will even occur on a particular metal sample. Long-term tests of copper alloys show that the average pit depth does not continually increase with extended times of exposure. Instead, pits tend to reach a certain limit beyond which little apparent increase in depth occurs. Of the copper alloys, the most pit resistant are the aluminum bronzes with less than 8% Al and the low-zinc brasses. Copper-nickels and tin bronzes tend to have intermediate pitting resistance, but the high-copper alloys and silicon bronzes are somewhat more prone to pitting.

Waterline attack is a term used to describe pitting due to a differential oxygen cell functioning between the well-aerated surface layer of a liquid and the oxygen-starved layer immediately beneath it. The pitting occurs immediately below the waterline.

Crevice corrosion occurs near a crevice formed by two metal surfaces or by a metal and a nonmetal, such as a lap joint or flange interface. Like pitting, the depth of attack appears to level off rather than to increase continually with time. This depth is usually less than that from pitting, and for most copper alloys, it will be less than 400 μm (0.016 in.).

For most copper alloys, the location of the attack will be outside but immediately adjacent to the crevice, due to the formation of metal ion concentration cells. Classic crevice corrosion resulting from oxygen depletion and attack within crevices is less common in copper alloys. Aluminum- and chromium-bearing copper alloys, which form more passive surface films, are susceptible to differential oxygen cell attack, as are aluminum alloys and stainless steels. The occurrence of crevice attack is statistical in nature, with the probability and its severity increasing if the area within a crevice is small compared to the area outside the crevice. Other conditions that will increase crevice attack are high water temperatures or water flow on the surface outside the crevice.

Local cell action similar to crevice attack may also result from the presence of foreign objects or debris, such as dirt, shells, or vegetation, or it may result from rust, permeable scales, or uneven accumulation of corrosion product on the metallic surface. Routine cleaning maintenance can sometimes control this type of attack.

Impingement

Various forms of impingement attack occur where gases, vapors, or liquids impinge on metal surfaces at high velocities, such as in condensers or heat exchangers. Rapidly moving turbulent water can strip away the protective films from copper alloys. When this occurs, the metal corrodes at a more rapid rate in an attempt to

reestablish this film, but because the films are being swept away as rapidly as they are being formed, the corrosion rate remains constant and high. The conditions under which the corrosion product film is removed are different for each alloy and are discussed in the section "Corrosion of Copper Alloys in Specific Environments" in this article.

Erosion-Corrosion. Undercut grooves, waves, ruts, gullies, and rounded holes characterize erosion-corrosion; it usually exhibits a directional pattern. Pits are elongated in the direction of flow and are undercut on the downstream side. When the condition becomes severe, it may result in a pattern of horseshoe-shaped grooves or pits with their open ends pointing downstream. As attack progresses, the pits may join, forming fairly large patches of undercut pits. When this form of corrosion occurs in a condenser tube, it is usually confined to a region near the inlet end of the tube where fluid flow is rapid and turbulent. If some of the tubes in a bundle become plugged, the velocity is increased in the remaining tubes; therefore, the unit should be kept as clean as possible. Erosion-corrosion is most often found with waters containing low levels of sulfur compounds and with polluted, contaminated, or silty saltwater or brackish water. The erosive action locally removes protective films, thus contributing to the formation of concentration cells and to localized pitting of anodic sites.

Cavitation occurs in a fluid when the flow is disturbed so as to create a local pressure drop. A vapor bubble will form and then collapse, applying a momentary stress of up to 1400 MPa (200 ksi) to the surface. It is theorized that this repeated mechanical work on the surface creates local deformation and fatigue that aids the removal of metal. This is in agreement with the observations that the harder alloys tend to have greater resistance to cavitation and that there is often an incubation period before the onset of cavitation attack. Of the copper alloys, aluminum bronze has the best cavitation resistance. Cavitation damage is confined to the area where the bubbles collapse, usually immediately downstream of the low-pressure zone. Impellers and propellers are prone to cavitation damage.

Impingement attack can be reduced through design changes that decrease fluid velocity, streamline the flow, eliminate low-pressure pockets, and remove entrained air in water boxes, injector nozzles, and piping. Proper materials selection will lessen the effect. Aluminum brasses or copper-nickels are more erosion resistant than the brasses or tin brasses. Erosion-resistant inserts at tube inlets and epoxy-type coatings are often effective repair methods in existing shell and tube heat exchangers. When contaminated waters are involved, filtering or screening the liquids and cleaning the surfaces can be very effective in minimizing impingement attack. The use of cathodic protection can lessen all forms of localized attack except cavitation.

Fretting

Fretting or fretting corrosion appears as pits or grooves in the metal surface that are surrounded or filled with corrosion product. Fretting is sometimes referred to as chafing, road burn, friction oxidation, wear oxidation, or galling.

Conditions for fretting include:

- Repeated relative (sliding) motion between two surfaces must occur. The relative amplitude of the motion may be very small (a few tenths of a millimeter).
- The interface is under load.
- Both load and relative motion are sufficient to produce deformation of the interface.
- Oxygen and/or moisture are present.

Fretting does not occur on lubricated surfaces in continuous motion, such as axle bearings, but instead on dry interfaces subject to repeated, small relative displacements. (There is a type of fretting, false brinelling, that occurs in bearings at rest.) A classic type of fretting occurs during shipment of bundles of mill products having flat faces.

Fretting can be controlled or eliminated by:

- Lubricating with low-viscosity, high-tenacity oils to reduce friction at the interface between the two metals and to exclude oxygen from the interface
- Separating the faying surfaces by interleaving an insulating material
- Increasing the load to reduce motion between faying surfaces; this may be difficult in practice, because only a minute amount of relative motion is necessary to produce fretting
- Decreasing the load at bearing surfaces to increase the relative motion between parts

Detailed information is available in the article "Forms of Mechanically Assisted Degradation" in *ASM Handbook*, Volume 13A, 2003.

Intergranular Corrosion

Intergranular corrosion is a rare form of attack that occurs most often in applications involving high-pressure steam. This type of corrosion penetrates the metal along grain boundaries—often to a depth of several grains—which distinguishes it from surface roughening. Mechanical stress is apparently not a factor in intergranular corrosion. The alloys that appear to be the most susceptible to this form of attack are Muntz metal, admiralty metal, aluminum brasses, and silicon bronzes. Additional information is provided in the article "Evaluating Intergranular Corrosion" in *ASM Handbook*, Volume 13A, 2003.

Dealloying

Dealloying is a corrosion process in which the more active constituent metal is selectively removed from an alloy, leaving behind a weak deposit of the more noble metal. Copper-zinc alloys containing more than 15% Zn are susceptible to a dealloying process called dezincification. Selective removal of zinc leaves a relatively porous and weak layer of copper and copper oxide in brass. Corrosion of a similar nature continues beneath the primary corrosion layer, resulting in gradual replacement of sound brass by weak, porous copper that would eventually penetrate the brass, weakening it structurally and allowing liquids or gases to leak through the porous mass.

Plug-type dealloying (Fig. 1) refers to the dealloying that occurs in local areas; surrounding areas are usually unaffected or only slightly corroded. In uniform-layer dealloying, the active component of the alloy is leached out over a broad area of the surface. Dezincification is the usual form of corrosion for uninhibited brasses in prolonged contact with waters high in oxygen and carbon dioxide (CO_2). It is frequently encountered with quiescent or slowly moving solutions. Slightly acidic water, low in salt content and at room temperature, is likely to produce uniform attack, but neutral or alkaline water, high in salt content and above room temperature, often produces plug-type attack.

Brasses with copper contents of 85% or more resist dezincification. Dezincification of brasses with two-phase structures is generally more severe, particularly if the second phase is continuous; it usually occurs in two stages: the high-zinc β phase, followed by the lower-zinc α phase.

Tin tends to inhibit dealloying, especially in cast alloys. Alloys C46400 (naval brass) and C67500 (manganese bronze), which are α-β brasses containing approximately 1% Sn, are widely used for naval equipment and have reasonably good resistance to dezincification. Addition of a small amount of phosphorus, arsenic, or antimony to admiralty metal (an all-α 71Cu-28Zn-1Sn brass) inhibits dezincification. Inhibitors are not entirely effective in preventing dezincification of the α-β brasses, because they do not prevent dezincification of the β phase.

Where dezincification is a problem, red brass, commercial bronze, inhibited admiralty metal, and inhibited aluminum brass can be successfully used. In some cases, the economic penalty of avoiding dealloying by selecting a low-zinc alloy may be unacceptable. Low-zinc alloy tubing requires fittings that are available only as sand castings, but fittings for higher-zinc tube can be die cast or forged much more economically. Where selection of a low-zinc alloy is unacceptable, inhibited yellow brasses are generally preferred.

Dealloying has been observed in other alloys. Dealloying of aluminum occurs in some copper-aluminum alloys, particularly with those having more than 8% Al. It is especially severe in alloys with continuous γ phase and usually occurs as plug-type dealloying. Nickel additions exceeding 3.5% or heat treatment to produce an $\alpha + \beta$ microstructure prevents dealloying. Dealloying of nickel in C71500 is rare, having been observed at temperatures over 100 °C (212 °F), low flow

conditions, and high local heat flux. Dealloying of tin in cast tin bronzes has been observed as a rare occurrence in hot brine or steam. Cathodic protection generally protects all but the two-phase copper-zinc alloys from dealloying. The mechanism of dealloying is explained in the article "Effects of Metallurgical Variables on Dealloying Corrosion" in *ASM Handbook*, Volume 13A, 2003.

Corrosion Fatigue

The combined action of corrosion (usually pitting corrosion) and cyclic stress may result in corrosion fatigue cracking. Like ordinary fatigue cracks, corrosion fatigue cracks generally propagate at right angles to the maximum tensile stress in the affected region. However, cracks resulting from simultaneous fluctuating stress and corrosion propagate much more rapidly than cracks caused solely by fluctuating stress. Also, corrosion fatigue failure usually involves several parallel cracks, but it is rare for more than one crack to be found in a part that has failed by simple fatigue. The cracks shown in Fig. 5 are characteristic of service failures resulting from corrosion fatigue.

Ordinarily, corrosion fatigue can be readily identified by the presence of several cracks emanating from corrosion pits. Cracks not visible to the unaided eye or at low magnification can be made visible by deep etching or plastic deformation or can be detected by eddy-current inspection. Corrosion fatigue cracking is often transgranular, but there is evidence that certain environments induce intergranular cracking in copper metals.

Copper and copper alloys resist corrosion fatigue in many applications involving repeated stress and corrosion. These applications include such parts as springs, switches, diaphragms, bellows, aircraft and automotive gasoline and oil lines, tubes for condensers and heat exchangers, and fourdrinier wire for the paper industry.

Copper alloys that have high fatigue limits and resistance to corrosion in the service environment are more likely to have good resistance to corrosion fatigue. Alloys frequently used in applications involving both cyclic stress and corrosion include beryllium-coppers, phosphor bronzes, aluminum bronzes, and copper-nickels. More information on corrosion fatigue is available in the section "Corrosion Fatigue" of the article "Mechanically Assisted Degradation" in *ASM Handbook*, Volume 13A, 2003.

Stress-Corrosion Cracking

Stress-corrosion cracking, traditionally called season cracking among copper alloys, occurs if a susceptible metal is subjected to the combined effects of sustained stress and certain chemicals, resulting in apparently spontaneous cracking. Stress-corrosion cracking is often intergranular (Fig. 6), but transgranular cracking may occur in some alloys in certain environments (Fig. 7).

Mechanism. Copper alloys crack in a wide variety of electrolytes. In some cases, the crack surfaces have the distinctive brittle appearance that is associated with SCC. It is also clear in many systems that cracking occurs at low threshold stresses only when certain environmental conditions exist. Variables that control this threshold stress in a specific environment include pH, oxygen concentration in the liquid, strength of the corrodent, potential of the metal, temperature, extent of cold work before the test, and minor alloying elements in the copper alloy.

A nonquantitative interpretation of SCC is that it occurs in those environmental/metal systems in which the rate of corrosion is low; the corrosion that does occur proceeds in a highly localized manner. Intergranular attack, selective removal of an alloy component, pitting, attack at a metal/precipitate interface, or surface flaws, when they occur in the presence of a surface tensile stress, may lead to a surface defect at the base of which the stress-intensity factor, K_I, exceeds the threshold stress intensity for SCC, K_{ISCC}, for that specific environment/alloy system under the conditions selected for the test or encountered in service. Whether or not a crack propagates depends on the specimen geometry and how the magnitude of the stress field at the crack tip changes as the crack develops. The critical factor is how the metal reacts at the crack tip. If the metallurgical structure or the kinetics of chemical corrosion at the crack tip is such that a small radius of curvature (sharp crack tip) is maintained at the crack tip, the crack will continue to propagate, because the local stress at the crack tip is high. High rates of corrosion at the crack tip, which lead to a large radius of curvature (blunt), will favor pitting rather than crack growth. Details of SCC mechanisms, crack initiation and growth, and SCC models are found in the article "Stress-Corrosion Cracking," in *ASM Handbook*, Volume 13A, 2003.

A sharp crack tip is favored by:

- Selective removal of one component of an alloy, with the resulting development of local voids that provide a brittle crack path
- Brittle fracture of a corrosion product coating at the base of a crack that continually reforms
- Attack along the interface of two discrete phases
- Intergranular attack that does not spread laterally
- Surface energy considerations that encourage intrusion of the environment (a liquid metal in particular) into minute flaws

Mattsson's solution, a medium containing ammonium sulfate [$(NH_4)_2SO_4$], ammonium hydroxide (NH_4OH), and copper sulfate ($CuSO_4$), is used by many researchers for studying the fundamentals of the SCC process caused by ammonia (NH_3) (Ref 1).

In a study of the chemistry and the electrochemistry of the brass-NH_3 system (Ref 2), cupric (Cu^{2+}) ammonium complex was concluded to be necessary for the occurrence of SCC

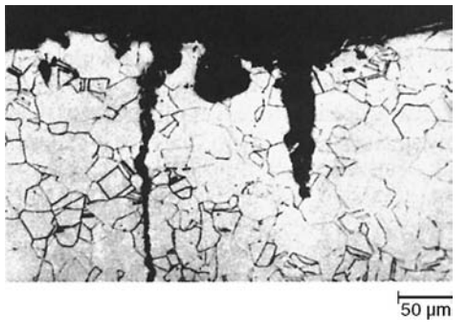

Fig. 5 Typical corrosion fatigue cracking of a copper alloy. Transgranular cracks originate at the base of corrosion pits on the roughened inner surface of a tube. Etched. Original magnification approximately 150×

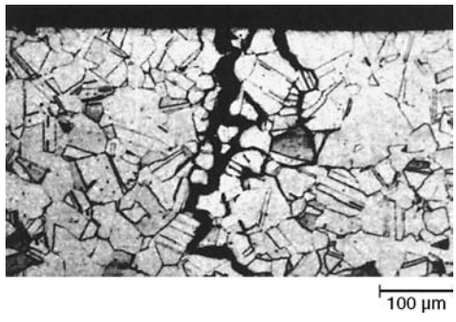

Fig. 6 Typical stress-corrosion cracking in a copper alloy. Intergranular cracking in Cu-27.5Zn-1.0Sn alloy tube, probably caused by mercury or ammonia. Specimen was etched in 50 mL HNO_3, 0.5 g $AgHNO_3$, and 50 mL H_2O. Original magnification approximately 100×

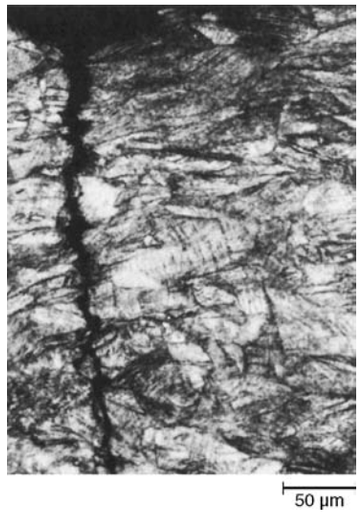

Fig. 7 Alloy 44300 (arsenical admiralty) tube, drawn, stress relieved, and bent 180° to induce transgranular stress-corrosion crack. Specimen was etched in 50 mL HNO_3, 0.5 g $AgHNO_3$, and 50 mL H_2O. Original magnification approximately 200×

under open-circuit conditions in oxygenated NH_3 solutions. This complex becomes a component in the predominant cathodic reaction:

$$Cu(NH_3)_4^{2+} + e^- \rightarrow Cu(NH_3)_2^+ + 2NH_3 \quad \text{(Eq 3)}$$

Equation 3 permits cracking by cyclic rupture of a Cu_2O film generated at the crack tip (Ref 3) or by a mechanism involving dezincification (Ref 4). Cracking can also occur in deoxygenated solutions in the absence of significant concentrations of the Cu^{2+} ions, provided the cuprous (Cu^+) complexes are available. It was suggested that the role of the Cu^+ complex is to provide a cathodic reaction, in this case allowing dezincification to occur. These findings are consistent with the recognition that SCC failures of brass are not limited to environments containing NH_3. See the section "Stress-Corrosion Cracking of Copper Alloys in Specific Environments" in this article.

Conditions Leading to SCC. Ammonia and ammonium compounds are the corrosive substances most often associated with SCC of copper alloys. These compounds are sometimes present in the atmosphere; in other cases, they are in cleaning compounds or in chemicals used to treat water in contact with the alloy. Both oxygen and moisture must be present for NH_3 to be corrosive to copper alloys; other compounds, such as CO_2, are thought to accelerate SCC in NH_3 atmospheres. Moisture films on metal surfaces will dissolve significant quantities of NH_3, even from atmospheres with low NH_3 concentrations.

While a specific corrosive environment and sustained stress are the primary causes of SCC, microstructure and alloy composition may affect the rate of crack propagation in susceptible alloys. Selecting the correct combination of alloy, forming process, thermal treatment, and metal-finishing process can control microstructure and composition. Although test results may indicate that a finished part is not susceptible to SCC, such an indication does not ensure complete freedom from cracking, particularly where service stresses are high.

Applied and residual stresses can both lead to failure by SCC. Susceptibility is largely a function of tensile stress magnitude. Stresses near the yield strength are usually required, but SCC can be initiated at 20% yield strength (Ref 5). In general, the higher the stress, the weaker the corroding medium must be to cause SCC. The reverse is also true: The stronger the corroding medium, the lower the required stress.

Sources of Stress. Applied stresses result from ordinary service loading or from fabricating techniques, such as riveting, bolting, shrink fitting, brazing, and welding. Residual stresses are of two types: differential-strain stresses, which result from nonuniform plastic strain during cold forming, and differential-thermal-contraction stresses, which result from nonuniform heating or cooling.

Residual stresses induced by nonuniform straining are primarily influenced by the method of fabrication. In some fabricating processes, it is possible to cold work a metal extensively and yet produce only a low level of residual stress. For example, die angle and amount of reduction influence residual stress in a drawn tube. Wide-angle dies (approximately 32°) produce higher residual stresses than narrow-angle dies (approximately 8°). Light reductions yield high residual stresses because only the surface of the alloy is stressed; heavy reductions yield low residual stresses because the region of cold working extends deeper into the metal. Most drawing operations can be planned so that residual stresses are low and susceptibility to SCC is negligible.

Residual stresses resulting from upsetting, stretching, or spinning are more difficult to evaluate and to control by varying tooling and process conditions. For these operations, SCC can be prevented more effectively by selecting a resistant alloy or by treating the metal after fabrication.

Alloy Composition. Brasses containing less than 15% Zn are highly resistant to SCC. Phosphorus-deoxidized copper and tough pitch copper rarely exhibit SCC, even under severe conditions. On the other hand, brasses containing 20 to 40% Zn are highly susceptible. Susceptibility increases only slightly as zinc content is increased from 20 to 40%.

There is no indication that the other elements commonly added to brasses increase the probability of SCC. Phosphorus, arsenic, magnesium, tellurium, tin, beryllium, and manganese are thought to decrease susceptibility under some conditions. Addition of 1.5% Si is known to decrease the probability of cracking.

Altering the microstructure cannot make a susceptible alloy totally resistant to SCC. However, the rapidity with which susceptible alloys crack appears to be affected by grain size and structure. All other factors being equal, the rate of cracking increases with grain size. The effects of structure on SCC are not sharply defined, primarily because they are interrelated with effects of both composition and stress.

Control Measures. Stress-corrosion cracking can be controlled, and sometimes prevented, by selecting copper alloys that have high resistance to cracking (notably, those with less than 15% Zn); by reducing residual stress to a safe level by thermal stress relief, which can usually be applied without significantly decreasing strength; or by altering the environment, such as by changing the predominant chemical species present or introducing a corrosion inhibitor.

Residual and assembly stresses can be eliminated by recrystallization annealing after forming or assembly. Recrystallization annealing cannot be used when the integrity of the structure depends on the higher strength of strain-hardened metal, which always contains a certain amount of residual stress. Thermal stress relief (sometimes called relief annealing) can be specified when the higher strength of a cold-worked temper must be retained. Thermal stress relief consists of heating the part for a relatively short time at low temperature. Specific times and temperatures depend on alloy composition, severity of deformation, prevailing stresses, and the size of the load being heated. Usually, time is from 30 min to 1 h and temperature is from 150 to 425 °C (300 to 795 °F). More details on stress relieving are available in the article "Heat Treating of Copper Alloys" in *Heat Treating*, Volume 4 of *ASM Handbook*, 1991.

Mechanical methods, such as stretching, flexing, bending, straightening between rollers, peening, and shot blasting, can also be used to reduce residual stresses to a safe level. These methods depend on plastic deformation to decrease dangerous tensile stresses or to convert them to less objectionable compressive stresses.

For information on testing the success of control methods and judging materials selection, see the article "Evaluating Stress-Corrosion Cracking" in *ASM Handbook*, Volume 13A, 2003, and specifically the section "Testing of Copper Alloys (Smooth Specimens)" in that article.

Corrosion of Copper Alloys in Specific Environments

Selection of a suitably corrosion-resistant material requires knowledge of the expected environment and the interaction of particular materials with all factors that influence corrosion. Operating records serve as a guideline, if the data are accurately recorded and interpreted. Results of short-term laboratory testing, simulated service tests, and in-service techniques are supportive in making materials selection decisions. Details of the advantages and limitations of these techniques are found in the Section "Corrosion Testing and Evaluation" of *ASM Handbook*, Volume 13A, 2003.

Uniform corrosion is the most reliable to predict from historical weight loss or dimensional change data. If damage occurs by pitting, intergranular corrosion, or dealloying, or if a thick adherent scale forms, corrosion rates calculated from a change in weight may be misleading. For these forms of corrosion, estimates of reduction in mechanical strength are often more meaningful. Corrosion fatigue and SCC are also potential sources of failure that cannot be predicted from routine measurements of weight loss or dimensional change. When corrosion occurs predominantly by pitting or some other localized form, or when corrosion is intergranular or involves the formation of a thick, adherent scale, direct measurement of the extent of corrosion provides the most reliable information. A common technique is to measure the maximum depth of penetration observed on a metallographic cross section through the region of interest. Statistical averaging of repeated measurements on multiple specimens may be warranted. Information gained in this manner

serves as a useful starting point for alloy selection. Operating experience may later indicate the need for a more discriminating selection.

Over the years, experience has been the best criterion for selecting the most suitable alloy for a given environment. The Copper Development Association (CDA) has compiled much field experience in the form of the ratings for wrought alloys shown in Table 3 and for cast alloys shown in Table 4. These tables should be used only as a guide; small changes in the environmental conditions sometimes degrade the performance of a given alloy from suitable to not suitable.

Whenever there is a lack of operating experience, whenever reported test conditions do not closely match the conditions for which alloy selection is being made, and whenever there is doubt as to the applicability of published data, it is always best to conduct an independent test. Field tests are the most reliable. Laboratory tests can be equally valuable, if operating conditions are precisely defined and accurately simulated in the laboratory. Long-term tests are generally preferred because the reaction that dominates the initial stages of corrosion may differ significantly from the reaction that dominates later. If short-term tests must be used as the basis for alloy selection, the test program should be supplemented with field tests so that the laboratory results can be reevaluated in light of true operating experience.

Atmospheric Exposure

Comprehensive tests conducted over a 20 year period under the supervision of ASTM International, as well as many service records, have confirmed the suitability of copper and copper alloys for atmospheric exposure (Table 5). These data support the fact that copper and copper alloys resist corrosion by industrial, marine, and rural atmospheres, except atmospheres containing NH_3 or certain other agents where SCC has been observed in high-zinc alloys (>20% Zn). The data should not be used to compare the current severity of the sites. Atmospheric cleanup initiated in the 1960s has resulted in the average sulfur dioxide concentration at an ASTM industrial site to be lower that the rural ASTM State College site (Ref 6). The copper metals most widely used in atmospheric exposure are C11000, C22000, C23000, C38500, and C75200. Alloy C11000 is an effective material for roofing, flashings, gutters, and downspouts.

The colors of copper alloys are often important in architectural applications, and color may be the primary criterion for selecting a specific alloy. After surface preparation, such as sanding or polishing, copper alloys vary in color from silver to yellow to gold to reddish shades. Alloys having the same initial color may show differences in color after weathering under similar conditions. Therefore, alloys having the same or nearly the same composition are usually used together for consistency of appearance in a specific structure.

Copper alloys are often specified for marine atmosphere exposures because of the attractive and protective patina formed during the exposure. In marine atmospheric exposures, this patina consists of a film of copper chloride or carbonate, sometimes with an inner layer of Cu_2O. The severity of the corrosion attack in marine atmospheres is somewhat less than that in industrial atmospheres but greater than that in rural atmospheres. However, these rates decrease with time.

Differences in corrosion rates exist between alloys, but these differences are frequently less than those caused by environmental factors. Thus, it becomes possible to classify the corrosion behavior of copper alloys in a marine atmosphere into two general categories: those alloys that corrode at a moderate rate and include high-copper alloys, silicon bronze, and tin bronze; and those alloys that corrode at a slower rate and include brass, aluminum bronze, nickel silver, and copper-nickel. The average metal loss, d, of the former group can be approximated by $d \approx t^{2/3}$; the latter group can be approximated by $d \approx t^{1/3}$, where t is exposure time. These relationships are shown as solid lines in Fig. 8.

Environmental factors can cause this median thickness loss to vary by as much as 50% or more in a few extreme cases. Figure 8 shows the extent of this variation as a pair of dashed lines forming an envelope around the median. Environmental factors that tend to accelerate metal loss include high humidity, high temperatures (either ambient or due to solar radiation), proximity to the ocean, long times of wetness, and the presence of pollutants in the atmosphere.

Metallurgical factors can also affect metal loss. Within a given alloy family, those with a higher alloy content tend to corrode at a lower rate. Surface finish also plays a role in that a highly polished metal will corrode slower than one with a rougher surface. Finally, design details can affect corrosion behavior. For example, designs that allow the collection and stagnation of rainwater will often exhibit wastage rates in the puddle areas that are more typical of those encountered in seawater immersions.

Certain copper alloys are susceptible to various types of localized corrosion that can greatly affect their utility in a marine atmosphere. Brasses and nickel silvers containing more than 15% Zn can suffer from dealloying. The extent of this attack is greater on alloys that contain higher proportions of zinc. In addition, these same alloys are subject to SCC in the presence of small quantities of NH_3 or other gaseous pollutants. Inhibited grades of these alloys are available that resist dealloying but are susceptible to SCC.

Alloys containing large amounts of manganese tend to be somewhat prone to pitting in marine atmospheres, as are the cobalt-containing beryllium-coppers. A tendency toward intergranular corrosion has been observed in silicon bronzes and aluminum brass, but its occurrence is somewhat sporadic.

On the whole, however, even under somewhat adverse conditions, the average thickness losses for copper alloys in a marine atmosphere tend to be very slight, typically under 20 μm (Fig. 8). Thus, copper alloys can be safely specified for applications requiring long-term durability in a marine atmosphere. Design considerations for the atmospheric use of copper alloys include allowance for free drainage of structures, the possibility of staining from runoff water, and the use of smooth or polished surfaces.

Soils and Groundwater

Copper, zinc, lead, and iron are commonly used in underground construction. Data compiled by the National Bureau of Standards (now National Institute of Standards and Technology) compared the behavior of these materials in soils of the following four types: well-aerated acid soils low in soluble salts (Cecil clay loam), poorly aerated soils (Lake Charles clay), alkaline soils high in soluble salts (Docas clay), and soils high in sulfides (Rifle peat). Corrosion data as a function of time for copper, iron, lead, and zinc exposed to these four types of soil are given in Fig. 9. Copper exhibits high resistance to corrosion by these soils, which are representative of most soils found in the United States. Where local soil conditions are unusually corrosive, it may be necessary to use some means of protection, such as cathodic protection, neutralizing backfill (limestone, for example), protective coating, or wrapping.

For many years, the National Bureau of Standards conducted studies on the corrosion of underground structures to determine the specific behavior of metals and alloys when exposed for long periods in a wide range of soils. Results indicate that tough pitch coppers, deoxidized coppers, silicon bronzes, and low-zinc brasses behave essentially alike. Soils containing cinders with high concentrations of sulfides, chlorides, or hydrogen ions (H^+) corrode these materials. In this type of contaminated soil, the corrosion rates of copper-zinc alloys containing more than approximately 22% Zn increase with zinc content. Corrosion generally results from dezincification. In soils that contain only sulfides, corrosion rates of the copper-zinc alloys decrease with increasing zinc content, and no dezincification occurs. Although not included in these tests, inhibited admiralty metals would offer significant resistance to dezincification.

Electric cables that contain copper are often buried underground. A study investigated the corrosion behavior of phosphorus-deoxidized copper (C12200) in four soil types: gravel, salt marsh, swamp, and clay (Ref 7). After 3 years of exposure, uniform corrosion rates were found to vary between 1.3 and 8.8 μm/yr (0.05 and 0.35 mil/yr). No pitting attack was observed. In general, the corrosion rate was highest for soils of lowest resistivity.

Table 3 Corrosion ratings of wrought copper alloys in various corrosive media

This table is intended to serve only as a general guide to the behavior of copper and copper alloys in corrosive environments. It is impossible to cover in a simple tabulation the performance of a material for all possible variations of temperature, concentration, velocity, impurity content, degree of aeration, and stress. The ratings are based on general performance; they should be used with caution, and then only for the purpose of screening candidate alloys.

The letters E, G, F, and P have the following significance:

E, excellent: resists corrosion under almost all conditions of service

G, good: some corrosion will take place, but satisfactory service can be expected under all but the most severe conditions.

F, fair: corrosion rates are higher than for the G classification, but the metal can be used if needed for a property other than corrosion resistance and if either the amount of corrosion does not cause excessive maintenance expense or the effects of corrosion can be lessened, such as by use of coatings or inhibitors.

P, poor: corrosion rates are high, and service is generally unsatisfactory.

Corrosive medium	Coppers	Low-zinc brasses (<15% Zn)	High-zinc brasses (≥15% Zn)	Special brasses	Phosphor bronzes	Aluminum bronzes	Silicon bronzes	Copper-nickels	Nickel silvers
Acetate solvents	E	E	G	E	E	E	E	E	E
Acetic acid(a)	E	E	P	P	E	E	E	E	G
Acetone	E	E	E	E	E	E	E	E	E
Acetylene(b)	P	P(b)	P	P	P	P	P	P	P
Alcohols(a)	E	E	E	E	E	E	E	E	E
Aldehydes	E	E	F	F	E	E	E	E	E
Alkylamines	G	G	G	G	G	G	G	G	G
Alumina	E	E	E	E	E	E	E	E	E
Aluminum chloride	G	G	P	P	G	G	G	G	G
Aluminum hydroxide	E	E	E	E	E	E	E	E	E
Aluminum sulfate and alum	G	G	P	G	G	G	G	E	G
Ammonia, dry	E	E	E	E	E	E	E	E	E
Ammonia, moist(c)	P	P	P	P	P	P	P	F	P
Ammonium chloride(c)	P	P	P	P	P	P	P	F	P
Ammonium hydroxide(c)	P	P	P	P	P	P	P	F	P
Ammonium nitrate(c)	P	P	P	P	P	P	P	F	P
Ammonium sulfate(c)	F	F	P	P	F	F	F	G	F
Aniline and aniline dyes	F	F	F	F	F	F	F	F	F
Asphalt	E	E	E	E	E	E	E	E	E
Atmosphere:									
Industrial(c)	E	E	E	E	E	E	E	E	E
Marine	E	E	E	E	E	E	E	E	E
Rural	E	E	E	E	E	E	E	E	E
Barium carbonate	E	E	E	E	E	E	E	E	E
Barium chloride	G	G	F	F	G	G	G	G	G
Barium hydroxide	E	E	G	E	E	E	E	E	E
Barium sulfate	E	E	E	E	E	E	E	E	E
Beer(a)	E	E	G	E	E	E	E	E	E
Beet-sugar syrup(a)	E	E	G	E	E	E	E	E	E
Benzene, benzine, benzol	E	E	E	E	E	E	E	E	E
Benzoic acid	E	E	E	E	E	E	E	E	E
Black liquor, sulfate process	P	P	P	P	P	P	P	G	P
Bleaching powder (wet)	G	G	P	G	G	G	G	G	G
Borax	E	E	E	E	E	E	E	E	E
Bordeaux mixture	E	E	G	E	E	E	E	E	E
Boric acid	E	E	G	E	E	E	E	E	E
Brines	G	G	P	G	G	G	G	E	E
Bromine, dry	E	E	E	E	E	E	E	E	E
Bromine, moist	G	G	P	F	G	G	G	G	G
Butane(d)	E	E	E	E	E	E	E	E	E
Calcium bisulfate	G	G	P	G	G	G	G	G	G
Calcium chloride	G	G	F	G	G	G	G	G	G
Calcium hydroxide	E	E	G	E	E	E	E	E	E
Calcium hypochlorite	G	G	P	G	G	G	G	G	G
Cane-sugar syrup(a)	E	E	E	E	E	E	E	E	E
Carbolic acid (phenol)	F	G	P	G	G	G	G	G	G
Carbonated beverages(a)(e)	E	E	E	E	E	E	E	E	E
Carbon dioxide, dry	E	E	E	E	E	E	E	E	E
Carbon dioxide, moist(a)(e)	E	E	E	E	E	E	E	E	E
Carbon tetrachloride (dry)	E	E	E	E	E	E	E	E	E
Carbon tetrachloride (moist)	G	G	F	G	E	E	E	E	E
Castor oil	E	E	E	E	E	E	E	E	E
Chlorine, dry(f)	E	E	E	E	E	E	E	E	E
Chlorine, moist	F	F	P	F	F	F	F	G	F
Chloracetic acid	G	F	P	F	G	G	G	G	G
Chloroform, dry	E	E	E	E	E	E	E	E	E
Chromic acid	P	P	P	P	P	P	P	P	P
Citric acid(a)	E	E	F	E	E	E	E	E	E
Copper chloride	F	F	P	F	F	F	F	F	F
Copper nitrate	F	F	P	F	F	F	F	F	F
Copper sulfate	G	G	P	G	G	G	G	E	G
Corn oil(a)	E	E	G	E	E	E	E	E	E
Cottonseed oil(a)	E	E	G	E	E	E	E	E	E
Creosote	E	E	G	E	E	E	E	E	E
Dowtherm “A”	E	E	E	E	E	E	E	E	E
Ethanol amine	G	G	G	G	G	G	G	G	G
Ethers	E	E	E	E	E	E	E	E	E
Ethyl acetate (esters)	E	E	G	E	E	E	E	E	E
Ethylene glycol	E	E	G	E	E	E	E	E	E
Ferric chloride	P	P	P	P	P	P	P	P	P
Ferric sulfate	P	P	P	P	P	P	P	P	P
Ferrous chloride	G	G	P	G	G	G	G	G	G
Ferrous sulfate	G	G	P	G	G	G	G	G	G
Formaldehyde (aldehydes)	E	E	G	E	E	E	E	E	E
Formic acid	G	G	P	F	G	G	G	G	G
Freon, dry	E	E	E	E	E	E	E	E	E
Freon, moist	E	E	E	E	E	E	E	E	E
Fuel oil, light	E	E	E	E	E	E	E	E	E
Fuel oil, heavy	E	E	G	E	E	E	E	E	E
Furfural	E	E	F	E	E	E	E	E	E
Gasoline	E	E	E	E	E	E	E	E	E
Gelatin(a)	E	E	E	E	E	E	E	E	E
Glucose(a)	E	E	E	E	E	E	E	E	E
Glue	E	E	G	E	E	E	E	E	E
Glycerin	E	E	G	E	E	E	E	E	E
Hydrobromic acid	F	F	P	F	F	F	F	F	F
Hydrocarbons	E	E	E	E	E	E	E	E	E
Hydrochloric acid (muriatic)	F	F	P	F	F	F	F	F	F
Hydrocyanic acid, dry	E	E	E	E	E	E	E	E	E
Hydrocyanic acid, moist	P	P	P	P	P	P	P	P	P
Hydrofluoric acid, anhydrous	G	G	P	G	G	G	G	G	G
Hydrofluoric acid, hydrated	F	F	P	F	F	F	F	F	F
Hydrofluosilicic acid	G	G	P	G	G	G	G	G	G
Hydrogen(d)	E	E	E	E	E	E	E	E	E
Hydrogen peroxide, up to 10%	G	G	F	G	G	G	G	G	G
Hydrogen peroxide over 10%	P	P	P	P	P	P	P	P	P
Hydrogen sulfide, dry	E	E	E	E	E	E	E	E	E
Hydrogen sulfide, moist	P	P	F	F	P	P	P	F	F

(continued)

(a) Copper and copper alloys are resistant to corrosion by most food products. Traces of copper may be dissolved and affect taste or color of the products. In such cases, copper alloys are often tin coated. (b) Acetylene forms an explosive compound with copper when moisture or certain impurities are present and the gas is under pressure. Alloys containing less than 65% Cu are satisfactory; when the gas is not under pressure, other copper alloys are satisfactory. (c) Precautions should be taken to avoid SCC. (d) At elevated temperatures, hydrogen will react with tough pitch copper, causing failure by embrittlement. (e) Where air is present, corrosion rate may be increased. (f) Below 150 °C (300 °F), corrosion rate is very low; above this temperature, corrosion is appreciable and increases rapidly with temperature. (g) Aeration and elevated temperature may increase corrosion rate substantially. (h) Excessive oxidation may begin above 120 °C (250 °F). If moisture is present, oxidation may begin at lower temperatures. (j) Use of high-zinc brasses should be avoided in acids because of the likelihood of rapid corrosion by dezincification. Copper, low-zinc brasses, phosphor bronzes, silicon bronzes, aluminum bronzes, and copper-nickels offer good resistance to corrosion by hot and cold dilute H_2SO_4 and to corrosion by cold concentrated H_2SO_4. Intermediate concentrations of H_2SO_4 are sometimes more corrosive to copper alloys than either concentrated or dilute acid. Concentrated H_2SO_4 may be corrosive at elevated temperatures due to breakdown of acid and formation of metallic sulfides and sulfur dioxide, which cause localized pitting. Tests indicate that copper alloys may undergo pitting in 90 to 95% H_2SO_4 at approximately 50 °C (122 °F), in 80% acid at approximately 70 °C (160 °F), and in 60% acid at approximately 100 °C (212 °F). (k) Wetting agents may increase corrosion rates of copper and copper alloys slightly to substantially when carbon dioxide or oxygen is present by preventing formation of a film on the metal surface and by combining (in some instances) with the dissolved copper to produce a green, insoluble compound.

Table 3 (continued)

Corrosive medium	Coppers	Low-zinc brasses (<15% Zn)	High-zinc brasses (≥15% Zn)	Special brasses	Phosphor bronzes	Aluminum bronzes	Silicon bronzes	Copper-nickels	Nickel silvers
Kerosine	E	E	E	E	E	E	E	E	E
Ketones	E	E	E	E	E	E	E	E	E
Lacquers	E	E	E	E	E	E	E	E	E
Lacquer thinners (solvents)	E	E	E	E	E	E	E	E	E
Lactic acid(a)	E	E	F	E	E	E	E	E	E
Lime	E	E	E	E	E	E	E	E	E
Lime sulfur	P	P	F	F	P	P	P	F	F
Linseed oil	G	G	G	G	G	G	G	G	G
Lithium compounds	G	G	P	F	G	G	G	E	E
Magnesium chloride	G	G	F	F	G	G	G	G	G
Magnesium hydroxide	E	E	G	E	E	E	E	E	E
Magnesium sulfate	E	E	G	E	E	E	E	E	E
Mercury or mercury salts	P	P	P	P	P	P	P	P	P
Milk(a)	E	E	G	E	E	E	E	E	E
Molasses	E	E	G	E	E	E	E	E	E
Natural gas(d)	E	E	E	E	E	E	E	E	E
Nickel chloride	F	F	P	F	F	F	F	F	F
Nickel sulfate	F	F	P	F	F	F	F	F	F
Nitric acid	P	P	P	P	P	P	P	P	P
Oleic acid	G	G	F	G	G	G	G	G	G
Oxalic acid(g)	E	E	P	P	E	E	E	E	E
Oxygen(h)	E	E	E	E	E	E	E	E	E
Palmitic acid	G	G	F	G	G	G	G	G	G
Paraffin	E	E	E	E	E	E	E	E	E
Phosphoric acid	G	G	P	F	G	G	G	G	G
Picric acid	P	P	P	P	P	P	P	P	P
Potassium carbonate	E	G	E	E	E	E	E	E	E
Potassium chloride	G	G	P	F	G	G	G	E	E
Potassium cyanide	P	P	P	P	P	P	P	P	P
Potassium dichromate (acid)	P	P	P	P	P	P	P	P	P
Potassium hydroxide	G	G	F	G	G	G	G	E	E
Potassium sulfate	E	E	G	E	E	E	E	E	E
Propane(d)	E	E	E	E	E	E	E	E	E
Rosin	E	E	E	E	E	E	E	E	E
Seawater	G	G	F	E	G	E	G	E	E
Sewage	E	E	F	E	E	E	E	E	E
Silver salts	P	P	P	P	P	P	P	P	P
Soap solution	E	E	E	E	E	E	E	E	E
Sodium bicarbonate	E	E	G	E	E	E	E	E	E
Sodium bisulfate	G	G	F	G	G	G	G	E	E
Sodium carbonate	E	E	G	E	E	E	E	E	E
Sodium chloride	G	G	P	F	G	G	G	E	E
Sodium chromate	E	E	E	E	E	E	E	E	E
Sodium cyanide	P	P	P	P	P	P	P	P	P
Sodium dichromate (acid)	P	P	P	P	P	P	P	P	P
Sodium hydroxide	G	G	F	G	G	G	G	E	E
Sodium hypochlorite	G	G	P	G	G	G	G	G	G
Sodium nitrate	G	G	P	F	G	G	G	E	E
Sodium peroxide	F	F	P	F	F	F	F	G	G
Sodium phosphate	E	E	G	E	E	E	E	E	E
Sodium silicate	E	E	G	E	E	E	E	E	E
Sodium sulfate	E	E	G	E	E	E	E	E	E
Sodium sulfide	P	P	F	F	P	P	P	F	F
Sodium thiosulfate	P	P	F	F	P	P	P	F	F
Steam	E	E	F	E	E	E	F	E	E
Stearic acid	E	E	F	E	E	E	E	E	E
Sugar solutions	E	E	G	E	E	E	E	E	E
Sulfur, solid	G	G	E	G	G	G	G	E	G
Sulfur, molten	P	P	P	P	P	P	P	P	P
Sulfur chloride (dry)	E	E	E	E	E	E	E	E	E
Sulfur chloride (moist)	P	P	P	P	P	P	P	P	P
Sulfur dioxide (dry)	E	E	E	E	E	E	E	E	E
Sulfur dioxide (moist)	G	G	P	G	G	G	G	F	F
Sulfur trioxide (dry)	E	E	E	E	E	E	E	E	E
Sulfuric acid 80–95%(j)	G	G	P	F	G	G	G	G	G
Sulfuric acid 40–80%(j)	F	F	F	P	F	F	F	F	F
Sulfuric acid 40%(j)	G	G	P	F	G	G	G	G	G
Sulfurous acid	G	G	P	G	G	G	G	F	F
Tannic acid	E	E	E	E	E	E	E	E	E
Tartaric acid(a)	E	E	G	E	E	E	E	E	E
Toluene	E	E	E	E	E	E	E	E	E
Trichloracetic acid	G	G	P	F	G	G	G	G	G
Trichlorethylene (dry)	E	E	E	E	E	E	E	E	E
Trichlorethylene (moist)	G	G	F	G	E	E	E	E	E
Turpentine	E	E	E	E	E	E	E	E	E
Varnish	E	E	E	E	E	E	E	E	E
Vinegar(a)	E	E	P	F	E	E	E	E	G
Water, acidic mine	F	F	P	F	G	F	F	P	F
Water, potable	E	E	G	E	E	E	E	E	E
Water, condensate(c)	E	E	E	E	E	E	E	E	E
Wetting agents(k)	E	E	E	E	E	E	E	E	E
Whiskey(a)	E	E	E	E	E	E	E	E	E
White water	G	G	G	E	E	E	E	E	E
Zinc chloride	G	G	P	G	G	G	G	G	G
Zinc sulfate	E	E	P	E	E	E	E	E	E

(a) Copper and copper alloys are resistant to corrosion by most food products. Traces of copper may be dissolved and affect taste or color of the products. In such cases, copper alloys are often tin coated. (b) Acetylene forms an explosive compound with copper when moisture or certain impurities are present and the gas is under pressure. Alloys containing less than 65% Cu are satisfactory; when the gas is not under pressure, other copper alloys are satisfactory. (c) Precautions should be taken to avoid SCC. (d) At elevated temperatures, hydrogen will react with tough pitch copper, causing failure by embrittlement. (e) Where air is present, corrosion rate may be increased. (f) Below 150 °C (300 °F), corrosion rate is very low; above this temperature, corrosion is appreciable and increases rapidly with temperature. (g) Aeration and elevated temperature may increase corrosion rate substantially. (h) Excessive oxidation may begin above 120 °C (250 °F). If moisture is present, oxidation may begin at lower temperatures. (j) Use of high-zinc brasses should be avoided in acids because of the likelihood of rapid corrosion by dezincification. Copper, low-zinc brasses, phosphor bronzes, silicon bronzes, aluminum bronzes, and copper-nickels offer good resistance to corrosion by hot and cold dilute H_2SO_4 and to corrosion by cold concentrated H_2SO_4. Intermediate concentrations of H_2SO_4 are sometimes more corrosive to copper alloys than either concentrated or dilute acid. Concentrated H_2SO_4 may be corrosive at elevated temperatures due to breakdown of acid and formation of metallic sulfides and sulfur dioxide, which cause localized pitting. Tests indicate that copper alloys may undergo pitting in 90 to 95% H_2SO_4 at approximately 50 °C (122 °F), in 80% acid at approximately 70 °C (160 °F), and in 60% acid at approximately 100 °C (212 °F). (k) Wetting agents may increase corrosion rates of copper and copper alloys slightly to substantially when carbon dioxide or oxygen is present by preventing formation of a film on the metal surface and by combining (in some instances) with the dissolved copper to produce a green, insoluble compound.

The use of copper components in systems for the disposal of nuclear waste underground is currently under investigation.

The corrosion rate of copper in quiescent groundwaters tends to decrease with time. This is due to the formation of a protective film, an example of which is shown in Fig. 10. The underlying layer consists of species from the groundwater as well as copper. This layer is brittle and is extensively cracked, permitting continued dissolution of copper ions into solution. In Fig. 10, some of these copper ions have precipitated on the underlying layer in the form of cupric hydroxychloride [$CuCl_2 \cdot 3(Cu(OH)_2)$] and copper oxide crystals. The corrosion layer is not truly passivating, and corrosion will continue, although at a reduced rate.

For copper and copper alloys, corrosion rate depends strongly on the amount of dissolved oxygen present. The data in Table 6 illustrate this point for both pure copper and Cu-10Ni in various synthetic groundwaters. These data are derived from experiments lasting from 2 to 4 weeks; therefore, they include the high initial rates of corrosion and do not represent long-term corrosion rates. However, they do serve to show

Table 4 Corrosion ratings of cast copper alloys in various media

The letters A, B, and C have the following significance: A, recommended; B, acceptable; C, not recommended

Corrosive medium	Copper	Tin bronze	Leaded tin bronze	High-leaded tin bronze	Leaded red brass	Leaded semi-red brass	Leaded yellow brass	Leaded high-strength yellow brass	High-strength yellow brass	Aluminum bronze	Leaded nickel brass	Leaded nickel bronze	Silicon bronze	Silicon brass
Acetate solvents	B	A	A	A	A	A	B	A	A	A	A	A	A	B
Acetic acid														
20%	A	C	B	C	B	C	C	C	C	A	C	A	A	B
50%	A	C	B	C	B	C	C	C	C	A	C	B	A	B
Glacial	A	A	A	C	A	C	C	C	C	A	B	B	A	A
Acetone	A	A	A	A	A	A	A	A	A	A	A	A	A	A
Acetylene(a)	C	C	C	C	C	C	C	C	C	C	C	C	C	C
Alcohols(b)	A	A	A	A	A	A	A	A	A	A	A	A	A	A
Aluminum chloride	C	C	C	C	C	C	C	C	C	B	C	C	C	C
Aluminum sulfate	B	B	B	B	B	C	C	C	C	A	C	C	A	A
Ammonia, moist gas	C	C	C	C	C	C	C	C	C	C	C	C	C	C
Ammonia, moisture-free	A	A	A	A	A	A	A	A	A	A	A	A	A	A
Ammonium chloride	C	C	C	C	C	C	C	C	C	C	C	C	C	C
Ammonium hydroxide	C	C	C	C	C	C	C	C	C	C	C	C	C	C
Ammonium nitrate	C	C	C	C	C	C	C	C	C	C	C	C	C	C
Ammonium sulfate	B	B	B	B	B	C	C	C	C	A	C	C	A	A
Aniline and aniline dyes	C	C	C	C	C	C	C	C	C	B	C	C	C	C
Asphalt	A	A	A	A	A	A	A	A	A	A	A	A	A	A
Barium chloride	A	A	A	A	A	C	C	C	C	A	A	A	A	C
Barium sulfide	C	C	C	C	C	C	C	C	B	C	C	C	C	C
Beer(b)	A	A	B	B	B	C	C	C	A	A	C	A	A	B
Beet-sugar syrup	A	A	B	B	B	A	A	A	B	A	A	A	B	B
Benzine	A	A	A	A	A	A	A	A	A	A	A	A	A	A
Benzol	A	A	A	A	A	A	A	A	A	A	A	A	A	A
Boric acid	A	A	A	A	A	A	A	B	A	A	A	A	A	A
Butane	A	A	A	A	A	A	A	A	A	A	A	A	A	A
Calcium bisulfite	A	A	B	B	B	C	C	C	C	A	B	A	A	B
Calcium chloride (acid)	B	B	B	B	B	B	C	C	C	A	C	C	A	C
Calcium chloride (alkaline)	C	C	C	C	C	C	C	C	C	A	C	A	C	B
Calcium hydroxide	C	C	C	C	C	C	C	C	C	B	C	C	C	C
Calcium hypochlorite	C	C	B	B	B	C	C	C	C	B	C	C	C	C
Cane-sugar syrups	A	A	B	A	B	A	A	A	A	A	A	A	A	B
Carbonated beverages(b)	A	C	C	C	C	C	C	C	C	A	C	C	A	C
Carbon dioxide, dry	A	A	A	A	A	A	A	A	A	A	A	A	A	A
Carbon dioxide, moist(b)	B	B	B	C	B	C	C	C	C	A	C	A	A	B
Carbon tetrachloride, dry	A	A	A	A	A	A	A	A	A	A	A	A	A	A
Carbon tetrachloride, moist	B	B	B	B	B	B	B	B	B	B	B	A	A	A
Chlorine, dry	A	A	A	A	A	A	A	A	A	A	A	A	A	A
Chlorine, moist	C	C	B	B	B	C	C	C	C	C	C	C	C	C
Chromic acid	C	C	C	C	C	C	C	C	C	C	C	C	C	C
Citric acid	A	A	A	A	A	A	A	A	A	A	A	A	A	A
Copper sulfate	B	A	A	A	A	C	C	C	C	B	B	B	A	A
Cottonseed oil(b)	A	A	A	A	A	A	A	A	A	A	A	A	A	A
Creosote	B	B	B	B	B	C	C	C	C	A	B	B	B	B
Ethers	A	A	A	A	A	A	A	A	A	A	A	A	A	A
Ethylene glycol	A	A	A	A	A	A	A	A	A	A	A	A	A	A
Ferric chloride, sulfate	C	C	C	C	C	C	C	C	C	C	C	C	C	C
Ferrous chloride, sulfate	C	C	C	C	C	C	C	C	C	C	C	C	C	C
Formaldehyde	A	A	A	A	A	A	A	A	A	A	A	A	A	A
Formic acid	A	A	A	A	A	B	B	B	B	A	B	B	B	C
Freon	A	A	A	A	A	A	A	A	A	A	A	A	A	B
Fuel oil	A	A	A	A	A	A	A	A	A	A	A	A	A	A
Furfural	A	A	A	A	A	A	A	A	A	A	A	A	A	A
Gasoline	A	A	A	A	A	A	A	A	A	A	A	A	A	A
Gelatin(b)	A	A	A	A	A	A	A	A	A	A	A	A	A	A
Glucose	A	A	A	A	A	A	A	A	A	A	A	A	A	A
Glue	A	A	A	A	A	A	A	A	A	A	A	A	A	A
Glycerin	A	A	A	A	A	A	A	A	A	A	A	A	A	A
Hydrochloric or muriatic acid	C	C	C	C	C	C	C	C	C	B	C	C	C	C
Hydrofluoric acid	B	B	B	B	B	B	B	B	B	A	B	B	B	B
Hydrofluosilicic acid	B	B	B	B	B	C	C	C	C	B	C	C	B	C
Hydrogen	A	A	A	A	A	A	A	A	A	A	A	A	A	A
Hydrogen peroxide	C	C	C	C	C	C	C	C	C	C	C	C	C	C

(continued)

(a) Acetylene forms an explosive compound with copper when moist or when certain impurities are present and the gas is under pressure. Alloys containing less than 65% Cu are satisfactory for this use. When gas is not under pressure, other copper alloys are satisfactory. (b) Copper and copper alloys resist corrosion by most food products. Traces of copper may be dissolved and affect taste or color. In such cases, copper metals are often tin coated.

Table 4 (continued)

Corrosive medium	Copper	Tin bronze	Leaded tin bronze	High-leaded tin bronze	Leaded red brass	Leaded semi-red brass	Leaded yellow brass	Leaded high-strength yellow brass	High-strength yellow brass	Aluminum bronze	Leaded nickel brass	Leaded nickel bronze	Silicon bronze	Silicon brass
Hydrogen sulfide, dry	C	C	C	C	C	C	C	C	C	B	C	C	B	C
Hydrogen sulfide, moist	C	C	C	C	C	C	C	C	C	B	C	C	C	C
Lacquers	A	A	A	A	A	A	A	A	A	A	A	A	A	A
Lacquer thinners	A	A	A	A	A	A	A	A	A	A	A	A	A	A
Lactic acid	A	A	A	A	A	C	C	C	C	A	C	C	A	C
Linseed oil	A	A	A	A	A	A	A	A	A	A	A	A	A	A
Liquors														
Black liquor	B	B	B	B	B	C	C	C	C	B	C	C	B	B
Green liquor	C	C	C	C	C	C	C	C	C	B	C	C	C	B
White liquor	C	C	C	C	C	C	C	C	C	A	C	C	C	B
Magnesium chloride	A	A	A	A	A	C	C	C	C	A	C	C	A	B
Magnesium hydroxide	B	B	B	B	B	B	B	B	B	A	B	B	B	B
Magnesium sulfate	A	A	A	A	B	C	C	C	C	A	C	B	A	B
Mercury, mercury salts	C	C	C	C	C	C	C	C	C	C	C	C	C	C
Milk(b)	A	A	A	A	A	A	A	A	A	A	A	A	A	A
Molasses(b)	A	A	A	A	A	A	A	A	A	A	A	A	A	A
Natural gas	A	A	A	A	A	A	A	A	A	A	A	A	A	A
Nickel chloride	A	A	A	A	A	C	C	C	C	B	C	C	A	C
Nickel sulfate	A	A	A	A	A	C	C	C	C	A	C	C	A	C
Nitric acid	C	C	C	C	C	C	C	C	C	C	C	C	C	C
Oleic acid	A	A	B	B	B	C	C	C	C	A	C	A	A	B
Oxalic acid	A	A	B	B	B	C	C	C	C	A	C	A	A	B
Phosphoric acid	A	A	A	A	A	C	C	C	C	A	C	A	A	A
Picric acid	C	C	C	C	C	C	C	C	C	C	C	C	C	C
Potassium chloride	A	A	A	A	A	C	C	C	C	A	C	C	A	C
Potassium cyanide	C	C	C	C	C	C	C	C	C	C	C	C	C	C
Potassium hydroxide	C	C	C	C	C	C	C	C	C	A	C	C	C	C
Potassium sulfate	A	A	A	A	A	C	C	C	C	A	C	C	A	C
Propane gas	A	A	A	A	A	A	A	A	A	A	A	A	A	A
Seawater	A	A	A	A	A	C	C	C	C	A	C	C	B	B
Soap solutions	A	A	A	A	B	C	C	C	C	A	C	C	A	C
Sodium bicarbonate	A	A	A	A	A	A	A	A	A	A	A	A	A	B
Sodium bisulfate	C	C	C	C	C	C	C	C	C	A	C	C	C	C
Sodium carbonate	C	A	A	A	A	C	C	C	C	A	C	C	C	A
Sodium chloride	A	A	A	A	A	B	C	C	C	A	C	C	A	C
Sodium cyanide	C	C	C	C	C	C	C	C	C	B	C	C	C	C
Sodium hydroxide	C	C	C	C	C	C	C	C	C	A	C	C	C	C
Sodium hypochlorite	C	C	C	C	C	C	C	C	C	C	C	C	C	C
Sodium nitrate	B	B	B	B	B	B	B	B	B	A	B	B	A	A
Sodium peroxide	B	B	B	B	B	B	B	B	B	B	B	B	B	B
Sodium phosphate	A	A	A	A	A	A	A	A	A	A	A	A	A	A
Sodium sulfate, silicate	A	A	B	B	B	B	C	C	C	A	C	C	A	B
Sodium sulfide, thiosulfate	C	C	C	C	C	C	C	C	C	B	C	C	C	C
Stearic acid	A	A	A	A	A	A	A	A	A	A	A	A	A	A
Sulfur, solid	C	C	C	C	C	C	C	C	C	A	C	C	C	C
Sulfur chloride	C	C	C	C	C	C	C	C	C	C	C	C	C	C
Sulfur dioxide, dry	A	A	A	A	A	A	A	A	A	A	A	A	A	A
Sulfur dioxide, moist	A	A	A	B	B	C	C	C	C	A	C	C	A	B
Sulfur trioxide, dry	A	A	A	A	A	A	A	A	A	A	A	A	A	A
Sulfuric acid														
78% or less	B	B	B	B	B	C	C	C	C	A	C	C	B	B
78% to 90%	C	C	C	C	C	C	C	C	C	B	C	C	C	C
90% to 95%	C	C	C	C	C	C	C	C	C	B	C	C	C	C
Fuming	C	C	C	C	C	C	C	C	C	A	C	C	C	C
Tannic acid	A	A	A	A	A	A	A	A	A	A	A	A	A	A
Tartaric acid	B	A	A	A	A	A	A	A	A	A	A	A	A	A
Toluene	B	B	A	A	A	B	B	B	B	B	B	B	B	A
Trichlorethylene, dry	A	A	A	A	A	A	A	A	A	A	A	A	A	A
Trichlorethylene, moist	A	A	A	A	A	A	A	A	A	A	A	A	A	A
Turpentine	A	A	A	A	A	A	A	A	A	A	A	A	A	A
Varnish	A	A	A	A	A	A	A	A	A	A	A	A	A	A
Vinegar	A	A	B	B	B	C	C	C	C	B	C	C	A	B
Water, acid mine	C	C	C	C	C	C	C	C	C	C	C	C	C	C
Water, condensate	A	A	A	A	A	A	A	A	A	A	A	A	A	A

(continued)

(a) Acetylene forms an explosive compound with copper when moist or when certain impurities are present and the gas is under pressure. Alloys containing less than 65% Cu are satisfactory for this use. When gas is not under pressure, other copper alloys are satisfactory. (b) Copper and copper alloys resist corrosion by most food products. Traces of copper may be dissolved and affect taste or color. In such cases, copper metals are often tin coated.

Table 4 (continued)

Corrosive medium	Copper	Tin bronze	Leaded tin bronze	High-leaded tin bronze	Leaded red brass	Leaded semi-red brass	Leaded yellow brass	Leaded high-strength yellow brass	High-strength yellow brass	Aluminum bronze	Leaded nickel brass	Leaded nickel bronze	Silicon bronze	Silicon brass
Water, potable	A	A	A	A	A	A	B	B	B	A	A	A	A	A
Whiskey(b)	A	A	C	C	C	C	C	C	C	A	C	C	A	C
Zinc chloride	C	C	C	C	C	C	C	C	C	B	C	C	B	C
Zinc sulfate	A	A	A	A	A	C	C	C	C	B	C	A	A	C

(a) Acetylene forms an explosive compound with copper when moist or when certain impurities are present and the gas is under pressure. Alloys containing less than 65% Cu are satisfactory for this use. When gas is not under pressure, other copper alloys are satisfactory. (b) Copper and copper alloys resist corrosion by most food products. Traces of copper may be dissolved and affect taste or color. In such cases, copper metals are often tin coated.

Table 5 Historic atmospheric corrosion of selected copper alloys

	Corrosion rates at indicated locations(a)											
	Altoona, PA		New York, NY		Key West, FL		La Jolla, CA		State College, PA		Phoenix, AZ	
Alloy	µm/yr	mils/yr	µm/yr	mils/yr	µm/yr	mils/yr	µm/yr	mils/yr	µm/yr	mils/yr	µm/yr	mils/yr
C11000	1.40	0.055	1.38	0.054	0.56	0.022	1.27	0.050	0.43	0.017	0.13	0.005
C12000	1.32	0.052	1.22	0.048	0.51	0.020	1.42	0.056	0.36	0.014	0.08	0.003
C23000	1.88	0.074	1.88	0.074	0.56	0.022	0.33	0.013	0.46	0.018	0.10	0.004
C26000	3.05	0.120	2.41	0.095	0.20	0.008	0.15	0.006	0.46	0.018	0.10	0.004
C52100	2.24	0.088	2.54	0.100	0.71	0.028	2.31	0.091	0.33	0.013	0.13	0.005
C61000	1.63	0.064	1.60	0.063	0.10	0.004	0.15	0.006	0.25	0.010	0.51	0.002
C65500	1.65	0.065	1.73	0.068	. . .	. . .	1.38	0.054	0.51	0.020	0.15	0.006
C44200	2.13	0.084	2.51	0.099	. . .	. . .	0.33	0.013	0.53	0.021	0.10	0.004
70Cu-29Ni-1Sn(b)	2.64	0.104	2.13	0.084	0.28	0.011	0.36	0.014	0.48	0.019	0.10	0.004

(a) Derived from 20 year exposure tests. Types of atmospheres: Altoona, industrial; New York City, industrial marine; Key West, tropical rural marine; La Jolla, humid marine; State College, northern rural; Phoenix, dry rural. (b) Although obsolete, this alloy indicates the corrosion resistance expected of C71500.

that deoxygenation of the solution results in at least an order of magnitude decrease in the short-term corrosion rate. It is also apparent from these data that, in aerated solutions at least, the addition of nickel decreases the uniform corrosion rate of copper. This is due to the formation of a more highly protective surface film.

The effects of salinity and temperature are less well understood. In general, increasing the total salinity of these groundwaters tends to increase their corrosiveness. However, it is not clear whether this is due to the sum effect of all the dissolved ions or of some of the species in particular. In open systems, it is difficult to distinguish the effect of temperature from that of dissolved oxygen, because the solubility of oxygen decreases with increasing temperature. The combination of these two opposing effects can lead to an apparent maximum in the corrosion rate at some intermediate temperature. Consequently, it is important that the rates refer to a constant dissolved-oxygen concentration when considering the effects of temperature.

Water

Freshwater. Copper is extensively used for handling freshwater. Seamless copper tubing, designated commercially as type K, L, and M in inch units, and type A, B, and C in metric units, is classified for water distribution service. All are UNS C12200. The largest single application of copper tubing is for hot- and cold-water distribution lines in homes and other buildings, although considerable quantities are also used in heating lines (including radiant heating lines for homes), drain tubes, and fire safety systems. The CDA (Ref 9) suggests, for reasons of excessive noise as well as possible erosion-corrosion, that the designer should limit the water velocity in hot- and cold-water distribution systems to 2.4 m/s (8 ft/s) for cold water and 1.5 m/s (5 ft/s) for water up to 60 °C (140 °F). Above 60 °C (140 °F), velocity should be limited to 0.6 to 0.9 m/s (2 to 3 ft/s).

Copper. Minerals in water combine with dissolved CO_2 and oxygen and react with copper to form a protective film. Therefore, the corrosion rate is low (5 to 25 µm/yr, or 0.2 to 1.0 mil/yr) in most exposures. In distilled water or very soft water, protective films are less likely to form; therefore, the corrosion rate may vary from less than 2.5 to 125 µm/yr (0.1 to 5 mils/yr) or more, depending on oxygen and CO_2 contents.

Copper-Zinc Alloys. The corrosion resistance of the brasses is good in unpolluted freshwater—normally 2.5 to 25 µm/yr (0.1 to 1.0 mil/yr). Corrosion rates are somewhat higher in non-scaling water containing CO_2 and oxygen. Uninhibited brasses of high zinc content (35 to 40% Zn) are subject to dezincification when used with stagnant or slowly moving brackish or slightly acid waters. On the other hand, inhibited admiralty metals and brasses containing 15% Zn or less are highly resistant to dezincification and are used very successfully in these waters. Inhibited yellow brasses are widely used in Europe and are gaining acceptance in North America. Alloy C68700 (arsenical aluminum brass, an inhibited 77Cu-21Zn-2Al alloy) has been successfully used for condenser and heat-exchanger tubes.

Copper-nickels generally have corrosion rates under 25 µm/yr (1 mil/yr) in unpolluted water. They are sometimes used to resist impingement attack where severe velocity and entrained-air conditions cannot be overcome by changes in operating conditions or equipment design.

Copper-silicon alloys (silicon bronzes) also have excellent corrosion resistance, and for these alloys, the amount of dissolved oxygen in the water does not influence corrosion significantly. If CO_2 is also present, the corrosion rate will increase (but not excessively), particularly at temperatures above 60 °C (140 °F). Corrosion rates for silicon bronzes are similar to those for copper.

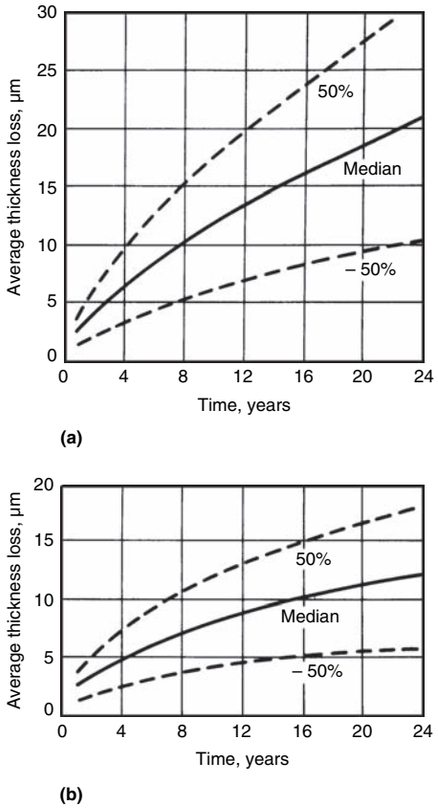

Fig. 8 Typical corrosion rates of representative copper alloys in a marine atmosphere. (a) Average data for copper, silicon bronze, and phosphor bronze. (b) Average data for brass, aluminum bronze, nickel silver, and copper-nickel

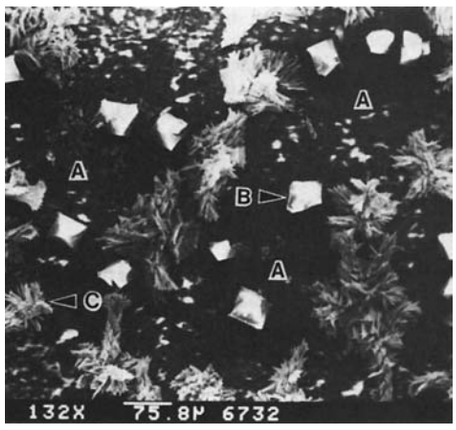

Fig. 10 Scanning electron micrograph of the corrosion product formed on C10100 in complex groundwater at 150 °C (300 °F). A, underlying film containing copper, silicon, calcium, chlorine, and magnesium; B, crystals of $CuCl_2 \cdot 3(Cu(OH)_2)$; C, crystals of CuO or Cu_2O. Courtesy of F. King and C.D. Litke

Copper-Aluminum Alloys. The aluminum bronzes have been used in many waters, from potable water to brackish water to seawater. Softened waters are usually more corrosive to these materials than hard waters. Alloys C61300 and C63200 are used in cooling tower hardware in which the makeup water is sewage effluent. Aluminum bronzes resist oxidation and impingement corrosion because of the aluminum in the surface film.

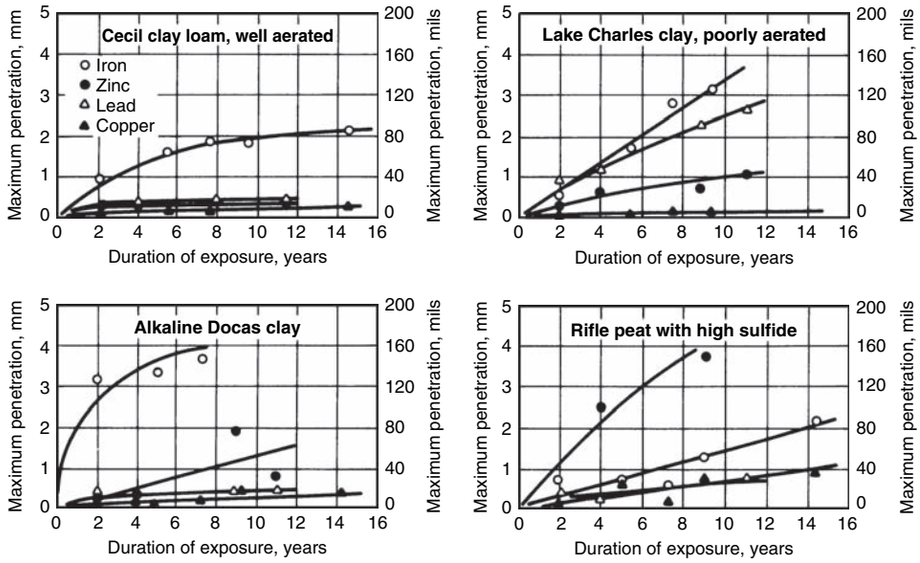

Fig. 9 Corrosion of copper, iron, lead, and zinc in four different soils

Steam. Copper and copper alloys resist attack by pure steam, but if much CO_2, oxygen, or NH_3 is present, the condensate is corrosive. Even though wet steam at high velocities can cause severe impingement attack, copper alloys are used extensively in condensers and heat exchangers. Copper alloys are also used for feedwater heaters, although their use in such applications is somewhat limited because of their rapid decline in strength and creep resistance at moderately elevated temperatures. Copper-nickels are the preferred copper alloys for the higher temperatures and pressures.

The working pressures of tubes and joints limit use of copper in systems handling hot water and steam. For example, copper tubing of 6.4 to 25 mm (1/4 to 1 in.) nominal diameter joined with 50Sn-50Pb solder can be used at temperatures to 120 °C (250 °F) and pressures to 585 kPa (85 psi). The working pressure at this temperature in tubing of the same size can be increased to 1860 kPa (270 psi) when the system is joined with 95Sn-5Sb solder. When the joining material is a brazing alloy with a melting point above 540 °C (1000 °F), the working pressure of the system is the working pressure of the annealed tubing. A few copper alloys have shown a tendency to fail by SCC when they are highly stressed and exposed to steam. Alpha aluminum bronzes that do not contain tin are among the susceptible alloys.

Steam condensate that has been properly treated so that it is relatively free of noncondensate gases, as in a power-generating station, is relatively noncorrosive to copper and copper alloys. Rates of attack in most such exposures are less than 2.5 µm/yr (0.1 mil/yr). Copper and its alloys are not attacked by condensate that contains a significant amount of oil, such as condensate from a reciprocating steam engine.

Dissolved CO_2, oxygen, or both significantly increase the rate of attack. For example, condensate with 4.6 ppm O, 14 ppm CO_2, and a pH of 5.5 at 68 °C (155 °F) caused an average penetration of 175 to 350 µm/yr (6.9 to

Table 6 Short-term corrosion rates of copper alloys in saline groundwaters

Alloy	Type of groundwater	Oxygen concentration, µg/g	Temperature		Corrosion rate		Ref
			°C	°F	µm/yr	mils/yr	
C10100	Synthetic	<0.1	150	300	15	0.6	(b)
	55 g/L TDS(a)	6	150	300	340	13.4	
Copper	Brine A	<0.1	250	480	70	2.8	8
	306 g/L TDS	600	250	480	1200	47.2	
	Seawater	<0.1	250	480	50	2	
	35 g/L TDS	1750	250	480	5000	197	
Cu-10Ni (C70600)	Brine A	<0.1	250	480	140	5.5	8
		600	250	480	400	15.7	
	Seawater	<0.1	250	480	70	2.8	
		1750	250	480	700	27.6	

(a) TDS, total dissolved solids. (b) F. King and C.D. Litke, unpublished research, 1985

13.8 mils/yr) when in contact with C12200 (phosphorus-deoxidized copper), C14200 (arsenical copper), C23000 (red brass), C44300 to C44500 (admiralty metal), and C71000 (copper-nickel, 20%). Steel tested under the same conditions was penetrated at approximately twice the rate given for the copper alloys listed previously, but tin-coated copper proved to be much more resistant and was attacked at a rate of less than 25 μm/yr (1 mil/yr). To attain the optimal service life in condensate systems, it is necessary to ensure that the tubes are installed with enough slope to allow proper drainage, to reduce the quantity of corrosive agents (usually CO_2 and oxygen) at the source by mechanical or chemical treatment of the feedwater, or to treat the steam chemically.

Modern power utility boiler feedwater treatments commonly include the addition of organic amines to inhibit the corrosion of iron components of the system by scavenging oxygen and increasing the pH of the feedwater. These chemicals, such as morpholine and hydrazine, decompose in service to yield NH_3, which can be quite corrosive toward some copper alloys. In the main body of well-monitored operating condensers, oxygen and NH_3 levels are quite low, and corrosion is usually mild. More aggressive conditions exist in the air-removal section. Abnormal operating conditions, tube leakage, and shutdown-startup cycles may also increase the corrosivity of the steam-side environment by raising the oxygen concentration. The corrosion resistance in laboratory tests of a number of copper alloys and low-carbon steel in both aerated (8 to 12 ppm O_2) and deaerated (100 to 200 ppb O_2) NH_3 solutions is illustrated in Fig. 11 and 12. In these tests, NH_3 enhanced the corrosion resistance of the copper-nickel alloys, modifying surface oxides by increasing nickel content. Elevated oxygen levels are generally more deleterious than elevated NH_3 levels. However, the elevated oxygen content minimally affected C71500. These laboratory data correlate well with field corrosion data from operating power plants (Table 7). Additional information on corrosion in power plant applications is available in the articles about corrosion in fossil and alternative fuel industries in this Volume.

Saltwater. An important use of copper alloys is in handling seawater in ships and tidewater power stations. Copper itself, although fairly useful, is usually less resistant to general corrosion than C44300 to C44500, C61300, C68700, C70600, or C71500. The superior performance of these alloys results from the combination of insolubility in seawater, erosion resistance, and biofouling resistance. The corrosion rates of copper and its alloys in relatively quiescent seawater are typically less than 50 μm/yr (2 mils/yr).

In the laboratory and in service, copper-nickel alloys C70600, C71500, C72200, and C71640 exhibit excellent corrosion resistance in seawater. Average corrosion rates for both C70600 and C71500 were shown to range from 2 to 12 μm/yr (0.08 to 0.5 mil/yr) (Ref 12). The long-term evaluations illustrated in Fig. 13 and 14 revealed corrosion rates less than 2.5 μm/yr (0.1 mil/yr) for both alloys after 14 years of exposure to quiescent and low-velocity seawater (Ref 13). Sixteen-year tests confirmed this same low corrosion rate (Ref 14).

Pitting Resistance. Alloys C70600 and C71500 both display excellent resistance to pitting in seawater. The average depth of the 20 deepest pits in C71500 observed at the end of the 16 year tests was less than 127 μm (5 mils) (Ref 14).

Chromium-modified copper-nickel alloys, developed for resistance to high-velocity seawater, were evaluated in both low- and high-velocity conditions. The quiescent and low-velocity performances of C72200, C70600, and C71500 were compared (Ref 15, 16); results showed uniform corrosion (5 to 25 μm/yr, or 0.2 to 1 mil/yr) on all three alloys. The chromium-containing alloys, however, were slightly more susceptible to localized attack in quiet seawater. Another study reported that the pitting behavior of C72200 is influenced by the presence of iron and chromium in or out of solid solution (Ref 17). The fraction of iron plus chromium in solution in C72200 must be kept higher than 0.7 to avoid pitting corrosion.

Velocity Effects. The corrosion resistance of copper alloys in flowing seawater depends on the growth and maintenance of a protective film or corrosion product layers. These alloys typically exhibit velocity-dependent corrosion rates. The more adherent and protective the film on a particular alloy, the higher its breakaway velocity (the velocity at which there is a transition from low to high corrosion rate) and the greater its resistance to impingement attack or erosion-corrosion.

Some of the earliest work on copper-nickel alloys demonstrated the beneficial effects of iron additions on seawater impingement resistance. The graphical summary of the effects of iron shown in Fig. 15 qualitatively illustrates the

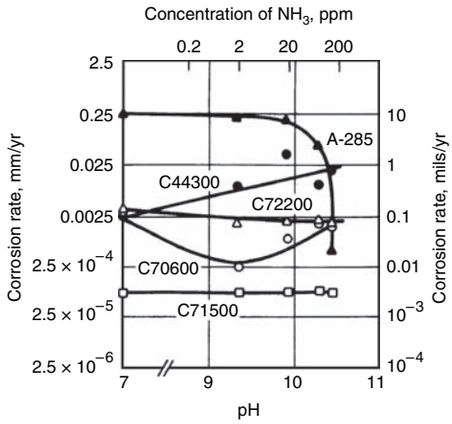

Fig. 11 Corrosion rates of copper alloys and low-carbon A-285 steel in aerated NH_3 solutions. Test duration: 1000 h. Source: Ref 10

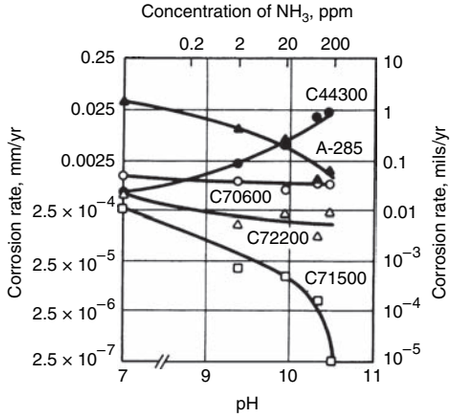

Fig. 12 Corrosion rates of copper alloys and low-carbon A-285 steel in deaerated NH_3 solutions. Test duration: 1000 h. Source: Ref 10

Table 7 Comparison of field and laboratory condensate corrosion of copper alloys

Data are weight loss measured after total exposure time, expressed as penetration rates

	Corrosion rate, μm/yr (mils/yr)					
	Field tests(a)			Laboratory tests(b)		
Alloy	Plant A	Plant B	Plant C	0 ppm NH_3	2 ppm NH_3	20 ppm NH_3
C71500	0.2 (0.0083)	0.1 (0.004)	0.4 (0.0151)	0.3 (0.012)	0.05 (0.002)	0.025 (0.001)
C72200	0.4 (0.016)	0.4 (0.016)	0.38 (0.015)	0.61 (0.024)	0.2 (0.008)	0.18 (0.007)
C70600	0.48 (0.019)	0.36 (0.014)	0.46 (0.018)	1.3 (0.053)	1.1 (0.043)	0.94 (0.037)
C44300	1.27 (0.05)	0.79 (0.031)	0.61 (0.024)	0.61 (0.024)	2.3 (0.09)	5.6 (0.22)
A285	6.2 (0.243)	10.4 (0.411)	2.6 (0.103)	38 (1.5)	8.3 (0.325)	4.6 (0.183)

(a) 2 year tests in hot wells at three plant sites (A, B, and C). Plant A, pH range of 8.9–9.7; typical pH of 9.1–9.3. Plant B, pH range of 9–10, typical pH of 9.3–9.6. (b) Laboratory data extrapolated from 1000 h tests in deaerated beakers. 0 pprn NH_3 solution, pH 7; 2 ppm NH_3 solution, pH 9.4; 20 ppm NH_3 solution, pH 10. Source: Ref 11

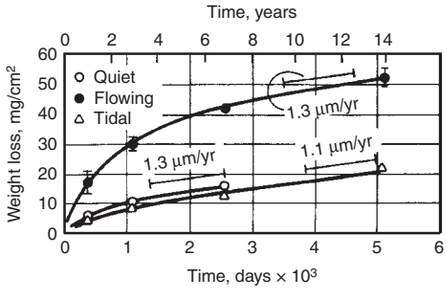

Fig. 13 Chronogravimetric curves for C70600 in quiet, flowing, and tidal seawater. Source: Ref 13

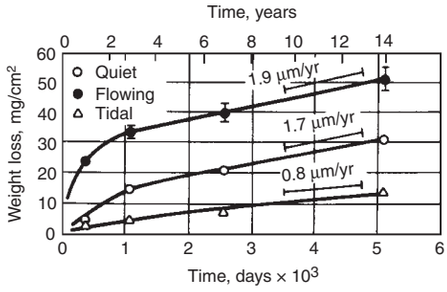

Fig. 14 Chronogravimetric curves for C71500 in quiet, flowing, and tidal seawater. Source: Ref 13

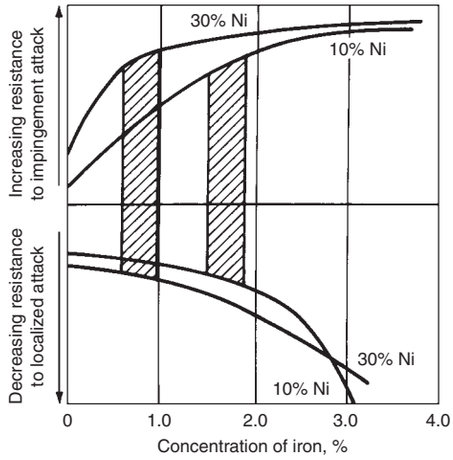

Fig. 15 Corrosion resistance of copper-nickel alloys as a function of iron content. Shaded areas indicate optimal iron contents for good balance between pitting resistance and impingement resistance. Source: Ref 18

balance between pitting resistance and impingement resistance that defines the optimal iron content for 90Cu-10Ni and 70Cu-30Ni at 1.5 and 0.5% Fe, respectively. The effects of manganese level in association with iron in copper-nickel alloys are also addressed in Ref 18. The relative beneficial effects of 2% Fe and 2% Mn in a 70Cu-30Ni alloy (C71640) are shown in Fig. 16, which indicates that the C71640 and C72200 alloys are markedly more resistant to erosion-corrosion than C70600 at velocities up to 9 m/s (30 ft/s). The chromium-modified copper-nickel alloys also provide increased resistance to impingement attack compared to Cu-Ni-Fe alloys. In jet impingement tests (Ref 16) on several copper-base alloys at impingement velocities as high as 10 m/s (33 ft/s), no measurable impingement attack was observed on alloys C72200 and C71900 at 4.6 m/s (15 ft/s) (Table 8).

The behaviors of several copper-nickel alloys, including C71640 and C72200, have been characterized under conditions simulating partial blockage of a condenser tube (Ref 19). In the 1 year natural seawater tests, enhanced erosion-corrosion resistance was observed for the C71640 and C72200 alloys as compared to C70600 and C71500. Some localized pitting and/or crevice corrosion associated with the nonmetallic blockage device was noted for C71640 and C72200, with no such attack occurring for the C70600 and C71500 alloys. Superior performance of the modified copper-nickel alloys C72200 and C71640 was also observed under severely erosive conditions in seawater containing entrained sand (Ref 20).

The combined results of laboratory impingement studies and service performance have produced maximum acceptable design velocities for condenser tube materials (Table 9). Erosion-corrosion was studied on the basis of fluid dynamics (Ref 21–23). Instead of defining the critical velocity for a material, which is difficult to relate to service conditions and which is specific to tubing diameter, the use of critical surface shear stress was advocated. This shear stress in a dynamic fluid system is a measure of the force applied by the moving fluid to the surface with which it interacts. It takes into account the changes in fluid density and kinematic viscosity with variations in temperature, specific gravity, and hydrodynamic parameters. Values of critical surface shear stress for several copper-base alloys are shown in Table 10.

Galvanic Effects. In general, the copper-base alloys are galvanically compatible with one another in seawater. The copper-nickel alloys are slightly cathodic (noble) to the nickel-free copper-base alloys, but the small differences in corrosion potential generally do not lead to serious galvanic effects unless unusually adverse anodic/cathodic area ratios are involved.

The data given in Table 11 demonstrate the increased attack of less noble carbon steel coupled to copper-nickel alloys (Cu-10Ni, C70600; Cu-30Ni, C71500), the increased attack on the copper-nickel alloys when coupled to more noble titanium, and the general compatibility of copper-nickel alloys with aluminum bronze (Cu-7Al, C61400). Coupling copper-nickel alloys to less noble materials affords protection to the copper-nickel that effectively reduces its corrosion rate, thus inhibiting the natural fouling resistance of the alloy.

Results of short-term galvanic couple tests between C70600 and several cast copper-base and ferrous alloys are listed in Table 12. The corrosion rate of cast 70Cu-30Ni was unaffected by coupling with an equal area of C70600, but some increased corrosion of other cast copper-base alloys was noted. Corrosion rates of cast stainless steels were reduced, with a resultant increase in the corrosion of C70600. Gray iron displayed the largest galvanic effect, while the corrosion rates of Ni-Resist (heat- and corrosion-resistant) cast irons nominally doubled. Although some caution should be exercised in using absolute values from any short-term tests, the relative degree of acceleration of corrosion from galvanic coupling was shown to be unaffected by extending some tests with Ni-Resist/C70600 couples to 1 year.

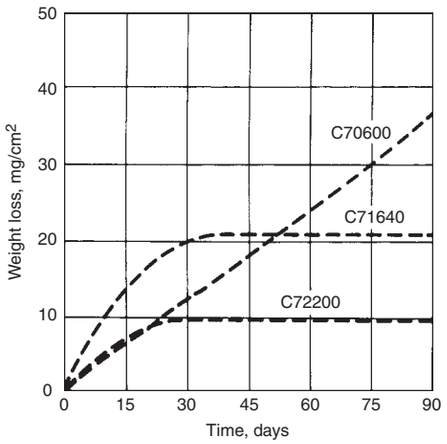

Fig. 16 Weight loss versus time curves for C70600, C71640, and C72200 exposed in seawater at a velocity of 9 m/s (30 ft/s). Source: Ref 18

Table 8 Summary of jet impingement test data for several copper alloys at three velocities

Test duration: 1–2 months; 10 to 26 °C (50 to 80 °F) seawater

	Impingement attack at velocity					
	4.6 m/s (15 ft/s)		6.8 m/s (22 ft/s)		9.8 m/s (32 ft/s)	
Alloy	mm/yr	mils/yr	mm/yr	mils/yr	mm/yr	mils/yr
C44300	1.8–4.8	71–189	Not tested		Not tested	
C68700	0.36–3	14.2–118	Not tested		Not tested	
C70600	0.12–2.16	4.7–85	0.36–1.56	14.2–61.4	1.56	61.4
C71500	0.12–1.08	4.7–42.5	0.36–6.84	14.2–269	1.68–2.04	66–80.3
C71900	No attack		0.12–0.36	4.7–14.2	1.08–1.44	42.5–56.7
C72200	No attack		0.12	4.7	No attack	

Source: Ref 16

Table 9 Accepted maximum tubular design velocities for some copper alloys for condenser tubes in seawater

Alloy	Maximum design velocity	
	m/s	ft/s
C12200	0.6–0.9	2–3
C44300	1.2–1.8	4–6
C60800, C61300	2.7	9
C68700	2.4	8
C65100, C85500	0.9	3
C70600	3.0–3.6	10–12
C71500	4.5–4.6	14.8–15
C72200	9.0	30

Effect of Oxygen, Depth, and Temperature. The corrosion of copper and copper-base alloys in clean seawater is cathodically controlled by oxygen reduction, with H^+ reduction being thermodynamically unfavorable. Dissolved oxygen retards corrosion by the promotion of a protective film on the copper alloy surface but increases the rate of corrosion by depolarizing cathodic sites and oxidizing Cu^+ ions to more aggressive Cu^{2+} ions. Other factors, such as velocity, temperature, salinity, and ocean depth, affect the dissolved oxygen content of seawater, thus influencing the corrosion rate. In general, oxygen concentration decreases with increasing salinity, temperature, and depth. These factors can vary with depth in a complex manner and also vary from location to location in the oceans of the world (Ref 24).

Although cathodic control by oxygen reduction suggests a strong dependence of corrosion rate on dissolved oxygen concentration, the growth of a protective oxide film on copper-nickel alloys minimizes the influence within the normally observed range of oxygen content found in seawater. Deep-ocean testing indicated that the corrosion rates of copper and copper-nickel alloys do not change significantly for dissolved oxygen contents between 1 and 6 mL/L of seawater and consequently were not significantly affected by variations in depth of exposure (Ref 24).

Short-term laboratory tests indicated only a small increase in corrosion rate with increasing temperature up to 30 °C (85 °F) (Ref 25). Long-term corrosion rate data from tests conducted at a coastal site near Panama (Ref 14) agree very well with long-term data for exposures in Wrightsville Beach, NC (Ref 13), where the seasonal temperature variation is 5 to 30 °C (40 to 85 °F).

Table 10 Critical surface shear stress for copper-base alloys in seawater

Alloy	Critical shear stress	
	Pa	psi
C12200	9.6	0.0014
C68700	19.2	0.0028
C70600	43.1	0.0063
C71500	47.9	0.007
C72200	296.9	0.043

Source: Ref 21

Final steady-state corrosion rates at both locations for C71500 ranged from 1 to 3 μm/yr (0.04 to 0.12 mil/yr).

In the last 30 years, desalination plant operations have provided data and experience for use of copper alloys that has extended the design life of these plants to 40 years (Ref 26). Copper-nickel alloys, C70600, C71500, and C71640 are used extensively. Inlet water temperatures have a great influence on the formation of protective films. In arctic waters (2 °C, or 35 °F), complete coverage by film of a C70600 specimen takes a week, whereas with inlet temperatures of 27 °C (80 °F), common in desalination plants located in Middle Eastern countries similar coverage occurs in a few hours (Ref 27). Within the flash desalination systems, the heat recovery, brine heater, and vapor-side components experience temperatures from 80 to 115 °C (175 to 240 °F). Alloy C70600 tubing is used in a majority of systems in these areas. In this temperature range, corrosion tests show that controlling water chemistry (bicarbonate alkalinity, dissolved oxygen, and pH) was a critical factor to controlling corrosion (Ref 28). In locations where the sand loading of water is high, C71640 is selected for use in the heat-recovery section for its resistance to erosion-corrosion (Ref 26).

Effect of Chlorine. Coastal power plants that use seawater as a coolant have long used chlorine to control fouling and slime formation. The effect of chlorination, both continuous and intermittent, on the corrosion of copper-nickel alloys was studied (Ref 29, 30). Continuous chlorine additions increased the corrosion rate of C70600 by a factor of 2. Intermittent chlorination at a higher level controlled fouling yet had no apparent effect on corrosion rates. A net reduction was noted in the corrosion rate of C71500 with continuous and most intermittent chlorine additions.

Seawater impingement tests were conducted on C70600, C71500, and C71640 with continuous additions of chlorine (and iron) (Ref 27). Additions of 0.5 to 4.0 mg/L of chlorine caused increased susceptibility to impingement attack on C70600 at a velocity of 9 m/s (30 ft/s). Addition of chlorine up to 4.0 mg/L had little effect on the impingement resistance of C71500. Figure 17 summarizes the results of these tests.

Polluted cooling waters, particularly in coastal harbors and estuaries, reportedly cause numerous premature failures of power station and shipboard condensers using copper-base alloys, including the copper-nickels. During the early 1950s, polluted waters were identified as the most important contributing factor in the failure of condenser tubes (Ref 31). Enforcement of strict pollution standards has dramatically reduced pollution in many harbors in recent years; however, accelerated attack of condenser tubes and seawater piping materials by polluted waters is still reported.

The attack of copper-containing materials by polluted seawater has been addressed in numerous test programs. The primary causes of accelerated attack of copper-base alloys in polluted seawater are (1) the action of sulfate-reducing bacteria, under anaerobic conditions (for example, in bottom muds or sediments), on the natural sulfates present in seawater and (2) the putrefaction of organic sulfur compounds from decaying plant and animal matter within seawater systems during periods of extended shutdown (Ref 32). Partial putrefaction of organic sulfur compounds may also result in the formation of organic sulfides, such as cystine or glutathione, which can cause pitting of copper alloys in seawater (Ref 33).

Alloys C70600 and C71500 have been found to be susceptible to sulfide-induced attack in aerated seawater containing sulfide concentrations as low as 0.01 mg/L (Ref 34). Subsequent tests showed that while both were subject to localized attack, C71500 was more resistant to

Table 11 Galvanic couple data for C70600 and C71500 with other materials in flowing seawater

2 year exposures of equal-area couples at a velocity of 0.6 m/s (2 ft/s)

Alloy	Corrosion rate	
	μm/yr	mils/yr
Uncoupled		
C70600	31	1.2
C71500	20	0.8
C61400	43	1.7
Carbon steel	330	13
Titanium	2	0.08
Coupled		
C70600	25	1
C61400	43	1.7
C70600	3	0.12
Carbon steel	787	31
C70600	208	8.2
Titanium	2	0.08
C71500	18	0.7
C61400	64	2.5
C71500	3	0.12
Carbon steel	711	28
C71500	107	4.2
Titanium	2	0.08

Table 12 Galvanic corrosion data for C70600/cast alloy couples in seawater

32 day tests of equal-area couples in seawater at 10 °C (50 °F). Velocity: 1.8 m/s (6 ft/s)

Alloy	Galvanic effect(a)	
	C70600	Other alloy
C70600	1.0	
Cast 90Cu-10Ni	0.8	1.6
Cast 70Cu-30Ni	0.9	1.0
85-5-5-5 (C83600)	0.9	1.5
M Bronze (C92200)	0.7	1.8
ACI CN7M stainless steel	1.5	0.6
ACI CF8M stainless steel	1.2	0.1
Gray iron	0.1	6.0
Ni-Resist type I(b)	0.4	2.1
Ni-Resist type II	0.3	2.6
Ni-Resist type D2	0.3	2.0

(a) Ratio of weight loss in couple to weight loss of an uncoupled control specimen. (b) Ni-Resist couple tests at 29 °C (85 °F)

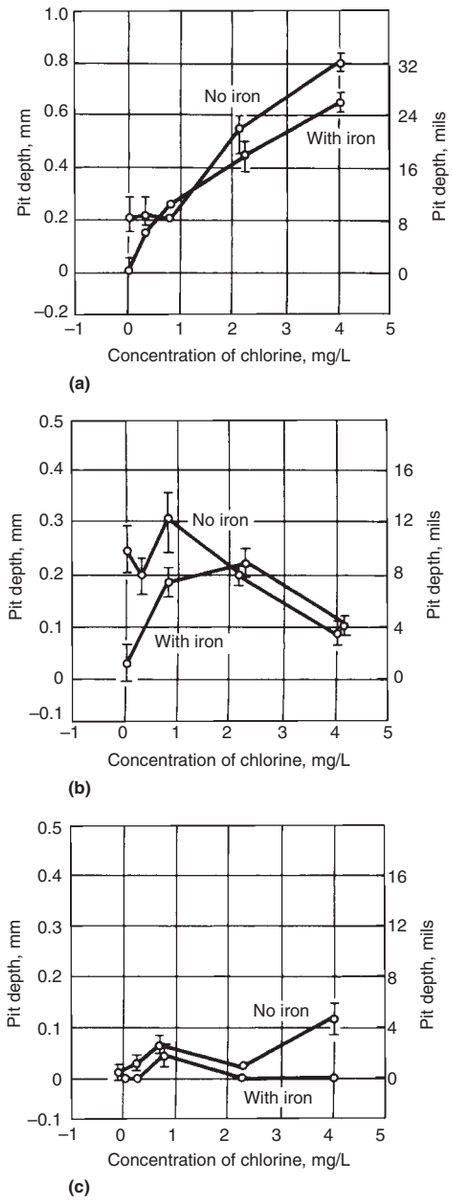

Fig. 17 Impingement attack versus chlorine levels for three copper alloys with the effect of a ferrous ion inhibitor. (a) C70600. (b) C71500. (c) C71640

long-term exposures to low concentrations of sulfide (Ref 35).

Inhibition of Corrosion. In some applications, adding iron to the seawater further enhances the corrosion resistance of copper alloys. This iron is introduced either through the addition of ferrous sulfate ($FeSO_4$) or by direct oxidation of a sacrificial iron anode either with or without an externally applied current.

The effectiveness of environmental iron additions against sulfide corrosion of copper-nickel alloys was evaluated (Ref 36, 37). Iron added continuously at a level of 0.2 mg/L by a stimulated iron anode was effective against low-level (0.01 mg/L) sulfide corrosion of both C70600 and C71500, although some attack was still observed. Corrosion, already actively proceeding, was significantly reduced, and the effects of additional low-level sulfide exposure were nullified by ferrous ion (Fe^{2+}) treatment. Intermittent injection of $FeSO_4$ for 2 h per day at 1.0 to 5.0 mg/L was not found effective against high sulfide levels (0.2 mg/L) but was effective in reducing corrosion at lower sulfide levels (0.01 to 0.04 mg/L). Additional work demonstrated that continuous low-level additions of $FeSO_4$ could counteract sulfide-accelerated corrosion of copper-nickel alloys (Fig. 18).

In the use of $FeSO_4$ or stimulated iron anodes to counteract sulfide-induced corrosion, it should also be considered that iron additions affect heat-exchanger efficiency. The continued use of iron additions can result in a significant buildup of scale on the tube surface. At high enough levels of iron addition, sufficient sludge or precipitate may develop to result in complete blockage of the heat-exchanger tubes. At lower levels of iron addition, a bulky deposit will develop on the tube surface that may also interfere with heat transfer. In a study of the increase in deposit formation and loss of heat transfer for aluminum brass in seawater with both intermittent and continuous Fe^{2+} ion dosing, it was recommended that some consideration be given to a gradual reduction in dosing levels after the initial film formation (Ref 39).

Other preventive measures can be taken to minimize the deleterious effects of sulfides (Ref 40–42). Elimination of decaying plant and animal life from inlet pipes and channels can alleviate the effects of sulfate-reducing bacteria. Initial design or operational procedures, such as eliminating stagnant legs in a piping system or careful use of screening and filtration systems, can yield a valuable return on investment. In one study, impingement tests were performed on C71500 in seawater containing 10 mg/L cystine (an organic sulfur compound) and varying amounts of an inhibitor, sodium dimethyldithiocarbamate (Ref 42). The results indicated a reduction in the depth of impingement attack. It was noted, however, that a 0.10% solution would be cost-prohibitive on a once-through basis but would be cost-effective if circulated through the shipboard piping system on first flooding and on shutting down. It was further noted that inhibitor injection is necessary only when the cooling water source is polluted estuarine seawater. Also see the article "Corrosion Inhibitors in the Water Treatment Industry" in *ASM Handbook,* Volume 13A, 2003.

Biofouling. Copper alloys, including the copper-nickels, have long been recognized for their inherent resistance to marine fouling. This fouling resistance is usually associated with macrobiological fouling, such as barnacles, mussels, and marine invertebrates of corresponding size. Service experience with shrimp trawlers and private yachts fabricated with C70600 or C71500 hulls has demonstrated excellent resistance to hard-shell fouling and an accompanying reduction in hull maintenance costs (Ref 41). Copper-nickel alloys have also performed successfully as seawater intake screens by virtue of their mechanical strength, corrosion resistance, and resistance to biofouling (Ref 42).

Research demonstrated that fouling was not observed on copper-nickel alloys containing 80% or more copper and that only incipient fouling was noted on the 70Cu-30Ni alloy (Ref 43, 44). More recent evaluations indicated approximately equivalent fouling resistance for C70600 and C71500 in 14 and 5 year exposures, respectively (Ref 13, 45). One investigation concluded that the fouling resistances of pure copper, C70600, and C71500 were virtually identical (Ref 45).

Studies of copper-nickel alloys found that some minimum copper solution rate from the corrosion process is required to prevent fouling (Ref 44). It was not established whether the effect was due to toxicity of copper ions released from the metal surface or to a continual sloughing off of corrosion products. Fouling was minimal on C71500 exposed for 14 years, during which time the corrosion rate approached 1.0 μm/yr (0.04 mil/yr) (Ref 13). It was further demonstrated that copper ions released from a bare C70600 surface offered no fouling protection to an adjacent painted surface (Ref 45). This work concluded that the duplex nature of corrosion products on copper alloy surfaces is responsible for fouling resistance. The initial film formed on copper alloys exposed to seawater is Cu_2O. This inherently fouling-resistant material subsequently oxidizes to $CuCl_2{\cdot}3(Cu(OH)_2)$, which does not appear to be as toxic to marine organisms. The $CuCl_2{\cdot}3(Cu(OH)_2)$ periodically sloughs off from the material surface, carrying with it many marine organisms that may have attached. This reexposes the adherent, toxic Cu_2O film and renews fouling resistance.

Whatever the mechanism, the resistance to fouling is a result of corrosion of the alloy. If this is suppressed by galvanic effects or impressed cathodic protection, fouling will not be prevented.

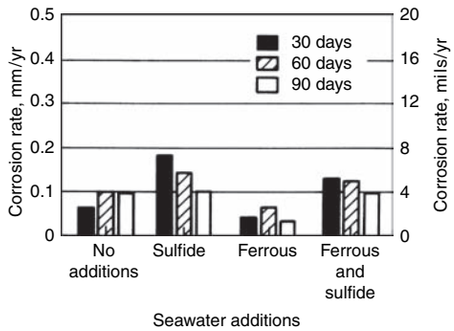

Fig. 18 Corrosion rates for C70600 exposed to seawater with additions of sulfide (0.05 mg/L) and/or Fe^{2+} (0.01 mg/L) ions. Source: Ref 38

Biofouling growth was studied on titanium and C70600 at 27 °C (80 °F) and at various velocities (Ref 46). Results (Fig. 19) indicated that the major fouling problem on titanium in the tests was silt particles bound by organic growths, while C70600 is fouled both by silt and corrosion products. Increasing velocity removes more of the silt and binding organisms but not the corrosion products. Because titanium does not produce corrosion products, the change in the fouling rate with increasing velocity was more dramatic. The behavior of C70600 suggested the periodic sloughing off of portions of the fouling layer previously noted (Ref 45). At sufficient velocities (1.8 and 2.4 m/s, or 6 to 8 ft/s), macroorganisms did not adhere to the C70600 surface, and heat-transfer resistance was due to corrosion products and entrapped particles. Fouling rates decrease by a factor of 10 on titanium with an increase in velocity from 0.6 to 2.4 m/s (2 to 8 ft/s) and decrease by a factor of 5 on C70600 for the same velocity range.

Other studies demonstrated the excellent resistance to fouling and resulting retention of heat-transfer efficiency in natural seawater of the copper alloys (Ref 47, 48). Figure 20 shows corrosion data for C70600 specimens. The relatively infrequent sponge ball mechanical cleaning did not increase corrosion of the C70600 compared to uncleaned controls. Mechanical cleaning was required much more frequently for the titanium in order to maintain a given level of heat-transfer efficiency. Intermittent chlorination did increase the initial corrosion rates, although the rates were comparable to uncleaned controls after approximately 90 days. By contrast, in other tests in which excessive mechanical cleaning was used in natural seawater, a significant acceleration of corrosion occurred with daily sponge ball cleaning at a rate of 12 passes/h (Ref 49).

Heat Exchangers and Condensers. The selection of material for condenser and heat-exchanger tubes necessitates a survey of service conditions, an examination of tubes previously used and evaluation of its service life, and a review of the type, form, and location of corrosion experienced in the unit or in similar units. Types of water and operating conditions vary widely, and any estimate of probable tube performance must be based on specific operating factors. The tubes of the various alloys discussed in this section provide satisfactory and economical performance for the services described.

Inhibited Admiralty Metal. (C44300, C44400, and C44500) has good corrosion resistance and is extensively used for tubing in various services, especially steam condensers cooled with fresh, salt, or brackish water. Admiralty metal tubes are also used for heat exchangers in oil refineries, in which corrosion from sulfur compounds and contaminated water may be very severe, and for feedwater heaters and heat-exchanger equipment as well as other industrial processes. Admiralty metal tubes are often used in equipment operating at temperatures of 200 °C (400 °F) or higher. Small amounts of phosphorus (0.02 to 0.06%) added to admiralty metal markedly increase dezincification resistance.

Inhibited aluminum brass (C68700) resists the action of high-velocity salt and brackish water and is commonly used for condenser tubes. The outstanding characteristic of C68700 is its high resistance to impingement attack. Tubes of this alloy are frequently recommended for use in marine and land power stations, in which cooling water velocities are high and inhibited admiralty metal tubes have failed because of impingement attack.

Aluminum Bronzes. Tube sheets made of C61300 and C63200 have been specified for coastal power station condensers. The aluminum bronzes of C61300, C63000, and C63200 in wrought form and C95400, C95500, and C95800 in cast form are extensively used in saltwater environments. They are used in Navy seawater systems and submarine systems in pumps, valves, heat exchangers, and structural components for mounting electronic gear and propulsion units and are even more widely used in minesweepers, for which their nonmagnetic characteristics are important. They are used in cast or wrought form for tube sheets and water boxes in saltwater evaporators and in seawater cooling loops in fossil and nuclear power plants. Corrosion rates are of the order of 10 to 50 μm/yr (0.4 to 2 mils/yr), depending on temperature and velocity, and generally decrease with time. Temper annealing is particularly important in the cast forms of these alloys when used in seawater.

Copper-nickel, 10% (C70600) exhibits excellent resistance to impingement attack; it appears to be inferior only to copper-nickel, 30%. It is also highly resistant to SCC. This alloy is

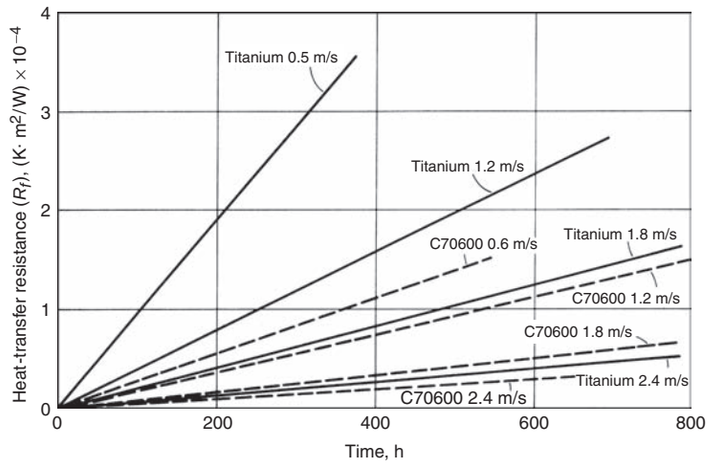

Fig. 19 Fouling rates (as measured by heat-transfer resistance, R_f) of C70600 and titanium as a function of seawater velocity. Source: Ref 46

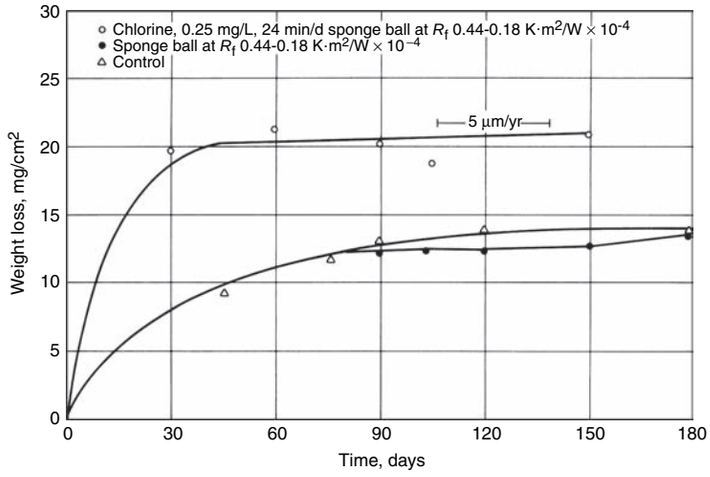

Fig. 20 Weight loss/corrosion data for C70600 cleaned by chlorinated sponge ball and sponge ball without chlorination

suitable for marine condenser tube installations in place of aluminum brass, especially where higher water velocities are encountered.

Copper-nickel, 30% (C71500) has, in general, the best resistance of any of the copper alloys to impingement attack and to corrosion by most acids and waters. It is being used in increasing quantities under severely corrosive conditions for which service lives longer than those of other copper alloys are desired. The United States Navy uses it for most shipboard condensers and heat exchangers.

Phosphorus-deoxidized coppers (C12000 to C12300) are extensively used in sugar refineries for condensers and evaporators. Deoxidized coppers are standard materials in the refrigeration industry and for transferring heat from steam to water or air, because of their excellent resistance to corrosion by freshwater and their high thermal conductivities.

Bimetal tubes are sometimes used to meet severe corrosion problems not handled adequately by tubes of a single metal or alloy. Two tubes of different alloys, one inside the other, form one integral tube. Copper may be the inner or outer layer, depending on the application.

Drain Tubes. Copper is used for waste and vent lines in drains. The first such installations were made in the mid-1930s, and since then, many municipalities have approved the use of copper drain lines. Development of Sovent fittings now enables construction of a single-stack drain system in high-rise buildings instead of the two-stack system formerly used.

Corrosion in Acids

Copper is widely employed for industrial equipment used to handle acid solutions. A fairly definite separation exists between those acids that can be handled by copper and those that cannot. In general, copper alloys are successfully used with nonoxidizing acids, such as CH_3COOH, H_2SO_4, HCl, and H_3PO_4, as long as the concentration of oxidizing agents, such as dissolved oxygen (air) and ferric (Fe^{3+}) or dichromate ions, is low. Broadly speaking, a thoroughly agitated or stirred solution or one into which a stream of air has been bubbled approaches air saturation and is therefore not a suitable acid medium for copper. Acids that are oxidizing agents in themselves, such as HNO_3; sulfurous (H_2SO_3); hot, concentrated H_2SO_4; and acids carrying such oxidizing agents as Fe^{3+} salts, dichromate ions, or permanganate (MnO_4^-) ions, cannot be handled in equipment made of copper or its alloys.

The corrosive action of a dilute (up to 1% acid) nonoxidizing acid on copper is relatively low; corrosion rates are usually less than 6 g/m^2/d (equivalent penetration rate: 250 μm/yr, or 10 mils/yr). This is true only of oxidizing acids when the concentration does not exceed 0.01%. At such low acid concentrations, aeration has little effect in either oxidizing or nonoxidizing acids.

Nonoxidizing acids with near-zero aeration have virtually no corrosive effect. Rates in 1.2 *N* H_2SO_4, HCl, and CH_3COOH are less than 0.1 g/m^2/d (4 μm/yr, or 0.15 mil/yr) in the absence of air. Figure 21 shows the general effect of various concentrations of oxygen on the corrosion rate of copper in these acids.

Except for HCl, nonoxidizing acids that contain as much air as is absorbed in quiet contact with the atmosphere are weakly corrosive. Rates generally range from 0.5 to 6 g/m^2/d (approximately 20 to 250 μm/yr, or 0.8 to 10 mils/yr).

Air-saturated solutions of nonoxidizing acids are likely to be strongly corrosive, with corrosion rates of 5 to 30 g/m^2/d (0.2 to 1.25 mm/yr, or 8 to 50 mils/yr). This rate is higher for HCl. The actual corrosion in any aerated acid depends on acid concentration, temperature, and other factors that are difficult to classify. Except in very dilute solutions, oxidizing acids corrode copper rapidly—usually at rates above 50 g/m^2/d (2.1 mm/yr, or 85 mils/yr). The reaction is independent of aeration.

The corrosion rates of three common acids are compared below (temperature and aeration are not specified):

	Corrosion rate		
Acid	g/m^2/d	mm/yr	mils/yr
32% HNO_3	5700	240	9450
Concentrated HCl	18	0.75	30
17% H_2SO_4	2	0.1	4

Phosphoric, CH_3COOH, tartaric, formic, oxalic, malic, and similar acids normally react comparably to H_2SO_4. Many of the copper alloys can be brazed with brazing rod of the same composition, which provides a joint that is approximately as corrosion resistant in acids as the base metal.

Factors that may accelerate corrosion vary from one plant to another, and it is advisable to conduct preliminary service or field tests under actual operating conditions before purchasing large quantities of an alloy. Corrosion-accelerating factors can then be evaluated. Selection of the most suitable material for use in a chemical process depends not only on corrosion resistance but also on such factors as continuing availability of the alloy in the desired form and size (which should be ensured before any alloy is given serious consideration).

The following corrosion data were obtained in tests made under various conditions for handling different acids and acid solutions. Because of the variety of factors affecting all chemical reactions, the values shown cannot be taken as absolute and should be considered only as trends.

Sulfuric Acid. The corrosion rate of C65500 (3% silicon bronze) in H_2SO_4 indicates that this alloy can be successfully used with solutions of 3 to 7096 H_2SO_4 (by weight) at temperatures of 25 to 70 °C (75 to 160 °F). Laboratory test results are shown in Fig. 22.

Rate of attack by H_2SO_4 varies with concentration (Table 13). The presence of copper or iron salts in acid solutions accelerates the corrosion rate of copper (Table 14).

Aluminum bronze C61300 (wrought) as well as C95200 and C95800 (cast) are used extensively in dilute (10 to 20%) H_2SO_4 service, particularly in steel-pickling acids. Because these alloys have good corrosion resistance and high mechanical properties, thinner sections can withstand the required loads. In general, the copper alloys are quite resistant to the environment, but when in contact with the steel being pickled, they are galvanically protected and in turn accelerate the cleaning action of the acid on the steels. In time, the iron salts are changed from Fe^{2+} to Fe^{3+} (oxidizing) form, and there is increased corrosion; therefore, filtering or elimination of the salts is beneficial. Also, open tanks made of copper for this medium will have a higher corrosion rate at the liquid level line because of higher oxygen concentration. Hydrochloric acid added to H_2SO_4 greatly increases the corrosion rate of copper alloys compared to that in either acid individually.

Phosphoric Acid (H_3PO_4). Copper and copper alloys are used in heat-exchanger tubes, pipes, and fittings for handling H_3PO_4, although the corrosion rates of some of these alloys may be comparatively high. Laboratory tests were

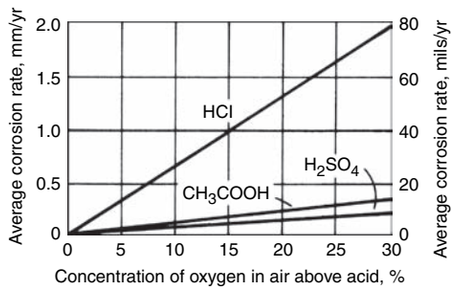

Fig. 21 Effect of oxygen on corrosion rates for copper in 1.2 *N* solutions of nonoxidizing acids. Specimens are immersed for 24 h at 24 °C (75 °F). Oxygen content of the solutions varied from test to test, depending on the concentration of oxygen in the atmosphere above the solutions.

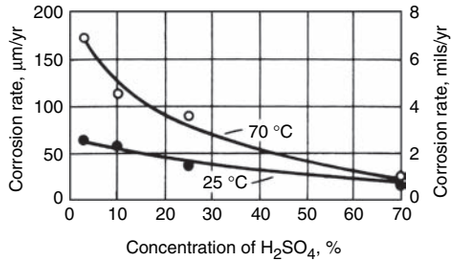

Fig. 22 Corrosion of C65500 in H_2SO_4 solutions. Specimens were immersed for 48 h at the indicated temperatures. The solution was not agitated or intentionally aerated.

performed on seven groups of copper alloys in aerated and unaerated acid, with specimens at the water line, in quiet immersion, and totally submerged. Acid concentrations ranged from 5 to 90%, and temperatures ranged from 20 to 85 °C (70 to 185 °F) except for the Cu-Al-Si alloy, which was tested only in 6.5% H_3PO_4 at 20 °C (70 °F) with specimens at the water line and in quiet immersion. Corrosion rates for the seven alloy groups were as follows:

	Corrosion rate	
Alloy type	mm/yr	mils/yr
Copper	0.55–3.7	22–146
Copper–zinc (70% Cu min)	0.13–7.0	5–280
Copper-tin	0.025–1.30	1–51
Copper-nickel	0.025–0.63	1–25
Copper-silicon	0.13–0.93	5–37
Copper-aluminum-iron	0.13–0.25	5–10
Copper-aluminum-silicon	0.28–2.4	11–94

In general, copper and copper alloys provide satisfactory service in handling pure H_3PO_4 solutions in various concentrations. The acid concentration seems to have less effect on the corrosion rate than the amount of impurities. The impure H_3PO_4 produced by the H_2SO_4 process may contain a markedly higher concentration of Fe^{3+}, SO_4^{2-}, sulfite (SO_3^{2-}), Cl^-, and fluoride (F^-) ions than acid produced by the electric furnace process. These ions increase the corrosion rate up to 150 times, which limits the service lives of copper alloys.

Pure H_3PO_4 produced by the electric furnace process contains only small quantities of impurities and is therefore only slightly corrosive to copper and its alloys. Inhibited admiralty metals C44300, C44400, and C44500 are suggested for solutions of pure H_3PO_4.

Accumulation of corrosion products on metal surfaces may also increase both the rate of corrosion and the possibility of pitting. Low-copper alloys, such as C46400 (naval brass), appear to form thin, adherent films of corrosion products. Copper, copper-silicon alloys, and other high-copper alloys form more voluminous, porous films or scales beneath which roughened or pitted surfaces are likely to be found.

The H_3PO_4 vapors that condense in electrostatic precipitators at approximately 120 °C (250 °F) are noticeably more corrosive than solutions of pure H_3PO_4 at the same or lower temperatures. The corrosion rates encountered in precipitators are so high that copper alloy wires will not give satisfactory service as electrodes. The high rate of corrosion is probably caused by an abundant supply of oxygen.

Although the corrosion rates of copper cooling tubes in H_3PO_4 condensation chambers are high (approximately 10 mm/yr, or 400 mils/yr), the rates are lower than those of some other materials. Therefore, the use of copper tubes is feasible for this application.

The previous discussion on the effect of H_3PO_4 on copper and its alloys emphasizes the value of keeping service records. Such records are valuable for anticipating repairs, making changes to minimize the effect of various factors, and selecting materials for replacement parts.

Hydrochloric acid (HCl) is one of the most corrosive of the nonoxidizing acids when in contact with copper and its alloys and is successfully handled only in dilute concentrations. The rates for C65800 in HCl of various concentrations are listed in Table 15. The corrosion rates for two nonstandard silicon bronzes were approximately the same as those for C65800.

The corrosion rate of copper-nickels in 2 *N* HCl at 25 °C (75 °F) may range from 2.3 to 7.6 mm/yr (90 to 300 mils/yr), depending on the degree of aeration and other factors. Specimens of C71000 (copper-nickel, 20%) in stagnant 1% HCl solutions at room temperature corrode at a rate of 305 μm/yr (12 mils/yr); in 10% HCl, 790 μm/yr (31 mils/yr).

Hydrofluoric acid (HF) is less corrosive than HCl and can be successfully handled by C71500 (copper-nickel, 30%), which has good resistance to both aqueous and anhydrous HF. Unlike some other copper alloys, C71500 is not sensitive to velocity effects. The data given in Table 16 were generated from laboratory tests in conjunction with the HF alkylation process in anhydrous acid.

Acetic Acid (CH_3COOH) and Acetic Anhydride [$(CH_3CO)_2O$]. Copper and copper alloys are successfully used in commercial

Table 13 Corrosion of copper alloys completely immersed in H_2SO_4 of various concentrations

	Average penetration for H_2SO_4 concentration of					
	30%		40%		50%	
Alloy	μm/yr	mils/yr	μm/yr	mils/yr	μm/yr	mils/yr
Exposure time 24–48 h, boiling at a pressure of 13.3 kPa (100 torr)						
C11000	670–700	26.4–27.6	487–700	19.2–27.6	660–792	26.0–31.2
C14200	640–670	25.2–26.4	487–548	19.2–21.6	610	24.0
C51000	640	25.2	395–457	15.6–18.0	915	36.0
C26000	...	...	...	...	...	...
Exposure time: 16–24 h, solution agitated						
C11000	60–245	2.4–9.6	18–60	0.7–2.4	60	2.4
C14200	92–335	3.6–13.2	nil	nil	50–60	2.0–2.4

	Average penetration for H_2SO_4 concentration of					
	60%		70%		80%	
Alloy	μm/yr	mils/yr	μm/yr	mils/yr	μm/yr	mils/yr
Exposure time: 24–48 h, boiling at a pressure of 13.3 kPa (100 torr)						
C11000	2195–2255	86.4–88.8	853–1067	33.6–42.0	39,630–166,420	1560–6552
C14200	2285–2377	90.0–93.6	945	37.2	67,310–527,300	2650–20,760
C51000	2957–3385	116.4–133.2	945–1067	37.2–42.0	60,660–62,080	2388–2444
C26000	...	...	580–793	22.8–31.2	72,850–206,050	2868–8112
Exposure time: 16–24 h, solution agitated						
C11000	60–92	2.4–3.6	1830–2745	72.0–108.0	39,370–40,890	1550–1610
C14200	15–60	0.6–2.4	2135	84.0	39,370–50,550	1550–1990

Table 14 Corrosion of copper in boiling 30% H_2SO_4 containing copper and iron salts

Copper, ppm	Average penetration		Iron, ppm	Average penetration		Iron and copper, ppm	Average penetration	
	μm/yr	mils/yr		μm/yr	mils/yr		μm/yr	mils/yr
0	60	2.4	0	122	4.8	0	13	0.5
20	183	7.2	28	122	4.8	20Cu + 28Fe	152	6.0
40	213	8.4	58	245	9.6	40Cu + 56Fe	244	9.6
80	243	9.6	112	427	16.8	80Cu + 112Fe	457	18.0
200	335	13.2	196	782	30.8	200Cu + 196Fe	730	28.8
280	360	14.2	280	975	38.4	280Cu + 280Fe	1005	39.6
360	427	16.8	364	1097	43.2	360Cu + 364Fe	1250	49.2
440	457	18.0	447	1280	50.4	440Cu + 447Fe	1525	60.0

Table 15 Corrosion of C65800 totally submerged in HCl

Size of specimens, 50 × 25 × 1.3 mm (2 × 1 × 0.050 in.); surface condition, pickled; velocity of solution, natural convection; aeration, none; duration of test, 48 h

HCl concentration, wt.%	Corrosion rate		
	g/m²/d	μm/yr	mils/yr
At 25 °C (75 °F)			
3	2.3	99	3.9
10	2.3	99	3.9
20	1.8	79	3.1
35	12.3	526	20.7
At 70 °C (160 °F)			
3	18.3	780	30.7
10	13.7	508	20.0
20	23.8	102	4.0
35	160.8	6860	270.1

processes involving exposure to CH_3COOH and related chemical compounds or in the manufacture of this acid. One plant kept records concerning the corrosion rate of C11000 used in two different CH_3COOH still systems. One still operated at 115 to 140 °C (240 to 285 °F) and handled a solution containing 50% CH_3COOH and approximately 50% $(CH_3CO)_2O$, with some esters also present. After operating for 663 h, the kettle showed an average penetration rate of 210 μm/yr (8.4 mils/yr). The rate was lower (60 μm/yr, or 2.4 mils/yr) for the bottom column and was lower yet (30 μm/yr, or 1.2 mils/yr) for the middle and top columns. A second still operating at 60 to 140 °C (140 to 285 °F) contained a 70% solution of CH_3COOH, the remainder being anhydride, esters, and ketones. After 1464 h, the kettle showed a corrosion rate of 120 μm/yr (4.8 mils/yr). The rate was only 30 μm/yr (1.2 mils/yr) for the middle and top columns.

In another field test, C11000 and C65500 coupons were placed in an CH_3COOH storage tank at ambient temperature. The stored solution contained 27% CH_3COOH, 1% butyl acetate, 70% H_2O, and small amounts of acetates, aldehydes, and other acids. During the 3984 h exposure, the specimens were immersed in the liquid phase 80% of the time and were in the vapor phase 20% of the time. The C11000 specimens showed a corrosion rate of 38 to 53 μm/yr (1.5 to 2.1 mils/yr); the C65500 specimens, 30 to 45 μm/yr (1.2 to 1.8 mils/yr).

The results of other field tests for C11000 and C65500 exposed in CH_3COOH mixtures are given in Tables 17 to 19. Test conditions involved various temperatures, concentrations, exposure times, locations in equipment, as well as the presence of other chemicals.

In laboratory tests at room temperature, C61300 and C62300 exhibited typical corrosion rates of 65 to 80 μm/yr (2.5 to 3.2 mils/yr) in 10 to 40% CH_3COOH. The copper-aluminum alloys are suitable for use in CH_3COOH and the range of aliphatic and aromatic organic acids. The addition of chlorine atoms to the organic molecule will not increase the tendency toward pitting or crevice corrosion. Alloy C61300 is extensively used for pressure and valve castings.

Hydrocyanic acid (HCN) is successfully handled by copper and copper alloys. Results of field tests for C11000 and C65500 are given in Tables 20 and 21.

Fatty Acids ($C_nH_{2n+1}COOH$) are organic acids of the aliphatic or open-chain structure. They are common in animal fats and vegetable fatty oils, and they attack copper alloys at somewhat higher rates than other organic acids, such as CH_3COOH or citric. Tests were conducted for 400 h in a copper-lined wooden splitting tank containing a mixture of approximately 60% fatty acids, 39% H_2O, and 1.17% H_2SO_4 heated to 100 °C (212 °F) and agitated violently with an open steam jet. Specimens of C71000 (copper-nickel, 20%) showed a corrosion rate of 64 μm/yr (2.6 mils/yr); specimens of C71500 (copper-nickel, 30%), 59 μm/yr (2.4 mils/yr) when submerged just below the liquid level in the tank. Similar specimens submerged 150 mm (6 in.) from the bottom of the tank showed corrosion rates of 178 and 185 μm/yr (7.0 and 7.3 mils/yr) for C71000 and C71500, respectively.

Oleic Acid. Copper and copper-zinc alloys are highly resistant to attack by pure oleic acid. However, oleic acid will attack these alloys when air and water are present. Temperature also

Table 16 Corrosion of wrought copper alloys in anhydrous HF

Temperature		Corrosion rate(a)					
		C51000		C44400		C71500	
°C	°F	μm/yr	mils/yr	μm/yr	mils/yr	μm/yr	mils/yr
16–27	60–80	510	20	255	10	180	7
27–38	80–100	480	18.8	480	18.8	...	...
82–88	180–190	1525	60	510	20	255	10

(a) These values are representative of results on copper alloys having high copper content, such as copper, aluminum bronze, silicon bronze and inhibited admiralty metal. Corrosion rates for C23000 are between those for C44400 and C51000.

Table 17 Corrosion of copper in CH_3COOH-$(CH_3CO)_2O$ mixtures

Copper alloy	Exposure time, h	Test conditions	Average penetration rate	
			μm/yr	mils/yr
C11000	1115	CH_3COOH-$(CH_3CO)_2O$-acetone mixture, 110 to 140 °C (230 to 285 °F)	483	19.0
	2952	Same as above	66–70	2.6–2.8
C65500	1115	Same as above	213	8.4
	2952	Same as above	70–90	2.8–3.6
C11000	1115	1 : 1 CH_3COOH-$(CH_3CO)_2O$ mixture, 130 to 145 °C (265 to 295 °F)	120–533	4.7–21.0
C65500	1115	Same as above	116–236	4.6–9.3
C11000	865	95% CH_3COOH-5% $(CH_3CO)_2O$, liquid phase, 120 °C (250 °F)	97–116	3.8–4.6
C11000 coupled to type 316 stainless steel	865	Same as above	102–216	4.0–8.5
C11000	865	95% CH_3COOH-5% $(CH_3CO)_2O$, vapor phase, 120 °C (250 °F)	102–104	4.0–4.1
C11000 coupled to type 316 stainless steel	865	Same as above	94–213	3.7–8.4
C11000	2448	50 : 50 CH_3COOH-$(CH_3CO)_2O$, 150 °C (300 °F)	84–90	3.3–3.6
C11000	2448	Essentially pure CH_3COOH	5	0.2

Table 18 Corrosion of C11000 in isopropyl ether-CH_3COOH mixtures

Concentration, %		Average penetration rate	
Isopropyl ether	CH_3COOH	μm/yr	mils/yr
Exposed 72 h at 60–65 °C (140–150 °F)			
93	7	40–50	1.6–2.0
85	15	18–20	0.7–0.8
Exposed 328 h at 20 °C (70 °F)			
93	7	100	4.0
85	15	13	0.5

Table 19 Corrosion of copper alloys in CH_3COOH

Alloy	Exposure time, h	Average penetration rate	
		μm/yr	mils/yr
$(CH_3CO)_2O$(a)			
C11000	2448(b)	60	2.4
	2448(c)	915–1100	36.0–43.2
C65500	2448(b)	60	2.4
	2448(c)	488–732	19.2–28.8
90% CH_3COOH(d)			
C11000, annealed	672	60	2.4
	816	30	1.2
C11000, cold worked	672	90	3.6
	792	90	3.6
Copper joint(e)	1512	183	7.2
	4000	120	4.8
Copper joint(f)	1512	183	7.2
	4000	120	4.8
45% CH_3COOH(g)			
C11000	1038	30 max	1.2 max
C65500	1038	30 max	1.2 max
Copper joint(f)	1038	30 max	1.2 max
25% CH_3COOH(h)			
C11000	432	274	10.8
	792	152	6.0

(a) Test specimens were exposed in stills separating CH_3COOH from $(CH_3CO)_2O$, (b) Top of column. (c) Kettle. (d) Test specimens were exposed in cycle feed lines at 30–50 °C (85–120 °F). (e) Joint brazed with BCuP-5 filler metal. (f) BAg filler metal. (g) Test specimens were exposed in the CH_3COOH recovery column, in which concentration of the acetic acid was 45% max. (h) Test specimens were exposed to crude by-product CH_3COOH (approximately 25% concentration) in pump suction line from storage tank.

Table 20 Corrosion of copper alloys in production of HCN

		Average penetration rate(a)							
		Stripping still		Top of HCN refining still		Base of HCN stripping still		Base of partial condenser	
Alloy	Exposure time, h	μm/yr	mils/yr	μm/yr	mils/yr	μm/yr	mils/yr	μm/yr	mils/yr
C11000	573	173–218	6.8–8.6	54–60	2.1–2.4	1033–1186	40.7–46.7	1534–14,170	60.4–558
	671	155–609	6.1–24.0	18–25	0.7–1.0	nil	nil	478	18.8
C65500	573	229–244	9.0–9.6	18–25	0.7–1.0	777–1145	30.6–45.1	1138–5385	44.8–212
	671	137–503	5.4–19.8	...	...	275	10.8	343	13.5

(a) All data from separate specimens; differences at similar locations imply expected variability.

Table 21 Corrosion of C11000 and C65500 in HCN solutions

			Average penetration rate	
Alloy	Exposure time, h	Test conditions	μm/yr	mils/yr
C11000	3144	Ethylene cyanohydrin residues, 70 °C (160 °F)	5–35	0.2–1.4
C11000	2232	Ethylene cyanohydrin residues, 30 to 90 °C (85 to 195 °F)	13	0.5
C65500	2232	Same as above	40	1.6
C11000	1621	Cyanohydrin stripping still products (kettle)	690	27
C65500	1621	Same as above	35	1.4

Table 22 Corrosion of copper alloys in contact with tartaric acid at 25 °C (75 °F)

	Corrosion rate	
Acid concentration,%	μm/yr	mils/yr
C26000 and C23000		
10	50 max	2 max
30	500–1250	20–50
50	500–1250	20–50
100	50 max	2 max
C71000		
5	25 max	1 max
C71300		
2	40	1.6

Table 23 Corrosion of copper and brass in NH_3

	Average penetration rate(a)			
	Liquid		Vapor	
Alloy	μm/yr	mils/yr	μm/yr	mils/yr
Anhydrous NH_3				
C11000	2.5	0.1	<2.5	<0.1
C26000	<2.5	<0.1	<2.5	<0.1
Anhydrous NH_3 plus 1% H_2O(b)				
C11000	<2.5	<0.1	<2.5	<0.1
C26000	2.5	0.1	<2.5	<0.1
Anhydrous NH_3 plus 2% H_2O(b)				
C11000	2.5	0.1	2.5	0.1
C26000	5.0	0.2	2.5	0.1

(a) Atmospheric temperature and pressure of 345 to 1035 kPa (50 to 150 psi) for 1600 h exposure. Specimens were placed at the top and bottom of 2 L bombs that were charged with NH_3. Pressure varied throughout the test, depending on temperature. Water was added to two of the bombs before charging with NH_3. (b) Any air present was probably depleted rapidly during initial stages of test.

influences the rate of attack. Copper and several copper alloys were tested in oleic acid at 25 °C (75 °F); C51000 and C61300 corroded at less than 50 μm/yr (2 mils/yr) compared with approximately 500 μm/yr (20 mils/yr) for C26000 and C65500.

Stearic acid, like all other fatty acids, attacks copper and copper alloys when moisture and air are present. Temperature and impurities also influence the rate of attack. Tests made at 25 to 100 °C (75 to 212 °F) in stearic acid showed corrosion rates of C11000, C26000, and C65500 to be in the range of 500 to 1250 μm/yr (20 to 50 mils/yr).

Tartaric Acid. Copper and its alloys corrode rather slowly when exposed to various concentrations of tartaric acid, as indicated by the laboratory test data given in Table 22.

Corrosion in Alkalis

Copper and its alloys resist alkaline solutions, except those containing NH_4OH or compounds that hydrolyze to NH_4OH or cyanides. Ammonium hydroxide reacts with copper to form soluble complex copper cations, but the cyanides react to form soluble complex copper anions. The rate of attack for copper-zinc alloys exposed to alkalis other than those specified previously is approximately 50 to 500 μm/yr (2 to 20 mils/yr) at room temperature under stagnant conditions but is approximately 500 to 1750 μm/yr (20 to 70 mils/yr) in aerated boiling solutions.

Alloy C71500 corrodes at less than 5 μm/yr (0.2 mil/yr) in 1 *N* to 2 *N* NaOH solutions at room temperature and the degree of aeration usually has no significant effect. This rate is two to three times as great as the rate in boiling solutions. Copper-tin alloys (phosphor bronzes) corrode at less than 250 μm/yr (10 mils/yr) in 1 *N* to 2 *N* NaOH solutions at room temperature and are apparently unaffected by aeration.

Copper and two grades of silicon bronze were tested in a 50% NaOH solution at 60 °C (140 °F) for 4 weeks. The specimens were bright rolled and degreased sheet measuring approximately 25 by 50 by 1.3 mm (1 by 2 by 0.05 in.). The solution was exposed to air (no additional aeration), and velocity was limited to natural convection. Alloy C11000 showed a corrosion rate of 1.7 g/m^2/day (70 μm/yr, or 2.8 mils/yr); C65100, 1.5 g/m^2/day (63 μm/yr, or 2.5 mils/yr); and C65500, 1.1 g/m^2/day (47 μm/yr, or 1.85 mils/yr).

Ammonium Hydroxide (NH_4OH). Strong solutions attack copper and copper alloys rapidly, as compared with the rates of attack by metallic hydroxides, because of the formation of a soluble complex copper-ammonium compound. However, in some applications, the corrosion of copper exposed to dilute solutions of NH_4OH is low. For example, copper specimens submerged in 0.01 *N* NH_4OH solution at room temperature for 1 week experienced weight loss of 1.5 m/m^2/day (60 μm/yr, or 2.5 mils/yr).

Ammonium hydroxide solutions also attack copper-zinc alloys. Alloys containing more than 15% Zn are susceptible to SCC when exposed to NH_4OH. The stress may be due to applied service loads or to unrelieved residual stresses. In quiescent 2 *N* NH_4OH solutions at room temperature, copper-zinc alloys corrode at 1.8 to 6.6 mm/yr (70 to 260 mils/yr), copper-nickel alloys at 0.25 to 0.50 mm/yr (10 to 20 mils/yr), copper-tin alloys at 1.3 to 2.5 mm/yr (50 to 100 mils/yr), and copper-silicon alloys at 0.75 to 5 mm/yr (30 to 200 mils/yr).

Anhydrous NH_3. Copper and its alloys are suitable for handling anhydrous NH_3 if the NH_3 remains anhydrous and is not contaminated with water and oxygen. In one test conducted for 1200 h, C11200 and C26000 each showed an average penetration of 5 μm/yr (0.2 mil/yr) in contact with anhydrous NH_3 at atmospheric temperature and pressure. Tests showed the rates of corrosion to be low in the presence of small amounts of water, but oxygen was probably excluded. Table 23 lists data on exposure for 1600 h. For any new installation, tests simulating the expected conditions are recommended.

Corrosion in Salts

Copper metals are widely used in equipment for handling saline solutions of various kinds, particularly those that are nearly neutral. Among these are the nitrates, sulfates, and chlorides of sodium and potassium. Chlorides are usually more corrosive than the other salts, especially in strongly agitated, aerated solutions.

Nonoxidizing acid salts, such as the alums and certain metal chlorides (magnesium and calcium chlorides) that hydrolyze in water to produce an acidic pH, exhibit essentially the same behavior as dilute solutions of the corresponding acids. Corrosion rates generally range from 2.5 to 1500 μm/yr (0.1 to 60 mils/yr) at room temperature, depending on the degree of aeration and the acidity. Table 24 lists test data for corrosion of copper in 30% calcium chloride

Table 24 Corrosion of C11000 in refrigeration brine

Brine	Inhibitor	Location	Corrosion rate	
			μm/yr	mils/yr
30% $CaCl_2$	None(a)	...	10	0.4
	$K_2Cr_2O_7$(b)	...	6.0	0.23
NaCl(c)	None; pH 10.5	Open brine tank	160	6.3
		Brine cooler outlet, rapid flow	360	14.2
		Cooler inlet	157	6.2
		Cooler outlet	250	9.8
	$Na_2Cr_2O_7$; pH 6.0 to 6.5	Brine tank for near main outlet	5	0.2
		Top of brine pump, high agitation	10	0.4
		Inside cooler tube	15	0.6
		Return line to storage tank	2.5	0.1
		Brine tank near agitator	2.5	0.1
		Brine tank for near main outlet	5	0.2

(a) Exposed for 325 days at –12 °C (10 °F). (b) Exposed for 372 days, cold. (c) Field test; 98 days at –15 °C (4 °F)

Table 25 Corrosion of copper alloys in alkaline saline solutions

Alloy family	Common name	Corrosion rate	
		μm/yr	mils/yr
Na_2SiO_3, Na_3PO_4, or Na_2CO_3			
Copper-zinc	Brass	50–125	2–5
Copper-tin	Phosphor bronze	<50	<2
Copper-nickel	Copper-nickel	2.5–40	0.1–1.5
NaCN			
Copper-zinc	Brass	250–500	10–20
Copper-tin	Phosphor bronze	875	35
Copper-nickel	Copper-nickel	500–2500	20–100

Table 26 Corrosion of copper alloys in amine system service

Alloy	Exposure time, h	Test conditions	Average penetration rate	
			μm/yr	mils/yr
C11000	1622	Coupons exposed in ethylenediamine refining still	nil–180	nil–7
C11000	1580	Aqueous ethylenediamine	25	1
C71500	1580	Same as above	75	3
C11000	806	Liquid vapor containing NH_3 and mono-, di-, and triethanol-amines; 90–156 °C (195–315 °F)	760	30
C65500	806	Same as above	790	31.2
C11000	1437	Liquid vapor containing NH_3 and mono-, di-, and triethanolamines; 180–195 °C (355–385 °F)	28	1.1
C65500	1437	Same as above	48	1.9
C11000	2622	Vapor phase of diethanolamine still containing mono-, di-, and triethanolamines; 180–195 °C (355–385 °F)	28	1.1
C26000	887	Denuded monoethanolamine (20%)	nil	nil
C26000 coupled to carbon steel	168	20% monoethanolamine (MEA) (4 mol CO_2 per mol MEA); 60 °C (140 °F)	4550	179
C44200	900	Lean solution of diethanolamine containing impurities	50	2
C26000	1440	Rich solution of monoethanolamine	330	13
Cl11000	1440	Same as above	Dissolved	Dissolved
C26000	1440	Lean solution of monoethanolamine	3000	118
C11000	1440	Same as above	11,500	454

($CaCl_2$) refrigeration brine with and without inhibitors.

Copper alloys can successfully handle neutral saline solutions. Consequently, these alloys are used in heat-exchanger and condenser equipment exposed to seawater. Corrosion rates of copper in NaCl brine are given in Table 24. These rates are not necessarily the same as those in seawater. There is renewed interest in brine as a secondary coolant to minimize primary refrigerants that may be potentially harmful to the environment.

Such alkaline salts as sodium silicate (Na_2SiO_3), sodium phosphate (Na_3PO_4), and sodium carbonate (Na_2CO_3) attack copper alloys at low but different rates at room temperature. On the other hand, alkali cyanide is aggressive and attacks copper alloys fairly rapidly, because it forms a soluble complex copper anion. Table 25 provides specific corrosion rates.

Oxidizing salts corrode copper and copper alloys rapidly; therefore, copper metals should not be used with oxidizing saline solutions, except those that are very dilute. Aqueous sodium dichromate ($Na_2Cr_2O_7$) solutions can be safely handled by copper alloys, but the presence of a highly ionized acid, such as H_2CrO_4 or H_2SO_4, may increase the corrosion rate several hundred times, because the dichromate acts as an oxidizing agent in acidic solutions. In one test, a copper-nickel corroded at 2.5 to 250 μm/yr (0.1 to 10 mils/yr) and a copper-tin alloy (phosphor bronze) at 5 μm/yr (0.2 mil/yr) when handling an aqueous $Na_2Cr_2O_7$ solution. The rate increased 200 to 300 times for both metals when H_2CrO_4 was added to the solution. In solutions containing Fe^{3+}, mercuric (Hg^{2+}), or stannic (Sn^{4+}) ions, a copper-nickel showed a corrosion rate of 27.4 mm/yr (1080 mils/yr), while copper-zinc and copper-tin alloys showed a still greater rate of 228 mm/yr (8980 mils/yr).

Salts of metals more noble than copper, such as the nitrates of mercury and silver, corrode copper alloys rapidly, simultaneously plating out the noble metal on the copper surface. Temperature and acidity influence the rate of attack. A film of mercury on high-zinc brass (more than 15% Zn) may cause intergranular cracking by liquid metal embrittlement (LME) if the alloy is under tensile stress, either residual or applied.

Corrosion in Organic Compounds

Copper and many of its alloys resist corrosive attack by most organic solvents and by organic compounds, such as amines, alkanolamines, esters, glycols, ethers, ketones, alcohols, aldehydes, naphtha, and gasoline. Although the corrosion rates of copper and copper alloys in pure alkanolamines and amines are low, they can be significantly increased if these compounds are contaminated with water, acids, alkalis, salts, or combinations of these impurities, particularly at high temperatures. Tables 26 to 32 list the results of corrosion testing of copper and a limited but representative variety of copper alloys in contact with various organic compounds under many conditions.

Gasoline, naphtha, and other related hydrocarbons in pure form will not attack copper or any of the copper alloys. However, in the manufacture of hydrocarbon materials, process streams are likely to be contaminated with one or more of such substances as water, sulfides, acids, and various organic compounds. These contaminants attack copper and its alloys. Corrosion rates for C44300 and C71500 exposed to gasoline are low (Table 33), and these two alloys are successfully used in equipment for refining gasoline. Table 34 lists corrosion rates for copper and for alloys exposed to contaminated naphtha in two different environments.

Creosote. Copper and copper alloys are generally suitable for use with creosote, although creosote attacks some high-zinc brasses. Alloys C11000, C23000, C26000, C51000, and C65500 typically corrode at rates less than 500 μm/yr (20 mils/yr) when exposed to creosote at 25 °C (75 °F).

Linseed Oil. Copper and its alloys are fairly resistant to corrosion by linseed oil. All of the alloys show some attack, but none exhibits corrosion severe enough to make it unsuitable for

Table 27 Corrosion of copper alloys in ester solutions

Alloy	Exposure time, h	Test conditions	Average penetration rate	
			μm/yr	mils/yr
Acetates				
C11000	400	Alkenyl acetate plus H_2SO_4	6100	240
C65500	400	Same as above	3050	120
	257	Allylidene diacetate; 110 °C (230 °F)	183–213	7.2–8.4
C11000	240	Butyl acetate plus 1% H_2SO_4	1625–4090	64–161
C65500	240	Same as above	2870	113
C11000	2328	2-chloroallylidene diacetate	5	0.2
C11000	250	Crude vinyl acetate; 110–150 °C (230–300 °F)	25	1.0
C71500	250	Same as above	7.5–125	0.3–5
C11000	550	Ethyl acetate plus 1.0% H_2SO_4	483	19
C65500	550	Same as above	400	16
C11000	991	Ethyl acetate reaction mixture; liquid; 90 °C (195 °F)	550	21.6
C62300	991	Same as above	395	15.6
C65500	991	Same as above	518	20.4
C11000	991	Ethyl acetate reaction mixture; vapor; 90 °C (195 °F)	5	0.2
C62300	991	Same as above	15	0.6
C65500	991	Same as above	13	0.5
C11000	2976	Ethyl acetoacetate	10	0.4
C65500				
Cold-worked	216	Isopropyl acetate	6700	264
Annealed	216	Isopropyl acetate	6100	240
	480	Isopropyl acetate process; liquid; 120 °C (250 °F)	300	12
C11000	519	Methylamyl acetate process; batch still coils; 115 °C (240 °F)	500–685	22–27
C65500	519	Same as above	280–300	11–12
C11000	519	Methylamyl acetate process; batch still down pipe; 115 °C (240 °F)	330	13
C65500	51	Same as above	300	12
C11000	1345	Methylamyl acetate process; batch still condenser; 30 °C (85 °F)	840–940	33–37
C65500	1345	Same as above	1400–1575	55–62
C63600	3312	Methylamyl acetate process; batch still coils; 95 °C (205 °F)	483	19
C51000	3312	Same as above	430–483	17–19
C60800	3312	Same as above	330	13
C51000	3312	Methylamyl acetate process; batch still downpipe; 95 °C (205 °F)	380–483	15–19
C63600	3312	Same as above	400–460	16–18
C60800	3312	Same as above	280	11
C11000	217	Refined isopropenylacetate; 98 °C (210 °F)	60	2.4
	2784	Vinyl acetate, inhibited	2.5	0.1
C11000	250	Vinyl acetate, process; 150–190 °C (300–375 °F)	355–400	14–16
C71500	250	Same as above	685–1250	27–49
C11000	768	Vinyl acetate process; batch still kettle	685–1170	27–46
C65500	768	Same as above	150–483	6–19
C11000	864	Same as above	2290–3500	90–138
C65500	864	Same as above	660–2160	26–85
Acrylates				
C11000	240	Acidified sodium acrylate containing 5% H_2SO_4; 49 °C (120 °F)	945	37.2
	254	Ethyl acrylate process; 130 to 150 °C (265 to 300 °F)	1220	48
C65500	254	Same as above	430	16.8
Cl1000	240	Isopropyl ether solution of acrylic acid (18%); 49 °C (120 °F)	18	0.7
	240	Sodium acrylate solution containing 1% NaOH; 49 °C (120 °F)	5	0.2
	240	Washings from isopropyl ether solution of acrylic acid; 49 °C (120 °F)	210	8.3
	240	Wet calcium acrylate	240	9.4
	504	2-ethylhexylacrylate process; 95 °C (205 °F)	230–275	9.0–10.8
C65500	504	Same as above	220–275	8.6–10.8
C11000	566	2-ethylhexylacrylate process; condensate tank; 30 °C (85 °F)	66–74	2.6–2.9
C51000	566	Same as above	60–86	2.4–3.4
C65500	566	Same as above	114–122	4.5–4.8
C11000	566	2-ethylhexylacrylate process; 120 °C (250 °F)	236–239	9.3–9.4
C51000	566	Same as above	264	10.4
C65500	566	Same as above	328–360	12.9–14.2
Benzoates				
C11000	1680	Butyl benzoate	nil	nil
	1296	Butyl benzoate process; circulating line; 40 °C (100 °F)	800–1025	31.4–40.4
C60800	1296	Same as above	1060	41.8
C65500	1296	Same as above	843–1090	33.2–42.8
C23000	1296	Same as above	790–1085	31.2–42.7
C22000	1296	Same as above	900–985	35.6–38.8
C11000	1296	Butyl benzoate process; 40 °C (100 °F)	280	11.1
C65500	1296	Same as above	350–400	13.7–15.7
C11000	1296	Butyl benzoate process; batch still kettle; 185 °C (365 °F)	7.5–38	0.3–1.5
C65500	1296	Same as above	7.5–25	0.3–1.0
C11000	1680	Methyl benzoate (refined)	2.5	0.1
C11000	1680	Methyl benzoate (copper-free)	7.5	0.3

this application. Alloys C11000, C51000, and C65500 showed corrosion rates less than 500 μm/yr (20 mils/yr) in linseed oil at 25 °C (75 °F). Alloy C26000 had a rate of 500 to 1250 μm/yr (20 to 50 mils/yr).

Benzol and Benzene. Alloys C11000, C23000, C26000, C51000, and C65500 tested in these materials at 25 °C (75 °F) had corrosion rates under 500 μm/yr (20 mils/yr).

Sugar. Copper is successfully used for vacuum-pan heating coils, evaporators, and juice extractors in the manufacture of both cane and beet sugar. Inhibited admiralty metals, aluminum brass, aluminum bronzes, and copper-nickels are also used for tubes in juice heaters and evaporators. Bimetal tubes of copper and steel have been used by manufacturers of beet sugar to counteract SCC of copper tubes caused by NH_3 from beets grown in fertilized soil. Table 35 lists the results of tests conducted on copper and copper alloys in a beet-sugar refinery.

Beer. Copper is extensively used in the brewing of beer. In one installation, the wall thickness of copper kettles thinned from an original thickness of 16 mm (5/8 in.) to 10 mm (3/8 in.) in a 30 year period. Brazing with BAg (copper-silver) filler metals eliminates the possibility that the alkaline compounds used for cleaning copper equipment will destroy joints by attacking tin-lead solders. Steam coils require more frequent replacement than any other component in brewery equipment. They have service lives of 15 to 20 years. The service lives of other copper items exposed to process streams in a brewery range from 30 to 40 years. Additional information on metals and alloys for this application is available in the article "Corrosion in the Food and Beverage Industry" in this Volume.

Sulfur compounds free to react with copper, such as H_2S, sodium sulfide (Na_2S), or potassium sulfide (K_2S), form CuS. Reaction rates depend on alloy composition; the alloys of highest resistance are those of high zinc content.

Strip tensile specimens of eight copper alloys were exposed in a fractionating tower in which oil containing 1.4% S was being processed. The results of this accelerated test are given in Table 36. These data show the suitability of the higher-zinc alloys for use with sulfur-bearing compounds. Alloy C28000 (60Cu-40Zn) showed good corrosion resistance, but C23000 (85Cu-15Zn) was completely destroyed.

Inhibited admiralty metals are also excellent alloys for use in heat exchangers and condensers that handle sulfur-bearing petroleum products and use water as the coolant. Alloys C44300, C44400, and C44500, which are inhibited toward dezincification by the addition of arsenic, antimony, or phosphorus to the basic 70Cu-29Zn-1Sn composition, offer good resistance to corrosion from sulfur as well as excellent resistance to the water side of the heat exchanger.

Table 28 Corrosion of C11000 and C65500 in ethers

Alloy	Exposure time, h	Test conditions	Average penetration rate	
			µm/yr	mils/yr
C11000	2784	γ-methylbenzyl ether, N2 atmosphere	2.5 max	0.1 max
C11000	2784	γ-methylbenzyl ether, air atmosphere	2.5 max	0.1 max
C11000	288	Recovered butyl ether	nil	nil
C65500	288	Same as above	2.5	0.1
C11000	94	Dichloro ethyl ether residues, 80 °C (175 °F)	183–915	7.2–36
C65500	94	Same as above	61–245	2.4–9.6
C11000	71	Crude dichloro ethyl ether, 80 °C (175 °F)	2130–3050	84–120
C65500	71	Same as above	1220–3050	48–120
C11000	70	Dichloro ethyl ether, 80 °C (175 °F)	150	6
C65500	70	Same as above	120	4.8
C11000	70	Dichloro ethyl ether, 100 °C (212 °F)	610	24
C65500	70	Same as above	245	9.6
C11000	70	Dichloro ethyl ether, boiling	183	7.2
C65500	70	Same as above	213	8.4

Table 29 Corrosion of copper alloys in ketones

Alloy	Exposure time, h	Test conditions	Average penetration rate	
			µm/yr	mils/yr
C11000	138	Phenylxylol ketone mixture	41–43	1.6–1.7
C65500	138	Same as above	76	3.0
C11000	163	Pentanedione mixture	46–91	1.8–3.6
C65500	163	Same as above	33–84	1.3–3.3
C12000	43	Diethyl ketone, 30 °C (86 °F)	nil	nil
C12000	42	Diethyl ketone, boiling	nil-7.6	nil-0.3
C12000	43	Methyl *n*-propyl ketone, 30 °C (85 °F)	nil	nil
C12000	42	Methyl *n*-propyl ketone, boiling	nil	nil
C11000	216	Methylamyl ketone, boiling	2.5	0.1
C11000	353	Methyl ethyl ketone, boiling	12.7	0.5
C11000	409	Phenylxylol ketone containing NaOH	457–518	18–20.4
C65500	409	Same as above	701–823	27.6–32.4
C11000	165	Acetone dispersion of cellulose acetate, 56 °C (135 °F)	10.2	0.4
C26000	165	Same as above	5.1	0.2

Table 30 Corrosion of copper alloys in aldehydes

Alloy	Exposure time, h	Test conditions	Average penetration rate	
			µm/yr	mils/yr
C11000	49	Boiling 2-ethylbutyraldehyde	33	1.3
C11000	112	Boiling butyraldehyde	33	1.3
C11000	1752	2-hydroxyadipaldehyde	20–23	0.8–0.9
C11000	168	Diethyl acetal mixture, 45 °C (115 °F)	60–120	2.4–4.8
C65500	168	Same as above	90–150	3.6–6.0
C26000	168	Same as above	90–150	3.6–6.0
C11000	70	2-ethyl–3–propylacrolein, 98 °C (210 °F)	33	1.3
C11000	168	Diacetoxybutyraldehyde, 160 °C (320 °F)	230–240	9.0–9.4
C65500	168	Same as above	75	3.0
C51000	168	Same as above	18–20	0.7–0.8
C11000	540	Propionaldehydc	1420–1550	56.0–61.0
C11000	216	Propionaldehyde, 190 °C (375 °F)	610–1220	24.0–48.0
C11000	443	Butylaldehyde	310	12.2
C51000	443	Same as above	360	14.2
C11000	2374	Same as above	165	6.5
C65500	2374	Same as above	20	0.8
C51000	2374	Same as above	10	0.4

Corrosion in Gases

Carbon dioxide (CO_2) and carbon monoxide (CO) in dry forms are usually inert to copper and its alloys, but some corrosion takes place when moisture is present. The rate of reaction depends on the amount of moisture. Because CO attacks some alloy steels, the high-pressure equipment used to handle this gas is often lined with copper or copper alloys.

Sulfur Dioxide (SO_2). Gases containing SO_2 attack copper in a manner similar to oxygen. The dry gas does not corrode copper or copper alloys, but the moist gas reacts to produce a mixture of oxide and sulfide scale. Table 37 lists the corrosion rates of some copper alloys in hot paper mill vapor that contains SO_2.

Hydrogen Sulfide (H_2S). Moist gas reacts with copper and copper-zinc alloys to form CuS. Alloys containing more than 20% Zn have considerably better resistance than lower-zinc alloys or copper. Hot, wet H_2S vapors corrode C26000, C28000, or C44300 at a rate of only 50 to 75 µm/yr (2 to 3 mils/yr), but the rate for C11000 and C23000 under the same conditions is 1250 to 1625 µm/yr (50 to 65 mils/yr).

Halogen Gases. When dry, fluorine, chlorine, bromine, and their hydrogen compounds are not corrosive to copper and its alloys. However, they are aggressive when moisture is present. The corrosion rates of copper metals in wet hydrogen compounds are comparable to those given for HF and HCl in Tables 15 and 16.

Hydrogen. Copper and its alloys are not susceptible to attack by hydrogen unless they contain copper oxide. Tough pitch coppers, such as C11000, contain small quantities of Cu_2O. Deoxidized coppers with low residual deoxidizer contents—C12000, for example—may contain Cu_2O but will contain less than the tough pitch coppers. These deoxidized coppers are not immune to hydrogen embrittlement. Deoxidized coppers with high residual deoxidizer contents, however, are not susceptible to hydrogen embrittlement, because the oxygen is tied up in complex oxides that do not react appreciably with hydrogen.

When oxygen-bearing copper is heated in hydrogen or hydrogen-bearing gases, the hydrogen diffuses into the metal and reacts with the oxide to form water, which is converted to high-pressure steam if the temperature is above 375 °C (705 °F). The steam produces fissures, which decrease the ductility of the metal. This condition is generally known as hydrogen embrittlement. Any degree of embrittlement can lead to catastrophic failure and therefore should be avoided; there is no safe depth of attack.

Figure 23 shows the depth of damage, or embrittlement, of C11000 after it has been heated in hydrogen at approximately 600 °C (1100 °F) for varying times. The reaction is especially important when oxygen-containing copper is bright annealed in reducing atmospheres containing relatively small amounts of hydrogen (1 to 1.5%). Annealing of tough pitch coppers in such atmospheres at temperatures much above 475 °C (900 °F) may lead to severe embrittlement, especially when annealing times are long. In fact, tough pitch coppers should not be exposed to hydrogen at any temperature if they will subsequently be exposed to temperatures above 370 °C (700 °F).

When tough pitch coppers are welded or brazed, the possibility of hydrogen embrittlement must be anticipated, and hydrogen atmospheres must not be used. Where copper must be heated in hydrogen atmospheres, an oxygen-free copper or deoxidized copper with high residual deoxidizer content should be selected. No hydrogen embrittlement problems have been encountered with these materials. Additional information on hydrogen damage in metals is available in the article "Hydrogen Damage" in *ASM Handbook*, Volume 13A, 2003.

Dry Oxygen. Copper and copper alloy tubing is used to convey oxygen at room temperature, as

Table 31 Corrosion of copper alloys in ethylene glycol solutions

Alloy	Exposure time, h	Test conditions	Average penetration rate, µm/yr	Average penetration rate, mils/yr
C11000	1344	Triethylene glycol solution, aerated; room temperature	nil	nil
Cl1000	2560	Triethylene glycol air-conditioning system; 175 °C (345 °F)	40	1.6
C26000	2560	Same as above	50	2.0
C11000	3320	Same as above	10	0.4
C26000	3320	Same as above	15	0.6
C11000	8328	Same as above	25	1.0
C26000	8328	Same as above	35	1.4
C11000	2880	Triethylene glycol air-conditioning system(a); 160 °C (320 °F)	7.5	0.3
C26000	2880	Same as above	7.5	0.3
C11000	5760	Same as above	2.5	0.1
C26000	5760	Same as above	2.5	0.1
C51000	2880	Ethylene glycol solution(b) plus 0.03% H_2S0_4; 99 °C (210 °F)	7.5–10	0.3–0.4
C60800	2880	Same as above	2.5–7.5	0.1–4.3
C63000	2880	Same as above	2.5–18	0.1–0.7
C65500	2880	Same as above	20–25	0.8–1.0
C11000	2400	Ethylene glycol solution(b) plus 0.03–0.05% H_2SO_4; second run; 99 °C (210 °F)	580	23
C61800	2400	Same as above	380	15
C70600	2400	Same as above	480	19
C71500	2400	Same as above	460	18
C11000	305	Glycol maleate, 79 °C (175 °F)	20	0.8

(a) 87–95% glycol. (b) 15% glycol, 85% H_2O

Table 32 Corrosion of copper alloys in alcohols

Alloy	Exposure time, h	Test conditions	Average penetration rate, µm/yr	Average penetration rate, mils/yr
C11000	503	Crude C-5 alcohols; 126–140 °C (260–285 °F)	7.5	0.3
C11000	210	Crude decyl alcohol; 175 °C (345 °F)	3–5	0.1–0.2
C11000	288	Primary decyl alcohol; 175 °C	15–45	0.6–1.8
C65500	288	Same as above	20–60	0.8–2.4
C44400	8160	Isopropanol and water; 118–145 °C (245–295 °F)	10–38	0.4–1.5
C23000	8160	Same as above	10–56	0.4–2.2
C11000	8160	Same as above	8–75	0.3–3.0
C65500	8160	Same as above	10–63	0.4–2.5
C11000	264	Allyl alcohol; refluxed at 88 °C (190 °F)	25	1
C11000	94	Methanol; boiling	nil	nil
C11000	46	Denaturing grade ethanol; boiling	25	1
C23000	165	2-ethyl–2-butyl–1,3 propanediol; 45 °C (115 °F)	5	0.2

in hospital oxygen service systems. When heated in air, copper develops a Cu_2O film that exhibits a series of interference tints (temper colors) as it increases in thickness. The colors associated with different oxide film thicknesses are:

Color	Film thickness, nm
Dark brown	37–38
Very dark purple	45–46
Violet	48
Dark blue	50–52
Yellow	94–98
Orange	112–120
Red	124–126

Black cupric oxide (CuO) forms over the Cu_2O layer as the film thickness increases above the interference color range.

Scaling results when copper is used at high temperatures in air or oxygen. At low temperatures (up to 100 °C, or 212 °F), the oxide film increases in thickness logarithmically with time.

Scaling rate increases irregularly with further increases in temperature and rises rapidly with pressure up to 1.6 kPa (12 torr). Above 20 kPa (150 torr) the rate of increase is steady. Beyond the interference color range, the growth rate of the oxide film is approximately defined by:

$$W^2 = kt \qquad \text{(Eq 4)}$$

where W is weight gain (or increase in equivalent thickness) per unit area, t is time, and k is a constant of proportionality. Values for k are given in Table 38. Different investigators report different oxidation rates, but those given in Ref 50 appear to be reliable.

Low concentrations of lead, oxygen, zinc, nickel, and phosphorus in copper have little influence on oxidation rate. Silicon, magnesium, beryllium, and aluminum form very thin insulating (nonconductive) oxide films on copper, which protect the metal surface and retard oxidation.

Stress-Corrosion Cracking of Copper Alloys in Specific Environments

Properly selected copper alloys possess excellent resistance to SCC in many industrial and chemical environments; nevertheless, cracking has been identified in a significant number of environments. In some cases, the conditions for cracking are very limited and exist only within a narrow range of pH values or a narrow range of potentials. In many cases, the experimental data are limited to a single alloy, and it is not known if the environment is generally deleterious to many copper alloys or to a restricted group of alloys. Data are summarized as follows for environments in which cracking has been recognized. Additional information is available in the references cited in this section; they should be consulted when selecting a copper alloy for a specific application.

Acetate Solution. Pure copper wire stressed beyond the yield strength was observed to crack in 0.05 *N* cupric acetate ($Cu(C_2H_3O_2)_2$) (Ref 51). Alloy C26000 is susceptible to cracking in the same solution, and the cracking rate under slow strain-rate conditions is a function of both pH and applied potential (Ref 52).

Amines. Alloy C26000 is susceptible to cracking in solutions of methyl amine, ethyl amine, and butyl amine when dissolved copper is present in the solution (Ref 53). Susceptibility is a maximum at a potential approximately 50 mV anodic from the rest potential. Tubing fabricated from C68700 exhibited cracks from the steam side of a condenser system after 3048 h of service in a desalination plant. The most likely cause of the cracking was an amine used as a water treatment chemical (Ref 54).

Ammonia. All copper-base alloys can be made to crack in NH_3 vapor, NH_3 solutions, ammonium ion (NH_4^+) solutions, NH_3 and NH_4^+ salts, and environments in which NH_3 is a reaction product. The rate at which cracks develop is critically dependent on many variables, including stress level, specific alloy, oxygen concentration in the liquid, pH, NH_3 or NH_4^+ concentration, copper ion concentration, and potential.

The first reports of environmentally induced cracking involved brass cartridge cases. It was called season cracking because the failures occurred during the rainy season in India when cartridges were stored in horse barns where they were exposed to ammonia vapors (Ref 55).

Table 33 Corrosion of C44300 and C71500 exposed to gasoline in a refinery

Service condition(a)	Temperature °C	Temperature °F	Average penetration rate µm/yr	Average penetration rate mils/yr
C44300				
Straight-run (untreated)				
Tower liquid(b)	121	250	1270 min	50 min
Storage(c)	4–27	40–80	63	2.5
Distilled tops from straight-run gasoline(d)	35	95	1270	50
Cracked gasoline (top tray in tower)(e)	204	400	15	0.6
Sweet gasoline vapor(f)	177	350	7.5	0.3
C71500				
Straight-run (untreated)				
Tower liquid(b)	121	250	180	7
Storage(c)	4–27	40–80	180	7
Distilled tops from straight-run gasoline(d)	35	95	1140	45
Cracked gasoline (top tray in tower)(e)	204	400	200	8
Sweet gasoline vapor(f)	177	350	10	0.4
Aviation gasoline (top of column)	121	250	2.5	0.1

(a) Gasoline or related hydrocarbons will not attack copper or its alloys. Attack depends on the type and amount of impurities in the gasoline, such as water, sulfides, mercaptans, aliphatic acids, naphthenic acids, phenols, nitrogen bases, and dissolved gases. (b) 100 lb of H_2S present per 1000 bbl of gasoline. (c) 0.02–0.03 g H_2S per liter of gasoline. (d) pH controlled by NH_3. (e) H_2S and HCl present. (f) Vacuum operation

Table 34 Corrosion of copper alloys in contaminated naphtha

Alloy	Corrosion rate µm/yr	Corrosion rate mils/yr
At 21 °C (70 °F)(a)		
C23000	230	9
C46400	50	2
C28000	75	3
C44200	200	8
C11000	1270	50
At 177 °C (350 °F)(b)		
C23000	2030	80
C46400	10	0.4
C28000	10	0.4
C44200	200	8

(a) The naphtha contained H_2S, H_2O, and HCl. (b) The naphtha contained H_2S, mercaptans, and naphthenic acids.

Table 35 Corrosion of copper alloys in beet-sugar solution

Alloy	Decrease in tensile strength, %, for test rack number(a) 1	2	3	4
C11000	0	4.0	3.5	0
C44300	2.0	9.5	11.5	2.5
C44400	0	3.0	6.0	0
C44500	4.5	9.0	12.5	5.5
C71000	1.0	4.5	7.0	0
C71500	0	5.0	8.0	0

(a) Corrosion specimens (0.8 mm, or 0.032 in. thick strips) were exposed in contact with beet-sugar solution for 100 days in normal refinery operations. Test racks 1 and 4 were at the finishing pan containing Steffen's filtrate; rack 2 was in the first-effect thin-juice evaporator; rack 3 was at the third body of the triple-effect evaporator.

Table 36 Corrosion of selected copper alloys in cracked oil containing 1.4% S

Alloy type	UNS number	Exposure time, days	Loss in tensile strength (a),% 360 °C (680 °F)	315 °C (600 °F)	285 °C (545 °F)	255 °C (490 °F)
Red brass, 85%	C23000	27	100(b)	100(c)	100	100
Muntz metal	C28000	27	12(b)	7.5(d)	1	1.5
Naval brass	C46400	24	...	1.5	0	2
Uninhibited admiralty metal	...	27	13(b)	6(c)	3	2
Antimonial admiralty metal	C44400	27	16.5(b)	6(c)	4	2.5
Aluminum brass	...	24	...	7	16	10
Copper-nickel, 30%	C71500	24	...	100	100	57
Silicon bronze, 3%	...	34	...	100	100	100

(a) Specimens 0.8×13 mm (0.032×0.50 in.) in cross section were exposed at different locations within a high-pressure fractionating column, each location having a characteristic average temperature. (b) 115 day exposure. (c) 26 day exposure. (d) Length of exposure unavailable

Table 39 provides a ranking of various copper alloys according to their relative SCC susceptibility in NH_3 environments.

Atmosphere. Many natural environments contain pollutants that, in the presence of moisture, may cause stress-corrosion problems (Ref 56). Sulfur dioxide, oxides of nitrogen, and NH_3 are known to induce SCC of some copper alloys. Chlorides may also cause problems. Atmospheric-exposure test data are summarized in Table 40. In these tests, 150 by 13 mm (6 by 1/2-in.) U-bend samples were stressed in the long-transverse direction. Bending around a 19 mm (3/4 in.) diameter mandrel produced the bend, and the legs of each specimen were held in nonconductive jigs during the test. The stress on the specimens was not determined. The stressed specimens were exposed in two industrial locations in New Haven, CT, and Brooklyn, NY, and in one marine location at Daytona Beach, FL.

Chlorate Solutions. Brass was observed to crack intergranularly and transgranularly when immersed in 0.1 to 5 *M* sodium chlorate ($NaClO_3$) solutions at pHs from 3.5 to 9.5 when subjected to slow straining (Ref 58). Crack velocities in 1 *N* $NaClO_3$ at pH 6.5 were 10^{-7} m/s at a crosshead speed of 10^{-4} cm/min (4×10^{-5} in./min) and 10^{-6} m/s at a crosshead speed of 10^{-3} cm/min (4×10^{-4} in./min).

Chloride Solutions. The service lives of copper alloys under cyclic stress are shorter in chloride solutions than in air. Slow strain-rate experiments have also shown that C26000 (Ref 59) and C44300 (Ref 60, 61) have lower fracture stresses in NaCl solutions when the metal is anodically polarized. The changes in fracture stress are insignificant relative to those in air in the absence of an applied potential.

Citrate Solutions. Alloy C72000 is sensitive to cracking in citrate solutions containing dissolved copper in the pH range of 7 to 11. The U-bend test specimens exhibited intergranular cracking (Ref 62).

Formate Solutions. Brass is susceptible to SCC in sodium formate ($NaCHO_2$) solutions at pHs exceeding 11 over a considerable range of applied potentials (Ref 52).

Hydroxide Solutions. Brass exhibits increased crack growth rates under slow strain-rate conditions when it is exposed to NaOH at pHs of 12 and 13. The rate of crack growth is a function of the applied potential (Ref 52).

Mercury and Mercury Salt Solutions. Stressed alloys and alloys with internal stress crack readily when exposed to metallic mercury or mercury salt solutions that deposit mercury on the surface of the alloy. This high sensitivity to mercury is the basis of an industry test for the detection of internal stresses in which the alloy is immersed in a solution of mercurous nitrate. Cracking in mercury is the result of LME, not stress corrosion. It does not indicate the SCC susceptibility of an alloy.

Nitrate Solutions. Transgranular cracking was observed on C44300 specimens immersed in naturally aerated 1 *N* sodium nitrate ($NaNO_3$) at

Table 37 Corrosion of copper alloys in hot paper mill vapor containing SO_2

Temperature, 200–220 °C (390–430 °F); atmosphere, 17–18% SO_2 plus 1–2% O_2; test duration, mainly 30 days but some longer

Alloy	Common name	Weight loss, $g/m^2/d$
90Cu-10Sn	Bronze	22.0
C61800	Aluminum bronze	26.4
C51100	Phosphor bronze	28.6
C73200	Nickel silver, 75–20	35.6
C52100	Phosphor bronze, 8% C	39.4
C65800	Silicon bronze	50.2
C77000	Nickel silver, 55–18	63.8
C75200	Nickel silver, 65–18	67.4
88.5Cu-5Sn-5Ni-1.5Si	Nickel bronze	70.5

pH 8 and a potential of 0.15 V versus standard hydrogen electrode (SHE). The fracture stress relative to air was 0.34 (Ref 60).

Copper alloy (Cu-23Zn-12Ni) wires measuring 0.6 mm (0.023 in.) in diameter and normally under a 6 g load and a positive potential in telephone equipment were observed to undergo SCC within 2 years (Ref 63). Laboratory tests suggested that nitrate salts were the cause. The phenomenon was duplicated in the laboratory by exposing the wires to such nitrate salts as zinc nitrate ($Zn(NO_3)_2$), ammonium nitrate (NH_4NO_3), calcium nitrate ($Ca(NO_3)_2$), and cupric nitrate ($Cu(NO_3)_2$) at high humidity; a potential was applied such that the wires were anodic to the normal corrosion potential. The wires were tested under a constant load of 386 MPa (56 ksi). Cracking also occurred in the absence of an applied potential when the nitrate concentration of the surface was high. Cracking did not occur in the presence of $(NH_4)_2SO_4$ and ammonium chloride (NH_4Cl) salts. Wires of Cu-20Ni did not crack under similar conditions.

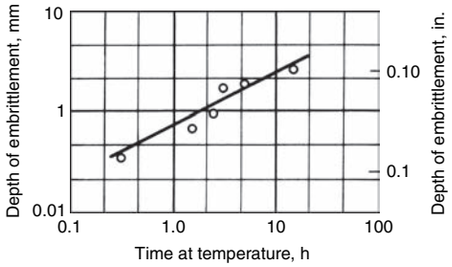

Fig. 23 Hydrogen embrittlement of tough pitch coppers heated in pure hydrogen at 600 °C (1100 °F)

Nitrite Solutions. Copper, 99.9 and 99.996% pure, exhibited transgranular cracking when subjected to a strain rate of 10^{-6} s^{-1} while immersed in 1 *M* sodium nitrite ($NaNO_2$) at a pH of 8.2 (Ref 64). The 99.9% Cu tested in solution showed an ultimate tensile strength of 160 MPa (23 ksi) and 25% elongation, as opposed to the 196 MPa (28.5 ksi) and 55% elongation obtained in air. Cracking in 1 *M* $NaNO_2$ was also observed in C26000, admiralty brasses, and C70600.

Solder. In one investigation of the susceptibility to cracking of copper alloys by various solders, a U-shaped tube was coated with solder at 400 °C (750 °F) and then immediately flattened between steel tools in a hand press (Ref 65). The sample was then examined for cracks. The data are given in Table 41.

Sulfur Dioxide. Brass is susceptible to SCC in moist air containing 0.05 to 0.5 vol% SO_2. In addition, pre-exposure of the brass to a solution of benzotriazole inhibits the cracking (Ref 66).

Sulfate Solutions. Stress-corrosion cracking of C26000 was observed in a solution of 1 *N* sodium sulfate (Na_2SO_4) and 0.01 *N* H_2SO_4 when the alloy was polarized at a potential of 0.25 V versus SHE and subjected to a constant strain (Ref 67).

Sulfide Solutions. National Association of Corrosion Engineers committee T-1F issued a report on the acceptability of various materials for valves for production and pipeline service (Ref 68). Bronze and other copper-base alloys are generally not acceptable for highly stressed

Table 38 Values of rate constant for oxide growth on unalloyed copper

Temperature		Rate constant *k*(a)	
°C	°F	Pure O_2	Air
400	750	4.4×10^{-8}	...
500	950	4.4×10^{-7}	...
600	1100	3.24×10^{-6}	...
700	1300	1.6×10^{-5}	8.03×10^{-6}
800	1475	8.69×10^{-5}	7.97×10^{-5}
900	1650	3.49×10^{-4}	3.36×10^{-4}
950	1750	7.30×10^{-4}	...
1000	1850	1.78×10^{-3}	1.35×10^{-3}

(a) For calculation of weight pin in g/m^2 from Eq 4 when time is measured in seconds

Table 39 Relative susceptibility to stress-corrosion cracking (SCC) of some copper alloys in NH_3

Alloy	Susceptibility index(a)
C26000	1000
C35300	1000
C76200	300
C23000	200
C77000	175
C66400	100
C68800	75
C63800	50
C75200	40
C51000	20
C11000	0
C15100	0
C19400	0
C65400	0
C70600	0
C71500	0
C72200	0

(a) 0, essentially immune to SCC under normal service conditions; 1000, highly susceptible to SCC, as typified by C26000

Table 40 Stress-corrosion cracking of wrought copper alloys in three atmospheres

		Time to failure, years			Crack morphology(a)		
UNS No.	Temper, % cold rolled	New Haven, CT	Brooklyn, NY	Daytona Beach, FL	New Haven, CT	Brooklyn, NY	Daytona Beach, FL
C11000	37	NF(b), 8.5	NF, 8.5	NF, 8.8	...	...	...
C19400	37	NF, 8.5	NF, 8.5	NF, 8.8	...	...	...
C19500	90	NF, 3.2	NF, 3.1	NF, 3.1	...	...	...
C23000	40	NF, 8.5	NF, 8.5	NF, 8.8	...	...	...
C26000	50	35–47 days	0–23 days	NF, 2.7	I	I	...
C35300	50	51–136 days	70–104 days	NF, 2.7	T + (I)	T + (I)	...
C40500	50	NF, 2.7	NT(c)	NT	...	...	...
C41100	50	NF, 2.7	NT	NT	...	...	...
C42200	37	NF, 8.5	NF, 8.5	NF, 8.8	...	...	...
C42500	50	NF, 2.7	NT	NT	...	...	...
C44300	10	NF, 2.7	NF, 2.7	NF, 2.7	...	...	...
	40	51–95 days	41–70 days	NF, 2.7	T	T	...
	40% + ordered(d)	51–67 days	33–49 days	NF, 2.7	T	T	...
C51000	37	NF, 8.5	NF, 8.5	NF, 8.8	...	...	...
C52100	37	NF, 5.7	NF, 5.7	NF, 5.7	...	...	...
C61900	40%, 9% β phase(e)	NF, 8.5	NF, 8.5	NF, 8.8	...	...	...
	40%, 95% β phase	NF, 8.5	NF, 8.5	NF, 8.8	...	...	...
C63800	50	NF, 5.7	NF, 5.7	NF, 5.7	...	...	...
C67200	Annealed	0–30 days	0–134 days	NF, 3.1	I	I	...
	50	0–30 days	0–22 days	18–40 days	I	I	I
C68700	10	517–540 days	2.3-NF 2.7	NF, 2.7	T	T	...
	40	221–495 days	311–362 days	NF, 2.7	T	T	...
	40% + ordered(d)	216–286 days	143–297 days	NF, 2.7	T	T	...
C68800	10	NF, 2.7	NF, 2.7	NF, 2.7	...	...	...
	40	4.7–NF 6.4	2.7–NF 6.4	NF, 6.4	T	T	...
	40% + ordered(d)	NF, 2.7	NF, 2.7	NF, 2.7	...	...	...
C70600	50	NF, 2.2	NF, 2.3	NF, 2.2	...	...	...
C72500	40	NF, 2.2	NF, 2.3	NF, 2.2	...	...	...
C75200	Annealed	NF, 3.2	NF, 3.1	NF, 3.1	...	...	...
	25	NF, 3.2	NF, 3.1	NF, 3.1	...	...	...
	50	NF, 3.2	NF, 3.1	NF, 3.1	...	...	...
C76200	Annealed	171–NF 3.2	672–NF 3.1	NF, 3.1	T	T	...
	25	142–173 days	236–282 days	NF, 3.1	T	T	...
	50	142–270 days	236–282 days	NF, 3.1	T	T	...
C76600	38	127–966 days	197–216 days	754-NF 8.8	T	T	T
C77000	Annealed	731–1003 days	337–515 days	NF, 3.1	T	T	...
	38	137–490 days	196–518 days	596–1234 days	T	T	T
	50	153–337 days	489–540 days	692–970 days	T	T	T
C78200	50	23–48 days	26–216 days	236–300 days	T + (I)	T + (I)	T

(a) I, intergranular; T, transgranular Parentheses indicate minor mode. (b) NF, no failures in time specified. (c) NT, not tested. (d) Heated at 205 °C (400 °F) for 30 min. (e) Normal structure for this alloy. Source: Ref 57

Table 41 Susceptibility of copper alloy tubes to cracking by solder

Solder applied at 400 °C (750 °F); specimens were immediately deformed and examined for cracks

	Alloy		
Solder	**80Cu–20Ni**	**97Cu–3Zn**	**70Cu–30Zn**
Lead	Shattered	Cracked	Cracked
97.5Pb–2.5Ag	Shattered	Uncracked	Cracked
95Pb–5Sn	Cracked	Uncracked	Cracked
80Pb–20Sn	Cracked	Uncracked	Uncracked
Grade B solder	Cracked	Uncracked	Uncracked
95Sn–5Sb	Uncracked	Uncracked	Uncracked

Source: Ref 65

parts in sour service. Some nickel-copper alloys are considered satisfactory.

Tungstate Solutions. Mild transgranular cracking of C44300 was observed in 1 *N* sodium tungstate (Na_2WO_4) at pH 9.4 and a corrosion potential of 0.080 V versus SHE. The fracture stress relative to that in air was 0.89, and the crack growth velocity was 2×10^{-9} m/s when a strain rate of 1.5×10^{-5} s^{-1} was used (Ref 60).

Water. Several cases of the SCC of admiralty brass heat-exchanger tubing are documented in Ref 69. The environments in which such SCC was observed included stagnant water, stagnant water contaminated with NH_3, and water accidentally contaminated with a nitrate. No cases were noted of SCC of the following alloys when used in heat-exchanger service: C70600, C71500, arsenical copper, C19400, and aluminum bronze.

Service data for various copper alloys used as condenser tubing are given in Ref 61. Reference 70 ranked susceptibility to SCC for alloys used as condenser tubes. In freshwater, admiralty brass was very susceptible, C19400 had low susceptibility, and C70600 and arsenical copper were resistant. In seawater, arsenic-aluminum brass bronze was susceptible, while C70600 and C71500 were resistant.

An instance of the SCC of a Cu-7Al-2Si stud from an extraction pump exposed to wet steam is discussed in Ref 70. Also in Ref 70 are examples of SCC failures of copper alloys in marine service. These include tubing, a lifeboat keel pin, brass bolts and screws, a brass propeller, a flooding valve, and aluminum bronze valve parts. Some of the failures were attributed to bird excreta that provided a source of NH_3.

Protective Coatings

Copper metals resist corrosion in many environments because they react with one or more constituents of the environment on initial exposure, thus forming an inert surface layer of protective reaction products. In certain applications, applying metallic or organic protective coatings may increase the corrosion resistance of copper metals. If the coating material is able to resist corrosion adequately, service life may depend on the impermeability, continuity, and adhesion to the basis metal of the coating. The electropotential relationship of the coating to the basis metal may be important, especially with metallic coatings and at uncoated edges. Tin, lead, and solder, used extensively as coatings, are applied by hot dipping or electroplating.

Tin arrests corrosion caused by sulfur. It is most effective as a coating for copper wire and cable insulated by rubber that contains sulfur. Lead-coated copper is primarily used for roofing applications, in which contact with flue gases or other products that contain dilute H_2SO_4 is likely. Tin or lead coatings are sometimes applied to copper intended for ordinary atmospheric exposure, but this is done primarily for architectural effect; the atmospheric-corrosion resistance of bare copper is excellent in rural, urban, marine, and most industrial locations. Additional information on the use of tin for corrosion resistance is available in the article "Corrosion of Tin and Tin Alloys" in this Volume.

Electroplated chromium is used for decoration, for improvement of wear resistance, or for reflectivity. Because it is somewhat porous, it is not effective for corrosion protection. Where corrosion protection is important, electroplated nickel is most often used as a protective coating under electroplated chromium. Additional information on the corrosion resistance of chromium plate is available in the article "Corrosion of Electroplated Hard Chromium" in this Volume.

Various organic coatings are applied to copper alloys to preserve a bright metallic appearance (see the article "Organic Coatings and Linings" in *ASM Handbook*, Volume 13A, 2003). Physical vapor deposition is also used on plumbing fixtures to preserve their luster.

Corrosion Testing

Aqueous Corrosion Testing. Testing and evaluation techniques are covered extensively in *ASM Handbook*, Volume 13A, 2003. One specific static procedure that has been applied to copper alloys in closed-container tests is the determination of the partitioning of the major alloying elements between the corrosion product and the solution (Ref 10, 71). In this procedure, the samples are exposed to the test solution for some time period, after which the sample is removed and the solution filtered to remove any particulate. The collected particulate is dissolved in an acidified solution and quantitatively analyzed for copper and other alloying elements of interest; a similar analysis is performed on the filtered solution. The corrosion product is then stripped from the copper alloy using an inhibited HCl solution and analyzed. The results indicate which alloying elements contribute to film formation and whether the element is more prone to go into solution rather than into the film. In addition, the amount of copper that has entered solution and the amount that is actually particulate that spalled off of the surface can be determined. These data are of significance with regard to heavy-metal ion contamination of water sources.

Dynamic Corrosion Tests. One of the major uses of copper alloys is the transport of aqueous solutions; consequently, a significant number of tests have been designed to examine the effects of dynamic conditions on the corrosion behavior of the materials in these environments. The tests, which range in complexity from simple recirculating loops to jet impingement apparatus, examine the effects of such variables as flow rate, heat-transfer conditions, and blockages, as well as various solution conditions. Of the systems developed, the flow loop is probably the most widely used test because it is easily constructed, requiring only a pump, ducting, and valves, and can incorporate a wide variety of test variables. Because of their simplicity, flow loops can be constructed on-site and tapped into process flow systems so that the actual operating environment can be used as the test environment. Descriptions of test loops are available in Ref 21, 35, and 72 to 75.

Tubular samples are the most easily tested in this system because they can be directly incorporated into the loop. As with any other corrosion test, the tube samples must be separated by insulating connectors to avoid galvanic effects; tube union fittings of plastic or flexible plastic hose clamped to the tubes are generally adequate. Flat samples can also be tested in flow loops by using special sample holders, such as those described in ASTM D 2688 (Ref 76) and in Ref 21, 72, 73, and 77.

A major variable that affects the corrosion behavior of copper alloys is solution velocity. The effect of flow rate on copper alloys has been examined by placing various diameters of the same tube material in series within a loop and pumping the solution through the loop at a constant pump speed (Ref 73). Velocity effects have also been studied in a parallel flow system with orifice size and header pressure controlled to produce various velocities simultaneously (Ref 21, 44). The effects of local velocity changes and crevices, conditions that arise in power plant condenser tubes because of lodged debris, have been examined by introducing artificial blockages into tubes (Ref 72). The blockage reduces the cross section of the tube, increasing local flow rate, and produces crevice corrosion conditions where it contacts the tube.

Heat-transfer effects have been studied by running test tubes through small steam condensers to ovens and pumping the test solution through the tubes. It should be noted that the conditions provided by this type of test are unlike those obtained when the bulk solution is heated before pumping it through the tubes. Heating the bulk solution may change the concentration of components throughout the solution, such as decreasing the oxygen concentration or promoting precipitation. Under heat-transfer conditions, these changes may only occur locally, resulting in different corrosion

behavior. Corrosion behavior can also be affected by the temperature gradient that exists between the tube wall and the solution under heat-transfer conditions, which is much larger than that of a heated solution passing through a tube surrounded by ambient air.

Loop tests are generally used to evaluate the corrosion rates of materials based on their weight loss over a period of time. Test duration depends in large measure on the aggressiveness of the solution and the sample thickness. However, for copper alloys in most aqueous solutions, the test duration should be at least 120 days in order to ensure attainment of steady-state corrosion rates.

When evaluating the samples that have been exposed to flowing systems, more than just the weight loss should be considered. Evidence of erosion should be sought, especially at leading edges and obstructions, and the depth of erosion should be monitored with respect to time. Evidence of pitting should also be looked for, and the depth of pitting as a function of time should be determined. Depth of crevice attack should be noted in samples with crevices, for example, at clamp sites. With regard to crevice corrosion in copper alloys, the attack usually occurs adjacent to the contact site; therefore, the contact site will generally be at the original thickness and can be used as a reference point when measuring the depth of attack.

Each alloy should also be examined for evidence of dealloying. This can generally be determined by metallographic examination of the cross section to see if a copper-rich layer at the sample surface is present. The material can also be mechanically tested to determine whether the mechanical properties have deteriorated with respect to a control sample. This type of testing, however, is generally performed only on materials that have not suffered from severe corrosion, which would obviously degrade the properties of the material.

Other dynamic systems, in addition to flow loops, have been developed primarily to evaluate the maximum flow rate that materials can withstand before erosion-corrosion occurs (Ref 78). An example of such a system is the jet impingement test (Ref 79). In this test, a high-velocity stream of solution is sprayed onto the specimen for some period of time, after which the depth of attack and the amount of surface area attacked are determined. Based on this evaluation, the relative erosion-corrosion resistance of various materials can be ranked.

The spinning-disk test is used to define the velocity that causes erosion in a material (Ref 79, 80). In this test, a disk of the material is immersed in the solution and rotated at a specific rate around the disk axis perpendicular to the plane of the disk. At the conclusion of the test, the sample is examined to determine the distance from the center of the disk, and therefore the velocity, at which erosion occurs.

One other test is used to examine the relative resistance of various materials to erosion by entrained particles in solution (Ref 20). In this test, silica sand of controlled size is introduced to the solution in which L-shaped samples are mounted on the periphery of a rotating disk.

Although any solution can be used in these dynamic test systems, most tests are conducted with seawater or freshwater. Natural waters, such as from the sea, rivers, or lakes, are used as test solutions, but their use is generally restricted by the location of the test facility. In addition, the compositions of natural waters vary not only with location but also with time, making a standardized test procedure difficult. To circumvent this problem for seawaters, substitute seawater (Ref 81) and a 3.4% NaCl solution have both been used. In general, these solutions are slightly more aggressive than natural seawaters; as a result, predictions of corrosion lifetimes based on data from these solutions are generally conservative with respect to actual performance.

A significant amount of work has recently been done on the behavior of copper alloys in sulfide-contaminated seawaters. An extensive bibliography is given in Ref 82. Either bubbling H_2S gas through the solution or adding a Na_2S solution adds sulfides to the seawater. In general, sulfide concentrations of the order of 1 ppm are sufficient to cause accelerated attack. For rapid corrosion to occur, the copper alloy must be exposed to a solution that contains oxygen as well as sulfide or must be alternately exposed to sulfide-bearing deaerated solutions followed by exposure to sulfide-free aerated solutions.

Because of the transient nature of sulfides in water, it is necessary to monitor the sulfide level in solution with time. Titration techniques are available for measuring the sulfide concentration, but these are generally time-consuming and tedious if continual monitoring is required. An alternative is the use of a sulfide-specific ion electrode, which provides accurate sulfide readings in substitute ocean water in much less time.

Atmospheric Testing. In a variety of applications, such as electrical and architectural components, the behavior of copper alloys when fully immersed in solution is not relevant with regard to their performance under various atmospheric conditions. Constant humidity and temperature chambers are used to evaluate the relative atmospheric behavior of the materials. The design, typical test environments, and a list of international standard test methods are described in the article "Cabinet Testing" in *ASM Handbook*, Volume 13A, 2003. As with aqueous tests under artificial conditions, the corrosion behavior determined in these tests is of value in providing a controlled means of ranking the test materials and a means of comparing test materials to standard materials.

Evaluation of tested specimens involves typical corrosion parameters, such as weight loss, depth of pitting, and crevice corrosion. In addition, patina (oxide film formation) is evaluated with regard to color, continuity, and film tenacity. After the specimen has been cleaned, evidence of dealloying should also be sought by examination of a metallographic cross section or by loss of mechanical properties (as compared to a control sample).

Atmospheric testing of copper alloys in natural environments is conducted to evaluate the behavior of the materials in industrial, rural, and marine atmospheres. International procedures are listed in the article "Simulated Service Testing in the Atmosphere" in *ASM Handbook*, Volume 13A, 2003. This article describes specimens, types of test racks, and analysis of data.

Stress-Corrosion Testing. Much of the early knowledge of the SCC tendencies of copper alloys was based on service experience. Such data were assimilated at laboratories involved in the development of copper alloys and were used to design alloys with greater resistance to SCC in specific environments. Some of this information reached the open literature. In other cases, researchers concerned with specific objectives, such as designing a desalination plant or operating power station, occasionally wrote summary articles in which they cited their experience with different alloy compositions. Such information is useful but qualitative, and the environmental constituents or conditions that led to the cracking are unknown.

In the past several decades, the study of SCC has been greatly accelerated, and materials scientists, physicists, chemists, metallurgists, and mechanical engineers have addressed the causes and mechanisms for the behavior. Laboratory studies under controlled conditions have been expanded, ASTM International has developed standardized tests, and laboratories have compared data. As a result, considerable quantitative information is now available in the literature. In some cases, this information is obtained with full knowledge of fracture mechanics principles. The methods of generating SCC data are numerous and include both static and dynamic tests.

In the static tests, the sample is put under tension by bending and restraining the sample or by mounting it in a tensile-testing machine. The data thus generated include time to first crack, time to fracture, or time to relax to a certain fraction (for example, 50 or 80%) of the unrestrained distance between the ends of the bent specimen. The data generated in this fashion allow comparison among different alloys, among different pretreatments, and among other experimental variables. The data are comparative within one data set but yield no absolute information.

Various NH_3 environments are widely used to test copper alloys, the most common being Mattsson's solution of pH 4.0, 7.2, and 10. Two other NH_3-base environments that produce very aggressive stress-corrosion conditions are a NH_3-0.5 *M* copper solution of pH 14, and a moist NH_3 test. The pH 14 solution is made by dissolving 3.18 g of copper powder in 1 L of 29.5% NH_4OH solution (typical reagent-strength NH_4OH). The moist NH_3 test requires

the construction of a chamber in which 100% relative humidity and a constant NH_3 gas concentration are maintained (Ref 83).

One of the simplest laboratory stress-corrosion tests that provide a significant amount of information is the U-bend test, in which the springback of the sample is measured over time in the test solution. Two sample sets of each material are produced in a manner similar to that described in Ref 84. One is placed in the test solution, and the other remains in the room environment as a control. A variety of test jigs are described in Ref 84; however, the legs of the jig must be compressed the same distance when the sample is removed and then replaced in the jig. A typical example of this type of jig is given in Ref 84.

The samples are placed in the jig, removed, and the springback between the legs measured; this is also done for the control samples. The samples are reinserted in the test jig and placed in the test solution. At periodic intervals, the samples are removed from the solution, taken from the jig, and the springback distance between the legs remeasured. Similar measurements are made on the air control samples. The test continues until either physical failure occurs— that is, if the sample breaks or if it no longer has enough tension to hold it in the jig—or some predetermined performance criteria are met, for example, 1000 h elapsed time or springback reduction to 80% of its initial value. At the conclusion of the test, the average change in percent springback for each material at each time is determined, taking into account the loss in springback that occurred as a result of stress relaxation based on springback measurements of the air control samples.

A constant percent springback versus time indicates that the material is not susceptible to SCC in the test solution over that time period. A decrease in percent springback with time indicates the SCC has occurred. This should be verified by optical examination for cracking as well as metallographic examination of the sample to determine the mode of cracking. An increase in percent springback indicates that the tension side of the sample dissolved at a faster rate than the compressive side due to stress-assisted dissolution. Examination will reveal that the specimen has thinned and that failure occurred because of overload, not cracking. This result indicates that the solution is too aggressive for SCC to occur and that another solution should be used to compare stress-corrosion behavior.

Dynamic Tests. Reently, there has been a move toward the use of dynamic tests, which yield values that can be quantitatively applied to the proposed mechanisms of SCC. Primary among these is the slow strain-rate technique, which produces test results faster than static methods. An excellent summary of the slow strain-rate technique and its applications to SCC is given in Ref 85. The International Organization for Standardization standard ISO 7539-7 provides a guide to this method (Ref 86).

ACKNOWLEDGMENTS

This article is a revision of the article "Corrosion of Copper and Copper Alloys," *Corrosion*, Vol 13, *ASM Handbook*, ASM International, 1987, p 610–640, by the ASM Committee on Corrosion of Copper, Chairman: Ned W. Polan, Olin Corporation; Members: Frank J. Ansuini, Consulting Engineer; Carl W. Dralle, Ampco Metal; Fraser King, Whiteshell Nuclear Research Establishment; W. W. Kirk, LaQue Center for Corrosion Technology, Inc.; T. S. Lee, National Association of Corrosion Engineers; Henry Leidheiser, Jr., Center for Surface and Coating Research, Lehigh University; Richard O. Lewis, Department of Materials Science and Engineering, University of Florida; and Gene P. Sheldon, Olin Corporation.

REFERENCES

1. E. Mattsson, *Electrochim Acta*, Vol 3, 1961, p 279
2. U. Bertucci and E.N. Pugh, in *Proceedings of the Ninth International Congress on Metallic Corrosion* (Toronto, Canada), Vol 1, National Research Council of Canada, June 1984, p 144
3. H.L. Logan, *J. Res. Natl. Bur. Stand.*, Vol 48, 1952, p 99
4. H. Leidheiser, Jr. and R. Kissinger, *Corrosion*, Vol 28, 1972, p 218
5. R.C. Newman, Stress-Corrosion Cracking Mechanisms, *Corrosion Mechanisms in Theory and Practice*, P. Marcus, Ed., Marcel Dekker, 2002, p 405
6. S.W. Dean, Corrosion Testing of Metals Under Natural Atmospheric Conditions, *Corrosion Testing and Evaluation*, STP 1000, ASTM, 1990, p 163
7. G.S. Haynes and R. Baboian, A Comparative Study of the Corrosion Resistance of Cable Shielding Materials, *Mater. Perform.*, Vol 18, 1979, p 45–56
8. J.W. Braithwaite and M.A. Molecke, Nuclear Waste Canister Corrosion Studies Pertinent to Geologic Isolation, *Nuc. Chem. Waste Man.*, 1980, p 37–50
9. "Understanding Copper Tube," Copper Development Association, Inc., 2004
10. N.W. Polan, G.P. Sheldon, and J.M. Popplewell, "The Effect of NH_3 and O_2 Levels on the Corrosion Characteristics and Copper Release Rates of Copper Base Condenser Tube Alloys Under Simulated Steam Side Conditions," Paper 81-JPGC-Pwr-9, Joint ASME/IEEE Power Generation Conference, Oct 1981
11. G.P. Sheldon and N.W. Polan, Field-Testing of Power Utility Condenser Tube Alloys, *J. Mater. Energy Syst.*, Vol 6 (No. 4), March 1985
12. A.H. Tuthill and C.M. Schillmoller, "Guidelines for Selection of Marine Materials," paper presented at the Ocean Science and Ocean Engineering Conference, Marine Technology Society, June 1965
13. K.D. Efird and D.B. Anderson, *Mater. Perform.*, Vol 14 (No. 11), 1975
14. C.R. Southwell, J.D. Bultman, and A.L. Alexander, *Mater. Perform.*, Vol 15 (No. 7), 1976
15. D.B. Anderson and F.A. Badia, *Trans. ASME*, Vol 95 (No. 4), 1973
16. D.B. Anderson and K.D. Efird, *Proceedings of the Third International Congress on Marine Corrosion and Fouling* (Gaithersburg, MD), National Bureau of Standards, Oct 1972
17. R.D. Schelleng, "Heat Treatment and Corrosion Resistance of Cr-Modified Cu-Ni," Technical Publication 949-OP, International Nickel Company, Nov 1976
18. C. Pearson, *Br. Corros. J.*, Vol 7, March 1972
19. N.W. Polan, M.A. Heine, J.M. Popplewell, and C.J. Gaffoglio, Paper 58, presented at Corrosion/82, National Association of Corrosion Engineers, 1982
20. N.W. Polan, M.A. Heine, and C.J. Gaffoglio, "Erosion Corrosion Resistance of Copper Alloys C72200 in Seawater Containing Entrained Sand," Paper 82-JPGC-Pwr-4, Joint ASME/IEEE Power Generation Conference, 1982
21. K.D. Efird, *Corrosion*, Vol 33 (No. 1), 1977
22. S. Sato and K. Nagata, *Sumitomo Light Met. Tech. Rep.*, Vol 19, July 1978
23. G. Bianchi, G. Fiori, P. Longhi, and F. Mazza, *Corrosion*, Vol 34 (No. 11), 1978
24. F.M. Reinhart, *Corrosion in Natural Environments*, STP 558, American Society for Testing and Materials, 1974
25. "Corrosion Resistance of Wrought 90/10 Copper-Nickel-Iron Alloy in Marine Environments," Marine Corrosion Bulletin 1, The International Nickel Co. Inc., 1975
26. A.H. Tuthill, B. Todd, and J. Oldfield, Experience with Copper Alloy Tubing, Waterboxes, and Piping in MSF Desalination Plants, *Proceedings of IDA World Congress on Desalination and Water Reuse* (Madrid, Spain), International Desalination Association, 1997
27. R. Francis, "Effects of Cooling Water Treatment on Ships' Condenser Tubes," Report A.1945, British Non-Ferrous Technology Center, Jan 1979
28. R.W. Ross, *Mater. Perform.*, Vol 18 (No. 7), 1979
29. W.C. Stewart and F.L. LaQue, *Corrosion*, Vol 8 (No. 8), 1952
30. F.L. LaQue, *Corrosion*, Vol 6 (No. 4), 1950
31. P.T. Gilbert, *Trans. IME*, Vol 66 (No. 1), 1954
32. K.D. Efird and T.S. Lee, *Corrosion*, Vol 35 (No. 2), 1979
33. J.F. Bates and J.M. Popplewell, Paper 100, presented at Corrosion/74, National Association of Corrosion Engineers, 1974

34. J.P. Gudas and H.P. Hack, Paper 93, presented at Corrosion/77, National Association of Corrosion Engineers, 1977
35. T.S. Lee, H.P. Hack, and D.G. Tipton, in *Proceedings of the Fifth International Congress on Marine Corrosion and Fouling* (Barcelona, Spain), Orsi, May 1980
36. H.P. Hack and J.P. Gudas, Paper 23, presented at Corrosion/78, National Association of Corrosion Engineers, 1978
37. H.P. Hack and J.P. Gudas, Paper 234, presented at Corrosion/79, National Association of Corrosion Engineers, 1979
38. H.P. Hack and T.S. Lee, *Shell and Tube Heat Exchangers*, American Society for Metals, 1982
39. S. Sato, Corrosion and Its Prevention in Copper Alloy Condenser Tubes Under Modern Conditions, *Rev. Coat. and Corr.*, Vol 1 (No. 2), 1973, p 139
40. T.H. Michels, W.W. Kirk, and A.H. Tuthill, *J. Mater. Energy Syst.*, Vol I (No. 12), 1979
41. J.L. Manzolillo, E.W. Thiele, and A.H. Tuthill, "CA-706 Copper-Nickel Alloy Hulls: The Copper Mariner's Experience and Economics," paper presented at the Society of Naval Architects and Marine Engineers, Nov 1976
42. F.J. Ansuini and K.L. Money, "Fouling Resistant Screens for OTEC Plants," paper presented at Fifth Ocean Thermal Energy Conversion Conference (Miami Beach, FL), Feb 1978
43. C.L. Bulow, *Trans. Electrochem. Soc.*, Vol 87, 1945
44. F.L. LaQue and W.F. Clapp, *Trans. Electrochem. Soc.*, Vol 87, 1945
45. K.D. Efird, *Mater. Perform.*, Vol 15 (No. 4), 1976
46. R.B. Ritter and J.W. Suitor, "Fouling Research on Copper and Its Alloys—Seawater Studies," Progress Report, Project 214B, International Copper Research Association, March 1976 to Feb 1978
47. R.O. Lewis, Paper 54, presented at Corrosion/82, National Association of Corrosion Engineers, 1982
48. G.P. Sheldon and N.W. Polan, The Heat Transfer Resistance of Various Heat Exchanger Tubing Alloys in Natural and Synthetic Seawaters, *J. Mater. Energy Syst.*, Vol 5 (No. 4), March 1984
49. D.G. Tipton, "Effect of Mechanical Cleaning on Seawater Corrosion of Candidate OTEC Heat Exchanger Materials," ANL/OTEC-BCM-018, National Bureau of Standards, June 1981
50. N.B. Pilling and R.E. Bedworth, *J. Inst. Met.*, Vol 29, 1923, p 529–582
51. E. Escalante and J. Kruger, *J. Electrochem. Soc.*, Vol 118, 1971, p 1062
52. R.N. Parkins and N.J.H. Holroyd, *Corrosion*, Vol 28, 1982, p 245
53. S.C. Sircar, U.K. Chattedee, S.K. Roy, and S. Kisku, *Br. Corros. J.*, Vol 9, 1974, p 47
54. A.J. Fiocco, Annual Report, 1967–1968, Office of Saline Water, Denver, CO, 1969, p 241
55. J.A. Beavers, Stress-Corrosion Cracking of Copper Alloys, *Stress-Corrosion Cracking: Material Performance and Evaluation*, R.H. Jones, Ed., ASM International, 1992, p 211
56. W.H.J. Vernon, *Trans. Faraday Soc.*, Vol 23, 1927, p 162; Vol 27, 1931, p 255
57. J.M. Popplewell and T.V. Gearing, *Corrosion*, Vol 31, 1975, p 279
58. A.V. Bobylev, "Intercrystalline Corrosion and Corrosion of Metals Under Stress," I.A. Levin, Ed., Consultants Bureau, 1962
59. V.K. Gouda, H.A. El-Sayed, and S.M. Sayed, in *Eighth International Congress on Metallic Corrosion* (Frankfurt, West Germany), Dechema, Frankfurt am Main, 1981, p 479
60. A. Kawashima, A.K. Agrawal, and R.W. Staehle, in *Stress Corrosion Cracking—The Slow Strain Rate Technique*, STP 665, American Society for Testing and Materials, 1979, p 266
61. J. Papamarcos, *Power Eng.*, Vol 89, July 1973, p 24
62. S.P. Nayak and A.K. Lahire, *Indian J. Technol.*, Vol 10, 1972, p 322
63. N. McKinney and H.W. Hermance, in *Stress Corrosion Cracking*, STP 425, American Society for Testing and Materials, 1967, p 274
64. S.P. Pednekar, A.K. Agrawal, H.E. Chaung, and R.W. Staehle, *J. Electrochem. Soc.*, Vol 126, 1979, p 701
65. R. Chadwick, *J. Inst. Met.*, Vol 97, 1969, p 93
66. J.B. Cotton, in *Second International Congress on Metallic Corrosion* (New York, NY), National Association of Corrosion Engineers, 1963, p 590
67. H.W. Pickering and P.J. Byrne, *Corrosion*, Vol 29, 1973, p 325
68. J.B. Greer and M.R. Chance, *Mater. Prot. Perform.*, Vol 12 (No. 3), 1973, p 41
69. S.D. Reynolds, Jr. and F.W. Pement, *Mater. Perform.*, Vol 13 (No. 9), 1974, p 2128
70. B.F. Peters, J.A.H. Carson, and R.D. Barer, *Mater. Prot.*, Vol 4 (No. 5), 1965, p 24
71. A.J. Brock and J.M. Popplewell, Paper 105, presented at Corrosion/79 (Atlanta, GA), National Association of Corrosion Engineers, U.S. Government Printing Office, March 1979
72. F.W. Fink and T.P. May, *Proceedings of the First International Symposium on Water Desalination*, Vol 1, 1965, p 432–438
73. W. Wolfe, Jr., and S.F. Hager, Paper G7-PWR-7, presented at Joint ASME/IEEE Power Generation Conference (Detroit, MI), Sept 1967
74. J.M. Popplewell and E.A. Thiele, Paper 30, presented at Corrosion/80 (Chicago, IL), National Association of Corrosion Engineers, March 1980
75. G.A. Gehring, Jr., R.L. Foster, and B.C. Syrett, Paper 76, presented at Corrosion/83 (Anaheim, CA), National Association of Corrosion Engineers, April 1983
76. "Standard Test Methods for Corrosivity of Water in the Absence of Heat Transfer (Weight Loss Methods)," D 2688, *Annual Book of ASTM Standards*, American Society for Testing and Materials
77. J.F. Bates and J.M. Popplewell, *Corrosion*, Vol 31 (No. 8), Aug 1975, p 267–275
78. B.C. Syrett, *Corrosion*, Vol 32 (No. 6), June 1976, p 242–252
79. F.L. LaQue and J.F. Mason, Jr., "The Behavior of Iron Modified 70–30 Copper-Nickel Alloy in Salt Water and in Some Petroleum Industry Environments," American Petroleum Institute, Division of Refining, May 1950
80. W.C. Stewart and F.L. LaQue, *Corrosion*, Vol 8 (No. 8), Aug 1952, p 259–277
81. "Standard Specification for Substitute Ocean Water," D 1141, *Annual Book of ASTM Standards*, American Society for Testing and Materials
82. P.T. Gilbert, *Mater. Perform.*, Vol 21 (No. 2), Feb 1982, p 47–53
83. J.M. Popplewell, *Corros. Sci.*, Vol 13, 1973, p 593
84. "Recommended Practice for Making and Using U-Bend Stress Corrosion Test Specimens," G 30, *Annual Book of ASTM Standards*, American Society for Testing and Materials
85. G.M. Ugiansky and J.H. Payer, Ed., *Stress Corrosion Cracking—The Slow Strain Rate Technique*, STP 665, American Society for Testing and Materials, 1979
86. "Corrosion of Metals—Stress Corrosion Testing, Part 7: Slow Strain Rate Testing," ISO 7539-7, International Organization for Standardization, 1989

SELECTED REFERENCES

Dealloying corrosion

- A.M. Beccaria et al., Dealloying of Cu-Ni Alloys in Natural Sea Water, *Br. Corros. J.*, Vol 24 (No. 1), 1989, p 49–52
- Dealloying, *Mater. Perform.,* May 2003, p 66
- H. Kaiser, Alloy Dissolution, *Corrosion Mechanisms,* F. Mansfeld, Ed., Marcel Dekker, 1987, p 85–118
- J.R. Martin et al., Dealloying of Cupronickels in Stagnant Seawater, Paper 314, presented at Corrosion 99, NACE International, p 1–8
- H.H. Rehan et al., Technical Note: Synergetic Effect of 8-Quinolinol and Benzotriazole on Preventing Dezincification of Alpha-Brass (35.9% Zinc) in Acid Chloride Solutions, *Corrosion*, Vol 58 (No. 4), p 299–302
- P.K. Rohatgi et al., Corrosion and Dealloying of Cast Lead-Free Copper Alloy-Graphite Composites, *Corros. Sci.*, Vol 42, 2000, p 1553–1571

Galvanic corrosion

- R. Baboian, Galvanic Series Can Mislead, *Mater. Perform.*, Vol 37 (No. 8), Aug 1998, p 70–71
- F. Bellucci, Galvanic Corrosion Between Nonmetallic Composites and Metals, Part I: Effect of Metal and of Temperature, *Corrosion*, Vol 47 (No. 10), Oct 1991, p 808–819
- F. Bellucci, Galvanic Corrosion Between Nonmetallic Composites and Metals, Part II: Effect of Area Ratio and Environmental Degradation, *Corrosion*, Vol 48 (No. 4), April 1992, p 281–291
- S.A. Campbell, G.J.W. Radford, C.D.S. Tuck, and B.D. Barker, Corrosion and Galvanic Compatibility Studies of a High-Strength Copper-Nickel Alloy, *Corrosion*, Vol 58 (No. 1), p 57–71
- R.A. Corbett, Galvanic Corrosion Can Occur at Same-Metal Couple, *Mater. Perform.*, Dec 1998, p 63–64
- C.R. Crowe and R.G. Kasper, Ionic Current Densities in the Nearfield of a Corroding Iron-Copper Galvanic Couple, *J. Electrochem. Soc.*, May 1986, p 879–887
- Editorial Staff, Protective Measures for Galvanic Corrosion of Cooling Tower, *Corros. Eng.*, Vol 42, 1993, p 77–81
- G.A. Gehring, Jr., Galvanic Corrosion in Power Plant Condensers, *Galvanic Corrosion*, STP 978, ASTM, p 301–309
- A.J. Griffin, et al., A Galvanic Series for Thin-Film Metallizations and Barrier Layers Commonly Used in the Microelectronics Industry, *J. Electrochem. Soc.*, Vol 141 (No. 3), March 1994, p 807–809
- R.G. Kasper, *Three-Dimensional Electric Field Predictions of an Iron-Copper Galvanic Couple*, Naval Underwater Systems Center, 1987, p 1–24
- R.G. Kasper and C.R. Crowe, Comparisons of Localized Ionic Currents as Measured from 1-D and 3-D Vibrating Probes with Finite-Element Predictions for an Iron-Copper Galvanic Couple, *Galvanic Corrosion*, STP 978, ASTM, p 118–135
- N. Masuko and T. Inoue, Dezincification of Corrosion Behaviors of Brass Materials in Galvanic Coupling with Pure Copper, *J. Jpn. Brass Res. Assoc.*, Vol 25, 1986, p 80–94
- G. Saleh Al Zaharani, B. Todd, and Oldfield, Bimetallic Joints in Multistage Flash Desalination Plants, *Galvanic Corrosion*, STP 978, ASTM, p 323–335
- J.R. Scully and H.P. Hack, Prediction of Tube-Tubesheet Galvanic Corrosion Using Finite Element and Wagner Number Analyses, *Galvanic Corrosion*, STP 978, ASTM, p 136–157
- J.R. Scully and H.P. Hack, *Prediction of Tube-Tubesheet Galvanic Corrosion Using Long Term Electrochemical Polarization Data*, David Taylor Research Center, p 1–35
- D.A. Shifler and D. Melton, "Control Measures to Mitigate Galvanic Corrosion," Paper 319, presented at Corrosion 99, NACE International, p 1–20

Galvanic corrosion in seawater

- H.I. Al Hossani et al., Galvanic Corrosion of Copper-Base Alloys in Contact with Molybdenum-Containing Stainless Steels in Arabian Gulf Water, *Desalin.*, Vol 109 (No. 11), March 1997, p 25–37
- D.J. Astley, Use of the Microcomputer for Calculation of the Distribution of Galvanic Corrosion and Cathodic Protection in Seawater System, *Galvanic Corrosion*, STP 978, ASTM, p 53–78
- D.M. Aylor, R.A. Hayes and L.S. Marshall, "Galvanic Corrosion Evaluation of High Performance Naval Seawater Valve Materials in Quiescent, Natural Seawater," Paper 00640, presented at Corrosion 2000, NACE International, p 640/1–27
- P.O. Gartland, R. Johnsen, and S. Valen, "How to Prevent Galvanic Corrosion in Seawater Piping Systems," Paper 496, NACE, 1996, p 1–17
- M. Shibata et al. Studies of Galvanic Corrosion of 90/10 Cu-Ni Clad Steel Plate in Seawater, *Proceedings of EVALMAT 89*, p 519–526
- B. Wallen and T. Andersson, "Galvanic Corrosion of Copper Alloys in Contact with a Highly Alloyed Stainless Steel in Seawater," Tenth Scandinavian Corrosion Congress (Stockholm), 1986, p 149–154

Atmospheric galvanic corrosion

- D.P. Doyle and T.E. Wright, Quantitative Assessment of Atmospheric Galvanic Corrosion, *Galvanic Corrosion*, STP 978, ASTM, p 161–173
- Y.M. Pachenko, P.V. Streklov, and T.B. Pustovskikh, Corrosion Tests of the Galvanic Coatings for the Ship Instruments in a Marine Climate; Part VI: The Decorative and Protective Properties and the Useful Life of Nickel, Copper-Nickel, and Copper-Nickel-Chromium Coatings, *Prot. Met.,* Vol 34 (No. 1), 1998, p 68–80
- A.M. Shams El Din and L. Wang, Galvanic Corrosion of Copper/Silver Contacts in Electrical Switches, *Br. Corros. J.,* Vol 28 (No. 4), 1993, p 271–278

Galvanic corrosion in salt solutions

- J. Garcia-Anton, A. Igual-Munoz, J.L. Guinon, V. Perez-Herranz, and J. Pertusa-Grau, Online Visualization of Corrosion Processes of Zinc and a Cu/Zn Galvanic Pair in Lithium Bromide Solutions, *Corrosion*, Vol 59 (No. 2), Feb 2003, p 172–180
- A. Igual-Munoz, J. Garcia-Anton, J.L. Guinon, and V. Perez-Herranz, Corrosion Behavior and Galvanic Studies of Brass and Bronzes in Aqueous Lithium Bromide Solutions, *Corrosion*, Vol 58 (No. 7), p 560–568
- D. Itzhak and T. Greenberg, Galvanic Corrosion of a Copper Alloy in Lithium Bromide Heavy Brine Environments, *Corrosion*, Vol 55 (No. 8)
- N. Masuko and T. Inoue, Galvanic Corrosion of Brass Coupled to Bronze Casting in Chloride Solutions, *J. Jpn. Copper Brass Res. Assoc.*, Vol 27, 1988, p 134–146
- L.I. Shuying and W. Chen, Galvanic Coupling Behavior on Carbon Steel/Red Copper in NaCl Media, *Corros. Sci. Prot. Tech.*, Vol 12 (No. 5), Sept 2000, p 300–302

Galvanic corrosion in condensers and heat exchangers

- G. Haynes and R. Baboian, "Galvanic Corrosion Behavior of Copper and Stainless Steel in Heat Exchanger Environments," SAE 1993 Vehicle Thermal Management Systems Conference, 29 March to 1 April 1993, p 321–331

Microbial corrosion and biofouling

- C.A. Powell, Preventing Biofouling with Copper-Nickel Alloys, *Mater. World*, Vol 2 (No. 4), April 1994, p 181–183
- H.M. Shalaby et al., Effects of Inorganic Sulphide and Ammonia on Microbial Corrosion Behaviour of 70Cu-30Ni Alloy in Sea Water, *Br. Corros. J.*, Vol 34 (No. 4), 1999, p 292–298
- E.F.C. Somerscales, Fundamentals of Corrosion Fouling, *Br. Corros. J.*, Vol 34 (No. 2), 1999, p 109–124
- J.K. Spelt et al., "Zebra Mussel Attachment," ICA Project 460, Department of Mechanical Engineering, University of Toronto, Toronto, Ontario, Feb 1992, p 1–13
- J.K. Spelt et al., "Zebra Mussel Attachment," ICA Project 460, Sept 1994, p 1–102
- G.W. Swain et al., "Composite Copper Alloys and Electrochemical Control Techniques for the Prevention of Biofouling," INCRA Report 461, p 1–21
- G.W. Swain et al., "Composite Copper Alloys and Electrochemical Control Techniques for the Prevention of Biofouling," final report, Jan 1993, p 1–43
- D. Wagner, "Microbiologically Influenced Pitting Corrosion of Copper Pipes, Final Report ICA Project 453-A, reference period 15 Feb 1992 to 14 Feb 1993, p 1–144

Microbial corrosion and biofouling in freshwater

- P. Angell, H.S. Campbell, and A.H.L. Chamberlain, "Microbial Involvement in Corrosion of Copper in Fresh Water," ICA Project 405, interim report, Aug 1990, p 1–62
- W.R. Fischer et al., Microbiologically Influenced Corrosion in Potable Water Installations—An Engineering Approach to

Developing Countermeasures, *Mater. Perform.*, Oct 1995, p 50–54
- G. Geesey, "Involvement of Biofilm Microorganisms in Pitting Corrosion of Copper Tubing Used for Water Service in Institutional Buildings," Project 413, final report, Montana State University, June 1993, p 2–19
- G.G. Geesey et al., "State of Knowledge of Microbially-Influenced Pitting Corrosion of Copper Tubing Used in Potable Water Systems of Institutional Buildings," Dec 1992, p 1–14
- D. Wagner, A.H.L. Chamberlain, W.R. Fischer, J.N. Wardnell, and C.A.C. Sequeira, Microbiologically Influenced Corrosion of Copper in Potable Water Installations—A European Project Review, *Mater. Corros.*, Vol 48, 1997, p 311–321
- D. Wagner et al., Copper Deterioration in a Water Distribution System of a County Hospital in Germany Caused by Microbially Influenced Corrosion, Part II: Simulation of the Corrosion Process in Two Test Rigs Installed in This Hospital, *Werkst. Korros.*, Vol 43, 1993, p 496–502
- J.T. Walker, "The Influence of Plumbing Material, Water Chemistry and Temperature on Biofouling of Plumbing Circuits with Particular Reference to the Colonisation of Legionalla Pneumophila," ICA Project 437B, annual report, Oct 1993, p 1–59
- J.T. Walker et al., "The Influence of Plumbing Tube Material, Water Chemistry, and Temperature on Biofouling of Plumbing Circuits with Particular Reference to the Colonisation of Legionalla Pneumophila, ICA Project 437A, annual report, Jan 1993, p 1–62
- J.T. Walker, C.W. Keevil, P.J. Dennis, J. McEvoy, and J.S. Colbourne, "The Influence of Water Chemistry and Environmental Conditions on the Microbial Colonisation of Copper Tubing Leading to Pitting Corrosion Especially in Institutional Buildings," ICA Project 407, final report, 1988–1990, p 1–64

Microbial corrosion and biofouling in seawater

- L.H. Boulton et al., "Controlling Biofouling on Ferry Hulls with Copper-Nickel Sheathing," Tenth International Congress on Marine Corrosion and Fouling, University of Melbourne, Feb 1999, p 73–87
- F. D'Souza et al., Analysis of Microfouling Products Formed on Metallic Surfaces Exposed in a Marine Environment, *Biofoul.*, Vol 19 (No. 2), 2003, p 95–107
- B.J. Little, P.A. Wagner, J.M. Jones, and M.B. McNeil, "Microbiologically Influenced Corrosion in Copper and Nickel Seawater Piping Systems," First Annual Naval Corrosion Control Workshop, 29–31 Oct 1990, Naval Oceanographic and Atmospheric Research Laboratory
- F. Mansfield and B. Little, Microbiologically Influenced Corrosion of Copper-Based Materials Exposed to Natural Seawater, *Electrochim. Acta.*, Vol 37 (No. 12), 1992, p 2291–2297
- C.A. Powell, "Corrosion and Biofouling Protection of Ship Hulls Using Copper-Nickel," International Conference on Marine Corrosion Prevention, 11–12 Oct 1994, p 1–14
- C.A. Powell, "Corrosion and Biofouling Resistance of Copper-Nickel in Offshore and Other Marine Applications," U.K. Corrosion and EuroCorr 1994, p 188–200
- C.A. Powell et al., "Copper-Nickel Alloys for Seawater Corrosion Resistance and Antifouling—A State of the Art Review," Paper 00627, Corrosion 2000, NACE International, p 1–17
- R.L. Townsin, The Ship Hull Fouling Penalty, *Biofoul.*, Vol 19 (Supplement), 2003, p 9–15
- E.E. Williams et al., Marine Biofouling Solutions for Closed Seawater Systems, *Sea Technol.*, June 1989, p 17–18

Microbial corrosion and biofouling in soil and groundwater

- C.J. Gaffoglio, Beating Biofouling with Copper-Nickel Alloys Offshore, *Sea Technol.*, June 1987, p 43–46
- Y. Kikuchi et al., "Microbiologically Influenced Corrosion of Copper in Ground Water," Paper 170, Corrosion 99, NACE International, p 1–14
- K.E.J. Miller, "Antifouling Composite Material, Copper Alloys in Marine Environments," Seamark Systems, United Wire Group PLC
- "90-10 Copper-Nickel for Resistance to Corrosion and Marine Biofouling," Publication 118, Copper Development Association, Dec 1996

Microbial corrosion and biofouling in condensers and heat exchangers

- J.R. Ibars et al., Biofouling and Microbiologically Influenced Corrosion in Admiralty Brass Heat Exchanger Tubes, *Proceedings of the Fourth International EFC Workshop on Microbial Corrosion*, Dep. de Ingeneria y Ciencia de los Materiales, Madrid, Spain, p 53–60
- A. Kawabe et al., Intergranular Corrosion Under Barnacles on Aluminum Brass Condenser Tubes, *Corros. Eng.*, Vol 37, 1988, p 105–111

Microbial corrosion and biofouling in organic chemicals

- B. Little, *Microbiologically Influenced Corrosion in Offshore Oil and Gas Systems*, Naval Research Laboratory, p 1–13

Pitting corrosion

- F.M. Al-Kharafi et al., Pitting of Copper Under Laboratory and Field Conditions, *Br. Corros. J.*, Vol 24 (No. 4), 1989, p 284–290
- P.E. Francis et al., Electrochemical Measurements of the Influence of Sulfate/Hydrogen Carbonate Ion Ratio on the Pit Initiation Process on Copper, *Proceedings of the 11th Corrosion Conference*, Associazione Italiana di Metallurgia, p 5.363–5.370
- T. Hamamoto et al., Case Studies on Pitting Corrosion of Copper Tubes, *J. Jpn. Copper Brass Res. Assoc.*, Vol 29, 29th meeting, 1990, p 101–108
- M. Jani and P. Diehl, A Farewell to Pitting, *Print. Circ. Fab.*, Vol 16 (No. 3), March 1993, p 40–41
- K. Kasahara et al., Case Studies of Pitting Corrosion of Copper Tubes in Central Hot-Water Supply Systems, *Corros. Eng.*, Vol 36, 1987, p 453–459
- K. Kasahara et al., Preventing Copper-Pipe Pitting in Central Hot Water Supply by Residual-Chlorine UV Photolysis, *Corros. Eng.*, Vol 37, 1988, p 361–370
- J.L. Nuttall, *Pitting Corrosion Eradication in Copper Tube*, IMI Yorkshire Copper Tube Ltd., International Tube Association, p 44–48
- Y. Ono, "Method of Preventing Pitting Corrosion," U.S. Patent 5,736,097, p 1–6
- W. Qafsaoui et al., Comparative Study of Inhibitive Efficiency of Different Triazole Derivatives on the Pitting Corrosion of Copper, *Proceedings of the Ninth European Symposium on Corrosion Inhibitors (9 SEIO)*, Ann. Univ. Ferrara, N.S., Sez. V, Suppl. N. 11, 2000
- W. Qafsaoui et al., Study of Different Triazole Derivative Inhibitors to Protect Copper against Pitting Corrosion, *J. Appl. Electrochemi*, Vol 30, 2000, p 959–966
- M. Sakai et al., The Reproduction of Moundless Pitting by Both Field Test and Laboratory Test, *J. Jpn. Res. Inst. Adv. Copper Based Mater. Technol.*, Vol 41 (No. 1), 2002, p 136–141
- Y. Sakai, Cause of Pitting Corrosion in Copper Tubes of Air Conditioning Coils in Open Heat-Storage Water Tank Systems, *Corros. Eng.*, Vol 40, 1991, p 721–732
- M. Sosa et al., Concentration Cells and Pitting Corrosion of Copper, *Corros. Sci.*, Vol 55 (No. 11), Nov 1999, p 1069–1076
- C. Taxen, *Pitting of Copper Moderately Oxidizing Conditions*, Swedish Corrosion Institute, Aug 1992, p 1–32
- Y. Yamada et al., Hazard Mapping for Pitting Corrosion of Copper Tube by Using Electric Conductivity, *Sumitomo Light Met. Tech. Rep.*, Vol 43 (No. 1), 2002, p 95–99
- Y. Yamada et al., Pitting Corrosion of Copper in Aqueous Solutions Containing Phosphoric Acid as an Inhibitor, *Corros. Eng.*, Vol 42, 1993, p. 675–684

Pitting corrosion in freshwater

- A. Cohen and J.R. Myers, Mitigating Copper Pitting Through Water Treatment, *J. AWWA*, Feb 1987, p 58–61
- R.A. Corbett, Well Water Causes Copper Pipe Pitting, *Mater. Perform.*, Nov 1998, p 61–63
- M. Edwards, The Pitting Corrosion of Copper, *J. AWWA*, July 1994, p 74–90
- M. Edwards et al., Inorganic Anions and Copper Pitting, *Corrosion*, Vol 50 (No. 5), May 1994, p 366–372
- P.F. Ellis II, "Pitting Corrosion in Domestic Copper Plumbing—The Rise and Fall of the Pitting Water Theory," Paper 00652, Corrosion 2000, NACE International, p 2–10
- R. Francis, Pitting of Corrosion of Copper in Fresh Waters, *Mater. Perform.*, Feb 1997, p 8
- T. Funjii, Localized Corrosion and Its Prevention for Copper in Water, *Trans. Natl. Res. Inst. Met. (Jpn.),* Vol 30 (No. 2), 1988, p 25–30
- G.C. Geesey et al., *Unusual Types of Pitting Corrosion of Copper Tubes Used for Water Service in Institutional Buildings,* International Copper Association, Ltd., 1993, p 1–30
- H.M. Halaby et al., A Morphological Study of Pitting Corrosion of Copper in Soft Tap Water, Corrosion, Vol 45 (No. 7), July 1989, p. 536–547
- T. Hamamoto et al., "Development of Anti-Pitting Corrosion Copper Alloy Tube in Hot Water Service, *J. Jpn. Copper Brass Res. Assoc.*, Vol 27 1988, p 182–208
- T. Hamamoto et al., Effect of Water Compositions on the Pitting Corrosion of Copper Tubes in Hot Water Service, *Sumitomo Light Met. Tech. Rep.*, p 16–21
- D.B. Kasul and L.A. Heldt, "Characterization of Pitting Corrosion of Copper Pipe Carrying Municipal Water," Paper 512, Corrosion 93, NACE International, p 1–7
- S. Komukai et al., Pitting Potential and Repassivation Potential of Copper Tubes in Hot Water, *Corros. Eng.*, Vol 43, 1994, p 245–256
- M. Linder, *Pitting Corrosion of Type III in Copper Cold Water Pipes—Causes and Countermeasures*, Swedish Corrosion Institute, May 1989
- J.R. Myers and A. Cohen, Pitting Corrosion of Copper in Cold Potable Water Systems, *Mater. Perform.*, Oct 1995, p 60–63
- J.R. Myers and A. Cohen, Soldering Flux-Induced Pitting of Copper Water Lines, *Mater. Perform.*, Vol 33 (No. 10), Oct 1994, p 62–63
- R. Riedl et al., Pitting Corrosion in Copper Water Pipes, *J. Inst. Mater. Prod. Technol.*, Vol 4 (No. 2), 1989, p 159–166
- R. Sandenberg, Pitting Corrosion of Copper Tubing in Domestic Waters, *Corros. Coatings, S. Afr.*, March 1993, p 4–12
- Y. Yamada, Pitting Corrosion of Copper Soft Tubes in Well Water, *Sumitomo Light Met. Tech. Rep.*, Vol 40 (No. 1), 1999, p 53–60
- T. Yamana et al., Pitting Corrosion in Copper Pipes for Hot Water Supply and Its Countermeasure, *J. Jpn. Res. Inst. Adv. Copper-Based Mater. Technol.*, Vol 41, 2002, p 127–130

Pitting corrosion in salt solutions

- J.P. Duthill et al., The Synergetic Effect of Chloride and Sulfate on Pitting Corrosion of Copper, *Corros. Sci.*, Vol 38 (No. 10), p 1839–1849
- W. Qasfaoui et al., Pitting Corrosion of Copper in Sulphate Solutions: Inhibitive Effect of Different Triazole Derivative Inhibitors, *J. Appl. Electrochem.*, Vol 31, 2001, p 223–231
- W. Qafsaoui, G. Mankowski, and F. Dabosi, The Pitting Corrosion of Pure and Low Alloyed Copper in Chloride-Containing Borate Buffered Solutions, *Corros. Sci.*, Vol 34 (No. 1), 1993, p 17–25
- S. Sathiyanarayanan et al., In Situ Grazing Incidence of X-Ray Diffractometry Observation of Pitting Corrosion of Copper in Chloride Solutions, *Corros. Sci.*, Vol 41, 1999, p 1899–1909

Pitting corrosion in soil and groundwater

- Takayuki et al., Electrochemical Evaluation of Influence of Surface Conditions and Oxygen Gas Partial Pressure on Pitting Corrosion of Copper Tubing in Artificial Ground Water, *J. Jpn. Res. Inst.*, Vol 41 (No. 1), 2000, p 142–147

Pitting corrosion in condensers and heat exchangers

- S. Suziki, Pitting Corrosion and Its Prevention of Copper Heat Exchanger Tubes for Water Heater, *J. Jpn. Res. Inst.*, Vol 41 (No. 1), 2000, p 148–151

Mechanically assisted corrosion fatigue

- R. Bagheri et al., Fatigue and Corrosion Fatigue of Beryllium-Copper Spring Materials, *ASTM J. Test. Eval.*, 1993, p 101–106
- J.I. Dickson et al., Corrosion-Fatigue Crack Propagation Behavior of Mn-Ni-Al Bronze Propeller Alloys, *J. Mater. Eng.*, Vol 10 (No. 1), 1988, p 45–56
- J.I. Dickson et al., Fatigue Propagation Behavior of Mn-Al-Ni Bronzes, *Proceedings of the Copper 91 International Symposium*, Vol 1 (Ottawa, Canada), 18–21 Aug 1991, p 251–266
- D.J. Duquette, Corrosion Fatigue, *Corrosion Mechanisms*, F. Mansfeld, Ed., Marcel Dekker, 1987, p 367–395
- C. Ramakrishna et al., Corrosion Fatigue Behavior of Some Copper Based Condenser Tube Materials in NH_4OH, *Pract. Met.*, Vol 28, 1991, p 15–24
- T. Yamasaki et al., *Corrosion Fatigue of Ultra-Fine Grain Copper Fabricated by Severe Plastic Deformation*, The Minerals, Metals and Materials Society, 2002, p 361–370

Stress-corrosion cracking in mechanically assisted corrosion

- D.C. Argawal, Stress Corrosion in Copper-Nickel Alloys: Influence of Ammonia, *Br. Corros. J.*, Vol 37 (No. 4), 2002, p 267–275
- G.L. Edgemon et al., "Comparison of TGSCC and Crevice in a Brass/Nitrite System," Paper 210, Corrosion 99, NACE International, p 1–19
- J.J. Hoffman et al., "Stress Corrosion Cracking Susceptibility of Aluminum-Silicon Bronze," Paper 03510, Corrosion 2003, NACE International, p 1–12
- W.L. Johnson, Stress Corrosion Cracking of Copper Pipes, *Armstrong World Industries*, 20 Nov 1987, p 1–16
- K. Kawano et al., Cracking of Hot-Water Supply Copper Tube, *Corros. Eng.*, Vol 43, 1994, p 449–453
- F. King, *The Potential for Stress Corrosion Cracking of Copper Containers in a Canadian Nuclear Fuel Waste Disposal Vault*, Whiteshell Laboratories, Pinawa, Manitoba, Canada, Sept 1996, p 1–82
- F. King et al., "The Stress Corrosion Cracking of Copper Containers for the Disposal of High Level Nuclear Waste," Paper 482, Corrosion 99, NACE International, p 1–31
- Mueller Brass Says Copper Not at Fault in Stress Corrosion Cracking Failures, *Air Conditioning, Heating and Refrigeration News*, Oct 8, 1990, p 28–29
- K. Pettersson et al., Stress Corrosion Crack Growth in Copper for Waste Canister Applications, *Mat. Res. Soc. Symp. Proc.*, Vol 608, 2000
- M.J. Pryor et al., The Mechanism of Stress Corrosion Cracking of Copper-Base Alloys, *Corros. Sci.*, Vol 30 (No. 2/3), 1990, p 267–291
- S.M. Sayed et al., Effect of Sulfide Ions on the Stress Corrosion Behavior of Al-Brass and Cu10Ni Alloys in Salt Water, *J. Mater. Sci.*, Vol 37, 2002, p 2267–2272
- S. Schwentenwein et al., "Stress Corrosion Cracking of Semi-Hard DHP-Copper Tubes in Potassium Nitrite Solution," Paper 02432, Corrosion 2002, NACE International, p 1–10
- A. Vinogradov et al., Corrosion, Stress Corrosion Cracking and Fatigue of Ultra-Fine Grain Copper Fabricated by Severe Plastic Deformation" *Ann. Chim. Sci. Mater.*, Vol 27 (No. 3), 2002, p 65–75
- S.-J. You et al., Stress Corrosion Cracking Properties of Environmentally Friendly Unleaded Brasses Containing Bismuth in Mattsson's Solution, *Mater. Sci. Eng. A*, Vol 345, 2003, p 207–214

Freshwater environment

- F.M. Al-Kharafi and H.M. Shalaby, Corrosion Behavior of Annealed and Hard-Drawn Copper in Soft Tap Water, *Corrosion*, Vol 51 (No. 6), June 1995, p 469–481
- M.M. Benjamin et al., *Chemistry of Corrosion Inhibitors in Potable Water*, AWWA Research Foundation, Feb 1990, p XVII-15
- B.P. Boffardi, Minimization of Lead Corrosion in Drinking Water, *NACE MP*, Aug 1990, p 45–49
- A.J. Brock, "Corrosion Evaluation of Copper Tubes Taken from Water Service Lines in Billings Montana," Olin Corporation, 8 Dec 1992
- R.S. Charlton, "Failures of Copper Potable Water Piping Due to Design, Materials and Poor Workmanship," Paper 01486, Corrosion 2001, NACE International, p 01486/1-01486/33
- A. Cohen, Corrosion by Potable Waters in Building Systems, *Mater. Perform.*, Aug 1993, p 56–61
- A. Cohen, Occurrence and Control of Corrosion in Copper Water Tube Systems, *Proceedings of the American Water Works Association*, 1994 Water Quality Technology Conference, 6–10 Nov 1994, p 1803–1809
- A. Cohen and J.R. Myers, Overcoming Corrosion Concerns in Copper Tube Systems, *Mater. Perform.*, Vol 35 (No. 9), Sept 1996, p 53–55
- A. Cohen and J.R. Myers, Water Treatment to Mitigate Corrosion of Copper Plumbing Systems, *Mater. Perform.*, Aug 1993, p 43–45
- H. Cruse et al., Corrosion of Copper in Potable Water Systems, *J. AWWA*, Vol 52, 1960, p 317–416
- Editorial Staff, Corrosion of Copper Tubing in Hot Water Supply Systems, *Corros. Eng.*, Vol 40, 1991, p 613–615
- H.P. Hack, Galvanic Corrosion of Piping and Fitting Alloys in Sulfide-Modified Seawater, *Galvanic Corrosion*, STP 978, ASTM, 1988, p 340–351
- R.A. Hoffman, J. Ziemianski, and S. Lamb, "Twenty-Year Test Program—Stainless Steel Piping in NYC Water—The Beginning," Paper 01490, *NACE International*, 2001, p 1–11
- H. Idrissi Chbibi, S. Audisio, J.C. Dupuy, and J.C. Bureau, Structure and Composition in Thin Films Formed during a Galvanic Corrosion of Copper and Brazings (Copper or Tin Alloys) in Water, *Proceedings of the Sixth International Conference on Secondary Ion Mass Spectrom*, 1987, p 1003–1006
- K. Ito et al., Corrosion of Copper and Adjacent Stainless Steel in Pure Water, *Corros. Eng.*, Vol 44 (No. 8), 1995, p 545–550
- J.G. Kim et al., Technical Note: Behavior of Unleaded Brasses Containing Bismuth in Potable Water, *Corrosion*, Vol 57 (No. 4), April 2001, p 291–294
- K. Minamoto et al., Corrosion Problems of Copper Tube in Hot-Water Supply Systems and Their Countermeasures, *Kobe Steel Eng. Rep.*, Vol 38 (No. 4), 1988, p 51–54
- J.R. Myers et al., Erosion-Corrosion of Copper Tube Systems by Domestic Waters, *Mater. Perform.*, Nov 1998, p 57–59
- T.M. Prakash et al., "Development of the Pipe Loop System for Determining Effectiveness of Corrosion Control Chemicals in Potable Water Systems," USA-CERL Technical Report N-88/12, Upgrading Army Water and Wastewater Treatment Plants, Aug 1988, p 1–56
- "Prevention and Control of Water-Caused Problems in Building Potable Water Systems," TPC 7 Publication, NACE International, 1995, p 1–71
- A. Sakamoto et al., Analysis of Corrosion Damage on Water Tap, *Corros. Eng.*, 1995, p 391–401
- A. Sakamoto et al., Erosion-Corrosion Tests on Copper Alloys for Water Tap Use," *Wear*, 1995, p 548–554
- E.A. Vik et al., Corrosion Monitoring Techniques Used in Water Supply Systems, *Br. Corros. J.*, Vol 25 (No. 2), 1990, p 108–114
- J. Wagner, Jr. et al., Corrosion on Building Water Systems, *Mater. Perform.*, Oct 1990, p 40–46

Saltwater environment

- D.C. Argawal, Effect of Ammoniacal Sea Water on Material Properties of Copper-Nickel Alloy, *Br. Corros. J.*, Vol 37 (No. 2), 2002, p 105–113
- J.A. Carew et al., Erosion Corrosion of Copper- and Nickel-Based Alloys in Polluted Sea Water, *Mater. Perform.*, April 1995, p 54–57
- R. Francis, Effects of Pollutants on Corrosion of Copper Alloys in Sea Water, Part 1: Ammonia and Chlorine, *Br. Corros. J.*, Vol 20 (No. 4), 1985, p 167–174
- R. Francis, Effect of Pollutants on Corrosion of Copper Alloys in Sea Water, Part 2: Sulphide and Chlorine, *Br. Corros. J.*, Vol 20 (No. 4), 1985, p 175–182
- R. Francis, The Effects of Chlorine on the Properties of Films on Copper Alloys in Sea Water, *Corros. Sci.*, Vol 26 (No. 3), 1986, p 205–212
- A. Igual-Munoz, J. Garcia-Anton, J.L. Guinon and V. Perez-Herranz, Corrosion Studies of Copper Alloys in Aqueous Lithium Bromide Solutions, *EUROCORR 2001 Congress Proceedings*, p 1–10
- C.A. Powell et al., "Copper Alloys for Marine Construction," International Workshop on Advanced Materials for Marine Construction, Feb 1997
- S.M. Sayed et al., Effect of Sulfide Ions on the Corrosion Behaviour of Al-Brass and Cu10Ni Alloys in Salt Water, *Mater. Chem. Phys.*, Vol 78, 2003, p 825–834
- P. Traverso et al., Effect of Sulphides on Corrosion of Cu-Ni-Fe-Mn Alloy in Sea Water, *Bri. Corros. J.*, Vol 29 (No. 2), 1994, p 110–114
- A.H. Tuthill, Guidelines for the Use of Copper Alloys in Seawater, *Mater. Perform.*, Sept 1987, p 12–22
- P. Wenschot, The Properties of Ni-Al Bronze Sand Cast Ship Propellers in Relation to Section Thickness, *Nav. Eng. J.*, Sept 1986, p 58–69

Soils and groundwater environments

- G. Camitz et al., "Corrosion of Copper in Swedish Soils," KI Report 1993:4, Swedish Corrosion Institute
- G. Camitz et al., "Corrosion Resistance of Copper in Swedish Soils," KI Report 2003 : 2E, Swedish Corrosion Institute
- A. Cohen and A.J. Brock, Water- and Soil-Side Corrosion of Copper Water Service Lines, *Mater. Perform.*, Vol 34 (No. 3), March 1995, p 51–57
- G. Haynes and R. Baboian, Field Corrosion Testing and Performance of Cable Shielding Materials in Soils, *NACE MP*, Sept 1989, p 68–74

Atmospheric corrosion

- R. Baboian, The Statue of Liberty Revisited, *ASTM Stand. News*, Vol 25 (No. 8), Aug 1997, p 16–21
- R. Baboian et al., Statue of Liberty Restoration: Ten Years Later, *Mater. Perform.*, Nov 1996, p 5–10
- T.S. Barron, "Architectural Uses of Copper—An Evaluation of Stormwater Pollution Loads and Best Management Practices," Palo Alto Regional Water Quality Control Plant, Palo Alto, CA, 2000
- B. Boulanger and N.P. Nikolaidis, Mobility and Aquatic Toxicity of Copper in an Urban Watershed, *J. Am. Water Resources Assoc. (JAWRA)*, Vol 39 (No. 2), April 2003, p 325–336
- Corrosion in Automotive Wiring, *Automot. Eng.*, March 1991, p 32–35
- S.D. Cramer, S.A. Matthes, B.S. Covino, Jr., S.J. Bullard, and G.R. Holcomb, Environmental Factors Affecting the Atmospheric Corrosion of Copper, *Outdoor Atmospheric Corrosion*, STP 1421, H.E. Townsend, Ed., ASTM International, 2002, p 245–264
- S.D. Cramer and L.G. McDonald, Atmospheric Factors Affecting the Corrosion of Zinc, Galvanized Steel, and Copper, *Corrosion Testing and Evaluation*, STP 1000, R. Baboian and S.W. Dean, Ed., American Society for Testing and Materials, 1990, p 208–224
- S.D. Cramer, L.G. McDonald, and J.W. Spence, Effects of Acidic Deposition on the Corrosion of Zinc and Copper, *Proceedings of the 12th International Corrosion Congress*, Vol 2, NACE International, 1993, p 722–733

- S.W. Dean and D.B. Reiser, Analysis of Long-Term Atmospheric Corrosion Results from ISO CORRAG Program, *Outdoor Atmospheric Corrosion*, STP 1421, H.E. Townsend, Ed., ASTM International, 2002, p 3–18
- D.R. Flinn, S.D. Cramer, J.P. Carter, D.M. Hurwitz, and P.J. Linstrom, Environmental Effects on Metallic Corrosion Products Formed in Short-Term Atmospheric Exposures, *Materials Degradation Caused by Acid Rain*, ACS Symposium Series 318, R. Baboian, Ed., American Chemical Society, 1986, p 119–151
- G. Haynes et al., Atmospheric Corrosion Behavior of Clad Metals, *Degradation of Metals in the Atmosphere*, STP 965, ASTM, p 145–190
- T.E. Graedel, Copper Patinas Formed in the Atmosphere, B II: Qualitative Assessment of Mechanisms, *Corros. Sci*., Vol 27 (No. 7), 1987, p 721–740
- T.E. Graedel, Copper Patinas Formed in the Atmosphere, B III: A Semi-Quantitative Assessment of Rates and Constraints in the Greater New York Metropolitan Area, *Corros. Sci*., Vol 27 (No. 7), 1987, p 741–769
- T.E. Graedel, K. Nassau, and J.P. Franey, Copper Patinas Formed in the Atmosphere, B I: Introduction, *Corros. Sci*., Vol 27 (No. 7), 1987, p 639–657
- W. He, I. Odnevall Wallinder, and C. Leygraf, A Comparison between Corrosion Rates and Runoff Rates from New and Aged Copper and Zinc as Roofing Materials, *Water, Air and Soil Pollution. Focus*, Vol 1, 2001, p 67–82
- W. He, I. Odnevall Wallinder, and C. Leygraf, A Laboratory Study of Copper and Zinc Runoff During First Flush and Steady-State Conditions, *Corros. Sci.*, Vol 43, 2001, p 127–146
- L.S. Hernandez et al., Protective Effect of the Corrosion Products Layers of Atmospheric Exposure, *Rev. Metal. Madrid*, Vol 38, 2002, p 108–116
- V.F. Hock et al., "Corrosion Mitigation and Materials Selection Guide for Military Construction in a Severely Corrosive Environment," USA-CERL Technical Report M-88/03, Corrosion Protection Selection Guide for Rapid Deployment, Joint Task Force Facilities, U.S. Army Corps of Engineers, Construction Engineering Research Laboratory, July 1988, p 1–143
- A.M. Horton, "Corrosion Effects of Electrical Grounding on Water Pipe," Paper 519, Corrosion 91, NACE International, p 1–20
- C. Karlen, I. Odnevall Wallinder, D. Heijerick, and C. Leygraf, Runoff Rates, Chemical Speciation and Bioavailability of Copper Released from Naturally Patinated Copper, *Environ. Pollut*., Vol 120 (No. 3), Dec 2002, p 691–700
- D. Knotkova, V. Kucera, S.W. Dean, and P. Boschek, Classification of the Corrosivity of Atmosphere—Standardized Classification System and Approach for Adjustment, *Outdoor Atmospheric Corrosion*, STP 1421, H.E. Townsend, Ed., ASTM International, 2002, p 109–124
- A. Kratschmer et al., The Evolution of Outdoor Copper Patina, *Corros. Sci*., Vol 44, 2002, p 425–450
- V. Kucera and E. Mattsson, Atmospheric Corrosion, *Corrosion Mechanisms*, F. Mansfeld, Ed., Marcel Dekker, 1987, p 211–284
- C. Leygraf and T.E. Graedel, *Atmospheric Corrosion*, Wiley-Interscience, 2000
- H.T. Michels, B. Boulanger and N.P. Nikolaidis, "Copper Roof Stormwater Runoff—Corrosion and the Environment," Paper 02225, Corrosion/2002, NACE International, 2002
- H.T Michels et al., Environmental Impact of Stormwater Runoff from a Copper Roof, *Mater. Perform*., Feb 2003, p 70–74
- M. Morcillo, Atmospheric Corrosion in Ibero-America: The Micat Project, *Atmospheric Corrosion*, STP 1239, ASTM, 1995, p 257–275
- M. Morcillo, E. Almeida, B. Chico, and D. de la Fuente, Analysis of ISO Standard 9223 (Classification of Corrosivity of Atmospheres) in the Light of Information Obtained in the Ibero-American Micat Project, *Outdoor Atmospheric Corrosion*, STP 1421, H.E. Townsend, Ed., ASTM International, 2002, p 59–72
- I. Odnevall Wallinder, T. Korpinen, R. Sundberg, and C. Leygraf, Atmospheric Corrosion of Naturally and Pre-Patinated Copper Roofs in Singapore and Stockholm—Runoff Rates and Corrosion Product Formation, *Outdoor Atmospheric Corrosion*, STP 1421, H.E. Townsend, Ed., ASTM International, 2002, p 230–244
- I. Odnevall Wallinder and C. Leygraf, A Study of Copper Runoff in an Urban Atmosphere, *Corros. Sci.*, Vol 39 (No. 12), 1997, p 2039–2052
- I. Odnevall Wallinder and C. Leygraf, Environmental Effects of Metals Induced by Atmospheric Corrosion, *Outdoor Atmospheric Corrosion*, STP 1421, H.E. Townsend, Ed., ASTM International, 2002, p 185–199
- I. Odnevall Wallinder, P. Verbiest, W. He, and C. Leygraf, Effects of Exposure Direction and Inclination on the Runoff Rates of Zinc and Copper Roofs, *Corros. Sci.*, Vol 42, 2000, p 1471–1487
- J. Tidblad et al., Acid Deposition Effects on Materials: Evaluation of Electric Contact Materials After 4 Years of Exposure, *Atmospheric Corrosion*, STP 1239, ASTM, 1995, p 11–25
- J. Tidblad, V. Kucera, A.A. Mikhailov, J. Henriksen, K. Kreislova, T. Yates, and B. Singer, Field Exposure Results on Trends in Atmospheric Corrosion and Pollution, *Outdoor Atmospheric Corrosion*, STP 1421, H.E. Townsend, Ed., ASTM International, 2002, p 34–47
- J. Tidblad, V. Kucera, A.A. Mikhailov, and D. Knotkova, Improvement of the ISO Classification System Based on Dose-Response Functions Describing the Corrosivity of Outdoor Atmospheres, *Outdoor Atmospheric Corrosion*, STP 1421, H.E. Townsend, Ed., ASTM International, 2002, p 73–87
- L. Veleva and M.A. Alpuche-Aviles, Time of Wetness (TOW) and Surface Temperature Characteristics of Corroded Metals in Humid Tropical Climate, *Outdoor Atmospheric Corrosion*, STP 1421, H.E. Townsend, Ed., ASTM International, 2002, p 48–58
- G. Wildsmith, Copper-Nickel Brake Lines, *Mater. Action*, Jan 1985, p 58–59

Organic chemicals

- H. Baba et al., Localized Corrosion of Copper in Wet Organic Acid Vapor, *Corros. Eng*., Vol 44, 1995, p 279–287
- A.Y. El-Etre, Natural Honey as Corrosion Inhibitor for Metals and Alloys, Part 1: Copper in Neutral Aqueous Solution, *Corros. Sci*., Vol 40 (No. 11), 1998, p 1845–1850
- U. Lechner-Knoblauch et al., Corrosion of Zinc, Copper and Iron in Contaminated Non-Aqueous Alcohols, *Electrochim. Acta*, Vol 32 (No. 6), 1987, p 901–907
- A. Lopez-Delgado et al., A Comparative Study on Copper Corrosion Originated by Formic and Acetic Acid Vapors, *J. Mater. Sci*., Vol 36, 2001, p 5203–5211
- J.M. Pandya, A Short Note on the Corrosion of Copper by Lemon Juice Containing Sweetener: Part II, *Bull. Electrochem*., Vol 16 (No. 3), March 2000, p 103–109
- V.B. Singh et al., Corrosion and Inhibition Studies of Copper in Aqueous Solutions of Formic Acid and Acetic Acid, *Corros. Sci*., Vol 37 (No. 9), 1995, p 1399–1410
- J.D. Talati et al., Corrosion of Copper by Malic Acid Containing Colourants and Sweetening Agents, *Indian J. Technol*., Vol 26, June 1988, p 278–284
- J.J. Vora et al., Corrosion Study of Tin-Lead Alloy and Brass by Tartaric and Citric Acids, *Trans. SAEST*, Vol 35 (No. 2), April–June 2000

Other

- M. Bakszt, Providing Solderability Retention by Means of Chemical Inhibitors, *Met. Finish*., Jan 1985, p 35–38
- A.J. Brock, *Corrosion of Copper and Its Alloys*, Metals Research Laboratories, Olin Corporation, New Haven, CT, p 115–150
- R.A. Corbett et al., "Ant-Nest Corrosion—Digging the Tunnels," Paper 00646, Corrosion 2000, NACE International, p 00646/1–00646/14
- V. Curicuta et al., Evaluation of the Tendency towards Formicary Type Corrosion of Copper Tubes in the Heat Exchangers for Air Conditioning, *Acta Tech. Napocensis*, Vol 45, 2002, p 696–701

- C.P. Dillon, Copper Alloys in Alkaline Environments, *Mater. Perform.*, Vol 35 (No. 2) Feb 1996, p 97
- P. Elliott et al., "Ant Nest Corrosion—Exploring the Labyrinth," Paper 342, Corrosion 99, NACE International, p 1–11
- A.S. Fabiszewski and J.J. Hoffman, "Failure of Brass Gas Cylinder Valves by Commercial Leak Detector Fluids," Paper 03512, Corrosion 2003, NACE International, p 1–13.
- T. Hamamoto et al., Formicary Corrosion of Copper Tubes by Organic Chlorinated Solvents, *Sumitomo Light Met. Tech. Rep.*, Vol 32 (No. 4), Oct 1991
- J.D. Hwang, B.J. Li, W.S. Hwang, and C.T. Hu, Comparison of Phosphor Bronze Metal Sheet Produced by Twin Roll Cast and Horizontal Continuous Casting, *J. Mater. Eng. Perform.*, Vol 7 (No. 4), Aug 1998, p 495–502
- F. King et al., "General Corrosion of Copper Nuclear Waste Containers," Paper 119, Corrosion 92, NACE International, p 1–28
- T. Matsuhima, Case Studies on the Causes and Cures of Corrosion in Building Equipment, *Corros. Eng.*, Vol 39, 1990, p 545–566
- K. Minimoto et al., Corrosion Behavior of Copper Tube, *J. Jpn. Copper Brass Res. Assoc.*, Vol 27, 1988, p 73
- C.H. Neff, "Corrosion and Metal Leaching," Illinois State Water Survey, p 1–19
- T. Notoya, Ant Nest Corrosion in Copper Tubing, *Corros. Eng.*, Vol 39, 1990, p 353–362
- T. Notoya et al., Ant Nest Corrosion in Copper Tubes and Its Classification, *J. Jpn. Copper Brass Res. Assoc.*, Vol 29, 1990, p 109–116
- T. Notoya et al., An Unusual Form of Corrosion in Copper Tubes, *Corros. Eng.*, Vol 37, 1988, p 97–99
- T. Notoya et al., Formicary Corrosion in Copper Tubes in Wet Atmospheric Conditions, *Sumitomo Light Met. Tech. Rep.*, Vol 30 (No. 3), p 123–128
- J.M. Steigerwald et al., Chemical Processes in the Chemical Mechanical Polishing of Copper, *Mater. Chem. Phys.*, Vol 41, 1995, p 217–228
- D. Wagner, W. Fischer, and G.J. Tuschewitzki, final report, ICA Project 453, 15 Feb 1991 to 14 March 1992, p 1–85
- K. Worgan et al., Performance Analysis of Copper Canister Corrosion Under Oxidizing of Reducing Conditions, *Mat. Res. Soc. Symp. Proc.*, Vol 353, 1995, p 695–702
- F. Zucchi et al., Fatty Acids as Inhibitors of Copper Corrosion in Chloride Solutions, *Proceedings of the Ninth European Symposium on Corrosion Inhibitors*, Ann. Univ. Ferrara, N.S., Sez. V. Suppl. 11, 2000

ASM Handbook, Volume 13B: Corrosion: Materials
S.D. Cramer, B.S. Covino, Jr., editors, p164-176
DOI: 10.1361/asmhba0003817

Corrosion of Cobalt and Cobalt-Base Alloys

COBALT ALLOYS are selected for applications requiring high strength in corrosive aqueous environments or in high-temperature environments. This article first addresses the alloys most suited for aqueous environments and then those suited for high temperatures. There are some alloys that are used in both environments.

Alloys Resistant to Aqueous Corrosion

Paul Crook, Haynes International, Inc.
Jim Wu, Deloro Stellite, Inc.

Something unique about the cobalt alloys was discovered by Elwood Haynes as he experimented with additions of chromium to iron, nickel, and cobalt in the early 1900s: They were very strong. Adding tungsten to these cobalt-chromium alloys made them even stronger and led to the introduction of a family of wear-resistant materials (the Stellite alloys) capable of operating in corrosive environments over a wide temperature range. Later in the 20th century, when materials were being sought for aircraft engine applications, the intrinsic strength of the cobalt-chromium system led to the development of several cast and wrought high-temperature cobalt alloys, some of which are still in use today. The high cost of cobalt, however, has limited their use to critical applications.

The original Stellite (Co-Cr-W) alloys were casting materials. However, they soon became popular for hardfacing critical surfaces subjected to wear, using welding as the means of application. Carbon, which was an impurity in the original alloys, is now a controlled ingredient that gives rise to an abundance of carbide precipitates in the microstructure of these alloys, imparting high resistance to abrasion. The resistance of these alloys to other forms of wear, such as galling and cavitation erosion, is attributed to the unusual characteristics of cobalt. These include an ability to transform under mechanical stress from a face-centered cubic (fcc) to a hexagonal close-packed (hcp) structure, a high twinning propensity, and a low stacking-fault energy.

The resistance to corrosion of the Co-Cr-W alloys and newer cobalt alloys stems from the effects of chromium, which enhances passivity in aqueous media and encourages the formation of protective oxide films at high temperatures. The aqueous corrosion resistance of these alloys is enhanced by the tungsten (and, in some cases, molybdenum) additions. However, in the high-carbon cobalt alloys, significant amounts of chromium and tungsten partition to the carbide precipitates, thus reducing their effective levels with regard to corrosion resistance.

The cobalt alloys considered resistant to aqueous corrosion fall generally into five categories: high-carbon Co-Cr-W alloys, low-carbon Co-Cr-Mo alloys, high-carbon Co-Cr-Mo alloys, low-carbon Co-Mo-Cr-Si (Tribaloy) alloys, and age-hardenable Co-Ni-Cr-Mo (Multiphase) materials. The compositions of several commercially important alloys from these groups are given in Table 1. Note that there is more than one version of alloy 6 (UNS R30006, R30016, R30106, W73006), the most widely used high-carbon Co-Cr-W material. The basic alloy 6 composition is used for castings and hardfacing consumables, such as wires, bare rods, coated electrodes, and powders. Alloy 6B (UNS R30016) is a wrought version. A powder metallurgy (P/M) version (UNS R30106), optimized for sinterability, is also available.

To harden the Co-Ni-Cr-Mo alloys, they are first cold worked. This generates either hcp platelets or an intersecting network of deformation twin platelets; there are conflicting views on the precise hardening mechanism (Ref 1, 2). Subsequent exposure of the materials to elevated temperatures, for example, between 430 and 650 °C (805 and 1200 °F) for MP35N, causes precipitates to form at the platelet boundaries, enhancing strength still further (Ref 1).

High-Carbon Co-Cr-W Alloys

Carbon has a profound influence on the properties of the high-carbon Co-Cr-W (Stellite) alloys. By causing carbides to form in the microstructure during solidification, carbon enhances hardness and resistance to low-stress abrasion but degrades ductility and corrosion resistance. To provide industry with various options, several high-carbon Co-Cr-W alloys have been developed through the years, the main difference being their carbon contents. For low-impact conditions, where high hardness is required, alloys with carbon contents as high as 3.2 wt% are available. Such alloys have low ductilities, and special techniques (such as careful substrate preheating and postdeposition cooling) are required when applying them as weld overlays. For more corrosive environments, where the hardness requirements are not so stringent, compositions such as alloy 6 (with 1 wt% C) are available. These are more amenable to weld overlay processes, although precautions are still necessary to attain crack-free deposits. The hot ductility of alloys containing approximately 1.6 wt% C or less is sufficient to allow some wrought processing, thus the existence of the wrought alloys 6B and 6K. Cold working and cold forming, however, are not possible with these materials.

The microstructures of the high-carbon Co-Cr-W alloys are complex. In cast and weld overlay form, those alloys with relatively low carbon and tungsten contents, such as alloy 6, exhibit hypoeutectic structures comprised of networks of chromium-rich M_7C_3 particles within the cobalt-rich solid solution (matrix). Sand-cast alloy 6 contains approximately 13 wt% of such carbides. Castings and weld overlays of those alloys with higher carbon and tungsten contents exhibit hypereutectic structures containing very large chromium-rich M_7C_3 particles, along with networks of smaller chromium-rich M_7C_3 and tungsten-rich M_6C precipitates. The proportion of carbides in sand-cast alloy 3 (2.4 wt% C) is approximately 30 wt% (Ref 3).

Although these carbide precipitates within the microstructure provide enhanced strength and low stress abrasion resistance, the outstanding wear characteristics of the Co-Cr-W alloys are due primarily to the properties of the cobalt-rich matrix, which has a metastable fcc structure in the as-cast or as-deposited condition.

Table 1 Nominal compositions of cobalt alloys resistant to aqueous corrosion

Family	Common name	UNS No.	Primary product forms	Composition, wt%									
				Co	Ni	Mo	Cr	Fe	W	Mn	Si	C	Other
High-carbon Co-Cr-W	1	R30001 W73001(a)	Welding consumables	bal	1.5	0.5	30	3(b)	13	0.5	1.3	2.5	...
	3	...	Castings	bal	3(b)	...	31	3(b)	12.5	1(b)	1(b)	2.4	...
	6	R30006 W73006(a)	Castings Welding consumables	bal	3(b)	1.5(b)	29	3(b)	4.5	1(b)	1.5(b)	1.2	...
	6B	R30016	Wrought	bal	2.5	1.5(b)	30	3(b)	4	1.4	0.7	1	...
	6K	...	Wrought	bal	3(b)	1.5(b)	30	3(b)	4.5	2(b)	2(b)	1.6	...
	12	R30012 W73012(a)	Castings Welding consumables	bal	3(b)	1(b)	29.5	3(b)	8.25	1(b)	1.2	1.5	...
	306	...	Welding consumables	bal	5	...	25	5(b)	1.5	1	1	0.55	Nb 7.5
	F	R30002	Welding consumables	bal	22.5	1(b)	25.5	6(b)	12	1	1.2	1.75	...
Low-carbon Co-Cr-Mo	21	R30021 W73021(a)	Castings Welding consumables	bal	2.75	5.5	27	3(b)	...	1(b)	1(b)	0.25	B 0.007(b)
	F 75	R30075	Castings	bal	1(b)	6	28.5	0.75(b)	0.2(b)	1(b)	1(b)	0.35(b)	Al 0.3(b) B 0.01(b) N 0.25(b)
	Ultimet	R31233	Wrought Welding consumables Castings	bal	9	5	26	3	2	0.8	0.3	0.06	N 0.08
	Vitallium	...	Castings	bal	...	6	30	...	...	0.75(b)	...	0.5(b)	...
High-carbon Co-Cr-Mo	706	...	Castings Welding consumables	bal	3(b)	5	29	3(b)	...	1.5(b)	1.5(b)	1.2	...
	706K	...	Wrought	bal	1.5	4.5	31	1.5	...	1	1	1.6	...
Low-carbon Co-Mo-Cr-Si	T-400	R30400	Welding consumables Thermal spray powders	bal	2(b)	29	8.5	1.5(b)	...	...	2.6	0.08(b)	...
	T-400C	...	Welding consumables Thermal spray powders	bal	...	27	14	...	...	...	2.6	...	...
	T-800	...	Welding consumables Thermal spray powders	bal	3(b) (Ni + Fe)	29	18	3(b) (Ni + Fe)	...	...	3.4	0.08(b)	...
	T-900	...	Welding consumables Thermal spray powders	bal	16	23	18	...	...	...	2.7	0.08(b)	...
Age-hardenable Co-Ni-Cr-Mo	MP35N	R30035	Wrought	bal	35	9.75	20	1(b)	...	0.15(b)	0.15(b)	0.025(b)	Ti 1(b)
	MP159	R30159	Wrought	36	bal	7	19	9	...	0.2(b)	0.2(b)	0.04(b)	Al 0.2 B 0.03(b) Nb 0.5 Ti 2.9

(a) Welding filler metal has slightly different composition. (b) Maximum value

This structure can transform and twin under the action of mechanical stress. As a result, work hardening rates are high, stresses can be accommodated without the onset of cracking, and fatigue crack propagation is restricted. Of course, the presence of carbides has a strong influence, particularly on the nucleation and propagation of mechanically induced cracks, so the matrix properties become less influential as the alloy carbon content (hence carbide volume fraction) increases. The types of wear to which the Co-Cr-W alloys are resistant include galling, fretting, cavitation erosion, and liquid droplet impingement erosion. All of these have a microfatigue component.

As to the general corrosion characteristics of the high-carbon Co-Cr-W alloys, these are strongly dependent on carbon content, because chromium, in particular, partitions to the carbide precipitates. Alloy 6, with a carbon content of 1 wt%, can be considered equivalent to the 300-type stainless steels in many corrosive media. As is discussed in the section "Environmental Cracking" in this article, the cobalt alloys are similar to the austenitic stainless steels in terms of their susceptibility to stress-corrosion cracking.

Low-Carbon Co-Cr-Mo Alloys

The Elwood Haynes patent covering the Co-Cr-W system (Ref 4) indicates that tungsten can be partially or wholly replaced by molybdenum. It was not until many years later, however, that the first Co-Cr-Mo material (a casting alloy for dental applications) was introduced. Named Vitallium alloy, it was to have a profound effect on the development of cobalt alloys for biomedical implants and, by chance, aerospace applications.

The development of Vitallium alloy (circa 1930) was a result of a search by the Austenal Laboratories for an alternate to gold for dentures. In a joint development with the Haynes Stellite Company, a castable Co-Cr-Mo composition, with a carbon content lower than that of the original Stellite alloys, was selected (Ref 5, 6). Interest in both the alloy and the casting method (known as investment casting) spread to the biomedical industry in the mid-1930s and then to the aircraft engine industry for turbocharger blades at the start of World War II. Fine-tuning of the Vitallium composition led to the ASTM F 75 alloy (UNS R30075), a material that is still widely used by the biomedical industry. Fine-tuning of the composition for aircraft engine use led to a family of cobalt superalloys, some of which are described in the section "Alloys Resistant to High-Temperature Corrosion" in this article.

One of the alloys to emerge from fine-tuning of the Vitallium composition was Stellite 21 alloy (UNS R30021). Over the years, this has become well established, in weld overlay form, for steam valve applications. A half-century after the introduction of Vitallium alloy, there was a further significant development in the field of corrosion-resistant Co-Cr-Mo alloys, namely, the introduction of Ultimet alloy (UNS R31233). This was an attempt to provide industry with an easily formed and welded wrought alloy, with high resistance to both aqueous corrosion and wear.

To minimize the precipitation of carbides in the grain boundaries of Ultimet alloy (these being deleterious to both corrosion resistance and mechanical properties), a carbon content lower than that of the F 75 alloy was used. Also, nitrogen was added to enhance strength and pitting resistance. More importantly, a significant nickel addition was used to provide a balance between ease of processing, formability, and

wear performance. Nickel stabilizes the high-temperature fcc structure in cobalt alloys and reduces their tendency to transform to hcp during cold working. Chromium and molybdenum have the opposite effect. For ease of processing and good formability, stability of the fcc phase is desirable. For optimal wear performance, a strong transformation tendency (in other words, a high transformation temperature) is desirable.

High-Carbon Co-Cr-Mo Alloys

Recently, a new family of high-carbon materials, containing molybdenum in place of tungsten, was developed (Ref 7). Molybdenum-rich carbide particles, in the form of M_6C, form readily in these materials on cooling. Together with chromium-rich M_7C_3 particles, these alloys have a high amount of carbide particles, resulting in improvement in abrasion resistance over the Co-Cr-W alloys. Another effect of replacing tungsten with molybdenum is the improvement of corrosion resistance in reducing acids. Pitting resistance is also increased.

As with the Co-Cr-W alloys, hot working is possible only if the carbon content is approximately 1.6 wt% or less, and cold working is not possible due to cracking. Alloy 706K (with a carbon content of 1.6 wt%) is hot rolled for making industrial cutting knives for use in corrosive media.

Low-Carbon Co-Mo-Cr-Si Alloys

These alloys are widely known as Laves-phase alloys because they are hardened not by the formation of carbides, but rather by the precipitation of Laves phase. In cobalt alloys, Laves phase typically involves cobalt, molybdenum, chromium, and silicon. Molybdenum and silicon partition strongly to the Laves phase, whereas chromium and cobalt partition only modestly. The fact that Laves phase is stable at high temperatures makes these alloys highly resistant to high-temperature degradation. Due to their high molybdenum contents (23 to 29 wt%) and significant chromium contents, these alloys are resistant to a variety of corrosive media.

There are several of these alloys containing 20 to 60 vol% of Laves phase, with Rockwell C hardnesses ranging from 48 to 58. Although the mechanical strength of this family of alloys is high, the ductility is low. They are used as castings, P/M parts, thermal-sprayed coatings, and weld overlays. No hot working is possible on these alloys. Hot isostatic pressing has been used to consolidate powders into a solid piece.

The precipitation of Laves phase is cooling-rate dependent. Therefore, the microstructure and properties vary with the manufacturing process. A high cooling rate, such as found in laser cladding, may result in a supersaturated microstructure with a reduced amount of Laves phase. On the other hand, investment casting allows the complete precipitation of Laves phase. Powder metallurgy processing, using rapidly cooled powders, can result in improved toughness.

Welding with these alloys requires extreme care to prevent cracking. Preheating, temperature uniformity, and slowly cooling are all keys to the success of weld overlaying these alloys.

Age-Hardenable Co-Ni-Cr-Mo Alloys

There are two important age-hardenable Co-Ni-Cr-Mo alloys, MP35N (UNS R30035) and MP159 (UNS R30159) alloys. They differ in their maximum operating temperature. The MP35N alloy is useful up to 400 °C (750 °F), while the MP159 alloy maintains high strength to approximately 600 °C (1110 °F). This difference relates to the type of precipitation reaction employed. Following cold work, precipitates of Co_3Mo form at platelet boundaries in MP35N alloy during age hardening (Ref 1, 8). In the case of MP159 alloy, the precipitation of gamma prime, $Ni_3(Al, Ti)$, at platelet boundaries is encouraged during age hardening by the addition of 3 wt% Ti.

There are differences of opinion as to the precise nature of the platelets formed in the microstructure of the age-hardenable (multiphase) materials during cold work. It was originally believed that the platelets resulted from the allotropic fcc-to-hcp transformation common in cobalt alloys. More recent studies indicate, however, that the platelets are finely spaced deformation twins (Ref 2). This is consistent with the fact that nickel and iron, the combined levels of which are approximately 35 wt% in these materials, are strong stabilizers of the fcc form of cobalt and suppress the formation of the hcp form during cold deformation.

As to the general characteristics of the age-hardenable Co-Ni-Cr-Mo alloys, high strength and general corrosion resistance are the main attributes. In particular, MP35N alloy has been shown to possess good resistance to environmental cracking in oilfield environments.

Product Forms

High-carbon Co-Cr-W alloys are applied by welding to critical industrial surfaces and are available in several welding consumable forms:

- Bare rods, for gas tungsten arc and oxyacetylene welding
- Coated electrodes, for shielded metal arc welding
- Tubular wires, for gas metal arc and submerged arc welding
- Powders, for plasma-transferred arc welding

The bare rods and the cores of the coated electrodes are typically made by continuous casting. The powders are normally made by gas atomization; this process results in spherical powders that flow easily. The tubular wires are normally made by tightly wrapping powdered alloying ingredients in a Co-5Fe (wt%) strip, made by P/M.

The high-carbon Co-Cr-W alloys are widely used in the form of castings. Many of these are investment cast, using high-frequency rollover furnaces. Others are sand or resin-shell cast. Powder metallurgy parts are also available in several high-carbon Co-Cr-W compositions. To enhance their sinterability, many P/M versions include boron.

Alloy 6B (UNS R30016) is a wrought version of alloy 6, available in the form of bars, plates, and sheets. All of the wrought processing is performed at high temperatures, using electroslag remelted ingots. Wrought processing results in discrete carbide particles in the microstructure, rather than continuous carbide networks, and a much more homogeneous matrix. These lead to enhanced ductility and improved resistance to aqueous corrosion (when compared with the cast version).

Ultimet alloy (UNS R31233), as a representative of the low-carbon Co-Cr-Mo system, is available in a very wide range of product forms. Available wrought forms include plates, sheets, bars, and solid wires (cold drawn from hot-worked rod coils). No tubes have been made from Ultimet alloy, however, due to the fact that the material work hardens so quickly and would therefore require an impractical number of intermediate anneals during tube processing. Most wrought products of Ultimet alloy are used in the solution-annealed condition. However, at least one major application (which requires a high yield strength) uses cold-reduced bars. Other important product forms of Ultimet alloy include castings (investment and sand castings, in particular) and gas-atomized powders, for plasma-transferred arc weld overlays and laser cladding.

The age-hardenable Co-Ni-Cr-Mo (Multiphase) alloys are wrought materials. Round products (bars, rods, tubes, and solid wires) are the most widely used, but flat products (sheets, strips, and plates) are also available. With these alloys, the microstructural condition (solution annealed, cold worked, cold worked and aged) is very important, and specifications covering the product forms and the different microstructural conditions exist.

Aqueous Corrosion Properties

Paul Crook, Haynes International, Inc.

The performance of cobalt alloys in aqueous environments encountered in commercial applications follows.

Hydrochloric Acid

Hydrochloric acid is one of the most extensively used chemicals within the chemical process and pharmaceutical industries. It is also one of the most aggressive. The high-carbon Co-Cr-W alloys, like the stainless steels, are only useful in dilute hydrochloric acid and at moderate temperatures. Naturally, the higher the carbon content of these alloys, the poorer is their performance in hydrochloric acid (because those elements that provide corrosion resistance partition to the carbide precipitates). Also, wrought products are more resistant than corresponding cast materials, because they are more homogeneous.

The effects of acid concentration and temperature on the resistance of alloy 6B (UNS R30016) to hydrochloric acid are indicated by the corrosion rates in Table 2.

Generally, a material is considered unacceptable for service if its corrosion rate exceeds 0.5 mm/yr (20 mils/yr); for some applications, where component dimensions are critical, 0.1 mm/yr (4 mils/yr) is considered the upper limit. These data indicate that alloy 6B is useful up to at least 66 °C (150 °F), at an acid concentration of 2 wt%, but is unsuitable (even at room temperature) in higher concentrations of hydrochloric acid.

Table 2 Corrosion rates for alloy 6B (UNS R30016) in hydrochloric acid

Acid concentration, wt%	Temperature		Corrosion rate	
	°C	°F	mm/yr	mils/yr
2	Room		<0.01	<0.4
	66	150	<0.01	<0.4
5	Room		1.6	63
	66	150	>25	>985
10	Room		2.74	108
	66	150	>25	>985
20	Room		2.36	93
	66	150	>25	>985

Those low-carbon Co-Cr-Mo alloys designed specifically to resist both aqueous corrosion and wear are much more resistant to hydrochloric acid, as indicated by the isocorrosion diagram for Ultimet alloy in Fig. 1. This diagram was constructed using interpolative mathematical techniques and laboratory data generated at many different concentration/temperature combinations. It indicates the regimes over which low (under 0.1 mm/yr, or 4 mils/yr), moderate (0.1 to 0.5 mm/yr, or 4 to 20 mils/yr), and high (over 0.5 mm/yr, or 20 mils/yr) corrosion rates can be expected.

Sulfuric Acid

Sulfuric acid is one of the most important industrial chemicals. It is used in the manufacture of fertilizers, detergents, plastics, synthetic fibers, and pigments and as a catalyst in the petroleum industry.

The high-carbon Co-Cr-W alloys possess moderate resistance to sulfuric acid. Alloy 6B (UNS R30016), for example, can withstand most concentrations of the acid at room temperature and is useful up to 66 °C (150 °F) in dilute sulfuric (Table 3). As with other acids, there is an inverse relationship between the carbon content of these alloys and their corrosion resistance, due to the partitioning of key elements to carbide precipitates in the microstructure.

Table 3 Corrosion rates for alloy 6B (UNS R30016) in sulfuric acid

Acid concentration, wt%	Temperature		Corrosion rate	
	°C	°F	mm/yr	mils/yr
2	Boiling		0.79	31
5	Boiling		2.31	91
10	Room		<0.01	<0.4
	66	150	<0.01	<0.4
	Boiling		3.99	157
30	Room		<0.01	<0.4
	66	150	<0.01	<0.4
	Boiling		>25	>985
50	Room		0.01	<0.4
	66	150	>25	>985
	Boiling		>25	>985
77	Room		0.02	0.8
	66	150	4.5	177
	Boiling		>25	>985

Ultimet alloy (UNS R31233), as a representative of the low-carbon Co-Cr-Mo system, has been tested extensively in sulfuric acid. The resulting isocorrosion diagram is shown in Fig. 2. Corrosion rates in the under 0.1 mm/yr (4 mils/yr) regime are generally very low. Together with the small 0.1 to 0.5 mm/yr (4 to 20 mils/yr) regime, this indicates the presence of protective films, then their breakdown at critical temperatures. The performance of Ultimet alloy in sulfuric acid is approximately equivalent to those of the 6 wt% Mo stainless steels and 20Cb-3 alloy (UNS N08020). Its performance is below that of the Ni-Cr-Mo (C-type) alloys, however.

Phosphoric Acid

There are two industrially important forms of phosphoric acid. Reagent-grade (pure) phosphoric acid is used in the food industry and is made from elemental phosphorus that is oxidized then reacted with water. Wet process phosphoric acid, which is made by reacting phosphate rock with sulfuric acid, is very important as the primary source of phosphorus in agrichemical fertilizers. This wet process acid contains many impurities (including chlorides) that increase its corrosivity.

Pure phosphoric acid is not as aggressive as the halogen acids (such as hydrochloric). The most widely used cast high-carbon Co-Cr-W material, alloy 6 (UNS R30006), for example, is capable of withstanding even high concentrations at 66 °C (150 °F), as indicated in Table 4. The low-carbon Co-Cr-Mo alloys possess even

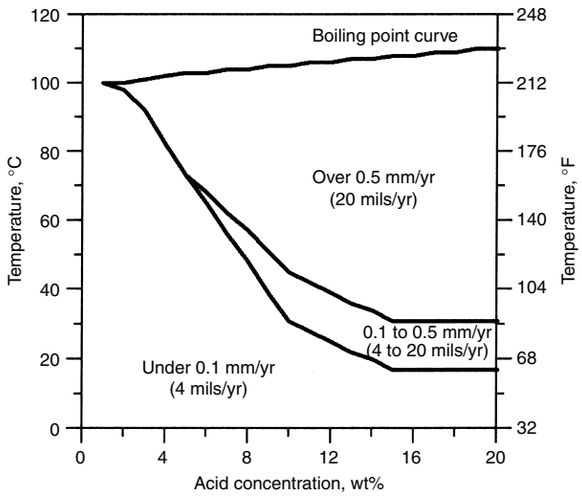

Fig. 1 Isocorrosion diagram for Ultimet alloy (UNS R31233) in hydrochloric acid

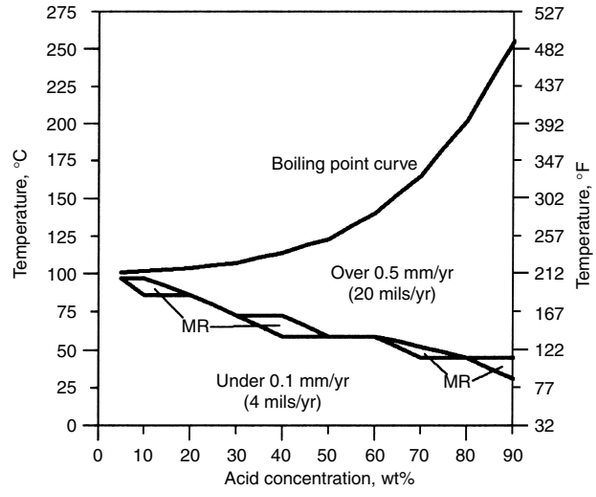

Fig. 2 Isocorrosion diagram for Ultimet alloy (UNS R31233) in sulfuric acid. MR, moderate regime (0.1 to 0.5 mm/yr, or 4 to 20 mils/yr)

higher resistance to pure phosphoric acid. Wrought Ultimet alloy (UNS R31233), for example, exhibits a corrosion rate of 0.01 mm/yr (0.4 mils/yr) or less in concentrations up to 85 wt% at 93 °C (200 °F) and in concentrations up to 30 wt% at boiling.

With regard to the performance of the cobalt alloys in wet process phosphoric acid, no data are available for the high carbon Co-Cr-W alloys. Ultimet alloy (low-carbon Co-Cr-Mo), however, has been tested in 30 and 40 wt% acid (these concentrations representing the P_2O_5 contents) at various temperatures. The resistance of Ultimet alloy was similar to that of the most widely used nickel composition for wet process acid service, G-30 alloy (UNS N06030). While not currently used in the agrichemical industry, these cobalt alloys could be a solution if a wear problem arises in this environment.

Hydrofluoric Acid

Data concerning the performance of the cobalt alloys in hydrofluoric acid are scarce. In fact, the only known study involved Ultimet alloy (UNS R31233) and yielded the results in Table 5. These data indicate strong concentration and temperature dependencies. Given that 0.5 mm/yr (20 mils/yr) is the generally accepted upper-use limit, it is evident that Ultimet alloy is only useful in hydrofluoric acid at low concentrations and temperatures.

The data in Table 5 were generated over a test period of 24 h and therefore should only be used as a guide. Also, condensing hydrofluoric acid can be more of a problem than the bulk liquid, due to a higher dissolved oxygen content; that can cause surface cracking in stressed nickel alloy components.

Nitric Acid

Nitric is a strong oxidizing acid for which chromium is a very beneficial alloying element. The performance of the cobalt alloys in nitric acid is therefore tied to the content of chromium in solid solution. In the case of the high-carbon alloys, the nominal chromium content can be misleading, because a significant quantity of chromium can partition to the carbides in the microstructure. Nitric acid data for the cast and wrought versions of the most widely used Co-Cr-W alloys are presented in Table 6. These results indicate that few problems exist at room temperature, but that high corrosion rates can be expected in boiling solutions at concentrations in excess of 40 wt%.

The low-carbon Co-Cr-Mo alloys possess high resistance to nitric acid, as illustrated in the iso-corrosion diagram for Ultimet alloy (UNS R31233) (Fig. 3). This indicates that the alloy can be used at all temperatures below the boiling point curve at concentrations up to at least 70 wt%, and that low corrosion rates of less than 0.1 mm/yr (4 mils/yr) can be expected at most concentration/temperature combinations.

Organic Acids

The organic acids do not ionize as readily as the inorganic (mineral) acids and are therefore less corrosive to metallic materials (Ref 9). As a result of their importance to the chemical process industries, acetic acid and formic acid are the most common organic test environments. Corrosion rates for alloy 6B (UNS R30006) in boiling solutions of these two acids are given in Table 7. From these data, it is evident that formic acid is much more corrosive than acetic acid. In fact, all of the corrosion rates exhibited by alloy 6B in boiling formic acid exceed 0.5 mm/yr (20 mils/yr), the generally accepted upper limit for use of a material.

Salts

The salts, especially the halides (chlorides, bromides, and fluorides), are very important in the chemical process industries. Although not very aggressive with regard to uniform corrosion, they can cause localized corrosion of a very destructive nature. Chlorides promote pitting, crevice attack (in gaps between components, or under deposits), and stress-corrosion cracking. The austenitic stainless steels are very prone to these forms of corrosion.

The resistance to pitting and crevice corrosion of alloy 6B (UNS R30016) from the high-carbon Co-Cr-W family and Ultimet alloy (UNS R31233) from the low-carbon Co-Cr-Mo group, in the presence of chlorides, is apparent from Table 8. The critical pitting temperature in Green Death is the lowest temperature at which pitting is observed in Green Death (a mixture of sulfuric and hydrochloric acids and ferric and cupric chlorides) in 24 h. The critical crevice

Table 4 Corrosion rates for alloys 6 (UNS R30006) and 6B (UNS R30016) in reagent-grade phosphoric acid

Acid concentration, wt%	Temperature		Corrosion rate			
			Alloy 6 sand cast		Alloy 6B wrought sheet	
	°C	°F	mm/yr	mils/yr	mm/yr	mils/yr
10	24	75	<0.01	<0.4	Not tested	
	66	150	<0.01	<0.4	Not tested	
	Boiling		<0.01	<0.4	<0.01	<0.4
30	Boiling		Not tested		0.05	2
50	Boiling		Not tested		0.48	19
70	Boiling		Not tested		0.58	23
85	24	75	<0.01	<0.4	Not tested	
	66	150	<0.01	<0.4	Not tested	
	Boiling		>25	>985	15.5	611

Table 5 Corrosion rates for Ultimet alloy (UNS R31233) in hydrofluoric acid

Temperature		Corrosion rate(a)							
		1%		3%		5%		10%	
°C	°F	mm/yr	mils/yr	mm/yr	mils/yr	mm/yr	mils/yr	mm/yr	mils/yr
20	68	Not tested		Not tested		Not tested		0.06	2.4
38	100	Not tested		0.01	0.4	0.06	2.4	Not tested	
52	125	Not tested		0.14	5.5	0.46	18	Not tested	
66	150	0.15	5.9	0.92	36	1.88	74	Not tested	
79	175	0.64	25	2.62	103	4.75	187	Not tested	

(a) Hydrofluoric acid concentration, wt%

Table 6 Corrosion rates for alloys 6 (UNS R30006) and 6B (UNS R30016) in nitric acid

Acid concentration, wt%	Temperature		Corrosion rate			
			Alloy 6 sand cast		Alloy 6B wrought sheet	
	°C	°F	mm/yr	mils/yr	mm/yr	mils/yr
10	24	75	<0.01	<0.4	Not tested	
	Boiling		Not tested		<0.01	<0.4
20	Boiling		0.04	1.6	Not tested	
30	Boiling		Not tested		0.15	5.9
40	24	75	<0.01	<0.4	Not tested	
50	Boiling		Not tested		>25	>985
70	24	75	<0.01	<0.4	Not tested	
	Boiling		Not tested		>25	>985

temperature is the lowest temperature at which crevice attack occurs in 72 h in 6 wt% ferric chloride. Ultimet alloy possesses very high resistance to these forms of corrosion. Indeed, its performance is similar to that of the Ni-Cr-Mo material C-22 alloy (UNS N06022). This result was not expected, given that Ultimet alloy contains only 5 wt% Mo and 2 wt% W, as compared with 13 and 3 wt%, respectively, in the case of C-22 alloy, and given that molybdenum and tungsten are known to be extremely beneficial to performance in chloride media. Alloy 6B exhibits reasonable resistance to pitting and crevice corrosion, relative to type 316L stainless steel (UNS S31603).

The chloride-induced stress-corrosion cracking resistance of the cobalt alloys is discussed in the section "Environmental Cracking" in this article.

Table 7 Corrosion rates for alloy 6B (UNS R30016) in boiling solutions of acetic and formic acids

Acid	Concentration, wt%	Corrosion rate mm/yr	Corrosion rate mils/yr
Acetic	10	<0.01	<0.4
	30	<0.01	<0.4
	50	<0.01	<0.4
	70	<0.01	<0.4
	99	<0.01	<0.4
Formic	10	0.51	20.1
	30	0.66	26
	50	1.19	46.9
	70	1.27	50
	88	0.58	23

Table 8 Critical pitting temperatures and critical crevice temperatures of selected alloys in Green Death and 6% ferric chloride

Common name	UNS No.	Critical pitting temperature in Green Death(a) °C	Critical pitting temperature in Green Death(a) °F	Critical crevice temperature in 6% ferric chloride °C	Critical crevice temperature in 6% ferric chloride °F
Alloy 6B	R30016	45	113	25	77
Ultimet alloy	R31233	120	248	65	149
Alloy 625	N06625	75	167	30	86
C-22 alloy	N06022	120	248	70	158
C-276 alloy	N10276	110	230	65	149
Type 316L stainless steel	S31603	25	77	<0	<32

(a) 11.5% H_2SO_4 + 1.2% HCl + 1% $FeCl_3$ + 1% $CuCl_2$

Seawater

The cobalt alloys possess good to excellent resistance to seawater. In fact, Stellite 306, a Co-Cr-W alloy modified by the addition of niobium (and with a carbon level of 0.55 wt%), has been used as a wear-resistant overlay material on the rudder bearings of ships. As to the effects of increasing carbon content within the Co-Cr-W system on performance in seawater, there are no relevant data.

With regard to the low-carbon Co-Cr-Mo alloys, Ultimet alloy (UNS R31233) has twice been included in seawater tests at the LaQue Corrosion Services laboratories at Wrightsville Beach, NC. The most recent study involved a wide range of materials (copper alloys, nickel alloys, titanium alloys, cobalt alloys, and stainless steels), the objective being to assess their crevice-corrosion performance, with a view to their use in seawater valves. The two cobalt alloys tested, Ultimet alloy and alloy 25 (a low-carbon Co-Cr-Ni-W alloy), were among the few metallic materials that exhibited no crevice attack in either quiescent or flowing seawater at 29 °C (84 °F).

The importance of a homogeneous microstructure, with regard to seawater resistance, was recently established electrochemically, using investment castings and hot isostatically pressed (HIPed) P/M products of alloy 6. This study used solutions of 3.5 wt% sodium chloride to simulate seawater and established that the more homogeneous HIPed material is considerably more resistant to localized attack, as measured by the breakdown potential. The results are summarized in Fig. 4.

Alkalis

The performance of the cobalt alloys in caustic environments is little understood. However, it is apparent from previous work (Ref 10) that several cobalt alloys are susceptible to stress-corrosion cracking in boiling 50% sodium hydroxide. A recent study of alloy 6B and Ultimet alloy in 50% sodium hydroxide at 93 and 107 °C (200 and 225 °F) indicates that the cobalt alloys are also prone to a phenomenon known as caustic dealloying, whereby certain alloying constituents are selectively leached from the surface of the material. Nickel alloys are also prone to this form of degradation in concentrated sodium hydroxide, at temperatures in excess of approximately 100 °C (212 °F).

Environmental Cracking

Paul Crook, Haynes International, Inc.

The high-carbon Co-Cr-W (Stellite) alloys are not amenable to cold working or cold forming. Therefore, it has not been possible to establish

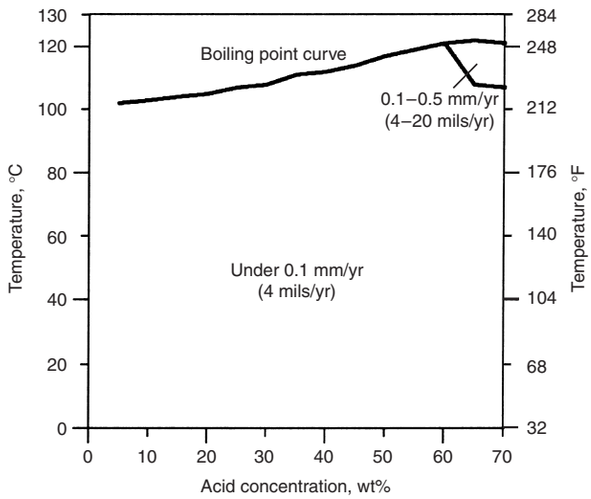

Fig. 3 Isocorrosion diagram for Ultimet alloy (UNS R31233) in nitric acid

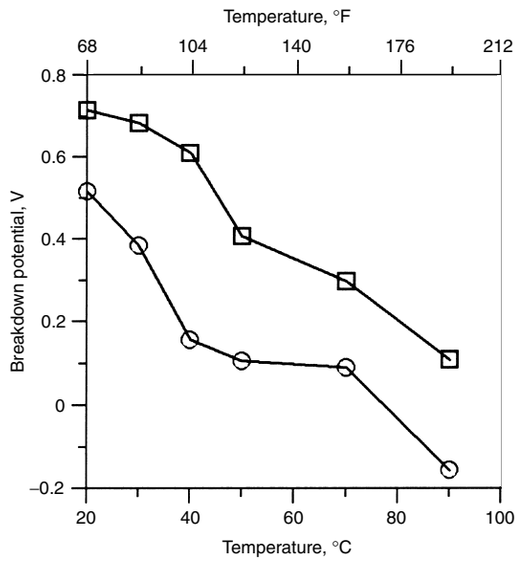

Fig. 4 Change in breakdown potential of alloy 6 (UNS R30006) in 3.5% NaCl as a function of temperature. Circles, cast alloy; squares, hot isostatically pressed alloy

their resistance to environmental cracking by conventional means, such as U-bend testing. However, data concerning chloride stress-corrosion cracking, sulfide stress cracking, and caustic stress cracking are available for the low-carbon Co-Cr-Mo and age-hardenable Co-Ni-Cr-Mo alloys.

Reference 10 indicates that the nickel content of the cobalt alloys is important to their environmental cracking resistance. This is not unexpected, given that nickel has the same positive effect on the austenitic stainless steels. The age-hardenable Co-Ni-Cr-Mo material MP-35N alloy (UNS R30035), with a 35 wt% Ni, resists stress-corrosion cracking in boiling magnesium chloride, whereas alloy 25 (a high-temperature cobalt alloy with 10 wt% Ni) is susceptible (Ref 10). These results are consistent with more recent data generated during the development of Ultimet alloy (which contains 9 wt% Ni). U-bend testing of this alloy, along with two austenitic stainless steels, in three different chloride environments gave the results in Table 9.

Although these results do not take into account the fact that Ultimet alloy is much stronger and work hardens much more rapidly than the stainless steels, they do indicate that Ultimet alloy is considerably more resistant to chloride stress-corrosion cracking than type 316L stainless steel.

The low-nickel cobalt alloy 21 (2.75 wt% Ni) has been tested in boiling magnesium chloride for stress-corrosion cracking (Ref 10). Cracking in 200 h or less was reported, using C-shaped samples stressed beyond the elastic limit.

Data concerning sulfide stress cracking of the cobalt alloys are sparse. However, for many years, the high-carbon Co-Cr-W alloys have been used as weld overlays for oilfield applications involving hydrogen sulfide and elemental sulfur at moderate temperatures. An appreciation of the sulfide stress cracking properties of the cobalt alloys, in the presence of hydrogen sulfide, can be gained from data developed for Ultimet alloy, as part of the approval process of NACE standard MR0175 (Ref 11).

At room temperature, tests were performed according to NACE standard TM0177 (Ref 12). This document defines sulfide stress cracking as a room-temperature phenomenon resulting from hydrogen embrittlement; cracking at elevated temperatures in environments containing hydrogen sulfide is defined as a form of stress-corrosion cracking. The TM0177 tests of Ultimet alloy involved 5% NaCl + 0.5% glacial acetic acid + water, saturated with H_2S, proof-ring apparatus, and samples coupled to carbon steel and stressed to the point of yield. Ultimet alloy did not crack in these tests, either in the annealed or cold-reduced (15%) conditions, indicating good resistance to hydrogen embrittlement.

At elevated temperatures, four-point bent-beam stress-corrosion tests of Ultimet alloy were performed, according to the recommendations of ASTM standard G 39 (Ref 13). This time, the test fixtures were also made from Ultimet alloy, to prevent galvanic effects. Again, the samples were stressed to the room-temperature yield point. The specimens sustained immersion in test environments of water + 20% NaCl + 0.517 MPa (75 psi) H_2S + 4.83 MPa (700 psi) CO_2, with and without 0.5 g/L sulfur. In the annealed condition, no cracking was observed after 720 h at either of the two test temperatures, 121 and 177 °C (250 and 350 °F). In the cold-reduced (15%) condition, Ultimet alloy was prone to cracking, even at 93 °C (200 °F). From this may be ascertained that the presence of the hcp structure (which occurs during cold working of the cobalt alloys) is detrimental to their stress-corrosion cracking resistance in the presence of hydrogen sulfide.

Interestingly, MP35N, which has a nickel content of 35 wt% and therefore a much reduced tendency to transform at a given level of cold work, has outstanding resistance to cracking in the presence of hydrogen sulfide. In the strengthened condition, it appears to be limited to a stress level of approximately 2000 MPa (290 ksi) at temperatures above 200 °C (392 °F) in deep sour wells (Ref 1).

Table 9 U-bend stress corrosion cracking test results

Common name	UNS No.	Solution(a)	Time to cracking, h
Ultimet	R31233	1	1008(b)
		2	1008(b)
		3	80
316L	S31603	1	168
		2	288
		3	72
20Cb-3	N08020	1	1008(b)
		2	1008(b)
		3	448

(a) Solution 1: water + 0.8% NaCl + 0.2% H_3PO_4, 141 °C (286 °F); Solution 2: water + 0.8% NaCl + 0.5% CH_3COOH, 141 °C (286 °F); Solution 3: water + 35% $MgCl_2$, 126 °C (259 °F). (b) Did not crack

Applications and Fabrication

Steve Matthews, Haynes International, Inc.
Jim Wu, Deloro Stellite, Inc.

Cobalt alloys are mainly chosen for applications where wear resistance is a primary consideration, especially in hostile environments. Examples include:

- Exhaust valves in many automotive engines were originally hardfaced with a cobalt alloy to lengthen their service lives. However, as a cost reduction measure, iron-base alloys have largely replaced cobalt alloys on the engine valves, except in certain high-performance engines where alloy F (UNS R30002), a cobalt alloy containing 22% Ni, is still used. In diesel engines, where the environment is more hostile and the temperature is higher than in gasoline engines, Tribaloy alloy T-400 (UNS R30400), a Laves-phase cobalt alloy, is still used on the valve trims. With the advent of turbochargers, which use exhaust gas to drive a turbine, alloy T-400 has become a preferred alloy for making the sliding parts, due to its high-temperature wear resistance. This alloy is also used in the form of thermal-sprayed coatings on certain components of gas turbines. The higher-chromium variant, T-400C, is another prime candidate for this type of application, especially when oxidation resistance is a consideration.
- In making glassware, cobalt alloys with good high-temperature and glass corrosion resistance are used to make plungers for forming molten glass into rough shapes. Any reaction between the plunger and the glass would result in defects, that could embrittle the glass.
- In the food and beverage canning industry, the lid-seaming rolls and chucks are made of high-carbon Co-Cr-W alloys to enable high-speed canning operations. The alloys are chosen for their wear resistance and corrosion from the beverage or contents, such as tomato juice.
- Cutting rayon fibers in the textile industry requires a knife material that resists wear from the cutting action and corrosion from the process fluid. The wrought alloys 6B (UNS R30016) and 706K are commonly used to make the knives.
- Molten metal attack on the pot hardware is a great concern in the galvanizing industry. Tribaloy T-800 alloy has been found to be the best choice for making the bearings on the rolls that carry steel sheets through the molten zinc bath.
- In refineries, cobalt alloys are widely used where high-temperature degradation and abrasion exist. In fluidized catalytic cracking units, riser nozzles experience high-speed flow of hydrocarbon feedstock at a high temperature. In the regeneration section, the air nozzles suffer erosion from catalyst particles in high-temperature steam, and here, cobalt alloys offer a longer service life than the stainless steels. In thermowells used to protect thermocouples from attack by process streams at high temperature, cobalt alloys are used either to make the casing or coat the casing by weld overlaying or thermal spraying.
- In oil drilling, the tricone drill bit bearings offer a unique challenge to materials selection. There is severe abrasion from the mud, and corrosion as well. High-carbon Co-Cr-W alloys are widely used to hardface the bearing surfaces. In deep-sea drilling, the combination of wear and corrosion by seawater calls for

high-carbon Co-Cr-W or Co-Cr-Mo alloys to make pump casings.

- Desalination can induce seawater corrosion of the processing equipment. Overlaying pump shafts with T-800 alloy can alleviate crevice and pitting attack in this application, as well as wear.
- In chemical processing, where both wear and corrosion are concerns, cobalt alloys are often chosen to battle the degradation. For example, in the case of a pump shaft suffering corrosion attack from phosphoric acid, as well as wear, a T-900 alloy weld overlay has been found to prolong the service life.
- In primary woodcutting, where both abrasion and corrosion are present, especially when cutting green wood, cobalt alloys are used to tip the saw teeth, to minimize downtime in sawmills. Saw tipping can be accomplished either by attaching a preformed tip made by P/M or by using a weld deposit, followed by grinding.
- Alloy F 75, from the low-carbon Co-Cr-Mo system, is commonly used to make prosthetic parts, due to its resistance to wear and corrosion by human body fluids. The alloy is also used to make partial dentures, which need to be able to stand the wear from chewing food and the corrosion from a mixture of food and saliva.

Hardfacing with the High-Carbon Co-Cr-W Alloys

The high-carbon Co-Cr-W alloys, which are resistant to both wear and aqueous corrosion, are typically used in the form of hardfacing deposits. Hardfacing is a term that describes the application of a material to the surface of a component by welding or thermal spraying, for the main purpose of reducing wear. Wear can be defined as the loss of material by abrasion, sliding wear, or erosion (solid particle, liquid droplet, slurry, or cavitation). These forms of wear are described in detail in Ref 14.

Table 10 lists advantages and disadvantages of commonly used hardfacing processes. Factors that influence the choice of a hardfacing process include the size and shape of the component, its composition, the area to be hardfaced, and dilution (intermixing of the substrate and overlay materials). Cobalt alloys are available in a variety of product forms for hardfacing (bare cast rod, coated electrodes, tubular wires, solid wires, and powder).

Most welding processes are readily adaptable to hardfacing, if proper techniques are implemented to prevent cracking of the deposit due to thermally induced stresses and to minimize base-metal dilution. The occurrence of thermally induced stresses can be minimized by the use of preheat, high interpass temperatures, and very slow cooling. The hardfacing of transformation-hardenable steels, such as type 410 stainless steel, can compound the stresses operating on the hardfacing deposit during cooling and can require special precautions to minimize cracking. Specifically, preheat and interpass temperatures should be maintained above the M_s temperature (the temperature at which austenite begins to transform to martensite) of the steel. Depending on the size and mass of the part, a postweld heat treatment immediately after hardfacing may also be required to minimize cracking. Three welding processes that have been extensively used for hardfacing with the high-carbon Co-Cr-W alloys are oxyacetylene, gas tungsten arc, and plasma-transferred arc.

The oxyacetylene process produces the lowest achievable base-metal dilution by welding (less than 5%); unfortunately, the process is relatively slow and time-consuming, depositing only approximately 1 kg/h (2.2 lb/h) of hardfacing deposit. Furthermore, the low-carbon Co-Cr-Mo alloys intrinsically do not have good oxyacetylene weldability. Alloy 6 (UNS W73006) can be deposited by oxyacetylene welding. However, special melting practices and compositional control are required during the manufacture of the cast rod in order to produce consumables that do not generate porosity during deposition.

Gas Tungsten Arc Welding (GTAW). Oxyacetylene methods have given way, in many cases, to GTAW processes, especially when hardfacing the austenitic stainless steels, which sensitize if exposed to a carburizing oxyacetylene flame. However, GTAW is a more intense heat source; therefore, more base-metal dilution (approximately 20%) can be expected. However, the overall dilution can usually be minimized by using two or more layers of hardfacing deposit. Hot cracking can be a potential problem in GTAW hardfacing. Hot cracking may be caused by high levels of deleterious elements, such as sulfur. Attempts to hardface a free-machining steel, such as type 303 (UNS S30300) or 303Se (UNS S30323), may result in hot cracking, because harmful elements to cobalt alloys can be introduced to the deposit through dilution.

The plasma-transferred arc process is characterized by the ideal combination of relatively low base-metal dilution (approximately 10%) and a relatively high deposition rate (up to 5 kg/h, or 11 lb/h). In the plasma-transferred arc process, powder is used as the consumable, rather than a cast welding rod. The process is mechanized rather than manual. A tungsten electrode, recessed into a torch body, generates a transferred arc to the workpiece. Plasma gas (usually argon) is ionized within the torch and exits through a constricted orifice. At this location, the hardfacing filler material is introduced in powder form through powder injection ports, assisted by an argon carrier gas. The powder particles melt completely and resolidify as a fusion-welded overlay. The weldability of cobalt alloy powders for plasma-transferred arc hardfacing is very good, and they will usually produce clean, smooth, sound deposits.

Hardfacing techniques that use welding as the method of deposition should always be selected to minimize dilution, for the obvious reason that excessive dilution compromises the metallurgical effectiveness of the hardfacing alloy. The deposition of cobalt alloys by thermal spray methods offers the advantage of no dilution, because most spray processes do not melt the substrate material. Cobalt hardfacing alloys in powder form can be deposited by the conventional flame spray process. The flame spray process is usually followed by a second fusing operation with an oxyacetylene torch. For this reason, cobalt alloys intended for spray and fuse deposition are modified with intentional additions of boron to lower the melting point and to allow for good fusing. Cobalt alloy powders that are not modified with boron can be deposited by high-energy thermal spray processes, such as plasma spray, detonation gun, or high-velocity oxyfuel. All three of these processes are designed

Table 10 Advantages and disadvantages of commonly used hardfacing processes and consumables

Process	Consumables(a)	Advantages	Disadvantages
Gas tungsten arc	CR	High-quality deposits	Relatively slow process
Shielded metal arc	CE, TW	Portability (field repair)	Slag removal and low deposit efficiency
Open arc	TW	High deposition rate	Spatter and rough deposits
Submerged arc	TW	High deposition rate and efficiency	High base-metal dilution
Gas metal arc	TW	Good quality and good deposition rate	Relatively high dilution
Oxyacetylene	CR, TW, P	Low dilution	Slow process
Plasma arc	CR, TW, P	Very smooth high-quality deposits	Some overspray (powder loss) with plasma-transferred arc process
Flame spray	P	Very smooth deposit (after fusing)	Maximum thickness of 3.2 mm (0.126 in.)
Plasma spray	P	No dilution, no distortion	Only thin coatings, not 100% dense
High-velocity oxy-fuel	P	High-quality dense coatings	Higher gas consumption than flame spray
Laser	P	High volume production capability	Very expensive equipment

(a) CR, cast rod; CE, coated electrode; TW, tubular wire; P, powder

to achieve an extremely high-velocity gas stream into which the powders are introduced. Powder particles pick up heat and kinetic energy from the high-velocity gas stream and are driven against the substrate surface; this produces an extremely dense coating. Coatings, however, never achieve full theoretical density, and some degree of porosity is intrinsic to this type of hardfacing. For maximum effectiveness in corrosion environments, thermal spray coatings are generally sealed with a suitable sealer, such as an epoxy.

Welding of Wrought Cobalt Alloys

The welding characteristics of wrought cobalt alloys are very similar to those of the wrought nickel alloys. Conventional fusion-welding processes can be used, although oxyacetylene welding is not recommended for joining cobalt alloys. Gas tungsten arc welding or gas metal arc welding will produce the most satisfactory results. The submerged arc welding process should be used with caution, because this process tends to use high heat-input parameters (high voltage and current) that can lead to weld metal solidification cracking. Regardless of the welding process selected, the development and qualification of a welding procedure specification is recommended. Cobalt alloys are generally welded using a filler-metal composition that matches the composition of the base material. Like low-carbon, corrosion-resistant nickel alloys, cobalt alloys have relatively good resistance to fusion-zone solidification cracking. The lower the carbon content, the greater the resistance to hot cracking. Sound welds are readily achieved when good welding practices are observed. These include thorough joint preparation and cleaning prior to welding. For cobalt alloys with carbon contents less than 0.15 wt%, preheat is not required, and weld interpass temperatures should be below 93 °C (200 °F) when possible.

Cobalt alloys are highly susceptible to copper contamination cracking. Molten copper will initiate liquid metal embrittlement in the heat-affected zone (Ref 15, 16). Care must be taken, therefore, to avoid copper contamination of the area to be welded, either from copper jigs and fixtures or from the use of copper wire cleaning brushes. Stainless steel wire brushes are recommended for interpass cleaning.

Cobalt alloys with relatively low nickel or iron contents (for example, Ultimet alloy, or UNS R31233) exhibit unique mechanical properties in the as-welded condition. Weldments are characterized by high strength and only moderate ductility, because of stress-induced structural transformations from fcc to hcp (Ref 17). Because the as-deposited weld metal possesses limited ductility, a 3T longitudinal bend test is recommended for weld procedure development. In this test, the weld is oriented longitudinally to the bend, and the bar is bent over a mandrel with a radius three times the specimen thickness. Furthermore, if cold forming of a weldment is necessary, a postsweld solution anneal at 1121 °C (2050 °F), followed by water quenching, is recommended prior to cold forming.

Alloys Resistant to High-Temperature Corrosion

Dwaine Klarstrom, Haynes International, Inc.

Cobalt alloys are industrially important for their resistance to certain types of high-temperature corrosion. For example, they have outstanding resistance to sulfidation and are generally superior to nickel alloys and stainless steels in this mode of attack.

The cobalt alloys are not as resistant to oxidation as the high-temperature nickel alloys. However, they are much more resistant to oxidation than stainless steels, and, with suitable alloying, they can be made quite resistant to oxidation attack. Likewise, the resistance of cobalt alloys to carburization and nitridation attack is not as good as that of the nickel alloys, but it is much better than that of the stainless steels.

Essentially all of the commercially important high-temperature cobalt alloys are solid-solution strengthened. In the past, there were many attempts to develop age-hardenable cobalt alloys. However, they were easily surpassed in terms of high-temperature strength by the age-hardenable nickel alloy compositions, and they never became commercially viable.

Some important cast and wrought high-temperature cobalt alloys are shown in Table 11. As is evident, most compositions contain nickel to provide a metastable or stable fcc structure. The good resistance of the alloys to oxidation and sulfidation is attributed to their chromium contents. Additions of aluminum are not used for this purpose, due to the formation of the brittle β-CoAl phase. High-temperature strength is imparted by significant additions of tungsten, along with carbon.

Cast alloys are used for nozzle guide vanes in gas turbine engines. The wrought alloys 25 (UNS R30605) and 188 (UNS R30188) are also used for gas turbine components such as combustors, afterburner parts, and brush seals. The use of alloy 6B (UNS R30016) for high-temperature corrosion applications is quite limited, due to its fabrication difficulties. However, it offers a unique combination of resistance to wear and high-temperature corrosion.

High-Temperature Corrosion Properties

Dwaine Klarstrom and Krishna Srivastava, Haynes International, Inc.

The effects of various modes of high-temperature corrosion are discussed.

Oxidation

To provide resistance to high-temperature oxidation, cobalt alloys rely on additions of chromium in the range of 20 to 30 wt% (Table 11). In the wrought compositions, small additions of manganese and silicon promote the formation of more protective spinel oxides. In the case of (UNS R30188), 188 alloy the addition of lanthanum has been used to increase the resistance of the protective scale to spallation.

Table 11 Nominal compositions of cobalt alloys resistant to high-temperature corrosion

		Composition, wt%									
Common name	UNS No.	Co	Ni	Mo	Cr	Fe	Mn	W	Si	C	Other
Cast alloys											
FX-414	...	bal	10.5	...	29.5	2	...	7	...	0.35	B 0.01
MAR-M 302	...	bal	...	...	21.5	...	...	10	...	0.85	B 0.005 Ta 9 Zr 0.2
MAR-M 509	...	bal	10	...	24	...	...	7	...	0.6	Ta 3.5 Zr 0.5 Ti 0.2
Wrought alloys											
6B	R30016	bal	2.5	1.5(a)	30	3(a)	1.4	4	0.7	1	...
25 (L-605)	R30605	bal	10	...	20	3(a)	1.5	15	0.4(a)	0.10	...
150	...	bal	...	...	28	20	0.65	...	0.75	0.08	...
188	R30188	bal	22	...	22	3(a)	1.25(a)	14	0.35	0.1	La 0.03

(a) Maximum value

Table 12 compares the oxidation behavior of two wrought cobalt alloys (25 and 188) with that of 230 alloy (UNS N06230), a well-known oxidation-resistant nickel alloy, in flowing air. In terms of average metal affected, there is little to choose between the alloys at 980 °C (1800 °F). However, at 1095 °C (2000 °F), 188 and 230 alloys exhibit significant advantages over 25 alloy, and above 1095 °C (2000 °F), the superiority of the nickel alloy is evident. The average metal affected represents half the difference in the thickness of the sample, due to metal loss, plus the average depth of internal attack.

A comparison of the same alloys under conditions of dynamic oxidation is shown in Table 13. These data indicate that 188 alloy is clearly superior to 25 alloy. This difference is principally due to its better resistance to oxide spallation, which, in turn, is due to the lanthanum addition. At 980 °C (1800 °F), 188 and 230 alloys have comparable resistance, but 230 alloy is significantly better at 1095 °C (2000 °F). Because there are many compositional similarities between 188 and 230 alloys, other than their base elements, these results imply that nickel is more advantageous than cobalt within the protective oxide scales, which are predominantly Cr_2O_3 but may include the spinels ($NiCr_2O_4$ and $CoCr_2O_4$) and/or the base-metal monoxides NiO and CoO.

Sulfidation

Cobalt sulfides will form in an environment comprising only H_2 and H_2S. Co-Co_4S_3 forms a low-temperature eutectic, that melts at 880 °C (1616 °F). Liquid sulfide products accelerate the corrosion rate greatly; therefore, cobalt alloys are unsuitable for use in such environments above approximately 850 °C (1560 °F). Sulfide scales are not protective. They contain many defects; therefore, diffusion rates of metal ions through sulfides are rapid. The kinetics of sulfidation, like those of oxidation, depend on metal ion diffusion and are parabolic in nature. However, the rate constants for sulfidation are several orders of magnitude higher than those for oxidation.

Fortunately, most industrial sulfur-bearing environments give rise to sulfidizing-oxidizing conditions, because they also contain gases such as H_2O, SO_2, CO, CO_2, and so on. Under such conditions, the chromium-bearing cobalt alloys develop protective oxide scales.

The magnitude of corrosion is determined by the environment, temperature, and the duration of exposure. A thermodynamic analysis is necessary to determine the partial pressures of sulfur and oxygen, which essentially define the environment at the temperature of concern. Knowing the partial pressures of sulfur and oxygen, it is possible to determine from phase stability diagrams whether a metal will form only sulfides, a mixture of sulfides and oxides, or just oxides. For complex alloys, such as those cobalt alloys in Table 11, such an analysis becomes extremely complicated, requiring the superimposition of several phase stability diagrams. References 18 and 19 provide an understanding of the underlying thermochemical principles.

Sulfidation data at 760, 871, and 982 °C (1400, 1600, and 1800 °F) for a variety of cobalt alloys, in a sulfidizing-oxidizing gas mixture comprised of 5% H_2, 5% CO, 1% CO_2, 0.15% H_2S, and balance argon, are reported in Tables 14 to 16 (Ref 20). Metal loss corresponds to half the difference in thickness of the sample, due to metal loss. The maximum metal affected corresponds to this plus the maximum depth of internal attack. The 556 alloy (UNS R30556) has an iron base but contains significant quantities of nickel (20 wt%), chromium (22 wt%), and cobalt (18 wt%). Ultimet alloy was described earlier in this article.

At 760 °C (1400 °F), none of the alloys tested showed excessive corrosion. At 871 °C (1600 °F), the partial pressure of oxygen increased a little, and the carbon activity went to 0. In the 215 h test, alloys 25, 6B, and Ultimet alloy exhibited excellent resistance to sulfidation. In the 500 h test, however, only alloy 6B showed excellent resistance. It is worth noting that alloy 6B contains 30 wt% Cr and only small amounts of nickel and iron. At 982 °C (1800 °F), only alloy 6B did not undergo catastrophic sulfidation.

Table 17 presents results from sulfidation tests in a SO_2-bearing oxidizing environment, comprising 10% SO_2, 5% O_2, 5% CO_2, and balance argon. The duration of all tests was 215 h. In these tests, the partial pressure of oxygen was substantially higher and that of sulfur much lower.

In this section, short-term (<500 h) sulfidation data have been reported for 556 and several cobalt alloys. These results should not be extrapolated to estimate the long-term performance of the alloys. However, the results are useful in discriminating the relative performance of the various alloys.

Carburization

Carburization refers to the ingress of carbon into a metal. This phenomenon occurs in many processing industries, in the presence of carbonaceous gases such as CO, CO_2, CH_4, and other hydrocarbons. Carbon is transferred to the metal surface, diffuses through the metal, and forms various carbides with the alloying elements. It is

Table 12 Oxidation data in flowing air

Common name	UNS No.	Average metal affected: 980 °C (1800 °F) µm	980 °C (1800 °F) mils	1095 °C (2000 °F) µm	1095 °C (2000 °F) mils	1150 °C (2100 °F) µm	1150 °C (2100 °F) mils	1205 °C (2200 °F) µm	1205 °C (2200 °F) mils
25	R30605	18	0.7	259	10.2	488	19.2	>963	>37.9
188	R30188	15	0.6	33	1.3	203	8.0	>551	>21.7
230	N06230	18	0.7	33	1.3	86	3.4	201	7.9

Test duration: 1008 h, with cycle to room temperature every 168 h

Table 13 Dynamic oxidation data

Common name	UNS No.	Average metal affected: 980 °C (1800 °F), 1000 h(a) µm	980 °C (1800 °F), 1000 h(a) mils	1095 °C (2000 °F), 500 h(a) µm	1095 °C (2000 °F), 500 h(a) mils
25	R30605	211	8.3	>635	>25
188	R30188	89	3.5	249	9.8
230	R06230	71	2.8	132	5.2

(a) Rapid cooled to room temperature every 30 min

Table 14 Sulfidation data for 556 and cobalt alloys at 760 °C (1400 °F)

$Ps_2 = 1.02\times10^{-7}$ atm; $Po_2 = 3.87\times10^{-22}$ atm; carbon activity = 0.16; test duration = 500 h

Common name	UNS No.	Metal loss µm	Metal loss mils	Maximum metal affected µm	Maximum metal affected Mils
150	...	157	6.2	239	9.4
556	R30556	91	3.6	168	6.6
188	R30188	122	4.8	165	6.5
6B	R30016	71	2.8	130	5.1

Source: Ref 20

Table 15 Sulfidation data for 556 and cobalt alloys at 871 °C (1600 °F)

$Ps_2 = 8.11\times10^{-7}$ atm; $Po_2 = 1.62\times10^{-19}$ atm; carbon activity = 0

Common name	UNS No.	Metal loss µm	Metal loss mils	Maximum metal affected µm	Maximum metal affected mils
Test duration, 215 h					
150	...	5	0.2	145	5.7
556	R30556	157	6.2	521	20.5
188	R30188	43	1.7	277	10.9
25	R30605	28	1.1	193	7.6
6B	R30016	8	0.3	79	3.1
Ultimet	R31233	0	0	76	3.0
Test duration, 500 h					
150	...	127	5.0	414	16.3
556	R30556	417	16.4	1013	39.9
188	R30188	Consumed		>546	>21.5
25	R30605	107	4.2	373	14.7
6B	R30016	5	0.2	91	3.6

Source: Ref 20

generally observed at temperatures greater than 800 °C (1470 °F) and a carbon activity less than 1. When the temperature is lower and the carbon activity is greater than 1, another mode of corrosion, namely metal dusting, occurs. See the section "Metal Dusting" in the article "Corrosion of Nickel and Nickel-Base Alloys" in this Volume.

Carburization is different from most other modes of high-temperature corrosion; the formation of internal carbides leads to metal degradation, embrittlement, and fracture. In this mode, metal loss due to scale formation does not occur; corrosion damage cannot be defined in terms of the sum of the metal loss and internal attack. Instead, the magnitude of carburization is defined by the mass carbon pickup (mg/cm^2) and the depth of carburization. The kinetics of carburization depend on the solubility and diffusivity of carbon at the operating temperature.

The solubility of carbon in cobalt alloys is higher than that in nickel alloys. High-temperature cobalt alloys contain many alloying elements, including chromium. Carburization thus always leads to the formation of various chromium carbides. As with the nickel alloys, cobalt alloys are protected from carburization by the formation of stable oxide scales.

Whether an alloy undergoes oxidation or carburization in a gas mixture at a given temperature is determined by the partial pressure of oxygen (the oxygen potential) and the carbon activity at that temperature. Reference 21 provides an understanding of the thermodynamic principles underlying carburization. At higher temperatures, typically greater than 1050 °C (1920 °F), oxide scales are stable in the following order: $Al_2O_3 > SiO_2 > Cr_2O_3$. For service below 1050 °C, chromia-forming alloys generally offer satisfactory life. However, for service above 1050 °C, alumina- or silica-forming alloys are preferred. Given that there are no alumina- or silica-forming cobalt alloys (they are all chromia forming), it follows that cobalt alloys are unsuitable for carburizing environments above 1050 °C.

Carburization data for several cobalt alloys are given in Table 18. All alloys were tested in a gaseous mixture comprised of 5% H_2, 5% CO, 5% CH_4, and balance argon (by volume). They were tested at 870 °C (1600 °F) and 930 °C (1700 °F) for 215 h and at 980 °C (1800 °F) for 55 h. The environment was characterized by a low oxygen potential and unit carbon activity. While the gaseous composition remained constant, the partial pressures of oxygen changed at different temperatures. The calculated equilibrium oxygen partial pressures at the test temperatures were as follows: at 870 °C, $Po_2 = 8.13 \times 10^{-23}$ atm; at 930 °C, $Po_2 = 2.47 \times 10^{-22}$ atm; and at 980 °C, $Po_2 = 6.78 \times 10^{-22}$ atm. From Table 18, it is evident that the magnitude of carbon pickup increased significantly at 980 °C (1800 °F), even though the duration of the test was much shorter.

Additional carburization data are shown in Table 19. In this instance, the test alloys were exposed to a gaseous mixture comprised of 5% H_2, 1% CH_4, and balance argon (by volume) at 980 °C for 55 h. The results are reported in terms of the mass carbon pickup and also the average and maximum depths of internal attack (penetration). The latter two were measured using an optical microscope. The oxygen potential for this environment was especially low, impurities being the only source of oxygen. The carbon activity for the environment, at the test temperature, equaled 1.

Comparison of Tables 18 and 19 indicates that, in the second environment (5% H_2 + 1% CH_4 + Ar), the magnitude of carbon pickup of the alloys was much higher, probably because the alloys did not have sufficient oxygen to form a protective scale.

Corrosion by Halogens

This primarily refers to corrosion by gaseous Cl_2/HCl and occurs in many industrial environments. Examples include coal combustion (less than 950 °C, or 1740 °F), mineral chlorination (300–900 °C, or 570–1650 °F), the production of ethylene dichloride (280–480 °C, or 540–900 °F), titanium dioxide production (900 °C, or 1650 °F), and waste incineration (approximately 900 °C, or 1650 °F) (Ref 23).

The amount of chlorine in the environment can range from approximately 0.01 vol% in coal combustion to approximately 2 vol% in hazardous waste incineration. Corrosion by Cl_2/HCl presents a very challenging problem; in contrast to oxides, metal chlorides are marked by low melting points and high vapor pressures. The melting point of $CoCl_2$ is 740 °C (1360 °F), and it reaches a partial pressure of 10^{-4} atm at 587 °C (1090 °F). Therefore, significant evaporation of metal chlorides will take place at service temperatures above 600 °C (1110 °F). The cobalt alloys are much less resistant to gaseous Cl_2/HCl environments than the nickel alloys, because the melting point of $CoCl_2$ is lower than that of $NiCl_2$. In the presence of oxygen, corrosion involves the formation of oxides as well as volatile chlorides. Corrosion data from Ref 24 and 25 for two cobalt-containing alloys, tested in Ar + 20 O_2 + 0.25 Cl_2 at various temperatures for 400 h, are given in Table 20. Corrosion data taken from Ref 26, for tests run in air + 2% Cl_2 at 900 °C for 50 h, are given in Table 21.

Elements such as tungsten and molybdenum are known to be detrimental to chloridation resistance. Cobalt alloys such as 25 and 188 both contain high tungsten contents (14 to 15 wt%). In oxidizing environments, this can lead to

Table 16 Sulfidation data for 556 and cobalt alloys at 982 °C (1800 °F)

$Ps_2 = 4.43 \times 10^{-6}$ atm; $Po_2 = 2.24 \times 10^{-17}$ atm; carbon activity = 0

Common name	UNS No.	Metal loss		Maximum metal affected	
		µm	mils	µm	mils
Test duration, 215 h					
556	R30556	25	1.0	381	15
188	R30188	20	0.8	123	4.8
6B	R30016	10	0.4	102	4.0
Test duration, 500 h					
556	R30556	Consumed		>1549	>61.0
188	R30188	Consumed		>533	>21.0
150	...	310	12.2	937	36.9
6B	R30016	94	3.7	157	6.2

Source: Ref 20

Table 17 Sulfidation data for 556 and cobalt alloys at 1093 °C (2000 °F)

$Po_2 = 4.92 \times 10^{-2}$ atm $Ps_2 = 3.73 \times 10^{-20}$ atm; carbon activity = 0; test duration = 215 h

Common name	UNS No.	Metal loss		Maximum metal affected	
		µm	mils	µm	mils
556	R30556	10	0.4	102	4
188	R30188	8	0.3	84	3.3
150	...	20	0.8	160	6.3
25	R30605	15	0.6	142	5.6
6B	R30016	15	0.6	130	5.1

Table 18 Carburization data for 556 and cobalt alloys

Common name	UNS No.	Mass carbon pickup, mg/cm^2		
		870 °C (1600 °F), 215 h	930 °C (1700 °F), 215 h	980 °C (1800 °F), 55 h
25	R30605	0.1	0.9	4.5
6B	R30016	0.2	0.8	1.5
556	R30556	0.4	1.0	1.3
188	R30188	0.5	1.1	2.7

Source: Ref 22

Table 19 Carburization data for 556 and cobalt alloys at low oxygen potential

Test duration = 55 h

Common name	UNS No.	Mass carbon pickup, mg/cm^2	Average internal penetration		Maximum internal penetration	
			µm	mils	µm	mils
188	R30188	6.2	732	28.8	787	31.0
556	R30556	7.9	831	32.7	884	34.8
Ultimet	R31233	5.4	655	25.8	686	27.0

the formation of highly volatile oxychlorides. Also, the high iron content of 556 alloy will lead to the formation of the low-melting-point chlorides $FeCl_2$ (676 °C, or 1249 °F) and $FeCl_3$ (303 °C, or 577 °F), which will contribute to the corrosion.

Corrosion by Molten Salts

An introduction to corrosion by molten salts is provided in the article "Corrosion of Nickel and Nickel-Base Alloys" in this Volume. For reasons of cost, cobalt alloys have not been popular in the heat treating industry. However, available experimental data indicate that cobalt alloys can be used in many applications. For example, one cobalt-base material (188 alloy) and one with a significant cobalt content (556 alloy) were subjected to field tests in $NaCl + KCl + BaCl_2$ at 840 °C (1540 °F) for one month. The total depths of attack, equal to the metal loss plus internal attack, were 0.69 mm/month (0.027 in./month) for 188 alloy, and 1.12 mm/month (0.044 in./month) for 556 alloy. The mechanism of attack was predominantly intergranular corrosion by the salt components, especially chlorine (Ref 27).

The results of laboratory testing in a sodium chloride salt bath at 840 °C for 100 h are given in Table 22. A fresh salt bath was used for each run, and air was used as the cover gas. Again, the corrosion attack was mainly intergranular, without discernible metal loss.

Two materials, 188 alloy and the Ni-Co-Cr HR-160 alloy (UNS N12160), have been tested in the atmosphere above a mixture of molten salts at 870 °C (1600 °F), that is, in the salt vapor. The mixture was comprised of 54% barium chloride, 27% potassium chloride, and 19% sodium chloride. The samples were held 150 mm (5.9 in.) above the salt bath, and the test duration was 173 h (8 h of exposure, with 22 cycles to room temperature). The calculated metal losses were 1.30 mm (51.2 mils) for 188 alloy and 0.25 mm (9.9 mils) for HR-160 alloy. In contrast, the metal loss for type 310 stainless steel (UNS S31000) was 1.80 mm (71 mils). Also, it was found that the average and maximum internal attacks for HR-160 alloy were 0.17 and 0.38 mm (6.7 and 15 mils), respectively.

Applications and Fabrication for High-Temperature Service

Lee Flower and Steve Matthews, Haynes International, Inc.

Wrought and cast cobalt alloys find wide use in aircraft gas turbines and airframe hot sections due to their high-temperature strength coupled with excellent resistance to high-temperature combustion environments. Cobalt alloys typically are used in static gas turbine engine components, such as fuel nozzles, brush seals, vanes, and combustor components. Near the engine exhaust in airframe applications, cobalt alloys are used in afterburner components, such as flameholders, and in nozzle assemblies. Cobalt alloys also are used in high-temperature rocket engine and automotive applications.

Forming and Annealing

Cold working is the preferred method of bending, drawing, and spinning wrought high-temperature cobalt alloys. In the annealed condition, they have excellent ductility, but the cobalt-rich matrix will tend to work harden more readily than the nickel alloys. Because of work hardening, more intermediate anneals may be required to produce the final shape. Intermediate annealing near the final annealing temperature, usually between 1180 and 1200 °C (2150 and 2200 °F), depending on the alloy, will restore the original ductility and allow further cold work. The strain introduced during cold deformation should exceed 10% cold work. Lower percentages of cold work can reduce the grain nucleation rate during recrystallization, leading to abnormally large grain growth. Final annealing should also be accompanied by water quenching, for heavy sections, or rapid air cooling, if the material thickness is less than 9.5 mm (0.375 in.). Vacuum annealing should employ an argon or helium gas quench.

Following heat treatment in an oxidizing atmosphere, the oxide films that form are more adherent than those associated with stainless steel. A molten caustic dip followed by acid pickling has been found to be most effective in final cleaning. Descaling should be performed at 480 °C (900 °F) in a commercial molten hydroxide salt bath. Subsequent acid pickling should be performed at 65 °C (150 °F) in a bath containing 20% nitric acid and 5% hydrofluoric acid, followed by water rinsing.

Welding Characteristics

The welding characteristics of the wrought cobalt alloys resistant to high-temperature corrosion are similar to those of the wrought alloys resistant to aqueous corrosion.

Following welding, the use of a postweld heat treatment is neither required nor prohibited. The use of a stress-relief temperature between 540 and 1120 °C (1000 and 2050 °F) is not recommended. These intermediate temperatures are not as effective in relieving residual stresses as a full solution anneal and will result in grain-boundary carbide precipitation, with consequent negative effects on mechanical properties and corrosion resistance.

ACKNOWLEDGMENTS

Stellite and Tribaloy are registered trademarks of Deloro Stellite, Inc. Multiphase, MP35N, and MP159 are registered trademarks of SPS Technologies, Inc. Ultimet, Hastelloy, C-22, and

Table 20 Corrosion in halogen-bearing environments

Test duration = 400 h

Temperature		Metal loss				Total depth			
		556 R30556		188 R30188		556 R30556		188 R30188	
°C	°F	µm	mils	µm	mils	µm	mils	µm	mils
800	1470	20.3	0.8	58.4	2.3	50.8	2.0	73.7	2.9
850	1560	20.3	0.8	25.4	1.0	78.7	3.1	264.2	10.4
900	1650	45.7	1.8	215.9	8.5	152.4	6.0	>355.6	>14.0
1000	1830	152.4	6.0	254.0	10.0	299.7	11.8	416.6	16.4

Total depth = Metal loss + average internal attack. Source: Ref 24, 25

Table 21 Corrosion in air + 2% chlorine at 900 °C (1650 °F)

Test duration = 50 h

Common name	UNS No.	Metal loss		Total depth	
		µm	mils	µm	mils
556	R30566	50.8	2.0	109.2	4.3
25	R30605	114.3	4.5	152.4	6.0

Source: Ref 26

Table 22 Corrosion of 556 and cobalt alloys in salt bath at 840 °C (1540 °F)

Test duration = 100 h

Common name	UNS No.	Total depth	
		mm	mils
188	R30188	0.051	2.0
25	R30605	0.064	2.5
556	R30556	0.066	2.6
150	...	0.076	3.0

G-30, 230, 556, and HR-160 are registered trademarks of Haynes International, Inc. 20Cb-3 is a registered trademark of Carpenter Technology Corp. Vitallium is a registered trademark of Stryker Howmedica Osteonics.

REFERENCES

1. J.P. Stroup, A.H. Bauman, and A. Simkovich, *Mater. Perform.,* June 1976, p 43–47
2. S. Lu, B. Shang, Z. Luo, R. Wang, and F. Zeng, *Metall. Mater. Trans. A,* Vol 31, Jan 2000, p 5–13
3. W.L. Silence, *Proceedings of Wear 1977* (St. Louis, MO), American Society of Mechanical Engineers, 1977, p 77–85
4. E. Haynes, U.S. Patent 1,057,423, April 1913
5. R.C. Feagin, *Incast,* Vol 5 (No. 2), 1992, p 8–13
6. R.D. Gray, *A History of the Haynes Stellite Company 1912–1972,* Cabot Corp., 1974
7. J.B.C. Wu and J.E. Redman, *Weld. J.,* Vol 73 (No. 9), 1994, p 63–68
8. J.M. Drapier, P. Viatour, D. Coutsouradis, and L. Habraken, *Cobalt,* Vol 49, Dec 1970, p 171–186
9. A.J. Sedricks, *Corrosion of Stainless Steels,* Wiley-Interscience, 1996, p 378–381
10. H.H. Uhlig and A.I. Asphahani, *Mater. Perform.,* Vol 18 (No. 11), 1979, p 9–20
11. "Petroleum and Natural Gas Industries—Materials for Use in H_2S-Containing Environments in Oil and Gas Production," NACE MR0175/ISO 15156-1, NACE International/ISO, 2001
12. "Laboratory Testing of Metals for Resistance to Sulfide Stress Cracking and Stress Corrosion Cracking in H_2S Environments," ANSI/NACE Standard TM0177, NACE International, 1996
13. "Preparation and Use of Bent-Beam Stress-Corrosion Test Specimens," G 39, ASTM International
14. P. Crook, *Mater. Perform.,* Vol 30 (No. 2), 1991, p 64–66
15. S.J. Matthews, M.O. Maddock, and W.F. Savage, *Weld. J.,* Vol 51 (No. 5), 1972, p 326–328
16. W.F. Savage, E.P. Nippes and M.C. Mushala, *Weld. J.,* Vol 57 (No. 5), 1978, p 145–152
17. S.J. Matthews, P. Crook, L.H. Flasche, and J.W. Tackett, *Weld. J.,* Vol 70 (No. 12), 1991, p 331–337
18. N. Birks and G.H. Meier, *Introduction to High Temperature Oxidation of Metals,* Edwin Arnold, 1983, p 10–30
19. P. Kofstad, *High Temperature Corrosion,* Elsevier Applied Science, 1988, p 428–464
20. S.K. Srivastava and J.E. Barnes, Internal Report 14675, Haynes International, 2003
21. H.J. Grabke, "Carburization—A High Temperature Corrosion Phenomenon," MTI Publication 52, MTI, 1998
22. G.Y. Lai, Internal Report 11620, Haynes International
23. P. Elliott, A.A. Ansari, and R. Nabovi, *High Temperature Corrosion in Energy Systems,* M.F. Rothman, Ed., TMS, 1985, p 437
24. M.J. McNallan, M.H. Rhee, S. Thongtem, and T. Hensler, Paper 11, Corrosion 85, NACE International, 1985
25. S. Thongtem, M.J. McNallan, and G.Y. Lai, Paper 372, Corrosion 86, NACE International, 1986
26. P. Elliott, A.A. Ansari, R. Prescott, and M.F. Rothman, Paper 13, Corrosion 85, NACE International, 1985
27. G.Y. Lai, M.F. Rothman, and D.E. Fluck, Paper 14, Corrosion 85, NACE International, 1985

ASM Handbook, Volume 13B: Corrosion: Materials
S.D. Cramer, B.S. Covino, Jr., editors, p177-194
DOI: 10.1361/asmhba0003818

Corrosion of Tin and Tin Alloys

TIN, a soft, brilliant white, low-melting metal, is widely known and characterized in the form of coating for steel, that is, tinplate, and as a component of solder. In the molten state, it reacts with and readily wets most of the common metals and their alloys. Because of its low strength, the pure metal is not regarded as a structural material and is rarely used in monolithic form. Rather, the metal is most frequently used as coating for other metals and in alloys to impart corrosion resistance, enhance appearance, or improve solderability. It also finds wide use in alloys, the most important of which are tin-base soft solders and bearing alloys and copper-base bronzes.

Pure Tin

Pure tin is subject to two phenomena that are sometimes confused with the corrosion process in the ordinary atmosphere. These are its low-temperature allotropic modification and its susceptibility to whisker growth. To avoid this confusion, these processes are discussed as follows.

Allotropic Modification. At temperatures from 13.2 °C (55.8 °F) to its melting point of 232 °C (450 °F), tin exists in a body-centered tetragonal structure commonly known as β-tin. Below 13.2 °C (55.8 °F), the β form can change to a diamond cubic structure known as α-tin, which lacks cohesion and appears as a friable gray powder. This is sometimes called the tin pest. This transformation does not occur spontaneously unless the tin is of extremely high purity and is exposed to subzero temperatures. The transformation can be accelerated by inoculating the β with α crystals or by deforming the β-tin at low temperatures (Fig. 1). Some details of the mechanisms and kinetics of this process are discussed in Ref 1.

The transformation is inhibited by the presence of small amounts of bismuth, antimony, or lead. Hot-dipped tin coatings and most electrodeposited coatings seem to be immune to this phenomenon, probably because of impurity effects. Thus, no traces of transformation were evident on hot-dipped tinplate cans after burial for 46 years in arctic snow or on electroplated tin coatings on refrigerator parts (Ref 2). However, transformation has occurred with thicker deposits; when such low-temperature exposure is anticipated, the incorporation of approximately 0.1% Bi is recommended to avoid the problem (Ref 3).

Tin Whiskers. Tin is subject to a form of recrystallization at room temperature that manifests itself as a growth of thin (1 to 2 μm, or 0.04 to 0.08 mil, diam), single-crystal filaments from the surface of tin coatings. These can begin to form in as little as 5 weeks and may grow at a rate up to 1 mm/mo (0.04 in./mo). Although the mechanism is not clearly understood, formation of tin whiskers appears to be favored by residual or applied stress, by the presence of a brass substrate, and by high-purity electrodeposited tin (Ref 4–6). The potential for whisker growth can be minimized, if not completely eliminated, by reflowing the tin coating or by incorporating 2 to 10% Pb into the electrodeposited tin.

Atmospheric Corrosion. In clean dry air, tin retains a bright appearance for many days. In one study, a light dulling was observed after 100 days, and a noticeable, faint yellow-gray tarnish film was seen after 150 days (Ref 7). However, it was also reported that the reflectivity of tin remains practically unchanged over long periods when the tin is washed with soap and water (Ref 8). Thus, at ordinary temperatures, the surface oxide film on tin is very thin and exhibits a very slow rate of growth. The rate of oxidation increases with temperature. Above 190 °C (375 °F), a film thickness sufficient to produce interference colors is reportedly produced in a few hours; at 210 °C (410 °F), this film thickness is produced in 20 min (Ref 2).

The results of a comprehensive 20 year study of the atmospheric corrosion resistance of bulk tin were reported by an ASTM International committee (Ref 9–13). Sheets of commercial 99.85% purity tin, measuring 230 by 300 mm (9 by 12 in.) were exposed at seven sites in the United States, including industrial, seacoast, and rural atmospheres. Results are listed in Table 1.

Ancient tin coins from Malaysia were found to be covered with successive layers of brown and gray scale that were principally stannic oxide (SnO_2) that contained sulfate plus traces of silica and iron (Ref 14). Examination of seventeenth and eighteenth century sarcophagi in Vienna revealed some evidence of deterioration that was suspected to be the tin pest. It was found, however, that the casting was porous and that air and moisture produced corrosion products of stannous oxide (SnO) and SnO_2, causing the observed swelling, blistering, and cracking.

Oxidation. At extremely low temperatures, the oxidation of tin is very superficial. In one investigation, resistivity measurements were used on tin condensation films formed at 1.5 to 300 K; in all cases, a step function indicating that the growth of tin oxide first began at 23 K was found (Ref 15). No further growth of the oxide was detected at 50 to 150 K.

The most comprehensive studies of interactions between tin and oxygen were those discussed in Ref 16 to 19, in which 99.994% pure foils and a vacuum microbalance were used to

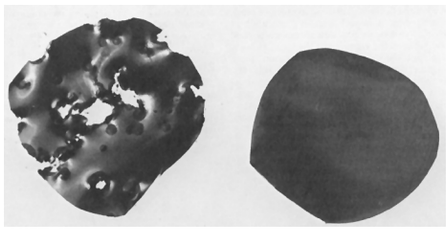

Fig. 1 Gray tin transformation on pure tin. Both samples were stored at −20 °C (−4 °F), but the sample on the left was bent at this temperature, and the other was left undisturbed.

Table 1 Corrosion of tin exposed in different environments for 10 and 20 years

	Average corrosion rate(a)			
	10 years		20 years	
Sample location	mm/yr	mil/yr	mm/yr	mil/yr
Heavy industrial	...	...	0.0017	0.067
Marine heavy industrial	...	...	0.0013	0.051
Marine (New Jersey)	0.0019	0.075	...	...
Marine (Florida)	0.0023	0.09	...	...
Marine (California)	...	...	0.0029	0.11
Semiarid	...	...	0.00044	0.017
Rural	0.00049	0.019	...	...

(a) Converted from weight loss data, assuming a tin density of 7.29 g/cm^3. Source: Ref 13

measure oxidation rates at oxygen pressures between 10^{-3} and 500 torr (0.13 and 6.7×10^{4} Pa) and temperatures from 150 to 220 °C (300 to 430 °F). The essential features of oxidation behavior were found to be explainable in terms of the microstructure of the oxide. With oxygen pressure under 1 torr (133 Pa), dendritic α-SnO crystallites grew at an increasing rate, with the rate-determining factor apparently being the dissociation of oxygen. Above 1 torr (133 Pa), the oxidation rate curves had a characteristic sigmoid shape, in which the initial stages corresponded to the lateral spread of oxide from numerous nuclei to form α-SnO platelets. Subsequent growth followed a logarithmic law and was consistent with control by tin diffusion through an oxide film under a parabolic or cubic law, while the formation of cavities in the oxide film progressively reduced the area through which diffusion could take place. For long oxidation times, the thick oxide film was subject to random fracture, leading to erratic results.

The oxidation of tin containing 0.17% Pb and 0.024% Sb was examined at 168 to 211.5 °C (335 to 413 °F) and oxygen pressures of 4 to 9 torr (533 to 1200 Pa) (Ref 20). These oxidation rate data were not significantly different from those given in Ref 16 to 19.

The effects of impurities on the oxidation rate of tin were also studied by using microbalance techniques under conditions similar to those described in Ref 16 to 19 (Ref 21). The results are summarized in Table 2. These results were later rationalized in terms of the relative thermodynamic stability of the oxides formed, as follows. If the oxide of the alloying element is less thermodynamically stable than SnO, the oxidation rate of the alloy remains unchanged for additions whose ions have the same valence as the tin. However, when the formal ionic charge of the alloying element exceeds that of the tin—for example, antimony, bismuth, iron, and titanium—then the oxidation rate of the tin increases. Those alloying elements forming an oxide more stable than SnO—for example, zinc, indium, phosphorus, and germanium—undergo preferential oxidation at the surface, thus inhibiting the oxidation of tin (Ref 22).

The oxidation rate of molten tin was studied at 400 to 800 °C (750 to 1470 °F) with oxygen pressures of 50 to 500 torr (6.7 to 67 kPa) (Ref 23). The rate varied greatly from specimen to specimen at any one temperature but was apparently linear under all conditions. The variability was attributed to crystal orientation in the oxide film, which was in apparent agreement with the results of other investigations (Ref 24). One researcher commented that another possibility is the continuous conversion of SnO to a nonprotective SnO_2 (Ref 25). In one experiment conducted at 800 °C (1470 °F), the initially formed jet-black film of SnO became incandescent at one end of a boat, and the incandescence traveled rapidly to the other end of the boat, leaving an orange coating.

Table 2 Effect of alloy additions of 0.1 at.% on the oxidation rate of tin at 190 °C (375 °F) and an oxygen pressure of 10 torr (1330 Pa)

Alloying element	Increase in weight after 1000 min, μg/cm²
Manganese	2.7
Antimony	2.5
Thorium	2.1
Bismuth	1.7
Iron	1.6
Lead	1.3
Nothing added	1.0
Cadmium	1.0
Phosphorus (0.5 at.%)	0.3
Zinc	0.2
Indium	0.1

Source: Ref 21

Another study investigated the effects of alloying additions at levels of 0.01, 0.1, and 1% on the oxidation of molten tin (Ref 26). Antimony, lead, bismuth, and copper had negligible effects, while higher concentrations of lead increased the temperature at which significant oxidation occurs. Magnesium, lithium, and sodium significantly increased the oxidation rate, but zinc, phosphorus, indium, and aluminum decreased the rate. The oxidation of an alloy containing 0.01% Al was approximately the same as that of pure tin at 425 °C (795 °F).

Other laboratory oxidation studies were concerned with tin in contact with air. The formation of an oxide film was shown in Ref 27 and 28, and weight increment curves were developed in Ref 29. In another study, the oxidation rate was determined to be linear after the first few days and was nonprotective (Ref 6). Lastly, the oxidation of tin and tinplate was investigated by using coulometric and x-ray techniques (Ref 30, 31). Up to 130 °C (265 °F), the oxidation followed a logarithmic rate law that tended to become parabolic at higher temperatures. At room temperature, the oxide film appeared to be amorphous, but at higher temperatures, α-SnO was detected, possibly with some SnO_2.

One study found that SnO forms on tin immediately above its melting point and that SnO_2 forms at higher temperatures (Ref 32). This effect was demonstrated by spot heating a piece of tinfoil (Ref 33). Stannic oxide was found at the center and was surrounded by SnO, which was in turn ringed with an amorphous oxide. According to other researchers, the disproportionation of SnO to tin and SnO_2 is a slow process, even at 300 °C (570 °F) (Ref 34). The need for extreme care in oxidation studies, especially with regard to surface preparation, was emphasized in Ref 22. This was demonstrated by using cathodic cleaning to show the effects of humidity (Ref 35). Minor impurities in tin also affect its oxidation behavior in air. Small amounts of indium, phosphorus, or zinc were found to slow the oxidation (Ref 30). In addition, traces of aluminum were shown to cause embrittlement as a result of intercrystalline attack (Ref 36). Antimony additions, however, counteracted this effect.

Reaction with Other Gases. Tin does not react with hydrogen or nitrogen below its melting point, nor is it reactive with dry ammonia (NH_3). Molten tin reacts with carbon dioxide (CO_2) as:

$$Sn + 2CO_2 \rightarrow SnO_2 + 2CO \qquad \text{(Eq 1)}$$

Above 650 °C (1200 °F), molten tin reacts with water vapor to form SnO_2 and hydrogen.

From 25 to 100 °C (75 to 212 °F), hydrogen sulfide (H_2S) has little apparent effect on tin, but above 100 °C (212 °F), stannous sulfide (SnS) forms. Stannous sulfide and stannic sulfide (SnS_2) are also formed by reacting tin with sulfur at high temperatures. Tin also reacts readily with SCl_2, S_2Cl_2, NOF, and hydrofluoric acid (HF). Tin is readily attacked by chlorine, bromine, and iodine at room temperature, but fluorine reactions become significant only above 100 °C (212 °F).

Water. In hot or cold distilled water, the only action of tin is the slow growth of an oxide film with a negligible amount of metal entering solution. Water that was freshly distilled in a tin was found to have less than 1 ppb Sn in solution (Ref 2). Storage in tin-lined or tinned copper tanks for 24 h produced, in the worst instances, only a few parts per billion, but in some cases, the tin content remained below 1 ppb.

In tapwater of 7.2 pH at 25 °C (75 °F), specimens of 99.99% cold-rolled tin showed a weight gain of 0.023 mg/dm²/d (1.2×10^{-4} mm/yr, or 0.004 mil/yr) in 50 days and the formation of an insoluble film (Ref 37). With harder tapwaters of 7.4 and 8.6 pH, weight losses of the order 0.046 and 0.01 mg/dm²/d (2.3×10^{-4} and 5×10^{-5} mm/yr, or 0.009 and 0.002 mil/yr), respectively, were incurred in 50 days. Precipitated carbonate was mainly responsible for localized waterline attack with hot and cold hard waters, because no attack occurred without the precipitate. Addition of 5% Sb to the tin prevented localized attack by hard water.

The results of corrosion test data on tin and several tin alloys in seawater under conditions of total immersion are shown in Table 3. It was also observed that application of a fairly thick 60Pb-40Sn alloy coating over copper will protect it from erosion by seawater at high velocity (Ref 38).

Acids. Tin may be corroded by acidic aqueous solutions of pH less than 3 or by less acidic solutions containing compounds that form stable complex ions with tin. The corrosion rate is also highly influenced by oxygen concentration and the presence of metallic impurities in the tin or by the acid that can concentrate on the surface and facilitate the cathodic half reaction.

Table 4 compares the corrosion rates for tin samples exposed vertically in various acids open to the air at 30 °C (85 °F). The greater weight loss over the 96 h period was largely attributed to the access of oxygen to the solutions.

The following general comments concern the effects of other acids (Ref 25). Hot hydrobromic (HBr) and hydroiodic (HI) acids rapidly attack tin, but the rate of attack is slow with HF. Tin is slowly attacked by $HClO_2$ and is readily attacked by $HClO_3$. Sulfurous acid (H_2SO_3) attacks tin,

but sodium acid sulfite ($NaHSO_3$) is noncorrosive. Pyrosulfuric acid ($H_2S_2O_7$) and chlorosulfonic acid (SO_2ClOH) react rapidly with tin; nitric acid (HNO_3) reacts rapidly with tin over a wide range of concentrations, and the reaction is complex.

Bases. Tin may be dissolved by alkaline solutions, with the production of soluble stannates or stannites. Corrosion will usually follow if the surface oxide layer can be dissolved; this will occur with pH greater than 12 and may occur at pH values down to 10. When corrosion is possible, its rate is governed by the temperature and the rate of arrival of oxygen or other oxidizing agents to the initial surface and is not greatly affected by the character of the alkali in long periods of immersion. However, in intermittent immersion, the corrosion rate is affected by the nature of the alkali and its concentration, because these affect the time for removal of the oxide film. The corrosion rates of tin in various alkaline solutions exposed to air at 60 °C (140 °F) are summarized in Table 5.

Hydrogen evolution does not occur on a tin surface in alkaline solutions. Thus, exclusion of oxidizing agents, including air, can provide complete protection unless the tin is in contact with another metal on which hydrogen evolution can occur. Additions of oxygen absorber can prevent corrosion even without the exclusion of air, but they must be replenished. Small additions of oxidizing agents to alkalis stimulate corrosion, but sufficiently large additions can be completely effective. Soluble chromates are particularly effective in this way. Saturated NH_3 solutions do not attack tin, but more dilute solutions behave like other alkaline solutions of comparable pH.

Other Liquid Media. Milk and milk products are usually nonreactive with tin, although a long period of stagnant contact may produce local corrosion (Ref 41). Sulfide solutions and materials containing sulfur dioxide (SO_2) as a preservative produce sulfide stains, but the rate of metal loss is low. Beer dissolves a trace of tin from freshly exposed metal. Although this may cause an objectionable haze in the beverage, the action usually ceases within a short period. To avoid this effect, the tin surfaces can be passivated by using alkaline chromate solutions.

Most organic liquids, including ethers, alcohols, ketones, esters, hydrocarbons, and chlorinated hydrocarbons, are inert toward tin in the absence of water (Ref 25). However, a reaction was reported between tin and lower alcohols at elevated temperatures, and when mineral acidity can arise, as with chlorinated hydrocarbons containing water, there may be some corrosion (Ref 42). Animal, vegetable, or mineral oils and fatty acids are also essentially inactive, and the absence of any catalytic action of tin on their oxidation makes tin or tin-coated vessels suitable for these products.

Galvanic Behavior. When immersed in electrical contact with a more noble metal, such as copper or nickel, tin is much more likely to be corroded, and any loss of metal will be faster, with an increase in the number of locally corroded spots in conditions favorable to local corrosion. However, contact with such metals as aluminum or zinc can prevent corrosion of tin entirely, and a tin coil or vessel can be protected by joining it to a strip of one of these metals. The galvanic-corrosion behavior of tin and tin-lead alloys in contact in seawater with numerous alloy steels and other structural materials is summarized in Table 6.

Passivation of Tin. Tin can be readily passivated with or without an applied potential. The solutions most frequently used are the strongly oxidizing chromate solutions, which produce a thin, tenacious oxide layer that is quite protective. This film is 4 to 5 nm (16×10^{-8} to 20×10^{-8} in.) thick when prepared by immersion in an alkaline chromate solution at 80 to 90 °C (175 to 195 °F) for 15 min (Ref 43). Anodic passivation with a current density of 500 A/dm^2 (32 A/in.^{2}) for 5 s in 0.5% sodium hydroxide (NaOH) forms a 30 nm (12×10^{-7} in.) thick film. In 0.005 *M* potassium chromate (K_2CrO_4) solution, SnO is oxidized to SnO_2 above a potential of 0.2 V versus a Ag/AgCl electrode, and the oxide continues to thicken even after the oxygen evolution potential is reached. The passivation behavior of tin in solutions of phosphoric acid (H_3PO_4) (Ref 44), NaOH (Ref 45), sodium borate ($NaBO_2$), and sodium carbonate (Na_2CO_3) has also been studied, and is reviewed in detail in Ref 25.

Soft Solders

Until the 1990s, most soft solders contained from 2 to 100% Sn, with the balance consisting of lead, although some special-purpose solders substituted silver or antimony for some or all of the lead. In 1990, concern for health and the effect of increasing quantities of discarded electronic items containing lead in landfills prompted legislation in the United States to encourage lead-free solders in these applications. In 1998, the European Union had similar directives to eliminate lead. Work on low-melting-point alternatives has met with success, but high-melting-point alternatives to lead-rich solders still need to be found. In the mid-1990s, the electronics industry used approximately 60,000 tonnes (66,000 tons) of lead-tin solder annually (Ref 46).

Table 3 Corrosion of tin and tin alloys totally immersed in seawater

Material	Form	Exposure time, years	Corrosion rate(a)		Test location
			mm/yr	mils/yr	
99.75 tin	Cast bar	4	0.0022	0.087	Bristol Channel
99.2 tin	Cast bar	4	0.0008	0.03	Bristol Channel
Babbitt alloy (Sn-7.4Sb-3.7Cu)	Cast plate	1.4	0.060	2.4	Kure Beach, NC
Solder (Sn-50Pb)	Sheet	0.5	0.075	2.95	Bogue Inlet, NC
Solder (Sn-60Pb on copper)	Plate	2.1	0.011	0.43	Kure Beach, NC

(a) Converted from weight loss data, assuming cast densities of 7.29 g/cm^3 for tin, 7.39 g/cm^3 for babbitt, 8.90 g/cm^3 for 50-50 solder, and 9.28 g/cm^3 for 40-60 solder. Source: Ref 38

Table 4 Corrosion rate of tin in 0.1 *N* acids at 30 °C (85 °F) exposed vertically in solutions open to air

Acid	Average corrosion rate(a)			
	24-h test		96-h test	
	mm/yr	mils/yr	mm/yr	mils/yr
Hydrochloric	0.40	15.7	0.30	11.8
Sulfuric	0.32	12.6	0.29	11.4
Phosphoric	0.03	1.2	0.01	0.4
Formic	0.34	13.4	0.25	9.8
Acetic	0.29	11.4	0.24	9.4
Oxalic	0.17	6.7	0.17	6.7
Citric	0.25	9.8	0.21	8.3
Malic	0.22	8.7	0.22	8.7
Lactic	0.24	9.4	0.21	8.3

(a) Converted from weight loss data, assuming a tin density of 7.29 g/cm^3. Source: Ref 39

Table 5 Corrosion rate of tin in alkaline solutions exposed to air at 60 °C (140 °F)

Concentration of solution, %	Corrosion rate(a)							
	Na_3PO_4		Na_2CO_3		Na_2SiO_3		NaOH	
	mm/yr	mils/yr	mm/yr	mils/yr	mm/yr	mils/yr	mm/yr	mils/yr
0.005	0.015	0.6	0.030	1.2	0.030	1.2	0.21	8.3
0.02	0.015	0.6	0.045	1.8	0.045	1.8	0.24	9.4
0.05	0.21	8.3	0.24	9.4	nil		0.21	8.3
0.10	0.23	9.1	0.26	10.2	0.015	0.6	0.20	7.9
0.15	0.24	9.4	0.27	10.6	0.075	2.95	0.20	7.9
0.20	0.26	10.2	0.27	10.6	0.090	3.5	0.21	8.3
0.25	0.26	10.2	0.27	10.6	0.12	4.7	0.24	9.4

(a) Converted from weight loss data, assuming a tin density of 7.29 g/cm^3. Source: Ref 40

Two features are particularly relevant to the corrosion behavior of solders with regard to their function as a joining material. First, fluxes are usually used, and, second, the solder exposure areas are usually much smaller than the area of the materials being joined.

By nature, fluxes function as oxide removers and may contain hygroscopic products that, if not removed, will promote corrosion. A mild flux, such as pure natural resin, is inactive at normal (room) temperatures and therefore has a harmless residue.

Table 6 Seawater corrosion of galvanic couples

□ The corrosion of the metal under consideration will be reduced considerably in the vicinity of the contact
○ The corrosion of the metal under consideration will be reduced slightly
△ The galvanic effect will be slight with the direction uncertain
■ The corrosion of the metal under consideration will be increased slightly
▲ The corrosion of the metal under consideration will be increased moderately
● The corrosion of the metal under consideration will be increased considerably

S Exposed area of the metal under consideration is small compared with the area of the metal with which it is coupled
E Exposed area of the metal under consideration is approximately equal to that of the metal with which it is coupled
L Exposed area of the metal under consideration is large compared to that of the metal with which it is coupled

Metal considered		Magnesium	Magnesium alloys	Zinc	Galvanized steel	Aluminum 5052	Aluminum 3004	Aluminum 1100	Alclad	Aluminum 3003	Aluminum 6053	Aluminum 6061	Cadmium	Aluminum 2017	Aluminum 2117	Aluminum 2024	Low-carbon steel	Wrought iron	Low-alloy steels	Cast iron	Low-alloy cast irons	4–6% Cr	Ni cast iron	12–14% Cr	Lead-tin solders	16–18% Cr steel	Lead	Tin	Muntz metal	Manganese bronze	Naval brass	Nickel	Yellow brass	Admiralty brass	Aluminum bronze	Red brass	Copper	Silicon bronze	Nickel silver	70-30 copper-nickel	Composition G bronze	Composition M bronze	Inconel	Silver solder	70-30 nickel-copper	25–30% Cr steel	Cr-Ni stainless steel	Cr-Ni-Mo stainless steel	Graphite
Low-carbon steel	S	□	□	□	□	□	□	□	□	□	□	□	□	□	□	□	△	▲	●	●	●	●	●	●	●	●	●	●	●	●	●	●	●	●	●	●	●	●	●	●	●	●	●	●	●	●	●	●
	E	□	□	○	○	□	□	□	□	□	□	□	□	□	□	□	△	△	■	■	■	■	▲	▲	▲	▲	▲	▲	▲	▲	▲	▲	▲	▲	▲	▲	▲	▲	▲	▲	▲	▲	▲	▲	▲	▲	▲	▲	▲
	L	○	○	○	○	○	○	○	○	○	○	○	○	○	○	○	△	△	■	■	■	■	■	■	■	■	■	■	■	■	■	■	■	■	■	■	■	■	■	■	■	■	■	■	■	■	■	■	■	■
Wrought iron	S	□	□	□	□	□	□	□	□	□	□	□	□	□	□	□	△	△	●	●	●	●	●	●	●	●	●	●	●	●	●	●	●	●	●	●	●	●	●	●	●	●	●	●	●	●	●	●	●	●
	E	□	□	○	○	□	□	□	□	□	□	□	□	□	□	□	△	△	■	■	■	■	▲	▲	▲	▲	▲	▲	▲	▲	▲	▲	▲	▲	▲	▲	▲	▲	▲	▲	▲	▲	▲	▲	▲	▲	▲	▲	▲
	L	○	○	○	○	○	○	○	○	○	○	○	○	○	○	○	○	△	■	■	■	■	■	■	■	■	■	■	■	■	■	■	■	■	■	■	■	■	■	■	■	■	■	■	■	■	■	■	■	■
Low-alloy steels	S	□	□	□	□	□	□	□	□	□	□	□	□	□	□	□	□	□	△	□	△	▲	●	●	●	●	●	●	●	●	●	●	●	●	●	●	●	●	●	●	●	●	●	●	●	●	●	●	●
	E	□	□	○	○	□	□	□	□	□	□	□	□	□	□	□	○	○	△	○	△	△	▲	▲	▲	▲	▲	▲	▲	▲	▲	▲	▲	▲	▲	▲	▲	▲	▲	▲	▲	▲	▲	▲	▲	▲	▲	▲	▲
	L	○	○	○	○	○	○	○	○	○	○	○	○	○	○	○	○	○	△	○	△	△	■	■	■	■	■	■	■	■	■	■	■	■	■	■	■	■	■	■	■	■	■	■	■	■	■	■	■	■
Cast iron	S	□	□	□	□	□	□	□	□	□	□	□	□	□	□	□	△	△	●	△	●	▲	●	●	●	●	●	●	●	●	●	●	●	●	●	●	●	●	●	●	●	●	●	●	●	●	●	●	●
	E	□	□	○	○	□	□	□	□	□	□	□	□	□	□	□	○	○	■	△	■	■	▲	▲	▲	▲	▲	▲	▲	▲	▲	▲	▲	▲	▲	▲	▲	▲	▲	▲	▲	▲	▲	▲	▲	▲	▲	▲	▲
	L	○	○	○	○	○	○	○	○	○	○	○	○	○	○	○	○	○	■	△	■	■	■	■	■	■	■	■	■	■	■	■	■	■	■	■	■	■	■	■	■	■	■	■	■	■	■	■	■	■
Low-alloy cast iron	S	□	□	□	□	□	□	□	□	□	□	□	□	□	□	□	□	□	△	□	△	▲	●	●	●	●	●	●	●	●	●	●	●	●	●	●	●	●	●	●	●	●	●	●	●	●	●	●	●
	E	□	□	○	○	□	□	□	□	□	□	□	□	□	□	□	○	○	△	○	△	△	▲	▲	▲	▲	▲	▲	▲	▲	▲	▲	▲	▲	▲	▲	▲	▲	▲	▲	▲	▲	▲	▲	▲	▲	▲	▲	▲
	L	○	○	○	○	○	○	○	○	○	○	○	○	○	○	○	○	○	△	○	△	△	■	■	■	■	■	■	■	■	■	■	■	■	■	■	■	■	■	■	■	■	■	■	■	■	■	■	■	■
4–6% Cr steel	S	□	□	□	□	□	□	□	□	□	□	□	□	□	□	□	□	□	▲	□	▲	△	●	●	●	●	●	●	●	●	●	●	●	●	●	●	●	●	●	●	●	●	●	●	●	●	●	●	●
	E	□	□	○	○	□	□	□	□	□	□	□	□	□	□	□	○	○	△	○	△	△	▲	▲	▲	▲	▲	▲	▲	▲	▲	▲	▲	▲	▲	▲	▲	▲	▲	▲	▲	▲	▲	▲	▲	▲	▲	▲	▲
	L	○	○	○	○	○	○	○	○	○	○	○	○	○	○	○	○	○	△	○	△	△	■	■	■	■	■	■	■	■	■	■	■	■	■	■	■	■	■	■	■	■	■	■	■	■	■	■	■	■
Nickel cast iron	S	□	□	□	□	□	□	□	□	□	□	□	□	□	□	□	□	□	□	□	□	□	△	●	●	●	●	●	●	●	●	●	●	●	●	●	●	●	●	●	●	●	●	●	●	●	●	●	●	●
	E	□	□	○	○	□	□	□	□	□	□	□	□	□	□	□	○	○	○	○	○	○	△	■	■	■	■	■	■	■	■	■	■	■	■	■	■	■	■	■	■	■	■	■	■	■	■	■	■	▲
	L	○	○	○	○	○	○	○	○	○	○	○	○	○	○	○	○	○	○	○	○	○	■	■	■	■	■	■	■	■	■	■	■	■	■	■	■	■	■	■	■	■	■	■	■	■	■	■	■	■
12–14% Cr steel	S	□	□	□	□	□	□	□	□	□	□	□	□	□	□	□	□	□	□	□	□	□	□	△	▲	●	●	●	△	△	●	●	●	●	●	●	●	●	●	●	●	●	●	●	●	●	●	●	●
	E	□	□	□	□	□	□	□	□	□	□	□	□	□	□	□	□	□	□	□	□	□	□	○	△	■	■	▲	■	■	▲	▲	▲	▲	▲	▲	▲	▲	▲	▲	▲	▲	▲	▲	▲	▲	▲	▲	▲
	L	○	○	○	○	○	○	○	○	○	○	○	○	○	○	○	○	○	○	○	○	○	○	○	△	■	■	■	■	■	■	■	■	■	■	■	■	■	■	■	■	■	■	■	■	■	■	■	■	●
Lead-tin solders	S	□	□	□	□	□	□	□	□	□	□	□	□	□	□	□	□	□	□	□	□	□	□	□	△	△	■	■	△	△	■	■	■	■	■	■	■	■	■	■	■	■	■	■	■	■	■	■	●
	E	□	□	□	□	□	□	□	□	□	□	□	□	□	□	□	□	□	□	□	□	□	□	□	△	△	△	△	△	△	△	△	△	△	△	△	△	△	△	△	△	△	△	△	△	△	△	△	▲
	L	○	○	○	○	○	○	○	○	○	○	○	○	○	○	○	○	○	○	○	○	○	○	○	△	△	△	△	△	△	△	△	△	△	△	△	△	△	△	△	△	△	△	△	△	△	△	△	▲
16–18% Cr steel	S	□	□	□	□	□	□	□	□	□	□	□	□	□	□	□	□	□	□	□	□	□	□	□	□	■	△	■	■	■	●	●	●	●	●	●	●	●	●	●	●	●	●	●	●	●	●	●	●
	E	□	□	□	□	□	□	□	□	□	□	□	□	□	□	□	□	□	□	□	□	□	□	□	□	△	△	△	▲	▲	▲	▲	▲	▲	▲	▲	▲	▲	▲	▲	▲	▲	▲	▲	▲	▲	▲	▲	●
	L	○	○	○	○	○	○	○	○	○	○	○	○	○	○	○	○	○	○	○	○	○	○	○	○	△	△	■	■	■	■	■	■	■	■	■	■	■	■	■	■	■	■	■	■	■	■	■	■	■
25–30% Cr steel	S	□	□	□	□	□	□	□	□	□	□	□	□	□	□	□	□	□	□	□	□	□	□	□	□	△	△	□	□	□	□	●	●	●	●	●	●	●	●	●	●	●	●	●	△	□	△	●	●
	E	□	□	□	□	□	□	□	□	□	□	□	□	□	□	□	□	□	□	□	□	□	□	□	□	△	△	○	○	○	○	■	■	■	■	■	■	■	■	■	■	■	■	■	△	○	△	●	●
	L	○	○	○	○	○	○	○	○	○	○	○	○	○	○	○	○	○	○	○	○	○	○	○	○	△	△	○	○	○	△	△	△	△	△	△	△	△	△	△	△	△	△	△	△	△	△	△	●
Austenitic Cr-Ni stainless steel	S	□	□	□	□	□	□	□	□	□	□	□	□	□	□	□	□	□	□	□	□	□	□	□	△	□	□	△	△	□	□	□	●	●	●	●	●	●	●	●	●	●	●	●	△	●	●	●	●
	E	□	□	□	□	□	□	□	□	□	□	□	□	□	□	□	□	□	□	□	□	□	□	□	□	△	△	○	○	○	△	○	■	■	■	■	■	■	■	■	■	■	■	■	△	■	●	●	●
	L	○	○	○	○	○	○	○	○	○	○	○	○	○	○	○	○	○	○	○	○	○	○	○	○	△	△	○	○	○	△	△	△	△	△	△	△	△	△	△	△	△	△	△	△	△	△	△	●
Austenitic Cr-Ni-Mo stainless steel	S	□	□	□	□	□	□	□	□	□	□	□	□	□	□	□	□	□	□	□	□	□	□	□	△	□	□	△	△	□	□	□	●	●	●	●	●	●	●	●	●	●	●	●	△	●	●	●	●
	E	□	□	□	□	□	□	□	□	□	□	□	□	□	□	□	□	□	□	□	□	□	□	□	□	△	△	○	○	○	△	○	■	■	■	■	■	■	■	■	■	■	■	■	△	■	●	●	●
	L	○	○	○	○	○	○	○	○	○	○	○	○	○	○	○	○	○	○	○	○	○	○	○	○	△	△	○	○	○	△	△	△	△	△	△	△	△	△	△	△	△	△	△	△	△	△	△	▲
Lead	S	□	□	□	□	□	□	□	□	□	□	□	□	□	□	□	□	□	□	□	□	□	□	□	□	■	△	■	■	■	■	■	■	■	■	■	■	■	■	■	■	■	■	■	■	■	■	■	●
	E	□	□	□	□	□	□	□	□	□	□	□	□	□	□	□	□	□	□	□	□	□	□	□	□	△	△	△	△	△	△	△	△	△	△	△	△	△	△	△	△	△	△	△	△	△	△	△	▲
	L	○	○	○	○	○	○	○	○	○	○	○	○	○	○	○	○	○	○	○	○	○	○	○	△	△	△	△	△	△	△	△	△	△	△	△	△	△	△	△	△	△	△	△	△	△	△	△	▲
Tin	S	□	□	□	□	□	□	□	□	□	□	□	□	□	□	□	□	□	□	□	□	□	□	□	△	△	■	■	■	■	■	■	■	■	■	■	■	■	■	■	■	■	■	■	■	■	■	■	●
	E	□	□	□	□	□	□	□	□	□	□	□	□	□	□	□	□	□	□	□	□	□	□	□	△	△	△	△	△	△	△	△	△	△	△	△	△	△	△	△	△	△	△	△	△	△	△	△	▲
	L	○	○	○	○	○	○	○	○	○	○	○	○	○	○	○	○	○	○	○	○	○	○	○	△	△	△	△	△	△	△	△	△	△	△	△	△	△	△	△	△	△	△	△	△	△	△	△	▲

Source: Ref 38

More powerful fluxes may consist of natural resin with additions—for example, chlorides and bromides—or mixtures of chlorides, H_3PO_4, and derivatives. Residues from such fluxes must usually be completely removed by mechanical wiping or with solvents.

The area effect can be minimized by coating the joined metals with tin or tin-lead alloys. However, the suitable design of joints and the formation of protective corrosion products over the solder often permit the satisfactory use of soldered joints in conditions that may at first appear hostile.

Simple binary tin-lead solders consist essentially of eutectic mixtures, and their corrosion behavior is similar to that for either metal, with the overall behavior similar to that of the predominant metal. Both metals are attacked by acids and alkalis, but the presence of lead, which forms many more insoluble compounds than tin, creates further possibilities for the formation of protective layers in near-neutral aqueous media. The addition of other elements has not been found to affect the corrosion resistance of tin-lead alloys appreciably (Ref 2). Also, the behavior of lead-free solders containing silver or antimony with tin does not differ greatly from that of pure tin.

Atmospheric Corrosion. Even small additions of lead to tin impair the retention of its bright reflective surface in common atmospheres. With increasing lead content, the appearance of soldered joints becomes increasingly dull, like that of lead. However, destructive corrosion (except effects from flux residues) is highly unusual. On rare occasions, within enclosed spaces, condensed pure water may extract lead, but more common causes of trouble are volatile organic acids. Acetic acid (CH_3COOH) vapors from wood or insulating materials and formic acid (HCOOH) or other acids that may come from insulating materials may attack lead-containing solders to produce a white incrustation and cause serious destruction of metal. Where such attack occurs, substitution of a solder with a higher tin content may eliminate the problem.

Lead-tin alloys used to make the pipes for historic organs in Europe have become more susceptible to corrosion recently. These centuries-old instruments may be affected by air pollution or by the acetic acid from oak wood used to build or restore parts of the organs. This corrosion is being investigated by a European Union-funded research project, Corrosion of Lead and Lead-Tin Alloys of Organ Pipes in Europe (COLLAPSE). The COLLAPSE group noted that the amount of tin varied in the pipes depending on the cost and availability of tin at the time of construction. Pipes with greater tin content generally experienced less corrosion. The introduction of central heating into the churches may also have been a factor in driving more acetic acid from the oak wood (Ref 47).

Contact of solder with other metals can impose a serious risk in conditions of exposure to sea spray or where pockets or crevices can trap moisture or flux residues. In most atmospheric conditions, the formation of lead sulfate ($PbSO_4$) protects the solder. However, in chloride pollution conditions, nickel, copper, and their alloys are likely to be more noble than the solder. Zinc tends to be strongly active to soft solders, but correctly designed zinc roof coverings appear to suffer no deterioration at the soldered joints (Ref 2).

The Sn-9Zn eutectic alloy is unsuitable for most electronic soldering applications, because it will corrode in chlorine-containing atmospheres and produce a conductive zinc chloride film (Ref 46).

Immersion. Natural waters and commercially treated waters that are aggressive to lead are likely to corrode solder at a rate that increases slowly, in proportion to its lead content, up to approximately 70% Pb, then more rapidly at higher lead contents. Selective dissolution of lead can also occur in distilled, demineralized, or naturally soft waters, causing serious weakening of joints (Ref 2). In the general run of commercial waters, the ability of lead to form insoluble oxides, sulfates, and carbonates usually protects solders against serious attack. Although rare, selective dissolution of tin has been reported during prolonged contact of solders with solutions of anionic surface-active agents.

When freshly exposed to water, solders are anodic to copper, but soldered joints in copper pipes are widely used without trouble in conventional commercial and domestic cold- and hot-water systems. Despite this generally good corrosion resistance, it has been demonstrated that, under adverse conditions, lead may be leached from the commonly used 50Sn-50Pb plumbing solder into water traveling through the pipe; this is a cause of increasing concern (Ref 48, 49). The lead content of water passing through soldered copper pipes is usually less than that recommended by various regulatory authorities, although higher values may be found in new installations and in some soft water areas (Ref 49). Public concern about all sources of lead in the human diet is well documented in numerous publications, and in some countries, including the United States, legislative action has been undertaken to prohibit the use of lead-containing solders and to tighten existing water quality standards (Ref 50).

Soldered joints in brass usually perform well in domestic waters, but good joint design is imperative. In automobile radiators in which there are no inhibitors, ethylene glycol, although not directly aggressive, does appear able to detach protective deposits that may form on soldered joints. Properly tested and approved inhibitors avoid this problem. Sodium nitrite ($NaNO_2$), which is used as an inhibitor for some metals, will attack solders and must be used in conjunction with sodium benzoate ($NaC_7H_5O_2$).

In seawater or uninhibited brines, the high conductivity and predominance of chloride makes galvanic action at a soldered joint more likely to continue destructively, and soldered joints in copper, nickel, and their alloys may need protection by coatings. Although tin or tin-coated metals can be used in contact with aluminum alloys even in saltwater, the soldering process introduces sufficient aluminum to the solder to render it susceptible to intergranular corrosion. If tin-zinc solders are used, the zinc can prevent the serious embrittling action, although some corrosion will still occur under moist conditions.

Pewter

By definition, modern pewter is an alloy that contains 90 to 98% Sn, 1 to 8% Sb, 0.25 to 3% Cu, and a maximum of 0.05% Pb and As (Ref 51). Material that conforms to these standards has approximately the same degree of corrosion resistance to ordinary atmospheres as pure tin. Alloys within this range are widely used for decorative items, containers, and flatware. Indoors, they retain a bright, white luster in the same manner as pure tin. Because contamination from fabrication residues can deteriorate the protective oxide, care should be exercised in removing residues of soldering fluxes and cleaning solutions. Regular, simple washing with a mild soap solution will ensure that the surface remains in good condition.

Pewter tankards and plates also have approximately the same degree of corrosion resistance to foods and drinks as tin does. With the normal contact time, the amount of tin dissolved by beer is insufficient to cause a haze. However, citrus juices or vinegar will etch a pewter surface if contact is maintained for more than an hour. Undisturbed neutral salt solutions may produce black spots and, later, local pitting. Strong alkaline cleaning agents may also etch the surface.

In years past, pewter alloys contained lead in sufficient quantities to affect its corrosion resistance significantly, for example, by producing a dark patina during atmospheric exposure. Modern pewter can be chemically treated to reproduce this patina. Several proprietary processes are available, including those based on immersion in iron chloride ($FeCl_3$) or sodium nitrate (Na_2NO_3) solutions or acidic solutions of copper and arsenic (Ref 52, 53).

Bearing Alloys

The most widely used babbitt-bearing alloys are usually classified as tin- or lead-base and have composition ranges within the following limits:

	Composition, %	
Alloy addition	Tin-base	Lead-base
Tin	65–91	0–20
Lead	0.35–18	63 (min)
Antimony	4.5–15	10–15
Copper	2–8	1.5 (max)

The tin-base alloys are much more corrosion resistant against the action of the acids contained or formed in lubricating oils (see the article "Tin and Tin Alloys" in *Properties and Selection: Nonferrous Alloys and Special-Purpose Materials,* Volume 2, *ASM Handbook,* 1990). An addition of as little as 3% Sn in lead appears to prevent corrosion from the development of oil acidity (Ref 54).

In some instances of marine use, the formation of a hard, crusty oxidation product has been observed on tin-rich bearings (Ref 55). When free access of saltwater to a bearing is possible, the cathodic relationship of the babbitt alloys to steel renders them unsuitable, and bearing alloys such as Zn-70Sn-1.5Cu are preferred (Ref 2).

Some aluminum-base alloys containing 5 to 40% Sn and 0.7 to 1.3% Cu have also found use as bearing alloys in automobiles. These alloys are manufactured using thermal treatments designed to produce structures that avoid a continuous network of the tin in order to obviate the risk of susceptibility to corrosion by the presence of moisture (Ref 56). With normal lubrication, the aluminum-tin alloys appear to be as fully resistant to corrosion as the tin-base babbitt alloys. The aluminum-tin alloys, however, are not suitable for exposure to wet conditions.

Other Tin Alloys

Tin-Copper. Alloys in this group are all copper-base and consist mainly of bronzes, gunmetal, and brass that contains tin additions. Understandably, their corrosion behavior in air is based on the behavior of copper, which tends to develop a layer of basic green salts (mainly sulfates), that is adherent, protective, and has a pleasing appearance. More information on the corrosion resistance of copper alloys is available in the article "Corrosion of Copper and Copper Alloys" in this Volume.

Atmospheric Corrosion. Early studies were conducted on Cu-6.3Sn-0.08P wire and Cu-6.3Sn-0.08P-0.5Zn sheet in rural, suburban, urban, industrial, and marine environments for 1 year (Ref 57). Evaluations included weight gains as well as changes in tensile strength and electrical resistance. The bronze samples ranked consistently high among the materials tested, as indicated by the tensile strength data shown in Table 7.

A more extensive study covering 20 years and seven sites compared the behavior of a variety of alloys, including phosphor bronze (Cu-7.85Sn-0.03P), admiralty brass (Cu-29.01Zn-1.22Sn), and a nickel-tin bronze (Cu-28.6Ni-1.04Sn-0.55Zn) (Ref 59). Weight changes were used to assess corrosion behavior, along with changes in electrical resistance and tensile strength. Some representative data are given in Table 8. Small tin additions also impart dezincification resistance to brass.

A similar study involved exposure of screen wire cloth at four sites for up to 9 years (Ref 60). A Cu-2Sn bronze was found to exhibit the lowest strength losses at all sites from a group of alloys that included brasses, aluminum bronze, and nickel-copper. Outstanding corrosion resistance of a Cu-2Sn bronze exposed to sulfur-bearing gases in railway tunnels was also reported (Ref 61).

Another investigation compared the behavior of five stainless steels and a low-alloy steel with that of a Cu-4.38Sn-0.36P bronze exposed at tropical inland and seacoast sites for 8 years (Ref 62). The coastal site was more aggressive toward the bronze, which showed higher weight losses at both sites than the stainless, but the low-alloy steel was more severely attacked. However, the bronze was free of pitting and suffered no loss in strength, which was not the case with some of the stainless steels. In Ref 63, these researchers summarized the results of 16 year exposures on three tin-containing alloys (Cu-4.38Sn-0.36P, Cu-39Zn-0.84Sn, and Cu-40Zn-1Fe-0.65Sn) exposed at marine, inland semirural, and two tropical sites. In general, the copper alloys resisted corrosion in the tropical zones, although less so at coastal sites as compared to inland sites. The tin-containing alloys were as good as, or slightly superior to, the other alloys.

More recent work by the same investigators included previous data plus additional information on the following cast bronzes: Cu-5Sn-5Pb-5Zn, Cu-6Sn-2Pb-3Zn-1Ni, Cu-9Sn-3Zn-1Ni, and Cu-3Sn-2Zn-6Ni (Ref 64). The conclusions were much the same as before. The later work included a study of the effect of coupling phosphor bronze to equal areas of numerous other metals, and this work indicated that the coastal sites were 4 to 8 times more aggressive than the inland sites. Evaluation of the effect of corrosion on the solderability of a Cu-2Sn-9Ni alloy was reported by workers at Bell Telephone, who found this material to be superior to both nickel-silver and an 8% Sn phosphor bronze (Ref 65).

Alloys in the Cu-Sn-Al system were evaluated, and those alloys containing at least 5% each of tin and aluminum were found to have good corrosion resistance in rural, urban, and industrial environments (Ref 66). The most promising material was Cu-5Sn-7Al. Another researcher noted that such alloys could be brittle, but that the addition of 1% Fe and 1% Mn overcame this difficulty without detracting from the corrosion resistance of the alloy (Ref 67).

Tin-Silver. In the mid-1930s, tin-silver alloys were assessed as potential replacements for sterling silver (silver-copper alloy) in decorative applications (Ref 68). In this work, a Ag-7.5Sn alloy was found to show improved corrosion resistance over pure silver in several environments. In a later extension of this work, alloys with up to 10% Sn were tested in atmospheres containing H_2S, SO_2, and indoor air as well as for resistance to salt and oxidation upon heating in air (Ref 69). Comparison to sterling silver showed the tin-silver alloys to be at least as good as the sterling alloys, and in some cases even better. Specifically, their resistance to chloride attack was considerably better, and less discoloration occurred upon heating in air. Also, preoxidation of the tin-silver alloys improved resistance to attack by sulfur-containing atmospheres.

Table 7 Tensile strength loss in copper alloys after exposure for 1 year in various environments

Environments included industrial, marine, rural, suburban, and urban locations; data are averages for all five environments.

Alloy	Strength loss, %
Tin bronze (6% Sn)	1.2
High-conductivity copper	2.4
Aluminum bronze (3.5% Al)	2.1
70-30 nickel-copper	3.2
60-40 copper-zinc	18.4
70-30 copper-zinc	8.6

Source: Ref 58

Table 8 Tensile strength loss in copper alloys after exposure for 10 years at four sites

	Strength loss, %			
Exposure site	Copper	Tin bronze (8% Sn)	70-30 copper-zinc	70 Cu-29Zn-1Sn
Heavy industrial	5.9	7.2	30.9	9.0
Marine, heavy industrial	6.3	8.0	28.2	7.9
Severe marine	7.6	5.7	8.0	2.5
Rural	3.1	3.1	3.2	2.2

Source: Ref 59

Tin and Tin-Alloy Coatings

Tin coatings can be applied by various processes, including hot dipping, electrodeposition, spraying, and chemical displacement. Electrodeposits can be matte or bright as plated, and matte deposits less than 8 μm (0.3 mil) thick can be brightened by momentary fusion. The latter fusion can be effected by conductive or resistive heating in air or by immersion in suitable oil.

In the standard electrodeposition process, alkaline stannate, acid sulfate, or fluoborate solutions are all widely used. The alkaline solutions give smooth, matte deposits, but the acid solutions usually require organic addition agents to produce smooth, coherent coatings. If improperly controlled, these agents can increase the risk of dewetting during soldering or flow melting.

The ranges of coating thicknesses that are practical for the various processes are as follows (Ref 2):

Process	Thickness	
	μm	mils
Chemical replacement	Trace–2.5	Trace–0.1
Flow-melted electrodeposition	0.4–7.5	0.02–0.3
Electrodeposition, general	2.5–75	0.1–2.9
Hot dipping	1.5–25	0.06–1
Spraying	75–350	2.9–13.6

Coatings applied by any method may contain pores that will expose the base metal. Porosity should be minimal for electrodeposited and hot-dipped coatings thicker than 15 μm (0.6 mil) (Ref 2). However, the behavior of the coating will be strongly influenced by the relative polarity of tin and substrate, by the nature of any intermetallic layers formed by reactions between these, and by the extremely low rate of corrosion of tin in alkaline and mildly acidic media in the absence of oxygen or other cathode depolarizers.

Because deposits less than approximately 12 μm (0.5 mil) thick are not likely to be pore free, the heaviest practical deposits should be used when tin is specified for corrosion resistance. Table 9 lists recommended tin coating thicknesses for quality tin coatings for various service conditions.

Tests conducted by the Metal Finishing Supplies Association (MFSA) showed that bright acid tin deposits generally perform better than the matte tin deposits in salt spray corrosion tests (Ref 70). However, no published specifications recognize any difference between the corrosion performance of these processes. Similarly, because tin is more noble than almost all of the commonly used base metals and undercoating metals, the MSFA recommends that the same tin coating thicknesses be applied to any of the common base metals. Also, the use of a copper or nickel undercoating does not justify the use of thinner tin deposits (Ref 70).

Tin Coatings on Steel. Tin on steel is widely used in packaging. The single most important product of this type is tinplate. Modern tinplate is a highly developed, sophisticated product that is produced at high speeds to yield a coiled, thin, low-carbon steel strip carrying a very thin (0.1 to 2 μm, or 0.004 to 0.08 mil) tin coating on each side. Because of the importance of tinplate, its preparation and properties as well as its performance as a container for food and food products are discussed in the section "Tinplate" in this article.

This section primarily deals with heavier tin coatings that are usually applied to individual components by batch processing for nonpackaging applications, such as food-processing equipment, electrical and electronic components, wire, and fasteners. Unless otherwise stated, these coatings, unlike tinplate, have not been subjected to fusion or reflow treatments and are therefore free of the iron-tin intermetallic layer, which can exert profound effects.

One study compared the behavior of 25 μm (1 mil) thick plated layers of tin, 80Sn-20Zn, and zinc on steel at three sites in Nigeria for 2 years (Ref 71). Samples were exposed at 30° to the horizontal, approximately 1.2 m (47 in.) above ground, facing south and in sheltered exposure where they were supported vertically inside a ventilated box. The test results are given in Table 10.

An evaluation of various protective coatings based on many years of testing is summarized in Ref 72, in which a 12 μm (0.5 mil) thick coating is concluded to be a practical minimum for reasonable protection of steel in a mild indoor exposure; for outdoors, the minimum coating thickness should be 50 μm (2 mils).

The Protective Coatings (Corrosion) Subcommittee of the Corrosion Committee of the British Iron and Steel Research Association reported test results after 12 years of exposure in an industrial area (Sheffield), two marine atmospheres (Colshot and Congella, South Africa), and a rural area with heavy rainfall (Flanwryted Falls) (Ref 73, 74). These data, listed in Table 11,

Table 9 Recommended tin coating thicknesses for typical applications

Service condition	Thickness range		Typical applications
	μm	mils	
Very mild (little or no exposure to atmospheric conditions)	1.3–2.5	0.05–0.1	Insulated copper wire; pistons and other lubricated machine components
Mild (exposure to relatively clean indoor atmospheres)	2.5–5.0	0.1–0.2	Connectors, wires, etc., plated primarily for immediate solderability or where storage periods are short
Moderate (exposure to average shop and warehouse atmospheres)	3.8–7.6	0.15–0.3	This range is considered best for parts that must be reflowed: connectors, circuit boards, wire, busbars; deposits heavier than 7.5 μm (0.3 mil) may dewet
	7.6–12.7	0.3–0.5	Connectors, fasteners, busbars, wire, transformer cans, chassis frames; adequate for good shelf life and in service
Severe (exposure to humid air, mildly corrosive industrial environments)	12.7–25.4	0.5–1.0	Connectors, wire, gas meter components, automotive air cleaners; adequate as a nitride stop-off
Very severe (exposure to seacoast atmospheres; contact with certain chemical corrosives)	25.4–127	1.0–5.0	Water containers; oil-drilling pipe couplings

Source: Ref 70

Table 10 Corrosion rate of 25 μm (1 mil) thick coatings on steel at three tropical sites after 2 years of exposure

Coating	Corrosion rate, full exposure test					
	Jungle		Town		Coast	
	μm/yr	mil/yr	μm/yr	mil/yr	μm/yr	mil/yr
Tin	0.18	0.007	1.02	0.04	3.02	0.12
80Sn-20Zn	0.46	0.018	1.35	0.053	2.87	0.113
Zinc	0.53	0.021	1.45	0.057	2.90	0.114
	Weight loss, sheltered exposure test mg/dm^2					
	Jungle		Town		Coast	
Tin	1.6		11.3		40	
80Sn-20Zn	9.3		15.5		23	
Zinc	16.5		10.7		18.1	

Source: Ref 71

Table 11 Summary of atmospheric corrosion tests on tin-coated steel at four exposure sites

Coating method	Sheffield		Flanwryted Falls		Colshot		Congella	
	T(a)	*L*(b)	*T*	*L*	*T*	*L*	*T*	*L*
Electrodeposited from stannate bath	0.076	>11.9	0.077	2.4	0.063	1.0	...	...
Hot-dipped	0.015	5.9	...	...	...	...	...	...
Sprayed by molten-metal pistol	0.023	1.5(c)	...	...	...	...	...	...
	0.031	5.9(c)	0.034	0.6	0.037	0.7(c)	0.041	0.9(c)
	0.067	>11.9	...	...	...	...	...	...
Sprayed by powder pistol	0.096	3.0	...	...	0.102	0.8	...	...

(a) *T*, coating thickness in mm. (b) *L*, lifetime in years of coating as determined by rust appearing on more than 5% of the specimen. (c) Average of duplicate results that did not agree well. Source: Ref 73, 74

indicated that tin deposited by any of several methods appeared more protective in the industrial area than at the other sites. This behavior was attributed to the production of protective corrosion products in the pores of the coatings. Similar observations have been reported (Ref 75), and similar evaluations have been conducted using accelerated corrosion tests and outdoor exposure in urban Berlin (Ref 76). One conclusion, based on 1 year of exposure, was that reflowing of tin coatings improved their corrosion resistance, except in salt spray exposure. Also, deposits from an acid electrolyte were said to be better than those from a stannate bath.

Additional atmospheric corrosion test results have been reported (Ref 77–80). In one study, data were summarized from 10 years of exposure for tin-plated steel in industrial, marine, and rural atmospheres that included estimates of the added cost of SO_2 pollution. Another study included tropical exposures of samples in China in two environments. In the first environment, samples were mounted at 45° outdoors facing south. In the second, the racks were sheltered from solar radiation, wind, and rain. Recommendations based on 58 months of testing were that matte tin coatings 25 μm (1 mil) thick should not be exposed to either environment for more than 1 year and that the life of similar coatings 32 μm (1.2 mils) thick would be less than 2 years (Ref 80). The general conclusion, based on results of most of the aforementioned outdoor studies, was that the corrosion resistance of tin coatings, that is, their protection of steel, was not very high (Ref 22). In addition, this is reflected in the international standard ISO 2093-1973 covering tin coatings, which carries the following tin coating thickness recommendations:

	Minimum tin thickness			
	On steel		On nonferrous metals(a)	
Type of service	μm	mils	μm	mils
Exceptionally severe	30	1.2	30	1.2
Severe	20	0.8	15	0.6
Moderate	12	0.5	8	0.3
Mild	4	0.2	4	0.2

(a) Except brass

Tin Coatings on Nonferrous Metals. Tin coatings are widely used on nonferrous substrates, usually for one or more of the following reasons:

- Improvement and retention of solderability
- Excellent compatibility (low toxicity) with foods
- Prevention of galvanic effects between dissimilar metals
- Low electrical resistance

Not surprisingly, copper and copper-base alloys are the most frequently tinned nonferrous materials. Tin tends to be more active than copper and copper alloys, including the intermetallic tin-copper compounds. Therefore, accelerated corrosion of the tin coating may be expected in aqueous environments. Indeed, this is sometimes evidenced by black spots on a tin coating that result from localized corrosion around discontinuities. Although normally associated with total aqueous immersion, these black spots can also appear on outdoor exposure involving cyclic condensation (Ref 22).

Deterioration of the solderability of tinned copper during aging has been studied by many researchers, and accelerated test procedures have been devised to simulate the effect (Ref 81–83). Similarly, changes in the contact resistance of tin coatings have been related to increases in the thickness of the oxide film on its surface (Ref 84).

Special mention should be made of the corrosion behavior of tin coatings on brass in ordinary atmospheres. Zinc diffuses through tin coatings fairly rapidly; significant zinc levels are reached on the surface of a coating thickness of 7.5 μm (0.3 mil) in approximately 1 year (Ref 34). Zinc at the surface oxidizes readily to form white corrosion products that adversely affect its solderability and contact resistance. To avoid such problems, a 2.5 μm (0.1 mil) thick barrier layer of either copper or nickel is recommended over the brass (Ref 85).

Immersion Tin Coating. Contrary to the standard electromotive force series of metals, tin can be applied by immersion (chemical displacement) on copper. This is done by using a cyanide or a thiourea type of solution.

An outstanding application is tinning of the inside of copper tubing. Such tubing in coil form is used in water coolers. The tin prevents delivery of greenish water from new coolers and eventually disappears. By then, the copper surface has become conditioned to deliver water appearing as it did when it entered the cooler.

Tin-cadmium alloy coatings for the corrosion protection of tin were first studied by plating duplex coatings of tin on cadmium and then heat treating. These and later electrodeposited surfaces (Ref 86) were found to have phenomenal resistance to salt spray tests, and they were successfully used for some time to protect the engine components of naval aircraft (Ref 87).

Tin-cadmium coatings resemble tin-zinc coatings in appearance and behavior. Because cadmium is less effective at sacrificially protecting steel exposed at pores, the optimal cadmium content in the coating ranges from 25 to 50%. The initial electrolyte development discussed in Ref 86 was followed by an investigation of a range of alloys; it was concluded that the alloys performed better than cadmium alone in marine environments (Ref 88). Another study found that the attack on tin-cadmium coatings by organic vapors was less than for pure cadmium (Ref 89). In addition, tin-cadmium was found to be superior to tin-zinc when in contact with jet fuels or in hot synthetic oils. This work was supplemented by that described in Ref 90, which suggests that tin-cadmium alloys, particularly with a chromate surface treatment, performed better than cadmium coatings of the same thickness.

More recently, tin-cadmium alloy coatings were shown to provide better corrosion resistance to steel than duplex coatings of tin and cadmium (Ref 91). Lastly, zinc or tin-zinc coatings were found to be more protective to steel in industrial atmospheres than tin on cadmium or cadmium on tin, but this behavior was reversed in a marine environment (Ref 92).

Tin-Cobalt Coatings. As expected, the properties of tin-cobalt electrodeposits are similar to those for tin-nickel. Intermetallic deposits of SnCo (Ref 93, 94) or SnCo mixed with Sn_2Co (Ref 95) have been produced, and proprietary plating systems have been patented. These deposits are bright and are similar to chromium plate; most studies of their performance have concerned systems of steel coated by nickel, with a thin film of tin-cobalt applied to obtain a bright finish.

An evaluation of tin-cobalt coatings for their resistance to salt spray, NH_3, and in copper-accelerated salt spray (CASS) tests revealed that the deposit was resistant to all of these environments and was more ductile than tin-nickel electrodeposits (Ref 96).

Two researchers also tested systems of nickel plus tin-cobalt in CASS and outdoor exposure tests (Ref 97, 98). Their conclusions were similar even though different baths were used and minor differences in the deposits were obtained. Thus, their corrosion resistance was comparable to that for a nickel-chromium system in all but the more severe conditions.

Corrosion tests on coatings of 0.2 μm (0.008 mil) tin-cobalt over duplex bright nickel were compared with the same thickness of chromium (Ref 99). The tin-cobalt appeared markedly inferior to chromium in outdoor exposure and wear resistance but was reasonably satisfactory as a substitute for decorative chromium for indoor use.

Tin-Copper Coatings. Tin alloys close to the Cu_3Sn intermetallic composition (40 to 45% Sn) were once used as a material for mirrors; hence the name speculum. These alloys resemble silver in brightness and appearance; they find some use as tableware and on bathroom fixtures but are not used outdoors, where they rapidly turn dull and gray. However, even the indoor corrosion resistance of the alloy is seriously impaired if the composition is not optimum (~42% Sn), and the subsequent need for close control of plating conditions has prevented large-scale development of the coating.

Tin-bronze deposits containing approximately 12% Sn were reported to be superior to copper as an undercoat for nickel-chromium coatings with regard to weathering behavior (Ref 100, 101). Some results were also reported with tin-copper coatings over steel in industrial and marine environments (Ref 102).

Tin-lead coatings with a wide range of composition are applied by hot dipping or electrodeposition. Steel strip coated with tin-lead

alloys by hot dipping and sold as sheet or coil carries the general designation of terneplate. The tin content varies from 2 to 20%. In general, the higher the tin content, the lower the porosity of the terneplate and therefore the greater the protection afforded to the substrate. Like tin coatings, tin-lead coatings do not offer any galvanic protection to steel in the atmosphere; protection against rusting depends on coating continuity and on the formation of protective corrosion products. A comparison of the behavior of a Pb-12Sn coating with pure tin and lead revealed that both lead-containing coatings developed white films believed to be $PbSO_4$ (Ref 73).

In a more comprehensive study, a range of electrodeposited tin-lead coatings obtained with different bath additives was evaluated (Ref 58). The performance of a Pb-5.5Sn coating in salt spray and outdoor testing was found to be superior to pure lead and lead-tin alloys containing tin additions of 7, 10, or 15%. The Pb-10Sn and Pb-15Sn alloys were comparable in behavior to pure tin. These results were partially supported by those of another study, which consisted of atmospheric exposures at three sites on electrodeposited lead and coatings of Pb-5Sn and Pb-14Sn (Ref 103). Superior protection was achieved with the tin-containing alloys at all sites, which included severe industrial, rural, and marine environments.

The results of tests on a number of commercial terneplate compositions in accelerated corrosion tests, SO_2, humidity, and salt spray as well as outdoor exposure in both industrial and marine environments are given in Ref 104. Performance was assessed largely on the degree of rusting of the underlying steel after 12 months of exposure. Lead-tin alloys showed greater resistance to chloride attack than lead-antimony alloys. It was also noted that coverage of the steel increased with the tin content of the alloy and that resistance of the coating to attack appeared to increase in both chloride-rich and humid conditions.

Tin-Nickel Coatings. Alloys containing 18 to 25% Ni can be deposited from a cyanide-stannate bath to give bright coatings with good resistance to HNO_3 (Ref 105). However, because of their high hardness and brittleness, no interest has been shown in these coatings. Similar results have been reported with a complex pyrophosphate bath (Ref 106). Primary commercial interest has centered on the intermetallic compound SnNi (containing approximately 67 wt% Sn), which is readily deposited from mixed chloride/fluoride electrolytes (Ref 107, 108).

The SnNi intermetallic is metastable and does not transform to a mixture of other intermetallics unless it is heated (Ref 109). The deposit is hard, bright, and has reasonable solderability. It also has good wear resistance and remarkable resistance to attack by a wide range of solutions. For these reasons, tin-nickel coatings have found use as decorative corrosion-resistant finishes for balance weights, drawing instruments, pistons in automobile braking systems, and some food contact applications. Recommended coating thicknesses for this alloy coating have been specified in ISO 2179 1972 as follows:

	Thickness	
Intended duty	μm	mil
Severe environments	25	1
Moderate environments	15	0.6
Mild environments	8	0.3

For coatings on steel intended for moderate or severe service, an undercoat of copper, tin, or bronze with a minimum thickness of 8 μm (0.3 mil) is also specified, and porosity tests are required.

Studies of tin-nickel coatings showed them to be unaffected by atmospheres containing SO_2 or H_2S (Ref 110–112). This work also indicated that these coatings retained their brilliance more readily than nickel-chromium in positions sheltered from rain. Similar conclusions were reached in other investigations (Ref 113, 114), taking into consideration the undercoatings used for both alloy deposits on steel. On the other hand, nickel-chromium deposits were reported as superior to tin-nickel in marine environments (Ref 115).

Within the past 10 years, studies of the corrosion resistance of tin-nickel deposits have centered on their effect on the electrical contact resistance of this alloy, either alone or with a thin coating of gold. The contact resistance of tin-nickel is sufficiently low to merit consideration for moderate-voltage applications (approximately 50 V), but too high for low-voltage uses. Several extensive studies have been reported in this field (Ref 116, 117). This effect on contact resistance is largely a result of the insulating passive film that forms on SnNi and the high hardness of the material. An excellent review of the work in this field is available in Ref 22. It is generally agreed that tin tends to concentrate at the surface of tin-nickel electrodeposits, but no adequate explanation of the oxidation behavior of this alloy is currently available.

The resistance to attack of the coating by various acids and chemicals has been studied, and the results are given in Table 12, which also compares these with coatings of tin and nickel (Ref 118). Generally, the results show that tin-nickel has a high resistance to attack by acids, alkalis, and several neutral salt solutions. This behavior is attributed to the presence of a passive air-formed film.

Tin-Zinc Coatings. The general shortage of cadmium after World War II led to an interest in the possibilities of tin-zinc coatings for the protection of steel. One of the first studies to explore this possibility compared the behavior of tin-zinc alloy coatings containing 8 to 72% Zn with that of electrodeposited coatings of tin, zinc, and cadmium and with hot-dipped zinc (Ref 119). Coatings 8 to 25 μm (0.3 to 1 mil) thick were compared to exposures to a humidity cabinet, salt spray, and hot water. Coating failure occurred as a result of zinc dissolution such that deposits containing low percentages of zinc did not protect the steel from rusting at pores, but coatings with more than 40% Zn soon developed voluminous white corrosion products at the surface. The best overall results were indicated for tin-zinc coatings with compositions near Sn-25Zn, which were superior to zinc and cadmium in salt spray and were superior to zinc but approximately equal to cadmium in the humidity test. This work also suggested that chromate passivation treatments improved the overall performance of tin-zinc coatings, making them less susceptible to staining by finger or grease marks.

Table 12 Corrosion resistance in various media of tin, nickel, and tin-nickel alloy

	Weight losses, mg			
Solution(a)	Tin	Nickel	Tin-nickel	Change in appearance of tin-nickel coating
1 *M* hydrochloric acid	61.5	41.5	24.8	Covered by adherent brown film
0.5 *M* sulfuric acid	19.5	25.6	14.5	Slightly darkened
1 *M* nitric acid	205.0	97.6	1.1	None
0.05 *M* sulfurous acid	0.2	725.0	0.5	None
1 *M* formic acid (pH 1.8)	22.1	35.5	nil	None
1 *M* acetic acid (pH 2.4)	22.2	43.6	0.6	Very slightly darkened
0.5 *M* oxalic acid (pH 1.1)	12.3	16.4	12.0	Etched on immersed area; dark stain at waterline
1 *M* lactic acid (pH 1.9)	18.0	17.8	2.1	None
0.5 *M* tartaric acid (pH 1.7)	10.6	10.0	0.5	None
0.3 *M* citric acid (pH 1.9)	12.0	19.2	0.4	None
0.5 *M* phenol (pH 2.3)	nil	0.3	nil	None
1 *M* sodium chloride	0.5	1.0	0.8	None
Seawater	1.4	0.3	1.0	. . .
0.3 *M* ferric chloride (pH 1.5)	290.0	303.0	2.3	None, except slight local action on edge
Sodium hypochlorite (40 g/L available chlorine)	1.3	625.0	22.0 and 67.0	Bottom edge badly etched; none elsewhere
Sodium hypochlorite (0.1 g/L available chlorine)	1.8	1.8	0.8	None
1 *M* sodium hydroxide	36.6	0.2	0.7	None

(a) Specimens (75×25 mm, or 3×1 in.) vertically suspended in solutions at 30 °C (85 °F) with a length of 58 mm (2.3 in.) immersed for 24 h. Source: Ref 118

This study was followed by a number of others that reached the same general conclusion about the usefulness of tin-zinc coatings for protecting steel against atmospheric corrosion (Ref 72, 76, 120, 121).

Another comprehensive study compared coating corrosion resistance in urban and marine environments (Ref 122). The order of merit (best to worst performance) in urban exposures was zinc, 50Sn-50Zn, 80Sn-20Zn, and cadmium. For marine exposures, 50Sn-50Zn and zinc were superior, while 80Sn-20Zn and cadmium performed approximately the same. Details on the results of the marine exposures are given in Table 13.

The effectiveness of tin-zinc coatings in protecting steel nuts and screws was studied by exposing these coatings to suburban, industrial, and marine environments in contact with aluminum plates (Ref 123). Although failure of the 80Sn-20Zn coating was indicated by rusting of the steel more quickly than with zinc or cadmium, the presence of the 80Sn-20Zn was observed to prevent rapid attack of the aluminum. Another advantage was the absence of hygroscopic products on the tin-zinc; that is, rings of moisture tended to form around the corrosion products on nuts and screws coated with zinc and cadmium, but this behavior was not noted with the 80Sn-20Zn.

Tin-zinc alloys have also been used to solder aluminum (Ref 124). Again, it was found that corrosion resistance of the solders in a tropical atmosphere was a function of zinc content. After nine months of exposure, the 80Sn-20Zn alloy appeared to be the most resistant to attack and had the best retention of strength.

In another study, contact resistance measurements were used to follow the progress of corrosion on binary alloys of tin with zinc, lead, antimony, and cadmium on steel in a rural outdoor atmosphere (Ref 125). It was noted that tin-zinc and tin-cadmium coatings maintained a lower contact resistance than equal thicknesses of tin, tin-lead, or tin-antimony alloys after two months of exposure.

Table 13 Relative ability of different coatings to prevent the rusting of steel in a marine atmosphere

	Months to first appearance of rust for coating thicknesses indicated, μm		
Coating	**7.5**	**12.5**	**25**
Zinc	18	33	36
Passivated zinc	18	18	36
50-50 tin-zinc	25	35	>48
Passivated 50-50 tin-zinc	29	35	>48
80-20 tin-zinc	9	18	36
Passivated 80-20 tin-zinc	13	21	36
Cadmium	8	21	34
Passivated cadmium	13	21	25
Tin	1	1	1

Source: Ref 122

The most recent studies with tin-zinc coatings explored the effects of four passivation treatments on the resistance to attack of a Sn-25Zn coating by a salt fog and in cyclic humidity (Ref 126). An electrolytic treatment using sodium dichromate ($Na_2Cr_2O_7$) was found to be superior to the others and was particularly outstanding in the salt fog. The other treatments, in decreasing order of merit, used passivation based on electrolytic molybdate, electrolytic tungstate, and nonelectrolytic chromate solutions.

Another investigation concluded that tin-zinc solders exhibit a significant decrease in shear strength after immersion in 3% sodium chloride (NaCl)-0.1% hydrogen peroxide (H_2O_2) solutions (Ref 124). However, other soft solders, including tin-cadmium and tin-antimony alloys, also behaved in the same manner.

Tinplate

As noted earlier, the term *tinplate* is reserved for a low-carbon steel strip product coated on both sides with a thin layer of tin. For almost 200 years, tinplate has been the primary material used to make containers (tin cans) for the long-term storage of food. Most of the tinplate manufactured is used to make food cans, and nearly all food cans are made of tinplate.

Modern tinplate is much more sophisticated than a simple coating of tin on steel. To achieve the demanding deep-drawing properties necessary for the production of can bodies for two-piece can manufacture, the steel base for tinplate is often continuously cast using the most current technology. Inclusions or other defects in the steel may otherwise cause breakage in the can-body drawing operation. Because the economics of canmaking depend on high-speed operation using a continuous coiled strip, such breakage cannot be tolerated due to the lost production time; therefore, the steel must be as clean as possible.

In preparing the base steel, the metal is processed to strip form, the final step being a cold reduction that brings the strip to a thickness that is typically from 0.15 to 0.50 mm (6 to 20 mils). Next, the strip is annealed and then temper rolled to obtain the desired mechanical properties. At the final stage of temper rolling, textured rolls can be used to produce a special surface finish for particular applications. A cold reduction in place of temper rolling yields a product that is termed double reduced.

The coiled steel is now ready for the tinplate line. It is first welded to the end of the previous coil to form a continuous strip for processing. The strip passes through cleaning and pickling sections to prepare it for plating, then immediately through the plating cells, where up to 11.2 g/m^2 (1 g/ft^2) of tin is deposited. Any one of three different electrolytes can be used, depending on the other details of the installation, and strip speeds typically approach 600 m/min (1970 ft/min). More details of tinplate production and commerce are available in Ref 127 to 130.

The production steps that typically follow plating create additional layers in the tinplate structure that significantly affect corrosion properties. Upon exiting the plating cells, the tinplate has a matte surface that is usually reflowed by momentarily melting the tin coating in a resistance or induction heating unit. In doing so, a thin layer of tin-iron intermetallic compound is formed at the tin/steel interface. Next, an extremely thin passivation film based on chromium oxide is created by immersion or spraying of chromic acid (H_2CrO_4) on the tinplate surface or by passing the tinplate through a solution of $Na_2Cr_2O_7$, with or without the simultaneous application of electrical current. Finally, a very thin, uniform layer of lubricant, usually either dioctyl sebacate or acetyl tributyl citrate, is electrostatically applied.

Therefore, as supplied to the can maker, the typical tinplate product consists of five layers, the innermost being a steel sheet approximately 200 to 300 μm (7.8 to 11.7 mils) thick. This steel is covered on each side with perhaps 0.08 μm (0.004 mil) of tin-iron intermetallic compound. The next layer is free tin that is perhaps 0.3 μm (0.012 mil) thick, with a passivation film of approximately 0.002 μm (0.00008 mil) and an oil film also approximately 0.002 μm (0.00008 mil) thick. All five layers affect corrosion behavior.

General Properties. Although the unique corrosion properties of tinplate have kept it the material of choice for food cans, other useful properties should be mentioned. Until a few years ago, all food cans were soldered, and tin coatings were used quite often for their excellent solderability. Can welding has recently replaced soldering, and the favorable electrical contact properties of tinplate have made it very amenable to high-speed resistance welding.

The strength of the steel base gives tin cans the durability to withstand the filling, sterilization, and transportation phases of processing. Because a wide range of mechanical properties is possible, the steel base properties can be adjusted, for example, to maximize strength and stiffness, to maximize ductility and elongation, or to minimize directional properties.

Corrosion Resistance in Sealed Cans. A cursory glance at a seawater galvanic series would lead one to expect tin to be more noble than steel. Therefore, with a very thin coating of tin, the rapid dissolution of iron at any plating pores, scratches, or other breaks in the coating would be anticipated, resulting in pitting corrosion and eventual perforation of the tinplate. Fortunately, inside the sealed can of food, the situation is very different.

The good performance of the tinplate food can begins with the ability of tin to form chemical complexes with a variety of organic liquids, especially those found in foodstuffs. This fact reverses the situation described in the preceding paragraph; therefore, tin becomes more active than steel and thus becomes a sacrificial anode,

greatly diminishing the rate of dissolution of the iron. Once in solution, the tin ions have a very strong inhibiting effect on iron dissolution, because the tin may actually plate out on the exposed steel to form a thin surface layer of tin-iron intermetallic that would be more noble than the steel surface it covers (Ref 25).

With the available atmospheric oxygen limited to only that in the headspace (the volume between the top of the contents and the bottom of the can lid), dissolution of tin is usually rapid only at the very beginning of storage, that is, until the cathodic reaction involving this small amount of oxygen has gone to completion. This effect is desirable because it provides quick protection of the steel. Too large a headspace, however, may allow too much tin to be dissolved, which would allow iron dissolution and probably hydrogen evolution. Hydrogen evolution usually leads to swells, or bulging can ends, a condition the consumer has come to recognize as the sign of can failure. A similar situation applies if a leak in the can allows the free entry of oxygen; the contents are spoiled by iron dissolution, but swelling is not expected to occur.

The small amount of tin dissolved in the food passes easily and quickly through the human body with no known effect, although there is circumstantial evidence that tin is an essential element for human well-being. Too much tin, that is, of the order of 1000 ppm, in the food may cause gastric distress in sensitive individuals. This distress lasts only as long as the irritant is present, and no permanent damage is expected. As a precaution, most governmental regulations limit the tin content of food containers to well below this threshold, typically at a level of approximately 250 ppm. This lower level is not known to have an effect on any individuals and appears to provide a substantial margin of safety while assuring the effectiveness of tin in preserving the food.

Until a decade ago, food cans were typically of three-piece soldered construction. Recent concerns over the lead content of foods, however, resulted in the abandonment of soldering in favor of welded construction or of two-piece (no side seam) fabrication, even though this source of lead was probably a small component in the overall human intake of lead. Both of these newer techniques appear to produce improved can integrity in general, although the soldered tinplate container is capable of many years of safe, stable shelf life. Soldered construction is still used for dry packs, in which the absence of a liquid food component eliminates the migration of lead into the packed product, and of course for nonfood items, because there is no reason to change from a successful time-tested production method.

Can Corrosion Problems. Even with nearly 200 years of experience and some of the strictest quality-control programs imaginable, the canning industry is not perfect. Although not at all common, failures tend to be serious when they occur, because the economics of efficient food production depend on large, rapid production runs. The slightest misjudgment can result in a problem during long-term storage.

The first consideration in matching a given food product to the appropriate can has always been the thickness of the tin coating, as indicated previously. Recent years have seen more extensive use of lacquers to provide an inert barrier against any metal dissolution (see the section "Lacquers" in this article). However, the inevitable defects in lacquer coverage make the tin coating the last defense against corrosion.

Tin is necessary for pale (uncolored or yellow) fruits and many vegetables to preserve the taste and color of the product. Suitable cans are made of plain (unlacquered) tinplate with a coating weight (the usual way of expressing the thickness) of 8.4 to 11.2 g/m^2 (0.8 to 1 g/ft^2). A special grade of tinplate called grade K uses an altered tin-iron intermetallic layer (probably thicker and more continuous over the tin/steel interface) to improve corrosion resistance with these products (Ref 2). Grade K tinplate then allows the use of tin coatings at the lower end of the thickness range.

Parenthetically, it may be mentioned that inorganic tin chemicals have been used as intentionally added preservatives for some food products that have been packed in containers other than tin cans. This fact emphasizes the importance of tin in preserving the organoleptic properties of foodstuffs.

Certain other vegetable packs, such as asparagus, green beans, and tomato-based products, would benefit from tin availability but are strong detinners. This rapid dissolution of tin may produce an unsightly interior can surface or tin levels above the regulatory limit. The usual remedy is to use lacquer as an inert barrier, but this practice involves the possibility of even more rapid and concentrated attack at any interior scratch or other defect in coverage. Double lacquering reduces this possibility. Dark fruit packs, such as cherries, behave similarly in that strong detinning may produce undesirable color changes, which can be controlled by double lacquering.

Dairy products can be stored in plain tinplate cans, but it is advisable to use a weak passivation film, because dark stains may be produced. Sodium dichromate ($Na_2Cr_2O_7$) and a sodium bicarbonate (Na_2CO_3) treatment have each proven successful for these packs.

A stronger-than-normal passivation film (or, more precisely, one with higher metallic chromium content) is used to prevent staining from sulfur, which is a naturally occurring contaminant of some meat products and soups, for example. Tin sulfide stains may be unsightly on the can interior surface or may be protective enough of the tin surface to reverse the tin-iron polarity and cause rapid iron dissolution. Too thick a passivation film may adversely affect lacquerability; therefore, again, correct specification and quality control are needed to produce the required product. An alternative is special lacquers containing zinc compounds that react with the sulfur to form less objectionable, nonstaining sulfides.

Sulfur can also have a deleterious effect if present as an impurity in the base steel, as can copper, phosphorus, and silicon. In these cases, impurity control in steelmaking provides a usable base material. Various tests are used to provide the suitability of the complete tinplate product (see the section "Corrosion Testing of Coatings" in this article).

Still another source of sulfur is as a residual chemical contaminant in the foodstuff. Nitrate contamination is also possible as plant uptake from fertilizers. Nitrates and certain other naturally occurring and additive organic compounds can act as cathode depolarizers, which, by increasing cathodic activity, require an increase in anodic activity, that is, tin dissolution, probably leading to early pack failure.

The wide variations in natural food products, even the same product produced in different locales, make it impossible to be more specific regarding container-product interactions. Tinplate makers and users always find it necessary to perform pack testing, that is, preparing larger samples of the canned product and observing their performance over several months of storage. Although this testing is expensive, there is no alternative, given the wide variations in product chemistry. A laboratory simulation test has recently been developed that may help in screening variables for subsequent pack testing (Ref 131).

Lacquers, also called enamels, are combinations of various resins modified with various additives (Table 14). These formulations (only the main ingredients are listed in Table 14) must produce an inert, protective film on the tinplate surface at a reasonable cost. To keep costs low, the lacquers must wet well over a surface that has received minimal preparation. In fact, cost is often one of the primary reasons for using lacquers, because they tend to substitute for the use of thicker tin coatings. In covering up so much of the sacrificial anode, however, the integrity of the lacquer film becomes extremely important in determining can performance due to the risk of more concentrated attack at defects.

Difficulties in lacquer application appear as eyeholing, which consists of roundish areas of uncovered tinplate surface in the cured coating. These eyeholes may occur singly or as parts of larger affected areas. They may be caused by incompatibility between the lacquer and the surface to be coated, either the oil that must be displaced or the passivation film to which the lacquer must adhere. Dust contamination or improper tinplate surface temperature are other possible causes. Heating the tinplate before lacquer is applied usually alleviates all of these potential problems.

Once successfully applied, the lacquer must adhere to the tinplate surface through processing and storage. It must not crack during mechanical deformation, as in a beading process in which circumferential expansions in the sidewall are used for strengthening. The lacquer must also

adhere through the heat-processing steps. If the lacquer cracks, there may be rapid attack in the crack. The tin layer under the crack is corroded away (undermining corrosion), causing collapse of the lacquer, widening of the crack, and exposure of the steel. Undermining corrosion may also cause failure after initiation at scratches or other lacquer defects that may occur during processing, transportation, or storage. Corrosion proceeds rapidly in such cracks because of their small relative areas. Therefore, lacquers are usually applied as two coats; additional coats are applied to particularly sensitive corrosion areas, such as the side seam in three-piece can technology.

Undermining corrosion becomes more severe with increased tin coating weights, because there is more of the readily dissolvable tin under the defect. Therefore, lacquer detachment is a greater possibility, leading to consumer complaints. As outlined previously, the use of thinner tin coatings to combat undermining corrosion also increases the possibility of pack failure due to iron dissolution.

External corrosion of tinplate cans follows more closely the classical galvanic behavior described previously. The ready availability of oxygen and the lack of complexing agents make the tin coating more noble, and the unprotected steel will readily rust at plating pores and scratches in the coating that expose the underlying base steel. Coils or sheets of tinplate in transit from tinplate production to canmaking, as well as unfilled cans, are equally susceptible to this kind of deterioration.

A thicker tin coating will provide improved protection by reducing the steel exposure through plating pores. The passivation film also helps to provide corrosion protection. Because both of these factors are usually limited by other considerations, special precautions are taken to minimize moisture and pollution exposure. Where water is an essential part of the processing, as in steam retorting of cans or the subsequent cooling, the water is deoxygenated and treated with corrosion control agents. Minimizing the time of exposure to water is also practiced, as is the use of wetting agents to promote drying of the cans.

The paper to be used for labels and the materials to be used for shipping containers must be carefully selected. The presence of chloride or sulfate compounds in the paper, for example, may create a serious corrosion problem during storage. Wooden shipping cases may release corrosive organic vapors, and these and other materials can promote moisture exposure during transit. Again, it is difficult to be specific, because various foods are packed and then shipped literally all around the world.

A special type of corrosion may occur during transportation or handling of the tinplate. Fretting corrosion results from the intimate contact of two tinned surfaces combined with small relative movements between the two. The rubbing together of the surface asperities produces erosion, and the increased surface area yields more oxidation. Oxide particles are formed, and they act as very effective abrasives to cause additional damage to the surface. Fretting corrosion, therefore, typically features fine spots of dark, embedded tin oxide particles in areas of the tinplate that were subjected to pressure, such as from steel strapping used to secure a bundle of tinplate sheets. The most effective preventive measure is to pack the tinplates so as to minimize the relative movement of the tinplate surfaces. One purpose of the lubricant applied to the tinplate is to reduce fretting corrosion.

Corrosion Testing of Coatings

The preceding sections point out the excellent corrosion resistance of tin and tin alloys and how this property is used to advantage by coatings on stronger structural metals, typically steel or a copper alloy. Because the tin is more noble than the base metal in normal environments, complete coverage of the base metal is important for preventing rapid attack at any pores in the coating. Therefore, porosity testing is valuable in predicting corrosion performance; however, because porosity tends to decrease with increasing coating thickness, thickness measurements often provide a more convenient indication of suitability.

In fact, most international and national specifications stipulate certain minimum coating thicknesses for anticipated service conditions. For example, ASTM B 545 specifies a minimum tin thickness of 5 μm (0.2 mil) for mild service conditions or where solderability is a primary concern (Ref 132). For exceptionally severe service conditions, such as where abrasion is combined with corrosion, the specification calls for a minimum tin thickness of 30 μm (1.2 mils). Between these extremes, for so-called normal conditions, 20 μm (0.8 mil) on steel or 8 μm (0.3 mil) on copper alloys is the specified minimum (Table 9).

The test methods described subsequently are suited only to the purpose for which they were designed. Corrosion resistance can only be defined relative to a metal and to a particular environment; it is not an absolute property (Ref 2).

Coating Thickness Measurements. Several commercial instruments are available for measuring tin and tin alloy coating thicknesses. They have been developed to satisfy the need for a nondestructive test, and each has advantages and disadvantages.

Perhaps the simplest are the magnetic methods, which require the base metal to be magnetic or ferromagnetic. The tests determine how the coating alters the strength of a magnetic field that is passed through the coating when a magnet is

Table 14 Main types of internal can lacquer

General type of resin and components blended to produce it	Flexibility	Sulfide-stain resistance	Typical uses	Comments
Oleo-resinous (drying oil and natural or synthetic resins)	Good	Poor	Acid fruits	Good general-purpose range at relatively low cost
Sulfur-resistant oleo-resinous (added ZnO)	Good	Good	Vegetables and soups (especially can ends or as topcoat over epoxy phenolic)	Not for use with acid products; possible intense green color with such vegetables as spinach
Phenolic (phenol or substituted phenol with formaldehyde)	Moderate-poor	Very good	Meat, fish, vegetables, and soups	Good at relatively low cost, but film thickness is restricted by flexibility
Epoxy-phenolic (epoxy resins with phenolic resins)	Good	Poor	Meat, fish, vegetables, soups, beer, and beverages (first coat)	Wide range of properties can be obtained by modifications
Epoxy-phenolic with ZnO (ZnO added)	Good	Good	Vegetables and soups (especially can ends)	Not for use with acid products; possible color change with some green vegetables
Aluminized epoxy-phenolic (metallic aluminum powder added)	Good	Very good	Meat products	Clean but rather dull appearance
Vinyl, solution (vinyl chloride-vinyl acetate copolymers)	Excellent	Not applicable	Spray on can bodies, roller coating on ends, as topcoat for beer and beverages	Free from flavor taints; sensitive to soldering heat and not usually suitable for direct application to tinplate
Vinyl, organosol, or plastisol (high-molecular-weight vinyl resins suspended in a nonsolvent)	Good	Not applicable	Beer and beverage topcoat on ends, bottle closures, drawn cans for sweets, pharmaceuticals, and tobacco	Same as for vinyl solutions, but giving a thicker, tougher layer
Acrylic (acrylic resin, usually pigmented white)	Very good in some ranges	Very good when pigmented	Vegetables, soups, and prepared foods containing sulfide stainers	Attractive, clean appearance of opened cans
Polybutadiene (hydrocarbon resins)	Moderate-poor	Very good if zinc-oxide is added	Beer and beverages first coat; vegetables and soups if with ZnO	Cost and therefore popularity depend on country

positioned on the coating surface. The force required to remove the magnet is proportional to the tin thickness. The accuracy of the determination is enhanced by the use of accurate standards of known coating thickness to which comparisons can be made. The surface condition of the test sample is obviously very important for accurate measurements, because the magnet is brought into contact with that surface.

The β backscatter method directs a beam of electrons (β particles) at the surface to be measured and detects particles scattered back in the direction of the source. This backscatter is in proportion to the coating thickness, and the instrument reads thickness after careful calibration to standards. The accuracy of the method relies on proper alignment of the source, sample, and backscatter collector, and periodic recalibration is important to allow for the gradual depletion of the radioactive source that generates the electron beam. Because the method does not require contact with the surface to be measured, it is particularly useful for high-speed continuous plating operations.

Somewhat similar is the x-ray fluorescence method, which directs x-rays onto the test sample and records secondary emissions that are caused by the excitation of the coating and/or base metal. The secondary emissions are not only in proportion to the coating thickness but are also characteristic of the coating alloy. X-ray fluorescence, therefore, provides a quick alloy analysis in addition to the coating thickness measurement. It also has the advantage of being noncontacting.

Among the destructive tests are the coulometric and microscopic methods. The coulometric test involves essentially a controlled stripping or deplating of the coated surface within an accurately determined area. An electrical current is applied through an electrolyte, resulting in anodic dissolution of the coating. When the coating is removed, a voltage change signals the end of the test. The amount of current passed through this small test cell is proportional to the amount of material removed and therefore implies a coating thickness.

In the microscopic method, the surface to be measured is simply sectioned and then examined optically. A direct measurement of the coating thickness is possible without using plated standards, but there is the potential problem of subjective evaluation. The other metallurgical observations that can be made on a cross section often constitute the reason for using this method.

A few other methods are available for coating thickness measurements. A micrometer can be used before and after application of the coating for thicker coatings. Gravimetric methods involve weighing parts before and after coating or before and after coating dissolution and then calculating an average thickness based on the weight difference (coating weight) and the surface area from which it was dissolved. A drop test involves a stream of droplets of, for example, trichloroacetic acid solution, applied to a specific spot at a certain rate until the coating is penetrated, with the time to penetration being an indication of the coating thickness. In all test methods, the thinness of the typical tin alloy coating makes it important to perform the test carefully.

Porosity and Rust Resistance Testing. Although thickness testing can be performed quickly to provide process control feedback, common industrial practice includes porosity testing of statistically selected samples. This testing can predict performance more accurately by revealing the extent of variations in coating coverage that may go unobserved in thickness testing, because the latter tends to give an average over an area. The porosity test often uses simulated service conditions, usually with some accelerating factor to provide results more quickly.

Although techniques have been devised for automated test evaluation, most porosity tests rely on a visual assessment of the results. Therefore, the corrosive medium is often selected to give a readily visible corrosion product. This choice facilitates the reporting of both the quantity and distribution of porosity, along with any abnormalities in coverage.

For tin coatings on steel, SO_2, ferricyanide, or ammonium thiocyanate (NH_4CNS) tests have been used, and either of the first two is suitable for testing tin-lead coatings on steel. Tin coatings on copper alloys can be evaluated by using SO_2 or ammonium persulfate ($(NH_4)_2S_2O_8$) tests. Tin-nickel coatings are tested in a manner similar to tin coatings.

The sample of the coated metal is exposed to the corrosive medium for a specified time, perhaps at an elevated temperature to accelerate the corrosive action. After exposure, the test panel is removed and examined for rust or corrosion product. The number of attacked pores per unit area or the percentage of attacked area compared to the total area is the criterion for evaluation.

Solderability. Because tin and tin alloy coatings are so widely used to provide long-term protection to a solderable surface, much effort has recently been devoted to developing solderability tests, including accelerated aging techniques to predict shelf life. Indeed, if the coating is applied molten or if a plated coating is reflowed (also called flow melting), a form of solderability test has already been done in the sense that wetting difficulties will have been revealed during processing.

The simplest solderability test is a vertical dip of the properly fluxed sample into a solder pot. After a typical dwell time of approximately 3 s, the sample is withdrawn, the coating is allowed to solidify, and the surface is visually inspected for evidence of good wetting.

The other solderability tests tend to be variations of this dip test. In the rotary dip test, the sample is fixed to the end of a rotating arm, which is aligned so that the sample is passed through the upper surface of a solder bath. This test physically simulates the relative motion of surface and bath as it may happen in a wave-soldering operation. By testing a series of samples, a minimum time for complete wetting can be established and compared to the required standards. Another popular solderability test, the surface tension balance test, is also a variation of the vertical dip test. The most significant difference is that the sample is suspended from an instrumented test rig that accurately records the forces that act on the sample during the dip into the solder pot. If wetting occurs, a force develops that attempts to pull the sample into the bath. The speed with which this force develops and its magnitude are two of the sensitive parameters often specified in standards for this test.

As indicated previously, accelerated aging techniques are under investigation. The problem is that the current solderability tests may give a good correlation to actual soldering behavior in the short term, but none can predict soldering performance weeks or months from the time of testing; the latter is almost always more important. Solderability tends to maintain a certain level over the shelf life of the part and then to degrade very quickly to an unacceptable level. Aging the samples in steam for 16 to 24 h seems to give tin or tin-lead coatings the correct temperature and moisture exposure to cause poor samples to degrade. This procedure has won some acceptance for estimating the effects of 6 months to 1 year of normal storage, but only for tin-base coatings.

Special Test for Tinplate. Because of its commercial importance, tinplate is subjected to several special tests. Coating weights (thicknesses) are often determined coulometrically, although some installations use β backscatter or x-ray fluorescence methods to obtain a quick continuous evaluation for process control. Porosity tests may involve the SO_2 or NH_4CNS tests mentioned in the section "Porosity and Rust Resistance Testing" in this article. Other tests determine the presence of tin oxides, the composition of the passivation film, and the coverage of the oil film, all of which are important for good corrosion performance. Several of the special tinplate tests are outlined as follows.

The Iron Solution Test (Ref 2). The tinplate sample is exposed to a solution containing sulfuric acid (H_2SO_4), H_2O_2, and NH_4CNS under controlled conditions. The amount of iron (in micrograms) dissolved during the fixed test period is termed the iron solution value. This value reflects to some extent the continuity of the coating; however, it may also be influenced by the quality of the steel, because the test solution was devised as one in which exposed steel is on the threshold of protection by tin.

The Pickle-Lag Test (Ref 2). The steel base of the tinplate is exposed to 6 *M* hydrochloric acid (HCl) under defined conditions, and the time before hydrogen is steadily evolved is measured. This time period (in seconds) is the pickle-lag value; the lower the value, the better. A high value is associated with subsurface oxidation during annealing, and it seems likely that this defect may influence both the continuity of the

coating and the continuity of the tin-iron alloy layer.

The Alloy-Tin Couple (ATC) Test (Ref 2). A sample of the tinplate from which the free tin layer has been removed, but with the tin-iron intermetallic layer intact, is coupled to a relatively large electrode of pure tin in deoxygenated grapefruit juice. The current flowing between the test sample and the tin electrode is measured; its value after 23 h is termed the ATC value. The purpose of this test is to assess the restraining effect of the tin-iron compound layer on the cathodic efficiency of the metal exposed when the free tin layer is dissolved from part of the surface. Thus, test results are affected by the continuity of the compound layer and by the characteristics of the steel.

The Tin Grain Size Test (Ref 2). The tin coating is lightly etched, and the size of the crystals revealed is expressed on the ASTM International Standard Scale for the grain size of nonferrous metals. Increased grain size is considered beneficial. This is based on experience without, as yet, support from experimental measurements, but the effect of this factor is most likely to be seen in the initial rate of tin dissolution. It has been shown that different crystal faces of tin have differing dissolution and oxidation rates, and perhaps the effects of crystal orientation and crystal size are associated. It is also possible that impurities segregated at the grain boundaries produce a change related to boundary length and thus to grain size.

Other Tests. A cysteine hydrochloride ($C_3H_7O_2NS \cdot HCl$) staining test measures the tendency toward sulfide staining. A heating test simulates stoving (baking) to reveal any tendency toward discoloration during that operation. Finally, a series of tests can be used to evaluate lacquerability and lacquer adhesion to the tinplate. Additional information on these specialized tests is available in Ref 2, 129, and 130.

ACKNOWLEDGMENT

This article is based on Daniel J. Maykuth and William B. Hampshire, Corrosion of Tin and Tin Alloys, *Corrosion,* Volume 13, *ASM Handbook,* ASM International, 1987, p 770–783.

REFERENCES

1. W.B. Burgers and L.J. Groen, *Faraday Soc. Discuss.,* Vol 23, 1957, p 183
2. S.C. Britton, *Tin Versus Corrosion,* Publication 510, Tin Research Institute, 1975
3. E.S. Hedges, *Tin and Its Alloys,* Edward Arnold, Ltd., 1960
4. S.C. Britton and M. Clarke, *Trans. IMF,* Vol 40, 1963, p 205
5. S.C. Britton, *Trans. IMF,* Vol 52, 1974, p 95
6. N.A.J. Sabbagh and H.J. McQueen, *Met. Finish.,* March 27, 1975
7. L. Kenworthy, *Trans. Faraday Soc.,* Vol 31, 1935, p 1331
8. L. Kenworthy and J.M. Waldram, *J. Inst. Met.,* Vol 55, 1934, p 247
9. W. Finkeldy, *Symposium on Outdoor Weathering of Metals,* American Society for Testing and Materials, 1934, p 69–87
10. Report of Committee B3, *Proc. ASTM,* Vol 34 (No. 1), 1934, p 221
11. Report of Committee B3, *Proc. ASTM,* Vol 35 (No. 1), 1935, p 1
12. G.O. Hiers, *Symposium on Outdoor Weathering of Metals,* American Society for Testing and Materials, 1946
13. G.O. Hiers and E. Minarcik, *Symposium on Atmospheric Corrosion of Nonferrous Metals,* STP 175, American Society for Testing and Materials, 1956, p 135
14. H.J. Plenderleith and R.M. Organ, *Studies Conserv.,* Vol 1, 1953, p 63
15. W. Ruehl, *Z. Phys.,* Vol 176, 1963, p 409
16. W.E. Boggs, R.G. Kachik, and G.E. Pellissier, *J. Electrochem. Soc.,* Vol 108 (No. 1), 1961
17. W.E. Boggs, P.S. Trozzo, and G.E. Pellissier, *J. Electrochem. Soc.,* Vol 108 (No. 1), 1961, p 13
18. W.E. Boggs, *J. Electrochem. Soc.,* Vol 108 (No. 2), 1961
19. W.E. Boggs, R.H. Kachik, and G.E. Pellissier, *J. Electrochem. Soc.,* Vol 111 (No. 6), 1964, p 636
20. C. Luner, *Trans. Met. Soc. AIME,* Vol 218 (No. 3), 1960, p 572
21. W.E. Boggs, R.H. Kachik, and G.E. Pellissier, *J. Electrochem. Soc.,* Vol 110 (No. 1), 1963, p 4
22. M.E. Warwick, *Atmospheric Corrosion of Tin and Tin Alloys,* Publication 602, Tin Research Institute, 1980
23. L.L. Bircumshaw and G.D. Preston, *Philos. Mag.,* Vol 21, 1936, p 686
24. J.H. Bilbrey, D.A. Wilson, and M.J. Spendlove, Publication 5181, *US Bur. Mines Rep. Invest.,* 1955
25. H. Leidheiser, Jr., *The Corrosion of Copper, Tin, and Their Alloys,* R.E. Krieger, 1979
26. W. Gruhl and V. Gruhl, *Metall,* Vol 6, 1952, p 177
27. A. Kutzelnig, *Z. Anorg. Allg. Chem.,* Vol 202, 1931, p 418
28. A. Kutzelnig, *Z. Electrochem.,* Vol 41, 1935, p 450
29. D.J. MacNaughton and E.S. Hedges, *Proceedings of the International Congress on Mining, Metallurgy, and Applied Geology,* 1935
30. S.C. Britton and K. Bright, *Metallurgia,* Vol 56, 1957, p 163
31. S.C. Britton and J.C. Sherlock, *Br. Corros. J.,* Vol 9, 1974, p 96
32. R.D. Jenkins, *Proc. Phys. Soc.,* Vol 47, 1935, p 107
33. R.K. Hart, *Proc. Phys. Soc.,* Vol 65B, 1952, p 955
34. J.C. Platteuw and G. Meyer, *Trans. Faraday Soc.,* Vol 52, 1956, p 1066
35. S.N. Shah and D.E. Davies, *First International Congress on Metallic Corrosion,* Butterworths, 1961, p 232
36. H.S. Rawdon, *Ind. Eng. Chem.,* Vol 19, 1927, p 613
37. T.P. Hoar, *J. Inst. Met.,* Vol 55, 1934, p 135–145
38. F.L. LaQue, Corrosion by Seawater, Behavior of Metals and Alloys in Seawater, *The Corrosion Handbook,* H.H. Uhlig, Ed., John Wiley & Sons, 1948, p 383–430
39. S.C. Britton, *Anti-Corrosion Manual,* Scientific Surveys, Ltd., 1958
40. C.L. Baker, *Ind. Eng. Chem.,* Vol 27, 1935, p 1358
41. O.F. Hunziker, W.H. Cordes, and B.H. Nissen, *J. Dairy Sci.,* Vol 12, 1929, p 140
42. A. Guillemin, *Ann. Chim.,* Vol 19, 1944, p 145
43. A.I. Levin, M.E. Prostakov, and V.P. Kochergin, *Zh. Prikl. Khim.,* Vol 33, 1960, p 2102
44. A. Ragheb and L.A. Kamel, *Corrosion,* Vol 18, 1962, p 153t
45. A.M.S. El Din and F.M.A. El Wahab, *Electrochim. Acta,* Vol 9, 1964, p 883
46. G. Humpston and D. Jacobson, *Principles of Soldering,* ASM International, 2004
47. M. Woods, Some of Europe's Historic Organs Suffer from Mysterious Corrosion, *The Toledo Blade,* April 25, 2005
48. Lead and Health, *Report of a DHSS Working Party on Lead in the Environment,* Her Majesty's Stationary Office, 1980
49. *Toxic Metals in Drinking Water,* Sierra Club, 1984
50. EEC Council Directive 15.7.80 Relating to the Quality of Water Intended for Human Consumption, *J. Eur. Comm.,* Vol L229, p 11
51. "Standard Specification for Modern Pewter Alloys," B 560-79, *Annual Book of ASTM Standards,* American Society for Testing and Materials
52. *Working with Pewter,* Publication 566, International Tin Research Institute, 1979
53. H. Schmidt and A. Niessen, *Blasberg-Mitteilungen,* Vol 22, 1971, p 10
54. Symposium on Lead-Base Babbitt Alloys, *Met. Prog.,* Vol 69, 1956, p 174
55. J.B. Bryce and T.G. Roehner, *Trans. IME,* Vol 73, 1961, p 377, 393
56. *Aluminum-Tin Alloy Bearings,* Publication 463, International Tin Research Institute, 1972
57. J.C. Hudson, *Trans. Faraday Soc.,* Vol 25, 1929, p 177
58. A.H. DuRose, *J. Electrochem. Soc.,* Vol 89, 1946, p 101
59. A.W. Tracey, *Symposium on Outdoor Weathering of Metals,* American Society for Testing and Materials, 1955, p 67

60. G.W. Quick, *J. Res. Natl. Bur. Stand.,* Vol 14, 1935, p 175
61. S.C. Britton, *J. Inst. Met.,* Vol 47, 1941, p 119
62. A.L. Alexander, C.R. Southwell, and B.W. Forgeson, *Corrosion,* Vol 17 (No. 7), 1961, p 97
63. C.W. Hummer, C.R. Southwell, and A.L. Alexander, *Mater. Prot.,* Vol 7 (No. 1), 1968, p 41
64. C.R. Southwell, J.D. Bultman, and A.L. Alexander, *Mater. Perform.,* Vol 15 (No. 7), 1976, p 9
65. D.M. Ward and P.A. Lovett, *Electron,* Jan 15, 1970
66. L. Habraken, C. Rogister, A. Davin, and D. Cousouradis, *Metall,* Vol 23 (No. 11), 1969, p 1148
67. Z. Ahmad, *Anti-Corros. Methods Mater.,* Vol 24 (No. 1), 1977, p 8
68. L.E. Price and G.J. Thomas, *J. Inst. Met.,* Vol 63, 1938, p 29
69. R. Duckett, D.A. Robins, and S.C. Britton, *Metallurgia,* Vol 65, 1962, p 291
70. "Quality Metal Finishing Guide—Tin and Tin Alloy Coatings," Vol 1 (No. 1), Metal Finishing Suppliers Association, 1977
71. S.C. Clarke and E. Longhurst, *First International Congress on Metallic Corrosion,* Butterworths, 1961, p 70
72. K.G. Compton, *Corrosion,* Vol 4, 1948, p 112
73. J.C. Hudson and T.H. Banfield, *J. Iron Steel Inst.,* Vol 154, 1946, p 229
74. J.C. Hudson and J.F. Stanners, *J. Iron Steel Inst.,* Vol 175, 1953, p 381
75. S.C. Britton, *Metall. Ital.,* Vol 46, 1954, p 89
76. M. Dettner, *Plating,* Vol 46 (No. 5), 1959, p 469
77. P.L. Speddin, *Australas. Corros. Eng.,* Vol 15 (No. 8), 1971, p 27
78. T. Biestek, *Pr. Inst. Mech.,* Vol 7 (No. 26), 1959, p 89
79. T. Biestek, *Pr. Inst. Mech.,* Vol 11, 1963, p 11
80. T. Biestek, *Met. Finish.,* Oct 1974, p 39
81. W.G. Bader and R.G. Baker, *Plating,* March 1973, p 242
82. M.L. Ackroyd, *A Survey of Accelerated Aging Techniques for Solderable Substrates,* Publication 531, International Tin Research Institute, 1976
83. C.A. MacKay, *Surface Finishes and Their Solderability,* Publication 561, International Tin Research Institute, 1979
84. H.B. Gibson, *Prod. Eng.,* Nov 1956, p 1
85. M.L. Ackroyd and C.A. MacKay, *Solders, Solderable Finishes, and Reflowed Coatings,* Publication 529, International Tin Research Institute, 1977
86. B.E. Scott and R.D. Gray, *Iron Age,* Vol 167 (No. 3), 1951, p 59
87. N.E. Promisel and G.S. Mustin, *Corrosion,* Vol 7, 1951, p 377
88. S.C. Britton and R.W. de Vere Stacpoole, *Trans. IMF,* Vol 32, 1955, p 211
89. B. Cohen, *Plating,* Vol 44 (No. 9), 1957, p 963
90. I.T. Turner, *Plating,* Vol 52, (No. 7), 1965, p 677
91. W. Beck and E.J. Janowsky, *J. Electrochem. Soc.,* Vol 109, 1962, p 496
92. F. Cook, J.K. Cosslet, R.W. Scott, and C.E.A. Shanahan, *Br. Corros. J.,* Vol 1 (No. 7), 1966, p 283
93. V. Sree and T.L. Rama Char, *Metalloberfläche,* Vol 15, 1961, p 301
94. M. Clarke, R.G. Elbourne, and C.A. MacKay, *Trans. IMF,* Vol 50 (No. 4), 1972, p 160
95. M. Clarke and R.G. Elbourne, *Electrochim. Acta,* Vol 16 (No. 11), 1971, p 1949
96. H. Miyashita and S. Kurihara, *J. Met. Finish. Soc. Jpn.,* Vol 21, 1970, p 79
97. J. Hyner, *Plat. Surf. Finish.,* Vol 64 (No. 2), 1977, p 33
98. J.D.C. Hemsley and M.E. Roper, *Trans. IMF,* Vol 57 (No. 2), 1979, p 77
99. J.W. Price, *Tin and Tin Alloy Plating,* Electrochemical Publications Ltd., 1983
100. F.A. Lowenheim, *Proc. Am. Electropl. Soc.,* Vol 44, 1957, p 1
101. W.H. Safranek and C.L. Faust, *Proc. Am. Electropl. Soc.,* Vol 41, 1954, p 201
102. H. Laub, *Werkst. Korros.,* Vol 15 (No. 6), 1964, p 437
103. A.K. Graham and H.C. Pinkerton, *Plating,* Vol 54 (No. 4), 1967, p 367
104. R. Smith, *Sheet Met. Ind.,* Vol 49 (No. 12), 1972, p 761; Vol 50 (No. 2), 1973, p 92
105. R.G. Monk and J.H.T. Ellingham, *Trans. Faraday Soc.,* Vol 31, 1935, p 1460
106. J.L. Rama Char and J. Vaid, *Electropl. and Met. Finish.,* Vol 14, 1961, p 367
107. *Electroplated Tin-Nickel Alloy,* Publication 235, International Tin Research Institute, 1968
108. J.W. Cuthbertson, N. Parkinson, and H.P. Rooksby, *J. Electrochem. Soc.,* Vol 100, 1953, p 107
109. R.F. Smart and D.A. Robins, *Trans. IMF,* Vol 37, 1960, p 108
110. S.C. Britton and R.M. Angles, *Trans. IMF,* Vol 29, 1953, p 26
111. S.C. Britton, D.G. Michael, and R.M. Angles, *Trans. IMF,* Vol 29, 1953, p 40
112. S.C. Britton, *Met. Ind.,* Vol 87 (No. 25), 1955, p 510
113. J. Chadwick, *Electroplating,* Vol 6 (No. 12), 1953, p 451
114. F.A. Lowenheim, W.W. Sellers, and F.X. Carlin, *J. Electrochem. Soc.,* Vol 105 (No. 6), 1958, p 338
115. R.M. Angles, *Tin-Nickel Alloy Plating,* International Nickel Company (Mond) Ltd., 1964
116. M. Antler, *Proceedings of the Conference on Corrosion Control by Coatings,* Lehigh University, 1978
117. M. Antler, M. Feder, C.F. Hornig, and J. Bohland, *Plat. Surf. Finish.,* Vol 63 (No. 7), 1976, p 30
118. S.C. Britton and R.M. Angles, *J. Electrodep. Tech. Soc.,* Vol 27, 1951, p 293
119. R.M. Angles and R. Kerr, *Engineering,* Vol 161, 1946, p 289
120. H. Heinemann, *Metalloberfläche,* Vol 6B, 1954, p 33
121. *Auto. Eng.,* 1955, p 75
122. S.C. Britton and R.M. Angles, *Metallurgia,* Vol 44, 1951, p 185
123. S.C. Britton and R.W. de Vere Stacpoole, *Metallurgia,* Vol 52, 1955, p 64
124. S.V. Lashko-Avakyan and N.F. Lashko, *Savarochnoe Proivodstvo,* Vol 5, 1961, p 13
125. S.L. Phillips and C.E. Johnson, *J. Electrochem. Soc.,* Vol 117, 1970, p 827
126. D.R. Cowieson and A.R. Schofield, *Passivation of Tin-Zinc Alloy Coated Steel,* Publication 661, International Tin Research Institute, 1985
127. W.E. Hoare, E.S. Hedges, and B.T.K. Barry, *The Technology of Tinplate,* Edward Arnold, 1965
128. *Steel Products Manual: Tin Mill Products,* American Iron and Steel Institute, 1979
129. *Guide to Tinplate,* Publication 662, International Tin Research Institute, 1983
130. E. Morgan, *Tinplate and Modern Canmaking Technology,* Pergamon Press, 1985
131. M.E. Warwick and W.B. Hampshire, *Laboratory Corrosion Tests and Standards,* STP 866, American Society for Testing and Materials, 1985, p 48
132. "Standard Specification for Electrodeposited Coatings of Tin," B 545, *Annual Book of ASTM Standards,* American Society for Testing and Materials

SELECTED REFERENCES

- O.A. Abu Zeid, Influence of Tin Addition on Corrosion Resistance of Aluminium Ion Platings, *Br. Corros. J.,* Vol 27 (No. 2), 1992, p 144–146
- A.A. Al-Suhybani, Corrosion of Tin in Nitric Acid Solutions, *Surf. Coat. Technol.,* Vol 34 (No. 4), June-July 1988, p 463–470
- A.A. Al-Suhybani, Effect of Some Inorganic Anions on Corrosion of Tin in Nitric Acid Solutions, *Br. Corros. J.,* Vol 24 (No. 3), 1989, p 204–210
- C.M.V.B. Almeida, T. Raboczkay, and B.F. Giannetti, Inhibiting Effect of Citric Acid on the Pitting Corrosion of Tin, *J. Appl. Electrochem.,* Vol 29 (No. 1), Jan 1999, p 123–128
- R.D. Armstrong, J.D. Wright, and T.M. Handyside, Impedance Studies into the Corrosion Protective Performance of a Commercial Epoxy Acrylic Coating Formed upon Tin Plated Steel, *J. Appl. Electrochem.,* Vol 22 (No. 9), Sept 1992, p 795–800
- D.A. Asbury and G.B. Hoflund, A Surface Study of the Oxidation of Polycrystalline Tin, *J. Vac. Sci. Technol. A,* Vol 5 (No. 4-II), July-Aug 1987, p 1132–1135

- F.H. Assaf, A. Sayed, and S.S. Abd El-Rehim, Effect of Halide Ions on the Corrosion of Tin in Some Fruit Acids, *Bull. Electrochem.,* Vol 7 (No. 10), Oct 1991, p 445–447
- M. Braic, S. Zamfir, M. Balaceanu, V. Braic, G. Pavelescu, A. Zamfir, and A. Vladescu, Corrosion Resistance of Tin Coated 316 Stainless Steel in Artificial Physiological Solution, *J. Optoelectron. Adv. Mater.,* Vol 5 (No. 2), June 2003, p 503–510
- G. Brunoro, G. Laguzzi, L. Luvidi, and C. Chiavari, Corrosion Evaluation of Artificially Aged 6 wt% Tin Bronze, *Br. Corros. J.,* Vol 36 (No. 3), 2001, p 227–232
- V. Brusic, D.D. DiMilia, and R.D. MacInnes, Corrosion of Lead, Tin and Their Alloys, *Third Electronic Materials and Processing Congress* (San Francisco, CA), ASM International, 1990, p 261–268
- V. Brusic, D.D. DiMilia, and R. MacInnes, Corrosion of Lead, Tin, and Their Alloys, *Corrosion,* Vol 47 (No. 7), July 1991, p 509–518
- S.S. Cha, K.H. Park, C.G. Woo, and W.S. Moon, Effects of Nickel Flash Coating on the Weldability and Corrosion Resistance of Lightly Tin Coated Steel, *J. Korean Inst. Met. Mater.,* Vol 31 (No. 11), Nov 1993, p 1440–1448
- C.Y. Chan, K.H. Khoo, Y.C. Chua, and S. Guruswamy, Potentiodynamic Studies of Tin Corrosion in Presence of Citrate and Bisulphate Ions in Aqueous Solutions of Varying pH, *Br. Corros. J.,* Vol 28 (No. 1), 1993, p 53–58
- V.I. Chernova and I.A. Gagauz, Effect of Current Conditions on Corrosion Resistance of Tin Plate, *Chernaya Metall. Byulleten Nauchno-Tekh.,* Vol 1–2, Jan-Feb 1999, p 59–60
- I.A. Chernyakhovskaya, S.V. Vilkul, R.I. Cherkasskij, and A.V. Kushnarev, Ways for Improving the Corrosion Resistance of Tin Plate at JSC Magnitogorsk Metallurgic Plant, *Proizvod. Prokata,* Vol 5, May 2000, p 19–21
- Corrosion of Tin and Tin Alloys, *Handbook of Corrosion Data,* 2nd ed., ASM International, 1995, p 49–50
- S.D. Cramer, and M.J. Baker, Monticello Roof Restoration, *Mater. Perform.,* Vol 32 (No. 10), Oct 1993, p 61–64
- P. De Padova, M. Fanfoni, R. Larciprete, M. Mangiantini, S. Priori, and P. Perfetti, A Synchrotron Radiation Photoemission Study of the Oxidation of Tin, *Surf. Sci.,* Vol 313 (No. 3), July 1, 1994, p 379–391
- A. Dieguez, A. Romano-Rodriguez, J.R. Morante, P. Nelli, L. Sangaletti, and G. Sberveglieri, Analysis of the Thermal Oxidation of Tin Droplets and Its Implications on Gas Sensor Stability, *J. Electrochem. Soc.,* Vol 146 (No. 9), Sept 1999, p 3527–3535
- P.H. Dionisio and I.J.R. Baumvol, The Influence of Tin Ion Implantation and Radiation-Enhanced Tin Diffusion on the Thermal Oxidation of a High-Carbon Steel, *Phys. Status Solidi (A),* Vol 101 (No. 1), May 1987, p 63–76
- N.I. Dolotov, A.B. Zil'berman, Yu.A. Il'in, A.V. Makhin, V.A. Moshnikov, and D.A. Yas'kov, Phase Analysis of Tin Thin Films during Oxidation in the Air, *Neorg. Mater.,* Vol 30 (No. 1), Jan 1994, p 83–86
- A.M. El-Kot, A.A. El-Aal, R. El-Sheikh, and A. Ghuzza, Corrosion Inhibition of Tin in HNO_3 and Effect of Chloride Ions, *Bull. Electrochem,* Vol 7 (No. 3), March 1991, p 114–118
- S.S.A. El Rehim, H.H. Hassan, and N.F. Mohamed, Anodic Behaviour of Tin in Maleic Acid Solution and the Effect of Some Inorganic Inhibitors, *Corros. Sci.,* Vol 46 (No. 5), May 2004, p 1071–1082
- S.S.A. El-Rehim, F. Taha, M.B. Saleh, and S.A. Mohamed, On the Pitting Corrosion of Tin by Sulphate Anion, *Corros. Sci.,* Vol 33 (No. 11), Nov 1992, p 1789–1796
- A. El Sayed, F.H. Assaf, and S.S. Abd El Rehim, Anodic Behaviour and Corrosion of Tin in Carboxylic Acid Solutions, *Bull. Electrochem.,* Vol 7 (No. 8), Aug 1991, p 345–347
- M. Fukushima, T. Yonesaki, K. Takizawa, and T. Susai, Improved Corrosion Resistance of a Heat Exchanger Using a Copper Tube Coated with Tin, *Hyomen Gijutsu (J. Surf. Finish. Soc. Jpn.),* Vol 51 (No. 11), Nov 2000, p 1165–1167
- K. Galic, N. Cikovic, S. Hamin, and K. Berkovic, Inhibition Efficiency of Natural Compounds on Tin Corrosion in Salt Solutions, EUROCORR 2001 (Lake Garda, Italy), *Congress Proceedings,* 2001
- K. Galic, M. Pavic, and N. Cikovic, The Effect of Inhibitors on the Corrosion of Tin in Sodium Chloride Solution, *Corros. Sci.,* Vol 36 (No. 5), May 1994, p 785–795
- K. Galic, M. Pavic, N. Cikovic, and K. Berkovic, Influence of Nitrite and Nitrate on Tin Corrosion in Sodium Chloride, *Proceedings Seventh European Symposium on Corrosion Inhibitors* (Ferrara, Italy), Vol 1, Universita degli Studi di Ferrara, Ferrara, Italy, 1990, p 701–710
- R. Guo, F. Weinberg, and D. Tromans, Pitting Corrosion of Passivated Beta-Tin Monocrystals, *Corrosion,* Vol 51 (No. 3), March 1995, p 212–222
- G.B. Hoflund and G.R. Corallo, Electron-Energy-Loss Study of the Oxidation of Polycrystalline Tin, *Phys. Rev. B, Condens. Matter,* Vol 46 (No. 11), Sept 15, 1992, p 7110–7120
- X.-Q. Huang, N. Li, and D.-Y. De, Effect of Crystal Orientation of Black Plate on Corrosion Resistance of Tinplate, *Mater. Prot. (China),* Vol 37 (No. 9), Sept 2004, p 1–3
- M.-Y. Huh, S.-H. Kim, J.-P. Ahn, J.-K. Park, and B.-K. Kim, Oxidation of Nanophase Tin Particles, *Nanostructured Mater.,* Vol 11 (No. 2), March 1999, p 211–220
- S. Jouen, B. Hannoyer, and O. Piana, Non-Destructive Surface Analysis Applied to Atmospheric Corrosion of Tin, *Surf. Interface Anal.,* Vol 34 (No. 1), Aug 2002, p 192–196
- W.S. Jun, P.S. Yun, and E.C. Lee, Leaching Behavior of Tin from Sn-Fe Alloys in Sodium Hydroxide Solutions, *Hydrometallurgy,* Vol 73 (No. 1–2), April 2004, p 71–80
- S. Khandekar, L. Vedula, and V. Malshe, Tin Corrosion Induced by Corrosive De-Ionized (DI) Water, *ISTFA 1999: Conference Proceedings from the 25th International Symposium for Testing and Failure Analysis,* ASM International, Nov 1999, p 141–143
- M. Kitada, Microstructures and Corrosion Behavior of Tin Thread Made in the Late Edo Period, *J. Jpn. Inst. Met.,* Vol 67 (No. 11), Nov 2003, p 661–667
- V. Kohutekova, D. Dadejovaa, and V. Vargova, Evaluation of the Corrosion Resistance of Thin Tin Coatings, *Koroze Ochr. Mater.,* Vol 45 (No. 3), 2001, p 58–64
- V.I. Kondrashov, N.A. Frolova, and V.S. Bezlyudnaya, Effect of Additives and Impurities in Metal on Tin Oxidation and Penetration into the Underside of Float-Glass, *Steklo Keram.,* Vol 3, March 2001, p 6–9
- E. Kulig, Aliphatic Acids as Corrosion Inhibitors, Part II: Corrosion of Lead and Tin in Sodium Chloride and Steel in Sulphuric Acid, *Ochr. Przed Koroz.,* Vol 30 (No. 8), Aug 1987, p 180–182
- L. Kumar, D.D. Sarma, S. Krummacher, XPS Study of the Room Temperature Surface Oxidation of Zirconium and Its Binary Alloys with Tin, Chromium and Iron, *Appl. Surf. Sci.,* Vol 32 (No. 3), July 1988, p 309–319
- K. Leyendecker, Corrosion Protection of Ferrous Metals Using Tin Alloy Coatings, *Galvanotechnik,* Vol 92 (No. 10), Oct 2001, p 2682–2688
- N. Li, Z. Wang, and D. Li, Study on High Temperature Oxidation of Tin Plate, *Gangtie Yanjiu Xuebao (J. Iron Steel Res.) (China),* Vol 12, July-Aug 2000, p 47–50
- Y. Li, B. Gao, X.-W. Dong, X.-P. Liu, G.-C. Li, and D.-P. Jin, Corrosion Resistance of Electrolytic Tin Plate Used for Food Cans and Its Testing Methods, *Mater. Prot. (China),* Vol 35 (No. 8), Aug 2002, p 20–23
- Y. Lu, Thermodynamics of Surface Corrosion of Solid Pure Lead, Tin and Their Alloys, *J. Univ. Sci. Technol. Beijing,* Vol 11 (No. 2), 1989, p 167–172
- Y. Lu, Surface Corrosion Kinetics of Solid Lead, Tin and Their Alloys, *J. Univ. Sci. Technol. Beijing,* Vol 13 (No. 5), Sept 1991, p 493–497
- P. Madakson, Effects of Tin Ion and Nitrogen Ion Implantation on the Oxidation of Titanium, *Mater. Sci. Eng.,* Vol 90, June 1987, p 205–212
- A. Mance, The Effect of Tin on the Anodic and Corrosion Behavior of Al-0.2% Ga Alloy in Sodium Chloride Solution, *J. Serb. Chem. Soc.,* Vol 55 (No. 3), 1990, p 171–178

- M. Marek, The Effect of Tin on the Corrosion Behavior of the Ag-Hg Phase of Dental Amalgam and Dissolution of Mercury, *J. Dent. Res.,* Vol 69 (No. 12), Dec 1990, p 1786–1790
- A.I. Marshakov and N.P. Chebotareva, Effect of Oxygen-Containing Oxidants on Tin Corrosion and Its Electrochemical Behavior in Acidic Solutions, *Prot. Met. (Russia),* Vol 28 (No. 6), Nov-Dec 1992, p 714–719
- A.I. Marshakov, N.P. Chebotaryova, and Yu.N. Mikhailovskii, Mechanism of Corrosion of Electronic Materials (Tin and Copper) under the Action of Oxygen-Containing Oxidizers, *Proceedings—Corrosion and Reliability of Electronic Materials and Devices* (Toronto, Canada), The Electrochemical Society, 1993, p 564–574
- S. Miyazaki, H. Yoshizawa, and H. Hori, Underfilm Corrosion of Dewy Spread Lightly Tin Coated Steel for Welded Can, *Trans. Iron Steel Inst. Jpn.,* Vol 27 (No. 5), 1987, p B131–B132
- Y. Mizutani, Corrosion Resistance in H_2SO_4 of Heat Diffusion Layers of Cast Irons Coated with Tin Plating, *J. Met. Finish. Soc. Jpn.,* Vol 37 (No. 6), 1986, p 313–315
- M. Mori, K. Miura, T. Sasaki, and T. Ohtsuka, Corrosion of Tin Alloys in Sulfuric and Nitric Acids, *Corros. Sci.,* Vol 44 (No. 4), April 2002, p 887–898
- J. Morita and M. Yoshida, Effects of Free Tin on Filiform Corrosion Behavior of Lightly Tin-Coated Steel, *Corrosion,* Vol 50 (No. 1), Jan 1994, p 11–19
- I.V. Murav'eva and Y.Y. Andreev, The Determination of the Tendency to Selective Corrosion for Aluminium and Tin Bronzes, *Izv. V.U.Z. Tsvetn. Metall.,* Vol 3, May-June 1999, p 57–60
- T.P. Murphy, Some Economic and Environmental Aspects of the Corrosion Behaviour of Tin and Its Alloys, *Proceedings—Progress in the Understanding and Prevention of Corrosion* (Barcelona, Spain), Vol I, The Institute of Materials, London U.K., 1993, p 696–711
- M. Natesan and S.V. Iyer, Corrosion Behaviour of Tin in Sulphuric Acid in the Presence of Acetylenic Alcohols, Oxalic Acid and Hexamine, *Trans. SAEST,* Vol 24 (No. 3), July-Sept 1989, p 1.47
- M. Natesan and S.V. Iyer, Corrosion Behaviour of Tin in 1*N* H_2SO_4 in Presence of Acetylenic Alcoholic Compounds, Hexamine and Oxalic Acid, *Bull. Electrochem.,* Vol 6 (No. 1), Jan 1990, p 16–1
- K. Ojima and Y. Taneda, Electron Microscopic Study on the Oxidation of Beta-Tin Irradiated by Electron Beam, *J. Mater. Sci.,* Vol 25 (No. 1B), Jan 1990, p 563–566
- E. Otero, J.A. Gonzalez, and M.E. Chacon, New Procedures for Determining Corrosion in the Head Space of Tin Plate Aerosol Containers, *Rev. Metal.,* Vol 26 (No. 3), May-June 1990, p 143–150
- A. Palmieri, A. Montanari, and G. Fasanaro, De-Tinning Corrosion of Cans Filled with Tomato Products, *Corros. Eng. Sci. Technol.,* Vol 39 (No. 3), Sept 2004, p 198–208
- V.A. Paramonov and N.G. Filatova, Passivation of Electrolytical Tin-Plate in Trivalent Chromium Solutions, *Prot. Met. (Russia),* Vol 40 (No. 3), May-June 2004, p 271–274
- P. Paulitsch and S. Wittmer, Tin Corrosion in Works of Art, *Mater.wiss. Werkst.tech.,* Vol 20 (No. 5), 1989, p 163–166
- A.P. Pchel'nikov, G.A. Bokov, A.V. Polunin, I.K. Marshakov, and V.V. Losev, Corrosion of Plain and Tin Beta-Brasses in Chloride Solutions, *Prot. Met. (Russia),* Vol 26 (No. 2), March-April 1990, p 176–180
- A.P. Pchelnikov, A.V. Polunin, and I.K. Marshakov, Dezincing of Tin Alpha Brass during Corrosion in Chloride Solutions, According to Results of Radiometry and Mossbauer Spectroscopy, *Prot. Met. (USSR),* Vol 22 (No. 1), Jan-Feb 1986, p 13–18
- S. Peter, R. Pintaske, and G. Hecht, Electronographic Phase Analysis of the Corrosion Products of Copper and Tin, *Korrosion,* Vol 18 (No. 1), 1987, p 39–50
- A. Preuss, B. Adolphi, and K. Drescher, Oxidation of Indium-48 Tin, *J. Electrochem. Soc.,* Vol 141 (No. 10), Oct 1994, p 2784–2788
- R. Raicheff, R. Slavov, and J. Marcheva, Effect of the Thickness of the $FeSn_2$ Layer on the Corrosion Resistance of Electrolytically Tin Plated Sheet Steel, *Proceedings—Sixth Symposium on Electroplating* (Budapest, Hungary), Technoinform, Budapest, Hungary, 1985, p 249–254
- J. Rawat and M.A. Quraishi, Corrosion of Tin in Fruit Juices and Its Inhibition, *Bull. Electrochem.,* Vol 19 (No. 10), Oct 2003, p 467–470
- S.A.M. Refaey, Passivation and Pitting Corrosion of Tin in Gluconate and the Effect of Halide Ions, *J. Appl. Electrochem.,* Vol 26 (No. 5), May 1996, p 503–507
- S.A.M. Refaey, The Corrosion and Passivation of Tin in Borate Solutions and the Effect of Halide Ions, *Electrochim. Acta,* Vol 41 (No. 16), July 31, 1996, p 2545–2549
- S.A.M. Refaey and G. Schwitzgebel, Electrochemical Impedance Spectroscopic Investigation of Dissolution, Passivation and Pitting Corrosion of Tin in Na_2CO_3 Solution and the Effect of Cl^- and I^- ions, *Appl. Surf. Sci.,* Vol 135 (No. 1–4), Sept 1998, p 243–253
- S.S.A. Rehim, S.M. Sayyah, and M.M. El Deeb, Corrosion of Tin in Citric Acid Solution and the Effect of Some Inorganic Anions, *Mater. Chem. Phys.,* Vol 80 (No. 3), June 26, 2003, p 696–703
- M. Renner and E. Altpeter, Contact Corrosion of Alloyed Rolled Tin (ZnCuTi), *Metall,* Vol 40 (No. 12), Dec 1986, p 1262–1268
- A. Roos and P. Hedenqvist, Corrosion Protection of Aluminum Surfaces Using Pyrolytic Tin Oxide, *Appl. Phys. Lett.,* Vol 59 (No. 1), July 1, 1991, p 25–27
- R. Sangiorgi, C. Senillou, and J.C. Joud, Study of the Superficial Oxidation of Liquid Tin by Auger Spectrometry and the Relation to the Surface Energy, *Vide, Couches Minces,* (Suppl. 243), Aug-Oct 1988, p 239–241
- T. Sasaki, R. Kanagawa, T. Ohtsuka, and K. Miura, Corrosion Products of Tin in Humid Air Containing Sulfur Dioxide and Nitrogen Dioxide at Room Temperature, *Corros. Sci.,* Vol 45 (No. 4), April 2003, p 847–854
- S.M. Sayyah, S.S. Abd El-Rehim, and M.M. El-Deeb, The Effect of Some Polymers on the Corrosion Behaviour of Tin in 1 *M* NaCl Solution, *Int. J. Polym. Mater.,* Vol 49 (No. 1), March 2001, p 59–80
- O. Semenova, H. Flandorfer, and H. Ipser, On the Non-Occurrence of Tin Pest in Tin-Silver-Indium Solders, *Scr. Mater.,* Vol 52 (No. 2), Jan 2005, p 89–92
- O. Seri and K. Tagashira, Influence of Cl^- Concentration on Galvanic Corrosion of Tin Plate and Aluminum Alloy 5052, *Boshoku Gijutsu (Corros. Eng.),* Vol 37 (No. 4), April 1988, p 212–217
- V.S. Sinyavskii, V.D. Val'kov, G.M. Toguzov, and L.S. Guzei, Effect of Added Tin on Corrosion and Electrochemical Behavior of Aluminum, *Prot. Met. (USSR),* Vol 23 (No. 5), Sept-Oct 1987, p 587–590
- V.S. Sinyavskii, V.D. Val'kov, G.M. Toguzov, and L.S. Guzei, Effect of Tin Additions on the Corrosion and Electrochemical Behavior of Aluminum, *Zashch. Met.,* Vol 23 (No. 5), 1987, p 801–805
- T. Sonoda, Y. Hayashi, and Y. Matsuda, Corrosion Resistance of Electroless Nickel-Phosphorus Plating Films Coated with Tin, *Hyomen Gijutsu (J. Surf. Finish. Soc. Jpn.),* Vol 47 (No. 1), Jan 1996, p 78–79
- S. Suzuki, Y. Yamada, T. Atsumi, K. Kawano, and O. Toriyama, Performance of the Tin Coated Copper Tube in the Water Service System in Which the Copper Plumbing Tubes Have Been Suffering from Corrosion, *Sumitomo Light Met. Tech. Rep.,* Vol 41 (No. 1), 2000, p 70–75
- S. Takeshi, K. Ryoji, and O. Toshiaki, In Situ IR-RAS Investigation of Corrosion of Tin in Air Containing H_2O, NO_2 and SO_2 at Room Temperature, *J. Univ. Sci. Technol. Beijing,* (English ed.), Vol 10 (No. 3), June 2003, p 35–38
- K. Takizawa, Y. Nakayama, K. Kurokawa, and H. Imai, Corrosion Behavior of Type 304 Stainless Steels Containing Tin in Sulfuric Acid Solution, *Boshoku Gijutsu (Corros. Eng.),* Vol 37 (No. 12), Dec 1988, p 732–739
- S. Tanaka, T. Aoki, M. Yoshida, Y. Iino, and S. Asai, Liquid Composition and Process for Treating Aluminum or Tin Cans to Impart

Corrosion Resistance and Mobility Thereto, U.S. Patent 5,370,909, Dec 6, 1994

- W.J. Tomlinson and M. Wedgburg, Corrosion of Zinc, Nickel, Electroless Nickel, Titanium, Tin, Magnesium and Cadmium in Simulated Concrete Solutions of pH 13.7 Containing Chloride, *J. Mater. Sci. Lett.,* Vol 7 (No. 3), March 1988, p 191–194
- D. Toshkovich, M.B. Rajkovich, and I. Chirich, Tin Plate Corrosion in Brine Solutions, *Zh. Prikl. Khim.,* Vol 75 (No. 11), Nov 2002, p 1843–1846
- V.K. Vaidyan, J.T. Abraham, P.V. Thomas, K.G. Gopchandran, and B. Joseph, Oxidation Mechanism Involved in Thin Tin Films, *Ind. J. Eng. Mater. Sci.,* Vol 3 (No. 3), June 1996, p 109–113
- M.L. Varsanyi, L. Sziraki, L. Kiss, and A. Vertes, Corrosion Study of Tin and Tin Alloys, *Proceedings—Eurocorr'87,* European Corrosion Meeting (Karlsruhe, Germany), DECHEMA, Germany, 1987, p 349–354
- V.S. Vasantha, M. Pushpavanam, and V.S. Muralidharan, Corrosion Resistant Tin Electrodeposit, *Bull. Electrochem.,* Vol 15 (No. 5–6), May-June 1999, p 215–218
- K. Wang, G. Oian, W. Lu, and N. Chen, Correlation between Potential-Time Curves of Constant-Current Anodic Dissolution and Corrosion, *Acta Metall. Sin. (China),* Vol 40 (No. 7), July 2004, p 759–762
- M. Wautelet, L. Baufay, M.C. Joliet, and R. Andrew, Laser-Induced Oxidation of Thin Tin Films, *Thin Solid Films,* Vol 129 (No. 3–4), July 26, 1985, p L67–L70
- J.F. Weaver, T.J. Campbell, G.B. Hoflund, and G.N. Salaita, Oxidation of Polycrystalline Tin by Hyperthermal Atomic Oxygen: An Investigation Using Electron Energy-Loss Spectroscopy, *J. Electron Spectrosc. Relat. Phenom.,* Vol 106 (No. 1), Jan 1, 2000, p 81–91
- B. Webling, Organic Metals: A New Class of Material for Electronics, Corrosion Protection, Part III: A Finish Revolution—Organic Metal plus Electroless Tin, *Galvanotechnik,* Vol 89 (No. 9), Sept 1998, p 3034–3040
- Z. Xia, N. Mu, and Y. Shi, Corrosion Behavior of Tin-Zinc Based Alloy Solder, *J. Chin. Soc. Corros. Prot.,* Vol 23 (No. 4), Aug 2003, p 234–238
- Y. Yomura, N. Ooniwa, and T. Adaniya, Effect of Anodic Oxidation Treatment Prior to Reflow on Uniformity of Tin Layer on Tinplate, *Tetsu-to-Hangane (J. Iron Steel Inst. Jpn.),* Vol 76 (No. 4), April 1990, p 598–605
- D.-W. Yuan, Rapid Oxidation of Liquid Metals: Tin and Zinc Systems, *Diss. Abstr. Int.,* Vol 53 (No. 5), Nov 1992
- D.-W. Yuan, R.-F. Yan, and G. Simkovich, Rapid Oxidation of Liquid Tin and Its Alloys at 600 to 800 °C, *J. Mater. Sci.,* Vol 34 (No. 12), June 15, 1999, p 2911–2920

ASM Handbook, Volume 13B: Corrosion: Materials
S.D. Cramer, B.S. Covino, Jr., editors, p195-204
DOI: 10.1361/asmhba0003819

Corrosion of Lead and Lead Alloys

Revised by Safaa J. Alhassan, International Lead Zinc Research Organization, Inc.

LEAD has such a successful record of service in exposure to the atmosphere and to water that its resistance to corrosion by these media is often taken for granted. Underground, thousands of kilometers of lead-sheathed cable and lead pipe give reliable long-term performance all over the world. In the chemical industry, lead is used in the corrosion-resistant equipment necessary for handling many chemicals. Batteries account for the largest use of lead and are the source of most recycled lead. General information on compositions, properties, and applications can be found in the article "Lead and Lead Alloys" in *Properties and Selection: Nonferrous Alloys and Special-Purpose Materials,* Volume 2 of *ASM Handbook,* 1990.

The Nature of Lead Corrosion

The corrosion of lead in aqueous electrolytes is an electrochemical process. The metal either enters the solution at anodic sites as metallic cations or is converted anodically to solid compounds. Both corrosion reactions can be represented by the reaction:

$$Pb - 2e^- \rightarrow Pb^{2+} \quad \text{(Eq 1)}$$

This oxidation reaction (standard oxidation potential, $E^\circ = 0.126$ V), which takes place at anodic sites, is accompanied by a reduction of some constituent in the electrolyte at cathodic sites. In neutral salt solutions, the cathodic reaction is the reduction of dissolved oxygen:

$$^1/_2O_2 + H_2O + 2e^- \rightarrow 2OH^- \quad \text{(Eq 2)}$$

In acid solutions free of oxygen, the corresponding cathodic reaction is:

$$2H^+ + 2e^- \rightarrow H_2 \quad \text{(Eq 3)}$$

The rate of corrosion is a function of the current flowing between the anodes and cathodes of the corrosion cell. Many factors and conditions can initiate or influence this flow of current. In the corrosion of a single metal, such as lead, local anodes and cathodes may be set up as a result of inclusions, inhomogeneities, stress variations, and differences in temperature. In galvanic corrosion, the anodic and cathodic sites are on different metals, with the less noble metal (anode) corroding in preference to the more noble metal (cathode).

In most environments, lead is cathodic to steel, aluminum, zinc, cadmium, and magnesium and therefore will accelerate the corrosion of these metals. With titanium, copper, silver, and passivated stainless steels, lead is the anode of the cell and suffers accelerated attack. In either case, the rate of corrosion is governed by the difference in potential between the two metals, the ratio of their areas, and their polarization characteristics.

The corrosion rate of lead is usually under anodic control, because the most important determinant generally is the solubility and other physical characteristics of the corrosion products formed at anodic sites. Most of these products are relatively insoluble lead salts that are deposited on the lead surface as impervious films, which tend to stifle further attack. The formation of such insoluble protective films is responsible for the high resistance of lead to corrosion by sulfuric (H_2SO_4), chromic (H_2CrO_4), and phosphoric (H_3PO_4) acids.

In general, anything that damages the protective film increases the corrosion rate. Factors that help create or strengthen the film reduce the corrosion rate. Therefore, the life of lead-protected equipment can be extended, for example, by washing it with film-forming aqueous solutions containing sulfates, carbonates, or silicates. This procedure is suggested for protecting lead when it will be in contact with corrosives that do not form protective films.

Forms of Corrosion. The corrosion of lead can take many forms. Lead exposed to the usual type of atmospheric attack will corrode uniformly. Pitting will occur under conditions of partial passivity or cavitation, which is the formation and collapse of gas bubbles at a liquid/metal interface.

In some cases, a combination of corrosion and other forms of deterioration, such as erosion, fatigue, and fretting, will cause damage much more severe than that caused by each form of attack working independently. Another type of accelerated corrosion can occur when lead is in contact with a corrosive environment and is subjected to a continuous load exceeding its creep strength. The process of creep will continually expose fresh surface to the corroding environment.

Intergranular corrosion is another form of attack on lead. It occurs at grain boundaries of lead generally in the cast form and can cause a significant loss in strength.

It is evident that the specific rate and form of corrosion that occur in a particular situation depend on many complex variables. However, in each of the four major environments discussed subsequently—water, atmosphere, underground, and chemical—certain factors have a determining influence on what form and rate lead corrosion will have.

Corrosion in Water

Distilled water free of oxygen and carbon dioxide (CO_2) does not attack lead. Distilled water containing CO_2 but not oxygen also has little effect on lead. The corrosion behavior of lead in distilled water containing dissolved CO_2 and dissolved oxygen depends on CO_2 concentration. This dependency, which causes many different reactions to take place in a narrow range of concentration, explains the contradictory nature of much of the corrosion data reported in the literature.

For example, lead steam coils that handle pure water condensate are not severely corroded in systems in which all condensate is returned to the boiler and negligible makeup water is used. However, if makeup water is used, dissolved oxygen can be introduced to the condensate, and corrosion can be severe. Carbon dioxide can also be generated from the breakdown of carbonates and bicarbonates in boiler water, decreasing the severity of corrosion of lead. The oxygen level in the makeup water is usually controlled by adding oxygen scavengers, such as hydrazine or sodium sulfite.

In general, the corrosion rate in natural and domestic waters depends on the degree of water hardness, which is primarily caused by calcium and magnesium salts in the water. However, environmental regulations do not permit the use of lead in the drinking water supply system despite the very low corrosion rate of lead and lead alloys in these environments. Water hardness in the form of salts, if present in at least

moderate amounts (>125 ppm), forms films on lead that adequately protect it against corrosive attack. Silicate salts present in the water increase both the hardness and the protective value of the film. In contrast, nitrate and chloride ions either interfere with the formation of the protective film or penetrate it; thus, they increase corrosion.

In soft, aerated natural and domestic waters, the corrosion rate depends on both the hardness and the oxygen content of the water. When water hardness is less than 125 ppm, corrosion rate, like the rate in distilled water, depends on the relative proportions of dissolved CO_2 and dissolved oxygen. Potable waters, which in the United States have a zero maximum containment level, often have hardness below 125 ppm and often contain considerable amounts of CO_2 and oxygen; thus, lead cannot be used for pipe or containers that handle potable waters. The U.S. Environmental Protection Agency calls for an action level of 0.015 mg/L of lead in drinking water. This problem of contamination limits the use of lead in such applications, even though from a service point of view, the corrosion rate is negligible.

The corrosion rates of chemical lead (99.9% Pb) in several industrial and domestic waters are presented in Table 1. It should be noted that corrosion rate is relatively low, even where water hardness is below 125 ppm. A corrosion rate for a freshwater is also included among the data for seawater in Table 2.

The corrosion of lead in seawater is relatively slight and may be retarded by incrustations of lead salts. Data on the performance of lead in seawater at several locations are given in Table 2. Comparison of two of the entries in this table shows that at the same tropical location (Panama), the corrosion rate of lead in freshwater is approximately one-fourth the rate in seawater.

Extensive service experience and laboratory testing have indicated that the corrosion rate of lead is generally quite low in a wide variety of waters. The only major applications in which lead cannot be used are those involving some pure waters containing oxygen and soft natural waters, especially if contamination is of concern. In contrast, as discussed previously, addition of calcium and magnesium salts further enhances the resistance of lead to corrosion by water.

Atmospheric Corrosion

In most of its forms, lead exhibits consistent durability in all types of atmospheric exposure, including industrial, rural, and marine (Table 3). The corrosion rate of lead in industrial environment (Altoona, PA) is 0.6 to 0.7 μm/yr (0.02 to 0.03 mils/yr) and 1.0 to 1.3 μm/yr (0.04 to 0.05 mils/yr) in marine environment (Kure Beach, NC). The corrosion rate of lead in a rural environment (State College, PA) is 1.0 to 1.4 μm/yr (0.04 to 0.06 mils/yr) in 2 years and 0.33 to 0.35 μm/yr (0.013 to 0.014 mils/yr) in 20 years. These three atmospheric environments are distinct because each involves different factors that promote corrosion. In rural areas, which are relatively free of pollutants, the only important environmental factors influencing corrosion rate are humidity, rainfall, and air flow. However, near or on the sea, chlorides entrained in marine air often exert a strong effect on corrosivity. In industrial environments, sulfur oxide gases and

Table 1 Corrosion of chemical lead in industrial and domestic waters

Total immersion

Type of water	Temperature, °C	Temperature, °F	Aeration	Agitation	Corrosion rate, μm/yr	Corrosion rate, mils/yr
Condensed steam, traces of acid	21–38	70–100	None	Slow	21.59	0.85
Mine water						
pH 8.3, 110 ppm hardness	20	68	Yes	Slow	6.60	0.26
160 ppm hardness	19	67	Yes	Slow	7.11	0.28
110 ppm hardness	22	72	Yes	Slow	6.35	0.25
Cooling tower water, oxygenated, from Lake Erie	16–29	60–85	Complete	None	134.6	5.3
Los Angeles aqueduct water, treated with chlorine and copper sulfate	Ambient		...	150 mm/s (0.5 ft/s)	9.65	0.38
Spray cooling water, chromate treated	16	60	Yes	...	9.4	0.37

Table 2 Corrosion of lead in natural waters

Location	Type of water	Type of test	Agitation	Corrosion rate, μm/yr	Corrosion rate, mils/yr	Ref
Bristol Channel	Seawater	Immersion approx. 93% of the time	...	12.7	0.50	1
Southampton Docks	Seawater	Half tide level	...	2.79	0.11	2
Gatun Lake, Panama	Tropical freshwater	Immersion	None	2.03	0.08	3
Fort Amador, Panama	Tropical Pacific Ocean	Immersion	Flowing(a)	9.14	0.36	4
Fort Amador, Panama	Tropical Pacific Ocean	Mean tide level	Flowing(a)	5.08	0.20	4
San Francisco Harbor	Seawater	Mean tide level	Flowing	10.67	0.42	4
Port Hueneme Harbor, CA	Seawater	Immersion	Flowing(b)	5.59	0.22	5
Kure Beach, NC	Seawater	Immersion	...	15.24	0.60	4

(a) At 150 mm/s (0.5 ft/s). (b) At 60 mm/s (0.2 ft/s)

Table 3 Corrosion of lead in various natural outdoor atmospheres

Location	Type of atmosphere	Duration of test, years	Type of lead	Corrosion rate, μm/yr	Corrosion rate, mils/yr	Ref
Altoona, PA	Industrial	10	Chemical	0.737	0.029	6, 7
			Pb-1Sb	0.584	0.023	6, 7
New York City	Industrial	20	Chemical	0.381	0.015	6, 7
			Pb-1Sb	0.330	0.013	6, 7
Sandy Hook, NJ	Seacoast	20	Chemical	0.533	0.021	6, 7
			Pb-1Sb	0.508	0.020	6, 7
Key West, FL	Seacoast	10	Chemical	0.584	0.023	6, 7
			Pb-1Sb	0.559	0.022	6, 7
LaJolla, CA	Seacoast	20	Chemical	0.533	0.021	6, 7
			Pb-1Sb	0.584	0.023	6, 7
State College, PA	Rural	20	Chemical	0.330	0.013	6, 7
			Pb-1Sb	0.356	0.014	6, 7
Phoenix, AZ	Semiarid	20	Chemical	0.102	0.004	6, 7
			Pb-1Sb	0.308	0.012	6, 7
Kure Beach, NC (25 m, or 80 ft site)	East coast, marine	2	Chemical	1.321	0.052	8
			Pb-6Sb	1.041	0.041	8
Newark, NJ	Industrial	2	Chemical	1.473	0.058	8
			Pb-6Sb	1.067	0.042	8
Point Reyes, CA	West coast, marine	2	Chemical	0.914	0.036	8
			Pb-6Sb	0.660	0.026	8
State College, PA	Rural	2	Chemical	1.397	0.055	8
			Pb-6Sb	0.991	0.039	8
Birmingham, England	Urban	7	99.96% Pb	0.939	0.037	9
			Pb-1.6Sb	0.102	0.004	9
Wakefield, England	Industrial	1	99.995% Pb	1.879	0.074	9
Southport, England	Marine	1	99.995% Pb	1.778	0.070	9
Bourneville, England	Suburban	1	99.995% Pb	1.956	0.077	9
Cardington, England	Rural	1	99.995% Pb	1.422	0.056	9
Cristobal, Panama	Tropical, marine	8	Chemical	1.346	0.053	3
Miraflores, Panama	Tropical, marine	8	Chemical	0.762	0.030	3

the minerals in solid emissions change the patterns of corrosion behavior considerably. However, the protective films that form on lead and its alloys are so effective that corrosion is insignificant in most natural atmospheres. The extent of this protection is demonstrated by the survival of lead roofing and auxiliary products after hundreds of years of atmospheric exposure. In fact, the metal is preserved permanently if these films are not damaged (Ref 10). A detailed review (Ref 11) reported that the aggressiveness and abundance of various potentially interacting anions produce a composite diagram of lead corrosion reactions and products for atmospheric laboratory exposures of lead involving H_2S, SO_2, CO_2, and Cl_2 gases. Depending on the characteristic of the environment, atmospheric corrosion products on lead customarily include anglesite ($PbSO_4$) and cerussite ($PbCO_3$). In addition to the products reported for exposed lead samples, it would not be surprising to find lead oxalates where oxalic acid is abundant, such as in fog droplets in urban areas (Ref 11).

Furthermore, lead runoff is an important issue because of the possible adverse effect on human health. Modern structures may use considerable quantities of lead for aesthetic purposes in the form of leaded-copper sheeting.

An analysis of precipitation runoff from high-purity lead sheets at unpolluted sites in Newport (marine) and Albany (rural), OR, found lead levels of 0.7 and 3.7 mg/L, respectively (Ref 12). The study also showed that lead corrosion films consisted mainly of lead carbonate and lead hydroxy carbonate that showed extensive cracking.

Antimonial lead, such as UNS 52760 (Pb-2.75Sb-0.2Sn-0.18As-0.075Cu), exhibits approximately the same corrosion rate in atmospheric environments as chemical lead (99.9% commercial-purity lead). However, the greater hardness, strength, and resistance to creep of antimonial lead often make it more desirable for use in specific chemical and architectural applications. The ability of some antimonial leads to retain this greater mechanical strength in atmospheric environments has been demonstrated in exposure tests in which sheets containing 4% Sb and smaller amounts of arsenic and tin were placed in semirestricted positions for 3 years. They showed less tendency to buckle than chemical lead, indicating that their greater resistance to creep had been retained.

Painting of lead coatings, especially terne metal (a coating containing 8 to 12% Sn, bal Pb), further raises their resistance to corrosion in outdoor environments. Terne metal has such good paint retention that one coat will far outlast two separate coats on plain steel.

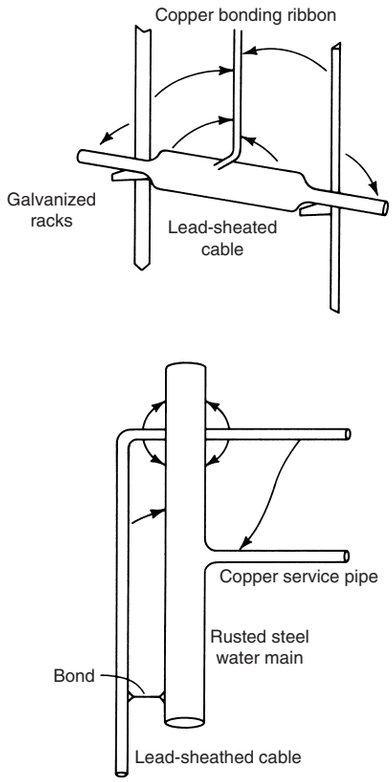

Fig. 1 Corrosion caused by galvanic coupling. Arrows indicate direction of current flow. Source: Ref 2

Corrosion in Underground Ducts

Lead is extensively used in the form of sheathing for power and communications cables because of its impermeability to water and its excellent resistance to corrosion in a wide variety of soil conditions. Cables are either buried directly in the ground or installed in ducts or conduits made of such materials as cement or vitrified clay.

Severe corrosion of lead in underground service (in ducts or directly in the soil) is the exception rather than the rule. However, because repair or replacement of underground components is difficult and expensive, proper corrosion protection is recommended in any underground

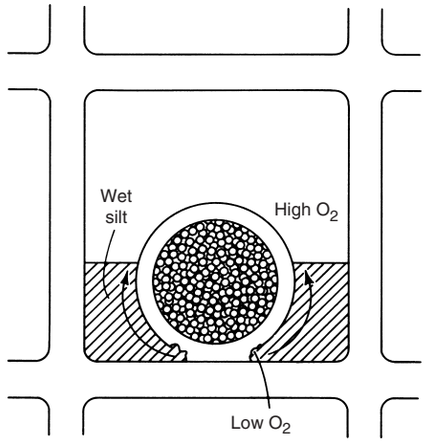

Fig. 2 Corrosion caused by differential aeration in a duct. Arrows indicate direction of current flow. Source: Ref 2

Table 4 Corrosion of lead alloys in various soils

Maximum exposure time: 11 years

	Chemical lead(a)				Tellurium lead(b)				Antimonial lead(c)			
	Corrosion rate		Max pit depth		Corrosion rate		Max pit depth		Corrosion rate		Max pit depth	
Type of soil	μm/yr	mils/yr	μm	mils	μm/yr	mils/yr	μm	mils	μm/yr	mils/yr	μm	mils
Cecil clay loam	<2.54	<0.1	457	18	<2.54	<0.1	406	16	<2.54	<0.1	229	9
Hagerstown loam	<2.54	<0.1	787	31	<2.54	<0.1	762	30	<2.54	<0.1	406	16
Lake Charles clay	7.62	0.3	2540	100	10.16	0.4	2718	107	10.16	0.4	2642	104
Muck	7.62	0.3	1321	52	7.62	0.3	1346	53	7.62	0.3	1295	51
Carlisle muck	5.08	0.2	508	20	5.08	0.2	533	21	2.54	0.1	305	12
Rifle peat	<2.54	<0.1	838	33	<2.54	<0.1	584	23	<2.54	<0.1	711	28
Sharkey clay	7.62	0.3	1778	70	7.62	0.3	1854	73	10.16	0.4	2261	89
Susquehanna clay	<2.54	<0.1	864	34	2.54	0.1	1016	40	2.54	0.1	356	14
Tidal marsh	<0.25	<0.01	305	12	<0.25	<0.01	203	8	<0.25	<0.01	152	6
Docas clay	<2.54	<0.1	635	25	<2.54	<0.1	432	17	<2.54	<0.1	483	19
Chino silt loam	<2.54	<0.1	381	15	<2.54	<0.1	508	20	<2.54	<0.1	178	7
Mohave fine gravelly clay	<2.54	<0.1	610	24	<2.54	<0.1	584	23	2.54	<0.1	406	16
Cinders	7.62	0.3	2159	85	7.62	0.3	1549	61	10.16	0.4	1168	46
Merced silt loam	<2.54	<0.1	610	24	<2.54	<0.1	406	16	<2.54	<0.1	229	9

(a) 0.056 Cu, 0.002 Bi, 0.001 Sb. (b) 0.08 Cu, 0.01 Sb, 0.043 Te. (c) 0.036 Cu, 5.3 Sb, 0.016 Bi. Source: Ref 19

service. Although the discussion that follows is based on preventive methods used for lead-sheathed cables, it is directly applicable in many ways to the underground behavior of other lead products, such as chemical service pipe.

The environment within ducts is often quite complex (Ref 10). It can include combinations of highly humid manhole and soil atmospheres, free lime leached from concrete, and alkalis formed by the electrolysis of salts in the water that seeps into ducts. Some of the factors involved in the corrosion of lead cable sheathing and how they relate to cable assembly and installation are discussed in Ref 13. Their influence in initiating or accelerating corrosion is described in Ref 13, with simple sketches used for illustration. Two of these factors—galvanic coupling and differential aeration—are discussed as follows.

Galvanic Coupling. Figure 1 illustrates two typical examples of contact between lead and other metals. In the presence of an electrolyte, such a dissimilar-metal couple forms a galvanic cell in which the more anodic metal is corroded. A difference in potential sufficient to cause corrosion may also arise when the surface of the lead is scratched to expose bright, active metal. In such cases, the exposed metal is the anode and is attacked.

Differential Aeration. Figure 2 illustrates differential-aeration corrosion. In this type of corrosion cell, areas exposed to low oxygen concentration tend to become anodic to areas exposed to higher oxygen concentrations. As shown, the amount of air able to penetrate the silt and reach the crevice where the cable sheath and the duct meet is less than the amount available at the upper surface of the sheath; this results in corrosion.

An actual example of differential-aeration corrosion is described in Ref 14. Lead-sheathed cable was pressed tightly against the inner surface of a tile duct, and water formed a meniscus extending from the sheathing surface to the tile. The area that was pressed against the tile did not corrode. However, an adjacent area, where the water was farthest from contact with air, corroded severely. The lead surface in contact with water closer to the air in the duct was the cathode.

Alkalinity is another factor that causes the corrosion of cable sheathing (Ref 15). Sheathing on cable installed in continuous concrete or asbestos cement ducts in concrete tunnels under waterways was found to be severely corroded. Analysis of water samples from these locations revealed that the corrosion had resulted from the presence of up to 1000 ppm of hydroxides.

Table 5 Solubility of lead compounds in water

Lead compound	Formula	Temperature °C	Temperature °F	Solubility, kg/m^3
Acetate	$Pb(C_2H_3O_2)_2$	20	68	433
Bromide	$PbBr_2$	20	68	8.441
Carbonate	$PbCO_3$	20	68	0.0011
Basic carbonate(a)	$2PbCO_3$, $Pb(OH)_2$	...	...	Insoluble
Chlorate	$Pb(ClO_3)_2$, H_2O	18	64	0.513
Chloride	$PbCl_2$	20	68	9.9
Chromate	$PbCrO_4$	25	77	0.000058
Fluoride	PbF_2	18	64	0.64
Hydroxide	$Pb(OH)_2$	18	64	0.155
Iodide	PbI_2	18	64	0.63
Nitrate	$Pb(NO_3)_2$	18	64	565
Oxalate	PbC_2O_4	18	64	0.0016
Oxide	PbO	18	64	0.017
Orthophosphate	$Pb_3(PO_4)_2$	18	64	0.00014
Sulfate	$PbSO_4$	25	77	0.0425
Sulfide	PbS	18	64	0.1244
Sulfite(a)	$PbSO_3$	...	...	Insoluble

(a) At room temperature. Source: Ref 21

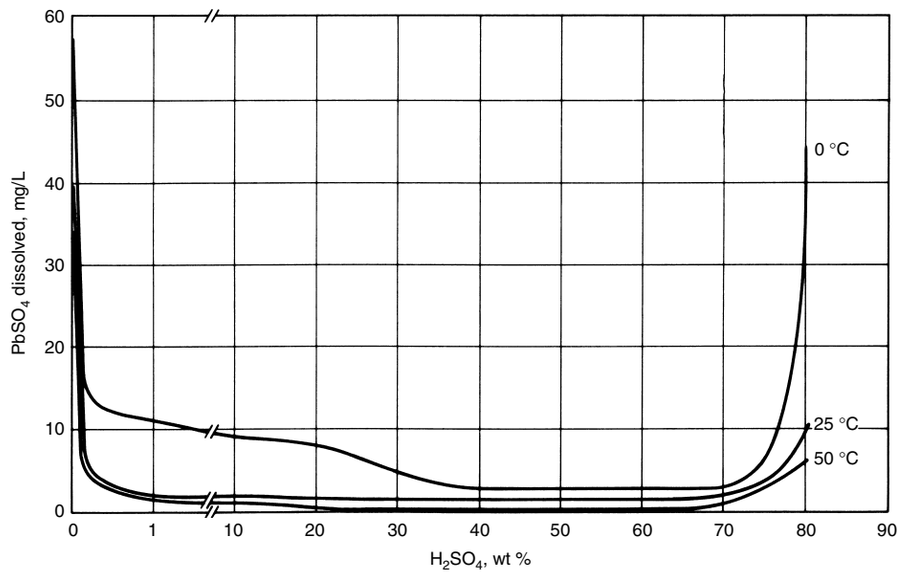

H_2SO_4, wt%	$PbSO_4$, dissolved, mg/L, at: 0 °C (32 °F)	25 °C (75 °F)	50 °C (120 °F)
0	33.0	44.5	57.7
0.005	8.0	10.0	24.0
0.01	7.0	8.0	21.0
0.10	4.6	5.2	13.0
1.0	1.8	2.2	11.3
10.0	1.2	1.6	9.6
20.0	0.5		8.0
30.0	0.4	1.2	4.6
60.0	0.4	1.2	2.8
70.0	1.2	1.8	3.0
75.0	2.8	3.0	6.6
80.0	6.5	11.5	42.0

Fig. 3 Solubility of lead sulfate in sulfuric acid

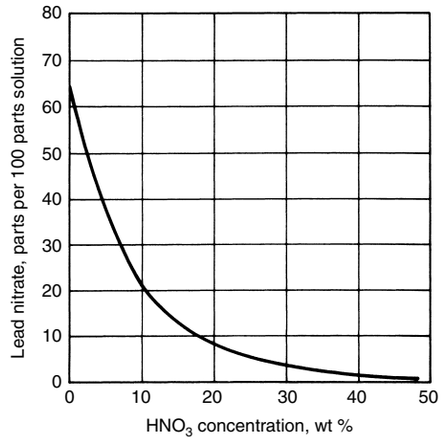

Fig. 4 Solubility of lead nitrate in nitric acid

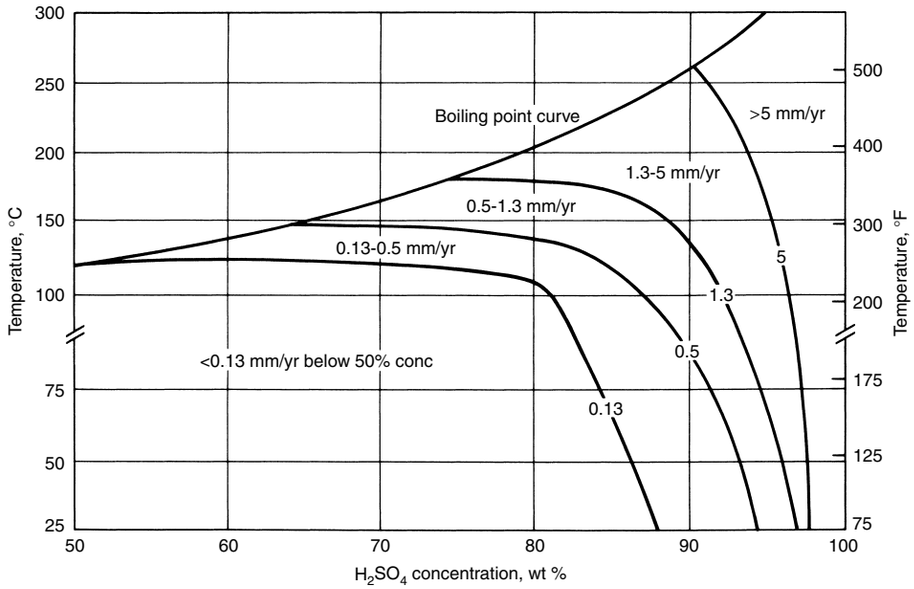

Fig. 5 Corrosion rate of lead in H_2SO_4. Source: Ref 22

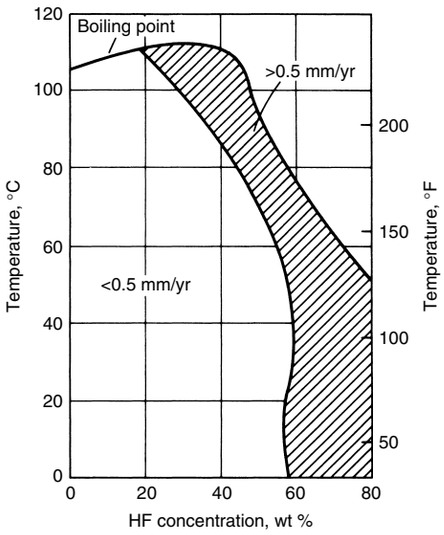

Fig. 6 Resistance of lead to corrosion in air-free hydrofluoric acid

Table 6 Corrosion of chemical lead in commercial phosphoric acid at 21 °C (70 °F)

Solution	Corrosion rate	
	µm/yr	mils/yr
20% H_3PO_4	86.4	3.4
30% H_3PO_4	124.5	4.9
40% H_3PO_4	144.8	5.7
50% H_3PO_4	162.6	6.4
85% H_3PO_4	40.6	1.6
80% H_3PO_4(a)	325.1	12.8

(a) Pure grade

Table 7 Corrosion of lead in hydrochloric acid at 24 °C (75 °F)

HCl concentration, %	Chemical lead		6% antimonial lead	
	µm/yr	mils/yr	µm/yr	mils/yr
1	610	24	840	33
5	410	16	510	20
10	560	22	1090	43
15	790	31	3810	150
20	1880	74	4060	160
25	4830	190	5080	200
35(a)	8890	350	13,720	540

(a) Commercially concentrated HCl

Table 8 Corrosion of lead in hydrochloric acid-ferric chloride mixtures at 24 °C (75 °F)

Solution	Chemical lead		6% antimonial lead	
	µm/yr	mils/yr	µm/yr	mils/yr
5% HCl + 5% $FeCl_3$	711	28	940	37
10% HCl + 5% $FeCl_3$	1041	41	1930	76
15% HCl + 5% $FeCl_3$	2235	88	4064	160
20% HCl + 5% $FeCl_3$	3810	150	4826	190

Table 9 Corrosion of lead in nitric acid

HNO_3 solution, %	Corrosion rate			
	24 °C (75 °F)		50 °C (122 °F)	
	µm/yr	mils/yr	µm/yr	mils/yr
1	3556	140	15,240	600
5	41,910	1650	46,990	1850
10	86,360	3400	88,646	3490

These alkaline water samples (pH 10.9 to 12.2) contained mainly calcium hydroxide. Sodium hydroxide was also found in some tunnels.

The source of the calcium hydroxide was incompletely cured concrete. Electrolysis of solutions of deicing salts that had seeped into the tunnels was believed to be the source of sodium hydroxide. The buildup in concentration occurred because seepage water was not being removed (the ducts had been designed to function without removal of seepage water). Proper drainage and use of completely cured, impervious concrete were suggested as corrective measures.

The process of passive film formation on lead in alkaline solutions and its breakdown were examined (Ref 16) and it was found that the anodic polarization curves exhibit three peaks that correspond to PbO, Pb_3O_4, and PbO_2 prior to the oxygen evolution reaction. It was also found that the addition of NO_3^- ions enhances the anodic dissolution of PbO and, at certain pitting potentials, causes the breakdown of the passivation layer itself. The critical potential was found to decrease linearly with both the logarithmic concentration of nitrate and temperature, while increasing the alkali concentration or the potential scan rate increased the pitting potential.

Stray currents can cause severe corrosion of lead pipe or lead cable sheathing. Stray currents are those that follow paths outside intended circuits. They may also be minor earth currents. Stray currents cause corrosion at the point where they leave the metal. Sources of stray currents include electric railway systems, grounded electric direct current power, electric welders, cathodic protection systems, and electroplating plants. Stray alternating currents are much less damaging than stray direct currents.

It has also been found that corrosion of lead cable sheathing in manhole water depends more on the magnitude and polarity of the potential between the ground and the lead sheathing than it does on the natural dissolved salts in the water. Corrosion is at a minimum when the sheathing is cathodic to the ground (Ref 17, 18). Proper grounding prevents this type of corrosion.

Other factors that can initiate the corrosion of lead sheathing include contact with acetic acid (in wooden ducts), microorganisms, and corroded steel-tape armor. Bacterial corrosion usually occurs when aeration is poor and mud, water, or organic matter is present. Bacteria capable of reducing sulfates to sulfides are the principal cause of attack. Microbial decomposition of the hydrocarbons present in cable coatings may also produce organic acids corrosive to lead. Corrosion of lead by corroded steel-tape armor can occur when the oxide coating formed on the steel is cathodic to lead.

Corrosion in Soil

Soils vary widely in physical and chemical characteristics and, consequently, in corrosive effect. More than 200 varieties of soil in the United States have been classified according to texture, color, and natural drainage. The physical properties of soils that most influence the corrosion of lead in underground service are those

that affect the permeability of the soil to air and water, because good drainage tends to minimize corrosion. Soils with coarse textures, such as sands and gravels, permit free circulation of air. Corrosion in such soils is approximately the same as in the atmosphere. Clays and silty soils generally exhibit fine texture and high water-holding capacity and therefore poor aeration and drainage.

Numerous chemical compounds are present in soils, but only those soluble in water play important roles in the corrosion of metals. For example, the calcareous nature of some Indiana soils influences corrosion through alkaline attack or the promotion of bacterial activity.

Considerable corrosion testing of lead and lead alloys in numerous soils has indicated that corrosion rate decreases with increasing particle size and that the distribution of anodic and cathodic areas depends on soil particle size, water activation value of the soil, soil pH, and duration of exposure. Test results also show that lead tends to become passive in soils regardless of water content; however, addition of sodium bicarbonate reactivates it.

The data in Table 4 show that in most soils the average corrosion rate of lead is low—from less than 2.5 to 10 μm (0.1 to 0.4 mil) per year. It should be noted, however, that the depth of pitting is often a more important measure of underground corrosion behavior than corrosion rate.

The most comprehensive investigation of corrosion of metals buried in soils was conducted by the National Bureau of Standards from 1910 to 1955 (Ref 19). This investigation included lead alloy pipe of three different compositions buried in 14 soils. Specimens were removed periodically; maximum exposure time was 11 years (Table 4).

Analysis of the data in Table 4 indicates that, in general, weight lost and maximum pit depth decrease with increasing aeration of the soil. For example, poor aeration caused severely deep pitting of the lead buried in Sharkey clay, in Lake Charles clay, and in cinders, but pitting of pipe buried in the well-aerated Cecil clay loam was shallow.

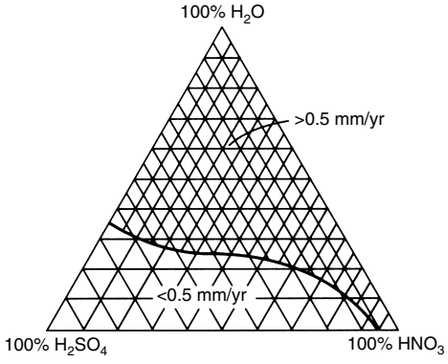

Fig. 7 Corrosion rates of lead in H_2SO_4-HNO_3-H_2O mixtures

Resistance to Chemicals

The excellent resistance of lead and lead alloys to corrosion by a wide variety of chemicals is attributed to the polarization of local anodes caused by the formation of a relatively insoluble surface film of lead corrosion products (Ref 20). The extent of protection depends on the compactness, adherence, and solubility of these films.

Solubilities of various lead compounds in water at room temperature are given in Table 5. These data are general indicators of the behavior of lead in solutions that promote the formation of these compounds. The solubility of a lead corrosion product, however, depends on the solution in which the lead is immersed. Therefore, the solubility of that corrosion product in water is not always an adequate indicator of its behavior in another solution. This fact is illustrated by the variation in solubility of lead sulfate ($PbSO_4$) in H_2SO_4 as acid concentration and temperature change (Fig. 3). The $PbSO_4$ film is less soluble in H_2SO_4 solutions than it is in water. Solubility drops to a minimum value at acid concentrations of 30 to 60% and then increases at higher concentrations. At intermediate concentrations, the sulfate film is so insoluble that corrosion is negligible.

Another example of the importance of the solubility relationship of the lead film to its environment is shown in Fig. 4. Lead nitrate ($Pb(NO_3)_2$) is quite soluble in dilute and intermediate-strength solutions of nitric acid (HNO_3) at room temperature. Lead is not resistant to corrosion under such conditions. However, above an HNO_3 concentration of 50%, $Pb(NO_3)_2$ is only slightly soluble, and lead is quite resistant to attack.

Increases in temperature generally increase corrosion rate (Fig. 3). This effect is primarily due to increases in film solubility.

Galvanic Corrosion. When lead is anodic to a metal to which it is coupled and a firm film develops on the lead, galvanic corrosion of the lead will be negligible. For example, when lead is galvanically connected to a copper or a copper alloy in a H_2SO_4, H_2CrO_4, or H_3PO_4 solution,

Table 10 Effect of nitric acid in sulfuric acid on the corrosion of lead at 118 °C (245 °F)

	Chemical lead		6% antimonial lead	
Solution	μm/yr	mils/yr	μm/yr	mils/yr
54% H_2SO_4 + 0% HNO_3	188	7.4	356	14
54% H_2SO_4 + 1% HNO_3	150	5.9	559	22
54% H_2SO_4 + 5% HNO_3	213	8.4	2896	114

Table 11 Corrosion of chemical lead with sulfuric-nitric mixed acids

	Corrosion rate			
	24 °C (75 °F)		50 °C (122 °F)	
Solution	μm/yr	mils/yr	μm/yr	mils/yr
78% H_2SO_4 + 0% HNO_3	25.4	1	50.8	2
78% H_2SO_4 + 1% HNO_3	76.2	3	304.8	12
78% H_2SO_4 + 3.5% HNO_3	91.4	3.6	457.2	18
78% H_2SO_4 + 7.5% HNO_3	101.6	4	889	35

Table 12 Corrosion of lead in hydrochloric acid-sulfuric acid mixtures

	Chemical lead				6% antimonial lead			
	24 °C (75 °F)		66 °C (150 °F)		24 °C (75 °F)		66 °C (150 °F)	
Solution	μm/yr	mils/yr	μm/yr	mils/yr	μm/yr	mils/yr	μm/yr	mils/yr
1% HCl + 9% H_2SO_4	130	5	230	9	130	5	300	12
3% HCl + 7% H_2SO_4	360	14	810	32	530	21	1040	41
5% HCl + 5% H_2SO_4	360	14	1070	42	530	21	1650	65
7% HCl + 3% H_2SO_4	410	16	1140	45	560	22	1880	74
9% HCl + 3% H_2SO_4	460	18	1190	47	760	30	2130	84
5% HCl + 25% H_2SO_4	250	10	560	22	560	22	860	34
10% HCl + 20% H_2SO_4	430	17	1070	42	2030	80	1470	58
15% HCl + 15% H_2SO_4	1040	41	1880	74	2290	90	4570	180
20% HCl + 10% H_2SO_4	2180	86	3050	120	2790	110	4570	180
25% HCl + 5% H_2SO_4	3560	140	4060	160	3810	150	5330	210
5% HCl + 45% H_2SO_4	1580	62	...	...	1350	53	...	...
10% HCl + 40% H_2SO_4	1650	65	...	...	2130	84	...	...
15% HCl + 35% H_2SO_4	1680	66	...	...	3050	120	...	...
20% HCl + 30% H_2SO_4	2130	84	...	...	3300	130	...	...
25% HCl + 25% H_2SO_4	3050	120	...	...	5330	210	...	...

Table 13 Effect of sulfuric acid on the corrosion of lead by fluosilicic acid at 45 °C (113 °F)

	Chemical lead		6% Sb lead	
Solution	μm/yr	mils/yr	μm/yr	mils/yr
5% H_2SiF_6	1346	53	1956	77
5% H_2SiF_6 + 5% H_2SO_4	229	9	356	14
10% H_2SiF_6	1626	64	2921	115
10% H_2SiF_6 + 1% H_2SO_4	2235	88	1930	76
1% H_2SiF_6 + 10% H_2SO_4	102	4	229	9

Table 14 Corrosion of lead in chemical process fluids

Fluids	Temperature °C	Temperature °F	Corrosion rate µm/yr	Corrosion rate mils/yr
Sulfation of oils with 25% sulfuric acid (66° Bé) at 60 °C (140 °F)				
Castor	...	...	76.2	3
Tallow	...	...	304.8	12
Olive	...	...	76.2	3
Cod liver	...	...	152.4	6
Neatsfoot	...	...	279.4	11
Fish	...	...	279.4	11
Vegetable	...	...	584.2	23
Peanut	...	...	457.2	18
Sulfonation with 93% sulfuric acid (66° Bé)				
Naphthalene	166	330	1143	45
Phenol	120	248	76.2	3
Washing and neutralization of sulfated and sulfonated compounds				
Sulfated vegetable oil + water wash—neutralized with sodium hydroxide	60	140	228.6	9
Naphthalene sulfonic acid + water wash—neutralized with caustic soda pH 3	70	158	990.6	39
Washing tallow with 2% by wt 60° Bé sulfuric acid	121	250	127	5
Storage of liquid alkyl detergent	...	...	7.62	0.3
Storage of 50% chlorosulfonic acid-50% sulfur trioxide	...	...	15.24	0.6
Mixing tank and crystallizer-saturated ammonium sulfate-5% sulfuric acid solution	47	116	25.4–127	1–5
Splitting				
Olive oil and 0.5% sulfuric acid (66° Bé)	88	190	279.4	11
Storage of split fatty acids	...	...	Liquid 20.32	Liquid 0.8
Storage of split fatty acids	...	...	Liquid level 304.8	Liquid level 12
Extraction of aluminum sulfate from alumina				
Bauxite + sulfuric acid—boiling	...	...	Liquid 406.4	Liquid 16
Bauxite + sulfuric acid—boiling	...	...	Vapor 127	Vapor 5
Alum evaporator	116	240	76.2	3
Tank for dissolving alum paper mill	49	120	406.4	16
Storage of 24% alum solution	...	...	15.24	0.6
Dorr settling tank				
19.5 sulfuric acid, 20% ferrous sulfate, 10% titanium oxide as $TiSO_4$	70	158	254	10
Evaporator				
Nickel sulfate solution	100	212	152.4	6
Zinc sulfate solution	107	225	152.4	6
Ammonium sulfate production				
Solution-saturated ammonium sulfate + 5% sulfuric acid	47	116	Mixing tank 25.4	Mixing tank 1
Solution-saturated ammonium sulfate + 5% sulfuric acid	47	116	Crystallizer 127	Crystallizer 5
Acid washing				
Lube oil-treatment with 25% sulfuric acid	104	220	635	25
Sludge oil + 15% sulfuric acid-steam treatment	...	...	508	20
Benzol (crude)-treatment with 3% sulfuric acid washed with water, neutralized with lime	60	140	152.4	6
Tar oil-treatment with 25% sulfuric acid, washed with water, neutralized with sodium hydroxide	77	170	609.6	24
Wet acid gases from regeneration of sulfuric acid	121	250	152.4	6
Polymerization				
Polymerization of butenes with 72% sulfuric acid	80	175	12.7	0.5
Polymerization of butenes with 72% sulfuric acid	80	175	356 pits	14 pits
Viscose rayon spinning bath				
Evaporator—6% sulfuric acid, 17% sodium sulfate, 30% other inorganic sulfates	40	104	127	5
Evaporator—concentrated bath of 20% sulfuric acid, 30% sodium sulfate	55	130	101.6	4
Vapors from spin bath evaporator	49	120	127	5
Spinning bath drippings	46	115	203.2	8
Storage-reclaimed spinning bath liquor	...	...	50.8	2
Pickling solution				
Brass and copper-sulfuric acid + 5% cupric sulfate	71	160	127	5

Source: Ref 23

the lead is protected by a firm film even though it is the anode in the galvanic cell. However, when the other metal is the anode and forms a protective film, galvanic corrosion of the lead may occur, and it is sometimes severe. Aluminum or magnesium will be severely corroded if coupled with lead in the presence of an electrolyte. If lead is coupled with Monel in a 6% H_2SO_4 solution, corrosion of the Monel will be accelerated.

A factor to be kept in mind is that environmental changes can reverse the galvanic positions of the two metals. For example, iron is anodic to lead in acids and cathodic to it in alkalis.

In general, galvanic corrosion of lead is significant only when the lead is coupled with a metal to which it is anodic, when an electrolyte is present, and when a firm film cannot be maintained; corrosion of metals anodic to lead seldom occurs. When galvanic corrosion of either lead or the dissimilar metal does occur, it is unlikely to be severe, because lead occupies a central position in the galvanic series.

Physical variables also influence the corrosion rate of lead in many situations. For example, if the flow velocity of a solution is above a critical point, it can completely erode the protective film, leaving only a clean lead surface exposed for continued attack. This is demonstrated by the rapid increase in corrosion of lead in 20% H_2SO_4 at velocities greater than 1.5 m/s (300 ft/min). The presence of foreign insoluble matter further aggravates this condition.

Fatigue stresses may also break the protective film on lead, repeatedly exposing lead to environmental attack. However, applied fatigue stresses no greater than the creep strength of lead do not significantly affect corrosion properties.

Quantitative Corrosion Data. It is important to remember when evaluating quantitative corrosion data that lead weighs more per unit of volume and is normally used in greater thicknesses than most other metals. The effects of these two factors should be considered in evaluating the data presented in this section.

Lead has high corrosion resistance to H_2CrO_4, H_3PO_4, H_2SO_4, and sulfurous (H_2SO_3) acids and is widely used in their manufacture and handling. Lead satisfactorily resists all but the most dilute solutions of H_2SO_4. It performs well at acid concentrations up to 95% at ambient temperatures, up to 93% at 150 °C (302 °F), and up to 85% at 220 °C (428 °F) (Fig. 5). Below a concentration of 5%, the corrosion rate increases, but it is still relatively low. In the lower range of acid concentration, antimonial lead is recommended.

Lead exhibits the same excellent corrosion resistance to higher concentrations of H_2CrO_4, H_2SO_3, and H_3PO_4 at elevated temperatures. Lead finds especially wide application in the manufacture of H_3PO_4 from phosphate rock when H_2SO_4 is used in the process. Corrosion rates are low for all acid concentrations up to 85% (Table 6). However, when in pure H_3PO_4 manufactured from elemental phosphorus, lead

shows a higher rate due to the absence of sulfates. The corrosion rate of 6% antimonial lead has been reported to be lower than that of chemical lead in a plant test using a solution containing 32% H_3PO_4, 0.4% H_2SO_4, and 1% chlorides at 88 °C (190 °F). In pure acid manufactured from elemental phosphor, lead corrodes at a higher rate because of the absence of sulfates.

Lead has fair corrosion resistance to dilute hydrochloric acid (HCl) (up to 15%) at 24 °C (75 °F); the corrosion rate increases at higher concentrations and at higher temperatures (Table 7). The presence of 5% ferric chlorides also accelerates corrosion (Table 8).

The resistance of lead to corrosion by hydrofluoric acid (HF) is only fair. However, lead is used to handle HF because it is the only low-priced metal that has adequate corrosion resistance. The corrosion rate in this acid (if it is free of air) is less than 510 μm/yr (20 mils/yr) for a wide range of temperatures and concentrations (Fig. 6).

Nitric, acetic, and formic acids in most concentrations corrode lead at rates high enough to preclude its use in these acids. However, although HNO_3 rapidly attacks lead when dilute, it has little effect at strengths of 52 to 70%. The same is true of HF and acetic acid.

Addition of H_2SO_4 to acids corrosive to lead often lowers the corrosion rate. For example, although HNO_3 in concentrations less than 50% is quite corrosive to lead (Table 9), in the presence of 54% H_2SO_4 the corrosion rate in 1% and 5% HNO_3 is quite low even at 118 °C (245 °F) (Table 10). Other concentrations of H_2SO_4 also lower the corrosion rate in HNO_3 (Table 11). The composition range of mixed H_2SO_4 and HNO_3 solutions for which chemical lead has a corrosion rate of less than 500 μm (20 mils) per year is shown in Fig. 7. Chemical lead is preferred over 6% antimonial lead for handling these mixtures of acids.

The corrosion rates of chemical lead and 6% antimonial lead in HCl and in fluosilicic acid are retarded by the presence of H_2SO_4 (Tables 12 and 13). Data on the corrosion of lead in chemical process fluids containing H_2SO_4 or closely related compounds are presented in Table 14.

Qualitative corrosion data serve to provide guidelines for screening suitable metals for chemical equipment. Laboratory test environments may not always simulate actual plant conditions, and there may be significant variations among plants manufacturing the same product. Therefore, it is often more helpful to be less specific when categorizing the corrosion rates of lead in various chemicals. Table 15 presents such less specific information and should be used only as a guide for determining whether further tests are warranted. Most of the data in Table 15 are for chemical lead. The corrosion rates of different grades of lead in the same chemical all normally fall within the same category. Therefore, no mention is made of variations in corrosion rate for other grades of lead.

Table 15 Corrosion rate of lead in chemical environments

For corrosion rate information on lead in other chemical environments, see the more extensive tables contained in *Lead for Corrosion Resistant Applications—A Guide*, Lead Industries Association, Inc., 295 Madison Avenue, New York, NY, 10017, 1974

Chemical	Temperature, °C	Temperature, °F	Concentration, %	Corrosion class(a)
Acetic acid	24	75	Glacial	B
Acetic anhydride	24	75	...	A
Acetone	24–100	75–212	10–90	A
Alcohol, ethyl	24–100	75–212	10–100	A
Alcohol, methyl	24–100	75–212	10–100	A
Aluminum chloride	24	75	0–10	B
Aluminum potassium sulfate	24–100	75–212	10–20	A
Aluminum potassium sulfate	24–100	75–212	20–100	B
Ammonia	24–100	75–212	10–30	B
Ammonium chloride	24	75	0–10	B
Ammonium hydroxide	27	80	3.5–40	A
Ammonium nitrate	24–49	75–120	10–30	D
Ammonium sulfate	24	75	...	B
Amyl acetate	24	75	80–100	B
Aniline	20	68	...	A
Antimony chloride	24	75	...	C
Arsenic trichloride	100–149	212–300	...	B
Barium chloride	24–100	75–212	10	B
Benzaldehyde	24	75	10–100	D
Benzene	24	75	...	B
Benzoic acid	24	75	...	D
Benzyl alcohol	24–100	75–212	...	B
Benzyl chloride	24–100	75–212	...	B
Beryllium chloride	100	212	...	D
Boric acid	24–149	75–300	10–100	B
Bromine	24	75	...	B
Butyric acid	24	75	10–100	D
Cadmium sulfate	24–100	75–212	10–30	A
Calcium bicarbonate	24	75	...	C
Calcium chloride	24	75	20	A
Calcium fluoride	24–100	75–212	...	B
Calcium nitrate	24	75	10	D
Calcium sulfate	24–100	75–212	10	B
Carbon disulfide	24–100	75–212	...	A
Carbonic acid	24	75	...	D
Cellulose acetate	24	75	...	A
Cellulose nitrate	24–100	75–212	...	B
Chloroacetic acid	24	75	...	B
Chloric acid	24	75	10	D
Chlorine	38	100	...	B
Chloroform	24–62	75–143	...	B
Chromic acid	24	75	...	B
Copper chloride	24	75	10–40	D
Creosote	24	75	90	D
Dichlorobenzene	24–100	75–212	10–100	B
Diethyl ether	24	75	...	B
Dioxane	24–100	75–212	...	B
Ethyl acetate	24–79	75–175	...	B
Ferric ammonium sulfate	24–100	75–212	10–20	A
Ferric chloride	24	75	20–30	D
Ferric sulfate	24–79	75–175	10–20	A
Ferrous chloride	24	75	10–30	C
Ferrous sulfate	24–100	75–212	10	B
Fluosilicic acid	45	113	10	D
Formaldehyde	24–52	75–125	20–100	B
Formic acid	24–100	75–212	10–100	D
Glycerol	24	75	...	B
Hydrazine	24	75	20–100	D
Hydriodic acid	24	75	10–50	D
Hydrobromic acid	24	75	10–70	D
Hydrochloric acid	24	75	0–10	C
Hydrogen peroxide	24	75	10–30	D
Isopropanol	24	75	...	A
Lead acetate	24	75	10–30	D
Lead chloride	24–100	75–212	...	B
Lithium hydroxide	24	75	...	D
Magnesium chloride	24	75	10–100	D

(continued)

(a) The four categories of the table are: A, <50 μm/yr (<2 mils/yr): negligible corrosion—lead recommended for use. B, <500 μm/yr (<20 mils/yr): practically resistant—lead recommended for use. (When the only information available is that "lead is resistant" to a certain chemical, that chemical was arbitrarily placed in this category.) C, 500–1270 μm/yr (20–50 mils/yr): lead may be used where this effect on life can be tolerated. D, >1270 μm/yr (>50 mils/yr): corrosion rate too high to merit any consideration of lead

Table 15 (continued)

Chemical	Temperature °C	Temperature °F	Concentration, %	Corrosion class(a)
Magnesium sulfate	24–100	75–212	10–60	B
Mercury	24	75	100	D
Methyl ethyl ketone	24–100	75–212	10–100	B
Nitrobenzene	24–52	75–125	. . .	B
Oxalic acid	24	75	20–100	D
Phenol	24	75	90	B
Phosphoric acid	24–93	75–200	. . .	B
Potassium chloride	8	47	0.25–8.0	B
Potassium hydroxide	24–60	75–140	0–50	B
Pyridine	24–100	75–212	10	B
Sodium acetate	25	77	4	B
Sodium bicarbonate	24	75	10	B
Sodium chloride	25	77	0.5–24	A
Sodium hydroxide	26	79	0–30	B
Sodium nitrate	24	75	10	D
Sodium sulfate	24	75	2–20	A
Stannous chloride	24	75	10–50	D
Zinc sulfate	35	95	. . .	B
Zinc chloride	79	175	25	B

(a) The four categories of the table are: A, <50 μm/yr (<2 mils/yr): negligible corrosion—lead recommended for use. B, <500 μm/yr (<20 mils/yr): practically resistant—lead recommended for use. (When the only information available is that "lead is resistant" to a certain chemical, that chemical was arbitrarily placed in this category.) C, 500–1270 μm/yr (20–50 mils/yr): lead may be used where this effect on life can be tolerated. D, >1270 μm/yr (>50 mils/yr): corrosion rate too high to merit any consideration of lead

Table 16 Melting characteristics and applications of tin-lead solders

Composition, %		Temperature Solidus		Temperature Liquidus		
Tin	Lead	°C	°F	°C	°F	Uses
2	98	270	518	312	594	Side seams for can manufacturing
5	95	270	518	312	594	Coating and joining metals
10	90	268	514	299	570	. . .
15	85	226	440	288	550	. . .
20	80	183	361	277	531	Coating and joining metals, or filling dents or seams in automobile bodies
25	75	183	361	266	511	Machine and torch soldering
30	70	183	361	255	491	. . .
35	65	183	361	247	477	General-purpose and wiping solder
40	60	183	361	238	460	Wiping solder for joining lead pipes and cable sheaths. For automobile radiator cores and heating units
45	55	183	361	227	441	Automobile radiator cores and roofing seams
50	50	183	361	216	421	General purpose. Most popular of all
60	40	183	361	190	374	Primarily used in electronic soldering applications in which low soldering temperatures are required
63	37	183	361	183	361	Lowest-melting (eutectic) solder for electronic applications

Tin-Lead Solder Alloys

Solders were based on the tin-lead system. Industrial solder alloys contain a combination of materials ranging from 100% Pb to 100% Sn, as demanded by the application. Each alloy has unique melting characteristics and load-carrying and temperature capabilities. Because electronic equipment is not recycled as efficiently as batteries, there are health concerns about discarded electronic equipment in landfills. Initiatives worldwide have sought to eliminate lead in solder for electrical and electronic equipment. There are exceptions where no substitutes are available, and, in some cases, implementation dates have been delayed (Ref 24).

Table 16 gives the melting temperatures of some tin-lead compositions and their respective applications. More detailed information on the compositions and melting characteristics of tin-lead solders can be found in the article "General Soldering" in *Welding, Brazing, and Soldering,* Volume 6 of *ASM Handbook,* 1993. Corrosion-related data of these alloys are also presented in the article "Corrosion of Tin and Tin Alloys" in this Volume.

Applications. Solder alloys containing less than 5% Sn are used for joining tin-plated containers and for automobile radiator manufacture. For automobiles, a small additional amount of silver is usually added to provide extra joint strength at automobile radiator operating temperatures. Solder alloys of 10Sn-90Pb and 20Sn-80Pb are also used in radiator joints. With compositions between 10Sn-90Pb and 25Sn-75Pb, care must be taken to avoid any kind of movement during the solidification phase to prevent hot tearing in solders with a wide freezing range.

Higher tin content solders at the 25Sn-75Pb and 30Sn-70Pb compositions have lower liquidus temperatures and can be used for joining materials with sensitivity to high temperature or where the wetting characteristics of the tin are important to providing sound soldering joints. Solder alloys in the composition range described previously are usually applicable to industrial products and generally are used in conjunction with inorganic fluxing materials.

The widely used general-purpose solder alloys contain 40 to 50% Sn. These solders are used for plumbing applications, electrical connections, and general soldering of domestic items. The 60Sn-40Pb and 63Sn-37Pb alloys are used most extensively in the electronic industries for both hand soldering and wave or dip applications. Sometimes, silver additions are made to alloys used in the electronics industries to reduce dissolution of silver-base coatings.

ACKNOWLEDGMENT

This article is a revision of the article by Jerome F. Smith, Lead Industries Association, Inc., "Corrosion of Lead and Lead Alloys", *Corrosion,* Volume 13, *ASM Handbook,* ASM International, 1987, p 784–792. Portions of that article were based on Chapters 5 and 6 of *Lead for Corrosion Resistant Applications—A Guide,* Lead Industries Association, Inc.

REFERENCES

1. J.N. Friend, The Relative Corrodibilities of Ferrous and Nonferrous Metals and Alloys—Part 1—The Results of Four Years of Exposure in Bristol Channel, *J. Inst. Met.,* Vol 39, 1928, p 111–143
2. J.N. Friend, The Relative Corrodibilities of Ferrous and Nonferrous Metals and Alloys—Part III—Results of Three Years Exposure at Southampton Docks, *J. Inst. Met.,* Vol 48, 1932, p 109–120
3. B.W. Forgeson et al., Corrosion of Metals in Tropical Environments, *Corrosion,* Vol 14, 1958, p 73t–81t
4. Guruswamy, *Engineering Properties and Applications of Lead Alloys,* Marcel Dekker, 2000
5. C.V. Brouilette, Corrosion Rates in Port Hueneme Harbor, *Corrosion,* Vol 14, 1958, p 352t–356t
6. G.O. Hiers and E.J. Minarcik, The Use of Lead and Tin Outdoors, *Symposium on Atmospheric Corrosion of Nonferrous Metals,* STP 175, American Society for Testing and Materials, 1955, p 135–140

7. Report of Subcommittee VI of ASTM Committee B-3 on Atmospheric Corrosion Tests of Nonferrous Metals and Alloys, in *ASTM Proceedings,* Vol 44, American Society for Testing and Materials, 1944, p 224
8. Report of Subcommittee VI of ASTM Committee B-3 on Atmospheric Corrosion Tests of Nonferrous Metals and Alloys, in *ASTM Proceedings,* Vol 62, American Society for Testing and Materials, 1962, p 216
9. J.N. Friend, The Relative Corrodibilities of Ferrous and Nonferrous Alloys—Part II—The Results of Seven Years Exposure to Air at Birmingham, *J. Inst. Met.,* Vol 42, 1929, p 149–155
10. R.M. Burns, Corrosion of Metals II—Lead and Lead Alloy Cable Sheathing, *Bell Syst. Tech. J.,* Vol 15, 1936, p 603–625
11. T.E. Graedel, Chemical Mechanisms for the Atmospheric Corrosion of Lead, *J. Electrochem. Soc.,* Vol 141 (No. 4), April 1994, p 922–927, with excerpts in *Atmospheric Corrosion,* C. Leygraf and T.E. Graedel, Ed., Wiley, 2000, p 295–304
12. S.A. Matthes, S.D. Cramer, B.S. Covino, Jr., S.J. Bullard, and G.R. Holcomb, Precipitation Runoff from Lead, *Outdoor Atmospheric Corrosion,* STP 1421, H.E. Townsend, Ed., ASTM, 2002, p 265
13. K.G. Compton, Factors Involved in Corrosion of Lead Cable Sheath, *Corrosion,* Vol 17, 1961, p 409t–412t
14. NACE Task Group T-4B-1, Cell Corrosion on Lead Cable Sheaths, *Corrosion,* Vol 12, 1956, p 257t–259t
15. R.I. Perry, Preventing Corrosion of Lead-Sheathed Power Cables in Concrete Tunnels, *Corrosion,* Vol 12, 1956, p 207t–212t
16. S.S. Abd El Rehim and N.F. Mohamed, Passivity Breakdown of Lead Anode in Alkaline Nitrate Solutions, *Corros. Sci.,* Vol 40 (No. 11), 1998, p 1883–1896
17. Y. Yamaguchi et al., Studies on Corrosion of Communication Cable Lead Sheath by Manhole Water, *Corros. Eng. (Jpn.),* Vol 5, 1956, p 302–306
18. NACE Technical Unit Committee T-4B, Corrosion of Lead Sheath in Manhole Water, *Corrosion,* Vol 14, 1958, p 85t–87t
19. M. Romanoff, "Underground Corrosion," NBS 579, National Bureau of Standards, April 1957, p 227
20. E.L. Littauer and H.C. Wesson, Lead and Lead Alloys, *Corrosion,* Vol 1, L.L. Shrier, Ed., John Wiley & Sons, 1963, p 4:68–4:85
21. R.C. Weast, Ed., *Handbook of Chemistry and Physics,* 45th ed., CRC Press, 1964
22. M.G. Fontana, *Ind. Eng. Chem.,* Vol 43, 1951, p 105A
23. G.A. Nelson, *Corrosion Data Survey,* National Association of Corrosion Engineers, 1967
24. G. Humpston and D. Jacobson, *Principles of Soldering,* ASM International, 2004, p 190

SELECTED REFERENCES

- E.E. Abd El Aal, Studies on the Pitting Corrosion of Lead in Carbonate Media, *Anti-Corros. Methods Mater.,* Vol 48 (No. 2), 2001, p 116–125
- V. Hock, K.W. Smothers, and J.L. Overman, "Evaluation of in-situ Pipe Coating Process for Mitigation of Lead and Copper in Drinking Water," Paper 03107, Corrosion/2003, NACE International, 2003
- I. Ivanov et al., Insoluble Anodes Used in Hydrometallurgy, Part I. Corrosion Resistance of Lead and Lead Alloy Anodes, *Hydrometallurgy,* Vol 57 (No. 2), 2000, p 109–124
- E. Rocca, C. Rapin, and F. Mirambet, "Inhibition of the Corrosion of Lead Artifacts in Atmospheric Conditions and by Acetic Acid Vapour: Use of Sodium Decanoate," *Corros. Sci.,* Vol 46 (No. 3), 2004, p 653–665

ASM Handbook, Volume 13B: Corrosion: Materials
S.D. Cramer, B.S. Covino, Jr., editors, p205-227
DOI: 10.1361/asmhba0003820

Corrosion of Magnesium and Magnesium-Base Alloys

Revised by Barbara A. Shaw and Ryan C. Wolfe, Pennsylvania State University

LOW DENSITY and high strength-to-weight ratio are usually the prime reasons for specifying the use of magnesium alloys in engineering designs. High stiffness-to-weight ratios, good castability, high thermal and electrical conductivity, and high damping capacity of magnesium alloys are also attractive properties. However, magnesium possesses a strong thermodynamic driving force for corrosion, and its surface film does not present a very protective kinetic barrier to corrosion. Despite these shortcomings, the interest in using magnesium alloys for a variety of applications is still high because of its weight advantage. Consumer uses of magnesium alloys include cases for personal electronics (laptop computers, cameras), luggage enclosures, handtools, frames for sunglasses, and even in space suits designed for use on Mars. The premier automotive use of magnesium is in the form of transmission casings; because these components are necessarily large structures, the weight savings realized with magnesium are substantial (20 to 25% over aluminum). Military uses for magnesium are extensive and include radar equipment, portable ground equipment, decoy flare ordnance, helicopter transmission and rotor housings, and in torpedoes.

In the past 20 years, numerous efforts have been made toward improving the corrosion properties of magnesium and magnesium alloys to make them more suitable for use in structural designs. In fact, the corrosion rate of newer magnesium alloys is similar to that of mild steel when used in suitable applications and adequately insulated from more noble metals (Ref 1). Coatings, control of impurities, alloying additions, inhibitors, and careful attention to design details (to address galvanic corrosion issues) are the primary ways in which the corrosion of magnesium and magnesium alloys are addressed.

Impurities, in particular, exacerbate corrosion by increasing the rate of hydrogen evolution. The tolerance limits for impurities such as iron, nickel, and copper in magnesium were quantified (Ref 1), as was the importance of manganese in mitigating these effects (Ref 2). Corrosion of magnesium can be reduced by the mere elimination of impurities, and improvements in corrosion resistance of many of the newer magnesium alloys are due to the careful control of impurities.

The electrochemical thermodynamics of magnesium can be visualized in the form of a Pourbaix diagram. Figure 1 is the potential-pH diagram of the magnesium-water system (Ref 3). Magnesium is shown to dissolve over a wide range of pH and potential. At high pH, the corrosion product film of magnesium hydroxide (brucite) that forms on the surface is only semiprotective. The film is of low density due to the platelike structure of magnesium hydroxide, allowing for the ingress of electrolyte to the metal underneath. In addition, the film undergoes compressive rupture due to the higher molar volume of magnesium hydroxide compared to metallic magnesium, resulting in the constant exposure of fresh metal (Ref 4). Thus, the region of presumed passivity in the Pourbaix diagram must be considered with skepticism.

The corrosion product film on magnesium causes the lustrous metal to assume a dull gray appearance when exposed to air. When observed under a transmission electron microscope, this film is shown to comprise of an outer layer and at least one inner layer near the magnesium metal/oxide interface (Ref 5–7). Native oxide films were found to be 20 to 50 nm (0.8 to 2 μin.) thick, while films grown at 65% relative humidity (RH) and 30 °C (85 °F) were 100 to 150 nm (4 to 6 μin.) thick. Films grown in distilled water for 48 h consisted of an inner cellular layer (0.4 to 0.6 μm, or 0.016 to 0.024 mil, thick) and a platelike outer layer (1.8 to 2.2 μm, or 0.071 to 0.087 mil, thick). The inner layer is assumed to be responsible for corrosion resistance. Improvements in corrosion resistance have been found to correlate with an increase in the concentration of the alloying element or its oxide in the passive film.

The measurement of magnesium corrosion by electrochemical methods is complicated by the negative difference effect. The negative difference effect is a unique and important aspect of magnesium corrosion. The negative difference effect is described by the observation that the rate of the cathodic reaction (hydrogen evolution) can increase even when the driving force for reduction decreases (by application of an anodic potential). In most cases, on application of potentials anodic to the open-circuit potential, the rate of the expected anodic reaction will increase, while the rate of the expected cathodic reaction would decrease. Four different theories for the negative difference effect are commonly described: the partially protective oxide theory, the monovalent magnesium ion theory, the particle undermining model, and the magnesium hydride model (Ref 1). Understanding the actual mechanism may lead to corrosion prevention methods in new magnesium alloys.

Galvanic corrosion plagues magnesium alloys. The origin of the problem is the large difference in potential between magnesium and most alloys with which it is coupled. One can

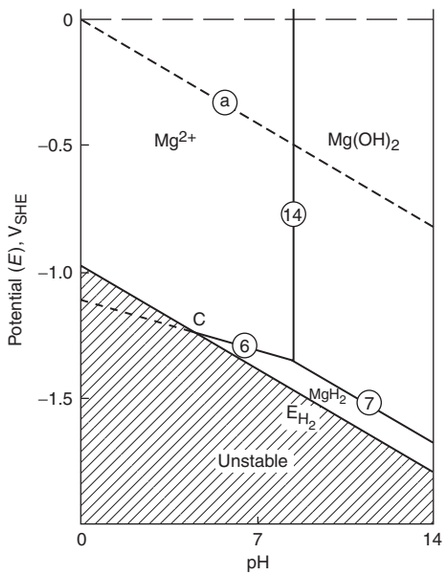

Fig. 1 Pourbaix diagram for magnesium as developed by Perrault. Source: Ref 3

also attribute galvanic corrosion to the oxidation of magnesium due to the occurrence of the supporting cathodic reaction on another metal. Still another way in which to view galvanic corrosion of magnesium is the corrosion due to magnesium being coupled with a metal that is more noble on the galvanic series. The meaning and effect of galvanic corrosion are the same regardless of the definition used.

There is also considerable interest in the use of magnesium alloys in metal-matrix composites (MMCs). This is a strenuous application for magnesium, considering the extreme galvanic nobility of many composite materials, such as graphite. In the case of AZ91 combined with alumina fibers, the corrosion rate of the MMC is 7 times higher than that of the bulk alloy, showing the paramount importance of galvanic effects (Ref 8). The microstructural as well as macroscopic effects of galvanic corrosion must be carefully regarded.

Environmental Factors

The information in this section is based on the behavior of unprotected metal. Improved resistance is obtained by using proper protection systems. The alloy composition also affects corrosion behavior.

Atmospheres. A clean, unprotected magnesium alloy surface exposed to indoor or outdoor atmospheres free from salt spray will develop a gray film that partly protects the metal from corrosion while causing only negligible losses in mechanical properties. Chlorides, sulfates, and foreign materials that hold moisture on the surface can promote corrosion and pitting of some alloys unless the metal is protected by properly applied coatings.

The surface film that ordinarily forms on magnesium alloys exposed to the atmosphere gives limited protection from further attack. Unprotected magnesium and magnesium alloy parts are resistant to rural atmospheres and moderately resistant to industrial and mild marine atmospheres, provided they do not contain joints or recesses that entrap water and thus promote the establishment of galvanic couples. Compositions of the corrosion products that form on magnesium vary from one location to another and from indoor to outdoor exposure. X-ray diffraction analysis of corrosion products scraped from magnesium ingots after 18 months of exposure in a rural atmosphere have shown the presence of various hydrated carbonates of magnesium, including $MgCO_3 \cdot H_2O$, $MgCO_3 \cdot 5H_2O$, and $3MgCO_3Mg(OH)_2 \cdot 3H_2O$. In an industrial atmosphere, hydrated and basic carbonates were found, together with magnesium sulfite ($MgSO_3 \cdot 6H_2O$) and magnesium sulfate ($MgSO_4 \cdot 7H_2O$). These analyses, in addition to similar analyses after shorter periods of exposure, indicate that the primary reaction in corrosion of magnesium is the formation of magnesium hydroxide, $Mg(OH)_2$, followed by a secondary reaction with carbonic acid to convert the hydroxide to a hydrated carbonate. In atmospheres contaminated with sulfur compounds, sulfites or sulfates may also be present in the corrosion product. The sulfates may be formed by the reaction of acidic sulfur-bearing gases with $Mg(OH)_2$ or $MgCO_3$.

Corrosion of magnesium alloys increases with RH. At 9.5% RH, neither pure magnesium nor any of its alloys exhibit evidence of surface corrosion after 18 months. At 30% RH, only minor corrosion may occur. At 80% RH, the surface may exhibit considerable corrosion. In marine atmospheres heavily loaded with salt spray, magnesium alloys require protection for prolonged survival.

Freshwater. In stagnant distilled water at room temperature, magnesium alloys rapidly form a protective film that prevents further corrosion. Small amounts of dissolved salts in water, particularly chlorides or heavy-metal salts, will break down the protective film locally, which usually results in pitting.

Dissolved oxygen plays no major role in the corrosion of magnesium in either freshwater or saline solutions. However, agitation or any other means of destroying or preventing the formation of a protective film leads to corrosion. When magnesium is immersed in a small volume of stagnant water, its corrosion rate is negligible. The magnesium ions that initially dissolve increase the pH of the solution and cause the precipitation of insoluble $Mg(OH)_2$. When the water is constantly replenished so that the solubility limit of $Mg(OH)_2$ is never reached, the corrosion rate may increase.

The corrosion of magnesium alloys by pure water increases substantially with temperature. At 100 °C (210 °F), the aluminum-zinc (AZ) alloys typically corrode at 0.25 to 0.50 mm/yr (10 to 20 mils/yr). Pure magnesium and alloy ZK60A corrode excessively at 100 °C (212 °F), with rates up to 25 mm/yr (1000 mils/yr). At 150 °C (300 °F), all magnesium alloys corrode excessively (Ref 9).

Salt Solutions. When exposed to magnesium-salt solutions, the corrosivities of chlorides were greater than that of bromides, which was greater than that of chlorates, as shown in Table 1. The lower corrosion rates in the 2 *M* solutions were attributed to concentration polarization.

Severe corrosion may occur in neutral solutions of salts of heavy metals, such as copper, iron, and nickel. Such corrosion occurs when the heavy metal, the heavy-metal basic salts, or both plate out to form active cathodes on the anodic magnesium surface.

Chloride solutions are corrosive because chlorides, even in small amounts, tend to break down the protective film on magnesium. Fluorides form insoluble magnesium fluoride and consequently are not appreciably corrosive. Oxidizing salts, especially those containing chlorine or sulfur atoms, are more corrosive than nonoxidizing salts, but chromates, vanadates, phosphates, and many others promote film formation and thus retard corrosion, except at elevated temperatures.

Acids and Alkalis. Magnesium is rapidly attacked by all mineral acids except hydrofluoric acid (HF) and chromic acid (H_2CrO_4). Hydrofluoric acid does not attack magnesium to an appreciable extent, because it forms an insoluble, protective magnesium fluoride film on the magnesium; however, pitting develops at low acid concentrations. With increasing temperature, the rate of attack increases at the liquid line, but to a negligible extent elsewhere.

Pure H_2CrO_4 attacks magnesium and its alloys at a very low rate. However, traces of chloride ion in the acid will markedly increase this rate. A boiling solution of 20% H_2CrO_4 in water is widely used to remove corrosion products from magnesium alloys without attacking the base metal. Magnesium resists dilute alkalis, and 10% caustic solution is commonly used for cleaning at temperatures up to the boiling point.

Organic Compounds. Aliphatic and aromatic hydrocarbons, ketones, ethers, glycols, and higher alcohols are not corrosive to magnesium and its alloys. Ethanol causes slight attack, but anhydrous methanol causes severe attack. The rate of attack in the latter is reduced by the presence of water. Gasoline-methanol fuel blends in which the water content equals or exceeds approximately 0.25 wt% of the methanol content do not attack magnesium (Ref 11).

Pure halogenated organic compounds do not attack magnesium at ambient temperatures. At elevated temperatures or if water is present, such compounds may cause severe corrosion, particularly those compounds having acidic reaction products.

Dry fluorinated hydrocarbons, such as the Freon (E.I. Du Pont de Nemours, Inc.) refrigerants, usually do not attack magnesium alloys at room temperature, but when water is present, they may stimulate significant attack. While fluorinated hydrocarbons may react violently with magnesium alloys at elevated temperatures, newer processes involving fluoronated ketones are being developed to protect molten magnesium from burning.

Table 1 Corrosion rates of magnesium and magnesium-aluminum alloys in various magnesium-salt solutions

	1 *M* solution, mg/cm²/day			2 *M* solution, mg/cm²/day		
Alloy	$Mg(ClO_4)_2$	$MgBr_2$	$MgCl_2$	$Mg(ClO_4)_2$	$MgBr_2$	$MgCl_2$
AZ31	9.2	142	289	4.2	117	264
AZ61	27	153	311	6.4	127	272
Mg	258	289	473	128	225	384

Specimens were immersed in the solutions for 5 h and the weight loss measured. Source: Ref 10

In acidic foodstuffs, such as fruit juices and carbonated beverages, attack of magnesium is slow but measurable. Milk causes attack, particularly when souring.

At room temperature, ethylene glycol solutions produce negligible corrosion of magnesium that is used alone or galvanically connected to steel; at elevated temperatures, such as 115 °C (240 °F), the rate increases, and corrosion occurs unless proper inhibitors are added. Measures should be taken to control the galvanic corrosion.

Gases. Dry chlorine, iodine, bromine, and fluorine cause little or no corrosion of magnesium at room or slightly elevated temperature. Even when it contains 0.02% H_2O, dry bromine causes no more attack at its boiling temperature (58 °C, or 136 °F) than at room temperature. The presence of a small amount of water causes pronounced attack by chlorine, some attack by iodine and bromine, and negligible attack by fluorine. Wet chlorine, iodine, or bromine below the dewpoint of any aqueous phase causes severe attack of magnesium. Water vapor in air or in oxygen sharply increases the rates of oxidation of magnesium and its alloys above 100 °C (212 °F), but boron trifluoride (BF_3), SO_2, and SF_6 are effective in reducing oxidation rates. The presence of BF_3 or SF_6 in the ambient atmosphere is particularly effective in suppressing high-temperature oxidation up to and including the temperature at which the alloy normally ignites.

The oxidation rate of magnesium in oxygen increases with temperature. At elevated temperature (approaching melting), the oxidation rate is a linear function of time. Cerium, lanthanum, calcium, and beryllium in the metal reduce the oxidation rate below that of pure magnesium. Beryllium additions have the most striking effects, protecting some alloys at temperatures up to the melting point over extended periods of time. Structural applications of magnesium alloys at elevated temperature are usually limited by creep strength rather than by oxidation.

Soils. Except when used as galvanic anodes, magnesium alloys have good corrosion resistance in clay or nonsaline sandy soils but have poor resistance in saline sandy soils.

Corrosion in Real and Simulated Environments

Structural applications of magnesium alloys usually involve environmental conditions ranging from indoor atmospheres (computer disk drive components and notebook computer housings) to intermittent salt splash (automotive clutch housings). Allowable corrosion in these applications may range from zero for disk drive parts or critical military and aerospace components to substantial for some automotive castings, provided there is no interference with function for a specified period. Magnesium alloys of controlled high purity have demonstrated the capability of withstanding these environments in properly designed assemblies. Designers, however, must have advance information about the type and magnitude of corrosion that can occur under particular service conditions.

The best sources of such information would be previous service experience or long-term data from tests in the actual environment. When these are lacking, accelerated corrosion tests, such as alternate (intermittent) immersion in saltwater or salt spray, are often used to compare the corrosion resistance of magnesium alloys to each other and to other metals. In addition, such tests are used to examine the relative merits of protective chemical treatments and coatings and the galvanic compatibilities of dissimilar metals with magnesium. The ASTM B 117 salt spray test (Ref 12) in particular is widely used and is firmly established as an acceptance test in many specifications. Magnesium is also subjected to various saltwater-based accelerated corrosion tests developed for special purposes. An important example is the proving ground cycle tests used by automobile manufacturers. Correlation has been established between proving ground cycle performance and vehicle corrosion in long-term service.

Corrosion Testing. Weight-loss and penetration measurements are the most common ways of assessing the corrosion resistance of magnesium and magnesium alloys. However, electrochemical techniques, such as polarization methods or electrochemical impedance spectroscopy, are often used to supplement weight-loss measurements and to evaluate corrosion mechanisms.

Potentiodynamic polarization curves for magnesium in 0.5 *M* sodium sulfate solutions having different values of pH are shown in Fig. 2. The anodic polarization shows active dissolution of magnesium over the entire pH range test, and the effect of pH seems minor over this range. Electrochemical impedance data for cast pure magnesium (99.98% purity) in sodium borate having a pH of 9.2 are presented in Fig. 3, which shows a single capacitance semicircle, indicative that the only process occurring is charge transfer.

For most metal systems, there is usually good quantitative agreement between weight-loss and electrochemical measurements. However, for magnesium metal, especially pure magnesium, this does not seem to be true. Figure 4 gives a comparison of corrosion rates of alloys in pH 9.2 sodium borate determined from electrochemical and gravimetric techniques. For pure magnesium, the weight-loss values are roughly an order of magnitude higher than predicted by electrochemical techniques. This is a result of the negative difference effect, which is the phenomenon described by the increase of hydrogen evolution upon anodic polarization. The hydrogen evolution reaction consumes the electrons generated by the corrosion of magnesium, resulting in a corrosion rate measurement that is lower that the actual corrosion rate.

Figure 5 shows the effect of current density on the negative difference for anodic dissolution of magnesium in sulfuric acid obtained by hydrogen-evolution rate. When there is no negative difference effect, the voltage is proportional to 6.97 *I*, where *I* is the current input. The deviation from linearity becomes more pronounced with increasing current density and decreasing acid concentration. The reasons for this effect have been extensively discussed in the literature (Ref 16) and explained as:

- Formation of metastable monovalent magnesium ions
- Loss of metal by disintegration (chunk effect)
- Damage to protective film, exposing active metal
- Formation of magnesium hydride

Specific Effects of Chloride Environments. Salt-based accelerated tests can provide useful

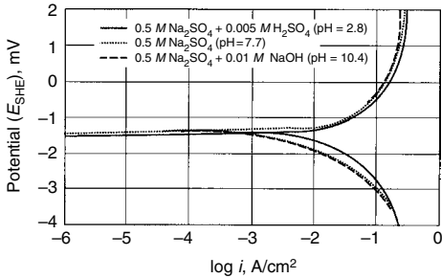

Fig. 2 Stationary potentiodynamic polarization curves of magnesium in 0.5 *M* Na_2SO_4 solutions having different levels of pH. Source: Ref 13

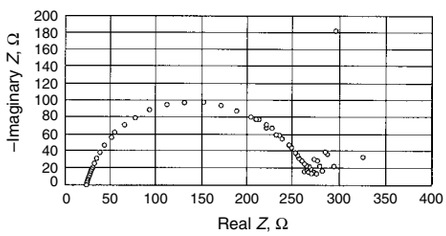

Fig. 3 Electrochemical impedance data for cast pure magnesium (99.9% pure) in pH 9.2 sodium borate presented in the Nyquist format. Source: Ref 14

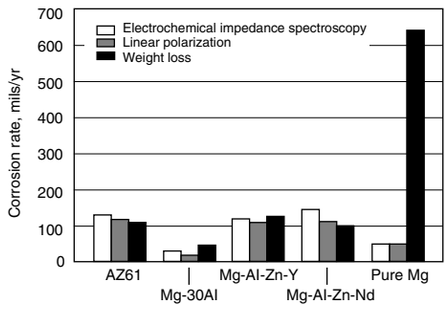

Fig. 4 Comparison of corrosion rates of pure magnesium (99.98% pure) and magnesium alloys determined by electrochemical and gravimetric techniques. Source: Ref 14

information on the performance of magnesium alloys and assemblies, both bare and coated, in saline environments. The results of such tests must be interpreted with care, however, and no attempt should be made to relate them to the behavior of magnesium in rural, urban, or industrial atmospheres in which chloride is not the controlling constituent of the environment.

The corrosion of magnesium alloys in saline solutions is governed by the concentration and distribution of the critical impurities of nickel, iron, and copper, whose presence in precipitated alloy phases creates active cathodic sites of low hydrogen overvoltage. The chloride ion further stimulates corrosion through its interference with protective-film formation and through the high solubility and acidic nature of magnesium chloride that accumulates at local anodic sites. The high conductivity of the chloride electrolyte also promotes the flow of corrosion current. If an adverse galvanic couple is introduced (by attaching a steel bolt to the magnesium, for example) and if the junction is bridged by saltwater, corrosion of magnesium is greatly accelerated, and alloy purity provides no defense. In a salt spray test, galvanic corrosion of magnesium in such an assembly would be excessive compared to that which would occur in a marine atmosphere or even under road salt splash conditions.

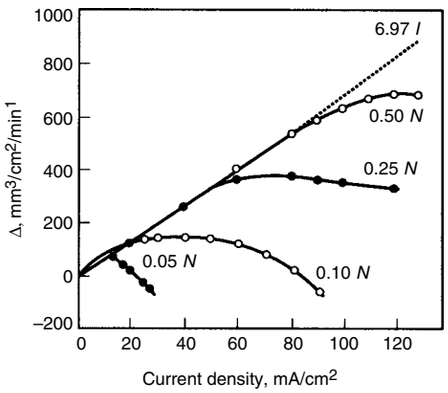

Fig. 5 Effect of current density on the negative difference for anodic dissolution of pure magnesium in various concentrations of sulfuric acid. Δ is the difference between hydrogen-evolution rate V_1, from an electrode without current flowing, and hydrogen-evolution rate V_2, from the same electrode with current flowing. When there is no negative difference effect, the voltage is proportional to 6.97 *I*, where *I* is the current input. Source: Ref 15

Corrosion Rates in Salt Spray, Salt-Immersion, and Natural Marine Environments. The marine atmosphere corrosion rate of magnesium-aluminum alloys is much smaller than the salt spray rate, but both rates are affected by the impurity content. Figures 6(a) and (b) show the effects of nickel, iron, and copper content on the corrosion of controlled-purity AZ91 die-casting alloy in a 10 day salt spray (5% NaCl, ASTM B 117) test and in a 2 year atmospheric exposure on the Texas Gulf Coast, respectively. Although the salt spray corrosion scale is 200 times larger than the marine atmospheric corrosion scale, some parallels can be drawn:

- Breakpoints relative to nickel and copper contamination are the same in both exposures (50 and 550 ppm, respectively).
- AZ91 corrosion remains low in both exposures over the iron contamination range studied (0.31% Mn alloy), confirming that the critical iron/manganese ratio (0.032 for this alloy) was not significantly exceeded.
- High-purity AZ91 alloy is shown in both exposures to have lower overall corrosion rates than carbon steel or die-cast aluminum 380.

Average corrosion rates found for three unprotected magnesium alloys in salt spray (20% NaCl), tidal-immersion, and marine atmospheres are presented in Fig. 7. The principal alloy and impurity constituents of the specimens tested are shown in Table 2.

The marine atmosphere and tidal-immersion exposures were conducted at the Naval Air Station, Norfolk, VA. The atmospheric panels were suspended directly over the water, 3 m (10 ft) above mean tide level, at an angle of 45° from the horizontal and facing east-southeast. The tidal-immersion panels were mounted vertically so that they were totally immersed in the water at high tide and totally exposed to atmosphere at low tide.

The salt spray and tidal-immersion results are in good agreement in rating the three alloys in order of actual corrosion rates. The atmospheric panels, even though directly above the water, sustained only a small fraction of the corrosion damage seen in the salt spray and tidal tests.

Good correlation in the ranking of the aluminum-zinc alloys between the salt spray cabinet test results and the immersion results is shown in Fig. 7, but this is often not the case with salt spray cabinet testing.

Caution should be exercised when comparing the relative performance of magnesium alloys of different families, for example, QE22 and ZE41, or when comparing magnesium with other metals. Figure 8 shows average corrosion rates over various exposure times for a standard alloy and a high-purity die-cast alloy in salt spray and in 5% NaCl continuous immersion.

There are also interactive effects of casting method and temper on corrosion rates obtained in salt-immersion tests. Table 3 shows the corrosion rate of gravity-cast AZ91 in 5 wt% NaCl solution. The alloy exhibits the highest corrosion resistance in the T6 condition, whereas treatment to the T4 temper leads to the largest weight loss. The mold temperature during casting, which affects the cooling rate, does not appear to have a significant influence on the corrosion rate.

Table 4 presents the pit-initiation results for cast magnesium-aluminum alloys in salt solution. The tolerance limit for Cl^- falls in the range of 2×10^{-3} to 2×10^{-2} *M* NaCl. Pure unalloyed magnesium shows exfoliation, in which individual grains were preferentially attacked along certain crystallographic planes.

Marine atmospheres also produce pitting corrosion in addition to general atmospheric corrosion. The fine pitting, which is commonly seen on exposure to marine atmosphere at the 24 m (80 ft) Kure Beach site, had little effect on

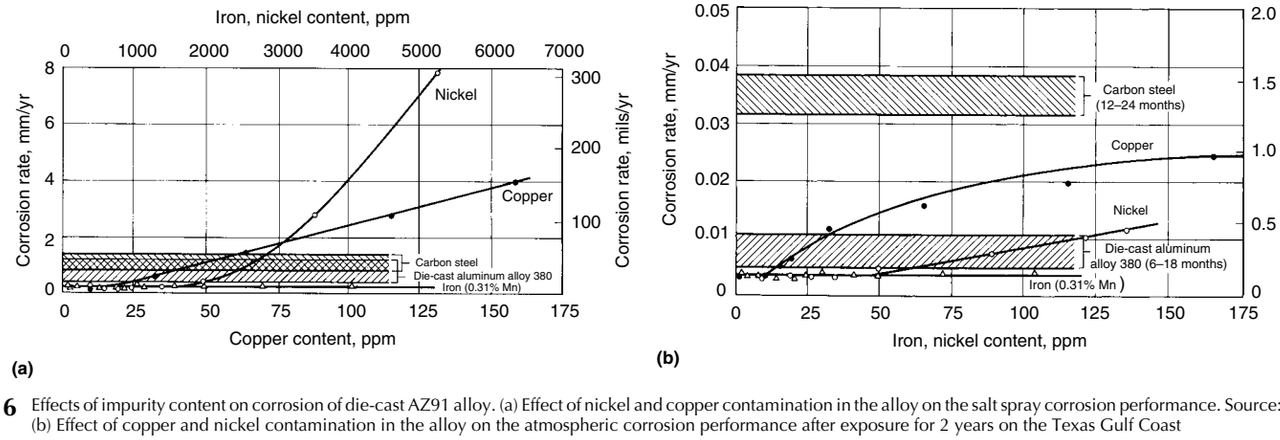

Fig. 6 Effects of impurity content on corrosion of die-cast AZ91 alloy. (a) Effect of nickel and copper contamination in the alloy on the salt spray corrosion performance. Source: Ref 17. (b) Effect of copper and nickel contamination in the alloy on the atmospheric corrosion performance after exposure for 2 years on the Texas Gulf Coast

the strength, but it did reduce the ductility (Fig. 9).

Influence of Galvanic Couples in Salt Spray and Marine Atmospheres. The combination of salt spray and dissimilar metals coupled to magnesium represents an extreme in accelerated corrosion testing. The disparity between such a test and a marine atmosphere exposure is illustrated in Fig. 10 and in Table 5. Figure 10 shows magnesium die-cast plates that were assembled with steel cap screws and nuts and exposed to salt spray (5% NaCl) for 10 days. Table 5 lists losses of tensile strength of AZ31B-H24 sheet with an original thickness of 4.8 mm (0.188 in.), coupled with various dissimilar-metal cleats and exposed for 13 months at Kure Beach, NC, at 24.4 m (80 ft) from the mean-tide point. Comparative data are shown for a rural and an urban-industrial test site. Saltwater immersion of steel/magnesium couples will produce nearly complete perforation failure of 4.8 mm (0.188 in.) magnesium panels in 10 days. However, it should be noted that the panels retained 88% of their tensile strength after 13 months.

Corrosion in Rural, Urban, and Industrial Atmospheres. In contrast to wet-chloride exposure, a rural atmosphere would probably cause negligible corrosion damage to the magnesium assembly referred to earlier. Some corrosion, still minor compared to that caused by saltwater, will occur in atmospheres containing significant acidic gas pollution, principally SO_2. These gases convert the insoluble hydroxide-carbonate films that form naturally on magnesium alloys into soluble bicarbonates, sulfites, and sulfates that can be washed away by rain. This increases the rate of weathering and can provide conductive electrolytic paths, allowing some galvanic corrosion to occur.

To simulate atmospheric exposure where chloride does not exert a controlling influence, various humidity tests have been used or proposed. Water fog and water-immersion tests are also used, primarily to evaluate the adhesion and blister resistance of organic coatings. Table 6 lists some simulated environmental tests and their intended purposes.

Magnesium-aluminum alloys, like most other metals, form protective films when exposed to the atmosphere. If CO_2 is present (in industrial atmospheres), the film is a mixture of hydrotalcite, $MgCO_3 \cdot 5Mg(OH)_2 \cdot 2Al(OH)_3 \cdot 4H_2O$, and hydromagnesite, $3MgCO_3 \cdot Mg(OH)_2 \cdot 3H_2O$. Due to hydrotalcite film formation, the magnesium-aluminum alloys are more tarnish resistant than other magnesium alloys when exposed to the atmosphere. Wrought magnesium-aluminum alloys show slightly higher corrosion rates than cast magnesium-aluminum alloys because the aluminum levels are usually lower than cast alloys (3 to 8% instead of 6 to 9%), and the purity of the alloys is often lower. In addition, wrought alloys are less isotropic, which may contribute to the higher corrosion rate.

Listed in Table 7 are the average corrosion rates reported for several magnesium alloys after 2.5 to 3 years of exposure at three different atmospheric test sites: a rural site (Midland, MI), an industrial site (Madison, IL), and a severe marine site (Kure Beach, NC). It can be seen that the alloy purity level (iron content) and the type of atmosphere affect the corrosion rate. The difference in corrosion rate between sheet and extrusions, however, was found to be negligible. Alloys not containing aluminum corroded at a somewhat higher rate than those of the AZ type; the ratios were approximately 2 to 1 in rural, 1.65 to 1 in industrial, and 1.25 to 1 in marine-rural exposure. Table 8 shows the composition of the

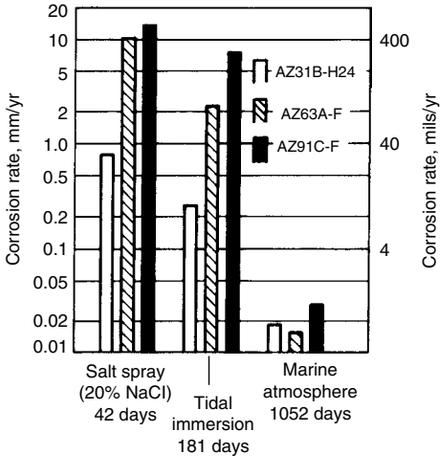

Fig. 7 Relative performance of magnesium alloys in saltwater exposures

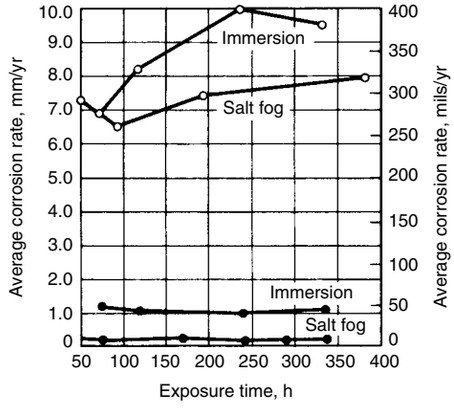

Analysis of die-cast plates, %		
	AM60A (○)	AZ91D (●)
Aluminum	6.2	9.7
Zinc	0.09	0.74
Manganese	0.22	0.19
Nickel	0.003	0.0018
Iron	0.005	0.006
Copper	0.03	0.0067

Fig. 8 Corrosion rates of die-cast magnesium in 5% NaCl salt spray and continuous-immersion exposures. Source: Ref 18

Table 3 Corrosion rate of gravity-cast AZ91 immersed in 5 wt% NaCl solution for 3 days

Temper	Mold temperature, °C	Mold temperature, °F	Corrosion rate, mg/cm²/day
F	400	750	1.1 ± 0.2
	350	660	1.4 ± 0.1
	250	480	2.0 ± 0.6
T4	400	750	3.6 ± 1
	350	660	1.8 ± 0.3
	250	480	2.7 ± 0.1
T6	400	750	0.5 ± 0.1
	350	660	0.4 ± 0.1
	250	480	0.4 ± 0.1

Source: Ref 19

Table 4 Pit-initiation results for wrought and cast magnesium alloys immersed in salt solutions for 24 h at room temperature

Alloy	Percentage of five coupons showing pitting in 0.1 *M* NaOH + 0.005 *M* NaCl	+ 0.01 *M* NaCl	+ 0.02 *M* NaCl
Wrought			
Magnesium A8	100(ex)	...	...
MA	0	100	...
M1	0	100	...
AZ31	0	0	100
AZ61	0	0	100
AZ91	0	0	100
Cast			
AM60B cold chamber	100	...	...
AM50 high purity	100	...	...
WE43	100	...	...
ZE41	100	...	...
ZE41A	100	...	...
A3A	100	...	...
EZ33	80	100	...
AZ92	40(ex)	60(ex)	100(ex)
AZ92A	40	100	...
AZ31	0	40	100
AZ91E	0	60	100
AZ91D hot chamber	0	80	100
AZ91	0	80	100
AM20 high purity	0	80	100
QE22	0	0	100
QE22A	0	0	100
AZ91D cold chamber	0	0	100

Note: ex, exfoliation. Source: Ref 20

Table 2 Principal alloy and impurity constituents in selected magnesium alloys

Alloy and temper	UNS No.	Form	Content, % Al	Zn	Mn	Si	Ni	Fe	Cu	Fe/Mn
AZ31B-H24	M11311	Sheet	2.6	1.0	0.51	0.0017	0.0005	0.0007	0.0019	0.0014
AZ63A-F	M11630	Sand cast	5.8	2.9	0.25	<0.05	<0.001	0.005	0.015	0.020
AZ91C-F	M11914	Sand cast	8.8	0.68	0.22	<0.05	<0.01	0.006	0.013	0.027

corrosion products on AZ31B-O alloy after 4 years of exposure to various atmospheres. It is deduced that aluminum ions concentrate in the film during weathering as the magnesium ions are leached away and form hydrotalcite on the top surface.

The data in Table 7 also show that of the alloys and forms tested, the combination having the best corrosion resistance in all three environments is cast AZ91C-T6 (10 ppm Fe). The alloys with the worst performance are ZE10A-O, EZ33A-T5/ZH62A-T5, and ZH62A-T5 in the rural, industrial, and marine exposures, respectively. Based on the average corrosion rates for all alloys at each of the rural, industrial, and marine-rural sites, the relative severity of the exposures is 1 to 2.1 to 1.7. Therefore, the industrial, SO_2-rich atmosphere is the most severe of the three sites.

Effect of SO_2 Pollution. Figure 11, prepared from data of the National Research Council of Canada, shows the effects of SO_2 pollution on the corrosion of ZK61A, AZ80A, and low-carbon steel. These effects may cause industrial atmospheres to corrode magnesium at average rates that are somewhat higher than those found in marine atmospheres (Table 7). The marine atmosphere poses a greater threat, however, for two reasons:

- Greater sensitivity of the marine corrosion rate to critical impurity content
- Greatly increased susceptibility to galvanic-corrosion damage by incompatible coupling of metals in a wet-chloride environment

These principles are demonstrated in Tables 5 and 9. Table 9 lists the corrosion rates of high- and low-iron samplings of AZ31 sheet and AZ91C-T6 castings at the three test sites represented in Table 7 plus a 20% NaCl salt spray test for the AZ91 castings. Table 5 assesses the relative galvanic damage to AZ31B-H24 caused by various cleat metals in rural, industrial, and marine exposures.

Indoor Atmospheres. Before the computer age, the reaction of magnesium alloys with indoor atmospheres was of concern primarily from the standpoint of appearance, not function. The widespread introduction of magnesium die castings into the computer disk drive environment has imposed strict new standards of surface stability on the metal because of the need to maintain a clean, particle-free atmosphere at the disk/head interface. The corrosion of magnesium alloys in indoor atmospheres increases with RH. At RHs up to approximately 80%, corrosion is very minor, resulting in the formation of a nearly invisible film of amorphous $Mg(OH)_2$. As humidity increases beyond this level, heavier tarnish films develop, the principal corrosion product now being crystalline $Mg(OH)_2$. In die castings, small traces of chloride residues from cover or refining fluxes may serve as nuclei for corrosion spots in humid air.

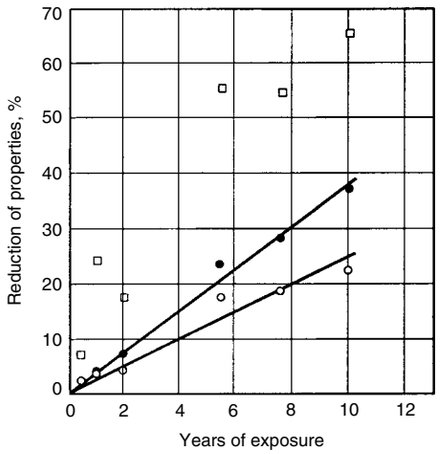

Fig. 9 Loss in mechanical properties of AZ31B-H24 alloy sheet at the 24 m (80 ft) marine site. Initial: 1.6 mm (0.063 in.) thick; 17.0% elongation; 255.8 MPa (37.1 ksi) ultimate tensile strength. ○, reduction in thickness as calculated from weight loss. ●, reduction in tensile strength. □, reduction in elongation. Source: Ref 21

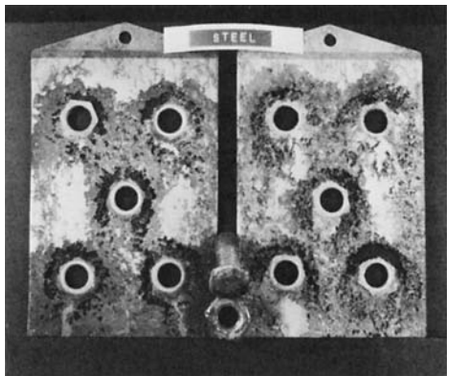

Fig. 10 Galvanic corrosion of AZ91D caused by bare steel fasteners during a 10 day exposure to 5% NaCl salt spray. Source: Ref 18

Table 5 Severity of galvanic attack on AZ31B-H24 sheet versus coupled metal cleat and exposure

	Relative loss of tensile strength(a)		
Cleat metal	Rural (State College, PA)	Urban-industrial (Newark, NJ)	Marine (Kure Beach, NC, 24.4 m, or 80 ft, site)
Aluminum alloy 5052	1.0	2.4	3.2
Aluminum alloy 7075	1.0	4.0	10.2
AISI type 304 stainless steel	1.8	6.8	18.0
Monel	2.2	8.8	21.4
Low-carbon steel	3.0	13.6	24.8
85-15 brass	3.6	14.2	30.4

(a) Aluminum alloy 5052 tested at State College, PA = 1.00. Source: Ref 21

Table 6 Accelerated or simulated environmental corrosion tests for magnesium alloys

Test condition	Used to evaluate
Humidity tests	
95% relative humidity, 38 °C (100 °F)	Flux inclusions, indoor tarnishing, filiform corrosion
100% relative humidity, 38 °C (100 °F), condensing (ASTM D 2247)	Paint adhesion and blistering, corrosion in rural (uncontaminated) atmospheres
Polluted atmosphere (DIN-50018-1960), 100% relative humidity, 40 °C (105 °F), Air + SO_2 + CO_2 for 8 h, then 16 h in air at room temperature	Corrosion and coating performance in industrial atmospheres
Water tests	
Water fog (ASTM D 1735), deionized water, 38 °C (100 °F)	Paint adhesion and blistering (roughly equivalent to condensing humidity)
Water immersion (ASTM D 870), deionized water, 38 °C (100 °F)	Paint adhesion and blistering (severe test)
Salt tests	
Salt spray (ASTM B 117), 5% NaCl, pH 6.5–7.2	Corrosion of magnesium alloys, impurity effects, surface treatments and coatings on the same substrate alloy, galvanic compatibilities of other materials with magnesium. Valid for chloride environments, with careful interpretation. A severe accelerated test
Salt immersion, 5% NaCl, 25 °C (75 °F), pH 10.5, intermittent or continuous immersion with mild air agitation	Same as salt spray
Copper-accelerated acetic acid salt spray (ASTM B 368), 5% NaCl, 1 g $CuCl_2 \cdot 2H_2O$ per 3.8 L, of solution, 49 °C (120 °F), pH 3.1–3.3	Plated coatings on magnesium
Salt spray-SO_2, 5% NaCl + SO_2, 35 °C (95 °F), pH 2.5–3.2. Naval Air Development Center	Naval aircraft materials (simulates sea spray plus ship stack gases)
Automotive proving ground test, repeated cycles of salt-mud splash, partial drying, and high-humidity storage	Magnesium alloys, bare or coated, for exposed automobiles and truck parts. Galvanic compatibilities. Simulates severe road deicing salts exposure

The strict requirements of these applications are being met by a combination of the following factors:

- Constant efforts by alloy producers and die casters to provide metal that is extremely low in nonmetallic inclusions
- Use of selected conversion coatings and proprietary protective coatings for supplementary surface stabilization

Accelerated tests involving cyclic humidity and temperature variation provide useful information for these applications, both on coating performance and by detection of any nonmetallic inclusions that may be present.

Table 7 Corrosion rates of magnesium alloys during atmospheric exposure for 2.5 to 3 years

		Rural		Industrial		Marine-rural	
UNS No.(a)	Alloy and temper	mm/yr	mils/yr	mm/yr	mils/yr	mm/yr	mils/yr
Sheet							
M11311	AZ31B-H24 (10 ppm Fe)	0.013	0.52	0.025	1.0	0.017	0.69
M11312	AZ31C-O (70 ppm Fe)(b)	0.012	0.46	0.025	1.0	0.038	1.5
M13310	HK31A-H24	0.018	0.73	0.030	1.2	0.016	0.64
M13210	HM21A-T8	0.020	0.80	0.032	1.3	0.022	0.88
M16100	ZE10A-O	0.022	0.88	0.030	1.2	0.028	1.1
Extrusions							
M11311	AZ31B-F	0.013	0.53	0.025	1.0	0.019	0.77
M13312	HM31A-F	0.018	0.70	0.035	1.4	0.020	0.80
M 16600	ZK60A-T5	0.017	0.66	0.032	1.3	0.025	1.0
Castings							
M11630	AZ63A-T4	0.0086	0.34	0.022	0.88	0.019	0.76
M11914	AZ91C-T6 (350 ppm Fe)(b)	0.0043	0.17	0.015	0.62	0.022	0.88
	AZ91C-T6 (10 ppm Fe)	0.0027	0.11	0.014	0.57	0.0064	0.25
M11920	AZ92A-T6	0.0094	0.37	0.020	0.80	0.025	1.0
M12330	EZ33A-T5	0.020	0.79	0.040	1.6	0.028	1.1
M13310	HK31A-T6	0.017	0.67	0.035	1.4	0.028	1.1
M13320	HZ32A-T5	0.015	0.61	0.038	1.5	0.028	1.1
M16620	ZH62A-T5	0.015	0.58	0.040	1.6	0.041	1.6
M16510	ZK51A-T5	0.014	0.57	0.035	1.4	0.025	1.0
Site average		**0.014**	**0.56**	**0.030**	**1.2**	**0.024**	**1.0**

(a) Possible UNS composition equivalent of the tested alloy is listed. In some cases, more than one UNS number is registered to an alloy designation. (b) Iron content would exceed specification. Source: Ref 21

Table 8 Composition of corrosion product on AZ31B-O alloy after 4 years atmospheric exposure

	Corrosion rate			% by x-ray diffraction			
Exposure site	mm/yr	mils/yr	Panel surface	Hydromagnesite(a)	Hydrotalcite(b)	Chloride, %	Sulfate, %
Kure Beach, NC, 24 m (80 ft) (marine-rural)	0.014	0.57	Top	50	50	0.070	0.14
			Bottom	100	0	0.031	0.18
Kure Beach, NC, 244 m (800 ft) (marine-rural)	0.012	0.50	Top	50	50	0.024	0.05
			Bottom	100	0	0.022	0.13
Midland, MI, (rural)	0.012	0.50	Top	50	50	0.006	0.36
			Bottom	100	0	0.011	0.57
Midland, MI, (industrial)	0.023	0.92	Top	25	75	0.016	1.2
			Bottom	75	25	0.010	4.5
Madison, WI, (industrial)	0.025	1.02	Top	25	75	0.016	1.0
			Bottom	75	25		3.3

(a) $3MgCo_3 \cdot Mg(OH)_2 \cdot 3H_2O$. (b) $Mg_6Al_2(OH)_{16}CO_3 \cdot 4H_2O$

Table 9 Corrosion rates versus exposure and iron content for AZ31 sheet and AZ91 castings

		Exposure and average corrosion rates							
		Rural		Industrial		Marine		20% NaCl spray	
Alloy(a)	Iron, ppm	mm/yr	mils/yr	mm/yr	mils/yr	mm/yr	mils/yr	mm/yr	mils/yr
(1)AZ31	70	0.012	0.5	0.025	1.0	0.038	1.5	...	...
(2)AZ31	10	0.013	0.51	0.025	1.0	0.018	0.7	...	...
Ratio of (1) to (2)	7	0.9	0.9	1.0	1.0	2.2	2.2	...	...
(3)AZ91	350	0.0043	0.17	0.016	0.6	0.022	0.87	95	3740
(4)AZ91	10	0.0028	0.11	0.014	0.55	0.0064	0.25	0.71	27.9
Ratio of (3) to (4)	35	1.5	1.5	1.1	1.1	3.5	3.5	134	134

(a) (1) AZ31C sheet. (2) AZ31B-H24 sheet. (3) AZ91C-T6 cast plate (Fe/Mn = 0.15). (4) AZ91C-T6 cast plate (Fe/Mn = 0.007). Source: Ref 21

Localized Corrosion Mechanisms

The previous discussion was, for the most part, about general or uniform corrosion where corrosion rates can be determined and are meaningful. Localized corrosion involves specific factors that determine the severity of the degradation.

Stress-Corrosion Cracking

Magnesium alloys containing more than a threshold value of 0.15 to 2.5% Al are susceptible to stress-corrosion cracking (SCC), and the tendency increases with aluminum content (reaching a maximum at approximately 6% Al) (Ref 16).

Effects of Alloy and Condition. Commercially pure magnesium is not susceptible to SCC when loaded up to its yield strength in atmospheric and most aqueous environments. The only reports of SCC of commercially pure magnesium have emanated from laboratory tests in which specimens were immersed in very severe corrosive solutions.

Aluminum-containing magnesium alloys have the highest SCC susceptibility, with the sensitivity generally increasing with increasing aluminum content, as illustrated in Fig. 12. An aluminum content above a threshold of 0.15 to 2.5% is reportedly required to induce SCC behavior, with the effect peaking at approximately 6% Al. In contrast, a study of magnesium-aluminum die-casting alloys revealed no significant increase in SCC susceptibility between 4 and 9% Al.

Zinc also induces SCC susceptibility in magnesium alloys, so it is not surprising that the aluminum- and zinc-bearing AZ alloys, which are the most commonly used magnesium alloys, have the greatest susceptibility to SCC. Alloys with higher aluminum content, such as AZ61, AZ80, and AZ91, can be very susceptible to SCC in atmospheric and more severe environments.

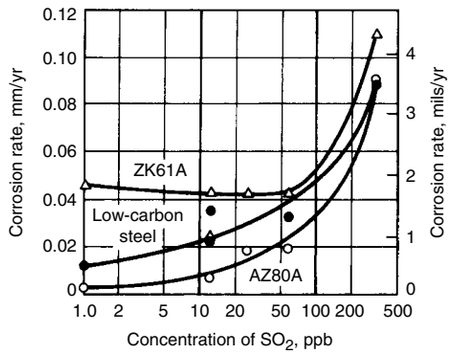

Fig. 11 Corrosion rates versus SO_2 pollution levels at six exposure sites. Rainfall at the sites ranged from 533 to 965 mm/yr (21 to 38 in./yr). Source: Ref 22

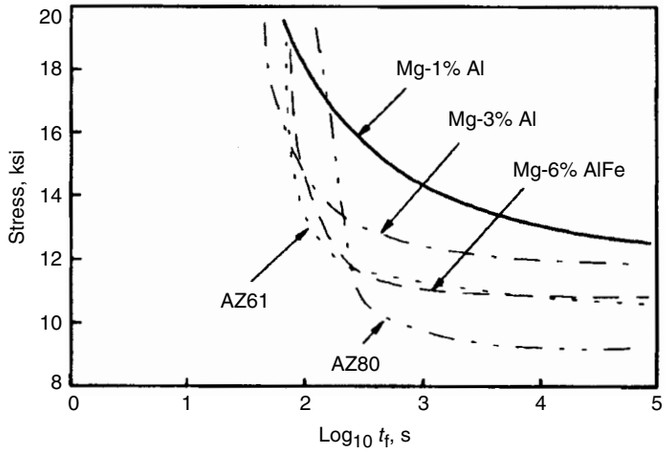

Fig. 12 Stress versus time to failure (t_f) for magnesium-aluminum alloys in aqueous 40 g/L NaCl + 40 g/L Na_2CrO_4. Source: Ref 23

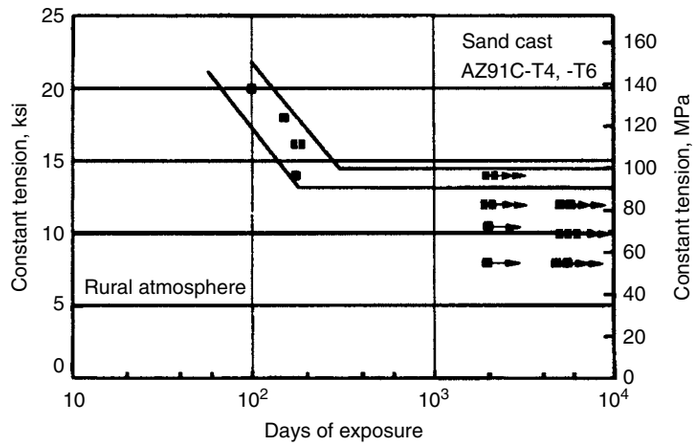

Fig. 13 Stress corrosion of sand-cast AZ91C (T4 and T6) in rural atmosphere. Source: Ref 24

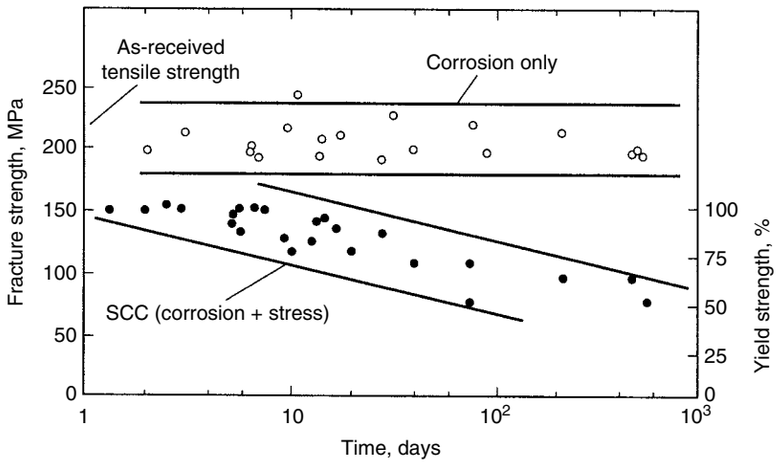

Fig. 14 Stress-corrosion cracking behavior of AZ91 in distilled water. Stress-corrosion cracking tests on standard ASTM B 577 die-cast tensile specimens were conducted on a dead-weight tension-loading apparatus. Source: Ref 25

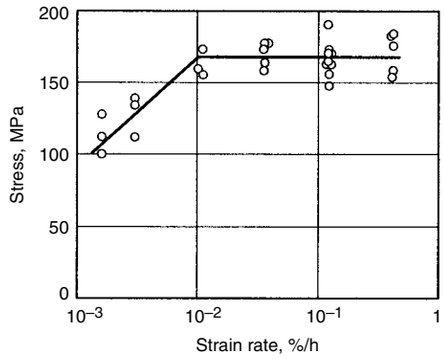

Fig. 15 Stress at fracture versus strain rate in slow-strain-rate SCC tests of AZ91. The specimens were partially immersed in distilled water. Strain was controlled with a linear ramp to maintain the desired strain rate. Source: Ref 25

For example, Fig. 13 and 14 show that AZ91 is quite susceptible to SCC in rural atmosphere, and very susceptible when partially immersed in distilled water, with fractures occurring at stresses at least 50% of the yield strength. The SCC fractures plotted in Fig. 14 generally occurred at, or very close to, the tip of the meniscus formed at the water-air interface. Figure 15 shows the stress at fracture versus strain rate in the slow-strain-rate SCC tests. Fracture stress during these tests was a function of strain rate when it was below 0.01%/h, indicating the effects of a rate-dependent SCC interaction. The mechanism may be a cathodically driven, film-rupture SCC process. The effect of immersion in an electrolytic solution ($NaCl + Na_2CrO_4$) is shown in Fig. 16.

In contrast to the magnesium alloys that contain higher amounts of aluminum, lower-aluminum AZ31 is generally more resistant. However, it too can suffer SCC under certain conditions (Fig. 17).

Magnesium-zinc alloys that are alloyed with either zirconium or rare earths, but not with aluminum, such as ZK60 and ZE10, have intermediate SCC resistance (Fig. 18). SCC has not been a serious problem in some applications. However, SCC can still occur in atmospheric environments at stresses as low as 50% of the yield strength, although life is significantly longer than for Mg-Al-Zn alloys.

Magnesium alloys that contain neither aluminum nor zinc are the most SCC resistant. Magnesium-manganese alloys, such as M1, are among the alloys with the highest resistance to SCC, and they are generally considered to be immune when loaded up to the yield strength in normal environments. In fact, SCC of Mg-Mn alloys has been reported only in tests involving stresses higher than the yield strength and/or exposure to very severe laboratory environments. Alloy QE22 is also resistant to SCC, exhibiting SCC thresholds at approximately 70 to 80% of the yield strength in rural-atmosphere tests.

Magnesium-lithium alloys are of commercial interest because of their higher stiffness and lower density compared with other magnesium alloys. Tests in humid air have resulted in SCC failures of Mg-Li-Al alloys, but SCC did not occur during testing of magnesium-lithium alloys strengthened with zinc, silicon, and/or silver instead of aluminum.

Iron is found in commercial magnesium alloys in small, residual amounts and, although iron is known to reduce general corrosion resistance, its effect on SCC remains unclear. Early investigations indicated that iron was associated with decreased SCC resistance in Mg-Al-Zn alloy. Later studies, however, found that iron had minimal or no effect.

The effects of other alloying elements have had limited study. It has been reported that additions of cadmium increase SCC susceptibility, while cerium, tin, lead, copper, nickel, and silicon have no effect. Other researchers, however, have indicated that the addition of cerium or tin to Mg-Al-Mn alloys somewhat increases SCC susceptibility.

Effects of Environment. Stress-corrosion cracking of magnesium alloys can occur in many environments. In general, the only solutions that do not induce SCC are either those that are nonactive to magnesium, such as dilute alkalies, concentrated hydrofluoric acid, and chromic acid, or those that are highly active, in which general corrosion predominates.

Air Environments. Exposure to normal atmospheric environments has been shown to produce SCC in susceptible magnesium alloys; such environments include rural, urban, industrial, and coastal conditions. Tests of identical materials at different sites—for example, seacoast versus rural and rural versus industrial—have produced nearly identical results, indicating that SCC severity is not necessarily associated with the corrosion severity of the environment.

Rainfall, dew, and high humidity accelerate SCC of magnesium alloys during atmospheric exposure, with failures often occurring during the drying period after a rain. Laboratory tests have shown that SCC occurs in indoor air only when the relative humidity exceeds 85 to 98%, with additions of oxygen or carbon dioxide slightly reducing this threshold.

Water Environments. Distilled water produces SCC in magnesium alloys during spraying or full, partial, or intermittent immersion. Dissolved oxygen accelerates SCC, and deaeration considerably retards or even prevents it. Rapid SCC has also been observed during seawater immersion.

Aqueous Solutions. The desire for an accelerated test to study SCC of magnesium alloys led to the development of an aqueous NaCl + K_2CrO_4 solution that produces very rapid cracking and a ranking of alloy susceptibility that appears to correlate with atmospheric tests. The aggressiveness of this solution is thought to result from the partial passivation of the magnesium by the chromate, which retards general corrosion but allows, or even promotes, local attack by the chloride. This electrolyte has remained very popular in laboratory studies of magnesium SCC, even though it has since been found to correlate poorly with service experience. In fact, no accelerated laboratory test has been developed that adequately predicts service life or the relative susceptibility of different alloys.

The addition of nitrate ions or carbonate ions to salt-chromate solutions inhibits SCC. This is believed to be associated with the formation of a stronger, more stable or more readily repaired passive film.

Magnesium SCC is also produced in many other *dilute* aqueous solutions, including (in approximate decreasing severity): NaBr, Na_2SO_4, NaCl, $NaNO_3$, Na_2CO_3, $NaC_2H_3O_2$, NaF, and Na_2HPO_4. Accelerated SCC has also been reported in dilute solutions of KF, KHF_2, HF, KCl, CsCl, NaI, KI, $MgCO_3$, NaOH, and H_2SO_4, HNO_3, and HCl acids.

Although pH can affect the general corrosion of magnesium alloys, a pH of between 1.05 and 11.5 has been found to have no effect on SCC susceptibility in a salt solution. However, when pH is greater than 12, magnesium alloys become very resistant to SCC. The pH of salt-chromate solutions has been reported to have an effect on whether the SCC crack path is intergranular or transgranular, although other studies have shown the path to be independent of pH.

Cathodic polarization has been shown in many studies to reduce, if not prevent, SCC of magnesium alloys in salt-chromate and other aqueous solutions. In a few cases, however, cathodic polarization was found to accelerate SCC.

Anodic polarization generally has been found to increase the SCC susceptibility of magnesium and magnesium alloys, although mixed behavior has also been reported. In single-phase magnesium-aluminum alloys, it was shown that high anodic potentials can produce a passive film that prevents SCC in a salt-chromate solution. In a multiphase alloy, however, the same conditions do not produce a protective film, and the electrochemical potential difference between the Mg17Al12 phase and matrix solid solution can promote pitting.

Service Failures. Despite the SCC sensitivity shown by magnesium alloys in laboratory tests, it has often been reported that service failures are rare and normally result from excessive residual stress produced during fabrication. In 1970, however, failures of several forged AZ80 French aircraft components were reported, apparently resulting from excessive assembly and residual stresses. Service failures of cast plus forged South African magnesium aircraft wheels have also been described. In addition, a comprehensive review of more than 3000 unclassified failure reports from aerospace companies, government agencies, and research laboratories in the United States and five Western European countries estimate that approximately 10 to 60 magnesium aerospace-component SCC service failures occurred each year from 1960 to 1970. Of this total, more than 70% involved either cast alloy AZ91-T6 or wrought alloy AZ80-F, both of which contain aluminum. In contrast, magnesium alloys without aluminum do not, in practice, have a stress-corrosion problem. The broad class of alloys containing zirconium are also sufficiently insensitive that SCC is not a problem in practice.

The fastest growing segment of the structural market for magnesium alloys is die castings, principally for automotive applications. The alloys involved contain from 2 to 9% Al, the most common being AZ91D alloy. These are the alloys that have been demonstrated in published literature to be most susceptible to SCC. The risk of SCC failure is of great concern in many of these applications, which involve safety-related components. Despite the variety of environmental conditions to which these components have been exposed, documented SCC failures have been rare. This has been attributed to low levels of actual applied stress, stresses due to imposed deflections being relieved by yielding and subsequent creep, and benign environmental conditions (Ref 27).

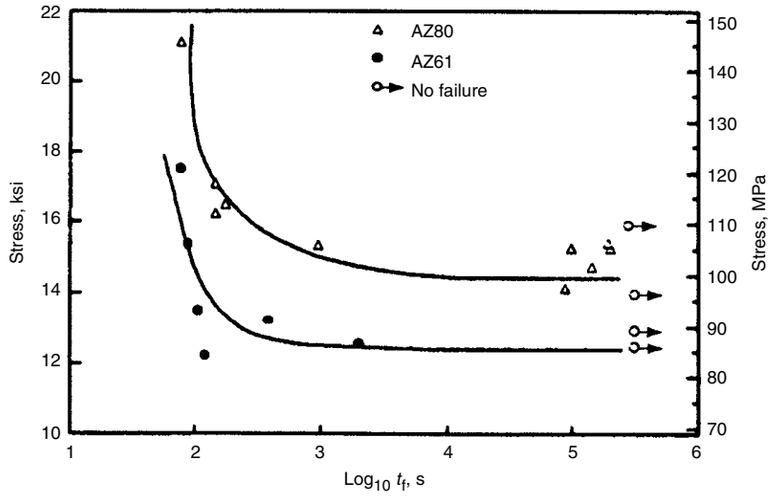

Fig. 16 Stress versus time to failure (t_f) for the two-phase alloys AZ80 (Mg-8.5Al-0.5Zn) and AZ61 (Mg-6Al-1Zn) in aqueous 40 g/L NaCl + 40 g/L Na_2CrO_4

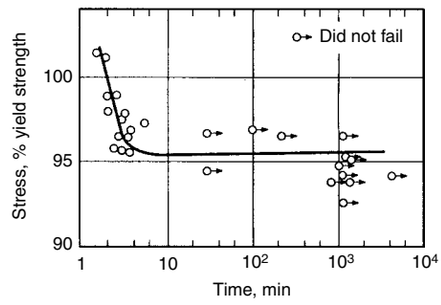

Fig. 17 Stress-corrosion cracking behavior of AZ31 in an aqueous solution of 3.5% NaCl + 2% K_2CrO_4. Source: Ref 26

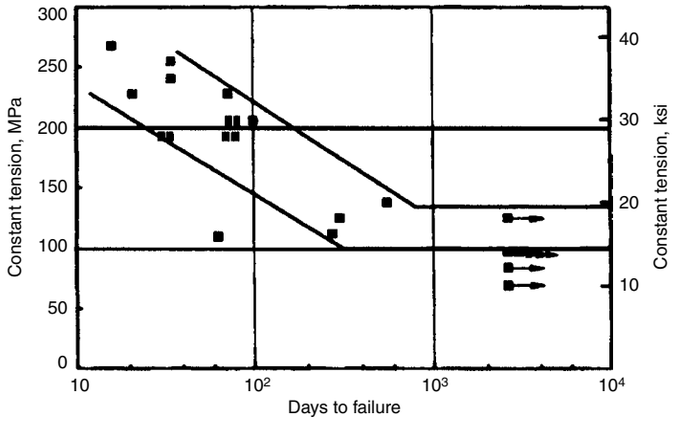

Fig. 18 Stress corrosion of ZK60A-T5 extrusion in rural atmosphere. Source: Ref 24

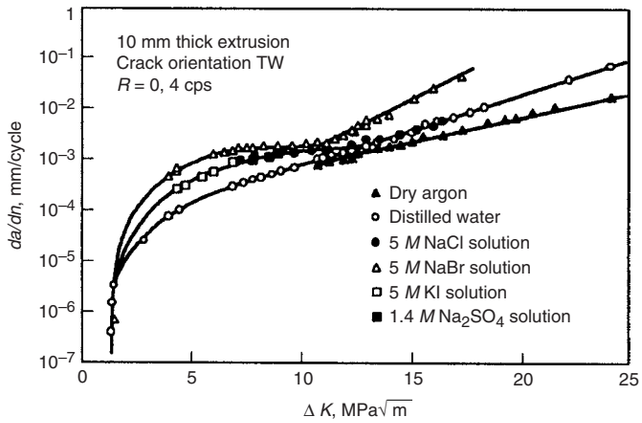

Fig. 19 Corrosion-fatigue-crack growth curves for ZK60A-T5 in different environments. Source: Ref 28

Under severe salt-spray test conditions in the presence of a galvanic couple, a bracket fracture suspected to be SCC was actually caused by stress concentration at notches generated by severe surface corrosion.

Corrosion Fatigue

Substantial reductions in fatigue strength are shown in laboratory tests using sodium chloride (NaCl) spray or drops. Such tests are useful for comparing alloys, heat treatments, and protective coatings. Effective coatings, by excluding the corrosive environment, provide the primary defense against corrosion fatigue.

A fundamental study of the corrosion fatigue of magnesium alloys is that of Speidel et al. on high-strength magnesium alloy ZK60A (Ref 28, 29) (Fig. 19). All magnesium alloys behave similarly with respect to environmentally enhanced subcritical crack growth, according to Speidel et al. They found that both stress-corrosion and corrosion-fatigue cracks propagate in a mixed transgranular-intergranular mode. They measured the corrosion-fatigue crack growth for all of the aqueous environments shown in Fig. 19 and compared the corrosion fatigue with stress-corrosion behavior. They found that:

- Corrosion-fatigue-crack-growth rate is accelerated by the same environments as those that accelerate stress-corrosion crack growth (i.e., sulfate and halide ions).
- The boundary between regions II and III in sodium bromide (NaBr) solutions of the *da/dn* versus ΔK curve is higher than the stress-corrosion threshold (K_{ISCC}), which occurs at a much lower stress intensity.
- There is a distinct boundary between regions II and III for all the media given in Fig. 19 (except dry argon). This boundary occurs at about the same stress intensity (~14 MPa$\sqrt{m}$) as K_{ISCC} in distilled water.

Table 10 How to design corrosion out of magnesium structures

Procedure	Method
Eliminate "sump" areas where trapped moisture is held in contact with metal.	• Design them out in the first place by careful attention to design of structure details. • Provide properly located drain holes. Minimum hole size approximately 3.2 mm (1/8 in.) to prevent plugging
Choose nonabsorbent, nonwicking materials to contact magnesium.	• Determine water absorption qualities of materials to be used. • Use epoxy and vinyl tapes and coatings, wax, or latex for protective barriers. • Avoid, if possible, use of wood, paper, cardboard, open-cell foams, and sponge rubbers.
Protect all faying surfaces.	• Use proper sealing materials (tapes, films, sealing compounds) on all faying surfaces. • Use primers. • Lengthen continuous liquid path to reduce galvanic current.
Use compatible metals.	• For magnesium-aluminum couples, 5000- and 6000-series alloys are most compatible. • For magnesium-steel couples, plate steel with zinc, 80%Sn-20%Zn, tin, or cadmium.
Select proper finishing systems.	• Choose chemical treatments, paints, plating on basis of service requirements. • Service-test system before setting up production run. • Use past experience in similar applications as guide to choice.

Galvanic Corrosion

Insufficient attention to galvanic corrosion has been one of the major obstacles to the growth of structural applications of magnesium alloys. Serious galvanic problems occur mainly in wet saline environments for the reasons described earlier. This form of localized corrosion is discussed in more detail.

As applied to uniform corrosion, outstanding improvements in saltwater corrosion resistance of magnesium alloys have been achieved by reducing the internal corrosion currents through strict limitations on the critical impurities of nickel, iron, and copper, as well as on the iron-to-manganese ratio.

Principles of Galvanic Corrosion. The conditions necessary for galvanic corrosion to occur are shown in Fig. 20. If only one of these factors is eliminated, galvanic corrosion can be prevented.

The basic principles of corrosion are fundamental to any design involving metals; the degree to which they can be employed properly determines the amount and the kind of finishing protection required in a given environment. These basic design principles are summarized briefly in Table 10 in their order of importance.

Details of these measures are treated in the section "Protection of Assemblies" in this article. It is useful, however, to review the basic principles governing the galvanic corrosion of magnesium and the relative compatibility of dissimilar metals with magnesium.

Relative Compatibility with Other Metals. All structural metals are cathodic to (more noble than) magnesium. The degree to which the corrosion of magnesium is accelerated under a given set of exposure conditions depends partly on the relative positions of the two metals in the electromotive force series or galvanic series (if available) but more importantly on how rapidly the effective potential of the couple is reduced by polarization as galvanic current flows. The principal polarization mechanism in a

magnesium couple in saltwater is the resistance to the formation and liberation of hydrogen gas at the cathode. Therefore, metals of low hydrogen overvoltage, such as nickel, iron, and copper, constitute efficient cathodes for magnesium and cause severe galvanic corrosion. Metals that combine active potentials with higher hydrogen overvoltages, such as aluminum, zinc, cadmium, and tin, are much less damaging, although not fully compatible with magnesium.

Because galvanic corrosion requires a continuous liquid path on the surface to provide electrolytic connection of the anode and the cathode, this form of corrosion is most severe in chloride splash, spray, and immersion conditions. Note that galvanic corrosion can also be a serious concern in chloride-bearing atmospheres. Data were compiled in tests at Kure Beach, NC, in which sheets of dissimilar metals were fastened to panels of AZ31B and AZ61A. The dissimilar metals were divided into five groups based on observed gradations of galvanic damage to magnesium. These ratings are summarized in Table 11. Electrolyte conductivity and composition play key roles in galvanic corrosion. Table 12 shows corrosion rates for a Mg-6%Al-3%Zn-0.2%Mn alloy coupled to a variety of other metals (of equal area) in 3% NaCl solution, Midland tap water, and distilled water and illustrates the influence of environment on galvanic corrosion. The galvanic corrosion of magnesium is substantially reduced when coupled to steel that has been coated with zinc, cadmium, or tin. The compatibility of AZ91 magnesium alloy with several different fasteners is presented in Fig. 21. The relative corrosion rates were determined from weight loss in a 10 day salt spray test.

Table 11 Relative effects of various metals on galvanic corrosion of magnesium alloys AZ31B and AZ61A exposed at the 24.4 and 244 m (80 and 800 ft) stations, Kure Beach, NC

Group	Alloys
1 (least effect)	Aluminum alloy 5052
	Aluminum alloy 5056
	Aluminum alloy 6061
2	Aluminum alloy 6063
	Alclad alloy 7075
	Aluminum alloy 3003
	Aluminum alloy 7075
3	Alclad alloy 2024
	Aluminum alloy 2017
	Aluminum alloy 2024
	Zinc
4	Zinc-plated steel
	Cadmium-plated steel
5 (greatest effect)	Low-carbon steel
	Stainless steel
	Monel
	Titanium
	Lead
	Copper
	Brass

Effects of Anode and Cathode Areas. The relative areas of the magnesium anode and the dissimilar-metal cathode have an important effect on the corrosion damage that occurs. A large cathode coupled with a small area of magnesium results in rapid penetration of the magnesium, because the galvanic current density at the small magnesium anode is very high, and anodic polarization in chloride solutions is very limited. This explains why painted magnesium should not be coupled with an active cathodic metal if the couple will be exposed to saline environments. A small break in the coating at the junction results in a high concentration of galvanic current at that point, unmitigated by any polarization. Unfavorable area effects can also be seen in the behavior of some proprietary coatings using aluminum or zinc powder. When used as a coating on a steel bolt attached to magnesium, the metallic pigment can present a very large effective surface area, which may be more detrimental than bare steel. Galvanic action is further accelerated if the metallic pigment contains such impurities as iron.

Effects of Minor Constituents on Compatibility of Aluminum with Magnesium. Aluminum alloys containing small percentages of copper (7000 and 2000 series and 380 die-casting alloy) may cause serious galvanic corrosion of magnesium in saline environments. Very pure aluminum is quite compatible, acting as a polarizable cathode; but when iron content exceeds 200 ppm, cathodic activity becomes significant (apparently because of the depolarizing effect of the intermetallic compound $FeAl_3$), and galvanic attack of magnesium increases rapidly with increasing iron content. The effect of iron is diminished by the presence of magnesium in the alloy (Fig. 22). This agrees with the relatively compatible behavior of aluminum alloys 5052, 5056, and 6061 shown in Table 11.

Cathodic Corrosion of Aluminum. Assessment of compatibility of aluminum alloys with magnesium alloys is complicated by the fact that aluminum can be attacked by the strong alkali generated at the cathode when magnesium corrodes sacrificially in static NaCl solutions. Such attack destroys compatibility in alloys containing significant iron contamination, apparently by exposing fresh, active sites with low overvoltage. The aluminum alloys having substantial magnesium content (5052 and 5056) are more resistant to this effect, but not completely so. The essential requirement for a fully compatible aluminum alloy, as indicated in Fig. 22, would be met by a 5052 alloy with a maximum of 200 ppm Fe or a 5056 alloy with a maximum of 1000 ppm Fe. Commercially produced 5052 alloy is permitted by specification to have a maximum (iron + silicon) content of 0.45% and may typically contain 0.3% Fe. In a severe exposure such as 5% NaCl immersion, this iron content, combined with the cathodic corrosion caused by the current from the magnesium, can render the 5052 alloy incompatible with magnesium. In most real situations, however, this extreme condition would not exist, and a 5052 washer under the head of a plated steel bolt in a magnesium assembly would reduce galvanic attack of the magnesium. For maximum effect of the washer, the linear distance along the aluminum from the bolt should be approximately 4.8 mm ($^3/_{16}$ in.).

Table 12 Corrosion of Mg-6Al-3Zn-0.2Mn alloy galvanically connected to selected other metals in various media

	Corrosion rate, mdd, at indicated separation distance					
	3% NaCl(a)					
Galvanically connected metal	Close contact	3.5 mm (0.14 in.)	20 mm (0.8 in.)	100 mm (3.9 in.)	Midland tap water(b), 3.5 mm (0.14 in.)	Distilled water(c), 3.5 mm (0.14 in.)
Steel	23,400	25,500	8,300	3,900	300	18
Aluminum alloy 2024	12,800	25,700	6,800	3,200	90	6
Nickel	18,800	22,400	6,600	...	210	19
Aluminum alloy 1100	14,500	15,600	4,100	...	40	4
Copper	8,500	8,200	3,700	...	90	15
Brass	7,100	4,000	2,500	1,700	60	14
Aluminum alloy 5056	...	1,900	...	...	10	3
Cadmium-plated steel	5,200	2,200	1,000	...	40	14
Zinc	6,200	1,300	900	700	30	8
Mg-1.5Mn	...	50	...	...	2	3
Mg-6Al-3Zn-0.2Mn	...	200	...	...	7	3

mdd, milligrams per square decimeter per day. Test parameters: Specimen size, 40 × 13 × 2 mm (1.5 × 0.5 × 0.08 in.); room temperature; relative areas, 1:1 (mounted face-to-face); aeration, natural convection; surface preparation, Aloxite 150 ground; volume of testing solution, 100 mL; velocity, quiescent. (a) Test duration, 3 h. (b) Test duration, 24 h. (c) Test duration, 4 days. Source: Ref 30

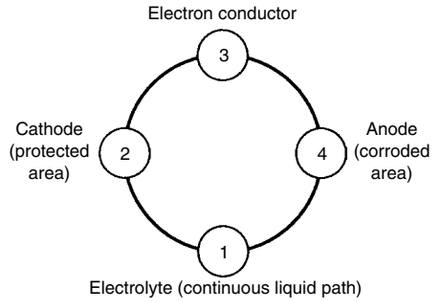

Fig. 20 The corrosion circle. 1, electrolyte (continuous liquid path, usually water in the form of condensate, salt spray, etc.). 2, cause (cathode—the cause of corrosion—the area through which electricity flows). 3, electron conductor (in a structure, usually a metal-to-metal contact, e.g., rivets, bolts, spot welds, etc.). 4, effect (anode—the surface or object that corrodes)

Cathodic corrosion of aluminum is much less severe in seawater than in NaCl solution, because the buffering effect of magnesium ions reduces the equilibrium pH from 10.5 to approximately 8.8 (Ref 32). The compatibility of aluminum with magnesium is accordingly better in seawater and is less sensitive to iron content.

Cathodic Damage to Coatings. Hydrogen evolution and strong alkalinity generated at the cathode can damage or destroy organic coatings applied to fasteners or other accessories coupled to magnesium. Alkali-resistant resins are necessary, but under severe conditions such as salt spray or salt immersion, the coatings may be simply blown off by hydrogen, starting at small voids or pores. Because of its severity, the salt spray test can lead to rejection of some fastener coatings that may provide useful benefits in real service environments. Salt spray cabinet tests should not be relied on exclusively to evaluate these coatings.

Compatibility of Plated Steel. Zinc, cadmium, or tin plating on steel all reduce galvanic attack of magnesium substantially compared to bare steel. This agrees with the more compatible potentials and/or the higher hydrogen overvoltages of the plated deposits. The relative merit of the three electroplates is generally considered to be (in decreasing order) tin, cadmium, zinc. The salt spray cabinet test is biased against zinc because zinc is rapidly removed from the steel substrate in this test medium due to general corrosion as well as cathodic attack when coupled with magnesium. This does not occur in many natural environments, and the failure of the salt spray cabinet test to rate zinc and cadmium plating properly in marine atmospheres is well known (Fig. 23).

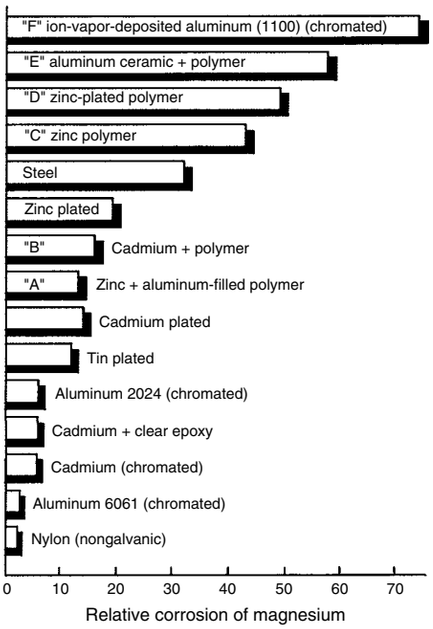

Fig. 21 Galvanic corrosion produced by dissimilar fasteners in AZ91D magnesium alloy. Reproduced from Ref 31 with permission of the International Magnesium Association, McLean, VA

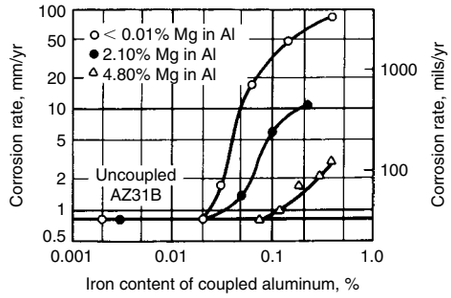

Fig. 22 Corrosion rates in 3% NaCl solution of magnesium alloy AZ31B coupled with aluminum containing varying amounts of iron and magnesium. The corrosion rate of uncoupled AZ31B is shown for comparison.

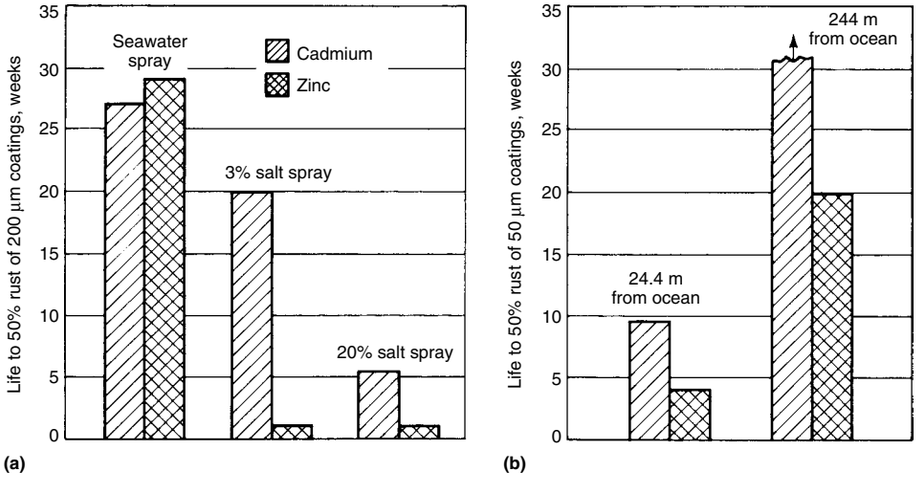

Fig. 23 Comparison of cadmium and zinc plate on steel in salt spray tests and in marine atmospheres. (a) 200 µm (8 mils) coating. (b) 50 µm (2 mils) coating. Source: Ref 33

Protection of Assemblies

A dissimilar metal in contact with magnesium will not by itself result in galvanic corrosion. For corrosion to occur, both surfaces must also be wetted by a common electrolyte. The degree to which precautions against galvanic corrosion are taken will depend on many factors, of which the operating environment is of primary importance.

For indoor use, where condensation is not likely, no protection is necessary. Even in some sheltered outdoor environments, magnesium components can give good service lives without special precautions against galvanic attack, provided other mitigating factors are present. These may include design elimination of water traps, good ventilation, component warmth, or the presence of an oil film.

For continuous outdoor use, during which magnesium assemblies may be wetted or subjected to salt splash or spray, precautions against galvanic attack must be taken. Although corrosive attack from any source can jeopardize the satisfactory performance of magnesium components, attack resulting from galvanic corrosion is probably the most detrimental. Under corrosive conditions, use of high-purity magnesium alloys will have no significant influence in reducing the effects of galvanic corrosion.

Magnesium-to-Magnesium Assemblies. For all practical purposes, galvanic corrosion between magnesium alloys is negligible. However, because joining two magnesium components almost invariably involves use of dissimilar-metal fasteners and the formation of a crevice at the joint, good assembly practice dictates that in corrosive conditions some precautions should be taken (Fig. 24). Magnesium faying or mating surfaces should be assembled using wet assembly techniques. Chromate-inhibited primers or sealing compounds are placed between the surfaces at the time of assembly. Sealing/jointing compounds of the polymerizing or nonpolymerizing type are preferred because they remain flexible and resist cracking. Polymerizing-type compounds are also used for caulking operations. In bolted

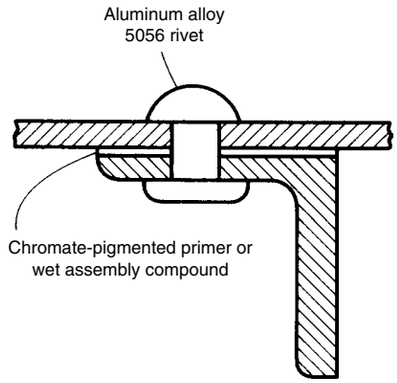

Fig. 24 Schematic of the proper method of protecting faying surfaces in magnesium-to-magnesium assemblies

assemblies, the retorquing of bolts shortly after assembly will help eliminate any joint relaxation problems. For additional protection, mating surfaces should be primed before assembly and painted after assembly.

Magnesium-to-Nonmetallic Assemblies. Although the joining of most nonmetallic materials, such as plastics and ceramics, to magnesium will not result in any potential corrosion hazard, there are some notable exceptions. Magnesium-to-wood assemblies present an unusual problem because of the water absorbency of wood and the tendency of the assemblies to leach out natural acids. To protect magnesium from attack, the wood should first be sealed with paint or varnish, and the faying surface of the magnesium treated as described previously for magnesium-to-magnesium assemblies. The joining of magnesium to carbon-fiber-reinforced plastics is another exception that, in the presence of a common electrolyte, could result in corrosion of the magnesium unless similar assembly precautions are observed.

Magnesium-to-Dissimilar-Metal Assemblies. Several techniques can be implemented to minimize or eliminate galvanic corrosion or, if breakdown occurs, to reduce its effect in magnesium-to-dissimilar-metal couples. These include:

- Elimination of the common electrolyte
- Reduction of the relative area of dissimilar metal present
- Minimization of the potential difference of the dissimilar metal
- Protection of the dissimilar metal and the magnesium from the common electrolyte

Good design can play a vital role in reducing the threat of galvanic corrosion (Fig. 25). Elimination of a common electrolyte may be possible by the provision of a simple drain hole or shield to prevent liquid entrapment at the dissimilar-metal junction. Alternatively, the location of screws or bolts on raised bosses may also help avoid common electrolyte contact, as would use of nylon washers, spacers, or similar moisture-impermeable gaskets. The use of studs in place of bolts will reduce the area of dissimilar metal exposed by up to 50%, provided the captive ends of the studs are located in blind holes.

The degree of attack resulting from galvanic corrosion is, among other things, proportional to the potential difference between the metals involved. Consequently, this should be reduced to a minimum by careful materials selection or the use of selected plating or coating of metals brought into contact with magnesium.

As discussed previously, dissimilar metals that are relatively compatible with magnesium are the aluminum-magnesium (5*xxx*-series) or aluminum-magnesium-silicon (6*xxx*-series) aluminum alloys, which should be used for washers, shims, fasteners (rivets and special bolts), and structural members, where possible. Other aluminum alloys, steels, titanium, copper, brass, monel, and so on, will corrode magnesium when coupled with it under corrosive conditions, and protection is therefore required.

Figure 26 indicates the relative severity of galvanic corrosion of die-cast AZ91D caused by

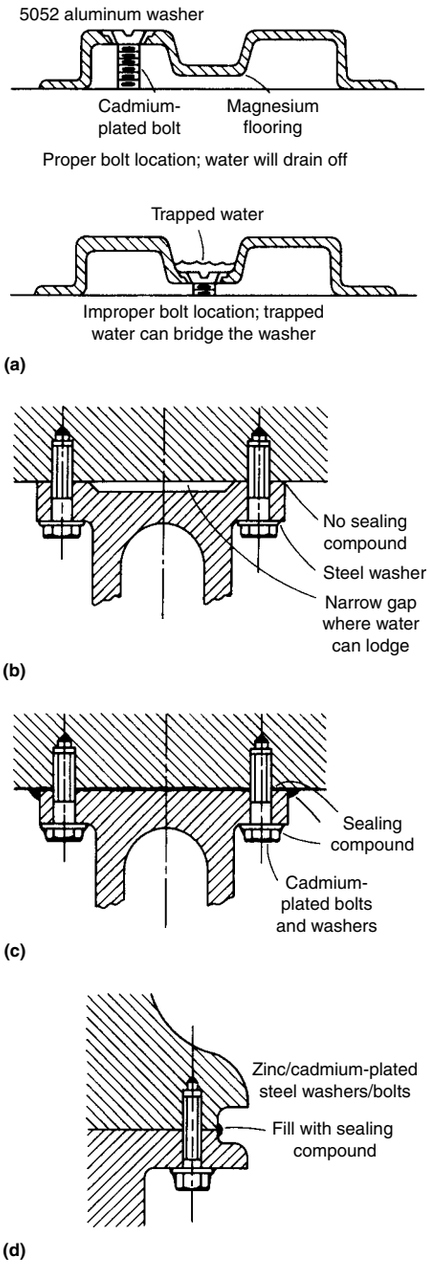

Fig. 25 Design considerations for reducing galvanic corrosion. (a) Proper bolt location. (b) Poor practice. (c) Good with no gap. (d) For use when direct metal-to-metal contact is required for electrical reasons

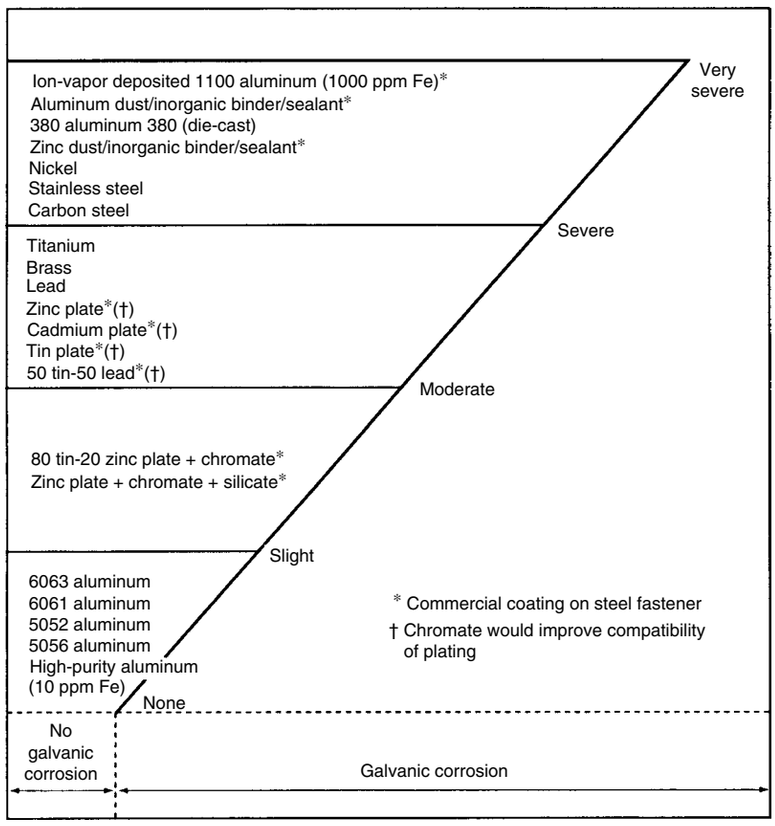

Fig. 26 Relative galvanic corrosion produced by dissimilar fasteners attached to AZ91D magnesium alloy (ASTM B 117 salt spray test). Source: Ref 34, 35

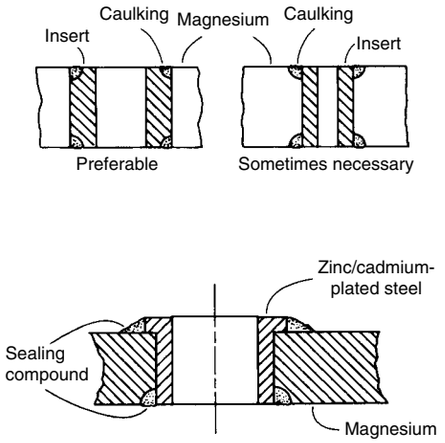

Fig. 27 Examples of good practice for bushing installations

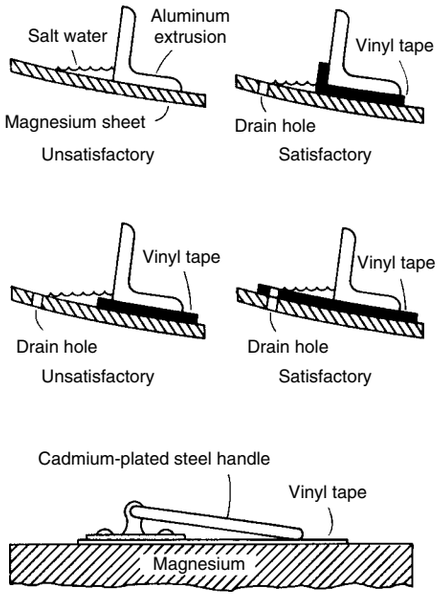

Fig. 28 Use of insulating tapes to avoid galvanic corrosion

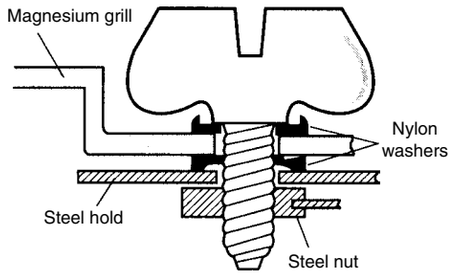

Fig. 29 Use of nylon washers to separate a magnesium automobile grill from a steel hood and hold-down screw and avoid galvanic corrosion

coupling with various dissimilar metals in salt spray (ASTM B 117). These ratings provide useful guidelines for selection, but they are not quantified because of the major influence of design factors and the difference between actual environmental conditions and the severe salt spray test (Ref 16).

Aluminum, zinc, cadmium, and tin are used to coat steel or brass components to reduce the galvanic couple with magnesium. Reducing the potential difference or plating using materials with high hydrogen overvoltages will help reduce galvanic corrosion under mildly corrosive environments but will have minimal effect in severe environments; additional precautions are required for corrosion protection.

Use of wet assembly techniques, as discussed previously, will eliminate galvanic corrosion in crevices. Caulking the metal junctions will increase the electrical resistance of the galvanic couple by lengthening the electrolytic path and thus reduce the degree of attack should it occur (Fig. 27). Vinyl tapes have also been used to separate magnesium from dissimilar metals or a common electrolyte and thus prevent galvanic attack (Fig. 28). Finally, painting the magnesium and, more important, the dissimilar metal after assembly will effectively insulate the two materials externally from any common electrolyte.

Fastener Selection. The design of bolted connections and the selection of fastener materials are critical decisions of magnesium assemblies exposed to saltwater. In rare instances, the problem can be completely avoided by the use of nonmetallic fasteners or insulating washers (Fig. 29). Where strength is adequate and the possibility of seizure is not a concern, fasteners made of compatible aluminum alloys (5*xxx* or 6*xxx* series) can limit galvanic corrosion. In the great majority of situations, mechanical requirements and cost factors dictate the use of steel fasteners having plated or other protective coatings. However, many proprietary coatings based on zinc or aluminum powders in organic or inorganic binders prove to be completely incompatible with magnesium in salt exposure. Phosphate coatings on steel bolts do not significantly reduce galvanic corrosion of magnesium.

A recent study compared several commercial fastener coatings with two types of heavy-duty polymer encapsulation for ability to reduce galvanic attack of die-cast AZ91D test plates in salt spray (Fig. 30). The most effective coating was nylon 11 electrostatically applied to the head surfaces of a socket-head bolt to a thickness of 0.20 to 0.25 mm (8 to 10 mils). This coating has performed satisfactorily on clamping bolts joining two halves of die-cast-magnesium four-wheel-drive transfer cases in light-truck applications. A high level of protection was also demonstrated in this study by the molded plastic caps and the nylon 11 coating to provide a substantial barrier to the flow of galvanic current through the electrolyte (Fig. 31).

In the category of electroplated coatings, zinc is fundamentally the most compatible with magnesium due to its position in the emf series and its polarization characteristics. Zinc-plating technology is highly developed, and zinc plating is economical. Specialized plating processes have been developed in which the zinc deposit is chemically augmented or alloyed with tin, nickel, or cobalt to improve the life of the coating in salt spray environments, where unmodified zinc tends to corrode rapidly. Four commercial modified zinc-alloy plates were included in the study (Fig. 32):

- Zinc plate + chromate + silicate (JS500)
- 80Sn-20Zn plate + chromate
- Zinc/7–13% Ni plate (Zincrolyte CLZ-Ni)

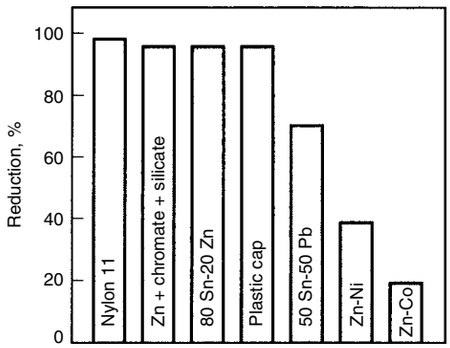

Fig. 30 Reduction of galvanic corrosion between magnesium-alloy AM608 (AZ91D) die-cast test plates and various coated steel fasteners, compared to bare steel fasteners. Tested for 200 h in continuous salt spray. Source: Ref 35

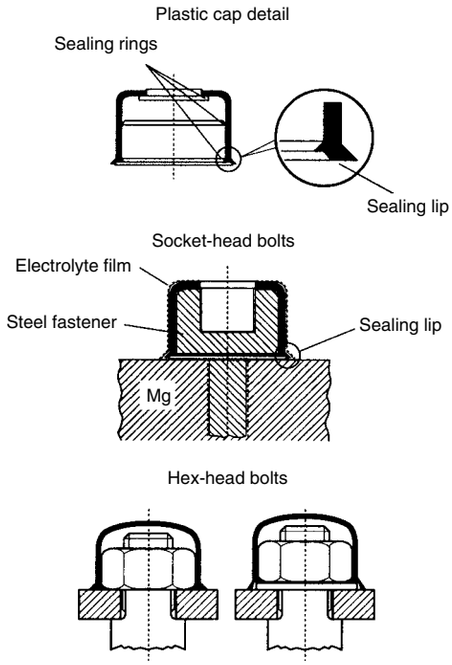

Fig. 31 Use of molded plastic caps on socket-head and hex-head bolts to avoid galvanic corrosion. Source: Ref 35

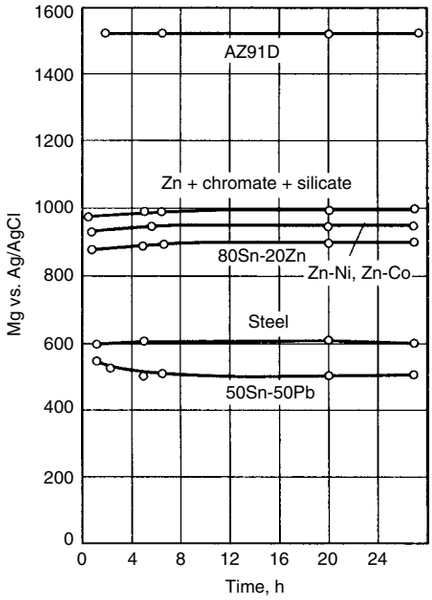

Fig. 32 Open-circuit potentials of plated steel and bare steel fasteners and die-cast AZ91D magnesium alloy against a Ag/AgCl reference electrode in 5% NaCl saturated with $Mg(OH)_2$. Source: Ref 35

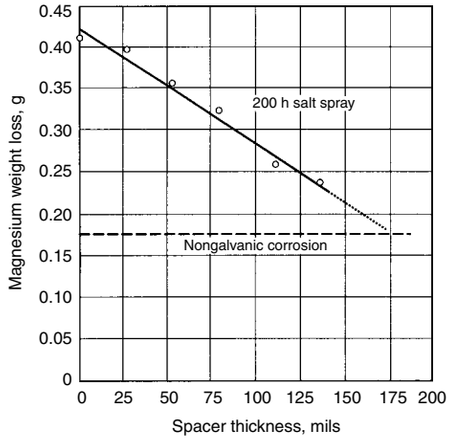

Fig. 33 Effect of spacer thickness on the galvanic corrosion of AZ91 magnesium coupled to cast iron disks through plastic spacers (200 h salt spray). Source: Ref 34

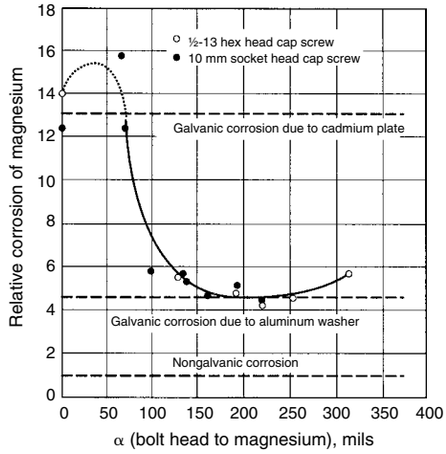

Fig. 34 Effects of aluminum-alloy washer size on the galvanic corrosion of AZ91 magnesium fastened with cadmium-plated bolts. α is a linear distance measured from the cadmium-plated bolt head to the magnesium surface via washer surface. 10 days salt spray exposure. ASTM B 117. Source: Ref 34

- Zinc/0.2–0.9% Co plate + supplements (Zincrolyte CLZ-Co)

The first two of these coatings reduced the magnesium corrosion by more than 90%. Predictably, the zinc-nickel and zinc-cobalt alloy deposits were much less effective, a consequence of the adverse cathodic activity of nickel and cobalt.

Also included in this study were steel bolts commercially plated with a deposit of 50Sn-50Pb. This coating reduced the galvanic attack of magnesium by approximately 70%, despite the fact that its open-circuit potential was approximately 100 mV more noble than that of steel. Figure 32 illustrates the important principle that it is the polarized potential that governs galvanic corrosion rather than the position of the dissimilar metal on the equilibrium emf series.

Washers. Properly selected and sized washers or spacers can contribute substantially to control of galvanic corrosion at magnesium/dissimilar-metal junctions. Insulating plastics are effective where their limited mechanical properties do not cause loss of clamping force. Aluminum 5052 or other compatible aluminum alloy is a preferred material for washers and spacers. A 5052 aluminum washer interposed between cast iron engine blocks and AZ91D magnesium clutch housings has successfully prevented galvanic attack of the magnesium under conditions of road-salt splash.

Table 13 shows the effect of washer, washer material, and surface treatment on salt spray galvanic corrosion of high-pressure die-cast AZ91B. The improved protection by zinc plating of the fastener as compared to simple black phosphate treatment is shown. The surface condition of the magnesium alloy, from untreated through chromating and anodizing, has little effect on the galvanic corrosion behavior.

Washers and spacers are used to increase the length of the electrolyte path that separates the dissimilar metals. Effect of spacer thickness on the galvanic corrosion (salt spray) of AZ91 coupled to cast iron disks through plastic spacers is shown in Fig. 33. The galvanic effect caused by contact with the cast iron disks disappears when the plastic spacer thickness exceeds 4.5 mm (0.175 in.). Figure 34 shows the effect of aluminum washer size on the galvanic corrosion (salt spray) of AZ91D fastened with cadmium-plated bolts. The galvanic effect due to the cadmium plate disappears when the excess diameter plus the washer thickness reaches 3.8 to 5.1 mm (0.150 to 0.200 in.) (approximately $^3/_{16}$ in.). For conservative design, the spatial separation provided by the washer or spacer should be at least 5 mm (200 mils).

It is important to note that even though the use of 5052 aluminum washers decreases the galvanic effect of AZ91D connected by cadmium-, tin-, or zinc-plated steel and bare steel in salt spray conditions, a different behavior is observed when immersed in salt solution. Table 14 shows the effects of 5052 aluminum washers with plated steel bolts in salt spray and saltwater-immersion tests. The results of 5 wt% NaCl immersion tests indicate that the washer was actually detrimental. It is reported that the ineffectiveness of the washers with plated bolts was associated with a high rate of cathodic attack on the aluminum compared to that which occurred in salt spray. Similarly, severe corrosion of AZ91D was observed (Table 15) in salt immersion when coupled with other aluminum-alloy contacts (5052, 1100, and 380), with proportionately severe cathodic corrosion of the aluminum. Magnesium assemblies are not deliberately subjected to saltwater immersion, but a situation approaching this could occur with unfavorable designs that allow accumulation of pools of saltwater at dissimilar junctions.

Table 13 Salt spray galvanic corrosion of pressure die-cast AZ91B effect of washer, washer material, and surface treatment

Assembly(a)			Corroded area around bolthead/washer		Maximum penetration	
Mg(b)	Bolt finish	Washer	mm	in.	mm	mils
A	Black phosphate	None	1030	41	2.3	92
B	Black phosphate	None	1030	41	2.8	112
A	Zn-plate(c)	None	250	10	1.7	68
A	Zn-plate(c)	Steel(c)	150	6	1.1	44
A	Zn-plate(c)	Al (6082)	40	1.6	0.6	24
B	Zn-plate(c)	None	330	13	1.6	64
B	Zn-plate(c)	Steel(c)	100	4	1.0	40
B	Zn-plate(c)	Al (6082)	20	0.8	1.3	52
C	Zn-plate(c)	None	320	12.6	2.1	84
C	Zn-plate(c)	Steel(c)	130	5	1.9	76
C	Zn-plate(c)	Al (6082)	20	0.8	0.7	28

(a) Magnesium alloys test panels with two M12 bolts (approx. 13 mm, or 0.5 in., diam) in each. (b) Treatment: A, none; B, yellow chromate; C, anodized HAE 15–20 μm (0.6–0.8 mil). (c) 25.4 μm (1 mil) zinc plate with yellow chromate posttreatment

Table 14 Effects of 5052 aluminum alloy washers with plated steel bolts in salt spray and saltwater immersion tests

	Relative weight losses of AZ91D	
Fastener unit	10 days salt spray	16 h immersion in 5% NaCl
Nylon	1.0 (0.28 g)	1.0 (0.07 g)
Cadmium plated, 5052 washer(a)	5.85	48.7
Tin plated, 5052 washer(a)	8.84	37.7
Zinc plated, 5052 washer(a)	15.82	39.9
Bare steel, 5052 washer(a)	6.81	326.0
Cadmium plated	14.0	26.7
Tin plated	11.8	17.6
Zinc plated	18.5	14.9
Bare steel	31.3	377.0
	Washer benefit factor(b)	
Bolt material	Salt spray	5% NaCl immersion
Zinc plated	1.17 (0.28)	0.37 (1.09)
Tin plated	1.33 (0.32)	0.47 (1.09)
Cadmium plated	2.39 (0.25)	0.55 (1.11)
Steel	4.60 (0.18)	1.16 (0.14)

(a) $1\frac{1}{4}$ in. outside diameter washer ($d = 317$ mils). (b) (Magnesium corrosion without washer)/(Magnesium corrosion with washer). Numbers in parentheses: weight loss of five 5052 washers. Source: Ref 34

Protective Coating Systems

Besides the previously mentioned metallic coatings, several inorganic and organic systems are available.

Inorganic Surface Treatments. A full range of chemical and electrochemical cleaning and surface pretreatments before application of paint finishes is available for magnesium. Whichever pretreatment is selected, it must be applied to a clean metal surface. In the case of magnesium, this implies the removal of oil, dirt, or grease, and more important, a surface free of other contaminants. Heavy-metal contamination arising from blasting, brushing, tumbling, lapping, and other abrasive operations is particularly detrimental, as is contamination from graphite-containing die-forming lubricants. The use of abrasive materials compatible with magnesium (high-purity alumina, silicon carbide, and glass, for example) will help ensure that heavy-metal pickup is kept to a minimum. Oil, dirt, and grease are removed by conventional solvent immersion or vapor-degreasing techniques using chlorinated solvents. Alkali cleaning in high-pH cleaners is also suitable. Oxides, die-forming compounds, and other surface contaminants are removed by a range of acid-pickling solutions. Details are given in Table 16. In addition, an electrochemical process known as fluoride anodizing will more effectively remove sand or heavy-metal contamination. This process is also applicable to finished work when dimensional losses cannot be tolerated. The primary function of dip or anodic coatings on magnesium is to provide a suitable surface to promote the adhesion of subsequent organic coatings. Conversion coatings should not be regarded as protective treatments in their own right unless they are to be exposed only to noncorrosive environments. Under these conditions, they will delay the onset

Table 15 Corrosion rates of magnesium and aluminum in galvanic couples 24 h immersion in 5% NaCl

	Average corrosion rate, mm/yr (mils/yr)	
Couple(a)	AZ91D	Aluminum
AZ91D, high-purity aluminum(b)	1.8 (71)	0.8 (31.5)
A91D, Al 5052	20.0 (788)	13.0 (512)
A91D, Al 1100	31.0 (1221)	59.0 (2325)
A91D, Al 380	73.0 (2876)	61.0 (2403)

(a) Exposed surface area 3×14 cm (1.2×5.5 in.) (both), 0.6 cm (0.24 in.) space between them. (b) Less than 10 ppm Fe. Source: Ref 34

Table 16 Some chemical cleaning treatments for magnesium alloys

		Operating conditions			Typical metal removal		
			Temperature				
Type	Composition(a)	Time, min	°C	°F	mm/surface	in./surface	Comments
Nitric acid	50–100 mL, 70% HNO_3, to 1 mL H_2O	$\frac{1}{2}$–$1\frac{1}{2}$	21–27	70–80	0.01–0.05	0.0004–0.002	General cleaning of rough castings, forgings, etc.
Acetic-nitrate	200 mL glacial acetic acid, 50 g $NaNO_3$ (sodium nitrate), to 1 L H_2O	$\frac{1}{2}$–1	21–27	70–80	0.012–0.025	0.0005–0.0009	Removal of mill scale and other surface contamination from wrought products
Chromic-nitrate	180 g CrO_3, 30 g $NaNO_3$, to 1 L H_2O	2–20	21–32	70–90	0.012–0.025	0.0005–0.0009	Removal of mill scale and graphite lubricants from wrought or founded products
Hydrofluoric-sulfuric	250 mL 60% HF, 31 mL 96% H_2SO_4, to 1 L H_2O	2–5	21–32	70–90	0.003	0.0001	Brightens die castings. Improves response to chemical pretreatment
Chromic-nitric-hydrofluoric	280 g CrO_3, 8 mL 60% HF, 25 mL 70% HNO_3, to 1 L H_2O	$\frac{1}{2}$–2	21–32	70–90	0.012–0.025	0.0005–0.0009	Removal of surface segregation from die castings to leave a smut-free surface. Improves response to chemical treatment
Chromic acid	100–200 g CrO_3, to 1 L H_2O	1–15	90–100	195–212	Negligible		Removal of oxides, corrosion product, and conversion coatings. Negligible metal removal, providing bath uncontaminated by chlorides, sulfates, etc. Use silver chromate addition to control chloride contamination.
Chromic-sulfuric	100 g CrO_3, 10 mL 96% H_2SO_4, to 1 L H_2O	Swab until clean	21–32	70–90	Negligible		Local removal of superficial corrosion product
Nitric-sulfuric	80 mL 70% HNO_3, 20 mL 96% H_2SO_4, to 1 L H_2O	10–15 s	21–32	70–90	0.05	0.002	Preliminary treatment for sand castings to remove surface-contaminating effects of blast cleaning
Nitric acid/hydrofluoric acid treatment	(1) 50–100 mL, 70% HNO_3, to 1 L H_2O (2) 100 mL 60% HF, to 1 L H_2O	Up to 2 min in (1), rinse, then 15 min in (2)	21–27	70–80	0.05	0.002	Removal of heavy-metal contamination from surface of rough castings. Second-stage immersion removes reprecipitated contaminants remaining after first-stage cleaning.
Fluoride, anodizing	150–250 g $NH_4F{\cdot}HF$ (ammonium bifluoride), to 1 L H_2O	ac anodize at 200 A/m^2 (0.13 A/in.^{2}) up to 120 V	30	85 max	Negligible		Supercleaning of heavy-metal-contaminated surfaces. Fluoride film formed requires removal in H_2CrO_4 before chemical pretreatment.

(a) Whenever water is specified, use deionized water

of natural surface oxidation and may provide a more visually attractive surface appearance.

Table 17 lists some of the treatments used worldwide, together with brief application details and uses. Some treatments are quick and inexpensive to use but may not provide as good a paint base as others. Consequently, their use should be restricted to mildly corrosive environments. Newer chromate-free approaches to inhibiting corrosion are presented elsewhere in this Volume.

Several hard-anodizing treatments are available for magnesium. They are No. 17 and HAE treatments (Table 18) and newer anodic treatments based on alkaline baths or plasma electrolytic techniques such as Tagnite. Both may be applied as thin (0.005 mm, or 0.0002 in.) or thick (0.038 mm, or 0.0015 in.) coatings, with the thicker treatments imparting wear and abrasion resistance. These coatings are porous and provide excellent bases for subsequent painting. However, particularly for the thicker films, conventional painting may not completely seal the anodic pores. Another anodized coating that is purported to offer improved corrosion resistance over the No. 17 and HAE treatments is the Tagnite coating process, which is being applied to magnesium castings for helicopter drive system components (Ref 36). To prevent the risk of subsurface lateral corrosion spread from a point of damage, resin impregnation is used for maximum serviceability in aggressive corrosive environments. Inorganic chemical posttreatments are sometimes used to impregnate the anodic film with corrosion inhibitors, but these treatments can be detrimental to subsequently applied organic coatings and are not as effective as resin impregnation.

Organic Coatings. Adhesion and subsequent corrosion protection to cleaned and pretreated magnesium surfaces are enhanced by the use of alkali-resistant paint systems. Paints based on epoxy, epoxy ester, phenolic, polyurethane, vinyl, acrylic, polyester, silicone, and epoxy silicone systems are generally suitable. Those based on linseed, soya or other oils, alkyds, or nitrocellulose are best avoided unless applied for decorative purposes only.

Table 17 Some chemical conversion coating treatments for magnesium alloys

Name	Bath composition(a)	Procedure	Appearance	Typical metal removal	Comments
Chrome pickle (acid chromate)	180 g $Na_2Cr_2O_7·2H_2O$ (sodium dichromate), 187 mL 70% HNO_3, to 1 L H_2O	1/2 to 2 min immersion at room temperature; allow to drain for 5–30 s; rinse in cold water, then hot water to aid drying	Golden yellow, often with iridescence	Up to 0.015 mm (0.0006 in.)	Applicable to all alloys and forms; mainly applied to wrought and die castings; good paint base
Modified chrome pickle	15 g $NaHF_2$ (sodium acid fluoride), 180 g $Na_2Cr_2O_7·2H_2O$, 10 g $Al_2(SO_4)_3·14H_2O$ (aluminum sulfate), 125 mL 70% HNO_3, to 1 L H_2O	1/2 to 2 min immersion at room temperature; allow to drain for 5 s; rinse in cold water, then hot water to aid drying	Yellow-red iridescence to gold	Up to 0.012 mm (0.0005 in.)	Particularly suited to treatment of die castings; prepickle in $HF·H_2SO_4$ mixture or hot alkaline clean; good paint base
Galvanic dichromate	(1) 50 g $NH_4F·HF$ (ammonium bifluoride) (or sodium or potassium bifluoride), to 1 L H_2O	Immerse in activator for 5 min and rinse	Dark brown to black	Negligible	Applicable to all alloys and forms; matte black film useful for optical applications; good paint base
	(2) 30 g $(NH_4)_2SO_4$ (ammonium sulfate), 30 g $Na_2Cr_2O_7·2H_2O$, 2.6 mL 0.880 NH_4OH, to 1 L H_2O	10 to 30 min immersion at 50–60 °C (120–140 °F) with parts coupled to low-carbon steel cathode; bath pH 5.6–6.2			
Dichromate	(1) 50 g $NH_4F·HF$, or 187 mL 60% HF, to 1 L H_2O	5 min immersion in activator at room temperature, except for AZ31 alloy, which should only be immersed for 1/2–1 min if HF activator is used; rinse thoroughly	Brassy to dark brown	Negligible	Applicable to most alloys and all forms; as-cast die-cast surfaces should be prepickled to remove skin segregation; excellent paint base
	(2) 180 g $Na_2Cr_2O_7·2H_2O$, 2.5 g CaF_2 or MgF_2 (calcium or magnesium fluoride), to 1 L H_2O	Immersion for 30 min in boiling solution (95 °C, or 205 °F, min); maintain pH 4.0–5.5; rinse and dry			
Chrome-manganese	100 g $Na_2Cr_2O_7·2H_2O$, 50 g $MnSO_4·5H_2O$ (manganese sulfate), 50 g $MgSO_4·7H_2O$ (magnesium sulfate), to 1 L H_2O	Up to 2 h immersion at room temperature, proportionately less at higher temperatures, e.g. 10 min at boiling; maintain pH 4.0–6.0; rinse and dry	Dark brown to black	Negligible	Applicable to most alloys and all forms; as-cast die-cast surfaces should be prepickled to remove skin segregation; excellent paint base
Dilute chromic acid	10 g CrO_3, 7.5 g $CaSO_4·2H_2O$ (calcium sulfate), to 1 L H_2O	Immerse or swab for 1–2 min; rinse and hot air dry	Brassy to brown	Negligible	For touch-up use or as complete treatment; moderate paint base; solution should be stirred or shaken vigorously before use
Iridite mag-coat	37.5 g proprietary Iridite 15 chromate compound. 58.5 mL 37% HCl, 0.26 mL proprietary wetting agent, to 1 L H_2O	Immerse or swab 15–30 s at 21–32 °C (70–90 °F); maintain pH 0.2–0.6; rinse thoroughly in cold water and hot air dry	Brown to dark brown	Slight, up to 0.003 mm (0.0001 in.)	For touch-up use or as complete treatment; as-cast surfaces should be prepickled in $H_2CrO_4·HNO_3·HF$ to remove skin segregation; good paint base
Parker phosphate	(1) Proprietary Parco Coater 2557	3 to 5 min immersion at 55–70 °C (130–160 °F) followed by hot water rinse, then immerse for 15–45 s in hot supplementary treatment and hot air dry	Gray to matte silver	Negligible	Paint base for mild environments only when applied to high-purity alloys; not recommended for corrosive environments; nonchromate-containing treatment
	(2) Proprietary Parcolene "Dilute"				
Amchem phosphate	(1) Proprietary, Prep-n-Cote 978	1 to 5 min immersion or spray at 38 °C (100 °F); water rinse; final rinse at 60 °C (140 °F) with Deoxylite	Light gray to beige	Negligible	Paint base for mild environments when applied to high-purity alloys; provides option of a chromium-free treatment
	(2) Deoxylite 41 (optional)				
Dilute chromate; NH35	2.5 g $NaHF_2$, 2.5 g $Na_2Cr_2O_7·2H_2O$, 3 g $MgSO_4·7H_2O$, 32 mL 65% HNO_3, to 2 L H_2O	Clean (alkaline bath/or solvent); water rinse; NH35 treat 20–30 s; water rinse and dry	Yellow to yellow-brown low-pressure castings; yellow-brown to matte gray on high-pressure die castings	0.002 mm (0.00008 in.)	A dilute chromate treatment developed primarily for high-pressure die-cast alloys; is near equivalent of standard chromates in both shelf life and paint base performance

(a) Whenever water is specified, use deionized water.

Inhibiting pigments, such as strontium or zinc chromates, are often incorporated into primer systems for magnesium. These slightly soluble compounds will release chromate ions to retard subsequent corrosion should the paint film be damaged. Chromate inhibitors are, however, not as effective on magnesium as on aluminum alloys, particularly under corrosive conditions. Primers containing metallic zinc, lead, or any other metallic pigmentation should not be used on magnesium.

The full range of application techniques can be used. These include brushing, dipping, solvent or electrostatic powder spray, and electrophoretic techniques. Multilayer compatible coatings of primer, filler, and topcoat systems will provide optimal protection in corrosive environments. Use of high-temperature stoving (baking) systems is also beneficial in developing maximum resistance to moisture permeability.

General Recommendations. Selection of a suitable protective scheme depends on many factors, especially the expected operational environment, design life, inspection and maintenance costs, the component cost, and of course the cost of original surface protection. For new applications, it is advisable to err on the side of overprotection until enough experience is gained to enable a more valued judgment to be made.

For indoor and similar noncorrosive environments, surface protection requirements are minimal and may range from none to simple chromate or phosphate conversion coatings with primer only or a decorative paint finish. Even under apparently more corrosive conditions, other mitigating factors, such as the use of high-purity alloys, good ventilation, component warmth, good design, and oil films, will enable magnesium components to be used with little or no protection.

For mildly or moderately corrosive environments, a chromate pretreatment followed by one coat of suitable primer and one or more coats of compatible finish should be applied. Under these conditions, the effect of galvanic couples, if present, should be considered, and some precautions taken, as previously outlined. It is expected that most commercial applications would be covered by this and the preceding general recommendations. (See the section "Industry-Proven Protection Systems" in this article.)

For moderately to severely corrosive environments, good-quality chromate conversion coatings or thin anodic pretreatments should be used. Chromate-inhibited epoxy primer systems, careful wet assembly procedures, and painting after assembly with primer and topcoat are recommended. Use of low-temperature baking paints is beneficial for improving humidity resistance (Fig. 35a).

For severely corrosive environments, for which maximum chemical, salt spray, and humidity resistance are required (Fig. 35b), specialized paints and coating techniques are used. Good-quality chromate or anodic pretreatments are required. Use of thick anodic coatings will also impart a measure of abrasion and damage resistance (Fig. 35c). Pretreatments should then be sealed with high-temperature baking organic resins. This is achieved by a process known as Surface Sealing (MIL-M-3171 section 3.9.3, MIL-M-46080), in which three coats of thinned resin are applied to a preheated component by spraying or, preferably, by dipping. Epoxy-resin systems are preferred (MIL-C-46079), although the technique would be beneficial for other high-temperature baking resins, such as phenolics and epoxy silicones.

After this foundation treatment, full wet assembly procedures, including caulking of joints, should be performed before application of a cold or low-temperature curing chromate-inhibited primer and a compatible topcoat system. For additional protection, a high-temperature baking paint system should be maintained throughout. The previous recommendations are necessarily very general in scope but represent the various protection schemes in worldwide use on magnesium.

Inhibitors

Uniform corrosion on pure magnesium has been drastically reduced by exposure to chromate (Ref 37) as well as dichromate, molybdate, and nitrate-containing solutions (Ref 38). Filiform corrosion is instead initiated on these alloys, suggesting formation of a protective surface film. Reduced chromium ions have been found in the uniform hydroxide layer but not in the filament corrosion product (which is probably MgO). Adding soluble chromates, neutral fluorides, or rare earth metal salts is effective in reducing magnesium-base metal corrosion. Inhibitors can even be incorporated into magnesium as metallic alloying elements, whose oxidation on gradual dissolution provides inhibiting effects.

Industry-Proven Protection Systems

Specific industries have developed systems for protecting magnesium.

Aerospace Applications. Even within this specialized area, many surface protection schemes that reflect the differing operational environments encountered are in use.

For military and helicopter applications, comprehensive protection schemes are required to achieve extended component life and to reduce maintenance costs. Such schemes, as recommended for severely corrosive environments in the previous section, are required, and indeed, are mandatory in certain countries. Full wet assembly procedures and the coating of all exposed surfaces are essential. These schemes

Table 18 Details of two hard-anodizing treatments for magnesium alloys

		Anodizing conditions				Coating buildup		
			Temperature					
Name	Bath composition(a)	Time, min	°C	°F	Coating appearance	mm	in.	Comments
HAE	135–165 g KOH, 34 g $Al(OH)_3$ (aluminum hydroxide), 34 g KF (potassium fluoride), 34 g Na_3PO_4 (trisodium phosphate), 20 g K_2MnO_4 (potassium manganate), to 1 L H_2O	8 min at 200 A/m^2 (0.13 A/in.^{2}) for thin coating (70 V)	15–30 max (cooling required)	60–85	Light tan (thin)	0.005	0.0002	Applicable to all alloys and forms. Thin coating provides excellent paint base. Thick coating provides excellent wear resistance and, if sealed with organic resins, provides superior corrosion protection as well. Process has good throwing power.
		60 min at 250 A/m^2 (0.16 A/in.^{2}) for thick coating (90 V) (ac anodize)			Dark brown (thick)	0.040	0.0016	
No. 17	240 g $NH_4F{\cdot}HF$, 100 g $Na_2Cr_2O_7{\cdot}2H_2O$, 90 mL 85% H_3PO_4, to 1 L H_2O	5 min at 200 A/m^2 (0.13 A/in.^{2}) for thin coating (70 V)	70–80	160–175	Light green (thin)	0.006	0.0002	Applicable to all alloys and forms. Thin coating provides excellent paint base. Thick coating gives good wear resistance and, if sealed with organic resins, provides superior corrosion protection. Process has excellent throwing power.
		25 min at 200 A/m^2 (0.13 A/in.^{2}) for thick coating (90 V) (ac anodize)			Dark green (thick)	0.030	0.0012	

(a) Whenever water is specified, use deionized water.

have given total protection for thousands of hours in various accelerated testing programs and will minimize corrosion spread.

For civil and other less aggressive aerospace applications, the protection schemes outlined for moderately corrosive environments are applicable. Good-quality aerospace paint systems should be used with wet assembly techniques.

Automotive Applications. The most notable automotive use of magnesium has undoubtedly been for the engine and transmission casings on the original Volkswagen Beetle. For this application, no protective treatment was required to obtain long and reliable service life because of the mitigating environmental factors previously outlined. More modern automotive applications include air cleaner covers, engine compartment grills, retractable headlight assemblies, clutch and brake pedal supports, and clutch and transmission housings. One of the more recent implementations of magnesium in the automotive industry is the use of alloy AM50 for the front-end support assembly for light-duty Ford trucks. For some applications, no protection is required. For others, where aesthetic appearance or corrosion protection is needed, the protective schemes outlined for mildly corrosive environments are suitable.

Cathodic electrophoretic epoxy primers applied to chromic acid pickled or dichromate pretreatments have proved effective, particularly in conjunction with high-purity AZ91D die castings. Electrostatic powder spray is used for topcoating. Specially designed fasteners incorporating nylon or plastic washers, sleeves, shims, and so on help reduce the risk of galvanic corrosion on exposed parts.

Some evaluations (Ref 39, 40), however, demonstrated that for structural underbody and road wheel applications, in which frequent exposure to water splash, stone impact damage, and the absence of mitigating environmental factors are problems, more comprehensive protection schemes may be required, together with protection against galvanic corrosion. Where applicable, use of underbody wax-type coatings can provide additional protection. It is expected that use of high-purity alloys will enable designers to specify many more magnesium automotive applications in the future.

Electronic and Computer Applications. Die-cast, investment-cast, and wrought magnesium components are used by computer and computer peripheral manufacturers for several applications where lightweight, low inertia, rigidity, and heat sink requirements preclude the use of other metals or plastics. The noncorrosive operational environment within the computer eliminates the need for galvanic-corrosion precautions.

For exterior housings, decorative surface treatments consisting of chromate pretreatment followed by textured epoxy powder coatings have proved satisfactory. Within disk drive units, where minute dust or other particles could cause disk or head failure, very thin (0.003 mm, or 0.0001 in.) specialized conformal coatings are applied to protect against atmospheric oxidation. Other similar commercial applications include housing or support frames in portable video equipment and a range of optical and medical electronic equipment.

Other Applications. Some magnesium applications may require surface protection against wear and corrosion. The use of resin-sealed hard-anodizing treatments, particularly thick HAE treatments, will provide excellent abrasion and corrosion resistance, but some applications (e.g., pulley wheels) will themselves cause excessive wear on other components. Under these conditions, dry-lubricant coatings are required. Nylon coatings applied by electrostatic powder or fluidized bed techniques onto chromated and suitably primed magnesium surfaces have proved effective for use in aircraft pulley control systems. Thick nylon coatings also offer good damage and erosion resistance. Other systems, based on fluorocarbon (Teflon, E.I. Du Pont de Nemours & Company, Inc.) impregnation of anodic pretreatments or resin-bonded solvent-based fluoropolymer coatings, are also effective in providing combined corrosion resistance and lubricity.

For high-temperature (above 200 °C, or 390 °F) applications, silicone-, epoxy-silicone-, and polyimide-based paints will provide effective corrosion-resistant coatings on magnesium. In environments where lubricants may be present, polyimide coatings are preferred, particularly when applied onto No. 17 anodic pretreatment.

There are a few applications in which magnesium components may be subjected to prolonged immersion or contact with corrosive electrolyte. In some systems, it may be possible to add corrosion-inhibiting agents to the electrolyte. Maintaining electrolyte pH above 10.5 or adding soluble chromates or neutral fluorides is effective in reducing magnesium-base metal corrosion. In other applications, comprehensive surface protection schemes and good maintenance are essential to achieve satisfactory service life. One such example is an atmospheric pressure deep-sea diving suit, the body and helmet of which are in magnesium alloy (Fig. 36). Surface protection consists of a thick HAE anodic film that is surface sealed with high-temperature stoving epoxy resin, full wet assembly procedures, and final painting with primer and topcoat. Coupled with good maintenance, this protection scheme has given satisfactory service between major overhaul intervals of 4 years.

Some special applications may require the metal plating of a magnesium component. Zinc and nickel can be directly plated onto magnesium from special electroless baths. Other metals may be electroplated from standard plating baths after surface cleaning, activation, zinc-immersion coating, and a copper strike. It should be

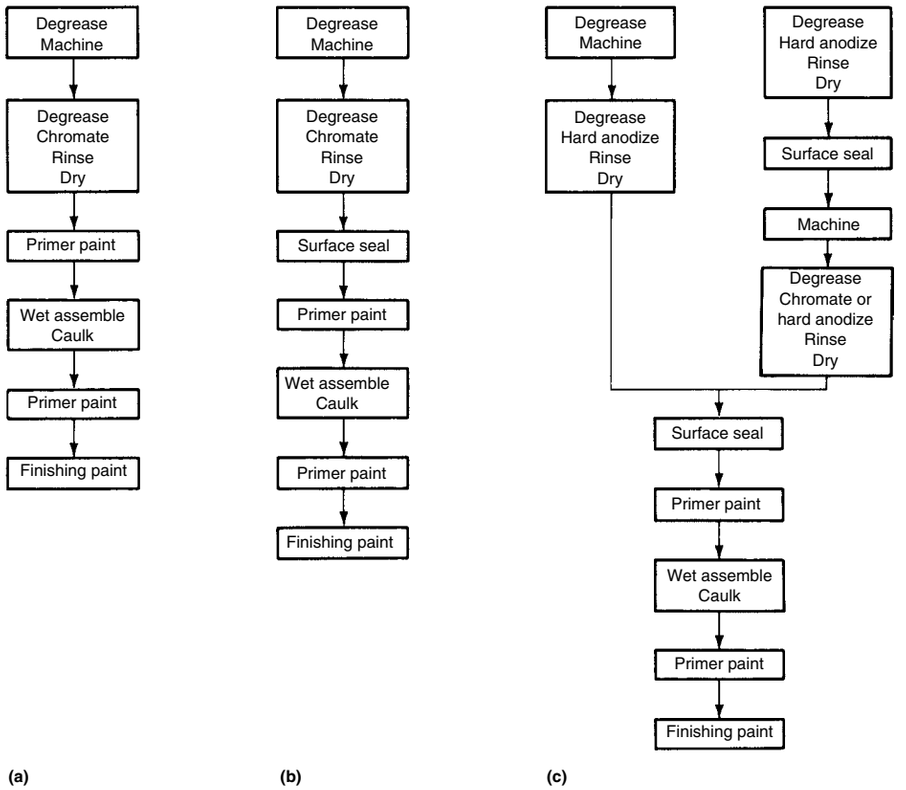

Fig. 35 Diagram of protection schemes for critical applications in corrosive environments. (a) For moderately corrosive environments. (b) For severely corrosive environments. (c) For severely corrosive environments with risk of abrasion or damage

emphasized that metal plating of magnesium is not a corrosion-protective coating and that plated components should not be exposed to severely corrosive environments. Plated magnesium die castings are suitable, however, for such applications as interior automotive door handles and window cranks, where it is necessary to combine weight reduction with strength durability and good appearance.

Novel Magnesium Alloys with Improved Corrosion Resistance

A number of methods are available for the production of novel or nonequilibrium magnesium alloys with substantially improved corrosion resistance. Included in these methods are new rheocasting processes (Ref 41), rapid solidification (RS) processes (Ref 42–45), ion implantation (Ref 46, 47), and vapor deposition (Ref 48–50). These processing methods typically enhance corrosion resistance by producing a more homogeneous microstructure, by increasing the solubility limits of alloying additions, or by some combination of both. One specific result of this is the reduction in the amount of corrosion-inducing second phases and precipitates. Reviews of the corrosion resistance of rapidly solidified magnesium alloys are available (Ref 30, 42). The significant reductions in corrosion rates that are possible as a result of RS processing are illustrated in Fig. 37. The benefits of nonequilibrium, rare earth alloying additions on the corrosion resistance of magnesium are further illustrated in Table 19 and Fig. 38 to 40 (Ref 48, 49).

Rapid Solidification. Quenching from the melt, melt block spinning, and some powder metallurgy techniques, for example, all qualify as nonequilibrium RS techniques. These techniques, among others, are aimed at extending the limits of solid solution and/or refining the microstructure, even to the extent of producing an amorphous alloy.

Extension of solid solubility in magnesium by RS has been accomplished with several elements. In one study alone, solubility limits in magnesium are extended for calcium, barium, strontium, aluminum, zinc, germanium, antimony, tellurium, cobalt, nickel, copper, yttrium, palladium, silver, platinum, gold, lanthanum, cerium, neodymium, samarium, europium, gadolinium, and ytterbium (Ref 51). Rapid solidification successfully extends the solid-solubility limits for these elements (as well as others) (Ref 4). For example, the maximum terminal solid-solubility extension of yttrium in magnesium was 9.7 at.%, compared to only 3.5 at.% at equilibrium.

Corrosion properties often benefit from extended solid-solution concentration afforded by RS. Gravimetric and hydrogen evolution methods have determined the effect of ternary neodymium, yttrium, nickel, copper, and silicon additions on the dissolution rate of magnesium-manganese; manganese decreased corrosion rate to values <0.025 mm/yr (<1 mil/yr) for Mg-Mn-Nd, while nickel and copper in Mg-Mn-Ni increased the corrosion rate (Ref 52). Nickel is not unanimously detrimental, however. Magnesium-aluminum-nickel alloys prepared by the rotation cylinder method showed noble corrosion potentials (–1.3 V_{SCE}) and low corrosion currents (30 μA/cm^2) (Ref 53).

A thorough review of the thermodynamic, kinetic, and microstructural bases of magnesium corrosion is presented in Ref 54. It was found that, in general, less-ordered surface films show better performance (especially in terms of localized corrosion) due to "better inherent breakdown resistance, higher ductility, and faster repassivation rates." In amorphous alloys, additionally, there are no grain boundaries to act as diffusion pathways to allow the ingress of oxygen or adverse solution species. In a separate publication (Ref 55), the authors specifically studied RS binary magnesium alloys of aluminum, zinc, lithium, calcium, and silicon. Electrochemical impedance spectroscopy was used to measure uniform corrosion rates in borate buffer, and anodic polarization showed that rapidly solidified AZ61 was better than the cast material. Aluminum was the only alloying addition found to decrease corrosion rate. Consistently, the structure and morphology of the corrosion products formed on the surfaces of splat-quenched Mg-16Al were found to be the key to decreasing corrosion rate (Ref 56). In contradiction, however, zinc has been found by other researchers to decrease corrosion current (Ref 57). Several publications have reported the benefits of various alloying elements, besides aluminum. A corrosion rate of 0.28 mm/yr (11 mils/yr) was observed for the yttrium-containing alloy $Mg_{91}Zn_2Al_5Y_2$, for example (Ref 58).

Laser cladding and powder metallurgy are two nonconventional RS techniques. Laser cladding involves a high-heat flux into a small area, resulting in very fast heating and cooling rates. In the case of Mg-2Zr and Mg-5Zr laser clad onto magnesium, anodic passive currents were 0.40 and 0.25 A/cm^2 (2.6 and 1.6 A/in.^{2}) versus 1.32 A/cm^2 (8.5 A/in.^{2}) for AZ91B (Ref 59). Laser cladding of zirconium also results in a more noble corrosion potential. Powder metallurgy alloys undergo RS during atomization of the source material to form metal powder. The powders are subsequently extruded, compacted, and sintered to form functional materials, often near the net shape of the final product being manufactured. There has been much development of magnesium, aluminum, and titanium alloys by RS powder metallurgy. Rapid solidification of magnesium-base powders yielded a corrosion rate of 0.25 mm/yr (10 mils/yr) in the case of Mg-Al-Zn-(Ce, Pr, Nd, or Y), with the surface film being enriched in the rare earth

Table 19 The benefits of rapid solidification (RS) and rare earth additions on corrosion rates of magnesium-aluminum alloys

	Corrosion rate	
Material	mm/yr	mils/yr
RS-MgAlZnSiMn	0.38	15
RS-MgZnAlY	0.2	8
RS-MgZnAlNd	0.28	11
AZ91HP-T6	2.1	82

Source: Ref 30

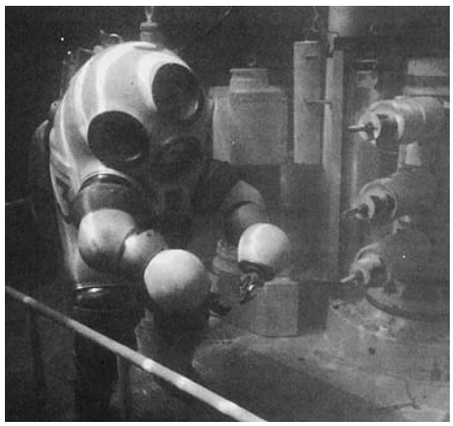

Fig. 36 Magnesium-bodied atmospheric deep-sea diving suit

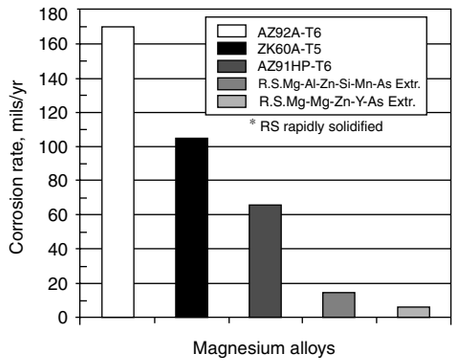

Fig. 37 Corrosion rates (1 mil/yr ≈ 25 μm/year) of rapidly solidified magnesium alloys tested in 3% NaCl at 21 °C (70 °F) compared with some commercial cast alloys. Extr, extruded. Source: Ref 30

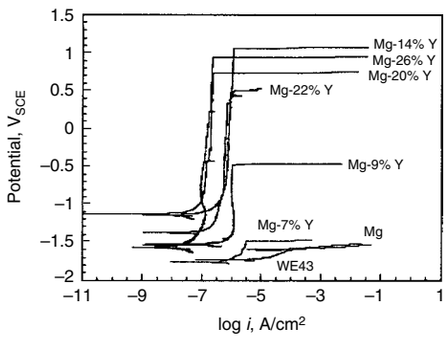

Fig. 38 Anodic potentiodynamic polarization behavior of the magnesium-yttrium alloys compared to alloy WE43 and pure magnesium generated in 0.1 *M* NaCl (initially adjusted to pH 12) at a scan rate of 0.05 mV/s

content (Ref 60). Extruded sections such as these also exhibited 15 to 40% higher compressive yield strength. Rapidly solidified powder metallurgy alloys $Mg_{91}Zn_2Al_5Y_2$ and $Mg_{92}Zn_2Al_5Nd_1$ have low corrosion rates of 0.2 and 0.28 mm/yr (8 and 11 mils/yr), respectively (Ref 61).

Microstructure can be refined to the extent of producing amorphous alloys, with appropriate compositions and cooling rates. Melt-spun amorphous $Mg_{65}Y_{10}Cu_{25}$ metallic glass was studied by x-ray diffraction (XRD), scanning electron microscopy (SEM), Auger electron spectroscopy (AES), x-ray photoelectron spectroscopy (XPS), atomic force microscopy (AFM), and differential scanning calorimetry (DSC) (Ref 62). The amorphous alloy showed better corrosion resistance than the crystalline, with a passive current of 50 $\mu A/cm^2$ and a breakdown potential of 1 V_{SCE}. The corresponding crystalline material exhibited a passive current density of 300 $\mu A/cm^2$, with a breakdown potential several hundred millivolts less noble.

Vapor deposition has allowed for the study of magnesium alloys that are unobtainable by conventional techniques. The corrosion rate of vapor-deposited magnesium-titanium alloys decreases for greater than 22 wt% Ti (Ref 63).

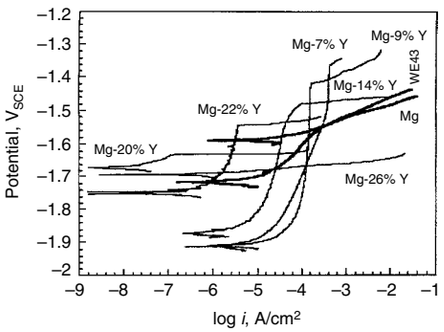

Fig. 39 Anodic potentiodynamic polarization behavior of the magnesium-yttrium alloys compared to alloy WE43 and pure magnesium. Tests were conducted in 0.1 *M* NaCl (initially adjusted to pH 8) at a scan rate of 0.2 mV/s.

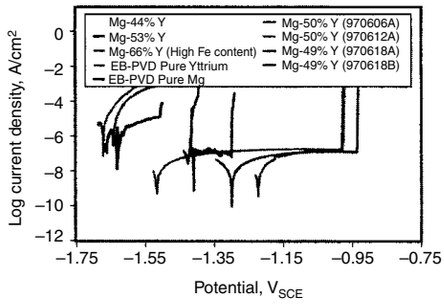

Fig. 40 Anodic polarization behavior of the second group of electron beam/physical vapor deposition (EB-PVD) magnesium-yttrium alloys in pH 12 buffered solution containing 0.1 *M* NaCl

Increasing the titanium content understandably makes the open-circuit potential more noble, discouraging galvanic corrosion. The corrosion resistance of magnesium-chromium, magnesium-manganese, and magnesium-titanium alloys also was assessed using total immersion tests (Ref 64). Manganese and titanium lowered the corrosion rate, while chromium raised it. The lowest corrosion rate was recorded for the magnesium-titanium alloy (0.3 milligrams per square decimeter per day, or mdd).

Other studies have taken advantage of the tremendous solid-solution solubility obtainable with vapor phase processing, particularly for such insoluble elements as zirconium. Vapor deposition of magnesium alloys with up to 10 wt% Zr resulted in columnar grains with porosity at the grain boundaries (Ref 65). Corrosion rates as low as 2.4 mdd were measured despite the high porosity. X-ray photoelectron spectroscopy suggests the formation of a zirconium oxide/hydroxide layer. These as well as other binary alloys are difficult to form when the melting temperature of the alloying element is higher than the boiling point of magnesium.

Numerous studies have recognized the benefit of vapor depositing magnesium with yttrium. In some studies, the breakdown potentials for magnesium-yttrium alloys were 2 V higher than for WE43 (Ref 66). These significant improvements were achieved in the anodic polarization behavior of magnesium by nonequilibrium alloying with 9 to 22 at.% Y (Ref 67). Many of these alloys were fabricated using the nonequilibrium technique of magnetron cosputter deposition. Lower passive current densities were commonly observed (Ref 68, 69).

Aluminum is a common and lightweight metal that exhibits good corrosion resistance in near-neutral solutions. In light of these features, aluminum is a very attractive potential alloying element for magnesium. Because of this, aluminum-magnesium alloys have been investigated vigorously. Thin-film analogs of aluminum precipitates made by flash evaporation have been analyzed by SEM, AFM, and AES (Ref 70). The $Mg(Zn, Cu, Al)_2$ intermetallics were active at the open-circuit potential (OCP) of 7*xxx* aluminum during OCP playback experiments. In an OCP playback experiment, the OCP is measured versus time, and, in a separate experiment, another material (such as an intermetallic that would be present) is polarized to the time-varying OCP of the parent material. Numerous aluminum-magnesium coatings have been prepared by unbalanced magnetron sputtering in order to enhance bombardment of the alloy (Ref 71). Higher substrate bias voltage (greater than −80 V) resulted in argon implantation (up to 20 at.%) and increased resputtering of magnesium. Aluminum-magnesium films formed on glass and quartz substrates by magnetron sputtering using an Al-5Mg casting alloy as a sputtering target were crystalline, with pronounced ⟨111⟩ texture of aluminum, and with breakdown potentials of the sputtered coatings being superior with respect to the cast alloy (Ref 72).

Corrosion of Bulk Vapor-Deposited Alloys

Although uncommon, physical vapor deposition (PVD) techniques have been used to produce bulk alloys. A magnesium-zirconium and an aluminum alloy are shown in Fig. 41 (Ref 73). Royal Aerospace Establishment alloy 72 is a vapor-deposited alloy that has been used on aerospace vehicles.

The PVD magnesium-vanadium alloys exhibit improved corrosion properties (Ref 75). Corrosion rates as low as 30 mdd were observed, with a strong basal texture and grain refinement of the alloy provided by the vanadium. Magnesium-vanadium solid-solution solubility limit was extended to 27 wt% V, beyond which corrosion rates increased due to the precipitation of vanadium (Ref 76). The increase in corrosion rate from the precipitation of pure vanadium dramatically increases the rate of corrosion product formation, consisting of hydromagnesite, $Mg(OH)_2$, MgH_2, MgO, and V_2O_4 (Ref 77). Other studies find no evidence of vanadium oxide in the surface film (Ref 75).

The PVD alloying behavior of magnesium with vanadium as well as zirconium has been considered. Greater stability of the zirconium oxide in air and zirconium hydroxide in chloride solution were the main reasons for the decreased corrosion of magnesium-zirconium alloys compared to magnesium-vanadium alloys (Ref 78).

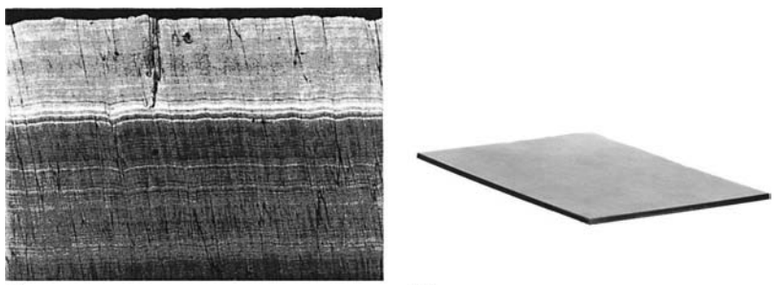

Fig. 41 Bulk physical vapor-deposited alloys. (a) As-deposited magnesium-zirconium. Source: Ref 74. (b) Extruded aluminum Royal Aerospace Establishment (RAE) alloy 72. The RAE alloy 72 is 3.2 mm (1/8 in.) thick.

A corrosion evaluation of 25 mm (1 in.) thick magnesium electron beam/PVD alloys containing titanium, vanadium, and zirconium has been conducted (Ref 79). Vapor deposition of zirconium with magnesium is uncannily beneficial to corrosion performance, suggesting a synergistic effect. As in all magnesium vapor-deposition processes, distillation of magnesium purifies the vapor. Corrosion rates with 8.6 wt% Zr were only 0.2 mdd. Another publication reports that PVD magnesium-zirconium alloys exhibit some of the lowest corrosion rates ever reported for magnesium alloys (Ref 80, 81). Corrosion rates from weight-loss data were 0.21 mdd for 2.44 at.% Zr (8.6 wt%) versus 21 mdd for WE43. The PVD magnesium-zirconium alloys up to 3.07 at.% Zr resulted in zirconium oxide coexisting with magnesium oxide/hydroxide in the surface film, with zirconium providing grain refinement by forming stable compounds with aluminum and manganese (e.g., Al_3Zr) (Ref 78).

Magnesium-titanium alloys produced in bulk form have shown thermal stability up to 500 °C (930 °F) by DSC. Optimal titanium concentration is approximately 22 wt%. Disruption of diffusion paths is important, especially because unchecked condensation can lead to the formation of large intercolumnar void networks (Ref 73). Disruption of void network growth can be accomplished by mechanically working in situ.

Metal-Matrix Composites

Low density, high elastic modulus, and increased thermal stability are some of the attractive attributes of magnesium metal-matrix composites. Consequently, magnesium composites containing boron, SiC, and graphite are of increasing interest, particularly in the aerospace industry (Ref 82). The literature on the corrosion of magnesium-base composites is sparse, however. Because of galvanic issues between magnesium and some reinforcements, such as graphite, special care needs to be exercised in the design and manufacturing of magnesium-base composites (Ref 8). Vapor-deposited, corrosion-resistant magnesium-yttrium metal-matrix composites hold promise for the future (Ref 83). Because much of the bulk volume is taken up by the composite solute, only small amounts of vapor-deposited material may be needed. This feature significantly reduces the amount of material that needs to be vapor deposited. Using vapor-deposited magnesium in a similar manner could make a bulk magnesium component more viable, because the vapor-deposited material comprises only a portion of the total volume.

ACKNOWLEDGMENTS

Much information in this article was adapted from the article Corrosion of Magnesium and Magnesium Alloys, *Corrosion,* Volume 13, *ASM Handbook,* 1987, by Allan Froats, Terje Kr. Aune, David Hawke, William Unsworth, and James Hillis. Parts were adapted from David L. Hawke, James E. Hillis, Mihiriban Pekguleryuz, and Isao Nakatsugawa, Corrosion Behavior, *ASM Specialty Handbook: Magnesium and Magnesium Alloys,* ASM International, 1999, p 194–210.

REFERENCES

1. G.L. Song and A. Atrens, *Adv. Eng. Mater.,* Vol 1 (No.1), 1999, p 11–33
2. J.D. Hanawalt, C.E. Nelson, and J.A. Peloubet, *Trans. AIME,* Vol 147, 1942, p 273–299
3. G.G. Perrault, *Electroanal. Chem. Interfac. Electrochem.,* Vol 51, 1974, p 107–119
4. F.H. Froes, Y. Kim, and S. Krishnamurthy, *Mater. Sci. Eng.,* Vol 117, 1989, p 19–32
5. J.H. Nordlien, S. Ono, and N. Masuko, *J. Electrochem. Soc.,* Vol 142 (No. 10), 1995, p 3320–3322
6. J.H. Nordlien, K. Nisancioglu, S. Ono, and N. Masuko, *J. Electrochem. Soc.,* Vol 143 (No. 8), 1996, p 2564–2572
7. J.H. Nordlien, K. Nisancioglu, S. Ono, and N. Masuko, *J. Electrochem. Soc.,* Vol 144 (No. 2), 1997, p 461–466
8. W.M. Chan, F.T. Cheng, et al., *Corros. Rev.,* Vol 16 (No. 1–2), 1998, p 43–52
9. M.R. Bothwell, in *The Corrosion of Light Metals,* John Wiley & Sons, 1967, p 84
10. R. Udhayan, N. Muniyandi, and P.B. Mathur, *Br. Corros. J.,* Vol 137, 1990, p 414
11. D.L. Hawke, Paper 860285, Society of Automotive Engineers, 1986
12. "Standard Method for Salt Spray (Fog) Testing," B 117, *Annual Book of ASTM Standards,* American Society for Testing and Materials
13. B. Mazurkiewicz, *Corros. Sci.,* Vol 23, 1983, p 687
14. G.L. Maker and J. Kruger, *J. Electrochem. Soc.,* Vol 137, 1990, p 414
15. W.J. James, M.E. Straumanis, B.K. Bhota, and J.W. Johnson, *J. Electrochem. Soc.,* Vol 110, 1963, p 1117
16. D.L. Hawke, J.E. Hillis, M. Repguleryuz, and I. Nakatsugawa, Corrosion Behavior, *ASM Specialty Handbook: Magnesium and Magnesium Alloys,* ASM International, 1999, p 194–210
17. J.E. Hillis and K.N. Reichek, Paper 860288, Society of Automotive Engineers, 1986
18. AMAX Magnesium, unpublished research
19. O. Lunder et al., *Corrosion,* Vol 45, 1989, p 741
20. V. Mitrovic-Scrpanovic and R.J. Brigham, *Corrosion,* Vol 48, 1992, p 780
21. H.P. Godard, W.P. Jepson, M.R. Bothwell, and R.L. Kane, Ed., *The Corrosion of Light Metals,* John Wiley & Sons, 1967
22. M.R. Bothwell, *The Corrosion of Light Metals,* John Wiley & Sons, 1967, p 291
23. J.A. Beavers, G.H. Koch, and W.E. Berry, "Corrosion of Metals in Marine Environments," Metals and Ceramics Information Center, Battelle Columbus Laboratories, July 1986
24. R.S. Busk, *Magnesium Products Design,* Marcel Dekker, 1987
25. W. Miller, *Mater. Res. Symp. Proc.,* Vol 125, 1988, p 253
26. H.I. Logan, What We Don't Know about Stress Corrosion Cracking. *The Coupling of Basic and Applied Corrosion Research—A Dialogue,* National Association of Corrosion Engineers, 1969, p 57–62
27. W.K. Miller, Internal General Motors Research Report MR 766, Nov 1982
28. M.O. Speidel, M.J. Blackburn, T.R. Beck, and J.A. Feeney, *Proc. Corrosion Fatigue: Chem. Mech. Microstructure,* Storrs, CT, 1971, p 324–325
29. M.O. Speidel, M.J. Blackburn, T.R. Beck, and J.A. Feeney, *Corrosion Fatigue: Chemistry, Mechanics and Microstructure,* O. Devereux et al., Ed., National Association of Corrosion Engineers, 1986, p 331
30. E. Ghali, Magnesium and Magnesium Alloys, *Uhlig's Corrosion Handbook,* R.W. Revie, Ed., John Wiley & Sons, Inc., 2000, p 823–824
31. D.L. Hawke, J.E. Hillis, and W. Unsworth, "Preventive Practice for Controlling the Galvanic Corrosion of Magnesium Alloys," Technical Committee, International Magnesium Association, 1988
32. M.R. Bothwell, *J. Electrochem. Soc.,* Vol 106, 1959, p 1021
33. F.L. LaQue, Corrosion Testing, *Proc. Am. Soc. Test. Mater.,* Vol 51, 1951, p 557
34. D.L. Hawke, Paper G-T87-004, SDCE 14th International Die-Casting Congress and Exposition (Toronto), May 1987
35. D.L. Hawke and T. Ruden, Paper 950429, Society of Automotive Engineers, 1995
36. G. Craig, in *Proceedings of the IMA Annual World Magnesium Conference,* International Magnesium Association, 1998
37. P. Schmutz, V. Guillaumin, et al., *J. Electrochem. Soc.,* Vol 150 (No. 4), 2003, p B99–B110
38. Q. Meng, T. Ramgopal, and G.S. Frankel, *Electrochem. Solid-State Lett.,* Vol 5 (No. 2), 2002, p B1–B4
39. F. Kaumle, N.C. Toemmeraas, and J.A. Bolstad, Paper 850420, Society of Automotive Engineers, 1985
40. P.A. Wickberg and R. Ericsson, Society of Automotive Engineers, 1985
41. P. Schmutz, S. Virtanen, L. Kocher, P.J. Uggowitzer, Corrosion Behavior of Novel Mg-Al Alloys Produced by Means of the New Rheocasting (NRC) Process, *Electrochem. Soc. Proc.,* Vol 2000-23, 2000
42. G.L. Makar and J. Kruger, Corrosion of Mg, *Int. Mater. Rev.,* Vol 38 (No. 3), 1993, p 138

43. G.L. Maker, "Effect of Alloying Elements on the Corrosion Resistance of Rapidly Solidified Mg Alloys," M.S. Thesis, The Johns Hopkins University, Baltimore, MD, 1988
44. P.L. Hagans, Science and Technology of Rapidly Quenched Alloys, M. Tenhover et al., Ed., *Mater. Res. Soc. Symp. Proc.,* Vol 80, 1987, p 113–120
45. C.F. Chang, S.K. Das, D. Raybould, and A. Brown, *Met. Powder Rep.,* Vol 41 (No. 4), 1986, p 302–308
46. S. Akavipat, C.E. Habermann, P.L. Hagans, and E.B. Hale, *Fundamental Aspects of Corrosion Protection by Surface Modification,* E. McCafferty et al., Ed., Electrochemical Society, 1984, p 52–61
47. P.L. Hagans, *41st World Magnesium Conf.* (Dayton, OH), International Magnesium Assoc., 1984, p 30–38
48. P.L. Miller, B.A. Shaw, R.G. Wendt, and W.C. Moshier, Assessing the Corrosion Resistance of Nonequilibrium Magnesium-Yttrium Alloys, *Corrosion,* Vol 52 (No. 12), 1995, p 922
49. K.L. Heidersbach, "An Evaluation of the Corrosion Performance of Mg-Y and Y-Mg Nonequilbrium," Ph.D. Thesis, The Pennsylvania State University, 1998
50. S.B. Dodd, S. Morris, R.W. Gardiner, R.M.D Brydson, S. Diplas, and P. Tsakiropoulos, Preliminary Corrosion Evaluation of Some Novel Bulk Electron Beam Evaporated Magnesium Alloys, *Corros. Rev.,* Vol 16 (No. 1–2), 1998, p 159–174
51. F. Hehmann, F. Sommer, and B. Predel, *Mater. Sci. Eng.,* Vol A125, 1990, p 249–265
52. D. Rugg, R.G.J. Edyvean, and H. Jones, *Mater. Sci. Technol.,* Vol 9 (No. 11), 1993, p 994–999
53. J.G. Kim, Y.S. Choi, et al., *Corrosion,* Vol 59 (No. 3), 2003, p 228–237
54. G.L. Makar, and J. Kruger, *Int. Mater. Rev.,* Vol 38 (No. 3), 1993, p 138–153
55. G.L. Makar, and J. Kruger, *J. Electrochem. Soc.,* Vol 137 (No. 2), 1990, p 414–421
56. C.B. Baliga and P. Tsakiropoulos, *Mater. Sci. Technol.,* Vol 9 (No. 6), 1993, p 513–519
57. D. Daloz, P. Steinmetz, and G. Michot, *Corrosion,* Vol 53 (No. 12), 1997, p 944–954
58. F.H. Froes, *MPR,* 1986, p 302–308
59. R. Subramanian, S. Sircar, and J. Maxumder, *J. Mater. Sci.,* Vol 26, 1991, p 951–956
60. C. Suryanarayana, S.F.H. Froes, S. Krishnamurthy, and Y. Kim, *Int. J. Powder Metall.,* Vol 26 (No. 2), 1990, p 117–129
61. C.F. Chang, S. K. Das, et al., *Light Met. Age,* 1989, p 12–20
62. U. Wolff, A. Gebert, et al., in *Ris½ International Symposium on Materials Science,* Ris½ National Laboratory, Roskilde, Denmark, 2001
63. K.R. Baldwin, S.B. Dodd, and R.W. Gardiner, in *Third International Magnesium Conference,* The Institute of Materials, 1997
64. K.R. Baldwin, D.J. Bray, G.D. Howard, and R.W. Gardiner, *Mater. Sci. Technol.,* Vol 12 (No. 11), 1996, p 937–943
65. S. Diplas, P. Tsakiropoulos, et al., in *Magnesium Alloys and Their Applications,* Werkstoff-Informationsgesellschaft mbH, Wolfsburg, Germany, 1998
66. P.L. Miller, B.A. Shaw, R.G. Wendt, and W.C. Moshier, *Corrosion,* Vol 51 (No. 12), 1995, p 922–931
67. P.L. Miller, B.A. Shaw, R.G. Wendt, and W.C. Moshier, *Corrosion,* Vol 49 (No. 12), 1993, p 947–950
68. P.L. Miller, Corrosion Characteristics of Nonequilibrium Magnesium-Yttrium Alloys, *Engineering Science,* The Pennsylvania State University, 1994, p 102
69. K.L. Heidersbach and B.A. Shaw, in *Symposium on Passivity and Its Breakdown,* The Electrochemical Society, 1997
70. T. Ramgopal, P. Schmutz, and G.S. Frankel, *J. Electrochem. Soc.,* Vol 148 (No. 9), 2001, p B348–B356
71. B.A. Shedden, M. Samandi, and B. Window, *Surf. Coat. Technol.,* Vol 97 (No. 1–3), 1997, p 557–563
72. V. Uksiene, K. Leinartas, et al., *Electrochem. Commun.,* Vol 4 (No. 10), 2002, p 747–752
73. S.B. Dodd and R.W. Gardiner, in *Third International Magnesium Conference,* The Institute of Materials, 1997
74. J.R. Wood, *JOM,* Vol 54 (No. 2), 2002, p 56–58
75. S. Diplas, P. Tsakiropoulos, and R.M.D. Brydson, *Mater. Sci. Technol.,* Vol 14 (No. 7), 1998, p 689–698
76. S. Diplas, P. Tsakiropoulos, et al., in *Third International Magnesium Conference,* The Institute of Materials, 1997
77. D.P. Tsakiropoulos, R.M.D. Brydson, and J.F. Watts, *Mater. Sci. Technol.,* Vol 14 (No. 7), 1998, p 699–711
78. S. Diplas, P. Tsakiropoulos, and R.M.D. Brydson, *Mater. Sci. Technol.,* Vol 15 (No. 12), 1999, p 1349–1357, 1373–1378
79. S.B. Dodd, S. Morris, et al., *Corros. Rev.,* Vol 16 (No. 1–2), 1998, p 159–174
80. S. Diplas, P. Tsakiropoulos, R.M.D. Brydson, and J.F. Watts, *Mater. Sci. Technol.,* Vol 15 (No. 12), 1999, p 1359–1372
81. S.B. Dodd, S. Morris, and R.W. Gardiner, in *Magnesium Alloys and Their Applications,* Werkstoff-Informationsgesellschaft mbH, Wolfsburg, Germany, 1998
82. S. Rawal, *JOM,* Vol 53 (No. 4), 2001, p 14–17
83. R.G. Wendt, W.C. Moshier, et al., *Corrosion,* Vol 50 (No. 11), 1994, p 819–826

SELECTED REFERENCES

- E.F. Emley, *Principles of Magnesium Technology,* Pergamon Press, 1966
- J.D. Hanawalt, C.E. Nelson, and J.A. Peloubet, Corrosion Studies of Magnesium and Its Alloys, *Trans. AIME,* Vol 147, 1942
- I. Lunder, T.K. Aune, and K. Nisancioglu, Paper 382, Corrosion/85, National Association of Corrosion Engineers, 1985
- R.B. Mears and C.D. Brown, *Corrosion,* Vol 1, 1945
- K.N. Reicheck, K.J. Clark, and J.E. Hillis, Paper 850417, Society of Automotive Engineers, 1985
- C. Suman, Paper 900794, Society of Automotive Engineers, 1990

ASM Handbook, Volume 13B: Corrosion: Materials
S.D. Cramer, B.S. Covino, Jr., editors, p228-251
DOI: 10.1361/asmhba0003821

Corrosion of Nickel and Nickel-Base Alloys

Paul Crook, Haynes International, Inc.

NICKEL ALLOYS are very important to industries that have to deal with aggressive chemicals and high-temperature conditions. Most nickel alloys are much more resistant than the stainless steels to reducing acids, such as hydrochloric, and some are extremely resistant to the chloride-induced phenomena of pitting, crevice attack, and stress-corrosion cracking (to which the stainless steels are susceptible). Nickel alloys are also among the few metallic materials able to cope with hot hydrofluoric acid.

Introduction to Alloys Resistant to Aqueous Corrosion

Paul Crook and Dwaine Klarstrom, Haynes International, Inc.
Jim Crum, Special Metals Corp.

The nickel alloys designed to resist aqueous corrosion can be categorized according to their major alloying elements. In addition to commercially pure nickel, which possesses high resistance to caustic soda and caustic potash, there are six important nickel alloy families: Ni-Cu, Ni-Mo, Ni-Cr, Ni-Cr-Mo, Ni-Cr-Fe, and Ni-Fe-Cr. Some of these families are strongly associated with certain trademarks. The nickel-copper materials, which are commonly used in seawater applications and in hydrofluoric acid, for example, are known as the Monel alloys. Likewise, the nickel-molybdenum materials are known as the Hastelloy B-type alloys, and the versatile Ni-Cr-Mo materials are known as the Hastelloy C-type alloys. The Inconel trademark is used for several Ni-Cr and Ni-Cr-Fe alloys, and the Incoloy name is associated with Ni-Fe-Cr materials. While these trademarks are still used by the companies that own them, many of the nickel alloys are now generic and available from multiple sources.

Many of the current wrought alloys are descended from casting materials developed during the early part of the 20th century. Some of these early casting materials are still in general use for pump and valve components and other intricate parts.

A listing of popular wrought and cast nickel alloys resistant to aqueous corrosion is provided in Table 1. The basic structure of these alloys, like that of nickel itself, is face-centered cubic (fcc). However, most are alloyed beyond the solubility limits to maximize corrosion resistance and require an annealing treatment (usually followed by water quenching) to minimize deleterious second phases. Such second phases can occur during reheating, as in weld heat-affected zones (HAZs), typically as grain-boundary precipitates. Modern wrought alloys, with their very low carbon and silicon contents, are quite stable and can be used in the as-welded condition with only a low risk of intergranular attack. Older cast alloys with higher carbon and silicon contents, however, are more prone to grain-boundary precipitation during welding and generally require postweld annealing.

The roles of the various elements in the nickel alloys are discussed for each alloy category, but a synopsis for the key elements follows:

- *Nickel:* This element is an ideal base because it not only possesses moderate corrosion resistance by itself, but it also can be alloyed with significant quantities of copper, molybdenum, chromium, iron, and tungsten, while retaining its ductile fcc structure. Some inherent properties imparted by nickel to its alloys are resistance to stress-corrosion cracking, resistance to caustic compounds, and resistance to hydrofluoric acid.
- *Copper:* The addition of copper to nickel enhances its resistance to reducing-acid media, in particular, hydrofluoric acid. Copper, even at levels as low as 1.5 to 2 wt%, is also very beneficial in sulfuric acid.
- *Chromium:* The role of chromium in the nickel alloys is the same as that in the stainless steels, that is, to participate in the formation of passive films. These films provide protection in a wide range of oxygen-bearing environments. A secondary role of chromium is to provide some strengthening of the solid solution.
- *Molybdenum:* The addition of molybdenum to nickel greatly enhances its nobility under active corrosion conditions. In particular, it provides high resistance to reducing chemicals, such as hydrochloric acid. In combination with chromium, it produces alloys that are extremely versatile (resistant to both oxidizing and reducing chemicals) and that can withstand chloride-induced pitting and crevice corrosion. Molybdenum also greatly increases the strength of the nickel-rich solid solution, by virtue of its large atomic size.
- *Tungsten:* This element behaves in the same way as molybdenum and is often used in combination with molybdenum. It is an even more effective solid-solution strengthener.
- *Iron:* The chief purpose of adding iron to the nickel alloys is to reduce their cost. However, it does provide benefits in concentrated sulfuric acid and in nitric acid, probably by contributing to the formation of passive films.

Commercially Pure Nickel

Commercially pure wrought nickel has good corrosion resistance and mechanical properties. A combination of good ductility and malleability, low hardness, a low work-hardening rate, and good weldability make the metal highly fabricable. Good low-temperature ductility and impact strength make it a useful material at cryogenic temperatures. Nickel is also noted for very good resistance to aqueous corrosion in certain environments. The most common product is nickel 200 (N02200). It contains 99.6% Ni with small amounts of iron, copper, manganese, silicon, and carbon. It has found a wide variety of applications involving caustic soda, water, nonoxidizing acids, alkaline salt solutions, chlorine, hydrogen chloride, fluorine, and

Table 1 Nominal compositions of nickel alloys resistant to aqueous corrosion

Family	Common name	UNS No.	Form	Composition, wt%											
				Ni	Cu	Mo	Cr	Fe	W	Mn	Si	C	Al	Ti	Other
Ni	200	N02200	Wrought	99.5	0.1	...	...	0.2	...	0.2	0.2	0.08	...	...	...
	201	N02201	Wrought	99.5	0.1	...	...	0.2	...	0.2	0.2	0.01	...	...	...
	301	N03301	Wrought (age hardenable)	96.5	0.1	...	...	0.3	...	0.2	0.5	0.2	4.4	0.6	...
Ni-Cu	400	N04400	Wrought	66.5	31.5	...	...	1.2	...	1	0.2	0.2	...	...	...
	K-500	N05500	Wrought (age hardenable)	66.5	29.5	...	...	1	...	0.8	0.2	0.1	2.7	0.6	...
	M-35-1	N24135	Cast	bal	29.5	...	...	3.5(a)	...	1.5(a)	1.25(a)	0.35(a)	...	...	Nb 0.5(a)
Ni-Mo	B	N10001	Wrought	bal	...	29.5	1.00(a)	6.00(a)	...	1.00	1.00	0.12(a)	...	...	Co 2.5(a)
	B-2	N10665	Wrought	69	0.5(a)	28	1(a)	2(a)	0.5(a)	1(a)	0.1(a)	0.01(a)	...	...	...
	B-3	N10675	Wrought	65(b)	0.2(a)	28.5	1.5	1.5	3(a)	3(a)	0.1(a)	0.01(a)	0.5(a)	...	...
	N-7M	N30007	Cast	bal	...	31.5	1(a)	3(a)	...	1(a)	1(a)	0.07(a)	...	...	...
Ni-Cr	600	N06600	Wrought	76	0.2	...	15.5	8	...	0.5	0.2	0.08	...	...	...
	625	N06625	Wrought	61	...	9	21.5	2.5	...	0.2	0.2	0.05	0.2	0.2	Nb + Ta 3.6
	690	N06690	Wrought	58(b)	0.5(a)	...	29	9	...	0.5(a)	0.5(a)	0.05(a)	...	...	...
	725	N07725	Wrought (age hardenable)	57	...	8	21	7.5	...	0.35(a)	0.2(a)	0.03(a)	0.35(a)	1.5	Nb 3.5
	FM 72	N06072	Filler Metal	bal	0.5(a)	...	44	0.5(a)	...	0.2(a)	0.2(a)	0.1(a)	...	0.7	...
	G-35	N06035	Wrought	58	0.3(a)	8.1	33.2	2(a)	0.6(a)	0.5(a)	0.6(a)	0.05(a)	0.4(a)	...	...
	Allcorr	N06110	Wrought	bal	...	10	31	...	2	...	...	0.02	0.25	0.25	Nb 0.4
Ni-Cr-Mo	C-4	N06455	Wrought	65	0.5(a)	16	16	3(a)	...	1(a)	0.08(a)	0.01(a)	...	0.7(a)	...
	C-22	N06022	Wrought	56	0.5(a)	13	22	3	3	0.5(a)	0.08(a)	0.01(a)	...	...	V 0.35(a)
	C-22HS	...	Wrought (age-hardenable)	61	0.5(a)	17	21	2(a)	1(a)	0.8(a)	0.08(a)	0.01(a)	0.5(a)	...	...
	C-276	N10276	Wrought	57	0.5(a)	16	16	5	4	1(a)	0.08(a)	0.01(a)	...	...	V 0.35(a)
	C-2000	N06200	Wrought	59	1.6	16	23	3(a)	...	0.5(a)	0.08(a)	0.01(a)	0.5(a)	...	...
	59	N06059	Wrought	bal	...	16	23	1.5(a)	...	0.5(a)	0.1(a)	0.01(a)	0.25	...	...
	686	N06686	Wrought	bal	...	16	21	5(a)	3.7	0.75(a)	0.08(a)	0.01(a)	...	0.15	...
	CW-2M	N26455	Cast	bal	...	16.25	16.25	2(a)	1(a)	1(a)	0.8(a)	0.02(a)	...	...	...
	CW-6M	N30107	Cast	bal	...	18.5	18.5	3(a)	...	1(a)	1(a)	0.07(a)	...	...	...
	CW-12MW	N30002	Cast	bal	...	17	16.5	6	4.5	1(a)	1(a)	0.12(a)	...	...	V 0.3
Ni-Cr-Fe	G-3	N06985	Wrought	44	2	7	22	19.5	1.5(a)	1(a)	1(a)	0.015(a)	...	...	Nb 0.5(a) Co 5(a)
	G-30	N06030	Wrought	43	2	5.5	30	15	2.5	1.5(a)	0.8(a)	0.03(a)	...	...	Nb 0.8 Co 5(a)
	G–50	N06950	Wrought	50(b)	0.5(a)	9	20	17	1(a)	1(a)	1(a)	0.015(a)	0.4(a)	...	Co 2.5(a), Nb 0.5(a)
	718	N07718	Wrought (age hardenable)	52.5	0.2	3	19	18.5	...	0.2	0.2	0.04	0.5	0.9	Nb + Ta 5.1
Ni-Fe-Cr	825	N08825	Wrought	42	2.2	3	21.5	30	...	0.5	0.2	0.03	0.1	0.9	...

(a) Maximum. (b) Minimum

molten salts. Nickel has relatively high electrical and thermal conductivity as well as a high Curie temperature and good magnetostrictive properties. This leads to use in many electrical and electronic applications. Minor variations of residual elements allow use in other specific applications, such as automotive spark plugs.

The low-carbon grade 201 (N02201) is used at elevated temperatures, at or above 315 °C (600 °F), where graphitization can occur in the higher-carbon material. As is the case with nickel-copper and other nickel alloys, commercially pure nickel can be age hardened by the addition of aluminum and titanium to form γ', a fcc compound $Ni_3(Al,Ti)$. Age-hardened nickel 301 (N03301) has high strength in addition to the corrosion resistance and electrical and magnetic properties of pure nickel. This material is often used in extrusion dies for plastics and magnetostrictive units under stress.

Nickel-Copper Alloys

Nickel and copper form a continuous solid solution in all proportions, making a variety of nickel-copper and copper-nickel alloys possible. These alloys are characterized by good strength, good ductility and weldability, and resistance to aqueous corrosion and stress-corrosion cracking in a variety of environments and applications. Nickel-copper alloys also have good electrical and thermal conductivity and have a Curie temperature in the ambient range. Specialized electrical and magnetic properties allow use in critical electrical, electronic, and other applications.

The first commercial and most common nickel-copper alloy in use was alloy 400 (N04400). This alloy was developed in 1905 and is still used in a wide variety of applications, such as seawater, non-oxidizing acids, hydrocarbon processing, water-fed heat exchangers, neutral and alkaline salts and alkali process equipment, industrial plumbing and valves, marine fixtures, petrochemical equipment, and pickling equipment. Small additions of aluminum and titanium to N04400 allow age hardening through the precipitation of fine particles of the fcc compound $Ni_3(Al,Ti)$, known as gamma prime. This age-hardenable material, N05500 (alloy K-500), is used for pump shafts and impellers, valves, oil well drill parts, springs, and fasteners.

Nickel and copper are alloyed with zinc to form nickel silvers, which are ductile and highly formable, have good corrosion resistance, can be worked to achieve a range of mechanical properties, and have an attractive white color. They are used for ornamental purposes and in silver-plated or uncoated tableware, electrical contacts, connections and springs, as well as formed and machined parts.

Nickel-Molybdenum Alloys

Nickel-molybdenum alloys are known for their excellent resistance to nonoxidizing (reducing) media, such as hydrochloric and sulfuric acids. The original B alloy (N10001) was invented in the 1920s, and it had a nominal composition of Ni-28Mo-5Fe-0.3 V, with a maximum carbon content of 0.05 wt% and a maximum silicon content of 1 wt%. The alloy was used successfully for many years, but it suffered an important drawback in that fabricated components required a solution heat treatment in order to avoid corrosion attack in the weld HAZs. Experimental work in 1958 to 1960 indicated that the corrosion resistance of the

alloy could be significantly improved by reducing the carbon, iron, and silicon levels (Ref 1, 2). However, the achievement of very low carbon levels on a production scale did not occur until the invention of the argon-oxygen decarburization melting process (Ref 3). This enabled the commercialization of an improved nickel-molybdenum material, B-2 alloy (N10665), in the early 1970s (Ref 4).

The new alloy lived up to expectations in terms of corrosion resistance, but it soon became apparent that the reductions in the residual alloying elements, especially iron, had adversely impacted its thermal stability. That is, the alloy became very susceptible to the Ni_4Mo transformation when it was exposed to the 650 to 750 °C (1200 to 1380 °F) temperature range. As a result of this embrittling transformation, cracking was encountered during some of the alloy manufacturing operations as well as during customer fabrication of components. In addition, a number of in-service cases of environmental cracking were observed. These were usually associated with weld HAZs.

In order to solve the embrittlement problems of B-2 alloy, without sacrificing its excellent corrosion resistance, a research program was undertaken that led to the development of B-3 alloy (N10675) (Ref 5). By carefully controlling additions of iron, chromium, and manganese, the equilibrium structure of the alloy was redirected toward the Ni_3Mo transformation, which is more sluggish than the Ni_4Mo transformation. This provides more time to effect a heat treatment without the risk of cracking. The new alloy is also more resistant to stress-corrosion cracking (Ref 6).

Additions of molybdenum to nickel impart a pseudopassive behavior to the resulting alloy in nonoxidizing acids, which gives it good resistance to corrosion (Ref 7). However, contamination of the environment with oxidizing ions such as Fe^{3+} or Cu^{2+} destroys this behavior and dramatically increases the corrosion rate (as discussed in the section "Hydrochloric Acid" in this article). Consequently, the nickel-molybdenum alloys should never be used where oxidizing conditions are known to exist.

Nickel-Chromium Alloys

Many materials within this category are useful not only to resist aqueous corrosion but also at high temperatures, where their chromium additions encourage the growth of protective oxide scales. A prime example is alloy 625 (N06625), which is used in many aggressive chemicals and hot, gaseous environments. While it is not quite as resistant to reducing acids as the Ni-Cr-Mo alloys, because of its lower molybdenum content, it is better than stainless steels in this respect. It also exhibits moderately high resistance to chloride-induced phenomena, such as pitting, crevice corrosion, and stress-corrosion cracking.

Alloy 600 (N06600) is used as an alternate to alloy 200 (N02200) in caustic environments, when the latter is not of sufficient strength. Alloy 600 was also used extensively in nuclear steam generators, until superseded by alloy 690 (N06690), which was found to be considerably more resistant to stress-corrosion cracking in pure water, at high temperatures.

Those nickel-chromium materials with very high chromium contents, such as N06072 (filler metal 72 with 44 wt% Cr), N06035 (G-35 alloy with 33.2 wt% Cr), and N06690 (alloy 690 with 29 wt% Cr), possess outstanding resistance to oxidizing aqueous environments, such as nitric acid and nitric-hydrofluoric acid mixtures.

Ni-Cr-Mo Alloys

The Ni-Cr-Mo materials are the most versatile of the nickel alloys designed to resist aqueous corrosion and are consequently the most widely used within the chemical process industries. They exhibit good resistance to both oxidizing and reducing media and possess exceptional resistance to chloride-induced pitting, crevice attack, and stress-corrosion cracking. They are also easily formed and welded into complex components.

The chromium contents of the Ni-Cr-Mo alloys range from approximately 15 to 25 wt%, while their molybdenum contents range from approximately 12 to 17 wt%. The primary function of chromium is to provide passivity in oxidizing acid solutions; this is also its main function in the stainless steels. Molybdenum greatly enhances the resistance of nickel to reducing acids, in particular hydrochloric, and increases the resistance to localized attack (pitting and crevice corrosion), perhaps because these forms of attack involve the local formation of hydrochloric acid. Molybdenum provides considerable strength to the fcc solid solution because of its atomic size.

Optional minor element additions include iron, tungsten, and copper. The primary purpose of including iron is to lessen the cost of furnace charge materials during melting. Interestingly, in the most recently developed Ni-Cr-Mo alloys, iron has been relegated to the role of an impurity, to increase the solubility of other more useful elements. Tungsten is sometimes used as a partial replacement for molybdenum. In fact, a specific tungsten-to-molybdenum ratio was shown to provide increased resistance to localized attack during the development of C-22 alloy (N06022).

Copper, which has so far been added to only one of the Ni-Cr-Mo alloys, is known to enhance resistance to both sulfuric and hydrofluoric acids. The mechanisms are poorly understood, but even at the 1.6 wt% level in C-2000 alloy (N06200), copper plating of samples has been observed in sulfuric acid. The mechanism in hydrofluoric acid may be one of augmentation of the fluoride films that are known to form on nickel alloys in this environment (Ref 8).

To maximize their corrosion resistance, the amounts of chromium, molybdenum, or other element added to the C-type alloys exceed their solubility limits at room temperature. In fact, the alloys are metastable below their solution-annealing temperatures of approximately 1050 to 1150 °C (1920 to 2100 °F). The extent of alloying is actually governed by the kinetics of second-phase precipitation, the design principle being that the alloys should retain their solution-annealed structures when water quenched and should not suffer continuous grain-boundary precipitation of deleterious second phases in weld HAZ.

As to the types of second-phase precipitate normally found in the C-type alloys, Ref 9 describes those observed in C-276 alloy (N10276), as follows:

- At temperatures between 300 and 650 °C (570 and 1200 °F), an ordered phase of the type A_2B, or, in this case, $Ni_2(Cr,Mo)$, occurs by long-range ordering. The precipitation reaction is described as being homogeneous, with no preferential precipitation at the grain boundaries or twin boundaries. The reaction is slow at lower temperatures within this range; it has been established, for example, that it takes in excess of 38,000 h for A_2B to form in C-276 alloy (N10276) at 425 °C (800 °F).
- At temperatures above 650 °C (1200 °F), three precipitate phases can nucleate heterogeneously at grain boundaries and twin boundaries. These are μ phase, M_6C carbide, and *P* phase. The μ phase is described as having a hexagonal crystal structure and an A_7B_6 stoichiometry. M_6C has a diamond cubic crystal structure, and *P* phase has a tetragonal structure. Reference 10 indicates that μ phase precipitates in C-276 alloy within the temperature range 760 to 1093 °C (1400 to 2000 °F), whereas M_6C carbide precipitates at temperatures between 650 and 1038 °C (1200 and 1900 °F). The same reference indicates that the kinetics of carbide formation are faster than those of μ phase.

To reduce the susceptibility of the alloys to the precipitation of M_6C, μ phase, and *P* phase, steps are taken during melting to minimize their carbon and silicon contents, silicon being a known promoter of intermetallic phases, such as μ. As to the effects of these second-phase precipitates on the properties of the C-type alloys, it is well known that the heterogeneous precipitates that occur at temperatures in excess of 650 °C (1200 °F) are detrimental to both corrosion resistance and material ductility. On the other hand, the homogeneous precipitation reaction that occurs at lower temperatures can be used to strengthen the C-type alloys while maintaining good ductility (Ref 11). Indeed, a Ni-Cr-Mo composition (C-22HS alloy) that can be strengthened by this mechanism in a short period of time (48 h) has recently been introduced.

Ni-Cr-Fe Alloys

Nickel-chromium-iron alloys comprise a large number of industrially important materials. Most of these alloys fall within the broad austenitic, γ-phase field of the ternary Ni-Cr-Fe phase diagram, and they are noted for good elevated-temperature strength, good workability, and resistance to corrosion and oxidation. Many of these alloys serve equally well in a wide range of both high-temperature and aqueous corrosion applications. The high nickel content provides metallurgical stability and corrosion resistance in reducing environments, while the chromium addition contributes to strength, oxidation resistance, and aqueous corrosion resistance in oxidizing environments.

Among the Ni-Cr-Fe alloys designed purely for resistance to aqueous corrosion are G-3 (N06985), G-30 (N06030), and G-50 (N06950) alloys. G-3 and G-50 alloys are popular for downhole tubulars in the oil and gas industries, while G-30 alloy was designed specifically for use, in tubular form, in wet process phosphoric acid evaporators in the agrichemical industry.

Ni-Fe-Cr Alloys

These materials bridge the gap between the high-nickel austenitic stainless steels and the Ni-Cr-Fe alloys. Their main advantage over the stainless steels is enhanced resistance to environmental cracking. One of the most commonly used Ni-Fe-Cr materials is alloy 825, which contains 2.2 wt% Cu to improve its resistance to sulfuric acid. This alloy is used in sulfuric acid, phosphoric acid, seawater, and in downhole oilfield environments.

For more about the effects of composition and microstructure on corrosion, see "Effects of Metallurgical Variables on the Corrosion of High-Nickel Alloys" in *ASM Handbook,* Volume 13A, 2003.

Product Forms

The primary differences between the wrought and cast materials are:

- The cast materials are inherently less homogeneous than wrought products, due to elemental segregation during solidification.
- Carbon and silicon contents are generally much higher in air-melted castings than in wrought products; this results in greater susceptibility to second-phase precipitation at alloy grain boundaries (i.e., sensitization).

Despite these limitations, castings are used extensively for intricately shaped components in valves, pumps, flowmeters, and the like. For small components, investment casting is the preferred casting technique. For larger components, sand casting is normal. Given their susceptibility to sensitization, however, it is important that nickel alloy castings are properly annealed and quenched prior to use. The annealing guidelines for these casting alloys are given in ASTM A 494 (Ref 12).

The demand for wrought nickel alloy products far exceeds that for castings. Wrought nickel alloys have been used for large reaction vessels, lengthy pipelines, and extensive flue gas scrubbing systems, for example. Common wrought forms include sheets, plates, bars, wires (for both welding and structural use), tubes, and pipes.- Many of these wrought products are covered by ASTM, American Society of Mechanical Engineers, and Technischen Überwachungs-Vereine specifications. Welding products are generally covered by American Welding Society specifications.

Aqueous Corrosion Properties

Paul Crook and Sabrina Meck, Haynes International, Inc.
Jim Crum, Special Metals Corp.
Raul Rebak, Lawrence Livermore Laboratory

The behavior of nickel alloys to corrosive media found in industrial settings is examined.

Hydrochloric Acid

If any one chemical is responsible for the widespread use of the nickel alloys within the chemical process industries, it is hydrochloric acid. This acid is used extensively in the manufacture of chlorinated compounds and is very aggressive to most stainless steels.

Of the various nickel alloys, those with the highest molybdenum contents possess the greatest resistance to hydrochloric acid. In particular, the nickel-molybdenum alloys are useful over wide ranges of concentration and temperature, provided the dissolved oxygen content of the acid is low and the acid contains no oxidizing impurities. The Ni-Cr-Mo alloys, although not quite as useful as the nickel-molybdenum materials in pure hydrochloric acid, are extremely tolerant of oxidizing impurities. Those nickel-chromium alloys with moderate molybdenum contents also exhibit useful resistance to hydrochloric acid.

Nickel alloys have been tested extensively in pure hydrochloric acid. From the results, isocorrosion diagrams have been created. These indicate the concentration and temperature regimes over which low (under 0.1 mm/yr, or 4 mils/yr), medium (0.1 to 0.5 mm/yr, or 4 to 20 mils/yr), and high (over 0.5 mm/yr, or 20 mils/yr) corrosion rates can be expected. Isocorrosion diagrams for nickel-molybdenum B-3 (N10675) alloy, nickel-chromium alloy 625 (N06625), and Ni-Cr-Mo C-2000 (N06200) alloy are shown in Fig. 1 to 3. These charts cover temperatures up to the boiling points and concentrations up to 20 wt%, the highest that is stable when boiling. To provide some perspective, the 0.1 mm/yr (4 mils/yr) lines for three stainless steels in hydrochloric acid are plotted in

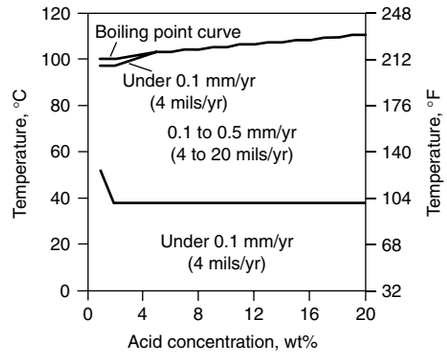

Fig. 1 Isocorrosion diagram for B-3 alloy in hydrochloric acid

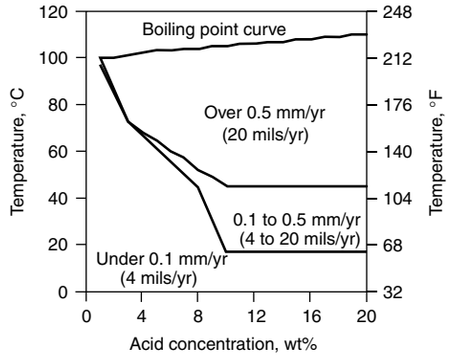

Fig. 2 Isocorrosion diagram for alloy 625 in hydrochloric acid

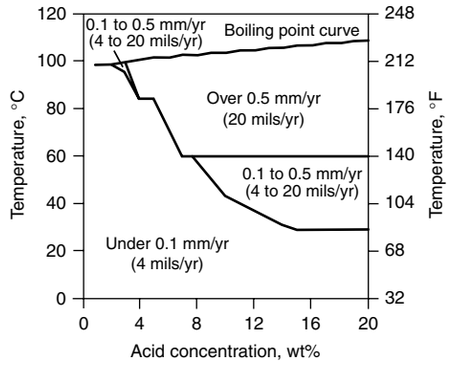

Fig. 3 Isocorrosion diagram for C-2000 alloy in hydrochloric acid

Fig. 4, alongside the corresponding line for C-2000 alloy. Type 316L stainless steel (S31603) and 20Cb-3 alloy (N08020) contain 2.5 wt% Mo, while 254SMO alloy (S31254) contains 6 wt% Mo. The plot indicates that molybdenum is beneficial to the stainless steels in hydrochloric acid. It also indicates how much more resistant the Ni-Cr-Mo alloys are.

The electrochemical characteristics of B-3 and C-2000 alloy in pure and impure hydrochloric acid have recently been studied in great detail. The tests were performed in deaerated 20 wt% hydrochloric acid at 25 °C (77 °F). Ferric ions were added (in the form of ferric chloride) as impurities, because these are commonly encountered within industrial systems, and they markedly affect electrochemical behavior of the alloys, even at parts per million (ppm) levels.

The potentiodynamic polarization curves generated for B-3 alloy in these studies are shown in Fig. 5 to 7. In deaerated, pure HCl, the electrochemical behavior of B-3 alloy is typical of activation polarization. That is, the electrochemical process appears to be controlled by the reaction step at the alloy/electrolyte interface.

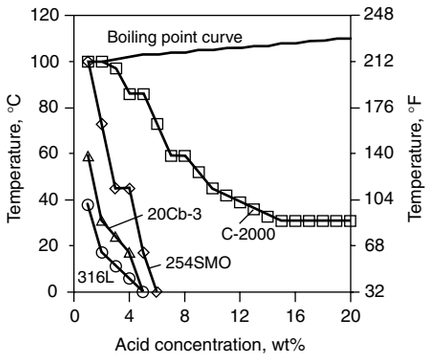

Fig. 4 Comparison of 0.1 mm/yr (4 mils/yr) lines of four alloys in hydrochloric acid

The cathodic reaction is hydrogen reduction, followed by the evolution of hydrogen gas at the surface of the alloy. In the anodic domain of the polarization curve B-3 alloy exhibited a short passive plateau, with a low passive current density of approximately 2×10^{-6} A/cm^2. This pseudopassive region is most likely due to the formation of molybdenum dioxide (MoO_2) and/or molybdenum trioxide (MoO_3) under the studied conditions (Ref 13).

As anticipated, knowing that the nickel-molybdenum alloys are intolerant to oxidizing contaminants, ferric ions had a marked effect on the electrochemical behavior of B-3 alloy. Indeed, the corrosion process appears to change from purely activation polarization (at 0 ppm impurity level) to purely concentration polarization (at the 1000 ppm impurity level), where the electrochemical reactions are controlled by mass transfer or diffusion-limited effects of the oxidizer (Fe^{3+}) at the reacting alloy surface, as seen from Fig. 7. As the ferric ion content was increased from 5 to 1000 ppm, the limiting current density (I_L) increased from approximately 1 to 1050 μA/cm^2, that is 1000 times more. As seen in Fig. 6, for ferric iron content of 100 ppm, I_L is approximately 100 μA/cm^2.

The corresponding potentiodynamic polarization curves for C-2000 alloy are also shown in Fig. 5 to 7. These curves indicate that the electrochemical characteristics of the Ni-Cr-Mo alloys are completely different from those of the nickel-molybdenum materials. The primary difference is that the Ni-Cr-Mo alloys exhibit large passive ranges, yielding low current densities and hence low corrosion rates.

The influence of oxidizing species (in this case, ferric ions) on the electrochemical behavior of the Ni-Cr-Mo alloys is very strong. With no ferric ions present (Fig. 5), C-2000 alloy exhibits typical active-passive behavior. In this case, the cathodic reaction is the reduction of hydrogen and the evolution of hydrogen gas from the surface. On the other hand, the increase in anodic current density (presence of the peak) is most likely due to the dissolution of the main element nickel to (Ni^{2+}) ions and possibly the oxidation of molybdenum (Mo) to (Mo^{3+}) and chromium (Cr) to (Cr^{3+}) ions. Interestingly, the electrochemical behavior of C-2000 alloy is similar at ferric ion contents of 5, 10, 25, and 50 ppm, and the additional electrochemical reaction is the reduction of ferric (Fe^{3+}) to ferrous (Fe^{2+}) ions, with no significant limiting current density (I_L).

At the intermediate concentrations of 100 and 250 ppm ferric ions, the corrosion behavior of C-2000 alloy changes markedly. The electrochemical process becomes influenced by concentration polarization of the oxidizer, yielding a significant I_L. Under such oxidizing conditions, brought about by the presence of high levels of ferric ions, it is believed that the first peak is most likely due to active dissolution of nickel (Ni) to (Ni^{2+}) along with chromium (Cr) to (Cr^{3+}) and/or molybdenum (Mo) to (Mo^{3+}). Conversely, the second peak is most likely related to the reduction of ferric to ferrous ions, followed by the formation of passive oxide films. The passive films are believed to be a mixture of chromium-molybdenum-rich oxides or hydroxides formed on the surface of the alloy. This is supported by recent studies that indicate that the presence of a segregated oxide film, which had an inner nickel/chromium-rich layer, was mainly responsible for the low passive currents on C-2000 alloy. A more effective barrier layer accompanied by molybdenum in the outer regions of the film resulted in a more resistive film (Ref 14–16).

At the highest ferric ion levels studied (500 and 1000 ppm), the electrochemical characteristics changed again. While C-2000 alloy still exhibits an active regime, the passivation process predominates. At these concentrations, the oxidizer acts as a strong cathodic depolarizer,

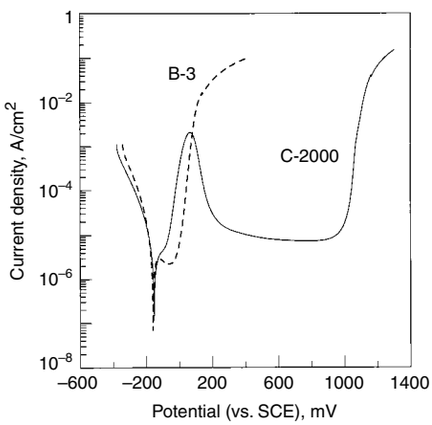

Fig. 5 Electrochemical behavior of C-2000 and B-3 alloys in pure deaerated 20% HCl solution with 0 ppm ferric ions at 25 °C (77 °F). SCE, saturated calomel electrode

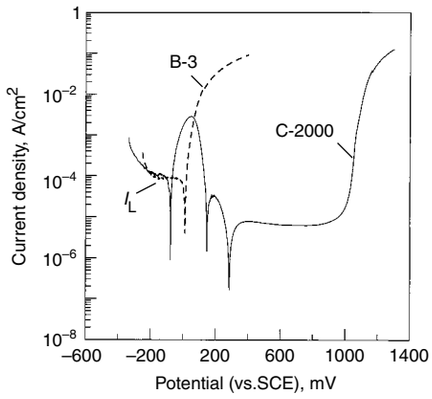

Fig. 6 Electrochemical behavior of C-2000 and B-3 alloys in deaerated 20% HCl solution with 100 ppm ferric ions, at 25 °C (77 °F). Limiting current density, $I_L \approx 10^{-4}$ A/cm^2. SCE, saturated calomel electrode

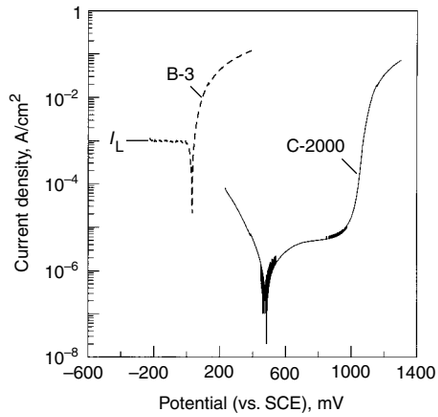

Fig. 7 Electrochemical behavior of C-2000 and B-3 alloys in deaerated 20% HCl solution with 1000 ppm ferric ions at 25 °C (77 °F). Limiting current density, $I_L \approx 10^{-3}$ A/cm^2. SCE, saturated calomel electrode

because the corrosion potential of the alloy shifted significantly toward more positive values, that is, over 400 mV/SCE (saturated calomel electrode). Consequently, the corrosion rate decreased significantly, and the influence of the limiting current density of the oxidizer, which increased the corrosion rate of the alloy for previous concentrations, as well as the active peaks, no longer exists at these higher concentrations (Fig. 7).

Irrespective of the ferric ion level, C-2000 alloy exhibits passive film breakdown (i.e., breakdown potential) at approximately 950 mV/SCE. Above this value, there is an increase in the current density, corresponding to the transpassive regime, which is characterized by the dissolution of the passive layer, often associated with higher oxidation states of the elements in the alloy such as (Ni^{3+}, Mo^{6+}, and Cr^{6+}), as well as the evolution of free oxygen from the decomposition of water.

The variation in the corrosion rates of B-3 and C-2000 alloys (from the electrochemical curves) versus the range of ferric ion concentrations used during this study is represented in Fig. 8. Even though both nickel alloys exhibited different characteristics, in terms of corrosion resistance, they experienced some similarities. In fact, in 20% hydrochloric acid without an oxidizer, B-3 and C-2000 alloys exhibited excellent corrosion resistance, that is, 2.5×10^{-3} and 0.01 mm/yr (0.1 and 0.4 mils/yr), respectively. Yet, the performance of the nickel-molybdenum alloy was four times better than that of the Ni-Mo-Cr alloy, which indicates that molybdenum is a beneficial alloying element in nickel alloys for reducing environments. Within the range of 5 to 25 ppm of the oxidizer, the corrosion rate of the two alloys was almost similar, because, even though an increase in corrosion rates was observed in both cases, this increase was slightly higher for B-3 alloy (0.05 to 0.5 mm/yr, or 2 to 20 mils/yr), whereas for C-2000 alloy this increase was from 0.04 to 0.3 mm/yr (1.6 to 12 mils/yr). At 50 ppm of the oxidizing species, C-2000 alloy showed a lower corrosion rate (0.4 mm/yr, or 16 mils/yr) than B-3 alloy (>1 mm/yr, or 40 mils/yr). Above 100 ppm, the nickel-molybdenum alloy corrosion rates continued to increase, from approximately 2 to 14 mm/yr (79 to 552 mils/yr), with the increase of the ferric ions (from 100 to 1000 ppm), while for the Ni-Cr-Mo alloy, this increase was observed only in the intermediate range of 100 and 250 ppm, and that is from 1 to 2.5 mm/yr (40 to 166 mils/yr). For the highest solution impurity concentration (>500 ppm ferric ions), the corrosion rate of C-2000 alloy decreased markedly to approximately 10^{-3} mm/yr (0.04 mils/yr), due to surface passivation. Hence, chromium is the key element in enhancing passivation in oxidizing conditions.

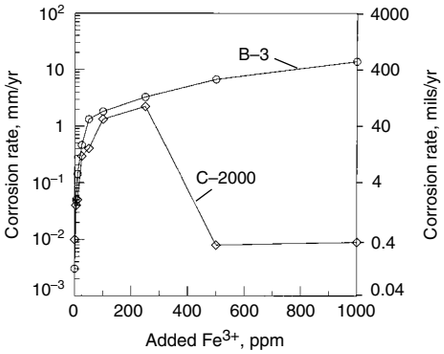

Fig. 8 Corrosion rates of B-3 and C-2000 alloys in deaerated 20% HCl solution versus added ferric ion concentrations at 25 °C (77 °F)

Sulfuric Acid

Although some stainless steels, notably those containing copper, such as 20Cb-3 alloy (N08020), offer good resistance to sulfuric acid, many industrial situations involving this acid require the use of the nickel alloys, some of which can withstand much higher solution temperatures.

The general corrosion characteristics of the Ni-Cu, Ni-Mo, Ni-Cr, Ni-Cr-Mo, and Ni-Fe-Cr alloys in pure sulfuric acid are evident from the isocorrosion diagrams shown in Fig. 9 to 13, respectively. These diagrams were compiled using hundreds of laboratory corrosion rate values at different concentrations and temperatures. The nickel-copper system is represented by alloy 400 (N04400), nickel-molybdenum by B-3 alloy (N10675), nickel-chromium by alloy 625 (N06625), Ni-Cr-Mo by C-2000 alloy (N06200), and Ni-Fe-Cr by 825 alloy (N08825). Notable are the extent of the <0.1 mm/yr (4 mils/yr) regime of the nickel-molybdenum alloys, and the narrow 0.1 to 0.5 mm/yr (4 to

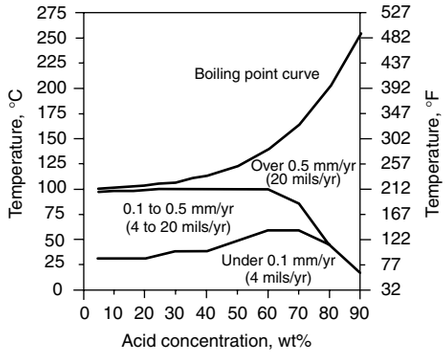

Fig. 9 Isocorrosion diagram for alloy 400 in sulfuric acid

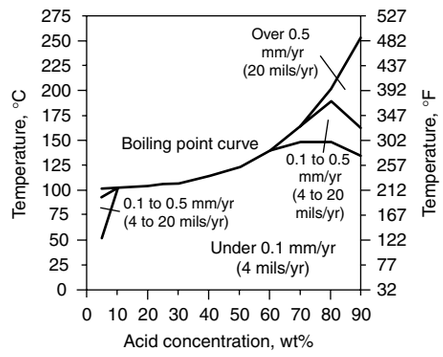

Fig. 10 Isocorrosion diagram for B-3 alloy in sulfuric acid

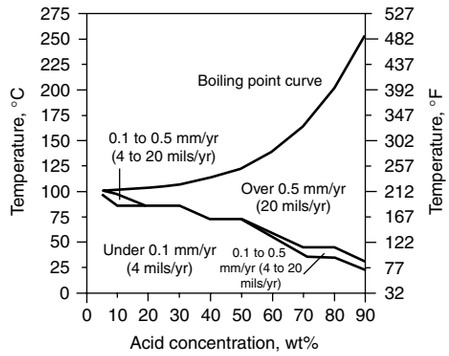

Fig. 11 Isocorrosion diagram for alloy 625 in sulfuric acid

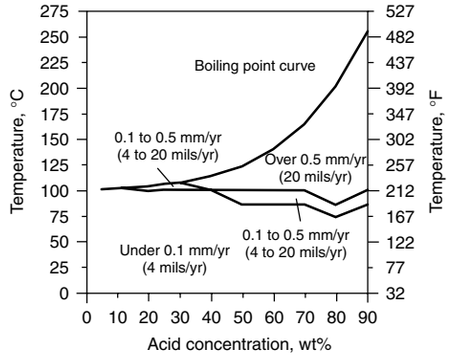

Fig. 12 Isocorrosion diagram for C-2000 alloy in sulfuric acid

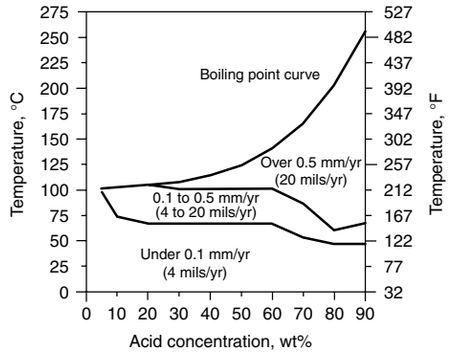

Fig. 13 Isocorrosion diagram for alloy 825 in sulfuric acid

20 mils/yr) regime of the Ni-Cr-Mo and Ni-Fe-Cr alloys. For perspective, the 0.1 mm/yr (4 mils/yr) line for C-2000 alloy is plotted alongside those for 316L (S31603), 254SMO (S31254), and 20Cb-3 alloy (N08020) in Fig. 14.

As with hydrochloric acid, the performance of the nickel alloys in sulfuric acid is strongly dependent on acid purity. Impurities or additions of an oxidizing nature enhance the performance of the chromium-bearing nickel alloys but degrade the performance of the nickel-molybdenum materials.

The electrochemical behavior of the nickel alloys in sulfuric acid is complex and very much dependent on the acid concentration. At low concentrations, the cathodic reaction is believed to be hydrogen evolution. At high concentrations, sulfuric acid is highly oxidizing, and mixed reactions appear to be occurring. It has been established that the chromium-bearing nickel alloys exhibit active-passive behavior in sulfuric acid over wide ranges of concentration and temperature (Ref. 17, 18).

It is known that copper benefits the performance of the nickel alloys at intermediate sulfuric acid concentrations (20 to 60 wt%) by virtue of a dissolution/plating reaction. It is also known that significant silicon contents can benefit the performance of the nickel alloys in very high concentrations of sulfuric acid (above 95 wt%), although such additions bring about metallurgical instability that limits their use.

Phosphoric Acid

Two types of phosphoric acid are widely used. The first is the pure, or food-grade, phosphoric acid, made from elemental phosphorus. The second is wet process phosphoric acid, which is made by reacting phosphate rock with sulfuric acid. This wet process acid is a very important industrial chemical, being the primary source of phosphorus for agrichemical fertilizers. Food-grade phosphoric acid is not very aggressive. On the other hand, wet process phosphoric acid is much more corrosive, because it contains numerous impurities, including unreacted sulfuric acid, various metallic ions, fluoride ions (although these tend to form complexes with the metallic ions), and chloride ions.

The Ni-Mo and Ni-Cr-Mo alloys possess high resistance to pure phosphoric acid. Only at high concentrations and temperatures approaching the boiling point do these alloys exhibit corrosion rates above 0.1 mm/yr (4 mils/yr). To illustrate this, the isocorrosion diagram for Ni-Cr-Mo C-2000 alloy is shown in Fig. 15.

With regard to wet process phosphoric acid, the main use of the nickel alloys has been in the concentration process, where the acid is taken through a series of evaporation steps, some involving metallic tubing. Typically, the concentration of the P_2O_5 component is raised from approximately 30 wt% (after rinsing and separation of the initial reaction products) to 54 wt%. Some companies concentrate the acid still further, to approximately 70 wt% P_2O_5, for ease of transportation.

As concentration increases, the impurity levels decrease. Thus, the corrosivity of wet process phosphoric acid is not directly related to concentration. Typically, corrosivity reaches a maximum between approximately 42 and 54 wt% P_2O_5. Within this concentration range, it has been found that high-chromium nickel alloys (such as G-30 alloy, from the Ni-Cr-Fe group, and G-35 alloy, from the nickel-chromium family) perform well, indicating that the acid is strongly oxidizing. Alloy 625 (from the nickel-chromium system) has been used successfully in 70% P_2O_5.

The corrosion rates of several alloys commonly used in wet process phosphoric acid (from a Florida producer) are given, as a function of temperature, in Fig. 16 and 17. Alloys 28 (N08028) and 31 (N08031) are austenitic stainless steels containing 27 wt% Cr and moderate molybdenum contents (3.5 and 6.5 wt%, respectively). From these data, it is evident that:

- The 42 wt% acid from this Florida plant is more corrosive than the 54 wt% acid.
- Of the alloys tested, G-30 alloy, with 30 wt% Cr, exhibits the highest resistance to these concentrations.

Wet process phosphoric acid also contains particulate matter. Therefore, it is common for deposits to build up in the evaporator tubes. If the chloride content of the acid is high, then under-deposit attack (a form of crevice corrosion) is possible. In this case, the molybdenum content of the alloy being used is important, because molybdenum enhances resistance to chloride-induced localized attack.

Hydrofluoric Acid

Hydrofluoric acid (HF) is a water solution of hydrogen fluoride. Hydrofluoric acid is used widely in diverse types of industrial applications; traditionally, it is used in pickling solutions in the metal industry, in the fabrication of chlorofluorocarbon compounds, as an alkylation agent for gasoline, and as an etching agent in the glass industry. In recent years, hydrofluoric acid has extensively been used in the manufacture of semiconductors and microelectronics during the wet chemical cleaning of silicon wafers.

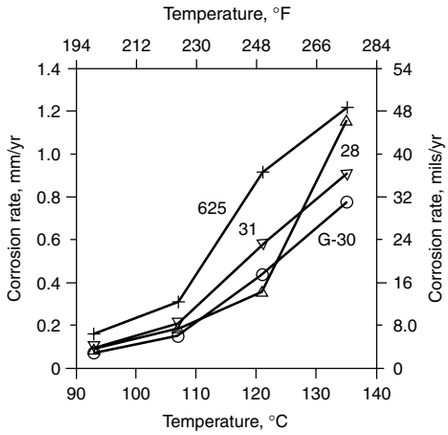

Fig. 16 Corrosion rates versus temperature in 42% wet process phosphoric acid

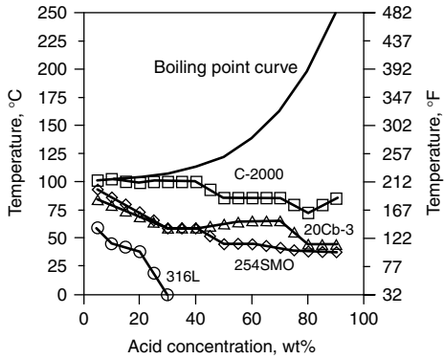

Fig. 14 Comparison of 0.1 mm/yr (4 mils/yr) lines in sulfuric acid

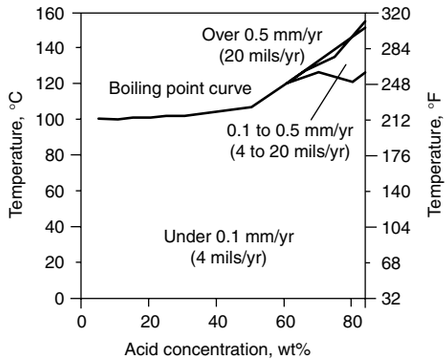

Fig. 15 Isocorrosion diagram for C-2000 alloy in phosphoric acid

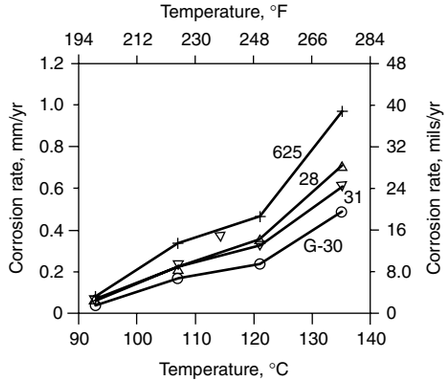

Fig. 17 Corrosion rates versus temperature in 54% wet process phosphoric acid

Hydrofluoric acid can be considered a reducing acid, and, although it is chemically classified as weaker than, for example, sulfuric or hydrochloric acids, it is extremely corrosive. This acid is also particularly toxic and poses a greater health hazard than most other acids. The corrosion behavior of metals in hydrofluoric acid has not been as systematically studied as it has for other common inorganic acids. This is largely because tests using hydrofluoric acid cannot be run in standard glass equipment and because of the toxic nature of this acid. Moreover, short-term weight-loss laboratory corrosion tests in hydrofluoric acid can be frustrating, because the results are not as reproducible as they are with other acids, such as sulfuric or hydrochloric. One of the reasons is because hydrofluoric acid commonly attacks the coupons used for testing in a nonuniform manner. That is, the corrosive power of this acid is not aimed toward uniform thinning but mostly to localized penetration below the surface of the metal in the form of thin cracks, voids, pits, trenches, and sometimes, intergranular attack. Figure 18 shows the cross section of a coupon of alloy 600 (N06600) exposed for 336 h to the vapor phase of a solution of 20% HF at 93 °C (200 °F). In cases where internal penetration occurs, as in Fig. 18, it is not recommended that corrosion rates based on weight-loss be used for materials selection.

The choices of engineering alloys to handle hydrofluoric acid are limited. Some nonmetallic materials such as polyethylene can be used. However, traditional materials, such as glass, and the reactive metals, such as titanium, zirconium, and tantalum, are readily attacked by hydrofluoric acid. Hydrofluoric acid will dissolve most oxides; therefore, any alloy reliant on a passive oxide film for protection against corrosion will not perform well in the presence of this acid.

Hydrofluoric acid at concentrations higher than 64% can be handled with carbon steel; however, at lower concentrations, this acid attacks steel rapidly (Ref 19, 20). Steels also may suffer embrittlement in the presence of hydrofluoric acid (Ref 20). Because nickel alloys offer moderate corrosion resistance over a wide range of acid concentrations and temperatures, they are a common choice for wet hydrofluoric acid (Ref 8, 21–26). For example, it has been reported that in solutions containing mixtures of hydrofluoric and nitric acids, high-chromium nickel materials such as G-30 alloy (N06030) perform well (Ref 22). Traditionally, the most popular nickel alloy used for hydrofluoric acid has been the copper-bearing alloy 400 (N04400), even though its corrosion resistance is greatly diminished by the presence of air or oxidizing salts (Ref 8, 19–21, 23–26). C-2000 alloy (N06200), which contains only 1.6 wt% Cu, has also been shown to perform well in hydrofluoric acid (Ref 26). It has been reported in the literature that the resistance to corrosion of engineering alloys in wet hydrofluoric acid is a consequence of the formation of insoluble fluoride salts on the surface of these alloys (Ref 19, 20, 23).

The two most useful alloys for hydrofluoric acid applications seem to be C-2000 and 400. The corrosion behavior of these two nickel alloys in hydrofluoric acid has been characterized regarding the effect of temperature, acid concentration, and testing time (Ref 26). Table 2 shows the uniform corrosion rate calculated by weight loss and the depth of attack by internal penetration, as a function of the temperature, and vapor versus liquid phase of exposure, for a testing time of 240 h. As the testing time increased from 24 to 240 h, the corrosion rate of C-2000 alloy in the vapor phase for 20% HF at both 79 and 93 °C (175 and 200 °F) markedly decreased, while in the liquid phase, the corrosion rate was almost independent of the testing time (Ref 26). On the other hand, under the same test conditions, the corrosion rate of alloy 400 in the liquid phase slowly increased as the test time increased. In the vapor phase, the corrosion rate of alloy 400 was high (2.5 to 10 mm/yr, or 100 to 400 mils/yr) and independent of the testing time.

As would be expected, as the acid concentration increased from 1 to 20%, the corrosion rates of both alloys increased; however, the effect was more pronounced for alloy 400, especially in the vapor phase. Both materials had similar corrosion rates at the lower temperatures of 38 and 52 °C (100 and 126 °F); however, as the temperature was raised to higher values, the corrosion rate of alloy 400 increased faster than the corrosion rate of C-2000 alloy, both in the vapor and liquid phases. Table 2 also indicates that the internal penetration in alloy 400 is high at all temperatures in the vapor phase. On the other hand, in the liquid phase, the internal penetration was higher for C-2000 alloy, mainly at 79 and 93 °C (175 and 200 °F).

From these results, it is evident that chromium is a beneficial element for vapor phase applications. It is also apparent that copper is the most beneficial alloying element for nickel alloys, while iron seems to be detrimental (Ref 26).

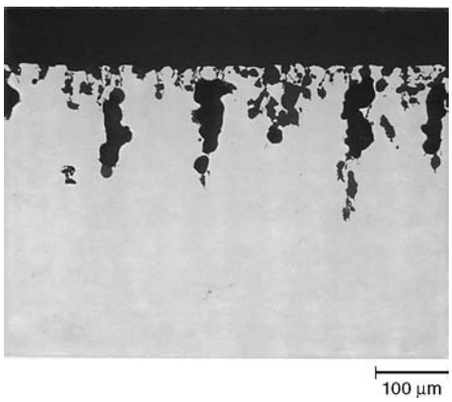

Fig. 18 Specimen of alloy 600 exposed for 336 h to the vapor phase of 20% HF solution at 93 °C (200 °F)

Hydrobromic Acid

The behavior of the nickel alloys in hydrobromic acid mirrors that in its sister compound, hydrochloric acid (HCl). As in HCl, those nickel alloys with high molybdenum contents provide

Table 2 Effect of temperature on the corrosion behavior of unstressed N04400 and N06200 coupons exposed in 20% hydrofluoric acid for 240 h

Common name	UNS No.	Temperature °C	Temperature °F	Phase(a)	Average corrosion rate mm/yr	Average corrosion rate mils/yr	Internal penetration, µm	Observations
400	N04400	38	100	L	0.27	10.6	13	Uniform corrosion, (b)
		38	100	V	1.15	45.3	241	IGA. Cracks at the perforated hole and edges
		52	126	L	0.46	18.1	13	Uniform corrosion, (b), GB etching
		52	126	V	3.31	130.4	622	Severe IGA. Some cracks from edges
		66	150	L	0.22	8.7	13	Uniform corrosion, (b)
		66	150	V	1.76	69.3	191	IGA. Cracks along drilled hole
		79	175	L	1.10	43.3	25	Uneven corrosion. GB etching
		79	175	V	7.59	299	356	Deep IGA
		93	200	L	2.06	81.2	25	Uneven corrosion. GB etching
		93	200	V	12.3	484.6	368	Deep IGA and uneven corrosion
C-2000	N06200	38	100	L	0.21	8.3	13	Uniform corrosion, (b)
		38	100	V	0.19	7.5	241	Uniform corrosion, (b), trace of copper on surface
		52	126	L	0.48	18.9	13	Uniform corrosion, (b), copper on surface
		52	126	V	0.36	14.2	13	Uniform corrosion, (b)
		66	150	L	0.85	33.5	38	Uneven general corrosion. Small dealloyed layer. Sample plated with copper and probably nickel
		66	150	V	0.85	33.5	13	Minimal corrosion. Sample plated with nickel and traces of copper
		79	175	L	0.67	26.4	102	Thin, lacelike penetration. Light copper color
		79	175	V	0.92	36.2	38	Shallow, isolated, lacelike penetration
		93	200	L	0.74	29.2	216	Thin, lacelike penetration
		93	200	V	0.69	27.2	64	Isolated, lacelike penetration. Green corrosion products

(a) L, liquid; V, vapor. (b) Roughness reported as internal penetration. IGA, intergranular attack; GB, grain boundary

the greatest resistance to hydrobromic acid. The nickel-molybdenum materials, for example, exhibit corrosion rates of less than 0.3 mm/yr (12 mils/yr) at concentrations up to 40 wt% (which is equivalent to 20 wt% HCl, on a molar basis) and temperatures up to the boiling points, provided the acid is pure. The Ni-Cr-Mo alloys are also useful over fairly large ranges of concentration and temperature; more importantly, they are tolerant of oxidizing impurities and additions.

A plot of the 0.1 mm/yr (4 mils/yr) lines for several Ni-Cr-Mo alloys in pure hydrobromic acid is presented in Fig. 19. These lines indicate the concentrations and temperatures at which a corrosion rate of 0.1 mm/yr (4 mils/yr) is expected, based on laboratory test results. Naturally, lower rates are expected below the lines. From Fig. 19, it is evident that there are considerable differences between some of the Ni-Cr-Mo alloys. In particular, the extent of the low-corrosion-rate regime (under 0.1 mm/yr, or 4 mils/yr) appears to be tied to the chromium content of the alloys, those with the highest chromium contents having the largest regimes.

Nitric Acid

Nitric acid is one of the few chemicals in which the stainless steels generally outperform the nickel alloys. This is because the acid is strongly oxidizing, and passive films form readily on the stainless steels due to their high iron and chromium contents.

The nickel alloys with the greatest resistance to nitric acid are those with high chromium levels. They are typically used when the nitric acid is mixed with halogen-bearing chemicals (for example, hydrofluoric acid). They are also useful in nitric systems cooled with chlorinated waters and in batch systems requiring resistance to other inorganic acids.

While the Ni-Fe-Cr alloys are among the most resistant of the nickel alloys to nitric acid, iron is not essential for good performance in this acid. High-chromium, low-iron compositions, such as Allcorr alloy (N06110) and G-35 alloy (N06035), exhibit corrosion rates of less than 0.1 mm/yr (4 mils/yr) over very wide ranges of concentration and temperature.

With regard to the widely used Ni-Cr-Mo alloys, their performance in nitric acid is strongly related to chromium content. C-276 alloy (N10276), for example, with 16 wt% Cr, is far less resistant to nitric acid than those Ni-Cr-Mo materials with higher chromium contents, such as alloy 686 (N06686) (21 wt% Cr), C-22 alloy (N06022) (22 wt% Cr), alloy 59 (N06059) (23 wt% Cr), and C-2000 alloy (N06200) (23 wt% Cr). To illustrate these differences, isocorrosion diagrams for C-276 alloy and C-2000 alloy in nitric acid are shown in Fig. 20 and 21, respectively.

Organic Acids

The organic acids are not as corrosive as the inorganic acids because they do not ionize as readily (Ref 27). Much of the corrosion data for nickel alloys and stainless steels in organic acids relates to acetic and formic acid. Of these, formic acid is much more corrosive as a result of its higher dielectric constant, and hence, it has a higher ionic dissolution tendency. The results of tests of nickel alloys in boiling acetic acid are given in Table 3; available corrosion rates for the same alloys in boiling formic acid are shown in Table 4. It is worthy of note that the corrosion rates in formic acid (albeit at different concentrations) are considerably higher than those in acetic acid, except in the case of B-2 alloy (N10665).

Among the most corrosive organic compounds are the sulfonic acids. These are widely used in the chemical process industries. In particular, methane sulfonic acid (MSA) is used as a catalyst for esterification and alkylation. Tests of stainless steels, nickel alloys, and reactive metal alloys (Ref 28) in 25% MSA at 95 °C (203 °F) indicated corrosion rates of less than 0.1 mm/yr (4 mils/yr) for only four of the test materials (C-22, or N06022, and G-30, or N06030, alloys, tantalum, and zirconium). Three alloys exhibited corrosion rates between 0.1 and 0.5 mm/yr (4 and 20 mils/yr) (B-2, or N10665, B-3, or N10675, and C-2000, or N06200, alloys). All other materials tested (alloys 200, or N02200, 400, or N04400, 625, or N06625, 825, or N08025, C-276, or N10276, and titanium) gave corrosion rates in excess of 0.5 mm/yr (20 mils/yr). Commercially pure nickel (alloy 200) and titanium experienced severe corrosion under these conditions.

The results of a more recent series of laboratory tests in MSA are given in Table 5. These results indicate a strong temperature dependency, especially for the Ni-Cr-Mo materials.

Salts

While the inorganic acids are the most aggressive chemicals commonly encountered, halide salts (that is, chlorides, fluorides, bromides, and iodides) are also of great concern, in a corrosion sense. Their effects are often insidious and unpredictable, leading to the premature failure of components. Most of these effects are related to ionic migration and ionic hydrolysis (to the respective halogen acids). Chlorides are by far the most common halide salts, and their promotion of stress-corrosion cracking (in austenitic stainless steels, in particular), pitting, and crevice attack is well known. Fluorides are less common but are very damaging to alloys of the reactive metals (titanium, zirconium, niobium, and tantalum).

The effects of the halide salts are often complicated by the metallic component. For example, ferric chloride is very influential, in a corrosion sense, because it contributes ferric ions (which are oxidizing) and chloride ions (which can migrate and hydrolyze) to any aqueous system. Even in strong solutions of hydrochloric acid (where the additional chloride ions are ineffectual), if there are sufficient ferric ions, the nature of the corrosion process will change, leading to much higher corrosion rates for alloys

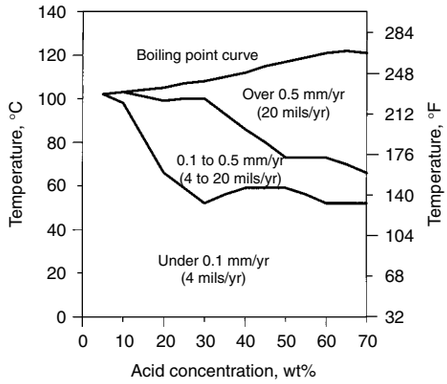

Fig. 20 Isocorrosion diagram for C-276 alloy in nitric acid

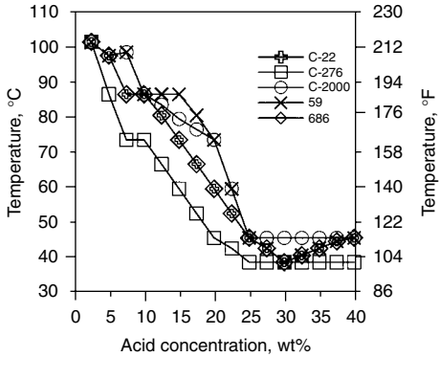

Fig. 19 Comparison of 0.1 mm/yr (4 mils/yr) lines in hydrobromic acid

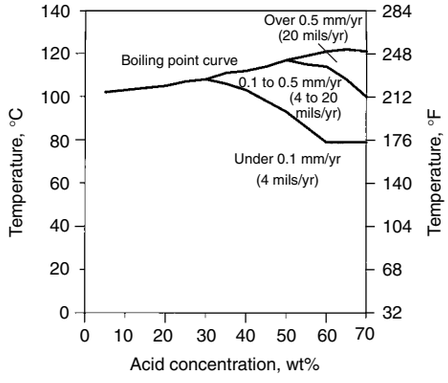

Fig. 21 Isocorrosion diagram for C-2000 alloy in nitric acid

that do not passivate or dramatically reducing the corrosion rates of passivating alloys, as discussed in the section "Hydrochloric Acid" in this article.

Ferric chloride is also a strong promoter of pitting and crevice corrosion, because the ferric ions create an oxidizing environment in which passive films can be established, while the chloride ions can damage the films and result in localized corrosion through migration and hydrolysis. The resistance to crevice corrosion of several nickel alloys is defined in Table 6, along with comparative data for several austenitic stainless steels. The critical crevice temperatures given in this table are the lowest at which crevice corrosion occurs, under laboratory conditions, in a solution containing 6 wt% ferric chloride and 1 wt% hydrochloric acid over 72 h. Higher values are better than lower ones. The excellent resistance of the Ni-Cr-Mo alloys to crevice attack is evident from this table, as are the benefits of a high molybdenum content in the austenitic stainless steels.

With regard to which halide ion has the greatest effect on susceptibility to localized attack, several nickel alloys have been subjected (Ref 30) to electrochemical (cyclic polarization) studies in molar solutions of NaCl, NaBr, NaF, and NaI, at 50 °C (122 °F). The results of these studies are summarized in Fig. 22, which indicates the repassivation potentials associated with each alloy and halide. Because repassivation potential is a measure of localized corrosion resistance, it can be deduced that:

- The effects are alloy specific, in the case of the bromide and chloride.
- Compositional effects are greatest in sodium chloride, where high chromium and high molybdenum contents appear to be beneficial.
- Compositional effects are minimal in sodium iodide and sodium fluoride solutions.
- The susceptibility of the nickel alloys to localized attack is generally greater in sodium fluoride than it is in sodium iodide.

Seawater

Nickel 200 (N02200), and alloy 400 (N04400), and nickel alloys containing chromium and iron are very resistant to flowing seawater, but in stagnant or very low-velocity seawater, pitting or crevice corrosion can occur, especially under fouling organisms or other deposits. In moderate- and high-velocity seawater or brackish water, alloy 400 is frequently used for pump and valve trim and transfer piping. It has excellent resistance to cavitation erosion and exhibits corrosion rates less than 0.025 mm/yr (1.0 mils/yr). Alloy 400 sheathing also provides economical seawater splash zone protection to steel offshore oil and gas platforms, pilings, and other structures. Although pitting can occur in alloy 400 under stagnant conditions, such pitting tends to slow down after fairly rapid initial attack and rarely exceeds 1.3 mm (0.05 in.) in depth.

Other nickel alloys containing chromium and molybdenum offer increased resistance to localized corrosion in stagnant seawater. The corrosion resistance of the nickel-copper and molybdenum-containing nickel alloys is compared to type 316 stainless steel (S31600) in ambient temperature stagnant seawater in Table 7. In this test, alloy 625 (N06625) was completely resistant to attack. Under crevice conditions, this alloy can be attacked, necessitating the use of even more highly alloyed materials.

Table 3 Corrosion rates for nickel alloys in boiling acetic acid

			Corrosion rate			
			10 wt% CH_3COOH		99 wt% CH_3COOH	
Common name	UNS No.	Alloy group	mm/yr	mils/yr	mm/yr	mils/yr
200	N02200	Ni	(a)	(a)	0.11	4.3
400	N04400	Ni-Cu	(a)	(a)	0.02	0.8
B-2	N10665	Ni-Mo	0.01	0.4	0.03	1.2
625	N06625	Ni-Cr	0.01	0.4	0.01	0.4
C-276	N10276	Ni-Cr-Mo	0.01	0.4	0.01	0.4
825	N08825	Ni-Fe-Cr	0.02	0.8	(a)	(a)

(a) Not tested

Table 4 Corrosion rates for nickel alloys in boiling formic acid

			Corrosion rate			
			40 wt% formic acid		88 wt% formic acid	
Common name	UNS No.	Alloy group	mm/yr	mils/yr	mm/yr	mils/yr
200	N02200	Ni	0.27	10.6	0.33	13
400	N04400	Ni-Cu	0.05	2.0	0.03	1.2
B-2	N10655	Ni-Mo	0.01	0.4	<0.01	<0.4
625	N06625	Ni-Cr	0.18	7.1	0.24	9.5
C-276	N10276	Ni-Cr-Mo	0.07	2.8	0.05	2.0
825	N08825	Ni-Fe-Cr	0.2	8.0	0.07	2.8

Table 5 Corrosion rates for nickel alloys in methane sulfonic acid

		Corrosion rate							
		20%, boiling		40%, 93 °C (200 °F)		40%, boiling		70%, 79 °C (175 °F)	
Common name	UNS No.	mm/yr	mils/yr	mm/yr	mils/yr	mm/yr	mils/yr	mm/yr	mils/yr
625	N06625	0.14	5.5	0.1	4	0.23	9.1	0.01	0.4
C-22	N06022	0.93	36	<0.01	<0.4	2.04	80.4	<0.01	<0.4
C-2000	N06200	0.58	23	<0.01	<0.4	0.81	32	<0.01	<0.4
G-30	N06030	0.75	30	<0.01	<0.4	0.84	33	<0.01	<0.4

Table 6 Critical crevice temperatures (CCTs) for nickel alloys and stainless steels

			CCT(a)	
Common name	UNS No.	Alloy group	°C	°F
316L	S31603	Stainless steel, 2.5% Mo	0	32
28	N08028	Stainless steel, 3.5% Mo	17.5	64
254SMO	S31254	Stainless steel, 6.25% Mo	30	86
G-30	N06030	Ni-Cr-Fe	37.5	100
G-35	N06035	Ni-Cr	45	113
C-276	N10276	Ni-Cr-Mo	55	131
C-22	N06022	Ni-Cr-Mo	80	176
C-2000	N06200	Ni-Cr-Mo	80	176

(a) ASTM G 48, method D (Ref 29)

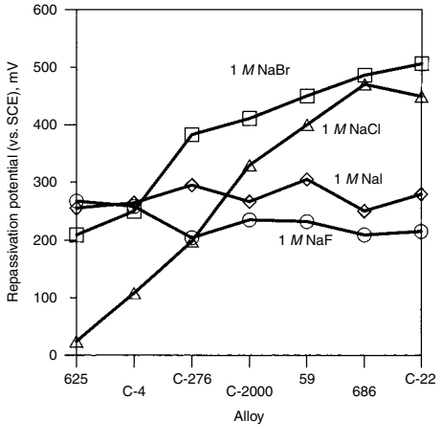

Fig. 22 Repassivation potentials for nickel alloys in 1*M* NaCl (triangle), 1*M* NaBr (square), 1*M* NaF (circle), and 1*M* NaI (diamond). Cyclic polarization at 50 °C (122 °F) and 0.5 mV/s

The results of testing in quiescent seawater with creviced specimens are given in Ref 31. Under these conditions, alloy 625 and even the more highly alloyed C-276 (N10276) are attacked. C-22 (N06022), 686 (N06686), 59 (N06059), and C-2000 (N06200) alloys, which contain higher levels of chromium, molybdenum, and/or tungsten, are resistant to attack. This class of materials is also required for hot seawater applications such as heat exchangers.

The age-hardenable alloy K-500 (N05500), with corrosion resistance similar to that of alloy 400, is frequently used for high-strength fasteners and pump and propeller shafting in freshwater and seawater applications. Other precipitation-hardened nickel-chromium alloys, such as 718 (N07718) and 725 (N07725), are also used. For combined high strength and optimal corrosion resistance, cold-worked alloy 686 is used for bolting and shafts.

Alkalis

Nickel 200 (N02200) and 201 (N02201) are used extensively in caustic production and processes involving all concentrations and temperatures of sodium hydroxide (NaOH) and potassium hydroxide (KOH). This resistance prevails even when these alkalis are molten. The lower-carbon nickel 201 is used at temperatures above 315 °C (600 °F), to avoid graphite precipitation. Isocorrosion curves for nickel 200 and 201 in sodium hydroxide solutions are shown in Fig. 23. Nickel 200 is used extensively in caustic evaporator service where dilute caustic is concentrated up to 50%. In this service, contaminants such as chlorates, hypochlorites, and chlorides can cause increased corrosion rates, especially under high-velocity conditions (Ref 32–35). Although nickel is resistant to most alkalis, it is not resistant to ammonium hydroxide (NH_4OH) solutions.

The resistance of nickel alloys to general corrosion and stress-corrosion cracking increases with increasing nickel content. In some caustic applications where higher strength or resistance to other corrodents is required, alloy 400 (N04400) from the nickel-copper system, alloy 600 (N06600) from the nickel-chromium system, and others are used. Alloys 400 and 600 are resistant to general corrosion over a wide range of temperatures and caustic concentrations. However, at the higher concentrations and temperatures, nickel alloys can suffer intergranular stress-corrosion cracking. Under these conditions, stress relieving may be necessary. Only nickel 200 and 201 are resistant to stress-corrosion cracking in caustic solutions up to and including molten caustic. Under severe conditions, nickel alloys containing molybdenum may be less resistant to caustic than those that do not contain molybdenum.

Alloys 600 and 800 (N08800) have been used extensively in nuclear steam generator service at approximately 300 °C (570 °F). In this service, resistance to caustic, which can be formed and concentrated at tube sheets, is of concern (Ref 36). The higher-chromium alloy 690 (N06690) is more resistant to stress-corrosion cracking under some conditions.

Recently, a phenomenon known as caustic dealloying has been experienced with the Ni-Mo and Ni-Cr-Mo alloys (Ref 37, 38). It appears that, at temperatures in excess of approximately 100 °C (212 °F), certain elements, notably molybdenum, can be selectively leached from these alloys in high concentrations of sodium or potassium hydroxide. The depths to which the microstructures are affected appear related to the molybdenum contents of the alloys, with the high-molybdenum B-type alloys being most affected. Potassium hydroxide is reported to be less aggressive than sodium hydroxide with regard to dealloying (Ref 37).

Table 7 Resistance of various alloys to stagnant seawater

		Maximum pit depth	
Common name	UNS No.	mm	mils
625	N06625	0	0
825	N08825	0.03	1
K-500	N05500	0.86	34
400	N04400	1.07	42.1
316	S31600	1.58	62.2

Environmental Cracking

Raul Rebak, Lawrence Livermore Laboratory

Environmentally assisted cracking (EAC) or environmentally induced cracking are general terms that include phenomena such as stress-corrosion cracking, hydrogen embrittlement, sulfide stress cracking, and liquid metal embrittlement. Environmentally assisted cracking refers to a phenomenon by which a normally ductile metal loses its toughness (elongation to rupture) when subjected to mechanical stresses in the presence of a specific corroding environment. For EAC to occur, three affecting factors must be present simultaneously: mechanical tensile stresses, a susceptible metal microstructure, and a specific aggressive environment. If any of these three factors is removed, EAC will not occur. To mitigate the occurrence of EAC, engineers may eliminate residual stresses in a component or limit its application to certain chemical environments. The term *environment* includes not only the chemical composition of the solution in contact with the component, but also other variables such as temperature and applied potential.

Nickel alloys are, in general, more resistant than stainless steels to EAC. Austenitic stainless steels, such as type 304 (S30400), suffer stress-corrosion cracking in the presence of hot aqueous solutions containing chloride ions. Because chloride ions are ubiquitous in most industrial applications, the use of stressed stainless steel parts is seriously limited. On the other hand, nickel alloys, such as C-276 (N10276), are practically immune to stress-corrosion cracking in the presence of hot chloride solutions and are therefore an excellent alternative. Nonetheless, nickel alloys are not immune to other types of EAC. There are several environments (such as hot caustic and hot hydrofluoric acid) that may produce embrittlement in nickel alloys (Ref 39). These are listed in Table 8. The conditions where nickel alloys suffer EAC are highly specific and therefore avoidable by proper design of the industrial components.

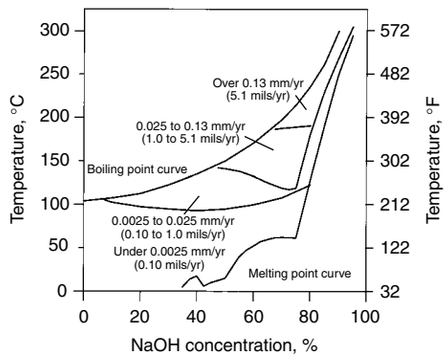

Fig. 23 Isocorrosion diagram for nickel 200 and 201 in NaOH

Commercially Pure Nickel

Commercially pure nickel 200 (N02200) is not susceptible to stress-corrosion cracking, except in the heavily cold-worked condition and in the presence of concentrated caustic solutions at temperatures in excess of 250 °C (480 °F). Commercially pure nickel is not susceptible to hydrogen embrittlement, because the solubility and diffusivity of hydrogen in nickel are low, and this material has low mechanical strength. The yield strength of annealed N02200 at room temperature is 190 MPa (27.6 ksi), the ultimate tensile strength is 465 MPa (67.4 ksi), the elongation to rupture is 50%, and the hardness is only 60 HRB.

Nickel-Copper Alloys

As in the case of N02200, alloy 400 (N04400) is not very susceptible to stress-corrosion cracking, probably because it has low mechanical strength. The yield strength of annealed alloy 400 at room temperature is 260 MPa (37.7 ksi), the ultimate tensile strength is

550 MPa (79.8 ksi), the elongation to rupture is approximately 50%, and the hardness is 72 HRB. Alloy 400 was found to be susceptible to stress-corrosion cracking in acidic solutions containing mercury salts, in liquid mercury, in hydrofluoric acid, and in fluosilicic acid (Ref 40). In hydrofluoric acid, the cracking is transgranular, and the highest susceptibility occurs in the vapor phase, especially in the presence of air (Ref 8). Reduction of aeration reduces the susceptibility to cracking in hydrofluoric acid. Using U-bend specimens, it has been reported that the crack propagation rate in alloy 400 exposed to the vapor phase of 20% hydrofluoric acid for 240 h decreased as the temperature increased from 66 to 93 °C (150 to 200 °F), probably because less oxygen was available in the vapor phase as the temperature increased (Ref 41). In the same study, U-bends of alloy 400 were found to be free from cracking while immersed in the liquid phase (Ref 26, 41).

It has also been reported (Ref 42) that highly stressed alloy 400 suffers stress-corrosion cracking in ammonia vapors at 300 °C (570 °F). Heat treatments that eliminate residual stresses and cold-worked microstructures greatly reduce the susceptibility of alloy 400 to all types of environmentally induced cracking.

Nickel-Molybdenum Alloys

Nickel-molybdenum alloys are resistant to chloride-induced cracking in boiling magnesium chloride solutions (Ref 43, 44). When B-2 (N10665) and, to a lesser extent, B-3 (N10675) alloys are exposed to temperatures in the range of 550 to 850 °C (1020 to 1560 °F), they lose ductility, due to a solid phase transformation that forms ordered intermetallic phases such as Ni_4Mo. The precipitation of these ordered phases changes the deformation mechanisms of the alloys, making them susceptible to EAC such as hydrogen embrittlement. In B-2 alloy, the precipitation of intermetallic phases can occur in the HAZ during welding. It has been reported (Ref 45) that B-2 alloy failed by intergranular stress-corrosion cracking of the HAZ when exposed to organic solvents containing traces of sulfuric acid at 120 °C (250 °F). It has also been reported (Ref 46) that B-2 alloy was prone to transgranular stress-corrosion cracking in the presence of hydroiodic acid above 177 °C (351 °F).

Stress-corrosion cracking studies of B (N10001), B-2, and B-3 alloys in acidic solutions were carried out under laboratory and plant conditions (Ref 47). The effects of the electrochemical potential, cold work produced by drilling, and two different aging processes (that would simulate welding and the subsequent cooling cycle) were investigated. At anodic potentials of 200 mV above the free corrosion potential, transgranular fissuring was found in all three alloys, for both mill-annealed and aged materials. At cathodic potentials of 100 and 400 mV below the free corrosion potential, intergranular cracking occurred only for the aged alloys. Because the amount of intergranular brittle cracking increased at the lower applied cathodic potential, this environmentally induced cracking was attributed to hydrogen embrittlement (Ref 47).

U-bend specimens of mill-annealed B-3 alloy were found (Ref 26) to suffer stress-corrosion cracking in the presence of the vapor and liquid phases of a 20% hydrofluoric acid solution at 66, 79, and 93 °C (150, 175, and 200 °F). The cracking susceptibility of B-3 alloy increased with the temperature, and the liquid phase was more aggressive than the vapor phase.

Ni-Cr-Mo Alloys

One of the major limitations of stainless steels is susceptibility to chloride-induced localized attack, such as crevice corrosion, pitting corrosion, and stress-corrosion cracking. The Ni-Cr-Mo alloys are the most resistant nickel alloys to the classic chloride-induced localized corrosion. In some cases, stress-corrosion cracking was reported in high-strength materials; however, cracking only occurred in very aggressive conditions, such as temperatures higher than 200 °C (390 °F), a pH lower than 4, and the presence of hydrogen sulfide (Ref 48). U-bend specimens of C-2000 (N06200), C-22 (N062022), and C-276 (N10276) alloys were not susceptible to cracking in boiling 45% $MgCl_2$ solution after 1008 h of testing (Ref 41). The C-276 and C-4 (N06455) alloys were free from cracking in a 25% NaCl solution at 232 °C (450 °F); however, these alloys were susceptible to cracking in a $MgCl_2$ solution of the same chloride content at the same temperature (Ref 43). The C-22 alloy was immune to stress-corrosion cracking in a 20.4% $MgCl_2$ solution up to 232 °C (450 °F), even in the 50% cold-worked condition and 50% cold-worked plus aged at 500 °C (930 °F) for 100 h.

Laboratory tests, using U-bend specimens in accordance with ASTM G 30 (Ref 49), have shown that Ni-Cr-Mo alloys such as C-276, C-22, and C-2000 alloys are susceptible to stress-corrosion cracking in wet hydrofluoric acid (in both the liquid and vapor phase). Typical results are shown for C-276 alloy in Fig. 24 (Ref 26, 41). The most resistant of the Ni-Cr-Mo alloys to cracking in wet hydrofluoric acid appears to be C-2000 alloy, probably because of the beneficial effect of its 1.6% Cu content. Counter to the behavior of alloy 400 (N04400), Ni-Cr-Mo alloys were less susceptible to cracking in the vapor phase than in the liquid phase, suggesting that the presence of chromium is beneficial for hydrofluoric acid vapor phase applications (Ref 41).

Nickel alloys are known to be susceptible to caustic cracking. Under slow strain-rate conditions, C-276 alloy was susceptible (Ref 50) to transgranular cracking in 50% $NaOH + H_2O$ at 147 °C (297 °F). On the other hand, C-shaped specimens of C-22 alloy, mill annealed and aged for 24 h at 677 °C (1251 °F), did not exhibit cracking after immersion in 50% NaOH solution at 147 °C (297 °F) for 720 h.

When Ni-Cr-Mo alloys are aged at temperatures higher than 600 °C (1110 °F) for long periods of time, second phases can occur within the microstructure, due to solid-state reactions. These solid-state reactions during aging reduce the ductility of Ni-Cr-Mo alloys. For example, for annealed C-276 alloy, the yield strength at room temperature is 360 MPa (52.2 ksi), the ultimate tensile strength is 807 MPa (117 ksi), and the elongation to rupture is 63%; however, for C-276 alloy aged for 16,000 h at 760 °C (1400 °F), the yield strength increases to 476 MPa (69 ksi), the ultimate tensile strength increases to 894 MPa (129.7 ksi), and the elongation to rupture decreases to 10%. It has been reported that aged C-276 alloy is susceptible to hydrogen-induced cracking in environments containing hydrogen sulfide (Ref 51, 52).

The Ni-Cr-Mo alloys were also found to suffer environmentally induced cracking in conditions associated with supercritical water oxidation. It has been reported (Ref 53–55) that both C-276 alloy and alloy 625 suffer intergranular cracking when exposed to various aqueous solutions in the vicinity of the critical point of water, 374 °C (705 °F).

Because of its excellent resistance to stress-corrosion cracking and other types of localized corrosion, C-22 alloy was selected by the U.S. Department of Energy to fabricate the inner walls of the high-level nuclear waste containers that are planned to be buried permanently at the

Table 8 Environments that may cause environmentally assisted cracking (EAC) in nickel alloys

Typical alloy			
Common name	UNS No.	Alloy group	Environments that may produce EAC
200	N02200	Commercially pure nickel	Not especially susceptible
400	N04400	Ni-Cu	Hydrofluoric acid (especially in the vapor phase containing oxygen)
B-3	N10675	Ni-Mo	Cathodic and anodic acidic solutions (especially near welds), wet hydrofluoric acid solutions
C-22	N06022	Ni-Cr-Mo	Hot caustic, supercritical water oxidation, hot liquid hydrofluoric acid solutions
C-276	N10276	Ni-Cr-Mo	
600	N06600	Ni-Cr	Hot water, hot caustic, high chloride with high temperature

Yucca Mountain site. As a result, the alloy is being extensively tested for its susceptibility to stress-corrosion cracking in a variety of environments. So far, the alloy has been found (Ref 56–59) to be extremely resistant to EAC in many different solutions at the corrosion potential, at test temperatures from ambient to 110 °C (230 °F).

Tests have been carried out using cyclic loading, constant load, and slow strain-rate tests in solutions from 14 molal $MgCl_2$ to basic saturated water and simulated acidified water. Similarly, U-bend specimens of C-22 alloy and other nickel alloys, such as C-4 (N06455), G-3 (N06985), 825 (N08825), and 625 (N06625), are being used to assess the stress-corrosion cracking susceptibility in a variety of environments (Ref 60). Gas tungsten arc welded and nonwelded U-bend specimens have been exposed for more than five years at the corrosion potential to the vapor and liquid phases of three different solutions (pH 2.8 to 10), simulating up to 1000 times the concentration of ground water, both at 60 and 90 °C (140 and 195 °F). None of these alloys have exhibited any indication of environmentally induced cracking (Ref 60).

C-22 alloy, on the other hand, was found to be susceptible to EAC when slow strain-rate testing was performed on mill-annealed specimens in hot, simulated concentrated water at anodic applied potentials (Ref 61, 62). Simulated concentrated water is a multiionic alkaline solution approximately 1000 times more concentrated than Yucca Mountain groundwater. It is likely that the presence of fluoride ions in this solution contributed to the cracking of C-22 alloy (Ref 62). The susceptibility to cracking was strongly dependent on the applied potential and the temperature of the solution. The highest susceptibility to EAC was found at approximately 90 °C (195 °F) at +400 mV in the saturated silver chloride electrode scale (Fig. 25). At the corrosion potential, C-22 alloy was free from EAC, even at 90 °C (195 °F). Similarly, at anodic applied potentials, C-22 alloy was free from EAC at ambient temperatures, and, as the temperature increased, the time to failure in the tests decreased (Fig. 26).

It has also been reported that C-22 alloy may suffer embrittlement when slowly strained under cathodic applied potentials or currents (Ref 62–64). The maximum susceptibility to cracking under cathodic conditions seemed to occur at ambient temperatures, suggesting a hydrogen-related failure mechanism.

Ni-Cr, Ni-Cr-Fe, and Ni-Fe-Cr Alloys

These families of nickel alloys include alloys 600 (N06600), 825 (N08825), 800 (N08800), and G-30 (N06030). Because alloy 600 has been used to fabricate the tubes of steam generators in nuclear power plants, it has been by far the most studied nickel alloy regarding its stress-corrosion cracking behavior, especially in hot water. Alloy 600 has been found to suffer stress-corrosion cracking in pure water at temperatures in excess of 300 °C (570 °F), both in service and in the laboratory.

As a result of their importance to the nuclear industry, the stress-corrosion cracking of alloys 600 and 690 (N06690) in pure water and in caustic solutions has been extensively researched in the last three decades (Ref 65, 66), and more than 1000 papers have been published on this subject. In general, alloy 690 is more resistant to stress-corrosion cracking than alloy 600, probably due to its higher chromium content (29%). The susceptibility to cracking of alloys 600 and 690 depends strongly on environmental factors such as the temperature, the level of tensile stresses, the presence of hydrogen gas, the solution pH and the electrochemical potential, and metallurgical factors, such as the amount of cold work and heat treatment. Stress-corrosion cracking in alloy 600 can be intergranular or transgranular.

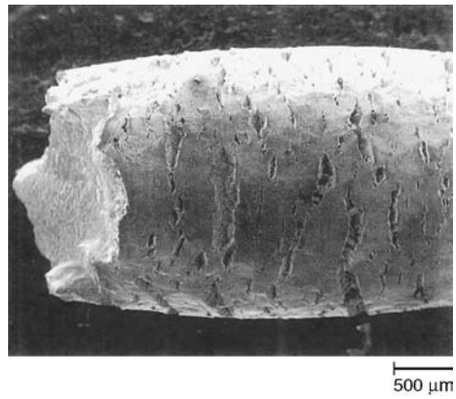

Fig. 25 C-22 alloy strained in 86 °C (187 °F) simulated concentrated water solution at +400 mV applied versus silver-saturated silver chloride potential

Fig. 24 Stress-corrosion cracking of C-276 alloy in HF solution

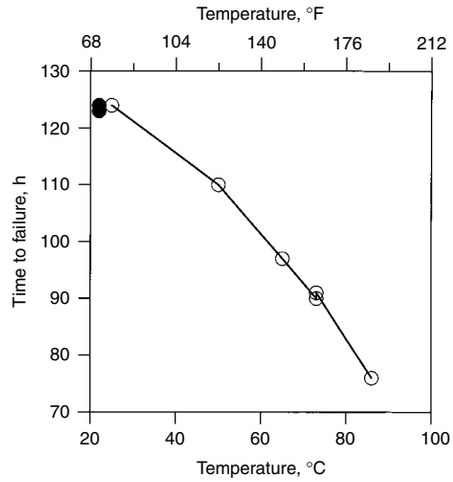

Fig. 26 Effect of temperature on the stress-corrosion cracking susceptibility of C-22 alloy in simulated concentrated water at an applied potential of +400 mV versus silver saturated silver chloride potential (open circles). Strain rate, 1.67×10^{-6} s^{-1}. Stress-corrosion cracking in air, solid circles

Alloy 600, like other nickel alloys, also suffers stress-corrosion cracking in hot caustic solutions at temperatures in the range of 150 to 200 °C (300 to 390 °F). Alloy 690, which has almost double the amount of chromium as alloy 600, has been found to be more resistant than alloy 600 to high-temperature cracking in pure water and in caustic solutions. As a result of its high nickel content (76%), alloy 600 is resistant to stress-corrosion cracking in chloride-containing solutions; however, alloy 600 is susceptible to localized attack in hydrofluoric acid-containing environments (Ref 8).

Alloy 800 is also used in the nuclear power generation industry. It has been shown that alloy 800 is also susceptible to caustic cracking (Ref 67) and even more susceptible than alloy 690, probably because of the higher chromium content of the latter (Ref 68). Alloy 825 is more resistant to stress-corrosion cracking than 316 stainless steel, due to its higher nickel content. Slow strain-rate tests and U-bend tests have shown, however, that alloy 825 is susceptible to transgranular stress-corrosion cracking in 45% $MgCl_2$ + water solutions at temperatures above 146 °C (295 °F).

Data on the stress-corrosion cracking behavior of G-30 alloy are scarce. It has been reported that G-30 components used in the industrial production of hydrofluoric acid suffered cracking (Ref 41). U-bend specimens of G-30 alloy did not crack after exposure for 500 h in a 45% $MgCl_2$ solution at 154 °C (309 °F). It has been found, however, that G-30 and other nickel alloys suffer cracking in the aggressive conditions encountered in supercritical water oxidation treatments.

Applications and Fabrication

Brian Baker, Special Metals Corp.
Paul Crook, Lee Flower, and
Mark Rowe, Haynes International, Inc.

Applications where the aqueous corrosion properties of nickel alloys are important factors in materials selection include the petroleum, chemical, and electrical power industries.

Petrochemical and Refining

A variety of iron- and nickel-base materials is currently used for equipment construction in petrochemical plants and refineries. Components include pressure vessel containment and piping, valves, fittings, transfer lines, and expansion bellows. The increasing use of sour crude coupled with the desire for greater throughput from existing equipment necessitate consideration of higher-alloyed materials.

Corrosion considerations for petrochemical and refining applications may be separated into two categories for simplicity: low temperature and high temperature. High-temperature corrosion considerations are discussed later. Low-temperature corrosion phenomena generally originate not due to the presence of the hydrocarbon-based process stream but to the existence of contaminants as well as process chemicals, including solvents, neutralizers, and catalysts. Compounds present in the process stream may include water, H_2S, HCl, HF, H_2SO_4, caustic, nitrogen compounds, and polythionic acid, as well as various organic acids, including naphthenic acid.

Naphthenic acid corrosion in distillation towers has been addressed through the use of molybdenum-containing materials. Alloys such as 825 (N08825), 25-6Mo (UNS N08926), and 317L (UNS S31703) are finding favor over 316 (UNS S31600) stainless steel. Another excellent material for resistance to severe naphthenic acid corrosion is alloy 625 (N06625) and its matching filler metal or 112 welding electrode (W86112). Overhead condensers and air coolers may encounter problems with polythionic acid stress-corrosion cracking; the same mode of attack may occur during shutdown of hydrotreating units as well. Here again, alloys such as 825 and 625 find applicability over austenitic stainless steels. Generally, an alloy should contain at least approximately 42% Ni to assure reliable resistance to chloride stress-corrosion cracking.

Chemical Processing

In the chemical process industries and in allied industries such as agrichemicals and pharmaceuticals, the nickel alloys are generally used as upgrades to the austenitic and duplex stainless steels, their main advantage being enhanced resistance to the inorganic halogen acids and halide salts.

At the heart of most chemical processes are reaction vessels. The use of the nickel alloys for reaction vessels and agitators is common where the robustness and heat-transfer characteristics of a metallic system are needed, and where the nickel alloys possess the necessary corrosion resistance. As has been discussed, each nickel alloy family has specific advantages. Commercially pure nickel (alloy 200), for example, is widely used for caustic soda and caustic potash. Alloy 400, from the nickel-copper group, is used in hydrofluoric acid. The nickel-molybdenum materials are used in pure hydrochloric and sulfuric acids. The Ni-Cr-Mo alloys are extremely versatile and suited to a wide range of acid/halide environments.

In addition to the piping, flanges, valves, and pumps associated with the transfer of chemicals to and from reaction vessels, metallic materials are important for the heating and cooling of chemicals. Both shell-and-tube and plate-frame heat exchangers are commonly made from the corrosion-resistant nickel alloys, especially where chloride-bearing cooling waters are involved.

Power Industry

Wrought nickel alloys are used routinely in wet flue gas desulfurization (FGD) systems that scrub coal-fired power plant flue gas. Nickel-chromium-molybdenum alloys are used for their resistance to sulfuric and mixed acids and their resistance to underdeposit corrosion caused by high chlorides. Typical FGD applications for wrought nickel alloys include absorbers, inlet and outlet ductwork, mist eliminators, reheaters, dampers, wet electrostatic precipitators, and chimney (stack) linings. Nickel alloys are employed as solid sheet and plate, welded sheet linings, roll-bonded clad plate, and explosion-bonded plate in FGD systems.

Nuclear power plants have used large quantities of Ni-Cr and Fe-Ni-Cr alloys since the beginning of the nuclear power program. In pressurized water reactors, alloys 600 (N06600) and 800 (N08800) were used for steam generator tubes, nozzles, and baffle plates. Alloy 600 has been replaced with the high-chromium alloy 690 (N06690), due to caustic and high-purity water failures of alloy 600. Age-hardenable alloy 718 (N07718) is also used for high-strength bolting and springs. These same nickel alloys are used to a lesser extent in boiling water reactors.

Fabrication

Forming and Annealing. Corrosion-resistant nickel alloys are readily hot worked, but some care is needed to achieve satisfactory results. In comparison to austenitic stainless steels, hot-working temperature ranges are narrower, melting temperatures are lower, hot strength is higher, strain-rate sensitivity is greater, thermal conductivity is less, and strain-hardening coefficients are greater. The best results can be achieved with moderate reductions per pass, frequent reheating, and relatively slow deformation rates. Solution annealing, followed by rapid cooling to room temperature, is recommended after hot working, to maximize corrosion resistance.

Cold working is the preferred method of forming the corrosion-resistant nickel alloys. Cold-working characteristics are similar to those of the austenitic stainless steels, with the exception that the nickel alloys have higher strength and work harden more rapidly than stainless steels. Severe cold-working operations should be conducted in multiple steps, with intermediate anneals to restore ductility.

Annealing of material that has received less than 10% reduction in area may result in an abnormally large grain size. Cold work generally does not affect resistance to uniform or pitting corrosion but may increase the likelihood of stress-corrosion cracking for susceptible combinations of alloy and environment.

Annealing most often consists of a solution-annealing treatment, which involves heating to a temperature where secondary carbides and intermetallic phases are dissolved, usually at approximately 1121 °C (2050 °F), followed by rapid cooling. Alloy manufacturers should be contacted for exact heat treatment temperatures for specific alloys. Rapid air cooling or water quenching is required for most alloys to avoid the grain-boundary precipitation of carbides or intermetallic phases on cooling, which can result in intergranular corrosion. Oxide scales should be removed prior to service. Scale is more adherent than on stainless steels, and its removal requires treatment in a molten caustic bath, followed by pickling in a hot solution of nitric and hydrofluoric acids. Alternatively, descaling can be conducted mechanically, by grit blasting or grinding. Pickling may be conducted to remove embedded iron or other impurities, after mechanical descaling.

Welding Considerations. As nickel replaces iron in alloys, the weld pool becomes less fluid, and weld penetration is reduced. Special attention is required to avoid lack of penetration and lack of fusion defects. It is always good practice to develop a qualified welding procedure, whether or not it is required by a code.

In comparison to welding steels and stainless steels, joints must be more open when welding nickel-base alloys, to compensate for reduced penetration and fluidity. V-groove included angles of approximately 70° are recommended. Root openings should be slightly greater, and land thickness should be less than for steels.

Nickel alloys are more susceptible than stainless steels to cracking caused by contamination with compounds of sulfur, phosphorus, or with low-melting-point metals. Standard preparation of new material involves removing any grease or oils, by wiping with a solvent, then removing the as-received surface with an abrasive. If material is known to have been exposed to sulfur compounds or low-melting-point metals, chemical cleaning methods may be required to remove the contamination, because grinding may smear contaminants into the surface. Thermal cutting methods, such as plasma arc, laser beam, or air carbon arc, may be used to prepare bevels, but the cut surfaces should be ground to bright metal prior to welding. Oxyfuel cutting is not effective on nickel alloys.

High-current and heat-input welding conditions increase the likelihood of problems such as sensitization and solidification cracking; therefore, the heat input should be kept at low to moderate levels. A maximum heat-input recommendation would be alloy and service-environment specific; thus, some engineering judgment is required. The same concerns that lead to the requirement of relatively low heat input also necessitate maintenance of relatively low interpass temperatures. Maximum interpass temperature recommendations vary between alloys and manufacturers, but maximum temperatures are usually between 90 and 200 °C (195 and 390 °F). The low fluidity of nickel-base filler metals may require manipulation or slight weaving to avoid steep toe angles that can lead to lack of fusion defects. Excessive weaving with a low travel speed produces high heat input and should be avoided. The low-carbon, low-silicon nickel-base alloys generally have good resistance to solidification cracking. The likelihood of solidification cracking can be minimized by favoring a convex weld bead crown and low-to-moderate current and travel speed.

Postweld heat treatment (PWHT) is usually not required for modern wrought nickel alloys with low carbon and silicon contents. Cast alloys, however, are more prone to precipitation in the HAZ, due to their higher carbon and silicon contents; thus, PWHT may be required. A postweld solution anneal, if practical, may have the beneficial effect of relieving residual stress and providing some homogenization of the weld metal. Stress-relief heat treatments below the solution-annealing temperature, at temperatures that are commonly used for steels, should not be used on nickel alloys, because grain-boundary precipitation can lead to sensitization or loss of ductility.

Passivation treatments used on some stainless steels are not usually required for nickel alloys. Slag, undercut, and other potential crevices should be removed, to avoid crevice corrosion. Grinding and polishing are sometimes used where low process contamination is needed, as in pharmaceutical or fine chemical production, but most welds are placed in service in the as-welded condition. Heat tint oxidation is not as harmful to nickel alloys as it is to stainless steels but can be removed by grinding or pickling.

Welding Processes. The highest-quality weld joints, with the best mechanical properties and corrosion resistance, can be achieved by using the inert gas welding processes. The maximum recommended welding current (nonpulsing) for gas tungsten arc welding is approximately 200 A. The maximum recommended welding current (nonpulsing) for gas metal arc welding (GMAW) is approximately 250 A. Both processes use bare wire welding consumables, which are covered by the American Welding Society (AWS) A5.14 specification (Ref 69).

The use of flux-bearing welding processes can offer improved deposition rates and bead profiles compared to the inert gas processes. The tensile strength of weld metal is usually not affected by use of a flux-bearing process, but impact toughness and ductility are somewhat reduced, in comparison to inert gas weldments, by the oxide inclusions that are inherent in flux-deposited weld metal. The corrosion resistance of flux-deposited weld metal is usually not degraded, assuming that the weld metal composition falls within the specified limits for the alloy. Some pickup of silicon from the flux is unavoidable and is allowed for in specifications such as AWS A5.11 (Ref 70).

Coated electrodes for shielded metal arc welding are covered by the AWS A5.11 specification. The maximum recommended welding current is approximately 180 A, with electrodes of diameter 4.8 mm (0.19 in.). Flux-cored arc welding is occasionally used to join corrosion-resistant nickel-base alloys. The compositional ranges and properties in the AWS A5.11 specification are sometimes referenced when purchasing these welding consumables.

Submerged arc welding (SAW) has been successfully used to join corrosion-resistant nickel-base alloys; however, this process should be used with caution, particularly with the highly alloyed Ni-Cr-Mo and Ni-Mo alloys. Potential problems include solidification cracking, microfissuring, modification of the weld metal composition, and sensitization. High welding currents will exacerbate all of these problems, so currents should be limited to approximately 250 A maximum. Low arc voltages will help to prevent pickup of silicon and loss of chromium, due to reaction with the flux; the recommended voltage is therefore approximately 26 to 28 V. Proper flux selection is critical to success. A highly basic, nonalloying flux is recommended. A procedure qualification that involves chemical analysis or corrosion testing of the weld metal, in addition to mechanical testing, should always be conducted when using SAW.

Filler-Metal Selection. Matching composition filler metals are available for most alloys and are selected in the majority of applications. Segregation of alloying elements occurs during the solidification of the weld metal. Dendrite cores are depleted in elements such as molybdenum and tungsten, while interdendritic areas are consequently enriched. The resulting nonuniform composition usually causes the weld metal to have higher uniform corrosion rates and less pitting resistance than matching-composition wrought alloys.

Excessive corrosion of the weld metal is usually only a problem when the selected alloy is subjected to an environment that is near the limit of the alloy useful range. Overalloyed filler metals may be selected in special cases, but the filler metal must be matched with the anticipated corrosive environment. For example, C-22 alloy (N06022) is sometimes used as an overalloyed filler metal for C-276 alloy (N10276) in hot chlorine bleach (an oxidizing environment where high chromium is beneficial), but C-22 alloy filler metal would suffer higher corrosion rates than matching C-276 alloy in pure hydrochloric acid (a reducing environment where high molybdenum is beneficial). Another common application of over-alloyed filler metals is the use of 625 or C-22 alloy

filler metals to join 6% Mo stainless steels in environments where pitting corrosion is a concern. However, there is no single, overalloyed filler metal that will provide the best performance under all conditions. Even when overalloyed filler metals are selected, localized corrosion of the unmixed zone is possible. Therefore, overalloyed filler metals are only selected in special cases where the combination is known to be effective.

Nickel alloys can be readily joined to steels and stainless steels by welding. The filler metal matching the nickel-base side of the joint is often a good choice for dissimilar metal welds. Alloy manufacturers should be contacted for specific recommendations.

Weld Overlays. A thin layer of corrosion-resistant alloy is often applied to steel to provide corrosion resistance at relatively low cost. The GMAW process is often selected for weld overlay applications. When depositing a corrosion-resistant weld metal onto steel, dilution from the steel can be minimized by favoring low welding currents and overlapping alloy weld beads by 50% or more. Stress-relief heat treatments that may be required for the steel base metal can reduce the corrosion resistance of alloy cladding; heat treatment requirements should be taken into account before undertaking a project.

Alloys Resistant to High-Temperature Corrosion

Dwaine Klarstrom, Haynes International, Inc.

Nickel alloys are industrially important for their resistance to certain types of high-temperature corrosion. For example, they have outstanding resistance to oxidation, and they are generally superior to iron- or cobalt-base alloys in this mode of attack. They have low solubilities for interstitial atoms, which makes them inherently more resistant to carburization and nitridation attack than other types of alloy. They also have good resistance to halogen-containing environments, due to the high melting points of the halogen compounds formed.

The compositions of several high-temperature nickel alloys are given in Table 9. These are grouped according to their primary elements: Ni-Cr, Ni-Cr-Mo, Ni-Cr-W, Ni-Co-Cr, Ni-Cr-Fe, Ni-Fe-Cr, and Ni-Mo. It is also useful to categorize the high-temperature nickel alloys by whether or not they can be age hardened. Age hardening is usually accomplished by the precipitation of fine, gamma prime or gamma double-prime particles in the microstructure. Gamma prime is a fcc A_3B compound, wherein A is predominantly nickel, and B is predominantly aluminum (sometimes in tandem with titanium). Gamma double prime is a body-centered tetragonal phase of the same composition, except that element B is predominantly niobium. Obviously, gamma prime requires significant alloying additions of aluminum (and possibly titanium), while gamma double prime requires substantial additions of niobium.

Use of the age-hardenable alloys is generally limited to gas turbine applications, where strength over well-defined temperature ranges and oxidation resistance are the chief requirements. For most other high-temperature corrosion applications, the solid-solution-strengthened nickel alloys are chosen because they are useful over much larger temperature

Table 9 Nominal compositions of nickel alloys resistant to high-temperature corrosion

Family	Common name	UNS No.	Form	Composition, wt%											
				Ni	Co	Mo	Cr	Fe	W	Mn	Si	C	Al	Ti	Other
Ni-Cr	80A	N07080	Wrought (age hardenable)	bal	2(a)	...	19.5	3(a)	...	1(a)	1(a)	0.1(a)	1.4	2.3	Cu 0.2(a)
	FM 72	N06072	Filler metal	bal	...	...	44	0.5(a)	...	0.2(a)	0.2(a)	0.1(a)	...	0.7	Cu 0.5(a)
	600	N06600	Wrought	76	...	...	15.5	8	...	0.5	0.2	0.08	...	...	Cu 0.2
	602 CA	N06025	Wrought	bal	...	...	25	9.5	...	0.1(a)	0.5(a)	0.2	2.1	0.15	Cu 0.1(a) Y 0.09 Zr 0.06
	625	N06625	Wrought	61	...	9	21.5	2.5	...	0.2	0.2	0.05	0.2	0.2	Nb + Ta 3.6
	625 LCF	N06626	Wrought	58(b)	1(a)	9	21.5	2.5	...	0.2	0.15(a)	0.03(a)	0.2	0.2	Nb + Ta 3.6
	671	...	Cast, powder metallurgy	bal	...	...	48	...	...	...	...	0.05	...	0.35	...
	690	N06690	Wrought	58(b)	...	...	29	9	...	0.5(a)	0.5(a)	0.05(a)	...	...	Cu 0.5(a)
	693 (53 MD)	N06693	Wrought	bal	...	...	29	4.25	...	...	0.5(a)	0.15(a)	3.25	...	Nb 1.5
	X-750	N07750	Wrought (age hardenable)	73	...	...	15.5	7	...	0.5	0.2	0.04	0.7	2.5	Cu 0.2 Nb + Ta 1
	214	N07214	Wrought	75	2(a)	0.5(a)	16	3	0.5(a)	...	0.2(a)	0.04	4.5	...	Y 0.01
Ni-Cr-Mo	S	N06635	Wrought	67	2(a)	15	16	3(a)	1(a)	0.5	0.4	0.2(a)	0.25	...	Cu 0.35(a) La 0.02 B 0.015(a)
Ni-Cr-W	230	N06230	Wrought	57	5(a)	2	22	3(a)	14	0.5	0.4	0.1	0.3	...	La 0.02
Ni-Co-Cr	HR-160	N12160	Wrought	37	29	1(a)	28	2(a)	1(a)	0.5	2.75	0.05	0.4(a)	0.5	...
	263	N07263	Wrought (age hardenable)	52	20	6	20	0.7(a)	...	0.4	0.2	0.06	0.6(a)	2.4(a)	Cu 0.2(a)
	617	N06617	Wrought	52	12.5	9	22	1	...	...	0.5	0.07	1.2	0.3	...
Ni-Cr-Fe	X	N06002	Wrought	47	1.5	9	22	18	0.6	...	1(a)	0.1	0.5(a)	...	...
	718	N07718	Wrought (age hardenable)	52.5	...	3	19	18.5	...	0.2	0.2	0.04	0.5	0.9	Cu 0.2 Nb + Ta 5.1
	45 TM	N06045	Wrought	45(b)	...	...	27.5	23	...	1(a)	2.75	0.09	0.2(a)	...	Cu 0.3(a) Rare earths 0.1
	RA 333	N06333	Wrought	45.5	3.3	3.3	25.5	bal	3.3	2(a)	1.2	0.08(a)	...	...	Cu 0.5(a)
	601	N06601	Wrought	60.5	...	...	23	15	...	...	0.5(a)	0.1(a)	1.4	...	...
Ni-Fe-Cr	706	N09706	Wrought (age hardenable)	41.5	...	...	16	40	...	0.2	0.2	0.03	0.2	1.8	Cu 0.2 Nb + Ta 2.9
	HR-120	N08120	Wrought	37	3(a)	1(a)	25	33	...	...	0.6	0.05	0.5(a)	...	Nb 0.7 N 0.2
Ni-Mo	242	N10242	Wrought (age hardenable)	65	1(a)	25	8	2(a)	...	0.8(a)	0.8(a)	0.03(a)	0.5(a)	...	Cu 0.5(a)

(a) Maximum. (b) Minimum

ranges and are more amenable to welding and fabrication. Many of the solid-solution-strengthened alloys have been tailored to resist specific forms of high-temperature corrosion, such as sulfidation.

Aluminum is sometimes added to the solid-solution-strengthened nickel alloys to enhance their oxidation resistance, through the promotion of external Al_2O_3 (alumina) films. Such is the case with 214 alloy (N07214). Normally, such alloys are used at temperatures beyond the gamma-prime solvus, to avoid precipitation-hardening complications.

In the sections to follow, the resistance of the nickel alloys to a variety of high-temperature corrosion modes of attack is described. Later sections cover specific applications. The fabrication issues associated with the high-temperature, solid-solution-strengthened nickel alloys are similar to those discussed in the previous section for the aqueous corrosion alloys.

High-Temperature Corrosion Properties

Dwaine Klarstrom and Krishna Srivastava, Haynes International, Inc.

The modes of high-temperature corrosion include oxidation, carburization, metal dusting, sulfidation, nitridation, corrosion by halogens, and corrosion by molten salts.

Oxidation

To provide resistance to high-temperature oxidation, most of the nickel alloys rely on additions of chromium. As shown in Table 9, the levels range from 8 to 48 wt%. Some of the alloys contain minor additions of silicon and manganese, to promote the formation of highly protective spinel oxides. Additions of rare earth elements, such as lanthanum and yttrium, can also be used to enhance the resistance of the oxide scales to spallation. As discussed, aluminum is a key addition to many nickel alloys, either to enable precipitation hardening or to form highly protective alumina films during high-temperature oxidation.

Oxidation attack consists of two major components: a loss of metal as the base material is converted into an oxide scale, and internal attack that may consist of intergranular attack, along with the formation of isolated internal oxides. The metal loss can further be described in terms of a continuous oxide scale and oxides lost by spallation, if thermal cycling is involved. For internal attack, if the exposure is in air, then internal nitrides can occur along with internal oxides. This is especially the case in Cr_2O_3-forming alloys, if significant oxide spallation has taken place, or if the alloy contains insufficient aluminum to form a continuous Al_2O_3 layer. The characterization of oxidation attack by measurement of weight changes during exposure does not give a complete description of the damage. Therefore, it is imperative to examine the exposed samples metallographically and to make measurements of the attack observed. In the sections to follow, oxidation attack is expressed as the average metal affected, which comprises metal loss plus average internal attack.

As one may expect, the degree of oxidation attack generally increases with increasing temperature. This is illustrated in Table 10 for tests of selected nickel alloys, carried out in flowing air, with cycling to room temperature every 168 h. At temperatures above 980 °C (1795 °F), volatile CrO_3 is formed, and the protective value of the Cr_2O_3 scale is degraded. This effect is especially evident in the data at 1205 °C (2200 °F). The very low values at all four temperatures for 214 alloy indicate that an Al_2O_3 oxide layer is highly protective.

Cycling to room temperature can have a marked effect on the extent of oxidation attack, due to spallation of the oxide scales. This is illustrated by the data shown in Table 11, which relate to different cycle times in flowing air at 1095 °C (2005 °F). Even though the lengths of the two tests were similar, the amount of damage for the shorter cycling time was much greater.

The amount of attack is even more severe for conditions representing a high-velocity combustion gas and a short cycle time. This type of (dynamic oxidation) test was designed to simulate the conditions in an aircraft gas turbine (Ref 71). The test rig burns a mixture of No. 1 and No. 2 fuel oils, with an air-to-fuel ratio of 50 to 1, to produce a combustion gas having a velocity of Mach 0.3. The samples are held in a rotating carousel that is withdrawn from the hot zone every 30 min and cooled with a blast of air for 2 min, after which it is inserted back into the hot zone. The results of such tests at 980 and 1095 °C (1795 and 2005 °F) are presented in Table 12. The greater severity of these tests can be appreciated by comparing the results to those given in Table 10.

Judgments should not be made about long-term behavior based on the results of short-term tests. Some materials can exhibit a phenomenon known as breakaway oxidation during prolonged exposure. For example, the data shown in Table 13 indicate that X (N06002) and HR-120 (N08120) alloys suffered catastrophic oxidation attack in long-term tests at 1205 °C (2200 °F). For X alloy, complete failure of the sample occurred in 120 days, and for HR-120 alloy, failure occurred in 330 days. Therefore, the data indicate that neither alloy is suitable for long-term service at temperatures above 1150 °C (2100 °F).

Carburization

Carburization refers to ingress of carbon into the metal. This phenomenon occurs in many processing industries, in the presence of carbonaceous gases such as CO, CO_2, CH_4, and other hydrocarbons. Carbon is transferred to the metal surface, diffuses through the metal, and forms various carbides with the alloying elements. It is generally observed at temperatures greater than 800 °C (1470 °F) and at carbon activities less

Table 10 Oxidation in flowing air for 1008 h at various temperatures

Common name	UNS No.	Average metal affected							
		980 °C (1795 °F)		1095 °C (2005 °F)		1150 °C (2100 °F)		1205 °C (2200 °F)	
		µm	mils	µm	mils	µm	mils	µm	mils
214	N07214	5	0.2	3	0.12	8	0.32	18	0.7
230	N06230	18	0.7	33	1.3	86	3.4	201	7.9
600	N06600	23	0.9	41	1.6	74	2.9	213	8.4
617	N06617	33	1.3	46	1.8	86	3.4	318	12.5
601	N06601	33	1.3	66	2.6	135	5.3	191	7.5
X	N06002	23	0.9	69	2.7	147	5.8	>899	>35.4

Table 11 Effect of cycle time on oxidation in flowing air at 1095 °C (2005 °F)

Common name	UNS No.	Average metal affected			
		168 h cycles for 1008 h test		25 h cycles for 1050 h test	
		µm	mils	µm	mils
214	N07214	3	0.1	25	0.98
230	N06230	33	1.3	86	3.4
600	N06600	41	1.6	185	7.28
617	N06617	46	1.8	267	10.5
601	N06601	66	2.6	297	11.7

Table 12 Dynamic oxidation data with a 30 min cycle

Common name	UNS No.	Average metal affected			
		980 °C (1795 °F) for 1000 h		1095 °C (2005 °F) for 500 h	
		µm	mils	µm	mils
214	N07214	25	0.98	30	1.2
230	N06230	71	2.8	132	5.2
600	N06600	312	12.3	495	19.5
617	N06617	249	9.8	>610	>24
601	N06601	76	3.0	>610	>24
X	N06002	142	5.6	328	12.9

than 1. When the temperature is lower and the carbon activity is greater than 1, another mode of corrosion, metal dusting, is observed.

Carburization is different from most other modes of high-temperature corrosion; the formation of internal carbides can lead to metal degradation, embrittlement, and fracture. In this mode, metal loss due to scale formation does not take place; corrosion damage cannot be defined in terms of the sum of the metal loss and internal attack. Instead, the magnitude of carburization is defined by the mass carbon gain (mg/cm^2) and the depth of carburization. The kinetics of carburization depend on the solubility and diffusivity of carbon at the temperature concerned.

The solubility of carbon in nickel alloys is low; therefore, the use of nickel alloys to resist carburizing environments is widespread. However, heat-resistant alloys invariably contain many alloying elements, such as chromium, aluminum, silicon, and so on. Carburization thus always leads to the formation of various chromium carbides. Nickel alloys are protected from carburization by stable oxide scales. Whether an alloy will undergo oxidation or carburization in a gas mixture at a given temperature is determined by the partial pressure of oxygen (oxygen potential) and the carbon activity at that temperature. Reference 72 defines the thermodynamic principles underlying carburization. Also see the several articles on fundamentals of gaseous corrosion and "High-Temperature Gaseous Corrosion Testing" in *ASM Handbook,* Volume 13A, 2003.

At higher temperatures, typically greater than 1050 °C (1920 °F), oxide scales are stable in the following order: $Al_2O_3 > SiO_2 > Cr_2O_3$. For service below 1050 °C (1920 °F), chromia-forming alloys offer satisfactory life. For service above 1050 °C (1920 °F), however, silica- or alumina-forming alloys are preferred. If the processing conditions alternate between carburizing and oxidizing, then chromium in the alloy would alternately oxidize and carburize. The carburization of oxides releases CO for subsequent oxidation, and the cycle continues. This phenomenon leads to what is known as green rot, named for the greenish chromium oxides on the fracture surface.

Carburization data for several commercial alloys are given in Table 14 (Ref 73). All alloys were tested in a gaseous mixture: 5% H_2, 5% CO, 5% CH_4, and balance argon (by volume). The environment was characterized by a low oxygen potential and unit carbon activity. While the gaseous composition remained constant, the partial pressures of oxygen changed with temperature. The calculated equilibrium oxygen partial pressures at the test temperatures were as follows: at 871 °C (1600 °F), $Po_2 = 8.13 \times 10^{-23}$ atm; at 927 °C (1700 °F), $Po_2 = 2.47 \times 10^{-22}$ atm; and at 982 °C (1800 °F), $Po_2 = 6.78 \times 10^{-22}$ atm.

The magnitude of carbon pickup increased significantly at 982 °C (1800 °F), even though the duration of the test was much shorter. Micrographs showing carburization for a set of nickel alloys at 982 °C (1800 °F) for 55 h are shown in Fig. 27. In the case of alloys 601 and 617, carburization penetrated to the center of the samples. Carburization leads to degradation of properties. The influence of carburizing exposure on the residual tensile and Charpy impact properties is given for a wide variety of alloys in Ref 74.

Another set of previously unpublished carburization data is presented in Table 15. In this instance, several alloys were exposed to a gaseous mixture of 5% H_2, 1% CH_4, and balance argon (by volume) at 982 °C (1800 °F) for 55 h. The results are reported in terms of the mass of carbon gain per unit area, the average internal penetration, and the maximum internal penetration. The latter two were measured using an optical microscope. The oxygen potential for this

Table 13 Oxidation in flowing air for 360 days with cooling to room temperature and weighing every 30 days

Common name	UNS No.	Average metal affected							
		980 °C (1795 °F)		1095 °C (2005 °F)		1150 °C (2100 °F)		1205 °C (2200 °F)	
		µm	mils	µm	mils	µm	mils	µm	mils
214	N07214	0	0	0	0	0	0	36	1.4
230	N06230	64	2.5	279	11.0	874	34.4	1626	64.1
HR-120	N08120	84	3.3	589	23.2	1118	44.0	Consumed	
X	N06002	71	2.8	666	26.2	1407	55.4	Consumed	
HR-160	N12160	348	13.7	780	30.7	1158	45.6	1598	62.9

Table 14 Carburization data for heat-resistant alloys

Common name	UNS No.	Carbon mass gain per unit area, mg/cm^2		
		871 °C (1600 °F) for 215 h	927 °C (1700 °F) for 215 h	982 °C (1800 °F) for 55 h
214	N07214	0.14	0.3	0.6
263	N07263	0.1	0.4	3.8
617	N06617	0.26	2.4	5.0
625	N06625	0.31	1.1	5.3
S	N06635	0.32	1.6	2.1
600	N06600	0.40	1.3	2.8
230	N06230	0.40	2.0	2.5
X	N06002	0.45	1.8	2.5
800H	N08810	0.48	1.0	1.0
601	N06601	NA	1.8	4.8

NA, not available. Source: Ref 73

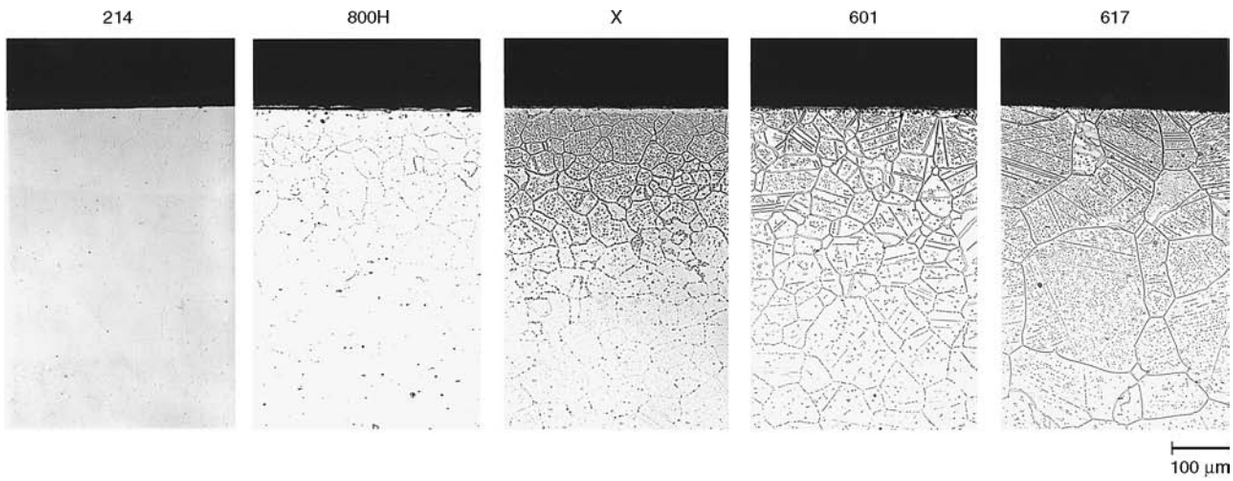

Fig. 27 Light micrographs showing typical carburized structures of several nickel alloys after testing at 982 °C (1800 °F) for 55 h in 5% H_2, 5% CO, and 5% CH_4 (balance argon). Amount of carbon penetration increases in alloys from left to right. Also see Table 14.

environment was very low, because the only source of oxygen was the impurities present in the gaseous mixture. The carbon activity for the environment at the test temperature equaled 1.

A cursory examination of the two tables shows that in the 5% H_2 + 1% CH_4 + argon environment, the gain of carbon for the test materials was much higher than that in the first environment. Apparently, the alloys did not have sufficient oxygen to form a protective scale in this environment. The 214 alloy, with its alumina-rich protective scale, showed the least propensity to carburize.

Metal Dusting

Metal dusting is a form of material degradation that occurs in a strongly carburizing environment in which the carbon activity is $\gg 1$ and the oxygen partial pressure is very low. It also mainly occurs (Ref 75) in the temperature range of 450 to 750 °C (840 to 1380 °F). The attack generally occurs in iron-, nickel-, and cobalt-base alloys and results in the formation of a dust composed of metal particles and carbon. Sometimes, oxides and carbide particles are included as well.

This high-temperature corrosion phenomenon is a particular problem in industrial processes such as ethylene pyrolysis, hydrogen reforming, ammonia synthesis, and steel surface carburization, in which the conditions required for metal dusting are met. A number of studies have been carried out to determine the compositional factors that provide good resistance to this form of attack (Ref 76–78).

Nickel-base alloys have a higher resistance to metal dusting, because their solubility of carbon is relatively low. High chromium levels (22 to 28%) give better resistance, perhaps because a protective oxide film is better able to form in the low-oxygen environment. Aluminum additions appear to be beneficial, due to the formation of Al_2O_3 films, but in environments having very low oxygen partial pressures, such protective layers cannot be readily formed. It appears that additions of molybdenum and tungsten are also beneficial, probably because they tie up carbon in the form of carbides and thereby delay the onset of metal dusting. Finally, additions of silicon have been shown to be effective in resisting metal dusting.

A standardized test for metal dusting has not been developed, because the conditions that produce it are quite varied. For nickel alloys, the attack has a very long period of incubation, which can last many thousands of hours. This is especially true if the levels of iron are low. The progression of the attack has been studied by periodically determining the rate of metal wastage during the test (Ref 75–77). After the incubation period, the rate of metal wastage increases dramatically and may show a slight decrease, as illustrated in Fig. 28. Eventually, pits may form to signify the onset of the metal dusting process, as shown in Fig. 29. A summary of metal wastage rates obtained for a very severe metal dusting environment is given in Table 16.

Because of the great diversity in metal dusting environments, no nickel alloy has yet been found that is completely resistant to attack.

Sulfidation

Nickel sulfides will form in an environment comprising only H_2 and H_2S. The compound Ni-Ni_3S_2 forms a low-temperature eutectic that melts at 635 °C (1175 °F). Liquid sulfide products accelerate corrosion rate greatly; therefore, nickel alloys are unsuitable for use in such environments above approximately 600 °C (1110 °F). Sulfide scales are not protective. They contain an abundance of defects; therefore, diffusion rates of metal ions through sulfides are much faster than through oxides. The kinetics of sulfidation, like those of oxidation, depend on metal ion diffusion and are parabolic in nature. However, rate constants for the sulfidation reaction are several orders of magnitude greater than those for the oxidation reaction.

Fortunately, most sulfur-bearing, high-temperature environments also contain gases such as H_2O, SO_2, CO, CO_2, and so on that give rise to sulfidizing-oxidizing conditions. Under such conditions, the chromium-containing nickel alloys derive their resistance from the formation of protective oxide scales, which are impervious to sulfur diffusion. Thus, sulfidation resistance, in such environments, depends on chromium alloying. Some high-temperature nickel alloys also contain significant amounts of aluminum or silicon, which can contribute to sulfidation resistance by forming an Al_2O_3- or SiO_2-rich sublayer.

The magnitude of corrosion is determined by the environment, temperature, and duration of exposure. A thermodynamic analysis is necessary to determine the partial pressures of sulfur and oxygen, which define the environment at the temperature of concern. Knowing the partial pressures of sulfur and oxygen, it is possible to determine from phase stability diagrams whether a metal will form only sulfides, a mixture of sulfides and oxides, or only oxides. For a nickel-chromium alloy, the superimposition of phase stability diagrams for chromium and nickel is necessary. Similarly, for an alloy based on the Ni-Cr-Si system, the superimposition of three phase stability diagrams is necessary, to identify the regions of stable phases. References 79 and

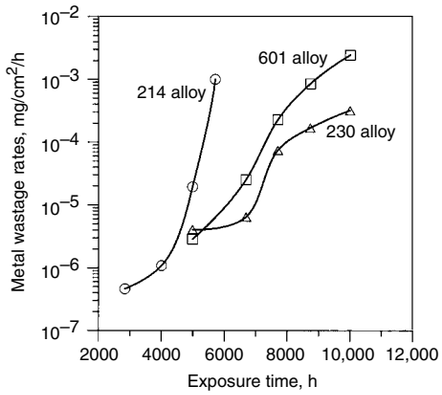

Fig. 28 Metal wastage rates as a function of time in 49% CO, 49% H_2, and 2% H_2O at 650 °C (1200 °F)

Fig. 29 Pitting attack in alloy 601

Table 15 Carburization data for heat-resistant alloys at low oxygen potential

Common name	UNS No.	Carbon mass gain, mg/cm²	Average internal penetration		Maximum internal penetration	
			µm	mils	µm	mils
214	N07214	0	0	0	0	0
617	N06617	2.6	384	15.1	419	16.5
HR-160	N12160	2.9	505	19.9	559	22.0
601	N06601	3.2	521	20.5	572	22.5
800H	N08810	3.6	803	31.6	940	37.0
X	N06002	5.8	526	20.7	559	22.0
230	N06230	5.8	584	23.0	648	25.5
600	N06600	7.2	1021	40.2	1067	42.0
HR-120	N08120	7.9	638	25.1	686	27.0

Table 16 Final metal wastage rates obtained for exposures in 49% CO, 49% H_2, and 2% H_2O at 650 °C (1200 °F)

Common name	UNS No.	Total exposure time, h	Final metal wastage rate, mg/cm²/h
HR-120	N08120	190	0.041
800H	N08810	925	0.0027
214	N07214	5707	0.0010
601	N06601	10,000	0.0025
230	N06230	10,000	0.00032
HR-160	N12160	10,000	(a)

(a) Attack too small for analysis

80 provide an understanding of the thermochemical principles involved.

Coal gasification is an important process, providing material challenges. Reference 81 describes the evaluation of alloys exposed to a gaseous environment, typical of coal gasification, comprising 0.9% CO, 22.2% H_2O, 1.1% H_2S, and balance H_2 at 600 °C (1110 °F). The results of this study are summarized in Table 17.

In this test, prediction of corrosion over a one year period indicated HR-160 alloy (N12160) to be the most sulfidation resistant, due to the presence of a continuous silica-rich layer that protected the substrate metal. The 45TM alloy (N06045) formed a friable external iron, nickel, and chromium sulfide scale; the corrosion attack could not be extrapolated. The MA956 alloy (S67956), an iron-base mechanical alloy, formed a discontinuous aluminum-rich oxide scale, that did not offer sufficient protection from sulfidation.

Sulfidation data are presented in Tables 18 to 20 for tests conducted in a gaseous environment comprising 5% H_2, 5% CO, 1% CO_2, 0.15% H_2S, and balance argon at 760, 871, and 982 °C (1400, 1600, and 1800 °F), respectively. While the gaseous composition was the same at each temperature, it should be noted that the partial pressures of sulfur and oxygen do not remain the same.

Most of the nickel alloys were consumed in the test at 760 °C (1400 °F). In the case of alloy 671, the high chromium content provides the protective oxide scale that enhances its sulfidation resistance. Also, the silica-rich scale that forms on HR-160 alloy (N12160) imparts its sulfidation resistance.

At 871 °C (1600 °F), the partial pressures of sulfur and oxygen changed slightly, and the carbon activity equaled 0. In tests at 871 °C (1600 °F), many nickel alloys were consumed or suffered a high degree of corrosion attack. Of note is the observation that alloy 671, which suffered only a modest degree of attack in the 215 h test, was consumed in the 500 h test.

Sulfidation data for tests in a SO_2-bearing oxidizing environment, 10% SO_2, 5% O_2, 5% CO_2, and balance argon, at 1093 °C (2000 °F) are shown in Table 21. The test duration for all tests was 215 h. The results show that in this environment, most of the alloys performed satisfactorily.

These results of short-term test data should not be extrapolated to estimate the long-term performance of the alloys. However, the results are useful in assessing the relative performance of various alloys.

Corrosion by Halogens

Corrosion by halogens refers to corrosion by gaseous Cl_2/HCl, which occurs in many industrial environments. Examples (Ref 82) include coal combustion (<950 °C, or 1740 °F), mineral chlorination (300 to 900 °C, or 570 to 1650 °F), the production of ethylene dichloride (280 to 480 °C, or 535 to 895 °F), titanium dioxide production (900 °C, or 1650 °F), and waste incineration (~900 °C, or 1650 °F). The amount of chlorine in the environment can range from ~0.01 vol%, in coal combustion, to ~2 vol%, in hazardous waste incineration.

Corrosion by Cl_2/HCl presents a very challenging problem; in contrast to oxides, metal chlorides are characterized by low melting points and high vapor pressures. Relative to many chlorides, the melting points of $NiCl_2$ (1030 °C, or 1885 °F) and $CrCl_3$ (1150 °C, or 2100 °F) are high; therefore, chromium-bearing nickel alloys are frequently used for corrosion protection in such environments. In the presence of oxygen, corrosion involves the formation of oxides as well as volatile chlorides.

Corrosion data from Ref 83 and 84, for a variety of nickel alloys and 800H (iron-nickel alloy, N08810) tested in argon, 20% oxygen, and 0.25% Cl at various temperatures for 400 h, are shown in Table 22. The superior resistance of 214 alloy (N07214) is attributed to the formation of a protective Al_2O_3 scale in this environment. Also, the presence of refractory elements, such as tungsten and molybdenum, is detrimental to chloridation resistance. Both S alloy (N06635) and C-276 alloy (N10276) contain significant amounts of molybdenum and exhibit poorer response. Reference 85 describes tests performed on many of the same nickel alloys in air + 2% Cl at 900 and 1000 °C (1650 and 1830 °F) for 50 h. The results are summarized in Table 23. Data describing the performance of the nickel alloys (including two aqueous corrosion-resistant Ni-Cr-Mo alloys) in air + 2% Cl, at lower temperatures, between 300 and 800 °C (570 and 1470 °F), are summarized in Table 24 (Ref 86).

For the alloys identified in Table 24, it is believed that due to lower testing temperatures and/or short periods of testing, protective scales are still not in place. This makes long-term prediction of the corrosion resistance in such environments very difficult.

The performance of several nickel alloys in 100% hydrogen chloride gas is summarized in Table 25 (Ref 87). The increase in the corrosion rate for HR-160 alloy (N12160) at higher temperatures is attributed to the high cobalt content of the alloy. It has been determined that the chromium-bearing nickel alloys, C-4 (N06455), 600 (N06600), and 625 (N06625), possess good resistance to gaseous HCl at temperatures up to 700 °C (1290 °F). It has been observed that Ni-Cr-Mo materials, such as the aqueous corrosion-resistant C-276 alloy and S alloy (N06635), are more resistant than X (N06002), 600, and 625 alloys.

Table 17 Sulfidation data in a coal gasification environment

600 °C (1110 °F); $P_{S_2} = 6.12 \times 10^{-10}$ atm; $P_{O_2} = 1.38 \times 10^{-25}$ atm; carbon activity = 0.18

		Attack after 2000 h				Predicted attack in 1 year			
		Mean metal affected(a)		Maximum metal affected(b)		Mean metal affected(a)		Maximum metal affected(b)	
Common name	UNS No.	µm	mils	µm	mils	µm	mils	µm	mils
HR-160	N12160	4	0.16	13	0.5	8	0.3	31	1.2
45TM	N0645	24	0.95	55	2.2	No prediction			
MA956	S67956	9	0.35	20	0.8	19	0.75	64	2.5

(a) Mean metal affected = metal loss + mean internal attack. (b) Maximum metal affected = metal loss + maximum internal attack

Table 18 Sulfidation data for heat-resistant alloys at 760 °C (1400 °F) for 215 h

$P_{S_2} = 1.02 \times 10^{-7}$ atm; $P_{O_2} = 3.87 \times 10^{-22}$ atm; carbon activity = 0.16

		Metal loss		Maximum metal affected(a)	
Common name	UNS No.	µm	mils	µm	mils
600	N06600	Consumed		>551	>21.7
601	N06601	Consumed		>749	>29.5
X	N06002	Consumed		>749	>29.5
671	N06671	10	0.4	86	3.4
HR-160	N12160	8	0.3	58	2.3

(a) Maximum metal affected = metal loss + maximum internal attack. For cases where the test coupon was consumed, the maximum metal affected is greater than one-half the coupon thickness.

Table 19 Sulfidation data for heat-resistant alloys at 871 °C (1600 °F)

$P_{S_2} = 8.11 \times 10^{-7}$ atm; $P_{O_2} = 1.62 \times 10^{-19}$ atm; carbon activity = 0

		Metal loss		Maximum metal affected(a)	
Common name	UNS No.	µm	mils	µm	mils
Test duration, 215 h					
230	N06230	Consumed		>495	>19.5
625	N06625	Consumed		>610	>24.0
800H	N08810	193	7.6	>762	>30.0
617	N06617	97	3.8	541	21.3
HR-120	N08120	160	6.3	516	20.3
671	...	36	1.4	188	7.4
HR-160	N12160	20	0.8	157	6.2
Test duration, 500 h					
617	N06617	Consumed		>648	>25.5
671	...	Consumed		>635	>25.0
601	N06601	399	15.7	881	34.7
HR-120	N08120	452	17.8	1189	46.8
800H	N08810	528	20.8	1443	56.9
HR-160	N12160	5	0.2	145	5.7

Maximum metal affected = metal loss + maximum internal attack. Where the test coupon was consumed, the maximum metal affected is greater than one-half the coupon thickness.

Corrosion by Molten Salts

The heat treating industry has been using salt pots and heat exchangers containing a variety of molten salts for a long time for heat treatments such as annealing, quenching, and tempering of metals and alloys. This causes the furnace equipment and other containment equipment in contact with the molten salts to suffer from high-temperature corrosion. Molten salt corrosion is also encountered in heat-transfer and energy-storage media used in solar energy and nuclear systems, fuel cells, high-temperature batteries, and metallurgical extraction processes.

Molten salts flux away the protective oxide scales from a metal surface, causing the corrosion to proceed by oxidation of the alloy, followed by dissolution of the oxide in the molten salt. Oxygen and water vapor present in the molten salts accelerate the kinetics of molten salt corrosion. The heat treating industry uses various compositions of neutral salt. Typical salt baths are $50NaCl + 50KCl$, $50KCl + 50Na_2CO_3$, $20NaCl + 25KCl + 55BaCl_2$, $25NaCl + 75BaCl_2$, and $21NaCl + 31BaCl_2 + 48CaCl_2$.

Field test results in $NaCl + KCl + BaCl_2$ at 840 °C (1545 °F) for one month are shown in Table 26. The mechanism of attack was predominantly intergranular corrosion by the salt components, especially chlorine (Ref 88). The results of laboratory testing in a sodium chloride salt bath, at 840 °C (1545 °F) for 100 h, are given in Table 27. A fresh salt bath was used for each run, and air was used as the cover gas. Again, the corrosion attack was mainly intergranular, without discernible metal loss.

Molten mixtures of nitrate-nitrite salts are also extensively used in the heat treat industry, in the temperature range of 150 to 600 °C (300 to 1110 °F). Reference 89 provides data for various alloys in an equimolar $NaNO_3$-KNO_3 salt bath at 675 °C (1250 °F) over 336 h, with an equilibrium nitrite concentration. A decrease was observed in the corrosion rate with the nickel content of the alloys tested. However, commercially pure nickel (N02200) exhibited a sharply higher corrosion rate. The results of tests at 675 and 700 °C (1250 and 1290 °F) in the sodium-potassium nitrate-nitrite salt for two test durations are shown in Table 28. The corrosion rates appear similar in the two tests. However, alloy 800 showed a sharp increase at the higher temperature.

Metals react with molten sodium hydroxide to form metal oxides, sodium oxide, and hydrogen. Commercially pure nickel possesses the highest resistance to molten sodium hydroxide.

Table 20 Sulfidation data for heat-resistant alloys at 982 °C (1800 °F)

$P_{S_2} = 4.43 \times 10^{-6}$ atm; $P_{O_2} = 2.24 \times 10^{-17}$ atm; carbon activity = 0

Common name	UNS No.	Metal loss		Maximum metal affected	
		µm	mils	µm	mils
Test duration, 215 h					
230	N06230	84	3.3	>572	>22.5
671	...	64	2.5	318	12.5
HR-160	N12160	64	2.5	211	8.3
Test duration, 500 h					
800H	N08810	315	12.4	>1481	>58.4
HR-120	N08120	414	16.3	1328	52.3
HR-160	N12160	541	21.3	1379	54.3

Table 21 Sulfidation data for heat-resistant alloys at 1093 °C (2000 °F) for 215 h

$P_{O_2} = 4.92 \times 10^{-2}$ atm; $P_{S_2} = 3.73 \times 10^{-20}$ atm; carbon activity = 0

Common name	UNS No.	Metal loss		Maximum metal affected	
		µm	mils	µm	mils
230	N06230	13	0.5	203	8.0
600	N06600	13	0.5	127	5.0
X	N06002	15	0.6	142	5.6
800H	N08810	13	0.5	178	7.0
625	N06625	25	0.98	229	9.0
601	N06601	15	0.6	180	7.1
617	N06617	89	3.5	279	11.0

Applications

Brian Baker and Jim Crum, Special Metals Corp.
Lee Flower, Haynes International, Inc.

High-temperature corrosive attack occurs in the petrochemical industry, in heat treating processing equipment, in power plants, and in gas turbines. See also the articles in this Volume that address these specific applications.

Petrochemical and Refining

High-temperature corrosion mechanisms of various types are encountered in petrochemical and refining applications. Sulfidation is frequently encountered. Contaminants containing organic sources of sulfur can convert or partially convert to hydrogen sulfide at sufficiently high temperatures (260 to 288 °C, or 500 to 550 °F). At temperatures below approximately 593 °C (1100 °F), nickel-base materials can perform well in hydrogen-sulfide-containing environments. Alloy 625 (N06625), with its niobium stabilization, can offer a good combination of sulfidation resistance to 593 °C (1100 °F) and resistance to stress-corrosion cracking in polythionic acid resulting from condensation during shutdown. The Fe-Ni-Cr alloys, such as 800 (N08800), 800H (N08810), and 800HT (N08811), are used for high-temperature sulfidation resistance and offer good performance in the absence of polythionic acid stress-corrosion cracking issues. Alloys in the same family but with higher chromium and silicon contents, such as 803 (S35045), 890 (N08890), HPM, and 353MA (S35315), and HR-120 alloy (N08160) (from the Ni-Fe-Cr family) offer admirable resistance to sulfidizing-oxidizing environments. Expansion joint bellows found in fluid catalytic crackers make use of nickel-base alloys such as 825 (N08825) and 625LCF (N06626) because of their combination of sulfidation resistance, strength, and fatigue properties.

Resistance to carburization and oxidation are important for steam methane reforming. The Fe-Ni-Cr alloys 800H and 800HT are commonly used for pigtails and headers collecting the reformer effluent. Components downstream or associated with the reformer may also encounter metal dusting. High-nickel alloys having substantial additions of scale-forming elements (chromium, silicon, and aluminium) perform well. Alloy 693 (N06693) excels in such environments; alloys 690 (N06690) and 601 (N06601) may offer good performance as well, depending on the severity of the environment. Weld overlaying with materials such as filler metal 72, with 44 wt% Cr, or filler metal 53MD, with 29 wt%

Table 22 Halogen corrosion data for heat-resistant alloys at 700 to 1000 °C (1290 to 1830 °F) for 400 h

Common name	UNS No.	Results, µm									
		700 °C (1290 °F)		800 °C (1470 °F)		850 °C (1560 °F)		900 °C (1650 °F)		1000 °C (1830 °F)	
		Metal loss	Total depth(a)	Metal loss	Total depth(a)	Metal loss	Total depth(a)	Metal loss	Total depth(a)	Metal loss	Total depth(a)
214	N07214	10.2	10.2	17.8	61.0	17.8	66.0	22.9	149.9	12.7	50.8
600	N06600	(b)	(b)	20.3	86.4	38.1	132.1	127.0	251.5	330.2	386.1
601	N06601	(b)	(b)	(b)	(b)	(b)	(b)	61.0	264.2	203.2	294.6
800H	N08810	25.4	33.0	22.9	45.7	30.5	96.5	43.2	190.5	203.2	424.2
X	N06002	(b)	(b)	(b)	(b)	(b)	(b)	99.1	218.4	317.5	434.3
S	N06635	78.7	81.3	144.8	149.9	223.5	256.5	315.0	353.1	419.1	472.4
C-276	N10276	33.0	45.7	66.0	71.1	162.6	175.3	299.7	345.4	419.1	449.6

(a) Total depth = metal loss + average internal attack. (b) Not tested

Cr, may be an attractive option as well. The Fe-Ni-Cr alloys 803 and 890 have been used with success as tubing in ethylene cracking furnaces, performing well by virtue of their good resistance to the carburizing-oxidizing environment and good elevated-temperature strength.

Heating and Heat Treating

Heating and heat treating furnace components and accessories may include belts, muffles, baskets, trays, hangers, tubes, and pots. Alloys used for constructing these components must have good corrosion resistance, thermal fatigue resistance, high-temperature strength, thermal stability, and fabricability. Heat treating operations may involve annealing, nitriding, carburizing, carbonitriding, sintering, and brazing. Contaminants may be present, originating from the combustion gases, residual cleaners, lubricants, binders (on or in the parts to be heat treated), brazing compounds, and so on. The presence of certain contaminants, which may include halides, sulfur-containing compounds, sodium, potassium, phosphorus, and so on, can result in significantly accelerated corrosion rates. Typical modes of corrosion found in heat treating operations include oxidation, carburization, sulfidation, nitridation, and molten salt corrosion.

For resistance to oxidation, carbon steels and alloy steels exhibit acceptable performance up to approximately 538 °C (1000 °F). At temperatures up to approximately 871 °C (1600 °F), austenitic and ferritic stainless steels, such as 304 (S30400), 309 (S30900), 310 (S31000), 316 (S31600), 321 (S32100), 347 (S34700), 430 (S43000), and 446 (S44600), exhibit acceptable performance. For long-term service at temperatures above 871 °C (1600 °F), however, materials containing higher nickel levels are generally required, to combat oxidation. Materials that develop tight chromia layers, sometimes in combination with an alumina or silica sublayer, provide enhanced service life. Alloys 601, 602CA (N06625), 617 (N06617), X, 230 (N06230), 800, 803, 890, HPM, 353MA, HR-120, and the cast Fe-Ni-Cr alloy HP (N08705) and its variants are in this category. Alloys 693 and 214 are capable of forming highly protective aluminum oxide scales at high temperatures.

Nickel-base alloys are considered to be more resistant to carburization than stainless steels, primarily due to the fact that the solubility and diffusivity of carbon in the nickel-base alloy matrix are much lower. Heat-resistant Fe-Ni-Cr alloys that find use in carburizing atmospheres include 800 (N08800), 330 (N08330), and DS (WNr 1.4862, 41Fe-37Ni-18Cr-2.3Si-1Mn). Again, materials that can form silicon oxide or aluminum oxide scales or subscales perform well in carburizing atmospheres (e.g., 330 and DS). Increased nickel content, such as in the silicon-containing RA333 alloy (N06333) or the aluminum-containing alloy 601, offers further enhancement in performance. Alloy 600, with a high nickel content and low chromium content, offers excellent performance as well. Nickel-base materials that are capable of forming a tight aluminum oxide scale, such as alloy 214, offer additional increases in performance in carburizing atmospheres.

Elevated-temperature sulfidation under reducing conditions is best countered by using iron- or cobalt-base materials. Sulfidation-oxidation problems, especially when coupled with other forms of corrosion, such as carburization or halide attack, can be countered by using Fe-Ni-Cr materials having sufficient scale-forming elements to afford protection, or by using nickel-chromium claddings (e.g., filler metal 72, or N06072, or alloy 671 powder co-extrusion) or castings (e.g., alloy 671).

Nitriding atmospheres challenge the capabilities of stainless steels at elevated temperatures, approximately 871 °C (1600 °F) and

Table 23 Corrosion data for heat-resistant alloys in air plus 2% Cl for 50 h

Common name	UNS No.	Metal loss		Total depth	
		µm	mils	µm	mils
900 °C (1650 °F)					
214	N07214	15.2	0.60	40.6	1.6
800H	N08810	25.4	1.0	109.2	4.3
600	N06600	50.8	2.0	127.0	5.0
601	N06601	5.1	0.2	132.1	5.2
625	N06625	101.6	4.0	177.8	7.0
C-276	N10276	154.9	6.1	205.7	8.1
230	N10276	33.0	1.3	208.3	8.2
617	N06617	96.5	3.8	299.7	11.8
1000 °C (1830 °F)					
214	N07214	25.4	1.0	50.8	2.0
601	N06601	50.8	2.0	203.2	8.0
800H	N08810	88.9	3.5	266.7	10.5

Source: Ref 85

Table 24 Average thickness and appearance of corrosion layers after 300 h exposure in air plus 2% Cl

Common name	UNS No.	300 °C (570 °F)	500 °C (930 °F)	650 °C (1200 °F)	800 °C (1470 °F)
800H	N08810	1–2 µm Pitlike near carbides	3–4 µm Fragile	2500 µm Very buckled	75 µm Buckled, fragile
45TM	N06045	1 µm Pitlike near carbides	6 µm Buckled	110 µm Fragile, porous, spalled in parts	110 µm Little buckled, spalled in parts
690	N06690	1–2 µm Pitlike	1–2 µm Little porous	6–7 µm Compact, little porous, spalled in parts	27 µm Compact, little porous, spalled in parts
59	N06059	1 µm Fingerlike corrosion	10 µm Layer with good adherence	10 µm Continuous layer, spalled off	36 µm Porous layer, big parts spalled off
C-2000	N06200	1 µm No corrosion attack detectable	20 µm Layer with good adherence	105 µm Leafy layer, spalled off	590 µm Porous layer
HR-160	N12160	1 µm	1 µm Very leafy layer with cracks	20 µm Porous layer with many cracks	30 µm Porous, leafy layer
214	N07214	1–2 µm	7–8 µm Leafy layer, some internal corrosion	9 µm Slightly leafy oxide scale consisting of Cr/Fe and Al oxides	1–2 µm Leafy oxides, spallation

Table 25 Corrosion of heat-resistant alloys in 100% hydrogen chloride gas

Common name	UNS No.	Temperature		Metal loss rate	
		°C	°F	mm/yr	mils/yr
201	N02201	685	1265	4.2	165
600	N06600	685	1265	7.5	296
HR-160	N12160	685	1265	7.0	276
214	N07214	685	1265	5.7	225
602CA	N06025	685	1265	28.6	1127
HR-160	N12160	735	1355	45.6	1797
201	N02201	785	1445	16.7	658
600	N06600	785	1445	26.4	1040
HR-160	N12160	785	1445	96.0	3782

Source: Ref 87

Table 26 Field test results in $NaCl + KCl + BaCl_2$ at 840 °C (1545 °F) for 1 month

Common name	UNS No.	Total depth(a)	
		mm/mo	mils/mo
X	N06002	0.96	37.8
S	N06635	1.02	40
214	N07214	1.80	71
600	N06600	2.44	96
601	N06601	>2.92	>115

(a) Total depth = metal loss + internal attack. Source: Ref 88

Table 27 Laboratory test results in a sodium chloride bath at 840 °C (1545 °F) for 100 h

Common name	UNS No.	Total depth	
		mm	mils
601	N06601	0.066	2.6
214	N07214	0.079	3.1
X	N06002	0.097	3.8
800H	N08810	0.109	4.3
625	N06625	0.112	4.4
617	N06617	0.122	4.8
230	N06230	0.140	5.5
S	N06635	0.168	6.6
600	N06600	0.196	7.7

Table 28 Corrosion rates of nickel alloys in nitrate-nitrite salt

Common name	UNS No.	Corrosion rate: 675 °C (1250 °F) for 1920 h, mm/yr	675 °C (1250 °F) for 1920 h, mils/yr	700 °C (1290 °F) for 720 h, mm/yr	700 °C (1290 °F) for 720 h, mils/yr
214	N07214	0.41	16	0.53	21
600	N06600	0.25	9.9	0.99	39
N	N10003	0.23	9.1	1.22	48
601	N06601	0.48	19	1.25	49
800	N08800	1.85	72.9	6.60	260

Source: Ref 89

above. The solubility of nitrogen in the high-nickel matrix, as for carbon, is very low. The presence of high levels of strong nitride formers, such as aluminum, titanium, niobium, and chromium, can prove detrimental at high temperatures. Alloy 600 (N06600), with its high nickel content and relatively low chromium content, has historically been a workhorse alloy in nitriding environments.

Molten cyanide, nitrate, chloride, and caustic salts may be used for tempering, annealing, hardening, carburizing, and other purposes at temperatures up to approximately 705 °C (1300 °F). Molten chloride salts are used at temperatures above approximately 704 °C (1300 °F); alloy 600 has been shown to be very effective in molten chloride.

Aircraft Gas Turbines

Wrought, cast, and powder-processed nickel alloys are widely used in aircraft gas turbines for both rotating and static components under extreme conditions related to combustion environments, that require high-temperature strength in combination with resistance to oxidation and other forms of high-temperature corrosion. Typical static gas turbine components include compressor, combustor, diffuser, and exhaust cases; combustor liners; turbine vanes; compressor and turbine seal rings; honeycomb and brush seals; turbine vanes; shrouds; fuel manifolds; pneumatic ducting; thermocouple sheaths; and fasteners. Typical rotating gas turbine components in nickel alloys include shafts, disks, and turbine blades.

Power Industry

Fossil fuel power plants use alloy 800 (N08800) reheater or superheater tubes for high-temperature strength and oxidation resistance when steel or stainless steel has unacceptable life. Under very severe conditions, firewall tubes can be weld overlayed with alloy 625 or C-22 alloy (Table 1). Also, cold-drawn, stress-relieved alloy 400 (N04400) has been used for over 40 years in feedwater heater service.

Nickel alloys are used extensively in the hot sections of land-based gas turbines for power generation. As compared with aircraft gas turbines, those based on land are more robust, due to fewer weight constraints. However, the material requirements are generally the same for both types of turbine. Materials commonly used in gas turbine applications include the solid-solution-strengthened 230 (N06230), 617 (N06617), and 625 LCF (N06626) alloys and the age-hardenable Nimonic 80A (N07080), 263 (N07263), 706 (N09706), 718 (N07718), and X-750 (N07750) alloys.

ACKNOWLEDGMENTS

Monel, Inconel, Incoloy, and Nimonic are registered trademarks of Special Metals Corp. Hastelloy, B-3, C-22, C-22HS, C-2000, G-30, G-35, G-50, 230, HR-120, and HR-160 are registered trademarks of Haynes International, Inc. Allcorr is a registered trademark of Allegheny Technologies, Inc. 20Cb-3 is a registered trademark of Carpenter Technology Corp. 254SMO is a registered trademark of Avesta Sheffield.

REFERENCES

1. G.N. Flint, *J. Inst. Met.,* Vol 87, 1959, p 303–310
2. G.N. Flint, *Metallurgia,* Vol 62, 1960, p 195–200
3. W.A. Krivsky, U.S. Patent 3,252,790, May 1966
4. F.G. Hodge and R.W. Kirchner, *Mater. Perform.,* Vol 15 (No. 8), 1976, p 40–45
5. D.L. Klarstrom, A New Ni-Mo Alloy with Improved Thermal Stability, *Proceedings of the 12th Intl. Corrosion Congress,* Sept 1993 (Houston, TX), NACE International, 1993
6. M.M. James, D.L. Klarstrom, and B. Saldanha, Stress-Corrosion Cracking of Nickel-Molybdenum Alloys, Paper 432, *Proceedings of Corrosion 96,* March 1996 (Houston, TX), NACE International, 1996
7. C.R. Brooks, J.E. Spruiell, and E.E. Standsbury, *Int. Met. Rev.,* Vol 29 (No. 3), 1984, p 210–248
8. S.J. Pawel, *Corrosion,* Vol 50 (No. 12), 1994, p 963–971
9. M. Raghavan, B.J. Berkowitz, and J.C. Scanlon, *Metall. Trans. A,* Vol 13, 1982, p 979–984
10. F.G. Hodge, *Corrosion,* Vol 29 (No. 10), 1973, p 375–383
11. L.M. Pike, D.L. Klarstrom, and M.F. Rothman, U.S. Patent 6,544,362, April 2003
12. "Specification for Castings, Nickel and Nickel Alloys," A 494/A 494M, *Annual Book of ASTM Standards,* Vol 01.02, ASTM International, 1999
13. M. Pourbaix, *Atlas of Electrochemical Equilibria in Aqueous Solutions,* NACE International, 1974, p 275–276
14. A.C. Lloyd, D.W. Shoesmith, N.S. McIntyre, and J.J. Noel, *J. Electrochem Soc.,* Vol 150, 2003, p B120–B130
15. A.C. Lloyd, J.J. Noel, N.S. McIntyre, and D.W. Shoesmith, *Electrochim. Acta,* Vol 49, 2004, p 3015–3027
16. A.C. Lloyd, D.W. Shoesmith, J.J. Noel, and N.S. McIntyre, International Symposium on Environmental Degradation of Materials and Corrosion Control in Metals, Metallurgical Society of Canada, 2003
17. N. Sridhar, *Mater. Perform.,* Vol 27 (No. 3), 1988, p 40–46
18. J.R. Crum, and M.E. Adkins, "Correlation of Alloy 625 Electrochemical Behavior with the Sulfuric Acid Isocorrosion Chart" Paper 299, presented at Corrosion 85, NACE International, 1985
19. M.G Fontana, *Corrosion Engineering,* 3rd ed., McGraw-Hill, 1986, p 353
20. T.F. Degnan, *Process Industry Corrosion — The Theory and Practice,* NACE International, 1986, p 275–282
21. "Materials for Receiving, Handling and Storing Hydrofluoric Acid," Publication 5A171, NACE International, 1995
22. E.M. Horn, P.E. Manning, and M. Renner, *Werkst. Korros.* Vol 43, 1992, p 191–200
23. S.W. Ciaraldi, R.M. Berry, and J.M. Johnson, Paper 98, presented at Corrosion 82, NACE International, 1982
24. C.M. Schillmoller, *Chem. Eng. Prog.* Nov 1998, p 49–54
25. J.R. Crum, G.D. Smith, M.J. McNallan, and S. Hirnyj, Paper 382, presented at Corrosion 99, NACE International, 1999
26. R.B. Rebak, J.R. Dillman, P. Crook, and C.V.V. Shawber, *Mater. Corros.,* Vol 52, 2001, p 289–297
27. A.J. Sedricks, *Corrosion of Stainless Steels,* Wiley-Interscience, 1996, p 378
28. B. Gaur and H.S. Srinivasan, *Br. Corros. J.,* Vol 34 (No. 1), 1999, p 63–66
29. "Test Method for Pitting and Crevice Corrosion Resistance of Stainless Steels and Related Alloys by the Use of Ferric Chloride Solution," G 48, *Annual Book of ASTM Standards,* ASTM International, 1999
30. N.S. Meck, P. Crook, and R.B. Rebak, *Electrochem. Soc. Proc.,* Vol 2002-13, 2002, p 355
31. D.M. Aylor, R.A. Hays, R.M. Kain, and R.J. Ferrara, "Crevice Corrosion Performance of Candidate Naval Ship Seawater Valve Materials in Quiescent and Flowing Natural Seawater," Paper 329, presented at Corrosion 99, NACE International, 1999
32. B.M. Barkel, Paper 13, presented at Corrosion 79, NACE International, 1979
33. J.R. Crum and W.G. Lipscombe, *Mater. Perform.,* Vol 25 (No. 4), 1986, p 9–12
34. J.R. Crum, and W.G. Lipscombe, Paper 23, presented at Corrosion 83, NACE International, 1983
35. M. Yasuda, F. Takeya, and F. Hine, *Corrosion,* Vol 39 (No. 10), 1983, p 399–405

36. A.R. McIlree and H.T. Michels, *Corrosion,* Vol 33 (No. 2), 1977, p 60–67
37. G.B. Chambers, *Stainl. Steel World,* Oct 2003, p 57–60
38. P. Crook, The Caustic Dealloying of Molybdenum-Bearing Nickel Alloys, to be presented at EUROCORR 2005 (Lisbon, Portugal), Sept 2005
39. J.R. Crum, E. Hibner, N.C. Farr, and D.R. Munasinghe, Chapter 7, *Casti Handbook of Stainless Steels and Nickel Alloys,* Casti Publishing, 2000, p 287
40. "Corrosion Engineering Bulletin," CEB-5, The International Nickel Company, 1968
41. R.B. Rebak, in *Environmentally Assisted Cracking: Predictive Methods for Risk Assessment and Evaluation of Materials, Equipment and Structures,* ASTM, 2000, p 289
42. G.J. Theus, R.H. Emanuelson, and J. Russell, Paper 209, presented at Corrosion 82, NACE International, 1982
43. J. Kolts, Paper 241, presented at Corrosion 82, NACE International, 1982
44. F.G. Hodge, *Corrosion and Corrosion Protection Handbook,* P.A. Schweitzer, Ed., Marcel Dekker, 1983, p 55
45. Y. Takizawa and I. Sekine, Paper 355, presented at Corrosion 85, NACE International, 1985
46. N. Sridhar and G.A. Cragnolino, *Stress-Corrosion Cracking,* ASM International, 1992, p 131
47. M. Nakahara and T. Shoji, *Corrosion,* Vol 52, 1996, p 634
48. J. Kolts, in *Corrosion,* Vol 13, *Metals Handbook,* 9th ed., ASM International, 1987, p 647
49. "Standard Practice for Making and Using U-Bend Stress-Corrosion Test Specimens," *Annual Book of ASTM Standards,* Vol 3.02, ASTM International, 1997
50. A.I. Asphahani, *Stress-Corrosion Cracking—The Slow Strain Rate Technique,* STP 665, ASTM, 1979, p 279
51. R.D. Kane, M. Watkins, D.F. Jacobs, and G.L. Hancock, *Corrosion,* Vol 33, 1977, p 309
52. N. Sridhar, J.A. Kargol, and N.F. Fiore, *Scr. Metall.,* Vol 14, 1980, p 1257
53. D.B. Mitton, S.-H. Zhang, M.S. Quintana, J.A. Cline, N. Caputy, P.A. Marrone, and R.M. Latanision, Paper 414, presented at Corrosion 98, NACE International, 1998
54. P. Kritzer, N. Boukis, and E. Dinjus, Paper 415, presented at Corrosion 98, NACE International, 1998
55. D.W. Alley and S.A. Bradley, Paper 03351, presented at Corrosion 2003, NACE International, 2003
56. P.L. Andreson, P.W. Emigh, L.M. Young, and G.M. Gordon, Paper 03683, presented at Corrosion 2003, NACE International, 2003
57. D.S. Dunn, Y.-M. Pan, and G.A. Cragnolino, Paper 02425, presented at Corrosion 2002, NACE International, 2002
58. Y.-M. Pan, D.S. Dunn, and G.A. Cragnolino, in *Environmentally Assisted Cracking: Predictive Methods for Risk Assessment and Evaluation of Materials, Equipment and Structures,* ASTM, 2000, p 273
59. J.C. Estill, K.J. King, D.V. Fix, D.G. Spurlock, G.A. Hust, S.G. Gordon, R.D. McCright, G.M. Gordon, and R.B. Rebak, Paper 02535, presented at Corrosion 2002, NACE International, 2002
60. D.V. Fix, J.C. Estill, G.A. Hust, L.L. Wong, and R.B. Rebak, Paper 04549, presented at Corrosion 2004, NACE International, 2004
61. K.J. King, J.C. Estill, and R.B. Rebak, *PVP,* Vol 449, American Society of Mechanical Engineers, 2002, p 103
62. K.J. King, L.L. Wong, J.C. Estill, and R.B. Rebak, Paper 04548, presented at Corrosion 2004, NACE International, 2004
63. S. Kesavan, Ph.D. dissertation, Ohio State University, 1991
64. K.M. Scammon, M.S. thesis, University of Central Florida, 1994
65. Z. Szklarska-Smialowska, and R.B. Rebak, *Control of Corrosion on the Secondary Side of Steam Generators,* NACE International, 1996, p 223
66. R.W. Staehle and J.A. Gorman, *Corrosion,* Vol 59, 2003, p 931
67. A. Mignone, M.F. Maday, A. Borello, and M. Vittori, *Corrosion,* Vol 46, 1990, p 57
68. W. Yang, Z. Lu, D. Juang, D. Kong, G. Zhao, and J. Congleton, *Corros. Sci.,* Vol 43, 2001, p 967
69. "Specification for Nickel and Nickel Alloy Bare Welding Electrodes and Rods,"A5.14, American Welding Society, 1997
70. "Specification for Nickel and Nickel Alloy Welding Electrodes for Shielded Metal Arc Welding," A5.11, American Welding Society, 1997
71. M.F. Rothman, "Oxidation Resistance of Gas Turbine Combustion Materials," Paper 85-GT-10, American Society of Mechanical Engineers, 1985
72. H.J. Grabke, "Carburization—A High Temperature Corrosion Phenomenon," Publication 52, MTI, 1998
73. G.Y. Lai, Internal Report 11620, Haynes International, Inc., 1984
74. M.F. Rothman, *Proceedings of the Ninth International Conference on Metallic Corrosion,* National Research Council of Canada, (Toronto, Canada), 1984
75. H.J. Grabke, R. Krajak, E.M. Müller-Lorenz, and S. Strauss, *Mater. Corros.,* Vol 47, 1996, p 495–504
76. D.L. Klarstrom, H.J. Grabke, and L.D. Paul, "The Metal Dusting Behavior of Several High Temperature Nickel Based Alloys," Paper 01379, presented at Corrosion 2001, NACE International, 2001
77. H.J. Grabke, E.M. Müller-Lorenz, J. Klöwer, and D.C. Agarwal, *Mater. Perform.,* Vol 37 (No. 7), 1998, p 58–63
78. B.A. Baker, G.D. Smith, V.W. Hartmann, L.E. Shoemaker, and S.A. McCoy, "Nickel-Base Material Solutions to Metal Dusting Problems," Paper 02394, presented at Corrosion 2002, NACE International, 2002
79. N. Birks and G.H. Meier, *Introduction to High Temperature Oxidation of Metals,* Edwin Arnold, 1983, p 10–30
80. P. Kofstad, *High Temperature Corrosion,* Elsevier Applied Science, 1988, p 428–464
81. T.P. Levi, J.F. Norton, and W.T. Bakker, *Mater. Corros.,* Vol 50, 1999, p 405–416
82. P. Elliott, A.A. Ansari, and R. Nabovi, *High Temperature Corrosion in Energy Systems,* M.F. Rothman, Ed., TMS, 1985, p 437
83. M.J. McNallan, M.H. Rhee, S. Thongtem, and T. Hensler, Paper 11, presented at Corrosion 85, NACE International, 1985
84. S. Thongtem, M.J. McNallan, and G.Y. Lai, Paper 372, presented at Corrosion 86, NACE International, 1986
85. P. Elliott, A.A. Ansari, R. Prescott, and M.F. Rothman, Paper 13, presented at Corrosion 85, NACE International, 1985
86. C. Schwalm and M. Schutze, *Mater. Corros.,* Vol 51, 2000, p 34–49, 73–79, 161–172
87. J.J. Barnes, Paper 446, presented at Corrosion 96, NACE International, 1996
88. G.Y. Lai, M.F. Rothman, and D.E. Fluck, Paper 14, presented at Corrosion 85, NACE International, 1985
89. J.W. Slusser, J.B. Titcomb, M.T. Heffelfinger, and B.R. Dunbobbin, *J. Met.,* Vol 37 (No. 6), 1985, p 24–27

SELECTED REFERENCE

- G.Y. Lai, *High-Temperature Corrosion of Engineering Alloys,* ASM International, 1990

ASM Handbook, Volume 13B: Corrosion: Materials
S.D. Cramer, B.S. Covino, Jr., editors, p252-299
DOI: 10.1361/asmhba0003822

Corrosion of Titanium and Titanium Alloys

Ronald W. Schutz, RMI Titanium Company

TITANIUM ALLOYS were originally developed in the early 1950s for aerospace applications in which their high strength-to-density ratios were especially attractive. Although titanium alloys are still vital to the aerospace industry for these properties, recognition of the excellent resistance of titanium to many highly corrosive environments, particularly oxidizing and chloride-containing process streams, has led to widespread nonaerospace (industrial) applications. Stemming from decreasing cost and increasing availability of mill and fabricated products, titanium and its alloys have become standard engineering materials for a host of common industrial applications (Ref 1, 2). In fact, a growing trend involves the use of high-strength aerospace-founded titanium alloys for industrial service in which the combination of high strength-to-density ratio and superior corrosion resistance is critical and desirable.

The objectives of this article are severalfold:

- Describing and characterizing the relevant modes of corrosion observed on titanium alloys
- Providing a comprehensive overview of the available corrosion database on titanium alloys, with references
- Providing basic explanations and insights relative to the corrosion behavior, and relevant application guidelines where available
- Offering practical strategies for expanding the useful corrosion resistance of titanium in corrosive environments

The designations and nominal compositions of commercial titanium alloys addressed in this article are listed in Table 1. The alloys listed in this table with a footnote indicator represent titanium alloys typically used in industrial service based primarily on their corrosion resistance. It is for this reason that the majority of corrosion data compiled in this article relate to these alloys. These range from no- or low-alloy-content single-phase alpha (α) or near-α (relatively small amount of beta, β, phase) titanium alloys to more highly alloyed, higher-strength α-β and metastable β alloys. The α phase consists of a hexagonal close-packed crystal structure, whereas the β phase is body-centered cubic. The remaining titanium alloys listed were primarily developed for aerospace purposes, where generally higher strength and, particularly, an improved strength-to-weight ratio were sought. Increased alloy strength is achieved via solid-solution alloying and stabilization of two-phase ($\alpha + \beta$) structures. With sufficient β-phase stabilization, many of these more highly alloyed α-β and metastable β grades may also be heat treated (i.e., aged) to much higher strengths. An extensive review of the metallurgy and corresponding properties of these commercial titanium alloys can be found in various handbooks (Ref 2–5).

Mechanism of Corrosion Resistance

The excellent corrosion resistance of titanium alloys results from the formation of very stable, continuous, highly adherent, and protective surface oxide films. Because titanium metal itself is highly reactive and has an extremely high affinity for oxygen, these beneficial surface oxide films form spontaneously and instantly when fresh metal surfaces are exposed to air and/or moisture. In fact, a damaged oxide film can generally reheal itself instantaneously if at least traces (that is, a few parts per million) of oxygen or water are present in the environment.

Table 1 Designation and nominal composition of commercial titanium alloys

Common alloy designation	ASTM grade	UNS designation	Nominal composition, wt%	Alloy type
CP 1(a)	1	R50250	Unalloyed titanium	α
CP 2(a)	2	R50400	Unalloyed titanium	α
CP 3(a)	3	R50550	Unalloyed titanium	α
CP 4	4	R50700	Unalloyed titanium	α
Ti-Pd(a)	7/11	R52400, R52250	Ti-0.15Pd	α
Ti-lean Pd(a)	16/17	R52402, R52252	Ti-0.06Pd	α
TIRU or TiRu(a)	26/27	R52404/R52254	Ti-0.1Ru	α
SMI-ACE(a)	30/31	...	Ti-0.3Co-0.05Pd	α
AKOT(a)	33/34	...	Ti-0.4Ni-0.015Pd-0.025Ru-0.15Cr	α
Grade 12(a)	12	R53400	Ti-0.3Mo-0.8Ni	α
Ti-3-2.5	9	R56320	Ti-3Al-2.5V	Near-α
Ti-3-2.5-Ru(a)	28	R56323	Ti-3Al-2.5V-0.1Ru	Near-α
Ti-3-2.5-Pd(a)	18	R56322	Ti-3Al-2.5V-0.06Pd	Near-α
Ti-6-2-1-1	...	...	Ti-6Al-2Nb-1Ta-0.8Mo	Near-α
Ti-5-2.5	6	R54250	Ti-5Al-2.5Sn	α
Ti-5-1-1-1	32	R55111	Ti-5Al-1Sn-1Zr-1V-0.8Mo	Near-α
Ti-8-1-1	...	R54810	Ti-8Al-1V-1Mo	Near-α
Ti-6-2-4-2-S	...	R54620	Ti-6Al-2Sn-4Zr-2Mo-0.1Si	Near-α
Ti-6-4	5	R56400	Ti-6Al-4V	α-β
Ti-6-4 ELI	23	R56407	Ti-6Al-4V (0.13 max O)	α-β
Ti-6-4-Ru(a)	29	R56404	Ti-6Al-4V-0.1Ru (0.13 max O)	α-β
Ti-550	...	...	Ti-4Al-2Sn-4Mo-0.5Si	α-β
Ti-6-6-2	...	R56620	Ti-6Al-6V-2Sn-0.6Fe-0.6Cu	α-β
Ti-6-2-4-6	...	R56260	Ti-6Al-2Sn-4Zr-6Mo	α-β
Ti-6-22-22	...	...	Ti-6Al-2Sn-2Zr-2Mo-2Cr-0.15Si	α-β
Ti-17	...	R58650	Ti-5Al-2Zr-2Sn-4Mo-4Cr	α-β
Ti-10-2-3	...	...	Ti-10V-2Fe-3Al	Near-β
Ti-5-5-5-3	...	...	Ti-5Al-5Mo-5V-3Cr	Near-β
Ti-15-3-3-3	...	...	Ti-15V-3Sn-3Cr-3Al	β
Ti Beta-C(a)	19	R58640	Ti-3Al-8V-6Cr-4Zr-4Mo	β
Ti Beta-C/Pd(a)	20	R58645	Ti-3Al-8V-6Cr-4Zr-4Mo-0.06Pd	β
Ti-13-11-3	...	...	Ti-3Al-13V-11Cr	β
Beta-21S(a)	21	R58210	Ti-15Mo-2.7Nb-3Al-0.25Si	β
Ti-15-5-3(a)	...	...	Ti-15Mo-5Zr-3Al	β
Ti-45Nb	...	...	Ti-45Nb	β

Note: ELI, extra-low interstitial. (a) Often used primarily for corrosion resistance

However, certain anhydrous conditions in the absence of a source of oxygen may result in titanium corrosion, because the protective film may not be regenerated if damaged.

The nature, composition, and thickness of the protective surface oxides that form on titanium alloys depend on environmental conditions. In most aqueous environments, the oxide is typically TiO_2 but may consist of mixtures of other titanium oxides, including TiO_2, Ti_2O_3, and TiO (Ref 6). High-temperature oxidation tends to promote the formation of the denser, more chemically resistant form of TiO_2 known as rutile, whereas lower temperatures often generate a less crystalline and protective form of TiO_2, anatase, or a mixture of rutile and anatase (Ref 6). In dilute reducing acids, a 20 to 100 Å multiplex film consisting of a hydrated titanium sesquioxide (Ti_2O_3) inner layer and a TiO_2 outer layer has been shown to form (Ref 7). Increasing redox potential favors TiO_2 formation, and increasing exposure temperature and/or time motivate conversion to the more stable rutile form of TiO_2. Although these naturally formed films are typically less than 10 nm thick (Ref 8) and are invisible to the eye, the TiO_2 oxide is highly chemically resistant and is attacked only by very few substances that include hot concentrated HCl, H_2SO_4, NaOH, and (most notably) HF. This thin surface oxide is also a highly effective barrier to hydrogen penetration of the alloy, as is discussed in a later section of this article.

Furthermore, the TiO_2 film, being an *n*-type semiconductor, exhibits increasing electronic conductivity with increasing temperature. As a cathode, titanium readily passes current and permits electrochemical reduction of ions in an aqueous electrolyte. On the other hand, very high resistance to anodic current flow (anodic polarization) across this passive oxide film can be expected in most aqueous solutions. Because the passivity of titanium stems from the formation of a stable oxide film, an understanding of the corrosion behavior of titanium is obtained by recognizing the conditions under which this oxide is thermodynamically stable. The Pourbaix (potential-pH) diagram for the titanium-water system at 25 °C (75 °F) is shown in Fig. 1 (Ref 9) and depicts the wide regime over which the passive TiO_2 film is predicted to be stable, based on thermodynamic (free-energy) considerations. Oxide stability over the full pH scale is indicated over a wide range of highly oxidizing to mildly reducing potentials, whereas oxide film breakdown and the resultant corrosion of titanium occur under reducing acidic conditions. Under strongly reducing (cathodic) conditions, titanium hydride formation is predicted. This range of oxide film stability and passivation is relatively insensitive to the presence of chlorides, explaining the high innate resistance of titanium to aqueous chloride environments (Ref 10).

Thus, successful use of titanium alloys can be expected in mildly reducing to highly oxidizing environments in which protective TiO_2 and/or Ti_2O_3 films form spontaneously and remain stable. On the other hand, uninhibited, strongly reducing acidic environments may corrode titanium, particularly as temperature increases. However, shifting the alloy potential in the noble (positive) direction by various means can induce stable oxide film formation, often overcoming the corrosion resistance limitations of titanium alloys in normally aggressive reducing acidic media. Effective strategies for expanding corrosion resistance, such as alloying titanium with more acid-resistant and/or noble elements, are discussed in greater detail in the final section of this article.

The nature of the oxide film on titanium alloys basically remains unaltered in the presence of minor alloying constituents; thus, small additions (<2 to 3%) of most commercially used alloying elements or variations in trace alloy impurities generally have little effect on the basic corrosion resistance of titanium in normally passive environments. For example, despite small differences in interstitial element (carbon, oxygen, and nitrogen) and iron content, all unalloyed grades of titanium possess the same useful range of resistance in environments in which corrosion rates are normally very low (Ref 11, 12). However, under active conditions in which titanium exhibits significant general corrosion (such as in strong reducing acid media), certain background elements may accelerate corrosion. Increasing the alloy iron and sulfur content, for example, increases corrosion rates when corrosion rates exceed ~0.10 mm/yr (3.9 mils/yr) (Ref 11, 12). Thus, minor variations in alloy chemistry may be of concern only under conditions in which the passivity of titanium is borderline or when the metal is actively corroding.

Weldments (Ref 12) and castings (Ref 13, 14) of most of the titanium alloys listed in Table 1 generally exhibit corrosion resistance similar to that of the unwelded, wrought counterparts. Because the same basic protective titanium oxide surface film forms regardless of microstructure, titanium weldments and associated heat-affected zones generally do not experience corrosion limitations in welded components when normal passive conditions prevail for the wrought metal. However, under marginal or actively corroding conditions (for corrosion rates >0.05 mm/yr, or 2.0 mils/yr), weldments may experience accelerated corrosion attack relative to the base metal, depending on alloy composition (Ref 12).

Forms of Corrosion and Related Test Methods

Titanium alloys, like other metals, are subject to corrosion in certain environments.

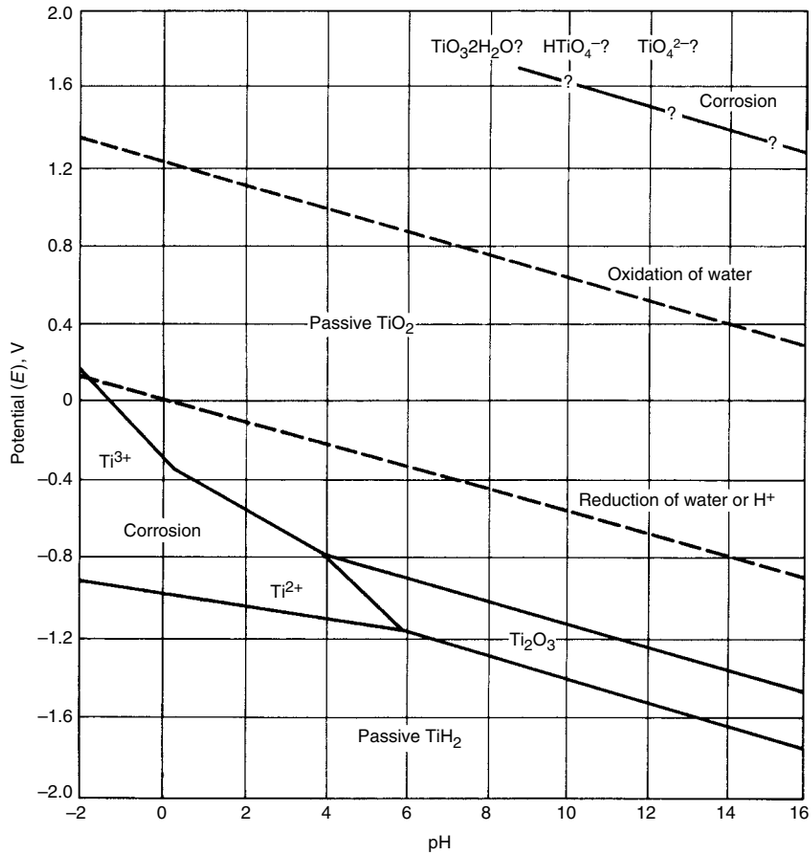

Fig. 1 Pourbaix (potential-pH) diagram for the titanium-water system at 25 °C (75 °F). Source: Ref 9

The primary forms of corrosion that have been observed on these alloys include general corrosion, crevice corrosion, anodic pitting, hydrogen damage, and stress-corrosion cracking. In any contemplated application of titanium, its susceptibility to degradation by any of these forms of corrosion should be considered. In order to understand the advantages and limitations of titanium alloys, each of these forms of corrosion is explained. Although they are not common limitations to titanium alloy performance, galvanic corrosion, corrosion fatigue, and erosion-corrosion are included for completeness.

General Corrosion

General corrosion is characterized by a relatively uniform attack over the exposed metal surface. At times, general corrosion in aqueous media may take the form of mottled, severely roughened metal surfaces that resemble localized attack. This uneven attack results from variations in the corrosion rate of localized surface patches due to localized masking of metal surfaces by process scales, corrosion products, or gas bubbles. When titanium is in the fully passive condition, corrosion rates are typically less than 0.02 mm/yr (0.8 mil/yr) and well below the 0.13 mm/yr (5 mils/yr) maximum corrosion rate commonly accepted by designers. This minimal acceptable corrosion is attributable to the finite oxidation (typically TiO_2 film growth) of titanium alloy surfaces. This oxide film growth manifests itself as colored surfaces and very slight weight gain by test coupons. As a result, titanium is generally designed with a zero corrosion allowance in normal passive environments.

General corrosion becomes a concern in reducing acid environments, particularly as acid concentration and temperature increase. In strong and/or hot reducing acids (in the absence of inhibitors), the oxide film of titanium can deteriorate and dissolve, and the unprotected metal is oxidized to the soluble trivalent ion ($Ti \rightarrow Ti^{3+} + 3e^-$). This ion has a characteristic violet color in acid solutions. If dissolved oxygen or other oxidizing species are present in hot acid, the Ti^{3+} ion is readily oxidized to the less soluble (pale yellow) Ti^{4+} ion, which may subsequently hydrolyze to form insoluble TiO_2 precipitates/scales. Titanium ion hydrolysis often produces highly colored metal surfaces, generating thin titanium oxide films that may inhibit subsequent corrosion. Gray-matte or dull silver surface finishes, produced by thin titanium hydride surface films, can also be observed in reducing acid exposures where severe corrosion attack has occurred.

General Corrosion Testing. General corrosion rates for titanium alloys can be determined from weight loss data, dimensional changes, and electrochemical methods (Ref 15). Electrochemical anodic and cathodic polarization testing is often used to supplement weight loss testing. Polarization testing can identify whether the alloy is truly fully passive or possibly metastable; this is often not discernible from weight loss tests alone. The immersion test procedures described in ASTM G 1 and G 31 apply, provided several modifications are observed (Ref 15, 16). These modifications focus on test sample surface preparation and posttest sample-cleaning procedures.

The type of surface finish tested should resemble the one expected in service. For titanium alloys, this will often be the pickled finish, although sandblasted or ground surfaces are also common. The initial degreasing of test samples should avoid chlorinated organic solvents (with higher-strength titanium alloys), anhydrous methanol, or hot alkaline cleaners, if possible. Acceptable cleaning solvents include methyl ethyl ketone, acetone, most alcohols, benzene, and most detergent solutions. The pickled finish can be prepared by pickling the metal in a 35 vol% HNO_3-5 vol% HF-60 vol% H_2O solution (based on 48 wt% HF and 70 wt% HNO_3 stock acids) at 20 to 55 °C (70 to 130 °F) for one minute or more. Typically, 0.003 to 0.025 mm (0.1 to 1.0 mils) of surface is removed in this process, depending on surface requirements. More dilute solutions, such as 12 vol% HNO_3-1 vol% HF-87 vol% H_2O, can also be used if slower pickling rates are desired. In any case, a minimum 7 to 1 HNO_3 to HF vol% ratio should be maintained to avoid excessive uptake of hydrogen in titanium alloys during pickling. After pickling, a quick rinse in deionized water leaves a shiny specimen that is ready for weighing after air drying. Blasted and abraded surfaces are prepared by procedures similar to those used for other metals. Steel or chilled-iron grit, which can smear/embed into titanium surfaces, should be avoided.

After laboratory or in situ test exposure, titanium samples can be coated with tenacious, insoluble corrosion product (TiO_2) films or scales, which require removal before final weighing. Because titanium oxides are not soluble in common mineral acids, very light (a several second exposure), fine grit blasting has been found to be most effective. If scaling consists of silicaceous, carbonaceous, sulfate, or other typical process stream deposits, then acids or alkaline solutions that are properly inhibited with oxidizing species must be used; common amine inhibitors are not effective on titanium. Recommended cleaning solutions for these scales are discussed in detail in Ref 1 and 15.

Serious consideration must be given to the presence of test medium contaminants that may significantly affect the corrosion rate of titanium. Metal ion contaminants or dissimilar-metal corrosion products can promote the passivity of titanium (see the section "Expanding the Corrosion Resistance of Titanium" later in this article). The degree of aeration and other background chemistry variables in the test media that influence alloy passivity in service must be taken into account in order to avoid deviated and/or misleading test results.

Immersion testing will generate weight loss data, or corrosion current measurements can be obtained from electrochemical polarization tests (ASTM G 3 and G 5). Corrosion rates in millimeters per year for titanium alloys can be calculated from weight loss data as follows:

$$\text{Corrosion rate (mm/yr)} = \frac{(8.76 \times 10^4)W}{(d)(A)(t)}$$

where d is the titanium alloy density (in grams per cubic centimeter), A is the sample surface area (in square centimeters), t is the exposure time (in hours), and W is the weight change (in grams).

Corrosion rates in millimeters per year can be calculated from electrochemical measurements by using the equation:

$$\text{Corrosion rate (mm/yr)} = \frac{(0.0033)(i_{corr})(\text{EW})}{d}$$

where i_{corr} is the measured corrosion current density (in milliamps per square centimeter), d is alloy density (in grams per cubic centimeter), and EW is the equivalent weight for titanium. The equivalent weight for titanium is approximately 16 under reducing acid conditions and 12 under oxidizing conditions. The value of i_{corr} is typically determined from Tafel slope extrapolation or linear polarization methods (Ref 17, 18).

Further guidance on corrosion testing of titanium can be found elsewhere (Ref 15).

Crevice Corrosion

Titanium alloys may be subject to localized attack in tight crevices exposed to hot (>70 °C, or 160 °F) chloride, bromide, iodide, fluoride, or sulfate-containing solutions. Crevices can stem from surface-adherent process stream deposits or scales, metal-to-metal joints (for example, poor weld joint design or tube-to-tubesheet joints), and gasket-to-metal flange and other seal joints (Ref 19, 20).

The mechanism for crevice corrosion of titanium is similar to that for stainless steels, in which oxygen-depleted reducing acid conditions develop within tight crevices (Ref 19). The model for crevice corrosion is illustrated in Fig. 2. Dissolved oxygen or other oxidizing species in the bulk solution are depleted in the restricted volume of solution in the crevice. Finite surface oxidation in crevices consumes these species faster than diffusion from the bulk solution can replenish them (Ref 19, 21). As a result, metal potentials within crevices become active (negative) relative to metal surfaces exposed to the bulk solution. This creates a macro electrochemical cell in which the crevices become anodic and corrode, and the surrounding more noble metal surface is the cathode.

Titanium chlorides formed within the crevice are unstable and tend to hydrolyze, forming hydrochloric acid (HCl) and titanium oxide/hydroxide corrosion products. Because of the

small, restricted volumes of solution within tight crevices, crevice pH levels as low as 0 to 1 can develop. These local reducing acidic conditions can result in severe and rapid localized active corrosion within crevices, depending on alloy resistance, temperature, and redox potential of the bulk solution.

Although dissolved oxidizing species such as oxygen, chlorine, ferric ion (Fe^{3+}), and cupric ion (Cu^{2+}) tend to effectively inhibit the general corrosion of exposed titanium surfaces, most of these species tend to accelerate the onset and propagation of titanium alloy crevice corrosion. These species are excellent cathodic depolarizers and thus accelerate cathodic reduction kinetics, which often are rate controlling. These cationic oxidizing species will not diffuse into the active crevice to inhibit attack. On the other hand, certain anionic oxidizing species, such as NO_3^-, ClO_3^-, OCl^-, CrO_3^{2-}, ClO_4^-, and MnO_4^-, can migrate into the crevice and inhibit crevice attack when present in halide solutions.

Crevice corrosion on titanium typically generates irregularly shaped pits (Fig. 3). Microstructural examination of hand-polished and etched sections of crevices often reveals a surrounding layer of precipitated titanium hydrides (Fig. 4). These are a by-product of hydrogen reduction at cathodic sites within and/or surrounding the crevice. Hydrides may not form around or within active crevices in aqueous media containing strong cathodic depolarizers (oxidants).

Although frequently interpreted as a pitting phenomenon, smeared surface iron pitting of unalloyed titanium in hot brines appears to be a special case of crevice corrosion (Ref 22). It results when iron, carbon steel, or low-alloy steel is gouged, scratched, smeared, or embedded into a titanium surface, breaching the titanium oxide film. During hot (>80 °C, or 175 °F) brine exposure, the embedded iron can either corrode off the surface and permit repassivation, or develop local acidic conditions if occluded by titanium metal smears or laps. Localized attack initiated by this mechanism creates a very characteristic circular pit morphology (Fig. 5) and can involve local hydrogen absorption. Pit initiation has not been observed with copper, nickel, or austenitic stainless steel alloys smeared into titanium surfaces. The titanium-palladium (Ti-Pd), titanium-ruthenium (Ti-Ru), and grade 12 alloys appear to be much more resistant to this form of localized attack.

Several highly effective strategies are available for preventing titanium alloy crevice corrosion and smeared iron pitting, as discussed in a subsequent section of this article. In all cases, the basic remedy aims at maintaining creviced metal surfaces at sufficiently noble potentials where titanium alloy passivity is assured (Ref 20).

Crevice corrosion testing of titanium alloys generally aims at determining go/no-go performance information. The rate of crevice corrosion is of little practical interest, because crevice attack is generally insidious and very rapid. Thus, crevice corrosion cannot be tolerated in any form. Many crevice test assemblies have been used, including the multiple-crevice serrated washer (ASTM G 78). Unfortunately, crevice corrosion initiation is not very reproducible, especially when pH and temperature conditions are marginal and few or no cathodic depolarizers are present.

Because the susceptibility of titanium to crevice corrosion increases dramatically as creviced surface area increases and crevice gap decreases, the larger sandwich-type crevice test assembly illustrated in Fig. 6 has proved to be most effective (Ref 15, 16). This approach typically employs an assembly consisting of 25 to 38 mm (1.0 to 1.5 in.) square flat sheet or plate specimen, with thin gasket sheets (typically virgin polytetrafluoroethylene, or PTFE) interspersed to provide the desired number of metal-to-metal and metal-to-gasket crevices per assembly.

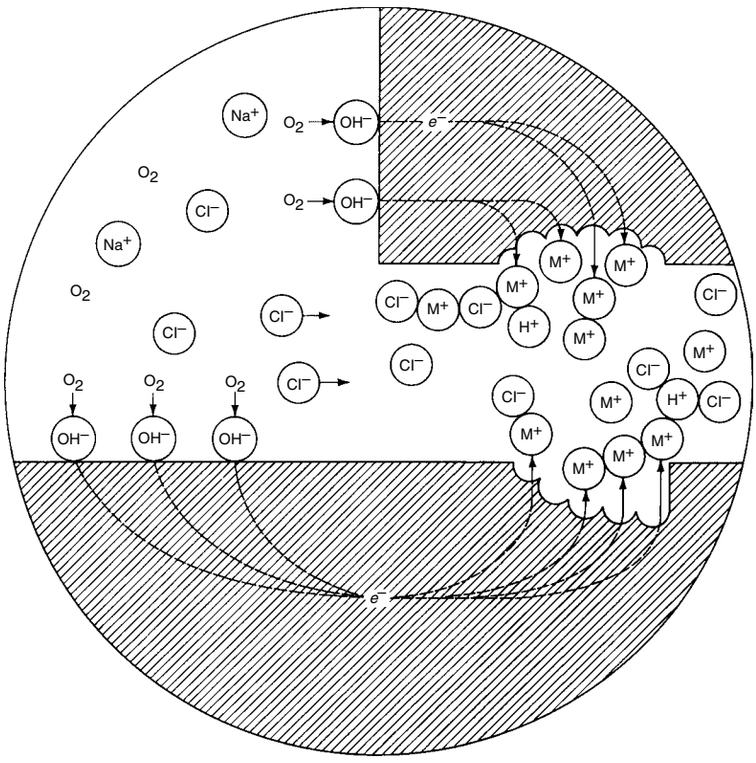

Fig. 2 Schematic showing the mechanism of crevice corrosion for titanium in aqueous chloride media

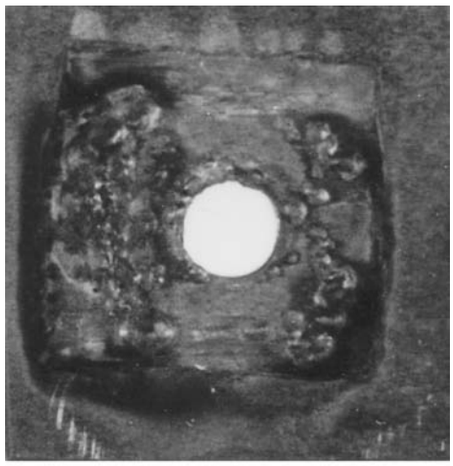

(a)

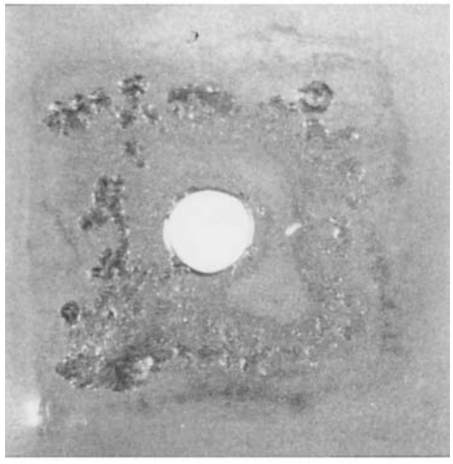

(b)

Fig. 3 Crevice corrosion attack of unalloyed titanium coupon surfaces within tight gasket-to-metal crevices after exposure to hot chloride brines. (a) Before cleaning. (b) After cleaning

This assembly is fastened together with a centerline titanium bolt and nut and tightened with a controlled torque in the range of 2.8 to 10.1 N · m (25 to 90 in · lb). Titanium assembly bolts are covered with an insulating PTFE sleeve or tapewrap to avoid galvanic interactions between coupons. Coupons must be flat and surfaces must be smooth to ensure tight, uniform crevice gaps. When only metal-to-metal crevices are of interest, the interspersed gaskets are omitted, and one generally torques the assembly up toward the high end of the range given. The preparation of crevice test coupons involves considerations similar to those described for general corrosion test coupons.

Although crevice corrosion can actually initiate after several hours of exposure, test duration should be a minimum of approximately 30 days (and preferably longer) in order to develop a sufficient degree of attack for detection and measurement purposes. Post-test evaluation of creviced coupons may require removal of titanium oxide/hydroxide corrosion products if crevice attack has occurred. Common mineral acids and reagents will not dissolve these tenacious deposits. Very light (≥120 grit and <5 to 8 s) sandblasting of the coupon will readily remove these scales and facilitate visual examination of pitted surfaces (ASTM G 46).

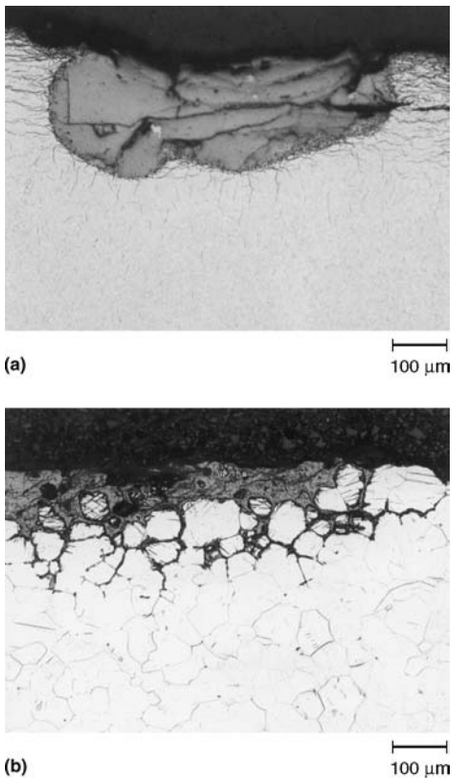

Fig. 4 Typical cross-sectional micrographs of crevice attack on unalloyed titanium in hot chloride brines. (a) More uniform crevice attack with hydride surface layer beneath TiO_2 cap. (b) Intergranular crevice attack beneath TiO_2 cap. Original magnification approximately 100×

Creviced coupon surfaces are often highly colored after exposure but reveal no visible pits after sandblasting. This is indicative of the very slight growth of a protective surface titanium oxide film, which is considered quite normal and acceptable from a performance standpoint. Slight coupon weight gain is often measured in this situation. In addition to visual examination and weight change measurements, monitoring of creviced specimen potential (Ref 23) and current (Ref 24) has been used to a limited extent to identify the initiation of titanium crevice corrosion. More comprehensive information on crevice corrosion testing of titanium is available elsewhere (Ref 15).

Pitting

Pitting is defined as localized corrosion attack occurring on openly exposed metal surfaces in the absence of any apparent crevices. Pitting occurs when the potential of the metal exceeds the anodic breakdown potential of the metal oxide film in a given environment. When the anodic breakdown (pitting) potential of the metal is equal to or less than the corrosion potential under a given set of conditions, spontaneous pitting can be expected.

Because of its protective oxide film, titanium exhibits anodic pitting potentials, E_b, that are very high (≫1 V); thus, pitting corrosion is generally not of concern for titanium alloys. For example, pitting potentials exceed +80 V versus the saturated calomel electrode (SCE) in sulfate and phosphate solutions and are typically in the +5 to +10 V range for chlorides. Although pitting is normally not a limiting factor in titanium performance, pitting potential values provide useful guidelines for titanium used in anode applications where impressed anodic potentials may be high, or where significant inadvertent stray currents exist.

The anodic pitting potential of titanium is dependent on alloy content, medium chemistry, temperature, potential scan rate, and, especially, surface condition. A more intrinsic alloy property is the repassivation (protection) potential, which is defined as the minimum potential at which pitting can be maintained (Ref 25).

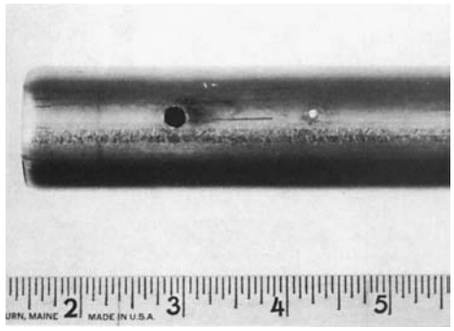

Fig. 5 Smeared surface iron pitting of unalloyed titanium tubing in hot brine service. Source: Ref 22

This pitting parameter is not sensitive to surface condition or measuring-technique artifacts, and it represents a more conservative design guideline than the anodic breakdown potential. The repassivation potentials of titanium alloys are also very high relative to the alloy corrosion potentials, and this explains why titanium alloys are generally resistant to pitting attack.

Pitting Potential Testing. The potentiostatic (constant potential) and potentiodynamic (potential scan) electrochemical techniques used on other metals to measure anodic pitting potential apply to titanium alloys as well (Ref 15, 18). Guidelines are described in ASTM G 3 and G 5. Determination of anodic pitting potential requires slow scan rates (≤0.5 mV/s) and consideration of the surface condition tested. For example, abraded or sandblasted sample finishes will exhibit significantly lower pitting potentials than as-pickled surfaces. Also, because of the relatively high pitting potential of titanium, a potentiostat with a potential scan range of at least −2 to +10 V (SCE) is generally required. Recommended auxiliary electrodes include high-density graphite, glassy carbon, or platinum.

Repassivation potentials are readily determined by using the galvanostatic method (Ref 25, 26) or the constant potential-surface scratch test (Ref 18, 25). The galvanostatic method involves impressing an anodic current density of approximately +200 mA/cm^2 (1290 mA/in.^{2}) on the specimen for at least several minutes before measuring the repassivation potential of the sample (Ref 15, 26). Reproducible, definitive repassivation potentials are often more difficult to derive by using reverse scan potentiodynamic techniques.

Hydrogen Damage

Titanium alloys are widely used in hydrogen-containing environments and under conditions in which galvanic couples or cathodic charging (impressed current) causes hydrogen to be evolved on metal surfaces. Although excellent performance is revealed for these alloys in most cases, hydrogen embrittlement has been observed.

The surface oxide film of titanium is a highly effective barrier to hydrogen penetration. Traces of moisture or oxygen in hydrogen-gas-containing environments very effectively

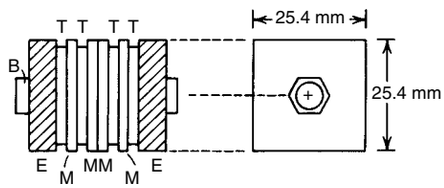

Fig. 6 Schematic of typical crevice corrosion test assembly used for titanium alloy sheet and plate samples. E, assembly and plates; M, alloy test coupons; T, PTFE sheet spacers; B, titanium bolt/nut

maintain this protective film, thus avoiding or limiting hydrogen uptake (Ref 27–29). On the other hand, anhydrous hydrogen gas atmospheres may lead to absorption, particularly as temperatures and pressures increase.

In α and α-β alloys, excessive hydrogen uptake can induce the precipitation of titanium hydride in the α phase. These acicular-appearing hydride platelets (Fig. 7, 8) are brittle and have been well characterized in the literature (Ref 28, 30–32). Small amounts of hydride precipitates are not detrimental from an engineering standpoint in most cases, but cause severe reduction in alloy ductility and toughness when present in greater amounts. For example, hydride precipitates can be observed in grade 2 titanium microstructures at hydrogen concentrations above approximately 40 to 100 ppm, depending on the amount of β phase present, but these precipitates do not result in gross embrittlement of grade 2 titanium until levels in excess of 500 to 600 ppm are achieved. Hydrides are observed at concentrations above ~400 ppm in grade 12 titanium and above 400 to 600 ppm in Ti-6-4, depending on microstructure and composition.

Although uniaxial tensile properties may experience little effect from increasing hydrogen levels, biaxial or triaxial stress properties, such as bend ductility, cup (cold-drawing) formability, and impact toughness, in α and near-α alloys are very sensitive to hydrogen levels (Ref 31–35). In α and, especially, α-β alloys, hydrogen contents above critical levels can result in sustained-load cracking, which dramatically reduces useful maximum service loads in notched or cracked components under slow strain rate or constant tensile load situations (Ref 31–37).

Beta titanium alloys have a very high solubility for hydrogen, such that embrittlement is generally not associated with hydride precipitation. Significant losses in ductility or formability may not occur below levels of several thousand parts per million of hydrogen (Ref 31, 38, 39). This enhanced tolerance to hydrogen decreases somewhat in the aged (high-strength) condition as more α phase is precipitated. This increased β alloy tolerance must be weighed against substantially higher hydrogen uptake rates that result from the much higher hydrogen diffusion coefficient in β titanium (Ref 38, 40).

Factors that can lead to hydrogen uptake and possible embrittlement of α titanium alloys in aqueous media have been identified from field and laboratory experience. The three general conditions that must exist simultaneously for the hydrogen embrittlement of α alloys are (Ref 29):

- A mechanism for generating nascent (atomic) hydrogen on a titanium surface. This may be from a galvanic couple, an impressed cathodic current, corrosion of titanium, or severe continuous abrasion of the titanium surface in an aqueous medium.
- Metal temperature above approximately 80 °C (175 °F), above which the diffusion rate of hydrogen into α titanium becomes significant (Ref 1, 41, 42)
- Solution pH less than 3 or greater than 12, or impressed potentials more negative than −0.75 V (versus Ag/AgCl reference electrode) (Ref 29, 43–47)

The key to preventing hydrogen embrittlement is simply to avoid one or more of these conditions.

Galvanic couples between titanium and certain active metals and excessive cathodic charging from impressed-current cathodic protection systems are the usual causes of excessive hydrogen absorption (Ref 47–49). In near-neutral electrolytes such as seawater, active metals such as zinc, aluminum, and, especially, magnesium can induce enhanced hydrogen uptake and embrittlement when coupled to titanium above approximately 75 to 80 °C (165 to 175 °F) (Ref 29, 50). A similar problem occurs when titanium is in galvanic contact with carbon steels or active stainless steels in aqueous sulfide media above this temperature (Ref 29). Similar to arsenic, antimony, and cyanide species, the sulfide acts as a hydrogen recombination poison (that is, prevents the recombination of atomic hydrogen) and accelerates hydrogen uptake in this situation.

No hydrogen uptake and embrittlement problems occur when titanium is coupled to fully passive materials in a given environment. Galvanically compatible materials may include other titanium alloys, resistant (passive) stainless steels, copper alloys, and nickel-base alloys, depending on conditions.

Cathodic charging of hydrogen onto unalloyed titanium surfaces is not recommended when temperatures exceed approximately 80 °C (175 °F). At metal temperatures below this level, thin surface hydride films may form on α titanium alloys (Fig. 8); however, these are usually not detrimental from the standpoint of corrosion or mechanical properties (Ref 51). However, very high cathodic current densities may lead to enhanced hydride film growth and eventual wall penetration and embrittlement even at room temperature (Ref 49). Near-α or α-β alloys are also susceptible at near-ambient temperatures (despite increased β-phase content), especially under sustained tensile stress (Ref 48). Practically speaking, impressed cathodic potentials on titanium should remain more noble than −1.0 and, preferably, −0.85 V (versus Ag/AgCl) in ambient-temperature seawater applications. Thermal oxide surface films on titanium appear to inhibit hydrogen uptake effectively under low-to-moderate cathodic charging conditions but can break down and become nonprotective at high current densities (Ref 52).

Hot alkaline conditions may also result in excessive hydrogen uptake and embrittlement of titanium alloys. The nascent hydrogen generated on titanium surfaces from small but finite general corrosion in hot (>80 °C, or 175 °F), strongly alkaline (pH ≥12) media appears to be responsible.

Hydrogen Testing. Testing to determine the susceptibility of a titanium alloy to hydrogen uptake and embrittlement should simulate conditions expected in service. Test exposures in hydrogen gas atmospheres must duplicate exact gas chemistry, particularly with respect to water and oxygen content. Mere traces of moisture, for example, will effectively inhibit hydrogen absorption by titanium in dry hydrogen gas and possibly cause test interference (Ref 28).

Galvanic coupling tests or cathodic charging tests can also be conducted to evaluate susceptibility to hydrogen uptake. For a given environment, an active metal (iron, aluminum, etc.) sample is galvanically coupled to the titanium alloy sample such that a specific anode-to-cathode surface area is established. Impressed cathodic charging tests are performed in electrolytic cells containing a specific electrolyte. A power supply (potentiostat or galvanostat) impresses a constant potential or current on the

Fig. 7 Micrograph of severely hydrided unalloyed titanium. Original magnification approximately 200×

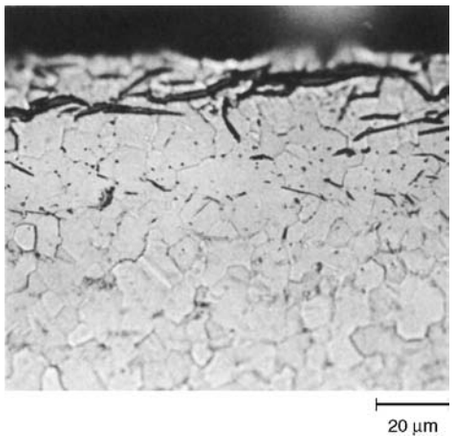

Fig. 8 Micrograph of unalloyed titanium sheet revealing a very thin, innocuous surface layer of titanium hydrides. Original magnification approximately 500×

cell such that the titanium is cathodic relative to an inert counterelectrode such as graphite or platinum. A reference electrode can also be used to control or to measure the polarization potential of the test cathode. A typical cathodic charging cell and test procedures are presented elsewhere (Ref 15, 16).

The surface condition of the coupon is a critical variable in all hydrogen uptake tests. Studies have shown that abraded or sandblasted surfaces absorb hydrogen more readily than as-pickled surfaces. Thickening of the surface oxide film by anodizing or thermal oxidation further retards absorption. The actual surface finish anticipated in service should be evaluated.

After test exposure, sample evaluation may involve tensile, notched tensile, bend, cold formability (for example, drawn cup), Charpy V-notch impact, and/or hydrogen analysis. Uniaxial, smooth-specimen tensile testing is generally of little value in diagnosing the subtle embrittling effects of hydrogen. Titanium alloys tend to exhibit susceptibility under biaxial or triaxial stress states; therefore, bend tests, cup tests, notched tensile, or loaded precracked fracture toughness tests are generally more sensitive to hydrogen effects. Impact toughness testing can be an especially sensitive indicator of hydrogen effects in α alloys, whereas slow strain rate or sustained-load methods are very suitable for α-β alloys (Ref 31, 34–36). Because hydrogen content has a relatively minor effect on alloy hardness, hardness testing is generally not used.

Hydrogen analysis of coupons is performed by the hot vacuum extraction method. In the hot vacuum extraction apparatus, a small sample is heated to 1100 to 1400 °C (2010 to 2550 °F) for several minutes to reversibly release the absorbed hydrogen, followed by evolved gas measurements. More information on testing titanium for hydrogen damage is available elsewhere (Ref 15).

Stress-Corrosion Cracking

Stress-corrosion cracking (SCC) is a fracture phenomenon caused by the combined factors of tensile stress, a susceptible alloy, and a corrosive environment. The metal normally shows no evidence of general corrosion attack, although slight localized attack in the form of pitting may also be visible in certain metals. Usually, only specific combinations of metallurgical and environmental conditions cause SCC. This is important because it is often possible to eliminate or reduce SCC susceptibility by modifying either the metallurgical characteristics of the metal and/or the makeup of the environment. Another important aspect of SCC is the requirement that tensile stress be present, such as those stemming from cold work, residual stresses from fabrication, and/or externally applied loads.

The key to understanding titanium alloy SCC is the observation that no apparent corrosion, either uniform or localized, usually precedes the cracking process (Ref 53, 54). As a result, it can sometimes be difficult to initiate cracking in certain laboratory tests (Ref 15, 55).

It is also important to distinguish between the two basic classes of titanium alloys. The first class, which includes the lower-strength industrial alloys (grades 1, 2, 9, 12, 28, and titanium-palladium/titanium-ruthenium alloys) is generally resistant to SCC except in a few specific environments. These specific environments include anhydrous methanol, nitrogen tetroxide (N_2O_4), red-fuming nitric acid, liquid or solid cadmium, or liquid mercury. The second class of titanium alloys, including the aerospace titanium alloys, has been found to be susceptible to several additional environments, most notably aqueous halide (e.g., chloride, bromide) solutions and certain halogenated organic compounds. However, this susceptibility is almost always associated with high stress concentrations typical of laboratory testing with loaded, precracked specimens or specimens very slowly strained to failure, and generally is not observed with loaded smooth or notched specimens. As such, the SCC susceptibility identified for these alloys is seldom observed in actual field applications.

Over the years, a variety of mechanisms or models have been proposed to explain SCC phenomena in titanium alloys (Ref 55–60). In general, the mechanisms fall into two broad categories. The first mechanism, anodic-assisted cracking, may begin where localized corrosion has occurred in the presence of a tensile stress. If corrosion is not so rapid as to allow the advancing crack tip to blunt, the crack will continue to advance into the metal and eventually lead to failure. Once a crack initiates, the balance among the crack tip corrosion rate, the crack tip environment, and the crack tip stress state is critical to crack propagation.

The second mechanism, hydrogen-assisted cracking, is said to occur by absorption of hydrogen near the crack tip. Hydrogen absorption leads to embrittlement of the metal ahead of the crack tip and promotes crack formation. The source of hydrogen is normally associated with anodic dissolution (that is, from the concurrent cathodic hydrogen-reduction reaction) at freshly exposed metal at the crack tip. As a result, anodic dissolution in the vicinity of the crack tip is normally required for this mechanism to operate. Obviously, this confuses the nature of the true mechanism, because the second mechanism relies to a certain extent on at least a portion of the first mechanism to generate the embrittling species. As a result, there has been on-going debate in the literature as to whether titanium SCC is governed by a cathodic or anodic mechanism. It is quite likely, given the tremendous diversity of cracking observations, that no single mechanism exists to explain SCC in titanium alloys.

Applicable SCC Test Methods. Test methods for assessing the SCC resistance of titanium alloys can be grouped into three basic categories (Ref 15, 55):

- *Category 1 tests:* Use smooth, statically loaded specimens, such as U-bend, C-ring, bent beam, and dead-loaded tensile specimens (described in ASTM G 30, G 38, G 39, and G 49, respectively)
- *Category 2 tests:* Fracture mechanics tests that use notched and precracked specimens that are statically or dynamically loaded, such as cantilever beam bend specimen, SE(B); compact tension, C(T), and double-cantilever beam specimens; and are conducted per ASTM E 399 guidelines
- *Category 3 tests:* Use smooth or notch tensile specimens that are dynamically loaded at relatively low strain rates, for which the slow strain rate tensile (SSRT) test (ASTM G 129) is the primary test method

Selection of a suitable SCC test method for titanium alloys is primarily determined by the nature of the stress-cracking data or design information desired and by the chemical nature of the test environment relative to the titanium alloy passivation. For simple go/no-go assessment of SCC with no quantitative cracking parameters, the least costly category 1 tests may be adequate if SCC initiation (incubation) periods are not too long. The data are typically considered in terms of sample stress versus time to failure, as shown in Fig. 9.

If fracture mechanics design information (i.e., threshold stress intensity to produce stress-corrosion cracking, K_{ISCC}, or stage I or II crack growth parameters) is required, then the more sophisticated, costly category 2 tests are the obvious choice. Precracked C(T)- or SE(B)-type specimens (ASTM E 399) may be either dead (constant) loaded to generate an increasing stress-intensity factor, K, field as the crack grows; loaded to increasing levels in a stepwise or continuously slow strain-rate fashion (increasing K field); or preloaded via wedge- or bolt-open loading, producing a decreasing K field as the crack grows (and finally arrests at the K_{ISCC} value). Because K_{ISCC} values for titanium alloys are stress and time dependent, as indicated in Fig. 9(b), it is vital that adequate time at each (constant or step) load level (or slow enough strain rate) be allowed to generate conservative K_{ISCC} results. For example, experience suggests that a minimum of 6 to 10 h holdtime at each increasing step load should be adequate.

Although SSRT testing (ASTM G 129) does not directly provide design/engineering parameters, it does represent a more rapid, highly discriminating, and conservative means of identifying existence and relative degree of SCC susceptibility in titanium alloys. This category 3 test is generally assessed as comparative ratios of test sample ductility (reduction in area) and/or time-to-failure values to those obtained from a reference sample test in air or inert gas. Final confirmation of susceptibility includes a thorough low- and high-magnification examination of specimen fracture surfaces for SCC indications (i.e., quasi-cleavage and/or intergranular/secondary cracking). The SSRT testing of

titanium alloys in aqueous and methanolic solutions indicates that discriminating, relevant strain rates lie within the 10^{-5} to 10^{-7}/s window (Ref 61–64).

Selection of SCC test method for titanium alloys should also be based on the particular type of environment to be tested. In environments where alloy repassivation (oxide film formation) is favored and where stage I subcritical cracking is generally not observed, category 2 and 3 tests are more discriminating than category 1 tests. This is the case for aqueous media, including saltwater and brines, and chlorinated organic solvents in which cracking failure of category 1 specimens is generally not observed at near-ambient temperatures. One must provide initial or continued local oxide film breakdown, such as in category 2 and 3 tests, to expeditiously initiate and manifest potential SCC tendencies in these alloys. Exceptions to this rule are those very few titanium alloys that may exist in highly sensitized metallurgical conditions. For example, the few titanium alloys susceptible to SCC in ambient neutral saltwater in stressed smooth or notched samples include step-cooled Ti-8-1-1 and the Ti-8Mn and Ti-13-11-3 alloys. Highly stressed category 1 test specimens may also be applicable for testing susceptible alloys in hot aqueous halides or chlorinated solvents, where higher temperatures may overcome SCC activation barriers within reasonable exposure periods.

For environments where stage 1 subcritical cracking behavior occurs and repassivation is not favored, category 1 tests may be preferred over category 2 and 3 tests for practical/cost reasons. These environments include methanol, red-fuming nitric acid, nitrogen tetraoxide, liquid/solid metals, molten salts, and hot salt. Note that category 2 testing is not physically applicable to the evaluation of solid metal embrittlement and hot salt SCC in these alloys.

Galvanic Corrosion

The coupling of titanium with dissimilar metals usually does not accelerate the corrosion of titanium. The exception is in strongly reducing environments in which titanium is severely corroding and not readily passivated. In this uncommon situation, accelerated corrosion may occur when titanium is coupled to more noble metals. In its normal passive condition, titanium is beneficially influenced by materials that exhibit more noble (positive) corrosion potentials. In this regard, graphite and various noble metals (such as platinum, palladium, ruthenium, iridium, and gold) provide anodic protection when coupled to titanium by further stabilizing the oxide film of titanium at more positive potentials (Fig. 1).

As shown in Table 2, the corrosion potential of titanium under normally passive conditions is quite noble but similar to stainless steel or nickel-base alloys in the passive condition. The insignificant potential difference between these passive engineering alloys generally means negligible galvanic interactions and good galvanic compatibility as long as passive conditions prevail for the alloys involved.

However, when titanium is coupled to a metal that is active in an environment, accelerated anodic attack of the active metal may result. The rate of accelerated attack depends on many factors, including the cathode-to-anode surface area ratio, concentration of dissolved cathodic depolarizers (for example, oxygen or atomic hydrogen), temperature, solution flow velocity, and medium chemistry. Depending on environmental conditions, active metals may include carbon or low-alloy steels, aluminum, zinc, magnesium, copper alloys, or stainless steels that are active (depassivated) or pitting. When galvanic corrosion is unacceptably high, consideration should be given to all-titanium component design, coupling to more compatible corrosion-resistant alloys, use of dielectric (insulating) joints, or controlled cathodic protection of the active metal.

As discussed in the section "Hydrogen Damage" in this article, attention should be

Table 2 Galvanic series in flowing natural seawater

At 24 °C (75 °F) at a velocity of 4 m/s (13 ft/s)

Material	Steady-state electrode potential, V versus saturated calomel electrode
Graphite	+0.25
Platinum	+0.15
Zirconium	−0.04
316 stainless steel (passive)	−0.05
304 stainless steel (passive)	−0.08
Monel alloy 400	−0.08
Hastelloy alloy C	−0.08
Titanium	−0.10
Silver	−0.13
410 stainless steel (passive)	−0.15
316 stainless steel (active)	−0.18
Nickel	−0.20
430 stainless steel (passive)	−0.22
Copper alloy C71500 (70Cu-30Ni)	−0.25
Copper alloy C70600 (90Cu-10Ni)	−0.28
Copper alloy 442 (admiralty brass)(a)	−0.29
G bronze	−0.31
Copper alloy	−0.32
Copper	−0.36
Copper alloy C46400 uninhibited naval brass	−0.40
410 stainless steel (active)	−0.52
304 stainless steel (active)	−0.53
430 stainless steel (active)	−0.57
Carbon steel	−0.61
Cast iron	−0.61
Aluminum alloy 3003-H	−0.79
Zinc	−1.03

(a) No longer listed by the Copper Development Association; admiralty brasses are now inhibited with small additions of arsenic (C44300), antimony (C44400), or phosphorus (C44500).

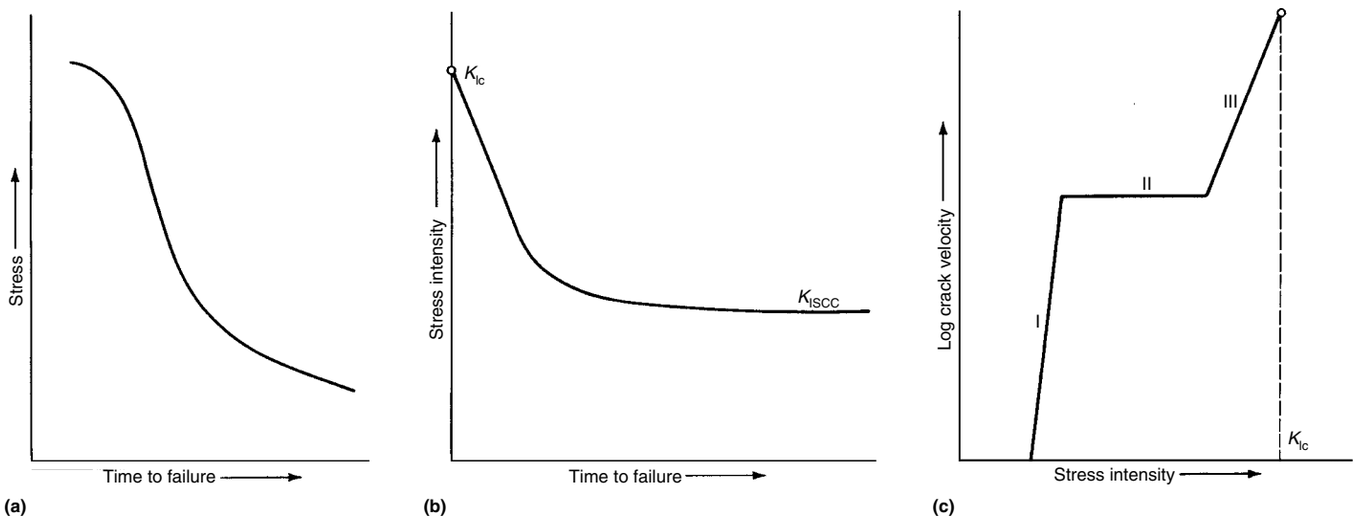

Fig. 9 Typical data representations for stress-corrosion cracking using category 1 and category 2 specimens. (a) Stress versus time to failure for category 1 specimens. (b) and (c) Stress intensity versus time to failure and crack velocity versus stress intensity for category 2 specimens. K_{Ic}, plane-strain fracture toughness; K_{ISCC}, threshold stress intensity to produce stress-corrosion cracking

given to possible excessive hydrogen uptake by titanium when it is galvanically coupled to active metals. This is of concern in α titanium alloys when temperatures exceed 80 °C (175 °F) in aqueous electrolytes, especially when hydrogen recombination poisons, such as sulfide, arsenous, or cyanide ions, are present.

Erosion-Corrosion and Corrosion Fatigue

Erosion-corrosion is defined as the acceleration in metal corrosion rate because of relative movement between a corrosive fluid and a metal surface. This form of attack is highly dependent on fluid velocity and is favored in areas where high local turbulence, impingement, or cavitation of the fluid occur on metal surfaces. Suspended solids in fluid can also result in abrasion, which can drastically accelerate metal removal.

In normal passive environments, the hard, tenacious TiO_2 surface film of titanium provides a superb barrier to erosion-corrosion. For this reason, titanium alloys can withstand flowing water or seawater velocities as high as 30 m/s (100 ft/s) with insignificant metal loss. The ability of the oxide film to repair itself when damaged and the intrinsic hardness of titanium alloys both contribute to their excellent resistance to erosion-corrosion. Therefore, inlet turbulence in shell and tube heat exchangers, entrained gas bubble impingement, and pump cavitation effects are generally not of concern in titanium tubing, piping, and other components.

Titanium alloys exhibit relatively high resistance to fluids containing suspended solids. Critical velocities for excessive metal removal depend on the concentration, shape, size, and hardness of the suspended particles, in addition to fluid impingement angle (Ref 65), local turbulence, and titanium alloy properties. The typically low concentrations of silt entrained in seawater are generally of little consequence, but continuous exposure to high-velocity slurries of hard particles can lead to finite metal removal. The harder, higher-strength titanium alloys generally offer improved erosion/abrasion resistance when marginal erosion of the softer unalloyed titanium grades is observed. When abrasive conditions are severe, application of hard surface coatings or treatments should be considered. In potential applications involving high-velocity slurries or suspended solids, it is advisable to conduct erosion tests whenever possible.

Titanium alloys also demonstrate superior resistance to cavitation in seawater (Ref 66, 67) compared to most marine alloys, making them attractive for brine/seawater pumps, impellers, agitators, and so on.

Corrosion fatigue refers to the reduction in fatigue resistance of a metal stemming from environmental exposure. Due to the ultrathin but highly protective and rehealable oxide film of titanium, the smooth and notched S-N fatigue life of the more common titanium alloys (Table 1) and their weldments is not significantly affected by water, seawater, and many other aqueous chloride media (Fig. 10) (Ref 68, 69). Fatigue crack growth (FCG) resistance, on the other hand, can be environmentally affected depending on titanium alloy composition, microstructure, and/or metallurgical condition. Parallel to relative alloy SCC susceptibility, most of the common, lower-medium-strength industrial titanium alloys exhibit little or no increase in FCG rate in aqueous halide media. The more corrosion- and crevice-resistant, higher-strength alloys can be expected to be corrosion-fatigue resistant as well.

Corrosion in Specific Media

The corrosion rate data reviewed in the following sections were generated from both laboratory and field tests and, in some cases, from actual equipment service. Most of these data were derived from weight change measurements involving varying exposure periods. Samples of plate and sheet in the fully annealed condition were typically tested, most frequently in as-pickled or as-ground surface conditions.

These corrosion rate values should be used as general indicators of corrosion resistance, but it must be recognized that corrosion rates can change with exposure time. For example, corrosion rates often decrease with exposure time in normal passive environments; this reflects the finite growth of the protective oxide film. In addition, these values do not always reveal whether the alloy is in a fully passive or stable condition. Therefore, supplemental electrochemical testing may be necessary when borderline passivity, such as in reducing environments, is suspected. These rates may not reflect the influence of solution flow velocity or the degree of media replenishment/depletion. Finally, it should be recognized that titanium alloy corrosion behavior can be highly sensitive to small, even trace, concentrations of various oxidizing or complexing species in normally aggressive, reducing, acidic environments. Therefore, it is necessary to take all trace species or background contaminants in the anticipated service (degree of aeration and so on) into account when deciding alloy suitability based on pure or simplified simulated medium chemistry. In cases in which the simulation of complex or variable media chemistry is difficult, in situ testing is recommended if possible. Additional corrosion rate data for various titanium alloys are compiled in the Appendixes of this article.

General Corrosion in Specific Media

Water and Seawater. Titanium and its alloys are fully resistant to water, all natural waters, and steam to temperatures in excess of 315 °C (600 °F) (Ref 70). Slight weight gain is usually experienced in these benign environments, along with some surface discoloration at higher temperatures from finite passive oxide film thickening. The immunity to attack of α alloys is observed regardless of dissolved oxygen level or in high-purity water, such as that used in nuclear reactor coolant systems (Ref 71–74). The typical contaminants encountered in natural water streams, such as iron and manganese oxides, sulfides, sulfates, carbonates, and chlorides (Ref 10), do not compromise the passivity of titanium. In media containing chloride levels greater than approximately several hundred parts per million (e.g., seawater) at temperatures above ~75 °C (170 °F), consideration should be given to possible crevice corrosion when tight crevices exist in service (see the section "Crevice Corrosion" in this article).

Titanium alloys exhibit negligible corrosion rates in seawater to temperatures as high as 260 °C (500 °F). As shown in Table 3, extremely low corrosion rates of unalloyed titanium and Ti-6Al-4V after 3 years of exposure in ambient seawater are indicated. Pitting and crevice corrosion will not occur in ambient seawater, even if marine deposits form and biofouling occurs. Titanium tubing exposed for 16 years to polluted and sulfide-containing seawater showed no evidence of corrosion (Ref 79). Similar reports of nil corrosion in ambient seawater have been reported for unalloyed titanium (Ref 80, 81) and various titanium alloys, such as Ti-6-4, Ti-5-2.5, Ti-13-11-3, Ti-6-2-1-1, and titanium-palladium (Ref 81–83). Exposure of titanium to marine atmospheres (Ref 81, 84), splash or tide zone, and soils also does not cause corrosion (Ref 75–78, 85). As indicated in

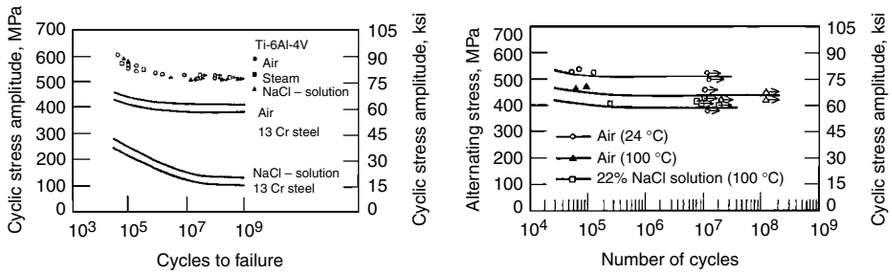

Fig. 10 Stress-number of cycles fatigue curves for Ti-6Al-4V in air and saltwater at 24 and 100 °C (75 and 212 °F), indicating excellent resistance to corrosion fatigue. Source: Ref 68, 69

the section "Erosion-Corrosion and Corrosion Fatigue" of this article, the excellent resistance of titanium to seawater is retained at relatively high flow velocities.

Unalloyed titanium welded tubing and piping has provided more than 40 years of outstanding service in seawater for the chemical, oil refining, desalination, and power industries. As a result of its immunity to ambient, natural seawater attack, titanium is considered to be the technically correct material for many critical marine applications, including many naval and offshore components.

Oxidizing Media. Titanium alloys are generally highly resistant to oxidizing media and oxidizing acids over a wide range of concentrations and temperatures. Common chemicals in this category include chromic, nitric, perchloric, and hypochlorous acids, and salts of these acids. Other oxidizing salts include thiosulfates, vanadates, permanganates, chromates, and molybdates. Corrosion rates at and below the boiling point of these aqueous salt solutions over the full range of concentration will typically be less than 0.02 mm/yr (0.8 mil/yr). Data for unalloyed titanium exposed in boiling chromic acid solutions are presented in Table 4.

Nitric Acid. Unalloyed titanium has been extensively used for handling and producing nitric acid in applications in which stainless steels have experienced significant uniform or intergranular attack (Ref 74, 86–88). Titanium offers excellent resistance over the full concentration range at subboiling temperatures. As temperatures exceed approximately 80 °C (175 °F), however, the corrosion resistance becomes highly dependent on nitric acid purity.

In hot, very pure solutions or vapor condensates of nitric acid, significant uniform corrosion rates may occur, particularly as temperatures increase. The data plotted in Fig. 11 and 12 show that the midrange HNO_3 concentrations (20 to 70 wt%) are most aggressive when full inhibition to attack is not achieved in relatively pure, refreshed solutions. In these situations, semiprotective titanium oxide surface films form that do not fully retard continued oxidation of the metal surface.

As the impurity levels increase in hot HNO_3 solutions, the resistance of unalloyed titanium improves dramatically. In particular, relatively small amounts of certain dissolved metallic species, including Si^{4+}, Cr^{6+}, Fe^{3+}, Ti^{4+}, or various platinum-group metal ions, can effectively inhibit the high-temperature corrosion of titanium in nitric acid (Ref 74, 87–93). This inhibitive effect is very potent, as shown in Fig. 13 and 14 for Cr^{6+} and Ti^{4+}, respectively (Ref 92), and in Table 5 for Ti^{4+} (Ref 91). Thus, titanium exhibits excellent resistance to recirculating nitric acid process streams, such as stripper reboiler loops (Table 6) in which steady-state levels of dissolved Ti^{4+} inhibitor are achieved. Hold tanks and stripper sumps are also good applications for similar reasons. Another good example of this inhibitive effect is the excellent performance of unalloyed titanium in evaporator reboilers and other components in the high-temperature metal-contaminated process streams used for U_3O_8 recovery (Ref 93–95).

The significant discrepancies and variations in titanium corrosion rates in hot HNO_3 media reported by investigators over the years appear to be the result of these inhibitive metal ion effects. Because titanium corrosion is inhibited by its own soluble corrosion product (Ti^{4+}), the titanium surface area to acid volume ratio, the test duration, and the rate of solution replenishment will all be critical to the rate obtained. The container material and acid purity (chemistry) will also be influential, as discussed in detail

Table 3 Corrosion of titanium in ambient seawater

Alloy	Ocean depth		Corrosion rate	
	m	ft	mm/yr	mils/yr
Unalloyed titanium	Shallow		8×10^{-7}	0.00003
	720–2070	2360–6800	$<2.5\times10^{-4}$	<0.01
	2–2070	6.5–6800	nil	
	1720	5640	4×10^{-5}	0.0015
Ti-6Al-4V	2–2070	6.5–6800	$<2.5\times10^{-4}$	<0.01
	1720	5640	8×10^{-6}	0.0003
	1720	5640	$<1\times10^{-3}$	<0.04

Source: Ref 74–78

Table 4 Corrosion of unalloyed titanium in chromic acid solutions

Concentration of CrO_3, wt%	Temperature		Corrosion rate	
	°C	°F	mm/yr	mils/yr
10	Boiling		0.003	0.12
15	24	75	0.005	0.2
	82	180	0.015	0.6
36.5	90	195	0.046	1.8
50	24	75	0.013	0.5
	82	180	0.025	1.0

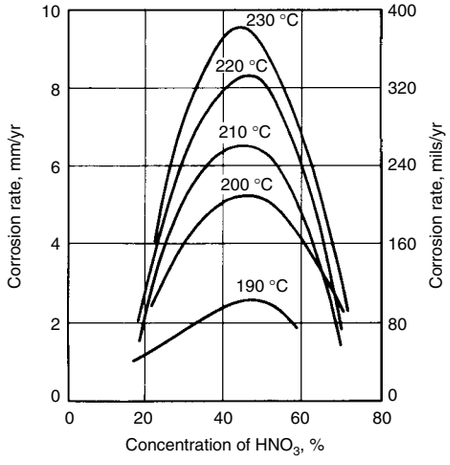

Fig. 11 Corrosion of unalloyed titanium in high-temperature HNO_3 solutions. Source: Ref 89

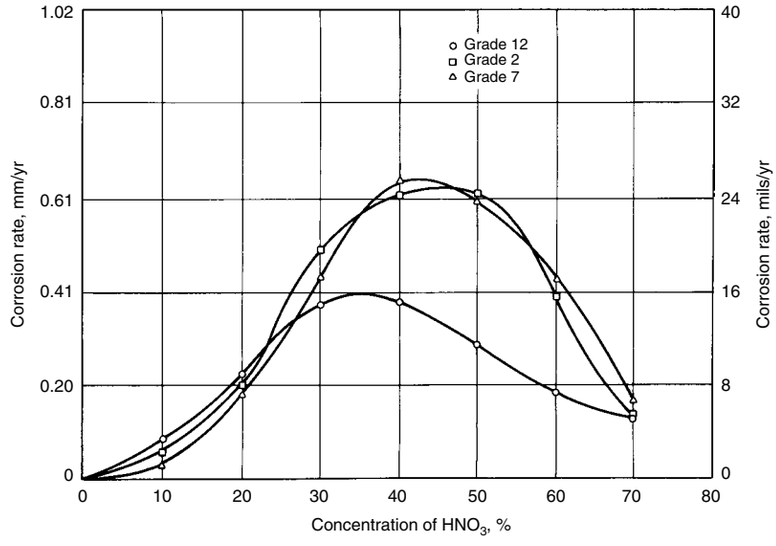

Fig. 12 Corrosion of titanium alloys in boiling, uninhibited HNO_3 solutions. Acid solutions were refreshed every 24 h for 96 h.

elsewhere (Ref 92, 96). Thus, it is vital that all design and operating factors must be taken into account when evaluating titanium for high-temperature concentrated HNO_3 service.

Limited corrosion testing of α-β and β titanium alloys in boiling HNO_3 indicates that increasing aluminum and/or β alloying elements tend to decrease corrosion resistance. The corrosion data for various titanium alloys listed in Table 7 show that low-alloy-containing α alloys are generally most resistant to hot HNO_3. Other studies have shown that high-purity (i.e., low iron and sulfur) unalloyed titanium does not experience the significant accelerated weldment attack in high-temperature HNO_3 that may be exhibited by the less pure unalloyed grades and the near-α alloys.

Fuming Nitric Acid. Titanium alloys exhibit good resistance to white-fuming nitric acid. However, dangerous and violent pyrophoric reactions may occur with titanium alloys exposed to red-fuming nitric acid or to nitrogen tetroxide (see the section "Gases" in this article). The attack is intergranular and results in a surface residue of finely divided titanium particles that are highly reactive. The critical variables are the nitrogen dioxide (NO_2) and water contents of the acid (Fig. 15) (Ref 97). Fuming nitric acid containing less than 1.4 to 2.0% water or more than 6% NO_2 may cause this rapid impact-sensitive reaction to occur (Ref 53, 97–101). Both water and NO are effective inhibitors to this attack, but increasing oxygen and NO_2 are detrimental in this situation. Corrosion rate data in red-fuming nitric acid for various alloys as a function of NO_2 and water content also can be found in Ref 6.

Peroxides. Although peroxides are generally oxidizing, titanium alloys can experience general corrosion in hydrogen peroxide solutions, depending on concentration, temperature, and pH. As shown in Table 8, titanium corrosion rates are minimal in dilute, slightly acidic, or

Table 5 Effect of dissolved Ti^{4+} on the corrosion rate of unalloyed titanium in boiling HNO_3 solutions

Titanium ion added, mg/L	Corrosion rate			
	40% HNO_3		68% HNO_3	
	mm/yr	mils/yr	mm/yr	mils/yr
0	0.75	29.5	0.81	32
10	...	...	0.02	0.8
20	0.22	8.7	0.06	2.4
40	0.05	2	0.01	0.4
80	0.02	0.8	0.01	0.4

Source: Ref 91

Table 6 Corrosion of grade 2 titanium and 304L stainless steel heating surfaces exposed to boiling 90% HNO_3

Metal temperature		Corrosion rate			
		Grade 2		Type 304L	
°C	°F	mm/yr	mils/yr	mm/yr	mils/yr
116	240	0.03–0.17	1.2–6.7	3.8–13.2	150–520
135	275	0.04–0.15	1.6–6	17.2–73.7	675–2900
154	310	0.03–0.06	1.2–2.4	18.3–73.7	720–2900

Source: Ref 87

Table 7 Corrosion of various titanium alloys in boiling HNO_3 solutions after 196 h

Titanium alloy	Corrosion rate at indicated HNO_3 concentration					
	25 wt%		45 wt%		70 wt%	
	mm/yr	mils/yr	mm/yr	mils/yr	mm/yr	mils/yr
Grade 1	0.15	6	0.39	15	0.08	3.1
Grade 7	0.17	6.7	0.38	14.9	0.07	2.8
Grade 12	0.18	7	0.27	10.6	0.06	2.4
Ti-6-2-1-1	0.39	15	0.73	28.7	0.21	8.3
Grade 9	0.18	7	0.54	21.3	0.10	4
Ti-550	0.83	32.6	1.14	44.9	0.30	12
Grade 5	0.67	26.4	0.86	33.8	0.02	0.8
Ti-6-2-4-6	4.3	170	5.7	224	0.78	30.7
Ti-10-2-3	0.48	18.9	1.2	47.2	0.07	2.8
Ti-3-8-6-4-4	1.13	44.5	3.6	141.7	1.46	57.5
Ti-5Ta	0.04	1.6	0.08	3.1	0.03	1.2

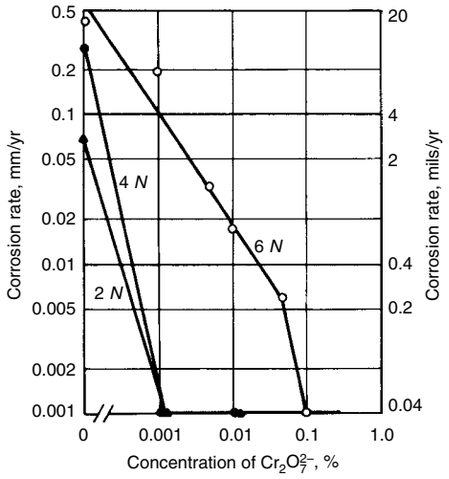

Fig. 13 Inhibitive effect of dissolved chromate ions on the corrosion of commercially pure titanium after 65 h in boiling HNO_3 solutions. Source: Ref 92

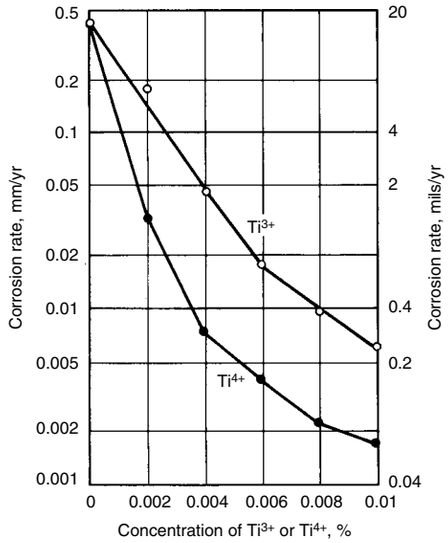

Fig. 14 Inhibitive effect of dissolved titanium ions on the corrosion of titanium after 65 h in boiling 6 *N* HNO_3 solutions. Source: Ref 92

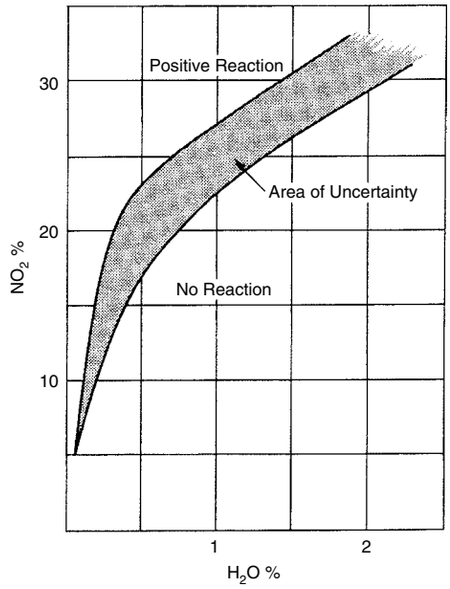

Fig. 15 Acid composition limits for avoiding rapid, pyrophoric reactions of titanium with red-fuming nitric acid. Source: Ref 97

Table 8 General corrosion of grade 2 titanium in hydrogen peroxide solutions

Medium	pH(a)	Temperature		Corrosion rate	
		°C	°F	mm/yr	mils/yr
5% H_2O_2	1	23	73	0.064	2.5
	4.3	23	73	0.013	0.5
	1	66	150	0.152	6
	4.3	66	150	0.061	2.4
5% H_2O_2 + 500 ppm Ca^{2+}	1	66	150	nil	
20% H_2O_2	1	66	150	0.686	27
20% H_2O_2 + 500 ppm Ca^{2+}	1	66	150	nil	
10 g/L H_2O_2 + 20 g/L NaOH	...	60	140	55.9	2200
3.5 g/L H_2O_2 + 10 g/L NaOH + 10 g/L Na_2SiO_3 + 0.5 g/L Na_3PO_4	...	60	140	nil	
0.75 g/L H_2O_2	11	70	160	0.42	16.5
0.2–0.3% H_2O_2	11.5	70	160	2.0	79
	12.0	70	160	8.7	342
0.2–0.3% H_2O_2 + 1 ppm Ca^{2+}	12.0	70	160	0.18	7
0.2–0.3% H_2O_2 + 50 ppm Ca^{2+}	12.0	70	160	0.46	18
0.2–0.3% H_2O_2	11.0	80	175	4.5	177
0.2–0.3% H_2O_2 + 10 ppm Ca^{2+}	11.0	80	175	0.0	0.0
0.2–0.3% H_2O_2 + 100 ppm Ca^{2+}	11.5	80	175	0.25	10
0.2–0.3% H_2O_2	12.0	80	175	10.2	400
0.2–0.3% H_2O_2 + 50 ppm Ca^{2+}	12.0	80	175	0.41	16
0.2–0.3% H_2O_2 + 100 ppm Ca^{2+}	11.0	85	185	0.12	4.7
0.05% H_2O_2	12.0	90	195	3.0	120
0.10% H_2O_2	11.0	90	195	2.0	79

(a) Acidic solutions were prepared with HCl additions. Source: Ref 102–106

Table 9 Corrosion of unalloyed titanium in solutions of oxidizing chlorine compounds

Reagent	Concentration, wt%	Temperature		Corrosion rate	
		°C	°F	mm/yr	mils/yr
Water saturated with chlorine	...	75	165	0.003	0.12
	...	88	190	0.002	0.08
	...	97	207	0.07	2.8
NaOCl	6	25	77	nil	
ClO_2 + HOCl	15	43	110	nil	
ClO_2 + steam	5	100	212	0.005	0.2
$Ca(OCl)_2$	2	100	212	0.001	0.04
	6	100	212	0.001	0.04
	18	25	77	nil	
HOCl + ClO_2 + Cl_2	17	38	100	nil	

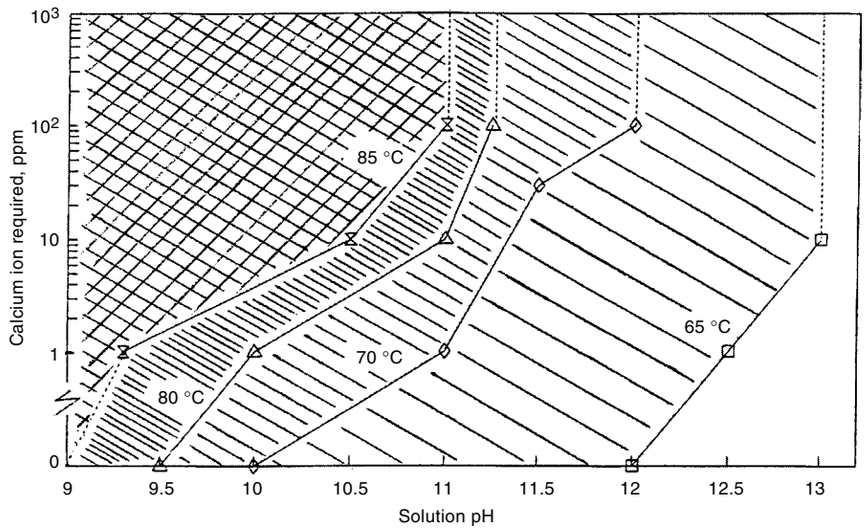

Fig. 16 Approximate limits for useful corrosion resistance (< 0.13 mm/yr, or 5.1 mils/yr) of grade 2 titanium in alkaline solutions containing up to 0.3 wt% H_2O_2. Source: Ref 104

near-neutral H_2O_2 solutions but increase dramatically under alkaline conditions (Ref 102–104). This stems from the formation of soluble titanium peroxide complexes from the perhydroxyl species generated in alkaline H_2O_2 media (Ref 102, 104–106), which prevents formation of an insoluble, protective surface oxide film on titanium. Fortunately, corrosion can be effectively inhibited by the naturally occurring presence and/or intentional addition of relatively minor concentrations of calcium (Table 8) or strontium or barium ions (Ref 102, 103). Figure 16 depicts some pH/temperature guidelines for using titanium in dilute H_2O_2 solutions, illustrating the potent inhibitive influence of Ca^{2+} ion level (Ref 104). Sodium silicate and hexametaphosphate additions (Ref 102), as well as Mg^{2+} ion, are also inhibitive to a lesser extent. The addition of certain chelating agents (e.g., ethylenediaminetetracetic acid, diethylenetriaminepentaacetic acid) to the Ca^{2+} ion containing peroxide solutions may compromise inhibition if added in excess (Ref 104).

Significant attack of titanium may also occur in highly concentrated (90%) H_2O_2 solutions.

Other Oxidizing Media. Titanium alloys exhibit outstanding resistance to solutions of oxidizing chlorine compounds over the full range of concentrations and to relatively high temperatures. Various data for unalloyed titanium are presented in Table 9. Titanium is highly resistant to wet chlorine gas, although a minimum water content must be present, depending on temperature, to maintain full passivity. This is discussed in more detail in the section "Gases" in this article. Titanium is unique among the common engineering alloys in its elevated resistance to general and pitting corrosion in oxidizing chloride environments (Ref 10), as well as bromine- and iodine-containing media. Halide salts of oxidizing metal cations also enhance the passivity of titanium alloys such that negligible corrosion rates can be expected. Prominent examples include $FeCl_3$, $CuCl_2$, and $NiCl_2$ solutions and their bromide counterparts.

Reducing Acids. The corrosion resistance of titanium alloys in reducing acid media is very sensitive to acid concentration, purity, temperature, and background chemistry, in addition to titanium alloy composition. When the temperature and/or concentration of strong reducing acid solutions exceed certain values, the protective oxide film of titanium can break down (i.e., depassivate), resulting in severe general corrosion. Strong reducing acids of concern include hydrochloric, sulfuric, hydrobromic, hydriodic, hydrofluoric, phosphoric, sulfamic, oxalic, and trichloroacetic acids.

Temperature-acid concentration guidelines for titanium grades 2, 7, and 12 in naturally aerated but pure (uninhibited) HCl, H_2SO_4, and H_3PO_4 solutions are presented in Fig. 17, 18, and 19, respectively. Supplemental titanium alloy corrosion data in these acids are provided in Tables 10 to 13 and in the Appendixes to this article. Corrosion rate profiles for various palladium- and ruthenium-enhanced titanium alloys

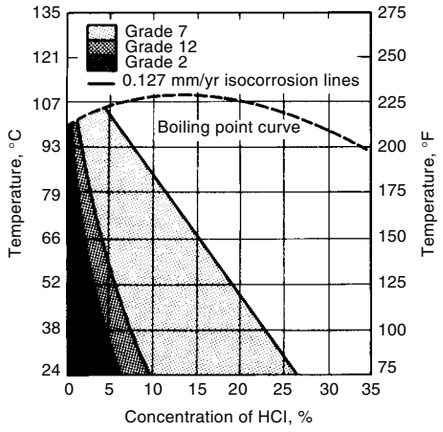

Fig. 17 Isocorrosion diagram for titanium alloys in pure, naturally aerated HCl solutions. 0.127 mm/yr (5 mils/yr) isocorrosion lines are shown.

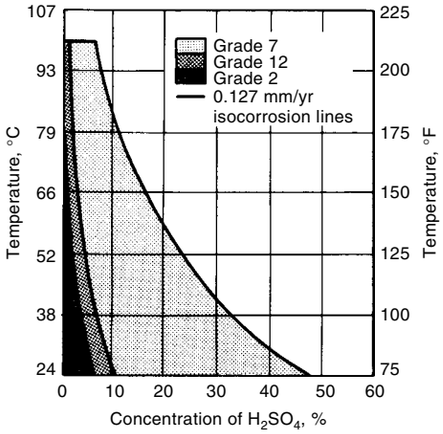

Fig. 18 Isocorrosion diagram for titanium alloys in pure, naturally aerated H_2SO_4 solutions. 0.127 mm/yr (5 mils/yr) isocorrosion lines are shown.

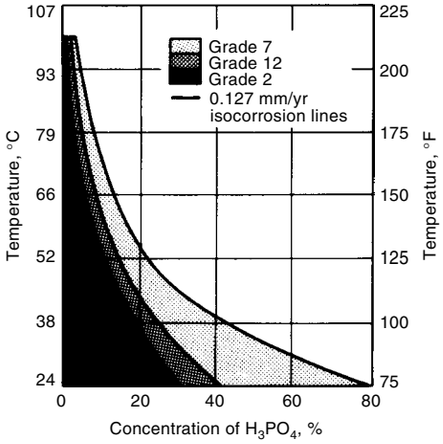

Fig. 19 Isocorrosion diagram for titanium alloys in pure, naturally aerated H_3PO_4 solutions. 0.127 mm/yr (5 mils/yr) isocorrosion lines are shown.

in boiling HCl media are presented in Fig. 20. Table 14 lists data for several alloys in HBr and HI solutions. Corrosion data for unalloyed titanium in highly concentrated and SO_3-fuming H_2SO_4 media can be found in Ref 6. It should be noted that the titanium-palladium (grades 7, 11, 16, 17) and titanium-ruthenium (grades 26, 27) alloys exhibit substantially greater resistance to dilute uninhibited reducing acids than other commercial titanium alloys. General corrosion rate profiles for as-annealed high-strength titanium alloys in uninhibited boiling HCl solutions are plotted in Fig. 21 to 23 (Ref 13). Figure 24 suggests that aging has little effect on the general resistance of a titanium alloy to HCl (Ref 13). The potent beneficial effect of palladium, ruthenium, and/or molybdenum alloying additions on titanium corrosion resistance is apparent from these results.

Table 10 Corrosion of grade 2 titanium in naturally aerated HCl solutions

Concentration of HCl, wt%	Temperature °C	Temperature °F	Corrosion rate mm/yr	Corrosion rate mils/yr
5	24	75	nil	
6	24	75	0.07	2.8
8	24	75	0.2	8
9	24	75	0.25	10
17.3	24	75	0.51	20
26	24	75	2.59	102
1.4	52	125	0.02	0.8
5.8	52	125	0.51	20
6	52	125	0.68	26.8
7	52	125	1.27	50
11.5	52	125	3.07	121
1	66	150	0.01	0.4
1.5	66	150	0.02	0.8
1.7	66	150	0.13	5
2	66	150	0.61	24
3	66	150	1	40
4.7	66	150	7.08	279
0.05	Boiling		0.02	0.8
0.1	Boiling		0.1	4
0.2	Boiling		0.23	9
0.4	Boiling		0.53	21
0.5	Boiling		0.84	33.1
1	Boiling		1.83	72

Table 11 Corrosion of grade 12 titanium in naturally aerated HCl solutions

Concentration of HCl, wt%	Temperature °C	Temperature °F	Corrosion rate mm/yr	Corrosion rate mils/yr
6	24	75	0.008	0.31
8	24	75	0.008	0.31
10	24	75	1.40	55
12	24	75	2.54	100
28.5	24	75	5.58	220
3	52	125	nil	
4	52	125	0.001	0.04
5.9	52	125	0.51	20
7	52	125	5.30	209
2.4	66	150	0.01	0.4
3.6	66	150	0.03	1.2
5.9	66	150	0.51	20
7	66	150	8.98	354
0.6	Boiling		0.025	1
1.7	Boiling		0.16	6.3
2	Boiling		0.51	20
2.5	Boiling		6.85	270

Hydrofluoric acid solutions can aggressively attack titanium alloys over the full range of concentrations and temperatures, because the fluoride ion (F^-) forms highly stable, soluble complexes with titanium. Although the addition of oxidizing species, such as HNO_3, will tend to reduce corrosion and retard hydrogen uptake in HF solutions, significant rates of attack still prevail. Inhibition of corrosion can be achieved in dilute acid fluoride solutions when an excess of complexing metal ions (e.g., Ca^{2+}, Mg^{2+}, Fe^{3+}, Al^{3+}, or Cr^{6+}) is present (Ref 101, 102, 107–109). In the absence of these complexing metal ions, solutions containing more than 20 to 30 ppm F^- may attack titanium when solution pH falls below 6 to 7.

Titanium alloys exhibit good resistance to most mildly reducing acid solutions whether they are inhibited or not. These environments include sulfurous acid, aqueous hydrogen sulfide solutions, boric acid, or carbonic acid. Near-nil corrosion rates can be expected over the full concentration range to temperatures well beyond their boiling points (Ref 110).

Inhibition of Reducing Acid Corrosion. Although strong reducing acids may seriously corrode titanium alloys in pure form, the presence of certain oxidizing species (cathodic depolarizers) in these acids can effectively inhibit general corrosion; this expands the useful range of application of these alloys. These species may be prime constituents of a process stream, naturally occurring background contaminants (such as dissolved oxygen), intentionally added inhibitors, or ferrous corrosion products.

The inhibitors commonly encountered in industrial service are listed in Table 15 (Ref 111, 112). Many of these effective inhibitors are multivalent metal ions in their highest valence

Table 12 Corrosion of grade 7 titanium in naturally aerated HCl solutions

Concentration of HCl, wt%	Temperature °C	Temperature °F	Corrosion rate mm/yr	Corrosion rate mils/yr
9	24	75	nil	
18	24	75	nil	
20	24	75	0.01	0.4
26.5	24	75	0.02	0.8
27	24	75	0.70	27.6
9	52	125	0.008	0.3
11.5	52	125	0.02	0.8
14.7	52	125	0.03	1.2
16.8	52	125	0.06	2.4
19	52	125	0.08	3.1
21.9	52	125	0.41	16.1
6	66	150	0.01	0.4
9.6	66	150	0.03	1.2
11.5	66	150	0.04	1.6
16.8	66	150	0.13	5.1
17	66	150	0.39	15.4
20.9	66	150	0.51	20
2	Boiling		0.025	1
3	Boiling		0.05	2
4	Boiling		0.10	4
6	Boiling		0.23	9
9	Boiling		0.51	20
16.8	Boiling		2.97	117

Table 13 Corrosion rates for welded and wrought titanium-ruthenium and titanium-palladium sheet in reducing acid media

Naturally aerated, 24 h exposure

			Corrosion rate											
			Grade 7				Grade 16				Grade 26			
	Temperature(a)		Base		Weld		Base		Weld		Base		Weld	
Acid solution	°C	°F	mm/yr	mils/yr	mm/yr	mils/yr	mm/yr	mils/yr	mm/yr	mils/yr	mm/yr	mils/yr	mm/yr	mils/yr
1% HCl	102	216	<0.01	<0.39	0.01	0.39	<0.01	<0.39	<0.01	<0.39	<0.01	<0.39	0.01	0.39
2% HCl	103	217	0.03	1.2	0.04	1.6	0.03	1.2	0.04	1.6	0.04	1.6	0.06	2.4
3% HCl	105	220	0.07	2.8	0.06	2.4	0.09	3.5	0.17	6.7	0.09	3.5	0.17	6.7
3% H_2SO_4	240	465	<0.01	<0.39	<0.01	<0.39	<0.01	<0.39	<0.01	<0.39	<0.01	<0.39	<0.01	<0.39

(a) Boiling point at atmospheric pressure

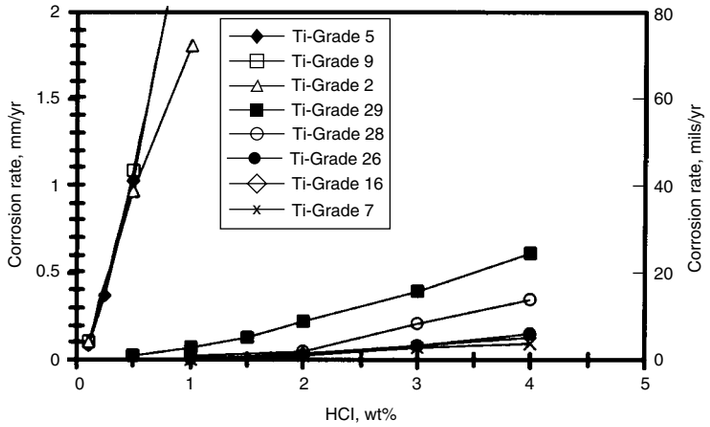

Fig. 20 Corrosion rate profiles for various palladium- and ruthenium-enhanced titanium alloys in boiling, naturally aerated HCl solutions

states. Inhibitor potency at levels as low as 100 ppm or below is typically observed, as indicated by the data presented in Table 16 (Ref 113) and those listed under the respective acids in the Appendixes to this article. The beneficial influence of minute ferric ion concentrations on the useful resistance of titanium grades 2, 7, and 12 in HCl media is shown in Fig. 25. Figure 26 (Ref 114) reveals how ferric ion additions dramatically expand the useful resistance of various titanium alloys in boiling HCl solutions. A substantial database on corrosion rate inhibition by ferric ion additions in various HCl media and temperatures can be found in Ref 114. Nitric acid or nitrate additions effectively inhibit titanium alloy corrosion on HCl media, whereas more limited inhibition is observed in H_2SO_4 and H_3PO_4 solutions containing nitric acid or nitrates.

Because the performance of titanium alloys in reducing acids is highly influenced by the presence of many inhibiting species, the nature and background chemistry of a reducing acid environment should be thoroughly examined before determining alloy suitability. Titanium is often selected for normally aggressive, high-temperature reducing acid solutions, such as hydrometallurgical acid-leach processes for treating ores to recover metallic values, because of the beneficial effect of these inhibitive metal ions (Ref 113).

Anodic protection is also an effective means of passivating and protecting titanium alloys in reducing acids. Table 17 shows that impressed anodic potentials can significantly reduce the corrosion rate of unalloyed titanium in various hot, dilute, or concentrated acids (Ref 115, 116). Generally, an increase in anodic potential will decrease corrosion rate as long as the anodic pitting (and repassivation) potentials are not exceeded for titanium in the electrolyte.

Salt Solutions. Titanium alloys are highly resistant to practically all salt solutions over the pH range of 3 to 11 and to temperatures well in excess of boiling. Titanium withstands exposure to solutions of chlorides (Ref 10, 117), bromides, iodides, sulfites, sulfates, borates, phosphates, cyanides, carbonates, bicarbonates, and ammonium compounds. Corrosion rate values for titanium alloys in these various salt solutions are generally less than 0.025 mm/yr (1.0 mil/yr) and can be found in the Appendixes to this article as reported by various sources (Ref 6, 117, 118).

Oxidizing anionic salts such as nitrates, hypochlorites, chlorites, chlorates, perchlorates, molybdates, chromates, permanganates, and vanadates further extend titanium alloy passivity into stronger acidic and alkaline solutions. Similar beneficial effects on the low-pH (acidic) side can be expected from oxidizing cationic salts, such as ferric, cupric, and nickelous chlorides or sulfates. In fact, titanium is often the most practical metal for handling hot, oxidizing, acidic chloride conditions.

Titanium alloys are frequently selected because of their superior resistance to the chlorides typically found in many process streams, brines, and seawater. In hot chloride media, susceptibility to pitting is usually not an issue, but crevice corrosion may be possible, depending on pH, temperature, and the specific alloy (see the section "Crevice Corrosion" in this article). Special attention must be given to nonoxidizing acidic or hydrolyzable salt solutions as temperatures and concentrations increase. To avoid general or localized HCl attack resulting from salt hydrolysis, special concentration-temperature guidelines for titanium should be observed for concentrated $AlCl_3$ (Ref 6, 117), $ZnCl_2$ (Ref 119), $MgCl_2$ (Ref 120), and $CaCl_2$ solutions. Guidelines for grades 2, 7, and 12 titanium in hot concentrated $MgCl_2$ and in concentrated sea salt and NaCl slurries are presented in Fig. 27 and 28, respectively, and in Fig. 29 for concentrated $CaCl_2$ brines. The titanium-palladium, titanium-ruthenium, grade 12, and higher (>3.5 wt%)-molybdenum-containing titanium alloys exhibit superior resistance to general and localized corrosion in these high-temperature acid salt solutions.

Alkaline Media. Titanium alloys are generally very resistant to alkaline media, including solutions of NaOH, KOH, $Ca(OH)_2$, $Mg(OH)_2$, and NH_4OH. Near-nil corrosion rates can be expected in boiling solutions of the latter three alkalis up to saturation. As shown in Table 18, titanium exhibits low corrosion rates in NaOH and KOH solutions at subboiling temperatures. However, significant increases in corrosion are noted as the concentrations of these two strong alkalis increase at higher temperatures. Potassium hydroxide tends to be more aggressive than sodium hydroxide under these conditions.

Although corrosion rates are relatively low in alkaline media, titanium alloys may experience excessive hydrogen pickup and eventual embrittlement under certain conditions. For α and near-α alloys, hydrogen embrittlement is possible when temperatures exceed 80 °C

(175 °F) and pH is 12 or more. The presence of dissolved oxidizing species in hot caustic solutions, such as chlorate, hypochlorite, molybdate, or nitrate compounds, can extend resistance to hydrogen uptake to higher temperatures.

Organic Compounds. As indicated in Table 19, titanium alloys are highly resistant to most organic compounds, including alcohols, ketones, ethers, aldehydes, and hydrocarbons. The traces of moisture (10 to 100 ppm) normally present in industrial organic process streams are sufficient to maintain the protective oxide film of titanium. Totally anhydrous organic streams may prevent oxide film repair and should be avoided. In the special case of anhydrous or near-anhydrous methanol, a minimum water content (on the order of several weight percent or more) is required to prevent depassivation and SCC, depending on the alloy (Ref 121). These forms of attack are aggravated by decreasing pH and/or halide concentration (Ref 55, 122–124). Higher-molecular-weight alcohols are generally benign toward titanium alloys.

Chlorinated hydrocarbons generally do not pose any problems for most titanium alloys (Table 19). A few high-strength alloys may be susceptible to SCC under specific circumstances (see the section "Stress-Corrosion Cracking" in this article). If significant quantities of water are also present, many chlorinated hydrocarbons may undergo hydrolysis to form HCl at higher temperatures. Titanium alloy performance will depend on the temperature and the extent of HCl formation and concentration in the aqueous phase.

Titanium alloys are generally very resistant to organic acids. Nil corrosion can be expected in concentrated solutions of very weak organic acids such as adipic, hydroxyacetic, acetic, terephthalic, tannic, stearic, maleic, tartaric, benzoic, butyric, and succinic acids to temperatures in excess of 100 °C (212 °F). As indicated in Table 20, corrosion rates can become significant in the stronger, nonaerated organic acids as acid concentration and temperature increase (Ref 6, 110, 117). These acids include formic, lactic, citric, trichloroacetic, and, especially, oxalic acid (see data in the Appendixes to this article). The titanium-palladium, titanium-ruthenium, and grade 12 alloys exhibit much greater resistance to these acids than unalloyed titanium.

Solution aeration is often sufficient to inhibit corrosion on unalloyed titanium in the stronger organic acids, such as formic, lactic, and citric (Ref 6). Addition of oxidizing species (Table 15) may also effectively inhibit corrosion in the more aggressive organic acids, such as oxalic.

Gases. The oxide film on titanium alloys provides an effective barrier to attack by most gases in wet or dry condition, including oxygen, nitrogen, dry HCl, SO_2, NH_3, HCN, CO_2, CO, and H_2S (Ref 125). This protection extends to temperatures in excess of 150 °C (300 °F). The outstanding resistance of titanium alloys to rural, marine, and urban atmospheric exposure has been documented (Ref 74, 84).

Titanium alloys experience no significant corrosion degradation in air, oxygen, or sulfur-bearing (Ref 125) gases below 300 °C (570 °F). Depending on alloy type and composition, excessive surface oxidation and eventual embrittlement may occur above ~550 °C (1020 °F) after prolonged, sustained exposure to air. Embrittlement results from enhanced diffusion of interstitial oxygen into the metal at the higher temperatures, such that time to failure depends on metal section thickness and state of stress. A brittle, oxygen-rich α-case surface layer forms initially, which grows in depth as a function of temperature and time. The diffusion rate for oxygen in α titanium is substantially less than that in β-phase titanium, to a degree that depends on temperature (Ref 38). Diffusion rates for nitrogen in titanium are substantially lower (Ref 6, 8), such that a protective titanium nitride film can be formed with minimal α case below ~650 °C (1200 °F).

Titanium alloys exhibit good oxidation resistance up to ~550 °C (1020 °F) due to formation of protective TiO_2 films. The growth of thermal oxide films on unalloyed titanium and Ti-6Al-4V with time in air at 400 to 700 °C (750 to 1290 °F) is profiled in Fig. 30 and 31, respectively. Below 200 °C (390 °F), logarithmic oxide growth behavior is typical (Ref 6, 128). Logarithmic dependence with time is also generally observed at 300 to 500 °C (570 to 930 °F), which transitions to parabolic at 500 to 700 °C (930 to 1290 °F) (Ref 6, 8, 126, 127, 129). On the other hand, a faster, cubic rate law was indicated for titanium oxidation in 0.10 MPa (1 atm) saturated steam at 400 to 550 °C (750 to 1020 °F) (Ref 130). Above 700 °C (1290 °F), linear growth rate behavior is typical, indicating little protective effect of the oxide. Studies have shown that alloying titanium with aluminum, silicon, significant chromium, and/or niobium decreases oxidation rates (Ref 6, 38, 128, 131), whereas iron, vanadium, and certain other β-stabilizing elements can aggravate oxidation. Various coating systems for inhibiting thermal oxidation of titanium alloys in air are reviewed elsewhere (Ref 131).

Although ignition or burning of common mill product forms in ambient air is generally not a concern, titanium may ignite and/or burn in rare situations where metal surface temperatures are maintained at or above the alloy melting point in air or oxygen gas. Ultrathin section or elevated

Table 14 Corrosion of titanium alloys in naturally aerated HBr and HI solutions

Acid	Concentration, wt%	Temperature °C	Temperature °F	Alloy grade	Corrosion rate mm/yr	Corrosion rate mils/yr
HBr	0.3	Boiling		2	nil	
	0.6	Boiling		2	0.003	0.12
	0.9	Boiling		12	0.008	0.32
	3.0	Boiling		2	1.45	57
	3.0	Boiling		12	0.013	0.5
	3.0	Boiling		7	0.010	0.4
	8.0	Boiling		7	0.094	3.7
	40	24	75	2	nil	
HI	10	Boiling		2	nil	
	57	24	75	2	0.15	6

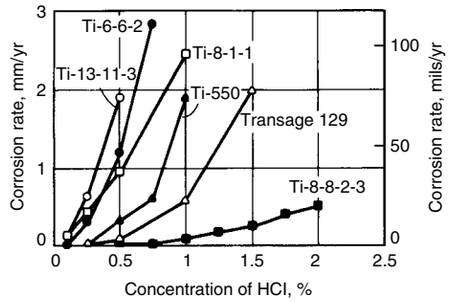

Fig. 21 Corrosion rate profiles for annealed titanium alloys in boiling, naturally aerated HCl solutions

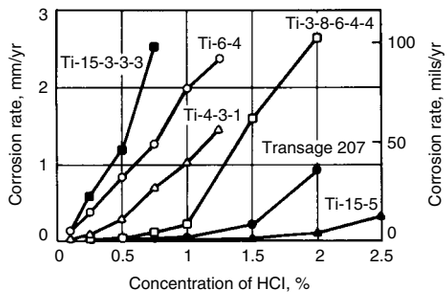

Fig. 22 Corrosion rate profiles for annealed titanium alloys in boiling, naturally aerated HCl solutions

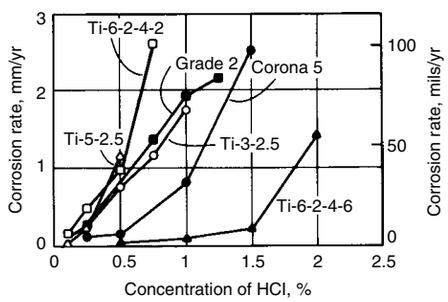

Fig. 23 Corrosion rate profiles for annealed titanium alloys in boiling, naturally aerated HCl solutions

surface-to-volume ratio forms (e.g., thin foils or powders) are most susceptible, because the exothermic heat of oxidation cannot be extracted quickly enough for the surface metal to resolidify and form a protective titanium oxide film. (Note: Molten titanium readily dissolves its own oxide film.) Ignition and burning in air is also possible in highly pressurized, high-velocity air, such as in gas turbine jet engine compressors. Ignition/burn testing in air has shown that titanium alloys containing at least 11 wt% Cr (e.g., Ti-13-11-3 and Alloy C [Ti-35V-15Cr]) are exceptionally burn resistant (Ref 38, 39).

Susceptibility to ignition/burning increases dramatically in enriched and pure oxygen gas compared to air. Figure 32 (Ref 132, 133) shows that ignition may occur when oxygen content exceeds 35 vol%. Thresholds for the ignition of unalloyed titanium in pure oxygen gas are plotted in Fig. 33 (Ref 133) as a function of pressure and temperature. Ignition thresholds for titanium in low-temperature gaseous oxygen are depicted in Fig. 34. Titanium alloys exhibit impact sensitivity in liquid oxygen (Ref 134). Note that ignition is not easily achieved unless the surface oxide film is mechanically damaged (i.e., fractured, heavily plastically strained, scratched) and fresh metal surfaces are exposed.

Recent ignition studies indicate that the highly corrosion-resistant Ti-45Nb alloy uniquely resists ignition in pure oxygen gas to pressures as high as ~3.1 MPa (0.45 ksi) at 250 °C (480 °F), compared to a pressure limit of ~1.7 MPa (0.25 ksi) for unalloyed titanium (Ref 38, 39, 135).

Ignition and burning of titanium alloys can be avoided in oxygen-rich atmospheres by proper equipment design, surface coatings, and/or avoidance of mechanical damage to exposed titanium surfaces (Ref 113). Recommended guidelines for preventing ignition of titanium powders have also been established (Ref 136).

Although titanium is the preferred metallic material for handling wet chlorine and bromine gas environments, rapid, dangerous, exothermic halogenation reactions may occur with titanium in dry chlorine and bromine gas environments. A minimum water content (or oxygen content) in these cases is necessary to maintain total alloy passivity, as indicated in Fig. 35 and 36 (Ref 137, 138). The critical water content depends on gas temperature and flow rate. Mechanical damage to metal surfaces to expose fresh metal facilitates reaction with dry chlorine, but thicker oxide films (e.g., thermal or anodized oxides) tend to retard initiation of the reaction. Titanium alloys cannot be fully passivated in liquid bromine because of the extremely low solubility of water in this medium.

Rapid, pyrophoric reactions with titanium alloys are also possible in anhydrous N_2O_4 gas atmospheres (Ref 97–99). Small water additions (Ref 139) or the presence of 0.6 to 1.0 wt% nitric acid effectively inhibit metal attack.

Liquid Metals and Fused Salts. Titanium exhibits good resistance to many liquid metals at moderately elevated temperatures, at which corrosion rate increases with temperature and flow rate (Ref 6, 74, 117). As shown in Table 21, these metals include molten aluminum, sodium, potassium, sodium-potassium mixtures, magnesium, tin, and lead. In contrast, useful performance of titanium in molten lithium, bismuth, zinc, gallium, cadmium, and mercury is limited to relatively low temperatures. Liquid mercury below 150 °C (300 °F) does not appear to affect titanium unless wetting of freshly exposed (mechanically damaged) surfaces occurs (Ref 74). As discussed in the sections on SCC, liquid and solid cadmium, silver, and mercury may cause embrittlement of titanium alloys.

Titanium exhibits relatively high rates of attack in molten chloride salts, increasing with

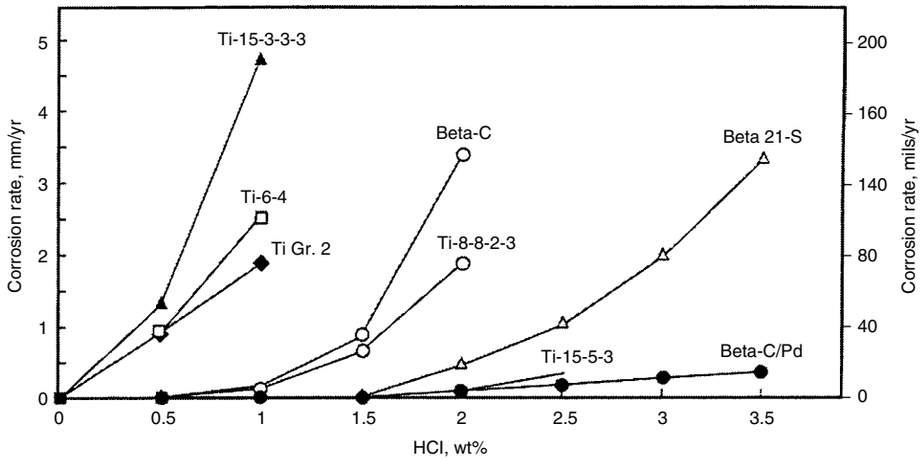

Fig. 24 Corrosion rate profiles in boiling HCl for several aged titanium alloys

Table 15 Species that inhibit the corrosion of titanium alloys in reducing acids

Inhibitor category	Species	Relative inhibitor potency
Oxidizing metal cations	Ti^{4+}, Fe^{3+}, Cu^{2+}, Hg^{4+}, Ce^{4+}, Sn^{4+}, VO_2^+	High
	Te^{6+}, Se^{6+}	High
	Te^{4+}, Se^{4+}, Ni^{2+}	Low
Oxidizing anions	ClO_4^-, $Cr_2O_7^{2-}$, MoO_4^{2-}, MnO_4^{2-}, WO_4^-, IO_3^-	Very high
	NO_3^-, SbO_3^-, VO_4^{3-}, VO_3^-	Very high
	NO_2^-, $S_3O_3^{2-}$	Moderate
Precious-metal ions	Pt^{2+}, Pt^{4+}, Pd^{2+}, Ru^{3+}, Ir^{3+}, Rh^{3+}, Au^{3+}	High
Oxidizing organic compounds	Picric acid, o-dinitrobenzene, 8-nitroquinoline, m-nitroacetanilide, trinitrobenzoic acid, and certain other nitro, nitroso, and quinone organics	Moderate-high
Others	O_2, H_2O_2, ClO_3^-, OCl^-	Moderate

Source: Ref 111, 112

Table 16 Effect of certain multivalent metal ions on the corrosion of titanium in boiling reducing acids

		Corrosion rate			
		Boiling 5% HCl		Boiling 10% H_2SO_4	
Inhibiting ion	Concentration of inhibiting ion, ppm	mm/yr	mils/yr	mm/yr	mils/yr
Fe^{3+} (ferric)	0	29	1142	>76.2	>3000
	100	0.025	1	0.208	8.2
	500	0.02	0.8	0.069	2.7
Cu^{2+} (cupric)	0	29	1142	>76.2	>3000
	100	0.033	1.3	0.419	16.5
	500	nil		0.361	14.2
Mo^{6+} (molybdate)	0	29	1142	>76.2	>3000
	100	nil		0.001	0.04
	500	nil		nil	
Cr^{6+} (chromate)	0	29	1142	>76.2	>3000
	100	nil		0.001	0.04
	500	nil		0.001	0.04
V^{5+} (vanadate, vanadyl)	0	29	1142	>76.2	>3000
	100	0.02	0.8	0.005	0.2
	500	0.008	0.3	0.005	0.2

Source: Ref 113

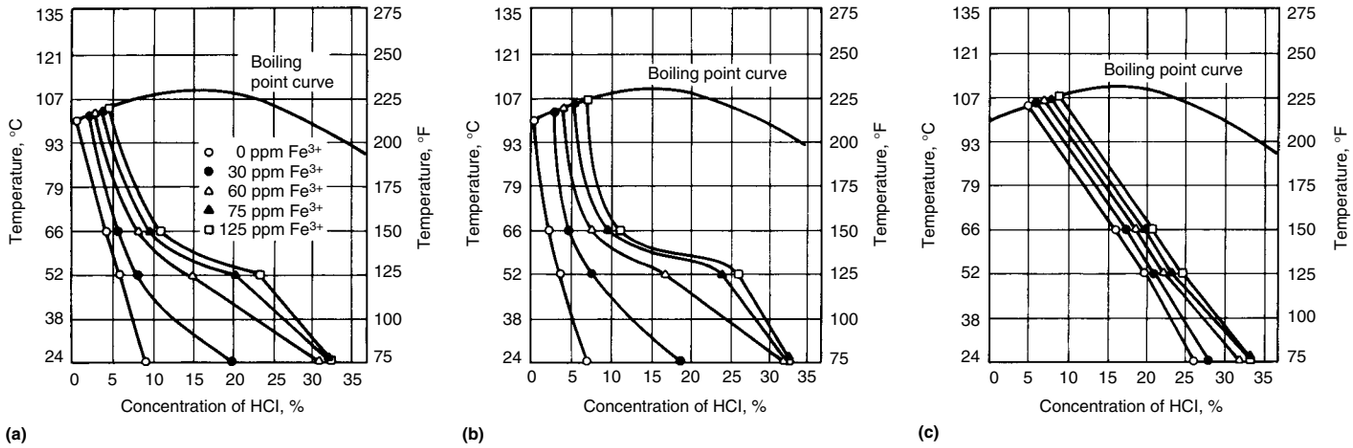

Fig. 25 Effect of minute ferric ion concentrations on the useful corrosion resistance of grades 2 (a), 12 (b), and 7 (c) titanium in naturally aerated HCl solutions. 0.127 mm/yr (5 mils/yr) isocorrosion lines are shown.

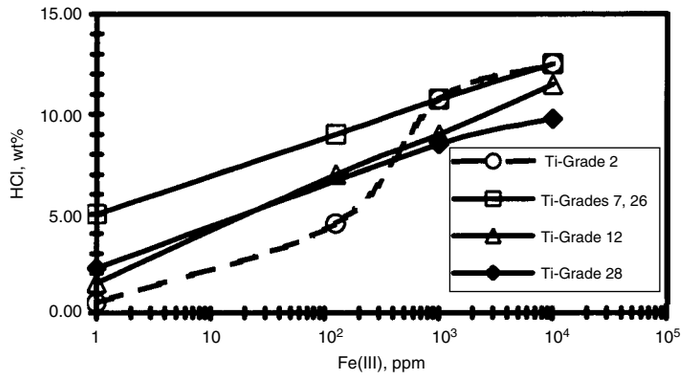

Fig. 26 Beneficial effect of ferric ion level on boiling HCl acid limits for various titanium alloys. 0.127 mm/yr (5 mils/yr) isocorrosion lines are shown. Source: Ref 114

Table 17 Effect of impressed anodic potentials on the corrosion of unalloyed titanium in hot reducing acids

Acid	Concentration, wt%	Temperature °C	Temperature °F	Applied potential, V versus standard hydrogen electrode	Corrosion rate mm/yr	Corrosion rate mils/yr	Reduction in corrosion rate
Sulfuric	40	60	140	+2.1	0.005	0.2	11,000×
	40	90	195	+1.4	0.07	2.8	896×
	40	114	237	+2.6	1.8	71	189×
	60	60	140	+1.7	0.035	1.4	662×
	60	90	195	+3.0	0.10	4	163×
Hydrochloric	37	60	140	+1.7	0.068	2.7	2080×
Phosphoric	60	60	140	+2.7	0.018	0.7	307×
	60	90	195	+2.0	0.5	20	100×
Formic	50	Boiling		+1.4	0.083	3.3	70×
Oxalic	25	Boiling		+1.6	0.25	10	350×
Sulfamic	20	90	195	+0.7	0.005	0.2	2710×

Source: Ref 115, 116

both temperature and the presence of oxygen. Aggressiveness of attack follows the order: KCl > NaCl > LiCl (Ref 6, 117). High rates of metal dissolution have also been reported in fused sodium carbonate, sodium hydroxide, sodium peroxide, and sodium bisulfate (Ref 117).

Crevice Corrosion in Specific Media

Titanium alloys generally exhibit superior resistance to crevice corrosion as compared to stainless steel and nickel-base alloys (Ref 140). Nevertheless, the susceptibility of titanium alloys to crevice corrosion should be considered when tight crevices exist in hot aqueous chloride, bromide, iodide, or sulfate solutions. Crevice test results indicate that the initiation of crevice corrosion often lacks reproducibility, consistency, and regularity. These test data must be judged relative to their statistical significance (that is, number of data points). Factors that affect crevice attack significantly include alloy composition, pH, temperature, halide concentration, presence of oxidizing species (cathodic depolarizers), sample surface condition, type of gasket, type of crevice (gasket-to-metal, metal-to-metal, deposit-to-metal), and the crevice geometry, particularly crevice gap (tightness) (Ref 19–21, 23, 141, 142).

Chlorides. The susceptibility of titanium alloys to crevice corrosion in hot, concentrated chloride solutions increases significantly as temperatures increase and pH decreases (Ref 19, 20). Figure 37 shows pH-temperature limits for the crevice corrosion of various titanium grades. These guidelines have been found to be applicable to most chloride salt solutions, including seawater, over a wide range of chloride concentrations (> several hundred parts per million). The limits presented for grade 2 are applicable to all unalloyed grades, whereas those for grade 7 similarly apply to all titanium-palladium and titanium-ruthenium grades (Ref 10).

Crevice attack of titanium alloys will generally not occur below a temperature of 70 °C (160 °F) regardless of solution pH or chloride concentration or when solution pH exceeds 10 regardless of temperature. As indicated in Fig. 37 and Table 22, grade 12 provides crevice corrosion resistance when brine pH falls between 3 and 11 to temperatures as high as 280 °C (535 °F) (Ref 143, 144). The titanium-palladium and titanium-ruthenium alloys extend this resistance to brine pH values as low as ~0.5, depending on brine composition and temperature (Ref 145–149). Uniquely, these alloys all fully resist crevice attack in chlorine-saturated NaCl brines at 90 °C (195 °F) and boiling 10% $FeCl_3$

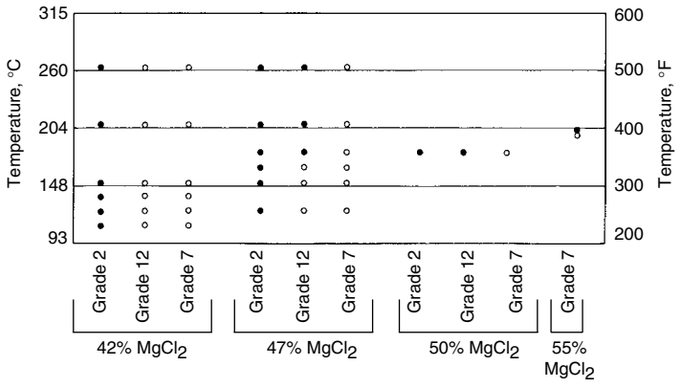

Fig. 27 Temperature guidelines for avoiding localized attack of grades 2, 7, and 12 titanium in concentrated $MgCl_2$ solutions in the absence of crevices. • denotes susceptibility to attack.

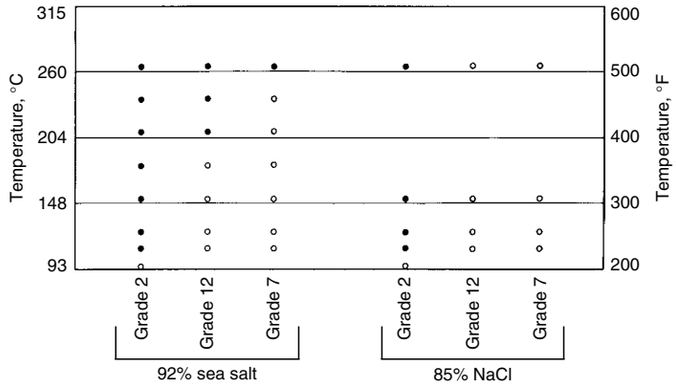

Fig. 28 Temperature guidelines for avoiding localized attack of grades 2, 7, and 12 titanium in pressure-bled tests in concentrated sea salt and NaCl slurries in the absence of crevices. • denotes susceptibility to localized attack.

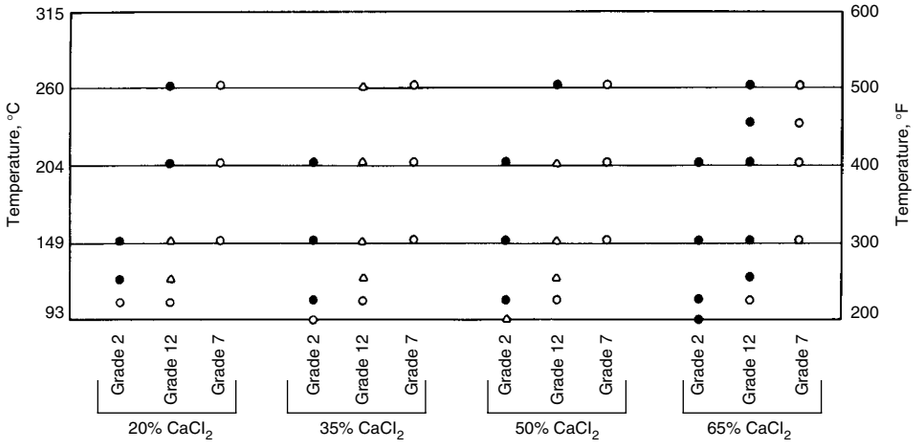

Fig. 29 Temperature guidelines for avoiding localized attack of grades 2, 7, and 12 titanium in concentrated $CaCl_2$ solutions in the absence of crevices. • denotes susceptibility to localized attack; Δ indicates incipient edge attack.

Table 18 Corrosion of unalloyed titanium in highly alkaline solutions

		Temperature		Corrosion rate	
Medium	**Concentration, wt%**	**°C**	**°F**	**mm/yr**	**mils/yr**
Ammonium hydroxide	28	26	79	0.002	0.08
	70	Boiling		nil	
Sodium carbonate	20	Boiling		nil	
Sodium hydroxide	28	25	75	0.003	0.12
	10	Boiling		0.02	0.8
	40	66	150	0.038	1.5
	40	93	200	0.064	2.5
	40	121	250	0.13	5
	50	66	150	0.018	0.7
	50–73	188	370	>1.1	>43.3
	73	110	230	0.05	2
	73	Boiling		0.13	5
Potassium hydroxide	10	Boiling		0.13	5
	25	Boiling		0.3	12
	50	25	75	0.010	0.4
	50	Boiling		2.7	106

Source: Ref 6, 74

solution under PTFE sheet gasketed crevices. These titanium-palladium/ruthenium alloys are considered to be the most crevice-corrosion-resistant titanium grades available commercially and are preferred for hot, low-pH salt solutions (Fig. 38).

The crevice corrosion resistance of grade 12 titanium was extensively tested in concentrated near-neutral NaCl, NaCl-$MgCl_2$, and NH_4Cl brines at high temperatures. Studies were conducted to assess this alloy for potential application in hypersaline geothermal brine (Ref 143), high-level nuclear waste storage (Ref 150), oil refineries (Ref 151), and salt evaporator brine heaters (Ref 144). In all cases, crevice testing involving PTFE gasket-to-metal and metal-to-metal crevices for extended periods revealed no evidence of significant attack to temperatures as high as 250 °C (480 °F). In saturated NH_4Cl solution, no gasket-to-metal or under-salt-deposit attack was noted to 177 °C (350 °F) and at pH 3 to 7.

It should be cautioned that deviations from normal crevice corrosion guidelines can be expected in certain acidic salts that may hydrolyze to form HCl at high temperatures when highly concentrated (Ref 119, 120). These salts include concentrated sea salt, $MgCl_2$, $CaCl_2$, $ZnCl_2$, and $AlCl_3$ (Fig. 27 to 29). The titanium-palladium and titanium-ruthenium alloys are generally most resistant in these situations (Ref 120).

The PTFE gasket-to-metal crevices of various high-strength titanium alloys were also tested in hot NaCl brines. The data, detailed in Ref 13, produced the ranking of alloy resistance shown in Table 23. Relative alloy crevice corrosion resistance generally parallels alloy resistance in reducing acid media. Titanium alloys containing at least 4 wt% Mo exhibit significantly increased crevice corrosion resistance in high-temperature NaCl media down to relatively low pHs. The beneficial effect of higher molybdenum content is confirmed in PTFE gasket-to-metal crevice tests performed on the Ti-3-8-6-4-4 alloy in hot sweet and sour brine conditions (Ref 62, 152, 153). This resistance is extended to even higher temperatures and/or lower pH by minor ruthenium or palladium alloy additions (Ref 38, 39, 61, 62, 153).

The crevice corrosion resistance of grade 9 titanium appears to be essentially the same as that for unalloyed titanium in hot NaCl brines. On the other hand, the greater aluminum content of the grade 5 alloy results in slightly reduced

crevice resistance as compared to unalloyed grades. The crevice threshold temperature limits for both of these alloys are dramatically elevated by minor ruthenium addition (i.e., grades 28 and 29 titanium), as depicted in Fig. 38 (Ref 39, 63, 146, 147, 154).

Studies have addressed the effect of chloride concentration on crevice corrosion initiation on unalloyed titanium (Ref 142). Threshold temperatures of 250, 200, and 150 °C (480, 390, and 300 °F) were indicated for chloride concentrations of 0.01, 0.1, and 1%, respectively, in neutral (pH 7) NaCl brine. Unpublished results suggest that 0.01% Cl^- at 90 °C (195 °F) and 0.10% Cl^- at 70 °C (160 °F) may be threshold conditions for crevice attack in aerated, pH 3 to 5 solutions given tight PTFE gasket-to-metal crevices.

Tests have shown that crevice tightness and area and type of gasket are critical to crevice corrosion initiation. The PTFE gasket-to-metal crevices are generally more susceptible to crack initiation than silicone rubber, neoprene rubber, asbestos, and polyvinyl chloride gasket-to-metal crevices (Ref 23, 141). Certain polymeric sealants, such as styrol-acrylic copolymer or methacrylate polymers, may significantly increase susceptibility to crevice attack, especially when the sealant contains chloride salts. On the other hand, metal-to-metal crevices are generally least susceptible to attack. In addition, it has been found that the incubation time for crevice corrosion in NaCl brine may be significantly reduced, and attack aggravated, by impressed anodic (positive) potentials (Ref 23, 141). As reviewed in the previous section on crevice corrosion, certain dissolved oxidizing species (cathodic depolarizers) in the brine may similarly decrease crevice attack incubation period and increase attack rate.

Bromides and Sulfates. Unpublished test results suggest that the pH-temperature guidelines for crevice corrosion of titanium in saturated NaCl (Fig. 37) are conservatively applicable in saturated NaBr solutions. However, rates of crevice attack are much lower than those in chloride at corresponding pHs and temperatures.

Crevice testing of unalloyed titanium in saturated Na_2SO_4 solutions revealed attack in neutral solutions at temperatures above 110 °C (230 °F) and only below pH 6 at 104 °C (220 °F), with no attack at 93 °C (200 °F) as low as pH 3. The PTFE gasket-to-metal crevices were also

Table 19 Corrosion of unalloyed titanium in organic media

Medium	Concentration, wt%	Temperature		Corrosion rate	
		°C	°F	mm/yr	mils/yr
Acetic anhydride	99–99.5	20 to boiling	70 to boiling	<0.13	<5
Adipic acid	0–67	204	400	<0.05	<2
Adipic acid + 20% glutaric acid + 5% acetic acid	25	200	390	nil	
Aniline hydrochloride	5–20	35–100	95–212	<0.001	<0.04
Benzene + HCl + NaCl	Vapor + liquid	80	175	0.005	0.2
Carbon tetrachloride	99–100	Boiling		0.003	0.12
Chloroform	100	Boiling		nil	
Chloroform + water	50	Boiling		0.12	4.7
Cyclohexane + traces formic acid	...	150	300	0.003	0.12
Ethyl alcohol	95	Boiling		0.013	0.5
Ethylene dichloride	100	Boiling		<0.13	<5
Formaldehyde	37	Boiling		<0.13	<5
Tetrachloroethylene	100	Boiling		nil	
Tetrachloroethylene + water	...	Boiling		0.13	5
Tetrachloroethane	100	Boiling		nil	
Trichloroethylene	99	Boiling		<0.13	<5

Source: Ref 6, 74, 117

Table 20 Corrosion of titanium alloys in various organic acids

Acid	Concentration, wt%	Alloy grade	Temperature		Corrosion rate	
			°C	°F	mm/yr	mils/yr
Acetic	0–99.5	2, 7, 12	Boiling		nil	
Adipic	67	2	240	465	nil	
Citric, aerated	10–50	2	100	212	0.01	0.4
Citric	50	2	Boiling		0.35	13.8
	50	7, 12	Boiling		0.01	0.4
Di- and mono-chloroacetic	100	2	Boiling		<0.013	<0.5
Formic, aerated	25–90	2	100	212	0.001	0.04
	25	2	Boiling		2.4	94.5
Formic	45	2	Boiling		11.0	433
	45	7, 12	Boiling		nil	
	10	2	Boiling		nil	
Lactic, aerated	10	2	Boiling		0.014	0.55
Lactic	10	2	100	212	0.048	1.9
	25	2	Boiling		0.028	1.1
	85–100	2	Boiling		0.01	0.4
Oxalic	0.5	2	60	140	2.4	94.5
	1	2	35	95	0.15	6
	10	7	Boiling		32.3	1272
Stearic	100	2	180	355	0.003	0.12
Tartaric	10–50	2	100	212	<0.013	<0.5
Terephthalic	77	2	225	435	nil	
Trichloroacetic	100	2	Boiling		14.6	575

Source: Ref 6, 110, 117

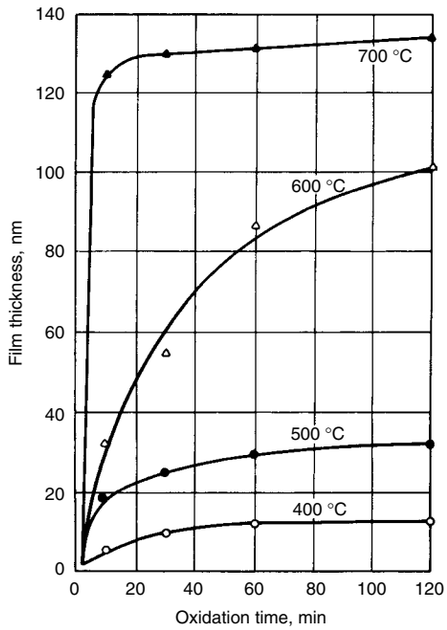

Fig. 30 Growth of thermal oxide films on unalloyed titanium in air. Source: Ref 126

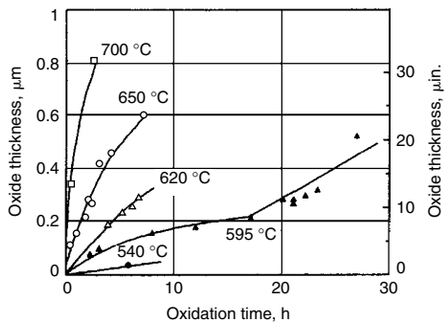

Fig. 31 Growth of thermal oxide surface films on Ti-6Al-4V in air. Source: Ref 127

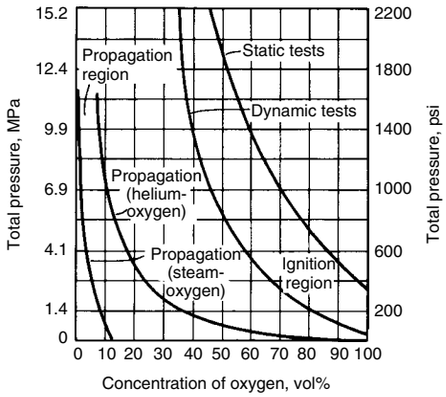

Fig. 32 Ignition and propagation limits for unalloyed titanium in various oxygen gas mixtures. Source: Ref 132, 133

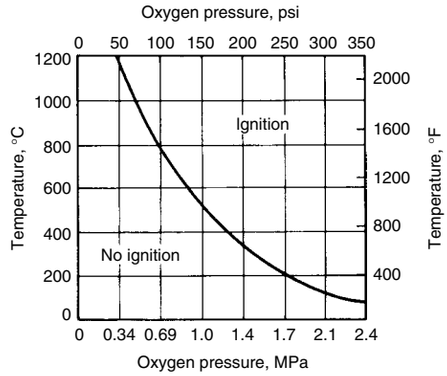

Fig. 33 Ignition limits for ruptured unalloyed titanium in pure oxygen gas atmospheres. Source: Ref 133

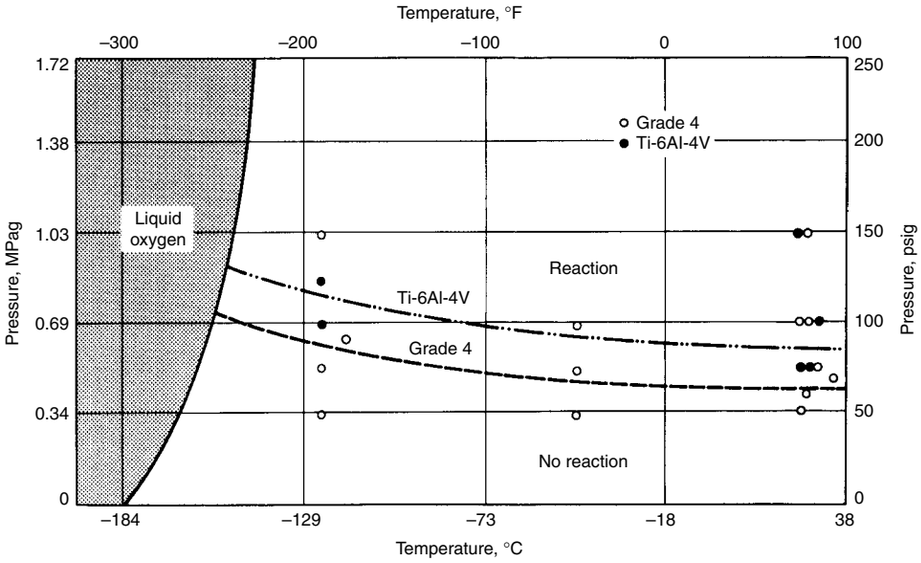

Fig. 34 Ignition limits for grade 4 titanium and Ti-6Al-4V alloy in low-temperature pure oxygen atmospheres. Source: Ref 74, 132

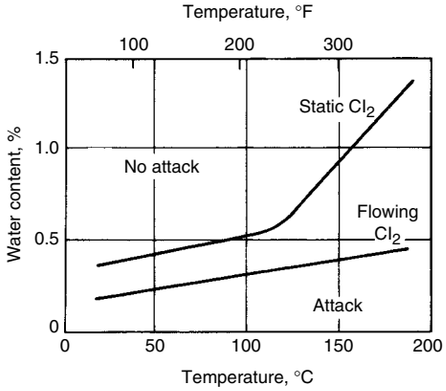

Fig. 35 Effect of temperature and gas flow on the critical water content required to passivate titanium in pure chlorine gas. Source: Ref 137

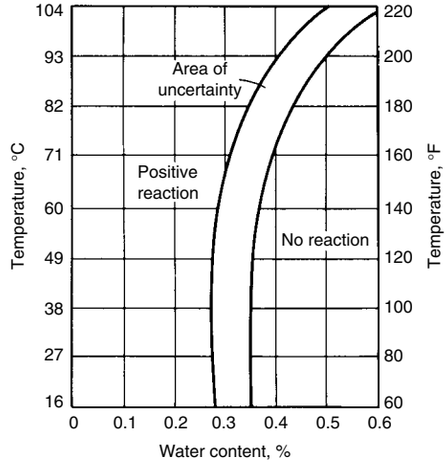

Fig. 36 Water content necessary to maintain passivity of unalloyed titanium in static chlorine gas atmospheres. Source: Ref 138

exposed to a simulated acid sulfate galvanizing solution for 38 days at temperatures of 66, 82, and 100 °C (150, 180, and 212 °F). The pH 1.3 solution consisted of 100 g/L Na_2SO_4, 120 g/L $ZnSO_4$, 0.6 g/L Fe^{3+} (as $Fe_2(SO_4)_3$), and 0.008% Cl^-. Grade 2 titanium proved to be fully resistant, except at the atmospheric boiling point. Titanium-palladium, titanium-ruthenium, and grade 12 titanium alloys resisted crevice attack under all conditions tested. All results suggest that crevice corrosion threshold temperatures in sulfate solutions are measurably higher, and rates of crevice attack are lower, than those in chloride brines.

Anodic Pitting in Specific Media

Anodic Breakdown Pitting. Titanium exhibits relatively high anodic breakdown potentials, E_b, in aqueous solution as compared to most engineering metals. This is the basis for its use as dimensionally stable anodes for chlor-alkali cells, anodes for recovery of metals or metal oxides from solutions, zinc and nickel plating anode baskets, aluminum anodizing racks, and platinum anode substrates for impressed-current cathodic protection systems. In sulfate and phosphate media, anodic pitting potentials of titanium alloys are typically in the range of +80 to +100 V (versus Ag/AgCl electrode). For this reason, dilute sulfuric and phosphoric acid solutions (and their salts) are typical electrolytes for anodizing titanium to grow protective surface oxides and/or produce colored surfaces.

In halide salt solutions, titanium alloys exhibit somewhat lower but yet reasonably high pitting potentials. Table 24 reveals that the anodic break down pitting potential decreases measurably with increasing temperature (Ref 155–158). Values of +9 to +10.5 V (versus Ag/AgCl) can be expected in room-temperature chloride solutions, decreasing to approximately +1.2 V at 175 to 250 °C (345 to 480 °F). These values are dependent on sample surface condition. For example, abraded or sandblasted surfaces exhibit

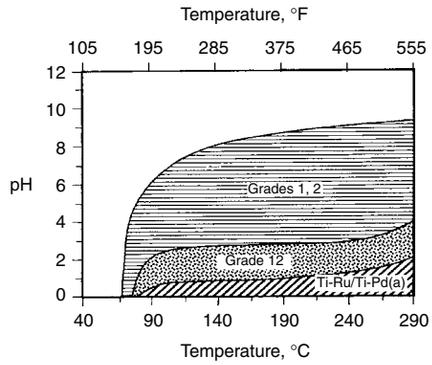

Fig. 37 Temperature-pH limits for crevice corrosion of titanium alloys in naturally aerated NaCl-rich brines (shaded areas indicate susceptibility to attack). (a) Includes grades 7, 11, 16, 17, 26, and 27. Source: Ref 10, 19, 143

Table 21 Corrosion of unalloyed titanium in liquid metals

Liquid metal	Temperature °C	Temperature °F	Corrosion rate mm/yr	Corrosion rate mils/yr
Bismuth-lead	300	570	<0.1	<4
	600	1110	0.13–1.3	5–50
Gallium	400	750	0.1	4
	450	840	>1.0	>40
Lithium	850	1560	0.1–1.0	4–40
Magnesium	750	1380	0.1	4
	850	1560	0.1–1.0	4–40
Lead	400	750	<0.13	<5
	600–950	1110–1740	0.1–1.0	4–40
Mercury	150	300	<0.1	<4
	150–300	300–570	0.1–1.0	4–40
Sodium, potassium	600	1110	<0.1	<4
	800	1470	0.1–1.0	4–40
	600	1110	<0.1	<4
Tin	350	660	<0.1	<4
	600	1110	0.1–1.0	4–40
Aluminum	750	1380	<0.1	<4
	850	1560	≫0.1	≫4
Cadmium	500	930	>1.0	>40
Zinc	445	830	≫1.0	≫40

Table 22 Resistance of titanium alloys to crevice corrosion in boiling salt solutions

Tight metal-to-gasket crevices

Solution	pH	Grades 1, 2	Grades 12, 28, 29	Grades 7, 16, 26
Saturated $ZnCl_2$	3.0	F	R	R
10% $MgCl_2$	4.2	F	R	R
10% $CaCl_2$	3.0	F	R	R
10% KCl	3.0	F	R	R
Saturated NaCl	3.0	F	R	R
Saturated NaCl + Cl_2	1–2	F	F	R
10% NH_4Cl	4.1	F	R	R
10% $FeCl_3$	0.6	F	F	R
10% Na_2SO_4	2.0	F	R	R

Note: F, crevice attack; R, resistant. Source: Ref 63, 144–148

somewhat lower values than as-pickled surfaces. In one study, increasing alloy aluminum content was shown to reduce anodic pitting potential in titanium alloys (Ref 155, 156). Pitting potentials were determined for a 20% NH_4Cl solution under stagnant and flowing (1 m/s, or 3.3 ft/s) conditions (Ref 159). Values were measured at +9 to +10 V at 20 to 40 °C (70 to 100 °F), decreasing into the range of +4.0 to +5.5 V at 120 °C (250 °F). Increased flow rate produced a minor negative effect on pitting potential. A relatively minor effect by pH and chloride concentration is also observed in NaCl brine (Ref 158).

Table 23 Ranking of titanium alloy crevice corrosion resistance

In naturally aerated NaCl brines at 90 to 150 °C (195 to 300 °F)

Alloy	Maximum pH at which attack occurred
Ti-6-4 (least resistant)	≥9
Grades 1, 2, 3, 9	≥8
Ti-550, Ti-6-22-22, Ti-4-3-1	3–4
Grade 12	2.5–3
Ti-6-2-4-6, Ti-3-8-6-4-4	2
Grades 28 and 29, Ti Beta-C/Pd, Beta-21S, Ti-15-5	0.8–1
All Ti-Pd and Ti-Ru alloys (most resistant)	<0.7

It was shown that pitting potentials of titanium can be raised in chloride solutions by addition of sulfate ions (Ref 160). Above a critical sulfate concentration, titanium exhibits pitting potential values similar to those obtained in pure sulfate media (Table 24).

As shown in Fig. 39, anodic pitting potential values are significantly lower in bromide solutions, and they decrease with increasing temperature. The dependence of pitting potential on bromide concentration at room temperature is given by (Ref 158): E_b (versus SCE) = 1.1 − 0.43 log (Br^-). At room temperature, anodic pitting potentials of +0.90 to +1.4 V have been reported for titanium grades 2 and 5 (Ref 155, 158). One study has reported values for grades 1, 2, and 3 titanium ranging between +1.8 to +2.2 V in 1% NaBr (pH 6) solution at room temperature, decreasing to +1.0 to +1.2 V at 100 °C (212 °F) (Ref 161). As Fig. 39 suggests, pitting potentials may fall to as low as +0.6 to +0.8 V at temperatures above approximately 140 °C (285 °F). Thus, pitting of titanium alloys may be possible in pure bromide solutions at higher temperature if highly oxidizing conditions prevail.

However, additions of various oxidizing anions may inhibit pitting in NaBr solutions by significantly raising anodic pitting potentials

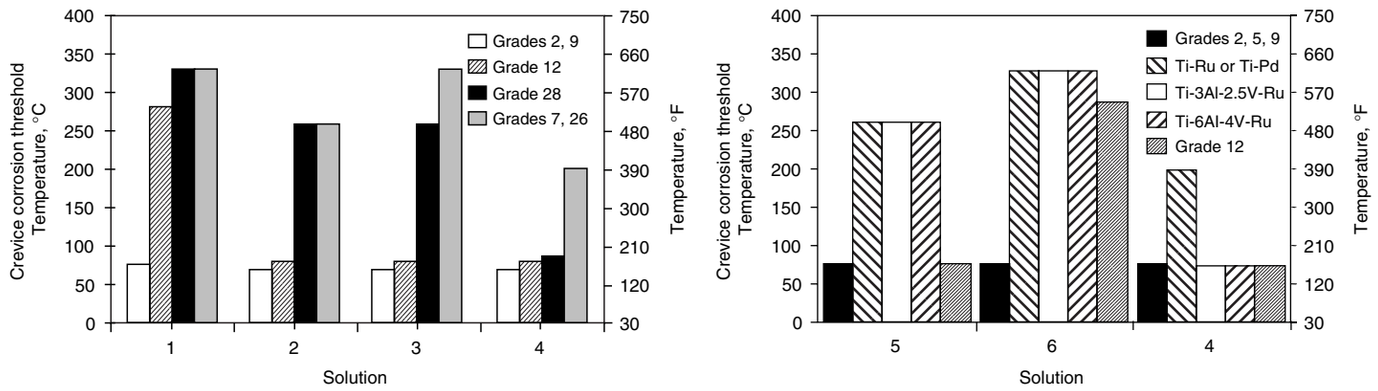

Fig. 38 Crevice corrosion threshold temperature limits for titanium alloys in various chloride/sulfate media. (a) ASTM grades in Solution 1, 20% NaCl, pH 3, naturally aerated; Solution 2, 20% NaCl, pH 1, naturally aerated; Solution 3, 30 g/L H_2SO_4 + 100 ppm Fe^{3+}; Solution 4, 10% $FeCl_3$ or Cl^{2-} saturated NaCl, pH 1–2. (b) Alloys in Solution 5, 20% NaCl, pH 2, naturally aerated; Solution 6, 25% NaCl, pH 3, deaerated; 4, as in (a). Source: Ref 63, 147, 149

(Ref 158). Critical concentrations of these inhibitive anions have been determined, and the relative efficiency of inhibition decreases in the order: $SO_4^{2-} > NO_3^- > CrO_4^{2-} > PO_4^{3-} CO_3^{2-}$.

Studies in room-temperature iodide solutions reveal anodic pitting potentials of +1.7 to +1.8 V, despite acidification (Ref 155, 162). Values near +0.5 V (versus SCE) are indicated above 40 to 50 °C (100 to 120 °F).

Repassivation Potentials. Repassivation (or protection potentials, E_{prot}) represent conservative measures of anodic pitting tendency, because they represent minimum potentials below which pitting cannot be sustained. The values presented in Table 25 (Ref 13, 26, 38, 146–148) suggest that titanium alloys will not experience spontaneous pitting attack in aqueous acidic chloride media, even if oxidizing species are present. Unalloyed titanium exhibits the highest E_{prot} value, which decreases as alloy aluminum (and most β alloying elements) content increases. Increasing iron content over the range of 0.02 to 0.20% results in a minor (several tenths of a volt) decrease in E_{prot} values in unalloyed titanium (Ref 11). Minor palladium or ruthenium alloy additions impart minimal negative influence on these potentials.

Like anodic pitting potentials, repassivation potentials are significantly lower in bromide and iodide media. Room-temperature values of +1.2 and +0.95 V are measured for grades 2 and 5 titanium, respectively (Ref 155), whereas values of +0.9 V in dilute KBr solutions have been reported (Ref 162). Repassivation potentials for grades 2 and 5 titanium in dilute room-temperature iodide solutions have been measured to be +1.8 and +1.5 V, respectively (Ref 155, 162).

Hydrogen Damage in Specific Environments

Gaseous Hydrogen. Absorption of hydrogen by titanium alloys in gaseous hydrogen is highly dependent on temperature, gas pressure, gas moisture or oxygen content, metal surface condition, alloy composition, and the nature of the surface oxide formed on the metal (Ref 163). In the absence of surface oxide film interferences, the hydrogen concentration in titanium is directly proportional to the square root of the hydrogen gas partial pressure (Ref 6, 164). Hydrogen absorption is a fully reversible process in that vacuum may remove absorbed hydrogen, given sufficient temperatures to promote kinetics and overcome oxide film diffusion barriers. The ability of anodic and thermal oxide films on titanium to retard hydrogen absorption significantly in high-temperature hydrogen gas has been demonstrated (Ref 163, 165).

As shown in Table 26 (Ref 28), absorption of hydrogen by grade 2 titanium in dry hydrogen gas dramatically increases as both pressure and temperature increase. These test data also reveal the protective effect of surface oxides (as-pickled and anodized surfaces) and the detrimental effect of iron surface contamination. Similar results for unalloyed titanium are given in Table 27 (Ref 165), in which hydrogen gas pressures of 4.1 to 6.2 MPa (600 to 900 psi) and temperatures of 100 to 300 °C (212 to 570 °F) were tested. These results also demonstrate the beneficial effects of gas moisture content. It has been shown that at least 2% H_2O content in 5.5 MPa (800 psi) hydrogen gas at 315 °C (600 °F) effectively retards hydrogen uptake in unalloyed titanium (Ref 28).

Cathodic Hydrogen Uptake. As discussed in the section "Hydrogen Damage" in this article, titanium may absorb hydrogen if there is a mechanism for generating atomic hydrogen on the metal surface. This mechanism may involve an impressed cathodic current, galvanic coupling to active metals, or severe, continuous mechanical damage of titanium surfaces. In these situations, the factors of potential, current density, metal temperature, solution pH and chemistry, and alloy composition and surface condition all significantly influence the rate at which hydrogen is absorbed (Ref 43–51).

Figure 40 (Ref 43, 44) shows that unalloyed titanium may absorb hydrogen in near-neutral brines (e.g., seawater) at 25 and 100 °C (75 and 212 °F) when cathodic potentials are more active

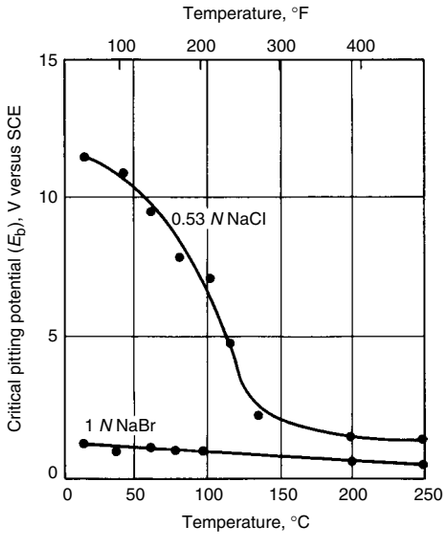

Fig. 39 Effect of temperature on the anodic pitting potential (E_b) of grade 2 titanium in dilute NaCl and NaBr solutions. SCE, saturated calomel electrode. Source: Ref 158

Table 24 Anodic breakdown pitting potentials, E_b, for titanium alloys in chloride solutions

Alloy grade	Solution	pH	Temperature °C	Temperature °F	E_b(a), V
2	1 *N* NaCl	7	25	75	+11.0
5	1 *N* NaCl	7	25	75	5.2
2	Saturated NaCl	1, 7	25	75	9.6
12	Saturated NaCl	1, 7	25	75	9.6
7	Saturated NaCl	1, 7	25	75	9.6
5	Saturated NaCl	1, 7	25	75	8.9
2	Saturated NaCl	1, 7	95	200	5.0–6.5
12	Saturated NaCl	1, 7	95	200	5.0–5.7
7	Saturated NaCl	1, 7	95	200	5.2–7.0
5	Saturated NaCl	1, 7	95	200	2.5–3.4
2	1 *N* NaCl	7	125	255	~4.4
2	1 *N* NaCl	7	150	300	~2.2
2	1 *N* NaCl	7	175	345	~1.2
2	1 *N* NaCl	7	200	390	~1.2
12	Seawater	8	245	475	2.3
12	O_2-saturated seawater	8	245	475	3.3
2	1 *N* KCl + 0.2 *M* H_2SO_4	...	25	75	80.0

(a) Measured versus Ag/AgCl reference electrode. Source: Ref 155–158

Table 25 Anodic repassivation (protection) potentials of titanium alloys in boiling chloride solutions

Alloy	Repassivation potential, V vs. Ag/AgCl: 5% NaCl/ pH 3.5	3% HCl
Grade 1	+7.7	+6.4
Grade 2	6.2	5.5
Grade 3	5.9	5.4
Grade 12	... (5.9)(a)	...
Grade 7 (Ti-0.15Pd)	7.1 (5.6)(a) (6.9)(b)	...
Grade 16 (Ti-0.05Pd)	7.1 (6.2)(b)	...
Grade 26 (Ti-0.1Ru)	6.7 (5.9)(b)	...
Ti-5-2.5	2.2	1.3
Ti-8-1-1	0.9	0.5
Grade 9 (Ti-3-2.5)	2.6	1.9
Grade 28 (Ti-3-2.5-Ru)	2.3 (2.3)(b)	...
Ti-6-2-4-2	1.8	1.7
Ti-4-3-1	2.2	1.7
Grade 23 (Ti-6-4 ELI)(c)	2.4	...
Ti-6-4	1.8	1.4
Grade 29 (Ti-6-4-Ru)	2.2	...
Ti-550	2.3	2.0
Ti-6-6-2	1.5	1.4
Ti-6-2-4-6	2.5	2.1
Ti-15-3-3-3	2.0	1.6
Ti-3-8-6-4-4 (Ti Beta-C)	2.7–3.3	2.3
Beta-21S	2.8	...
Ti-13-11-3	2.7	2.3
Beta III	7.5	7.2
Ti-8-8-2-3	2.1	2.1
Ti Beta-C/Pd	3.3	...
Ti-15-5	5.8	5.3

(a) In boiling saturated NaCl solution. (b) Gas tungsten arc weld metal. (c) ELI, extra-low interstitial. Source: Ref 13, 26, 38, 146–148

(negative) than −0.75 V versus SCE. This charging produces only thin, innocuous surface hydride films (Fig. 8) on unalloyed titanium as long as potentials remain more noble (more positive) than −1.0 V and temperatures are below 80 °C (175 °F). For example, grade 2 titanium galvanically coupled to aluminum alloy 6063 in a process water electrolyte at 65 °C (150 °F) generated surface hydrides only. However, accelerated hydriding of unalloyed titanium may occur at impressed potentials cathodic (negative) to −1.0 V even at room temperature (Ref 47–49). The potential threshold indicated in Fig. 40 applies to a-β and β titanium alloys as well; however, significantly higher rates of hydrogen absorption and penetration can be expected at any given temperature under hydrogen charging conditions. This results from the significantly higher solubility and diffusion coefficients for hydrogen in the β phase (Ref 38, 40). Sustained tensile stress on grades 9 and 12 titanium U-bends coupled to aluminum-zinc anodes in ambient seawater (−1.05 V versus Ag/AgCl) resulted in surface hydriding and cracking (Ref 48). The increased volume fraction of β phase in the Ti-6Al-4V and Ti-6Al-4V-0.1Ru alloys provided enhanced tolerance to hydride formation and cracking in these seawater charging tests (Ref 48, 166).

Increasing temperature and decreasing pH have both been shown to accelerate significantly the rate of hydrogen absorption of titanium alloys during cathodic charging (Ref 41, 46, 51, 167–169). These studies indicate that the rate of hydrogen absorption and surface hydride layer growth initially follow a parabolic rate law; this suggests that hydrogen diffusion is rate controlling at temperatures less than and equal to 100 °C (212 °F) (Ref 49, 170). Linear rate behavior has been observed in long-term charging exposures (Ref 51). Dramatic increases in hydrogen absorption rate during cathodic charging are noted when electrolyte pH levels are reduced to 2 or below (Ref 28, 29, 41, 51, 167). On the other hand, the inverse solubility of protective calcareous deposit coatings formed during cathodic charging (aluminum-zinc anode at −1.05 V) of titanium alloys in seawater dramatically inhibits hydrogen absorption as temperature increases (Ref 47, 166).

The presence of hydrogen recombination poisons, such as sulfide, arsenate, antimony, or cyanide species, substantially increases hydrogen uptake during charging (Ref 167). This effect of sulfide has been observed in a few oil refinery heat exchangers in which grades 2 or 12 titanium tubes were galvanically coupled to carbon steel tubesheets and components in hot (≥80 °C, or 175 °F) sulfide-containing aqueous process streams (Ref 1). Severe hydriding (Fig. 7) and eventual embrittlement of the tubes occurred. Elimination of the detrimental couple with the active metal (steel) has been achieved by designing with more galvanically compatible passive alloys (including all-titanium design) and/or use of dielectric joints. In comparison, grade 2 titanium galvanically coupled to carbon steel in neutral sulfide-free electrolytes results in very minor increases in hydrogen uptake to temperatures as high as 120 °C (250 °F) (Ref 29, 46). Note that galvanic hydrogen embrittlement of titanium does not occur in hot sour hydrocarbon-dominated streams (i.e., with minimal and/or discontinuous water phase).

The surface condition of titanium also influences hydrogen absorption rates during cathodic charging. Studies consistently reveal that as-pickled and as-received surfaces are much less amenable to hydrogen uptake than abraded, vapor-blasted, or sandblasted surfaces (Ref 29, 41, 50). Furthermore, anodized and, particularly, thermally oxidized surfaces are highly effective barriers to hydrogen uptake in titanium during charging (Ref 44, 52).

Stress-Corrosion Cracking in Specific Media

In the following sections, SCC of titanium alloys in a variety of environments is discussed. Although the protective oxide film of titanium exhibits a high degree of chemical stability and resistance in many aggressive environments, even to the extent that essentially no corrosion occurs, SCC has been identified in several environments. Table 28 lists the environments that are known to have caused SCC and those corresponding titanium alloys that were reported to be susceptible. The environmental parameters and metallurgical factors that influence SCC susceptibility are discussed in the following sections.

Red-Fuming Nitric Acid. The first reported observation of titanium SCC occurred in red-fuming nitric acid (Ref 97, 98). This is acid greater than 86% HNO_3 with dissolved nitrogen oxides imparting a reddish color. Cracking was observed for commercially pure titanium in a room-temperature environment containing 20% NO_2. Later, investigators found that SCC occurred in as little as 6.5% NO_2 with less than 0.7% H_2O. Intergranular cracking was observed on smooth specimens, which indicates the high sensitivity to SCC in this medium (Fig. 15). In addition to unalloyed titanium, cracking was observed on Ti-8Mn and Ti-6Al-4V, even in red-fuming HNO_3 without free NO_2. Studies showed that 1.5 to 2.0% H_2O or 1% NaBr inhibits SCC (Ref 97, 98).

Nitrogen Tetroxide. As titanium use in aerospace increased, it was found that titanium alloys were highly resistant to corrosion attack in

Table 26 Hydrogen absorption in grade 2 titanium after 96 h exposure in pure, dry hydrogen

Temperature		Hydrogen pressure		Hydrogen absorption, ppm			
°C	°F	MPa	psi	Freshly pickled	Pickled +2 mo air exposure	Iron-contaminated	Anodized
149	300	Atmospheric		0	0	0	0
149	300	2.76	400	58	20	174	0
149	300	5.52	800	28	0	117	0
315	600	Atmospheric		0	0	0	0
315	600	2.76	400	2586	6911	5951	516
315	600	5.52	800	4480	10,550	13,500	10,000

Source: Ref 28

Table 27 Hydrogen absorption in unalloyed titanium after 14 day exposures

Sample condition	Hydrogen absorption, ppm		
	Dry hydrogen	Moist hydrogen	Hydrogen + CO_2
As-received	58	1	4
Iron-contaminated	780	21	125
Copper-contaminated	27	5	5
Platinum-contaminated	...	...	770
Anodized	9	2	3

Source: Ref 165

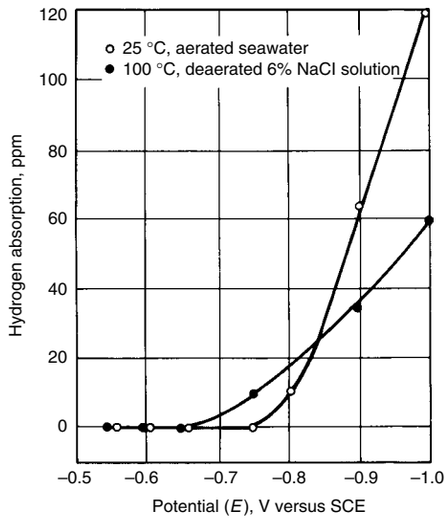

Fig. 40 Cathodic potential thresholds for absorption of hydrogen by unalloyed titanium in neutral brines. SCE, saturated calomel electrode. Source: Ref 43, 44

nitrogen tetroxide (N_2O_4), an oxidizer used in conjunction with hydrazine rocket fuels. Unfortunately, SCC was rather dramatically revealed in an explosion during proof testing of a Ti-6Al-4V storage vessel. The vessel that exploded had been exposed to N_2O_4 at 40 °C (100 °F) at a stress level of 620 MPa (90 ksi). Testing revealed that titanium alloys would crack in NO-free N_2O_4 (that is, N_2O_4 with excess dissolved oxygen, or red N_2O_4) but would not crack in NO-containing N_2O_4 (oxygen-free, or green N_2O_4) (Ref 55, 139).

Methanol. Unlike other engineering metals, titanium and zirconium alloys are highly susceptible to SCC in anhydrous or near-anhydrous methanol liquid and vapor (Ref 55). Titanium alloys that are generally susceptible to SCC in aqueous media, such as the more highly alloyed grades containing >5 wt% Al and/or higher interstitial levels (e.g., Ti-6-4, Ti-8-1-1), tend to exhibit intergranular stage I cracking and predominantly transgranular stage II cracking modes in dry methanol. Aged, coarse-grained Ti-3-8-6-4-4 and grades 28 and 29 titanium exhibit this mode of cracking (Ref 64, 171, 172). On the other hand, intergranular cracking is primarily observed in the unalloyed grades 1 and 2 and in certain β alloys, such as Ti-13-11-3 and aged, fine-grained Ti-3-8-6-4-4 (Ref 171). Methanolic stress cracking can occur rapidly (within hours) at relatively low tensile stresses at or near room temperature, depending on conditions.

Methanolic SCC stems from the reaction of methanol with titanium metal to form a soluble, non-protective titanium methoxide ($Ti(OCH_3)_4$) (Ref 55, 64), whereby passive TiO_2 film reformation is not possible. Once local metal dissolution achieves a critical flaw size under tensile stress, interactive overload/dissolution cycles occur at the crack tip. It has long been debated to what extent absorbed atomic hydrogen generation versus anodic dissolution at the crack tip influences methanolic SCC.

Fortunately, water addition to dry methanol represents an extremely effective, potent, and practical inhibitor for titanium alloy SCC. The presence of sufficient water in methanol (or other oxygen-containing species) promotes full repassivation via TiO_2 film formation. The beneficial, inhibitive influence of increasing water content in room-temperature methanol is illustrated for unalloyed titanium and Ti-6Al-4V in Fig. 41 and 42, respectively (Ref 122, 123, 173). These category 1 SCC test data reveal the following:

- Increasing the halide content decreases time to failure.
- Higher halide concentrations increase this critical water level where maximum SCC susceptibility occurs.
- Minimal water additions up to a critical level can decrease time to failure.
- Water levels greater than this critical level reduce and can fully inhibit methanolic SCC.

Additions of acids, oxidizing species or certain metal ions, and impressed potential can dramatically influence methanolic SCC on titanium alloys (Ref 55). Acidification with HCl, H_2SO_4, or acetic acid substantially decreases time to failure and the minimum water level required for complete inhibition (Ref 123, 174). Similar acceleration of SCC (anodic dissolution and cracking rates) has been observed with additions of strong oxidizers such as halogens (Cl_2, Br_2, I_2) or metal ions of gold, iron, copper, mercury, and especially palladium (Ref 55, 173–175). On the other hand, nitrate (Ref 172) and sulfate ions (Ref 172), NaF, and 0.1 *M* Al^{3+}, Zr^{4+}, Cd^{+}, and Sn^{2+} ion additions act to inhibit stage II transgranular SCC in titanium alloys (Ref 173, 176). Anodic polarization generally increases SCC susceptibility and cracking rates in methanol/halide mixtures, whereas cathodic polarization diminishes susceptibility. Impressed cathodic potentials more negative than −250 mV (versus Ag/AgCl) prevented intergranular cracking on unalloyed titanium (Ref 177), whereas transgranular cracking was fully arrested on titanium alloys at impressed potentials negative to −1.0 V (SCE) (Ref 53, 55).

Contrary to aqueous SCC behavior, the maximum SCC susceptibility of titanium in methanol liquid and vapor is somewhere near room temperature, and it diminishes substantially as the temperature increases above this point. The critical level of water required to fully inhibit SCC at higher temperatures drops substantially in α-β and β titanium alloys (Ref 64, 171).

Practical guidelines for conservative minimum water content required in methanol to prevent SCC on various commercial titanium alloys (at room temperature) are offered in Table 29. In hydrocarbon production, this water inhibition strategy is readily and practically achieved by adding available fresh/natural waters or seawater directly to anhydrous commercial methanol prior to well injection and titanium alloy component exposure (Ref 64, 121, 171).

Other Alcohols. Titanium alloy susceptibility rapidly diminishes with increasing alcohol carbon atom chain size (i.e., molecular weight) (Ref 55). Most common industrial titanium alloys, including unalloyed titanium and Ti-6Al-4V, are generally considered to be resistant to

Table 28 Environments known to promote stress-corrosion cracking of commercial titanium alloys

Environment	Temperature °C	Temperature °F	Titanium alloys with reported susceptibility
Oxidizers			
Nitric acid (red-fuming)	Room temperature		Ti, Ti-8Mn, Ti-6Al-4V, Ti-5Al-2.5Sn
Nitrogen tetroxide (no excess NO)	30–75	85–165	Ti-6Al-4V
Organic compounds			
Methyl alcohol (anhydrous)	Room temperature		All commercial grades
Monomethylhydrazine	Room temperature		Ti-8Al-1Mo-1V, Ti-6Al-4V (solution treated and aged)
Ethyl alcohol (anhydrous)	Room temperature		Ti-8Al-1Mo-1V, Ti-5Al-2.5Sn
Ethylene glycol	Room temperature		Ti-8Al-1Mo-1V
Methylene chloride, trichloroethylene, carbon tetrachloride	Room temperature		Ti-8Al-1Mo-1V, Ti-5Al-2.5Sn
	>150	>300	Ti-3Al-8V-6Cr-4Zr-4Mo
Freons (fluorinated hydrocarbons)	Room temperature		Ti-8Al-1Mo-1V, Ti-5Al-2.5Sn, Ti-6Al-4V
Chlorinated diphenyl	315–370	600–700	Ti-5Al-2.5Sn
Hot salt			
Chloride and other halide salts/residues	230–430	450–805	Most commercial alloys, except ASTM grades 1, 2, 7, 9, 11, 12, 16, 17, 26–29
Metal embrittlement			
Cadmium (solid + liquid)	25–600	75–1110	Ti-8Mn, Ti-13V-11Cr-3Al, grade 2, Ti-6Al-4V
Mercury (liquid)	Room temperature		Grade 4, Ti-6Al-4V, Ti-8Al-1Mo-1V
	370	700	Ti-13V-11Cr-3Al, Ti-8Al-1Mo-1V
Silver (solid) and AgCl	204–470	400–880	Ti-7Al-4Mo, Ti-5Al-2.5Sn, Ti-6Al-6V-2Sn
Ag-5Al-2.5Mn (braze alloy)	343	650	Ti-6Al-4V, Ti-8Al-1Mo-1V, Ti-5Al-2.5Sn
Gold (solid)	232	450	Ti-6Al-6V-2Sn
Miscellaneous			
Seawater/NaCl solution	Room temperature		Unalloyed Ti (with >0.25% O), Ti-3Al-11Cr-13V, Ti-5Al-2.5Sn, Ti-8Mn, Ti-6Al-4V, Ti-6Al-6V-2Sn, Ti-7Al-2Nb-1Ta, Ti-4Al-3Mo-1V, Ti-8Al-1Mo-1V, Ti-6Al-Sn-4Zr-6Mo
Distilled water	Room temperature		Ti-8Al-1Mo-1V, Ti-5Al-2.5Sn, Ti-11.5Mo-6Zr-4.5Sn
Moist chlorine gas	288	550	Ti-8Al-1Mo-1V
10% HCl	240–400	465–750	Ti-5Al-2.5Sn, Ti-8Al-1Mo-1V
LiCl, KBr, and Na_2SO_4 solution (0.6 *M*)	Room temperature		Ti-6Al-4V, Ti-6Al-6V-2Sn
Molten chloride/bromide salts	300–500	570–930	Ti-8Al-1Mo-1V

SCC in all alcohols other than methanol. However, addition of halogens (e.g., Cl_2, Br_2, I_2) or other strong oxidizers ($FeCl_3$) to various anhydrous alcohols can induce SCC in all titanium alloys (Ref 122, 124), requiring increased water levels for SCC inhibition. The highly susceptible Ti-8Al-1Mo-1V alloy uniquely experiences cracking in non-halogen/halide-containing anhydrous ethanol and ethylene glycol (Ref 55).

Halogenated Hydrocarbons. Widespread use of titanium alloys in the aerospace industry has prompted considerable study of SCC in halogenated hydrocarbons common to aerospace processing in the past. Stress-corrosion cracking of certain titanium alloys has been identified in the following halogenated hydrocarbons:

- Carbon tetrachloride
- Methylene chloride
- Methylene iodide
- Trichloroethylene
- Trichloroethane
- Trichlorofluoromethane
- Trichlorofluoroethane
- Octafluorocyclobutane

In most of these environments, precracked specimens (category 2) are required to identify SCC.

Stress-corrosion cracking in carbon tetrachloride (CCl_4) was first noted on Ti-8Al-1Mo-1V (Ref 178, 179), with a threshold stress intensity to produce SCC (K_{ISCC}) approximately the same as that observed in 3.5% NaCl solution. Crack velocities in CCl_4 were approximately 10 times faster than those in methanol. Slow strain-rate (category 3) testing also showed that Ti-5Al-2.5Sn was susceptible to SCC in CCl_4 at stresses approaching the tensile strength of the alloy.

The other hydrocarbons listed were found to cause cracking in Ti-8Al-1Mo-1V and Ti-5Al-2.5Sn alloys, which are also known to be susceptible to SCC in distilled water (Ref 178, 180). No other alloys were found to be similarly affected.

Freons include any of a number of fluorinated hydrocarbons commonly used as refrigerants. The Ti-8Al-1Mo-1V and Ti-5Al-2.5Sn alloys and Ti-6Al-4V in the solution-treated and aged condition have been found to exhibit threshold stress intensities in commercial freons below those in air (Ref 53, 55, 180).

Hot Salts. In the late 1950s, cracking of α titanium alloys was discovered during routine laboratory creep testing. The failure was eventually traced to chlorides from fingerprints on the specimen surface. These findings were reproduced in several laboratory studies for a host of titanium alloys. Nearly all titanium alloys were found to be susceptible to this hot salt SCC phenomenon (termed hot salt cracking), with the exception of unalloyed titanium. Although there was a great deal of concern in regard to numerous existing aerospace applications similar to this laboratory environment, no service failure on titanium alloys has been attributed to hot salt cracking to date.

A more complete description of hot salt cracking and its mechanism can be found in the literature (Ref 55, 181–189). Hot salt cracking is primarily influenced by temperature, stress, time, alloy composition, and metallurgical condition. Cracking is observed in the temperature range from 285 to 425 °C (545 to 800 °F). In general, susceptibility increases with stress and/or temperature and does not occur below 260 °C (500 °F) or above 540 °C (1000 °F). Cracking is normally characterized by extensive branching and is not necessarily associated with the regions of highest stress intensity; therefore, category 2 or 3 specimens are not required to initiate cracking. Because it is often difficult to initiate cracks in precracked notches, statically loaded

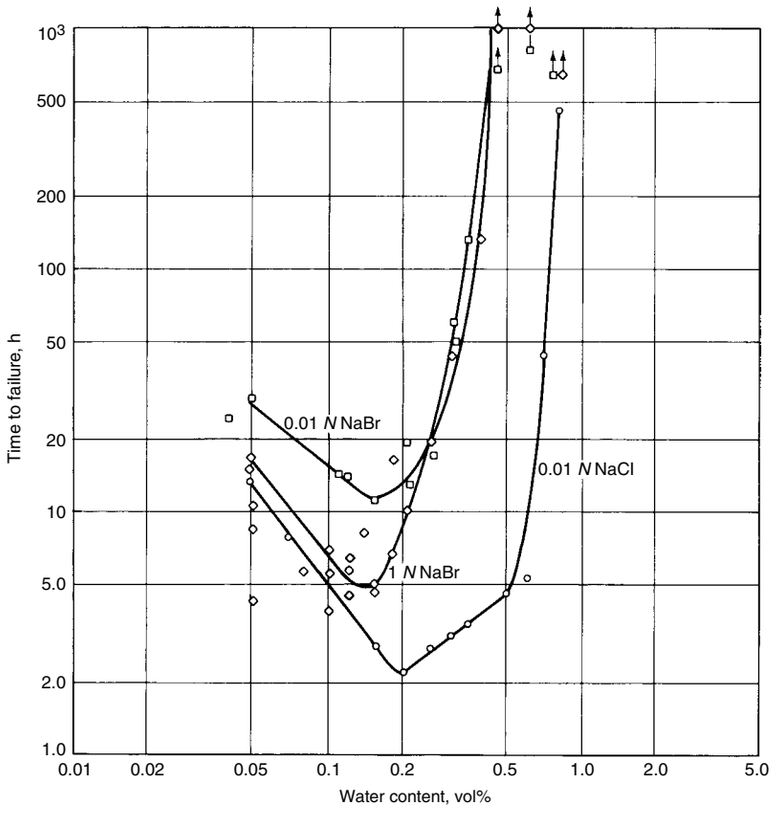

Fig. 41 Effect of bromide and chloride additions on stress-corrosion cracking of commercially pure titanium in methanol/water solutions at room temperature. Source: Ref 123

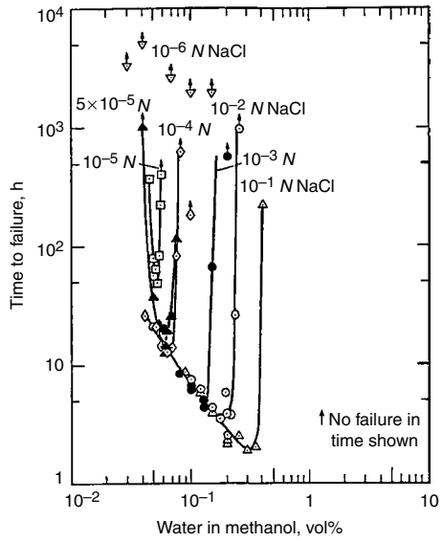

Fig. 42 Effect of chloride concentration and water content on the stress-corrosion cracking susceptibility of Ti-6Al-4V in room-temperature methanol. Cold rolled and annealed. Tested at 75% yield strength. Source: Ref 173

Table 29 Minimum water content required in methanol to prevent stress-corrosion cracking of titanium alloys at room temperature

Titanium alloy	Minimum water content required, wt%	
	Short-term/ intermittent exposure	Sustained exposure
Unalloyed (grades 1, 2)	1.5	2.0
Ti-0.3Mo-0.8Ni (grade 12)	2.0	2.0
Ti-3Al-2.5V (grade 9)	2.0	2.0
Ti-3Al-2.5V-Ru (grade 28)	2.5	3.0
Ti-6Al-4V (grades 5, 23)	3.0	3.0
Ti-6Al-4V-Ru (grade 29)	5.0	10.0
Ti Beta-C (grade 19)	5.0	10.0

Source: Ref 121

smooth specimens (category 1) have been used in most of the laboratory investigations.

The alloys that are most susceptible to hot salt cracking are α or near-α alloys with more than 3.5% Al, such as Ti-5Al-2.5Sn and Ti-8Al-1Mo-1V. Unalloyed titanium appears to be immune (Ref 190), and it is assumed that the highly resistant titanium-palladium and titanium-ruthenium alloys and most ruthenium- or palladium-enhanced titanium alloys are all highly resistant as well. Alpha-beta alloys are less susceptible to cracking, although alloys with high aluminum contents are most susceptible. Alloys with higher molybdenum content, such as Ti-4Al-3Mo-1V, are most resistant (Ref 183). Zirconium and most β-isomorphous alloying elements (e.g., molybdenum, tantalum, niobium, and vanadium) improve resistance. The combined effect of time, temperature, and stress is shown in the Larsen-Miller diagram in Fig. 43 for several alloys, from which it is evident that alloy type and microstructural condition are also important.

Oxygen has been reported as necessary for hot salt cracking. At least one study has shown that cracking will not occur in Ti-5Al-2.5Sn when the environmental pressure is reduced below 10 microns (Ref 183). Although the role of water (moisture) has not been clearly established, it appears that water is also a necessary environmental component in the cracking process (Ref 184, 185).

Chloride, bromide, and iodide salts have all been shown to produce similar cracking, whereas fluoride and hydroxide salts have not. The cation associated with the salt has been reported to affect cracking susceptibility. Attack severity has been shown to increase as follows (Ref 184, 185):

$$MgCl_2 > SrCl_2 > CsCl > CaCl_2 > KCl > BaCl_2 > NaCl > LiCl$$

Table 30 categorizes titanium alloys with respect to their susceptibility to hot salt cracking (Ref 55, 191).

Cracking is normally intergranular in nature but depends largely on alloy type. Alpha alloys exhibit both transgranular and intergranular fracture, depending on whether the material was annealed above or below the β transus, respectively. Alpha-beta alloys exhibit predominantly intergranular fracture (Ref 185, 187, 190, 192).

From a practical standpoint, hot salt cracking appears to be a phenomenon that is restricted to the laboratory, with no in-service failure reported thus far. This may stem from the critical, complex relationship between environment (including salt deposit morphology and composition), stress level, exposure time, temperature, and alloy type required for attack to initiate.

Molten Salts. Ti-8Al-1Mo-1V appears to be the only titanium alloy tested for SCC in molten salt environments. Cracking has been observed in pure chloride and bromide eutectic melts at temperatures between 300 and 500 °C (570 and 930 °F). In general, increasing temperature increases crack velocity. Cathodic protection has been observed to inhibit or stop cracking.

Nitrate salts below 125 °C (255 °F) do not induce cracking even when Cl^-, Br^-, or I^- anions are present. Cracking in pure molten nitrates at higher temperatures can occur only when halides are present (Ref 55).

Liquid/Solid Metal Embrittlement. Titanium alloys may experience premature failure and brittle fracture when stressed while in intimate contact with certain metals in liquid and/or solid forms (Ref 53, 139, 193–200). These metals include cadmium, mercury, silver, cesium, gallium, gold, and possibly zinc.

Liquid metal embrittlement (LME) in liquid cadmium has been reported for the Ti-8Mn, Ti-13V-11Cr-3Al, and grade 2 titanium alloys. Dramatic reductions in both elongation and strength were observed in the 325 to 400 °C (620 to 750 °F) range, which were very dependent on strain rate (Ref 55). Penetration of the TiO_2 oxide film by the liquid cadmium appears to be the critical factor, with cracking predominantly intergranular.

Liquid mercury has produced embrittlement in the grade 4, Ti-13V-11Cr-3Al, Ti-6Al-4V, Ti-8Al-1Mo-1V, and Ti-8Mn alloys (Ref 55, 197). Ti-8Al-1Mo-1V exhibits both intergranular stage I and transgranular stage II cracking behavior, with microstructural influences paralleling those observed in methanol and aqueous media.

Exposure of stressed U-bend and C-ring samples of grades 2, 12, 19, and 29 (Ref 55) in liquid mercury reveals no cracking tendencies to temperatures as high as 232 °C (450 °F). These static tests have shown that the surface oxide film of titanium is not wetted by liquid mercury,

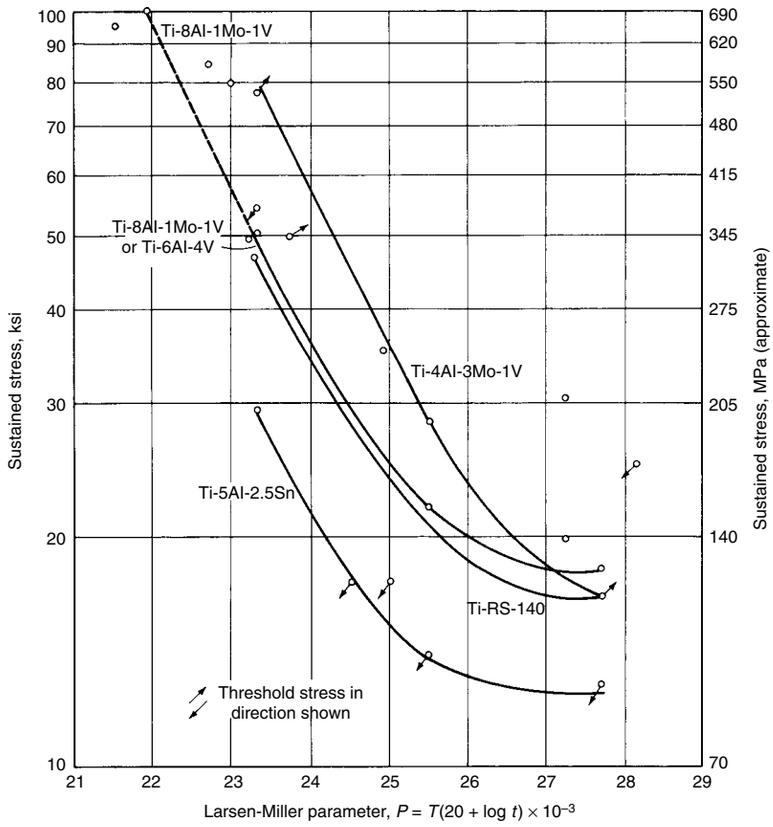

Fig. 43 Larsen-Miller plot for hot salt cracking of several annealed α-β titanium alloys. *T* is temperature (°R), and *t* is exposure time (hours).

Table 30 Relative resistance of titanium alloys to hot salt stress-corrosion cracking

Resistance	Titanium alloy
Least resistant	Ti-5Al-2.5Sn
	Ti-5Al-5Sn-5Zr
	Ti-8Al-1Mo-1V
	Ti-8Mn
Moderately resistant	Ti-5Al-5Sn-5Zr-1Mo-1V
	Ti-6Al-4V
	Ti-6Al-6V-2Sn
	Grade 4
	Ti-13V-11Cr-3Al
Highly resistant	Ti-4Al-3Mo-1V
	Ti-2.25Al-1Mo-11Sn-5Zr-0.25Si
	Ti-3Al-8V-6Cr-4Zr-4Mo (Ti Beta-C)
	Ti-8Mo-8V-2Fe-3Al
	Ti-11.5Mo-6Zr-4.5Sn
Immune	Grades 1, 2, 7, 9, 12, 16, 17, 26, 27, 28

Source: Ref 55, 191

thereby precluding amalgamation and embrittlement. However, cracking failure may be induced when oxide films of stressed samples are severely mechanically damaged (heavily scraped or scratched or slowly plastically strained above the yield point) while immersed in the liquid metal. Thermal nitride (Ref 55) or enhanced oxide film barriers (achieved through anodizing or thermal oxidation) may offer improved resistance to LME in mercury, unless the film is physically compromised.

Liquid metal embrittlement has also been reported for titanium (Ref 195) exposed to silver brazing alloys (Ref 198, 199) and molten zinc (Ref 55). Similar to high-temperature mercury, degradation of titanium alloy properties in molten zinc, cesium, and gallium is generally the result of titanium dissolution and diffusion of the metal along grain boundaries to form brittle phases.

Solid Metal Embrittlement (SME). Early reported incidences of SME stemmed from investigations of cracked titanium alloy jet engine compressor disks involving cadmium- and silver-plated fasteners (Ref 198). Studies that followed confirmed that embrittlement could be induced at temperatures well below the melting point of the metal (Ref 55, 195, 196). In the case of cadmium, SME has been shown to occur in Ti-6Al-4V, Ti-13V-11Cr-3Al, and Ti-8Al-1Mo-1V from room temperature up to the melting point of cadmium (321 °C, or 610 °F) (Ref 195). The cadmium must be smeared or pressed (beyond the yield point) into the highly stressed titanium alloy surface at loads exceeding the yield stress for brittle failure to occur. Simply stressing cadmium-coated titanium is not sufficient to initiate cracking. Increasing temperature and stress level decrease time to cracking and increase crack depth (Ref 195).

Any barrier film or coating that inhibits direct bearing contact of cadmium onto titanium alloy surfaces can avert cadmium embrittlement. For example, sprayed or vapor-deposited aluminum coatings, organic coatings, dry film lubricants, and/or oxidized surfaces on titanium may provide effective protection, depending on bearing loads.

Intergranular embrittlement of Ti-6Al-6V-2Sn has also been reported in contact with cadmium, gold, and silver (Ref 200). Thresholds for silver and gold were 204 and 232 °C (400 and 450 °F), respectively. No embrittlement was stimulated by nickel or copper metal to temperatures as high as 287 °C (550 °F).

Pure silver and silver brazing alloys have also induced SME of Ti-8Al-1Mo-1V, Ti-7Al-4Mo, and Ti-5Al-2.5Sn (Ref 198) at temperatures of 468 and 343 °C (875 and 650 °F), respectively. The presence of silver chloride stimulates SME more aggressively in titanium alloys than in pure silver. The perceived SME threshold for Ti-6Al-4V in contact with silver is approximately 340 °C (645 °F).

Compatibility of titanium alloys in contact with solid zinc metal has not been well defined or documented. There are vague indications that some susceptibility to SME may be possible (Ref 55). It should be pointed out that, practically speaking, the likelihood of incurring SME of titanium alloys in most applications is very low. This is because the problem metal must be smeared at extreme bearing loads and plastically embedded into the titanium surface while the titanium is loaded in tension to well above 50% of the yield strength.

Aqueous Environments. A wide range of susceptibility of titanium alloys to SCC in halide-containing aqueous media has been observed that depends on an interaction of metallurgical, mechanical, and environmental factors (Ref 53, 55, 60). Generally speaking, susceptibility in aqueous media is primarily limited to chloride-, bromide-, and/or iodide-containing solutions and is mainly observed in tests or situations where high stress intensities (i.e., highly loaded, precracked test specimens, such as category 2, or very slow, sustained plastic straining test specimens, such as category 3) are involved. Titanium alloys may be categorized into four types of SCC behavior based on their level of susceptibility in near-ambient aqueous halide solutions (Ref 55):

- *Type 0:* Includes alloys that are resistant to aqueous SCC, such as the unalloyed grades 1, 2, and 3 (below 0.2 wt% O), all titanium-palladium and titanium-ruthenium alloys, and grades 9, 12, 18, 19 (when not highly aged), 20, 21, 28, and 29
- *Type 1:* Includes alloys that have good SCC resistance and require a highly loaded precrack to exhibit any susceptibility (i.e., $K_{ISCC} < K_{Ic}$, or plane-strain fracture toughness). Loaded smooth or notched configurations will not produce SCC. Examples include Ti-6Al-4V extra-low interstitial (ELI) (see the discussion of metallurgical factors in this section), mill-annealed or duplex-annealed Ti-6Al-4V, or highly aged Ti-38644 in neutral brines.
- *Type 2:* Includes relatively few alloys of mild-to-moderate susceptibility that require a loaded notch or precrack to reveal cracking susceptibility. Examples include mill-annealed Ti-8Al-1V-1Mo and Ti-5Al-2.5Sn in neutral saltwater.
- *Type 3:* Includes the very few titanium alloys that are highly susceptible to SCC, for which even a loaded smooth configuration (e.g., category 1 test specimen) can induce cracking. Examples include step-cooled Ti-8Al-1Mo-1V, and Ti-8Mn and Ti-13V-11Cr-3Al alloys in neutral salt solutions.

Fortunately, because most commercial, industrial titanium alloys display type 0 or 1 SCC behavior, the SCC susceptibility identified in lab testing has rarely been experienced in actual field service.

Stemming from past critical aircraft, submersible, and offshore marine service applications, a substantial SCC database for titanium alloys in ambient neutral saltwater has been established. Table 31 (Ref 53, 55, 201) lists K_{Ic} versus K_{ISCC} values for various commercial alloys derived from category 2 test specimens, to provide an indication of degree of SCC susceptibility.

Environmental Factors. Discounting metallurgical effects, susceptibility of titanium alloys to SCC in aqueous media primarily depends on the type and concentration of halide species, pH, temperature, and/or metal potential in the solution. As depicted in Fig. 44, increasing halide concentration increases alloy cracking velocity and reduces K_{ISCC}, depending on degree of alloy susceptibility (Ref 55, 202, 203). Interestingly, several alloys in sensitized conditions have even exhibited SCC in distilled water, including step-cooled Ti-8Al-1Mo-1V, Ti-5Al-2.5Sn, and aged Ti-11.5Mo-6Zr-4.5Sn (Ref 53).

Other ionic species can have a neutral or an inhibitive effect on SCC in halide solutions if the alloy is not highly susceptible. These species include NO^{3-}, SO_4^{2-}, F^-, OH^-, CrO_4^{2-}, and PO_4^{3-} (Ref 55). Oxidizing cations such as Fe^{3+} and Cu^{2+} may raise K_{ISCC} values in the more susceptible alloys (Ref 53, 55). On the other hand, significant concentrations of ferric chloride induced SCC in grade 29 titanium exposed to high-temperature (>150 °C, or 300 °F) chloride brine (Ref 204).

The potential of the metal can influence SCC behavior in susceptible titanium alloys. Significant cathodic and anodic polarization can increase K_{ISCC} and inhibit SCC. This is illustrated in Fig. 45 (Ref 55) for several β titanium alloys in ambient KCl solutions, whereby maximum susceptibility occurs just cathodic to the alloy corrosion potential. Similar behavior was reported for Ti-6Al-4V-0.05Pd in sour brine at 232 °C (450 °F) (Ref 205) and for α-β alloys in various ambient halide solutions (Ref 178). In the more susceptible Ti-13-11-3 β alloy, crack velocity increases linearly with anodic polarization (Ref 202).

The aggravating influence of acidification and/or increasing metal potential on titanium alloy stress cracking velocity in halide solutions is depicted in Fig. 46 (Ref 53, 55). In more acidic solutions, cathodic polarization will not stop propagating cracks. Lowering pH decreases alloy K_{ISCC} and increases crack velocity at constant potential, whereas SCC behavior in alkaline halide solutions mimics that in neutral media (Ref 55, 206, 207).

The influence of temperature depends on the alloy susceptibility to halide SCC. Type 0 alloys, which are inherently resistant to halide SCC, tend to retain this resistance to relatively high temperatures. In fact, the upper temperature limit for these alloys in halide solutions often coincides with that for crevice corrosion. The type 1 and 2 alloys that are mildly SCC susceptible suffer lower K_{ISCC} values and higher stage II cracking rates with increasing temperature. The highly susceptible alloys, such as Ti-8Al-1Mo-1V, exhibit temperature-independent K_{ISCC} values (Ref 53, 55, 208), with crack velocities that increase with temperature.

Table 31 Fracture toughness data for titanium alloys tested in air and 3.5% NaCl solution at 25 °C (75 °F)

Alloy	Thickness mm	Thickness in.	Heat treatment(a)	Yield strength MPa	Yield strength ksi	K_{Ic} or K_c(b) MPa$\sqrt{m}$	K_{Ic} or K_c(b) KSi$\sqrt{in.}$	K_{ISCC} or K_{SCC}(c) MPa$\sqrt{m}$	K_{ISCC} or K_{SCC}(c) KSi$\sqrt{in.}$
Grade 1	19.0	0.75	MA	...	...	58	53	57	52
Grade 2	19.0	0.75	MA	...	...	66	60	66	60
Grade 3	19.0	0.75	MA	...	...	79	72	75	68
Grade 4	19.0	0.75	MA	...	...	99	90	58	53
Ti-5Al-2.5Sn	12.7	0.50	MA	869	126	97	88	33	30
	12.7	0.50	βA-WQ	869	126	131	119	41	37
Ti-5Al-2.5Sn (ELI)(d)	9.7	0.38	MA	827	120	108	98	45	41
Ti-8Al-1Mo-1V	12.7	0.50	MA	1000	145	53	48	22	20
	12.7	0.50	DA	930	135	110	100	35	32
	12.7	0.50	MA-WQ	841	122	>110	>100	46	42
	12.7	0.50	β-ST-WQ	869	126	>110	>100	>110	>100
Ti-6Al-2Sn-4Zr-2Mo	12.7	0.50	STA	1048	152	58	53	30	27
Ti-6Al-4V (standard grade)	12.7	0.50	MA	945	137	66	60	38	35
	12.7	0.50	DA	917	133	77	70	57	52
	12.7	0.50	STA	1100	160	52	47	27	25
	12.7	0.50	β-STA	1070	155	77	70	49	45
Ti-6Al-4V ELI (0.05 O_2)(d)	19.0	0.75	α-β rolled	820	119	...	...	71–119	65–108
	19.0	0.75	β-rolled	738	107	...	...	85–110	77–100
Ti-6Al-4V ELI (0.07 O_2)(d)	19.0	0.75	α-β rolled	862	125	...	...	75–84	68–76
	19.0	0.75	β-rolled	786	114	...	...	82–98	75–89
Ti-6Al-4V ELI (0.11 O_2)(d)	19.0	0.75	α-β rolled	910	132	...	...	53–64	48–58
	19.0	0.75	β-rolled	807	117	...	...	76–86	69–78
Ti-6Al-4V ELI (0.12 O_2)(d)	20.0	0.79	βA	814	118	115	105	94 (81)(e)	86 (74)(e)
Ti-6Al-4V (0.15 O_2)	19.0	0.75	α-β rolled	945	137	...	...	45–51	41–46
	19.0	0.75	β-rolled	869	126	...	...	59–62	54–56
Ti-6Al-4V-Ru (grade 29)	20.0	0.79	βA	814	118	101	92	99 (92)(e)	90 (84)(e)
Ti-4Al-3Mo-1V	12.7	0.50	MA	862	125	126	115	115	105
	12.7	0.50	DA	862	125	137	125	132	120
	12.7	0.50	β-STA	965	140	104	95	77	70
Ti-7Al-4Mo	12.7	0.50	MA	993	144	80	73	34	31
	12.7	0.50	STA	1151	167	40	36	29	26
Ti-6Al-6V-2Sn	12.7	0.50	MA	1083	157	66	60	22	20
	12.7	0.50	STA	1170	170	49	45	33	30
	12.7	0.50	β-STA	1048	152	77	70	49	45
Ti-6Al-2Sn-4Zr-6Mo	12.7	0.50	MA	1100	160	60	55	22	20
	12.7	0.50	DA	1035	150	88	80	49	45
Ti-11.5Mo-6Zr-4.5Sn	12.7	0.50	β-STA	1035	150	71	65	27	25
Ti-8Mo-8V-3Al-2Fe	12.7	0.50	β-STA	1248	181	55	50	34	31
	12.7	0.50	β-STA	1035	150	67	61	42	38
	12.7	0.50	β-STA	1415	205	22	20	22	20
Ti-3Al-8V-6Cr-4Zr-4Mo	12.7	0.50	β-STA	1331	193	55	50	41	37
	14.2	0.56	β-STA	1262	183	38	35	38	35
Ti-13V-11Cr-3Al	12.7	0.50	β-ST	827	120	>110	>100	38	35
	12.7	0.50	β-STA	1100	160	77	70	33	30

(a) MA, mill annealed; βA, beta annealed; DA, duplex annealed; ST, solution treated; STA, solution treated and aged; WQ, water quenched. (b) K_{Ic}, plane-strain fracture toughness; K_c, plane-stress fracture toughness. (c) K_{ISCC} or K_{SCC}, threshold stress intensity to produce stress-corrosion cracking. (d) ELI, extra-low interstitial. (e) Naturally aerated seawater at 95 °C (205 °F). Source: Ref 53, 55, 201

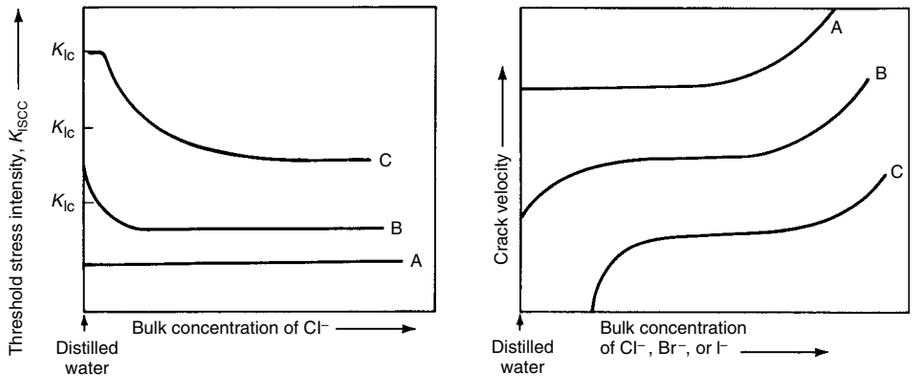

Fig. 44 Effect of halide ion concentration on K_{ISCC} and crack velocity in aqueous solutions. A, highly susceptible; B, moderately susceptible; C, slightly susceptible. K_{Ic}, plane-strain fracture toughness

Sour/Hydrogen Sulfide Environments. Stemming from their inherent nonreactivity with H_2S, sulfides, and elemental sulfur species, most commercial titanium alloys are generally not susceptible to sulfide stress corrosion (SSC) at any known temperature. The exceptional resistance of titanium to H_2S-rich brines is of particular relevance to production and drilling of deep, hot sour hydrocarbon wells, where high-temperature H_2S and/or CO_2-pressurized chloride brines limit well component alloy options. As such, extensive SSC, SCC, and crevice corrosion laboratory testing has been conducted on numerous titanium alloys considered for hot sour well service.

Table 32 provides guidance concerning practical temperature limits for various commercial titanium alloys in deaerated sour chloride brines. Many of these alloys are approved under the NACE MR01-75 standard for sour service and are not limited by H_2S and CO_2 partial pressure and/or elemental sulfur content. In fact, it is chloride SCC and/or crevice corrosion (and not SSC) that dictate the practical temperature limits for these alloys.

Metallurgical Factors. In addition to environmental factors, SCC susceptibility in titanium alloys is also highly dependent on alloy composition and final product metallurgical/processing condition (i.e., grain structure/size, phase type/morphology/volume fraction, and/or

crystallographic texture). For α and α-β alloys, increasing interstitials (i.e., high oxygen equivalency), aluminum, and/or tin content tend to increase susceptibility to aqueous halide SCC (Ref 55). In unalloyed titanium, oxygen levels above 0.20 to 0.25 wt% promote SCC (Ref 201), relating to a transition from wavy to lower-energy planar slip (Ref 53, 55, 60). As such, the K_{Ic} equals K_{ISCC} for grade 2 titanium (typically 0.12 to 0.16% O_2) in ambient saltwater, whereas higher-oxygen (and total interstitials) grades 3 or 4 titanium can exhibit K_{ISCC} values substantially below these in air (Table 31). Aluminum content above 4.5 to 5.0 wt% increases susceptibility due to the increased tendency to form the low-ductility, highly ordered Ti_3Al (alpha-2) phase. As alpha-2 volume fraction increases within the temperature range of 400 to 700 °C (750 to 1290 °F) (Ref 211), alloy K_{ISCC} decreases and crack velocities increase. This is why a final product anneal at temperatures above 718 °C (1325 °F) may be advisable to maximize SCC resistance in these higher-aluminum-containing alloys. The detrimental influence of increasing aluminum in titanium alloy SCC (e.g., Ti-8Al-1Mo-1V) in saltwater is evident in Fig. 47 (Ref 55, 172). Increasing oxygen, nitrogen, carbon, and/or tin further aggravate this phenomenon.

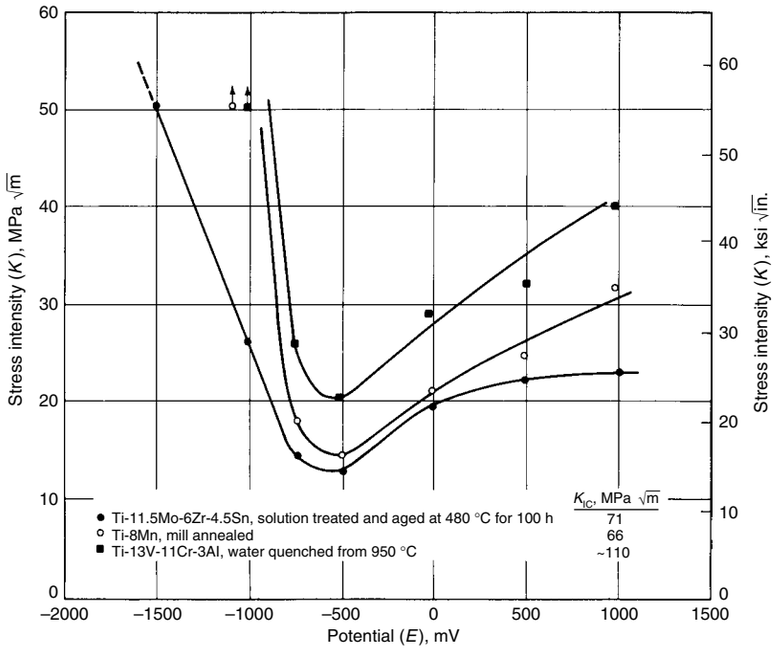

Fig. 45 Stress-corrosion cracking of β-titanium alloys as a function of potential in 0.6 *M* KCl at 24 °C (75 °F). Source: Ref 55

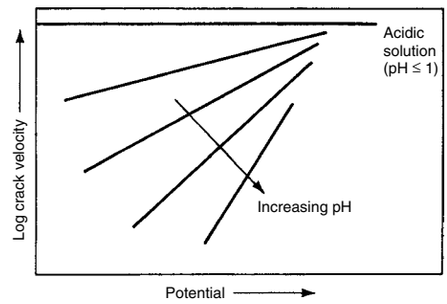

Fig. 46 Stage II crack velocity as a function of pH and potential in aqueous solutions. Source: Ref 53

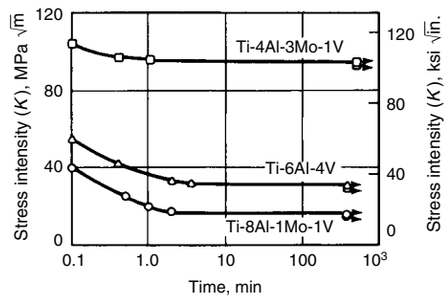

Fig. 47 Effect of alloy composition on stress-corrosion cracking resistance of mill-annealed titanium alloys in aqueous 3.5% NaCl solution at 24 °C (75 °F). Source: Ref 172

Table 32 Maximum environmental limits for titanium alloys in sour hydrocarbon production fluids and sour brines

		Maximum limits							
							Temperature		
ASTM grade	Product forms (condition)(a)	NaCl, wt%	H_2S, psia	CO_2, psia	Elemental S, g/L	Minimum pH	°C	°F	Reference
Grade 2(b)	All (MA)	>25(c)	NL	NL	NL	3.0	75	165	125
Grade 12(b)	All (MA)	>25(c)	NL	NL	NL	3.0	280	535	143
Grade 9	All (MA)	>25(c)	NL	NL	NL	3.0	75	165	...
Grade 28(b)	All (MA or TB)	>25(c)	NL (1000)(d)	NL (500)(d)	NL (1)(d)	2.3	330(d)	625(d)	63
Grade 5	All (MA)	>25(c)	NL	NL	NL	3.0	75	165	...
Grade 23	All (MA or TB)	>25(c)	NL	NL	NL	3.0	75	165	...
Grade 29(b)	All (MA or TB)	>25(c)	NL (1000)(d)	NL (500)(d)	NL (1)(d)	2.3	330(d)	625(d)	63, 154
Ti6246(b)	All (duplex or triplex annealed)	>25(c)	NL (150)(d)	NL (150)(d)	NL	2.6	232	450	205, 209
Grade 19 (Ti Beta-C)(b)	Tubulars (cold-pilgered + STA)	>25(c)	NL (1000) (d)	NL (500)(d)	NL (1)(d)	2.6	177–190	351–374	61, 205, 210
	Tubulars (extruded + STA)	>25(c)	NL (1000)(d)	NL (500)(d)	NL (1)(d)	2.6	163–177	325–351	...
	Forgings (STA)	>25(c)	NL (1000)(d)	NL (500)(d)	NL (1)(d)	2.6	163–177	325–351	...
Grade 20 (Ti Beta-C/Pd)	Tubulars (cold-pilgered + STA)	>25(c)	NL (1000)(d)	NL (500)(d)	NL (20)(d)	2.5	246–274	475–525	61, 62
	Tubulars (extruded + STA)	>25(c)	NL (1000)(d)	NL (500)(d)	NL (1)(d)	2.5	215–246	420–475	...
	Forgings (STA)	>25(c)	NL (1000)(d)	NL (500)(d)	NL (1)(d)	2.5	215–246	420–475	...

NL, no limit indicated or known. (a) MA, mill annealed; TB, transformed beta (acicular alpha); STA, solution treated and aged. (b) Approved under NACE MR01-75 standard for sour service. (c) Up to the chloride saturation limit. (d) Documented test level but with no limit revealed in test. Source: Ref 121

Improved SCC resistance in α and α-β titanium alloys has been achieved through formulation of extra-low interstitial (ELI) grades of some alloys. These ELI grades typically limit maximum oxygen levels to 0.11 to 0.13 wt% while also limiting maximum carbon, nitrogen, and/or aluminum content. The enhanced K_{ISCC} values achievable with ELI Ti-6Al-4V (grade 23) versus standard Ti-6Al-4V (grade 5) in ambient saltwater, for example, are revealed in Table 31 and Fig. 48 (Ref 121).

In α-β and β alloys, isomorphous β-phase stabilizing elements, such as molybdenum, vanadium, niobium, and tantalum (and zirconium), generally mitigate or eliminate aqueous halide SCC. On the other hand, the β-eutectoid alloying additions, such as iron, manganese, chromium, silicon, and copper, tend to degrade alloy SCC resistance (Ref 55). Increasing hydrogen content may also diminish SCC resistance in near-α and α-β alloys (Ref 53, 55). Substantial improvements in titanium alloy SCC resistance are achieved by minor ruthenium or palladium additions (Ref 61–63, 147, 153, 154). As shown by grades 20, 28, and 29 titanium listed in Table 32, alloy SCC (and crevice corrosion) thresholds in sweet and sour brines are well in excess of 200 °C (390 °F) (Ref 63, 147).

Phase structure is also vital in dictating SCC behavior, such that degree of susceptibility directly relates to grain size, α- or β-phase volume fraction, and α-phase mean free path (Ref 55, 60). Increasing α grain size in α and α-β alloys generally increases SCC susceptibility. Typically, SCC in susceptible α and α-β alloys manifests as a predominately transgranular (quasi-cleavage) mode of fracture. Because β phase can act as a ductile, SCC-resistant crack arrestor, increased β-phase volume fraction (especially when it surrounds α phase) is often beneficial. Stemming from the significant crystallographic texture (i.e., typically basal transverse) developed during substantial unidirectional forging or rolling below the alloy β transus, α and α-β alloys often exhibit pronounced orientation(s) for stress-corrosion fracture path. A preferred α-phase cleavage plane (and hydride habit-plane) at ~15° to the basal (0001) plane commonly predominates, resulting in the following directional SCC susceptibilities: TL > SL > LT. See the article "Evaluating Stress-Corrosion Cracking" in *ASM Handbook,* Volume 13A, 2003, p 591, Fig. 28, for orientation of specimens.

A transformed-β structure (produced by processing or annealing above the alloy β transus) dramatically enhances both air and saltwater toughness (K_{ISCC}) by randomizing crystallographic texture and defraying crack tip stress intensity via increased crack path tortuosity (Ref 53, 55, 60). In other words, either Widmanstätten (basketweave)- or colony-type transformed β (acicular α) structures elevate K_{Ic} and K_{ISCC} values (while reducing crack growth rates) relative to mill-annealed equiaxed α-β structures. This is indicated in Fig. 48 for Ti-6Al-4V, and for various alloys in Table 31.

In β alloys, the β phase may be susceptible to either transgranular or intergranular SCC, depending on alloy composition, grain size, and metallurgical condition (Ref 55, 60). The high-eutectoid-element-containing Ti-13-11-3 and Ti-8Mn alloys are very susceptible in all conditions. β phase stabilized by molybdenum, vanadium, niobium, and/or tantalum is highly resistant to aqueous SCC in both aged and, especially, unaged conditions. Increased aging, producing increasing volume fractions of the more susceptible α-phase precipitates, can increase susceptibility (e.g., lower SCC temperature thresholds and/or K_{ISCC} values). In particular, aging at lower temperatures to produce very fine α precipitates and elevated strengths may substantially diminish resistance.

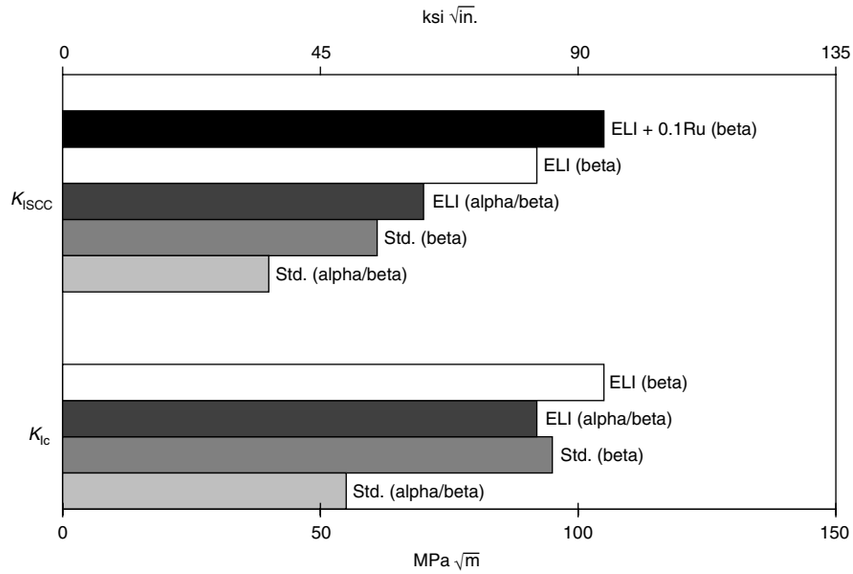

Fig. 48 Typical air (K_{Ic}) and saltwater (K_{ISCC}) fracture toughness values for Ti-6Al-4V-based alloys in various conditions. Alpha-beta is equiaxed α-β structure; beta is transformed-beta structure; ELI is extra-low interstitial. Source: Ref 121

Galvanic Corrosion in Specific Media

In their normal passive condition, titanium alloys are most often the cathode when galvanically coupled to most common engineering alloys in service. As a result, galvanic corrosion of titanium is very rare and occurs only under very unusual conditions. This rare situation could occur in a medium such as a strong reducing acid, in which titanium is actively corroding. In this case, coupling to a more active metal (Ref 212) or a more noble metal could accelerate titanium alloy corrosion only if full passivation is not achieved. Coupling titanium alloys to a more noble material is most often very beneficial, resulting in establishing passivity when titanium is marginally active (corroding) or further maintaining passivity of titanium at more noble potentials (Fig. 1). This form of anodic protection explains the excellent galvanic compatibility of titanium with noble metals (e.g., platinum-group metals) and graphite composites in most environments, including seawater.

Titanium alloys exhibit relatively noble corrosion potentials in the many environments in which full passivity is achieved (Table 2). Similar data in natural seawater from other sources indicate that corrosion potentials for titanium and its alloys fall in the range of +0.1 to −0.3 V versus SCE (Ref 43, 46, 213–215). Deaeration, increasing temperature (Ref 215), and sunlight (Ref 216) were all shown to cause a slight shift in titanium corrosion potential in the active direction. On the other hand, growth of thin biofilms on titanium surfaces in ambient natural seawater and freshwaters can induce subtle ennoblement (from biometabolic cathodic catalysis), similar to that experienced by other corrosion-resistant alloys (Ref 217, 218).

In all cases, these referenced sources reveal that titanium exhibits corrosion potentials that are very similar to those of other corrosion-resistant alloys in the passive condition, including the stainless steels and Ni-Cr-Mo alloys. The minor potential differences between these resistant alloys result in very small, benign galvanic interactions as long as passive alloy conditions exist. Thus, galvanic compatibility can be expected in most environments when a titanium alloy is coupled to another resistant alloy, assuming both exist in a fully passive condition. The data in Table 33 for stainless steel and nickel-base alloys coupled to titanium in marine environments support this point (Ref 76).

However, when a titanium alloy is coupled to a metal that is active (corroding or pitting) in an environment, accelerated anodic attack of the

active metal may ensue. Depending on the environment, active metals may include carbon steel, aluminum, zinc, copper alloys, or stainless steels that are active or pitting.

Galvanic corrosion of various copper alloys when coupled to commercially pure titanium in ambient-temperature seawater is graphically depicted in Fig. 49 and 50. These sources and others reveal a wide variation in the extent of galvanic corrosion of copper alloys and steel (Ref 45, 76, 219–221). The degree of galvanic attack depends on many (often interacting) factors, including cathode-to-anode surface area ratio, concentration of dissolved cathodic depolarizers such as oxygen and atomic hydrogen, temperature (Ref 46, 219), media flow velocity and flow characteristics (that is, turbulence, angle of impingement), and media chemistry. The presence of sulfide, increasing cathode-to-anode area, oxygen content, and flow velocity all aggravate the galvanic attack of copper alloys in seawater. As shown in Fig. 51, deaeration of NaCl brines drastically reduces galvanic attack (compare with Fig. 49). Galvanic interactions between titanium and a wide array of engineering alloys in flowing seawater are surveyed in Ref 81.

As a result of the relatively high cathodic polarization resistance (2.6×10^6 ohm · cm^2) and significant hydrogen overvoltage of titanium in ambient seawater, the cathodic behavior of titanium is similar to that of the 18-8 stainless steels (Ref 222). Therefore, the galvanic effects of titanium on active metals are quite similar to those for 18-8 stainless, as observed in salt spray tests (Ref 223), and often not as detrimental as those of Ni-Cr-Mo alloys. Although these cathode characteristics tend to mitigate galvanic current, they also result in increased cathodic current throwing power in conductive electrolytes; therefore, the effective surface area of titanium involved in a galvanic couple may be quite large. For example, studies show that the effective length of titanium (and stainless steel) condenser tubing involved in the galvanic attack of copper alloy tubesheets in seawater is in excess of 6 m (20 ft) (Ref 219, 222). This differs significantly from the two-tube diameter effective zone length rule used for copper alloys in seawater. Thus, significant cathodic polarization of titanium may occur in aqueous electrolytes that have limited or no dissolved oxygen (e.g., natural seawater or deaerated well brines), when coupled to a more active metal. This often leaves the galvanic couple in cathodic control.

Effective design strategies for limiting or avoiding galvanic attack of active metals include (Ref 47, 121, 221):

- Coupling to more compatible (passive) alloys (including all-titanium design)
- Use of dielectric (insulating) joints between dissimilar metals
- Cathodic protection of the active metal by either impressed current or sacrificial anode means (Ref 46, 219, 221) (while avoiding excessive cathodic charging of titanium surfaces)
- Coating of titanium (cathode) surfaces (e.g., nonconductive, bonded polymer coatings or sheathing, or anodic metal coating such as aluminum physical vapor deposition coatings) to limit the cathode-to-anode surface area ratio

Erosion-Corrosion in Specific Media

Unalloyed titanium and grade 5 titanium have both been shown to withstand silt-free flowing seawater to velocities as high as 30 m/s (100 ft/s) (Ref 43, 224–228). In fact, high-speed water wheel tests in seawater indicate erosion rates for grade 5 titanium of approximately 0.013 mm/yr (0.5 mil/yr) at 46 m/s (150 ft/s) (Ref 226). Jet impingement tests also involving seawater velocities of 46 m/s (150 ft/s) reveal rates of 0.03 to 0.06 mm/yr (1.2 to 2.4 mils/yr) for unalloyed titanium, with values of approximately 0.03 mm/yr (1.2 mils/yr) for welded and unwelded Ti-6Al-4V samples alike (Ref 228). Extremely low erosion rates are also reported for grade 2 titanium at various seawater locations, as shown in Table 34 (Ref 68). The superior erosion-corrosion resistance of titanium has also been reported in other media (Ref 110).

Studies involving sand and emery particle-laden seawater indicate satisfactory erosion-corrosion resistance to flow rates of approximately 6 m/s (20 ft/s) (Ref 76). Data generated from rotating disk tests are presented in Table 35 (Ref 68). The immunity of titanium to erosion-corrosion in silt-laden seawater flowing at approximately 2 m/s (6.5 ft/s) has been demonstrated in more than 40 years of power plant surface condenser tube service (Ref 76, 79). The outstanding resistance of titanium alloys to cavitation damage has also been documented (Ref 66, 67, 227, 229). As expected, the harder, higher-strength titanium alloys are more cavitation resistant (Ref 230).

Testing in a hypersaline geothermal brine further demonstrated the superior erosion-corrosion characteristics of titanium alloys (Ref 143, 231). Expanded brine (104 °C, or 220 °F; pH 2.5 to 4.5) impinged on high-strength ferrous, nickel, cobalt, and titanium alloy samples at a velocity of 240 m/s (800 ft/s). Ti-6Al-4V uniquely experienced no detectable erosive wear after 120 h.

The relative erosion resistance of unalloyed titanium was investigated in two special versions of a rotating drum test involving erosive wear by wet TiO_2 filter cake solids and feed slurry (Ref 232). Titanium exhibited minor metal loss, being measurably superior to the steels, stainless steels, and nickel alloys tested. Superior erosion-corrosion resistance of titanium compared to Hastelloy alloy C was noted in a high-velocity gas scrubber venturi device in which a chloride-rich solution was used to scrub hot (315 °C, or 600 °F) process gas (Ref 232).

Erosion-corrosion testing in coal-water slurries representative of those associated with coal-washing plants also affirmed the superior performance of unalloyed titanium as compared to carbon steel, Ni-hard cast iron, and stainless steel alloys (Ref 233). Test results revealed that titanium was inert to attack to slurry velocities of 5 m/s (16 ft/s) but that types 304 and 316, alloy 904L, and type 440C stainless steels exhibited significant wear above 2 m/s (6.5 ft/s). Unalloyed titanium that was thermally oxidized at 700 °C (1290 °F) provided full wear resistance to velocities as high as 8 m/s (26 ft/s) in these rotary tests.

Table 33 Corrosion rates of various metals galvanically coupled to titanium in marine exposures

	Corrosion rate after indicated exposure, mm/yr (mils/yr)				
	193 days at half tide			56 months in sea air	
Coupled material	Uncoupled	Coupled(a)	Coupled(b)	Uncoupled	Coupled(b)
Alclad 2024-T3	0.015 (0.6)	0.03 (1.2)	0.043 (1.7)	0.001 (0.04)	0.007 (0.28)
Copper	0.013 (0.5)	0.023 (0.9)	0.025 (1)	0.002 (0.08)	0.006 (0.24)
Low-carbon steel	0.15 (6)	0.31 (12.2)	0.43 (17)	0.156 (6.1)	. . .
Monel alloy 400	0.025 (1)	0.003 (0.12)	0.003 (0.12)	nil	0.001 (0.04)
Inconel alloy 600	nil	nil	nil	nil	nil
AISI type 302 stainless steel	0.002 (0.08)	nil	0.003 (0.12)	nil	nil
AISI type 316 stainless steel	nil	nil	nil	nil	nil

(a) Area ratio of titanium to other metal: 1 to 7. (b) Area ratio of titanium to other metal: 7 to 1. Source: Ref 76

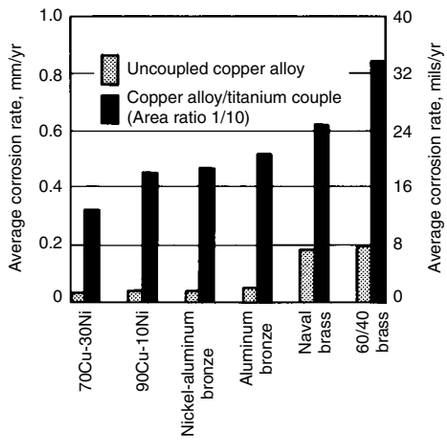

Fig. 49 Corrosion of various copper alloys that were galvanically coupled to titanium in aerated seawater at 25 °C (77 °F). Compare with Fig. 51. Source: Ref 43, 46

Extensive erosion-corrosion testing of Ti-6Al-4V, Ti-5Al-2.5Sn, and Ti-7Al-4Mo alloys has been conducted in high-velocity wet stream environments for application in low-pressure steam turbine blading in power plants. These alloys have demonstrated superior resistance to 403 stainless steel (12 to 13% Cr steel) in operating turbines and in water droplet erosion and water jet impingement tests (Ref 69). Full erosion resistance of Ti-6Al-4V blades to velocities of 440 to 530 m/s (1450 to 1740 ft/s) at 10% steam moisture has been noted in turbines. Studies suggest useful erosion resistance of Ti-6Al-4V in approximately 8 and 11% steam moisture to 549 m/s (1800 ft/s) and 488 m/s (1600 ft/s), respectively. Single-shot water jet impingement testing has shown that annealed Ti-7Al-4Mo alloy is significantly more erosion resistant than 12% Cr steel, 303 stainless steel, or Stellite alloy 6 at jet velocities of 610 and 915 m/s (2000 and 3000 ft/s).

Although titanium is highly resistant to high-velocity steam erosion, several cases of substantial steamside droplet erosion have been reported on certain grade 2 titanium tubes in power plant surface condensers. This outside surface erosion of the tube has been limited to isolated, outer-row areas in the cold end of turbine steam condensers located in very cold climates, such as Scandinavia in the winter. The colder tubeside cooling waters increase steam condensation and flow velocities. The degree and rate of steam droplet erosion is directly influenced by drop velocity and size and the amount of impinging water droplets. Erosion occurs when substantial condensed steam droplets impinge on the tube surface at sonic velocities (115 to 200 m/s, or 375 to 660 ft/s). Remedial measures include installation of harder, higher-strength titanium alloy or stainless steel outer-row tube shields, increasing cooling water temperatures, modifying shellside inlet steam flow, and/or incorporating condensate collectors.

Corrosion Fatigue

As indicated in Fig. 10, the smooth or notched stress-number of cycles fatigue life of the more common titanium alloys (Table 1) and their weldments is not significantly affected by water, seawater, and many other aqueous chloride media (Ref 68, 69, 234, 235). These alloys typically exhibit smooth fatigue run-out stress to tensile strength ratios in the range of 0.5 to 0.6, which remain unchanged in 3.5% sodium chloride (NaCl) solutions and in seawater (Ref 69, 234, 236).

In regard to fatigue crack growth (FCG), certain halide-rich media (such as saltwater) may enhance crack growth rates and/or lower stress-intensity factor range (ΔK) threshold values in those titanium alloys that are also known to be susceptible to SCC in that media (i.e., $K_{ISCC} < K_{Ic}$) (Ref 237, 238). Thus, unalloyed grades 1 and 2; most titanium alloys containing $\leq$4.5 wt% Al; palladium- or ruthenium-enhanced, higher molybdenum, and ELI alloys are generally highly FCG resistant in these aqueous environments (Ref 237, 239). Along with composition, metallurgical condition (microstructure and crystallographic texture) strongly influences FCG behavior in titanium alloys (Ref 237, 238, 240). Parallel to effects on alloy SCC susceptibility in aqueous halides, improved FCG resistance and $\Delta K_{threshold}$ values for the Ti-6Al-4V alloy, for example, are achieved by selecting the ELI version and/or processing to achieve a transformed β (acicular α) instead of the typical mill-annealed (equiaxed α-β) microstructure. The higher-strength molybdenum-rich (such as Ti Beta-C, Beta 21S) and/or ruthenium- or palladium-enhanced (grade 20, 28, 29) titanium alloys offer excellent SCC and FCG resistance in higher-temperature sweet or sour chloride brines (Ref 63, 121).

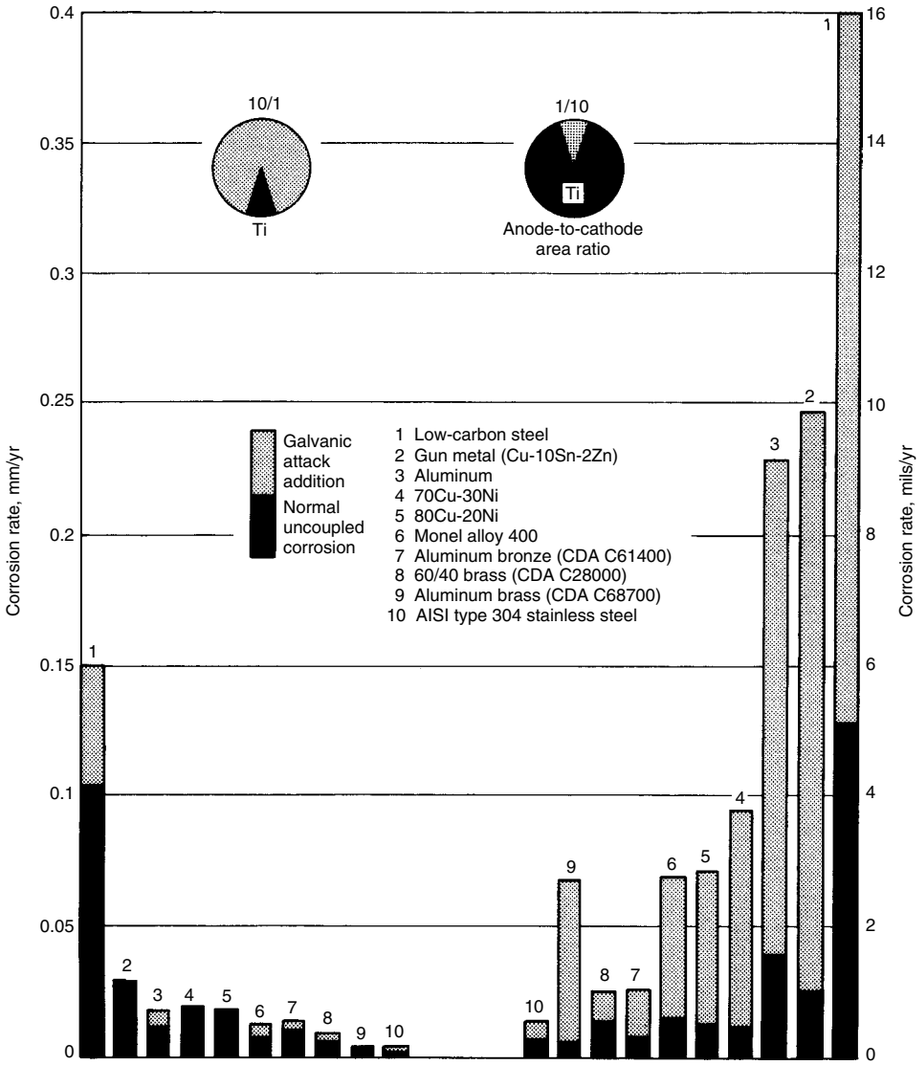

Fig. 50 Corrosion of dissimilar metals coupled to titanium in flowing ambient-temperature seawater. Source: Ref 68

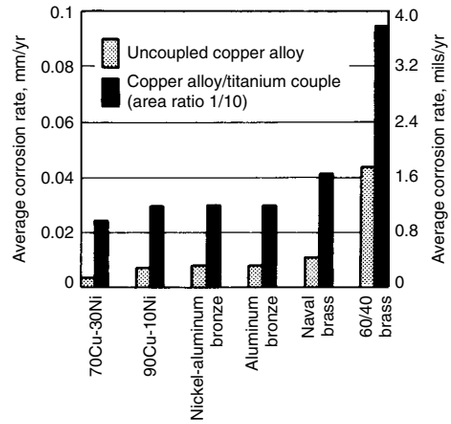

Fig. 51 Corrosion of copper alloys that were galvanically coupled to titanium in boiling, deaerated 6% NaCl at 100 °C (212 °F). Compare with Fig. 49, which shows corrosion rates in aerated seawater. Source: Ref 46

Expanding the Corrosion Resistance of Titanium

Although titanium is highly resistant to a rather wide range of environments, ranging from highly oxidizing to mildly reducing and acidic to basic (Fig. 1), it does exhibit definite limitations in strong reducing acid media. This reducing acid media primarily includes (uninhibited) HCl, HBr, HI, H_2SO_4, H_3PO_4, and oxalic and sulfamic acid solutions, which become increasingly corrosive as concentration and/or temperature increase. These same reducing acid limitations are responsible for crevice and stress-corrosion limitations for titanium and its alloys in aqueous halide media, where strong reducing (deaerated) acidic conditions can develop deep within crevices and cracks (Ref 19, 21, 23), especially as temperatures increase.

General Corrosion Resistance

Fortunately, numerous proven methods for overcoming the limitations of titanium under strong reducing acid conditions can be practically invoked, depending on the service/process paradigm. The first five methods, listed subsequently, enhance passivation of titanium by shifting its potential in the noble (positive) direction out of the active region (Fig. 1, 52), where the protective TiO_2 film is stable (Ref 6, 147, 241–245):

- Alloying titanium with noble metals (e.g., platinum-group metals), which facilitates cathodic depolarization by catalyzing the hydrogen reduction step in acid solutions (Fig. 52)
- Alloying titanium with more thermodynamically stable, acid-resistant elements (e.g., molybdenum, zirconium, tantalum, niobium)
- Addition or presence of soluble oxidizing ions or compounds (cathodic depolarizers) in the acid media (e.g., Fe^{3+}, O_2, Cl_2, NO_3^-) (Table 15)
- Noble metal surface treatments (e.g., platinum-group metal coatings or enriched/modified surfaces)
- Anodic protection via impressed positive potentials from an external power source or from direct galvanic coupling with a noble metal (e.g., a platinum-group metal)
- Thermal oxidation or nitriding of titanium surfaces

Alloying. Perhaps the most effective and conservative means of extending titanium resistance into reducing acid environments has been through selective alloying. Beneficial alloying elements for titanium primarily include ≥0.04 wt% Pd, ≥0.08 wt% Ru, ≥4.0 wt% Mo, and/or ≥0.5 wt% Ni (Ref 6, 13, 147, 148, 241, 245–248). Other less common alloying elements that are effective at much higher levels include niobium (≫10 wt%), tantalum (≥5 wt%), and/or zirconium (>8 to 10 wt%). Of these, very minor (of the order of 0.1 wt%) additions of the platinum-group metals (palladium and/or ruthenium) have been widely and cost-effectively used to dramatically enhance reducing acid, crevice, and/or stress-corrosion resistance in α, α-β, and β titanium alloys (Ref 147, 209, 249). These additions generally have no significant effect on mechanical, physical, and metallurgical properties of the base alloy. Commercial palladium/ruthenium-enhanced alloys include the titanium ASTM grades 7, 11, 13–18, 20, 24–31, 33, and 34 (Table 1). Minor nickel additions to titanium together with minor palladium, ruthenium, or molybdenum levels also provide expanded reducing acid resistance (e.g., ASTM grades 12–15, 25, 30, 31, 33, 34, 15R) (Ref 147, 148, 205, 209, 250).

Commercial α-β and β titanium alloys containing 3.5 to 15.0 wt% Mo also offer substantially improved reducing acid, crevice, and/or stress-corrosion resistance. These alloys include ASTM grades 19, 20, and 21, and Ti-550, Ti-6-2-4-6, Ti-17, Ti-5-5-5-3, and Ti-15-5-3 alloys (Table 1). Minor palladium or ruthenium additions to molybdenum-containing titanium alloys (Ref 6, 147, 245, 248) further expand these application windows.

Inhibitor Additions. Various oxidizing ions or compounds, listed in Table 15, dramatically expand the useful resistance of titanium in reducing acid solutions. Most of these inhibitors are very potent, such that as little as 20 to 100 ppm are effective, depending on acid concentration and temperature. These inhibitors may be added to once-through or recycled process streams.

Although a totally different mechanism and not acid solution related, minute/minor additions of water to dry (anhydrous) environments may be required to achieve/maintain titanium passivity. This inhibitive strategy is highly effective in anhydrous organic solvents, dry/reagent methanol, red-fuming nitric acid, dry hydrogen or chlorine gas, and nitrogen tetroxide. Guidelines for minimum water additions to these environments are presented in this article.

Noble Metal Surface Treatments. Platinum-group metals such as platinum and palladium have been electroplated, ion plated, ion implanted, or thermally diffused onto/into titanium alloy surfaces to improve reducing acid resistance (Ref 251, 252). This strategy can be effective but can have practical limitations, such as cost, equipment size/geometry issues, and so on. Ion-plated platinum or gold surface films offer significant improvements in titanium alloy oxidation resistance to temperatures as high as 650 °C (1200 °F) (Ref 253, 254).

Table 34 Erosion-corrosion of grade 2 titanium in seawater at various locations

Location	Flow rate m/s	Flow rate ft/s	Type of test	Test duration, months	Erosion-corrosion rate mm/yr	Erosion-corrosion rate mils/yr
Brixham Sea	9.8	32	Model condenser	12	0.003	0.12
Kure Beach, NC	1	3.3	Ducting	54	7.5×10^{-7}	0.00003
	8.5	28	Rotating disk	2	1.3×10^{-4}	0.005
	9	29.5	Micarta wheel	2	2.8×10^{-4}	0.01
	7.2	23.6	Jet impingement(a)	1	5×10^{-4}	0.02
Wrightsville Beach, NC	1.3	4.3	...	6	1×10^{-4}	0.004
	9	29.5	Micarta wheel	2	1.8×10^{-4}	0.007
Mediterranean Sea	7.2	23.6	Jet impingement(a)	0.5	0.5 mg/day	...
Dead Sea	7.2	23.6	Jet impingement(a)	0.5	0.2 mg/day	...

(a) Included air. Source: Ref 68

Table 35 Erosion-corrosion of grade 2 titanium in seawater containing suspended solids

Flow rate m/s	Flow rate ft/s	Seawater suspension	Test duration, h	Erosion-corrosion rate mm/yr	Erosion-corrosion rate mils/yr
7.2	23.6	No solids	10,000	nil	
2.0	6.5	40 g/L of 60-mesh sand	2000	0.0025	0.1
2.0	6.5	40 g/L of 10-mesh emery	2000	0.0125	0.5
3.5	11.5	1% 80-mesh emery	17.5	0.0037	0.15
4.1	13.5	4% 80-mesh emery	17.5	0.083	3.3
7.2	23.6	40% 80-mesh emery	1	1.5	60

Source: Ref 68

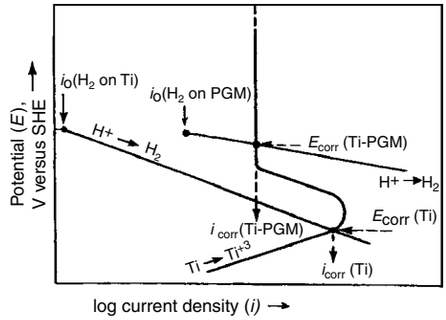

Fig. 52 Evans diagram showing how alloying titanium with palladium or ruthenium achieves passivation in reducing acids via cathodic depolarization. SHE, standard hydrogen electrode; PGM, platinum-group metal. Source: Ref 147

Anodic Protection. Titanium alloys can be effectively passivated and protected from corrosion in strong reducing acid solutions by anodic protection. Sustained applied positive metal potentials in the range of +0.7 to +4.0 V (versus standard hydrogen electrode) are usually sufficient to achieve full passivation of titanium in many acids (Table 17). These positive potentials are impressed by either a controlled direct current power supply or by galvanic coupling to a noble metal such as a platinum-group metal (e.g., platinum, palladium, ruthenium, iridium) (Ref 6). Although limited use of anodic protection by impressed currents has been made in strong H_2SO_4 and H_3PO_4 solutions, wherein anodic pitting potentials for titanium are very high, the added system costs and challenges with complex component geometries and stray currents have inhibited wide-scale use. Also, alternating wet/dry surfaces or vapor phases are not protected by this method.

Thermal Oxidation or Nitriding. Protective thermal oxide films can form when titanium is heated in air at temperatures of 600 to 800 °C (1110 to 1470 °F) for 2 to 10 min. The rutile TiO_2 film formed measurably improves resistance to dilute reducing acids as well as absorption of hydrogen under cathodic charging (Ref 52, 159, 165) or gaseous hydrogen conditions (Ref 163). Corrosion studies in hot, dilute HCl solutions have confirmed its superior protective benefits as compared to as-pickled, polished, or anodized surfaces on unalloyed titanium (Ref 52, 255). Resistance to corrosion and hydrogen uptake in molten urea at 200 °C (390 °F) was achieved by thermal oxidation of titanium (Ref 159, 256). Enhanced protection from dry chlorine gas attack can also be expected. As with anodizing, thermal oxidation offers no improvements in titanium resistance exposed to highly alkaline or oxidizing aqueous media.

Although the thermal oxide has proved to be protective in relatively short-term tests in dilute reducing acids, long-term performance has not been fully demonstrated. Mechanical damage and plastic strain of thermally oxidized components must be avoided for effective protection. The oxide has been successfully applied on tubing and small components, but may be impractical for large components or where component distortion may occur during the thermal treatment cycle.

Surface films of titanium nitrides and carbides are highly resistant to reducing acids. Studies have shown that the dense, adherent titanium nitride films produced by reactive plasma ion plating provided superior protection in deaerated H_2SO_4 solutions when compared to several other film-forming methods (Ref 256). Methods of applying nitride surface films to titanium and its alloys (Ref 252, 257) include ion implantation, ion plating, sputter deposition, or thermal diffusion (with or without plasma assistance in nitrogen gas, or in a molten cyanide bath). Due to cost and limitations of film application and inherent thin-film performance limitations, these films are generally not used solely for corrosion resistance. The improved wear resistance offered by these hard films is generally the primary incentive (Ref 252).

Crevice Corrosion Resistance

The crevice corrosion resistance of titanium alloys can be dramatically expanded by the following strategies (Ref 20, 147):

- Alloying titanium with certain noble metals and/or acid-resistant elements
- Noble metal surface treatments
- Other metallic and/or metal oxide coatings
- Thermal oxidation
- Noble alloy contact
- Surface pickling (to remove smeared-in surface iron)

Alloying. Because the crevice corrosion resistance of titanium alloys tends to parallel their general corrosion resistance in reducing acids, the same alloying element strategies discussed prior for expanding general corrosion resistance are directly applicable. Thus, alloying titanium with certain noble, more acid-resistant metals, such as palladium, ruthenium, molybdenum, or nickel, is commonly used to enhance titanium alloy crevice corrosion resistance (Ref 13, 20, 39, 137, 145, 147, 148, 249, 250, 258). Therefore, commercial titanium alloys that exhibit superior crevice corrosion resistance include ASTM grades 7, 11–18, 20, 24–31, 33, and 34 (Table 1). Other molybdenum-containing crevice-corrosion-resistant alloys include ASTM grades 19, 20, and 21, and Ti-550, Ti-6-2-4-6, Ti-17, Ti-5-5-5-3, and Ti-15-5-3 alloys.

Selection of a more resistant titanium alloy is generally preferred from a long-term reliability, cost, and practical standpoint over surface treatment strategies for less resistant titanium alloys (particularly for equipment involving large, complex, inaccessible surfaces). On the other hand, localized surface treatments may be cost-effective when very heavy alloy wall sections or highly localized surface application are involved, and/or when it is necessary to expeditiously upgrade certain existing unalloyed titanium equipment components.

Noble Metal Films. Coatings of noble metals and/or their oxides offer significant improvements in the crevice corrosion resistance of titanium. In fact, these treatments can offer crevice resistance approaching that of the titanium-palladium or titanium-ruthenium alloys. The most common noble metals applied to titanium surfaces are palladium, platinum, and ruthenium, and their oxides. Thermal diffusion coatings of palladium (Ref 251), platinum, iridium, and ruthenium are readily applied by firing in an air furnace after coating titanium with modified metal chloride solutions (Ref 252, 259). The resultant (0.1 to 10 μm, or 0.004 to 0.4 mil, thick) coating is typically a mixture of titanium and platinum-group metal oxides, depending on firing temperature (Ref 251). Thermal palladium surface treatments have been successfully used in titanium-tubed oil refinery heat exchangers (Ref 260).

Other methods of applying these platinum-group metals on titanium surfaces include electroplating, brush plating, and ion implantation (Ref 20, 252). Electroplating or brush plating provides precious metal layer thicknesses of the order of 0.01 mm (0.4 mil). Brush plating is a special technique for achieving localized electroplating of surfaces (Ref 261). Palladium implantation generates palladium-rich surface layers of the order of 0.5 μm (0.02 mil) or less, which has been shown to be effective in hot, concentrated chloride brines (Ref 262).

Other Metallic Coatings. The application of certain metals and their oxides within titanium alloy crevices can effectively inhibit crevice corrosion initiation in hot chloride media. These metals include nickel and copper, their oxides, and the Fe_2O_3 and MoO_3 oxides (Ref 20, 263, 264). In finely powdered form, these materials can be painted on creviced titanium surfaces in slurry form. Alternatively, these powders can be formulated into sealants, such as silicone or ethylene propylene diene monomer (EPDM) rubber. For example, a 5 wt% addition of nickel metal/NiO powder (50/50) blended into EPDM gaskets for chlor-alkali cell anode components is known to prevent the crevice corrosion of unalloyed titanium in hot, low-pH, chlorine-saturated NaCl brines. It has been shown that unalloyed titanium anodized in a molybdate solution also provides crevice-corrosion-resistant metal surfaces (Ref 264).

Thermal Oxidation. Crevice corrosion resistance is afforded from thermal oxide films formed when titanium alloys are heated in air to 500 to 800 °C (930 to 1470 °F) for 2 to 10 min. Increasing the temperature (or time) within this range results in thicker, more protective oxide films. In hot NaCl brines, thermally oxidized titanium has proved its superior resistance to anodized or as-pickled titanium in both metal-to-metal and metal-to-gasket crevices (Ref 20, 52, 141). Avoidance of mechanical damage or plastic metal strain is necessary for good protection. Thermal oxide films may exhibit limitations at higher temperatures and in low-pH brine, and they are better considered for situations in which only borderline crevice conditions exist for unalloyed titanium.

Noble Alloy Contact. Crevice corrosion of unalloyed titanium or other titanium alloys may be averted in certain metal-to-metal crevice situations. If a more noble alloy is one member of the metal-to-metal crevice, the titanium metal surface can be anodically protected by the galvanic couple achieved in the crevice (Ref 20). More noble metals include the platinum-group metals and more resistant titanium alloys, such as titanium-palladium, titanium-ruthenium, or copper alloys. For example, it is well known that unalloyed titanium tubes that are expanded into copper alloy tubesheets resist tube joint crevice corrosion in high-temperature seawater (Ref 43, 46). Similarly, the more noble

titanium-palladium or titanium-ruthenium alloys will protect unalloyed titanium with which it is in direct contact, providing similar crevice resistance to that of the titanium-palladium or titanium-ruthenium alloy. For example, a titanium-palladium-to-unalloyed-titanium mating metal crevice will resist crevice attack in boiling chlorine-saturated NaCl brines, where an unalloyed titanium-to-unalloyed-titanium mating crevice would undergo severe crevice corrosion. This principle also applies to noble-alloy-treated titanium surfaces in contact with untreated unalloyed titanium.

Surface Pickling. If the presence of galled-in or smeared-in surface iron is suspected on titanium equipment, it should removed to prevent possible pitting or hydrogen uptake in titanium exposed to hot chloride brines (Ref 22). This surface iron contamination can be removed with a light (1 to 3 min) pickle in near-ambient-temperature 35 vol% HNO_3-5 vol% HF or 12 : 1 HNO_3-HF solution, followed by water flushing. This procedure will remove less than 0.03 mm (1.2 mils) from the titanium alloy surface. Studies have shown that pickling in dilute HNO_3-HF solutions is much more effective in removing surface iron contamination than either anodizing or strong nitric acid exposures (Ref 52).

ACKNOWLEDGMENT

This article is adapted from Corrosion of Titanium and Titanium Alloys by Ronald W. Schutz and David E. Thomas, *Corrosion*, Vol 13, *ASM Handbook,* ASM International, 1987, p 669–706.

Appendix 1: General Corrosion Data for Unalloyed Titanium

This appendix is a compilation of general (i.e., uniform) corrosion rate values for unalloyed titanium (ASTM grades 1 to 4). These values were derived from various published sources cited in the references and from unpublished laboratory tests. These data should be used only as a preliminary guideline for alloy performance. Rates may vary depending on changes in solution chemistry, temperature, exposure time, ratio of metal surface to solution volume, solution replenishment rate, flow velocity, and other factors. Also, total alloy suitability cannot be assumed from these values alone, because other forms of corrosion, such as localized attack, stress corrosion, or hydrogen embrittlement, may be limiting. The text should be consulted to assess overall alloy suitability more thoroughly for a given set of environmental conditions. In complex, variable, and/or dynamic environments, in situ testing may provide more reliable data. In Table 36, solution constituent concentrations are in weight percent, temperatures are given in degrees centigrade, and corrosion rates are reported in millimeters per year (mm/yr). Unless otherwise stated, it should be assumed that solutions were tested in the naturally aerated condition.

Table 36 General corrosion rates for unalloyed titanium

Medium	Concentration, wt%	Temperature, °C	Corrosion rate, mm/yr
Acetaldehyde	75	149	0.001
	100	149	nil
Acetate, *n*-propyl	...	87	nil
Acetic acid	99.7	204	nil
	5–99.7	124	nil
	33–vapor	Boiling	nil
	99	Boiling	0.003
	65	121	0.003
	58	130	0.381
	99.7	124	0.003
Acetic acid + 3% acetic anhydride	Glacial	204	1.02
Acetic acid + 1.5% acetic anhydride	Glacial	204	nil
Acetic acid + 0.011% Cl^-	31.2	Boiling	0.259
	62.0	Boiling	0.272
Acetic acid + 5% formic acid	58	Boiling	0.457
Acetic anhydride	100	21	0.025
	100	150	0.005
	99.5	Boiling	0.013
Adipic acid + 15–20% glutaric + 2% acetic acid	25	199	nil
Adipic acid	67	240	nil
Adipylchloride and chlorobenzene solution	...	...	nil
Adiponitrile	Vapor	371	0.008
Aluminum chloride, aerated	10	100	0.002
	25	100	3.15
Aluminum chloride	10	100	0.002
	10	150	0.03
	25	60	nil
	25	100	6.55
Aluminum chloride + 3.6% HCl + 0.7% HNO_3 + 0.3% H_3PO_4	8	Boiling	0.002
Aluminum	Fused metal	677	164.6
Aluminum fluoride	Saturated	Room	nil
Aluminum nitrate	Saturated	Room	nil
Aluminum sulfate	Saturated	Room	nil
	10	80	0.05
	10	Boiling	0.12
Aluminum sulfate + 1% H_2SO_4	Saturated	Room	nil
Ammonium acid phosphate	10	Room	nil
Ammonium aluminum chloride	Molten	350–380	Very rapid attack
Ammonia, anhydrous	100	40	<0.127
Ammonia, steam, water	...	222	11.2
Ammonium acetate	10	Room	nil
Ammonium bicarbonate	50	100	nil
Ammonium bisulfite, pH 2.05	Spent pulping liquor	71	0.015
Ammonium carbamate	50	100	nil
Ammonium chloride	Saturated	100	<0.013
Ammonium chlorate	300 g/L	50	0.003
Ammonium fluoride	10	Room	0.102
Ammonium hydroxide	28	Room	0.003
	28	100	nil
Ammonium nitrate	28	Boiling	nil
Ammonium nitrate + 1% nitric acid	28	Boiling	nil
Ammonium oxalate	Saturated	Room	nil
Ammonium perchlorate	20	88	nil
Ammonium persulfate, pH 11	10	Boiling	nil
Ammonium sulfate	10	100	nil
Ammonium sulfate + 1% H_2SO_4	Saturated	Room	0.010
Aniline	100	Room	nil
Aniline + 2% $AlCl_3$	98	158	>1.27
Aniline hydrochloride	5	100	nil
	20	100	nil
Antimony trichloride	27	Room	nil
Aqua regia	3:1	Room	nil
	3:1	80	0.86
	3:1	Boiling	1.12
Aqua regia + 0.2% $FeCl_3$	3:1	Boiling	0.734
	3:1	79	0.211
Aqua regia + 0.02% $FeCl_3$	3:1	Boiling	0.604
	3:1	79	0.198
Arsenous oxide	Saturated	Room	nil
Barium carbonate	Saturated	Room	nil
Barium chloride	5	100	nil
	20	100	nil
	25	100	nil
Barium hydroxide	Saturated	Room	nil
Barium nitrate	10	Room	nil
Barium fluoride	Saturated	Room	nil
Benzaldehyde	100	Room	nil

(continued)

Table 36 (continued)

Medium	Concentration, wt%	Temperature, °C	Corrosion rate, mm/yr
Benzene (traces of HCl)	Vapor and liquid	80	0.005
	Liquid	50	0.025
Benzene	Liquid	Room	nil
Benzoric acid	Saturated	Room	nil
Bismuth	Molten	816	High
Bismuth/lead	Molten	300	Good resistance
Boric acid	Saturated	Room	nil
	10	Boiling	nil
	18	Boiling	nil
Bromine	Liquid	30	Rapid attack
Bromine, moist	Vapor	30	<0.003
Bromine gas, dry	...	21	Rapid attack
Bromine-water solution	...	25	nil
Bromine in methyl alcohol	5.0	25	19.2 (stress-corrosion cracking possible)
N-butyric acid	Undiluted	Room	nil
Calcium bisulfite	Cooking liquor	26	0.001
Calcium carbonate	Saturated	Boiling	nil
Calcium chloride	5	100	0.005
	10	100	0.007
	20	100	0.015
	55	104	0.001
	60	149	<0.003
	62	154	0.406
	73	175	0.80
Calcium hydroxide	Saturated	Room	nil
	Saturated	Boiling	nil
Calcium hypochlorite	2	100	0.001
	6	100	0.001
	18	21	nil
	Saturated	21	nil
Carbon dioxide	100	...	Excellent
Carbon tetrachloride	99	Boiling	0.005
	Liquid	Boiling	nil
	Vapor	Boiling	nil
Carbon tetrachloride + 50% H_2O	50	25	0.005
Chlorine gas, wet	>0.7 H_2O	Room	nil
	>0.95 H_2O	140	nil
	>1.5 H_2O	200	nil
Chlorine saturated water	Saturated	97	nil
Chloride gas, dry	<0.5 H_2O	Room	May react
Chlorine dioxide	5	82	<0.003
Chlorine dioxide + HOCl, $H_2O + Cl_2$	15	43	nil
Chlorine dioxide in steam	5	99	nil
Chlorine dioxide	10	70	0.03
Chlorine monoxide (moist)	Up to 15	43	nil
Chlorine trifluoride	100	30	Vigorous reaction
Chloracetic acid	30	82	<0.127
	100	Boiling	<0.127
Chlorosulfonic acid	100	Room	0.312
Chloroform	Vapor and liquid	Boiling	0.000
Chloroform + 50% H_2O	50	25	0.000
Chloropicrin	100	95	0.003
Chromic acid	10	Boiling	0.003
	15	24	0.006
	15	82	0.015
	50	24	0.013
	50	82	0.028
Chromic acid + 5% nitric acid	5	21	<0.003
Citric acid	10	100	0.009
	25	100	0.001
	50	60	0.000
	50	Boiling	0.127–1.27
	672	149	Corroded
Citric acid (aerated)	50	100	<0.127
Copper nitrate	Saturated	Room	nil
Copper sulfate	50	Boiling	nil
Copper sulfate + 2% H_2SO_4	Saturated	Room	0.018
Cupric carbonate + cupric hydroxide	Saturated	Ambient	nil
Cupric chloride	20	Boiling	nil
Cupric chloride (continued)	40	Boiling	0.005
	55	118	0.003
Cupric cyanide	Saturated	Room	nil
Cuprous chloride	50	90	<0.003
Cyclohexylamine	100	Room	nil
Cyclohexane (plus traces of formic acid)	...	150	0.003
Dichloroacetic acid	100	Boiling	0.007
Dichlorobenzene + 4–5% HCl	...	179	0.102
Diethylene triamine	100	Room	nil
Ethyl alcohol	95	Boiling	0.013
	100	Room	nil
Ethylene dichloride	100	Boiling	0.005–0.127
Ethylene dichloride + 50% water	50	25	0.005
Ethylene diamine	100	Room	nil
Ferric chloride	10–20	Room	nil
	1–30	100	0.000–0.004
	10–40	Boiling	0.00–0.02
	50	150	0.003
Ferric sulfate	10	Room	nil
Ferrous chloride + 0.5% HCl	30	79	0.006
Ferrous sulfate	Saturated	Room	nil
Fluoboric acid	5–20	Elevated	Rapid attack
Fluorine, commercial	Gas	−109	0.864
Fluorine, HF free	Liquid	−196	0.011
	Gas	−196	0.011
Fluorosilicic acid	10	Room	47.5
Formaldehyde	37	Boiling	nil
Formamide vapor	...	300	nil
Formic acid, aerated	10	100	0.005
	25	100	0.001
	50	100	0.001
	90	100	0.001
Formic acid	9	50	<0.127
	10	Boiling	1.68
	25	100	2.44
	50	Boiling	3.36
Furfural	100	Room	nil
Gluconic acid	50	Room	nil
Glycerin	...	Room	nil
Hydrogen chloride, gas	Air mixture	25–100	nil
Hydrochloric acid, aerated	1	60	0.004
	2	60	0.016
	5	60	1.07
	1	100	0.46
	5	35	0.01
	10	35	1.02
	20	35	4.45
Hydrochloric acid	0.1	Boiling	0.10
	1	Boiling	1.8
Hydrochloric acid + 4% $FeCl_3$ + 4% $MgCl_2$	19	82	0.51
Hydrochloric acid + 6% $FeCl_3$ + 9% $MgCl_2$	22	82	11.07
Hydrochloric acid + 4% $FeCl_3$ + 4% $MgCl_2$ + Cl_2 saturated	19	82	0.46
Hydrochloric acid, chlorine saturated	5	190	<0.025
	10	190	28.5
Hydrochloric acid + 0.02% Cl_2	36	25	0.432
Hydrochloric acid			
+1% HNO_3	5	40	nil
+1% HNO_3	5	95	0.091
+5% HNO_3	5	40	0.025
+5% HNO_3	5	95	0.030
+10% HNO_3	5	40	nil
+10% HNO_3	5	95	0.183
+3% HNO_3	8.5	80	0.051
+5% HNO_3	1	Boiling	0.074
Hydrochloric acid + 63.6% KNO_3	7.7	90	0.132
Hydrochloric acid			
+2.5% $NaClO_3$	10.2	80	0.009
+5.0% $NaClO_3$	10.2	80	0.006
Hydrochloric acid			
+0.5% CrO_3	5	38	nil
+0.5% CrO_3	5	95	0.031

(continued)

Table 36 (continued)

Medium	Concentration, wt%	Temperature, °C	Corrosion rate, mm/yr
+1% CrO_3	5	38	0.018
+1% CrO_3	5	95	0.031
Hydrochloric acid			
+0.05% $CuSO_4$	5	38	0.040
+0.05% $CuSO_4$	5	93	0.091
+0.5% $CuSO_4$	5	38	0.091
+0.5% $CuSO_4$	5	93	0.061
+1% $CuSO_4$	5	38	0.031
+1% $CuSO_4$	5	93	0.091
+5% $CuSO_4$	5	38	0.020
+5% $CuSO_4$	5	93	0.061
+0.05% $CuSO_4$	5	Boiling	0.064
+0.5% $CuSO_4$	5	Boiling	0.084
Hydrochloric acid			
+0.05% $CuSO_4$	10	66	0.025
+0.20% $CuSO_4$	10	66	nil
+0.5% $CuSO_4$	10	66	0.023
+1% $CuSO_4$	10	66	0.023
+0.05% $CuSO_4$	10	Boiling	0.295
+0.5% $CuSO_4$	10	Boiling	0.290
Hydrochloric acid + 0.1% $FeCl_3$	5	Boiling	0.01
Hydrochloric acid + 1 g/L Ti^{4+}	10	Boiling	0.000
Hydrochloric acid + 5.8 g/L Ti^{4+}	20	Boiling	0.000
Hydrochloric acid + 18% H_3PO_4 + 5% HNO_3	18	77	0.000
Hydrochloric acid + 10% H_2SO_4 + 0.3% Cu^{2+}	10	93	1.13
Hydrofluoric acid	1	26	127
Hydrofluoric acid, anhydrous	100	Room	0.127–1.27
Hydrofluoric-nitric acid 5 vol% HF-35 vol% HNO_3	...	25	452
Hydrofluoric-nitric acid 5 vol% HF-35 vol% HNO_3	...	35	571
Hydrogen peroxide	3	Room	<0.127
	6	Room	<0.127
	30	Room	<0.305
Hydrogen peroxide + 2% NaOH	1	60	55.9
Hydrogen peroxide, pH 4	5	66	0.061
Hydrogen peroxide, pH 1	5	66	0.152
Hydrogen peroxide, pH 1	20	66	0.69
Hydrogen peroxide, pH 11	0.08	70	0.42
Hydrogen sulfide (water saturated)	...	21	<0.003
Hydrogen sulfide, steam, and 0.077% mercaptans	7.65	93–110	nil
Hydroxy-acetic acid	...	40	0.003
Hypochlorous acid + ClO and Cl_2 gases	17	38	0.000
Iodine, dry or moist gas	...	25	0.1
Iodine in water + potassium iodide	...	Room	nil
Iodine in alcohol	Saturated	Room	Pitted
Lactic acid	10–85	100	<0.127
	10	Boiling	<0.127
Lead	...	816	Attacked
	...	324–593	Good
Lead acetate	Saturated	Room	nil
Linseed oil, boiled	...	Room	nil
Lithium, molten	...	316–482	nil
Lithium chloride	50	149	nil
Magnesium	Molten	760	Limited resistance
Magnesium chloride	5–20	100	<0.010
	5–40	Boiling	0.005
Magnesium hydroxide	Saturated	Room	nil
Magnesium sulfate	Saturated	Room	nil
Manganous chloride	5–20	100	nil
Maleic acid	18–20	35	0.002
Mercuric chloride	1	100	0.000
	5	100	0.011
	10	100	0.001
	Saturated	100	0.001
Mercuric cyanide	Saturated	Room	nil
Mercury	100	Up to 38	Satisfactory
	100	Room	nil
	...	371	3.03
Methyl alcohol	91	35	nil
	95	100	<0.01
Mercury + iron	...	371	0.079
Mercury + copper	...	371	0.063
Mercury + zirconium	...	371	0.033
Mercury + magnesium	...	371	0.083
Monochloroacetic acid	30	80	0.02
	100	Boiling	0.013
Nickel chloride	5	100	0.004
	20	100	0.003
Nickel nitrate	50	Room	nil
Nitric acid, aerated	10	Room	0.005
	30	Room	0.004
	40	Room	0.002
	50	Room	0.002
	60	Room	0.001
	70	Room	0.005
	10	40	0.003
	20	40	0.005
	30	50	0.015
	40	50	0.016
	50	60	0.037
	60	60	0.040
	70	70	0.040
	40	200	0.610
	70	270	1.22
	20	290	0.305
Nitric acid	35	80	0.051–0.102
	70	80	0.025–0.076
	17	Boiling	0.076–0.102
	35	Boiling	0.127–0.508
	70	Boiling	0.064–0.900
Nitric acid, not refreshed	5–60	35	0.002–0.007
	5–60	60	0.01–0.02
	30–50	100	0.10–0.18
	5–20	100	0.02
	30–60	190	1.5–2.8
	70	270	1.2
	20	290	0.4
	70	290	1.1
Nitric acid, white fuming	Liquid or vapor	Room	nil
	...	82	0.152
	...	122	<0.127
	...	160	<0.127
Nitric acid, red fuming	<Approx. 2% H_2O	Room	Ignition sensitive
	>Approx. 2% H_2O	Room	Not ignition sensitive
Nitric acid	40	Boiling	0.63
+0.01% $K_2Cr_2O_7$	40	Boiling	0.01
+0.01% CrO_3	40	Boiling	0.01
+0.01% $FeCl_3$	40	Boiling	0.68
+1% $FeCl_3$	40	Boiling	0.14
+1% $NaClO_3$	40	Boiling	0.31
+1% $NaClO_3$	40	Boiling	0.02
+1% $Ce(SO_4)_2$	40	Boiling	0.10
+0.1% $K_2Cr_2O_7$	40	Boiling	0.016
Nitric acid, saturated with zirconyl nitrate	33–45	118	nil
Nitric acid + 15% zirconyl nitrate	65	127	nil
Nitric acid + 179 g/L $NaNO_3$ and 32 g/L NaCl	20.8	Boiling	0.127–0.295
Nitric acid + 170 g/L $NaNO_3$ and 2.9 g/L NaCl	27.4	Boiling	0.483–2.92
Oxalic acid	1	35	0.03
	5	35	0.13
	1	Boiling	107
	25	60	11.9
	Saturated	Room	0.508
Perchloroethylene + 50% H_2O	50	25	nil
Perchloryl fluoride + liquid ClO_3	100	30	0.002
Perchloryl fluoride + 1% H_2O	99	30	Liquid 0.290
	...	...	Vapor 0.003
Phenol	Saturated solution	25	0.102
Phosphoric acid	10–30	Room	0.020–0.051
	30–80	Room	0.051–0.762
	5.0	66	0.005
	6.0	66	0.117

(continued)

Table 36 (continued)

Medium	Concentration, wt%	Temperature, °C	Corrosion rate, mm/yr
Phosphoric acid (continued)	0.5	Boiling	0.094
	1.0	Boiling	0.266
	12	25	0.005
	20	25	0.076
	50	25	0.19
	9	52	0.03
	10	52	0.38
	5	Boiling	3.5
	10	80	1.83
Phosphoric acid + 3% nitric acid	81	88	0.381
Phosphorus oxychloride	100	Room	0.004
Phosphorus trichloride	Saturated	Room	nil
Photographic emulsions	...	...	<0.127
Phthalic acid	Saturated	Room	nil
Potassium bromide	Saturated	Room	nil
Potassium chloride	Saturated	Room	nil
	Saturated	60	nil
Potassium dichromate	Saturated	Room	nil
Potassium ethyl xanthate	10	Room	nil
Potassium ferricyanide	Saturated	Room	nil
Potassium hydroxide + 13% potassium chloride	13	29	nil
Potassium hydroxide	50	29	0.010
	10	Boiling	<0.127
	25	Boiling	0.305
	50	Boiling	2.74
	50 anhydrous	241–377	1.02–1.52
Potassium iodide	Saturated	Room	nil
Potassium permanganate	Saturated	Room	nil
Potassium perchlorate	20	Room	0.003
	0–30	50	0.003
Potassium sulfate	10	Room	nil
Potassium thiosulfate	1	Room	nil
Propionic acid	Vapor	190	Rapid attack
Pyrogallic acid	355 g/L	Room	nil
Salicylic acid	Saturated	Room	nil
Seawater	...	24	nil
Seawater, 4.5 year test	...	Ambient	nil
Sebacic acid	...	240	0.008
Silver nitrate	50	Room	nil
Sodium	100	To 1100 (593)	Good
Sodium acetate	Saturated	Room	nil
Sodium aluminate	25	Boiling	0.091
Sodium bifluoride	Saturated	Room	Rapid
Sodium bisulfate	Saturated	Room	nil
	10	66	1.83
Sodium bisulfite	10	Boiling	nil
	25	Boiling	nil
Sodium bromide	0–saturated	≤100	<0.005
Sodium carbonate	25	Boiling	nil
Sodium chlorate	Saturated	Room	nil
Sodium chlorate + 80–250 g/L NaCl	0–721 g/L	40	0.003
Sodium chloride	Saturated	Room	nil
Sodium chloride, pH 7	23	Boiling	nil
Sodium chloride, pH 1.5	23	Boiling	nil
Sodium chloride, pH 1.2	23	Boiling	0.71
Sodium chloride, pH 1.2, some dissolved chlorine	23	Boiling	nil
Sodium citrate	Saturated	Room	nil
Sodium cyanide	Saturated	Room	nil
Sodium dichromate	Saturated	Room	nil
Sodium fluoride	Saturated	Room	0.008
Sodium fluoride, pH 7	1	Boiling	0.001
Sodium fluoride, pH 10	1	Boiling	0.001
Sodium fluoride, pH 7	1	204	0.000
Sodium hydrosulfide + sodium sulfide and polysulfides	5–12	110	<0.003
Sodium hydroxide	5–10	21	0.001
	10	Boiling	0.021
	28	Room	0.003
	40	80	0.127
	50	57	0.013
	50	Boiling	0.051
	73	129	0.178
	50–73	188	>1.09
	50	38	0.023
Sodium hypochlorite	6	Room	nil
Sodium hypochlorite + 15% NaCl + 1% NaOH	1.5–4	66–93	0.030
Sodium nitrate	Saturated	Room	nil
Sodium perchlorate	900 g/L	50	0.003
Sodium phosphate	Saturated	Room	nil
Sodium silicate	25	Boiling	nil
Sodium sulfate	10–20	Boiling	nil
	Saturated	Room	nil
Sodium sulfide	10	Boiling	0.027
	Saturated	Room	nil
Sodium sulfite	Saturated	Boiling	nil
Sodium thiosulfate	25	Boiling	nil
Sodium thiosulfate + 20% acetic acid	20	Room	nil
Soils, corrosive	...	Ambient	nil
Stannic chloride	5	100	0.003
	24	Boiling	0.045
Stannic chloride, molten	100	66	nil
Stannic chloride	100	35	nil
	Saturated	Room	nil
Steam + air	...	82	nil
Steam + 7.65% hydrogen sulfide	...	93–110	nil
Stearic acid, molten	100	180	0.003
Succinic acid	100	185	nil
	Saturated	Room	nil
Sulfanilic acid	Saturated	Room	nil
Sulfamic acid	3.75 g/L	Boiling	nil
	7.5 g/L	Boiling	2.74
	10%	25	nil
Sulfamic acid + 0.375 g/L $FeCl_3$	7.5 g/L	Boiling	0.030
Sulfur, molten	100	240	nil
Sulfur monochloride	...	202	>1.09
Sulfur dioxide, dry	...	21	nil
Sulfur dioxide, water saturated	Near 100	Room	0.003
Sulfur dioxide gas + small amount SO_3 and approximately 3% O_2	18	316	0.006
Sulfuric acid, aerated	1	60	0.008
	3	60	0.013
	5	60	4.83
	10	35	1.27
	40	35	8.64
	75	35	1.07
	75	Room	10.8
	1	100	0.005
	3	100	23.4
	Concentrated	Room	1.57
	Concentrated	Boiling	5.38
	1	100	7.16
	3	100	21.1
Sulfuric acid	1	Boiling	17.8
	5	Boiling	25.4
Sulfuric acid + 4 g/L $NaClO_3$ + 5 g/L NaCl	30	49	0.013
Sulfuric acid + 2 *M* $NaClO_3$ + Na_2SO_4 (saturated)	9 *N*	80–90	0.013
Sulfuric acid + 0.25% $CuSO_4$	5	95	nil
	30	38	0.061
	30	95	0.088
Sulfuric acid + 0.5% $CuSO_4$	30	38	0.067
	30	95	0.823
Sulfuric acid + 1.0% $CuSO_4$	30	38	0.020
	30	95	0.884
Sulfuric acid + 1.0% $CuSO_4$	30	Boiling	1.65
Sulfuric acid + 5% Cu^{2+} + 0.1% Fe^{3+}	18	54	0.020
Sulfuric acid + 6% $CuSO_4$	20	63	0.050
	20	79	0.119
	30	63	0.061
	30	82	0.315
Sulfuric acid + 0.5% CrO_3	5	95	nil
	30	95	nil
Sulfuric acid + 5% CrO_3	30	Boiling	0.018
Sulfuric acid vapors	96	38	nil
	96	66	nil
	96	200–300	0.013
Sulfuric acid + 10% HNO_3	90	Room	0.457

(continued)

Table 36 (continued)

Medium	Concentration, wt%	Temperature, °C	Corrosion rate, mm/yr
Sulfuric acid + 50% HNO_3	50	Room	0.635
Sulfuric acid + 70% HNO_3	30	Room	0.102
Sulfuric acid + 90% HNO_3	10	Room	nil
Sulfuric acid + 90% HNO_3	10	60	0.011
Sulfuric acid + 95% HNO_3	5	60	0.005
Sulfuric acid + 50% HNO_3	50	60	0.399
Sulfuric acid + 20% HNO_3	80	60	1.59
Sulfuric acid saturated with chlorine	45	24	0.003
	62	16	0.002
	5, 10	190	<0.025
	82	50	>1.19
Sulfuric acid + 4 g/L Ti^{4+}	40	100	nil
Sulfuric acid + titanic sulfate (saturated)	20–26	50–100	0.152
Sulfurous acid	6	Room	nil
Tannic acid	25	100	nil
Tartaric acid	10–50	100	<0.127
	10	60	0.003
	25	60	0.003
	50	60	0.001
	10	100	0.003
	25	100	nil
	50	100	0.0121
Terephthalic acid	77	218	nil
Tetrachloroethane, liquid and vapor	100	Boiling	0.001
Tetrachloroethylene + H_2O	...	Boiling	0.127
Tetrachloroethylene	100	Boiling	nil
Tetrachloroethylene, liquid and vapor	100	Boiling	0.001
Titanium tetrachloride	99.8	300	1.57
Trichloroacetic acid	100	Boiling	14.6
Trichloroethylene	99	Boiling	0.003–0.127
Trichloroethylene + 50% H_2O	50	25	0.001
Uranium chloride	Saturated	21–90	nil
Uranyl ammonium phosphate filtrate + 25% chloride + 0.5% fluoride + 1.4% ammonia + 2.4% uranium	20.9	165	<0.003
Uranyl nitrate containing 25.3 g/L Fe^{3+}, 6.9 g/L Cr^{3+}, 2.8 g/L Ni^{2+}, 4.0 *M* HNO_3 + 1.0 *M* Cl	120 g/L	Boiling	nil
Uranyl sulfate + 3.1 *M* Li_2SO_4 + 100–200 ppm O_2	3.1 *M*	250	<0.020
Uranyl sulfate + 3.6 *M* Li_2SO_4, 50 psi oxygen	3.8 *M*	350	0.006–0.432
Urea + 32% ammonia + 20.5% H_2O, 19% CO_2	28	182	0.079
Water, degassed	...	316	nil
Water, river, saturated with chlorine	...	93	nil
X-ray developer solution	...	Room	nil
Zinc chloride	5	Boiling	nil
	20	104	nil
	50, 75	150	nil
	75	150	0.06
	75	200	Rapid pitting
	80	173	2.1
Zinc sulfate	Saturated	Room	nil

Appendix 2: General Corrosion Data for Titanium Alloys

Table 37 is a compilation of general (i.e., uniform) corrosion rate values for commercial titanium alloys other than the unalloyed grades (see Appendix 1 for unalloyed titanium data). These values were derived from various published sources cited in the references and from unpublished laboratory tests. These data should be used only as a preliminary guideline for alloy performance. Rates may vary depending on changes in solution chemistry, temperature, ratio of metal surface to solution volume, solution replenishment rate, flow velocity, exposure time, and other factors. Total alloy suitability cannot be assumed from these values alone, because other forms of corrosion, such as localized attack, stress corrosion, or hydrogen embrittlement, may be limiting. The text should be consulted to assess overall alloy suitability more thoroughly for a given set of environmental conditions. In complex, variable, and/or dynamic environments, in situ testing may provide more reliable data. In the following table, solution constituent concentrations are in weight percent, temperatures are given in degrees centigrade, and corrosion rates are reported only in millimeters per year (mm/yr). Unless otherwise stated, it should be assumed that solutions were tested in the naturally aerated condition.

Table 37 General corrosion rates for commercial titanium

Medium	Alloy	Concentration, wt%	Temperature, °C	Corrosion rate, mm/yr
Acetic acid	Grade 12	99.7	204	nil
	Grade 9	99.7	Boiling	nil
Acetic acid, deaerated	Grade 28	10	204	0.000
Acetic acid + 5% formic acid	Grade 12	58	Boiling	nil
Acetic acid + 10% formic acid, deaerated	Grade 28	10	204	0.000
Acetic acid + 5% NaCl, deaerated	Grade 28	10	204	0.000
Acetic acid + 0.5% HBr	Grade 7	85	200	<0.01
	Grade 26	85	200	<0.01
	Grade 16	85	200	<0.01
Acetic acid + 1.5% acetic anhydride	Grade 7	Glacial	204	0.051
	Grade 12	Glacial	204	0.203
Acetic acid + 3.0% acetic anhydride	Grade 7	Glacial	204	1.52
	Grade 12	Glacial	204	12.7
Acetic anhydride	Grade 7	100	149	0.015
	Grade 12	100	149	0.003
Ammonium hydroxide	Grade 12	30	Boiling	nil
Aluminum chloride	Grade 12	10	Boiling	nil
	Grade 7	10	100	<0.025
	Grade 7	25	100	0.025
Aluminum chloride + 3.6% HCl + 0.7% HNO_3 + 0.3% H_3PO_4	Grade 7	8	Boiling	0.005
Ammonium chloride	Grade 12	10	Boiling	nil
Ammonium hydroxide	Grade 9	8, 28	150	nil
Aqua regia	Grade 7	3:1	Boiling	1.18
	Grade 9	3:1	Boiling	2.11
	Grade 12	3:1	Boiling	4.61
	Grade 16	3:1	Boiling	1.40
	Grade 9	3:1	Boiling	1.29
	Grade 9	3:1	25	0.015
Aqua regia + 0.2% $FeCl_3$	Grade 7	3:1	Boiling	0.650
	Grade 9	3:1	Boiling	2.06
	Grade 12	3:1	Boiling	2.94
	Grade 16	3:1	Boiling	0.782
Aqua regia + 0.02% $FeCl_3$	Grade 7	3:1	Boiling	0.96
	Grade 7	3:1	79	0.206
	Grade 9	3:1	Boiling	1.37
	Grade 9	3:1	79	0.485
	Grade 12	3:1	Boiling	4.37
Boric acid	Grade 12	18	Boiling	0.000
	Grade 26	18	Boiling	0.002

(continued)

Table 37 (continued)

Medium	Alloy	Concentration, wt%	Temperature, °C	Corrosion rate, mm/yr
Calcium chloride	Grade 7	62	150	nil
	Grade 7	73	177	nil
Chlorine, wet	Grade 7	. . .	25	nil
Chromic acid	Grade 7	10	Boiling	nil
	Grade 9	10	Boiling	0.008
	Grade 9	30	Boiling	0.053
	Grade 9	50	Boiling	0.26
Citric acid	Grade 7	50	Boiling	0.025
	Grade 12	50	Boiling	0.013
	Grade 9	50	Boiling	0.38
Ferric chloride	Grade 7	10	Boiling	nil
	Grade 12	10	Boiling	nil
	Ti-5Ta	10	Boiling	nil
	Grade 7	30	Boiling	nil
	Ti-6-4	10	Boiling	nil
	Ti-3-8-6-4-4	10	Boiling	nil
	Ti-10-2-3	10	Boiling	nil
	Ti-6-2-4-6	10	Boiling	0.06
	Ti-550	10	Boiling	nil
	Grade 9	10	Boiling	nil
	Ti-6-2-1-0.8	10	Boiling	nil
Formic acid, nitrogen-sparged	Grade 9	25	35	<0.13
Formic acid	Grade 9	25	88	<0.13
	Grade 9	10	Boiling	3.32
	Grade 9	50	Boiling	7.1
	Grade 18	10	Boiling	0.00
	Grade 18	50	Boiling	3.38
	Grade 16	10	Boiling	<0.003
	Grade 16	20	Boiling	0.008
	Grade 16	50	Boiling	0.01
	Grade 12	45, 50	Boiling	nil
	Grade 7	10	Boiling	<0.003
	Grade 7	20	Boiling	0.008
	Grade 7	50	Boiling	0.01
	Grade 7	45	Boiling	nil
	Grade 26	10	Boiling	<0.003
	Grade 26	20	Boiling	0.008
	Grade 13	20	Boiling	0.016
	Grade 30	20	Boiling	0.016
	Grade 33	20	Boiling	0.010
	Ti-6-4	10	Boiling	3.53
	Ti-6-4	50	Boiling	8.0
	Ti-6-2-4-6	50	Boiling	0.62
	Ti-3-8-6-4-4	50	Boiling	0.98
	Ti-5Ta	50	Boiling	3.16
	Ti-550	50	Boiling	0.02
	Grade 12	90	Boiling	0.56
	Grade 7	90	Boiling	0.056
Formic acid, deaerated	Grade 28	10	204	0.000
Hydrochloric acid	Ti-15-3-3-3	0.5	Boiling	1.35
	Ti-15-3-3-3	1.0	Boiling	4.75
	Ti-550	0.5	Boiling	0.056
	Ti-550	1.0	Boiling	0.64
	Beta-21S	1.0	Boiling	0.00
	Beta-21S	1.5	Boiling	0.00
	Beta-21S	2.0	Boiling	0.46
	Beta-21S	3.0	Boiling	2.03
	Ti-6-2-4-6	0.5	Boiling	nil
	Ti-6-2-4-6	1.0	Boiling	0.03
	Ti-6-2-4-6	1.5	Boiling	0.26
Hydrochloric acid, aerated	Ti-6-2-4-6	pH 1	Boiling	0.01
Hydrochloric acid	Ti-10-2-3	0.5	Boiling	1.10
	Ti-10-2-3	1.0	Boiling	2.66
	Ti-3-8-6-4-4 (solution treated and aged, or STA)	0.5	Boiling	0.003
	Ti-3-8-6-4-4 (STA)	1.0	Boiling	0.10
	Ti-3-8-6-4-4 (STA)	1.5	Boiling	0.86
	Ti-3-8-6-4-4 (STA)	2.0	Boiling	3.43
	Grade 20 (STA)	1.0	Boiling	0.00
	Grade 20 (STA)	2.0	Boiling	0.10
	Grade 20 (STA)	3.0	Boiling	0.30
Hydrochloric acid, aerated	Ti-3-8-6-4-4	pH 1	Boiling	nil
Hydrochloric acid	Ti-45Nb	0.5	Boiling	0.00
	Ti-45Nb	1.0	Boiling	0.007
	Ti-45Nb	2.0	Boiling	0.013
	Ti-45Nb	3.0	Boiling	0.023
	Ti-5Ta	0.5	Boiling	0.013
	Ti-5Ta	1.5	Boiling	2.10
	Ti-6-4	0.25	Boiling	0.37
	Ti-6-4	0.50	Boiling	1.02
	Ti-6-4	1.0	Boiling	2.80
Hydrochloric acid, aerated	Ti-6-4	pH 1	Boiling	0.60
Hydrochloric acid	Grade 9	0.5	Boiling	0.98
	Grade 9	1.0	Boiling	2.60
	Grade 9	1.5	Boiling	5.13
	Grade 9	1	88	0.009
	Grade 9	3	88	3.10
Hydrochloric acid, deaerated	Grade 7	2	82	0.013
	Grade 7	3	82	0.013
	Grade 7	5	82	0.051
	Grade 7	10	82	0.419
Hydrochloric acid	Grade 9	1	Boiling	2.79
Hydrochloric acid, aerated	Grade 9	5	35	0.001
Hydrochloric acid, nitrogen saturated	Grade 9	5	35	0.185
Hydrochloric acid	Ti-6-2-1-0.8	0.5	Boiling	0.020
	Ti-6-2-1-0.8	1.0	Boiling	1.07
	Grade 29	0.50	Boiling	0.03
	Grade 29	1.0	Boiling	0.08
	Grade 29	1.5	Boiling	0.13
	Grade 29	2.0	Boiling	0.22
	Grade 29	3.0	Boiling	0.41
	Ti-15-5-3	1.0	Boiling	0.00
	Ti-15-5-3	2.0	Boiling	0.08
	Ti-15-5-3	2.5	Boiling	0.33
	Grade 7	0.5	Boiling	nil
	Grade 7	1.0	Boiling	0.008
	Grade 7	1.5	Boiling	0.03
	Grade 7	5.0	Boiling	0.23
	Grade 12	0.5	Boiling	nil
	Grade 12	1.0	Boiling	0.04
	Grade 12	1.5	Boiling	0.25
	Grade 28	0.5	Boiling	0.002
	Grade 28	1.0	Boiling	0.026
	Grade 28	1.5	Boiling	0.060
	Grade 28	2.0	Boiling	0.106
	Grade 28	3.0	Boiling	0.193
	Grade 28	4.0	Boiling	0.340
Hydrochloric acid, hydrogen saturated	Grade 7	1–15	25	<0.025
	Grade 7	20	25	0.102
	Grade 7	5	70	0.076
	Grade 7	10	70	0.178
	Grade 7	15	70	0.33
	Grade 7	3	190	0.025
	Grade 7	5	190	0.102
	Grade 7	10	190	8.9
Hydrochloric acid, oxygen saturated	Grade 7	3, 5	190	0.127
	Grade 7	10	190	9.3
Hydrochloric acid, chlorine saturated	Grade 7	3, 5	190	<0.03
	Grade 7	10	190	29.0
Hydrochloric acid, aerated	Grade 7	1, 5	70	<0.03
	Grade 7	10	70	0.05
	Grade 7	15	70	0.15
Hydrochloric acid + 4% $FeCl_3$ + 4% $MgCl_2$	Grade 7	19	82	0.49
Hydrochloric acid + 4% $FeCl_3$ + 4% $MgCl_2$, chlorine saturated	Grade 7	19	82	0.46
Hydrochloric + 14.4% $MgCl_2$ + 7.7% NaCl + 6.5% $MgSO_4$	Grade 7	7.4	65	1.47
	Grade 16	7.4	65	3.27
	Grade 26	7.4	65	7.28
Hydrochloric acid + 0.10% $FeCl_3$	Grade 7	19	71	0.135
+ 0.10% $FeCl_3$	Grade 16	19	71	0.107
+ 0.10% $FeCl_3$	Grade 26	19	71	0.119
+ 5 g/L $FeCl_3$	Grade 7	10	Boiling	0.279

(continued)

Table 37 (continued)

Medium	Alloy	Concentration, wt%	Temperature, °C	Corrosion rate, mm/yr
Hydrochloric acid (continued)				
+16 g/L $FeCl_3$	Grade 7	10	Boiling	0.076
+16 g/L $CuCl_2$	Grade 7	10	Boiling	0.127
+ 2 g/L $FeCl_3$	Grade 12	4.2	91	0.058
+ 0.2% $FeCl_3$	Grade 9	1	Boiling	0.005
+ 0.2% $FeCl_3$	Grade 9	5	Boiling	0.033
+ 0.2% $FeCl_3$	Grade 9	10	Boiling	0.305
+ 0.1% $FeCl_3$	Grade 9	5	Boiling	0.008
+ 0.1% $FeCl_3$	Ti-550	5	Boiling	0.393
+ 0.1% $FeCl_3$	Ti-6-2-4-6	5	Boiling	0.068
+ 0.1% $FeCl_3$	Ti-10-2-3	5	Boiling	0.008
+ 0.1% $FeCl_3$	Grade 28	8.5	Boiling	0.139
+ 0.1% $FeCl_3$	Ti-3-8-6-4-4	5	Boiling	0.018
+ 0.1% $FeCl_3$	Ti-5Ta	5	Boiling	0.020
+ 0.1% $FeCl_3$	Ti-6-4	5	Boiling	0.015
+ 0.25 g/L Fe^{3+}	Grade 7	20	Boiling	6.2–22.0
+ 0.50 g/L Fe^{3+}	Grade 7	20	Boiling	1.9
+ 0.1% $FeCl_3$	Ti-6-2-1-0.8	5	Boiling	0.051
+ 0.1% $FeCl_3$	Grade 7	5	Boiling	0.013
+ 0.1% $FeCl_3$	Grade 12	5	Boiling	0.020
+1.0% $FeCl_3$	Grade 28	7.5	Boiling	0.013
+1.0% $FeCl_3$	Grade 28	9.0	Boiling	0.061
Hydrochloric acid + 10% H_2SO_4 + 0.3% Cu^{2+}	Grade 7	10	93	1.14
Hydrochloric acid + 18% H_3PO_4 + 5% HNO_3	Grade 7	18	77	nil
Hydrochloric acid + 63.6% KNO_3	Grade 7	7.7	90	0.087
Hydrochloric acid + 0.1% Na_2MoO_4	Grade 28	10	Boiling	0.025
Hydrochloric acid + 0.1% Na_2MoO_4	Grade 28	15	Boiling	33.6
Hydrochloric acid +1% Na_2MoO_4	Grade 28	10	Boiling	0.000
Hydrochloric acid +1% Na_2MoO_4	Grade 28	15	Boiling	0.236
Hydrochloric acid + 0.5% Ti^{4+}	Grade 28	10	Boiling	0.000
Hydrochloric acid + 0.5% Ti^{4+}	Grade 28	15	Boiling	0.000
Hydrochloric acid +1% $KSbO_3 \cdot 3H_2O$	Grade 28	10	Boiling	0.000
Hydrochloric acid +1% $KSbO_3 \cdot 3H_2O$	Grade 28	15	Boiling	0.523
Hydrofluoric acid + 0.25% Ti^{3+}	Ti-6-4	5.0	30–35	6,350
Hydrofluoric acid + 0.50% Ti^{3+}	Ti-6-4	5.0	30–35	2,030
Hydrofluoric acid +1.00% Ti^{3+}	Ti-6-4	5.0	30–35	1,270
Hydrofluoric acid +12% HNO_3	Ti-6-4	3.0	60	19,040
Hydrofluoric acid +12% HNO_3	Grade 29	3.0	49	7,340
Hydrofluoric acid + 8% HNO_3	Grade 29	3.0	49	7,340
Hydrofluoric acid + 35% HNO_3	Grade 29	5.0	49	1,670
Hydrogen peroxide, pH 1	Grade 7	5	23	0.062
Hydrogen peroxide, pH 4	Grade 7	5	23	0.010
Hydrogen peroxide, pH 1	Grade 7	5	66	0.127
Hydrogen peroxide, pH 4	Grade 7	5	66	0.046
Hydrogen peroxide + 500 ppm Ca^{2+}, pH 1	Grade 7	5	66	nil
Hydrogen peroxide + 500 ppm Ca^{2+}, pH 1	Grade 7	20	66	0.76
Hydrogen peroxide, pH 1 + 5% NaCl	Grade 7	20	66	0.008
Magnesium chloride	Grade 7	Saturated	Boiling	nil
Methyl alcohol	Grade 9	99	Boiling	nil
Oxalic acid	Grade 7	1	Boiling	1.14
Nitric acid	Grade 9	10	Boiling	0.084
	Grade 9	30	Boiling	0.497
	Grade 28	40	Boiling	0.739
Phosphoric acid	Grade 12	25	25	0.019
	Grade 12	30	25	0.056
	Grade 12	45	25	0.157
	Grade 12	8	52	0.02
	Grade 12	13	52	0.066
	Grade 12	15	52	0.52
	Grade 12	5	66	0.038
	Grade 12	7	66	0.15
	Grade 12	0.5	Boiling	0.071
	Grade 12	1.0	Boiling	0.14
	Grade 7	40	25	0.008
	Grade 7	60	25	0.07
	Grade 7	15	52	0.036
	Grade 7	23	52	0.15
Phosphoric acid (continued)	Grade 7	8	66	0.076
	Grade 7	15	66	0.104
	Grade 7	0.5	Boiling	0.050
	Grade 7	1.0	Boiling	0.107
	Grade 7	5.0	Boiling	0.228
Polymaleic acid	Grade 12	5.0	232	0.007
Potassium hydroxide	Grade 9	50	150	9.21
Seawater	Grade 9	...	Boiling	nil
Sodium chloride, pH 1	Grade 9	Saturated	93	nil
Sodium fluoride, pH 7	Grade 12	1	Boiling	0.001
Sodium fluoride, pH 7	Grade 7	1	Boiling	0.002
Sodium hydroxide	Grade 9	50	150	0.49
Sodium sulfate, pH 1	Grade 7	10	Boiling	nil
Sulfamic acid	Grade 12	10	Boiling	11.6
	Grade 12	10	25	nil
	Grade 7	10	Boiling	0.37
	Grade 7	10	25	nil
Sulfuric acid	Grade 5	pH 1.0	70	2.28
	Grade 12	9	24	0.003
	Grade 12	9.5	24	0.006
	Grade 12	10	24	0.38
	Grade 12	3.5	52	0.013
	Grade 12	3.75	52	1.73
	Grade 12	2.75	66	0.015
	Grade 12	3.0	66	1.65
	Grade 12	0.75	Boiling	0.003
	Grade 12	1.0	Boiling	0.91
	Grade 12	1.0	204	0.91
	Grade 7	1.0	204	0.005
	Grade 7	2.0	204	nil
	Grade 7	3.0	240	0.025
	Grade 7	5.0	240	0.028
	Grade 26	3.0	240	<0.01
	Grade 16	3.0	240	0.00
	Grade 16	5.0	240	0.70
	Grade 18	3.0	240	0.08
	Grade 18	5.0	240	3.01
	Grade 9	0.5	Boiling	8.48
	Grade 28	1.0	Boiling	0.071
	Grade 28	2.0	Boiling	0.327
Sulfuric acid, nitrogen saturated	Grade 7	5	70	0.15
	Grade 7	10	70	0.25
	Grade 7	1, 5	190	0.13
	Grade 7	10	190	1.50
Sulfuric acid, oxygen saturated	Grade 7	1–10	190	0.13
Sulfuric acid, chlorine saturated	Grade 7	10	190	0.051
	Grade 7	20	190	0.38
Sulfuric acid, nitrogen saturated	Grade 7	10	25	0.025
	Grade 7	40	25	0.23
Sulfuric acid, aerated	Grade 9	5	35	0.025
Sulfuric acid, nitrogen saturated	Grade 9	5	35	0.405
Sulfuric acid	Grade 7	2.0	Boiling	0.096
	Grade 7	3.0	Boiling	0.178
	Grade 7	4.0	Boiling	0.330
	Grade 7	6.0	Boiling	0.584
	Ti-3-8-6-4-4	1	Boiling	nil
	Ti-3-8-6-4-4	5	Boiling	1.85
Sulfuric acid, aerated	Grade 7	10	70	0.10
	Grade 7	40	70	0.94
Sulfuric acid + 4 g/L $NaClO_3$ + 5 g/L NaCl	Grade 7	30	49	0.007
Sulfuric acid + 2 *M* $NaClO_3$ + Na_2SO_4 (saturated)	Grade 7	9 *N*	80–90	0.008
	Grade 16	9 *N*	80–90	0.012
Sulfuric acid + 5 g/L $Fe_2(SO_4)_3$	Grade 7	10	Boiling	0.178
Sulfuric acid +16 g/L $Fe_2(SO_4)_3$	Grade 7	10	Boiling	<0.03
Sulfuric acid +16 g/L $Fe_2(SO_4)_3$	Grade 7	20	Boiling	0.15
Sulfuric acid +15% $CuSO_4$	Grade 7	15	Boiling	0.64
Sulfuric acid + 3% $Fe_2(SO_4)_3$	Ti-3-8-6-4-4	50	Boiling	<0.03
Sulfuric acid +1 g/L $FeCl_3$	Ti-3-8-6-4-4	10	Boiling	0.15
Sulfuric acid + 0.1% Fe^{3+}	Grade 28	8.5	Boiling	0.084
Sulfuric acid +1.0% Fe^{3+}	Grade 28	9.75	Boiling	0.042
Sulfuric acid +10 g/L $FeCl_3$	Grade 28	70 g/L	260	0.010
Sulfuric acid + 0.81% $FeCl_3$	Grade 7	25	Boiling	0.75
Sulfuric acid + 50 g/L $FeCl_3$	Ti-3-8-6-4-4	10	Boiling	0.05
Sulfuric acid +1% $CuSO_4$	Grade 7	30	Boiling	1.75

(continued)

Table 37 (continued)

Medium	Alloy	Concentration, wt%	Temperature, °C	Corrosion rate, mm/yr
Sulfuric acid + 6% $CuSO_4$	Grade 7	20	79	0.107
Sulfuric acid + 5% Cu^{2+} + 0.1% Fe^{3+}	Grade 7	18	54	0.020
Sulfuric acid + 100 ppm Cu^{2+} + 1% thiourea (deaerated)	Grade 7	1	100	nil
Sulfuric acid + 100 ppm Cu^{2+} + 1% thiourea (deaerated)	Grade 12	1	100	0.23
Sulfuric acid + 1000 ppm Cl^-	Grade 7	15	49	0.015
Sulfuric acid + 1.8% Cl^-	Grade 7	31 g/L	255–275	0.003
(30% Ni laterite ore slurry)	Grade 12	31 g/L	255–275	0.005
(vapor phase)	Grade 26	31 g/L	255–275	<0.001
Sulfuric acid + 1.8% Cl^-	Grade 7	31 g/L	255–275	0.018
(30% Ni laterite ore slurry)	Grade 12	31 g/L	255–275	0.044
(liquid phase)	Grade 26	31 g/L	255–275	0.008

REFERENCES

1. R.W. Schutz, Titanium, *Process Industries Corrosion—The Theory and Practice,* National Association of Corrosion Engineers, 1986, p 503
2. "Titanium and Its Alloys," Course 27, Metals Engineering Institute, ASM International
3. *Aerospace Structural Metals Handbook,* Mechanical Properties Data Center, U.S. Department of Defense, 1985
4. R. Boyer, G. Welsch, and E. Collings, Ed., *Materials Properties Handbook: Titanium Alloys,* ASM International, 1994
5. *Titanium Alloys Handbook,* MCIC-HB-02, Metals and Ceramics Information Center, Department of Defense Information Analysis Center, Dec 1972
6. N.D. Tomashov and P.M. Altovskii, "Corrosion and Protection of Titanium," Government Scientific-Technical Publication of Machine-Building Literature (Russian translation), 1963
7. K. Shimogori et al., Analysis of Passive Film on Titanium Formed in Dilute HCl Solutions at Elevated Temperatures, *Titanium and Titanium Alloys: Scientific and Technological Aspects,* Vol 2, Plenum Publishing Corp., 1982, p 881–890
8. V.V. Andreeva, Behavior and Nature of Thin Oxide Films on Some Metals in Gaseous Media and in Electrolyte Solutions, *Corrosion,* Vol 20, 1964, p 35–46
9. M. Pourbaix, *Atlas of Electrochemical Equilibria in Aqueous Solutions,* National Association of Corrosion Engineers, 1974, p 217
10. R.W. Schutz, Utilizing Titanium to Successfully Handle Chloride Process Environments, *Can. Min. Metall. Bull.,* Vol 95 (No. 1065), 2002, p 84–88
11. R.W. Schutz, J.S. Grauman, and J.A. Hall, Effect of Solid Solution Iron on the Corrosion Behavior of Titanium, *Titanium—Science and Technology,* Proceedings of the Fifth International Conference on Titanium, Deutsche Gesellschaft für Metallkunde e.V., Oberursel, Germany, 1985, p 2617–2624
12. L.C. Covington and R.W. Schutz, Effects of Iron on the Corrosion Resistance of Titanium, *Industrial Applications of Titanium and Zirconium,* STP 728, American Society for Testing and Materials, 1981, p 163–180
13. R.W. Schutz and J.S. Grauman, Fundamental Corrosion Characterization of High-Strength Titanium Alloys, *Industrial Applications of Titanium and Zirconium: Fourth Volume,* STP 917, American Society for Testing and Materials, 1986, p 130–143
14. J. Newman, Fighting Corrosion with Titanium Castings, *Chem. Eng.,* June 4, 1979
15. R. Baboian, Ed., *Corrosion Tests and Standards: Application and Interpretation,* 2nd ed., ASTM International, Jan 2005, p 598–612
16. R.W. Schutz and L.C. Covington, Guidelines for Corrosion Testing of Titanium, *Industrial Applications of Titanium and Zirconium,* STP 728, American Society for Testing and Materials, 1981, p 59–70
17. S.W. Dean, Jr., Electrochemical Methods of Corrosion Testing, *Electrochemical Techniques for Corrosion,* National Association of Corrosion Engineers, 1977, p 52–60
18. E.L. Liening, Electrochemical Corrosion Testing Techniques, *Process Industries Corrosion,* National Association of Corrosion Engineers, 1986, p 85–122
19. R.W. Schutz, Understanding and Preventing Crevice Corrosion of Titanium Alloys—Part 1, *Mater. Perform.,* Oct 1992, p 57–62
20. R.W. Schutz, Understanding and Preventing Crevice Corrosion of Titanium Alloys—Part II, *Mater. Perform.,* Nov 1992, p 54–56
21. J.C. Griess, Jr., Crevice Corrosion of Titanium in Aqueous Salt Solutions, *Corrosion,* Vol 24 (No. 4), April 1968, p 96–109
22. L.C. Covington, Pitting Corrosion of Titanium Tubes in Hot Concentrated Brine Solutions, *Galvanic and Pitting Corrosion—Field and Laboratory Studies,* STP 576, American Society for Testing and Materials, 1976, p 147–154
23. M. Kobayashi et al., Study on Crevice Corrosion of Titanium, *Titanium '80—Science and Technology,* Vol 4, The Metallurgical Society, 1980, p 2613–2622
24. B.M. Ikeda, R.C. Styles, M.G. Bailey, and D.W. Shoesmith, The Effect of Material Purity on Crevice Corrosion of Titanium in NaCl Solution, *Compatibility of Biomedical Implants Conference Proceedings,* The Electrochemical Society, Inc., May 1994, p 368–380
25. L. Szklarska-Smialowska and M. Janik-Czachor, *Corros. Sci.,* Vol 11, 1971, p 901–914
26. R.W. Schutz and J.S. Grauman, Compositional Effects on Titanium Alloy Repassivation Potential in Chloride Media, *Advances in Localized Corrosion,* Proceedings of the Second International Conference on Localized Corrosion, H.S. Isaacs, U. Bertocci, J. Kruger, and S. Smialowska, Ed., National Association of Corrosion Engineers, 1990, p 335–337
27. J.B. Cotton, *Chem. Eng. Prog.,* Vol 66 (No. 10), 1970, p 57
28. L.C. Covington, "Factors Affecting the Hydrogen Embrittlement of Titanium," Paper 59, Corrosion/75, National Association of Corrosion Engineers, April 1975
29. L.C. Covington, *Corrosion,* Vol 35 (No. 8), Aug 1979, p 378–382
30. V.A. Livanov et al., "Hydrogen in Titanium," Israel Program for Scientific Translation Ltd., Catalog 2163, Daniel Davey and Company, Inc., 1965
31. N.E. Paton and J.C. Williams, Effect of Hydrogen on Titanium and Its Alloys, *Titanium and Titanium Alloys—Source Book,* American Society for Metals, 1982, p 185–207
32. R.R. Boyer and W.F. Spurr, Characteristics of Sustained-Load Cracking and Hydrogen Effects in Ti-6Al-4V, *Metall. Trans. A,* Vol 9, Jan 1978, p 23–29
33. R. Bourcier and D. Koss, *Acta Metall.,* Vol 32 (No. 11), 1984, p 2091–2099
34. G.A. Lenning et al., Effect of Hydrogen on Alpha Titanium Alloys, *Trans. AIME,* Oct 1956, p 1235
35. C.M. Craighead et al., Hydrogen Embrittlement of Beta-Stabilized Titanium Alloys, *Trans. AIME,* Aug 1956, p 923
36. D.A. Meyn, Effect of Hydrogen on Fracture and Inert-Environment Sustained Load Cracking Resistance of Alpha-Beta Titanium Alloys, *Metall. Trans.,* Vol 5, Nov 1974, p 2405

37. G.R. Yoder, C.A. Griffis, and T.W. Crooker, "Sustained-Load Cracking of Titanium—A Survey of 6Al-4V Alloys," NRL Report 7596, Naval Research Laboratory, Washington, D.C., Aug 24, 1973
38. R.W. Schutz, Environmental Behavior of Beta Titanium Alloys, *JOM,* July 1994, p 24–29
39. R.W. Schutz, Developments in Titanium Alloy Environmental Behavior, *Proc. Eighth World Conf. on Titanium, Titanium '95—Science and Technology,* Institute of Materials, 1996, p 1860–1870
40. W.R. Holman et al., Hydrogen Diffusion in a Beta Titanium Alloy, *Trans. AIME,* Vol 233, Oct 1965, p 1836
41. I.I. Phillips, P. Pool, and L.L. Shreir, Hydride Formation During Cathodic Polarization of Ti.-II. Effect of Temperature and pH of Solution on Hydride Growth, *Corros. Sci.,* Vol 14, 1974, p 533–542
42. R.L. Jacobs and J.A. McMaster, Titanium Tubing: Economical Solution to Heat Exchanger Corrosion, *Mater. Prot. Perform.,* Vol 11 (No. 7), July 1972, p 33–38
43. "Get More Advantages by Applying Titanium Tubing not Only for Power Plants but also for Desalination Plants!!," Technical Brochure, Japan Titanium Society, May 1984
44. H. Satoh, T. Fukuzuka, K. Shimogori, and H. Tanabe, "Hydrogen Pickup by Titanium Held Cathodic in Seawater," Second International Congress on Hydrogen in Metals (Paris), June 1977
45. S. Sato, K. Nagata, and M. Nagayama, "Experiences of Welded Titanium Condenser Tubes in Japan," Technical Research Laboratory, Sumitomo Light Metal Industries Ltd.
46. T. Fukuzuka, K. Shimogori, H. Satoh, and F. Kamikubo, "Corrosion Problems and Countermeasures in MSF Desalination Plant Using Titanium Tube," Kobe Steel Ltd., 1985
47. P.O. Gartland, F. Bjørnas, and R.W. Schutz, "Prevention of Hydrogen Damage of Offshore Titanium Alloy Components by Cathodic Protection Systems," Paper 477, Corrosion/97, National Association of Corrosion Engineers, 1997
48. G.Venkataraman and A.D. Goolsby, "Hydrogen Embrittlement in Titanium Alloys from Cathodic Polarization in Offshore Environments, and its Mitigation," Paper 554, Corrosion/96, National Association of Corrosion Engineers, 1996
49. J.P. Fulford, R.W. Schutz, and R.C. Lisenbey, "Characterization of Titanium Condenser Tube Hydriding at Two Florida Power and Light Company Plants," Paper 87-JPGC-Pwr-F, Joint ASME/IEEE Power Generation Conference, Oct 4–8, 1987, American Society of Mechanical Engineers
50. L.A. Charlot and R.E. Westerman, Low-Temperature Hydriding of Zircaloy-2 and Titanium in Aqueous Solutions, *Electrochem. Technol.,* Vol 6 (No. 3–4), March/April 1968
51. J. Lee and P. Chung, "A Study of Hydriding of Titanium in Seawater Under Cathodic Polarization," Paper 259, Corrosion/86, National Association of Corrosion Engineers, March 1986
52. R.W. Schutz and L.C. Covington, *Corrosion,* Vol 37 (No. 10), Oct 1981, p 585–591
53. B.R. Brown, "Stress Corrosion Cracking in High Strength Steels and in Titanium and Aluminum Alloys," Naval Research Laboratory, 1972
54. I.R. Lane, Jr., J.L. Cavallaro, and A.G.S. Morton, *Stress Corrosion Cracking of Titanium,* STP 397, American Society for Testing and Materials, 1966
55. R.W. Schutz, Stress-Corrosion Cracking of Titanium Alloys, *Stress-Corrosion Cracking,* R.H. Jones, Ed., ASM International, 1992, p 265–297
56. T.R. Beck, Electrochemical Aspects of Titanium Stress-Corrosion Cracking, *Proceedings of Conference—Fundamental Aspects of Stress-Corrosion Cracking,* National Association of Corrosion Engineers, 1969, p 605
57. T.R. Beck and E.A. Grens, An Electrochemical Mass-Transport-Kinetic Model for Stress-Corrosion Cracking of Titanium, *J. Electrochem. Soc.,* Vol 116 (No. 2), 1969, p 117
58. D.T. Powell and J.C. Scully, Stress-Corrosion Cracking of Alpha Titanium Alloys at Room Temperature, *Corrosion,* Vol 24 (No. 6), 1968, p 151
59. G. Sanderson, D.T. Powell, and J.C. Scully, The Stress-Corrosion Cracking of Ti Alloys in Aqueous Chloride Solutions at Room Temperature, *Corros. Sci.,* Vol 8, 1968, p 473
60. R.J.H. Wanhill, Aqueous Stress-Corrosion in Titanium Alloys, *Br. Corros. J.,* Vol 10, 1975, p 69
61. R.W. Schutz, M. Xiao, and T.A. Bednarowicz, "Stress Corrosion Behavior of the Ti-3Al-8V-6Cr-4Zr-4Mo Titanium under Deep Sour Gas Well Conditions," Paper 51, Corrosion/92, National Association of Corrosion Engineers, 1992
62. R.W. Schutz, M. Xiao, and J.W. Skogsberg, Stress Cracking and Crevice Corrosion Resistance of Pd-Enhanced Ti-38644 Titanium Alloy Products in Deep Sour Gas Well Environments, *Proc. 12th Int. Corros. Cong.,* Vol 4, 1993, p 2506–2519
63. R.W. Schutz, "Performance of Ruthenium-Enhanced Alpha-Beta Titanium Alloys in Aggressive Sour Gas and Geothermal Well Produced-Fluid Brines," Paper 32, Corrosion/97, National Association of Corrosion Engineers, 1997
64. R.W. Schutz, J.M. Horrigan, and T.A. Bednarowicz, "Stress Corrosion Behavior of Ru-Enhanced Alpha-Beta Titanium Alloys in Methanol Solutions," Paper 261, Corrosion '98, National Association of Corrosion Engineers, 1998
65. N. Gat and W. Tabakoff, Effects of Temperature on the Behavior of Metals Under Erosion by Particulate Matter, *J. Test. Eval.,* Vol 8 (No. 4), 1980, p 177–186
66. B.A.B. McDougall and A. Neville, "Understanding Wear/Corrosion Interactions in Tribo-Corrosion of Titanium and Its Alloys," Paper 03265, Corrosion/2003, National Association of Corrosion Engineers, 2003
67. J.F.G. Condé, Some Naval and Marine Applications of Titanium, *Designing with Titanium,* Proceedings of the International Conference organized by the Metals Technology Committee of The Institute of Metals, in collaboration with Deutsche Gesellschaft für Metallkunde and the Société Française de Métallurgie, 1986, p 205
68. J.B. Cotton and B.P. Downing, Corrosion Resistance of Titanium to Seawater, *Trans. Inst. Marine Eng.,* Vol 69 (No. 8), 1957, p 311
69. R.I. Jaffee, G. Luetjering, and T. Rust, Application of Ti-6Al-4V as Steam Turbine Blading Material, *Titanium '80—Science and Technology,* Proceedings of the Fourth International Conference on Titanium (Kyoto, Japan), Metallurgical Society of AIME, May 1980, p 477–488
70. P.C. Hughes and I.R. Lamborn, Contamination of Titanium by Water Vapour, *J. Inst. Met.,* Vol 89, 1960–1961, p 165
71. C.R. Breden, *Met. Prog.,* Vol 64, 1953, p 194
72. S.C. Datski, Report ANL 5354, U.S. Atomic Energy Commission, 1954
73. D. Schlain, "Corrosion Properties of Titanium," Bulletin 619, U.S. Bureau of Mines, 1964
74. R.L. Kane, The Corrosion of Titanium, *The Corrosion of Light Metals,* The Corrosion Monograph Series, John Wiley & Sons, 1967
75. F.M. Reinhart, "Corrosion of Materials in Hydrospace, Part III, Titanium and Titanium Alloys," Technical Note N-921, U.S. Naval Civil Engineering Laboratory, Sept 1967
76. H.B. Bomberger, P.J. Cambourelis, and G.E. Hutchinson, Corrosion Properties of Titanium in Marine Environments, *J. Electrochem. Soc.,* Vol 101, 1954, p 442
77. W.L. Wheatfall, "Metal Corrosion in Deep-Ocean Environments," Research and Development Phase Report 429/66, U.S. Navy Marine Engineering Laboratory, Jan 1967
78. M.A. Pelensky, J.J. Jawarski, and A. Gallaccio, Air, Soil, and Sea Galvanic Corrosion Investigation at Panama Canal Zone,

Galvanic and Pitting Corrosion—Field and Laboratory Studies, STP 576, American Society for Testing and Materials, 1967, p 94
79. L.C. Covington, W.M. Parris, and D.M. McCue, "The Resistance of Titanium Tubes to Hydrogen Embrittlement in Surface Condensers," Paper 79, Corrosion/79, National Association of Corrosion Engineers, March 1976
80. K.O. Gray, *Mater. Prot.,* Vol 3 (No. 7), 1964, p 46
81. J.A. Beavers et al., Chapter 3, *Corrosion of Metals in Marine Environments,* MCIC-86-50, Metals and Ceramics Information Center, Battelle-Columbus Division, July 1986
82. F.M. Reinhart and J.F. Jenkins, "Corrosion of Alloys in Hydrospace—189 Days at 5,900 Feet," Final Report NCEL-TN-1224, U.S. Naval Civil Engineering Laboratory, April 1972, p 4
83. F.M. Reinhart and J.F. Jenkins, "The Relationship Between the Concentration of Oxygen in Seawater and the Corrosion of Metals," U.S. Naval Civil Engineering Laboratory, 1971, p 562–577
84. L.C. Covington and R.W. Schutz, "Resistance of Titanium to Atmospheric Corrosion," Paper 113, Corrosion/81, National Association of Corrosion Engineers, April 1981
85. B. Sanderson and M. Romanoff, Performance of C.P. Titanium in Corrosive Soils, *Mater. Prot.,* April 1969, p 29–32
86. C.R. Bishop, Corrosion Tests at Elevated Temperatures and Pressures, *Corrosion,* Vol 19, Sept 1963, p 308–314
87. T.F. Degnan, Materials for Handling Hydrofluoric, Nitric and Sulfuric Acids, *Process Industries Corrosion,* National Association of Corrosion Engineers, 1975, p 229
88. E.E. Millaway, Titanium: Its Corrosion Behavior and Passivation, *Mater. Prot. Perform.,* Jan 1965, p 16–21
89. H. Keller and K. Risch, The Corrosion Behavior of Titanium in Nitric Acid at High Temperatures, *Werkst. Korros.,* Vol 9, 1964, p 741–743
90. A. Takamura, K. Arakawa, and Y. Moriguchi, Corrosion Resistance of Titanium and Titanium-5% Tantalum Alloys in Hot Concentrated Nitric Acid, *The Science, Technology and Applications of Titanium,* R.I. Jaffee and N.E. Promisel, Ed., Pergamon Press, 1970, p 209
91. S.H. Weiman, *Corrosion,* Vol 22, April 1966, p 98–106
92. H. Satoh, F. Kamikubo, and K. Shimogori, Effect of Oxidizing Agents on Corrosion Resistance of CP Titanium in Nitric Acid Solution, *Titanium—Science and Technology,* Proceedings of the Fifth International Conference on Titanium, Deutsche Gesellschaft für Metallkunde e.V., Oberursel, Germany, 1985, p 2649–2655
93. M.W. Wilding and B.F. Paige, "Survey on Corrosion of Metals and Alloys in Solutions Containing Nitric Acid," Report ICP-1107, Allied Chemical Corporation, Idaho Chemical Programs, Dec 1976
94. C.E. Stevenson, "Idaho Chemical Processing Plant—Technical Progress Report for January thru March 1958," IDO-14443, Allied Chemical Corporation, Sept 1958
95. R. Villemez and C. Millet, Evaluation of Alloys for Nuclear Waste Evaporators, *Mater. Perform.,* July 1980, p 19–25
96. D.E. Thomas, Titanium Alloy Corrosion Resistance in Nitric Acid Solutions, *Titanium 1986—Products and Applications,* Vol 1, Proceedings of the Technical Program from the 1986 International Conference, Titanium Development Association, 1986
97. L.L. Gilbert and C.W. Funk, Explosions of Titanium and Fuming Nitric Acid Mixtures, *Met. Prog.,* Nov 1956, p 93–96
98. H.B. Bomberger, Titanium Corrosion and Inhibition in Fuming Nitric Acid, *Corrosion,* Vol 13 (No. 5), May 1957, p 287–291
99. R.L. Wallner et al., *Mater. Prot.,* Jan 1965, p 55–56
100. W.K. Boyd, "Stress Corrosion Cracking of Titanium Alloys—An Overview," International Symposium on Stress Corrosion Mechanisms in Titanium Alloys, Georgia Institute of Technology, Jan 1971
101. J.B. Rittenhouse and C.A. Popp, Inhibition of Corrosion in Fuming Nitric Acid, *Corrosion,* Vol 14, June 1958, p 283–284
102. T.M. Sigulovskaya et al., Corrosion-Electrochemical Behavior of Titanium and Its Alloys in Alkaline Solutions of Hydrogen Peroxide, UDC 620.193.01, *Zashch. Met.,* Vol 12 (No. 4), July/Aug 1976, p 363–367
103. L. Clerbois and L. Plumet, Process for Inhibiting the Corrosion of Equipment Made of Titanium, U.S. Patent 4,372,813, 1983
104. R.W. Schutz and M. Xiao, Expanded Windows for Titanium Use in the Pulp/Paper Peroxide Bleach Plant, *J. Test. Eval.,* Vol 24 (No. 2), March 1996, p 119–122
105. J. Been and D. Tromans, Titanium Corrosion in Alkaline Hydrogen Peroxide, *Corrosion,* Vol 56 (No. 8), 2000, p 809–818
106. D.L. Reichert, "Corrosion Behavior in Hydrogen Peroxide Bleaching Solutions," Paper 467, Corrosion/96, National Association of Corrosion Engineers, 1996
107. D.E. Thomas and E.B. Bomberger, The Effect of Chlorides and Fluorides on Titanium Alloys in Simulated Scrubber Environments, *Mater. Perform.,* Nov 1983, p 29–36
108. N.G. Thompson, G.H. Koch, and B.C. Syrett, "Effect of Trace Elements on the Polarization Behavior of Alloys in FGD Environments," Paper 37, Corrosion/85, National Association of Corrosion Engineers, March 1985
109. F. Mansfeld, S.L. Jeanjaquet, M. Kendig, D.O. Raleigh, and K. Fertig, "The Effects of Trace Elements on Corrosion in Total Immersion and in Wet/Dry Conditions," Paper 38, Corrosion/85, National Association of Corrosion Engineers, March 1985
110. D.W. Stough, F.W. Fink, and R.S. Peoples, "The Corrosion of Titanium," Report 57, Titanium Metallurgical Laboratory, Battelle Memorial Institute, 1956
111. J.A. Petit et al., *Corros. Sci.,* Vol 21 (No. 4), 1981, p 279–299
112. V.P. Gupta, Process for Decreasing the Rate of Titanium Corrosion, U.S. Patent 4,321,231, 1982
113. R.W. Schutz and L.C. Covington, Hydrometallurgical Applications of Titanium, *Industrial Applications of Titanium and Zirconium: Third Conference,* STP 830, American Society for Testing and Materials, 1984, p 29–47
114. R.L. Porter and B.J. Saldanha, "Effect of Fe(III) Levels on the Corrosion Resistance of Titanium Alloys in HCl Solutions," Paper 03453, Corrosion/2003, National Association of Corrosion Engineers, 2003
115. J.C. Cotton, *Chem. Eng. Prog.,* Vol 66 (No. 10), 1970, p 57
116. J.B. Cotton, *Chem. Ind.,* Vol 3, Jan 1958, p 68–69
117. R.L. LaQue and H.R. Copson, *Corrosion Resistance of Metals and Alloys,* 2nd ed., ACS Monograph, Reinhold, 1963, p 646–661
118. F.W. Fink and W.K. Boyd, "The Corrosion of Metals in Marine Environments," DMIC Report 245, Defense Materials Information Center, Battelle Memorial Institute, May 1970
119. R.E. Smallwood, Corrosion of Titanium and Zirconium Alloys in Zinc Chloride Solutions, *Industrial Applications of Titanium and Zirconium,* STP 728, American Society for Testing and Materials, 1981, p 147–162
120. R.W. Schutz and J.S. Grauman, "Localized Corrosion Behavior of Titanium Alloys in High Temperature Seawater Service," Paper 162, Corrosion/88, National Association of Corrosion Engineers, 1988
121. R.W. Schutz, "Guidelines for Successful Integration of Titanium Alloy Components into Subsea Production Systems," Paper 01003, Corrosion 2001, National Association of Corrosion Engineers, 2001
122. C.M. Chen, H.B. Kirkpatrick, and H.L. Gegel, "Cracking of Titanium Alloys in Methanolic and Other Media," International Symposium on Stress Corrosion Mechanisms in Titanium Alloys, Georgia Institute of Technology, Jan 1971
123. E.G. Haney and W.R. Wearmouth, Effect of Pure Methanol on the Cracking of

Titanium, *Corrosion,* Vol 25 (No. 2), Feb 1969, p 87
124. A.J. Sedriks and J.S.A. Green, Stress Corrosion of Titanium in Organic Liquids, *J. Met.,* April 1971, p 48
125. B.J. Hanson, Behavior of C.P. Titanium in Hydrogen Sulfide Atmospheres at Elevated Temperatures, *Industrial Applications of Titanium and Zirconium: Third Conference,* STP 830, American Society for Testing and Materials, 1984, p 19–28
126. T. Fukuzuka et al., On the Beneficial Effect of the Titanium Oxide Film Formed by Thermal Oxidation, *Titanium '80—Science and Technology,* Vol 4, The Metallurgical Society, p 2783–2792
127. R. Boyer, G. Welsch, and E. Collings, Ed., *Materials Properties Handbook: Titanium Alloys,* ASM International, 1994, p 501
128. C. Coddet et al., Oxidation of Titanium Base Alloys for Application in Turbines, *Titanium '80—Science and Technology,* Vol 4, The Metallurgical Society, 1980, p 2755–2764
129. D. David et al., A Structural and Analytical Study of Titanium Oxide Thin Films, *Titanium '80—Science and Technology,* Vol 4, The Metallurgical Society, 1980, p 2811–2817
130. T. Moroishi and Y. Shida, Oxidation Behaviour of Titanium in High Temperature Steam, *Titanium '80—Science and Technology,* Proceedings of the Fourth International Conference on Titanium (Kyoto, Japan), The Metallurgical Society, May 1980, p 2773–2782
131. C. Leyens, Oxidation and Protection of Titanium Alloys and Titanium Aluminides, *Titanium and Titanium Alloys,* C. Leyens and M. Peters, Ed., Wiley-VCH Verlag GmbH & Co. KGaA, Weinheim, Germany, 2003, p 187–230
132. J.D. Jackson, W.K. Boyd, and P.D. Miller, "Reactivity of Metals with Liquid and Gaseous Oxygen," DMIC Memorandum 163, Defense Materials Information Center, Battelle Memorial Institute, Jan 1963
133. F.E. Littman, F.M. Church, and E.M. Kinderman, A Study of Metal Ignitions—I. The Spontaneous Ignition of Titanium, *J. Less-Common Met.,* Vol 3, 1961, p 367–378
134. J.D. Jackson et al., Technical Report 60-258, Wright Air Development Center, Battelle Memorial Institute, June 1960
135. P.W. Krag and H.R. Henson, *Materials Selection for Sulfide Pressure Oxidation Autoclaves,* STP 1197, American Society for Testing and Materials, 1993, p 168–180
136. "Standard for the Production, Processing, Handling, and Storage of Titanium," NFPA 481-1982, National Fire Protection Association
137. H.B. Bomberger, *Industrial Applications of Titanium and Zirconium: Third Conference,* STP 830, American Society for Testing and Materials, 1984, p 143–158
138. E.E. Millaway and M.H. Klineman, Factors Affecting Water Content Needed to Passivate Titanium in Chlorine, *Corrosion,* Vol 23 (No. 4), 1972, p 88
139. J.D. Jackson and W.K. Boyd, "Corrosion of Titanium," DMIC Memorandum 218, Defense Materials Information Center, Battelle Memorial Institute, Sept 1966
140. R.W. Schutz and J.S. Grauman, *Mater. Perform.,* Vol 25 (No. 4), April 1986, p 35–42
141. H. Satoh et al., Effect of Gasket Materials on Crevice Corrosion of Titanium, *Titanium—Science and Technology,* Proceedings of the Fifth International Conference of Titanium, Deutsche Gesellschaft für Metallkunde e.V., Oberursel, Germany, 1985, p 2633–2639
142. K. Shimogori and Mitarbeiter, Crevice Corrosion of Titanium in NaCl Solutions in the Temperature Range 100 to 250 °C, *J. Jpn. Inst. Met.,* Vol 44 (No. 6), 1978, p 567–572
143. R.W. Schutz, Performance and Application of Titanium Alloys in Geothermal Brine Service, *Mater. Perform.,* Vol 24 (No. 1), Jan 1985, p 39–47
144. R.W. Schutz, J.A. Hall, and T.L. Wardlaw, "TI-CODE 12, An Improved Industrial Alloy," Japan Titanium Society 30th Anniversary International Symposium, Japan Titanium Society, Aug 1983, p 72–88
145. Y. Shida and S. Kitayama, Effect of Pd Addition on the Crevice Corrosion Resistance of Titanium, *Sixth World Conference on Titanium,* Part IV, P. Lacombe, R. Tricot, and G. Béranger, Ed., 1988, p 1729
146. R.W. Schutz, "Defining the Corrosion Performance Window for Grade 28 Titanium," Paper 455, Corrosion 2003, National Association of Corrosion Engineers, 2003
147. R.W. Schutz, Platinum Group Metal Additions to Titanium: A Highly Effective Strategy for Enhancing Corrosion Resistance, *Corrosion,* Vol 59 (No. 12), 2003, p 1043–1057
148. R.W. Schutz and R.L. Porter, Comparative Corrosion Resistance of Commercial Ru- and Pd-Modified C.P. Titanium Alloys, *Ti 2003—Science and Technology,* Vol IV, Proceedings of the Tenth World Conference on Titanium, Wiley-VCH Verlag GmbH & Co. KGaA, Weinheim, Germany, 2004, p 2099
149. R.W. Schutz, *Platin. Met. Rev.,* Vol 40 (No. 2), 1996, p 54–61
150. J.A. Ruppen, R.S. Glass, and M.A. Molecke, Titanium Utilization in Long-Term Nuclear Waste Storage, *Titanium for Energy and Industrial Applications,* The Metallurgical Society, 1981, p 355–369
151. W.J. Neill, Experience with Titanium Tubing in Oil Refinery Heat Exchangers, *Mater. Perform.,* Sept 1980, p 57–63
152. D.E. Thomas et al., Beta-C: An Emerging Titanium Alloy for the Industrial Marketplace, *Industrial Applications of Titanium and Zirconium: Fourth Volume,* STP 917, American Society for Testing and Materials, 1986, p 144–163
153. R.W. Schutz and M. Xiao, Enhancing Corrosion Resistance of the Ti-38644 Alloy for Industrial Applications, *Titanium '92—Science and Technology,* Vol 3, TMS-AIME, 1993, p 2095
154. R.W. Schutz, R.L. Porter, and J. Horrigan, *Corrosion,* Vol 56 (No. 11), 2000, p 1170–1178
155. H.J. Raetzer-Scheive, *Corrosion,* Vol 34 (No. 12), Dec 1978, p 437–442
156. F.A. Posey and E.G. Bohlmann, *Desalin.,* Vol 3, 1967, p 268
157. J.W. Braithwaite, N.J. Magnani, and J.W. Munford, "Titanium Alloy Corrosion in Nuclear Waste Environments," Paper 213, Corrosion/80, National Association of Corrosion Engineers, 1980
158. T. Koizumi and S. Furuya, *Titanium—Science and Technology,* Vol 4, Proceedings of the Second International Conference, Plenum Press, 1973, p 2383–2393
159. F. Kamikubo, H. Satoh, and K. Shimogori, Corrosion of Titanium and Its Prevention in a Fertilizer Plant, *Titanium—Science and Technology,* Proceedings of the Fifth International Conference on Titanium, Deutsche Gesellschaft für Metallkunde e.V., Oberursel, Germany, 1985, p 1173
160. I. Dugdale and J.B. Cotton, *Corros. Sci.,* Vol 4, 1964, p 397
161. F. Kamikubo et al., Effects of a Small Amount of Impurity Elements on Pitting Potential of C.P. Titanium in Sodium Bromide Solutions, *Metallic Corrosion,* Vol 2, Proceedings of the Eighth International Congress on Metallic Corrosion, Deutsche Gesellschaft für Chemisches Apparatewesen e.V., 1981, p 1378–1383
162. T.R. Beck, *J. Electrochem. Soc.,* Vol 120, 1973, p 1310
163. G.R. Caskey, Jr., The Influence of a Surface Oxide Film on Hydriding of Titanium, *Hydrogen in Metals,* I.M. Bernstein and A.W. Thompson, Ed., Materials/Metalworking Technology Series, American Society for Testing and Materials, 1974, p 465–474
164. E.A. Gulbransen and K.F. Andrew, *Trans. Am. Inst. Mining Met. Engrs.,* Vol 185, 1949, p 174
165. J.B. Cotton and J.G. Hines, Hydriding of Titanium Used in Chemical Plant and Protective Measures, *The Science, Technology and Application of Titanium,* Pergamon Press, 1970, p 150–170
166. M. Seiersten, T.G. Eggen, L. Lunde, and T. Rogne, "Hydrogen Absorption in Cathodically Polarized Titanium Alloys,"

Paper OMAE2002-28580, 21st International Conference on Offshore Mechanics and Arctic Engineering (Oslo, Norway), ASME, 2002
167. Z.A. Foroulis, Factors Influencing Absorption of Hydrogen in Titanium from Aqueous Electrolytic Solutions, *Titanium '80—Science and Technology,* Vol 4, The Metallurgical Society, 1980, p 2705–2711
168. L.C. Covington and N.G. Feige, A Study of Factors Affecting the Hydrogen Uptake Efficiency of Titanium in Sodium Hydroxide Solutions, *Localized Corrosion—Cause of Metal Failure,* STP 516, American Society for Testing and Materials, 1972, p 222–235
169. I. Phillips et al., *Corros. Sci.,* Vol 12, 1972, p 855–866
170. R. Gruner, B. Streb, and E. Brauer, Hydrogen in Titanium, *Titanium—Science and Technology,* Proceedings of the Fifth International Conference on Titanium, Deutsche Gesellschaft für Metallkunde e.V., Oberursel, Germany, 1985, p 2571
171. R.W. Schutz and M. Xiao, "Stress Corrosion Behavior of Ti-38644 Titanium Alloy Products in Methanol Solutions," Paper 148, Corrosion '93, National Association of Corrosion Engineers, 1993
172. W.F. Czyrklis and M. Levy, Stress Corrosion Cracking Susceptibility of β Titanium Alloy 38-6-44, *Corrosion,* Vol 32 (No. 3), March 1976, p 99–102
173. E.G. Haney and P. Fugassi, Titanium Behavior in Methanol-Water-Chloride Solutions—Effect of Cations, *Proceedings of an International Symposium on Stress Corrosion Mechanisms in Titanium,* co-sponsored by Georgia Institute of Technology and NACE International, Jan 1971
174. L.K. Mori, A. Takamura, and T. Shimose, Stress-Corrosion Cracking of Ti and Zr in HCl-Methanol Solutions, *Corrosion,* Vol 22 (No. 2), Feb 1966, p 29–31
175. A.J. Sedriks and J.A.S. Green, Stress-Corrosion Cracking and Corrosion Behavior of Titanium in Methanol Solutions: Effect of Metal Ions in Solution, *Corrosion,* Vol 25 (No. 8), 1969, p 324
176. E.G. Haney and P. Fugassi, Inhibition of Methanol Cracking of Ti-6Al-4V Foil: Effect of Pretreatments with Aqueous Solutions of Electrolytes, *Corrosion,* Vol 27, Jan 1971, p 46–48
177. B.S. Hickman, J.C. Williams, and H.L. Marcus, Transgranular and Intergranular Stress-Corrosion Cracking of Titanium Alloys, *Aust. Inst. Met.,* Vol 14 (No. 3), 1969, p 138
178. T.R. Beck and M.J. Blackburn, Stress-Corrosion Cracking of Titanium Alloys, *AIAA J.,* Vol 6 (No. 2), 1968, p 326
179. "Accelerated Crack Propagation of Titanium by Methanol, Halogenated Hydrocarbons, and Other Solutions," DMIC Memorandum 228, Defense Metals Information Center, Battelle Memorial Institute, March 1967, p 16–50
180. C.C. Seastrom and R.A. Gorski, "The Influence of Fluorocarbon Solvents on Titanium Alloys, Accelerated Crack Propagation of Titanium by Methanol, Halogenated Hydrocarbons, and Other Solutions," DMIC Memorandum 228, Defense Metals Information Center, Battelle Memorial Institute, March 1967, p 20
181. J.D. Jackson and W.K. Boyd, "The Stress-Corrosion and Accelerated Crack Propagation Behavior of Titanium and Titanium Alloys," DMIC Technical Note, Defense Metals Information Center, Battelle Memorial Institute, Feb 1966
182. *Stress-Corrosion Cracking of Titanium,* STP 397, American Society for Testing and Materials, 1965
183. A.J. Hatch, H.W. Rosenberg, and E.F. Erbin, Effect of Environment on Cracking in Titanium Alloys, *Stress-Corrosion Cracking of Titanium,* STP 397, American Society for Testing and Materials, 1965
184. H.L. Logan, Studies of Hot-Salt Cracking of the Titanium-8% Al-1% Mo-1% V Alloy, *Proceedings of Conference—Fundamental Aspects of Stress-Corrosion Cracking,* National Association of Corrosion Engineers, 1969, p 662
185. H.L. Logan, M.J. McBee, G.M. Ugiansky, C.J. Bechtoldt, and B.T. Sanderson, Stress-Corrosion Cracking of Titanium, *Stress-Corrosion Cracking of Titanium,* STP 397, American Society for Testing and Materials, 1965, p 215
186. S.P. Rideout, R.S. Ondrejcin, M.R. Louthan, and D.E. Rawl, The Role of Moisture and Hydrogen in Hot-Salt Cracking of Titanium Alloys, *Proceedings of Conference—Fundamental Aspects of Stress-Corrosion Cracking,* National Association of Corrosion Engineers, 1969, p 650
187. R.V. Turley and C.H. Avery, Elevated Temperature Static and Dynamic Sea-Salt Stress Cracking of Titanium Alloys, *Stress-Corrosion Cracking of Titanium,* STP 397, American Society for Testing and Materials, 1965, p 1
188. S.P. Rideout, R.S. Ondrejcin, and M.R. Louthan, Hot-Salt Stress-Corrosion Cracking of Titanium Alloys, *The Science, Technology and Application of Titanium,* Pergamon Press, 1970
189. G. Sanderson and J.C. Scully, The Stress Corrosion of Titanium Alloys in Aqueous Magnesium Chloride Solution at 154 °C, *Corrosion,* Vol 24 (No. 3), 1968, p 75
190. M.A. Donachie, W.P. Danesi, and A.A. Pinkowish, Effect of Salt Atmosphere on Crack Sensitivity of Commercial Titanium Alloys at 600 °F–900 °F, *Stress-Corrosion Cracking of Titanium,* STP 397, American Society for Testing and Materials, 1965, p 179
191. W.K. Boyd, Stress-Corrosion Cracking of Titanium and Its Alloys, *Proceedings of Conference—Fundamental Aspects of Stress-Corrosion Cracking,* National Association of Corrosion Engineers, 1969, p 593
192. D.E. Piper and D.N. Fager, The Relative Stress-Corrosion Susceptibility of Titanium Alloys in the Presence of Hot-Salt, *Stress-Corrosion Cracking of Titanium,* STP 397, American Society for Testing and Materials, 1965, p 31
193. "Examination of Cracks in Titanium-Alloy Compressor Disc, Westinghouse Electric Corporation, Aviation Gas Turbine Division, Caused by Molten Cadmium," Memorandum Report, Titanium Metallurgical Laboratory, Battelle Memorial Institute, Feb 1956
194. W.M. Robertson, Embrittlement of Titanium by Liquid Cadmium, *Metall. Trans.,* Vol 2, 1970, p 68
195. D.N. Fager and W.F. Spurr, Solid Cadmium Embrittlement: Titanium Alloys, *Corrosion,* Vol 26 (No. 10), Oct 1970, p 409
196. D.A. Meyn, Solid Cadmium Cracking of Titanium Alloys, *Corrosion,* Vol 29 (No. 5), May 1973, p 192
197. J.B. Hollowell, J.G. Dunleavy, and W.K. Boyd, "Liquid-Metal Embrittlement," DMIC Technical Note, Defense Metals Information Center, Battelle Memorial Institute, April 1965
198. R.E. Duttweiler, R.R. Wagner, and K.C. Antony, An Investigation of Stress-Corrosion Failures in Titanium Compressor Components, *Stress-Corrosion Cracking of Titanium,* STP 397, American Society for Testing and Materials, 1966, p 152
199. G. Martin, Investigation of Long-Term Exposure Effects Under Stress of Two Titanium Structural Alloys, *Stress-Corrosion Cracking of Titanium,* STP 397, American Society for Testing and Materials, 1965, p 95
200. R.E. Stoltz and R.H. Stulen, Solid Metal Embrittlement of Ti-6Al-6V-2Sn by Cadmium, Silver, and Gold, *Corrosion,* Vol 35 (No. 4), April 1979, p 165
201. S.R. Seagle, R.R. Seeley, and G.S. Hall, The Influence of Composition and Heat Treatment on Aqueous Stress Corrosion of Titanium, *Applications Related Phenomena in Titanium Alloys,* STP 432, American Society for Testing and Materials, 1967, p 170
202. T.R. Beck, Stress-Corrosion Cracking of Titanium Alloys: II. An Electrochemical Mechanism, *J. Electrochem. Soc.,* Vol 115, 1968, p 890
203. D.N. Fager and W.F. Spurr, Some Characteristics of Aqueous Stress Corrosion in

Titanium Alloys, *Trans. ASM,* Vol 61, 1968, p 283
204. R.W. Schutz and E. van der Lingen, Characterization of the Ti-6Al-4V-Ru Alloy for Application in the Energy Industry, *Proc. Eurocorr '97 Congress,* Vol 1, 1997, p 259–265
205. M. Ueda, T. Kudo, S. Kitayama, and Y. Shida, "Corrosion Behavior of Titanium Alloys in a Sulfur-Containing H_2S-CO_2-Cl^- Environment," Paper 271, Corrosion/90, National Association of Corrosion Engineers, 1990
206. D.A. Litvin and B. Hill, Effect of pH on Sea-Water Stress-Corrosion Cracking of Ti-7Al-2Cb-1Ta, *Corrosion,* Vol 26 (No. 3), 1970, p 89
207. H.A. Johanson, G.B. Adams, and P. Van Rysselberghe, *J. Electrochem. Soc.,* Vol 104, 1957, p 339
208. M.J. Blackburn and J.C. Williams, Metallurgical Aspects of Stress-Corrosion Cracking of Titanium Alloys, *Proceedings of Conference—Fundamental Aspects of Stress-Corrosion Cracking,* National Association of Corrosion Engineers, 1969, p 620
209. S. Kitayama, Y. Shida, M. Ueda, and T. Kudo, "Effect of Small Pd Addition on the Corrosion Resistance of Ti and Ti Alloys in Severe Gas and Oil Environment," Paper 52, Corrosion/92, National Association of Corrosion Engineers, 1992
210. D.E. Thomas and S.R. Seagle, Stress Corrosion Cracking Behavior of Ti-38-6-44 in Sour Gas Environments, *Titanium—Science and Technology,* Proceedings of the Fifth International Conference on Titanium, Deutsche Gesellschaft für Metallkunde e.V., Oberursel, Germany, 1985, p 2533–2540
211. R.D. Briggs, Effect of Cooling Rate from Mill Annealing Temperature on Stress Corrosion Threshold of Titanium 6Al-4V ELI Beta Annealed, *Advances in the Science and Technology of Titanium Alloy Processing,* I. Weiss, R. Srinivasan, P.J. Bania, D. Eylon, and S.I. Semiatin, Ed., The Minerals, Metals and Materials Society, 1997, p 413–420
212. D. Schlain et al., Galvanic Corrosion Behavior of Titanium and Zirconium in Sulfuric Acid Solutions, *J. Electrochem. Soc.,* Vol 102 (No. 3), March 1955, p 102–109
213. T.S. Lee, Preventing Galvanic Corrosion in Marine Environments, *Chem. Eng.,* April 1, 1985, p 89–92
214. T.S. Lee, E.W. Thiele, and J.H. Waldorf, The Effect of Seawater Velocity on Corrosion Potentials of Materials, *Mater. Perform.,* Nov 1984, p 44–46
215. C.A. Smith and K.G. Compton, *Corrosion,* Vol 31 (No. 9), Sept 1975, p 320–326
216. J. Symonds, "The Influence of Sunlight on the Behavior of Galvanic Couples Between Ti and Cu-Base Alloys in Seawater," Oceanic Engineering Report 82-26, Westinghouse Electric Company, Oceanic Division, Feb 1982
217. R. Holthe, E. Bardal, and P.O. Gartland, Time Dependence of Cathodic Properties of Materials in Seawater, *Mater. Perform.,* June 1989, p 16–23
218. S.C. Dexter and H.-J. Zhang, "Biofilm Effects on Corrosion Potentials in Water Systems," EPRI Contract RP2939-4, Nuclear Power Division, Electric Power Research Institute, Dec 1990
219. G.A. Gehring, Jr. and R.J. Kyle, "Galvanic Corrosion in Steam Surface Condensers Tubed with Either Stainless Steel or Titanium," Paper 60, Corrosion/82, National Association of Corrosion Engineers, March 1982
220. G.A. Gehring, Jr. and J.R. Maurer, "Galvanic Corrosion of Selected Tubesheet/Tube Couples Under Simulated Seawater Condenser Conditions," Paper 202, Corrosion/81, National Association of Corrosion Engineers, April 1981
221. H.T. Hack and W.L. Adamson, "Analysis of Galvanic Corrosion Between a Titanium Condenser and a Copper-Nickel Piping System," Report 4553, David W. Taylor Naval Ship Research and Development Center, Jan 1976
222. G.A. Gehring, Jr. et al., "Effective Tube Length—A Consideration on the Galvanic Corrosion of Marine Heat Exchanger Materials," Corrosion/80, National Association of Corrosion Engineers, 1980
223. D.W. Stough, F.W. Fink, and R.S. Peoples, "The Galvanic Corrosion Properties of Titanium and Titanium Alloys in Salt-Spray Environments," TML Memorandum, Battelle Memorial Institute, Oct 1957
224. G.J. Danek, Jr., The Effect of Seawater Velocity on the Corrosion Behavior of Metals, *Naval Eng. J.,* Vol 78 (No. 5), 1966, p 763
225. C.F. Hanson, *Titanium—Science and Technology,* Vol 1, Pergamon Press, 1973, p 145
226. J.A. Davis and G.A. Gehring, Jr., *Mater. Perform.,* Vol 14 (No. 4), 1975, p 32–39
227. D.F. Hasson and C.R. Crowe, Titanium for Offshore Oil Drilling, *J. Met.,* Vol 34 (No. 1), 1982, p 23–28
228. A.E. Hohman and W.L. Kennedy, *Mater. Prot.,* Vol 2 (No. 9), Sept 1963, p 56–68
229. W.L. Williams, *J. Am. Soc. Naval Eng.,* Vol 62, Nov 1950, p 865–869
230. J.Z. Lichtman, *Corrosion,* Vol 17, 1961, p 119
231. A. Goldberg and R. Kershaw, "Evaluation of Materials Exposed to Scale-Control/Nozzle-Exhaust Experiments at the Salton Sea Geothermal Field," VCRL-52664, Lawrence Livermore Laboratory, Feb 1979
232. R.P. Lee, *Mater. Perform.,* July 1976, p 26–32
233. G. Hoey and J. Bednar, *Mater. Perform.,* Vol 22 (No. 4), April 1983, p 9–14
234. J.P. Doucet et al., Corrosion Fatigue Behavior of Ti-6Al-4V for Marine Application, *Titanium 1986—Products and Applications,* Vol 1, Proceedings of the Technical Program from the 1986 International Conference, Titanium Development Association, 1986
235. A.G.S. Morton, "Mechanical Properties of Thick Plate Ti-6Al-4V," MEL Report 266/66, U.S. Navy Marine Engineering Laboratory, Jan 1967
236. R. Ebara et al., Corrosion Fatigue Behavior of Ti-6Al-4V in NaCl Aqueous Solutions, *Corrosion Fatigue: Mechanics, Metallurgy, Electrochemistry, and Engineering,* STP 801, American Society for Testing and Materials, 1983, p 135–146
237. J.K. Gregory and H.-G. Brokmeier, "The Influence of Texture and Microstructure on Corrosion-Fatigue in Ti-6Al-4V," GKSS 94/E/35, GKSS-Forschungszentrum Geesthacht GmbH, Geesthacht, Germany, 1994
238. J.K. Gregory, Fatigue Crack Propagation in Titanium Alloys, *Handbook of Fatigue Crack Propagation in Metallic Structures,* Vol 1, A. Carpinten, Ed., Elsevier Science B.V., The Netherlands, 1994, p 281–323
239. T.P. Wilks, K.N. Strafford, and P.K. Datta, Fatigue Crack Growth in Titanium and Its Alloys: The Effect of Oxygen Content, Environment and R-Ratio, *Sixth World Conference on Titanium,* Part 1 (Cannes, France), P. Lacombe, R. Tricot, and G. Béranger, Ed., 1988, p 331–337
240. G.R. Yoder, L.A. Cooley, and T.W. Crooker, Effects of Microstructure and Frequency on Corrosion-Fatigue Crack Growth in Ti-8Al-1Mo-1V and Ti-6Al-4V, *Corrosion Fatigue: Mechanics, Metallurgy, Electrochemistry, and Engineering,* STP 801, T.W. Crooker and B. Leis, Ed., American Society for Testing and Materials, 1983, p 159–174
241. H.B. Bomberger and L.F. Plock, Methods Used to Improve Corrosion Resistance of Titanium, *Mater. Prot.,* June 1969, p 45–48
242. M. Stern and H. Wissenberg, The Influence of Noble Metal Alloy Additions on the Electrochemical and Corrosion Behavior of Titanium, *J. Electrochem. Soc.,* Vol 106 (No. 9), Sept 1959, p 759
243. M. Stern, Corrosion-Resistant Alloys, U.S. Patent 3,063,835, 1962
244. N.D. Thomashov et al., Corrosion and Passivity of the Cathode-Modified Titanium-Based Alloy, *Titanium and Titanium Alloys—Scientific and Technological Aspects,* Vol 2, Plenum Press, 1982, p 915–925

245. N. Thomashov, R. Al'tovskii, and G. Chernova, Passivity and Corrosion Resistance of Titanium and Its Alloys, *J. Electrochem. Soc.,* Vol 108, Feb 1961, p 113–119
246. M. Stern and C.R. Bishop, The Corrosion Behavior of Titanium-Palladium Alloy, *Trans. ASM,* Vol 52, 1960, p 239
247. A.J. Sedriks, Further Observations on the Electrochemical Behavior of Ti-Ni Alloys on Acidic Chloride Solutions, *Corrosion,* Vol 29 (No. 2), 1973, p 64
248. M. Stern and C. Bishop, The Corrosion Resistance and Mechanical Properties of Titanium-Molybdenum Alloys Containing Noble Metals, *Trans. ASM,* Vol 54, Sept 1961, p 286–298
249. R.W. Schutz and M. Xiao, Optimized Lean-Pd Titanium Alloys for Aggressive Reducing Acid and Halide Service Environments, *Proc. 12th Int. Corros. Cong.,* Vol 3A, 1993, p 1213
250. S. Kitayama, Y. Shida, and M. Oshiyama, *Sumitomo Search,* Vol 41 (No. 1), 1990, p 23–32
251. T. Fukuzuka, K. Shimogori, H. Satoh, and F. Kamikubo, Protection of Titanium Against Crevice Corrosion by Coating with Palladium Oxide, *Titanium '80—Science and Technology,* The Metallurgical Society, 1980, p 2631–2638
252. R.W. Schutz, Surface Treatments for Expanding Titanium Alloy Application Limits: An Overview, *Surface Performance of Titanium,* J.K. Gregory, H.J. Rack, and D. Eylon, Ed., The Minerals, Metals, and Materials Society, 1997, p 1–22
253. S. Fujishiro and D. Eylon, *Thin Solid Films,* Vol 54, 1978, p 309–315
254. S. Fujishiro and D. Eylon, *Metall. Trans. A,* Vol 11, Aug 1980, p 1261–1263
255. T. Fukuzuka et al., *Industrial Applications of Titanium and Zirconium,* STP 728, American Society for Testing and Materials, 1981, p 71–84
256. A. Erdemir et al., *Mater. Sci. Eng.,* Vol 69, 1985, p 89–93
257. P. Sioshansi, Surface Modification by Ion Implantation, *Mach. Des.,* March 20, 1966
258. A. Takamura, Corrosion Resistance of Ti and a Ti-Pd Alloy in Hot, Concentrated Sodium Chloride Solutions, *Corrosion,* Oct 1967, p 306–313
259. K. Shimogori et al., Chemical Apparatus Free from Crevice Corrosion, U.S. Patent 4,154,897, 1979
260. K. Suzuki and Y. Nakamoto, *Mater. Perform.,* June 1981, p 23–26
261. S. Senderoff, Brush Plating, *Prod. Finish.,* Dec 1955
262. P. Munn and G. Wolf, *Mater. Sci. Eng.,* Vol 69, 1985, p 303–310
263. L.C. Covington, The Role of Multivalent Metal Ions in Suppressing Crevice Corrosion of Titanium, *Titanium—Science and Technology,* Vol 4, Proceedings of the Second International Conference, Plenum Press, 1973, p 2395–2403
264. T. Moroishi and H. Miyuki, Effect of Several Ions on the Crevice Corrosion of Titanium, *Titanium '80—Science and Technology,* The Metallurgical Society, 1980, p 2623–2630

ASM Handbook, Volume 13B: Corrosion: Materials
S.D. Cramer, B.S. Covino, Jr., editors, p300-324
DOI: 10.1361/asmhba0003823

Corrosion of Zirconium and Zirconium Alloys

Te-Lin Yau, Te-Lin Yau Consultancy
Richard C. Sutherlin, ATI Wah Chang, An Allegheny Technologies Company

ZIRCONIUM was identified by the German chemist Martin Heinrich Klaproth in 1789. It took another 135 years for Anton E. van Arkel and J.H. de Boer, of Einhoven, Holland, to develop the iodide decomposition process to make a pure, ductile metal. The iodide crystal bar process continues to be a method for purifying titanium, zirconium, and hafnium, even though it is slow and expensive.

In the 1940s, several groups of scientists and engineers were investigating zirconium and other metals and alloys for nuclear reactors. A suitable structural material with good corrosion/oxidation resistance, resistance to irradiation damage, and transparency to thermal neutrons to sustain the nuclear reaction was needed to clad nuclear fuel. Zirconium seemed to meet these requirements; however, only a few hundred pounds of zirconium were produced in the United States in 1945, and it cost more than $136/kg ($300/lb). Consequently, there was a great interest in developing a process that could produce a large quantity of zirconium at a much lower cost.

In 1945, developmental work on zirconium was initiated at the U.S. Bureau of Mines in Albany, Ore., under Dr. William Justin Kroll's technical direction. Dr. Kroll had already developed a production process for titanium by the reduction of titanium tetrachloride with magnesium in an inert atmosphere. A similar process for zirconium was developed by 1947 at a pilot plant with a weekly capacity of 27 kg (60 lb) of zirconium sponge.

About the time of Kroll's work, Dr. Kaufman of Massachusetts Institute of Technology and Dr. Pomerance of Oak Ridge National Laboratory discovered that zirconium, as occurring in nature, was combined with hafnium, and that it is the hafnium that gives zirconium a high level of neutron absorption. When the hafnium is removed, zirconium has a very low thermal neutron absorption cross section. Admiral Hyman Rickover, who directed the U.S. Navy Nuclear Propulsion Program, immediately chose zirconium for the naval reactor. This decision stimulated research and development programs to advance zirconium technology in production, zirconium/hafnium separation, property information, fabrication, and applications.

Crystal bar zirconium or zirconium produced from sponge was not ideal because of its inconsistent corrosion and oxidation resistance in high-temperature water and steam. This abnormal behavior was attributed to the presence of minor impurities, such as nitrogen and carbon. Various alloy development programs were established in the early 1950s to examine the effects of adding various elements to zirconium. Independent discoveries by Battelle Memorial Institute and Iowa State College revealed that tin was the most beneficial alloying element. The Zr-2.5-Sn alloy was named Zircaloy-1 and was recommended for the *Nautilus* reactor. By 1952, data showed that Zircaloy-1 had an increasing rate of corrosion over time. An urgent search for a new alloy began.

Fortunately, Bettis Atomic Power Laboratory already had an active program of corrosion tests for several zirconium-base alloys. Included was one ingot accidentally contaminated with a small amount of stainless steel. Test results revealed the beneficial effects of iron, nickel, and chromium. Quickly, Zircaloy-2, the Zr-1.5Sn-0.12Fe-0.1Cr-0.05Ni alloy, was developed and specified for the *Nautilus* reactor in August 1952.

One of the limiting factors for Zircaloy-2 in a reactor was identified to be its absorption of hydrogen during corrosion in high-temperature water. Bettis Atomic Power Laboratory eventually discovered that replacing nickel with iron produced an alloy that cut hydrogen absorption in half. This alloy was named Zircaloy-4. The effect of nickel on corrosion remains controversial. Nevertheless, both of the Zircaloys are important materials for nuclear applications.

Demand for zirconium rose for submarines, and with the nuclear power industry on the horizon, lower-cost commercial sources, including Carborundum Metals, National Distillers Products, NRC Metals, and Wah Chang, were developed. Wah Chang was contracted to provide zirconium at just less than 5/kg ($10/lb) in April 1956.

By 1958, the chemical processing industry began to use zirconium because of its excellent resistance to a broad range of corrosives and because of its biocompatibility. Zirconium is also used in medical applications, such as surgical tools and instruments, and for stitches in brain operations. Zirconium is a beneficial alloying element for iron-, copper-, magnesium-, aluminum-, molybdenum- and titanium-base alloys. Zirconium is useful as a getter because of its ability to combine with gases at elevated temperatures. Along with niobium, zirconium is superconductive at low temperatures and is used to make superconductive magnets.

In the nuclear power industry, stainless steel was used to clad uranium dioxide fuel for the first generation of reactors, but by 1965, zirconium alloys were the predominant cladding material for water-cooled reactors, launching a widespread effort to develop strong, corrosion-resistant zirconium alloys. Noticeably, the Ozhennite alloys were developed in the former USSR for use in pressurized water and steam. These alloys contain tin, iron, nickel, and niobium, with a total alloy content of 0.5 to 1.5%. The Zr-1Nb alloy also is used in the Soviet Union for pressurized water and steam service. Researchers at Atomic Energy of Canada Limited took a lead from the Russians' zirconium-niobium alloys and developed the Zr-2.5Nb alloy. This alloy is strong and heat treatable. It is used in either a cold-worked condition or a quenched-and-aged condition.

Zirconium is often stated to be a rare or exotic metal. To the contrary, zirconium is plentiful and is ranked 19th in abundance of the chemical elements occurring in the earth's crust. It is more abundant than common metals such as nickel, copper, chromium, zinc, lead, and cobalt. The most important source for zirconium is zircon ($ZrSiO_4$), which appears in several regions throughout the world in the form of beach sand. Availability should not be a major concern in selecting zirconium for most applications (Ref 1–3).

General Characteristics

There are two major categories for zirconium and its alloys: nuclear and nonnuclear, as listed in Table 1. They all have low alloy contents. They are based on the alpha structure, that is, the hexagonal close-packed lattice, with dilute additions of solid-solution strengthening and alpha-stabilizing elements such as oxygen and tin. However, in niobium-containing alloys, there is the presence of some niobium-rich beta particles of the body-centered cubic lattice.

One of the major differences between nuclear and nonnuclear zirconium alloys is the hafnium content. Nuclear grades of zirconium alloys are virtually free of hafnium (not greater than 100 ppm). Nonnuclear grades of zirconium alloys are permitted to have 4.5% Hf but normally have less. Hafnium has an enormous effect on absorbing thermal neutrons and is suitable for nuclear reactor control rods. It has a minor effect on zirconium mechanical and chemical properties.

The major use of nuclear-grade zirconium tubing is for nuclear fuel rod cladding, guide tubes, pressure tubes, and ferrule spacer grids. Flat materials, such as sheets and plates, are used for spacer grids, water channels, and channel boxes for nuclear fuel bundles. Bars are used for nuclear fuel rod end plugs.

For nonnuclear applications, product forms include ingots, forgings, pipes, tubes, plates, sheets, foils, bars, wires, castings, and clad materials. They are used to construct corrosion-resistant equipment such as heat exchangers, condensers, vaporizers, reactors, columns, piping systems, pumps, valves, and packing for industries, including chemical processing, petrochemical, food, pharmaceutical, and waste management. Industry standards, such as ASTM International specifications, exist for the various product forms of zirconium for nuclear and commercial applications. International standard ISO 10270, "Corrosion of Metals and Alloys—Aqueous Corrosion Testing of Zirconium Alloys for Use in Nuclear Power Reactors," provides a corrosion test procedure, and other ISO and EN standards provide welding specifications.

Physical and Mechanical Properties. Zirconium is a lustrous, grayish-white, ductile metal. The physical and mechanical properties of zirconium are given in the article "Zirconium and Hafnium" in *Properties and Selection: Nonferrous Alloys and Special-Purpose Alloys,* Volume 2, of *ASM Handbook,* 1990, p 661–669. For engineering purposes, interesting features of zirconium are:

- Lower density than iron- and nickel-base stainless alloys
- Low coefficient of thermal expansion; approximately two-thirds that of titanium, one-third that of type 316 stainless steel, and approximately one-half that of Monel
- High thermal conductivity; 30% more than that of stainless alloys

These features allow zirconium to be fabricated into compact, efficient equipment.

As indicated in Table 1, Zircaloy-2 and Zircaloy-4 contain nominally 1.5% Sn. Zircaloy-4 has more iron but no nickel for the purpose of minimizing hydrogen pickup. Both alloys are popular in water-moderated reactors, such as boiling water and pressurized water reactors. The Zr-2.5Nb alloy is used in heavy-water-moderated reactors, such as the Canadian deuterium-uranium reactors.

Of the nonnuclear grades, Zr700, with an oxygen content of less than 1000 ppm, has improved bondability in explosive cladding applications and deep-drawing applications. Zr702 is commercially pure zirconium and is most popular for corrosion-resistant applications. Zr705 is preferred when strength is an important factor.

Because recyclable material is generated in the nuclear industry, a major impurity (not listed in Table 1) is tin. The use of recycled Zircaloys lowers the cost of nonnuclear alloys and keeps mechanical properties consistent. The elevated tin content may affect corrosion properties in certain environments. Also, there is not enough demand in nonnuclear applications to support the production of Zr704, so, for nonnuclear applications, Zircaloy-2 or Zircaloy-4 may be substituted for Zr704.

Zirconium and hafnium form solid solutions at all concentrations. The counterparts of nuclear and nonnuclear grades of zirconium alloys are interchangeable in mechanical properties. However, specification requirements for nuclear materials are more extensive than those for nonnuclear materials. Mechanical properties for nonnuclear grades are listed in Tables 2 and 3. Zr705 is the strongest alloy with improved formability. Furthermore, Zr700 and Zr706, with low oxygen content, are suitable for severe forming applications, such as explosive cladding and deep drawing.

Table 4 indicates that the fatigue limits of zirconium alloys are very notch sensitive. Figures in the article in *Properties and Selection: Nonferrous Alloys and Special-Purpose Alloys,* Volume 2 of *ASM Handbook,* 1990, show that the tensile strength of zirconium alloys decreases quickly with increasing temperature, and Zr702 and Zr705 creep at low temperatures and stresses. These are important factors to consider for zirconium equipment to be used at elevated temperatures.

Microstructures. The reader is encouraged to read the article "Metallography and Microstructures of Zirconium, Hafnium, and Their Alloys," in *Metallography and Microstructures,* Volume 9 of *ASM Handbook,* 2004. Typical microstructures for the parent metal, heat-affected zone (HAZ), and weld metal of annealed zirconium alloys are shown in Fig. 1 to 3.

Zr702 is unalloyed and primarily exists as an alpha grain structure at room temperature. It exhibits an equiaxed alpha structure, as shown in Fig. 1(a). Most elements have very low solubility in zirconium. Oxygen, titanium, hafnium, and scandium are the few exceptions. Zirconium tends to react with many elements to form

Table 1 Nuclear and nonnuclear grades of zirconium alloys

		Composition, wt%									
Alloy design	**UNS No.**	**Zr + Hf(a)**	**Hf(b)**	**Sn**	**Nb**	**Fe**	**Cr**	**Ni**	**Fe + Cr**	**Fe + Cr + Ni**	**O(b)**
Nuclear grades											
Zircaloy-2	R60802	...	0.01	1.20–1.70	...	0.07–0.2	0.05–0.15	0.03–0.08	...	0.18–0.38	...
Zircaloy-4	R60804	...	0.01	1.20–1.70	...	0.18–0.24	0.07–0.13	...	0.28–0.37	...	...
Zr-2.5Nb	R60901	...	0.01	...	2.40–2.80	...	...	...	...	...	...
Nonnuclear wrought grades											
Zr700	R60700	99.2	4.5	...	...	...	...	...	0.2(b)	...	0.10
Zr702	R60702	99.2	4.5	...	...	...	...	...	0.2(b)	...	0.16
Zr704	R60704	97.5	4.5	1.0–2.0	...	...	...	...	0.2–0.4	...	0.18
Zr705	R60705	95.5	4.5	...	2.0–3.0	...	...	...	0.2(b)	...	0.18
Zr706	R60706	95.5	4.5	...	2.0–3.0	...	...	...	0.2(b)	...	0.16
Nonnuclear casting grades											
Zr702C	...	98.8	4.5	...	...	...	...	...	0.3(b)	...	0.25
Zr704C	...	97.1	4.5	1.0–2.0	...	...	...	...	0.3(b)	...	0.3
Zr705C	...	95.1	4.5	...	2.0–3.0	...	...	...	0.3(b)	...	0.3

(a) Minimum. (b) Maximum

intermetallic compounds during the production stage. One of the major impurities in zirconium is iron. Consequently, the most visible second-phase particles in Fig. 1(a) are zirconium-iron compounds. There may be fine chromium and nickel particles incorporated into these compounds that are well distributed in the alpha structure.

Tin may be another major impurity in Zr702 and may also form compounds with zirconium. However, the solubility of tin in zirconium is much higher than that of iron in zirconium. The zirconium-tin compounds, if present, are difficult to see in metallographic examination. Moreover, metallographic examination can be used to identify other compounds, including hydrides, carbides, nitrides, silicides, and phosphides, when they are present in meaningful amounts.

With little impedance from impurities in Zr702, grains in the HAZ grow to much larger sizes, with an acicular structure (Fig. 1b). Weld metal exhibits a Widmanstätten structure, as shown in Fig. 1(c). Welding has a great effect on the morphology of second-phase particles, which affects the corrosion of zirconium in certain conditions. This is discussed in the next section.

Like Zr702, Zircaloys or Zr704 exhibit an equiaxed alpha structure in the parent metal (Fig. 2a), pronounced acicular alpha structure in the HAZ (Fig. 2b), and a Widmanstätten structure in the weld metal (Fig. 2c).

The Zr-2.5Nb alloy or Zr705 exhibits a two-phase structure. It has much finer grain structure than that of the alpha alloys, as shown in Fig. 3. It contains both the alpha-zirconium phase and the beta-niobium phase in the parent metal (Fig. 3a). The HAZ has a mild change in structure, as shown in Fig. 3(b). The weld metal has a fine acicular structure of alpha zirconium and beta niobium (Fig. 3c).

Chemical and Corrosion Properties. Zirconium is a highly reactive metal, as evidenced by its potential of −1.53 V versus the standard hydrogen electrode (SHE) at 25 °C (77 °F). For comparison, the potentials for chromium, iron, and nickel are −0.74, −0.44, and −0.25 V, respectively. Zirconium is also a highly corrosion-resistant metal and has a strong affinity for oxygen. In an oxygen-containing medium such as air, water, or carbon dioxide, zirconium spontaneously reacts with oxygen at ambient temperature and below to form an adherent, protective oxide film on its surface. This film is self-healing and protects the base metal from chemical and mechanical attack at temperatures to 350 °C (660 °F). As a result, zirconium resists attack in most acids, salt solutions, alkaline solutions, and organic media. Zirconium is particularly suitable for handling reducing acids, which is difficult for most passive alloys.

Protective oxide films are difficult to form on the surface of zirconium in a few media, such as hydrofluoric acid, concentrated sulfuric acid, and certain dry organic halides. Consequently, zirconium is not suitable for handling these media.

In addition, zirconium is susceptible to localized corrosion, such as pitting and stress-corrosion cracking in chloride solutions under oxidizing conditions. However, zirconium is not susceptible to crevice corrosion in chloride solutions, because the condition in a crevice is normally reducing. However, zirconium is susceptible to crevice corrosion in fluoride solutions and sulfuric acid. Readers are encouraged to obtain detailed information from the review articles (Ref 4–7).

Variables Affecting Corrosion

Oxide Films. Zirconium behaves much like other passive metals, such as titanium, iron, nickel, and chromium, relying on passive oxide film for corrosion resistance. However, zirconium is unique in several aspects in the formation and properties of its oxide film.

First, the growth of the zirconium oxide film results entirely from the migration of the O^{2-}

Table 2 ASTM International requirements for the room-temperature mechanical properties of zirconium alloys

Alloy	Minimum tensile strength, MPa	Minimum tensile strength, ksi	Minimum yield strength (0.2% offset), MPa	Minimum yield strength (0.2% offset), ksi	Minimum elongation, %	Bend test radius(a)
Zr700	380(b)	55	305(b)	44	20	5*T*
Zr702	380	55	207	30	16	5*T*
Zr704	414	60	240	35	14	5*T*
Zr705	552	80	380	55	16	3*T*
Zr706	510	74	345	50	20	2.5*T*

(a) Bend tests are not applicable to material more than 4.75 mm (0.187 in.) thick. *T* is the thickness of the bend test specimen. (b) Maximum

Table 4 The 10^7 fatigue limits for zirconium alloys

Alloy	Fatigue limit, Smooth, MPa	Fatigue limit, Smooth, ksi	Fatigue limit, Notched, MPa	Fatigue limit, Notched, ksi
Iodide Zr	145	21	55	8
Zircaloys or Zr705 (annealed 2 h at 732 °C, or 1350 °F)	283	41	55	8
Zr-2.5%Nb (aged 4 h at 566 °C, or 1050 °F)	290	42	55	8

Table 3 ASME mechanical requirements for Zr702 and Zr705 used for unfired pressure vessels

Material form and condition	ASME specification number	Alloy grade	Tensile strength, MPa	Tensile strength, ksi	Minimum yield strength, MPa	Minimum yield strength, ksi	Maximum allowable stress in tension for metal temperature not exceeding °C (°F): −4 to 40 (25 to 100), MPa	−4 to 40 (25 to 100), ksi	95 (200), MPa	95 (200), ksi	150 (300), MPa	150 (300), ksi	205 (400), MPa	205 (400), ksi	260 (500), MPa	260 (500), ksi	315 (600), MPa	315 (600), ksi	370 (700), MPa	370 (700), ksi
Plate, sheet, strip	SB 551	702	359	52	207	30	108	16	84.3	12.2	70.1	10.2	62.4	9.0	47.9	6.9	40.3	5.8	35.5	5.1
		705	552	80	379	55	158	23	128	19	111	16	98.2	14.2	88.6	12.8	81.2	11.8	77.6	11.3
Seamless tubing	SB 523	702	359	52	207	30	108	16	84.3	12.2	70.1	10.2	62.4	9.0	47.9	6.9	40.3	5.8	35.5	5.1
		705	552	80	379	55	158	23	128	19	111	16	98.2	14.2	88.6	12.8	81.2	11.8	77.6	11.3
Welded tubing(a)	SB 523	702	359	52	207	30	92.1	13.4	76.9	11.2	63.7	9.2	52.9	7.7	43.3	6.3	35	5	30.9	4.5
		705	552	80	379	55	134	19	111	16	94.7	13.7	83.8	12.2	75.5	10.9	69.4	10.1	66	9.6
Forgings	SB 493	702	359	52	207	30	108	16	84.3	12.2	77	11	62.4	9.0	47.9	6.9	40.3	5.8	35.5	5.1
		705	552	80	379	55	158	23	128	19	111	16	98.2	14.2	88.6	12.8	69.4	10.1	77.6	11.3
Bar	SB 550	702	359	52	207	30	108	16	84.3	12.2	77.2	11.2	62.4	9.0	47.9	6.9	40.3	5.8	35.5	5.1
		705	552	80	379	55	158	23	128	19	111	16	98.2	14.2	88.6	12.8	81.2	11.8	77.6	11.3
Seamless pipe	SB 658	702	359	52	207	30	108	16	84.3	12.2	76.9	11.2	62.4	9.0	47.9	6.9	40.3	5.8	35.5	5.1
		705	552	80	379	55	158	23	128	19	111	16	98.2	14.2	88.6	12.8	81.2	11.8	77.6	16.3
Welded pipe(a)	SB 658	702	359	52	207	30	92.1	13.4	76.9	11.2	63.7	9.2	52.9	7.7	43.3	6.3	35	5	30.9	4.5
		705	552	80	379	55	134	19	111	16	94.7	13.7	83.5	12.1	75.5	10.9	69.4	10.1	66	9.6

(a) 0.85 factor used for welded product

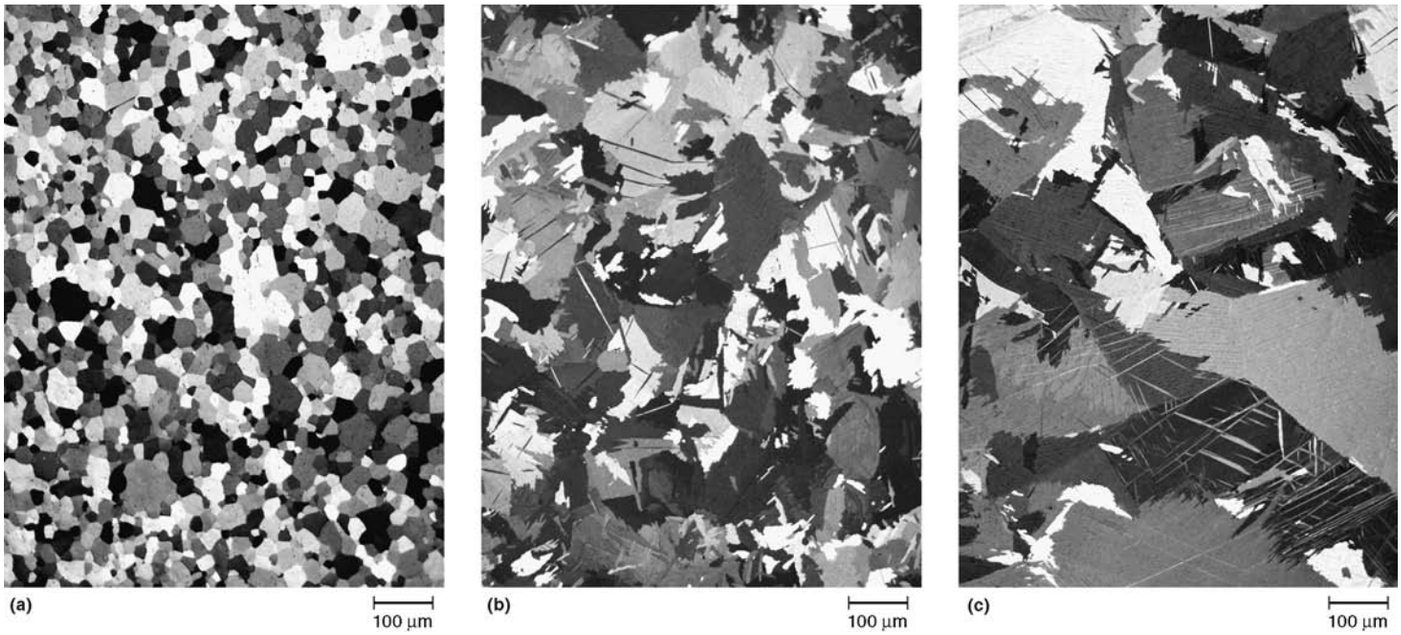

Fig. 1 Microstructure of Zr702. (a) Parent metal. (b) Heat-affected zone. (c) Weld metal. Original magnification: 100×

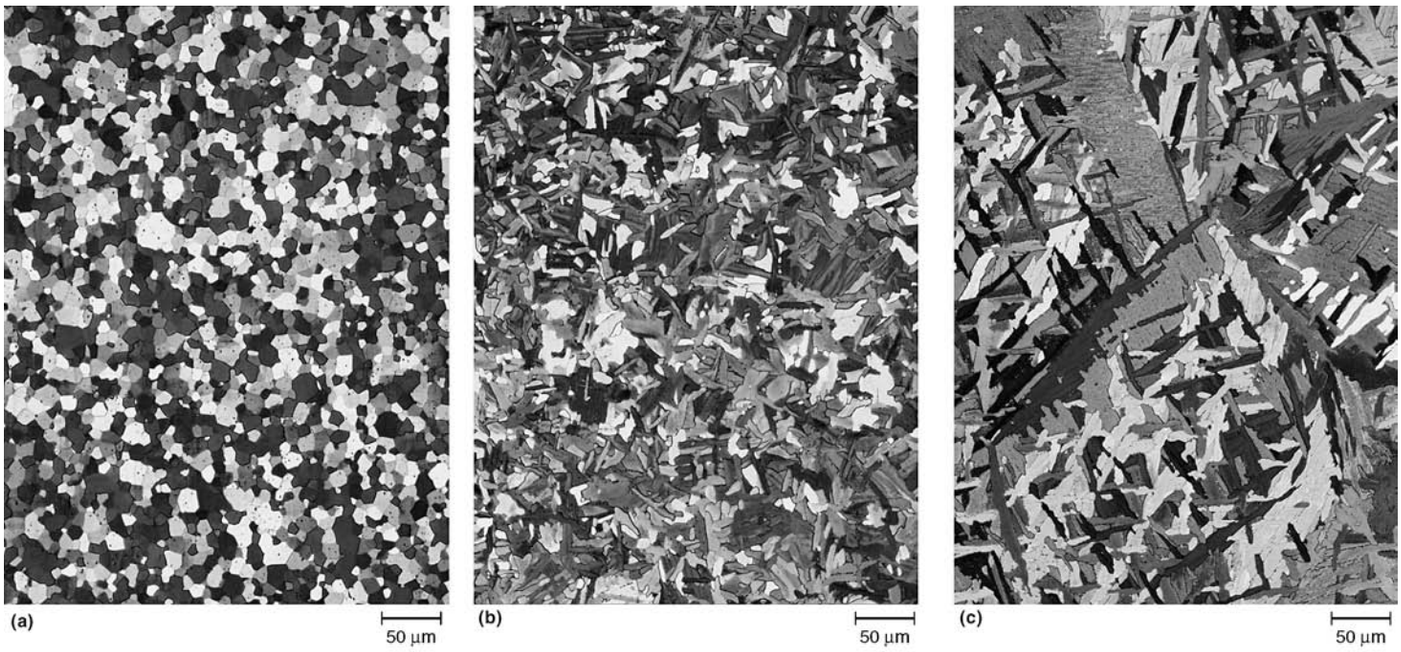

Fig. 2 Microstructure of Zircaloy-4 or Zr704. (a) Parent metal. (b) Heat-affected zone. (c) Weld metal. Original magnification: 200×

ion (Ref 8). That is, a new layer of oxide film continues to form at the metal/oxide interface. The first layer will form spontaneously because of the reactive nature of zirconium and its strong affinity for oxygen. Additional layers will form at much reduced and decreasing rates, resulting from the protective power of the first and additional layers. This also implies that zirconium can conveniently heal any damage done at the metal/oxide interface, provided that the damage is done in an oxygen-containing environment. Very often, there is a thin layer of protective oxide film at the interface, even if or when the outer layer is porous and not so protective.

Second, the oxide film on zirconium is most likely ZrO_2. The existence of oxygen derivatives of zirconium in valence states other than four may be possible but is doubtful (Ref 9). However, the passive films on most passive metals can be oxides in valency of various states. For example, the oxide film on titanium can be the most protective TiO_2 film formed in oxidizing media, or a much less protective film, such as TiO, Ti_2O_3, and their mixture formed in reducing media.

Third, ZrO_2 is a compound that is closer to insulators than to semiconductors. The chemical

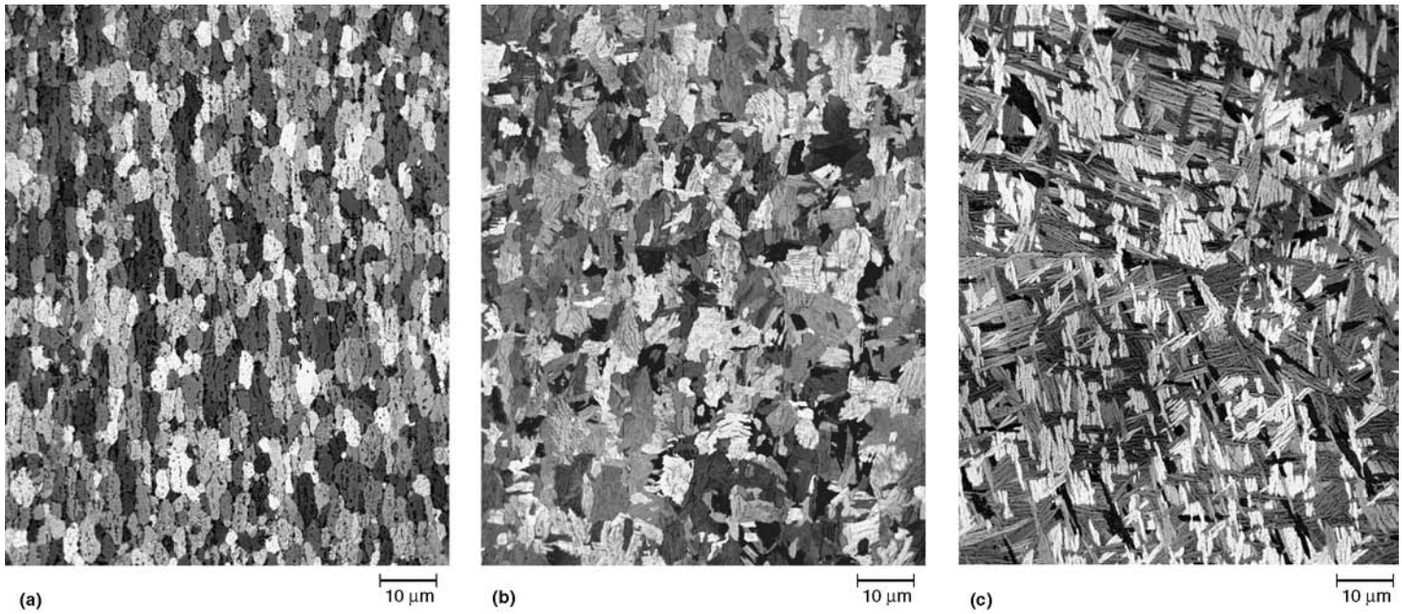

Fig. 3 Microstructure of the Zr-2.5Nb alloy or Zr705. (a) Parent metal. (b) Heat-affected zone. (c) Weld metal. Original magnification: 1000×

bonding between zirconium and oxygen is very strong at 6.6 eV per equivalent. The transport of current through the film becomes increasingly difficult as the film grows. It can proceed at areas such as grain boundaries and atomic defect sites. The film could become less protective with increasing thickness due to an increase in grain boundaries and defects. Thick, protective oxide films may form under well-controlled conditions, which are discussed later.

Accepting ZrO_2 as the compound for the passive film on zirconium does not lead to a total agreement among researchers. After all, ZrO_2 has three different crystalline structures: cubic (c), tetragonal (t), and monoclinic (m). Normally, (c), (t), and (m) ZrO_2 are stable at temperatures between 2680 and 2370 °C (4860 and 4300 °F), between 2370 and 1240 °C (4300 and 2260 °F), and below 1240 °C (2260 °F), respectively. The crystalline structure of the zirconium passive film is also unique.

The film formed on zirconium during anodic polarization in a phosphoric solution is (m) ZrO_2, identical to the natural zirconium ore baddeleyite (Ref 10). According to Ref 11, the anodic film is (c) ZrO_2 in the case of polarization in 0.1 *N* HNO_3; in dilute H_2SO_4 or a borate solution, the film is primarily amorphous but contains some (c) ZrO_2. Cox (Ref 12) states that the passive film formed on zirconium in H_2SO_4 is predominantly (c) structure with traces of the (m) structure.

The oxide film formed on zirconium alloys in water and steam is just as complicated as the preceding process. The oxide scales are known to be predominately (m) ZrO_2; however, it has been shown that the oxide layer is under high compressive stress, which may stabilize the oxide in its tetragonal form (Ref 13, 14). Studies by Raman spectroscopy and x-ray diffraction have shown that the oxide is a mixture of both (t) and (m) ZrO_2 structures (Ref 15, 16). Godlewski et al. (Ref 15), using tapered samples, have shown that in Zircaloy-4 and Zr-1%Nb alloys, ~40% of the oxide film near the oxide/metal interface has (t) structure, and the proportion of (t) decreases to ~15% as the distance from the interface increases beyond ~600 nm. Using the reflection high-energy electron diffraction technique on the Zr-2.5%Nb alloy, Khatamian and Lalonde (Ref 17) detected a mixture of nearly (−c), (−t), and (m) structures for films of 200 nm thick or less, and the (m) structure for the outer layers of films thicker than 800 nm.

It appears that protective oxide films can be (m), (t), (c), or their mixtures. It would be incorrect to assume that zirconium and its alloys have to have, for example, (t) ZrO_2 to be corrosion and oxidation resistant. After all, to form, for example, (t) ZrO_2 at a temperature between 1240 and 2370 °C (2240 and 4300 °F) cannot protect zirconium. All three forms of zirconium oxide are approximately equally inert. Which one forms on the surface of zirconium depends on temperature, alloying elements, environmental composition, and the state of stress in the film. Regardless of its structure, as long as the film is compact and adherent, it is protective.

Effects of Water. Water is the essential ingredient in the aqueous corrosion of most metals and alloys. The presence of water in many chemicals makes them much more corrosive to common metals and alloys. For example, in order to use steel in many applications, water needs to be removed from process streams.

With few exceptions, water is the best friend of zirconium. A major reason for using zirconium in the nuclear industry is its excellent resistance in water and steam. Zirconium is one of few metals that has the capability to react with water to form a protective oxide film. Zirconium exhibits this capability better in water than in air. This capability even extends into highly reducing conditions such as hydrochloric and dilute sulfuric acids. Other passive metals and alloys, such as titanium and stainless steels, would require the presence of an oxidant such as oxygen for the formation of protective oxide films.

Zirconium may become vulnerable in certain water-free environments, such as organic solutions. Without water, zirconium is not able to repair any damage made to the protective film. Hence, the reactive nature of zirconium will be exposed to corrosive attack. The addition of small amounts of water may stop this.

Exceptions include the presence of water, which makes chlorine and fluorine corrosive to zirconium. Unlike titanium, zirconium resists attack by dry chlorine, because titanium may even ignite in dry chlorine. Zirconium is susceptible to local attack in wet chlorine, which can be regarded as an oxidizing chloride solution. Water-containing fluorine is corrosive to both titanium and zirconium.

Effects of Temperature. Zirconium is regarded as both a reactive and refractory metal because of its high melting point of 1852 °C (3365 °F). However, zirconium is not suitable for high-temperature applications because of its reactivity. Zirconium reacts with many metallic and nonmetallic elements at elevated temperatures, which is why zirconium needs a clean surface and argon shielding in welding. Heat treatments may be done in air, but only with a clean surface. For example, a fingerprint on a zirconium surface may result in local breakaway oxidation, as seen in Fig. 4.

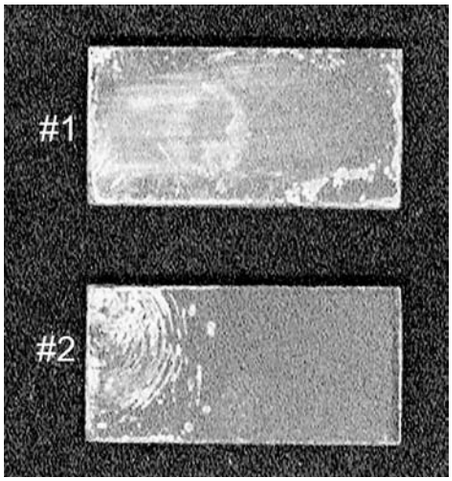

Fig. 4 Effect of a fingerprint on zirconium after heating at 760 °C (1400 °F) for 30 min

Zirconium may be used for long-term services when the temperature is at 350 °C (660 °F) or lower. Here, zirconium corrosion does not show a strong dependence on temperature in compatible environments. For example, the corrosion rate of zirconium changes little in nitric acid and dilute sulfuric acid as the temperature increases within this limit. With increasing temperature, the corrosion rate of zirconium may increase but so does the film formation rate. The net change remains small.

In noncompatible media, such as hydrofluoric acid and concentrated sulfuric acid, the corrosion rate of zirconium increases rapidly with increasing temperature.

Effects of pH. Thermodynamically, zirconium behaves like most passive metals in acidic and alkaline solutions, as shown in Fig. 5 (Ref 9). Zirconium dioxide or hydrated zirconium dioxide dissolves as ZrO^{2+} when the pH is less than or equal to 3.5 and as Zr^{4+} when the pH is less than or equal to −1.03. Dissolving as ZrO^{2+} is expected to be much slower than dissolving as Zr^{4+}. Zirconium dioxide retains most of its protective capability until the pH is less than −1.03. Zirconium oxide protects zirconium until the pH is at least 13. In fact, zirconium is one of few metals that exhibits excellent corrosion resistance over such a wide range of pH. Zirconium equipment has been used in processes that cycle between strong acids and strong alkalis. In this aspect, zirconium is more unique than other high-performance materials, such as titanium, tantalum, glass, and polytetrafluoroethylene (PTFE), which are poor in strong alkalis.

The pH has some effect on the solubility of the oxide film on zirconium, but the effect is not dramatic. Practically, the corrosion resistance of zirconium has little dependence on pH over a wide range (Ref 18). Zirconium dioxide is virtually insoluble in neutral water. It dissolves slightly as the pH increases or decreases, as long as pH is not extreme. Slight dissolution conditions for zirconium oxides may have some beneficial effects that are discussed later.

However, pH change may alter the corrosive nature of impurities in a solution. Two important impurities to be considered are ferric ion and fluoride ion. Ferric ion is a common, well-known oxidizing ion that induces pitting on metals and alloys in halide solutions. Fluoride ion has the capability to interfere with oxide formation even at low temperatures.

Normally, ferric ion exists in solutions when the pH is less than or equal to 2.5 and when the solution potential exceeds 0.771 V versus SHE (Ref 9). In a nonaerated acid, iron corrodes to yield ferrous ions that are too reducing to induce pitting on most metals and alloys. Ferrous ion tends to become ferric ion in the presence of oxygen. Zirconium resists pitting in iron-containing chloride solutions when the pH is 3 or greater (Ref 19). To control the pitting of zirconium in copper-containing chloride solutions, the pH needs to be 5 or greater (Ref 20).

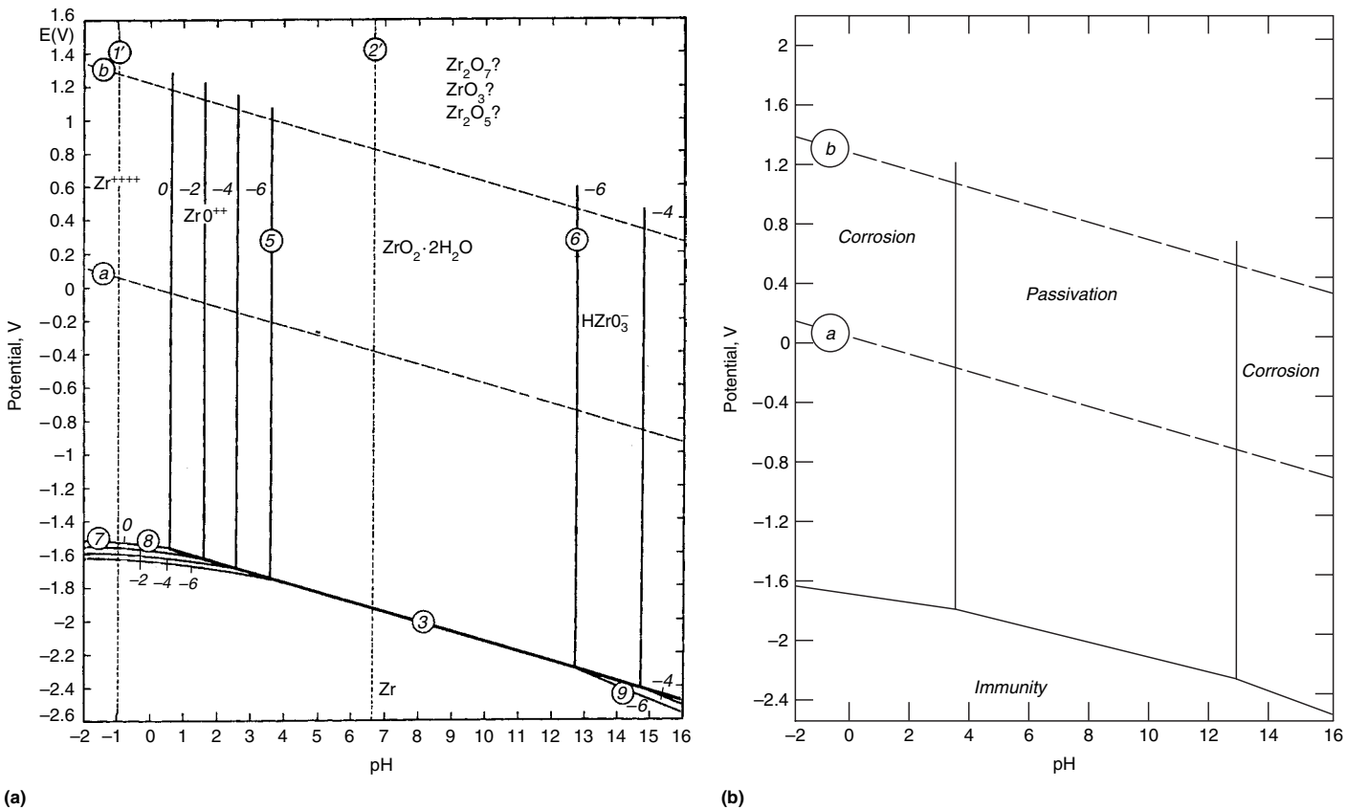

Fig. 5 Potential-pH diagrams. (a) Zirconium in water at 25 °C (75 °F). (b) Theoretical conditions of corrosion, immunity, and passivation of zirconium at 25 °C (75 °F). (Kinetically, passivation may be extended to pH = − 1.03.)

Moreover, there are reducing agents and oxygen scavengers that can be used as inhibitors to pitting by preventing the formation of ferric ions. As an example, zirconium corrodes in boiling 18% HCl+1% $FeCl_2$ as ferrous ions are oxidized to ferric ions. This is visible as the solution color changes from green to brown. Zirconium does not corrode when this solution is purged with hydrogen plus the addition of 1 g/L $SnCl_2$. With the help from these reducing agents, ferrous ions stay as ferrous ions (Ref 20), and, as a result, zirconium does not corrode.

Furthermore, the corrosivity of fluoride solutions may change dramatically with changing pH. Zirconium is totally defenseless in hydrofluoric acid at all concentration and temperature. It forms soluble zirconium complex ions in the acid. Although zirconium is not suitable for handling fluoride solutions, it has some resistance to certain fluoride solutions, such as calcium and sodium fluorides, when the pH is high enough and the temperature is low enough. The corrosion rate of zirconium in saturated calcium fluoride at pH 5 and 90 °C (195 °F) is nil (less than 0.025 mm/yr, or 1 mil/yr). The corrosion rates of zirconium in saturated sodium fluoride (pH is congruent to 7.4) are nil at 28 °C (80 °F) but greater than 1270 μm/yr (50 mils/yr) at 90 °C (195 °F). One major difference between calcium and sodium fluorides is their solubility in water. At room temperature, the solubility of calcium and sodium fluorides is 2 and 4300 ppm, respectively. Hot solutions with many dissolved fluoride ions could be corrosive to zirconium. However, the concentration of dissolved fluoride ions is not always proportional to the concentration of the added fluoride salt.

In a mixed solution of a chloride and a fluoride sharing a common cation, the solubility product, K_{sp}, of the difficult soluble salt cannot exceed a constant. For example, the K_{sp} of CaF_2, that is, $[Ca^{+2}]\times[F^-]^2$, in water at 26 °C (79 °F) is 3.95×10^{-11}. It is obvious that F^- ions tend to precipitate as CaF_2 when the concentration of Ca^{+2} increases. That is, CaF_2 is less soluble in water when $CaCl_2$ is also present, as indicated in Table 5.

Thermodynamically, hydrofluoric acid exists when the pH is less than or equal to 3.18 (Ref 9). Dissolved fluoride ions will be converted into hydrofluoric acid when the pH is lowered to less than 3.18. The solution then becomes vigorously corrosive to zirconium, regardless of temperature, with decreasing pH.

Table 5 Dissolved fluoride ions in mixed solutions

Solution					
$CaCl_2$, %	$MgCl_2$, %	F^- (NaF), ppm	F^- (CaF_2), ppm	pH	F^- in water, ppm
0.2	0.1	200	100	1	198
0.2	0.1	200	100	3	19
2.0	1.0	200	2800	1	91
2.0	1.0	200	2800	3	18
6.6	3.3	200	9800	1	68
6.6	3.3	200	9800	3	9

Zirconium is not recommended for handling fluoride-containing acids, unless the fluoride ion is complexed (Ref 21). Nevertheless, there are overlooked fluoride sources existing in the process (Ref 22). For example, technical-grade phosphoric acid may contain several thousand parts per million of fluoride ion, which is often not indicated in the specification. Food-grade phosphoric acid clearly gives the maximum fluoride content, typically less than 5 ppm. Other overlooked sources include contaminated waters, recycled acids, fluxes, and fluorinated compounds.

Pitting

Like other passive metals and alloys, zirconium is susceptible to pitting in all halide solutions except fluoride (Ref 23). Zirconium is vulnerable to general corrosion in fluoride solutions, and its susceptibility to pitting is greatest in chloride solutions. It decreases as the halide ion becomes heavier. The reversed order is the case for titanium, which is highly resistant to pitting in chloride solutions but is vulnerable to pitting in iodide solutions.

The pitting potentials of zirconium in 1 *N* solutions of Cl^-, Br^-, and I^- are 380, 660, and 910 mV_{SHE}, respectively. These potentials decrease gradually with increasing concentration and decrease rapidly in concentrated halide solutions (Ref 24). Other factors, such as pH (Ref 24), temperature (Ref 24), alloying element (Ref 25), and film quality (Ref 26), also affect pitting potential under certain conditions. The major concern for zirconium is pitting in chloride solutions.

Figure 6 illustrates the electrochemical behaviors of zirconium and stainless steel. In chloride-free solutions, zirconium is more corrosion resistant than stainless steel and most other passive alloys. In chloride-containing solutions, the advantage of zirconium disappears under an oxidizing condition. Zirconium may have a slightly higher pitting potential than stainless steel in chloride solutions. It pits at a much higher rate than stainless steel under a constant potential condition.

Zirconium does not pit in most chloride solutions, such as seawater and underground fluids, because its corrosion potential is often lower than the pitting potential (Ref 27, 28). The presence of oxidizing ions, such as ferric and cupric ions, in acidic chloride solutions may increase the corrosion potential to exceed the pitting potential. Therefore, pitting may occur. The standard potentials of several reduction/oxidation pairs are given in Table 6, which includes oxidizing ions other than ferric and cupric ions.

Pitting may also occur when there is an applied anodic potential or when zirconium is coupled with a noble material, such as graphite or platinum.

For iron, the dissolved oxygen in a chloride solution is enough to cause pitting due to its low pitting potential. For zirconium, the oxidizing power needs to be stronger than that of the cupric ion for inducing pitting. Then, there must be enough oxidizing ions in chloride solutions for pitting to occur. According to the mixing potential theory, the solution potential does not reach or exceed the pitting potential when there

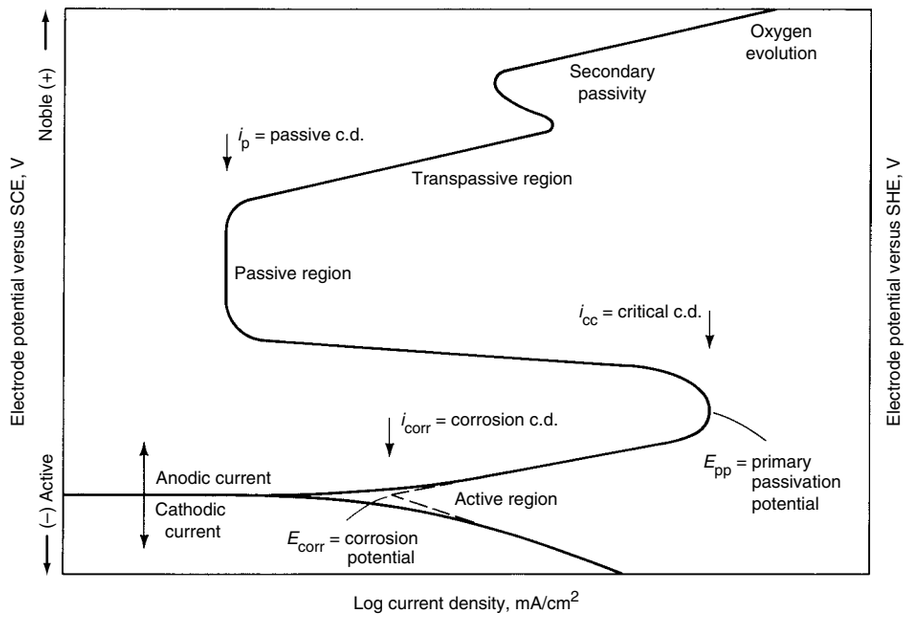

Fig. 6 The electrochemical behavior of stainless steel and zirconium. Solid line, common features found in stainless steel; broken line, common features found in zirconium in chloride-free dilute solutions, in chloride-free concentrated solutions, and in chloride-containing solutions. SCE, saturated calomel electrode; SHE, standard hydrogen electrode; c.d., current density

Table 6 Reduction/oxidation pairs

Reduction/oxidation pair	Standard potential versus SHE, V
Am^{4+}/Am^{3+}	2.18
$H_2O_2+H^+/H_2O$	1.77
Cl_2/Cl^-	1.36
Pd^{2+}/Pd	0.987
Pu^{4+}/Pu^{3+}	0.970
Fe^{3+}/Fe^{2+}	0.771
Cu^+/Cu	0.521
Cu^{+2}/Cu	0.337
Cu^{+2}/Cu^+	0.153
Sn^{4+}/Sn^{2+}	0.150
H^+/H_2	0.0
Sn^{2+}/Sn	−0.136
Fe^{2+}/Fe	−0.440

SHE, standard hydrogen electrode

are not enough oxidizing ions. Below the minimum amount of oxidizing ions, the presence of oxidizing ions may actually enhance the oxide formation process. The required minimum amount of oxidizing ions for inducing pitting depends on chloride concentration, pH, temperature, and other factors. It is not established but appears to range from a few parts per million in concentrated hydrochloric acid to 1000 ppm or more in dilute chloride solutions.

Pit initiation is complicated and not fully understood but is assumed to be the result of a unique type of anodic reaction. A model for the corrosion process within a pit after passing the initiation stage is discussed in Ref 29.

Considering the pitting of a metal in an aerated sodium chloride solution, rapid dissolution occurs within the pit, while oxygen reduction takes place on adjacent surfaces. In the presence of ferric ions, the reduction of ferric ion to ferrous ion is an additional reduction reaction. The rapid dissolution of metal within the pit tends to produce an excess of positive charge in this area, resulting in the migration of chloride ions to maintain electroneutrality. Thus, in the pit there is a high concentration of metal chloride. As a result of the hydrolysis of metal chloride, a high concentration of hydrogen ions is created. Both hydrogen and chloride ions stimulate the dissolution of most metals and alloys, and the pitting growth rate increases with time. These changes are not particularly harmful to zirconium.

In fact, after the creation of a pit, the condition becomes increasingly favorable for zirconium. Zirconium has the capability to form an oxide film in a reducing acid. After the reduction of some oxidizing ions, the driving force for pitting weakens with time. At a certain point, the pitting process stops due to the oxide formation at the pit. Often, zirconium has shallow pits covered with oxide films.

Pitting is an autocatalytic process for most metals and alloys but not for zirconium. Because of the ability of zirconium to form an oxide in low-pH solutions and the oxygen migration for film formation, oxygen moves to where a repair is needed. Pitting stops when the driving force weakens. Monitoring pitting by the electrochemical noise technique, on-going pitting slows down and then stops as a ferric chloride solution is diluting (Ref 30).

The presence of oxidizing ions in chloride solutions may induce localized corrosion on zirconium. Ferric and cupric ions are the most common and well known. There are also some strong oxidants, such as ions of noble metals, that, although rare, may also induce pitting on zirconium. Furthermore, ions of noble metals may be reduced to metal plating on the surface of zirconium, creating the galvanic effect.

When the pitting of zirconium is caused by an applied potential or galvanic coupling, the pit may continue to grow. At a constant potential above the pitting potential, the pit generation rate is always higher than the pit repassivation rate (Ref 26).

Nitrate and sulfate ions can inhibit the pitting of zirconium under certain conditions (Ref 20, 31, 32). Corrosion control measures for pitting and other types of corrosion are discussed in a later section.

Crevice Corrosion

In chloride solutions, zirconium is among the most resistant to crevice corrosion. Zirconium is not subject to crevice corrosion even in low-pH chloride solutions or chlorine gas. This can be rationalized by the model for crevice corrosion as given in Ref 29. In the initial stage of crevice corrosion, metal dissolution and oxygen reduction occur uniformly over the entire surface, including the interior of the crevice. After a short interval, the oxygen within the crevice is depleted because of its confinement, so oxygen reduction ceases within the crevice while metal dissolution continues. This tends to produce an excess of positive charge in the solution, which is necessarily balanced by the migration of negative chloride ions into the crevice. At the same time, positively charged ions, such as Fe^{3+}, stay outside the crevice. Similar to the pitting process, metal chloride dissociates into an insoluble hydroxide and a free acid ($H^+ + Cl^-$). In addition, the condition within crevices is too reducing to have ferric ions. These changes are actually favorable for zirconium. Consequently, zirconium is not susceptible to crevice corrosion in chloride solutions. Crevice corrosion tests done according to ASTM International and NACE International test methods have been performed to look for crevice corrosion, and none has been observed.

To follow the same model, zirconium would be susceptible to crevice corrosion in fluoride solutions. Crevice corrosion at the contact between zirconium and PTFE would be a special case. PTFE is an inert material and releases few fluoride ions when it is produced by the pressurized process. It can also be produced from recycled materials by remelting. Recycled PTFE is not as stable as virgin PTFE and may release large amounts of fluorides. Crevice corrosion of zirconium under PTFE gaskets occurred several times in acids when recycled PTFE or a less stable type of fluoropolymer had been used.

Furthermore, zirconium is susceptible to crevice corrosion in dilute sulfuric acid when the acid is allowed to concentrate within the crevice.

Intergranular Corrosion

Zirconium does not alloy as well as other more common materials. It is miscible only with titanium, hafnium, and scandium. Most elements have very low solubility in zirconium and form intermetallic compounds. Iron is the major, most visible impurity in zirconium. Zirconium-iron compounds are the most important to consider.

Depending on thermomechanical history, zirconium-iron compounds distribute in zirconium in several ways (Ref 33). Mill products typically have the uniform distribution of fine particles. Grain boundaries also are favorite sites for these particles to precipitate. More importantly, these particles tend to be spheroidal under the annealed condition. These particles become elongated in the HAZ and the weld metal under the as-welded condition, as shown in Fig. 7. When there are enough elongated particles, they tend to form interconnected networks and are not as corrosion resistant as zirconium in most environments. Consequently, the HAZ and the weld metal are susceptible to intergranular corrosion in media such as concentrated sulfuric and hydrochloric acids.

Heat treatment can be used to modify the morphology of the second-phase particles in the HAZ and the weld metal. Heating at 770 °C (1420 °F) is effective, as shown in Fig. 8. After heat treatment, elongated particles become spheroidal particles similar to those in the parent metal. The resistance of zirconium to intergranular corrosion is, therefore, greatly improved.

Stress-Corrosion Cracking

Zirconium and its alloys resist stress-corrosion cracking (SCC) in many environments, such as NaCl, $MgCl_2$, NaOH, and H_2S, which are strong SCC-inducing agents on common metals and alloys. Zirconium service failures resulting from SCC are few in chemical applications. The high SCC resistance of zirconium can be attributed to its high repassivation rate. In the presence of water or oxygen, any breakdown in the surface oxide film is quickly healed.

The environments known to cause SCC of zirconium include $FeCl_3$, $CuCl_2$, halogen or halide-containing methanol and certain other organics, concentrated HNO_3, liquid mercury or cesium (Ref 34), and 64 to 69% H_2SO_4 (Ref 35). Control measures for the SCC of zirconium include:

- Avoiding high sustained tensile stresses
- Modifying the environment by changing pH, concentration, or adding an inhibitor

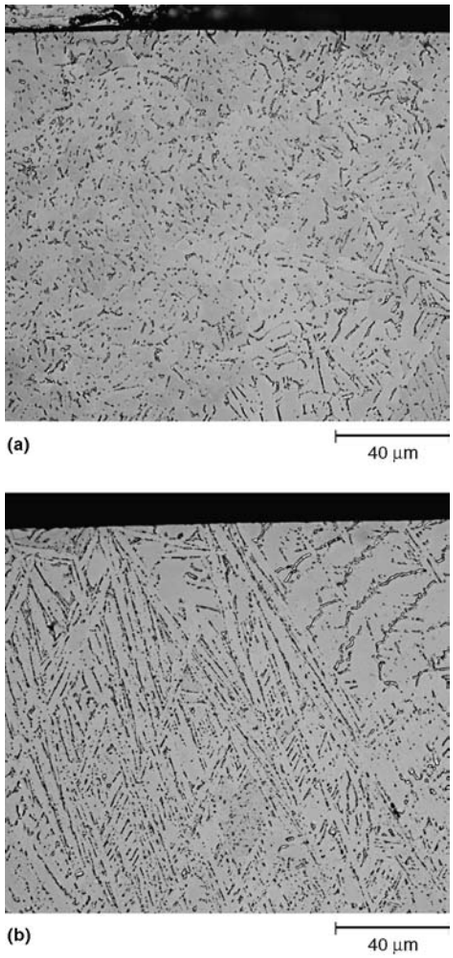

Fig. 7 Micrographs of as-welded Zr702. (a) Heat-affected zone. (b) Weld metal. Original magnification 825×

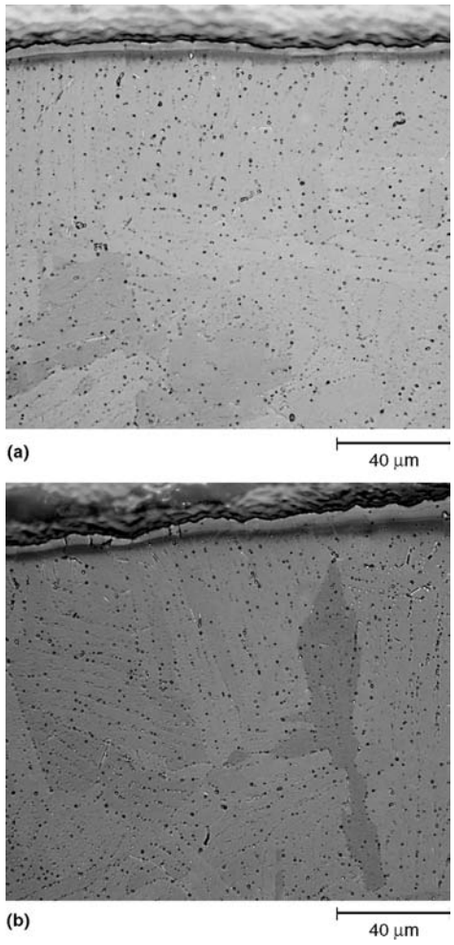

Fig. 8 Micrographs of welded Zr702 heat treated at 770 °C (1420 °F) for 1 h. (a) Heat-affected zone. (b) Weld metal. Original magnification 825×

- Maintaining a high-quality surface film—one low in impurities, defects, and mechanical damage
- Applying a small cathodic potential or coupling with a more active material
- Insulating the contact between zirconium and a noble material, such as graphite and platinum
- Shot peening

Delayed Hydride Cracking

Hydrogen is the lightest element. Yet, because of its mobility and reactivity, hydrogen finds many ways to cause external and internal damage in most metals and alloys. See the article "Hydrogen Damage" in *ASM Handbook,* Volume 13A, 2003. One process is delayed hydride cracking (DHC) in certain hydride-forming metals. The DHC of zirconium is discussed in Ref 36.

Certain metals, such as titanium and zirconium, that form brittle hydrides can fail by two embrittlement processes. One process is a reduction in the fracture toughness of the metal due to the presence of a high concentration of hydride platelets that have their in-plane dimensions in the crack growth direction. The second process is DHC, which is the result of a mechanism of crack initiation and slow propagation.

In DHC, hydrogen diffusion in the metal is required. Gradients of concentration (C_x), temperature (T), and stress (σ) are all important factors in controlling diffusivity, as given in the general diffusion equation:

$$J = \frac{DC_x}{RT}\left[RT\frac{d\ln C_x}{dx} + \frac{Q^*}{T}\frac{dT}{dx} - \frac{V^*}{3}\frac{d\sigma}{dx}\right]$$

where J is hydrogen flux, D is diffusivity of hydrogen at any point x, R is the gas constant, Q^* is the heat of transport of hydrogen in metal, V^* is the volume of transport of hydrogen in metal, and σ is positive for tensile stress and negative if compressive.

That is, hydrogen is driven by three forces to an area of lower concentration, colder temperature, and higher tensile stresses. Because DHC may occur at low temperatures in a matrix of uniformly distributed hydrogen, its mechanism is believed to be as follows: Stress gradients at stress concentration sites attract hydrogen, resulting in local hydride precipitation, growth, and reorientation. When the growing hydride reaches some critical size, the hydride either cleaves, or the hydride-matrix interface opens up to nucleate a crack. Once a crack has nucleated, propagation occurs by repeating the same process at the crack tip and, as such, is a discontinuous process. It should be noted that the formation of hydrides is not a necessary requirement for this mechanism to operate, as is the case in delayed hydrogen embrittlement in high-strength steels.

Stress and stress gradient are two necessary requirements for DHC to occur, and, fortunately, they are controllable. High stresses without gradients will not induce DHC. Hydrogen cannot move when high stresses are uniformly distributed in the structure. High-stress gradients are needed to move hydrogen but cannot be created without high stresses. High stresses are also required in fracturing hydrides.

It is estimated that hydrogen can hardly move from stress gradients generated by stressing up to 240 MPa (35 ksi). The common ASME requirement for unfired pressure vessels is to set the maximum allowable stresses at one-fourth the tensile strength at the operating temperature. As indicated in Table 3, the maximum allowable design stresses for zirconium alloys 702 and 705 are much lower than 200 MPa (29 ksi). Consequently, DHC should not occur when ASME requirements are met.

Due to its low coefficient of thermal expansion, residual stresses from welding are typically below the yield points. Nevertheless, residual stresses greater than 240 MPa (35 ksi) are possible. Minimum ASTM International yield requirements, however, for Zr702, Zr704, and Zr705 at room temperature are 210, 240, and 380 MPa (30, 35, and 55 ksi), respectively. This implies that only Zr705 is likely to retain high enough stresses from welding to become susceptible to DHC. Practically, this has been the case.

Stress-relieving treatment is one of the most effective measures in preventing DHC, a time-dependent process. It takes considerable time for hydrogen to reach the highly stressed area and to precipitate out as hydride platelets. The platelets must grow large enough for cracking to occur. Depending on many factors, it sometimes takes 2 years for DHC to happen, but 5 weeks after welding is the shortest known period for Zr705 to suffer DHC at room temperature. This provides a base for the *Boiler and Pressure Vessel Code of the ASME* (Ref 37):

> "Within 14 days after welding, all products of zirconium Grade R60705 shall be heat-treated at 1000 °F–1100 °F (538 °C–593 °C) for a minimum of 1 hr for thicknesses up to 1 in. (25.4 mm) plus $^1/_2$ hr for each additional inch of thickness. Above 800 °F (427 °C), cooling

shall be done in a closed furnace or cooling chamber at a rate not greater than 500 °F/hr (260 °C/hr) divided by the maximum metal thickness of the shell or head plate in inches but in no case more than 500 °F/hr. From 800 °F, the vessel may be cooled in still air."

Effects of Surface Condition

Corrosion is a surface phenomenon, so the existing surface condition is an important factor in the initiation and propagation of localized corrosion. The corrosion resistance of zirconium is not affected by common surface features, such as scratch and heat tint, but may be degraded by embedded particles, such as iron and silicon carbide, in oxidizing chloride solutions. As indicated in Fig. 9, zirconium with different surface conditions has a wide range of rest potential in a hydrochloric acid solution (Ref 20). The potential of pickled zirconium is low and stays low. The potential of zirconium with SiC-abraded surface increases quickly to reach the breakdown potential. In chloride solutions, it is preferred for zirconium to have a low potential that is below the breakdown potential. Pitting is therefore avoided. Zirconium with a clean, smooth surface is expected to have the optimal resistance to localized corrosion, including pitting, SCC, and DHC.

Galvanic Corrosion

An electrochemical potential difference usually exists between two dissimilar metallic or nonmetallic conductors when they are electrically connected in an electrolyte. An electric current is generated in the electrolyte between these two conductors. Consequently, the less corrosion-resistant conductor (the anode) will corrode faster, and the more corrosion-resistant conductor (the cathode) will corrode more slowly, as compared with the behavior of these conductors when they are not in contact. This form of corrosion is called galvanic corrosion. The area ratio between the anode and the cathode is an important factor in galvanic corrosion. It is preferable to have a small cathode with a large anode. Insulating dissimilar materials whenever practicable could be effective in preventing galvanic corrosion.

With the naturally occurring oxide film, zirconium assumes a noble potential in most environments. As an example, the galvanic series in seawater is given in Table 7. It can be seen that zirconium is close to the nobility of noble materials. Because zirconium is more corrosion resistant than most materials in a wide range of corrosives, zirconium is likely the cathode in most cases. The material in contact with zirconium could corrode at a much faster rate.

However, in incompatible environments, such as hydrofluoric acid and concentrated sulfuric acid, zirconium may assume an active potential. Moreover, zirconium may be activated at vulnerable sites when it is in contact with a noble material in chloride solutions. Graphite and carbides in the powder form can be very effective in promoting galvanic corrosion on zirconium, because a small amount of powder may produce a very large cathodic area. The effect of coupling with graphite on the corrosion of zirconium in boiling 20% HCl is shown in Table 8. It is evident that the effect can be dramatic when the surface area of graphite is significantly larger than that of zirconium.

Galvanic effect from carbon-base materials is common in chemical equipment, due to their popularity and the availability of various forms. Carbon-base materials are being used as structural materials, gaskets, additives to lubricants, and so on. Galvanic effects induced by carbon-base materials should be appraised not just for zirconium but also for other common metals and alloys.

Microbiologically Induced Corrosion

Regardless of whether the presence of living organisms is the primary reason or just a contributor to corrosion, microbiologically induced corrosion (MIC) can cause damage to equipment in contact with natural waters. Results of long-term tests in natural waters indicate that zirconium is immune to MIC.

Most organisms are sulfate-reducing bacteria. Metabolic processes may produce corrosives, such as sulfuric acid, inorganic or organic sulfides, and organic acids. Common metals and alloys have a high affinity for sulfur and its compounds. As a result, metabolic products simply make it too corrosive for common metals and alloys. Conversely, zirconium has little affinity for sulfur and its compounds. Zirconium resists attack by most inorganic and organic acids as well. Metabolic products are not corrosive to zirconium.

In addition, changes in oxygen potential, salt concentration, and pH from organisms do not degrade the corrosion resistance of zirconium. Cathodic depolarization associated with anaerobic growth is unfavorable to certain metals and alloys but not to zirconium.

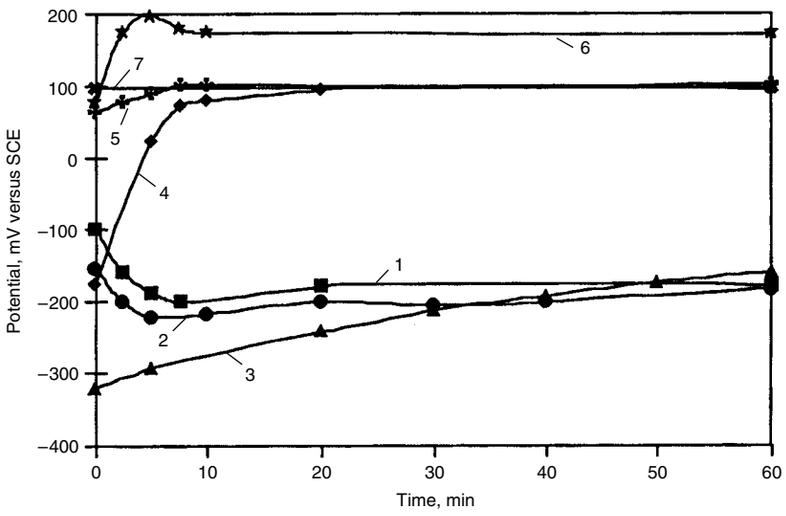

Fig. 9 Surface effect on the rest potential of Zr702 in 10% HCl plus 500 ppm ferric ion at 30 °C (85 °F). Rest potential is given in volts versus the saturated calomel electrode (SCE). (1) pickled; (2) pickled and scratched with broken glass; (3) polished with 1 μm alumina (Al_2O_3); (4) polished with 600-grit SiC; (5) polished with 600-grit Al_2O_3; (6) air annealed; (7) E_{crit}, the potential that initiates pitting

Table 7 Galvanic series in seawater

Cathodic (noble)
Platinum
Gold
Graphite
Titanium
Silver
Zirconium
Type 316, 317 stainless steels (passive)
Type 304 stainless steel (passive)
Type 410 stainless steel (passive)
Nickel (passive)
Silver solder
Cupronickel (70 : 30)
Bronzes
Copper
Brasses
Nickel (active)
Naval brass
Tin
Lead
Type 316, 317 stainless steels (active)
Type 304 stainless steel (active)
Cast iron
Steel or iron
Aluminum 2024
Cadmium
Aluminum (commercially pure)
Zinc
Magnesium and its alloys
Anodic (active)

Erosion-Corrosion

Erosion is accelerated corrosion resulting from the conjoint action of corrosion and erosion in the presence of a moving corrosive fluid. This type of attack is highly dependent on fluid flow rate and corrosivity. It is particularly prevalent in areas where high local turbulence, impingement, or cavitation of the fluid occurs on metal surfaces. Suspended solids in fluid result in abrasion that may drastically accelerate metal removal.

In compatible environments, zirconium forms a hard, tenacious ZrO_2 surface film that provides an excellent barrier to erosion-corrosion. Also, zirconium can quickly repair damage done to the film in environments containing oxygen. Consequently, zirconium can withstand many corrosives at high flow rates. A corrosion test loop was constructed to investigate the effects of flow rate and heat flux on the corrosion of zirconium tube specimens (Ref 38). There was no effect when the test conditions are 50% sulfuric acid at 166 °C (330 °F) flowing at 2.1 m/s (7 ft/s).

Many passive alloys have difficulty forming protective films on their surfaces in sulfuric acid. They are vulnerable to erosion-corrosion in the acid. This is seen in Fig. 10 (Ref 39). In a sulfuric-acid-based mixture, the corrosion of zirconium is insensitive to increasing rotation speed up to 10,000 rpm. On the other hand, the corrosion of a Ni-Cr-Mo-W alloy C-276 increases continuously from low speed to high speed under the same test conditions.

Fretting Corrosion

Fretting corrosion results from the combined effects of wear and corrosion and takes place when vibration contact is made at the interface of tight-fitting, highly loaded surfaces, such as between the leaves of a spring or in rolling-contact bearings. Factors affecting fretting corrosion include contact load, amplitude, frequency, temperature, and corrosivity of the environment.

Fretting corrosion is a concern for zirconium, because zirconium is a soft and reactive metal. It occurs when zirconium protective oxide film is mechanically damaged or removed. Measures should be taken to control fretting corrosion. Fretting corrosion on zirconium may be avoided by proper design and fabrication or through the addition of a heavy oxide coating to eliminate mechanical factors. This coating drastically reduces friction and prevents the removal of the protective oxide layer.

Table 8 Effect of graphite coupling on the corrosion of zirconium in boiling 20% HCl after four weeks of exposure

Specimen area						
Graphite		Zirconium		Area ratio graphite/zirconium	Corrosion rate	
cm^2	$in.^2$	cm^2	$in.^2$		mm/yr	mils/yr
...	...	31.0	4.8	0	0.013	0.5
5.9	0.9	31.0	4.8	0.19	0.013	0.5
24.8	3.8	5.0	0.8	4.96	0.0173(a)	0.7(a)
27.0	4.2	2.5	0.4	10.8	0.239(a)	9.4(a)

(a) Localized corrosion. Source: Ref 20

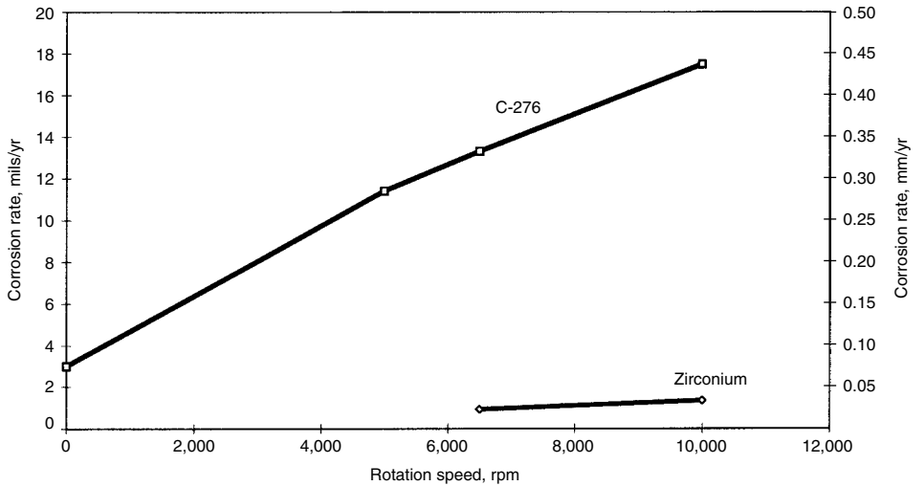

Fig. 10 Results of rotating cylinder electrode tests in a mixture of sulfuric acid, organic acids, and water at 100 °C (212 °F) compared to Ni-Cr-Mo-W alloy C-276

Effects of Tin Content in Zirconium

Zircaloy recycling is a major source for zirconium in making zirconium alloys. There may be more than 2000 ppm tin in Zr702 without violating the chemical requirements given in Table 1. Advantages of using Zircaloy recycle include consistent mechanical properties, improved corrosion/oxidation resistance in water and steam, reduction in cost, and material conservation. While small amounts of tin may be beneficial or acceptable for Zr702, high tin content will degrade corrosion resistance. Because of the mechanical strength advantage over Zr702, Zircaloys have been used to make fittings for corrosive applications. Zircaloy fittings have failed in hot glacial acetic acid after 3 weeks to 5 months of service (Ref 40). Zr702 and Zr705 are known to be highly compatible with acetic acid. The failures are attributed to the high tin content (~1.4%) in the alloys.

Zircaloys were developed for improved corrosion properties in water and steam. The tin addition was intended to offset the harmful effects from impurities such as nitrogen in zirconium, and initially, the nitrogen content in zirconium was typically higher than 40 ppm. However, the nitrogen content of the present Zircaloys is lower, and tin is found to be a harmful alloying element. Corrosion resistance in 400 °C (750 °F) steam improves with decreasing tin content from 1.41 to 0.09% in the Zircaloy-4-based alloy (Ref 41). It should be noted that the test temperature is much higher than the operating temperature of zirconium equipment in most corrosive applications. The tin effect is expected to decrease with decreasing temperature.

Results of 28 day tests show that the presence of greater than 3000 ppm tin is much more critical to zirconium in boiling sulfuric acid than in boiling acetic, hydrochloric, and nitric acids. The critical tin content in zirconium for sulfuric acid service seems to be between 2000 and 3000 ppm (Ref 42). Although tin is reasonably soluble in zirconium, the distribution of tin in zirconium is much more irregular than that of oxygen in zirconium (Ref 42). To take the fluctuation into consideration, the target point for the tin content in Zr702 should be set at 1500 ppm, if 2000 ppm proves to be the limit for the alloy in sulfuric acid service (Ref 42). Recently generated data seem to support this recommendation (Ref 43). Samples of Zr702 with 1400 ppm tin outperform those of Zr702 with 2400 ppm tin in sulfuric acid solutions at elevated temperature (Ref 43).

Corrosion mechanisms for the tin effect are discussed in Ref 41 and 42. A small amount of tin is soluble in zirconium, but because the atomic radius of tin is slightly larger than that of zirconium, tin is not very mobile in zirconium. There may be preferred sites, such as grain boundaries, for tin to settle. The distribution of tin is not as uniform as that of oxygen in zirconium. Furthermore, tin is not as reactive as zirconium. When both zirconium and tin are exposed

to oxygen, zirconium will quickly react with oxygen to protect tin from being oxidized. The oxide film formed at low temperatures is expected to be almost all zirconium oxide. There must be an enriched layer of tin at the metal/oxide interface. When the oxide film grows at a high temperature, tin tends to diffuse into the oxide film, likely through grain boundaries. The higher the tin content, the more tin will diffuse into the oxide film. Tin will be oxidized to form particles of tin oxides in the oxide layer. The particle size of tin oxides would be larger with a higher tin content. A high corrosion rate is possible when tin-enriched areas are exposed to a corrosive. Tin effects may not show up in short-term tests and tend to be irregular.

Corrosive Environments

Water and Steam. Zirconium has excellent corrosion and oxidation resistance in water and steam at temperatures exceeding 300 °C (570 °F). Zirconium has a great capability to take oxygen from water to form a protective oxide film. It retains this capability even in highly reducing media, such as hydrochloric acid and dilute sulfuric acid. Most passive metals form protective oxide films in aqueous solutions only when the solutions are somewhat oxidizing. Consequently, zirconium is uniquely suitable for nuclear applications, because water-cooled reactors operate with oxygen- or hydrogen-charged coolant at temperatures from 286 to 350 °C (547 to 660 °F).

However, corrosion and oxidation of unalloyed zirconium in high-temperature water and steam were found to be irregular (Ref 44, 45) and are related to variations in the impurity content of the metal. Nitrogen and carbon impurities are particularly harmful. The oxidation rate of unalloyed zirconium increases markedly when nitrogen and carbon concentrations exceed 40 and 300 ppm, respectively (Ref 44, 45). The irregular behavior of unalloyed zirconium stimulated alloy development programs. Zircaloy-2, Zircaloy-4, Zr-2.5Nb, and Zr-1Nb are the most important alloys developed for nuclear applications, because they are more reliable and predictable for use in hot water and steam, in addition to being stronger.

As compared to unalloyed zirconium, Zircaloy-2 has an improved character in oxide formation at elevated temperatures. A tightly adherent oxide film forms on this alloy at a rate that is at first quasi-cubic but, after an initial period, undergoes a transition to linear behavior. Unlike the white, porous oxide films on unalloyed zirconium, the oxide film on Zircaloy-2 remains dark and adherent throughout transition and in the posttransition region.

Zircaloy-4 differs in composition from Zircaloy-2 by having a slightly higher iron content but no nickel. Both variations are intended for reducing hydrogen pickup with little effect on corrosion resistance in reactor operation. For example, in water at 360 °C (680 °F), hydrogen pickup for Zircaloy-4 is approximately 25% of theoretical, or less than half that for Zircaloy-2. In addition, hydrogen pickup for Zircaloy-4 is less sensitive to hydrogen overpressure than that for Zircaloy-2. For both alloys, hydrogen pickup is greatly reduced when dissolved oxygen is present in the medium (Ref 44).

The Zr-2.5Nb alloy is considered somewhat less resistant to corrosion than the Zircaloys, with exceptions. Nevertheless, the Zr-2.5Nb alloy is suitable for many applications, such as pressure tubes in the primary loops of some reactors. Furthermore, the corrosion resistance of the Zr-2.5Nb alloy can be substantially improved by heat treatments (Ref 45, 46). In addition, the Zr-2.5Nb alloy is superior to the Zircaloys in steam at temperatures above 400 °C (750 °F) (Ref 46).

However, unalloyed zirconium does not seem to have as irregular behavior in common waters as in pure water. Common waters, such as city water, river water, and seawater, are used as the cooling medium in the chemical processing industry. They have much higher levels of impurities than water used in the nuclear industry. Very often, one side of zirconium equipment faces a corrosive environment, and the other side faces cooling water. The highest temperature has been approximately 300 °C (570 °F), and the longest time is more than 20 years. Zirconium has performed well in these waters.

The major difference between pure water and common waters is their corrosivity. Assuming the formed oxide film on unalloyed zirconium in pure water is totally insoluble, the oxide film will continue to grow. Eventually, too much stress will build up within the film, due to the big volume difference between the metal and the oxide. The densities of zirconium and (m) ZrO_2 are 6.49 and 5.73 g/cm^3, respectively. When the oxide film becomes too thick, it is difficult to stay compact and breaks down at weak spots.

The very slight dissolving power of common waters on the oxide film could relieve some of the built-up stress and keep the oxidation process in better balance. Then, the irregular behavior of unalloyed zirconium in common waters is avoided.

A unique example regarding the chemical processing industry includes two zirconium heat exchangers retired from a urea plant after continual service for 20 years. The tubes looked like new and were used to build yet another heat exchanger. The watersides of the tubes were covered with very thin oxide films without any sign of breakaway oxidation after 20 years of use.

Saltwaters. Zirconium has excellent corrosion resistance to seawater, brackish water, and polluted water. The advantages of zirconium in saltwaters include its insensitivity to variation in factors such as chloride concentration, pH, temperature, velocity, crevice, and sulfur-containing organisms. The effects of pH when there are some iron ions in saltwater were discussed earlier.

Zr702 specimens, welded and nonwelded, with and without a crevice attachment, were placed in the Pacific Ocean at Newport, Ore., for up to 129 days and had nil corrosion rates. Marine biofouling was observed; however, no attack was found beneath the marine organisms or within the crevices.

Laboratory tests were performed on specimens of Zr702 and Zr704 in boiling seawater for 275 days and in 200 °C (390 °F) seawater for 29 days. Both alloys resisted general corrosion, pitting, and crevice corrosion.

U-bend specimens, with and without steel coupling, of Zr702, nickel-containing Zr704 (Zircaloy-2), and nickel-free Zr704 (Zircaloy-4) were tested in boiling seawater for 365 days. No cracking was observed during the test period. Overstressing of the tested U-bends indicated that all specimens, except one, remained ductile. The exception was the welded nickel-containing Zr704 with steel coupling, which showed some hydrogen and oxygen absorption (Ref 28). Chemical analyses and metallographic examinations on other U-bends did not reveal any evidence of hydrogen absorption and hydride formation. Results of chemical analyses are given in Table 9. These results support that the presence of nickel in zirconium promotes hydrogen pickup.

Sulfur and its compounds are often present in underground fluids, such as oil, natural gas, and geothermal fluids. Although zirconium is a reactive metal, it has very little affinity for sulfur and consequently has excellent corrosion resistance to sulfur and its compounds. It requires a high temperature (700 to 900 °C, or 1290 to 1650° F) for zirconium to react with sulfur vapor or hydrogen sulfide to yield sulfides. Moreover, there is no instance of zirconium-sulfur bonds forming in aqueous systems (Ref 47, 48). Practically, zirconium is immune to sulfide stress cracking.

Sulfuric acid is the most important sulfur compound and is the most important acid for use in the manufacture of many chemicals. For example, the acid is used as a dehydrating agent, an oxidizing agent, an absorbent, a catalyst, and a

Table 9 Hydrogen and oxygen analyses of zirconium-steel coupled U-bend test specimens

365 day test in boiling seawater

Specimen	Condition	Hydrogen/oxygen content, ppm	
		Hydrogen	Oxygen
Zr702-steel	Unwelded	6	1350
Zr704 (nickel-containing)-steel	Unwelded	8	1480
Zr704 (nickel-free)-steel	Unwelded	9	1440
Zr702-steel	Welded	8	1250
Zr704 (nickel-containing)-steel	Welded	450	5000
Zr704 (nickel-free)-steel	Welded	5	1480

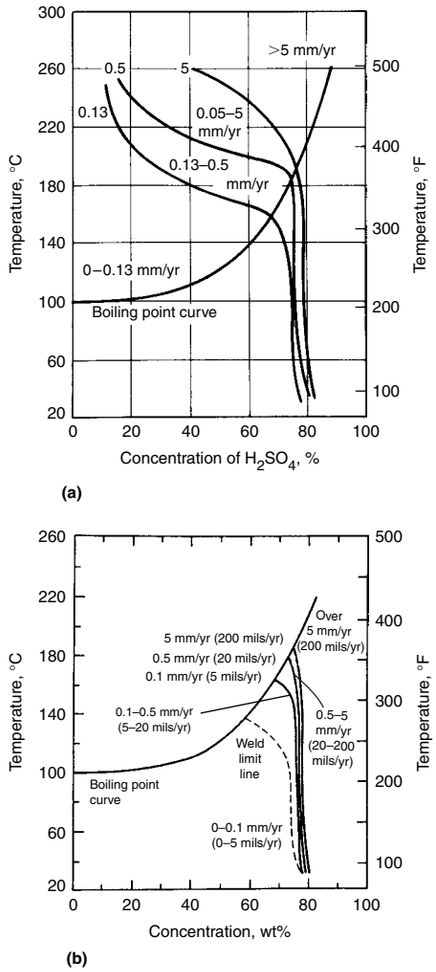

Fig. 11 Isocorrosion diagrams of zirconium in sulfuric acid. (a) Early data on ungraded zirconium. (b) Zr-702

reagent in chemical syntheses. These highly versatile capabilities can be attributed to the complicated nature of this acid. Sulfuric acid is corrosive, with a continuously changing character. It changes from the reducing nature of dilute acid to the oxidizing nature of concentrated acid. The reactivity of sulfur compounds and the difficulty of forming protective oxide films under reducing condition make common passive metals vulnerable to corrosion in dilute acid. In fact, hot, dilute acid is a pickling solution for steel and stainless steel. Solutions become increasingly oxidizing at or above 65%. The usefulness of passive metals and alloys depends strongly on acid concentration, temperature, aeration, and other impurities.

Zirconium and its alloys are straightforward in their corrosion resistance to sulfuric acid, as shown in Fig. 11 to 13 (Ref 49). Published data for zirconium before the establishment of Zr702 were collected to construct Fig. 11(a). Corrosion data generated at Wah Chang are used to construct Fig. 11(b) to 13 for ASTM International grades. It should be noted that isocorrosion curves are normally constructed based on the results of laboratory tests conducted under well-controlled conditions. The curves should be used to understand the corrosion behavior of the alloys rather than to predict the performance of the alloys in actual service. There are many factors, including impurities in the alloys and environments, equipment design and fabrication, operating conditions, and maintenance, that affect the performance of the alloys.

Zirconium and its alloys resist attack by sulfuric acid at all concentrations up to 70%. The major difference among these grades is near the boiling region when the acid concentration is greater than 60%. In this region, Zr702 outperforms Zr704 and Zr705. In 70 to 80% sulfuric acid, the corrosion resistance of zirconium and its alloys depends strongly on temperature. In higher concentrations, the corrosion rate of zirconium and its alloys increases rapidly with concentration due to the formation of nonprotective zirconium sulfate film.

There are three regions in Fig. 11(a) that are attractive for using zirconium in sulfuric acid services. The first region is dilute sulfuric acid, $\leq$10%, at elevated temperatures. In this region, the temperature limit for zirconium is well above 200 °C (390 °F). The second region is hot 10 to 45% sulfuric acid. In this region, zirconium is highly stable in the passive state. It can tolerate many oxidizing impurities and some chlorides. The third region is 45 to 70% sulfuric acid, where zirconium stays corrosion resistant when factors such as acid concentration and impurities are closely monitored and controlled within the limitations.

The corrosion behavior of zirconium can be further examined from electrochemical measurements. The anodic polarization curves of zirconium in 4.9 to 72.5% sulfuric acid at near-boiling temperature are shown in Fig. 14. As indicated in Fig. 14, zirconium experiences a passive-to-transpassive transition in sulfuric acid with an increasing potential. Zirconium does not have the active region in sulfuric acid as is the case with common metals and alloys. The very high transpassive (breakdown) potentials in dilute sulfuric acid are also seen. This indicates zirconium can tolerate large amounts of oxidizing agents, such as ferric, cupric, and nitrate ions, in dilute sulfuric acid. For example, there is no effect on zirconium in a steel pickling application, even after a few percent of iron dissolves in dilute sulfuric acid, provided that chlorides are not present.

In >20% sulfuric acid, the breakdown potential of zirconium decreases noticeably with increasing concentration. There still is a visible passive region for zirconium in 65% sulfuric acid. This means zirconium can tolerate some amounts of strong oxidizing agents in $\leq$65%

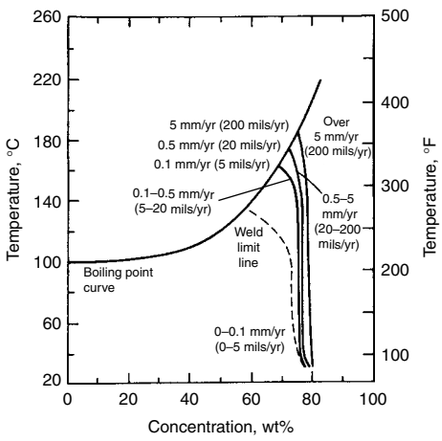

Fig. 12 Isocorrosion diagram of Zr704 in sulfuric acid

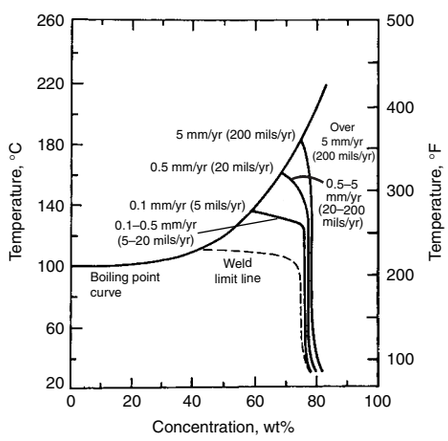

Fig. 13 Isocorrosion diagram of Zr705 in sulfuric acid

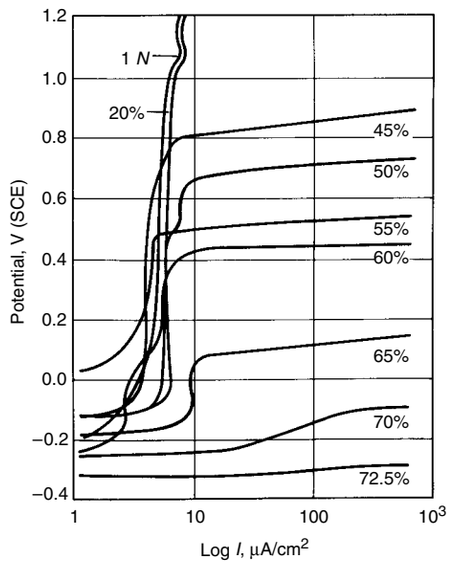

Fig. 14 Anodic polarization curves for Zr702 in sulfuric acid at near-boiling temperature. Applied potential is given in volts versus the saturated calomel electrode (SCE)

sulfuric acid (Ref 50). In >65% sulfuric acid, zirconium becomes sensitive to the presence of oxidizing agents. Figure 15 illustrates the effect of the presence of 200 ppm of various oxidizing agents on zirconium in >65% sulfuric acid.

The acid concentration limit is very important when zirconium is used to process sulfuric acid in the marginal-concentration region (60% or more). In less than 65% sulfuric acid, although the vapor is almost entirely water, the concentration shows little change in a pressurized system. However, acid concentration can change significantly because, for example, of imperfect sealing of a system. Acid concentration can easily change in a vacuum system, because the water vapor is continuously removed.

When the acid concentration limit is exceeded, zirconium may corrode rapidly. Under certain conditions, a pyrophoric surface layer may be formed on zirconium. The pyrophoric surface layer on zirconium formed in 77.5% sulfuric acid plus 200 ppm ferric ion at 80 °C (175 °F) consisted of γ-hydride, zirconium sulfate, and fine metallic particles. The combination of γ-hydride and metallic particles is suggested to be responsible for the pyrophoricity (Ref 51). Treating in hot steam can be used to eliminate this tendency to spontaneously combust when exposed to air.

As shown in Fig. 11(b) to 13, the resistance of zirconium in >55% sulfuric acid is somewhat degraded when welded. Zirconium weld metal may corrode preferentially and can be attributed to the morphology of the second-phase particles, as previously discussed. Heat treatment at 775 ± 15 °C (1425 ± 27 °F) for 1 h per 25.4 mm (1 in.) of thickness can be used to restore the corrosion resistance of weld metal.

The presence of chlorides in sulfuric acid does not degrade corrosion resistance unless oxidizing ions are also present. When heavy metal ions and halide ions coexist in sulfuric acid, the optimal acid concentration range for zirconium is 60 to 65%. Sulfate ion possesses a mild inhibitive effect on the pitting of zirconium in chloride solutions. In ≤1% chloride solution, a minimum $[SO_4^{2-}]/[Cl^-]$ ratio of ≥42 is needed for inhibition (Ref 20). The more sulfate ions in the solution, the more oxidizing ions zirconium can tolerate before pitting occurs. Figure 16 can be used as a guide when chloride ions and oxidizing ions coexist. Table 10 indicates that sulfuric acid of approximately 60% concentration would be the optimal range for Zr702 to face the coexistence of chloride ions and oxidizing ions.

Halides. Zirconium resists attack by most halides, including halogen acids. Exceptions include hydrofluoric (HF) acid and oxidizing chloride solutions. It has been discussed that surface condition greatly affects the corrosion of zirconium in oxidizing chloride solutions. Zirconium has some corrosion resistance in certain fluorides when the pH is high enough. For example, a few parts per million fluoride ions in city or groundwater have little effect on corrosion resistance. However, a few parts per million hydrofluoric acid will noticeably increase the general corrosion of zirconium.

Nevertheless, zirconium and its alloys have very limited usefulness in fluoride-containing solutions. The concern is general corrosion but not pitting. Zirconium and its alloys exhibit low corrosion rates in fluoride solutions only when the temperature is low enough and the pH is high enough. They are totally defenseless in HF-containing solutions. Hydrofluoric acid exists when the pH is less than 3.18. This does not mean that all fluoride ions will be converted into hydrofluoric acid when the pH is less than 3.18, at least not immediately. The effect of pH on the corrosion of zirconium in fluoride-containing solutions is shown in Table 11 (Ref 52).

In recent years, it appears that the chance to have some fluorides in the process stream has increased. Fluorides may come from often overlooked sources (Ref 21, 22) that include recycled chemicals and PTFE. For example,

Table 10 Inhibiting effect of SO_4^{2-} on the corrosion of zirconium in boiling H_2SO_4 containing $FeCl_3$

Medium	Temperature		Corrosion rate(a)	
	°C	°F	mm/yr	mils/yr
40% H_2SO_4 + 2% $FeCl_3$	115	240	5(b)	199(b)
50% H_2SO_4 + 2% $FeCl_3$	124	255	2	80
55% H_2SO_4 + 2% $FeCl_3$	131	270	2.1	83
60% H_2SO_4 + 2% $FeCl_3$	141	285	0.66	26
70% H_2SO_4 + 2% $FeCl_3$	166	330	0.84	33

(a) Calculated from four 1 day cycles. (b) Localized corrosion

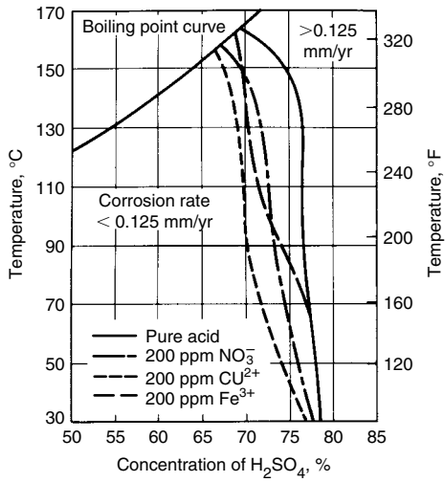

Fig. 15 Effect of various oxidizing ions on the 0.125 mm/yr (4.9 mils/yr) isocorrosion line for Zr702 in sulfuric acid

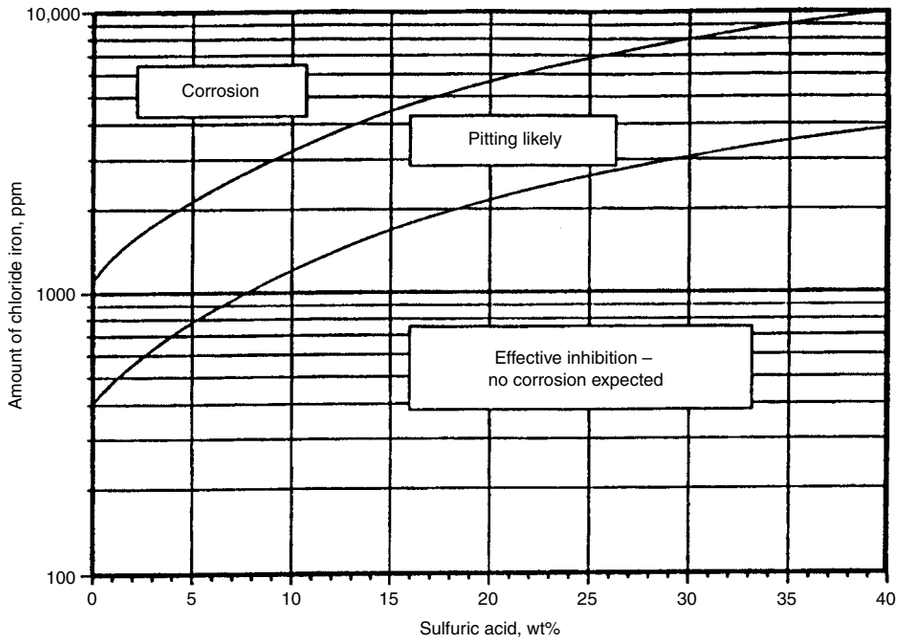

Fig. 16 Chloride allowable for Zr702 in sulfuric acid in the oxidizing condition

recycled sulfuric acid may contain more than 100 ppm fluoride ions (Ref 21). When zirconium equipment faces fluoride-containing acids, inhibitors that form strong fluoride complexes should be added for protection (Ref 21). Effective inhibitors include zirconium sponge, soluble zirconium chemicals, and phosphorous pentoxide. Table 12 gives the results of the effects of certain inhibitors on zirconium corrosion in fluoride-containing solutions.

However, the presence of an acidic fluoride solution is not always bad for zirconium. It counteracts the effect of an oxidizing agent. That is, it makes an oxidizing solution less oxidizing or even reducing. Consequently, zirconium is less vulnerable to pitting and SCC in fluoride-containing acids (Ref 20).

Unlike titanium and tantalum, the corrosion resistance of zirconium in halides increases in the order of chloride, bromide, and iodide. Unless the condition is oxidizing, zirconium is very corrosion resistant in chloride solutions, including strong hydrochloric acid. Oxidizing conditions include the presence of oxidizing agents, coupling with a noble material and applied anodic potential.

Zirconium and its alloys are highly corrosion resistant in up-to-saturated chloride solutions at temperatures to 250 °C (480 °F). This resistance changes little with changing temperature and pH when the pH is greater than or equal to 1. Within this range, the passive film on zirconium and its alloys hardly dissolves.

Zirconium and its alloys are susceptible to pitting in ferric-chloride-containing solutions. However, ferric ion does not exist in chloride solutions under all conditions. For ferric ions to exist in solution, the pH must be less than 2.5. The solution also must be free of reducing agents. Ferric ions show harmful effects on zirconium only in very acidic solutions, such as hydrochloric acid.

Without the presence of oxidizing agents, zirconium is one of the most corrosion-resistant metals to hydrochloric acid. As shown in Fig. 17, zirconium is totally resistant to attack in all concentrations of hydrochloric acid. Normally, stainless alloys can be considered only for handling very dilute and/or low-temperature hydrochloric acid. Zirconium would outperform stainless alloys in hydrochloric acid. Moreover, zirconium is not as susceptible to hydrogen embrittlement in hydrochloric acid as tantalum.

Although hydrochloric acid is reducing, the anodic polarization curves of zirconium still do not have an active region (Fig. 18). This corrosion property explains the resistance of zirconium to crevice corrosion in chloride-containing solutions.

However, Fig. 18 shows that zirconium may suffer pitting and/or SCC when it is anodically polarized to a potential at or exceeding the pitting potentials. The same types of corrosion problems can be developed in hydrochloric acid when strong oxidizing agents are present. Figure 19 illustrates the detrimental effect of ferric ions in 20% HCl at 100 °C (212 °F). The presence of ferric ions polarizes the zirconium surface to a potential exceeding the pitting potential. Thus, local breakdown of the passive surface at preferred sites occurs, and a condition develops that favors pitting and/or SCC.

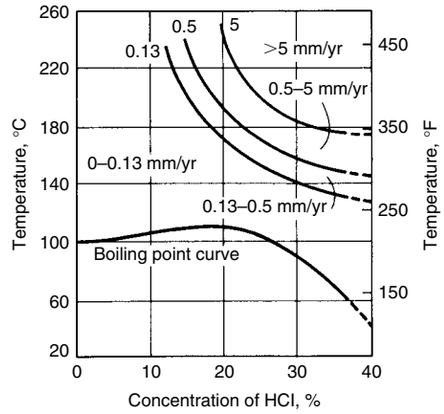

Fig. 17 Isocorrosion diagram of Zr702 in hydrochloric acid

Table 11 Corrosion of Zr702 in fluoride-containing solutions at 80 °C (175 °F) after four 1 day cycles

Solution						Corrosion rate	
$CaCl_2$, %	$MgCl_2$, %	F (as NaF), ppm	F (as CaF_2), ppm	P_2O_5, ppm	pH	mm/yr	mils/yr
0.2	0.1	200	100	...	1	8.79	346
0.2	0.1	200	100	...	3	0.17	6.7
0.2	0.1	200	100	1200	1	3.54	139
0.2	0.1	...	300	...	1	8.79	346
0.2	0.1	...	300	1200	1	0.39	15.4
2.0	1.0	200	2800	...	1	2.87	113
2.0	1.0	200	2800	...	3	0.01	0.4
2.0	1.0	200	2800	800	1	0.13	5.1
2.0	1.0	...	300	...	1	3.71	146
2.0	1.0	...	300	1200	1	0.01	0.4
6.6	3.3	200	9800	...	1	1.92	75.6
6.6	3.3	200	9800	...	3	0.01	0.4
6.6	3.3	200	9800	800	1	0.00	0.00
6.6	3.3	...	300	...	1	1.02	40.2
6.6	3.3	...	300	1200	1	0.02	0.8

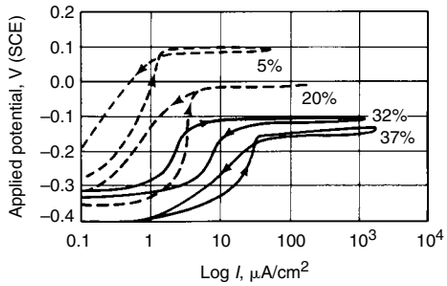

Fig. 18 Anodic polarization curves for Zr702 in hydrochloric acid at near-boiling temperature. Applied potential is given in volts versus the saturated calomel electrode (SCE)

Table 12 Effect of zirconium sponge or phosphorous pentoxide on the corrosion of Zr702 in fluoride-containing solutions

		Temperature		Corrosion rate	
Medium	Inhibitor	°C	°F	mm/yr	mils/yr
7.2% AlF_3 + 0.5% HF	None	90	195	>25	>1000
	16% Zr sponge	90	195	<0.03	<1
0.2% $CaCl_2$ + 0.1% $MgCl_2$ + 620 ppm CaF_2; pH 1	None	80	175	9	350
	1200 ppm P_2O_5	80	175	0.4	15
2% $CaCl_2$ + 1% $MgCl_2$ + 620 ppm CaF_2; pH 1	None	80	175	4	150
	1200 ppm P_2O_5	80	175	<0.03	<1
6.6% $CaCl_2$ + 3.3% $MgCl_2$ + 620 ppm CaF_2; pH 1	None	80	175	1.0	40
	1200 ppm P_2O_5	80	175	<0.03	<1
90% HNO_3 + 200 ppm HF	None	25	75	>25	>1000
	800 ppm Zr sponge	25	75	0.03	1

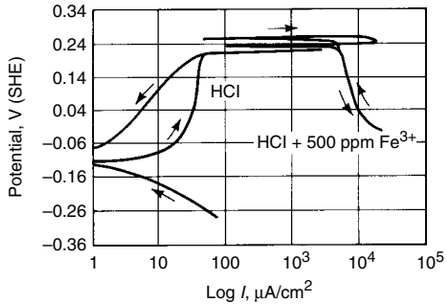

Fig. 19 Effect of 500 ppm ferric ions on the anodic polarization of Zr702 in 20% hydrochloric acid at 100 °C (212 °F). Potential is given in volts versus the standard hydrogen electrode (SHE).

Maintaining zirconium at a potential in its passive region, which is arbitrarily set at 50 to 100 mV below the corrosion potential, can counteract the detrimental effects resulting from the presence of ferric ions.

Nitric Acid. Due to its passivating power, nitric acid is not considered to be a difficult acid for passive metals and alloys to handle. However, nitric acid becomes highly corrosive when its temperature is high or when impurities, such as heavy-metal ions, are present. The passivating power favors the formation of oxide films but may also cause the passive films to break down.

Zirconium is considerably more suitable than most passive alloys for handling nitric acid, particularly when the acid is hot, impure, and/or variable in concentration. Under certain conditions, zirconium is even more resistant than the noble metals to the acid. Zirconium temperature limit is somewhat higher than that of the noble metals. Traces of chloride ion may lead to rapid attack of noble metals but not of zirconium.

The excellent corrosion resistance of zirconium in nitric acid has been recognized for more than 30 years (Ref 53–55). Below the boiling point and at 98% nitric acid, and up to 250 °C (480 °F) and at 70% nitric acid, the corrosion rate of zirconium is less than 0.13 mm/yr (5 mils/yr) (Fig. 20).

Zirconium is normally susceptible to pitting in acidic oxidizing chloride solutions. However, nitrate ion is also an inhibitor for the pitting of zirconium because of its passivating power. The minimum $[NO_3^-]/[Cl^-]$ molar ratio required to inhibit pitting of zirconium is between 1 (Ref 31, 54, 55) and 5 (Ref 56). Results of tests indicate that zirconium resistance is not degraded in up to 70% nitric acid with dissolved 1% ferric chloride, 1% sodium chloride, 1% seawater, 1% ferric ion, or 1% stainless steel at 204 °C (400 °F) (Ref 57). Still, the presence of an appreciable amount of HCl should be avoided, because zirconium is not resistant to aqua regia.

In the production of nitric acid, ammonia is oxidized with air over platinum catalysts. The resulting nitric oxide is further oxidized into nitrogen dioxide, then absorbed in water to form nitric acid. Acid of up to 70% concentration is produced at temperatures up to 204 °C (400 °F) by the process. Zirconium is one of very few materials that is suitable for this process when the temperature is near the high end.

The polarization curves of zirconium in nitric acid are shown in Fig. 21. Again, zirconium has the passive-to-transpassive transition similar to that which occurs in sulfuric acid. However, corrosion potentials are noble because of the oxidizing nature of nitric acid. As indicated in the aforementioned test results, common oxidizing agents, such as ferric ions, do not affect the corrosion resistance of zirconium in nitric acid. The polarization curves do suggest that zirconium may be susceptible to SCC in concentrated nitric acid. This is shown by the low passive-to-transpassive potential. This is consistent with the observation of SCC in U-bend specimens in greater than 70% nitric acid (Ref 58). The slow strain-rate technique reveals zirconium susceptibility to SCC in less than 70% nitric acid (Ref 59). Results of C-ring tests indicate that zirconium specimens will have a long life when they are stressed below the yield point (Ref 58). Stress-corrosion cracking of zirconium can be controlled by avoiding high, sustained tensile stresses (Ref 60).

Additional concerns include the accumulation of chlorine gas in the vapor phase and the presence of fluorides. Chlorine gas may be generated by the oxidation of chlorides by nitric acid. Areas that can trap chlorine gas should be avoided for zirconium equipment when chlorides are present in nitric acid. The corrosion of fluoride-containing nitric acid solutions can be controlled by adding an inhibitor, such as zirconium sponge or zirconium nitrate, to convert fluoride ions into noncorrosive complex ions.

Phosphoric acid is less corrosive than other mineral acids. Many materials demonstrate useful resistance in phosphoric acid, at least at low temperatures. Corrosion rates often increase with temperature and impurities in the acid. Areas such as the liquid-level line or the condensing zone are particularly vulnerable to corrosive attack.

Figure 22 shows that zirconium resists attack in phosphoric acid at concentrations up to 55% and temperatures exceeding the boiling point. Above 55% phosphoric acid, the corrosion rate of zirconium increases with temperature. The most interesting area for zirconium would be dilute acid at elevated temperatures.

Figure 23 gives the anodic polarization curves of zirconium in phosphoric acid at the near-boiling temperatures. As concentration increases, the passive range diminishes gradually, and the passive current increases progressively. It appears that zirconium passivates more slowly in phosphoric acid than in other mineral acids.

If phosphoric acid contains more than a trace of fluoride ions, attack on zirconium may occur. Because fluoride compounds are often present in

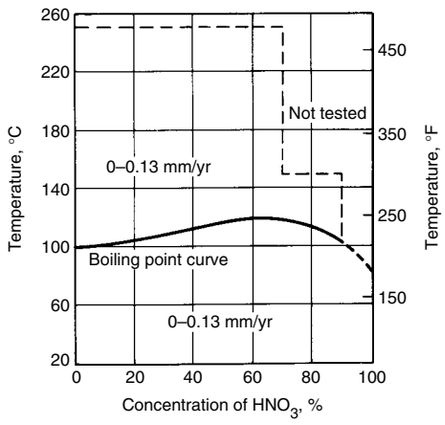

Fig. 20 Isocorrosion diagram of Zr702 in nitric acid

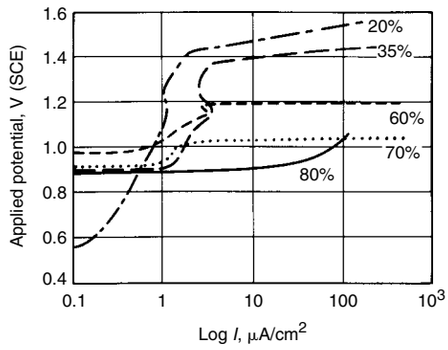

Fig. 21 Anodic polarization curves for Zr702 in nitric acid at near-boiling temperature. Applied potential is given in volts versus the saturated calomel electrode (SCE)

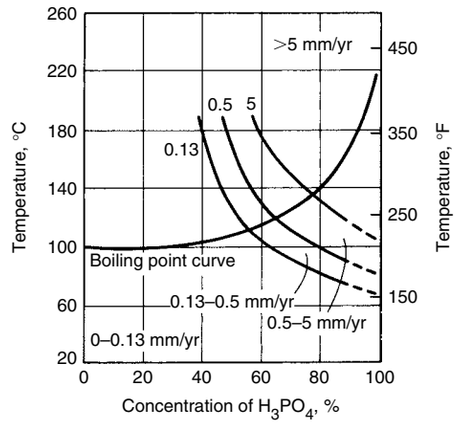

Fig. 22 Isocorrosion diagram of Zr702 in phosphoric acid

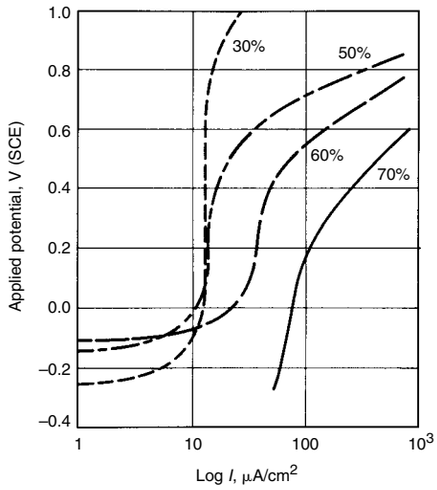

Fig. 23 Anodic polarization curves for Zr702 in phosphoric acid at near-boiling temperature. Applied potential is given in volts versus the saturated calomel electrode (SCE).

Table 13 Corrosion of zirconium in certain mixed acids

Test solution, wt%		Temperature, °C	Corrosion rate	
			mm/yr	mils/yr
1% H_2SO_4	99% HNO_3	RT, 100	0.0015	0.06
10% H_2SO_4	90% HNO_3	RT, 100	WG(a)	WG(a)
14% H_2SO_4	14% HNO_3	Boiling	0.0025	0.1
25% H_2SO_4	75% HNO_3	100	3.8	150
50% H_2SO_4	50% HNO_3	RT	0.016	0.63
68% H_2SO_4	5% HNO_3	Boiling	50.8	2000
68% H_2SO_4	1% HNO_3	Boiling	0.28	11
75% H_2SO_4	25% HNO_3	RT	6.6	260
88% H_3PO_4	0.5% HNO_3	RT	0.0	0.0
88% H_3PO_4	5% HNO_3	RT	WG(a)	WG(a)
Aqua regia	...	RT	Dissolved	Dissolved
20% HCl	20% HNO_3	RT	Dissolved	Dissolved
10% HCl	10% HNO_3	RT	Dissolved	Dissolved
7.5% H_2SO_4	19% HCl	Boiling	0.013	0.5
34% H_2SO_4	17% HCl	Boiling	0.008	0.3
40% H_2SO_4	14% HCl	Boiling	0.005	0.2
56% H_2SO_4	10% HCl	Boiling	0.05	2.0
60% H_2SO_4	1.5% HCl	Boiling	0.025	1.0
69% H_2SO_4	1.5% HCl	Boiling	0.13	5.0
69% H_2SO_4	4% HCl	Boiling	0.38	15.0
72% H_2SO_4	1.5% HCl	Boiling	0.51	20.0

(a) WG, weight gain

phosphoric acid, the acid specification is important when zirconium equipment is involved. For example, food grades contain little fluoride ion, while technical grades may contain tens to thousands parts per million fluoride ions.

Other Inorganic Acids. Zirconium resists chromic acid up to 30% at temperatures to 100 °C (212 °F) (Ref 61). It is not suitable for handling certain chrome-plating solutions that contain fluoride catalysts.

Zirconium is also resistant to certain mixed acids that include sulfuric-nitric, sulfuric-hydrochloric and phosphoric-nitric mixtures. The sulfuric acid concentration must be below 70% (Ref 54, 55, 62, 63).

Zirconium is aggressively attacked in 1 to 3 volume mixtures of nitric and hydrochloric acids (aqua regia). In the volume mixture, zirconium is attacked more slowly than in the aqua regia (Ref 54, 55). In mixtures greater than the 3 to 1 ratio, zirconium becomes resistant. Data for some mixed-acid systems are given in Table 13.

Hydrogen peroxide is a unique and important covalent peroxide. Many of its physical properties resemble those of water, but it differs chemically. It is not as stable as water. It decomposes into water and oxygen upon heating or in the presence of numerous catalysts, particularly salts of such metals as iron, copper, manganese, nickel, or chromium. Explosion may occur, resulting from catalytic decomposition. Often, small amounts of stabilizers, for example, tin salts and phosphates, are needed to suppress peroxide decomposition.

Hydrogen peroxide can be corrosive even to highly corrosion-resistant metals and alloys, such as titanium. In fact, titanium is one of the worst materials for handling hydrogen peroxide solutions. One reason is that hydrogen peroxide has the capability of forming peroxide complex compounds by attacking metals and alloys. These compounds may be soluble and are not as protective as oxide films.

As indicated in Table 6, hydrogen peroxide possesses a high oxidizing power. Its oxidizing power is higher than those of other well-known oxidizing agents, such as ferric ion and chlorine. Unlike ferric ion, hydrogen peroxide retains its oxidizing power in either acidic or basic solutions.

Zirconium is regarded as one of the best materials for hydrogen peroxide service (Ref 64, 65). Its corrosion resistance in this medium is excellent. It does not produce active ions to catalytically decompose hydrogen peroxide. It has few problems for use in the production of hydrogen peroxide, because it is essential to keep impurities out of process streams.

Nevertheless, zirconium is susceptible to pitting in oxidizing chloride solutions, and hydrogen peroxide is an oxidizer. Zirconium may pit in hydrogen peroxide solutions even when drops of hydrochloric acid are added for acidification (Ref 66). It should be noted that zirconium is fully compatible with other acidic peroxide solutions when acids such as sulfuric acid are added.

Surface conditions have a great influence on pitting. Good surface finish can effectively suppress the pitting of zirconium in ferric chloride and chlorine solutions. This is expected to be the case for the pitting of zirconium in chloride-containing peroxide solutions.

Alkaline Solutions. Zirconium resists attack in most alkalis, which include sodium hydroxide, potassium hydroxide, calcium hydroxide, and ammonium hydroxide (Ref 61, 67, 68). This makes zirconium distinctly different from some other high-performance materials, such as titanium, tantalum, glass, graphite, and PTFE, which are attacked by strong alkaline solutions. Moreover, steel and stainless steel, which may have low corrosion rates in alkaline solutions, are subject to SCC at certain concentrations and temperatures.

U-bends of Zr702 were tested in boiling 50% sodium hydroxide. During the test period, the concentration changed from 50 to approximately 85%, and temperature increased from 150 to 300 °C (300 to 570 °F). The PTFE washers and tubes used to make the U-bends dissolved. However, the zirconium U-bends remained ductile and did not show any cracks after 20 days.

Coupons of Zr702 were tested in a white liquor, paper-pulping solution, which contains sodium hydroxide and sodium sulfide, at 125, 175, and 225 °C (255, 345, and 435 °F). All coupons had corrosion rates of less than 0.025 mm/yr (1.0 mil/yr). In the same solution, graphite and glass both corroded at 100 °C (212 °F). Zr702 also exhibited resistance to SCC in simulated white liquor (Ref 69).

Salt Solutions. Zirconium resists most salt solutions, which include halogen, nitrate, carbonate, and sulfate (Ref 62, 63). Corrosion rates are typically very low at temperatures at least up to the boiling point. Solutions of strong oxidizing chloride salts, such as ferric and cupric chlorides, are examples of the few exceptions. In strong oxidizing chloride solutions, zirconium performance depends on surface conditions. Zirconium is quite pitting resistant when it has a good surface finish, such as the pickled surface.

Zirconium is considerably more resistant to chloride SCC than are stainless steels (Ref 34). For example, U-bends of Zr702 do not fail in boiling 42% magnesium chloride. Another attractive property of zirconium is its high resistance to crevice corrosion. Zirconium is not subject to crevice corrosion even in acidic chloride solutions at elevated temperatures. No attack was observed on zirconium in a salt spray environment (Ref 70).

Urea. In 1828, urea became the first organic compound synthesized from an inorganic material (ammonium cyanate). This changed the concept that organic compounds must be associated with living organisms. Today, urea is produced commercially in vast amounts from ammonia and carbon dioxide. These two materials are combined to form ammonium carbamate, followed by the dehydration of the ammonium carbamate. In order to have a high conversion rate, reactions have to take place at elevated temperatures and pressures. The reactants, particularly the carbamate solution, are too corrosive for stainless alloys unless oxygen is injected carefully for passivation.

One of the earliest applications of zirconium was in the production of urea. Certain zirconium vessels and heat exchangers have been in service for more than 30 years and show no signs of corrosion. Zirconium has been recognized as the most corrosion-resistant metal for urea-synthesis service (Ref 71, 72). Stainless alloys corrode in urea-synthesis conditions at rates exceeding 2 mm/yr (79 mils/yr) (Ref 71). Even silver has a high corrosion rate at 0.76 mm/yr (30 mils/yr). Although titanium does not corrode much, it

exhibits several problems, such as erosion (Ref 72) and hydrogen embrittlement (Ref 73).

The high corrosion rates of stainless steels can be reduced, provided oxygen is present for passivation, so oxygen injection has become popular as the corrosion-control measure in urea plants.

In recent years, zirconium has become popular again. The driving force for renewed interest in zirconium is the concern about heavy metals in fertilizers. To protect the environment, allowables for the presence of heavy-metal salts in fertilizers are being tightened. Stainless steel equipment still corrodes with the oxygen injection, so the corrosion resistance and nontoxicity of zirconium is attractive.

Acetic Acid. The importance of acetic acid in the organic chemistry industry is comparable to that of sulfuric acid in the inorganic chemistry industry. Acetic acid is extensively used in a variety of organic syntheses. Millions of tons of the acid are produced annually, and production capacity is on the rise to meet the increasing demand. In order to ensure a high-quality product and to minimize downtime and the cost of equipment replacement, materials selection for acetic acid service must be thorough.

Acetic acid can effectively acidify aqueous solutions, increasing their corrosivity. It is not highly corrosive at low temperatures. Many materials, including wood, rubber, aluminum, copper, stainless steels, and titanium, have been used in acetic acid service with different degrees of success. Corrosion problems arise due to variations in acid concentration, temperature, solution impurities or catalysts, and heat transfer (Ref 74).

For over 40 years, zirconium has been recognized as one of the most versatile materials for acetic acid service (Ref 74–77). Zirconium has nil corrosion rates (<0.025 mm/yr, or 1.0 mil/yr) in most acetic acid media to at least 260 °C (500 °F). In fact, acetate ions have a mildly inhibitive effect on the localized corrosion of zirconium in halide solutions. Conditions that lead to corrosion are few. They include very dry acid (<650 ppm water) and the presence of copper ions in the acid (Ref 78).

Zirconium has become an important material for the production of acetic acid through the reaction of methanol and carbon monoxide. This technology has been studied for more than 40 years but was not commercialized until the 1970s, when the corrosion problems of structural materials were managed. This reaction must proceed at high temperature (150 °C, or 300 °F, or greater) and high pressure (3.3 to 6.6 MPa, or 0.48 to 0.96 ksi) in the presence of a halide as the catalyst. The crude acid produced is first separated from the catalyst and then dehydrated and purified in an azeotropic distillation column. The final product is highly pure acetic acid, allowing it to be used in food and pharmaceutical applications. Factors inducing corrosion problems on stainless alloys include:

- An intermediate acid concentration
- An elevated temperature
- The presence of highly corrosive methanol and iodides

Process equipment materials were evaluated (Ref 75, 76), and zirconium was identified as the most corrosion resistant. Zr702 and Zr705 are often used to construct process equipment, such as reactors, columns, heat exchangers, pumps, valves, piping systems, trays, and packings. Modern acetic acid plants can use more than 91 metric tons (100 tons) of zirconium per plant.

Nevertheless, in certain tests, zirconium exhibited pitting and high corrosion rates in mixtures of acetic acid and acetic anhydride when copper ions were present. Copper ions seem to play a catalytic role in the corrosion process. It is undesirable for zirconium equipment to be exposed to acetic acid contaminated with copper ions. Copper ions may come from corrosion of upstream equipment made of copper-containing alloys. They may also be added as catalysts in certain processes.

Formic Acid. The dielectric constant of formic acid is much higher than that of acetic acid, that is, 56.1 versus 6.2 at 25 °C (75 °F). Formic acid is more easily ionized than acetic acid. Therefore, formic acid is expected to be much more corrosive than acetic acid.

Indeed, formic acid attacks many common metals and alloys. Steel is attacked rapidly by this acid at all concentrations, even at ambient temperatures. Aluminum, copper, and their alloys show fair resistance to the acid only at ambient temperatures. If the acid is free of oxygen and other oxidants, the corrosion resistance of copper improves toward higher temperatures. Stainless alloys have some serious limitations. Type 304 stainless steel resists only 1 to 2% formic acid at boiling. Type 316 stainless steel is attacked by hot formic acid in the intermediate concentrations. Nickel-base alloys may corrode at high rates in the acid with the presence of certain impurities, such as halides, and under heat-transfer conditions. Titanium and its alloys are useful in formic acid service under certain conditions. They are not consistent, due to factors such as aeration and water content. Compared to the mentioned alloys, zirconium is versatile and corrosion resistant in most formic acid solutions (Ref 79).

Zirconium has played a key role in the commercialization of the Leonard/Kemira process (Ref 80, 81). In this process, CO gas contacts methanol in the presence of a catalyst to form methyl formate in a reactor. The methyl formate is hydrolyzed in the presence of a catalyst to yield formic acid and methanol, which are separated by distillation. The methanol is recycled to the first stage of the process. Factors such as elevated temperatures and pressures and the presence of water and catalyst make common materials, including glass lining, resin and plastic coatings, and stainless alloys, inadequate as structural materials for this process. Zirconium proves to be the most economical structural material for use in the main equipment for this process.

Other Organic Environments. Acetic and formic acids are among the most corrosive organic acids. As expected, zirconium has excellent corrosion resistance in most organic environments. Exceptions are certain halide-containing organic solutions (e.g., impure methanol) and organic halides (e.g., dichloroacetic and trichloroacetic acids).

Zirconium has been extensively tested in organic-cooled reactors where the coolant consists of mixtures of high-boiling aromatic hydrocarbons, for example, terphenyls (Ref 82). These coolants are noncorrosive to zirconium. However, early experiments in the organic coolants indicated that hydriding was a major concern. It was found that chlorine impurity in the coolants was the reason for hydriding. Elimination of the chlorine and maintenance of a good surface oxide film by ensuring the presence of some water (>50 ppm) alleviate the hydriding problem.

Indeed, the combination of a lack of water and the presence of halogens or halides is the common reason for zirconium to corrode in organic environments. For example, the addition of some water suppresses zirconium susceptibility to SCC in alcohol solutions with halides (Ref 83–85).

On one hand, zirconium shows excellent corrosion resistance in many chlorinated carbon compounds, such as carbon tetrachloride and dichlorobenzene, at temperatures up to 200 °C (390 °F). On the other hand, zirconium is poor in certain chlorinated organic chemicals, such as acetyl halides, even at ambient temperatures.

It is well known that certain organic halides are very corrosive to metals in the absence of water and oxygen. Metals can directly incorporate into these compounds to form intermetallic compounds. The reactions were investigated extensively by Grignard during the early 1900s. Today, organometallic halides are termed Grignard reagents. Unsaturated organic compounds and alkyl, aryl, and vinyl halides are commonly used to react with metals in the preparation of organometallic compounds. They are potentially corrosive to metals, including zirconium.

From the corrosion point of view, organic halides can be classified into three groups, that is, watersoluble, water insoluble, and water incompatible:

- Water-soluble halides, such as aniline hydrochloride, chloroacetic acid, and tetrachloroethane, are not corrosive to zirconium. More active halides, such as dichloroacetic and trichloroacetic acids, are corrosive to zirconium. Corrosion rates of zirconium in these two acids at boiling are greater than 500 and 1250 μm/yr (20 and 50 mils/yr), respectively. Water addition and stress relieving could be effective in controlling the corrosion of zirconium in water-soluble halides.
- Water-insoluble halides, such as trichloroethylene and dichlorobenzene, are not corrosive to zirconium, likely because of their

stability. They do not dissolve in nor exclude water. They and water can be physically mixed together.

- Water-incompatible halides, such as acetyl chloride, may be highly corrosive to zirconium. They are not just unstable but also react violently with water. There is no chance for water to be present in these types of halides, which are the most undesirable organic compounds for zirconium to handle.

Gases. Zirconium forms a visible oxide film in air at approximately 200 °C (390 °F). The oxidation rate becomes high enough to produce a loose, white scale on zirconium at temperatures above 540 °C (1000 °F). At temperatures above 700 °C (1290 °F), zirconium can absorb oxygen and become embrittled after prolonged exposure.

Zirconium reacts more slowly with nitrogen than with oxygen, because it has a higher affinity for oxygen than for nitrogen. Also, a layer of oxide film normally protects zirconium from reacting with nitrogen. However, once nitrogen penetrates through the oxide layer, it diffuses into the metal faster than oxygen because of its smaller size. Clean zirconium starts the nitriding reaction in ultrapure nitrogen at approximately 900 °C (1650 °F). Temperatures of 1300 °C (2370 °F) are needed to fully nitride zirconium. The nitriding rate can be enhanced by the presence of oxygen in the nitrogen or on the metal surface.

The oxide film on zirconium provides an effective barrier to hydrogen absorption up to 760 °C (1400 °F), provided that small amounts of oxygen are also present in hydrogen for healing damaged spots in the oxide film. In an all-hydrogen atmosphere, hydrogen absorption will begin at a much lower temperature (310 °C, or 590 °F). Zirconium will ultimately become embrittled by forming zirconium hydrides. Hydrogen can be removed from zirconium by prolonged vacuum annealing at temperatures above 760 °C (1400 °F).

The corrosion and oxidation of zirconium and its alloys in steam are of special interest to nuclear power applications. The alloys can be exposed for prolonged period without pronounced attack at temperatures up to 425 °C (795 °F). In the 360 °C (680 °F) steam, up to 350 ppm chloride and iodide ions, 100 ppm fluoride ions, and 10,000 ppm sulfate ions are acceptable for zirconium in general applications but not in nuclear power applications.

Zirconium is stable in ammonia up to approximately 1000 °C (1830 °F), in most gases (carbon monoxide, carbon dioxide, and sulfur dioxide) up to approximately 300 to 400 °C (570 to 750 °F), and in dry halogens up to approximately 200 °C (390 °F). At elevated temperatures, zirconium forms volatile halides. The corrosion resistance of zirconium in wet chlorine depends on surface condition. Zirconium is susceptible to pitting in wet chlorine unless it has been properly cleaned.

Molten Salts and Metals. Zirconium resists attack in some molten salts. It is very resistant to corrosion by molten sodium hydroxide to temperatures above 1000 °C (1830 °F) and is also fairly resistant to potassium hydroxide. The oxidation properties of zirconium in nitrate salts are similar to those in air.

Zirconium resists some types of molten metals, but the corrosion resistance is affected by trace impurities such as oxygen, hydrogen, or nitrogen. It has a corrosion rate less than 25 μm/yr (1.0 mil/yr) in liquid lead to 600 °C (1110 °F), lithium to 800 °C (1470 °F), mercury to 100 °C (212 °F), and sodium to 600 °C (1110 °F). The molten metals known to attack zirconium include aluminum, zinc, bismuth, and magnesium. Table 14 gives zirconium corrosion resistance in several molten metal systems (Ref 86).

Effects of Fabrication on Corrosion

The corrosion performance of materials will largely depend on fabrication practices. Corrosion failures of zirconium equipment exposed to certain environments can often be prevented by using alternate methods of design, fabrication (including welding), or by specific heat treatment processes and techniques. Final surface treatment methods can also be applied to modify a surface finish or remove impurities from a surface for improved corrosion resistance.

Table 14 Corrosion of zirconium in some liquid metals

	Melting temperature		Temperature, °C (°F)		
Liquid metal	°C	°F	300 (570)	600 (1110)	800 (1470)
Bi	271.3	520.3	Unknown	Poor	Poor
Bi-In-Sn	60	140	Unknown	Poor	Unknown
Bi-Pb	125	257	Good	Limited	Unknown
Bi-Pb-In	70	158	Unknown	Poor	Unknown
Bi-Pb-Sn	97	207	Good	Limited	Unknown
Ga	298	568	Limited	Poor	Poor
Hg	−38.4	−37.1	Poor	Poor	Unknown
Li	180.5	356.9	Good	Limited	Limited
Mg	650	1202	. . .	Poor(a)	Unknown
Na, K, or NaK	12.3–97.9	54.1–208.2	Good	Good	Unknown
Pb	327.4	621.3	Good(a)	Limited	Limited
Sn	231.9	449.4	Good	Unknown	Unknown

(a) At its melting point

During standard fabrication processes, the surface of the material can be embedded with particles that may affect the corrosion resistance of the zirconium. This may occur when the material is conditioned using an abrasive grinding stone, shot- or gritblasted, or polished. In addition, embedding of particles could occur when materials are improperly transported or formed or when tubes are rolled into a tubesheet. This is especially a problem if the zirconium equipment is to be placed in halogen acids.

Because zirconium is a relatively soft metal, abrasive grinding stones may embed aluminum oxide or silicon carbide particles in the material surface, causing preferred sites for corrosion. Abrasive grinding operations performed on zirconium should be followed by conditioning with a clean stainless steel brush, clean draw file, or rotary carbide burr to remove any abrasive particles embedded on the surface. If the final part is blasted for a cosmetic appearance, steel shotblast should not be used, because the shot will embed into the material surface, causing potential localized corrosion failures, especially if used in an acidic chloride environment. If steel shot is used, it must be followed by acid pickling or chemical cleaning to remove embedded iron particles.

If other alloys are fabricated near the zirconium vessel, potential sources for embedded particles include grinding and weld spatter of foreign material. For this reason, it is recommended that the zirconium equipment not be welded and fabricated in an area where other materials are being ground, welded, or torch cut. If a zirconium vessel is fabricated in a bay where other materials are being fabricated, then the area should be surrounded by protective barriers and kept clean. Any weld spatter should be removed by stainless steel brushing, grit or glass bead blasting, or light grinding.

It is recommended that hydrostatic expansion be performed when zirconium tubes are expanded into a tubesheet and prior to welding. This minimizes the potential for embedded particles on the inside diameter of the tube surface, caused during roller expansion as a result of improperly cleaned roller expansion tooling. Corrosion failures in halogen acid environments have been identified where roller expansion of tubes was used. Embedded particles may cause localized pitting attack of the tubes and eventual penetration of the tube wall. For halogen acid applications, all final equipment surfaces exposed to the corrosive environment should be free of iron contamination.

Any tooling used for the fabrication of zirconium should be thoroughly cleaned to remove any contamination left by previous materials. Tooling used for welding or conditioning such as grinding stones, wire brushes, and draw files, should be dedicated for zirconium only. Color coding of the ancillary tooling is recommended to minimize the potential for cross contamination.

Forming and Handling Defects. When zirconium is handled or moved using a forklift and/

or lifting straps, protective coverings should be used to prevent the steel from being smeared into the zirconium metal surface. Forklift blades and steel straps will also cause scratches, scrapes, and surface defects that could be detrimental when it is exposed to subsequent forming operations and to certain corrosive environments. To minimize pickup of steel and other metal particles, it is recommended whenever possible to cover the forming dies with a protective covering, such as leather, rubber, or some other type of noncontaminating material. This will also minimize the potential for surface damage caused by the steel tooling.

Welding. Generally, zirconium welds exhibit similar corrosion resistance to nonwelded areas, except when used at the higher concentrations of sulfuric acid. Improper welding processes, however, can affect the mechanical and corrosion properties of zirconium. Interstitial element pickup, such as hydrogen, nitrogen, oxygen, and carbon in welds, will generally not increase the corrosion rate of zirconium. These interstitials may, however, reduce the ductility of the metal and cause premature mechanical failures. Nitrogen contamination caused by plasma cutting with nitrogen gas may increase the corrosion rate of zirconium in nitric acid environments. If any type of cutting operation is performed (oxyacetylene, plasma, or laser), the heat-affected zone should be removed by grinding or machining prior to welding. Waterjet cutting should be used for the cutting of zirconium, where possible, to avoid the potential for contamination caused by the heat input. The waterjet cut should also be conditioned, because this process uses an abrasive (such as garnet) that will embed into the zirconium surface.

Heat Treatment. Improper heat treatment can result in damage to zirconium in a way that could be deleterious to corrosion resistance. Zirconium can be damaged during heat treatment if the material is placed in a non-oxidizing (reducing) atmosphere. A reducing (excess hydrogen) atmosphere will cause the zirconium to absorb hydrogen and may affect the corrosion resistance. Before heat treatment, the zirconium vessel must be thoroughly cleaned of any surface impurities to prevent contamination during elevated-temperature annealing.

When zirconium is cold formed and then heated into the full annealing temperature range of 649 to 788 °C (1200 to 1450 °F), critical grain growth may occur. The grain structure will enlarge in the areas where 2 to 10% strain energy or cold work has been placed. Cold work of this degree can occur in some cases where plate has been brake press formed into pipe or elbows. On many occasions, formed pipe is stress relieved at 550 °C (1020 °F) for 0.5 h per 2.54 cm (1 in.) of thickness to relieve the stresses caused by forming and welding. The recrystallized large grains are surrounded by fine grains (unworked areas). These areas can be either on the outer metal surface that was in tension or on the inner surface that was in compression and will have large grains with large grain boundaries. These areas may be more susceptible to intergranular attack in higher concentrations of sulfuric acid.

Chemical Cleaning. If zirconium equipment is to be used in halogen acids, it is recommended that it be cleaned by chemical cleaning to remove any embedded iron during fabrication. This process should be done by a chemical cleaning company experienced in the cleaning of a reactive metal. Smooth and clean surfaces will have the optimal corrosion resistance, where rough surfaces are more likely to have surface imperfections that could initiate premature corrosion attack, especially in the more severe environments. Before any equipment is placed in any corrosive media, it should be cleaned thoroughly to remove oils, grease, paint, and other surface debris.

Protection Measures

Zirconium oxide, which forms on the surface of zirconium, is among the most insoluble compounds in a broad range of corrosives. This film, although very thin, provides excellent protection for zirconium from corrosion in most media. When the film is mechanically damaged, it will regenerate itself. For corrosion resistance, there is no need to thicken the film before zirconium equipment is placed in a corrosive medium.

Enhanced Oxide Films. It is desirable to preoxidize zirconium for meeting heavy mechanical duties. Properly oxidized zirconium has a much-improved performance against sliding forces, although it can be damaged by striking action. Oxidized zirconium pump shafts are an example of common applications. Bolts and nuts are often oxidized for the purpose of preventing galling.

Several methods for forming thick layers of oxide films are available. They include anodizing, autoclaving in hot water or steam, oxidation in air or oxygen, and formation in molten salts.

Anodizing forms a very thin film (<0.5 μm, or 0.02 mil). The surface of zirconium with anodized films appears in different colors, varying through the entire spectrum. The thickness of the film is in the range of the wavelengths of visible light. Consequently, because of interference of this light, only certain wavelengths are selectively reflected through the film from the zirconium metal underneath. Because the selected wavelengths depend on the thickness of the film, the change in color observed with increasing voltage indicates that the film is growing in thickness. Nevertheless, the film is formed at ambient temperatures. It does not have the adhesion to the underlying metal of thermally produced films. Anodized films look beautiful but have very limited capability to protect the metal from mechanical damage.

Autoclaving in hot water or steam is a common practice for determining corrosion resistance in the nuclear industry. In this method, the uniform film of high integrity is formed in pressurized (19 MPa, or 2.8 ksi) deionized water at 360 °C (680 °F) for 14 days or in high-purity steam (10 MPa, or 1.5 ksi) at 400 °C (750 °F) for 1 to 3 days. In addition to improving corrosion resistance, the rate of hydrogen absorption is greatly reduced. Oxidation in air or oxygen is the most common method used in the chemical processing industry. In fact, a thick layer of film is formed during the final stress relief of a component in air at 550 °C (1020 °F) for 0.5 to 4 h. This film ranges from a straw yellow through an iridescent blue or purple to a powdery tan or light gray. This treatment does not result in significant penetration of oxygen into the metal, but it does form an oxide layer that is diffusion bonded to the base metal.

Oxidation in air or oxygen under well-controlled conditions can produce high-quality films on zirconium. The formed films serve as an excellent bearing surface against a variety of materials. For example, a layer of black film forms on a cleaned zirconium component in air at 550 °C (1020 °F) for 4 to 6 h (Ref 87) or in a fluidized bed using oxygen during the oxide formation period but using an inert gas during the heating and cooling periods (Ref 88). The resultant oxide layer is approximately 5 and 20 μm, respectively. It is equivalent to sapphire in hardness and is diffusion bonded to the base metal. The oxide layer can be damaged by a striking force, but it serves as an excellent surface for sliding contact.

Film formation in molten salts would be useful for small components. In this process, a zirconium subject is treated in fused sodium cyanide containing 1 to 3% sodium carbonate or in a eutectic mixture of sodium and potassium chlorides with 5% sodium carbonate (Ref 89). Treatment is carried out at a temperature ranging from 600 to 800 °C (1110 to 1470 °F) for up to 50 h. The thickness of oxide film formed by this method is 20 to 30 μm (0.8 to 1.2 mil). This film greatly improves resistance to abrasion and galling over thick oxide films grown by many other methods.

Surface Conditioning. Figure 9 shows the effect of surface condition on the rest potential of zirconium in 10% HCl plus 500 ppm Fe^{3+} at 30 °C. (85 °F). Air annealing yields rest potentials nobler than the pitting potential, E_{crit}, due to the formed thick oxide during annealing. This does not mean that pitting will occur if the film quality is good. This does put thick oxide-coated materials in a position vulnerable to pitting, particularly when there is an anodically applied potential. Surfaces abraded with either 600-grit SiC or Al_2O_3 cloth reach the pitting potential quickly and have short pit initiation times. This can be attributed to the presence of embedded particles resulting from rough polishing. Pickled and finely polished surfaces have rest potentials below the pitting potential. They are very resistant to pitting even in oxidizing chloride solutions. This can be attributed to surface homogeneity that favors general corrosion but not localized corrosion. Results of immersion tests indicate that pickled zirconium performs well in boiling 10% $FeCl_3$ and in ClO_2 (Ref 20,

30). It is well known that zirconium with a normal surface finish is unsuitable for handling these solutions.

Electrochemical Protection. Zirconium exhibits a passive-to-transpassive transition with increasing potential in all mineral acids except hydrofluoric acid (Ref 90). The commonly observed active node, as shown in Fig. 6 for many metal-acid systems, is not observed for zirconium.

Consequently, zirconium performs well in most reducing media. This can be attributed to the ability of zirconium to take oxygen from water to form a stable passive film. Most passive metals and alloys would need some oxidizing power, such as the presence of oxygen, for them to form passive films. In fact, zirconium is one of the best metals for handling reducing media. On the other hand, zirconium may experience corrosion problems, such as pitting and SCC, under oxidizing conditions. These problems can be controlled by converting the oxidizing condition to a more reducing condition by various means.

Electronically, by impressing a potential that is arbitrarily 50 to 100 mV below its corrosion potential, zirconium becomes corrosion resistant in oxidizing chloride solutions (Ref 91, 92). Tables 15 and 16 demonstrate the benefits of electrochemical protection in controlling pitting and SCC. Table 15 shows that the general corrosion rates of unprotected zirconium in oxidizing chloride solutions may be low. However, the penetration rates are much higher than the general corrosion rate. Electrochemical protection eliminates this local attack. As indicated in Table 16, unprotected U-bends of welded zirconium cracked in all but one case shortly after exposure. Protected U-bends resisted cracking for the 32 day test interval in all but one acid concentration. Thus, electrochemical protection offers an improvement to the corrosion properties of zirconium in oxidizing chloride solutions.

This technique is also applicable to control the SCC of zirconium in concentrated nitric acid (Ref 60). Because of the strong oxidizing power of the acid, zirconium exhibits a noble corrosion potential. Also, there is a large difference between the corrosion potential and the critical potential to cause SCC. It is desirable to control the potential of zirconium a few hundred millivolts below the corrosion potential or at 740 mV_{SHE}.

Other Measures. Ferric and cupric ions are the common oxidizing agents experienced in the chemical processing industry. Cupric ion is more detrimental than ferric ion in promoting the general corrosion and pitting of zirconium in acidic chloride solutions. Tables 17 and 18 demonstrate the effect of pH, welding, and heat treatment on the corrosion of zirconium in cupric-ion-containing solutions. The corrosion problems of zirconium in these solutions can be controlled by adjusting the pH to 6 or higher (Table 17) or by high-temperature heat treatment (Table 18). In ferric-ion-containing solutions, it is sufficient to adjust the pH to 3 or higher.

Various inhibitors, such as nitrate, sulfate, and stannous ions, can be used to control the pitting of zirconium in chloride solutions (Ref 20). Furthermore, the solution potential of an oxidizing solution can be lowered when a small amount of hydrofluoric acid is added (Ref 20, 60). Therefore, hydrofluoric acid can be used to control pitting and SCC of zirconium in oxidizing solutions, such as concentrated nitric acid and ferric chloride solutions. Because hydrofluoric acid is very corrosive to zirconium, the corrosivity of this acid can be neutralized by adding a complexing agent, such as zirconium sponge or zirconium compounds.

Tensile stresses provide a driving force not just for SCC but also for other types of corrosion to occur. Lowering residual stresses by a stress-relieving treatment is useful in controlling pitting as well.

Industrial Applications of Zirconium and Its Alloys

Zirconium and its alloys are being used as structural materials in fabricating columns, reactors, heat exchangers, vaporizers, pumps,

Table 15 Corrosion of protected and unprotected Zr702 in HCl solutions containing 500 ppm Fe^{3+}

Test duration: 32 days

				Corrosion rate			
		Temperature		Unprotected		Protected(a)	
Medium	Acidity	°C	°F	mm/yr	mils/yr	mm/yr	mils/yr
10% HCl	3 *N*	60	140	0.18	7.1	<0.0025	<0.1
		102	215	1.3	51	<0.0025	<0.1
Spent acid (15% Cl^-)	5 *N*	65	150	0.9	36	<0.0025	<0.1
		80	175	0.9	36	<0.0025	<0.1
20% HCl	6 *N*	60	140	0.09	3.6	<0.0025	<0.1
		107	225	1.5	59	<0.0025	<0.1

(a) Protected means specimens were protected electrochemically; see text for details.

Table 16 Time to failure of welded Zr702 U-bend specimens in HCl solutions containing 500 ppm Fe^{3+}

		Temperature		Time to failure, days	
Medium	Acidity	°C	°F	Unprotected	Protected
10% HCl	3 *N*	60	140	0.1	NF
		102	215	0.1	NF
Spent acid (15% Cl^-)	5 *N*	65	150	0.3	NF
20% HCl	6 *N*	60	140	NF	NF
		107	225	0.1	NF
28% HCl	9 *N*	60	140	2	NF
		94	200	0.1	NF
32% HCl	10 *N*	53	125	1	32
		77	170	0.1	20
37% HCl	12 *N*	30	85	0.3	NF
		53	125	1	NF

NF, no failure

Table 17 Corrosion of zirconium in boiling NaCl solutions containing 500 ppm Cu^{2+}

Test consisted of seven 1 day runs

		Average corrosion rate			
		Unwelded specimens		Welded specimens	
Concentration of NaCl, %	pH	mm/yr	mils/yr	mm/yr	mils/yr
3.5	1	0.053(a)	2.1(a)	0.59(a)	23.6(a)
25	1	0.04	1.6	0.55(a)	21.7(a)
3.5	4.8	0.009(a)	0.38(a)	0.6(a)	23.8(a)
25	4	0.025	1	0.56(a)	21.9(a)
3.5	5	0.018	0.7	0.64(a)	25.3(a)
25	5	nil		nil	
3.5	6	nil		nil	
25	6	nil		nil	
3.5	7.5	nil		nil	
25	7.5	nil		nil	

(a) Pitting

Table 18 Effects of heat treatment on the corrosion of sandblasted and pickled zirconium in boiling NaCl solutions containing 500 ppm Cu^{2+}

Test consisted of seven 1 day runs; Cu^{2+} was added as $CuCl_2$

		Average corrosion rate			
		3.5% NaCl		25% NaCl	
Specimen type	Metallurgical condition	mm/yr	mils/yr	mm/yr	mils/yr
Unwelded	Sandblasted and pickled	0.007(a)	0.27(a)	0.024(a)	0.98(a)
Welded	Sandblasted and pickled	0.011(a)	0.45(a)	0.033(a)	1.3(a)
Welded	Heated to 760 °C (1400 °F), air cooled	0.0025(a)	0.1(a)	0.006(a)	0.23(a)
Welded	Heated to 760 °C (1400 °F), water quenched	0.0025(a)	0.1(a)	0.004(a)	0.17(a)
Welded	Heated to 870 °C (1600 °F), air cooled	0.0033	0.13	0.006(a)	0.23(a)
Welded	Heated to 870 °C (1600 °F), water quenched	0.0033	0.13	0.004(a)	0.17(a)
Welded	Heated to 980 °C (1800 °F), air cooled	0.005	0.2	0.007	0.27
Welded	Heated to 980 °C (1800 °F), water quenched	0.005	0.2	0.007	0.27

(a) Pitting

piping systems, valves, and agitators for the chemical processing industry.

Sulfuric-Acid-Containing Processes. Zirconium was used in H_2O_2 manufacturing by the electrolysis of acid sulfates. This production process was very corrosive. At one time, graphite equipment was standard for this process. The FMC plant in Vancouver, Wash., found that zirconium was superior to graphite and used zirconium equipment to produce up to 90% H_2O_2. The average maintenance-free life of the heat exchanger was 10 years; graphite exchangers failed after 12 to 18 months of service. The graphite equipment failure was attributed to the leaching of the binder from the graphite by the 35% H_2SO_4 feed, which created a porous condition and ultimately caused failure.

The experience of zirconium in peroxide production led to the replacement of the graphite heat exchangers with zirconium shell-and-tube exchangers in the manufacturing of acrylic films and fibers. In this application, the H_2SO_4 concentration was as high as 60% at 150 °C (300 °F). Hydrogen peroxide is becoming a preferred oxidant because of its environmentally friendly nature. It has made inroads into many industrial applications, and its consumption is increasing. It is, however, not a stable chemical. It can be catalytically decomposed by many heavy-metal ions. The decomposition reaction is wasteful and may create a condition for fire or explosion. Certain peroxide solutions are corrosive as well. Zirconium is one of very few metals that is highly compatible with a broad range of peroxide solutions. It is corrosion resistant. It does not produce active ions to catalytically decompose peroxide.

Another major application in H_2SO_4 concerns the manufacture of methyl methacrylate and methacrylic acid. The system at the Rohm and Haas plant in Deer Park, Texas, includes pressure vessels, columns, heat exchangers, piping systems, pumps, and valves made from zirconium. A zirconium unit, which was built more than 20 years ago, is still in service.

Zirconium is also widely used for column internals and reboilers in the manufacture of butyl alcohol. The operating conditions are 60 to 65% H_2SO_4 at temperatures to boiling and slightly above. Zirconium may corrode under upset conditions of elevated concentrations and when such impurities as Fe^{3+} are present. Zirconium has been used in H_2SO_4 recovery and recycle systems in which fluorides are not present and the acid concentration does not exceed 65%. A major application for zirconium is in iron and steel pickling, using hot 5 to 40% H_2SO_4.

Rayon is a manmade textile fiber, and most of today's rayon is made by the viscose process. Equipment made of graphite was popular for use in the H_2SO_4-affected areas of this process yet is vulnerable to breakdowns. Avtex Fiber, Inc. began experimenting with zirconium equipment in 1970. The excellent performance of zirconium prompted Avtex to convert more pieces of equipment to zirconium, which included 10 acid evaporators, 14 shell-and-tube heat exchangers, and 12 bayonet heat exchangers. In addition to dramatically reducing maintenance costs and downtime, the zirconium equipment improved operating efficiency and lowered overall energy costs.

Hydroxyacetic acid (HAA), also known as glycolic acid, can be produced in a synthetic process other than being extracted from natural sources. Under high pressure (30 to 90 MPa, or 4.4 to 13 ksi) and temperature (160 to 200 °C, or 320 to 390 °F), formaldehyde reacts with carbon monoxide and water in the presence of an acidic catalyst, such as sulfuric acid, to form HAA. DuPont could not rely on a silver lining for reliable service in this process, because silver showed poor erosion resistance in the piping system. There were cases of blowouts in the piping due to failure of the lining. By the mid-1980s, zirconium lining was evaluated when other materials, such as glass, ceramic, stainless alloys, and titanium, were found unsuitable. Zirconium is well known for its corrosion resistance in weak sulfuric acid at temperatures up to and above 260 °C (500 °F). An eight month field test at DuPont indicated that a zirconium tube would not corrode in the most severe service section of the process. The excellent resistance of zirconium to erosion is also apparent, and consequently, DuPont replaced silver lining with zirconium lining in piping sections more than five years ago. It was estimated that zirconium lining would last at least three times as long as silver lining.

Halide-Containing Processes. Zirconium has many applications in HCl, such as the production of concentrated HCl and polymers. Zirconium heat exchangers, pumps, and agitators have been used for more than 15 years in an azo dye coupling reaction. In addition to being very corrosion resistant in this medium, zirconium does not plate out undesirable salts that would change the color and stability of the dyes.

Lactic acid is commercially produced either by fermentation or by synthesis. The synthetic process is based on lactonitrile, which is prepared by reacting acetaldehyde with hydrogen cyanide at up to 200 °C (390 °F). Lactonitrile is then hydrolyzed in the presence of HCl to yield lactic acid. In the HCl-affected areas, suitable materials are limited. Glass-lined materials are prone to breakdowns. Stainless alloys corrode and introduce toxic materials to the process stream. Titanium and its alloys are susceptible to crevice corrosion in hot chloride solutions. Zirconium is ideal for this process. Because lactic acid is produced as a fine chemical, contamination has to be prevented in all areas. Oxidizing HCl conditions resulting from the presence of ferric or cupric ions are avoided. Moreover, zirconium is highly resistant to crevice corrosion in chloride solutions. Since the 1970s, zirconium equipment has provided excellent service in lactic acid production.

Other applications in HCl include the breaking down of cellulose in the food industry and the polymerization of ethylene chloride, which is carried out in HCl and chlorinated solvents.

Zirconium and its alloys have been identified to offer the best prospects, from a cost standpoint, as materials for an HI decomposer in hydrogen production. They resist attack by HI media (gas or liquid) from room temperature to 300 °C (570 °F). Most stainless alloys have adequate corrosion resistance to HI only at low temperatures.

Nitric-Acid-Containing Processes. There is an increasing interest in the use of zirconium for HNO_3 service. For example, because of the high degree of concern over safety, zirconium is chosen as the major structural material for the critical equipment used to reprocess spent nuclear fuels.

In most HNO_3 service, stainless steel has been the workhorse for decades. The excellent compatibility between zirconium and HNO_3 was not thought to be needed. This situation changed when nitric acid producers started to modernize their technology in the late 1970s.

Conventionally, HNO_3 is manufactured by oxidation of ammonia with air over platinum

catalysts. The resulting nitric oxide is further oxidized into nitrogen dioxide and then absorbed in water to form HNO_3. Acid of up to 65% concentration is produced by this process. Higher-concentration acid is produced by distilling the dilute acid with a dehydrating agent.

Before the l970s, dual-pressure processes were the dominant means of HNO_3 production. A typical dual-pressure process operates the converter at approximately 500 kPa (0.07 ksi) and the absorber at approximately 1100 kPa (0.16 ksi). In the late 1970s, Weatherly, Inc. introduced a high monopressure process that operates at 1300 to 1500 kPa (0.19 to 0.22 ksi). The advantages of this new process include:

- Greater productivity due to higher operating pressure
- Smaller equipment, resulting in a lower capital cost
- Higher energy-recovery capabilities

The new process was first tried in 1979 when Mississippi Chemical Corp. in Yazoo City, Miss., retrofit their existing plant with a new compressor system to increase pressure for greater productivity and energy efficiency. It was at this point that severe corrosion problems were discovered.

Prior to the upgrade, the cooler condenser was constructed of type 304L stainless steel tubesheets and type 329 stainless steel tubes. Under the previous operating conditions, the cooler condenser had experienced some corrosion, which was managed by plugging tubes and replacing the unit every three to four years. Shortly after the upgrade, with an operating temperature and pressure of 200 °C (390 °F) and 1035 kPa (0.15 ksi), 10% of the type 329 stainless steel tubes were found to be leaking. This condenser was replaced with a unit using type 310L stainless steel, which had to be replaced after 13 months of operation. The original condenser with new tubes of improved-grade 329 stainless steel replaced the 310L unit. Mississippi Chemical Corp. began looking for alternatives.

In an attempt to find a solution to this problem, autoclave tests were conducted on many newer types of stainless steels and zirconium in solutions up to 204 °C (399 °F) and at concentrations up to 65%. Clearly, zirconium was the only suitable material for the monopressure process. Corrosion rates of zirconium coupons were consistently below 25 μm/yr (1.0 mil/yr). The next step was to test zirconium tubes in service. Several tubes were installed into a rebuilt stainless steel condenser. They were destructively examined after 13 months and showed no signs of corrosion. Zirconium tubes were then placed in another condenser for one year. Once again, there were no signs of corrosion.

Consequently, Mississippi Chemical Corp. replaced its stainless steel cooler condenser with one constructed from zirconium tubes and zirconium/304L stainless steel explosion-bonded tubesheets. This unit contains more than 18 km (11 miles) of zirconium tubing. In service since 1984, the zirconium unit has already outperformed the stainless steel predecessors. Thereafter, several zirconium cooler condensers have been built for other HNO_3 producers.

Monopressure plants are not the only ones to use zirconium as a solution to corrosion problems. Certain plants use a distillation process to increase the acid concentration. The acid is passed through a reboiler and enters a distillation column to drive off water for concentrating the acid. In 1982, Union Chemicals Corp. replaced the bottom portion of each of two distillation columns and the tube bundles of each of two reboilers. The lower parts of the columns had been constructed originally with type 304L stainless steel, which experienced corrosion problems.

Titanium was tried but also failed. While glass-lined steel did not have the corrosion problems experienced by type 304L stainless steel and titanium, the maintenance costs were found to be unacceptable. Zirconium provides significantly improved corrosion resistance without adding maintenance costs. Zirconium also solved corrosion problems in the reboilers. Prior to the installation of zirconium tube bundles, both 304L and titanium tube bundles had failed in less than 18 months of operation.

With proper design and fabrication, zirconium susceptibility to SCC can be suppressed in highly concentrated HNO_3. For example, an Israeli chemical plant uses zirconium tubes in a U-tube cooler that processes bleached HNO_3 at concentrations between 98.5 and 99%. The unit cools the acid from 70 to 75 °C (160 to 165 °F) to 35 to 40 °C (95 to 105 °F). Previously, U-tube coolers were made from aluminum, which failed in 2 to 12 weeks. The zirconium unit has been in service for more than 2 years, operating 24 h a day, 6 days a week.

Adipic acid is produced primarily for use in the manufacture of nylon-6,6. Major commercial routes to make adipic acid involve the use of HNO_3 in the oxidation of cyclohexanol or oxidized cyclohexane at elevated temperatures. Because of the excellent performance of zirconium in the production of HNO_3, it has started to find its way into adipic acid plants.

Safety

Zirconium is low in toxicity and is not known to be a carcinogen. The permissible exposure limit for zirconium set by various health agencies is 5 mg/m^3. For comparison, the limit for iron is 1 mg/m^3.

One major concern is the reactivity of zirconium. Under most conditions, the reactivity works toward the advantage of zirconium. This reactivity allows zirconium to react spontaneously with oxygen to form a protective film that suppresses its reactivity. Consequently, zirconium can be safely used under most conditions. Nevertheless, unsafe situations may develop when this reactive nature is overlooked.

Heat of formation for zirconium dioxide at 25 °C (75 °F) is 1101.3 kJ (1043.9 Btu). It is potently exothermic. The generated heat can be easily absorbed by a large piece of zirconium. After the oxide film is formed, the oxidation rate will decrease quickly and pose no problems. However, when the heat is generated at a very small area, ignition may occur. Care should be exercised in handling fine materials including powder, sponge, machine chips, and thin foils. Ignition of fine materials will result in a very rapid, high-temperature fire that can be extinguished by using dry salt or sand. Attempts to extinguish a large zirconium fire with water will only result in scavenging of the oxygen atoms in the water molecules by the burning zirconium, leaving the hydrogen molecules to act as an additional fuel or explosion source. These very large fires should be allowed to burn out by themselves.

It is normally safe to handle a large piece of zirconium. Still, ignition may occur when this piece experiences an enhanced oxidation reaction in a confined space. Under this condition, generated heat cannot easily dissipate, leading to escalated oxidation reaction, and ignition becomes possible.

Furthermore, when the corrosion resistance of zirconium is grossly exceeded in certain environments, pyrophoric films may form on its surface (Ref 51). These environments include concentrated sulfuric acid and ferric-chloride-containing solutions that may induce massive localized corrosion. Consequently, the solid surface is broken down into tiny pieces that contain corrosion products and unreacted zirconium particles. When unreacted particles are fine enough, ignition may occur. This pyrophoricity can be neutralized by treating it with steam (Ref 51). Unreacted particles will oxidize in steam to become a stable oxide or covered with a thick layer of oxide film. Treating time is approximately 20 min when the steam temperature is 250 °C (480 °F). A longer time is needed when a lower-temperature steam is used.

Conclusions

Zirconium and its alloys can spontaneously form a layer of inert oxide films on their surfaces in an oxygen-containing environment. They retain this capability even in highly reducing environments, such as hydrochloric acid and dilute sulfuric acid, which are difficult for many passive alloys to form protective oxide films. They are also excellent for chloride-free oxidizing solutions such as nitric acid. Consequently, zirconium and its alloys have been successfully used in many corrosive conditions in the chemical processing industry for decades. They are used in many harsh environments and applications. They corrode at very low rates in media from strong acids to strong alkaline solutions. Media that attack zirconium include

hydrofluoric acid, concentrated sulfuric acid, and certain dry organic halides.

Characteristics of corrosion behavior of zirconium are:

- All zirconium alloys are low in alloying contents. They all are protected by zirconium oxide films. Zirconium and its alloys are very close in corrosion resistance in a wide range of environments, with some subtle differences. The corrosion difference among zirconium alloys becomes readily visible when the condition nears the upper limit. For example, the difference is small in dilute sulfuric acid but large when the acid concentration is greater than 60%.
- Zirconium and its alloys resist localized corrosion, such as pitting, crevice corrosion, and SCC, in all chloride solutions except the highly oxidizing chlorides. It has been noted that zirconium and its alloys are vulnerable to ferric chloride pitting, but this requires bulk pH values below 2.5. Above this value, the ferric ion does not exist. Corrosion will not occur in crevices either, even when the pH is low, because the condition is too reducing for the ferric ion to exist.
- Zirconium and its alloys are resistant to crevice corrosion in chloride solutions. They are susceptible to crevice corrosion in fluoride solutions and sulfuric acid.
- A good surface finish is effective in controlling pitting, SCC, and delayed hydride cracking of zirconium.
- It is important not to forget that zirconium is a reactive metal. There are safety-related issues, including ignition, to consider when this reactive nature is exposed.

REFERENCES

1. "Zirconium: Its Production and Properties," USBM Bulletin 561, U.S. Bureau of Mines, 1956
2. H.G. Rickover, L.D. Geiger, and B. Lustman, "History of the Development of Zirconium Alloys for Use in Nuclear Reactors," TID-26740, U.S. GPO, U.S. Energy Research and Development Administration, Division of Naval Reactors, 1975
3. J.H. Schemel, *ASTM Manual on Zirconium and Hafnium,* STP 639, ASTM, 1977
4. T.L. Yau and R.T. Webster, Zirconium, *Process Industries Corrosion—Theory and Practice,* NACE, 1986, p 529
5. T.L. Yau and R.T. Webster, Corrosion of Zirconium and Hafnium, *Corrosion,* Vol 13, *Metals Handbook,* 9th ed., ASM International, 1987, p 707
6. T.L. Yau, Corrosion of Zirconium, *Corrosion Engineering Handbook,* Marcel Dekker, 1996, p 195
7. T.L. Yau, "Zirconium Meeting the Challenges of the New Millennium," Paper 01331, Corrosion 2001 (Houston, TX), NACE International, 2001
8. J.L. Whitton, *J. Electrochem. Soc.,* Vol 115, 1968, p 58
9. M. Pourbaix, *Atlas of Electrochemical Equilibria in Aqueous Solutions,* Pergamon Press, 1966, p 223
10. W.G. Burgers, A. Claassen, and J. Zernike, *Z. Phys*., Vol 74, 1932, p 593
11. A. Charlesby, Ionic Current in Thin Films of Zirconium Oxide, *Acta Metall*., Vol 1, 1953, p 340–347
12. B. Cox, Factors Affecting the Growth of Porous Anodic Oxide Films on Zirconium, *J. Electrochem. Soc*., Vol 117, 1970, p 654–663
13. D.H. Bradhurst and P.M. Heuer, The Influence of Oxide Stress on the Breakaway Oxidation of Zircaloy-2, *J. Nucl. Mater.,* Vol 37, 1970, p 35–47
14. C. Roy and G. David, X-Ray Diffraction Analyses of Zirconia Films on Zirconium and Zircaloy-2, *J. Nucl. Mater.,* Vol 37, 1970, p 71–81
15. J. Godlewski, J.P. Gros, M. Lambertin, J.F. Wadier, and H. Weidinger, *Raman Spectroscopy Study of the Tetragonal-to-Monoclinic Transition in Zirconium Oxide Scales and Determination of Overall Oxygen Diffusion by Nuclear Microanalysis of* O^{18}, STP 1132, ASTM, 1991, p 416
16. J. Godlewski, *How the Tetragonal Zirconia is Stabilized in the Oxide Scale That Is Formed on a Zirconium Alloy Corroded at 400 °C in Steam,* STP 1245, ASTM, 1994, p 663
17. D. Khatamian and S.D. Lalonde, Crystal Structure of Thin Films Grown on Zr-Nb Alloys Studied by RHEED, *J. Nucl. Mater.,* Vol 245 (No. 1), 1997, p 10–16
18. M.L. Brown and G.N. Walton, A Comparison of the Polarization Behavior of Zirconium and Its Alloys, *J. Nucl. Mater.,* Vol 58, 1975, p 321–335
19. T.L. Yau, *Corrosion,* Vol 38 (No. 12), 1982, p 615
20. T.L. Yau and M.A. Maguire, Control of Localized Corrosion of Zirconium in Oxidizing Chloride Solutions, *Advances in Localized Corrosion,* NACE, 1990, p 311
21. T.L. Yau, "Chemical Impurities Create New Challenges in Material Selection," *Outlook,* Vol 9 (No. 4), 1988, p 4
22. T.L. Yau and D.R. Holmes, "Fluorides from Overlooked Sources," presented at Corrosion Applications Conference, 7–12 Sept 2003 (Coeur d'Alene, ID), ATI Wah Chang, An Allegheny Technologies Company
23. Y.M. Kolotyrkin, Electrochemical Behavior of Metals during Anodic and Chemical Passivation in Electrolytic Solutions, Proc. *First Int. Cong. on Metallic Corrosion,* 1961 (London), 1962, p 10–20
24. M. Maguire, *The Pitting Susceptibility of Zirconium in Aqueous* Cl^-, Br^-, *and* I^- *Solutions,* STP 830, ASTM, 1984, p 175
25. G. Cragnolino and J.R. Galvele, Anodic Behavior and Pitting of Zirconium and Zircaloy-4 in Aqueous Solutions of Sodium Chloride, *Passivity of Metals,* The Electrochemical Society, 1974, p 1053–1057
26. T. Shibato and M.A.M. Ameer, Stochastic Process of Pit Generation on Zirconium with an Anodic Oxide Film, *Corros. Sci.,* Vol 33, 1992, p 1633–1643
27. T.L. Yau, "Zirconium versus Corrosive Species in Geothermal Fluids," Paper 140, Corrosion 84, NACE, 1984
28. T.L. Yau, "Corrosion Properties of Zirconium in Chloride Salt Solutions," Paper 26, Corrosion 83, NACE, 1983
29. M.G. Fontana, *Corrosion Engineering,* 3rd ed., McGraw-Hill, 1986
30. J. Fahey, D.R. Holmes, and T.L. Yau, Evaluation of Localized Corrosion of Zirconium in Acidic Chloride Solutions, *Corrosion,* Vol 53 (No. 1), 1997, p 54
31. G. Jangg, R.T. Webster, and M. Simon, *Werkst. Korros.,* Vol 29, 1978, p 16
32. M. Maraghini, G.G. Adams, and P.V.J. Russelberghe, *J. Electrochem. Soc.,* Vol 101, 1954, p 400
33. T.L. Yau and R.T. Webster, The Effect of Iron on the Corrosion Resistance of Zirconium, *Corrosion,* Vol 39, 1983, p 218
34. T.L. Yau, Stress-Corrosion Cracking of Zirconium Alloys, *Stress-Corrosion Cracking: Materials Performance and Evaluation,* R.H. Jones, Ed., ASM International, 1992, p 299
35. B.J. Fitzgerald and T.L. Yau, "The Mechanism and Control of Stress Corrosion Cracking of Zirconium in Sulfuric Acid," Paper 092, 12th International Corrosion Congress, 19–24 Sept 1993 (Houston, TX), NACE International
36. T.L. Yau and R.T. Webster, "Delayed Hydride Cracking of Zirconium Alloys," Paper No. 250, Corrosion/95, NACE, 1995
37. *Boiler and Pressure Vessel Code of the ASME,* Section VIII, Division 1, Subsection C, UNF-56, (d), American Society of Mechanical Engineers, 1992, p 183
38. T.L. Yau and R.T. Webster, *Corrosion Test Loop,* STP 866, ASTM, 1985, p 36–47
39. J.G. Nelson, private communication, 28 April 2000
40. R. Haffpauir, J. Hsieh, M. Coles, and C. Wong, The Effects of Tin and Nickel on the Corrosion Resistance of Zirconium Alloys in Glacial Acetic Acid Service, *1997 Zirconium—Organics Conference Proceedings,* ATI Wah Chang, An Allegheny Technologies Company, 1998, p 29
41. K. Takeda and H. Anada, *Mechanism of Corrosion Rate Degradation due to Tin,* STP 1354, ASTM, 2000, p 592
42. T.L. Yau, Effect of Tin Content in Zirconium, *Corrosion Solutions Conference Proceedings,* ATI Wah Chang, An Allegheny Technologies Company, 2001, p 255
43. D.R. Holmes, "Tin in Zirconium 702—Effect in Sulfuric Acid Applications," presented at Corrosion Applications Conference, 7–12 Sept 2003 (Coeur d'Alene,

ID), ATI Wah Chang, An Allegheny Technologies Company
44. S. Kass, The Development of the Zircaloys, *Corrosion of Zirconium Alloys,* STP 368, ASTM, 1964, p 3
45. D.E. Thomas, Corrosion in Water and Steam, *Metallurgy of Zirconium,* B. Lustman and F. Kerze, Jr., Ed., McGraw-Hill, 1955
46. S.B. Dalgaard, Corrosion and Hydriding Behavior of Some Zr-2.5Nb Alloys in Water, Steam and Various Gases at High Temperature, *Proceedings of the Conference on Corrosion Reactor Materials,* Vol 2, International Atomic Energy Association, 1962, p 159
47. W.M. Latimer, *The Oxidation States of the Elements and Their Potentials in Aqueous Solutions,* Prentice Hall, 1952, p 270
48. W.B. Blumenthal, *Zirconium Compounds,* National Lead Co., TAM Division, 1969
49. D.R. Knittel and R.T. Webster, *Corrosion Resistance of Zirconium and Zirconium Alloys in Inorganic Acids and Alkalies,* STP 728, ASTM, 1981, p 191
50. T.L. Yau, *Effects of Impurities in H_2SO_4 on the Corrosion Resistance of Zirconium,* STP 830, ASTM, 1984, p 203
51. T.L. Yau, *Methods to Treat Pyrophoric Films on Zirconium,* STP 830, ASTM, 1984, p 124
52. T.L. Yau, Performance of Zirconium and Columbium in Simulated FGD Scrubber Solutions, *Corrosion in Desulfurization Systems,* NACE, 1984
53. C.R. Bishop, *Corrosion,* Vol 19, 1963, p 308t
54. V.V. Andreeva and A.I. Glukhova, *J. Appl. Chem.,* Vol 11, 1961, p 390
55. V.V. Andreeva and A.I. Glukhova, *J. Appl. Chem.,* Vol 12, 1962, p 457
56. M. Maraghini, G.G. Adams, and P.V.J. Russelberghe, *J. Electrochem. Soc.,* Vol 101, 1954, p 400
57. T.L. Yau, *Zirconium for Nitric Acid Solutions,* STP 917, ASTM, 1986, p 57
58. T.L. Yau, *Corrosion,* Vol 39, 1983, p 167
59. J.A. Beavers, J.C. Griess, and W.K. Boyd, *Corrosion,* Vol 36, 1981, p 292
60. T.L. Yau, *Corrosion,* Vol 44, 1988, p 745
61. S.M. Shetlon, "Zirconium: Its Production and Properties," USBM Bulletin 561, U.S. Bureau of Mines, 1956
62. L.B. Golden, I.R. Lane, Jr., and W.L. Acherman, *Ind. Eng. Chem.,* Vol 44, 1952, p 1930
63. L.B. Golden, I.R. Lane, Jr., and W.L. Acherman, *Ind. Eng. Chem.,* Vol 45, 1953, p 782
64. R. Bloom, Jr., L.E. Weeks, and C.W. Raleigh, *Corrosion,* Vol 16, 1960, p 164t
65. T.L. Yau, Zircadyne Succeeds Where Other Materials Fail: A Study of Stability and Corrosivity of Hydrogen Peroxide, *Outlook,* Vol 12 (No.1), 1991, p 3
66. T.L. Yau, *TAPPI J.,* Vol 74 (No.3), 1991, p 155
67. P.L. Gegner and W.L. Wilson, *Corrosion,* Vol 15, 1959, p 341t
68. C.M. Graighead, L.A. Smith, and R.I. Jaffee, "Screen Tests on Metals and Alloys in Contact with Sodium Hydroxide at 1,000 and 1,500 °F," U.S. Energy Commission Report BMI-707, Battelle Memorial Institute, Nov 1951
69. T.L. Yau, *Mater. Perform.,* Vol 32 (No. 6), 1993, p 65
70. L.B. Golden, *Zirconium and Zirconium Alloys,* American Society for Metals, 1953
71. D.W. McDowell, *Chem. Eng.,* Vol 26, May 1974, p 96
72. C. Miola and H. Richter, *Werkst. Korros*., Vol 43, 1992, p 396
73. P.E. Krystow, *Chem. Eng. Prog.,* Vol 67 (No. 4), 1971, p 59
74. "Corrosion Resistance of Nickel-Containing Alloys in Organic Acids and Related Compounds," Publication 1285, Nickel Development Institute, Toronto, Canada, 1979
75. H. Togano and K. Osato, *Boshoku Gijutsu,* Vol 10 (No. 13), 1961, p 529
76. T. Shimose, A. Takamura and S. Segawa, *Boshoku Gijutsu,* Vol 15 (No. 2), 1966, p 49
77. T.L. Yau, *Outlook,* Vol 8 (No. 3), 1987, p 2
78. T.L. Yau, Performance of Zirconium and Zirconium Alloys in Organics, *J. Test. Eval.,* Vol 24 (No. 2), 1996, p 110
79. T.L. Yau, *Outlook,* Vol 9 (No. 3), 1988, p 6
80. J.D. Leonard, Euorpean Patent 5,998, 12 Dec 1979
81. Kemira Specifies Zircadyne 702 for Use in a Formic Acid Application, *Outlook,* Vol 11 (No. 1), 1990, p 1
82. B. Cox, *Advances in Corrosion Science and Technology,* Vol 5, Plenum Press, 1976, p 173
83. K. Mori, A. Takamura, and T. Shimose, *Corrosion,* Vol 22, 1966, p 29
84. P.K. De, K. Elayaperumal, and J. Balschandra, *Corros. Sci*., Vol 11, 1971, p 579
85. B. Cox, Reports AECL-3551, 3612, and 3799, Atomic Energy of Canada Ltd
86. R.F. Koenig, "Corrosion of Zirconium and Its Alloys in Liquid Metals," Report KAPL-982, U.S. Atomic Energy Commission, 1 Oct 1953
87. R.D. Watson, "Oxidized Zirconium as a Bearing Material in Water Lubricated Mechanism," Report CRE-996, Atomic Energy of Canada, 1960
88. W.E. Kemp, Noblizing: Creating Tough, Wear Resistant Surfaces on Zirconium, *Outlook,* Vol 11 (No. 2), 1990, p 4
89. J. Haygarth and L. Fenwick, Improved Wear Resistance of Zirconium by Enhanced Oxide Films, *Thin Solid Films,* 1984, p 351
90. M.A. Maguire and T.L. Yau, "Electrochemical Properties of Zirconium in Mineral Acids," Paper 265, Corrosion 86, NACE, 1986
91. T.L. Yau and M.A. Maguire, *Corrosion,* Vol 40, 1984, p 289
92. T.L. Yau and M.A. Maguire, *Corrosion,* Vol 41, 1985, p 397

SELECTED REFERENCES

- M.G. Fontana, *Corrosion Engineering,* 3rd ed., McGraw-Hill, 1986
- F.I. LaQue and H.R. Copson, Ed., *Corrosion Resistance of Metals and Alloys,* 2nd ed., Reinhold, 1963
- J.H. Schemel, *ASTM Manual on Zirconium and Hafnium,* STP 639, ASTM, 1977
- L.L. Shreir, R.A. Jarman, and G.T. Burstein, Ed., *Corrosion,* 3rd ed., Butterworth/Heinemann, 1994

ASM Handbook, Volume 13B: Corrosion: Materials
S.D. Cramer, B.S. Covino, Jr., editors, p325-336
DOI: 10.1361/asmhba0003824

Corrosion of Niobium and Niobium Alloys

Richard C. Sutherlin and Ronald A. Graham, ATI Wah Chang, An Allegheny Technologies Company

NIOBIUM AND NIOBIUM ALLOYS have been used in a number of industrial and aerospace applications for over 40 years. Niobium use primarily includes rocket and jet engine applications, alloying of steels and superalloys, sodium vapor highway lighting, superconductors, anodic protection devices for steel bridge structures, and chemical processing equipment.

Niobium alloys for rocket and jet engines operate at very high temperatures, exceeding 1093 °C (2000 °F), and these alloys retain fairly high strengths at these temperatures. Some of the alloys used in these applications include C-103, C-129Y, Cb-752, WC-3009, and FS-85 (Ref 1). Niobium has many of the same properties as tantalum, its sister metal, but it is approximately one-half the density of tantalum. A common characteristic of both niobium and tantalum is their interaction with the reactive elements hydrogen, oxygen, nitrogen, and carbon at temperatures above 300 °C (570 °F). These reactions will cause severe embrittlement. Consequently, at elevated temperatures, the metal must be protectively coated or used in vacuum or inert atmospheres.

Niobium is commonly used as an alloying element for steels and nickel-base superalloys, such as alloys 625 and 718, where it strengthens by solid-solution formation, carbide precipitation, and coherent phase formation. In carbon steels, high-strength low-alloy (HSLA) steels, and stainless steels, niobium is an important microalloying element that improves fabricability, weldability, creep resistance, and thermal fatigue resistance (Ref 2).

Niobium has excellent compatibility with liquid metals such as sodium, potassium, lithium, and uranium. It is used in sodium vapor lamps because of its excellent resistance to metallic sodium, in either vapor or molten form. A niobium alloy component holds the metallic sodium, which is heated to 875 to 925 °C (1607 to 1697 °F) (Ref 3).

Niobium has also been used for over 20 years in cathodic protection devices for oil drilling rigs, ship hulls, bridges, and underground storage tanks. These cathodic protection devices, such as platinum-clad niobium anodes, use an impressed current to force the corroding structure to become a cathode. These anodes provide a cost-effective method to protect structures from galvanic corrosion (Ref 4, 5).

For chemical processing, niobium resists a wide variety of corrosive environments. These environments include mineral acids, many organic acids, liquid metals, and most salt solutions. One application is the heating of hydrochloric acid, using niobium steam-heating coils, to pickle carbon steel. Another application for niobium is for overhead condenser and heat-recovery sections of nitric acid and fertilizer production facilities. Niobium has also been considered for use in the pharmaceutical industry, where corrosion of any level is undesirable. Niobium has also been used in the evaporators in the chrome plating industry to resist the hot, concentrated chromic acid media (Ref 6). Niobium resists the chromic acid environment, even when small amounts of free fluorides are present. Niobium is one of the more resistant materials in applications where fluoride-contaminated solutions are present (Ref 7). Applications in other corrosive environments include bromine and hydrogen peroxide. Niobium has also been used during the past 10 years in the form of rupture disks for chemical applications. The use of niobium in this application has decreased the cost of the rupture disks significantly over other material choices, including alloy B-2 and tantalum (Ref 8, 9). The high-nickel alloy B-2 had a slight corrosion rate and failed prematurely, while the tantalum was much more costly than niobium.

Niobium Alloys

There are several niobium alloys that are corrosion resistant in severe applications. These alloys include Nb-1Zr, Nb-55Ti, Nb-50Ta, and Nb-40Ta. Nb-1Zr (UNS R04251 or R04261, reactor or commercial grade) is a corrosion-resistant niobium alloy with corrosion resistance similar to that of pure niobium, except with higher strength imparted by the addition of zirconium. In most applications where pure niobium is used, Nb-1Zr can be applied using higher design-strength allowables. Nb-1Zr is also considered for use in heat exchangers for hydrochloric acid pickling of steel.

Nb-55Ti (or Ti-45Nb, titanium grade 36) has been used in the Loprox process, a wet oxidization process for organic materials in an aqueous waste stream to improve biodegradability (Ref 10). The Loprox process requires materials that can survive 200 °C (390 °F) and pressures of 2.0 MPa (290 psi) while injecting pure oxygen into an acidified waste stream. Pure titanium offers corrosion resistance as adequate as that of Nb-55Ti but is potentially self-ignitable under the process conditions. The addition of niobium reduces the propensity for ignition and improves the corrosion resistance. Nb-55Ti has been used in oxygen injectors, in piping systems, and in a pressure vessel (Ref 11).

Tantalum is more resistant than niobium to almost all process streams, with the exception of some complex fluoride plating baths where it is preferred over tantalum (Ref 12). The performance of niobium-tantalum alloys in boiling 70% sulfuric acid is reported in Ref 13. The tantalum-rich alloys showed a decrease in corrosion rate with increasing exposure time, as was found for pure tantalum and pure niobium. Nb-50Ta and Nb-40Ta showed a constant or increasing corrosion rate as time increased. The corrosion rate of niobium will increase with hydrochloric acid concentration and diminish initially with time, due to the formation of superficial oxide films (Ref 14). In niobium-tantalum alloys, it was demonstrated that in sulfuric acid solutions, as the tantalum composition increases, the corrosion rate will improve. The corrosion rate of pure niobium in 10 *N* HCl solutions decreased with time (Ref 15). This has occurred in other laboratory testing, showing that niobium initially sees a higher corrosion rate in the first few days, and then the corrosion rate decreases and stabilizes over time. The corrosion rate of tantalum-rich alloys, such as Ta-40Nb, is much lower than would be expected for a simple mixture for niobium and tantalum, where corrosion is proportional to niobium content. Ta-40Nb could be considered for service in 70% sulfuric acid at 165 °C (330 °F) (Ref 16).

Mechanisms of Corrosion Resistance

Niobium, like other refractory metals, derives its corrosion resistance from a readily formed,

adherent, passive oxide film, Nb_2O_5. Similar to titanium, niobium will also form lower or suboxide films (NbO and NbO_2) under reducing conditions. The stoichiometry of the oxide film will depend on the media that the niobium is exposed to. The oxide film can be composed of a single oxide (Nb_2O_5, NbO, or NbO_2) or a mixture of the three. The oxide film will exist in a lower valence state under reducing conditions. Typically, the presence of oxidizing impurities in the environment will improve the corrosion resistance of niobium.

Films of amorphous niobium oxides are only a few nanometers thick. They form according to the following reaction sequences:

$$Nb + H_2O \rightarrow NbO + 2H^+ + 2e^-$$
$$NbO + H_2O \rightarrow NbO_2 + 2H^+ + 2e^-$$
$$2NbO_2 + H_2O \rightarrow Nb_2O_5 + 2H^+ + 2e^-$$

Niobium reacts readily with water to form a niobium oxide. If the oxide forms a thin, compact film, as is the case in pure water and many dilute solutions, corrosion resistance is excellent. In the presence of complexing agents, such as fluoride ion in H_2SO_4 or HCl and potentially other environments, the corrosion behavior is dominated by the dissolution of the oxide layer. Niobium also forms a very stable, adherent oxide film under anodic conditions. This oxide film has a very high dielectric constant and a high electrochemical breakdown potential. In seawater, the breakdown potential of niobium is 115 V as compared to other more common reactive/refractory materials, such as titanium (9 V). The oxide layer also helps to reduce hydrogen pickup. Monatomic hydrogen is easily absorbed into bare niobium metal, and if the oxide layer fails in aqueous solutions, niobium will suffer embrittlement.

The Pourbaix (potential-pH) diagram for the niobium-water system represents the conditions of thermodynamic stability of niobium, which can exist in the presence of water and in aqueous solutions that do not contain substances capable of forming soluble complexes or insoluble compounds with niobium. Figure 1 shows a potential-pH equilibrium diagram for the niobium-water system at 25 °C (77 °F) (Ref 17). This figure also shows the theoretical conditions for immunity and passivation of niobium.

The region where niobium monoxide (NbO) forms on niobium shows the oxide to be thermodynamically unstable (between lines 1 and 2). This oxide state would be in the presence of water or acid and in neutral or basic solutions. At any pH, the oxide tends to decompose water by the evolution of hydrogen. Under these conditions, NbO will become oxidized to a higher oxide state (Ref 18).

In the region where niobium dioxide (NbO_2) is formed, below line *a*, this compound is thermodynamically unstable in the presence of water and aqueous solutions at any pH. Theoretically, this oxide species will decompose water with the evolution of hydrogen. In this process, the NbO_2 will become oxidized to niobium pentoxide (Nb_2O_5).

In the region where niobium pentoxide (Nb_2O_5) is formed, shown on the Pourbaix diagram between lines *a* and *b*, the compound is thermodynamically stable in the presence of water and noncomplexing acid, alkaline, and neutral solutions. This oxide can be attacked in concentrated hydrofluoric acid, with the formation of fluorinated or oxyfluorinated complexes.

According to the potential-pH equilibrium diagram, niobium pentoxide can be reduced to a lower oxide (such as NbO_2 or NbO) or to metallic niobium. It may not be possible to accomplish this reduction, however, by electrochemical means in the presence of noncomplexing solutions.

General Corrosion in Specific Media. Except for hydrofluoric acid, niobium is resistant to most mineral and organic acids at temperatures to 100 °C (212 °F). In certain applications, the corrosion properties of niobium are similar to those of tantalum; however, niobium is generally more dependent on the temperature and acid purity than tantalum. Niobium shows lower resistance than tantalum to the more aggressive acidic media, such as hot, concentrated mineral acids. Niobium generally has excellent resistance to oxidizing acids, such as nitric acid, but may be subject to hydrogen embrittlement in reducing acids, such as hydrochloric acid, at high concentrations and temperatures. Like tantalum, niobium is susceptible to hydrogen embrittlement if cathodically polarized by either galvanic coupling or by impressed potential. In addition to being very stable, the anodic niobium oxide film has a high dielectric constant and a high breakdown potential. These properties, coupled with its electrical conductivity, have led to the use of niobium as a substrate for platinum-group metals in impressed-current cathodic protection anodes.

Corrosion in Waters. Niobium is fully resistant to water, either natural or pure, and to high-temperature water and steam. Niobium reacts with water to form niobium oxide. There is a direct transition from immunity to passivity without an intermediate region where corrosion occurs, as indicated by the Pourbaix (potential-pH) diagram in Fig. 1.

Acid Solutions. Niobium is resistant to most organic and mineral acids at concentrations and temperatures below 100 °C (212 °F). This list of acids includes the halogen acids hydrochloric (HCl), hydriodic (HI), and hydrobromic (HBr) in addition to nitric acid (HNO_3), sulfuric acid (H_2SO_4), and phosphoric acid (H_3PO_4). Niobium is completely resistant in dilute sulfurous acid (H_2SO_3) at 100 °C (212 °F). In concentrated

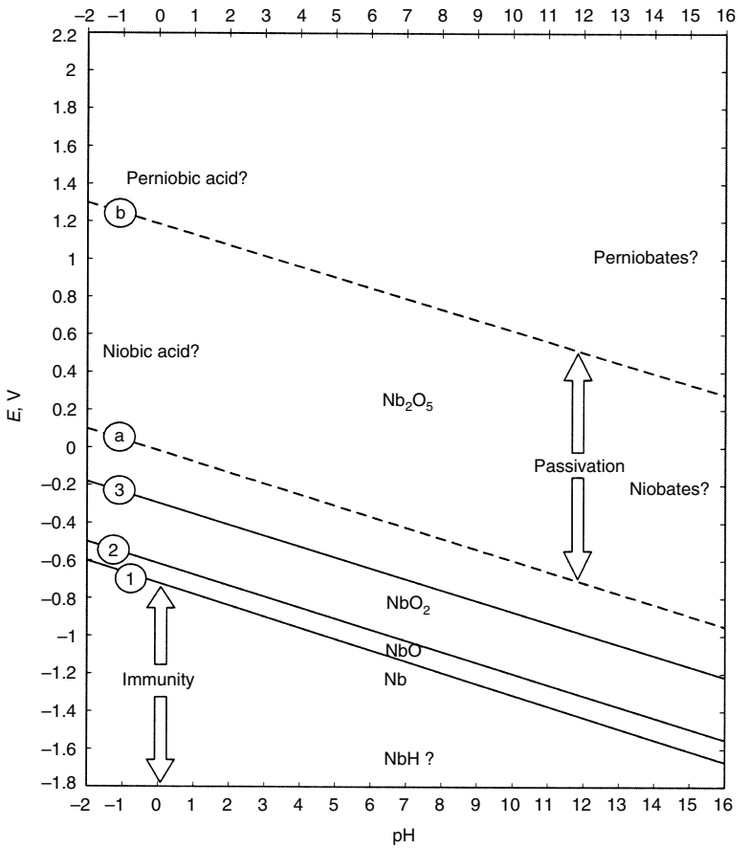

Fig. 1 Potential-pH equilibrium diagram for niobium-water at 25 °C (75 °F)

sulfuric acid at the same temperature, niobium has a corrosion rate of 0.25 mm/yr (10 mils/yr). Niobium is completely resistant in HNO_3, having a corrosion rate of 0.025 mm/yr (1 mil/yr) in 70% HNO_3 at 250 °C (480 °F). In chromium plating solutions, niobium experiences only a slight weight change, and in the presence of small amounts of fluoride (F^-) catalyst, niobium exceeds the corrosion resistance of tantalum in that application. Niobium is inert in mixtures of HNO_3 and HCl. It has a corrosion rate of less than 0.025 mm/yr (1 mil/yr) in aqua regia at 55 °C (130 °F). In boiling 40 and 50% H_3PO_4 with small amounts of F^- impurity (5 ppm), niobium has a corrosion rate of 0.25 mm/yr (10 mils/yr). Niobium, like most reactive and refractory metals, is susceptible to attack in hydrofluoric acid.

Hydrochloric acid is an important mineral acid used in many industrial processes, including acid pickling, chemical cleaning, pharmaceutical production, and chemical processing. Niobium and niobium alloys have excellent resistance in hydrochloric acid environments in concentrations from room temperature to above boiling as well as higher concentrations and lower temperatures. Hydrochloric acid is a highly reducing acid. Niobium is susceptible to hydrogen pickup in a reducing acid such as hydrochloric acid, especially at the higher concentrations and higher temperatures. The addition of strong oxidizers such as ferric ions (Fe^{3+}), cupric ions (Cu^{2+}), or nitric acid to hydrochloric acid, however, increases the corrosion resistance of niobium, particularly in higher concentration and higher temperature ranges. Generally, niobium does not require aeration for its corrosion resistance, but aeration, like oxidizing impurities, may improve its resistance in hydrochloric acid environments.

There may be numerous candidate materials when the hydrochloric acid is below the boiling point. Few materials, however, will resist hydrochloric acid at concentrations above the boiling temperature. Figure 2 shows an isocorrosion curve of various reactive and refractory metals tested in pure hydrochloric acid. As the isocorrosion curve indicates, niobium alloys have good resistance to hydrochloric acid solutions above the boiling point at the lower concentrations. Nb-1Zr, an alloy with 1% Zr added for strength, has slightly less resistance in hydrochloric acid than that of pure niobium. Although niobium and niobium alloys show low corrosion rates at temperatures even well above the boiling point, they may begin to pick up hydrogen at temperatures above the boiling point. This hydrogen absorption at elevated temperatures will cause embrittlement.

Table 1 indicates corrosion data for niobium and niobium alloys in pure hydrochloric acid. This table includes both welded and nonwelded samples at concentrations up to 37% and temperatures exceeding the boiling point. This table also compares the corrosion resistance of both niobium and Nb-1Zr in pure hydrochloric acid as well as acid with various impurities. It has been shown in extensive laboratory testing that the presence of oxidizing impurities will improve the corrosion resistance of niobium. Table 2 shows the effect of ferric ion in hydrochloric acid. The effect of ferric ion in HCl will, however, be more pronounced in the lower concentrations of acid than that of the higher concentrations. As the acid concentrations increase, the ferric ion has little effect in protecting the niobium from attack. Welded niobium and niobium alloys will also have similar resistance to nonwelded niobium alloys in the lower concentrations, but as the acid concentration exceeds approximately 10%, the welded samples will experience a slightly higher corrosion rate.

Many common materials of construction are considered corrosion resistant if their corrosion rate is less than 0.125 mm/yr (5 mils/yr). A corrosion allowance of this rate is generally acceptable for most materials. Due to the higher cost of niobium compared with other more common materials of construction, niobium alloy tubes are typically designed with very thin-wall or sheet thickness, 0.4 to 0.5 mm (0.015 to 0.020 in.). This is a reason that the desired corrosion rate for niobium equipment in service is less than 0.05 mm/yr (2 mils/yr). Although equipment has been installed in applications where the corrosion rate of niobium has exceeded 0.05 mm/yr (2 mils/yr), it is recommended that whenever possible, the niobium corrosion rate be less. Figure 3 shows an isocorrosion curve for niobium alloys where the corrosion rate is less than 0.05 mm/yr (2 mils/yr).

Electrochemical measurements help us to better understand the effect of alloy composition, acid impurities, acid temperature, and acid concentration. These methods accelerate the corrosion process so that the effects of process variables can be determined rapidly. To investigate the effect of these factors, the addition of oxidizing impurities and the increase in temperature were evaluated by electrochemical testing on niobium and niobium alloys. As mentioned previously, the presence of an oxidizing impurity such as ferric ion in HCl improves the corrosion resistance of niobium. Once a minimum ferric ion content is present in hydrochloric acid, the corrosion resistance is improved. Ferric ion impurities as low as 70 ppm at temperatures up to 100 °C (212 °F) in 5 *N* HCl and up to 60 °C (140 °F) in 10 *N* HCl will improve the corrosion resistance of niobium over that in pure hydrochloric acid (Ref 15).

Figure 4 shows a series of potentiodynamic curves for niobium and Nb-1Zr with 500 and 1500 ppm ferric chloride added to 20% hydrochloric acid. These scans show that niobium and Nb-1Zr react almost identically to the presence of ferric in hydrochloric acid. It is also apparent that 500 ppm ferric and 1500 ppm ferric have the same beneficial effect on niobium and Nb-1Zr in this environment. The passive current density virtually cannot be distinguished between the two alloys.

To compare the behavior of niobium and Nb-1Zr as a function of temperature, electro-

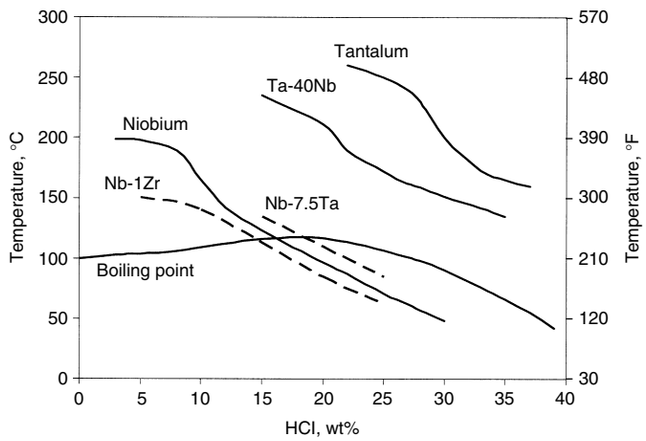

Fig. 2 Isocorrosion curve of reactive and refractory metals in pure hydrochloric acid, 0.13 mm/yr (5 mils/yr) lines

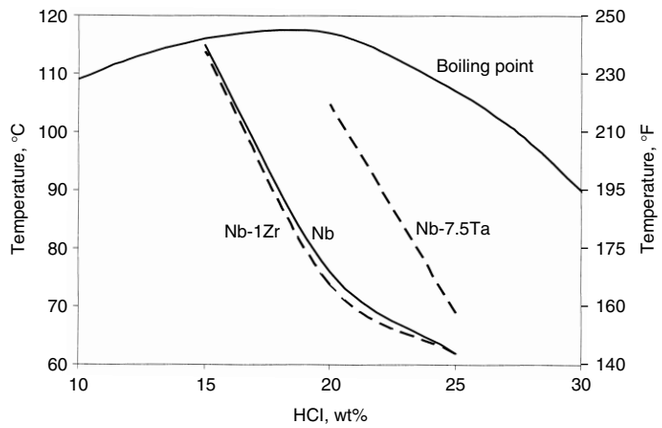

Fig. 3 Isocorrosion curves of niobium alloys in hydrochloric acid, 0.05 mm/yr (2 mils/yr) lines

Table 1 Corrosion of niobium alloys in aqueous hydrochloric acid

HCl, wt%	Test duration, days	Specimen condition(a)	Temperature °C	Temperature °F	Corrosion rate Nb mm/yr	Corrosion rate Nb mils/yr	Corrosion rate Nb-1Zr mm/yr	Corrosion rate Nb-1Zr mils/yr	Impurities	Comments
5	7	NW	50	122	nil	nil	...	...	...	...
	7	NW	60	140	0.001	0.04	...	...	...	...
	7	NW	80	176	0.002	0.08	...	...	...	...
	3-4	NW	100	212	0.015/0.0025	0.6/0.1	0.0025/0.005	0.1/0.2	...	...
	3-4	W	100	212	0.0025/0.005	0.1/0.2	0.0025/0.005	0.1/0.2	...	...
	7	NW	170	338	0.019	0.7	...	...	...	...
	7	NW	180	356	0.007	0.3	...	...	...	...
	7	NW	190	374	0.017	0.7	...	...	...	...
10	7	NW	50	122	...	...	nil	nil	...	...
	7	NW	60	140	...	...	nil	nil	...	...
	7	NW	70	158	...	...	nil	nil	...	...
	7	NW	80	176	...	...	0.0025	0.1	...	...
	7	NW	100	212	...	...	0.005	0.2	...	...
	2	NW	105	221	<0.025	<1	...	...	...	...
	2	NW	105	221	<0.025	<1	...	...	...	...
	1	NW	105	221	0.052	2.0	...	...	35% ferrous chloride + 2% ferric chloride	...
	1	NW	105	221	0.132	5.2	...	...	35% ferrous chloride + 2% ferric chloride	Argon sparge
	2-4-2	W	105	221	0.01/0.005/0.012	0.4/0.2/0.4	...	...	...	pH = 0.5 (pitting)
	2-4-2	NW	105	221	0.015/0.005/0.012	0.5/0.2/0.4	...	...	200 ppm ferric chloride	...
	2-4-2	W	105	221	0.012/0.005/0.009	0.4/0.2/0.3	...	...	200 ppm ferric chloride	...
	2-4-2	NW	105	221	0.015/0.009/0.009	0.5/0.3/0.3	...	...	1% ferric chloride	...
	2-4-2	W	105	221	0.012/0.005/0.009	0.4/0.2/0.3	...	...	1% ferric chloride	Cracks in welds
	2-4-2	NW	105	221	0.012/0.009/0.009	0.4/0.3/0.3	...	...	2% ferric chloride	...
	2-4-2	W	105	221	0.012/0.005/0.009	0.4/0.2/0.3	...	...	2% ferric chloride	Cracks in welds
	7	NW	210	392	...	...	5.8	229	...	...
11	22	NW	70	158	0.002	0.08	...	...	60% phenol	Vapor
	22	NW	70	158	0.001	0.04	...	...	60% phenol	Liquid
15	7	W	93	199	0.055	2.2	0.06	2.4	15% ferrous chloride	...
	7	W	93	199	0.04	1.6	0.04	1.6	15% ferric chloride	Cracked when bent 90°
	4	W	177	350	0.52	20	0.396	16	1000 ppm ferric chloride	...
	4	W	177	350	14	552	9.38	370	1500 ppm ferric chloride	Embrittlement
	7	W	177	350	14.9	587	12.4	489	500 ppm ferric chloride	Embrittlement
	4	W	177	350	10.8	426	10.2	402	500 ppm ferric chloride	Embrittlement
	7	W	177	350	5.79	228	13.9	548	1000 ppm ferric chloride	Embrittlement
	7	W	100	212	0.012	0.5	0.012	0.5	500 ppm ferric chloride	...
	7	W	100	212	0.015	0.6	0.018	0.7	1000 ppm ferric chloride	...
	7	W	100	212	0.012	0.5	0.012	0.5	1500 ppm ferric chloride	...
	7	W	60	140	0.003	0.1	0.003	0.1	500 ppm ferric chloride	...
	7	W	60	140	0.003	0.1	0.003	0.1	1000 ppm ferric chloride	...
	7	W	60	140	0.006	0.2	0.003	0.1	1500 ppm ferric chloride	...
18	<1	W	150	302	2.77	109	...	...	...	Vapor
	<1	W	150	302	3.44	136	...	...	...	Liquid
	3-2	NW	105	221	0.15/0.15	5.8/5.9	...	...	1% ferric chloride + 1g Sn	...
20	7	NW	60	140	0.055	2.2	0.058	2.3	500 ppm ferric	...
	7	NW	60	140	0.07	2.8	0.082	3.2	1000 ppm ferric	...
	7	NW	60	140	0.037	1.5	0.036	1.4	1500 ppm ferric	...
	7	NW	100	212	0.067	2.6	0.033	1.3	500 ppm ferric	...
	7	NW	100	212	0.067	2.6	0.109	4.3	1000 ppm ferric	...
	7	NW	100	212	0.079	3.1	0.076	3.0	1500 ppm ferric	...
	7	W	93	199	0.046	1.8	0.043	1.7	25% ferrous chloride + 2% ferric chloride	...
	7	W	93	199	0.14	5.5	0.149	5.9	15% ferrous chloride	...
	7	W	93	199	0.155	6.1	0.171	6.7	15% ferric chloride	...
25	7	NW	100	212	0.366	14	0.378	15	500 ppm ferric	...
	7	NW	100	212	0.256	10	0.274	11	1000 ppm ferric	...
	7	NW	100	212	0.396	16	0.366	14	1500 ppm ferric	...
	7	NW	60	140	0.009	0.4	0.006	0.2	500 ppm ferric chloride	...
	7	NW	60	140	0.006	0.2	0.006	0.2	1000 ppm ferric chloride	...
	7	NW	60	140	0.006	0.2	0.006	0.2	1500 ppm ferric chloride	...
	7	W	177	350	11.8	465	13.44	530	500 ppm ferric chloride	Embrittlement
	7	W	177	350	13.5	532	12.5	493	1000 ppm ferric chloride	Embrittlement
30	3	NW	70	158	...	...	1.61	63	...	...
	3	W	70	158	...	...	1.71	67	...	...
35	1	NW	127	260	3.29	130	...	...	...	...
	7	NW	25	77	nil	nil	...	...	1 : 7 with hydrogen peroxide + chlorine sparge	...
37	14	NW	60	140	0.104	4.1	...	...	8 g/L ferric chloride	...

(a) W, welded; NW, nonwelded

chemical scans were developed in 25% HCl at 80 and 100 °C (175 and 212 °F). The potentiodynamic plots in Fig. 5 show the similarity between niobium and Nb-1Zr in pure hydrochloric acid. Niobium tends to have a slightly lower current density, indicating lower corrosion rates, than Nb-1Zr does under identical conditions. Notice the progression of higher current densities for both niobium and Nb-1Zr as the temperature increases from 80 to 100 °C (175 to 212 °F). These data show that the corrosion resistance of niobium is very dependent on temperature, because as the temperature increases, the current density and corrosion rate increase.

Pure niobium has been shown to be a candidate material for use in hydrochloric acid pickling applications in the form of steam heating coils. In addition to pure niobium, the alloy Nb-1Zr is an ideal candidate for use in steel pickling applications due to a similar corrosion resistance as pure niobium and the additional solid-solution strengthening imparted by the zirconium. At the higher concentrations of hydrochloric acid and at the lower concentrations at the higher temperatures, niobium and niobium alloys may suffer with hydrogen pickup and possible embrittlement. For this reason, it is extremely important that the temperature of the tube surface, not the bath temperature, be considered as the application temperature.

Table 2 Effect of ferric ion on the corrosion rate of niobium and Nb-1Zr

Temperature		HCl,	Ferric (Fe^{3+})	Corrosion rate			
				Nb		Nb-1Zr	
°C	°F	wt%	concentration, ppm	mm/yr	mils/yr	mm/yr	mils/yr
60	140	20	0	<0.025	<1	<0.025	<1
		20	500	0.046	1.8	0.048	1.9
		20	1000	0.058	2.3	0.069	2.7
		20	1500	0.030	1.2	0.030	1.2
		25	0	0.0381	1.5	0.033	1.3
		25	500	0.008	0.3	0.005	0.2
		25	1000	0.005	0.2	0.005	0.2
		25	1500	0.005	0.2	0.005	0.2
100	212	20	0	0.101	4	0.127	5
		20	500	0.056	2.2	0.028	1.1
		20	1000	0.056	2.2	0.091	3.6
		20	1500	0.066	2.6	0.064	2.5
		25	0	0.203	8	0.228	9
		25	500	0.304	12	0.314	12.4
		25	1000	0.215	8.5	0.228	9
		25	1500	0.329	13	0.304	12

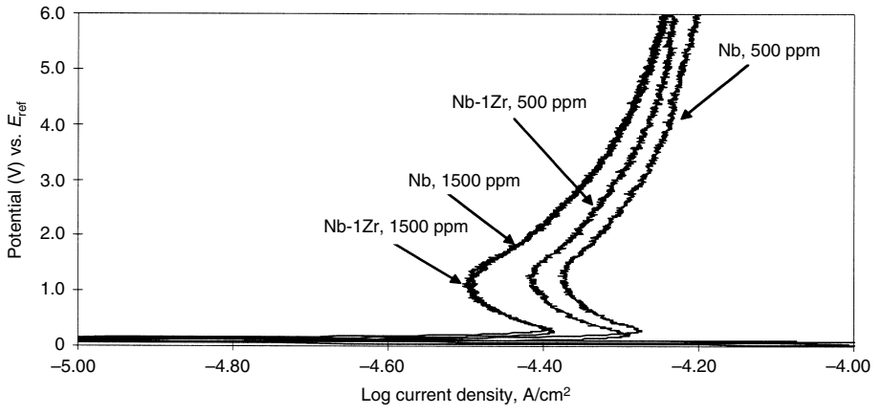

Fig. 4 Potentiodynamic scan results of niobium and Nb-1Zr in 20% HCl at 100 °C (212 °F) with ferric ion. Saturated calomel electrode with scan rate of 0.3 mV/s

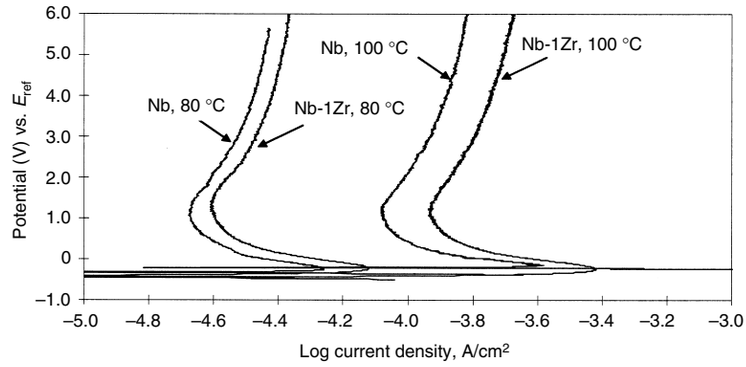

Fig. 5 Potentiodynamic scan results of niobium and Nb-1Zr in 25% HCl at various temperatures. Scan rate of 0.3 mV/s

Nitric Acid Environments. Niobium will exhibit excellent corrosion resistance in an oxidizing acid such as nitric acid. Table 3 shows corrosion data of niobium in nitric acid environments. Niobium has a corrosion rate of <0.025 mm/yr (1 mil/yr) in 70% HNO_3 at 250 °C (480 °F). Niobium has good stress-corrosion cracking resistance in 97% HNO_3 at 250 °C (480 °F) in the welded and non-welded condition. See Table 4 for U-bend testing of niobium in nitric acid.

Sulfuric Acid Solutions. Niobium and its alloys generally have good resistance in sulfuric acid environments, primarily at the lower concentrations and lower temperatures. Table 5 shows the corrosion resistance in various concentrations and temperatures. In most solutions, welded niobium exhibits a similar corrosion resistance to that of nonwelded niobium, except at the higher concentrations and temperatures. The corrosion resistance of niobium increases under the oxidizing conditions in sulfuric acid with Fe^{3+}, Cu^{2+}, Cr^{3+}; in sulfuric/nitric acid mixtures; sulfuric/phosphoric acid mixtures; or sulfuric/hydrochloric acid mixtures. Table 6 shows the effect of ferric or cupric ions on the corrosion rate of niobium in boiling sulfuric acid. This information demonstrates the dramatic effect of oxidizing impurities on the corrosion resistance in sulfuric acid. From the limited amount of information available, the surface condition (i.e., pickled surface) has not been found to have a major effect on improvement of the corrosion resistance of niobium. At room temperature, niobium is resistant up to approximately 95% sulfuric acid concentration, but care should be taken due to the potential hydrogen absorption of niobium at the higher concentrations. Figure 6 shows an isocorrosion curve for niobium as compared to other reactive and refractory metals (Ref 19).

Alkaline Solutions. Niobium is resistant and has a corrosion rate of less than 0.025 mm/yr (1 mil/yr) in most aqueous alkaline solutions at room temperature. Niobium is, however, severely attacked at elevated temperatures by hot alkalis and may be embrittled in concentrated alkalis even at ambient temperature. At higher temperatures, even when the corrosion rate is not

excessive, niobium can be embrittled at low concentrations (5%) of sodium hydroxide (NaOH) and potassium hydroxide (KOH). Table 7 shows the corrosion of niobium in alkaline solutions. The poor resistance of niobium in alkaline media is believed to be due to the formation of hexaniobate salts, $M_8Nb_6O_{19}{\cdot}18H_2O$ (where M is lithium, sodium, or potassium), which are soluble in aqueous alkaline solutions (Ref 20, 21). Embrittlement of niobium is caused by the absorption of hydrogen. Niobium alloys, such as Nb-1Zr, have a resistance similar to that of pure niobium in alkaline environments.

Salt Solutions. Niobium has excellent corrosion resistance to most salt solutions. Niobium will not, however, resist those salt solutions that tend to hydrolyze to form alkalis. Like tantalum, niobium is embrittled in salts, such as sodium and potassium carbonates and phosphates that hydrolyze to form alkaline solutions. Niobium is also resistant to chloride solutions, even with oxidizing agents present. Niobium does not corrode in 10% ferric chloride ($FeCl_3$) to the boiling temperature. Niobium exhibits resistance similar to tantalum in salt solutions. Table 8 provides the corrosion resistance of niobium in many common salt solutions as well as some more complex media.

Organic Acids. Niobium shows good resistance to many types of organic environments. These environments include acetic acid, citric acid, formaldehyde, formic acid, lactic acid, tartaric acid, and trichloroethylene. Table 9 shows examples of organic media in which niobium has been tested. Niobium is currently being used with excellent results in the acetic acid process for rupture disks.

Gases. Niobium has a high solubility for oxygen, nitrogen, and hydrogen. These gas atoms occupy interstitial locations. As hydrogen is dissolved, the level will eventually exceed the terminal solid-solution limit, causing niobium hydrides to precipitate. Hydrides are brittle and create internal stress raisers that fail under low applied loads. In solution, oxygen and nitrogen are potent hardeners and will significantly decrease the ductility of the metal. Because the oxides have a larger molecular volume than the base metal, oxygen forms surface oxides that spall and are nonprotective.

The oxides of niobium have a relatively high vapor pressure compared with the base metal, and under conditions of low oxygen pressures and high temperature, the loss of metal via evaporation of the oxides can be substantial. The kinetics of oxygen uptake can be divided into three regions as a function of time: a linear region where oxygen dissolves without oxide formation, a parabolic region associated with the formation of a protective NbO_2 layer and NbO growing into the metal, and another linear region where the formation of porous Nb_2O_5 on top of NbO_2 occurs. At temperatures greater than 1600 °C (2910 °F), evaporation of NbO occurs.

The hydrides of niobium exist over a broad range of compositions (Ref 20). Homogenous solid solutions (alpha phase) exist at compositions up to Nb-0.1H. Beyond this hydrogen concentration, a second beta phase appears. The alpha + beta phases coexist between Nb-0.1H and Nb-0.9H. Beyond those compositions, the system again becomes homogeneous until the monohydride NbH forms. The crystal structure of the alpha phase is a body-centered cubic structure while that of the beta phase is orthorhombic. At temperatures above 150 °C (300 °F), the miscibility gap disappears. A dehydride exists as an unstable compound and, at low pressures, decomposes by loss of hydrogen into the monohydride.

Niobium will oxidize in air above 200 °C (390 °F). The reaction, however, does not become rapid until above red heat at approximately 500 °C (930 °F). At 980 °C (1795 °F), the oxidation rate in air is 430 mm/yr (17 in./yr). In pure oxygen, air oxidation is extremely rapid at 390 °C (735 °F). Oxygen diffuses freely through the metal, which causes embrittlement. Niobium reacts with nitrogen above 350 °C (660 °F), with water vapor above 300 °C (570 °F), with chlorine above 200 °C (390 °F), and with carbon dioxide, carbon monoxide, and hydrogen above 250 °C (480 °F). At a temperature of 100 °C (212 °F), niobium is inert in most common gases such as bromine, chlorine, nitrogen, hydrogen, oxygen, carbon dioxide, and sulfur dioxide (wet or dry).

Miscellaneous Chemical Environments. Niobium has good resistance in a variety of miscellaneous corrosive environments, including hydrogen peroxide, bromine, phosphoric acid, and chromic acid. Many materials are resistant to dry bromine, but moist bromine is extremely corrosive to many materials. Niobium is one of the few materials that resists corrosive attack of dry and wet bromine at temperatures even as high as 100 °C (212 °F) (Ref 22). Niobium has also been considered for use in highly oxidizing solutions, such as those found in chemical wastes and scrubber environments. Niobium did not suffer pitting or crevice attack when exposed to simulated scrubber environments. Table 10 shows the corrosion resistance of niobium in a number of miscellaneous environments.

Liquid Metals. Niobium has excellent resistance to many types of liquid metals. The presence of excessive amounts of nonmetallic impurities (e.g., gases) may reduce the resistance of niobium to these liquid metals. Because liquid metals are excellent heat-transfer media, they can be used in very compact thermal systems, such as fast breeder reactors, reactors for space vehicles, and fusion reactors. Niobium resists attack by sodium vapor at high temperatures and pressures. For this reason, Nb-1Zr alloy is used as end caps for high-pressure sodium vapor lamps used for highway lighting. Table 11 shows the corrosion resistance of niobium to selected liquid metals.

Galvanic Effects. Niobium is susceptible to hydrogen embrittlement if it is polarized cathodically by galvanic coupling or by chemical attack. For this reason, niobium cannot be protected cathodically. However, if niobium is polarized anodically, it forms a very stable passive film that protects the metal from corrosion. This property, combined with good electrical conductivity (13% that of copper) and good mechanical properties, has led to the use of niobium as a substrate metal for platinum in impressed-current cathodic protection anodes.

Table 3 Corrosion of niobium in aqueous nitric acid solutions

HNO_3, wt%	Test duration, days	Specimen condition(a)	Temperature °C	Temperature °F	Corrosion rate(b) Nb mm/yr	Nb mils/yr	Nb-1Zr mm/yr	Nb-1Zr mils/yr
10	3-4	NW	102	216	0.001/0.0025	0.04/0.1	...	...
	3-4	W	102	216	0.008/0.005	0.3/0.2	0.005/0.0025	0.2/0.1
	3-4	NW	102	216	...	...	GW/0.008	GW/0.3
65	3-4	NW	121	250	0.007/0.0025	0.3/0.1	0.005/0.012	0.2/0.5
	3-4	W	121	250	0.018/0.008	0.7/0.3	...	...
	2-6-4	NW	121	250	GW/0/0.0127	GW/0/0.5	...	...
70	3-4	NW	250	482	0.025/0.1	1.0/4.0	...	...
98.5	2-4-2	NW	40	104	0/0.002/0	0/0.1/0	...	...
	2-4-2	W	40	104	0/0.002/0.007	0/0.1/0.3	...	...

(a) W, welded; NW, nonwelded. (b) GW, gained weight

Table 4 Results of U-bend tests on niobium

Media	Specimen condition(a)	Temperature °C	Temperature °F	Impurity	Test duration, days	Corrosion rate mm/yr	Corrosion rate mils/yr	Result
11% hydrochloric acid	NW	70	158	60% phenol	14	0.001	0.04	No crack
97% nitric acid	NW	40	104	...	14	0.025	<1	No crack
	W	40	104	...	14	0.025	<1	No crack
	NW	40	104	...	14	0.025	<1	No crack
	W	40	104	...	14	0.025	<1	No crack

(a) W, welded; NW, nonwelded

Table 5 Corrosion of niobium alloys in sulfuric acid solutions

H_2SO_4, wt%	Alloy	Specimen condition(a)	Temperature		Impurity	Test duration, days	Corrosion rate(b)		Comment
			°C	°F			mm/yr	mils/yr	
1	Nb	NW	Boiling		65% nitric acid	2-4-2	0.028/0.008/0.028	1.1/0.3/1.1	Embrittled
3	Nb	NW	Boiling		65% nitric acid	2-4-2	0.003/0.005/0.003	0.1/0.2/0.1	Embrittled
5	Nb	NW	Boiling		65% nitric acid	2-4-2	0.041/0.020/0.036	1.6/0.8/1.4	...
10	Nb	NW	Boiling		75% nitric acid	2-4-2	0.008/0.008/0.013	0.3/0.3/0.5	...
	Nb	NW	Boiling		78% nitric acid	2-4-2	0.005/0.003/0.008	0.2/0.1/0.3	...
	Nb	NW	Boiling		80% nitric acid	2-4-2	0.003/0.003/0.005	0.1/0.1/0.2	...
14	Nb	NW	Boiling		36% nitric acid	2	0.102	4	...
	Nb	W	Boiling		36% nitric acid	2	0.079	3.1	...
15	Nb	NW	Boiling		35% nitric acid	2-4-2	0.099/0.058/0.094	3.9/2.3/3.7	...
	Nb	NW	Boiling		45% nitric acid	2-4-2	0.099/0.071/0.102	3.9/2.8/4.0	...
	Nb	NW	Boiling		45% nitric acid	2	0.117	4.6	...
	Nb	W	Boiling		45% nitric acid	2	0.086	3.4	...
	Nb	NW	Boiling		49% nitric acid	2-4-2	0.102/0.071/0.096	4.0/2.8/3.8	...
	Nb	NW	Boiling		63% nitric acid	2-4-2	0.028/0.030/0.025	1.1/1.2/1.0	...
	Nb	NW	Boiling		67% nitric acid	2-4-2	0.013/0.015/0.010	0.5/0.6/0.4	...
	Nb	NW	Boiling		70% nitric acid	2-4-2	0.005/0.005/0.008	0.2/0.2/0.3	...
20	Nb	NW	Boiling		50% nitric acid	2-4-2	0.084/0.076/0.079	3.3/3/3.1	Loose black oxide
	Nb	NW	Boiling		55.6% nitric acid	2-4-2	0.046/0.038/0.036	1.8/1.5/1.4	...
	Nb	NW	Boiling		60% nitric acid	2-4-2	0.028/0.028/0.023	1.1/1.1/0.9	...
	Nb	NW	Boiling		...	2-4-2	0.094/0.109/0.076	3.7/4.3/3	...
23	Nb	NW	Boiling		28% nitric acid	2	0.145	5.7	...
	Nb	W	Boiling		28% nitric acid	2	0.119	4.7	...
	Nb	NW	Boiling		37% nitric acid	2	0.160	6.3	...
	Nb	W	Boiling		37% nitric acid	2	0.132	5.2	...
30	Nb	NW	Boiling		25% nitric acid	2-4-2	0.155/0.132/0.190	6.1/5.2/7.5	...
	Nb	NW	Boiling		33% nitric acid	2-4-2	0.132/0.127/0.170	5.2/5.0/6.7	...
	Nb	NW	Boiling		40% nitric acid	2-4-2	0.112/0.099/0.099	4.4/3.9/3.9	...
40	Nb	NW	Boiling		11% nitric acid	2-4-2	0.173/0.168/0.241	6.8/6.6/9.5	...
	Nb	NW	Boiling		2% ferric chloride	2-4-2	0.218/0.406/0.127	8.6/16/5	...
	Nb	NW	Boiling		2% nitric acid	2-4-2	0.168/0.208/0.223	6.6/8.2/8.8	...
	Nb	NW	Boiling		5% nitric acid	2-4-2	0.170/0.178/0.231	6.7/7/9.1	...
	Nb	NW	Boiling		8% nitric acid	2-4-2	0.173/0.178/0.239	6.8/7/9.4	...
	Nb	NW	Boiling		...	2-4-2	0.431/0.355/0.381	17/14/15	...
	Nb-1Zr	NW	Boiling		...	2-4	0.558/0.533	22/21	...
50	Nb	NW	50	122	20% nitric acid	2-4-2	0/0/0	0/0/0	...
	Nb	W	50	122	20% nitric acid	2-4-2	0.003/0.003/0	0.1/0.1/0	Cracks in weld
	Nb	NW	80	176	20% nitric acid	2-4-2	0.005/0.005/0	0.2/0.2/0	Few pits, cracks in weld
	Nb	W	80	176	20% nitric acid	2-4-2	0.003/0.010/0.005	0.1/0.4/0.2	...
	Nb	NW	82	180	50% phosphoric acid	2-4-2	0.066/0.063/0.046	2.6/2.5/1.8	...
	Nb	W	82	180	50% phosphoric acid	2-4-2	0.066/0.056/0.056	2.6/2.2/2.2	...
	Nb	NW	123	253	...	7	0.279	11	pH = 0.1
	Ti-45Nb	NW	123	253	...	7	3.55	140	pH = 1
	Nb	NW	Boiling		2% ferric chloride	2-4-2	0.193/0.170/0.170	7.6/6.7/6.7	pH = 1
	Nb	NW	Boiling		...	2-4-2	>5.076	>200	pH = 0.5
60	Nb	NW	25	77	...	2-4-2	GW/0.025/0.003	GW/1/0.1	...
	Nb	NW	Boiling		1% copper powder	2-4-2	0.736/0.609/0.787	29/24/31	Scaled finish
	Nb	NW	Boiling		1% copper powder, iron powder	2-4-2	0.761/0.584/0.761	30/23/30	pH = 1.5
	Nb	NW	Boiling		1% ferric chloride	1-1-1-1	0.330/0.508/0.254/0.254	13/20/10/10	Pickled surface
	Nb	NW	Boiling		1% iron powder	2-4-2	1.421/1.345/1.371	56/53/54	pH = 1.5
	Nb	NW	Boiling		10,000 ppm ferric chloride	1-1-1-1	0.381/0.381/0.305/0.305	15/15/12/12	...
	Nb	NW	Boiling		100 ppm ferric chloride	1-1-1-1	0.761/0.558/0.584/0.635	30/22/23/25	...
	Nb	NW	Boiling		1000 ppm cupric chloride	1-1-1-1	0.584/0.635/0.660/0.660	23/25/26/26	Pickled surface
	Nb	NW	Boiling		1000 ppm ferric chloride	1-1-1-1	0.508/0.254/0.508/0.508	20/10/20/20	...
	Nb	NW	Boiling		1000 ppm ferric chloride	1-1-1-1	0.533/0.558/0.533/0.558	21/22/21/22	Pickled surface
	Nb	NW	Boiling		200 ppm ferric chloride	1-1-1-1	0.863/0.609/0.685/0.685	34/24/27/27	...
	Nb	NW	Boiling		...	2-4-2	0.685/0.761/0.888	27/30/35	Scaled finish
62	Nb	NW	135	275	450 ppm nitric acid	2-4-2	0.558/1.04/0.533	22/40/21	Pickled surface
	Nb	W	135	275	450 ppm nitric acid	2-4-2	0.635/1.269/0.533	25/50/21	Pickled surface
64	Nb	NW	100	212	4% nitric acid	2-4-2	0.028/0.030/0.036	1.1/1.2/1.4	Pickled surface
	Nb	W	100	212	4% nitric acid	2-4-2	0.053/0.038/0.036	2.1/1.5/1.4	Pickled surface
65	Nb	NW	25	77	...	2-4-2	0.003/0/GW	0.1/0/GW	...
	Nb	NW	153	307	...	2-4-2-4	2.157/2.030/2.107/2.183	85/80/83/86	...
	Nb	NW	Boiling		1% copper powder	2-4-2	1.015/0.660/1.04	40/26/40	...
	Nb	NW	Boiling		1% copper powder, 1% iron powder	2-4-2	0.838/0.914/0.964	33/36/38	...
	Nb	NW	Boiling		1% iron powder	2-4-2	1.904/2.107/2.284	75/83/90	...
	Nb	NW	Boiling		10,000 ppm cupric chloride	1-1-1-1	0.660/0.711/0.863/0.763	26/28/34/29	...
	Nb	NW	Boiling		10,000 ppm ferric chloride	1-1-1-1	0.635/0.635/0.533/0.457	25/25/21/18	Heat treated, 400 °C (750 °F), 2 h
	Nb	NW	Boiling		10,000 ppm ferric chloride	1-1-1-1	0.508/0.508/0.508/0.508	20/20/20/20	...
	Nb	NW	Boiling		100 ppm ferric chloride	1-1-1-1	2.583/2.583/1.523/1.269	100/100/60/50	...
	Nb	NW	Boiling		1000 ppm cupric chloride	1-1-1-1	1.015/0.914/1.015/1.066	40/36/40/42	...

(continued)

(a) W, welded; NW, nonwelded. (b) GW, gained weight

Table 5 (continued)

H_2SO_4, wt%	Alloy	Specimen condition(a)	Temperature °C	Temperature °F	Impurity	Test duration, days	Corrosion rate(b) mm/yr	Corrosion rate(b) mils/yr	Comment
65 (continued)	Nb	NW	Boiling		1000 ppm ferric chloride	1-1-1-1	1.066/0.838/0.838/0.914	42/33/33/36	Heat treated, 300 °C (570 °F), 2 h
	Nb	NW	Boiling		1000 ppm ferric chloride	1-1-1-1	0.939/0.964/1.015/0.964	37/38/40/38	...
	Nb	NW	Boiling		200 ppm cupric chloride	1-1-1-1	2.487/2.411/3.046/2.792	98/95/120/110	...
	Nb	NW	Boiling		200 ppm ferric chloride	1-1-1-1	1.269/1.091/1.091/1.015	50/43/43/40	Heat treated, 400 °C (750 °F), 4 h
	Nb	NW	Boiling		200 ppm ferric chloride	1-1-1-1	2.411/1.954/1.878/1.777	95/77/74/70	...
	Nb	NW	Boiling		...	2-4	3.223/3.046	127/120	...
68	Nb	NW	135	169	300 ppm nitric acid	2-4-2	0.482/0.838/0.431	19/33/17	...
	Nb	W	135	169	300 ppm nitric acid	2-4-2	0.533/1.168/4.340	21/46/171	...
70	Nb	NW	25	77	...	2-4-2	GW/0.015/0.005	GW/0.6/0.2	...
	Nb	NW	100	212	15% chromic acid	2-4	0.020/0.112	0.8/4.4	...
	Nb	W	100	212	15% chromic acid	2-4	0.020/0.160	0.8/6.3	...
	Nb	NW	Boiling		1% copper powder	2-4-2	1.447/1.523/2.030	57/60/80	...
	Nb	NW	Boiling		1% copper powder, iron powder	2-4-2	1.701/1.675/1.904	67/66/75	...
	Nb	NW	Boiling		1% iron powder	2-4-2	5.076/3.299/3.553	200/130/140	...
	Nb	NW	Boiling		10 ppm cupric chloride	1-1	2.284/>5.076	90/>200	...
	Nb	NW	Boiling		10,000 ppm ferric chloride	1-1-1-1	3.046/1.624/1.244/1.701	120/64/49/67	...
	Nb	NW	Boiling		100 ppm cupric chloride	1-1	3.147/2.538	124/100	...
	Nb	NW	Boiling		1000 ppm cupric chloride	1-1-1-1	1.345/1.396/2.134/2.234	53/55/84/88	...
	Nb	NW	Boiling		1000 ppm ferric chloride	1-1-1-1	2.792/2.792/3.553/3.807	110/110/140/150	...
	Nb	NW	Boiling		10,000 ppm cupric chloride	1-1-1-1	1.497/2.030/1.777/1.726	59/80/70/68	...
	Nb	NW	Boiling		200 ppm ferric chloride	1-1-1-1	3.807/2.157/3.807/>5.076	150/85/150/>200	Liquid
	Nb	NW	Boiling		3% chromic acid	20 min	1.574	62	...
	Nb-1Zr	NW	Boiling		3% chromic acid	20 min	2.843	112	...
	Nb-1Zr	NW	Boiling		3% chromic acid	20 min	2.843	112	Vapor
	Nb	NW	Boiling		3% nitric acid	20 min	1.777	70	...
	Nb	NW	Boiling		...	2-4-2	>5.076/>5.076/>5.076	>200/>200/>200	...
	Nb	NW	Boiling		...	1-1	>5.076/>5.076	>200/>200	...
72	Nb	NW	110	230	3% nitric acid	2-4-2	0.053/0.061/0.051	2.1/2.4/2	Liquid
74	Nb	NW	93	199	10% nitric acid	6	0.041	1.6	...
	Nb	W	93	199	16% nitric acid	3	0.114	4.5	...
	Nb	NW	93	199	16% nitric acid	2-3	0.051/0.038	2/1.5	...
	Nb	NW	93	199	5% nitric acid	6	0.132	5.2	...
	Nb	W	110	230	3% nitric acid	2-4-2	0.074/0.066/0.053	2.9/2.6/2.1	Vapor
75	Nb	NW	25	77	...	2-4-2	0.003/0/0	0.1/0/0	...
	Nb	NW	Boiling		10,000 ppm ferric chloride	1-1-1-1	2.360/2.690/0.964/2.157	93/106/38/85	...
	Nb	NW	Boiling		100 ppm ferric chloride	1	>5.076	>200	...
	Nb	NW	Boiling		1000 ppm ferric chloride	1	>5.076	>200	...
	Nb	NW	Boiling		200 ppm ferric chloride	1	>5.076	>200	...
	Nb	NW	Boiling		...	2	>5.076	>200	...
76	Nb	NW	93	199	10% nitric acid	6	0.041	1.6	...
	Nb-1Zr	NW	93	199	10% nitric acid	6	0.102	4	...
	Nb	NW	93	199	16% nitric acid	3	0.038	1.5	...
	Nb-1Zr	NW	93	199	16% nitric acid	2-3	0.102/0.051	4/2	...
	Nb	NW	93	199	5% nitric acid	6	0.132	5.2	...
	Nb-1Zr	NW	93	199	5% nitric acid	6	0.279	11	...
77.5	Nb	NW	Boiling		10,000 ppm ferric chloride	1-1-1-1	>5.076/>5.076/>5.076/4.822	>200/>200/>200/190	...
	Nb	NW	Boiling		1000 ppm ferric chloride	1-1-1	>5.076/>5.076/>5.076	>200/>200/>200	...
	Nb	NW	Boiling		...	1-1	>5.076/>5.076	>200/>200	...
	Nb	NW	Boiling		200 ppm ferric chloride	1-1	>5.076/>5.076	>200/>200	...
80	Nb	NW	25	77	...	2-4-2	GW/0.013/0.003	GW/0.5/0.1	...
	Nb	NW	Boiling		...	1	>5.076	>200	...
90	Nb	NW	25	77	...	2-4-2	0/0.013/0.003	0/0.5/0.1	...
98	Nb	NW	25	77	...	2-4-2	0/0.013/0.005	0/0.5/0.2	...
	Nb-1Zr	W	25	77	...	2-4	0.020/0.003	0.8/0.1	...
	Nb-1Zr	W	114	237	...	2-4	0.609/0.533	24/21	...
	Nb	NW	Boiling		...	0.5	>5.076	>200	...

(a) W, welded; NW, nonwelded. (b) GW, gained weight

Niobium-platinized anodes are used in high-resistivity waters and other environments that require high driving potential to obtain good current distribution. In this application, niobium has an advantage over tantalum due to its lower cost. The cost can be further decreased by using a composite electrode with a copper core, which increases the conductivity of the anodes.

The galvanic series in seawater can be found in Table 8 in the article "Corrosion of Zirconium and Zirconium Alloys" in this Volume. Niobium is located between type 316

and type 304 stainless steels. From noble to active, the order is type 316, yellow brass, niobium, tantalum, tungsten, and type 304 stainless steel (Ref 23).

Localized Corrosion. Niobium is highly resistant to localized attacks, such as pitting, crevice corrosion, and stress-corrosion cracking (SCC). The presence of heavy-metal ions in reducing acids will improve the corrosion resistance of niobium. Also, as shown in Table 10, niobium does not suffer pitting or crevice corrosion in simulated scrubber solutions (Ref 24).

In one laboratory study, niobium did not exhibit SCC in 90% HNO_3 at room temperature using the slow strain-rate technique or in liquid bromine using U-bend specimens (Ref 25). However, with particular types of surface contamination and preparation, niobium (like tantalum) was found to be sensitive to crevice corrosion at anodic potentials below those normally regarded as safe (Ref 26). Table 4 shows results of U-bend ring tests in nitric acid and hydrochloric acid solutions.

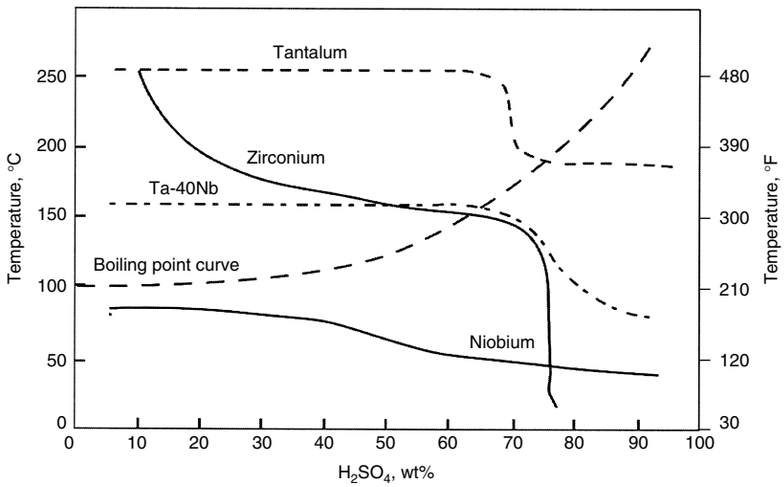

Fig. 6 Isocorrosion curve of reactive and refractory metals in sulfuric acid, 0.13 mm/yr (5 mils/yr) lines

Table 6 Corrosion of niobium in boiling sulfuric acid with $FeCl_3$ or $CuCl_2$ impurities

	$FeCl_3$ impurity			$CuCl_2$ impurity		
		Corrosion rate			Corrosion rate	
H_2SO_4, wt%	Concentration, ppm	mm/yr	mils/yr	Concentration, ppm	mm/yr	mils/yr
60	0	0.74	29	0	0.74	29
	100	0.63	25	100	...	...
	200	0.71	28	200	...	...
	1000	0.43	17	1000	0.63	25
	10,000	0.38	15	10,000	0.41	16
65	100	1.32	52	100	...	...
	200	0.96	38	200	2.79	110
	1000	0.91	36	1000	1.02	40
	10,000	0.56	22	10,000	0.74	29
70	0	6.32	249	0	6.3	249
	10	8.41	331	10	3.96	156
	100	9.07	357	100	2.56	101
	200	8.43	332	200	7	276
	1000	3.02	119	1000	1.78	70
	10,000	1.93	76	10,000	1.77	69

Table 7 Corrosion of niobium in alkaline media

				Corrosion rate				
		Temperature		Nb		Nb-1Zr		
Media	Concentration, wt%	°C	°F	mm/yr	mils/yr	mm/yr	mils/yr	Comment
NaOH	1–40	25	77	0.125	5.0	...		...
	1–10	98	209	...		0.86	34	Embrittled
KOH	5–40	25	77	...		...		Embrittled
	1–5	98	209	...		...		Embrittled

All specimens are nonwelded.

Applications

Niobium, like tantalum, is able to be fabricated into many types of chemical process equipment. Equipment that includes niobium components are reactor vessels, columns, shell and tube heat exchangers, plate and frame heat exchangers, bayonet heaters, thermowells, rupture disks, and spargers. Because niobium is not approved for use under the ASME Boiler and Pressure Vessel Code, it must be used as a liner or in a pressure-containing envelope. In most applications, niobium is used as a thin liner material.

Chemical and Petrochemical Processing. Niobium retains excellent corrosion resistance in liquid bromine, even when saturated with moisture. Niobium-base materials can be used to make equipment designed to produce or transport liquid bromine (Ref 27).

Niobium would be well suited for handling hot, concentrated HNO_3. Niobium may be considered for the highly oxidizing solutions expected in chemical wastes, scrubber environments, and mining solutions.

Because of recent advancements in cladding techniques, the corrosion resistance and mechanical properties of niobium are now more affordable and easily used. Thin layers (i.e., 0.25 mm, or 0.01 in.) of niobium sheet can be clad to common metals such as steel by using various cladding techniques, including explosive bonding.

Niobium is an important metal in the chrome plating industry as an evaporator to recover spent chromic acid. Niobium was found to withstand hot, concentrated chromic acid media, particularly where fluoride ions were present. Niobium is generally known to have the highest resistance to attack by fluoride ions among reactive and refractory metals.

Pharmaceutical Industry. Niobium has been considered for use in the pharmaceutical industry because of its corrosion resistance in a variety of unique solutions (Ref 28). It is reported that niobium can be applied to applications in many severe corrosive environments, such as the pharmaceutical industry.

Mineral Processing Wet Oxidization Process. Nb-55Ti (titanium grade 36) has shown resistance in high-oxygen-pressure leaching of gold and nickel ores (Ref 11). The niobium significantly increases the threshold oxygen pressure and process temperature for ignition compared to commercially pure (CP) titanium. Nb-55Ti is used in high-pressure gas vents, oxygen lances, and valves.

Nuclear Applications. Niobium is used in certain fast breeder reactors because of its compatibility with uranium and liquid sodium/potassium. Because niobium also has a low neutron cross section, it can be alloyed with

Table 8 Corrosion of niobium in aqueous salt solutions

Media	Concentration, wt%	Temperature °C	Temperature °F	Corrosion rate mm/yr	Corrosion rate mils/yr
$AlCl_3$	25	Boiling		0.005	0.2
$Al_2(SO_4)_3$	25	Boiling		nil	
$AlK(SO_4)_2$	10	Boiling		nil	
$CaCl_2$	70	Boiling		nil	
	0.2% with 0.1% $MgCl_2$ + 200 ppm NaF + 200 ppm CaF_2	80	176	0.025	1.0
	0.2% with 0.1% $MgCl_2$	80	176	0.25	10
	2% with 1% $MgCl_2$ + 200 ppm NaF + 2800 ppm CaF_2	80	176	0.025	1.0
	2% with 1% $MgCl_2$	80	176	0.125	5.0
	6.6% with 3.3% $MgCl_2$ + 200 ppm NaF + 9800 ppm CaF_2	80	176	0.025	1.0
	6.6% with 3.3% $MgCl_2$	80	176	0.025	1.0
$Cu(NO_3)_2$	40	Boiling		nil	
$CuSO_4$	40	104	219	0.025	1.0
$FeCl_3$	10	25–boiling	77–boiling	nil	
$HgCl_2$	Saturated	Boiling		0.0025	0.1
H_2SiF_6	10	90	194	5.0	200
HSO_3NH_2	10	Boiling		0.025	1.0
K_2CO_3	1–10	25	77	0.025	1.0
	10–20	98	208	Embrittle	
K_2PO_4	10	25	77	0.025	1.0
$MgCl_2$	47	Boiling		0.025	1.0
NaCl	Saturated and pH = 1	Boiling		0.025	1.0
	5% with 0.5% acetic acid	100	212	nil	
Na_2CO_3	10	25	77	0.025	1.0
	10	Boiling		0.025	1.0
$NaHSO_4$	40	Boiling		0.125	5.0
NaOCl	6	50	122	0.125	5.0
Na_3PO_4	5–10	25	77	0.025	1.0
NH_4Cl	40	Boiling		0.025	1.0
NH_2SO_3H	10	Boiling		0.025	1.0
$NiCl_2$	30	Boiling		nil	
$Ni(NO_3)_2$	40	104	219	0.025	1.0
$ZnCl_2$	40–70	Boiling		nil	
$ZrCl_4$	70	Boiling		nil	
	88	Boiling		nil	

zirconium for use in the cladding of nuclear fuel rods.

Platinized Niobium Anodes for Cathodic Protection. The high anodic breakdown potential and good electrical conductivity and mechanical properties of niobium have led to its use as a substrate material for platinized electrodes in impressed-current cathodic protection systems for reinforced steel bridge structures (Ref 4). Niobium was chosen as a substrate material due to its excellent inert-oxide-forming properties, which provide dimensional stability in this application. The platinized niobium wire used in the bridge protection systems has an estimated life of over 50 years.

Sodium Gas Discharge Lamps. Because of the high corrosion resistance of niobium to liquid sodium, the Nb-1Zr alloy is used in sodium vapor lamps to hold metallic sodium, which is heated to 871 to 927 °C (1600 to 1700 °F). The intense heat creates a vapor that, when channeled through a quartz tube, generates light (Ref 3). The ductility of the Nb-1Zr enables the material to be easily fabricated into tight-tolerance parts.

Microalloying Element in Steels and Nickel-Base Alloys. Niobium is one of the most effective microalloying elements in steels. Additions of niobium in steel, depending on the grade, will improve grain refinement, retardation of recrystallization, and precipitation hardening and will promote scavenging of the iron matrix (in interstitial-free steels). Niobium is also recognized as a major alloying element in the production of superalloys.

Miscellaneous Applications. Niobium is finding use in components for satellite launch vehicles and spacecraft and in the production of superconducting devices. Niobium alloys are

Table 9 The corrosion of niobium in organic solutions

Media	Alloy	Specimen condition(a)	Temperature °C	Temperature °F	Impurity	Test duration	Corrosion rate(b) mm/yr	Corrosion rate(b) mils/yr	Comment
30% oxalic acid	Nb	W	Boiling		...	20 min	1.7	67	Liquid
	Nb-1Zr	NW	Boiling		...	20 min	2.4	95	Liquid
40% methanesulfonic acid	Nb	NW	60	140	...	2 d	0.0	0	Liquid
	Nb	NW	60	140	500 ppm ceric nitrate	2 d	GW	GW	Liquid
	Nb	NW	60	140	500 ppm ceric sulfate	2 d	0.003	0.1	Liquid
	Nb	W	60	140	...	2 d	0.003	0.1	Liquid
	Nb	W	60	140	500 ppm ceric citrate	2 d	0.000	0	Liquid
	Nb	W	60	140	500 ppm ceric sulfate	2 d	0.003	0.1	Liquid
50% acetic acid	Nb-1Zr	NW	Boiling		...	3–4 d	0.0076/GW	0.3/GW	Liquid
	Nb-1Zr	W	Boiling		...	3–4 d	0.01/GW	0.4/GW	Liquid
Glacial acetic acid	Nb	NW	40	104	HCl and chlorine gas sparge	18 h/11 d	0.0126/GW	0.5/0.7	Liquid
	Nb	NW	40	104	HCl and chlorine gas sparge	18 h/11 d	0.0076/0.0126	0.3/0.5	Vapor
	Nb	NW	80	176	HCl and chlorine gas sparge	18 h	0.020	0.8	Liquid
	Nb	NW	80	176	HCl and chlorine gas sparge	18 h	0.008	0.3	Vapor
	Nb	NW	100	212	HCl and chlorine gas sparge	18 h	0.020	0.8	Vapor
	Nb	NW	100	212	HCl and chlorine gas sparge	18 h	0.013	0.5	Liquid
	Nb	NW	Boiling		HCl and chlorine gas sparge	18 h	>5.1	>200	Vapor
	Nb	NW	Boiling		HCl and chlorine gas sparge	18 h	>5.1	>200	Liquid
	Nb	W	40	104	HCl and chlorine gas sparge	18 h/11 d	GW/2.3	GW/90	Liquid
	Nb	W	40	104	HCl and chlorine gas sparge	18 h/11 d	GW/>5.1	GW/>200	Vapor
	Nb	W	80	176	HCl and chlorine gas sparge	18 h	GW	GW	Liquid
	Nb	W	80	176	HCl and chlorine gas sparge	18 h	GW	GW	Vapor
	Nb	W	100	212	HCl and chlorine gas sparge	18 h	GW	GW	Vapor
	Nb	W	100	212	HCl and chlorine gas sparge	18 h	GW	GW	Liquid
	Nb	W	Boiling		HCl and chlorine gas sparge	18 h	>5.1	>200	Vapor
	Nb	W	Boiling		HCl and chlorine gas sparge	18 h	>5.1	>200	Liquid

(a) W, welded; NW, nonwelded. (b) GW, gained weight

Table 10 Corrosion of niobium in miscellaneous solutions

Media	Test duration	Specimen condition(a)	Temperature °C	Temperature °F	Corrosion rate(b) mm/yr	Corrosion rate(b) mils/yr	Impurities
10% aluminum potassium sulfate	2-4-2 d	NW	Boiling		GW/GW/GW	GW/GW/GW	...
50% aluminum chloride	2-4-2 d	NW	116	241	0.056/0.018/0.0025	2.2/0.7/0.1	...
40% ammonium chloride	2-4-2 d	NW	Boiling		GW/0.015/0.007	GW/0.6/0.3	...
	...	NW	20	70	nil	nil	...
Bromine	...	NW	20	70	0.025	1	...
	1-6 d	NW	25	77	0/0.0025	0/0.1	...
50% chromic acid	1-6 d	W	25	77	0/0.0025	0/0.1	...
Chrome plating solutions	...	NW	92	198	0.125	5	25% CrO_3, 12% H_2SO_4, H_2O
	...	NW	92	198	0.125	5	17% CrO_3, 2% Na_5SiF_6, trace H_2SO_4, H_2O
40% copper sulfate	2-4-2 d	NW	Boiling		0.05/0.01/0.0025	2/0.5/0.1	...
37% formaldehyde	4 d	NW	Boiling		0.01	0.4	...
10% hydrofluoric	2.5 h	NW	90	194	3.8	150	...
silicic acid	2.5 h	W	90	194	3.8	150	...
30% hydrogen peroxide	2-4-2 d	NW	25	77	0.007/0.01/0.015	0.3/0.5/0.6	...
	2-4-2 d	NW	Boiling		0.17/0.08/0.15	6.8/3.2/6	...
30% nickel chloride	2-4-2 d	NW	Boiling		0/0.0076/GW	0/0.3/GW	...
30% oxalic acid	20 min	W	Boiling		1.7	67	...
10% sodium carbonate	2-4-2 d	NW	25	77	0.015/0.01/0.01	0.6/0.4/0.5	...
	2-4-2 d	NW	Boiling		0.7/0.4/0.3	28/17/12	...
33% sodium sulfide	10 d	NW	Boiling		>5	>200	...
47% magnesium chloride	2-4 d	NW	Boiling		0.01/0.04	0.5/1.6	...
Mercuric chloride (saturated)	2-4-2 d	NW	Boiling		0.01/0.012/0.02	0.4/0.5/0.8	...
40% nickel nitrate	2-4-2 d	NW	Boiling		0.04/GW/GW	1.7/GW/GW	...
50% phosphoric acid	2-4-2 d	NW	30	86	GW/GW/GW	GW/GW/GW	...
	2-4-2 d	NW	90	194	0.086/GW/0.05	3.4/GW/2	...
85% phosphoric acid	2-4-2 d	NW	30	86	GW/GW/GW	GW/GW/GW	...
	2-4-2 d	W	88	190	0.02/0.02/0.015	1/1/0.6	...
9% sodium sulfide	4 d	NW	Boiling		>5	>200	...
50,000 mg/L chloride + 1000 ppm fluoride	1 d	NW	55	131	0.07	2.7	30% $CaCl_2$, 30% NaCl, 20% $MgCl_2$, 20% KCl, NaF, SO_2 bubble
	1 d	W	55	131	0.07	2.7	30% $CaCl_2$, 30% NaCl, 20% $MgCl_2$, 20% KCl, NaF, SO_2 bubble
50,000 mg/L chloride + 5000 ppm fluoride	1 d	NW	55	131	0.23	9.3	30% $CaCl_2$, 30% NaCl, 20% $MgCl_2$, 20% KCl, NaF, SO_2 bubble
	1 d	W	55	131	0.25	10	30% $CaCl_2$, 30% NaCl, 20% $MgCl_2$, 20% KCl, NaF, SO_2 bubble
Simulated scrubber solution	8 d	NW	110	230	0.018	0.7(c)	7 vol% H_2SO_4, 3 vol% HCl, 1% $FeCl_3$, 1% $CuCl_2$
	8 d	NW	110	230	0.12	4.8(c)	7 vol% H_2SO_4, 3 vol% HCl, 1% $FeCl_3$, 1% $CuCl_2$

(a) W, welded; NW, nonwelded. (b) GW, gained weight. (c) No pitting or crevice corrosion observed

used for rocket nozzles on satellite launch vehicles and spacecraft (Ref 29). Because niobium is easily oxidized at elevated temperatures, it must be coated for this use. Aluminide and silicide coatings are used for this purpose. Niobium alloys, such as Nb-55Ti, are used in the aircraft industry. Nb-55Ti requires approximately 25% of the buckling force necessary to head a CP titanium rivet of the same size and is stronger than CP titanium at temperatures in excess of 316 °C (600 °F).

A recent application for Nb-55Ti is for flanges and helium vessels to support high-purity superconducting cavities in radio frequency (RF) linear accelerators (Ref 30, 31). Nb-55Ti flanges have been shown to withstand heat treatments of 1400 °C (2550 °F), where stainless steel flanges would deform while losing mechanical strength. Also, the Nb-55Ti can be electron beam welded directly to the high-purity niobium RF cavities.

Table 11 Corrosion of niobium in liquid metals

Niobium is resistant to attack below the indicated temperatures.

Molten metal	Temperature °C	Temperature °F
Bismuth	<510	<950
Gallium	<400	<750
Lead	<850	<1560
Mercury	<660	<1220
Sodium	<1000	<1830
Potassium	<1000	<1830
Sodium-potassium	<1000	<1830
Thorium-magnesium eutectic	<850	<1560
Uranium	<1400	<2550
Zinc	<450	<840

REFERENCES

1. J. Hebda, Niobium Alloys and High Temperature Applications, *Proceedings of the International Symposium Niobium 2001,* 2–5 Dec 2001 (Orlando, FL), TMS, p 243–259
2. L. Meyer, History of Niobium as a Micro-alloying Element, *International Symposium Niobium 2001 Proceedings,* 2–5 Dec 2001 (Orlando, FL), TMS
3. Miniature Niobium Tubular Parts Help Brighten the Night, *Outlook,* Vol 9 (No. 2), 1988
4. Platinized Niobium Anodes Halt the Tide of Corrosion on Two Bridges, *Outlook,* Vol 7 (No. 2), 1986
5. Columbium Fights Corrosion in Cathodic Protection Devices, *Outlook,* Vol 6 (No. 2), 1985
6. Niobium Evaporator Resists Corrosion in Chromic Acid Recovery Process, *Outlook,* Vol 8 (No. 4), 1987
7. T.-L. Yau and D.R. Holmes, Fluorides from Overlooked Sources, *Proceedings of the Corrosion Applications Conference 2003,*

7–11 Sept 2003 (Coeur d'Alene, ID), ATI Wah Chang, p 23–28
8. R.M. Gibbs and B.J. Sanders, Niobium Solves a Rupture Disk Corrosion Problem, *Proceedings of the Corrosion Solutions Conference 2001,* 9–13 Sept 2001 (Sunriver, OR), Wah Chang, p 281–286
9. Q&A—Safety Valves and Rupture Disks, *Outlook,* Vol 22 (No. 4) 4th quarter 2001, p 5
10. A. Dannmeyer, T-45Nb: A Material of Construction for Wet Oxidation Processes, *Reactive Metals in Corrosive Applications Conference Proceedings,* J. Haygarth and J. Tosdale, Ed., 12–16 Sept 1999 (Sunriver, OR), Wah Chang, 2000, p 21–29
11. First Miss Strikes Gold with Nb-55Ti Alloy, Solves Long-Standing Autoclave Problem, *Outlook,* Vol 13 (No. 3), 1992
12. T.-L. Yau, Reactive and Refractory Alloys, *Environmental Effects on Engineered Materials,* Russel Jones, Ed., Marcel Dekker, Inc., 2001, p 170
13. D. Lupton, W. Schreiber, and E. Heitz, Corrosion Behavior of Tantalum and Possible Substitute Materials under Extreme Conditions, *Metallic Corrosion Proceedings,* Eighth International Congress on Metallic Corrosion, DECEMA, Frankfurt, 1981, p 1441–1446
14. A. Robin and J. Rosa, Corrosion Behavior of Niobium, Tantalum, and Their Alloys in Hot Hydrochloric and Phosphoric Acid Solutions, *Int. J. Refract. Met. Hard Mater.,* Vol 18 (No. 1), 2000, p 13–21
15. B.S. Covino, Jr., J.P. Carter, and S.D. Cramer, The Corrosion Behavior of Niobium in Hydrochloric Acid Solutions, *Corrosion,* Vol 36 (No. 10), 1980, p 554–558
16. D. Lupton, F. Aldridge, and K. Shulze, Niobium in Corrosive Environments, *Niobium Proceedings of the International Symposium,* TMS, 1983, p 533–561
17. M. Pourbaix, *Atlas of Electrochemical Equilibria in Aqueous Solutions,* Pergamon Press, 1966
18. J. Van Muyler, N. de Zoubov, and M. Pourbaix, Electromechanical Behavior of Niobium, Potential-pH Equilibrium Diagram for the System Nb-H_2O, at 25 °C, *CEBELCOR* Rapports Techniques (No. 53), June 1957, p 1–11
19. M. Coscia and M. Renner, Defining Ta Operating Limits in H_2SO_4, *Ind. Heat.,* Oct 2003
20. F. Fairbrother, The Chemistry of Niobium and Tantalum, *Topics in Inorganic Chemistry and General Chemistry,* P. Robinson, Ed. Monograph 10, Elsevier, 1967
21. I. Tingley and R. Rogers, *Corrosion,* Vol 21 1965, p 132
22. *Mater. Des. Eng.,* Vol 54, 1961, p 121
23. C.M. Forman and E.A. Verchot, U.S. Missile Command Report RS-TR-67-11, 1967
24. T.L. Yau, Performance of Zirconium and Columbium in Simulated FGD Scrubber Solutions, *Corrosion in Desulfurization Systems, Corrosion,* NACE, 1984
25. Teledyne Wah Chang Albany, unpublished research
26. P.C.S. Hayfield, "Electrochemical Properties of Niobium in Impressed Current Cathodic Protection," Paper 103, presented at Corrosion/81, National Association of Corrosion Engineers, 1981
27. Columbium Shows Excellent Results in Severe Corrosion Applications, *Outlook,* Vol 2 (No. 2), 1981
28. M. Coscia, *Tantalum and Niobium Materials for the Pharmaceutical Industry,* Tantalum Press Monitor, 1996
29. Niobium Alloy C-103/Aerospace Applications, *Outlook,* Vol 21 (No. 2), 2000
30. Innovator Gravitates to Niobium for Superconducting Cavity Experiments, *Outlook,* Vol 23 (No. 2), 2000
31. Uniformity Key in Producing Superconducting Magnets for Brookhaven Collide, *Outlook,* Vol 16 (No. 4), 1995

SELECTED REFERENCES

- W.T. Bachman, Don't Overlook Refractory Metals for Corrosive Environments, *Mater. Des. Eng.,* Vol 64 (No. 6), 1966, p 106–108
- C.R. Bishop, *Corrosion,* Vol 14, 1963, p 308
- R.H. Burns, F.S. Shuker, and P.E. Manning, Industrial Applications of Corrosion-Resistance Tantalum, Niobium, and Their Alloys, *Refractory Metals and Their Industrial Applications,* STP 849, R.E. Smallwood, Ed., ASTM, 1984, p 50–69
- J. Chelius, Use of the Refractory Metals in Corrosive Environment Services, *Mater. Eng. Q.,* Vol 7 (No. 3), 1967, p 57–59
- Columbium: What Is It Used For?, *Outlook,* Vol 5 (No. 2), 1984
- Evans Uses Niobium to Make Small Parts Solve Tough Problems, *Outlook,* Vol 10 (No. 1), 1989
- C.A. Hampel, Refractory Metals: Tantalum, Niobium, Molybdenum, and Tungsten, *Ind. Eng. Chem.,* Vol 53 (No. 2), Feb 1961, p 90–96
- HOH Selects Niobium for Use in Consumer Water Purification System, *Outlook,* Vol 9 (No. 1), 1988
- C. Mosheim, *Utilization of Niobium and Tantalum in Chemical Processing Industries,* Tantalum-Niobium Study Center, Chemical Processing Directions International
- A. Robin, *Int. J. Refract. Met. Hard Mater.,* Vol 15 (No. 5–6), 1997, p 317–323
- R.E. Smallwood, Use of Refractory Metals in Chemical Process Industries, *Refractory Metals and Their Industrial Applications,* STP 849, R.E. Smallwood, Ed., ASTM, 1984, p 106–114
- J. van Muylder and M. Pourbaix, Technical Report 53, Centre Belge d'Etude de la Corrosion, 1959
- R.T. Webster, Niobium in Industrial Applications, *Refractory Metals and Their Industrial Applications,* STP 849, R.E. Smallwood, Ed., ASTM, 1984, p 18–27

ASM Handbook, Volume 13B: Corrosion: Materials
S.D. Cramer, B.S. Covino, Jr., editors, p337-353
DOI: 10.1361/asmhba0003825

Corrosion of Tantalum and Tantalum Alloys

TANTALUM is one of the most versatile corrosion-resistant metals known. It combines the inertness of glass with the strength and ductility of low-carbon steel and with a much higher heat-transfer capability than glass. The relatively high cost of tantalum has been a limiting factor in its use, but where premium corrosion resistance is important, the cost can be justified. Fabrication techniques, in which thin linings of tantalum are used in chemical processing equipment, result in equipment that has the acid corrosion resistance provided by tantalum but at a much lower cost than an all-tantalum construction.

The long life and reliability of tantalum equipment in severe-corrosion applications can offset its higher initial cost. Table 1 lists numerous applications for tantalum in the chemical processing industry and in other industries.

Most tantalum, (approximately 60%) is used in electronics, with tantalum capacitors being the largest application by far. The constant drive for smaller portable electronic devices with high reliability has increased the demand for tantalum capacitors. The dielectric is tantalum oxide, and the capacitor packaging protects the tantalum from the environment, so this article does not dwell on this application.

The most common compositions of tantalum are unalloyed cast (UNS R05200) and unalloyed sintered (UNS R05400); tungsten alloyed, Ta-2.5W (UNS R05252); and Ta-10W (UNS R05255). Ta-2.5W is selected for greater low-temperature mechanical strength than pure tantalum, and Ta-10W has superior high-temperature strength (service up to 2480 °C, or 4500 °F). Tantalum is processed as a powder that can be sintered or remelted using an electron beam or vacuum arc. Ta-40Nb (UNS R05240) provides higher tensile and yield strength than pure tantalum, while retaining much of the chemical resistance at a lower cost.

Mechanism of Corrosion Resistance

The outstanding corrosion resistance and inertness of tantalum are attributed to a very thin, impervious, protective oxide film that forms on exposure of the metal to slightly anodic or oxidizing conditions (Ref 1). Although tantalum pentoxide (Ta_2O_5) is the usual oxide form, suboxides may also exist in transition between the base metal and the outer film (Ref 2). It is only when these oxide films react with or are penetrated by a chemical reagent that attack occurs on the underlying metal substrate. A visible, continuous oxide film can be formed on tantalum by electrolytic anodizing in an acid solution such as dilute phosphoric acid (H_3PO_4). This film has a high dielectric constant, which prevents the flow of direct current from tantalum to an electrolyte when the metal is made anodic. The high stability of the oxide film makes tantalum valuable for capacitor and rectifier applications. For corrosion applications, pickling in a solution of HF/HNO_3/H_2O or HF/H_2SO_4/H_2O will also produce a continuous oxide film.

Tantalum occupies a position toward the electropositive end of the electromotive force series and thus tends to become cathodic in the galvanic cell circuit formed by contact with almost all other metals. Because of this cathodic behavior, atomic hydrogen, which may be liberated, can be absorbed by the tantalum and result in hydrogen embrittlement. Stray voltages can also cause this undesired effect. Therefore, when used in chemical processing equipment, tantalum must be protected from becoming cathodic so that the material will not become embrittled. Hydrogen embrittlement and methods for minimizing its effect are discussed later in this article.

Corrosion in Specific Media

Because tantalum is resistant to a wide range of acids, salts in solution, and organic chemicals at elevated temperatures, tantalum has a primary application as a material of construction in the chemical processing industry. The corrosion resistance of tantalum in media important to the chemical processing industry follows.

Water. Tantalum is not attacked by freshwater, mine waters (which are usually acidic), or seawater. Tantalum shows no corrosion in deionized water at 40 °C (100 °F) (Ref 3). For tantalum equipment exposed to boiler waters and condensates, the alkalinity must be controlled. The pH should be less than 9 and preferably no more than 8. No failures caused by exposure of tantalum to steam condensate have ever been recorded. Tantalum is used in many cases at saturated steam pressures above 1035 kPa (150 psi) at temperatures of 185 °C (365 °F) and is considered resistant to saturated steam below 250 °C (480 °F) at a pressure of 3.9 MPa (560 psi).

Acids. The chemical properties of tantalum are similar to those of glass. Like glass, tantalum is immune to attack by almost all acids except HF (Table 2). Reactions conducted in the laboratory in glass equipment can be transferred to plant operations in tantalum equipment with complete assurance that the equipment will be free from corrosion, that the product will not become contaminated, and that undesired side reactions will not occur.

Tantalum is not attacked by such agents as sulfuric acid (H_2SO_4), nitric acid (HNO_3), hydrochloric acid (HCl), aqua regia, perchloric acid ($HClO_4$), chlorine, bromine, hydrobromic acid (HBr) or any of the bromides, phosphoric acid (H_3PO_4) when free of the F^- ion, nitric oxides, chlorine oxides, hypochlorous acid (HClO), organic acids, and hydrogen peroxide (H_2O_2) at ordinary temperatures. It is attacked, even at room temperature, by strong alkalis (e.g., NaOH), HF, and free sulfur trioxide (SO_3) (as in fuming H_2SO_4). Table 3 compares the corrosion resistance of tantalum and other resistant metals in various acids.

Sulfuric Acid. Tantalum is highly resistant to corrosion by H_2SO_4 in all concentrations up to approximately 98%. It is inert to dilute acid even at boiling temperatures and is not attacked by concentrated acids at temperatures below 150 °C (300 °F). A slow, uniform attack by concentrated H_2SO_4 begins on tantalum at approximately 175 °C (345 °F). However, the corrosion by hot, concentrated H_2SO_4 is uniform, and at a temperature as high as 200 °C (390 °F), tantalum can be successfully used with 98% H_2SO_4 (Fig. 1) and, under certain conditions, in 99% H_2SO_4 at temperatures as high as 230 °C (445 °F) (Ref 4, 5).

Fuming H_2SO_4 (oleum) attacks the metal much more rapidly than the concentrated acid does (Fig. 1), but the attack on tantalum by either concentrated H_2SO_4 or oleum is uniform over

Table 1 Applications for tantalum equipment

Product	Operation	Industry	Equipment	Remarks
Acetic acid, crude	Recovery from wood distillate	Chemical	Bayonet heaters, condensers	...
Aluminum chloride	Concentration	Chemical	Bayonet heaters, condensers	Condensers for HCl recovery
Amino acids	Digesting proteins in HCl	Chemical, breweries, distilleries, food	Bayonet heaters, condensers, complete plants	See glutamic acid, mono-sodium glutamate
Ammonium chloride, crude	Concentration from gas house liquors	Gas and coke	Bayonet heaters, heat exchangers	...
Ammonium chloride, pure	Concentration before crystallizing	Chemical	Heat exchangers	High pressure
Ammonium nitrate	Concentration	Chemical	Heat exchangers	...
Aqua regia	Ore solution, stainless steel pickling	Chemical, steel	Bayonet heaters, heat exchangers, pickling tank coils	...
Aviation gasoline	Butane isomerization	Petroleum	Anhydrous HCl plants	...
Benzoic acid	Hydrolysis from benzyl chloride	Chemical, pharmaceutical	HCl absorbers	Recovery of by-product HCl
Benzyl chloride	Chlorination of toluene	Chemical	HCl absorbers	Recovery of by-product HCl
Bromine, crude	Steam and bromine condensation	Chemical	Condensers	...
Bromine, pure	Purification from chlorine and organics	Chemical	Boilers, condensers, complete purification plants	...
Bromides, organic	Bromination	Pharmaceutical	Condensers	Both reflux and product condensers
Chloral	HCl absorption	Chemical	HCl absorbers	Recovery of by-product HCl
Chlorine	Brine cooling	Chemical	Heat exchangers	...
Chloroacetic acid	HCl absorption	Chemical	HCl absorbers	Recovery of by-product HCl
Chlorobenzene, also monochloro-benzene and paradichloro-benzene	Chlorinator operation HCl absorption	Chemical	Condensers, HCl absorbers	Recovery of by-product HCl
Chromic acid	Heating solutions	Electroplating	Coils, heat exchangers	...
Diphenyl chloride	HCl absorption	Chemical	HCl absorbers	Recovery of by-product HCl
Detergents (chlorinated)	HCl absorption	Chemical	HCl absorbers	Recovery of by-product HCl
Ethyl ether	Heating alcohol reactor	Pharmaceutical, chemical	Bayonet heaters, single and multiple	...
Ethyl bromide	Alcohol bromination	Chemical	Special HBr reactor; anhydrous HBr plant	...
Ethyl chloride	Alcohol chlorination	Chemical	Special HCl reactor; anhydrous HCl plant	...
Ethyl gasoline	Tetraethyl lead production	Chemical, petroleum	Heaters, coolers, condensers, anhydrous HCl plant	...
Ethylene dibromide	Ethyl gas stabilizer, ethylene bromination	Chemical	Condensers, bromide plants	...
Ethylene dichloride	Chlorination	Chemical	Condensers	...
Ethylene glycol	Reactor, sulfuric acid concentrator	Chemical	Bayonet heaters, multiple	...
Ferric chloride	Dissolving concentration	Chemical	Bayonet heaters, single and multiple	...
	Sewage treatment	Sanitary districts	Bayonet heaters, flow regulator parts, thermometer wells	Heaters to warm storage tanks
Formic acid	Distillation	Chemical	Condensers	...
Fuming HNO_3	Distillation	Chemical	Multiple bayonet heaters, condensers	...
Glutamic acid	Digesting gluten in HCl, vacuum evaporation of HCl, recovery of HCl	Chemical	Bayonet heaters, single and multiple; condensers; synthetic HCl plants	...
Halogens (except fluorine)	Chlorine, bromine, iodine generators and recovery systems	Chemical, pharmaceutical	Bayonet heaters, coils, condensers, regulator parts, thermometer wells	...
Hydrobromic acid	Generation	Chemical	Bayonet heaters, coils, condensers, synthetic HBr plants	...
Hydrochloric acid	Production, purification, recovery, processing	Chemical, pharmaceutical, food	Bayonet heaters, heat exchangers, coils, condensers, HCl absorbers, synthetic HCl plants, acid coolers, gas coolers, chlorine burners, strippers, thermometer wells	...
Hydrochloric acid C. P.	Distillation	Chemical	Bayonet heaters, coils, condensers, complete stills	...
Hydrochloric acid, anhydrous	Production	Chemical	Absorbers, coolers, strippers, chlorine burners, complete plants	...
Hydriodic acid	Generation and recovery	Chemical, pharmaceutical	Bayonet heaters, coils, condensers	...
Hydrogen chloride	Production	Chemical	Absorbers, coolers, strippers, chlorine burners, complete plants	...
Hydrogen peroxide	Hydrolysis, concentration	Chemical	Bayonet heaters, heat exchangers	...
Iodine	Recovery from sour brines	Chemical	Coils	...
Isobutane	Isomerization for aviation gasoline	Petroleum	Anhydrous HCl plants	...
Isopropyl alcohol	Concentration of H_2SO_4	Chemical, petroleum	Bayonet heaters, multiple	...
Lactic acid	Distillation purification	Chemical, pharmaceutical	Bayonet heaters, condensers	...
Magnesium bromide	Concentration	Chemical	Bayonet heaters, coils	...
Magnesium chloride	Concentration	Chemical	Heat exchangers	...
Methyl chloride	Methanol chlorination	Chemical	Coils, condensers, complete units	...
Methyl ethyl ketone	Recovery of by-product HCl	Chemical	HCl absorbers	...
Mono-sodium glutamate	Glutamic hydrochloride production	Chemical, food	Bayonet heaters, condensers, complete plants	...
Muriatic acid pickling	Heating, pickling tanks	Steel, metal working	Coils	...
Nitric acid	Distillation, recovery	Chemical	Bayonet heaters, single and multiple; condensers	...
Nitroglycerin	Nitration, HNO_3 recovery	Chemical, explosive	Condensers, thermometer wells	...
Nitrosyl bromide	Recovery, handling	Chemical	Condensers, pipe and fittings	...
Nitrosyl chloride	Generation, recovery	Chemical	Pipe and fittings	...
Oakite (tri-sodium phosphate)	Cleaning and degreasing metals	Metal working	Bayonet heaters, coils	...
Pentachlor phenol	Chlorination	Chemical	HCl absorbers	Recovery of by-product
Perchloric acid	Generation, concentration	Chemical	Coils, condensers	...
Persulfuric acid	Electrolysis, recovery	Chemical	Bayonet heaters, electrode supports	...
Phenol (carbolic acid)	Chlorination, hydrolysis	Chemical, plastic	Bayonet heaters, HCl absorbers	Tantalum equipment used in Raschig process

(continued)

Table 1 (continued)

Product	Operation	Industry	Equipment	Remarks
Phosphoric acid	Concentration	Chemical, food	Bayonet heaters	Tantalum can be used only when fluorine content is below 10 ppm.
Phosgene	Generation	Chemical	Bayonet heaters, condensers	...
Pickling liquors	Heating, pickling tanks	Metal working, steel	Coils	Tantalum used with HCl, HNO_3, or mixtures of them
Plating	(See chromic acid)	...	...	...
Polystyrene	Recovery of by-product HCl	Chemical, plastic	HCl absorbers	...
Rayon (viscose process)	...	...	Bayonet heaters, spinneret cups, thermometer wells	...
Silver nitrate	Recovery	Photographic	Heat exchangers	...
Smokeless powder	Nitration, HNO_3 and H_2SO_4 recovery	Chemical equipment	Bayonet heaters, condensers, thermometer wells	...
Sulfuric acid	Concentration	Chemical, petroleum	Bayonet heaters	...
Styrene	Recovery of by-product HCl	Chemical, plastic	HCl absorbers	...
Sulfuric acid	Concentration, recovery	Chemical, petroleum, pharmaceutical	Bayonet heaters, single and multiple	...
Tartaric acid	Reactor concentrator	Chemical, pharmaceutical, food	Bayonet heaters, multiple	...
Tetraethyl lead	Production	Chemical, petroleum	Heaters, coolers, condensers, anhydrous HCl plants	...
T.N.T (Tri-nitrotoluene)	Nitration, HNO_3 and H_2SO_4 recovery	Chemical, explosive	Bayonet heaters, condensers, thermometer wells	...
Tri-sodium phosphate	Cleaning and degreasing metals	Metal working	Bayonet heaters, coils	...
Vinyl chloride	Chlorination	Chemical, plastic	Anhydrous HCl plants	...

the surface. The presence of impurities does not increase the corrosion rate of tantalum in H_2SO_4. In general, no failures due to hydrogen embrittlement have been reported for tantalum chemical processing equipment used in H_2SO_4 service unless additional factors such as fatigue loading, or mechanical damage are present. However, under special laboratory test conditions, hydrogen embrittlement can be induced in tantalum (Ref 7).

Phosphoric Acid. Figure 2 shows the corrosion rate of tantalum exposed to various concentrations of reagent-grade (chemically pure) H_3PO_4 at the boiling temperature and at 190 °C (375 °F). Figure 2 also shows the boiling point curve of H_3PO_4 as a function of concentration. Tantalum exhibits superior resistance to boiling H_3PO_4 at all concentrations. At temperatures in excess of boiling, the superiority of tantalum is evident. Data for 85% H_3PO_4 are included in Fig. 1. If the H_3PO_4 contains more than a few parts per million of F^- ion, however, as is frequently the case with commercial acid, attack on the tantalum may occur.

In one study, the corrosion resistance of commercially pure tantalum to a mixture of H_3PO_4, potassium chloride (KCl), and water initially containing 60 to 260 ppm F^- was evaluated at 120 °C (250 °F) and at atmospheric pressure (Ref 9). Corrosion rates calculated from the test data were of the order of 0.0005 to 0.15 mm/yr (0.02 to 6 mils/yr), indicating good corrosion resistance.

Hydrochloric Acid. Specific corrosion tests and many industrial applications show that tantalum is completely inert to HCl in all concentrations under atmospheric pressure to at least 121 °C (250 °F) (Ref 4). This has been demonstrated by long industrial experience. Bayonet heaters, probes stuck into the medium to be heated, that were fabricated from tantalum with a wall thickness as thin as 0.33 mm (0.013 in.) have been in continuous industrial use in HCl distilling units for over 20 years without being attacked. However, there have been instances where hydrogen embrittlement without signs of corrosive attack has occurred in tantalum when exposed to solutions of HCl and methanol.

Figure 3 shows the corrosion rate of tantalum in HCl over the concentration range from 1 to 35%. Figure 4 shows a plot of the corrosion rate of tantalum in 20, 32, and 37% HCl as a function of temperature. Additions of HNO_3 and ferric or cupric chlorides ($FeCl_3$ or $CuCl_2$) to HCl tend to improve corrosion resistance.

Tests indicate that tantalum resists HCl at all temperatures and concentrations to 190 °C (375 °F). At concentrations near 30% and at 190 °C (375 °F), some tendency toward hydrogen embrittlement has been noted. This possibility should be considered when handling concentrated solutions of acid above the boiling point. The tendency was not noted at or below the boiling point of HCl solutions.

Nitric Acid. Tantalum is inert to HNO_3 solutions in all concentrations and at all temperatures to boiling. The presence of Cl^- in HNO_3 does not reduce the corrosion resistance of the metal to this acid. Figure 5 shows the corrosion rate of tantalum in HNO_3 concentrations ranging from 1 to 70%.

The corrosion rate of tantalum to HNO_3 at subboiling temperature is less than 0.4 μm/yr (0.015 mil/yr) for most concentrations and temperatures. In general, the use of tantalum at these temperatures would not be economical, considering the resistance offered by stainless steels. At temperatures near and above the normal boiling point of HNO_3, the superior resistance of tantalum becomes pronounced. Corrosion testing of tantalum for equipment to be used at these temperatures is recommended. Tantalum has been successfully used for years to handle fuming HNO_3 at service conditions up to 5.5 MPa (800 psig) and 315 °C (600 °F) in chemical processing equipment.

Hydrofluoric acid is the best solvent for tantalum. The rate of attack varies from slow for dilute acid to rapid for concentrated solutions. The rate of attack by HF can be greatly accelerated by the addition of HNO_3 and other oxidizing agents, such as H_2O_2. Metallographic etchants use this recipe. Embrittlement of the metal due to the absorption of atomic (nascent) hydrogen can occur when the metal is attacked by HF. However, when sufficient HNO_3 is present, hydrogen embrittlement does not occur, even after nearly all of the tantalum is dissolved, for example, by severe pickling. The rate of hydrogen absorption is greatly reduced in dilute HF if the tantalum is made positive by impressing 2 to 10 V on the material in an electrolytic cell. Embrittlement by hydrogen does not occur when tantalum is made positive. In solutions of HF, which prevent the formation of the protective oxide film, tantalum is less noble than zinc, manganese, aluminum, and zirconium (Ref 10).

Attack on tantalum apparently does not occur in chromium plating baths containing F^- (Ref 11). In one test, a corrosion rate of 0.0005 mm/yr (0.02 mil/yr) was observed on a sample placed in a chromium plating bath for $2\frac{1}{2}$ months. The solution contained 40% chromium trioxide (CrO_3) and 0.5% F^- ion at a temperature of 55 to 60 °C (130 to 140 °F). In another 4-day exposure, a corrosion rate of 0.005 mm/yr (0.2 mil/yr) occurred in a bath containing 250 g/L (33 oz/gal) CrO_3, 1.5 g/L (0.20 oz/gal) H_2SO_4, and 3 g/L (0.40 oz/gal)

Table 2 Effects of acids on tantalum

Acid	Concentration, %	Temperature, °C (°F)	Code(a)
Acetic acid	5–99.5	Room to boiling	E
Acetic acid, glacial	99.7	Room to boiling	E
Acetic acid vapor	0–100	Room to boiling	E
Acetic anhydride	99	Room	E
Aqua regia	3 HCl, 1 HNO_3	Room to 77 (170)	E
Arsenic acid	90	Room	E
Benzoic acid	5	Room	E
	Saturated	Room	E
Boric acid	5	Room to boiling	E
	10	Room to boiling	E
	Saturated	Room	E
Butyric acid	5	Room	E
Carbolic acid	Saturated	Room	E
	...	...	E
Chloroacetic acid	30	Room to 82 (180)	E
	100	Room to boiling	E
Chloric acid	...	Room	E
Chlorosulfonic acid	10	...	E
Chromic acid	5–50	Room to boiling	E
Citric acid	5	Room	E
	10–25	Room to boiling	E
Citric acid (nonaerated)	50	Room to 100 (212)	E
Citric acid (aerated)	50	Room to 100 (212)	E
Citric acid	Concentrated	Room to boiling	E
Dichloroacetic acid	100	Room to 100 (212)	E
	100	Room to boiling	E
Fatty acids	...	...	E
Fluoboric acid	5–20	Elevated	NR
Fluorosilicic acid	10	Room	NR
Formic acid (still)	5	Room to 66 (150)	E
Formic acid (nonaerated)	10–50	Room to boiling	E
Formic acid (aerated)	10–90	Room to 100 (212)	E
Gallic acid	5	Room to boiling	E
Hydrobromic acid	0–100	Room to boiling	E
Hydrochloric acid (nonaerated)	5–20	Room to 35 (95)	E
Hydrochloric acid (aerated)	5–20	Room to 35 (95)	E
Hydrochloric acid	All	Room to 71 (160)	E
Hydrochloric acid fumes	Concentrated	Room to 38 (100)	E
Hydrocyanic acid	...	...	E
Hydrofluoric acid	5–48	Room	NR
Hydrofluoric acid (anhydrous)	100	Room	NR
Hydrofluoric acid vapors	...	Room	NR
Hydrofluoric-nitric acid	1 HF:15 HNO_3	Room	NR
Hydrofluosilicic acid	5	Room	V
Hydrofluosilicic acid vapors	...	100 (212)	NR
Hydroxyacetic acid	...	Room to 40 (105)	E
Lactic acid	5	Room to 66 (150)	E
	10–100	Room to boiling	E
Malic acid	...	Room and hot	E
Methyl-sulfuric acid	0–100	Room to 150 (300)	E
Molybdic acid	5	Room	E
Muriatic acid	...	Room	E
Nitric acid	5	Room	E
Nitric acid (continued)	10–40	Room to 100 (212)	E
	50–65	Room to boiling	E
	69.5	Room to 100 (212)	E
Nitric acid (white fuming)	90	Room to 82 (180)	E
Nitric acid	95	Room	E
Nitric acid	Concentrated	Room to boiling	E
Nitric acid	Fuming	Room	E
Nitrous acid	5	Room	E
Oleic acid	...	Room	E
Oxalic acid	1	Room to 38 (100)	E
	5	Room to 35 (95)	E
	10	Room to boiling	E
	0.5–25	Room to 60 (140)	E
	Saturated	Room to 93 (200)	E
Perchloric acid	0–100	Room to 150 (300)	E
Phenol (carbolic acid)	Saturated	Room	E
Phosphoric acid	1	Room	E
Phosphoric acid	5	Room to 100 (212)	E
Phosphoric acid (still)	10	Room to 175 (350)	E
Phosphoric acid (agitated)	10	Room	E
Phosphoric acid (aerated)	10	Room	E
Phosphoric acid	5–30	Room	E
Phosphoric acid	35–85	Room	E
Phosphoric acid	85	Room to 38 (100)	E
Phosphoric-sulfuric + $CuSO_4$	$15H_3PO_4$-$10H_2SO_4$	Room to 66 (150)	E
Picric acid	Concentrated	...	E
Propionic acid vapor	...	190 (375)	E
Pyrogallic acid	...	...	E
Salicylic acid	...	Room	E
Stearic acid	Concentrated	Room to 93 (200)	E
Succinic acid	...	Molten	E
Sulfuric acid	1–5	Room to 60 (140)	E
	5	Room to 60 (140)	E
	10	Room to boiling	E
	15	Room	E
	50	Room to boiling	E
	Concentrated	Room to 150 (300)	E
	Concentrated	Boiling	NR
	Fuming	Room	NR
Sulfuric acid vapors	96	Room to 150 (300)	E
Sulfuric anhydride	Dry	Room	NR
Sulfuric-nitric acid	90–10	Room	E
	70–30	Room	E
	50–50	Room to 60 (140)	E
	30–70	Room	E
	10–90	Room to 60 (140)	E
Sulfurous acid	6	Room	E
	Saturated	Room to 190 (375)	E
Sulfurous spray	...	Room	E
Tannic acid	10	Room to 66 (150)	E
	25	Room to 100 (212)	E
Tartaric acid	10	Room to 100 (212)	E
	25	Room to 100 (212)	E
	50	Room to 100 (212)	E

(a) E, no attack; V, variable, depending on temperature and concentration; NR, not resistant

of F^- ion at 55 °C (130 °F). Complex ion formation between chromium and F^- ions is thought to explain the reduced activity of F^-.

Corrosion rates were determined on several construction materials, including tantalum in HNO_3 plus HF mixtures (Ref 12). These studies were related to tests of various candidate materials for fuel element processing. Tantalum showed some promise but was not entirely satisfactory. Its possible use was considered restricted to low fluoride concentrations and temperatures below boiling.

Acid Mixtures. Tests were conducted to determine the suitability of tantalum to either hot or cool mixed solutions of HCl, H_2SO_4, and potassium hydrogen sulfate ($KHSO_4$). The test temperature ranged from the boiling point of the solution, 115 to 120 °C (235 to 250 °F). The corrosion rate of the tantalum based on 4 days of exposure was 0.001 mm/yr (0.04 mil/yr). Examination of the sample after the test indicated no apparent discoloration. There were no visible signs of attack, and the sample remained ductile after the test. The very slight weight loss reported was believed to have been caused by physical scraping on the sample. Thus, tantalum exhibited excellent corrosion resistance to this mixture.

Corrosion rates were also determined on tantalum exposed to a mixture of concentrated H_2SO_4, HNO_3, and HCl at temperatures ranging from 200 to 270 °C (390 to 520 °F) (Ref 13). Corrosion rates were reduced by a factor of 3 compared to the rate in H_2SO_4 alone. When only HCl or water was added, the corrosion rate was reduced only slightly. When HNO_3 was added alone, the corrosion rate was the same as when HCl and HNO_3 were both added. Thus, the oxidizing effect of HNO_3 reduced the tantalum corrosion rate.

Other Acids and Reagents. Over the temperature range commonly used in solution processes, tantalum is inert to sulfur and phosphorus chlorides, diphenyl and diphenyl oxide, and hydrogen sulfide (H_2S).

Hypochlorites do not affect tantalum unless they are strongly alkaline. The same is true of all chlorides, bromides, and iodides. Fluorides, however, will attack tantalum.

A detailed corrosion study was conducted in a chlorine dioxide (ClO_2) plant for pulp bleaching in an effort to secure useful information on the performance of various metals and alloys in this service (Ref 14). Tantalum was among the materials tested, and it showed no corrosion attack in any of the tests.

Salts. Tantalum is not attacked by dry salts or by salt solutions at any concentration or temperature unless HF is liberated when the salt dissolves or unless a strong alkali is present. Salts that form acidic solutions have no effect on tantalum. However, fused sodium hydrosulfate ($NaHSO_4$) or $KHSO_4$ dissolves tantalum (Ref 11), Table 4 gives compatibility data for tantalum in numerous salts.

Alkalis. Sodium hydroxide (NaOH) and potassium hydroxide (KOH) solutions do not dissolve tantalum but tend to destroy the metal by formation of successive layers of surface scale. The rate of the destruction increases with concentration and temperature. Damage to tantalum equipment has been experienced unexpectedly when exposed to strong alkaline solutions for prolonged periods during cleaning and maintenance.

Tantalum is attacked, even at room temperature, by concentrated alkaline solutions and is dissolved by molten alkalis. However, tantalum is fairly resistant to dilute alkaline solutions. In one long-term exposure test in a paper mill, tantalum suffered no attack in a solution with a pH of 10.

A study using change in electrical resistivity to measure corrosion rates found that tantalum wire totally immersed in 10% NaOH solution at room temperature for 210 days corroded at the rate of 0.24 μm/yr (0.01 mil/yr). A similar rate occurred in 10% NaOH at 100 °C (212 °F). In the latter case, there was some local effect at the points where the wire left the solution and entered submerged rubber stoppers in the sides of the corrosion vessel; this accounted for most of the weight loss. In another study (Ref 4), tantalum sheet was exposed to solutions of 5 to 10% NaOH at temperatures of 66 to 100 °C (151 to 212 °F). Corrosion rates as high as 0.76 μm/yr (0.03 mil/yr) were measured, along with extreme hydrogen embrittlement.

Tantalum has been used as anode baskets in a number of silver cyanide barrel platers for several years of service life, and although the solutions are quite alkaline with free KOH, the tantalum has remained bright and ductile, with no failures occurring. The tantalum anode

Table 3 Corrosion resistance of tantalum and other metals to acids

Solution	Temperature °C	Temperature °F	Test duration, days	Corrosion rate: Tantalum mm/yr	Tantalum mils/yr	Niobium mm/yr	Niobium mils/yr	Zirconium mm/yr	Zirconium mils/yr	Titanium mm/yr	Titanium mils/yr
HCl, 18%	19–26	65–80	36	nil		nil		2.3 μm	0.09(a)	0.11	4.5
HCl, 37%	19–26	65–80	36	nil		0.003	0.12	2 μm	0.08	17.7	698
HCl, 37%	110	230	7	nil		0.1	4(b)	0.48	18.75	Not tested	
HNO_3, conc	19–26	65–80	36	nil		nil		nil		1.3 μm	0.05
$1HNO_3{\cdot}2HCl$	19–26	65–80	35	nil		0.5 μm	0.02	Very soluble		5.3 μm	0.21
$1HNO_3{\cdot}2HCl$	50–60	120–140	1	nil		0.025	1	Very soluble		Not tested	
H_2SO_4, 20%	95–100	205–212	4	nil		0.5 μm	0.02	4.6 μm	0.18	Not tested	
H_2SO_4, 50%	19–26	65–80	35	nil		Not tested		nil		0.053	2.1
H_2SO_4, 98%	19–26	65–80	36	nil		0.5 μm	0.02	Very soluble		1.2	46.8
H_2SO_4, 98%	21	70	. . .	nil		Not tested		Not tested		Not tested	
H_2SO_4, 98%	145	295	30	nil		4.6	180(b)	Very soluble		Very soluble	
H_2SO_4, 98%	175	345	30	0.25 μm	0.01	Not tested		Not tested		Not tested	
H_2SO_4, 98%	200	390	30	0.04	1.5	Not tested		Not tested		Not tested	
H_2SO_4, 98%	250	480	6 h	0.74	29	Not tested		Not tested		Not tested	
H_2SO_4, 98%	300	570	Not stated	8.7	342	Not tested		Not tested		Not tested	
H_3PO_4, 85%	19–26	65–80	36	nil		0.5 μm	0.02	0.5 μm	0.02(b)	0.17	6.75
$FeCl_3$, 10%	19–26	65–80	36	nil		nil		0.01	0.42(c)	0.76 μm	0.03

(a) Became brittle. (b) Tarnished. (c) Uneven corrosion

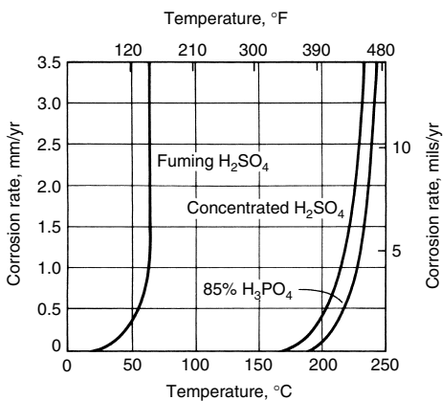

Fig. 1 Corrosion rates of tantalum in fuming H_2SO_4 (oleum), concentrated H_2SO_4, and 85% H_3PO_4. Source: Ref 6

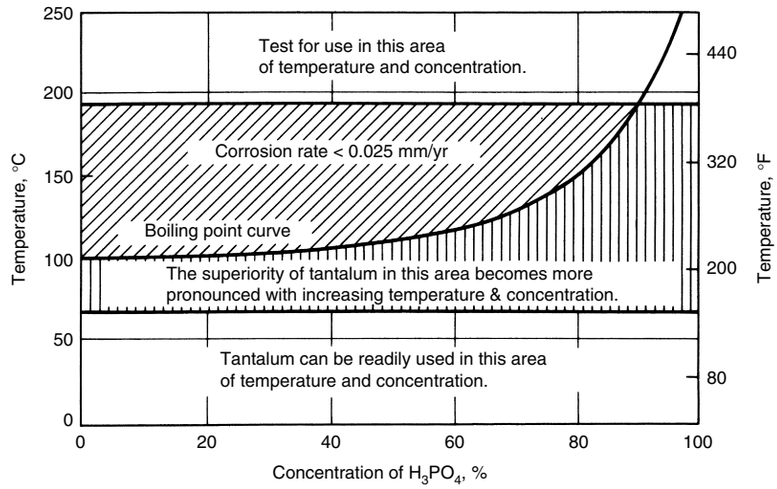

Fig. 2 Corrosion resistance of tantalum in H_3PO_4 at various concentrations and temperatures. Source: Ref 7, 8

basket is protected by the positive voltage of the cell itself.

Organic Compounds. In general, tantalum is completely resistant to organic compounds and is used in heat exchangers, spargers, and reaction vessels in several important organic reactions, particularly when corrosive inorganics are involved. These include solutions of phenol and of acetic, lactic, and oxalic acids. Table 5 lists the compatibility of tantalum in numerous corrosive environments, including many organic compounds.

Most organic salts, gases, alcohols, ketones, alkaloids, and esters have no effect on tantalum. Specific exceptions, however, should be made for reagents that may hydrolyze to HF or contain free SO_3 or strong alkalis. One important exception was noted in Ref 15, which states that mixtures of anhydrous methanol with chlorine, bromine, or iodine cause pit-type corrosion on tantalum at 65 °C (150 °F). This is of particular interest because tantalum is not attacked individually by methanol, the halogens involved, or the product, methyl halide, even at somewhat higher temperatures. Also, pit-type corrosion on tantalum is rare.

Reagents, Foods, and Pharmaceuticals. The immunity of tantalum to corrosion also ensures freedom from product contamination and undesired side reactions in the processing of fine chemicals, foods, and pharmaceuticals.

Body Fluids and Tissues. Tantalum is thought to be completely inert to body fluids and tissues. Bone and tissue are not thought to recede from tantalum, which makes it attractive as an implant material for the human body. Tantalum is used for bone repair and prosthetic devices, suture wire, cranial repair plates, and wire gauze for abdominal muscle support in hernia-repair surgery (Ref 16). A highly porous tantalum biomaterial called Trabecular Metal that is 99 wt% Ta and 1 wt% C has excellent biocompatibility and an elastic modulus that is similar to bone. The textured surface makes it attractive to bone (osteophilic) (Ref 17). (Please consult with current studies before considering tantalum for biomedical applications.)

Carbon, Boron, and Silicon. Tantalum reacts at elevated temperatures directly with carbon, boron, and silicon to form Ta_2C and TaC, TaB and TaB_2, and $TaSi_2$, respectively, although other binary compounds of these elements have been reported (Ref 11). These compounds are characterized by metallic appearance and properties, high melting point, and high hardness.

Phosphorus. Tantalum phosphides, TaP and TaP_2, are formed by heating tantalum filings in phosphorus vapor at 750 to 950 °C (1380 to 1740 °F) (Ref 11).

Sulfur. Tantalum reacts with sulfur or H_2S at red heat to form tantalum sulfide (Ta_2S_4). Tantalum sulfide is also formed when Ta_2O_5 is heated in H_2S or carbon disulfide (CS_2). Little or no data are available on the effect of solutions of sulfides, such as those of the alkali and alkaline earth metals, but the highly alkaline nature of these compounds indicates that they probably corrode tantalum to some degree.

Selenium and Tellurium. Tantalum is attacked by selenium and tellurium vapors at temperatures of 800 °C (1470 °F) and higher. In contrast, there is little or only slight attack on the metal by liquid selenides and tellurides of yttrium, the rare earths, and uranium at temperatures of 1300 to 2100 °C (2370 to 3810 °F), and tantalum is considered to be a satisfactory material in which to handle these intermetallic compounds.

Gases. The solubility of oxygen in tantalum, as determined by an x-ray technique, is shown by curve B in Fig. 6.

The conversion of tantalum into oxide was shown to occur by the nucleation and growth of small plates along the {100} planes of the body-centered cubic (bcc) metal (Ref 19, 20). The kinetics of the oxidation of tantalum were studied at temperatures to 1400 °C (2550 °F) and at pressures ranging from less than 1 to over 40 atm (100 to 4050 kPa) (Ref 18). The reaction was found to be initially parabolic, with a transformation to a linear rate after a period of time.

Increasing the temperature not only increases the rate of oxidation of tantalum but also decreases the time before the reaction changes from parabolic to linear behavior. At a moderately high temperature (approximately 500 °C, or 930 °F), this transition occurs almost at once. Under a pressure of 1 atm (100 kPa) of oxygen, tantalum oxidizes rapidly and catastrophically at a temperature of 1300 °C (2370 °F). At slightly lower temperatures (1250 °C, or 2280 °F), the specimen oxidizes linearly at a high rate for a short period of time, then oxidizes catastrophically.

The effects of pressure on the oxygen-tantalum reaction have been established and can be summarized as follows: tantalum oxidizes linearly from 500 to 1000 °C (930 to 1830 °F) at all pressures between 1.3 and 4137 kPa (0.19 and 600 psi). From 600 to 800 °C (1110 to 1480 °F), the oxidation rate shows a pronounced increase in rate with oxygen pressures above 100 kPa (14.7 psi). Another investigator found that at a higher temperature (1000 °C, or 1830 °F), the rate tends to vary as the square root of pressure

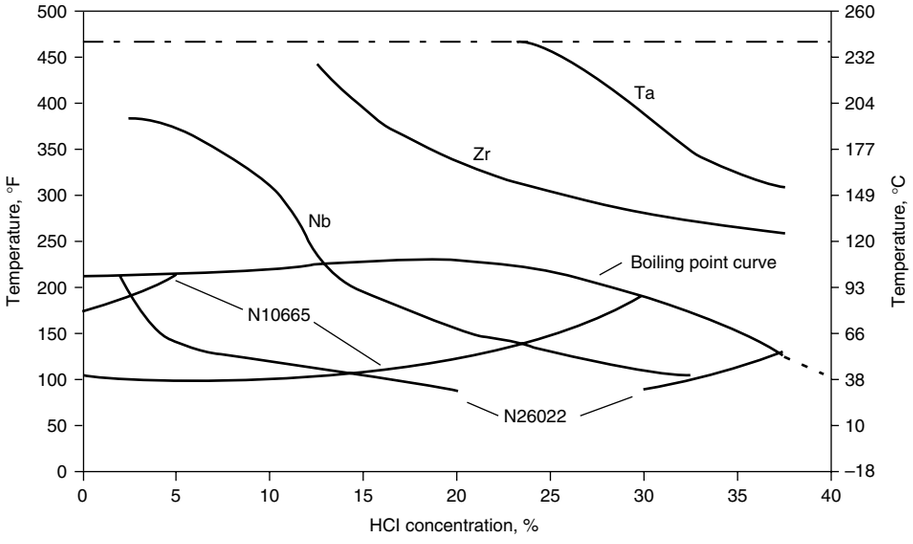

Fig. 3 Isocorrosion diagram comparing tantalum with other materials in HCl as a function of HCl and temperature. Lines represent 127 μm/yr (5 mils/yr). Courtesy of H.C. Starck Inc.

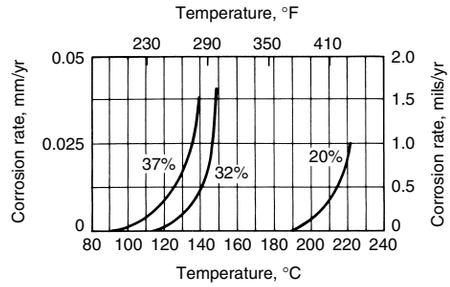

Fig. 4 Corrosion rates of tantalum in HCl of various concentrations

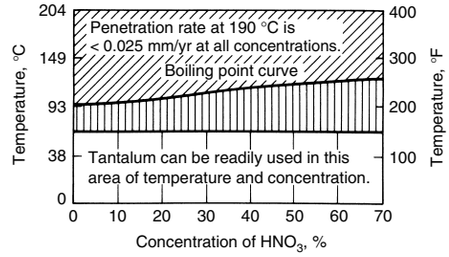

Fig. 5 Corrosion resistance of tantalum in HNO_3 at various concentrations and temperatures. Source: Ref 7, 8

Table 4 Effects of salts on tantalum

Salt	Concentration, %	Temperature, °C (°F)	Code(a)
Aluminum acetate	Saturated	Room	E
Aluminum chloride	5	Room	E
Aluminum chloride (aerated)	5–10	Room to 60 (140)	E
Aluminum chloride	25	Room to 100 (212)	E
Aluminum fluoride	5	Room	NR
	Saturated	Room	NR
Aluminum hydroxide	Saturated	...	E
Aluminum potassium sulfate (alum)	2	Room	E
	10	Room to boiling	E
Aluminum sulfate	10–saturated	Room to boiling	E
Ammonium acid phosphate	10	Room	E
Ammonium alum	...	...	E
Ammonium alum (slightly ammoniacal)	...	...	E
Ammonium bicarbonate	50	Room to 100 (212)	E
Ammonium bromide	5	Room	E
Ammonium carbonate	50	Room to 100 (212)	E
Ammonium carbonate (aqueous)	50	Room to boiling	E
Ammonium carbonate	All	Room to hot	E
Ammonium chloride	1	Room	E
	10–50	Room to boiling	E
Ammonium fluoride	10	Room	NR
Ammonium hydroxide	...	...	V
Ammonium monosulfate	...	...	E
Ammonium nitrate	0–100	Room to 150 (300)	E
Ammonium oxalate	5	Room	E
Ammonium persulfate	5	Room	E
Ammonium phosphate	5	Room	E
Ammonium sulfate (aerated)	1	Room	E
	5	Room to 100 (212)	E
Ammonium sulfate	10	Room to 100 (212)	E
Ammonium sulfate	Saturated	Room to boiling	E
Ammonium sulfite	Saturated	Room to boiling	E
Amyl acetate	...	...	E
Aniline hydrochloride	5	Room	E
	20	Room to 38 (100)	E
Antimony trichloride	...	Room	E
Barium carbonate	Saturated	Room	E
Barium chloride	5 to saturated	Room	E
	5	Room to 100 (212)	E
	20	Room to 100 (212)	E
	25	Room to boiling	E
Barium hydroxide	Saturated	...	E
Barium hydroxide·8H_2O	Saturated	Room	E
Barium nitrate	Aqueous solution	Room to hot	E
Barium sulfate	...	Room	E
Butyl acetate	...	Room	E
Calcium bisulfite	...	Room	E
Calcium carbonate	Saturated	Room to boiling	E
Calcium chlorate	Dilute	Room to hot	E
Calcium chloride	5–20	Room to 100 (212)	E
	28	Room to boiling	E
	Concentrated	Room	E
Calcium hydroxide	10–saturated	Room to boiling	E
Calcium hypochlorite	2–saturated	Room to boiling	E
Calcium sulfate	Saturated	Room	E
Copper acetate	Saturated	Room	E
Copper carbonate	Saturated	...	E
Copper chloride (agitated, aerated)	1	Room	E
Copper chloride (agitated)	5	Room	E
Copper chloride (aerated)	5	Room	E
Copper cyanide (electroplating solution)	...	Room	E
Copper cyanide	Saturated	Room to boiling	E
Copper nitrate	1–saturated	Room	E
Copper sulfate	5	Room	E
	Saturated	Room to boiling	E
Cupric carbonate-cupric hydroxide	Saturated	Room	E
Cupric chloride	20–50	Room to boiling	E
Cupric cyanide	Saturated	Room	E
Cupric nitrate	...	Room to 40 (105)	E
Cuprous chloride	50	Room to 90 (195)	E
Ferric chloride (still)	1–50	Room to boiling	E
Ferric chloride (agitated)	5	Room	E
Ferric chloride (aerated)	5	Room	E
Ferric hydroxide	...	Room	E
Ferric nitrate	1–5	Room	E
Ferric sulfate	1–saturated	Room	E
Ferrous chloride	...	Room	E
Ferrous sulfate	Dilute	Room	E
Ferrous ammonium citrate	...	...	E
Fluoride salts	Variable	Variable	V
Hydrogen bromide	...	...	E
Hydrogen peroxide	3–30	Room	E
	...	Room to boiling	E
Hydrogen iodide	...	...	E
Hydrogen sulfide	Dry	Room	E
	Saturated H_2O	Room	E
Hyposulfite soda (hypo)	...	...	E
Lactic acid salts	...	Room	E
Lead acetate	Saturated	Room	E
Magnesium carbonate	...	...	E
Magnesium chloride (still)	1–5	Room to hot	E
Magnesium chloride	5–40	Room to boiling	E
Magnesium hydroxide	Saturated	Room	E
	Thick suspension	Room	E
Magnesium nitrate	...	...	E
Magnesium sulfate	5	Room to hot	E
	Saturated	Room	E
Manganese carbonate	...	...	E
Manganese chloride	10–50 (Aqueous)	Room to boiling	E
Manganous chloride	5–20	Room to 100 (212)	E
Mercuric bichloride	0.07	Room	E
Mercuric chloride	1–saturated	Room to 100 (212)	E
Mercuric cyanide	Saturated	...	E
Mercurous nitrate	...	...	E
Nickel chloride	5–20	Room to 100 (212)	E
Nickel nitrate	10	Room	E
Nickel nitrate plus 6% H_2O	50	Room	E
Nickel sulfate	10	Room	E
Phosphoric anhydride	Dry	Room	E
Phosphorus trichloride	...	...	E
	Saturated	Room	E
Phthalic anhydride	...	...	E
Potassium bichromatic (neutral)	...	Room	E
Potassium bromide	5–saturated	Room	E
Potassium carbonate	1	Room	E
Potassium chlorate	...	...	E
Potassium chloride	1–36	Room to boiling	E
	Saturated	Room	E
Potassium cyanide	...	...	E
Potassium dichromate (neutral)	...	...	E
Potassium ferricyanide	5–saturated	Room	E
Potassium ferricyanide plus 5% NaCl	0.5	Room	E
Potassium ferrocyanide	5	Room	E
Potassium hydrate	...	...	E
Potassium hydroxide	5	Room	E
	27–50	Boiling	NR
Potassium iodide	Saturated	Room	E
Potassium iodide—iodine	...	...	E
Potassium iodide plus 0.1% Na_2CO_3	Saturated	Room	E
Potassium nitrate	5	Room	E
Potassium oxalate	...	...	E
Potassium permanganate (neutral)	...	...	E
Potassium pyrosulfate	...	Molten	NR
Potassium sulfate	1–5	Room to hot	E
	10	Room	E
Potassium sulfide	...	...	E
Potassium thiosulfate	1	Room	E
Silver bromide	...	...	E
Silver chloride	...	...	E
Silver cyanide	...	...	E
Silver nitrate	50	Room	E
Sodium acetate (moist)	5	Room	E
Sodium acetate	Saturated	Room	E
Sodium aluminate	25	Room to boiling	E
Sodium benzoate	...	...	E
Sodium bicarbonate	All	Room to 66 (150)	E
Sodium bichromate (neutral)	...	...	E
Sodium bisulfate	Solution	...	E
	10–25	Room to boiling	E
	Saturated	Room	E
	...	Molten	NR
Sodium borate	...	...	E
Sodium bromide	5	Room	E
Sodium carbonate	10–25	Room to boiling	E
	All	Room	E

(continued)

(a) E, no attack; V, variable, depending on temperature and concentration; NR, not resistant

Table 4 (continued)

Salt	Concentration, %	Temperature, °C (°F)	Code(a)
Sodium chlorate	10–25	Room	E
	Saturated	Room	E
Sodium chloride (still)	5	Room to 40 (105)	E
Sodium chloride (aerated)	20	Room	E
Sodium chloride	29	Room to boiling	E
	Saturated	Room to boiling	E
Sodium citrate	Saturated	Room	E
Sodium cyanide	Saturated	Room	E
Sodium dichromate	Saturated	Room	E
Sodium ferricyanide	...	...	E
Sodium ferrocyanide	...	...	E
Sodium fluoride	5–saturated	Room	NR
Sodium hydrosulfite	...	...	E
Sodium hydroxide	10–saturated	Room	NR
	10	Boiling	NR
	25	Room to boiling	NR
	40	80 (175)	NR
Sodium hypochlorite	6	Room	E
Sodium hyposulfite	Dilute	Room	E
Sodium lactate	...	...	E
Sodium nitrate	All	Room	E
Sodium nitrite	...	...	E
	Saturated	Room	E
Sodium peroxide	...	100 (212)	V
Sodium phosphate	5–saturated	Room	E
Sodium pyrosulfate	...	Molten	NR
Sodium silicate	...	...	E
	25	Room to boiling	E
Sodium sulfate (still)	5	Room	E
Sodium sulfate	10–20	Room to boiling	E
	Saturated	Room	E
Sodium sulfide	10	Room to boiling	E
	Saturated	Room	E
Sodium sulfite	5	Room	E
	10–saturated	Room to boiling	E
Sodium thiosulfate	10–25	Room to boiling	E
Sodium thiosulfate—acetic acid	20	Room	E
Stannic chloride	5	Room to 100 (212)	E
	24	Room to boiling	E
	100	Molten	E
Stannous chloride	5–saturated	Room	E
Sulfur chloride	Dry	...	E
Sulfuryl chloride	...	...	E
Thionyl chloride	...	...	E
Tin salts	...	...	E
Titanium tetrachloride	...	...	E
Zinc chloride (still)	5	Room to boiling	E
Zinc chloride	10	Room to boiling	E
	20	Room to 100 (212)	E
	Saturated	Room	E
Zinc sulfate	5–saturated	Room	E
	25	Room to boiling	E

(a) E, no attack; V, variable, depending on temperature and concentration; NR, not resistant

below 100 kPa (14.7 psi). At any one temperature between 500 and 800 °C (930 and 1480 °F), the rate of oxidation approaches a limiting rate as the pressure increases.

The presence of a few atomic percent of oxygen in tantalum increases electrical resistivity, hardness, tensile strength, and modulus of elasticity but decreases elongation and reduction of area, magnetic susceptibility, and corrosion resistance to HF (Ref 21). When one realizes that 1 at.% O in tantalum equals 892 ppm, the effect of very small contents of oxygen on the properties is evident. Tantalum is used as a getter in vacuum tubes to absorb outgases released on heating to maintain a high vacuum. It is used as a getter in vacuum furnaces to capture oxygen and hydrogen.

Nitrogen. The solubility of nitrogen in tantalum is shown by curve B in Fig. 7. It was found that tantalum dissolves 4 at.% N at 1000 °C (1830 °F) and that the solubility decreases rapidly with decreasing temperature. Other researchers indicated that the room-temperature solubility limit was 5.5 at.% for a stable solid solution and 7.7 at.% for a metastable solid solution (Ref 11, 18).

Below 800 °C (1470 °F), the tantalum-nitrogen reaction was reported to be cubic by one investigator, or parabolic by another (Ref 18). In the latter case, the nonlinear behavior of the Arrhenius plot of parabolic rate constants below 600 °C (1110 °F) suggests that the reaction does not obey a parabolic rate law. In contrast, an Arrhenius plot of cubic rate constants, although showing a wide range of scatter, was stated to be linear (Ref 21).

Above 800 °C (1470 °F), the reaction is parabolic, with rate constants increasing uniformly as temperature increases. Although both investigators agree on the rate law followed in this temperature region, neither their initial weight gain versus time data nor their rate constants are in agreement.

As in the case of oxygen in tantalum, the presence of nitrogen in only a few atomic percent concentration increases hardness, tensile strength, and electrical resistivity and decreases elongation and density. One atomic percent N_2 in tantalum equals 780 ppm N_2.

Air. The kinetics of the reaction of tantalum with air can be regarded as an extension of the reaction of tantalum with oxygen, because tantalum forms oxides preferentially over nitrides. The rate law governing the initial period of the reaction has not been established, but by analogy to the oxygen-tantalum reaction, it may be linear (with a rate constant differing from that of subsequent linear oxidation rates), parabolic, or logarithmic, depending on temperature and pressure conditions. Tantalum is quite stable in air at 250 °C (480 °F) and below; at 300 °C (570 °F), it shows a tarnish after 24 h of exposure. The rate of corrosion, as measured by weight gain, increases rapidly at higher temperatures. At 500 °C (930 °F), the white oxide, Ta_2O_5, begins to form. Figure 8 shows a plot of weight gain versus temperature (Ref 11, 18).

After a certain amount of time, ranging from over 6 h at 400 °C (750 °F) to less than 2 min at 900 °C (1650 °F), the reaction was said to become linear (Ref 22). The possibility was expressed that, at high temperatures or after extended exposure at low temperature, the linear oxidation data may also fit one of the other rate laws.

Protection against Oxidation. Although proposed environments for tantalum and tantalum alloy applications involve gases ranging from carbon dioxide (CO_2) to halides, most of the interest centers on applications that will expose the metals to either oxygen or air at an elevated temperature. A great deal of work has been done in an effort to understand the reactions involved and to develop methods to protect the metal against attack. Although nitrogen in air may in some cases be deleterious, oxygen attack is usually seen as the mechanism of failure under low loads at elevated temperatures. Consequently, most attempts to protect tantalum against elevated-temperature gas attack have focused on imparting resistance to the base metal.

If any degree of oxidation resistance is to be imparted to tantalum, two approaches are:

- Form a denser, more adherent oxide film by alloy additions to the tantalum that alter and modify the oxide phase
- Provide a protective coating to inhibit oxygen attack on the tantalum. Coatings include silicides, aluminides, and noble metals (Ref 23)

The use of silicide coatings to protect tantalum substrates is also described in the article "Ceramic Coatings and Linings" in *Surface Engineering,* Volume 5, *ASM Handbook,* 1994.

Other than by oxidation, tantalum structures may also fail in high-temperature service because of embrittlement by diffusion of an environmental gas into a subsurface layer of the base metal. Protection against this contamination is achieved by the same techniques as used against surface oxidation, although the actual agents are often different. Because oxidation and contamination are both symptoms of the same basic problem, most work on contamination has been done as part of a larger effort on oxidation.

Hydrogen. Tantalum dissolves a considerable amount of hydrogen at comparatively low

Table 5 Effects of miscellaneous corrosive reagents on tantalum

Medium	Concentration, %	Temperature, °C (°F)	Code(a)
Acetone	...	Boiling	E
Air	...	Below 300 (570)	E
	...	Above 300 (570)	NR
Amines	...	...	E
Aniline	Concentrated	Room	E
Baking oven gases	...	...	E
Beer	...	...	E
Benzene	...	Room	E
Benzol	...	Hot	E
Bleaching powder	Solution	Hot	V
Blood (meat juices)	...	Cold	E
Body fluids	...	...	E
Borax	...	Fused	NR
Bromine	Dry	Below 300 (570)	E
	Wet	...	E
Bromine water	...	Room	E
Buttermilk	...	Room	E
Carbon bisulfide	...	Room	E
Carbon tetrachloride	99	Boiling	E
	Liquid	Boiling	E
	Pure	Room	E
	5–10 aqueous solution	Room	E
Chlorinated brine	...	...	E
Chlorinated hydrocarbons	...	...	E
Chlorinated water	Saturated	Room	E
Chlorine dioxide	...	180 (355)	E
Chlorine gas	Dry	Up to 250 (480)	E
	Moist (1.5% H_2O)	Up to 375 (705)	E
	Moist (30% H_2O)	Up to 400 (750)	E
Chloroform	...	Room	E
Chromium plating bath	...	Room	E
Cider	...	Room	E
Coffee	...	Boiling	E
Copal varnish	...	...	E
Cream of tartar	...	...	E
Creosote (coal tar)	...	Hot	E
Crude oil	...	...	E
Developing solutions	...	Room	E
Distillery wort	...	...	E
Dyewood, liquor	...	Room	E
Ether	...	Room	E
Ethyl acetate	...	...	E
Ethyl chloride	5	Room	E
Ethyl sulfate	...	...	E
Ethylene chloride	...	Room	E
Ethylene dibromide	...	...	E
Ethylene dichloride	100	Boiling	E
Flue gases	...	...	E
Fluorine	...	Room	NR
Food pastes	...	...	E
Formaldehyde	...	Room	E
Formaldehyde plus 2.5% H_2SO_4	50	158 (315)	E
Fuel oil	...	Hot	E
Fuel oil (containing H_2SO_4)	...	Hot	E
Fruit juices	...	Room	E
Furfural	...	...	E
Gasoline	...	...	E
Glauber's salt	Solution	Hot	E
Glue, dry	...	Room	E
Glue, solution acid	...	Hot	E
Glycerine	...	Room	E
Gypsum	...	...	E
Hydrocarbons	...	...	E
Hydrogen	...	Up to 300 (570)	E
Ink	...	...	E
Iodine	...	Up to 300 (570)	E
Idoform	...	...	E
Kerosene	...	Room	E
Ketchup	...	Room	E
Lard	...	Room	E
Linseed oil	...	...	E
Lye (caustic)	34	110 (230)	NR
Lysol	...	100 (212)	E
Mayonnaise	...	Hot and cold	E
Meats (unsalted)	...	Room	E
Mash	...	Hot	E
Methylene chloride	40	Room to boiling	E
Milk	Fresh or sour	Hot or cold	E
Mine water, acid	...	...	E
Molasses	...	...	E
Mustard	...	Room	E
Naphtha	...	...	E
Nitre cake	...	Fused	NR
Nitric oxides	...	...	E
Nitrosyl chloride	...	...	E
Nitrous oxide	Dry	...	E
Oils, crude	...	Hot and cold	E
Oils, mineral, vegetable	...	Hot and cold	E
Organic chlorides	...	...	E
Oxygen	...	Up to 300 (570)	E
Paraffin	...	Molten	E
Paregoric compound	...	...	E
Petroleum ether	...	...	E
Phenol	...	...	E
Phenolic resins	...	...	E
Pine tar oil	...	...	E
Potash	Solution	Hot	NR
Quinine bisulfate (dry)	...	...	E
Quinine sulfate (dry)	...	...	E
Rosin	...	Molten	E
Sal ammoniac	20	Boiling	E
Salt	Saturated	Room	E
Salt brine	Saturated	Hot	E
Salt water	...	...	E
Sewage	...	...	E
Soaps	...	Room	E
Soy bean oil	...	...	E
Starch	Solution	...	E
Steam	...	...	E
Sugar juice	...	...	E
Sulfur, dry	...	Molten	E
Sulfur, wet	...	...	E
Sulfur dioxide	Dry	Room	E
	Moist	Room	E
Sulfur trioxide	Dry	Room	NR
Tomato juice	...	Room	E
Turpentine oil	...	...	E
Tung oil	...	...	E
Varnish	...	...	E
Vegetable juices	...	...	E
Vegetable oil	...	Hot and cold	E
Vinegar	Still	Room	E
	Agitated	Room	E
	Aerated	Room	E
	Fumes	...	E
Vinegar and salt	...	...	E
Water	...	...	E
	...	Hot	E
	Salt	...	E
	Sea	...	E
Whiskey	...	...	E

(a) E, no attack: V, variable, depending on temperature and concentration; NR, not resistant

temperatures (Ref 11, 18). The maximum limit of solubility is 50 at.%.

Although tantalum generally does not react with molecular hydrogen below 250 °C (480 °F), it can absorb 740 times its own volume of hydrogen at red heat. However, it was reported that tantalum containing dissolved oxygen can absorb molecular hydrogen at room temperature when it is undergoing deformation. Tantalum containing more than 100 ppm (by weight) of hydrogen begins to lose its ductility (Ref 16).

Atomic hydrogen can be absorbed by tantalum, even at room temperature. Therefore, chemical equipment should be insulated from stray currents. In a few commercial cases, the metal is made electrolytically positive to prevent the liberation and absorption of atomic hydrogen on its surface.

Absorption of hydrogen is accompanied by an expansion of the bcc crystal lattice. When such material is heated to approximately 800 °C (1470 °F) or more in a high vacuum, it loses essentially all of its hydrogen. When permanent damage to the metal has not occurred, annealing

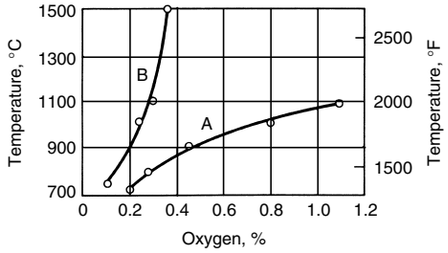

Fig. 6 Solubility of oxygen in niobium and tantalum. Curve A, niobium; curve B, tantalum. Source: Ref 18

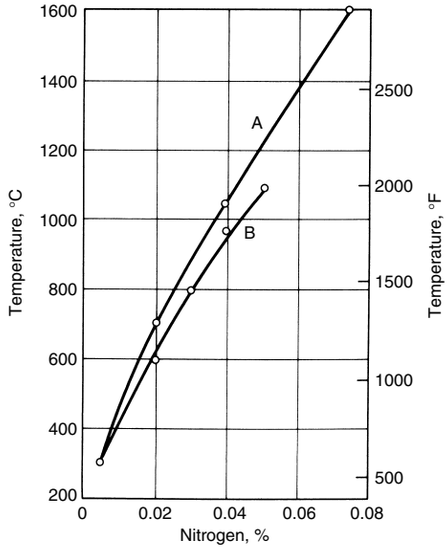

Fig. 7 Solubility of nitrogen in niobium and tantalum. Curve A, niobium; curve B, tantalum. Source: Ref 18

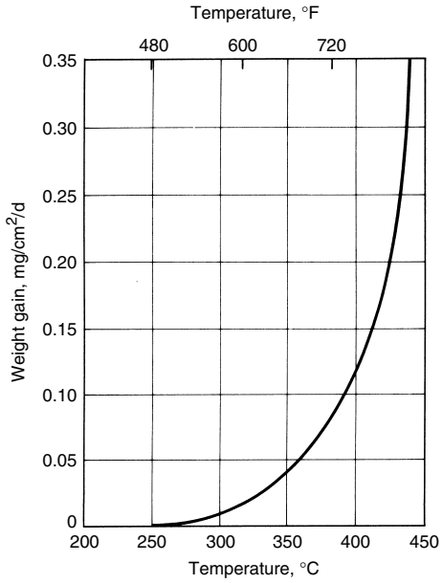

Fig. 8 Corrosion rate of tantalum in air as a function of temperature

or degassing at 800 °C (1470 °F) or higher temperature restores the metal to its original condition. In addition to decreasing the ductility, strength, and density of tantalum, the presence of hydrogen increases the hardness and the electrical resistivity.

Water Vapor. It is known from industrial practice that tantalum is not affected adversely when heated with steam at pressures to 1380 kPa (200 psig), corresponding to a temperature of 200 °C (390 °F). It has been reported that at temperatures above 1125 °C (2057 °F), water is decomposed by tantalum, with adsorption of oxygen by the metal and evolution of hydrogen. At 925 °C (1700 °F) and lower temperatures, the reaction is negligibly slow.

Halogens. Fluorine attacks tantalum at room temperature. Tantalum is totally inert to wet or dry chlorine, bromine, and iodine to 150 °C (300 °F), and these elements dissolved in solutions of salts or acids likewise have no effect. Chlorine begins to attack tantalum at approximately 250 °C (480 °F).

The reaction is rapid at 450 °C (840 °F), and it occurs instantaneously at 500 °C (930 °F). The presence of water vapor sharply decreases corrosion by chlorine so that the maximum temperatures at which tantalum is sufficiently resistant to chlorine containing 1.5 to 30% H_2O for chemical equipment applications are 375 and 400 °C (705 and 750 °F), respectively. Bromine attacks tantalum at 300 °C (570 °F), and iodine begins to attack at approximately the same temperature (Ref 6, 11).

Carbon Dioxide and Carbon Monoxide. Tantalum is corroded by dry CO_2 at 810 kPa (8 atm) and 500 °C (930 °F). Tantalum reacts with CO_2 at 1100 °C (2010 °F) to form Ta_2O_5, and with carbon monoxide (CO) at the same temperature to form TaO. The latter reverts to Ta_2O_5 when exposed to oxygen (Ref 11, 18).

The oxidation rates of tantalum in various partial pressures of CO_2 in the temperature range of 700 to 950 °C (1290 to 1740 °F) were measured with a gravimetric balance (Ref 24). Oxidation involved a surface-controlled reaction associated with the formation of a nonprotective layer of Ta_2O_5. Below 720 °C (1330 °F), there was a change in the rate-determining mechanism, and above 830 °C (1525 °F), the linear rate was preceded by a complex region of nonlinear oxidation behavior. The linear oxidation of tantalum has been explained quantitatively in terms of CO_2 absorption, followed by a rate-controlling surface reaction. The initial absorption has been expressed both as an equilibrium process and as a steady-state reaction.

Nitrogen Monoxide and Nitrous Oxide. Below approximately 1125 °C (2050 °F), the reaction rate of nitrogen monoxide (NO) (as a 5% mixture in argon) with tantalum cannot be detected (Ref 11). As the temperature is increased, the reaction takes place with increasing rapidity, rising from 0.0065% area loss per second at 1195 °C (2180 °F) to 0.076% at 1457 °C (2660 °F) (Ref 25).

The oxidation by nitrous oxide (N_2O) on evaporated films of niobium, tantalum, and titanium was studied in the temperature range of 195 to 435 K (Ref 26). For tantalum, fast dissolution absorption of N_2O occurred at 195 K, accompanied by N_2 evolution. Some incorporation of N_2O also occurred. The rate of N_2O absorption was found to depend on the pressure of the reacting gas.

Other Reactive Gases. Although little published data appear to exist on the subject, it is expected that tantalum would react at some elevated temperature with oxygen-containing gaseous compounds, such as sulfur dioxide (SO_2) and nitrogen dioxide (NO_2) (Ref 22). With such hydrocarbons as benzene or naphthalene, tantalum reacts at temperatures from 1700 to 2500 °C (3090 to 4530 °F) to form tantalum carbide.

Inert Gases. Helium and argon do not react with tantalum, even at its melting point. These gases are used as an inert atmosphere for arc melting and welding the metal. Tantalum will react with trace amounts of oxygen, nitrogen, hydrogen, and carbon in inert gases.

Liquid Metals. Tantalum and some tantalum-base alloys exhibit good resistance to many liquid metals (Ref 7, 11, 27). Table 6 lists the effect of various liquid metals on tantalum. Tantalum materials exhibit remarkable resistance to several liquid metals, even to high temperatures (900 to 1100 °C, or 1650 to 2010 °F) in the absence of oxygen or nitrogen.

The severity of attack on tantalum by liquid metals may be markedly increased by increasing temperature. Because operating temperatures somewhat in excess of 700 °C (1290 °F) are desirable in many cases, refractory metals, including tantalum and niobium, seem to be particularly promising materials of construction for containing liquid metals.

Aluminum. Tantalum reacts rapidly with aluminum to form the stable compound tantalum aluminide (Al_3Ta) (Ref 11).

Bismuth. Tantalum reacts little with bismuth at temperatures below 1000 °C (1830 °F) and exerts no detrimental effects on the stress-rupture properties of tantalum at 815 °C (1500 °F); but it causes some intergranular attack at 1000 °C (1830 °F) (Ref 7, 28).

Calcium. Tantalum is only slightly attacked by calcium at 1200 °C (2190 °F). A crucible with a wall thickness of 0.15 mm (5.8 mils) was reduced to 0.13 mm (5.3 mils) after 12 days of exposure to calcium at 1200 °C (2190 °F) (Ref 11).

Cesium. Similar lack of corrosion resistance to cesium was found for tantalum as reported for niobium. Refluxing capsule tests indicated surface dissolution and severe attack after 720 h at 980 and 1370 °C (1800 and 2500 °F) (Ref 29).

Gallium. The resistance of tantalum to molten gallium is considered to be good at temperatures to 450 °C (840 °F) but poor at temperatures above 600 °C (1110 °F).

Lead. Tantalum is highly resistant to liquid lead at temperatures to 1000 °C (1830 °F), with a rate of attack of less than 0.025 mm/yr

(1 mil/yr). It exhibits no detrimental effects when stress-rupture tests are conducted in molten lead at 815 °C (1500 °F) (Ref 7).

Lithium. Tantalum possesses good resistance to molten lithium at temperatures to 1000 °C (1830 °F) (Ref 7, 27, 30, 31). Tantalum capability with lithium is similar to that of niobium in that corrosion resistance depends on oxygen concentration. Tantalum metal will exhibit good corrosion resistance to lithium as long as the oxygen concentration of the tantalum is maintained below 100 to 200 ppm.

Ta-9.6W-2.4Hf-0.01C alloy, oxygen contaminated to 500 ppm and welded in argon, was exposed to lithium at 750 and 1200 °C (1380 and 2190 °F) for 100 h. Evaluation indicated no attack in the weld areas; however, intergranular penetration was observed in the base metal of both alloys. Heat treatment at 1315 °C (2400 °F) eliminated the attack. In addition, a method of inhibiting the corrosion of tantalum by liquid lithium at temperatures above 1000 °C (1830 °F) by the addition of 0.15 to 1.5 at.% Si to the lithium is discussed in Ref 32.

Magnesium and Magnesium Alloys. Tantalum is unattacked by molten magnesium at 1150 °C (2100 °F) (Ref 11).

Mercury. The limited amount of corrosion testing of refractory metals in mercury is summarized as follows. The results for tantalum are consistent with the solubility information (Ref 33).

In static tests, tantalum exhibited good resistance to mercury at temperatures to 600 °C (1110 °F). Refluxing capsule tests showed no attack of tantalum up to 760 °C (1400 °F). The corrosion resistance of tantalum to mercury was further documented in a two-phase natural-circulation loop test that ran for 19,975 h with a boiling temperature of 650 °C (1200 °F) and superheat temperature of 705 °C (1300 °F).

Posttest evaluation of the loop revealed no corrosion. As a result of the inertness of tantalum to mercury attack demonstrated in this long-term experiment, tantalum was evaluated as a replacement material for Croloy 9M steel in a mercury boiler (Ref 27). Results of other tests of tantalum in mercury are described in Ref 33 and 34.

Potassium. The compatibility of tantalum and potassium at 600, 800, and 1000 °C (1110, 1470, and 1830 °F) was studied in static capsule tests (Ref 35). As the oxygen concentration of potassium was increased, the amount of tantalum in the potassium was also found to increase. The results indicated the formation of an unidentified ternary oxide phase that is either nonadherent or dissolved when the potassium is dissolved for chemical analysis. When the tantalum specimens contained oxygen above a certain threshold concentration, potassium penetrated the tantalum, and intergranular, as well as transgranular, attack was observed. The threshold levels for intergranular attack at the test temperatures were found to be 500, 700, and 1000 ppm O, respectively. The mechanism of attack was believed to be the formation of a ternary oxide phase.

Silver. Tantalum is only slightly attacked by silver at 1200 °C (2190 °F); a tantalum crucible tested in silver at this temperature for 35 days showed a loss in wall thickness of 0.02 mm (0.8 mil).

Sodium has little effect on tantalum at temperatures to 1000 °C (1830 °F), but oxygen contamination of sodium causes increases in corrosion. Sodium does not alloy with tantalum (Ref 7).

The presence of oxygen in liquid sodium leads to slight weight loss of tantalum in flowing systems. In addition, extensive intergranular and transgranular attack of tantalum by sodium was observed. This attack was attributed to the high (390 ppm) oxygen concentration of the tantalum before exposure to the sodium.

The compatibility of Ta-8W-2Hf and Ta-10W with static sodium was demonstrated in capsules tested at 1315 °C (2400 °F) for 6271 and 300 h, respectively. No corrosion was found in either alloy.

Tellurium. Corrosion of candidate construction materials for stills to extract radioactive polonium-210 from bismuth by distillation at temperatures of 450 to 950 °C (840 to 1740 °F) was investigated (Ref 30, 36). Tellurium, which is chemically similar to polonium, was used as a nonradioactive substitute for polonium. Of the materials investigated, tantalum appeared to be the most satisfactory from the standpoint of fabricability and long-term corrosion resistance. Tantalum was corroded at rates up to 0.5 μm/h (0.02 mil/h) during the initial 100 to 200 h of exposure; the rate decreased to less than 0.05 μm/h (0.002 mil/h) after 400 h for concentrations of tellurium of less than 30% in bismuth.

Thorium-Magnesium. In static tests, the thorium-magnesium eutectic had no appreciable effect on tantalum at 1000 °C (1830 °F). No measurable corrosion of tantalum by the thorium-magnesium eutectic was noted in dynamic tests for 28 days with a temperature range of 700 to 840 °C (1290 to 1545 °F) (Ref 7). Extensive tests on components for molten-metal fuel reactors revealed that tantalum is a satisfactory material for several thousand hours of service in high-temperature circulating loops containing a molten magnesium-thorium alloy having a composition in the range of the magnesium-rich eutectic (Ref 11).

Uranium and Plutonium Alloys. Short-term tests indicated that the practical upper limit for tantalum as a container material for uranium is approximately 1450 °C (2640 °F). However, attack below this temperature is also significant, because a tantalum crucible with a wall thickness of 1.5 mm (0.06 in.) was completely corroded within a test period of 50 h at 1275 °C (2325 °F) (Ref 7). Other investigations showed that tantalum is not attacked by uranium-magnesium and plutonium-magnesium alloys at 1150 °C (2100 °F) (Ref 11). Extensive tests on components for molten-metal fuel reactors revealed that tantalum is a satisfactory material for several thousand hours of service in several liquid-metal environments (Ref 11).

Zinc is reported to wet and attack tantalum, the surface of which is abraded in zinc at 440 °C (825 °F); also, molten zinc attacks tantalum at significant rates at temperatures above 450 °C (840 °F) (Ref 11). Tantalum showed appreciable attack from molten zinc at 750 °C (1380 °F) (Ref 18). However, one industrial zinc producer observed excellent corrosion resistance at 500 °C (930 °F) (Ref 11). The maintenance of

Table 6 Effects of molten metals on tantalum

Metal	Remarks	Temperature, °C (°F)	Code(a)
Aluminum	Forms Al_3Ta	Molten	NR
Antimony	...	to 1000 (1830)	NR
Bismuth	...	to 900 (1650)	E
Cadmium	...	Molten	E
Gallium	...	to 450 (840)	E
Lead	...	to 1000 (1830)	E
Lithium	...	to 1000 (1830)	E
Magnesium	...	to 1150 (2100)	E
Mercury	...	to 600 (1110)	E
Potassium	...	to 900 (1650)	E
Sodium	...	to 900 (1650)	E
Sodium-potassium alloys	...	to 900 (1650)	E
Zinc	...	to 500 (930)	E/V
Tin	...	...	V
Uranium	...	...	V
Mg-37Th	In helium	to 800 (1470)	S
Bi-5 to 10U	In helium	to 1100 (2010)	S
Bi-5U-0.3Mn	In helium	to 1050 (1920)	S
Bi-10U-0.5Mn	In helium	to 1160 (2120)	S
Al-18Th-6U	Failed	to 1000 (1830)	NR
U-10Fe	Failed	to 900 (1650)	NR
U-Cr (eutectic)	Failed	to 900 (1650)	NR
YSb-intermetallic compound	...	1800–2000 (3270–3630)	S
YBi-intermetallic compound	...	1800–2000 (3270–3630)	S
ErSb-intermetallic compound	...	1800–2000 (3270–3630)	S
LaSb-intermetallic compound	...	1800–2000 (3270–3630)	S
Plutonium-cobalt-cerium	...	to 650 (1200)	V

(a) E, no attack; S, satisfactory; V, variable, depending on temperature and concentration; NR, not resistant

the oxide film on the tantalum may account for the latter result.

Other Molten Metals. The intermetallic compounds YSb, ErSb, LaSb, and YBi have little effect on tantalum at 1800 to 2000 °C (3270 to 3630 °F), but antimony vapor severely attacks tantalum at temperatures of 1000 °C (1830 °F) and higher (Ref 11).

Hydrogen Embrittlement, Galvanic Effects, and Cathodic Protection of Tantalum

Hydrogen embrittlement of tantalum was observed when it was exposed to concentrated H_2SO_4 at 250 °C (480 °F) or to concentrated HCl at 150 °C (300 °F) (Ref 37).

Failures due to hydrogen embrittlement have occurred in some severe aqueous acid media in chemical industry applications where tantalum was, or became, electrically coupled to a less noble material, such as low-carbon steel. Under these conditions, tantalum became the cathode in the galvanic cell thus created.

Because of the presence of stray currents, tantalum may become a cathode in the system and consequently may absorb and become embrittled by atomic hydrogen in the electrolytic cell (galvanic cell). The presence of stray current can result from induction from adjacent lines, leakages, variable ground voltages, and other sources. Although stray voltages may be transient, absorbed hydrogen is cumulative in its effect on producing hydrogen embrittlement of tantalum.

For applications of pure tantalum in aggressive acids at high temperatures, hydrogen embrittlement rather than uniform corrosion attack is the crucial concern (Ref 7, 37). References cited in Ref 37 propose a specific mechanism for hydrogen embrittlement of tantalum based on stress-induced hydride precipitation.

Several methods have been used or proposed to reduce hydrogen embrittlement of tantalum (Ref 7, 38–40).

- Complete electrical isolation of tantalum from all metals in the system. For additional protection, the insulated tantalum may be connected to a positive direct current source (approximately 15 V), while the negative is connected to some other metallic part, which is exposed to the solution in the vessel or to ground.
- Addition of a selected oxidizing agent to the solution
- Coupling the tantalum surface to a noble metal, such as electroplated platinum spots
- Anodizing the tantalum

Galvanic Effects. If tantalum is the cathode in a galvanic couple, hydrogen embrittlement can prove disastrous (Ref 7). If tantalum is the anode in such a cell, anodization occurs so readily that no damage occurs, and galvanic current quickly drops to a very low value. In couples of tantalum with platinum, silver, copper, bismuth, antimony, molybdenum, nickel, lead, tin, zinc, and aluminum, tantalum was initially the more electronegative member of the couple (except for zinc and aluminum). However, galvanic current rapidly decayed as the tantalum spontaneously anodized. In HF, tantalum was again more noble than zinc and aluminum and was more active than platinum, silver, copper, antimony, nickel, and lead. The latter six couples result in high steady-state currents, because tantalum dissolves rather than anodizes in fluoride solution. The anomalous behavior of tantalum when coupled with bismuth or iron in HF is apparently attributable to the formation of insoluble fluorides on the surfaces of the bismuth or iron electrodes.

Time is an important factor in determining whether tantalum will be damaged by galvanic effects (Ref 41). In practice, it is dangerous to depend on laboratory tests to provide information on whether tantalum is anodic in a given galvanic couple. In results reported in Ref 41, tantalum was cathodic to aluminum in dilute NaC1, HCl, and NaCl after times of 0.5 and 60 min. When tantalum was coupled to certain of the other metals—notably Hastelloy B, nickel, and lead—the polarity of the tantalum reversed with time in some electrolytes from anodic to cathodic. When tantalum is cathodic, or becomes cathodic, hydrogen embrittlement can occur. In probably all of the couples, tantalum would become cathodic if given sufficient time (Ref 41). The conclusion is drawn that it is highly desirable to prevent galvanic cell formation by providing adequate electrical insulation.

Cathodic Protection. Applying low-overvoltage elements, such as platinum and other noble metals, to tantalum and other metals has received further attention in efforts to develop improved anodes for cathodic protection (Ref 42). The first of the precious-metal-containing anodes to become commercial was platinum or platinum alloy on a titanium substrate. The uniqueness of this concept was not that of platinum, which has been used as an electrode material for many years, but the nature of titanium (or tantalum) itself. Titanium and tantalum have a very adherent, nonporous inert oxide film that will not transfer current unless the electrode-to-electrode potential reaches a certain value. With proper treatment, this oxide film can be removed, and a very thin layer of platinum can be applied to the titanium (or tantalum) surface. Any unplatinized surface will reoxidize, leaving a surface that will pass current from the platinized areas but not from the oxidized areas. Platinum electroplated spots are a commercially accepted technique to reduce potential hydrogen embrittlement through galvanic effects. Current industrial practices use tantalum-to-platinum area ratios no greater than 10,000 to 1, with ratios of 1000:1 to 2000:1 being more common.

The commonly used precious metal and anode materials are lead-platinum bielectrodes, platinized titanium, platinized niobium, and platinized tantalum. The latter two substrates allow greater applied voltage to the anode system. Like platinized titanium anodes, the mechanism for successful operation of the platinized niobium or platinized tantalum anodes is the valvelike nature of the oxide film on the niobium or tantalum substrates. Niobium in such anodes operates to a breakdown voltage of 40 to 50 V, but tantalum will operate up to 200 V. For both materials, the resistivity of the alloys used is approximately one-third that of titanium, which is said to give better anode characteristics (Ref 42).

Corrosion Resistance of Tantalum-Base Alloys

The outstanding corrosion resistance found for certain low-substitutional alloy content tantalum-base alloys, notably tantalum-molybdenum, is described (Ref 37). Data found in the literature on the corrosion resistance of other tantalum-base alloys are also summarized.

Tantalum-Tungsten Alloys. Samples of 0.18 to 0.75 mm (0.007 to 0.03 in.) thick strip or sheet of the following materials were exposed for selected times in concentrated (95.5 to 98%) H_2SO_4 at chosen temperatures ranging from 175 to 200 °C (345 to 390 °F):

- Tantalum, electron beam (EB) melted
- Tantalum, powder metallurgy
- Ta-2.5W-0.15Nb
- Ta-5W
- Ta-10W

Some tests on EB-melted tantalum and Ta-2.5W-0.15Nb were conducted on materials in the as-rolled, stress-relieved, and fully recrystallized conditions. The average corrosion rates observed in these tests are listed in Table 7. Corrosion rate as a function of tungsten content is plotted in Fig. 9 for additional tests on EB-melted tantalum, Ta-2.5W-0.15Nb, Ta-5W, and Ta-10W exposed to concentrated H_2SO_4 at 180 and 210 °C (360 and 410 °F).

The corrosion behavior of substitutional tantalum-molybdenum, tantalum-tungsten, tantalum-niobium, tantalum-hafnium, tantalum-zirconium, tantalum-rhenium, tantalum-nickel, tantalum-vanadium, tantalum-tungsten-molybdenum, tantalum-tungsten-niobium, tantalum-tungsten-hafnium, and tantalum-tungsten-rhenium alloys was studied in various corrosive media, including concentrated H_2SO_4 at 200 and 250 °C (390 and 480 °F) (Ref 37). Figure 10 gives corrosion data in 95% H_2SO_4 for several binary tantalum alloys. Tantalum became embrittled in concentrated H_2SO_4 at 250 °C (480 °F). Additions of tungsten reduced the corrosion rate and hydrogen absorption, but additions of molybdenum and rhenium were more effective in reducing both effects. Additions of niobium and vanadium had only a slight influence on the corrosion rate of tantalum;

lower-valence elements, such as hafnium, increased the corrosion rate (Ref 37).

Hydrochloric Acid. Samples of recrystallized sheet of EB-melted tantalum and Ta-2.5W-0.15Nb were exposed in the same test in a tantalum autoclave to concentrated (37 to 38%) HCl at 100 °C (212 °F) for 24 h. The corrosion rates of these materials were:

	Corrosion rate	
Alloy	mm/yr	mils/yr
Tantalum	0.04	1.6
Ta-2.5W-0.15Nb	0.023	0.9

Researchers in other tests also found that tantalum and substitutional tantalum-base alloys became hydrogen embrittled in concentrated HCl at 150 °C (300 °F) (Ref 37).

Nitric Acid. Samples of unalloyed, EB-melted tantalum and Ta-2.5W-0.15Nb were exposed to concentrated (70%) HNO_3 for 3 days at approximately 200 °C (390 °F). Following this test, neither material showed any measurable weight loss. Additional tests on Ta-2.5W-0.15Nb tested in 70% HNO_3 at approximately 200 °C (390 °F) for 72 h in an autoclave reactor gave the following corrosion rates for material in three metallurgical conditions:

	Corrosion rate	
Condition	μm/yr	mils/yr
As-rolled	0.1	0.0038
Stress relieved	0.04	0.0016
Fully recrystallized	0.038	0.0015

Other Aqueous Media. The Ta-10W binary solid-solution alloy has been used in some applications, such as pump and valve parts, for which a material appreciably harder and stronger than the pure metal is desired. For example, Ta-10W alloy is used as an insert in the plug of a tantalum-lined split-body valve to give a hard-plug-to-soft-seat combination when used with a tantalum seat.

The Ta-10W alloy is of interest as a repair metal for glass-lined steel equipment because it is of much higher strength than unalloyed tantalum. Consequently, corrosion tests were conducted on the Ta-10W alloy in various environments (Ref 43).

Figure 11 shows the corrosion rate as a function of H_2SO_4 concentration for tests at 205 and 230 °C (400 and 450 °F). These data indicate that either unalloyed tantalum or Ta-10W alloy can be used at 230 °C (450 °F) to handle H_2SO_4 in concentrations below 90%. Although the corrosion rates at 205 °C (400 °F) are similar for the two materials, on the basis of this graph, the corrosion weight loss of the Ta-10W alloy is approximately twice that of unalloyed tantalum at 230 °C (450 °F) in H_2SO_4 over the concentration range of 70 to 90%.

Little or no weight loss occurred below 175 °C (350 °F) in HCl, even at 30% concentration. At 190 °C (375 °F), a small amount of attack was detected, with that for the Ta-10W alloy being more severe.

In the HNO_3 corrosion tests, even up to 175 °C (350 °F) in concentrations to 60%, it was concluded that neither the tantalum nor the Ta-10W alloy showed any perceptible loss in weight (Ref 44). No comments were made regarding the small weight gains observed in most cases.

Tests were also conducted in 5% NaOH solution at 100 °C (212 °F). Considerable weight losses occurred on both the unalloyed tantalum and the alloy under caustic conditions. The difference, if any, in the corrosion rates of the two materials appears small.

The NaOH corrosion test was conducted because tantalum is known to be susceptible to caustic embrittlement; therefore, it was desired to determine whether the Ta-10W alloy suffered embrittlement also. Unalloyed tantalum showed approximately a 25% increase in yield strength, and a 10% increase was attributed to a pickup of interstitial elements (oxygen, nitrogen, and hydrogen), although chemical analyses of the materials before and after exposure were not conducted. With the Ta-10W alloy, the exposure to 5% NaOH at 100 °C (212 °F) produced embrittlement, as evidenced by the premature fracture in the tensile test. Reportedly, such embrittlement was not evident on the sample of the Ta-10W alloy to which a platinum spot had been welded before the test. The corrosion resistance of tantalum-tungsten alloys was also studied in 50% KOH at 30 and 80 °C (85 and 175 °F), 20% HF at 20 °C (70 °F), and KOH:$3K_3Fe(CN)_6$ mixture (concentration not given) (Ref 11). In the hydroxide solutions, a maximum corrosion rate was obtained at approximately 60 at.% Ta. Although the alloy system reportedly represents a continuous series of solid solutions, a maximum electrical resistance also was found at the same composition.

In 20% HF solution, the tantalum-tungsten alloy system essentially exhibits the relatively low corrosion rates associated with tungsten, except when the tantalum concentration exceeds 80 at.%, at which concentration the corrosion increases markedly. Alloys containing more than 18% W show no corrosion in 20% HF, thus

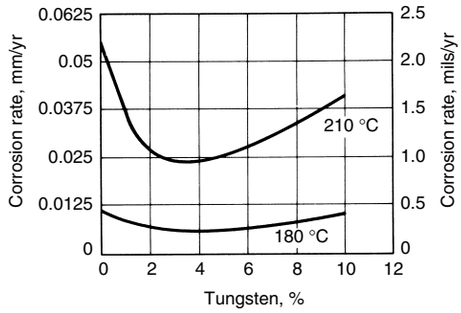

Fig. 9 Corrosion rate versus tungsten content for tantalum-tungsten alloys exposed to concentrated H_2SO_4 at 180 and 210 °C (360 and 410 °F)

Table 7 Corrosion rates for tantalum materials exposed to concentrated H_2SO_4 at 175 to 200 °C (345 to 392 °F)

		Temperature			Corrosion rate	
Material	Metallurgical condition	°C	°F	Exposure, days	mm/yr	mils/yr
Ta, electron beam melted	Recrystallized	175	345	60	0.005	0.189
Ta, P/M	Recrystallized	175	345	60	0.0055	0.217
Tantaloy 63(a)	Recrystallized	175	345	60	0.0058	0.229
	As-rolled	181	360	7	0.0026	0.104
	Stress-relieved	181	360	7	0.0022	0.087
	Recrystallized	181	360	7	0.0022	0.087
Ta, electron beam melted	As-rolled	199	390	3	0.018	0.72
	Recrystallized	199	390	3	0.024	0.96
Tantaloy 63(a)	As-rolled	199	390	3	0.0048	0.19
	Stress-relieved	199	390	3	0.0043	0.17
	Recrystallized	199	390	3	0.0045	0.18
Ta, electron beam melted	Recrystallized	200	392	32	0.057	2.24
Ta, P/M	Recrystallized	200	392	32	0.058	2.27
Tantaloy 63(a)	Recrystallized	200	392	32	0.029	1.15
	Recrystallized	200	392	13	0.03	1.24
Ta-5W	Recrystallized	200	392	13	0.034	1.34
Ta-10W	Recrystallized	200	392	13	0.05	1.98

Note: P/M, powder metallurgy. (a) UNS R05252

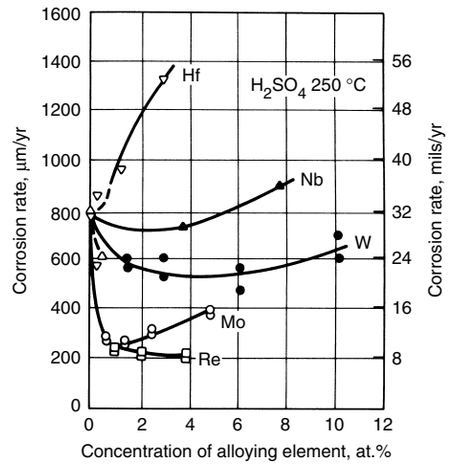

Fig. 10 Influence of alloying elements on the corrosion rate of binary tantalum alloys exposed 3 days to 95% H_2SO_4 at 250 °C (480 °F). Source: Ref 37

offering an advantage over pure tantalum. Other tests have been conducted on tantalum and tantalum-tungsten alloys having tungsten contents ranging from 8.7 to 20.4% in 20% HF. This work showed that tantalum and tantalum-tungsten alloys containing less than approximately 20% W were more susceptible to attack by 20% HF than was previously reported.

Tantalum-tungsten alloys showed little improvement over tantalum when tested in the $KOH:3K_3Fe(CN)_6$ mixture.

Combined Reagents. In a proposed dehydrator application, the exposure was to be to an environment containing 61.5% HNO_3 plus 7% magnesium nitrate ($Mg(NO_3)_2$) at 115 °C (240 °F). Although no significant corrosion on tantalum would be expected on exposure to the separate reagents, tests were conducted on the mixture to determine corrosion rates. Base metal and weldment specimens of tantalum and Ta-2.5W-0.15Nb were used. Within the precision of the weight measurements, no specimen of either tantalum or Ta-2.5W-0.15Nb showed any weight loss in these corrosion tests.

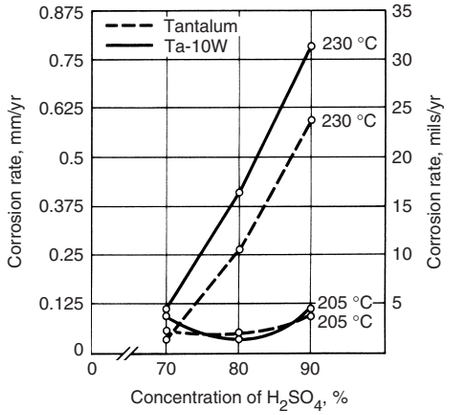

Fig. 11 Corrosion rate versus concentration for tantalum and Ta-10W alloy exposed to H_2SO_4 at various temperatures. Source: Ref 43

Table 8 Corrosion rates of tantalum-molybdenum alloys in concentrated H_2SO_4 at 150 °C (300 °F)

Solutions were saturated with oxygen.

	Average corrosion rate, mg/cm²/day	
Tantalum in molybdenum, at.%	Concentrated H_2SO_4 (98%)	Concentrated HCl (37%)
0	0.008	0.018
10.1	0.009	0.017
20.1	0.008	0.018
30.0	0.010	0.009
40.0	0.009	0.010
50.0	0.000	0.010
61.2	0.000	0.000
71.5	0.000	...
82.8	0.000	0.000
91.4	0.000	0.000
100.0	0.000	0.000

Phosphoric Acid plus Residual Hydrofluoric Acid. The use of tantalum in H_3PO_4, other than the high-purity food-grade acid, has always been questioned, because fluoride compounds are usually present. The observation has been made in several publications and bulletins that the presence of a small amount of HF (< 5 ppm) in commercial H_3PO_4 causes severe corrosion of tantalum (Ref 45). Therefore, tantalum has not been considered resistant to H_3PO_4 containing more than a trace of F^- ion.

In one test, a sample of Ta-2.5W-0.15Nb was exposed to a wet-process H_3PO_4 at an average temperature of 155 °C (310 °F) for a total of 283.5 h. Following the corrosion exposure, the sample (0.64 mm, or 0.025 in., thick) was fully ductile and withstood bending flat on itself with no evidence of cracking. There was no indication of corrosion on the surface of the specimen, and metallographic examination of a cross section of the specimen showed no evidence of corrosion attack. The weight loss data for the exposure equated to a corrosion penetration rate of 0.004 mm/yr (0.15 mil/yr). These data suggested that the tantalum alloy showed good corrosion resistance to the hot wet-process H_3PO_4.

Tantalum-Molybdenum Alloys. Corrosion resistance was studied on tantalum-molybdenum alloys that form a continuous series of solid solutions (Ref 7). The entire alloy system is extremely corrosion resistant, and the corrosion resistance of tantalum is generally retained when the alloy contains more than approximately 50% Ta. Table 8 gives weight loss data for tantalum-molybdenum alloys in concentrated H_2SO_4 and concentrated HCl at 150 °C (300 °F).

Tantalum-Niobium Alloys. Corrosion tests were conducted in hot and cold concentrated HCl and H_2SO_4 on alloys having various proportions of tantalum and niobium (Ref 46). The corrosion rates increased roughly in proportion to the niobium content in the alloy. Even though the 95Ta-5Nb alloy showed excellent resistance in all exposures, the attack was three times that obtained on pure tantalum. Additional corrosion data on binary tantalum-niobium alloys are given in Ref 47 and 48.

Other data were reported on corrosion tests of binary tantalum-niobium alloys and ternary alloys based on the tantalum-niobium system (Ref 49). Tests on the materials were carried out in 75% H_2SO_4 at 185 °C (365 °F), in 70% H_2SO_4 at 165 °C (330 °F), in 75% H_2SO_4 at room temperature, and in 20% HCl at room temperature. The tantalum-niobium alloys containing approximately 60% or more tantalum appeared promising for boiling 70% H_2SO_4. Ternary alloys containing elements of groups IV, V, and VI with tantalum and niobium did not offer any advantages in fabricability, and the addition of zirconium, hafnium, chromium, and vanadium lowered the corrosion resistance.

Data for Ta-40Nb in HCl acid are found in Fig. 12 and are compared to unalloyed tantalum. There is no corrosion below the boiling point curve, but Ta-40Nb rates of corrosion are higher than for pure tantalum at temperatures above it.

A comparison of unalloyed tantalum and Ta-40Nb in sulfuric acid is made in Fig. 13.

Tantalum-Titanium Alloys. Considerable data have been accumulated on the corrosion resistance of tantalum-titanium alloys (Ref 7). Dilution of tantalum with titanium shows

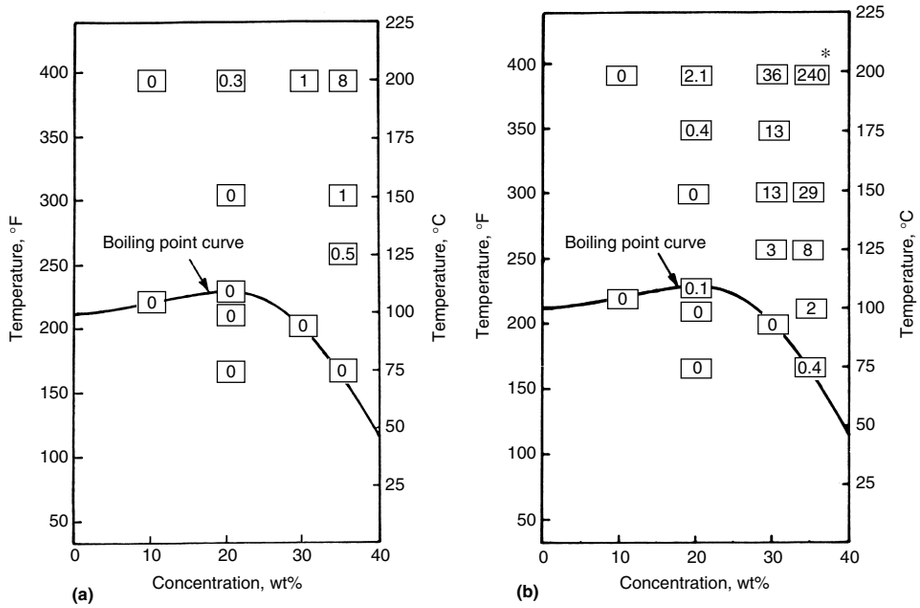

Fig. 12 Corrosion resistance in HCl as affected by concentration and temperature. The values in the boxes are the corrosion rate in mils/yr. No measurable corrosion is 0. (a) Unalloyed tantalum. (b) Ta-40Nb. Hydrogen embrittlement was noted (*). Adapted from Ref 50

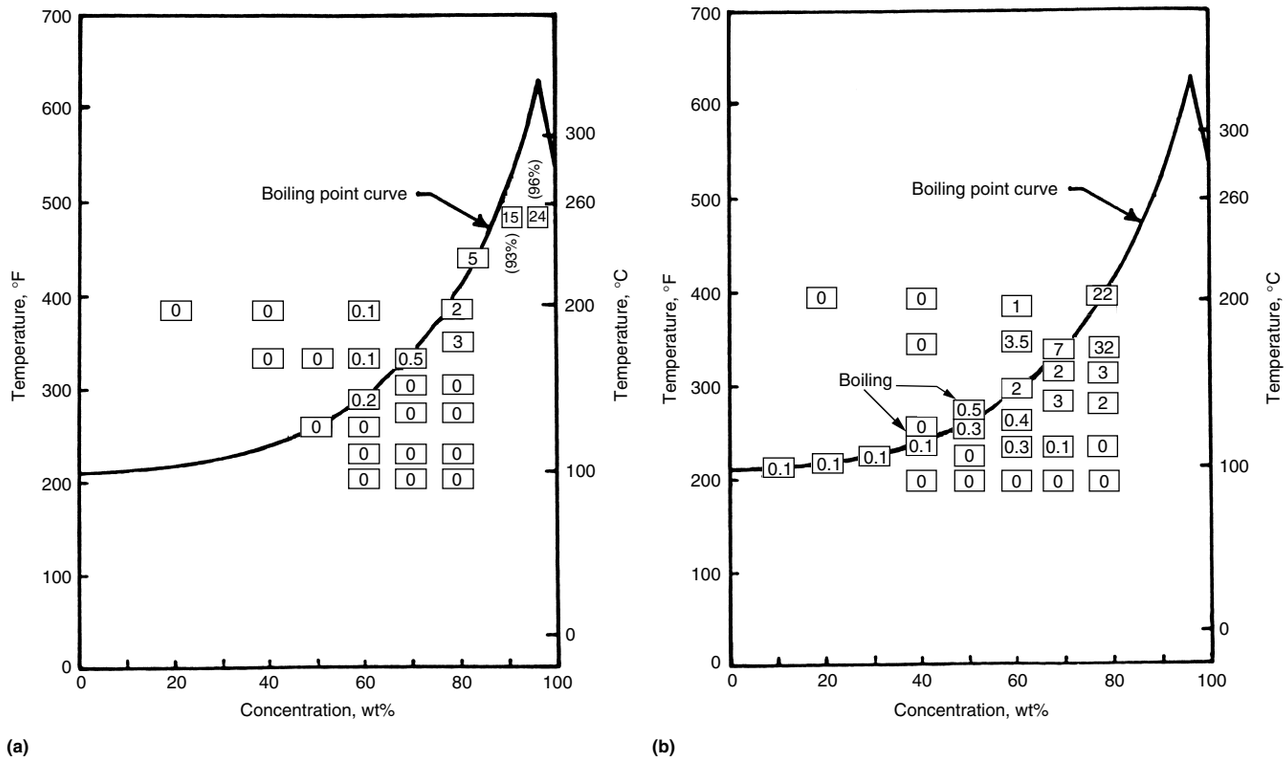

Fig. 13 Corrosion resistance in H_2SO_4 as affected by concentration and temperature. The values in the boxes are the corrosion rate in mils/yr. No measurable corrosion is 0. (a) Unalloyed tantalum. (b) Ta-40Nb. Adapted from Ref 50

considerable promise for the possibility of providing a lower-cost alloy with corrosion resistance almost comparable to that of tantalum in some selected environments. In addition to dilution with a lower-cost material, the resulting marked reduction in density is particularly advantageous because corrosion applications generally require materials on a volume rather than a weight basis. Corrosion tests in 10 to 70% HNO_3 at the boiling point and at 190 °C (375 °F) (in sealed glass tubes) were conducted on tantalum-titanium alloys ranging from pure tantalum to Ta-90Ti. All of these materials showed excellent behavior, with corrosion rates less than 0.025 mm/yr (1 mil/yr) and no indication of embrittlement.

Hydrogen embrittlement may occur when this alloy system is exposed to reducing corrosive conditions in tests conducted in sealed capsules. The tendency for hydrogen damage is markedly decreased as the tantalum concentration is increased (Ref 11).

Ternary Alloys. The corrosion behavior of alloys in the Ti-Ta-Nb system in 5% HCl at 100 °C (212 °F) was investigated (Ref 44). The corrosion rate dropped by a factor of 1.5 to 2 times less than that of titanium with a total of 15 to 20% Nb or Ta in the alloy. At 20 to 30% additions of these elements, the corrosion rate dropped by a factor of 10 to 70 times less than that of titanium. Tantalum increased the corrosion resistance of the alloys more effectively than niobium did.

The role of the structural factor in increasing the corrosion resistance of the titanium-tantalum-chromium and titanium-chromium alloys in a 5% HCl solution at 100 °C (212 °F) was demonstrated (Ref 51). The corrosion rate of quenched alloys was 2 to 10 times or more lower than that of annealed alloys. As the tantalum content increases, the corrosion rate decreases for both quenched and annealed alloys. The ternary alloys with a tantalum-to-chromium ratio of 3 to 1 and binary titanium-tantalum alloys with 20% more tantalum were found to have good corrosion resistance.

Other Tantalum Alloys. It has been observed that the presence of a small amount of iron or nickel, for example, in a tantalum weld makes that site subject to approximately the same acid attack as would be experienced by iron or nickel alone (Ref 11). Galvanic action, as well as simple chemical attack, is undoubtedly involved.

ACKNOWLEDGMENT

This article is adapted from Corrosion of Tantalum by Mortimer Schussler (retired) and Charles Pokross, Fansteel Inc., that appeared in *Corrosion,* Volume 13, *ASM Handbook,* 1987. That article was adapted with permission from *Corrosion Data Survey on Tantalum,* 2nd ed., Fansteel Inc., 1985. We thank Paul Aimone and Kurt Moser for reviewing this material.

REFERENCES

1. J. Chelius, Use of Refractory Metals in Corrosive Environment Service, *Mater. Eng. Q.,* Aug 1957, p 57–59
2. R.B. Flanders, Try Tantalum for Corrosion Resistance, *Chem. Eng.,* Dec 17, 1979
3. B.A. Johnson, "Corrosion of Metals in Deionized Water at 38 °C," Technical Memorandum TM X-1791, National Aeronautics and Space Administration, March 10, 1969
4. P. Aimone and E. Hinshaw, "Tantalum Materials in the CPI for the Next Millennium," Paper 01330, Corrosion Expo 2001, NACE International
5. M. Coscia and M.H.W. Renner, Corrosion of Tantalum and Tantalum-2.5% Tungsten in Highly Concentrated Sulfuric Acids, *Mater. Perform.,* Jan 1998
6. D.F. Taylor, "Tantalum: Its Resistance to Corrosion," Paper presented at the Chicago Section, The Electrochemical Society, May 4, 1956

7. M. Stern and C.R. Bishop, Corrosion and Electrochemical Behavior, *Columbium and Tantalum,* F.T. Sisco and E. Epremian, Ed., John Wiley & Sons, 1963
8. "Tantalum, Corrosion Data, Comparative Charts and Coating Characteristics," General Technologies Corporation
9. A. Alon, M. Schor, and A. Vromen, Corrosion Resistance of Ta to Mixture of Phosphoric Acid and Potassium Chloride at 120 C, *Corrosion,* Vol 22 (No. 1), Jan 1966
10. *Corrosionomics,* Vol 5 (No. 5), Fansteel Inc., 1960, p 5
11. C.A. Hampel, Ed., Tantalum, *Rare Metals Handbook,* 2nd ed., Reinhold, 1967
12. W.T. Edwards, Aqueous Corrosion in the Atomic Energy Industry, *First International Congress on Metallic Corrosion,* 1962
13. J. Vehlow and H. Geisert, "Tantalum Corrosion under Wet Incineration Conditions: Influence of the Dosing Components and Study of Welded Specimens," Paper presented at International Corrosion Conference, Sept 6, 1981
14. H.O. Peeple and R.L. Adams, Jr., A Corrosion Study in a Chlorine Dioxide Pulp Bleaching Plant, reprinted from *TAPPI,* Vol 38 (No. 1), Jan 1955, copyright 1955 by Technical Association of the Pulp and Paper Industry, reprinted with permission
15. E. Rabald, *Werkst. Korros.,* Vol 12, 1961, p 695–698
16. D.F. Taylor, Tantalum and Tantalum Compounds, *Encyclopedia of Chemical Technology,* Vol 19, 2nd ed., John Wiley & Sons, 1969, p 630–652
17. D.J. Medlin, S. Charlebois, D. Swarts, R. Shetty, and R. Poggie, Metallurgical Characterization of a Porus Tantalum Biomaterial (Trabecular Metal) for Orthopaedic Implant Applications, *Adv. Mater. Process.,* Dec 2003, p 31–32
18. F.E. Bacon and P.M. Moanfeldt, Reaction with the Common Gases, *Columbium and Tantalum,* F.T. Sisco and E. Epremian, Ed., John Wiley & Sons, 1963
19. E. Gebhardt and H.D. Seghezzi, *Z. Metallkd.,* Vol 50, 1959, p 248
20. R. Bakish, *J. Electrochem. Soc.,* Vol 105, 1958, p 71
21. F.F. Schmidt, W.D. Klopp, W.M. Albrecht, F.C. Holden, H.R. Ogden, and R.I. Jafee, Technical Report WADD-TR-59-13, United States Air Force, 1959
22. W.M. Albrecht and W.D. Goode, Jr., Publication BMI-1360, Battelle Memorial Institute, July 6, 1959
23. J.B. Hallowell, D.J. Maykuth, and H.R. Ogden, Silicide Coatings for Tantalum and Tantalum-Base Alloys, *Refractory Metals and Alloys III: Applied Aspects,* Vol 30, Part 2, American Institute of Mining, Metallurgical, and Petroleum Engineers, Dec 1963
24. K.J. Richards and M.E. Wadsworth, Oxidation Kinetics of Tantalum in Carbon Dioxide, *Trans. AIME,* Vol 230, Feb 1964, p 33–38
25. M. Farber, A.J. Darnell, and D.M. Ehrenberg, *J. Electrochem. Soc.,* Vol 102, 1955, p 446–453
26. J.M. Saleh and M.H. Matloob, Oxidation of Titanium, Tantalum, and Niobium Films by Oxygen and Nitrous Oxide, *J. Phys. Chem.,* Vol 76 (No. 24), 1974, p 2486–2489
27. E.E. Hoffman and R.W. Harrison, The Compatibility of Refractory Metals with Liquid Metals, *Refractory Metals and Alloys: Metallurgy and Technology,* I. Machlin, R.T. Begley, and E.D. Weisert, Ed., Proceedings of Metallurgy and Technology of Refractory Metals Symposium (Washington, D.C.), April 25–26, 1968, Plenum Press, 1968
28. E.C. Miller, Chapter 4, *Liquid Metals Handbook,* Atomic Energy Commission, Department of the Navy, 1952, p 144–183
29. W.D. Manly, *Corrosion,* Vol 12, 1956, p 336t–342t
30. P. Cybulskis, "Review of Metals Technology, Liquid Metals," Metals and Ceramics Information Center, Dec 21, 1973
31. R.H. Cooper and E.E. Hoffman, *Refractory Alloy Technology for Space Nuclear Power Applications,* Oak Ridge National Laboratory, Aug 10–11, 1983
32. J.Y.N. Wang, Method of Inhibiting the Corrosion of Tantalum by Liquid Lithium at High Temperatures, U.S. Patent 3,494,805, 1970
33. J.R. Weeks, "Liquidus Curves and Corrosion of Fe, Cr, Ni, Co, V, Cb, Ta, Ti, Zr in 500–750 C Mercury," revised and expanded version of a paper presented at the 20th NACE Conference, National Association of Corrosion Engineers, March 9–13, 1974
34. L.B. Engel, Jr. and R.W. Harrison, "Corrosion Resistance of Tantalum, T-111, and Cb-1Zr to Mercury at 1200 F," Contractor Report CR-1811, National Aeronautics and Space Administration, May 1971
35. R.L. Klueh, "Effect of Oxygen on the Corrosion of Niobium and Tantalum by Liquid Lithium," Report ORNL TM-4069, Oak Ridge National Laboratory, March 1973
36. W.R. Kanne, Jr., Corrosion of Metals by Liquid Bismuth-Tellurium Solutions, *Corrosion,* Vol 29, Feb 1973, p 75–82
37. L.A. Gypen, M. Brabers, and A. Deruyttere, Corrosion Resistance of Tantalum Base Alloys, Elimination of Hydrogen Embrittlement in Tantalum by Substitutional Alloying, *Werkst. Korros.,* Vol 35, 1984, p 37–46
38. Tantalum and Galvanic Action, *Corrosionomics,* Fansteel Inc., March 1957
39. T. Fukuzuka, K. Shimogori, H. Satok, and F. Kamikulo, Inhibition of Corrosion and Hydrogen Embrittlement of Tantalum in Concentrated Sulfuric Acid Solutions at Elevated Temperatures by Additions of N-O Compounds, *Boshoku Gijutsu (Corros. Eng.),* Vol 30 (No. 6), June 1981, p 327–336
40. N. Kagarva, K. Yamanmoto, R. Sasano, T. Kusakabe, and Y. Moriya, Method for Preventing Corrosion and Hydrogen Embrittlement of Tantalum-Made Equipment Handling Hot Concentrated Sulphuric Acid Therein, U.S. Patent 4,356,148, 1982
41. R. Wehrmann, Oxidation-Reduction Potential of Tantalum, *Corrosionomics,* Fansteel Inc., Sept 1956
42. E.W. Dreyman, Precious Metal Anodes: State of the Art, *Mater. Protect. Perform.,* Vol 11 (No. 9), Sept 1972, p 17–20
43. B.G. Staples and W.S. Galloway, Jr., Recent Results of Testing Corrosion Performance of 90-10 Tantalum-Tungsten Alloy, Pfaudler Reprint 581, reprinted from *Mater. Protect.,* Vol 7 (No. 7), July 1968, p 34–39
44. N.D. Tomashov, T.V. Chukalovskaya, et al., "Investigation of the Corrosion Resistance of Alloys of the Ti-Ta-Nb Systems," translation of the Foreign Technology Division, Air Force Systems Command, FTD-HT-149-74
45. *Corrosionomics,* Vol 3 (No. 1), Fansteel Inc., 1958
46. G.L. Miller, *Tantalum and Columbium,* Academic Press, 1959
47. A.V. Mosolov, I.D. Nefedova, and I.Y. Klinov, Corrosion and Electrochemical Behavior of Niobium-Tantalum Alloys in HCl at Elevated Temperatures and Pressures, *Z. Metallov.,* Vol 4 (No. 3), May–June 1968, p 248–251 (in English)
48. A.P. Gulyaev and I.Y. Georgieva, Corrosion Resistance of Binary Niobium Alloys, *Z. Metallov.,* Vol 1 (No. 6), Nov–Dec 1965, p 652–657 (in English)
49. D. Lupton and F. Aldinger, Possible Substitutes for Tantalum in Chemical Plant Handling Mineral Acids, *Trends in Refractory Metals, Hard Metals, and Special Materials and Their Technology,* Proceedings of the 10th Plansee Seminar (Reutte, Austria), 1981, p 101–130
50. R.H. Burns and F.S. Shuker, Jr., Industrial Applications of Corrosion-Resistant Tantalum, Niobium, and Their Alloys, *Refractory Metals and Their Industrial Applications,* STP 849, ASTM, 1984, p 59–60
51. N.D. Tomashov, G.P. Chernova, et al., "Investigation of the Structure and Corrosion Behavior of Alloys in the Ti-Ta-Cr Systems," translation of the Foreign Technology Division, Air Force Systems Command, FTD-HT-150-74

SELECTED REFERENCES

- P. Aimone and E. Hinshaw, "Tantalum Materials in the CPI for the Next Millennium," Corrosion/2001 (Houston, TX), March 11–16, 2001, NACE International, 2001
- P. Aimone and K. Moser, "Working with Tantalum and Tantalum Alloys," Corrosion/

2003 (San Diego, CA), March 16–20, 2003, NACE International, 2003

- H. Diekmann and U. Gramberg, Tantalum as a Construction Material in the Chemical Industry, *Tantalum-Niobium Int. Study Center Bull.,* Vol 78, June 1994, p 2–5
- C. Friedrich, P. Kritzer, N. Boukis, G. Franz, and E. Dinjus, The Corrosion of Tantalum in Oxidizing Sub- and Supercritical Aqueous Solutions of HCl, H_2SO_4 and H_3PO_4, *J. Mater. Sci.,* Vol 34 (No. 13), July 1, 1999, p 3137–3141
- A. Robin, Corrosion Behaviour of Tantalum in Sodium Hydroxide Solutions, *J. Appl. Electrochem.,* Vol 33 (No. 1), Jan 2003, p 37–42
- C.E.D. Rowe, The Use of Tantalum in the Process Industry, *JOM,* Vol 49 (No. 1), Jan 1997, p 26–28
- J.A. Shields and C. Rowe, Molybdenum and Tantalum Offer Competitive Edge in Hostile Environments, *Ind. Heat.,* Vol 68 (No. 1), Jan 2001, p 51–52, 69
- D. Zhang, Q. Lin, Q. Fei, H. Zhao, G. Kang, and M. Geng, Corrosion Behavior of Tantalum and Its Nitride in Alkali Solution, *Rare Met. (Engl. Ed.),* Vol 22 (No. 4), Dec 2003, p 276–279

ASM Handbook, Volume 13B: Corrosion: Materials
S.D. Cramer, B.S. Covino, Jr., editors, p354-359
DOI: 10.1361/asmhba0003826

Corrosion of Hafnium and Hafnium Alloys

D.R. Holmes, ATI Wah Chang, Allegheny Technologies

HAFNIUM is element number 72. It resides in group IVA of the periodic table with titanium and zirconium. Hafnium is always associated with zirconium in minerals such as zircon and baddeleyite, usually in the range of 1 to 5%. The chemical similarity between hafnium and zirconium is more pronounced than between any other two elements in the periodic table, except the inert gases. This similarity in chemistry of hafnium and zirconium makes separation extremely difficult. Along with zirconium, hafnium forms intermetallic compounds with most metallic elements, except the alkali metals and some alkaline earths (Ref 1). Hafnium is obtained as a by-product of the extraction process to produce hafnium-free nuclear-grade zirconium. Commercial hafnium typically contains 0.2 to 4.5% Zr. The van Arkel-de Boer (iodine) process is used to obtain hafnium purities of greater than 99.99%. Annual world consumption of hafnium was approximately 60 tons in 2003 (Ref 2).

Hafnium was first identified by x-ray analysis in 1923 by Coster and von Hevesy in Copenhagen, Denmark. Von Hevesey and Jantzen were the first to separate hafnium from zirconium by repeated recrystallization of fluoride salts. The name hafnium comes from the Latin name for Copenhagen, which is Hafnia. Van Arkel and de Boer were the first to produce metallic hafnium. Their process of passing hafnium tetraiodide vapor over a heated filament is the basis for the refining process used today to produce higher-purity hafnium metal.

With a standard reduction potential of −1.72 V versus the normal hydrogen electrode at 24 °C (75 °F), hafnium is more reactive than either titanium (−1.63 V) or zirconium (−1.53 V). This high chemical reactivity allows a thin, tenacious protective oxide layer to form when exposed to most chemical environments. Like other reactive metals, hafnium resists attack by many chemicals as long as this thin oxide layer is not penetrated by reactants. Oxide layers can also be developed by anodizing and by treatment in steam autoclaves and in air at elevated temperatures. The most commonly formed oxide is hafnium dioxide (HfO_2). Because of its high melting point of 2222 °C (4032 °F), hafnium may be considered refractory.

In addition to the inherent corrosion resistance of hafnium, other properties make hafnium useful in chemical equipment. It is relatively easy to form and join, sufficiently strong, ductile, and wear resistant to withstand the abuse of industrial applications. Its coefficient of thermal expansion is approximately 60% lower than that of 304 stainless steel at ambient temperature, and its thermal conductivity is approximately 40% higher at ambient temperature (Ref 3).

Hafnium appears to be nontoxic. Haygarth and Graham state that "there seems to be no report of the metal, or its alloys with nontoxic constituents, causing physiological reaction" (Ref 3). Like zirconium, dissolved hafnium ions are colorless—an important attribute for some applications.

Production

Because hafnium is always associated with zirconium, two main processes have been used to separate hafnium from zirconium. A European producer uses an extractive distillation process, while in the United States a liquid-liquid extraction is the preferred method. Two primary operational methods of metal production are also possible. The Kroll process is the primary reduction process used in the United States, while in Europe an electrowinning process is preferred. Ullman gives a detailed description for each of these processes (Ref 4).

Highest-purity metal is obtained by using the van Arkel-de Boer process, also known as the iodine bar or crystal bar process. In this process, hafnium sponge produced by the Kroll process is loaded into a cylindrical Ni-Cr-Fe vessel. The vessel lid contains insulated electrical lines from which a hafnium wire filament, in a hairpin shape, is suspended. Iodine is added to the vessel, which is then evacuated and heated to vaporize the iodine. Volatile hafnium tetraiodide forms and diffuses to the central hafnium filament, which is resistance heated to 1200 to 1500 °C (2200 to 2700 °F). The tetraiodide thermally dissociates at the hot filament, depositing hafnium and releasing iodine to react again with the sponge feed. This cycle continues until the efficiency diminishes (Ref 4, 5). Under conditions optimized for hafnium transfer, interstitial impurities such as oxygen, carbon, and nitrogen are left behind, along with some of the impurity metals. Electron beam melting is also effective in purifying hafnium. In this process, hafnium is slowly double-melted under high vacuum. This process removes impurities having partial pressures at the surface of the melt greater than the vapor pressure of hafnium, which is approximately 0.1 Pa (0.75 μm Hg) at 2500 K (4040 °F). The more volatile metallic impurities, such as iron, manganese, and aluminum, along with chlorine, are moved. Only the higher-melting-point metals, such as tantalum and tungsten, are not removed. To get the highest purity possible, the van Arkel-de Boer process and electron beam melting are used in sequence.

The United States Government allows the export of high-hafnium (0.2% or greater) commercial-grade (nonnuclear) zirconium (UNS R60702) to most countries. This level of hafnium content prevents commercial-grade zirconium from being modified for use in nuclear production facilities. This requirement limits the amount of hafnium metal available for other uses.

Physical and Mechanical Properties of Hafnium

Hafnium is often considered for the same applications as zirconium, because of their very similar physical and chemical characteristics. In fact, Clark (Ref 1) states that other than the higher transition temperatures ($\alpha \rightarrow \beta$) for hafnium, the only other chemical and physical property showing a major difference between these elements is the density. Both zirconium and hafnium exhibit anisotropy; their mechanical properties depend on the direction in which they are measured. Table 1 gives the physical properties of hafnium, while Table 2 gives the mechanical properties.

Chemical Properties. The ionic radii of zirconium and hafnium are almost identical, due to the lanthanide contraction. This results in very similar chemical properties between the two metals. As a result, a review of the chemical behavior of zirconium can be a useful indicator of the chemical behavior of hafnium (Ref 4).

Table 1 Physical properties of hafnium

Property	Value
Atomic number	72
Atomic weight	178.49
Density, kg/m^3 (lb/in.^{3})	13.31×10^3 (0.481)
Modulus of elasticity, MPa (ksi)	
At 294 K (70 °F)	13.7×10^4 (2.00×10^4)
At 533 K (500 °F)	10.6×10^4 (1.54×10^4)
At 644 K (700 °F)	9.5×10^4 (1.38×10^4)
Magnetic susceptibility per g at 298.2 K (77.4 °F)	0.42×10^{-6}
Hall effect at 25 °C (77 °F), Vm/AT	-1.62×10^{-12}
Spectral emissivity, 1750–2300, $e_{0.65u}$	0.40
Electron emission, A/m^2	
At 1900 K (2960 °F)	4.80×10
At 2000 K (3140 °F)	2.62×10^2
At 2100 K (3320 °F)	1.23×10^3
At 2200 K (3500 °F)	4.85×10^3
Work function, J	6.25×10^{-19}
Thermal neutron absorption cross section, barns	104
Crystal structure	
Alpha phase	Hexagonal close-packed
Beta phase	Body-centered cubic
Alpha-to-beta transformation temperature, K (°F)	2033 (3200)
Melting point, K (°F)	2500 (4041)
Boiling point, K (°F)	4875 (8312)
Coefficient of linear thermal expansion, (m/m)/K, at 273–1273 K (32–1830 °F)	5.9×10^{-6}
Thermal conductivity, W/m · K	
At 298 K (77 °F)	23
At 373.2 K (212.4 °F)	22.4
Specific heat, J/kg · K, at 298.2 K (77.4 °F)	117.0
Vapor pressure, Pa	
At 2040 K (3215 °F)	10^{-5}
At 2280 K (3645 °F)	10^{-4}
Electrical resistivity, Ω · m, at 298.2 K (77.4 °F)	3.51×10^{-7}
Temperature coefficient of electrical resistivity, Ω · m/K, at 298.2 K (77.4 °F)	3.82×10^{-11}
Latent heat of fusion, J/kg	1.35×10^5
Latent heat of vaporization, J/mol	
At 298.2 K (77.4 °F)	7.02×10^5
At 1000 K (1340 °F)	6.99×10^5
At 2000 K (3140 °F)	6.96×10^5
Hardness	
Brinell, MN/m^2	1700
Mohs	5.5
Vickers, MN/m^2	1760

Source: Ref 6

Specifications and Standards. Hafnium comes in two grades: grade R1 for nuclear applications (low zirconium) and grade R3 for commercial applications and alloying. Higher-quality material can be produced by the crystal bar process. Grade R3 hafnium is available in specific grades from 0.5 to 4.5% Zr content (Ref 6). No Unified Numbering System number has been assigned to hafnium. ASTM B 776, "Standard Specification for Hafnium and Hafnium Alloy Strip, Sheet, and Plate" (Ref 7), includes chemistry requirements. Table 3 gives the chemical composition of three grades of hafnium.

Aqueous Corrosion Testing of Hafnium and Hafnium Alloys

It is not the purpose of this article to describe the recommended procedure for corrosion testing. Reactive-metals corrosion testing, specifically zirconium and hafnium, is, however, sufficiently different from stainless steels, nickel-base alloys, and more common materials of construction to warrant a few comments.

Testing procedure ASTM G 2, "Corrosion Testing of Products of Zirconium, Hafnium and Their Alloys in Water at 360 °C (680 °F) or Steam at 400 °C (750 °F)," is specifically directed at zirconium and hafnium and their alloys for use by the nuclear industry (Ref 8). Different test methods are required for the commercial chemical processing industry. Reference 9 is specifically designed for testing of zirconium in commercial aqueous environments; hafnium would require the same guidelines. ASTM G 31, "Practice for Laboratory Immersion Corrosion Testing of Metals," may also be adapted for corrosion testing of hafnium. The subject of corrosion testing of reactive metals is also covered by Yau (Ref 10). Surface condition is more important with hafnium than with many other metals. In hydrochloric acid applications, for instance, a well-pickled surface is recommended. Pickling removes impurities, specifically embedded iron, from the surface and removes other surface imperfections where pitting may be initiated. Pickling hafnium requires a solution of 3 to 7% hydrofluoric acid (48% concentration) with 25 to 59% nitric acid (70% concentration) and the balance of water. Heat treatment for weldments may also be beneficial for corrosion resistance in specific applications. Heat treatments may be either a solution anneal requiring high temperatures or a stress anneal at lower temperatures. The choice of heat treatment depends on the specific environment and application.

For corrosion tests involving stress-corrosion or environmental cracking, such as tensile, U-bend, or C-ring specimens, consideration should be given to the anisotropy in hafnium. Specimen properties such as thermal expansion, yield strength, tensile elongation, and bend ductility depend on the orientation of mill products. Anisotropy is a characteristic of zirconium, titanium, and hafnium but not of niobium or tantalum. Table 2 gives examples of changes in mechanical properties between materials tested in the longitudinal and transverse directions.

Welding of reactive metals for corrosion samples also requires some care. Although commonly welded, hafnium and other reactive metals are very sensitive to contamination by oxygen, nitrogen, hydrogen, and carbon during the welding process.

Hafnium can be sensitive to minor impurities in corrosive environments. The presence of fluoride in low-pH solutions is particularly damaging to hafnium and other reactive metals. The data in Table 4 indicate the effect of fluoride in nitric acid solutions. Fluoride contamination can come from unexpected sources, such as boiling chips and the breakdown of some fluorinated polymers (Ref 13). Beyond this, oxidizers such as ferric ion (Fe^{3+}) in hydrochloric acid environments may pose a problem

Table 2 Typical mechanical properties for fully annealed products

Temperature			Ultimate tensile strength		Yield strength (0.02% offset)		Elongation in 5 cm (2 in.), %
°C	°F	Test direction	MPa	ksi	MPa	ksi	
Rod							
RT		Longitudinal	483	70	241	35	25
315	600	Longitudinal	310	45	124	18	40
Plate							
RT		Longitudinal	469	68	193	28	25
RT		Transverse	448	65	310	45	25
315	600	Longitudinal	367	53	124	18	45
315	600	Transverse	234	34	165	24	48
Strip							
RT		Longitudinal	448	65	172	25	30
RT		Transverse	448	65	376	55	30
315	600	Longitudinal	376	55	97	14	45
315	600	Transverse	241	35	165	24	50

RT, room temperature. Source: Ref 6

Table 3 Chemical composition of hafnium grades and crystal bar

Element	Composition		
	Grade R1, wt%	Grade R3, wt%	Crystal bar, ppm
Aluminum	0.010	0.050	70
Chromium	0.010	0.050	20
Copper	0.010	...	25
Iron	0.050	0.0750	250
Molybdenum	0.0020	...	5
Nickel	0.0050	...	50
Niobium	0.010	...	...
Silicon	0.010	0.050	50
Tantalum	0.020	...	...
Tin	0.0050	...	...
Titanium	0.010	0.050	50
Tungsten	0.0150	0.0150	10
Uranium	0.0010	...	5
Vanadium	0.0050	...	...
Zirconium	(a)	(a)	(a)
Hafnium	bal	bal	bal
Carbon	0.015	0.025	0.0030
Hydrogen	0.0025	0.0050	...
Nitrogen	0.010	0.0150	0.0010
Oxygen	0.040	0.130	0.0100

(a) Zirconium content varies. Source: Ref 6, 7

for the corrosion resistance of hafnium. Because of its high reactivity, hafnium will generally be the cathode in most galvanic couples. This will accelerate the corrosion of the anode component and allow hydrogen buildup in the cathode (hafnium) component of the cell. For this reason, care must be exercised in the use of dissimilar wire or bolting systems when placing hafnium coupons in multicoupon test racks. Any suspension system must be well insulated to get meaningful corrosion rates. The effect of impurities generated by corrosion of other metals contained on the test rack may affect the corrosion of hafnium. With few precautions, any standard test method and coupon configuration can be used or adapted for use with hafnium.

Aeration is not generally needed to passivate hafnium in aqueous environments. Hafnium forms a protective oxide film in the presence of even small amounts of water. The oxide film developed on hafnium also forms an effective barrier to erosion under normal conditions. For more abrasive conditions, a heat treatment at 566 °C (1051 °F) for 1 to 4 h in air may be helpful in reducing erosion.

Corrosion Resistance of Hafnium

In aqueous solutions, hafnium is soluble in hydrofluoric acid (HF) and concentrated sulfuric acid (H_2SO_4). Hafnium is resistant to dilute hydrochloric acid (HCl) and sulfuric acid. Hafnium is unaffected by nitric acid (HNO_3) in all concentrations. Aqua regia dissolves hafnium. The addition of small amounts of soluble fluoride salts in other acidic solutions can result in an appreciable increase in corrosion rates. Researchers report no corrosion for hafnium in hypochlorite ($HClO_4$) solutions and hydriodic acid (HI) at room temperature (Ref 14). Pourbaix gives some indication of possibly higher corrosion rates for hafnium in substances that can form soluble complexes or insoluble salts; fluorinated, oxalic, and salicylic complexes are specifically mentioned (Ref 15). Nielson states that the tendency of hafnium to form inorganic complexes with anions decreases in the following order: $OH^- > F^- > PO_4^{3-} > CO_3^{2-} > SO_4^{2-} > NO_3^- \approx Cl^- > ClO_4^-$ (Ref 4). Data presented in the tables that should be considered only as a guide for potential applications. As with all materials, corrosion performance should be determined in situ in the actual process stream, because even small process impurities may have a profound impact on corrosion in a particular application. The corrosion resistance of hafnium in various media is given in Table 5.

Table 6 gives the corrosion behavior of hafnium in some mixed acid solutions. Because hafnium is not resistant to aqua regia, caution should be exercised when applying hafnium in mixed acids involving hydrochloric acid and nitric acid.

Corrosion in Specific Media

Water and Steam. Hafnium is superior to commercial zirconium (UNS R60702) and zircaloys (UNS R60804 and R60802), which are nuclear grades of zirconium, in corrosion resistance in water at elevated temperatures to 450 °C (840 °F). Table 7 gives weight gains in standard corrosion tests in water at 360 °C (680 °F) and 2690 psi (18.5 MPa).

Hydrochloric Acid. In hydrochloric acid, hafnium has slightly higher corrosion rates than zirconium. In 10 and 37% acid at 35 °C (95 °F), for instance, hafnium will experience corrosion rates of 0.007 and 0.033 mm/yr (0.3 and 1.3 mils/yr), respectively (Ref 11). Surface finish is an important factor to consider for corrosion resistance in hydrochloric acid environments. Surface impurities such as iron may have a substantial impact on pitting resistance.

Nitric Acid. Hafnium is resistant to all concentrations of nitric acid, including fuming nitric

Table 4 Corrosion of hafnium in nitric acid solutions

Concentration of nitric acid	Temperature, °C	Temperature, °F	Condition	Duration of testing, days	Corrosion rate, mm/yr	Corrosion rate, mils/yr
10%(a)	35	95	Unknown	14	0.008	0.3
30%	BP(b)		Nonwelded	8	0	0
30%+1% NaCl	BP(b)	240	Nonwelded	8	0	0
50%	115	240	Nonwelded	8	0	0
50%+1% NaCl	115	240	Nonwelded	8	0	0
70%	116	240	Nonwelded	8	0	0
70%+1% NaCl	116	240	Nonwelded	8	0	0
70%	116	240	Nonwelded	8	0	0
70%	116	240	Welded	8	0	0
30%+50 ppm fluoride(c)	80	176	Nonwelded	1	1.8	73
30%+100 ppm fluoride(c)	80	176	Nonwelded	1	3.2	126
50%+50 ppm fluoride(c)	80	176	Nonwelded	1	2.8	113
70%+50 ppm fluoride(c)	80	176	Nonwelded	1	5.1	202
Fuming HNO_3	35	95	Nonwelded	14	0.01	0.43

(a) Ref 11. (b) BP, boiling point. (c) Added as hydrofluoric acid. Source: Ref 12

Table 5 Average corrosion rates of hafnium in various boiling solutions

Medium	Exposure time, days	Corrosion rate, mm/yr	Corrosion rate, mils/yr
Seawater	10	0	0
Saturated sodium chloride (NaCl) at pH 1	21	<0.0025	<0.1
Saturated sodium chloride (NaCl) at pH 1 with crevice device attached	21	<0.0025(a)	<0.1(a)
3% sodium chloride (NaCl) (alternate immersion)	7	0	0
70% calcium chloride ($CaCl_2$)	10	0	0
40% hydrobromic acid (HBr)	10	0.025(b)	1.0(b)
48% hydrobromic Acid (HBr)	10	0.025	1.0
40% cupric nitrate ($Cu(NO_3)_2$)	10	0	0
40% sodium bisulfate ($NaHSO_4$)	10	1.1	44
10% sulfamic acid (NH_2SO_3H)	10	0	0
25% aluminum sulfate ($Al_2(SO_4)$)	10	0	0
70% zinc chloride ($ZnCl_2$)	10	0	0
88% zinc chloride ($ZnCl_2$)	10	0	0.1
20% hydrochloric acid (HCl)	8	0.005	0.2
60% phosphoric acid (H_3PO_4)	8	0.22	8.5
85% phosphoric acid (H_3PO_4)	1	>200	>7900
Hydrogen sulfide (H_2S) in water	12	0	0
Sour gas (vapor)	18	0	0

(a) No pitting or crevice attack. (b) Pitting. Source: Ref 12

Table 6 Corrosion rates of hafnium in mixed acid solutions at 35 °C (95 °F)

Medium	Exposure time, days	Corrosion rate, mm/yr	Corrosion rate, mils/yr
$HCl + H_2SO_4$ (1 : 1)	14	0.0	0.5
$HCl + HNO_3$ (1 : 1)	14	3.3	130
$H_2SO_4 + HNO_3$ (1 : 1)	14	4.7	185

Source: Ref 6

Table 7 Corrosion of hafnium in high-temperature water

Material	Weight gain, mg/dm^2, 28 days	Weight gain, mg/dm^2, 56 days
Zircaloy(a)	20–22	25–28
Hafnium	3–6	5–7(b)

(a) Nuclear grade of zirconium containing iron, chromium, nickel, and tin as important alloy additions. (b) Estimated range; test not run on routine basis. Source: Ref 12

acid. Table 4 gives corrosion information for both welded and nonwelded materials. As with most solutions, the presence of fluoride ions in nitric acid will greatly increase the corrosion of hafnium.

Sulfuric acid is an environment where hafnium could see more use. Zirconium is a suitable material of construction for acid concentrations up to 70 to 75% at boiling temperatures. Above 80%, materials of construction that can be used include some stainless steels and carbon steels. In the range of 70 to 80% acid concentration, hafnium is more corrosion resistant than zirconium. Table 8 gives corrosion rates for other temperatures and concentrations of sulfuric acid. Table 9 gives data showing the effect of ferric ions on the corrosion of hafnium in various sulfuric acid concentrations.

Alkalis. Hafnium appears to have a very high resistance to corrosion by strong alkali solutions. Potassium hydroxide solutions do not attack hafnium until the concentration reaches 70 wt%, and then only at near-boiling temperatures. Sodium hydroxide is more aggressive toward hafnium. An upper limit appears to approximately 38% concentration at boiling temperatures. The presence of a weld does not appear to alter the corrosion resistance to a significant degree. Table 10 gives the corrosion resistance of hafnium in various alkali solutions.

Organics. The only reported corrosion information for hafnium in an organic solution is testing performed in acetic acid. No significant corrosion was reported at room temperature; the duration of testing was not given (Ref 14).

Molten Metals. Hafnium is superior to zirconium and zircaloy in molten alkali metals. In lithium, zirconium is rated good to 300 °C (570 °F) and limited to 600 °C (1110 °F). In sodium at 500 °C (930 °F), hafnium is as resistant as stainless steel, the corrosion rate being 1.2 mg/cm^2 · yr, or 0.001 mm/yr (0.04 mils/yr) (Ref 11).

Gases. Hafnium begins to react slowly with air or oxygen to form hafnium oxide at approximately 400 °C (750 °F), with nitrogen to form nitrides at approximately 900 °C (1650 °F), and rapidly with hydrogen at approximately 700 °C (1290 °F) to form hydrides. Hydrogen can be readily removed from hafnium by heating in a vacuum at 900 °C (1650 °F). The oxides and nitrides formed at these elevated temperatures tend to remain at the surfaces; however, hydrogen diffuses rapidly and forms hydrides throughout the metal. Oxides, nitrides, and hydrides all lead to impaired ductility. Hafnium (containing 2.5 wt% Zr) has a high reaction rate with nitrogen but less than that for titanium and zirconium (Ref 11). Hafnium reacts with carbon at >500 °C (930 °F) (Ref 5). At elevated temperatures, hafnium will react with boron, sulfur, and silicon, while halogens react directly to form tetrahalides. As a comparison, hafnium, at 740 °C (1360 °F), reacts with air at approximately the same rate as zirconium but at one-half the rate of zirconium at 900 °C (1650 °F) (Ref 11).

Table 8 Corrosion of hafnium in sulfuric acid solutions

Acid concentration, %	Temperature °C	Temperature °F	Condition	Duration of testing, days	Corrosion rate mm/yr	Corrosion rate mils/yr
60	140	284	Nonwelded	8	0	0
60	140	284	Welded	8	0	0
65	110	230	Nonwelded	1	0.03	1
65	154	310	Nonwelded	9	0.03	1
65	151	303	Nonwelded	8	0	0
65	151	303	Welded	8	0	0
70	165	329	Nonwelded	8	0.05	2
70	165	329	Welded	8	0.05	2
70	120	248	Nonwelded	8	0	0
70	120	248	Welded	8	0	0
70	180	356	Nonwelded	8	0.1	4
70	110	230	Nonwelded	1	0.03	1
75	185	365	Nonwelded	4	0.2	8
75	185	365	Nonwelded	4	0.5	20
75	185	365	Welded	8	0.13	5
75	182	360	Nonwelded	8	0.13	5
75	150	302	Nonwelded	12	0.03	1
75	100	212	Nonwelded	12	0	0
80	202	396	Nonwelded	7	1.8	70
80	204	400	Nonwelded	4	3	118
80	200	392	Nonwelded	7	2.2	86
80	150	302	Nonwelded	4	0.97	38
80	80	176	Nonwelded	2	1.7	66
80	80	176	Welded	2	1.1	42
80	65	149	Nonwelded	2	1.6	64
80	65	149	Welded	2	2.4	95
80	50	122	Nonwelded	11	0.03	1
80	50	122	Welded	11	0.1	4
80	50	122	Nonwelded	8	0.1	4
80	50	122	Welded	8	0.4	16
80	21	70	Nonwelded	8	0.13	5
80	21	70	Welded	8	0.05	2
85	210	410	Nonwelded	1	>5	>200
85	210	410	Welded	1	>5	>200
85	21	70	Nonwelded	1	>5	>200
85	21	70	Welded	1	>5	>200

Source: Ref 12

Table 9 Corrosion of hafnium in sulfuric acid containing Fe^{3+}

Acid concentration plus Fe^{3+}	Temperature °C	Temperature °F	Condition	Duration of testing, days	Corrosion rate mm/yr	Corrosion rate mils/yr
65% +1000 ppm	151	305	Nonwelded	2–4–2	0.05–0.01–0.05	2–0.4–2
65% +1000 ppm	151	305	Welded	2–4–2	0.04–0.01–0	1.6–0.4–0.1
70% +1000 ppm	165	330	Nonwelded	2–4–2	0.06–0.2–0	2.4–7.9–0.1
70% +1000 ppm	165	330	Welded	2–4–2	0.07–0.02 – 0.02	2.8–0.8–0.8
75% +1000 ppm	185	365	Nonwelded	2–4–2	1.5–0.65–0.68	59–26–27
75% +1000 ppm	185	365	Welded	2–4–2	1.2–0.6–0.6(a)	47–24–24(a)
85% +200 ppm	21	70	Nonwelded	1	>5	>200
85% +200 ppm	21	70	Welded	1	>5	>200

(a) Localized attack. Source: Ref 16

Table 10 Corrosion of hafnium in alkaline solutions

Solution concentration	Condition	Temperature °C	Temperature °F	Duration of testing, days	Corrosion rate mm/yr	Corrosion rate mils/yr
Sodium hydroxide 38%	Nonwelded	115	240	3	0.15	6
Sodium hydroxide 38%	Welded	115	240	3	0.2	8
Sodium hydroxide 50%	Nonwelded	140	284	4	0.67	27
Sodium hydroxide 50%	Welded	140	284	4	0.63	25
Sodium hydroxide 50%	Nonwelded	35	95	14	0.005	0.2
Potassium hydroxide 50%	Nonwelded	BP(a)		4	0	0
Potassium hydroxide 50%	Welded	BP(a)		4	0	0
Potassium hydroxide 70%	Nonwelded	170	338	2	0.15	6
Potassium hydroxide 70%	Welded	170	338	2	0.15	6

(a) BP, boiling point. Source: Ref 12

Forms of Corrosion

Galvanic Corrosion. Hafnium is a very noble (cathodic) metal, probably similar in ranking to silver and zirconium on the galvanic series for seawater. With few exceptions, when hafnium is galvanically coupled with another metal, the other metal will become the anode and suffer an increase in corrosion as a result of the couple. Although the corrosion rate of hafnium will remain low, its mechanical properties can suffer from hydrogen pickup as a result of the couple with the less noble metal.

Crevice Corrosion. Hafnium appears to be resistant to crevice corrosion in saturated sodium chloride solutions. Table 5 indicates a limited tendency for pitting attack in other saturated chloride solutions and as a result of exposure to other halide salts.

Pitting Corrosion. Hafnium appears to be resistant to pitting in a wide variety of solution compositions. Pitting appears to be limited to hydrobromic acid (Table 5) and to high concentrations of sulfuric acid containing additions of ferric ion (Table 9).

Corrosion of Hafnium Alloys

Hafnium-Zirconium Alloys. The hafnium-zirconium system is one of the few metallic systems in which thermochemical properties are almost ideal. That is, hafnium and zirconium can form isomorphous alloys for all ratios of the components. Moreover, hafnium and zirconium exhibit similar excellent corrosion-resistant properties, although they differ greatly in neutron absorption. Therefore, hafnium-zirconium alloys offer a broad range of neutron absorption for special applications in which corrosion resistance and neutron absorption are both important.

Hafnium alloys with 2.9, 17.3, 42.4, 59.5, and 81.4% Zr were evaluated for their corrosion resistance in various media. All of the alloys exhibited low corrosion rates (<0.0025 mm/yr, or 0.1 mil/yr) in the following boiling solutions: 30% HNO_3 with or without 19% NaCl, 50% HNO_3 with or without 1% NaCl, and 70% HNO_3 with or without 1% NaCl. Transverse-cut U-bend specimens of these alloys were tested in 90% HNO_3 at room temperature for 60 days. No cracking was observed.

Table 11 Corrosion of hafnium-zirconium alloys in boiling 20% HCl + 200 ppm Fe^{3+}

	Average corrosion rate				
	First test (2 days)		Second test (4 days)		Pitting ranking (a)
Alloy	mm/yr	mils/yr	mm/yr	mils/yr	
Hf-2.9Zr	0.19	7.4	0.058	2.3	2
Hf-17.3Zr	0.18	7.0	0.053	2.1	5
Hf-47.4Zr	0.22	8.7	0.053	2.1	4
Hf-59.5Zr	0.09	3.5	0.036	1.4	1
Hf-81.4Zr	0.13	5.1	0.058	2.3	3

Note: Fe^{3+} added as $FeCl_3$. (a) 1, best; 5, worst

The pitting resistance of these alloys was evaluated in boiling 20% HCl containing 200 ppm Fe^{3+} (as $FeCl_3$) and in chlorine-gas-saturated water. Test results are given in Tables 11 and 12. Although all alloys showed some pitting in these oxidizing chloride solutions, Hf-59.5Zr appeared to have the highest pitting resistance.

Hafnium-Tantalum Alloys. All hafnium-tantalum alloys tested exhibit no significant corrosion in boiling $\leq$70% nitric acid with or without 1% sodium chloride (Table 13). The tensile strength of hafnium-tantalum alloys increases with increasing tantalum concentration. Average tensile strengths of hafnium, Hf-1Ta, Hf-3Ta, and Hf-5Ta are 480, 520, 560, and 690 MPa (70, 75, 81, and 100 ksi), respectively (Ref 17).

Applications

The limited availability of hafnium leaves very little material for uses other than nuclear applications and as an alloying element.

Alloy Component. The primary use of hafnium is as an alloying element in nickel-base superalloys. These include cast nickel-base alloys such as MM 002, IN-713 Hf (MM 004), B-1900 Hf (MM 007), René 80 Hf, René 125 Hf (MM 005), MAR-M 200 Hf (MM 009), MAR-M 246 Hf (MM 006), MAR-M 247 (MM 0011), and CM 247LC. Each of these alloys contains from 0.05 to 2% Hf. Single-crystal alloys CMSX-3, CMSX-4, and CMSX-6 use 0.05 to 0.1% Hf in their formulation. In these alloys, hafnium serves as a strong carbide former and provides improved grain-boundary ductility and increased oxidation resistance (Ref 18).

Hafnium is also used in several niobium- and tantalum-base alloys to increase strength at high temperature. The niobium-base alloys are C-103 (Nb-10Hf-1Ti) and C-129Y (Nb-10Hf-0.07Y). These alloys are used in turbojet and rocket engine parts. Alloys such as WC-3015 (Nb-30Hf-1.5Zr-15W) and WC-3009 (Nb-30Hf-1.5Zr-9W) are used in applications requiring high-temperature strength and oxidation resistance. Hafnium provides dispersed particle strengthening and solid-solution strengthening in niobium-base alloys (Ref 4). Tantalum-base alloys also use hafnium as an important alloying element. Alloys T-111 (Ta-8W-2Hf-0.003C), T-222 (Ta-9.6W-2.4Hf-0.012C), and Astar 811-C (Ta-8W-1Re-1Hf-0.25C) are used to make honeycomb-type heat shields for use in re-entry vehicles and for fasteners for high-temperature conditions. Hafnium is also an important addition to certain titanium, tungsten, and molybdenum alloys where, along with carbon, it forms second-phase dispersions.

Nuclear. The second major use of hafnium is in control rods for nuclear reactors. Hafnium is used in pressurized light water reactors used primarily to power naval vessels (Ref 5). The combination of excellent hot water corrosion resistance, good ductility, and good machinability, along with a large neutron absorption cross section, makes hafnium ideal for this application. Hafnium has been proposed as separator sheets to allow closer spacing of spent nuclear fuel rods in interim holding ponds, because of it superior neutron absorption capabilities (Ref 5). Hafnium absorbs both thermal

Table 12 Corrosion of hafnium-zirconium alloys in boiling water saturated with chlorine gas

	Average corrosion rate				
	First test (2 days)		Second test (4 days)		Pitting ranking(a)
Alloy	mm/yr	mils/yr	mm/yr	mils/yr	
Hf-2.9Zr	0.015	0.6	0.005	0.2	3–4
Hf-17.3Zr	<0.0025	<0.1	0.005	0.2	3–4
Hf-47.4Zr	<0.0025	<0.1	<0.0025	<0.1	2
Hf-59.5Zr	0	0	<0.0025	<0.1	1
Hf-81.4Zr	<0.0025	<0.1	<0.0025	<0.1	5

(a) 1, best; 5, worst

Table 13 Corrosion of hafnium-tantalum alloys at 120 °C (248 °F)

		Corrosion rate	
Alloy	Corrodant concentration	mm/yr	mils/yr
Hf-1Ta	70% nitric acid	0	0
	70% nitric acid + 1% NaCl	0	0
	20% HCl + 200 ppm Fe^{3+}	0.08(a)	3.1(a)
Hf-3Ta	70% nitric acid	0	0
	70% nitric acid + 1% NaCl	0	0
	20% HCl + 200 ppm Fe^{3+}	0.09(a)	3.5(a)
Hf-5Ta	70% nitric acid	0	0
	70% nitric acid + 1% NaCl	0	0
	20% HCl + 200 ppm Fe^{3+}	0.04(a)	1.6(a)

Note: Samples both as-received and vacuum annealed at 816 °C (1500 °F) for 45 min were tested. No appreciable difference in corrosion rate was detected. Fe^{3+} added as $FeCl_3$. Corrosion rate is the average of the results from 3 to 48 h test periods. (a) Some corrosion at edges. Source: Ref 12

and epithermal neutrons, and its absorption cross section decreases only slowly after long periods of neutron irradiation. The combination of high corrosion resistance in nitric acid and high neutron absorption cross section allows hafnium to be used in spent fuel reprocessing plants that utilize nitric acid. The unique properties of hafnium help avoid criticality in this application (Ref 17).

Chemical Processing Industry. While hafnium has good corrosion resistance, zirconium has similar corrosion properties, costs less, is approximately half as dense, and is more available.

Other uses for hafnium are in the production of specialty chemicals, including borides, tetrahydridoborates, carbides, halides, nitrides, hydrides, sulfides, carbonates, acetates, and oxides. These are discussed in detail by Nielsen (Ref 5). It is also used in plasma arc metal-cutting tips, high-temperature ceramics, tool bits, and sputtering targets.

REFERENCES

1. R.J.H. Clark, *The Chemistry of Titanium, Zirconium and Hafnium,* Pergamon Press, 1973, p 419–490
2. J.B. Hedrick, "Mineral Industry Surveys: Zirconium and Hafnium," Mineral Commodity Summaries, U.S. Geological Survey, Jan 2003
3. J.C. Haygarth and R.A. Graham, *Review of Extraction, Processing, Properties and Applications of Reactive Metals,* B. Mishra, Ed., TMS, 2000, p 1–71
4. R.H. Nielsen, Hafnium and Hafnium Compounds, *Ullman's Encyclopedia of Industrial Chemistry,* 5th ed., Vol A12, VCH Verlagsgesellschaft mbH, 1989, p 559–569
5. R.H. Nielsen, Hafnium and Hafnium Compounds, *Encyclopedia of Chemical Technology,* 4th ed., Vol 12, Kirk-Othmer, 1994, p 863–881
6. "Hafnium Brochure," Wah Chang, an Allegheny Technologies Company, Albany, OR, 1987
7. "Standard Specification for Hafnium and Hafnium Alloy Strip, Sheet, and Plate," B 776, *Annual Book of ASTM Standards 02. 04,* ASTM, 1996
8. "Corrosion Testing of Products of Zirconium, Hafnium, and Their Alloys in Water at 680 °F (633 K) or in Steam at 750 °F (673 K)", G-2 (G2M), *Annual Book of ASTM Standards 03.02,* ASTM International, 1999
9. T.-L. Yau, J.A. Andrews, R. Henson, and D.R. Holmes, Practice for Conducting Corrosion Tests on Zirconium and Its Alloys, Corrosion Tests and Evaluation, *Silver Anniversary Volume,* STP 1000, R. Baboian and S.W. Dean, Ed., ASTM, 1990, p 303–311
10. R. Baboian, Ed., *Corrosion Tests and Standards, Application and Interpretation,* ASTM, 1995, p 507–510
11. D.E. Thomas and E.T. Hayes, Ed., *The Metallurgy of Hafnium,* United States Atomic Energy Commission, 1960, p 282
12. Corrosion tests conducted at Wah Chang, an Allegheny Technologies Company, Albany, OR
13. T.-L. Yau and D. Holmes, "Fluorides from Overlooked Sources," presented at the Corrosion Applications Conference (Coeur d' Alene, ID), Wah Chang, an Allegheny Technologies Company, 2003
14. R. Herold, Hafnium, *Metall,* Vol 26 (No. 7), July 1972 (in German)
15. M. Pourbaix, *Atlas of Electrochemical Equilibria in Aqueous Solutions,* Pergamon Press, 1966, p 230–233
16. J.H. Schemel, *Manual on Zirconium and Hafnium,* STP 639, American Society for Testing and Materials, 1977
17. T.-L. Yau, Hafnium: A Unique Metal with Uncommon Properties Finds New Applications, *Outlook,* Vol 10 (No. 2), Wah Chang, an Allegheny Technologies Company, 1989, p 3–5
18. *Properties and Selection: Irons, Steels, and High-Performance Alloys,* Vol 1, *ASM Handbook,* ASM International, 1990, p 982

SELECTED REFERENCES

- W.W. Allison, "Zirconium, Zircaloy and Hafnium Safe Practice Guide for Shipping, Storing, Handling and Scrap Disposal," WAPD-TM-17, Bettis Atomic Power Laboratory, Pittsburgh, PA, 1960
- R.J.H. Clark, D.C. Bradley, and P. Thornton, The Chemistry of Titanium, Zirconium and Hafnium, *Pergamon Texts in Inorganic Chemistry,* Vol 19, Pergamon Press, 1973
- K.L. Komaraek, Ed., *Hafnium: Physico-Chemical Properties of Its Compounds and Alloys,* International Atomic Energy Agency, Vienna, 1981
- *Metallography and Microstructures,* Vol 9, *ASM Handbook,* American Society for Metals, 1985, p 497–502
- *National Fire Codes,* Vol 13, NFPA 482M, National Fire Protection Association, Boston, MA, 1978
- E. Negishi and T. Takahashi, *Aldrichim. Acta,* Vol 18 (No. 2), 1985, p 31–48
- C.R. Tipton, Jr., Ed., *Reactor Handbook,* 2nd ed., Interscience Publishers, Inc., 1960, p 783–789
- B. Venugopal and T.D. Luckey, *Metal Toxicity in Mammals: Chemical Toxicity of Metals and Metalloids,* Vol 2, Plenum Press, 1978
- P.C. Wailes, R.S.P. Coutts, and H. Weigold, *Organometallic Chemistry of Titanium, Zirconium, and Hafnium,* Academic Press, Inc., 1974
- "Welding Brochure," Wah Chang, an Allegheny Technologies Company, Albany OR

ASM Handbook, Volume 13B: Corrosion: Materials
S.D. Cramer, B.S. Covino, Jr., editors, p360-369
DOI: 10.1361/asmhba0003827

Corrosion of Beryllium and Aluminum-Beryllium Composites

Warren J. Haws, Brush Wellman, Inc.

BERYLLIUM, like aluminum, is a thermodynamically reactive metal that forms a thin, well-bonded oxide layer on the surface at room temperature. Of the structural metals, only magnesium is more reactive. The oxide film on beryllium is approximately 10 nm (0.4 μin.) thick at room temperature, with this thickness being achieved in approximately 2 h. This thin layer of oxide provides a natural protection against atmospheric oxidation, similar to the oxide layer of aluminum, titanium, and zirconium. Beryllium is unique among the alkaline earth metals in providing this characteristic. This oxidation protection is effective up to 600 °C (1110 °F), while above 800 °C (1470 °F), the oxide formed has a tendency to spall.

Health and Safety

Handling beryllium and aluminum-beryllium composites in solid form and in finished parts poses no special health risk. Like many industrial materials, beryllium-containing materials may pose a health risk if the recommended safe-handling practices are not followed. Inhalation of airborne beryllium may cause a serious lung disorder in susceptible individuals. The degree of hazard varies, depending on the form of the product, how it is processed and handled, as well as the amount of beryllium in the product. The Occupational Safety and Health Administration (OSHA) has set mandatory limits on occupational respiratory exposures. Read and follow the guidance in the manufacturer's material safety data sheet before working with this material.

Effects of Impurities and Composite Composition

Beryllium is available in pure form in alloys, and as a composite with aluminum.

Beryllium. There are currently four major grades of beryllium (commonly referred to as pure beryllium) commercially available for structural applications today (Table 1). There are two other grades of high-purity beryllium that are used for foil applications, principally as windows for radiation sources and detectors. For the structural grades, oxygen (BeO), aluminum, iron, and silicon are intentionally controlled to achieve the desired mechanical properties. Beryllium oxide in these grades ranges from 0.5% to approximately 2%, depending on the grade, and has no effect on the corrosion behavior of pure beryllium.

Aluminum, iron, silicon, and magnesium are present at between 100 and 1000 ppm and are not generally a major contributor to the corrosion behavior of pure beryllium. Aluminum is present as free aluminum and/or as the $AlFeBe_4$ compound at the grain boundaries. Iron is present in one or more of the following forms: solid solution in beryllium, precipitated as a beryllide ($FeBe_{11}$) within the grains, or as the $AlFeBe_4$ compound at the grain boundaries. The form of the aluminum and iron is determined by the hold temperature and cooling rate during heat treatment. Silicon is mainly a grain-boundary constituent, but the exact nature of its form is not known.

Carbon is the only elemental impurity that presents special corrosion issues and is discussed later. Table 1 lists the compositions of the four structural grades for intentionally controlled elements and major impurities. All other impurity elements in beryllium are typically less than 100 ppm.

Aluminum-Beryllium Composites. Two aluminum-beryllium composites are currently produced commercially, AlBeMet 162 and AlBeMet 140 (Brush Wellman, Inc). These composites contain 62 wt% Be (the original Lockalloy material) and 40 wt% Be, respectively. Because these composites solidify as eutectic microstructures containing aluminum and beryllium phases with virtually no solubility of either element in the other, they also have the same self-protection mechanism against atmospheric oxidation.

The aluminum is the matrix, and the beryllium is the reinforcement. Aluminum-beryllium composites are made by inert gas atomization from a molten alloy. The input aluminum is 1100 alloy, and the input beryllium is typical of the pure beryllium grades. Carbon is the only impurity element that presents special corrosion issues, with behavior in the composite similar to its behavior in pure beryllium. The other issue with aluminum-beryllium composites is the potential galvanic corrosion that may occur in these composites. The difference between the aluminum and beryllium electrode potential is small (in seawater, for example), which minimizes the driving force for the galvanic effect; however, the rate of this reaction has not been studied in detail.

Alloys. Beryllium is an alloying element in the copper-beryllium group of alloys. See the article "Corrosion of Copper and Copper Alloys" in this Volume.

Corrosion of Beryllium in Air

Even though beryllium is commonly referred to as being self-protective against atmospheric oxidation, there are four major conditions that can cause beryllium to corrode in air:

- Beryllium carbide particles exposed at the surface
- Surface contaminated with halide, sulfate, or nitrate ions
- Surface contaminated with other electrolyte fluids
- Atmosphere that contains halide, sulfate, or nitrate ions

All of these conditions have a common factor: moisture in the air. Corrosion of pure beryllium or aluminum-beryllium composites can and does occur in air if moisture condenses on the metal surface. This type of corrosion is essentially a subset of aqueous corrosion.

One study demonstrated the noncorroding nature of pure water vapor when the beryllium surface was uncontaminated and free of exposed Be_2C inclusions (Ref 1). Polished, uncoated specimen coupons were subjected to an atmosphere of air plus 95% relative humidity at 40 °C (100 °F) for 30 days, with a result of no apparent

corrosive attack. Neither microscopic examination nor weight gain measurements indicated corrosive attack on any of the specimens.

Beryllium carbide will react in the presence of moisture at room temperature. The reaction occurs very slowly and forms a white exfoliated beryllium oxide (BeO) powder, with an accompanying large volume expansion, according to the following reaction:

$$Be_2C + 2H_2O \rightarrow 2BeO + CH_4$$

with methane as a gaseous product. The following reaction:

$$Be_2C + 4H_2O \rightarrow 2Be(OH)_2 + CH_4$$

is generally believed to be an intermediate step in arriving at the final BeO product. This is consistent with the observed formation of a white gelatinous product from the reaction of Be_2C in an aqueous environment.

These reactions were first reported in 1955 (Ref 2). In work performed at Oak Ridge National Laboratory in 1947, white corrosion products and blisters were observed to form on the surface of extruded beryllium that had been exposed for approximately 6 months to the local humid air. The corrosion products were caused by carbide inclusions that were parallel to the extrusion axis. Similar corrosion attack has been observed on finished precision-machined components during shelf storage.

An instrument-grade material, in service in a controlled gas environment containing a fixed value of relative humidity, exhibited corrosion in the form of spotty white buildup and disruption of the surface. This type of corrosion was experimentally duplicated with carbide-seeded beryllium subjected to the same type of environment. In addition, beryllium that exhibits flowery corrosion spots during extended air storage was also found to yield a similar pattern of corrosion attack within hours of immersion in an aqueous bath.

A study of a large atypical carbide inclusion (13 mm, or 0.5 in., disk) corroding in a humid air environment during storage (Ref 3) resulted in the fracture of a large piece of beryllium from the component, caused by the volume expansion of the corrosion product.

The corrosion of a metallographic mount containing a Be-Be_2C composite, from a fusion research project, over a 6 month period caused the mount to split apart from the volume expansion. The corrosion product was piled 12 mm (0.5 in.) high on the mount, illustrating the volume expansion of the corrosion product.

The carbon typically present in commercial beryllium today is uniformly distributed as fine carbide particles roughly 1 μm (0.04 mil) in size and not likely to cause mechanical damage to the component; however, blistering and disruption of beryllium at the edges of Be_2C inclusions can occur.

Surface contamination is the second major condition that can lead to corrosion of beryllium and aluminum-beryllium in a humid air environment. Halides, sulfates, and nitrates remaining on the surface of beryllium, after the evaporation of fluids containing the ions, can become very concentrated, with a small amount of water condensation from a humid atmosphere providing a condition for corrosion at active sites. Failure to clean a beryllium surface that has come in contact with these ions, or an improper rinsing and drying operation, can result in localized deposits of these contaminants.

Common fluids that could contain these ions include cutting oils and fluids, tap water, chlorine-contaminated water, and chlorinated solvents. In general, it is best to avoid the use of fluids containing these ions. Where the use of these fluids cannot be avoided, minimizing the contact time with beryllium surfaces is recommended. In addition, proper rinsing and drying is recommended to eliminate evaporation of ion-containing fluids from the beryllium surface.

Plastic piping, used to avoid metallic contamination of the rinse system, has been found to be a source of chloride ions that resulted in the corrosion of beryllium components during storage.

Salt residue not adequately removed from a molten-salt dip-brazed aluminum-beryllium chassis was activated during a humidity test. The chassis suffered significant corrosion during this test when the salt residue dissolved in the condensed water on the metal, producing a concentration of chloride ions. Galvanic corrosion also occurred during this test, because the part was supported by a stainless steel rack, and the dissolved salt provided a suitable electrolyte.

Contamination can also occur after proper cleaning and drying, from fluids splashing or dripping onto the beryllium surface. Another source of surface contamination in beryllium is fingerprints. The corrosive nature of fingerprints causes them to be etched into the beryllium surface when subjected to a humid environment. This causes cosmetic issues on finished or semifinished parts as well as problems in etching or applying coatings to the surface. Fingerprinted surfaces need to be removed by mechanical abrasion before most chemical treatments.

In addition to the general aqueous corrosion that can occur as a result of halides, sulfates, and nitrates, there is also the potential for galvanic corrosion if the metal is touching a dissimilar metal and the solution is bridging both metals.

Electrolyte solutions that come in contact with beryllium and aluminum-beryllium composites and are allowed to dry on the surface can reactivate in the presence of humid air in the same manner as halides, sulfates, and nitrates. Even though the chemicals in the electrolytes may not attack the beryllium or aluminum-beryllium composites, there is the potential for galvanic corrosion, as described in the previous paragraph.

Atmospheric contamination is the fourth major condition that can lead to corrosion of beryllium or aluminum-beryllium composites in air. Atmospheric contamination can be from natural sources, such as salt from the sea, or from manmade sources, such as exhaust from industrial smokestacks. However, any fumes containing halide, sulfate, or nitrate ions (or any chemical species that can transform to these ions) that condense on the metal surface can cause corrosion. Rainwater and salt air from the ocean are two well-known sources of airborne contamination.

Rainwater has been recognized as a potential source of corrosive agents that can be inadvertently introduced into a protective environment through atmospheric transport or through leaky structures. Table 2 lists the corrosive agents commonly found in rainwater.

Inadvertent admission of atmospheric moisture into silos and launch control centers of missile systems has been cited as the cause of most of the general corrosion problems associated with the metals contained in these structures (Ref 4). Despite the fact that corrosion problems have been encountered in missile silos, the use of a humidity-controlled environment has generally been effective in protecting most components from corrosion.

The open atmosphere above the ocean provides a site of unusually high salt content. The natural salt concentration above the sea can increase by as much as 50 times due to the high winds during storms. In addition, the mist generated by a moving vessel can add to the corrosion problem. Severe corrosion of the beryllium brake shoe pads of bombers on military aircraft carriers has been reported. The brake shoes were typical of those that have performed well for years on the C5A military transport in less corrosive environments. The salt-laden environment of the aircraft carrier caused the brake pads to pit and become covered with corrosion products. Beryllium brake pads are no longer used in this application.

Table 1 Specification and typical compositions of four grades of beryllium

S, structural grade; I, instrument grade; O, optical grade

Chemical composition (by weight)	S-200F	S-65C	I-220C	O-30
Be, % (min)	98.5 (99.2)	99.0 (99.4)	98.0 (98.5)	99.0 (99.4)
BeO, % (max)	1.5 (1.0)	1.0 (0.65)	2.2 (1.85)	0.5 (0.35)
Al, ppm (max)	1000 (500)	600 (320)	1000 (70)	700 (450)
C, ppm (max)	1500 (800)	1000 (300)	1500 (300)	1200 (500)
Fe, ppm (max)	1300 (1100)	800 (750)	1500 (700)	1200 (1050)
Mg, ppm (max)	800 (350)	600 (100)	800 (100)	700 (300)
Si, ppm (max)	600 (300)	600 (250)	800 (200)	700 (300)

Note: Typical values are shown in parentheses.

Salt in the air can also cause problems on land in coastal areas, extending many miles inland. The effect can vary, depending on distance from the ocean, wind velocity, and wind direction. Proper processing, handling, and storage of beryllium and aluminum-beryllium composites in these areas are essential to preventing corrosion damage.

Aqueous Corrosion of Beryllium

Beryllium that is clean and free of surface impurities has very good resistance to attack in low-temperature high-purity water. The corrosion rate in good-quality water is typically less than 0.025 mm/yr (1 mil/yr) (Ref 5). Beryllium has been reported to perform without problems for 10 years in slightly acidified demineralized water in a nuclear test reactor (Ref 3, 6). This high-purity water environment also produced no evidence of accelerated corrosion with the beryllium galvanically coupled with stainless steel or aluminum.

Ionic Solutions. Beryllium is susceptible to attack, primarily in the form of localized pitting, when exposed to impure water (Ref 7). Chloride (Cl^-) and sulfate ions (SO_4^{2-}) are the most critical contaminants in aqueous corrosion. Because these contaminants are present in tap water, most processing specifications warn against its use. Even etching solutions should not be prepared using tap water. In cases where tap water is used for rinsing, the final rinses should be performed immediately in deionized water to ensure that the Cl^- or SO_4^{2-} impurities are not retained on the subsequently dried metal surface. Aluminum-beryllium reacts similarly to pure beryllium under these conditions, but aluminum is also present on exposed surfaces to act as a cathode.

The pitting of beryllium in aqueous baths containing Cl^- or SO_4^{2-} ions occurs as the result of a galvanic cell between the impurities and the base metal, beryllium (Ref 8). Because beryllium is anodic to all common metals except magnesium, zinc, and manganese, the beryllium area surrounding the impurities (other than magnesium, zinc, and manganese) is rapidly attacked, creating a pit, while the impurity is cathodically protected. This reaction progresses until the impurity is fully undercut and falls out of the beryllium.

Based on the purity of beryllium today, pitting is usually visible only microscopically. Macroscopic pitting becomes a problem only when large inclusions are present due to powder-handling problems in the manufacture of beryllium.

There are reports that pits are observed in areas associated with concentrations of iron, aluminum, and silicon (Ref 9–11). For aluminum and silicon, these observations are consistent with the fact that these metals have virtually no solubility in beryllium and are known to segregate to the grain boundaries, where they are concentrated and can react to form a pit. Iron, however, is present within the beryllium grains in either solid solution or precipitated as $FeBe_{11}$. It can also concentrate in grain boundaries as precipitated $AlFeBe_4$. Both $AlFeBe_4$ and $FeBe_{11}$ act as cathodes when galvanically coupled with beryllium in an ionic solution. Because these compounds are generally believed not to be chemically active, they will not dissolve but will remain at grain boundaries until the corrosion of beryllium around them causes them to fall out. Thus, iron can be observed within pits located either within grains or at grain boundaries.

A study on the effects of the surface finish of beryllium on aqueous corrosion showed that the magnitude of attack for various types of surfaces in extended exposures reached approximately the same value: 0.0025 to 0.005 mm/yr (0.1 to 0.2 mil/yr). The specimen surface conditions included as-machined, pickled in chromic-phosphoric (H_2CrO_4-H_3PO_4) acid after machining, and machined and annealed in vacuum for 1 h at 825 °C (1515 °F). In the short term, however, the tests showed that the pickled specimens corroded at a higher rate than the other specimens. This was probably the result of a fresh, clean surface provided by the pickling process.

Several studies have been performed more recently that are more quantitative in nature and allow for a better understanding of the mechanisms of corrosion and pitting in beryllium.

Polarization data and open-circuit potential measurements were used to make mixed-potential predictions of the electrochemical activity of the beryllides in commercial grades of beryllium (Ref 12). Angle-resolved x-ray photoelectron spectroscopy was used to characterize the oxide film on as-prepared and postimmersion samples.

Table 2 Corrosive agents in rainwater

Agent and source	Location	Concentration, ppm
Chloride (Cl^-) ions, major source is sea spray	Over sea or near coastlines	Average 2–20; with extreme winds, may increase up to 100
	500 miles or more inland	Average 0.1–0.2 but sometimes higher than 1.0
Sulfate (SO_4^{2-}) ions; major sources in industrial areas	Large cities, industrial areas	Average 10–50; higher under extreme conditions such as smog
	Other areas	1–5
Nitrate (NO_3^-) ions	Over land	0.5–5
Hydrogen ions (pH)	Over land	Average approximately 5; may decrease to 3 near industrial centers

Beryllium was observed to exhibit a passivity breakdown dependent on voltage, chloride concentration, and pH in an electrochemical study of beryllium in buffered and unbuffered chloride solutions (Ref 13). This work theorized but could not confirm that the barrier layer was beryllium oxide.

The passive behavior of beryllium was studied in a variety of aqueous solutions, using electrochemical measurements, solution analyses, and electron microscopy (Ref 14). Beryllium exhibited passive behavior in some solutions and pitting corrosion in other solutions. The passive film was identified as microcrystalline BeO.

It is well known that surface defects, such as twins, microcracks, and pits, in beryllium compromise mechanical properties in beryllium. A quantitative study was performed to determine the effect of pitting corrosion on bend test specimens (Ref 15). Both modulus and failure strength increased as the concentration of chloride increased. These properties were supported by the change in the nature of pitting from localized deep pitting (low concentration) to uniform shallow pitting (high concentration). Scanning electron microscopy, atomic force microscopy, and potentiodynamic polarization experiments were also conducted to provide supportive evidence for the differences in the pitting behavior of the beryllium with different NaCl concentrations.

Several electrochemical studies of corrosion have been performed on single-crystal beryllium (Ref 16–19). Dramatic differences in cyclic polarization and pitting were observed.

Galvanic corrosion can occur when beryllium contacts most other metals in the presence of an electrolyte. Such situations arise in mechanical joints that use threaded inserts, screws and bolts, washers, and bolted assemblies of different metals. Electrical isolation and coatings can mitigate this problem.

Galvanic corrosion is also possible in welded beryllium. Beryllium is difficult to weld because it is highly susceptible to cracking. An aluminum-silicon filler alloy is typically used to prevent cracking. This aluminum-rich weld zone provides the opportunity for galvanic corrosion between beryllium and the weld zone. An investigation of galvanic corrosion between beryllium and the aluminum-silicon weld material showed cathodic protection of the weld zone and anodic dissolution of the beryllium, which included some pitting (Ref 20). Beryllium precipitate in the weld zone did dissolve, but no corrosion of the aluminum-silicon matrix was observed.

Microbial corrosion can occur when microorganisms grow on a metal surface in the presence of moisture. In a study of microbial-influenced corrosion, uncoated beryllium samples exhibited degradation of mechanical properties when exposed to marine *Pseudomonas* bacteria (Ref 21). Application of a self-assembled silane monolayer on the surface of the beryllium was found to prevent degradation of mechanical properties.

Chlorinated Solvents. Pitting caused by chlorinated solvents in contact with beryllium is a well-known phenomenon. The pitting mechanism, however, was not well understood. An x-ray photoelectron spectroscopic study of beryllium exposed to chlorinated solvents concluded that the chlorinated solvents react with the beryllium metal surface to produce chlorides (Ref 22). A mechanism was proposed that explains the loss of the protective oxide, allowing the reaction to occur.

Acid solutions are commonly used to etch machined beryllium components to remove the effects of machining damage from the surface. Both the high residual stress stored in surface twins and the surface microcracks resulting from this stress can lower the mechanical properties of beryllium. The industry-standard etching solution is known as the 2-2-2 etch: 2 vol% concentrated HNO_3, 2 vol% concentrated H_2SO_4, and 2 vol% diluted (48%) HF. All etching solutions should be prepared with distilled water. Metal removal rate is approximately 2.5 to 6.5 μm/min (0.1 to 0.25 mil/min) at room temperature with fresh acid. Total metal removal is typically 75 to 125 μm (3 to 5 mils) per surface. A natural micropitting of the surface is expected. Excessive pitting/cratering may develop at greater than 125 μm (5 mils) removal.

For heavier metal removal, such as chemical milling, a solution containing 6 to 20 vol% H_2SO_4 and 0.5 to 1.0 vol% HF at room temperature is recommended. This etch is fast and has the advantage that it is a leveling etch, which removes scratches and dings rather than deepening them. A final light etch using 45 vol% HNO_3-1 vol% HF is required to remove the smut caused by the H_2SO_4.

Beryllium must be thoroughly rinsed and dried after any etching process to prevent corrosion of the active surfaces. Neutralizing the surface with mildly alkaline solutions followed by thorough rinsing and drying is sometimes desirable. While tap water can be used for an intermediate rinse, final rinsing should be performed immediately, using copious amounts of deionized water. Techniques such as cascade rinsing or spray rinsing from top to bottom can be used. Special care should be taken to ensure that corners, holes, and cavities are thoroughly rinsed. Drying is performed in vacuum at approximately 93 °C (200 °F) or by dipping in acetone. Another useful technique is to rinse in hot water, with sufficient time to heat the beryllium. The high specific heat of the beryllium will dry the metal surface when it is removed from the rinse.

Beryllium carbide particles at the surface will react in aqueous solutions in the same manner as the reaction in humid air. Unlike metallic impurities, Be_2C does not require the presence of any other ions to corrode. The reaction takes place even in distilled water. Carbon control has improved over the last 20 years; thus, the problem of corrosion due to Be_2C particles is greatly reduced.

Stress-Corrosion Cracking

Extensive information on the behavior of beryllium under the combined effects of stress and chemical environment is not readily available (Ref 23–25). The first reported work involved the use of extruded material in water containing 0.005 *M* hydrogen peroxide (H_2O_2) with pH values ranging from 6 to 6.5 at 90 °C (195 °F) (Ref 23). No evidence of cracking was noted, even though stresses up to 90% of the yield strength were used. Stress corrosion has been reported on cross-rolled sheet when synthetic seawater was used as the test medium (Ref 24). Studies of time-to-failure versus applied stress revealed that the time decreased from 2340 to 40 h as the applied stress was increased from 8.4 to 276 MPa (1.22 to 40 ksi), or 70% of yield strength. Failure appeared to be closely associated with random pitting attack. Certain pits appeared to remain active and promote severe localized attack.

Stress-corrosion cracking (SCC) testing of aluminum-beryllium was performed by the European Space Agency (Ref 26) in accordance with ECSS-Q-70-37A (Ref 27). Three types of aluminum-beryllium material were tested: extruded (longitudinal and transverse direction), hot isostatic pressing (HIP) consolidated, and electron beam welded HIP. Specimens stressed at 75% of the 0.2% yield strength were immersed in 3.5% NaCl solution for 10 min and dried for 50 min every hour for 30 days. Unstressed control specimens were tested with the stressed specimens. None of the specimens failed during the SCC test. Metallographic inspection showed no evidence of SCC. This material was graded as class 1 (has high resistance) with respect to SCC.

High-Temperature Corrosion

Elevated-temperature exposure of beryllium that has been studied includes gaseous and liquid metal corrosion.

High-Temperature Gas Oxidation. The oxidation of beryllium exposed to gases at high temperature has been studied for applications in gas-cooled reactor systems (Ref 28–33). Oxide films were found to protect beryllium in dry oxygen at temperatures up to 650 °C (1200 °F) with exposure times up to 300 h (Ref 30). Above that temperature, oxidation increased rapidly. There was some evidence that the oxide film cracked and rehealed during exposure. High-temperature oxidation was also studied in water vapor and moist oxygen (Ref 31). One study showed that carbide inclusions were oxidized preferentially at 700 °C (1290 °F) (Ref 32). Another study examined the oxidation of beryllium at 927 to 1293 °C (1700 to 2360 °F) (Ref 33).

High-temperature oxidation in carbon dioxide and carbon monoxide atmospheres has also been studied (Ref 34–37).

High-Temperature Steam Exposure. The behavior of beryllium exposed to steam at high temperature is important for first-wall and blanket applications in fusion reactors. The reaction rate of 88% dense beryllium (low-quality plasma sprayed) was determined to be 200 times greater than that of fully dense beryllium (high-quality plasma sprayed) (Ref 38). This work was performed over a 600 to 1230 °C (1110 to 2250 °F) temperature range. Kinetic data were obtained for the reaction of beryllium in air and in steam as a function of temperature (Ref 39). These data confirmed the existence of two oxidation mechanisms as a function of temperature. Steam reactivity of beryllium pebbles and beryllium powder at elevated temperatures showed complex behavior primarily dependent on the test temperature (Ref 40).

Liquid metal corrosion has been studied for cooling systems in land- and space-based nuclear reactors. The resistance of beryllium to liquid sodium or sodium-potassium alloy (NaK) is excellent as far as attack by the molten metal or mass transfer is concerned. Beryllium, however, reduces sodium oxide (as it reduces most oxides), forming beryllium oxide, which is nonadherent in rapidly flowing sodium. Thus, the reaction will proceed as long as there is sodium oxide present. Cold trapping alone will not sufficiently remove the oxygen (Ref 41). However, cold trapping followed by calcium deoxidation of the liquid metal reduced the corrosion rate to acceptable levels (Ref 42).

Darwin and Buddery (Ref 43) discuss the performance of beryllium in a number of other liquid metal systems. They indicate that the resistance of beryllium to molten magnesium, zinc, cadmium, mercury, gallium, tin, lead, antimony, and bismuth is generally good, while resistance to molten calcium and aluminum is poor. The compatibility of a molten lead/lithium alloy in contact with beryllium is addressed in Ref 44.

In-Process, Handling, and Storage Corrosion Problems and Procedures

In addition to in-service corrosion issues with beryllium and aluminum-beryllium composites, care must also be taken to prevent corrosion during processing, handling, and storage. Corrosion during processing can result in problems such as loss of tolerance, visual cosmetic issues, degradation of mechanical properties, and poor coating adherence. Most of the specified practices used by manufacturers and users result from experience gained in processing and handling of components. Improper handling, inadequate control of chemical and rinse baths, and improper storage or packaging procedures are the primary causes of in-process corrosion problems.

In-Process Problems and Procedures

There are several corrosion mechanisms that are common but avoidable when processing beryllium.

Water. One of the most common caveats in handling beryllium and aluminum-beryllium composites is to avoid contact by tap water. Pitting or surface corrosion will occur in beryllium when allowed to stand in tap water or when rinsed with tap water and allowed to stand in a damp atmosphere while drying. Because most people are aware of this issue, most problems with tap water are due to inadvertent contact. Water leaking from a pipe or valve or a small leak in a roof can go undetected, contaminate a surface, and lead to corrosion.

Chloride ions from sources other than tap water can also lead to pitting attack in aqueous baths. Chlorinated solvents used to remove oils and greases present problems when the solvent is carried into a cleaning bath on an as-machined surface. The fact that chloride ions are introduced into rinse water from the walls of polyvinyl chloride piping illustrates the need to pay attention to details with respect to the entire system when dealing with aqueous solutions that come in contact with beryllium.

Galvanic corrosion can occur during the electrical discharge machining (EDM) of both beryllium and aluminum-beryllium. This can be minimized by fixturing the component so the EDM fluid does not puddle where the part is in contact with the metal fixture. Chemical conversion coatings have been used to protect aluminum-beryllium from corrosion during EDM operations.

Galvanic corrosion has occurred during the etching of beryllium and was traced to soft copper from the jaws of a machining clamp that had smeared onto the hard beryllium surface.

A beryllium x-ray window, brazed in a stainless steel frame, suffered significant pitting corrosion in less than 5 min of metallographic polishing. The electrolyte solution used in polishing allowed galvanic corrosion to occur between the beryllium and the stainless steel. The window was reground and polished successfully using a nonelectrolyte solution.

Fingerprint contamination of in-process parts is another common problem. Certain atmospheric conditions cause the salt in a fingerprint to seriously etch a beryllium surface. In addition to causing cosmetic issues, the etched fingerprint may cause a critically sized finished component to be rejected or to fail due to poor coating adherence. Complete removal of all evidence of fingerprints is strongly recommended before any etching or coating process.

Etching Problems. Micropitting of an etched beryllium or aluminum-beryllium surface is natural and cannot be prevented. The objective during etching is to prevent microscopic imperfections from becoming macrodefects visible to the naked eye and likely to affect the mechanical behavior of the metal. Most problems that occur during etching can be traced to an unclean or improperly cleaned surface, to contamination of the acid baths, or to the wrong choice of etchant.

Cleaning. The metal surface must be clean of oxides in order to obtain a uniform initiation and a uniform rate of attack during the process. The oxides are best removed using a mechanical process, such as machining, sanding, or grinding. Heat treating a finished part in vacuum prior to etching can produce nonuniform etching if the oxide film has variable thickness across the part. Sometimes, a geometric pattern of machine tool marks will appear after etching a part machined to precision tolerance. This problem occurs when the part has been rough machined, stress relieved, and finish machined with very light cuts to the final dimensions prior to etching. The rough machining step leaves deep grooves that oxidize during the stress relief, even when carried out in a good vacuum. If the finish machining operation does not remove sufficient metal to clean up all of the rough machining tool marks, the oxidized bottoms of the grooves from rough machining will be close to the surface. These grooves may not be visible due to their fineness or because smeared metal from the finish machining has covered them. The etching process reveals the grooves from the rough machining, because heavy oxide films dissolve at a slower rate than the metal. The solution to this problem is to reduce the depth of cut at the end of the rough machining step, minimizing the depth of the grooves after rough machining.

Organic contamination should be removed using nonchlorinated organic solvents only. Vapor degreasing is a commonly used technique. Alkaline cleaners are also excellent for removing organic contaminants. A clean beryllium surface should not exhibit a water break, an area where there is no wetting.

After cleaning, the surface should not be touched with bare hands. Clean white cotton, nylon, polyethylene, or rubber gloves are usually used. If anything else is touched with the gloves, a clean pair should be put on before touching the beryllium again.

Acid Contamination. The most notorious cause of macropit formation in etched beryllium surfaces is the presence of chloride ions. Etching solutions should be prepared with chloride-free water. Hydrochloric acid or chloride salts should not be part of the composition of the etching reagent.

Replacing acid solutions should be done on a regular basis. Continuously adding fresh acid to a spent acid solution can cause etching problems.

Acid solutions contaminated with other metal ions can cause significant corrosion problems. Beryllium will chemically displace most metals from solution, resulting in the plating of the metal onto the beryllium surface. In doing so, it forms a galvanic cell, and pitting can occur. This can also occur when acid solutions have been used on other metals or when the acid solution has etched significant beryllium to cause a significant increase in the metal ion content of the solution.

The metal removal rate is also influenced by the concentration of dissolved beryllium in the etchant. As the beryllium concentration increases, the dissolution rate decreases, even if the hydrogen ion content is maintained by replenishing the acid.

In both cases, completely replacing the acid solution on a regular basis eliminates contamination problems.

Acid Bath. Choosing the correct etchant is essential to preventing macropitting problems during etching. In general, the 2-2-2 etch can be used for most light removal (up to approximately 125 μm, or 5 mils). If the material has slight surface imperfections, such as porosity, scratches, or gouges, the acid can cause them to grow larger. This can become a significant problem when more than 125 μm (5 mils) is removed per surface. The H_2SO_4-HF solution discussed earlier is a better choice when a large amount of removal is required or when the material contains surface imperfections. This H_2SO_4-HF solution has also been used to remove pits and craters created by an improper etch. A final light etch using HNO_3-HF must be performed to remove the smut caused by the H_2SO_4.

Other Contact. Careful thought should be given to all materials that come in contact with beryllium. By taking the proactive stance of understanding the chemical composition of these materials, corrosion problems can be avoided.

Incomplete removal of dye penetrant solution for nondestructive testing has been reported to cause localized attack if it is merely wiped off the surface. Because the dye penetrant solution seeps out of crevices very slowly, this problem is usually not discovered until well after the occurrence.

Precision components that cannot be acid etched but are lapped to final size are susceptible to corrosion as a result of unremoved microcracks. Improper lapping of the part to remove only a few micrometers (tenths of a mil) of stock can cause smearing of metal and trapping of contaminants in microcracks, which can cause corrosion of the component at a later time. A free-cutting diamond paste is recommended as the lapping agent for this type of operation.

Contact with apparently dry materials has also been found to cause corrosion of beryllium. Beryllium was etched when placed on an inspection bench on which a rubberized mesh was used to prevent nicking and scratching of finished parts.

Corrosion occurred on small beryllium components inserted into plastic shop-routing folders when photocopied routing sheets were in direct contact the components.

Handling and Storage Corrosion Problems and Procedures

In handling and packaging beryllium components for shipment or storage, it is important to maintain a clean surface, avoid humid environments, and avoid contact with solid materials that are not compatible with beryllium.

Handling of beryllium parts with bare hands is often done and is not harmful when the part is in a rough or semifinished stage. In general, a finish-machined surface, even if it is to be acid etched to remove machine-damaged surface

material, should not be handled with bare hands. A fingerprint left on the surface for some time, during which it may etch the beryllium, may retard the beneficial aspects of the acid-etching treatment or at least may provide a questionable artifact after etching. Fingerprints that have etched the beryllium adversely affect conversion or passivation coatings by disrupting the continuity and effectiveness of the coating.

The common practice in handling finished and semifinished parts (or when fingerprinting is unacceptable) is to use protective gloves. White cotton, nylon, polyethylene, or rubber gloves are usually used. It is important to maintain cleanliness of the gloves to ensure that contaminants are not transferred to the beryllium from the gloves.

Packaging for Shipment. Polyethylene bags are extensively used by industry as protective containment and as barriers to contact between beryllium and its surrounding. A desiccant in a permeable container is often placed inside the polyethylene bag to remove undesirable moisture. Because the desiccant has limits on the amount of moisture it can remove, the part being placed in the bag should be clean and dry. An argon gas purge of the interior of the bag is often used as a means of displacing the moisture initially present. An effective seal at the bag opening is provided by an integrally molded interlocking seal, overlapping and taping, or sealing the bag with heat.

Molded foam, formed plastic foam, and contoured fiber-type insulation materials are typical means of supporting and protecting large beryllium structures or components against mechanical damage inside a shipping container. When support is desired in all directions (to protect the part if the container is overturned), a molded upper closure is used to totally encase the structure with supporting material. However, in almost every case, a polyethylene bag provides an effective separator between beryllium and the contacting support material.

The importance of isolating beryllium from other packing materials cannot be stressed enough. In one case, a molded styrofoam support used for shipment of a complex satellite boom caused severe localized etching of the beryllium at points of pressure contact. While the beryllium part was not shipped in direct contact with the styrofoam, the part had been laid on the foam after being removed from its polyethylene bag for inspection. Evidence suggests the etching resulted from attack by chemical compounds contained in the styrofoam packing materials.

Celotex insulating board (composed of 80 wt% sugarcane fiber, 10 wt% paper, and 10 wt% starch), which is used as a packing material, was studied to assess the risk of corrosion when dust from the material and moisture from the air contact a beryllium surface (Ref 45). The packing material is known to contain aggressive anions, including chloride.

Storage of beryllium components while awaiting assembly or use can be safely accomplished under the conditions used for shipment, that is, in a compatible container made of metal or polyethylene with a desiccant to maintain a dry storage atmosphere. In high-humidity conditions, particularly near coastal regions, long-term storage has been successfully accomplished by placing material in a cabinet with a light bulb to keep the interior at approximately 50 °C (120 °F). A room or chamber with humidity control is also effective in preventing corrosion of beryllium components during storage periods of several years. The following points should be considered in safely storing components for extended periods of time:

- Ensure that the component entering storage is free of corrosion-causing contaminants
- Maintain a moderately dry and noncondensing environmental atmosphere
- Ensure against contact with materials of nonproven compatibility

Corrosion-Protection Surface Treatments and Coatings

The types of coatings used on beryllium and aluminum-beryllium belong to these major categories:

- Chemical conversion coatings
- Anodized coatings
- Plated coatings
- Organic coatings
- Plasma-sprayed coatings

General summaries of the coatings developed for beryllium in the 1960s are contained in Ref 3, 46, and 47. Specific processing parameters for the application of these coatings will vary, depending on the material being coated. Most coating vendors consider their coating processing parameters proprietary. Individual coaters may also have their own proprietary procedures for cleaning, but the goal should be the same: a clean surface capable of being coated and delivering consistent performance. There are many coating vendors but only a few with experience in coating beryllium-containing materials. Choosing a coating vendor with experience in coating beryllium materials will help avoid potential problems.

Early evaluation of coatings was performed using the ASTM B 117 salt fog test or a humidity test to determine the relative effectiveness of corrosion protection. In addition, wipe testing of the surface is now performed to assess the relative effectiveness of corrosion protection.

Surface Preparation. For any type of coating, preparation of the specimen surface is critical in achieving an adherent coating. The three major steps in surface preparation are degreasing, acid etch, and activation dip. It is preferred that the process continues uninterrupted from the degreasing to the coating. It is possible to dry the part after degreasing or etching, if necessary. However, the part must remain wet between the activation and coating steps (for processes that involve dipping into a solution). If there is an interruption of the process, the procedure should restart at the etching step. One approach for the precoating preparation is detailed as follows. Other approaches can be used if they accomplish the goal of a clean, oxide-free surface capable of being coated.

Degreasing is performed to remove organic contaminants. A common problem is incomplete removal of the marking or layout ink used by the machinist. The majority of these marks should be removed during this process. Vapor degreasing using a dry solvent is effective in removing organic soils. Samples are exposed to solvent vapors for 30 min, with a periodic spray of clean liquid solvent. The parts are heated by the solvent vapor and must be cooled before continuing. Room-temperature degreasing can also be performed using a toluene (or other solvent), followed by a thorough rinse with (dry) acetone to remove any adhering toluene film. Organic contamination can be removed using alkaline solutions.

The primary purpose of the acid-etch step is the removal of inorganic contamination, mainly beryllium oxide. The industry-wide standard mixture of 40% nitric acid and 2% hydrofluoric acid is excellent for this purpose. No evidence of the marking or layout ink used by the machinist should be observed after this step. Two short etches of 20 s each, with a distilled water rinse in between, is better than one long etch. A thorough rinse in distilled water finishes this step.

The final step is an activation step. This step is optional, because good coatings may be obtained without performing it. However, this step adds a level of robustness to the coating process. The activating solution is prepared by diluting 83 mL of concentrated ammonium hydroxide with distilled water to 375 mL. The solution is neutralized to a pH of 6.4 with glacial acetic acid and cooled to room temperature. Finally, 4.2 g of ammonium fluoride are added to the solution, which is then diluted to a final volume of 500 mL. A vigorous reaction occurs when a beryllium sample is introduced into this solution. However, no dimensional changes have been measured after 2.5 h of immersion. The part is removed after a 1 min dip in the activating solution, immediately rinsed in distilled water, and placed in the coating solution. It is unknown if the activating solution has been used to preclean aluminum-beryllium parts for coating.

Chemical conversion coatings or chemical films refer to a number of coatings, including chromate, phosphate, phosphate-chromate, and oxalate. These coatings are applied by a simple dip treatment in solutions of the desired chemistry. Of the various conversion coating chemistries listed previously, chromate coating provides the best corrosion protection for beryllium and aluminum-beryllium composites. Of the available chromate conversion coating solutions, Alodine (MacDermid Acumen) and Iridite (Amchem Products) provide good results. Conversion coating solutions containing sulfuric acid should be avoided.

In the United States, the coating for beryllium or aluminum-beryllium composites is typically specified as MIL-C-5541, even though this specification was written for conversion coating of aluminum alloys.

The coatings are extremely thin, typically 0.013 mm (0.5 mil) thick, and not generally electrically insulating. Thickness is varied by dip time. Typical dip time is approximately 6 min.

Conversion coatings are soft when first deposited and can be damaged if not properly dried. The recommended drying time is 24 h.

Because chemical films are created from reactions with the base metal surface, abrasion of the coating could produce fine particulates that could become airborne (see the section "Health and Safety" in this article).

Several nonchromium replacements for the chromate conversion coating have been developed and have shown equivalent corrosion protection for aluminum alloys. Evaluation of these coatings for both beryllium and aluminum-beryllium composites is planned in the near future.

A chromate conversion coating can be used by itself for light-duty corrosion protection or as a substrate for application of organic paints, epoxy primers, or, more recently, powder coatings for improved corrosion protection. The structure of the conversion coating provides better paint adhesion than is possible on bare metal. The overcoats also help mitigate the potential problem of beryllium-containing particulates being released from the surface with light abrasion.

Beryllium Substrate. Chromate conversion coatings provide reasonable protection for beryllium during handling and storage and against attack by salt-containing environments for moderately long time periods. One investigation demonstrated the ability of a chromate-type coating on S-100 beryllium to hold up well in a 100% relative humidity (RH) test involving fifty 6 h cycles at 75 °C (170 °F) and in a 5% salt spray test for a period of 120 h (Ref 48).

Another study found that a passivation chromate treatment applied to a type of beryllium that showed susceptibility to white spot formation in moist air was very effective in improving resistance to such attack (Ref 49). The treatment involved a 30 min dip in a solution consisting of 25% H_3PO_4, 25% (saturated) solution of potassium chromate (K_2CrO_4), and 50% deionized water. Specimen life in 100% RH at 70 °C (160 °F) increased from 1 day to 10 to 14 days because of the passivation treatment.

A chromate conversion coating is reported to prevent the oxidation of beryllium up to 927 °C (1700 °F) (Ref 48).

A chromate conversion coating provided adequate protection of beryllium heat sinks on land-based military brake systems for many years. Carrier-based aircraft required a better corrosion protection scheme, which is described in the section on plating.

Aluminum-Beryllium Substrate. Chromate conversion coatings applied to aluminum-beryllium provide some corrosion protection in less hostile salt environments but do not pass the MIL-C-5541 salt fog test requirements for chemical films. One vendor has been able to produce a chemical film coating that not only passed the 168 h test but also passed a 500 h salt fog test by using a proprietary surface preparation technique. This coating has also been used to reduce corrosion during wire EDM machining.

Fluoride Coatings. A BeF_2 coating was produced by treating beryllium in fluorine above 520 °C (970 °F), resulting in a glassy-appearing water-insoluble coating. The structure of the coating is of the rhombic tridymite type. This type of coating was shown to be very effective in resisting corrosion in chloride-containing water and in distilled water (Ref 50). Coatings 0.2 and 1.2 μm (0.008 and 0.05 mil) thick were unchanged after 3000 h in distilled water at room temperature. A 0.2 μm (0.008 mil) thick coating provided effective protection in water containing a 150 ppm concentration of Cl^- ion.

Anodized Coating. Beryllium and aluminum-beryllium can be anodized using processes similar to those used for anodizing aluminum (MIL-A-8625F). Only chromic anodization (type 1) can be performed on these materials. Sulfuric anodize (type 2) and hard anodize (type 3) cannot be performed, because the solutions attack the beryllium surface. Anodizing solutions containing sulfuric acid should be avoided with beryllium and aluminum-beryllium.

The anodized coating is typically called out on drawings as a U.S. Navy specification OD-58710 for beryllium. MIL-A-8625F type 1 is typically called out for aluminum-beryllium, even though the specification does not apply specifically to aluminum-beryllium.

The anodized coatings are electrically insulating, except when measured using mercury contact.

Because anodized coatings are created by the reactions with the base metal, abrasion of the coating could produce fine particulates that could become airborne (see the section "Health and Safety" in this article).

Anodization can be used by itself for corrosion protection or used as a substrate for application of organic paints, epoxy primers, or, more recently, powder coatings for improved corrosion protection. The structure of the anodized coating provides better paint adhesion than is possible on bare metal. These overcoats also help mitigate the potential problem of beryllium-containing particulates being released from the surface with light rubbing or abrasion.

Beryllium Substrate. Anodization has been shown to improve the resistance of beryllium to corrosion in normally corrosive aqueous solutions and to oxidation in air at elevated temperature. In synthetic seawater, unprotected beryllium corrodes at a rate approximately 21 times that of anodized beryllium. At elevated temperature in air, unprotected beryllium oxidizes at rates greater than 100 times that of anodized beryllium.

Chromic acid/nitric acid anodic coatings have been found to protect beryllium effectively in environments for the following times (Ref 3):

- 2400 h in a humidity cabinet
- 3 months at 40 °C (100 °F) in tap water
- 2000 h in ASTM salt spray test

No evidence of pitting, staining, or other attack was observed after the tests. In another study, an approximately 5 μm (0.2 mil) thick anodic coating produced in a 1% H_2CrO_4 solution and sealed in boiling water produced no corrosion after exposure to 5% salt fog spray at 40 °C (100 °F) for 30 days (Ref 1).

Anodic coatings can provide protection from breakaway oxidation at temperatures up to 1200 °C (2190 °F). No additional weight gain was observed after approximately 20 h of exposure at 700 °C (1290 °F) and after 50 h of exposure at 817 °C (1500 °F). Oxidation occurs at 1030 °C (1890 °F) after 60 h of exposure, but the effective rate of oxidation is 100 times less than unprotected beryllium. Samples were also exposed to air with 1% moisture at 800 °C (1470 °F) for over 1000 h without evidence of attack. At higher temperatures, the normally dark anodic film turns the alabaster white of beryllium oxide.

Nitric acid (HNO_3), chromic acid (H_2CrO_4), potassium dichromate ($K_2Cr_2O_7$), sodium chromate (Na_2CrO_4), sodium dichromate ($Na_2Cr_2O_7$), and sodium hydroxide (NaOH) are common ingredients in many anodizing bath formations. A chromic acid bath produces a more uniform and denser anodized coating compared to other formulations.

Bath temperature is typically approximately room temperature. A lower anodizing bath temperature (< 5 °C, or 40 °F) will produce a more dense coating. Increasing the bath temperature produces a less dense coating. Bath temperatures exceeding 55 °C (130 °F) are not recommended.

A short rinse (20 to 30 s) in deionized water at 80 °C (175 °F) is followed by a 2 to 5 min rinse in deionized water at room temperature. A double rinse in acetone followed by a vacuum bakeout for 2 h minimum at 135 to 150 °C (275 to 300 °F) is recommended. Postanodizing treatments have included boiling water and sodium silicate solutions. Beryllium is typically not treated with any postanodizing solution treatments.

Anodizing in nondissolving-type electrolytes, such as oxalic acid, tartaric acid, and sodium silicate solutions, produces a very thin anodic film. The film provides little high-temperature protection and probably only light-duty corrosion protection.

Anodized films vary in thickness from 2.5 μm (0.1 mil) to several mils, depending on solution type, applied voltage, current density, bath temperature, and time of treatment. The as-applied anodized coat is either amorphous or crystalline BeO so fine that it cannot be detected as crystalline by x-ray diffraction. On heating above 850 °C (1560 °F), the coating is converted to crystalline BeO. By altering the temperature of

the anodization process, it is possible to grow a film that would show crystalline BeO by x-ray diffraction in the as-deposited state.

The appearance of the anodized coating is smooth, hard, uniform, and black. The color is black even though beryllium oxide is white, due to the fine particle size of the anodize film. If a glossy finish is desired, surfaces must be finish machined and lapped prior to anodizing. Minimal etching to activate the surface for anodization should be performed. A black matte appearance can be achieved by increasing etch time prior to anodization. The matte finish is probably the result of micropitting created by the nitric-hydrofluoric etching. Removal of only 2.5 μm (0.1 mil) with the acid etch is needed to produce the matte finish. A more distinct matte finish can be obtained with additional metal removal.

Beryllium oxide is the principal component in the anodized film. Chemical analysis has shown the chromium content of the film to be on the order of 10,000 ppm.

Anodized coatings are used in the mirror industry, where beryllium is used for its light weight, its high modulus of elasticity, and its high specific heat and thermal conductivity. Anodized coatings are selected for their high thermal emissivity and absorptivity values. Room-temperature solar absorptance of anodized beryllium is 0.95, and room-temperature total normal emittance is 0.85. The corrosion resistance of the anodized coating is an added benefit in this application. An anodized coating applied before lapping spherical mirror surfaces has been found to provide protection against pitting corrosion at the unlapped edge of the mirror. The lapping compound tends to move to the rim of the lens structure, where it will readily attack uncoated beryllium if allowed to stand even for relatively short periods of time.

Aluminum-Beryllium Substrate. Chromic anodization of aluminum-beryllium is more difficult than pure beryllium but is being done successfully. If done improperly, the resultant coating is a black smut on the surface that easily rubs off with very light contact. This problem has been solved by using several approaches. In one case, an anodized coating was produced that passed the 336 h salt fog test using a proprietary surface preparation technique. In another case, by Alumiplate (Alumiplate, Inc.) coating the aluminum-beryllium surface first, an anodized coating passed the 336 h salt fog test. In a third case, the smut problem was solved through process control measures. No data were available regarding salt fog corrosion testing of this last material.

The anodized color ranges from gray to black, depending on surface finish prior to coating and other processing conditions. Anodized aluminum-beryllium can be dyed various colors, similar to anodized aluminum alloys.

Chemical removal of the anodized coating on aluminum-beryllium leaves a film on the surface that prevents reanodization. Vapor honing to remove 8 to 12 μm (0.3 to 0.5 mil) produces a surface with minimal material removal that can be reanodized.

Sealing the anodized coating with an electrolyte solution is not recommended, because corrosion can occur during the sealing process. Topcoating with epoxy, paint, or powder coat will improve the corrosion resistance and minimize health and safety issues.

Plated Coatings. Beryllium and aluminum-beryllium can be plated to provide corrosion protection and for other specific performance requirements. A variety of metals have been electrodeposited successfully onto beryllium, including nickel, silver, copper, chromium, cadmium, iron, tin, and gold. While direct plating onto an activated beryllium surface can be done, electrodeposition of metals onto beryllium can be accomplished reliably only through a surface pretreatment that includes a zincate immersion coating. Complete coating coverage produces the best corrosion results; thus, multiple immersions in the zincate solution are recommended.

Both electroless and electrolytic nickel are used for light corrosion protection, wear resistance, and electrical contact/grounding. Cadmium can be plated over the nickel to improve corrosion resistance. Electrolytic nickel plating is also used to improve the polishability of mirrors used in the visible range. Aluminum, silver, or gold are plated over the nickel plating for these applications. A potential problem with nickel plating (as well as with most other metal platings) is that a galvanic cell is created wherever the coating is scratched. This cell has a large cathode/small anode ratio that will concentrate the corrosion attack along the scratch line.

Aluminum has been electroplated from an organic solution (Alumiplate) on both beryllium and aluminum-beryllium and has also been ion vapor deposited (IVD) on aluminum-beryllium. The advantage of these two coatings is that subsequent chromate conversion coating or anodization of the Alumiplate or IVD surfaces does not contain beryllium compounds. The other advantage is that these coatings can be hard anodized, while both uncoated beryllium and aluminum-beryllium cannot be hard anodized.

Manganese plating was developed to provide cathodic protection of beryllium brake segments used in carrier-based aircraft (Ref 51). Without the manganese coating, beryllium was in contact with steel and formed a galvanic couple in the presence of saltwater. Manganese was determined to be anodic to beryllium and acted as the sacrificial anode in the same environment.

A proprietary co-plated binary alloy has been used on beryllium to provide magnetic shielding.

A double zincate coating is required prior to electroless nickel plating. The Alumiplate process requires a zincate coating followed by a nickel strike prior to plating. The IVD process does not require any preplating preparation after the cleaning steps.

Nickel plating is performed on many different types of beryllium and aluminum-beryllium parts. Nickel plating has shown variable results in salt fog testing, which may be due to nonuniform processes or variations in coating thickness. Nickel plating with a cadmium overcoat passes the 96 h salt fog test.

Alumiplate coating on aluminum-beryllium has been used on heat flow modules for proprietary noncorrosion performance requirements. Chromic anodized and hard anodized coatings over Alumiplate-coated AlBeMet specimens have passed a 500 h salt fog corrosion test. Alumiplate coatings on beryllium have been experimentally evaluated with encouraging results. The IVD coating process has been evaluated only on aluminum-beryllium testpieces. Salt fog corrosion testing of this coating did not match that of the Alumiplate coating, which may be due to the more porous structure of the IVD coating.

Organic Coatings. Organic paint coatings are used for general corrosion protection or when an electrically insulating barrier between the beryllium or aluminum-beryllium component and another metallic structure is required to prevent galvanic attack. These coatings can be applied over a cleaned metal surface but form a better bond with the substrate when applied over a chemical conversion coating or anodized surface.

Organic coatings include paints, epoxy primers, and, more recently, powder coatings for improved corrosion protection. An advantage of organic coatings is that field repair is easy, should the coating become nicked or scratched.

An electrodeposited paint coating added over a passivation coating was found to provide suitable protection for beryllium structures requiring long-term storage capability (Ref 49). The black anodizing treatment yielded a coating that became troublesome because of scratching and chipping and the need for additional protection of uncoated sites where electrical contacts were attached.

A polyvinyl butyrol phosphating primer was evaluated for the Navy for atmospheric protection of several metals, including beryllium (Ref 52). A two-coating system was recommended for storage periods of 8 to 10 months in open atmospheric exposure.

An epoxy primer has been effective for general protection of sheet and tubular components in communications satellite platform structures. The primer is used on all exposed surfaces, and all individually-coated components are joined by adhesive bonding or mechanical fasteners. The primer is applied immediately after a flash etching of the surfaces to be coated and is cured by baking. The primer system of protection was selected to satisfy the requirement of years-duration storage capability for the fabricated structure.

Thermal- and Plasma-Sprayed Coatings. Aluminum oxide and tungsten carbide have been flame sprayed onto beryllium and lapped to a mirror finish for air bearings in guidance systems. Surface preparation for this type of coating violates the fundamental rule, "Do not use hydrochloric acid." The deep, intergranular

attack of this acid provides a rough surface to which the flame-sprayed coating can attach.

Chromium carbide has been plasma sprayed onto aluminum-beryllium for wear and corrosion resistance. An overcoat containing no cadmium was applied for corrosion resistance. Tabor abrasion tests were performed on specimens using a 500 g load for 4000 cycles. The specimens were then subjected to a 500 h salt fog test. The coating was not abraded through to the aluminum-beryllium substrate, and the specimens passed a 500 h salt fog test.

REFERENCES

1. C.B. Gilpin and T.L. Mackay, "Corrosion Research Studies on Forged Beryllium," AFML-TR-66-294, Air Force Materials Laboratory, Jan 1967
2. J.L. English, Corrosion of Beryllium in Air, *The Metal Beryllium,* D.W. White, Jr. and J.E. Burke, Ed., American Society for Metals, 1955, p 530–532
3. A.J. Stonehouse and W.W. Beaver, Beryllium Corrosion and How to Prevent It, *Mater. Prot.,* Vol 4, 1965, p 24–28
4. L.E. Gatzek, "Corrosion Control of Missiles in Long-Term Silo Environments," paper presented at the National Aeronautics and Space Engineering Meeting, Oct 5–9, 1964 (Los Angeles, CA)
5. J.N. Wanklyn and P.J. Jones, The Aqueous Corrosion of Reactor Metals, *J. Nucl. Mater.,* Vol 6 (No. 3), 1962, p 291–329
6. P.D. Miller and W.K. Boyd, Beryllium Deters Corrosion—Some Do's and Don'ts, *Mater. Eng.,* Vol 68 (No. 1), 1968, p 33–36
7. J.L. English, Corrosion of Beryllium in Water, *The Metal Beryllium,* D.W. White, Jr. and J.E. Burke, Ed., American Society for Metals, 1955, p 533–548
8. T.L. Mackay and C.B. Gilpin, *Corros. Met.,* Vol 6, 1968, p 235–240
9. J.L. English, Report ORNL-772, United States Atomic Energy Commission, 1951
10. A.M. Kinan et al., "The Significance of Inclusion/Precipitates in Beryllium," paper presented at 1972 WESTEC Conference (Los Angeles, CA), American Society for Metals, March 1972
11. H.A. Moreen and A.G. Gross, Jr., "Pitting Corrosion in Beryllium," unpublished report, Boeing North America, Inc., Autonetics and Missle Systems Division
12. M.A. Hill, R.J. Hanrahan, C.L. Haertling, R.K. Schulze, and R.S. Lillard, Influence of Beryllides on the Corrosion of Commercial Grades of Beryllium, *Corrosion,* Vol 59 (No. 5), May 2003, p 424–435
13. A. Venugopal, D.D. Macdonald, and R. Varma, Electrochemistry and Corrosion of Beryllium in Buffered and Unbuffered Chloride Solutions, *J. Electrochem. Soc.,* Vol 147, (No. 10), Oct 2000, p 3673–3679
14. E. Gulbrandsen and A.M.J. Johansen, Study of the Passive Behaviour of Beryllium in Aqueous Solutions, *Corros. Sci.,* Vol 36 (No. 9), Sept 1994, p 1523–1536
15. R.U. Vaidya, M.A. Hill, M. Hawley, and D.P. Butt, Effect of Pitting Corrosion in NaCl Solutions on the Statistics of Fracture of Beryllium, *Metall. Mater. Trans. A,* Vol 29 (No. 11), Nov 1998, p 2753–2760
16. M.A. Hill, J.F. Bingert, and R.S. Lillard, The Relationship between Crystallographic Orientation and the Passivity and Breakdown of Beryllium, *Electrochem. Soc. Series,* Vol 98 (No. 17), 1999, p 265–273
17. J.R. Friedman and J.E. Hanafee, "Corrosion/Electrochemistry of Monocrystalline and Polycrystalline Beryllium in Aqueous Chloride Environment," Lawrence Livermore National Laboratory Report UCRL-ID-137482, Jan 2000
18. R.S. Lillard, Factors Influencing the Transition from Metastable to Stable Pitting in Single-Crystal Beryllium, *J. Electrochem. Soc.,* Vol 148 (No. 1), Jan 2001, p B1–11
19. R.S. Lillard, Relationships between Pitting Corrosion and Crystallographic Orientation, An Historical Perspective, *Electrochem. Soc. Series,* Vol 2002 (No. 13), 2002, p 334–343
20. M.A. Hill, R.S. Lillard, and D.P. Butt, "Galvanic Corrosion of Beryllium Welds," Report LA-UR-97-3163, Aging, Compatibility, and Stockpile Stewardship Conference, Sept 30 to Oct 2, 1997 (Albuquerque, NM), Sandia National Laboratories
21. R.U. Vaidya, S.M. Brozik, A. Deshpande, L.E. Hersman, and D.P. Butt, Protection of Beryllium Metal against Microbial Influenced Corrosion Using Silane Self-Assembled Monolayers, *Metall. Mater. Trans. A,* Vol 30 (No. 8), Aug 1999, p 2129–2134
22. J.C. Birkbeck, N.L. Kuehler, D.L. Williams, and W.E. Moddeman, X-Ray Photoelectron Spectroscopic Examinations of Beryllium Metal Surfaces Exposed to Chlorinated Solvents, *Surf. Interface Anal.,* Vol 27 (No. 4), April 1999, p 273–282
23. H.L. Logan and H. Hessing, "Summarizing Report of Stress Corrosion of Beryllium," NBS-6, National Bureau of Standards, Dec 1955
24. R.A. Miller et al., *Corrosion,* Vol 23, 1967, p 11–14
25. C.M. Packer, "Stress Corrosion Cracking of Beryllium," Report LMSC-288140, General Research in Materials and Propulsion, Section 6, Lockheed Corporation, Jan 1960; also LMSD-49735.
26. E. Semerad, T. Gross, and H. Lichtl, "Stress-Corrosion Cracking Testing of AlBeMet 162, Extruded, HIP and EB Weld," Metallurgy Report 3276, European Space Agency, Noordwijk, The Netherlands, Jan 2002
27. "Determination of the Susceptibility of Metals to Stress-Corrosion Cracking," ECSS-Q-70-37A, European Space Agency, 1998
28. E.A. Gulbransen and K.F. Andrew, The Kinetics of the Reactions of Beryllium with Oxygen and Nitrogen and the Effect of Oxide and Nitride Films on Its Vapor Pressure, *J. Electrochem. Soc.,* Vol 97, 1950, p 383–385
29. D. Cubicciotti, The Oxidation of Beryllium at High Temperatures, *J. Am. Chem. Soc.,* Vol 72 (No. 5), May 1950, p 2084–2086
30. D.W. Aylmore, S.J. Gregg, and W.B. Jepson, The High Temperature Oxidation of Beryllium, Part I: In Dry Oxygen, *J. Nucl. Mater.,* Vol 2 (No. 2), 1960
31. D.W. Aylmore, S.J. Gregg, and W.B. Jepson, The High Temperature Oxidation of Beryllium, Part IV: In Water Vapor and Moist Oxygen, *J. Nucl. Mater.,* Vol 3 (No. 2), 1961
32. W.B. Jepson, J.B. Warburton, and B.L. Myatt, The High Temperature Oxidation of Beryllium and the Fate of Beryllium Carbide Inclusions, *J. Nucl. Mater.,* Vol 10 (No. 2), 1963
33. W.G. Bradshaw and E.S. Wright, "Reaction Kinetics of High Temperature Corrosion of Beryllium in Air," Paper 25, Conference on Metallurgy of Beryllium, Institute of Metals, (London), Oct 1961
34. S.J. Gregg, R.J. Hussey, and W.B. Jepson, The High Temperature Oxidation of Beryllium, Part II: The Reaction with CO_2 and CO, *J. Nucl. Mater.,* Vol 2 (No. 2), 1960
35. W.J. Werner and H. Inouye, "The Reactions of Beryllium with Wet Carbon Dioxide," Paper 32, Conference on Metallurgy of Beryllium, Institute of Metals, (London), Oct 1961
36. T. Raine and J.A. Robinson, The Corrosion of Beryllium with Calcium in CO_2, *J. Nucl. Mater.,* Vol 5 (No. 3), 1962
37. V.D. Scott and G.V.T. Ranzetta, Electron Metallography of the Corrosion of Beryllium and Beryllium-Calcium Alloys, *J. Nucl. Mater.,* Vol 9 (No. 3), 1963
38. G.R. Smolik, B.J. Merrill, and R.S. Wallace, Implications of Beryllium: Steam Interactions in Fusion Reactors, Proceedings of the Fifth International Conference on Fusion Reactor Materials ICFRM-5, Nov 17–22, 1991 (Clearwater, FL), Minerals, Metals and Materials Society, ASM International and Atomic Energy Society Japan; *J. Nucl. Mater.,* Vol 191–194, part A, Sept 1992, p 153–157
39. F. Druyts, B. Beaumont, G. Tonon, B. de Gentile, and P. Libeyre, Determination of Be/Air and Be/Steam Reactivities with TG/DTA, Symposium on Fusion Technology 1998 (Marseille France), Vol 1–2 (No. 1744), Euratom-CEA, p 1597–1600
40. R.A. Anderl, R.J. Pawelko, G.R. Smolik, F. Scaffidi Argentina, and D. Davydov, Steam Chemical Reactivity of Be Pebbles and Be Powder, *Fusion Technol.,* Vol 38 (No. 3), Nov 2000, p.283–289; Fourth International Workshop on Beryllium Technology for

Fusion, Sept 15–17, 1999 (Karlsruhe, Germany), International Energy Agency
41. F.L. Bett and A. Droycott, "The Compatability of Beryllium with Liquid Sodium and NaK in Dynamic Systems," Paper 1091, Second United Nations Conference on the Peaceful Uses of Atomic Energy, 1958
42. W.W. Kendall, "Corrosion of Beryllium in Flowing Sodium," U.S. AEC Report GEAP-3333, Jan 15, 1960
43. G.E. Darwin and J.H. Buddery, Reactions with Corrosive Environments, *Beryllium,* Butterworths Scientific Publications, London, 1960, p 259–262
44. H. Feuerstein, H. Graebner, J. Oschinski, and S. Horn, Compatibility of Refractory Metals and Beryllium with Molten Pb-17Li, Proceedings of the 1995 Seventh International Conference on Fusion Reactor Materials, ICFRM-7, Sept 25–29, 1995 (Obninsk, Russia), Institute of Physics and Power Engineering; *J. Nucl. Mater.,* Vol 233–237B, Oct 1996, p 1383–1386
45. M.A. Hill, R.S. Lillard, and D.P. Butt, "Corrosion of Beryllium Exposed to Celotex and Water," Aging, Compatibility, and Stockpile Stewardship Conference, Sept 30 to Oct 2, 1997 (Albuquerque, NM), Sandia National Laboratories
46. J.G. Beach, "Electrodeposited, Electroless, and Anodized Coatings on Beryllium," Memorandum 197, Defense Materials Information Center, Sept 1, 1964
47. "Corrosion of Beryllium," Report 242, Defense Materials Information Center, Dec 11, 1967
48. J. Booker and A.J. Stonehouse, Chemical Conversion Coatings Retard Corrosion of Beryllium, *Mater. Prot.,* Vol 8 (No. 2), 1969, p 43–47
49. S.J. Morana, "Surface Passivation Coating for Beryllium Metal," paper presented at the Air Force Materials Laboratory 15th Anniversary Corrosion of Military and Aerospace Equipment Technical Conference, May 23–25, 1967
50. P.M. O'Donnell, Beryllium Fluoride Coating as a Corrosion Retardant for Beryllium, *Corros. Sci.,* Vol 7, 1967, p 717–718
51. R.M. Paine and A.J. Stonehouse, "A Corrosion Protection System for Beryllium in Aircraft Brake Applications," Brush Wellman Technical Report TR-584, Dec 1976; also presented at Corrosion'77, March 14–18, 1977 (San Francisco, CA), National Association of Corrosion Engineers
52. G. Ya Terlo, "Protection of Steel and Light Alloys with Polyvinyl Butyral Phosphatizing Primers," VL-023, AD628185, Department of the Navy, 1966

SELECTED REFERENCES

- P.P. Budnikov, R.A. Belyaev, P.L. Volodin, N.A. Rakhalin, V.A. Furaev, and M.I. Tumbakova, Corrosion of Aluminum and Beryllium Oxides in Gaseous Ammonia at Temperatures of 200 to 800 C, *Zh. Prikl. Khim.,* Vol 44 (No. 1), Jan 1971, p 54–59; English translation in *J. Appl. Chem. USSR,* Vol 44 (No. 1), part 1, Jan 1971, p 51–55
- B.V. Cockeram, and G. Wang, The Pesting of Intermetallic Compounds, *Oxidation and Corrosion of Intermetallic Alloys,* Purdue University, HTMIAC/CINDAS, 1996, p 333–350
- W.E. Dalton, Passivation of Beryllium in an Ultrasonic Field, *Plat. Surf. Finish.,* Vol 70 (No. 5), 1983, p 106–107
- I.N. Ganiev, K.O. Odinaev, A.A. Safarov, and K.M. Nazarov, Corrosion-Electrochemical Behavior of Aluminum-Beryllium Alloys with Yttrium, Lanthanum, and Cerium, *Russ. J. Appl. Chem.,* Vol 73 (No. 2), Feb 2000, p 235–237
- M. Pourbaix, *Atlas of Electrochemical Equilibria in Aqueous Solutions,* Pergamon Press, 1974, p 132–138
- M. Seki, T. Yamanishi, W. Shu, M. Nishi, T. Hatano, M. Akiba, H. Takeuchi, K. Nakamura, M. Sugimoto, K. Shiba, S. Jitsukawa, and E. Ishitsuka, Development of Fusion Nuclear Technologies at Japan Atomic Energy Research Institute, *Fusion Sci. Technol.,* Vol 42 (No. 1), July 2002, p 50–61
- G.F. Tikhinskij and G.I. Volokita, Beryllium Foils for Devices and Physical Experiments, *Prib. Tekh. Eksp.,* No. 5, Sept–Oct 1994, p 191–195

ASM Handbook, Volume 13B: Corrosion: Materials
S.D. Cramer, B.S. Covino, Jr., editors, p370-384
DOI: 10.1361/asmhba0003828

Corrosion of Uranium and Uranium Alloys

Jennifer A. Lillard and Robert J. Hanrahan, Jr., Los Alamos National Laboratory

URANIUM as an industrial material is limited to areas where its nuclear properties and/or high density are required. Due to the high value of many applications and the reactivity of uranium, there have been numerous studies of uranium corrosion in both dry and aqueous environments. This article reviews general corrosion of uranium and its alloys under atmospheric and aqueous exposure as well as with gaseous environments. Reaction rates for general corrosion and oxidation are dependent on the surface area available for reaction and are therefore normalized to the surface area of the specimen. The exception is reactions that only occur at isolated sites on a specimen (e.g., pitting). In this case, the surface normalized rate underestimates local penetration rates. Stress-corrosion cracking and hydrogen embrittlement of uranium are discussed briefly. In view of its catastrophic nature, a detailed review of the corrosion of uranium in hydrogen (hydriding) has also been included. Protection of uranium using plating and surface modification is discussed, with particular emphasis on techniques that have proved successful in industrial applications. Finally, storage conditions and environmental, health, and safety considerations are briefly addressed.

The corrosion properties of uranium are minimal, but uranium is often used in radiation shields, counterweights, and armor-piercing kinetic energy penetrators because of its high density (68% greater than lead) and ease of fabrication. Uranium has moderate strength and ductility and can be cast, formed or machined, and welded by standard methods. Pure uranium metal and uranium alloys have also been used as nuclear fuel in plutonium production reactors. Uranium corrodes in room-temperature air at a rate slightly less than that of cast iron. The corrosion rate increases exponentially as temperature and humidity increase. At temperatures below about 200 °C (390 °F), the primary corrosion product is nominally UO_2, and if hydrogen is present or is generated during corrosion, UH_3 can form. Additionally, aqueous electrochemical polarization can produce UH_3 directly or hydrated UO_3. At temperatures above about 200 °C (390 °F), U_3O_8 becomes the primary corrosion product.

Similar to the group IV metals, uranium forms colorful interference films in the early stages of oxidation that can be correlated with the thickness of the oxide. Larson found that as uranium oxide thickness increased, the observed film color changed in the following order: silver, yellow, red brown, violet, blue, second-order silver, second-order yellow, and gray (Ref 1). Caution must be exercised, however, because the second-order colors appear the same as first-order and yet represent significantly different thicknesses. Many of the alloys of uranium under atmospheric conditions grow scales to characteristic thickness in the interference regime and therefore are often identified by their color (e.g., U-0.75Ti often appears blue and U-6Nb is often blue or gold).

The corrosion resistance of uranium can be increased by adding alloy elements. Alloys are generally still susceptible to corrosion, particularly pitting in salt solutions and galvanic corrosion. The major uranium alloys can all trace their history back to work during the 1940s, which was devoted to the development of metallic nuclear fuels for reactors. As a consequence, virtually all of the common uranium alloys have reasonable corrosion resistance. Uranium is most commonly alloyed with elements that stabilize the γ phase such as titanium, niobium, molybdenum, zirconium, and vanadium, and their properties are summarized below. Pure uranium has also been used in reactors by roll cladding with aluminum (Ref 2). The corrosion resistance of uranium-aluminum alloys was therefore studied extensively in the 1950s.

U-0.75Ti is used when strength and ductility are important. The alloy is more resistant to corrosion than unalloyed uranium, but still suffers significant oxidation accompanied by hydrogen production in vapor and aqueous environments, especially when galvanically coupled to more noble metals. Small amounts of hydrogen can embrittle the alloy. Because hydrogen is generated as a result of atmospheric and aqueous solution corrosion, the alloy is susceptible to environmentally assisted cracking. Protective coatings are often employed to reduce corrosion.

U-6Nb is commonly used for applications requiring good corrosion resistance and ductility. It is less susceptible to environmental embrittlement than U-0.75Ti and other alloys. Alloys with 8 to 12 wt% Nb have excellent corrosion resistance, but they also have higher strengths and are therefore more susceptible to environmental cracking. Uranium-niobium alloys are most corrosion resistant when used in the gamma quenched condition and can undergo low-temperature phase transformations. Hence, the applications of U-6Nb are limited to near ambient temperatures.

Uranium-molybdenum alloys are not as widely used as uranium-titanium and uranium-niobium alloys because they do not perform as well as other alloys. For example, U-2Mo is less corrosion resistant and more susceptible to environmental cracking than U-6Nb; U-10Mo has good corrosion resistance, but it exhibits severe environmental assisted cracking and residual stress. U-10Mo was extensively investigated as a fuel material for pressurized water reactors (PWRs) because it is not susceptible to the low-temperature phase transformations observed in U-6Nb.

Ternary, quaternary, and higher-order alloys show improved corrosion resistance. These alloys include U-7.5Nb-2.5Zr (Mulberry), U-0.5Nb-0.5Mo-0.5Zr-0.5Ti ($^1/_2$ quad), U-0.75Nb-0.75Mo-0.75Zr-0.75Ti ($^3/_4$ quad), U-1Nb-1Mo-1Zr-1Ti (1 quad), and U-1Nb-1Mo-1Zr-1Zr-0.5Ti-0.5V (1 quint). They do not exhibit significantly better strength-ductility combinations, quench-rate insensitivity, or resistance to environmentally assisted cracking and thus have limited application.

Aqueous Corrosion

Corrosion of uranium in aqueous solutions has been widely studied but can been difficult to interpret due to large variations in corrosion rates under similar test conditions. Uranium corrosion is very sensitive to the nature and concentration of dissolved gases and to impurities in the metal. For this reason, much of the early corrosion work was carried out using boiling water. This section looks at the dependence of uranium and uranium alloy corrosion on microstructure, alloying, solution chemistry, and temperature as well as galvanic interactions between uranium, its alloys, and other metals.

As with any metal, thermodynamics and kinetics govern the rate and type of corrosion. The Pourbaix diagram for uranium in water (Fig. 1, Ref 3) predicts stable, room-temperature phases based on electrochemical thermodynamics.* If the electrochemical potential and solution pH are known, the Pourbaix diagram will show the equilibrium phase of uranium (e.g., UO_2 is expected at pH 7 and -1 V_{SCE}, SCE is the saturated calomel reference electrode). However, the kinetics of a reaction may be so slow that the equilibrium phase is not reached. Furthermore, the diagram is only valid in the absence of substances that can form insoluble salts or soluble complexes. Electrochemical polarization techniques and weight loss/gain are commonly used to measure the kinetics of corrosion and to determine some of the parameters important in localized corrosion. The Pourbaix diagram and polarization techniques are used in the discussions that follow to better understand results of time-dependent weight-loss techniques as they apply to uranium and uranium alloy corrosion.

Microstructure and Alloying

Microstructural effects on uranium corrosion were reported as early as the 1950s (Ref 4, 5). Two observations were significant. First, corrosion rate was found to depend on impurity content, particularly iron and carbon (Ref 4). Second, corrosion rate could be reduced by quenching from the γ phase where impurities generally have a higher solubility (Ref 5). For this reason, elements that stabilize the uranium γ phase (e.g., Ti, Mo, Nb, and Zr) have been used to develop corrosion-resistant alloys. For example, weight-loss data in air-exposed water show that the corrosion rate decreases from about 3 μm/yr (0.12 mil/yr) for uranium (Ref 6) to about 0.5 μm/yr (0.02 mil/yr) for U-6Nb (Ref 7).

Uranium alloys are produced by vacuum induction or vacuum arc melting methods, and corrosion properties are often sensitive to cooling rate and postfabrication heat treatment. Heat treatment generally occurs at approximately 800 °C (1470 °F) (in the γ region) to put the alloying elements into solid solution; alloys are then allowed to slowly cool to allow diffusional decomposition or are quenched to form supersaturated metastable phases (Ref 8). Slow cooling does not significantly increase corrosion resistance (Fig. 2) because alloy-free, α uranium regions form. Quenching or quenching and aging, on the other hand, can significantly increase corrosion resistance. Corrosion resistance is lost if alloys are overaged because regions of the α phase form.

The oxides of uranium and it alloys also play a large role in corrosion resistance, and both the microstructure and composition are important. Generally, alloy elements are incorporated into the oxide and make it more resistant to corrosion or more "passive." For example, in uranium-niobium alloys, the presence and amount of Nb_2O_5 in the oxide have a direct effect on the susceptibility and rate of alloy corrosion. Results show that higher niobium alloys produce compact, passive oxides (Ref 10, 11).

Screening of a wide number of alloys for corrosion resistance was carried out using boiling water corrosion tests (Ref 12, 13). Niobium, molybdenum, zirconium, titanium, nickel, silicon, and aluminum all increased boiling water corrosion resistance. Vanadium required alloying above 1 wt% for improved corrosion resistance (Ref 6). Corrosion resistance was further increased when the alloys were heat treated in the γ region.

Waber examined more than 20 alloys and found some additions had no effect or were detrimental (Ref 6). Antimony, beryllium, copper, and tantalum provided no significant increase in corrosion resistance. Chromium protected uranium in boiling water, but protection was lost in chloride solutions. Bismuth and tin additions formed pyrophoric phases. Cerium, rhodium, and ruthenium increased the corrosion rate. Some elements showed synergistic effects (e.g., U-Nb-Zr), but their corrosion resistance was sensitive to heat treatment. The most commonly used and studied alloys contain Ti, Nb, Mo, (Nb + Zr), and (Nb + Mo + Zr + Ti), and further discussion is limited to these alloys.

Solution Chemistry

The behavior of uranium and uranium alloys in an electrolyte will depend on the pH of the solution and dissolved gases and salts.

Dissolved Gases. Atmospheric gas, dissolved in the solution, can alter the solution chemistry and corrosion behavior of uranium and its alloys. The most significant differences are observed between inert or reducing and oxidizing (e.g., oxygen) conditions. For uranium, this difference can affect the corrosion rate by over an order of magnitude (Ref 13). When oxygen is dissolved in solution, uranium corrosion is remarkably slowed compared to either inert or reducing gases. The corrosion rate of unalloyed uranium is about 300 μm/yr (12 mils/yr) in hydrogen-saturated water and about 8 μm/yr (0.3 mil/yr) in air-saturated water at 50 °C (120 °F) (Ref 6).

Electrochemical polarization scans are a good way to look at the effect a dissolved gas has on corrosion kinetics. The difference in uranium polarization scan behavior for argon and air is shown in Fig. 3. Figure 3(a) shows that uranium in a neutral buffer solution that is purged with air has a corrosion potential (E_{corr}) of -0.5 V_{SCE}, and when it is purged with inert argon or "deaerated," E_{corr} is much lower, -1.2 V_{SCE}. The corrosion product at E_{corr} can be predicted from the Pourbaix diagram in Fig. 1. For this case, the predicted product for the aerated (pH 7.2, -0.5 V_{SCE}) and deaerated (pH 7.2, -1.2 V_{SCE}) conditions is the same, UO_2. However, the aerated and deaerated values are at opposite ends of the UO_2 region. For the aerated case, the value is in a region where the oxidation state transitions from +4 to +6, which would result in a mixed oxidation state and hyperstoichiometric UO_2. For the deaerated case, near-stoichiometric UO_2 is expected.

An important consideration for aerated and deaerated solutions is the cathodic reaction. For the air-purged solution, E_{corr} is at a potential where oxygen reduction is the primary cathodic reaction (Eq 1). For the argon-purged condition, E_{corr} is at a potential where water reduction is the primary cathodic reaction (Eq 2):

$$O_2 + 2H_2O + 4e^- \rightarrow 4OH^- \quad \text{(oxygen reduction)} \qquad \text{(Eq 1)}$$

$$2H_2O + 2e^- \rightarrow H_2 + 2OH^- \quad \text{(water reduction)} \qquad \text{(Eq 2)}$$

The corrosion rate depends on the kinetics of the anodic and cathodic reactions, and Fig. 3(a) suggests that the corrosion rate of uranium is slower when air (or oxygen) is dissolved in solution. The reverse scan (Fig. 3b) shows that there is an anodic nose between the E_{corr} values for air-purged and argon-purged solutions. In

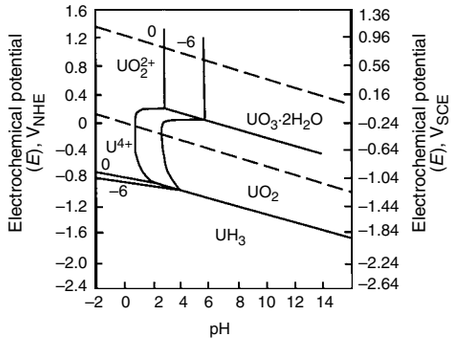

Fig. 1 Simplified Pourbaix diagram for uranium in water at 25 °C (77 °F). V_{NHE}, voltage vs. normal hydrogen electrode. V_{SHE}, voltage vs. standard hydrogen electrode. See Ref 3 for full diagram.

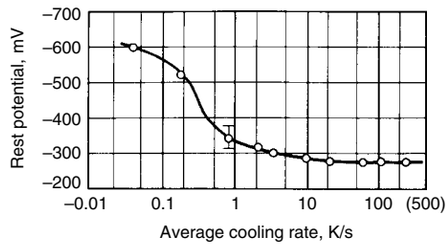

Fig. 2 Effects of cooling rate on rest potential of U-6Nb in 0.001 *M* KCl. Less negative corrosion potential (E_{corr}) values, which are observed at fast cooling rates, are generally associated with increased corrosion resistance. The error bar indicates the uncertainty in the potential measurement. Source: Ref 9

*There are two Pourbaix diagrams shown for uranium in Ref 3. The diagram in Fig. 1 is the equilibrium diagram. The second diagram in Ref 3 does not consider UH_3 or hydrated UO_3, but is useful for pitchblende, which has U_3O_8 as its main constituent, and for considering the slow kinetics of electrochemical UH_3 formation in aqueous solutions.

air, E_{corr} is at a point on the nose where the current density is low, and in argon E_{corr} is at a point on the nose where the current density is high. Also, the potential region where the current density is low on the anodic nose is small. This anodic control of uranium corrosion is important because small perturbations from equilibrium in aerated systems can cause an increase in corrosion rate.

Waber demonstrated the corrosion-rate dependence on dissolved oxygen by placing a cover glass near the uranium surface and immersing it in water. The uranium near the edge of the glass, where oxygen was readily available, was relatively unattacked, but the uranium in the oxygen-depleted region near the center of the glass was deeply pitted (Ref 4). Waber also observed the anodic control of uranium corrosion by observing the effects of dissolved oxygen and addition of cupric ions (Ref 6).

In addition to showing the effects of oxygen on E_{corr} and reaction rate, Fig. 3(a) shows two distinct regions of anodic behavior. Just above E_{corr}, the current density, i, is low and is the passive current density associated with predicted formation of UO_2. At just above 0.2 V_{SCE}, i increases to above 10^{-5} A/cm^2 and is associated with the predicted formation of hydrated UO_3.

Similar corrosion behavior is observed in uranium alloys. They generally undergo a decrease in E_{corr} when changing from aerated to deaerated conditions. Depending on the alloy and the solution, they may or may not show an increase in corrosion rate when changing from aerated to deaerated conditions. The absolute values of E_{corr} and relative change in E_{corr} depend on the alloy composition. Data for uranium-niobium alloys are shown in Table 1. Although E_{corr} changes for aerated/deaerated solutions and with alloy composition, it varies little between oxygen-saturated solutions and air-equilibrated solutions for uranium and uranium-niobium alloys (Ref 14), which indicates that the corrosion rate is relatively insensitive to the amount of oxygen in solution. Note also that E_{corr} increases as alloy content increases.

Solution pH. In addition to dissolved gas, corrosion of uranium depends significantly on solution pH. The Pourbaix diagram (Fig. 1) indicates corrosion in acidic environments (pH <3) with the formation of soluble ions U^{3+}, U^{4+}, and UO_2^{2+}. In mildly acidic solutions ($3 <$pH <5) solid UO_2 should begin to form but will probably be nonprotective. In neutral to alkaline solutions, solid UO_2 should form, which may or may not be protective. Electrochemical data for uranium show that E_{corr} decreases from -0.73 V_{SCE} at pH 0.55 to -1.27 V_{SCE} at pH 9.6 (Ref 15). From E_{corr} alone, it is not clear whether or not the UO_2 formed at pH 9.6 is protective.

Evidence for the protective nature of the oxide, which is probably UO_2, in mildly alkaline solutions is shown in Fig. 4. The figure shows the polarization scan behavior for uranium in buffered, room-temperature solutions ranging in pH from 0.5 to 13.6 (Ref 10). It also shows that uranium passivity is greatest at about pH 10.7. In highly alkaline solutions, an anodic nose is observed at about 0 V_{SCE} (Ref 10, 16, 17) and probably corresponds to the change from UO_2 to hydrated UO_3 as the stable phase. Surface science measurements of oxides grown at 0.6 V_{SCE} confirm hydrated UO_3 formation (Ref 11).

Alloy elements enhance uranium passivity, but solution pH can affect alloy effectiveness. Figure 5 shows the effect of niobium content on polarization scan behavior in neutral solution (Ref 10). The figure shows regions where the current density, i, is relatively constant. These regions of constant current are associated with film (e.g., oxide) growth. If the current density is low (less than ~10^{-5} A/cm^2), the oxide is considered protective and the current density is called "passive." If the current density is high, the oxide is not protective and the current density will be referred to as the "film-limited anodic current density." Above about 0 V_{SCE}, unalloyed uranium has a high film-limited anodic current density in neutral solution, but even small niobium additions increase the corrosion resistance so that the anodic current densities are considered passive. Figure 6 shows how niobium content affects the film-limited anodic current density as a function of pH (Ref 10). In neutral solutions, the alloy current densities were about one order of magnitude lower than for unalloyed uranium, and in mildly acidic solutions, alloy current densities were about two orders of magnitude lower. Niobium additions enhanced passive behavior in acidic and neutral solutions by the formation and enrichment of Nb_2O_5 in the oxide (Ref 10, 11). Niobium was not as effective at enhancing passivity in alkaline solutions because uranium shows an inherent increase in passivity in mild alkaline solutions while the oxide of niobium becomes less protective in alkaline solutions.

Table 1 Comparison of corrosion potential (E_{corr}) for U-Nb alloys in air-purged (aerated) and argon-purged (deaerated) solution

pH 7.2 buffer solution (0.5 *M* boric acid + 0.05 *M* sodium borate)

	E_{corr}, V_{SCE}	
Alloy(a)	Air purged	Argon purged
U	−0.51	−1.15
U-2Nb	−0.66	−0.82
U-4Nb	−0.51	−0.73
U-6Nb	−0.53	−0.68
U-8Nb	−0.46	−0.72
Nb	(b)	−0.72

(a) Designation based on wt%. (b) Not determined

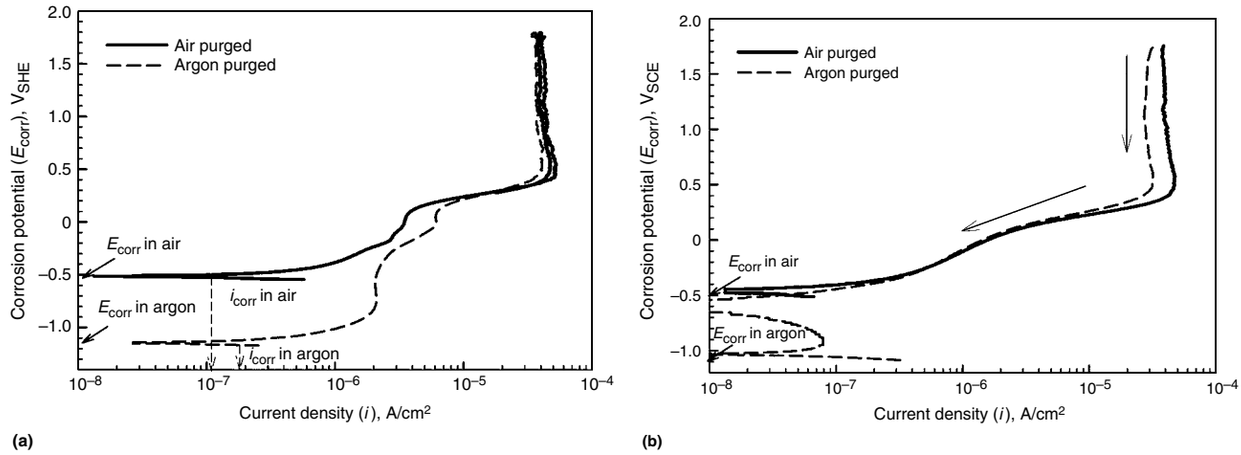

Fig. 3 Forward (a) and reverse (b) anodic polarization scans for uranium in neutral buffer solution (7.2 pH, 0.5 *M* boric acid plus 0.05 *M* sodium borate) showing the effect of oxidizing and inert gas environments on corrosion potential (E_{corr}) and anodic kinetic behavior.

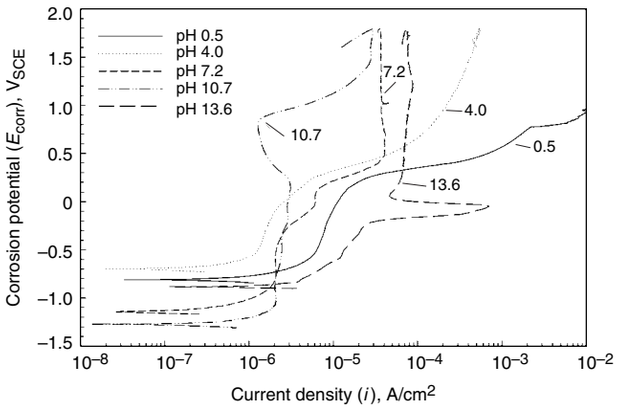

Fig. 4 Effect of pH on uranium polarization scan behavior in room-temperature, argon-purged solutions. Data from Ref 10

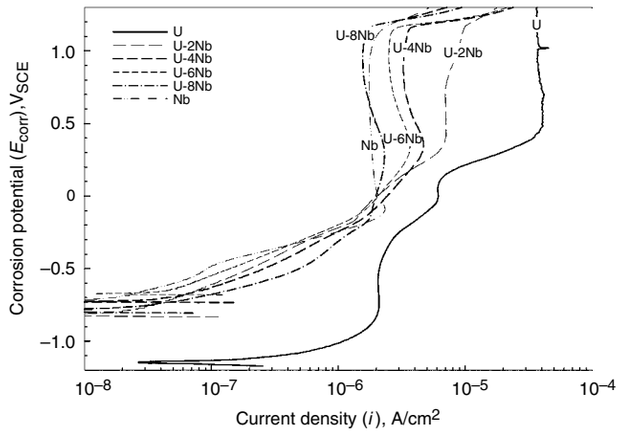

Fig. 5 Effect of Nb additions on uranium corrosion, measured by polarization scans in Ar-purged, neutral buffer solutions at room temperature. Data from Ref 10

Other uranium alloys also exhibit better effectiveness in acidic solutions than in alkaline solutions. Uranium-titanium and uranium-molybdenum alloys increase the corrosion resistance in acidic solutions. Levy and Zabielski observed a decrease in the passive current density of about two orders of magnitude for U-1.76Ti, U-3.41Ti, U-1.8Mo, and U-3.75Mo in 1 *N* H_2SO_4 (Ref 16). In alkaline environments, however, polarization scan data show that U-0.75Ti, U-7.5Nb-2.5Zr (Mulberry), and U-1.4Zr do not significantly increase corrosion resistance (Ref 18).

Salt Solutions. When no aggressive anions are present, uranium corrosion is relatively uniform; however, when chloride is present in solution, uranium corrosion occurs by localized attack (Fig. 7a). The localized corrosion sites in unalloyed uranium are not hemispherical pits. Instead, they have a central area where corrosion initiated and "fingers," which grew during corrosion propagation. The pits also are covered. That is, light grinding of the sample in Fig. 7(a) showed the fingers were much wider just under the surface. The pitting potential of uranium in 0.1 *M* NaCl (Ar purged) is approximately −0.03 V_{SCE}. This value varies somewhat and is lower if corrosion initiates at large defects. Additions of Nb increase E_{corr}, but do not significantly increase the pitting potential in 0.1 *M* NaCl (Table 2). Similar behavior was observed for uranium-titanium and uranium-molybdenum alloys, with the exception of U-3.75Mo, which showed a slight increase in pitting potential (Ref 16).

Although the pitting potential does not change, the pit size and number change as niobium content increases. For example, after potentiodynamic polarization uranium had 1 corrosion pit per 0.1 cm^2 area, U-4Nb had ~15 smaller pits per 0.1 cm^2 area, and U-6Nb had the smallest pits with ~40 pits per 0.1 cm^2 (Fig. 7). The figure also shows that as alloy content increases, the corrosion pit shape becomes more hemispherical. Therefore, niobium does not increase the resistance of uranium to pit initiation (as chromium does in stainless steel). Instead, niobium additions affect pit propagation by making the corrosion less localized (i.e., the pits will be more shallow and there will be more of them).

Results similar to those in NaCl have been observed in seawater. In ASTM artificial seawater at 25 °C (77 °F), uranium showed deep pitting with a maximum corrosion rate of 0.01 mg/cm^2·h (Ref 19). This corrosion rate is lower than what is observed in water; however, the corrosion was in the form of pits and the localized penetration rate would be much higher. In the same study, pitting corrosion was observed on uranium exposed to distilled water and some of those pits penetrated the metal at 3 mm/yr (0.12 in./yr) (Ref 19).

Macki and Kochen measured similar weight loss rates for uranium in ASTM artificial seawater at 20 °C (68 °F) (Ref 20). When uranium was exposed to acidic chloride (0.1 *N* HCl), they observed over an order of magnitude increase in corrosion rate. Alloy additions significantly decreased the corrosion rate, and weight loss generally decreased in the following order: U > U-4.5Nb > U-6Nb > [U-8Nb, U-7.5Nb-2.5Zr, and U-10Mo] (Ref 20). Figure 8 summarizes the measured corrosion rates for chloride-containing solutions as a function of alloy content.

Very little chloride is required to cause pitting corrosion on uranium alloys, but common inhibitors sometimes prevent pitting. For example, pitting corrosion occurred on uranium-titanium and uranium-molybdenum in chloride solutions at concentrations as low as 0.005 *M*, but chromates, sulfates, and nitrates at sufficient concentration inhibited pitting at the low chloride concentrations (Ref 16). The nature of the halide also plays a role in corrosion rate. Waber found that fluoride ions greatly increase the corrosion rate compared to chloride ions. The corrosion rate of U-6Nb in 1% NaCl at 178 °C (350 °F) was about 0.003 mg/cm^2·h, but in 1% NaF the corrosion rate increased to 12 mg/cm^2·h (Ref 6).

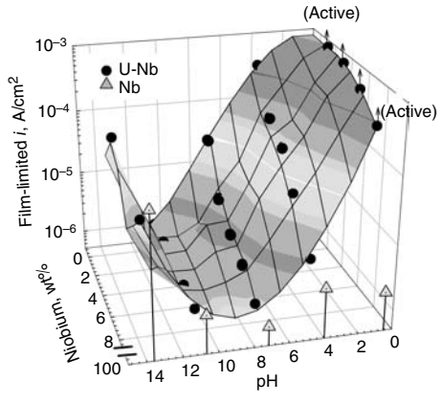

Fig. 6 Nb additions to uranium decrease corrosion susceptibility as measured by the film-limited anodic current density. Nb additions are most effective in neutral and slightly acidic solutions. Data from Ref 10

Temperature

As is the case with most metals, corrosion rates of uranium and its alloys increase with increasing temperature. As temperature is increased from 25 to 70 °C (77 to 158 °F) E_{corr} decreased slightly for uranium and its alloys in air-purged 0.1 *N* HCl (Table 3) (Ref 14). A decrease in E_{corr} for a given uranium alloy generally corresponds to an increase in corrosion rate. Reviews of early project data showed an exponential increase in uranium corrosion rate as temperature was increased in hydrogen-saturated and air-purged water, steam, and dilute hydrogen peroxide (Ref 6, 13, 21). A linear regression to literature data gives the following rate for uranium reaction in deaerated water at temperatures between 20 and 300 °C (68 and 570 °F) (Ref 22):

$$k = 5.03 \times 10^9 \exp\left[\frac{-66.4 \pm 2.0\,\text{kJ/mol}}{RT}\right] \quad \text{(Eq 3)}$$

where R is the gas constant, T is temperature, and k is corrosion rate in mg (U)/cm^2·h.

A second effect of temperature on uranium corrosion is that the amount of oxygen that can be dissolved in solution decreases as temperature increases. Therefore, the inhibiting effect of oxygen on uranium corrosion should decrease as the temperature increases. Measurements of uranium corrosion rates in hydrogen-saturated water were over an order of magnitude greater than in air-saturated water at 50 °C (122 °F), but were nearly equal at 100 °C (212 °F) (Fig. 9) (Ref 6).

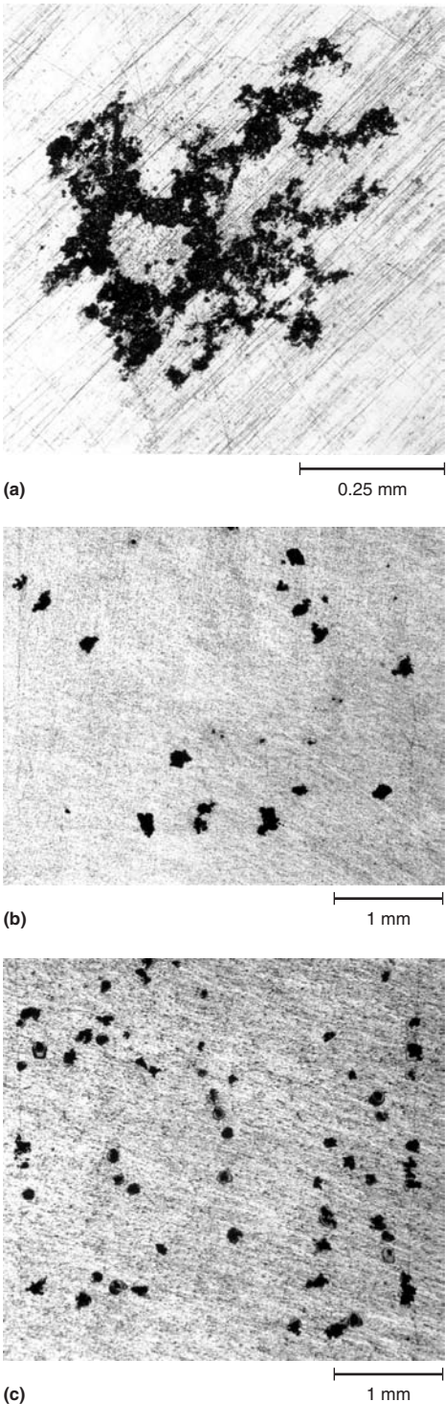

Fig. 7 Corrosion pits observed on (a) uranium, (b) U-4Nb, and (c) U-6Nb after anodic polarization scans in 0.1 *M* NaCl (room temperature, Ar-purged)

Galvanic Interactions

When uranium or its alloys are in contact with other metals, a galvanic corrosion cell may be created. If there is electrical contact and an electrolyte, there will be a driving force for corrosion of one of the metals. The driving force is proportional to the difference in the E_{corr} values of the metals, and the metal with the more negative E_{corr} value will corrode. The corrosion rate will depend not only on the metals in contact but also on the electrolyte solution. For example, alloyed uranium generally has better corrosion resistance than unalloyed uranium in neutral to acidic solutions; however, unalloyed uranium can have greater corrosion resistance than alloyed uranium in some alkaline solutions. Corrosion resistance also depends on oxygen dissolved in solution. Therefore, the rate and even which material is the anode or cathode may change as solution pH or aeration changes. Corrosion rate will also depend on the ratio of the cathode and anode areas. For example, if the cathode area is large and the anode area is small, the anode will corrode at an accelerated rate.

Early reports found that, in water, uranium galvanically corroded when it was coupled to stainless steel (Ref 21). When coupled to aluminum, uranium was initially cathodic but, after 50 h, uranium became anodic and corroded at 1.3 times the uncoupled rate (Ref 21). E_{corr} data in 25 °C (77 °F) ocean water support this observation with E_{corr} for aluminum 7178 at −0.800 V_{SCE}, uranium at −0.795 V_{SCE}, and 304 stainless steel at −0.250 V_{SCE} (Ref 14). Uranium is also corroded by uranium-niobium alloys, uranium-molybdenum, and Mulberry (U-7.5Zr-2.5Nb) in seawater (Ref 14). Some metals were anodic to uranium in seawater and reduced the short-term corrosion rate. When coupled to aluminum, beryllium, or beryllium plus stainless steel, the corrosion rate of uranium in seawater was reduced and the corrosion shifted from localized to general (Ref 19).

Although uranium alloys are more corrosion resistant than unalloyed uranium they still suffer from galvanic corrosion. Uranium-niobium alloys are corroded in 0.1 *N* HCl by Ti-6Al-4V, U-10Mo, Mulberry, and 304 stainless steel (Ref 14). Low uranium-niobium alloys will corrode when coupled to high alloys (e.g., U-4Nb will galvanically corrode when coupled to U-6Nb) (Ref 14).

Experiments on U-0.75Ti in ASTM seawater showed the alloy galvanically corroded when coupled to AISI 4340 steel and 7075-T6 aluminum (Ref 23). The same study showed that magnesium alloy ZK60A-T5 (UNS M16600) protected U-0.75Ti, and 4340 (UNS G43400) steel with a zinc chromate conversion coating protected the alloy for a limited time. U-0.75Ti

Table 2 Room-temperature pitting data for U and U-Nb in 0.1 *M* NaCl, argon purged solution

Alloy(a)	E_{corr}, V_{SCE}	E_{pit}, V_{SCE}	i_{pass}, 10^{-6} A/cm^2
U	−1.15	−0.03	2
U-4Nb	−0.66	−0.04	1
U-6Nb	−0.57	−0.01	0.7
U-8Nb	−0.63	−0.03	0.9
Nb	−0.23	(b)	2

E_{corr}, corrosion potential; E_{pit}, pitting potential; i_{pass}, passive current. (a) Designation based on wt%. (b) No pitting observed, transpassive oxygen evolution at approximately 1.2 V_{SCE}

Table 3 Comparison of corrosion potential (E_{corr}) for U-Nb alloys in air-purged 0.1 *N* HCl at 25 and 70 °C (77 and 158 °F)

	E_{corr}, V_{SCE}	
Alloy(a)	25 °C (77 °F)	70 °C (158 °F)
U	−0.755	−0.790
U-4.5Nb	−0.475	−0.600
U-6Nb	−0.420	−0.465
U-8Nb	−0.400	−0.445
U-7.5Nb-2.5Zr (Mulberry)	−0.340	−0.410
U-10Mo	−0.190	−0.240

(a) Designation based on wt%

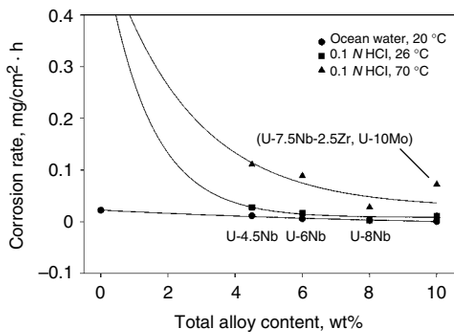

Fig. 8 Corrosion rates as a function of total alloy content for uranium alloys in various chloride-containing solutions exposed to air. Data from Ref 20

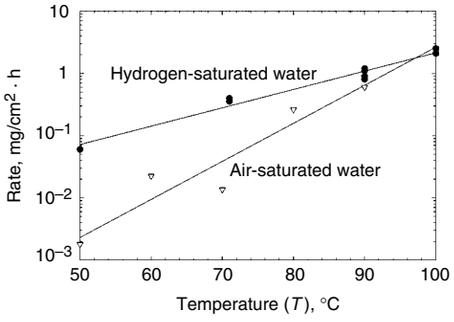

Fig. 9 Weight-loss rate as a function of temperature for uranium in hydrogen-saturated and air-saturated water. The rates converge at approximately 100 °C (212 °F). Data from Ref 6

showed a threefold increase in corrosion rate in distilled water when coupled to tungsten, and tungsten-reinforced uranium composites corroded 1.3 times faster than unalloyed uranium (Ref 24).

Winkel and Childs performed a comprehensive study of the galvanic corrosion of uranium, uranium alloys, and many other metals in nonaerated acidic, neutral, alkaline, and chloride solutions at 29 °C (84 °F) (Ref 25). Their data show a significant effect of solution pH on galvanic corrosion of uranium and its alloys. For example, in acidic, neutral, and chloride solutions, U-6Nb is significantly cathodic to uranium; however, in pH 11.3 carbonate solution, U-6Nb is anodic when coupled to uranium.

Although uranium and uranium alloy galvanic corrosion depends on solution pH, aeration, and salt content, Fig. 10 shows general trends in the driving force for uranium galvanic corrosion in room-temperature, neutral, chloride solutions. Negative values indicate the material is anodic to uranium.

Atmospheric Corrosion

Atmospheric corrosion of uranium is commonly divided into oxidation in dry air or oxygen, water vapor, and oxygen-water vapor mixtures. These are all discussed in this section because one or more of these conditions may apply to the atmospheric corrosion of uranium depending on the particular storage conditions. Hydriding, which is another condition that may apply in atmospheric corrosion of uranium, is discussed separately due to the unique mechanism and morphology of hydride corrosion of uranium.

Oxidation of Uranium in Dry Air or Oxygen

The oxidation of uranium is reviewed by Ref 22 and 26 to 30. The reaction of uranium with oxygen is typically described in the net reaction:

$$U + \frac{2+x}{2}O_2 \rightarrow UO_{2+x} \qquad \text{(Eq 4)}$$

The value of x is a product of the atmosphere (oxygen activity), temperature, and time. The value of x therefore varies as a function of the particular oxidizing species (oxygen, CO_2, and CO mixtures) or mixtures thereof. As the oxide scale grows, the outer layers in contact with the oxide/gas interface gradually increase in oxygen content. Early work reported values of x in Eq 4 between 0.2 and 0.4 (Ref 31, 32). More recent work, however, has measured x between 0.06 and 0.1 (Ref 28, 33, 34). The oxide spalls off of the surface at a thickness of approximately 1 μm (25 mils), leading to a reinitialization of the process. The spalling of oxide results in the linear kinetics characteristic of the steady-state oxidation of uranium. In fact, the linear kinetics are really a series of short parabolic steps approximated by a straight line. For temperatures between 38 and 300 °C (100 and 570 °F), the rate of uranium oxidation in dry air was derived from literature data by Hilton (Ref 22) and is expressed by Eq 5, which is also shown in Fig. 11.

$$k = 1.46 \times 10^7 \exp\left[\frac{-71.3 \pm 2.1\ \text{kJ/mol}}{RT}\right] \qquad \text{(Eq 5)}$$

where R is the gas constant, T is temperature, and k is the rate of mass increase in mg/cm^2·h. At high temperatures, uranium oxidation behavior becomes more complex as shown by the data of various investigators (Ref 32, 36–41) in Fig. 12.

Uranium in Water Vapor

The reaction rate of uranium with water vapor is much faster than that with dry air or oxygen and has been reviewed by numerous authors (Ref 22, 26, 42, 43). In the absence of oxygen, uranium reacts in the presence of water vapor to form UO_{2+x}, where x is between 0 and 0.1, and hydrogen. Hydrogen is formed as atomic hydrogen adsorbed to the surface. Most of the atomic hydrogen will recombine to form gas, but some will be absorbed into the lattice. The amount of hydrogen gas measured is typically between 1 and 13% less than predicted and is believed to be trapped hydrogen and/or hydride (Ref 31, 44). The oxide is black, has a face-centered cubic (fcc) crystal structure, and readily flakes off the uranium surface (Ref 29, 31, 35, 45). Depth profiling with isotopically labeled water showed that the water adsorbed last produces the oxide nearest the metal (Ref 46). Positron annihilation techniques showed that an oxygen species migrates through complex oxygen interstitial defects to form oxide (Ref 29).

Uranium oxidation rates in water vapor have been measured by various researchers (Ref 35, 45, 47–51). The weight-gain rate for uranium oxidation in unsaturated water vapor at temperatures between 30 and 80 °C given by (Ref 35):

$$k = 4.0 \times 10^8\, r^{1/2} \exp\left[\frac{-64.9\ \text{kJ/mol}}{RT}\right] \qquad \text{(Eq 6)}$$

where r is the fractional relative humidity (e.g., $r = 0.5$ at 50% RH), R is the gas constant, and T is temperature. The units of k in Eq 6 and 7 are mg/cm^2·h. For 100% RH and temperatures between 20 and 100 °C (68 and 212 °F), the rate is given by (Ref 27):

$$k = 4.3 \times 10^7 \exp\left[\frac{-57.7\ \text{kJ/mol}}{RT}\right] \qquad \text{(Eq 7)}$$

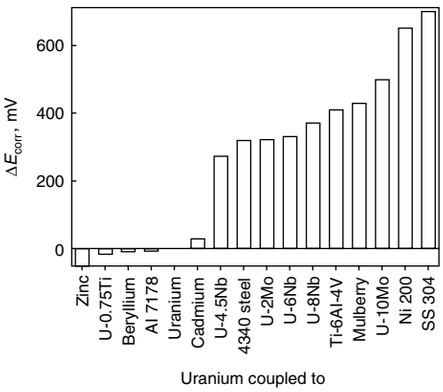

Fig. 10 A comparison of the driving force for galvanic corrosion of uranium couples in neutral, chloride-containing solutions. A negative driving force indicates uranium is the cathodic member of the couple. E_{corr}, corrosion potential. Based on data from Ref 14, 19, and 25

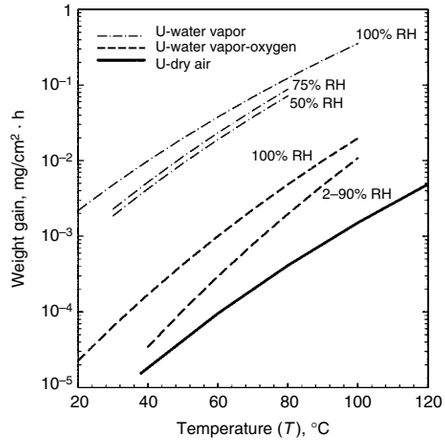

Fig. 11 Summary of uranium oxidation rates in dry air, oxygen-water vapor, and water vapor as a function of temperature. Based on equations in Ref 22 for U-O_2; Ref 35 for U-H_2O; Ref 27 for U-H_2O, 100% RH; Ref 22 for U-O_2-H_2O and for U-O_2-H_2O, 100% RH

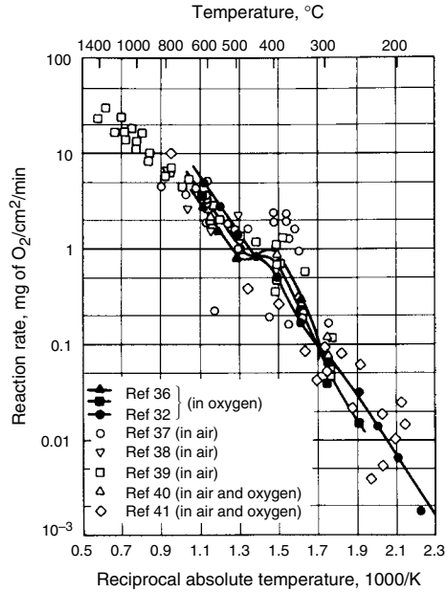

Fig. 12 Oxidation rates of uranium in dry air and oxygen

The oxidation rates in water vapor from Eq 6 and 7 are shown in Fig. 11. A regression analysis in a more recent review found that for temperatures between 20 and 302 °C (68 and 575 °F) and water vapor pressure below 101 kPa (14.6 psi), the weight-gain rate follows (Ref 22):

$$k = 1.31 \times 10^5 p^{1/2} \exp\left[\frac{-46.6 \pm 0.7\,\text{kJ/mol}}{RT}\right] \quad \text{(Eq 8a)}$$

where p is the water vapor partial pressure expressed in kPa, and k is in units of mg $(\text{kPa})^{1/2}/\text{cm}^2 \cdot \text{h}$. In terms of fractional relative humidity (RH):

$$k = 1.28 \times 10^9 r^{1/2} \exp\left[\frac{-68.0 \pm 0.1\,\text{kJ/mol}}{RT}\right] \quad \text{(Eq 8b)}$$

and R is the gas constant, T is temperature, and k is in units of $\text{mg/cm}^2 \cdot \text{h}$. Equations 6 and 8 give similar results at low temperatures, but diverge somewhat at higher temperatures (Fig. 13). The reaction mechanism is discussed in the next section.

Uranium in Oxygen-Water Vapor Mixtures

This condition is the most typical of atmospheric oxidation of uranium. The reaction rate falls between that of oxygen and water vapor, and the kinetics and mechanism have been widely studied (Ref 4, 22, 26, 28, 43, 45, 47, 52–54). In oxygen-water vapor systems or air-water vapor systems below about 200 °C (392 °F), uranium reacts to form an fcc oxide, UO_{2+x}, where x is between 0.2 and 0.4. (Ref 27, 53, 55). When oxygen is present, the reaction rate is significantly reduced, and the oxide formed is initially more adherent than that formed in pure water vapor. Given enough time, however, the uranium oxide formed in oxygen-water vapor mixtures will flake off of the substrate as plates (Fig. 14).

The reduction in oxidation rate is observed even at very low partial pressures of oxygen (Fig. 15). For small amounts of moisture in oxygen-containing environments (below about 2% RH), there is a strong dependence of reaction rate on water vapor pressure (Ref 27, 31, 33, 52, 53). At intermediate oxygen and water vapor pressures, the reaction rate is, for practical purposes, independent of oxygen content or water vapor pressure (Ref 52, 53).

The oxidation rate of uranium in oxygen-water vapor for temperatures between 40 and 100 °C (104 and 212 °F) and RH between 11 and 75% has been found to follow (Ref 53):

$$k = 7.6 \times 10^{13} \exp\left[\frac{-110\,\text{kJ/mol}}{RT}\right] \quad \text{(Eq 9)}$$

where R is the gas constant, T is temperature, and the gain rate k is in units of $\text{mg/cm}^2 \cdot \text{h}$. More recent work (Ref 22), which includes data from 20 to 200 °C (68 to 392 °F) and 2 to 90% RH, fit the data to:

$$k = 1.10 \times 10^{11} \exp\left[\frac{-92.9 \pm 4.8\,\text{kJ/mol}}{RT}\right] \quad \text{(Eq 10)}$$

Equations 9 and 10 are plotted in Fig. 16 along with literature data for comparison. For the case of 100% RH and temperatures between 20 and 100 °C (68 and 212 °F), the rate can be expressed by (Ref 22):

$$k = 1.16 \times 10^9 \exp\left[\frac{-76.9 \pm 7.0\,\text{kJ/mol}}{RT}\right] \quad \text{(Eq 11)}$$

Equation 11 is very similar to equations derived by Ritchie (Ref 27) and Pearce (Ref 43). Equations 10 and 11 are plotted in Fig. 11 for comparison to the rates in water vapor and dry air/oxygen.

In closed oxygen-water vapor systems, the rate of oxidation varies with time. When uranium is introduced into the system there is an initial period where equilibration takes place and the reaction is parabolic. After equilibration, there are two distinct regions representing different uranium oxidation rates (Fig. 17). In the first region, (a), uranium reacts with water and oxygen with no significant formation of hydrogen gas (Ref 45, 55). In the second region, (b), oxygen has been depleted, and uranium reacts with essentially deaerated water and hydrogen gas is evolved (Ref 45, 55). Measurements of the oxidation rates show that, after oxygen is consumed, the oxidation rate is up to 100 times faster (Ref 55). Spalling of the oxide is observed at the same time as the rate increase (Ref 45). Many explanations for the slower reaction rate when oxygen is present have been published. Most

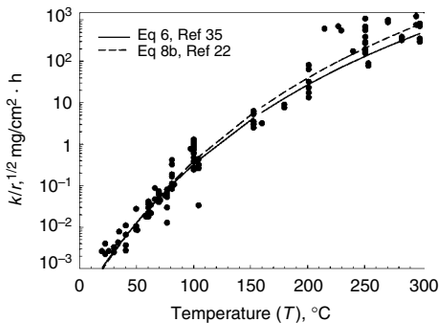

Fig. 13 Summary of literature data and derived expressions for uranium oxidation weight-gain rate, in water vapor with vapor pressures less than 101 kPa (14.6 psi) and temperatures between 20 and 302 °C (68 and 575 °F). Based on Ref 22

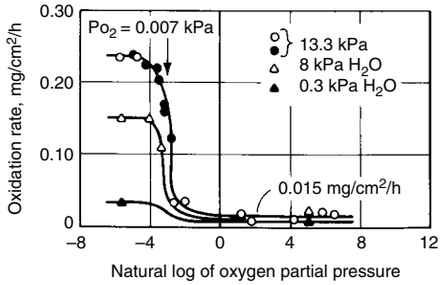

Fig. 15 Oxidation rate of uranium versus oxygen pressure in water vapor at 100 °C (212 °F). Source: Ref 29

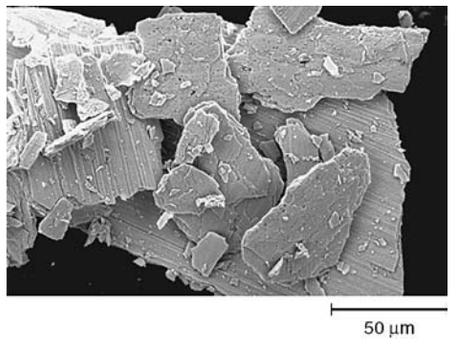

Fig. 14 Scanning electron micrograph of oxide plates that flaked off of uranium that was stored in air for more than 10 years

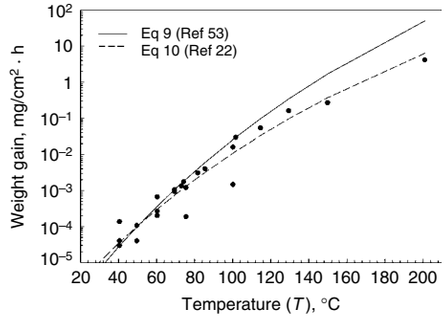

Fig. 16 Summary of literature data and derived expressions for uranium oxidation rate of weight gain in oxygen-water vapor systems at temperatures less than 302 °C (575 °F) and relative humidity between 2 and 90%. Based on Ref 22 and 53

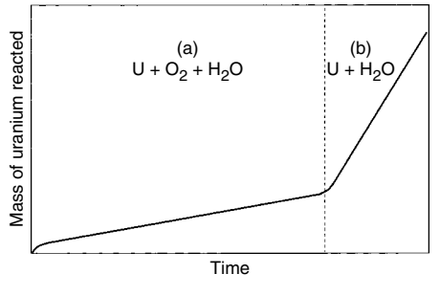

Fig. 17 Mass of reacted uranium over time shows (a) the inhibiting effect oxygen has on corrosion rate and (b) the increase in rate after oxygen is consumed for uranium in a closed oxygen-water vapor system. Based on Ref 45 and 55

relate the slower oxidation rate to a chemisorbed oxygen layer and/or a less defective oxide (Ref 28, 52, 55). Isotopic surface science studies have shown that it is not a chemisorbed layer or oxide diffusion barrier that slows the reaction (Ref 56) and that both oxygen and water react simultaneously to form the oxide (Ref 52). The slower kinetics can be understood by looking at the electrochemical cell that forms when uranium is exposed to water vapor.

In humid environments, a thin layer of water forms on a material surface and sets up an electrochemical cell (Ref 57). Therefore, uranium oxidation in water vapor environments is electrochemical corrosion, which is governed by anodic and cathodic reactions. The anodic reaction is the oxidation of uranium whereby uranium gives up electrons and UO_{2+x} is formed. To maintain charge neutrality, the cathodic reaction must consume the electrons generated by oxidation. In water-containing systems, the two predominant cathodic reactions are oxygen reduction and hydrogen evolution.

When oxygen and water are present, the primary cathodic reaction is oxygen reduction (Eq 1): oxygen and water react with four electrons to form hydroxide ions. The hydroxide undergoes further reaction, and the overall reaction for uranium oxidation in water vapor and oxygen can be written as:

$$U + O_2 + 3H_2O \rightarrow UO_2 + 3OH^- + 3H^+ \quad \text{(Eq 12)}$$

Although both oxygen and water participate in the reaction, this reaction depletes only oxygen from the system. The OH^- and H^+ in Eq 12 will recombine to form H_2O with no net loss of water. This reaction is consistent with observations that both O_2 and H_2O participate in the reaction, but no water is consumed during the period of "inhibition."

After the oxygen is depleted from the system, the system becomes the same as the uranium-water vapor system, and the cathodic reaction changes to hydrogen evolution (Eq 2). The overall reaction is:

$$U + 5H_2O \rightarrow UO_2 + 4H_{ads} + 3OH^- + 3H^+ \quad \text{(Eq 13)}$$

In this reaction, water is consumed and adsorbed hydrogen (H_{ads}) is formed. H_{ads} may combine to form H_2 gas or may be absorbed into the oxide and/or metal substrate, which is consistent with observations that hydrogen gas is detected in the system after oxygen depletion but at a level that is less than theoretically predicted.

Another aspect of the electrochemical nature of the oxygen-water vapor reaction with uranium is that aqueous electrochemical data can also be applied to this system. The aqueous data show that the uranium corrosion rate is under anodic control. The rate of the anodic reaction, which is lower when oxygen is present (Fig. 3), controls the corrosion rate. Therefore, the rate-controlling step is somewhere in the anodic reaction, which can include the formation of intermediate species. The anodic reactions of uranium are complex and are not yet well understood (Ref 58).

The proposed electrochemical reactions also explain results from oxygen isotope studies. According to Eq 1 and 12, $^{18}O_2$ would be reduced to $^{18}OH^-$; $^{18}OH^-$ would then further react and could form $H_2{}^{18}O$, $U^{18}O_2$ and/or $U^{18}O^{16}O$. Isotope studies have shown that these three ^{18}O compounds are observed. Baker found that the water was enriched with ^{18}O after oxygen was consumed (Ref 55). Another $^{18}O_2$ study analyzed time-interval gas samples from the system; ^{18}O was not observed in the water vapor (Ref 45). However, according to the electrochemical model, $^{18}O_2$ would react to form $^{18}OH^-$, which would mainly stay in the adsorbed water layer on the uranium surface and would not likely be detected by gas sampling.

Additionally, various studies using isotopes have also shown that it is an oxygen-containing species (Ref 29, 46, 52, 59) that migrates through complex oxygen interstitial sites (Ref 29) in the oxide to form new uranium oxide, not uranium ions migrating through the oxide to react at the water/oxide interface. These observations agree with defect models that show UO_{2+x} has complex oxygen interstitial defects (Ref 28, 60, 61).

Oxidation of Uranium Alloys

The objective of alloying of uranium has been principally intended to improve corrosion or oxidation resistance. The few exceptions to this rule are the high-strength uranium alloys such as U-0.75wt%Ti, which is used in penetrators (Ref 62) and in alloys containing a small amount of a second element such as chromium or vanadium as an α grain refiner. The elements most often used to obtain improved oxidation resistance and/or mechanical properties from uranium are the group IV elements niobium, zirconium, titanium, and molybdenum, as well as aluminum and copper.

Uranium Alloys in Water Vapor and Oxygen-Water Vapor Mixtures. Oxidation rates in water vapor can be reduced by orders of magnitude by alloying uranium. The alloy, U-0.75Ti, which is desirable for its high strength, has only slightly better oxidation resistance in water vapor. Molybdenum additions below about 5 wt% also have little to no effect on uranium oxidation. Additions of 10% Mo, on the other hand, result in significant improvement of oxidation resistance. Niobium additions improve water vapor oxidation resistance, and the improvement increases with increasing niobium content. Figure 18 compares uranium and uranium alloy oxidation resistance in 100% relative humidity N_2 (Ref 63). The figure shows the rate of hydrogen gas produced, which is proportional to the oxidation rate, as a function of alloy addition. The significant decrease for alloys with greater than 10 at.% additions should be viewed with caution. Highly alloyed materials are usually γ phase, which has high hydrogen solubility, so the measured hydrogen rate is lower than the actual hydrogen generation rate.

The presence of oxygen in water vapor further slows the oxidation of uranium alloys. For example, uranium oxidation occurs at 1.2×10^{-2} mg/cm^2·h in 2.7 kPa (0.39 psi) water vapor and 0.67 kPa (0.097 psi) oxygen at 100 °C (212 °F), but the U-0.75Ti oxidation rate is only 3.7×10^{-3} mg/cm^2·h in 2.0 kPa (0.29 psi) water vapor and 0.13 kPa (0.02 psi) oxygen at 140 °C (284 °F) (Ref 64). The oxidation rate is even lower for uranium-niobium alloys. U-6Nb heat treated to the α″ phase, which is the monoclinic distortion of α, reacted at $^1/_{500}$ the rate of unalloyed uranium in moist air, and two-phase U-6Nb (α + γ) reacted at $^1/_{20}$ to $^1/_{200}$ the rate of uranium (Ref 65).

High-Temperature Oxidation. Uranium alloys are generally not used in high-temperature service because they tend to always form a mixed scale of uranium oxides and oxides of the alloying elements (Ref 36, 66–69). Nonetheless, the high-temperature oxidation of uranium alloys is observed in hot processing of these metals and, of course, in conditions where the alloys are exposed in fires. The high-temperature oxidation of uranium alloys is reviewed by Cathcart (Ref 70). As in atmospheric oxidation, the growth of scales on uranium alloys proceeds principally via anion diffusion through hyperstoichiometric UO_2. As a result, the oxide scale tends to grow outward and develop extremely high stresses that result in cracking and spallation. Because of the very low oxygen activity maintained in the uranium oxide scale, the alloying elements (notably Nb and Zr) are often found in the scale as only partially oxidized metal, the distribution of which largely reflects the microsegregation of the original alloy. This phenomenon is thought to contribute to the "explosive" behavior of uranium alloys pickled in concentrated nitric acid (Ref 71). The uranium dioxide that forms the majority of the scale rapidly dissolves in nitric acid, leaving behind a layer of finely divided niobium and/or zirconium that reacts explosively with the acid. Therefore, it is strongly advised that pickling not be used to remove thick

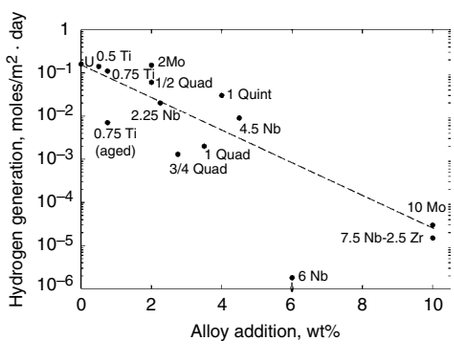

Fig. 18 Rate of hydrogen generation versus alloy addition for uranium alloys exposed to 100% RH nitrogen gas at 75 °C (167 °F). Data from Ref 63

scales from uranium alloys, rather that they be mechanically cleaned prior to any acid cleaning.

Hydriding

The product of the reaction between hydrogen gas and uranium is nearly stoichiometric uranium hydride, UH_3. The preparation of this compound was the subject of the first report within the field of metallurgy produced at the Los Alamos Laboratory during the Manhattan project, although this work was not published in the open literature until 1947 (Ref 72). UH_3 is the only stable phase formed between uranium and hydrogen. It is reported to exist in two forms, α and β UH_3. Both the α and β forms share the same crystal structure (PM_3M), but the α is the lower-density phase. The nomenclature used for these phases would imply that the α phase could be obtained from the β phase on cooling; however, α UH_3 is in fact metastable at all temperatures (Ref 73).

The kinetics of the uranium-pure hydrogen reaction have been the subject of many studies and are well characterized (Ref 42, 73–81). In the reaction between hydrogen and bulk uranium metal at constant temperature and pressure, paralinear kinetics are observed. Under these conditions, the reaction is extremely rapid relative to any other corrosion phenomenon observed in uranium. Because of the large difference in density between uranium metal and uranium hydride, the hydride product spalls off of the surface of the uranium. Consequently, the initiation period of the reaction (discussed below) is followed by a transition to a linear rate. At longer times, a faster linear rate is observed due to the breakup of the substrate and consequent increase in surface area. Finally, a decreasing rate is observed as the available uranium is consumed. The kinetics are dependent on the strength of the material, so in order to obtain reproducible kinetics it has been shown that it is necessary to use well-annealed material with properties similar to those of as-cast uranium. Figure 19 (Ref 82) illustrates typical initiation kinetics on bulk uranium with a native oxide present. Figure 20 (Ref 82) shows the overall linear reaction kinetics as a function of pressure and temperature for well-annealed uranium. Note that at higher temperatures the rates decrease as the dissociation pressure of the hydride becomes comparable to the applied hydrogen pressure.

The initiation of the uranium-hydrogen reaction has been the subject of some controversy. While early studies identified an "induction period" prior to the reaction initiating, most later studies maintain that this is a product of low gas purity. In high-purity hydrogen, the reaction begins immediately (Ref 4, 73, 75, 83). It has been reported that, in order for the induction period to be eliminated at temperatures below 100 °C (212 °F) it is also necessary to "sensitize" the surface with an anneal at 200 to 600 °C (390 to 1100 °F) (Ref 73, 76). It has recently been demonstrated that, at the temperature of the sensitization treatments, a range of chemical species characteristic of hyperstoichiometric uranium dioxide exposed to air are evolved (such as CO_x or H_2O) (Ref 84). This implies the presence of excess oxygen, OH^-, and carbonate or carbide/carboxide in the native oxide, all of which have been shown to "inhibit" the uranium-hydrogen reaction, although the mechanism of inhibition varies. The kinetics of the initiation stage have been reported by Brill (Ref 85).

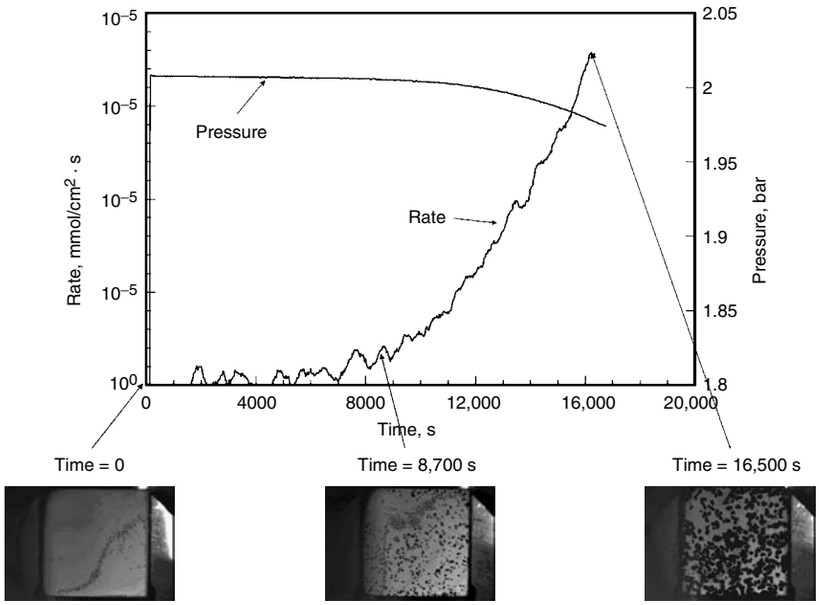

Fig. 19 The initial reaction rate of uranium bearing an air-formed oxide with hydrogen gas at 25 °C (77 °F) exhibits a cubic dependence on time. The inset micrographs show that, as time progresses, hydride sites grow and new sites are initiated. Crown copyright—used by permission. Source: Ref 82

Most studies have reported that the reaction initiates at discrete sites on the surface of the metal, the number and distribution of which have been observed to vary with surface preparation, grain size, purity, inclusion size, and inclusion distribution, among other variables (Ref 86–91). The kinetics vary considerably with the metallurgical condition of the specimen, notably the reaction is slower with cold-worked material than in as-cast or annealed metal (Ref 92). This effect has been explained by the growth rate of the hydride being dependent on the resistance of the metal to deformation (flow stress) as the pits nucleate and grow below the metal surface (Ref 79). This phenomenon is significant and is often overlooked in mechanisms proposed for the hydriding of uranium. Mechanisms that postulate a reaction limited to the surface of the uranium are difficult to reconcile with the inverse relationship between strength and hydride growth in uranium, since the hydride itself is not coherent with the metal and has no strength. The Condon model predicts that the nucleation occurs below the surface of the metal in a hydrogen-saturated region (Ref 79). This phenomenon has recently been observed in the form of blisters that develop in the early stages of hydriding (Ref 93).

There have been a number of studies on the nature of the sites where the hydride nucleates (Ref 87, 88, 94, 95). Owen and Scudamore (Ref 87) identified inclusions as nucleation sites. They also determined that the nucleation rate decreases as the native oxide film grows. Bloch et al. (Ref 88) conducted hydrogen exposures at 133 kPa (1000 torr) and 150 to 250 °C (300 to 480 °F) with unalloyed uranium and U-0.1Cr. They specifically excluded carbides as nucleation sites, but associated nucleation with random sites in preferential areas such as grain boundaries, slip lines, scratches, and so forth. This study showed extensive attack at all of these sites. A "pitting-type" attack was identified as occurring at temperatures below 130 °C (266 °F) by coalescence of several nuclei into a single pit growing into the metal. At higher

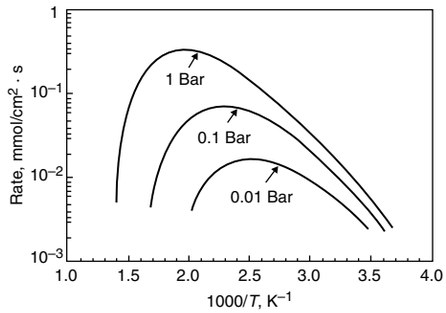

Fig. 20 Hydriding rates in uranium exhibit a strong dependence on temperature and hydrogen pressure and are illustrated here for a liner reaction front. As temperature increases, the dissociation pressure of the hydride approaches the applied hydrogen pressure and the reaction rate falls to 0. Crown copyright—used by permission. Source: Ref 82

temperatures, the growth appeared to be more of a "lateral spread" type. Moreno et al. (Ref 95) investigated uranium and U-0.1Cr exposed to hydrogen at 50 °C (122 °F). They sensitized their samples at 600 °C (1112 °F). Very rapid attack was observed at grain boundaries, inclusions, and twins. They attributed this to transport through the oxide along planar defects formed during oxide growth in the annealing stage.

Regardless of the precise nucleation site, it has been demonstrated that the initial stage of precipitation of uranium hydride on oxidized uranium occurs below the surface. This results in blisters that subsequently rupture and result in pits on the surface of the uranium (Ref 93). Once ruptured, the pits continue to grow until they cover the entire surface of the component or all of the available hydrogen is consumed. The product of the uranium-hydrogen reaction is a very fine powder that is extremely pyrophoric (Ref 96, 97). Hydriding and dehydriding of uranium is a convenient process for the production of uranium powder.

It has been reported that at low partial pressures of hydrogen (on the order of 1 torr, or 0.1 kPa) uranium with a thin surface layer of oxide does not initiate hydriding (Ref 98). This phenomenon suggests that a threshold pressure may be required to maintain a sufficient hydrogen activity at the metal/oxide interface to dissolve hydrogen in the uranium prior to the initiation of hydriding.

In the presence of mixtures of hydrogen and other oxidants, the kinetics of the reaction are considerably slower (Ref 99). This is due to a combination of the effects discussed previously, inhibition caused by the formation of surface species such as uranium carbonate, and differential diffusion and geometry effects in the case of large or nonuniform components.

Electrochemically Generated Hydrogen

Electrochemical polarization can produce uranium hydriding in aqueous solutions at room temperature. Uranium and U-2Nb hydrided in acidic, neutral, and alkaline buffer solutions when potentials were in the UH_3 potential-pH region, which is shown in Fig. 1. The reaction was relatively slow, and samples that were exposed for about 1 h were only ~20% covered with hydrided material. Attempts to hydride U-4Nb, U-6Nb, and U-8Nb were unsuccessful.

Figure 21 shows typical hydride morphology after cathodic electrochemical polarization. The hydrides were black in color and were raised above the uranium surface. Hydriding was localized, and initiation of the hydrides occurred near, but not on, inclusions (Fig. 21a). Hydride growth often occurred preferentially along grain boundaries (Fig. 21b).

Environmentally Assisted Cracking

Uranium and uranium alloys, particularly those with high strength, are often susceptible to environmentally assisted cracking (EAC). Environmentally assisted cracking is observed in aqueous chloride solutions, hydrogen environments, and even in atmospheric air. A thorough review of uranium alloy EAC has been written by Eckelmeyer (Ref 100); therefore, this discussion only briefly reviews cracking due to chloride and hydrogen environments. In general, unalloyed uranium and moderately alloyed uranium (e.g., U-6Nb) are more resistant to environmental degradation of mechanical properties than dilute alloys (e.g., U-0.75Ti) or highly alloyed uranium (e.g., U-7.5Nb-2.5Zr).

The most sensitive and conservative method for quantifying EAC susceptibility is a rising-load, fracture mechanics test, which employs precracked specimens. The stress intensity (K_{ISCC}) at crack initiation and the crack growth rate as a function of K_{ISCC} can be measured. This method is conservative because it uses precracked specimens, which will give the lowest initiation K_{ISCC}. The method is sensitive to differences in alloy, heat treatment, and environment because these differences often change crack growth rates more than the initiation K_{ISCC}.

Stress-Corrosion Cracking

Stress-corrosion cracking (SCC) is the brittle failure of an alloy when it is exposed to a corrosive environment and tensile stress. Stress-corrosion cracking is often characterized by multiple, branching cracks, and it can be suppressed by cathodic polarization.

Studies show a significant decrease in the fracture properties of U-0.75Ti (Ref 101, 102), U-4.5Nb (Ref 103), U-6Nb (Ref 104), U-7.5Nb-2.5Zr (Ref 105), and polynary uranium alloys (Ref 101), in moist air and chloride environments due to SCC. Stress-corrosion cracking typically occurs intergranularly, along prior γ grain boundaries. These alloys even suffer degradation in humid air: the moist air plane-strain fracture toughness, K_{Ic}, can be on the order of 50% lower than the dry air K_{Ic} value.

In high-chloride environments (above 500 ppm), cracking is sometimes observed in the absence of any stress (Ref 103, 105). This type of crack propagation is due to stresses created by the wedging force of the higher-volume corrosion product at the crack tip.

Hydrogen Embrittlement

Hydrogen embrittlement occurs when hydrogen diffuses into the alloy and causes brittle failure under tensile stress. Sources of hydrogen can be from the gas environment or the result of electrochemical reactions such as corrosion, electroplating, cleaning and pickling, or cathodic protection. Hydrogen is commonly introduced into uranium and its alloys during processing, either by heating in molten salt baths or by heat treatment in moist atmospheres.

Unlike in SCC, unalloyed uranium and lean uranium alloys are most susceptible to hydrogen embrittlement due to the low hydrogen solubility of the α phase. Hydrogen embrittlement is also more pronounced in lean alloys because they tend to have higher strengths. The critical hydrogen concentration for significant degradation in uranium and its alloys can be as low as 0.5 ppm by weight. For example, U-0.75Ti with hydrogen contents of 0.06 and 0.16 ppm showed little decrease in reduction in area; however, U-0.75Ti containing 1.14 ppm H had a significant decrease, with a reduction in area of only a few percent (Ref 106). U-0.75Ti and lean alloys can

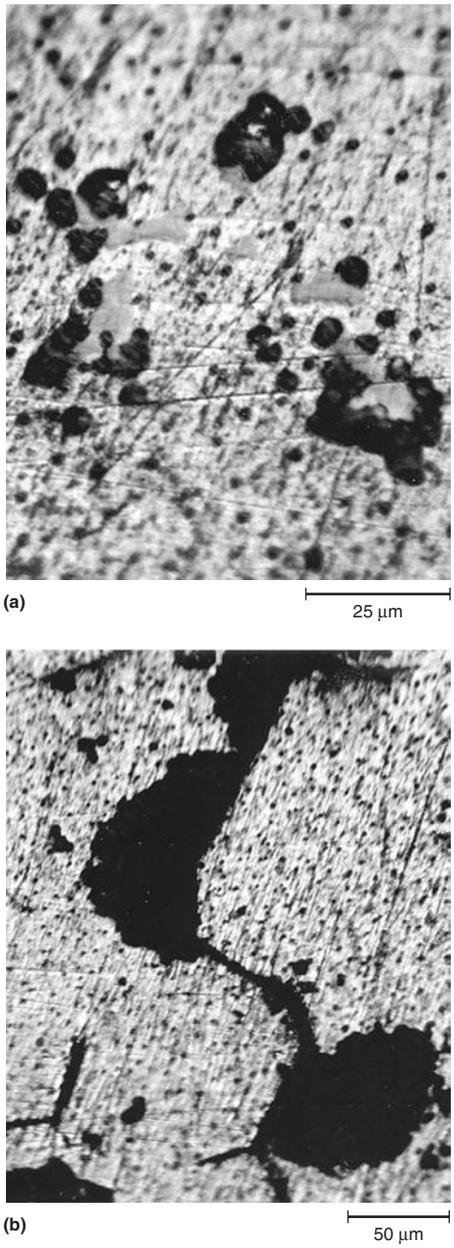

Fig. 21 Hydrides observed on U-2Nb after cathodic polarization at −3.5 V_{SCE} in pH 7.2 borate buffer solution (Ar purged). (a) Hydrides initiate near, but not on, carbide inclusions. (b) Hydride growth often follows grain boundaries.

even undergo HE due to residual stresses from quenching or welding.

Hydrogen embrittlement in uranium and uranium alloys that is a result of processing can be all but eliminated by vacuum heat treatment and thermal or mechanical stress relief. Lean uranium alloys in particular benefit from stress relief because they can retain high residual stress.

Protective Coatings and Surface Modification

Oxide, organic, and metallic coatings have been tested on uranium and lean uranium alloys for improved corrosion resistance. Of the numerous coating systems investigated, the most successful are electroplating (principally of nickel), cladding, and ion plating (both with aluminum). Organic and ceramic coatings and surface modification techniques, such as preoxidation and ion implantation, have also been investigated with varying degrees of success.

Protective Oxides

Both thermally grown and anodically grown oxides have been investigated as protective oxides on uranium and U-0.75Ti. Protective oxides are attractive because they do not change the surface finish of the metal, and they are also hard and adherent. Although they can delay the onset of corrosion, they do not provide any additional corrosion resistance once corrosion has initiated.

In the late 1960s, thermal oxides were grown using a controlled oxygen atmosphere and temperatures near 625 °C (1155 °F) (Ref 107). Corrosion testing showed that thermal oxides could delay the onset of corrosion for up to several hundred hours at 100% relative humidity at 95 °C (203 °F). However, once corrosion initiated, the rate was the same as for unprotected uranium. The most protective oxides were blue in color and were hydrophobic; that is, when they were dipped into water, the water did not wet the surface (Ref 108).

Similar results were observed for anodically grown oxides. Oxides were grown in solutions of ammonium borate, ethanol, ethylene glycol, and combinations thereof, but they did not provide long-term corrosion protection (Ref 109). A nonaqueous solution was used to grow oxides on U-0.75Ti, but they did not show any additional increase in corrosion resistance (Ref 110).

Organic Coatings

Organic coatings or paint work well for corrosion protection when the environment is only mildly corrosive and the substrate is somewhat corrosion resistant (e.g., coated aluminum cans for food or beverages). Water, given enough time, will permeate through an organic coating, and organic coatings can easily be scratched or damaged. Because uranium is easily corroded, organic coatings are not ideal for long-term corrosion protection in aggressive environments.

Orman and Walker (Ref 111) examined a wide range of coatings that represented the three major curing mechanisms. They compared the effectiveness of a single coat against multiple coats and even added an aluminum powder to try to reduce water permeability. Corrosion rates were measured in water-saturated air at various temperatures. Of the systems examined, only an aluminum-pigmented, styrene-butadiene lacquer provided significant protection at temperatures up to 40 °C (105 °F) (Ref 111).

Although lean uranium alloys have somewhat better corrosion resistance, organic coatings performed marginally on them as well. Specimens of U-4.2Nb that were α-aged and then coated with epoxy primer and polyurethane showed no severe corrosion in unscratched areas after a 90 day salt fog test; however, severe corrosion was observed in areas where the coating was intentionally scratched (Ref 112). Also, U-2Mo coated with both thermoplastic and thermosetting acrylic resins using water and solvent vehicles showed a delay in corrosion initiation, but long-term corrosion rates were at least as high as the uncoated material (Ref 113). Monochlorotrifluoroethylene over an epoxy paint on U-0.75Ti had good corrosion protection in moderate humidity environments, but not in high humidity environments (Ref 114).

It is clear from these results that organic coatings should only be used on uranium and lean alloys for short times where conditions are only mildly aggressive. If storage is short-term, a coating that is easily removed may be used. For example, uranium was successfully stored for several months under room-temperature, atmospheric conditions by applying a thin coating of watch oil (Ref 115).

Metallic Plating and Surface Modification

Metallic coatings are the most common method for increasing the corrosion resistance of unalloyed uranium and lean uranium alloys. These coatings are often applied in applications where uranium and lean alloys will form galvanic couples with more noble metals. There are several processes for applying metallic coatings on uranium: electroplating, ion implantation, and physical vapor deposition.

Electroplating nickel on uranium provides increased corrosion resistance and was developed at Los Alamos National Laboratory and Battelle Memorial Institute in the 1960s (Ref 116, 117). The Batelle process removed a large amount of uranium from the surface. The Los Alamos process did not remove as much metal and included a chemical etch that created a good mechanical bond (e.g., Fig. 22). The drawback to the process was that metallic tin, which resulted from a displacement reaction during an alcohol-stannous chloride etch, had to be mechanically removed as part of the process.

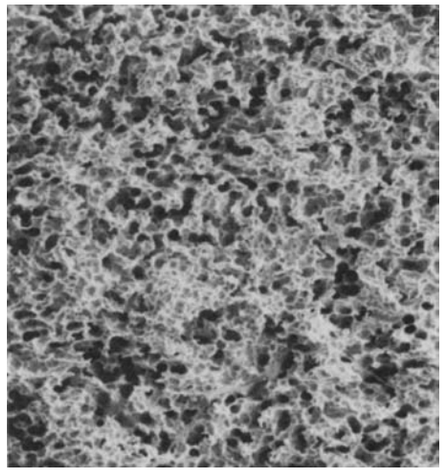

(a)

(b)

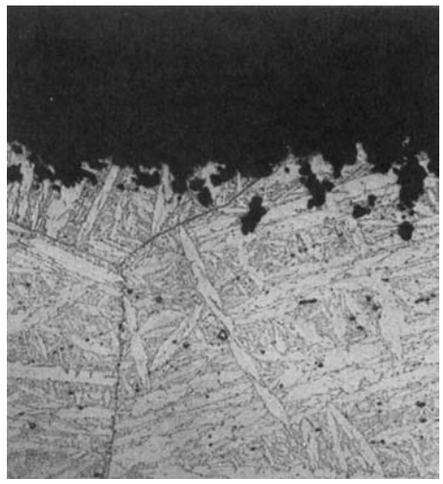

(c)

Fig. 22 Surface morphology (a) and (b) and cross section (c) of U-0.75Ti after chemical etching. The recesses extending into the base metal facilitate adherence of the electroplate and provide enhanced corrosion protection. Original magnification: (a) and (c) 300 ×, (b) 1000 ×

Improvements, made at Sandia Laboratories, eliminated mechanical removal of tin (Ref 118, 119). Because of recent regulations and waste reduction, this process is slightly different from the original process:

1. Ultrasonic clean in an aqueous, alkaline detergent to degrease.
2. Caustic soak in sodium hydroxide at 80 °C for 5 to 10 min.
3. Water rinse.
4. Pickle in 50 vol% nitric acid at room temperature until oxide is removed.
5. Water rinse.
6. Etch in ferric chloride hexahydrate (1.34 g/mL) at 32 ± 1 °C for about 20 min. The water content of this solution is critical to the etch rate. An alternate solution is 40 g/L $CuCl_3 + 2$ mL/L HF for 1 min (requires operator expertise).
7. Double rinse in water.
8. Pickle in 30 vol% nitric acid at room temperature.
9. Water rinse.
10. Apply a noncyanide copper strike (optional).
11. Nickel sulfamate plate (160 to 220 A/m^2).

The process yields better results if the noncyanide copper strike (step 10 above) is applied. The older processes used trichloroethylene to clean the surface, but aqueous, ultrasonic cleaners are now used. Also, a pumice scrub was used in addition to the caustic soak to remove oxide; however, it creates a potential operator contamination hazard and is not needed for good results.

Nickel coatings of 6 to 8 μm (0.24 to 0.31 mil) thickness significantly reduced the uranium corrosion rate (Fig. 23), but a coating thickness greater than 50 μm (1.97 mils) would be required for good, long-term corrosion resistance in moist nitrogen (Ref 120, 121). Because nickel is noble to uranium and lean uranium alloys (Fig. 10), any breach or defect in the coating will cause accelerated, galvanic corrosion to the substrate. Therefore, nickel or any noble metal coating should be used with caution. A better option is a multilayer plate that incorporates a sacrificial layer. When zinc and zinc-chromate conversion overplates are applied to a nickel layer, thinner nickel thicknesses are required for protection of U-0.75Ti (Ref 122, 123).

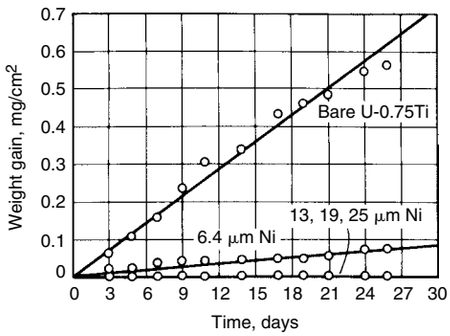

Fig. 23 Oxidation, as measured by weight gain, as a function of time for nickel-plated U-0.75Ti in air at 10% relative humidity and 105 °C (220 °F)

Another consequence of electroplated, nickel coatings is hydrogen generation and uptake during plating. This is of special concern in highly susceptible alloys such as U-0.75Ti. Hydrogen uptake from nickel electroplating is concentrated at the surface and generally does not affect tensile properties of bulk specimens tested in air (Ref 120). However, if the nickel coating is thin, tensile properties are reduced in water or water vapor due to accelerated corrosion at coating defects (Ref 120).

Adhesion of electroplated nickel coatings is good due to mechanical interlocking between uranium and nickel, but high temperatures can affect adhesion. Specifically, the uranium-nickel bond is susceptible to reduced bond strength at temperatures above about 350 °C (660 °F), and brittle intermetallic phases form at long times and higher temperatures (Ref 124).

Ion Implantation. Another method for applying metallic coatings is ion implantation. The corrosion protection provided by ion-implanted coatings depends on the coating structure that results from various process parameters, including deposition rate, bias voltage, substrate cleanliness, contaminants, and interdiffusion of substrate and coating materials (Ref 125, 126). The advantages of this process over electroplating include no hydrogen uptake, excellent coating adherence, uniform thickness, and the ability to plate aluminum or, any other species, most of which cannot be accomplished electrochemically. The disadvantages include cost, possible surface heating, which may affect mechanical properties, and part geometry/thickness effects due to line-of-sight application, although this can be overcome by using plasma implantation techniques.

Aluminum and molybdenum are the most commonly studied elements for ion implantation on uranium. Aluminum ion-implanted onto uranium provided good humid-air corrosion resistance at temperatures below about 75 °C (165 °F) through the formation of a uranium-aluminum intermetallic layer (Ref 126). Ion-implanted molybdenum on U-0.75Ti had a beneficial effect on pitting resistance in acidic and alkaline chloride solutions, but not in neutral chloride solution, (Ref 127).

Ion implantation has also been investigated as a means to suppress interactions between metals and hydrogen gas. Implantation of oxygen resulted in much delayed hydride initiation and localized hydride pits compared to as-polished uranium, which exhibited fairly rapid initiation and uniform hydriding (Ref 128). The same study showed that implantation of carbon instead of oxygen produced a similar delay in initiation, but a larger area on the carbon-implanted surface participated in the hydride reaction. In a later study, carbon and nitrogen were implanted separately into uranium, with the result that both oxidation and hydriding were suppressed (Ref 129–131). These results are especially interesting insofar as they relate to the effects of impurities on the corrosion of uranium. The most common impurities in uranium are carbon, nitrogen, and oxygen, usually in the form of cubic inclusions based on UC. The fact that uniform layers of these elements actually decrease reactivity with oxygen and hydrogen suggests that the inclusions themselves, which are composed of these elements, are unlikely to act as nucleation sites for pitting corrosion.

Physical Vapor Deposition. Metallic coatings can also be applied by the physical vapor deposition (PVD) process. In PVD, the source material is either evaporated and then deposited or sputtered and then deposited. A wider variety of metals, including alloys, can be applied using the sputter method. Physical vapor deposition by sputtering provides excellent adhesion, but can cause substrate heating and is expensive.

The corrosion resistance of PVD coatings ranging in thickness from 3 to 13 mm (0.12 to 0.51 in.) was examined electrochemically in aerated 3.5% NaCl solution (Ref 132). For all thicknesses studied, the coatings were porous, and only sacrificial coatings of zinc, magnesium, aluminum-zinc, and aluminum-magnesium provided protection. Coatings with noble metals, such as nickel, titanium, aluminum, and TiN, would need to be thicker and defect-free to provide protection. Another study confirmed that sacrificial aluminum-zinc on U-0.75Ti provided better corrosion protection and adhesion than a noble, multilayer coating of TiN/Ti/TiN, which will corrode if there are coating defects (Ref 132).

Storage of Uranium

Proper storage and handling of uranium to minimize corrosion is somewhat counter-intuitive. Uranium produces hydrogen in reactions with H_2O, except when oxygen is present. The solubility of hydrogen in uranium alloys tends to increase with alloy content, so while the tendency to precipitate the hydride decreases, more hydrogen may dissolve in the metal, which could have a detrimental effect on the material properties. Consequently, for most cases, the best option for storing uranium metal is in well-ventilated metal containers that allow the continued reaction with air and do not lead to low-oxygen conditions, which will result in accelerated corrosion. Alternatively, if it is necessary to avoid corrosion entirely, the metal should be stored in sealed cans that have been thoroughly dried and backfilled with ultrahigh-purity, dry, inert gas. Uranium metal that has been stored in sealed containers for many years without any known provision for the removal of moisture must be suspected of having some fraction of hydride present. Because the hydride is pyrophoric when exposed to air,

this material should be treated with extreme caution. The pyrophoricity of uranium compounds formed on old metallic nuclear fuel stored under poor conditions has recently been reported (Ref 96).

Environmental, Safety, and Health Considerations

Special care should be observed when handling uranium due to its mild radioactivity, chemical toxicity, and pyrophoricity. The primary radiological hazards associated with uranium are alpha and beta emission. Alpha radiation mainly poses an internal radiation hazard, so any process that may produce ingestible particulate should be designed with appropriate engineering controls. Exposure to beta radiation can easily be minimized by increasing distance and shielding (safety glasses, gloves, and plastic shields, for example). Uranium is a heavy metal, and as such, can cause damage to internal organs when ingested. Finely divided uranium, uranium oxide, and uranium hydride are pyrophoric and must be handled carefully to avoid fire. As the material becomes more finely divided, the surface area available for reaction increases, which results in more mass being consumed per unit time, resulting in a more energetic fire. Therefore, uranium or uranium alloys that have corroded and have loose oxide need to be handled carefully. Finally, uranium-niobium and uranium-zirconium alloys can become explosive after immersion in acid. Immersion of heavily oxided, two-phase uranium-niobium or uranium-zirconium in nitric acid can produce a black surface film that will explode when triggered by a spark or mechanical shock, even after being dried (Ref 71). Because of the radioactivity and toxicity of uranium, disposal is strictly regulated. Additional information on uranium safety can be found in Ref 133 and 134.

ACKNOWLEDGMENTS

The authors would like to especially thank Richard Bramlett and Randall Edwards at the Los Alamos National Laboratory for their guidance on the current practice of uranium cleaning and electroplating; Larry Weirick, the author of the article on this subject in the ninth edition of Volume 13; and Pallas Papin for the uranium oxide SEM images.

REFERENCES

1. D.T. Larson, L.A. Lott, and D.L. Cash, *Appl. Opt.,* Vol 12, (No. 6), 1973, p 1271–1275
2. J.P. Howe, The Metallurgy of Reactor Fuels, *Progress in Nuclear Energy,* H.M. Finniston and J.P. Howe, Ed., McGraw Hill, 1956, p 481–510
3. M. Pourbaix, *Atlas of Electrochemical Equilibria,* National Association of Corrosion Engineers, 1974
4. J.T. Waber, "A Review of the Corrosion Behavior of Uranium," LA-2035, Los Alamos National Laboratory, April 1956
5. J.E. Draley and J.W. McWhirter, "Effects of Metal Purity and Heat-Treatment on the Corrosion of Uranium in Boiling Water," ANL-5029, Argonne National Laboratory, April 1953
6. J.T. Waber, "A Review of the Corrosion of Uranium and Its Alloys," LA-1524, Los Alamos National Laboratory, Nov 1952
7. A.G. Ritchie et al., "Long Term Studies of the Corrosion of Uranium-6% Niobium Alloy," SWC Research Note No. 2/15, Atomic Weapons Research Establishment, April 1986
8. K.H. Eckelmeyer, Uranium and Uranium Alloys, *Properties and Selection: Nonferrous Alloys and Special-Purpose Materials,* Vol 2, *ASM Handbook,* ASM International, 1990, p 670–682
9. K.H. Eckelmeyer, A.D. Romig, and L.J. Weirick, *Metall. Trans. A,* Vol 15A, 1984, p 1319–1330
10. J.A. Lillard, et al., Electrochemically-Grown Oxides on U-Nb Alloys, *Oxide Films,* K. Hebert, et al., Ed., The Electrochemical Society, 2000, p 100–111
11. D. Kelly et al., *J. Vac. Sci. Technol. A (Vacuum, Surfaces, and Films)—47th International Symposium of AVS,* Vol 19 (No. 4), 2001, p 1959–1964
12. V.B. Kishinevski, L.I. Gomozov, and O.S. Ivanov, Corrosion Resistance in Water of Some Alloys of Uranium with Zirconium, Niobium and Molybdenum, *Physical Chemistry of Alloys and Refractory Compounds of Thorium and Uranium,* O.S. Ivanov, Ed., U.S. Atomic Energy Commission, 1972
13. J.W. McWhirter and J.E. Draley, "Aqueous Corrosion of Uranium and Alloys: Survey of Project Literature,'' ANL-4862, Argonne National Laboratory, May 1952
14. J.M. Macki and R.L. Kochen, "The Galvanic Corrosion Behavior of Uranium Alloys in Hydrochloric Acid and Ocean Water," RFP-1592, Rocky Flats Plant, Feb 1971
15. G.H. Jenks, "Electrochemistry of Uranium and Uranium Alloys in Aqueous Solutions," ORNL-4651, Oak Ridge National Laboratory, June 1971
16. M. Levy and C.V. Zabielski, Electrochemical Behavior of Some Binary and Polynary Uranium Alloys, *Physical Metallurgy of Uranium Alloys,* J.J. Burke et al., Ed., Brook Hill Publishing, 1976, p 897–947
17. X.G. Fu et al., *Rare Met. Mater. Eng.,* Vol 30 (No. 5), 2001, p 262–266
18. J.S. Bullock, Electrochemical Studies of Uranium Alloy Corrosion, *Physical Metallurgy of Uranium Alloys,* J.J. Burke et al., Ed., Brook Hill Publishing, 1976, p 847–895
19. C.L. Peterson, "A Limited Evaluation of the Corrosion of Uranium and Weapon-Associated Metals in Substitute Ocean Water," LA-3590-MS, Los Alamos National Laboratory, July 1966
20. J.M. Macki and R.L. Kochen, "The Corrosion Behavior of Uranium-Base U-Nb, U-Nb-Zr, and U-Mo Alloys in Hydrochloric Acid and Ocean Water," RFP-1586, Dow Chemical Company, Feb 1971
21. J.T. Waber, "An Analysis of Project Data on the Corrosion of Uranium in Various Media," LA-1381, Los Alamos National Laboratory, Dec 1948
22. B.A. Hilton, "Review of Oxidation Rates of DOE Spent Nuclear Fuel," DOE/SNF/REP-054, INEEL, Sept 2000
23. J.F. McIntyre, E.P. Lefeave, and K.A. Musselman, *Corros.,* Vol 44, (No. 8), 1988, p 502–510
24. P.P. Trzaskoma, *J. Electrochem. Soc.,* Vol 129, (No. 7), 1982, p 1398–1402
25. J.R. Winkel and E.L. Childs, "Galvanic Corrosion of Metals and Coatings When Coupled to Uranium in Severe Environments," RFP-3486, Rocky Flats Plant, Aug 1982
26. S. Orman, Oxidation of Uranium and Uranium Alloys, *Physical Metallurgy of Uranium Alloys,* J.J. Burke et al., Ed., Brook Hill Publishing, 1974, p 815–833
27. A.G. Ritchie, *J. Nucl. Mater.,* Vol 102, 1981, p 170–182
28. C.A. Colmenares, *Progress in Solid State Chemistry,* Vol 15, (No. 4), 1984, p 257–364
29. C.C. Colmenares, R. Howell, and T. McCreary, "Oxidation of Uranium Studied by Gravimetric and Positron Annihilation Techniques," UCRL-85549, Lawrence Livermore National Laboratories, April 1981
30. S. Orman, "Oxidation of Uranium in Water and Water Vapor," O 25/64, Atomic Weapons Research Establishment, 1964
31. M.M. Baker, L.N. Less, and S. Orman, *Trans. Faraday Soc.,* Vol 62, 1966, p 2513–2524
32. L. Leibowitz et al., *J. Electrochem. Soc.,* Vol 108, 1961, p 1155–1161
33. R.J. Pearce and P. Kay, "The Reaction of Uranium in the $U-O_2-H_2O$ and $U-H_2O$ Systems," TPRD/0954/R87, Central Electricity Generating Board, Berkeley Nuclear Laboratories, 1987
34. G.C. Allen, I.R. Trickle, and P.M. Tucker, *Philos. Mag. B,* Vol 43, (No. 4), 1981, p 689–703
35. A.G. Ritchie et al., *J. Nucl. Mater.,* Vol 140, 1986, p 197–201
36. L. Baker and J.D. Bingle, *J. Nucl. Mater.,* Vol 20, 1966, p 11–21
37. J.W. Isaacs and J.N. Wanklyn, "The Reaction of Uranium with Air at High

Temperatures," AERE-R-3559, Atomic Energy Research Establishment, Dec 1960
38. W.J. Megaw et al., *J. Nucl. Energy, Parts A/B,* Vol 15, 1961, p 176–184
39. R.K. Hilliard, "Oxidation of Uranium in Air at High Temperatures," U.S. Atomic Energy Commission Contract Report No. HW-58022, General Electric Co., Hanford Atomic Products Operation, 1958
40. A.F. Bessonov and V.G. Blasov, *Phys. Met. Metallogr.,* Vol 12, 1961, p 89–94
41. J.E. Antill and P. Murray, Reactions Between Fuel Elements and Gaseous Coolants, *Progress in Nuclear Energy, Ser. IV, Technology, Engineering and Safety,* C.M. Nicholls, Ed., Pergamon Press, 1960, p 65–86
42. W.M. Albrecht and M.W. Mallet, *J. Electrochem. Soc.,* Vol 103, (No. 7), 1956, p 404–409
43. R.J. Pearce, "A Review of the Rates of Reaction of Unirradiated Uranium in Gaseous Atmospheres," RD/B/6231/R89, Central Electricity Generating Board, Berkely Nuclear Laboratories, 1989
44. J.T. Waber and S.F. Waber, "The Reaction of Uranium with Purified Water," LAMS-1841, Los Alamos National Laboratory, Dec 1961
45. L.J. Weirick, "The Oxidation of Uranium in Low Partial Pressures of Oxygen and Water Vapor at 100 C," SAND83-0618, Sandia National Laboratories, June 1984
46. S.S. Cristy and J.B. Condon, Investigation of Metal Corrosion Mechanisms Using Stable Isotopes with the Ion Microprobe, *Secondary Ion Mass Spectroscopy: SIMS VI,* A. Benninghoven et al., Ed., Wiley, 1988, p 151–153
47. T.F. Kondo, F.H. Beck, and M.G. Fontana, *Corrosion,* Vol 30, 1974, p 330–339
48. J.H. Grimes and J.R. Morris, "Uranium Corrosion Studies, Part 2. The Rate of Reaction of Polish Uranium and Water Vapor at Various Temperatures," AWRE O-68/65, Atomic Weapons Research Establishment, 1965
49. V.J. Corcoran et al., "The Water Vapor Corrosion of Uranium and Its Prevention," AWRE O-42/65, Atomic Weapons Research Establishment, 1965
50. D.J. Trimble, "Reaction Rate Constant for Uranium in Water and Water Vapor," HNF-2853, Duke Engineering & Services Hanford, 1998
51. J. Abrefah and R.L. Sell, "Oxidation of K-West Spent Nuclear Fuel in Moist Helium Atmosphere," PNNL-12167, Pacific Northwest National Laboratory, 1999
52. G.W. McGillivray, D.A. Geeson, and R.C. Greenwood, *J. Nucl. Mater.,* Vol 208, 1994, p 81–97
53. A.G. Ritchie, R.C. Greenwood, and S.J. Randles, *J. Nucl. Mater.,* Vol 139, (No. 2), 1986, p 121–136
54. T.C. Totemeier, "A Review of the Corrosion and Pyrophoricity Behavior of Uranium and Plutonium," ANL/ED/95-2, Argonne National Laboratory, June 1995
55. M.M. Baker, L.N. Less, and S. Orman, *Trans. Faraday. Soc.,* Vol. 62, 1966, p 2525–2530
56. J.B. Condon, S.S. Cristy, and J.R. Kirkpatrick, "Final Progress Report—Uranium Reactions with Water Vapor," Y/DU-0274, Oak Ridge Y-12 Plant, April 1983
57. C. Leygraf and T. Graedel, *Atmospheric Corrosion,* Wiley-Interscience, 2000, p 354
58. S. Kihara et al., *Pure Appl. Chem.,* Vol 71 (No. 9), 1999, p 1771–1807
59. S.S. Cristy and J.B. Condon, Application of SIMS to the Study of a Corrosion Process—Oxidation of Uranium by Water, *Secondary Ion Mass Spectroscopy: SIMS V,* A. Benninghoven, Ed., Springer-Verlag, 1986, p 405–408
60. P. Kofstad, *Nonstoichiometry, Diffusion and Electrical Conductivity in Binary Metal Oxides,* Wiley-Interscience, 1972, p 382
61. R.H. Howell, C. Colmenares, and T. McCreary, *J. Less Common Met.,* Vol 98, 1984, p 267–278
62. D.J. Sandstrom, "A Review of the Early AP Penetrator Work at LASL Which Led to the Selection of U-3/4 Ti Alloy," LA-UR-76-1614, Los Alamos National Laboratory, 1976
63. N.J. Magnani, "The Reaction of Uranium and Its Alloys with Water Vapor at Low Temperatures," SAND-74-0145, Sandia Laboratories, Aug 1974
64. C.J. Greenholt and L.J. Weirick, *J. Nucl. Mater.,* Vol 144, 1987, p 110–120
65. A.G. Ritchie et al., "The Atmospheric Corrosion of Uranium-6%Niobium Alloy," CXD Memo No. 879, Atomic Weapons Research Establishment, Nov 1985
66. S. Barnartt, R.G. Charles, and E.A. Gulbransen, *J. Electrochem. Soc.,* Vol 103 (No. 9), 1956, p C203
67. S. Barnartt, R.G. Charles, and E.A. Gulbransen, *J. Electrochem. Soc.,* Vol 104 (No. 4), 1957, p 218–221
68. T. Matsui and T. Yamada, *J. Nucl. Mater.,* Vol 210 (No. 1/2), 1994, p 172–177
69. T. Matsui et al., *J. Nucl. Mater.,* Vol 199 (No. 2), 1993, p 143–148
70. J.V. Cathcart, Gaseous Oxidation of Uranium Alloys, *Physical Metallurgy of Uranium Alloys,* J.J. Burke et al., Ed., Brook Hill Publishing, 1976, p 775–813
71. R.L. Jackson and W.L. Johns, "Explosive Nature of Uranium-Base Niobium Alloys after Immersion in Nitric Acid," RFP-1575, Rocky Flats Plant, Dec 1970
72. J.E. Burke and C.S. Smith, *J. Am. Chem. Soc.,* Vol 69 (No. 10), 1947, p 2500–2502
73. J.B. Condon and E.A. Larson, *J. Chem. Phy.,* Vol 59 (No. 2), 1973, p 855–864
74. W.M. Albrecht and M.W. Mallet, *J. Electrochem. Soc.,* Vol 105 (No. 10), 1958, p 610–611
75. R.M. Alire et al., *J. Chem. Phys.,* Vol 52, (No. 1), 1970, p 37–46
76. J. Bloch and M. Mintz, *J. Alloys Cmpd.,* Vol 241 (No. 1/2), 1996, p 224–231
77. J.L. Stakebake, *J. Electrochem. Soc.,* Vol 126 (No. 3), 1979, p 495–496
78. J. Bloch and M. Mintz, *J. Alloys Cmpd., International Symposium on Metal Hydrogen Systems: Fundamentals and Applications,* Vol 253, 1997, p 529–541
79. J.B. Condon, *J. Phys. Chem.,* Vol 79 (No. 4), 1975, p 392–397
80. G.L. Powell, W.L. Harper, and J.R. Kirkpatrick, *J. Less-Common Met.,* Vol 172, 1991, p 116–123
81. G.L. Powell et al., *Z. Physik. Chem.—Int. J. Res. Phys. Chem. Chem. Phys.—3rd International Symposium on Metal-Hydrogen Systems: Fundamentals and Applications,* Vol 181, 1993, p 275–282
82. J. Glascott, *Discovery, Sci. Technol. J. AWE,* No. 6, 2003, p 16–27
83. J. Bloch et al., *J. Less-Common Met.,* Vol 139 (No. 2), 1988, p 371–383
84. D.F. Teter, R.J. Hanrahan, and C.J. Wetteland, "Urainum Hydride Nucleation Kinetics: Effects of Oxide Thickness and Vacuum Outgassing," LA-UR-01-5287, Los Alamos National Laboratory, 2001
85. M. Brill, J. Bloch, and M. Mintz, *J. Alloys Compd.,* Vol 266 (No. 1/2), 1998, p 180–185
86. R. Arkush et al., *J. Alloys Compd.,* Vol 244 (No. 1/2), 1996, p 197–205
87. L.W. Owen and R.A. Scudamore, *Corros. Sci.,* Vol 6, 1966, p 461–468
88. J. Bloch et al., *J. Less-Common Met.,* Vol 103 (No. 1), 1984, p 163–171
89. J. Bloch, E. Swissa, and M.H. Mintz, *Z. Phys. Chem.,* Vol 164, 1989, p 1193–1198
90. Y. Ben-Eliyahu, M. Brill, and M. Mintz, *J. Chem. Phys.,* Vol 111 (No. 13), 1999, p 6053–6060
91. R. Hanrahan, M. Hawley, and G. Brown, *Materials Research Society Symposium Proceedings—Symposium on Hydrogen in Semiconductors and Metals,* Materials Research Society, Vol 513 1998, p 43–48
92. J. Bloch and M.H. Mintz, *J. Less-Common Met.,* Vol 166 (No. 2), 1990, p 241–251
93. J. Bingert et al., *J. Alloys Compd.,* Vol 365 (No. 1–2), 2004, p 138–148
94. M. Balooch and A.V. Hamza, *J. Nucl. Mater.,* Vol 230 1996, p 159–170
95. D. Moreno et al., *J. Nucl. Mater.,* Vol 230 (No. 2), 1996, p 181–186
96. G. Powell, Reaction of Oxygen with Uranium Hydride, *TMS Annual Meeting,* TMS, 2004
97. T.C. Totemeier, Technical Investigation of a Pyrophoric Event Involving Corrosion Products from HEU ZPPR Fuel Plates, *Embedded Topical Meeting on DOE Spent Nuclear Fuel and Fissile Material Management,* American Nuclear Society, 2000

98. D.F. Teter and R.J. Hanrahan, "Effects of Surface Conditions and Thermomechanical Processing on Uranium Hydride Kinetics," LA-UR-03-5044, Los Alamos National Laboratory, 2003
99. C.E.G. Board, "Reaction of Uranium with Moist Hydrogen," Report 1987
100. K.H. Eckelmeyer, Environmentally Assisted Cracking of Uranium Alloys, *Stress-Corrosion Cracking,* R.H. Jones, Ed., ASM International, 1992, p 313–328
101. W.F. Czyrklis and M. Levy, *Corrosion,* Vol 30 1974, p 181
102. N.J. Magnani, *J. Nucl. Mater.,* Vol 54 (No. 1), Nov 1974, p 108-116
103. N.J. Magnani, *J. Nucl. Mater.,* Vol 42, 1972, p 271
104. N.J. Magnani, "Stress Corrosion Cracking of Uranium-Niobium Alloys," SAND78-0439, Sandia National Laboratories, 1978
105. N.J. Magnani, Hydrogen Embrittlement and Stress-Corrosion Cracking of Uranium and Uranium Alloys, *Advances in Corrosion Science and Technology,* M.G. Fontana and R.W. Staehle, Ed., Plenum Press, 1976
106. B.C. Odegard, K.H. Eckelmeyer, and J.J. Dillon, The Embrittlement of U-0.8%Ti by Absorbed Hydrogen, *Hydrogen Effects on Material Behavior,* N.R. Moody and A.W. Thompson, Ed., TMS, 1990, p 775–784
107. G.S. Petit et al., "Formation of Corrosion-Resistant Oxide Film on Uranium," K-1778, Oak Ridge Gaseous Diffusion Plant, 1969
108. G.S. Petit, "Formation of Corrosion-Resistant Oxide Film on Uranium," K/TL-613, Oak Ridge Gaseous Diffusion Plant, Oct 1976
109. O. Flint, J.J. Polling, and A. Charlesby, *Acta Metall.,* Vol 2, 1954, p 696
110. L.J. Weirick, Protective Coatings for Uranium Alloys, *Physical Metallurgy of Uranium Alloys,* J.J. Burke et al., Ed., Brook Hill Publishing, 1974
111. S. Orman and P. Walker, *J. Oil Colour Chem. Assoc.,* Vol 48, 1965, p 233
112. J.M. Macki and R.L. Kochen, "The Corrosion and Stress-Corrosion Cracking of Painted U-4.2wt%Nb," RFP-1891, Rocky Flats Plant, Aug 1972
113. C.E. Miller, "Producibility Study, Cartridge 20MM, DS Mk 149," Final Report, Olin Energy Systems Operations, Olin Corporation, Dec 1974
114. C.A. Colmenares, "Aluminum and Polymeric Coatings for Protection of Uranium," UCID-19970, Lawrence Livermore National Laboratory, Dec 1983
115. L. Kayler, Los Alamos National Laboratory, private communication, 2004
116. J.K. Gore and R. Seegmiller, *Plating,* Vol 50, 1963, p 215
117. J.G. Beach and C.L. Faust, "Electroplates on Thorium and Uranium for Corrosion Protection and to Aid Joining," BMI-1537, Battelle Memorial Institute, Aug 1961
118. P.D. Anderson, P.R. Coronado, and L.M. Berry, "Method of Preparing a Uranium Article for a Protective Coating," U.S. Patent 3,341,350, 1967
119. J.W. Dini and P.R. Coronado, *Trans. IMF,* Vol 47, 1969, p 1
120. H.R. Johnson, J.W. Dini, and S.W. Zehr, On the Embrittlement of Uranium and U-0.8Ti Alloy by Hydrogen and Water, *Hydrogen in Metals,* I.M. Bernstein and A.W. Thompson, Ed., American Society for Metals, 1974, p 325–343
121. J.W. Dini, H.R. Johnson, and C.W. Schoenfelder, *Nucl. Technol.,* Vol 28 (No. 2), 1976, p 249–255
122. L.J. Weirick and D.L. Douglass, *Corrosion,* Vol 36 (No. 6), 1976, p 209
123. L.J. Weirick, "Evaluation of Metallic Coatings for the Corrosion Protection of a Uranium—3/4 Weight Percent Titanium Alloy," SLL-73-5024, Sandia National Laboratories, Feb 1974
124. J.W. Dini, H.R. Johnson, and J.R. Helms, *J. Nucl. Mater.,* Vol 45 (No. 4), 1973, p 343–346
125. C.M. Egert and D.G. Scott, *J. Vac. Sci. Technol. A,* Vol 5 (No. 4), 1987, p 2724–2727
126. R.D. Bland, *Electrochem. Technol.,* Vol 6 1968, p 272
127. K.-S. Lei, F. Chang, and M. Levy, "Effect of Molybdenum Ion Implantation on the Pitting Corrosion of Depleted Uranium-0.75 Titanium Alloy," ARL-TR-144, US Army Research Laboratory, July 1993
128. R.G. Musket, *Nucl. Instrum. Meth. Phys. Res.,* Vol B40/41, 1989, p 591–594
129. R. Arkush, M. Mintz, and N. Shamir, *J. Nucl. Mater.,* Vol 281 (No. 2/3), 2000, p 182–190
130. R. Arkush et al., *J. Alloys Compd.—International Symposium on Metal-Hydrogen Systems, Fundamentals and Applications (MH2000),* Vol 330/332, 2002, p 472–475
131. R. Arkush et al., *J. Alloys Compd.,* Vol 340, 2002, p 122–126
132. F. Chang, M. Levy, and B. Jackman, *Surf. Coat. Technol.,* Vol 48, 1991, p 31–39
133. "Occupational Health Guideline for Uranium and Insoluble Compounds," U.S. Department of Health and Human Services, 1978
134. "Guide of Good Practices for Occupational Radiation Protection in Uranium Facilities," DOE-STD-1136-2000, U.S. Department of Energy, Aug 2000

ASM Handbook, Volume 13B: Corrosion: Materials
S.D. Cramer, B.S. Covino, Jr., editors, p385-401
DOI: 10.1361/asmhba0003829

Corrosion of Precious Metals and Alloys

Revised by Gaylord D. Smith, Special Metals Corporation

THIS ARTICLE characterizes the corrosion resistance of the precious metals: ruthenium, rhodium, palladium, silver, osmium, iridium, platinum, and gold. The elements are listed in order of their atomic number as found in periods 5 and 6 and group VIII and IB of the periodic table. These metals—also called noble, based on their positive position relative to a hydrogen electrode and in recognition of their resistance to chemical reaction, especially oxidation—offer corrosion resistance that is unmatched in base metals and alloys. The available information on the corrosion resistance of each element varies widely. Generally, more data are available for the more abundant, more easily fabricated elements. Silver and platinum have been evaluated in more environments than the other elements. Conversely, very little data are available for the intractable elements, osmium and ruthenium.

For each element, the general fabricability of the metal is briefly defined. More detailed information on fabricability is available in Ref 1 to 3. Fabrication characteristics and physical properties are found in the article "Properties of Precious Metals," *Properties and Selection: Nonferrous Alloys and Special-Purpose Materials,* Volume 2, *ASM Handbook,* 1990. This will aid in assessing the relevance of any particular noble metal to a given application. Atomic, structural, and physical properties can also play an important role in the use of any element or alloy in a given environment. Table 1 lists selected physical and mechanical properties for all of the noble metals. Corrosion data are divided into several categories, including high-temperature oxidation. These data follow a general summary of the performance of each element. For comparative purposes, certain tables have common corrosive environments in each table for each element. This should aid the reader in finding the optimal element or alloy for any given type of common corrosive environment. Much of these data were originally presented in different corrosion units. This information has been standardized in units of millimeters per year (mils per year). Virtually all the corrosion results are based on short-duration tests, so the information is intended to serve principally as a guide of expected results, because short-term results do not always reliably predict longer-term corrosion rates. The corrosion resistance of the pure or principal element is given in the tables but this is still relevant to the performance of many of their available commercial alloys. Effects of some alloying elements, when significant, are mentioned in the text.

Corrosion data for the noble metals have been summarized for the various elements in the past (Ref 1, 3–10). Some of these data are in conflict and some are in question. A best effort has been made to present the most reliable corrosion rate. The references cited will frequently contain additional detail in specific incidences.

Because of the high cost of the noble metals, a corrosion rate of approximately 0.05 mm/yr (2 mils/yr) was selected as an arbitrary practical upper limit of an acceptable corrosion rate. In severe environments, where a noble metal must be used and a higher corrosion rate can be tolerated, an upper limit of 0.25 mm/yr (10 mils/yr) may be acceptable. Most of the corrosion data presented here are in either of these two categories. For many design applications, more rigorous limits and knowledge of the actual corrosion rate and type are required. For these applications, a more rigorous search of the literature or actual laboratory/field testing is warranted.

Silver

Fabrication. Next to gold, silver is the most easily fabricated metal in the periodic table. It is very soft and ductile in the annealed condition. Silver is available in a large variety of product forms, including sheet, strip, foil, bar, wire, and shaped extrusions. Although silver work hardens, it is easily annealed in air above approximately 300 °C (570 °F). Silver is readily fusion welded—preferably by argon arc welding, because an oxyhydrogen flame can embrittle silver through gas absorption. Silver can be soldered by a number of silver- or tin-base solders. It can also be hammer peened to form strong joints.

Silver is commonly clad to copper, nickel, and steel alloys by either brazing or solid-phase bonding. Silver-lined tubing can be fabricated by expanding silver tubing inside the base metal tubing.

Atomic, Structural, and Physical Properties. Silver has several distinctions in the ranking of properties:

- Silver has the lowest density of the noble metal group of elements.
- Silver has the lowest melting point of all the noble metals.
- The thermal conductivity of silver is the highest of all the elements near room temperature.
- The room-temperature electrical resistance of silver is the lowest of all the elements.
- The standard electrode potential for silver ($Ag \leftrightarrow Ag^{+} + e^{-}$) is $+0.79$ V and is exceeded only by gold and the platinum group metals.

Mechanical Properties. Annealed silver has relatively low yield and tensile strengths, but appreciable strength can be induced through cold working. Tensile strength can be increased from 124 to 186 MPa (18 to 27 ksi) for annealed material to approximately 310 MPa (45 ksi) following 50 to 80% cold work. Silver loses strength rapidly above room temperature and, accordingly, is used with caution if high-temperature service is contemplated. Silver cladding is being successfully used to extend the useful temperature range of silver and its alloys.

Corrosion Resistance. Extensive reviews of the corrosion resistance of silver are available in the literature (Ref 1, 4–6, 8).

The corrosion resistance of silver depends on purity; much of the data presented here is for 999 fine silver (the fineness of silver is the pure silver content per 1000 parts of alloy). Silver can be used in hydrochloric acid (HCl), but results can be unsatisfactory under strongly aerating conditions when the concentration of acid and the temperature are increased. The halide acids, with the exception of hydrofluoric acid (HF), passivate silver under favorable conditions by forming a stable protective film. Silver-lined vessels are used for the bromination of organic materials, but hydrobromic acid (HBr) exposure is limited to room temperature and a maximum of 14% acid. Similarly, silver is restricted to room-temperature exposure in dilute hydroiodic acid (HI). Nitric acid (HNO_3) that contains traces of nitrous acid attacks silver vigorously. Hot, concentrated

Table 1 Selected properties of the noble metals

Property	Metal							
	Platinum	Palladium	Iridium	Rhodium	Osmium	Ruthenium	Gold	Silver
Atomic number	78	46	77	45	76	44	79	47
Atomic weight, amu	195.09	106.4	192.2	102.905	190.2	101.07	196.967	107.87
Crystal structure(a)	fcc	fcc	fcc	fcc	hcp	hcp	fcc	fcc
Electronic configuration (ground state)	$5d^9 6s$	$4d^{10}$	$5d^7 6s^2$	$4d^8 5s$	$5d^6 6s^2$	$4d^7 5s$	$5d^{10} 6s$	$4d^{10} 5s^1$
Chemical valence	2,4	2,4	3,4	3	4,6,8	3,4,6,8	1,3	1,2,3
Density at 20 °C (70 °F), g/cm^3 (lb/in.^{3})	21.45 (0.774)	12.02 (0.434)	22.65 (0.818)	12.41 (0.448)	22.61 (0.816)	12.45 (0.449)	19.32 (0.697)	10.49 (0.378)
Melting point, °C (°F)	1769 (3216)	1554 (2829)	2447 (4437)	1963 (3565)	3045 (5513)	2310 (4190)	1064.4 (1948)	961.9 1763.4
Boiling point, °C (°F)	3800 (6870)	2900 (5250)	4500 (8130)	3700 (6690)	5020 ± 100 (9070 ± 180)	4080 ± 100 (7375 ± 180)	2808 (5086)	2210 (4010)
Electrical resistivity, μΩ · cm at 0 °C (32 °F)	9.85	9.93	4.71	4.33	8.12	6.80	2.06	1.47
Linear coefficient of thermal expansion, μin./in./°C	9.1	11.1	6.8	8.3	6.1	9.1	14.16	19.68
Electromotive force versus Pt-67 electrode at 1000 °C (1830 °F), mV	...	−11.457	12.736	14.10	...	9.744	12.34(b)	10.70(c)
Tensile strength, MPa (ksi)								
As-worked wire	207–241 (30–35)	324–414 (47–60)	2070–2480(d) (300–360)	1379–1586(d) (200–230)	... ...	496 (72)(d)	207–221 (30–32)	290 (42)
Annealed wire	124–165 (18–24)	145–228 (21–33)	1103–1241 (160–180)	827–896 (120–130)	... ...	... ...	124–138 (18–20)	125–186 (18.2–27)
Elongation in 50 mm (2 in.), %								
As-worked wire	1–3	1.5–2.5	15–18(d)	2	...	3(d)	4	3–5
Annealed wire	30–40	29–34	20–22	30–35	...	...	39–45	43–50
Hardness, HV								
As-worked wire	90–95	105–110	600–700(d)	...	...	...	55–60	...
Annealed wire	37–42	37–44	200–240	120–140	300–670	200–350	25–27	25–30
As-cast	43	44	210–240	...	800	170–450	33–35	...
Young's modulus at 20 °C (70 °F) GPa (10^6 psi)								
Static	171 (24.8)	115 (16.7)	517 (75)	319 (46.5)	558 (81)	414 (60)	77 (11.2)	74 (10.8)
Dynamic	169 (24.5)	121 (17.6)	527 (76.5)	378 (54.8)	...	476 (69)	...	...
Poisson's ratio	0.39	0.39	0.26	0.26	...	...	0.42	0.37(e)

(a) fcc, face-centered cubic; hcp, hexagonal close-packed. (b) At 800 °C (1470 °F). (c) At 700 °C (1290 °F). (d) Hot worked. (e) Annealed. Source: Engelhard Industries Division, Engelhard Corporation

(60%) sulfuric acid (H_2SO_4) also attacks silver rapidly, as does 95% acid at room temperature. Phosphoric acid (H_3PO_4) can be handled at all concentrations and temperatures of 160 to 200 °C (320 to 390 °F). The corrosion resistance of silver in acids is given in Table 2. The Pourbaix diagram for silver is given in Ref 11. Silver is not attacked by water or steam to 600 °C (1110 °F).

Silver is resistant to dry and moist chlorine, due to the formation of a compact and pore-free film of silver chloride through which ambipolar diffusion of silver ions and electrons takes place. Silver is resistant to dry bromine but is not resistant to iodine and fluorine unless it is cathodically protected (Table 3). Silver is resistant to many hydroxide, sulfate, carbonate, nitrate-bisulfate, and halide salt solutions but is attacked by others (Table 4).

Table 5 lists corrosion rate data for silver in nearly 100 organic compound environments. Silver is satisfactory for use in nearly 90% of these environments. Several of the organics for which silver is not recommended did not attack silver; rather, silver affected the organic compound, such as certain fats and the essential oils. This is also true for hydrogen peroxide and hydrazine. Silver is attacked by organic amines and by ammoniacal solutions of copper acetate. The inertness of silver in many organic environments makes it the material of choice, especially where high product purity is essential.

Silver is attacked by most fused bisulfates, cyanides, halides, phosphates, and peroxides but is not attacked at temperatures below 500 °C (930 °F) by sodium hydroxide and at slightly lower temperatures by potassium, cesium, and rubidium hydroxides. All the low-melting molten metals attack silver, including mercury, sodium, potassium, lead, tin, bismuth, and indium. The corrosion resistance of silver in various gases is given in Table 6.

Oxidation. Silver is resistant to dry and moist air at ordinary temperatures. At slightly elevated temperatures, silver may form a thin film of silver oxide. Above approximately 455 °C (850 °F), any silver oxide present will dissociate at atmospheric pressure, leaving the surface clean once again. However, molten silver dissolves appreciable quantities of oxygen, which can result in considerable internal porosity upon resolidification as the oxygen is rejected from the lattice. Oxygen diffuses more freely through solid silver than through any metal. This fact has made it feasible to internally oxidize certain alloying elements, such as magnesium, in order to dispersion strengthen silver in, for example, the Ag-10MgO alloy used for electrical contacts. The information on oxygen in silver is reviewed in Ref 12. The causes and characteristics of sulfur-induced tarnish on silver and silver-rich alloys are reviewed in Ref 6. Sulfur in air will tarnish silver items, as will sulfur in eggs, wool, and rubber products.

Silver is blackened by ozone, with the maximum rate of attack at 220 to 250 °C (430 to 480 °F); the black tarnish disappears above approximately 455 °C (850 °F). Silver can be exposed to carbon monoxide to 300 °C (570 °F), to hydrogen to 700 °C (1290 °F), and to nitrogen to 500 °C (930 °F). At red heat, sulfur dioxide and sulfur trioxide rapidly attack silver. This attack becomes progressively worse with temperatures beginning at or near room temperature (Table 6).

The relatively poor strength of silver at elevated temperatures has minimized its use at high temperatures. However, silver-plated bearings are used in jet engines because of the improved lubricity and thermal conduction the silver contributes.

Alloying of Silver for Corrosion Applications. Sterling silver contains a minimum of 92.5% Ag. Although the remainder is unrestricted, it is usually copper. Because copper is soluble in silver to the extent of approximately 4%, sterling silver is commonly a duplex alloy.

The copper in solid solution has little effect on corrosion resistance, but the duplex microstructure may be a source of galvanic attack in strong electrolytes, such as seawater. However, this effect is rare in most environments. At slightly elevated temperatures, the copper is selectively oxidized. In this regard, copper does adversely affect the tarnish resistance of silver. However, copper additions to silver improve the strength of the metal, an attribute that is exploited in making cooling coils for beer and other foodstuff manufacturers. In general, base metal alloying does little to improve the corrosion resistance of silver. Most alloying of silver with base metals is done to change mechanical properties and melting point.

Some electrical contacts have been made with a 60 to 70% Ag alloy containing up to 30% Au. A ternary Au-24Ag-6Pt alloy is extensively used in telephone equipment. Silver-gold binary alloys are used for jewelry and dental applications as well (Ref 13–17). Alloys of silver containing 3 to 10% Pd are used for electrical contact materials. It should be noted that the alloy Pd-23Ag, because of its dimensional stability and high hydrogen permeability, has found acceptance as a diffusion membrane for the production of ultrapure hydrogen. Alloys in the Ag-Au-Pd ternary field possess excellent high-temperature oxidation resistance, favorable brazing characteristics, and a wide range of fusion temperatures from the melting point of silver (961.9 °C, or 1763.4 °F) to that of palladium (1554 °C, or 2829 °F).

Corrosion Applications of Silver. The use of silver and silver-rich alloys in jewelry, coinage, and sterling ware is well known. Also of commercial significance are the uses of silver in manufacturing and processing equipment within the food, chemical, and pharmaceutical industries. Silver has been used for decades within the food industry to maintain purity and freedom from metallic taste. Silver is resistant to many organic acids, salts, compounds, and foodstuffs and is used to manufacture, concentrate, and evaporate these products. Silver equipment has been used for handling syrups, fruit juices, beer, cider, white vinegar, jellies, gelatin, fatty acids, and essential oils, as well as autoclaves, mixing vessels, boiling pans, storage vats, and transfer equipment. Similarly, in the pharmaceutical industry, silver equipment is used to produce certain fine chemicals, hormones, and vitamins.

The chemical industry frequently uses silver-lined process equipment to minimize corrosion. Silver is used in apparatus to synthesize

Table 2 Corrosion of silver in acids

Acid	Temperature °C	Temperature °F	Corrosion rate mm/yr	Corrosion rate mils/yr
Acetic, all concentrations	Boiling		<0.05	2
Acetylsalicylic, all concentrations	Boiling		<0.05	2
Aqua regia	Room		Potential dissolution(a)	
Arsenic	Room		Dissolution	
Ascorbic, all concentrations	Room		<0.05	2
Benzoic, all concentrations	130	265	<0.05	2
Boric, salt	Boiling		<0.05	2
Butyric	Boiling		<0.05	2
Carbonic, all concentrations	Room		<0.05	2
Chloric, all concentrations	Room		Attacked	
Chlorotoluene-sulfonic	Room		<0.05	2
Chromic, all concentrations	100	212	<0.05	2
Citric, to 30% concentration	Boiling		<0.05	2
Crotonic	Boiling		<0.05	2
Fatty acids	400	750	<0.05	2
Fluorosilicic	65	150	<0.05	2
Formic, pure	Boiling		<0.05	2
Gluconic, all concentrations	Boiling		<0.05	2
Glycerophosphoric, to 50%	Boiling		<0.05	2
Hydrogen selenide	Room		Attacked	
Hydrogen sulfide	Room		Attacked	
Hydrobromic, below 14%	Room		<0.05	2
Hydrochloric, %				
5 (limited aeration)	100	212	0.035	1.4
5 (strong aeration)	Room		0.04	1.6
15 (limited aeration)	Room		0.007	0.28
15 (strong aeration)	Room		0.085	3.3
25 (limited aeration)	Room		0.14	5.5
25 (strong aeration)	Room		0.36	14.2
36 (limited aeration)	Room		0.07	2.8
36 (strong aeration)	100	212	2.5	100
Hydrofluoric, below 50%	Boiling		<0.05	2
Hydroiodic, dilute	Room		<0.25	10
Hypochlorous	Room		Attacked	
Isovaleric, all concentrations	Boiling		<0.05	2
Lactic	Boiling		<0.05	2
Laevulinic, all concentrations	Boiling		<0.05	2
Monochloroacetic, all concentrations	Boiling		<0.05	2
Nitric	Room		Rapid dissolution	
Nitrous	Room		Dissolution	
Oxalic	Boiling		<0.05	2
Phenylacetic, all concentrations	Boiling		<0.05	2
Phosphoric, %				
5	102	215	0.003	0.12
45	60	14	nil	
45	110	230	0.007	0.28
67	60	140	0.004	0.16
67	125	255	0.02	0.8
85	60	140	0.002	0.08
85	140	285	0.048	1.9
85	160	320	0.306	12
Phthalic, pure	Boiling		<0.05	2
Picric, pure	125	255	<0.05	2
Propionic	Boiling		<0.05	2
Pyridine-carboxylic, pure	Room		<0.05	2
Salicylic, all concentrations	Boiling		<0.05	2
Stearic, pure	160	320	<0.05	2
Sulfuric, %				
10	Boiling		0.003	0.12
50	Boiling		0.034	1.3
60	Boiling		0.88	34.6
95	Room		0.14	5.5
Sulfurous, all concentrations	90	195	<0.05	2
Tartaric, all concentrations(b)	100	212	<0.05	2

(a) Attack will occur whenever silver chloride film is ruptured. (b) Oxygen increases attack in dilute tartaric acid at room temperature

Table 3 Corrosion of silver in halogens

Halogen	Temperature °C	Temperature °F	Corrosion rate mm/yr	Corrosion rate mils/yr
Chlorine, dry(a)	100	212	Slight >0.05	2
Chlorine, moist or in solution	100	212	<0.05	2
Saturated chlorine in water	Room		<0.05	2
Bromine, dry(a)	Room		<0.05	2
Bromine, in methanol	Room		>0.05, <0.5	2.20
Bromine, in glacial acetic acid	50	120	<0.05	2
Iodine, dry	Room		Dissolution	
Iodine, moist or in solution	Room		Dissolution	
Fluorine, dry(b)	Room		Very slight attack	

(a) Halogen attack accelerates with increasing temperature, especially with moisture present. (b) Can be used as cathode to 250 °C (480 °F) for electrolysis of potassium fluoride plus HF to produce fluorine

Table 4 Corrosion of silver in salts and other environments

Environment	Temperature °C	Temperature °F	Corrosion rate mm/yr	Corrosion rate mils/yr
Alum, all concentrations	Boiling		<0.05	2
Aluminum chloride, all concentrations(a)	Boiling		<0.05	2
Aluminum fluoride, all concentrations	Boiling		<0.05	2
Aluminum sulfate, all concentrations	Boiling		<0.05	2
Ammonium chloride, all concentrations	Boiling		<0.05	2
Ammonium hydroxide(b)	Room		<0.05	2
Ammonium nitrate, <20%	Room		<0.05	2
Ammonium phosphate, all concentrations	Boiling		<0.05	2
Ammonium sulfate, all concentrations	Boiling		<0.05	2
Ammonium thiocyanate, pure	100	212	<0.05	2
Antimony pentachloride, pure	90	195	<0.05	2
Barium chloride, all concentrations	Boiling		<0.05	2
Barium chloride, all concentrations	Room		<0.05	2
Barium peroxide, all concentrations	Room		Attacked	
Bismuth oxide, all concentrations	Room		Slight attack	
Calcium bisulfite, pure	Boiling		<0.05	2
Calcium carbonate, all concentrations	Room		Slight attack	
Calcium chloride, all concentrations	100	212	<0.05	2
Calcium hydroxide, all concentrations	100	212	<0.05	2
Calcium sulfate, all concentrations	100	212	<0.05	2
Calcium sulfide, all concentrations	Room		Blackens	
Cesium hydroxide, all concentrations	500	930	<0.05	2
Cupric chloride, all concentrations	100	212	Attacked	
Cupric nitrate, all concentrations	Room		<0.05	2
Cupric sulfate, all concentrations	Room-boiling		<0.05	2
Cupric sulfate in sodium chloride	100	212	Attacked	
Cuprous chloride, all concentrations	100	212	Attacked	
Cuprous nitrate, all concentrations	100	212	Attacked	
Cuprous sulfate, all concentrations	100	212	Attacked	
Dyes, acid chromium	Boiling		<0.05	2
Ferric alum, all concentrations	100	212	Attacked	
Ferric chloride, <5%	Room		<0.05	2
Ferrous sulfate, all concentrations(c)	Room		<0.05	2
Fluorosilicate, all concentrations	100	212	<0.05	2
Hydrogen peroxide, all concentrations	Room		Peroxide decomposed	
Hydrogen sulfide, all concentrations	Room		Blackened	
Lithium chloride, all concentrations	Boiling		<0.05	2
Magnesium chloride, all concentrations	120	250	<0.05	2
Magnesium chloride, melt	710	1310	Attacked	
Mercuric chloride, all concentrations	Room		Not recommended	
Nitrosyl chloride, dry	Room		<0.05	2
Phosphorus chlorides, pure	Boiling		<0.05	2
Potassium bisulfate, all concentrations	Boiling		<0.05	2
Potassium bromide, all concentrations	200–400	390–750	<0.05	2
Potassium carbonate, all concentrations	Boiling		<0.05	2
Potassium chlorate, all concentrations	Boiling		<0.05	2
Potassium cyanide, concentrated, in air	Room		Attacked	
Potassium dichromate, all concentrations	Boiling		<0.05	2
Potassium ferrocyanide, all concentrations	Room		Attacked	
Potassium hydroxide, all concentrations(b)	300	570	<0.05	2
Potassium hydroxide, melt(b)	350	680	<0.05	2
Potassium nitrate, all concentrations	Boiling		<0.05	2
Potassium nitrate, melt	335	635	Attacked	
Potassium perborate, all concentrations(d)	50	120	<0.05	2
Potassium permanganate, all concentrations	Boiling		Attacked	
Potassium peroxide, melt	100	212 above melting point	Attacked	
Potassium persulfate, all concentrations	Room		Attacked	
Potassium sulfate, all concentrations	Boiling		<0.05	2
Sodium bisulfate, melt	400	750	Attacked	
Sodium bisulfites, all concentrations	100	212	<0.05	2
Sodium carbonate	Boiling		<0.05	2
Sodium chloride, all concentrations	Boiling		<0.05	2
Sodium chromate, all concentrations	Boiling		<0.05	2
Sodium cyanide, all concentrations	Room		Attacked	
Sodium fluorosilicate, pure	100	212	<0.05	2
Sodium hydroxide, <95%	Boiling		<0.05	2
Sodium hydroxide, melt(b)(e)	500	930	<0.05	2
Sodium hypochlorite, all concentrations	Room		<0.05	2
Sodium hypochlorite plus sodium chloride, saturated solution	Room		<0.05	2
Sodium nitrate, all concentrations	Boiling		<0.05	2
Sodium perborate, all concentrations	50	120	<0.05	2
Sodium perchlorate, all concentrations	Boiling		<0.05	2
Sodium perchlorate, melt	480	900	Attacked	
Sodium peroxide, melt	400	750	Attacked	
Sodium phosphates, all concentrations	Boiling		<0.05	2
Sodium silicates, all concentrations	Boiling		<0.05	2
Sodium sulfate, all concentrations	Boiling		<0.05	2
Sodium sulfide, all concentrations	Room		Slight attack	
Sodium thiosulfate, all concentrations	Room		<0.05	2
Stannic ammonium chloride, all concentrations	Boiling		<0.05	2
Stannic chloride, all concentrations	Boiling		<0.05	2
Sulfuryl chloride, dry and wet	300	570	<0.05	2
Thionyl chloride, dry or wet	Boiling		<0.05	2
Uranyl nitrate, all concentrations	Boiling		<0.05	2
Zinc chloride, all concentrations	Boiling		<0.05	2

(a) Provided oxidizing agents are not present. (b) Air must be excluded. (c) Attacked upon heating. (d) Causes deterioration of potassium perborate. (e) Mass transfer possible above 600 °C (1110 °F)

urea from ammonia and carbon dioxide. Dye manufacturers use silver to handle aniline, ethyl chloride, boric acid, iodine, formaldehyde, magnesium chloride, magnesium sulfate, and zinc oxide. Silver-lined equipment is used to dehydrate glacial acetic acid and to process and store acetic anhydride in the rayon industry and phenol in the synthetic coatings industry. Highly refined acid products, such as phthalic acid made from hardwood distillation, can be processed in silver-lined stills. Silver vessels are often used to produce highly corrosive writing inks. Silver condensers are used to produce high-purity methyl acetone. High-purity sodium and potassium hydroxide are concentrated to the anhydrous melt in silver pans, and commercial grades of these products are also concentrated in silver-lined continuous vacuum evaporators operating at over 315 °C (600 °F). Silver-tubed condensers are used for condensing 70% HF from the hot hydrogen fluoride vapors formed during the hydrofluorination of uranium. Silver metering equipment is employed in disperse wet chlorine gas in water purification installations. The chemical industry uses equipment made from silver to produce fluorophosphoric acid and salts. Rupture disks for emergency relief of pressure in chemical-processing equipment are frequently made of silver.

The use of silver to produce mirrors is based on the relative inertness of silver in air as well as its high and uniform reflectivity in the visible light range. Silver-containing electrical contacts and batteries derive their utility from the chemical nobility and stability of silver, although in relay contacts the formation of silver sulfide, whose resistance increases as the current decreases, imposes restraints on the use of silver and its alloys in this field.

Gold

Fabrication. Gold is a highly malleable element that does not work harden significantly at room temperature. It is available for industrial use in all product forms, including thin strip and leaf, tubing, and fine wire. It is readily fabricated into finished-product forms and claddings. Gold is easily fusion or hammer welded. Soft soldering is not recommended. Gold can be deposited in thin films and fabricated on the nanometer scale for electronic components.

For jewelry, the common unit of gold content is the carat (commonly spelled karat in the United States). This is the proportion of gold in alloy in twenty-fourths. Au 18 karat item is 18/24 or 75% Au.

Mechanical Properties. Annealed gold is extremely soft (25 to 27 HV) at room temperature and is relatively low in tensile strength (125 to 138 MPa, or 18 to 20 ksi). Cold-worked wire cannot be strengthened much above 207 MPa (30 ksi). Because of the low strength of gold, the use of gold cladding on stronger base metals is common. Gold cannot be used as a structural material at elevated temperatures because of creep of the metal. Gold rupture disks usually are not used above 80 °C (175 °F).

Table 5 Corrosion resistance of silver in organic compounds

Environment	Temperature °C	Temperature °F	Corrosion rate mm/yr	Corrosion rate mils/yr
Acetaldehyde, pure	200–400	390–750	<0.05	2
Acetic anhydride, all concentrations	Boiling		<0.05	2
Acetone, pure	Boiling		<0.05	2
Acetylene dichloride, wet and acid	Boiling		<0.05	2
Ethyl alcohol, all concentrations	Boiling		<0.05	2
Amyl acetate, pure	Boiling		<0.05	2
Amyl alcohol, pure	Boiling		<0.05	2
Aniline, pure	Boiling		<0.05	2
Benzaldehyde, pure and aqueous	Boiling		<0.05	2
Benzene, pure	Boiling		<0.05	2
Benzotrifluoride, pure	Boiling		<0.05	2
Benzyl chloride, pure	180	355	<0.05	2
-bromoisovaleryl bromide, pure	100	212	<0.05	2
-bromoisovaleryl urea, pure	Melting point		<0.05	2
Butyl acetate, pure	Boiling		<0.05	2
Butyl alcohol, pure	Boiling		<0.05	2
Carbon tetrachloride, dry and wet	Boiling		<0.05	2
Chlorobenzene, pure	Boiling		<0.05	2
Chlorocresols, all concentrations	Boiling		<0.05	2
Chloroform, dry or wet	Boiling		<0.05	2
Chlorohydrins, pure	Boiling		<0.05	2
Chloronitrobenzenes, pure	Boiling		<0.05	2
Chlorotoluene, pure	Boiling		<0.05	2
Coniferyl alcohol, all concentrations	80	175	<0.05	2
Copals, pure and wet	400	750	<0.05	2
Copper acetate, neutral solutions	100	212	<0.05	2
Copper acetate, ammoniacal solutions	Room		Attacked	
Coumarin, pure	100	212	<0.05	2
Cresols, pure	Boiling		<0.05	2
Dextrose, all concentrations	Boiling		<0.05	2
Dialkyl sulfates, pure	Boiling		<0.05	2
Dibutyl phthalate, pure	Boiling		<0.05	2
Dimethylaniline, pure	Boiling		<0.05	2
Diphenyl, pure	400	750	<0.05	2
Essential oils, pure(a)	Boiling		<0.05	2
Ether, pure	Boiling		<0.05	2
Ethyl acetate, pure	Boiling		<0.05	2
Ethyl benzene, pure	136	277	<0.05	2
Ethylene dibromide, wet and acid products	Boiling		<0.05	2
Ethylene dichloride, wet and acid products	Boiling		<0.05	2
Fats pure	300	570	<0.05	2
Fatty acids, pure	400	750	<0.05	2
Formaldehyde, all concentrations	Boiling		<0.05	2
Furfural, wet and slightly acid	Boiling		<0.05	2
Gelatin, pure	Boiling		<0.05	2
Glycerol, pure	Boiling		<0.05	2
Guanidine nitrate, all concentrations	Room		Not recommended	
Guinolines, pure	Boiling		<0.05	2
Guinone, inorganic solvent and pure	100	212	<0.05	2
Hexachloroethane, dry and moist	187	369	<0.05	2
Hexamethylene tetramine, all concentrations(b)	Room		<0.05	2
Hydrazine, pure	Room		Not recommended	
Hydroguinone, pure	Boiling		<0.05	2
Isoborneol acetate, pure	Boiling		<0.05	2
Isobutyl chloride, dry and wet	Boiling		<0.05	2
Limonene, pure	Boiling		<0.05	2
Methyl alcohol, pure	Boiling		<0.05	2
Methylamines, aqueous	Room		Attacked	
Methyl chloride, dry and wet	300	570	<0.05	2
Methylene chloride, dry and wet	Boiling		<0.05	2
Methylglycol, pure	Boiling		<0.05	2
Milk, pure(c)	Boiling		<0.05	2
Nitrobenzene, pure	Boiling		<0.05	2
Nitrocellulose, in water or alcohol	Room		<0.05	2
Nitrophenols, pure	Boiling		<0.05	2
Nitrotoluenes, pure	Boiling		<0.05	2
Pentachloroethane, wet, dry, and acid	Boiling		<0.05	2
Phenol, all concentrations	Boiling		<0.05	2
Phthalic anhydride, pure	Boiling		<0.05	2
Potassium acetate, all concentrations	Boiling		<0.05	2
Quinine sulfate, all concentrations	70	160	<0.05	2
Sodium acetate, all concentrations	Boiling		<0.05	2
Sodium acetate, melt	400	750	<0.05	2
Sodium bisulfate, all concentrations	Boiling		<0.05	2
Sodium formate, all concentrations	Boiling		<0.05	2
Sodium isovalerate, all concentrations	Boiling		<0.05	2
Sodium isovalerate, melt with sodium hydroxide	290	555	<0.05	2
Sodium methylate, all concentrations in alcohol or ether	100	212	<0.05	2
Sodium pentachlorophenolate, all concentrations	Boiling		<0.05	2
Sodium phenolate, all concentrations	Boiling		<0.05	2
Sodium salicylate, all concentrations	Boiling		<0.05	2
Sodium tartrates, all concentrations	Boiling		<0.05	2
Sorbital, all concentrations	Boiling		<0.05	2
Sorbose, all concentrations	Boiling		<0.05	2
Toluene, pure	Boiling		<0.05	2
Toluenesulfonyl chlorides, pure	Boiling		<0.05	2
Triethanolamine, mixture with diethylene glycol	Room		<0.05	2
Vinyl chloride, pure	200	390	<0.05	2

(a) Silver may taint the flavor of fats. (b) Solutions must be free of air and ammonia. (c) Silver may impart metallic taste

Corrosion Resistance. Pure gold essentially owes its corrosion resistance to the low chemical affinity of the element. Passive film protection, such as occurs for silver in halide environments, is rare.

Table 7 gives the corrosion resistance of gold in acids. Gold is very resistant to H_2SO_4 to 250 °C (480 °F), and attack above this temperature may be primarily dependent on available oxygen. Gold is also resistant to concentrated HCl to its boiling point and to HNO_3 concentrations of up to 50% at the boiling point. However, hot mixtures of HNO_3 and H_2SO_4 will rapidly attack gold, as will aqua regia and hydrogen cyanide (with oxygen present). Mixtures of HCl, HBr, and HI with HNO_3 are extremely corrosive to gold. Mixtures of HF and HNO_3 are not corrosive to gold. Gold is resistant to most other acids. The anodic dissolution and corrosion of gold is reviewed in Ref 18.

Gold is generally attacked by wet or dry gaseous halogens. Only dry fluorine and wet or dry iodine can be handled by gold, and then only within limitations (Table 8). Gold, second only to platinum, is resistant to dry hydrogen chloride to 870 °C (1600 °F), to oxygen to its melting point, to ozone to 100 °C (212 °F), to phosgene at room temperature, and to sulfur dioxide, dry and wet, to 600 °C (1110 °F) (Table 9).

Gold is not attacked by most inorganic salts in solution for their typical conditions of use (Table 10). Exceptions are the solutions of alkali cyanide and peroxide. Most alkali and alkaline melts as nitrates, hydroxides, and bisulfates will eventually attack gold but only at elevated temperatures. The corrosion resistance of gold in over 40 organic compounds is given in Table 11. In all cases, gold was found to be resistant enough for commercial use.

Gold is attacked by all low-melting alloys, including mercury, sodium, potassium, lead, tin, bismuth, and iridium. The standard electrode potential for gold ($Au \leftrightarrow Au^+ + e^-$) is +1.68 V, the highest of all precious metals.

Oxidation Resistance. Gold does not oxidize at any temperature up to its melting point but may possess an absorbed layer of oxygen on the surface. Gold and its alloys greater than 14 karat are usually not susceptible to tarnish by hydrogen sulfide, sulfur, or other nonoxidized sulfur compounds. Tarnish is a superficial corrosion that darkens the surface.

Corrosion Applications. Gold is primarily used for its decorative appearance in jewelry, coinage, dentistry, and gold leaf. Because of its softness and lack of resistance to halogens, its use in chemical applications, even as gold-lined apparatus, is somewhat limited. Gold is resistant to nonoxidizing H_3PO_4 and

phosphates; therefore, it is used for lining autoclaves handling phosphate mixtures to 500 °C (930 °F). In the production of zirconium by the iodide process, gold closure gaskets are used to handle dry iodine vapors at 500 °C (930 °F). The use of gold-lined equipment to perform hydrochlorinations and hydrofluorinations of organic compounds in the chemical industry has been established. Laboratory ware fabricated from an Au-10Pt alloy is frequently used in place of platinum.

The stability of gold, coupled with its ability to reflect infrared radiation, has made it a popular glass window coating for energy conservation. Gold-base brazing alloys are used in critical aerospace and chemical equipment applications. Electroplated gold is used for its stability in electrical applications, such as connectors, relay switches, and contacts. Gold-silver-copper alloys are used for pen nibs and for slip rings and brushes in electrical instruments. Gold-palladium-iron alloys are used for potentiometer wire. A gold-palladium-iron alloy having a high resistivity and a negative temperature coefficient of resistance has been used as a resistor and potentiometer wire.

Table 6 Corrosion of silver in gases

Gas	Temperature °C	Temperature °F	Corrosion rate mm/yr	Corrosion rate mils/yr
Acetylene, dry	Room		Risk of explosion	
Ammonia, pure	190	375	<0.05	2
Ammonium chloride, vapor	200	390	Attacked	
Carbon dioxide, pure	Room		<0.05	2
Carbon monoxide, pure	300	570	<0.05	2
Hydrogen, pure	700	1290	<0.05	2
Hydrogen chloride dry(a)	430	805	<0.05	2
Nitric oxide, pure	Room		Attacked	
Nitric tetroxide, pure	Room		<0.05	2
Nitrogen, pure	500	930	<0.05	2
Oxygen, pure(b)	100	212	<0.05	2
Ozone, with 98% oxygen	Room		<0.05	2
Steam, pure(c)	600	1110	<0.05	2
Sulfur dioxide, pure	Red heat		Attacked	
Sulfur trioxide, pure	Red heat		<0.05	2

(a) Silver is protected by a layer of silver chloride that forms rapidly on the surface. (b) Attack becomes appreciable at 200 °C (390 °F). (c) Without pressure

Platinum

Fabrication. Platinum is a soft, ductile, white metal, and like other face-centered cubic (fcc) metals, it can be readily hot or cold worked. Hot working is typically begun at 1000 °C (1830 °F), with reductions per pass as great as 50% being possible. Cold work is usually performed with reductions of 10% per pass and intermediate annealing after 75% reduction in thickness. Wire processing is similarly performed. Platinum can be processed bare into leaf and wire as small as 2.5 μm (0.1 mil). Pure platinum can be annealed in a short time at 600 to 700 °C (1110 to 1290 °F). Alloys require higher temperatures. Platinum can be annealed in air, but other atmospheres, such as nitrogen, argon, and helium, can also be used without damage. Platinum is readily fusion or resistance welded. Platinum can be electrodeposited on base metals.

Mechanical Properties. Platinum work hardens at approximately the same rate as copper or silver; the mechanical properties obtained are strongly influenced by the purity of the platinum. The hardness and tensile strength are in the range of 37 to 42 HV and 124 to 165 MPa (18 to 24 ksi) for annealed material. The tensile strength of annealed platinum wire versus temperature is given in Table 12.

Corrosion Resistance. The exceptional corrosion resistance of platinum is extensively covered in the literature (Ref 1, 7, 10). Platinum is one of the few metals that is unaffected by atmospheric exposure, even in sulfur-bearing industrial atmospheres.

Platinum is resistant to corrosion by single acids (Table 13), alkalis, aqueous solutions of common salts (Table 14), and organic materials (Table 15). The potential-pH diagram for platinum as defined by Pourbaix shows that platinum at 25 °C (75 °F) is immune to attack at all but the lowest pH levels and high redox potentials (Ref 11). Even at elevated temperatures, platinum is resistant to dry hydrogen chloride and sulfurous gases (Table 16). Platinum is resistant to most halogen gases at room temperature, with dry and moist bromine being the exception

Table 7 Corrosion of gold in acids

Acid	Temperature °C	Temperature °F	Corrosion rate mm/yr	Corrosion rate mils/yr
Acetic, glacial	100	212	<0.05	2
Aqua regia	Room		Rapid dissolution	
Arsenic, all concentrations	Room		<0.05	2
Chlorosulfonic, all concentrations	Boiling		<0.05	2
Chlorotoluene-sulfonic, all concentrations	Boiling		<0.05	2
Citric, 20%	Boiling		<0.05	2
Citric, 30%	Boiling		<0.05	2
Crotonic, all concentrations	Boiling		<0.05	2
Fatty acids, pure	Boiling		<0.05	2
Glycerophosphoric, 1 to 50%	Boiling		<0.05	2
Hydrobromic, specific gravity 1.7	Room		<0.05	2
Hydrochloric, 36%	Room-100	212	<0.05	2
Hydrofluoric, 40%	Room		<0.05	2
Hydrogen sulfide, moist	Room		<0.05	2
Hydroiodic, specific gravity 1.75	Room		<0.05	2
Isovaleric, all concentrations	Boiling		<0.05	2
Lactic, all concentrations	Boiling		<0.05	2
Laevulinic, all concentrations	Boiling		<0.05	2
Nitric, %				
1–50	Boiling		<0.05	2
70	Room		>0.05	2
70	Boiling		0.15	6
Oxalic, all concentrations	Boiling		<0.05	2
Phenol-2,4-disulfonic, all concentrations	100	212	<0.05	2
Phthalic, pure	Boiling		<0.05	2
Picric, pure	125	255	<0.05	2
Propionic, all concentrations	Boiling		<0.05	2
Pyridine, all concentrations	Boiling		<0.05	2
Pyridine-carboxylic, all concentrations	150	300	<0.05	2
Salicylic, all concentrations	Boiling		<0.05	2
Stearic, pure	Boiling		<0.05	2
Sulfuric, all concentrations	250	480	<0.05	2
Sulfurous, all concentrations	100	212	<0.05	2
Tartaric, all concentrations	Boiling		<0.05	2

Table 8 Corrosion of gold in halogens

Halogen	Temperature °C	Temperature °F	Corrosion rate mm/yr	Corrosion rate mils/yr
Bromine, all concentrations, dry and wet	Room		Attacked	
Chlorine, dry	Room		0.3	12
	120	250	0.7	27.6
	150	300	1.5	60
	175	345	3.0	120
	205	400	30.5	1200
Chlorine, wet	Room		Attacked	
Fluorine, dry	<500	930	<0.05	2
Iodine, dry and wet	Room		<0.05	2
Iodine, dry and wet	>50	120	Attacked	
Iodine, 5% in alcohol	Room		Attacked	

Table 9 Corrosion of gold in various gases

Gas	Temperature °C	Temperature °F	Corrosion rate mm/yr	Corrosion rate mils/yr
Hydrogen chloride, dry	870	1600	<0.05	2
Ozone, with 98% oxygen	100	212	<0.05	2
Phosgene	Room		<0.05	2
Steam	800	1470	<0.05	2
Sulfur dioxide, dry and wet	600	1110	<0.05	2

(Table 17). Platinum is also essentially inert to many molten salts, and it resists the action of fused glasses if oxidizing conditions are maintained.

Aqua regia and mixtures of HCl and oxidizing agents will attack platinum, as will free halogens and selenic acid to some degree at elevated temperatures. A number of low-melting metals, including lead, tin, antimony, zinc, and arsenic, will readily alloy with and attack platinum at their melting temperatures. Low-melting phases are formed with silicon, phosphorus, bismuth, and boron, and salts or compounds of these metals can be detrimental at high temperatures under reducing conditions.

As an anode, platinum will resist attack in a wide variety of alkaline, neutral, and mild acid solutions (Ref 19). There is attack in strong HCl. If an alternating current is applied to platinum electrodes, attack will occur in cyanide and in some acid solutions. The standard electrode potential ($Pt \leftrightarrow Pt^{2+} + 2e^-$) is approximately +1.2 V at 25 °C (75 °F).

Effect of Alloying on Corrosion Resistance. Alloys containing up to 25% Pd in platinum have essentially the same corrosion resistance as platinum and are not discolored by heating in air.

The corrosion resistance of the entire binary series of rhodium-platinum alloys is excellent, with corrosion resistance tending to improve with higher rhodium contents. For example, a 10% addition of rhodium to platinum reduces the corrosion rate in 36% HCl at 100 °C (212 °F) from 0.2 mm/yr (8 mils/yr) to 0 and the attack of 100 g/L ferric chloride ($FeCl_3$) at 100 °C (212 °F) from 16.7 to 0.2 mm/yr (660 to 8 mils/yr). Alloys containing less than approximately 20% Rh can be hot or cold worked, while those containing between 20 and 40% Rh must be hot worked prior to cold working. The practical limit for workability is approximately 40% Rh.

Iridium and ruthenium additions to platinum result in corrosion resistance similar to that obtained through rhodium additions. However, the ranges for working are slightly more restrictive for iridium and much more limiting for ruthenium. All the alloys of the gold-platinum binary system remain quite corrosion resistant. Alloys containing more than 60% Ag are rapidly attacked by HNO_3 and $FeCl_3$ and are tarnished by exposures to industrial atmospheres.

Nickel additions rapidly harden platinum and gradually reduce the nobility of platinum. Up to 50% Cu can be added to platinum while still retaining its resistance to HNO_3.

Platinum can be used as a minor alloying element in the base metals titanium and chromium. Platinum additions as small as 0.1% greatly increase the resistance of these base metals to HCl and H_2SO_4.

Oxidation Resistance. Platinum is outstanding in its resistance to oxidation, remaining untarnished upon heating in air at all temperatures and retaining its metallic luster up to the melting point. At temperatures above approximately 750 °C (1380 °F), an extremely small but measurable weight loss occurs because of the formation of a volatile oxide, probably PtO_2, and because of volatilization of the metal. The loss due to oxide formation is the greater of the two effects as higher temperatures are reached, and it is influenced by such factors as oxygen pressure, atmosphere flow rate, degree of saturation of the atmosphere with the oxide, and the geometry of the system (Ref 20, 21). A comparison of the oxidation resistance of platinum with that of a number of other high-melting metals is given in Fig. 1.

Alloys with more than 5% Rh or Ir are slowly oxidized in air at temperatures between 750 °C (1380 °F) for rhodium, 900 °C (1650 °F) for iridium, and 1150 °C (2100 °F) with the formation of a superficial blue-black film. At higher temperatures, the film decomposes, and the alloy becomes bright again. Above approximately 800 to 900 °C (1470 to 1650 °F), both alloy systems lose mass because of the volatilization of oxides formed on the surface and the preferential volatilization of the alloying element. Iridium-containing alloys have greater volatilization rates at a given temperature than rhodium-containing platinum alloys. When heated in air, ruthenium is selectively oxidized from ruthenium-platinum alloys, although less vigorously than osmium.

Corrosion Applications. Pure platinum, as well as platinum containing small amounts of rhodium, gold (5%), or iridium, is used for crucibles and other laboratory ware. The first major use of platinum was in laboratory ware and, to a certain extent, in chemical equipment, particularly for stills and condensers in the concentration of H_2SO_4. Today, laboratory apparatus and ware made from platinum and other noble metals are extensively used in analytical control work (fusions, ignitions, ashing) and research demanding corrosion resistance at room and elevated temperatures. Platinum crucibles are used for the production of large synthetic crystals. The chemical industry uses platinum for constructing heating and cooling coils, evaporation apparatus, stills, and autoclaves. Corrosion-resistant platinum rupture disks are used for the protection of pressure vessels handling corrosive materials. Platinum electrodes are used for the electrolytic production of hydrogen peroxide and per-salts, such as perchlorates,

Table 10 Corrosion of gold in salts

Salt	Temperature		Corrosion rate	
	°C	°F	mm/yr	mils/yr
Aluminum sulfate, 10%	100	212	<0.05	2
Ferric chloride in HCl solutions	Room		<0.25	10
Magnesium chloride, all concentrations	Boiling		<0.05	2
Mercuric chloride, 10%	100	212	50.0	2000
Nitrosyl chloride, dry	Room		<0.05	2
Potassium bisulfate, all concentrations	Boiling		<0.05	2
Potassium bromide, all concentrations	Boiling		<0.05	2
Potassium carbonate, all concentrations	Boiling		<0.05	2
Potassium chlorate, all concentrations	Boiling		<0.05	2
Potassium dichromate, all concentrations	Boiling		<0.05	2
Potassium hydroxide, all concentrations	300	570	<0.05	2
Potassium hydroxide, melt	360	680	<0.05	2
Potassium iodide, with iodine	Room		Attacked	
Potassium nitrate, all concentrations	Boiling		<0.05	2
Potassium permanganate, all concentrations	Boiling		<0.05	2
Potassium peroxide, melt	380	715	Attacked	
Potassium sulfate, all concentrations	Boiling		<0.05	2
Sodium bisulfate, all concentrations	Boiling		<0.05	2
Sodium bisulfate, melt	400	750	<0.05	2
Sodium bisulfites, all concentrations	100	212	<0.05	2
Sodium carbonate, all concentrations	Boiling		<0.05	2
Sodium chloride, all concentrations	Boiling		<0.05	2
Sodium chromate, all concentrations	Boiling		<0.05	2
Sodium cyanide, all concentrations	Room		Attacked	
Sodium hydroxide, <90%	Boiling		<0.05	2
Sodium nitrate, all concentrations	Boiling		<0.05	2
Sodium perborate, all concentrations	50	120	<0.05	2
Sodium phosphates, all concentrations	Boiling		<0.05	2
Sodium silicates, all concentrations	Boiling		<0.05	2
Sodium sulfate, all concentrations	Boiling		<0.05	2
Sodium sulfide, all concentrations	Boiling		<0.05	2
Sodium sulfite, all concentrations	Boiling		<0.05	2
Stannic ammonium chloride, all concentrations	Boiling		<0.05	2
Stannic chloride, all concentrations	Boiling			
Strontium nitrate, all concentrations	Boiling		<0.05	2
Sulfur monochloride, pure	Boiling		<0.05	2
Sulfuryl chloride, dry and wet	300	570	<0.05	2
Thionyl chloride, dry or wet	Boiling		<0.05	2
Uranyl nitrate, all concentrations	Boiling		<0.05	2
Zinc sulfate, 10%	100	212	<0.05	2

because they have a high oxygen overvoltage and do not corrode or affect the purity of the product. In addition, platinum electrodes can be used for cathodic protection in seawater and in chlorine production (Ref 22).

Platinum and, preferably, Pt-5Rh or Pt-10Rh are used in woven screen form to catalytically oxidize ammonia to HNO_3. Platinum, platinum-rhodium, and other platinum-base alloys are used in large quantities by the glass industry for molds, nozzles, and spinnerets.

A large percentage of the platinum market is used by the automotive industry in catalytic converters. It is also used in spark plugs and sensors. Depending on economics and catalyst performance requirements, other metals of the platinum group, such as palladium and rhodium, are used in the catalytic converters.

A platinum-silver membrane was used in the first practical alkaline fuel cells. Platinum is still used in phosphoric-acid fuel cells. See the article "Fuel Cells" in *ASM Handbook,* Volume 13A, 2003.

The platinum resistance thermometer and the 90%Pt-Pt thermocouple are used to define the International Practical Temperature Scale between 13.81 K and 630.74 °C and between 630.74 °C and 1064.43 °C (freezing point of gold), respectively. In commercial practice, the rhodium platinum-platinum thermocouple is regularly used to 1400 °C (2550 °F) and under special conditions to as high as 1600 °C (2910 °F).

Because of its tarnish resistance, platinum is used in the jewelry, dental, medical implant, and electrical contact fields. Platinum-containing aluminide coatings are gaining favor as turbine blade and vane coatings (Ref 23).

Palladium

Fabrication. In many respects, the fabricability of palladium resembles that of platinum and gold, which are closely associated with palladium in the periodic table. Like other fcc metals, palladium is ductile and can be readily hot or cold worked. Palladium can withstand drastic working and forming operations and, like gold, can be processed into leaf as thin as 0.1 μm (4 μin.). Many wrought and fabricated forms of palladium and its commercial alloys are readily available, including sheet and strip, bar and wire, and shaped extrusions. Palladium and some alloys are easily electroplated.

Physical Properties. Palladium, with a density of 12.02 g/cm^3 (0.434 lb/in.^{3}), is the lightest of the platinum-group metals. It also has the lowest melting point of the platinum metal group (1554 °C, or 2829 °F).

Mechanical Properties. Palladium work hardens at approximately the same rate as platinum; the annealed hardness increases from 40 HV to approximately 105 HV after a 50% reduction in thickness. Similarly, the tensile strength increases from 207 MPa (30 ksi) annealed to approximately 379 MPa (55 ksi) after a 50% reduction in thickness to 448 MPa (65 ksi) following a 75% reduction. The tensile strength of annealed palladium wire decreases progressively with increasing temperature, as shown in Table 12. Creep and stress rupture properties are reviewed in Ref 24 and 25.

Corrosion Resistance. Palladium is generally resistant to corrosion by most single acids, alkalis, and aqueous solutions of many common salts (Ref 9) (Tables 18, 19). It is not attacked at room temperature by H_2SO_4, HCl, HF, acetic, or oxalic acids but may be attacked at 100 °C (212 °F) or when air is present. Nitric and hot H_2SO_4 attack palladium, as do $FeCl_3$ and hypochlorite solutions, chlorine, bromine, and, to a negligible extent, iodine. Table 20 lists the resistance of palladium to halogens at room temperature. Palladium is readily corroded anodically in HCl or acid chloride solutions. As an electrode for cathodic protection use in seawater, palladium corrodes at a rate of 8.6 g/A · yr at a current density of 540 A/m^2 (50 A/ft^2). The current efficiency is 0.05%. In binary palladium-platinum alloys, the corrosion rate in this application becomes equal to that of platinum if the palladium content is less than 20%. Cyanide solutions containing an oxidizing agent are

Table 11 Corrosion of gold in organic compounds

Compound	Temperature °C	Temperature °F	Corrosion rate mm/yr	Corrosion rate mils/yr
Acetylene dichloride, wet and acid	Boiling		<0.05	2
Aniline, pure	Boiling		<0.05	2
C-bromoisovalerty bromide, pure	100	212	<0.05	2
Chloronitrobenzenes, pure	Boiling		<0.05	2
Copper acetate, neutral solutions	100	212	<0.05	2
Cresols, pure	Boiling		<0.05	2
Dextrose, all concentrations	Boiling		<0.05	2
Dimethylaniline, pure	Boiling		<0.05	2
Diphenyl, pure	400	750	<0.05	2
Essential oils, pure	Boiling		<0.05	2
Ether, pure	Boiling		<0.05	2
Ethylene dibromide, wet and acid products	Boiling		<0.05	2
Ethylene dichloride, wet and acid products	Boiling		<0.05	2
Glycerol, pure	Boiling		<0.05	2
Guinine sulfate	Boiling		<0.05	2
Guinolines, pure	Boiling		<0.05	2
Hydroguinone, all concentrations	Boiling		...	...
Isoborneol acetate, pure	Boiling		<0.05	2
Isobutyl chloride, dry and wet	Boiling		<0.05	2
Limonene, pure	Boiling		<0.05	2
Methyl alcohol, pure	Boiling		<0.05	2
Methyl chloride, dry and wet	300	570	<0.05	2
Methylglycol, pure	Boiling		<0.05	2
Milk, pure	Boiling		<0.05	2
Nitrobenzene, pure	Boiling		<0.05	2
Nitrotoluenes, pure	Boiling		<0.05	2
Pentachloroethane, wet, dry, and acid	Boiling		<0.05	2
Phenol, all concentrations	Boiling		<0.05	2
Phenylhydrazine, all concentrations	100	212	<0.05	2
Phthalic anhydride, pure	Boiling		<0.05	2
Potassium acetate, all concentrations	Boiling		<0.05	2
Pyridine, all concentrations	Boiling		<0.05	2
Sodium acetate, all concentrations	Boiling		<0.05	2
Sodium bisulfate, all concentrations	Boiling		<0.05	2
Sodium formaldehyde sulphoxylate, all concentrations	90	195	<0.05	2
Sodium formate, all concentrations	Boiling		<0.05	2
Sodium formate, melt	260	500	<0.05	2
Sodium isovalerate, all concentrations	Boiling		<0.05	2
Sodium isovalerate, melt with sodium hydroxide	290	555	<0.05	2
Sodium phenolate, all concentrations	Boiling		<0.05	2
Sorbital, all concentrations	Boiling		<0.05	2
Sorbose, all concentrations	Boiling		<0.05	2
Toluene, pure	Boiling		<0.05	2
Triethanolamine, pure and all concentrations	Boiling		<0.05	2
Vinyl chloride, pure	500	930	<0.05	2

Table 12 Effect of temperature on the tensile strength of annealed platinum and palladium wires

1.3 mm (0.05 in.) diam wire annealed at 1100 °C (2010 °F) for 5 min

Test temperature °C	Test temperature °F	Tensile strength Platinum MPa	Tensile strength Platinum ksi	Tensile strength Palladium MPa	Tensile strength Palladium ksi
20	70	138	20	193	28
200	390	117	17	169	24.5
400	750	90	13	125	18
600	1110	76	11	88	13
800	1470	55	8	57	8
1000	1830	28	4	26	4

useful for metallographic etching. Benari describes the corrosion of palladium in dimethylsulphoxide and water solutions by Fe(III) and Cu(II) (Ref 26).

At high temperatures, molten salts such as sodium peroxide, hydroxide, and carbonate attack palladium, but the molten nitrate does not. Hydrogen sulfide at temperatures above 600 °C (1110 °F) attacks the metal and produces a low-melting phase. The standard electrode potential ($Pd \leftrightarrow Pd^{2+} + 2e^-$) is approximately +0.83 V at 25 °C (75 °F).

Effect of Alloying Elements on Corrosion Resistance. The addition of 2% Pt to palladium makes the alloy resistant to the jewelers' HNO_3 drop test used to determine equivalency with gold alloys, and the addition of 10% Pt to palladium makes it completely resistant to HNO_3. In $FeCl_3$ solution (100 g/L), 10% Pt decreases the room-temperature corrosion rate of palladium from 11.9 to 8.6 mm/yr (469 to 339 mils/yr). A 30% Pt addition further decreases the corrosion rate to 1.8 mm/yr (71 mils/yr).

Both iridium and rhodium are quite effective in improving the corrosion and tarnish resistance of palladium. Palladium alloys with 2% Ir or Rh are resistant to the HNO_3 drop test, and alloys with 10% of either element are untarnished by industrial sulfur-bearing atmospheres. The addition of up to 10% Ru only slightly improves the corrosion resistance of palladium. Alloys containing more than 10% Au are resistant to tarnish by industrial sulfur-bearing environments, and those with more than 20% Au are resistant to HNO_3 and HCl. Atmospheric corrosion of palladium-silver claddings is described in Ref 27. The effect of saliva is described in Ref 16. The anodic characteristics of amorphous Pd-Ir-P alloys in hot concentrated NaCl solution is given in Ref 28.

Table 13 Corrosion of platinum in acids

Acid	Temperature		Corrosion rate	
	°C	°F	mm/yr	mils/yr
Acetic, all concentrations	Boiling		<0.05	2
Acetylsalicylic, all concentrations	Boiling		<0.05	2
Aqua regia	Room		Rapid dissolution	
Ascorbic, all concentrations	Boiling		<0.05	2
Benzoic, all concentrations	130	265	<0.05	2
Benzene sulfonic, pure	Room		<0.05	2
Boric, saturated	Boiling		<0.05	2
Butyric, all concentrations	Boiling		<0.05	2
Carbonic, pure	1400	2550	<0.05	2
Chloric, all concentrations	Room		<0.05	2
Chlorosulfonic, all concentrations	Boiling		<0.05	2
Chlorotoluene-sulfonic, all concentrations	Boiling		<0.05	2
Citric, <20% concentrations	Boiling		<0.05	2
Citric, 30% concentrations	Boiling		<0.05	2
Crotonic, all concentrations	Boiling		<0.05	2
Fatty, pure	400	750	<0.05	2
Fluorosilicic (10% hydrofluoric, 5% fluorosilicic)	Boiling		<0.05	2
Formic, pure	Boiling		<0.05	2
Gluconic, all concentrations	Boiling		<0.05	2
Glycerophosphoric, 1–50% solution	Boiling		<0.05	2
Hydrobromic, fuming	Room		<0.25	10
	100	212	4.8	189
Hydrochloric, 36%	Room		nil	
	100	212	<0.25	10
Hydrofluoric, 40%	Room		nil	
Hydrogen sulfide, pure	1000	1830	<0.05	2
Hydroiodic, specific gravity 1.75	Room		<0.25	10
	100	212	13.7	539
Isovaleric, all concentrations	Boiling		<0.05	2
Lactic, all concentrations	Boiling		<0.05	2
Laevolinic, all concentrations	Boiling		<0.05	2
Monochloroacetic, all concentrations	Boiling		<0.05	2
Nitric, 70%	Room		<0.25	10
Nitric, 95%	Room-100	212	nil	
Nitrosyl-sulfuric, pure	100	212	<0.05	2
Oxalic, all concentrations	Boiling		<0.05	2
Phenol-2,4-disulfonic, all concentrations	100	212	<0.05	2
Phenylacetic, all concentrations	Boiling		<0.05	2
Phosphoric, 100 g/L	100	212	nil	
Phthalic, pure	Boiling		<0.05	2
Picric, pure	125	255	<0.05	2
Propionic, all concentrations	Boiling		<0.05	2
Pyridine, all concentrations	Boiling		<0.05	2
Pyridine-carboxylic, all concentrations	150	300	<0.05	2
Salicylic, all concentrations	Boiling		<0.05	2
Stearic, pure	Boiling		<0.05	2
Sulfuric	Room-100	212	nil	
Sulfurous, all concentrations	100	212	<0.05	2
Tartaric, all concentrations	Boiling		<0.05	2

The corrosion resistance of binary palladium-nickel or cobalt alloys is intermediate between that of the component metals and can be raised to levels above those of gold alloys by the addition of platinum, rhodium, or iridium in quantities of from 5 to 20%. Small additions of palladium (0.15 to 0.20%) to titanium may have been found to be effective in improving its corrosion resistance. In such corrosive media as boiling HCl, an almost hundredfold increase in corrosion resistance is obtained. Similar effects in chromium have also been observed.

Oxidation Resistance. Palladium is not tarnished by dry or moist air at ordinary temperatures. At temperatures in the range of 400 to 790 °C (750 to 1450 °F), a thin oxide film forms in air. At higher temperatures, the superficial oxide decomposes to give off oxygen, leaving a clean metal surface.

At temperatures above approximately 1000 °C (1830 °F), the behavior of palladium in air or oxygen is complicated by the interplay of two phenomena: the solution of oxygen in palladium (which increases the weight) and the loss of metal by volatilization (which decreases the weight). The mass change data for palladium oxidized in air over the temperature range 700 to 1400 °C (1290 to 2550 °F) are given in Fig. 1. The oxidation of palladium (thin oxide film formation) can be eliminated by alloying with 75% Pt (Ref 29, 30). Because palladium lacks an oxide film above 1000 °C (1830 °F), the volatilization losses will depend on rate of flow of the gas stream over the surface of the metal (Ref 31–33).

Corrosion Applications. Palladium is a frequently used component of automobile emission catalytic converters. It is sometimes used in place of platinum for economic reasons. Although it is more subject to poisoning by sulfur and lead than platinum, it may improve emission control for diesel engines. Pure wrought or electroplated palladium is used for electrical contacts and relays. Palladium and palladium-rich alloys, because of their freedom from tarnish, perform with high reliability and low electrical noise, even with low contact forces. Many alloys containing palladium have been developed to meet specific contact requirements. A list of platinum and palladium alloys is given in Table 6 of the article "Electric Contact Materials," *Properties and Selection: Nonferrous Alloys and Special-Purpose Materials,* Volume 2, *ASM Handbook,* 1990. The palladium content provides the noble metal characteristics; other metals are added for improved hardness, electrical resistance, or economy.

Palladium does not stain or discolor porcelain that is fired on it, and palladium-rich alloys are used as supports in porcelain overlay dental restorations (Ref 34). In the jewelry field, palladium hardened with a few percent of ruthenium or rhodium provides a light, white, tarnish-free alloy suitable for such articles as watch cases, brooches, and settings for gems. Palladium is an exceptionally effective whitener for gold; the addition of as little as 15% produces

Table 14 Corrosion of platinum in salts

Salt	Temperature °C	Temperature °F	Corrosion rate mm/yr	Corrosion rate mils/yr
Alum, all concentrations	Boiling		<0.05	2
Aluminum chloride, all concentrations	Boiling		<0.05	2
Aluminum fluoride, all concentrations	Boiling		<0.05	2
Aluminum sulfate, 100 g/L	Room-100	212	nil	
Aluminum sulfate, all concentrations	Boiling		<0.05	2
Ammonium chloride, all concentrations	Boiling		<0.05	2
Ammonium nitrate, all concentrations	Boiling		<0.05	2
Ammonium persulfate, all concentrations	60	140	<0.05	2
Ammonium phosphate, all concentrations	Boiling		<0.05	2
Ammonium sulfate, all concentrations	Boiling		<0.05	2
Ammonium thiocyanate, pure	Boiling		<0.05	2
Antimony pentachloride, pure	100	212	<0.05	2
Barium chloride, all concentrations	Boiling		<0.05	2
Calcium hypochlorite, all concentrations	Room		<0.05	2
Calcium bisulfite, pure	Boiling		<0.05	2
Calcium chloride, all concentrations	100	212	<0.05	2
Calcium sulfate, pure	To red heat		<0.05	2
Calcium sulfide, all concentrations	100	212	<0.05	2
Calcium tungstate, pure	800	1470	<0.05	2
Calcium tungstate, all concentrations	Boiling		<0.05	2
Carnallite, pure	500	930	<0.05	2
Carnallite, all concentrations	Boiling		<0.05	2
Carnallite, saturated solution	Boiling		<0.05	2
Cupric chloride, 100 g/L	Room		nil	
Cupric sulfate, 100 g/L	100	212	nil	
Ferric chloride, 100 g/L	Room		<0.25	10
	100	212	16.7	657
Ferrous sulfate, all concentrations	Room		<0.05	2
Fluorosilicate, all concentrations	100	212	<0.05	2
Lithium chloride, all concentrations	Boiling		<0.05	2
Magnesium chloride, all concentrations	Boiling		<0.05	2
Magnesium sulfate, all concentrations	100	212	<0.05	2
Mercury chloride, all concentrations	Boiling		<0.05	2
Nitrosyl chloride, dry	Room		<0.05	2
Phosphorus chlorides, pure	Boiling		<0.05	2
Potassium bisulfate, all concentrations	Boiling		<0.05	2
Potassium bisulfate, melt	200–400	390–750	<0.05	2
Potassium bromide, all concentrations	Boiling		<0.05	2
Potassium bromide, melt	760	1400	<0.05	2
Potassium carbonate, all concentrations	Boiling		<0.05	2
Potassium carbonate, melt(a)	900	1650	<0.05	2
Potassium chlorate, all concentrations(b)	Boiling		<0.05	2
Potassium cyanide, 50 g/L	Room		<0.25	10
	100	212	14	55
Potassium dichromate, all concentrations	Boiling		<0.05	2
Potassium ferricyanide, all concentrations	Boiling		<0.05	2
Potassium ferrocyanide, all concentrations	Boiling		<0.05	2
Potassium hydroxide, all concentrations	300	570	<0.05	2
Potassium hydroxide, melt(a)	300	570	<0.05	2
Potassium nitrate, all concentrations	Boiling		<0.05	2
Potassium nitrate, melt	335	635	Attacked	
Potassium permanganate, all concentrations	Boiling		<0.05	2
Potassium peroxide, all concentrations	100	212	<0.05	2
Potassium peroxide, melt	380	715	Attacked	
Potassium persulfate, all concentrations	60	140	Attacked	
Potassium sulfate, all concentrations(c)	Boiling		<0.05	2
Potassium sulfate, melt	Melting point		<0.05	2
Sodium bisulfate, all concentrations	Boiling		<0.05	2
Sodium bisulfate, melt	400	750	<0.05	2
Sodium bisulfites, all concentrations	100	212	<0.05	2
Sodium carbonate, all concentrations	Boiling		<0.05	2
Sodium carbonate, melt	860	1580	<0.05	2
Sodium chloride, all concentrations	Boiling		<0.05	2
Sodium chloride, melt(d)	800	1470	<0.05	2
Sodium chromate, all concentrations	Boiling		<0.05	2
Sodium cyanide, all concentrations	Room		<0.05	2
Sodium formaldehyde sulfoxylate, all concentrations	90	195	<0.05	2
Sodium formate, all concentrations	Boiling		<0.05	2
Sodium formate, melt	260	500	<0.05	2
Sodium fluorosilicate, all concentrations	100	212	<0.05	2
Sodium hydroxide, <90% pure	Boiling		<0.05	2
Sodium hydroxide, melt	350	660	<0.05	2
Sodium hypochlorite, all concentrations	100	212	<0.05	2
Sodium hypochlorite + sodium chloride, saturated solution	100	212	<0.25	10
Sodium nitrate, all concentrations	Boiling		<0.05	2
Sodium perborate, all concentrations	50	120	<0.05	2
Sodium percarbonate, all concentrations	50	120	<0.05	2
Sodium perchlorate, all concentrations	Boiling		<0.05	2
Sodium perchlorate, melt	480	900	Attacked	
Sodium peroxide, all concentrations	Boiling		<0.05	2
Sodium peroxide, melt	400	750	<0.05	2
Sodium phosphates, all concentrations	Boiling		<0.05	2
Sodium silicates, all concentrations	Boiling		<0.05	2
Sodium sulfate, all concentrations	Boiling		<0.05	2
Sodium sulfide, all concentrations	Boiling		<0.05	2
Sodium sulfide, melt	700	1290	<0.05	2
Sodium sulfite, all concentrations	Boiling		<0.05	2
Sodium thiocyanate, all concentrations	Boiling		<0.05	2
Sodium thiocyanate, melt	300	570	<0.05	2
Sodium thiosulfate, all concentrations	Boiling		<0.05	2
Stannic ammonium chloride, all concentrations	Boiling		<0.05	2
Stannic chloride, all concentrations	Boiling		<0.05	2
Strontium nitrate, all concentrations	Boiling		<0.05	2
Sulfite cooking liquor, pH 13	Boiling		<0.05	2
Sulfur monochloride, pure	Boiling		<0.05	2
Sulfuryl chloride, dry and wet	300	570	<0.05	2
Thionyl chloride, dry or wet	Boiling		<0.05	2
Uranyl nitrate, all concentrations	Boiling		<0.05	2

(a) Platinum is attacked if strong oxidizers are present. (b) Platinum-iridium anodes used to electrolytically manufacture potassium chlorate. (c) Provided reducing agents are not present. (d) Provided no ammonia is present

a satisfactory white color. In contrast to the great increase in hardness and working difficulties encountered when gold is whitened by other metals, the white gold-palladium alloys are ductile and readily worked.

Palladium alloys are well suited for the construction of fine wire precision resistors because of their ductility, corrosion resistance, and the range of electrical resistivities available. Alloys with exceptionally low temperature coefficients of electrical resistivity have been developed for applications as potentiometer resistor wire. An alloy that is widely used for this is Pd-40Ag, which has a resistivity of 42 $\mu\Omega \cdot$ cm in the as-worked condition and a temperature coefficient of only 0.00003/°C (0.00005/°F) in the temperature range 0 to 100 °C (32 to 212 °F).

Metallic films fired on glass or ceramic substrates are of interest for thin-film resistors. For this application, palladium-gold resistance films can be produced by the thermal decomposition of resinate mixtures. In another process, a mixture of finely ground low-melting glass and palladium and silver powders is fired on the substrate. Thin-film resistors made in this manner do not exhibit a critical resistance/composition dependence.

In general, brazing alloys containing palladium exhibit exceptional wettability, good flow and gap-filling characteristics, freedom from the tendency to attack and erode base metals, good ductility, and other desirable brazing qualities. The palladium-containing brazing alloys have proved useful for dissimilar-metal or metal-to-ceramic joints, for extremely thin sheet metal assemblies, and for assemblies that must withstand extreme service temperatures. The alloys can be used to braze a wide range of base metals, including low-alloy and stainless steels; nickel-, cobalt-, and copper-base alloys; and refractory metals such as tungsten and molybdenum. They are consequently gaining a significant place in the gas turbine, jet engine, air frame, missile, nuclear, and electronic industries.

Gold-palladium alloys are used for thermal fuses to prevent temperature override in furnaces. The range of melting temperatures possible with the different gold-palladium combinations (1063 to 1552 °C, or 1945 to 2825 °F), the narrow melting range of the alloys,

Table 15 Corrosion of platinum in organic compounds

Environment	Temperature °C	Temperature °F	Corrosion rate mm/yr	Corrosion rate mils/yr
Acetaldehyde, pure	200–100	390–750	<0.05	2
Acetic anhydride, all concentrations(a)	Boiling		<0.05	2
Acetone, pure	Boiling		<0.05	2
Acetylene, dry	600	1110	Becomes spongy	
Acetylene dichloride, wet and acid	Boiling		<0.05	2
Ethyl alcohol, all concentrations	Boiling		<0 05	2
Amyl acetate, pure	Boiling		<0.05	2
Amyl alcohol, pure	Boiling		<0.05	2
Aniline, pure	Boiling		<0.05	2
Benzaldehyde, pure and aqueous	Boiling		<0.05	2
Benzene, pure	Boiling		<0.05	2
Benzotrifluoride, pure	Boiling		<0.05	2
Benzyl chloride, pure	180	355	<0.05	2
Butyl acetate, pure	Melting point		<0.05	2
Butyl alcohol, pure	Boiling		<0.05	2
Carbon bisulfide, pure	Boiling		<0.05	2
Carbon tetrachloride, dry and wet	Boiling		<0.05	2
Chloramine(s), all concentrations	Boiling		<0.05	2
Chlorobenzene, pure	Boiling		<0.05	2
Chlorocresols, all concentrations	Boiling		<0.05	2
Chloroform, dry or wet	Boiling		<0.05	2
Chlorohydrins, pure	Boiling		<0.05	2
Chloronitrobenzenes, pure	Boiling		<0.05	2
Chlorotoluene, pure	Boiling		<0.05	2
Copper acetate, neutral solutions	100	212	<0.05	2
Cresols, pure	Boiling		<0.05	2
Dextrose, all concentrations	Boiling		<0.05	2
Dibutyl phthalate, pure	Boiling		<0.05	2
Dichlorodifluoromethane, pure	600	1110	<0.05	2
Dimethylaniline, pure	600	1110	<0.05	2
Diphenyl, pure	400	750	<0.05	2
Essential oils, pure	Boiling		<0.05	2
Ether, pure	Boiling		<0.05	2
Ethyl acetate, all concentrations	Boiling		<0.05	2
Ethyl benzene, pure	135	275	<0.05	2
Ethylene dibromide, wet and acid products	Boiling		<0.05	2
Ethylene dichloride, wet and acid products	Boiling		<0.05	2
Fatty acids, pure	400	750	<0.05	2
Formaldehyde, all concentrations	500	930	<0.05	2
Furfural, wet and slightly acid	Boiling		<0.05	2
Gelatin, pure	Boiling		<0.05	2
Glycerol, pure	Boiling		<0.05	2
Guanidine nitrate, all concentrations	Room		<0.05	2
Guinine sulfate, all concentrations	Boiling		<0.05	2
Guinolines, pure	Bailing		<0.05	2
Guinone, inorganic solvent and pure	100	212	<0.05	2
Hexachloroethane, dry and moist	187	370	<0.05	2
Hydrazine, <50% solution	Room		<0.05	2
Hydroquinone, all concentrations	Boiling		<0.05	2
Isoborneol acetate, pure	Boiling		<0.05	2
Isobutyl chloride, dry and wet	Boiling		<0.05	2
Limonene, pure	Boiling		<0.05	2
Methyl alcohol, pure	Boiling		<0.05	2
Methylamines, all solutions and gaseous	Room		<0.05	2
Methyl chloride, dry and wet	300	570	<0.05	2
Methylene chloride, dry and wet	Boiling		<0.05	2
Methylglycol, pure	Boiling		<0.05	2
Milk, pure	Boiling		<0.05	2
Nitrobenzene, pure	Boiling		<0.05	2
Nitrocellulose, in water or alcohol	Room		<0.05	2
Nitrotoluenes	Boiling		<0.05	2
Pentachloroethane, wet, dry, and acid	Boiling		<0.05	2
Phenol, all concentrations	Boiling		<0.05	2
Phenyl hydrazine, all concentrations	100	212	<0.05	2
Phenylmercuric acetate, pure and all concentrations	Melting point		<0.05	2
Phthalic anhydride, pure	Boiling		<0.05	2
Potassium acetate, all concentrations	Boiling		<0.05	2
Pyridine, all concentrations	Boiling		<0.05	2
Sodium acetate, all concentrations	Boiling		<0.05	2
Sodium acetate, melt	400	750	<0.05	2
Sodium bisulfate, all concentrations	Boiling		<0.05	2
Sodium formaldehyde sulphoxylate, all concentrations	90	195	<0.05	2
Sodium formate, all concentrations	Boiling		<0.05	2
Sodium formate, melt	260	500	<0.05	2
Sodium isovalerate, all concentrations	Boiling		<0.05	2
Sodium isovalerate, melt with sodium hydroxide	290	555	<0.05	2
	Boiling		<0.05	2
Sodium methylate, all concentrations in alcohol or ether	100	212	<0.05	2
Sodium pentachlorophenolate, all concentrations	Boiling		<0.05	2
Sodium phenolate, all concentrations	Boiling		<0.05	2
Sodium salicylate, all concentrations	Boiling		<0.05	2
Sodium tartrates, all concentrations	Boiling		<0.05	2
Sorbital, all concentrations	Boiling		<0.05	2
Sorbose, all concentrations	Boiling		<0.05	2
Toluene, pure	Boiling		<0.05	2
Toluenesulfonyl chlorides, all concentrations	Boiling		<0.05	2
Triethanolamine, pure and all concentrations	Boiling		<0.05	2
Vinyl chloride, pure	500	930	<0.05	2

(a) Platinum-gold alloys perform better than pure platinum

and their corrosion and oxidation resistance make them well suited for this service.

Rhodium

Fabrication. Rhodium powder can be consolidated either by powder metallurgy techniques or by melting. Powder compacts are sintered by air, inert atmospheres, hydrogen, or vacuum at approximately 1200 °C (2190 °F).

The melting of rhodium requires careful control of atmospheric conditions because liquid rhodium will dissolve a large quantity of oxygen, which is rejected upon solidification. If conditions are reducing, the rhodium may become contaminated through reduction of the refractory crucibles. A satisfactory technique for the production of small rhodium ingots is electron beam or argon arc melting on a water-cooled copper hearth.

Sintered or cast rhodium ingots can be worked down to thin strip or fine wire. The fabrication of these wrought forms requires an initial hot working at a temperature of 1200 °C (2190 °F) or higher, but subsequently, the temperature can be dropped. At thinner gages, the metal can be cold worked. During cold work, the rhodium should be given stress-relief anneals at 600 to 800 °C (1110 to 1470 °F), but complete annealing should be avoided because recrystallized metal is less ductile than metal with a fibrous structure. Moderate amounts of cold work (up to 40 to 50%) can be given between stress-relief anneals.

Physical Properties. Rhodium is characterized by:

- High specular reflectivity
- The highest electrical conductivity of all the platinum-group metals
- The highest thermal conductivity of all the platinum-group metals
- A high melting point: 1963 °C (3565 °F)
- A density of 12.41 g/cm^3 (0.448 lb/in.^{3}), approximately 58% that of platinum

Mechanical Properties. The hardness of wrought rhodium in the annealed condition averages approximately 130 HV. Therefore, rhodium is harder than platinum or palladium (each approximately 40 HV).

Rhodium work hardens rapidly. A 15% reduction by cold rolling increases hardness to 300 HV. The hardness of annealed rhodium decreases progressively with increasing temperature; hardness falls from approximately 120 HV at room temperature to 80 HV at 600 °C (1110 °F) and to less than 50 HV at 1100 °C (2010 °F). The tensile strength of annealed rhodium is 827 to 896 MPa (120 to 130 ksi), while a tensile strength of 1379

to 1517 MPa (200 to 220 ksi) is obtainable in cold-drawn wire.

Corrosion Resistance. Rhodium is resistant to corrosion by nearly all aqueous solutions at room temperature, including concentrated acids (Ref 35), but it is slowly attacked by solutions of sodium hypochlorite. In wrought or cast form, it is unattacked at 100 °C (212 °F) by concentrated HCl, HNO_3, and aqua regia, but it is attacked slowly by concentrated H_2SO_4 and by HBr (Table 21). Table 22 lists corrosion rates of rhodium in other environments. Rhodium can be used for insoluble anodes in electrolytic processes in which evolution of oxygen and chlorine occurs. When alternating current is used, however, rhodium is dissolved fairly readily in a number of electrolytes.

Rhodium is unattacked by chlorine at room temperature, but it may be attacked at elevated temperatures. It is generally more resistant to the halogens than platinum, although it is less resistant than iridium (Table 23). In the massive form, it is attacked slowly by molten sulfur, but finely divided metal may react violently. Rhodium is resistant to wet or dry gaseous sulfur dioxide vapors to 1000 °C (1830 °F) if elemental sulfur is not present.

Rhodium is resistant to attack by some molten salts. Rhodium crucibles have been used at 1620 °C (2950 °F) for growing calcium tungstate single crystals by the Czochralski technique.

Rhodium is attacked to varying extents by fused alkalis under oxidizing conditions; the rate of corrosion is comparable to that of platinum. It is corroded fairly rapidly by alkali cyanides and fused sodium bisulfate.

At temperatures 200 °C (360 °F) above their melting points, gold, silver, mercury, cesium, potassium, sodium, and gallium have negligible corrosive action on rhodium, but unlike iridium and ruthenium, rhodium is rapidly dissolved by lead and bismuth. The standard electrode potential of rhodium ($Rh \leftrightarrow Rh^{2+} + 2e^-$) is approximately +0.6 V at 25 °C (75 °F).

Oxidation Resistance. Rhodium does not tarnish in air at room temperature, even in the most severe atmospheric conditions, but heating in air at temperatures above approximately 600 °C (1110 °F) will produce a thin oxide film that is visible as a dark discoloration. The weight change due to oxidation at these temperatures is negligible even after prolonged heating.

The oxide decomposes at approximately 1100 °C (2010 °F) in air at normal pressure and at slightly higher temperatures in oxygen. At higher temperatures, rhodium dissolves some oxygen and simultaneously reacts with it to form a volatile oxide. The volatile oxide is formula rhodium dioxide (Ref 33).

The vapor pressure of rhodium dioxide is directly proportional to the partial pressure of oxygen in the atmosphere. It is slightly less than that of the corresponding platinum oxide at temperatures below 1200 °C (2190 °F), but at higher temperatures the reverse is true.

Corrosion Applications. Rhodium is principally used as an alloying element in conjunction with platinum and palladium. Rhodium-containing platinum alloys are used for crucibles, furnace windings, thermocouple elements, linings for glass extrusion nozzles and spinnerets, and woven screen oxidation catalysts for production of HNO_3 from ammonia. Rhodium is used to harden palladium in jewelry applications. It also increases the corrosion resistance. Similarly, rhodium increases the hardness and corrosion resistance of nickel.

As the element, rhodium is electroplated for a number of decorative and nontarnishing uses, including jewelry, reflective mirrors, and electrical contacts. Rhodium is also vacuum deposited on glass to produce mirrors with high reflectivity and chemical stability. Thin coatings of rhodium on glass make an excellent gray filter.

Iridium

Fabrication. Pure iridium is not readily amenable to conventional fabrication and is generally used as an alloying element. However, iridium powder can be consolidated by conventional powder metallurgy techniques or by melting. Powder compacts are preferably sintered in vacuum at 1500 °C (2730 °F) before forging, rolling, swaging, or other hot-working operations for consolidation. Melting can be carried out in an argon arc furnace on a water-cooled copper hearth or by induction heating in a zirconia crucible, again in an argon atmosphere. In both cases, iridium powder is the raw material, which is preferably first briquetted and vacuum sintered into a partially consolidated material.

Sintered or cast iridium has working characteristics that are similar to those of tungsten and therefore requires considerable care in the early stages of processing. Initial breakdown of cast or sintered shapes is done in the temperature range of 1200 to 1500 °C (2190 to 2730 °F).

Subsequent drawing to wire is performed by warm working at 600 to 750 °C (1110 to 1380 °F), which is below the recrystallization temperature. Such wire has a fibrous structure, a hardness of 600 to 700 HV, and useful tensile strength and ductility. Drawing at lower temperatures leads to a rapid increase in hardness and splitting of the wire. Drawing of material that has been fully recrystallized by annealing results in frequent breakage.

Iridium can also be rolled at 600 to 750 °C (1110 to 1380 °F) into strip with the fibrous

Table 16 Corrosion of platinum in gases

Gas	Temperature		Corrosion rate	
	°C	°F	mm/yr	mils/yr
Ammonia, with oxidant(a)	950	1740	<0.05	2
Ammonia, pure	Elevated		Nitridation	
Carbon dioxide, no reductant present	1400	2550	<0.05	2
Carbon monoxide, no reductant present	1400	2550	<0005	2
Hydrogen, pure	1000	1830	<0.05	2
Hydrogen chloride, dry(b)	1200	2190	<0.1	4
Hydrogen sulfide, moist	Room		Blackened(c)	
Nitrogen dioxide			<0.05	2
Ozone, with 98% oxygen	100	212	<0.05	2
Steam	600	1110	<0.05	2
Sulfur dioxide, dry and wet	600	1110	<0.05	2

(a) Use of platinum-rhodium alloys is preferred for ammonia oxidation (loss is < 250 mg of platinum/ton of nitric acid). (b) Corrosion rate is increased by the presence of steam or oxidizing agent. (c) Platinum is blackened but unattacked in hydrogen sulfide to 1000 °C (1830 °F).

Table 17 Corrosion of platinum in halogens at room temperature

Halogen	Corrosion rate	
	mm/yr	mils/yr
Chlorine, dry	<0.25	10
Chlorine, moist	<0.25	10
Saturated chlorine in water	nil	
Bromine, dry	3.5	138
Bromine, moist	2.0	80
Saturated bromine in water	nil	
Iodine, dry	<0.25	10
Iodine, moist	nil	
Iodine in alcohol, 50 g/L	nil	

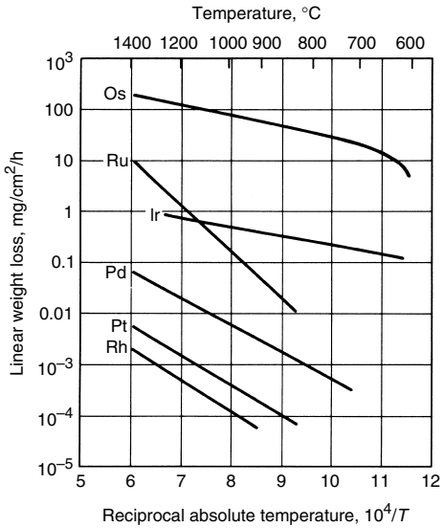

Fig. 1 Weight losses of platinum-group metals oxidized in air

structure characteristic of drawn wire. In addition, iridium can be rolled at higher temperatures (1200 to 1500 °C, or 2190 to 2730 °F) to yield a product with an equiaxed structure and hardness of approximately 400 HV. In general, worked material that has a fibrous structure is preferred because it has better ductility and strength.

Warmed-worked iridium does not exhibit a sharp recrystallization temperature. Some softening occurs upon heat treatment at 700 °C (1290 °F), but it is necessary to heat to a minimum of 1000 °C (1830 °F) or higher temperatures before full recrystallization occurs.

Physical Properties. Interesting features of iridium include:

- Iridium has the distinction of being the heaviest element known, with a density of 22.65 g/cm^3 (0.818 lb/in.^{3}).
- Next to osmium, iridium has the highest melting point of the platinum-group metals, 2447 °C (4437 °F).
- The modulus of elasticity of iridium is one of the highest for an element, 517 GPa (75,000 ksi).

Mechanical Properties. Iridium shows a high degree of work hardening compared with other fcc metals. The hardness of annealed iridium increased by 250 HV with 20% cold reduction, as compared to an increase of 30 HV for pure platinum worked to a similar degree. The very small amounts of the impurities segregated at the grain boundaries may be the cause of the rapid work-hardening behavior. The excellent high-temperature strength properties of iridium place it in the category of the refractory metals.

Corrosion Resistance. Iridium is the most corrosion-resistant metal known. It is completely unattacked by the common mineral acids at normal and high temperatures and by cold and boiling aqua regia (Table 24) (Ref 36). It is the most resistant of the platinum metals to the halogens, as shown in Table 25. It is slightly attacked by fused sodium and potassium hydroxides and by fused sodium bicarbonate. Iridium is resistant to anodic corrosion in aqueous electrolytes but may be attacked in aqueous potassium cyanide, HCl, and ammonium carbonate solutions under the action of an alternating current. The corrosion resistance of iridium in other environments is shown in Table 26. Iridium can be dissolved by aqua regia under pressure by heating to 250 to 300 °C (480 to 570 °F). Iridium is resistant to wet or dry gaseous sulfur dioxide to 1000 °C (1830 °F) if elemental sulfur is not present.

Iridium shows excellent resistance to attack by a wide range of molten metals. Iridium is unattacked by gallium, lithium, potassium, sodium, indium, mercury, and bismuth at temperatures up to 200 °C (360 °F) above their respective melting points under an atmosphere of argon. It is only slowly attacked by molten lead, tellurium, cadmium, antimony, tin, calcium, silver, and gold. On the other hand, the metal is readily attacked by molten copper, aluminum, zinc, and magnesium. The standard electrode potential of iridium ($Ir \leftrightarrow Ir^{3+} + 3e^-$) is approximately +1.0 V at 25 °C (75 °F).

Iridium is unattacked by lithium, sodium, potassium, bismuth, gallium, lead, silver, and gold at up to 200 °C (360 °F) above the respective melting points of these metals (Ref 37). It is also unattacked by mercury up to 550 °C (1020 °F). Iridium is not wetted by lithium, sodium, potassium, bismuth, gallium, and lead at these test temperatures, although at 400 °C (720 °F) above its melting point, gallium does wet iridium, and there is some surface attack. Gold and silver wet iridium and form continuous films over both the inside and outside of the sintered crucible.

Tellurium, cadmium, and tin attack iridium at all temperatures above their melting points, along with the formation of intermediate compounds at the interface. These compounds have some protective value for the iridium, although they are brittle and do not adhere well to the iridium. Antimony also reacts with iridium to form an intermetallic compound, but this compound does not seem to adhere to the iridium and has no protective action.

Table 18 Corrosion of palladium in acids

Acid	Temperature °C	Temperature °F	Corrosion rate mm/yr	Corrosion rate mils/yr
Aqua regia	Room		Rapid dissolution	
Hydroiodic, specific gravity 1.75	Room		65.7	2587
Hydrobromic, fuming	Room		161.2	6346
Hydrochloric, 36%	Room		<0.25	10
	100	212	1.3	51
Hydrofluoric, 40%	Room		nil	
Nitric, 70%	Room		61.3	2413
Nitric, 95%	100	212	Rapid dissolution	
Phosphoric, 100 g/L	100	212	<0.25	10
Hydrochloric, specific gravity 1.6	Room		nil	
	100	212	2.5	100
Sulfuric, concentrated	Room		<0.25	10
	100	212	1.6	63
Acetic acid, glacial	Room		<0.25	10

Table 19 Corrosion of palladium in common salts and other environments

Environment	Temperature °C	Temperature °F	Corrosion rate mm/yr	Corrosion rate mils/yr
Hydrogen sulfide, moist	Room		nil	
Sodium hypochlorite + sodium chloride, saturated solution	Room		1.8	71
	100	212	14.9	587
Ferric chloride, 100 g/L	Room		11.9	469
	100	212	Rapid dissolution	
Potassium cyanide, 50 g/L	Room		1.6	63
	100	212	62.7	2469
Mercuric chloride, solution	100	212	nil	
Cupric chloride, 100 g/L	Room		<0.25	10
Cupric sulfate, 100 g/L	100	212	nil	
Aluminum sulfate, 100 g/L	Room		nil	
	100	212	nil	

Table 20 Corrosion of platinum in halogens at room temperature

Halogen	Corrosion rate mm/yr	Corrosion rate mils/yr
Chlorine, dry	1.1	43
Chlorine, moist	14.0	551
Saturated chlorine in water	<0.25	10
Bromine, dry	24.5	965
Bromine, moist	25.0	984
Saturated bromine in water	27.7	1090
Iodine, dry	<0.25	10
Iodine, moist	<0.25	10
Iodine in alcohol, 50 g/L	<0.25	10

Table 21 Corrosion of rhodium in acids

Acid	Temperature °C	Temperature °F	Corrosion rate mm/yr	Corrosion rate mils/yr
Aqua regia	Boiling		nil	
Hydroiodic, specific gravity 1.75	100	212	nil	
Hydrobromic, fuming	100	212	2.2	87
Hydrochloric, 35%	100	212	nil	
Hydrofluoric, 40%	Room		nil	
Nitric, 95%	100	212	nil	
Phosphoric, 100 g/L	100	212	nil	
Sulfuric, concentrated	100	212	<0.25	10
Acetic acid, glacial	100	212	nil	

Table 22 Corrosion of rhodium in common salts and other environments

Environment	Temperature °C	Temperature °F	Corrosion rate mm/yr	Corrosion rate mils/yr
Hydrogen sulfide, moist	Room		nil	
Sodium hypochlorite + sodium chloride, saturated solution	Room		<0.25	10
	100	212	<0.25	10
Ferric chloride, 100 g/L	100	212	nil	
Mercuric chloride, 100 g/L	100	212	nil	
Cupric sulfate, 100 g/L	100	212	nil	
Aluminum sulfate, 100 g/L	100	212	nil	

Table 23 Corrosion of rhodium in halogens at room temperature

Halogen	Corrosion rate mm/yr	Corrosion rate mils/yr
Chlorine, dry	nil	
Chlorine, moist	nil	
Saturated chlorine in water	nil	
Bromine, dry	nil	
Bromine, moist	nil	
Saturated bromine in water	nil	
Iodine, dry	nil	
Iodine, moist	<0.25	10
Iodine in alcohol, 50 g/L	<0.25	10

Molten copper, calcium, and zinc at all temperatures penetrate iridium intergranularly; this is followed by the dissolution of iridium in these liquid metals. Copper, in particular, penetrates very rapidly into the iridium. Magnesium and aluminum attack iridium very rapidly by uniform diffusion at the interface; the solid solution so formed then dissolves in the liquid metal.

Oxidation Resistance. Iridium does not tarnish at room temperature, but heating in air at temperatures above approximately 600 °C (1110 °F) will produce a thin oxide tarnish. At temperatures of 1000 °C (1830 °F) and higher, iridium loses weight through the formation of a volatile oxide, which is reported to be either iridium sesquioxide, iridium trioxide, or iridium dioxide (Ref 38–40). The weight loss as a function of time is linear, because base metal is continually exposed to the attacking air. The linear mass change for all the platinum metals is plotted in Fig. 1. Although the weight loss in air is much greater for iridium than for platinum, iridium is the only metal with a sufficiently high melting point that can be used unprotected in air at temperatures up to 2300 °C (4170 °F) without catastrophic failure.

Table 24 Corrosion of iridium in acids

Acid	Temperature		Corrosion rate	
	°C	°F	mm/yr	mils/yr
Aqua regia	Room-boiling		nil	
Hydroiodic, specific gravity 1.75	Room-100	212	nil	
Hydrobromic, specific gravity 1.7	100	212	nil	
Hydrochloric, 36%	100	212	nil	
Hydrofluoric, 40%	Room		nil	
Nitric, 95%	100	212	nil	
Phosphoric	100	212	nil	
Sulfuric, concentrated	Room-100	212	nil	
Acetic acid, glacial	100	212	nil	

Table 25 Corrosion of iridium in halogens at room temperature

Halogen	Corrosion rate	
	mm/yr	mils/yr
Chlorine, dry	nil	
Chlorine, moist	nil	
Bromine, dry	nil	
Bromine, moist	<0.25	10
Saturated bromine in water	nil	
Iodine, dry	nil	
Iodine, moist	nil	
Iodine in alcohol, 50 g/L	nil	

Table 26 Corrosion of iridium in other environments

Environment	Temperature		Corrosion rate	
	°C	°F	mm/yr	mils/yr
Hydrogen sulfide, moist	Room		nil	
Sodium hypochlorite + sodium chloride, saturated solution	100	212	<0.25	10
Ferric chloride, 100 g/L	100	212	nil	
Mercuric chloride, solution	100	212	nil	
Cupric sulfate, 100 g/L	100	212	nil	
Aluminum sulfate, 100 g/L	100	212	nil	

Corrosion Applications. Except for the use of pure iridium as high-performance sparkplug electrodes and for very high-temperature crucibles used in the preparation of single crystals of certain optical and electronic glasses, iridium is largely used for hardening and increasing the corrosion resistance of platinum and palladium. In platinum, which in the fully annealed state has a tensile strength of 131 MPa (19 ksi), a 10% Ir addition increases tensile strength to 414 MPa (60 ksi); a 35% Ir addition increases tensile strength to 965 MPa (140 ksi). Platinum-iridium alloys are used for prosthetics and other biomedical devices. The electrochemical and corrosion behavior of an iridium-palladium oxide electrode is characterized in Ref 41.

In addition to hardening platinum, iridium greatly enhances its corrosion resistance, particularly in environments involving nascent chlorine, aqua regia, and similar corrosives. Because of their exceptional resistance to corrosion and tarnish, platinum-iridium alloys containing up to 30% Ir have been used in:

- Chemical plants handling extremely corrosive materials
- Electrical contacts exposed to severe environments and where extreme reliability of chlorine is required
- Jewelry, surgical tools, and implants (catheters, microelectrodes, and pacemaker components)
- Primary standards of length and weight. (When the meter was defined by a physical bar in 1889, a platinum-iridium bar was used as the standard.)

Iridium is also an effective hardener for palladium, and it imparts corrosion resistance. Although not so widely applied as their platinum counterparts, the palladium alloys have been used for jewelry and electrical contacts.

Iridium alloys containing up to 60% Rh have been proposed for high-temperature thermocouples. The couple iridium versus Ir-40Rh is regarded as one of the most satisfactory for use in oxidizing atmospheres at temperatures as high as 2100 °C (3810 °F).

The naturally occurring alloy osmiridium (30 to 65% Os balance iridium) has been widely used for the tipping of fountain pen nibs, for instrument pivots, and for similar applications requiring high hardness and extreme resistance to wear and corrosion. Recently, osmiridium has been replaced by a wide variety of complex synthetic alloys containing, among others, the refractory metals, together with iridium, ruthenium, osmium, rhodium, and platinum.

Iridium-tungsten alloys have been principally developed for springs required to operate at high temperatures. These springs have excellent relaxation properties at temperatures up to 800 °C (1470 °F).

Small additions of iridium are very effective in improving the corrosion resistance of titanium. As with the other platinum-group metals, addition of as little as 0.1% Ir increases the corrosion resistance of titanium to nonoxidizing acids a hundredfold. Similar improvements have been reported for chromium containing 0.5% Ir. Iridium-base alloys are undergoing evaluation as gas turbine blade and vane coatings (Ref 42).

Ruthenium

Fabrication. Wrought forms of ruthenium are limited. Those products that are available are generally fabricated by powder metallurgy techniques. The ruthenium powder is obtained from the refining process. Hot working can be accomplished at 1150 to 1500 °C (2100 to 2730 °F), although rolling of bar to strip can be performed in the range of 1050 to 1250 °C (1920 to 2280 °F) to minimize grain growth and edge cracking due to large grain size. Cold rolling of ruthenium is very limited because of the low ductility of the metal. The metal work hardens rapidly and requires frequent intermediate anneals.

Single-crystal ruthenium, prepared by electron beam zone refining, shows a relatively high degree of ductility when compared to polycrystalline material. However, the material work hardens rapidly, and upon annealing, it reverts to a polycrystalline state and exhibits low ductility.

Atomic, Structural, and Physical Properties. A high melting point (2310 °C, or 4190 °F), a moderate density of 12.45 g/cm^3 (0.45 lb/in.^{3}), and a Young's modulus of 414 GPa (60,000 ksi) characterize ruthenium. In relation to other metals of the platinum group, ruthenium bears closest resemblance to osmium and, like it, has a hexagonal close-packed (hcp) structure. Some of these properties will vary according to the degree of preferred orientation present in the material.

Mechanical Properties. The hardness of ruthenium varies considerably according to the orientation of the hexagonal lattice. The hardness of sintered bar, swaged at 1500 °C (2730 °F) with a 45% reduction in area and subsequently annealed at the same temperature, is in the range of 400 to 450 HV on longitudinal sections and 250 to 300 HV on transverse sections.

The tensile strength of a polycrystalline sintered bar, swaged with a 45% reduction in area at 1500 °C (2730 °F) and subsequently annealed at the same temperature, is 496 MPa (72 ksi), and the elongation is 3%. High-temperature tensile tests carried out in air indicate a steady decrease in strength with increasing temperature and a maximum in elongation and reduction of area in the temperature range of 750 to 900 °C (1380 to 1650 °F).

Corrosion Resistance. Ruthenium is resistant to attack by cold and hot acid solutions, including aqua regia, and, in this respect, is superior to platinum (Table 27). However, its

resistance to attack under certain oxidizing conditions is not as high as that of platinum. Therefore, it is attacked fairly rapidly by sodium hypochlorite. Saturated aqueous solutions of chlorine and bromine and alcoholic solutions of iodine attack the metal slowly (Table 28). It is dissolved fairly rapidly as an anode in a large number of electrolytes and more rapidly by alternating current electrolysis (Ref 43). Ruthenium is attacked by fused alkaline hydroxides, carbonates, and cyanides and is attacked very rapidly by fused sodium peroxide. The corrosion resistance of ruthenium in other environments is given in Table 29. The behavior of ruthenium anodes in base is reviewed in Ref 44.

Ruthenium exhibits good resistance to attack by molten lithium, sodium, potassium, copper, silver, and gold when it is heated in an atmosphere of argon. No solution attack by these metals occurs up to 100 °C (180 °F) above their melting points, although grain-boundary penetration is observed with sintered and unworked ruthenium. It is also resistant to attack by molten lead, and up to 700 °C (1290 °F), attack by liquid bismuth is extremely slight. The solubility of ruthenium in bismuth at this temperature is 0.029%, and at 1200 °C (2190 °F), it is 0.016%.

Ruthenium is unattacked by lithium, sodium, potassium, gold, silver, copper, lead, bismuth, tin, tellurium, indium, cadmium, calcium, and gallium at temperatures up to 200 °C (360 °F) above the melting points of the respective metals (Ref 37). Gold, silver, and copper flow readily over the surface of ruthenium but do not wet it. Ruthenium is also unattacked by mercury at temperatures to 550 °C (1020 °F). Ruthenium is apparently unattacked at lower temperatures by gallium, but there is some attack at temperatures 400 °C (720 °F) above the melting point of gallium. Similarly, bismuth dissolves ruthenium very slowly at 700 °C (1290 °F), with the dissolution occurring uniformly at the ruthenium surface.

Ruthenium is attacked by molten aluminum or zinc at all temperatures above their melting points. This attack appears to consist of uniform dissolution of the surface and does not result in the formation of intermetallic compounds or grain-boundary penetration. On the other hand, attack by magnesium and antimony occurs with the formation of an intermetallic compound at the interface, which appears to have some protective value.

Oxidation Resistance. Ruthenium does not tarnish at room temperature, even in heavily polluted atmospheres, but when heated in air or oxygen to temperatures approaching 800 °C (1470 °F), it oxidizes to form a surface film of ruthenium dioxide. Between this temperature and 1150 °C (2100 °F), there is simultaneous formation of a volatile oxide, probably ruthenium monoxide and ruthenium dioxide. At higher temperatures, only ruthenium monoxide is formed. The vapor pressure of the monoxide when formed on heating ruthenium in pure oxygen at temperatures in the range of 1200 to 1400 °C (2190 to 2555 °F) has been found to follow the approximate relationship:

$$\log_{10} P = \frac{11{,}100}{T} + 4.83$$

where T is the absolute temperature, and P is the pressure in atmospheres (Ref 21). The actual rate of weight loss upon heating the metal in air will depend on a number of factors, including the geometric form of the sample under test and the degree of movement of the surrounding atmosphere. The mass change of ruthenium in air in comparison with the other platinum metals is given in Fig. 1.

Corrosion Applications. Because of the lack of wrought forms of ruthenium that can be readily fabricated, the applications of ruthenium in corrosive environments are limited. High-ruthenium alloys containing other platinum metals or base metals have been used for electrical contacts and for severe wear-resistance applications, such as tips for fountain pen nibs and for nonmagnetic instrument pivots. High hardness and excellent resistance to corrosion are the prime virtues of these alloys. Ruthenium-dioxide-coated titanium is an effective anode in chlorine-manufacturing cells.

Ruthenium is added to platinum and palladium as a hardener. A 5% addition of ruthenium to annealed platinum will increase the hardness from 40 to 130 HV; similarly, the hardness of annealed palladium can be increased from 40 to 90 HV. The work-hardening rate of these metals is also increased by the addition of ruthenium.

Small additions of ruthenium have also been found to be effective in improving the corrosion resistance of titanium. As a cost-reduction measure, the titanium industry has developed two grades of Ti-0.1%Ru with properties similar to the more expensive titanium-palladium grades. These precious-metal-containing grades outperform commercial-grade titanium in hot halide and sulfate environments, particularly in inhibiting crevice corrosion (Ref 45, 46).

Table 27 Corrosion of ruthenium in acids

Acid	Temperature °C	Temperature °F	Corrosion rate mm/yr	Corrosion rate mils/yr
Aqua regia	100	212	nil	
Hydroiodic, 60%	100	212	nil	
Hydrobromic, 62%	100	212	nil	
Hydrochloric, 36%	100	212	nil	
Hydrofluoric, 49%	Room		nil	
Nitric, 95%	100	212	nil	
Sulfuric, 95%	100	212	nil	

Table 28 Corrosion of ruthenium in halogens at room temperature

Halogen	Corrosion rate mm/yr	Corrosion rate mils/yr
Saturated chlorine in water	1.3	51
Chlorine, dry	nil	
Chlorine, moist	nil	
Saturated bromine in water	1.0	40
Bromine, dry	nil	
Bromine, moist	nil	
Iodine, dry	nil	
Iodine, moist	nil	
Iodine in alcohol, 50 g/L	1.0	40

Table 29 Corrosion of ruthenium in salts and other environments at 100 °C (212 °F)

Environment	Corrosion rate mm/yr	Corrosion rate mil/yr
Hydrogen sulfide, moist, at room temperature	nil	
Sodium hypochlorite + sodium chloride, saturated solution	Moderate attack	
Ferric chloride, 100 g/L	nil	
Mercuric chloride, 100 g/L	44.0	1732
Aluminum sulfate, 100 g/L	nil	

Osmium

Fabrication. Osmium is an element that is essentially impossible to fabricate except by powder metallurgy, and even with powder metallurgy techniques, extreme care must be used. Arc melting must be done under vacuum or inert atmospheres.

Atomic, Structural, and Physical Properties. Osmium has the highest melting point (approximately 3045 °C, or 5515 °F) and the second-highest density (22.57 g/cm^3, or 0.815 lb/in.^{3}) of the platinum-group metals. Osmium is similar in many properties to ruthenium and, like ruthenium, has a hcp crystal structure. The principal physical properties of the element are given in Table 1. Some of these properties will vary according to the degree of preferred orientation present in the test specimen.

Mechanical property data on osmium are scarce. The annealed hardness of osmium is 300 to 670 HV (Ref 47). This makes osmium the hardest of the platinum-group metals.

Corrosion Resistance. Compared to other elements in the platinum-group metals, osmium has relatively modest corrosion resistance. The element is attacked by aqua regia and the oxidizing acids but is resistant to HCl and H_2SO_4 (Table 30). Osmium is attacked by the halogens at room temperature (Table 31), and the attack becomes progressively worse upon heating. Osmium is dissolved fairly rapidly in sodium hypochlorite at room temperature and in $FeCl_3$ at 100 °C (212 °F) (Table 32). Osmium burns in the vapor of sulfur and phosphorus and is attacked by molten alkali hydrosulfates, potassium hydroxide, and oxidizing agents. Osmium powder readily absorbs considerable amounts of hydrogen.

Oxidation Resistance. Osmium powder will slowly oxidize, even at room temperature, to form osmium tetroxide. Osmium tetroxide boils at 130 °C (265 °F) and is extremely toxic.

Table 30 Corrosion of osmium in acids

	Temperature		Corrosion rate	
Acid	°C	°F	mm/yr	mils/yr
Aqua regia	Boiling		Rapid dissolution	
Hydroiodic, specific gravity 1.75	100	212	3.7	148
Hydrobromic, specific gravity 1.7	100	212	1.8	72
Hydrochloric, 36%	Room		nil	
Hydrochloric, 36%	100	212	<0.25	10
Hydrofluoric, 40%	Room		nil	
Nitric, 95%	100	212	Rapid dissolution	
Phosphoric, concentrated	100	212	nil	
Sulfuric, concentrated	100	212	nil	

Table 31 Corrosion of osmium in halogens at room temperature

	Corrosion rate	
Halogen	mm/yr	mils/yr
Chlorine, dry	<0.25	10
Bromine, dry	4.1	161
Iodine, dry	<0.25	10

Table 32 Corrosion of osmium in salts and in other environments

	Temperature		Corrosion rate	
Environment	°C	°F	mm/yr	mils/yr
Hydrogen sulfide, moist	Room		<0.25	10
Sodium hypochlorite + sodium chloride, saturated solution	Room		Rapid dissolution	
Ferric chloride, 100 g/L	100	212	3.0	120

Corrosion Applications. Osmium is the rarest of the platinum-group metals; annual worldwide production amounts to only a few thousand ounces. Some of this production is for medical applications. A principal use of osmium is in the manufacture of hard, nonrusting pivots for instruments, phonograph needles, tipping the nibs of fountain pens, and certain types of electrical contacts. Alloys containing at least 60% Os or osmium plus ruthenium in conjunction with another platinum-group metal are usually used in these applications.

Anodic Behavior of the Noble Metals

Under anodic conditions in nitrate and cyanide solutions, silver is readily dissolved. This behavior is the basis of numerous silver electroplating baths. Silver becomes passive in most halide and hydroxide solutions because of the formation of a silver halide layer and a silver oxide layer, respectively. In sulfate solution, silver first forms a passive film of sulfate, but on application of a higher potential, the sulfate becomes an oxide that can be reduced again to silver sulfate at a potential even lower than that required for the initial sulfate film formation.

Gold dissolves readily when it is made anodic in chloride solution containing an oxidizing agent (Ref 18). Only under conditions of low acid concentration or high current densities will the surface gradually become passivated by an absorbed layer of oxygen. In H_2SO_4, gold initially dissolves as Au^+, but the surface gradually becomes passivated by a layer of gold hydroxide.

Platinum and iridium are capable of carrying high current densities in certain acidic and alkaline solutions but can become passivated with difficulty by absorbed oxygen (Ref 48). This film formation is accelerated by the superimposition of an alternating current on the direct current. The low solubility of platinum has made it a valuable commercial anode material for the electrolytic production of persulfates and perchlorates, electroplating anodes, and cathodic protection. Platinum loses less than 0.6 mg/A · yr over a current density range of 540 to 5400 A/m^2 (50 to 500 A/ft^2) in flowing seawater, and less than 1 g per ton of chlorine produced in the electrolysis of brine. In strong HCl solutions, platinum may be attacked, particularly if the temperature is raised. Rhodium becomes anodically passive in HCl. Conversely, palladium is readily dissolved anodically in acid chloride solutions and under certain neutral chloride conditions. Ruthenium metal is dissolved anodically in both HCl and H_2SO_4. The anodic dissolution of osmium in acid media is reviewed in Ref 49 and 50.

Small additions of the noble metals, particularly palladium and platinum, can substantially lower the corrosion rate of such metals as titanium, stainless steel, and chromium (Ref 46). This is achieved through the noble metal additions by their cathodic reduction of dissolved oxygen or hydrogen ions, permitting larger current densities and higher positive potentials in the anodic regions of the surface. To be effective, this higher potential must move the metal into a passive condition; otherwise, the corrosion rate will be accelerated. The technique works well for many base metal alloys in H_2SO_4.

ACKNOWLEDGMENT

This article is based on the article "Corrosion of the Noble Metals," by Gaylord D. Smith and Edward Zysk, that appeared in *Corrosion,* Volume 13, *ASM Handbook,* 1987.

REFERENCES

1. G.W. Walkiden, The Noble Metals, *Corrosion—Metal/Environmental Reactions,* Vol 1, 2nd ed., L.L. Sheir, Ed., Newnes-Butterworths, 1979, p 6.3–6.23
2. C.R. Marsland, The Fabrication of Silver and Silver-Base Alloys, *Silver—Economics, Metallurgy and Use,* A. Butts and C.D. Cox, Ed., D. Van Nostrand, 1967, p 310–321
3. E.M. Wise, *Gold,* D. Van Nostrand, 1964
4. R.H. Leach, Silver and Silver Alloys, *The Corrosion Handbook,* H.H. Uhlig, Ed., John Wiley & Sons, 1948, p 314–320
5. A. Butts and J.M. Thomas, Corrosion Resistance of Silver and Silver Alloys, *Silver in Industry,* L. Addicks, Ed., Reinhold, 1940, p 357–400
6. A. Butts, The Chemical Properties of Silver, *Silver—Economics, Metallurgy and Use,* D. Van Nostrand, 1967, p 123–136
7. E.M. Wise, Platinum Group Metals and Alloys, *The Corrosion Handbook,* H.H. Uhlig, Ed., John Wiley & Sons, 1948, p 299–313, 699–718
8. R.F. Vines, Noble Metals, *Corrosion Resistance of Metals and Alloys,* 2nd ed., F.L. LaQue and H.R. Copson, Ed., ACS Monograph Series, No. 158, Reinhold, 1963, p 601–621
9. E.M. Wise, Corrosion Behavior of Palladium, *Palladium—Recovery, Properties and Uses,* Academic Press, 1968, p 21–28
10. E. Rabald, *Corrosion Guide,* 2nd ed., Elsevier, 1968
11. M.J.N. Pourbaix, *Atlas of Electrochemical Equilibria in Aqueous Solutions,* 2nd ed., NACE, 1974
12. J.C. Chaston, Oxygen in Silver, *Silver—Economics, Metallurgy and Use,* A. Butts and C.D. Cox, Ed., D. Van Nostrand, 1917, p 304–309
13. M.C. Bernard et al., Reduction of Silver Tarnishing and Protection against Subsequent Corrosion, *Corros. Sci.,* in press
14. P.R. Mezger et al., The Corrosion Behaviour of Palladium-Silver-Ceramic Alloys, *Dent. Mater.,* Vol 5 (No. 2), March 1989, p 97–100
15. N. Horasawa et al., The Effect of Recasting on Corrosion of a Silver-Palladium Alloy, *Dent. Mater.,* Vol 20 (No. 4), 4 May 2004, p 352–357
16. L. Joska et al., The Mechanism of Corrosion of Palladium-Silver Binary Alloys in Artificial Saliva, *Biomaterials,* Vol 26 (No. 14), May 2005, p 1605–1611
17. H.J. Mueller et al., Electrochemical Characterization and Immersion Corrosion of a Consolidated Silver Dental Biomaterial, *Biomaterials,* Vol 22, (No. 19), 1 Oct 2001, p 2635–2646
18. A.T. Kuhn et al., Anodic Dissolution, Oxygen Reduction and Corrosion of Gold Alloys, *Surf. Technol.,* Vol 13 (No. 1), May 1981, p 17–31
19. D.A.J. Rand, A Study of the Dissolution of Platinum, Palladium, Rhodium and Gold Electrodes in 1 *M* Sulphuric Acid by Cyclic Voltammetry, *J. Electroanal. Chem.,* Vol 35, March 1972, p 209–218
20. J.S. Hill and H.J. Albert, Loss of Weight of Platinum, Rhodium and Palladium at High

Temperatures, *Englehard Ind. Tech. Bull.,* Vol 4 (No. 2), 1963, p 59–63
21. J.C. Chaston, Reaction of Oxygen with the Platinum Metals: I-The Oxidation of Platinum, *Platin. Met. Rev.,* Vol 8 (No. 2), 1964, p 50–54
22. I.K. Igumenov et al., Corrosion Testing of Platinum Metals CVD Coated Titanium Anodes in Seawater-Simulated Solutions, *Desalination,* Vol 136, (No. 1–3), 1 May 2001, p 273–280
23. B.A. Pint, J.A. Haynes, K.L. More, and I.G. Wright, "The Use of Model Alloys to Understand and Improve the Performance of Pt-Modified Aluminide Coatings," Tenth International Symposium on Superalloys, 19–23 Sept 2004 (Champion, PA), TMS
24. E.P. Sadowski, Stress-Rupture Properties of Some Platinum and Palladium Alloys, Part I, *Metallurgical Society Conferences,* Vol II, The Metallurgical Society, 1961, p 465–476
25. H.J. Albert, D.J. Accinno, and J.S. Hill, Stress-Rupture Properties of Some Platinum and Palladium Alloys, Part II, *Metallurgical Society Conferences,* Vol II, The Metallurgical Society, 1961, p 476–482
26. M.D. Benari et al., The Corrosion of Silver, Copper, Palladium and Gold by Fe(III) and Cu(II) in Dimethylsulphoxide and Water Solutions, *Electrochimi. Acta,* Vol 36, (No. 3–4), 1991, p 479–488
27. C.A. Haque et al., Atmospheric Corrosion of Clad Palladium-Silver Alloys: Film Growth and Contamination Effects, *Corros. Sci.,* Vol 22 (No. 10), 1982, p 939–949
28. M. Hara et al., Anodic Characteristics of Amorphous Palladium-Iridium-Phosphorus Alloys in a Hot Concentrated Sodium Chloride Solution, *J. Non-Cryst. Solids,* Vol 54, (No. 1–2), Jan–Feb 1983, p 85–100
29. E.D. Zysk, Noble Metals in Thermometry—Recent Developments, *Englehard Ind. Tech. Bull.,* Vol 5 (No. 3), 1964, p 69–99
30. E. Raub and W. Plate, The Solid State Reactions Between the Precious Metals or Their Alloys and Oxygen at High Temperatures, *Z. Metall.,* Vol 48, 1957, p 529–539
31. W. Betteridge and D.W. Rhys, High-Temperature Oxidation of Platinum Metals and Their Alloys, *Proceedings of the First International Congress on Metallic Corrosion,* Butterworths, 1962, p 186–192
32. J.C. Chaston, Reaction of Oxygen with the Platinum Metals III—The Oxidation of Palladium, *Platin. Met. Rev.,* Vol 9 (No. 4), 1965, p 126–129
33. C.B. Alcock and G.W. Hooper, Thermodynamics of the Gaseous Oxides of the Platinum-Group Metals, *Proc. R. Soc. (London) A,* Vol 254, p 551–561
34. P.R. Mezger et al., The Corrosion Behaviour of High-Palladium Porcelain-Bonding Alloys, *J. Dent.,* Vol 17 (No. 1), Feb 1989, p 33–37
35. J.M. Martinovic et al., Nature of the Rhodium Rest Potentials in Oxygen Saturated Aqueous Solutions, *Electrochim. Acta,* Vol 34 (No. 5), 10 May 1989, p 671–676
36. J. Llopis et al., Passivation of Iridium in Hydrochloric Acid Solutions, *Electrochim. Acta,* Vol 9 (No. 1), 1 Jan 1964, p 103–111
37. D.W. Rhys and E.G. Price, Resistance of Iridium and Ruthenium to Attack by Liquid Metals, *Englehard Ind. Tech. Bull.,* Vol V (No. 2), 1964, p 37–42
38. R.W. Douglass and R.J. Jaffee, Elevated-Temperature Properties of Rhodium, Iridium and Ruthenium, *Proc. ASTM,* Vol 62, 1962, p 627
39. H. Schafer and N.J. Heitland, Equilibrium Measurements in the System Iridium-Oxygen: Gaseous Iridium Trioxide, *Z. Anorg. Allg. Chem.,* Vol 304, 1960, p 249–265
40. W.L. Phillips, Jr., Oxidation of the Platinum Metals in Air, *Trans. ASM,* Vol 57, 1964, p 33–37
41. Y.-P. Lee et al., Electrochemical and Corrosion Behaviour of Iridium-Palladium Oxide Electrode Prepared by Electrochemical Methods, *Corros. Sci.,* Vol 35 (No. 1–4), 1993, p 387–389
42. H. Murakami, A. Suzuki, F. Wu, P. Kuppusami, and H. Harada, "Application of Ir-Base Alloys to Novel Oxidation Resistant Bond-Coatings," Tenth International Symposium on Superalloys, 19–23 Sept 2004 (Champion, PA), TMS
43. J. Llopis et al., Anodic Corrosion of Ruthenium in Hydrochloric Acid Solutions, *Electrochim. Acta,* Vol 10 (No. 11), Nov 1965, p 1045–1055
44. L.D. Burke et al., The Behaviour of Ruthenium Anodes in Base, *J. Electroanal. Chem.,* Vol 103 (No. 2), 12 Nov 1979, p 179–187
45. E. van den Lingen et al., The Cathodic Modification Behaviour of Ruthenium Additions to Titanium in Hydrochloric Acid, *Corros. Sci.,* Vol 43 (No. 3), 3 March 2001, p 577–590
46. C.S. Brossia and G.A. Cragnolino, Effect of Palladium on the Corrosion Behaviour of Titanium, *Corros. Sci.,* Vol 46 (No. 7), 7 July 2004, p 1693–1711
47. R.F. Vines, *The Platinum Metals and Their Alloys,* The International Nickel Company, Inc., 1941
48. F. Colom et al., Anodic Corrosion of Iridium in the LiCl + KCl Eutectic Melt, *J. Electroanal. Chem.,* Vol 290 (No. 1–2), 10 Sept 1990, p 105–118
49. F. Colom, Anodic Film Formation on Osmium Electrodes in Strong Acid Solutions—Voltammetric Studies, *J. Electroanal. Chem.,* Vol 89 (No. 2), 25 May 1978, p 397–406
50. F. Colom, Anodic Dissolution of Osmium in Acid Media, *J. Electroanal. Chem.,* Vol 73 (No. 3), 10 Nov 1976, p 303–315

SELECTED REFERENCE

- L.S. Brenner, T. Suzuki, K. Meguro, and S. Tanaka, *Precious Metals Science and Technology,* International Precious Metals Institute, 1991

ASM Handbook, Volume 13B: Corrosion: Materials
S.D. Cramer, B.S. Covino, Jr., editors, p402-417
DOI: 10.1361/asmhba0003830

Corrosion of Zinc and Zinc Alloys

X. Gregory Zhang, Teck Cominco Metals Ltd.

ZINC is twenty-third among the elements in relative abundance in the earth's crust, at 0.013%. However, zinc is one of the most used metals, ranking fourth in worldwide production and consumption behind iron, aluminum, and copper (Ref 1).

Zinc is silvery blue-gray with relatively low melting (419.5 °C, or 787.1 °F) and boiling (907 °C, or 1665 °F) points. The strength and hardness of unalloyed zinc are greater than tin or lead but appreciably less than aluminum or copper. Pure zinc, however, cannot be used in applications under mechanical stress because of its low creep resistance. It recrystallizes rapidly after deformation at room temperature and thus cannot be work hardened at room temperature. The temperature for recrystallization and creep resistance can be increased through alloying (Ref 2).

Applications of Zinc

The applications of zinc can be divided into six categories: coatings, casting alloys, alloying element in brass and other alloys, wrought zinc alloys, zinc oxide, and zinc chemicals (zinc dust, powder, salts). The most important use of zinc is for corrosion protection of steel, mainly in the form of coatings, due to the excellent corrosion performance of zinc-coated steel in natural environments. Nearly one-half of all zinc produced is consumed for this purpose. Cast zinc products are mainly produced by the die-casting process, which can turn out complex, very accurate components requiring little or no final machining. Die-cast products are used for automotive parts, household appliances and fixtures, office and computer equipment, and building hardware. Rolled zinc products can have a variety of compositions and be in the form of sheet, strip, foil, plate, rod, and wire. Rolled zinc sheet is widely used in the building construction for roofing, cladding, gutters, rainwater pipes, and flashings. The main commercial use of zinc powder is as anode material for alkaline batteries. Zinc dust is used as a reagent for producing chemicals, in metal refining processes, as a component for making zinc-rich paints, and as an additive for plastics.

Zinc is alloyed for different applications. The binary zinc alloy systems of commercial interest are:

- 95Zn-5Al and 55Al-45Zn, major coating alloys
- 96Zn-4Al, zinc die-casting alloy
- Zn-Cu, with up to 45% Zn, are brass alloys
- Zn-Fe, includes the phases making up galvanized coatings
- Zn-Pb, plays an important role in some pyrometallurgical extraction processes

Ternary and quaternary systems involving these alloys, with additions of such elements as nickel, magnesium, titanium, and cadmium, are also of commercial importance.

Zinc is essential for the normal healthy growth and reproduction of plants, animals, and humans (Ref 1). A wide range of human health problems is related to a zinc deficiency. The use of zinc compounds in medicine and agriculture, although very small in quantity, has gained recognition in recent years in addressing the zinc deficiency in both crop and human nutrition (Ref 3).

Zinc Coatings. Through galvanizing, metal spraying, sacrificial anodes, zinc-dust paints, and other methods, zinc-protected steels are widely used in automobiles, building structures, reinforced concrete, roofing, and other domestic and industrial structures. The protection of zinc-coated steel is due primarily to the much better corrosion resistance of zinc. In most natural environments, zinc corrodes by a factor of 10 to 100 times slower than steel (Ref 2). A unique feature of zinc coatings is the extra protection provided by galvanic action between the zinc coating and the substrate steel at places where the coating is damaged and the steel is exposed.

The many types of zinc and zinc alloy coatings can be classified according to coating composition and production methods (Ref 4, 5). By chemical composition, zinc-base coatings are categorized as pure zinc, zinc-iron, zinc-aluminum, zinc-nickel, zinc-aluminum-magnesium, and zinc composites. In terms of methods, zinc coatings can be produced by hot dipping, electroplating, mechanical bonding, sherardizing, and thermal spraying (metallizing). The hot dipping process may be continuous or batch. See the articles "Continuous Hot Dip Coatings" and "Batch Process Hot Dip Galvanizing" in *ASM Handbook,* Volume 13A, 2003. Typical applications for zinc and its alloy-coated steel sheet products cover a wide range in the construction, automotive, utility, and appliance industries, as shown in Table 1.

Coating Processes. Hot dip galvanizing, either continuous or batch, is a process by which an adherent coating of zinc and zinc-iron alloys is produced on the surface of iron or steel products by immersion in a bath of molten zinc. In general, an article to be galvanized is cleaned, pickled, and fluxed in a batch process, or heat

Table 1 Typical applications of zinc-coated steel products

Coatings	Typical applications
Continuous galvanized coatings	
Zn and Zn-5Al	Roofing, culverts, housing, appliances, autobody panels and components, nails, guy wire, rope, utility wire, and fencing
Zn-Fe	Autobody panels and structural components
Zn-Ni and Zn-Co	Autobody panels and structural components, housing, appliances, and fasteners
Zn-55Al	Roofing, siding, ductwork, culverts, mufflers, tailpipes, heat shields, ovens, toasters, chimneys, and silo roofs
Zn-Al-Mg	Construction products
Batch galvanized	
Various alloys	Structural steel for power generating plants, petrochemical facilities, heat exchangers, cooling coils, water treatment facilities, and electrical transmission towers and poles. Bridge structural members, culverts, corrugated steel pipes, and arches. Reinforcing steel for concrete. Highway guard rails, lighting stands, and sign structures. Marine pilings and rails. Architectural applications of structural steel, lintels, beams, columns, and related building materials
Thermal spray	
Zn-15Al	Large structures that are not suitable for batch galvanizing, such as bridge superstructures

Source: Ref 4, 5

treated in a reducing atmosphere in a continuous galvanizing process, to remove surface oxide. It is then immersed in a bath of molten zinc for a time sufficient for it to wet and alloy with zinc, after which it is withdrawn and cooled.

The coating produced in this way is bonded to the steel by a series of zinc-iron alloy layers with a layer of almost pure zinc on the surface. The engineering properties of the coating depend on the physical and chemical nature of the zinc-iron intermetallic layers formed. The thickness and composition of the layers depend on the immersion time and bath composition, which vary in the batch and continuous processes. The coating produced by a batch process is relatively thicker and has clearly distinguishable alloy layers, while that of the continuous process is thinner and has only a very thin and sometimes invisible alloy layer at the coating/steel interface. The thickness, structure, and quality of galvanized zinc coatings depend on many operational factors, particularly the surface condition of the steel and the chemistry of the steel and the molten zinc bath.

In addition to pure zinc coatings, a number of zinc alloy coatings that offer better corrosion performance have been developed, among them Galvanneal, Galvalume (BIEC International, Inc.), and Galfan (International Lead Zinc Research Organization). Galvanneal is a zinc-iron alloy coating obtained by annealing hot dipped sheet. Galvalume (55Al-1.5Si-43.5Zn) has a microstructure consisting of an outer layer and a thin intermetallic layer that bonds the outer layer to the steel. Galfan, 95Zn-5Al and a small amount of mischmetal, has a multiphase microstructure that is characteristic of its composition, exhibiting a lamellar structure of alternating zinc-rich and aluminum-rich phases. More recently, some magnesium-alloyed zinc-coated steel sheets have been developed for specialized applications (Ref 6, 7). For example, new alloy coatings with a composition of Zn-6Al-3Mg and Zn-11Al-3Mg-0.2Si are being used in the construction industry (Ref 6, 8).

Electroplating is another common galvanizing method used mainly for high-surface-quality thinner coatings. These coated products are generally painted (automotive bodies and household appliances). Owing to its versatility, electroplating has been extensively used with new zinc alloy coatings (zinc, zinc-iron, zinc-cobalt, and zinc-nickel). The plating process generally comprises three stages: degreasing and cleaning, electroplating, and posttreatment. Electroplating can be a batch or a continuous process.

Postgalvanizing surface treatment is commonly applied to freshly galvanized steel products to prepare the surface for manufacturing processes such as forming or painting or to provide short-term protection during handling, storage, and transportation (Ref 2). A number of surface treatment processes are commonly used in the industry, such as phosphating, chromating, oiling, thin polymer coating, and variations and combinations thereof.

Phosphating is a surface treatment process with a solution of phosphoric acid and other chemicals for metals such as iron, zinc, and aluminum and their alloys. The reaction between the surface of the metal and the solution results in the formation of an integral layer of insoluble crystalline phosphate. Phosphating on zinc-coated steels is used mainly to prepare metal surfaces for painting. Phosphate coatings provide uniformity in surface texture and increased surface area and, when used as a base for paint, promote good adhesion, increase the resistance of the paint to humidity and water soaking, and eventually increase the corrosion resistance of the painted system. They can also serve the role of lubricants in the forming process of some applications.

Chromating to provide short-term stain or corrosion protection has been the most commonly used posttreatment process for galvanized steel products (Ref 9). Chromating is a process in which an aqueous solution of chromic acid, chromium salts, and mineral acids is used to produce a thin conversion coating on a metal surface. The chemical reaction between the metal and the solution causes the dissolution of the metal and the formation of a protective film containing complex chromium and metal compounds. Since its introduction in the mid-1930s, the chromating process has become the most widely used process for postgalvanizing surface treatment of zinc products. However, due to environmental concerns, great efforts have been made in the industry to develop new processes to reduce the environmental impact of the chromating process (Ref 10). One measure the galvanizing industry has taken is to use very weak chromate solutions for wet-storage stain prevention. Also, many chromium-free organic and inorganic thin films have been developed in recent years, particularly in continuous galvanizing (Ref 10, 11). Unlike chromating, in which the processing conditions and procedures are largely the same from operation to operation, these thin-film processes may vary greatly in material composition and processing conditions and procedures.

Corrosion Performance

There is a wealth of information on the corrosion and electrochemical behavior of zinc and its alloys in various environments, particularly in atmospheres in which they are most widely used. Much of this information has been systematically compiled in a book (Ref 2) and on a website (Ref 12). Information in this article is treated in a general way; interested readers are encouraged to consult the original sources for details.

Electrochemical Characteristics. Zinc has electrochemical properties that are important in the production and applications of zinc, including electrowinning in zinc refining and electroplating in the production of zinc coatings, zinc batteries for energy storage, and coatings and anodes for corrosion protection. The electrochemical properties that are important to the performance of zinc coatings for corrosion protection of steel are the favorable position in the electromotive force (emf) fast series, dissolution/deposition kinetics, large overpotential for hydrogen evolution, and formation of a porous, tenacious corrosion product film (Ref 2). The favorable position in the (emf) series (lower than iron but not too low) allows zinc to act as a sacrificial anode when galvanically coupled with steel; the fast reaction kinetics allow a large galvanic protection distance; the large overpotential for hydrogen reaction is the reason that zinc is stable in aqueous environments; and the formation of a porous, tenacious corrosion product film provides zinc with high corrosion resistance without losing the effect of galvanic protection. Among the metallic elements in the periodic table, this set of electrochemical properties, in its combined effect, is unique to zinc.

The corrosion of zinc is an electrochemical process in which zinc is oxidized with simultaneous reduction of hydrogen ions or dissolved oxygen in the electrolyte. The oxidation follows the reaction:

$$Zn \rightarrow Zn^{2+} + 2e^- \qquad \text{(Eq 1)}$$

The chemical potential Nernst equation is:

$$E^0 = -0.763 + 0.0295 \log [Zn^{2+}] \ V_{SHE} \qquad \text{(Eq 2)}$$

The standard potential of this reaction is $-0.763\ V_{SHE}$, which is 0.315 V more negative than iron and 0.9 V more positive than aluminum in the electromotive series.

Figure 1 shows the Pourbaix diagram of zinc in aqueous solutions. The solid lines, calculated from Eq 1, assuming 10^{-4} *M* Zn^{2+} in the solution, define the stability regions of the different solid and dissolved zinc species and thus the condition for zinc corrosion and passivation.

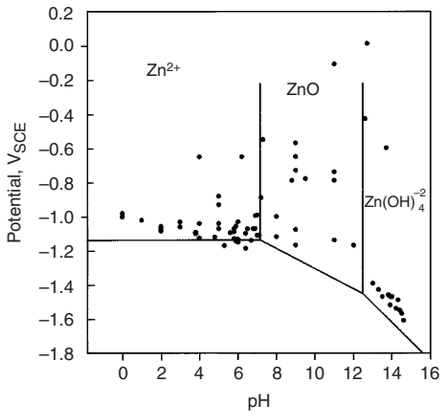

Fig. 1 Corrosion potentials experimentally determined in various solutions with respect to pH. The solid line indicates the reversible potential, which is calculated from the Nernst equation, assuming 10^{-4} *M* Zn^{2+} in the solution. SCE stands for saturated calomel electrode, the potential of which is 0.236 V positive of the standard hydrogen elctrode.

Also plotted in the figure are the corrosion potentials reported in different studies on zinc or zinc coatings as functions of pH (Ref 2). It can be seen that the corrosion potentials experimentally measured in the pH range of 4 to 8 are close to the theoretical values. However, the corrosion potentials in acidic and alkaline solutions are somewhat higher than the reversible potential value, indicating that the zinc electrode at the corrosion potential is anodically polarized from its reversible value. Part of the deviation of the corrosion potential from the reversible value may result from a concentration of Zn^{2+} in these solutions higher than 10^{-4} *M*, at least near the surface where the zinc ions from the dissolution reaction may accumulate. The corrosion potential in slightly alkaline solutions, from pH of approximately 8 to 12, in which ZnO is the stable form, can be much higher than the reversible value due to the formation of a surface oxide, which, depending on the specific conditions, results in various degrees of passivation.

Because the kinetics of the electrochemical reactions and the surface state determine the rate and form of corrosion in a given circumstance, the corrosion potential values, along with the equilibrium potential values and their variation with pH, shown in Fig. 1, are fundamental for understanding the corrosion behavior of zinc under different conditions.

Atmospheric corrosion occurs when a surface is wet due to rain, fog, or condensation. Atmospheric corrosion is a complex process involving a large number of interacting and constantly varying factors, such as weather conditions, air pollutants, and material conditions. The combined effect of these factors results in a great variation in corrosion rates, as shown in Fig. 2. The corrosion rate of zinc in atmospheric environments may vary from approximately 0.1 μm/yr (0.004 mil/yr) in indoor environments to as high as more than 10 μm/yr (0.4 mil/yr) in industrial or marine environments—2 orders of magnitude. The corrosion rate is lowest in dry, clean atmospheres and highest in wet, industrial atmospheres. Seacoast atmospheres, not in direct contact with salt spray, are mildly corrosive to zinc. Locations nearer seawater, subject to salt spray, have higher corrosion rates. Atmospheres are conventionally defined as rural, industrial, urban, and marine. The typical range of corrosion rates of zinc in each of these categories is (Ref 8, 13):

Rural	0.2 to 2 μm/yr (0.008 to 0.08 mil/yr)
Marine (outside the splash zone)	0.5 to 10 μm/yr (0.02 to 0.4 mil/yr)
Urban and industrial	0.8 to 8 μm/yr (0.03 to 0.3 mil/yr)

Except for the initial years, the corrosion loss of zinc is generally observed to be almost linear with respect to time (Ref 14). The corrosion rate in the initial period of exposure tends to be higher than that after several years of exposure. For a given location, the yearly average corrosion rate may vary, because atmospheric conditions, such as the amount of rain or the pollution level, change from year to year.

Table 2 ranks the atmospheric corrosivity of different locations for steel and zinc around the world (Ref 15). The corrosivity of atmospheres from one location to another varies by as much as a factor of 100 for zinc and 500 for steel. The data indicate that the corrosion rate of zinc in most atmospheres is at least ten times lower than that of steel, which accounts for the use of galvanized steel. The steel/zinc loss ratio data of Table 2, plotted in Fig. 3, show that the ratio increases with increasing corrosion rate of steel, suggesting that the more corrosive an atmosphere is to steel, the more benefit derived from using zinc coatings.

Table 3 compares the corrosion rate of zinc and other common metals in various atmospheres. Zinc has a lower corrosion rate than iron and cadmium in all atmospheres, is lower than copper in industrial atmospheres, and is lower than tin and magnesium in marine and rural atmospheres.

Figure 4 shows that, for a given thickness, the life of coatings produced by different processes does not vary significantly. It has been reported that zinc-coated steel wire of different diameters has a coating life directly proportional to the coating thickness, largely irrespective of the method used to produce the coating (Ref 2).

The most corrosive pollutant to zinc in air is sulfur dioxide. The rate is dependent on time of wetness, which is affected by relative humidity (RH) and temperature (Ref 14, 16). Other air pollutants, such as NO_x, have a relatively less significant effect on the corrosion of zinc, largely due to the much lower content of these species in the air (Ref 17). The level of pollution in many developed countries has been considerably reduced over the years because of environmental awareness and regulations; similar trends have generally been found for reduced corrosion rates of many metals. For example, the corrosion rate of zinc has been found to be lower in the 1980s and 1990s than in the 1960s and 1970s (Ref 18).

Near the seacoast, where the major pollutants in the air are chloride salts, the corrosion rate of zinc is high. Figure 5 shows that the corrosion rate decreases with distance from the seacoast, because the salt content in the air drops significantly with distance from the sea (Ref 19). In general, at distances greater than 1 km (0.6 mile) from the seashore, the corrosion rate of zinc is close to that measured inland.

In addition to RH, rainfall, and temperature, other climatic factors, such as wind and solar radiation, may also affect condensation and the rate of drying as well as the amount of contaminants and corrosion products retained on the surface. The initial climatic conditions at the time of exposure exert marked effects on the corrosion of zinc. Long-lasting rainfall or a RH near 100% during the first days tends to cause a higher corrosion rate.

Data from field-testing programs, such as in Table 2, account for the macroscopic effect of atmospheric environments; namely the factors determined by the general climate and pollution of a geographic area. Other small-scale factors, such as the distance from the ground, orientation of the samples, rain shielding, and distance to local contaminant sources, may also significantly affect the corrosion rate.

The corrosion rate is higher on the skyward surface than on the groundward surface, even though the wetting time is longer on the groundward surface. This may be attributed to the effect of rain and the retention of larger amounts of pollutants on the skyward surface (Ref 20). Figure 6 shows the effect of rain sheltering on corrosion rate in four typical environments (Ref 21). Sheltering reduced the corrosion rate by 3.8 times in rural, 2.4 times in urban, and 2.2 times in industrial environments. The fact that the corrosion rate under sheltered conditions in the marine environment was increased by 1.4 times is due to the lack of rain to wash away the deposited seasalt.

The highway environment experienced by automobiles and highway structures is particularly aggressive, due to splashed water that may contain sand, minerals, and deicing salts. In one study, the corrosion rate of zinc coatings in an undervehicle environment was found to be approximately 8.5 μm/yr (0.33 mil/yr), which is comparable to the corrosion rate in a relatively severe marine atmospheric environment (Ref 22).

In an indoor atmosphere, the corrosion rate of zinc is very low, typically below 0.1 μm/yr

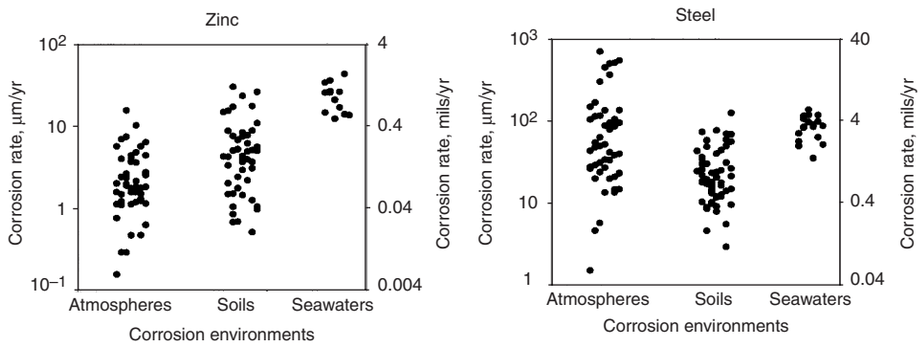

Fig. 2 Corrosion rates of zinc and steel in atmosphere, soil, and seawater. Source: Ref 13

(0.004 mil/yr), making galvanized steel a long-lasting material for indoor applications such as residential housing. The low corrosion rate in indoor environments, if they are properly insulated from outdoor environments, appears to have little correlation to the corrosivity of outdoor environments, as observed in various types of environments at different geographic locations worldwide (Ref 2). Generally, in an indoor environment, a visible tarnish film forms slowly, starting at spots where dust particles have fallen on the surface. Over a period of time, such films grow gradually until the surface has lost much of its original luster. The appearance and the degree of corrosive attack are related to RH. Relative humidity of up to approximately 70% has little influence on corrosion. Above 70%, corrosion activity may occur, because moisture precipitates on the surface, especially on that covered with zinc corrosion products and contaminants.

The effect of alloying elements on the atmospheric corrosion performance of zinc is complex. Some elements may be beneficial in one situation while harmful in another, while others have little effect. The effect may depend on the combination of alloying elements present.

Lead has little effect on the corrosion of zinc when synergistic effects with other elements are absent. It has been found that there are no significant differences in corrosion rates among different grades of zinc with lead concentrations of 0.0055, 0.049, and 0.84% after 20 years of atmospheric exposure. Copper has been found to have a beneficial effect on the atmospheric corrosion resistance of galvanized coatings. The addition of up to 0.82% Cu increased the corrosion resistance by as much as 20% in a two year industrial exposure test. However, copper-bearing zinc is more likely than unalloyed zinc to develop distinct pits due to corrosion. Small additions of tin (from 0.27 to 0.96%) to a galvanizing bath have been reported to have very little effect on the atmospheric corrosion rate. The addition of 0.08% V slightly increases the corrosion resistance of galvanized coatings. Galvanized coatings containing 0.04% Mg have been found to demonstrate no significant differences in coating life in various atmospheres.

Aluminum is a widely used alloying element for zinc. When present in small quantities (0.3%), aluminum significantly reduces the atmospheric corrosion resistance, but the addition of a small amount of copper was found to offset the effect of aluminum. For higher concentrations (>1% Al), the atmospheric corrosion resistance of zinc coatings increases with aluminum content. Two major commercial zinc-aluminum alloy coatings, Galfan and Galvalume, have been developed for more corrosion-resistant steel sheets. Table 4

Table 2 Ranking of corrosivity in 45 locations for steel and zinc after two years' exposure

Specimen size: 102 by 152 mm (4 by 6 in.)

Ranking			Weight loss, g		
Steel	Zinc	Location	Steel	Zinc	Loss ratio steel/zinc
1	1	Norman Wells, NWT, Canada	0.73	0.07	10.3
2	2	Phoenix, AZ, USA	2.23	0.13	17.0
3	3	Saskatoon, SK, Canada	2.77	0.13	21.0
4	4	Esquimalt, Vancouver Island, BC, Canada	6.50	0.21	31.0
5	15	Detroit, MI, USA	7.03	0.58	12.2
6	5	Fort Amidor Pier, Panama	7.10	0.28	25.2
7	11	Morenci, MI, USA	9.53	0.53	18.0
8	7	Ottawa, ON, Canada	9.60	0.49	19.5
9	13	Potter County, PA, USA	10.0	0.55	18.3
10	31	Waterbury, CT, USA	11.0	1.12	9.8
11	10	State College, PA, USA	11.2	0.51	22.0
12	28	Montreal, PQ, Canada	11.4	1.05	10.9
13	6	Melbourne, Australia	12.7	0.34	37.4
14	20	Halifax (York Redoubt), NS, Canada	13.0	0.70	18.5
15	19	Durham, NH, USA	13.3	0.70	19.0
16	12	Middletown, OH, USA	14.0	0.54	26.0
17	30	Pittsburgh, PA, USA	14.9	1.14	13.1
18	27	Columbus, OH, USA	16.0	0.95	16.8
19	21	South Bend, PA, USA	16.2	0.78	20.8
20	18	Trail, BC, Canada	16.9	0.70	24.2
21	14	Bethlehem, PA, USA	18.3	0.57	32.4
22	33	Cleveland, OH, USA	19.0	1.21	15.7
23	8	Miraflores, Panama	20.9	0.50	41.8
24	29	London(Battersea), England, UK	23.0	1.07	21.6
25	24	Monroeville, PA, USA	23.8	0.84	28.4
26	35	Newark, NJ, USA	24.7	1.63	15.1
27	16	Manila, Philippine Islands	26.2	0.66	39.8
28	32	Limon Bay, Panama	30.3	1.17	25.9
29	39	Bayonne, NJ, USA	37.7	2.11	17.9
30	22	East Chicago, IN, USA	41.1	0.79	52.1
31	9	Cape Kennedy (3.2 km, or 2 miles, from ocean), FL, USA	42.0	0.50	84.0
32	23	Brazos River, TX, USA	45.4	0.81	56.0
33	40	Pilsey Island, England, UK	50.0	2.50	20.0
34	42	London (Stratford), England, UK	54.3	3.06	17.8
35	43	Halifax (Federal Building), NS, Canada	55.3	3.27	17.0
36	38	Cape Kennedy (55 m, or 60 yd, from ocean; 18 m, or 60 ft, elevation), FL, USA	64.0	1.94	33.0
37	26	Kure Beach (250 m or 800 ft, lot), NC, USA	71.0	0.89	80.0
38	36	Cape Kennedy (55 m, or 60 yd, from ocean; 9 m, or 30 ft, elevation), FL, USA	80.2	1.77	45.5
39	25	Daytona Beach, FL, USA	144.0	0.88	164.0
40	44	Widness, England, UK	174.0	4.48	39.0
41	37	Cape Kennedy (55 m, or 60 yd, from ocean, ground level), FL, USA	215.0	1.83	117.0
42	34	Dungeness, England, UK	238.0	1.60	148.0
43	17	Point Reyes, CA, USA	244.0	0.67	364.0
44	41	Kure Beach (25 m, or 80 ft, lot), NC, USA	260.0	2.80	93.0
45	45	Galeta Point Beach, Panama	336.0	6.80	49.4

Source: Ref 15

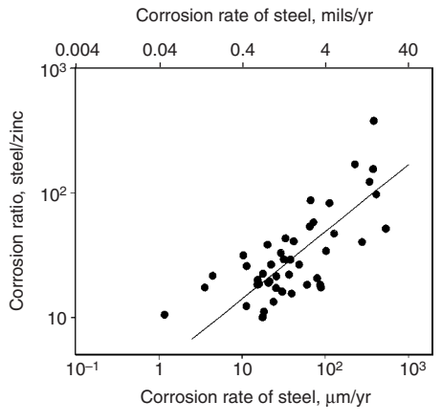

Fig. 3 Corrosion rate ratios of steel/zinc as a function of the corrosion rate of steel in atmospheric environments. The correlation is significant at 99.9% confidence level. Source: Ref 13

Table 3 A comparison of typical corrosion rates of zinc and other common commercial metals

Metal	Industrial	Marine	Rural
Zinc	1	1	1
Cadmium	2	2	2.4
Tin	0.23	1.6	1.9
Aluminum	0.13	0.3	0.09
Copper	2.4	0.72	0.38
Lead	0.07	0.3	0.28
Nickel	...	0.6	1.1
Antimony	0.06	...	...
Magnesium	0.31	1.8	1.9
Iron	30	50	15

Note: Corrosion rate is relative to zinc, which is taken as 1. Source: Ref 2

compares the corrosion resistance of galvanized, Galfan, and Galvalume coatings. In general, Galfan is approximately two times more corrosion resistant than a galvanized coating, and Galvalume is two to four times more corrosion resistant than a galvanized coating. The corrosion of zinc-aluminum alloys proceeds through several stages. First, the zinc preferentially dissolves, leaving an aluminum-rich porous structure. During this stage, the steel is cathodically protected. After the zinc is depleted in the coating, depending on the compactness of the remaining structure and the type of atmosphere, red rust may start to form, because the aluminum may be passivated and hence is cathodic to steel. The zinc-aluminum alloy system has been further expanded by the addition of magnesium to produce ternary alloy coatings for special applications (Ref 6, 7). The reported increased corrosion performance is related to the altered structure of the corrosion product due to the presence of magnesium.

Corrosion Mechanism. The high corrosion resistance of zinc-coated steel is attributed to barrier protection and cathodic protection. Barrier protection is the primary protection mechanism, because the majority of the surface area of a galvanized product is covered with the zinc coating, while galvanic protection is secondary and occurs only at places where the zinc coating is not present.

The galvanic action of zinc-coated steel with the coating partially removed under a thin moisture layer (e.g., atmospheric environments) is schematically represented in Fig. 7. There are five regions across the surface. On the zinc side, the surface area away from the zinc/steel boundary experiences only normal corrosion (no galvanic corrosion), and the narrow region at the boundary corrodes galvanically. On the steel side, there are three regions: a region next to the zinc, measured by protection distance, in which the steel is fully cathodically protected; a region where the steel is partially protected; and a region further away from the zinc where the steel is not cathodically protected and corrodes normally.

The high corrosion resistance of zinc coatings in atmospheric environments is associated with the compactness and tenacity of the corrosion products formed on the surface of zinc. During atmospheric corrosion, the corrosion products formed initially are loosely attached to the surface but gradually become more adherent and denser, resulting from the wetting and drying cycles of the weathering process. After the formation of this corrosion product layer, further corrosion can proceed only within the pores where the zinc surface is not sealed by the corrosion products, while the rest of the surface area, which is sealed by the corrosion products, is protected from corrosion. This is a dynamic process. With time, some pores become sealed by newly formed corrosion products, while some pores are opened due to dissolution of the corrosion products. This corrosion mechanism, in simplified form, is illustrated in Fig. 8. The low

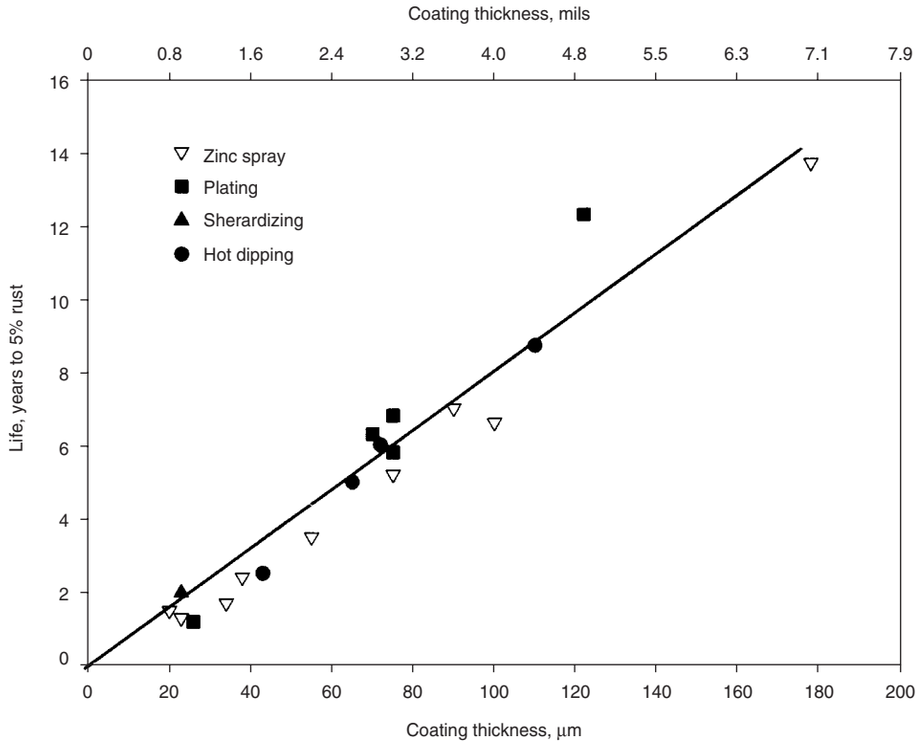

Fig. 4 Effect of coating thickness and coating methods on coating life in industrial atmospheres

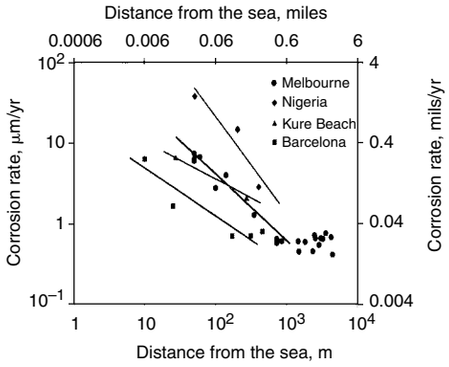

Fig. 5 Corrosion rate as a function of distance from the sea at four different geographic locations

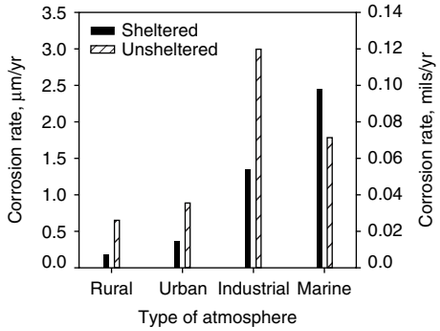

Fig. 6 Corrosion loss of zinc plates exposed for five years in different types of atmospheres under sheltered and unsheltered conditions. Source: Ref 21

Table 4 Corrosion losses for galvanized steel, Galfan, and Galvalume after one year exposure in four different atmospheric environments

	Corrosion loss							
	Galvanized		Galfan				Galvalume	
			Min		Max			
Environment	μm	mils	μm	mils	μm	mils	μm	mils
Rural	1.0	0.04	0.3	0.012	1.0	0.04	0.3	0.012
Urban	3.0	0.12	0.7	0.03	1.4	0.06	0.6	0.024
Marine	2.4	0.09	1.4	0.06	2.8	0.11	1.1	0.043
Severe marine	5.4	0.21	2.8	0.11	3.8	0.15	2.6	0.10

corrosion rate observed in atmospheric environments is described as:

$$R = ra/A \qquad \text{(Eq 3)}$$

where R is the observed corrosion rate, averaged over the entire surface; r is the actual corrosion rate on an active zinc surface unsealed by corrosion products; a is the area of active zinc surface; and A is the area of the entire surface.

Because a is small compared to A, the observed rate R is low even though the actual corrosion rate r within the pores may be much higher. Thus, the more compact the corrosion product layer, as determined by the corrosion environment, the smaller the active surface area within the pores and the smaller the observed corrosion rate.

The value of a, and thus the observed corrosion rate of zinc, depends on the physical and chemical natures of zinc corrosion products, which depend on environmental conditions and change over time. The more compact and continuous the corrosion product layer, the smaller the active surface area within the pores and the smaller the observed corrosion rate. Thus, the performance of galvanized steel in various environments depends largely on the tendency to form compact and tenacious corrosion products that have a small a. The corrosion rates will be high under conditions where tenacious and compact corrosion products cannot form. For example, wet-storage stain formed under continuous wetting is loose, having a large a, and thus is not protective.

Corrosion products are the solid phases formed as a result of the interaction between the metal substrate and the environment. The white rust on zinc is a corrosion product. The physical characteristics of the zinc corrosion products play a more important role in corrosion protection than the chemical composition. Also, the physical characteristics, such as the morphology, are, in general, more difficult to define than the chemical characteristics, partly due to the extremely rich morphological details of corrosion products and partly due to the lack of convenient examination methods. The morphology of corrosion products can vary greatly, depending on conditions, as shown in Fig. 9.

Many zinc compounds have been identified in the corrosion products formed in different types of atmospheres. However, for a specific atmosphere, only certain compounds dominate. Generally, among the zinc compounds, oxides, hydroxides, and carbonates are most often found in corrosion products (Ref 24). Zinc sulfate ($ZnSO_4 \cdot nH_2O$) and basic zinc sulfate ($Zn_4SO_4(OH)_6 \cdot nH_2O$) are also found. In seacoast areas, zinc hydroxy chloride ($Zn_5(OH)_8Cl_2 \cdot H_2O$) is also a major compound.

The formation sequence of the major zinc compounds found in corrosion products is given in Fig. 10. On exposure, the zinc surface is covered quickly with zinc hydroxide, which is gradually converted to zinc carbonate. Within one month of exposure, almost all major zinc compounds can be detected in the corrosion products. In the more severe marine and industrial atmospheres, the formation of chloride and

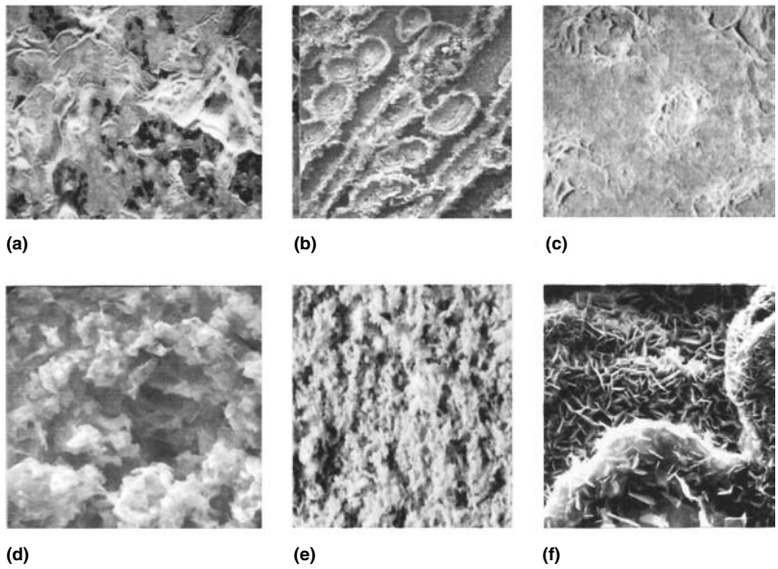

Fig. 9 Examples that show the morphological diversity of the corrosion products that form under various environmental conditions. (a) After standard salt spray test (continuous spraying with 5% NaCl solution). (b) After cyclic corrosion test with 17.5 min of spraying with 0.001 M $Na_2(SO)_4$, 2.5 min of 100% humidity, and 10 min of air drying. (c) After atmospheric exposure. (d) After immersion in water. (e) After exposure in a sealed box containing water (100% humidity). (f) After a cyclic test with 10 min of spraying with 0.001 M $Na_2(SO)_4$, 30 min of 100% humidity, and 20 min of air drying

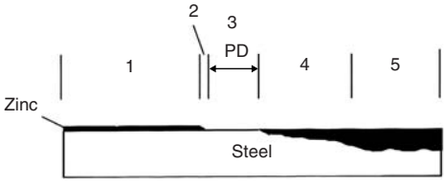

Fig. 7 Schematic illustration of the different regions on a partially zinc-coated steel surface. 1, normal corrosion only; 2, mainly galvanic corrosion; 3, full cathodic protection; 4, partial cathodic protection; and 5, normal corrosion with no cathodic protection. The protection distance (PD) is indicated. Source: Ref 23

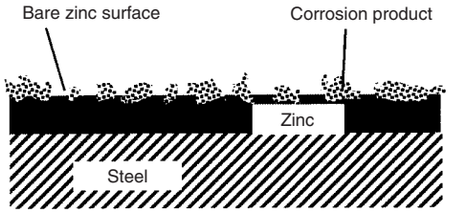

Fig. 8 Schematic illustration of the corrosion mechanism of galvanized steel

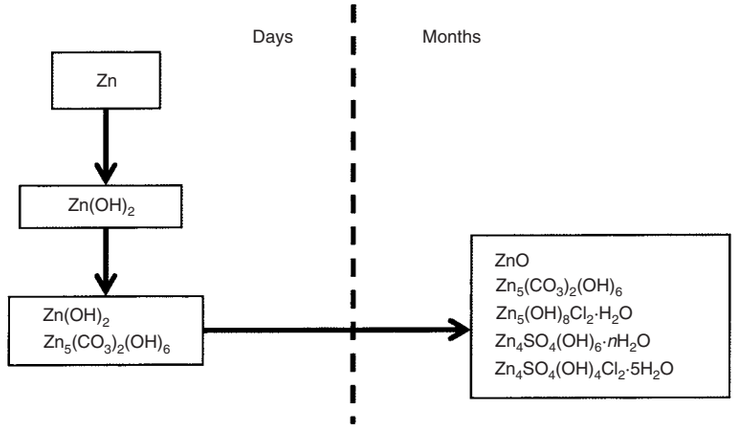

Fig. 10 Sequence of formation of major zinc compounds in the corrosion products formed in different corrosion environments

sulfate compounds can be very rapid, occurring within one day. As corrosion continues, the various zinc compounds generally increase in quantity but may also disappear due to transformation into different compounds, depending on the specific environmental factors. The specific types of compounds and the time needed for their formation depend on the specific conditions of the environment.

Dissolution of Corrosion Products and Zinc Runoff. Corrosion of zinc in the atmosphere proceeds through formation of solid corrosion products to dissolution of the corrosion products. The rainwater that is collected by and runs over a zinc surface plus the dissolved/particulate substances, including zinc, is the runoff. Figure 11 shows the amount of zinc runoff from zinc specimens exposed at an urban site in Stockholm, Sweden (Ref 25). Both corrosion rate and runoff rate decreased with time during the period. However, runoff rate was found to increase from 23% of total corroded metal at the eighth week of exposure to 60% at the 48th week.

In general, the amount of dissolved and particulate zinc in runoff water relative to the amount of corrosion is approximately 30 to 60% during relatively short exposure and 50 to 90% in long exposure (Ref 25, 26). This means that, at an early stage of exposure, most corrosion products are retained on the surface and are carried away as runoff at a later stage, which is in agreement with the two-step corrosion model. The amount of runoff is affected by many environmental factors, such as the amount of rain, intensity, pH, pollutants in the air, and wetting and drying pattern. Thus, the amount of zinc runoff relative to the amount of corrosion will vary significantly with atmospheric environment, as has been reported (Ref 2, 26). It has been found that during one rain episode, zinc concentration in runoff water is initially higher compared to a later stage; it tends to increase with increasing rain acidity but decreases with the intensity of rain. There is also a correlation between the amount of SO_2 in the air and the zinc runoff rate.

Efforts have been made in recent years to improve the understanding of the impact of zinc corrosion products when they enter the environment. The amount of zinc released through corrosion is small compared to the natural presence of zinc, and recent studies have explained the absence of observed effects on the environment.

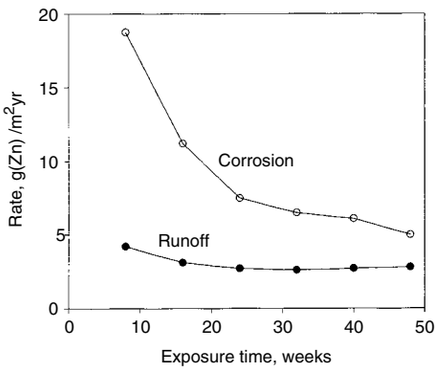

Fig. 11 Zinc runoff rate from samples exposed for 48 weeks at an urban site in Stockholm, Sweden. Source: Ref 25

The fate and potential effects of zinc runoff entering aquatic ecosystems is dependent on many different factors. The uncomplexed or free metal ion of trace metals (e.g., Zn^{2+}) is considered to be the bioavailable form that can result in toxicity. However, it is well known that water chemistry parameters such as pH, dissolved organic carbon, and hardness can all significantly affect (e.g., reduce) the bioavailability/toxicity of metals such as zinc (Ref 27). These environmental factors must be considered in both the immediate runoff water and the receiving water. Only a portion of the zinc in runoff water is in the dissolved/ionic form, and the speciation of the zinc can further change from the major cations and anions, such as calcium, magnesium, sodium, SO_4, and chlorine, that are generally present in runoff water (Ref 28). The water body receiving the runoff will have different water chemistry parameters present (e.g., pH, dissolved organic carbon), affecting the speciation and bioavailability/toxicity of zinc. Also, there typically is a large dilution effect, depending on the volume and/or flow of the receiving water body. Further, runoff traveling even short distances to the receiving water can be altered significantly from changes in partitioning and speciation as it passes over/through different substrates (e.g., concrete, pavement, soil). In conclusion, the site-specific characteristics of the runoff and receiving waters must all be taken into account to determine if any potential impacts may occur to organisms in the aquatic ecosystem in question.

Similar natural processes limit the impact of zinc corrosion products in soils, and studies have shown that soil chemistry parameters can limit and control the bioavailability/toxicity of zinc to plants and invertebrates, even at relatively high concentrations (Ref 29). Further, although elevated concentrations of zinc may build up in soils from a corrosion source after long periods of time, these elevated levels are only found in close proximity (i.e., at or around the base) to the source, thus limiting the exposure to a small and localized area.

Corrosion testing is an essential part of materials development, life prediction, materials selection, and quality control (Ref 30–32). Generally, results from corrosion testing conducted under field conditions are reliable, because they provide direct information regarding the corrosion performance of the tested materials, but field testing is often not practical because of the length of time involved. To shorten the testing time, many corrosion tests run under simulated conditions are used for various materials/application environments. Laboratory corrosion tests are efficient and flexible but give results that are generally difficult to correlate to performance in the field.

Zinc and its alloy coatings are known to be corrosion resistant in a range of natural environments. However, they may not perform well in comparison to other materials in many laboratory accelerated tests, such as the salt spray test. In a systematic investigation of laboratory corrosion tests for zinc-coated steels, the ratio of the corrosion rate of steel to that of zinc has been used as a quantitative measure of relevance of a corrosion test to field performance (Ref 32). It is based on the premise that a relevant test will accelerate corrosion similarly for different materials, such as steel and zinc.

Figure 12 shows the corrosion rates and corrosion rate ratios obtained for a number of different laboratory tests. Clearly, tests 1 to 6 are not relevant tests for atmospheric environments, because the corrosion ratios of steel to zinc in atmospheric environments are higher than 20 (Fig. 2, 3). In particular, it has long been known that test 6, the ASTM standard salt spray test, which gives a ratio of less than 2, is not a relevant test. The use of concentrated salt and the lack of cyclic drying are the main factors causing the differences. This is reasonable because the salt content in the moisture formed under atmospheric conditions is much lower than 5% NaCl, and drying cycles are part of natural exposure in almost all atmospheric environments. On the other hand, test 8, with a low solution concentration of 0.01 *M* NaCl and a 0.5 h drying period after every 0.25 h of spray, is a more relevant test for steel and zinc products, because it generates a corrosion ratio within the range observed in natural environments.

The fundamental reason that corrosion ratios vary with testing conditions is due to the different effects of those conditions on the formation of corrosion products on the two metals. The rust on steel, due to its porous nature, lack of adherence to the surface, and catalytic effect for cathodic reactions, has little protective effect on the steel surface beneath. On the contrary, it may enhance corrosion by acting as a reservoir for water, thus increasing time of wetness, or as a catalyst for oxygen reduction. On the other hand, the corrosion products formed on zinc surfaces in most natural environments are compact and tenacious and thus provide protection to the zinc surface. The compactness and tenacity of zinc corrosion products strongly depend on the environmental conditions. For example, the effect of periodic drying increases the compactness of the corrosion products of zinc but not those of steel and therefore results in a significantly increased corrosion ratio.

Because the corrosiveness of natural corrosion environments is determined by many interacting factors, it is extremely difficult to exactly simulate the conditions of these environments in laboratories. However, it is essential that a relevant corrosion test simulate the most important conditions for a particular corrosion environment. Every corrosion test has a set of conditions to generate specific corrosion phenomena for a specific metal alloy. There is no intrinsically bad test or good test, in a general sense, and every test

can be a good test if it generates results relevant to the specific application conditions. Immersion tests are good tests for corrosion in water or solutions. Continuous salt spray may provide a close simulation of the condition in a spray zone of a seacoast but is not a good test for corrosion in atmospheric environments. For atmospheric environments, dilute salt spray, in addition to cyclic drying, produces more realistic results. Ideally, one needs to have a specific corrosion test for each specific material/application combination. The corrosion ratio of steel to zinc is a simple measurable parameter that is useful for evaluating the relevance of corrosion tests to actual field performance.

Corrosion Rate Prediction. Because the corrosion rate of galvanized steel varies greatly from one geographic location to another, the ability to predict the specific corrosion rate and life of a zinc coating in a given application environment is important for effective application of zinc-coated steels.

Historically, there have been a number of approaches to predicting the life of galvanized steels in atmospheric environments. These include the general value, mapping, ISO CORRAG, regression, and neural network methods. The general value method has been a common method for estimating the life of galvanized steels. Because it uses only four to six values to classify the diverse atmospheric environments rather subjectively, it is no longer adequate in today's marketplace. In the mapping method, corrosion rates of materials in a geographic area are determined and used in the form of maps, notably in the United Kingdom and Australia (Ref 33). Although most reliable, its usefulness is limited to the areas where such mapping is available. The ISO CORRAG method is an environmental corrosivity classification system that was developed by the International Organization for Standardization (Ref 34). Although this method is widely used, it is still a rather approximate estimation, using only five ranges to account for the 2 orders of magnitude in the variation of corrosion rates. In the regression method, mathematical functions are formulated based on the statistical analysis of historical data with respect to certain factors (Ref 35–38). Large uncertainty may be associated, mainly due to the fact that these models use presumed functions, while the real function for atmospheric corrosion is unknown.

Most recently, the neural network method has been used for predicting the corrosion rate of metals. Using neural network methodology, an Internet-based software program, "Zinc Coating Life Predictor," has been developed for prediction of the specific corrosion rate of zinc in an atmospheric environment, based on commonly available weather and air pollution data (Ref 39). This software has been available on the Internet because 2001 from the websites of a number of organizations, including American Galvanizers Association, International Zinc Association, and Teck Cominco Metals Ltd.

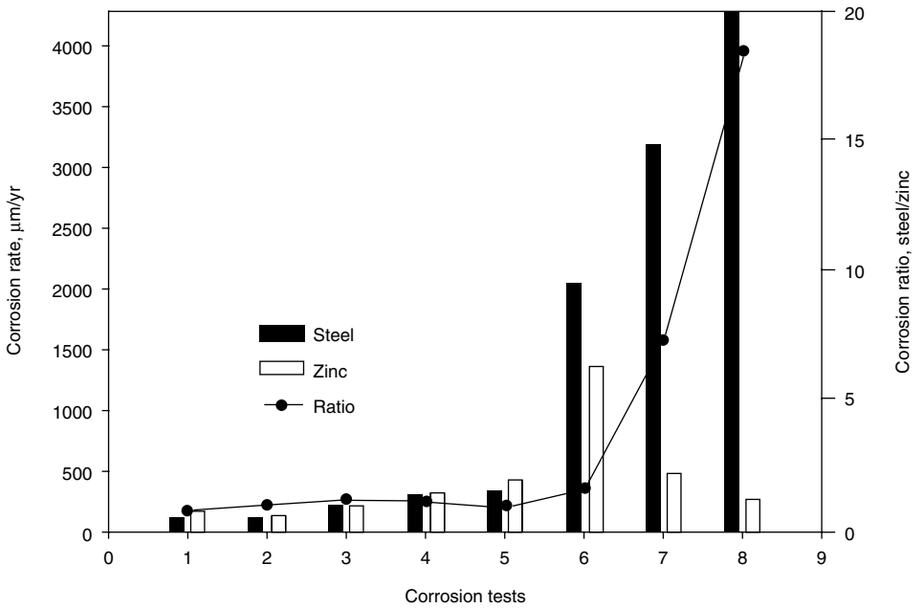

Tests	
Test No.	**Type**
1	Deionized water immersion
2	5% NaCl immersion
3	0.01 *M* NaCl immersion
4	Deionized water spray
5	100% humidity
6	5% NaCl spray
7	0.01 *M* NaCl spray
8	0.25 h spray (0.01 *M* NaCl) + 0.5 h dry

Fig. 12 Corrosion rates of steel and zinc and the corrosion rate ratio between the two materials in different corrosion tests. Source: Ref 32

Corrosion in Waters, Solutions, Soils, and Other Environments

In distilled water at room temperature and open to air, zinc corrodes with the formation of pits. The formation of these pits depends on the oxygen content of the water. When the water is depleted of oxygen, there is little corrosion, and when oxygen pressure is high, the corrosion is of a uniform type.

As shown in Table 5, the corrosion rate in different hard waters can vary significantly. In general, the corrosion rate of zinc is lower in hard water than in soft or distilled water. Flowing water causes more corrosion than still water. The presence of trace amounts of copper in water can substantially increase the corrosion of zinc. As little as 0.1 ppm copper causes a definite increase in the corrosion rate (Ref 40). With concentrations of copper up to 0.3 ppm, the corrosion rate is proportional to the concentration of copper.

The corrosion rate of zinc in seawater is between 20 and 70 µm/yr (0.8 and 2.8 mils/yr), varying with location, length of exposure, and type of zinc. It is generally much higher at the beginning of exposure and decreases with time.

The corrosion processes of zinc in solutions are greatly influenced by the nature of the anions present. Table 6 lists the corrosion rates of zinc in

Table 5 Corrosion rates of zinc and zinc coatings immersed in various types of waters

	Corrosion rate	
Solution	**µm/yr**	**mils/yr**
Mine water, pH 8.3, 110 ppm hardness, aerated	31	1.2
Mine water, 160 ppm hardness, aerated	30	1.18
Mine water, 110 ppm hardness, aerated	46	1.8
Demineralized water	137	5.4
River water, moderately soft	61–97	2.4–3.8
River water, treated by chlorination and copper sulfate	64–81	2.5–3.2
Tapwater, pH 5.6, 170 ppm hardness, aerated	142	5.6
Spray cooling water, chromate treated, aerated	15	0.59
Hard water	16	0.63
Soft water	15	0.59
Seawater in Pacific Ocean	70	2.8
Seawater in Bristol Channel	64	2.5
Seawater at Eastport, ME	28	1.1
Seawater at Kure Beach, NC	28	1.1
Seawater at Panama	21	0.8

Source: Ref 2

solutions of different compositions. The particularly low values in phosphate and chromate solutions are due to the formation of passive films on the zinc surfaces. In neutral solutions, with chemical agents that are not electrochemically reactive and that do not form insoluble salts or complex ions with zinc, the corrosion rate of zinc is not very different from that in distilled water.

In the absence of reducing or passivating agents, the corrosion of zinc in aqueous solutions is determined primarily by the pH of the solutions. The corrosion rate of zinc in water of pH 6 to 12 is relatively low, primarily due to the formation of passive corrosion products on the surface of the zinc (Ref 41). At pH values lower than 6 or higher than 12, the corrosion rate increases substantially. Figure 13 shows the corrosion loss measured for various chemical solutions as a function of pH (Ref 38). The pH dependence of the corrosion rates of zinc in sulfate, chloride, and benzoate is similar to that in water, that is, relatively low in solutions near neutral or slightly alkaline and high in acidic or strong alkaline solutions. In phosphate solutions, corrosion is inhibited between pH 4 to 12, due to the formation of a less soluble and more protective zinc phosphate film. In chromate solutions, the corrosion of zinc is inhibited almost in the entire pH range of 1 to 13, due to the formation of a passive chromate-incorporated chromium/zinc oxide film.

Table 6 Corrosion rates of zinc in different solutions in the neutral pH range

Solution	Duration	Rate of corrosion	
		µm/yr	mils/yr
Distilled water	4 weeks	46	1.8
Distilled water	1 month	55	2.2
0.1 *N* benzoate	4 weeks	59	2.3
0.1 *N* NaCl	4 weeks	62	2.4
0.1 *N* Na_3PO_4	4 weeks	1.8	0.07
0.1 *N* Na_2ClO_4	4 weeks	0.4	0.016
5 g/L NaCl	2 months	90	3.5
5 g/L KCl	2 months	92	3.6
5 g/L $NaNO_3$	6 months	18	0.71
5 g/L K_2SO_4	2 months	52	2.0
8% $Na_2SO_4 \cdot 10H_2O$	1 month	83	3.3
5% NaCl	3 weeks	89	3.5
3% Na_2SO_4	1 day	144	5.7

Source: Ref 2

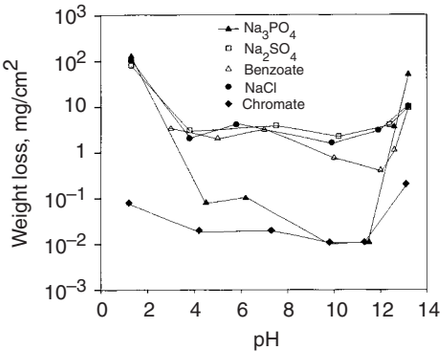

Fig. 13 Effect of pH on weight loss of zinc in 0.1 *N* solutions of different salts for four weeks. Source: Ref 38

Soils. The corrosion rate of zinc varies drastically among the soils, as shown in Table 7, because soils vary in chemical and physical properties. For example, the pH of soil may vary from as low as 2.6 to as high as 10.2, and the electrical resistance from less than 100 Ω to nearly 100 kΩ. Also, because soil is a highly inhomogeneous environment, both microscopically (at the dimension of a clay particle) and macroscopically (at the dimension of a rock), corrosion in soil is seldom uniform across the metal surface.

The factors that may affect the corrosion of zinc and galvanized steel in soils are numerous, but the correlation between the corrosion behavior and the various factors is rather poor. In general, the corrosion rates tend to be lower in soils with very high resistivity. There is little correlation between corrosion rate and soil pH, which is an indication of the very complex nature of soil corrosion (Ref 2). Poorly aerated soils tend to be more corrosive to zinc. Soils of fair to good aeration but containing high concentrations of chlorides and sulfates tend to induce deep pitting. Also, muddy clay and peat (as compared to sand) are, in general, more corrosive to zinc (Ref 42).

Painted products include both coil painted and painted in product forms. These are commonly referred to as a duplex system. Painted galvanized steels, due to superior corrosion performance and versatility in surface finishing, have been widely used in automotive bodies, appliances, wall panels, building roofs, and so on. In particular, the use of painted galvanized steel starting late in the 1980s has greatly improved the corrosion life of automotive bodies and is responsible for the virtual disappearance of rusty cars.

The corrosion process occurring on painted metal is very different from that on unpainted metal. Typically, corrosion of painted metals is characterized as perforation corrosion or cosmetic corrosion. Cosmetic corrosion is an attack that is initiated at the exterior surface, usually at regions where the paint is damaged. Cosmetic corrosion is usually related to red rust, paint creep, and chipping. Corrosion of a painted steel sheet that initiates at an interior surface of a car body panel, penetrates the sheet, and eventually shows through as rust at the exterior exposed surface is known as perforation corrosion (Ref 43). It often occurs at locations that are difficult to clean, phosphate, or coat, such as lapped parts and hem flanges, or at crevices that collect dirt, salt, and moisture.

Cosmetic corrosion is most commonly evaluated by measuring the length of underpaint creeping. It is sometimes evaluated also by the extent of rust formation or paint loss. Many factors, such as coating composition, coating thickness, surface treatment, test condition, type of paint damage, and type of paint, can affect the cosmetic corrosion of painted steels. Data from a field survey have shown that, in general, steel panels coated with zinc or zinc alloy coatings have much slower underpaint creep than cold rolled steel (Ref 44). The creep resistance of zinc- and zinc-alloy-coated steels increases with coating weight.

In general, underpaint corrosion starts at places where the paint is damaged. The process begins with corrosion of the coating or with paint delamination, followed by corrosion of the substrate and, with time, leads to perforation of the steel. For cold rolled steel, the corrosion products built up at the corrosion front may mechanically delaminate the paint. Delamination can occur at

Table 7 Corrosion rates of zinc coatings in soils at different geographic locations in the United States

No. (a)	Soil type	Location	Soil resistance, Ω-cm	pH	Corrosion rate(b)	
					µm/yr	mils/yr
1	Allis silt loam	Cleveland, OH	1215	7.0	11.8	0.46
2	Bell clay	Dallas, TX	684	7.3	1.5	0.059
3	Cecil clay loam	Atlanta, GA	30,000	5.2	1.7	0.067
4	Chester loam	Jenkintown, PA	6670	5.6	7.9	0.31
5	Dublin clay adobe	Oakland, CA	1345	7.0	7.7	0.30
6	Everett gravelly sandy loam	Seattle, WA	45,100	5.9	0.5	0.02
7	Maddox silt loam	Cincinnati, OH	2120	4.4	10.8	0.43
8	Fargo clay loam	Fargo, ND	350	7.6	3.2	0.13
9	Genesee silt loam	Sidney, OH	2820	6.8	5.0	0.20
10	Gloucester sandy loam	Middleboro, MA	7460	6.6	5.2	0.20
11	Hagerstown loam	Loch Raven, MD	11,000	5.3	3.7	0.15
12	Hanford fine sandy loam	Los Angeles, CA	3190	7.1	2.2(c)	0.09(c)
13	Hanford very fine sandy loam	Bakersfield, CA	290	9.5	3.7	0.15
14	Hempstead silt loam	St. Paul, MN	3520	6.2	1.1	0.04
15	Houston black clay	San Antonio, TX	489	7.5	1.5	0.06
16	Kalmia fine sandy loam	Mobile, AL	8290	4.4	4.2	0.17
17	Keyport loam	Alexandria, VA	5980	4.5	14.8(d)	0.58(d)
19	Lindley silt loam	Des Moines, IA	1970	4.6	2.9	0.11
20	Mahoning silt loam	Cleveland, OH	2870	7.5	4.9	0.19

(a) Original identification. (b) Average coating thickness, 121 µm (4.8 mils). (c) Sheet specimens. (d) Coating corroded completely, and the data included the corrosion of steel. Source: Ref 2, 42

different interfaces in a paint-coating-steel system, depending on the material and environmental conditions. The causes of the delamination at the corrosion front can be physical, anodic, cathodic, mechanical, or combinations thereof. The predominant cause in a specific corrosion situation can be due to variations in paints, coatings, phosphates, and test conditions (Ref 43–45).

Concrete. The use of galvanized steel rebar as concrete reinforcement has been one of the remedies to alleviate the corrosion problems of steel rebar in concrete caused by water and chloride permeation into the concrete (Ref 2). When galvanized steel is covered with a good-quality concrete free of chloride, the corrosion rate is very low (Ref 46). The corrosion rate is higher when concrete contains a high level of chloride salts. According to a field investigation on galvanized steel-reinforced concrete structures in different marine locations, the corrosion rates of galvanized rebar are, in most cases, at or below 0.5 μm/yr (0.02 mil/yr) (Table 8).

There are large amounts of data in the published literature on the corrosion performance of galvanized rebar in concrete (Ref 2). Most of these data are from laboratory-simulated testing environments. The data from natural exposure tests, the only reliable information for predicting the life of galvanized reinforced concrete structures, are rather limited. Particularly, there is a lack of conclusive data from heavy deicing salt environments in which protection of reinforced steel is most needed. The available field data generally suggest that galvanized steel reinforcement provides longer life compared to black steel, which is not always in agreement with the data from studies using simulated test conditions (Ref 47).

Organic Solvents. Reactivity of metals in organic solvents depends on the type and structure of the organic compound. Figure 14 shows that the corrosion rate varies greatly with the type of solvents (Ref 48). It also shows that the corrosion rate (slope of curves) of zinc is much higher in some solvents while much lower in others than that in water. Table 9 and Fig. 14 show that the corrosion rate of zinc is higher in methanol than in ethanol (Ref 49). The addition of formic acid, sodium formate, acetic acid, and sodium acetate results in an increase in the corrosion rate. Formic acid causes more corrosion than acetic acid, due to the higher acid strength of formic acid.

Viscosity is a major factor in determining the corrosion rate of zinc in organic solvents containing small amounts of acid (Ref 48). The corrosion processes in solvents containing small amounts of contaminants are usually diffusion controlled due to the fact that viscosity determines the diffusion coefficient. This explains why the corrosion rate for zinc in primary alcohols containing 0.01 *M* HCl decreases with increasing chain length of the alcohol. Corrosion rate does not appear to be a direct function of the solubility of zinc in solvents. Additionally, neither the dissociation level of the dissolved acid nor the electrolytic conductivity has been found to have a predominant effect on the corrosion rate.

Gaseous environment corrosion is governed by principles similar to those for atmospheric corrosion but has its own special features (Ref 40). As in normal atmospheres, the amount of moisture plays an important role in gaseous corrosion. Depending on the kinds of gases and their concentrations, the critical RH required for corrosion may vary. Also, depending on whether an electrolyte is formed, the corrosion can be of an electrochemical or chemical nature. Dry air has little effect on zinc at room temperatures, but oxidation occurs rapidly above 200 °C (390 °F) (Ref 1).

In hydrogen sulfide gas, the corrosion rate of zinc compared to other common metal alloys is low. The corrosion rate of zinc in a moving mixture of SO_2, water vapor, and air is rather high but reduces with exposure (Ref 50, 51). When zinc is enclosed with other materials that may release vapors in the enclosure, direct contact with these materials causes more corrosion than merely being exposed in the vapor released by these materials (Ref 52). The corrosion rate of galvanized steel over sealed aqueous solutions of several organic acids is much higher than that over water (Ref 53). Table 10 shows the corrosion rates of zinc in a sealed chamber containing different woods at 35 °C (95 °F). The corrosivity of wood is due to the production of acetic acid and, in lesser amounts, formic acid (Ref 52).

Table 8 Average corrosion rate of zinc coatings on galvanized steel rebar inside concrete in marine environments

Structure	Age, yr	Cover		Sample Cl^- location(a)	Corrosion loss			
		cm	in.		wt%	kg/m^3	μm/yr	mils/yr
Longbird Bridge	23	10	4	Above HT	0.19	4.4	0.2	0.008
St. George Dock	12	8	3	Above HT	0.27	6.4	1.1	0.04
	10	6	2.4	Above HT	0.22	4.6	0.5	0.02
	7	13	5	Above HT	0.14	3.0	0.29	0.01
Hamilton Dock	10	5	2.0	Near MT	0.08	1.9	0.5	0.02
	10	6	2.4	Above HT	0.14	3.6	0.8	0.03
Bermuda Yacht Club	8	7	2.8	Below HT	0.16	3.7	0.0	0.0

(a) HT, high tide; MT, mean tide. Source: Ref 46

Corrosion Forms

Metallic corrosion has different forms or mechanisms (general corrosion, galvanic corrosion, pitting corrosion, stress-corrosion cracking, intergranular corrosion). The most common form of corrosion encountered by zinc and its alloys is general (uniform) corrosion. Pitting corrosion and intergranular corrosion are less common for zinc and its alloys; they may occur under certain specific conditions. Stress-corrosion cracking is generally not encountered by zinc products that are normally used for non-structural applications. Wet-storage stain is a common concern in the galvanizing industry and is a type of general corrosion. The corrosion forms that are encountered in zinc coatings are described as follows.

Galvanic action is a particularly important process for applications of zinc and zinc alloys, whether as a coating, an anode, or a zinc-dust paint. In most situations, unlike many other metals, the corrosion of zinc due to galvanic action is desirable, because it results in protection of the coupled metal, usually steel. The unique role of zinc in galvanic protection is mainly due to its low position in the galvanic series. Because of its relatively low self-corrosion rate and lack of full passivation in many common environments, it is also an efficient sacrificial anode for protection of steel structures in many situations.

Galvanic Series and Polarity. When two dissimilar metals in electrical contact with each other are exposed to an electrolyte, a galvanic

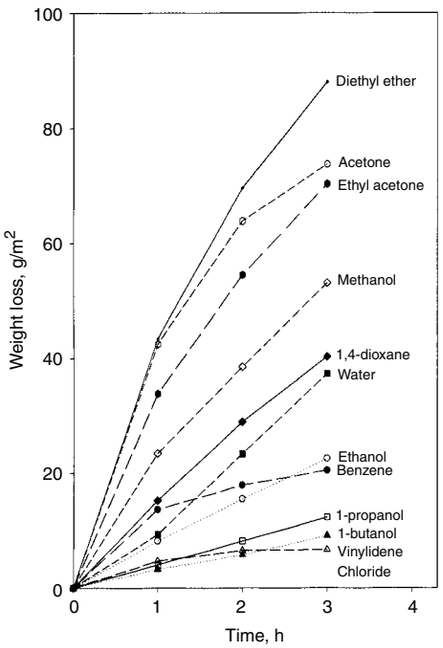

Fig. 14 Zinc corrosion in various organic solvents containing 0.05 mol/L HCl compared to water. Source: Ref 48

Table 9 Corrosion of zinc in the presence of different solvents, gases, and contaminants at room temperature

Contaminant, mol/L	Corrosion rate(a), g/m²h								
	H_2O			CH_3OH			C_2H_5OH		
	N_2	O_2	Air	N_2	O_2	Air	N_2	O_2	Air
0	...	...	0.09	0.01	0	0	0	0	0
50 ppm Cl^-	0.01	0.18	...	0.14	0.01	0	0	...	...
CH_3COONa									
0.1	0.02	...	...	0.38	0.67	...	0.03	0.03	...
CH_3COOH									
0.1	1.29	...	...	4.2	7.0	11.7	0.17	2.8	3.51
0.05	...	...	0.87	3.93	...	1.06	2.8	...	...
0.01	...	...	...	0.62	0.28	0.43	0.62	...	...
0.005	...	...	...	...	0.16	0.21	0.29	...	...
0.001	...	...	...	...	0.13	0.03	0.02	...	...
HCOONa									
0.1	...	...	...	0.46	0.3	...	0.01	0	...
HCOOH									
0.1	...	...	...	3.9	5.5	9.7	0.17	0.08	0.13
0.05	...	...	...	...	0.24	...	...	...	...
0.01	...	...	...	...	0.20	...	...	...	...
0.005	...	...	...	...	...	0.29	...	...	...
0.001	...	...	...	...	0.07	...	...	...	...

(a) 0 corresponds to weight loss rates < 0.01 g/m²h. Corrosion rates in g/m²h nearly correspond to mm/yr. Source: Ref 49

Table 10 Corrosion losses of iron and zinc enclosed with wood at 35 °C (95 °F) for 32 days

Wood(a)	Relative humidity, %	Corrosion loss			
		Iron		Zinc	
		µm	mils	µm	mils
Oak	100	10.57	0.42	15.42	0.61
	84	1.37	0.05	10.47	0.41
Beech	100	3.02	0.12	3.00	0.12
	84	0.53	0.02	4.33	0.17
Ash	100	3.16	0.12	3.00	0.12
	84	0.53	0.02	4.33	0.17
Maple	100	1.04	0.04	1.53	0.06
	84	0.48	0.02	4.22	0.17
Spruce	100	0.58	0.02	0.40	0.02
	84	0.03	0.001	0.46	0.02
Poplar	100	1.12	0.04	5.20	0.20
	84	0.07	0.003	6.37	0.25

(a) Veneer. Source: Ref 52

current flows from one to the other. Galvanic corrosion is that part of the corrosion that occurs to the anodic member of such a couple and is directly related to the galvanic current by Faraday's law. The polarity and direction of galvanic current flow between two connected bare metals is determined by the thermodynamic reversible potentials of the metals. The metal that has the higher or more positive reversible potential in the electromotive force series is the cathode in the galvanic couple. In real situations, owing to the formation of a surface oxide or a salt film on the surface, or owing to differences in the local electrolytes around the two coupled metals, the polarity may be different from that predicted by the electromotive series. A metal surface can exhibit different potentials in different electrolytes, as shown in Fig. 15. Thus, a galvanic series is environment-specific because the relative position of each metal changes with solution. A galvanic series of some commercial metals and alloys in seawater is found in the article "Corrosion of Zirconium and Zirconium Alloys" in this Volume.

Materials Factors. The extent of galvanic corrosion of a metal does not, in general, correlate with the potential difference between the coupled metal alloys (Ref 54). Table 11 shows that, although the potential difference between steel and zinc is much less than that between stainless steel and zinc and between Ti-6Al-4V and zinc, the amount of galvanic corrosion is much larger in the zinc/steel couple than in the other two couples (Ref 55, 56). This indicates that the difference in corrosion potentials for uncoupled metals is not a reliable indicator of the extent of galvanic corrosion. As indicated by Table 11, zinc corrosion is greater when zinc is coupled with 4130 steel than with copper, although the potential difference between zinc and steel is smaller than that between zinc and copper. In these situations, other factors, such as reaction kinetics and formation of corrosion products, are the rate-determining factors in the galvanic corrosion.

The addition of alloying elements to zinc changes its electrochemical properties, such as electrode potential, dissolution kinetics, oxygen and hydrogen reduction overpotentials, and formation of solid-surface films (Ref 54, 57). In general, the additions of small amounts of alloying elements cause little change to the corrosion potential of zinc. With the additions of alloying elements to approximately 10%, the potential of the zinc alloy may change by 50 to 100 mV, usually to a more noble value than pure zinc (Table 12).

The corrosion potential of an alloy in an electrolyte is a function of time. It tends to change to more positive values with the length of immersion time because, in most cases, the preferential dissolution of zinc causes an enrichment of the more noble elements on the surface. The polarization behavior of zinc can also be significantly affected by alloying. High polarization resistance is normally not desirable for zinc when it is used for galvanic protection of steel, because a large polarization of the zinc anode reduces the amount of current available for the polarization of steel.

The effect of anode and cathode areas on galvanic corrosion depends on the type of control over the system. If the galvanic system is under cathodic control, variation in the area of the anode will have little effect on the total amount of corrosion, but variation of the cathodic area will significantly change the corrosion rate.

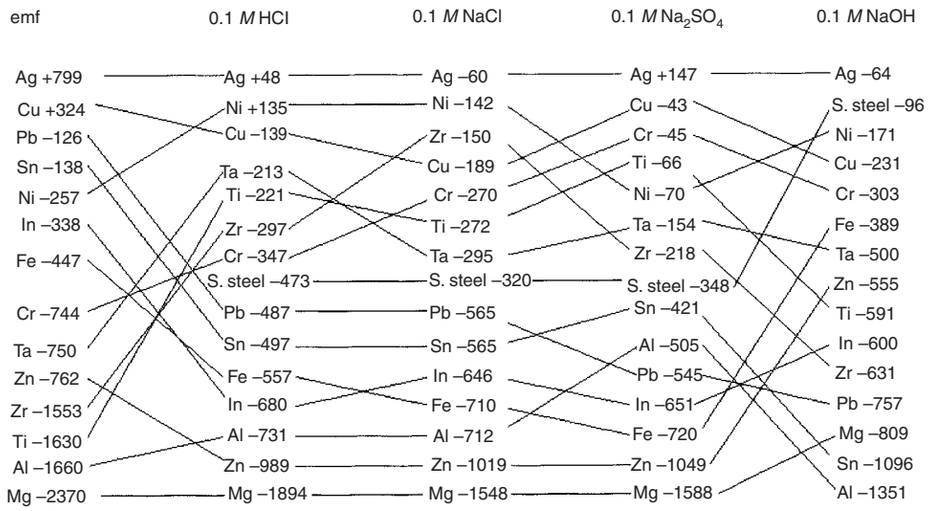

Fig. 15 Corrosion potentials (mV_{SCE}) of metals after 24 h immersion in four solutions, compared with the electromotive force series. Sample surface area approximately 1 cm² (0.16 in.²) polished with 600-grade emery paper, solutions open to air at room temperature. Source: Ref 54

The opposite occurs if the system is under anodic control.

Environmental Factors and Polarity Reversal. Galvanic action of a bimetallic couple depends on the surface condition of the metals, which, in turn, is determined by environmental conditions. A metal surface exhibits different potentials in different electrolytes (Fig. 15). A galvanic series is environment-specific because the relative position of each metal changes with solution.

The conductivity of the electrolyte is a very important factor, because it determines the distribution of galvanic corrosion across the anode surface. When conductivity is high, as in seawater, the galvanic corrosion of the anodic metal is distributed uniformly across the surface. As the conductivity decreases, galvanic corrosion becomes concentrated in a narrow region near the junction. The total galvanic corrosion is usually less in a poorly conductive electrolyte than in a highly conductive one.

The physical position of a galvanic couple in solution can also affect the galvanic action between coupled metals (Ref 58, 59). One important solution factor is the thickness of thin-layer electrolytes that are encountered in atmospheric environments. The thickness of an electrolyte affects corrosion processes in several different ways. First, it affects the lateral resistance of the electrolyte and thus affects the potential and current distribution across the surface of the coupled metals. Secondly, it affects the transport rate of oxygen across the electrolyte layer and thus the rate of cathodic reaction. Thirdly, it changes the volume of the electrolyte and the solvation capacity of the electrolyte and thus affects the formation of corrosion products.

Formation of a surface film, whether a salt film or an oxide film, may not only affect the rate of galvanic corrosion but may also affect the polarity of the galvanic couple. The corrosion products formed on the zinc surface, in the pH range of 9 to 13, have varying degrees of compactness and can result in passivation of the zinc surface (Ref 60, 61). The presence of certain ionic species, such as carbonate, phosphate, and chromate, can enhance the formation of a passive film in a broader pH range (Ref 38). As a result of passivation, the potential of zinc can shift to more positive values and thus change its galvanic behavior when coupled with another metal. Typically, if a stable and compact zinc oxide is formed, the zinc electrode may show a potential more noble than -0.5 V_{SCE}.

When the potential of zinc rises to such a value, polarity reversal of galvanized steel can occur. It commonly occurs in hot water and diluted solutions but does not occur in distilled water up to 65 °C (150 °F). Also, without the presence of oxygen, it does not occur in hot water (Ref 2).

The presence of certain ionic species is often responsible for the reversal. In hot water containing oxygen, sulfates and chlorides decrease, whereas bicarbonates and nitrates increase the probability of reversal. In the absence of oxygen, zinc is always found to be anodic to the steel. Additions of even small amounts (up to 20 ppm) of calcium salts or silicates can also decrease the probability of reversals. The pH of the solutions in which reversal occurs is usually slightly basic.

Polarity reversal observed in hot water and solutions is primarily due to the ennoblement of zinc, because the potential of the steel is relatively unaffected by changes in the temperature. In general, the enoblement of zinc:

- Only occurs in certain waters and solutions; it occurs readily in the presence of bicarbonate and less readily, or not at all, in the presence of chloride or sulfate.
- Requires oxygen
- Increases with increasing temperature for a given solution

Atmospheric and Soil Environments. Galvanic corrosion of galvanized steel occurs in areas where the coating is damaged and the steel beneath is exposed, such as at cuts or scratches. At these areas, the exposed steel is cathodically protected, while the surrounding zinc coating is galvanically corroded. However, in most cases for galvanized steel, the amount of coating loss due to galvanic corrosion, compared to normal corrosion, is small, because the exposed areas of bare steel are usually too small to cause significant corrosion of the relatively much larger zinc surface area. As a result, the atmospheric corrosion rate of galvanized zinc coatings, including galvanic and normal corrosion, is usually very similar to that of uncoupled zinc.

Galvanic corrosion can, however, be a significant contributor to the total corrosion of zinc in atmospheres when it is connected to other metals of similar size. Data in Table 13 show the galvanic corrosion rate of zinc wires when coupled to bolts of various metals in different atmospheres (Ref 56). Depending on the connected metal and the type of atmosphere, the galvanic corrosion can be as much as five times the normal corrosion of zinc in a rural atmosphere and three times that in a marine atmosphere (Ref 62, 63).

Table 11 Galvanic corrosion rate of zinc coupled with various alloys

Tested in 3.5% NaCl solution for 24 h

	Corrosion rate(a)				
	A		B		
Coupled alloy	μm/yr	mils/yr	μm/yr	mils/yr	ΔV(b), mV
Zinc	0	0	101	3.98	0
Stainless steel 304	244	9.61	705	27.8	905
Nickel	990	39.0	1390	54.8	817
Copper	1065	41.9	1450	57.1	811
Ti-6Al-4V	315	12.4	815	32.1	729
Tin	320	12.6	810	31.9	435
4130 steel	1060	41.7	1550	61.1	483
Cadmium	600	23.6	660	26.0	258

(a) A, measured as galvanic current; B, measured as weight loss. (b) Potential difference between zinc and the coupled metal before testing. Samples of zinc and coupled alloys were of equal size, 20 cm^2 (3.1 $in.^2$). Source: Ref 55

Table 12 Corrosion potential of zinc alloys in solutions

Alloy	Solution	E_{SCE}, V
Steel	NaCl, Na_2SO_4	−0.55 to −0.65
Zinc	NaCl, Na_2SO_4	−1.00 to −1.10
5% Al	3% NaCl	−1.04 to −1.07
55% Al	1 *N* Nacl	−0.99 to −1.05
10% Fe	0.1 *M* NaCl	−0.97 to −0.95
25% Fe	0.1 *M* NaCl	−0.95
50% Fe	0.1 *M* NaCl	−0.72
25% Mn	3% NaCl	−1.05
10% Cr	5% NaCl	−0.95
10% Ti	5% NaCl	−1.00
10% Mg	5% NaCl	−1.10
10% Ni	5% NaCl	−0.90 to −1.00
20% Ni	3.5% NaCl	−0.7
10% Cu	3.5% NaCl	−0.85 to −1.02
40% Cu	3.5% NaCl	−0.4
10% Co	5% NaCl	−1.02

Source: Ref 2

Table 13 Galvanic corrosion rate of zinc coupled with other common metals in different atmospheres

	Corrosion rate					
	Rural		Urban		Marine	
Coupled alloy	μm/yr	mils/yr	μm/yr	mils/yr	μm/yr	mils/yr
Zinc freely exposed	0.5	0.02	2.4	0.09	1.3	0.05
Mild steel	3.0	0.12	3.3	0.13	3.9	0.15
Stainless steel	1.1	0.04	1.8	0.07	2.0	0.08
Copper	2.2	0.09	2.0	0.08	3.2	0.13
Lead	1.6	0.06	2.4	0.09	3.4	0.13
Nickel	1.5	0.06	1.9	0.07	2.8	0.11
Aluminum	0.4	0.02	1.1	0.04	1.1	0.04
Anodized aluminum	0.9	0.04	1.9	0.07	1.0	0.04
Tin	1.0	0.04	2.6	0.10	2.4	0.09
Chromium	0.7	0.03	1.4	0.06	1.9	0.07
Magnesium	0.02	0.0008	0.04	0.002	1.1	0.04

Source: Ref 56

Galvanic action is most significant in marine atmospheres because of the high conductivity of seawater. In a marine atmosphere, the galvanic corrosion rate of zinc is found to increase at the beginning of exposure and then remain at a relatively constant value. Rain, compared to other types of moisture, is particularly effective in causing galvanic corrosion. It has been found that the galvanic corrosion rate is several times that of normal corrosion rates in an open exposure, while they are similar when under a rain shelter, due to the fact that the electrolyte layer formed by rain is thicker and has a smaller lateral electric resistance.

There are many sources in soils that can affect the electrochemical behavior of metal alloys and therefore the galvanic actions between the alloys. The zinc electrode potential can vary hundreds of millivolts, depending on the type of soil (Ref 42). It has been reported in a study by the National Bureau of Standards (now the National Institute of Standards and Technology) that the amount of galvanic corrosion of zinc generally increased with decreasing soil resistivity. However, the degree of galvanic protection for steel is lower in a soil of higher resistivity.

Galvanic Protection of Steel. The galvanic corrosion of zinc generally results in galvanic protection of the coupled alloy. It was reported that galvanic action reduced the corrosion of steel by 40 times in industrial, 230 times in humid industrial, and 300 times in seacoast industrial atmospheres using discs of zinc and steel clamped together, exposing an annular area of each metal. The reduction was only approximately three times in rural atmospheres, largely due to the relatively non-conductive nature of the moisture.

The protection distance (PD) or throwing power of galvanic action, as illustrated in Fig. 7, is the width of the steel between the steel edge next to the zinc and the line of critical potential value, below which the steel is considered to be cathodically protected (Ref 23). The NACE International criterion for cathodic protection of steel is -780 mV_{SCE}) (Ref 64).

Figure 16 shows the PD values determined for galvanic samples with zero separation distance under various environmental conditions. The data indicate that PD varies greatly with corrosion environments. The PD, based on color examination of samples tested under exposure in 100% RH, was close to zero, because the steel surface was almost fully covered with red rust. The very small value of PD was due to the extremely high resistance of the very thin moisture layer formed on the surface under the humid condition. A large PD, approximately 5 mm (0.2 in.), was observed under a full immersion test in deionized water. The immersion condition, although in high-resistivity water, provided considerable galvanic action between the two metals.

The PD increased from 0.2 mm (8 mils) under a cyclic spray with deionized water to 0.6 mm (24 mils) with tapwater, indicating the effect of increased conductivity of the spraying solution. The PD was 1.6 mm (63 mils) under the 5% salt spray and 1.3 mm (51 mils) under 0.001 *M* Na_2SO_4 spray. The fact that the PD value obtained under 5% salt spray was only slightly larger than that under the much less conductive 0.001 *M* Na_2SO_4 spray may indicate a much larger galvanic current in the 5% salt solution.

The surface activity of zinc plays an important role in determining galvanic action. This is shown in Fig. 17, which is the result of theoretical modeling (Ref 65). When the activity of a zinc surface is very low, such as at a passive surface, PD is practically zero; the entire exposed steel surface is not protected. As zinc surface activity increases to a certain value, PD starts to increase with increasing surface activity. On the other hand, galvanic current increases with the increasing surface activity of zinc. Unlike PD, it does not level off at a high zinc surface activity.

For a given environmental condition, there is a given range of zinc surface activity within which the exposed steel surface is protected effectively (with a relatively large PD and moderate galvanic current). This explains the fact that there is no galvanic protection for an exposed steel surface when the zinc surface is in a passive condition, as may occur in some hot waters.

The data in Fig. 17 can also be used to explain the differences in galvanic properties between varied commercial zinc-aluminum-alloy-coated sheet products. Under normal environmental conditions, the surface activity decreases from galvanized to Galfan to Galvalume to aluminum-coated steel, as qualitatively marked by the arrows in Fig. 17. There are significant differences in PD and galvanic current for these materials. On one end, the pure zinc coating (galvanized steel) has the largest PD and galvanic corrosion rate of the coating. On the other end, aluminum-coated steel has the lowest PD and corrosion rate. This is why zinc-coated steel, due to its large PD, is widely used in atmospheric environments and aluminum-coated steel is not, because, having insignificant PD, it offers very little galvanic protection. Galfan and Galvalume have surface activity and thus galvanic properties between that of zinc and aluminum and are used in situations where high corrosion resistance and moderate galvanic protection are preferred.

Sacrificial Anode. Zinc is a common material for making sacrificial anodes. Historically, zinc anodes have been used mostly in seawater applications. They are also used for the cathodic protection of hot water tanks, fuel storage tanks, concrete rebar, and underground steel structures. Anodes can be designed according to composition, shape, size, and position for specific applications.

When zinc is used as an anode material in an electrolyte of low resistivity, compared to other anode materials such as aluminum and magnesium, it has the advantages of high efficiency and little hydrogen evolution. Owing to the small self-corrosion rate in most natural environments, the zinc anode has a high galvanic efficiency, 95 to almost 100%, because zinc suspended in seawater or buried in the ground does not corrode rapidly by self-corrosion. Another advantage of zinc as an anode material is its generally low overpotential for anodic dissolution. Because the overpotential on the anode is low, most of the potential difference between zinc and steel is available to polarize the steel. In some situations, the smaller potential difference between zinc and steel, compared to aluminum and magnesium, has the advantage of not causing overprotection, which would cause hydrogen evolution on the steel and a high anode consumption rate (Ref 2).

When a zinc anode is employed in the cathodic protection of a steel ship hull in seawater, an empirical rule is to employ one unit of zinc anode area for 100 units of surface area of a painted steel hull, and one to five units for bare surface area. According to such a rule, the zinc anode consumption rate is approximately 0.5 to 1.0 kg/yr per square meter (0.1 to 0.2 lb/yr per square foot) of painted steel surface. The presence of iron in a zinc anode, even in very small amounts, for example, 0.001%, is harmful to the performance of the anode. The presence of iron causes a reduction of current output and ennoblement of the anode potential due to the formation of an insulating dissolution product film on the surface of the anode. The addition of aluminum can reduce the effect of iron in the zinc anode.

Zinc-Rich Paint. Steels can also be protected by zinc-rich paints, in which the zinc dust not only serves as a binder material but also provides some galvanic protection to the painted steel (Ref 2). For zinc-rich coatings, three conditions

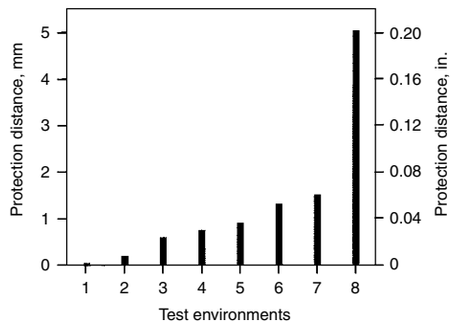

Tests	
Test No.	**Type**
1	100% relative humidity + dry
2	Deionized water spray + 100% relative humidity + dry
3	Tapwater spray
4	Atmospheric exposure
5	Tapwater spray + 100% relative humidity + dry
6	0.001 *M* Na_2SO_4 spray + 100% relative humidity + dry
7	Salt spray test
8	Deionized water immersion

Fig. 16 Protection distance of a planar steel/zinc galvanic couple under various environmental conditions. Source: Ref 23

must be satisfied for the galvanic process to occur:

- The zinc particles in the coating must be in electrical contact with each other.
- The zinc particles must be in electrical contact with the steel.
- A continuous electrolyte must exist between the zinc particles and the steel.

These conditions imply that the galvanic protection of steel by zinc-rich coatings improves with increasing amounts of zinc. Thus, high zinc contents, higher than 70%, are needed for good galvanic protection of steel. Galvanic action of the zinc dust is usually effective in the early stage, because the oxidized zinc particles cause a gradual loss of the electrical continuity between the dust particles in the interior of the paint and the steel. However, the transformation of the zinc particles from metallic form to oxide form exerts a sealing effect on the paint and adds more resistance to the permeation of aggressive agents from the environment.

Pitting is not a common form of corrosion in zinc applications (Ref 2). In atmospheric environments, pitting corrosion has seldom been reported as the main cause of failure of zinc products. In soil, pitting may result from the nonuniform nature of corrosion in this environment, and the extent varies significantly, depending on the chemical composition and texture of the soil (Ref 42). Pitting may occur in distilled water under an immersed condition.

Pitting is a rather common form of corrosion for zinc in hot water and can be a serious problem for galvanized steel hot water tanks. In hot soft water, pitting corrosion is likely to lead to rapid penetration of galvanized coatings because of the reversal of polarity for zinc/steel galvanic couples in hot water. In hot hard water, the corrosion is likely to be stifled by the deposition of a protective scale, depending on the heating method. The presence of copper in the water was found to enhance the pitting corrosion of galvanized coatings in hot water (Ref 40).

Intergranular corrosion has been observed to occur on zinc alloys in different environments: atmosphere, water, solution, and concrete. Zinc of high purity is not susceptible to intergranular corrosion (Ref 66). The presence of other elements, particularly aluminum, as alloying elements or impurities is necessary to cause intergranular corrosion. Table 14 shows the intergranular corrosion rates of zinc-aluminum alloys of different compositions in steam or hot water. Intergranular corrosion is observed to occur in a concentration range between 0.03 and 50% Al and is most severe at approximately 0.2% Al, as shown in Fig. 18. When aluminum concentration is higher than 0.03%, the aluminum precipitates at the grain boundaries and is responsible for the increased corrosion rate at the grain boundaries. Below 0.03% Al, intergranular corrosion does not occur. For zinc alloys containing an aluminum concentration higher than 0.03%, the aluminum precipitates at the grain boundaries and is responsible for the increased corrosion rate at the grain boundaries.

The presence of impurities is not required for the occurrence of intergranular corrosion on zinc-aluminum alloys. However, the presence of other metal impurities can greatly influence the intergranular corrosion rate of zinc-aluminum alloys. More specifically, according to the experimental results, magnesium, copper, gold, nickel, platinum, and cobalt are beneficial, while tin, thallium, indium, lead, bismuth, mercury, cadmium, and sodium are harmful (Ref 66). Molybdenum, zirconium, titanium, barium, silicon, beryllium, tellurium, lithium, antimony, and silver are found to have little effect. Table 15 shows the effects of some harmful elements on the intergranular corrosion of Zn-0.1Al alloy exposed to 95 °C (205 °F) water vapor.

Heat treatment generally affects intergranular corrosion, because it influences the amount of grain boundaries and the extent of grain-boundary segregation. Stress, particularly tensile stress, can also affect intergranular corrosion. Temperature is the most significant of the environmental factors. Alkaline environments

Table 14 Intergranular penetration rates of some zinc alloys in different environments

% Al	Environment	Duration, day	Rate	
			mm/day	mils/day
0.075	95 °C (205 °F) water vapor	10	0.02	0.8
0.1	95 °C (205 °F) water vapor	10	0.018	0.7
4	95 °C (205 °F) water vapor	10	0.033	1.3
20	95 °C (205 °F) water vapor	10	0.028	1.1
21.1	100% RH at 50 °C (120 °F)	42	0.002	0.08
0.1	95 °C (205 °F) tapwater	...	0.1	3.9

RH, relative humidity. Zinc purity, 99.99%. Source: Ref 2, 66

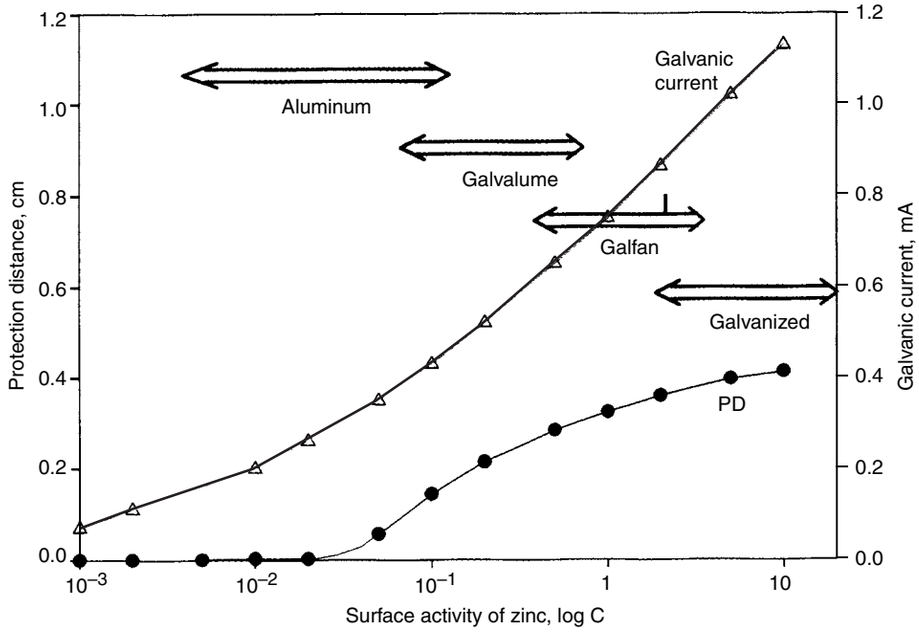

Fig. 17 Results from theoretic modeling on protection distance (PD) and galvanic current as a function of surface activity of zinc. The length of the arrows in the figure illustrates qualitatively the possible variation of surface activity of these different materials that may be involved in normal applications.

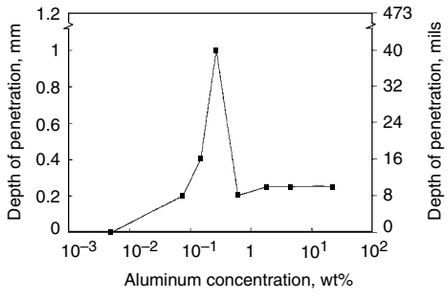

Fig. 18 Average depth of intergranular corrosion penetration of zinc-aluminum alloys as a function of aluminum concentration in water vapor at 95 °C (205 °F) for ten days. Source: Ref 64

Table 15 The increase of grain-boundary corrosion rate in a Zn-0.1Al alloy with addition of 0.01 at.% of harmful impurity elements to the alloy

Impurity element	Increase in corrosion rate, %
Tin	400
Lead	300
Bismuth	260
Cadmium	250
Mercury	50
Thallium	50

Source: Ref 66

are also the most aggressive in intergranular corrosion of zinc-aluminum alloys (Ref 66). Between pH 5 and 10, the corrosion penetration rate is almost constant. Below pH 5, it decreases with decreasing pH. At pH values above 10, it increases drastically with increasing pH.

As a result of intergranular corrosion, the strength of zinc alloys can be drastically reduced. It has been reported, for example, that for an alloy containing more than 0.05% Al after ten days of exposure in 95 °C (205 °F) water vapor, there is practically no mechanical strength left.

Wet-storage stain is a term used to describe the zinc corrosion products formed on galvanized steel surfaces during periods of storage and transportation. It is voluminous, white, powdery, and bulky and is formed when closely packed galvanized articles are stored under damp and poorly ventilated conditions.

White corrosion products may have a wide range of appearances and morphology, as shown in Fig. 9. The crevices formed between the articles can attract and absorb moisture and retain the wetness more readily than the surface area exposed to the open air. The nonprotective characteristic of such a corrosion product can be described with the mechanistic model illustrated in Fig. 8.

The moisture necessary for the formation of wet-storage stain originates in various ways. It may result from direct exposure to rain or seawater or from condensation caused by atmospheric temperature changes. Close packing can result in moisture being retained by capillary action between the surfaces in contact, because drying is delayed by the lack of circulating air. Under sustained wetting, a fluffy white rust is formed. Due to this loose nature, it has little barrier effect on the access of solution to the zinc metal and also prolongs the time of wetness.

Wet-storage stain discolors the galvanized steel surface and, in some situations, can seriously affect the appearance of the galvanized steel articles. However, it is generally not harmful to the long-term corrosion performance (Ref 67). Wet-storage stain can be prevented by properly stacking and storing galvanized products under dry and ventilated conditions. In addition, surface treatments can be applied to freshly galvanized articles to enhance corrosion resistance. Among surface treatment processes, chromating has been most widely used in the galvanizing industry as an effective surface treatment to prevent wet-storage stain from forming during storage or transportation. Due to environmental concerns, chromium-free surface treatment processes have been developed to replace the chromating process (Ref 10, 11).

REFERENCES

1. International Zinc Association, www.iza.com, accessed Feb 2005
2. X.G. Zhang, *Corrosion and Electrochemistry of Zinc,* Plenum, 1996
3. "Zinc Health," website sponsored by the International Zinc Association, www.zinc-health.org, accessed Feb 2005
4. H.E. Townsend, Continuous Hot Dip Coatings, *Surface Engineering,* Vol 5, *ASM Handbook,* ASM International, 1994, p 339–348
5. D. Wetzel, Batch Hot Dip Galvanized Coatings, *Surface Engineering,* Vol 5, *ASM Handbook,* ASM International, 1994, p 360–371
6. T. Tsujimura, A. Komatsu, and A. Andoh, Influence of Mg Content in Coating Layer and Coating Structure on Corrosion Resistance of Hot-Dip Zn-Al-Mg Alloy Coated Steel Sheet, *Proceedings of Galvatech '01* (Brussels, Belgium), 2001, p 145
7. S. Tanaka, K. Honda, A. Takahashi, Y. Morimoto, M. Kurosaki, H. Shindou, K. Nishimura, and M. Sugiyama, The Performance of Zn-Al-Mg-Si Hot-Dip Galvanized Steel Sheet, *Proceedings of Galvatech '01* (Brussels, Belgium), 2001, p 153
8. H. Nomura, Y. Kimata, and H. Kanai, Corrosion Resistance of Prepainted Zn-11%Al-3%Mg-0.2Si Coated Steel Sheet, *Proceedings of Galvatech '04* (Chicago, IL), Assoc. for Iron and Steel Technology, 2004, p 763
9. P.L. Hagans and C.M. Haas, Chromate Conversion Coatings, *Surface Engineering,* Vol 5, *ASM Handbook,* ASM International, 1994, p 405–411
10. P. Carlsson, U. Bexell, and S.E. Hornstrom, Corrosion Behavior of Aluzink with Different Passivation Treatment, *Proceedings of Galvatech '01* (Brussels, Belgium), 2001, p 670
11. N. Yoshimi, S. Ando, A. Matsuzaki, T. Kubota, and M. Yamashita, Newly Developed Chromium-Free Thin Organic Coated Steel Sheets with Excellent Corrosion Resistance—Trend in Coated Steel Sheets for Electrical Appliances, *Proceedings of Galvatech '01* (Brussels, Belgium), 2001, p 655
12. "Zinc Corrosion Information System," Teck Cominco Metals Ltd., www.teckcominco.com, accessed March 2005
13. X.G. Zhang, Corrosion Ratios of Steel to Zinc in Natural Corrosion Environments, *Corrosion,* Vol 55, 1999, p 787
14. H. Guttman, Effects of Atmospheric Factors on the Corrosion of Rolled Zinc, *Metal Corrosion in the Atmosphere,* STP 435, ASTM, 1968, p 223–239
15. Corrosiveness of Various Atmospheric Test Sites as Measured by Specimens of Steel and Zinc, *Metal Corrosion in the Atmosphere,* STP 435, ASTM, 1968, p 360–391
16. F.H. Haynie and J.B. Upham, Effects of Atmospheric Sulfur Dioxide on the Corrosion of Zinc, *Mater. Prot. Perform.,* Vol 9 (No. 8), 1970, p 35–40
17. T.E. Graede, Corrosion Mechanisms for Zinc Exposed to the Atmosphere, *J. Electrochem. Soc.,* Vol 136 (No. 4), 1989, p 193–203
18. P.A. Baedecker, E.O. Edney, P.J. Moran, T.C. Simpson, and R.S. Williams, "Effects of Acidic Deposition on Materials," Report 19, State-of-Science/Technology, National Acid Precipitation Assessment Program, May 1990
19. M. Morcillo, M. Almeida, B.M. Rosales, J. Uruchurtu, and M. Marrocos, Ed., *Corrosion y Proteccion de Metales en Las Atmosferas de Iberoamerica (Corrosion and Protection of Metals in the Atmospheres of Spanish America*), Programa CYTED (Madrid, Spain), 1998, p 283
20. R.A. Legault, Atmospheric Corrosion of Galvanized Steel, *Atmospheric Corrosion,* W.H. Ailor, Ed., John Wiley & Sons, Inc., 1982, p 607–613
21. E. Johansson and J. Gullman, Corrosion Study of Carbon Steel and Zinc, *Atmospheric Corrosion,* STP 1239, W.W. Kirk and H.H. Lawson, Ed., ASTM, 1995, p 240
22. R.J. Neville, A Test for Undervehicle Corrosion Resistance, *Automotive Corrosion by Deicing Salts,* R. Baboian, Ed., NACE International, 1981, p 182–218
23. X.G. Zhang, Galvanic Protection Distance of Zinc-Coated Steels under Various Environmental Conditions, *Corrosion,* Vol 56, 2000, p 139
24. I. Odnevall, "Atmospheric Corrosion of Field Exposed Zinc," Ph.D. thesis, Royal Institute of Technology, Stockholm, Sweden, 1994

25. W. He, "Atmospheric Corrosion and Runoff Processes on Copper and Zinc Roofing Materials," Ph.D. thesis, Royal Institute of Technology, Sweden, 2002
26. S.D. Cramer, L.G. McDonald, and J.W. Spence, Effects of Acidic Deposition on the Corrosion of Zinc and Copper, *Proceedings of 12th International Corrosion Congress,* Vol 2, NACE International, 1993, p 722
27. H. Allen and D. Hansen, The Importance of Trace Metal Speciation to Water Quality Criteria, *Water Environ. Res.,* Vol 68, 1996, p 42–54
28. J. Forster, Variability of Roof Runoff Quality, *Water Sci. Technol.,* Vol 39, 1999, p 137–144
29. H.E. Allen, Ed., *Bioavailability of Metals in Terrestrial Ecosystems: Importance of Partitioning for Bioavailability to Invertebrates, Microbes, and Plants,* SETAC, Pensacola, FL, 2002
30. S.B. Lyon, G.E. Thompson, and J.B. Johnson, *Materials Evaluation Using Wet-Dry Mixed Salt Spray Tests,* STP 1134, No. 396, ASTM, 1992, p 20–31
31. C.H. Simpson, C.J. Ray, and B.S. Skerry, Accelerated Corrosion Testing of Industrial Maintenance Paints Using a Cyclic Corrosion Weathering Method, *J. Prot. Coatings Linings,* May 1991, p 27–36
32. X.G. Zhang, J. Hwang, and W.K. Wu, Corrosion Testing of Steel and Zinc, *Proceedings of Galvatech '98* (Tokyo, Japan), 1998
33. G.A. King, Corrosivity Mapping—A Novel Tool for Materials Selection and Asset Management, *Mater. Perform.,* Jan 1995, p 6
34. "Corrosion of Metals and Alloys—Corrosivity of Atmospheres—Classification," ISO 9223, International Organization for Standardization, 1992
35. V. Kucera, S. Haagenrud, L. Atteraas, and J. Gullman, Corrosion of Steel and Zinc in Scandinavia with Respect to the Classification of the Corrosivity of Atmospheres, *Degradation of Metals in the Atmosphere,* S.W. Dean and T.S. Lee, Ed., STP 965, ASTM, 1982, p 264
36. D. Knotkova, P. Boschek, and K. Kreislova, *Results of ISO CORRAG Program: Processing of One-Year Data in Respect to Corrosivity Classification,* STP 1239, W.W. Kirk and H.H. Lawson, Ed., ASTM, 1995, p 38
37. S. Feliu, M. Morcillo, and S. Feliu, The Prediction of Atmospheric Corrosion from Meteorological and Pollution Parameters, Part I: Annual Corrosion, *Corros. Sci.,* Vol 34, 1993, p 403
38. K.F. Lorking, "The Corrosion of Zinc," Metallurgy Report 67, Department of Supply, Australian Defence Scientific Service, Melbourne, Australia, May, 1967
39. X.G. Zhang, S. Alhassan, and F.E. Goodwin, "Predicting Zinc Coating Life on Internet," NACE/2004 Conference, NACE International, 2004
40. L. Kenworthy, The Problem of Copper and Galvanized Iron in the Same Water System, *J. Inst. Met.,* Vol 69, 1943, p 67–90
41. B.E. Roetheli, G.L. Cox, and W.B. Littreal, Effect of pH on the Corrosion Products and Corrosion Rate of Zinc in Oxygenated Aqueous Solutions, *Met. Alloys,* Vol 3 (No. 3), 1932, p 73–76
42. M. Romanoff, "Underground Corrosion," Circular 579, U.S. National Bureau of Standards, 1957
43. H.E. Townsend, "Coated Steel Sheets for Corrosion-Resistant Automobiles," Paper 416, Corrosion '91 Conference, March 11–15, 1991 (Cincinnati, OH), NACE International
44. Y. Ito, K. Hayashi, C. Kato, and Y. Miyoshi, A Study on Simulated and Accelerated Corrosion Test Methods for Automotive Precoated Steel Sheet, *Proceedings, International Conference on Zinc and Zinc Alloy Coated Steel Sheet,* Galvatech '89, Sept 5–7, 1989 (Tokyo, Japan), p 503–510
45. C.R. Shastry and H.E. Townsend, Mechanisms of Cosmetic Corrosion in Painted Zinc and Zinc-Alloy-Coated Sheet Steels, *Corrosion,* Vol 45 (No. 2), 1989, p 103–118
46. K.W.J. Treadaway, B.L. Brown, and R.N. Cox, Durability of Galvanized Steel in Concrete, *Corrosion of Reinforcing Steel in Concrete,* STP 713, ASTM, 1980, p 102–131
47. P. Hronsky, Corrosion Behavior of Metallic Materials in Organic Media Containing Hydrogen Chloride, *Corrosion,* Vol 37 (No. 3), 1981, p 161–170
48. S.W.K. Morgan, *Zinc and Its Alloys and Compounds,* John Wiley & Sons, Inc., 1985
49. U. Lechner-Knoblauch and E. Heitz, Corrosion of Zinc, Copper and Iron in Contaminated Non-Aqueous Alcohols, *Electrochim. Acta,* Vol 32 (No. 6), 1987, p 901–907
50. I.L. Rozenfeld, *Atmospheric Corrosion of Metals,* NACE International, 1972
51. W. McLeod and R.R. Rogers, The Nature of Corrosion of Zinc by Sulfurous Acid at Ordinary Temperatures, *Corrosion,* Vol 25 (No. 2), 1969, p 74–76
52. D. Knotkova-Cermakova and J. Vlckova, Corrosive Effect of Plastics, Rubber and Wood on Metals in Confined Spaces, *Br. Corros. J.,* Vol 6 (No. 1), 1971, p 17–22
53. L.E. Helwig and J.E. Bird, Protection of Galvanized Coatings from Attack by Organic Acid Vapors, *Met. Finish.,* Vol 71 (No. 11), 1973, p 45–48, 52
54. X.G. Zhang, Galvanic Corrosion, *Uhlig's Corrosion Handbook,* 2nd ed., R.W. Revie, Ed., John Wiley & Sons, Inc., 2000, p 137
55. F. Mansfeld and J. Kenkel, Laboratory Studies of Galvanic Corrosion, Part I: Two-Metal Couples, *Corrosion,* Vol 31 (No. 8), Aug 1975, p 298–302
56. V. Kucera and E. Mattsson, Atmospheric Corrosion of Bimetallic Structures, *Atmospheric Corrosion,* W.H. Ailor, Ed., John Wiley & Sons, Inc., 1982, p 561–574
57. E.A. Anderson, Zinc and Zinc Coatings, *Corrosion Resistance of Metals and Alloys,* 2nd ed., F.L. Laque and H.R. Copson, Ed., Reinhold Publishing Co., 1963, p 223
58. D. Massinon and D. Thierry, "Rate Controlling Factors in the Cosmetic Corrosion of Coated Steels," Paper 574, Corrosion' 91 Conference, March 11–15, 1991, NACE International
59. D. Massinon and D. Dauchelle, Recent Progress Towards the Understanding of Underfilm Corrosion of Coated Steels Used in the Automotive Industry, *Proceedings, International Conference on Zinc and Zinc Alloy Coated Steel Sheet,* Galvatech '89, Sept 5–7, 1989 (Tokyo, Japan), p 585–595
60. B.E. Roetheli, G.L. Cox, and W.B. Littreal, Effect of pH on the Corrosion Products and Corrosion Rate of Zinc in Oxygenated Aqueous Solutions, *Met. Alloys,* Vol 3 (No. 3), 1932, p 73–76
61. K.G. Boto and L.F.G. Williams, Rotating Disc Electrode Studies of Zinc Corrosion, *J. Electroanal. Chem.,* Vol 77, 1977, p 1–20
62. D.P. Doyle and T.E. Wright, Quantitative Assessment of Atmospheric Galvanic Corrosion, *Galvanic Corrosion,* STP 978, ASTM, 1988, p 161–171
63. A.K. Dey, A.K. Sinha Mahapatra, D.K. Khan, A.N. Mukherjee, R. Narain, K.P. Mukherjee, and T. Banerjee, Interim Report on Atmospheric Corrosion Studies under Marine Atmosphere, *NML Tech. J. (India),* Vol 8 (No. 4), 1966, p 11–16
64. "Impressed Current Cathodic Protection of Internal Submerged Surfaces of Carbon Steel Water Storage Tanks," RP0388-90, NACE International, 1990
65. X.G. Zhang and A.Q. Xing, Galvanic Action of Zinc-Coated Steel—Fundamentals and Practical Applications, *Proceedings of Galvatech '04* (Chicago, IL), Assoc. for Iron and Steel Technology, 2004, p 1017
66. L.P. Devillers, "The Mechanism of Aqueous Intergranular Corrosion in Zinc-Aluminium Alloys," Ph.D. thesis, University of Waterloo, 1974
67. "Wet Storage Stain," American Hot Dip Galvanizers Association, 1984

SELECTED REFERENCES

- E.A. Anderson and C.E. Reinhard, Zinc, *The Corrosion Handbook,* H.H. Uhlig, Ed., John Wiley & Sons, Inc., 1948, p 331–346
- K.V. Brix, Fate and Effect of Zinc from Stormwater Runoff, *Proceedings of Galvatech '04* (Chicago, IL), Assoc. for Iron and Steel Technology, 2004, p 815
- G.L. Cox, Effect of Temperature on the Corrosion of Zinc, *Ind. Eng. Chem.,* Vol 23 (No. 8), 1931, p 902–904

ASM Handbook, Volume 13B: Corrosion: Materials
S.D. Cramer, B.S. Covino, Jr., editors, p418-421
DOI: 10.1361/asmhba0003831

Corrosion of Brazed and Soldered Joints

Manish Dighe, HI TecMetal Group

CORROSION is often thought of as rusting, the process of deterioration undergone by a metal when it is exposed to air or water. However, corrosion reactions are actually much broader in scope. Whereas rusting involves the corrosion of iron or steel, other materials also suffer deterioration when they react with the environment. In a wider sense, corrosion can be defined as any reaction between a material, whether this be a metal, plastic, or ceramic, and its environment, resulting in a reduction in the ability of the material to perform the service for which it was intended.

This article primarily addresses various forms of corrosion observed in brazed and soldered joints, their causes, the role of proper brazing procedures in controlling corrosion, and the corrosion resistance of various brazing alloy systems. Corrosion of weldments is discussed in the articles "Corrosion of Carbon Steel Weldments," "Corrosion of Stainless Steel Weldments," and "Corrosion of Nonferrous Alloy Weldments" in *ASM Handbook,* Volume 13A, 2003. Design aspects of mechanical joints are discussed in the article "Designing to Minimize Corrosion" also in *ASM Handbook,* Volume 13A, 2003.

Fundamentals of Corrosion of Joints

In the case of soldered/brazed/welded joints, variables such as the materials being joined, the filler metal and fluxes used, and the geometry, orientation, and environment all play important roles in the corrosion behavior of the joint. Inasmuch as corrosion can cause degradation, structural or functional failure, and lead to equipment or plant downtime for replacement or repair, corrosion is expensive. A great deal of time and economic resources are spent to protect components. Corrosion occurs on practically all metals in a wide variety of environments. Reactions occur in liquids such as aqueous solutions, molten salts, molten metals, and in air, oxygen, or other gaseous compounds at ambient or elevated temperatures.

The effects of diffusion and alloying with the base metal during brazing/soldering/welding (and during service) also influence compatibility. For this reason, each brazing filler metal class must be considered in conjunction with the various base materials commonly brazed with it. For specific applications, surveillance testing in actual or simulated systems should be performed in order to model actual service conditions.

Corrosion of Soldered Joints

Soldering is a widely used low-temperature joining technique applied to a wide variety of metals. Soldering is a process generally carried out at temperatures below 450 °C (840 °F) and often is accomplished in air without a protective atmosphere. In many cases, soldering is used to join dissimilar metals or nonferrous metals. Soldering achieves its strength from the wetting of the surface of the part to be joined. There is minimal interaction between the base metal and the solder alloy. A soldered joint is a mechanical joint and not a metallurgical joint. In most cases, due to the low temperatures involved, fluxes are needed to clean up the surface to be joined. Because there are rarely any controlled atmospheres involved, the cleaning has to be done solely by the flux. These fluxes are highly reactive materials, designed to react with the base metal and to remove the oxide layer on the surface. Thus, the flux must be chemically very active to accomplish the cleaning action. Most of the fluxes are chloride- or fluoride-base compounds. These compounds dissociate at the soldering temperature, react with the metal surface, and help in cleaning the surface by reducing the surface oxides. As a result, most of the corrosion associated with soldered joints is due to the use of improper or insufficient cleaning methods to remove the fluxes.

Materials that are commonly soldered include copper and copper alloys, aluminum, and low-carbon steels. Although copper and aluminum have good corrosion resistance due to the formation of an oxide layer, flux, if not completely removed, may continue to react with the oxide layer. Thus, the base metal is continuously exposed to the atmosphere and the flux, resulting in severe local corrosion attack over time. Prevention of this type of attack includes the use of proper solvents to remove the flux, and rinsing the joint with clean water. In many cases (for example, steel alloys), a further step is required to instill some corrosion resistance to the base metal. This may include the application of rust-preventive solutions or coatings to the soldered part. In most cases, prevention of corrosion in soldered joints involves proper cleaning, proper selection of flux and flux removal, and use of soldering alloys that have corrosion resistance to meet the requirements.

Corrosion of Brazed Joints

Brazing is a widely used manufacturing technique due to its adaptability, applicability to dissimilar materials, and strength levels meeting or exceeding those of base materials. Brazing is a high-temperature joining process, usually above 450 °C (840 °F). In addition to the mechanical bonding between the base material and the braze alloy, there is also a metallurgical bonding that occurs, resulting in very high joint strengths. Due to the chemical difference and interaction between the base material and the braze alloy, there is a possibility of corrosion if proper care is not taken during the selection of materials.

Ceramics as well as metals are brazed. Structural ceramics can be categorized as either monolithic materials or ceramic-matrix materials. Such ceramic-based materials are widely used in automotive, aerospace, and energy applications. In many cases, ceramic-to-ceramic or ceramic-to-metal brazing is required. Many applications where ceramic materials are selected include exposure to high-temperature corrosive environments. As a result, high-temperature corrosion behavior of ceramic braze joints is critical. Ceramics, by themselves, are highly corrosion- and oxidation-resistant materials, but the brazing alloys often have inferior corrosion resistance. The braze filler alloys may form intermediate phases with the ceramic or the matrix material (in the case of composites), altering the chemical composition locally. This can affect the corrosion in two ways. The new phase formed may be much less corrosion resistant than the ceramic or the braze filler alloy; or the different chemistries may form a galvanic cell, increasing the chances of corrosion. Various techniques used for

ceramic brazing include (but are not limited to) active metal brazing techniques, nonmetallic glass brazing techniques, and eutectic brazing. In addition, much research is being done to develop newer techniques. Ceramics have very low surface energy, which means that there is no thermodynamic driving force for interface formation (wetting).

The active metal brazing technique is based on the observation that addition of certain elements, such as titanium and aluminum, to the conventional braze alloys, such as copper-silver eutectic composition, increases the surface energy of the ceramics, resulting in better wetting of the surface and adherence to structural ceramics and graphite. In the case of oxide ceramics, elements having a strong affinity for oxygen, such as titanium, aluminum, hafnium, and silicon, promote better adhesion with the ceramic. In the case of nonoxide ceramics, such as carbides and nitrides, elements showing strong interactions with carbon and nitrogen increase the surface energy and wetting of the ceramic surface. In the case of active metal brazing, it is very important to choose a braze filler metal composition with good corrosion resistance to the anticipated corrodants, taking into consideration the final application of the ceramic.

Brazed joint design can also greatly influence corrosion response, often by means of mechanical effects such as complicating stress factors. Brazed joint performance is improved when the joint is designed so that the braze, when stressed, is placed in shear or compression rather than tension. The stress and corrosion resistance of the brazed joint improve with increasing braze length or depth. Unless specified, the joint design of the braze discussed in this article typically shows the effect of corrosion only; the joint is not load bearing. Examples include lap joints and T-joints.

The types of corrosion that affect brazed joints are often similar to those that act on the base metals and their alloys. Brazed joints experience attack caused by environmental and geometric factors, selective attack due to the microstructure or composition of the brazed joint, galvanic corrosion, high-temperature corrosion, and occasional cracking complicated by corrosion.

The materials, stress condition, and service conditions determine which corrosion mechanisms are involved. Certain types of corrosion occur more frequently because of conditions that are inherent to brazing. For example, galvanic corrosion is often of concern because the brazed joint consists of a bond between dissimilar base and filler metals. If the braze is immersed in an electrolyte, galvanic corrosion may occur. The electrolyte may be simply water and could be in the form of dew.

Types of Corrosion. Most common types of corrosion seen in monolithic materials are also seen in braze assemblies. The following sections explain these major types of corrosion as applied to brazed assemblies. The fundamentals and evaluation of these types of corrosion are detailed in *Corrosion: Fundamentals, Testing, and Protection,* Volume 13A, *ASM Handbook,* 2003.

General corrosion, also called uniform corrosion, usually results from improper selection of the braze alloy for the service environment. In most cases, uniform corrosion occurs when the braze alloy is exposed to environments in which it has inherently low corrosion resistance. Stainless steel parts are widely brazed using copper as a braze alloy under vacuum, dissociated ammonia, or pure hydrogen atmospheres. If such a copper-brazed assembly is exposed to an environment containing nitric acid, it will result in uniform corrosion of the braze alloy. Although stainless steel has decent resistance to nitric acid, copper is eaten away by nitric acid. The acid will uniformly dissolve copper as a braze alloy, resulting in failure of the braze assembly. This type of corrosion can be easily prevented by careful study and selection of the braze alloy.

Pitting refers to corrosion of a metal surface in the form of cavities. The amount and severity of pitting is more difficult to predict than uniform corrosion and even more difficult to design against. In some cases, pits can initiate at locations of specific chemical compositions, such as manganese-silicon inclusions in steels. If such inclusions are formed during the brazing operation due to interaction of the braze alloy and the base metal, there is a potential for pitting corrosion.

Selective Dealloying. Many brazed joints consist of two or more phases. Sometimes, one or more of the phases are subjected to selective attack. Occasionally, an element is selectively leached from the braze. An example is the leaching (removal) of phosphorus from nickel-phosphorus brazed joints during liquid metal service. Other areas selectively attacked due to structure or composition differences are grain or phase boundaries, precipitates, or the compositionally depleted matrix material immediately surrounding them.

The same mechanism is involved with the removal of aluminum from copper-aluminum, cobalt from cobalt alloys, nickel from copper-nickel, or the separation of silver-gold alloys. In an example involving a silver braze (Ag-15.6Cu-19.9Zn-18.5Cd), both zinc and cadmium were removed. After corrosion, the brittle, spongy residue contained 66.3% Ag, 16.5% Zn, and 13.8% Cd. Selective attack is less likely under uniform high-velocity flow conditions because of decreased opportunity for concentration buildups.

Galvanic Corrosion. In simple terms, galvanic corrosion is a type of corrosion that is initiated or aided by electrical contact between two dissimilar metals. This type of corrosion also requires an electrolyte to complete the electrical circuit. A galvanic series is a very useful tool in assessing the potential for galvanic corrosion in a braze system in a specific environment. See the reference material at the back of this Volume. The list ranks the metals according to their galvanic potential. The higher the alloy or metal on this list, the better the resistance to galvanic corrosion. While using this series, it should be remembered that the galvanic series deals with only a portion of the corrosion phenomenon and provides the standard oxidation-reduction potentials as compared to a standard solution. The galvanic potentials may change in different solutions and concentrations. Hence, the galvanic series should be used with care, and some experimentation in actual conditions should be conducted for verification.

In the case of braze systems, galvanic corrosion can occur, because two metals or alloys are always involved. It is unwise to combine a small area (that is, the braze) of the anodic member of a couple with a large area (base metal) of the cathodic member. The reverse relationship is usually not hazardous, unless corrosion is selective toward a phase in the braze or toward the interface. In addition, the braze alloys or the base metals may not be homogeneous and may have multiple phases. This situation can also have a potential for galvanic corrosion. Galvanic corrosion is often the result of poor design and the improper selection of materials and can be prevented by proper attention to the microstructure, the application environment, and the galvanic series.

As an example of galvanic corrosion, consider a stainless steel or nickel alloy brazed with nickel-phosphorus eutectic brazing alloy. Phosphorus is a melting-point depressant and forms a low-melting eutectic with nickel at 910 °C (1670 °F) with approximately 11% P. After the brazing operation, the joint microstructure consists of Ni_3P intermetallic in a matrix of nickel. The Ni_3P has inferior mechanical and corrosion properties and can form a galvanic cell with the surrounding nickel in some electrolytes, resulting in galvanic corrosion. Proper diffusion heat treatments are required after the brazing operation to diffuse the phosphorus in the base metal and to reduce the amount of intermetallics in the joint. Figure 1 shows the scanning electron microscopy image of the joint structure.

Intergranular Attack. Most engineering materials consist of grains separated by grain boundaries. These grain boundaries can be locations of differences in chemical composition, such as alloying element segregation or second-phase precipitation. An example is the carbide precipitation in austenitic stainless steels during sensitization. It is also a well-established fact that diffusion occurs faster along the grain boundaries than through the bulk of the grains. During brazing, such diffusion of the braze alloy occurs along the grain boundaries in the base metal and can result in the formation of second-phase particles along the grain boundaries. The second-phase particles will have a different corrosion response than the base metal. The grain-boundary region may corrode faster when exposed to a corrosive medium in such a situation. One such example is the brazing of nickel alloys with a boron-containing braze alloy. In Fig. 2, UNS N06617 (Inconel 617) was brazed with UNS N99620 (AMS 4777), a braze alloy

containing Ni-Cr-B. The boron from the braze alloy diffuses along the grain boundaries into the Inconel 617 base metal. This boron combines with nickel to form nickel boride along the grain boundaries. This second phase can deteriorate the corrosion resistance in some alloys.

Interfacial Corrosion. A brazed joint may be susceptible to interfacial corrosion, depending on a number of factors. The types of base and filler metals, the brazing technique (such as using flux or using a vacuum), and the service environment influence the likelihood of attack. Several of these mechanisms interact, depending on the particular environmental circumstances, to result in interfacial corrosion.

Interfacial corrosion is most commonly seen in stainless steels brazed with silver brazing alloys. Such a process usually involves the use of flux, which makes the problem worse. The interfacial corrosion problem is more prominent in martensitic and low-nickel-containing ferritic stainless steels. Using nickel-containing braze alloys and employing fluxless brazing techniques, such as hydrogen atmospheres or furnace brazing techniques, can reduce the chances of interfacial corrosion.

Role of Proper Brazing Procedures in Minimizing Corrosion

The severity of corrosion of brazed joints is governed by many variables. To minimize the risk of corrosion failure of brazed assemblies, proper understanding of the base metal, braze alloy, brazing atmosphere, brazing fluxes, postheat treatment, and application environment is required. The risk of corrosion can be minimized by proper part and joint design, correct selection of the braze alloy and brazing atmosphere, and proper postcleaning and heat treating operations.

Joint Design. In designing a joint that is to be brazed, geometries that minimize corrosion are preferred. For example, if an assembly is to be pickled, the internal geometry of the entire assembly should allow complete exchange of the pickling and cleaning solutions.

If a lap joint is to be fabricated, the possibility of the buildup of a stagnant solution at the leading edge of the joint should be considered. In a butt joint, the efficiency of the joint is maximized by making sure the joint has no discontinuities such as entrapped flux, voids, incomplete joining, or porosity. These discontinuities, in addition to impairing the structural integrity of the joint, may enhance the susceptibility of the joint to corrosion. Entrapped flux may lead to high-temperature corrosion, whereas incomplete joining may lead to crevice corrosion.

The distribution of the stress as evenly as possible in the joint is also important in joint design. If the stress is concentrated, the likelihood of stress-corrosion cracking exists.

Materials Selection. The selection of the materials to be used in the fabrication of a brazed joint must involve a consideration of the potential for corrosion in addition to the factors routinely considered, such as liquidus temperature and strength. In particular, the appropriate galvanic series for the particular service environment should be consulted if available. Standard galvanic series, such as the one for seawater located in the back of this Volume, may serve as a guide. Also, attention should be paid to the susceptibility of certain materials to other types of corrosion, such as selective (dealloying) attack and general attack. The service environment and selected materials dictate the potential for corrosion.

Brazing Process Selection. Brazing processes are classified based on the heating method used to elevate the part to the brazing temperature, and the protective atmosphere. Thus, most common brazing processes include furnace brazing (with atmospheres of hydrogen, nitrogen, argon, exothermic, endothermic, or dissociated ammonia), vacuum brazing, induction brazing, and torch brazing. The choice of brazing process depends on the base material, part size, part geometry, and braze alloy. For example, small parts usually work well in continuous furnace brazing, because they heat up very quickly. On the other hand, parts that are big and have intricate geometry should be slowly heated at a controlled rate to prevent excessive thermal stresses during heating and cooling. Excessive stresses due to fast and nonuniform heating can cause stress-corrosion cracking during the brazing operation.

Actual brazing temperatures should be decided after consulting the phase diagram and continuous cooling transformation diagram for the material in question. For example, brazing of stainless steel should not be carried out in the temperature range of 538 to 954 °C (1000 to 1750 °F), because carbide precipitation occurs in this temperature range, and this reduces the corrosion resistance of stainless steel.

Furnace or induction heating may be used to maintain a uniform temperature distribution around the joint to prevent the formation of stresses from nonuniform thermal expansion and contraction, thus avoiding the tendency for stress cracking. Generally, vacuum brazing is used for larger parts where high temperatures are involved. Vacuum brazing prevents oxidation of the surface and degasses the assemblies before brazing. In addition, the use of flux is usually not required, thus reducing the cleaning and flux-removal operation after the brazing operation.

Many times, the negative effects of the brazing process can be eliminated or minimized by a proper postbraze heat treatment. The corrosion resistance of the material is strongly influenced by the microstructure of the braze and base material. Hence, proper control of the braze microstructure is required. For example, effects such as sensitization of stainless steel can be eliminated by using a fast cooling once the part reaches the temperature below the braze solidification temperature.

Final Cleaning. After brazing, the brazed joint must be cleaned to remove flux residue and any oxide scale formed during the brazing process. Flux removal is particularly important because flux residues are often chemically active, and if not removed, they could cause corrosion.

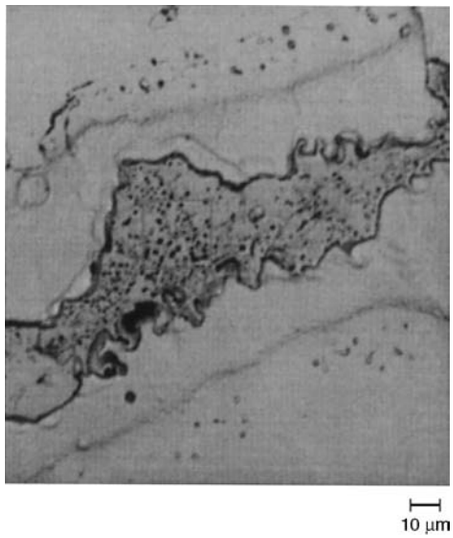

Fig. 1 Nickel phosphide intermetallic in the braze joint under scanning electron microscopy. Original magnification 400×. Courtesy of HI TecMetal Group

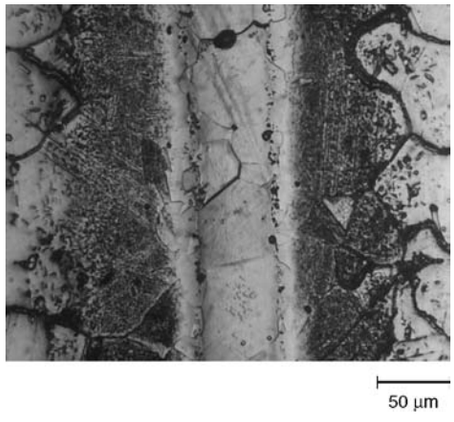

Fig. 2 UNS N06617 (Inconel 617) brazed with UNS N99620 (AMS 4777) under vacuum at 1038 °C (1900 °F). The structure shows borides at the grain boundaries in the base metal. Original magnification 200×. Courtesy of HI TecMetal Group

Corrosion Resistance of Particular Brazing Alloy Systems

The corrosion resistance of brazed joints involves the corrosion resistance of the base metals and filler metals individually and collectively. The corrosion resistance of various common filler metals is discussed in this section.

Silver-base braze alloys are widely used in the industry to join metals such as titanium, zirconium, copper, steel, and stainless steels. They are also used for dissimilar-metal joining. Silver braze alloys can be brazed in air (with flux) and with torch, induction, or furnace. In general, silver braze alloys have good corrosion resistance. These brazing filler metals are not suitable for strong acids for extended periods. They behave well for short times, thus making it possible to acid clean or pickle assemblies brazed with silver. Silver-brazed parts have decent high-temperature corrosion resistance. Silver-brazed parts can be used at temperatures up to 427 °C (800 °F). When brazing stainless steels with silver alloys, the use of flux is usually required. In addition, stainless steel parts brazed with silver have a tendency for interfacial corrosion.

Copper-Base Filler Metals. As a brazing filler metal, the material cost of copper is much less than silver and hence more suitable for large-volume brazing. The energy cost is higher, however, because copper brazing is done at much higher temperatures, usually at 1121 °C (2050 °F). This requires the use of a protective atmosphere and control to prevent oxidation. Thus, copper brazing has to be performed in a controlled atmosphere furnace. The most common atmospheres used are hydrogen, dissociated ammonia, and exothermic.

Many studies of the corrosion resistance of copper-base filler alloys have been made on joints involving stainless steel. Copper filler alloys containing significant amounts of zinc (such as naval brass welding and brazing rod, RBCuZn, similar to UNS C4700) or phosphorus (such as copper-phosphorus brazing filler metal, BCuP, similar to UNS C55180) are not recommended for the joining of stainless steels, because brittle compounds tend to form at the interface between the braze and the base metal. The combination of copper-base brazing filler metals and stainless-steel-base metals is particularly susceptible to liquid metal embrittlement, especially if the assembly is held at brazing temperature for too long.

When copper-base filler metals are used to braze stainless steel, care should be taken to cool the assembly through the carbide sensitization range (538 to 927 °C, or 1000 to 1700 °F) as quickly as possible. The dezincification of copper-zinc filler metals may occur under certain circumstances.

Nickel-Base Filler Metals. Brazed joints produced with nickel-base filler metals are used at temperatures ranging from −200 °C (−328 °F) to above 1200 °C (2192 °F). The characteristics of nickel make it a good starting point for developing brazing filler metals to withstand high service temperatures. Nickel is ductile, and with proper alloying additions such as chromium, it has excellent strength and oxidation resistance as well as corrosion resistance at elevated temperatures. Nickel braze alloys contain phosphorus, silicon, and boron as melting-point-lowering elements. These elements also have a tendency to form nickel-base intermetallics during the brazing operation. These intermetallics have low melting points and also have different high-temperature corrosion behavior as compared to pure nickel. Prolonged diffusion treatment is required to diffuse the phosphorus, boron, and silicon into the base metal in order to reduce the amount of intermetallics in the braze joint. Such diffusion treatments are performed immediately after the brazing operation or as a part of the brazing operation itself. This step minimizes the amount of second phases in the braze joint, thereby lowering the susceptibility to localized corrosion mechanisms discussed in the earlier sections.

Aluminum-Base Filler Metals. Aluminum-silicon braze alloys are widely used to braze aluminum. Brazing of aluminum requires the use of fluxes. This makes most postcleaning operations very critical, because the highly active and hygroscopic flux residue may cause corrosion by absorbing moisture. These fluxes can be removed by immersion in boiling water.

Aluminum braze alloys are also used to join titanium alloys. Although there is a galvanic potential difference between aluminum and titanium, in reality, the risk of galvanic corrosion is greatly reduced due to the formation of passive oxide layers on titanium and aluminum.

Manganese-base filler metals are generally alloyed with nickel when used with stainless steels and nickel-base alloys. Most results published on the corrosion behavior of manganese-nickel filler metals indicate that this system exhibits poor corrosion resistance in high-temperature environments.

Precious-Metal-Base Filler Alloys. Gold filler alloys are used in vacuum and high-temperature heat-resisting applications (e.g., electronics and engine components), because they are generally free from volatiles and have exceptional resistance to oxidation and other types of corrosion. Gold brazing alloy BAu-4 (UNS P00820), when used to braze stainless steel or other Fe-Ni-Co-base heat-resistant alloys, is resistant to oxidation by air and sulfur-bearing gases up to 816 °C (1500 °F).

SELECTED REFERENCE

- *NACE Corrosion Engineers Handbook,* 3rd ed., NACE International, 2002

ASM Handbook, Volume 13B: Corrosion: Materials
S.D. Cramer, B.S. Covino, Jr., editors, p422-429
DOI: 10.1361/asmhba0003832

Thermal Spray Coatings for Corrosion Protection in Atmospheric and Aqueous Environments

Seiji Kuroda, National Institute for Materials Science
Andrew Sturgeon, TWI, Ltd.

CORROSION PREVENTION by the application of thermal spray coatings has a history dating back to the 1940s. When applied to large infrastructures such as bridges, highway rail, and light and sign supports, their use requires a relatively high initial application cost compared to competitive technologies such as painting and galvanizing. As the expected life of these structures becomes longer, typically 50 years and more, the life-cycle cost consideration is a more widely accepted criterion for structural design, materials selection, and judging the merits of corrosion prevention and maintenance methods. Also, environmental regulations now require paints and other treatments to contain significantly lower volatile organic compounds (VOCs), whereas thermal spraying is essentially a zero-VOCs process. In these respects, thermal spray coatings are an attractive alternative to paint systems that can offer longer service life and are suitable as a maintenance upgrade for existing structures. In addition, thermal spray coatings can provide protection to smaller engineering components, such as tanks, pumps, impellers, ship equipment, architectural products, and many other items. Thermal-sprayed coatings of zinc, aluminum, and their alloys have a proven history in service and in tests of providing long-term corrosion protection of steel in various natural environments. This information is accumulated and incorporated into industrial standards and assists the user in the selection of coating materials and the posttreatment most suitable for a particular environment. Dense barrier-type coatings of various corrosion-resistant alloys can be fabricated using the high-velocity oxyfuel (HVOF) spray processes, but the corrosion resistance of the coating itself in aqueous solutions does not yet match that of the wrought materials. This article is intended to give the reader a general technical background of thermal spray coatings used for corrosion protection in atmospheric and aqueous environments. It covers coating types and application methods, with reference to industrial standards and some established application examples. Also see the article "Thermal Spray Coatings" in *ASM Handbook,* Volume 13A, 2003, for additional information about quality control of the process, plasma spray, and applications of polymers and ceramics.

Coating Types

There are two approaches for the corrosion prevention of steel structures using thermal spray coatings. The first approach is to spray metallic coatings that can provide cathodic protection to the underlying steel substrate as well as act as a barrier layer. The spray metals include zinc, aluminum, and alloys such as zinc-aluminum and aluminum-magnesium that have a corrosion potential less noble than that of steel. When the steel surface is covered with such metals, it does not corrode, even if pores exist in the coating. The coating is acting as a sacrificial anode, and the steel is cathodically protected. The term *metallizing* is often used as an equivalent expression for thermal spraying when describing these types of coatings, and the coatings are usually referred to as thermal spray zinc (TSZ) or thermal spray aluminum (TSA).

The second approach is to spray dense, low-porosity coatings of corrosion-resistant materials such as stainless steels, titanium, or nickel-base alloys, such as nickel-chromium, alloy C278 or alloy 625. These metals and alloys are expected to form a very thin (usually less than 0.1 μm, or 0.004 mils), compact oxide film on the surface, called a passive film that inhibits reaction of the coating with the environment. Here, the coating acts as a barrier layer on the steel surface. If there is through-coating porosity, any moisture that penetrates through the pores can cause galvanic corrosion at the coating-substrate interface, usually with the substrate being anodic to the coating. This is an undesirable situation, because the corrosion rate at the interface is accelerated by the coupling effect, often with rapid corrosion of the substrate and loss of coating adhesion.

The sacrificial coatings of TSA and TSZ have a long history of development and evaluation, both in the laboratory and in industry. The barrier-type coatings of corrosion-resistant alloys have been used in various industries for the corrosion protection of engineering components but are at a developmental stage for the corrosion protection of steel infrastructures requiring long service life. The recent availability of new spraying processes such as HVOF is believed to offer the potential to fabricate extremely dense coatings with high corrosion resistance.

Aluminum Coatings and Zinc Coatings

The TSA and TSZ coatings are usually sprayed onto large structures using flame and electric arc-based processes, and with the coating material supplied in wire form to the spray gun. There are standards for the composition and diameter of these wires: ISO 14919 (Ref 1) and AWS C2.25/C2.25M (Ref 2). Among these, four classes of materials—zinc, aluminum, Zn-15Al, and Al-5Mg—are specified for the general purpose of corrosion protection in ISO 2063 (Ref 3).

Alloys with other compositions, as well as composite coatings, can be used for corrosion protection, but their use has been limited. One way to fabricate composite coatings is to simultaneously feed wires of different materials, such as zinc and aluminum, to the arc spraying gun. The molten droplets of the two metals mix on the substrate and form a composite coating called a pseudoalloy. Another route is to use cored wires filled with powders. Oxide powders

are used to enhance wear resistance of the coating. The in situ synthesis of various intermetallic compounds by the reaction between the sheath metal and the filler powder is also possible (Ref 4, 5).

Figure 1 shows the pH dependence of corrosion rates of zinc and aluminum in NaCl aqueous solution (Ref 6). Corrosion of zinc proceeds significantly faster in low-pH acidic environments, whereas aluminum corrodes more readily in high-pH alkaline environments. This behavior influences the selection of coating type to be used. Table 1 presents the minimum thickness of thermal spray coatings of zinc, Zn-15Al, aluminum, and Al-5Mg recommended for different environments (Ref 3). Zinc is not recommended for industrial areas where acid rain is expected. These recommendations are based on a large number of field exposure tests carried out globally over many years, as is described in a later section.

In the United States and northern Europe, zinc and the Zn-15Al alloy are commonly used to coat steel bridges rather than TSA. The reasons cited for this are that TSZ is lower in cost and somewhat easier to spray than aluminum or Al-5Mg. The TSZ is also said to be more forgiving of the surface preparation quality. A typical coating system consists of 100 μm (4 mils) of thermal-sprayed zinc, followed by an etch primer and a vinyl resin sealer.

In Japan, there is a preference for TSA coatings, with an increasing number of aluminum-coated bridges in the coastal regions. Because aluminum forms a very thin and tight passive oxide film on its surface in the pH range of 4 to 8.5, its corrosion rate is low in such coastal environments. Another reason is that TSA can have good adhesion to steel substrates. However, when the coating is damaged and the steel substrate exposed, the capability of a TSA coating to protect the exposed steel (often referred to as the throwing power) is significantly less than for TSZ (Ref 7). Alloying of aluminum with zinc, and also sometimes with a third element, has been studied to increase the durability of the coating while maintaining its throwing power (Ref 8, 9). In severely corrosive marine atmospheres, aluminum or Zn-15Al coatings are preferred.

The TSA in combination with a sealer or a paint system is widely used in Europe to provide long-term corrosion protection of steel structures on North Sea oil and gas installations, both offshore and onshore. In the last 10 years, arc-sprayed Al-5Mg has been used almost exclusively as the coating material. The prepared steel surface is coated with 200 to 400 μm (8 to 16 mils) of Al-5Mg and then usually painted with an organic coating, such as epoxy, urethane, or acrylic. This coating system has shown a good combination of long-term stability in marine environments while providing sufficient cathodic protection to the underlying steel substrate to prevent corrosion.

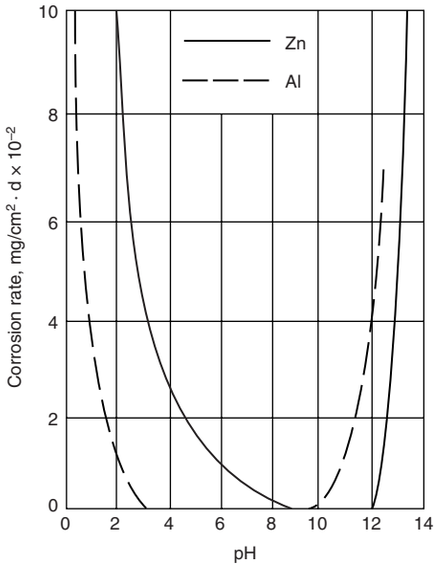

Fig. 1 Corrosion rate of zinc and aluminum in NaCl aqueous solution as a function of pH

Thermal Spray Application Methods for TSA and TSZ Coatings

Application of a thermal spray coating onto a steel structure consists of three steps: surface preparation, coating deposition by thermal spraying, and postspray treatment.

Substrate surface preparation is a critical step in the thermal spraying process. Table 2 shows the International Organization for Standardization (ISO) and the Society for Protective Coatings (SSPC) standards relating to the blasting process, abrasive materials, and assessment

Table 1 Minimum thicknesses recommended for different purposes according to ISO 2063

	Metal thickness(a), μm							
	Zinc		Aluminum		Al-5Mg		Zn-15Al	
Environment	Unpainted	Painted	Unpainted	Painted	Unpainted	Painted	Unpainted	Painted
Saltwater	NR(b)	100	300	150	250	200	NR(b)	100
Freshwater	200	100	200	150	150	100	150	100
Urban environment	100	50	150	100	150	100	100	50
Industrial environment	NR(b)	100	200	100	200	100	150	100
Marine atmosphere	150	100	200	100	250(c)	200(c)	150	100
Dry indoor environment	50	50	100	100	100	100	50	50

(a) To convert to mils, multiply by 0.03937. (b) NR, not recommended. (c) Offshore application. Source: Ref 3

Table 2 Standards for surface preparation

Standard	Title
Blasting	
ISO 8504	"Preparation of Steel Substrates before Application of Paints and Related Products—Surface Preparation Methods—Part 2: Abrasive Blast-Cleaning" (There are three parts.)
Abrasive materials	
ISO 11124	"Preparation of Steel Substrates before Application of Paints and Related Products—Specifications for Metallic Blast-Cleaning Abrasives—Part 1: General Introduction and Classification" (There are four parts.)
ISO 11125	"Preparation of Steel Substrates before Application of Paints and Related Products—Test Methods for Metallic Blast-Cleaning Abrasives—Part 1: Sampling" (There are seven parts.)
ISO 11126	"Preparation of Steel Substrates before Application of Paints and Related Products—Specifications for Nonmetallic Blast-Cleaning Abrasives—Part 1: General Introduction and Classification" (There are ten parts.)
ISO 11127	"Preparation of Steel Substrates before Application of Paints and Related Products—Test Methods for Nonmetallic Blast-Cleaning Abrasives—Part 1: Sampling" (There are seven parts.)
SSPC-AB 1	"Mineral and Slag Abrasives"
SSPC-AB 2	"Cleanliness of Recycled Ferrous Metallic Abrasives"
SSPC-AB 3	"Ferrous Metallic Abrasive"
Assessment	
ISO 8501	Preparation of Steel Substrates before Application of Paints and Related Products—Visual Assessment of Surface Cleanliness—Part 1: Rust Grades and Preparation Grades of Uncoated Steel Substrates and of Steel Substrates after Overall Removal of Previous Coatings (There are four parts.)
ISO 8502	"Preparation of Steel Substrates before Application of Paints and Related Products—Tests for the Assessment of Surface Cleanliness" (There are twelve parts.)
ISO 8503 Part 1	"Preparation of Steel Substrates before Application of Paints and Related Products—Surface Roughness Characteristics of Blast-Cleaned Steel Substrates—Part 1: Specifications and Definitions for ISO Surface Profile Comparators for the Assessment of Abrasive Blast-Cleaned Surfaces" (There are five parts.)
SSPC-VIS 1	"Guide and Reference Photographs for Steel Surfaces Prepared with Dry Abrasive Blast Cleaning"
SSPC SP 5/NACE 1	"White Metal Blast Cleaning"
SSPC SP 10/NACE 2	"Near-White Metal Blast Cleaning"

ISO, International Organization for Standardization; SSPC: The Society for Protective Coatings; NACE, NACE International

of the blasted surface. The surface preparation begins with blast cleaning to achieve the required degree of cleanliness, normally, level Sa 2.5 according to ISO 8501-1 or SP 10 according to SSPC. For all immersion and marine service, more complete removal of rust (Sa 3 or SP 5) may be required. The difference between SP 5, "White Metal Blast Cleaning," and SP 10, "Near-White Metal Blast Cleaning," is that a white metal blast removes all the mill scale, rust, oxides, corrosion products, and other foreign matter from the surface. Near-white metal blasting allows light shadows, slight streaks, or minor discolorations to remain on no more than 5% of each unit area of surface.

The blasted surface must have a sharp, angular profile, usually with a depth greater than 60 μm (2.4 mils). This profile is the anchor tooth pattern to which the particles of spray metal adhere, forming a mechanical bond between the coating and substrate. In order to achieve the surface as specified and to ensure good adhesion of the spray coating applied thereafter, there are several practical matters to consider, such as the type and size of grit, the temperature and humidity of the atmosphere, the holding period or time between blast cleaning and spraying, and the appearance of rust bloom. These issues should be clearly defined in the coating specifications. Compliance with the detailed specifications is necessary to avoid errors that can lead to poor coating application and premature coating failure.

The most commonly used blasting materials include alumina, chilled iron, angular steel, silicon carbide, and garnet. The selection of blasting material and the size is based on the type, grade, and surface condition of the steel to be cleaned, the type of blast-cleaning system employed, the finished surface to be produced (cleanliness and roughness), and whether the abrasive will be recycled. When the abrasive is recycled, a procedure to maintain the size and cleanliness of the abrasive needs to be followed. Clean, dry compressed air must be used for blasting. The use of moisture separators, oil separators, traps, or other equipment may be necessary.

In order to assess the cleanliness of the blasted surface, reference photos for visual comparison are included in ISO 8501-1 and SSPC-VIS 1-89. For the assessment of the surface profile of blast-cleaned steel, a reference plate with different grades of roughness, called a comparator, may be used. Other procedures use a stylus instrument or replica tapes. Because of the dust generated during abrasive blast cleaning, operators must be provided with appropriate protection. Also, the blasting media should not be allowed to escape from the application site to the environment and must be treated in accordance with the industrial wastes regulations.

Monitoring and control of the atmosphere during and after blast cleaning is very important. The surface temperature of the steel substrate should be higher than the dewpoint by at least 3 °C (5 °F) in order to avoid water condensation on the surface, which will degrade the adhesion of the spray coating. The procedures to inspect the blast-cleaned surface before spraying must be clearly defined, with, ideally, the thermal sprayer responsible for the surface preparation. In areas where significant chloride contamination of the steel surface is likely, such as in coastal regions, the amount of soluble salt contaminants on the steel should be determined and the salts removed prior to blast cleaning. Similarly, degreasing or pressure washing may be necessary prior to abrasive blasting.

Arc and Flame Spraying Processes. The term *thermal spray* covers several application methods. Electric arc spraying and flame spraying using wire consumables are the most suitable methods for applying coatings of zinc, aluminum, and their alloys to steel structures. These methods are simple, they can be used on-site, and they offer relatively high coverage rates compared to other thermal spray processes. Wire consumables are also more economical and easier to handle than powders. A more detailed description of these spray processes can be found elsewhere (Ref 10). Electric arc spraying (Fig. 2) is performed by feeding two electrically conducting metal wires toward each other. An electric arc is produced at the wire tips. The arc melts the metal wires, and a high-pressure air line is used to atomize and then spray the fine droplets onto the steel surface. In flame spraying (Fig. 3), a metal wire is melted in a gas flame and then air sprayed onto the steel surface.

The rate of coating application is a major cost factor and an important consideration in equipment selection. The traverse speed of the spray gun over the substrate surface will vary, depending on the operator and coating specification. A gun traverse speed of approximately 0.5 m/s (20 in./s) is typical, with upper spray rates for aluminum being approximately 20 kg/h (44 lb/h) and that for zinc being 50 kg/h (110 lb/h). This corresponds to a coverage rate of approximately 50 m^2/h (540 ft^2/h) for a 150 μm (6 mils) thick coating.

Modern arc spray units can apply a 50 mm (2 in.) wide band of coating, 75 μm (3 mils) thick, at a traverse rate of 0.5 m/s (20 in./s). This compares to an airless spray unit moving at approximately 0.5 m/s (20 in./s) when applying 150 μm (6 mils) of wet paint in a band up to 450 mm (18 in.) wide. The application rate of thermal spray coatings is, at best, only 5% that of conventional organic coatings. Such comparisons can be misleading, however, as they do not include mixing, thinning, equipment setup, cleaning, and the curing cycle, which are time-consuming steps in applying organic coatings. The application of thermal spray coatings normally requires fewer steps, saving considerable time.

A notable trend in the United States is the development of wire arc spraying equipment capable of spraying thicker wires, such as 4.8 mm ($^3/_{16}$ in.) diameter. This offers significant improvement in terms of application speed and cost. With such a large-diameter wire, a deposition rate of 75 kg/h (165 lb/h) with deposition efficiency at 68% for pure zinc has been reported (Ref 11). Acceptance of such large-wire spraying has been limited until recently, partly due to the greater surface roughness of these coatings, which absorbs more sealant and topcoat paint, together with a less acceptable appearance.

Posttreatment. Arc and flame spray coatings usually contain numerous pores, some of which are closed and the rest connected from the coating surface to the substrate. Natural sealing can be achieved by oxidation of the metallic coating under normal environmental exposure conditions, when the resulting oxides, hydroxides, and/or basic salts are not soluble in this environment. It is often beneficial to apply an organic sealant to close these pores. Penetration of sealant into the spray coating becomes more difficult with time after spraying. This is due to the adsorption of moisture on the pore surface, which can lead to the formation of corrosion product within the pores. As a consequence, it is often recommended that any posttreatment, in particular, the application of organic sealants, is completed within the same day as the thermal spray coating application. Sealant materials include acrylic, epoxy, phenolic, silicone, urethane, and vinyl resins. They should be diluted properly to assure good wetting and penetration into the porosity present in the coating. Typically, the sealant coat is applied to give a 0.06 mm (2 mils) dry-film thickness. A cross section through a typical arc-sprayed and sealed TSA coating is shown in Fig. 4.

The effect that sealing has on the thickness change of thermal-sprayed zinc, Zn-13Al, and aluminum coatings exposed in a splash-zone environment is shown in Fig. 5 (Ref 7). Coating thickness was measured by an electromagnetic

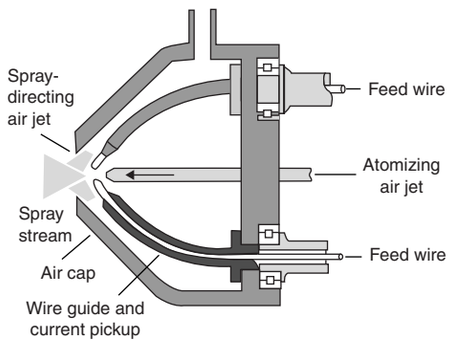

Fig. 2 Schematic of arc spraying process

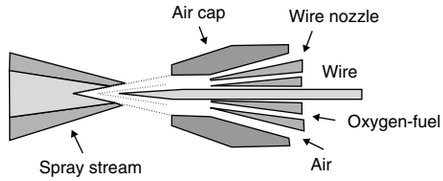

Fig. 3 Schematic of wire flame spraying process

thickness tester. It is believed that the thickness values increased over the years, mostly due to the formation of corrosion products on the surface and within the pores of the spray coatings. The rate of increase was dependent on the coating material as well as the sealant type. Coatings of zinc showed the most rapid increase in thickness and started to show heavy rusting after 5 to 6 years. The thickness of a Zn-13Al coating without sealing almost doubled over 16 years. By sealing the Zn-13Al coating, the rate of thickness increase was dramatically reduced, with the steel still protected from corrosion. Aluminum coatings in both the as-sprayed and sealed condition showed little increase in thickness over the years. Sealing has the effect of slowing down the penetration of water and seasalt into the coatings and hence prolonging coating life. It is not always possible to state the benefits of sealing quantitatively, but the appearance of spray metal coatings is also improved by sealing. There is no requirement for a measurable layer of sealant, but the sealant should be applied until absorption is complete. From the corrosion-prevention viewpoint, painting or topcoating is seldom required, except to give a specific color to the surface for aesthetic reasons.

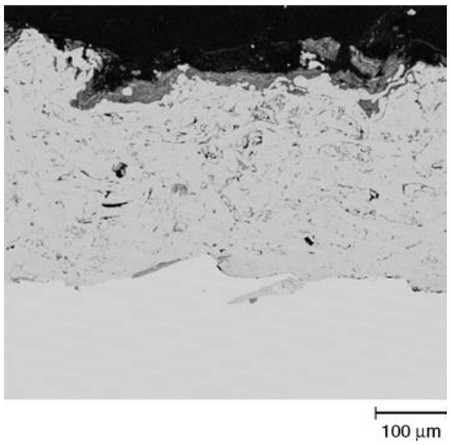

Fig. 4 Cross section of arc-sprayed coating of aluminum with sealant. Courtesy of TWI, Ltd.

Field Exposure Tests of TSA and TSZ Coatings

Field exposure tests are regarded as the most reliable method to estimate the longer-term performance of spray coatings in service environments. For atmospheric and marine exposure tests, there are international standards to be observed (Ref 12).

The major field exposure tests of thermal spray coatings conducted around the world are summarized in Fig. 6. Small test panels have been used for selection of coatings, but steel pipe piles or model steel structures are also used for more realistic testing. One of the earliest exposure tests was undertaken by the British Iron and Steel Research Association (1940 to 1952) and included metallic coatings of zinc, aluminum, cadmium, lead, and tin prepared by thermal spraying, electroplating, and hot dipping (Ref 13). Atmospheric test sites included rural, coastal, and industrial areas. Marine immersion testing was also included. An important result obtained from these tests was that the life of a coating, as defined by the period when rust covered 5% of the surface area, was roughly proportional to the coating thickness, regardless of the application processes. The relationship between the life and the coating thickness of zinc and aluminum coatings at a site in Sheffield, United Kingdom, is shown in Fig. 7. Life of a zinc coating was shown to be significantly shorter in the severe industrial areas.

A subsequent exposure trial tested various alloy and composite coatings, including zinc-aluminum and aluminum-magnesium, in marine and industrial atmospheres (Ref 14). Prealloyed or mixed powders with various compositions were flame sprayed onto small steel substrates (50 by 75 mm, or 2 by 3 in.) to a thickness of approximately 80 μm (3 mils). After 10.5 years of exposure, it was reported that zinc-aluminum alloys and composites of approximately a 50 to 50 composition were the best performers. One set of specimens still remains at the Kure Beach exposure site in the United States, 250 m (800 ft) from the ocean, and it has been subsequently reported that aluminum and aluminum-rich coatings perform better over the long term at this location (Ref 15).

The 19 year exposure test carried out by the American Welding Society is by far the largest, with more than 4200 testpieces tested in various atmospheric and seawater immersion environments (Ref 16). Coatings were wire flame-sprayed zinc and aluminum with a thickness range from 80 to 460 μm (3 to 18 mils), with and without sealing. The sealants included wash primer, aluminum vinyl, and chlorinated rubber. Coarse- and fine-grained silica as well as cast iron grit were used as abrasive for sandblast cleaning of the steel substrate prior to coating application. Major results included:

- Aluminum coating with a thickness of 80 to 150 μm (3 to 6 mils), with or without sealing, protected the steel substrate in seawater, severe marine, and industrial atmospheres.
- For 19 year protection life, zinc coatings without sealing required at least 300 μm (12 mils) thickness in seawater and 230 μm (9 mils) in marine and industrial atmospheres; the latter can be reduced to 80 to 150 μm (3 to 6 mils) with appropriate sealing.
- Pretreatment did not significantly affect the coatings performance.
- Chlorinated rubber is not a good sealant for zinc or aluminum coatings.

Carbon steel pipe piles for marine construction with thermal-sprayed zinc, aluminum, and alloy coatings have been tested and compared with other protective coatings and linings (Ref 7, 17–20). Corrosion rate varied significantly along the pipe pile length, depending on the surrounding environment. The rate was approximately 0.1 to 0.2 mm/yr (0.004 to 0.008 mil/yr) in seawater but can be several times higher in the splash zone (Ref 21). If the pipe pile is only protected in the areas exposed to splash and tidal zones, the coating is consumed very rapidly by its sacrificial action with respect to the adjacent bare steel in the seawater (Ref 19). The pipe pile should be totally covered with the thermal spray coating or used in combination with sacrificial anodes or impressed current to cathodically protect the uncoated immersed steel. In

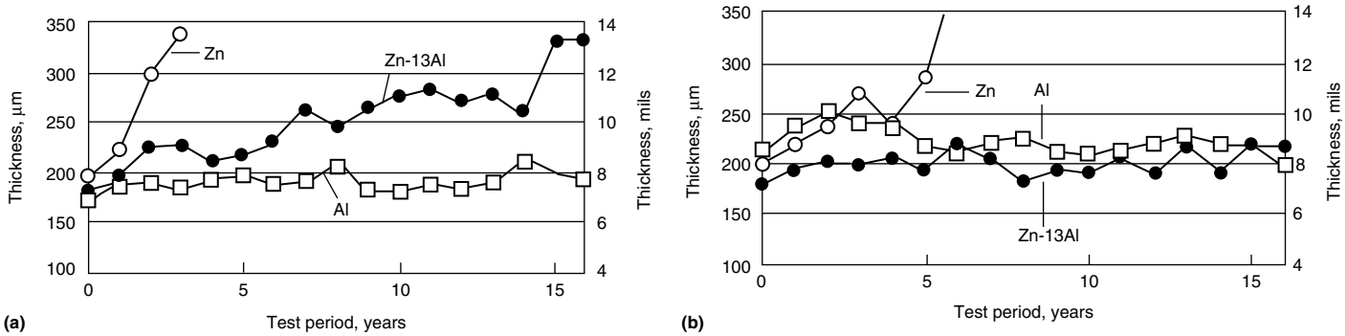

Fig. 5 Effects of sealing on the thickness changes of thermal spray coatings in the splash zone. (a) No sealing. (b) Sealed

long-term tests conducted in the United States and Japan, TSA coatings with a thickness of approximately 150 μm (6 mils) provided protection over 15 years in both immersion and splash conditions, whereas TSZ coatings with a similar thickness lost protection capability after several years (Ref 7, 18). One problem associated with a TSA coating is its inferior cathodic protection, compared to TSZ coatings (Ref 7), over sharp edges or exposed steel substrate where the coating is damaged.

Application History of TSA and TSZ Coatings for Corrosion Prevention

In the United States (Ref 22), the Federal Highway Administration has demonstrated that thermal spraying is a valuable and proven technology for corrosion control. In 1984, the Rhode Island Department of Transportation was the first to metallize a bridge in the United States. This project was the Acorn Street Bridge in downtown Providence and was a replacement of an old bridge. The thermal spraying was done partly in a shop and partly on-site. The steel was coated with TSZ, sealed, and finished with a topcoat. The Department of Transportation in Ohio followed a short time later, coating several existing bridges in central Ohio with TSZ. The first bridge was in a rural setting in Morrow County and was coated with TSZ, sealed with epoxy, then coated with an epoxy intermediate coat and a urethane topcoat in 1985. The Mile 135 bridge on Interstate I-71 north of Columbus was coated with zinc in 1988. Over 20,000 m^2 (215,000 ft^2) of the substructure of Castleton Bridge over the Hudson River near Albany, NY, was sprayed with Zn-15Al in 2001. The Mile 73 overpass bridge for the CSX rail line on I-71 near Columbus, OH, was metallized with TSZ in 2001.

In the northern United States, deicing salt used on highways during the winter causes severe corrosion of steel rebars in reinforced concrete structures. Corrosion prevention using thermal spray coatings has been developed and tested in existing bridges. A TSZ is applied on the blast-cleaned surface of concrete and acts as the anode to the impressed current between the steel rebars. Necessary current density for such protection has been shown to be 2.2 mA/m^2 (0.2 mA/ft^2), and the coating life has been estimated as a function of electrical charge transmitted across the coating/concrete interface until the coating adhesion is significantly lost. Typical lifetime for such cathodes is estimated at approximately 27 years (Ref 23).

The use of thermal spray coatings for corrosion control of production risers, tethers, flare booms, and other equipment on offshore platforms has increased over the last several years. Other applications include corrosion control of subsea production system flow pipes and land-based flowlines with thermal insulation. In June 1984, the Hutton tension leg platform was installed in water 146 m (480 ft) deep in the North Sea. The tethers, risers, and flare boom were all TSA coated. The background and several reports on this TSA coating application have been published (Ref 24, 25). The coating was flame-sprayed aluminum sealed with two coats of vinyl on the tethers and silicone on the risers. One tether was removed in 1986, and a production riser was removed in 1987 for inspection. There were distinct differences in the TSA coating on the production risers and the tethers, with the vinyl sealant on the tethers blistering, while that on the riser did not. Despite the blisters, the TSA coating was in excellent condition, with no measurable reduction in coating thickness or evidence of corrosion damage to the substrate. Visual inspections of the splash zone also revealed no deterioration in coating quality or performance or any corrosion damage. High-pressure waterjetting was used to remove fouling to enable better inspection (no antifouling coating was applied). This strong mechanical impact did not cause any coating deterioration.

Based on the good experience with TSA coatings on the Hutton platform, TSA was used for splash-zone protection on nine platforms in the southern North Sea, installed between 1987 and 1988. The splash-zone coatings were typically 200 μm (8 mils) thick, with a polyvinyl butyral etch primer overcoated with polyurethane. Pinholes occurred in the polyurethane if the etch primer was not used. Subsequent annual splash-zone inspections have revealed no damage to the TSA, and the sealer has performed well. A TSA was also selected to protect the risers on the Jolliett platform in the Gulf of Mexico in 1989, and no visual damage of the coating was observed after 13 years of service.

More recent examples of TSA coatings applied to give corrosion protection in severe offshore environments include the Shell Sheerwater jackets (5000 m^2, or 54,000 ft^2) and the Mobile Sable Islands (10,000 m^2, or 108,000 ft^2) over five platforms. For the Shell Sheerwater jackets, the coating systems comprised 200 μm (8 mils) of TSA followed by an epoxy sealant and epoxy-acrylic topcoat.

Kanmon Bridge, the first long-span suspension bridge in Japan, was constructed in 1973, connecting the mainland Honshu with the Kyushu district. The bridge was protected from corrosion by TSZ, with six layers of painted

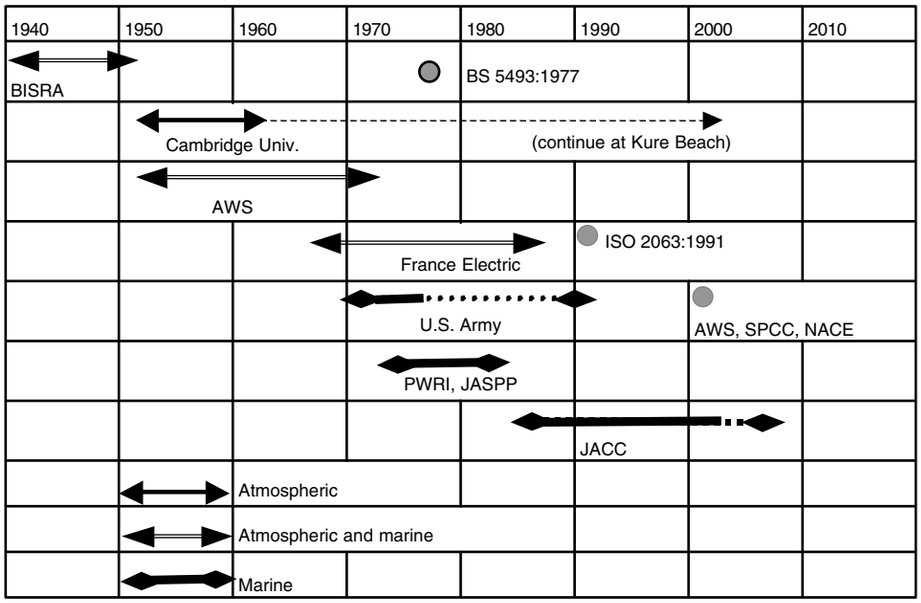

Fig. 6 Summary of important field exposure tests of thermal-sprayed coatings in the world. BISRA, British Iron and Steel Research Association; BS, British Standard; AWS, American Welding Society; ISO, International Organization for Standardization; SPCC: The Society for Protective Coatings; NACE, NACE International; PWRI, Public Works Research Institute; JASPP, Japan Association for Steel Pipe Piles; JACC, Japan Association of Corrosion Control

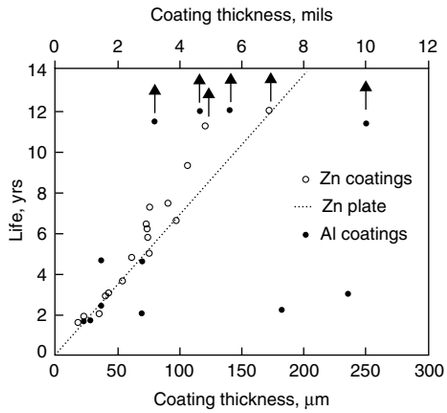

Fig. 7 Relationship between the lives of zinc and aluminum coatings and the coating thickness in a severe industrial atmosphere (Sheffield, United Kingdom)

topcoat. Thermal spray coatings have not been used for subsequent other large-scale bridges due to the high cost, except for small areas such as the inspection girder. Since the mid-1990s, an increasing number of smaller steel bridges and port facilities in coastal areas have been protected with sealed TSA. The most recent large-scale application of thermal spray coatings in Japan is for the urban highway route No. 5 in Fukuoka. During the first term of its construction, more than 200,000 m^2 (2.15×10^6 ft^2) of steel structures such as girders and piers supporting the highway were thermal sprayed, and approximately 500,000 m^2 (5.4×10^6 ft^2) will be sprayed in total when completed. Two types of coating systems have been adopted for this construction. One is thermal-sprayed Zn-15Al, finished with an inorganic sealant. The other coating system is based on co-spraying zinc and aluminum wires simultaneously to form a pseudoalloy coating that is then sealed. Thermal spray was selected to achieve a longer maintenance cycle. This was essential, because the cost of maintenance and repair is prohibitively high in such a densely populated urban area with high traffic levels.

Dense Barrier Coatings by High-Velocity Spraying Processes

High-velocity oxyfuel (HVOF) spraying is a relatively new process being considered for coatings of corrosion-resistant alloys that act as barrier layers on less resistant substrates. The HVOF process produces coatings with much lower levels of porosity compared to arc and flame spraying. The HVOF spraying process is based on oxyfuel combustion at high pressure inside a spray gun to produce a high-velocity jet. A schematic of the HVOF spray gun is shown in Fig. 8. This jet is used to heat and accelerate a powder consumable to high velocity, which then impacts on a substrate to build up the coating. There are several types of HVOF equipment available commercially. The fuel for combustion is a gas such as ethylene, methane, acetylene, and hydrogen, or a liquid fuel such as kerosene. The very high velocity of the powder particles results in a dense coating structure with porosity usually below 2%. Such low-porosity coatings have been achieved for corrosion-resistant alloys, including stainless steels 304, 316L, and nickel-base alloys such as C276 and 625. The coating microstructures obtained depend on the HVOF system type and the spray conditions used to prepare the coating. In all cases, the coating microstructures are different than those seen for these materials in their wrought form. Unlike the sacrificial anode-type coatings of TSZ and TSA, elimination of through porosity in the barrier layer coating type is of critical importance. In wet conditions, corrosion of the substrate surface can be accelerated by the galvanic coupling between the more noble coating and the less noble substrate, which will lead to premature debonding of the coating. Of next importance is control of oxidation of the powder material during spraying. Oxidation degrades the corrosion resistance of the deposited coating by creating regions depleted in alloying elements, such as chromium and nickel.

The HVOF-sprayed coatings can be prepared with low levels of oxide and porosity. An example of a cross section through a coating of nickel alloy prepared with the HVOF process is shown in Fig. 9. The coating shows an inhomogeneous microstructure dominated by interparticle (splat) boundaries, often depleted in alloy elements, and by the presence of thin oxide films at these splat boundaries (Ref. 26). The HVOF-sprayed coatings are found to exhibit different corrosion behavior compared to the corresponding alloy in wrought materials.

Corrosion Performance of Dense HVOF Spray Coatings. The corrosion performance of dense HVOF coatings in aqueous environments can be difficult to evaluate. If the porosity level is very small, typically below 0.5 vol%, penetration of water through the coating may take a long time. Reliance on immersion methods to compare corrosion behavior requires long test durations (often 60 days or longer), with a qualitative visual judgment of any corrosion attack. Electrochemical test techniques, such as that described by ASTM G 61(Ref 27) and based on cyclic potentiodynamic polarization methods, are used to quickly determine susceptibility to corrosion of wrought iron- or nickel- base alloys in aqueous chloride-containing environments. More recently, such techniques have also been applied to thermal-sprayed metallic coatings (Ref 28) to provide a relatively quick method to rank their resistance to corrosion. When the spray coating is porous—higher than 1 vol%—the influence of the substrate on corrosion should be taken into account when interpreting the results. For denser HVOF coatings, the results are likely to be dominated by the corrosion resistance of the coating itself.

Using this approach, the electrochemical corrosion characteristics of coatings of corrosion-resistant alloys sprayed onto low-carbon steel using commercially available HVOF systems have been investigated in seawater and other aqueous solutions (Ref 29). Some examples of typical polarization curves obtained by this test method in artificial seawater for HVOF-sprayed stainless steel 316L and alloy 625 coatings, and the respective materials in bulk wrought form, are shown in Fig. 10 and 11. Only the forward scan is shown for clarity. Coatings with corrosion potentials closer to the values of the corresponding wrought material and lower anodic currents at a given potential are taken to have better resistance to corrosion. Such coatings would be expected to provide greater protection to the underlying steel substrate if completely dense.

The results of these tests suggest that high-quality HVOF-sprayed coatings of nickel alloy

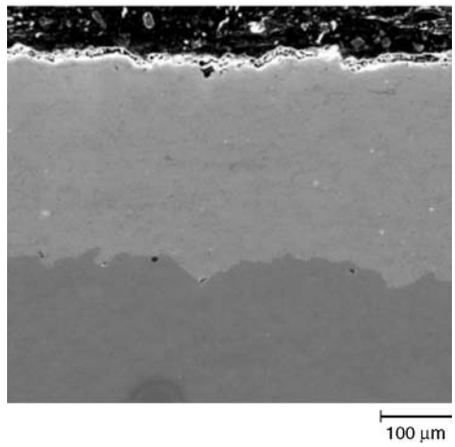

Fig. 9 Cross section of high-velocity oxyfuel-sprayed coating of nickel alloy 625. Courtesy of TWI, Ltd.

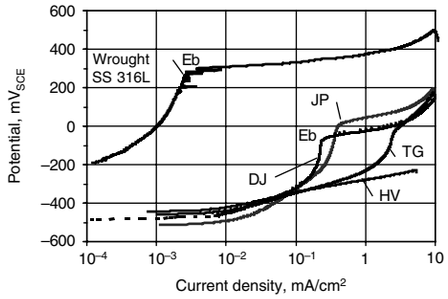

Fig. 10 Examples of anodic polarization curves obtained for high-velocity oxyfuel (HVOF)-sprayed coatings of 316L in deaerated artificial seawater solution. Typical processes include DJ, Diamond Jet hybrid (Sulzer Metco); JP, JP5000 (Tafa/Praxair); TG, TopGun HVOF systems (Miller Thermal); and HV, high-velocity flame spray system. Courtesy of TWI, Ltd.

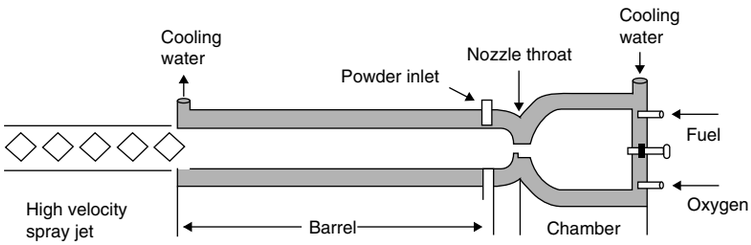

Fig. 8 Schematic of high-velocity oxyfuel spraying process

with composition similar to alloy 625 can provide significantly better corrosion resistance and, consequently, better protection to a steel substrate than similar high-quality HVOF coatings of stainless steel. All the HVOF-sprayed coatings of stainless steel 316L exhibit a significantly lower rest potential and show a much more rapid rise in anodic current density as potential is increased, compared to wrought 316L (Fig. 10). The coatings also show an apparent breakdown potential at approximately 0 mV_{SCE}, considerably lower than that seen for the wrought alloy. As shown in Fig. 11, all the nickel alloy 625 coatings have higher anodic current densities at potentials below approximately 400 mV_{SCE} than the nickel alloy in wrought form. These results again suggest that a HVOF-sprayed nickel alloy coating does not match the corrosion resistance of the same alloy in its wrought form when in a seawater environment.

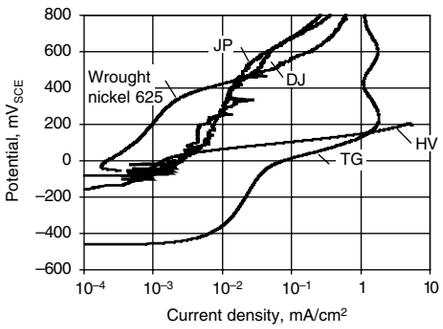

Fig. 11 Examples of anodic polarization curves obtained for high-velocity oxyfuel (HVOF)-sprayed coatings of nickel alloy 625 in deaerated artificial seawater solution. Typical processes include DJ, Diamond Jet hybrid; JP, JP5000; TG, TopGun HVOF systems; and HV, high-velocity flame spray system. Courtesy of TWI, Ltd.

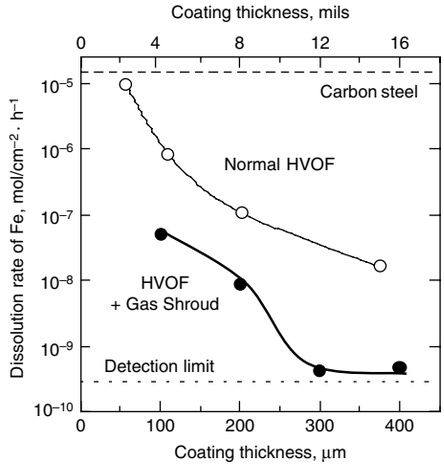

Fig. 12 Amount of through porosity in high-velocity oxyfuel (HVOF)-sprayed Hastelloy C coatings as a function of coating thickness. Through porosity was evaluated by the dissolution rate of iron ions from the carbon steel substrate.

Efforts to achieve denser coatings with less oxidation of the coating have been made by improving the HVOF processes. An earlier study reports success in petroleum plants by the use of a gas shroud to control the atmosphere surrounding the spray particles as they travel from the spray gun to the substrate (Ref 30, 31). A more recent study demonstrated the ability to produce dense, low-oxide coatings without through-coating porosity by controlling the atmosphere surrounding the spray particles in flight while still attaining the very high particle velocity typical of HVOF spraying (Ref 32, 33). The relationship between the amount of through-coating porosity in alloy C278 coatings and coating thickness is shown in Fig. 12 for a commercial HVOF spray gun and with a gas shroud attachment. Alloy C278 is a nickel alloy and has a superior corrosion resistance, especially against crevice corrosion, in seawater compared to 316L stainless steel. Coated specimens were immersed in 0.5 *M* HCl aqueous solution for long durations, and iron ions present in the test solution, dissolved from the steel substrate, were measured by inductively coupled plasma (ICP) emission spectroscopy analysis. The results of these tests showed that the through-coating porosity decreased significantly with increase in coating thickness, but there still remains detectable through-coating porosity when the coating was sprayed using the normal HVOF process. It should be noted that the porosity of alloy C278 coatings obtained by the commercial HVOF spray gun was below the detection limit of mercury porosimeter (0.3 vol% in this case) and protected the steel substrate for more than 3 months in a laboratory immersion test in aerated artificial seawater. With the gas shroud attachment, through porosity was reduced to the detection limit of the ICP analysis. Based on these tests, HVOF coatings with a thickness of 400 µm (16 mils) were selected for longer-term marine exposure tests.

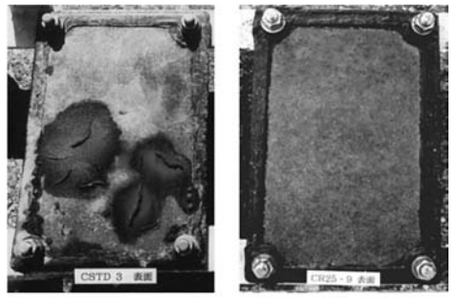

Fig. 13 Appearance of high-velocity oxyfuel (HVOF)-sprayed Hastelloy C coatings on steel plates after 3 months in seawater. (a) Coating sprayed by a commercial HVOF. (b) Coating sprayed by the improved HVOF process with a gas shroud

The appearance of alloy C278 coatings immersed in seawater at a test site facing the Pacific Ocean washed by vigorous waves for three months is shown by the samples in Fig. 13. Even though the coating produced by the commercial HVOF process performed well in the laboratory immersion test, it was penetrated by seawater, and corrosion had started. The results of the marine exposure test of alloy C278 coatings sprayed by using commercial HVOF equipment, HVOF with the gas shroud, and coatings sprayed with commercial HVOF and then heat treated in vacuum at 1050 °C (1920 °F) for 1 h are summarized in Fig. 14. The coatings produced with the commercial HVOF process lasted for 3 months in the tidal and immersed zones, but coating life was longer than a year in the splash zone. The coatings produced with the HVOF process using the gas shroud attachment protected the steel substrate for approximately 1 year in seawater and approximately 2 years in the tidal zone. In the splash zone, the coating life is in excess of 2 years, with the test still in progress. Generally, the coatings exposed at the splash zone have a longer life. The heat treated coatings provided very good corrosion protection in all the zones, with a life

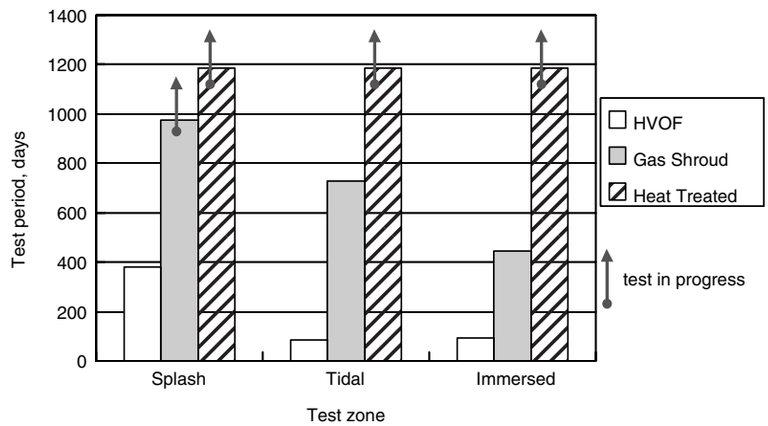

Fig. 14 Period to failure (appearance of rusting on the coating surface) for high-velocity oxyfuel (HVOF)-sprayed Hastelloy C coatings on a steel substrate. The HVOF denotes a commercial HVOF; heat treatment was carried out in vacuum at 1050 °C (1920 °F) for 1 h.

greater than 2 years. The results indicate that the elimination of through-coating porosity must be achieved, and a coating material with good resistance against crevice corrosion should be selected for such applications. The latter is because the spray coating has a rough surface and a more inhomogeneous microstructure, with the potential for microcrevices at the coating surface.

Even though significant progress has been made in this field with the development of the HVOF spraying process, the industrial need is for coatings that can provide a protection life in seawater of 50 years, which is yet to be shown possible.

The Future Use of Thermal Spray Coatings

Thermal spray coatings of zinc, aluminum, and their alloys have a proven history in providing long-term corrosion protection of steel in various natural environments. As the concept of life-cycle cost becomes a more widely accepted requirement, thermal spray coatings will be a more attractive choice for steel structures that require protection against corrosion for many years. There now exists a large amount of information from exposure tests conducted worldwide. This information and the case histories of applications are being accumulated and incorporated into industrial standards and will assist the user in the selection of coating materials and the post-treatment most suitable for a particular environment.

Dense barrier-type coatings of corrosion-resistant alloys using the HVOF spraying processes have not yet achieved the corrosion resistance in aqueous solutions of that of the wrought form of the same materials. Depending on the environment and the coating material, a minimum amount of the residual porosity or thin oxide films at the intersplat boundary can be detrimental. Further improvement of the HVOF process, including the use of gas shrouds and the development of new processes such as cold spraying, is expected to further improve coating quality in the near future.

REFERENCES

1. "Thermal Spraying—Wires, Rods and Cords for Flame and Arc Spraying—Classification—Technical Supply Conditions," ISO 14919, International Organization for Standardization, 2001
2. "Specification for Thermal Spray Feedstock, Solid and Composite Wire and Ceramic Rods," AWS 2.25/2.25M, American Welding Society, 2002
3. "Metallic and Other Inorganic Coatings—Thermal Spraying—Zinc, Aluminium and Their Alloys," ISO 2063, International Organization for Standardization, 2005
4. S. Dallaire and H. Levert, *Surf. Coat. Technol.,* Vol 50 (No. 3), 1992, p 241–248
5. Y. Tsunekawa, M. Hiromura, and M. Okumiya, *J. Therm. Spray Technol.,* Vol 9 (No. 1), 2000, p 83–89
6. G. Itoh, *Fushoku Kagaku To Boushoku Gijutsu (Corrosion Science and Protection Technology),* revised edition, Corona Publishing, 1979, p 62 (in Japanese)
7. S. Kuroda, J. Kawakita, M. Takemoto, and Thermal Spray Committee of Japan Association of Corrosion Control, Marine Exposure Tests of Thermal Sprayed Coatings in Japan, *Proceedings of International Thermal Spray Conference 2003,* (Orlando, FL), ASM International, May 2003, p 343–352
8. T. Lester, D.J. Kingerley, S.J. Harris, and S.P. Matthews, Thermally Sprayed Composite Coatings for Enhanced Corrosion Protection of Steel Structures, *Proceedings of International Thermal Spray Conference,* 1998, ASM International, p 49–55
9. M. LeClercq and R. Bensimon, Combined Paper: New Zinc-Based Alloy for Metallizing, *Proceedings of Eighth International Thermal Spray Conference,* American Society for Metals, 1976, p 417–429
10. M.L. Berndt and C.C. Berndt, Thermal Spray Coatings, *Corrosion: Fundamentals, Testing, and Protection,* Volume 13A, *ASM Handbook,* ASM International, 2003, p 803–813
11. F.S. Rogers, Benefits and Technology Developed to Arc Spray $^{3}/_{16}''$ (4.8 mm) Diameter Wires Used for Corrosion Protection of Steel, *Proceedings of Int. Thermal Spray Conference 2000,* (Montreal, Quebec, Canada), ASM International, p 691–695
12. "Standard Practice for Exposing and Evaluating Metals and Alloys in Surface Seawater," G 52-88, ASTM, reapproved 1993
13. J.C. Hudson and J.F. Stanners, *J. Iron Steel Inst.,* Vol 175, 1953, p 381–390
14. T.P. Hoar and O. Radovici, Zinc-Aluminum Sprayed Coatings, *Proceedings of Sixth Int. Conf. Electrodeposition and Metal Finishing,* (London), *Int. Soc. Met. Finish. Trans.,* Vol 42, 1964
15. R.M. Kain and E.A. Baker, Marine Atmospheric Corrosion Museum Report on the Performance of Thermal Spray Coatings on Steel, *Testing of Metallic and Inorganic Coatings, Special Technical Publication,* Vol 947, American Society for Testing and Materials,1987, p 211–234
16. "Corrosion Tests of Flame-Sprayed Coated Steel, 19-Year Report," AWS C2.14-74, American Welding Society
17. A. Kumar and D. Wittmer, *Mater. Perform.,* Vol 18 (No. 12), 1979, p 9–19
18. A. Beitelman, V.L. Van Blaricum, and A. Kumar, Performance of Coatings in Seawater, A Field Study, *Corrosion,* Vol 439, 1993, p 1–15
19. M. Makita, Y. Mori, and R. Tanaka, The Corrosion and Protection of Steel Pipe Piles in Natural Seawater, *Corros. Marina,* 1980, p 381–393
20. S. Kuroda and M. Takemoto, Ten-Year Interim Report of Thermal Sprayed Zn, Al and Zn-Al Coatings Exposed to Marine Corrosion by Japan Association of Corrosion Control, Proceedings of International Thermal Spray Conference 2000, *Thermal Spray: Surface Engineering via Applied Research,* C.C. Berndt, Ed., ASM International, p 1017–1024
21. M. Schumacher, Ed., *Seawater Corrosion Handbook,* Noyes Data Corporation, 1979, p 13
22. S.D. Cramer, B.S. Covino, Jr., S.J. Bullard, G.R. Holcomb, and J.T. Butler, Metalizing for Corrosion Prevention on Concrete and Steel Bridges, *A Survey Report on the Corrosion Prevention Technology by Thermal Spraying,* Japan Association of Corrosion Control, 2002, p 144
23. B.S. Covino, S.J. Bullard, G.R. Holcomb, S.D. Cramer, G.E. McGill, and C.B. Cryer, *Corrosion,* Vol 53 (No. 5), 1997, p 399–411
24. T. Rosbrook, W.H. Thomason, and J.D. Byrd, Review of the Performance of Flame Sprayed Aluminium Coatings Used on Subsea Components, *Mater. Perform.,* Vol 28 (No. 9), Sept 1989, p 34–38
25. K.P. Fischer, W.H. Thomason, T. Rosbrook, and J. Murali, Performance History of Thermally Sprayed Coatings in Offshore Service, *Mater. Perform.,* Vol 34 (No. 4), March 1995, p 27–35
26. H. Edris, D.G. McCartney, and A.J. Sturgeon, Microstructural Characterization of High Velocity Oxy-Fuel Sprayed Coatings of Inconel 625, *J. Mater. Sci.,* Vol 32 (No. 4), 1997, p 863–872
27. "Conducting Cyclic Potentiodynamic Polarization Measurements for Localized Corrosion Susceptibility of Iron-, Nickel-, and Cobalt-Based Alloys," G 61, *Annual Book of ASTM Standards,* Vol 03.02, ASTM
28. A.J. Sturgeon and D. Buxton, The Electrochemical Corrosion Behaviour of HVOF Sprayed Coatings, *Proceedings of the International Thermal Spray Conference and Exhibition,* (Montreal, Canada), ASM International, May 2000
29. A.J. Sturgeon, "The Corrosion Behaviour of HVOF Sprayed Stainless Steel and Nickel Alloy Coatings in Artificial Seawater," Corrosion 2003, (San Diego, CA), NACE International, March 2003
30. L.N. Moskowitz, *J. Therm. Spray Technol.,* Vol 1 (No. 1), 1993, p 21–29
31. R.P. Krepski, "Thermal Spray Coatings Applications in the Chemical Process Industries," MTI Publication 42 for NACE International, 1994
32. J. Kawakita, T. Fukushima, S. Kuroda, and T. Kodama, *Mater. Trans.,* Vol 44, 2003, p 253–258
33. J. Kawakita, S. Kuroda, T. Fukushima, and T. Kodama, *Sci. Technol. Adv. Mater.,* Vol 4, 2003, p 281–289

ASM Handbook, Volume 13B: Corrosion: Materials
S.D. Cramer, B.S. Covino, Jr., editors, p434-441
DOI: 10.1361/asmhba0003833

Corrosion of Electroplated Hard Chromium

Allen R. Jones, Atotech

HARD CHROMIUM plated parts have chromium coatings more than approximately 1.2 μm (0.05 mil) thick. Parts that are plated with less than this amount are referred to as decorative applications. Electroplated chromium protects substrates by acting as a barrier coating as opposed to a sacrificial coating, such as zinc. Chromium is more electrochemically active than steel; however, it forms a dense self-healing oxide layer on its surface. Chromium can be passivated, or the oxide layer can be formed by exposure to air or by immersion in room-temperature oxidizing acids. Electroplated chromium is chemically resistant to most compounds and offers excellent corrosion protection in various environments. It is especially useful in applications that also require wear resistance.

Corrosion of Chromium Electrodeposits

Coatings protect a substrate by forming a barrier or by being sacrificial. The electrochemical series predicts that chromium is more base or active than zinc, a sacrificial coating. However, chromium metal rapidly reacts with air or oxidizers to form a thin chromium oxide film. This surface chromium oxide film is very passive or noble. If scratched, this passive film automatically heals in the air. Electrodeposited chromium coatings have a Knoop (100 g) microhardness of between 900 and 1100 kg/mm^2. Chromium is the hardest as-deposited electrodeposit. This combination of self-healing and coating hardness provides a good barrier in abrasive environments.

The protective chromium oxide resists high-temperature corrosion and has a desirable Pilling-Bedworth (PB) ratio of 2. The PB ratio is the ratio of the metal oxide volume divided by the metal volume. Pilling-Bedworth values of less than 1 result in an oxide that does not completely cover the surface (Ref 1, 2). A PB ratio of more than 1 is necessary but not sufficient to predict corrosion resistance. Some oxides with ratios of more than 1 are not protective. Additional information about the PB ratio is available in the article "Gaseous Corrosion Mechanisms" in *ASM Handbook,* Volume 13A, 2003.

Microribbons or Microcracks. Chromium electrodeposits are not homogenous, because they contain microribbons. Microcracks are formed by stress relief in the chromium during plating and are filled in by plating with material that contains more oxide and less metallic chromium than the bulk, producing microribbons. Microcracks may form due to the spontaneous decomposition of chromium hydride to form chromium metal and hydrogen. *Microribbons* is a more accurate and descriptive term than the classical term *microcracks,* which is a misnomer. Microribbons are not voids but are ribbons of a three-dimensional network of areas that are more electrochemically active than the bulk of the chromium. They are like ribbons in that they are long, very narrow, and are solid material uniformly distributed throughout the chromium coating. Microcracks only exist on the surface of the chromium where they have not been plated in. When chromium electrodeposits are etched in hydrochloric acid or etched anodically, the microribbons are attacked before the bulk of the chromium and become visible as microcracks. The tensile stress in most electroplated chromium deposits increases with deposit thickness until microcracks are formed (Ref 3, 4). The microcracks decrease the stress in the deposit as the thickness of the deposit increases. Stress is inversely proportional to the number of microcracks (microribbons). Crack-free deposits are highly stressed and softer than microribboned (microcracked) chromium deposits.

Microribbons are present in most electroplated hard chromium deposits. Figure 1 shows typical microribbon structures after etching. The density of microribbons in chromium deposits varies from 0 to more than 1200 ribbons/cm (3000 ribbons/in.), primarily depending on bath chemistry, current density, and temperature. The number of microribbons increases with the concentration of catalyst in the plating bath. After etching a deposit with a high microribbon density (Fig. 1a), the depth of a microribbon was less than 8 μm (0.3 mil) on a deposit 130 μm (5 mils) thick, with ribbon counts of approximately 800 ribbons/cm (2000 ribbons/in.). The depth and width of microribbons decrease as the microribbon density increases. Additional information on microribbons and their formation are reported in the literature (Ref 5).

Because chromium protects substrates by forming a barrier, the coatings must be thicker than the microribbon depth to provide good corrosion resistance. Microribbons are not detrimental to corrosion resistance, as may be expected. There are two reasons for this. First, the microribbons are not voids but are areas with a structure and composition that are different from those of the bulk. Microribbons contain more chromium oxide, which increases the deposit microhardness. Second, the microribbons distribute the corrosion over a larger area, decreasing corrosion penetration of the coating. This is similar to the use of microcracked or microdiscontinuous chromium coatings over nickel in decorative coatings.

Optimizing Corrosion Resistance

The corrosion resistance of a 25 μm (1 mil) thick hard chromium electrodeposit, as determined by neutral salt spray test (NSST), should be 10 to 500 h to red rust. This large range of NSST hours can be attributed to the large number of steps and variables involved in the total process. The main steps fall into the areas of pretreatment, electroplating, and postplating treatment. If any one of these areas is deficient, then the corrosion performance of the product is significantly reduced. These three processes can be viewed as a chain where each process is a link. The weak link will decrease the overall corrosion performance. Improvements in one process cannot overcome large deficiencies in one of the other processes. Interactions occur between the processes. Optimization of the corrosion performance should start with the area that needs the most improvement, because this gives the

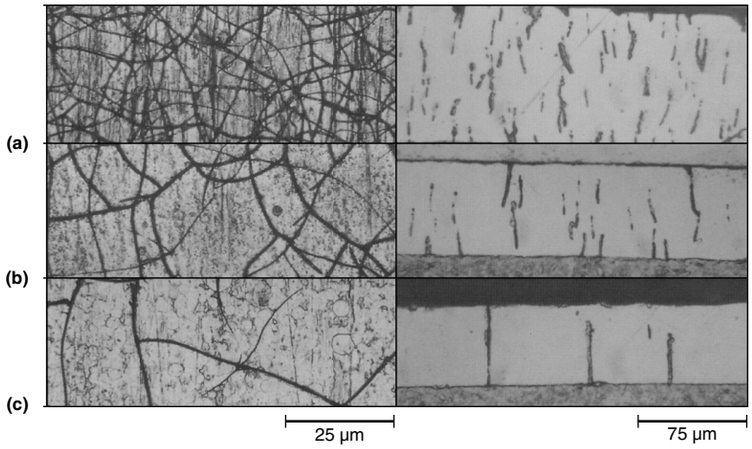

Fig. 1 Micrographs of surfaces (left) and cross sections (right) of anodically etched chromium deposits from (a) high-efficiency etch-free, (b) fluoride, and (c) conventional baths. The samples were plated under typical conditions for each bath. The cross sections were polished prior to etching. Etching was performed in a solution of 100 g/L NaOH at room temperature. Current density on surface: 46 A/dm^2 for 2 min. Electroetch on cross section: a few seconds at 4 V. Etched surface view, original magnification 600×. Etched cross section, original magnification 200×

biggest return (improved corrosion performance) on investment (time, resources, and money). If two of the three processes are at between 80 and 90% of optimum and the remaining process is only 50% of optimum, then the system optimization should start with the process that is only at 50% of optimum.

The corrosion resistances in NSST results are relative within each experiment or reference. Hours of NSST results may not be comparable between experiments or references due to variations in substrate, pretreatment, electroplating, and postplating treatment. Trends or rankings with respect to pretreatments, electroplating chemistries or conditions, and postplating treatments are reproducible.

A detailed analysis of unpublished and published corrosion data (Ref 6) has shown that any process change in the pretreatment or plating steps that would be expected to reduce nodulation leads to better corrosion performance. Large nodules can be removed (picked out) by finishing to form pits (Ref 7). This occurs because the cohesion between the nodule and the bulk of the chromium is less than the cohesion of the chromium within the nodule or bulk chromium. This weak bond may exist, partially, even in small nodules and could be a corrosion pathway to the substrate. The plated parts should be examined for nodules before postfinishing. The presence of significant nodules suggests that optimization should be done on the pretreatment and plating processes. Processes should be designed to give the least amount of nodules. Any process changes must be made with consideration for productivity.

Pretreatments. The main steps for pretreatment processing are shown in Table 1. The goal of the pretreatment is to make a smooth and uniform surface. Each step of the pretreatment process is discussed subsequently, with examples of problems that can be encountered.

Substrate quality is very important, because inclusions can lead to pretreatment problems and can cause plating defects. Inclusions can be classified as physical and chemical. Both types may result in plating defects such as pits or nodules. Physical inclusions, such as hard particles or voids, cause defects by mechanical means. Defects can be microscopic and can be obscured by grinding or honing but may be exposed in the chemical pretreatment processes. Defects in the substrate that cause pits or atypical cracking expose the substrate metal to corrosive media (Ref 8). Gas pits are usually caused by particles in or on the substrate surface that have a low hydrogen overvoltage, such as graphite or carbon particles. The low hydrogen overvoltage promotes the evolution of hydrogen gas in preference to chromium deposition. These pits can occur on overetched cast iron parts and on reworked parts that have not been baked after stripping. Chemical inclusions interact with the cleaning, etching, or plating processes to cause defects. Sulfur-bearing inclusions can cause pits by overcatalyzing the bath at the inclusion site. Inclusions can etch differently than the bulk of the substrate and produce a nonuniform deposit.

Case Depth. Heat treating a suitable ferrous substrate by means of electromagnetic induction and quenching will increase its hardness to a given depth. A hard surface can be finished better than a soft substrate. The harder substrate also improves the mechanical performance of the chromium coating. Hard and soft areas react very differently in an anodic etch, which is used to improve adhesion to the substrate. The case depth should be uniform so that the surface chemistry will react uniformly in the anodic etch, commonly referred to as reverse etching. When the case depth is shallow and variable, a nonuniform surface will be produced after reverse etching.

Grinding and polishing should produce a smooth surface with no or only small steel substrate slivers. The surface should have only small defects or defects that will be removed in the cleaning and etching cycle. Mechanical finishing was shown to be important in obtaining good corrosion resistance (Ref 9). Surface roughness can be quantified by many parameters. The most common are the average roughness (arithmetic mean deviations of the profile), R_a; the average peak-to-valley height in five sampling lengths, R_z; and the maximum peak-to-valley height (total roughness), R_t. The values of the parameters are $R_a < R_z < R_t$. The parameter R_z is often used for describing the surface to be plated, because it better quantifies defects that are important to plating. Naik (Ref 9) showed that if the substrate surface roughness parameter, R_z, was reduced from 1.2 to 1.0 μm (0.05 to 0.04 mil), the NSST hours of plated samples increased from less than 70 to between 180 and 410 h. Jones (Ref 10) demonstrated that substrates with equal R_a's may not produce the same surface finish after plating. Table 2 shows that although the part with a factory finish has a low R_a, it is much rougher after plating than a part finished with 400- and 600-grit paper to a comparable prefinish R_a value. The factory finish contained many bentover slivers that were raised during the pretreatment or plating process and produced roughness and nodules. Substrate brightness is not a good measure of surface finish, because brightness is determined by optical reflection (wavelength of light) and microscopic roughness, whereas larger defects are more important during electrodeposition.

Cleaning steps include demagnetization, cleaning, and rinsing. Demagnetizing parts will reduce the iron particle concentration in the plating bath. Iron particles in the plating bath can cause large nodules. Cleaning is usually done in alkaline solutions with or without current. The cleaning should be designed to remove oils, dirts, smuts, and oxides. Inadequate cleaning can cause pits and nodules. Up to 50% of the dirt is removed in the rinse water after the cleaner has loosened the dirt. Rinse water should be warm and contain less than 3% of the cleaner. The rinse should remove the alkaline film from the

Table 1 Processing steps and conditions for hard chromium plating

Step	Process or condition
Pretreatment	Substrate quality
	Case depth
	Grinding/polishing
	Cleaning
	Etching
Electroplating	Chemistry
	Temperature
	Current density
	Deposit thickness
	Contamination
Posttreatment	Grinding
	Superfinishing
	Buffing

substrate. Excessive cleaner contamination of the plating bath can partially neutralize the plating solution.

Anodic etching is typically the last step before plating most steel substrates. Anodic etching or reverse etching is usually accomplished in chromic acid but can be done in sulfuric acid. Other acid immersion treatments can also be used. The type of etching can significantly improve the corrosion resistance of the plated part (Ref 10). Table 3 shows that pretreatment B, which used a high-coulomb etch, produced a smoother part with much better corrosion resistance than the part prepared using pretreatment A. Jones (Ref 10) showed that to produce the least number of nodules, the reverse-etch coulombs should be either low (100 C/dm^2) or high (3000 C/dm^2). Anodic etch in the plating bath will increase the impurities (iron from the substrate) as well as the voltage required for deposition.

Electroplating. Commercially, hard chromium is deposited from three types of baths: conventional, fluoride mixed-catalyst, and high-efficiency etch-free. All of the baths contain sulfate (SO_4^{2-}) and chromium (VI) oxide, commonly referred to as chromic acid (CrO_3). The sulfate and fluoride compounds act as catalysts. The high-efficiency etch-free bath contains a nonhalide catalyst. Chromium cannot be electrodeposited from an aqueous CrO_3 solution unless one or more catalysts are present. Depending on which catalysts are present and the plating parameters, between 10 and 30% of the cathodic current will be used to reduce hexavalent chromium (Cr^{6+}) to chromium metal. In the fluoride process, a high concentration of fluoride compound must be used to obtain a high microribbon density; unfortunately, this causes severe substrate etching in the low-current-density areas. Excessive catalyst concentration will also decrease the cathodic chromium efficiency. The properties of the electrodeposits are influenced by the type of catalyst, the ratio of CrO_3 to the catalysts, bath impurities, plating temperature, and current density.

The best corrosion resistance is obtained from a chromium deposit having the highest microribbon density, with the smallest number and smallest size of nodules after plating. For a chromium coating with a high microribbon density, the corrosion current is distributed over a larger area, thereby reducing the corrosion rate at any one site and increasing the corrosion resistance of the coating. Figure 1 shows that as the microribbon density increases, the microribbon width and depth decrease. The microribbons in Fig. 1 were etched to make them visible.

The three chemistries used in hard chromium plating exhibit many differences in performance, but the main attribute that affects corrosion resistance is the microribbon density of the deposit. Typical microribbon density of deposits from a conventional bath is between 0 and 500/cm, a fluoride bath is between 500 and 1000/cm, and a high-efficiency etch-free bath is between 1000 and 2000/cm. Figure 2 shows the corrosion performance of 25 μm (1 mil) thick deposits plated from the three different bath types (Ref 11). All samples were plated under optimal conditions for each bath. Corrosion testing was performed according to ASTM B 117. These samples and the samples in Fig. 3 were pretreated as follows: polishing with 600-grit silicon carbide; 15 s, 15 A/dm^2 (1 A/in.^{2}) anodic electroclean; water rinse; 5 s immersion in room-temperature 5% hydrochloric acid; water rinse; and 5 s, 15 A/dm^2 reverse etch in the plating bath. The parts did not have any posttreatment. After 200 h of NSST exposure, 18% of the conventional deposits, 58% of the fluoride deposits, and 87% of the high-efficiency

Table 2 Surface roughness of parts processed with different pretreatment grinding

		Average roughness (R_a)			
		Before plating		After plating	
Finish	Appearance	μm	mil	μm	mil
Factory	Bright	0.079	0.0031	0.46	0.02
400- and 600-grit SiC	Semibright; grind lines visible	0.084	0.0033	0.14	0.006

Source: Ref 10

Table 3 Corrosion performance of 35 μm (1.4 mils) thick chromium deposits with different pretreatments

The samples were tested as plated with no postfinishing.

Performance	Pretreatment A	Pretreatment B
Process description	Anodic electroclean, cold water rinses, immersion in 5% sulfuric acid at room temperature for 15 s, cold water rinses	Anodic electroclean, cold water rinses, anodic etch in bath for 1 min at 60 A/dm^2
Surface roughness after plating		
R_a, μm (mil)	0.53 (0.02)	0.18 (0.007)
R_z, μm (mil)	3.9 (0.15)	1.7 (0.07)
Time in NSST to red rust, h	24–48	96–122

Note: Abbreviations are found in the text. Source: Ref 10

Table 4 Corrosion rates of chromium deposits with different postfinishing

	Chromium corrosion rate (a)	
Sample	μm/yr	mils/yr
As-plated	24	0.95
Coarse polish only	3.3	0.13
Fine polish only	8.2	0.32
Coarse and fine polish	0.4	0.016

(a) Rates are based on the corrosion current (i_{corr}) in 3% NaCl. Source: Ref 15

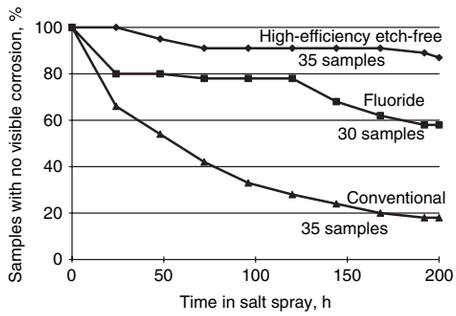

Fig. 2 Effect of plating bath type on the corrosion resistance of chromium. The chromium deposit thicknesses were 25 μm (1 mil), and the corrosion testing was conducted according to ASTM B 117. Samples were electroplated from high-efficiency etch-free, fluoride, and conventional baths under optimal conditions for each chemistry. The samples were tested as plated without any postfinishing. Source: Ref 11

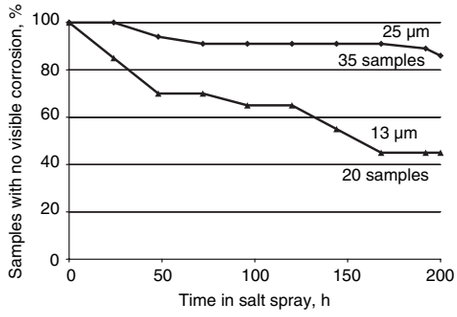

Fig. 3 Effect of plating bath type on the corrosion resistance of chromium. The chromium deposit thicknesses were 13 and 25 μm (0.5 and 1 mil), and the corrosion testing was conducted according to ASTM B 117. Samples were electroplated from a high-efficiency etch-free bath under optimal conditions. The samples were tested as plated without any postfinishing. Source: Ref 11

etch-free deposits were not corroded. The corrosion resistance of deposits 13 μm (0.5 mil) thick, plated from the three baths, had the same ranking as for the 25 μm (1 mil) thick deposits. These data show that as the microribbon density increases, the corrosion resistance of the deposit increases. The improved corrosion performance of the deposits may also be partially attributed to the capability of the high-efficiency etch-free and fluoride baths to plate deposits that are smoother and less nodular than deposits from a conventional bath. Naik (Ref 9) reports that the deposits from a high-efficiency etch-free bath have more corrosion resistance and more microribbons than deposits from a conventional bath.

Temperature. The residual stress and microribbon density are low at low plating temperatures. At plating temperatures of 40 °C (105 °F) and above, the residual stress increases, and microcracking occurs. Above 60 °C (140 °F),

Table 5 Corrosion resistance of electroplated chromium deposits immersed in various acids

Acid	Concentration, %	Temperature		Corrosion rate		Acid	Concentration, %	Temperature		Corrosion rate	
		°C	°F	mm/yr	mils/yr			°C	°F	mm/yr	mils/yr
Acetic	10	12	55	nil		Naphthionic	Saturated	12	55	nil	
		58	135	0.38	15			58	135	nil	
	100	12	55	nil		Nitric	10	12	55	nil	
		58	135	0.20	8			58	135	0.30	12
Anthranilic	Saturated	12	55	nil			100	12	55	nil	
		58	135	nil				58	135	0.13	5
Anthraquinone 2-sulfonic	10	12	55	nil		Nitrobenzoic (meta)	Saturated	12	55	nil	
		58	135	0.03	1.2			58	135	nil	
Arsenic	10	12	55	nil		Nitrocinnamic (meta)	Saturated	12	55	nil	
		58	135	0.28	11			58	135	nil	
Benzene, sulfonic	10	12	55	nil		Oleic	100	12	55	nil	
		58	135	0.05	2			58	135	nil	
Benzoic	Saturated	12	55	nil		Oxalic	10	12	55	nil	
		58	135	nil				58	135	0.03	1.2
Butyric	10	12	55	nil		Palmitic	100	12	55	nil	
		58	135	0.15	6			58	135	nil	
Carbolic (phenol)	Saturated	12	55	nil		Perchloric	10	12	55	0.03	1.2
		58	135	nil				58	135	1.07	42
Chloric	10	12	55	0.40	16	Phenolsulfonic (ortho)	10	12	55	nil	
Chlorine Acid	...	...	...	Attacked				58	135	0.66	26
Chromic	...	...	...	Slow attack		Phenylacetic	Saturated	12	55	nil	
Cinnamic	Saturated	12	55	nil				58	135	0.03	1.2
		58	135	nil		Phosphoric	10	12	55	0.03	1.2
Citric	10	12	55	nil				58	135	0.86	34
		58	135	0.18	7		85	12	55	nil	
Dichloroacetic	10	12	55	nil				58	135	0.05	2
		58	135	1.57	62	Phosphoric (crude)	28	81	180	Attacked	
Dinitrobenzoic (3,5)	Saturated	12	55	nil			60	81	180	Slight attack	
		58	135	0.03	1.2	Phthalic	Saturated	12	55	nil	
Formic	10	12	55	nil				58	135	0.08	3
		58	135	30.48	1200	Picric	Saturated	12	55	nil	
Fumaric	Saturated	12	55	nil				58	135	nil	
		58	135	nil		Propionic	10	12	55	nil	
Furoic (pyromucic)	10	12	55	nil				58	135	0.13	5
		58	135	nil		Pyrogallic	10	12	55	nil	
Gluconic	10	12	55	nil				58	135	nil	
		58	135	nil		Pyruvic	10	12	55	nil	
Glycollic	10	12	55	nil				58	135	nil	
		58	135	0.58	23	Salicylic	Saturated	12	55	nil	
Hydrobromic	10	12	55	0.03	1.2			58	135	0.05	2
		58	135	4.72	186	Stearic	100	12	55	nil	
Hydrochloric	...	...	...	Rapid attack				58	135	nil	
Hydrofluoric	10	12	55	25.4	1000			340	645	Resistant	
Hydroiodic	10	12	55	nil		Succinic	10	12	55	0.03	1.2
		58	135	0.38	15			58	135	0.25	10
Lactic	10	12	55	nil		Sulfanilic	Saturated	12	55	0.03	1.2
		58	135	0.15	6			58	135	0.20	8
Maleic	10	12	55	nil		Sulfobenzoic (ortho)	10	12	55	nil	
		58	135	0.46	18			58	135	3.28	129
Malic	10	12	55	0.05	2	Sulfuric	10	12	55	0.28	11
		58	135	0.23	9			58	135	254	10,000
Malonic	10	12	55	0.03	1.2		100	12	55	0.76	30
		58	135	0.36	14			58	135	1.75	69
Mandelic (amygdalic)	Saturated	12	55	nil		Tannic	10	12	55	nil	
		58	135	0.03	1.2			58	135	nil	
Mixed acid 36% HNO_3, 61% H_2SO_4, 3% H_2O	100	12	55	nil		Tartaric	10	12	55	nil	
		58	135	0.03	1.2			58	135	0.10	4
Monochloroacetic	10	12	55	nil		Toluene, sulfonic (para)	10	12	55	nil	
		58	135	0.08	3			58	135	nil	
Mucic	Saturated	12	55	nil		Trichloroacetic	10	12	55	0.03	1.2
		58	135	nil				58	135	2.62	103
Naphthalene 2,7 disulfonic	10	12	55	nil		Uric	...	...	...	Resistant	
		58	135	0.03	1.2						

Source: Ref 30, 31

the stress and microribbon density decrease (Ref 12) in some chemistries at typical current densities. Residual stress is high on the chromium surface, decreases at the center of the coating, and then increases at the coating-substrate interface (Ref 13). The high stress on the surface is probably due to the reduced cracking in the outer surface.

Current Density. For deposits plated from a high-efficiency etch-free bath, as the current density decreased from 46 to 23 A/dm^2 (3 to 1.5 A/in.^{2}), the corrosion resistance of the deposit increased (Ref 11). This improved corrosion resistance is probably related to the reduced nodulation that occurs at lower current densities. Plating at low current density reduces productivity, so a balance must be made between productivity and corrosion-resistance requirements.

Deposit Brightness. For a particular plating chemistry, as-plated chromium deposits that are bright typically contain an optimum microribbon density. For a particular current density, if the temperature is too low, then the deposit will appear frosty. Conversely, if the temperature is too high, then the deposit will appear dull. All plating chemistries have an optimum temperature and current density range combination that will produce bright deposits.

Coating Thickness. Corrosion resistance increases as the deposit thickness is increased. Figure 3 shows that as the chromium thickness of the high-efficiency etch-free deposit increases, the corrosion resistance increases (Ref 11). Naik (Ref 9) also showed that if the deposit thickness increases from 10 to 20 μm (0.4 to 0.8 mil), then the deposit corrosion resistance increases from 10 to 100 h to 190 to 390 h of NSST. Increasing the coating thickness by a factor of 2 increased the corrosion resistance by 4 to 19 times and decreased the corrosion variability of the sample. These data show that deposit thickness has a large effect on corrosion resistance. One reason is that as the deposit thickness increases, the corrosion path to the substrate is longer and more discontinuous.

Plating bath contaminants, such as iron, nickel, and copper ions; iron particles; nitrate, phosphate, and hydroxide ions, can decrease corrosion resistance of the deposition. The ions of iron, nickel, and copper have a cumulative effect and, at high concentrations, make a deposit nodular, which will decrease the corrosion resistance of the deposit. Iron particles are usually slivers that are narrow and long, approximately 2 by 5 μm (0.08 by 0.2 mil). When current is applied to the part, it becomes an electromagnet and attracts iron particles. This means that iron may stick through the chromium coating after postfinishing. Nitrate and phosphate contamination causes the deposit to become dull gray in appearance. Dull deposits usually have fewer microribbons and would therefore have less corrosion resistance than a bright deposit. When a bath is heavily contaminated with sodium hydroxide, the microribbon density decreases. The sodium hydroxide source is electrolytic or soak alkaline cleaners. Bath contamination from cleaners usually will not be a problem if good rinsing is used after the cleaner.

Additional Deposit Properties Influencing Corrosion. Hardness is related to microribboning, which is related to corrosion. Microribboned chromium coatings have hardnesses between 850 and 1050 HK (100 gf load). Microribbon-free deposits can have hardnesses as low as 300 to 600 HK (Ref 4). According to one study, as deposit hardness increases or crystal size decreases, the rate of attack by sulfuric acid (H_2SO_4), hydrochloric acid (HCl), and CrO_3 decreases (Ref 14).

Microribbon-free thick chromium deposits can be plated from special chemistries under specific conditions. However, these deposits are highly stressed and not as hard as microribboned chromium. Microribbon-free deposits may form macrocracks with aging or when exposed to mechanical or thermal stress. Deposits with macrocracks will have exposed substrate and very poor corrosion resistance.

Postplating Treatments. The main post-treatment of hard chromium deposits is mechanical finishing. The mechanical finishing is often used to machine parts to the proper size after plating. Table 4 shows the importance of proper post-finishing (Ref 15). Mechanical

Table 6 Corrosion resistance of electroplated chromium deposits immersed in salt solutions

		Temperature		Corrosion rate	
Salt	Concentration, %	°C	°F	mm/yr	mils/yr
Alum	...	...	...	Resistant	
Aluminum chloride	10	12	55	nil	
		58	135	0.08	3
Aluminum sulfate	10	12	55	nil	
		58	135	0.20	8
Amino G salt	Saturated	12	55	0.03	1.2
		58	135	0.38	15
Ammonium chloride	10	12	55	nil	
		58	135	0.10	4
Barium chloride	10	12	55	nil	
		58	135	0.03	1.2
Calcium chloride	10	12	55	nil	
		58	135	nil	
Calcium hypochlorite	10	12	55	0.05	2
		58	135	0.89	35
Chromic chloride	10	12	55	nil	
		58	135	0.08	3
Cupric chloride	10	12	55	0.38	15
Cupric nitrate	10	12	55	0.05	2
		58	135	0.18	7
Cupric sulfate	...	...	...	Resistant	
Ferric chloride	10	12	55	nil	
		58	135	0.41	16, pitting
Ferrous chloride	10	12	55	nil	
		58	135	0.14	5.5
Magnesium chloride	10	12	55	nil	
		58	135	nil	
Manganese chloride	10	12	55	nil	
		58	135	nil	
Mercuric chloride	10	12	55	2.01	79, pitting
Potassium chloride	10	12	55	nil	
		58	135	nil	
Scheaffer salt	Saturated	12	55	nil	
		58	135	0.15	6
Sodium benzene sulfonate	10	12	55	nil	
		58	135	nil	
Sodium carbonate	...	...	...	Resistant	
Sodium chloride	10	12	55	nil	
		58	135	nil	
Sodium formate	10	12	55	nil	
		58	135	nil	
Sodium hydrosulfite	10	12	55	nil	
		58	135	nil	
Sodium hydroxide	10	12	55	nil	
		58	135	nil	
Sodium phenol sulfonate	10	12	55	nil	
		58	135	0.03	1.2
Sodium sulfate	10	12	55	nil	
		58	135	0.05	2
Stannous chloride	10	12	55	nil	
		58	135	0.89	35
Strontium chloride	10	12	55	nil	
		58	135	nil	
Zinc chloride	10	12	55	nil	
		58	135	0.03	1.2

Source: Ref 30, 31

Table 7 Corrosion resistance of electroplated chromium deposits in miscellaneous environments

Environment	Concentration, %	Temperature °C	Temperature °F	Corrosion rate mm/yr	Corrosion rate mils/yr
Acid green	10	12	55	nil	
		58	135	0.08	3
Aminophenol (meta)	Saturated	12	55	nil	
		58	135	0.03	1.2
Aniline hydrochloride	10	12	55	0.03	1.2
		58	135	0.58	23
Bakelite during molding	...	...	...	Resistant	
Beer and wort	...	...	...	Resistant	
Beet sugar juice	...	...	...	Resistant	
Benzyl chloride	Saturated	12	55	nil	
		58	135	nil	
	100	12	55	nil	
		58	135	nil	
Biscuit dough	...	...	...	Resistant	
Brass, molten	...	...	...	Resistant	
Brine, neutral	...	...	...	Resistant	
Bronze, aluminum, molten	...	...	...	Resistant	
Carbonaceous material, hot	...	...	...	Resistant	
Carbon tetrachloride	Saturated	12	55	nil	
		58	135	nil	
	100	12	55	nil	
		58	135	nil	
Chlorobenzene	Saturated	12	55	nil	
		58	135	nil	
	100	12	55	nil	
		58	135	nil	
Chloroform	Saturated	12	55	nil	
		58	135	nil	
	100	12	55	nil	
		58	135	nil	
Chlorohydroquinone	10	12	55	nil	
		58	135	0.003	
Chlorophenol (ortho)	Saturated	12	55	nil	
		58	135	0.03	1.2
Cyanides, fused	...	...	...	Resistant	
Ebonite during molding	...	...	...	Resistant	
Fruit acids	...	...	...	Generally resistant	
Glass, molten	...	...	...	Resistant	
Glue, hot	...	...	...	Resistant	
Milk	...	...	...	Resistant	
Nitrophenol (para)	Saturated	12	55	nil	
		58	135	0.03	1.2
Oil, crude	...	...	...	Resistant	
Oils, essential	...	...	...	Resistant	
Paper pulp suspension	...	12	55	nil	
		58	135	nil	
Phthalimide	Saturated	12	55	nil	
		58	135	0.03	1.2
Printing ink	...	...	...	Resistant	
Resins, synthetic	...	...	...	Resistant	
Thiourea (during molding)	...	...	...	Resistant	
Vinyl (during molding)	...	...	...	Resistant	
Rubber (during vulcanizing)	...	...	...	Resistant	
Soap	...	...	...	Resistant	
Steam	...	...	...	Resistant	
Steam (superheated)	...	...	...	Resistant	
Succinimide	Saturated	12	55	nil	
		58	58	0.03	1.2
Sugar	...	...	...	Resistant	
Sulfite liquors	...	Below boiling		Resistant	
Sulfur (in petrol)	...	...	...	Resistant	
Tar	...	...	...	Resistant	
Tartrazine	10	12	55	nil	
		58	135	0.15	6
Tetrachlorobenzene	Saturated	12	55	nil	
		58	135	nil	
Vegetable oil acid	...	...	...	Generally resistant	
Water, deep well	...	...	...	Resistant	
Water, sea	...	...	...	Resistant	
Zinc, molten	...	...	...	Attacked	

Source: Ref 30, 31

finishing improves the corrosion resistance of the deposit compared with the as-plated condition. However, proper finishing is as important after plating as it is before plating. Coarse finishing alone results in a rough surface. The use of only fine polishing probably leaves areas where the chromium is in the as-plated condition. The combination of coarse and fine polishing increases the deposit corrosion resistance by 60 times compared with the as-plated sample. Polishing decreases the deposit surface area and makes the surface a more equipotential surface that corrodes at a slower rate than an unfinished surface. Naik (Ref 9) showed that by using superfinishing, the corrosion resistance of deposits increased from less than 70 h to 180 to 420 h of NSST. Buffing, with or without buffing compounds, is frequently used after grinding. Buffing compounds are composed of fine abrasive media and greases, oils, or waxes. Optimal corrosion resistance of the system is obtained when post-finishing, like prefinishing, proceeds in a series of steps from coarse to fine media.

The as-plated sample in Table 4 has a corrosion rate that would correspond to approximately a 9000 h life for a coating 25 μm (1.0 mil) thick in 3% NaCl solution. This lifetime far exceeds what would be expected based on NSST data. The electrochemical measurements appear to measure the bulk uniform initial corrosion rate and demonstrate the inherent corrosion resistance of electroplated chromium. The NSST for electroplated chromium is a porosity and defect test.

Chromium is often plated on hardened steel parts, and these parts will retain some of the hydrogen that is codeposited with the chromium and occluded in the steel. It is often necessary to

Table 8 Corrosion resistance of electroplated chromium in various gases

Gas	Temperature °C	Temperature °F	Corrosion rate
Air, gas works	...		Resistant
Air, hot oxidizing	...		Resistant
Air, hot reducing	...		Resistant
Air, nitric acid works	...		Resistant
Air, normal	...		Resistant
Ammonia	...		Resistant
Carbon monoxide	...		Resistant
Carbon dioxide	...		Resistant
Chlorine, dry	<300	<570	Resistant
Chlorine, wet	...		Attacked
Coal gas	...		Resistant
Hydrogen sulfide	...		Resistant
Oxygen	>1200	>2190	Oxidizes
Petroleum and diesel fuel combustion products, hot	...		Resistant
Steam	...		Resistant
Steam, superheated	...		Resistant

Source: Ref 30, 31

bake parts made with very hard substrates after plating in order to reduce hydrogen embrittlement. Baking will affect corrosion in two ways. First, it will develop (open up) the outermost microribbon layer. Second, if the temperature is sufficient (370 °C, or 700 °F), it will reduce the stress in the deposit (Ref 3). This reduced stress will decrease stress-corrosion cracking (SCC). Stress-corrosion cracking occurs at pits or grooves in the coating caused by differences in potentials at the bottom of the groove. The bottom of the groove will be dissolved anodically and will deepen the groove (Ref 16).

In one study, diamond compacting and baking in oil after plating improved the corrosion resistance of electrodeposited chromium (Ref 17). Diamond smoothing at forces of 10 and 15 kgf (22 and 33 lbf) after baking improved the corrosion resistance of 9 to 25 μm (0.35 to 1 mil) thick and 50 to 80 μm (2 to 3 mils) thick chromium coatings relative to samples that were not smoothed. Chromium-plated samples baked in oil were much more corrosion resistant than samples baked in air. Both methods sealed pores or outer microcracks in the chromium, which improved the corrosion resistance. Superfinishing techniques seal microcracks and enhance corrosion resistance (Ref 18). Superfinishing is more effective on high-microribbon-density coatings, because the microribbons are narrower than in coatings with lower microribbon densities. Mechanical recompression of electrodeposited chromium improves corrosion resistance (Ref 19).

Grinding of a chromium-plated part to finished dimensions should be performed with adequate cooling and lubrication. Excessive forces and heat may cause macrocracking of the chromium down to the substrate metal. Coarse grinding will promote SCC.

The passivation of chromium by exposure to air or by immersion in an oxidizing acid will significantly improve its corrosion resistance (Ref 20). In one study, nitrogen ion implantation of a chromium-plated molding tool improved the corrosion resistance of the part to molding gases and fluids and increased its service life by more than four times (Ref 21). Postplating treatments are extensively discussed in Ref 22.

Duplex Coatings

A duplex chromium coating is the combination of chromium on another coating. The inner layer is typically nickel and must be hard enough to prevent an anvil effect in wear applications. Anvil effect describes a mechanical force applied to a thin hard coating that is on a softer coating or substrate, which results in cracking of the hard coating and penetration and deformation of the inner coating or substrate. Electroless nickel and electrolytic deposits are used under chromium deposits. A heat treated chromium-nickel coating on type 304 stainless steel reduced SCC (Ref 23). Hard chromium has been used as the inner and outer layer; after grinding the first layer to remove all nodules, another hard chromium layer is deposited. This produces a corrosion-resistant duplex chromium coating. Crack-free chromium has been used as the inner layer, but these layers have the potential to macrocrack and reduce the corrosion resistance of the system. Attention must be given to the activation prior to chromium plating to ensure adhesion of the chromium to the inner layer.

Corrosion-Resistance Data

Corrosion of hard chromium deposits usually begins at microcracks or intersections of microcracks (Ref 20). After moderate acid attack in hydrochloric, sulfuric, or acetic acid, the corrosion reveals the microribbon pattern. Attack will continue on to all of the chromium, and the microribbon pattern will no longer be visible. The corrosion of chromium in sodium chloride (NaCl) solutions will produce mounds of corrosion products. When these mounds are removed, concentric rings define the attacked area. The center and outside areas are unattacked.

The corrosion resistance of chromium-plated 40 Ch steel (SAE 5140) in stratal water from oil wells was comparable to high-alloy steels and superior to low-alloy steels (Ref 24). In concrete corrosion testing, heat treated chromium-plated steel requires a shorter heat treatment time and has a higher tolerable chloride limit than pack chromized steel (Ref 25). Moist sulfur dioxide corrosion testing compared 316L steel to various coatings, including chromium and nickel-chromium duplex coatings with and without heat treatments (Ref 26). Several of the duplex coatings approached the corrosion resistance of 316L steel. Chromium coatings of 0.1 and 0.3 μm (0.004 and 0.012 mil) thickness significantly improved the corrosion resistance of a chromium alloy steel exposed to chloride and fluoride containing volcanic ash (Ref 27). Chromium-plated steel is resistant to a gas mixture of iodine, hydrogen iodide, and water up to temperatures of 500 °C (930 °F) (Ref 28).

Chromium-plated steel with and without a diffusion treatment at 1000 °C (1830 °F) resists corrosion by sodium polysulfides (Na_2S_4, Na_2S_5) and sulfur at temperatures to 440 °C (825 °F). In a 12 month static test, chromium-diffused samples (plating thickness: 50 to 200 μm, or 2 to 8 mils) performed better than the as-plated samples (Ref 29). Tables 5 to 8 provide detailed data on the corrosion of hard chromium in various media.

Applications

Electrodeposited chromium is used in a wide variety of applications and environments. Reference 31 includes a listing of 38 industrial categories with 315 specific applications of electroplated chromium. The corrosion resistance of electroplated chromium is important in wear applications. The wear resistance of a part will decrease if corrosion occurs on a wearing surface, for example, on automotive shocks and struts. Industrial applications in which chromium is not exposed directly to aggressive chemicals may expose chromium coatings to elevated temperature and corrosive environments, such as combustion products.

Electroplated chromium for atmospheric-corrosion applications should be between 20 and 30 μm (0.8 and 1 mil) thick. For corrosion resistance in chemical exposures, electroplated chromium should be 50 to 75 μm (2 to 3 mils) thick.

Electroplated chromium is attacked at 58 °C (135 °F) in formic acid (HCOOH), hydrobromic acid (HBr), HCl, perchloric acid ($HClO_4$), H_2SO_4, and trichloroacetic acid (CCl_3COOH) and is attacked at 12 °C (55 °F) in hydrofluoric acid (HF). Hot (58 °C, or 135 °F) solutions of ferric chloride ($FeCl_3$), mercuric chloride ($HgCl_2$), and stannous chloride ($SnCl_2$) attack electroplated chromium more severely than most other salt solutions.

REFERENCES

1. S.A. Bradford, Corrosion in Gases, *Corrosion,* Vol 13, *Metals Handbook,* 9th ed, ASM International, 1987, p 64–65
2. B. Zhang, Improving IC Yield with Protective Ceramics, *Semicond. Int.* June 1, 2000
3. J.E. Stareck, E.J. Seyb, and A.C. Tulumello, *Plating,* Vol 41, 1954, p 1171–1182
4. A. Bremmer, P. Burkhead, and C. Jennings, *J. Res. Natl. Bur. Stand.,* Vol 40, 1948, p 31–59, RP, 1954
5. A.R. Jones, *Plat. Surf. Finish.,* Vol 76 (No. 4), 1989, p 62–66
6. M. Kuramoto, Y. Kobayshi, and J. Nagasawa, *Proceedings of the Thirty-Second Japan Congress on Materials Research,* The Society of Materials Science, 1989, p 120–126
7. A.R. Jones, *AESF Hard Chromium Plating Workshop Proceedings,* American Electroplaters and Surface Finishers Society, Inc., 1992, p 13–31
8. H. Chessin, E.C. Knill, and E.J. Seyb, Jr., *Plat. Surf. Finish.,* Vol 70, 1983, p 24–29
9. D. Naik, *AESF Chromium Colloquium,* American Electroplaters and Surface Finishers Society, Inc., 1994, p 89–97
10. A.R. Jones, *AESF Chromium Colloquium,* American Electroplaters and Surface Finishers Society, Inc., 1994, p 99–118
11. K.R. Newby, *Interfinish 92 Surface Finishing Congress* (Sao Paulo, Brazil), IUSF, FIESP, and SINDISUPER, 1992, p 1089–1103

12. F. Durut, P. Benaben, B. Forest, and J. Rieu, *Met. Finish.,* Vol 96 (No. 3), 1998, p 52–60
13. J. Pina, A. Dias, M. Francois, and J.L. Leburn, *Surf. Coat. Technol.,* Vol 96, 1997, p 148–162
14. M. Cymboliste, *Trans. Electrochem. Soc.,* Vol 73, 1938, p 353–363
15. Plating Process Evaluation Using Electrochemical Corrosion Techniques, *Electrochemical Corrosion Newsletter II,* EG&G Princeton Applied Research, 1983
16. A.K. Graham, Ed., *Electroplating Engineering Handbook,* 3rd ed., Van Nostrand Reinhold, 1971, p 408–409
17. E.Y. Beider, E.V. Plaskeev, G.N. Petrova, and S.M. Pankratov, *Prot. Met.,* (Russia), Vol 20 (No. 1), 1984, p 127–129
18. Y. Kobayashi, J.I. Nagasawa, T. Sasaki, and Y. Hirose, *Mater. Sci. Res. Int.,* Vol 9, 2003, p 94–101
19. K. Schreck, "Producing a Corrosion-Proof Surface on Workpieces," U.S. Patent PCT Int. Appl. WO 85/3090, 1985
20. N. Hackerman and D.I. Marshall, *Trans. Electrochem. Soc.,* Vol 89, 1946, p 195–205
21. Combined Ion Implantation and Hard Chrome Plating Gives Ten Times Tool Life, *Prod. Finish.,* Vol 39 (No. 5), 1986, p 14
22. F.A. Lowenheim, Ed., *Modern Electroplating,* 3rd ed., John Wiley & Sons, 1974, p 112–114
23. H. Kamide, H. Sato, and Y. Tanaka, *J. Jpn. Inst. Met.,* Vol 58, 1994, p 1294–1298
24. K.T. Kakhramanov, N.S. Fataliev, A.L. Podshibyakina, A.I. Alieva, and Z.R. Fattaeva, *Chem. Pet. Eng. (Russia)* (English trans. of *Khim. Neft. Mashinostr.*), Vol 27, 1991, p 101–103
25. N.S. Rengaswamy, *Trans. Indian Inst. Met.,* Vol 51 (No. 5), 1998, p 249–254
26. R.C. Leu and L. Alting, *Br. Corros. J.,* Vol 25 (No. 3), 1990, p 171–173
27. O. Yamazaki and T. Ogushi, *Zairyo-to-Kankyo (Corros. Eng.),* Vol 40 (No. 12), 1991, p 801–805
28. Y. Imai, Y. Kanda, et al., *Boshoku Gijutsu (Corros. Eng.),* Vol 31 (No. 11), 1982, p 714–721
29. A. Wicker, "Corrosion of Chromium-Coated Steel in Sodium Polysulfide Environments," Report EPRI-EM-2947, Electric Power Research Institute, 1983
30. H.H. Uhlig, *The Corrosion Handbook,* John Wiley & Sons, 1948, p 825–828
31. P. Morisset, *Chromium Plating,* Robert Draper, 1954, p 179–183, 260–271

SELECTED REFERENCES

- E.W. Brooman, Chromium Alloy Plating, *Surface Engineering,* Vol 5, *ASM Handbook,* ASM International, 1994, p 270–273
- J.P. Greenwood, *Hard Chromium Plating,* Robert Draper, 1964
- F.A. Lowenheim, Ed., *Modern Electroplating,* 3rd ed., John Wiley & Sons, 1974
- P. Morisset, *Chromium Plating,* Robert Draper, 1954

ASM Handbook, Volume 13B: Corrosion: Materials
S.D. Cramer, B.S. Covino, Jr., editors, p442-446
DOI: 10.1361/asmhba0003834

Corrosion of Clad Metals

Robert Baboian, RB Corrosion Service

CLAD METALS are metallurgical materials systems consisting of two or more metals or alloys that are metallurgically bonded to form a single material. They are part of a large group of materials termed composites. As shown in Fig. 1, clad metals are categorized as bonded metal-metal laminar composite systems that can be fabricated by several processes. They are also referred to as sandwich metals, metal laminates, and multimetals. Clad metals can be provided in plate, strip, tube, rod, and wire form.

The use of clad metal systems dates back to 3000 B.C., when gold was used to cover bronze. Hammering was the method usually used for cladding. Even today, clad metals—including platinum- and gold-clad (gold-filled) systems—are widely used in the jewelry industry. In approximately 300 B.C., laminated swords fabricated by hammer cladding were stronger, lighter, and more durable than the ones made with a monometal. Modern cladding processes originated in the early 1800s, when English craftsmen developed the Old Sheffield process for cladding silver (or gold) to another metal. This was the first use of the roll-bonding process.

This article describes the principal cladding processes, methods of calculating properties of clad metals, how to design clad metals, and discusses six categories of clad metal systems designed for corrosion control.

The Cladding Process

The cladding process is generally differentiated from other bonding processes, such as brazing and welding, by the fact that none of the metals to be joined is molten when a metal-to-metal bond is achieved. Also, there are no intermediate layers, such as adhesives. The principal cladding techniques include cold roll bonding, hot roll bonding, hot pressing, explosion bonding, and extrusion bonding (Fig. 1). Regardless of the technique used, the bond is achieved by forcing clean oxide-free metal surfaces into intimate contact; this causes a sharing of electrons between the metals. Gaseous impurities diffuse into the metals, and nondiffusible impurities consolidate by spheroidization. All the techniques involve some form of deformation to break up surface oxides and to create metal-to-metal contact, and some form of heat in order to accelerate diffusion. The techniques differ in the amount of deformation and heat used to form the bond and in the method of bringing the metals into intimate contact. Cold and hot roll bonding apply primarily to sheet (less than 5 mm, or 0.2 in., thick), but explosion bonding is usually restricted to thicker gages (up to several inches).

Most engineering metals and alloys can be clad by using one or more of these techniques. As many as 100 different metal combinations with up to 15 layers have been cold roll bonded. Clad combinations that have been commercially produced on a large scale are shown in Fig. 2.

Certain combinations are more difficult to bond. Table 1 categorizes a number of cladding combinations by degree of difficulty in bonding.

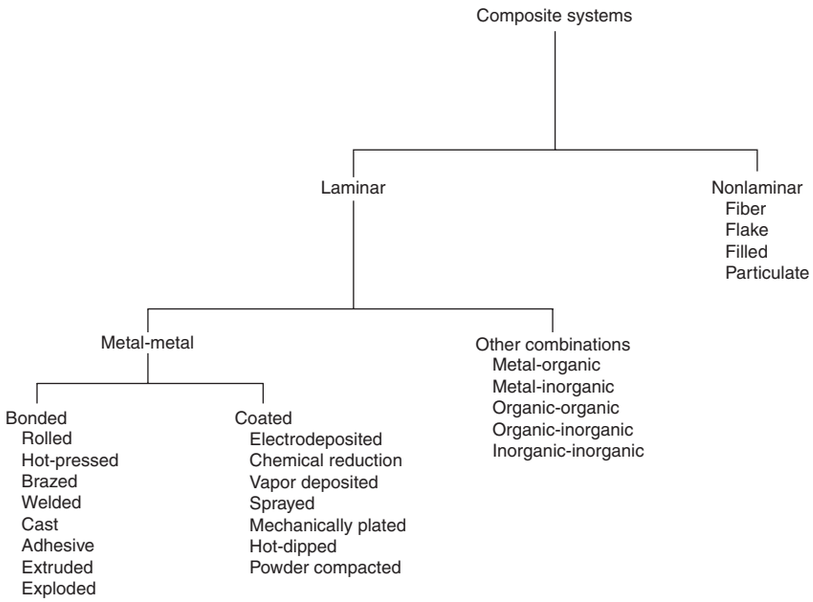

Fig. 1 Categorization of clad metals as bonded metal-metal laminar composite systems

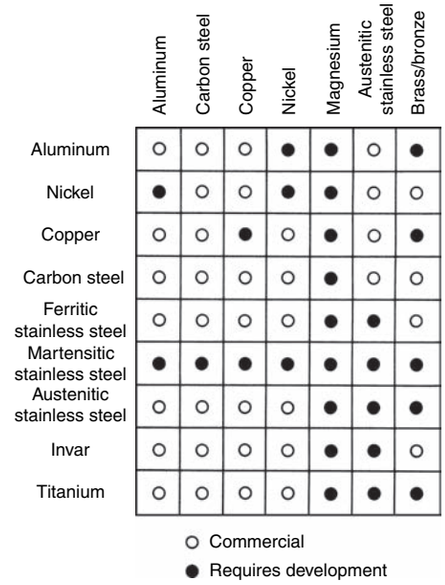

Fig. 2 High-volume commercially available clad metals

Table 1 Categorization of clad metals by degree of difficulty in bonding

In most cases, when a metal is named, alloys of that metal also apply.

Easy to bond
Copper/steel
Copper/nickel
Copper/silver
Copper/gold
Aluminum/aluminum alloys
Tin/copper
Tin/nickel
Gold/nickel
Difficult to bond
Copper/aluminum
Aluminum/carbon steel
Stainless steel/aluminum
Copper/tantalum, niobium, titanium
Titanium/carbon steel, stainless steel
Stainless steel/carbon steel
Aluminum/nickel
Nickel/steel
Copper/stainless steel
Manganese/nickel/copper
Copper/manganese
Silver/manganese
Silver/steel
Uranium/zirconium
Zirconium/copper, steel, stainless steel
Platinum/nickel, copper, steel
Tantalum/niobium
Impractical to bond
Gold/aluminum
Zirconium/aluminum
Cobalt/aluminum
Impossible to bond
Beryllium/anything
Chromium/anything

The degree of difficulty is not based on how some combinations are routinely bonded by companies. It is based on the complexity of the process and required equipment. Some of the properties that affect the bonding process include ductility, nature and stability of oxide films (for example, the ratio of hardness between the film and the metal itself), and the tendency to form intermetallic compounds. Because bonding processes commonly use large amounts of reduction, alloys with greater ductility are more easily clad. Metals and alloys with virtually no ductility, such as beryllium and chromium, are impossible to bond. Metals and alloys that form tenacious oxide films are generally more difficult to bond. These include stainless steels, aluminum alloys, and the refractory metals. However, there are exceptions, such as when the oxide film on the metal surface is very thin and dense and its hardness is much higher than that of the base metal. Finally, some combinations of metals are thermally unstable and form brittle intermetallic compounds above a certain temperature. These combinations can be clad but require stringent control of process variables to avoid the formation of intermetallic compounds, unless compounding is a desirable result.

Properties of Clad Metals

In the absence of measured data, properties of clad metals can be calculated using the rule of mixtures. Thus, a weighted combination of the properties of the components is used according to the following equation:

$$X = aA + bB + \cdots$$

where X is the property of clad metal, a is the volume fraction of component A, A is the property of component A, b is the volume fraction of component B, and B is the property of component B.

This simple equation can apply to the approximation of density, tensile strength, yield strength, thermal expansion (normal to surface), thermal conductivity (parallel to surface), and electrical conductivity (parallel to surface). When calculating properties such as thermal and electrical conductivities normal to the clad metal surface, the general equation for the rule of mixtures is as follows:

$$X = \frac{1}{\frac{a}{A} + \frac{b}{B} + \cdots}$$

Equations for other properties, such as modulus of elasticity in bending, and thermal properties, such as flexivity, thermal deflection, and thermal force, are also available (see Selected References) but are more complex than the rule of mixtures.

Designing with Clad Metals

The choice of a material for a particular application depends on such factors as cost, availability, appearance, strength, fabricability, electrical or thermal properties, mechanical properties, and corrosion resistance. Clad metals provide a means of designing into a composite material specific properties that cannot be obtained in a single material. The early use of clad metals in the jewelry industry combined the aesthetics of precious metals with the low-cost strength of base metals. These materials systems are currently being used for electrical and electronics applications, such as contacts and connectors with selectively clad (inlay) precious metals for low electrical contact resistance and high reliability.

Clad metals can provide properties not available in a monolithic material at any cost. The best example is thermostat bimetals. An alloy with a high coefficient of thermal expansion is clad to an alloy with a low coefficient of thermal expansion. When heated, the resulting bimetal will bend about its neutral axis. Thermostat bimetals are used in various temperature-sensing devices, including motor protectors, circuit breakers, automotive chokes, vent dampers, and room thermostats.

Clad metal coinage is another example of materials with unique properties. These materials are used throughout the world for coins because of the specific requirements of electrical conductivity and density for discrimination in coin machines. Choice of alloys and cladding ratio are varied to produce a coin with specific properties. For example, the U.S. dime and quarter coins are composed of a cupronickel-copper-cupronickel sandwich. This material is corrosion resistant in the coinage environment and provides the properties required for coinage. In addition, recovery of scrap after coin stamping simply involves melting and reuse after adjusting the composition.

Clad metals can be designed with a unique coefficient of linear expansion by cladding two or more alloys in a symmetrical configuration. Specific examples are copper-clad Invar (iron-nickel alloy) wire for glass-to-metal seals and copper-clad Invar (Cu/Invar/Cu) strip that matches the coefficient of expansion of ceramics for leadless semiconductor chip carriers. Different expansion rates can be obtained by varying the cladding ratio in the wire or strip materials.

Self-brazing materials, such as copper-clad stainless steel (Cu/SS/Cu) and copper-clad steel (Cu/steel/Cu), provide another example of the unique properties designed into a clad material. Multilayer heat exchangers are fabricated from these materials by simply stacking the layers of clad material and furnace brazing the entire assembly.

A final example of a unique clad system is the brass-clad steel used in bullet jackets. In this case, the brass cladding provides the drawability that allows steel to be used as a bullet jacket with improved strength, aerodynamics, and resistance to stress-corrosion cracking.

Designing Clad Metals for Corrosion Control

Clad metals designed for corrosion control can be categorized according to the following systems:

- Noble metal clad systems
- Corrosion barrier systems
- Sacrificial metal systems
- Transition metal systems
- Complex multilayer systems
- Clad diffusion alloys

Proper design is essential for providing maximum corrosion resistance with clad metals. This section discusses the basis for designing clad metals for corrosion resistance.

Noble metal clad systems are materials having a relatively inexpensive base metal covered with a corrosion-resistant metal. Selection of the substrate metal is based on the properties required for a particular application. For example, when strength is required, steel is frequently chosen as the substrate. The cladding metal is chosen for its corrosion resistance in a particular environment, such as seawater, sour gas, high temperature, and automotive. The corrosion

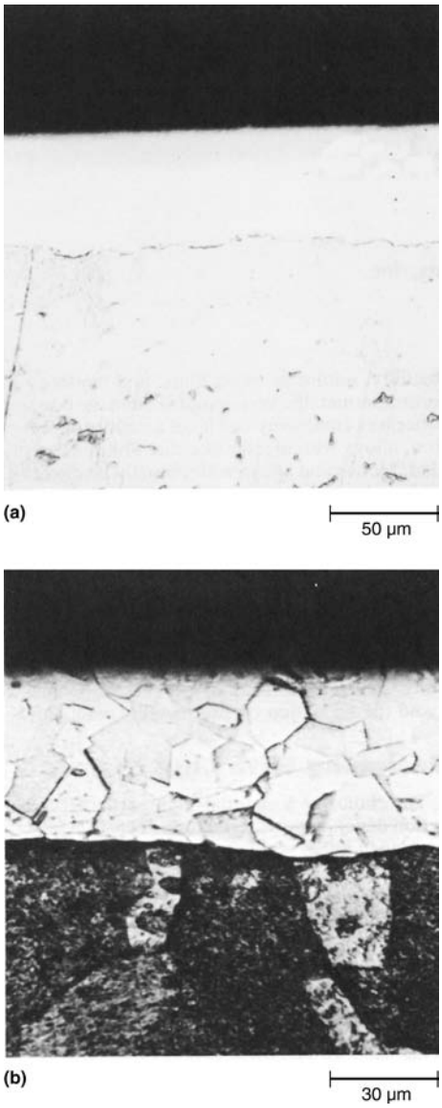

Fig. 3 Micrographs of cross sections of type 304 stainless steel clad carbon steel. (a) As polished. Original magnification 300×. (b) Polished and etched. Original magnification 500×

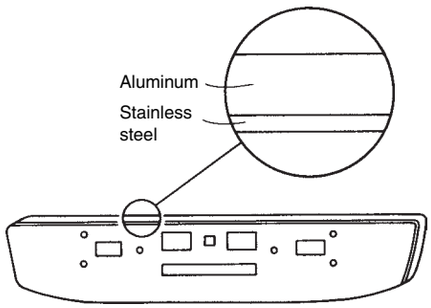

Fig. 4 Stainless steel clad aluminum truck bumper material that combines the corrosion resistance of stainless steel with lightweight aluminum

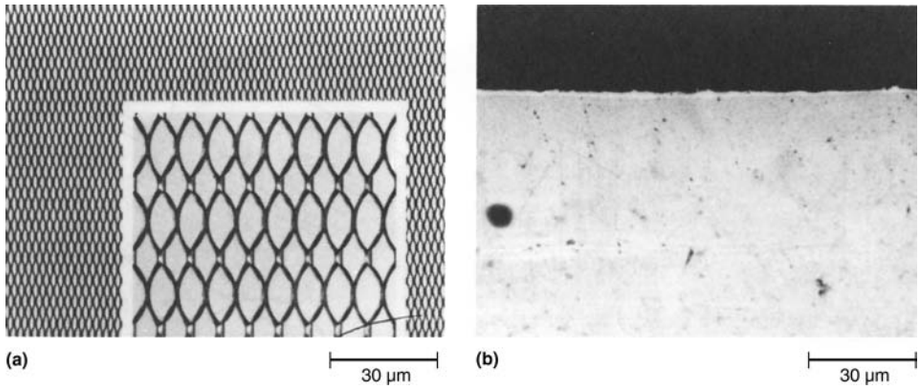

Fig. 5 Platinum-clad niobium, used widely as an anode material in electroplating and in impressed-current cathodic protection. (a) Expanded anode. (b) Cross section showing 1 μm (0.04 mil) thick platinum cladding on a niobium substrate. Original magnification 500×

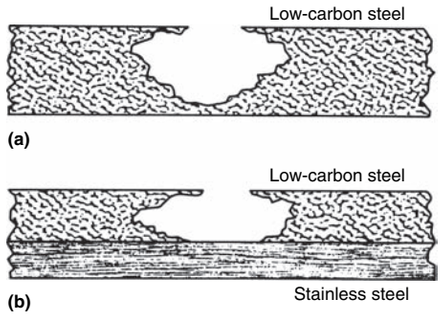

Fig. 6 Illustrations of the corrosion barrier principle. (a) Solid carbon steel. (b) Carbon steel clad stainless steel

resistance of this clad metal category is based on the cladding metal and the fact that the base metal is not exposed to the environment.

A wide range of corrosion-resistant alloys clad to steel substrates has been used in industrial applications. One example is type 304 (UNS S30400) stainless steel clad to steel. Figure 3 shows cross sections of this material. The uniformity of the bond interface is apparent in Fig. 3(a), and in the polished-and-etched condition (Fig. 3b), the metallographic structure of the stainless steel is clearly visible. The grain structure is analogous to that of annealed stainless steel strip.

Clad metals of this type are typically used in the form of strip, plate, and tubing. The noble metal cladding ranges from commonly used stainless steels, such as type 304, to high-nickel alloys, such as Inconel 625 (UNS N06625). These clad metals find various applications in the marine, chemical-processing, power, and pollution control industries. Specific uses include heat exchangers, reaction and pressure vessels, furnace tubes, tubes and tube elements for boilers, scrubbers, wallpaper for the pollution control industry, and other systems involved in the production of chemicals.

Another group of commonly used noble metal clad metals uses aluminum as a substrate. For example, in stainless steel clad aluminum truck bumpers (Fig. 4), type 301 (UNS S30100) or 302 (UNS S30200) stainless steel cladding provides a bright corrosion-resistant surface that also resists the mechanical damage (stone impingement) encountered in service. The aluminum provides a substrate with a high strength-to-weight ratio. This materials system provides an optimal combination of weight, appearance, and durability against road damage and corrosion.

A wide range of precious metals is clad to lower-cost materials. Platinum-clad niobium consists of a thin layer of the precious metal bonded to a niobium substrate. This clad material, available in strip, wire, and rod form, is used as an anode for impressed-current cathodic protection (Fig. 5) and for such other applications as electroplating and desalination. Gold that is clad to such substrate materials as brass is widely used in wire, strip, and tube form. The most familiar example is the gold-filled writing instrument (pens and pencils), which consists of gold clad to brass.

Corrosion Barrier Systems. The combination of two or more metals to form a corrosion barrier system is most widely used where perforation caused by corrosion must be avoided. Low-carbon steel and stainless steel are susceptible to localized corrosion in chloride-containing environments and may perforate rapidly. When steel is clad over the stainless steel layer, the corrosion barrier mechanism prevents perforation. Localized corrosion of the stainless steel is prevented; the stainless steel is protected galvanically by the sacrificial corrosion of the steel in the metal laminate. Therefore, only a thin pore-free layer is required. This mechanism of corrosion resistance is shown schematically in Fig. 6.

The example shown in Fig. 7 of carbon steel clad to type 304 stainless steel demonstrates how perforation is avoided in seawater compared to solid type 304 stainless steel. This material can be used for tubing and for wire in applications requiring strength and corrosion resistance.

Carbon steel cannot be used when increased general corrosion resistance of the outer cladding

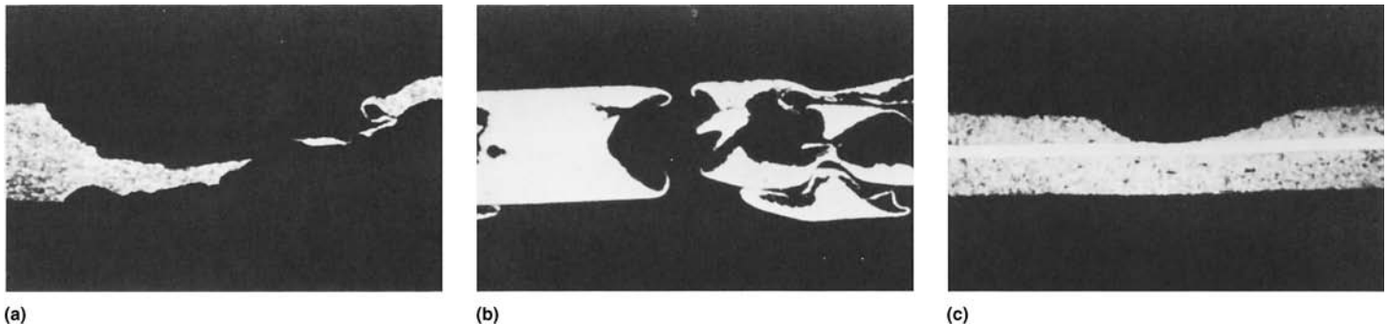

Fig. 7 Micrographs of cross sections of materials after 18 months of immersion in seawater at Duxbury, MA. (a) Low-carbon steel. (b) Type 304 stainless steel. (c) Carbon steel clad type 304 stainless steel

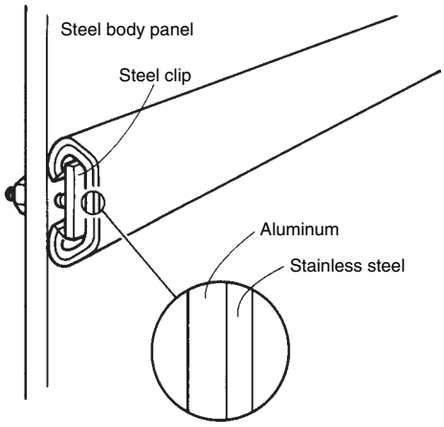

Fig. 8 Stainless steel clad aluminum automotive trim provides sacrificial corrosion protection to the auto body while maintaining a bright corrosion-resistant exterior surface.

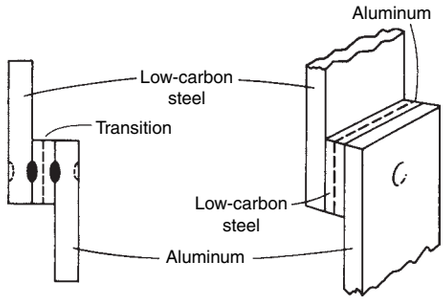

Fig. 9 Illustration of a steel-clad aluminum transition material insert used for joining aluminum to carbon steel

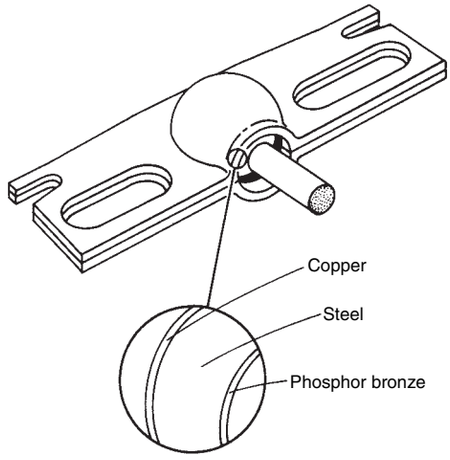

Fig. 10 Clad metal windshield wiper socket, which consists of copper-clad, steel-clad phosphor bronze

is required. A low-grade stainless steel with good resistance to uniform corrosion but poor resistance to localized corrosion can be selected. In seawater service, type 304 stainless steel that is clad to a thin layer of Hastelloy C-276 (UNS N10276) provides a substitute for solid Hastelloy C-276. In this corrosion barrier system, localized corrosion of the type 304 stainless steel is arrested at the C-276 alloy interface.

The most widely used clad metal corrosion barrier material is copper-clad stainless steel (Cu/430 SS/Cu) for telephone and fiber optic cable shielding. In environments in which the corrosion rate of copper is high, such as acidic or sulfide-containing soils, the stainless steel acts as a corrosion barrier and thus prevents perforation, while the inner copper layer maintains high electrical conductivity of the shield.

Sacrificial metals, such as magnesium, zinc, and aluminum, are in the active region of the galvanic series and are extensively used for sacrificial corrosion protection. The location of the sacrificial metal in the galvanic couple is an important consideration in the design of a system. By cladding, the sacrificial metal may be located precisely for efficient cathodic protection.

One of the classic applications for cold roll bonded materials is stainless steel clad aluminum for automotive trim (Fig. 8). The stainless steel exterior surface provides corrosion resistance, high luster, and abrasion and dent resistance, and the aluminum on the inside provides sacrificial protection for the painted auto body steel and for the stainless steel.

The largest application for hot roll bonded materials—Alclad aluminum—also falls into this category. In this case, a more active aluminum alloy is bonded to a more noble aluminum alloy. In service, the outer clad layer of aluminum corrodes sacrificially and protects the more noble aluminum substrate.

Transition Metal Systems. A clad transition metal system provides an interface between two incompatible metals. It not only reduces galvanic corrosion where dissimilar metals are joined but also allows welding techniques to be used when direct joining is not possible.

The principle of a clad transition metal is illustrated in Fig. 9. In this example, aluminum is joined to low-carbon steel through a steel-clad aluminum transition metal. Steel and aluminum form brittle intermetallic compounds at welding temperatures and are therefore difficult to weld directly. The clad transition metal insert allows steel to be welded to steel and aluminum to aluminum; the actual bond between the steel and the aluminum occurs in the clad transition. In addition, the dissimilar-metal crevice is eliminated, which reduces susceptibility to galvanic corrosion.

This concept has been applied commercially in a number of applications. Roll-bonded copper-clad aluminum has been deep drawn into transition tubes for joining aluminum and copper refrigeration tubing. Explosion-bonded steel-clad aluminum has been used to weld aluminum superstructures to steel ship hulls and aluminum bus bars to steel electrodes in aluminum smelting plants. Because of the increased use of aluminum on automobiles, steel-clad aluminum transition materials are being used for spot welding steel to aluminum in such applications as steering wheels and door components. This material is also being used to avoid galvanic corrosion between steel and aluminum in vehicle suspension systems.

Complex Multilayer Systems. In many cases, materials are exposed to dual environments; that is, one side is exposed to one corrosive medium, and the other side is exposed to a

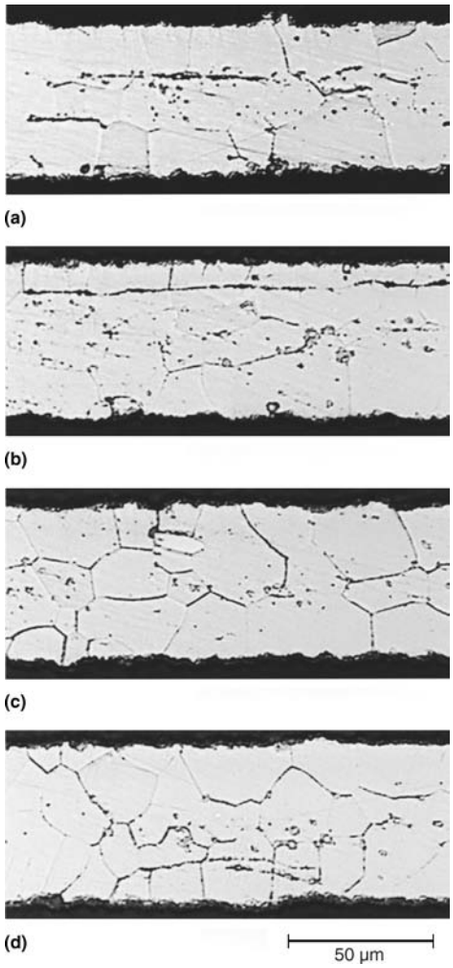

Fig. 11 Microstructure in cross sections of preoxidized and in situ diffused samples annealed at 950 °C (1740 °F) in air for the times indicated. (a) A2, 20 min. (b) A3, 30 min. (c) A4, 60 min. (d) A5, 120 min. Source: L. Chen and B. Jha

different one. A single material may not be able to meet this requirement, or a critical material may be required in large quantity.

Clad metals provide an ideal solution to the materials problem of dual environments. For example, in automobile windshield wiper sockets (Fig. 10), wear resistance is required on the mating surface, atmospheric-corrosion resistance is required on the external surface, and high strength is required and incorporated into the design. Multilayer phosphor-bronze-clad, steel-clad copper is used in this application. The phosphor bronze provides the required bearing surface, copper provides atmospheric-corrosion resistance, and steel provides the required strength.

In the application of small battery cans and caps, copper-clad, stainless steel clad nickel (Cu/SS/Ni) is used where the external nickel layer provides atmospheric-corrosion resistance and low contact resistance. The copper layer on the inside provides the electrode contact surface as well as compatible cell chemistry. The stainless steel layer provides strength and resistance to perforation corrosion.

Other examples include the titanium-clad, copper-clad nickel (Ti/Cu/Ni) bipolar electrode used in fuel cells. Titanium is required on the anode side, nickel provides a hydrogen barrier on the cathode side, and copper provides electrical and thermal conductivity. Tantalum-clad, copper-clad nickel (Ta/Cu/Ni) is used for capacitor cans. Tantalum provides internal corrosion resistance, nickel provides external atmospheric-corrosion resistance and low contact resistance, and copper provides electrical and thermal conductivity.

Clad Diffusion Alloys. Alloying by cladding and thermal diffusion has emerged as a new technology to provide materials with high-temperature corrosion/oxidation resistance. The process involves bonding the components having required compositions, followed by in situ thermal diffusion alloying processes. The technology is useful when an alloy has specific desirable properties but the alloy is brittle. Thus, fabricability of the material is limited. The cladding and diffusion processes provide a material with increased workability. In addition, the clad material can be fabricated to the desired configuration and then thermally diffused to form the alloy.

One example is the development of an oxidation-resistant Fe-Cr-Al metallic substrate for catalytic converters. Pure aluminum is roll bonded to both sides of ferritic stainless steel and then processed to foil thickness. The foil is then fabricated to form the converter structure. After the necessary converter fabrication process, the Fe-Cr-Al alloy is obtained by in situ diffusion alloying. For the example of pure aluminum clad to Fe22Cr, Fig. 11 shows the microstructure in cross sections of in situ diffused samples annealed at 950 °C (1740 °F) in air.

ACKNOWLEDGMENT

This article is adapted from R. Baboian and G. Haynes, "Corrosion of Clad Metals," *Corrosion,* Volume 13, *ASM Handbook,* ASM International, 1987, p 887–890.

SELECTED REFERENCES

- R. Baboian, Designing Clad Metals for Corrosion Control, *Trans. SAE,* Vol 81, 1973, p 1763
- R. Baboian, Conservation of Critical Materials with Clad Metal Systems, *Mater. Perform.,* Vol 33, 1984, p 13
- R. Baboian, Speller Award Lecture, Design of Materials Systems and Devices for Corrosion Control, *Mater. Perform.,* Vol 27 (No. 5), May, 1988
- R. Baboian, Clad Metal Systems for Automobiles, *Automotive Corrosion and Protection,* R. Baboian, Ed., NACE International, 1992
- R. Baboian, Clad Metal Systems for Corrosion Resistance, *Proceedings of the Third Annual ESD Conference on Advanced Coatings Technology* (Ann Arbor, MI), Nov 1993, ESD, The Engineering Society
- L. Chen and B. Jha, Cost Effective FeCrAl Alloys by Roll-Bonding and In Situ Diffusion Alloying for Catalytic Converters Used for Exhaust Gas Emission Control, *Processing and Fabrication of Advanced Materials XII,* T. Srivatsan and R. Varin, Ed., ASM International, 2004
- R.G. Delagi, Designing with Clad Metals, *Mach. Des.,* Vol 52 (No. 27), Nov 20, 1980
- G. Haynes and R. Baboian, "Atmospheric Corrosion of Clad Aluminum Materials," Paper 422, Corrosion/87, NACE International, 1987
- G. Haynes and R. Baboian, *Atmospheric Corrosion Behavior of Clad Metals,* STP 965, ASTM International, 1988, p 145–190
- M. Karavolis and R. Baboian, Clad Metals in Brazed Heat Exchanger Applications, Paper 931083, *Proceedings of the Vehicle Thermal Management Systems Conference,* SAE International, 1993
- A. Pocalyko, Explosion Clad Plate for Corrosion Service, *Mater. Prot.,* June 1965
- R.D. Sisson, Ed., *Coatings and Bimetallics for Aggressive Environments,* American Society for Metals, 1985

ASM Handbook, Volume 13B: Corrosion: Materials
S.D. Cramer, B.S. Covino, Jr., editors, p447-475
DOI: 10.1361/asmhba0003835

Corrosion-Resistant Powder Metallurgy Alloys

Barbara Shaw, Penn State University

POWDER METALLURGY (P/M) COMPONENTS produced from corrosion-resistant alloys constitute a relatively small, but rapidly growing, segment of the P/M market. Applications for corrosion-resistant P/M alloys, especially stainless steel alloys, span a variety of industries including aerospace, automotive, chemical processing, medical, and recreational. Stainless steels, nickel-base superalloys, and titanium and titanium-base alloys are the primary corrosion-resistant P/M alloys in use today. Among these, P/M stainless steels currently find the widest range of applications.

The corrosion resistance of stainless steels (SS) and nickel-base superalloys can be attributed to the natural, protective oxide layer (passive film) that forms on the surfaces of these metals. This protective oxide film is subject to localized breakdown, allowing pitting, crevice corrosion, and/or intergranular corrosion of the underlying substrate. Sintered stainless steels and nickel-base superalloys also derive their corrosion resistance from protective surface oxide films. However, in the case of the sintered metals, inherent pores/crevices are part of the material. Depending on their dimensions, these pores can act as initiation sites for breakdown of the protective oxide leading to the establishment of crevice corrosion.

Pitting resistance, especially in wrought stainless alloys, is often increased by the addition of passivity-enhancing elements to the base alloy. For wrought stainless steels, passivity is typically enhanced through the addition of molybdenum, nickel, or more chromium. These same alloying additions also enhance the pitting resistance of P/M stainless steels. While passivity-enhancing alloying additions also increase crevice-corrosion resistance, they are often not completely effective, and significant alteration of crevice dimensions (increasing its width and/or decreasing its depth), or total elimination of the crevice, is needed to deter crevice corrosion. Another form of localized attack to which corrosion-resistant alloys are susceptible is intergranular corrosion. This form of degradation is commonly encountered in wrought stainless steels and is the result of microstructural differences in composition in the grain-boundary region of the alloy. These unwanted compositional differences result in what is called a sensitized microstructure, and they are usually the result of improper heat treating or welding of the alloy. Powder metallurgy alloys can acquire sensitized microstructures during welding or, for unwelded components, as a result of the sintering/cooling cycle used to produce the alloy.

Susceptibility to pitting, crevice corrosion, and intergranular corrosion is typically evaluated by exposure testing or through the use of one or more electrochemical test methods. Exposure tests provide information on the number of pit or crevice sites present on the specimen surface and the maximum pit or crevice depth or weight loss resulting from attack of sensitized regions of a microstructure. Electrochemical test methods indicate how the passive characteristics of one alloy compare to those of another and provide insight into the mechanisms responsible for corrosion. Parameters that are frequently used to assess passive behavior include the pitting potential, the protection potential, and the passive current density.

Much of the corrosion literature for P/M alloys, including corrosion-resistant alloys, consists of simple immersion and salt-spray cabinet test results. Data from these tests can provide useful information for some simple systems and will be included in this article; however, the results of these tests are often not discriminating enough to separate similar types of alloys, and they do not provide information concerning the nature or mechanisms of corrosion in P/M alloys. In fact, the mechanism of degradation in an artificial environment, such as the salt-fog chamber, is often quite different than the operative mechanism in a natural environment. This difference in mechanism could lead to design decisions based on totally inappropriate data. Electrochemical test methods provide another means for evaluating corrosion resistance, and they can also be used to elucidate important mechanistic information. The corrosion of P/M alloys is often interpreted in simplistic terms; however, in reality the corrosion of sintered stainless steels, nickel-base superalloys, and titanium and titanium-base alloys is more likely the result of somewhat complicated electrochemical interactions. An understanding of these interactions and the mechanisms of corrosion is essential to the continued development of corrosion-resistant P/M alloys and exploitation of their inherent processing advantages. This understanding can only come from carefully planned and executed experiments.

In the following sections, the corrosion characteristics of P/M stainless steels and nickel-base superalloys are presented and discussed. Whenever possible, the corrosion data for P/M alloys are compared to that of their wrought counterparts, and a wide array of test results is presented.

Evaluating the Corrosion Resistance of P/M Alloys

A wide array of experimental techniques are currently being used to assess the corrosion resistance of P/M alloys. These tests range from simple laboratory exposure studies in open containers to more sophisticated electrochemical approaches aimed at gaining insight into the underlying mechanism(s) of P/M alloy corrosion. This section introduces several of the more commonly employed tests and provides specific examples of the use of these methods in evaluating the corrosion resistance of P/M stainless steels. More detailed information on corrosion testing, in general, is available in *Corrosion: Fundamentals, Testing, and Protection,* Volume 13A of the *ASM Handbook,* and in *Annual Book of Standards,* Volume 3.02, of the ASTM standards.

Results from Exposure Testing

Exposure tests are commonly used for ranking the performance of a group of related alloys and assessing quality control. Ideally, these tests should be conducted in actual service environments. Unfortunately, very few references in the literature cite service or environmental exposure

test results for P/M materials; instead, much of the P/M literature cites results from immersion and salt-spray cabinet testing.

Immersion Test Results. Most immersion test results found in the P/M literature are for exposures in either acid or chloride environments. The concentration of the aggressive species (i.e., chloride or hydrogen ions) in these immersion tests is typically greater than that expected during actual service. The increased concentration of the aggressive species serves to accelerate the test; however, the degree of acceleration is unknown and no real consensus exists on the best concentration to use. Several investigators have used a 5% NaCl solution for the chloride exposures. Immersion test results have been reported in a number of acid solutions including 1% HCl, 30% H_2SO_4, 10% HNO_3, and 20% HNO_3, at ambient and elevated temperatures. Unfortunately, no single acid electrolyte is used consistently.

Erroneous results can occur when using wrought alloy specimen preparation practices on P/M specimens. Surface polishing prior to testing, for example, can produce erroneous results because polishing tends to distort or close off surface pores that might normally be present on the surface of the actual component. The method of cleaning and degreasing porous P/M materials prior to testing is another practice that needs to be considered carefully. Degreasing, a practice that is routinely used for wrought specimens, can trap liquids in the pores of P/M specimens and care must be taken to remove this liquid prior to the initiation of a test. As with all corrosion exposure tests, it is advisable to test P/M specimens with surfaces similar to those anticipated for service conditions.

Evaluation of P/M specimens after exposure testing is a subject of some controversy. Typically, a rating system is used that involves visually assessing the amount of surface staining or corrosion on a test coupon and categorizing its degradation in one of four ways:

- A, no attack of the surface, categorized as 0% attack
- B, attack of 1% or less of the surface
- C, attack of 1 to 25% of the surface
- D, attack of more than 25% of the surface

A photographic chart showing a series of stainless steel specimens after exposure to a 5% NaCl solution and characterization using the A through D rating system (Ref 1) is shown in Fig. 1. Another way of using the data acquired from such an inspection is illustrated in Fig. 2, which shows a plot of the percentage of replicate specimens holding a particular rating versus the log of the time of exposure (Ref 1). This plot reveals that the mean life of a 316L P/M specimen immersed in 5% NaCl solution, accepting no surface rust or staining, is approximately 80 h (the intersection of the 50% line with the 1% surface rust/stain curve). If 1% surface rust/stain is acceptable, then the mean life is extended to longer than 300 h. If 1 to 25% surface rust/stain is acceptable, the mean life is extended to more than 1000 h. Corrosion-resistance data for a few different stainless steels, in terms of the hours needed to attain up to 1% surface rust or stain ("B" rating on Klar's scale), is presented in Table 1 (Ref 2). Not surprisingly, the more highly alloyed stainless steels exhibited the best performance. Because strict adherence with the first category in Klar's rating scheme (no rust or rust stain) is difficult to achieve for P/M specimens, this category is often broadened to allow for the first spot of rust or stain on the specimen surface. Some researchers find it more convenient to use 0.1% rust or rust stain for this first category instead of no attack (Ref 3–5).

Measurement of weight loss following exposure or immersion in a corrosive media is a standard method used for assessing corrosion resistance. While weight-loss measurements are relatively straightforward and easy to apply to wrought metals, they can be more difficult to apply to P/M materials because of their inherent porosity. Porosity traps the test solution and the corrosion products within the pores, making it difficult to accurately record small weight losses, even when elaborate cleaning and drying procedures are employed. Most researchers have been successful in obtaining meaningful weight-loss values for porous P/M alloys after immersion testing in acid solutions, but weight losses in less aggressive solutions (such as 0.1 *M* NaCl or 5% NaCl) are not available. Figure 3 (Ref 6) shows weight-loss data for P/M 316L stainless steel as a function of sintering atmosphere, after immersion in a 10% HNO_3 solution for 24 h. Following testing, the specimens in this study were rinsed three times in distilled water and dried in a box oven at a temperature less than 100 °C (212 °F). The drying was continued until the point where no further water evaporation was detected in the weight-loss measurements. A more elaborate cleaning and drying procedure, employed after similar testing, is described in

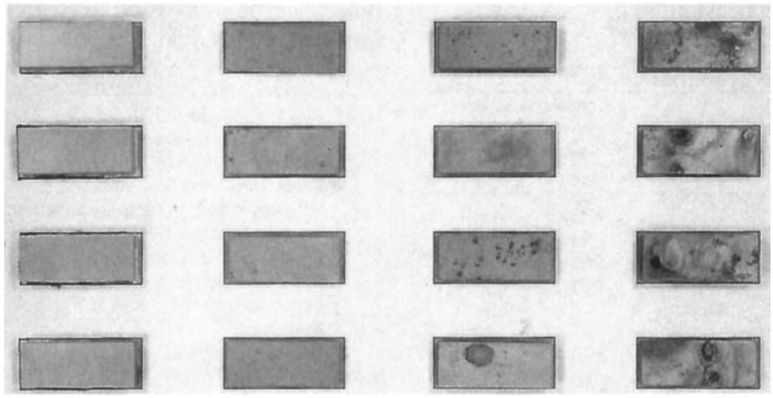

Fig. 1 Photographic chart of sintered stainless steel transverse rupture specimens tested in 5% aqueous NaCl by immersion. Definition of ratings: A, sample free from any corrosion; B, up to 1% of surface covered by stain or rust; C, 1 to 25% of surface covered by rust; D, more than 25% of surface covered by rust. Source: Ref 1. Courtesy of Prasan Samal, OMG Americas

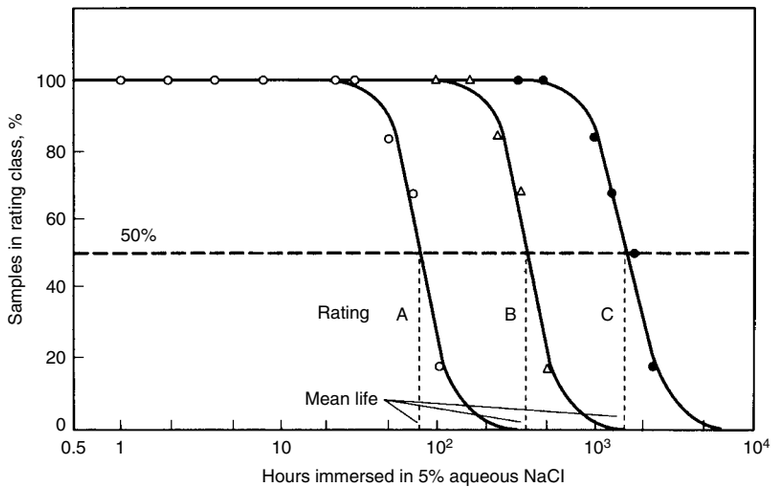

Fig. 2 Plot of percentages of replicate specimens with a given rating versus immersion time. Source: Ref 1

Ref 7 and is outlined in Table 2. Researchers occasionally report weight gains following corrosion testing; however, the utility of such values in assessing corrosion resistance is unknown and is, perhaps, not of much value.

Provided that the density of the material, the exposed surface area, and the time of exposure are known, the conversion of weight-loss data into corrosion-penetration rates is accomplished by the relationship:

$$\text{mm/yr} = 87.6\ w/dAt \qquad \text{(Eq 1)}$$

where d is the density in g/cm^3, w is the weight loss in mg, A is the surface area in cm^2, and t is the time in hours.

The application and design life of the part will determine a tolerable rate. In general, corrosion-penetration rates can be qualified as (Ref 8):

Penetration rate		
mm/yr	mils/yr	Rating
<0.02	<0.8	Outstanding
0.1–0.5	4–20	Good
0.5–1	20–40	Fair
1–5	40–200	Poor

An example of corrosion rate data for 304L and 316L wrought and P/M sintered stainless steel after immersion in 0.5 M H_2SO_4, as a function of immersion time and sintering conditions, is presented in Table 3 (Ref 9). The wrought alloys clearly exhibited the lowest corrosion rates, followed by the vacuum sintered alloys. As is the case here, weight-loss data are sometimes reported in the units of mg/dm^{2}day (mdd) or g/dm^{2}day (gdd). Conversion between these two corrosion rate measures and penetration rate is:

$$\text{mm/yr} = 56.6\,\text{mdd/alloy specific gravity}$$

or

$$\text{mm/yr} = 0.0566\,\text{gdd/alloy specific gravity} \qquad \text{(Eq 2)}$$

Elevated-temperature or boiling acid solutions are often used to assess susceptibility of wrought stainless steels to intergranular corrosion, and procedures for this type of testing are covered in ASTM A 262 and A 763. Because the solutions called for in these ASTM are quite aggressive to porous P/M specimens, a variety of modifications have been employed by investigators to reduce the aggressiveness of the specified solutions. These modifications include reducing the time of the test, reducing the concentration of the acid, and/or reducing the temperature of the solution. Unfortunately, no consensus on the appropriate approach for intergranular corrosion testing of P/M alloys has been reached. Weight-loss values for both P/M and wrought 434L and 409 stainless steels after testing according to ASTM method A 763 practice Z are presented in Table 4 (Ref 10). Practice Z of ASTM A 763 calls for exposure of the test specimens in a boiling solution of 6 wt% $CuSO_4 + 16$ wt% H_2SO_4 for a period of 24 h. In this test, the specimens are embedded in copper shot that is poured into the bottom of the test flask. The standard practice Z calls for 180° bending of the tested specimen, because weight loss for wrought specimens is often not large enough to determine corrosion rates. In the case of P/M parts, however, weight loss was found to be effective in measuring corrosion rates and, while 180° bending of the P/M specimens was possible prior to testing, bend testing resulted in fracture after only a few degrees of bending. Examination of the specimens after intergranular corrosion testing, via ASTM A 763 practice Z, revealed uniform corrosion of the P/M alloys in addition to the anticipated grain-boundary

Table 1 Sintering conditions, chemical analysis, and corrosion resistances of hydrogen-sintered stainless steel

Specimens held 45 min at 1127 °C (2060 °F)

		Sintering conditions				Properties of sintered parts				
		Dew point		Cooling rate,	Density,	Composition, wt%			Corrosion resistance (5% aqueous NaCl by immersion)	
Alloy	Sample No.	°C	°F	°C/min	g/cm^3	N	O	C	B-rating(a), h	% of maximum
316L(b)	1	−32	−25	540	6.7–6.8	0.04	0.21	0.033	2	~24
	2								50	
	3								60	
	4								80	
	5	−32	−25	54	6.7–6.8	0.03	0.21	0.032	1	~12
	6								1	
	7								30	
	8								60	
316LSC(c)	9	−40	−40	187	6.7	0.06	0.21	0.045	1800	~60
	10								1800	
	11								1800	
	12	−44	−45	187	6.8	0.04	0.19	0.043	1200	~100
	13								2900	
	14								2900	
	15								2900	
317L	16	−44	−45	187	6.75	0.04	0.24	0.052	600	~17
	17								200	
	18								1600	
	19								1600	
20Cr-17Ni-5Mo	20	−44	−45	187	6.7	0.05	0.15	0.049	6000	~100
	21								6000	
	22								6000	
	23								>6000	
	24	−40	−40	187	6.7	0.07	0.14	0.11	7800	~100
	25								7800	
	26								7800	

(a) Average of hours specimens are in test solution until 1% of surface is covered by stain or rust. (b) L, low carbon. (c) LSC, copper and tin are prealloyed into 316L powder. Source: Ref 2

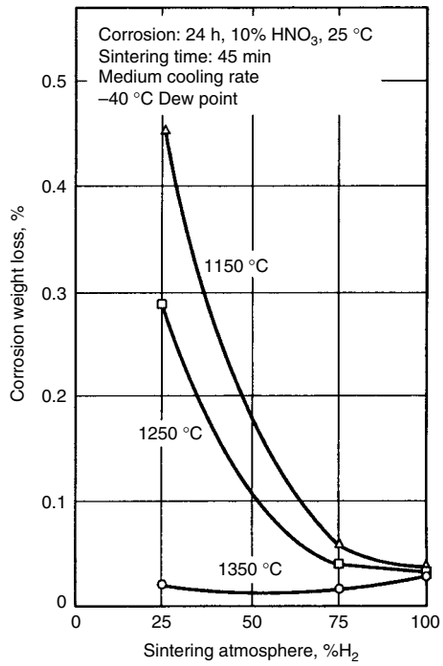

Fig. 3 Corrosion weight loss for 316L in 10% HNO_3 shown as a function of the sintering atmosphere for three sintering temperatures. Source: Ref 6

Table 2 Procedure used to clean P/M specimens after acid exposure testing

Step No.	Procedure
1	Heat P/M samples to 70 °C
2	Submit samples to a vacuum of (−100 kPa) to evaporate solution in the pores
3	Repeat steps 1 and 2 two times
4	Fill pores of the P/M samples with distilled water to wash out the pores
5	Repeat steps 1 and 2 three times
6	Impregnate samples with ethyl alcohol to absorb water
7	Repeat steps 1 and 2 once
8	Store in a dessicator

Source: Ref 7

attack, as Fig. 4 reveals for a P/M 434 alloy. After modifying this test method by reducing the concentration of sulfuric acid, as suggested in Ref 10, weight losses were reduced to the values reported in Table 5. Examination of the specimens after testing revealed that corrosion was predominantly along the grain boundaries, as the scanning electron micrograph in Fig. 5 reveals.

Another means of quantifying the degree of corrosion of a metal is to measure the amount of corroded material that is in solution following immersion for a given period of time. A colorimetric method for evaluating the corrosion of P/M stainless steels, which utilizes a commercially available test kit, has been described in Ref 11. In this method, the iron concentration in solution is measured as a function of time using a commercial test kit containing self-filling ampoules, activator solutions, and a photometer. First, a sample of the test solution is placed in a sample cup and an activator, a solution containing a mixture of thioglycolic acid and ammonia, is added to the solution. The activator dissolves most forms of particulate iron and reduces ferric (Fe^{3+}) ions within the solution to ferrous (Fe^{2+}) ions. The partially evacuated ampoule containing an acidic, buffered solution of 1,10-phenanthroline is inserted into the test solution, and its tip is snapped allowing both solutions to mix and fill the ampoule. After mixing, the ampoule is then inserted into a calibrated photometer and the transmission of light is measured by percentage. Iron content in parts per million (ppm), within the range of 0.01 to 7.6 ppm is then calculated based on a conversion chart provided with the test kit. Examples of the average total iron concentration measured as a function of exposure time for a variety of sintered stainless alloys exposed to a 5 wt% NaCl solution are presented in Table 6 (Ref 11). In each case, specimens of identical dimensions were exposed to 400 mL of a 5 wt% NaCl solution in closed containers, and the values reported were the average of five readings. A nearly linear iron dissolution rate was observed for most of the alloys during the eight-day test, as Fig. 6 illustrates (Ref 11). Good correlation was noted between the results of the colorimetric test and salt-spray and 5% NaCl immersion tests (Ref 12), as Fig. 7 and 8 reveal. Immersion testing can also be used in conjunction with other experimental methods, such as mechanical tests, to assess corrosion resistance. Table 7 illustrates the results from such a test conducted on sintered 316L stainless steel specimens (Ref 13). Prior to mechanical testing via a three-point loading transverse rupture test, the specimens in this study were immersed in a 5% NaCl solution at 20 °C (70 °F). Three sintering atmospheres were evaluated, and some of the specimens were passivated in acid solutions prior to chloride exposure. Under the sintering conditions used (laboratory alumina tube furnaces, no purification of the gaseous atmospheres, and dew points in the range of −40 to −60 °C, or −40 to −75 °F, upon entering the furnace), only the vacuum sintered specimens showed resistance to corrosion. These data also reveal that the two passivating treatments were detrimental to corrosion resistance. Strengths of specimens sintered in vacuum and

Table 3 Properties and corrosion rates of sintered type 304L and 316L stainless steels

Code	Sintering atmosphere	Sintering temperature, °C	Volume mass, $(kg/m^3)\times10^3$	Rockwell hardness, HRB	Porosity total, %	Pore size average, μm	Corrosion rates(a) Immersion time 7 days	14 days	21 days
304L									
W	...	...	...	...	...	...	2.5×10^{-2}	1.2×10^{-2}	3.4×10^{-2}
A	Vacuum	1200	6.52	44	12.0	1.99	2.1×10^{-1}	1.2×10^{-1}	4.0×10^{-1}
B	N_2+H_2	1120	6.39	72	11.7	1.25	7.2×10^{-1}	3.7×10^{-1}	7.3×10^{-1}
C	N_2+H_2	1190	6.43	78	10.9	0.79	1.4	9.3×10^{-1}	1.3
316L									
W	...	...	...	...	...	...	1.8×10^{-3}	9.2×10^{-4}	6.1×10^{-4}
A	Vacuum	1200	6.43	38	10.4	0.98	1.2×10^{-1}	6.9×10^{-2}	2.1×10^{-1}
B	N_2+H_2	1120	6.34	63	12.7	0.98	1.8	1.5	1.6
C	N_2+H_2	1190	6.36	69	11.4	0.79	2.3	2.0	2.3

(a) $(g/dm^2\times day)$ in 0.5 *M* H_2SO_4. $T = 25$ °C, of wrought (W) and sintered samples (A, B, C). Source: Ref 9

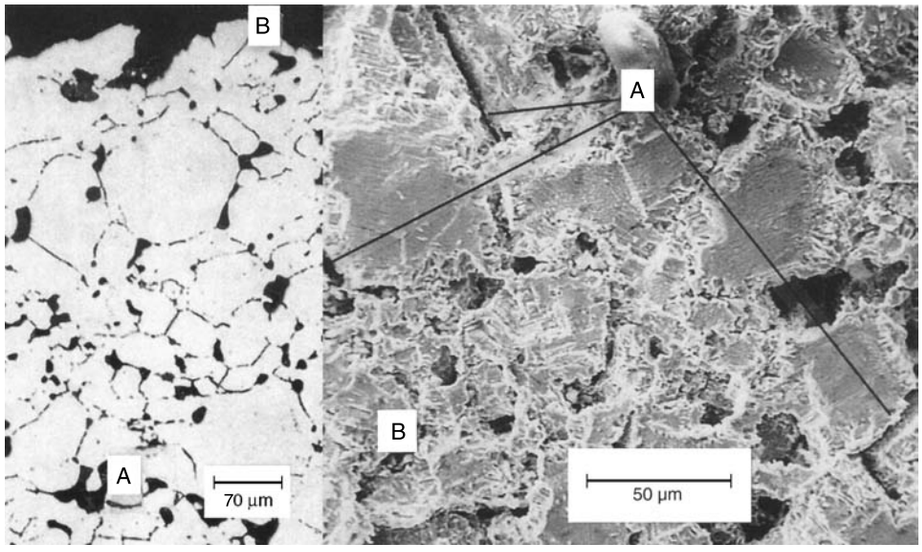

(a) (b)

Fig. 4 Two views of a 1290 °C (2350 °F) sintered P/M 434L specimen subjected to ASTM A 763 practice Z that reveals regions of: A, subsurface intergranular attack; and B, surface uniform attack. (a) Metallographic cross section. (b) Scanning electron micrograph of the surface

Table 4 Average intergranular corrosion rates via ASTM A 763 practice Z

Specimen	Density, g/cm^3	Sintering temperature °C	Sintering temperature °F	Corrosion rate(a), mm/month
P/M434L	7.00	1200	2200	4.68
	7.20	1290	2350	3.77
Wrought 434L	...	...	...	2.47
P/M 409Cb	6.90	1200	2200	63.01(b)
	7.07	1290	2350	23.06
Wrought 409	7.73	...	...	19.83
Welded wrought 409	...	...	...	12.37
Welded P/M 434L	...	1200	2200	2.73
	...	1290	2350	3.66

(a) Average of two tests. (b) After testing, pieces of the specimen were so badly dissolved that they could not be collected. Source: Ref 10

Table 5 Average intergranular corrosion rates for P/M and wrought 434 and 409 according to modified ASTM A 763

Specimen	Sintering temperature °C	Sintering temperature °F	Corrosion rate(a), mm/month
P/M 409Cb	1290	2350	1.22
Wrought 409	...	...	0.226
P/M 434L	1290	2350	0.231
Wrought 434L	...	...	0.002(b)

(a) Average of three tests. (b) The weight losses used to calculate corrosion rates were within the expected error range of the balance. Source: Ref 10

in hydrogen were similar. A similar investigation using a 20% NaCl solution, in lieu of the 5% solution, found that the corrosion resistance of 316L stainless steel was the same as reported in Table 7 (Ref 13).

Ferric Chloride and Ferroxyl Exposures. The ferric chloride test method, ASTM G 48, for characterizing the resistance of wrought stainless steels and related alloys to pitting and crevice corrosion is sometimes used for evaluating P/M materials. While this method may be useful in assessing the susceptibility of wrought materials to crevice corrosion, its use for evaluating crevice-corrosion susceptibility in sintered stainless steel alloys is questionable because these materials already contain inherent crevices. Applying a crevice former to a specimen that already contains a crevice may facilitate the initiation of crevice corrosion. Because crevice width and length are critical factors in establishing crevice corrosion, the application of one crevice on top of another seriously alters the intent and validity of the original test. However, if the ferric chloride solution is simply being used as an aggressive oxidizing solution and no crevice formers are used, such as the test described in ASTM G 48 method A, then the data for P/M specimens may be of value.

It should be noted that some researchers have found that exposures in the 6% $FeCl_3$ solution suggested in ASTM G 48 are too aggressive for the characterization of sintered stainless steels. An alternative solution that has been used for exposure studies is a hexacyanoferrate solution (ferroxyl) that may or may not contain added chloride (Ref 14). A benefit of this solution, in addition to being an oxidizing agent, is that it can be used as an indicator of contamination by iron because the solution turns blue in the presence of ferrous ions. A typical test involves exposure to the hexacyanoferrate solution for 24 h and a visual inspection of the specimens using the following rating scale (Ref 14):

Category	Amount of attack	Visual inspection results
0	No attack	No blue spots
1	Light attack	Very weak blue spots without growth
2	Moderate attack	Blue spots with slow growth—no needle growth or large accumulation of blue dye
3	Severe attack	Blue spots with growth—needle growth or accumulation of the corrosion product on the surface

An example of the results obtained on sintered 316L stainless steel (produced under different sintering conditions) and a few wrought stainless steels (which were tested with an artificial crevice formed by an O-ring) are provided in Table 8 (Ref 14). The pitting potential as reported in Table 8 is a characteristic potential such that pits are stable at potentials noble to the pitting potential, and pits will grow if potential is noble to the repassivation potential, which is less than the pitting potential. See the article "Pitting Corrosion" in Volume 13A, *ASM Handbook,* for further details.

Salt-Spray Cabinet Test Results. Despite the controversy that exists concerning the applicability of salt-spray cabinet exposure results compared to natural environments, the test remains a standard in many communities. In relation to other types of corrosion data for P/M materials, a substantial amount of salt-spray cabinet data exists. In fact, when conducted according to ASTM B 117, this test is probably the most commonly used experiment for assessing corrosion in P/M metals and alloys. Examples of the times needed to notice 0.1% surface rust for a variety of stainless steels after salt-spray cabinet testing are presented in Table 9 (Ref 3). An inspection at 100 h revealed no attack of wrought 316L specimens. Similar data, obtained using the Klar rating system, for sintered 304L, regular 316L, special 316L alloys, and SS 100 alloys after ASTM B 117 testing for times in excess of 1000 h are presented in Fig. 9 (Ref 11).

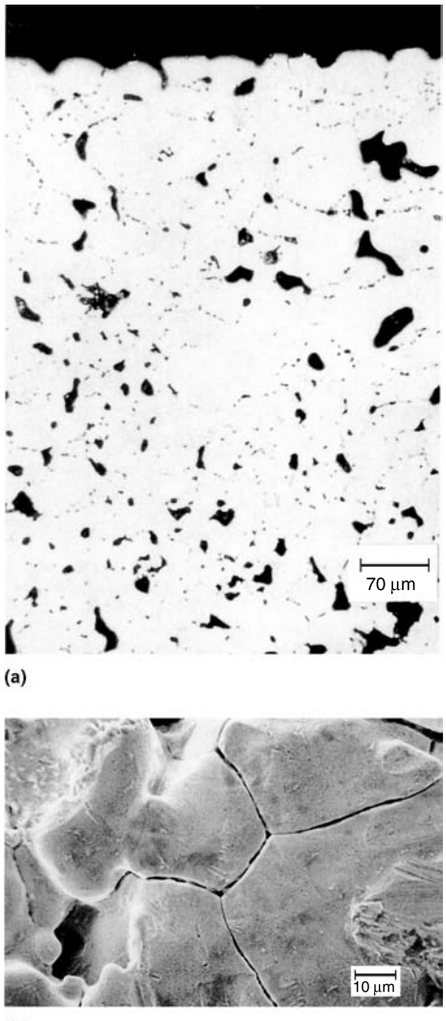

Fig. 5 Two views of a 1290 °C (2350 °F) sintered P/M 434L specimen subjected to the modified intergranular test. (a) Metallographic cross section showing subsurface intergranular attack and no uniform surface attack. (b) Scanning electron micrograph of the surface revealing intergranular attack and no attack of grain interiors

Electrochemical Testing

As stated earlier, electrochemical methods of corrosion testing yield information concerning corrosion mechanisms as well as information on corrosion rates. Because of their inherent porosity, some special issues arise in the electrochemical testing of sintered P/M materials. These issues include alteration of surface porosity resulting from polishing, insufficient removal of degreasing solvents from pores prior to testing, unknown or unreported surface areas, and increased time needed to establish steady-state conditions. Irrespective of the particular electrochemical test being conducted, care should be exercised in addressing each of the aforementioned issues.

Open-Circuit Potential versus Time. Prior to initiating an electrochemical test, it is customary to monitor the open circuit or corrosion potential for a period of time. Monitoring of the potential should be conducted for a long enough period of time to ensure that steady-state conditions exist between the metal and its environment. The length of time needed to establish a steady-state open-circuit potential can vary from a few minutes to several weeks, depending on the particular metal/environment combination. Important information concerning the nature of corrosion can sometimes be determined from open-circuit potential versus time behavior. Comparison of open-circuit potential versus time behavior for wrought and P/M alloys of the same nominal composition typically reveals lower potentials for the P/M alloys—indicating a more active electrochemical state, as Fig. 10 reveals for porous 316L sintered stainless steel (Ref 15, 16). Open-circuit potential behavior can also provide an indication of the role that alloying additions play in altering corrosion resistance. The data in Fig. 11 show that the addition of either nickel, platinum, or palladium to sintered stainless steel increases the open-circuit potentials of the alloy, suggesting that these alloying additions enhance passivity, at least temporarily (Ref 17). In some cases, the initial open-circuit potential versus time behavior for P/M materials reveals significant instabilities, supposedly resulting from the infiltration of solution into the porous alloy, as shown in Fig. 12 (Ref 18). Instabilities such as these, despite their origin, are the reason that the open-circuit potentials are monitored prior to initiating electrochemical experiments that rely on steady-state behavior, such as polarization tests.

Polarization experiments are the most commonly used electrochemical methods for assessing corrosion behavior. Of specific interest

in the study of corrosion-resistant P/M materials are the following polarization techniques: anodic polarization, cyclic polarization, polarization resistance, and electrochemical potentiokinetic reactivation. Prior to a discussion of electrochemical corrosion testing of P/M materials, it is necessary to briefly review some basic information concerning polarization curves and to define a few terms related to polarization behavior and passivity. The reader is encouraged to consult Ref 19 for more detailed information.

Figure 13 shows anodic polarization behavior for an active/passive metal (Ref 20). With regard to corrosion-resistant P/M alloys, anodic polarization curves provide useful information concerning the potential range over which a material is passive, the amount of protection afforded by the film, the susceptibility to pitting, and the ease with which passivity is obtained. Starting at the open-circuit potential and moving in the anodic direction, many metals undergo an initial period of active dissolution, prior to passive film formation, as the potential is scanned in the positive direction. The current density just prior to the onset of passive film formation is termed the "critical current density" and is often denoted by i_{crit}. The potential marking the onset of passivity is termed the primary passivation potential and it is denoted by E_{pp}. Passivity is observed in the region of the anodic polarization curve where the current density drops significantly. It is desirable for passivity to extend over a broad potential range and for the current density in this range, termed the passive current density (i_p), to be very low (typically, a few $\mu A/cm^2$ or less). If aggressive species, such as chloride ions, are not present, then the end of the passive region of the curve is determined by the onset of transpassive dissolution of the film or the initiation of another anodic reaction, such as oxygen evolution, on the specimen surface. The passive film is subject to pitting corrosion when chloride or another aggressive species is present. The onset of pitting is marked by a sudden increase in the current density—the potential where this increase occurs is called the pitting potential, E_{pit}, or the breakdown potential, E_{bd}. The higher the pitting potential, the less susceptible the material is to pitting. It should be noted that the pitting potential as measured in a potentiodynamic polarization experiment is a function of scan rate. As a result, care must be exercised in picking a scan rate to ensure that a slow enough scan rate is being used to maintain steady-state conditions at the metal electrolyte interface and to allow for the induction time needed for the onset of pitting. In a polarization curve, such as the one shown in Fig. 13, the potential provides the driving force for a reaction to occur and the current density (the current/surface area of the specimen) is a measure of the corrosion rate (Ref 20). For some metal/solution combinations, the protective passive film is present on the metal surface initially and polarization is not required for its formation. The term "self-passivating" is used to describe such metals, and their polarization behavior is illustrated in Fig. 14 (Ref 20).

Anodic polarization curves for wrought and P/M 434L stainless steel in 0.1 *M* NaCl are presented in Fig. 15 (Ref 18). In this particular example, the current density was based on the apparent surface area of the specimen rather than the actual wetted surface area of the specimen. Measurement of the actual wetted surface area would be needed for precise determination of current-related polarization characteristics, such as the passive current density and critical current density. In addition, the actual wetted surface area is needed for an accurate determination of the corrosion rate. Unfortunately, much of the P/M electrochemical corrosion literature fails to measure and/or report actual surface areas. As a result, care must be taken when basing judgments on variations in current density (i_p, i_{crit}, or i_{corr}) of an order of magnitude or less, unless the actual surface area of the specimen was measured. Anodic polarization characteristics (i_p, i_{crit}, E_{pit}, E_{corr}) are often summarized in tabular form, as shown in Table 10 for wrought and sintered 316L stainless steel (Ref 1).

Because E_{pit} is subject to scan rate effects and is a stochastic parameter, other more conservative parameters are often used to characterize the safe upper potential bounds for use of a passive metal. The most frequently used parameter in this category is the protection potential (E_{prot}). A cyclic polarization experiment in which the potential scan direction is reversed after reaching a predetermined critical current or potential is used to determine the protection potential, as shown in Fig. 16

Table 6 Total iron concentrations after immersion testing in 400 mL of 5 wt% NaCl solution

Sintering conditions and resulting properties of stainless steel samples							Average total iron concentration in solution(c), ppm		
				Surface, wt%					
Designation	Alloy	Sintering conditions(a)	Sintered density(b), g/cm^3	C	N	O	1 day	4 days	8 days
304N2	304 SS	1316 °C DA(d)	6.32	0.002	0.550	0.170	1.18	5.28	↑
304N29	304 SS	1316 °C DA(d)	6.90	0.016	0.560	0.190	0.61	4.01	6.33
304L	304 SS	1288 °C Vac	6.31	0.002	0.010	0.220	0.57	4.19	7.44
304L9	304 SS	1288 °C Vac	6.89	0.004	0.010	0.200	0.20	1.57	3.92
304N2LSC	304 LSC	1316 °C DA(d)	6.49	0.006	0.220	0.180	↓	↓	↓
304N2LSC9	304 LSC	1316 °C DA(d)	6.91	0.010	0.220	0.150	↓	↓	0.12
304L LSC9	304 LSC	1288 °C Vac	6.92	0.006	0.078	0.450	↓	0.12	0.50
304N2 PLUS	304 PLUS	1316 °C DA(d)	6.40	0.008	0.140	0.170	↓	↓	↓
304L PLUS	304 PLUS	1288 °C Vac	6.41	0.004	0.044	0.280	0.15	0.19	0.20
316N2	316 SS	1316 °C DA(d)	6.54	<0.001	0.570	0.150	1.13	4.06	7.17
316N29	316 SS	1316 °C DA(d)	6.83	0.010	0.430	0.190	1.37	3.57	5.53
316L	316 SS	1288 °C Vac	6.46	0.007	0.007	0.250	0.18	0.42	0.48
316L 9	316 SS	1288 °C Vac	6.86	0.006	0.014	0.230	↓	0.50	1.62
316N2LSC	316 LSC	1316 °C DA(d)	6.45	0.008	0.180	0.100	↓	↓	↓
316N2LSC 9	316 LSC	1316 °C DA(d)	6.87	0.010	0.210	0.210	↓	↓	0.03
316L LSC	316 LSC	1288 °C Vac	6.49	0.002	0.052	0.120	↓	0.33	0.76
316L LSC 9	316 LSC	1288 °C Vac	6.63	0.005	0.091	0.250	↓	0.06	0.52
316N2 PLUS	316 PLUS	1316 °C DA(d)	6.42	0.004	0.110	0.120	↓	↓	↓
316L PLUS	316 PLUS	1288 °C DA(d)	6.45	0.007	0.045	0.150	↓	↓	↓
316X	316 SS	1288 °C Vac	6.65	0.005	0.001	0.295	↓	↓	0.10
316X LSC	316 LSC	1288 °C Vac	6.69	0.006	0.002	0.174	↓	↓	0.03
316X PLUS	316 PLUS	1288 °C Vac	6.47	0.007	0.008	0.215	↓	↓	↓
100N2	20Cr-17Ni-5Mo	1316 °C DA(d)	6.29	0.006	0.820	0.039	1.88	4.39	5.70
100N29	20Cr-17Ni-5Mo	1316 °C DA(d)	6.82	0.010	0.610	0.054	0.78	3.45	4.16
100L	20Cr-17Ni-5Mo	1288 °C Vac	6.25	<0.001	0.011	0.140	↓	↓	↓
100L 9	20Cr-17Ni-5Mo	1288 °C Vac	6.71	<0.001	0.011	0.140	↓	↓	↓
100X	20Cr-17Ni-5Mo	1288 °C Vac(e)	6.72	0.007	0.001	0.144	↓	↓	↓

(a) DA, dissociated ammonia: Vac, vacuum. (b) Density was measured with oil impregnation per ASTM B 328. (c) ↑, above the detection range; ↓, below the detection range. (d). Actual furnace atmosphere was 91.8 vol% D.A. + 8.2 vol% N_2. (e) Followed by a hold at 1150 °C for 10 min. Source: Ref 12

(Ref 21). Pourbaix originally defined the E_{prot} as the potential at which the current on the reverse scan returns to a low value. This low value is traditionally reported as the potential at which the reverse scan intersects the forward scan. Cyclic polarization experiments are frequently conducted on P/M materials, and an example of the difference in protection potential observed between wrought and porous 316L stainless steel is shown in Fig. 17 (Ref 15).

A few types of electrochemical measurements can be used to determine corrosion rates, as discussed in Ref 19. One of these methods, polarization resistance, involves polarizing the specimens a few millivolts above and below the open-circuit potential and measuring the current response. The data are plotted using linear scales, and the slope of the potential versus current density data at the open-circuit potential ($\Delta E/\Delta i$) is taken as illustrated in Fig. 18. This slope is called the polarization resistance, R_p, and it is inversely proportional to the corrosion current density:

$$i_{corr} = (1/2.3R_p)[(b_a + b_c)/(b_a + b_c)] \qquad \text{(Eq 3)}$$

where b_a is the anodic Tafel slope and b_c is the cathodic Tafel slope (both with units of V/decade. This can be used for the corrosion rate:

$$\text{Corrosion rate} = (3.26 \times 10^{-3})(i_{corr})(EW)/d \qquad \text{(Eq 4)}$$

where EW is the equivalent weight of the metal or alloy in grams, d is the density of the metal or alloy in g/cm^3, and i_{corr} is the corrosion current density in mA/cm^2. A comparison of polarization resistance values for P/M and wrought 316 and 304 stainless steels is shown in Fig. 19 (Ref 9).

Sensitization in stainless steels can be evaluated by two electrochemical potentiokinetic reactivation methods (EPR): the single-loop method (SL-EPR) and the double-loop method (DL-EPR). A more detailed description of intergranular corrosion testing is offered in Ref 22. The SL-EPR method is a rather time-consuming test because, in addition to the electrochemical experiment, the grain-boundary area of the specimen must be determined.

The DL-EPR method was developed as a more rapid and reliable means of assessing susceptibility to intergranular corrosion. In the double-loop method, the potential is scanned (at a rate of 6 V/h) in the anodic direction from the open-circuit potential to +300 mV versus a saturated calomel electrode (mV SCE). At +300 mV, the direction of the scan is reversed and the potential is decreased (at the same scan rate) until the corrosion potential is reached. Susceptibility to sensitization is determined from the ratio of the maximum current on the reverse scan (I_r) to that measured on the forward scan (I_a), as illustrated in Fig. 20. The I_r/I_a ratios have been correlated with the step, dual, and ditch structures observed during oxalic acid etch screening of wrought stainless steels to identify sensitization. These three structures are presented in Fig. 21. Step structures (Fig. 21a) are free of grain-boundary attack resulting from sensitization. If the grain boundaries contain enough carbides to encircle the grain completely, then grains are undermined upon exposure to the etch and a ditch structure is observed (Fig. 21b). If the ditches do not completely encircle the grains (Fig. 21c), then a dual classification is used to describe the structure. Current ratios in the double-loop EPR test in the

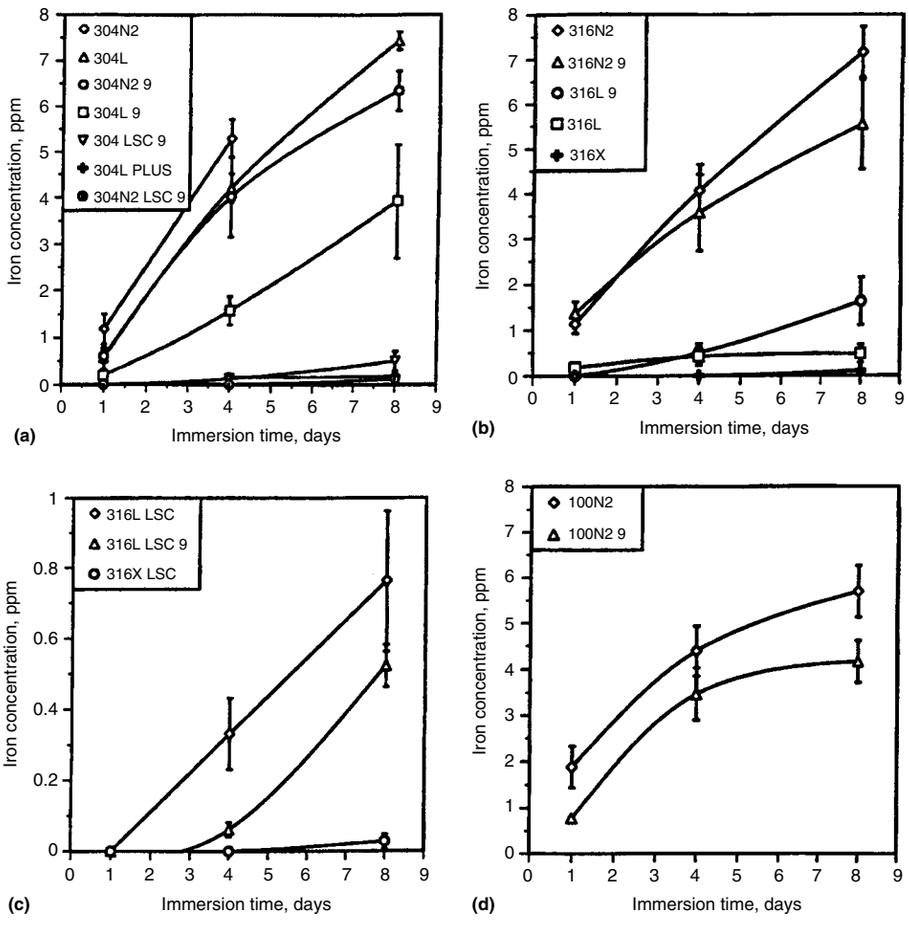

Fig. 6 Total dissolved iron in solution for alloys showing detectable concentrations after 1, 4, and 8 days. (a) 304 alloys. (b) 316 regular alloys. (c) 316 special alloys. (d) SS 100 (20Cr-17Ni-5Mo) alloys. Source: Ref 11

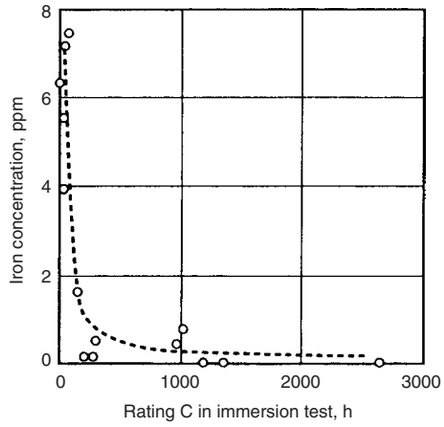

Fig. 7 Correlation between results of the colorimetric test for various alloys after eight days and the corresponding times to achieve a C rating in a 5 wt% NaCl immersion test. Source: Ref 11

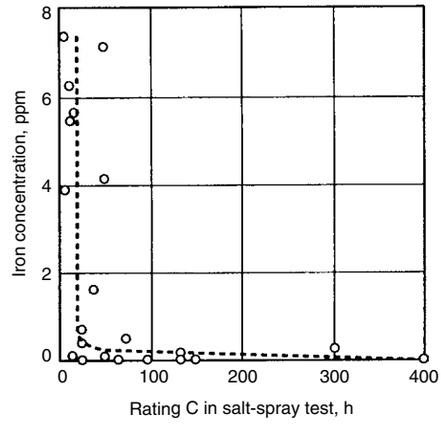

Fig. 8 Correlation between results of the colorimetric test for various alloys after eight days and the corresponding times to achieve a C rating in the salt-spray test. Source: Ref 11

Table 7 Corrosion tests on 316L sintered stainless steel specimens exposed to 5% NaCl solution at 20 °C

Specimens were sintered in various atmospheres at 1150 °C (2100 °F) for 1 h. Passivation 1 was carried out for 30 min at 80 °C (175 °F) in a 16 vol% HNO_3 nitric acid solution. Passivation 2 was carried out for 60 min at 70 °C (160 °F) in a 40 vol% HNO_3 solution.

	Properties after sintering but before corrosion testing					Properties after corrosion testing			
	Transverse rupture strength					Transverse rupture strength			
Sintering atmosphere	MPa	ksi	Angle of bend, degrees	Treatment after sintering	Period, days	MPa	ksi	Angle of bend, degrees	Appearance
Vacuum	460	67.0	>111(a)	None	4	425	61.6	>107(a)	No attack
					15	450	65.1	>109(a)	No attack
				Passivation 1	4	430	62.3	100	Slight rusting
					15	440	63.8	108	Slight rusting
				Passivation 2	4	432	62.8	91	Slight rusting
					15	437	63.4	95	Slight rusting
Hydrogen	515	74.6	112	None	4	475	68.9	44	Rusted
					15	460	66.8	55	Rusted
				Passivation 1	4	480	69.8	80	Rusted
					15	470	68.2	62	Rusted
				Passivation 2	4	380	55.3	45	Rusted
					15	469	68.1	60	Rusted
Dissociated ammonia	730	106.1	17	None	4	657	95.3	14	Rusted
					15	700	101.4	12	Rusted
				Passivation 1	4	655	95.1	17	Rusted
					15	650	94.2	10	Rusted
				Passivation 2	4	729	105.8	16	Rusted
					15	665	96.8	15	Rusted

(a) Specimen did not break. Source: Ref 13

Table 8 Ferroxyl test results for P/M and wrought stainless steels

		Visual rating(a) in ferroxyl test with chlorine added (% Cl^-)			Pitting potential(b), mV SCE
AISI No.	Type, treatment	0.05%	0.10%	0.50%	
316L	P/M, 1120 °C 20 min, dissociated ammonia (−27 °C)	3	3	...	75
	P/M, 1250 °C 30 min, H_2 (−35 °C)	...	1	3	250
	P/M, 1120 °C 30 min, H_2 (−70 °C)	...	0	3	375
	P/M, 1120 °C 120 min, H_2 (−70 °C)	...	0	3	375
	P/M, 1250 °C 120 min, H_2 (−70 °C)	...	0	1	600
431	Wrought	3	3	...	270
303	Wrought	3	3	...	325
304	Wrought	1	3	...	470
316	Wrought	...	1	2	590

(a) Rating scale, see in-text table. 0.1% Cl^-, pH 5, 30 °C, 5 mV/min. Source: Ref 14

Table 9 Salt-spray cabinet test results for P/M stainless steels

P/M material designation				Corrosion tests(a)	
Type	Ames	MPIF(b)	Density, g/cm^3	A, hours to 0.1% stain	B, hours to 1% stain
303	SFN-Cr18-N11-64	SS-303N-125	6.4	20	1–5 (200–500)
	SFAN-Cr18-N11-66	SS-303N2–35	6.6	20	N/A
	SFA-Cr18-N11-70	Approx SS-303L-12	7.0	24	N/A
304	SFN-Cr19-N10-64	SS-304N1–30	6.4	20	50–100 (500–1200)
	SFAN-Cr19-N10-66	SS-304N2–33	6.6	20	N/A
	SFA-Cr19-N10-70	Approx SS-304L-13	7.0	24	N/A
316	SFN-Cr17-N12-M1-64	SS-31NI-25	6.4	20	200–500 (500–1500)
	SFAN-Cr17-N12-M1-66	SS-316N2–33	6.6	20	N/A
	SFA-Cr17-N12-M1-70	Approx SS-316L-15	7.0	24	N/A
410	SFAN-Cr12-67	Approx SS-410–90HT	6.7	5	N/A
	SFA-Cr12-70		7.0	5	N/A
420	SFAN02-Cr12-67	Approx SS-410–90HT	6.7	5	N/A
434	SFA-Cr17-M1-70		7.0	24	N/A
632	SFA-Cr16-NS-M1-70		6.9	22	N/A

(a) A. 5% aqueous Nacl salt spray, per ASTM B 117; B. 5% aqueous NaCl immersion, per ASTM G 31. N/A, data not available. (b) MPIF, Metal Powder Industries Federation. Source: Ref 3

range of 0.0001 to 0.001 correspond to step structures, ratios of 0.001 to 0.05 correspond to dual structures, and ratios of 0.05 to 0.3 correspond to ditch structures.

Double-loop EPR curves for P/M 316L stainless steels with and without sensitized microstructures are shown in Fig. 22 (Ref 14). In this example, the sensitized microstructures in curves in Fig. 22(b) and (c) resulted from high nitrogen contents and liquid phase sintering using a boron addition, topics that are discussed in more detail in subsequent sections of this article.

P/M Stainless Steels

It was stated earlier that the corrosion resistance of the metals and alloys that are considered in this article is a result of the protective passive film that forms on their surfaces. This is certainly true for stainless steels, whose passive characteristics result from the alloying of iron with chromium. For wrought alloys, the influence of chromium concentration on the passivity of iron in a 2 *N* H_2SO_4 solution at 90 °C (195 °F) is shown in Fig. 23 (Ref 20). As the chromium content is increased, the primary passivation potential, E_{pp}, the critical current density, i_{crit}, and the passive current density, i_p, are reduced—extending the potential region over which the alloy is passive, reducing dissolution of the alloy, and enabling the alloy to become self-passivating, respectively. When chloride is present, chromium increases the pitting potential, as revealed in Fig. 24 (Ref 20).

Figure 23 clearly shows that a significant improvement in passivity occurs as the chromium content approaches 12%. While there is some debate over the minimum chromium content needed to call an iron-base alloy a stainless steel, most consider that at least 12% is needed to enhance passivity and, thus, corrosion resistance significantly. Passivity results from the presence of a stable, protective oxide barrier on the alloy surface. For stainless steels, this protective barrier is largely composed of chromium oxide and significantly limits dissolution of the underlying metal. Corrosion resistance in stainless steels is compromised when the chromium concentration of the alloy, or any part of its microstructure, falls below a threshold concentration of 10 to 12%.

The primary difference in the corrosion resistance of wrought and P/M stainless steels is due to the inherent porosity of the P/M materials. Of special concern with regard to the corrosion resistance of sintered stainless steels is their susceptibility to localized breakdown of the passive film in the form of crevice corrosion, pitting, intergranular corrosion, and stress-corrosion cracking. Development of corrosion-resistant sintered stainless steels depends on increasing one's understanding of how passivity is attained and sustained in porous metals.

Despite the fact that P/M stainless steel production accounted for only 2% of the overall

U.S. stainless steel market in 1993, research on the corrosion resistance of these alloys has been increasing, and it is obvious that an enormous opportunity exists for their future development and utilization. To date, the compositions of commercial P/M stainless steels have been largely based on those of their wrought counterparts. A listing of the currently produced commercial, water-atomized P/M stainless steel alloys is presented in Table 11. As stated earlier, applications for these P/M alloys are wide ranging with austenitic grades accounting for approximately two-thirds of the total usage. Table 12 summarizes a number of the current applications for the P/M stainless alloys identified in Table 11. It should be noted that automotive applications, especially exhaust systems, are responsible for much of the recent, increased interest in and demand for corrosion-resistant P/M stainless steel alloys.

Early P/M stainless steel developmental efforts were aimed at improving powder atomization and compacting properties, while interest in enhanced corrosion resistance has been more recent. In fact, the understanding of the corrosion of P/M stainless steels and the concomitant development of corrosion-resistant P/M alloys (specifically, P/M alloys that have been especially developed for their corrosion resistance) is still rudimentary. Several factors are responsible for the differences between the corrosion resistance of P/M stainless steels and their wrought counterparts. Next to the properties of the powder itself (which needs to have carbon, oxygen, and nitrogen levels less than or equal to values of 0.02%, 0.2%, and 0.03%, respectively), the chief factor governing the production of corrosion-resistant P/M alloys is the sintering process. Several sintering variables are of significant importance in the production of corrosion-resistant P/M alloys. Inadequate dissipation of lubricant results in the incorporation of unwanted carbides, and low sintering temperatures encourage chromium nitride formation; both conditions can deplete the alloy of the chromium needed to maintain passivity and aid in the establishment of microgalvanic cells in the microstructure. Insufficient cooling rates contribute to chromium carbide and chromium nitride formation. High dew points encourage oxide formation that has been associated with diminished corrosion resistance. Carbon and iron contamination from furnaces leads to carbide formation and iron incorporation in the alloy. Sintering atmospheres can either promote or degrade corrosion resistance; vacuum and hydrogen atmospheres typically yield the best results, and dissociated ammonia usually produces the worst results. Unfortunately, a significant portion of the literature on the corrosion of P/M alloys, stainless steels included, lacks specific details concerning processing conditions, making performance comparisons among different alloy groups difficult or impossible.

Austenitic stainless steels owe their corrosion resistance to chromium, nickel, and other passivity-enhancing alloying additions such as molybdenum. As stated earlier, chromium is the primary element responsible for the corrosion resistance of stainless steels. Nickel stabilizes the austenitic structure and promotes repassivation, especially in reducing environments. Molybdenum stabilizes the passive film, especially in combination with chromium, and improves pitting and crevice-corrosion resistance.

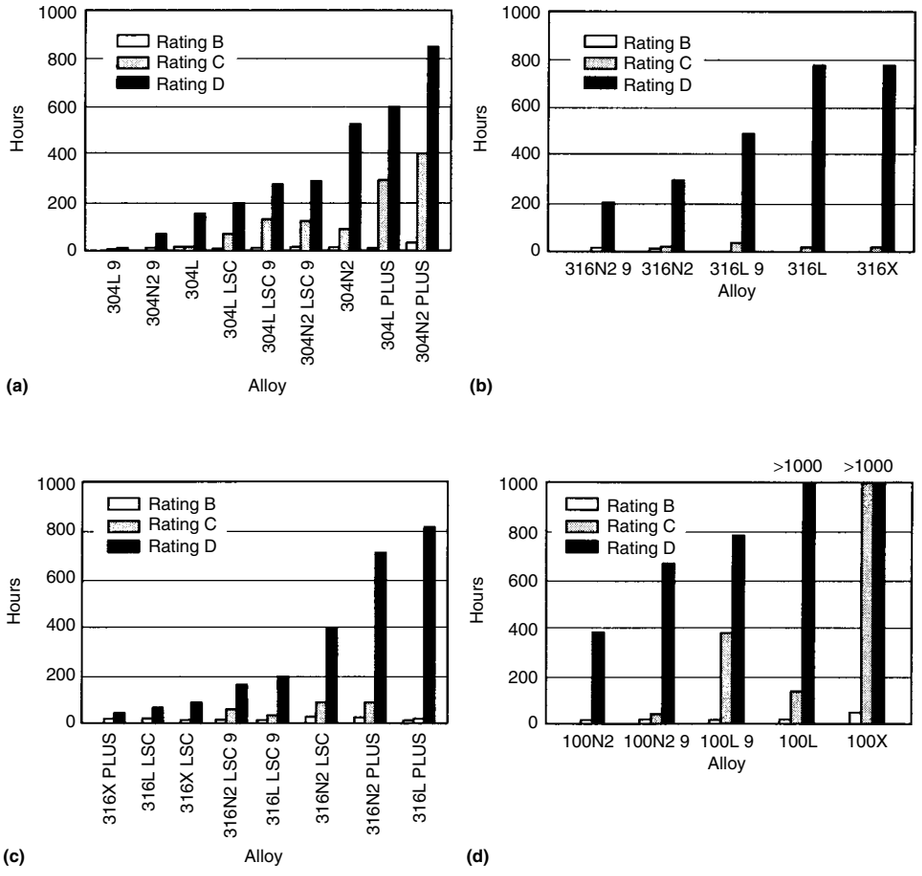

Fig. 9 Salt-spray test results (>1000 h). (a) 304 alloys. (b) 316 regular alloys. (c) 316 special alloys. (d) SS 100 alloys. B rating, attack of 1% or less of the surface; C rating, attack of 1 to 25% of the surface; D rating, attack of more than 25% of the surface. Source: Ref 11

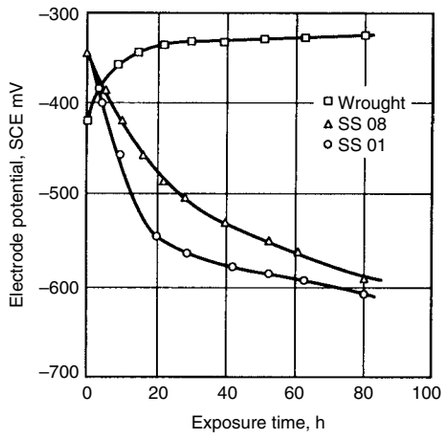

Fig. 10 Variation in open-circuit electrode potential with time for wrought and P/M 316L stainless steel in a 3% NaCl solution. Source: Ref 15

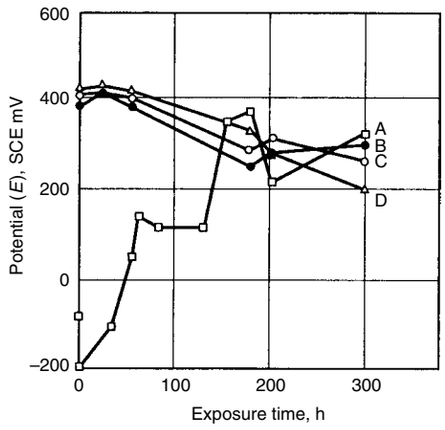

Fig. 11 Open-circuit potential of various passive hot-pressed and sintered samples in 1 *N* H_2SO_4 solution at ambient temperature: A, 316 stainless steel; B, 316 stainless steel containing an additional 0.5 wt% Ni; C, 316 stainless steel containing 2 wt% Pt; D, 316 stainless steel containing 2 wt% Pd. Source: Ref 17

Nitrogen enhances the strength and corrosion resistance of austenitic wrought stainless steels, but is linked to sensitization in stainless steels. These elements, and a few others, influence polarization behavior and enhance passivity in wrought alloys in the manner depicted in Fig. 25 (Ref 20).

Intergranular corrosion of 300 series stainless steels has long been associated with sensitization resulting from welding or improper heat treating. If the alloys are held in the temperature range of 550 to 850 °C (1020 to 1560 °F), carbides can form at the grain boundaries depleting the alloy adjacent to the grain boundary of chromium, as the chromium profile for a sensitized 304 stainless steel shown in Fig. 26 reveals (Ref 23). The region adjacent to the grain boundary with the lower chromium content has a lower corrosion resistance than either the precipitates at the grain boundary or the rest of the grain. These areas of dissimilar chromium concentration can result in the establishment of localized galvanic cells within the microstructure that lead to corrosion of the chromium-depleted regions adjacent to grain boundaries, as Fig. 27 illustrates. In P/M alloys, sensitization can occur during sintering as well as during welding operations. Stainless steel alloys with carbon and nitrogen contents that approach 0.03% have been shown to form chromium precipitates at the grain boundaries (Ref 23). In addition, sintering or cooling (especially from 870 to 425 °C, or 1600 to 800 °F) in an atmosphere that contains nitrogen can lead to the formation of chromium nitrides. When these chromium carbides and chromium nitrides form, they deplete the adjacent microstructure of chromium. Hence, a galvanic interaction ensues between the more corrosion-resistant, high-chromium concentration regions of the microstructure and the less-corrosion-resistant, chromium-depleted regions.

As revealed in Table 12, the 300-series alloys account for the largest percentage of applications for stainless P/M alloys. Among wrought stainless steels, 304L is the most commonly used alloy because of its excellent corrosion resistance and lower cost compared to other austenitic stainless steels. To date, 316L is the most commonly used P/M stainless steel because of its improved corrosion resistance in comparison to sintered 304L stainless steel. Low-carbon-grade alloys are essential for P/M stainless components because of sensitization that can accompany the sintering process.

Corrosion data for 300 series P/M stainless steels is largely centered on the susceptibility of these alloys to pitting/crevice corrosion, intergranular corrosion, and processing-induced degradation. This last item is the subject of the next section of this article. It must be stated that while there is an expanding base of literature on the subject of corrosion of sintered stainless steels, a number of studies fail to mention important details related to either processing or testing of the alloys.

Processing details such as dew-point temperatures, sintering and delubing times, and information related to cooling of the alloys are often missing. All of these items are critical to the production of corrosion-resistant stainless steels, and the lack of such information limits the utility of a number of the studies that have been

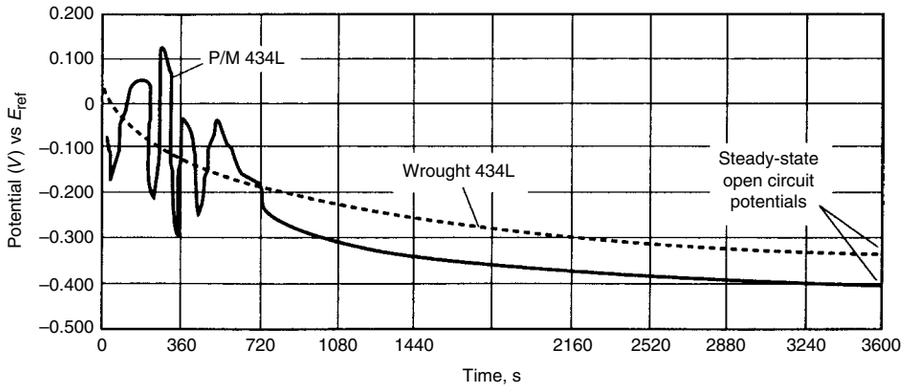

Fig. 12 Open-circuit potential versus time data for wrought 434L and P/M 434L sintered at 1290 °C (2350 °F). Source: Ref 18

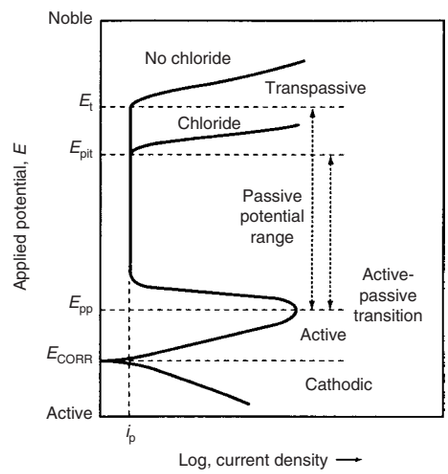

Fig. 13 Polarization curve for a stainless steel in a sulfuric acid solution. E_t, transpassive potential; E_{corr}, corrosion potential. Source: Ref 20

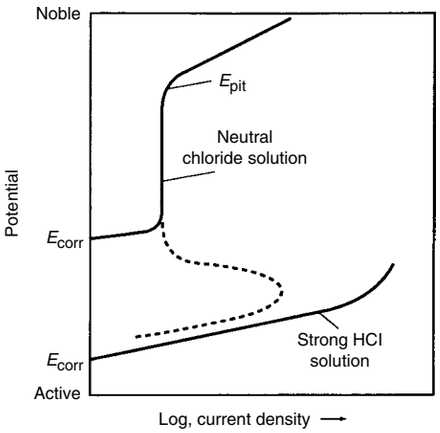

Fig. 14 Anodic polarization curves for stainless steel in a neutral chloride solution showing self-passivating behavior (top curve, solid line) and active dissolution in a strong hydrochloric acid solution (bottom curve). Source: Ref 20

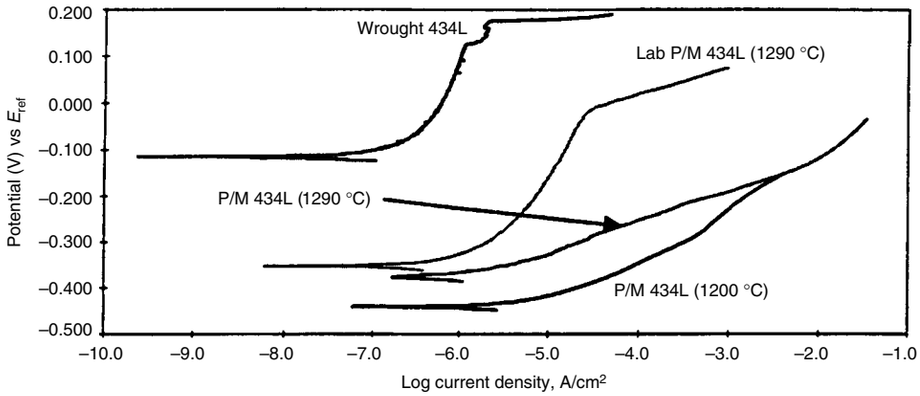

Fig. 15 Anodic potentiodynamic polarization scans for wrought 434L, laboratory-sintered P/M 434L sintered at 1290 °C (2350 °F), P/M 434L sintered in an industrial furnace at 1200 °C (2200 °F), and P/M 434L sintered in an industrial furnace at 1290 °C (2350 °F). Source: Ref 18

Table 10 Data obtained from anodic polarization testing of sintered 316L, raw 316L powder, and wrought 316 as a function of sintering conditions

Electrochemical properties were measured in 0.1% Cl^-, pH 5, 30 °C, with a scan rate of 5 mV/min.

	H_2 (−30 °C)				H_2 (−70 °C)				Vacuum					
	1120 °C		1250 °C		1120 °C		1250 °C		1120 °C		1250 °C			
Sintering(a)	30 min	120 min	30 min	120 min	30 min	120 min	30 min	120 min	30 min	120 min	30 min	120 min	Raw 316L powder	Wrought 316L
Density, g/cm^3	6.62	6.68	6.71	6.84	6.62	6.68	6.71	6.84	6.67	6.73	6.76	6.86	...	8.00
Nitrogen, ppm	400	320	220	60	470	190	110	70	410	220	90	20	700	...
Oxygen, ppm	2400	2400	2200	1500	2300	2000	1900	1700	2200	2200	2100	1800	1900	...
Carbon, ppm	230	220	190	130	240	250	170	110	60	60	20	10	180	300
i_{crit}, μA/cm^2	150	90	87	83	10	10	7	9	4	7	8	9	...	0
i_p, μa/cm^2	29	21	28	19	14	10	12	11	9	13	12	7	...	0.5
E_{pit}, mV SCE	250	243	243	333	345	370	330	395	368	410	363	405	...	665(b)
E_{stp}, mV SCE	269	213	188	163	238	275	188	163	263	238	175	150	...	538(c)
NSS 1, h	36	60	48	24	1392	1278	1260	1512	1056	1008	420	240	...	1512
NSS 2, h	13	24	13	2	1512	1140	1260	60	1512	1008	324	24	...	...

E_{stp} stepwise polarization. NSS: time to corrosion in neutral salt-spray test: 1, no pretreatment: 2, specimens filled with test solution. (a) Measured with a creative-free electrode. (b) Measured with a creviced electrode. Source: Ref 1

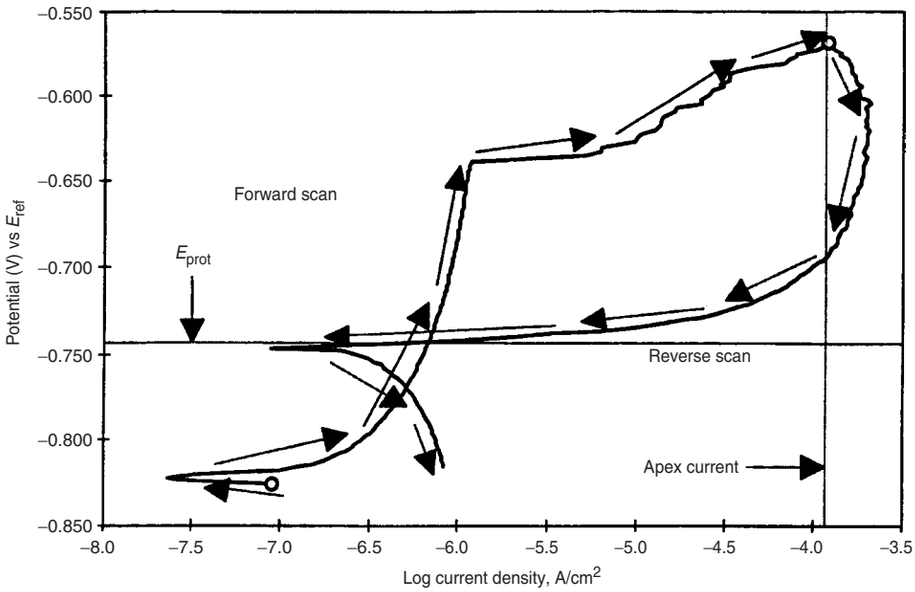

Fig. 16 Sample cyclic polarization curve with labeled values and regions E_{prot}, protection potential. Source: Ref 21

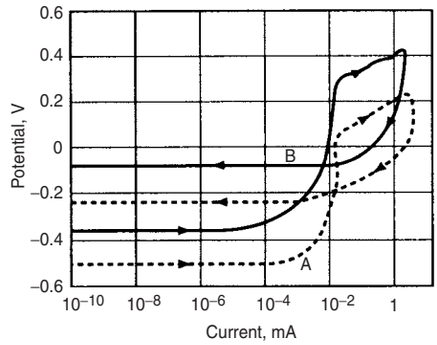

Fig. 17 Anodic potentiodynamic polarization curves for 316L stainless steel. A, P/M specimen; B, wrought specimen. Source: Ref 15

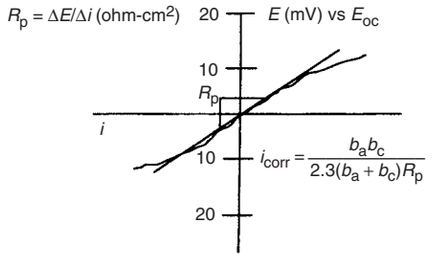

Fig. 18 Sample polarization resistance data showing determination of corrosion current density, i_{corr}, from R_p. The slope at E_{oc} is called the polarization resistance, R_p. The Tafel slopes, b_a and b_c, must be obtained from anodic and cathodic polarization experiments or estimated.

conducted. Testing details that are sometimes neglected include surface area measurements (needed for determining corrosion rates), test specimen preparation and test cleaning procedures, and the inclusion of wrought counterparts or control materials in test plans. This information is especially important because sintered alloys contain porosity. Corrosion resistances of a variety of austenitic stainless steel P/M alloys are shown in Table 13 (Ref 1) and Table 14 (Ref 14).

Mechanical properties of 316L stainless steel as a function of some of the more important processing parameters are presented in Fig. 28 to 30. As these figures reveal, nitrogen-containing atmospheres result in the absorption of considerable amounts of nitrogen, which increases strength, decreases ductility, and, as is seen in the following paragraphs, influences P/M alloy corrosion resistance.

Ferritic and Martensitic Stainless Steels. The 400 series alloys are typically less heavily alloyed than the austenitic grades and, as a result, they usually exhibit inferior corrosion resistance. In addition to the lower pitting and crevice-corrosion resistance resulting from lower concentrations of passivity enhancing elements, ferritic stainless steels are also more susceptible to sensitization and intergranular corrosion. Ferritic stainless steels exhibit a greater affinity for sensitization than austenitic stainless steels because the solubility limit of carbon in the austenite phase is greater than in the ferrite phase. Hence, the precipitation of carbides is more prevalent in ferritic microstructures (Ref 18).

Influence of Processing Parameters on the Corrosion Resistance of P/M Stainless Steels

Influence of Iron or Steel Contamination on Corrosion Resistance. It should come as no surprise that the corrosion resistance of P/M stainless steels is seriously degraded if iron or steel particles become incorporated into the

alloy. The potential difference between iron or steel and stainless steel is typically on the order of several hundred millivolts and easily results in the establishment of galvanic or dissimilar metal corrosion within the contaminated component. There are numerous possible contamination sources: contamination of the initial powder at the supplier; inadvertent introduction during mixing/blending, feeding, or pressing operations; incorporation of airborne particles during processing or storage; and inadequate furnace cleaning. Cleanliness is of the utmost importance and separate or dedicated equipment is often used for the production of stainless components. Figure 31 shows an example of the appearance of iron-contaminated sintered 316L stainless steel after exposure to a 5% NaCl solution. Rusting became apparent within minutes of exposure to the chloride-containing solution.

Corrosion resulting from iron or steel contamination is perhaps the worst and, ironically, most avoidable corrosion problem encountered with P/M stainless steels. A concentrated copper sulfate solution can be used to easily detect iron, or an iron alloy, present in a stainless steel powder or on the surface of a sintered part. Dissolved copper from a copper sulfate solution readily plates out on the anodic (lower potential) iron sites, making them easy to see at low magnification.

Influence of Lubricant and Carbon. As Fig. 32 suggests (Ref 23), carbide formation (especially, chromium carbide formation) with concomitant sensitization is an issue when the carbon content of an austenitic stainless steel exceeds 0.03%. In order to resist intergranular corrosion, water-atomized stainless steel powders have carbon contents greater than 0.03%. Unfortunately, other sources of carbon are associated with processing sintered stainless steels. These sources include the carbon resulting from inadequate organic lubricant dissipation and carbon contamination (soot) from insufficiently cleaned furnaces. Microstructures from two sintered 316L stainless steels, one below and one above the critical 0.03% concentration, are shown in Fig. 33. Thin, undecorated grain boundaries are observed in the low-carbon stainless steel, whereas heavily decorated grain boundaries are observed for the high-carbon stainless steel. In insufficiently cleaned furnaces, loose, adherent soot can fall onto the surface of stainless steel parts or moisture from the sintering atmosphere can react with soot and form carbon monoxide and carburize the stainless steel. If care is not taken to limit the uptake of carbon, sensitization of the microstructure can occur and severely compromise the overall corrosion resistance of the alloy. The influence of carbon content on the pitting potential for a number of different sintered stainless steels is shown in Fig. 34 (Ref 14). Sensitization can be minimized with proper lubricant dissipation, a clean furnace, and low initial carbon concentration in the powder. It should be noted that when optimal sintering conditions are used, differences in corrosion resistance have not been noted as a function of lubricant type, as Table 15 reveals (Ref 24).

Carbon contents in excess of 0.03% can be of benefit when stainless steels are vacuum sintered. In vacuum sintering, the excess carbon is used for the reduction of some oxides on the water-atomized stainless steel, improving strength, ductility, and corrosion resistance. Microstructures of vacuum sintered 430L stainless steel with and without the addition of 0.2% graphite are shown in Fig. 35. The graphite-containing stainless steel exhibited clean grain boundaries, while the alloy without graphite had grain boundaries containing carbides.

Influence of Nitrogen and Sintering Atmosphere. Dissociated ammonia is a commonly used sintering atmosphere because it costs less than other sintering atmospheres. However, sintering in dissociated ammonia usually leads to the pickup of nitrogen by the stainless steel—a factor that can enhance susceptibility to corrosion in a manner analogous to that observed with chromium carbide formation. For wrought stainless steels, enhanced passivity is observed with increased nitrogen content. However, if chromium nitrides precipitate, the sensitized stainless steel is susceptible to intergranular corrosion. Equilibrium solubilities for nitrogen in austenitic stainless steels with different chromium contents are presented in Fig. 36. The concentration of dissolved nitrogen depends on

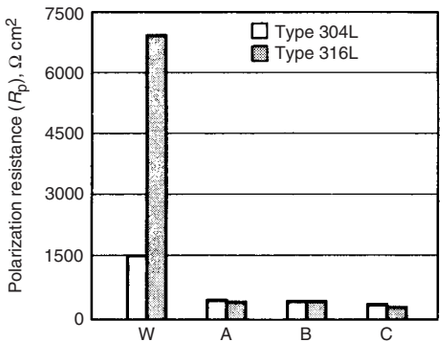

Fig. 19 Polarization resistance, R_p, values for wrought (W) and sintered (A, B, C). A, B, and C correspond to the same sintering conditions as shown in Table 3. Type 304L and 316L samples in 0.5 *M* H_2SO_4 solution at $T = 25$ °C (77 °F). A, B, and C correspond to the same sintering conditions as shown in Table 3. Source: Ref 9

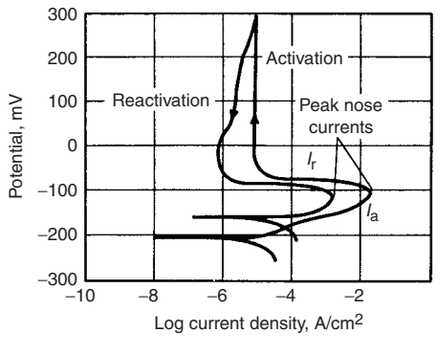

Fig. 20 *I-V* curve typical of a double-loop electrochemical potentiokinetic reactivation experiment

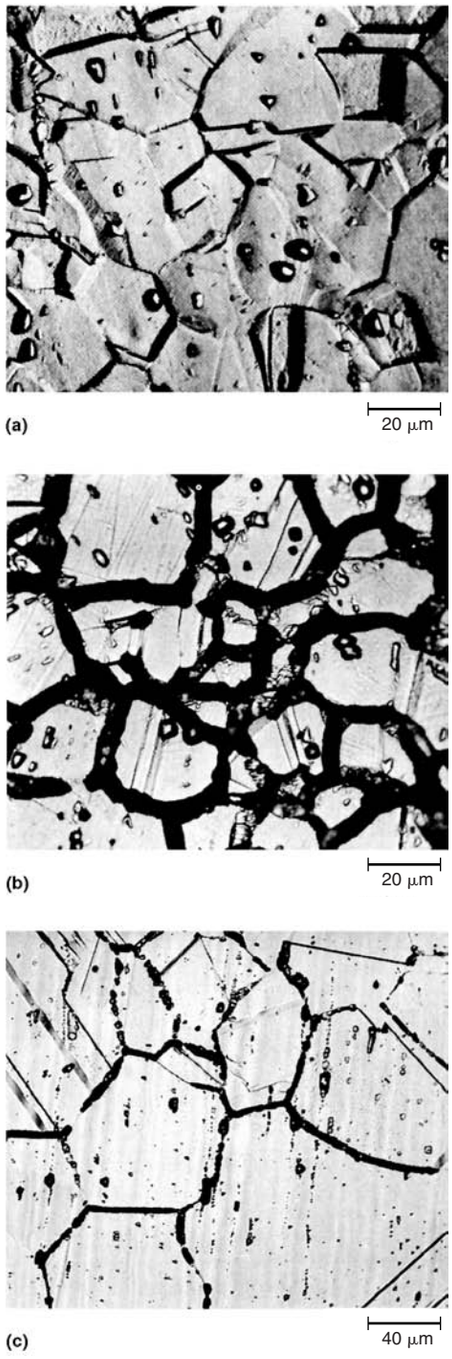

Fig. 21 Oxalic acid etch screening. (a) Oxalic acid etch (Original magnification: 500×). Step structure. Etched 1 A/cm^2 for 1.5 min. (b) Oxalic acid etch (Original magnification: 500×). Ditch structure. Etched 1 A/cm^2 for 1.5 min. (c) Oxalic acid etch (Original magnification: 250×). Dual structure. Etched 1 A/cm^2 for 1.5 min. Source: Ref 22 reprinted with permission

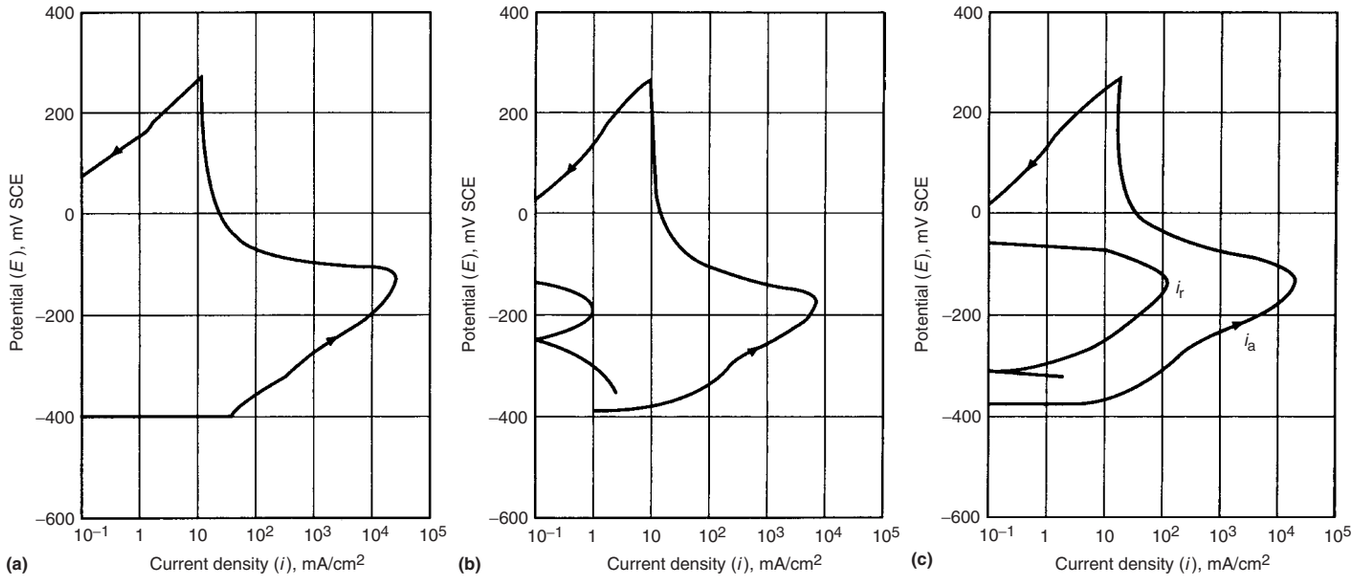

Fig. 22 Polarization curves for 316L P/M steels obtained by the DL-EPR technique in 0.5 *M* H_2SO_4 + 0.1 *M* KSCN (30 °C, or °F). (a) Steel without sensitization. (b) Sensitized steel with 1850 ppm N. (c) Liquid phase sintered steel with addition of boron. Source: Ref 14

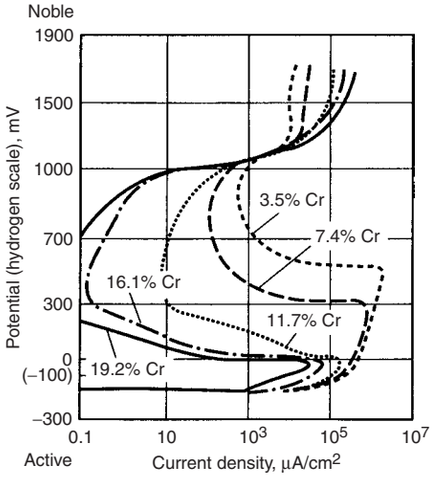

Fig. 23 Effect of chromium content of FeNiCr alloys on their anodic polarization behavior in 2*N* H_2SO_4 at 90 °C (195 °F). The nickel content was in the range of 8.3 to 9.8%. Source: Ref 20

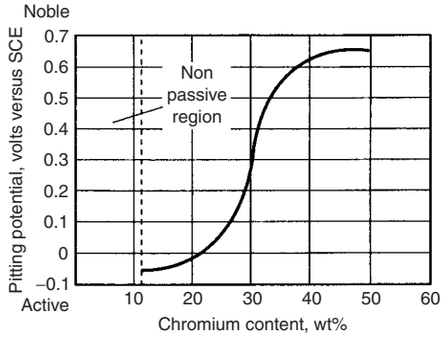

Fig. 24 Effect of chromium content on pitting potential of FeCr alloys in deaerated 0.1 *N* NaCl at 25 °C (77 °F). Source: Ref 20

the amount of nitrogen in the atmosphere, the sintering temperature, and the cooling rate of the sintered alloy. An example of the influence of nitrogen concentration in the sintering atmosphere on the corrosion resistance of 316L stainless steel is shown in Table 16 (Ref 14). These results reveal that up to the point where supersaturation associated with sensitization occurs, no significant difference in corrosion behavior was noted. In addition, these results show that the EPR test is very sensitive to the identification of nitride formation. Reference 26 reported that chromium nitrides were not present in 316L when its nitrogen content was lower than 0.4 wt%. This point is supported by the weight-loss data after exposure to 10% HNO_3 (as a function of absorbed nitrogen content) for sintered 316L stainless steel shown in Fig. 37 (Ref 3). The data presented in this figure were obtained using several sintering atmospheres.

An example of the influence of temperature on dissolved nitrogen concentration is shown in Fig. 38 (Ref 13). The data in this figure were obtained by continuously measuring weight gain during heating in dry nitrogen (nitrogen containing 0.01% water and 1% water). In the 700 to 1000 °C (1300 to 1800 °F) range a large absorption of nitrogen occurs. A maximum of 9 mg N per gram of stainless steel was absorbed—24 mg/g would be required to convert all of the chromium in the alloy to Cr_2N (Ref 13).

An example of the influence of cooling rate, and hence the dissolved nitrogen concentration, on the corrosion rate of 316L stainless steel is shown in Table 17 (Ref 13). While the rate of heating had no influence on corrosion of the alloy, cooling rates in excess of 100 °C/s (180 °F/s) inhibited or eliminated corrosion. Chromium nitride sensitization with concomitant loss of corrosion resistance is not limited to 316L stainless steel. Other stainless steels (both 300 and 400 series alloys) are subject to loss of corrosion resistance when nitrogen-containing sintering atmospheres are used. Table 2 shows weight-loss data for sintered 304L and 316L stainless steels as a function of sintering atmosphere and revealed that nitride formation lowered corrosion resistance (weight loss after 5% NaCl exposure).

Influence of Oxygen and Water Vapor/Dew Point. The influence of oxygen on the corrosion resistance of sintered stainless steels can, perhaps, best be understood by visualizing the structure of the as-sintered material. The as-received powders contain oxygen, much of which resides on the surface of the powder. Reduction of these oxides in industrial furnaces is not always complete, and the grain-boundary oxides within the as-sintered structure provide paths for easier corrosion of the alloy. The role these grain-boundary oxides play in the corrosion of sintered metals is likely similar to the role that such oxides play in the degradation of thermal sprayed coatings (Ref 27, 28). Upon cooling, high oxygen affinity elements oxidize when they reach the metal-oxide equilibrium temperature, and the water content (dew point) of the atmosphere determines the stability of the oxides according to Fig. 39. This figure reveals that the oxides are more easily formed at lower temperatures. The negative effect of high dew point on the corrosion resistance of sintered

Table 11 Compositions of commercial P/M stainless steels

	Chemical composition (b), wt%										
Material designation (a)	**Fe**	**Cr**	**Ni**	**Mn**	**Si**	**S**	**C**	**P**	**Mo**	**N**	**Nb**
Austenitic grades											
SS-303N1, N2	bal	17.0–19.0	8.0–13.0	0–2.0	0–1.0	0.15–0.30	0–0.15	0–0.20	. . .	0.20–0.60	. . .
SS-303L	bal	17.0–19.0	8.0–13.0	0–2.0	0–1.0	0.15–0.30	0–0.03	0–0.20	. . .	0–0.03	. . .
SS-304N1, N2	bal	18.0–20.0	8.0–12.0	0–2.0	0–1.0	0–0.03	0–0.08	0–0.045	. . .	0.20–0.60	. . .
SS-304L	bal	18.0–20.0	8.0–12.0	0–2.0	0–1.0	0–0.03	0–0.03	0–0.045	. . .	0–0.03	. . .
SS-316N1, N2	bal	16.0–18.0	10.0–14.0	0–2.0	0–1.0	0–0.03	0–0.08	0–0.045	2.0–3.0	0.20–0.60	. . .
SS-316L	bal	16.0–18.0	10.0–14.0	0–2.0	0–1.0	0–0.03	0–0.03	0–0.045	2.0–3.0	0–0.03	. . .
Ferritic grades											
SS-409L	bal	10.5–11.75	. . .	0–1.0	0–1.0	0–0.03	0–0.03	0–0.04	. . .	0–0.03	8XC-0.80
SS-430N2	bal	16.0–18.0	. . .	0–1.0	0–1.0	0–0.03	0–0.08	0–0.04	. . .	0.20–0.60	. . .
SS-430L	bal	16.0–18.0	. . .	0–1.0	0–1.0	0–0.03	0–0.03	0–0.04	. . .	0–0.03	. . .
SS-434N2	bal	16.0–18.0	. . .	0–1.0	0–1.0	0–0.03	0–0.08	0–0.04	0.75–1.25	0.20–0.60	. . .
SS-434L	bal	16.0–18.0	. . .	0–1.0	0–1.0	0–0.03	0–0.03	0–0.04	0.75–1.25	0–0.03	. . .
Martensitic grades											
SS-410	bal	11.5–13.5	. . .	0–1.0	0–1.0	0–0.03	0–0.25	0–0.04	. . .	0.20–0.60	. . .
SS-410L	bal	11.5–13.5	. . .	0–1.0	0–1.0	0–0.03	0–0.03	0–0.04	. . .	0–0.03	. . .

(a) These designations follow the code of MPIF Standard 35, which was adopted by ASTM B 783. Not all the materials listed are specified in ASTM B 783. N1, N2, nitrogen alloyed; L, low carbon. (b) Maximum unless a range is specified. Other elements: total by difference equals 2.0% maximum, which may include other minor elements added for specific purposes

Table 12 Applications for P/M stainless steels

Part	Alloy
Aerospace	
Seatback tray slides	316L
Galley latches	316L
Jet fuel refueling impellers	316L
Foam generators	316L
Agriculture	
Fungicide spray equipment	316L
Appliances	
Automatic dishwasher components	304L
Automatic washer components	304L
Garbage disposal components	410L
Pot handles	316L
Coffee filters	316L-Si
Electric knives	316L
Blenders	303L
Can opener gears	410L
Automotive	
Rearview mirror mounts	316L, 434L
Brake components	434L
Seat belt locks	304L–434L
Windshield wiper pinions	410L
Windshield wiper arms	316L, 434L
Manifold heat control valves	304L, 434L
Exhaust system flanges	304L, 434L
Coupling for a water pump	316L
Solenoid spacer for fuel injector	316L
Sealing washer for water pump	420L
ABS rings	434L
Building and construction	
Plumbing fixtures	316L
Spacers and washers	316L
Sprinkler system nozzles	316L
Shower heads	316L
Window hardware	304L, 316L
Thermostats	410L
General construction	303L
Electrical and electronic	
Limit switches	410L
G-frame motor sleeves	303L
Rotary switches	316L
Magnetic clutches	410L, 440A
Battery nuts	830
Electrical testing probe jaws	316L

Part	Alloy
Hardware	
Lock components	304L, 316L
Threaded fasteners	303L
Fasteners	316L
Quick-disconnect levers	303L, 316L
Industrial	
Water and gas meter parts	316L
Filters, liquid and gas	316L-Si
Recording fuel meters	303L
Fuel flow meter devices	410L
Pipe flange clamps	316L
High polymer filtering	316L-Si
Jewelry	
Coins, medals, medallions	316L
Watch cases	316L
Watch band parts	316L
Marine	
Propeller thrust hubs	316L
Cam cleats	304L
Medical	
Centrifugal drive couplings	316L
Dental equipment	304L
Hearing aids	316L
Anesthetic vaporizers	316L
Office equipment	
Office furniture hardware	304L, 316L
Recreation and leisure	
Fishing rod guides	304L, 316L
Fishing rod gear ratchets	316L
Photographic equipment	316L
Soft drink vending machines	830, 316L
Travel trailer water pumps	316L
Computers	
Support frame for computer CPU	303L
Bearing holder for hard disk	304L
Pulley for computer application	316L
Bearing housing for hard disk	410L
Chemical	
Filters	304L-Si, 316L
High-corrosion resistance filters	830
Cartridge assemblies	316L-Si

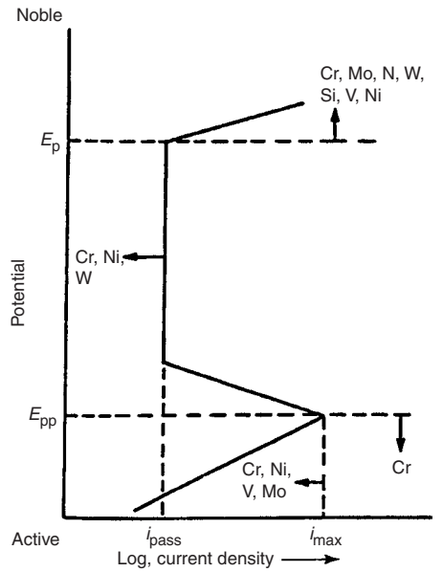

Fig. 25 Summary of the effect of alloying elements in stainless steels on the anodic polarization behavior. Source: Ref 20

316L stainless steel is further shown by the data in Table 18.

A number of investigators have observed decreased corrosion resistance with increasing oxygen content (Ref 14, 18, 24, 29). Figure 40 reveals that the pitting potential of P/M 316L stainless steel is found to decrease with increasing oxygen content (Ref 24). Immersion data in a 5% NaCl solution shows an identical trend, as seen in Fig. 41. High dew points (greater than −34 °C, or −29 °F) resulted in high oxygen concentrations within sintered alloys, leading to a reduction in mechanical properties and corrosion resistance. This is not surprising in light of the type of microstructure that is attained in

high dew point sintering atmospheres and illustrated in Fig. 42 (Ref 22). The P/M 316L stainless steel specimen shown in Fig. 42 exhibited a lack of interparticle bonding, resulting from the high grain boundary oxides, that led to poor mechanical and corrosion properties. Immersion data for sintered 316L stainless steel in a 5% NaCl solution, as a function of water vapor content of the hydrogen sintering atmosphere, is shown in Table 19 (Ref 30). When the water vapor content was 45 ppm or lower, no corrosion was noted after eight days of exposure.

Influence of Sintering Temperature, Sintering Time, and Cooling Rate. Improved electrochemical corrosion resistance has been noted for sintered 316L stainless steel with increased sintering time, as Table 20 reveals (Ref 24). These improvements in corrosion resistance were attributed to the reduced nitrogen, oxygen, and carbon levels observed for the specimens after the longer sintering time. Carbon, oxygen, and CO, H_2O, and CH_4 concentrations in a hydrogen sintering gas as a function of time at temperature are presented in Fig. 43. The significant influence of cooling rate on corrosion resistance is shown in Table 17. When there is sufficient water vapor to cause corrosion with slow cooling, it appears that a fast cooling rate (200 °C/min, or 360 °F/min) retards corrosion, as shown in Table 21 (Ref 13).

Influence of Porosity/Alloy Density. Sintered stainless steels are used in low-density forms (e.g., in filters) and in a wide variety of forms requiring higher-density alloys. The literature on P/M stainless steels in acid solutions reveals that corrosion resistance improves with increasing density, as Fig. 44 shows (Ref 31). In saline solutions the situation is not as clear—some researchers have reported that increasing density is beneficial, while others have reported it to be detrimental. These discrepancies are believed to be a result of differences, from study to study, in pore morphology and alloy density. This point is illustrated in Fig. 45, which shows

Table 13 Corrosion resistances of sintered and wrought austenitic stainless steels

Sintered stainless steels	Corrosion test(a)	Corrosion resistance rating(b), h	Sintered density, g/cm³	Comments				
				Sintering atmosphere(c)	Sintering temperature °C	Sintering temperature °F	Sintering time, min	Type of furnance(d)
303L	I	5	6.7–6.8	DA	1150	2100	60	L
303L SC(e)	I	500	6.7–6.8	DA	1150	2100	60	L
304L	I	100	6.7–6.8	DA	1150	2100	60	L
316L	I	500	6.7–6.8	DA	1150	2100	60	L
	I	...	6.7–6.9	Vac	1205	2200	60	L
	NSS	...	6.7	H_2	1150	2100	30	Ind
	NSS	...	6.3	H_2	1150	2100	30	Ind
	NSS	...	6.6–6.7	Vac	1120	2050	30	L
303LSC(e)	I	500	6.7–6.8	DA	1150	2100	60	L
	I	1700	6.7–6.9	Vac	1205	2200	60	L
317	I	4400	6.7–6.9	Vac	1205	2200	60	L
	NSS	...	6.7	H_2	1150	2100	30	Ind

(a) I, (by immersion in 5% NaCl: NSS, neutral salt-spray test (ASTM B 117: ISO 4540–1980(E)). (b) Time in hours until 1% of surface of specimen is covered with stain or rust. (c) H_2, hydrogen; DA, dissociated ammonia; Vac, vacuum; (d) L. laboratory; Ind. industrial; (e) Proprietary grades of SCM Metal Products. Source: Ref 1

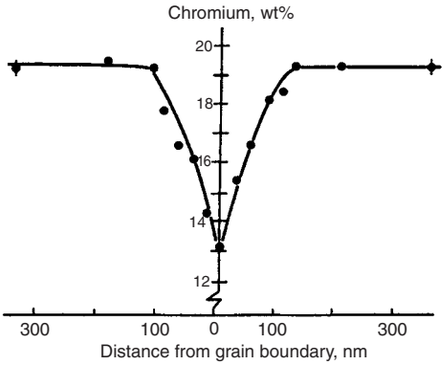

Fig. 26 Chromium concentration profile across a grain boundary between $M_{23}C_6$ carbides in type 304 (0.039% C) stainless steel heat treated for 10 h at 700 °C (1290 °F). Source: Ref 23

Table 14 Corrosion properties of sintered steels produced from prealloyed powders (–100 mesh) with different alloy compositions

Sintering, °C/min	Type	PRE	E_{pit}(a), mV SCE	E_{stp}(b), mV SCE	NSS1, h	NSS2, h
1120/30/H_2	316L	25	500	225	600	8
	317L	30	725	725	>1500	9
	18-18-6(c)	37	275	275	48	4
	SS-100(d)	37	575	400	>1500	9
	17-25-8(e)	42	550	425	>1500	9
1250/120/H_2	317L	25	500	150	96	7
	317L	30	500	350	14	6
	18-18-6	37	450	275	50	5
	SS-100	37	>800	>800	>1500	10
	17-25-8	42	675	450	355	8

PRE, Pitting resistance equivalent (%Cr + 3.3% Mo + 16% N) in wt%; NSS1, time to first sign of corrosion, salt-spray test in 5% NaCl; NSS2, rust rating after 1500 h of testing where 10 = no corrosion and 0 = surface half covered with corrosion products. (a) 0.1%Cl^-, pH 5, 30 °C, 5 mV/min. (b) 0.1% Cl^-, pH 5, 30 °C. 25 mV/8 h. (c) 18.3% Cr, 18.3% Ni, 5.6% Mo, 1.7% Cu, 1.3% Sn. 0.78% Si, 0.23% Mn, bal Fe. (d) 20% Cr, 17.0% Ni, 5.0% Mo, 0.75% Si. >0.15% Mn, bal Fe. (e) 16.3% Cr, 24.3% Ni, 7.7% Mo, 0.81% Si, 0.25% Si, bal Fe. Source: Ref 14

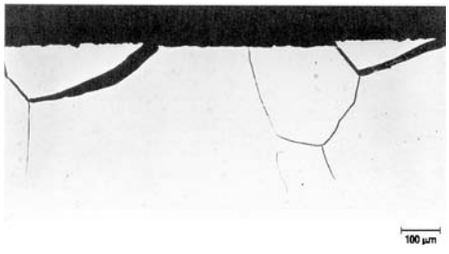

Fig. 27 Intergranular attack in a sensitized austenitic alloy produced by exposure to a boiling sulfuric acid-ferric sulfate solution. Prolonged exposure causes grains to detach from surface. Original magnification 100×. Source: Ref 23, reprinted with permission

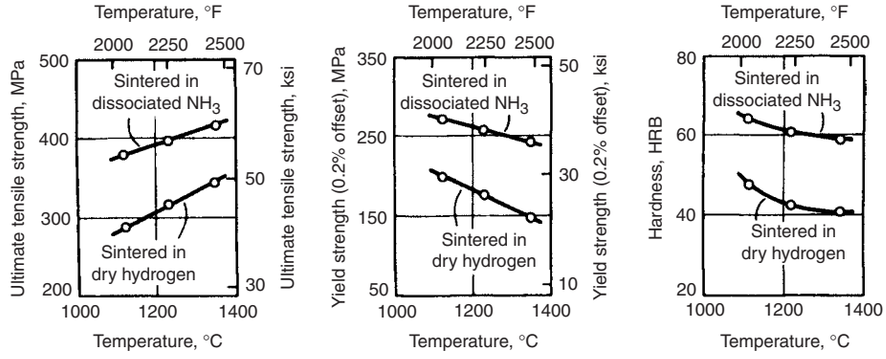

Fig. 28 Effect of sintering temperature on tensile and yield strengths and apparent hardness of type 316L stainless steel. Parts (density: 6.85 g/cm³) were sintered for 30 min in various atmospheres

the corrosion resistance of sintered 316L stainless steels as a function of density (Ref 1, 32). At low sintered densities, the network of pores, including boundary oxides and particle boundaries, is rather open and discourages the formation of the occluded cell environment associated with crevice-corrosion initiation in stainless steels. At relatively high sintered densities, this network is tighter and encourages both the establishment of an aggressive environment within the crevice and a high potential drop down the crevice. At very high sintered densities, crevice-corrosion susceptibility decreases as the porous network is closed off with increasing alloy density. Data showing the percentage of open pores as a function of sintered density and the resulting time to first rust during salt-spray exposure are presented in Table 20 (Ref 24).

In the corrosion literature for wrought alloys, it is well recognized that the aspect ratio of a crevice (the ratio of its width to its length) is a critical parameter in the establishment of crevice corrosion. Figure 46 illustrates that for narrow crevice gaps, crevice corrosion initiates at shallow depths, whereas, for wider crevice gaps, attack initiates deeper within the crevice (Ref 23). As a result, narrow and/or long crevices are likely initiation sites for crevice corrosion. In sintered stainless steels the inherent porous nature of the material provides a narrow tortuous electrolyte path that both encourages crevice-corrosion initiation and sustains its propagation.

Several changes occur in the occluded cell environment of a crevice during the initiation stages of crevice corrosion: oxygen depletion within the crevice that establishes a separation of anodic and cathodic sites (where the cathode is largely outside the crevice and the anode is inside the crevice), a lowering of the pH of the solution within the crevice by hydrolysis reactions, and migration of chloride into the crevice to maintain charge neutrality. For some of the less heavily alloyed stainless steels, the reduction in E_{pit} resulting from the increased chloride concentration is enough to initiate crevice corrosion, as the schematic polarization curve and mixed potential analysis in Fig. 47 reveal (Ref 33). The crossover point in the mixed potential analysis indicates dissolution of the metal within the

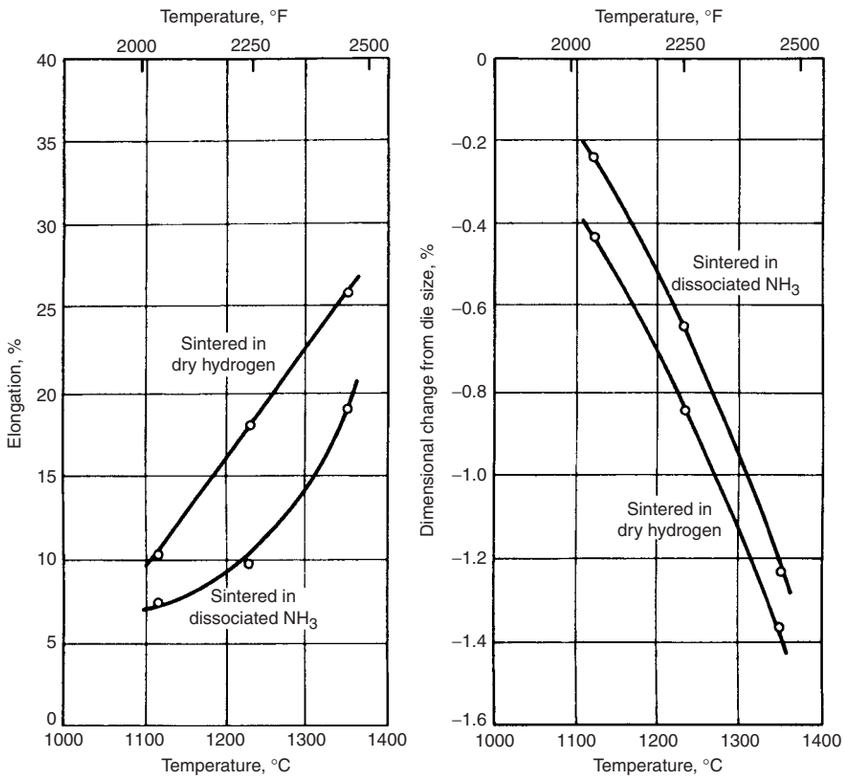

Fig. 29 Effect of sintering temperature on elongation and dimensional change during sintering of type 316L stainless steel. Parts (density: 6.85 g/cm^3) were sintered for 30 min in various atmospheres.

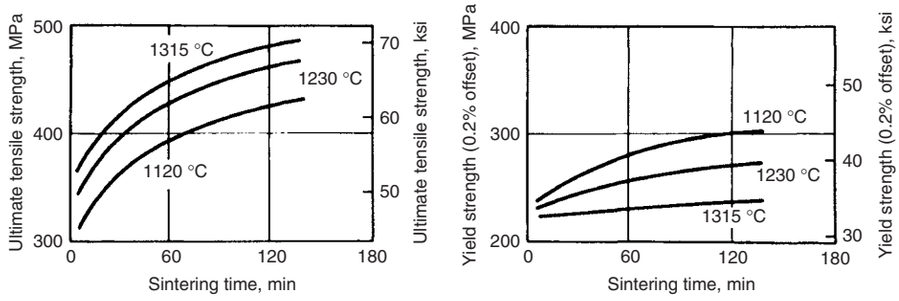

Fig. 30 Effect of sintering time on tensile and yield strengths of type 316L stainless steel. Parts were pressed to 6.85 g/cm^3 and sintered at various temperatures in dissociated NH_3.

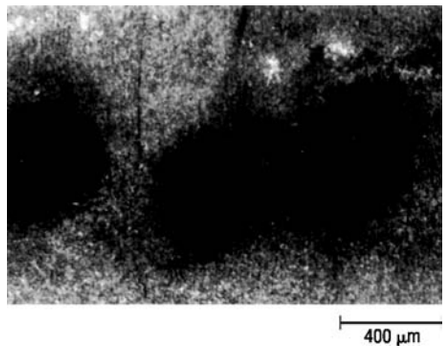

Fig. 31 Small circles of rust around iron particles embedded in the surface of sintered type 316L stainless steel after testing in 5% aqueous NaCl. Original magnification: 35×

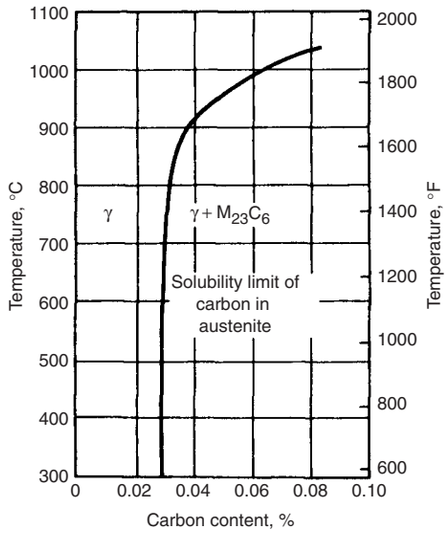

Fig. 32 Solid solubility of carbon in an austenitic stainless steel. Source: Ref 23

crevice via a pitting type of attack. Changes in the anodic polarization behavior for the stainless steel within the crevice, resulting from acidification and increase in chloride ion concentration of the crevice solution, are illustrated in Fig. 48 (Ref 33).

As the aggressive nature of the crevice solution increases, i_{crit}, E_{pp}, and i_p increase, while E_{bd} decreases. A mixed potential analysis of crevice-corrosion initiation (using the cathodic polarization behavior for the stainless steel in the environment outside of the crevice and the anodic polarization behavior for the stainless steel in the environment inside the crevice) is depicted in Fig. 49 (Ref 33). This analysis reveals that when the potential drop associated with the tortuous electrolyte path of a crevice exceeds a certain value, IR^* in this illustration, crevice corrosion is initiated by active dissolution of the metal in the crevice. While the mechanisms just described were proposed for wrought materials containing intentional or unintentional crevice formers, such as O-rings or gaskets, they are equally applicable to P/M materials containing inherent porosity. In fact, the extremely tortuous path provided by the pores, oxides, and particle boundaries in a sintered stainless steel provide what could be viewed as the ultimate geometry for establishing and, perhaps, even studying crevice corrosion. Clearly, by gaining a better understanding of the influence that processing parameters play in establishing pore morphologies susceptible to crevice corrosion, it will be possible to alter pore morphology to discourage crevice-corrosion initiation.

Another means of altering the susceptibility of sintered stainless steels to crevice attack is to alter alloy composition. By altering alloy

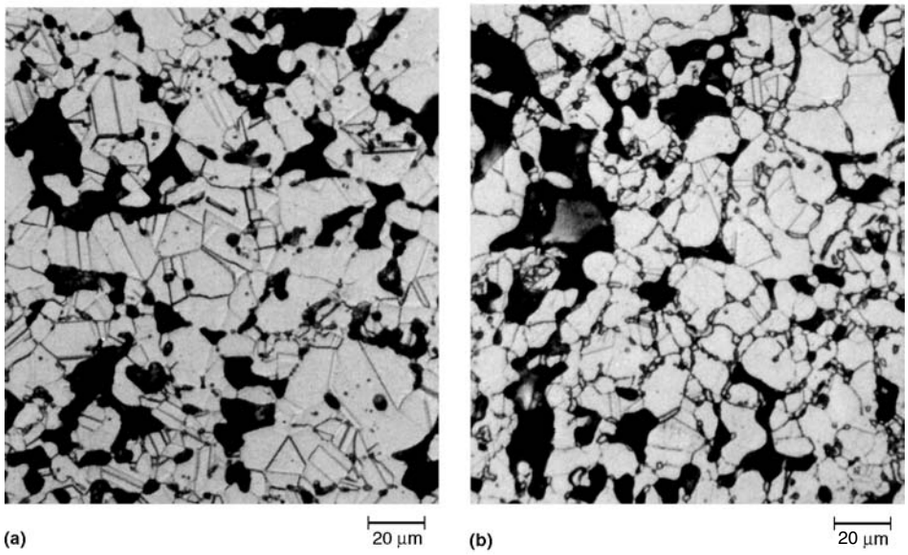

Fig. 33 Microstructures of type 316L stainless steel sintered in hydrogen at 1150 °C (2100 °F). (a) Low carbon content. (b) Excessive carbon content. Both 400× (original magnification)

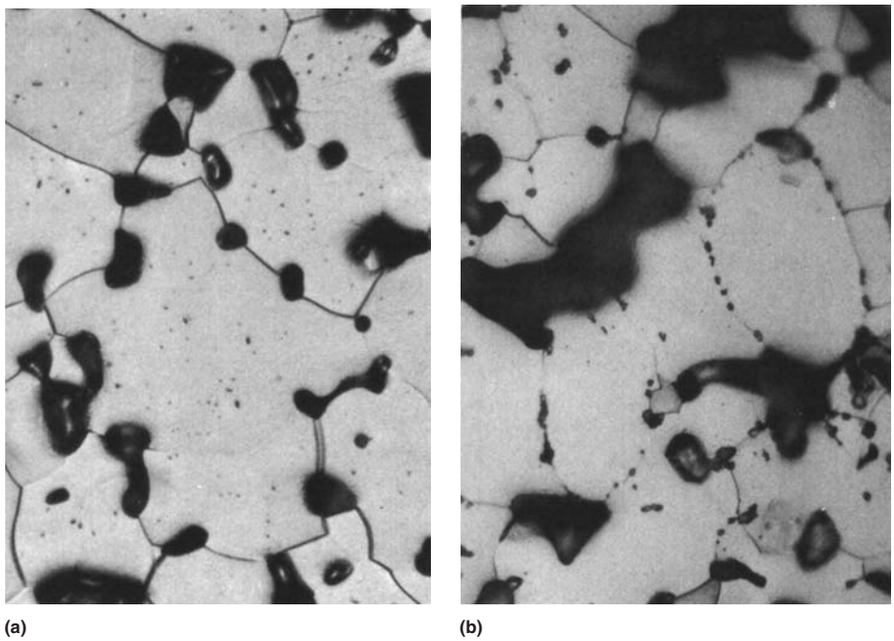

Fig. 35 Cross sections of vacuum-sintered (30 min at 1330 °C, or 2430 °F) type 430L stainless steel. (a) No oxides are present in grain boundaries after addition of 0.2% graphite. (b) Small, gray, rounded oxide particles in grain boundaries (no graphite added)

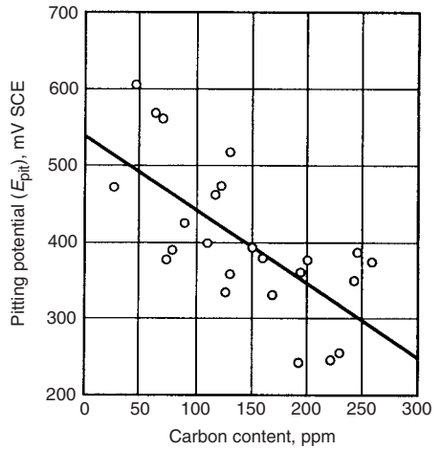

Fig. 34 Influence of carbon concentration on the pitting potential for a number of different materials. Source: Ref 14

Table 15 Effect of binder/lubricant on the corrosion resistance of sintered 316L stainless steel in deaerated 1000 ppm Cl buffered with acetate at 30 °C (pH=5)

The dew point of the gas atmospheres in the furnace was approximately −30 °C.

Binder(a)	Sintering, °C/min	Atmosphere	i_p, A/cm^2	E_{pit}, mV SCE	Salt spray, h
A	1120/20	DA	45	65	20
M			18	230	24
A	1160/45	H_2	3	455	30
M			2	400	620
A	1250/30	H_2	16	230	24
M			16	230	24
A	1120/30	Vacuum	4	390	500
M			4	380	500
A	1200/50	Vacuum	8	475	560
M			5	425	560
A	1295/30	Vacuum	2	405	240
M			2	500	330

(a) A, Acrawax (ethylene bis-stearamide); M, Metallub (multicomponent). Source: Ref 24

composition, the hydrolysis reactions responsible for lowering the pH within the crevice can be influenced, and these changes can be used to discourage crevice-corrosion initiation, as Fig. 50 reveals (Ref 32). The enhanced crevice-corrosion resistance of the 317L and 20Cr-17Ni-5Mo alloys is attributed to their higher molybdenum concentrations. It should be noted that the addition of molybdenum does not make these alloys immune to crevice corrosion because it is possible to initiate crevice corrosion in neutral pH crevice environments without the presence of chloride when the aspect ratio of the crevice is severe enough; it simply makes initiation more difficult.

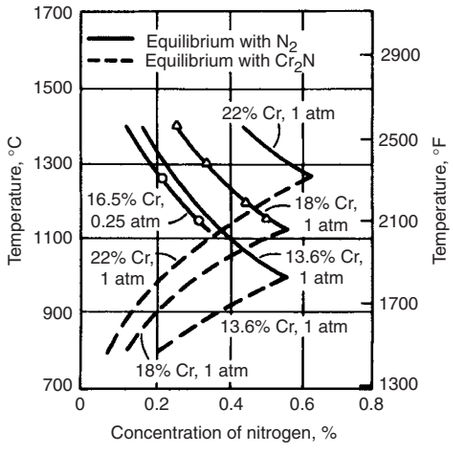

Fig. 36 Solubility of nitrogen in austenitic stainless steel in equilibrium with gaseous nitrogen or Cr_2N. Source: Ref 25

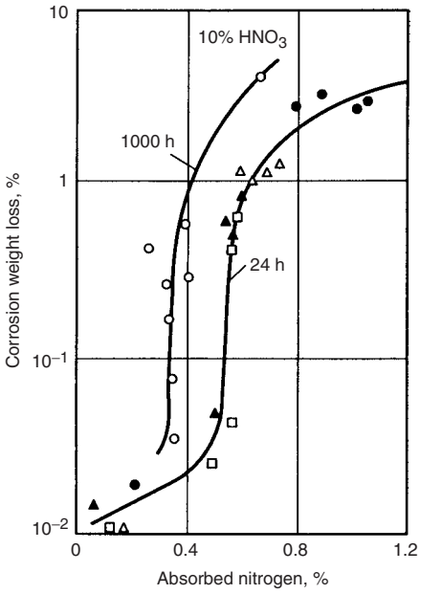

Fig. 37 Effect of the absorbed nitrogen content during sintering on the corrosion resistance of 316L stainless steel sintered at 1150 °C (2100 °F) in several atmospheres; corrosion rate is given in terms of weight loss resulting from immersion in 10% HNO_3. Source: Ref 3

Approaches Used to Improve the Corrosion Resistance of Sintered Stainless Steels. A variety of means have been employed to improve the corrosion resistance of sintered stainless steels—some of which simply alter the number of open pores, others are aimed at both

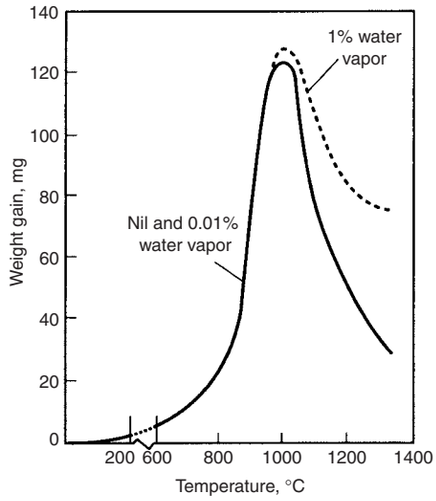

Fig. 38 Increase in weight of specimens heated in nitrogen containing various amounts of water vapor. Source: Ref 13

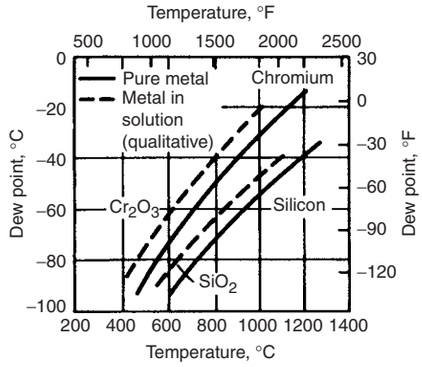

Fig. 39 Redox curves for chromium and silicon alone and in solution. Source: Ref 25

Table 16 Corrosion properties of 316L stainless steel sintered in hydrogen or nitrogen/hydrogen mixtures

Sintering, °C/min	Nitrogen content in atm, %	Nitrogen, ppm	i_{crit}(a), μA/cm²	i_p(a), μA/cm²	E_{pit}(a), mV SCE	E_{stp}(b), mV SCE	NSS1, h	NSS2, h	I_r/I_a(c) ×1000
1120/30	0	360	10	11	375	100	>1500	8	0.0
	5	1710	11	11	475	350	>1500	9	0.7
	10	2100	10	11	525	350	>1500	9	7.2
	25	5670	330	34	325	225	24	4	28.9
1250/120	0	20	8	10	600	375	990	8	0.0
	5	1350	11	9	550	300	864	6	0.0
	10	1850	10	12	600	375	240	3	0.1
	25	7180	400	160	−25	−25	24	2	390

(a) 0.1% Cl^-, pH 5, 30 °C, 5 mV/min. (b) 0.1% Cl^-, pH 5, 30 °C, 25 mV/8h. (c) EPR test in 0.5 *M* H_2SO_4 + 0.01 *M* KSCN, 30 °C. Source: Ref 14

Table 17 Influence of heating and cooling rates on the corrosion resistance of 316L stainless steel specimens sintered at 1150 °C in dissociated ammonia

Heating rate, °C/min	Cooling rate, °C/min	Weight increase, mg/g	Result of corrosion test in 5% NaCl solution
22	22	3.3	Corroded in 1 day
67	67	2.5	Corroded in 1 day
22	100	3	Slight attack in 4 days
5	200	2.9	No attack in 5 days(a)
22	200	3	No attack in 5 days
200	200	2.3	No attack in 5 days

(a) Test continued to 12 days with no attack. Source: Ref 13

Table 18 Corrosion properties of 316L stainless steel sintered in hydrogen with a dew point of −35 or −70 °C at different combinations of time and temperature

Sintering, °C/min	i_{crit}(a), μA/cm² at dew point:		i_p(a), μA/cm² at dew point:		E_{pit}(a), mV SCE at dew point:		NSS1, h at dew point		NSS2, h at dew point	
	−35 °C	−70 °C	−35 °C	−70 °C	−35 °C	−70 °C	−35 °C	−70 °C	−35 °C	−70 °C
1120/30	150	10	29	11	250	375	36	>1500	5	9
1250/30	105	7	20	12	325	325	288	1260	4	8
1120/120	120	10	25	10	325	375	48	1272	5	7
1250/120	83	4	19	9	325	500	24	96	1	7

(a) 0.1% Cl^-, pH 5, 30 °C, 5 mV/min. Source: Ref 14

reducing the number of open pores and enhancing passivity of the alloy. These approaches include the following finishing processes: tumbling, grinding and shot blasting, passivating treatments, liquid phase sintering, double pressing and sintering, and the addition of alloying elements, such as copper, tin, and noble metals (Ref 34).

One group of researchers evaluated the influence of several finishing processes on the anodic polarization behavior of P/M 316L stainless steel in a 0.1 *N* NaCl/0.4 *N* $NaClO_4$ solution (ASTM B 627). As shown in Fig. 51, the investigation revealed the following results: tumbling likely smears the pores and is ineffective at improving corrosion resistance; coining/sizing introduces residual stresses in the surface of the alloy that may increase corrosion; grinding, turning, and shot blasting can seal surface pores and improve corrosion resistance; and thermal and chemical passivation processes can alter the thickness and/or composition of the passive film, thus enhancing corrosion resistance (Ref 3). In another investigation, thermal passivation in the range of 325 to 500 °C (615 to 930 °F) for 30 min also showed promise for enhancing passivity, and thus corrosion resistance, of sintered 316L stainless steel exposed to a 1 *N* H_2SO_4 solution, as Fig. 52 reveals (Ref 35).

Closing of porosity through operations such as double pressing and double sintering (DPDS), while expensive, has been found to significantly reduce the amount of open porosity and yield anodic polarization behavior in aggressive acid solutions similar to that of wrought materials. Figure 53 shows anodic polarization data for wrought and hot pressed and hot sintered 316 stainless steel in 1 *N* H_2SO_4 (Ref 29). When a DPDS operation is used, a P/M 316 stainless steel alloy of nominal composition exhibits a degree of passivity almost identical to that of

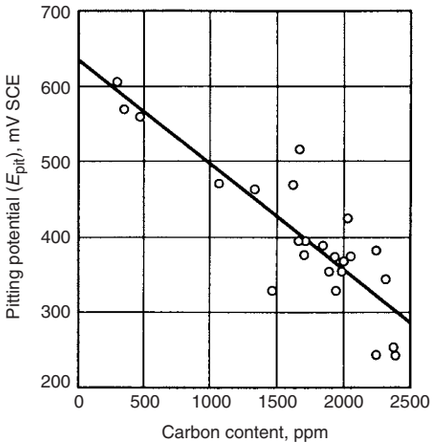

Fig. 40 Influence of the oxygen content on the pitting potential for a number of different materials of sintered AISI 316L. Source: Ref 24

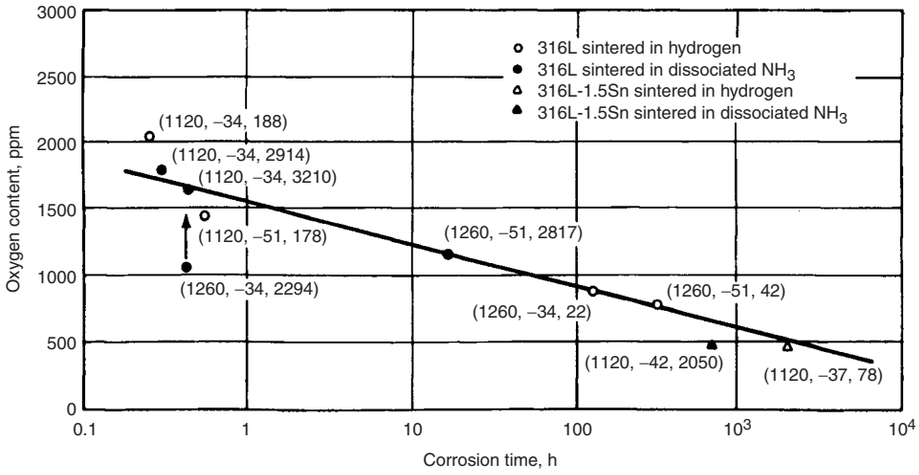

Fig. 41 Effect of oxygen content on corrosion resistance of sintered type 316L and tin-modified type 316L (sintered density: 6.65 g/cm^3; cooling rate: 75 °C/min, or 135 °F/min). Parenthetical values are sintering temperature (°C), dew point (°C), and nitrogen content (ppm), respectively. Time indicates when 50% of specimens showed first sign of corrosion in 5% aqueous NaCl. Source: Ref 16, 30

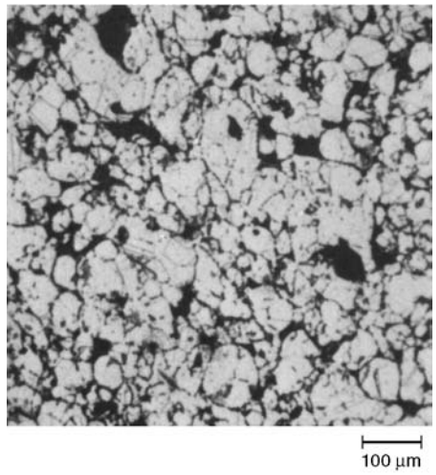

Fig. 42 Microstructure of type 316L stainless steel sintered in a high-dew-point atmosphere. Oxygen content: 5100 ppm; sintered density: 7.5 g/cm^3. Etched with Marble's reagent. Original magnification: 200×

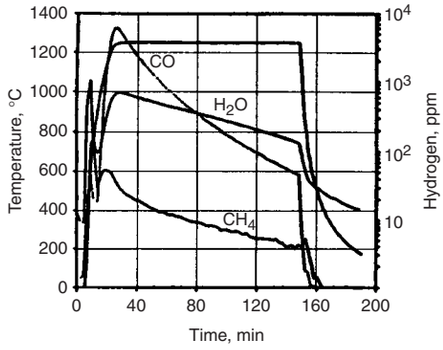

Fig. 43 Gas composition and progress of reactions for a sintering experiment performed with pure hydrogen. Source: Ref 14

Table 19 Effect of water-vapor content of the sintering atmosphere on the corrosion resistance of stainless steel specimens sintered at 1150 °C in hydrogen

Water-vapor content, ppm	Result of corrosion test in 5% NaCl solution
30	No attack in 8 days
45	No attack in 8 days(a)
90	Rusted after 3 days
110	Stained in 3 h
150	Rusted in 1½ h

(a) Test continued to 14 days with no attack. Source: Ref 13

Table 20 Effect of sintering temperature and time on the corrosion resistance of sintered 316L stainless steel

The materials were sintered in hydrogen with a dew point of −70 °C

Sintering, °C/min	Open pores, %	Nitrogen, %	Oxygen, %	Carbon, %	i_p, A/cm^2	E_{pit}, mV SCE	Salt spray, h
1120/30	17.4	380	2230	250	3.4	383	>1500
1250/30	16.3	110	1980	130	3.1	357	>1500
1120/240	15.8	70	1640	130	3.0	508	>1500
1250/240	13.8	20	450	70	1.8	561	260

Source: Ref 24

wrought 316 (Ref 36). Another, more thorough, means for reducing or eliminating open porosity in P/M materials is liquid phase sintering. Sintering additives such as boron, NiB, BN, and CrB have been found to be effective in producing dense microstructures with enhanced salt-spray corrosion resistance, as Table 22 reveals (Ref 14). Unfortunately, sensitized microstructures, as evidenced by the high I_r/I_a ratio listed in Table 22 are a by-product of liquid phase sintering (Ref 14). Careful development of liquid phase sintering additives for stainless steels will be needed in order to produce dense alloys that are not susceptible to intergranular corrosion. Injection molding also shows promise for producing dense P/M alloys with enhanced corrosion resistance. Figure 54 compares weight-loss values for injection-molded and wrought 14-4PH stainless steel as a function of exposure time in either full-strength chlorine bleach or a 10% $FeCl_3$ solution (Ref 37). The injection-molded P/M compacts had densities of 96 to 97% of the wrought density and exhibited weight losses comparable to those of the wrought 17-4PH stainless steel.

A number of alloying additions or infiltrants have been explored as means for enhancing passivity in P/M stainless steels. Among the most popular are copper and tin. Infiltration of P/M 316L and 304L alloys with either copper or bronze has been observed to increase corrosion resistance in boiling and room-temperature acid solutions (see Fig. 55). As this figure reveals, similar results were noted for the bronze and copper in the room-temperature acid, while the bronze infiltrant gave the best results in the boiling acid. Enhanced corrosion resistance was attributed to the elimination of open-connected porosity and the effect of the alloying. It should be noted that in both cases the infiltrants diffused either partially (bronze at all infiltration percentages and copper at the 6% infiltration level) or totally (copper at 4 and 6% infiltration levels) into the matrix. When both copper and tin are prealloyed into the powder, the alloys are marketed with an "LSC" designation. In Table 1 the beneficial influence of copper alloying additions in the 316LSC on the corrosion resistance of

Table 21 Effect of cooling rate on the corrosion resistance of 316L stainless steel specimens sintered at 1150 °C in a hydrogen atmosphere containing 100 ppm water vapor

Heating rate, °C/min	Cooling rate, °C/min	Result of corrosion test in 5% NaCl solution
5	22	Corroded in 2 days
200	67	Attack started after 1 day; severe attack after 8 days
200	200	No attack after 3 days; slight staining after 5 days

Source: Ref 13

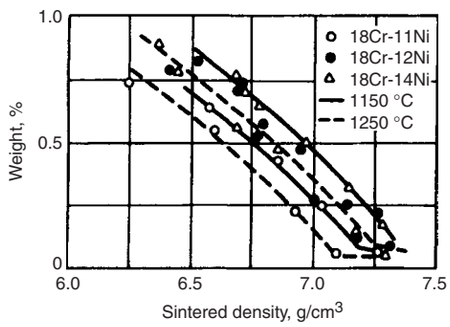

Fig. 44 Relationship between sintered density and weight loss of three austenitic stainless steels in 40% HNO_3 solution. Source: Ref 31

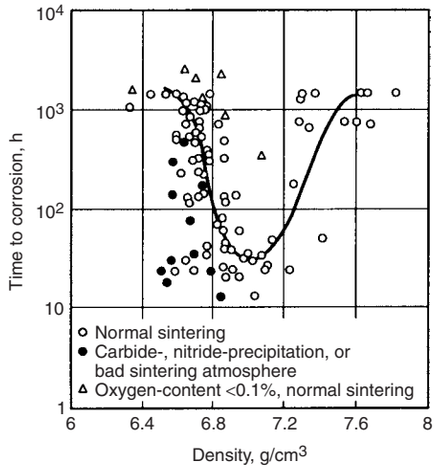

Fig. 45 Effect of sintered density upon corrosion resistance of sintered 316 type alloys. Source: Ref 1, 32

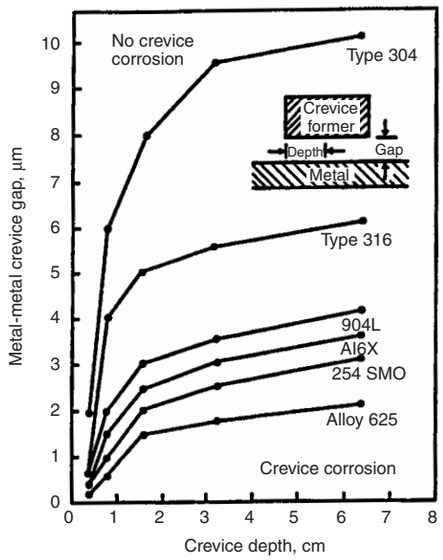

Fig. 46 Effect of crevice gap and depth on the initiation of crevice corrosion in various stainless steels and alloy 625. The gaps and depths below and to the right of the curve for each material define crevice geometries where initiation of crevice corrosion is predicted by the mathematical model of T.S. Lee and R.M. Kain, NACE Corrosion 83 Conference proceeding paper 69, 1983. Source: Ref 23

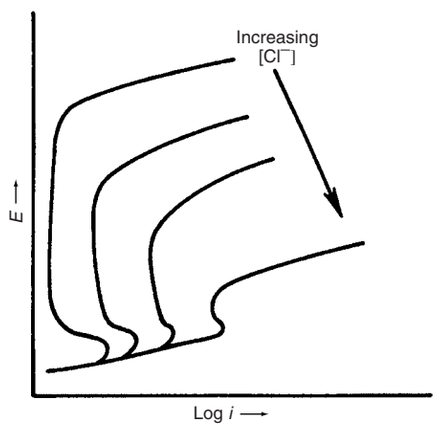

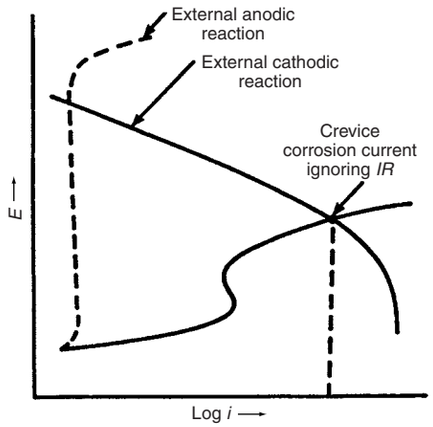

Fig. 47 Crevice-corrosion initiation resulting from lowering of E_{pit} with increasing chloride concentration. Source: Ref 33

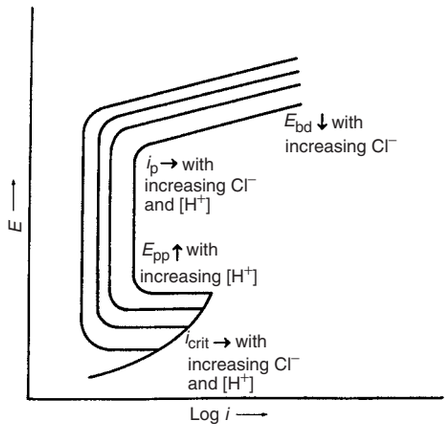

Fig. 48 Changes in anodic polarization behavior that occur as the environment in the crevice becomes increasingly aggressive. Source: Ref 33

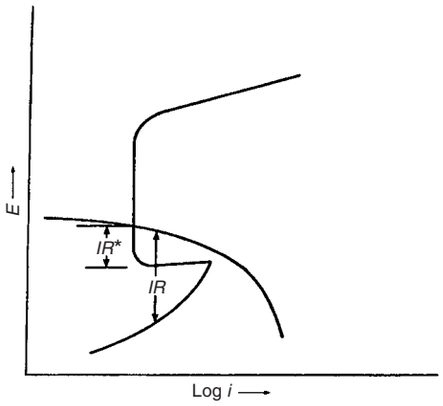

Fig. 49 Crevice-corrosion initiation by an *IR*-induced mechanism. When the *IR* drop down the crevice exceeds *IR**, crevice corrosion initiates. Source: Ref 33

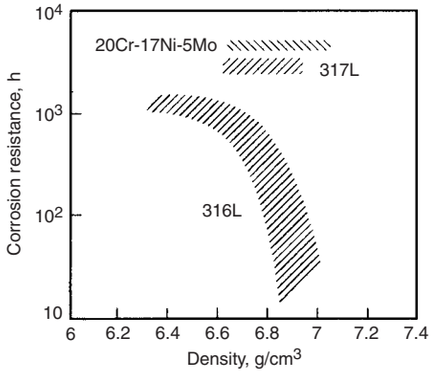

Fig. 50 Effect of density on corrosion resistance of sintered austenitic stainless steel. Source: Ref 32

Table 22 Corrosion properties of liquid phase sintered 316L steels with the addition of boron-base sintering additives

All stainless steels were sintered at 1250 °C for 60 to 120 min in pure hydrogen.

Additive	Density, g/cm³	Open pores, %	E_{stp}(a), mV SCE	NSS1, h	NSS2, h	$I_r/I_a \times 10^3$
None	6.86	8.2	150	96	7	0.0
0.2% B (−38 μm)	7.83	0.1	500	>1500	10	4.4
1% BN (−63 μm)	7.61	0.2	400	762	9	2.5
1% NiB (−38 μm)	7.67	0.1	525	>1500	10	3.8
1% CrB (−38 μm)	7.64	0.1	550	>1500	10	2.5

(a) 0.1% Cl^-, pH 5, 30 °C, 25 mV/8 h. Source: Ref 14

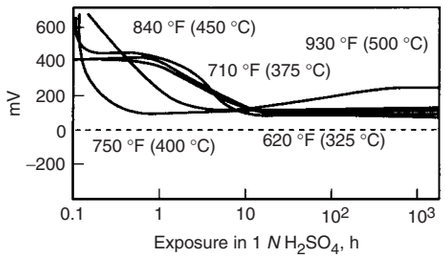

Fig. 52 Rest (open-circuit) potential measurements for sintered 316L thermally prepassivated at temperatures between 325 and 500 °C (615 and 930 °F). Source: Ref 35

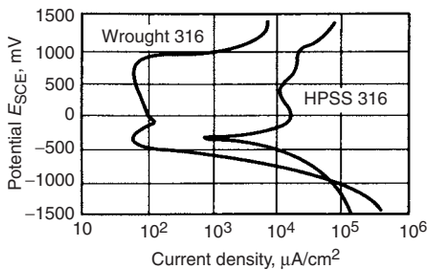

Fig. 53 Potentiodynamic polarization curves of samples tested in H_2SO_4, scanning rate 2 mV/S (1 *N* H_2SO_4). Source: Ref 29

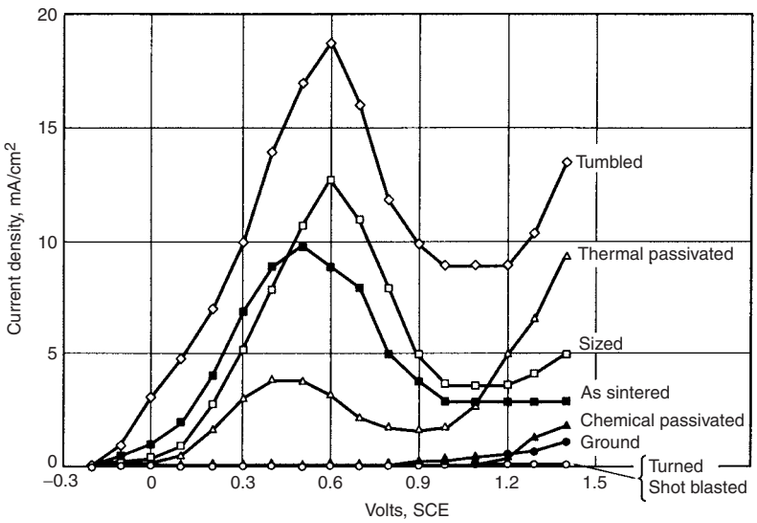

Fig. 51 Anodic potentiodynamic polarization curves for 316L stainless steel in 0.1 *N* NaCl/0.4 *N* $NaClO_4$ as a function of surface finishing. Source: Ref 3

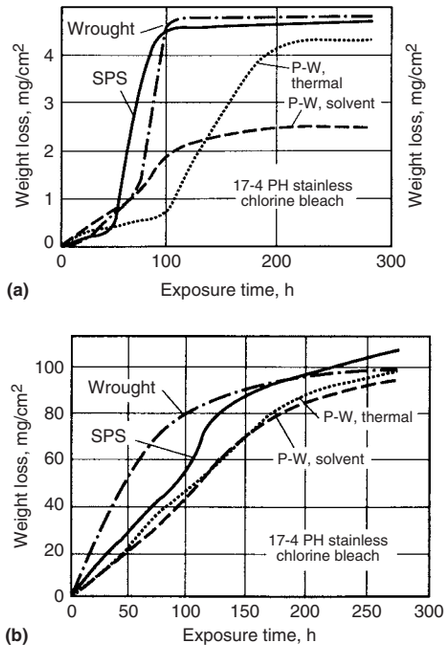

Fig. 54 Comparison of the corrosion weight loss versus exposure time in (a) ferric chloride and (b) chlorine bleach tests at room temperature. P-W, polymer wax binder, 69% paraffin wax, 20% polypropylene, 10% carnauba wax, 1% stearic acid; SPS, 73% acetanilide, 18% polystyrene, and 9% stearic acid. Source: Ref 37

316L stainless steel is seen. Additional data supporting the beneficial influence of copper alloying additions on hot pressed and sintered 316 stainless steel are provided in Fig. 55 (Ref 38). The improved passivity of the copper-containing alloys is attributed to its depolarizing influence on the oxygen reduction reaction. Depolarization of the cathodic, oxygen-reduction reaction enables the alloys to passivate more easily. Figure 56 shows the benefits of tin additions to the polarization behavior of 316 stainless steel (Ref 39). The addition of tin decreases the passive and critical current densities of the hot-pressed specimens by two orders of magnitude. Improvements in corrosion resistance, such as the ones just described, led to the development of copper- and tin-modified stainless steel powder chemistries, which are currently being marketed under the trademarks of Ultra 303L, Ultra 304, and Ultra 316. The

enhanced corrosion resistance of these alloys, when compared to those of nonmodified 303L, 304L, and 316L, is evident in Fig. 55 and 56.

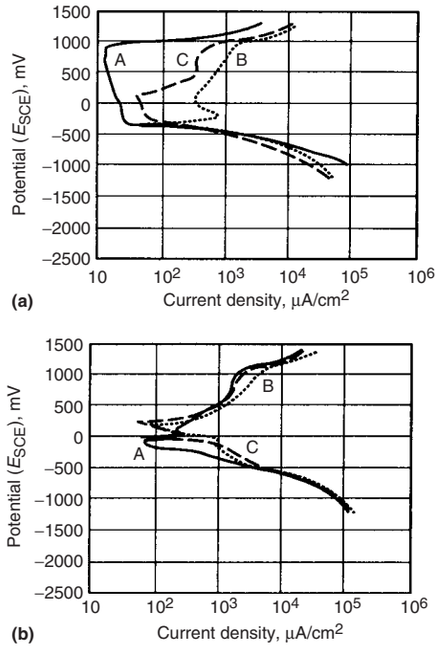

Fig. 55 Potentiodynamic polarization curves of as-received samples tested in 1 *N* H_2SO_4, scanning rate 1 mV/s. (a) A, wrought plate stainless steel of type 316; B, hot pressed sintered stainless steel; C, hot pressed and sintered stainless steel containing 0.25% Cu. (b) A, Hot pressed and sintered stainless steel containing 1 wt% Cu; B, hot pressed and sintered stainless steel containing 3 wt%; C, hot pressed and sintered stainless steel containing 5 wt% Cu. Source: Ref 38

The improved corrosion resistance for 316LSC compared to that of nonmodified 316L is presented in Fig. 57.

As this section has revealed, a number of processing variables exert a strong influence on the corrosion resistance of sintered stainless steels. A listing of the most important variables and their impact on corrosion performance is presented in Table 23.

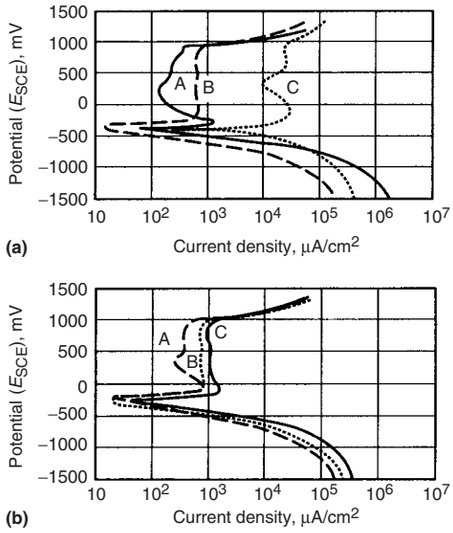

Fig. 56 Potentiodynamic polarization curves of samples tested in 5 *N* H_2SO_4, scanning rate 2 mV/s. (a) A, Wrought plate stainless steel of type 316; B, 2 wt% Sn; C, HPHS 316. (b) Hot pressed and sintered sample containing A, 3 wt% Sn; B, 2 wt% Sn; C, 0.5 wt% Sn. Source: Ref 39

P/M Superalloys

Development of P/M superalloys began in the 1960s with the search by the aerospace industry (and later the electric power industry) for stronger high-temperature alloys in order to operate engines at higher temperatures and thus improve fuel efficiency.

Initially, lower production costs were a major objective in exploring the P/M approach. Later, specific advantages were linked to the P/M approach. These consisted of the use of more complex and greater volume fractions of dispersoids, reduced segregation, improved workability, and the reduced cost of consolidating superalloy powders, particularly of oxide-dispersion-strengthened (ODS) superalloys,

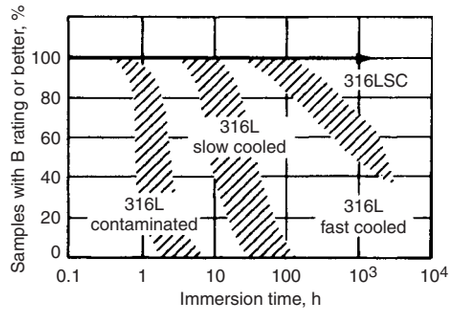

Fig. 57 Typical corrosion behavior or regular and copper-tin modified (type 316LSC) sintered type 316L stainless steel sintered in dissociated NH_3 under various conditions of cooling and contamination. B rating indicates that <1% of the specimen surface is covered by stain. Testing of the modified stainless steel was terminated after 1500 h. Source: Ref 25

Table 23 Effect of iron, carbon, nitrogen, and oxygen on corrosion resistance of sintered austenitic stainless steels

Variable	Origin of problem	Effect on corrosion resistance	Suggested solutions
Iron	Contamination of prealloyed powder with iron or iron-base powder at powder or parts producer's facility	Lowering of corrosion resistance by more than 99% due to galvanic corrosion	Utmost cleanliness at both powder and parts producer's manufacturing facilities, preferably separate and dedicated equipment and facilities
Carbon	Inadequate lubricant removal; carburizing sintering atmosphere soot in sintering furnace; high-carbon powder	Inferior resistance to intergranular corrosion	Use L-grade designation of stainless steel powder. Ensure adequate lubricant removal (before sintering). Use clean soot-free sintering furnace and carbon-free sintering atmospheres; carbon content of sintered part should be ≤0.03%.
Nitrogen	Sintering in dissociated NH_3 or other nitrogen-containing atmosphere combined with slow cooling	Inferior resistance to intergranular corrosion	Reduce percentage of nitrogen in sintering atmosphere. Use fast cooling of parts, preferably > 150 to 200 °C/min (> 270 to 360 °F/min) through critical temperature range (700 to 1000 °C, or 1290 to 1830 °F). Use higher sintering temperature. Use intermediate dew points (−37 to −45 °C, or −35 to −50 °F) in cooling zone of furnace. Use tin-modified stainless steel powders.
Oxygen	Excessive oxygen in powder, excessive dew point of sintering atmosphere; slow cooling after sintering	Inferior resistance to general corrosion	Use low oxygen content powder, preferably < 2000 ppm. Control dew point within sintering furnace to ensure reducing conditions. Fast cooling, preferably > 200 °C/min (360 °F/min) For nitrogen-containing atmospheres, use dew point of −37 to −45 °C (−35 to −50 °F) in cooling zone. For sintering in H_2, ensure that water vapor content of atmosphere is below 50 ppm.
Density of sintered part	High sintered density	Inferior resistance to crevice corrosion	Use lower density to increase pore size and circulation of corrodent. In acidic environments, corrosion resistance improves with increasing density due to a decrease of specific surface area.

through the development of suitable forging techniques (Ref 40). Efforts are also underway to exploit the advantages of microcrystallinity and extended solid solutions of rapid solidification technology.

Uses and State of Commercialization. Table 24 summarizes the uses of P/M superalloys as components in aircraft engines. Other uses of P/M superalloys include nuclear reactors, heat exchangers, furnaces, sour gas well equipment, and other high-temperature applications.

Manufacturing of P/M Superalloys. An important prerequisite for making P/M superalloys that possess reliable dynamic properties is the use of clean powders. Years of intensive work were spent in identifying and controlling the problems related to unclean powders. Today, argon and vacuum (also known as soluble gas process) atomization, as well as atomization by the rotating electrode process, are known to be suitable for producing powders with the required low oxygen content and low degree of contamination. The so-called prior particle boundary (PPB) problem, that is, the presence of carbides segregated at PPBs, was solved through the development of low-carbon alloys. Special equipment is used for removing ceramic particles and particles containing entrapped argon. Some of these problems are minimized or avoided in ODS alloys made by mechanical alloying. In mechanical alloying, elemental and master alloy powders as well as refractory compounds are mechanically alloyed by high-energy milling (Ref 42, 43).

Two established powder consolidation techniques for P/M superalloys are hot isostatic pressing (HIP) and isothermal forging. Both P/M methods permit the manufacture of so-called near-net-shape parts with attendant improved material use and reduced machining costs. Powder metallurgy forging exploits the improved forgeability deriving from the higher incipient melting temperature and reduced grain size of P/M material. Hot compaction by extrusion leads to very fine grain size, improved hot ductility, and superplasticity.

Depending on the application of a superalloy part, the powder consolidation process can be controlled in order to yield either a fine or a coarse grain size. Fine grain size is preferred for intermediate temperatures (up to approximately 700 °C, or 1290 °F) because of its higher strength and ductility at these temperatures. For high-temperature blade and vane applications, however, a large grain size (ASTM 1 to 2) provides superior creep strength due to reduced grain-boundary sliding. Grain coarsening of ODS alloys is achieved through special heat treatments after consolidation (Ref 40).

Compositions and Properties. Table 25 shows the compositions of the best known P/M superalloys. Many have the same compositions as cast alloys but are manufactured similarly to wrought alloys. The important P/M superalloys—IN-100, René 95, and Astroloy—were adapted in the P/M process by reducing their carbon content and by adding stable carbide formers to eliminate the problem of PPB carbides. To facilitate HIP, alloy compositions were modified to increase the temperature gap between the γ' solvus (above which HIP has to be carried out for increasing grain size) and the solidus temperature.

Oxidation. Nickel-, cobalt-, and iron-base superalloys use the selective oxidation of aluminum or chromium to develop oxidation resistance (Ref 44). These alloys are therefore often referred to as Al_2O_3 or Cr_2O_3 formers depending on the composition of the oxide scale that provides protection. Alloy composition, surface conditions, gas environment, and cracking of the oxide scale affect the selective-oxidation process (Ref 44). Figure 58 shows the development of superalloys in terms of the progress achieved against high-temperature oxidation.

Cyclic oxidation causes protective scales of Al_2O_3 and Cr_2O_3 to crack and spall. Regeneration of the scales will eventually result in the complete depletion of chromium and aluminum. The length of time for which superalloys are Al_2O_3 or Cr_2O_3 formers under given conditions is very important because of the subsequent appearance of less protective oxides.

Figures 59 and 60 show comparisons of the oxidation resistances of superalloys with and without oxide dispersions. Many studies have confirmed the beneficial effect of dispersed oxides on oxidation resistance. The lower oxidation rates of ODS alloys have been attributed to the reduced time required to form a continuous Cr_2O_3 scale due to the presence of dispersed oxides, which act as nuclei for oxidation (Ref 47). Based on marker studies with platinum, one investigation attributed the beneficial effect of oxide dispersions to the predominant, inward diffusion of oxygen ion (O^{2-}) and a slowdown of the chromic ion (Cr^{3+}) diffusion (Ref 48). The latter may be caused by the blocking of the dispersions in the Cr_2O_3 scale. With the dispersed oxides becoming dissolved in the scale, it

Table 24 Aerospace applications of P/M superalloys

P/M superalloy	Component	Engine	Aircraft/ manufacturer	Reason for using P/M technology: Cost reduction	Reason for using P/M technology: Improved properties
IN-100	Turbine disks, seals, spacers	F-100	Pratt & Whitney	X	X
René 95	Turbine disks, cooling plate	T-700	Helicopter/G.E	...	...
	Turbine disks, compressor shaft	F-404	F-18 Fighter	X	...
	Vane	F-404	G.E.	...	...
	High-pressure turbine blade retainer, disks, forward outer seals	F-101	...	X	...
Astroloy	High-pressure turbine disks	JTSD-17R Turbofan	...	X	...
Merl 76	Turbine disks	Turbofan	...	X	X
Inconel MA-754	Turbine nozzle vane	F-404	F-18 Fighter	...	X
	High- and low-pressure turbine vanes	Selected engines	...	...	X
Stellite 31	Turbine blade dampers	TF30-P100	USAF F-111F	X	...
Inconel MA-6000E	Turbine blades	TFE 731	...	...	X

Source: Ref 41

Table 25 Nominal compositions of several P/M superalloys

UNS No.	Alloy	Composition, % C	Cr	Mo	W	Th	Ti	Nb	Co	Al	Hf	Zr	B	Ni	Fe	V	Y_2O_3
N13100	In-100	0.07	12.5	3.2	...	...	4.3	...	18.5	5.0		0.04	0.02	bal	...	0.75	...
...	René 95	0.07	13.0	3.5	3.5	...	2.5	3.5	8.0	3.5	...	0.05	0.01	bal	...	...	...
...	MERL 76	0.02	12.4	3.2	...	...	4.3	1.4	18.5	5.0	0.4	0.06	0.02	bal	...	...	...
...	AF 115	0.05	10.5	2.8	6.0	...	3.9	1.7	15.0	3.8	2.0	...	...	bal	...	...	...
...	PA 101	0.1	12.5	...	4.0	4.0	4.0	...	9.0	3.5	1.0	...	...	bal	...	...	...
N13017	Astroloy M	0.04	15.0	5.0	...	...	3.5	...	17.0	4.0	...	0.04	0.025	bal	...	...	...
N07754	MA 754	0.05	20.0	...	...	...	0.5	...	...	0.3	...	...	...	bal	...	...	0.6
S67956	MA 956	...	20.0	...	...	...	0.5	...	...	4.5	...	...	...	...	bal	...	0.5
...	MA 6000	0.05	15.0	2.0	4.0	2.0	2.5	...	...	4.5	...	0.15	0.01	bal	...	...	1.1
R30031	Stellite 31	0.5	25.5	...	7.5	...	...	...	rem	...	...	...	...	10.5	2.0	...	...

also appears possible that trivalent ions, such as yttrium (Y^{3+}) and lanthanum (La^{3+}), will reduce the number of vacant cation sites, thus lowering the diffusivity of Cr^{3+}.

Dispersed oxides may also improve scale adhesion because of the thinner scale or because of increased porosity or smaller grain size in the oxide scale (Ref 46). It was reported that at 1300 °C (2370 °F) the outer regions of the Al_2O_3 film of MA 956 (Fe-20Cr-4.5Al-0.5Ti-0.5Y_2O_3) became enriched with titanium, giving rise to a continuous layer of titanium-rich oxide (Ref 49). Pegging of the oxide by titanium carbide particles and the irregular metal/oxide interface is said to contribute to the good spalling resistance of the alloy.

In oxidation tests in air and in an inert atmosphere at 1260 °C (2300 °F) for MA 754 (Ni-20Cr-0.5Ti-0.5Y_2O_3-0.3Al-0.05C), Ni-20Cr (cast/wrought), and an ODS nickel-chromium alloy, subsurface porosity was attributed to the oxidation of chromium and aluminum (Kirkendall porosity), and thermally induced porosity was excluded as a cause (Ref 50). This type of porosity decreases with improving oxidation resistance of the alloy.

The importance of chromium and grain size on fatigue crack growth is demonstrated in Table 26, which lists fatigue crack growth rates for different alloys. Results of cyclic oxidation tests at 1100 °C (2010 °F) for MA 956, TD-NiCr, and Hastelloy X are given in Table 27. The superior resistance of MA 956 is attributed to a very stable Al_2O_3 film and parabolic oxidation for more than 500 h. Tables 28 and 29 list sulfidation and carburization resistance data for MA 956. As in the case of oxidation, the alloy shows marked superiority to the other alloys tested. Tables 30 and 31 provide similar data for alloy MA 6000E (Ni-15Cr-4.5Al-4W-2Mo-2Ta-2.5Ti-1.1Y_2O_3) (Ref 51). The functions of the various alloying elements are:

- Aluminum, titanium, and tantalum for γ' hardening
- Y_2O_3 for high-temperature strength and stability
- Aluminum and chromium for oxidation resistance
- Titanium, tantalum, chromium, and tungsten for sulfidation resistance
- Tungsten and molybdenum for solid-solution strengthening

Hot Corrosion. The requirement of hot corrosion resistance of superalloys derives from the use of sodium- and sulfur-containing fuels and the presence of salt in the air necessary for combustion. Under such conditions, combustion gases often leave deposits of sulfates or chlorides with metallic constituents of sodium, calcium, magnesium, or potassium on the surfaces of superalloys. The resulting corrosion problems

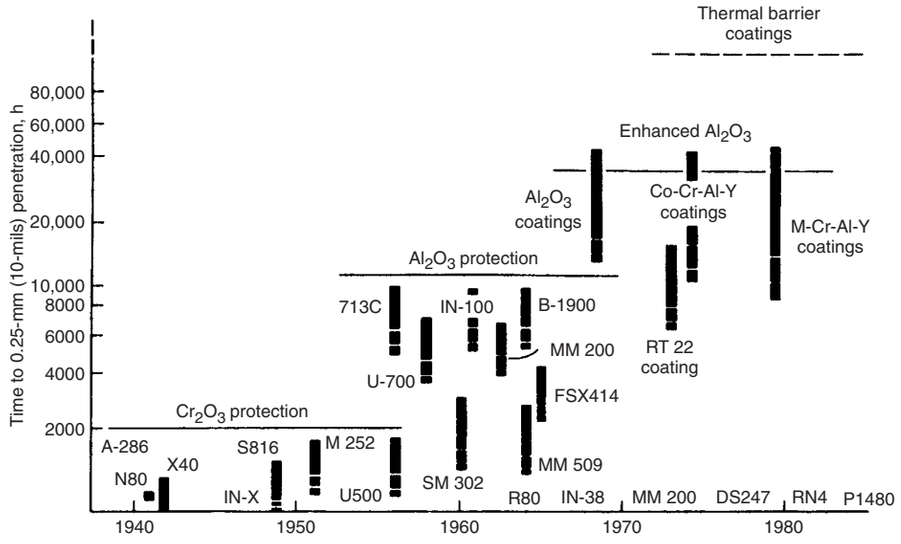

Fig. 58 Advancing steps in the protection of superalloys against oxidation of high temperatures showing life (in h) to 0.25 mm (10 mils) penetration of 980 °C (1800 °F). Source: Ref 45

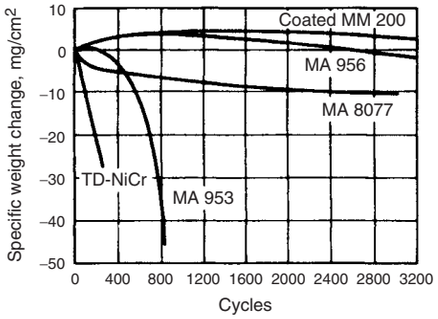

Fig. 60 Cyclic oxidation of ODS alloys MA 956, MA 8077, MA 953, and TD-NiCr compared to that of coated alloy MM 200. Testing conditions: held at 1100 °C (2010 °F) for 1 h and cooled by a 3 min air blast. Source: Ref 46

Table 26 Relative increase in fatigue crack growth rates after 15 min at 650 °C (1200 °F)

$\Delta K = 30$ MPa$\sqrt{m}$ (27 ksi$\sqrt{in.}$)

Alloy	Relative increase in crack growth rates	Grain size, μm	Chromium content, %
René 95 after HIP + forge	242	50–70	12.8
IN-100	43.4	4–6	12.0
HIP-consolidated MERL 76	41.5	15–20	12.0
NASA II B-7	335	4–6	8.9
HIP-consolidated Astroloy	3.3	50–70	15.1
Waspaloy	4.0	40–150	19.3
Astroloy after HIP + forge	3.5	50–100	14.7

Source: Ref 46

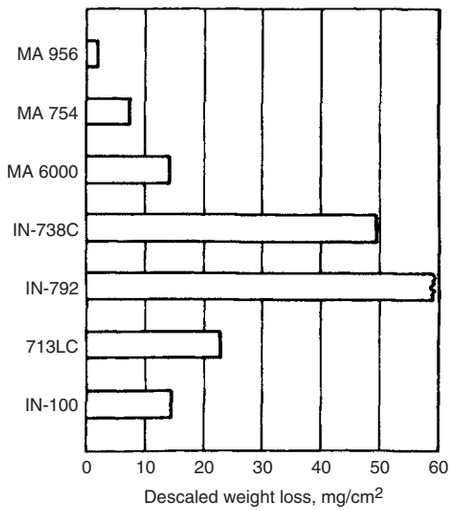

Fig. 59 Comparison of the oxidation resistance of ODS alloys MA 956, MA 754, and MA 6000 with that of other superalloys. Testing conditions: 504 h at 1100 °C (2010 °F) in air containing 5% H_2O. Temperature was cycled between test temperature and room temperature every 24 h. Source: Ref 46

Table 27 Cyclic oxidation resistance of superalloys at 1100 °C (2010 °F)

504 h test in atmosphere of air containing 5% H_2O; temperature cycled between 1100 °C (2010 °F) and room temperature every 24 h

Alloy	Weight change, mg/cm²		Metal loss, μm	Maximum attack, μm
	Undescaled	Descaled		
MA956	0.99	−1.57	2	15
TD-NiCr	−4.66	−12.52	20	33
Hastelloy X	−11.81	−20.62	50	256

Source: Ref 51

Table 28 Sulfidation resistance of superalloys at 925 °C (1700 °F)

312 h test in burner rig with air-to-fuel ratio of 30 to 1; fuel contained 0.3% S and 5 ppm seawater. Temperature cycle: 58 min at temperature, followed by 2 min cool to room temperature

Alloy	Weight change, mg/cm²		Metal loss, μm	Maximum attack, μm
	Undescaled	Descaled		
MA956	1.04	−0.17	5	18
TD-NiCr	−1.69	−11.57	25	129
Hastelloy X	−2.25	−6.83	33	132

Source: Ref 51

Table 29 Carburization resistance of superalloys at 1095 °C (2000 °F)

100 h test in atmosphere of hydrogen containing 2% methane

Alloy	Weight change, mg/cm²		Metal loss, μm	Maximum attack, μm
	Undescaled	Descaled		
MA956	0.07	−0.42	10	10
Incoloy 800	33.74	29.89	132	7615
Aloy 814	0.82	−0.73	13	363

Source: Ref 51

Table 30 Sulfidation resistance of superalloys at 925 °C (1700 °F)

Tested in burner rig with air-to-fuel ratio of 30 to 1; fuel contained 0.3% S and 5 ppm seawater. Temperature cycle 58 min at temperature, followed by 2 min cool to room temperature

Alloy	Exposure time, h	Descaled weight loss, mg/cm²	Maximum attack, μm
MA 6000E	312	−11.11	24
IN-100	48	−367.36	169
Alloy 713LC	168	−488.63	328
IN-738C	312	−9.73	28

Source: Ref 51

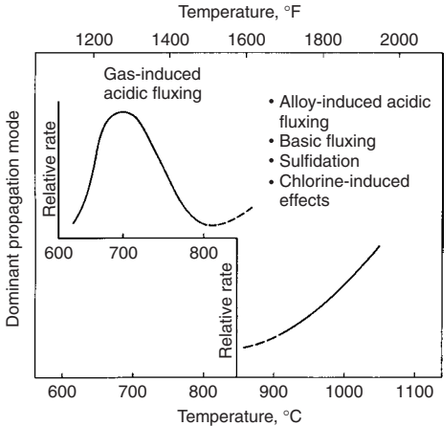

Fig. 61 Temperature regimes over which different propagation modes are most prevalent

are particularly severe if these condensed phases are liquid. Hot corrosion may occur in gas turbines, boiler tubes, and incinerators. Typically (and similar to what happens in pure oxidation), hot corrosion of superalloys occurs in two stages: a slow rate initiation stage, followed by a propagation stage of rapid degradation. The difference, compared to oxidation, is that the conditions causing hot corrosion simply shorten the time in which superalloys form protective Al_2O_3 or Cr_2O_3 scales by selective oxidation (Ref 44). Factors affecting the length of the initiation stage (at the end of the initiation stage, the superalloy must be removed from service because of the start of excessive corrosion) include alloy composition, alloy fabrication conditions, gas composition and velocity, deposit composition and its physical state, amount of deposit, temperature, temperature cycles, erosion, and specimen geometry.

When a protective scale dissolves into a liquid deposit, so-called fluxing reactions can occur with the appearance of other basic or acidic nonprotective reaction products. Propagation may also be caused by components from the deposit that can accumulate in the deposit or the alloy and thus cause a nonprotective scale to form. Chlorine and sulfur produce such effects, and hot corrosion caused by the latter is known as sulfidation. Figure 61 shows the temperature ranges over which the various hot corrosion propagation modes are important.

Some superalloys corrode in several modes. For example, hot corrosion of IN-738 proceeds by alloy-induced acidic fluxing, but is preceded by other propagation modes, including a basic fluxing mode. The higher chromium content alloys IN-738 and IN-939 were developed to improve the hot corrosion resistance of

Table 31 Cyclic oxidation resistance of superalloys at 1100 °C (2010 °F)

504 h test in air containing 5% H_2O; temperature cycled from 1100 °C (2010 °F) to room temperature every 24 h

Alloy	Descaled weight change, mg/cm²
MA 6000E	−14.12
IN-100	−7.27
Alloy 713LC	−22.08
IN-738C	−49.51

Source: Ref 51

Table 32 Dependence on carbide microstructure of creep crack growth rates of alloy IN-750 in four environments

Grain-boundary carbide microstructure	Crack growth rate (*da/dt*)(a), mm/min			
	Helium	Air	Helium + 4% methane	Helium + 3% SO_2
Blocky	7×10^{-4}	1.95×10^{-2}	7×10^{-4}	1.5×10^{-1}
Cellular	1.15×10^{-3}	2.6×10^{-3}	3.1×10^{-3}	1.3×10^{-1}
None	7×10^{-4}	6.3×10^{-2}	7×10^{-4}	1.6×10^{-1}

(a) $K = 35$ MPa$\sqrt{m}$(32 ksi$\sqrt{in.}$). Source: Ref 46, 55

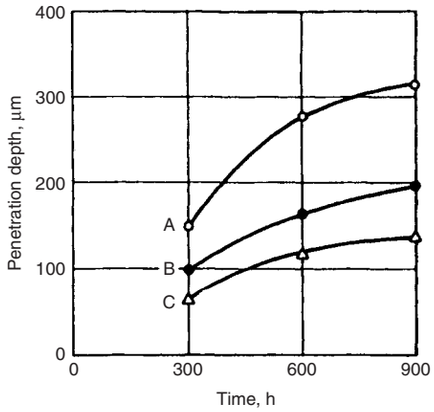

Fig. 62 Comparison of resistance of alloy IN-738LC in hot (850 °C, or 1560 °F) gases. A, IN-738LC; B, IN-738LC with Y_2O_3 dispersion, annealed at 1270 °C (2320 °F); C, IN-738LC with Y_2O_3 dispersion, annealed at 1100 °C (2010 °F). Source: Ref 40

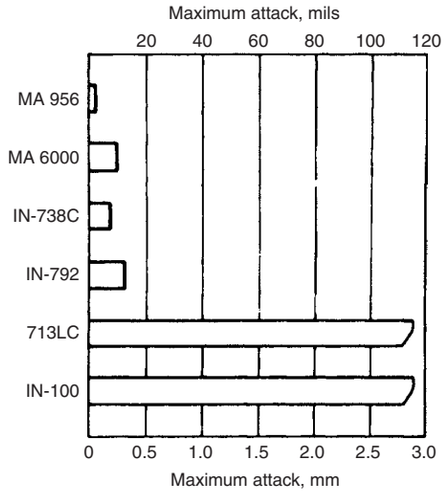

Fig. 63 Comparison of the corrosion resistance of MA 6000 and MA 956 with that of other superalloys. Tested in a burner rig for 312 h using a 30-to-1 air-to-fuel ratio. Fuel contained 0.3% S and 5 ppm seawater, and specimens were held at temperature for 58 min of each hour, then cooled 2 min with an air blast. Source: Ref 46

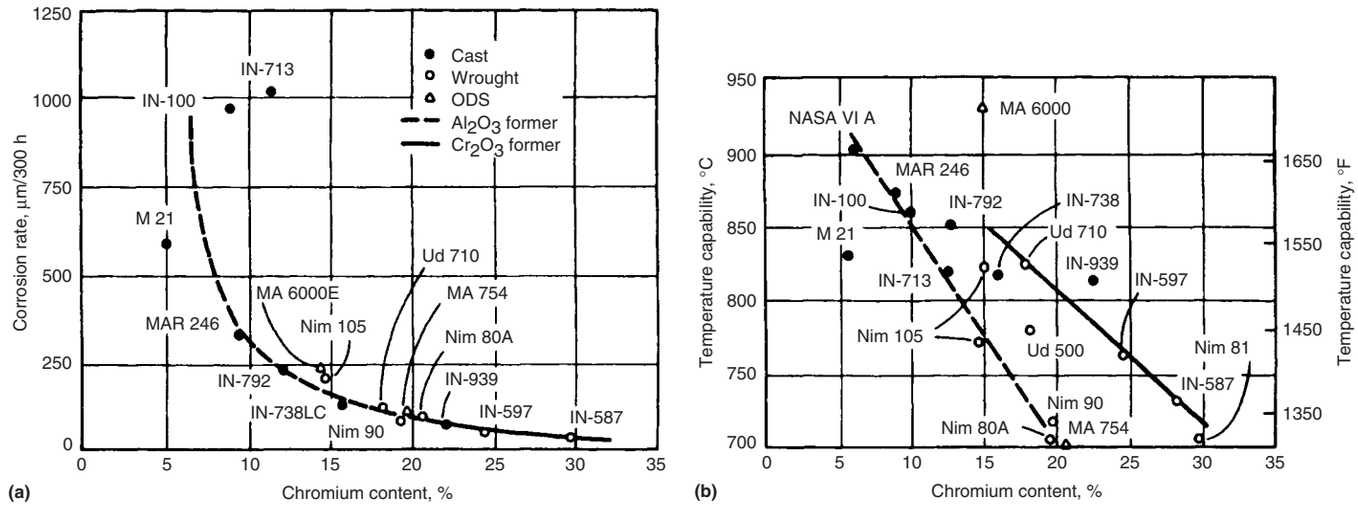

Fig. 64 Corrosion rate (a) and temperature capability (b) of MA 6000, MA 754, and non-ODS superalloys as a function of chromium content. A stress of 200 MPa (29 ksi) was applied to the specimens during the 10,000 h test. Source: Ref 46

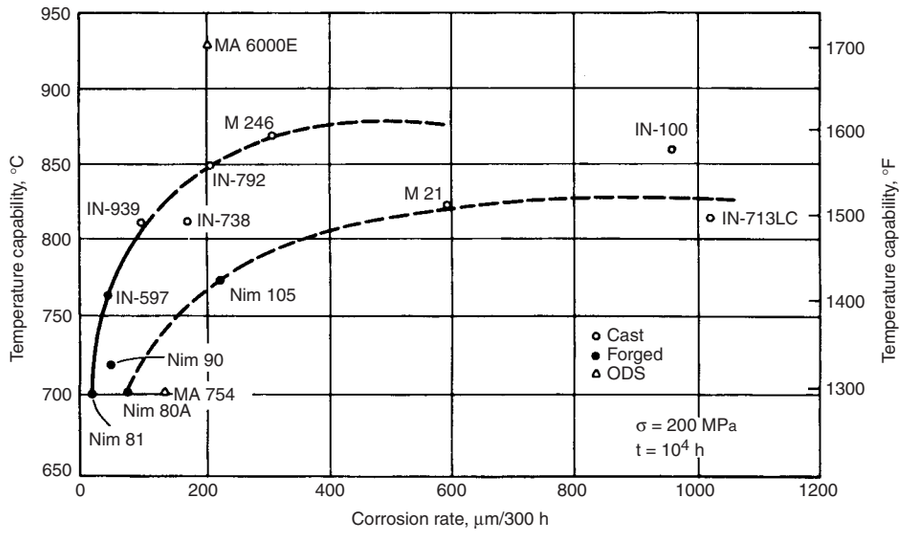

Fig. 65 Temperature capability as a function of corrosion rate for various superalloys. Same data as in Fig 64. Source: Ref 46

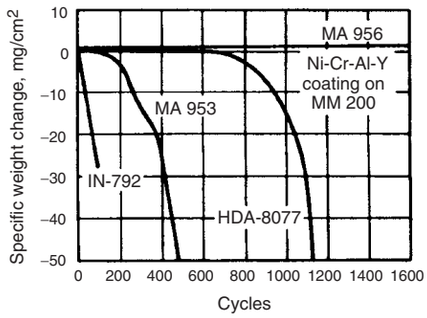

Fig. 66 Hot corrosion of alloys MA 953, HDA 8077, and MA 956 compared to that of some non-ODS alloys. Test conditions: 900 °C (1650 °F), 1 h, followed by a 3 min air blast, 5 ppm sea salt. Source: Ref 46

land-based gas turbines. Carbide stabilization through tungsten and tantalum additions and delay of $M_{23}C_6$ formation in service were expected to allow the large chromium content to impart improved hot corrosion resistance. Increasing the chromium and decreasing the Al_2O_3, however, lowered γ' solution temperatures and strength, which necessitated the use of coatings. The use of coatings led to the current use of enhanced aluminum, that is, carefully balanced coating alloys (based on nickel, iron, or cobalt with chromium, aluminum, and other active elements). Generally, all superalloy load-bearing parts used at very high temperatures under dynamic conditions are coated (Ref 45). Nevertheless, coatings generally last longer on more corrosion-resistant base materials.

In a model study, IN-738 was used to demonstrate the effect of grain size and Y_2O_3 dispersions on hot corrosion behavior (Ref 52). Under gas turbine simulated hot gas corrosion test conditions at 850 and 950 °C (1560 and 1740 °F) (Fig. 62), the presence of a Y_2O_3 dispersion lowered the corrosion rate. At 950 °C (1740 °F), a finer grain size further reduced the corrosion rate, which was thought to be mainly due to a higher diffusion rate of chromium and aluminum. The effect of the dispersion was predominant at 850 °C (1560 °F). Reduced sulfate formation at 850 °C (1560 °F) was attributed to the likely formation of yttrium oxysulfide.

In a study of the oxidation and hot corrosion resistance of P/M LC Astroloy and IN-100, isostatically pressed samples were found to be moderately attacked in a sulfate-chloride environment and heavily corroded by pure sodium sulfate (Na_2SO_4) (Ref 53). Heat treatment and the use of coarse powder (62 to 150 μm for Astroloy and 88 to 200 μm for IN-100) lowered the susceptibility to catastrophic corrosion. Additions of yttrium to IN-100 improved the corrosion resistance in pure sulfate, but were detrimental when NaCl was present. Therefore, yttrium additions to IN-100 cannot be recommended for marine turbines. It was concluded that in many cases impregnation coatings must be considered for components made of IN-100 alloys.

As a part of an evaluation of improved alloys for use in oil and gas drilling at depths of 6100 m

(20,000 ft), HIP nickel-base alloy Inconel 625 was studied in a simulated deep, hot, sour cell environment (Ref 54). The alloy demonstrated resistance to pitting and crevice corrosion, sulfide stress cracking, chloride stress-corrosion cracking (SCC), and elevated-temperature anodic stress cracking. Hot isostatically pressed Inconel 625 exhibited essentially the same corrosion resistance as wrought Inconel 625.

Fatigue and Creep Crack Growth. Fatigue crack growth rates of nickel-base superalloys measured at frequencies above 0.1 Hz, at intermediate temperatures, and at an intermediate stress intensity range, ΔK, were found to be several times higher than those measured in inert atmospheres (Ref 55). The buildup of corrosion products with decreasing ΔK, however, was thought to enhance crack closure, thus reducing the effective stress intensity range and leading to fatigue thresholds higher than those in inert environments.

Table 32 shows creep crack growth rates of IN-750 with various grain-boundary carbide microstructures (Ref 46, 55). Aggressive environments (helium + 3% SO_2 and air) produce order of magnitude increases over the rates in inert gas. In general, the reaction of both oxide dispersoid-free P/M superalloys and cast and wrought superalloys to aggressive environments is similar. This suggests that crack growth is governed mainly by microstructure and alloy chemistry.

Oxide-Dispersion-Strengthened (ODS) Alloys. Mechanical alloying has removed many constraints on the development of new superalloys. Many new ODS alloys were designed specifically for corrosion resistance because alloying requirements for precipitation strengthening can be greatly reduced. Superior creep, corrosion, and erosion resistance at high temperatures have been claimed to enable the use of lower-grade fuels (Ref 56). Figures 63 to 66 show the corrosion resistances of ODS alloys MA 956, MA 6000, and MA 754 compared to several conventional superalloys.

Coatings for ODS Alloys. As mentioned previously, for extended high-temperature service, superalloys require additional protection through coatings. The use of aluminide coatings appears to be unsatisfactory due to the development of subsurface Kirkendall porosity and early spalling of the protective scale. Kirkendall porosity decreases with increasing aluminum content of the substrate alloy as well as with decreasing grain size (Ref 56). Only limited information exists on the properties of Cr-Al-Y coatings (Ref 46) and on diffusion barrier coatings (Ref 57–60).

ACKNOWLEDGMENTS

This article is adapted from the article by Barbara Shaw that appeared in *Powder Metal Technologies and Applications,* Volume 7, *ASM Handbook,* 1998. Much of the data of Dr. Erhard Klar was used in this review, and the author would like to acknowledge him and thank him for this contribution. The author would also like to thank Michael Baran for the contribution of his work on ferritic stainless steels.

REFERENCES

1. E. Klar and P.K. Samal, *Powder Metals, Corrosion Tests and Standards Manual,* R. Baboian, Ed., ASTM, 1995, p 551–557
2. E. Klar and P.K. Samal, Effect of Density and Sintering Variables on the Corrosion Resistance of Austenitic Stainless Steels, *Advances in Powder Metallurgy and Particulate Materials,* Vol 3, M. Phillips and J. Porter, Ed., Metal Powder Industries Federation, American Powder Metallurgy Institute, 1995, p 3–17
3. C. Molins, J.A. Bas, J. Planas, and S.A. Ames, P/M Stainless Steel: Types and Their Characteristics and Applications, *Advances in Powder Metallurgy and Particulate Materials,* Vol 5, J.M. Capus, Ed., Plenum Press, 1992, p 345–357
4. J.A. Bas, J. Peñafiel, A. Bolarin, and M.P. Latre, Determination Methods of the PM Stainless Steels Corrosion Resistance, *Advances in Powder Metallurgy and Particulate Materials,* Plenum Press, p 47–59
5. D. Itzhak and E. Aghion, An Anodic Behavior Study of an Analogical Sintered System of Austenitic Stainless Steel in H_2SO_4 Solution, *Corros. Sci.,* Vol 24 (No. 2), 1984, p 145–152
6. G. Lei, R.M. German, and H.S. Nayar, Corrosion Control in Sintered Austenitic Stainless Steels, reprinted from *Progress in Powder Metallurgy,* Vol 39, Metal Powder Industries Federation, 1984, p 55–74
7. A. Tremblay and R. Angers, *Corrosion Resistance of 316L P/M Stainless Steel, Advances in Powder Metallurgy and Particulate Materials—1994,* Vol 7, C. Lall and A.J. Neupaver, Ed., Metal Powder Industries Federation, American Powder Metallurgy Institute, p 225–237
8. D.A. Jones, *Principles and Prevention of Corrosion,* 2nd ed., Prentice Hall, 1996
9. G. Scavino, E. Angelini, M. Rosso, and F. Rosalbino, Comparison of Corrosion Resistance Properties of PM Steels, *Computer Methods and Experimental Measurements for Surface Treatment Effects,* Computational Mechanics Publications, 1993, p 337–346
10. M. Baran, A.E. Segall, B.A. Shaw, et al., "Evaluation of P/M Ferritic Stainless Steel Alloys for Automotive Exhaust Applications," presented at the P/M Tec '97 Conf. (Chicago, IL), Metal Powder Industries Federation, June 1997
11. D.W. Yuan, J.R. Spirko, and H.I. Sanderow, Colorimetric Corrosion Testing of P/M Stainless Steel, *Int. J. Powder Metall.,* Vol 33 (No. 2), 1997
12. D.W. Yuan, T. Prucher, and H.I. Sanderow, "An Evaluation of the Relative Corrosion Resistance of P/M Stainless Steel Alloys," Technical Paper No. 950391, Society of Automotive Engineers, 1995
13. R.L. Sands, G.F. Bidmead, and D.A. Oliver, The Corrosion Resistance of Sintered Austenitic Stainless Steel, *Modern Developments in Powder Metallurgy,* Vol 2, H.H. Hausner, Ed., Plenum Press, 1966, p 73–83
14. E. Maahn, S.K. Jensen, R.M. Larsen, and T. Mathiesen, Factors Affecting the Corrosion Resistance of Sintered Stainless Steel, *Advances in Powder Metallurgy and Particulate Materials,* Vol 7, C. Lall, Ed., Plenum Press, 1994, p 253–271
15. T. Raghu, S.N. Malhotra, and P. Ramakrishnan, Corrosion Behavior of Porous Sintered Type 316L Austenitic Stainless Steel in 3% NaCl Solution, *Corrosion,* Vol 45 (No. 9), 1989, p 698–704
16. D.H. Ro and E. Klar, Corrosion Behavior of P/M Austenitic Stainless Steels, *Modern Developments in Powder Metallurgy,* Vol 13, H.H. Hausner, Ed., Plenum Press, 1980, p 247–287
17. P. Peled and D. Itzhak, The Surface Composition of Sintered Stainless Steel Containing Novel Alloying Elements Exposed to a H_2SO_4 Environment, *Corros. Sci.,* Vol 32 (No. 1), 1991, p 83–90
18. M. Baran, "An Evaluation of a P/M Ferritic Stainless Steel Automotive Exhaust Flange," Master's dissertation, The Pennsylvania State University, 1997
19. F. Mansfeld, Electrochemical Methods of Corrosion Testing, *Corrosion: Fundamentals, Testing, and Protection,* Vol 13A, *ASM Handbook,* ASM International, 2003, p 446–462
20. A.J. Sedriks, Effects of Alloy Composition and Microstructure on the Passivity of Stainless Steels, *Corrosion,* Vol 42 (No. 7), 1986, p 376–388
21. L. Campbell, "Corrosion Behavior of an Alumina-Reinforced Aluminum Metal Matrix Composite," Baccalaureate thesis, The Pennsylvania State University, 1996
22. M.A. Streicher, *Corrosion Tests and Standards Manual,* R. Baboian, Ed., ASTM, 1995, p 197–217
23. A.J. Sedriks, *Corrosion of Stainless Steels,* 2nd ed., John Wiley & Sons, 1996
24. E. Maahn and T. Mathiesen, Corrosion Properties of Sintered Stainless Steel, *U.K. Corrosion Proc.* (Manchester, U.K.), Vol 2, Institute of Corrosion, 1991, p 1–15
25. M.A. Pao and E. Klar, Corrosion Phenomena in Regular and Tin-Modified P/M Stainless Steels, *Progress in Powder Metallurgy,* H.S. Nayar, S. Kaufman, and K.E. Meiners, Ed., Metal Powder Industries Federation, 1984, p 431–444
26. K. Frisk, A. Johansson, and C. Lindberg, Nitrogen Pick Up During Sintering Stainless

Steel, *Advances in Powder Metallurgy and Particulate Materials,* Vol 3, J.M. Capus and R.M. German, Ed., Metal Powder Industries Federation, 1992, p 167
27. B.A. Shaw and G.S. Morton, "Thermal Spray Coatings—Marine Performance and Mechanisms," ASM International Thermal Spray Technology Proc. of the National Thermal Spray Conf. (Cincinnati, Ohio), Oct 24–27,1988, ASM International
28. B.A. Shaw, "Characterization of the Corrosion Behavior of Aluminum, Zinc and Zinc-Aluminum Thermal Spray Coatings," Master's dissertation, Johns Hopkins University, 1985
29. D. Itzhak and E. Aghion, Corrosion Behavior of Hot-Pressed Austenitic Stainless Steel in H_2SO_4 Solutions at Room Temperature, *Corros. Sci.,* Vol 23 (No. 10), 1983, p 1085–1094
30. E. Klar, M. Svilara, C. Lall, and H. Tews, Corrosion Resistance of Austenitic Stainless Steels Sintered in Commercial Furnaces, *Advances in Powder Metallurgy and Particulate Materials—1992,* Vol 5, J.M. Capus and R.M. German, Ed., Metal Powder Industries Federation, American Powder Metallurgy Institute, p 411–426
31. F.M.F. Jones, The Effect of Process Variables on the Properties of Type 316L Powder Compacts, *Progress in Powder Metallurgy,* Vol 30, Metal Powder Industries Federation, 1970, p 25–50
32. E. Klar and P.K. Samal, Optimization of Vacuum Sintering Parameters for Improved Corrosion Resistance of P/M Stainless Steels, *Advances in Powder Metallurgy and Particulate Materials,* Vol 7, C. Lall, Ed., Plenum Press, 1994, p 239–251
33. B.A. Shaw, "Crevice Corrosion of a Ni-Cr-Mo-Fe Alloy in Natural and Chlorinated Seawater," Ph.D. dissertation, Johns Hopkins University, 1988
34. P. Peled and D. Itzhak, The Effect of Noble Alloying Elements Ag, Pt, and Au on the Corrosion Behavior of Sintered Stainless Steel in an H_2SO_4 Environment, *Corros. Sci.,* Vol 28 (No. 10), 1988, p 1019–1028
35. M.H. Tikkanen, Corrosion Resistance of Sintered P/M Stainless Steels and Possibilities for Increasing It, *Scand. J. Metall.,* Vol 11, 1982, p 211–215
36. P. Peled and D. Itzhak, The Corrosion Behavior of Double Pressed, Double Sintered Stainless Steel Containing Noble Alloying Elements, *Corros. Sci.,* Vol 30 (No. 1), 1990, p 59–65
37. R.M. German and D. Kubish, Evaluation of Injection Molded 17-4 PH Stainless Steel Using Water Atomized Powder, *Int. J. Powder Metall.,* Vol 29 (No. 1), 1993, p 47–62
38. D. Itzhak and P. Peled, The Effect of Cu Addition on the Corrosion Behavior of Sintered Stainless Steel in H_2SO_4 Environment, *Corros. Sci.,* Vol 26 (No. 1), 1986, p 49–54
39. D. Itzhak and S. Harush, The Effect of Sn Addition on the Corrosion Behavior of Sintered Stainless Steel in H_2SO_4, *Corros. Sci.,* Vol 25 (No. 10), 1985, p 883–888
40. G.H. Gessinger, Recent Developments in Powder Metallurgy of Superalloys, *Powder Metall. Int.,* Vol 13 (No 2), 1981, p 93–101
41. R.F. Singer, Recent Developments and Trends in High Strength P/M Materials, *Powder Metall. Int.,* Vol 17 (No. 6), 1985, p 284–288
42. L.R. Curwick, The Mechanical Alloying Process: Powder to Mill Product, *Frontiers of High-Temperature Materials,* J.S. Benjamin, Ed., Proc. International Conference on Oxide Dispersion Strengthened Superalloys by Mechanical Alloying, Inco Alloy Products, 1981, p 3–10
43. J.S. Benjamin and T.E. Volin, The Mechanism of Mechanical Alloying, *Metall. Trans.,* Vol 5, 1974, p 1929–1934
44. F.S. Pettit and G.H. Meier, Oxidation and Hot Corrosion of Superalloys, *Superalloys, 1984,* M. Gell et al., Ed., Proc. the Fifth International Symposium on Superalloys, The Metallurgical Society, 1984, p 651–687
45. C.T. Sims, A History of Superalloy Metallurgy for Superalloy Metallurgists, *Superalloys, 1984,* M. Gell et al., Ed., Proc. the Fifth International Symposium on Superalloys, The Metallurgical Society, 1984, p 309–419
46. G.H. Gessinger, *Powder Metallurgy of Superalloys,* Butterworths, 1984
47. J. Stringer, B.A. Wilcox, and P.I. Jaffee, *Oxid. Met.,* Vol 5, 1972, p 11
48. C.S. Giggins and F.S. Pettit, The Oxidation of TD Ni Cr (Ni-20 Cr-2 Vol. pct ThO_2) Between 900 and 1200 C, *Metall. Trans.,* Vol 2, 1971, p 1071–1078
49. F. Perry, Oxide-Dispersion-Strengthened P/M Alloys Produced for Severe Service Applications, *Ind. Heat.,* Vol 49 (No. 5), May 1982, p 22–25
50. J.H. Weber and P.S. Gilman, Environmentally Induced Porosity in Ni-Cr Oxide Dispersion Strengthened Alloys, *Scr. Metall.,* Vol 18, 1984, p 479–482
51. J.H. Weber, *High Temperature Oxide Dispersion Strengthened Alloys,* Proc. 25th National SAMPE Symposium and Exhibition Society for the Advancement of Material and Process Engineering, 1980, p 752–763
52. G.H. Gessinger, *High Temperature Alloys for Gas Turbines,* D. Coutsouradis et al., Ed., Applied Science, 1978, p 817
53. P.L. Antona, A. Bennani, P. Cavalloti, and O. Ducati, Heat Treatments and Oxidation Behavior of Some P/M Ni-Base Superalloys, *European Symposium on Powder Metallurgy,* Vol 1, Jernkontoret Activity Group B, 1978, p 137–142
54. W.K. Uhl, M.R. Pendley, and S. McEvoy, "Evaluation of HIP Nickel-Base Alloys for Extreme Sour Service," Paper 219, presented at Corrosion/84, New Orleans, LA, National Association of Corrosion Engineers, April 1984
55. S. Floreen, Effects of Environment on Intermediate Temperature Crack Growth in Superalloys, *Proc. AIME Symposium* (Louisville, KY), American Society of Mining, Metallurgical, and Petroleum Engineers, 1981
56. G.A.J. Hack, Inconel Alloy MA 6000–A New Material for High Temperature Turbine Blades, *Met. Powder Rep.,* Vol 36 (No. 9), Sept 1981, p 425–429
57. D.H. Boone, D.A. Crane, and D.P. Whittle, *Thin Solid Films,* Vol 84, 1981, p 39
58. F.R. Wermuth and A.R. Stetson, NASA CR-120852, National Aeronautics and Space Administration, 1971
59. M.A. Gedwill, T.K. Glasgow, and LS. Levine, "A New Diffusion Inhibited Oxidation Resistant Coating for Superalloys," NASA TM 82687, National Aeronautics and Space Administration, 1981
60. T.K. Glasgow and G.J. Santoro, Oxidation and Hot Corrosion of Coated and Bare Oxide Dispersion Strengthened Superalloy MA 755E, *Oxid. Met.,* Vol 15 (No. 314), April 1986, p 251–276

SELECTED REFERENCES

- L. Fedrizzi, A. Molinari, F. Deflorian, A. Tiziani, and P.L. Bonora, Corrosion Study of Industrially Sintered Copper Alloyed 316L Austenitic Stainless Steel, *Br. Corros. J.,* Vol 26 (No. 1), 1991, p 46–50
- M. Hanada, Y. Takeda, N. Amano, et al., Development of a PM Sensor Ring for Use in an Antilock Brake System, *Met. Powder Rep.,* Vol 44 (No. 10), 1989, p 695–698
- C. Lall and M. Svilar, The Corrosion Resistance of P/M Stainless Steels and Selected Alloys in Methanol-Based Fuels, *P/M Steels,* J.M. Capus, Ed., Vol 5, Plenum Press, 1992, p 427–435
- G. Lei and R.M. German, Corrosion of Sintered Stainless Steels in a Sodium Chloride Solution, *Modern Developments in Powder Metallurgy,* E.N. Aqua, Ed., Vol 16, Plenum Press, p 261–275
- G. Lei, R.M. German, and H.S. Nayar, Influence of Sintering Variables on the Corrosion Resistance of 316L Stainless Steel, *Powder Metall. Int.,* Vol 15 (No. 2), 1983, p 70–76
- S.N. Malhotra and P. Ramakrishnan, Corrosion Behavior of PM Stainless Steel Filters, *Met. Powder Rep.,* 1991, p 48–51
- T. Mathiesen and E. Maahn, Evaluation of Sensitization Phenomena in Sintered Stainless Steels, *Powder Metallurgy World Congress (PM)* (Paris), Vol 3, Les Editions de Physique, 1994, p 2089–2092

- H.S. Nayar, R.M. German, and W.R. Johnson, The Effect of Sintering on the Corrosion Resistance of 316L Stainless Steel, *Progress in Powder Metallurgy,* Vol 37, Metal Powder Industries Federation, p 1–7
- P. Peled, S. Harush, and D. Itzhak, The Effect of Ni Addition on the Corrosion Behavior of Sintered Stainless Steel in H_2SO_4, *Corros. Sci.,* Vol 28 (No. 4), 1988, p 327–332
- J.R. Pickens, Techniques for Assessing the Corrosion Resistance of Aluminum Powder Metallurgy Alloys, *Rapidly Solidified Powder Aluminum Alloys,* ASTM, 1986 p 381–409
- J.H. Reinshagen and T.J. Bockius, Stainless Steel Based P/M Alloys with Improved Corrosion Resistance, *Advances in Powder Metallurgy and Particular Materials,* Metal Powder Industries Federation, Vol 3, 1995, p 19–30
- J.H. Reinshagen and G.D. Flick, Improved Corrosion Resistant Stainless Steel Based P/M Alloys, *Advances in Powder Metallurgy and Particulate Materials—1996,* Metal Powder Industries Federation, Vol 5, 1995, p 61–71
- J.H. Reinshagen and A.J. Neupaver, Fundamentals of P/M Stainless Steels, *Advances in Powder Metallurgy,* Vol 2, Plenum Press, 1989, p 283–295
- F. Velasco, J.R. Ibars, J.M. Ruiz-Roman, et al., Improving the Corrosion Resistance of Power Metallurgy Austenitic Stainless Steels through Infiltration, *Corrosion,* Vol 52 (No. 1), 1996, p 47–52

ASM Handbook, Volume 13B: Corrosion: Materials
S.D. Cramer, B.S. Covino, Jr., editors, p476-489
DOI: 10.1361/asmhba0003836

Corrosion of Amorphous Metals

John R. Scully and Ashley Lucente, University of Virginia

AMORPHOUS, or glassy, metal systems have been extensively studied since their introduction (Ref 1) for their unique structural, mechanical, electronic, magnetic, and corrosion properties (Ref 2, 3). These alloys can be produced by such techniques as liquid quenching, molecular deposition, or external action, and they retain a disordered structure resembling the liquid. As such, they have no long-range order. There is, however, short-range order over a few atomic distances (as found in the liquid state). Recently, medium-range order has been investigated. This has prompted the use of the terms *glassy* or *vitreous* to distinguish them from materials that are truly amorphous on the atomic scale.

Glassy metals have seen practical applications that exploit many of these properties, but they are also interesting as model materials for probing the influence of atomic structure and chemical composition on the corrosion process. In the fully amorphous state, they contain none of the classical crystalline or chemical defects found in crystalline solids, such as grain boundaries, dislocations, stacking faults, and second-phase particles, and they are chemically and structurally homogeneous.

Older glassy alloys were produced from two or more transition metals, for example, copper-zirconium and nickel-niobium, or from a combination of metals and metalloids, such as iron, nickel, and chromium containing boron, phosphorus, silicon, or carbon. A key aspect of metallic glasses is the critical temperature for cooling to retain the amorphous state. Very high cooling rates (>10^5 K/s) are often required to retain the highly metastable glassy state in some glassy alloys, chiefly those of the metal-metalloid compositions. Although the temperature decrease in quenching from the liquid to the solid is not large, the rate of heat extraction is very high and requires at least one dimension of the resulting alloy to be very small. Because of this requirement, many binary metal and metal-metalloid glassy metals produced by liquid quenching are typically in the form of ribbons, wires, and filaments. However, so-called bulk metallic glasses can be produced with much lower critical cooling rates. Significantly, the critical glass-formation cooling rates are as low as 1 K/s in some of these alloys (Ref 2–4). Thus, three-dimensional structures can be produced that are entirely amorphous. This new class of bulk amorphous and partially nanocrystalline-amorphous alloys has recently been produced over a broad range of alloy compositions (Ref 3–9). Most are either pseudo-binary or pseudo-ternary alloys with compositions characterized as $ETM_{100-x-y}\,LTM_xSM_y$. The meaning of this notation is: ETM, early transition metal (such as zirconium, titanium, niobium, yttrium, lanthanum, scandium); LTM, late transition-metals elements (such as iron, copper, cobalt, nickel, manganese); and SM, simple metal (such as aluminum, magnesium, beryllium) (Ref 4). These alloys exhibit a large supercooled region and high glass-forming abilities, indicated by a large difference between liquidus temperatures and glass transition temperatures (Ref 2, 10, 11). The critical glass-formation cooling rates are as low as 1 K/s in some of these alloys (Ref 4, 6, 7, 12). One implication of such slow critical cooling rates, the low viscosity of the undercooled liquid state, and lack of a phase transformation on solidification is that amorphous components of centimeter-scale dimensions can be fabricated (Ref 4, 6, 11, 13). Thus, the term *bulk metallic glasses* is appropriately applied to such alloys. These alloys are notably stable when reheated from the as-quenched condition and can be heat treated into the undercooled liquid state for fabrication of complex shapes using injection molding technologies used for polymers (Ref 4, 6).

Zirconium-, magnesium-, and aluminum-base amorphous-nanocrystalline alloys have been reported that exhibit excellent specific strengths (Ref 14–19) and other interesting properties (Ref 20, 21). In the 1980s, high-strength bulk magnesium alloys of the type Mg-TM-RE (TM, transition metal, such as nickel, copper, or zinc; RE, rare earth metal, such as yttrium, cerium, or neodymium) were developed (Ref 22). These alloys offer the possibility of superior strength with good corrosion resistance. Corrosion resistance in a magnesium alloy represents a grand challenge that could possibly be accomplished via the formation of a homogeneous single-phase system with alloying elements that either promote passivity in neutral and acidic environments or increase resistance to local halide-induced corrosion. Amorphous alloys offer this possibility.

The formation of an amorphous single phase in aluminum-base alloys having more than 50 at.% Al was also reported (Ref 23). As-spun Al-Fe-Si, Al-Fe-Ge, and Al-Mn-Si alloys containing an amorphous structure were discovered (Ref 24, 25). These very brittle amorphous alloys were followed by the discovery of amorphous Al-Ni-Si and Al-Ni-Ge systems with good ductility in bending (Ref 26). Since the discovery of the ductile aluminum-base amorphous alloys, a number of ternary amorphous alloy systems—Al-IV-V group TM, Al-VII and VIII group TM (Ref 27, 28), Al-RE-VII* and VIII group TM (Ref 5, 16), and Al-RE binary alloys (Ref 5, 29, 30)—have been investigated. Recently, the glass-formation mechanism of aluminum-base alloys has been studied extensively by various techniques (Ref 31–34). One of those showed the formation of ductile aluminum-base metallic glasses without RE elements, starting from a ternary eutectic composition of $Al_{75}Cu_{17}Mg_8$. A fully amorphous structure was achieved in this alloy when 2 to 8 at.% Ni was added.

Synthesis of Metallic Glasses

A critical rate of cooling exists that separates glass forming and crystal forming. Forming amorphous metals by quenching from the liquid phase generally requires cooling rates on the order of 10^5 to 10^6 K/s (Ref 35). Recent advances in the production of bulk metallic glasses have reduced this rate by orders of magnitude. An example is Zr-Ti-Be, where a critical cooling rate as low as 1 K/s has been achieved (Ref 36). Techniques for producing glassy metals can be divided into three main groups (Ref 37).

Liquid phase quenching involves rapid solidification from the melt under a particular set of conditions, such as cooling rate and sample dimensions, that precludes the formation of the stable equilibrium structure. This is achieved

*Rare earth elements include the group 1 to 5 lanthanides plus lanthanum. Scandium and yttrium are often included for practical reasons. Refer to periodic table in the Reference Information of this Volume.

by producing a cooling rate greater than the critical cooling rate required to reach the glass transition temperature prior to crystallization. This includes thermal spray methods (Ref 35, 38, 39).

Atomic or molecular deposition involves growth from the vapor phase, such as chemical and physical vapor deposition and sputtering, or from a liquid phase, such as electroless deposition (Ref 40) and electrodeposition, to form the desired alloy. These techniques have higher effective cooling rates than liquid quenching processes; therefore, they allow the formation of glassy alloys that cannot be produced by rapid liquid quenching.

External action techniques are a third set of techniques that rely on such procedures as mechanical deformation, irradiation, and cold spray methods to form the metastable glassy alloy. Ion implantation, ion beam mixing, and laser pulsing, for example, can produce amorphous surface layers on bulk crystalline substrates. The latter two groups of techniques—molecular deposition and external action techniques—have the advantage of being able to produce considerably thicker alloys, but they typically require considerably more time for completion of the process. Research on glassy alloy corrosion in the past few years has expanded to include developing means for using these alloys in practical applications. Therefore, research has accelerated in such areas as laser surface remelting (Ref 41, 42), ion implantation (Ref 43), sputter deposition, electrodeposition, and chemical vapor deposition. See, for example, the articles "Surface Modification Using Energy Beams" (ion implantation and laser surface processing are discussed) and "CVD and PVD Coatings" in *ASM Handbook,* Volume 13A, 2003.

Devitrification and Structural Relaxation

When subjected to elevated temperatures, devitrification will occur in many metallic glasses, which results in changes in properties. The glass transition temperature is, of course, a function of the alloy composition; therefore, some alloys are suitable for use at temperatures substantially above ambient. A variety of microstructures can be formed in partially devitrified metallic glasses, depending on the details of the metallurgical processes. Devitrification of an amorphous alloy can proceed by several routes, including primary crystallization, eutectoid crystallization, and polymorphous crystallization (Ref 44, 45). Figure 1 shows a free-energy versus composition diagram that summarizes many of the devitrification routes that are possible when a fully amorphous alloy is heated.

Regardless of the exact devitrification route, the equilibrium-stable final crystalline state in many cases consists of a solute-lean, crystalline α phase in equilibrium with one or more solute-rich intermetallic phases, such as β and γ, as shown in Fig. 1. Polymorphous crystallization, indicated by the arrow labeled "c" in Fig. 1, is a relatively rare case in which the transformation from the glass phase to a crystalline phase occurs without a change in composition. Eutectoid crystallization occurs when two crystalline phases of substantially different compositions grow simultaneously within the amorphous matrix. This devitrification path is indicated with the arrows labeled "b" in Fig. 1. Primary crystallization occurs when isolated solute-lean crystals, often of nanometer dimensions, grow in a remaining amorphous matrix, as shown by the arrow labeled "a" in Fig. 1. Such nanocrystals are typically enriched in the majority alloying element, adapt the crystal structure of this alloying element, and reject solutes that may be beneficial to the corrosion resistance. The rejected solute is concentrated in the remaining amorphous matrix, and compositional gradients are possible at the matrix-nanocrystal interface. Such amorphous-nanocrystalline alloys often exhibit a high density of nanocrystals, on the order of $10^{22}/m^3$, that can comprise 40 vol% of the composite alloy. Hence, nearly 40% of the surface area of amorphous-nanocrystalline alloys may also consist of majority alloying element-rich sites of nearly random orientation with a lattice parameter close to that of the bulk majority element. Notably, such amorphous-nanocrystalline composite alloys exhibit greater specific strengths than conventional polycrystalline alloys (Ref 17, 19). However, these materials differ from fully nanocrystalline materials with nanometer grain sizes in at least three respects:

- Isolated crystals embedded in an amorphous matrix lack grain-boundary triple points with their associated defective structure.
- The remaining amorphous matrix surrounding a nanocrystal can collect slowly diffusing solute that is rejected from newly formed nanocrystals.
- The crystalline phase does not form a continuous path through the material.

In addition, relaxation of glasses can occur when quenched glasses are heated below the glass transition temperature, T_g, and the dynamic recrystallization temperature. Relaxation of the quenched glass toward a more ideal form can result in topological and compositional short-range ordering (Ref 46) that can change corrosion properties at the nm scale (Ref 47). Structural and compositional relaxation of amorphous materials is well known and produces structural and compositional changes in a glass phase (Ref 48). The coordination number (CN) and short-range order (SRO) of amorphous solid metals and even liquid metals are often dictated by the CN of the majority (host) atom in the crystalline state (Ref 1). For instance, amorphous palladium-silicon alloys have a CN of 11.6 instead of 12 as in face-centered cubic (fcc) palladium, and the average distance of neighbors is 0.28 nm instead of 0.275 nm (Ref 1). Therefore, the arrangement is not completely random, and SRO exists. Molecular dynamics studies also show that melt temperature, quench rate, and annealing can lead to the formation of clusters of atoms in the amorphous state, giving rise to a medium-range order as well as the aforementioned SRO (Ref 49). Annealing of amorphous nickel has led to the formation of tetrahedral clusters within the amorphous state. X-ray absorption fine structure methods have been used to compare as-quenched, glassy $Al_{91}La_9$ to both annealed counterparts and the final crystalline phase La_3Al_{11} (Ref 50). Coordination, disorder, and lattice parameter change with annealing of the amorphous phase. Moreover, compositional and structural SRO has been observed in ternary amorphous alloys on annealing of as-quenched amorphous alloys. In the case of Fe-Ni-B alloys, chemical nonuniformity in the bulk amorphous matrix was observed on the nanometer scale, and development of mechanical brittleness was attributed to this phenomenon (Ref 51). In Fe-Ni-P-B alloys, when the spatial distributions of nickel and iron are changed, magnetic properties are significantly altered (Ref 52). Short-range order and clustering of aluminum and iron were observed in aluminum-rich metallic glasses with a substructure substantially different from random packing (Ref 31, 53). The change in nearest-neighbor atomic environment and lattice parameter can change electrochemical properties (Ref 54). Global electrochemical kinetics were altered by chemical heterogeneity during relaxation of Ni-Pd-Si glasses (Ref 55). Nanometer-scale corrosion-induced porosity of the amorphous substrate was observed on a heat treated amorphous-nanocrystalline Al-Ni-Y alloy in an acidic environment that destabilized

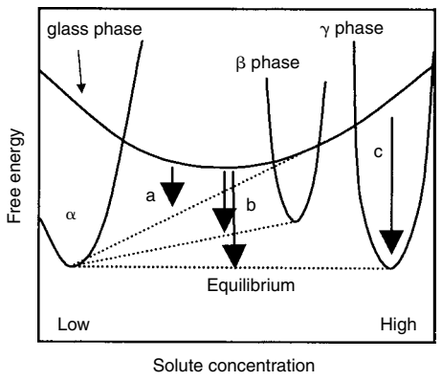

Fig. 1 Hypothetical free-energy curves for a metallic glass alloy indicating a glass phase as well as three distinct crystalline phases. The arrows indicate hypothetical devitrification paths: (a) primary, (b) eutectoid, and (c) polymorphous. The eutectoid devitrification route could be characterized by equilibrium between either a solute-lean α phase and a solute-rich metastable phase or a solute-rich equilibrium phase. A final equilibrium structure may be characterized by equilibrium between a solute-lean and a solute-rich phase. Source: Adapted from Ref 45

protective passive oxide films (Ref 47). Such behavior was not observed in the as-quenched version of the same amorphous alloy, which resisted depassivation and porosity development in the same solution. However, global electrochemical properties, such as resistance to micrometer-sized pit formation and stabilization, were not degraded in both Al-Ni-Y and Al-Co-Ce alloys when the as-quenched structure was relaxed (Ref 47, 56).

Mechanisms of Corrosion Resistance

Many glassy metals exhibit extremely good corrosion resistance, but there is controversy over the exact mechanism(s) responsible for such improvement over crystalline counterparts. There are several possibilities for explaining the difference in corrosion behavior between amorphous and crystalline metals. The good corrosion resistance of single-phase glasses is often attributed to structure, composition, as well as structural and compositional homogeneity. Glassy metals are free from such defects as the grain boundaries and second-phase particles that are present in crystalline metals. Corrosion often occurs preferentially at such defect sites; therefore, glassy metals may be expected to exhibit better corrosion resistance than crystalline alloys. The galvanic corrosion associated with chemical inhomogeneities, such as second-phase particles, is also impossible in glassy metals. Because dissolution occurs preferentially at active sites, including kinks, ledges, steps, and grain boundaries, and because there are fewer long-range defects in an amorphous alloy, a lower exchange current density may be expected for metal dissolution in the case of amorphous alloys. It is also possible that defects such as grain boundaries, second-phase particles, and other structural defects serve as initiation sites for localized corrosion such as pitting. According to this theory, the so-called weakest-link defect is responsible for pit formation (i.e., initiation and growth of pits to the micrometer-sized scale). The notion of a weak link at a critical defect that is responsible for pit initiation is a popular theory in local corrosion. The theory even applies to crystalline solid-solution alloys such as fcc stainless steels, where good pitting resistance is attributed to chromium and molybdenum in solid solution, and weakened corrosion resistance is attributed to inclusions (Ref 57). Such alloys suffer from reduced pitting resistance when pit initiation sites, such as Mn(Fe,Cr)S inclusions, are large (Ref 58). Indeed, pitting corrosion resistance is enhanced when such inclusions are small or even eliminated from body-centered cubic (bcc) or fcc solid-solution alloys without the need for the presence of an amorphous structure (Ref 59). For instance, the pitting resistance of an Fe-Cr-Ni alloy was increased enormously when high-purity crystalline Fe-Cr-Ni alloys were sputter deposited from a type 304 stainless steel target (Ref 60).

Another theory links the improved resistance of amorphous alloys to their ability to promote amorphous oxide formation. In high-temperature gas, vitreous or amorphous oxides offer improved oxidation resistance due to the absence of oxide grain boundaries, which provide a rapid diffusion path for concentration-gradient-driven ion movement (Ref 61, 62). In the case of metal passivity in aqueous solutions, ion transport is mostly driven by the electric field across the oxide film. The lack of oxide grain boundaries may lower ion migration rates, rendering the passive film more protective (Ref 61–63). The rapid transport and accumulation of cation vacancies at the oxide/metal interface is one theory accounting for oxide breakdown (Ref 64). Moreover, vitreous oxides on amorphous alloys perform well due to enhanced bond flexibility, because the vitreous or amorphous material can rearrange to accommodate lattice mismatch and strain between the oxide and the metal (Ref 63, 65). As a result of this flexibility, almost all surface atoms can bond with oxygen or OH^- without requiring an optimal epitaxial relationship between the ordered metal substrate and oxide. Intolerable changes in oxide/metal misfit strain with halide incorporation is another theory accounting for the rupture of protective oxide films on metals (Ref 66). The improved corrosion resistance associated with the addition of 18% Cr to crystalline iron is attributed, in part, to a change in the protective oxide structure from a well-oriented spinel structure at 0 to 12% Cr to a noncrystalline structure at 18% Cr (Ref 63). This disordering has been shown by low-energy electron diffraction (Ref 67) and scanning tunneling microscopy (Ref 68). A retardation in ionic transport may occur, because noncrystalline films have fewer defects or grain boundaries to enhance ionic movement. In summary, desirable amorphous oxide/amorphous alloy properties include defect minimization, film ductility, bond flexibility, and efficient, rapid film repassivation, which all contribute to the enhanced corrosion resistance (Ref 63, 65).

An alternative explanation for improved corrosion resistance is linked to the ability of these metastable alloys to form supersaturated solid solutions in one or more alloying elements. Such compositions may not be accessible by conventional ingot metallurgy processes. In some binary alloys, the corrosion resistance of the solid solution takes on the excellent corrosion properties of the most resistant element, assuming it is present in sufficient concentration. For instance, polycrystalline aluminum may be alloyed with transition metals to supersaturated solid-solution concentrations exceeding equilibrium solubilities. This has been a successful approach for improving localized corrosion resistance (Ref 69–73). Here, the native oxide formed on crystalline aluminum is already amorphous, and the main benefits of nonequilibrium alloying derive from two broad concepts. Alloying elements available in solid solution may be incorporated into the oxide film to enhance its resistance to halide chemisorption and/or penetration (Ref 69, 71). Alternatively, alloying elements in the underlying metallic substrate may reduce pit dissolution rates as a function of electrochemical potential (Ref 73), increase the severity of critical depassivating pit solutions, or result in oxidized solute with limited solubility in the pit environment. An interesting variation of the effect of alloying on corrosion properties surrounds the possible effects of solute on cathodic properties. A metal-metalloid glassy metal typically contains of the order of 20 at.% metalloids. The exchange current density for proton or water reduction reaction may be lower on the metalloid surface than on the metal. If it is assumed that the anodic kinetics do not change with metalloid additions, the Evans diagram predicts a decrease in corrosion current (i_{corr}) and a more active corrosion potential (E_{corr}).

Regarding structure, slight changes in the lattice parameter and coordination number for a metal in an amorphous state compared to its crystalline counterpart could theoretically induce large changes in electrochemical properties relevant to corrosion. For instance, amorphous palladium-silicon alloys have a coordination number of 11.6 instead of 12 as in fcc palladium, and the average distance of neighbors is 0.28 nm instead of 0.275 nm (Ref 1). The change in nearest-neighbor atomic environment and lattice parameter may change electrochemical properties. For instance, the kinetics of the oxygen reduction reaction change with platinum lattice parameter (Ref 54).

Thus, the effect of the amorphous structure, the chemical and structural homogeneity, and the possibility of forming unique chemical compositions not typical of near-equilibrium crystalline alloys must all be considered as factors that could affect the corrosion properties of metallic glasses. Unfortunately, structure cannot be changed independent of composition in most metallic glasses, and compositions cannot be varied over a broad range while still maintaining a fully amorphous state. These issues have long been an obstacle to more complete mechanistic understanding of metallic glass corrosion behavior.

Corrosion Behavior of Fully Amorphous and Partially Devitrified Metallic Glasses: A Historical Review

The first published information on the corrosion behavior of metallic glasses appeared in 1974 (Ref 74), and it concerned the Fe-Cr-P-C alloy system. Figure 2 shows the corrosion rates of $Fe_{70}Cr_{10}P_{13}C_7$ and $Fe_{65}Cr_{10}Ni_5P_{13}C_7$ metallic glasses and a typical type 304 stainless steel in hydrochloric acid (HCl) of various concentrations at 30 °C (85 °F). It also includes data from Ref 75 obtained under similar test conditions. The corrosion rates, calculated from gravimetric

measurements, were relatively large for the stainless steel because of pitting attack, but the rates for the metallic glasses were so low that they could not be detected even after immersion for 168 h. This early work illuminated the distinct differences in corrosion behavior between crystalline stainless steel and iron-base metal-metalloid glasses.

Other early research includes work that appeared in 1976 (Ref 76, 77). Figure 3 shows the relative corrosion rates in 1 *N* sodium chloride (NaCl) of crystalline iron-chromium alloys as compared to those of glassy Fe-$Cr_xP_{13}C_7$ alloys, where *x* ranges between 2 and 10 at.%. The corrosion rates of the crystalline alloys were approximately 0.6 mm/yr (24 mils/yr) and were largely unaffected by chromium content as a result of pitting corrosion. Conversely, the glassy alloys exhibited a sharp decrease in corrosion rate with increasing chromium content, with an undetectable rate occurring above 8 at.% Cr. Pitting did not occur on the glassy alloys, even those with only a few atomic percent of chromium.

In another study, the anodic polarization behavior of glassy $Fe_{25}Ni_{40}Cr_{15}P_{16}B_4$ and $Fe_{40}Ni_{40}P_{16}B_4$ alloys was compared in sulfuric acid (H_2SO_4) with and without NaCl additions. The presence of chromium facilitated passivation over a broad potential range. Thermal crystallization of the metallic glasses caused the corrosion rates during anodic polarization to increase sharply, especially in the presence of chloride ion (Cl^-). It was concluded that crystallization probably decreased corrosion resistance by introducing chemical and structural heterogeneities into the alloys.

Studies such as those summarized previously emphasized the excellent resistance to uniform and localized corrosion that could be obtained with certain types of metallic glasses. Results of these studies stimulated additional research into broader compositional ranges. Research during the late 1970s focused primarily on the transition metal-metalloid compositions, although some work was also initiated on metal-metal systems, such as copper-zirconium. Regarding the former compositional class of glassy alloys, research addressed the effects of phosphorus, boron, silicon, and carbon, which are added to stabilize the glassy structure.

These additive elements strongly influence the corrosion behavior of glassy alloys, as shown in Fig. 4 for $Fe_{70}Cr_{10}B_{13}X_7$ and $Fe_{70}Cr_{10}P_{13}X_7$ alloys (Ref 78). Specifically, in acidic solutions, the corrosion rates of the alloy system containing phosphorus as the major metalloid are 2 orders of magnitude lower than those of the alloy system with boron as the major metalloid. In addition, the corrosion rate of the glassy iron-chromium alloy progressively decreased by the addition of silicon, boron, carbon, and phosphorus in 0.1 *N* H_2SO_4. The addition of chromium without phosphorus to the glassy alloys is relatively ineffective in reducing corrosion rates, as evident from the $Fe_{70}Cr_{10}B_{13}C_7$ and $Fe_{70}Cr_{10}B_{13}Si_7$ alloys. Thus, phosphorus was identified as the single most effective metalloid element among phosphorus, carbon, silicon, and boron for improving the corrosion resistance of glassy iron-base alloys containing chromium. The combination of metalloids that is most effective in providing corrosion resistance in glassy iron-chromium alloys is phosphorus and carbon.

It was also recognized that the corrosion behavior of glassy alloys is strongly influenced by additions of metallic elements, especially those that form films on the alloy surface, that is, film-former additions. Figure 3 shows an early example of the strong beneficial effect of chromium additions to an iron-base glassy alloy. The effect of chromium content on the corrosion rates of glassy Ni-Cr-$P_{15}B_5$ alloys in 10% ferric chloride ($FeCl_3$) is apparent in Fig. 5, which shows that an undetectably small corrosion rate was attained with 7 at.% Cr (Ref 79). A large variety of other metal additions have also been investigated. For example, such elements as titanium, manganese, niobium, vanadium, tungsten, and molybdenum can benefit the corrosion resistance of Fe-$Cr_3P_{13}C_7X$ alloys in 1 *N* HCl (Ref 80).

Corrosion research involving metal-metalloid systems soon led to research with metal-metal glasses. One study characterized the corrosion behavior of copper-zirconium and copper-titanium alloys in H_2SO_4, HCl, HNO_3, and NaOH (Ref 81). In all of the solutions except NaOH, the crystalline and glassy copper-titanium alloys exhibited corrosion rates lower than those of pure copper, and in all cases, the corrosion resistance of the glassy alloy was better than that of the crystalline alloy. The glassy alloys in these compositional systems are not unusually corrosion resistant; in fact, neither the crystalline nor glassy forms of the alloys were more corrosion resistant than pure titanium or pure zirconium. This fact suggests that the corrosion resistance of the glassy alloys is the result of the presence of the passivating element (titanium or zirconium), not the presence of the glassy state. In another investigation, several alloys in the copper-zirconium system were examined in H_2SO_4 electrolyte (Ref 82). It was shown that the copper-zirconium alloys remained resistant to corrosion regardless of whether they were devitrified to a single-phase or

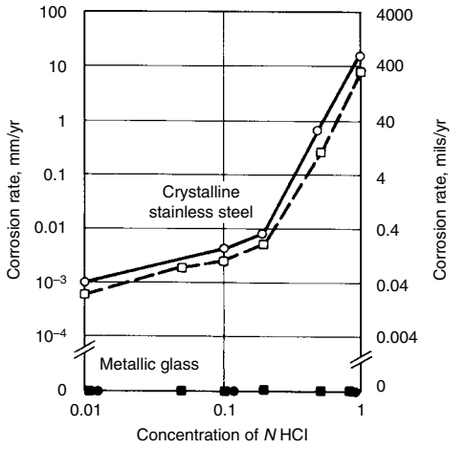

Fig. 2 Comparison of the corrosion rates of metallic glasses and crystalline stainless steel as a function of HCl concentration at 30 °C (85 °F). No weight changes of the metallic glasses of $Fe_{70}Cr_{10}P_{13}C_7$ were detected by a microbalance after immersion for 200 h. Open/closed circles, Ref 74; open/closed squares, Ref 75

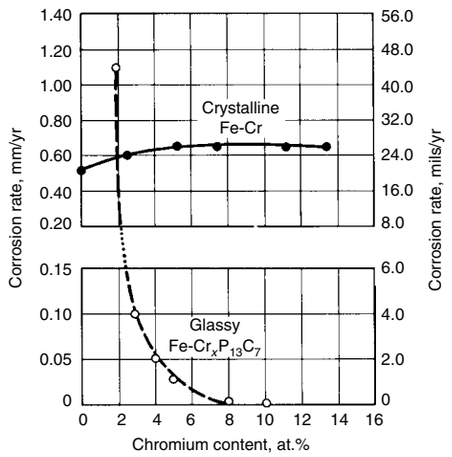

Fig. 3 Comparison of the corrosion rates of glassy Fe-$Cr_xP_{13}C_7$ alloys and crystalline iron-chromium alloys in 1 *N* NaCl solution at 30 °C (85 °F). Source: Ref 76

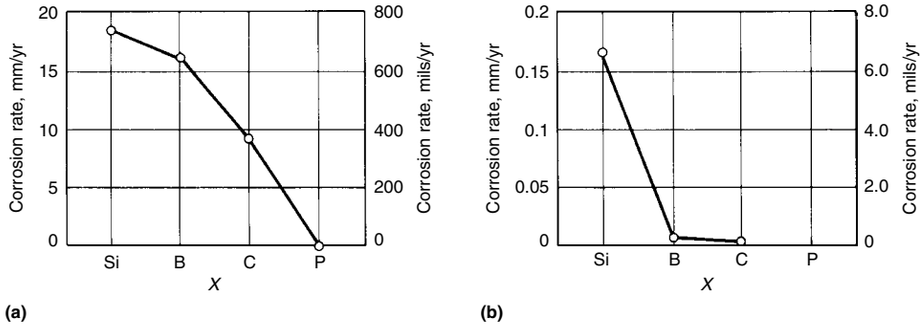

Fig. 4 Average corrosion rates estimated from the weight loss of amorphous $Fe_{70}Cr_{10}B_{13}X_7$ and $Fe_{70}Cr_{10}P_{13}X_7$ alloys in 0.1 *N* H_2SO_4 at 30 °C (85 °F), where (a) *X* is silicon, boron, carbon, and phosphorus, and (b) *X* is silicon, boron, and carbon. Source: Ref 78

a multiphase equilibrium microstructure; however, the glassy state was approximately 20% more corrosion resistant than the devitrified state.

Since the early work with iron-base metal-metalloid glasses, the field of study has been extended to include many alloy systems. The effect of metalloid additions on corrosion behavior is reasonably well characterized, and theories have been proposed to explain the beneficial effect of phosphorus on corrosion (Ref 78). The influence on corrosion behavior of a wide variety of other elemental additions is continuing to be evaluated, and many such additions increase corrosion resistance. Strong effects are seen by the classical film formers, such as chromium, titanium, and molybdenum, but alloying elements that raise pitting potentials may operate by lowering active dissolution rates or other means.

General Corrosion Behavior of All Classes of Amorphous Alloys

Glassy alloys can be grouped into three major categories with intrinsically different corrosion behaviors. The first group includes the transition metal-metal binary alloy systems, such as copper-zirconium, nickel-titanium, and nickel-niobium, as well as binary alloys in the aluminum-refractory metal and Al-TM type. The second class consists of TM-metalloid alloys. These alloys are usually iron-, nickel-, or cobalt-base systems, may contain film formers (such as chromium and titanium), and normally contain approximately 20 at.% P, B, Si, and/or C as the metalloid component. The third group of alloys studied includes the recently developed ETM-LTM-SM, SM-TM-RE, and assorted SM-TM-*X* alloys. These alloys can contain a RE and/or TM and SM elements. The grand challenge with respect to general corrosion is to impart passivity to active metals (i.e., magnesium), improve or extend the range of environments where passivity is seen (i.e., aluminum), and lower passive dissolution rates.

Transition Metal-Metal Binary Alloys. Research in the transition metal-metal systems indicates that corrosion resistance is sometimes determined by the behavior of the more corrosion-resistant component of the alloy. For example, in an investigation of the corrosion behavior of copper-zirconium alloys, the potentiodynamic polarization behavior of the alloys exhibited characteristics of both components, but the corrosion resistance of the alloy was not superior to the more passive material (zirconium) (Ref 83). Other alloys, including copper-titanium, copper-zirconium, and nickel-titanium, have demonstrated that the corrosion behavior of the transition metal-metal class of glassy metals is also determined almost completely by the more corrosion-resistant component. Thus, the corrosion resistance in some transition metal-metal alloy systems is apparently the result of the presence of a key passivating element in substitutional solid solution, not the glassy structure.

The work on copper-zirconium also examined the effect of alloy structure (Ref 83). By choosing the proper alloy composition ($Cu_{60}Zr_{40}$), the researchers devitrified the glassy alloy to a single-phase $Cu_{10}Zr_7$ and found a slight improvement in corrosion resistance when the material was in the glassy state. They worked with a series of copper-zirconium alloys and found that whether or not the alloy forms a single-phase or multiphase alloy on devitrification has very little effect on the general corrosion resistance. This leads to the conclusion that, at least in this alloy system, structure plays a secondary role in establishing general corrosion resistance. Local corrosion resistance was not investigated.

In other cases, the corrosion performance of amorphous binary alloys is superior to that of their component crystalline elements. Alloys such as chromium-niobium (Ref 84), chromium-titanium (Ref 85), chromium-zirconium (Ref 84), and chromium-tantalum (Ref 84) showed general corrosion rates in HCl solutions lower than those of both pure elements. An interesting point is that some alloying additions decrease the general corrosion rates regardless of the microstructure. For example chromium-tantalum and chromium-niobium alloys can be produced over a range of compositions, but only certain intermediate compositions form a homogeneous amorphous alloy. Corrosion resistance increases with tantalum additions regardless of structure, as shown in Fig. 6. For instance, Cr-89Ta and Cr-81Zr, which form supersaturated solid-solution single-phase crystalline alloys because the solute concentration is beyond the amorphous range, both showed a corrosion rate similar to what was seen for the fully amorphous alloys with slightly less solute. This again suggests that it is the composition and homogeneity of the supersaturated solid solution, not necessarily the amorphous structure, that improves the general corrosion resistance of many amorphous alloys. This behavior should be compared with the case of local corrosion where local nonuniformities at a critical size play a key, if not dominant, role in determining corrosion resistance.

Transition Metal-Metalloid Alloys. The second class of glassy alloys consists of TM-metalloid elements. This family includes iron-, nickel-, and cobalt-base alloys containing

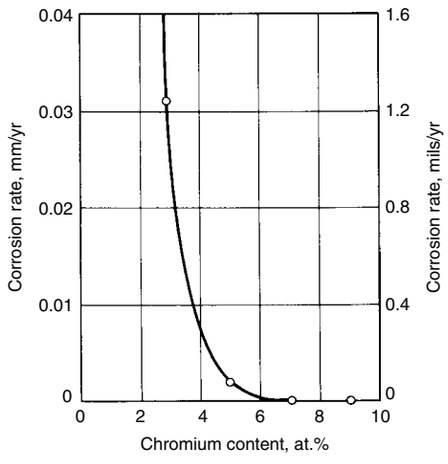

Fig. 5 Effect of the chromium content on the corrosion rates of amorphous Ni-Cr-$P_{15}B_5$ alloys in 10% $FeCl_3 \cdot 6H_2O$ at 30±1 °C (85 ±2 °F). The corrosion rate was estimated from weight loss during immersion for 168 h. Source: Ref 79

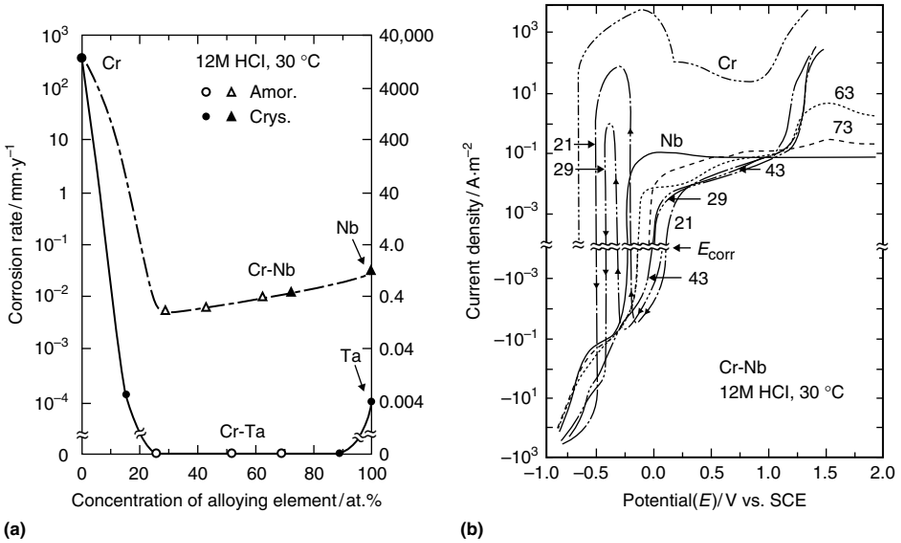

Fig. 6 Sputter-deposited chromium-niobium and chromium-tantalum alloys. (a) Corrosion rates of alloys compared to pure chromium, niobium, and tantalum. (b) Polarization curves of sputter-deposited chromium-niobium alloys and pure chromium and niobium. The number corresponds to the atomic percent of niobium in the chromium-niobium alloy. SCE, saturated calomel electrode. Source: Ref 84

combinations of phosphorus, boron, carbon, and silicon as the metalloid constituents. These alloys can be formed as binary systems, such as nickel-phosphorus and iron-boron, or they may be considerably more complex, such as Fe-Ni-P-B quaternary systems. In addition to the base metal, they often contain appreciable concentrations of film formers to promote passivity, for example, the Fe-Ni-Cr-P-B system. They derive their corrosion resistance from the same type of processes as crystalline alloys, namely the development of a passive film. The significant difference between corrosion-resistant glassy alloys and their crystalline counterparts, such as stainless steels, is that the level of chromium necessary to promote passivity can be considerably less in the glassy alloys.

Figure 3 shows a comparison between the corrosion rates of crystalline iron-chromium alloys and amorphous Fe-Cr-P-C alloys as a function of chromium concentration. At low chromium levels, the amorphous alloy corrodes at a higher rate than the crystalline material. However, at slightly higher chromium levels (4 at.%), there is a significant decrease in the corrosion rate of the glassy alloy, but the crystalline material is essentially unchanged. At an intermediate level of 8 at.% Cr, no corrosion of the glassy alloy was detected by weight loss experiments after immersion for 168 h. It was also found that the concentration of HCl, which has a profound effect on corrosion behavior of crystalline alloys, had no effect on corrosion of the glassy Fe-Cr-P-C or Fe-Ni-Cr-P-C alloy systems, which exhibited no weight loss after exposure for 168 h (Ref 76).

Figure 7 shows the effect of chromium concentration on the corrosion behavior of iron-, nickel-, and cobalt-base alloys. In all cases, the corrosion rate decreases with increasing chromium concentration and becomes vanishingly small at some level of chromium. In addition, the Fe-Cr-P-C alloy system, which exhibits the highest corrosion rate at low chromium contents, exhibits no weight loss in immersion tests with a chromium concentration as little as 8 at.%. This behavior supports the theory that, when an alloy contains a strong film former, the higher the initial reactivity of the alloy, the more rapidly the film former can be accumulated at the interface, and the more rapid the rate of passivation (Ref 80). The corrosion behavior of nickel-base (Ref 79) and cobalt-base (Ref 87) glassy alloys is very similar to that of the iron-base systems, and it is also a strong function of chromium concentration.

In one investigation, ion implantation was used to make glassy Fe-Cr-P alloys in which the chromium level varied from 6 to 18 at.% (Ref 88). An interaction between chromium and phosphorus was observed, which suggests a mechanism for the passivation of these amorphous alloys. Specifically, at low chromium levels, phosphorus implantation degrades passivity and induces pitting. At high chromium concentrations, there is a slight improvement in passivation, although the crystalline and amorphous alloys are both spontaneously passive and exhibit current densities of the order of 1 $\mu A/cm^2$. However, at intermediate chromium levels (8 to 10 at.%), there is a profound benefit from the phosphorus implantation. At these intermediate levels, there is a decrease in current density relative to the unimplanted alloy, namely 4 orders of magnitude for the $Fe\text{-}Cr_{10}P$ alloy. In fact, the $Fe\text{-}Cr_{10}P$ alloy exhibits current decay characteristics similar to an Fe-18Cr crystalline alloy. This research indicates that there is a critical chromium concentration required to provide passivity and that below this level, the combination of phosphorus and the amorphous structure increases the initial dissolution rate. Also, below the critical chromium level, there is insufficient chromium for passivation; therefore, pitting is observed. Above this critical chromium concentration, phosphorus and the glassy structure increase the initial dissolution rate, cause a rapid accumulation of chromium in the passive film, and result in an increased rate of passivation.

One study examined the influence of alloying elements on the corrosion behavior of iron-chromium-base alloys (Ref 86). Figure 8 shows current decay transients for glassy $Fe_{70}Cr_{10}B_{13}X_7$ alloys (*X* is silicon, carbon, or phosphorus) that were polarized in the passive region and abraded under potentiostatic control to produce the repassivation transients. The glassy alloy containing phosphorus exhibited the highest initial current, the most rapid repassivation kinetics, and the lowest passive current density.

Thus, the most effective elements in providing corrosion resistance are chromium and phosphorus. Published concepts concerning chromium and phosphorus appear to be consistent with existing data, but the relative effects of structure and composition on corrosion behavior remain to be quantified.

Amorphous SM-TM-RE Alloys and Other SM-TM-*X* Alloys. The general corrosion behavior of a variety of Al-TM-RE alloys has been investigated in acidic and basic solution over a range in pH values. In both Al-Fe-Gd and Al-Co-Ce alloys, the passive dissolution rate of the fully amorphous alloy was slightly faster in aqueous solutions of acidic pH than in the case of pure

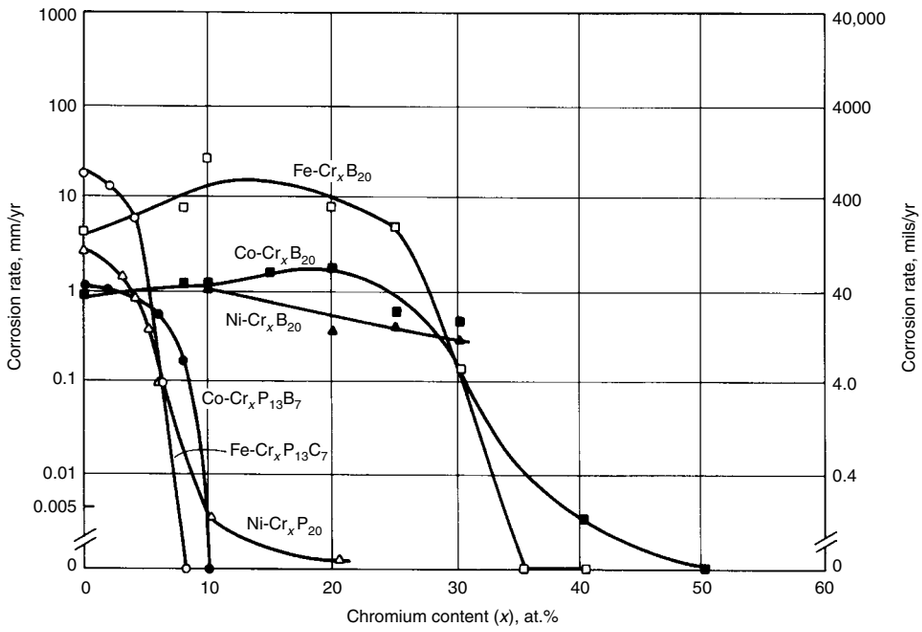

Fig. 7 The influence of chromium content on the corrosion rates of iron-, cobalt-, and nickel-base alloys in 1 *N* HCl. Source: Ref 86

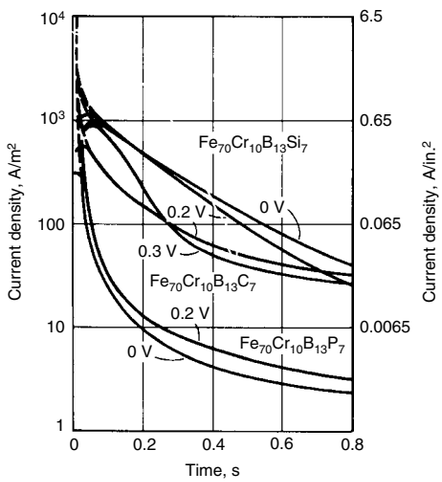

Fig. 8 Current density transients for glassy $Fe_{70}Cr_{10}B_{13}X_7$ alloys following mechanical abrasion of specimen surfaces during anodic polarization at constant potentials in 0.1 *N* H_2SO_4. *X* denotes minor metalloid content, and potentials (saturated calomel electrode) are indicated in the figure. Source: Ref 86

polycrystalline aluminum (Ref 56, 89). However, a slightly TM-RE-enriched passive film was evident, and passive current densities were considerably reduced in alkaline pH. This was attributed to the relative insolubility of iron, cobalt, gadolinium, and cerium oxides and hydroxides relative to aluminum oxide at alkaline pH levels, and the ability of the TM and RE elements to passivate over a range of potentials at high pH. In the case of Al-Co-Ce in 0.6 *M* NaCl solutions adjusted to acidic pH values, the amorphous alloys displayed a passive current density (i_{pass}) that was 2 to 3 times greater than that of the high-purity aluminum samples. In contrast, the passive current density of the alloys was significantly lower than that of high-purity aluminum in alkaline solutions at pH > 10. There were no detectable differences in the current densities over a range of near-neutral pH values. Hence, the amphoteric nature of aluminum was improved by rendering it passive in alkaline environments through the use of Al-TM-RE alloys, as shown in Fig. 9.

The passive current densities of partially devitrified aluminum-base alloys, heat treated to form primary aluminum-rich crystals embedded in an amorphous matrix, exhibited only slight or no significant deviation from the as-quenched amorphous material when similarly tested over a range of pH values. General corrosion properties after devitrification to form transitional and equilibrium phases in an amorphous matrix have not been investigated.

The general corrosion behavior of several Mg-Y-Cu glasses has also been reported (Ref 90, 91). Amorphous alloys exhibit the lowest corrosion rates in neutral or weakly acidic solutions and the greatest ability to passivate, compared to crystalline multiphase variants. Passivation did depend on the specific ion present in solution, but passivity could be considerably improved compared to pure magnesium.

Zirconium-base metallic glasses are more resistant to general corrosion than type 304 stainless steel in some acids. They can exhibit improved passivity as a function of valve metal components (Ref 81). Zirconium-base bulk metallic glasses that have been partially devitrified can exhibit improved mechanical properties but, nickel-zirconium, copper-zirconium, and icosahedral quasi-crystalline phases degrade passivity in acid environments (Ref 92).

Localized Corrosion Behavior of All Classes of Amorphous Alloys

One of the most outstanding characteristics regarding the corrosion behavior of certain metallic glasses is their ability to resist localized corrosion. In this article, the term *localized corrosion* refers to pitting and crevice attack. (Stress-assisted forms of corrosion, such as stress-corrosion cracking and hydrogen embrittlement, are discussed in another section in this article.) In many cases, this resistance to localized attack extends over wide ranges of oxidizing potential and pH and to alloy compositions that would be considered lean in film-former elements compared to conventional crystalline stainless steels.

Metal-Metal Binary Alloys. Alloying aluminum with transition metals such as chromium (Ref 93), zirconium (Ref 94, 95), titanium (Ref 95, 96), niobium (Ref 95), molybdenum (Ref 95), tungsten (Ref 95), and tantalum (Ref 95) to form amorphous alloys decreases the passive current density and increases the pitting potential of the amorphous alloys. The open-circuit potential, passive current density, and pitting potential of the resulting alloys are generally between those of the component elements and improve with an increase in the amount of the alloying element. The pitting resistance changes with devitrification in a way that is dependent on the types and sizes of the phases formed. This can be seen clearly in aluminum-chromium (Ref 93). In Al-35Cr, which undergoes a near-polymorphous transformation to $Al_{17}Cr_9$, the open-circuit potential decreases with devitrification, but the pitting potential stays the same. In Al-16Cr, neither the open-circuit nor pitting potential changes with either structural relaxation or devitrification to form two aluminum-rich intermetallic phases (Al_4Cr and $Al_{13}Cr_2$) in an Al(Cr) matrix. However, the passive current density decreases with devitrification. The Al-43Cr alloy has completely different behavior. The pitting potential does change with devitrification. A heat treatment to form bcc Cr(Al) and $Al_{17}Cr_9$ produces a higher pitting potential than the amorphous alloy, but other forms (with additional metastable phases or larger grains) have lower pitting potentials. In addition, it was found that the relative dissolution rates of the various devitrified states of this alloy changed with time in solution, suggesting that some phases may be preferentially dissolved. An alloy with more chromium, Al-51Cr, was mostly bcc Cr(Al) in the as-sputtered state and had a pitting potential close to that of Al-16Cr. The pitting potential of Al-51Cr increased when heat treated to decrease the amount of aluminum in bcc Cr(Al) and form additional aluminum-chromium intermetallic phases, but decreased when the size of the intermetallic phases increased. A critical size was not determined.

The improvement in the pitting resistance of some Al-TM alloys may be due to the presence of beneficial alloying elements, not the amorphous state. The localized corrosion resistance of crystalline aluminum has been successfully improved by nonconventional alloying methods to achieve supersaturated solid-solution concentrations (Ref 69–73). Here, the native oxide formed on crystalline aluminum is already amorphous, and the main benefits of nonequilibrium alloying derive from two broad concepts. Alloying elements available in solid solution may be incorporated into the oxide film to enhance its resistance to halide chemisorption and/or penetration (Ref 69, 71). Alternatively, alloying elements in the underlying metallic substrate may reduce pit dissolution rates as a function of electrochemical potential (Ref 97), increase the severity of critical depassivation pit solutions, or result in oxidized solute with limited solubility in the pit environment (Ref 98).

The pitting resistance of nickel-zirconium alloys has been found to be a function of not only the alloy composition but also the fabrication method. The passive current density of both Ni-60Zr and Ni-75Zr was lower than that of pure zirconium, but their pitting potentials were also lower (Ref 99). The pitting potential increased with increasing zirconium content of the alloy. The pitting potentials were different on different sides of a melt-spun ribbon (Ref 100–102). Sputtered alloys did not suffer pitting under conditions in which melt-spun alloys of the same composition did (Ref 102).

As discussed previously, amorphous chromium-zirconium alloys are quite resistant to general corrosion in acids. However, when the

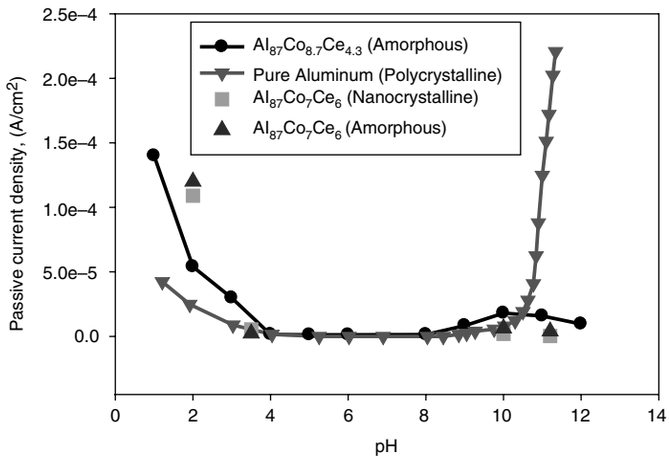

Fig. 9 Passive current densities for high-purity aluminum and amorphous alloys of the Al-Co-Ce system, including heat treated material, in solution adjusted to various pH values using 1 *M* HCl or 1*M* NaOH as neccesary. Source: Ref 56

zirconium content of the amorphous alloy is greater than 51%, the alloys undergo pitting under anodic polarization (Ref 103). The pitting potential decreases with increasing zirconium content. The pitting potential also changes with devitrification of the alloy to form primary hexagonal close-packed (hcp) zirconium crystals embedded in an amorphous matrix and, at higher temperatures, intermetallic Cr_2Zr (Ref 103). Heat treatment of Cr-60Zr increases the pitting potential, even when it leads to complete crystallization to hcp zirconium and Cr_2Zr with a grain size of ~16 nm. However, in Cr-67Zr, the pitting potential initially increases with heat treatment temperature, then decreases. The oxide-bridging model has been used to explain this observation. The buildup of a corrosion-resistant alloying element in the remaining amorphous phase allows for an increase in the concentration of this alloying element in the oxide. This protective oxide may be able to cover small nanocrystals, effectively eliminating the impact of the surface heterogeneity on the atomistic processes governing breakdown. Thus, partial devitrification would lead to an overall improvement in the pitting resistance of the material. A critical nanocrystal diameter of ~20 nm was proposed to be the maximum size that can be covered by the continuous oxide; devitrified states with phases larger than this were found to be more susceptible to pitting.

Metal-Metalloid Alloys. It has been proposed that the excellent resistance of certain glassy alloys to uniform and localized corrosion results from their enhanced chemical reactivity relative to conventional stainless alloys (Ref 104, 105). Transient repassivation experiments with glassy $Fe_{70}Cr_{10}P_{13}C_7$ and crystalline type 304 stainless steel in acidified chloride electrolyte showed a higher initial reactivity on the glassy alloy after abrasion and a more rapid rate of repassivation. These experiments demonstrated that there is a synergistic effect between chromium and phosphorus in transition metal-metalloid glasses such that the maximum resistance to localized corrosion exists when these two elements are both present. The excellent resistance to localized corrosion may result from the rapid reformation of a passive film at regions where it is damaged by mechanical or electrochemical means, combined with enrichment of Cr^{3+} species in the film.

Research cited earlier in this article concerning the use of ion implantation to make Fe-Cr-P alloys (Ref 88) demonstrated that the synergistic effect of chromium and phosphorus is a strong function of the chromium concentration. Potentiostatic polarization experiments in acidic chloride solutions showed behavior that was a strong function of chromium concentration. At low chromium levels, phosphorus implantation induced pitting, but at high chromium levels (18 at.%), a slight improvement in passivation was observed. At intermediate levels (10 to 12 at.%), substantial improvement in the passive film was obtained through phosphorus implantation. It was proposed that when the alloy contains small amounts of chromium, there is not enough chromium to passivate the alloy, and when the phosphorus stimulates the initial dissolution, the alloy becomes susceptible to pitting. As the chromium concentration increases, there is sufficient chromium for passivation, and the phosphorus promotes the accumulation of chromium and a very protective passive film.

The work summarized in Fig. 3 and described previously in this article indicates that iron-base glasses with only several atomic percent of chromium very effectively resist pitting in chloride-containing solutions. Polarization curves of glassy alloys obtained in 1 *N* NaCl do not show a characteristic pitting potential; rather, they exhibit stable passivity until the onset of transpassivity. In addition, results from the study discussed in connection with $Fe_{25}Ni_{40}Cr_{15}P_{16}B_4$ showed that the passive range in 1 *N* H_2SO_4 plus 0.1 *N* NaCl is not interrupted by pitting but extends to transpassivity (Ref 77). In another study, increasing the chromium content from 0 to 16 at.% in a series of Fe-Ni-Cr-P-B alloy systems facilitated passivation in acidified 1 *N* NaCl, but pitting was not observed on any alloy polarized below the transpassive potential region (Ref 106). Polarization at transpassive potentials caused numerous pits to form that penetrated the filament. These pits were noncrystallographic in shape.

Chromium was shown to be very effective in conferring pitting resistance, such as for the glassy alloys Fe-$Cr_xB_{13}C_7$ and Fe-$Cr_xB_{13}Si_7$ in 3%NaCl (Ref 104, 105). With chromium levels of 2 and 5 at.%, both alloy types pitted at potentials slightly anodic to the free corrosion potential of approximately −0.6 V_{SCE}. The addition of 8 at.% Cr extended the pitting resistance to approximately 1 V_{SCE}, which is an extremely aggressive condition for alloys containing such a low level of chromium. By contrast, type 304 stainless steel contains approximately 18 wt% Cr, yet its pitting potential is several hundred millivolts less positive than that of these glassy alloys. Approximately 7 at.% Cr was sufficient to prevent pitting of Ni-Cr-P-B alloy systems in 10% $FeCl_3 \cdot H_2O$ at 30 °C (85 °F) (Ref 79). Glassy $Fe_{73}Cr_7P_{15}B_5$ passivated spontaneously in 1 *N* HCl. Surface analysis by x-ray photoelectron spectroscopy showed that chromium and phosphorus were enriched and nickel depleted in the alloy substrate beneath the passive film. Figure 10 compares the effect on corrosion rate of adding chromium or titanium to Ni-(Cr,Ti)-P_{20} glasses. Chromium is more effective than titanium in conferring corrosion resistance, and the chromium-containing alloys exhibited a stronger tendency for spontaneous passivation. The corrosion rate decreased approximately logarithmically with increasing chromium or titanium up to approximately 10 and 7 at.%, respectively (Ref 107).

Molybdenum benefits the pitting resistance of glassy alloys and crystalline steels. The addition of molybdenum to glassy Fe-$Mo_xP_{13}C_7$ alloys suppressed pitting and decreased the critical current density for passivation and the passive current density (Ref 108). As little as 4 at.% Mo prevented pitting in 1 *N* HCl, and small additions of molybdenum were more effective than chromium in decreasing corrosion rates. Molybdenum has been shown to facilitate the formation of a passive hydrated chromium or iron oxyhydroxide film through its enrichment in the corrosion product layer during active dissolution (Ref 109). The enrichment assists the accumulation of the passivating species in the film by lowering the dissolution rate of the species; the molybdenum-rich product subsequently dissolves and thus leaves little molybdenum behind in the film.

Titanium, tantalum, molybdenum, and tungsten were incorporated by high-rate sputter deposition into alloys of the general composition M_1-M_2, where M_1 is titanium, tantalum, molybdenum, or tungsten, and M_2 is rhenium, iron, cobalt, nickel, or copper (Ref 110). Tungsten-iron and titanium-copper resisted pitting corrosion up to 2.5 V_{SCE} in chloride solutions of pH 1 and 7. Addition of tungsten to Fe-$W_xP_{13}C_7$ increased the critical pitting potential, E_{crit}, to above 2 V_{SCE} at $x = 6$ at.%, but $x = 10$ at.% caused transpassive dissolution at 1 V_{SCE}. Addition of tungsten to commercial type 304 stainless steel by sputtering stabilized the glassy structure and increased E_{crit} in chloride electrolyte (Ref 111).

One study investigated the effects of the alloying additions titanium, zirconium, vanadium, niobium, chromium, molybdenum, tungsten, manganese, cobalt, nickel, copper, ruthenium, rhodium, palladium, and platinum in the glassy alloy Fe-*X*-$P_{13}C_7$ (Ref 112). All elements except manganese decreased the corrosion rate in H_2SO_4, HCl, HNO_3, and NaCl solutions. Although the base alloy, Fe-$P_{13}C_7$, did not passivate, additions of any of the preceding elements

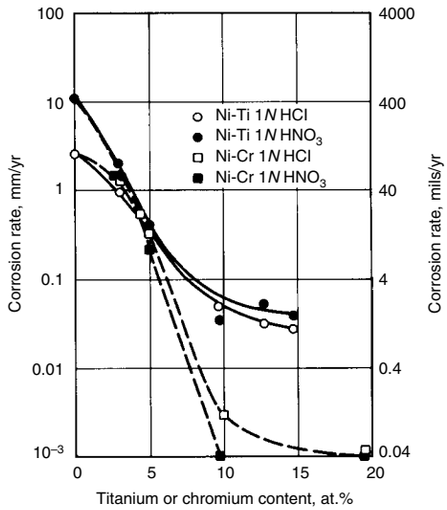

Fig. 10 Changes in corrosion rates of glassy Ni-Ti-P_{20} and Ni-Cr-P_{20} alloys measured in 1 *N* HCl and 1 *N* HNO_3 at 30 ± 1 °C (85 ± 2 °F) as a function of the titanium or chromium content. Source: Ref 107

at levels from 0.5 to several atomic percent enabled passivation to occur during anodic polarization in 0.1 *N* H_2SO_4. Chromium was most effective, and molybdenum and titanium also were very beneficial. Pitting was not observed in 3% NaCl for those alloys that passivated. The alloys that did not passivate, such as Fe-Co-$P_{13}C_7$, also did not pit, but they dissolved uniformly.

One investigation examined the resistance of glassy alloys to crevice corrosion in acidic solutions containing Cl^- ion. Crevice corrosion was studied as a means of circumventing the need for initiating localized corrosion; that is, crevice corrosion behavior was considered to represent more a measure of the resistance to propagation, rather than initiation, of localized corrosion (Ref 106). Introducing microcracks into Fe-Ni-Cr-P-B glassy alloy filaments by cold rolling was found to cause susceptibility to a transient form of crevice attack; however, the crevices widened into pit-shaped cavities and then passivated spontaneously (Ref 113). Subsequent research with an electrochemical cell consisting of a prepared crevice instrumented with microreference and pH electrodes showed that the glassy alloy possessed a strong tendency to passivate, even under the aggressive conditions of low pH, low dissolved oxygen concentration, and oxidizing potential that prevail within crevices (Ref 114). The conclusion was that the alloy resisted crevice attack because of its strong ability to passivate, which in turn stifled propagation. This resistance to crevice corrosion could be expected to extend to other glassy TM-metalloid compositions containing both a film former and phosphorus.

Glassy nickel-phosphorus is another alloy system that has been recently investigated and that appears to resist chloride-induced corrosion (Ref 114). In fact, the *E*-log(*i*) behavior is virtually identical in both chloride-containing and chloride-free electrolytes. A form of chemical passivity has been proposed to explain the corrosion behavior. Passivation in the nickel-phosphorus system is due to the formation of an ionic barrier layer, not to the formation of a classical passive oxide film. This barrier layer consists of hypophosphite ion adsorbed on the nickel-phosphorous surface, which may in turn be hydrogen bonded to an outer layer of water molecules. This barrier layer inhibits the transport of water to the surface and thus prevents hydration of nickel, which is the first step in the nickel dissolution process.

Amorphous SM-TM-RE Alloys and Other SM-TM-*X* Alloys. Various amorphous Al-Fe-Gd, Al-Co-Ce, Al-Ni-Gd, and Al-Ni-Y alloys formed at compositions greater than approximately 85 at.% Al have all exhibited good resistance to pit stabilization in 0.6 *M* NaCl solution, as shown in Fig. 11 and 12 (Ref 56, 115, 116).

Pitting and repassivation potentials were both raised several hundred millivolts compared to pure polycrystalline aluminum. Upon low-temperature heat treatment, these alloys all form isolated, solute-lean, aluminum-rich fcc nanocrystals by a primary crystallization process from the fully amorphous state (Fig. 13). The key result was that the excellent resistance to metastable pitting and pit stabilization seen in the fully amorphous condition were not lost in the nanocrystalline-amorphous state in the case of such small nonuniformities, as shown in Fig. 14.

A critical defect size for pitting of nanocrystalline-amorphous aluminum-based glasses is under investigation. These materials were expected to behave like a composite consisting of pure aluminum sites dispersed on an amorphous surface. Because both bulk high-purity poly- and single-crystalline fcc aluminum exhibit far inferior local corrosion properties compared to the fully amorphous Al-TM-RE alloy (Ref 56, 115, 116), the corrosion resistance of the nanocrystalline-amorphous material was expected to be inferior to that of its fully amorphous precursor. However, both pit initiation and stabilization are shown to be hindered (Ref 117, 118). This is a noteworthy finding in the field of pitting corrosion, that solute-lean nanophases embedded in an amorphous matrix resist corrosion despite a density approaching $10^{22}/m^3$. Moreover, many of these amorphous-nanocrystalline variants consist of up to 40 vol% fcc aluminum but still resist corrosion compared to bulk aluminum. The good corrosion resistance of the amorphous Al-TM-RE alloy was completely eliminated in the fully crystalline equilibrium state. The latter was expected because iron, nickel, and cobalt, as well as gadolinium and cerium, have limited solubility in bulk polycrystalline fcc aluminum. In addition, the fcc aluminum phase is continuous, and intermetallic phases are formed. All three of these factors can contribute to a decrease in the localized corrosion resistance. A second significant result was that nanometer-diameter solute-rich (e.g., intermetallic) precipitates behaved similarly to solute-lean (aluminum-rich) nanocrystals when embedded in an amorphous matrix. These sites also did not act as pit initiation sites. It should be noted that these nanocrystal sites are not selectively corroded prior to potential-driven pitting,

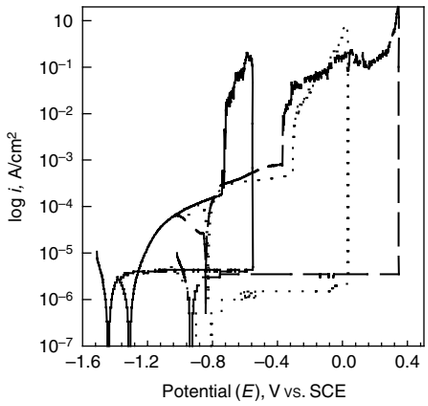

Fig. 11 *E*-log(*i*) plot for fully amorphous (dotted line) and amorphous-nanocrystalline $Al_{90}Fe_5Gd_5$ alloy (dashed line) compared to high-purity polycrystalline aluminum (solid line). SCE, saturated colomel electrode. Source: Ref 117

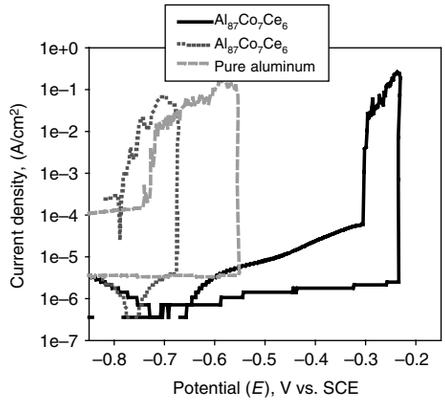

Fig. 12 Potentiodynamic scans conducted on fully amorphous (solid line) and fully crystalline, following 550 °C (1020 °F) isothermal heat treatment (dotted line), $Al_{87}Co_7Ce_6$ alloys compared to polycrystalline aluminum (dashed line) in deaerated 0.6 *M* NaCl solution. SCE, saturated calomel electrode. Source: Ref 56

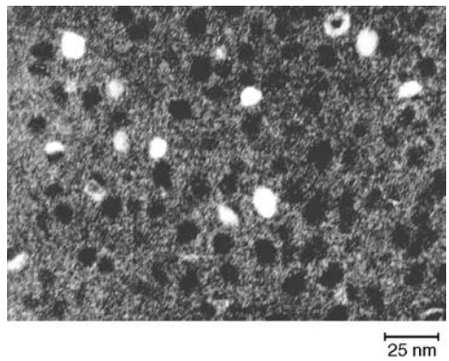

Fig. 13 Dark-field transmission electron micrograph of partially nanocrystalline-amorphous matrix $Al_{90}Fe_5Gd_5$ illiustrating the distribution of aluminum-rich nanocrystals in the remaining amorphous matrix after heat treatment at 150 °C (300 °F) for 25 h. Source: Ref 117, 118

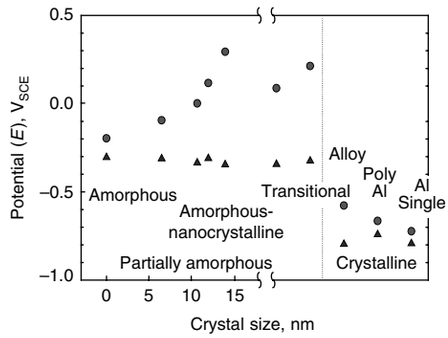

Fig. 14 Changes in the median pitting (E_{pit}) and repassivation (E_{rp}) potentials of $Al_{90}Fe_5Gd_5$ with devitrification. E_{pit} and E_{rp} for polycrystalline and single-crystal 99.999% Al are included for comparison. Source: Ref 118

because aluminum oxide is thermodynamically stable at the near-neutral pH associated with the 0.6 *M* NaCl solution.

Concerning Mg-TM-RE alloys, pitting potentials have been raised in alkaline NaCl-containing environments where magnesium is passive but exhibits an extremely negative pitting potential (Ref 119, 120). Approximately 11 at.% Ni promotes the formation of amorphous magnesium-nickel, as shown in Fig. 15. Notably, binary magnesium-nickel alloys raise pitting potentials, particularly when fully amorphous (Fig. 16) (Ref 119). Fully amorphous Mg-Cu-Y and Mg-Ni-Nd alloys performed even better than magnesium-nickel binary alloys in fast potentiodynamic scans with both raised pitting potentials and lowered passive current densities (Fig. 17) (Ref 120). Y_2O_3 was detected in the inner layer of passive films (Fig. 18). However, these alloying additions raise open-circuit potentials considerably, even in the fully amorphous state.

Concerning the pitting resistance of zirconium-base bulk metallic glasses, the pitting resistance of pure zirconium is already reasonably good in comparison to magnesium and aluminum (albeit inferior to other valve metals such as titanium and niobium). The localized corrosion resistance upon creation of the amorphous state tends to be similar to its crystalline state (Ref 121). A related interesting feature is the possible degradation in bulk zirconium-base glasses due to undesired casting defects.

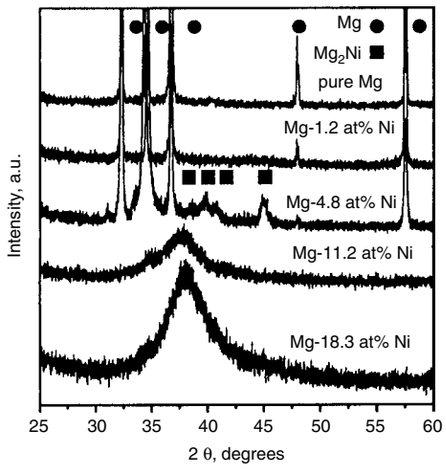

Fig. 15 X-ray diffraction results on pure magnesium and magnesium-nickel alloys showing the transition with increasing nickel from magnesium to magnesium plus Mg_2Ni and then to an amorphous structure. Source: Ref 119

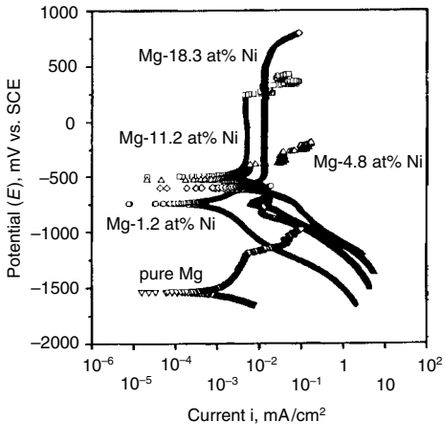

Fig. 16 *E*-log(*i*) data for pure polycrystaline magnesium compared to magnesium-nickel alloys shown in Fig. 15. The Mg-18.3%Ni alloy is fully amorphous. SCE, saturated calomel electrode. Source: Ref 119

Environmental Cracking Behavior

The environmentally induced fracture of glassy alloys, namely hydrogen embrittlement and stress-corrosion cracking (SCC), is discussed in this section. Details on the mechanisms of these phenomena can be found in the articles "Stress-Corrosion Cracking" and "Hydrogen Damage" in *ASM Handbook,* Volume 13A, 2003.

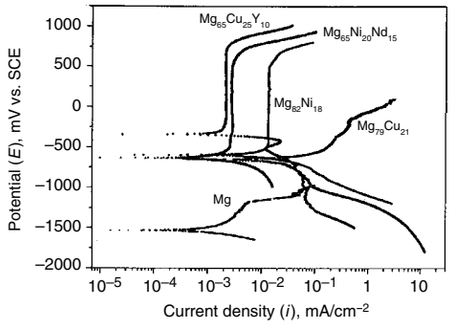

Fig. 17 *E*-log(*i*) measurements of melt-spun ternary $Mg_{65}Ni_{20}Nd_{15}$ and $Mg_{65}Cu_{25}Y_{10}$ as well as binary $Mg_{82}Ni_{18}$ and $Mg_{79}Cu_{21}$ ribbons in 0.01 *M* NaCl (pH 12) electrolyte at a scan rate of 1.0 mV/s. Pure magnesium is shown for comparison. SCE, saturated calomel electrode. Source: Ref 120

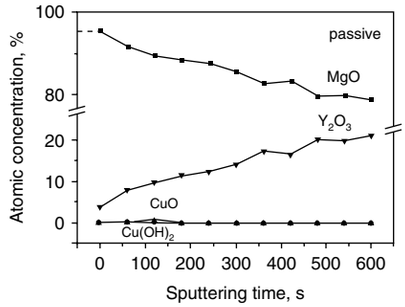

Fig. 18 Sputter-depth profile results for passive film grown on $Mg_{65}Cu_{25}Y_{10}$ from x-ray photoelectron spectroscopy, assuming the metal peaks are from the metal beneath the surface oxide layer. Source: Ref 120

Regarding SCC, one of the first reported experiments on the SCC of glassy alloys concerned $Ni_{49}Fe_{29}P_{14}B_6Al_2$ (Ref 122). Loading to 75% of the fracture stress in air in 3.5 *N* NaCl solution resulted in a slow, presumably SCC fracture region and a final, fast fracture region. However, another theory is that the fracture of this alloy was actually induced by hydrogen (Ref 123). In another case, the SCC behavior of a glassy $Fe_{32}Ni_{36}Cr_{14}P_{12}B_6$ alloy in boiling magnesium chloride ($MgCl_2$) at 125 °C (255 °F) was studied by means of constant extension-rate tensile tests and constant strain tests (Ref 124). Stress-corrosion cracking occurred at the corrosion potential and anodic overpotentials, and slight cathodic polarization prevented SCC. Examination of the fracture surfaces led to the conclusion that localized corrosion enhances hydrogen entry and subsequent embrittlement. The SCC behavior of glassy Fe-Cr-Ni-P-C alloy systems in acidic chloride solutions was investigated with constant extension-rate tensile tests (Ref 125). Hydrogen embrittlement occurred at cathodic polarizations up to −300 mV relative to the corrosion potential. In the passive potential region, no cracking occurred in neutral NaCl solutions and in acidic solutions at low Cl^- concentrations. Fracture stress decreased only when the specimens were strained in strong acidic solutions containing Cl^-, and this phenomenon was also attributed to hydrogen embrittlement. The tendency of glassy $Fe_{40}Ni_{40}P_{14}B_6$ to undergo SCC and hydrogen embrittlement in acidic electrolytes was also studied (Ref 126). Cathodic polarization of elastically stressed specimens in 1 *M* HCl resulted in failure by hydrogen embrittlement. Specimens immersed in aqueous $FeCl_3$ solution at the free corrosion potential failed by SCC, as did those that were anodically polarized in 1 *M* HCl. These specimens were covered by an iron oxide film, and selective leaching (dealloying of nickel from pits and cracks) occurred. $Fe_{74.5}Ni_{10}Si_{3.5}B_9C_2$ was also found to be susceptible to SCC and hydrogen-induced cracking, albeit by different fracture modes. Failure time and fracture stress in NaCl were reduced by anodic polarization, and a quasi-cleavage-type fracture mode was observed. Others have suggested hydrogen embrittlement, as discussed subsequently (Ref 123, 127, 128).

In corrosion fatigue studies of a zirconium-base metallic glass, the fatigue crack growth rate (*da*/*dN*) was increased over 3 orders of magnitude, and the threshold stress-intensity factor range (ΔK_{th}) was significantly reduced in a NaCl solution compared to tests in air. In fact, one of the largest increases in *da*/*dN* ever reported for any metallic system was seen for this alloy in the NaCl environment compared to moist air. The fundamental reasons remain unclear, except that cyclic blunting and sharpening in air was replaced by brittle fracture (Ref 129).

Hydrogen Embrittlement. Although classical SCC (defined as cracking caused directly by anodic dissolution at the crack tip) of glassy

alloys apparently occurs, hydrogen embrittlement is a common mode of environmentally assisted failure in aqueous electrolytes, due to the propensity for proton and water reduction at crack tips. Hydrogen embrittlement of glassy alloys has been observed during bending or tensile tests during or after hydrogen charging in the following alloys:

- $Fe_{80}P_{13}C_7$ and $Fe_{70}Cr_{10}P_{13}C_7$ (Ref 127)
- $Fe_{32}Ni_{36}Cr_{14}P_{12}C_6$ (Ref 130)
- $Fe_{49.5}Cr_{7.5}Ni_{23}P_{13}C_7$ and $Fe_{53}Cr_7Ni_{20}P_{14}C_6$ (Ref 125)
- $Fe_{78}B_{13}$,Si_9, $Fe_{81}B_{13.5}Si_{3.5}C_2$, $Fe_{66}Co_{18}B_{15}Si$, and $Fe_{77}B_{16}Cr_2Si_5$ (Ref 131)

As shown in Fig. 19, the stress-strain curve of a $Fe_{49.5}Cr_{7.5}Ni_{23}P_{13}C_7$ glassy alloy exhibits almost completely elastic behavior in air and in various acid chloride solutions, suggesting limited plastic deformation. The fracture strain decreased to approximately 30% of that in air as a result of charging the specimen with hydrogen. Local corrosion at the open-circuit and even passive potentials can produce hydrogen and thus create embrittlement; fractographic evidence and the return of ductility by baking after corrosion were cited as evidence for this claim (Ref 123).

Electrodeposited amorphous alloys are often extremely brittle compared to rapidly solidified counterparts, and this could be attributed to codeposited hydrogen. However, internal voids in porous electrodeposits may be more detrimental than internal hydrogen (Ref 132).

Although it appears that hydrogen embrittlement is more common than SCC as the environmentally assisted failure mode for glassy alloys, the detailed mechanism of the hydrogen embrittlement of transition metal-metalloid alloys is uncertain. At cathodic potentials in deaerated solutions, the principal cathodic reaction produces hydrogen by the following reaction sequence: $2H^+ + 2e^- \rightarrow H_2$, which can be separated into a proton reduction step and a hydrogen adatom-adatom combination step. Elements such as phosphorus, sulfur, arsenic, and antimony poison the reaction $H_{ads} + H_{ads} \rightarrow H_2$; thus, they increase the concentration of adsorbed (ads) hydrogen on the electrode surface and consequently the flux of atomic hydrogen absorbed through the surface into the bulk alloy. Because phosphorus is commonly found in TM-metalloid glassy alloys, it would seem likely that these phosphorus-containing alloys may have a large tendency toward absorbing hydrogen from the electrolyte and consequently a significant tendency toward hydrogen embrittlement. Augmenting this tendency would be the very high strength and limited ductility characteristic of this compositional class of glassy alloys. However, the detrimental role of metalloid segregation, at least to grain boundaries, would be absent, and intergranular fracture is, of course, eliminated in the fully amorphous alloys that lack grain boundaries.

Studies of hydrogen permeation through glassy phosphorus-containing nickel-base alloys concluded that phosphorus increases the rate of hydrogen absorption relative to that for pure nickel (Ref 83). Moreover, hydrogen transport can be faster in fully amorphous alloys compared to partially crystalline counterparts due to an absence of microstructural traps (Ref 133). However, large quantities of hydrogen may be absorbed, possibly owing to increased free volume (Ref 134). Another researcher characterized the effects of metalloid additions on the susceptibility to hydrogen embrittlement of glassy Fe-$Cr_5Mo_{12}X$ and Fe-$Cr_{10}Mo_{12}X$ (where X is 18C, 20B, or 13P-7C) in 1 N HCl, 0.5 N NaCl, and 1 N H_2SO_4 (Ref 123). Although phosphorus is an effective hydrogen recombination poison, alloys containing this element showed a lower susceptibility to hydrogen embrittlement. (The alloys containing carbon were the most susceptible.) This lower susceptibility was ascribed to the higher rate of repassivation of phosphorus-containing alloys; because the corrosion rate was decreased, the amount of hydrogen produced by the open-circuit corrosion reaction and that absorbed into the alloys should also be lowered.

The damage process mechanism for hydrogen in metallic glasses remains uncertain. Hydrogen is known to increase the relaxation time for viscous flow and retard atomic arrangements associated with the viscous flow process that enables plastic deformation (Ref 135). Such retarded viscous flow at a crack tip could help contribute to brittle fracture. The conventional rationale that brittle fracture occurs when the cleavage stress becomes lower than some shear stress required for viscous flow may apply to these situations.

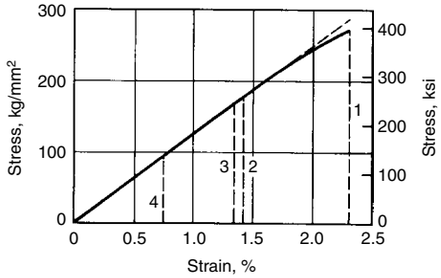

Fig. 19 Stress-strain behavior of glassy $Fe_{49.5}Cr_{7.5}Ni_{23}P_{13}C_7$ alloy at various potentials in air and in solution at a strain rate of $4.2 \times 10^{-6} s^{-1}$. Line 1: in air; line 2: in 5 N $H_2SO_4 + 0.1$ N NaCl, corrosion potential (E_{corr}) = −20 mV; line 3: in 5 N $H_2SO_4 + 0.1$ N NaCl, E_{corr} = +500 mV; line 4: in 5 N $H_2SO_4 + 0.1$ N NaCl, E_{corr} = −500 mV. Source: Ref 125

Conclusion

Amorphous metals are being studied extensively due to their unique physical, mechanical, magnetic, as well as electrochemical properties. A recent advance has been the development of so-called bulk amorphous alloys that should enable a wider application of amorphous materials, given the possibility of critical cooling rates as low as 1 K/s. In addition to their significance as novel materials with possible excellent corrosion properties, amorphous metals and partially devitrified amorphous metals with compositions similar to conventional alloys may be used as model materials for understanding the effects of both structural and chemical homogeneity and nonuniformities on corrosion mechanisms.

Amorphous materials appear to owe their good corrosion resistance to a variety of causes, and some controversy still exists regarding the exact operative explanation in each metallic glass system. Amorphous structure; structural and chemical homogeneity with the associated lack of defects, such as intermetallic phases, inclusions, grain boundaries and dislocations; promotion of amorphous oxide formation via an amorphous substrate; as well as alloying with beneficial elements to high nonequilibrium levels that would be beyond equilibrium solubility limits or supersaturated in crystalline states have each been cited as the cause for good corrosion resistance. In iron-base alloys, chromium and phosphorus additions act synergistically to improve the general corrosion and pitting resistance. These alloys are passive in aggressive environments, even when the chromium levels are much lower than the level required to confer passivity in conventional crystalline stainless steels. This is likely due to the effects of phosphorus and the homogeneous structure. In general, the addition of both a film former and phosphorus leads to good corrosion resistance in iron-base alloys.

In some cases, the amorphous structure alone does not appear to impart good corrosion resistance. Instead, it may be the ability to add passivating elements into solid solution beyond conventional limits and the compositional and structural homogeneity that lead to good general corrosion resistance. This is particularly clear in chromium-tantalum and chromium-niobium alloys in which the corrosion resistance of a variety of crystalline or amorphous single-phase alloys is better than both alloying elements, regardless of whether the alloy is amorphous or crystalline.

Several amorphous zirconium-base glasses with very low critical cooling rates have been developed in recent years. These bulk glasses exhibit good corrosion resistance in the fully amorphous state, but devitrification to form many different types of precipitates degrades the passivity. The localized corrosion resistance of these alloys is similar to that of the crystalline state.

Amorphous aluminum- and magnesium-base alloys show significant improvement in localized corrosion resistance over the pure elements, which are thermodynamically predisposed toward corrosion. This appears to be due to the addition of beneficial alloying elements that may be incorporated into the oxide, making it passive

over a broader range in pH and rendering it more protective. These alloying elements also may alter the potential dependence of alloy dissolution or alter the solution chemistry required to maintain pit growth under otherwise passive conditions. Interestingly, these beneficial effects are not diminished by partial devitrification of the amorphous alloy.

Several studies have examined the effects of partial and complete devitrification on the corrosion resistance of several classes of glassy alloys. In general, partial devitrification to form nanometer-sized crystalline precipitates does not significantly diminish the good corrosion resistance of the amorphous material. The exact behavior appears to be a function of the chemistry and size of the phases formed. Structural relaxation also appears to affect the nanoscale corrosion processes of the glasses.

Hydrogen embrittlement and SCC have been observed in several glassy alloys, but the exact damage mechanisms remain unclear. It is likely that the effects of alloying additions (particularly phosphorus for hydrogen embrittlement) and the amorphous structure interact in complex ways in these alloys to yield many different results, depending on the alloy composition. Dissolved hydrogen can also affect viscous plastic deformation behavior in ways other than those considered in the case of crystalline materials that undergo deformation by plastic slip and twinning.

ACKNOWLEDGMENTS

Support from the National Science Foundation under DMR-0204840 and the Air Force Office of Scientific Research under grant F49602-01-1-0352 are gratefully acknowledged. Helpful discussions with G.J. Shiflet are greatly appreciated. Portions of this article have been adapted from N. Robert Sorensen and Ronald B. Diegle, Corrosion of Amorphous Metals, *Corrosion,* Volume 13, *Metals Handbook,* 9th ed., ASM International, 1987, P 864–870.

REFERENCES

1. P. Duwez, *ASM Trans.,* Vol 60, 1967, p 607
2. Y.H. Kim, A. Inoue, and T. Masumoto, *Mater. Trans., JIM,* Vol 31, 1990, p 747
3. H.S. Chen, Metallic Glasses Update, *Micromechanics of Advanced Materials: A Symposium in Honor of Professor James Li's 70th Birthday,* S.N.G. Chu, P.K. Liaw, R.J. Arsenault, K. Sadananda, K.S. Chan, W.W. Gerberich, C.C. Chau, and T.M. Kung, Ed., The Minerals, Metals and Materials Society, 1995, p 295–300
4. W.L. Johnson, *Mater. Sci. Forum,* Vol 225–227, 1996, p 35–50
5. A. Inoue, K. Ohtera, and T. Masumoto, *Jpn. J. Appl. Phys.,* Vol 27, 1988, p L736–L739, L1796
6. T. Masumoto, *Mater. Sci. Eng. A,* Vol 179/180, 1994, p 8–16
7. Y. He, S.J. Poon, and G.J. Shiflet, *Science,* Vol 241, 1988, p 1640–1642
8. R.W. Cahn, *Nature,* Vol 341, 1989, p 183–184
9. Y. He, J. Chen, G.J. Shiflet, and S.J. Poon, *Philos. Mag. Lett.,* Vol 61, 1990, p 297–303
10. A. Peker and W.L. Johnson, *Appl. Phys. Lett.,* Vol 63, 1993, p 2342–2344
11. A. Inoue, T. Zhang, and T. Masumoto, *Mater. Trans., JIM,* Vol 31, 1990, p 177–183, 425–428
12. Y. He, S.J. Poon, and G.J. Shiflet, *Scr. Metall.,* Vol 22, 1988, p 1813–1816
13. A. Inoue, T. Zhang, and N. Nishiyama, *Mater. Trans., JIM,* Vol 34, 1993, p 1234–1237
14. Y. He, G.M. Dougherty, G.J. Shiflet, and S.J. Poon, *Acta Metall. Mater.,* Vol 41, 1993, p 337–343
15. A. Inoue, T. Nakamura, and N. Nishiyama, *Mater. Trans., JIM,* Vol 33, 1992, p 937–945
16. A. Inoue, K. Ohtera, A.-P. Tsai, and T. Masumoto, *Jpn. J. Appl. Phys.,* Vol 27, 1988, p L280, L479–L482
17. H. Chen, Y. He, G.J. Shiflet, and S.J. Poon, *Scri. Metall. Mater.,* Vol 25, 1991, p 1421–1424
18. G.J. Shiflet, Y. He, and S.J. Poon, *J. Appl. Phys.,* Vol 64, 1988, p 6863–6865
19. G.S. Choi, Y.H. Kim, H.K. Cho, A. Inoue, and T. Masumoto, *Scr. Metall. Mater.,* Vol 33, 1995, p 1301–1306
20. C.J. Gilbert, V. Schroeder, and R.O. Ritchie, *Metall. Mater. Trans. A,* Vol 30, 1999, p 1739–1753
21. C.J. Gilbert and R.O. Ritchie, *Appl. Phys. Lett.,* Vol 71, 1997, p 476–478
22. A. Inoue and T. Masumoto, *Mater. Sci. Eng. A,* Vol 6, 1991, p 133
23. A. Inoue, A. Kitamura, and T. Masumoto, *J. Mater. Sci.,* Vol 16, 1981, p 1895
24. R.O. Suzuki, Y. Komatsu, K.E. Kobayashi, and P.H. Shingu, *J. Mater. Sci.,* Vol 18, 1983, p 1195
25. A. Inoue, Y. Bizen, H.M. Kimura, M. Yamamoto, A.P. Tsai, and T. Masumoto, *J. Mater. Sci. Lett.,* Vol 6, 1987, p 811
26. A. Inoue, M. Yamamoto, H.M. Kimura, and T. Masumoto, *J. Mater. Sci. Lett.,* Vol 6, 1987, p 194
27. A.P. Tsai, A. Inoue, and T. Masumoto, *Metall. Trans. A,* Vol 19, 1988, p 1369
28. A.P. Tsai, A. Inoue, and T. Masumoto, *J. Mater. Sci. Lett.,* Vol 7, 1988, p 805
29. A. Inoue, K. Ohtera, T. Zhang, and T. Masumoto, *Jpn. J. Appl. Phys.,* Vol 27, 1988, p L1583
30. A. Inoue, T. Zhang, K. Kita, and T. Masumoto, *Mater. Trans., JIM,* Vol 30, 1989, p 870
31. H.Y. Hsieh, B.H. Toby, T. Egami, Y. He, S.J. Poon, and G.J. Shiflet, *J. Mater. Res.,* Vol 5, 1990, p 2807–2812
32. A.N. Mansour, C.P. Wong, and R.A. Brizzolara, *Phys. Rev. B,* Vol 50, 1994, p 12401
33. L. Zhang, Y.S. Wu, X.F. Bian, H. Li, W.M. Wang, J.G. Li, and N. Lun, *J. Phys., Condens. Matter,* Vol 11, 1999, p 7959
34. F.Q. Guo, S.J. Enouf, S.J. Poon, and G.J. Shiflet, *Philos. Mag. Lett.,* Vol 81 (No. 3), 2001, p 203–211
35. H.J. Kim, K.M. Lim, B.G. Seong, and C.G. Park, Amorphous Phase Formation of Zr-Based Alloy Coating by HVOF Spraying Process, *J. Mater. Sci.,* Vol 36 (No. 1), 2001, p 49–54
36. W.L. Johnson, Bulk Glass-Forming Metallic Alloys: Science and Technology, *Mater. Res. Soc. Bull.,* Vol 24, 1999, p 42–56
37. H. Jones, *Proceedings of the Second International Conference on Rapidly Quenched Metals,* N.J. Grant and B.C. Giessen, Ed., Elsevier, 1976
38. F. Otsubo, H. Era, T. Uchida, and K. Kishitake, Formation of Amorphous Fe-Cr-Mo-8P-2C Coatings by the High Velocity Oxy-Fuel Process, *J. Therm. Spray Technol.,* Vol 9 (No. 4), 2000, p 494–498
39. A.H. Dent, A.J. Horlock, D.G. McCartney, and S.J. Harris, *J. Therm. Spray Technol.,* Vol 8 (No. 3), 1999, p 399
40. D. Mencer, *J. Alloy. Comp.,* Vol 306, 2000, p 158–162
41. P. Fischer, A. Blatter, V. Romano, and H.P. Weber, *Appl. Phys. A,* Vol 80, 2005, p 489–492
42. D. Carvalho, S. Cardoso, and R. Vilar, *Scr. Mater.,* Vol 37 (No. 4), 1997, p 523–527
43. Z.Y. Al-Tamimi, W.A. Grant, and P.J. Grundy, *Vacuum,* Vol 34 (No. 10), 1994, p 861–865
44. M.G. Scott, in *Amorphous Metallic Alloys,* F.E. Luborsky, Ed., Butterworths, 1983, p 144–168
45. U. Köster and P. Weiss, *J. Non-Cryst. Solids,* Vol 17, 1975, p 359
46. H.S. Chen, Structural Relaxation in Metallic Glasses, *Amorphous Metallic Alloys,* F.E. Luborsky, Ed., Butterworth Monographs in Materials, 1983, p 169–186
47. R.A. Bley, J.R. Scully, and J.W.P. Hsu, Microstructure Dependence of Nanometer Corrosion in Al-Ni-Y Glassy Alloys, *Philos. Mag. Lett.,* Vol 80 (No. 2), 2000, p 85–94
48. T. Egami, *Mater. Res. Bull.,* Vol 13, 1978, p 557–562
49. V.A. Likhachev, A.I. Mikhailin, and L.V. Zhigilei, *Philos. Mag. A,* Vol 69, 1994, p 421–436
50. A. Rubshtein, Y. Rosenberg, A. Frenkel, V. Manov, E. Veliyulin, A. Voronel, and E.A. Stern, *Mater. Sci. Forum,* Vol 179, 1995, p 839–844
51. P.G. Zielinski and D.G. Ast, *J. Non-Cryst. Solids,* Vol 61–62, 1984, p 1021–1026
52. J. Piller and P. Haasen, *Acta Metall.,* Vol 30, 1982, p 1–8

53. H.Y. Hsieh, T. Egami, Y. He, S.J. Poon, and G.J. Shiflet, *J. Non-Cryst. Solids,* Vol 135, 1991, p 248–254
54. J.A. Poirier and G.E. Stoner, *J. Electrochem. Soc.,* Vol 141, 1994, p 425–430
55. Y. Masumoto, A. Inoue, A. Kawashima, K. Hashimoto, A.P. Tsai, and T. Masumoto, *J. Non-Cryst. Solids,* Vol 86, 1986, p 121–136
56. M.E. Goldman, N. Ünlü, G.J. Shiflet, and J.R. Scully, *J. Electrochem. Solid State Lett.,* Vol 8 (No. 2), 2005
57. G.S. Eklund, *J. Electrochem. Soc.,* Vol 121, 1974, p 467
58. H. Bohni, S. Matsch, T. Suter, and J.O. Parks, Initiation and Stability of Local Corrosion Processes on Stainless Steel, *ECS Proc.,* Vol 99-27, 1999, p 483–493
59. T. Suter and H. Bohni, *Electrochim. Acta,* Vol 43, 1998, p 2843
60. M.P. Ryan, N.J. Laycock, H.S. Isaacs, and R.C. Newman, *J. Electrochem. Soc.,* Vol 146, 1999, p 91–97
61. F.P. Fehlner, in *Passivity of Metals,* R.P. Frankenthal and J. Kruger, Ed., The Electrochemical Society, 1978, p 137
62. F.P. Fehlner and N.F. Mott, *Oxid. Met.,* Vol 2, 1970, p 59
63. A.G. Revesz and J. Kruger, in *Passivity of Metals,* R.P. Frankenthal and J. Kruger, Ed., The Electrochemical Society, 1978, p 137
64. L.F. Lin, C.Y. Chao, and D.D. Macdonald, *J. Electrochem. Soc.,* Vol 128, 1981, p 1194
65. T.P. Hoar, *J. Electrochem. Soc.,* Vol 117, 1970, p 17C
66. N. Sato, *Electrochim. Acta,* Vol 19, 1971, p 1683
67. C.L. McBee and J. Kruger, *Electrochim. Acta.,* Vol 17, 1972, p 1337
68. M.P. Ryan, R.C. Newman, and G.E. Thompson, *J. Electrochem. Soc.,* Vol 141, 1994, p L164
69. P. Natishan, *J. Electrochem. Soc.,* Vol 135 (No. 2), 1988, p 321
70. G.D. Davis, B.A. Shaw, B.J. Rees, and M. Ferry, *J. Electrochem. Soc.,* Vol 140, 1993, p 951
71. W.C. Moshier, *J. Electrochem. Soc.,* Vol 134, 1987, p 2677
72. B.A. Shaw, G.D. Davis, T.L. Fritz, B.J. Rees, and W.C. Moshier, *J. Electrochem. Soc.,* Vol 137, 1990, p 1317
73. G.S. Frankel, M.A. Russak, C.V. Jahnes, M. Mirzamaani, and V.A. Brusic, *J. Electrochem. Soc.,* Vol 136, 1989, p 1243
74. M. Naka, K. Hashimoto, and T. Masumoto, *J. Jpn. Inst. Met.,* Vol 38, 1974, p 38
75. Y. Waseda and K.T. Aust, *J. Mater. Sci.,* Vol 16, 1981, p 2337
76. M. Naka, K. Hashimoto, and T. Masumoto, *Corrosion,* Vol 32, 1976, p 146
77. R.B. Diegle and J.E. Slater, *Corrosion,* Vol 32, 1976, p 155
78. M. Naka, K. Hashimoto, and T. Masumoto, *J. Non-Cryst. Solids,* Vol 28, 1978, p 403
79. K. Hashimoto, M. Kasaya, K. Asami, and T. Masumoto, *Corros. Eng.,* Vol 26, 1977, p 445
80. K. Hashimoto, M. Naka, J. Noguchi, K. Asami, and T. Masumoto, in *Proceedings of the Fourth International Conference on Passivity,* R.P. Frankenthal and J. Kruger, Ed., The Electrochemical Society, 1978, p 156–169
81. M. Naka, K. Hashimoto, and T. Masumoto, *J. Non-Cryst. Solids,* Vol 30, 1978, p 29
82. J.C. Turn and R.M. Latanision, *Corrosion,* Vol 39, 1983, p 271
83. R.M. Latanision, J.C. Turn, and C.R. Compeau, in *Proceedings of the Third International Conference on Mechanical Behavior of Metals,* Vol 2, 1979, p 475
84. J.H. Kim, E. Akiyama, H. Habazaki, A. Kawashima, K. Asami, and K. Hashimoto, *Corros. Sci.,* Vol 34, 1993, p 1817, 1947
85. J.H. Kim, E. Akiyama, H. Yoshioka, H. Habazaki, A. Kawashima, K. Asami, and K. Hashimoto, *Corros. Sci.,* Vol 34, 1993, p 975
86. K. Hashimoto, "Supplement to the Scientific Report of the Research Institutes of Tohoku University," A 201–216, Tohoku University, 1980
87. M. Naka, K. Hashimoto, K. Asami, and T. Masumoto, *Proceedings of the Third International Conference on Rapidly Quenched Metals,* B. Cantor, Ed., The Metals Society, 1978, p 449
88. N.R. Sorensen, R.B. Diegle, and S.T. Picraux, *J. Mater. Res.,* Vol 1 (No. 6), 1986, p 752
89. R.G. Buchheit, Jr., G.E. Stoner, and G.J. Shiflet, Corrosion Behavior of an Al-Fe-Gd Metallic Glass in Aqueous Environments, *Proc. of the Sym. on the Application of Surface Analysis to Environment Materials Interactions,* D.R. Baer, C.R. Clayton, and G.D. Davis, Ed., ECS PV 91-7, 1991, p 490
90. R.V. Rao, U. Wolff, S. Bauneck, J. Eckert, and A. Gerbert, *J. Mater. Res.,* Vol 18, 2003, p 97
91. A. Gebert, U. Wolff, S. Bauneck, J. Eckert, and L. Schultz, *Mater. Sci. Eng. A,* Vol 299, 2001, p 125–135
92. U.K. Mudali, S. Scudino, U. Kühn, J. Eckert, and A. Gebert, *Scr. Mater.,* Vol 50, 2004, p 1379–1384
93. M. Mehmood, E. Akiyama, H. Habazaki, A. Kawashima, K. Asami, and K. Hashimoto, *Corros. Sci.,* Vol 41, 1999, p 477
94. H. Yoshioka, H. Habazaki, A. Kawashima, K. Asami, and K. Hashimoto, *Corros. Sci.,* Vol 32, 1991, p 313
95. H. Yoshioka, Q. Yan, H. Habazaki, A. Kawashima, K. Asami, and K. Hashimoto, *Corros. Sci.,* Vol 31, 1990, p 349
96. Q. Yan, H. Yoshioka, H. Habazaki, A. Kawashima, K. Asami, and K. Hashimoto, *Corros. Sci.,* Vol 32, 2001, p 327
97. G.S. Frankel, R.C. Newman, C.V. Jahnes, and M.A. Russak, *J. Electrochem. Soc.,* Vol 140, 1993, p 2192
98. Z. Szklarska-Smialowska, *Corros. Sci.,* Vol 33, 1992, p 1193
99. K. Asami, H. Habazaki, K. Kawashima, and K. Hashimoto, *Corros. Sci.,* Vol 34, 1993, p 445
100. B.-P. Zhang, A. Kawashima, H. Habazaki, K. Asami, and K. Hashimoto, *Corros. Sci.,* Vol 39, 1997, p 2005
101. M. Janik-Czachor, *Corrosion,* Vol 49, 1993, p 763
102. A. Kawashima, W.P. Yu, B.P. Zhang, H. Habazaki, K. Asami, and K. Hashimoto, *Mater. Trans., JIM,* Vol 38, 1997, p 443
103. M. Mehmood, B.-P. Zhang, E. Akiyama, H. Habazaki, A. Kawashima, K. Asami, and K. Hashimoto, *Corros. Sci.,* Vol 40, 1998, p 1
104. M. Naka, K. Hashimoto, and T. Masumoto, "Scientific Report of the Research Institutes of Tohoku University," A-26, Tohoku University, 1979, p 283
105. K. Hashimoto, M. Naka, and T. Masumoto, "Scientific Report of the Research Institutes of Tohoku University," A-26, Tohoku University, 1976, p 48
106. R.B. Diegle, *Corrosion,* Vol 35, 1979, p 250
107. M. Naka, K. Hashimoto, and T. Masumoto, 1703rd Report, Research Institute for Iron, Steel, and Other Metals, 1980, p 156
108. M. Naka, K. Hashimoto, and T. Masumoto, *J. Non-Cryst. Solids,* Vol 29, 1978, p 61
109. K. Asami, M. Naka, K. Hashimoto, and T. Masumoto, *J. Electrochem. Soc.,* Vol 127, 1980, p 2130
110. R. Wang, Abstract 80-2, *Extended Abstracts,* The Electrochemical Society, 1980, p 620
111. R. Wang, paper presented at the Fall Meeting (Pittsburgh, PA), The Metallurgical Society, Oct 1980
112. M. Naka, K. Hashimoto, and T. Masumoto, *J. Non-Cryst. Solids,* Vol 31, 1979, p 355
113. T.M. Devine, *J. Electrochem. Soc.,* Vol 124, 1977, p 38
114. R.B. Diegle, *Corrosion,* Vol 36, 1980, p 326
115. J.E. Sweitzer, J.R. Scully, R.A. Bley, and J.W.P. Hsu, *Electrochem. Solid State Lett.,* Vol 2, 1999, p 267–270
116. J.E. Sweitzer, G.J. Shiflet, and J.R. Scully, *Electrochim. Acta,* Vol 48, 2003, p 1223–1234
117. A.M. Lucente, G.J. Shiflet, and J.R. Scully, in *Critical Factors in Localized Corrosion IV,* S. Virtanen, Ed., ECS PV 2002-24, 2002, p 295–309
118. A.M. Lucente, G.J. Shiflet, and J.R. Scully, in *Pits and Pores: Formation, Properties and Significance for Advanced Materials,* P. Schmuki, Ed., Oct 2004, Proc. of Electrochemical Society, 2005
119. H.B. Yao, Y. Li, A. Lee, J. Chai, and J.S. Pan, *Electrochim. Acta,* Vol 46, 2001, p 2649–2657
120. H.B. Yao, Y. Li, and A. Wee, *Electrochim. Acta,* Vol 48, 2003, p 2641–2650

121. W.H. Peter, R.A. Buchanan, C.T. Liu, P.K. Liaw, M.L. Morrison, J.A. Horton, C.A. Carmichael, Jr., and J.L. Wright, *Intermetallics,* Vol 10, 2002, p 1157–1162
122. C.A. Pampillo, *J. Mater. Sci.,* Vol 10, 1975, p 1194
123. A. Kawashima, K. Hashimoto, and T. Masumoto, *Corrosion,* Vol 36, 1980, p 577
124. R.F. Sandenbergh and R.M. Latanision, *Corrosion,* Vol 41, 1985, p 369
125. A. Kawashima, K. Hashimoto, and T. Masumoto, *Corros. Sci.,* Vol 16, 1976, p 935
126. M.D. Archer and R.J. McKim, *J. Mater. Sci.,* Vol 18, 1983, p 1125
127. M. Nagumo and T. Takahashi, *Mater. Sci. Eng.,* Vol 23, 1976, p 257
128. J.X. Guo, J.X. Li, L.J. Qiao, K.W. Gao, and W.Y. Chu, *Corros. Sci.,* Vol 45, 2003, p 735–745
129. V. Schroeder, C.J. Gilbert, and R.O. Ritchie, *Mater. Sci. Eng. A,* Vol 317, 2001, p 145–152
130. R.K. Viswanadham, J.A.S. Green, and W.G. Montague, *Sci. Metall.,* Vol 10, 1976, p 229
131. K. Habib and A. Al-Hashem, *Corros. Sci.,* Vol 35, 1993, p 571–576
132. R.L. Zeller and U. Landau, *J. Electrochem. Soc.,* Vol 137, 1990, p 1107
133. M. Hara and R.M. Latanision, *Corros. Sci.,* Vol 37, 1995, p 865–875
134. A.J. Maeland, L.E. Tanner, and G.G. Libowitz, *J. Less-Common Met.,* Vol 74, 1980, p 279
135. D. Suh and R. Duaskardt, in *Hydrogen Effects on Materials Behavior and Corrosion Deformation Interactions,* N.R. Moody, Ed., TMS, 2003, p 183

ASM Handbook, Volume 13B: Corrosion: Materials
S.D. Cramer, B.S. Covino, Jr., editors, p490-512
DOI: 10.1361/asmhba0003837

Corrosion of Intermetallics

P.K. Datta, H.L. Du, and J.S. Burnell-Gray, Advanced Materials Research Institute, Northumbria University, United Kingdom
R.E. Ricker, National Institute of Standards and Technology

IN MANY APPLICATIONS of structural materials—aerospace, automobiles, power generation—increasing demands are being made for materials with temperature capabilities greater than those of superalloys. Intermetallics with higher melting points can replace superalloys with inadequate melting points (Ref 1–3). Intermetallics, characterized by strong, predominantly metallic bonding between unlike atoms, are situated between superalloys and ceramics. From bonding comes crystal structure, ordering, high strength at low and high temperature, and low ductility. Low fracture strain and poor fracture toughness (K_{Ic}) of the intermetallics stem from their complex crystal structures, large Burgers vectors (a crystal vector that defines the amount and direction of atomic displacement associated with dislocation motion in a crystal), high lattice stresses, inadequate slip systems, inability to promote cross slip, and lack of grain-boundary cohesion. The influence of such factors on the corrosion behavior is not insignificant. Stress generation during the scale growth, scale spallation during thermal cycling, stress corrosion and corrosion fatigue, and finally, cationic and anionic transports influencing the corrosion kinetics are all likely to be affected by these substructure defects. Thus, the corrosion behavior of the intermetallics stems from their inherent immunity or susceptibility to corrosion and from the modifications in macroscopic parameters, such as grain size, stoichiometry, grain-boundary design, microalloying, and second-phase incorporation, to increase the number of slip and to hence confer improvement of K_{Ic} and fracture strain.

This article reviews the progress that has been made in understanding the corrosion behavior of intermetallics. Such understanding is essential for the modeling of the corrosion processes and for devising a strategy to create corrosion protective systems by alloy and coating design.

The main emphasis is on the high-temperature corrosion properties of intermetallics, but information on aqueous corrosion is also reviewed due to the realization that aqueous corrosion can seriously compromise intermetallics usefulness. In the area of high-temperature corrosion, the discussion is centered on aluminides and silicides, while the aqueous corrosion review is concentrated on fundamental factors that make the aqueous corrosion of an intermetallic phase different from that of a homogeneous alloy or of the constituents in pure elemental form. Thermodynamic principles in the context of high-temperature corrosion, information on oxidation, sulfidation, hot corrosion of NiAl-, FeAl-, and TiAl-based intermetallics, and silicides are included. Aqueous corrosion is divided into two main topics: thermodynamic consideration, ordering influencing kinetics, stress-cracking corrosion, and hydrogen embrittlement; and practical issues of dealing with the corrosion problems.

High-Temperature Corrosion of Intermetallics

Three major types of high-temperature corrosion are oxidation, sulfidation, and hot corrosion. Oxidation involves solely the formation of an oxide scale. Sulfidation is concerned with the development of scales consisting of sulfide or sulfides. Materials exposed to environments containing other contaminants, in addition to oxygen and sulfur, can cause the development of complex scales containing oxides and sulfides, termed hot corrosion. The article "High-Temperature Gaseous Corrosion" in *ASM Handbook,* Volume 13A, 2003, will assist in understanding the fundamentals of high-temperature corrosion as well as the testing methods cited in this article.

General Principles

Important aspects of high-temperature corrosion are the processes of scale formation and scale degradation. Two additional modes of degradation that confer susceptibility of materials to high-temperature corrosion are intergranular corrosion and scale vaporization.

The scaling process in high-temperature corrosion involves the formation of a thermodynamically stable corrosion product (a scale) that separates the surface of the material from the aggressive environment. Although the following discussion begins with basic principles, these principles are very important and useful to understanding the formation of oxide/sulfide scales and the high-temperature corrosion mechanisms of intermetallics.

The formation of a defect-free, coherent and adherent scale containing lattice defects capable of sustaining only cationic and anionic transport allows progressive scale thickening and diffusion-controlled parabolic kinetics. Linear kinetics predominate in the case of an inherently nonprotective scale caused by the presence in the scale of inappropriate defect structures, physical defects, or by stress-induced scale spallation. A complex scaling process characterizes alloy corrosion accompanying the formation of a multiphase, multilayered scale; each layer grows in a parabolic rate with different rate constants. This steady-state scale development is often proceeded by the competitive processes of nucleation and growth of transient corrosion products dictating the mode and nature of subsequent scale growth.

Equilibrium thermodynamics, although not predictive, allow an assessment of the nature of the possible reaction products, whether or not significant evaporation or condensation of a given species is likely, and the conditions under which a given product can react with a condensed deposit. See the article "Thermodynamics of Gaseous Corrosion" in *ASM Handbook,* Volume 13A, 2003. The standard free energies of formation (ΔG°) of oxides and sulfides as a function of temperatures and the corresponding dissociation pressures of the oxides and sulfides are conveniently summarized in the form of Ellingham/Richardson diagrams, as illustrated in Fig. 1 and 2 (Ref 4). Along the ordinates are plotted values of ΔG° for the oxides and sulfides and of the partial molar free energy of oxygen and sulfur, while the temperature is plotted along the abscissa. The values of ΔG° refer to the standard free energies of formation of oxides and sulfides per mole of oxygen or sulfur, for example, $^4/_3Al + O_2 = {}^2/_3Al_2O_3$.

In an environment containing oxygen and sulfur, the following reactions need to be considered for a divalent metal, M:

$$M + {}^1/_2O_2 = MO \qquad \text{(Eq 1)}$$

$$M + {}^1/_2S_2 = MS \qquad \text{(Eq 2)}$$

The equilibrium oxygen and sulfur partial pressures are defined by the following relations:

$$p_{O_2}^{1/2} = \exp\left(\frac{\Delta G^\circ_{MO}}{RT}\right) \qquad \text{(Eq 3)}$$

$$p_{S_2}^{1/2} = \exp\left(\frac{\Delta G^\circ_{MS}}{RT}\right) \qquad \text{(Eq 4)}$$

Equations 3 and 4 allow the establishment of the conditions necessary for oxidation or sulfidation; however, a further reaction must be considered, namely:

$$MS + {}^1/_2O_2 = MO + {}^1/_2S_2 \qquad \text{(Eq 5)}$$

with the equilibrium condition:

$$p_{S_2}^{1/2}/p_{O_2}^{1/2} = \exp\left(\frac{\Delta G^\circ_{MS}}{RT} - \frac{\Delta G^\circ_{MO}}{RT}\right)\frac{a_{MS}}{a_{MO}} \qquad \text{(Eq 6)}$$

If unit activities are assumed for the phases MS and MO, Eq 6 can be reduced to:

$$p_{S_2}^{1/2}/p_{O_2}^{1/2} = \exp\left(\frac{\Delta G^\circ_{MS}}{RT} - \frac{\Delta G^\circ_{MO}}{RT}\right) \qquad \text{(Eq 7)}$$

Examination of Eq 3, 4, and 7 permits the identification of various limiting situations concerning the type of surface corrosion products that may be formed:

- If $(p_{O_2})_{gas} > (p_{O_2})_{eq}$ and $(p_{S_2})_{gas} < (p_{S_2})_{eq}$, then MO is the only stable surface phase.
- If $(p_{O_2})_{gas} < (p_{O_2})_{eq}$ and $(p_{S_2})_{gas} > (p_{S_2})_{eq}$, then MS is the only stable surface phase.
- If $(p_{O_2})_{gas} > (p_{O_2})_{eq}$ and $(p_{S_2})_{gas} > (p_{S_2})_{eq}$, then both MO and MS should be stable and form as surface products.

However, reference to Eq 7 indicates that only one phase will form, depending on which of the following conditions prevails:

- $(p_{S_2}/p_{O_2})_{gas} > (p_{S_2}/p_{O_2})_{eq}$. This condition will cause Eq 5 to proceed to the left, and MS will be the stable phase, where the metal is in contact with the gas.
- $(p_{S_2}/p_{O_2})_{gas} < (p_{S_2}/p_{O_2})_{eq}$. In this case, MO will be the stable phase, and Eq 5 will proceed to the right.

If the equilibrium partial pressures of the oxidants in the environment are known, a thermodynamic stability diagram can be constructed for a given temperature, as shown in Fig. 3 (Ref 5). Such a thermodynamic diagram gives the stability range for all relevant phases, in this case, metal, oxide, and sulfide, at a given temperature. The boundaries are calculated from thermodynamic data for the relevant reactions. The line between the oxide and sulfide remains unchanged by activity changes in the alloy. The corrosion conditions, that is, the oxygen and sulfur pressures in a given gas atmosphere, represent a point on the diagram.

The fields in the schematic thermodynamic stability diagram are indicated:

- A, metal is the only stable phase.
- B, oxide is the only stable phase.
- C, sulfide is the only stable phase.

It should be stated that although the gas equilibrium can be calculated readily for many gas mixtures at a given temperature and pressure, in many cases, even at temperatures as high as 1000 °C (1830 °F), gas equilibrium is not established. Furthermore, it should be noted that as soon as the metal surface is either partially or completely covered by the corrosion product, corrosion would then not be exclusively determined by thermodynamics. The kinetic factors, such as diffusivity of the different alloying elements and of the reactive species (oxygen, sulfur), as well as the morphological features of the scales formed significantly influence the degradation mechanisms of high-temperature corrosion. The analysis leading to this conclusion is based on the Wagner model (Ref 6) for the selective oxidation of an active element in a binary alloy to form a continuous external scale in the absence of transient oxidation. See the article "Kinetics of Gaseous Corrosion Processes," in *ASM Handbook,* Volume 13A, 2003. According to the Wagner theory, a continuous external layer of oxide should form on a binary (A-B) alloy when the solute concentration in the alloy exceeds a critical atom fraction (N_B^{crit}), as expressed as:

$$N_B^{crit} = \left\{\frac{\pi g^*}{3} N_O^{(S)} \frac{D_O V_m}{D_B V_{Ox}}\right\}^{1/2} \qquad \text{(Eq 8)}$$

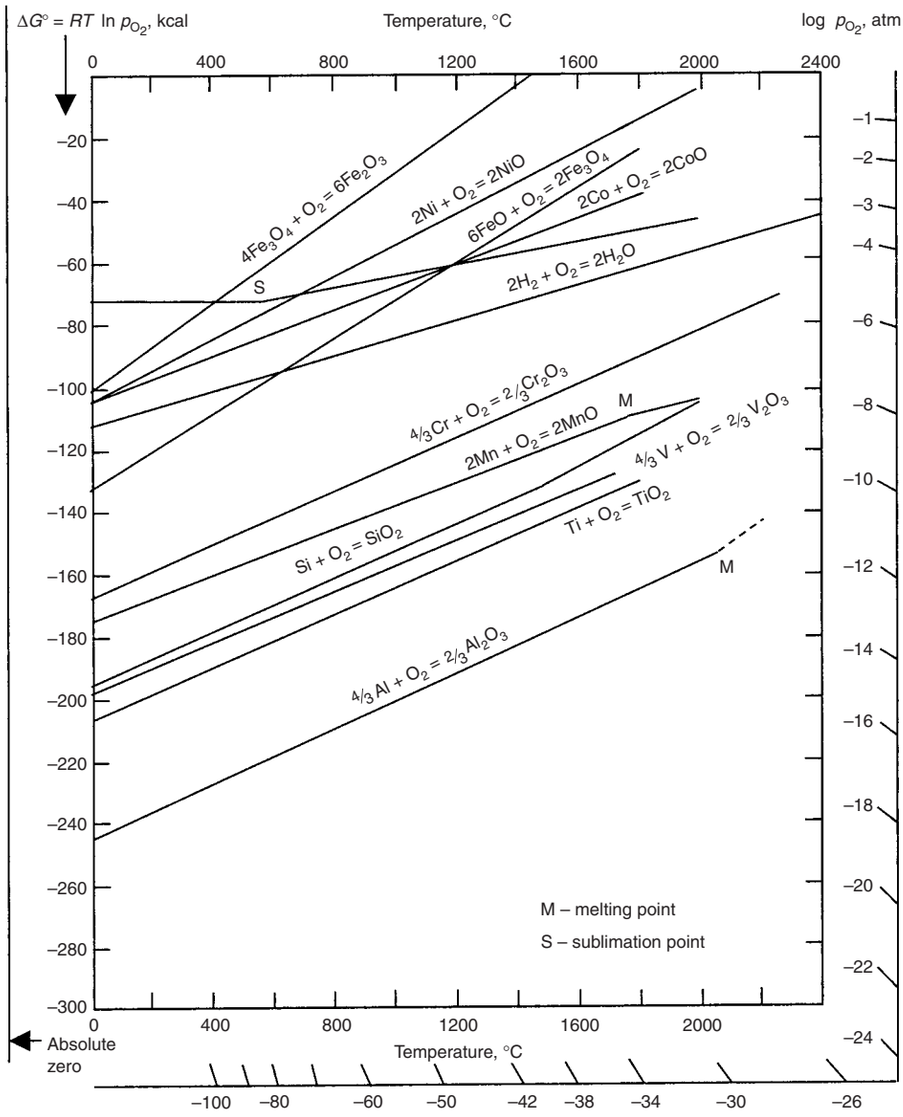

Fig. 1 Standard free energies of formation for selected oxides as a function of temperature and oxygen partial pressure. Source: Ref 4

where $N_O^{(S)}$ is the oxygen solubility in the alloy; D_O and D_B are the diffusivities of oxygen and solute in the alloy; V_m and V_{Ox} are the molar volumes of alloy and oxide, respectively; and g^* is the critical volume fraction of oxide scale. It is evident that if $N_O^{(S)}$ and D_O are very high, N_B^{crit} will also be high. If the ($N_O^{(S)}$) and/or (D_O) of oxygen in the alloy are reduced, the value of N_B^{crit} can also be significantly reduced. Long-term stability of the protective scale requires that the flux of solute to the alloy/scale interface remains large enough to prevent oxides of A from becoming stable. Pettit (Ref 7), for example, found that there are two critical concentrations for the formation of alumina scales on nickel-aluminum alloys: one value required for development of the alumina scale, and a larger value required for maintaining its stability.

When high-temperature alloys (usually based on nickel, cobalt, or iron) containing a number of elements are exposed to oxygen at elevated temperatures, oxidation may be anticipated in accordance with a design rationale. Thus, certain elements (such as chromium, aluminum, and silicon) with high affinities for oxygen may be expected to oxidize in preference to those derived from the base metals with high dissociation pressures. This process of selective oxidation is the concept for developing oxidation-resistant alloys (Ref 8–10). In particular, the composition of the alloy is chosen such that the stable oxide is the one that provides the most effective protective barrier. The oxides Cr_2O_3, Al_2O_3, SiO_2, and possibly BeO are of primary interest because they exhibit low diffusivities for both cations and anions and are also highly stable. Usually, alumina is an excellent barrier to oxygen at temperatures below 1300 °C (2370 °F), but at higher temperatures, oxygen permeation through silica occurs at a slower rate.

References 11 and 12 have a comprehensive review of the process of sulfidation. Compared to oxidation, sulfidation is characterized by faster kinetics and the formation of scales with complex defective morphologies. Sulfidation is particularly severe in high-p_{S_2} and low-p_{O_2} environments. Table 1 indicates the problems of designing sulfidation-resistant alloys and coatings. The parabolic rate constant (k_p) for the sulfidation of three elements, iron, cobalt, and nickel, that form the basis of many high-temperature oxidation-resistant alloys is typically 10^{-6} to 10^{-7} $g^2/cm^4/s$ at 640 to 800 °C (1180 to 1470 °F) and is several orders of magnitude higher than their oxidation k_p ($\sim 10^{-11}$ to 10^{-8} $g^2/cm^4/s$) at 800 to 1000 °C (1470 to 1830 °F). It is equally important to note that the k_p value for the sulfidation of chromium ($\sim 10^{-8}$ $g^2/cm^4/s$) at 750 °C (1380 °F) is significantly higher than that ($\sim 10^{-13}$ $g^2/cm^4/s$) at 800 °C (1470 °F) for the formation of Cr_2O_3, an important component in the development of many oxidation-resistant alloys. In contrast, the refractory metals (vanadium, molybdenum, niobium, and tungsten), together with zirconium and hafnium, display low rates of sulfidation. These elements, when incorporated in sulfidation-resistant materials, are likely to enhance the resistance to sulfidation, particularly under reducing conditions (Table 2).

Enhanced sulfidation resistance can be achieved by employing the same principles used in increasing the oxidation resistance of materials. The incorporation of appropriate elements into the base materials undergoing selective sulfidation leads to the development of a barrier layer capable of sustaining lower ionic transport rates. While selective sulfidation to form a

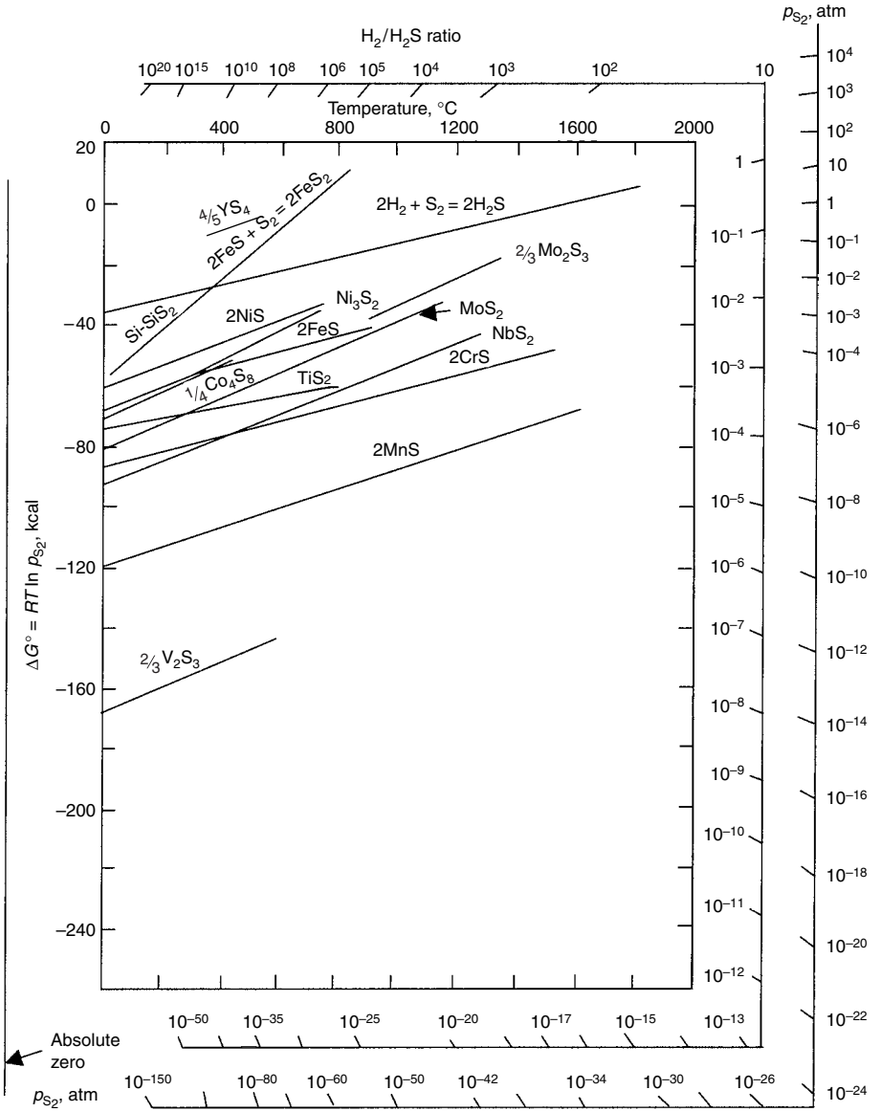

Fig. 2 Standard free energies of formation for selected sulfides as a function of temperature and sulfur partial pressure. Source: Ref 4

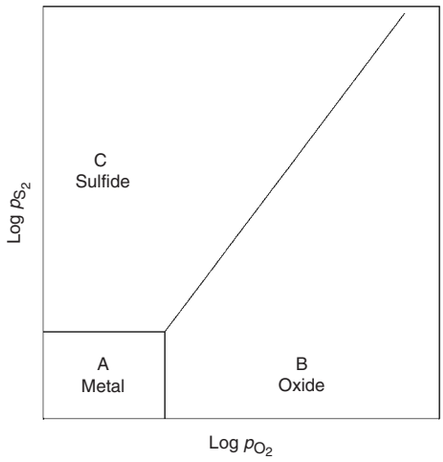

Fig. 3 Schematic of a thermodynamic stability diagram showing the stable ranges where oxide or sulfide can be formed at a given temperature. Source: Ref 5

sulfide barrier layer will be governed by the free energy of formation, the kinetics of this selective process, and hence the overall rate of sulfidation, will be controlled by the defect structure of the sulfides (Table 3), their ability to support fast or slow diffusion rates as measured by self-diffusion coefficients (Table 4), and the melting points and mechanical stability indicated by the Pilling-Bedworth ratio. See the article "High-Temperature Gaseous Corrosion" in *ASM Handbook,* Volume 13A, 2003.

Ni_3Al and NiAl

Figure 4 shows the binary NiAl phase diagram (Ref 13). NiAl possesses the ordered cubic B2 (cP2) CsCl crystal structure (Ref 1, 13). This structure exists over the composition range of 45 to almost 60 at.% Ni. NiAl is strongly ordered, even above 0.65 T_m (where T_m is the melting point), with an intrinsic disorder parameter of less than 5×10^{-3}. The B2 structure is stable for large deviation from stoichiometry, and significant long-range order has been reported. NiAl not only has the highest melting point of any compound in the NiAl system but also is the most stable. This high degree of thermodynamic stability and the existence of a wide phase field make NiAl relatively easy to fabricate in a range of forms, from fine homogeneous powders to single crystals.

For four decades, NiAl has been extensively studied as a potential structural material in the aerospace industry due to (Ref 1, 13):

- High melting point (1638 °C, or 2980 °F), as shown in Fig. 4, which is nearly 300 °C (540 °F) higher than the melting temperature of conventional superalloys
- Low density (5.35 to 6.50 g/cm^3); the density for the stoichiometric composition is 5.85 g/cm^3, roughly two-thirds that of typical nickel-base superalloys
- Good environmental resistance; the parabolic rate constant is very low, even in compositions with up to 60 at.% Ni, and is typically 2 orders of magnitude lower than for typical nickel-base superalloys
- High thermal conductivity
- Attractive modulus
- Metal-like properties above a modest ductile-to-brittle transition temperature
- Low raw materials cost
- Relatively easy processing (conventional melting, powder, metal forming)

However, two principal drawbacks exist for unalloyed NiAl: poor toughness and damage tolerance at room temperature, and inadequate strength and creep resistance at elevated temperatures.

Ni_3Al has an $L1_2$ ordered and face-centered cubic crystal structure (Ref 1) that can be maintained up to 1395 °C (2545 °F) (Fig. 4). Its unit cell contains four atoms, with three nickel

Table 1 Sulfidation and oxidation parabolic rate constants, k_p, of selected metals

	Sulfidation				Oxidation (p_{O_2} ~10^5 Pa)		
	Temperature				Temperature		
Metal	°C	°F	k_p, g^2/cm^4/s	p_{S_2}, Pa	°C	°F	k_p, g^2/cm^4/s
Al	500	930	1.0×10^{-12}	10^5	1000	1830	1.0×10^{-14}
Ti	750	1380	4.5×10^{-12}	10^{-1}	800	1470	3.3×10^{-10}
Zr	750	1380	2.7×10^{-12}	10^{-1}	800	1470	6.6×10^{-11}
Hf	750	1380	7.4×10^{-12}	10^{-1}	800	1470	3.3×10^{-11}
V	750	1380	2.3×10^{-10}	10^{-1}	...	...	Linear
Nb	750	1380	8.2×10^{-13}	10^{-1}	...	...	...
Cr	750	1380	1.9×10^{-8}	10^{-1}	800	1470	1.0×10^{-13}
Mo	750	1380	2.6×10^{-12}	10^{-1}	...	...	Linear
W	750	1380	2.0×10^{-9}	10^{-1}	...	...	Linear
Fe	800	1470	2.0×10^{-7}	10^5	800	1470	5.5×10^{-8}
Ni	640	1185	1.6×10^{-6}	10^5	1000	1830	9.1×10^{-11}
Co	800	1470	6.7×10^{-6}	10^5	900	1650	2.0×10^{-8}

Source: Ref 11

Table 2 Parabolic rate constants, k_p, of selected metals and alloys

	Temperature		Atmosphere, Pa		
Metal or alloy	°C	°F	p_{S_2}	p_{O_2}	k_p, g^2/cm^4/s
V	750	1380	10^{-1}	10^{-18}	2.3×10^{-10}
Nb	750	1380	10^{-1}	10^{-18}	8.2×10^{-13}
Mo	750	1380	10^{-1}	10^{-18}	2.6×10^{-12}
Fe-20Nb	700	1290	10^3	...	8.4×10^{-8}
Fe-30Nb	700	1290	10^3	...	3.5×10^{-8}
Ni-20Nb	700	1290	10^3	...	7.7×10^{-7}
Ni-30Nb	700	1290	10^3	...	1.3×10^{-7}
Co-20Nb	700	1290	10^3	...	1.6×10^{-7}
Co-30Nb	700	1290	10^3	...	5.9×10^{-8}
Fe-20Mo	700	1290	10^3	...	8.4×10^{-8}
Fe-30Mo	700	1290	10^3	...	3.5×10^{-8}
Ni-20Mo	700	1290	10^3	...	1.0×10^{-7}
Ni-30Mo	700	1290	10^3	...	1.5×10^{-8}
Co-20Mo	700	1290	10^3	...	4.4×10^{-8}
Co-30Mo	700	1290	10^3	...	2.0×10^{-9}
Co-20Cr-3.5Al-1Y-5V	750	1380	10^{-1}	10^{-18}	3.4×10^{-9}
Co-20Cr-3.5Al-1Y-5Nb	750	1380	10^{-1}	10^{-18}	3.1×10^{-9}
Co-20Cr-3.5Al-1Y-5Mo	750	1380	10^{-1}	10^{-18}	4.3×10^{-9}
Co-20Cr-3.5Al-1Y-5W	750	1380	10^{-1}	10^{-18}	8.9×10^{-9}
Co-20Cr-3.5Al-1Y-10V	750	1380	10^{-1}	10^{-18}	7.2×10^{-10}
Co-20Cr-3.5Al-1Y-10Nb	750	1380	10^{-1}	10^{-18}	1.8×10^{-9}
Co-20Cr-3.5Al-1Y-10Mo	750	1380	10^{-1}	10^{-18}	6.2×10^{-9}

Source: Ref 11

Table 3 Physico-chemical properties of sulfides of certain metals

	Pilling-Bedworth ratio	Defect structure	Melting point	
Sulfide			°C	°F
Al_2S_3	2.60	n-type	1099	2010
TiS_2	1.11	n-type	1999–2099	3630–3810
ZrS	1.91	n-type	1549	2820
HfS	...	...	2100–2273 (estimated)	3810–4123 (estimated)
V_2S_3	...	n-type	1799–1999	3270–3630
NbS_2	...	n-type	...	...
TaS_2	2.42	n-type	999	1830
Cr_2S_3	2.50 (CrS)	n/p-type	1550	2820 (CrS)
MoS_2	3.54	n-type	1457	2655
WS_2	3.47	n-type	>1800	>3270
FeS	2.50	p-type	1189	2172
Co_9S_8	2.37	p-type	1080	1975
NiS	2.50	p-type	796	1465

Source: Ref 11

Table 4 Self-diffusion coefficients (D_M) of cations in some metal sulfides and oxides

	Temperature		
Material	°C	°F	D_M, cm^2/s
Sulfide			
$Cu_{2+y}S$	650	1200	5.15×10^{-5}
$Co_{1-y}S$	720	1330	7.0×10^{-7}
$Ni_{1-y}S$	800	1470	1.4×10^{-8}
$Fe_{1-y}S$	800	1470	3.5×10^{-7}
Cr_2S_3	1000	1830	1.0×10^{-7}
Al_2S_3	600	1110	1.0×10^{-13}
Oxide			
$Cu_{2-y}O$	1000	1830	1.7×10^{-8}
$Co_{1-y}O$	1000	1830	1.9×10^{-9}
$Ni_{1-y}O$	1000	1830	1.0×10^{-11}
$Fe_{1-y}O$	800	1470	1.3×10^{-8}
Cr_2O_3	1000	1830	1.0×10^{-12}
Al_2O_3	1000	1830	1.0×10^{-16}

Source: Ref 11

atoms occupying face-centered positions and with one aluminum atom at corner positions. Ni_3Al has a homogeneous phase field of approximately 3 at.% around its stoichiometric composition, which is very important for alloy design. With off-stoichiometric compositions, antisite substitutions are formed on both nickel-rich and aluminum-rich sides of Ni_3Al. This is quite different from B2-NiAl, where antisite defects are stable in the nickel-rich side and vacancies are formed in the aluminum-rich side.

Oxidation. In the oxidation of nickel aluminides, Al_2O_3 grows in different modifications, depending on the oxidation temperatures. At lower temperatures and/or in the early stages of oxidation, the metastable oxides γ-Al_2O_3, δ-Al_2O_3, and θ-Al_2O_3 develop. These types of alumina contain a high concentration of cation vacancies. In the early stages of oxidation, the cubic oxides γ-Al_2O_3 and δ-Al_2O_3 have been observed on zirconium-doped NiAl (Ref 14). Later, they transform to the monoclinic θ-Al_2O_3 (Ref 15), and finally, the transformation to α-Al_2O_3 takes place (Ref 14–17). The cubic alumina modifications and their transformation to θ-Al_2O_3 were observed at lower temperatures (800 to 1000 °C, or 1470 to 1830 °F). The transformation to α-Al_2O_3 was observed at higher temperatures (1000 °C, or 1830 °F, and over).

The oxidation of NiAl generally results in the formation of a protective alumina surface scale. The formation of protective α-Al_2O_3 scale can be controlled by favorable alloying additions. The formation of pores and voids beneath the scale leads to a decrease in the area of coherence. Especially in NiAl with nickel excess, aluminum depletion by Al_2O_3 growth causes rapid diffusion of nickel into the material. Loss of nickel and aluminum beneath the scale leads to void nucleation and growth at the oxide/metal interface. Void formation also most probably occurs at other heterogeneities, for example, grain boundaries, which may allow oxygen ingress at grain boundaries, and intergranular oxidation of NiAl may occur. Intergranular oxidation can be followed or accompanied by internal oxidation of NiAl. NiAl with high aluminum content and multiphase alloys are much less susceptible to intragranular and internal oxidation attack (Ref 18).

It is found that the oxide scales forming on Ni_3Al at $T \geq 1000$ °C (1830 °F) in air consist of transiently equiaxed $NiO/NiAl_2O_4$ or γ-Al_2O_3 above a columnar α-Al_2O_3 protective layer (Ref 19–21). Thus, the steady-state oxidation mechanism is governed by transport through α-Al_2O_3 grain boundaries, although the results may vary depending on the oxidizing conditions (Ref 22, 23). The steady-state oxide scales formed on binary Ni_3Al are usually not adherent. Steady-state oxide scales are typically columnar-grained α-Al_2O_3. Temperatures below 1000 °C (1830 °F), low oxygen partial pressures (less than the NiO/Ni_3Al dissociation pressure), and high-humidity environments favor the formation of transition Al_2O_3 (Ref 19, 24).

The benefits of active element additions to NiAl are well documented in the literature (Ref 25–30). The inclusion of elements such as yttrium and hafnium will have a number of beneficial results, such as decreasing the oxide growth rate, decreasing voids at the oxide/substrate interface, increasing the mechanical properties of the oxide, and acting as sulfur getters. The effects of the ion implantation of yttrium on the oxidation behavior of β-NiAl after isothermal and thermal cycling at temperatures ranging from 1000 to 1300 °C (1830 to 2370 °F) is demonstrated in Ref 31. The use of ion implantation as a method of adding active elements has been reported to have several advantages over other processes. These include a decrease in segregation of the active elements to the grain boundaries of the substrate and the deposition of a thin layer onto the sample surface in the case of higher doses. At a level of 2×10^{14} Y^+/cm^2, the addition has been found to have little effect. However, at a level of 2×10^{16} Y^+/cm^2, the yttrium has been shown to promote the adherence of the alumina scale and to decrease the oxidation rate.

The effects of noble metals on the oxidation behavior of nickel aluminide coatings were extensively reported (Ref 32–34). Whether used as an environmental coating (Ref 35) or as a bond coat for thermal barriers (Ref 36, 37), platinum aluminides offer a higher level of protection than that afforded by standard aluminide coatings. This is due to the beneficial interaction between platinum and aluminum, which helps to promote and maintain the protective scale (Ref 38). First, a stable platinum oxide is not formed at the operating temperatures of the turbines (Ref 39), and second, aluminum is very mobile in platinum-rich phases, whereas other elements have to competitively diffuse relatively slowly to the oxide/coating interface (Ref 40). In essence, the platinum helps to create a reservoir of aluminum in the outer portion of the coating. This in turn promotes a more slowly grown, compact, and adherent alumina scale, which enables platinum aluminides to offer a greater level of protection in oxidizing and corrosive environments than standard aluminides (Ref 41). Palladium-modified aluminides have been reported to have better mechanical properties than platinum aluminides and yet still offer a comparable level of corrosion resistance (Ref 42), whereas the addition of rhodium is thought to increase both coating stability and oxidation resistance (Ref 43). However, the performance of iridium-modified aluminides has rarely been reported in the open literature. Iridium exhibits relatively low oxidation rates, compared to other refractory metals, and is known to have a low oxygen diffusivity (Ref 44). Iridium is less expensive than platinum, and investigations of IrAl intermetallics have found that they have potential as alumina formers (Ref 45, 46).

Sulfidation. The high-temperature sulfidation behavior of nickel aluminides has been shown to be strongly influenced by the alloy and gas compositions. The sulfidation behavior of four nickel-aluminum alloys containing 25 to 45 at.% Al studied (Ref 47) over the temperature range of 750 to 950 °C (1380 to 1740 °F) in a gas mixture of H_2/H_2S (0.1 to 10 vol%) has been reported to follow parabolic kinetics. Double-layered scales consisting of an outer layer of Ni_3S_2 and an inner layer of $NiAl_{3.5}S_{5.5}$ form on all alloys regardless of the aluminum content, indicating insignificant influence of aluminum content on sulfidation rate. However, the low oxygen partial pressure in $H_2/H_2S/H_2O$ mixtures has been shown to significantly influence the sulfidation behavior; severe attack by rapid internal oxidation destroys all the alloys except Ni25Al (25 at.% Al), with the internal oxidation zone consisting of a mixture of γ'-Ni_3Al and Al_2O_3. On the alloys containing 36 and 45 at.% Al, local attack occurs, with fast-growing pocks

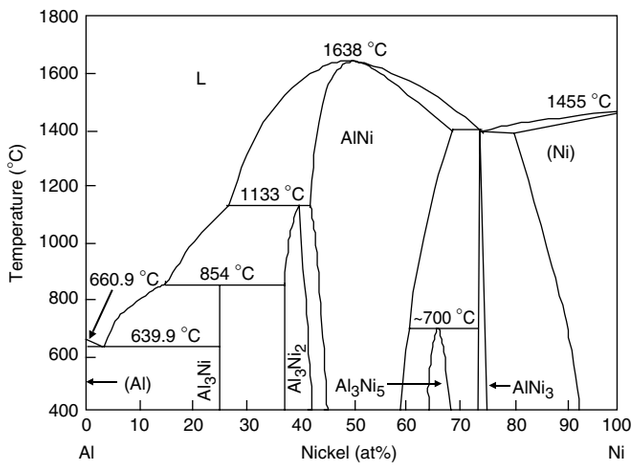

Fig. 4 The binary nickel-aluminum phase diagram

forming after an incubation period. An interruption of the H_2S gas flow stops internal oxidation; virtually no internal oxidation occurs in flowing H_2/H_2O atmospheres. These facts indicate that H_2S is essential for triggering and maintaining the internal oxidation of the nickel aluminides.

The effects of H_2S concentration on the sulfidation behavior of Ni_3Al at 875 °C (1605 °F) in several H_2/H_2S gas mixtures ranging from 0.16 to 4.7 vol% H_2S are demonstrated in Fig. 5 (Ref 3). Also shown for comparison are weight-change data for oxidation of the alloy in an air environment. The weight-change data indicate that at H_2S levels up to 0.75 vol%, the reaction rate follows a parabolic behavior, and at H_2S levels of 1.5 vol% or higher, the weight-change data exhibit accelerated corrosion. At low levels of H_2S (0.16 and 0.38 vol%) in the gas phase, the sulfidation rates become similar to the oxidation rates in an air environment. As the H_2S level increases, the sulfidation rate increases, and at ~1.5 vol% H_2S, liquid Ni-Ni_3S_2 eutectic forms, and accelerated corrosion ensues. At a H_2S level of 4.7 vol%, the calculated rate constant for sulfidation is 8.7×10^{-10} $g^2/cm^4/s$, which is ~4 orders of magnitude larger than the rate constant for the oxidation of the alloy. At higher sulfur levels, the weight-change curves show an accelerated rate for longer times, due primarily to a decrease in the reaction surface area produced as the reaction front advances deeper into the alloy.

Hot corrosion studies of the NiAl intermetallics are very few. An investigation of hot corrosion (Ref 48) on a Ni_3Al alloy at 605, 800, and 1000 °C (1120, 1470, and 1830 °F) demonstrates the significant effect of temperature. The specimens coated with 1 ± 0.1 mg/cm^2 of Na_2SO_4-Li_2SO_4 and then exposed to a 1% SO_2/air gas mixture have indicated highest weight gain at 1000 °C (1830 °F) and least weight gain at 800 °C (1470 °F). It is proposed that NiO oxide formation consumes oxygen in the molten salt. The consumption of oxygen locally reduces the oxygen potential and increases the sulfur partial pressure in the molten salt. As the sulfur partial pressure reaches the equilibrium partial pressure region of NiS_x and/or AlS_x, NiS_x and/or AlS_x forms at the salt/alloy interface through sulfidation reaction. The consumption of sulfur decreases the sulfur potential, and oxygen partial pressure increases in the molten salt. This leads to the formation of NiO again. This mechanism also suggests that NiO and NiS_x and/or AlS_x are produced simultaneously. Because the produced sulfide is thermodynamically unstable when the oxygen potential increases, it is possible for the sulfides to convert into oxides (NiO, Al_2O_3, and $NiAl_2O_4$) through the necessary reactions. There are two possibilities for the formation of spinel phase, which is produced either through the reaction of aluminum and nickel with oxygen in the molten salt or through the evolution of sulfides.

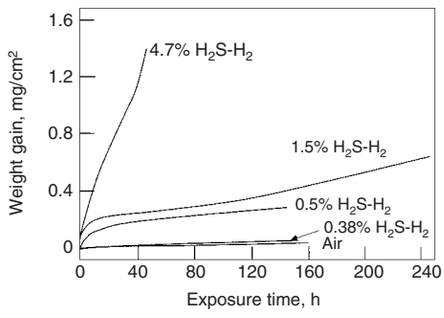

Fig. 5 Thermogravimetric test data for sulfidation of Ni_3Al at 875 °C (1605 °F). Source: Ref 3

Fe_3Al and FeAl

The iron aluminides, mainly Fe_3Al and FeAl, are of interest for many land-based applications because of their appropriate mechanical properties, ease of fabrication, excellent oxidation and corrosion resistance, conservation of strategic elements, low density, and low cost. Moreover, FeAl is characterized to possess good resistance to catalytic coking, carburization, sulfidation, and wear. Therefore, iron aluminides are being developed for use as structural materials and/or as cladding for conventional engineering alloys. Figure 6 presents the phase diagram of the iron-aluminum binary system (Ref 1). In the iron aluminide system, the alloys of interest are of composition Fe_3Al and FeAl. It is reported (Ref 3) that the crystal structure of Fe_3Al is $D0_3$ or B2, while FeAl has the B2 structure. The melting point temperatures of Fe_3Al and FeAl are 1520 and 1250 °C (2770 and 2280 °F), respectively, and densities are 6.72 and 5.56 g/cm^3, respectively. However, the Young's modulus values for Fe_3Al and FeAl are 140.6 and 260.4 GPa (20 and 38×10^6 psi), respectively, and the stiffer intermetallic has a tendency to be much more brittle. Their tensile strength also compares favorably with many ferritic and austenitic steels. However, Fe_3Al and FeAl are susceptible to environmental embrittlement in the presence of water vapor, although the degree of sensitivity of Fe_3Al appears to be less than FeAl. Limited ductility at ambient temperatures and a sharp drop in strength at above 600 °C (1110 °F) have been major deterrents to their acceptance for many structural applications.

Oxidation of FeAl-base intermetallic alloys usually shows different behavior in air and oxygen atmospheres (Ref 49); the oxidation rates of Fe-37Al oxidized in ambient air are higher than in oxygen at 1000 to 1200 °C (1830 to 2190 °F), with a double-layered oxide scale forming on the surface of Fe-37Al specimens during oxidation. In the case of air oxidation, the outer layer consists of convoluted whiskers of α-Al_2O_3, while the inner layer is comprised of $Al_2O_3 + AlN$. A convoluted α-Al_2O_3 layer with the inner layer consisting of Al_2O_3 is the result of oxidation in pure oxygen. It is believed that the nitrogen ions in Al_2O_3 and the growth of whisker oxides cause an increase of the oxidation rate in air.

Doping with yttrium, zirconium, and yttrium + zirconium has a strong influence on the

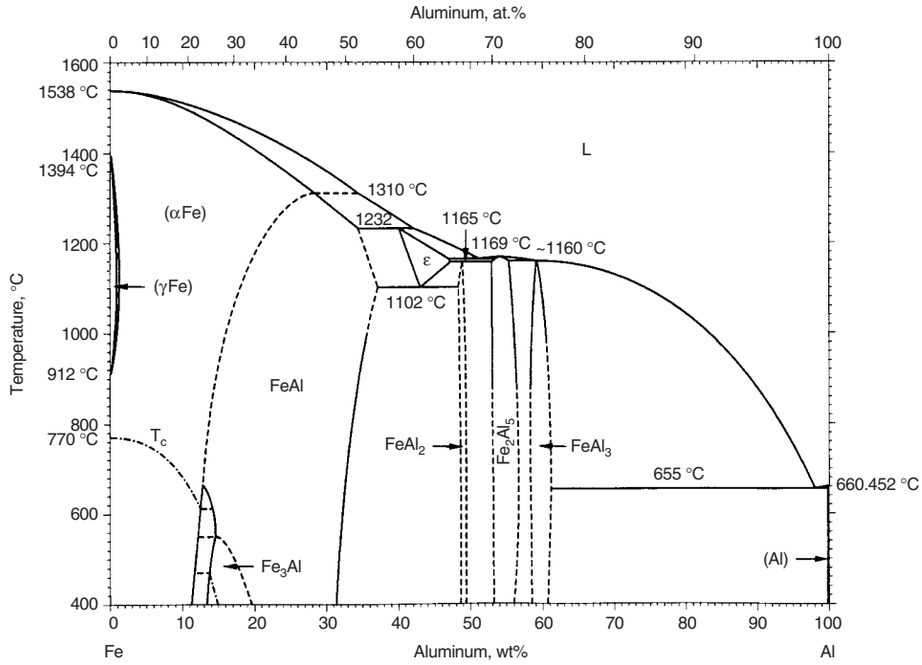

Fig. 6 The binary iron-aluminum phase diagram. Source: Ref 1

oxidation kinetics of Fe-37Al intermetallics. Yttrium additions to Fe-37Al decrease the oxidation rates at 1000 to 1200 °C (1830 to 2190 °F). Fe-37Al-0.1Y-0.2Zr revealed lower oxidation rates at 1100 and 1200 °C (2010 and 2190 °F) than Fe-37Al but not at 1000 °C (1830 °F). Fe-37Al with zirconium demonstrated higher oxidation rates than Fe-37Al. Fe-37Al-0.8Zr exhibits a lower oxidation rate at 1100 and 1200 °C (2010 and 2190 °F) than Fe-37Al-0.3Zr. The effects of the reactive elements on the isothermal oxidation of Fe-37Al can be classified into different groups. The compact oxide scale formed on the doped Fe-37Al reduces the oxidation rate. Reactive elements form special oxides that have faster growth rates than the aluminum oxides. Furthermore, reactive elements, such as yttrium or yttrium + zirconium, increase the transformation temperature of θ-Al_2O_3 to α-Al_2O_3. The scale growth on undoped FeAl is influenced by the cation and anion short-circuit diffusion. The scale growth on doped FeAl is controlled mainly by anion short-circuit diffusion. The oxide grain size has been observed to have significant effects on the effective diffusion coefficient of the scales formed on the undoped Fe-37Al but not on the yttrium-doped Fe-37Al alloys (Ref 50, 51). The results obtained from the studies of oxidation kinetics of the intermetallic phase β-FeAl in the temperature range of 800 to 1100 °C (1470 to 2010 °F) (Ref 52) demonstrate that at temperatures >900 °C (1650 °F), the initially formed metastable aluminum oxides are converted to adherent and slow-growing α-Al_2O_3 scales.

Parabolic kinetics after a period of transient θ-Al_2O_3 scale formation characterizes the oxidation behavior of Fe-40Al-1Hf, Fe-40Al-1Hf-0.4B, and Fe-40Al-0.1Zr-0.4B (at.%) alloys at 900, 1000, and 1100 °C (1650, 1830, 2010 °F) (Ref 53). The isothermally grown scales are associated with a propensity toward massive scale spallation due to both extensive rumpling from growth stresses and an inner layer of HfO_2. Spallation in cyclic oxidation for 200 one-hour cycles produced little degradation at 900 or 1000 °C (1650 or 1830 °F), but caused significant spallation at 1100 °C (2010 °F) in the form of small segments of the outer scale. The major difference in the cyclic oxidation of the three FeAl alloys mentioned previously is increased initial spallation for FeAl + zirconium and boron. Although these FeAl alloys indicate many similarities to NiAl alloys, they are generally less oxidation resistant. It is believed that this stems from the presence of nonoptimal levels of dopants and larger thermal-expansion mismatch stresses.

It is reported (Ref 54) that the addition of a reactive element (RE)—yttrium (usually) and/or hafnium—significantly improves the oxide adherence of Fe_3Al over the range of temperature from 900 to 1100 °C (1650 to 2010 °F) for up to 240 h. Without RE additions, the Al_2O_3 scales developed on Fe_3Al alloys become convoluted, with the growth of the oxide scale being controlled by a mixed-diffusion mode of aluminum and oxygen transport. Reduced aluminum diffusion and the formation of a flat scale growing mainly by the inward transport of oxygen are associated with adding REs, especially yttrium. The reduction in the transport of aluminum in RE-doped Fe_3Al alloys, reducing the Fe_3Al alloy rate of oxidation, probably stems from the segregation of the RE to the scale/alloy interface. Extensive intergranular oxidation of the yttrium-containing Fe_3Al alloys has been observed, probably due to the segregation of yttrium (not hafnium) to the alloy grain boundaries. The detrimental effect of excessive hafnium content on the oxide growth is believed to be due to the formation of hafnium-rich oxide particles facilitating inward scale growth, leading to the formation of localized oxide-thickening "pegs" and the eventual formation of less protective oxide, especially under thermal cycling.

Sulfidation. The results obtained from the sulfidation experiments conducted on several sets of iron aluminides at temperatures between 400 and 1000 °C (750 and 1830 °F) (Ref 55) are shown in Fig. 7, giving thermogravimetric data for ternary iron aluminide tested in a 1.35 vol% H_2S/H_2 gas mixture at 650, 875, and 1000 °C (1200, 1605, and 1830 °F). Also shown in the figure are data for type 310 stainless steel oxidized in air at 1000 °C (1830 °F) and sulfidized in the 1.35 vol% H_2S/H_2 gas mixture at 875 °C (1605 °F). Figure 8 shows some scanning electron micrographs of surfaces of Fe_3Al and type 310 stainless steel specimens after sulfidation. The temperature dependence of the morphologies of surface sulfides on the Fe_3Al probably results from the variable thermodynamic activity of sulfur in the exposure environment, with the activity being lowest at 1000 °C (1830 °F) and highest at 650 °C (1200 °F) (H_2S concentration in the gas was kept constant). In the scales on the Fe_3Al consisting of (Fe,Al) sulfides and iron sulfides, the relative proportion of the former to the latter decreases with decreased temperature. The scale on the type 310 stainless steel is predominantly (Fe,Cr) sulfides with some nodules of iron sulfide.

Comparative studies have been conducted on the sulfidation resistance of Fe_3Al and several chromia- and alumina-forming alloys in oxygen/sulfur mixed-gas environments (Ref 55, 56). Thermogravimetric studies on oxidation of iron-base alloys with differing aluminum concentrations and Fe_3Al alloys show that a minimum aluminum level of 12 wt% is needed to develop a continuous alumina scale that is resistant to sulfur attack. A detailed comparison has been made of the corrosion performance of alumina- and chromia-forming alloys exposed to oxygen/sulfur mixed-gas environments.

The results obtained from the high-temperature corrosion behavior of FeAl (42 at.% Al) intermetallics in a mixture gas (95% N_2 + 5% H_2) plus 1% H_2S at 600 °C (1110 °F) show excellent corrosion resistance for FeAl in this atmosphere; the mass gain of FeAl remains <0.15 mg/cm^2 after exposure to the atmosphere for 90 h at 600 °C (1110 °F). The depth profile of x-ray photoelectron spectroscopy analysis indicates the formation of the double-layered scale: a layer of a mixture of FeS and Al_2O_3 on the top surface and an Al_2O_3 layer on the bottom (Ref 57).

The corrosion behavior of Fe-28Al and Fe-18Al-10Nb (at.%) over the temperature range of 700 to 900 °C (1290 to 1650 °F) in a $H_2/H_2S/H_2O$ gas mixture with varying sulfur partial pressures of 10^{-2} to 10^3 Pa and oxygen partial pressures of 10^{-19} to 10^{-15} Pa is characterized, in general, by parabolic kinetics, although two-stage kinetics are noted in some cases. The steady-state parabolic rate constants increase with increasing temperature. Based on the equivalent addition (28 at.%) of alloying elements, Fe-18Al-10Nb exhibits a better corrosion resistance, being approximately 2 to 4 orders of magnitude lower than Fe-28Al (depending on temperature). The scales formed on Fe-28Al consist of mostly FeS, α-Al_2O_3, and minor $FeAl_2S_4$, while the scales formed on Fe-18Al-10Nb consist of mostly α-Al_2O_3, Nb_3S_4, Nb_2O_5, and minor Fe_xNbWS_2 ($FeNb_2S_4/FeNb_3S_6$) at $T \leq 800$ °C (1470 °F) and of α-Al_2O_3, Nb_3S_4, and Fe_xNbS_2 at 900 °C (1650 °F). Significantly reduced corrosion rates follow the formation of Al_2O_3 and Nb_3S_4 (Ref 58, 59).

The minimum aluminum concentration needed to resist sulfidation and oxidation in $H_2S/H_2/H_2O$ environments was established in Ref 60; alloys containing ≥18% Al are uniquely resistant to H_2S-containing environments at 800 °C (1470 °F). Chromium adversely affects the corrosion resistance in this mixed-gas environment, although this effect is partially offset by the addition of molybdenum. Zirconium and yttrium have no significant influence on the corrosion rate under the same temperature and environmental conditions. Investigations (Ref 61) on the effects of yttrium, hafnium, and yttrium + hafnium on the sulfidation behavior of Fe_3Al at 900 °C (1650 °F) in a $H_2S/H_2/H_2O$ environment demonstrate that additions of the RE confer significantly increased sulfidation resistance

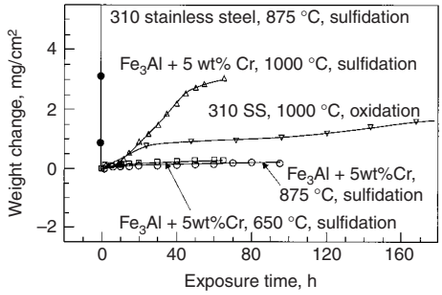

Fig. 7 Thermogravimetric test data for chromium-containing Fe_3Al exposed to 1.35 vol% H_2S/H_2 gas mixture at 650, 875, and 1000 °C (1200, 1605, and 1830 °F). Also shown are data for oxidation (at 1000 °C, or 1830 °F) and sulfidation (at 875 °C, or 1605 °F) for type 310 stainless steel. Source: Ref 3

to Fe_3Al. However, the combined addition of yttrium + hafnium compromises the benefit to the sulfidation-resistance enhancement. It is interesting to note that a superlattice of MnS formed on the sulfidized Fe_3Al with the addition of yttrium and hafnium, as revealed in Fig. 9.

Hot Corrosion. Important information on the hot corrosion behavior of FeAl intermetallics comes from the studies on binary iron aluminide, Fe-25Al (at.%), at 827, 952, and 1057 °C (1521, 1746, and 1935 °F) (Ref 62). The results obtained from hot corrosion studies conducted by coating the specimen surfaces with 2.5 ± 0.2 mg/cm^2 of Na_2SO_4 prior to exposure in pure oxygen show parabolic rate constants. The faster kinetics in the initial stages of oxidation are thought to be related to the formation of θ-Al_2O_3 and the slower kinetics in the later stages of oxidation to the formation of α-Al_2O_3, with the overall rate of hot corrosion being higher than that of oxidation at all the temperatures. The presence of α-Fe_2O_3 in addition to alumina is indicated by x-ray diffraction (XRD) analysis of the scales present on the surface of the samples after hot corrosion. Fourier transform infrared spectra from the spalled scales in hot corrosion divulge the presence of α-Al_2O_3, α-Fe_2O_3, and sulfate. Cross-sectional microscopy reveals pitted metal/scale interfaces in hot corrosion conditions, with the pits containing aluminum sulfide. Sulfides are also identified along the grain boundaries in the intermetallic near the scale/metal interface.

Ti_3Al and TiAl

Recent research and development efforts on Ti_3Al and TiAl ordered intermetallics, which are potential candidates for the structural materials in aerospace and automobile industries, have resulted in considerable improvement in their mechanical and metallurgical properties. The binary titanium-aluminum phase diagram is given in Fig. 10. Intermetallic materials with improved properties—superior specific stiffness and strength—over conventional titanium-base alloys in the intermediate temperature range of 600 to 800 °C (1110 to 1470 °F) have been developed. Among other properties, high-temperature strength (up to 800 MPa, or 116 ksi, ultimate tensile strength at 700 °C, or 1290 °F), creep resistance (typically primary ~1% strain after 500 h), and fatigue resistance (typically 480 MPa, or 70 ksi, runout following turning, and 730 MPa, or 106 ksi, after high-speed milling) make γ-titanium aluminides ideal materials for weight-critical components subject to medium temperatures (up to 800 °C, or 1470 °F)/fluctuating stress. The main advantage for the use of γ-TiAl is weight saving, because it is typically half the density of alternative nickel-base superalloys. High stiffness (~130 GPa, or 19×10^6 psi, at 700 °C, or 1290 °F) is a further advantage (Ref 63, 64). The maximum useful service temperature for γ-TiAl appears to be limited to 800 °C (1470 °F) today; however, future applications are targeting operating temperatures >800 °C (1470 °F). At these temperatures, titanium aluminides will be subjected to severe environmental attack, particularly oxidation during service. Clearly, to achieve such enhanced high-temperature capability, it is essential to devise strategies based on alloy development and/or protective coating design. Such strategies must be underpinned by a thorough understanding of the corrosion behavior of these intermetallics.

Oxidation behavior of TiAl and TiAl-base materials displays a complex pattern (Ref 65–68). The formation of a slow-growing, adherent, and protective Al_2O_3 scale is much more difficult in TiAl intermetallics than in disordered titanium-aluminum alloys and in NiAl (Ref 69, 70).

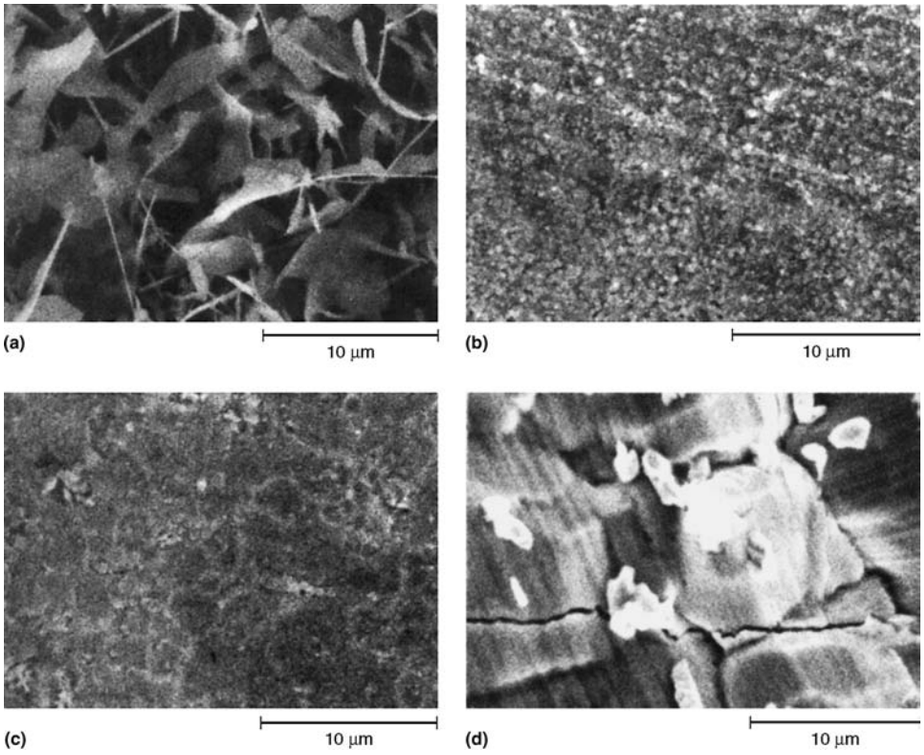

Fig. 8 SEM micrographs of surface of Fe_3Al and type 310 stainless steel after sulfidation exposure to a H_2/1.35 vol% H_2S gas mixture. Fe_3Al at (a) 650 °C (1200 °F), (b) 875 °C (1605 °F), and (c) 1000 °C (1830 °F); (d) type 310 stainless steel at 875 °C (1605 °F). Source: Ref 3

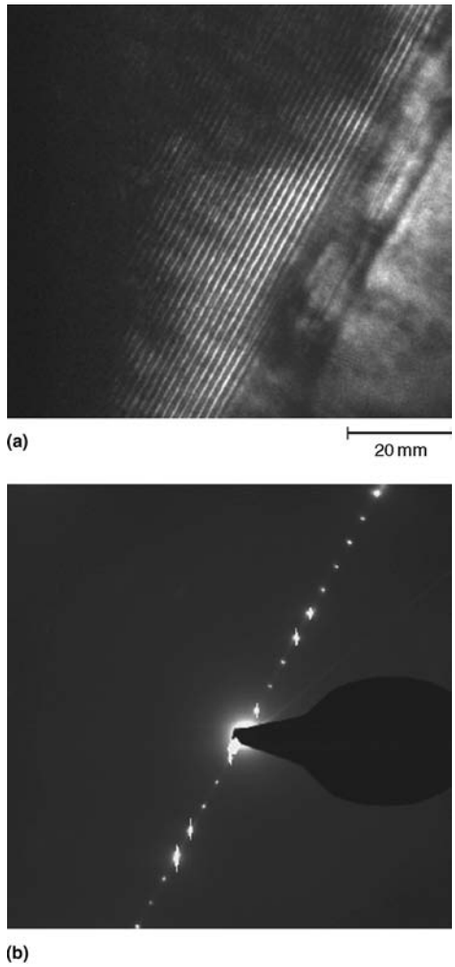

Fig. 9 Superlattice layer formed on the sulfidized Fe_3Al + yttrium-hafnium alloy in a $H_2/H_2S/H_2O$ environment at 900 °C (1650 °F) for 240 h. (a) Dark-field image. (b) Electron diffraction pattern. Source: Ref 61

The difficulty in the development of Al_2O_3 scale in TiAl intermetallics is associated with the retardation in the selective oxidation of aluminum. The thermodynamic imperative in promoting the formation of both titanium and aluminum oxides leads to the development of scale layering comprised of $TiO_2/Al_2O_3/TiO_2$. The number of layers formed is influenced by temperature, time, and the partial pressure of oxygen.

In order to understand the oxidation mechanisms from a fundamental point of view, the authors (Ref 71) have carried out nanoscale studies of the early stages of the oxidation behavior of TiAl, allowing nanoscale information on the scaling processes to be obtained. A two-stage strategy was used. The first stage involved scanning tunneling microscopy (STM)/scanning tunneling spectroscopy (STS) investigations of TiO_2(110)-(1 by 1) surface in order to establish "fingerprints" for the identification of the products formed during oxidation of TiAl. In the second stage, a TiAl intermetallic alloy was studied by STM/STS after repeated sputtering and heating (to provide ideal surfaces) in both low- and high-oxygen potential environments. For TiO_2, it was found that the oxygen vacancies produced created additional defect states in the band gap of stoichiometric TiO_2 (Fig. 11b). This state can be taken as the fingerprint for the reduced TiO_2 surface, indicating the presence of Ti_2O_3. The energy for this state, estimated from the STS measurement, is in agreement with previous results (Ref 71).

Following oxidation at room temperature with 100 Langmuir oxygen, the TiAl surface, with well-developed terraces, ledges, and kinks, shows islands of oxides of nanometer size and monolayer height (Fig. 11a). The tunneling spectroscopy results recorded on these islands show the semiconducting character and peaks at ~1 eV below the Fermi level (SS) on the normalized tunneling conductance dI/dV curves (Fig. 11b). This curve resembles the curve obtained for TiO_2 where surface states (SS) were created due to the formation of Ti_2O_3. Thus, the curves in Fig. 11(b) confirm the nucleation of Ti_2O_3 in a low-oxygen-pressure environment and clearly show that oxidation of TiAl begins with the formation of Ti_2O_3. Surface morphology of the TiAl alloy after exposure to a high-(atmospheric) oxygen-potential environment is shown in Fig. 12(a). The current/potential (I/V) curve recorded on this surface (Fig. 12b) reveals asymmetric shape and shows that the tunneling current is higher for the positive polarization of the sample than for the negative voltage of the same value. Furthermore, a well-defined suppression of the tunneling current, that is, presence of the $I(V) \approx 0$ region in the −1.5 to 0.8 eV energy range, is observed. This type of asymmetry and suppression of the tunneling current can be explained by the presence of TiO_2 material on the surface as amorphous TiO_2 and can be regarded as a 3 eV band-gap binary oxide (suppression of the tunneling current), with the Fermi level shifted toward the valence band (asymmetry of the tunneling current) (Ref 71). Such fundamental information is essential to studying the initial stages of scale growth and explaining the rapid diffusion observed during the onset of oxide nucleation.

Exposure of Ti_3Al alloys to oxygen at high temperature leads to both oxidation and dissolution in the alloy. High oxidation resistance would be expected if a protective Al_2O_3 layer could be formed by selective oxidation. However, Al_2O_3 is only slightly more stable than TiO, and the activity of titanium is much higher than that of aluminum in Ti_3Al (Ref 72). Thus, TiO is the stable oxide in contact with Ti_3Al, and further oxidation leads to nonprotective formation of rutile, TiO_2. The oxidation behavior is complex, leading to a layered oxide scale structure with TiO_2 on the outside and oxides with higher metal content underside, including Al_2O_3 (Ref 73). Besides scale formation at the surface, oxygen diffuses into Ti_3Al as a solute, because Ti_3Al has a comparatively high solubility for oxygen. This leads to embrittlement, increased strength, decreased ductility, and crack formation at the surface (Ref 74).

Molybdenum, tantalum, and niobium increase the oxidation resistance to such an extent that the

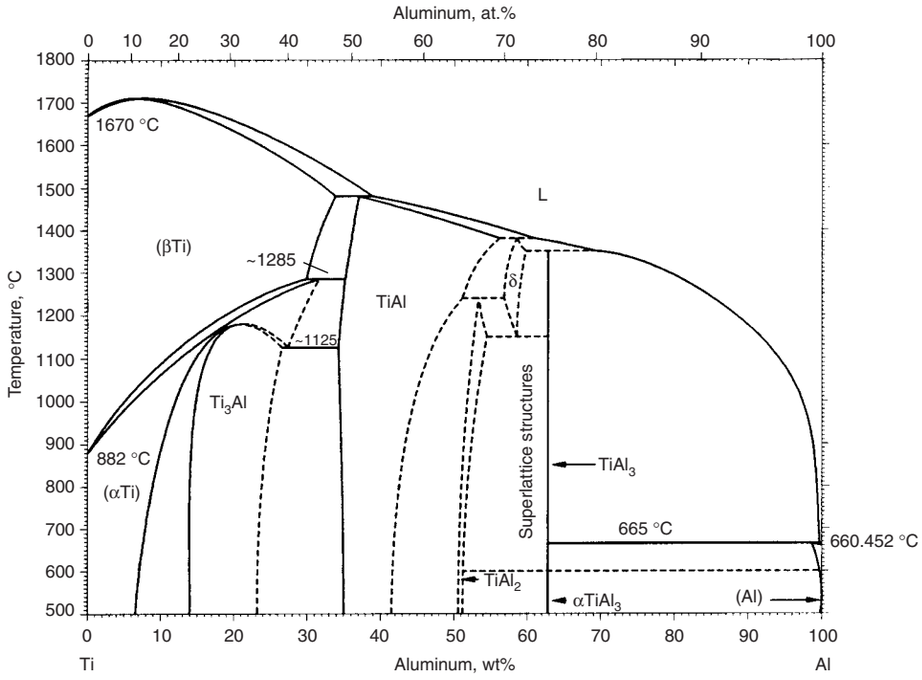

Fig. 10 The binary titanium-aluminum phase diagram

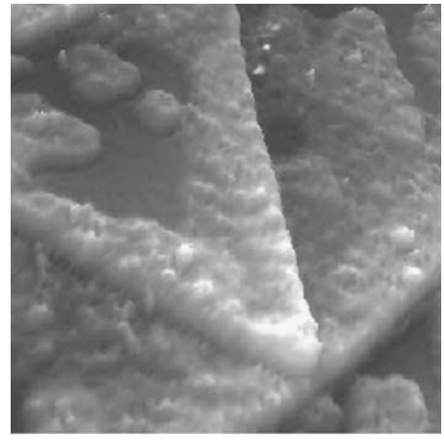

(a)

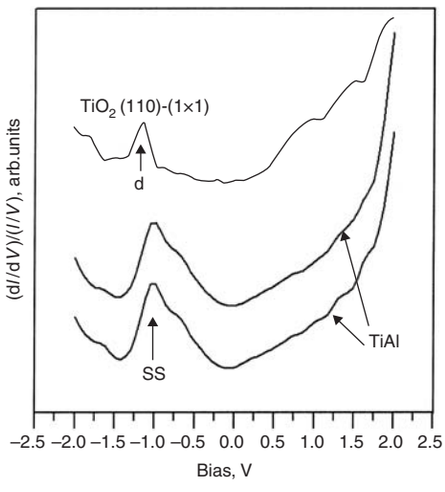

(b)

Fig. 11 (a) 175 nm × 175 nm scanning tunneling microscopy topography and (b) (dI/dV)/(I/V) curves for TiAl after exposure to environment with 100 Langmuir oxygen (1 Langmuir is 10^{-6} torr · s) SS, surface state. Source: Ref 71

obtained rate constants are intermediate between those of TiO_2 and Al_2O_3 formers (Ref 75). The obtained oxidation resistances remain too low and limit the application of Ti_3Al-base alloys at high temperature. Therefore, coating of these alloys is necessary.

The oxidation resistance of γ-TiAl is higher than α_2 due to the higher aluminum content but still orders of magnitude lower than that of Al_2O_3 formers. The oxidation resistance of TiAl relies on the formation of a protective Al_2O_3 layer that is only slightly more stable than TiO, with further oxidation producing nonprotective rutile. Thus, oxidation is a problem for TiAl alloys that have been optimized with respect to mechanical behavior.

The majority of the studies on oxidation behavior of TiAl intermetallics involved experiments in air. In general, it is found that faster oxidation kinetics are promoted in air than in oxygen (Ref 76–81). In Ref 82, the oxidation behavior of Ti-52Al (at.%) at 900 °C (1650 °F) in various atmospheres, including air and pure oxygen gas and also in oxygen mixed with different (2, 10, 90, 98, and 100%) nitrogen-containing atmospheres, was studied, and it was concluded that while a protective alumina scale was developed in pure O_2, the nitrogen-containing atmospheres do not promote the formation of a continuous alumina scale; instead, intermixed TiO_2/Al_2O_3 nodules are detected. The density of these nodules has been found to increase with increasing nitrogen concentration in the reactive atmosphere. Reference 83 attributes the fast oxidation of TiAl in air to nitridation. The mechanism by which nitrogen adversely affects the oxidation behavior is still not yet satisfactorily understood. In contrast, the oxidation results of titanium-aluminum in Ref 84 in air and Ar/O_2 atmospheres show beneficial effects of nitrogen for Ti-48Al-5Nb at 900 °C (1650 °F). The enhancing effect of nitrogen was attributed to the elimination of internal oxidation of the niobium-containing alloy, which has been found to occur during exposure in Ar-20%O_2. However, in the same study at 900 °C (1650 °F), the detrimental effect of nitrogen was also observed for Ti-50Al.

Using commercial gases (O_2, Ar-21%O_2, Ar-1%O_2, He-1%O_2, and argon containing impurities such as CO_2, N_2, H_2O, and H_2), the influence of the partial pressure of oxygen on the oxidation behavior of γ-TiAl was studied. The results show the lowest oxidation at 1000 °C (1830 °F) in pure O_2 and then increasing with decreasing oxygen partial pressure (Ref 85). The observed oxidation kinetic results in argon showing the highest mass gain at the same exposure temperature can be attributed to the presence of other oxidants present in the argon, such as CO_2, H_2, and H_2O. In fact, the rapid increase of the weight gain of the experimental material in the argon atmosphere probably stems from the presence of water vapor (H_2O). Such results are not consistent with those obtained from other studies on the effects of the partial pressures of oxygen (Ref 86). The oxidation rate of TiAl-V in pure oxygen has been found to be higher than in Ar-1%O_2 at 900 °C (1650 °F). The investigation of transport processes indicates the formation of protective Al_2O_3 increasing with the increase of oxygen partial pressure in the reactive atmosphere.

It is possible to predict the alloying element concentration, the temperature, and the oxygen partial pressure of the atmosphere in which preferential oxidation of the alloying element can initially occur, provided that appropriate thermodynamic data are available. An oxidation mechanism has been proposed by the authors (Ref 87) for the oxidation of an intermetallic alloy, Ti-46.7Al-1.9W-0.5Si, in air at 750 to 950 °C (1380 to 1740 °F). The minimum activities of titanium and aluminum required to form the relevant TiO_2 and Al_2O_3 can be calculated if the oxygen partial pressure (0.21 atm) and experimental temperatures (750, 850, and 950 °C, or 1380, 1560, and 1740 °F) are known. The free energies of formation (joule/mole) for TiO_2 and Al_2O_3 (Ref 88) are given by:

$$\Delta G^{\circ}_{T,TiO_2} = -910{,}000 + 173\,T \qquad \text{(Eq 9)}$$

$$\Delta G^{\circ}_{T,Al_2O_3} = -1{,}676{,}000 + 320\,T \qquad \text{(Eq 10)}$$

where T is the experimental temperature in Kelvin. The calculated results of minimum activities of aluminum and titanium to form Al_2O_3 and TiO_2 are listed in Table 5. Detailed calculations for the titanium-aluminum binary system (Ref 89) show that the activity of titanium is slightly higher than the aluminum activity in the Ti-46.7Al-1.9W-0.5Si alloy. It appears that the addition of tungsten and silicon does not significantly alter the situation concerning the activity of titanium and aluminum. Thus, the preferential formation of TiO_2 is predicted during exposure to both environments. The discontinuous nature of the TiO_2 layer at the early stages of oxidation, observed in this study, may be attributed to the two-phase nature of the microstructure of the alloy, which implies that the activities of titanium and aluminum varied depending on the location of the phases on the alloy surface, and it was difficult for TiO_2 to form in certain areas.

During the initial exposure of the Ti-46.7Al-1.9W-0.5Si alloy to air at the experimental temperatures, the high oxygen partial pressure promotes the formation of TiO_2, according to the reaction:

$$Ti(s) + O_2(g) = TiO_2(s) \qquad \text{(Eq 11)}$$

The formation of TiO_2 changes the balance of the activities of titanium and aluminum and the oxygen partial pressure between the TiO_2 layer and the substrate. The reduction of titanium activity then leads to the development of an Al_2O_3 layer:

$$2Al(s) + {}^3/_2O_2(g) = Al_2O_3(s) \qquad \text{(Eq 12)}$$

This development of an Al_2O_3 layer in turn leads to the formation of a titanium-enriched zone

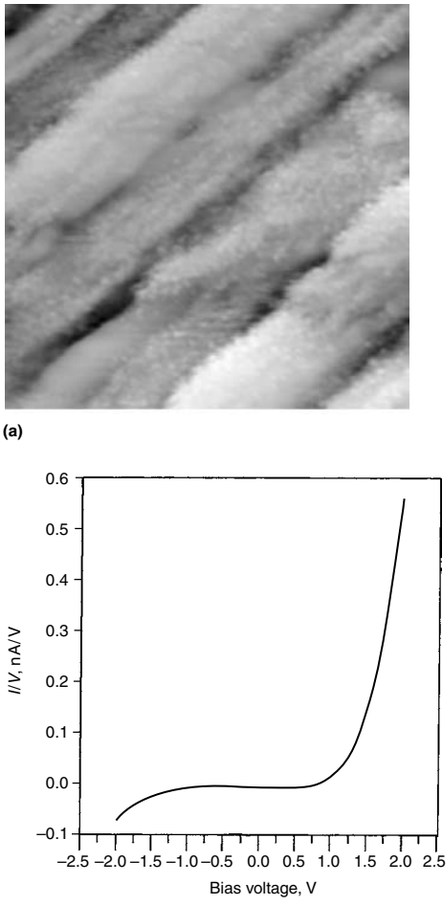

Fig. 12 (a) 300 nm × 300 nm scanning tunneling microscopy topography and (b) *I/V* curve for oxidized TiAl after exposure to atmospheric environment. Source: Ref 71

Table 5 The minimum activities of titanium and aluminum to form TiO_2 and Al_2O_3

0.21 atm of oxygen partial pressure at temperatures given

		Activity, minimum		
Metal	**Symbol**	**750 °C (1380 °F)**	**850 °C (1560 °F)**	**950 °C (1740 °F)**
Aluminum	a_{Al}	1.19×10^{-34}	7.72×10^{-31}	1.18×10^{-27}
Titanium	a_{Ti}	1.77×10^{-37}	2.44×10^{-33}	7.05×10^{-30}

beneath the Al_2O_3 layer. At the same time, nitrogen migrates through the Al_2O_3 layer to this titanium-enriched zone from the external atmosphere, which creates a favorable circumstance for the following reaction to take place:

$$Ti(s) + {}^1/_2N_2(g) = TiN(s) \qquad \text{(Eq 13)}$$

Thus, a TiN layer is formed beneath the Al_2O_3 layer. In the meantime, oxygen species also diffuse inward to the interface between the Al_2O_3 layer and the TiN layer, allowing a buildup of the oxygen partial pressure. When the oxygen partial pressure reaches a certain level, TiN became unstable, favoring the following reaction:

$$TiN(s) + O_2(g) = TiO_2(s) + {}^1/_2N_2(g) \qquad \text{(Eq 14)}$$

The released nitrogen migrates inward via the TiN layer. The nitrogen partial pressure gradually increases at the TiN/substrate interface, and the nitrogen species, encountering titanium from the substrate, allows the reaction (Eq 13) to take place again. This gives rise to the formation of a titanium-depleted zone, demonstrated by the existence of a $TiAl_2$ band beneath the TiN layer. The oxidation mechanisms of the Ti-46.7Al-1.9W-0.5Si alloy in air are schematically described in Fig. 13. It is apparent that the thickness of the TiO_2 layer increases with exposure time, as does the thickness of the TiN layer as nitrogen migrates inward from the external environment. However, it is not clear why AlN does not develop between the TiN and $TiAl_2$ band, because the affinities of aluminum and titanium to nitrogen are very close (Ref 88). This can probably be attributed to the faster self-diffusion of titanium in the TiAl substrate than that of aluminum (Ref 90); TiN became the kinetically favored product.

Sulfidation. Information on the high-temperature sulfidation behavior of titanium-aluminum intermetallics is not extensive. Some work has been reported on the response of titanium-aluminum-base materials, such as Ti-54Al and Ti-48Al-2Nb-2Mn, after exposure at 900 °C (1650 °F) to mixed-gas environments with a fixed p_{O_2} (10^{-14} Pa) and with p_{S_2} values of 0.0016, 0.11, and 1.6 Pa (Ref 91). The results from this study indicate parabolic kinetics at all p_{S_2} values for sulfidation of the alloys. After some uncertainties at the early stages of sulfidation, prolonged exposure (168 h at 900 °C, or 1650 °F) indicates that the greatest resistance to sulfidation occurs at the highest p_{S_2} (Fig. 14, 15).

In the initial stages of exposure, the high affinity of oxygen for titanium and aluminum leads to development of an outer layer of TiO_2, beneath which an Al_2O_3 layer forms. Sulfur diffuses through the TiO_2 and Al_2O_3 layers and reaches the substrate/scale interface, where the p_{O_2} is low enough to promote the formation of TiS_2 and Al_2S_3 (and NbS_2 in the case of Ti-48Al-2Nb-2Mn). Clearly, the presence of high p_{S_2} in the bulk environment provides a higher driving force for sulfur migration that then supports a higher sulfur flux and favors the formation of sulfides of alloy constituents. Accordingly, a mixed layer of sulfides and oxides develops in the high-p_{S_2} atmosphere, thicker than in the low-p_{S_2} environment, thereby providing higher resistance to sulfidation.

In summary, the superior sulfidation resistance of Ti-54Al and Ti-48Al-2Nb-2Mn can be ascribed to several aspects of the scaling processes. First, the development of an inner layer of sulfides (TiS_2, Al_2S_3, NbS_2) provides an effective barrier to cation transport. The presence of refractory metal sulfide, NbS_2, is known to cause significant improvement in the sulfidation resistance of the intermetallic alloy (Ref 92). Furthermore, sulfidation resistance of Ti-54Al stems from the formation of a $TiAl_3$ layer at the scale/substrate interface by the diffusion of titanium after the development of TiO_2 and TiS_2. Titanium released from the dissociation of TiS_2 is likely to promote a thick $TiAl_3$ layer, thus imparting further resistance to sulfidation.

The oxidation/sulfidation behavior of another intermetallic alloy, Ti-56.6Al-1.4Mn-2Mo, with duplex and lamellar microstructure has been investigated by the authors (Ref 93) in $H_2/H_2S/H_2O$ ($p_{S_2} = 0.1$ Pa; $p_{O_2} = 10^{-12}$ Pa) at 750 °C (1380 °F) and ($p_{S_2} = 0.1$ Pa; $p_{O_2} = 10^{-14}$ Pa)

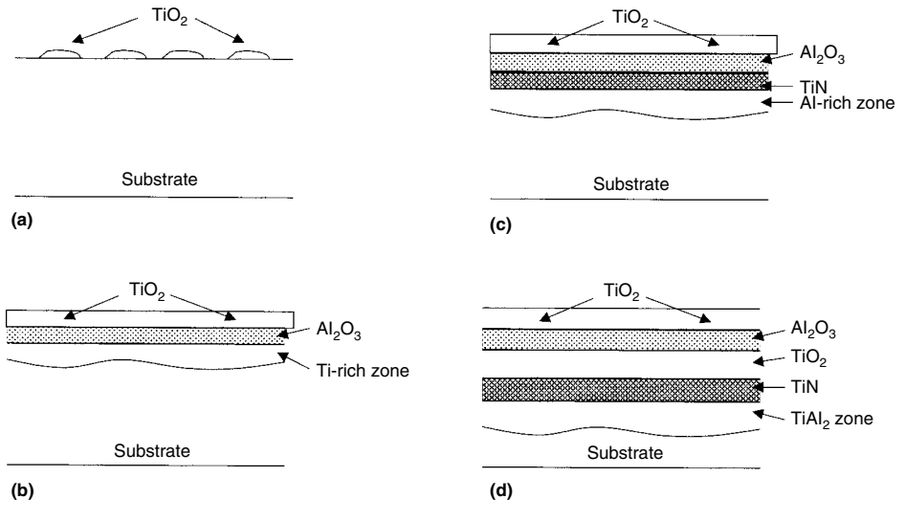

Fig. 13 Schematic illustration of the mechanism controlling oxidation of Ti-46.7Al-1.9W-0.5Si in air between 750 and 950 °C (1380 and 1740 °F). (a) Islands of TiO_2 form. (b) Al_2O_3 layer and titanium-rich zone form, and TiO_2 grows. (c) TiN layer develops in titanium-rich zone, and aluminum-rich zone forms. (d) TiN layer oxidizes and shifts inward, and TiO_2 and Al_2O_3 layers and $TiAl_2$ zone grow. Source: Ref 87

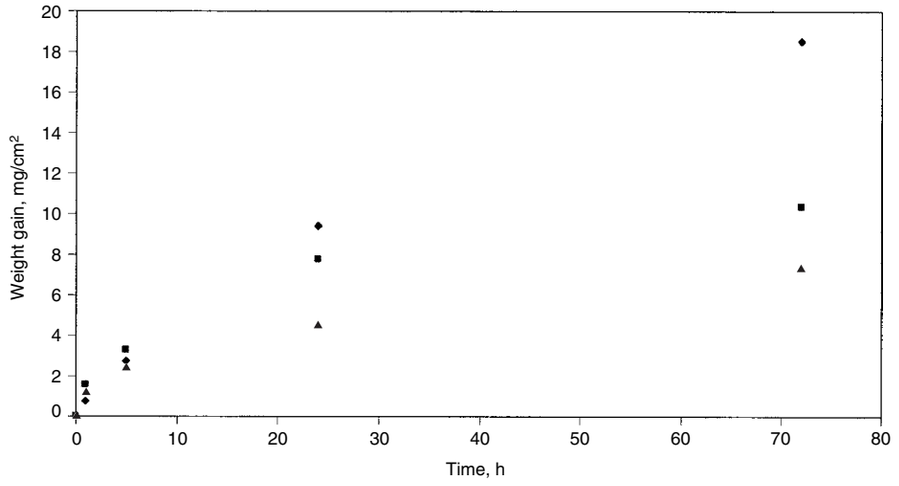

Fig. 14 Sulfidation kinetics for Ti-54Al at 900 °C (1650 °F) for three mixed gases. Partial pressure (p_{O_2}), 10^{-14} Pa. Partial pressures (p_{S_2}): diamond, 0.0016 Pa; square, 0.11 Pa; triangle, 1.6 Pa. Source: Ref 91

at 900 °C (1650 °F). The results of weight-gain/time data show parabolic kinetics ($k_p = 10^{-12}$ g^2/cm^{-4}/s) at 750 °C (1380 °F) and cubic kinetics at 900 °C (1650 °F) and the absence of significant effect on the corrosion behavior of increased exposure temperature, with scaling pattern development resembling that of the Ti-Al-Nb-Mn alloy, that is, with an outermost TiO_2/inner Al_2O_3 layer and base-element sulfides forming between the oxide layers and the substrate.

The enhanced corrosion resistance observed at 900 °C (1650 °F) compared to that at 750 °C (1380 °F) follows from the differences in the defect structures. Both oxygen vacancies and interstitial titanium ions are important point defects (Ref 8), with interstitial titanium ions predominating at low p_{O_2}, and high temperature, whereas oxygen vacancies predominate at high p_{O_2} and low temperature. At low p_{O_2}, many interstitial titanium ions are expected in TiO_2, and hence, an increase in p_{O_2} would result in a decreased number of interstitial ions. Reducing the interstitial titanium ions would decrease the transport of titanium through TiO_2. The temperature change between 750 and 900 °C (1380 and 1650 °F) may not significantly alter the diffusion of titanium and oxygen ions in these alloys. The increased oxygen pressure will increase the oxygen vacancies in TiO_2 and thereby increase the inward diffusion of oxygen and promote Al_2O_3, imparting a slow corrosion rate for both materials.

Further work by the authors (Ref 94) on the oxidation and sulfidation behavior of Ti-46.7Al-1.9W-0.5Si alloy in an $H_2/H_2S/H_2O$ atmosphere yielding high sulfur ($p_{S_2} \sim 1.2 \times 10^{-1}$ Pa) and low oxygen ($p_{O_2} \sim 1.2 \times 10^{-15}$ Pa) potentials at 850 °C (1560 °F) shows protective kinetics with a parabolic rate constant of 6×10^{-11} g^2/cm^4/s. Morphological analysis reveals the development of a multilayered scale consisting of a top rutile (TiO_2) layer, a continuous layer of α-Al_2O_3 beneath the rutile layer, and a TiS layer containing scattered pure tungsten particles. It is suggested that fast outward diffusion of titanium within the substrate results in the formation of a zone of high concentration of aluminum ($TiAl_3$ and $TiAl_2$) between the scale and substrate, as illustrated in Fig. 16.

Work by the same group (Ref 95) has been successful in increasing the sulfidation resistance of TiAl by the deposition of high-aluminum-concentration titanium aluminide (e.g., $TiAl_3$). The oxidation/sulfidation kinetics data of uncoated and $TiAl_3$-coated Ti-46.7Al-1.9W-0.5Si in a $H_2/H_2S/H_2O$ atmosphere at 850 °C (1560 °F) show increased high-temperature corrosion resistance of the Ti-46.7Al-1.9W-0.5Si alloy by the $TiAl_3$ coating. Both coated and uncoated samples underwent oxidation/sulfidation following a parabolic rate law with parabolic rate constants of 2.38×10^{-13} g^2/cm^4/s and 7.36×10^{-11} g^2/cm^4/s, respectively. It is indicated that the deposition of the $TiAl_3$ coating increases the corrosion resistance of Ti-46.7Al-1.9W-0.5Si by more than 2 orders of magnitude.

Hot corrosion behavior of TiAl-base materials is discussed by considering the response of three titanium-aluminum intermetallics—Ti-48Al, Ti-48Al-2Cr, and Ti-52Al—to exposure to 80 wt% $Na_2SO_4 + 20$ wt% NaCl-containing environments at 800 °C (1470 °F). Hot corrosion and scale spallation took place during the 200 h tests. Ti-52Al showed the best corrosion resistance among the three alloys. It is believed that the high aluminum content and single γ-TiAl phase played a role, forming an aluminum-rich oxide scale with relatively good protective ability. Ti-48Al-2Cr also showed better corrosion resistance than Ti-48Al. The latter suffered a high corrosion rate and severe scale spallation. Three different exposure methods were used to study hot corrosion in salt-containing environments. These represent different service conditions. Among these methods, suspending the specimens in salt vapor appeared to be the most reliable method for kinetic studies. The influential factors are relatively easy to control. When using the salt-deposition method, the spallation of the salt film at the early stage needs to be considered. The immersion method showed the severest hot corrosion. Crucible materials and corrosion products dissolve into the molten salts, further complicating the reactions (Ref 96).

Hot corrosion tests (Ref 97) on Ti_3Al, Ti-44Al, Ti-48Al, Ti-52Al, Ti-48Al-2Cr, and Ti_3Al-11Nb (at.%) intermetallics were conducted in a salt mixture of 80 wt% $Na_2SO_4 + 20$ wt% NaCl with a melting point of approximately

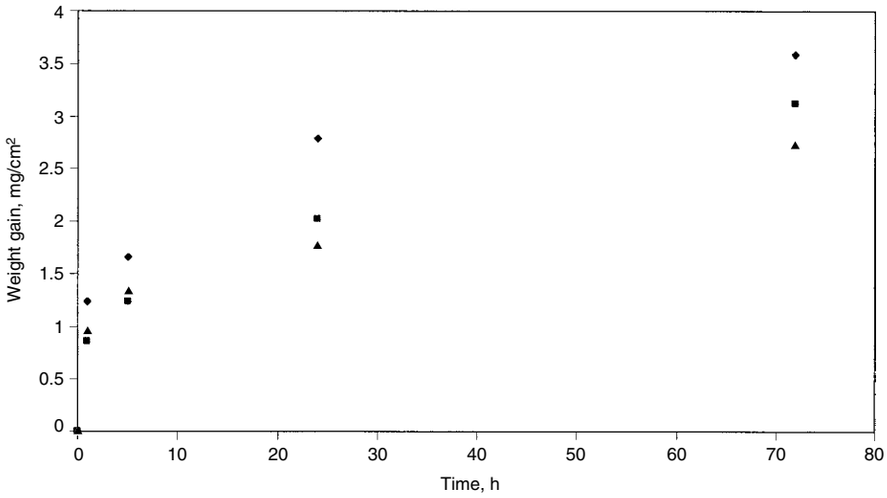

Fig. 15 Sulfidation kinetics for Ti-48Al-2Nb-2Mn at 900 °C (1650 °F) for three mixed gases. Partial pressure (p_{O_2}), 10^{-14} Pa. Partial pressure (p_{S_2}): diamond, 0.0016 Pa; square, 0.11 Pa; triangle, 1.6 Pa. Source: Ref 91

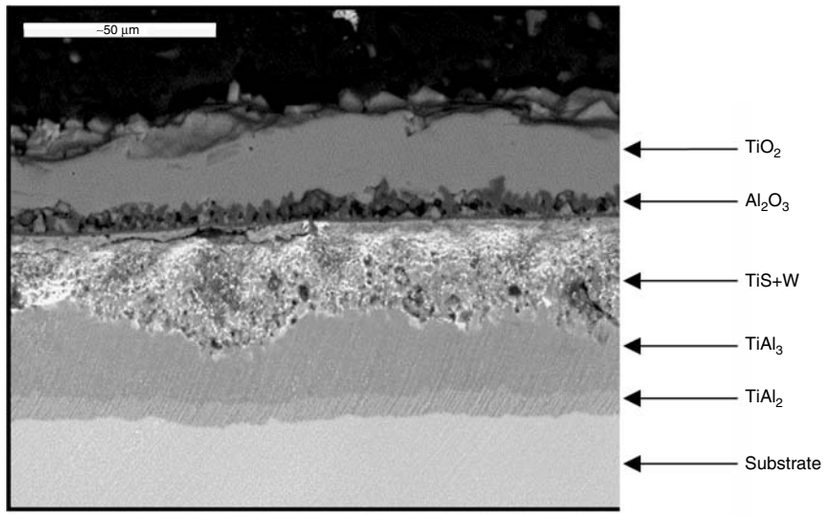

Fig. 16 SEM micrograph for exposed Ti-46.7Al-1.9W-0.5Si in $H_2/H_2S/H_2O$ atmosphere at 850 °C (1560 °F) for 240 h. Source: Ref 94

700 °C (1290 °F). The specimens were suspended in the salt vapor at 800 °C (1470 °F). It was found that the hot corrosion resistance generally increased with increasing aluminum content. Ti-48Al-2Cr showed the best corrosion resistance due to its relatively high aluminum content and chromium addition. Ti_3Al-11Nb unexpectedly showed poor corrosion resistance. It is suggested that the niobium addition may accelerate the formation of sulfide at the interface, playing a detrimental role in the corrosion process.

The effect of reactively sputtered Al_2O_3 and enamel coatings on oxidation and hot corrosion behaviors of TiAl was investigated at 900 °C (1650 °F). Isothermal oxidation testing indicated that both coatings were very effective in reducing the oxidation rate of γ-TiAl. Cyclic oxidation testing indicated that reactive-sputtered Al_2O_3 coating had little effect in improving the cyclic oxidation resistance of TiAl due to the spallation of Al_2O_3 coating. However, enamel coating exhibited an excellent positive effect on cyclic oxidation of TiAl. The enamel coating was very adherent to the substrate, and neither cracks nor spallation appeared in the coatings during cyclic oxidation. Furthermore, the hot corrosion behavior of TiAl with enamel coating was evaluated in $(Na,K)_2SO_4$ melts at 900 °C (1650 °F). The results showed that the enamel coating was very stable in $(Na,K)_2SO_4$ melts and was very effective in protecting TiAl from hot corrosion attack (Ref 98).

The hot corrosion behavior of Ti-50Al, Ti-48Al-2Cr-2Nb, and Ti-50Al-10Cr alloys was investigated in $(Na,K)_2SO_4$ and $Na_2SO_4 + NaCl$ melts (Ref 99). TiAl intermetallics showed much better hot corrosion resistance in $(Na,K)_2SO_4$ at 900 °C (1650 °F) than the nickel-base superalloy K38G. Two types of corrosion products formed on Ti-50Al: Some areas were covered with a continuous Al_2O_3 scale, whereas other areas formed a mixed $Al_2O_3 + TiO_2$ scale; TiS existed at the scale/alloy interface. A mixed $Al_2O_3 + TiO_2$ scale developed on Ti-48Al-2Cr-2Nb, and no sulfide was found beneath the scale. An adherent Al_2O_3 scale, however, formed on Ti-50Al-10Cr, which provided excellent hot corrosion resistance. All three alloys suffered severe hot corrosion in $Na_2SO_4 + NaCl$ melts at 850 °C (1560 °F). A mixed $Al_2O_3 + TiO_2$ scale was generated on all three alloys, and many voids and pits existed in the scale/alloy interface.

Silicides

Silicides form an important class of structural intermetallics, so their high-temperature corrosion response is of interest. High-temperature capabilities of silicides are much higher than those of aluminides, allowing working temperatures greater than 1400 °C (2550 °F). Such operating temperatures are needed for improving the thermal efficiency and reliability of energy-conversion systems and advanced engine systems (Ref 100). The use of currently available alloys, such as nickel-base single-crystal superalloys, is limited to temperatures of ~1100 °C (2010 °F). Superalloys derive their intrinsic strength by reinforcement with γ'-Ni_3Al precipitates, but these tend to coarsen and ultimately dissolve as the temperature increases beyond 1100 °C (2010 °F). Aluminide alloys based on NiAl, which are currently under development, have the potential for use up to 1200 °C (2190 °F). The melting temperature (T_m) of a material for structural applications at 1400 °C (2550 °F) needs to be >2000 °C (3630 °F), so that, at most, 0.75 T_m is reached during service, and appreciable high-temperature strength is maintained. Of the available potential systems, refractory silicides, such as $MoSi_2$ and $NbSi_2$, are widely recognized as potential structural and coating materials because of their high melting points, good mechanical strength, high thermal and electrical conductivities, and promising oxidation resistance at elevated temperature due to the formation of a self-passivating, glassy silica (SiO_2) layer. However, the use of silicides for high-temperature applications poses problems. The problems associated with the oxidation of silicides are well known, and so far, there have been limited studies on the sulfidation of silicides.

Oxidation. Molybdenum silicides ($MoSi_2$ and Mo_5Si_3) possess excellent oxidation resistance at >1000 °C (1830 °F). However, it was observed (Ref 101–103) that $MoSi_2$ showed accelerated oxidation behavior, resulting in so-called "pesting" in the temperature range between 400 and 650 °C (750 and 1200 °F), whereby the $MoSi_2$ disintegrates to powder. The pest degradation is associated with dissociative oxidation to form SiO_2 and MoO_3. The MoO_3 vapor pressure begins to increase within the pest degradation temperature regime such that much of the MoO_3 formed tends to sublime with time as temperatures increase. The poor oxidation resistance of molybdenum is generally assumed to be due to the instability of its related oxide phase (MoO_3). However, niobium appears to be less critically limited in this respect. Nb_2O_5 is nonvolatile below 1370 °C (2500 °F) (Ref 104); therefore, the latter would be expected to, and indeed does, perform relatively well under oxidizing conditions.

A great deal of research has been conducted worldwide to achieve protective oxidation of molybdenum silicides by the addition of a third element, such as aluminum, boron, germanium, tungsten, tantalum, titanium, zirconium, or yttrium (Ref 105–108). All of these elements form oxides that are more stable than SiO_2, and it is thought that the effect of their scavenging for oxygen may accelerate the scaling process of SiO_2 and thereby prevent or minimize molybdenum oxide formation. The addition of these elements, aluminum in particular, reportedly reduces pesting by the formation of an amorphous Mo-Si-Al-O phase in the initial cracks and voids (Ref 107). However, the growth rates for the oxides of any of these third element additions (at low concentration) are fairly low and comparable to that of MoO_3 and may not fully minimize pesting attack for molybdenum silicides at low temperature. The protectivity of $NbSi_2$ in oxidizing environments may be compromised by the simultaneous formation of SiO_2 and Nb_2O_5 due to the high solubility of oxygen in $NbSi_2$ and the close affinities of silicon and niobium for oxygen.

Sulfidation. A comprehensive review of the sulfidation behavior of intermetallics (Ref 100) found the Mo_5Si_3-type intermetallics in a 1.5 vol% H_2S/H_2 gas mixture and compared the sulfidation resistance with relevant oxidation performance in air. Figure 17 shows the thermogravimetric test data obtained at several temperatures for oxidation and sulfidation of a boron-containing Mo_5Si_3. The data imply a protective scaling of the alloy at 500 °C (930 °F) under oxidizing conditions, not because of SiO_2 formation, but because the volatilization rate of molybdenum oxide is negligible. At temperatures of 800 and 1200 °C (1470 and 2190 °F), the curves demonstrate a sharp drop in specimen weight for ~2 h, after which a plateau is reached and the weight changes little during 50 h of additional exposure, indicating a protective scale. The morphology of the scale after oxidation at 800 °C (1470 °F) has been observed to consist of a light-colored MoO_2 phase and a dark gray silicon-rich oxide; the scale after oxidation at 1200 °C (2190 °F) consists predominantly of silicon-rich oxide and almost pure molybdenum particles. The surface layer shows significant cracking and peeling and appears to remain highly plastic, as indicated by curling rather than spalling of the oxide layer. Such degradation of the oxide layer can expose interior molybdenum silicide to additional oxidation, and the sequential processes of oxidation and peeling can continue without offering oxidation protection for the alloy over long periods of exposure. The thermogravimetric test data obtained during sulfidation of the material reveal an approximately one order of magnitude smaller decline in specimen weight than in the data obtained during oxidation. It is not clear as to the cause for the initial drop in weight, except that the possible presence of residual moisture in the gas mixture can lead, in the early stages of exposure, to the formation of volatile oxides such as MoO_3 and/or SiO (especially in the reducing condition used in the experiments) before the development of sulfide reaction products. Figure 18 provides scanning electron micrographs of surfaces of boron-containing Mo_5Si_3 alloy after sulfidation at 500, 800 and 1100 °C (930, 1470, and 2010 °F) in a 1.5 vol% H_2S/H_2 gas mixture. After exposure at 500 °C (930 °F), the specimen surface shows isolated regions of molybdenum sulfide but no gross oxidation. After 800 °C (1470 °F) exposure, the specimen exhibits a greater coverage of the surface with molybdenum sulfide, whereas after exposure at 1100 °C (2010 °F), it shows almost complete coverage by molybdenum sulfide. These preliminary results indicate that the intermetallic

material based on molybdenum silicide can develop protective sulfide scales during service in reducing environments at elevated temperatures.

Recently, the sulfidation behavior of $CrSi_2$, WSi_2, $NbSi_2$, Nb_5Si_3, $MoSi_2$, and Mo_5Si_3 for up to 240 h in a $H_2/H_2S/H_2O$ environment that yields an oxygen potential of 1.2×10^{-15} Pa and a sulfur potential of $\sim 6.8 \times 10^{-1}$ Pa at 850 °C (1560 °F) was investigated (Ref 109). The sulfidation kinetics of all silicides (Fig. 19) show that all performed extremely well in this aggressive atmosphere. $CrSi_2$ shows the least sulfidation resistance, which is consistent with poor sulfidation resistance of chromium (Ref 11). On the other hand, the silicon content in silicides also plays an important role to resist sulfidation attack; the high silicon concentration significantly increases the sulfidation resistance. For example, the sulfidation rates of $MoSi_2$ and $NbSi_2$ are 1 order of magnitude slower than Mo_5Si_3 and Nb_5Si_3, respectively, as shown in Table 6.

A protective SiO_2 scale observed on all exposed silicides is responsible for the prevention of further severe environmental attack, as presented in Fig. 20. However, Cr_2S_3 and NbS_2 were also formed on the exposed $CrSi_2$ and Nb_5Si_3, indicated by XRD and electron dispersive x-ray data. It is interesting to note that only nodular Cr_3S_3 is formed on exposed $CrSi_2$, and a continuous layer of Cr_2S_3 failed to form even after 240 h exposure. Cross-sectional scanning electron microscopy observation showed that the Cr_2S_3 nodules virtually destroyed the underlying SiO_2. In contrast, a continuous and uniform NbS_2 layer developed. The SiO_2 layer still existed and effectively protected the substrate.

Hot Corrosion. Only very limited research on hot corrosion of silicides has been conducted. In the mid-1950s, it was shown that silicon-containing high-alloy steels had the best resistance against V_2O_5 melts at 925 °C (1700 °F); silicon and chromium appear to be the most promising combination of elements for the best hot corrosion resistance of heat-resistant alloys (Ref 110). It also is reported (Ref 111–113) that silicon-containing overlay coatings on nickel- and iron-base alloys show improved resistance against high-temperature oxidation and hot corrosion in the temperature range of 700 to 1000 °C (1290 to 1830 °F). Siliconized turbine blades coated by chemical vapor deposition processes as well as plasma spray tested (Ref 114–116) at 710 °C (1310 °F) for 30,000 h in a burner gas containing 0.4% S, 15 ppm sodium, and 5 ppm vanadium, reveal the least attack. These materials have been demonstrated to be extremely resistant against hot corrosion and show promise of higher lifetimes for turbine blades.

Silicon-containing coatings with a matrix consisting of the saturated γ solid-solution $Ni_6Cr_2Si_2$ and that also contain intermetallics of complex tantalum silicides as precipitates show great promise as protective layers for nickel-base alloys, with improved oxidation and hot corrosion resistance from the hot corrosion tests at 1000 °C (1830 °F) for up to 4000 h in burner gas with intermediate dipping in Na_2SO_4 and V_2O_5 melts. From silicon diffusion data, lifetimes greater than 10,000 h at 1000 °C (1830 °F) can be realized (Ref 117).

However, it is reported that there is evidence that silica or silicon-rich scales may be attacked under basic fluxing conditions. $MoSi_2$ has been shown to be very resistant to attack by NaCl and V_2O_5 but does dissolve in Na_2CO_3 and Na_2SO_4 (Ref 118). Burner rig test specimens made of hot-pressed $MoSi_2$, heated for 4 min

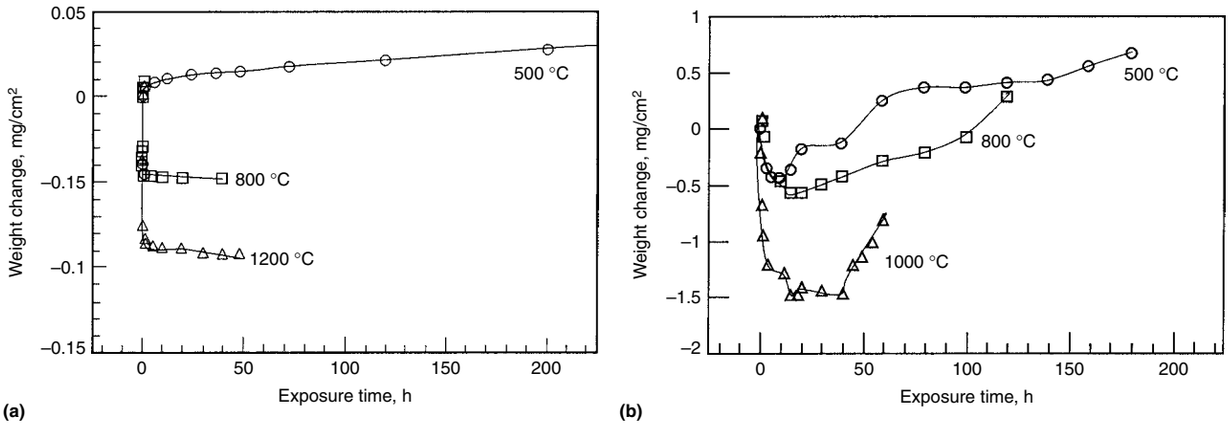

Fig. 17 Weight-change data during (a) oxidation in air and (b) sulfidation in 1.5 vol% H_2S/H_2 gas mixture for boron-containing Mo_5Si_3 after exposure at several temperatures. Source: Ref 100

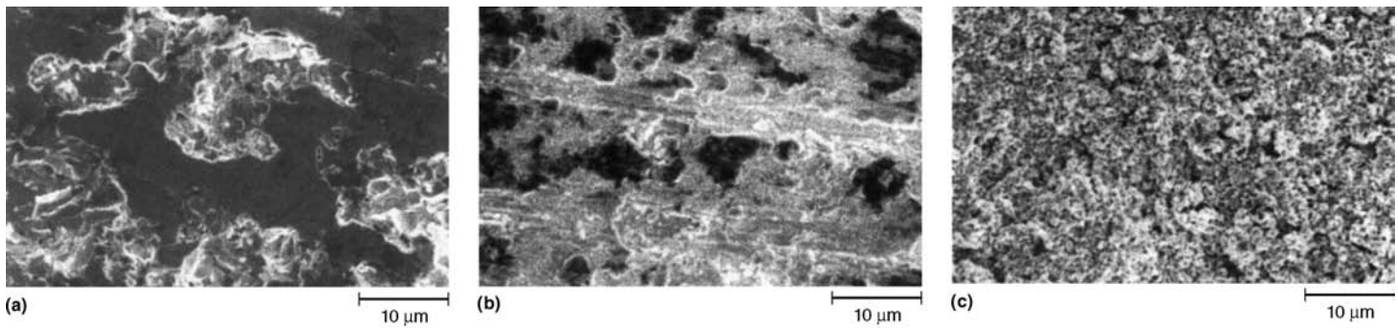

Fig. 18 SEM micrographs of surface of boron-containing Mo_5Si_3 after sulfidation in 1.5 vol% H_2/H_2S gas mixture at (a) 500 °C (930 °F), (b) 800 °C (1470 °F), and (c) 1100 °C (2010 °F). Source: Ref 100

intervals to 1000 to 1200 °C (1830 to 2190 °F) and then sprayed with 1 to 10% salt solutions of NaCl, Na_2CO_3, and Na_2SO_4, remain relatively unaffected after 20 h. The addition of acidic species, such as HCl, to the burner rig gas has been shown to significantly reduce dissolution in alkaline salts.

Other Intermetallics

The following intermetallics show interesting response to oxidation and may be useful as coating materials.

Noble-Metal-Containing Intermetallics: Platinum-Aluminum, Iridium-Aluminum, and Ruthenium-Aluminum Systems. Platinum-aluminum intermetallics favor the exclusive formation of Al_2O_3 and show stoichiometry-dependent oxidation kinetics and scale morphology; the overall growth rate is extremely small at 1450 °C (2640 °F) (Ref 119, 120). Pt_2Al, Pt_5Al_3, and $PtAl_2$ all display ridged oxide morphology.

Iridium-aluminum intermetallics require ~55% Al to form a protective Al_2O_3 scale at 1300 to 1800 °C (2370 to 3270 °F) (Ref 121, 122).

Ruthenium-aluminum intermetallics and their alloys containing chromium and ytttrium develop a protective Al_2O_3 scale at 1250 °C (2280 °F); high oxide vapor pressures are a limiting factor (Ref 123, 124). CrAl and Cr_2Al form a protective Al_2O_3 layer at 1000 to 1200 °C (1830 to 2190 °F) (Ref 125), with yttrium addition improving the scale adhesion. Aluminum-deficient Cr_2Al develops a chromium-rich scale, allowing N_2 ingress and leading to the formation of a nonprotective nitride-containing subscale.

Beryllide intermetallics with low densities and melting temperatures owe their good high-temperature oxidation resistance to the formation of a stable compact BeO scale (Ref 126, 127). In water-vapor-containing atmosphere, the protectiveness is lost due to the formation of volatile Be(OH). The lack of ductility and toxicity of BeO are additional problems.

Aqueous Corrosion

High-temperature structural applications are the main driving forces for the development of intermetallic compounds, and corrosion research has focused on degradation in the high-temperature gases of these environments. However, low-temperature aqueous corrosion of intermetallic compounds is of interest for four reasons. First, high-temperature materials will not always be at high-temperatures. Damage caused by low-temperature corrosion during fabrication or shutdown could result in catastrophic failures in service. This includes exposure to maintenance fluids or fire-extinguishing compounds as well as water or humid air and can be of particular concern for compounds susceptible to hydrogen-induced cracking in humid air. Second, there may be low- or intermediate-temperature applications where intermetallic compounds have superior properties to the alloys currently used. In many cases, intermetallic compounds will have lower densities and higher strengths than competing alloys and may have better resistance to fatigue, wear, corrosion, or a combination of these. Third, there are many fabrication processes, heat treatments, and joining methods that result in the formation of intermetallic compounds. Because heterogeneous nucleation is preferred, these phases tend to nucleate and grow at critical locations, such as grain boundaries and interphase bondings, and may limit performance if they have poor corrosion resistance. Fourth, because intermetallic compounds are frequently very hard or brittle at ambient temperatures, understanding corrosion could enable the creation of inexpensive electrochemical fabrication methods. Electropolishing, acid saw cutting, and electrochemical machining are examples of fabrication processes that use corrosion reactions to produce finished parts or surface finishes.

Aqueous corrosion of intermetallic compounds is influenced by the same factors that determine the corrosion performance of normal metallic alloys. In addition, there is a vast number of intermetallic compounds and environments that may cause corrosion of these compounds, most of which have not been studied. However, aqueous corrosion research has been conducted on a number of intermetallic compounds for low-temperature structural applications, but most of this research has been conducted on nickel, iron, and titanium aluminides. More detailed reviews of this research can be found in the literature (Ref 128–132). Some research has been conducted on other intermetallic phases that form during heat treatment or joining of metals, but this section does not attempt to cover this literature (Ref 133, 134). Here, the fundamental factors that make the

Table 6 Parabolic rate constants (k_p) for sulfidation of silicides at 850 °C (1560 °F)

Material	k_p, $g^2/cm^4/s$
$CrSi_2$	1.1×10^{-12}
WSi_2	2.7×10^{-14}
$NbSi_2$	8.7×10^{-14}
Nb_5Si_3	5.1×10^{-13}
$MoSi_2$	2.4×10^{-14}
Mo_5Si_3	1.0×10^{-13}

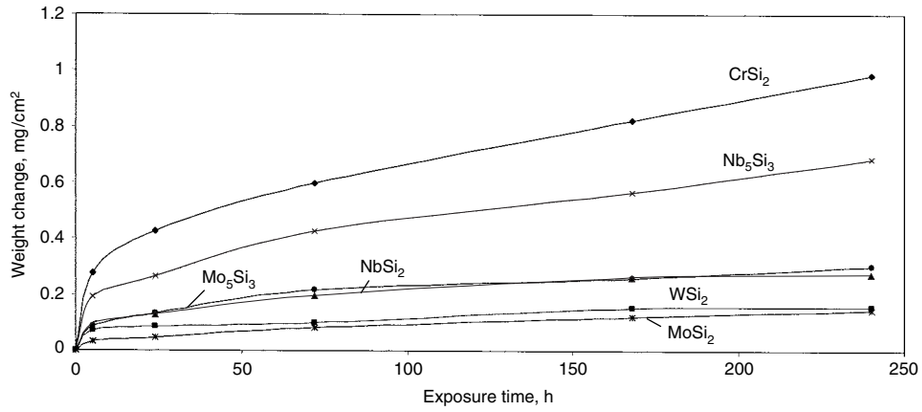

Fig. 19 Oxidation and sulfidation of silicides at 850 °C (1560 °F). Source: Ref 109

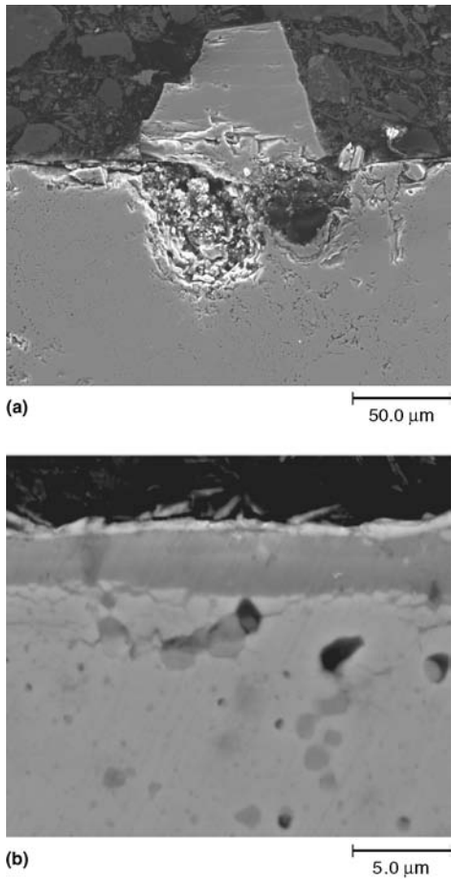

Fig. 20 SEM micrographs of exposed $CrSi_2$ and Nb_5Si_3 in $H_2/H_2S/H_2O$ environment at 850 °C (1560 °F). (a) $CrSi_2$. (b) Nb_5Si_3. Source: Ref 109

aqueous corrosion of an intermetallic phase different from that of a homogeneous alloy or of the constituents in pure elemental form are emphasized.

Basic Considerations

When a homogeneous solid solution of two or more species order on a lattice to form an intermetallic compound, three factors are altered that may influence the corrosion rates and stress-corrosion cracking behavior of the resulting phase:

- Chemical activity (thermodynamics)
- Physical arrangement of atoms (ordering-influenced kinetics)
- Deformation (slip character, stress-corrosion cracking, and hydrogen embrittlement)

Thermodynamic Considerations. When two or more elements are mixed to form a solid solution, the chemical activity of the species in this solution differs from that of the same species in pure elemental form. The literature on metallurgical thermodynamics has measured these activities and developed methods for estimating them and calculating phase diagrams. Currently, commercial software packages are available for making these calculations. If the energy of dissimilar interatomic bonds is lower, on average, than similar bonds, then the solid solution will tend to lower its energy by becoming ordered, with specific species on specific lattice sites (typically, when the elements have significantly different electronegativities). Of course, this ordering reaction also alters the chemical activity of the various species in the intermetallic phase. Taking these thermodynamic changes into consideration and remembering that when etching metallurgical structures, the intermetallic phases become observable due to a difference in the dissolution rates, it is not uncommon for investigators to assume that intermetallic compounds will have significantly better corrosion properties than similar alloys. While this may be true in some cases, it should be kept in mind that most corrosion-resistant engineering alloys rely on passivity for resistance to corrosion and not nobility. That is, they usually have a large overpotential (excess free energy) driving corrosion and rely on the formation of a thin, continuous, and protective film of corrosion products to protect the underlying microstructure from corrosion. In fact, a large overpotential can be beneficial because it may speed the reformation and sealing of the passive film when it becomes ruptured by chemical or mechanical means. Fortunately, while the energy of ordering is sufficient to drive the ordering reaction at heat treating temperatures, the change in the chemical potentials of the species during ordering is usually small compared to the free-energy changes that drive corrosion reactions. During ordering, thermodynamic changes occur and alter the chemical potentials of the species, but the magnitude of these changes is usually insufficient to produce fundamentally different corrosion behavior (such as the transition from active to noble or passive).

While this may seem disappointing, it is actually a very important deduction in terms of making first-order approximations of the corrosion behavior of intermetallic compounds in aqueous environments. First-order approximations of corrosion behavior are usually done through the use of electrochemical equilibrium diagrams of the type first proposed and made popular by Pourbaix and co-workers (Ref 135). These diagrams are essentially plots that identify the lowest energy phase that can form between an element and water as a function of electrode potential and pH. See the article "Potential versus pH (Pourbaix) Diagrams" in *ASM Handbook,* Volume 13A, 2003. Because the electrode potential is determined by the free energy for the chemical reactions between the elemental species and water, one should calculate a new diagram for each element in the intermetallic phase that takes into account chemical potential changes and the possibility of forming corrosion product phases that incorporate two or more of the species in the intermetallic phase (for example, $NiAl_2O_4$ for NiAl or Ni_3Al). Figure 21 provides examples of electrochemical equilibrium diagrams calculated for copper and tin that show the changes in the equilibrium boundaries for the various intermetallic phases that can form in the copper-tin system (Ref 136). By examining these diagrams, it can be seen that the magnitude of the changes in the equilibrium boundary for the various phases is of the order of 10 to 100 mV, which could be a small percentage of the corrosion driving force. Therefore, while calculation of diagrams is preferred, first-order approximations of behavior for monolithic structural applications can be made from the electrochemical equilibrium diagrams of the pure elemental species, which are readily available in published atlases (Ref 135). On the other hand, identifying phase-etching behavior in a

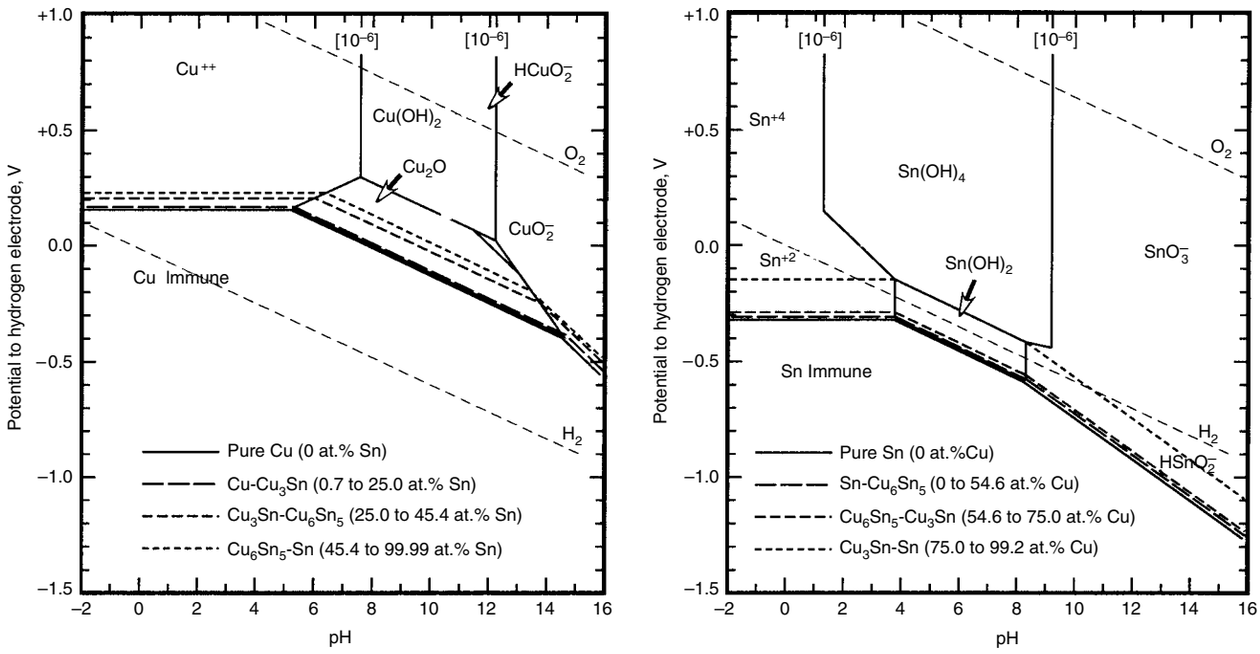

Fig. 21 Electrochemical equilibrium diagrams for copper and tin comparing equilibria for pure elemental form to that in various intermetallic compounds. Lines are drawn for the chemical potentials for equilibrium between two phases. The equilibria between ions and insoluble oxides or hydroxides are unaltered by substrate ordering.

microstructure containing different intermetallic phases or the phase that corrodes first in a weld or solder joint contaminated with flux residue may benefit greatly from calculations of this type (Ref 133, 134). Figure 22 shows the equilibrium diagrams for nickel and aluminum; the shift in the equilibrium lines to correct for the chemical potentials of nickel and aluminum in nickel aluminide are added as dashed lines (Ref 137). By examining these diagrams, it can be seen that the equilibrium line for nickel has shifted so little that the change is not resolvable as a separate line from the pure nickel line. On the other hand, the aluminum equilibrium line has shifted dramatically toward more noble potentials, but it is still significantly active compared to either the hydrogen or oxygen reduction reactions, so that both will still occur spontaneously and cause corrosion or passivity. Because corrosion reactions are usually mass transport rate limited at these large overpotentials (driving forces), these changes in the driving force probably produce no significant changes in corrosion behavior under service conditions. However, the kinetics of dissolution or passivation could be influenced by the imposition of particular species as nearest neighbors in the ordered structure.

Ordering-Influenced Kinetics. While the influence of ordering on thermodynamics is well known and can be calculated, the influence of ordering on the kinetics of dissolution and passivation is less well understood. In the case of a binary solid-solution alloy with a completely random distribution of the two different species on the lattice sites, one may assume that the more active species will tend to be selectively removed from the surface, leaving a surface enriched with the more noble species. In some cases, the surface layer becomes porous, which enables the removal of the active species to much greater depths into the alloy, leaving behind a dealloyed layer that is a mechanically weak spongelike network of pores. Dealloying corrosion, as this is known, is covered in the article "Effects of Metallurgical Variables on Dealloying Corrosion" in *ASM Handbook,* Volume 13A, 2003. However, dealloying typically arises above a specific concentration known as the parting limit and occurs most commonly in alloys of two or more species with significantly different electronegativities (gold-copper, copper-zinc) (Ref 138, 139). Based on the assumption that the parting limit is the atomic concentration where random distribution allows for the formation of a continuous percolation path of the active species through the solid, it is estimated that parting should occur at concentrations above approximately 18 mol fraction, which corresponds with the experimental results (Ref 140). Intermetallic compounds frequently exceed these concentration and electronegativity difference requirements without exhibiting dealloying (decomposition and dealloying), although dealloying does appear to occur in some cases, such as the copper-bearing grain-boundary precipitates in Al-Li-Cu alloys (Ref 141, 142). Because ordering does not usually alter thermodynamic conditions enough to modify corrosion behavior, as discussed previously, then this observation indicates that atomic arrangement influences the kinetics of dissolution and lends support to the percolation analysis of Ref 120. Of course, this would mean that the type and stoichiometry of the intermetallic structure will also be important and that the copper deposits found outside pits and cracks in Al-Li-Cu alloys may be pieces of the dealloyed intermetallic phase broken off by the hydrogen gas bubbles generated in the cathodically active copper-rich sponge and not dissolved and reprecipitated copper.

The $L1_2$ structure of A_3B-type intermetallic compounds frequently forms in binary face-centered cubic solid solutions (such as Ni_3Al and Ni_3Fe). In this structure, the B-type atoms are surrounded with only A-type nearest neighbors. As a result, these systems are excellent candidates for investigating the ability of ordering to induce stoichiometric limitations on dissolution rates. If the A-type atoms are the more noble in the structure, as is the case in the compounds identified previously, then the dissolution rate of the more active species is limited to the rate it becomes exposed by dissolution of the more noble species. Electrochemical measurements were conducted on Ni_3Al in a wide range of solutions without observing any evidence of dealloying (Ref 143). Figure 23 is an example of the current measured as this compound is dissolved anodically with closed-loop control of potential as the potential is increased in sulfuric acid (Ref 137, 143, 144). At this pH, this compound corrodes actively at open circuit but passivates when anodically polarized. Included in this figure is the current measured on pure nickel. By examining this figure, it can be seen that ordering in Ni_3Al appears to block aluminum dissolution until nickel dissolution starts, at which point the current created by dissolution

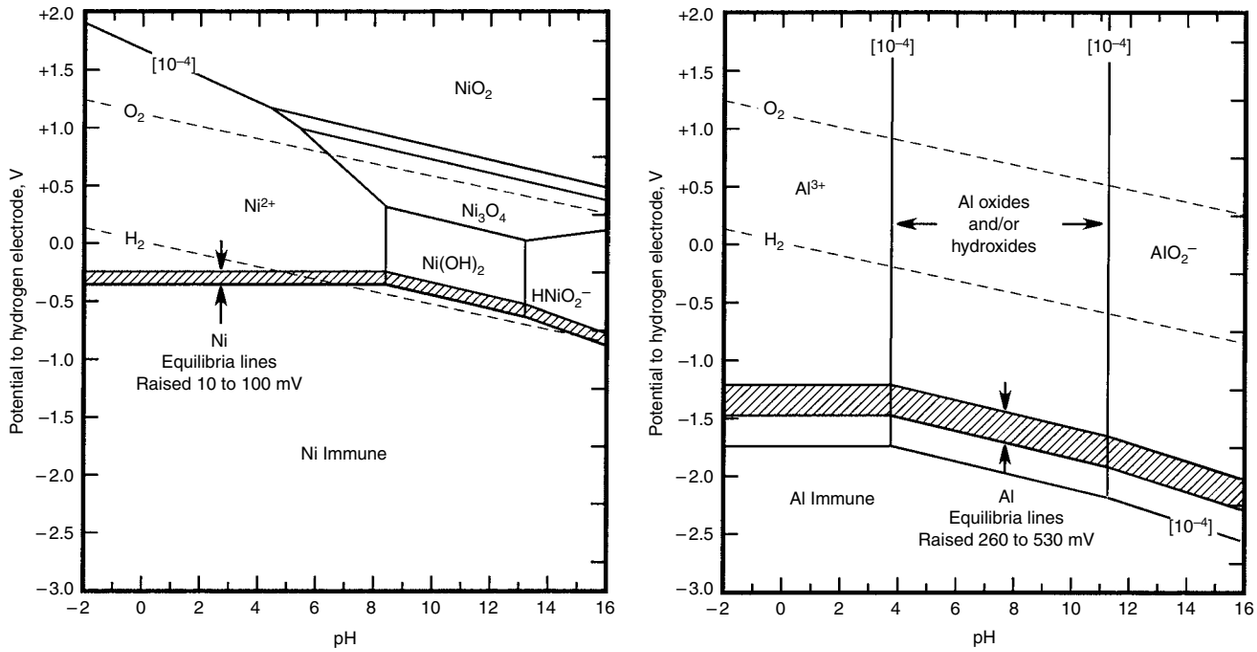

Fig. 22 Electrochemical equilibrium diagram for nickel and aluminum showing the influence of $L1_2$ ordering (Ni_3Al) on nickel and aluminum dissolution and passivation reactions. The potential ranges for the aluminide correspond to the aluminum concentration range from 0.2 to 0.3 mol fraction. The dashed lines illustrate the range of water stability from oxygen to hydrogen evolution, and it can be seen that ordering has not significantly altered the position of the nickel and aluminum equilibria relative to these reactions.

increases slightly more rapidly on the intermetallic until the onset of passivity, after which lower currents are observed on the aluminide. Clearly, aluminum dissolution, which could cause hydrogen evolution, absorption, and embrittlement, is limited to the stoichiometric ratio and determined by the rate of nickel dissolution (Ref 144).

Another way to examine this issue is to suddenly expose the bare and reactive surface of an intermetallic compound to a solution while measuring the potential with a reference electrode that has a potential fixed on the hydrogen electrode scale and therefore allows for direct measurement of the thermodynamic driving forces. When a bare surface is exposed rapidly to a solution in this manner, anodic reactions start immediately, while the mass transport required by cathodic reactions delays their initiation for a few milliseconds. Theoretically, this will result in the potential of the sample becoming more negative until the potential for equilibrium with the chemical potential of the species dissolving from the intermetallic compound is reached (Ref 145–148). When an experiment of this type was performed on Ni_3Al, the potential did not go below that predicted for nickel in Fig. 23, as shown in Fig. 24 (Ref 144). This does not indicate that aluminum is not dissolving, only that at potentials near the equilibrium potential for nickel dissolution, where there is still a large overpotential driving aluminum dissolution and the net nickel dissolution rate is approaching 0, the charge created by aluminum dissolution is not enough to overwhelm the nickel oxidation-and-reduction-exchange current density.

Deformation, Slip Character, Stress-Corrosion Cracking, and Hydrogen Embrittlement. When a random solid solution becomes ordered, it creates a specific arrangement of atomic nearest neighbors that lowers the energy of the solid. When a dislocation passes through this solid, it breaks this arrangement and creates a higher-energy region on the slip plane behind it, where the nearest neighbors of the atoms are not of the preferred type, until a second dislocation passes and returns the region to the original configuration. This antiphase region between the two dislocations is analogous to a stacking fault, where, instead of a dislocation decomposing into two partial dislocations connected by a stacking fault, there is now a superdislocation that is two dislocations connected by an antiphase domain boundary. As in the case of stacking faults, the formation of antiphase domain boundaries limits cross slip and promotes less homogeneous planar slip. Limiting cross slip reduces the ability of the solid to accommodate slip at grain boundaries where the slip planes of the adjacent grains are not aligned and promotes the formation of dislocation pileups and cracks (Ref 149). The limited ductility of many intermetallic phases has been attributed to this phenomenon, and the beneficial influence of boron on the ductility of many intermetallic compounds has been attributed to the influence of this addition on order and slip in the grain-boundary region as well as to a beneficial influence on grain-boundary cohesive forces (Ref 150, 151). Of course, hydrogen and stress-corrosion cracking are both known to promote intergranular fracture. As a result, the influence of hydrogen produced by cathodic charging on the ductility of Ni_3Al (+200 ppm boron) was studied (Ref 152), and it was found that cathodic hydrogen lowered the ductility of this material dramatically and changed the fracture mode from ductile transgranular to intergranular. Similarly, the influence of potential and pH on the ductility of Ni_3Al (+200 ppm boron) was studied (Ref 153, 154), with the conclusion that in any solution or pH, intergranular fracture and low ductility resulted whenever the potential of the sample became low enough to produce hydrogen, as shown in Fig. 25. Because most intermetallic compounds have at least one component that has a chemical potential that is active with respect to the potential required to spontaneously produce hydrogen by decomposition of water, investigators have found that most intermetallic compounds can be embrittled by exposure to humid air. This has created questions

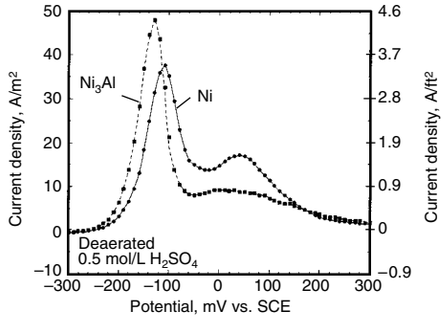

Fig. 23 Comparison of the current density produced by dissolution of nickel and nickel aluminide in deaerated sulfuric acid. SCE, saturated calomel electrode

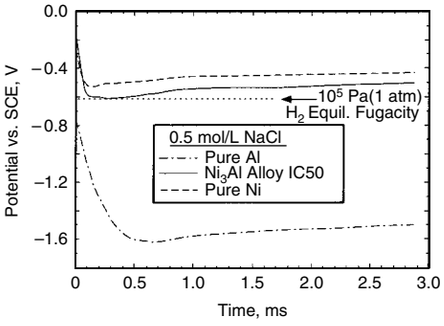

Fig. 24 Potential transients during and following the generation of fresh bare surface by scratching of nickel, aluminum, and nickel aluminide in 0.5 mol/L NaCl, with the hydrogen evolution potential for this environment indicated SCE, saturated calomel electrode

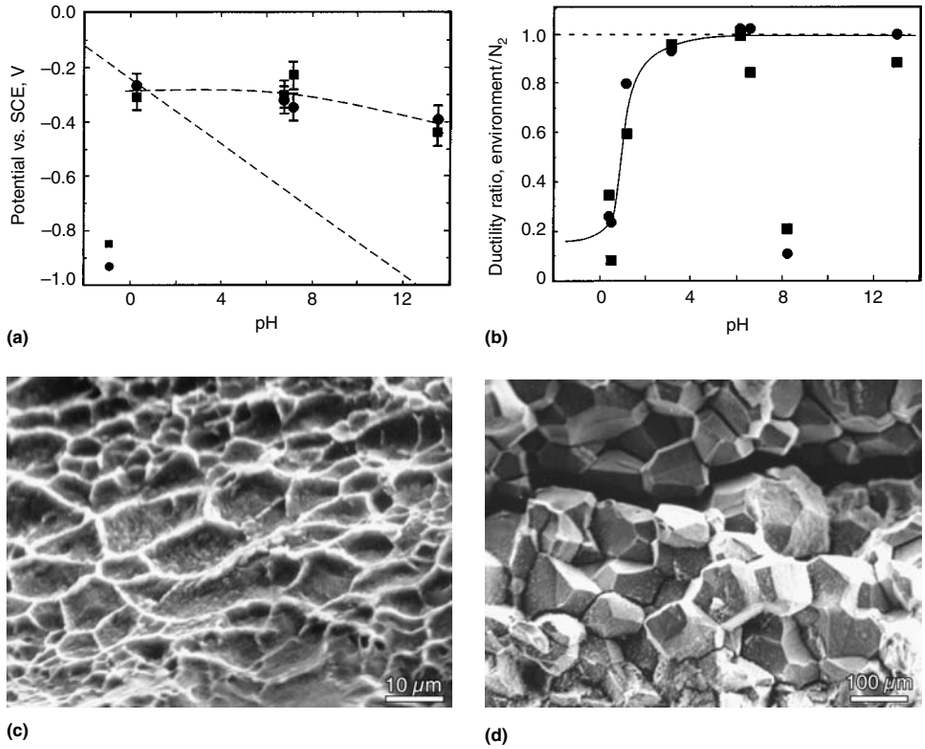

Fig. 25 Slow strain-rate tensile test results for free corrosion (open-circuit) conditions in different pH environments, showing that when (a) the free corrosion potentials reach the point where hydrogen evolution is thermodynamically possible, then (b) the ductility drops, and (c) the fracture mode changes from ductile microvoid coalescence to (d) intergranular. (c) 0.5 mol/L Na_2So_4, 6.5 pH. (d) 0.5 mol/L H_2SO_4, 0.7 pH. SCE, saturated calomel electrode

about whether the low ductility usually observed in room-temperature laboratory experiments on these types of materials is an inherent property, an environmental effect, or a combination of both (Ref 154, 155–157).

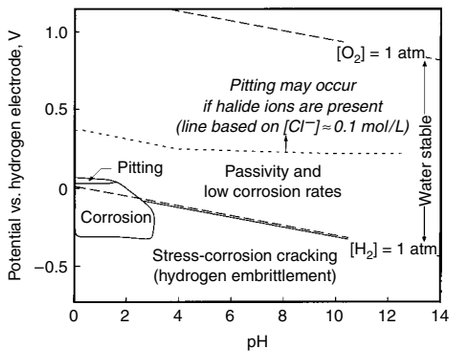

Fig. 26 Corrosion-mode diagram for nickel aluminide (Ni_3Al) in aqueous solutions, as estimated from electrochemical experiments

Practical Understanding

The objective of corrosion research is to convert scientific understanding into practical alloy selection and design guidelines. The understanding of aqueous corrosion of intermetallic compounds is not to the point where one can do this unequivocally, and thorough testing to evaluate performance should be conducted for any application. This testing should include out-of-service conditions as well as in-service conditions. References 158, and 159 have recommended the use of corrosion-mode diagrams to guide alloy selection for corrosive applications in a manner similar to the deformation mechanism maps of Ref 160 to 162. These diagrams are essentially electrochemical equilibrium diagrams where the modes of corrosion failure observed are plotted instead of the calculated equilibrium phase. An example of one of these diagrams is shown in Fig. 26 for Ni_3Al (Ref 163). By examining this figure, it can be seen that this intermetallic compound is passive over most of the range of potentials and pH that water is thermodynamically stable. It is interesting to note that while the chemical potential of aluminum in this solid is sufficient to cause hydrogen evolution, no evidence of hydrogen embrittlement was observed in any solution until the potential of the bulk sample reached that required for hydrogen evolution. Also interesting is the ability of Ni_3Al to exhibit passivity at a much lower pH than that predicted by the equilibrium diagram of Fig. 23, but nickel also shows passivity at anomalously low pH (Ref 145). Table 7 shows the corrosion rates determined for nickel aluminide alloys in a variety of different solutions, and Table 8 lists similar data for iron aluminide as determined by Ref 164 and 165. The corrosion rates in this table reflect the

Table 7 Average corrosion penetration rates for nickel aluminide alloys in various aqueous solutions

Calculated from continuous 200 h exposure mass-loss data

	Concentration		Penetration, µm/d (mils/d)					
			Exposure at 25 °C (75 °F)			Exposure at 95 °C (205 °F)		
Aqueous solution	mol/L	Mass%	IC-50(a)	IC-218(b)	IC-221(c)	IC-50(a)	IC-218(b)	IC-221(c)
Sulfuric acid	1	9	0.14 (0.006)	0.14 (0.006)	0.20 (0.008)	>34 (1.3)(d)	21 (0.8)	>60 (2.4)(d)
	18	96	0.49 (0.02)	0.42 (0.02)	0.42 (0.02)	4.7 (0.19)	1.3 (0.05)	1.4 (0.06)
Hydrochloric acid	1	4	0.35 (0.01)	0.20 (0.008)	0.20 (0.008)	35 (1.4)	>37 (1.5)(d)	77 (3.0)
	12	37	8.4 (0.03)	13 (0.51)	26 (1.02)	>35 (1.4)(d)	>35 (1.4)(d)	93 (3.7)(d)
Nitric acid	1	6	30 (1.2)	>111 (4.4)(e)	37 (1.5)	>36 (1.4)(d)	>37 (1.5)(d)	21 (0.83)
	8	40	>850 (33.5)(f)	0.07 (0.003)	0.20 (0.008)	>33 (1.3)(d)	3.1 (0.12)	3.9 (0.15)
	16	70	4.4 (0.17)	0.07 (0.003)	0.20 (0.008)	>36 (1.4)(d)	4.1 (0.16)	14 (0.55)
Hydrofluoric acid	1	2	0.20 (0.008)	0.20 (0.008)	0.20 (0.008)	>37 (1.5)(d)	>34 (1.3)(d)	28 (1.1)
Phosphoric acid	1	10	0.14 (0.006)	0.14 (0.006)	0.14 (0.006)	>33 (1.3)(d)	>36 (1.4)(d)	52 (2.0)
Oxalic acid	1	10	0.07 (0.003)	0.07 (0.003)	0.07 (0.003)	(g)	0.20 (0.008)	0.28 (0.011)
Acetic acid	1	6	0.20 (0.008)	0.014 (0.0006)	0 (0)	0.28 (0.01)	0.28 (0.011)	0.28 (0.011)
Sodium chloride	0.6	3.5	0.014 (0.0006)	0.014 (0.0006)	0.007 (0.0003)	0.014 (0.0006)	(g)	(g)
Sodium hydroxide	10	30	0.028 (0.001)	0.014 (0.0006)	0.014 (0.0006)	(g)	(g)	(g)
Ammonium hydroxide	10	18	0.42 (0.02)	0.020 (0.0008)	0.014 (0.0006)	(g)	(g)	(g)
Ferric chloride	0.2	20	>410 (16.1)(h)	>320 (12.6)(i)	62 (2.5)	>36 (1.4)(d)	>34 (1.3)(d)	>79 (3.1)(d)

Alloy compositions in mass fraction: (a) IC-50, 11.3% Al, 0.6% Zr, 0.02% B, bal Ni. (b) IC-218, 8.5% Al, 7.8% Cr, 0.8% Zr, 0.02% B, bal Ni. (c) IC-221, 8.5% Al, 7.8% Cr, 1.7% Zr, 0.02% B, bal Ni. (d) Total dissolution in <200 h. (e) Total dissolution in <65 h. (f) Total dissolution in <8 h. (g) Very small mass gain. (h) Total dissolution in <17 h. (i) Total dissolution in <24 h. Source: Ref 164, 165

Table 8 Cavitating water-jet erosion test for nickel and iron aluminide compared to other materials

Material	Erosion rate, mg/h	Relative erosion rate(a)
Nickel aluminide (IC-50, cold worked)	1.4	0.04
Nickel aluminide (IC-221)	2.5	0.08
Nickel aluminide (IC-218)	2.9	0.09
Nickel aluminide (IC-50)	4.1	0.1
Nickel aluminide (IC-50, plasma weld overlay)	7.0	0.2
Stellite 21 (stick)	7.3	0.2
Iron aluminide	11.6	0.4
Nitronic 60 bar stock	12.8	0.4
Aluminum oxide ceramic plate	18.4	0.6
308 stainless steel overlay (stick)	31.6	1.0
Carbon steel (cold-rolled bar)	32.3	1.0
304 stainless steel plate	33.2	1.1
Aluminum bronze	84.4	2.7

Water-jet pressure, 41 MPa (6000 psi). (a) Erosion rate/rate for 308 stainless steel. Source: Ref 164, 165

Table 9 Average corrosion penetration rates for iron aluminide (Fe_3Al) alloys in aqueous solutions at room temperature

		Concentration, penetration, µm/d (mils/d)			
Solution	mol/L	FA-84(a)	FA- 129(b)	FAL-Mo(c)	304L(d)
HCl	1	430 (17)	52 (2.5)	14 (0.55)	9.7 (0.38)
H_2SO_4	0.5	400 (15.7)	72 (2.8)	120 (4.7)	0.014 (0.0006)
HNO_3	1	160 (6.3)	3.5 (0.14)	1.4 (0.06)	0.007 (0.0003)
NaOH	1	0.042 (0.002)	0.021 (0.0008)	0.056 (0.002)	0.007 (0.0003)
$Na_2S_2O_3$	1	7.8 (0.31)	9.9 (0.39)	2.6 (0.10)	0.004 (0.0002)
$Na_2S_4O_6$	1	21 (0.83)	6.5 (0.26)	6.5 (0.26)	0.020 (0.0008)
Acetic acid	1	0.20 (0.008)	0.014 (0.0006)	0 (0)	0.28 (0.011)
NaCl	0.6	0.19 (0.008)(e)	0.13 (0.005)(e)	0.11 (0.004)	<0.007 (0.0003)
Seawater (synthetic)	...	0.07 (0.003)(e)	0.07 (0.003)(e)	0.06 (0.002)	<0.007 (0.0003)

Alloy compositions in mass fraction: (a) FA-84, 28% Al, 2% Cr, 0.05% B, bal Fe. (b) FA-129, 28% Al, 5% Cr, 0.5% Nb, 0.2% C, bal Fe. (c) FAL-Mo, 28% Al, 5% Cr, 1% Mo, 0.08% Zr, 0.04% B, bal Fe. (d) 304L, 18–22% Cr, 8–12% Ni, 2% Mo (max), 0.03% S (max), 1% Si (max), 0.045% P (max), 0.03% C (max), bal Fe. (e) Localized corrosion initiated within 24 h

behavior indicated by the corrosion-mode diagram for Fig. 25. Perhaps the most interesting low-temperature applications for intermetallic compounds require resistance to wear and corrosion combined. These applications require a combination of strength and corrosion resistance, and as shown in Table 9, intermetallic compounds have this combination and can exhibit many times better resistance to these combined failure mechanisms than existing alloys.

This article was not written to provide a catalog of the corrosion response of the numerous varieties of intermetallics. Instead, the emphasis is placed on generic principles governing the corrosion phenomena of intermetallics and then focusing on the corrosion response of selected structural intermetallics. Some of the information presented here originated from the authors' own research in this area. Lack of space has forced the authors to be selective in choosing the topics. Consequently, such areas as interdiffusion modeling in closed and open corrosion systems and modeling of scale spallation have been excluded.

REFERENCES

1. N.S. Stoloff and V.K. Sikka, Ed., *Physical Metallurgy and Processing of Intermetallic Compounds,* Chapman & Hall, 1996
2. T.A. Kircher and E.L. Courtright, *Mater. Sci. Eng. A,* Vol 155 (No. 1–2), 1992, p 67–74
3. P.K. Datta, K. Natesan, and J.S. Burnell-Gray, Coatings Technology, *Intermetallic Coatings and Coatings for Intermetallics, Intermetallic Compounds: Principles and Practice, Vol 3, Progress,* J.H. Westbrook and R.L. Fleischer, Ed., John Wiley & Sons Ltd., 2002, p 561–588
4. F.D. Richardson and J.H. Jeffes, *JISI,* Vol 171, 1952, p 165
5. H.J. Grabke, High Temperature Corrosion in Multi-Reactant Gaseous Environments, *High Temperature Materials Corrosion in Coal Gasification Atmospheres,* J.F. Norton, Ed., Elsevier Applied Science Publishers, 1984, p 59–82
6. C. Wagner, *Z. Elektrochem.,* Vol 63, 1959, p 772
7. F.S. Pettit, *Trans. Metall. Soc. AIME,* Vol 239, 1967, p 1296–1305
8. P. Kofstad, *High Temperature Corrosion,* Elsevier Applied Science, London and New York, 1988
9. N. Birks, G.H. Meier, and F.S. Pettit, *JOM,* Vol 39 (No. 12), 1987, p 28–31
10. D.L. Douglass, P. Kofstad, and G.C. Wood, *Oxid. Met.,* Vol. 45 (No. 5–6), 1996, p 529–620
11. K.N. Strafford and P.K. Datta, *Mater. Sci. Technol.,* Vol 5 (No. 8), 1989, p 765–779
12. P.K. Datta, H.L. Du, D. Jenkinson, J.S. Burnell-Gray, and K.N. Strafford, *The Design of Sulphidation Resistant Materials: State-of-the-Art and Future Prospects,* Elsevier Science BV (Netherlands), 1998, p 176–187
13. J.H. Westbrook and R.L. Fleischer, Ed., *Intermetallic Compounds: Structural Applications and Intermetallic Compounds,* John Wiley & Sons Ltd., 2000
14. G.C. Rybicki and J.L. Smialek, *Oxid. Met.,* Vol 31 (No. 3–4), 1989, p 275–304
15. A. Steiner and K.L. Komarek, *Trans. Metall. Soc. AIME,* Vol 230 1964, p 786
16. F.H. Stott and G.C. Wood, *Mater. Sci. Eng. A,* Vol 87 (No. 1–2), 1987, p 267–274
17. M.W. Brumm and H.J. Grabke, *Corros. Sci.,* Vol 33 (No. 11), 1992, p 1677–1690
18. H.J. Grabke, M.W. Brumm, and B. Wagemann, *Mater. Corros.,* Vol 47 (No. 12), 1996, p 675–677
19. E. Schumann, G. Schnotz, U. Salzberger, and M. Rühle, Oxidation of Single-Crystal γ-Ni_3Al at Low Oxygen Partial Pressure, *High-Temperature Ordered Intermetallics IV,* Vol 213, L.A. Johnson, D.P. Pope, and J.O. Stiegler, Ed., Materials Research Society, 1991, p 951–956
20. J. Doychak and M. Rühle, *Oxid. Met.,* Vol 31 (No. 5–6), 1989, p 431–452
21. K. Natesan, *Oxid. Met.,* Vol 30 (No. 1–2), 1988, p 53–83
22. J.L. Smialek and G.H. Meier, *Superalloys II,* C.T. Sims, N.S. Stoloff, and W.C. Hagel, Ed., Wiley, New York, 1989, p 293–326
23. R.T. Haasch, A.M. Venezia, and C.M. Loxton, *J. Mater. Res.,* Vol 7 (No. 6), 1992, p 1341–1349
24. J.A. Horton, J.V. Cathcart, and C.T. Liu, *Oxid. Met.,* Vol 29 (No. 3–4), 1988, p 347–365
25. G. Fisher, P.K. Datta, J.S. Burnell-Gray, W.Y. Chan, and J.C. Soares, *Surf. Coat. Technol.,* Vol 110 (No. 1–2), 1998, p 24–30
26. E. Schumann, J.C. Young, M. Rühle, and M.J. Graham, *Oxid. Met.,* Vol 46 (No. 1–2),1996, p 37–49
27. J. Jedlinski and G. Borchardt, *Oxid. Met.,* Vol 36 (No. 3–4),1991, p 317–337
28. B.A. Pint, J.R. Martin, and L.W. Hobbs, *Oxid. Met.,* Vol 39 (No. 3–4), 1993, p 167–195
29. B.A. Pint, M. Treska, and L.W. Hobbs, *Oxid. Met.,* Vol 47 (No. 1–2), 1997, p 1–20
30. I. Rommerskirchen and V. Kolarik, *Mater. Corros.,* Vol 47 (No. 11), 1996, p 625–630
31. J. Jedlinski and S. Mrowec, *Mater. Sci. Eng.,* Vol 87 (No. 1–2),1987, p 281–287
32. H. Todd, U.S. Patent 3,494,748, Feb 10, 1970
33. R. Strieff and D.H. Boone, *J. Mater. Eng.,* Vol 10 (No. 1) 1988, p 15–26
34. R.G. Wing and I.R. McGill, *Platin. Met. Rev.,* Vol 25 (No. 3), 1981, p 94–105
35. J.R. Nicholls and D.J. Stephenson, *Metals and Mater.,* Vol 7 (No. 3), 1991, p 156–163
36. T.N. Rhys-Jones, *Corros. Sci.,* Vol 29 (No. 6), 1989, p 623–646
37. B.M. Warnes and D.C. Punola, *Power Generation Technology, International Review of Primary Power Production,* Sterling Publishing, 1995, p 207
38. H.M. Tawancey, N.M. Abbas, and T.N. Rhys-Jones, *Surf. Coat. Technol.,* Vol 49, 1991, p 1–7
39. H. Jehn, *J. Less Common Met.,* Vol 100, 1984, p 321–339
40. J. Schaffer, G.M. Kim, G.H. Meier, and F.S. Pettit, *The Role of Active Elements in the Oxidation Behaviour of High Temperature Metals and Alloys,* Elsevier, Amsterdam, 1991, p 231
41. H.M. Tawancey, N. Sridar, B.S. Tawabin, and N.M. Abbas, *J. Mater. Sci.,* Vol 27 (No. 23), 1992, p 6463–6474
42. P.C. Patnaik, *Advances in High Temperature Structural Materials and Protective Coatings,* NRC Canada 1994, p 164
43. T.E. Strangman and P.A. Solfest, U.S. Patent 4,880,614, Nov 14, 1989
44. H. Hosada, T. Takahashi, M. Takehara, T. Kingetsu, and H. Masumoto, *Mater. Trans.,* Vol 38 (No. 10), 1997, p 871–878
45. W.M. Clift, K.F. McCarty, and D.R. Boehme, *Surf. Coat. Technol.,* Vol 47 (No. 1), 1990, p 29–40
46. K.N. Lee and W.L. Worrell, *Oxid. Met.,* Vol 32 (No. 5–6), 1989, p 357–369
47. B. Schramm and W. Auer, *Mater. Corros.,* Vol 47 (No. 12), 1996, p 678–684
48. W.H. Lee and R.Y. Lin, *Mater. Chem. Phys.,* Vol 77 (No. 1), 2002, p 86–96
49. W. Gao and C.H. Xu, *High Temp. Mater. Process.,* Vol 19, 2000, p 379–387
50. C.H. Xu, W. Gao, and Y.D. He, *Scr. Mater.,* Vol 42, 2000, p 975–980
51. W. Gao, C.H. Xu, and H. Gong, *Intermetallics,* Vol 8, 2000, p 769–779
52. I. Rommerskirchen, B. Eltester, and H.J. Grabke, *Mater. Corros.,* Vol 47, 1996, p 646–649
53. J.L. Smialek, J. Doychak, and D.J. Gaydosh, *Oxid. Met.,* Vol 34, 1990, p 259–275
54. A.A. Aljarany, "Studies of the Degradation Behaviour of Fe_3Al and γ-TiAl Intermetallics," Ph.D. thesis, Northumbria University, 2002
55. K. Natesan, *Proc. Seventh Annual Conf. on Fossil Energy Materials,* ORNL/FMP-93, Oak Ridge National Laboratory, 1993, p 249
56. K. Natesan and R.N. Johnson, *Proc. Second Int. Conf. Heat-Resistant Materials,* K. Natesan, P. Ganesan, and G. Lai, Ed., ASM International, 1995, p 591
57. W. Gao and C.H. Xu, *High Temp. Mater. Process.,* Vol 18, 1999, p 351–362
58. W. Kai, S.H. Lee, D.L. Chiang, and J.P. Chu, *Mater. Sci. Eng. A,* Vol 258, 1998, p 146–152
59. W. Kai, M.T. Chang, C.D. Liu, D.L. Chiang, and J.P. Chu, *Mater. Sci. Eng. A,* Vol 329–331, 2002, p 734–744
60. J.H. DeVan and P.F. Tortorelli, *Mater. High Temp.,* Vol 11, 1993, p 30–35

61. H.L. Du, P.K. Datta, J.S. Burnell-Gray, and J. Bernardi, Microscopy of Sulphidised Fe_3Al, *J. Mater. Sci.,* in press
62. D. Das, R. Balasubramaniam, and M.N. Mungole, *J. Mater. Sci.,* Vol 37, 2002, p 1135–1142
63. C.M. Austin, T.J. Kelly, K.G. McAllister, and J.C. Chesnutt, *Struct. Intermetallics,* 1997, p 413–425
64. T. Tetsui, *Curr. Opin. Solid State Mater. Sci.,* Vol 4 (No. 3), 1999, p 243–248
65. R.A. Perkins and G.H. Meier, *Proc. Industry-University Advanced Materials Conference,* F.W. Smith, Ed., Denver, 1991, p 92
66. J.L. Smialek and D.L. Humphrey, *Scr. Metall. Mater.,* Vol 26 (No. 11), 1992, p 1763–1768
67. G. Welsh and A.I. Kaveci, *Oxidation of High Temperature Intermetallic,* T. Grobstein and J. Doychak, Ed., The Minerals, Metals and Materials Society, 1989
68. G. Welsh, S. Freidman, and A. Kahveci, *Microscopy of Oxidation,* M.J. Bennett and G.W. Lorimer, Ed., Institute of Materials, London, 1991
69. H.L. Du, P.K. Datta, D.B. Lewis, and J.S. Burnell-Gray, *Corros. Sci.,* Vol 36 (No. 4), 1994, p 631–642
70. G. Fisher, P.K. Datta, and J.S. Burnell-Gray, *Surf. Coat. Technol.,* Vol 113 (No. 3), 1999, p 259–267
71. H.L. Du, P.K. Datta, Z. Klusek, and J.S. Burnell-Gray, Nanoscale Studies of the Early Stages of Oxidation of TiAl-Based Alloy, *Oxid. Met.,* Vol 62 (No. 3–4), 2004, p 175–193
72. G.H. Meier and F.S. Pettit, *Mater. Sci. Eng. A,* Vol 153, 1992, p 548–560
73. Y. Shida and H. Anada, *Corros. Sci.,* Vol 35, 1993, p 945–953
74. D.W. McKee, Oxidation and Protection of Ti_3Al-Based Intermetallic Alloys, *High-Temperature Ordered Intermetallic Alloys V,* Materials Research Society, 1993, p 953–958
75. Z. Liu and G. Welsch, *Metall. Trans. A,* Vol 19, 1988, p 1121–1125
76. W.B. Retallick, M.P. Brady, and D.L. Humphrey, *Intermetallics,* Vol 6 (No. 4), 1998, p 335–337
77. S. Frangini, A. Mignone, and F. DeRiccadis, *J. Mater. Sci.,* Vol 29, 1994, p 714–720
78. S.A. Kekare and P.B. Aswath, *J. Mater. Sci.,* Vol 32, 1997, p 2485–2499
79. V. Shemet, H. Hoven, and W.J. Quadakkers, *Intermetallics,* Vol 5 (No. 5), 1997, p 311–320
80. J. Geng, G. Gantner, P. Oelhafen, and P.K. Datta, *Appl. Surf. Sci.,* Vol 158, 2000, p 64–74
81. S.K. Varma, A. Chan, and R.N. Mahapatra, *Oxid. Met.,* Vol 55 (No. 5–6), 2001, p 423–435
82. G.H. Meier, F.H. Pettit, and S. Hu, *High Temperature Corrosion,* Les Embiez, France, 1992; *Proc. J. Phys. IV,* Vol 3, 1993, p 395
83. N.S. Choudhury, H.C. Graham, and J.W. Hinze, *Proceeding of High Temperature Alloys,* Z.A. Foroulis and F.S. Pettit, Ed., The Electrochemical Society, 1976, p 99
84. N. Zheng, W.J. Quadakkers, A. Gil, and H. Nickel, *Oxid. Met.,* Vol 44, 1995, p 477–499
85. S. Taniguchi, Y. Tachikawa, and T. Shibata, *Mater. Sci. Eng. A,* Vol 232 1997, p 47–54
86. S. Becker, A. Rahmel, M. Schorr, and M. Schurtz, *Oxid. Met.,* Vol 38 (No. 5–6), 1992, p 425–464
87. H.L. Du, A. Aljarany, K. Klusek, P.K. Datta, and J.S. Burnell-Gray, Effects of Oxygen Partial Pressures on the Oxidation Behaviour of Ti-46.7Al-1.9W-0.5Si between 750 and 950 °C, *Corros. Sci.,* Vol 47 (No. 7), 2005, p 1706–1723
88. D.R. Gaskell, *Introduction to Metallurgical Thermodynamics,* Hemisphere Publishing Corporation, 1981
89. H.L Du, P.K. Datta, A.L. Dowson, and M. Jacobs, Effects of Sulfur Partial Pressures on Degradation Behaviour of TiAl in $H_2/H_2S/H_2O$ Environments at 900 °C, *Oxid. Met.,* in press
90. Defects and Diffusion in Metals—Annual Retrospective II, D.J. Fisher, Ed., Scitec Publications, 1999
91. P.K. Datta, J.S. Burnell-Gray, H.L. Du, A.L. Dowson, and M.H. Jacobs, *Proc. World Ceramics Congress and Forum on New Materials,* (Florence, Italy), World Scientific Publishing Co., 1998
92. H.L. Du, P.K. Datta, J.S. Gray, and K.N. Strafford, *Corros. Sci.,* Vol 36, 1994, p 99–112
93. H.L. Du, P.K. Datta, J. Leggett, J.R. Nicholls, J.C. Bryar, and M.H. Jacobs, The Influence of Processing Route on the Oxidation/Sulphidation of a Ti-48Al-2Nb-2Mn Intermetallic Alloy at 750 and 900 °C, *Advances in Surface Engineering, Vol I, Proc. Conf. on Advances in Coatings and Surface Engineering for Corrosion and Wear Resistance and Other Applications,* (Newcastle upon Tyne, U.K.), Royal Society of Chemistry 1996, p 53–66
94. H.L. Du, P.K. Datta, D. Griffin, A. Aljarany, and J.S. Burnell-Gray, *Oxid. Met.,* Vol 60, 2003, p 29–46
95. H.L. Du, S.R. Rose, Z.D. Xiang, and P.K. Datta, *Mater.wiss. Werkst.tech.,* Vol 34, 2003, p 421–426
96. K. Zhang, Z. Li, and W. Gao, *Mater. Lett.,* Vol 57, 2002, p 834–843
97. K. Zhang, Z. Li, M.A. Hodgson, and W. Gao, *High Temp. Mater. Process.,* Vol 21, 2002, p 167–175
98. Z. Tang, F. Wang, and W. Wu, *Mater. Sci. Eng. A,* Vol 276, 2000, p 70–75
99. Z. Tang, F. Wang, and W. Wu, *Oxid. Met.,* Vol 51, 1999, p 235–250
100. K. Natesan and P.K. Datta, Sulphidation Behaviour, *Intermetallic Coatings and Coatings for Intermetallics, Intermetallic Compounds: Principles and Practice, Vol 3, Progress,* J.H. Westbrook and R.L. Fleischer, Ed., John Wiley & Sons Ltd., 2002, p 707–719
101. P.J. Meschter, *Metall. Trans. A,* Vol 23, (No. 6), 1992, p 1763–1772
102. Y.Q. Liu, G. Shao, and P. Tsakiropoulos, *Intermetallics,* Vol 9 (No. 2), 2001, p 125–136
103. T.E. Tietz and J.W. Wilson, *Behaviour and Properties of Refractory Metals,* Stanford University Press, 1965
104. R. Mitra and V.V. Rama Rao, *Mater. Sci. Eng. A,* Vol 260, 1999, p 146–160
105. B.V. Cockeram, G. Wang, and R.A. Rapp, *Mater. Corros.,* Vol 46, 1995, p 207–217
106. K. Yanagihara, K. Przybylski, and T. Maruyama, *Oxid. Met.* Vol 47 (No. 3–4), 1997, p 277
107. T.C. Chou and T.G. Nieh, *JOM,* Vol 45 (No. 12), 1993, p 15–21
108. R.E. Regan, W.A. Baginski, and C.A. Krier, *Ceram. Bull.,* Vol 46, 1967, p 502–508
109. H.L. Du, P.K. Datta, R. Cutting, and J.S. Burnell-Gray, "Sulphidation Behaviour of Siliconised Mo and Nb by Pack Cementation at 850 °C," presented at the International Conference on Metallurgical Coatings and Thin Films, ICMCTF 2004, April 19–23, 2004 (San Diego, CA), American Vacuum Society
110. E. Fitzer and J. Schwab, *Corrosion,* Vol 12, 1956, p 455–464
111. E. Fitzer, W. Nowak, and H. Mäurer, *Arch. Eisenhüttenwes.,* Vol 49, 1978, p 211–216
112. E. Fitzer, W. Nowak, and H.J. Mäurer, *Materials and Coatings to Resist High Temperature Corrosion,* D.R. Holmes and A. Rahmel, Ed., Applied Science Publishers, London, 1978, p 313–331
113. E. Fitzer, H.J. Mäurer, W. Nowak, and J. Schlichting, *Thin Solid Films,* Vol 64, 1979, p 305–319
114. P. Felix and E. Erdos, *Werkst. Korros.,* Vol 23, 1972, p 627–636
115. E. Erdos, M. Semlitsch, and P. Felix, Z. *Werkstofftech.,* Vol 3, 1972, p 193–197
116. M. Villat and P. Felix, *Tech. Rundsch. Sulzer,* Vol 58, 1976
117. I. Daimer, E. Fitzer, and I. Schlichting, *Thin Solid Films,* Vol 84, 1981, p 119–125
118. E. Fitzer and I. Schlichting, *High Temperature Corrosion,* R.A. Rapp, Ed., NACE-6, National Association of Corrosion Engineers, 1981, p 604
119. H.J. Felten and F.S. Pettit, *Oxid. Met.,* Vol 10, 1976, p 189–223
120. J.S. Sheasby and D.B. Jory, *Oxid. Met.,* Vol 12, 1978, p 527–539
121. K.N. Lee and W.L. Worrell, *Oxid. Met.,* Vol 32, 1989, p 357–369
122. T.C. Chou, *J. Mater. Res.,* Vol 5, 1990, p 378–384

123. R.L. Fleischer, *Platin., Met. Rev.,* Vol 36, 1992, p 139–145
124. D.W. McKee and R.L. Fleischer, *High Temperature Ordered Intermetallics IV,* Vol 213, L.A. Johnson, D.P. Pope, and J.O. Stiegler, Ed., Materials Research Society, 1991, p 969–974
125. E.J. Felten, *Trans. Metall. Soc. AIME,* Vol 245, 1969, p 1349–1355
126. R.M. Paine, A.J. Stonehouse, and W.W. Beaver, *Corrosion,* Vol 20, 1964, p 307–313
127. E.A. Aitken, *Intermetallic Compounds,* J.H. Westbrook, Ed., Wiley, 1967, p 491–516
128. R.A. Buchanan, J.G. Kim, R.E. Ricker, and L.A. Heldt, *Oxidation and Corrosion of Intermetallic Alloys,* G.E. Welsch and P.D. Desai, Ed., Purdue University, HTMIAC/CINDAS, 1996, p 351–419
129. R.A. Buchanan, J.G. Kim, R.E. Ricker, and L.A. Heldt, *Physical Metallurgy and Processing of Intermetallic Compounds,* N.S. Stoloff and V.K. Sikka, Ed., Chapman and Hall, 1996
130. D.J. Duquette, *Mater. Sci. Eng. A,* Vol 198 (No. 1–2), 1995, p 205–211
131. N.S. Stoloff, M. Shea, and A. Castagna, *Environmental Effects on Advanced Materials,* R.H. Jones and R.E. Ricker, Ed., The Minerals, Metals and Materials Society, 1991, p 3–19
132. N.S. Stoloff, C.T. Liu, and S.C. Deevi, *Intermetallics,* Vol 8, 2000, p 1313–1320
133. R.G. Buchheit, R.K. Boger, M.C. Carroll, R.M. Leard, C. Paglia, and J.L. Searles, *JOM,* Vol 53, 2001, p 29–33, 36
134. U. Bertocci, W.J. Boettinger, C.A. Handwerker, and S.M. Hues, *Corrosion and Reliability of Electronic Materials and Devices,* R.B. Comizzoli and J.D. Sinclair, Ed., *Vol. Proc. of the Second Int. Sym.,* The Electrochemical Society, 1992, p 99–118
135. M. Pourbaix, *Atlas of Electrochemical Equilibria in Aqueous Solutions,* NACE International, 1974
136. R.E. Ricker and U. Kattner, NIST, Gaithersburg, MD, communication to D. Wang, Lehigh Univ., 1997
137. R.E. Ricker, *International Symposium on Nickel and Iron Aluminides: Processing, Properties and Applications,* S.C. Deevi, V.K. Sikka, P.J. Maziasz, and R.W. Cahn, Ed., ASM International, 1997, p 253–263
138. H.H. Uhlig, *Corrosion and Corrosion Control,* 2nd ed., John Wiley & Sons, 1971
139. M.G. Fontana and N.D. Greene, *Corrosion Engineering,* McGraw-Hill Book Co., 1978
140. K. Sieradzki, R.R. Corderman, K. Shukla, and R.C. Newman, *Philos. Mag. A,* Vol 59, 1989, p 713–746
141. R.G. Buchheit, M.A. Martinez, and L.P. Montes, *J. Electrochem. Soc.,* Vol 147, 2000, p 119–124
142. R.G. Buchheit, L.P. Montes, M.A. Martinez, J. Michael, and P.F. Hlava, *J. Electrochem. Soc.,* Vol 146, 1999, p 4424–4428
143. U. Bertocci, R.E. Ricker, D.E. Hall, P.V. Madsen, and J.L. Fink, *Corros. Sci.,* Vol 31, 1990, p 471–478
144. R.E. Ricker, *Mater. Sci. Eng. A,* Vol 198, 1995, p 231–238
145. W. Latimer, *Oxidation Potentials,* 2nd ed., Prentice Hall, 1952
146. T. Hagyard and J.R. Williams, *Trans. Faraday Soc.,* Vol 57, 1961, p 2288–2294
147. A.A. Adams and R.T. Foley, *Corrosion,* Vol 31, 1975, p 84
148. M.R. Stoudt, A.K. Vasudevan, and R.E. Ricker, *Corrosion Testing of Aluminum Alloys,* STP 1134, V.S. Agarwala and G. Ugiansky, Ed., ASTM, 1992
149. R.G. Davies and N.S. Stoloff, *Philos. Mag.,* Vol 12, 1965, p 297–304
150. R.G. Davies and N.S. Stoloff, *Trans. AIME,* Vol 230, 1964, p 391–395
151. G.M. Camus, N.S. Stoloff, and D.J. Duquette, *Acta Metall.,* Vol 37, 1989, p 1497–1501
152. A.K. Kuruvilla and N.S. Stoloff, *Scr. Metall.,* Vol 19, 1985, p 83–87
153. R.E. Ricker, D.E. Hall, and J.L. Fink, *Scr. Metall. Mater.,* Vol 24, 1990, p 291–296
154. R.E. Ricker, M.R. Stoudt, and J.L. Fink, *Hydrogen Embrittlement of Ductile Nickel Aluminide during Corrosion in Aqueous Solutions,* TMS/AIME, 1990
155. C.T. Liu, E.H. Lee, and C.G. McKamey, *Scr. Metall.,* Vol 23, 1989, p 875–880
156. C.T. Liu and W.C. Oliver, *Scr. Metall. Mater.,* Vol 25, 1991, p 1933–1937
157. C.T. Liu and N.S. Stoloff, *Diffusion in Ordered Alloys,* The Minerals, Metals and Materials Society, 1993, p 223–246
158. R.W. Staehle, *Mechanisms of Environment Sensitive Cracking of Materials,* P.R. Swann, F.P. Ford, and A.R.C. Westwood, Ed., The Metals Society, London, U.K., 1977, p 574–602
159. R.W. Staehle, *Environment-Induced Cracking of Metals,* Vol 10, R.P. Gangloff and M.B. Ives, Ed., NACE International, 1989, p 561–612
160. M.F. Ashby, C. Gandhi, and D.M.R. Taplin, *Acta Metall.,* Vol 27, 1979, p 699–729
161. R.J. Fields, T. Weerasooriya, and M.F. Ashby, *Metall. Mater. Trans. A,* Vol 11, 1980, p 333–347
162. C. Gandhi and M.F. Ashby, *Acta Metall.,* Vol 27, 1979, p 1565–1602
163. R.E. Ricker, *JOM,* Vol 47, 1995, p 32–35
164. R.A. Buchanan and J.G. Kim, "Aqueous Corrosion Characteristics of Nickel Aluminides: Final Report," Univ. of Tennessee, final report to Nickel Development Institute, 1988
165. R.A. Buchanan and J.G. Kim, "Aqueous Corrosion of Iron Aluminides," Univ. of Tennessee, report to Oak Ridge National Laboratory, 1989

SELECTED REFERENCES

- M. Bachorczyk, M. Danielewski, P.K. Datta, and R. Filipek, Model of Heterogeneous Reaction Controlled by Diffusion, *J. Molecular Liq.,* Vol 86, 2000, p 61
- M. Bachorczyk, M. Danielewski, P.K. Datta, R. Filipek, and G. Fisher, Computer Simulations of Heterogeneous Reactions Controlled by Diffusion in Modified Aluminide Coatings on a Nickel-Based Superalloy, *Solid State Phenom.,* Vol 72, 2000, p 53–58
- M. Berlanga, J.L. González-Carrasco, M.A. Montealegre, and M.A. Muñoz-Morris, Oxidation Behaviour of Yttria Dispersion Strengthened Fe40Al Alloy Foils, *Intermetallics,* Vol 12, 2004, p 205–212
- P.K. Datta, R. Filipek, and M. Danielewski, Interdiffusion Issues in Pt-Modified NiAl Coatings, *Defect Diffus. Forum,* Vol 203–295, 2002, p 47–60
- V. Gauthier, F. Dettenwanger, and M. Schutze, Oxidation Behavior of γ-TiAl Coated with Zirconia Thermal Barriers, *Intermetallics,* Vol 10, 2002, p 667–674
- D. Griffin, A. Daadbin, and P.K. Datta, Deformation and Fracture, during Cooling, of the Alumina Scale Developed on Fe_3Al, *Surf. Coat. Technol.,* Vol 126, 2000, p 142–151
- J. Kumpfert, Intermetallic Alloys Based on Orthorhombic Titanium Aluminide, *Adv. Eng. Mater.,* Vol 3, 2001, p 851–864
- F. Lang, Z. Yu, S. Gedevanishvili, S.C. Deevi, and T. Narita, Effect of Pre-Oxidation on the Corrosion Behaviour of Fe-40Al Sheet in a N_2-11.2O_2-7.5CO_2-500 ppm SO_2 Atmosphere at 1273 K, *Intermetallics,* Vol 11, 2003, p 129–134
- M.K. Lei, X.P. Xhu, and X.J. Wang, Oxidation Resistance of Ion-Implanted γ-TiAl-Base Intermetallics, *Oxid. Met.,* Vol 58, 2002, p 361–374
- Z. Li, W. Gao, J. Liang, and D.L. Zhang, Oxidation Behaviour of Ti_3Al-TiC Composites, *Mater. Lett.,* Vol 57, 2003, p 1970–1976
- Z. Li, W. Gao, M. Yoshihara, and Y. He, Improving Oxidation Resistance of Ti_3Al and TiAl Intermetallic Compounds with Electro-Spark Deposit Coatings, *Mater. Sci. Eng. A,* Vol 347, 2003, p 243–252.
- Z. Liu and T. Narita, The Effect of Water Vapor on the Oxidation Behaviour of γ-TiAl-Ag Coatings at 1073 K in Air, *Intermetallics,* Vol 11, 2003, p 795–805.
- X.K. Meng, H. Shen, H. Vehoff, S. Mathur, and A.H.W. Ngan, Fractography, Elastic Modulus, and Oxidation Resistance of Novel Metal-Intermetallic Ni/Ni_3Al Multilayer Films, *J. Mater. Res.,* Vol 17, 2002, p 790–796
- S. Naka, M. Thomas, and T. Khan, Potential and Prospects of Some Intermetallic Compounds for Structural Applications, *Mater. Sci. Technol.,* Vol 8, 1992, p 291–298
- E.C.T. Ramos, G. Silva, A.S. Ramos, C.A. Nunes, and C.A.R.P. Baptista, Microstructure and Oxidation Behaviour of Ti-Si-B Alloys, *Mater. Sci. Eng. A,* Vol 363, 2003, p 297–306

- M. Schutze, Z. Schumacher, F. Dettenwanger, U. Hornauer, E. Richter, E. Wieser, and W. Moller, The Halogen Effect in the Oxidation of Intermetallic Titanium Aluminides, *Corros. Sci.,* Vol 44, 2002, p 303–318
- J.L. Smialek, J.A. Nesbitt, C.A. Barrett, and C.E. Lowell, Cyclic Oxidation Testing and Modeling, a NASA Lewis Perspective, *Eur. Fed. Corros. Pub.,* Vol 27, 1999, p 148–168
- V. Supatarawanich, D.R. Johnson, and C.T. Liu, Effects of Microstructure on the Oxidation Behaviour of Multiphase Mo-Si-B Alloys, *Mater. Sci. Eng. A,* Vol 344, 2003, p 328–339
- Third International Symposium on Structural Intermetallics, Sept 23–27, 2001 (Jackson Hole, WY), The Minerals, Metals and Materials Society
- F. Wu, H. Murakami, and H. Harada, Cyclic Oxidation Behavior of Iridium-Modified Aluminide Coatings for Nickel-Base Single Crystal Superalloy TMS-75, *Mater. Trans.,* Vol 44, 2003, p 1675–1678
- Z.D. Xiang and P.K. Datta, Deposition of Si Modified Aluminide Coatings on Nickel Base Superalloys by Pack Cementation Process, *Mater. Sci. Technol.,* Vol 19, 2003, p 935–942
- Z.D. Xiang, S.R. Rose, and P.K. Datta, Oxidation Resistance of Diffusion Coatings Formed by Pack-Codeposition of Al and Si on γ-TiAl, *J. Mater. Sci.,* Vol 39, 2004, p 2099–2106
- H. Yokota, T. Kudoh, and T. Suzuki, Oxidation Resistance of Boronized $MoSi_2$, *Surf. Coat. Technol.,* Vol 169–170, 2003, p 171–173
- L. Zhao and E. Lugscheider, High Velocity Oxy-Fuel Spraying of a NiCoCrAlY and an Intermetallic NiAl-TaCr Alloy, *Surf. Coat. Technol.,* Vol 149, 2002, p 231–235

ASM Handbook, Volume 13B: Corrosion: Materials
S.D. Cramer, B.S. Covino, Jr., editors, p513-525
DOI: 10.1361/asmhba0003838

Corrosion of Cemented Carbides

CEMENTED CARBIDES consist of hard refractory metal compounds that have a lower-melting-temperature ductile metal binder or cement. Internationally, the term *hardmetal* is used in preference to the term *cemented carbides,* which is used almost exclusively in the United States. Figure 1 shows microstructures of both the basic tungsten carbide-cobalt (WC-Co) materials and materials containing titanium carbide (TiC) and tantalum carbide (TaC). Table 1 indicates the physical properties of the commonly available refractory metal or hardmetal carbides used to make cemented carbides. Only two—WC and TiC—are used as true base compound materials that comprise over 50% of the composition. Tungsten carbide base materials are by far the most predominant and have been in widespread use for more than 70 years. They were originally used as early as 1916 (Ref 3–5). During this time, it was found that WC could be combined with cobalt to make a high-hardness, wear-resistant, strong material. This material was initially used in dies for drawing tungsten filament wires instead of expensive diamond dies.

The first key to the successful development of cemented carbides was that these refractory metal compounds, particularly WC, are best produced as powders. In fact, the only logical way to produce tungsten is the hydrogen reduction of WO_3 or ammonium paratungstate powder into tungsten metal powder. The carburization of tungsten to WC also results in a fine powder. The second key was the discovery of the eutectic system WC-Co (Fig. 2). Liquid-phase sintering is possible well below the melting point of the WC and even below the melting point of cobalt.

Cemented WC is produced by mixing from 3 wt% or less up to as much as 30 wt% of cobalt metal powder with a balance of WC powder. The mixed powders are ball milled, generally in volatile solvents, for times ranging from a few hours to as long as 7 days. Alternatively, the powders are milled in an attritor for 1 to 10 h.

A suitable transient binder is added to the powder, which is then pelletized and pressed to form the shape. Finally, the part is sintered at temperatures between 1300 and 1600 °C (2370 and 2910 °F), most often in vacuum. Because a liquid phase is formed during sintering, virtually 100% density is achieved. More information on the production of cemented carbides is available in the article "Powder Metallurgy Cermets and

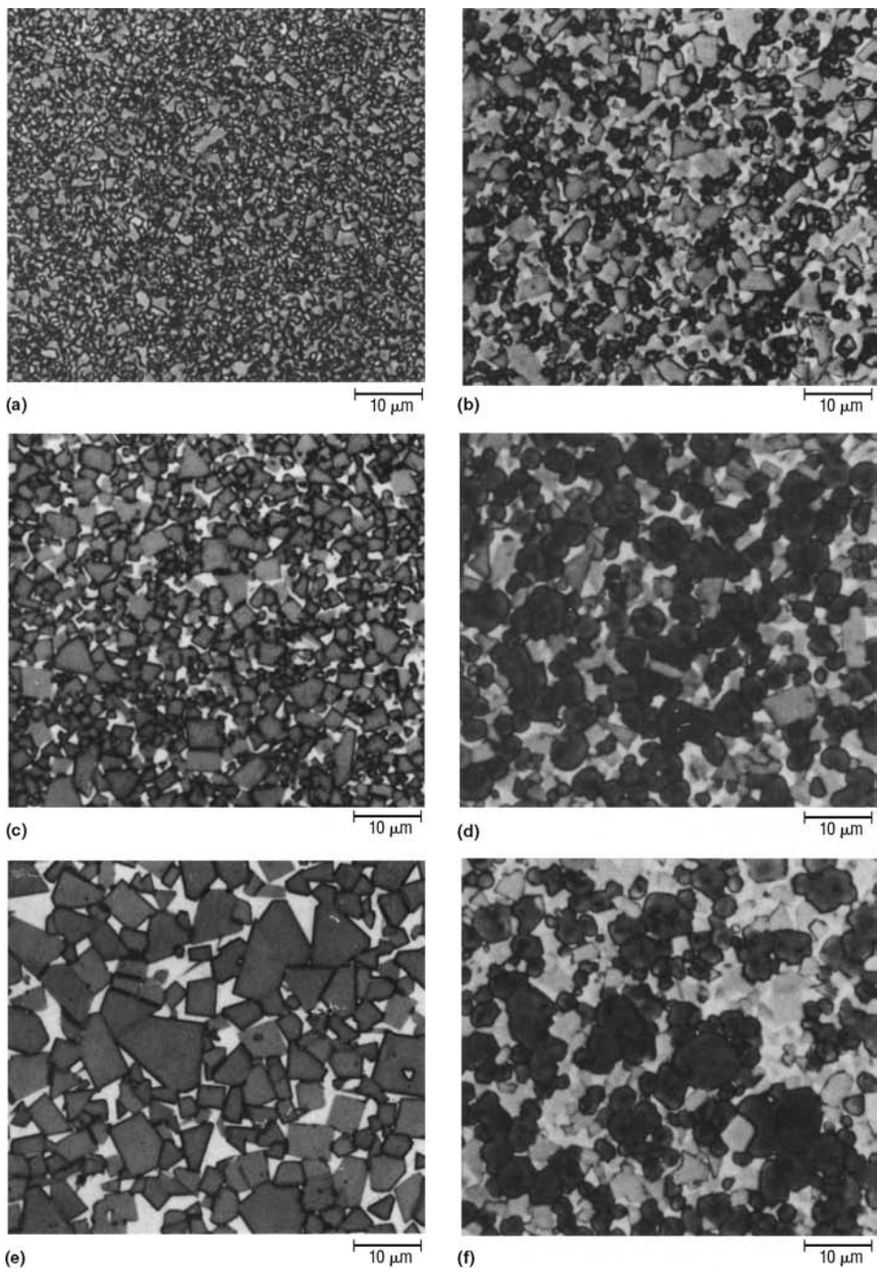

Fig. 1 Microstructures of WC-Co (a, c, and e) and WC-TaC-TiC-Co (b, d, and f) cemented carbides. In a, c, and e, the white areas are cobalt binder phase. In b, d, and f, the darker, more rounded grains are the $W_xTa_yTi_zC$ cubic solid-solution γ phase. (a) and (b) Fine grain structures. (c) and (d) Medium grain structures. (e) and (f) Coarse grain structures. Original magnification all 1500×. Source: Ref 1, 2

Cemented Carbides" in *Powder Metal Technologies and Applications,* Volume 7, *ASM Handbook,* 1998.

Effect of Composition on Properties

The two most common variables in cemented carbides are the cobalt or binder content and the grain size. As shown in Fig. 3, increased grain size decreases hardness, and increased cobalt content also decreases hardness (Ref 6). Increased contents of cobalt or other binders, however, are necessary to increase strength. As shown in Fig. 4, transverse rupture strength increases with increased cobalt content, to a maximum at approximately 15 to 18% Co (Ref 6). Very high impact strength requires very high cobalt contents (up to 25 or 30 wt%) and coarse-grain carbide. In corrosion applications, however, the binder content ranges from virtually nil (there are some so-called "binderless" compositions that actually contain 1 to 2% binder) up to approximately 10%, with exceptions running up to 15% binder.

Cemented carbides are not selected for corrosion applications per se. They are extremely important in corrosion conditions in which high hardness, wear resistance, or abrasion resistance is required. When this is the case and the selection of a cemented carbide is logical, the corrosion-resistant properties are examined. For ordinary corrosion resistance, many metals and ceramics are better choices, but when wear resistance is also a requirement, the cemented carbide is needed.

Binder Composition and Content. The corrosion resistance of cemented carbides is based on the two very different components. The cobalt binder has very poor corrosion and oxidation resistance, and the WC has excellent corrosion resistance and good oxidation resistance. Alternate binders, such as nickel, have better corrosion resistance than cobalt and are used in spite of their lower hardness and strength. Nickel is a superior binder for cemented TiC and therefore is used in all cemented TiC materials regardless of the need for hardness and strength. In some applications, cemented TiC shows superior corrosion resistance, and in other applications, cemented WC is better.

The addition of nickel to the usual cobalt binder used for WC, or the substitution of it entirely for cobalt, always improves corrosion resistance. There is, however, a sacrifice in strength, hardness, and wear resistance. A chromium addition also enhances corrosion resistance.

The most important variable in the corrosion of cemented carbides is the binder content. Because the binder corrodes more than the carbide, the smaller the amount of binder the better. On the other hand, decreasing the binder decreases the strength.

Carbides. Additions of TaC and TiC to the WC-Co materials are common for the compositions used for machining steel. These additives give the carbide crater resistance. Cratering on the top of a metal-cutting insert is the result of a physicochemical reaction. The addition of TaC and/or TiC will slow this reaction; indeed, it has been found that TaC also enhances the outright chemical corrosion resistance of these materials.

Other additives, such as chromium carbide (Cr_2C_3), molybdenum carbide (Mo_2C), niobium carbide (NbC), and vanadium carbide (VC), are often added in small quantities as grain growth inhibitors. Little has been published about their effect on corrosion, but chromium has been shown to be a beneficial binder additive to WC-Ni binder compositions (Ref 7). Vanadium carbide and Mo_2C will probably have a weakening effect on the strength of a WC-base hardmetal.

For TiC-base hardmetals, Mo_2C is invariably added to the composition, but there are no known studies of the effect of molybdenum on corrosion resistance. The molybdenum has always been added to enhance the liquid-phase sintering of the TiC-base compositions. In general, these compositions have been made for their hardness and strength characteristics, with corrosion resistance being a secondary consideration. Most recent TiC-base compositions have titanium nitride (TiN) added, and this has been shown to improve the corrosion resistance (Ref 8).

Perhaps it is not surprising that compositions developed primarily for machining should show improved corrosion resistance. In machining, there is heat with resultant oxidation and often corrosion-like mechanisms. Thus, some of the improved machining compositions also show better corrosion behavior. On the other hand, optimal corrosion resistance is obtained by tailoring the composition and amount of the binder phase. This can result in lower-strength materials with limited usefulness in machining applications.

Because carbon is the basis of cemented carbides, its variation within a given composition is very important to properties and corrosion resistance. Figure 5 shows the range of carbon content allowable in the simple WC-Co compositions as cobalt content is varied (Ref 9–11).

Table 1 Physical properties of carbides used in the manufacture of cemented carbides

Carbide	Micro-hardness, kg/mm^2	Melting point °C	Melting point °F	Density, g/cm^3
TiC	3200	3200	5790	4.94
VC	2950	2830	5125	5.71
HfC	2700	3890	7030	12.76
ZrC	2560	3530	6385	6.56
NbC	2400	3500	6330	7.80
Cr_2C_3	2280	1895	3440	6.66
WC	2080	2600	4710	15.67
Mo_2C	1950	2675	4850	9.18
TaC	1790	3780	6835	14.50

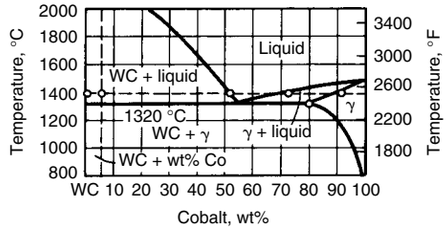

Fig. 2 Quasi-binary phase diagram for the WC-Co system

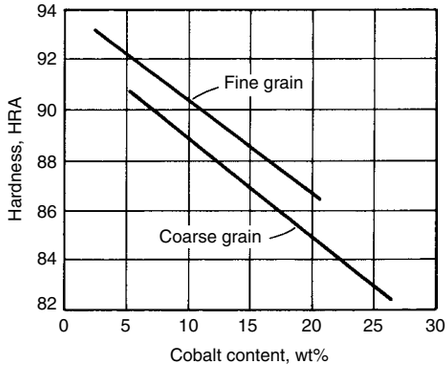

Fig. 3 Effect of cobalt content and grain size on the hardness of WC-Co cemented carbides

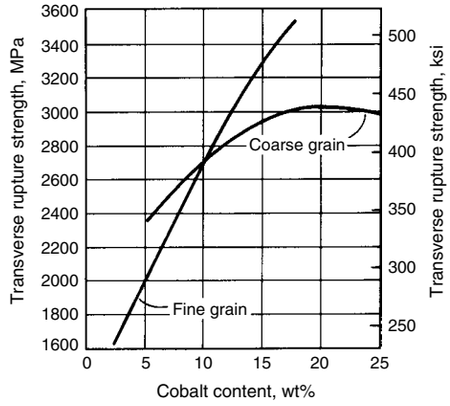

Fig. 4 Effect of cobalt content and grain size on the transverse rupture strength of WC-Co cemented carbides

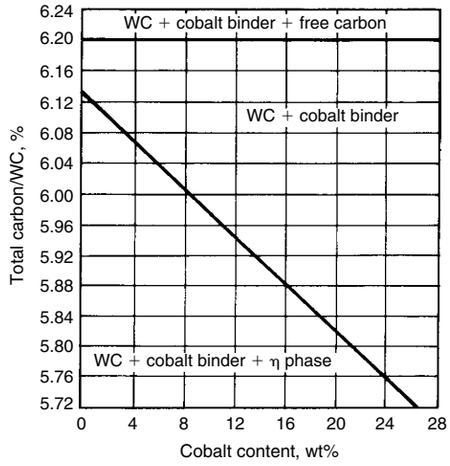

Fig. 5 Effect of cobalt content and carbon content on the phases present in WC-Co cemented carbides

Corrosion-resistant compositions have three problems:

- The lower the cobalt or binder content, the better the resistance to corrosion, but this limits the safe zone, in which neither carbon porosity nor η phase (hard, brittle M_6C or $M_{12}C$ intermetallics) exists.
- The lower the carbon content, the better the corrosion resistance, but falling into the η-phase zone results in embrittlement of the material.
- The addition of alternate binders, such as nickel, decreases the safe zone.

Table 2 C-grade classification of cemented carbides

C-grade	Application category
Machining of cast iron, nonferrous, and nonmetallic materials	
C-1	Roughing
C-2	General-purpose machining
C-3	Finishing
C-4	Precision finishing
Machining of carbon and alloy steels	
C-5	Roughing
C-6	General-purpose machining
C-7	Finishing
C-8	Precision finishing
Nonmachining applications	
C-9	Wear surface, no shock
C-10	Wear surface, light shock
C-11	Wear surface, heavy shock
C-12	Impact, light
C-13	Impact, medium
C-14	Impact, heavy

In making corrosion-resistant cemented carbides, manufacturers must be aware of these problems and limitations. Information on the metallography and microstructures of these materials is available in the article "Cemented Carbides: Metallographic Techniques and Microstructures" in *Metallography and Microstructures,* Volume 9, *ASM Handbook,* 2004.

Applications of Cemented Carbides

The major applications of cemented carbides involve environments that are inherently corrosive. For example, the major use of cemented carbides is for metal-cutting (machining) applications. In these applications, extreme heat is generated and the tool temperature rises whether or not coolants are used, and in those cases in which coolants are used, the corrosive attack of the coolant is a factor in the performance of the cutting tool. In general, however, very little heed is paid to this factor; cemented carbides are more often chosen for their wear resistance in such applications as mining and oil well drilling. There is a corrosive environment in mining (Ref 12) and oil well drilling; the natural waters and other fluids involved are often very corrosive. Other well-known examples in which cemented carbide perform in a corrosive environment include balls for ballpoint pens and dental drills. In both of these examples, the corrosion resistance of the most frequently used WC-6Co composition was serendipitous. The material was selected for its wear resistance. It just happens to have good corrosion resistance in the saline and ink solutions. The dulling of cemented carbide saw tips used for sawing green or unseasoned wood is a corrosive as well as a wear phenomenon (see the section "Saw Tips and Corrosion" in this article).

Table 3 Some physical properties of corrosion-resistant cemented carbide grades

Properties of a carbon steel, a tool steel, and a cast cobalt alloy are included for comparison.

Special attributes	Proprietary designation	Nominal composition, wt%							Hardness, HRA	Density, g/cm³	Transverse rupture strength		Abrasion resistance factor(a)	Coefficient of thermal expansion, μm/m · K	Thermal conductivity	
		WC	Co	TaC	TiC	Ni	Cr	Mo_2C			MPa	ksi			W/m · k	cal/cm · s · °C
Abrasion-resistant, wear, and structural grades																
Maximum abrasion resistance	GU-2(b)	96.5	3	0.5	...	...	...	...	93.3	15.30	1655	240	1.8	4.9	125.5	0.30
	PWX(b)	94.0	5.5	0.5	...	...	...	...	92.5	15.05	2137	310	2.1	5.2	108.8	0.26
	A(b)	94.0	6.0	...	...	...	...	...	91.8	15.00	2206	320	3.4	5.5	104.6	0.25
	B(b)	91.0	9.0	...	...	...	...	...	90.8	14.70	2758	400	6.8	5.5	96.2	0.23
	BB(b)	87.0	13.0	...	...	...	...	...	89.5	14.28	3103	450	17	6.2	87.9	0.21
Toughness	GU-1(b)	81.5	18.0	0.5	...	...	...	...	88.4	13.84	3448	500	32	6.8	83.7	0.20
Gall resistance	474(b)	79.0	12	9	...	...	...	...	89.6	14.29	2241	325	16.5	5.8	87.9	0.21
	GG(b)	60.0	12	28	...	...	...	...	89.0	14.09	2069	300	18	7.1	83.7	0.20
Oxidation resistance	Titan 80(b)	...	...	...	74	12.5	...	13.5	93.0	5.63	1379	200	22	7.8	16.7	0.04
	Titan 60(b)	...	...	...	70.5	17.5	1.0	11.0	91.7	5.71	1724	250	28	8.4	16.7	0.04
	Titan 50(b)	...	...	...	66.5	22.5	1.0	10.0	...	...	...	...	...	...	...	...
Special corrosion resistance	K602(c)	88.2	1.8	10.0	...	...	...	...	94.3	15.6	759	110	...	4.9	...	...
	K701(c)	85.8	10.1	...	...	...	4.1	...	92.0	14.0	1138	165	...	6.5	62.8	0.15(d)
	K703(c)	93.3	5.8	...	...	...	0.9	...	91.5	14.7	1931	280	...	4.5	...	...
	K714(c)	88.4	6.1	4.5	1.0	...	...	...	92.5	13.1	1827	265	1.8(d)	4.0	...	...
	K801(c)	93.7	...	0.3	...	6.0	...	...	90.0	14.8	2103	305	17(d)	5.6	96.2	0.23(d)
	K803(c)	89.0	...	...	1.0	10.0	...	...	91.0	14.4	2000	290	...	5.6	...	...
Grades for heading and forming dies																
Impact resistance	HD-15(b)	85.0	15	...	...	...	...	...	87.4	14.10	3172	460	30	6.5	83.7	0.20
	HD-20(b)	80.0	20	...	...	...	...	...	85.3	13.60	3103	450	45	6.8	83.7	0.20
	HD-25(b)	75.0	25	...	...	...	...	...	83.5	13.15	2965	430	65	7.5	83.7	0.20
Gall resistance	HD-20T(b)	75.0	20	5	...	...	...	...	85.3	13.55	2896	420	46	7.1	83.7	0.20
	HD-25T(b)	70.0	25	5	...	...	...	...	83.5	13.15	2827	410	67	7.8	83.7	0.20
Mining grades																
Strength and impact resistance	575(b)	94.0	6	...	...	...	...	...	90.8	15.00	2413	350	8.1	4.9	104.6	0.25
	569(b)	90.0	10	...	...	...	...	...	88.6	14.51	2930	425	13	5.8	104.6	0.25
	783(b)	89.0	11	...	...	...	...	...	88.1	14.41	3103	450	19	5.8	104.6	0.25
	502(b)	88.0	12	...	...	...	...	...	87.6	14.31	2965	430	21	6.2	104.6	0.25
Noncarbide metals																
Carbon steel	...	...	...	...	...	...	...	...	To 79	7.8	To 1379 (tensile strength)	200	>140	14.8	50.2	0.12
T1 tool steel	...	...	...	...	...	...	...	...	To 87	8.7	3448	500	70	12.6	...	...
Cast Co-Cr-W alloy	...	...	...	...	...	...	...	...	To 83	8.6	2069	300	110	13–16	...	...

(a) Determined in accordance with ASTM B 657 (Ref 2). The lower the number, the better the resistance to abrasion. (b) Adamas designation (former). (c) Kennametal designation (now Hertel Kennametal). (d) Values estimated from available data. Source: Ref 14, 15

Examples of the use of cemented carbide in true corrosion applications include the following:

- Ballpoint pen balls
- Dental drills and burrs
- Surgical and orthodontic tweezers, pliers, and clamps
- Valve seats
- Valve balls and valve stems
- Valve and shaft seals (seal rings)
- Spray nozzles
- Pulverizing hammers
- Compressor plungers
- Bearings
- Cage mills
- Ball mill linings and balls
- Internal parts in industrial meters

The article "Powder Metallurgy Cermets and Cemented Carbides" in *Powder Metal Technologies and Applications,* Volume 7, *ASM Handbook,* 1998, contains more information on applications for cemented carbides.

Selection of Cemented Carbides for Corrosion Applications

The selection of cemented carbides is a difficult problem for the user, because there is no universally accepted classification system on the part of the producers. The most commonly used systems are given here. Attempts have been made to standardize with regard to metal-cutting applications. The International Organization for Standardization (ISO) standard 513 addresses application of carbides for machining by chip removal (Ref 13). It is widely used in Europe and most other parts of the industrial world. The ISO standard does not include hardmetal used for wear, percussion tools, mining, or wire-drawing dies. In the United States, an application-oriented C-grade system is used (Table 2). Carbide manufactures provide reference to both systems.

The reason for the multiple designations of the same composition is that one designation may be for cutting tools, another for wear parts or dies, and another for mining. Composition may vary among manufacturers. For example, if one producer establishes a WC-25Co composition, another producer will make and market a grade with 24% Co, and another a product with 26% Co. Despite these differences, Table 3 lists the properties of various representative grades by nominal composition for corrosion applications. Reference 16 contains more complete data on any grade, and manufacturers can be consulted for more information.

In addition to small differences in cobalt content from one manufacturer to another, there are small differences in minor additives and in grain size. For example, with the 6% Co grades, there are two basic grain size classes—fine and coarse—but these two are not precisely the same from one manufacturer to another. Some have a slightly finer or coarser size within the defined category of fine and coarse (Ref 17). Another factor is the intentional addition of minor elements such as tantalum, titanium, vanadium, chromium, and molybdenum as grain growth inhibitors or the inadvertent introduction of minor amounts of these and other elements in the raw materials or through recycling. These elements affect hardness and strength and cannot be discounted in the selection of a cemented carbide for corrosion applications.

Other processing variables also affect properties and performance. Among the important results of processing variables is the amount of porosity in the final cemented carbide product. In some cases, the porosity is negligible, and theoretical density is achieved. In other cases, porosity is present. This can be rated in accordance with ISO 4505 (Ref 18) or ASTM B 276 (Ref 19), both of which are based on the same standard micrographs. The ultimate in freedom from porosity is achieved by hot isostatic pressing. This operation, when carried out properly at approximately 138 MPa (20 ksi) and at temperatures of 1200 to 1400 °C (2190 to 2550 °F), has no detrimental or beneficial effect on the cemented carbide except for the removal of the last vestiges of porosity.

Corrosion in Aqueous Media

The corrosion of cemented carbides is based on the solubility of the key ingredients used in the various compositions. Although some alloying occurs, the solubility of the WC or TiC in cobalt or nickel is very limited. The main alloying in the WC-Co compositions is primarily based on the addition of TiC, TaC, and NbC, which form cubic-phase solid solutions with WC.

Table 4 shows the relative solubilities of the chief constituents of cemented carbides in various media. Tungsten carbide is insoluble in most acids as well as in basic and salt solutions. It is soluble only in very strong mixtures of nitric acid plus hydrochloric acid ($HNO_3 + HCl$) and HNO_3 plus hydrofluoric acid (HF). Cobalt and nickel show the same significant solubility in all acids. Even so, the nickel binder compositions show somewhat less attack in some acid solutions than the cobalt binder alloys. From this elementary information, it is obvious that the lower the binder content, the less the corrosion.

Corrosion of cemented carbides, therefore, is generally based on the surface depletion of the binder phase such that at the surface region only a carbide skeleton remains; because the applications are invariably for wear or abrasion, this skeleton is rapidly worn away. At low

Table 4 Relative solubilities in acids and bases of the basic constituents of cemented carbides

	Medium and solubility(a)						
Constituent	Dilute HNO_3	HCl	H_2SO_4	$20HNO_3$-60HCl-$20H_2O$	$25HNO_3$-25HF-$50H_2O$	Alkali solutions	Salt solutions
Cobalt	V	Sl	Sl	V	V	I	I
Nickel	V	Sl	Sl	V	V	I	I
WC	I	I	I	S	S	I	I
TaC	I	I	Sl?(b)	S	S	I	I
TiC	S	I	I	S	S	I	I

(a) Solubility: V, very soluble; Sl, slightly soluble; I, insoluble; S, soluble (b) Data from Ref 20 and 21 are contradictory. Source: Ref 20, 21

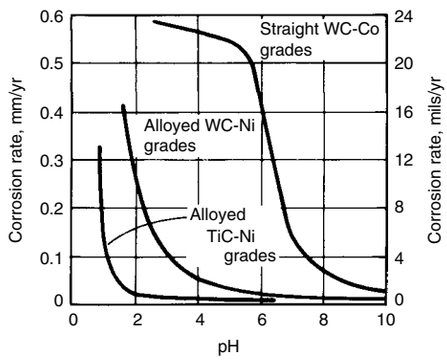

Fig. 6 Corrosion rate of various cemented carbide grades as a function of pH. Source: Ref 22

Table 5 Corrosion resistance of cemented carbides in various media at room temperature

	Corrosion resistance(a)	
Medium	WC-Co cemented carbides	TiC-Ni cemented carbides
Acid salts in water	E	E
Neutral salts in water	V	E
Alkalis		
KOH in water	F-G	F-P
NaOH in water	V	E
NH_3 in water	F	E
Weak acids	G	G-E
Distilled water	E	E
Seawater	V	E
Organic solvents, including acetone, alcohols, gasoline, benzene, carbon tetrachloride, and ethylene glycol	E	E

(a) Corrosion resistance: E, excellent; V, very good; F, fair; G, good; P, poor

Table 6 Corrosion resistance of cemented carbides in various media

Data for two austenitic stainless steels are included for comparison.

Medium	Chemical designation	Concentration, %	Temperature, °C (°F)	pH	Type of cemented carbide/corrosion resistance(a)					Stainless steels(b)	
					WC-Co	TiC-NiMo	WC-Ni	WC-CoCr	WC-TaC-Co	Type 302	Type 316
Acetic acid, unaerated	CH_3COOH	4	Room	...	C	B	B	B	A	...	...
Acetic acid (glacial), unaerated	CH_3COOH	99.8	Room	...	C	C	B	A	A	...	...
Acetone	$(CH_3)_2CO$	...	Room	...	A	A	A	A	A	A	A
Alcohols	...	...	Room	...	A	A	A	A	A	...	...
Ammonia, anhydrous	NH_3	...	...	...	B	B	B	B	A	...	...
Argon gas	Ar	...	...	...	A	A	A	A	A	...	...
Benzene, liquid	C_6H_6	...	Room	...	A	A	A	A	A	...	...
Carbon tetrachloride	CCl_4	Pure	Room	...	A	A	A	A	A	...	...
Chlorine gas, dry	Cl	...	Room	...	C	C	C	C	B	...	...
Chlorine gas, wet	$Cl \cdot H_2O$	...	Room	...	D	C	C	D	B	...	...
Citric acid	$C_3H_4(OH)(COOH)_3$	5	Room	1.7	C	A	A	...	...	A	A
Citric acid	$C_3H_4(OH)(COOH)_3$	5	60 (140)	1.7	D	A	B	...	...	A	A
Copper sulfate solution	$CuSO_4$	0.01	Room	6	C	A	A	...	...	A-C	A-C
Copper sulfate solution	$CuSO_4$	0.01	70 (160)	6	D	A	A	...	...	A-C	A-C
Digester liquor, black	...	...	66 (150)	...	B	B	B	B	A	...	...
Esters	...	...	Room	...	A	A	A	A	A	...	...
Ethanol	C_2H_5OH	96	Room	...	A	A	A	...	...	A	A
Ethylene glycol	$C_2H_6O_2$	...	Room	...	A	A	A	A	A	...	...
Ferrous sulfide	FeS	Slurry in water	Room	...	C	C	C	C	A	...	...
Fluorine, liquid	F	...	−188 (−305)	...	...	B	...	...	...	...	...
50% formaldehyde, 50% alcohol	...	...	Room	...	C	Uncoupled B Coupled C(c)	C	C	A	...	...
Formic acid	HCOOH	5	Room	...	C	A	C	...	...	A	A
Formic acid	HCOOH	5	60 (140)	1.8	D	A	...	...	...	B	A
Freon gas	$C_2Cl_3F_3/CH_2Cl_3$	...	Room	...	A	A	A	A	A	...	...
Gasoline	...	...	Room	...	A	A	A	A	A	...	...
Helium, liquid	He	...	−269 (−450)	...	A	A	A	A	A	...	...
Hydrochloric acid	HCl	0.5	Room	1	D	C	C	...	...	C	A
Hydrochloric acid	HCl	0.5	60 (140)	1	D	C	C	...	...	D	A
Hydrochloric acid	HCl	10	Room	...	D	D	D	...	...	D	C
Hydrochloric acid	HCl	37	Room	...	D	D	D	D	A	...	...
Hydrochloric acid	HCl	37	100 (212)	...	D	D	D	D	B	...	...
Hydrofluoric acid, anhydrous	HF	...	Room	...	B	B	B	B	A	...	...
Hydrofluoric acid	HF	1–60	Room	...	D	D	D	D	D	...	...
Hydrogen, liquid	H	...	253 (488)	...	A	A	A	A	A	...	...
Kerosene	...	...	Room	...	A	A	A	A	A	...	...
Magnesium bisulfite digester liquor	$MgHSO_3$	...	Room	...	B	B	B	B	A	...	...
Methane, liquid	CH_4	...	162 (342)	...	A	A	A	A	A	...	...
Methanol, anhydrous	CH_3OH	...	Room	...	A	A	A	A	A	...	...
Methanol, 20% water	CH_3OH/H_2O	...	Room	...	A	A	A	A	A	...	...
Nitric acid	HNO_3	0.5	Room	1.1	D	C	A	...	...	A	A
Nitric acid	HNO_3	5	Room	...	D	D	D	D	B	...	...
Nitric acid	HNO_3	...	100 (212)	...	D	D	D	D	B	...	...
Nitric acid	HNO_3	10	Room	...	D	B	C	...	...	A	A
Nitrogen, liquid	N	...	196 (385)	...	A	A	A	A	A	...	...
Oil, crude (sand, saltwater, high in sulfur)	...	...	Room	...	C	C	C	C	A	...	...
Oxalic acid	$(COOH)_2 \cdot 2H_2O$	5	Room	1	A-B	A	A	...	...	A	A
Oxalic acid	$(COOH)_2 \cdot 2H_2O$	5	60 (140)	1	B-C	A	...	...	...	B	A
Oxygen, liquid	O	...	183 (361)	...	A	A	A	A	A	...	...
Perchloric acid	$HClO_4$	0.5	Room	1.3	C-D	A	C	...	...	D	...
Perchloric acid	$HClO_4$	0.5	60 (140)	1.3		D	A	D	...	D	D
Phosphoric acid	H_3PO_4	5	Room	1.2	D	B	C	...	...	A	A
Phosphoric acid	H_3PO_4	85	Room	...	D	C	C	D	A	...	...
Crude phthalic acid and anhydride	C_6H_4-1.2$(COOH)_2$/ C_6H_4-1.2$(CO)_2O$	...	250–280 (480–535)	...	C	C	B	C	A	...	...
Sodium carbonate	Na_2CO_3	5	Room	12	A	A	A	...	...	A	A
Sodium carbonate	Na_2CO_3	5	60 (140)	12	A	A	A	...	...	A	A
Sodium chloride	NaCl	3	Room	7	A-B	A	A	...	...	A	A
Sodium chloride	NaCl	3	60 (140)	7	A-B	A	A	...	...	A	A
Sodium cyanide	NaCN	10	Room	...	D	D	D	D	A	...	...
Sodium hydrogen sulfate	$NaHSO_4$	5	Room	1.2	C-D	A	A-B	...	...	D	A
Sodium hydrogen sulfate	$NaHSO_4$	5	60 (140)	1.2	D	C	C-D	...	...	D	A
Sodium hydroxide	NaOH	5	Room	14	A	A	A	...	...	A	A
Sodium hydroxide	NaOH	5	60 (140)	14	B	A	A	...	...	A	A
Sodium hydroxide	NaOH	40	Room	16	A	A	A	...	...	A	A
Sodium hydroxide	NaOH	40	60 (140)	16	A	A	A	...	...	A	A
Steam, superheated	H_2O	...	600 (1110)	...	A	A	A	A	A	...	...

(continued)

(a) A, highly resistant, negligible attack; B, resistant, light attack; C, poor resistance, medium attack; D, not resistant, not suitable. This table should be used only as a guide. Many factors, such as temperature variations, changes in chemical environment, purity of solutions, and stress or loading conditions, may invalidate these recommendations. Tests under operating conditions should be made (b) Results were obtained under laboratory conditions in pure solutions and are classified with reference to corrosion resistance only (c) Coupled to brass. Source: Ref 22, 23

Table 6 (continued)

Medium	Chemical designation	Concentration, %	Temperature, °C (°F)	pH	Type of cemented carbide/corrosion resistance(a)					Stainless steels(b)	
					WC-Co	TiC-NiMo	WC-Ni	WC-CoCr	WC-TaC-Co	Type 302	Type 316
Sulfuric acid	H_2SO_4	0.5	Room	1.2	C-D	A	B-C	...	...	C	A
Sulfuric acid	H_2SO_4	0.5	60 (140)	1.2	D	D	D	...	...	D	A
Sulfuric acid	H_2SO_4	5	Room	...	C	B	C	C	A	...	...
Sulfuric acid	H_2SO_4	5	100 (212)	...	D	C	C	D	A	...	...
Sulfuric acid	H_2SO_4	10	Room	0	D	D	B	...	...	D	A
Sulfuric acid	H_2SO_4	10	60 (140)	0	D	D	...	...	...	D	D
Sulfur, liquid	S	100	130 (265)	...	A	A	...	...	...	...	A
Water, boiler feed	H_2O	...	66 (150)	...	B	C	A	A	A	...	...
Water, fresh, distilled, purified	H_2O	...	Room	...	A	A	A	A	A	...	...
Water, tap	H_2O	...	Room	...	B	A	B	B	A	...	...
Water, sea	...	...	Room	...	B	B	B	...	A	...	...

(a) A, highly resistant, negligible attack; B, resistant, light attack; C, poor resistance, medium attack; D, not resistant, not suitable. This table should be used only as a guide. Many factors, such as temperature variations, changes in chemical environment, purity of solutions, and stress or loading conditions, may invalidate these recommendations. Tests under operating conditions should be made (b) Results were obtained under laboratory conditions in pure solutions and are classified with reference to corrosion resistance only (c) Coupled to brass. Source: Ref 22, 23

Table 7 Corrosion of WC-Co cemented carbides in mineral acids

Corrosion rates for type 304 stainless steel are shown for comparison.

Cobalt content, wt%	Weight loss mg/mm²							
	37% HCl			5% HCl, 10% H_2SO_4				
	Room temperature		100 °C (212 °F)	100 °C (212 °F)	Room temperature	5% H_2SO_4 100 °C (212 °F)	10% HNO_3 Room temperature	5% HNO_3 100 °C (212 °F)
	10 h	100 h	10 h	20 h	200 h	20 h	20 h	20 h
5.5	0.001	0.015	0.05	0.01	0.020	0.10	0.02	0.02
6	0.003	0.02	0.01	0.02	0.030	0.20	0.10	0.15
9	0.005	0.03	0.2	0.08	0.033	0.25	0.20	Destroyed
13	0.01	0.05	0.04	0.12	0.036	0.35	Destroyed	Destroyed
15	0.015	0.13	1.8	0.15	0.040	0.40	Destroyed	Destroyed
Type 304 stainless steel	1.2	Destroyed	Destroyed	1.2	0.18	Destroyed	None	None

Source: Ref 24

Table 8 Properties of corrosion-resistant cemented carbide grades as a function of grade number

See Fig 7 to 14 for the corrosion resistance of 12 of these grades in various media.

Proprietary designation	Grade number(a)	Composition symbol(a)	Composition, wt%				Others	Hardness		Density, g/cm³	Transverse rupture strength	
			WC	Ni	Co	Cr		HV (30 gf load)	Converted to HRA		MPa	ksi
H03T(b)	1	WC-3Co	96.7	...	3	...	0.3TaC	1850	92.9	15.3	1400	203
H10T(b)	2	WC-6Co	94.5	...	5.5	...	(c)	1730	92.4	15.0	1900	276
H30T(b)	3	WC-9Co	90.4	...	9	...	0.2TiC, 0.4TaC	1450	90.7	14.6	2000	290
H40T(b)	...	...	88	...	12	...	(c)	1340	89.7	14.3	2600	377
K701(d)	4	WC-10Co-4Cr	85.8	...	10.1	4.1	...	1645	92.0	14.0	1140	165
WC6Ni(b)	5	WC-6Ni	94	6	...	...	...	1400	90.2	15.0	1500	218
WC9Ni(b)	6	WC-9Ni	91	9	...	...	...	1150	87.6	14.6	1800	261
TCR10(b)	7	WC-6NiCr	94	5.7	...	0.3	...	1520	91.2	14.8	2000	290
TCR30(b)	8	WC-9NiCr	91	8.5	...	0.5	...	1420	90.4	14.4	2500	363
H032(e)	...	WC-10TaC-3NiCoCr	87	1.5	1	0.5	10TaC	2000	93.3	15.3	1300	189
H031(e)	13	WC-20TaC-3NiCoCr	77	1.5	1	0.5	20TaC	1940	93.1	14.9	1430	207
V492(e)	9	WC-40TaC-3NiCoCr	57	1.5	1	0.5	40TaC	2000	93.3	14.9	1400	203
H035(e)	10	WC-40NbC-3NiCoCr	57	1.5	1	0.5	40NbC	1870	92.9	11.1	1280	186
V455(e)	11	WC-40TaC-9NiCoCr	50	4	4	1	41TaC	1450	90.7	14.2	1850	268
V473(e)	12	WC-40NbC-9NiCoCr	50	4	4	1	41NbC	1400	90.2	14.5	1750	254
TWF18(b)	...	...	...	18	...	...	66TiC, 16Mo_2C	1470	90.8	6.0	1270	184

(a) Used to refer to grades in Fig. 7 to 14. (b) Metallwerk Plansee grade designation. (c) Depending on the reference used these grades are sometimes shown with small additions of TaC and TiC (d) Kennametal designation (e) Metallwerk Plansee experimental designation. Source: Ref 7 and 27

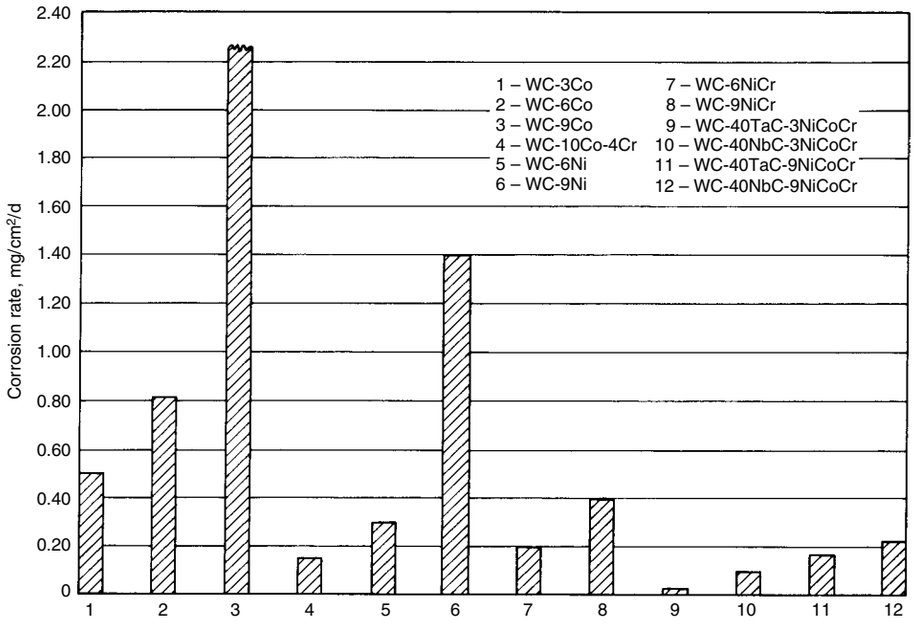

Fig. 7 Corrosion resistance of cemented carbides in 22% HCl at room temperature. See Table 8 for properties of these grades, and Fig. 8 to 14 for corrosion resistance in other media. Source: Ref 7, 27

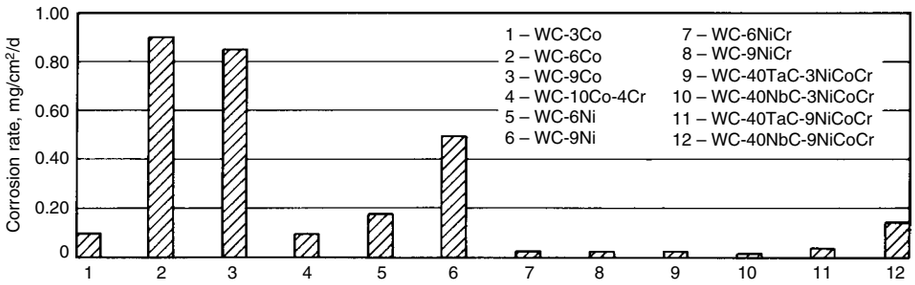

Fig. 8 Corrosion resistance of cemented carbides in 37.8% HNO_3 at room temperature as a function of grade. See Table 8 for properties of these grades. Source: Ref 7, 27

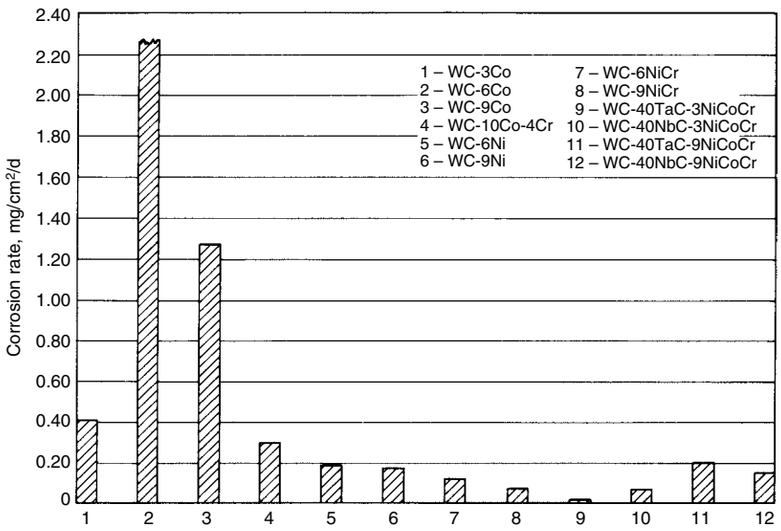

Fig. 9 Corrosion resistance of cemented carbides in 9.8% H_2SO_4 at room temperature as a function of grade. See Table 8 for properties of these grades. Source: Ref 7, 27

binder-phase contents, the rate of attack is diminished, and in conditions in which the corrosion is not too severe, the reduced binder content will be beneficial. In more severe corrosion, however, the use of a cobalt binder is prohibited, and the WC-Co grade is simply not resistant enough. In these cases, certain corrosion-resistant grades should be used. The most common of these are WC with nickel alloy binders and TiC-Ni-Mo_2C-base cemented carbide. Figure 6 shows the corrosion rate as a function of pH for these different types of cemented carbides tested in buffered solutions. These tests included a final surface wear treatment by tumbling in order to obtain a true value of the depth of the corroded surface.

As can be seen in Fig. 6, straight WC-Co grades are resistant down to pH 7. This is also valid for WC-Co grades containing cubic carbides such as TiC, TaC, and NbC. The highest corrosion resistance is obtained for certain alloyed TiC-Ni grades, which are resistant down to approximately pH 1, but compared to the straight WC-Co grades, they are less tough and have lower thermal conductivity. They also have the disadvantages of being difficult to grind and braze; therefore, they are used only in specific applications.

In many corrosion-wear situations, the proper choice is specially alloyed WC-Ni grades, which are resistant down to pH 2 to 3. Even in certain solutions with pH values less than 2, they have proved to be resistant to corrosion. Because WC is the hard principal constituent and because nickel and cobalt are similar metals in many respects, their mechanical and thermal properties are comparable to those of the straight WC-Co grades.

The pH value is one of the most important parameters when determining the corrosivity of a medium, but other factors such as temperature and electrical conductivity also have a great influence. The latter is dependent on the ion concentration, that is, the amount of dissolved salts in the solution. Thus, one cannot define the corrosivity of a certain medium in a simple way, and accordingly, no general rules that are valid in all situations can be given. However, Table 5 gives general guidelines for the corrosion resistance of WC-Co and TiC-Ni cemented carbides in various room-temperature media. Table 6 gives compatibility data for several types of cemented carbides in aqueous media at various temperatures, and Table 7 lists weight loss as a function of cobalt content for cemented carbides in mineral acids.

In general, it can be stated that the corrosion of cemented WC is fair to good in a limited way in all acids except HNO_3. The corrosion resistance of cemented TiC is excellent in phosphoric acid (H_3PO_4), boric acid, and picric acid and is somewhat better than cemented WC in HCl or sulfuric acid (H_2SO_4). Cemented TiC is poor in HNO_3. As expected, increasing the cobalt content to increase strength significantly decreases the corrosion resistance (Table 7). The same situation exists in virtually all corrosive

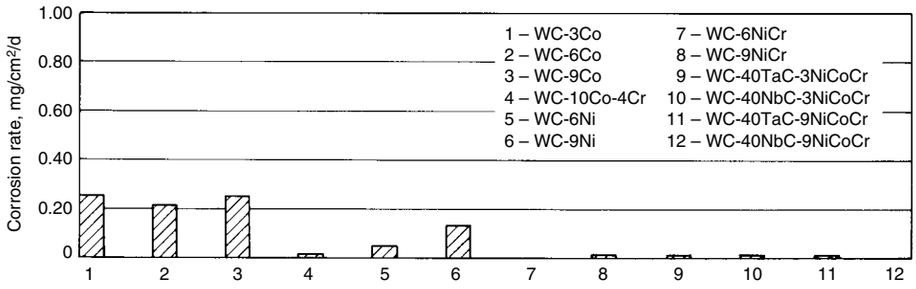

Fig. 10 Corrosion resistance of cemented carbides in 6% acetic acid at room temperature as a function of grade. See Table 8 for properties of these grades. Source: Ref 7, 27

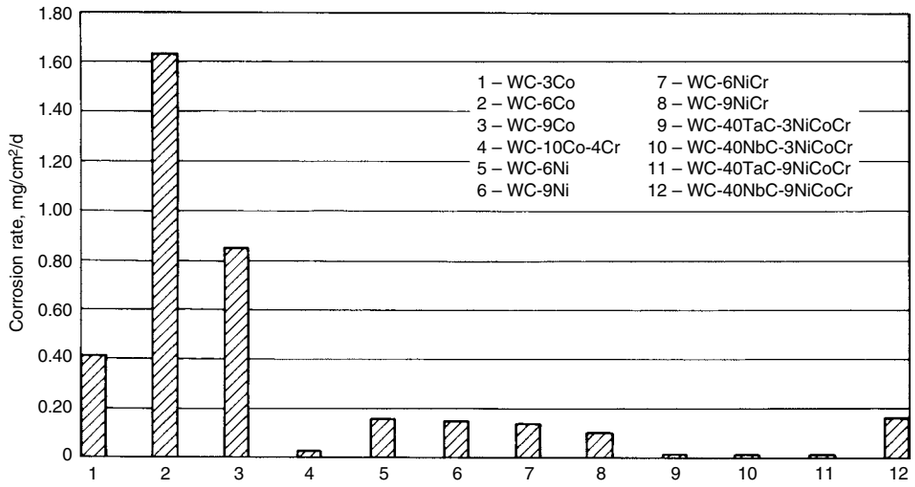

Fig. 11 Corrosion resistance of cemented carbides in 6.5% H_3PO_4 at room temperature as a function of grade. See Table 8 for properties of these grades. Source: Ref 7, 27

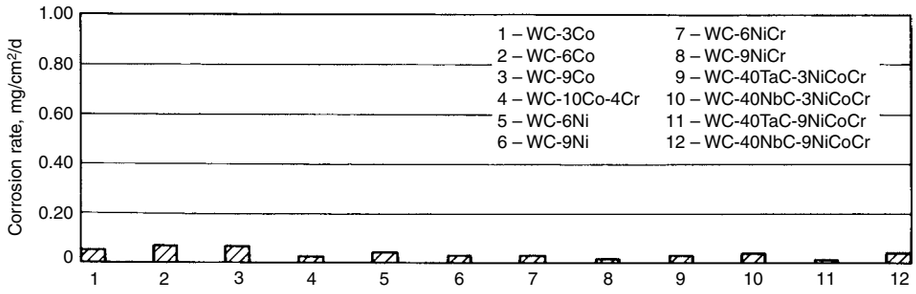

Fig. 12 Corrosion resistance of cemented carbides in 4% NaOH at room temperature as a function of grade. See Table 8 for properties of these grades. Source: Ref 7, 27

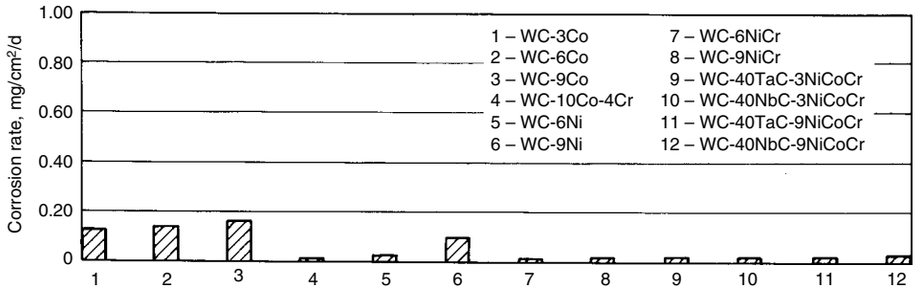

Fig. 13 Corrosion resistance of cemented carbides in 2.9% NaCl at room temperature as a function of grade. See Table 8 for properties of these grades. Source: Ref 7, 27

environments, and because the same effect is seen for abrasion resistance, it is recommended that the minimum cobalt content be used for all wear and corrosion applications. This means that for a given application, the hardest grade that will give adequate strength, impact resistance, and resistance to chipping should be chosen.

Special Corrosion-Resistant Grades. To obtain corrosion resistance above and beyond that available with the regular WC-Co and TiC-Ni grades, the special corrosion-resistant grades are used. These always result in a sacrifice in strength, hardness, and/or abrasion resistance, as shown in Table 3. On the other hand, the corrosion-resistant grades do offer significant benefits in corrosion resistance in many media (Table 6). These grades include the WC + Ni binder, the WC + Co-Cr binder, and the so-called binderless WC, which generally contains approximately 10% TaC and between 1 and 2% Co. In addition, there are other special grades, such as the 0.1 to 1.0% Pt addition patented as an improvement toward ink corrosion resistance in ballpoint pen balls (Ref 25).

Sintered cemented carbide compositions based on more than 50% Cr_2C_3 for corrosion resistance are also mentioned in patents (Ref 26) and the literature (Ref 3–5). These are generally not commercially viable and are brittle materials; therefore, they cannot compete with the ceramic materials, such as silicon carbide, silicon nitride, aluminum oxide, boron nitride, and the whisker-reinforced ceramics, which have superb corrosion resistance. Where impact and chipping are not problems, these ceramic materials are a better choice than the cemented carbides. The cemented carbides have the advantage, however, in strength, impact resistance, thermal conductivity, and often greater ease of manufacture.

The best work from the 1980s showing the performance of the special corrosion-resistant compositions compared to the standard compositions and even some experimental compositions is that done at Metallwerk Plansee (Ref 7, 27). Table 8 lists the properties of these grades; for convenience, the proprietary designations are given, and the grades are also noted by composition, such as WC-10Co-4Cr. Grades are also listed by a grade number that can be used when referring to Fig. 7 to 14.

Figure 7 shows the corrosion of the 12 different compositions listed in Table 8 in 22% HCl at room temperature. Grades 1 to 3 (WC-3Co, WC-6Co, and WC-9Co, respectively) illustrate the increase in corrosion rate that results from increasing cobalt binder content. The nickel binders (grades 5 and 6; WC-6Ni and WC-9Ni, respectively) are an improvement, but again, the increase in binder content increases the corrosion rate. Of the more exotic compositions, grades 4 (WC-10Co-4Cr) and 7 (WC-6NiCr) are viable choices for limited use in HCl at room temperature. The best of the experimental compositions is grade 9 (WC-40TaC-3NiCoCr); it has greater strength and higher

hardness. If additional strength is needed above grade 9, grade 11 (WC-40TaC-9NiCoCr) is a good choice with the increased binder content, but as is generally the case, this results in a loss of corrosion resistance.

Figure 8 shows the same type of information for 38% HNO_3 at room temperature. In general, corrosion is lower, but again, the higher-cobalt WC-Co compositions (grades 2 and 3) are not suitable, nor is the WC-9Ni composition (grade 6). Grade 5 (WC-6Ni) is marginal in HNO_3, but grades 1 and 4 are still better. On the other hand, the commercially available grades 7 and 8 (WC-6NiCr and WC-9NiCr, respectively) show very limited corrosion attack that is virtually equal to that of three of the four experimental grades; the commercial alloys in this case have better strength.

The basic cemented carbides are attacked most severely by H_2SO_4 (Fig. 9). Some of the WC-Ni or WC-NiCr commercial compositions can tolerate limited use. However, the experimental grade 9 (WC-40TaC-3NiCoCr) provides exceptional corrosion resistance.

Figure 10 shows that many compositions are available for use in acetic acid with little corrosion. Attack in H_3PO_4 is relatively rapid only on the WC-Co compositions (Fig. 11).

Figures 12 and 13 show the suitability of all of the compositions listed in Table 8 in sodium hydroxide (NaOH) and sodium chloride (NaCl), respectively. In NaCl, there is significant benefit in choosing a nickel binder cemented carbide (for example, grade 5, WC-6Ni) if the loss in strength can be tolerated.

Figure 14 shows the resistance to erosion-corrosion of different cemented carbide compositions in a slurry of artificial seawater and sand. It follows the pattern of benefit for the use of nickel binders in saline applications. The best of the WC-Co compositions is obviously the one with the lowest binder content (grade 1, WC-3Co). It shows a rate, however, more than 10 times greater than the experimental grade 9 (WC-40TaC-3NiCoCr), and both have the same transverse rupture strength and equivalent hardness. For a commercial composition, the grade 8 (WC-9NiCr) cemented carbide shows excellent performance, with one-half the rate of attack of the low-cobalt composition (grade 1, WC-3Co) and much higher transverse rupture strength.

Some of the same data are shown in Fig. 15 and 16 to compare the relative corrosion of the different compositions in various media. These tests were performed at room temperature, and solution concentrations are the same as those in Fig. 7 to 14. In Fig. 16, the cemented carbides are also compared to an Fe-20Cr-32Ni alloy; the superiority of the experimental WC-40TaC-3NiCoCr cemented carbide is evident. As with corrosion test data, care must be taken not to extrapolate these to different solution concentrations and temperatures. It would be logical to assume, for example, that the WC-40TaC-3NiCoCr alloy would always outperform WC-3Co in these media at different concentrations and temperatures, but the validity of this assumption must be verified through further testing.

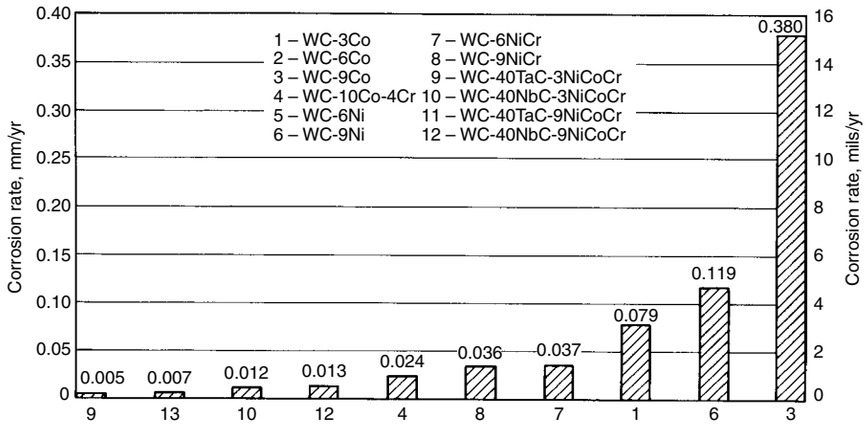

Fig. 14 Resistance to erosion-corrosion of cemented carbides in a room-temperature slurry of artificial seawater and sand as a function of grade. See Table 8. Source: Ref 7, 27

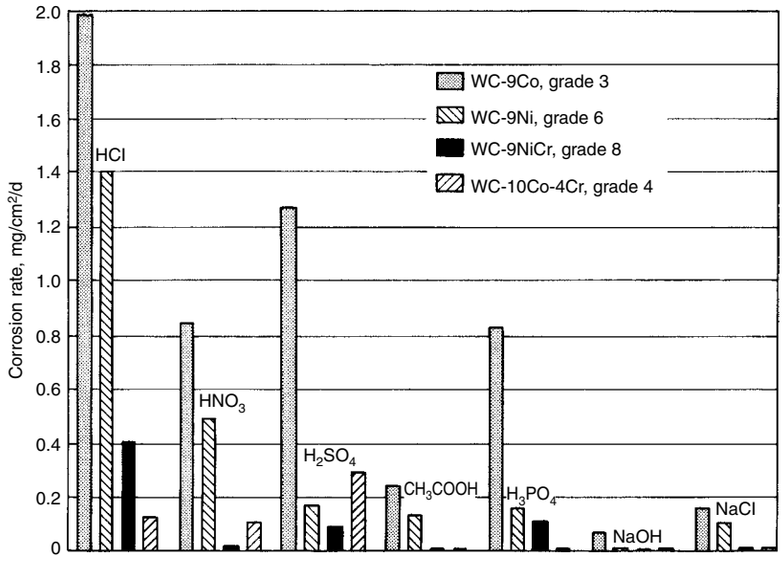

Fig. 15 Corrosion resistance of four commercial cemented carbide compositions in aqueous media at room temperature. Source: Ref 27

Corrosion in Warm Acids and Bases. The corrosion rate of various cemented carbide compositions in warm (50 °C, or 120 °F) acids is shown in Table 9. The straight WC-Co compositions show rapid attack in dilute H_2SO_4 and HNO_3, and little attack in those concentrated acids. Although the corrosion rate is lower in HCl, it is obvious that these compositions are not suitable for use in warm or hot acid solutions. The TiC-6.5Ni-5Mo composition is quite good in H_2SO_4, moderately good in HCl, and very poor in HNO_3. Several of the binderless compositions and the TaC-base cemented carbide show very acceptable corrosion resistance in these warm acids. These results are to be expected, because the cobalt and nickel binders are completely soluble in these acids.

The corrosion rates of various cemented carbides in basic solutions at 50 °C (120 °F) are quite a different matter, as shown in Table 10. Although corrosion does proceed, it is slow enough to demonstrate the utility of even the WC-Co compositions in such applications as seal rings in these basic solutions.

Galvanic Corrosion. The resistance to galvanic corrosion of various cemented carbides coupled to type 316 stainless steel has been investigated (Ref 29). Immersion testing of uncoupled specimens was also performed for comparison. Compositions of the materials tested are given in Table 11.

The apparatus used for the galvanic-corrosion testing is shown in Fig. 17. Figure 18 shows the corrosion rates of the materials in the immersion test. The binderless WC-3TiC-2TaC alloy performed the best, followed by the TiC-base

cermet, the WC-Ni-CrMo alloy, the sintered cobalt-base alloy, and the WC-6Co alloy. The logarithm of weight loss plotted against the logarithm of time yielded the linear weight loss curves in this test. Based on this, it was postulated that the movement of electrons between cemented carbide and stainless steel is the rate-determining factor in galvanic corrosion. Table 12 compares the corrosion rates of the materials in the immersion and galvanic tests. For most of the alloys tested, the rate of galvanic corrosion is greater than the corrosion rate in the simple immersion test. It is thought that the larger the potential difference between the cemented carbide and the stainless steel, the greater the difference between the corrosion rates obtained in the immersion test and in the galvanic-corrosion test.

Figure 19 shows cross sections of specimen rings after the galvanic corrosion test. Corrosion proceeded inward from the surface that contacted the seawater in the WC-6Co alloy (Fig. 19a). The investigators postulated that the electrode potential is large and that electrons would move smoothly between the cemented carbide and the contacting stainless steel; therefore, attack proceeded according to the galvanic-corrosion mechanism. In the case of the binderless WC-3TiC-2TaC alloy (Fig. 19b), corrosion is very slight even after 1 year. The TiC-base cermet (Fig. 19c) shows corrosion only on the inner side surface (the side contacting the Teflon, (DuPont PTFE fluoropolymer); see Fig. 17. In the sintered cobalt-base alloy and the WC-Ni-CrMo alloy (Fig. 19c and d), corrosion proceeded from the corner that contacted both the seawater and the stainless steel. It was postulated that the electrode potential and the distance of electron movement were smaller than those for the WC-6Co alloy. Based on the results of these tests, either the binderless alloy or the TiC-base alloy should be acceptable for this type of application.

Crevice Corrosion. The same investigators also reported on the crevice-corrosion resistance of cemented carbides in seawater with specimens of type 316 stainless steel, Teflon and silicon carbide adjacent to the cemented carbide specimens (Ref 29). Of the five compositions tested, only the WC-6Co specimen showed any significant attack after 1 year. The attack was moderate and progressed the least against the silicon carbide and the most against the stainless steel (Ref 29).

Table 9 Corrosion rates of cemented carbides immersed in various acids at 50 °C (120 °F) for 72 h

	Corrosion rate, mg/cm²/d								
	HCl, %			H_2SO_4, %			HNO_3, %		
Composition	5	10	37	10	50	98	5	10	50
WC-6Co	2.29	2.43	0.79	8.72	2.82	0.72	13.50	1.45	0.16
WC-9Co	2.55	1.96	1.92	12.70	5.05	0.72	25.60	6.48	0.18
WC-8Ni-2Mo-3Cr	0.07	0.01	+0.01	5.01	0.76	0.01	5.71	1.23	0.11
WC-5TaC	+0.02	nil	0.05	+1.03	0.23	0.02	+0.02	0.03	0.15
WC-2TaC-3TiC	0.06	nil	+0.02	+1.02	0.33	0.06	0.35	0.08	0.12
WC-47NbC-15TiC-9Ni-4Mo	1.06	0.98	0.14	5.31	0.51	0.52	8.07	1.35	0.24
TaC-4Co-3Ni-1Cr	0.09	0.02	0.22	2.03	0.41	0.51	0.09	0.05	0.01
TaC-23TiC-3Co-2Ni-1Cr	0.26	0.59	1.03	1.98	0.48	0.43	8.04	5.12	6.35
TiC-6.5Ni-5Mo	0.59	1.73	4.91	0.17	0.35	0.39	35.20	19.80	68.2

Source: Ref 28

Table 10 Corrosion rates of cemented carbides immersed in NaOH, KOH, and NaOCl at 50 °C (120 °F) for 72 h

	Corrosion rate, mg/cm²/d				
	NaOH, %		KOH, %		
Composition	5	10	5	10	NaOCl
WC-6Co	+0.75	+0.85	0.39	0.30	1.44
WC-9Co	+0.83	+0.88	0.24	0.28	2.35
WC-8Ni-2Mo-3Cr	+0.09	+0.11	0.08	0.09	1.12
WC-5TaC	+0.89	+0.92	0.18	0.18	+0.15
WC-2TaC-3TiC	+0.87	+0.90	0.20	0.20	+0.13
TaC-4Co-3Ni-1Cr	+0.71	+0.68	0.11	0.14	0.05

Source: Ref 28

Table 11 Compositions and properties of galvanic corrosion test specimens

			Transverse rupture strength	
Specimen	Composition, wt%	Hardness, HRA	MPa	ksi
WC-6Co	WC-6Co	91.0	2400	348
WC-3TiC-2TaC alloy	WC-3TiC-2TaC	92.9	1200	174
TiC-base cermet	TiC-10Tin-2 $5Mo_2C$-15Ni	91.5	1500	218
Sintered cobalt-base alloy	Co-Cr-W-C	85.5	1400	203
WC-NiCrMo alloy	WC-3TiC-1.5 ($Cr_3C_2Mo_2C$)-15Ni	89.0	2100	305

Source: Ref 29

Oxidation Resistance of Cemented Carbides

The ordinary WC-Co cemented carbides are reasonably resistant to oxidation in air up to approximately 650 to 700 °C (1200 to 1290 °F). The constituent affected the fastest is WC, which will oxidize to WO_3. In oxygen, the temperature limit is lower, and rapid deterioration will occur at approximately 500 °C (930 °F). Even in air, however, the practical temperature limit for WC-Co compositions for any length of time is 500 to 600 °C (930 to 1110 °F). Nonetheless, these compositions do stand up, for example, in cutting tools in which localized higher temperatures at the cutting tip will be encountered. The addition of both or either TiC or TaC to the WC-Co compositions increases the oxidation resistance somewhat and is undoubtedly also related to the improvement found for these additions for machining steel. In applications in which oxidation resistance combined with wear resistance is required, as in hot glass forming and shearing tools, the addition of TiC and/or TaC to the basic WC-Co is of little benefit. The TiC-Mo_2C-Ni compositions have clearly superior oxidation resistance and can be used at temperatures up to 900 °C (1650 °F), at which point they start to oxidize fairly rapidly. At the lower temperature, the TiC-base compositions form a tight adherent oxide film that tends to

Table 12 Corrosion rates of uncoupled immersion and galvanic corrosion test specimens

	Corrosion rate, g/m²/d	
Specimen	Immersion test	Galvanic test
WC-6Co alloy	4.2	16.67
WC-3TiC-2TaC alloy	0.6	0.03
TiC-base cermet	0.2	0.58
Sintered cobalt-base alloy	0.3	4.77
WC-NiCrMo alloy	0.2	1.71

Source: Ref 29

resist rapid attack. This behavior difference is analogous to the behavior difference between cobalt and nickel alone, but WC is also more readily oxidized than TiC.

Saw Tips and Corrosion

Cemented carbides are in widespread use in slitter saws, which are used to saw all types of metals, composites, lumber, and many other materials. Small saw blades are sometimes manufactured from a single piece of carbide; larger blades, which may run up to 2 m (6 ft) in diameter, more commonly use cemented carbide tips brazed onto the steel saw body. The heavy-duty chain saws used in the lumber industry also have carbide teeth. Selection of cemented carbides for these applications is invariably based on the need for excellent wear resistance and toughness. Basic WC-Co compositions are almost always used.

The rapid dulling of saws in such applications, however, is attributable to corrosive as well as abrasive conditions. For example, one investigation studied the corrosion of WC cutting tools used to cut western red cedar (Ref 30). Tests were performed to determine the relative rates of attack of WC and cobalt in substances extracted from western red cedar, which has a higher content of such substances than other commercial lumber species. Because the WC was not attacked, it was concluded that the cobalt binder content should be reduced to minimize attack. Alternatively, the cobalt binder could be replaced with another binder material, such as nickel; however, such a substitution would result in a serious loss of strength. Thus, the solution to this particular problem is not a simple one, and western red cedar is still being sawed primarily with WC-Co cemented carbide compositions.

It was also suggested that the carbide be coated with TiC, TiN, or Al_2O_3 (or a combination of these). To date, these coatings are not used in such applications because of the need for resharpening and because of the difficulties of brazing a coated tip.

Coating of Cemented Carbides

This widely used process has been primarily applied to metal-cutting tools. Certain special applications can be cited, such as the coating of cemented WC watch cases with TiN to form a hard, corrosion-resistant gold-colored watch case (bezel). Clearly, the potential exists to use these thin (2 to 10 μm, or 0.08 to 0.4 mil) coatings on wear- and corrosion-resistant parts. The limitation is that the coating must be very thin to avoid spalling or chipping.

Coating is most commonly done by chemical vapor deposition (CVD), and this process gives a wide range of possible coating materials. In addition to the common TiN, TiC, Al_2O_3,

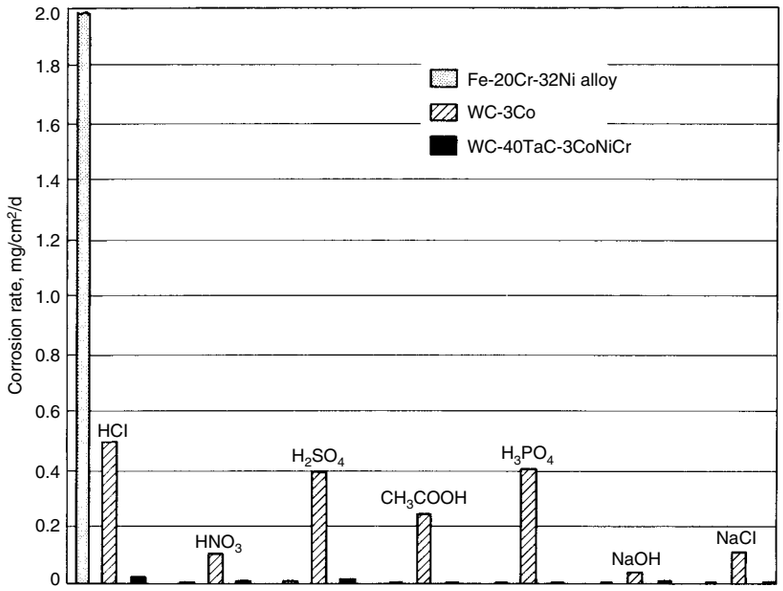

Fig. 16 Comparison of the corrosion resistance of a commercial WC-3Co cemented carbide and two experimental compositions in aqueous media. Source: Ref 27

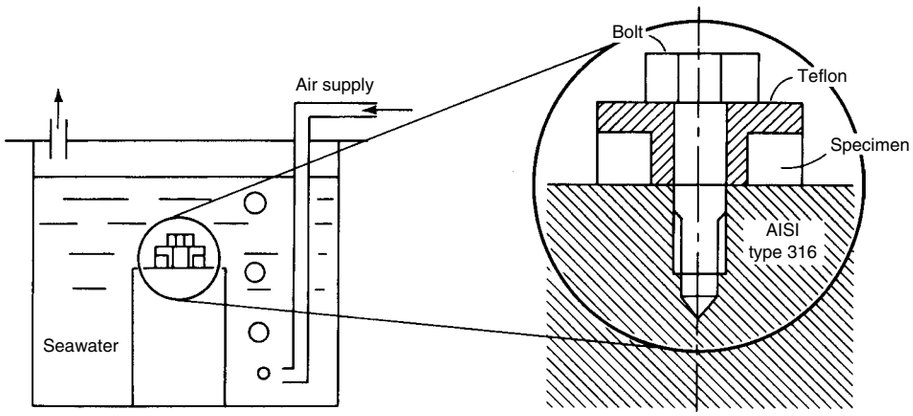

Fig. 17 Schematic of experimental apparatus used to study galvanic corrosion of cemented carbides in seawater. Source: Ref 29

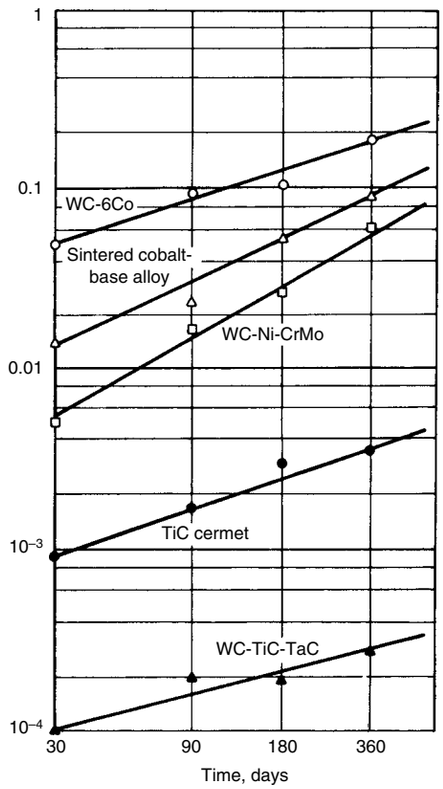

Fig. 18 Corrosion weight loss as a function of time for uncoupled test specimens from Ref 29

perfectly feasible coating materials include hafnium carbide (HfC), hafnium nitride (HfN), zirconium carbide (ZrC), zirconium nitride (ZrN), TaC, and NbC. The state of the art includes all combinations of TiC, TiN, Al_2O_3, and titanium carbonitride (TiCN), with limited commercial use of HfN and TaC as coating materials. Chemical vapor deposition is generally performed at 900 to 1100 °C (1650 to 2010 °F). Titanium nitride is coated at lower temperatures, down to perhaps 700 °C (1290 °F), in less used commercial apparatus.

Physical vapor deposition (PVD) has the advantage of being done at lower temperatures, down to perhaps 500 °C (930 °F), but it is a line-of-sight process that generally requires rotation of the parts being coated. Deposition rates for PVD are much lower than those of CVD, and PVD equipment is more expensive. Physical vapor deposited coatings have also been limited commercially to TiN, usually at thicknesses of 3 μm (0.12 mil) or less. More information on the corrosion and wear resistance of coatings applied by these methods is available in the article "CVD and PVD Coatings," in Volume 13A, *ASM Handbook,* 2003.

Although there are few applications in which cemented carbides are used solely for corrosion resistance, it is essential to recognize the availability of the coated carbides. Coatings of TiN, TiC, or Al_2O_3 can impart important corrosion and oxidation resistance to cemented carbides.

Special Surface Treatments

Considerable work has been done to enhance the surface properties of cemented carbides (Ref 31–33), but it generally has been derived from surface modification processes developed for other metals. These surface treatments include boriding, nitriding, and ion implantation. Most of the treatments have been used to enhance resistance to wear, abrasion, or erosion. The benefits, if any, of such treatments in increasing resistance to oxidation and corrosion are not yet well documented. Nevertheless, these processes may have potential in special applications.

ACKNOWLEDGMENT

This article is adapted from Herbert S. Kalish, "Corrosion of Cemented Carbides," *Corrosion,* Volume 13, *ASM Handbook,* 1987, p 846–858.

REFERENCES

1. "Hardmetals—Metallographic Determination of Microstructure," ISO 4499, International Organization for Standardization, 1978
2. "Standard Method for Determination of Microstructure in Cemented Carbides," B 657, *Annual Book of ASTM Standards,* American Society for Testing and Materials
3. P. Schwarzkopf and R. Kieffer, *Cemented Carbides,* Macmillan, 1960
4. R. Kieffer and F. Benesovsky, *Hartmetalle* (Hard Metals), Springer Verlag, 1965
5. C. Goetzel, *Treatise on Powder Metallurgy,* Vol I to III, Interscience, 1949
6. H.S. Kalish, Some Plain Talk About Carbides, *Mfg. Eng. Mgmt.,* Vol 71 (No. 1), July 1973
7. E. Kny, T. Bader, C. Hohenrainer, L. Schmid, and R. Glätzle, Korrosionsresistente, hochverschlei ß feste Hartmetalle, *Werkst. Korros.,* May 1986
8. H. Suzuki et al., *Choukougoukin to Syouketu Koushitu Goukin,* Tokyo, Maruzen, 1986, p 514
9. J. Gurland and P. Bardzil, Relation of Strength, Composition, and Grain Size of

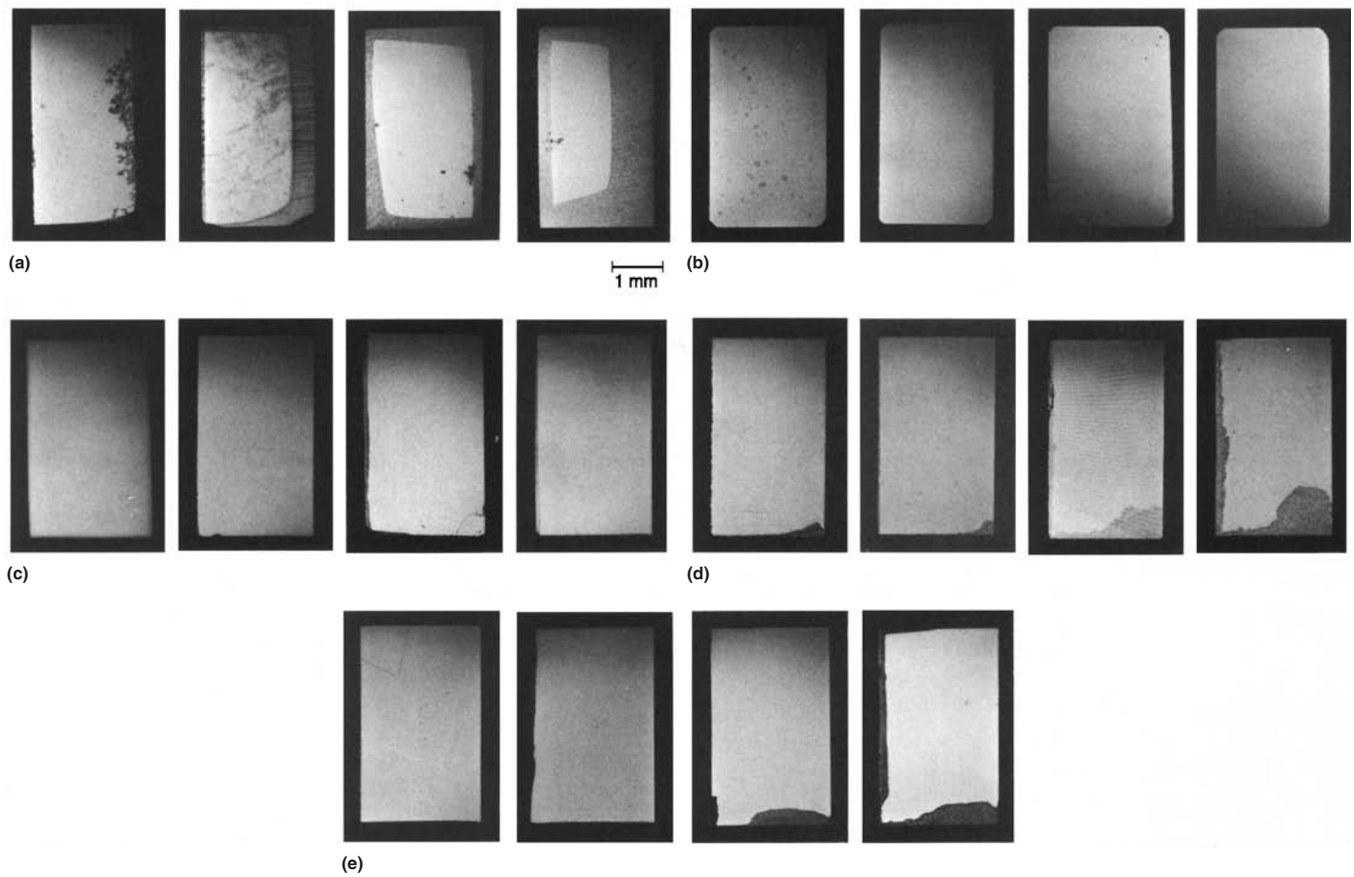

Fig. 19 Cross sections of galvanic-corrosion test specimens after (left to right) 1 month, 3 months, 6 months, and 12 months. (a) WC-6Co alloy. (b) WC-3TiC-2TaC binderless alloy. (c) TiC-base cermet. (d) Sintered cobalt-base alloy. (e) WC-NiCrMo alloy. Source: Ref 29

Sintered WC-Co Alloys, *J. Met.,* Feb 1955, p 311–315
10. H. Suzuki, Variation in Some Properties of Sintered Tungsten Carbide-Cobalt Alloys with Particle Size and Binder Composition, *Trans. Jpn. Inst. Met.,* Vol 7, 1966, p 112
11. H.S. Kalish, Carbide Grade Classifications—What They Mean, *Mfg. Eng. Mgmt.,* Vol 76 (No. 1), 1976
12. R.S. Montgomery, The Mechanism of Percussive Wear of Tungsten Carbide Composites, *Wear,* 1968, p 309–329
13. "Classification and Application of Hard Cutting Materials for Metal Removal with Defined Cutting Edges—Designation of the Main Groups and Groups of Application," ISO 513, International Organization for Standardization, 2004
14. Published and unpublished data, Adamas Carbide Corporation
15. *Properties and Proven Uses of Kennametal Hard Carbide Alloys,* Kennametal, Inc., 1976
16. K.J.A. Brookes, *World Directory and Handbook of Hardmetals,* 6th ed., 1996
17. "Evaluating Apparent Grain Size and Distribution of Cemented Tungsten Carbide," B 390, *Annual Book of ASTM Standards,* American Society for Testing and Materials
18. "Hardmetals—Metallographic Determination of Porosity and Uncombined Carbon," ISO 4505, International Organization for Standardization, 1978
19. "Standard Test Method for Apparent Porosity in Cemented Carbides," B 276, *Annual Book of ASTM Standards,* American Society for Testing and Materials
20. R.C. Weast, Ed., *Handbook of Chemistry and Physics,* 67th ed., CRC Press, 1986
21. E.K. Storms, *Refractory Carbides,* Academic Press, 1967
22. Published data, Sandvik Coramant
23. Published data, Kennametal, Inc.
24. A. Hara and Y. Saito, Corrosion and Oxidation Resistance of "Igetalloy," *Sumitomo Elec. Tech. Rev.,* No. 13, Jan 1970
25. Corrosion Resistant Binder for Tungsten Carbide Materials and Titanium Carbide Materials, U.S. Patent 3,628,921, 1971
26. Sintered Alloys of a Chromium Carbide Tungsten Carbide–Nickel System, U.K. Patent 1202844, 1970
27. E. Kny and L. Schmid, *New Hardmetal Alloys with Improved Erosion and Corrosion Resistance,* Metallwerk Plansee
28. K. Takao and K. Terasaki, Chemical Resistance of Various Cemented Carbides, *Nippon Tungsten Rev.,* Vol 10, 1977
29. Y. Masumoto, K. Takechi, and S. Imasato, Corrosion Resistance of Cemented Carbide, *Nippon Tungsten Rev.,* Vol 19, 1986
30. E. Kirbach and S. Chow, Chemical Wear of Tungsten Carbide Cutting Tools by Western Redcedar, *Forest Prod. J.,* Vol 26 (No. 3)
31. H. Ito and Y. Mohashi, Corrosion-Resistant Cemented Carbides by Chromium Diffusion Methods, *Nippon Tungsten Rev.,* Vol 6, Sept 1973
32. H.S. Kalish, Method of Forming a Hard Surface on Cemented Carbides and Resulting Article, U.S. Patent 3,744,979, 1973
33. Materials Development Corporation, Medford, MA

SELECTED REFERENCES

- O.A. Drobysheva and V.N. Latyshev, Interaction of a Hard Alloy and a Cutting Fluid, *Fiz. Khim. Mekh. Mater.,* Vol 8 (No. 3), May-June 1972, p 38–40
- A.L. Echtenkamp, "Combating Corrosion/Wear with the Hard Carbide Alloys," Paper presented at the ASLE/ASME Lubrication Conference (Minneapolis, MN), American Society of Lubrication Engineers, Oct 1978
- S. Imasato, S. Sakaguchi, and Y. Hayashi, Effect of Cr, C on Corrosion Resistance of WC-Ni-Cr Cemented Carbide, *J. Jpn. Soc. Powder Powder Metall.,* Vol 45 (No. 3), 1998, p 265–270
- S. Imasato, S. Sakaguchi, and Y. Hayashi, Research of Corrosion Properties by Potentiostatic Polarization of WC-Ni-Cr_3C_2 Cemented Carbide, *J. Jpn. Soc. Powder Powder Metall.,* Vol 47 (No. 5), 2000, p 541–546
- S. Imasato, S. Sakaguchi, T. Okada, and Y. Hayashi, Effect of NaCl Concentration and Aqueous Solution on Corrosion Resistance of Cemented Carbide, *J. Jpn. Soc. Powder Powder Metall.,* Vol 49 (No. 4), 2002, p 264–269
- S. Imasato, S. Sakaguchi, T. Okada, and Y. Hayashi, Effect of WC Grain Size on Corrosion Character of WC-Co Super-Hard Alloy, *2000 Fall Meeting of the Japan Society of Powder and Powder Metallurgy,* Japan Society of Powder and Powder Metallurgy, 2000, p 186
- S. Imasato, S. Sakaguchi, K. Sugano, and Y. Hayashi, Corrosion Behavior of WC-Ni-Cr Cemented Carbide in NaOH Solution, *J. Jpn. Soc. Powder Powder Metall.,* Vol 46 (No. 4), 1999, p 402–408
- S. Imasato, K. Tokumoto, and S. Sakaguchi, Microstructures, Mechanical and Corrosion Properties of WC-(0-16) Mass% Cr_3C_2-15 Mass% Ni Cemented Carbides, *J. Jpn. Soc. Powder Powder Metall.,* Vol 51 (No.1), 2004, p 3–9
- G. Mori and S. Sutthiruangwong, Influence of Refractory Metal Carbide Addition on Corrosion Properties of Cemented Carbides, *Mater. Manuf. Process.,* Vol 20 (No. 1), 2005, p 47–56
- G. Mori, H. Zitter, A. Lackner, and M. Schretter, Influencing the Corrosion Resistance of Cemented Carbides by Addition of Cr_2C_3, TiC and TaC, *15th International Plansee Seminar 2001 Proceedings,* Plansee Holding AG, Austria, 2001, p 15
- G. Mori, H. Zitter, S. Mitsche, and A. Lackner, Influence of Cr_3C_2, TiC and TaC on Corrosion Behaviour and of Cemented Carbides at Different pH Values, *EURO PM2001 Proceedings,* Vol 1, European Powder Metallurgy Association, 2001, p 121–127
- K. Nakahara, S. Imasato, S. Sakaguchi, and Y. Hayashi, Corrosion Behavior of Sintered Hard Alloys, *J. Jpn. Soc. Powder Powder Metall.,* Vol 49 (No. 4), 2002, p 257–263
- S. Raghunathan, R. Caron, J. Friederichs, and P. Sandell, Tungsten Carbide Technologies, *Adv. Mater. Process.,* Vol 149 (No. 4), 1996, p 21–23
- E. Suganuma, Electrochemical Behaviour of Cemented Carbide, *Bull. Yagamata Univ. Eng.,* Vol 11 (No. 2), March 1971
- S. Sutthiruangwong and G. Mori, Corrosion Properties of Co-Based Cemented Carbides in Acidic Solutions, *Int. J. Refract. Met. Hard Mater.,* Vol 21 (No. 3-4), 2003, p 135–145
- G. VerWeyst, Corrosion-Resistant Tooling for Metal-Forming Operations, *Lubr. Eng.,* Vol 41 (No. 6), June 1985, p 370–374

ASM Handbook, Volume 13B: Corrosion: Materials
S.D. Cramer, B.S. Covino, Jr., editors, p526-542
DOI: 10.1361/asmhba0003839

Corrosion of Metal-Matrix Composites

L.H. Hihara, The University of Hawaii at Manoa

METAL-MATRIX COMPOSITES (MMCS) are metals that are reinforced with fibers, monofilaments (MF), or particles (P) that usually are stiff, strong, and lightweight. The fibers and particles can be metal (such as tungsten), nonmetal (such as carbon or boron), or ceramic (such as silicon carbide or alumina). The purpose for reinforcing metals with fibers or particles is to create composites that have properties more useful than that of the individual constituents. For example, fibers and particles are used in MMCs to increase stiffness (Ref 1), strength (Ref 1), and thermal conductivity (Ref 2) and to reduce weight (Ref 1), thermal expansion (Ref 3), friction (Ref 4), and wear (Ref 5). The selection of the matrix metal and reinforcement constituent is usually based on how well the combination interacts to achieve desired properties. Interaction of the MMC with the environment is normally a secondary consideration, and therefore, it is not uncommon for MMCs to have lower resistance to corrosion than their monolithic-matrix alloys.

The earliest literature on the corrosion of MMCs, which appeared in the late 1960s, was primarily on boron MF/aluminum (B_{MF}/Al) MMCs. In the early 1970s, corrosion literature on graphite fiber/aluminum (Gr/Al) MMCs appeared; in the late 1970s, alumina fiber/aluminum (Al_2O_3/Al) and magnesium MMCs were discussed. Silicon carbide/aluminum (SiC/Al) MMCs literature emerged in the early 1980s, and then a wider variety of MMCs, such as lead, depleted uranium, and stainless steel, was addressed.

This article discusses the background of MMCs; general parameters affecting MMC corrosion; corrosion characteristics of aluminum, magnesium, titanium, copper, stainless steel, lead, depleted uranium, and zinc MMCs; and corrosion control of MMCs. In this document, the reinforcement content in MMCs is given in volume percent unless stated otherwise. Symbols used in this article, some of which are unique to composites, are listed in Table 1.

Background

Development of continuous-reinforced and discontinuous-reinforced MMCs began approximately in the 1960s. Examples include B_{MF}/Al MMCs (Ref 6), tungsten monofilament/copper (W_{MF}/Cu) MMCs (Ref 7), and B_{MF}/titanium MMCs (Ref 8). Aluminum MMCs were reinforced with Al_2O_3 (Ref 9–12) and SiC whiskers (Ref 13). In the 1970s, graphite fiber/aluminum MMCs were developed and aluminum MMCs were reinforced with SiC particles (Ref 3). Today, aluminum MMCs are the most widely available.

Continuous-reinforced MMCs are metals reinforced with fibers or monofilaments that generally have enhanced properties in comparison to discontinuous-reinforced MMCs. Disadvantages of continuous-reinforced MMCs are anisotropic properties and significantly higher material and fabrication costs. The reinforcement diameter generally varies from 10 μm fibers to 150 μm monofilaments (Fig. 1).

Discontinuous-reinforced MMCs are metals reinforced with particulates, which generally result in relatively modest property enhancements in comparison to continuous-reinforced MMCs. Advantages of discontinuous-reinforced MMCs include isotropic properties and lower material and fabrication costs. Reinforcement volume percents range from approximately 15 to 25% for structural MMCs (Fig. 2a) and greater than 30% for electronic-grade MMCs (Fig. 2b) used in electronic packaging. The particle-size distribution can be relatively uniform in structural MMCs but highly varied in electronic-grade MMCs to increase the reinforcement volume fraction. The high reinforcement loading in electronic-grade MMCs is necessary to reduce the coefficient of thermal expansion to levels closer to that of electronic materials such as silicon and gallium arsenide.

Parameters Affecting MMC Corrosion

The presence of the reinforcement fibers and particles and the processing associated with MMC fabrication can cause accelerated corrosion of the metal matrix as compared to corrosion of the unreinforced matrix alloys. Accelerated corrosion may originate from electrochemical and chemical interaction between MMC constituents, microstructural effects, and from problems related to processing. Interphases and reinforcements may undergo chemical degradation that cannot be assessed using electrochemical methods. The unique microstructure of MMCs can influence corrosion by inducing segregation, dislocation generation, and microcrevice formation. Processing may leave residual contaminants in MMC microstructures, resulting

Table 1 Nomenclature and units

Symbol	Meaning
B_{MF}	Boron monofilament
B_{MF}^{E}	B_{MF} electrode with monofilament ends exposed
B_{MF}^{S}	B_{MF} electrode with monofilament circumferential surface exposed
BORSIC	Silicon carbide-coated boron fiber
CVD	Chemical vapor deposition
DU	Depleted uranium
E_{appl}	Applied potential
E_{pit}	Pitting potential
g	Gaseous state
Gr	Graphite
Gr^{E}	Graphite electrode with fiber ends exposed
HP	Hot pressed
i	Current density
i_{corr}	Corrosion current density
i_{galv}	Galvanic current density
l	Liquid state
MMC	Metal-matrix composite
MPT	Mixed-potential theory
PVD	Physical vapor deposition
s	Solid state
SCE	Standard calomel electrode
σ	Standard deviation
SiC_{MF}	Silicon carbide monofilament
SiC_{MF}^{E}	SiC_{MF} electrode with monofilament ends exposed
SiC_{MF}^{S}	SiC_{MF} electrode with monofilament circumferential surface exposed
SiC_p	Silicon carbide particles
SiC_w	Silicon carbide whiskers
Si_P	Silicon particles
Subscript "p"	Particles (e.g., SiC_p)
Subscript "w"	Whiskers (e.g., SiC_w)
Superscript "E"	Electrode with fiber or monofilament ends exposed (e.g., SiC_{MF}^{E})
Superscript "S"	Electrode with fiber or monofilament circumferential surface exposed (e.g., SiC_{MF}^{S})
t	Thickness
vol%	Volume percent
V_{SCE}	Volts versus a standard calomel electrode
W_{MF}	Tungsten monofilament
wt%	Weight percent
X_C	Cathodic area fraction
ρ	Resistivity

in unexpected forms of corrosion. The primary sources of MMC corrosion that are discussed include:

- Galvanic corrosion between MMC constituents
- Chemical degradation of interphases and reinforcements
- Microstructure-influenced corrosion
- Processing-induced corrosion

Galvanic Interaction between MMC Constituents

Galvanic corrosion between the matrix, reinforcements, and interphases is a primary concern. The degree of galvanic corrosion depends on the matrix alloy; the environment; the reinforcement electrochemistry, resistivity, and area fraction; and interphases.

Matrix-Metal Effects. Galvanic corrosion in MMCs reinforced with conductive noble reinforcements is a concern in environments in which the matrix metal corrodes actively. For example, 6061-T6 Al would have galvanic-corrosion rates approximately 3 orders of magnitude higher than that of Ti-15V-3Cr-3Sn-3Al (Ti-15-3) if reinforced with an equal area fraction of graphite fibers and exposed to aerated 3.15 wt% NaCl (Fig. 3). The passivation of Ti-15-3 prevents its galvanic-corrosion rate from exceeding the passive current density (Fig. 3). For a galvanic couple with equal matrix and reinforcement area fractions, the intersection of the anodic polarization curve of the matrix metal and the cathodic polarization curve of the reinforcement indicates the magnitude of the galvanic-corrosion current density (*i*).

Environmental Effects. The electrolyte may also have significant effects on galvanic-corrosion rates. Chlorides and dissolved oxygen in the electrolyte are usually significant. In alloys that exhibit some degree of passivity, galvanic-corrosion rates could normally be kept in check if cathodic reinforcements cannot polarize the matrix alloys to their pitting potentials. This is demonstrated for aluminum in aerated chloride-free 0.5 *M* Na_2SO_4 (Fig. 4) and deaerated 3.15 wt% NaCl (Fig. 5). The passivation of aluminum (Fig. 4) prevents the galvanic current from exceeding the passive aluminum current density. In Fig. 5, hydrogen evolution on cathodic reinforcements is not sufficient to polarize aluminum to its pitting potential. In aerated chloride-containing environments, the galvanic-corrosion rate of aluminum MMCs increases dramatically, as shown with polarization diagrams (Fig. 6).

Reinforcement Effects. The reinforcement electrochemistry, resistivity, and area fraction can have significant effects on MMC corrosion.

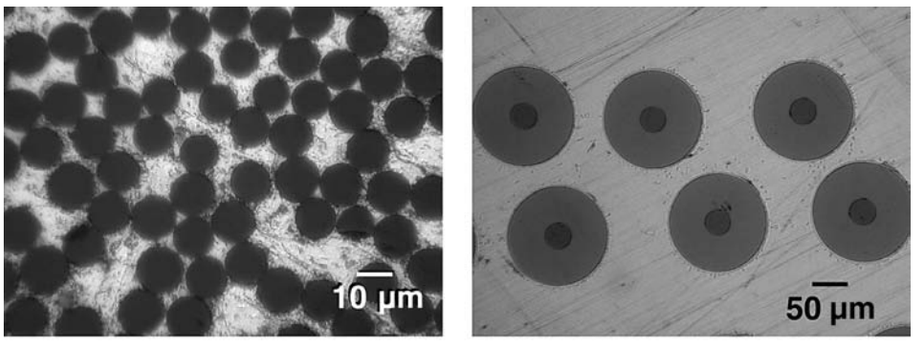

Fig. 1 Diameter of continuous-reinforcement range from 10 μm (a) microstructure of alumina fiber/aluminum metal-matrix composite (MMC) to 150 μm (b) SiC_{MF}/Ti-15-3 MMC

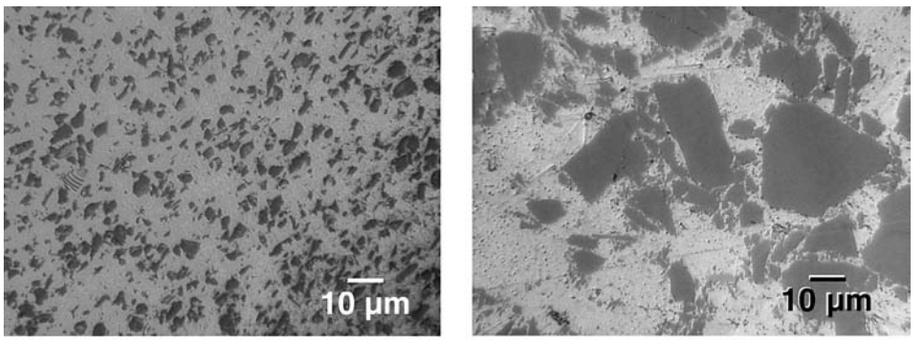

Fig. 2 Range in amount of reinforcement. (a) SiC_P/6061-T6 Al metal-matrix composite (MMC) with 15 vol% reinforcement. (b) Si_P/Al MMC with 43 vol% reinforcement

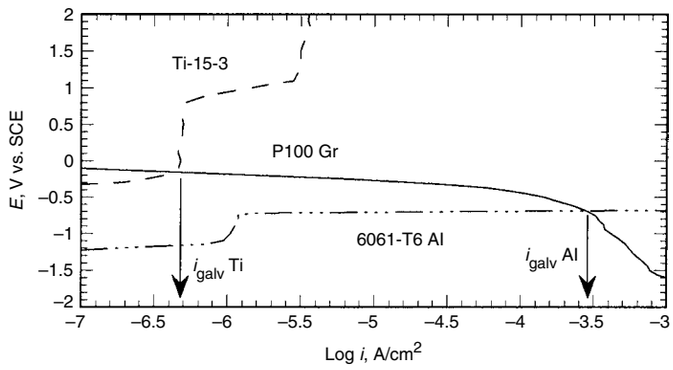

Fig. 3 Anodic polarization diagrams of Ti-15-3 (Ref 14, 15) and 6061-T6 Al (Ref 16) in deaerated 3.15 wt% NaCl at 30 °C (86 °F). Cathodic polarization diagram of P100 Gr fibers (Ref 16) in aerated 3.15 wt% NaCl at 30 °C (86 °F). Scan rate, 0.1 mV/s. *E*, potential; SCE, standard calomel electrode; *i*, current density

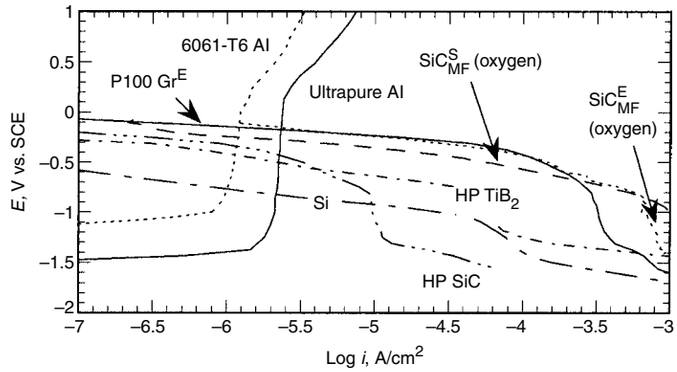

Fig. 4 A collection of anodic polarization curves of ultrapure aluminum (99.999 wt%) (Ref 16), and 6061-T6 Al (Ref 16), and cathodic polarization curves of P100 Gr^E (Ref 16), hot-pressed (HP) SiC (Ref 16), HP TiB_2 (Ref 17), and silicon (Ref 18) exposed to aerated 0.5 M Na_2SO_4 at 30 °C (86 °F). The $SiC_{MF}{}^E$ (Ref 19) and $SiC_{MF}{}^S$ (Ref 19) electrodes were exposed to oxygenated solutions. Scan rate, 0.1 mV/s. Superscript "E" denotes fiber ends exposed; superscript "S" denotes fiber surface exposed.

Reinforcement Electrochemistry. In cases where galvanic corrosion is under cathodic control, the type of reinforcement may significantly affect the rate of galvanic corrosion. For example, in aluminum MMCs, the galvanic-corrosion rates between 6061-T6 Al and various reinforcements would rank from highest to lowest in aerated 3.15 wt% NaCl as follows (Fig. 6): P100 Gr > carbon-cored $SiC_{MF}{}^{E}$ > tungsten-cored $B_{MF}{}^{E}$ > HP SiC > HP TiB_2 > Si. (P100 Gr is graphite fiber with 6.89 × 10^5 MPa, or 100 × 10^6 psi, elastic modulus. Superscripts "S" and "E" denote the surface and ends of the monofilaments, respectively. HP is hot pressed.) It should also be noted that ceramic reinforcements may vary in purity and structure, and some reinforcements are in themselves composites. For example, SiC monofilaments have carbon-rich outer layers and carbon cores, and their polarization diagrams have a stronger resemblance to P100 Gr^E than HP SiC. The orientation of the reinforcements may also affect electrochemical behavior. The SiC monofilaments have carbon cores, and boron monofilaments have tungsten cores. The polarization behavior of the circumferential surface of the monofilaments is different compared to the behavior of the ends of the monofilaments that expose the carbon and tungsten cores (Fig. 6). Compare cathodic curves for $SiC_{MF}{}^{S}$ versus $SiC_{MF}{}^{E}$, and $B_{MF}{}^{S}$ versus $B_{MF}{}^{E}$ (Fig. 6).

The composition of the reinforcement is important to the extent that it affects the kinetics of hydrogen evolution and oxygen reduction.

Reinforcement Resistivity. Many reinforcement materials are either semiconductors (SiC and silicon) or insulators (Al_2O_3 and mica). For reinforcements with very high resistivities, large ohmic losses through the reinforcement may limit galvanic corrosion significantly (Fig. 7). The cathodic curves were generated using the Tafel equation for P100 graphite fiber with the fiber ends exposed (Gr^E) (Ref 17) to aerated 3.15 wt% NaCl at 30 °C (86 °F) and incorporating a term for ohmic loss, $i\rho t$, through the electrode (Ref 21).

$$E_{appl}\ (V_{SCE}) = -0.67 - 0.081 \times \log\ i + i\rho t \qquad \text{(Eq 1)}$$

The ohmic loss term $i\rho t$ corresponds to a planar electrode having a thickness t, a resistivity ρ, and a one-dimensional current flow through the thickness.

The effect of ohmic losses through the particle can be demonstrated by plotting Eq 1 for various values of resistivity, ρ, for a fixed particle size (Fig. 7). In Eq 1, the thickness, t, of the material was taken to be equal to 5 μm, which is on the order for that of reinforcement particles used in MMCs. The polarization diagrams in Fig. 7 demonstrate that at very high resistivities, the galvanic-current density becomes insignificant. Figure 7 is based on a fixed particle size, but note that the critical resistivity to limit the galvanic-corrosion rate below a particular level is also dependent on the size of the reinforcement. Hence, if ohmic losses are to limit galvanic corrosion, the resistivity of the reinforcement has to be increased as the particle size decreases. For example, at a current density of 10^{-4} A/cm^2, an ohmic drop of 10 mV would result from either a 10 μm particle having a resistivity of 10^5 Ω · cm or from a 1 μm particle having a resistivity of 10^6 Ω · cm. If the reinforcements that are used in MMCs are not of high purity, resistivities may drop significantly, allowing galvanic corrosion to ensue. For example, SiC/Al MMCs are fabricated from both high-purity green SiC and lower-purity black SiC, depending on the application. The resistivity of SiC may vary by approximately 18 orders of magnitude, depending on its purity (Ref 22). Boron monofilaments are many times more conductive than pure boron, due to tungsten and tungsten borides in the core (Ref 23). In fact, many reinforcement materials have resistivities that are not high enough to stifle galvanic corrosion. The resistivities of some reinforcement materials are shown in Table 2 (Ref 21).

The aforementioned treatment for the ohmic losses through reinforcement particles should only be considered as an approximation, because one-dimensional current flow was assumed. In the actual case, the ohmic drop through the edges of the particle could be much less than through the thickness.

Reinforcement Area Fraction. The galvanic-corrosion rate increases with the area fraction of the reinforcement. This is demonstrated using the polarization diagrams of 1100 Al and P100 Gr^E (Ref 16) in Fig. 8 (Ref 21). The cathodic curve for P100 Gr^E shifts to higher currents as its area fraction is increased, causing the galvanic current with 1100 Al to increase. Because the galvanic couple with aluminum is under cathodic control and aluminum does not polarize significantly in the pitting regime, the catchment area principle (Ref 27) can be used to determine i_{galv} as a function of the area fraction of the cathodic reinforcement (Ref 16):

$$i_{galv} = i_C \cdot (X_C/1-X_C) \qquad \text{(Eq 2)}$$

The parameter i_{galv} is the dissolution current density of the matrix (i.e., i_{galv}/anode area); i_C is the current density of the cathode area; X_C is the area fraction of the cathode; and $1-X_C$ is the area fraction of the anode. The value of i_C can be set equal to the current density of the cathodic constituents in the pitting regime of aluminum. Ultrapure aluminum, 1100 Al, and 6061-T6 Al should have similar galvanic-corrosion behavior, because their anodic polarization diagrams are similar in the pitting regime. Values of i_C were read from Fig. 6. By plotting Eq 2, a graph (Fig. 9) was generated from which i_{galv} of ultrapure aluminum, 1100 Al, or 6061-T6 Al can be obtained as a function of the area fraction of P100 Gr^E, $SiC_{MF}{}^{E}$, $B_{MF}{}^{E}$, HP SiC, HP TiB_2, and silicon for exposure to aerated 3.15 wt% NaCl at 30 °C (86 °F). Figure 9 shows that to sustain a galvanic-corrosion rate equal to the normal corrosion rate of 6061-T6 Al, it would take less than 0.05 area fraction of P100 Gr^E or $SiC_{MF}{}^{E}$,

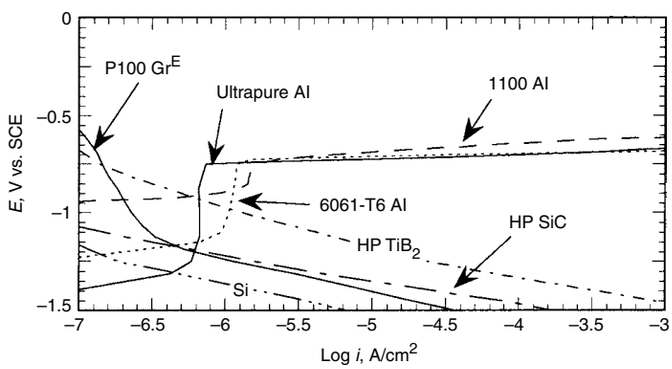

Fig. 5 A collection of anodic polarization diagrams of ultrapure aluminum (99.999 wt%) (Ref 16), 1100 Al (Ref 18), and 6061-T6 Al (Ref 16), and cathodic polarization diagrams of P100 Gr^E (Ref 16), hot-pressed (HP) SiC (Ref 16), HP TiB_2 (Ref 17), and silicon (Ref 18) exposed to deaerated 3.15 wt% NaCl at 30 °C (86 °F). Scan rate, 0.1 mV/s

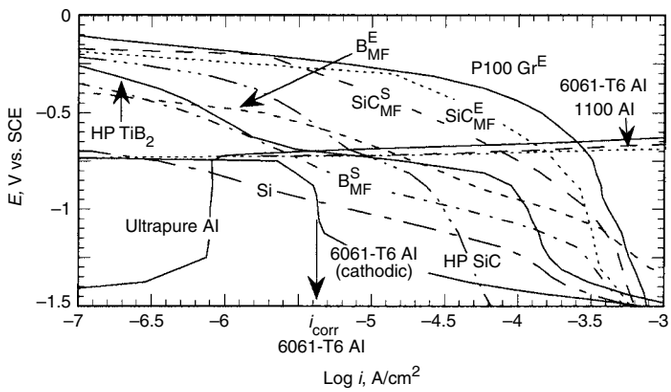

Fig. 6 A collection of anodic polarization diagrams of ultrapure aluminum (99.999 wt%) (Ref 16), 1100 Al (Ref 18), and 6061-T6 Al (Ref 16), and cathodic polarization diagrams of P100 Gr^E (Ref 16) hot-pressed (HP) SiC (Ref 16), HP TiB_2 (Ref 17), $SiC_{MF}{}^{E}$ (Ref 20), $SiC_{MF}{}^{S}$ (Ref 20), silicon (Ref 18), $B_{MF}{}^{E}$ (Ref 21), and $B_{MF}{}^{S}$ (Ref 21) exposed to aerated 3.15 wt% NaCl at 30 °C (86 °F). Scan rate, 0.1 mV/s

between 0.2 and 0.3 area fraction of $B_{MF}{}^{E}$ and HP SiC, approximately 0.5 area fraction of TiB_2, and more than 0.9 area fraction of silicon. It should be noted for those reinforcements that i_C was read in the diffusion-limited regime for oxygen reduction; galvanic-corrosion rates could increase with additional convection.

Interphase Effects. The prior discussion has focused on predicting galvanic-corrosion rates based on the electrochemical behavior of virgin reinforcement constituents. It should be emphasized, however, that the study of the actual MMC is essential to fully characterize the galvanic-corrosion behavior. During MMC fabrication, reactions between the reinforcement and matrix or precipitation of compounds may lead to the formation of an interphase or intermetallics at the reinforcement-matrix interface. If the interphase or intermetallic is a better cathode than the reinforcement, then galvanic corrosion could be more severe than that predicted based on the virgin constituents. Studies have shown that there are many different types of interphase compounds and intermetallics, but few studies have focused on their effect on galvanic corrosion in MMCs. In one case (Ref 28), an interphase in a B_{MF}/Al MMC was responsible for galvanic corrosion. Galvanic currents could not be measured between virgin boron monofilaments and 2024 Al or 6061 Al in 3.5 wt% NaCl solutions but were measurable between the aluminum alloys and $B_{MF}{}^{S}$ that were extracted from the matrix. The extracted boron monofilaments were enveloped by a 4 μm thick layer of aluminum boride. Galvanic currents measured between the aluminum alloys and aluminum boride were similar to those between the alloys and the extracted boron monofilaments. When the layer of aluminum boride was removed from the extracted boron monofilaments, the galvanic current ceased, indicating that the aluminum boride interphase is necessary for galvanic corrosion. In addition, B_{MF}/Al MMCs were noble to the matrix alloy and active to the extracted boron monofilaments and aluminum boride, which coincides with the mixed-potential theory. The corrosion rate of B_{MF}/Al MMCs also increased with the content of boron monofilaments, connoting that corrosion rates increase as aluminum-boride cathodic sites increase.

Chemical Degradation of Interphases and Reinforcements

Degradation of MMCs may also occur by chemical reactions that cannot be directly assessed by electrochemical analysis. Reinforcement phases and interphases may undergo chemical degradation that cannot be predicted, for example, with the aid of anodic polarization diagrams. A very important chemical degradation problem in aluminum MMCs is the hydrolysis of the Al_4C_3 interphase. Aluminum carbide degradation may affect both graphite-fiber- and SiC-reinforced MMCs. Reinforcement phases may also experience other forms of degradation. It has been reported that mica particles in mica/aluminum MMCs undergo exfoliation.

Aluminum Carbide Hydrolysis. Aluminum carbide may form by the reaction of aluminum and carbon (Ref 29):

$$4Al(l) + 3C(s) = Al_4C_3(s) \qquad \text{(Eq 3)}$$

and by the reaction of aluminum and SiC (Ref 30):

$$4Al(l) + 3SiC(s) = Al_4C_3(s) + 3Si(s) \qquad \text{(Eq 4)}$$

The formation of Al_4C_3 is substantial in Gr/Al MMCs during processing if temperatures are significantly higher than the liquidus temperature. At lower temperatures, Al_4C_3 formation can be controlled (Ref 31). Formation of Al_4C_3 was also reported in a Gr/Mg (1 wt% Al) MMC produced by squeeze casting. The Al_4C_3 formation resulted from heat treatments at 500 °C (932 °F) (Ref 32). Aluminum carbide also forms at SiC-Al interfaces if the silicon activity in liquid aluminum is low (Ref 30). On exposure to moisture, Al_4C_3 hydrolyzes, liberating methane gas by the reaction:

$$Al_4C_3(s) + 12H_2O(l) = 4Al(OH)_3(s) + 3CH_4(g) \qquad \text{(Eq 5)}$$

The rate of Al_4C_3 hydrolysis is approximately 1% per hour for hot-pressed Al_4C_3 (78% of theoretical density, and porous) exposed to pure water at 30 °C (86 °F) (Fig. 10) (Ref 17). Methane evolution has also been detected from Gr/Al MMCs containing Al_4C_3 (Ref 33, 34). The hydrolysis of Al_4C_3 in Gr/Al MMCs leaves fissures at fiber-matrix interfaces (Ref 34). The hydrolysis of Al_4C_3, therefore, could result in

Table 2 Resistivities of selected materials

Material	Resistivity, Ω · cm	Temperature °C	Temperature °F	Notes	Ref
Alumina	$>10^{14}$	30	86	99.7 wt% Al_2O_3	24
Dense alumina	10^{10}	30	86	96 wt% $Al_2O_3 + MgO + SiO_2$	24
Mica	10^{13}–10^{17}	...	...	Muscovite ($KAl_3Si_3O_{10}(OH)_2$)	25
SiC	10^{-5}–10^{13}	...	...	Depending on purity	22
Boron	6.7×10^{5}	25	77	Pure	26
Silicon	10^{-2}–10^{5}	...	...	Depending on purity	24
P100 Gr fiber	2.5×10^{-4}	...	...	Thornel	1
P55S Gr fiber	7.5×10^{-4}	...	...	Thornel	1
$SiC_{MF}{}^{E}$	4×10^{-2}	25	77	(a)(b)	21
$SiC_{MF}{}^{S}$	2×10^{-2}	25	77	(b)(c)	...
$B_{MF}{}^{E}$	2×10^{-1}	25	77	(a)(d)	...
$B_{MF}{}^{S}$	5×10^{-1}	25	77	(c)(d)	...

(a) E: Electrical contact was made with the end of the monofilament, exposing the core. (b) SiC has a carbon core. (c) S: Electrical contact was made with only the circumferential surface of the monofilament, excluding the core. (d) Boron has a tungsten core.

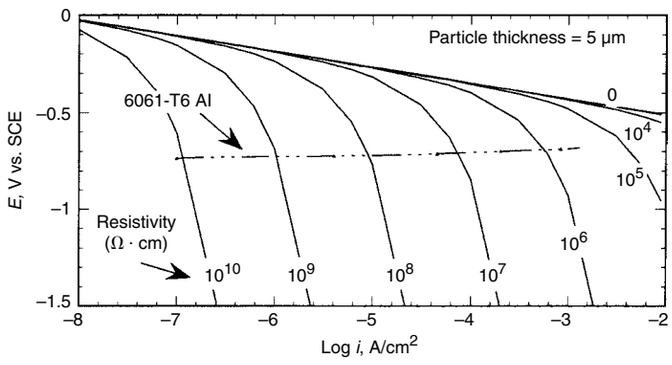

Fig. 7 Plots of the Tafel equation for oxygen reduction on P100 Gr^E incorporating the effect of hypothetical ohmic losses based on various resistivities (Eq 1) in aerated 3.15 wt% NaCl at 30 °C (86 °F) (Ref 21). The anodic polarization diagram of 6061-T6 Al (Ref 16) is also shown. Scan rate, 0.1 mV/s

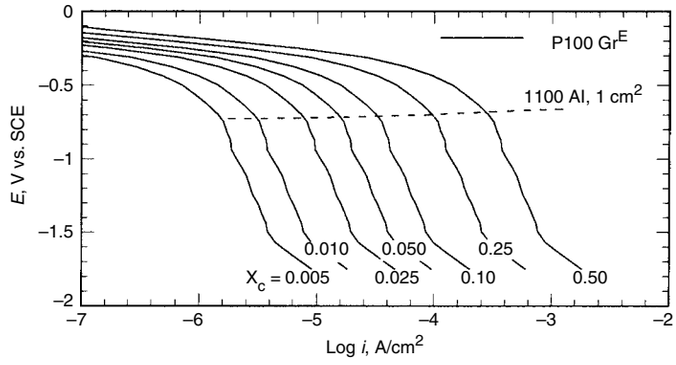

Fig. 8 Anodic polarization diagram of 1100 Al and cathodic polarization diagrams of P100 Gr^E (Ref 16) showing the effect of the P100 Gr^E area fraction X_C on the galvanic current in aerated 3.15 wt% NaCl at 30 °C (86 °F). Scan rate, 0.1 mV/s. Source: Ref 21

rapid penetration into the MMC microstructures through fiber-matrix interfaces. There is a possibility that these fissures may also lead to other secondary corrosion problems, such as pitting and crevice corrosion.

Mica Degradation. Mica/aluminum MMCs have been developed for potential use in applications where good antifriction, seizure resistance, and high damping capacity are required (Ref 35). Muscovite ($KAl_3Si_3O_{10}(OH)_2$) mica particles that are less than approximately 70 μm in size are used in mica MMCs (Ref 36). During exposure to nondeaerated 3.5 wt% NaCl solutions, the mica particles appeared to have absorbed moisture, swelled, and then exfoliated (Ref 37).

Microstructure-Influenced Corrosion

Corrosion in MMCs may be influenced by microstructural features due to the presence of the reinforcements. Intermetallic phases may form around reinforcements by solute rejection during solidification (Ref 38). Differences in the coefficient of thermal expansion between reinforcements and matrices can lead to the generation of dislocations (Ref 39) during heating and cooling of MMCs. High dislocation density may possibly lead to higher corrosion in some metals (Ref 40). The reinforcement particles left in relief resulting from matrix corrosion may form fissures, leading to crevice-type corrosion (Ref 41, 42).

Intermetallics may have potentials and corrosion resistances different than the matrix. Table 3 shows potentials of intermetallics and some aluminum alloys (Ref 43). Noble and inert intermetallics may induce galvanic corrosion of the matrix, as discussed previously, and are not addressed here. Active intermetallics and those with high corrosion rates may corrode and leave fissures or crevices on dissolution. The Al_8Mg_5 and Mg_2Si intermetallics have been reported to provide corrosion paths along fiber-matrix interfaces in Al_2O_3/Al MMCs (Ref 44). Pits in Al_2O_3/Al MMCs exposed to NaCl solutions containing H_2O_2 have been attributed to corrosion of $MgAl_3$, which is rapidly attacked at low potentials (Ref 45). In mica/aluminum MMCs, a dendritic phase that was probably Mg_2Al_3 or Al_8Mg_5 and spheroidized $CuMgAl_2$ was preferentially attacked in nondeaerated 3.5 wt% NaCl (Ref 46).

Dislocation Density. The high strengths of particulate MMCs in comparison to their monolithic alloys are generated by high dislocation densities caused by a mismatch in the coefficient of thermal expansion between reinforcement and matrix (Ref 39). Higher dislocation densities may increase corrosion rates in some metals, but the primary driving force may not be caused by an increase in strain energy. The increase in free energy due to cold working of steel is too small to account for higher corrosion rates (Ref 40). Instead, higher corrosion rates observed for steel are probably caused by the segregation of solute atoms to imperfection sites that lower the hydrogen overvoltage (Ref 40). In aluminum, heavy cold working of monolithic aluminum can change intergranular attack to general corrosion in industrial boiler applications (Ref 47). Based on the previous observations, high dislocation densities may affect the corrosion of MMCs (Ref 21). It has been suggested that corrosion near the SiC-Al interface in SiC/Al MMCs could be caused by high dislocation density due to a mismatch of the coefficient of thermal expansion between SiC and aluminum (Ref 48, 49).

Reinforcement-Induced Microcrevice Corrosion. The physical presence of the reinforcements may also have secondary effects on MMC corrosion. During immersion, aluminum MMCs will undergo significant corrosion in the open-circuit condition even in chloride-free electrolytes that passivate the MMCs during anodic polarization. The formation of localized corroded regions in aluminum MMCs (for example, Fig. 11 and 12a) usually appears after several days of immersion (Ref 41, 42). The reinforcements, which are inert in comparison to the matrix, are left in relief as the matrix corrodes leaving behind a network of fissures (Fig. 11, 12a) that becomes either acidified (Ref 42) or alkalinized (Fig. 12b) (Ref 50), preventing matrix passivation. The localized anodic and cathodic regions are many times larger than the individual reinforcement particle size.

Processing-Induced Corrosion

Corrosion problems that do not directly arise from the reinforcement, the matrix alloy, or their interaction are usually induced by processing. Examples are corrosion of diffusion bonds and corrosion due to microstructural chlorides. The B_{MF}/Al and Gr/Al MMCs have been fabricated using techniques where aluminum foils, filaments, and precursor wires are consolidated by diffusion bonding. If the diffusion bonds are of low integrity or contaminated, severe corrosion damage may result.

Low-Integrity Diffusion Bonds. Open-circuit potentials of B_{MF}/Al MMCs were active to that of their monolithic-matrix alloys in aerated NaCl solutions (Ref 51, 52). That was not expected, because open-circuit potentials of boron monofilaments were noble to that of the monolithic-matrix alloy. Based on the mixed-potential theory, it was expected that the MMCs would equilibrate to potentials between that of the noble boron monofilaments and the monolithic-matrix alloy. To investigate the origin of this discrepancy, the open-circuit potentials of hot-pressed stacks of aluminum foil processed in the same way as the MMC (but without the boron monofilaments) (Ref 52) were measured. The open-circuit potentials of the hot-pressed aluminum stacks were active to that of the MMCs and the monolithic aluminum (Ref 52). The only difference between the hot-pressed stacks of aluminum foil and the monolithic aluminum was crevices in the diffusion bonds between adjacent foils. The crevices, which are sources of additional anodic sites, polarized the stacks to active potentials.

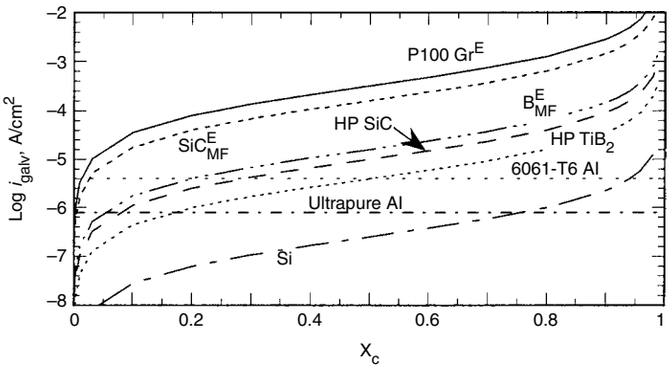

Fig. 9 Graphs showing the galvanic-corrosion current density i_{galv}, of ultrapure aluminum (99.999 wt%), 1100 Al, or 6061-T6 Al as a function of the area fraction X_C of P100 Gr^E, $SiC_{MF}{}^E$, $B_{MF}{}^E$, hot-pressed (HP) SiC, HP TiB_2, and silicon for exposure to aerated 3.15 wt% NaCl at 30 °C (86 °F). The horizontal dashed lines represent the normal corrosion rates of ultrapure aluminum and 6061-T6 Al.

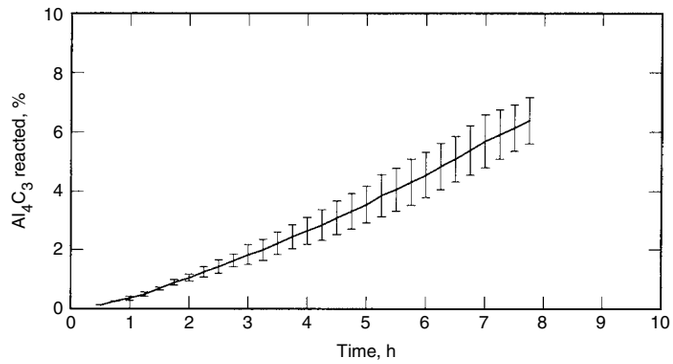

Fig. 10 Plot showing the percent of hot-pressed Al_4C_3 hydrolyzed as a function of time when exposed to pure water at 30 °C (86 °F) (Ref 17). The Al_4C_3 was porous and 78% of theoretical density. The hydrolysis rate was assessed by measuring the volume of water displaced by CH_4 gas. The curve is the average value of three experiments, with standard deviation error bars, $+/-\sigma$.

Microstructural Contaminants. Some types of Gr/Al MMC samples processed by the TiB_2 vapor deposit method (Ref 53) have been susceptible to severe corrosion (Ref 54, 55) due to microstructural chlorides (Ref 56) that were inadvertently introduced by $TiCl_4$ and BCl_3 gases during processing. The corrosion of these composites can be relatively unpredictable and cause catastrophic failures in environments where corrosion is not generally expected. Seemingly identical composites, but from different lots, stored in air-conditioned laboratory air for over 10 years show dramatic difference in corrosion behavior (Fig. 13a, b). The presence of microstructural chlorides induces corrosion in the Gr/Al MMCs even in chloride-free environments (Ref 55). An anodic polarization diagram was constructed using the mixed-potential theory (MPT) and the polarization diagrams of 6061-T6 Al and P100 Gr exposed to 0.5 M Na_2SO_4 (Ref 55) (Fig. 14). The MPT-generated diagram (Fig. 14) shows that a 6061-T6 Al matrix should passivate during the anodic scan. The anodic polarization diagram of an actual Gr/6061-T6 Al MMC processed by the TiB_2 vapor deposit method, however, showed that pitting is induced by microstructural chlorides at a potential of approximately -0.6 V_{SCE}. The polarization diagram of a Gr/1100 Al MMC processed by pressure infiltration, which does not use chlorides, resembles that of the MPT-generated diagram (Ref 34) (Fig. 14). Other types of MMCs, such as particulate silicon/aluminum MMCs (Fig. 15) and SiC_{MF}/Ti-15-3 (Fig. 16), that do not exhibit processing-induced corrosion problems also show polarization behavior, as predicted by the MPT.

Table 3 Solution potentials of second-phase constituents and aluminum alloys

Material	Potential(a), V_{SCE}
Silicon	−0.26
Al_3Ni	−0.52
Al_3Fe	−0.56
Al_2Cu	−0.73
Al_6Mn	−0.85
Al_8Mg_5	−1.24
1100 Al	−0.83
6061-T6 Al	−0.83

(a) Potential measured in solution consisting of 58.5 g NaCl and 9 mL of 30 wt% H_2O_2 per liter of solution at 25 °C (77 °F). Source: Ref 43

Corrosion of MMC Systems

The corrosion behavior of specific aluminum, magnesium, titanium, copper, stainless steel, lead, depleted uranium, and zinc MMCs systems is discussed.

Aluminum MMCs

Aluminum is a reactive metal with a high driving force to revert back to its oxide, but it generally has good resistance to aqueous corrosion in near-neutral solutions, due to the formation of a passive film (Ref 57). In acidic and basic solutions, the passive film is not thermodynamically stable, and thus, corrosion rates are high (Ref 57). Aluminum pits in halide-containing solutions, and the pitting potential (E_{pit}) is linearly dependent on the logarithm of the halogen anion concentration (Ref 58). However, in order for aluminum to pit in the open-circuit condition, it must be polarized to potentials noble to E_{pit} by a cathodic reaction. Proton and oxygen reduction are two possible cathodic reactions, but in neutral chloride-containing solutions, oxygen reduction is necessary to initiate pitting. Pits do not nucleate on aluminum in the open-circuit condition if solutions are deaerated (Ref 59). In aerated solutions, ultrapure aluminum (99.99 wt%), which is a poor catalyst for oxygen reduction, does not pit in the open-circuit condition. The slow oxygen-reduction kinetics on ultrapure aluminum are believed to be caused by the high resistivity of aluminum oxide which restricts electron migration through the passive film (Ref 27, 60). In aluminum alloys, however, noble precipitates and conducting reinforcements can polarize the alloy to E_{pit} in aerated solutions. Corrosion studies have been conducted on aluminum MMCs reinforced with boron monofilaments, graphite fiber, SiC, Al_2O_3, and mica. Corrosion of diffusion bonds, stress corrosion, and corrosion fatigue are also discussed.

Boron/aluminum MMCs have been used as tubular struts in the midfuselage structure of the space shuttle, which resulted in a 44% weight savings over the aluminum alloys planned in the original design (Ref 61).

Boron monofilaments consist of polycrystalline boron with a core of tungsten and tungsten borides, which form during processing (Ref 23). The B_{MF}/Al MMCs are usually fabricated by diffusion bonding boron monofilaments between aluminum foils (Ref 62). Aluminum borides (i.e., AlB_{12} and AlB_2) have been found at B_{MF}-matrix interfaces (Ref 63).

Although pure boron is an insulator, the conductivity of boron monofilaments is many orders of magnitude greater than that of pure boron, due to tungsten and tungsten borides in the core (Ref 23) (Table 2). Hence, boron monofilaments conduct cathodic currents, but the magnitude is dependent on the exposed region of the monofilaments. The ends of the boron monofilaments, which expose the tungsten core, support higher cathodic currents compared to the circumferential surface in aerated 3.15 wt% NaCl solutions (Fig. 6). Interphase formation on boron monofilaments may also increase corrosion rates. The corrosion rate of B_{MF}/Al MMCs increases when the boron-monofilament content is increased (Ref 28), suggesting that corrosion rates increase as boron-monofilament cathodic sites increase. Preferential sites of attack have also been documented as diffusion-bonded B_{MF}-foil and foil-foil interface regions (Ref 28, 51, 52).

Graphite/aluminum MMCs with continuous fiber graphite are known to have high specific tensile strength and stiffness in the direction of the fiber axis, but limitations of shear, compression, and transverse strengths generally precluded their use in structural applications (Ref 3). The high thermal conductivity, negative

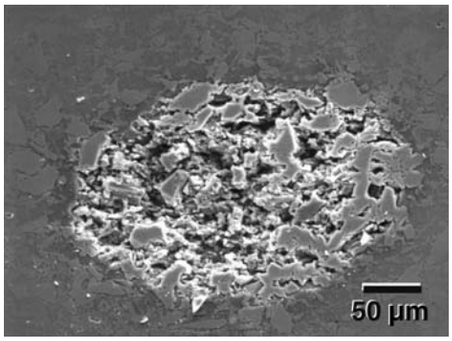

Fig. 11 Scanning electron microscope micrograph of localized corrosion on silicon/aluminum metal-matrix composite (MMC) after exposure to aerated 0.5 M Na_2SO_4 at 30 °C (86 °F) for 120 h in the open-circuit condition (Ref 41). Notice the formation of microcrevices by silicon particles in relief. This silicon/aluminum MMC passivates in 0.5 M Na_2SO_4 during anodic polarization.

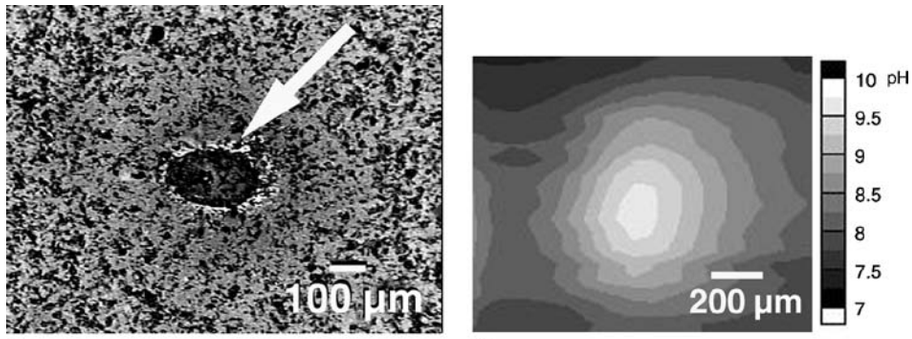

Fig. 12 Reinforcement-induced microcrevice corrosion. (a) In situ light micrograph of silicon/aluminum metal-matrix composite immersed in aerated 0.5 M Na_2SO_4 at 30 °C (86 °F) in the open-circuit condition. Region of localized corrosion at center (arrow). (b) The pH profile over that same region. Notice alkalinization over the corroded region. Source: Ref 50

coefficient of thermal expansion, and high stiffness of graphite, however, have made ultralow expansion Gr/Al MMCs ideal for thermally stable space structures. The Gr/Al MMCs have been used as antenna booms for the Hubble telescope (Ref 3). Particulate Gr/Al MMCs have also been developed for potential use in tribological applications due to good resistance to wear and seizure (Ref 64–65).

Graphite has a relatively small domain of thermodynamic stability in potential-pH space, but under normal conditions of temperature and pressure, it is relatively stable in water (Ref 66). Graphite is also an electrical conductor and efficient cathode in aerated solutions (Fig. 6), promoting galvanic corrosion in Gr/Al MMCs. In aerated solutions, the main driving force for galvanic corrosion is oxygen rather than proton reduction (Ref 67).

Another cause of degradation in Gr/Al MMCs is the presence of the Al_4C_3 interphase, which can form by the reaction of aluminum and carbon (Ref 29, 31) during processing and readily decomposes in water (Fig. 10) (Ref 17) to produce CH_4 and aluminum hydroxide ($Al(OH)_3$) (Ref 33).

Microstructural chloride contaminants have also been associated with accelerated corrosion (Ref 55) in some Gr/Al MMCs fabricated by the TiB_2 vapor deposit method (Ref 53) (compare Fig. 13a and b). The presence of the microstructural chlorides induces pitting in the MMC, as determined by polarization diagrams (Fig. 14), and appears to be significantly more deleterious than the large galvanic driving force inherent to the graphite-aluminum couple. Also see the section "Microstructural Contaminants" in this article.

Silicon carbide/aluminum MMCs are reinforced with SiC particles (P) (Fig. 2a), whiskers (W), fibers, or monofilament. In 1988, an aluminum tube in the catamaran *Stars and Stripes '88* was replaced by a lighter SiC_P/Al MMC tube having a 30.5 cm (12 in.) outer diameter (Ref 3). The SiC_P/Al MMCs have also been used in drive shafts, brake rotors, and brake drums in automobiles; fan exit guide vanes, ventral fins, actuator end glands (Fig. 17), and fuel access covers in aircraft; and a variety of bicycle components and golf clubs (Ref 68). The SiC_P/Al MMCs with reinforcement content exceeding 30 vol% are also used as electronic-packaging materials (Ref 69). Lightweight mirrors for telescopes have also been fabricated from SiC_P/Al MMC foam (Ref 70).

The electrical resistivity of SiC depends on its purity. It ranges from approximately 10^{-5} to 10^{13} Ω · cm (Ref 22). Thus, in the unpure state, the resistivity of SiC can be rather low. Some SiC_{MF} also have carbon cores and carbon-rich surfaces with resistivities on the order of 10^{-2} Ω · cm (Ref 21) (Table 2). Consequently, in aqueous solutions, SiC can serve as an inert electrode for proton and oxygen reduction. Depending on the type of SiC, galvanic corrosion with aluminum is possible.

The degree of galvanic corrosion is strongly dependent on the type of SiC reinforcement. Figure 6 shows the anodic polarization diagrams of ultrapure aluminum, pure aluminum, and 6061-T6 Al, with the cathodic polarization diagrams of 6061-T6 Al, HP SiC, and SiC monofilament (with either carbon cores or carbon-rich surface exposed) in aerated 3.15 wt% NaCl. The galvanic current density between aluminum and the SiC reinforcements (of equal surface area) is estimated by the intersection of the anodic aluminum and cathodic SiC polarization diagrams (Fig. 6). Figure 6 shows that the galvanic current density of 6061-T6 Al coupled to HP SiC of equal surface area is approximately twice the normal corrosion current density (i_{corr}) of 6061-T6 Al. When 6061-T6 aluminum is coupled to SiC monofilament (of equal surface area), i_{galv} is approximately 25 times greater than i_{corr} of 6061-T6 Al. The influence of the carbon core and carbon-rich surface of the SiC monofilament is clearly seen in Fig. 6 where the polarization diagram of the SiC monofilament has a stronger resemblance to that of pitch-based graphite than that of HP SiC (Ref 21). Galvanic current between Nicalon SiC fibers and an aluminum alloy was also measured in an aerated NaCl

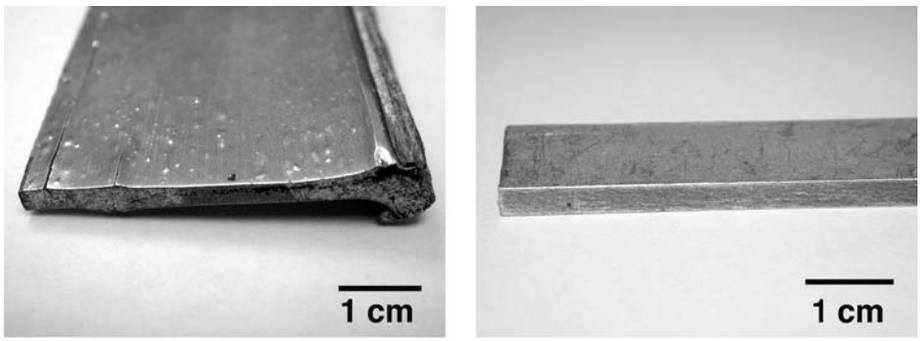

Fig. 13 Behavioral difference in seemingly similar composites from different lots. (a) Gr/6061-T6 Al metal-matrix composite (MMC), fabricated by the TiB_2 vapor deposit method, disintegrating in laboratory air after more than 10 years exposure. (b) Gr/Al MMC, processed by the same method, with over 10 years exposure in laboratory air but with no visual signs of degradation

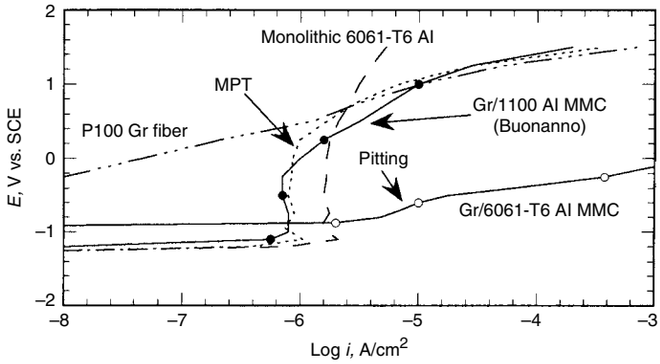

Fig. 14 Anodic polarization diagrams of P100 Gr, monolithic 6061-T6 Al, and an actual P100 Gr (50 vol% fiber)/6061-T6 Al metal-matrix composite (MMC) exposed to deaerated 0.5 M Na_2SO_4 at 30 °C (86 °F); scan rate, 0.1 mV/s (Ref 55). The discrepancy between the polarization diagram generated by the mixed-potential theory (MPT) and that of the P100 Gr/6061-T6 Al MMC is due to microstructural chlorides. Also, notice data (closed circle data points) from Gr (65 vol% fiber)/1100 Al MMC fabricated by pressure infiltration (Ref 34) exposed to 0.5 M Na_2SO_4 at 30 °C (86 °F); scan rate, 0.167 mV/s. The polarization diagram of Gr/1100 Al MMC corresponds to that of the MPT.

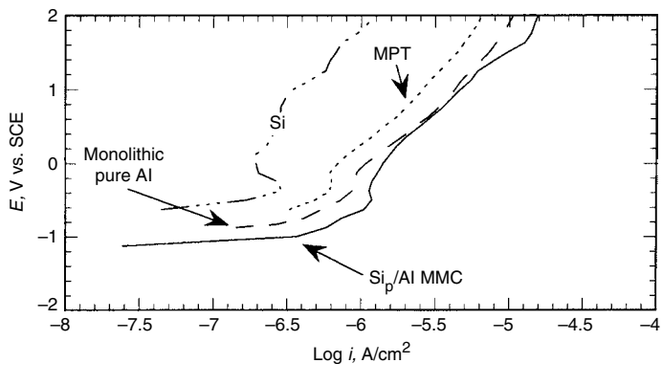

Fig. 15 Anodic polarization diagrams of silicon, pure aluminum, an Si_P/Al metal-matrix composite (MMC), and that generated with the mixed-potential theory (MPT) exposed to deaerated 0.5 M Na_2SO_4 at 30 °C (86 °F). Scan rate, 0.1 mV/s. Source: Ref 41

solution (Ref 71), but the galvanic current was only 15% of that between carbon fiber and the aluminum alloy.

Experimental results have generally indicated that the corrosion rate of particulate and whisker SiC/Al MMCs is higher than the monolithic-matrix alloy (Ref 72–74), and increases with SiC content (Ref 75) in aerated chloride-containing environments. Weight-loss data of SiC_P/6092-T6 Al MMCs showed an increase in the corrosion rate as the SiC content increased from 5, 10, 20, and 40 to 50 vol% for various 90 day humidity chamber tests (Ref 76). At the 50 vol% SiC content level, the corrosion rate for a MMC with high-purity, high-resistivity green SiC was noticeably lower than that of the MMC with low-resistivity black SiC (Ref 76). The black SiC is likely to support more cathodic currents, leading to higher corrosion rates in comparison to green SiC. The resistivity of the SiC may be the cause for conflicting results in the literature. For example, no obvious evidence of galvanic corrosion was found in SiC/6061 Al MMCs with 17 to 27 vol% SiC particles (Ref 77).

The presence of SiC particles does not have a significant effect on aluminum passive current densities (Ref 78, 79) and pitting potentials (Ref 71, 77, 78, 80–85), indicating that the presence of SiC particles does not degrade the pitting resistance of passive films on aluminum, as gaged by pitting potentials. The polarization diagrams (Fig. 18) show very little variation in pitting potentials for SiC_P/6092 Al MMCs ranging in SiC content from 5 to 50 vol% (Ref 76). Pit morphology, however, is indirectly affected by the presence of SiC particles. Pits on SiC_W/Al MMCs were notably more numerous and much smaller in size (Ref 86) compared to pits on wrought and powder-compacted monolithic alloys during anodic polarization in 0.1 N NaCl. The pits nucleated at intermetallic particles (not SiC), which are smaller and more numerous in the MMCs than in the monolithic-matrix alloys (Ref 86). Apparently, SiC whiskers (Ref 86) and particles (Ref 77) enhance the precipitation of the intermetallic phases. Pitting has also been observed at dendrite cores (Ref 87) and near eutectic silicon (Ref 84, 88) and intermetallic particles (Ref 88) in various SiC/Al MMCs.

Due to the influence of the microstructure, the corrosion behavior of particulate SiC/Al MMCs is also sensitive to processing. Processing conditions and the presence of SiC particles can affect void content (Ref 89), dislocation density (Ref 90), and the precipitation of active phases (Ref 91) in aluminum matrices. Certain solution heat treatments and high extrusion ratios improved corrosion resistance of a 20 vol% SiC_P/7091 Al MMC (Ref 89). Extrusion improved the corrosion resistance of cast MMCs by reducing the amount of pores and agglomerates of SiC particles (Ref 92). Corrosion resistance was also improved by a finer, more homogenous distribution of secondary phases at the T4 temper in comparison to the O and F tempers (Ref 93). It has been suggested that corrosion near the SiC-Al interface could be caused by high dislocation density due to a mismatch of the coefficient of thermal expansion between SiC and aluminum (Ref 21, 48, 49), segregation of alloying elements to the SiC-Al interface (Ref 94), or the formation of Al_4C_3, which hydrolyzes in water. Aluminum carbide has been identified as a source of corrosion for MMCs reinforced with particles (Ref 95) and SiC Nicalon fibers (Ref 71).

The formation of microcervices caused by reinforcement particles left in relief as the matrix corrodes (Fig. 11) also exacerbates corrosion by localized acidification and alkalinization of the solution in SiC_P/6092-T6 Al MMCs (Ref 42). The aluminum matrix loses its ability to passivate when the solution becomes either acidic or alkaline.

Alumina/Aluminum MMCs. Particles and both short and continuous Al_2O_3 fibers have been used to reinforce aluminum alloys. Characteristic properties of Al_2O_3/Al MMCs are low weight, high-temperature tensile and fatigue strengths, low thermal conductivity and expansion, and superior wear resistance. In the automotive industry, short-fiber Al_2O_3/Al MMCs have been used to replace cast iron components such as pistons (Ref 96, 97), engine blocks (Ref 96), cylinder heads (Ref 96), and brake calipers and rotors (Ref 96). Continuous-fiber Al_2O_3/Al MMCs, having high strength, high damping capacity, and low thermal expansion, are used for automotive push rods, brake calipers, and load-carrying wires in aluminum conductor cables (Ref 98) (Fig. 19).

The resistivity of Al_2O_3 (99.7 wt% pure) is greater than approximately $10^{14}\ \Omega \cdot cm$ (Ref 24), and therefore, galvanic corrosion between Al_2O_3 fibers and aluminum is unlikely. The Al_2O_3/pure Al MMCs have excellent corrosion resistance due to a lack of galvanic action with the Al_2O_3 fibers and a minimal amount of cathodic sites, such as those from conducting interphases and intermetallic precipitates. Only slight corrosion damage was observed on Al_2O_3/pure Al MMCs exposed to marine atmosphere 0.5 miles from the coastline for an 11 month period (Fig. 20a, b).

The Al_2O_3 reinforcements usually do not have significant effects on pitting potentials (Ref 71, 80, 82–84, 99) in chloride solutions. The anodic polarization diagrams of various 6092-T6 Al MMCs, including that of an Al_2O_3/6092-T6 Al MMC, are very similar (Fig. 18) for a 3.15 wt% NaCl solution (Ref 76). Passive current densities below the pitting potential have been reported to increase with Al_2O_3 content (Ref 99), although this may be related to processing. Passive current densities for a particulate Al_2O_3/6092-T6 Al MMC are consistent with other MMCs in sodium sulfate solutions (Ref 76) and in chloride solutions under the pitting potential (Fig. 18). Microbial corrosion was also reported to be more significant on particulate MMCs in comparison to the monolithic alloy, indicating that the Al_2O_3/Al-matrix interface or Al_2O_3 particles may have aided biofilm formation (Ref 100).

Formation of interphases incorporating aluminum, oxygen, and alloying elements has been observed in some Al_2O_3/Al MMCs. Thin layers of $Li_2O \cdot 5Al_2O_3$ (Ref 72) and $MgAl_2O_4$ (Ref 45) have been found to envelop continuous

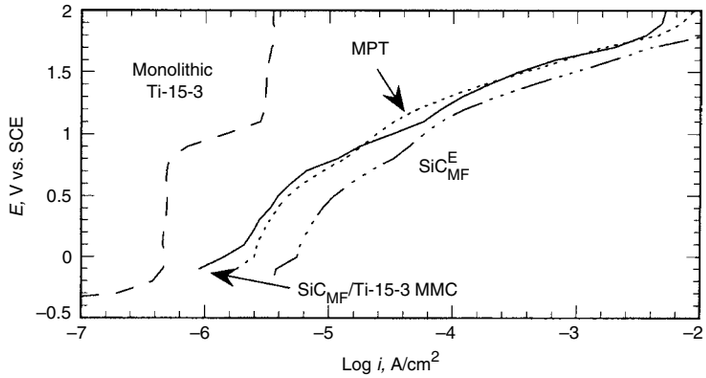

Fig. 16 Anodic polarization diagrams of SiC_{MF}^{E}, Ti-15-3, an actual SiC_{MF}/Ti-15-3 metal-matrix composite (MMC), and that generated with the mixed-potential theory (MPT) exposed to deaerated 3.15 wt% NaCl at 30 °C (86 °F). Scan rate, 0.1 mV/s. Source: Ref 14

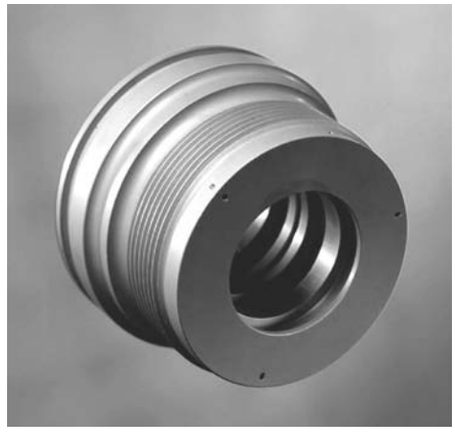

Fig. 17 Hydraulic actuator end gland for aircraft. The component is a machined extrusion of SiC_p (15 vol%)/2009Al-T4 metal-matrix composite. Photo courtesy of DWA Aluminum Composites

Al_2O_3 fibers in various types of Al_2O_3/Al MMCs. The presence of these interphases, however, was not suspected of inducing corrosion.

Preferential corrosion near fibers (Ref 45, 101, 102) and particles (Ref 84, 102, 103) is sometimes noticed in chloride-containing solutions. The presence of intermetallics and segregation of alloying elements may contribute to localized corrosion near reinforcements. In a 2 wt% Mg aluminum alloy MMC, iron and high levels of magnesium (10 wt%) were detected near fibers (Ref 45). It was suspected that the presence of magnesium originated from Mg_2Al_3. Pitting near fibers was attributed to corrosion of Mg_2Al_3, which is rapidly attacked at low potentials (Ref 45). The Al_8Mg_5 and Mg_2Si intermetallics have been also reported to induce corrosion in Al_2O_3/Al MMCs (Ref 44).

Mica/aluminum MMCs have been developed for potential use in applications where good antifriction, seizure resistance, and high damping capacity are required (Ref 35).

Muscovite ($KAl_3Si_3O_{10}(OH)_2$) mica particles that are less than approximately 70 μm in size are used in mica MMCs (Ref 36). Galvanic corrosion between aluminum and muscovite should not be a problem, because muscovite is an insulator with resistivities that range from approximately 10^{13} to 10^{17} Ω · cm (Ref 25). Muscovite is insoluble in cold water (Ref 104); however, it has been reported that muscovite particles have a tendency to absorb moisture and then swell (Ref 37).

Mica particles were cast in various aluminum alloys (Ref 37, 46). In 3.5 wt% NaCl solutions, the presence of mica particles depressed pitting potentials by approximately 20 to 30 mV in comparison to the monolithic-matrix alloys. Corrosion behavior was also affected by the precipitation of secondary phases. In some cases, precipitates were preferentially attacked. Pits around and away from mica particles, interfacial corrosion of the mica-matrix interface, and exfoliation of mica particles were also observed.

Stress-corrosion cracking in aluminum MMCs with continuous and discontinuous reinforcement has been studied.

Continuous-Reinforced MMCs. Stress-corrosion cracking studies for the immersed state have been conducted on aluminum MMCs reinforced with unidirectional graphite fibers (Ref 105), boron monofilaments (Ref 51), and Nextel 440 (Al_2O_3, SiO_2, B_2O_3) fibers (Ref 106). Stresses were applied either parallel or perpendicular to the fiber axis of unnotched specimens. The Gr/6061 Al MMCs were stressed parallel to the fiber axis in natural seawater. At high stresses, failure was stress dependent and occurred in less than 100 h. At lower stresses, failure was primarily caused by extensive corrosion and therefore was relatively independent of stress levels. The B_{MF}/2024 Al MMCs stressed parallel to the fiber axis at 80% fracture strength in a NaCl solution did not fail in 1000 h but failed after 500 h when H_2O_2 was added to the NaCl solution. Extensive intergranular matrix corrosion and broken filaments at random sites were observed. The monolithic-matrix alloy failed within 10 h under similar conditions. For B_{MF}/2024 Al MMCs stressed perpendicular to the fiber axis at 90% yield strength in the NaCl and NaCl with H_2O_2 solutions, failure occurred by intergranular matrix corrosion and separation at diffusion-bonded fiber-matrix interfaces. Failure times decreased with increasing boron-monofilament content. For the Nextel fiber 6061 Al MMCs, specimens were exposed to a pH 2 NaCl solution in the stressed and unstressed states (Ref 106). To assess damage, the composite strength was measured before and after exposure. The prevailing mode of failure was attributed to extensive corrosion along the fiber-matrix interface and not to stress-corrosion cracking.

Two types of aluminum MMCs reinforced with SiC-coated boron monofilament (BORSIC$_{MF}$) (Ref 107) were exposed to synthetic seasalt spray at 95 °C (203 °F) and nearly 100% relative humidity, then stressed to 689 MPa (100 ksi) along the fiber axis by three-point bending. The BORSIC$_{MF}$/6061 Al MMCs showed general corrosion attack without preference to tensile regions, whereas BORSIC$_{MF}$/2024 Al MMCs showed approximately a 2-to-1 depth-of-attack ratio comparing the tensile to the compressive surfaces, which may have been related to specimen orientation. Unlike the 6061 Al MMCs, the corrosion resistance of the 2024 Al MMC was sensitive to heat treatment.

Discontinuous-Reinforced MMCs. Stress-corrosion cracking studies for alternate exposure and immersion in NaCl solutions have been conducted on aluminum MMCs reinforced with Al_2O_3 particles (Ref 108), and SiC particles (Ref 108–110) and whiskers (Ref 108). The Al_2O_3/2014 MMC was susceptible to stress-corrosion cracking while subjected to three-point beam bending and alternate exposure and continuous immersions in a NaCl solution (Ref 108). Under the same conditions, however, the 6061 Al MMCs reinforced with SiC_p and SiC_w were not susceptible to stress-corrosion cracking (Ref 108). Similarly, SiC_p/2024 MMCs were not prone to stress-corrosion cracking under constant strain at 75% of ultimate tensile strength while exposed to an aerated NaCl solution (Ref 109). Slow strain-rate tension testing of SiC_p/2024 MMCs indicated that the MMC lost up to 10% of failure strength compared to exposure in air (Ref 110).

Corrosion fatigue has been studied in aluminum MMCs reinforced with graphite fibers (Ref 105), SiC whiskers (Ref 111–114), and SiC particles (Ref 112, 115). Processing conditions and type of reinforcement affect corrosion-fatigue behavior. Unnotched Gr/6061 Al MMCs were exposed to natural seawater and stressed parallel to the fiber axis. The MMCs were processed with either silica (SiO_2)-coated or TiB_2-coated graphite fibers. For a given stress amplitude, the TiB_2-type MMC had the longest corrosion-fatigue life, followed by the SiO_2 type and the monolithic-matrix alloy. At low stress amplitudes corresponding to longer exposure times, the SiO_2-type MMC suffered premature failure due to extensive corrosion. In SiC/Al MMCs, fatigue crack rates of compact-tension specimens are usually higher in NaCl solutions as compared to air (Ref 111) or argon (Ref 115). Loading frequency affects corrosion-fatigue crack rates (Ref 115), but no consistent trends were observed. Fatigue (Ref 111) and corrosion-fatigue (Ref 115) crack rates are influenced by loading and extrusion or rolling direction. The

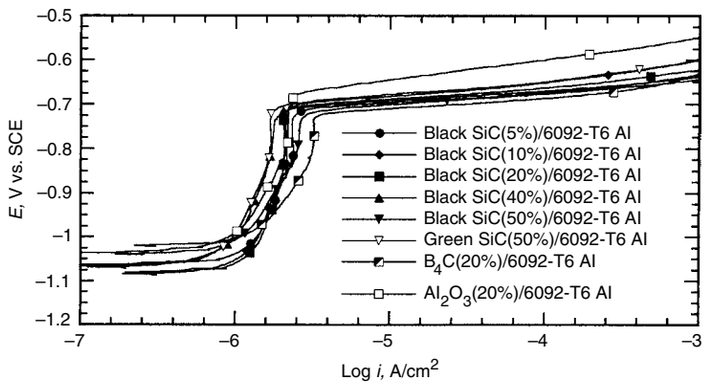

Fig. 18 Only a slight variation in potential is noted in this collection of anodic polarization diagrams as the volume content of various discontinuous reinforced 6092-T6 Al metal-matrix composites (MMCs) varies from 5 to 50%. The MMCs were exposed to 3.15 wt% NaCl at 30 °C (86 °F); scan rate, 1 mV/s. Source: Ref 76

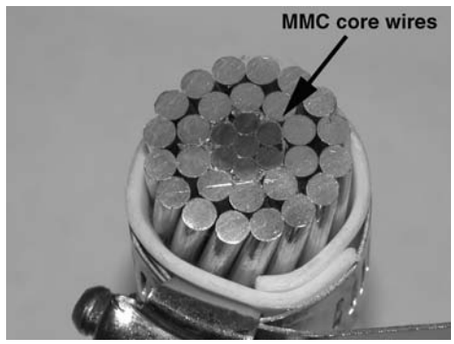

Fig. 19 Aluminum conductor composite-reinforced cable specimen. Note the seven inner Al_2O_3/Al metal-matrix composite (MMC) core wires

nucleation of a crack was also observed at the bottom of a corrosion pit (Ref 114). The shape of the reinforcement constituent may also have significant effects on stress-corrosion and corrosion fatigue, based on modeling that considers crack-tip strain rate (Ref 113). The model predicts that crack rates are reduced by increasing the reinforcement constituent 1-to-*d* ratio, implying that MMCs reinforced with whiskers are more resistant to stress-corrosion and corrosion fatigue than those reinforced with particles. This is in agreement with results on SiC_W/6061 Al MMCs that were found to have longer corrosion-fatigue lives than SiC_P/6061 Al MMCs in salt-ladened moist air (Ref 112).

Magnesium MMCs

Very light composites can be fabricated from magnesium, which is one of the lightest structural metals (density, 1.7 g/cm^3). Magnesium, however, is also the most active structural metal in the electromotive series (Ref 40), and has a very high tendency to corrode, making it particularly susceptible to galvanic corrosion when in contact with noble reinforcement constituents. Dissolved oxygen in solution does not significantly affect the corrosion of magnesium (Ref 40). Corrosion rates are highly dependent on metallic purity (Ref 40). Noble impurity elements that have low hydrogen overvoltages (e.g., iron, nickel, cobalt, and copper) (Ref 47) serve as efficient cathodic sites, which accelerate the corrosion rate of magnesium. In seawater, ultrapure magnesium corrodes at the rate of 0.25 mm/yr (0.01 in./yr), but commercial magnesium corrodes at approximately 100 to 500 times faster due to impurities (Ref 40). Because the corrosion rate of magnesium is highly dependent on the presence of cathodic sites, the incorporation of noble fibers and particles into magnesium MMCs can result in severe galvanic corrosion. Corrosion studies have been conducted on magnesium MMCs reinforced with B_{MF}, graphite fibers, SiC_{MF}, and Al_2O_3 fibers. The stress-corrosion cracking behavior of an Al_2O_3/Mg MMC has also been investigated.

Boron/Magnesium MMCs. The general properties of boron monofilaments discussed in the section "Boron/Aluminum MMCs" in this article also apply here. Pure boron is an insulator, and, accordingly, galvanic currents were unmeasurable between pure boron and magnesium in NaCl solutions (Ref 116, 117). Galvanic currents, however, were measurable between virgin tungsten-core boron monofilaments, with cores either shielded or exposed, coupled to pure magnesium (Ref 117) and an alloy (Ref 116). Galvanic currents were higher when tungsten cores were exposed (Ref 116, 117), because pure tungsten is an effective cathode (Ref 116). The measurable galvanic currents between magnesium and virgin boron monofilaments with tungsten cores shielded indicated that the outer layer of the monofilaments consisted of tungsten boride and not of pure boron (Ref 117). In addition, boron monofilaments extracted from the matrix supported cathodic current densities that were approximately five times that of virgin boron monofilaments (Ref 116). Corrosion rates of actual B_{MF}/Mg alloy (MA2–1) MMCs in 0.005 and 0.5 N NaCl solutions were 12.5 and 81.7 g/m^2/day, respectively, which were approximately six times the values of the monolithic-matrix alloy in respective environments.

Graphite/Magnesium MMCs. The general properties of graphite fibers found in graphite/aluminum MMCs also apply here. Figure 21 shows the cathodic polarization diagrams of pitch-based graphite (cross section exposed) in deaerated and aerated 3.15 wt% NaCl, with the anodic polarization diagrams of pure magnesium and ZE41A magnesium in deaerated and oxygenated 3.15 wt% NaCl. It should be noted that solution oxygenation does not have significant effects on anodic polarization curves of pure magnesium and ZE41A. Galvanic-corrosion rates with graphite fiber will increase in aerated solutions. In addition, galvanic corrosion of magnesium is cathodically controlled (Fig. 21), and therefore, galvanic-corrosion rates should increase with increasing area fraction of cathodic reinforcement material. Galvanic-corrosion current densities increased from approximately 0.3×10^{-3} to 0.6×10^{-3} A/cm^2 (based on magnesium area) as the graphite-to-magnesium area ratio was increased from 0.25 to 0.44 (Ref 120). The galvanic couples consisted of AZ31B magnesium alloy and pitch-based graphite fiber with fiber ends and circumferential fiber surface exposed to an aerated, borated-boric acid solution of 8.4 pH containing 1000 ppm NaCl. Actual MMCs immersed in air-exposed 0.001 N NaCl suffered severe degradation within five days (Ref 120). Comparisons between a Gr (40 vol%)/AZ91C Mg MMC and monolithic AZ91C Mg showed that the MMC open-circuit potential was approximately 0.3 V more noble and the corrosion rate 40 times greater than that of the monolithic alloy in a deaerated 50 ppm chloride solution (Ref 121). Even in relatively dry conditions, such as that in air-conditioned environments, a Gr/AZ91C/AZ31B Mg MMC disintegrated over a 15 year period (Fig. 22).

Silicon Carbide/Magnesium MMCs. The general properties of SiC given for SiC/Al MMCs also apply here. Galvanic corrosion between magnesium and SiC depends to a large degree on the type of SiC reinforcement and on the presence of dissolved oxygen in solution. Figure 21 shows anodic polarization diagrams of pure magnesium and ZE41A magnesium, with cathodic polarization diagrams of hot-pressed SiC and SiC monofilament, with carbon-rich circumferential surface exposed, in deaerated and aerated 3.15 wt% NaCl solutions. Galvanic-corrosion rates (as determined by the mixed-potential theory) are greater in aerated solutions due to oxygen reduction (Ref 19, 122). Galvanic-corrosion rates are lower for couples with hot-pressed SiC as opposed to the SiC_{MF}. Studies conducted on particulate ZC71 magnesium alloy reinforced with 12 vol% SiC particles ranging in size up to approximately 20 μm did not show preferential attack between SiC particles and the matrix in salt spray tests (Ref 123). Instead, macroscopic anodic and cathodic regions developed. Corrosion spread over the MMC surface much more rapidly than on the monolithic alloy, but the local corrosion rates were approximately only three times greater on the MMC. The authors (Ref 123) speculated that the higher corrosion rates on the MMCs could have been caused by iron contamination of the magnesium matrix during processing in a steel crucible. Studies on a model MMC consisting of high-purity magnesium and well-separated SiC particles exposed to 3.5 wt% NaCl also did not show evidence of galvanic corrosion between the particles and matrix (Ref 124).

Alumina/Magnesium MMCs. The general properties of Al_2O_3 given for Al_2O_3/Al MMCs also apply here. Galvanic corrosion should not be expected between magnesium and Al_2O_3, because Al_2O_3 is an insulator. The corrosion rates of a continuous-fiber Al_2O_3/AZ91C MMC (Ref 125) were approximately 100 times greater than that of the matrix alloy in 3.5 wt% NaCl at 25 °C (77 °F), but similar to that of the matrix

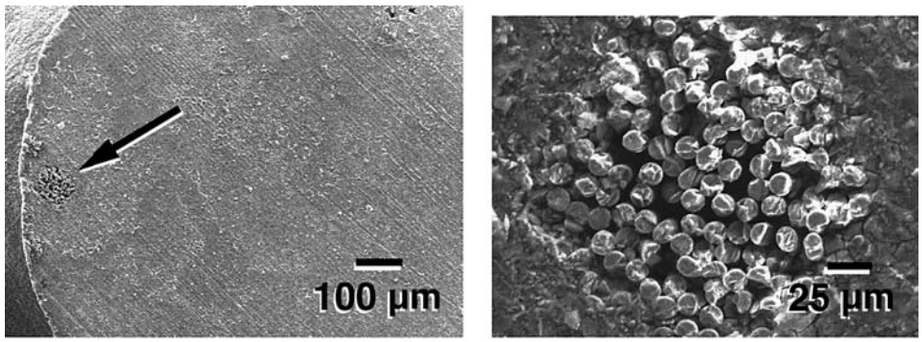

Fig. 20 Scanning electron microscope micrographs of an Al_2O_3/Al metal-matrix composite wire exposed to marine atmosphere 0.5 miles from the coastline for an 11 month period. Corrosion damage was minimal, and the region indicated with an arrow in (a) represents the worst damage. (b) Enlargement of area indicated by the arrow in (a)

alloy in distilled water at 20 °C (68 °F). The tremendously higher corrosion rates of the composites in the chloride solution appear to be caused by the presence of the Al_2O_3 fibers. Although galvanic corrosion is not expected between magnesium and Al_2O_3, it could be possible with conducting interphases or precipitates, which potentially could form due to the presence of the Al_2O_3 fibers. The open-circuit potential of a continuous-fiber Al_2O_3/AZ91C MMC was more noble than that of the matrix alloy in 50 ppm Cl^- solutions (Ref 126), indicating that noble precipitates or interphases could have been present.

Stress-corrosion tests (Ref 127) of continuous-fiber Al_2O_3/ZE41A Mg MMC in a NaCl-potassium chromate (K_2CrO_4) solution showed that notched and unnotched specimens stressed parallel to the fiber axis and exposed for approximately 100 to 1000 h in the NaCl-K_2CrO_4 solution retained approximately 90% of the strength in air. The matrix alloy and the MMC with the stress direction aligned perpendicular to the fiber axis retained only approximately 40 to 60% of the strength in air.

Titanium MMCs

Titanium MMCs are being developed for aerospace, commercial, and biomedical applications. Titanium MMCs reinforced with SiC monofilament (Fig. 1b) have utility in high-temperature applications requiring strong, lightweight materials (titanium density, 4.5 g/cm^3). Structural SiC_{MF}/Ti MMCs have been used in prototype drive shafts, turbine-engine discs, compressor discs, and hollow fan blades and were also candidate materials for the skin of the National Aerospace Plane (Ref 128). Discontinuous-reinforced titanium MMCs are candidate materials for gears, bearings, and shafts (Ref 129). Porous, particulate titanium MMCs have potential use as surgical implant materials, owing to the compatibility of titanium and bone growth (Ref 130). Porous titanium is a good surgical implant material, because bone growth is enhanced by the relatively low elastic modulus of titanium, and bone ingrowth is allowed by the porous structure. Porous titanium, however, has poor tribological properties, and therefore, MMCs that incorporate graphite to reduce friction and titanium carbide to improve wear resistance are of interest (Ref 130).

Graphite/titanium MMCs were processed and heat treated to fabricate a titanium carbide (TiC)/graphite/porous titanium MMC (Ref 130). Polarization tests were conducted in 0.9 wt% NaCl and lactated Ringer's solution for in vitro use. The anodic polarization current densities of the MMCs were significantly higher than that of pure monolithic titanium, which passivated. The authors attributed the higher corrosion rates of the TiC/graphite/Ti MMC to its porosity, which may have prevented complete passivation of the titanium matrix. Another possibility for the higher current densities could be the oxidation of graphite particles (see the following section).

Silicon Carbide/Titanium MMCs. Corrosion studies on titanium alloy Ti-15V-3Cr-3Sn-3Al (Ti-15-3) (Ref 14) and titanium aluminide α_2-Ti_3Al (14 wt% Al, 21 wt% Nb, balance titanium) (Ref 131) reinforced with SiC monofilament have been conducted. The corrosion behavior of SiC_{MF}/Ti-15-3 MMC was investigated in 3.15 wt% NaCl. There was excellent agreement in the polarization diagrams of the actual MMC and that of a model using the polarization diagrams of the individual constituents and the mixed-potential theory (Fig. 16). The matrix passivated, and the carbon cores and carbon-rich outer surface of the SiC monofilaments oxidized. During anodic polarization, graphite fibers oxidize to CO_2 (Ref 55). Zero-resistance ammeter studies showed that galvanic currents between the Ti-15-3 matrix and SiC monofilaments were negligible. Based on the polarization diagrams, the galvanic current density cannot exceed that of the passive current density of Ti-15-3. The corrosion behavior of the SiC_{MF} α_2-Ti_3Al (Ref 131) was somewhat similar to that of the SiC_{MF}/Ti-15-3 MMC (Ref 14), with the exception that the α_2-Ti_3Al matrix is less resistant to pitting. During anodic polarization, the SiC_{MF} α_2-Ti_3Al pitted at approximately 1 V_{SCE} in 0.5 N NaCl, which was approximately 0.5 V less than that of the monolithic-matrix alloy. Some matrix pitting and crevice corrosion around the SiC monofilaments was also observed after anodic polarization. The galvanic current density of the SiC_{MF} α_2-Ti_3Al MMC was negligible and limited to the passive current density of the α_2-Ti_3Al matrix (Ref 131).

Titanium Carbide/Titanium MMCs. Particulate titanium carbide/pure titanium (TiC/Ti) MMCs were fabricated by cold isostatic pressing followed by sintering (Ref 132). No interphase products were identified in the MMC after processing. Composites reinforced with 2.5, 5, 10, and 20 vol% TiC were anodically polarized in deaerated 2 wt% HCl in the temperature range of 50 to 90 °C (120 to 190 °F). The passive current density for pure titanium was approximately 10^{-5} A/cm^2 throughout the temperature range. Generally, dissolution currents for the TiC/Ti MMCs increased with increasing temperature and TiC content and, at worst-case scenario, were approximately 20 times higher than that of pure titanium. Microscopy revealed that the titanium matrix was virtually uncorroded, whereas the TiC particles underwent some degradation.

Titanium Diboride/Titanium MMCs. Particulate titanium diboride/pure titanium (TiB_2/Ti) MMCs were fabricated by cold isostatic pressing followed by sintering (Ref 132). The TiB interphase products were identified in the MMC after processing. Composites reinforced with 2.5, 5, 10, and 20 vol% TiB_2 were anodically polarized in deaerated 2 wt% HCl in the temperature range of 50 to 90 °C (120 to 190 °F). Dissolution currents for the TiB_2/Ti MMCs increased with increasing temperature and TiB_2 content. In the worst case, the dissolution current density of the MMC was approximately 2 orders of magnitude higher than that of pure titanium. As in the case of the TiC/Ti MMCs, the titanium matrix was virtually uncorroded; however, the TiB_2 particles and TiB interphase were corroded significantly.

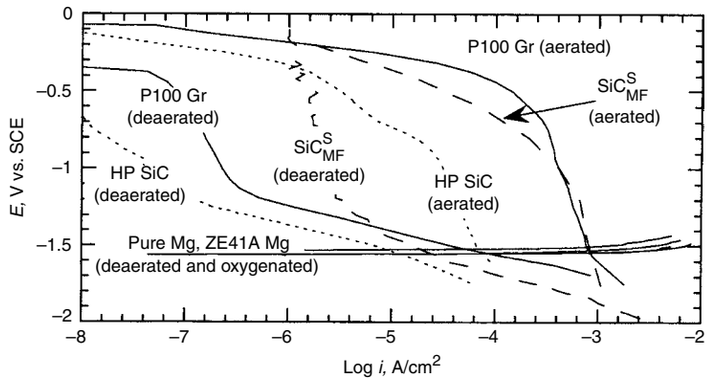

Fig. 21 Anodic polarization diagrams of pure magnesium and ZE41A Mg (Ref 118) in deaerated and oxygenated 3.15 wt% NaCl at 30 °C (86 °F), 0.1 mV/s scan rate, are plotted with a collection of cathodic polarization diagrams of P100 graphite (Ref 16), hot-pressed SiC (Ref 16) and SiC_{MF} (Ref 119), circumferential surface exposed, in deaerated and aerated 3.15 wt% NaCl at 30 °C (86 °F), 0.1 mV/s scan rate

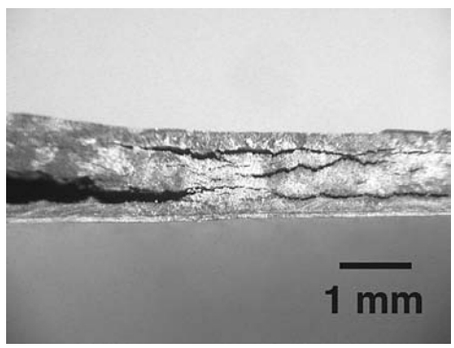

Fig. 22 Gr/AZ91C/AZ31B Mg metal-matrix composite disintegrating in laboratory air after 15 years exposure

Copper MMCs

Copper MMCs have been investigated for use in marine, electronic, and thermal applications. Copper is relatively heavy, with a density of 8.96 g/cm^3. Reinforcements are typically chosen to impart strength and stiffness, reduce weight, enhance thermal and electrical properties, improve machinability, and enhance wear resistance. Initial studies (Ref 133) were conducted on a wide variety of experimental copper and copper alloy MMCs reinforced with graphite, SiC, TiC, silicon nitride, boron carbide, and Al_2O_3 for marine applications. The MMCs generally showed corrosion behavior that was similar to that of the monolithic alloys, although corrosion rates were higher for some of the MMCs. More recent studies have focused on copper MMCs for electronic, thermal, and tribological applications.

Graphite/copper MMCs have been reinforced with graphite particles and fibers. The particulate MMCs have been developed for sliding electrical contact materials (Ref 134), and improved machinability for lead-free copper alloys (Ref 135). Fiber-reinforced MMCs have been developed for applications requiring reduced weight and high thermal conductivity (Ref 136). Highly graphitized fibers have very high thermal conductivity, exceeding that of silver (Ref 3).

The corrosion behavior was studied for pure copper MMCs reinforced with 1.2 to 40 vol% graphite particles and 50 vol% of graphite fibers in deaerated and aerated 3.5 wt% NaCl solutions (Ref 137). The corrosion potential of the particulate-reinforced MMCs became more noble with increasing graphite content in both the deaerated and aerated solutions, as would be expected by increasing the content of the noble graphite particles. The corrosion potential of the graphite fiber (50 vol%)/Cu MMC was approximately as noble as the MMC with 40 vol% graphite particles in the aerated solution but was significantly more active than the particulate composite in the deaerated solution. This finding could be expected, because oxygen-reduction kinetics is normally diffusion-limited in aerated solutions, but hydrogen evolution kinetics depend on the substrate and could be different on the graphite fibers when compared to the graphite particles in deaerated solutions. The corrosion potentials of UNS C90300 copper alloy (with 1 wt% Ti additive to increase graphite wettability) MMCs reinforced with 1 to 10 vol% graphite particles also increased with increasing graphite content in an aqueous solution containing ferric chloride, copper sulfate, and hydrochloric acid (Ref 135).

Silicon Carbide/Copper MMCs. The corrosion behavior of pure copper MMCs reinforced with 0, 5, 10, and 20 vol% SiC particles was examined in a 5 wt% NaCl solution (Ref 138). Porosity in the materials ranged from 2.2 to 3.5% and generally increased with increasing SiC content. Corrosion potentials became more active, and corrosion current densities increased with increasing SiC content. Decreasing corrosion potentials would not be expected with increasing SiC content if SiC served as efficient cathodes. The corrosion morphology indicated that there was significant corrosion at SiC-copper interfaces. Voids caused by porosity and by SiC-copper interfaces both increased with increasing SiC content. Hence, the decrease in corrosion potential with increasing SiC content is likely to have been caused by an increase in anodic currents from voids and SiC-copper interfaces.

Alumina/Copper MMCs. The corrosion behavior of copper MMCs reinforced with 2.7 vol% Al_2O_3 was examined in deaerated and aerated 3.5 wt% NaCl (Ref 139). The corrosion potentials of the MMC were slightly more active (i.e., 0.01 to 0.02 V) than monolithic pure copper. The corrosion rates of the MMCs were comparable to monolithic copper. A galvanic effect with Al_2O_3 is not expected, due to its insulative nature.

Stainless Steel MMCs

Sintered particulate composites consisting of ferritic 434L stainless steel and Al_2O_3 particles have been developed for potential application in chemical-processing plants, turbine blades, and heat exchanger tubes (Ref 140–142). Austenitic 316L stainless steels reinforced with Al_2O_3 and Y_2O_3 have also been investigated for enhanced strength and wear resistance (Ref 143).

Alumina/Stainless Steel MMCs. The corrosion behavior of sintered Al_2O_3/434L MMCs and sintered 434L alloy without Al_2O_3 particles was examined (Ref 140–142). The volume percent of Al_2O_3 particles in these materials ranged from 0 to 8%. The effect of small amounts of titanium and niobium alloying elements on corrosion resistance was also investigated. Galvanic corrosion between 434L stainless steel and Al_2O_3 should not occur, because the latter is an insulator. In 1 N H_2SO_4 (Ref 140–142), there was no strong correlation between Al_2O_3 content and corrosion behavior. One of the few generalities that could be made was that passive-current densities were within an order of magnitude of 1 mA/cm^2 for almost all materials. In the 5 wt% NaCl solutions, i_{corr} of the MMCs was less than 10 μA/cm^2 (Ref 141). On polarization, all materials displayed active corrosion behavior in the NaCl solutions.

Particulate 316L stainless steel MMCs (Ref 143), fabricated using powder metallurgy, were reinforced with 3, 4, and 5 wt% Al_2O_3 and additions of 2 wt% chromium diboride (CrB_2) or 1 wt% boron nitride (BN) for sintering aids. The density of the MMCs ranged from 86 to 96% of the theoretical value. Unreinforced 316L specimens were also fabricated using powder metallurgy without sintering aids, resulting in 85% of theoretical density. Less porosity was present in the reinforced MMCs as compared to the unreinforced pure 316L specimen. The test samples were immersed in 10 wt% sulfuric acid (H_2SO_4) at room temperature for 24 h, 1 wt% hydrochloric acid (HCl) at room temperature for 24 h, and boiling 10 wt% nitric acid (HNO_3) for 8 h. The pure, unreinforced 316L specimens passivated in the 10 wt% H_2SO_4 solution, whereas the corrosion rate of the MMC generally increased with increasing Al_2O_3 content to a maximum value of approximately 4 mm/yr (0.16 in./yr). The MMCs performed better than the unreinforced 316L specimen in the 1 wt% HCl solution but worse than the unreinforced specimen in the boiling nitric acid solution. There was no strong correlation between Al_2O_3 content in the MMCs and the corrosion rates in the 1 wt% HCl and boiling 10 wt% HNO_3 solutions.

Yttria/Stainless Steel MMCs. Yttria (Y_2O_3) is an insulator and galvanic effects are not expected. The 316L stainless steel specimens discussed previously (Ref 143) were also reinforced with 3, 4, and 5 wt% Y_2O_3 and additions of 2 wt% chromium diboride (CrB_2) or 1 wt% boron nitride (BN) for sintering aids. In all solutions (i.e., sulfuric, hydrochloric, and nitric acid solutions), the Y_2O_3-reinforced MMCs exhibited reduced corrosion resistance as compared to the Al_2O_3-reinforced MMCs. The Y_2O_3 MMCs were sintered to 88 to 96% of theoretical density, and the Al_2O_3 MMCs were sintered to 86 to 92% of theoretical density. The Y_2O_3 particles also showed better bonding to the matrix, probably forming a complex $YCrO_3$ oxide, as compared to the Al_2O_3 particles. It is possible that the formation of the reaction layer around the Y_2O_3 particles may have depleted chromium from the matrix, resulting in reduced corrosion resistance, as compared to the Al_2O_3-reinforced MMCs.

Lead MMCs

Lead is a relatively heavy metal with a density of 11.4 g/cm^3. Lead MMCs, therefore, are normally developed for applications where a combination of its structural, physical, and chemical properties is important. The corrosion behavior of pure lead MMCs in simulated lead-acid battery environments has been studied to assess the feasibility of using these composites as positive electrode grids in place of conventional lead-base alloy grid materials. Lead can be alloyed with elements such as arsenic, antimony, or calcium to increase strength and stiffness. These elements, however, reduce corrosion resistance. Monolithic pure lead has very good corrosion resistance in lead-acid battery environments (which consists of sulfuric acid solutions) but is heavy and lacks sufficient mechanical strength. Pure lead, therefore, has been reinforced with strong, lightweight fibers in hopes of achieving the goals of increasing strength, reducing weight, and retaining the corrosion resistance of pure lead (Ref 144–146). For other applications, discontinuous-reinforced lead-antimony alloy MMCs were also studied in sodium chloride solutions (Ref 147).

To simulate corrosion in lead-acid battery environments, lead MMCs reinforced with Al_2O_3, carbon, SiC, and glass-quartz fibers of various volume percents (Ref 144–146) have been anodically polarized at 1.226 V (versus mercury/mercurous sulfate reference electrode) in sulfuric acid solutions (of 1.285 specific gravity) at 50, 60, and/or 70 °C (120, 140, and/or 160 °F). At 1.226 V, lead and water are oxidized to lead dioxide (PbO_2) and molecular oxygen (O_2), respectively (Ref 148, 149). Approximately one-third of the total anodic current is consumed in the oxidation of lead under these conditions (Ref 146). Poor bonding between Al_2O_3 fibers and the matrix allowed the electrolyte to diffuse into fiber-matrix interfaces, leading to accelerated corrosion (Ref 144) and swelling of the composite due to corrosion-product buildup (Ref 146). The graphite fibers were also subjected to oxidation (Ref 145).

Lead (80 wt%)-antimony (20 wt%) alloy MMCs reinforced with 1 to 5 wt% zircon ($ZrSiO_4$) particles (Ref 147) were exposed to a 1 N NaCl solution. Zircon should not induce galvanic corrosion. Weight loss measurements, made over a 72 h period, showed that the corrosion rate of the MMCs increased with increasing zircon content.

Depleted Uranium MMCs

Tungsten fiber/depleted uranium (W/DU) MMCs are the antithesis of the lightweight MMCs and were developed to create high-density materials. Uranium has a density of 18.9 g/cm^3.

Depleted uranium corrodes galvanically when coupled to tungsten fibers in air-exposed 3.5 wt% NaCl solutions at room temperature (Ref 150). The open-circuit potential of tungsten fiber (−0.25 V_{SCE}) is noble to that of the DU alloy (−0.80 V_{SCE}). The open-circuit potentials of the W/DU MMC and galvanic couples consisting of tungsten fiber and DU alloy of equal areas are −0.78 and −0.77 V_{SCE}, respectively, and fall between those of tungsten fibers and the DU alloy. The galvanic-corrosion current density measured between equal areas of tungsten fibers and the DU alloy was equal to approximately 4×10^{-5} A/cm^2. In a 30 day exposure test in the NaCl solution, the W/DU MMC lost 43.56 mg/cm^2, which was approximately 1.3 times that of the DU alloy.

Zinc MMCs

Zinc MMCs have been developed (Ref 151) for potential use as bearing materials. Zinc has a density of 7.14 g/cm^3. Zinc alloy ZA-27 MMCs were cast with 1, 3, and 5 wt% graphite particles ranging in sizes from 100 to 150 μm. Zinc alloys are known to have excellent wear and bearing characteristics (Ref 152). The zinc MMCs were resistant to corrosion in SAE 40-grade lubricant that had been in service for 6 months in an internal combustion engine. In 1 N HCl, the corrosion rates of the MMCs decreased with time.

Corrosion Protection of MMCs

Corrosion of metals can be prevented with the use of protective coatings and inhibitors. The type of coating (impervious, inhibitive, or cathodically protective) will depend on the type of exposure anticipated (Ref 153). A proven coating system for an alloy may not be suitable for a MMC of that alloy however. Poor adhesion and wettability between the coating and reinforcement or differences in the electrochemical properties of the alloy and MMC may render a proven system ineffective for the MMC. Other coating techniques, such as anodization, could also be ineffective or even deleterious to the MMC. Anodization, which is frequently used for aluminum alloys, could destroy a Gr/Al MMC by oxidizing the graphite fibers to CO_2 (Ref 17). Inhibitors are normally used in closed systems. Inhibitors intended for monolithic alloys should be used with MMCs only after ample examination.

Graphite/aluminum MMCs have been coated with some success. The coatings have been primarily applied to the monolithic surface foils that encase the diffusion-bonded packs of precursor Gr/Al MMC wires. The corrosion resistance of the composites usually mimics that of the monolithic alloys until the surface foils are penetrated, exposing the subcutaneous Gr/Al MMC precursor wires. Corrosion occurs at an accelerated rate once the precursor wires are exposed. A few studies have been conducted on applying protection to the exposed graphite/aluminum structure.

Organic Coatings. Polyurethane, chlorinated rubber, and epoxy provided protection for aluminum surface foils on Gr/Al MMCs exposed to marine environments (Ref 154). Epoxy (Ref 155), and epoxy/polyamide (Ref 155, 156) coatings also showed promise in a NaCl solution, based on electrochemical impedance spectroscopy studies.

Inorganic Coatings. Diamond-like coatings have been deposited directly on the graphite fiber/aluminum-matrix structures in Gr/Al MMCs but provided only short-term corrosion protection in NaCl solutions (Ref 157).

Coatings from chemical vapor deposition (CVD) and physical vapor deposition (PVD) did not provide protection to aluminum surface foils on Gr/Al MMCs due to coating defects, which were initiation sites for corrosion (Ref 154). Corrosion initiated at coating flaws in composites coated with CVD nickel, CVD chromium carbide, PVD nickel plus chromium, and PVD titanium exposed to marine environments. When coatings were free of defects, however, such as in composites electroplated with nickel, protection was very good (Ref 154). It should be noticed, however, that metal coatings more noble than aluminum (e.g., the nickel coating used previously) could result in accelerated corrosion by intensified galvanic corrosion of aluminum exposed at coating breaches due to large surrounding cathodic regions. Accordingly, it was reported that electroless nickel coatings that contained breaches accelerated corrosion of Gr/Al MMCs exposed to marine environments (Ref 158, 159).

Graphite/aluminum MMCs have also been protected with cladding and electrodeposited coatings. Titanium and nickel claddings were susceptible to delamination from the Gr/Al MMC substrates along exposed edges in marine environments (Ref 154). Electrodeposited aluminum/manganese on electroless nickel-coated aluminum surface foils provided good corrosion protection of Gr/Al MMC plates if the composite edges were sealed with epoxy so that the Gr/Al microstructure was not exposed (Ref 158).

Anodization. Sulfuric acid anodization of surface aluminum foils followed by sealing in sodium dichromate provided good protection for Gr/Al MMC plates in marine environments when the plate edges were sealed with epoxy to prevent exposure of the Gr/Al microstructure (Ref 158). The anodized coatings, however, can thin with exposure time (Ref 159).

Chemical Conversion Coatings. Chromate/phosphate conversion coatings on surface aluminum foils provided good protection for Gr/Al MMC plates in marine environments when the plate edges were sealed with epoxy so that the Gr/Al microstructure was not exposed (Ref 158). Chemical passivation by cerium chloride ($CeCl_3$) was also explored to increase the pitting resistance of aluminum oxide films (Ref 160). It is believed that the coatings suppress the oxygen reduction reaction on the metal surface (Ref 161). The cerium chloride passivation treatment delayed the initiation of pitting on surface foils of Gr/Al MMCs exposed to NaCl solutions.

Inhibitors. Zinc ions were studied as a means to inhibit the oxygen reduction reaction on graphite. Galvanic-corrosion current densities of P100 graphite fiber/6061-T6 Al galvanic couples were reduced by 10 to 100 times using 10 ppm of Zn^{+2} as a cathodic inhibitor in aerated 3.15 wt% NaCl solution at 30 °C (86 °F). The galvanic current densities were reduced to levels in deaerated conditions (Ref 162).

Silicon Carbide/Aluminum MMCs. Various types of coatings have been used on SiC/Al MMCs for corrosion protection. Coatings are applied directly to the SiC/aluminum structure, because these MMCs are not usually fabricated with surface foils.

Organic Coatings. Epoxy coatings provided protection to SiC_w/6061-T6 Al MMCs in marine environments (Ref 158) and also showed promise in NaCl solutions, based on electrochemical impedance spectroscopy studies (Ref 155).

Inorganic Coatings. Alumina plasma-sprayed coatings and 1100 Al flame-sprayed coatings on SiC_w/6061-T6 Al MMCs provided corrosion protection in marine environments (Ref 158).

Anodization. The formation of hardcoats on SiC/Al MMCs by anodization in sulfuric acid solutions improved pitting resistance in deaerated NaCl solutions, as gaged by E_{pit} values (Ref 163, 164). Hardcoats increased E_{pit} for SiC_w MMCs with 2024 Al and 6061 Al matrices and for SiC_p MMCs with pure aluminum matrices (Ref 164). The hardcoat has been found to cover both matrix and SiC whiskers, but SiC content in the hardcoat is much less than that in the metal substrate, and it is unclear whether the SiC whiskers are oxidized or undercut (Ref 163). Scanning electron microscope analyses showed that relatively few surface whiskers are left undamaged during sulfuric acid anodization of SiC_w/Al MMCs, indicating that some whiskers are oxidized (Ref 165). Silicon carbide whiskers protruding from the matrix also cause nonuniformities in the anodized layer (Ref 158). Films formed on the SiC_p/pure aluminum MMCs are also much less uniform in comparision to the continuous films formed on monolithic aluminum (Ref 164).

Thin, compact barrier coatings formed by anodization in ammonium tartrate solutions did not significantly affect pitting potentials for SiC_w/6061 Al MMCs (Ref 163).

Limited success has been achieved with anodization for long-term corrosion protection. The SiC_w/Al MMCs that were either sulfuric acid anodized or chromic acid anodized and then exposed to marine environments pitted after 30 days exposure (Ref 158). The SiC/Al MMCs that were sulfuric acid anodized were susceptible to crevice corrosion (Ref 156) and pitting (Ref 166) in NaCl solutions, whereas their monolithic-matrix alloys were not susceptible for similar or longer time periods.

Chemical Conversion Coatings. Cerium-base conversion coatings have been investigated for use on various SiC/Al MMCs (Ref 160, 167). Corrosion rates of SiC_p (20 vol%)/6013 Al MMCs were lower in NaCl solutions that contained $CeCl_3$ as an additive as opposed to $CeCl_3$-free solutions (Ref 167). The SiC/Al MMCs that were chemically passivated in $CeCl_3$ (Ref 160) were susceptible to crevice corrosion in NaCl solutions, whereas their monolithic-matrix alloys were immune.

Al_2O_3/Al MMCs Chemical Conversion Coatings. Cerium-base conversion coatings have been investigated for use on Al_2O_3/6061 Al MMCs. The effectiveness of the coatings was dependent on $CeCl_3$ concentrations (Ref 168) and surface pretreatments (Ref 169). Best results were obtained when specimens were alkaline etched, boiled in water, and then treated with $CeCl_3$.

Other Concerns

There are many additional concerns regarding the corrosion of MMCs in comparison to their monolithic-matrix alloys. Certain MMC systems have inherent corrosion problems. Graphite/aluminum MMCs, for example, are subjected to high galvanic-corrosion rates in addition to being highly susceptible to Al_4C_3 formation. In contrast, galvanic corrosion between titanium and SiC is negligible in SiC_{MF}/Ti MMCs. Prudence should be used, however, when making generalities about corrosion behavior for a specific MMC group, such as SiC/Al, because MMC corrosion behavior may vary significantly due to the quality of the reinforcement and matrix alloy; the manufacturing technique, such as powder metallurgy or casting; postthermomechanical processing; and other factors. Hence, it will be difficult to obtain a corrosion database of corroborating and consistent corrosion behavior for a specific MMC group until standards are developed for the manufacture and processing of MMCs.

REFERENCES

1. J.W. Weeton, D.M. Peters, and K.L. Thomas, *Guide to Composite Materials,* ASM International, 1987, p 2–2
2. G.B. Park and D.A. Foster, in *International Technical Conference Proceedings,* SUR/FIN'90, July 1990 (Boston, MA), American Electroplaters and Surface Finishers Society, Inc.
3. W.C.J. Harrigan, Metal Matrix Composites, *Metal Matrix Composites: Processing and Interfaces,* Academic Press, 1991, p 1–16
4. Y. Liu et al., in *Conference Proceedings,* ICCM/8, Society for the Advancement of Material and Process Engineering (SAMPE), 1991
5. T. Lim et al., in *Conference Proceedings,* ICCM/8, Society for the Advancement of Material and Process Engineering (SAMPE), 1991
6. R.J. Hill and W.F. Stuhrke, The Preparation and Properties of Cast Boron-Aluminum Composites, *Fibre Sci. Technol.,* Vol 1 (No. 1), 1968, p 25–42
7. A. Kelly and W.R. Tyson, Tensile Properties of Fibre-Reinforced Metals: Copper/Tungsten and Copper/Molybdenum, *J. Mech. Phys. Solids,* Vol 13 (No. 6), 1965, p 329–338
8. F. Galasso and J. Pinto, Compatibility of Silicon Carbide Coated Boron Fibers in a Titanium Matrix, *Fibre Sci. and Technol.,* Vol 2 (No. 2), 1969, p 89–95
9. S.S. Brenner, *J. Appl. Phys.,* Vol 33, 1962, p 33
10. S.S. Brenner, *J. Met.,* Vol 14 (No. 11), 1962, p 808
11. W.H. Sutton, Whisker Composite Materials—A Prospectus for the Aerospace Designer, *Astronaut. Aeronaut.,* Aug 1966, p 46
12. W.H. Sutton and J. Chorn, *Met. Eng. Q.,* Vol 3 (No. 1), 1963, p 44
13. A.P. Divecha, P. Lare, and H. Hahn, "Silicon Carbide Whisker Metal Matrix Composites," AFML-TR-69-7, Air Force Materials Laboratory 1969
14. L.H. Hihara and C. Tamirisa, Corrosion of SiC Monofilament/Ti-15-3-3-3 Metal-Matrix Composites in 3.15 wt.% NaC1, *Mater. Sci. Eng. A,* Vol 198, 1995, p 119–125
15. C. Tamirisa, "Corrosion Behavior of Silicon-Carbide Reinforced Titanium 15–3 Metal-Matrix Composite in 3.15 wt% NaC1," Hawaii at Manoa, Honolulu, HI, 1993
16. L.H. Hihara and R.M. Latanision, *Corrosion,* Vol 48 (No. 7), 1992, p 546–552
17. L.H. Hihara, *Corrosion of Aluminum-Matrix Composites,* Massachusetts Institute of Technology, Cambridge, MA, 1989
18. Z.J. Lin, "Corrosion Study of Silicon-Aluminum Metal-Matrix Composites," Hawaii at Manoa, Honolulu, HI, 1995
19. L.H. Hihara and P.K. Kondepudi, *Corros. Sci.,* Vol 36, 1994, p 1585–1595
20. L.H. Hihara and R.M. Latanision, Corrosion of Metal Matrix Composites, *Int. Mater. Rev.,* Vol 39 (No. 6), 1994, p 245–264
21. L.H. Hihara, Corrosion of Aluminum-Matrix Composites, *Corros. Rev.,* Vol 15 (No. 3–4), 1997, p 361–386
22. N. Ichinose, *Introduction to Fine Ceramics,* John Wiley and Sons, Ltd., 1987, p 50–52
23. A.M. Tsirlin, in *Strong Fibres,* Vol 1, *Handbook of Composites,* W. Watt and B.V. Perov, Ed., Elsevier Science Publishers B.V., 1985, p 155–199
24. R.E. Bolz and G.L. Tuve, in *CRC Handbook of Tables for Applied Engineering Science,* CRC Press, 1973, p 262–264
25. H.R. Clauser, *The Encyclopedia of Engineering Materials and Processes,* Reinhold Publishing Corporation, 1963, p 429
26. N.N. Greenwood and A. Earnshaw, *Chemistry of the Elements,* Pergamon Press, Ltd., 1984
27. U.R. Evans, Metallic Corrosion, *Passivity and Protection,* Arnold, London, 1937, p 364, 513–516
28. S.L. Pohlman, *Corrosion,* Vol 34, 1978, p 156–159
29. H.J. Becher, in *Handbook of Preparative Inorganic Chemistry,* Vol 1, G. Brauer, Ed., Academic Press, 1963, p 832
30. T. Iseki, T. Kameda, and T. Maruyama, *J. Mater. Sci.,* Vol 19, 1984, p 1692–1698
31. E.G. Kendall, in *Metal Matrix Composites,* K.G. Kreider, Ed., Academic Press, 1974, p 319–397
32. I.W. Hall, *Scr. Metall.,* Vol 21, 1987, p 1717–1721
33. K.I. Portnoi et al., *Poroshk. Metall.,* Vol 2 (No. 218), 1981, p 45–49
34. M.A. Buonanno, *The Effect of Processing Conditions and Chemistry on the Electrochemistry of Graphite and Aluminum Metal Matrix Composites,* Massachusetts

Institute of Technology, Cambridge, MA, 1992
35. P.K. Rohatgi, R. Asthana, and S. Das, *Int. Mater. Rev.,* Vol 31, 1986, p 115
36. D. Nath, R.T. Bhat, and P.K. Rohatgi, *J. Mater. Sci.,* Vol 15, 1980, p 1241–1251
37. D. Nath and T.K. Namboodhiri, *Composites,* Vol 19, 1988, p 237–243
38. A. Mortensen, J.A. Cornie, and J. Flemings, *J. Met.,* Vol 40, 1988, p 12
39. R.J. Arsenault, in *Metal Matrix Composites: Mechanisms and Properties,* R.K. Everett and R.J. Arsenault, Ed., Academic Press, 1991, p 79
40. H.H. Uhlig and R.W. Revie, *Corrosion and Corrosion Control,* 3rd ed., John Wiley and Sons, Inc. 1985, p 123, 354
41. L.H. Hihara and Z.J. Lin, "Corrosion of Silicon/Aluminum Metal-Matrix Composites," Sixth Japan International SAMPE Symposium and Exhibition, 26–29 Oct 1999 (Tokyo, Japan), Society for the Advancement of Material and Process Engineering
42. L.H. Hihara, H. Ding, and T. Devarajan, "Corrosion-Initiation Sites on Aluminum Metal-Matrix Composites," U.S. Army Corrosion Summit 2004 (Cocoa Beach, FL), U.S. Army, 2004
43. E.H. Hollingsworth and H.Y. Hunsicker, in *Corrosion,* Vol 13, *ASM Handbook,* ASM International, 1987, p 583
44. N.K. Bruun, and K. Nielsen, in "Metal Matrix Composites—Processing, Microstructure and Properties," 12th Risø International Symposium on Materials and Science, Risø National Laboratory, Denmark, 1991
45. J.Y. Yang and M. Metzger, Abstract 155, in *Extended Abstracts,* (Denver, CO), The Electrochemical Society, Oct 1981
46. D. Nath and T.K. Namboodhiri, *Corros. Sci.,* Vol 29, 1989, p 1215–1229
47. G. Butler and H.C.K. Ison, *Corrosion and Its Prevention in Waters,* Robert E. Krieger Publishing, 1978, p 91, 149
48. Z. Ahmad, P.T. Paulette, and B.J.A. Aleem, Mechanism of Localized Corrosion of Aluminum-Silicon Carbide Composites in a Chloride Containing Environment, *J. Mater. Sci.,* Vol 35, 2000, p 2573–2579
49. H.-Y. Yao and R.-Z. Zhu, Interfacial Preferential Dissolution on Silicon Carbide Particulate/Aluminum Composites, *Corrosion,* Vol 54 (No. 7), 1998, p 499–503
50. H. Ding and L.H. Hihara, Localized Corrosion of Silicon/Aluminum Metal-Matrix Composites Examined Using Scanning Vibrating Electrode Techniques, Journal of the Electrochemical Society, 2005 (to be published)
51. A.J. Sedriks, J.A. Green, and D.L. Novak, *Metall. Trans.,* Vol 2, 1971, p 871–875
52. A.V. Bakulin, V.V. Ivanov, and V.V. Kuchkin, *Zashch Met.,* Vol 14 (No. 1), 1978, p 102–104
53. W.C.J. Harrigan and R.H. Flowers, in *Failure Modes in Composites IV,* J.A. Cornie and F.W. Crossman, Ed., The Metallurgical Society of AIME, 1979, p 319–335
54. L.H. Hihara, "Corrosion Mechanisms of Metal-Matrix Composites," Seventh Japan International SAMPE Symposium and Exhibition, 13–16 Nov 2001 (Tokyo, Japan), Society for the Advancement of Material and Process Engineering
55. L.H. Hihara and R.M. Latanision, *Corrosion,* Vol 47, 1991, p 335–341
56. L.H. Hihara and R.M. Latanision, *Mater. Sci. Eng. A,* Vol 126, 1990, p 231–234
57. E. Deltombe, C. Vanleugenhaghe, and M. Pourbaix, in *Atlas of Electrochemical Equilibria in Aqueous Solutions,* M. Pourbaix, Ed., National Association of Corrosion Engineers, 1974, p 168–176
58. J.R. Galvele, in *Passivity of Metals,* R.P. Frankenthal and J. Kruger, Ed., The Electrochemical Society, Inc., 1978, p 285–327
59. W. Hubner and G. Wranglen, in "*Current Corrosion Research in Scandinavia*," Fourth Scandinavian Corrosion Congress (Helsinki), Scandinavian Corrossion Congress, 1964
60. M.J. Pryor and D.S. Keir, *J. Electrochem. Soc.,* Vol 102, 1955, p 605–607
61. M.E. Buck and R.J. Suplinskas, in *Engineered Materials Handbook on Composites,* ASM International, 1987, p 851–857
62. M.M. Schwartz, *Composite Materials Handbook,* McGraw-Hill, Inc., 1984
63. W.H. Kim, M.J. Koczak, and A. Lawley, in *Proceedings of the 1978 International Conference on Composite Materials,* ICCM/2 (Toronto, Canada), The Metallurgical Society of AIME, 1978
64. V.G. Gurbunov, V.D. Parshin, and V.V. Pamin, *Russ. Cast. Prod.,* 1974
65. N.A.P. Rao et al., *Tribol. Int.,* Vol 13, 1980, p 171
66. J. Van Muylder and M. Pourbaix, in *Atlas of Electrochemical Equilibria in Aqueous Solutions,* M. Pourbaix, Ed., National Association of Corrosion Engineers, 1974, p 449–457
67. D.L. Dull, W.C.J. Harrigan, and M.F. Amateau, "The Effect of Matrix and Fiber Composition on Mechanical Strength and Corrosion Behavior of Graphite-Aluminum Composites," final report, The Aerospace Corporation, El Segundo, CA, 1977
68. *Aluminum Metal-Matrix Composites Consortium,* http://www.almmc.com, April, 2002
69. *DWA Aluminum Composites,* Chatsworth, CA, 2004
70. "*Stablcel*," Advanced Composite Materials Corporation, Greer, SC
71. S.L. Coleman, V.D. Scott, and B. McEnaney, Corrosion Behaviour of Aluminium-Based Metal Matrix Composites, *J. Mater. Sci.,* Vol 29, 1994, p 2826–2834
72. M. Metzger and S.G. Fishman, *Ind. and Eng. Chem., Prod. Res. Dev.,* Vol 22, 1983, p 296–302
73. H. Sun, E.Y. Koo, and H.G. Wheat, Corrosion Behavior of SiC_p/6061 Al Metal Matrix Composites, *Corrosion,* Vol 47 (No. 10), 1991, p 741–753
74. O.P. Modi et al., Corrosion Behaviour of Squeeze-Cast Aluminum Alloy-Silicon Carbide Composites, *J. Mater. Sci.,* Vol 27, 1992, p 3897–3902
75. K.D. Lore and J.S. Wolf, in *Extended Abstracts,* (Denver, CO), The Electrochemical Society, 1981
76. G.A. Hawthorn and L.H. Hihara, "Out-Door and Laboratory Corrosion Studies of Aluminum Metal-Matrix Composites," U.S. Army Corrosion Summit 2004 (Cocoa Beach, FL), U.S. Army, 2004
77. A.J. Griffiths and A. Turnbull, An Investigation of the Electrochemical Polarisation Behaviour of 6061 Aluminum Metal Matrix Composites, *Corros. Sci.,* Vol 36 (No. 1), 1994, p 23–35
78. P.P. Trzaskoma, E. McCafferty, and C.R. Crowe, *J. Electrochem. Soc.,* Vol 130, 1983, p 1804–1809
79. S.L. Golledge, J. Kruger, and C.M. Dacres, in *Extended Abstracts,* (Las Vegas, NV), The Electrochemical Society, Oct 1985
80. Y. Shimizu, T. Nishimura, and I. Matsushima, Corrosion Resistance of Al-Based Metal Matrix Composites, *Mater. Sci. Eng. A,* Vol 198, 1995, p 113–118
81. D.M. Aylor and P.J. Moran, *J. Electrochem. Soc.,* Vol 132, 1985, p 1277–1281
82. G.W. Roper and P.A. Attwood, Corrosion Behaviour of Aluminum Matrix Composites, *J. Mater. Sci.,* Vol 30, 1995, p 898–903
83. C. Monticelli et al., Application of Electrochemical Noise Analysis to Study the Corrosion Behavior of Aluminum Composites, *J. Electrochem. Soc.,* Vol 142 (No. 2), 1995, p 405–410
84. P.C.R. Nunes and L.V. Ramanathan, Corrosion Behavior of Alumina-Aluminum and Silicon Carbide-Aluminum Metal-Matrix Composites, *Corrosion,* Vol 51 (No. 8), 1995, p 610–617
85. G.E. Kiourtsidis, S.M. Skolianos, and E.G. Pavlidou, A Study on Pitting Behaviour of AA2024/SiC_p Composites Using the Double Cycle Polarization Technique, *Corros. Sci.,* Vol 41, 1999, p 1185–1203
86. P.P. Trzaskoma, *Corrosion,* Vol 46, 1990, p 402–409
87. G.E. Kiourtsidis and S.M. Skolianos, Corrosion Behavior of Squeeze-Cast Silicon Carbide-2024 Composites in Aerated 3.5 wt.% Sodium Chloride, *Mater. Sci. Eng. A,* Vol 248, 1998, p 165–172

88. M.M. Buarzaiga and S.J. Thorpe, Corrosion Behavior of As-Cast, Silicon Carbide Particulate-Aluminum Alloy Metal-Matrix Composites, *Corrosion,* Vol 50 (No. 3), 1994, p 176–185
89. R.C. Paciej and V.S. Agarwala, *Corrosion,* Vol 44, 1988, p 680–684
90. S.R. Nutt and J.M. Duva, *Scr. Metall.,* Vol 20, 1986, p 1055–1058
91. J. England and I.W. Hall, *Scr. Metall.,* Vol 20, 1986, p 697–700
92. M.S. Bhat, M.K. Surappa, and H.V. Sudhaker Nayak, Corrosion Behaviour of Silicon Carbide Particle Reinforced 6061/A1 Alloy Composites, *J. Mater. Sci.,* Vol 26 (No. 18), 1991, p 4991–4996
93. Z. Ahmad and B.J. Abdul Aleem, Effect of Temper on Seawater Corrosion of an Aluminum-Silicon Carbide Composite Alloy, *Corrosion,* Vol 52 (No. 11), 1996 p 857–864
94. W.N.C. Garrard, The Corrosion Behaviour of Aluminum-Silicon Carbide Composites in Aerated 3.5% Sodium Chloride, *Corros. Sci.,* Vol 36 (No. 5), 1994, p 837–851
95. J.K. Park and J.P. Lucas, Moisture Effect on SiC_p/6061 A1 MMC: Dissolution of Interfacial $A1_4C_3$, *Scr. Mater.,* Vol 37 (No. 4), 1997, p 511–516
96. *Saffil,* http://www.Saffil.com/ecoform1.htm, May 2002
97. T. Donomoto et al., Paper 830252, SAE Technical Paper Series, Society of Automotive Engineers, 1983
98. "Metal Matrix Composites," 3M Corp., http://www.3m.com/market/industrial/mmc/, Nov 17, 2004
99. C.-K. Fang, C.C. Huang, and T.H. Chuang, Synergistic Effects of Wear and Corrosion for $A1_20_3$ Particulate-Reinforced 6061 Aluminum Matrix Composites, *Metall. Mater. Trans. A,* Vol 30, 1999, p 643–651
100. R.U. Vaidya et al., Effect of Microbiologically Influenced Corrosion on the Tensile Stress-Strain Response of Aluminum and Alumina-Particle Reinforced Aluminum Composite. *Corrosion,* Vol 53 (No. 2), 1997, p 136–141
101. V.S. Agarwala, Abstract 15, *Extended Abstracts,* (Montreal, Canada), The Electrochemical Society, May 1982
102. L. Bertolini, M.F. Brunella, and S. Candiani, Corrosion Behavior of a Particulate Metal-Matrix Composite, *Corrosion,* Vol 55 (No. 4), 1999, p 422–431
103. J.M.G. DeSalazar et al., Corrosion Behaviour of AA6061 and AA7005 Reinforced with Al_2O_3 Particles in Aerated 3.5% Chloride Solutions: Potentiodynamic Measurements and Microstructure Evaluation, *Corros. Sci.,* Vol 41, 1999, p 529–545
104. R.C. Weast, *CRC Handbook of Chemistry and Physics,* 67th ed., CRC Press, 1986, p B-116
105. D.A. Davis, M.G. Vassilaros, and J.P. Gudas, *Mater. Perform.,* 1982 p 38–42
106. D.W. Berkeley, H.E.M. Sallam, and H. Nayeb-Hashemi, The Effect of pH on the Mechanism of Corrosion and Stress Corrosion and Degradation of Mechanical Properties of AA6061 and Nextel 440 Fiber-Reinforced AA6061 Composites, *Corros. Sci.,* Vol 40 (No. 2/3), 1998, p 141–153
107. L.E. Dardi and K.G. Kreider, in *Composite Materials: Testing and Design (Third Conference),* STP 546, American Society for Testing and Materials, 1974, p 269–283
108. C. Monticelli et al., Stress Corrosion Cracking Behaviour of Some Aluminum-Based Metal Matrix Composites, *Corros. Sci.,* Vol 39 (No. 10–11), 1997, p 1949–1963
109. G.E. Kiourtsidis and S.M. Skolianos, Stress Corrosion Behavior of Aluminum Alloy 2024/Silicon Carbide Particles (SiC_p) Metal Matrix Composites, *Corrosion,* Vol 56 (No. 6), 2000, p 646–653
110. H.-Y. Yao, Effect of Particulate Reinforcing on Stress Corrosion Cracking Performance of a SiC_p/2024 Aluminum Matrix Composite, *J. Compos. Mater.,* Vol 33 (No. 11), 1999, p 962–970
111. S.S. Yau and G. Mayer, *Mater. Sci. Eng.,* Vol 42, 1986, p 45–47
112. D.F. Hasson et al., in *Failure Mechanisms in High Performance Materials,* J.G. Early, T.R. Shives, and J.H. Smith, Ed., Cambridge University Press, 1984, p 147–156
113. R.H. Jones, in *Environmental Effects on Advanced Materials,* R.H. Jones and R.E. Ricker, Ed., The Minerals, Metals and Materials Society, 1991, p 283–295
114. K. Minoshima, I. Nagashima, and K. Komai, Corrosion Fatigue Fracture Behaviour of a SiC Whisker-Aluminum Matrix Composite under Combined Tension-Torsion Loading, *Fatigue Fract. Eng. Mater. Struct.,* 1998, p 1435–1446
115. R.F. Buck and A.W. Thompson, in *Environmental Effects on Advanced Materials,* R.H. Jones and R.E. Ricker, Ed., The Minerals, Metals and Materials Society, 1991, p 297–313
116. M.A. Timonova et al., *Mettalloved. Termi. Obrab. Met.,* Vol 11, 1980, p 33–35
117. V.F. Stroganova and M.A. Timonova, *Metalloved. Termi. Obrab. Met.,* 1978, p 44–46
118. P.K. Kondepudi, Corrosion Behavior of Magnesium Matrix Composites, *Mech. Eng.,* 1992
119. L.H. Hihara, Metal-Matrix Composites, *Corrosion Tests and Standards: Application and Interpretation,* R. Baboian, Ed., ASTM, 1995, p 531–542
120. P.P. Trzaskoma, *Corrosion,* Vol 42, 1986, p 609–613
121. W.F. Czyrklis, Paper 196, *Conference Proceedings of Corrosion 85,* (Boston, MA), National Association of Corrosion Engineers, 1985
122. L.H. Hihara and P.K. Kondepudi, *Corros. Sci.,* Vol 34, 1993, p 1761–1772
123. C.A. Nunez-Lopez et al., The Corrosion Behaviour of Mg Alloy ZC71/SiC_p Metal Matrix Composite, *Corros. Sci.,* Vol 37 (No. 5), 1995, p 689–708
124. C.A. Nunez-Lopez et al., An Investigation of Microgalvanic Corrosion Using a Model Magnesium-Silicon Carbide Metal Matrix Composite, *Corros. Sci.,* Vol 38 (No. 10), 1996, p 1721–1729
125. M. Levy and W.F. Czyrklis, in *Extended Abstracts,* (Denver, CO), The Electrochemical Society, Oct 1981
126. W.F. Czyrklis, "Corrosion Evaluation of Metal Matrix Composite FP/Mg AZ91C," 1983 Tri-Service Corrosion Conference, (Annapolis, MD), U.S. Naval Academy, 1983
127. J.M. Evans, *Acta Metall.,* Vol 34, 1986, p 2075–2083
128. D. Hughes, *Aviat. Week Space Technol.,* 28 Nov 1988, p 91
129. S. Ranganath, A Review on Particulate-Reinforced Titanium Matrix Composites, *J. Mater. Sci.,* Vol 32, 1997, p 1–16
130. D.J. Blackwood et al., Corrosion Behaviour of Porous Titanium-Graphite Composites Designed for Surgical Implants, *Corros. Sci.,* Vol 42, 2000, p 481–503
131. H.M. Saffarian and G.W. Warren, Aqueous Corrosion Study of α_2-Ti_3A1/SiC Composites, *Corrosion,* Vol 54 (No. 11), 1998, p 877–886
132. B.S. Covino, Jr. and D.E. Alman, Corrosion of Titanium Matrix Composites, *Proceedings of the 15th International Corrosion Congress,* (Madrid, Spain), Viajes Iberia Congresos, 2002
133. D.M. Aylor, Corrosion of Metal Matrix Composites, *Corrosion,* Vol 13, *ASM Handbook*, ASM International, 1987, p 859–863
134. H.L. Marcus, W.F. Weldon, and C. Persad, Technical Report Contract N62269-85-C0222, University of Texas at Austin, 1987
135. P.K. Rohatgi et al., Corrosion and Dealloying of Cast Lead-Free Copper Alloy-Graphite Composites, *Corros. Sci.,* Vol 42, 2000, p 1553–1571
136. R. Taylor and Y. Qunsheng, "Thermal Transport in Carbon Fibre-Copper and Carbon Fibre/Aluminum Composites," ICCM/8, Society for the Advancement of Material and Process Engineering (SAMPE), 1991
137. H. Sun, J.E. Orth, and H.G. Wheat, Corrosion Behavior of Copper-Based Metal-Matrix Composites, *J. Met.,* Sept 1993, p 36–41
138. Y.-F. Lee, S.-L. Lee, and J.-C. Lin, Wear and Corrosion Behaviors of SiC_p Reinforced Copper Matrix Composite Formed

by Hot Pressing, *Scand. J. Metall.,* Vol 28, 1999, p 9–16
139. H. Sun and H.G. Wheat, Corrosion Study of $A1_20_3$ Dispersion Strengthened Cu Metal Matrix Composites in NaCl Solutions, *J. Mater. Sci.,* Vol 28, 1993, p 5435–5442
140. S.K. Mukherjee, A. Kumar, and G.S. Upadhyaya, *Br. Corros. J.,* Vol 20, 1985, p 41–44
141. S.K. Mukherjee, A. Kumar, and G.S. Upadhyaya, *Powder Metall. Int.,* Vol 17, 1985, p 172–175
142. S.K. Mukherjee and G.S. Upadhyaya, *Mater. Chem. Phys.,* Vol 12, 1985, p 419–435
143. F. Velasco et al., Mechanical and Corrosion Behaviour of Powder Metallurgy Stainless Steel Based Metal Matrix Composites, *Mater. Sci. Technol.,* Vol 13 (No. 10), 1997, p 847–851
144. C.M. Dacres et al., *J. Electrochem. Soc.,* Vol 128, 1981, p 2060–2064
145. J.C. Viala, M. El Morabit, and J. Bouix, *Mater. Chem. Phys.,* Vol 13, 1985, p 393–408
146. C.M. Dacres, R.A. Sutula, and B.F. Larrick, *J. Electrochem. Soc.,* Vol 130, 1983, p 981–985
147. K.H.W. Seah et al., Corrosion Behaviour of Lead Alloy/Zircon Particulate Composites, *Corros. Sci.,* Vol 39 (No. 8), 1997, p 1443–1449
148. J. Burbank, *J. Electrochem. Soc.,* Vol 106, 1959, p 369
149. J. Burbank, A.C. Simon, and E. Willihnganz, in *Advances in Electrochemistry and Electrochemical Engineering,* P. Delahay, Ed., Wiley Interscience, 1971, p 157
150. P.P. Trzaskoma, *J. Electrochem. Soc.,* Vol 129, 1982, p 1398–1402
151. K.H.W. Seah, S.C. Sharma, and B.M. Girish, Corrosion Characteristics of ZA-27-Graphite Particulate Composites, *Corros. Sci.,* Vol 39 (No. 1), 1997, p 1–7
152. W. Smith, *Structure and Properties of Engineering Alloys,* 2nd ed, McGraw-Hill, 1993
153. C.G. Munger, *Corrosion Prevention by Protective Coatings,* National Association of Corrosion Engineers, 1984
154. J.H. Payer and P.G. Sullivan, in *Bicentennial of Materials, Eighth National SAMPE Technical Conference,* Society for the Advancement of Material and Process Engineering, 1976
155. S. Lin, H. Shih, and F. Mansfeld, Corrosion Protection of Aluminum Alloys and Metal Matrix Composites by Polymer Coatings, *Corros. Sci.,* Vol 33 (No. 9), 1992, p 1331–1349
156. F. Mansfeld and S.L. Jeanjaquet, *Corros. Sci.,* Vol 26, 1986, p 727–734
157. B. Wielage et al., Corrosion Protection of Carbon Fibre Reinforced Aluminum Composite by Diamondlike Carbon Coatings, *Mater. Sci. Technol.,* Vol 16, 2000, p 344–348
158. D.M. Aylor and R.M. Kain, Assessing the Corrosion Resistance of Metal Matrix Composite Materials in Marine Environments, in *Recent Advances in Composites in the United States and Japan,* STP 864, J.R. Vinson and M. Taya, Ed., American Society for Testing and Materials, 1983, p 632–647
159. D.M. Aylor, R.J. Ferrara, and R.M. Kain, *Mater. Perform.,* Vol 23, 1984, p 32–38
160. F. Mansfeld et al., *Corrosion,* Vol 45, 1989, p 615–630
161. B.R.W. Hinton, D.R. Arnott, and N.E. Ryan, *Mater. Forum,* Vol 9, 1986, p 162
162. L.H. Hihara and R.M. Latanision, Galvanic Corrosion of Aluminum-Matrix Composites, *Corrosion,* 1991
163. P.P. Trzaskoma and E. McCafferty, *Aluminum Surface Treatment Technology,* R.S. Alwitt and G.E. Thompson, Ed., The Electrochemical Society, 1986, p 171–177
164. J. Hou and D.D.L. Chung, Corrosion Protection of Aluminum-Matrix Aluminum Nitride and Silicon Carbide Composites by Anodization, *J. Mater. Sci.,* Vol 32, 1997, p 3113–3121
165. C.R. Crowe, D.G. Simons, and M.D. Brown, in *Extended Abstracts,* (Denver, CO), The Electrochemical Society, 1981
166. S. Lin et al., Corrosion Protection of Al/SiC Metal Matrix Composites by Anodizing, *Corrosion,* Vol 48 (No. 1), 1992, p 61–67
167. Z. Ahmad and B.J.A. Aleem, Degradation of Aluminum Metal Matrix Composites in Salt Water and Its Control, *Mater. Des.,* Vol 23, 2002, p 173–180
168. P. Traverso, R. Spiniello, and L. Monaco, Corrosion Inhibition of Al 6061 T6/Al_2O_{3p} 10% (v/v) Composite in 3.5% NaCl Solution with Addition of Cerium (III) Chloride, *Surf. Interface Anal.,* Vol 34, 2002, p 185–188
169. A.S. Hamdy, A.M. Beccaria, and P. Traverso, Corrosion Protection of Aluminum Metal-Matrix Composites by Cerium Conversion Coatings, *Surf. Interface Anal.,* Vol 34, 2002, p 171–175

SELECTED REFERENCES

- R.H. Jones, Metal Matrix Composites, *Environmental Effects on Engineered Materials,* R.H. Jones, Ed., Marcel Dekker, Inc., 2001, p 379–390
- K.A. Lucas and H. Clarke, *Corrosion of Aluminum-Based Metal Matrix Composites,* Research Studies Press, Ltd., England, and John Wiley & Sons, Inc., 1993
- P.P. Trzaskoma, Corrosion, *Metal Matrix Composites: Mechanisms and Properties,* E.R.K. and R.J. Arsenault, Ed., Academic Press, 1991, p 383–404

ASM Handbook, Volume 13B: Corrosion: Materials
S.D. Cramer, B.S. Covino, Jr., editors, p545-546
DOI: 10.1361/asmhba0003840

Introduction to Environmental Performance of Nonmetallic Materials

David C. Silverman, Argentum Solutions, Inc.

WHEN PEOPLE THINK OF CORROSION, they sometimes attribute such degradation to only metals and alloys. However, metals and alloys are not the only materials that deteriorate in an environment. A significant number of containment, protective, structural, and mechanical applications are fulfilled by alternative nonmetallic materials. Those who work to combat materials degradation fully appreciate both the extensive use of these alternative materials and the fact that they, too, can degrade with time, sometimes with catastrophic effect. No general classification exists as to what constitutes a nonmetallic material. Such materials include elastomers, plastics, resins, glass, wood, organic coatings, concrete, refractories, and ceramics. Indeed, sometimes the demarcation between nonmetals and metals is not distinct, because some nonmetals may duplicate properties found in metals. Sometimes, the interaction of nonmetallic materials with environments, both how the properties of the nonmetallic material are affected and how they affect the environment, are less clearly understood than those of metals. This Section has been developed to aid in filling some of these gaps in knowledge. The materials discussed are thermosetting resins, elastomers, rubber linings, protective coatings, ceramics, refractories, and concrete. While not all materials could be covered, the goal is to present information and further references for some of the more commonly used nonmetallic materials. In addition to reading these articles, individuals interested in obtaining a first-pass indication of chemical resistance of a wide array of nonmetallic materials can refer to the general resistance tables provided in the Selected References section of this introduction. However, caution is warranted when using such tabulations, because some of the tabulated information may be incorrect, or the variables in the actual environment may not match the tabulated conditions. Specific testing for chemical and mechanical compatibility is usually warranted before any nonmetallic material is placed into a specific service.

Thermosetting Resins and Resin-Matrix Composites

Glass-fiber-reinforced plastics are a composite material containing both resin-rich and combined resin-glass layers. No single resin can effectively handle every environment. Several families of resins exist, and within each family are subsets determined by moieties attached to the resin polymer backbone. Chemical resistance of the resin itself tends to be determined by a combination of the backbone polymer and the unique moieties added to the backbone. Such properties of the final fabricated component as chemical resistance, abrasion resistance, ability to retard fire, and structural integrity of the finished component are uniquely determined by the chemistry of the resin, fillers added, additional veils and topcoats, and the overall fabrication procedure. Thus, more than a cursory knowledge of these thermosetting resins is required in order to properly specify both the resin and fabrication requirements for a given application. The article "Environmental Performance of Thermosetting Plastics and Resin-Matrix Composites" provides an overview of the various resin backbones, moieties, fillers, and veils available and how environmental resistance is affected by them.

Elastomers

Elastomers are a group of macromolecular materials that (at room temperature) return rapidly to their initial dimensions and shapes after substantial deformation by weak stresses and the subsequent release of such stresses. Most of the more commonly used elastomers are thermoset resins. That is, they have cross linkages that impart "memory" so they return to their original dimensions. A number of chemistries exist, including natural and synthetic rubbers, fluoroelastomers, polyurethane rubbers, and silicon- and oxygen-bearing rubbers. Within each family are subsets, each with different chemical and mechanical properties. These elastomers are created in a process known as compounding in which other ingredients are homogeneously mixed with the raw elastomers to impart specific properties. The quantity and quality of each additive significantly impacts the part performance, because the chemical environment to which the part is exposed can extract the additives differently. Identical elastomers within the same generic family name may perform vastly different in the same service because of differences in compounding. The article "Environmental Performance of Elastomers" describes the chemistry of elastomers, the additives introduced in compounding, and the resulting effect on chemical and mechanical compatibility. In addition, the article provides an overview of the test procedures most useful in determining both chemical and mechanical compatibility with service requirements.

Rubber Linings

Natural and synthetic rubber can be applied as sheet materials to provide a cost-effective way of protecting (usually) steel from chemical attack. Chemical resistance is determined by a complex combination of the type of rubber used and the curing done after installation. If curing (vulcanization) is performed, the degree of curing depends on the rubber used and the end use. Understanding the effect of both rubber chemistry and postinstallation cure on chemical compatibility and structural integrity is important when specifying the appropriate lining. The article "Environmental Performance of Rubber Linings" provides an overview of their compatibility with frequently encountered environments. It describes the commonly used polymers, their strengths and weaknesses with respect to type of service, and the specific linings that seem to perform well in specific industries.

Protective Coatings

Application of coatings remains one of the most common and effective methods of protecting materials from environmental degradation. The coating must remain intact to provide such protection. Coating integrity tends to be influenced by a combination of factors, including:

- Chemical compatibility between the coating and the environment in contact with it
- Permeation of the environment into and through the coating to the substrate, followed by reaction with the coating, substrate, or both
- Adhesion of the coating, which often depends on the quality of the surface preparation prior to application of the coating
- Thickness of the coating or multiple coatings, especially to minimize pinholes or thinned areas

Indeed, in practice, poor surface preparation and insufficient thickness account for a significant number of coating failures. The article "Degradation of Protective Coatings" concentrates on environmental factors that influence coating integrity, such as:

- Indoor and outdoor heating and cooling, with subsequent formation of condensation
- Ultraviolet and other radiation from the sun
- Heating effects on bond stability within the coating
- Permeation by water and other organic or inorganic chemicals and their effect on both the coating and coating-substrate interface
- Internal and external mechanical stresses imparted during curing and by the subsequent application
- Mildew and marine fouling and their effect on coating integrity

Ceramics and Refractories

Although sometimes grouped together because of some similarities in the compounds that comprise these classes, ceramic materials and refractories differ in applications. Ceramics are used as structural substitutes for alloys in high-temperature environments, such as heat exchangers in the process industries and gas turbines in the aerospace and power-generation industries. Some typical ceramics are zirconia, thoria, silicon nitride, boron nitride, and silicon carbide. Refractories are used as lining materials for heat and mass containment in high-temperature processing equipment such as furnaces and kilns. Some typical examples are silica, alumina, chromium oxide, calcium oxide, silicon nitride, and silicon carbide. Minimizing corrosion of refractories and ceramics requires proper materials selection in terms of chemical, thermal, and mechanical compatibility; proper installation and fabrication; and proper control of the process in which the material is functioning. Acid-base reactions play a significant role in the degradation of refractory materials. Some of the factors influencing corrosion resistance are porosity, texture, presence of additives to decrease oxidation of, for example, carbon, and presence of a chemically vapor-deposited layer. The article "Performance of Ceramics in Severe Environments" provides an overview of corrosion types and causes. Consideration is given to the effects of various types of oxidation reactions, water vapor interaction, impurities in the ceramic, and molten salts. The article "Performance of Refractories in Severe Environments" provides an overview of the theory behind corrosion of refractories, appropriate tests to evaluate propensity for attack, and the specific applications in such diverse areas as steel, glass, aluminum, and chemical-resistant applications.

Concrete

Concrete has two components: aggregates (usually sand, gravel, or crushed rock) and paste (cement plus water) to hold the aggregate together. The quality of any concrete depends on the quality of the paste and aggregate and the bond between the two. Concrete can degrade by a number of chemical and physical mechanisms. Chemical mechanisms include reaction between the aggregate and alkali, reaction between lime and calcium aluminate in the paste and sulfates in alkaline soil, reaction with soluble salts in seawater, and reaction with atmospheric carbon dioxide. Physical mechanisms include hydraulic pressure caused by freeze/thaw cycles, osmotic pressure caused by differences in purity between water in the pores and pure water, thermal shock, and supercooling because of deicing salts. The article "Environmental Performance of Concrete" discusses the properties of concrete, their desirable properties, the causes of concrete degradation, and how these degradation issues can be addressed with old and new technology.

SELECTED REFERENCES

- *Chemical Resistence of Plastics and Elastomers,* 3rd ed., William Andrew Publishing/ Plastics Design Library, 2001
- *Corrosion Data Survey—Nonmetals Section,* NACE International, 1983
- K.M. Pruett, Ed., *Chemical Resistance Guide for Elastomers,* Compass Publications, 1994
- K.M. Pruett, Ed., *Chemical Resistance Guide for Plastics,* Compass Publications, 2000
- P.A. Schweitzer, Ed., *Corrosion Resistance Tables,* Marcel Dekker, Inc., 1995

ASM Handbook, Volume 13B: Corrosion: Materials
S.D. Cramer, B.S. Covino, Jr., editors, p565-578
DOI: 10.1361/asmhba0003842

Performance of Ceramics in Severe Environments

Nathan S. Jacobson, Dennis S. Fox, James L. Smialek, Elizabeth J. Opila, and Christopher Dellacorte, NASA Glenn Research Center
Kang N. Lee, Cleveland State University/NASA Glenn Research Center

CERAMICS are generally stable to higher temperatures than most metals and alloys. Thus, the development of high-temperature structural ceramics has been an area of active research for many years. While the dream of a ceramic heat engine still faces many challenges, niche markets are developing for these materials at high temperatures. In these applications, ceramics are exposed not only to high temperatures but also to aggressive gases and deposits. This article reviews the response of ceramic materials to these environments in terms of corrosion mechanisms, the relative importance of a particular corrodent, and, where available, corrosion rates. The focus is on structural ceramics and composites, which are differentiated from refractories by generally higher densities and higher load-bearing capabilities as well as by their application as a structural component in a larger system.

Most of the corrosion information available for ceramics concerns silicon carbide (SiC) and silicon nitride (Si_3N_4) monolithic ceramics. These materials form a stable film of silica (SiO_2) in an oxidizing environment. This article discusses the oxidation of these materials, the effects of other corrodents such as water vapor and salt deposit, and the oxidation and corrosion of other ceramics—precurser-derived ceramics, ceramic-matrix composites, ceramics that form oxide scales other than silica, and oxide ceramics. Many of the corrosion issues can be mitigated with refractory oxide coatings, and the current status of this active area of research is given.

Ultimately, the concern of corrosion is loss of load-bearing capability. The effects of corrosive environments on the strength of ceramics, both monolithic and composite, are considered, as is the high-temperature wear of ceramics, another important form of degradation at high temperatures.

The durability of ceramics is studied with a variety of techniques. Isothermal oxidation studies in air can be carried out in a simple box furnace. Formation of a protective surface oxide results in a weight gain, with oxidation kinetics determined by weight gain as a function of time. Alternatively, these kinetics can be derived from oxide thicknesses measured as a function of time via optical (Ref 1) and electron-optical techniques. Tube furnaces allow the use of controlled exposure environments. Thermogravimetic analysis (TGA) permits weight change to be continuously monitored (Ref 2). Thermal cycling can be introduced to more accurately model a real application. High-velocity, hydrocarbon-fueled burner rigs subject potential engine materials to an environment that closely approximates actual operating conditions. After these exposures, samples are typically analyzed with a variety of techniques, including optical microscopy, x-ray diffraction, and scanning electron microscopy, to determine composition and morphology of the corrosion products.

High-Temperature Oxidation and Corrosion of Silica-Forming Ceramics

High-temperature oxidation is examined under constant temperature and cyclic conditions. The effects of water vapor, impurities, and molten salts are discussed.

Isothermal Oxidation. This section reviews the kinetics of SiO_2 formation on silicon, SiC, and Si_3N_4 in oxygen:

$$Si(s) + O_2(g) = SiO_2(s) \quad \text{(Eq 1)}$$

$$SiC(s) + {}^3/_2O_2(g) = SiO_2(s) + CO(g) \quad \text{(Eq 2)}$$

$$Si_3N_4(s) + 3O_2(g) = 3SiO_2(s) + 2N_2(g) \quad \text{(Eq 3)}$$

Figure 1 illustrates the formation of a protective oxide scale. The amount of oxide formed can be described in three ways: the net weight change of the sample, the thickness of the oxide formed, and the surface recession of the starting material. Conversion of these quantities is given in Table 1, assuming the loss of carbon or nitrogen from SiC and Si_3N_4, respectively. Figure 2 illustrates typical parabolic TGA results for high-purity SiC and Si_3N_4 at 1300 °C (2370 °F) in pure oxygen. The raw data for this plot were taken as weight gain, while the plot is in the form of scale thickness to provide a comparison between the two materials. The parabolic oxidation rate constant (k_p) is given for each material.

A good deal can be learned from the oxidation of pure silicon to form surface SiO_2. This process has been extensively studied by the semiconductor industry (Ref 4) and is relatively well understood. The oxidation of silicon is briefly summarized to provide a basis for the discussion of SiC and Si_3N_4 oxidation.

Silicon oxidation is described by the reaction given in Eq 1. Kinetic data can be accurately described with the linear-parabolic model of Deal and Grove (Ref 4):

$$x^2 + Ax = B(t + \tau) \quad \text{(Eq 4)}$$

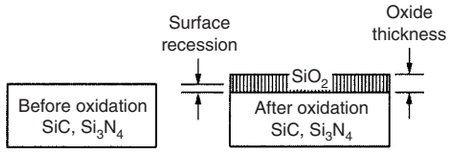

Fig. 1 Schematic of oxidation of a monolithic ceramic illustrating scale growth and substrate recession

Table 1 Conversion of scale thickness to weight gain and to recession for silicon, SiC, and Si_3N_4

Material(a)	Scale thickness, μm	Weight gain, mg/cm²	Recession, μm
Si-SiO_2 (am)	1	0.1173	0.4406
Si-SiO_2 (cr)	1	0.1237	0.4647
SiC-SiO_2 (am)	1	0.0733	0.4564
SiC-SiO_2 (cr)	1	0.0773	0.4813
Si_3N_4-SiO_2 (am)	1	0.0489	0.4974
Si_3N_4-SiO_2 (cr)	1	0.0516	0.5245

(a) am, amorphous; cr, cristobalite

where x is the thickness of the oxide, t is the exposure time, τ is a shift in time to correct for the initial oxide layer, and A and B are constants related to the linear and parabolic rate constants. At short times, Eq 4 reduces to:

$$x \cong \frac{B}{A}(t+\tau) \qquad \text{(Eq 5)}$$

Thus, the quantity B/A is the linear rate constant, which is also designated as k_L. It is generally agreed that in the early stages of oxidation, the rate-controlling step is the chemical reaction given in Eq 1. The linear rate constant can be fit to a standard Arrhenius expression:

$$\frac{B}{A} = \left(\frac{B}{A}\right)_0 \exp\left(\frac{Q_L}{RT}\right) \qquad \text{(Eq 6)}$$

where $(B/A)_0$ is the pre-exponential factor, Q_L is the activation energy for the linear rate constant, R is the gas constant, and T is the absolute temperature. Table 2 lists a fit for some measured silicon linear rate constants. At longer times, Eq 4 simplifies to:

$$x^2 \cong Bt \qquad \text{(Eq 7)}$$

where the quantity B is the parabolic rate constant, which is also designated as k_p. In this case, the rate-controlling step is diffusion through the oxide scale. Similarly, the parabolic rate constant can be expressed with an Arrhenius rate expression:

$$B = B_0 \exp\left(\frac{Q_P}{RT}\right) \qquad \text{(Eq 8)}$$

where B_0 is the pre-exponential factor, and Q_P is the activation energy for the parabolic rate constant. These are given in Table 2.

Silica exists in crystalline as well as amorphous forms. Consider first the amorphous form that grows on silicon in pure oxygen at temperatures less than 1200 °C (2200 °F). The network of silicon and oxygen atoms is sufficiently open so that there are channels for diatomic oxygen to permeate the silica. Based on this concept, Deal and Grove (Ref 4) derived the following expression for the parabolic rate constant:

$$B = \frac{2D_{eff}C^*}{N_1} \qquad \text{(Eq 9)}$$

where D_{eff} is the effective diffusion coefficient for permeation, C^* is the equilibrium concentration of oxidant in the oxide, and N_1 is the number of oxidant molecules incorporated into a unit volume of the oxide layer. Using the permeation rates of diatomic oxygen through amorphous silica, measured by Norton (Ref 6), Deal and Grove were able to derive the oxidation rates of silicon. These calculated rates show good agreement with measured parabolic rates.

Figure 3 is a standard Arrhenius plot of silicon oxidation compared to the oxidation rates for alloys that form other common protective oxides—alumina (Al_2O_3) (Ref 7) and chromia (Cr_2O_3) (Ref 8). This illustrates the unique properties of the silica scale. Note that the rates of silica formation are very low. More importantly, the activation energy for silica growth is low, because permeation of oxygen through the silica network does not involve bond breaking, as a lattice diffusion process would. Thus, the data indicate that SiO_2 is one of the best protective oxides in a pure oxygen environment.

Oxidation of SiC also follows linear-parabolic kinetics. The linear rate constant has been measured by only a few investigators and is listed in Arrhenius form in Table 2. Linear regimes are observable only at temperatures less than approximately 1200 °C (2200 °F). Oxidation occurs via the following reactions:

$$SiC(s) + {}^3/_2O_2(g) = SiO_2(s) + CO(g) \qquad \text{(Eq 10a)}$$

$$SiC(s) + 2O_2(g) = SiO_2(s) + CO_2(g) \qquad \text{(Eq 10b)}$$

Motzfeld (Ref 9) was the first to point out that the oxidation rates of SiC should be 1.5 to 2 times slower than the oxidation rates of silicon, due to the additional oxygen needed to oxidize the carbon, as shown in Eq 10(a) and (b), respectively. This has been verified experimentally (Ref 1, 9). Further, as indicated in Table 2, the activation energy for the parabolic rate constants of silicon and SiC are similar, suggesting a permeation mechanism for diffusion control through the SiO_2 scale.

One important observation with SiC is the oxidation rate dependence on crystallographic orientation (Ref 1). The reasons for this are controversial. Harris (Ref 10) suggested this occurs only during the linear oxidation period and is due to different chemical reaction rates. Costello and Tressler (Ref 11) and Zheng et al. (Ref 12) observed this during the parabolic regime. Ramberg et al. (Ref 1) saw evidence of a silicon oxycarbide subscale, which may influence the diffusion rate, although its existence has not been clearly established.

At short times and at temperatures below ~1200 °C (2200 °F), the thermally grown SiO_2 film is amorphous. A number of factors lead to

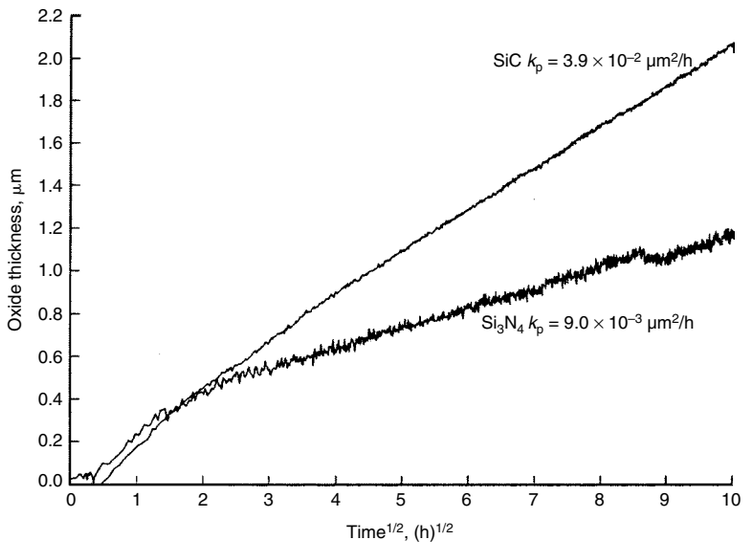

Fig. 2 Oxidation kinetics for chemical vapor deposited (CVD) SiC and CVD Si_3N_4 at 1300 °C (2370 °F) in oxygen. These data were taken with thermogravimetric analysis technique and converted to oxide thicknesses. k_p designates the parabolic rate constant. Source: Ref 3

Table 2 Linear and parabolic oxidation rate constants for silicon, SiC, and Si_3N_4 in dry oxygen

Compound	Linear oxidation rate (B/A)(a), μm/h	Temperature, K	Reference	Parabolic oxidation rate (B)(a), μm^2/h	Temperature, K	Reference
Silicon	8.713×10^6 exp (−195,800/RT)	973–1473	4	1296.05 exp(−124,000/RT)	1073–1473	4
Single-crystal SiC—fast	1.09×10^5 exp (−159,000/RT)	1073–1373	1	864 exp(−99,300/RT)	1073–1373	1
Single-crystal SiC—slow	...	...	...	8.94×10^7 exp(−292,000/RT)	1073–1373	1
CVD polycrystalline SiC(b)	...	...	...	285 exp(−117,800/RT)	1473–1773	3
CVD polycrystalline Si_3N_4(b)	...	...	...	5.363×10^9 exp(−363,900/RT)	1473–1773	3
SN282 Si_3N_4	...	...	...	2.16×10^5 exp(−204,600/RT)	1473–1673	16
AS 800 Si_3N_4	...	...	...	3560 exp(−131,900/RT)	1473–1673	16

(a) The gas constant R = 8.314 J/mol · K. T is the temperature in K. The given temperature is the applicable range. (b) CVD, chemical vapor deposited

crystallization of SiO_2, including longer exposure times, higher exposure temperatures, and impurities. A key question becomes the effect of crystallinity on oxidation rates. Ogbuji (Ref 13) has performed oxidation experiments of SiC at 1300 °C (2370 °F) with an in situ, long-term anneal to transform the scale from amorphous to crystalline. Oxidation rates decrease by a factor of ~30× upon crystallization. Further, even though crystalline scale occupies a portion of the total scale, new amorphous scale is continually growing. Thus, crystallization decreases oxidation rates but only by a small amount. This contrasts with Al_2O_3 scales where crystallization from the θ phase to the α phase leads to a two order of magnitude decrease in oxidation rates (Ref 14).

The discussion thus far has been based on test results of coupons and plates of silicon and SiC. Generally, the oxidation rates of powders scale accordingly with surface area (Ref 15). However, nanoparticles of silicon (20 to 500 nm) have been shown to oxidize more slowly than expected (Ref 5). The observed rates do not fit the classical models (Ref 4), and the reasons for the slower oxidation rates remain an interesting question.

Table 2 also lists oxidation rates for chemical vapor deposited (CVD) and additive-containing Si_3N_4 (Ref 3, 16). It is instructive to first examine high-purity Si_3N_4 and compare its rate to that of silicon and SiC. The oxidation rate of Si_3N_4 is slower than that of SiC (Fig. 2) and has a different activation energy than that of silicon and SiC. This suggests that a different oxidation process occurs, although the exact mechanism has been an area of some controversy. High-purity Si_3N_4 forms an intermediate silicon oxynitride layer of composition Si_2N_2O. The role of this intermediate is still unclear. Some investigators (Ref 17) believe it acts as a diffusion barrier, leading to the slower reaction rates; other investigators (Ref 18) believe it contributes to mixed diffusion/chemical reaction control of the oxidation process. Ogbuji and Jayne (Ref 19) show evidence that the silicon oxynitride, written as $SiN_{2-x}O_{2+x}$, is actually a graded composition from Si_3N_4 to SiO_2. They propose that oxidation occurs in this material as a progressive oxygen-for-nitrogen substitution.

Most commercial forms of Si_3N_4 contain additives, typically refractory oxides, to promote densification. It has been shown that the effects of these impurities dominate oxidation (Ref 20–22). In these cases, movement of the additive cation (e.g., Mg^{2+} or Y^{3+}) outward into the growing oxide film is the rate-controlling step for oxidation. Typically, these materials oxidize faster than high-purity Si_3N_4, as shown in Table 2. Many commercial forms of SiC also contain additives. In general, boron and carbon additives in SiC lead to materials with oxidation rates comparable to those of high-purity SiC (Ref 11); however, refractory oxide additives lead to materials with more rapid oxidation rates (Ref 23).

Cyclic Oxidation. The discussion thus far has dealt with isothermal oxidation. However, many applications involve thermal cycling. This leads to stress from the thermal expansion mismatch between the substrate and the growing oxide scale. Figure 4 is a plot of the thermal expansion of crystalline SiO_2 (cristobalite), SiC, Si_3N_4, and amorphous SiO_2 (Ref 24). As noted, for most practical applications, the scale will contain at least some amount of crystalline SiO_2. Assuming a stress-free scale at temperature, the larger thermal expansion of the crystalline SiO_2 means that on cooling, the scale on a SiC or Si_3N_4 substrate will be in tension. This leads to cracks on cooling, but these cracks heal in the next temperature increase. This behavior is in contrast to superalloys where the oxide is in compression on cooling, leading to oxide buckling and spallation. Thus, cyclic oxidation behavior of SiC and Si_3N_4 tends to be good, as illustrated in Fig. 5 (Ref 25, 26).

Corrosion of Silica-Forming Ceramics by Water Vapor. Many high-temperature environments contain water vapor. In general, combustion of hydrocarbon fuels in air leads to an environment with ~10% water vapor (Ref 24). At 1 bar total pressure, this is ~0.1 bar water vapor, and it scales accordingly to higher total pressures. The effects of water vapor on silica-forming ceramics must be understood to use these materials in such environments.

The fundamental studies of pure silicon are again helpful to understand the effect of water vapor on SiC and Si_3N_4 oxidation. Deal and Grove (Ref 4) have shown that silicon oxidizes more rapidly in water vapor. The diffusivity of water vapor in silica is less than the diffusivity of oxygen in silica; however, the solubility of water vapor in silica is considerably higher than that of oxygen. According to Eq 9, this leads to a net increase in oxidation rate. A similar effect is observed for SiC oxidation (Ref 27).

A second important effect of water vapor is that it can transport impurities from the environment to the sample (Ref 27). As is discussed subsequently, the oxidation of silica-forming ceramics is quite susceptible to secondary elements. Thus, the study of water vapor effects requires a clean furnace, for example, a silica furnace tube and preheating of any alumina parts to remove sodium impurities.

Perhaps the most important effect of water vapor at high temperatures is the formation of volatile species from the thermally grown SiO_2 scale (Ref 28, 29):

$$SiO_2(s) + H_2O(g) = SiO(OH)_2(g) \qquad \text{(Eq 11)}$$

$$SiO_2(s) + 2H_2O(g) = Si(OH)_4(g) \qquad \text{(Eq 12)}$$

Thus, as the scale grows, it is also volatilized by the water vapor in the gas stream. This leads to paralinear kinetics where the scale grows according to a parabolic rate law, and the scale volatilizes according to a linear rate. The parabolic rate constant, k_p, has been discussed in an earlier section. In a flowing gas, volatilization is limited by the boundary layer. The rate of scale removal is linear with time according to the following expression for laminar flow over a flat plate (Ref 30):

$$k_L = 0.664\,(\mathrm{Re})^{0.5}(\mathrm{Sc})^{0.33}\frac{D\rho_v}{L} \qquad \text{(Eq 13)}$$

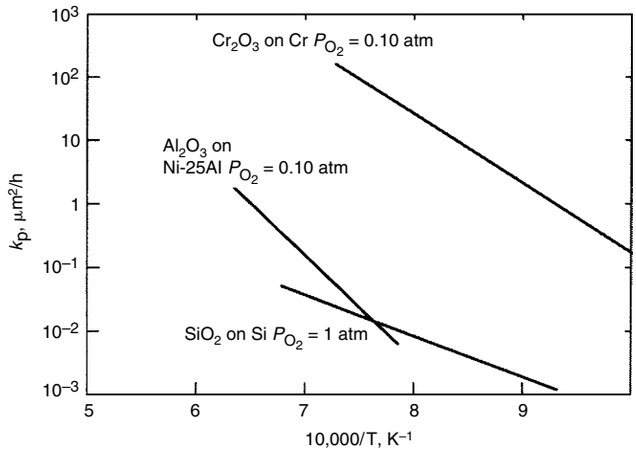

Fig. 3 Arrhenius plot showing comparison of silica growth rate on silicon (Ref 4) to those of growth rate of Cr_2O_3 on chromium (Ref 8) and Al_2O_3 on nickel-aluminum (Ref 7)

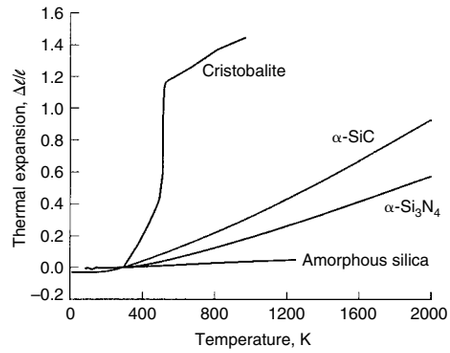

Fig. 4 Coefficient of thermal expansion for cristobalite and amorphous SiO_2, SiC, and Si_3N_4. Adapted from Ref 24

where k_L is the linear rate constant, Re is the Reynolds number, Sc is the Schmidt number, D is the interdiffusion coefficient of the volatile specie [primarily $Si(OH)_4(g)$] in the boundary layer, ρ_v is the density of the volatile specie in the boundary layer, and L is a characteristic dimension of the specimen.

Combined parabolic growth kinetics and linear volatilization kinetics lead to:

$$\frac{dx}{dt} = \frac{k_p}{x} - k_L \qquad \text{(Eq 14)}$$

where x is the scale thickness, and t is time. Figure 6 illustrates this behavior via TGA measurements in a 50% O_2/50% H_2O environment (Ref 26) at 1200 °C (2200 °F). The SiO_2 specimen shows a linear weight loss. Both the SiC and Si_3N_4 initially show a weight gain, followed by a weight loss at a rate similar to that of the SiO_2 specimen. Note the initial weight gain of SiC is greater than that of Si_3N_4 due to the faster oxidation rate of SiC. It is important to note that over long times, both substrates will exhibit greater recession as a result of this oxidation/volatilization process, relative to parabolic oxidation alone.

The previous description of scale volatility can be extended to a hydrocarbon fuel burner (Ref 31–33). Figure 7 illustrates some kinetic results for SiC under these conditions. These weight losses are primarily due to the volatility of the SiO_2 film according to Eq 12. From Eq 13, the key dependences on velocity, temperature, and pressure can be extracted:

$$k_L \propto \frac{v^{0.5}}{P_{total}^{0.5}} P_{Si(OH)_4} \propto v^{0.5} P_{total}^{1.5} \qquad \text{(Eq 15)}$$

where v is the gas velocity, P_{total} is the total pressure, and $P_{Si(OH)_4}$ is the partial pressure of $Si(OH)_4(g)$. According to Eq 12, $P_{Si(OH)_4}$ is proportional to the square of water vapor pressure, which is proportional to the total pressure for hydrocarbon fuel burners. This fact leads to the simplified expression on the right side of Eq 15. The linear rate constant would be expected to have an exponential dependency on temperature as the vapor pressure, $P_{Si(OH)_4}$, varies exponentially with temperature.

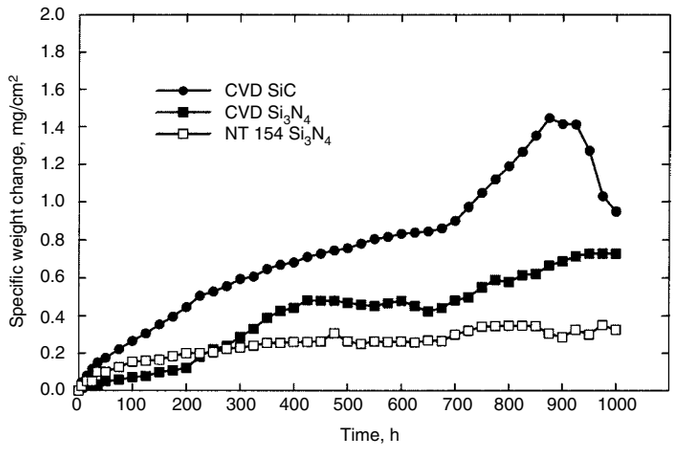

Fig. 5 Cyclic oxidation weight-change kinetics for SiC and Si_3N_4 in air at 1300 °C (2370 °F) with 5 h cycles. NT 154 Si_3N_4 contains approximately 4 wt% Y_2O_3. CVD, chemical vapor deposited. Adapted from Ref 25

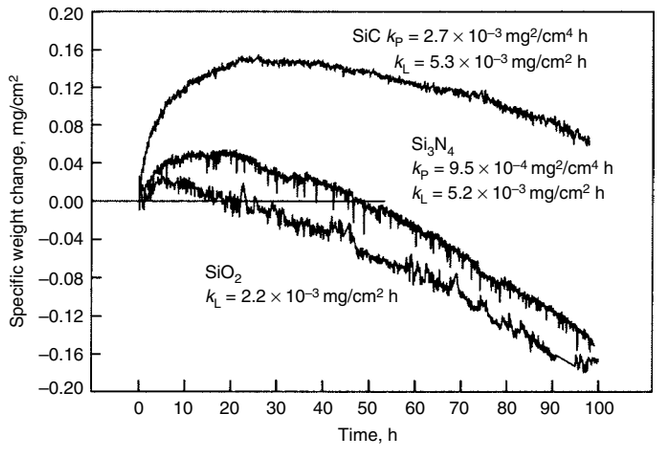

Fig. 6 Volatilization of SiO_2 and paralinear behavior of chemical vapor deposited (CVD) SiC and CVD Si_3N_4 in 50% H_2O/50% O_2 at 1200 °C (2200 °F) and a flow rate of 4.4 cm/s (1.7 in./s). Source: Ref 26

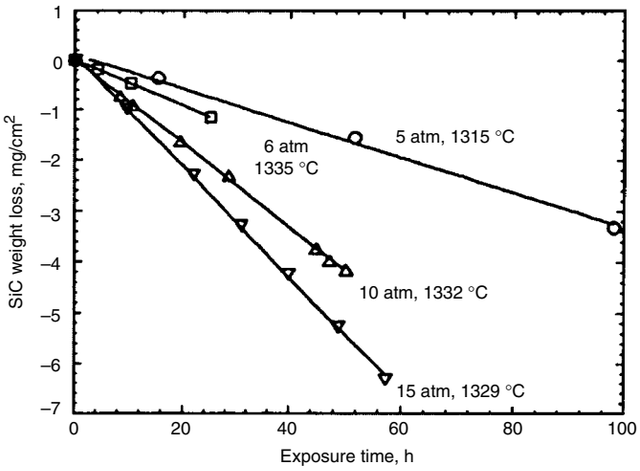

Fig. 7 Weight loss of chemical vapor deposited SiC in a fuel-lean high-pressure burner rig with gas velocities of 20 m/s (790 in./s). Adapted from Ref 31

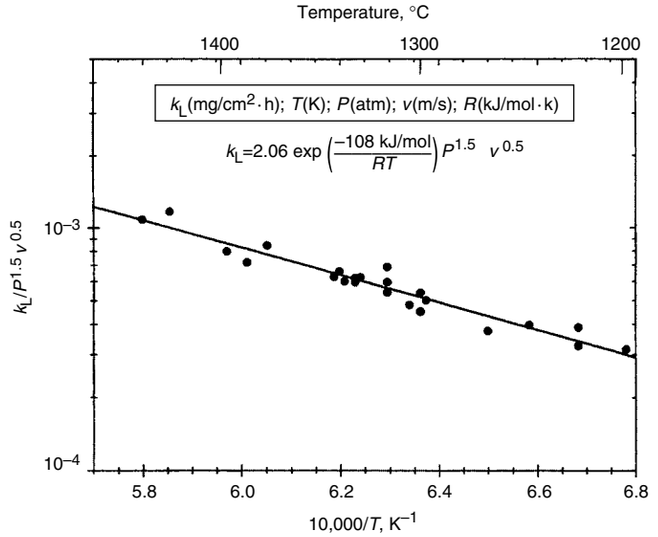

Fig. 8 SiC recession rates in a pressurized burner under fuel-lean conditions of 1200 to 1450 °C (2200 to 2640 °F), 4 to 15 atm, and 10 to 27 m/s (394 to 1063 in./s). Adapted from Ref 31

The normalized Arrhenius representation of k_L in Fig. 8 (Ref 31) was obtained from multiple linear regression over a range of pressure, gas velocity, and temperature test conditions, yielding an empirical weight-loss equation in a form similar to Eq 15:

$$k_L = 2.06 \exp\left(\frac{-108\ \text{kJ/mol}}{RT}\right) P_{\text{total}}^{1.5} v^{0.5} \quad \text{(Eq 16)}$$

where k_L is in mg/cm^2 · h, R is the gas constant 8.314 J/mol · K, T is temperature in degrees K, P is pressure in atmospheres, and v is velocity in meters per second.

Equivalent relationships were measured for recession of SiC in micrometers per hour, represented by multiplying Eq 16 by 2.9. Recession rates for three types of SiC composites were found to be equivalent to CVD SiC or sintered SiC (Ref 34). The volatility rates determined for CVD and sintered Si_3N_4 were both found to be 1.8 times those of SiC, with no apparent effect of additives or the oxynitride interface layer (Ref 35).

Equation 16 must be modified to include slightly different water vapor contents in actual turbine engines (changes in fuel-to-air ratio and/or water injection). By normalizing to the calculated equilibrium water content in the burner rig (0.10 to 0.12 atm), Eq 16 can be rewritten in general form as:

$$k_L = 177 \exp\left(\frac{-108\ \text{kJ/mol}}{RT}\right) \frac{P_{H_2O}^2 v^{0.5}}{P_{\text{total}}^{0.5}} \quad \text{(Eq 17)}$$

Active Oxidation. In addition to condensed-phase SiO_2, silicon-base ceramics also form a stable volatile suboxide, SiO(g). In a flowing gas stream at low oxygen partial pressures, formation of SiO(g)—known as active oxidation—can be a rapid mode of degradation (Ref 36, 37):

$$Si(s) + {}^1/_2O_2(g) = SiO(g) \quad \text{(Eq 18)}$$

$$SiC(s) + O_2(g) = SiO(g) + CO(g) \quad \text{(Eq 19)}$$

$$Si_3N_4(s) + {}^3/_2O_2(g) = 3SiO(g) + 2N_2(g) \quad \text{(Eq 20)}$$

It is essential to delineate the conditions when SiO_2 formation (passive oxidation) no longer occurs and a transition to SiO(g) formation (active oxidation) occurs. There are many studies of these transitions in the literature.

It is again useful to begin with an understanding of the active/passive transition for silicon, as discussed by Wagner (Ref 36). An important point is the difference between the active-to-passive and passive-to-active transitions, with the former generally several orders of magnitude of pressure greater than the latter. As oxidant pressure is gradually raised, silicon first oxidizes to SiO(g) and eventually undergoes an active-to-passive transition when SiO_2(s) forms. Wagner derives this based on the condition that there be sufficient oxygen to form the SiO(g) required by the equilibrium between silicon and SiO_2:

$${}^1/_2Si(s) + {}^1/_2SiO_2(s) = SiO(g) \quad \text{(Eq 21)}$$

Wagner assumes that the flux of oxygen approaching the bare silicon surface is boundary-layer limited and develops expressions for the partial pressure of oxygen for active-to-passive transition, $P^t_{O_2}$, based on this.

On the other hand, the passive-to-active transition occurs as pressure is gradually decreased to the point where SiO_2(s) decomposes:

$$SiO_2(s) = SiO(g) + {}^1/_2O_2(g) \quad \text{(Eq 22)}$$

Thus, a transition oxygen pressure can be calculated from the aforementioned equation.

This general approach has been extended to SiC and Si_3N_4 by a number of investigators (Ref 26, 37–45). Conditions for scale/substrate equilibrium analogous to Eq 21 can be written as:

$$SiC(s) + 2SiO_2(s) = 3SiO(g) + CO(g) \quad \text{(Eq 23)}$$

$$Si_3N_4(s) + 3SiO_2(s) = 6SiO(g) + 2N_2(g) \quad \text{(Eq 24)}$$

Figure 9 illustrates the transitions for SiC with the two boundaries indicated (defined by Eq 22 and 23 given previously) listed and experimental data presented from selected studies wherein active oxidation occurs. There is a good deal of research in this interesting phenomenon, and many theories exist on the details of the transitions. However, the important issue is that at low oxidant pressures, SiC and Si_3N_4 are not stable and can rapidly degrade due to volatile SiO(g) formation.

Related to active oxidation is the actual reaction of the SiO_2 scale and SiC or Si_3N_4 substrate at very high temperatures, according to Eq 23 and 24 (Ref 46). This is near the melting point of the SiO_2 scale (1996 K), which is well above the useful application temperature of these ceramics. These reactions lead to extensive gas generation and scale bubbling and could lift the oxide scale.

Effects of Low-Level Impurities. In various applications, low levels of metallic impurities are very common. These can induce crystallization of amorphous silica. In addition, alkali cations necessarily provide additional oxygen anions and act as network modifiers, creating nonbridging oxygen anions that open up the structure of the silica network. This translates to higher oxygen permeation rates. Small amounts of sodium cations will increase oxidation rates by an order of magnitude (Ref 47–49).

Recent studies (Ref 50, 51) indicate that optimized levels of implanted aluminum can counter this effect of sodium by bridging the oxygen anions. This leads to lower oxidation rates and more uniform SiO_2 scale morphologies. In addition, aluminum implanted ions can decrease the oxidation rates of additive-containing Si_3N_4 (Ref 51). As discussed previously, outward diffusion of the additive cations, such as Mg^{2+}, is rate controlling. It appears that aluminum retards this outward diffusion at temperatures of 1000 °C (1830 °F) or less. However, at higher temperatures, the effect is limited due to the appearance of liquidlike phases.

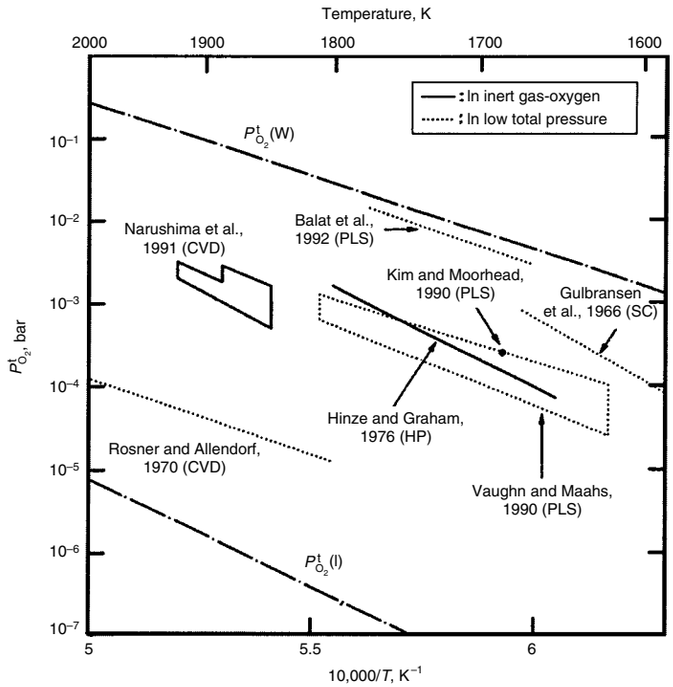

Fig. 9 Measured and calculated active/passive transitions. The upper boundary $P^t_{O_2}$(W) was calculated from Wagner's approach (Eq 23 and Ref 36), and the lower boundary $P^t_{O_2}$(I) was calculated from Eq 22 and Ref 36. Results are for the various types of SiC shown: chemical vapor deposited (CVD), pressureless sintered (PLS), single crystal (SC), and hot pressed (HP). Adapted from Ref 38

Molten Salt Corrosion. In many practical situations, such as heat engines and heat exchangers, condensed phase deposits will form. The most important type of deposit is sodium sulfate (Na_2SO_4), which forms from the combination of sodium impurities in the air or fuel with sulfur impurities in the fuel (Ref 52):

$$2NaCl(g) + SO_2(g) + 0.5O_2(g) + H_2O(g) = Na_2SO_4(l) + 2HCl(g) \quad \text{(Eq 25)}$$

This type of deposit-induced corrosion is termed hot corrosion, and there is a large amount of literature on the hot corrosion of metals (Ref 53, 54). In addition to Na_2SO_4-induced hot corrosion, other deposits, such as calcium sulfate, sodium vanadate, and oxide slags, can induce corrosion (Ref 26). The focus here is on Na_2SO_4-induced corrosion; however, the basic principles discussed carry through to other systems.

Hot corrosion attack occurs in two steps: (1) deposition and (2) corrosive attack. Generally, Na_2SO_4 is most corrosive above its melting point, 1157 K (1623 °F), but below the dewpoint. The dewpoint is related to sulfur and sodium contents together with the total pressure. Dewpoints can be calculated using a free-energy minimization code (Ref 55) and are shown in Fig. 10 (Ref 24, 56). In general, the range of Na_2SO_4 attack is narrow, typically only 100 K (180 °F), with higher pressures increasing the dewpoint and temperature range, but it can be quite severe when it does occur.

A laboratory simulation of deposition and corrosive attack is challenging, and various methods have been used. Important issues include continuous deposition as well as temperature, pressure, and velocity effects. The closest simulation to a heat engine is a fuel burner seeded with salt to form Na_2SO_4 (Ref 57). However, such tests are expensive, and it is difficult to control all parameters. The most common laboratory test is airbrushing an aqueous Na_2SO_4 solution on the sample and allowing the water to evaporate and leave a thin film of Na_2SO_4. The sample is exposed in a furnace, ideally with a set pressure of SO_3 (or SO_2/O_2) to establish a fixed activity of Na_2O (Ref 58). Such a test is easily conducted and allows accurate control of parameters, but a one-time deposition of Na_2SO_4 may not be an adequate simulation of an actual heat engine situation. Other laboratory tests involve a two-zone furnace, where a container of salt is heated in one zone and the sample is placed in a downstream zone (Ref 59). Such tests are more complex but create a more realistic continuous deposition situation.

Hot corrosion is generally described both by a sulfidation and/or an oxide fluxing mechanism (Ref 54). Condensed-phase silicon sulfide is not a thermodynamically stable compound, so the sulfidation mechanism is not applicable to silicon-base ceramics. However, the process is described very well by an oxide fluxing mechanism. The reactive component of Na_2SO_4 is Na_2O, formed by:

$$Na_2SO_4(l) = Na_2O(s) + SO_3(g) \quad \text{(Eq 26)}$$

Consider the acid/base properties of oxides (Ref 60). A low thermodynamic activity of Na_2O [$a_{(Na_2O)}$], set by a high partial pressure of SO_3 [$P_{(SO_3)}$], is termed an acidic molten salt. A high thermodynamic activity of Na_2O, set by a low $P_{(SO_3)}$, is termed a basic molten salt. Given a $P_{(SO_3)}$, the thermodynamic activity of Na_2O follows from the free energy for Eq 26 (Ref 61).

$$\Delta G = 526{,}500 - 118T = -RT \ln K_p = -RT \ln a_{(Na_2O)} P_{(SO_3)} \quad \text{(Eq 27)}$$

where K_p is the equilibrium constant.

SiO_2 is a strongly acidic oxide (Ref 60), and it reacts readily with basic Na_2O:

$$2SiO_2(s) + Na_2O(s) = Na_2O \cdot 2(SiO_2)(l) \quad \text{(Eq 28)}$$

Figure 11 is a calculated phase diagram for the Na_2O-SiO_2 system and indicates the various sodium silicates formed at a particular temperature and activity of Na_2O, using the free-energy minimization code and databases described in Ref 61. Consider the bold line between the most silica-rich sodium silicates and silica. This boundary provides a convenient method to predict dissolution of silica. If the $P_{(SO_3)}$ over the Na_2SO_4 deposit leads to $a_{(Na_2O)}$ greater than that given by the boundary in the figure, then dissolution will occur. This method has been used in a model situation in a burner to predict the behavior of quartz and fuels with different sulfur levels. The higher-sulfur fuel (diesel) led to a low $a_{(Na_2O)}$ and hence limited attack, whereas, the lower-sulfur fuel (such as jet A) led to a higher $a_{(Na_2O)}$ and hence dissolution (Ref 56). While the use of higher-sulfur fuels is not a practical way to control corrosion, it does confirm and illustrate the mechanism described by Eq 26 and 28.

The concept of acid/base reactions with oxides is central to understanding hot corrosion of ceramics. It has been shown that free carbon will drive sodium sulfate more basic, by creating a larger concentration and therefore larger activity of Na_2O (Ref 56). This is important because many ceramics contain carbon. In general, SiC tends to corrode more readily than Si_3N_4 in Na_2SO_4, primarily because the carbon drives the Na_2SO_4 more basic.

Equation 28 indicates the conversion of a solid, protective SiO_2 film to a liquid sodium silicate. Transport rates of oxygen through the liquid sodium silicate are much faster than transport of oxygen through solid SiO_2, so the underlying SiC or Si_3N_4 oxidizes readily, creating more SiO_2 for dissolution. Hot corrosion is best described by coupling of Eq 2 or 3 with Eq 28. With a one-time deposition of a basic Na_2O-containing deposit, it has been shown that these reactions continue until the liquidus boundary of $Na_2O \cdot x(SiO_2)(l)/SiO_2(s)$ is reached (Ref 62). After the corrosion products are enriched in SiO_2 to reach this boundary (Fig. 11), the reaction slows. The resultant $Na_2O \cdot x(SiO_2)/SiO_2/SiC$ structure is shown in Fig. 12. However, in a continuous deposition situation, there is no limit on the coupled oxidation/dissolution reactions. This leads to very thick scales and substantial consumption of the ceramic. Figure 13 is a macro-view of two coupons of SiC—one oxidized in a burner with no added salt and one oxidized with 2 ppm sodium. Note the very thick sodium silicate layer on the second coupon.

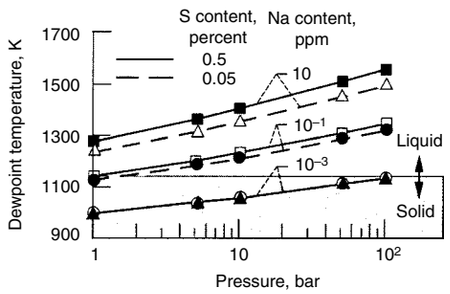

Fig. 10 Calculated dewpoints for sodium sulfate deposition as a function of sodium and sulfur content in the fuel. Source: Ref 24

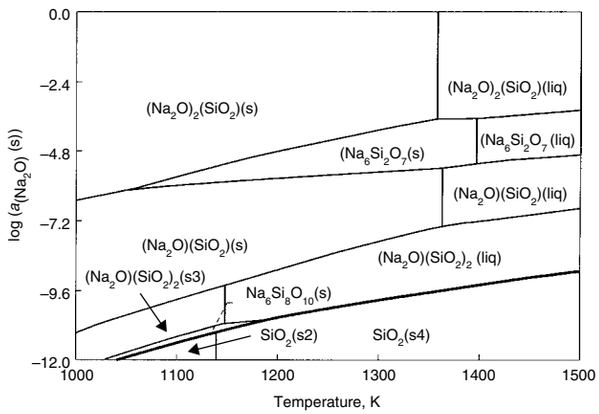

Fig. 11 Calculated phase diagram for Na_2O-SiO_2 showing phases as a function of Na_2O activity and absolute temperature. The critical boundary for stability of SiO_2 is in the lower portion of the diagram (bold line). Note that SiO_2(s2) is quartz, and SiO_2(s4) is tridymite.

As Figure 13 suggests, the kinetics of this process are rapid due to the presence of a liquid film. The thick film suggests rates of consumption several orders of magnitude greater than pure oxidation. Sun et al. (Ref 59) have performed controlled experiments on the corrosion of Si_3N_4, using $NaNO_3$ as a source of Na_2O. They found linear reaction rates, indicating that diffusion is so rapid that the interface oxidation reaction controls the rate.

Other deposits result in similar behavior. The major issue is that basic salt or slag deposits dissolve SiO_2 and lead to consumption of SiC and Si_3N_4. This has been observed with basic oxide slags from coal (Ref 63). In these low-oxygen situations, localized metal silicides also form from reaction of the silicon component with iron and nickel.

Oxidation of Precursor-Derived Ceramics, Composites, and Non-Silica-Forming Ceramics

Silicon carbonitrides are a new class of amorphous ceramic materials derived from polymer precursors. With the addition of boron, glass transition temperatures are as high as 1800 °C (3300 °F) (Ref 64). Initial oxidation kinetic studies of these materials by weight-change methods alone suggested extremely low oxidation rates (Ref 65). However, it is important to recognize that weight gains alone do not indicate oxidation behavior, because concurrent volatilization of boron, carbon, and nitrogen constituents would reduce the measured weight gains (Ref 66, 67). Also, in their present state, these materials are porous, so the effects of internal oxidation must be understood (Ref 64). Finally, inhomogenieties lead to nonuniform oxidation behavior. Nontheless, there are methodical studies (Ref 66) of these materials that separate the various contributions to observed weight losses. These indicate that the oxidation rates are comparable to those of high-purity SiC and Si_3N_4. As processing of these materials improves, more systematic studies of this interesting class of materials should be possible.

Oxidation of Silica-Forming Composites. The monolithic ceramics discussed thus far are generally low-toughness materials; that is, they show limited resistance to failure from a pre-existing crack. A variety of composite materials based on silica-forming ceramics have been developed with the goal of increasing toughness (Ref 68, 69). These include various types of fiber or particulate reinforcements, although the largest increase in toughness is attained with continuous fiber reinforcements. The matrix may be SiC or Si_3N_4; the fibers are typically high-strength SiC or carbon. The fibers deflect matrix cracks, which increases toughness. However, the fibers must not bond with the matrix. Carbon fibers do not bond with a SiC matrix, while SiC fibers are typically coated with either graphitic carbon or boron nitride (BN) to prevent bonding. Thus, the system contains both slowly oxidizing phases (SiC, Si_3N_4) and rapidly oxidizing phases (carbon or BN). Understanding the oxidation behavior of these complex systems is essential to their application.

Consider first the situation of carbon-fiber-reinforced SiC. Several investigators (Ref 70, 71) have shown that at low temperatures (<800 °C, or 1500 °F), oxidation is controlled by the chemical reaction rate of oxygen with carbon. At intermediate temperatures (800 to 1100 °C, or 1500 to 2000 °F), diffusion through cracks becomes rate controlling. At the highest temperatures (>1100 °C, or 2000 °F), the matrix is sealed due to SiO_2 formation. Reaction control leads to more uniform attack of the carbon fibers throughout the material, whereas diffusion control leads to localized attack of the carbon fibers near the composite surface.

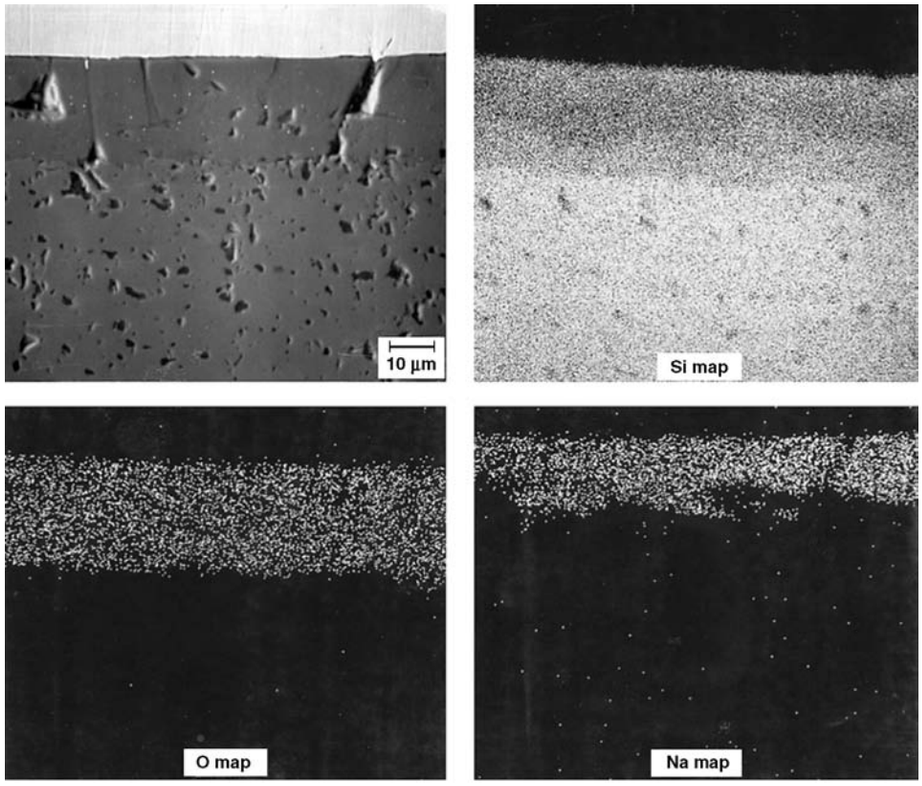

Fig. 12 Polished cross section showing microstructure for sintered SiC (boron, carbon additives) plus one-time deposition of Na_2CO_3 as a source of Na_2O after 48 h at 1000 °C (1830 °F) in 0.1% CO_2/O_2. The elemental maps indicate a layered $Na_2O \cdot x(SiO_2)/SiO_2/SiC$ structure. Source: Ref 24

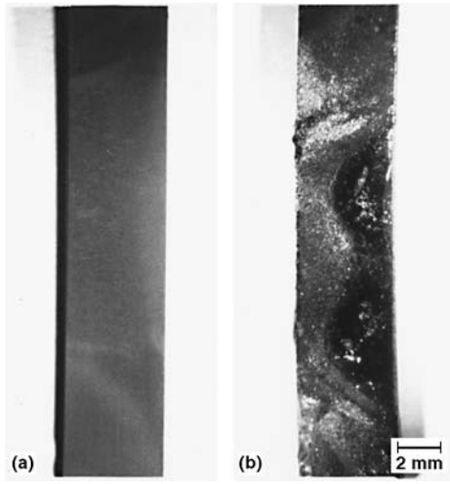

Fig. 13 Optical micrographs of sintered SiC (boron, carbon additives) after exposure in a jet fuel burner rig at 1273 K. (a) 46 h with no sodium. (b) 13.5 h with a sodium-chloride-seeded flame. Source: Ref 24

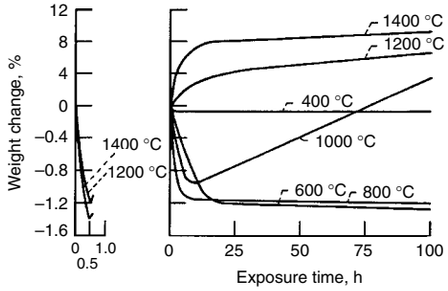

Fig. 14 Thermogravimetric oxidation curves for a SiC fiber/Si_3N_4 matrix composite in flowing oxygen. Note the weight losses at the lower temperatures and protective behavior at the higher temperatures. Source: Ref 72

Figure 14 illustrates weight-loss curves for a composite of carbon-coated SiC fibers in a Si_3N_4 matrix (Ref 72). Note that at 1400 and 1200 °C, (2600 and 2200 °F), oxidative attack of the carbon coating is rapid, yet the composite rapidly seals due to SiO_2 formation. At 1000 °C (1830 °F), oxidative attack is less rapid, and at 600 and 800 °C (1100 and 1500 °F), the composite does not appear to seal. Filipuzzi et al. have modeled oxidation of carbon-coated SiC fibers in a SiC matrix (Ref 73, 74). They developed an analytical model for diffusion of oxygen into the pore between the matrix and fiber, created as the carbon-fiber coating oxidizes. They included the growth of silica on the matrix and fiber, which eventually seals the pore. Their analysis indicates that thinner fiber coatings give better performance.

In theory, BN fiber coatings should be an improvement over carbon coatings, because the oxidation product of BN is not volatile:

$$2BN(s) + 1.5O_2(g) = B_2O_3(l) + N_2(g) \quad \text{(Eq 29)}$$

However, the problem here is the liquid B_2O_3 product. The $B_2O_3(l)$ can further react with SiO_2 to form low-melting silicates, or it can react with water vapor to form highly stable volatile boron hydroxides (Ref 75). This is illustrated in Fig. 15, which shows liquid borosilicate products formed in dry oxygen, and the absence of BN coating due to oxidation/volatilization in humid air.

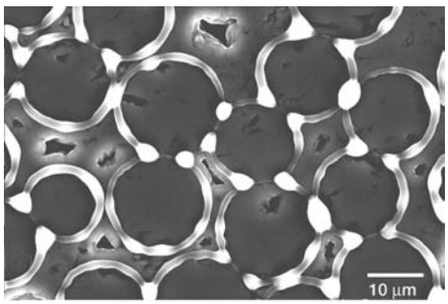

(a)

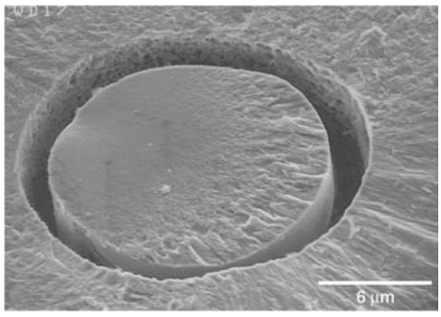

(b)

Fig. 15 Micrographs illustrating two types of behavior observed for oxidation of a SiC fiber/BN coating/SiC matrix composite. (a) Borosilicate glass formation after 100 h in oxygen at 816 °C (1500 °F). (b) Volatilization of BN due to reaction with water after oxidation at 500 °C (930 °F) in humid air. Source: Ref 75

The high toughness of these ceramic-matrix composites (CMCs) makes them one of the most promising high-temperature materials. However, understanding and mitigating their oxidation properties remains a critical issue.

Oxidation and Corrosion of Non-Silica-Forming Nitrides, Carbides, and Borides. In dry oxygen, aluminum nitride (AlN) oxidizes at rates comparable to nickel-aluminum alloys (Ref 76). However, even small amounts of water vapor lead to rapid oxidation due to the formation of 20 to 100 nm micropores in the alumina scale. This issue has limited the application of AlN ceramics.

As noted, BN is a potential fiber coating in CMCs. It has been shown that the oxidation rates are quite dependent on such factors as porosity, oxygen content, and crystallinity of the starting material (Ref 77). The BN oxidizes to B_2O_3, which is not a desirable protective oxide, due to its low melting point and high reactivity with water vapor.

Transition-metal carbides, nitrides, and borides have a number of important properties, including high melting points, hardness, wear resistance, and high-temperature strength. However, these form oxides with high-oxygen diffusivities and short circuit oxygen paths such as cracks and pores. The range of recession rates is given in Fig. 16 (Ref 78). More details can be found in a recent review and the references contained therein (Ref 26).

Corrosion of Oxide Ceramics

In general, oxides are the most stable ceramics. Useful oxide ceramics include silica, alumina (Al_2O_3), mullite ($3Al_2O_3 \cdot 2SiO_2$), various stabilized zirconia (ZrO_2) compositions, and composites with either oxide or nonoxide reinforcements in an oxide matrix. Luthra and Park (Ref 79) have shown that SiC-reinforced Al_2O_3 oxidizes rapidly at temperatures of 1375 to 1575 °C (2505 to 2865 °F) to form a complex reaction-product mixture.

The interaction of common oxides with water vapor has been reviewed (Ref 80) with volatilization rates in the following order: $SiO_2 > Al_2O_3 > ZrO_2$. The following thermodynamic data (Ref 29, 81, 82) can be used to estimate the vapor pressure of the primary volatile specie:

$$SiO_2(s) + 2H_2O(g) = Si(OH)_4(g)$$
$$\Delta G = -RT \ln K_p = 56{,}700 + 66.2T \quad \text{(Eq 30a)}$$

$$0.5Al_2O_3(s) + 1.5H_2O(g) = Al(OH)_3(g)$$
$$\Delta G = -RT \ln K_p = 210{,}600 - 7.7T \quad \text{(Eq 30b)}$$

$$ZrO_2(s) + H_2O(g) = ZrO(OH)_2(g)$$
$$\Delta G = -RT \ln K_p = 434{,}100 - 87.6T \quad \text{(Eq 30c)}$$

where ΔG is the free-energy change, R is the gas constant, T is the absolute temperature, and K_p is the equilibrium constant.

The effect of deposits on oxide ceramics has been reviewed by Pettit et al. (Ref 83). In general, the effects are less than those from deposit-induced corrosion on metals or silica-forming ceramics. Deposits of Na_2SO_4 lead to grain-boundary attack of Al_2O_3. Stabilized zirconias are used as coatings for both metals and ceramics. An important issue here is the possible attack of the stabilizing oxide by vanadate deposits (Ref 84).

Environmental Barrier Coatings

Environmental barrier coatings (EBCs) protect silica-forming ceramics and composites from attack by corrosive species in combustion environments (Ref 85). The key requirements for a successful EBC (Ref 86) include environmental stability, especially in water vapor;

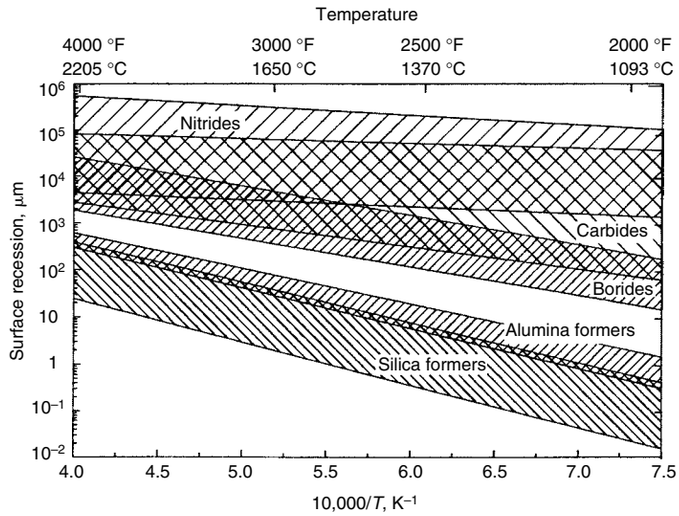

Fig. 16 Surface recession in 100 h from isothermal oxidation for various ceramics, classified according to the protective oxide formed. Adapted from Ref 78

coefficient of thermal expansion (CTE) that matches the substrate; chemical compatibility with the substrate; phase stability; and low thermal conductivity. Table 3 lists the CTE of SiC, Si_3N_4, and current EBC materials (Ref 87). A low thermal conductivity is needed to minimize coating thickness. Table 4 lists the thermal conductivity of current EBC materials in their hot-pressed forms. No material has yet been identified that satisfies all the requirements. As a result, current EBCs have multi-layers in which each layer has a specific role.

Processing. Currently, plasma spraying is the most successful and most widely used process to apply EBCs (Ref 86–88). The process is relatively cost-effective and can readily deposit both metals and ceramics with a wide range of compositions. Plasma-sprayed coatings typically exhibit excellent strain tolerance due to layered microstructures and high porosity. One limitation is the difficulty in applying coatings on complex structures and on small inner surfaces due to the line-of-sight nature of this process. Electron beam physical vapor deposition has been used with great success for processing thermal barrier coatings (TBCs) for metallic components in various heat engines, signifying its potential for EBC processing. Other coating processes being explored include chemical vapor deposition (CVD) (Ref 89, 90), sol-gel, and slurry coating (Ref 91). The non-line-of-sight nature of these processes allows the application of EBCs on complex-shaped components.

Performance of the EBCs by material type is given in the following sections.

Table 3 Coefficient of thermal expansion (CTE) of silicon-base ceramics and environmental barrier coating materials

Material	CTE, 10^{-6}/°C
SiC	4.5–5.5
Si_3N_4	3–4
Si	3.5–4.5
Mullite(a)	5–6
BSAS(b)	4–5
Y_2SiO_5	5–6
Sc_2SiO_5	5–6
Er_2SiO_5	5–7
Yb_2SiO_5	3.5–4.5

(a) $3Al_2O_3$-$2SiO_2$. (b) BSAS, barium-strontium-aluminosilicate. (1-x) BaO-xSrO-Al_2O_3-$2SiO_2$, for $0 \leq x \leq 1$

Table 4 Thermal conductivity of hot-pressed environmental barrier coating materials

At 200 to 1400 °C (400 to 2600 °F), determined by a high-heat-flux laser rig

Material	Thermal conductivity, W/m · K
YSZ(a)	2.2–2.9
Mullite	2.2–2.8
BSAS(b)	2.5–3.0
Mullite + BSAS	2.0–2.3
Y_2SiO_5	1.6–1.9
Sc_2SiO_5	2.3–3.5
Yb_2SiO_5	1.3–1.4
Er_2SiO_5	1.4–1.5

(a) Yttria-stabilized zirconia, $0.045(Y_2O_3)\cdot 0.955(ZrO_2)$. (b) BSAS, barium-strontium-aluminosilicate

Mullite and Mullite Plus Barium-Strontium-Aluminosilicate (BSAS). Mullite has a good CTE match and chemical compatibility with SiC and Si_3N_4 ceramics (Ref 85–88) and therefore constitutes a key component in most current EBCs. Conventional plasma-sprayed mullite coatings contain a significant amount of metastable, amorphous phase due to the rapid cooling of molten mullite during solidification on a cold substrate (Ref 88). A subsequent exposure of the mullite coating to a temperature above ~1000 °C (1830 °F) causes crystallization of the amorphous phase. Shrinkage accompanies the crystallization, leading to cracking and delamination of the mullite coating. A modified plasma spray process enables the deposition of crystalline mullite coating, which dramatically improves its crack resistance and adherence (Ref 88). A plasma-sprayed mullite coating on SiC showed improved resistance to Na_2SO_4-induced corrosion as compared to uncoated SiC (Ref 92). A CVD mullite showed similar results (Ref 93). Further improvement in the crack resistance of plasma-sprayed mullite coatings is achieved by adding a second-phase BSAS (Ref 86, 94). The improved crack resistance of the mullite plus BSAS composite coating is attributed to the reduced coating tensile stress from the low-modulus BSAS phase (Ref 95). Introduction of a silicon bond coat further enhances the durability of the mullite coating by improving its adherence (Ref 86, 94). The relatively high silica activity of mullite (0.3 to 0.4) causes the selective volatilization of silica and the partial recession of mullite in high-velocity combustion environments (Ref 96).

Mullite/Yttria-Stabilized Zirconia (YSZ). A water-vapor-resistant overlay coating is applied over the mullite coating, where the overlay coating provides water vapor stability while the mullite coating provides the adherence. YSZ is a logical candidate for a topcoat because it has been successfully used as a TBC for metallic components in gas turbine engines, indicating its water vapor stability. Figure 17 compares the weight change of SiC, plasma-sprayed mullite-coated SiC, and plasma-sprayed mullite/YSZ-coated SiC in a high-pressure burner rig (1230 °C, or 2250 °F; 6 atm; gas velocity 24 m/s, or 79 ft/s) (Ref 96). Note the absence of weight loss in the mullite/YSZ-coated SiC, indicating the water vapor stability of YSZ in a high-velocity combustion environment. However, there are critical disadvantages of YSZ, including a high CTE and sintering. The stress due to the CTE mismatch and sintering causes severe cracking, which provides an easy path for water vapor penetration, resulting in rapid oxidation and premature coating delamination (Ref 95).

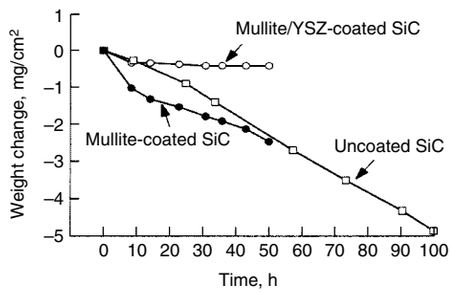

Fig. 17 Weight loss for coated and uncoated SiC in pressurized burner rig at 6 atm and 1230 °C (2250 °F). Weight losses are due to formation of volatile hydroxides. YSZ, yttria-stabilized zirconia. Source: Ref 96

Mullite/BSAS and Mullite Plus BSAS/BSAS. The BSAS has a low silica activity, a low CTE, and a low modulus (~100 GPa, or 14.5×10^6 psi)—key attributes for a successful EBC. The low silica activity leads to stability in water vapor, while the low CTE and low modulus lead to a low EBC stress. These EBCs exhibit dramatically improved durability compared to the mullite/YSZ environmental barrier coating. Figure 18 shows a cross section of plasma-sprayed silicon/mullite plus 20 wt% BSAS/BSAS on a SiC/SiC composite after 1000 h at 1316 °C (2401 °F) (1 h cycles) in 90% H_2O-bal O_2 furnace testing (Ref 87). The EBC maintained excellent adherence and crack resistance. Pockets of glass developed within the BSAS topcoat. These EBCs were applied on SiC/SiC composite combustor liners for Solar Turbine Centaur 50S gas turbine engines under the Department of Energy Ceramic Stationary Gas Turbines Program (Ref 97, 98). One engine used by Texaco in Bakersfield, CA, successfully completed a 14,000 h field test (~1250 °C, or 2280 °F, maximum combustor liner temperature).

However, BSAS still tends to volatilize at high velocities and high temperatures. The EBC on Solar Turbine engines suffered significant BSAS recession in some areas after the 14,000 h test (Ref 98). Another key issue is the chemical reaction between BSAS and the silica thermally grown on the silicon bond coat. The BSAS-silica reaction produces a low-melting (~1300 °C, or 2370 °F) glass, causing EBC degradation and premature failure at temperatures above ~1300 °C (2370 °F) (Ref 94). Therefore, it is desirable to avoid the BSAS second phase in the mullite layer for long-term exposures at high temperatures (>1300 to 1350 °C, or 2370 to 2460 °F).

Mullite/RE_2SiO_5 and Mullite Plus BSAS/Rare Earth Monosilicate (RE_2SiO_5). Some rare earth (RE) silicates are excellent EBC topcoat materials due to their low CTE, phase stability, and low silica activity. Volatility data (Ref 87, 99) indicate that rare earth monosilicates (RE_2SiO_5) are significantly less volatile than BSAS in water vapor, by at least an order of magnitude, while the volatility of rare earth disilicates ($RE_2Si_2O_7$) is similar to that of BSAS. Figure 19 shows a cross section of plasma-sprayed silicon/mullite/Yb_2SiO_5 on a SiC/SiC composite (1000 h) at 1380 °C (2515 °F) (1 h cycles) in 90% H_2O-bal O_2. The EBC maintained crack resistance and superb adherence to this substrate, as well as to Si_3N_4.

BSAS. As indicated earlier, BSAS is reactive with the silica thermally grown on SiC or Si_3N_4, forming a low-melting eutectic (melting point

~1300 °C, or 2370 °F). This chemical reaction causes the buildup of a thick reaction zone and pore formation at the BSAS/substrate interface, which renders a single layer of this material unsuitable for an EBC.

RE_2SiO_5, $RE_2Si_2O_7$, and Ta_2O_5. Plasma-sprayed RE_2SiO_5 (Ref 87) and Ta_2O_5-base EBC (Ref 100) show good adherence on silicon-base ceramics under thermal cycling in air. However, these coatings do not maintain the adherence in water vapor environments. Consequently, the substrate suffers rapid oxidation, forming a thick and sometimes porous scale. The CVD Ta_2O_5 is unstable in an environment containing Na_2SO_4, rapidly reacting to form $NaTaO_3$, which subsequently interacts destructively with the underlying Si_3N_4 substrate to form a molten phase (Ref 101).

Water Vapor Resistance of Candidate EBC Materials. As noted, one of the key issues in development of suitable oxide EBCs is water vapor resistance. As discussed in an earlier section, the necessary thermodynamic data are only available for a few oxides. However, screening-type studies have been done for a range of systems using high-water-content furnaces or pressurized burner rig tests. These are summarized in Table 5. This table indicates the superior performance of hafnia and zirconia compounds, followed by rare earth hafnates or zirconates, and then rare earth monosilicates. Rare earth disilicates are near the midrange of the spectrum, as are barium aluminosilicate, alumina, aluminum titanate, and aluminum silicate. Finally silica, chromia, and boria are among the common oxides most rapidly attacked by water vapor and are provided as a lower reference point. It should also be noted that this table is a summary of data from several sources using different techniques and represents the current state of understanding. Nonetheless it provides some general guidelines in the development of EBCs.

It is generally agreed that silicon-base ceramics and composites will require some type of EBC for engine/combustion-environment applications. The development of such coatings is still an active area of research.

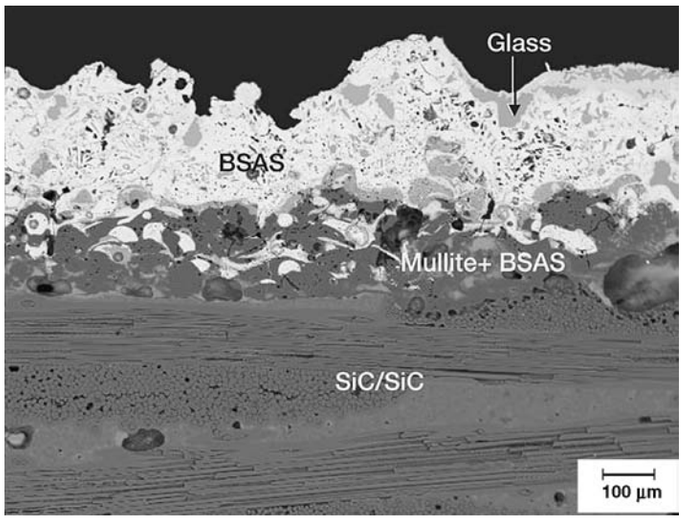

Fig. 18 Cross section of a silicon/mullite plus barium-strontium-aluminosilicate (BSAS)/BSAS coating on a SiC fiber/SiC matrix composite after furnace exposure in 90% H_2O/O_2 for 1000 h at 1316 °C (2401 °F) (1 h cycles). Source: Ref 87

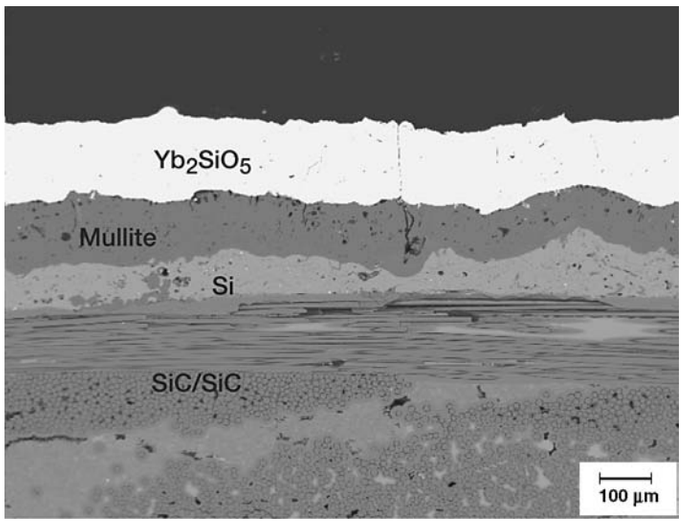

Fig. 19 Cross section of a silicon/mullite/Yb_2SiO_5 coating on a SiC fiber/SiC matrix composite after furnace exposure in 90% H_2O/O_2 for 1000 h at 1380 °C (2516 °F) (1 h cycles), showing good adherence, crack resistance, and environmental stability

Effects of Oxidation and Corrosion on Mechanical Properties

Current silicon nitrides have room-temperature flexural strengths of 600 to 800 MPa (90 to 120 ksi) (Ref 110, 111), with sintered α-SiC at ~400 MPa (60 ksi) (Ref 112). Because these ceramics are inherently brittle, strength is a function of surface morphology. After 4500 h at 1200 °C (2192 °F), sintered α-SiC exhibits a strength increase due to flaw healing, while alumina-containing SiC experiences a 50% strength loss due to pitting and oxide penetration along the grain boundaries (Ref 113). Oxidized Si_3N_4 has exhibited short-term strength increases due to blunting of crack tips, although at longer exposure times strength decreases due to

Table 5 Approximate order of water vapor resistance for environmental barrier coating candidate oxides

Oxide	Reference
Most water vapor resistant	
HfO_2	102
ZrO_2 [YSZ]	96, 102–105
$2(Lu_2O_3) \cdot 3(ZrO_2)$	106
$2(Y_2O_3) \cdot 3(ZrO_2)$	106
$3(Yb_2O_3) \cdot 5(Al_2O_3)$	103
$3(Y_2O_3) \cdot 5(Al_2O_3)$ (yttrium-aluminum-garnet)	103, 104
$Lu_2O_3 \cdot SiO_2$	87, 105
$Yb_2O_3 \cdot SiO_2$	87, 105
$Y_2O_3 \cdot SiO_2$	87, 105
$Al_2O_3 \cdot TiO_2$	102
$2(Lu_2O_3) \cdot 3(HfO_2)$	102
$Lu_2O_3 \cdot 2(SiO_2)$	102, 105, 106, 107
$Y_2O_3 \cdot 2(SiO_2)$	103, 106, 108
$Yb_2O_3 \cdot 2(SiO_2)$	87, 102, 103, 107
$Ba(Sr)O \cdot Al_2O_3 \cdot 2(SiO_2)$ (barium-strontium-aluminosilicate)	87, 94
$SrO \cdot Al_2O_3 \cdot 2(SiO_2)$ (strontium-aluminosilicate)	87, 94
Al_2O_3	33, 102, 103, 105, 107–109
$3(Al_2O_3) \cdot 2(SiO_2)$ (mullite)	96, 97, 102–105, 107
TiO_2	102
$CaO \cdot 2(Yb_2O_3) \cdot 3(SiO_2)$	102, 107
$x(CeO_2) \cdot (ZrO_2)$	108
SiO_2	28, 29, 31, 33, 108
Cr_2O_3	80
Least water vapor resistant	

Table 6 Friction and wear summary for pin-on-disk sliding of ceramics

Pin material	Disk material	Test temperature °C	Test temperature °F	Friction coefficient	Average wear coefficient, $mm^3/N \cdot m$	Observed wear mode	Reference
Al_2O_3	Al_2O_3	25	75	0.84	10^{-7}	Microfracture	129
Al_2O_3	Al_2O_3	1000	1830	0.50	10^{-7}	Microfracture	129
SiC	SiC	25	75	0.75	10^{-7}	...	...
SiC	SiC	1000	1830	0.77	10^{-5}	Oxide-layer removal	129
Si_3N_4	Si_3N_4	25	75	0.60	10^{-5}	Microfracture	128
Si_3N_4	Si_3N_4	1000	1830	0.70	10^{-2}	Oxide-layer removal	128
Al_2O_3-SiC_w(a)	Al_2O_3-SiC_w(a)	25	75	0.74	10^{-7}	Microfracture	132
Al_2O_3-SiC_w(a)	Al_2O_3-SiC_w(a)	1200	2190	0.58	10^{-6}	Microfracture oxidation	132
ZrO_2	ZrO_2	25	75	0.68	10^{-4}	Microfracture	133
ZrO_2	ZrO_2	800	1470	0.65	10^{-4}	Microfracture	133

(a) Al_2O_3-SiC_w is alumina with 25 vol% silicon carbide whiskers added.

oxidation pit formation (Ref 114). High-temperature oxidative environments can also adversely affect crack growth and enhance creep (Ref 115). Sintering additives play a major role in oxidation rate and mechanical properties. An addition of 12.5 wt% Lu_2O_3 to Si_3N_4 significantly improves its high-temperature ($\geq$1400 °C, or 2552 °F) strength due to formation of a high-temperature grain-boundary phase that extensively crystallizes during processing (Ref 116).

As discussed earlier, both active oxidation to SiO(g) and water vapor reactions to form $Si(OH)_4$(g) lead to material consumption. After 20 h at 1400 °C (2552 °F) and a $P(O_2) = 1.5 \times 10^{-5}$ MPa, α-SiC exhibits a 50% reduction in strength due to pit formation from active oxidation (Ref 45). In a high velocity combustion rig, the surface oxide is continually swept away by its reaction with water vapor. For Si_3N_4 after 100 h at 1400 °C (2550 °F), exposure with 5 bar total pressure in a natural gas burner (and corresponding water vapor content) results in strength reductions of 20 to 70% (Ref 111).

Corrosion of SiC by molten salts, either by thin films (Ref 117) or continuous deposition (Ref 118), results in surface pit formation and resultant strength loss. Pits occur where gas bubbles form at the substrate/liquid silicate interface, continually exposing the substrate to corrosion. Burner rig hot corrosion of a yttrium-containing Si_3N_4 results in modification of near-surface grain boundaries and subsequent strength loss (Ref 119).

Due to the complex nature of CMCs, differing modes of attack occur as a function of temperature. As discussed, the major issue with continuous fiber-reinforced CMCs is the easily oxidizable second phase (e.g., carbon or BN). If the second phase is exposed to oxygen and/or water vapor due to a crack or discontinuous outer protective oxide, degradation will occur. Stress-rupture life of a crack-free, as-produced SiC/SiC composite with BN fiber interphase at 815 °C (1499 °F) in air under 140 MPa (20 ksi) tensile load is 50 h. Stress-rupture life of the precracked material under the same conditions was less than 5 h (Ref 120). For a carbon-fiber-reinforced SiC matrix, attack of the fiber has an adverse effect on stress-rupture behavior (Ref 121). The effect of environment on mechanical properties of CMCs is a critical area of research.

High-Temperature Wear of Advanced Ceramics

The brittle nature of most monolithic ceramics has largely precluded their use in applications where high tensile stresses occur. One such example is in dry sliding contact, where high-friction forces can result in significant tensile stresses, even under modest loads, leading to fracture and subsequent wear (Ref 122). The development in recent decades of advanced ceramics with engineered microstructures has resulted in markedly improved strength and toughness properties (Ref 123). Certain ceramics, such as silicon nitride, achieve excellent toughness by tailoring the grain size and composition of grain-boundary phases (Ref 124). Others, such as alumina, are strengthened by the addition of secondary phases based on zirconia and silicon carbide whiskers intended to enhance favorable residual compressive stresses and to deflect and halt crack propagation (Ref 125). The engineering promise of advanced ceramics has been further enhanced by improved finishing technologies capable of generating precise and complex part geometries with significantly reduced flaw sizes. The emergence of these new ceramics in the early 1980s enabled consideration of several demanding high-temperature applications.

Two such applications involved heat engine components: ceramic gas turbines and adiabatic diesels (Ref 126, 127). Tribological, or friction and wear, properties are important characteristics for these and other applications involving sliding contact at high temperatures under dry, nonlubricated conditions. Unfortunately, extensive and reliable data regarding the high-temperature tribological properties of advanced ceramics have not been available, due to a lack of

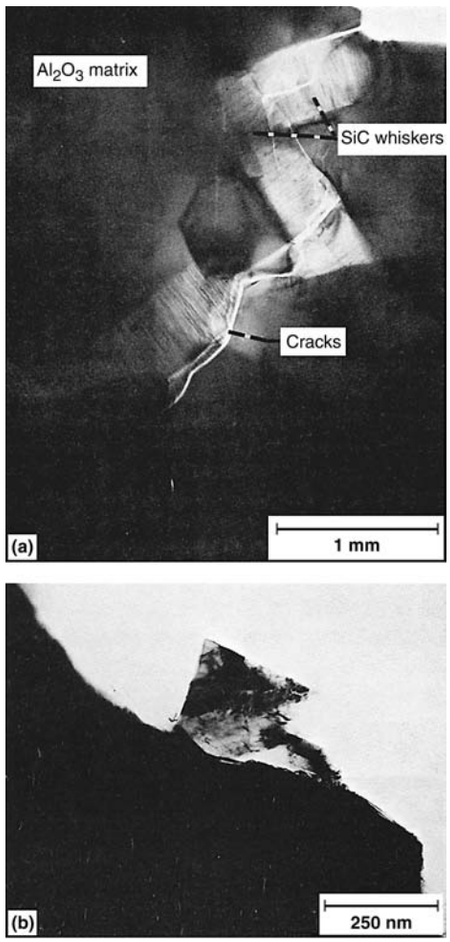

Fig. 20 Transmission electron microscopy micrographs of (a) cracks and (b) faceted wear debris following room-temperature sliding of an Al_2O_3-SiC_w whisker-reinforced ceramic composite. Source: Ref 134

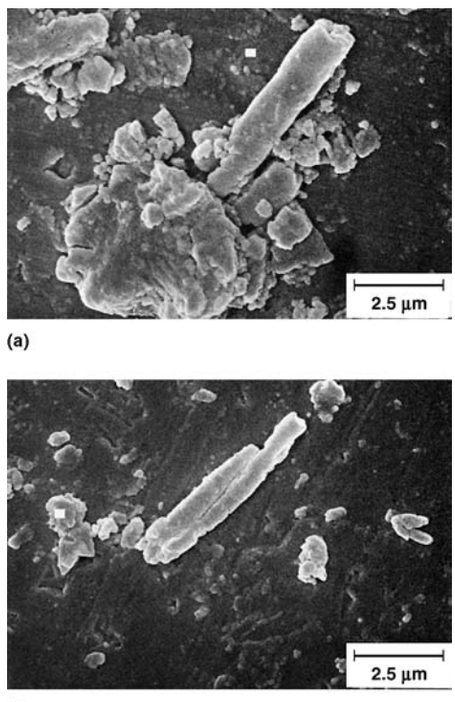

Fig. 21 Ceramic wear debris formed from oxide layer removal on Al_2O_3-SiC_w disk specimen following 1200 °C (2192 °F) sliding in air. Source: Ref 134

suitable test capabilities and lack of characterization of these newer ceramics and composites.

Initially, many in the research community hypothesized that advanced ceramics may exhibit favorable high-temperature friction and wear properties because of their high hot hardness and achievable low surface roughness characteristics. This concept was loosely based on the premise that friction and wear, for self-mated steel for instance, was due to local surface asperity interactions in which contact points of surfaces resulted in local hot spots, adhesive welding, and material oxidation. Therefore, it was considered that the hard, smooth, and chemically nonreactive ceramics would not suffer from such wear mechanisms.

More recent tribological studies of many classes of nitride, carbide, oxide, and composite ceramics, however, have revealed that, in general, ceramics exhibit high friction and wear in nonlubricated, high-temperature sliding contacts (Ref 128–133). Table 6 summarizes measured friction and wear factor coefficients for a variety of ceramics from self mated ceramic pin-on-disk tests at temperatures from 25 up to 1200 °C (75 up to 2192 °F). Typical tests are 1 hr for a total sliding distance of 9.7 km (6.0 mi). Observed steady-state friction coefficients range from approximately 0.5 to 1.0 or above. Often during initial sliding, especially at room temperatures, lower values are observed. Typically, these are attributed to surface contamination and adsorbed layers being quickly removed by the sliding process, leading to the higher steady-state friction values. Wear factor coefficients, defined as the wear volume (cubic meters) per distance slid (meters) per load (newtons), are also very high but, as is typical for wear data, are more scattered and range from approximately 10^{-7} to 10^{-2} $mm^3/N \cdot m$. By comparison, oil-lubricated steel sliding results in friction coefficients of 0.1 or less and wear factors less than 10^{-9} $mm^3/N \cdot m$.

Microscopic analyses of worn ceramic surfaces reveal two major modes of wear: brittle fracture and tribo-oxidative wear. High friction coefficients during sliding generate high tensile stresses in the wake of the contact area (Ref 134). If sufficiently large flaws exist, cracks form, grow, and ultimately lead to faceted wear debris formation. Figure 20 shows such features. Brittle wear predominates at lower temperatures for all ceramics, and at high temperatures, brittle behavior is a common feature for oxide materials such as alumina. Nitride- and carbide-containing ceramics, however, when sliding at high-temperature in air form complex and often glassy oxide surface layers that are removed by the sliding counterface, revealing fresh, nonoxidized surfaces. These then oxidize, resulting in an oxidative-type wear process. The wear debris from these tests is often characterized by smeared oxide layers and sometimes even rolled-up layered debris. Figure 21 shows an example of such oxide layer wear debris. In both cases, brittle fracture or oxide layer removal, wear rates are high.

Notwithstanding their poor self-lubricating properties, ceramics possess useful thermal, physical, and chemical properties enabling their use in high-temperature applications, provided their shortcomings are accommodated. For instance, using silicon nitride at lower temperatures in the presence of oil has enabled long-life diesel engine components, such as fuel injectors and valve train components. The generally high stiffness and low density of ceramic materials also reduce dynamic forces in high-speed components such as bearing balls. Hybrid ceramic bearings using silicon nitride rolling elements and steel races are capable of significantly higher speeds than comparable all-steel bearings under oil-lubricated conditions. Further, if contact loads can be sufficiently reduced, friction coefficients of 0.5 or higher can be tolerated in order to take advantage of the excellent chemical inertness and dimensional stability of ceramics. Finally, efforts are underway to add self-lubricating materials such as graphite and boron nitride to ceramics to mitigate high friction and wear without adversely affecting strength and other properties. As these research efforts progress, advanced ceramics will find ever-increasing applications in engineering and technology.

REFERENCES

1. C.E. Ramberg, G. Cruciani, K.E. Spear, R.E. Tressler, and C.E. Ramberg, Jr., *J. Am. Ceram. Soc.,* Vol 79 (No. 11), 1997, p 2897–2911
2. D.S. Fox, *J. Am. Ceram. Soc.,* Vol 81 (No. 4), 1998, p 945–950
3. L.U.J.T. Ogbuji and E.J. Opila, *J. Electrochem. Soc.,* Vol 142 (No. 3), 1995, p 925–930
4. B.E. Deal and A.S. Grove, *J. Appl. Phys.,* Vol 36 (No. 12), 1965, p 3770–3778
5. R. Okada and R. Iijima, *Appl. Phys. Lett.,* Vol 58 (No. 15), 1991, p 1662–1663
6. F.J. Norton, *Nature,* Vol 171, 1961, p 701
7. F.S. Pettit, *Trans. Met. Soc. AIME.,* Vol 239, 1967, p 1296–1302
8. W.C. Hagel, *Trans. ASM,* Vol 56, 1963, p 583–599
9. K. Motzfeld, *Acta Chem. Scand.,* Vol 18, 1964, p 1696–1706
10. R.C.A. Harris, *J. Am. Ceram. Soc.,* Vol 58 (No. 1/2), 1984, p 7–9
11. J.A. Costello and R.E. Tressler, *J. Am. Ceram. Soc.,* Vol 64 (No. 6), 1986, p 674–681
12. Z. Zheng, R.E. Tressler, and K.E. Spear, *J. Electrochem. Soc.,* Vol 137 (No. 3), 1990, p 854–858
13. L.U.J.T. Ogbuji, *J. Am. Ceram. Soc.,* Vol 80 (No. 6), 1997, p 1544–1550
14. G.C. Rybicki and J.L. Smialek, *Oxid. Met.,* Vol 31 (No 3/4), 1989, p 275–304
15. D. Das, J. Farjas, and P. Roura, *J. Am. Ceram. Soc.,* Vol 87 (No. 7), 2004, p 1301–1305
16. D.S. Fox, E.J. Opila, Q.N. Nguyen, D.L. Humphrey, and S. Lewton, *J. Am. Ceram. Soc.,* Vol 86 (No. 8), 2003, p 1256–1261
17. H. Du, R.E. Tressler, K.E. Spear, and C.G. Pantano, *J. Electrochem. Soc.,* Vol 136 (No. 5), 1989, p 1527–1536
18. K.L. Luthra, *J. Am. Ceram. Soc.,* Vol 74 (No. 5), 1991, p 1095–1103
19. L.U.J.T. Ogbuji and D.T. Jayne, *J. Electrochem. Soc.,* Vol 140 (No. 3), 1993, p 759–766
20. D. Cubicciotti and K.H. Lau, *J. Am. Ceram. Soc.,* Vol 61 (No. 11–12), 1978, p 512–517
21. D. Cubicciotti and K.H. Lau, *J. Electrochem. Soc.,* Vol 126 (No. 10), 1979, p 1724–1728
22. P. Andrews and F.L. Riley, *J. Eur. Ceram. Soc.,* Vol 7, 1991, p 125–132
23. S.C. Singhal and F.F. Lange, *J. Am. Ceram. Soc.,* Vol 58 (No 9–10), 1975, p 433–435
24. N.S. Jacobson, *J. Am. Ceram. Soc.,* Vol 76 (No. 1), 1993, p 3–28
25. E.J. Opila, D.S. Fox, and C.A. Barrett, Cyclic Oxidation of Monolithic SiC and Si_3N_4 Materials, *Ceram. Eng. Sci. Proc.,* Vol 14 (No. 7–8), 1993, p 367–374
26. E.J. Opila and N.S. Jacobson, Corrosion of Ceramic Materials, *Materials Science and Technology: A Comprehensive Treatment, Corrosion and Environmental Degradation,* Vol II, M. Schu?tze, Ed., Wiley-VCH, 2000, p 327–388
27. E.J. Opila, *J. Am. Ceram. Soc.,* Vol 77 (No. 3), 1994, p 730–736
28. E.J. Opila and R.E. Hann, Jr., *J. Am. Ceram. Soc.,* Vol 80 (No. 1), 1997, p 197–205
29. N.S. Jacobson, E.J. Opila, D.L. Myers, and E.H. Copland, Thermodynamics of the Gas Phase Species in the Si-O-H System, *J. Chem. Therm.,* in press
30. W.M. Kays and M.E. Crawford, *Convective Heat and Mass Transfer,* McGraw-Hill, 1980, p 139, 197
31. R.C. Robinson and J.L. Smialek, *J. Am. Ceram. Soc.,* Vol 82 (No. 7), 1999, p 1817–1825
32. E.J. Opila, J.L. Smialek, R.C. Robinson, D.S. Fox, and N.S. Jacobson, *J. Am. Ceram. Soc.,* Vol 82 (No. 7), 1999, p 1826–1834
33. I. Yuri and T. Hisamatsu, "Recession Rate Prediction for Ceramic Materials in Combustion Gas Flow," GT2003-38886, ASME Turbo Expo 2003, American Society of Mechanical Engineers, 2003
34. R.C. Robinson and J.L. Smialek, Durability of Ceramic Matrix Composites in Combustion Environments, *Electrochemical Society Proceedings,* Vol 99-38, M. McNallan, E. Opila, T. Maruyama, and T. Narita, Ed., Electrochemical Society, 2000, p 407–417
35. J.L. Smialek, R.C. Robinson, E.J. Opila, D.S. Fox, and N.S. Jacobson, *Adv. Compos. Mater.,* Vol 8 (No. 1), 1999, p 33–45

36. C. Wagner, *J. Appl. Phys.,* Vol 29 (No. 9), 1958, p 1295–1297
37. S.C. Singhal, *Ceramurgia Int.,* Vol 2 (No. 3), 1976, p 123–130
38. T. Narushima, T. Goto, T. Hirai, and Y. Iguchi, *Mater. Trans., JIM,* Vol 38 (No. 10) 1997, p 821–835
39. D.E. Rosner and H.D. Allendorf, *J. Chem. Phys.,* Vol 74 (No. 9), 1970, p 1829–1839
40. W.L. Vaughn and H.G. Maahs, *J. Am. Ceram. Soc.,* Vol 73 (No. 6), 1990, p 1540–1543
41. J.W. Hinze and H.C. Graham, *J. Electrochem. Soc.,* Vol 123 (No. 7), 1976, p 1066–1073
42. E.A. Gulbransen, K.F. Andrew, and F.A. Brassart, *J. Electrochem. Soc.,* Vol 113 (No. 12), 1966, p 1311–1314
43. M. Balat, G. Flamant, G. Male, and G. Pichelin, *J. Mater. Sci.,* Vol 27 1992, p 697–703
44. T. Narushima, T. Goto, Y. Iguchi, and T. Hirai, *J. Am. Ceram. Soc.,* Vol 74 (No. 10) 1991, p 2583–2586
45. H.-E. Kim and A.J. Moorhead, *J. Am. Ceram. Soc.,* Vol 73 (No. 7), 1990, p 1868–1872
46. N.S. Jacobson, K.N. Lee, and D.S. Fox, *J. Am. Ceram. Soc.,* Vol 75 (No. 6), 1992, p 1603–1611
47. E.J. Opila, *J. Am. Ceram. Soc.,* Vol 78 (No. 4), 1995, p 1107–1110
48. V. Pareek and D.A. Shores, *J. Am. Ceram. Soc.,* Vol 74 (No. 3), 1991, p 556–563
49. Z. Zheng, R.E. Tressler, and K.E. Spear, *Corros. Sci.,* Vol 33 (No. 4), 1992, p 545–556, 569–580
50. Y. Cheong, P. Mukundhan, H. Du, and S.P. Withrow, *J. Am. Ceram. Soc.,* Vol 83 (No. 1), 2000, p 154–160, 161–165
51. P. Mukundhan, H. Du, and S.P. Withrow, *J. Am. Ceram. Soc.,* Vol 85 (No. 4), 2002, p 865–872
52. F.J. Kohl, C.A. Stearns, and G.C. Fryburg, Sodium Sulfate: Vaporization Thermodynamics and Role in Corrosive Flames, *Metal-Slag-Gas Reactions and Processes,* Z.A. Foroulis and W.W. Smeltzer, Ed., The Electrochemical Society, 1975, p 649–664
53. R.A. Rapp, *Corros. Sci.,* Vol 42 (No. 10), 1986, p 568–577
54. F.S. Pettit and C.S. Giggins, Hot Corrosion, *Superalloys II,* C.T. Sims, N.S. Stoloff, and W.C. Hagel, Ed., Wiley, 1987, p 327–354
55. S. Gordon and B.J. McBride, "Computer Program for Calculation of Complex Chemical Equilibrium Compositions, Rocket Performance, Incident and Reflected Shocks, and Chapman-Jouguet Detonations," NASA SP-273, 1971
56. N.S. Jacobson, *Oxid. Met.,* Vol 31 (No 1/2), 1989, p 91–103
57. D.L. Deadmore, C.E. Lowell, and F.J. Kohl, *Corros. Sci.,* Vol 19, 1979, p 371–378
58. N.S. Jacobson and J.L. Smialek, *J. Am. Ceram. Soc.,* Vol 68 (No. 8), 1985, p 432–439
59. T. Sun, G.R. Pickrell, and J.J. Brown, Jr., *J. Am. Ceram. Soc.,* Vol 77 (No. 12), 1994, p 3209–3214
60. H. Flood and T. Fo?rland, *Acta Chem. Scand.,* Vol 1, 1947, p 592–604
61. C.W. Bale, P. Chartrand, S.A. Degterov, G. Eriksson, K. Hack, R. Ben Mahfoud, J. Melancon, A.D. Pelton, and S. Petersen, *CALPHAD,* Vol 26 (No. 2), 2002, p. 189–228
62. M.I. Mayer and F.L. Riley, *J. Mater. Sci.,* Vol 13, 1978, p 1319–1328
63. M.K. Ferber, J. Ogle, V.J. Tennery, and T. Henson, *J. Am. Ceram. Soc.,* Vol 68 (No. 4), 1985, p 191–197
64. R. Raj, L. An, S. Shah, R. Riedel, C. Fasel, and H.-J. Kleebe, *J. Am. Ceram. Soc.,* Vol 84 (No. 8), 2001, p 1803–1810
65. H. P. Baldus, and M. Jansen, *Angew. Chem. Int. Ed. Engl.,* Vol 36, 1997, p 328–343
66. A. Muller, P. Gerstel, E. Butchereit, K.G. Nickel, and F. Aldinger, *J. Eur. Ceram. Soc.,* Vol 24 (No. 12), 2004, p 3409–3417
67. N.S. Jacobson, E.J. Opila, and K.N. Lee, *Curr. Opin. Solid State Mater. Sci.,* Vol 5 2001, p 301–309
68. A.G. Evans, *J. Am. Ceram. Soc.,* Vol 73 (No. 2), 1990, p 187–206
69. R. Naslain, *Adv. Compos. Mater.,* Vol 8, 1999, p 3–16
70. F. Lamouroux, G. Camus, and J. Thebault, *J. Am. Ceram. Soc.,* Vol 77 (No. 8), 1994, p 2049–3057
71. M.C. Halbig and J.D. Cawley, Modeling the Environmental Effects on Carbon Fibers in a Ceramic Matrix at Oxidizing Conditions, *Proceedings of the 24th Annual Cocoa Beach Conference,* Ceram. Eng. and Sci Proceedings Vol 21 (No. 3.2) American Ceramic Society, 2000, p 219–226
72. R.T. Bhatt, "Oxidation Effects on the Mechanical Properties of SiC Fiber-Reinforced Reaction-Bonded Silicon Nitride Matrix Composites," NASA TM 102360, 1989
73. L. Filipuzzi, G. Camus, R. Naslain, and J. Thebault, *J. Am. Ceram. Soc.,* Vol 77 (No. 2), 1994, p 459–466
74. L. Filipuzzi and R. Naslain, *J. Am. Ceram. Soc.,* Vol 77 (No. 2), 1994, p 467–480
75. N.S. Jacobson, G.N. Morscher, D.R. Bryant, and R.E. Tressler, *J. Am. Ceram. Soc.,* Vol 82 (No. 6), 1999, p 1473–1482
76. E. Opila, N. Jacobson, D. Humphrey, T. Yoshio, and K. Oda, The Oxidation of AlN in Dry and Wet Oxygen, *Electrochemical Society Proceedings,* Vol 98-9, P.Y. Hou, M.J. McNallan, R. Oltra, E.J. Opila, and D.A. Shores, Ed., The Electrochemical Society, 1998, p 430–437
77. N.S. Jacobson, S. Farmer, A. Moore, and H. Sayir, *J. Am. Ceram. Soc.,* Vol 82 (No. 2), 1999, p 393–398
78. N.J. Shaw, J.A. DiCarlo, N.S. Jacobson, S.R. Levine, J.A. Nesbitt, H.B. Probst, W.A. Sanders, and C.A. Stearns, "Materials for Engine Applications Above 3000 °F—An Overview," NASA TM 100169, 1987
79. K.L. Luthra and H.D. Park, *J. Am. Ceram. Soc.,* Vol 73 (No. 4), 1990, p 1014–1023
80. E.J. Opila and N.S. Jacobson, Volatile Hydroxide Species of Common Protective Oxides and Their Role in High-Temperature Corrosion, *Electrochemical Society Proceedings,* Vol 96–26, R.A. Rapp, D.A. Shores, and P.Y. Hou, Ed., Electrochemical Society, 1997, p 269–280
81. A. Hashimoto, *Geochim. Cosmochim. Acta,* Vol 56, 1992, p 511–532
82. O.H. Krikorian, *High Temp.-High Press.,* Vol 14, 1982, p 387–397
83. F.S. Pettit, G.H. Meier, and J.R. Blachere, Oxide Ceramics, *Environmental Effects on Engineered Materials,* R.H. Jones, Ed., Marcel Dekker, 2001, p 351–374
84. R.L. Jones, "Vanadate-Sulfate Melt Thermochemistry Relating to Hot Corrosion of Thermal Barrier Coatings," NRL/MR/6170—97-8103, Naval Research Laboratory, 1997
85. K.N. Lee, H. Fritze, and Y. Ogura, Coatings for Engineering Ceramics, *Progress in Ceramic Gas Turbine Development,* Vol 2, M. van Roode, M. Ferber, and D.W. Richerson, Ed., ASME Press, 2003, p 641–664
86. K.N. Lee, *Surf. Coat. Technol.,* Vol 133–134, 2000, p 1–7
87. K.N. Lee, D.S. Fox, and N.P. Bansal, *J. Eur. Ceram. Soc.,* Vol 25, 2005, p 1705–1715
88. K.N. Lee, R.A. Miller, and N.S. Jacobson, *J. Am. Ceram. Soc.,* Vol 78 (No. 3), 1995, p 705–710
89. S.N. Basu, P. Hou, and V.K. Sarin, *Int. J. Refract. Met. Hard Mater.,* Vol 16, 1998, p 343–352
90. J.A. Haynes, M.J. Lance, K.M. Cooley, M.K. Ferber, R.A. Lowden, and D.P. Stinton, *J. Am. Ceram. Soc.,* Vol 83 (No. 3), 2000, p 657–659
91. J.I. Federer, *J. Mater. Eng.,* Vol 12, 1990, p 141–149
92. N.S. Jacobson, K.N. Lee, and Y. Yoshio, *J. Am. Ceram. Soc.,* Vol 79 (No. 8), 1996, p 2161–2167
93. W.Y. Lee, K.L. More, and Y.W. Bae, *J. Am. Ceram. Soc.,* Vol 79 (No. 9), 1996, p 2489–2492
94. K.N. Lee, D.S. Fox, J.I. Eldridge, D. Zhu, R.C. Robinson, N.P. Bansal, and R.A. Miller, *J. Am. Ceram. Soc.,* Vol 86 (No. 8), 2003, p 1299–1306
95. K.N. Lee, J.I. Eldridge, and R.C. Robinson, Residual Stresses and Their Effects on the Durability of Environmental Barrier Coatings for SiC Ceramics, *J. Am. Ceram. Soc.,* in press

96. K.N. Lee, *Trans. ASME,* Vol 122, 2000, p 632–636
97. H.E. Eaton, G.D. Linsey, E.Y. Sun, K.L. More, J.B. Kimmel, J.R. Price, and N. Miriyala, "EBC Protection of SiC/SiC Composites in the Gas Turbine Combustion Environment—Continuing Evaluation and Refurbishment Considerations," 2001-GT-0513, ASME Turbo Expo 2001, American Society of Mechanical Engineers, 2001
98. K.L. More, P.F. Tortorelli, L.R. Walker, J.B. Kimmel, N. Miriyala, J.R. Price, H.E. Eaton, E.Y. Sun, and G.D. Linsey, "Evaluating Environmental Barrier Coatings on Ceramic Matrix Composites after Engine and Laboratory Exposures," 2002-GT-30630, ASME Turbo Expo 2002, American Society of Mechanical Engineers, 2002
99. K.N. Lee, Multilayer Article Characterized by Low Coefficient of Thermal Expansion Outer Layer, U.S. Patent 6,759,151, 2004
100. C.M. Weyant, K.T. Faber, J.D. Almer, and J.V. Guibeen, *J. Am. Ceram. Soc.,* Vol 13 (No. 1), 2004, p 51–56
101. W.Y. Lee, Y.W. Bae, and D.P. Stinton, *J. Am. Ceram. Soc.,* Vol 78 (No. 7), 1995, p 1927–1930
102. S. Ueno, D.D. Jayaseelan, and T. Ohji, *Int. J. Appl. Technol.,* Vol 1 (No. 4), 2004, p 362–373
103. H. Klemm, M. Fritsch, and B. Schenk, Corrosion of Ceramic Materials in Hot Gas Environment, *Ceram. Eng. Sci. Proc.,* Vol 25 (No. 3–4), E. Lara-Curzio and M.J. Readey, Ed., 2004, p 463–468
104. Y. Harada, T. Suzuki, K. Hirano, N. Nakagawa, and Y. Waku, Effect of Water Vapor in Degradation of In-Situ Single-Crystal Oxide Eutectic Composites, *Fifth International Conference on High Temperature Ceramic Matrix Composites,* M. Singh, R.J. Kerans, E. Lara-Curzio, and R. Naslain, Ed., American Ceramic Society, 2004, p 389–394
105. H. Nakayama, K. Aoyama, M. Yamamoto, H. Sumitomo, K. Okamura, T. Yamamura, and M. Sato, Evaluation of Environmental Barrier Coatings for CRCC in the High-Water-Vapor-Pressurized Environments at High Temperatures, *Fifth International Conference on High Temperature Ceramic Matrix Composites,* M. Singh, R.J. Kerans, E. Lara-Curzio, and R. Naslain, Ed., American Ceramic Society, 2004, p 613–618
106. T. Ohji, "Enviromental Barrier Coating on Silicon Nitride; Challenges and Critical Issues," presented at the 28th International Conference and Exposition on Advanced Ceramics and Composites (Cocoa Beach, FL), American Ceramic Society, 2004
107. S. Ueno, N. Kondo, D.D. Jayaseelan, T. Ohji, and S. Kanzaki, High Temperature Hydro Corrosion Resistance of Silica Based Oxide Ceramics, 2003-GT-38878, Proceedings of IGTI2003 ASME Turbo Expo 2003, American Society of Mechanical Engineers
108. I. Yuri, T. Hisamatsu, S. Ueno, and T. Ohji, "Exposure Test Results of $Lu_2Si_2O_7$ on Si_3N_4 Substrate," GT2004-54277, ASME Turbo Expo 2004, American Society of Mechanical Engineers, 2004
109. S. Ueno, D.D. Jayaseelan, N. Kondo, T. Ohji, and S. Kanzaki, *J. Mater. Sci.,* Vol 39, 2004, p 6627–6629
110. S.R. Choi, J.M. Pereira, L.A. Janosik, and R.T. Bhatt, *Mater. Sci. Eng. A,* Vol 379, 2004, p 411–419
111. H. Klemm, *J. Eur. Ceram. Soc.,* Vol 22, 2002, p 2735–2740
112. Datasheet B-1045, Saint-Gobain Ceramics, Niagara Falls, NY, 2003, p 3
113. P.F. Becher, *J. Am. Ceram. Soc.,* Vol 66 (No. 8), 1983, p C120–C121
114. T.E. Easler, R.C. Bradt, and R.E. Tressler, *J. Am. Ceram. Soc.,* Vol 65 (No. 6), 1982, p 317–320
115. R.E. Tressler, Environmental Effects on Long Term Reliability of SiC and Si_3N_4 Ceramics, *Corrosion and Corrosive Degradation of Ceramics,* R.E. Tressler and M. McNallen, Ed., The American Ceramic Society, 1989, p 99–124
116. S. Guo, N. Hirosaki, Y. Yamamoto, T. Nishimura, and M. Mitomo, *J. Am. Ceram. Soc.,* Vol 86 (No. 11), 2003, p 1900–1905
117. J.L. Smialek and N.S. Jacobson, *J. Am. Ceram. Soc.,* Vol 69 (No. 10), 1986, p 741–752
118. D.S. Fox and J.L. Smialek, *J. Am. Ceram. Soc.,* Vol 73 (No. 2), 1990, p 303–311
119. D.S. Fox, M.D. Cuy, and T.E. Strangman, *J. Am. Ceram. Soc.,* Vol 80 (No. 11), 1997, p 2798–2804
120. G.N. Morscher and J.D. Cawley, *J. Eur. Ceram. Soc.,* Vol 22 (No. 14–15), 2002, p 2777–2788
121. M.J. Verrilli, E.J. Opila, A. Calomino, and J.D. Kiser, *J. Am. Ceram. Soc.,* Vol 87 (No. 8), 2004, p 1536–1542
122. D.W. Richerson, L.J. Lindberg, W.D. Carruthers, and J. Dahn, Contact Stress Effects in Si_3N_4 and SiC Interfaces, *Ceram. Eng. Sci. Proc.,* Vol 2, 1981, p 578–588
123. C.H.E. Helms and S.R. Thrasher, *Engineering Applications of Ceramic Materials,* American Society for Metals, 1985
124. M.N. Gardos and R.G. Hardisty, *Tribol. Trans.,* Vol 36 (No. 4), 1993, p 653–660
125. P.F. Becher and T.N. Tiegs, *Adv. Ceram. Mater.,* Vol 3, 1988, p 148
126. R. Kamo and W. Bryzik, *Lubr. Eng.,* Vol 48 (No. 10), 1992, p 809–815
127. "Advanced Gas Turbine (AGT) Powertrain System Development for Automotive Applications," Semiannual Progress Report Number 1, NASA Report CR-165175, Garret Turbine Engine Company, 1980
128. A. Skopp, M. Woydt, and K.H. Habig, *Tribol. Int.,* Vol 23 (No. 3), 1990, p 189–199
129. H. Wang, Y. Kimurs, and K. Okada, Sliding Friction and Wear of Ceramics at Elevated Temperatures up to 1000 °C, *Proc. Jpn. Int. Tribol. Conf.,* 1990, p 1389–1394
130. J.R. Gomes, M.I. Osendi, P. Miranzo, F.J. Oliveira, and R.F. Silva, *Wear,* Vol 233–235, 1999, p 222–228
131. C. Melandri, M.G. Gee, G. de Portu, and S. Guicciardi, *Tribol. Int.,* Vol 28 (No. 6), 1995, p 403–413
132. C. Dellacorte, Tribological Character of SiC-Whisker Reinforced Al_2O_3 at Elevated Temperatures, *Friction and Wear of Ceramics,* C.S. Jahanmir, Ed., Marcel-Dekker, Inc., 1994, p 225–259
133. H.E. Sliney and C. Dellacorte, *Lubr. Eng.,* Vol 50 (No. 7), 1993, p 571–576
134. C. Dellacorte, S.C. Farmer, and P.O. Book, "Experimentally Determined Wear Behavior of an Al_2O_3-SiC Composite from 25 to 1200 °C," NASA TM 102549, 1990

SELECTED REFERENCES

- N.S. Jacobson, *J. Am. Ceram. Soc.,* Vol 76 (No. 1), 1993, p 3–28
- N.S. Jacobson, D.S. Fox, J.L. Smialek, E.J. Opila, P.F. Tortorelli, K.L. Moore, K.G. Nickel, T. Hirata, M. Yoshida, and I. Yuri, Corrosion Issues for Ceramics in Gas Turbines, *Ceramic Gas Turbine Component Development and Characterization.,* M. van Roode, M.K. Ferber, and D.W. Richerson, Ed., ASME Press, 2003, p 607–640
- T. Narushima, T. Goto, T. Hirai, and Y. Iguchi, *Mater. Trans., JIM,* Vol 38 (No. 10), 1997, p 821–835
- K.G. Nickel and Y.G. Gogotsi, Corrosion of Hard Materials, *Handbook of Ceramic Hard Materials,* Vol 1, R. Riedel, Ed., Wiley-VCH, 2000, p 140–182
- E.J. Opila and N.S. Jacobson, Corrosion of Ceramic Materials, *Materials Science and Technology: A Comprehensive Treatment, Corrosion and Environmental Degradation,* Vol II, M. Schu?tze, Ed., Wiley-VCH, 2000, p 327–388

ASM Handbook, Volume 13B: Corrosion: Materials
S.D. Cramer, B.S. Covino, Jr., editors, p579-588
DOI: 10.1361/asmhba0003843

Environmental Performance of Concrete

William C. Panarese, Portland Cement Association

PORTLAND CEMENT CONCRETE has low environmental impact, versatility, durability, and economy, which make it the most abundant construction material in the world. In the United States more than 300 million m^3 (400 million yd^3) of ready-mixed concrete is used each year in airports, roads, bridges, stadiums, low- and high-rise buildings, dams, homes, and numerous other structures.

Concrete is a mixture of two main components: aggregate and paste. The paste binds the aggregates (usually sand and gravel or crushed stone) into a rocklike mass as the paste hardens through the chemical reaction of the cement and water.

The paste is composed of water and entrapped air or purposely entrained air, and sometimes chemical admixtures. The paste constitutes about 25 to 40% of the total volume of concrete. Figure 1 shows the range of component volume.

Because aggregates make up about 60 to 75% of the total volume of concrete, their selection is important. Aggregates should consist of particles with adequate strength and resistance to environmental conditions and should not contain *materials that will cause deterioration* of the concrete. A continuous gradation of aggregate particle sizes is desirable for efficient use of the paste. The quality of any concrete depends on the quality of the paste and aggregate and the bond between the two. In properly made concrete, each particle of aggregate is coated completely with paste, and all of the spaces between aggregate particles are filled completely with paste.

Durability of concrete is based on its ability to resist weathering action, chemical attack, and abrasion while maintaining its desired engineering properties. The ingredients, proportioning of those ingredients, interactions between the ingredients, placing and curing practices, and the severity of the environment determine the durability and useful life of the concrete.

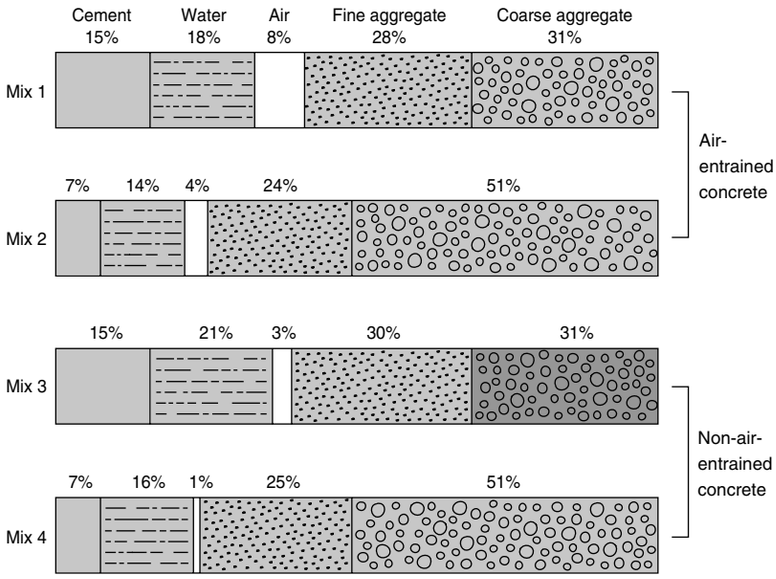

Fig. 1 Range in proportions of materials used in concrete (by absolute volume). Mixes 1 and 3 represent rich mixes with small-size aggregates. Mixes 2 and 4 represent lean mixes with large-size aggregates.

Types and Causes of Concrete Degradation

The exceptional durability of portland cement concrete is a major reason for its wide use. Material limitations, poor design and construction practices, and severe exposure conditions can cause concrete to deteriorate, resulting in aesthetic, functional, or structural problems. Following are potential causes of concrete deterioration and the factors that influence them.

Corrosion of reinforcing steel and other embedded metals is the leading cause of deterioration in concrete. When steel corrodes, the resulting rust (iron oxide) occupies a greater volume than the steel does. This expansion creates tensile stresses in the concrete that can eventually cause cracking, delamination, and spalling (Fig. 2). Corrosion of embedded metals in concrete can be reduced greatly by placing crack-free concrete with low permeability and sufficient concrete cover over the metal. Low-permeability concrete can be attained by decreasing the water to cementitious materials ratio of the concrete and by the use of pozzolans and slag admixtures (Ref 1). These admixtures reduce the corrosion rate even after it initiates. Minimum concrete cover requirements for different exposure conditions are set by building codes (Ref 2). Additional measures to mitigate corrosion of steel reinforcement in concrete include coating of reinforcement with epoxy resin and the use of sealers and membranes on the concrete surface.

Alkalinity. The alkaline environment of concrete—a pH of 12 to 13—protects the steel. At this high pH level, a thin oxide layer forms on the

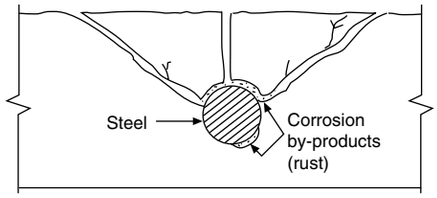

Fig. 2 The expansion of corroding steel creates tensile stresses in the concrete, which can cause cracking, delamination, and spalling.

steel surface, preventing further reaction. Steel corrosion is not an issue in the majority of concrete structures. However, corrosion can occur when the passivity layer is destroyed; this destruction occurs when the alkalinity of the concrete is reduced or when the chloride concentration in concrete is increased to a certain level.

Chlorides. Exposure of reinforced concrete to chloride ions is the primary cause of premature corrosion of steel reinforcement. The intrusion of chloride ions—present in deicing salts, seawater, and some admixtures—into reinforced concrete can cause steel corrosion if oxygen and moisture are also available to sustain the reaction. Chlorides dissolved in water can permeate through sound concrete or reach the steel through cracks. Table 1 shows the maximum permissible water-soluble chloride-ion content for prestressed and reinforced concretes in various exposure conditions (Ref 2).

Carbonation occurs when carbon dioxide from the air penetrates the concrete and reacts with hydroxides, such as calcium hydroxide, to form carbonates (Ref 3). In the reaction with calcium hydroxide, calcium carbonate is formed. This reaction reduces the pH of the pore solution in the concrete to as low as 8.5, a level at which the passive film on the steel is not stable.

Carbonation is generally a slow process. In high-quality concrete, it has been estimated that carbonation will proceed at a rate up to 1.0 mm (0.04 in.) per year. The amount of carbonation is increased significantly in concrete with a high water-to-cement ratio, low cement content, short curing period, low strength, and a highly permeable or porous paste.

Carbonation of concrete lowers the amount of chloride ions needed to promote corrosion. In new concrete with a pH of 12 to 13, about 7000 to 8000 ppm of chlorides are required to start corrosion of embedded steel. If, however, the pH is lowered to a range of 10 to 11, the chloride threshold for corrosion is significantly lower—at or below 100 ppm (Ref 4). Like chloride ions, however, carbonation destroys the passive film on the reinforcement but does not influence the rate of corrosion.

Galvanic corrosion can occur when two metals are in contact within concrete because each metal has a unique electrochemical potential. This situation can occur in balconies where embedded aluminum railings are in contact with the reinforcing steel (Ref 5). Following is a list of metals in order of their electrochemical activity in concrete:

Active or anodic
Zinc
Aluminum
Steel
Iron
Nickel (active)
Tin
Lead
Brass
Copper
Bronze
Stainless steel (passive)
Gold
Noble or cathodic

When two metals are in contact in an active electrolyte, the more active metal corrodes.

Freeze-Thaw Deterioration. When water freezes, it expands about 9%. As the water in moist concrete freezes, it produces pressure in the capillaries and pores of the concrete. If the pressure exceeds the tensile strength of the concrete, the cavity will dilate and rupture. The accumulative effect of successive freeze-thaw cycles and disruption of paste and aggregate can eventually cause expansion and cracking, scaling, and crumbling of the concrete (Fig. 3).

Air Entrainment. The severity of freeze-thaw exposure varies with climate. The resistance of concrete to freezing and thawing in a moist condition is improved significantly by the use of intentionally entrained air (Ref 6). The tiny entrained air voids act as empty chambers in the paste for the migrating water to enter, thus relieving the pressure in the capillaries and pores and preventing damage to the concrete. Concrete with a low permeability (that is, a low water-cement ratio and high compressive strength) is better able to resist freeze-thaw cycles. Recommended concrete air-content requirements, water-cement ratios, and compressive strengths for various exposure conditions are given in Ref 2 and 7.

Deicing chemicals used for snow and ice removal, such as sodium chloride, can aggravate freeze-thaw deterioration. In addition, because salt absorbs moisture, it keeps the concrete more saturated, increasing the potential for freeze-thaw deterioration. However, properly designed and placed air-entrained concrete can withstand deicers for many years. Deicers containing ammonium nitrate and ammonium sulfate should be prohibited because they rapidly attack and disintegrate concrete.

Freezing Temperatures. Concrete gains very little strength at low temperatures (Ref 8), so freshly placed concrete must be protected against freezing until the degree of saturation of the concrete has been reduced sufficiently by cement hydration. The time at which this reduction is accomplished corresponds roughly to the time required for the concrete to attain a compressive strength of 3.5 MPa (0.5 ksi) (Ref 9). Concrete that is to be exposed to deicers should attain a strength of 28 MPa (4 ksi) prior to repeated cycles of freezing and thawing (Ref 10).

Chemical Attack. Concrete performs well when exposed to various atmospheric conditions, water, soil, and many chemicals. However, chemical environments that degrade even high-quality concrete are given in Table 2. Concrete is rarely attacked by solid, dry chemicals. To produce significant attack, aggressive chemicals must be in solution and have a certain minimum concentration (Ref 11).

Acids. In general, portland cement concrete does not have good resistance to acids. In fact, no hydraulic cement concrete, regardless of its composition, will hold up for long if exposed to a solution with a pH of 3.0 or lower. However, some weak acids can be tolerated, particularly if the exposure is occasional. Acid rain, which often has a pH of 4 to 4.5, can etch concrete slightly, usually without affecting the performance of the exposed surface.

Acids react with the calcium hydroxide of the hydrated portland cement. In most cases, the chemical reaction forms water-soluble calcium compounds, which are then leached away by aqueous solutions (Ref 12). To minimize or prevent deterioration from acid attack, surface protective treatments are available (Ref 11, 12). Properly cured concretes with reduced permeability experience a slightly lower rate of attack from acids.

Salts and alkalis also can be a problem. The chlorides and nitrates of ammonium, magnesium, aluminum, and iron cause concrete deterioration, those of ammonium producing the most damage. Most ammonium salts are destructive because, in the alkaline environment of concrete, they release ammonia gas and hydrogen ions. These are replaced by dissolving calcium hydroxide from the concrete. The result is a leaching action, much like acid attack. Strong alkalis (over 20%) also can cause concrete degradation (Ref 13).

Sulfates can attack concrete by reacting with hydrated compounds in the hardened cement. Naturally occurring sulfates of sodium, potassium, calcium, or magnesium are sometimes found in soil or dissolved in groundwater. These reactions can induce sufficient pressure to

Table 1 Maximum chloride ion (Cl^-) content of concrete

Type of member	Maximum water-soluble chloride ion (Cl^-) content in concrete, % by mass of cement
Prestressed concrete	0.06
Reinforced concrete exposed to chloride in service	0.15
Reinforced concrete that will be dry or protected from moisture in service	1.00
Other reinforced concrete construction	0.30

Source: Ref 2

Fig. 3 Freeze-thaw cycles can cause scaling of concrete surfaces as shown on this pavement.

disrupt the cement paste, resulting in loss of cohesion and strength.

Environmental conditions have a great influence on sulfate attack. Seawater also contains sulfates, but seawater is not as severe an exposure as sulfates in groundwater (Ref 14, 15). Arid areas have a particular problem. Sulfate attack is greater in concrete exposed to wet/dry cycling. When water evaporates from concrete, sulfates can accumulate at the surface, increasing the sulfate's concentration and its potential for causing damage.

Resistance to sulfates is best achieved by using a low water-to-cement ratio and cement with a limited amount of tricalcium aluminates (Ref 16). ASTM C 150 type II cement contains less than 8% C_3A and type V contains less than 5% (Ref 17). ASTM C 1157 type MS cement (moderate sulfate resistant) and type HS cement (high sulfate resistant) can also be used (Ref 18), as well as moderate sulfate-resistant cements meeting ASTM C 595 (Ref 19).

Table 2 Chemicals that deteriorate concrete

Promote rapid deterioration of concrete
Aluminum chloride
Calcium bisulfite
Hydrochloric acid (all concentrations)(a)
Hydrofluoric acid (all concentrations)
Nitric acid (all concentrations)
Sulfuric acid, 10%–80%(a)
Sulfurous acid
Promote moderate deterioration of concrete
Aluminum sulfate(a)
Ammonium bisulfate
Ammonium nitrate
Ammonium sulfate(a)
Ammonium sulfide
Ammonium sulfite
Ammonium superphosphate
Ammonium thiosulfate
Castor oil
Cocoa bean oil(a)
Cocoa butter(a)
Coconut oil(a)
Cottonseed oil(a)
Fish liquor(b)
Mustard oil(a)
Perchloric acid, 10%
Potassium dichromate
Potassium hydroxide (>20%)
Rapeseed oil(a)
Slaughterhouse waste(c)
Sodium bisulfate
Sodium bisulfite
Sodium hydroxide (>20%)
Sulfite liquor
Sulfuric acid, 80% oleum(a)
Tanning liquor (if acid)
Zinc refining solutions(d)

(a) Sometimes used in food processing or as food or beverage ingredient. Ask for advisory opinion of Food and Drug Administration regarding coatings for use with food ingredients. (b) Contains carbonic acid, fish oils, hydrogen sulfide, methylamine, brine, and other active materials. (c) May contain various mixtures of blood, fats and oils, bile and other digestive juices, partially digested vegetable matter, urine, and manure, with varying amounts of water. (d) Usually contains zinc sulfate in sulfuric acid. Sulfuric acid concentration may be low (about 6% in "low current density" process) or higher (about 22 to 28% in "high current density" process)

Studies have shown that some pozzolans and ground-granulated blast-furnace slags increase the life expectancy of concrete exposed to sulfates (Ref 20, 21). Good results have been obtained with fly ash meeting the requirements of ASTM C 618 Class F (Ref 1). Slags should conform to ASTM C 989 (Ref 22). However, some pozzolans, especially some Class C fly ashes, decrease sulfate resistance. Therefore, pozzolans chosen to improve sulfate resistance should be tested to confirm their behavior. Reference 23 provides the requirements for concrete exposed to sulfates.

Alkali-Aggregate Reaction (AAR). In most concrete, aggregates are chemically inert. However, some aggregates react with the alkali hydroxides in concrete, causing expansion and cracking over a period of many years. This AAR has two forms: alkali-silica reaction (ASR) and alkali-carbonate reaction (ACR).

Alkali-silica reaction is of more concern because aggregates containing reactive silica materials are more common. In ASR, aggregates containing certain forms of silica will react with alkali hydroxide in concrete to form a gel that swells as it draws water from the surrounding cement paste or the environment. In absorbing water, these gels can swell and induce enough expansive pressure to damage concrete.

Typical indicators of ASR are random map cracking and, in advanced cases, closed joints and attendant spalled concrete (Fig. 4). Cracking due to ASR usually appears in areas with a frequent supply of moisture, such as close to the waterline in piers, near the ground behind retaining walls, near joints and free edges in pavements, or in piers or columns subject to wicking action.

Alkali-silica reaction can be controlled using certain mineral admixtures (Ref 24). Silica fume, fly ash, and ground-granulated blast-furnace slag have reduced ASR significantly. Class F fly ashes have reduced reactivity expansion up to 70%, or more, in some cases. In addition, lithium compounds have been shown to effectively reduce ASR (Ref 25). Although potentially reactive aggregates exist throughout North America, ASR distress in concrete is not that common because of the measures taken to control it. It is also important to note that not all ASR gel reactions produce destructive swelling.

Fig. 4 Typical indicators of alkali-silica reactivity are map cracking and, in advanced cases, closed joints and attendant spalled concrete.

Alkali-carbonate reactions are observed with certain dolomitic rocks. Dedolomitization, the breaking down of dolomite, is normally associated with expansion. This reaction and subsequent crystallization of brucite may cause considerable expansion. The deterioration caused by ACR is similar to that caused by ASR; however, ACR is relatively rare because aggregates susceptible to this phenomenon are less common and are usually unsuitable for use in concrete for other reasons.

Abrasion, Erosion, and Cavitation. Abrasion damage occurs when the surface of concrete is unable to resist wear caused by rubbing and friction. As the outer paste of a concrete surface wears, the fine and coarse aggregate are exposed; abrasion coupled with impact will cause additional degradation that is related to the aggregate-to-paste bond strength and hardness of the aggregate. The two most damaging forms of abrasion occur on vehicular traffic surfaces and in hydraulic structures, such as dams, spillways, and tunnels.

Abrasion of floors, pavements, and other traffic surfaces are the result of production operations or vehicular traffic. Many industrial floors are subjected to abrasion by steel or other hard-wheeled traffic, which can cause significant rutting and joint damage. Tire chains and studded snow tires can cause considerable rutting on concrete pavements. Compressive strength is the most important factor controlling the abrasion resistance of concrete, and hard aggregate is more wear resistant than soft aggregate. In addition, a hard-steel-troweled surface resists abrasion better than a surface that has not been troweled resists. Figure 5 shows results of abrasion tests on concretes of different compressive

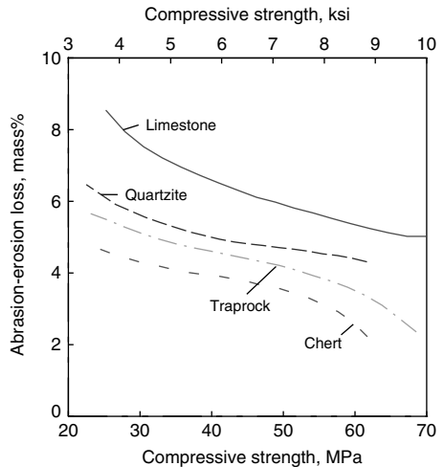

Fig. 5 Effect of compressive strength and aggregate type on the abrasion resistance of concrete. High-strength concrete made with a hard aggregate is highly resistant to abrasion (Ref 26, 27).

strengths and aggregate types (Ref 26, 27). The service life of warehouse floors subjected to hard-wheeled traffic abrasion is increased greatly by the use of special hard or tough aggregates used in toppings or dry-shakes (Ref 28).

Erosion damage in hydraulic structures is caused by the abrasive effects of water-borne silt, sand, gravel, rocks, ice, and other debris impinging on the concrete surface. Although high-quality concrete can resist high-water velocities for many years with little or no damage, the concrete may not withstand the abrasive action of debris grinding or repeatedly impacting on its surface.

In such cases, abrasion erosion ranging from a few millimeters (inches) to several meters (feet) has resulted, depending on flow conditions. Dam spillway aprons, stilling basins, sluiceways, drainage conduits or culverts, and tunnel linings are particularly susceptible to abrasion erosion. As is the case with traffic wear, erosion damage in hydraulic structures can be reduced by using strong concrete with hard aggregates.

Cavitation is damage caused by the formation and collapse of vapor bubbles in liquid. In hydraulic structures, bubbles form where the local pressure drops, causing the water to vaporize at the prevailing fluid temperature. The vapor cavities collapse, causing very high instantaneous pressures that impact on concrete surfaces, causing pitting, noise, and vibration.

Once cavitation damage has altered water flow substantially, other degradation mechanisms come into play. Fatigue due to vibration, rushing water striking irregular surfaces, and mechanical failure due to vibrating reinforcing steel can cause significant concrete damage. Although proper materials selection can increase the resistance of concrete to cavitation, the solution is to design hydraulic structures with flow patterns that reduce or eliminate cavitation.

Fire and Heat. Concrete performs exceptionally well at the temperatures encountered in most applications. Nonetheless, when exposed to fire or unusually high temperatures, concrete can lose strength and stiffness. The effect of high temperatures on the compressive strength, flexural strength, and modulus of elasticity of cured concrete has been determined by various investigators (Ref 29). Modulus of elasticity is the most sensitive to elevated temperature, followed by flexural strength and compressive strength. Many factors influence the performance of concrete at elevated temperatures. Numerous studies (Ref 30–34) have found these general trends:

- Concrete that undergoes thermal cycling suffers greater loss of strength than concrete that is held at a constant temperature, although much of the strength loss occurs in the first few cycles.
- Concrete that is under design load while heated loses less strength than unloaded concrete loses. The reason: imposed compressive stresses inhibit development of cracks that would be free to develop in unrestrained concrete.
- Concrete that is allowed to cool before testing loses more compressive strength than concrete that is tested hot.
- Concrete containing limestone and calcareous aggregates performs better at high temperatures than concrete containing siliceous aggregates.
- Strength loss is not proportional to compressive strength of concrete.
- Concrete with a higher aggregate-cement ratio suffers less reduction in compressive strength; however, the opposite is true for modulus of elasticity.
- If residual water in the concrete is not allowed to evaporate, compressive strength is greatly reduced. If heated too quickly, concrete can spall as the moisture tries to escape.

Restraint to Volume Changes. Concrete changes slightly in volume because of fluctuations in moisture content and temperature of the concrete. Restraint to volume changes, especially contraction, can cause cracking if the tensile stresses that develop exceed the tensile strength of the concrete.

Plastic shrinkage cracking can occur when water evaporates from the surface of freshly placed concrete faster than it is replaced by water bleeding to the surface. Because of the restraint provided by the concrete below the drying surface layer, tensile stresses develop in the weak, stiffening plastic concrete, resulting in shallow cracks of varying length and depth. Plastic shrinkage cracking can be curtailed by taking measures to prevent rapid water loss from the concrete surface; such measures include, for example, using fog nozzles, plastic sheeting, windbreaks, sunshades, or placing concrete at night when it is cooler with no sun.

Drying shrinkage cracking occurs because almost all concrete is mixed with more water than is needed to hydrate the cement. Much of the excess water evaporates, causing the concrete to shrink. Restraint to this shrinkage, provided by the subgrade, reinforcement, or other parts of the structure, causes tensile stresses to develop that may exceed the tensile strength of the hardened concrete. Restraint to drying shrinkage is the most common cause of concrete cracking (Fig. 6). Since drying shrinkage cracking is almost inevitable, control joints are placed in concrete to predetermine their location and to conceal any cracks. Drying shrinkage can be limited by minimizing the water content of concrete and maximizing the coarse aggregate content.

Thermal cracking might occur because concrete expands when heated and contracts when cooled. An average value for the coefficient of thermal expansion of concrete is 10×10^{-6}/°C (5.5×10^{-6}/°F). This amounts to a length change of about 5 mm in 10 m ($^2/_3$ in. in 100 ft) of concrete when concrete is subjected to a rise or fall of 50 °C (90 °F). Thermal expansion and contraction of concrete varies with factors such as aggregate type, cement content, water-cement ratio, temperature range, concrete age, and relative humidity. Of these factors, aggregate type has the greatest influence (Ref 35). To minimize the effects of temperature variations, designers should allow for thermal movement by providing proper expansion or isolation joints and correct detailing.

Overload and Impact. Properly designed and constructed concrete members are usually strong enough to support the loads for which they are intended. Nevertheless, overloading can occur for a variety of reasons: a change in use of a structure without proper structural upgrade; unintentional overloading; and other unusual circumstances, such as earthquakes beyond specified design (a classic example of overloading of concrete structures).

Overload damage can occur during construction when concrete has not yet reached design strength. Early removal of formwork or the storage of heavy materials or operation of equipment on and around the structure can result in the overloading of certain concrete elements. A common error occurs when precast concrete members are not properly supported during transport and erection. Errors in post-tensioned construction, such as improperly timed or sequenced strand release, can also cause overload cracking.

Impact damage is another form of overload. A common form of impact damage occurs at slab edges of joints in industrial floors (Ref 28). Even in properly designed reinforced concrete, load-induced tensile stresses can occur. This point is readily acknowledged and accepted in concrete design. Current design procedures use reinforcing steel to not only carry tensile loads but to obtain both an adequate distribution of cracks and a reasonable limit on crack width.

Loss of support beneath concrete structures usually is caused by settlement or the washing out of soils and subbase support materials. This loss can cause a variety of problems in concrete structures, from cracking and performance problems to structural failure. Loss of support can also occur during seismic events. During construction, inadequate formwork support or premature removal of forms cause loss of support.

Fig. 6 Restraint to drying shrinkage is the most common cause of concrete cracking.

Curling is a common problem related to loss of support in floor slabs (Ref 28). Curling is the rise of the edges and corners of a slab due to differences in the moisture content or temperature between the top and bottom of a slab. The top dries out or cools and contracts more than the wetter, warmer bottom. Curling results in a loss of contact between the slab and its subbase and can lead to cracking, slab deflection, joint deterioration, and problems with vehicular traffic.

Surface defects can occur on the surfaces of formed concrete (for example, walls and columns) or finished concrete (for example, floors and pavements). Many of these defects are avoidable by using proper materials and construction practices, while others are difficult to eliminate.

Air voids in formed surfaces, also known as *bug holes,* are small cavities that form in the vertical surface during placing and consolidation of formed concrete (Fig. 7). They can be up to 25 mm (1 in.) wide but are usually no more than 15 mm ($^9/_{16}$ in.) wide. These defects are more likely to occur when sticky or stiff concrete mixes of low workability are used. Such mixes may have an excessive amount of fine aggregate, entrapped air, or both. Improper use of vibrators and form-release agents also may contribute to the bug hole problem.

Honeycomb in formed surfaces occurs when mortar fails to fill all the spaces between coarse aggregate particles in concrete. Congested reinforcement, segregation, and insufficient fine aggregate content can contribute to the problem. Higher concrete slumps and proper vibration will assist in preventing honeycomb by increasing the flowability of the concrete.

Cold joints in formed surfaces are discontinuities in concrete members resulting from an excessive delay between placements of two successive lifts of concrete. In other words, visible lines in the surface indicate the presence of a joint where one layer of concrete had hardened before subsequent concrete was placed. Aside from their appearance, cold joints can be a concern if they allow moisture penetration or if the loss of tensile strength of the concrete across the joint is deemed detrimental to the performance of the structure.

Delamination in finished surfaces (slabs) occurs when air and bleed water become trapped under a prematurely finished (densified) mortar surface. The trapped air and bleed water separate the uppermost 3 to 6 mm ($^1/_8$ to $^1/_4$ in.) layer of mortar from the underlying concrete. Delamination is very difficult to detect during finishing and becomes apparent after the concrete surface has dried and the delaminated area crushes out under traffic.

Blisters are a smaller and more noticeable form of delamination; they form at the concrete surface due to trapped air and bleed water. The primary cause of delamination: finishing the slab surface before bleeding is complete.

Dusting of finished slab surfaces is the development of a fine, powdery material that easily rubs off the surface of hardened concrete. It is the result of a thin, weak surface layer, called *laitance,* which is composed of water, cement, and fine particles. The finishing operations of floating and troweling with bleed water on the surface are the usual causes of dusting. Other causes include using a too-wet mix, spreading dry cement over the surface to accelerate finishing, and allowing rapid drying of the surface.

Popouts in finished surfaces are fragments of aggregates that break out of the surface of concrete, leaving a hole usually 6 to 50 mm ($^1/_4$ to 2 in.) in diameter (Fig. 8). The cause of a popout usually is a piece of porous rock having a high rate of absorption and relatively low specific gravity. As the offending aggregate absorbs moisture or freezes under moist conditions, it swells, creating internal pressures sufficient to rupture the concrete surface. Pyrite, hard-burned dolomite, coal, shale, soft fine-grained limestone, or chert commonly cause popouts.

Subsidence cracks in finished surfaces may develop over embedded items, such as reinforcing steel, as the concrete settles or subsides (Fig. 9). Subsidence cracking results from insufficient consolidation (vibration), high slumps (overly wet concrete), or a lack of adequate concrete cover over embedded items.

Crazing in finished surfaces is a maplike pattern of fine cracks that do not penetrate much below the surface and are usually of cosmetic concern only. They are barely visible, except when the concrete is drying after the surface has been wet. Preventing excessive evaporation during placement and proper curing can prevent crazing. Reference 36 provides additional information about surface defects in slabs.

Addressing Durability with the Prescriptive Approach

Durability of concrete can be addressed by two approaches. The first is known as the *prescriptive approach,* where designers specify materials, proportions, and construction methods based on fundamental principles and practices that exhibit satisfactory performance. The second is called the *performance approach,* where designers identify functional requirements such as strength, durability, and volume changes and rely on concrete producers and contractors to develop concrete mixtures to meet those requirements. The prescriptive approach is based on what one might call "old technologies" because these requirements have been known for many years. Following are some prescriptive principles and practices that improve resistance to degradation (Ref 11):

- Water-cement ratio (w/c), or the water-cementitious materials ratio (where applicable), should not exceed 0.45 by weight (0.40 for corrosion protection of embedded metal in reinforced concrete). For severe conditions, w/c often range from 0.25 to 0.35.
- Cement content should be at least 335 kg/m^3 (564 lb/yd^3) of cementitious material for concrete exposed to corrosive environments.
- Cement type should be suited to the exposure. There are eight types of portland cement specified by ASTM (Ref 17), and there are other blended, modified, and special purpose cements (Ref 18, 19, 37–43). Some, such as sulfate-resistant cement, are formulated to prevent specific attack (Ref 11). Sulfate-resistant cements, like other portland or

Fig. 7 Surface air voids, called *bug holes,* are small cavities of entrapped air bubbles in the surface of formed concrete.

Fig. 8 Some aggregates absorb water and, upon freezing, expand to produce a popout.

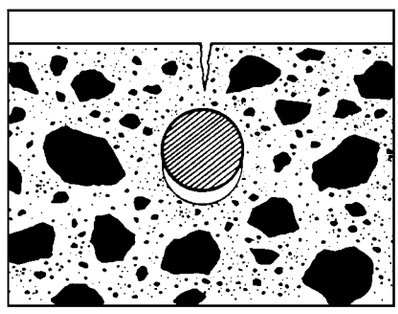

Fig. 9 Subsidence cracks can develop over reinforcing steel as the concrete settles or subsides.

blended hydraulic cements, are not resistant to most acids or other highly corrosive substances.
- Aggregates that are not prone to freeze-thaw deterioration, chemical attack, or AAR should be used. References 11 and 24 offer guidance on susceptibility to AAR.
- Mixing water should not contain impurities that can impair basic concrete properties or reduce resistance to chemical attack (Ref 44, 45). Water that is safe to drink is safe for use in concrete.
- Air entrainment in the proper amount—dependent on exposure conditions and maximum aggregate size—should be used (Ref 2). Air entrainment makes concrete resistant to deicers and scaling due to freezing and thawing; it also improves sulfate resistance, watertightness, and workability.
- Mixing must be thorough and should continue until the concrete is uniform in appearance with all materials evenly distributed. Mixtures containing silica fume may require a longer mixing period to thoroughly distribute the admixture.
- Workability requires the avoidance of mixes that are so harsh and stiff that honeycombing may occur and mixes so fluid that excess bleed water rises to the surface. Slump (a measure of the consistency of freshly mixed concrete) should generally be 50 to 125 mm (2 to 5 in.). If necessary, water reducers and superplasticizers can be used to make mixes more workable (higher slump).
- Finishing of slabs should not begin until all bleed water has left the surface. Supplementary cementitious materials, such as fly ash, slag, silica fume, or blended cements, may affect the bleeding characteristics of concrete. For instance, silica fume mixtures bleed very little and slag mixtures may bleed longer due to the retarding effect slag has on setting time. Placing concrete at the proper temperature helps control finishing operations.
- Jointing, the proper use of isolation, contraction, and construction joints, helps control cracking. Contraction joints in slabs on ground should be spaced about 30 times the slab thickness. In some cases, joints must be sealed with a sealant capable of enduring the environment. Water stops, if used, must be placed properly. Special construction methods, such as the use of heavily reinforced slabs or post-tensioned slabs, are helpful in reducing the number of joints in areas where joints are undesirable.
- When curing, either additional moisture should be supplied to the concrete during the early hardening period or the concrete should be covered with a water-retaining material. Curing compounds may be used but not on surfaces that are to receive protective surface treatments. Concrete should be kept moist and above 10 °C (50 °F) for the first week or until the desired strength is achieved. Longer curing periods increase concrete's resistance to corrosive substances.
- Chemical admixtures, such as water reducers (Ref 46) and superplasticizers (Ref 47), can be used to reduce the water-cement ratio, resulting in reduced permeability and less absorption of corrosive materials into concrete. Polymer admixtures, such as styrene-butadiene latex, greatly reduce the permeability of concrete to many corrosive substances. Admixtures containing chloride should not be used for reinforced or prestressed concrete, although corrosion inhibitors are available to reduce chloride-induced steel corrosion. Shrinkage-reducing admixtures can reduce the formation of shrinkage cracks through which aggressive materials penetrate concrete.
- Supplementary cementitious materials, such as fly ash and metakaolin (Ref 1), slag (Ref 22), and silica fume (Ref 48), reduce permeability and by-produce additional cementitious compounds that increase strength. Dosages for these materials by weight of cementitious material range from 15 to 40% for fly ash, 35 to 50% for slag, and 50% for silica fume.

Addressing Durability with the Performance Approach

During the last several decades, advances in concrete technology have widened the application and use of this material. New developments in admixture technology include high-performance concrete (HPC) (Ref 49–51), self-consolidating concrete (SCC) (Ref 52), high-strength concrete (HSC) (Ref 53–57), fiber-reinforced concrete (FRC) (Ref 58–61), and numerous special types of concrete (Ref 7). In order to ensure adequate durability, performance-based specifications are used. Designers specify the functional requirements such as strength, density, permeability, and volume stability depending on project requirements. A brief discussion of these innovative technologies follows.

High-performance concrete exceeds the properties and constructability of normal concrete. Special ingredients, mixing, placing, and curing practices may be needed to produce and handle HPC. Extensive performance tests usually are required to demonstrate compliance with specific project needs.

High-performance concrete characteristics are developed for particular applications and environments, such as in tunnels, bridges, roads, streets, and tall structures (Fig. 10). Properties that may be required include:

- High strength
- High early strength
- High modulus of elasticity
- High abrasion resistance
- High durability and long life in severe environments
- Low permeability and diffusion
- Self consolidation
- Resistance to chemical attack
- High resistance to frost and deicer scaling damage
- Toughness and impact resistance
- Volume stability

Typically, HPC concretes have a low w/c (0.20–0.45). Plasticizers are used to make these concretes fluid and workable. High-performance concrete usually has a higher strength than normal concrete; however, strength is not always the primary required property. A normal strength concrete with very high durability and very low permeability is considered to have high-performance properties. It has been demonstrated that 40 MPa (6 ksi) HPC for bridges could be economically made while meeting durability factors for air-void system and resistance to chloride penetration (Ref 62).

Table 3 lists materials often used in high-performance concrete and why they are selected. High-performance concrete specifications ideally should be performance oriented. Unfortunately, many specifications are a combination of performance requirements, such as permeability or strength limits, and prescriptive requirements, such as air-content limits or dosage of supplementary cementitious material (Ref 63).

Self-Consolidating Concrete. The construction industry has always longed for a high-performance concrete that can flow into tight spaces without requiring vibration. The need for this technology has grown over the years as

Fig. 10 The Two Union Square building in Seattle, WA, used concrete with a design compressive strength of 131 MPa (19 ksi) in its steel tube and concrete composite columns.

designers specify more heavily reinforced concrete members and ever more complex formwork. Until recently, the industry used superplasticizing admixtures in conventional mixes in an attempt to duplicate the advantages of a true self-consolidating concrete. This allowed the use of 200 mm (8 in.) slump concrete, or more, but some vibration was still required for adequate consolidation. While high doses of superplasticizer create a very fluid concrete that flows readily, the mixes often segregate because the mortar is too thin to support the weight of the coarse aggregate. The key to creating SCC is to produce a very flowable mortar that still has a viscosity high enough to support the coarse aggregate. Today, new advances in admixtures and mix proportioning are making SCC a reality. Developed in Japan during the 1980s, this technology is now gaining considerable attention in Europe and North America (Ref 52).

High-Strength Concrete. The definition of HSC has changed over the years as strengths have increased. Most HSC applications are designed for compressive strengths of 70 MPa (10 ksi) or greater. To get these strengths, stringent application of the best practices is required. Compliance with strict guidelines and commendations for preconstruction laboratory and field-testing is essential (Ref 64).

Traditionally, the specified strength of concrete has been based on 28 day test results. However, in high-rise buildings, where HSC is commonly used, the process of construction is such that the structural elements in lower floors are not fully loaded for periods of a year or more. For this reason, compressive strengths based on 56 or 91 day test results are commonly specified; this achieves significant economy in material costs. The time dependence of compressive strength is seen in Fig. 11. When later-age strengths are specified, supplementary cementitious materials usually are incorporated into the concrete. This produces additional benefits in the form of reduced heat generation during cement hydration.

With the use of low-slump or no-slump mixtures, high-compressive-strength concrete has been produced routinely under careful control in precast and prestressed concrete plants for decades (Ref 65). These stiff mixes are placed in rugged forms and consolidated by prolonged vibration or shock methods. However, typical cast-in-place concrete uses more fragile forms that do not permit the same compaction procedures; hence, more workable concretes with superplasticizers usually are necessary to achieve the required compaction and to avoid segregation and honeycomb.

Fiber-Reinforced Concrete. Fibers have been used in construction materials for centuries. The last three decades have seen a growing interest in the use of fibers in ready-mixed concrete, precast concrete, shotcrete, plaster, and stucco. Steel, plastic, glass, and natural material (such as wood cellulose) fibers are available in a variety of shapes, sizes, and thicknesses. They may be round in cross section or flat, crimped, and deformed with typical lengths of 6 to 150 mm (0.25–6 in.) and with thicknesses ranging from 0.005 to 0.75 mm (0.0002 to 0.03 in.).

Fibers are added to concrete during mixing. Like any composite, factors that control the performance of FRC are the physical properties of the fibers and matrix and the strength of the bond between fibers and matrix. Although the basic principles are the same, there are several characteristic differences between conventional reinforcement and fiber systems:

- Fibers are generally distributed throughout the entire cross section of a member, whereas reinforcing bars or wires are placed only where required.
- Most fibers are relatively short and closely spaced as compared with reinforcing bars or wires.
- It is generally not possible with achieve the same ratio of area of reinforcement to area of concrete using fibers as compared with a network of reinforcing bars or wires, without reducing workability and affecting fiber dispersion.

Fibers are typically added to concrete in low-volume dosages (often less than 1%) and have been shown to be effective in reducing plastic shrinkage cracking. Fibers do not significantly alter the free shrinkage of concrete; however, at high-enough dosages they can increase the resistance to cracking and decrease crack widths (Ref 66).

Special types of concrete are those with unusual properties or those produced by unusual techniques. Table 4 lists many special types of concrete made with portland cement and some made with binders. In many cases, the name describes the use, property, or condition of the concrete. Brand names are not given here, but some of these special concretes are identified by brand name. Some of these special concretes were discussed previously; following are brief descriptions of others.

Structural lightweight concrete is similar to normal weight concrete except that it has a lower density. It may be made with all lightweight aggregates or with a combination of lightweight and normal-weight aggregates. Most of the structural lightweight concrete used today is of the sanded variety made with coarse lightweight aggregate and natural sand. ASTM C 567 (Ref 68) provides a test for density. This concrete is used to reduce the dead load weight of floors in high-rise buildings.

Insulating lightweight concrete has an oven dry density of 800 kg/m^3 (50 lb/ft^3) or less. It is made with cementitious materials, water, air, and with or without aggregate and chemical admixtures. The oven dry density ranges from 240 to 800 kg/m^3 (15–50 lb/ft^3) with a 28 day compressive strength between 0.7 and 7 MPa (0.1 and 1 ksi). Cast-in-place insulating concrete is used primarily for thermal and sound insulation, roof decks, fill for slabs cast on grade, leveling courses for floors or roofs, firewalls, and underground thermal conduit linings.

Table 3 Materials used in high-performance concrete

Material	Primary contribution/desired property
Portland cement	Cementing material/durability
Blended cement	Cementing material/durability; high strength
Fly ash	Cementing material/durability; high strength
Slag	Cementing material/durability; high strength
Silica fume	Cementing material/durability; high strength
Calcined clay	Cementing material/durability; high strength
Metakaolin	Cementing material/durability; high strength
Calcined shale	Cementing material/durability; high strength
Superplasticizers	Flowability
High-range water reducers	Reduce water to cement ratio
Hydration control admixtures	Control setting
Retarders	Control setting
Accelerators	Accelerate setting
Corrosion inhibitors	Control steel corrosion
Water reducers	Reduce cement and water content
Shrinkage reducers	Reduce shrinkage
Alkali-silica reaction (ASR) inhibitors	Control ASR
Polymer/latex modifiers	Durability
Optimally graded aggregate	Effective use of binder/strength and durability

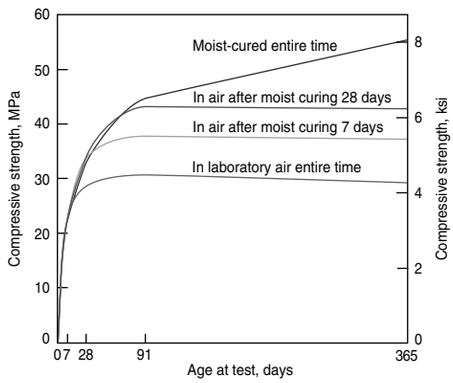

Fig. 11 Concrete strength increases with age as long as moisture and a favorable temperature are present for hydration of the cement. The effect of moisture during cure is evident.

Moderate-strength lightweight concrete has a density of 800 to 1900 kg/m^3 (50–120 lb/ft^3) oven dry and compressive strength of approximately 7 to 15 MPa (1–2.2 ksi). It is made with cementitious materials, water, air, and with or without aggregates and chemical admixtures. At lower densities, it is used as fill for thermal and sound insulation of floors, walls, and roofs and is referred to as *fill concrete*. At higher densities, it is used in cast-in place walls, floors and roofs, and for precast wall and floor panels. More information can be found in committee reports of the American Concrete Institute (Ref 69–71).

Autoclaved cellular concrete (ACC) is a special type of lightweight building material also known as *autoclaved aerated concrete*. It is manufactured from a mortar consisting of pulverized siliceous material (sand, slag, or fly ash), cement, and water; to this material a gas-forming agent, such as aluminum powder, is added. The chemical reaction of aluminum and alkaline water forms hydrogen gas, which expands the mortar; 0.5 to 1.5 mm (0.02–0.06 in.) diameter macropores form. After casting this mixture into forms, the material is pressure steam cured (autoclaved) for a period of 6 to 12 h at 190 °C (374 °F) and 1.2 MPa (0.17 ksi). After autoclaving, the hardened mortar matrix consists of calcium silicate hydrates.

This porous mineral building material has densities from 300 to 1000 kg/m^3 (19–63 lb/ft^3) and compressive strength 2.510 MPa (0.300–0.500 ksi). Due to the high macropore content—up to 80 vol%—ACC has a thermal conductivity of only 0.15 to 0.20 W/(m · K) (1–1.4 Btu · in./[h · ft^2 · °F]). Autoclaved cellular concrete is manufactured into blocks, wall panels, roof and floor slabs, and lintels for construction of residential and commercial buildings (Ref 70–73).

High-density (heavyweight) concrete has density to 6400 kg/m^3 (400 lb/ft^3). Heavyweight concrete is used for radiation shielding, counterweights, and other applications where high density is important. Where space requirements are not important, normal-weight concrete is more economical, but where space is limited, heavyweight concrete shields against x-rays, gamma rays, and neutron radiation more efficiently. High-density aggregates such as barite, ferrophosphorus, goethite, hematite, ilmenite, limonite, magnetite, steel punchings, or shot are used (Ref 74, 75).

Mass concrete is defined (Ref 67) as: "any large volume of cast-in-place concrete with dimensions large enough to require that measures be taken to cope with the generation of heat and attendant volume change to minimize cracking." Mass concrete includes not only low-cement-content concrete used in dams and other massive structures but also moderate- to high-cement-content concrete in large structural members of bridges and buildings. Mass concrete placements require special considerations to reduce heat of hydration and the resulting temperature rise to avoid damaging the concrete. Excessive temperatures and temperature differences throughout a concrete placement can result in thermal cracking (Ref 76).

Precast and Prestressed Concrete. Precast concrete is cast in forms in a controlled environment and allowed to achieve a specified strength prior to placement on location. Prestressed concrete is concrete in which compressive stresses are induced by high-strength steel tendons or bars in a concrete element. These stresses will balance the tensile stresses that will occur in the element during service.

Prestressing is accomplished in two ways: for pretensioning, usually done in a plant, the tendons are placed and tensioned before the concrete is placed; for posttensioning, usually done at the job site, tendons or bars are positioned before the concrete is placed and tensioned after the concrete has cured, hardened, and reached a specified strength.

Precast and prestressed concrete offers advantages for all types of structures (Ref 77). Precast elements are economical and of high quality; they have greater permanence than other building materials. Colored and textured precast panels often are used as the skin of a building and can also serve as structural elements (Ref 78).

Table 4 Special types of concrete

Made with portland cement	
Architectural concrete	Nailable concrete
Autoclaved cellular concrete	No-slump concrete
Centrifugally cast concrete	Polymer-modified concrete
Colloidal concrete	Pervious (porous) concrete
Colored concrete	Pozzolan concrete
Controlled-density fill	Precast concrete
Cyclopean (rubble) concrete	Prepacked concrete
Dry-packed concrete	Preplaced aggregate concrete
Epoxy-modified concrete	Reactive-powder concrete
Exposed-aggregate concrete	Recycled concrete
Ferrocement	Roller-compacted concrete
Fiber concrete	Sawdust concrete
Fill concrete	Self-compacting concrete
Flowable fill	Shielding concrete
Flowing concrete	Shotcrete
Fly-ash concrete	Shrinkage-compensating
Gap-graded concrete	Silica-fume concrete
Geopolymer concrete	Soil-cement
Heavyweight concrete	Stamped concrete
High-early-strength concrete	Structural lightweight
High-performance concrete	Superplasticized concrete
High-strength concrete	Terrazzo
Insulating concrete	Tremie concrete
Latex-modified concrete	Vacuum-treated concrete
Low-density concrete	Vermiculite concrete
Mass concrete	White concrete
Moderate-strength lightweight	Zero-slump concrete
Made without portland cement	
Acrylic concrete	Magnesium phosphate concrete
Aluminum phosphate concrete	Methyl methacrylate (MMA) concrete
Asphalt concrete	Polyester concrete
Calcium aluminate concrete	Polymer concrete
Epoxy concrete	Potassium silicate concrete
Furan concrete	Sodium silicate concrete
Gypsum concrete	Sulfur concrete
Latex concrete	

Most of the definitions of these special concretes appear in Ref 67.

Sustainability

Sustainable development is a topic of growing importance. Also known as "green building," sustainable construction makes it possible to use our natural resources efficiently while still acknowledging the desire for growth. Sustainability balances current and future needs. Since the population will continue to increase, sustainability will help balance the economic, social, and environmental impact of actions we take to create the built environment.

A few facts highlight dramatically the need to modify the way we design and construct buildings. Research has shown that buildings in the United States use 40% of the nation's material resources and 39% of its annual energy consumption. Even more telling is the fact that U.S. buildings use almost three times the energy of its European counterparts in similar climates (Ref 79); there is a definite imbalance.

Green building programs are becoming popular; the U.S. government is adopting them, and an increasing number of states are offering tax benefits for them. The U.S. government defines green buildings as those that:

- Demonstrate the efficient use of energy, water, and materials
- Limit impact on the outdoor environment
- Provide a healthier indoor environment

Concrete buildings offer a number of advantages: They are durable and have the longest lifespan of any traditional construction material; they are energy efficient in manufacture and use; are made of locally available raw materials; they do not rust, rot, or burn, and require less energy and resources over time to repair or replace. For more information about the sustainable benefits of concrete, see Ref 80–83.

REFERENCES

1. "Standard Specification for Coal Fly Ash and Raw or Calcined Natural Pozzolan for Use as a Mineral Admixture in Concrete," C 618-03, *Annual Book of ASTM Standards,* ASTM International, 2003
2. "Building Code Requirements for Structural Concrete," ACI 318-02, American Concrete Institute, Farmington Hills, MI, 2002
3. G.J. Verbeck, "Carbonation of Hydrated Portland Cement," Research Department Bulletin RX087, Portland Cement Association, Skokie, IL, 1958
4. R. Montani, Concrete's Forgotten Enemy, *Concrete Repair Digest,* Dec 1995/Jan 1996, p 330–333
5. M. McGovern, Combating Balcony Corrosion, *Concrete Technology Today,* CT012, Portland Cement Association, Skokie, IL, July 2001 p 1–2
6. W. Lerch, "Basic Principles of Air-Entrained Concrete," T-101, Portland Cement Association, Skokie, IL, 1960

7. S.H. Kosmatka, B. Kerkhoff, and W.C. Panarese, *Design and Control of Concrete Mixtures,* EB001, 14th ed., Portland Cement Association, Skokie, IL, 2002
8. P. Klieger, "Effect of Mixing and Curing Temperature on Concrete Strength," Research Department Bulletin RX103, Portland Cement Association, Skokie, IL, 1958
9. T.C. Powers, "Prevention of Frost Damage to Green Concrete," Research Department Bulletin RX148, Portland Cement Association, Skokie, IL, 1962
10. P. Klieger, "Curing Requirements for Scale Resistance of Concrete," Research Department Bulletin RX082, Portland Cement Association, Skokie, IL, 1957
11. B. Kerkhoff, "Effects of Substances on Concrete and Guide to Protective Treatments," IS001, Portland Cement Association, Skokie, IL, 2001
12. "Guide to Durable Concrete," ACI 201.2R-92, American Concrete Institute, Farmington Hills, MI, 1992
13. "A Guide to the Use of Waterproofing, Dampproofing, Protective, and Decorative Barrier Systems for Concrete," ACI 515.1R-79, American Concrete Institute, Farmington Hills, MI, 1979
14. D. Stark, "Long-Time Performance of Concrete in a Seawater Exposure," RP337, Portland Cement Association, Skokie, IL, 1995
15. D. Stark, "Long-Term Performance of Plain and Reinforced Concrete in Seawater Environments," Research and Development Bulletin RD119, Portland Cement Association, Skokie, IL, 2001
16. D. Stark, "Performance of Concrete in Sulfate Environments," PCA Serial No. 2248, Portland Cement Association, Skokie, IL, 2002
17. "Standard Specification for Portland Cement," C 150-04, *Annual Book of ASTM Standards,* ASTM International, 2004
18. "Standard Performance Specification for Hydraulic Cement," C 1157-03, *Annual Book of ASTM Standards,* ASTM International, 2003
19. "Standard Specification for Blended Hydraulic Cement," C 595-03, *Annual Book of ASTM Standards,* ASTM International, 2003
20. D. Stark, "Longtime Study of Concrete Durability in Sulfate Soils," Research and Development Bulletin RD086, Portland Cement Association, Skokie, IL, 1982
21. D. Stark, "Durability of Concrete in Sulfate-Rich Soils," Research and Development Bulletin RD097, Portland Cement Association, Skokie, IL, 1989
22. "Standard Specification for Ground Granulated Blast-Furnace Slag for Use in Concrete and Mortars," C 989-04, *Annual Book of ASTM Standards,* ASTM International, 2004
23. "Types and Causes of Concrete Deterioration," IS536, Portland Cement Association, Skokie, IL, 2002
24. J.A. Farny and S.H. Kosmatka, "Diagnosis and Control of Alkali-Aggregate Reactions in Concrete," IS413, Portland Cement Association, Skokie, IL, 1997
25. D. Stark, "Lithium Salt Admixtures—An Alternative Method to Prevent Expansive Alkali-Silica Reactivity," RP307, Portland Cement Association, Skokie, IL, 1992
26. "Standard Test Method for Abrasion Resistance of Concrete (Underwater Method)," C 1138-97, *Annual Book of ASTM Standards,* ASTM International, 2003
27. T.C. Liu, "Abrasion Resistance of Concrete," *J. American Concrete Inst*., Farmington Hills, MI, Sept-Oct 1981, p 341–350
28. J.A. Farny, "Concrete Floors on Ground," EB075, Portland Cement Association, Skokie, IL, 2001
29. D.R. Lankard, D.L. Birkimer, F.F. Fondriest, and M.J. Snyder, *"The Effects of Moisture Content on the Constitution and Structural Properties of Portland Cement Concrete Exposed to Temperatures up to 500 °F,* Battelle Memorial Institute, Columbus, OH, 1968
30. M.S. Abrams, "Behavior of Inorganic Materials in Fire," Research and Development Bulletin RD067, Portland Cement Association, Skokie, IL, 1979
31. M.S. Abrams, "Compressive Strength of Concrete at Temperatures to 1600 °F," Research and Development Bulletin RD016, Portland Cement Association, Skokie, IL, 1973
32. M.S. Abrams, "Performance of Concrete Structures Exposed to Fire," Research and Development Bulletin RD060, Portland Cement Association, Skokie, IL, 1977
33. M.S. Abrams, and D.L. Orals, "Concrete Drying Methods and Their Effect on Fire Resistance," Research Department Bulletin RX181, Portland Cement Association, Skokie, IL, 1965
34. A.H. Gustaferro, M.S. Abrams, and Albert Litvin, "Fire Resistance of Lightweight Insulating Concretes," Research and Development Bulletin RD004, Portland Cement Association, Skokie, IL, 1970
35. R.E. Davis, A Summary of the Results of Investigations Having to do with Volumetric Changes in Cements, Mortars, and Concretes Due to Causes Other Than Stress, *Proceedings of the American Concrete Institute,* Vol 26, American Concrete Institute, Farmington Hills, MI, 1930, p 407–443
36. "Concrete Slab Surface Defects: Causes, Prevention, Repair," IS177, Portland Cement Association, Skokie, IL, 2001
37. "Portland Cement," M 85-00, American Association of State Highway and Transportation Officials (AASHTO), Washington, D.C, 2000
38. "Standard Specification for Masonry Cement," C 91-03a, *Annual Book of ASTM Standards,* ASTM International, 2003
39. "Standard Specification for Plastic (Stucco) Cement," C 1328-03a, *Annual Book of ASTM Standards,* ASTM International, 2003
40. "Standard Specification for Expansive Hydraulic Cement," C 845-96, *Annual Book of ASTM Standards,* ASTM International, 2003
41. "Specification for Cements and Materials for Well Cementing," API Specification 10A, American Petroleum Institute (API), Washington, D.C, 2002
42. "Standard Specification for Air-Entraining Additions for Use in the Manufacture of Air-Entraining Hydraulic Cement," C 226-02, *Annual Book of ASTM Standards,* ASTM International, 2003
43. "Standard Specification for Functional Additions for Use in Hydraulic Cements," C 688-00, *Annual Book of ASTM Standards,* ASTM International, 2003
44. D.A. Abrams, "Tests of Impure Waters for Mixing Concrete," Structural Materials Research Laboratory Bulletin 12, Lewis Institute, Chicago, IL, 1924 (available through Portland Cement Association, Skokie, IL, library)
45. H.H. Steinour, "Concrete Mix Water—How Impure Can It Be?," Research Department Bulletin RX119, Portland Cement Association, Skokie, IL, 1960
46. "Standard Specification for Chemical Admixtures for Concrete," C 494-04, *Annual Book of ASTM Standards,* ASTM International, 2004
47. "Standard Specification for Chemical Admixtures for Use in Producing Flowing Concrete," C 1017-03, *Annual Book of ASTM Standards,* ASTM International, 2003
48. "Standard Specification for Use of Silica Fume for Use as a Mineral Admixture in Hydraulic-Cement Concrete, Mortar, and Grout," C 1240-03a, *Annual Book of ASTM Standards,* ASTM International, 2003
49. H.G. Russell, ACI Defines High-Performance Concrete, *Concrete International,* American Concrete Institute, Farmington Hills, MI, Feb 1999, p 56–57
50. "High-Performance Construction Materials and Systems," Technical Report 93-5011, American Society of Civil Engineers, New York, April 1993
51. J.A. Bickley and D. Mitchell, *A State-of-the-Art Review of High Performance Concrete Structures Built in Canada: 1990–2000,* Cement Association of Canada, Ottawa, Canada, May 2001
52. M. McGovern, Going with the Flow, *Concrete Technology Today,* CT022, Portland Cement Association, Skokie, IL, July 2002, p 1, 2, and 8
53. H.G. Russell, Long-Term Properties of High-Strength Concretes, *Concrete*

Technology Today, PL933, Portland Cement Association, Skokie, IL, Nov 1993, p 3
54. R.G. Burg and A.E. Fiorato, "High-Strength Concrete in Massive Foundation Elements," Research and Development Bulletin RD117, Portland Cement Association, Skokie, IL, 1999
55. R.G. Burg and B.W. Ost, "Engineering Properties of Commercially Available High-Strength Concretes (Including Three-Year Data)," Research and Development Bulletin RD104, Portland Cement Association, Skokie, IL, 1994
56. R.G. Burg, M.A. Caldarone, G. Detwiler, D.C. Jansen, and T.J. Willems, Compression Testing of HSC: Latest Technology, *Concrete International,* American Concrete Institute, Farmington Hills, MI, Aug 1999, p 67–76
57. J.A. Farny and W.C. Panarese, "High-Strength Concrete," EB114, Portland Cement Association, Skokie, IL, 1994
58. "State-of-the-Art Report on Fiber Reinforced Concrete," ACI 544.1R-96, American Concrete Institute, Farmington Hills, MI, 1997
59. "Fiber Reinforced Concrete," SP039, Portland Cement Association, Skokie, IL, 1991
60. W.C. Panarese, Fiber: Good for the Concrete Diet? *Civil Engineering,* American Society of Civil Engineers, New York, May 1992, p 44–47
61. G.E. Monfore, "A Review of Fiber Reinforcement of Portland Cement Paste, Mortar and Concrete," Research Department Bulletin RX226, Portland Cement Association, Skokie, IL, 1968
62. J.A. Bickley and R. Fung, *Optimizing the Economics of High-Performance Concrete,* a Concrete Canada and Canadian Cement Industry Joint Research Project, Cement Association of Canada, Ottawa, Canada, 2001
63. C.F. Ferraris and C.L. Lobo, Processing of HPC, *Concrete International,* American Concrete Institute, Farmington Hills, MI, April 1998, p 61–64
64. "Guide to Quality Control and Testing of High-Strength Concrete," ACI 363.2R-98, American Concrete Institute, Farmington Hills, MI, 1998
65. P. Klieger, "Early-High-Strength Concrete for Prestressing," Research Department Bulletin RX091, Portland Cement Association, Skokie, IL, 1958
66. S.P. Shah, W.J. Weiss, and W. Yang, Shrinkage Cracking—Can It Be Prevented? *Concrete International,* American Concrete Institute, Farmington Hills, MI, April 1998, p 51–55
67. *"Cement and Concrete Terminology,"* ACI 116R-00, American Concrete Institute, Farmington Hills, MI, 2000
68. "Standard Test Method for Determining Density of Structural Lightweight Concrete," C 567-00, *Annual Book of ASTM Standards,* ASTM International, 2003
69. Guide for Cast-in-Place Low-Density Concrete," ACI 523.1R-92, American Concrete Institute, Farmington Hills, MI, 1992
70. "Guide for Precast Cellular Concrete Floor, Roof, and Wall Units," ACI 523.2R-96, American Concrete Institute, Farmington Hills, MI, 1996
71. "Guide for Cellular Concretes above 50 pcf and for Aggregate Concretes above 50 pcf with Compressive Strengths Less Than 2500 psi," ACI 523.3R-93, American Concrete Institute, Farmington Hills, MI, 1993
72. Autoclaved Cellular Concrete—the Building Material of the 21st Century, *Concrete Technology Today,* PL912, Portland Cement Association, Skokie, IL, July 1991, p 1–3
73. B. Sauber, Mobile Demonstration Plant Will Produce Fly Ash-Based Cellular Concrete, *Concrete Technology Today,* PL921, Portland Cement Association, Skokie, IL, March 1992, p 1–3
74. "Standard Specification for Aggregates for Radiation-Shielding Concrete," C 637-98a (2003), *Annual Book of ASTM Standards,* ASTM International, 2003
75. "Standard Descriptive Nomenclature of Constituents of Aggregates for Radiation-Shielding Concrete," C 638-92 (2002), *Annual Book of ASTM Standards,* ASTM International, 2003
76. J. Gajda and M.G. VanGeem, Controlling Temperatures in Mass Concrete, *Concrete International,* Vol 24 (No. 1), Jan 2002, p 58–62
77. *Architectural Precast Concrete,* Precast/Prestressed Concrete Institute, Chicago, IL, 1989 (available from Portland Cement Association, Skokie, IL, as LT150)
78. "Tilt-Up Concrete Buildings," PA079, Portland Cement Association, Skokie, IL, 1989
79. D. Shepherd, Concrete Thinking for a Sustainable World, *Concrete Technology Today,* CT041, Portland Cement Association, Skokie, IL, March 2004, p 5
80. "Building Green with Gray Concrete," IS311, Portland Cement Association, Skokie, IL, 2003
81. "Concrete: Sustainability and Life Cycle," CD033, Portland Cement Association, Skokie, IL, 2003
82. "Concrete Builds the Sustainable Movement," RP417, Portland Cement Association, Skokie, IL, 2003
83. "Building Green with Concrete: Points for Concrete in LEED (Leadership in Energy and Environmental Design)," IS312, Portland Cement Association, Skokie, IL, 2003

ASM Handbook, Volume 13B: Corrosion: Materials
S.D. Cramer, B.S. Covino, Jr., editors, p589-599
DOI: 10.1361/asmhba0003844

Degradation of Protective Coatings

Kenneth B. Tator, KTA-Tator, Inc.

PAINTS AND PROTECTIVE COATINGS are by far the most common means of protecting materials from deterioration. Besides protection, coatings add color, beautify, provide light reflectivity, camouflage, reflect heat, absorb heat, and provide other functions. The generic types, functions, characteristics, and processes of corrosion-protective coatings are described in the articles "Introduction to Coatings and Linings," "Organic Coatings and Linings," and "Paint Systems" in *ASM Handbook,* Volume 13A, 2003.

To function, the protective coating must remain intact and adherent on the surface to which it has been applied. Failure occurs when the coating no longer fulfills the intended purpose. Ultimately, all coatings will fail, but sometimes premature failure, that is, unexpected excessive coating deterioration over a relatively short period of time, occurs. The most common reasons for premature failure are poor surface preparation of the substrate prior to application of the coating, or insufficient thickness of the applied coating. In the author's opinion, these two factors likely account for over 75% of all coating failures. Other less common but still prevalent causes are misspecification or misuse of the coating system (use in an environment for which it was not intended or formulated). Finally, although often alleged, misinformation or batching errors during the manufacture of a coating do occur.

It is important to recognize that the overwhelming vast majority of all protective coatings perform admirably. Premature coating failure is extremely rare. It is estimated that less than $^{1}/_{100}$ of 1% of coatings fail prematurely.

In the United States in 1997, 5.56 billion liters (1.47 billion U.S. gallons) of coatings were used (Ref 1). Most of the total yearly amount is successfully specified and applied to a properly prepared surface and to the appropriate thickness. These coatings perform as intended but, over time, deteriorate and lose their protective or aesthetic function as a result of aging combined with exposure to aggressive environments.

This article focuses on coating degradation resulting from the environmental interaction with the coating, rather than degradation resulting from human actions such as improper specification, deficient surface preparation, poor application, insufficient film thickness, insufficient drying or curing, and other abnormalities during application.

The environmental influences that may result in deterioration are:

- Energy (solar radiation, heat and temperature variation, nuclear radiation)
- Permeation (moisture, solvent retention, chemical, and oxygen)
- Stress (drying and curing—internal stress; vibration—external stress; impact and abrasion)
- Biological influences (microbiological and macrobiological, such as mildew and marine fouling)

These environmental influences may act in combination, with unpredictable aggressive results.

Before discussing the effects of an aggressive environment on coating, it is useful to understand what a coating is at the atomic level. Various atoms combine to form molecules. To form a coating, molecules of the constituents must form a resin that, after application, will result in a durable protective layer on a surface. The resin may convert from a liquid to a hardened film by the evaporation of solvents or water without changing chemically, or a chemical reaction may occur. The paint is usually filled with pigments to give it strength, opacity, and color.

Deterioration of a properly applied protective coating begins at the atomic level, and degradation processes continually affect the molecules that constitute the resin and pigment in the coating. In time, as the coating is exposed to the environment, it can become stressed such that it loses physical and mechanical properties, resulting in discoloration, cracking, peeling, loss of adhesion, and loss of function or suitability. If a coating protects 15 to 20 years or more, the cumulative effect of these stresses is called old age. Statistically, most atoms are stable in this time period. Individual atoms do not change with time, except by nuclear decay or nuclear fission or fusion reactions. Therefore, polymers, resins, and formulated protective coatings should not age either, unless they are affected by their environment in such a way that the polymers break into smaller parts, a process called chain scission. When this happens, the resins comprising the coating lose their environmental resistance, and the coating system, in time, fails to function as intended. It is the environmental influences on the molecules, resins, and pigments of the coating system that are discussed herein.

Molecular Composition of a Polymer

In a dried film, coatings are composed primarily of resins and pigments. The pigments, for the most part, strengthen the film, provide opacity and color, and, in some cases, provide protection by anodic means or corrosion inhibition. The film-forming organic or inorganic resin that holds the pigment particles together and provides adhesion to the substrate contributes the greatest effect to the environmental resistance of a coating system.

When describing most protective coatings, terms such as *epoxy, polyurethane, alkyd,* and *silicate* are used. These are generic descriptions of the resin or binder. The principal resins used in protective coatings are described in the articles "Organic Coatings and Linings" and "Zinc-Rich Coatings," in *ASM Handbook,* Volume 13A, 2003. The chemical structural formulas for many of the resins are provided in these articles. For example, the structural formula for a bis-A epoxy is shown in Fig. 1.

The structural formula depicts each atom of carbon, hydrogen, and oxygen in the molecule. The lines between each of the atoms indicate the chemical bonds between the atoms. These

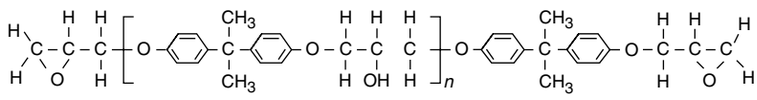

Fig. 1 Bis-A epoxy resin structure

electronic bonds hold the atoms together to form a molecule. The number of lines (or bonds) extending from each atom reflect the valence of that particular atom. Hydrogen, for example, always has only one line (or bond) extending to another atom, whereas carbon usually has four lines or bonds. The valence of hydrogen is one and that of carbon is four. In some cases, carbons form a ring structure, where the electrons that form the bond are shared loosely between a carbon atom and its carbon neighbors. Such an arrangement is depicted in Fig. 1 as a benzene ring structure. The valencies of some of the more common atoms used in protective coatings are presented in Table 1. Positive valence numbers were used to describe the combining capacity of elements in the 19th century, before atomic structure and the electronic basis for chemical bonding were known.

Atomic Structure. For elementary substances, the smallest particle is called an atom. Atoms consist of a nucleus of positively charged protons and neutral neutrons surrounded by one or more shells of small, negatively charged electrons. The nature of the element depends on the number of protons, which is the atomic number. Isotopes of an element have the same number of protons but differ in neutrons. The number of electrons in the outer shell of a neutral atom determines its valence. The number of protons and neutrons in the nucleus determines its atomic weight (for all practical purposes, the mass weight of an electron is negligible). Atoms with eight electrons in the outer shell (or, in some cases, two electrons in the outer shell) are most stable and unreactive. In metallic elements, such as sodium, aluminum, zinc, and iron, valence electrons are donated for bonding. In other elements, such as oxygen and chlorine, electrons are accepted. The electrons in some atoms, such as carbon, nitrogen, and silicon, may be donated or accepted, depending on the nature of the bonding that takes place.

Table 1 Atomic valencies

Element	Symbol	Valency	Names of valency state
Hydrogen	H	1	...
Potassium	K	1	...
Sodium	Na	1	...
Silver	Ag	1	...
Chlorine	Cl	1	...
Bromine	Br	1	...
Iodine	I	1	...
Magnesium	Mg	2	...
Calcium	Ca	2	...
Barium	Ba	2	...
Zinc	Zn	2	...
Boron	B	3	...
Aluminum	Al	3	...
Carbon	C	4	...
Silicon	Si	4	...
Copper	Cu	1 or 2	Copper (I) or cuprous Copper (II) or cupric
Mercury	Hg	1 or 2	Mercury (I) or mercurous Mercury (II) or mercuric
Gold	Au	1 or 3	Gold (I) or aurous Gold (III) or auric
Oxygen	O	2	...
Iron	Fe	2 or 3	Iron (II) or ferrous Iron (III) or ferric
Cobalt	Co	2 or 3	Cobalt (II) or cobaltous Cobalt (III) or cobaltic
Lead	Pb	2 or 4	Lead (II) or plumbus Lead (IV) or plumbic
Nickel	Ni	2 or 4	Nickel (II) or nickelous Nickel (IV) or nickelic
Sulfur	S	4 or 6	Sulfur (IV) or sulfurous Sulfur (VI) or sulfuric
Nitrogen	N	3 or 5	Nitrogen (III) or nitrous Nitrogen (V) or nitric
Chromium	Cr	2, 3, or 6	Chromous (2), chromic (3)

Chemical bonding generally consists of the transfer of electrons from a donor to an acceptor atom (ionic bonding), a sharing of electrons between two atoms (covalent bonding), or a continuum between transfer and sharing (coordinate covalent bonding). Ionic bonding occurs between metals, metal oxides, and salts of metals. Covalent bonding consists of a sharing of electrons in order to establish stability in two or more atoms. Covalent bonding is most common with nonmetallic elements, in particular with the carbon atom. Most bonding that exists within a coating film consists of covalent bonding between atoms comprising the molecular polymer of that film. All the bonds depicted in Fig. 1 are covalent bonds.

Polymers. A molecule consists of two or more atoms held together by chemical bonds. The properties of the molecule or the specific group of bonded atoms determine how it is classified. For the most part, metals are ionically bonded and have properties that differentiate them from the nonmetals. Nonmetals are principally covalently bonded and can be generally categorized as organic or inorganic materials. Inorganic nonmetallic materials do not contain the carbon atom, while organic materials do.

Coating resins are almost exclusively organic materials. There are some exceptions, notably silicones and silicates, that form the binders for very high-temperature-resistant coatings and inorganic zinc-rich coatings, respectively.

The molecular structure of most coatings consists of high-molecular-weight materials with a number of repeating units, called "mers," thus the terms *polymer* (many "mers" of different types forming a resin) or *monomer* (many "mer" units of the same type forming a resin). Polymers can be a relatively simple straight chain material of either low molecular weight (a relatively small number of atoms) or very high molecular weight (a great number of atoms). They can also be branched in a fashion similar to branches stemming outward from the trunk of a tree.

A polymer solution may consist of billions of polymer segments of constituent materials, all with different molecular weights, sizes, and shapes. At elevated temperatures (above the melting point), the polymer melt is a liquid, and while the attractive bonding forces within the molecule are sufficient to hold the molecule together, the bonding forces are insufficient to hold different molecules to each other. However, as the solution cools and the liquid solidifies, heat energy is lost such that molecular vibrations slow down, and the attractive force between portions of different molecules becomes sufficient to hold adjacent molecules together in a loose symmetry, resulting in a solid. These intermolecular attractive forces are principally a variety of polar attractive or dispersion forces within the family called van der Waals forces. Although these forces are not nearly as strong as the ionic or covalent bonding forces between atoms of a molecule, they are sufficiently strong to hold molecules together at temperatures below the melting point. The van der Waals forces of attraction between adjacent molecules can hold an amorphic (shapeless) polymer mass together in order to form a solid. If the polymer mass is of such a size and constituency that these forces can pull it into a close and symmetrical alignment, areas of crystallinity may develop within a polymeric structure.

Molecular orientation of most paints and coatings, when dried, consists of closely symmetrical, crystalline-oriented molecular structures within a larger, randomly oriented, amorphous molecular mass. If molecules have a simple and regularly ordered structure, they may naturally fit and pack together well, and that closely aligned structure gives rise to molecular crystallinity. Crystallinity of a coating molecule is generally undesirable, because the oriented crystalline structure leads to close, dense packing, and high impermeability resulting in an inability to be dissolved by solvents. Additionally, the close, dense packing leads to brittleness and a lack of flexibility or toughness in most polymers. However, some specific coatings, such as polyethylene and fluoropolymers (Teflon, E.I. Dupont de Nemours & Co., Inc.), are highly crystalline but also tough and flexible and make good inert coatings. Their method of application is usually by heating and extruding or by specially treating the substrate, not by the brush, roller, or spray techniques most often used for less crystalline coating materials.

Amorphous molecular orientations are less ordered, often random, and have greater toughness, impact resistance, and flexibility. Cross linking is often induced into amorphous materials in order to increase the molecular weight, provide rigidity of the molecular structure, and increase resistance to permeating moisture and chemicals. Cross-linked molecules change during film formation and are called thermoset materials (they "set" with heat). They do not soften and melt on reapplication of heat; rather, the thermoset structure will retain its rigidity and shape until decomposition occurs at an elevated temperature. Thermoplastic materials (uncross linked) do not change during film formation and will soften with increasing temperature until the material melts and forms a liquid. The melting point of a thermoplastic material is generally very close, within a few degrees, of the initial softening point of the material. Thermoplastic coatings include asphalts, coal tars, and some acrylic materials. Most high-performance, chemically resistant coatings are cross-linked thermosets, including epoxies, polyurethanes, and alkyds.

For a cross-linked thermoset, additional exposure to increasing temperature changes the

material from a relatively hard, glossy molecular structure to a softer, rubbery structure. The temperature at which this transition occurs is also a range but usually wider, generally 2 to 5 °C (5 to 10 °F) or more, and the material does not melt or liquefy. On application of additional heat, no other significant change occurs until darkening and discoloration or a charring thermo-decomposition occurs. The temperature at which the transition occurs from the glassy to the rubbery stage is called the glass transition temperature (T_g). All cross-linked coatings have their greatest toughness and flexibility above T_g, but they are also much more prone to permeation by moisture, solvents, and chemicals. Accordingly then, most coating materials are formulated with a T_g that is sufficiently higher than temperatures expected to be encountered during the normal service life of the coating. Susceptibility to permeation at temperatures above the T_g is compensated for by formulation, pigmentation, and increased cross linking.

The resin of an organic film, consisting of megamolecules or polymers, has interspersed within it discrete particles of pigment and other additives that ultimately constitute the solid portion of the film (that which remains after all volatiles have been lost). It is this resin/pigment combination that deposits onto, adheres to, and takes the shape of the object to which it is applied and provides the barrier or coating on steel, concrete, wood, plastic, and other metal or nonmetal surfaces. It protects the underlying substrate from the vagaries of the service environment into which the object will be placed.

Environmental Effects Resulting in Coating Deterioration

Characterizing an outdoor environment is a daunting task. The environment at one end of a bridge may be different than that at another end and different than the center span suspended over water or high in the air. Similarly, an exterior environment at the top of a building may be different than that near the bottom of the building, relative to sunlight, wind intensity and direction, and temperature. Ships hauling cargos have different environments, not only within the cargo tanks but above and below the waterline.

The International Organization for Standardization (ISO) has defined principal environments for coatings. The environmental categories and descriptions are presented in Table 2. In addition, the standard discusses metal loss per year for each category as well as time of wetness; special conditions, such as corrosion inside buildings and corrosion in box girders; and various stresses, such as chemical, mechanical, condensation, temperature, and stress combinations.

The Society for Protective Coatings (SSPC) (Ref 3) has also defined environmental zones for coating systems, as presented in Table 3.

These environmental descriptions are somewhat similar, to the extent that they progress from a relatively mild, noncorrosive environment to a relatively aggressive environment. The more benign, mild environments are generally warmer, dryer, and less polluted. The more severe environments generally have more moisture or are in immersion and have salts or chemical constituents.

Moisture, salts, and chemicals are primary influences of the corrosion process on most materials. The degrading-influence categories (energy related, permeation effects, mechanical stress, and biological influences) are not all-inclusive and are not mutually exclusive. In most environments, a combination of environmental influences is present to varying degrees, along with perhaps other influences not mentioned. It is the synergistic effect of the combinations of these and other environmental influences that degrades the coating or, for that matter, any material, resulting in loss of suitability for its intended purpose. Each of these environmental categories is discussed.

Energy-Related Degradation

Energy acting on a coating can degrade a material by breaking or interfering with the chemical bonds holding the resin (or a molecule) together and to a substrate. In virtually every case, the influence of increased energy makes an organic molecule more susceptible to degradation by other environmental influences.

Solar Energy. The sun is composed of 91.2% hydrogen and 7.8% helium gas. The remaining 1% is comprised of oxygen, carbon, silicon, iron, magnesium, neon, sulfur, and calcium. Each element is important because its presence contributes to the solar light spectrum received on earth. The sun emits energy created by the thermonuclear fusion of hydrogen into helium. The sun's core contains more helium (65%) than hydrogen because of this conversion. It is estimated that the remaining hydrogen should last another 4 billion years. Variations in the sun's activity affect the wavelength of emitted radiation. Changes in ultraviolet (UV) light radiation are more pronounced than those of other ranges

Table 2 ISO Corrosivity categories and examples of typical environments

Corrosivity category	Exterior environment	Interior environment
Atmospheric categories		
C1 very low	. . .	Heated buildings with clean atmospheres, i.e., offices, shops, schools, hotels
C2 low	Atmospheres with low levels of pollution. Mostly rural areas	Unheated buildings where condensation may occur, e.g., depots, sports halls
C3 medium	Urban and industrial atmospheres, moderate sulfur dioxide pollution. Coastal areas with low salinity	Production rooms with high humidity and some air pollution, e.g., food-processing plants, laundries, breweries, dairies
C4 high	Industrial areas and coastal areas with moderate salinity	Chemical plants, swimming pools, coastal ship- and boatyards
C5-I very high (industrial)	Industrial areas with high humidity and aggressive atmosphere	Buildings or areas with almost permanent condensation and with high pollution
Categories for water and soil		
Im 1	Freshwater	River installations, hydro-electric plants
Im 2	Sea or brackish water	Harbor areas with structures such as sluice gates, locks, jetties; offshore structures
Im 3	Soil	Buried tanks, steel piles, steel pipes

Source: Ref 2

Table 3 SSPC Environmental zones for coating systems

Zone	Description and comment
0	Dry interiors where structural steel is embedded in concrete, encased in masonry, or protected by membrane or noncorrosive contact type of fireproofing
1A	Interior, normally dry (or temporary protection). Very mild (oil-based paints last 6 years or more)
1B	Exteriors, normally dry (includes most areas where oil-based paints last 6 years or more)
2A	Frequently wet with freshwater. Involves condensation, splash, spray, or frequent immersion (oil-based paints last 5 years or less)
2B	Frequently wet by saltwater. Involves condensation, spray, or frequent immersion (oil-based paints last 3 years or less)
2C	Freshwater immersion
2D	Saltwater immersion
3A	Chemical atmospheric exposure, acidic (pH 2.0 to 5.0)
3B	Chemical atmospheric exposure, neutral (pH 5.0 to 10.0)
3C	Chemical atmospheric exposure, alkaline (pH 10.0 to 12.0)
3D	Chemical atmospheric exposure, presence of mild solvents, and intermittent contact with aliphatic hydrocarbons and their derivatives (mineral spirits, lower alcohols, glycols, etc.)
3E	Chemical atmospheric exposure, severe. Includes oxidizing chemicals, strong solvents, extreme pHs, or combinations of these with high temperatures

Source: Ref 3

of radiation. The distribution of emitted energy is such that 9% is in the UV region, 45% is in the visible range, and the remaining 46% is in the infrared range (Ref 4). However, the energy emitted by the sun is attenuated by the earth's atmosphere and variability within that atmosphere (in particular, ozone absorption and scattering of solar radiation by clouds, moisture, and other small molecules). Figure 2 depicts the solar spectrum as emitted and as absorbed on the earth's surface (Ref 4). Figure 3 shows the electromagnetic spectrum of radiation types (Ref 5).

Electromagnetic radiation with the shortest wavelength (λ) has the greatest energy. However, the shorter λ is more readily absorbed and has less penetrating effect than longer λ. Radio waves can be transmitted over long distances, compared to television and radar with shorter λ, which allows transmission generally along a line-of-sight. Gamma radiation and x-ray radiation are not found in solar radiation but result from bombardment of certain elements with electrons or from radioactive decay. These high-energy shortwave radiations are powerful enough to ionize gases, readily cleave chemical bonds, and induce potentially deadly chemical changes in human and animal tissues.

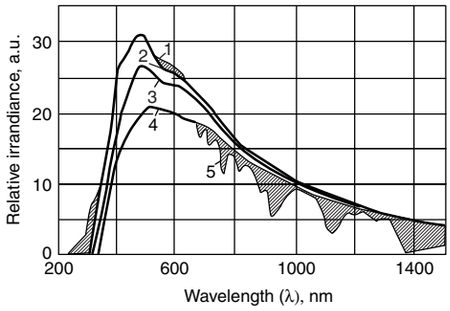

Fig. 2 Spectral changes in sunlight by absorption and scattering in the atmosphere. Curve 1, incident light above stratosphere (extraterrestrial radiation). Curve 2, modification by ozone absorption in stratosphere and troposphere. Curve 3, spectrum after Rayleigh scattering by small molecules. Curve 4, spectrum modified by aerosol (cloud) scattering and absorption (excluding water). Curve 5, spectrum after moisture-related scattering and absorption. Albedo units, a.u., are dimensionless. Albedo is the fraction of incident light or radiant energy that is scattered or reflected by a system of particles. Source: Ref 4

Ultraviolet light (λ, 10 to 400 nm), a naturally occurring energy from the sun, has a shorter wavelength than visible light (λ, 400 to 780 nm) and accordingly is more energetic. Ultraviolet light has sufficient energy to disrupt and break covalent bonds of organic molecules. The UV light range is divided into three subcategories: UV A (λ, 320 to 400 nm), UV B (λ, 280 to 320 nm), and UV C (λ, 10 to 280 nm). It was believed that the detrimental effects of UV radiation on paints started at 295 nm and extended to approximately 400 nm. However, recent experience has shown that there is sufficient radiation and penetration of UV light as low as 280 nm to cause deterioration of paint. Ultraviolet radiation below 280 nm is not considered detrimental, because it is generally absorbed by moisture and other small molecules in the atmosphere and therefore is of little consequence. Moreover, it has little ability to penetrate the surface of an organic material. Frequencies of radiation most harmful to polymeric systems are those from the blue part of the visible light spectrum and the near-UV light spectrum. The longer wavelengths are not energetic enough to harm molecules, and most of the other potentially harmful high-frequency rays are screened by the earth's atmosphere.

Breaking of molecular bonds and formation of free radicals by UV energy result in a shorting of the molecular chain of atoms (or polymer) and, accordingly, a reduction in molecular weight. Glass allows visible light to pass without any absorption but is opaque to the shorter wavelengths of UV light and reduces the transmission of UV light of longer wavelengths. Accordingly, materials exposed behind glass retain their color and last longer than those exposed in an exterior solar environment. However, fading and embrittlement of plastics and other materials on long-term interior exposure still occur in indoor environments exposed to sunlight. The UV energy that is transmitted through glass is still sufficient to degrade and fade coatings over time. It is generally accepted that radiation in the visible range and higher is nondetrimental to most paints, organic materials, and plant or animal tissues.

The effect of solar radiation and UV deterioration on polymers varies with location and altitude. Higher altitudes have higher levels of UV light. Additionally, they may be drier, and, accordingly, there will be less radiation absorption by moisture in the atmosphere. Similarly, an arid environment has clearer skies, and UV degradation may be more pronounced. Smog, dust, and atmospheric pollution will both absorb and scatter UV radiation, lessening its detrimental effect on the ground. However, while combinations of moisture, smog, and chemical contamination from industrial environments may reduce UV damage, the synergistic effect of these atmospheric materials on a polymer may be much greater than that of UV radiation alone. Ultraviolet radiation in combination with water on a surface (which concentrates the radiation) provides perhaps the greatest potential for UV-polymeric degradation.

Radiant solar energy in the form of light photons excites certain electrons in the molecules of a resin. Depending on the wavelength and frequency of the radiation, only certain electrons are affected. Excess electron energy as a result of UV photon excitation is dissipated by fluorescence, phosphorescence, and, most importantly, a cascading down of the electronic energy into vibrational and rotational energy of a molecular electrical bond. If sufficient energy is absorbed by the bond, it may break. Molecular groups with double bonds, such as carbon-to-carbon, carbon nitrogen, and carbon oxygen, absorb UV energy, and their electrons are lifted into higher energy levels. When these electrons decay to lower energy states, energy is released in the form of vibrations, which may cause a bond to break and create free radicals. Free radicals result when a chemical bond is broken. A covalent bond may break in either of two ways: the atoms previously joined by the bond share the electrons (homolytic dissociation), or the more electronegative of the atoms retains the electrons (heterolytic dissociation) (Ref 6). These two types of dissociations are represented by:

$$\text{Homolytic dissociation } A{:}B \rightarrow A^{\bullet} + {}^{\bullet}B$$

$$\text{Heterolytic dissociation } A{:}B \rightarrow A^{+} + {:}B^{-}$$

Heterolytic dissociation produces ions, which are electrically charged atoms or molecules. A negatively charged ion has more electrons than protons, and a positively charged ion has more protons than electrons. Such electrically charged atoms or molecules are polar and can dissociate from one another when placed in a water solution. The high dielectric constant or insulating property of pure water enables the polar molecules to separate and exist

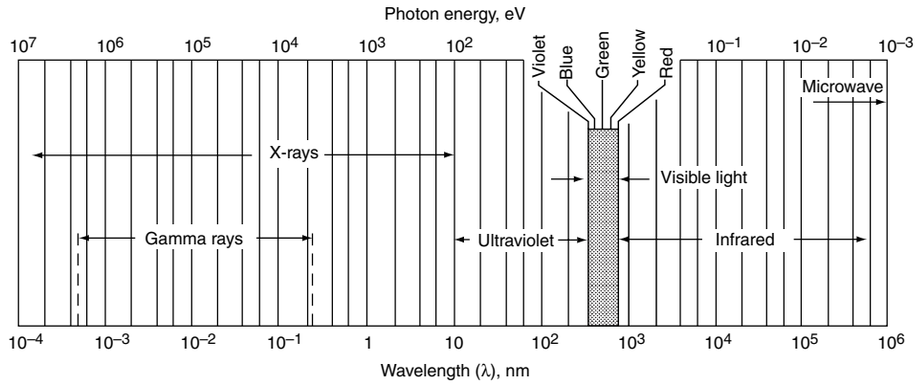

Fig. 3 Electromagnetic spectrum and energy of radiation. Source: Ref 5

separately in solution. Water itself is very weakly dissociated and forms hydrogen and hydroxide ions:

$$(H_2O)\ HOH \rightarrow H^+ + OH^-$$

Homolytic dissociation likely occurs if the two fragments are equally electronegative. This produces neutral atoms or groups, each with an unsatisfied valency or unpaired valency electron. Such groups are known as free radicals. Most free radicals are highly reactive and recombine either with each other or other free radicals to form chemical bonds.

If the free radicals are so reactive, why don't they all recombine? If, after separation, the free radicals are held in a relatively confined area and maintain close proximity to each other, recombination is likely. If the molecular structure is crystalline and has relatively tight, rigid chains in close proximity, or if the free radical is in an aromatic ring or in a very tightly and closely cross-linked molecular structure, it will be difficult for the free radical ends of the molecule to separate sufficiently after the break in the bond occurs. Accordingly, the free radicals will remain in close proximity and will likely recombine.

However, if the molecular chains are somewhat flexible and the temperature is sufficiently high that there is vibrational and rotational movement of molecules of the polymer, the free radicals on opposite ends of the broken bond may become so separated that they will not recombine. A radical may pick up a hydrogen from an adjacent chain upon the breaking of that bond and therefore transfer the radical to another portion of the chain. If the free radicals are on a flexible molecule that is moving around quite rapidly, there is a high probability that the radical will pick off a hydrogen of its own chain, five or seven carbon atoms back along the chain. Then, there will be a transfer of the radical to a position away from the chain and a termination of activity at the chain end. The newly formed free radical may pick up another hydrogen somewhere else or react with a monomer or react elsewhere to continue growth. Free-radical reactions result in chain scission (breaking of the molecular chain), depolymerization (reducing a polymeric chain to its monomer units), branching (a short growth at a free-radical site), self cyclization (forming a circular molecule by joining with another portion of the backbone of a molecule), and the formation of double bonds.

All of these free-radical reactions, which occur billions of times in material exposed to UV, will shorten the molecular chains, reduce their flexibility, and increase permeability of the molecule and resin, thus degrading it. Certain resins, such as an epoxy and particularly an amine cross-linked epoxy, are very susceptible to UV degradation. Exposure to even relatively low amounts of sunlight is sufficient, in many cases, to cause a chalking deterioration of the surface of the resin or paint. This chalk is composed of pigment particles and broken segments of the colorless molecular resin that refract light to give a white appearance.

Certain other resins, notably aliphatic polyesters, acrylics, and polyurethanes, are mostly transparent to UV light and allow UV energy to pass through them with no molecular absorption. Accordingly, there is no deterioration to these resins when exposed to UV light. Conversely, resins containing chromophores, or materials that absorb UV light at specific wavelengths, are more susceptible to UV light deterioration. Ketones and aldehydes (both containing the C=O group) are particularly active light absorbers, breaking down to form peroxides, which are strong oxidants and may cause further molecular breakdown. These materials are sometimes used as a polymerizing medium for some resins and may become incorporated into the resin by a chain transfer mechanism. Other chromophores and their characteristic absorption wavelengths are listed in Table 4.

Pigments in a paint, particularly inorganic pigments, will absorb and dissipate UV light, scatter it, or both, thereby lessening the deteriorating effect of the UV radiation. Platelike pigments, such as leafing aluminum, are particularly good reflectors and are opaque to visible and UV light. Zinc and zinc oxides are particularly good UV absorbers, and the UV energy is dissipated as heat within the coating with little, if any, detrimental effect. Carbon black is also a good UV absorber, also dissipating the UV radiation as heat. Titanium dioxide is an excellent white hiding pigment (and because of this is widely used in most industrial and commercial paints). However, it also is a good UV absorber and, in combination with water on a surface and in the presence of atmospheric oxygen, may accelerate UV deterioration of a coating resin. Both rutile TiO_2 and particularly the lesser-used anatase crystal lose an electron from a higher-energy valency band. Both the transferred electron and the hole in the valency band from the transfer are very active. The electron acts as a reducing agent and will add itself to any suitable group of atoms within a molecule. The electron deficiency, or hole, is a strong oxidant and seeks to take up other electrons. If the electron and hole are deep within the pigment particle, recombination usually takes place, and no deteriorating effect occurs. However, if the combination is at the pigment surface or near the molecular surface, oxygen may take up the electron, generating an oxygen free radical. The electron deficiency may be similarly satisfied by removal of an electron from a hydroxyl (−OH) group, generating a hydroxyl radical. Both of these radicals may attack other molecular groups in the resin, particularly at the TiO_2-resin interface, causing deterioration.

Hindered amine light stabilizers (HALS) are a variety of commercial and patented chemistries with hindered amines in the molecular backbone or as reaction products of phosphites, siloxanes, and hydrobenzenephenones. HALS cannot absorb UV radiation but instead function by their ability to terminate any free radicals formed as a result of UV light absorption. The use of HALS, in combination with UV absorbers, provides paint formulators a means to protect against UV degradation.

Heat Energy. The addition of heat to a material increases the vibrations of atoms within molecules. This increase in energy is rather uniform throughout the molecules, in contrast with radiation. Both UV and nuclear radiation affect only certain electrons in the atoms of the molecule. Other electrons on other atoms remain unaffected.

If the applied heat is of sufficient intensity, the molecular vibrations increase to such a degree that a bond may break. When that happens, free radicals are formed, and they will react as previously described. Again, the end result is a decrease of molecular weight of the chains comprising the resin of the coating; a reduction of the tensile strength, modulus of elasticity, and toughness; and the potential introduction or formation of reactive polar groups that may cause changes in compatibility and electrical and optical behavior of the polymer. Additionally, introduction of light-absorbing groups (chromophores) may cause discoloration and internal cyclization of polymer chains, resulting in hardening and a decrease in toughness. Free-radical initiation may also cause cross linking between hitherto independent macromolecules, which, in excess, may reduce impact strength and create brittleness. Energy in the form of UV light may pass through some aliphatic resins (acrylics, polyurethanes, polyesters) with little or no effect or be absorbed in other molecular combinations without breaking bonds. In the latter case, vibrational and rotational movement between atoms is increased, and the energy is dissipated as heat, which is generally harmless to the molecular structure. However, where absorbed heat energy is high enough, bonds may break, and free radicals may be formed. In a rigid, dense, closely packed, immovable solid resin or polymer, the free radicals may recombine with little effect on the molecule. However, in most cases, particularly in paints and most plastics, the structure is not rigid enough to allow immediate recombination of free radicals, and a variety of unanticipated secondary and tertiary reactions often occurs, resulting in a shortening of the molecular weight

Table 4 Absorptive wavelengths of chromophores

Chromophore	Absorptive wavelength, nm
C=C	162
C≡C	182, 220
C≡N	167
C=O	295
N=O	665
Cl	173
O–H	166
Benzene ring (aromatic)	255
C–H	150

Source: Adapted from Ref 4

of the resin molecule and other detrimental side effects, all resulting in deterioration and loss of properties.

Again, pigments within the paint or near the paint exterior surface may reflect heat and minimize damage to the resin. Color is a major influence in heat absorption, and darker colors will absorb more heat than lighter colors.

Permeation Effects

Permeation of a coating by moisture and chemicals in a service environment is a major factor in the deterioration of the coating. Coatings are specifically formulated and tested to resist certain environments in immersion or in the atmosphere. Pigments and resins must be carefully chosen for their resistance to a given set of environmental conditions, and they must also be compatible with each other. The following permeating species and mechanisms are discussed subsequently: moisture, solvents, chemicals, gases, and ions.

Moisture Permeation. The water molecule, H_2O, is a relatively small molecule in weight and size compared to other molecules commonly encountered in an environment. Water, in liquid or vapor form, is present in most all exterior environments, so coatings must be resistant to the effects of water penetration.

Water is also polar; the shared electron pairs in the covalent bond can be considered displaced. As a result, its oxygen atom has a slight negative charge and can attract hydrogen atoms with a slight positive charge (or any other atoms or groups of atoms with positive charges). Because of this polarity, water has an affinity for other polar groups within a resin molecule. Moreover, its small size enables it to readily permeate molecular interstices and microscopic pores, holidays, cracks, and defects inherent in almost any coating system. Water vapor can move in and out of porous materials with ease, as long as there is a driving force causing its movement.

What driving forces cause water movement? Simply placing a material in water will provide sufficient pressure from the head (depth) of the water, even though the immersion is relatively shallow. Water molecules, because of their relatively small size, can pack tightly and therefore are quite dense compared to many liquids and all gases. In immersion, there is sufficient capillary attraction (the wicking of water into a narrow pore opening, driven by wetting and hydrogen bonding meniscus attractions) pulling the water into the pore. Additionally, water head pressure may also aid water migration into cracks, crevices, pinholes, and microscopic fissures inherent in any coating system. Water, in permeating a coating, may fill any free space left by solvents and other materials that may have migrated from the coating during application and curing. Due to the polarity of the water molecule, water may be drawn into the coating if there are any polar solvents, polar groups, or polar materials retained in the film. Thus, the presence of ester groups:

ether linkages:

carboxyl groups:

and other polar groups within a coating resin may draw water into the paint. An electric potential applied across the coating film, such as cathodic protection or that resulting from a corrosion cell, can induce or accelerate the permeation of water into a coating. This phenomenon is called electroendosmosis. Additionally, corrosion-inhibiting pigments (chromates, borates, molybdates), due to their water solubility, may draw water through the coating film in an osmotic process. These pigments require water to partially dissolve the metal inhibitor, which then can wet and passivate the underlying steel or aluminum metal substrate.

Finally, rust deposits, dirts, salts, and other contaminants remaining on a surface may prevent bonding of the paint and establish osmotic driving forces, further promoting water permeation. At areas where paint adhesion is relatively poor, cross linking is less dense, or agglomerations of pigments are not completely wetted by the organic binder, water may collect and pool, causing a swelling of the film and additional water penetration. Water-soluble salts, including sodium chloride, calcium chloride, and other chlorides (found in marine environments and in deicing salts), and sulfates (from acid rains) are notorious for causing osmotic blistering of coatings in immersion service and accelerated rates of corrosion in atmospheric service if they are allowed to remain on a substrate before painting or between coats of paint.

Once water enters the paint film, the small water molecules have the ability to penetrate between and within molecular chains comprising the organic resin and the interstices between the resin and pigment, if the pigment is not completely wetted by the resin. As the water molecule penetrates, it separates loose bonds holding the resin particles together, such as polar bonds, and becomes attracted to and swells the molecule at sites of covalent bonds that are polar. This swelling forces the bonds even further apart, diminishing their tightness and close packing. The volume of the coating increases due to the water intrusion. Some films increase 20 to 50% in volume when in contact with water. (Ref 7), but most properly formulated and pigmented resins used for immersion or exterior environments do not increase their weight more than 2 to 3% after lengthy water contact. The swelling caused by the coating film may separate polar bonds and other weak forces holding the molecule together and to the substrate, such that polar attractions, so necessary to coating film adhesion/cohesion, no longer occur. Additionally, the oxygen of the water molecule may be attracted to and replace what otherwise would have been a polar attraction between two long-chain resin molecules, or between a resin molecule and the substrate. When this happens, the charge between the molecules is terminated, and attraction to water molecules by each chain end occurs instead. The dried coating film, when wetted and saturated with water, becomes plasticized and swollen. Wet adhesion of most coatings is substantially less than dry adhesion. When the film dries out, dry adhesion often re-establishes but usually not to the same extent as it was before moisture saturation.

The phenomenon of swelling by moisture penetration into a coating film occurs with virtually all coating materials except those that are extremely tightly cross linked with a high cross-link density (such as some phenolic epoxies or phenolic coatings formulated for water resistance) or other tightly cross-linked coating materials (such as the fluoropolymers). These materials are relatively impervious to water permeation, penetration, and swelling due to their dense molecular cross linking or the tight polar bonding between molecular chains.

Heating increases molecular movement, enabling more rapid water penetration. Conversely, cooling, particularly below the T_g, reduces molecular movement and retards water permeation.

Solvent Retention. Solvents are not found in most environments, and the presence of a solvent in a paint film occurs, for the most part, as a result of solvent addition to the resin when manufacturing the paint. Solvents are added to reduce resin viscosity, thinning it for application purposes. Upon drying and curing, the solvent must volatilize from the coating into the atmosphere in a timely manner. If sufficient solvent volatilization does not occur and solvent is retained in the film, the coating may remain soft and plasticized, because the relatively large solvent molecules separate resin molecules from adjacent resin molecules. Bonding that may otherwise occur cannot be done, because the bonding moieties (chemical groups) are not close enough for attraction to occur. Moreover, many solvents are somewhat polar, particularly the oxygenated solvents (including the ketones, esters, and alcohols). These solvents are generally used to dissolve polar or somewhat polar resins, and hydrogen bonding to other polar groups of the resin retards or keeps the solvents from completely evaporating from the resin. Hydrogen bonding is the attraction of the oxygen atom in a molecule to nearby hydrogen atoms in other molecules. Retained polar solvents may draw water into the resin. This is particularly a problem with slowly evaporating alcoholic solvents, such as the glycol ethers. Coatings used in immersion service, particularly for the interior of deionized water or freshwater storage tanks, will

often blister due to retained solvents. This is a problem on tank bottoms, because the tank bottom is cooled by the earth (acting as a heat sink), while the tank sidewalls are warmed by the sun and air convection. The warmer temperatures assist in volatilization of solvents, while the cooler temperatures of the tank bottom result in a slower evaporation of retained solvents in the paint film. The entrapped solvents may draw water into the coating at the bottom of the tank, causing osmotic blistering. This may be a problem not only on tank bottoms but anywhere a heat sink may occur, such as exterior steel supports, cradles, or bracing. Baking or heating of tank interior coatings is often done to ensure solvent evaporation from the paint film and to elevate the temperature above the T_g to attain a higher cross-linking density of the chemically reacted coating resin.

Chemical Permeation. Coatings are widely used to protect against chemical attack on a variety of different substrates and in a variety of different chemical environments. The widespread use of coatings for such protection attests not only to the diversity of coating formulations but the inherent capability of resin and pigment technologies, when combined, to form a coating that resists chemical attack in diverse environments.

In the simplest sense, chemical attack may be categorized as that by acids and bases. The strength of an acid or base is a simple function of the degree of dissociation of the chemical into hydrogen ions, H^+ (acids), or hydroxyl ions OH^- (alkalis or bases). Acidic or alkaline strength is measured on the logarithmic pH scale, which is a scale with each number being ten times greater than the preceding number. A pH of 3 is ten times more acidic than a pH of 4, for example. A pH of 7 is exactly neutral, while 1 is strongly acidic and 13 is strongly basic or alkaline. However, water, salts, and solvents (all of neutral pH) can dramatically affect and degrade a coating. This type of neutral degradation is described elsewhere in this article.

For all practical purposes, the medium in which the acid or alkaline dissociation occurs is water. Even very small amounts of water are sufficient to dissolve and disassociate most chemical compounds into their acidic or basic constituents. At the molecular level, when such dissociation occurs and the acid or base comes in contact with a coating material, chemical attack can take place.

However, many chemicals are hygroscopic and will attract and react with water. Examples are most sulfur chemicals, including sulfuric acid, sulfamic acid, and sodium sulfide; sodium and potassium hydroxides; sodium carbonate; zinc chloride; most salts, such as sodium, potassium, and zinc chlorides; and many solvents, in particular the alcohols and glycols.

Acid Attack. Inorganic mineral acids, such as hydrochloric, sulfuric, and nitric acids, dissociate completely in water. Organic acids, such as carboxylic acids, formic acid, and butyric acid, do not completely dissociate and, as a consequence, are considered weaker acids. However, even these acids can aggressively attack most coating systems.

Acid gases, such as sulfur dioxide (SO_2), sulfur trioxide (SO_3), and nitrogen oxides (NO_X), react with moisture in the air in the form of precipitation or condensation to form sulfuric and nitric acids. Even carbon dioxide (CO_2), as a normal constituent of the atmosphere, reacts with moisture to form weak carbonic acid (H_2CO_3).

Chemical attack on a coating by condensation is more aggressive than that by precipitation such as acid rain. Moisture containing acidic constituents that condenses on the surface usually evaporates as the substrate warms during the day. As the moisture evaporates, the acids within the condensation droplet concentrate and more aggressively attack the substrate on which the condensation resides. Acid rain, on the other hand, will be diluted by successive rainfall, and the chemical contamination may be diluted or even washed from the surface.

The chemicals thus deposited, however, attack and cleave chemical bonds that are susceptible to deterioration. Chemical groups specifically vulnerable to acidic attack and cleavage are ether, urea, and urethane linkages, where cleavage occurs by a reaction of the hydrogen ion.

Alkaline Attack. Strong alkalis, such as sodium, potassium, and calcium hydroxides, will attack susceptible chemical groups in coatings. Perhaps the most widespread type of alkaline attack is saponification, the alkaline attack of the ester linkage of drying oils used in most oil-based coatings and alkyds. The attack may occur when oil-containing coatings or alkyd resins are applied over concrete, which contains alkali salts. When combined with water, these form caustic hydroxide ions. In a similar fashion, application of oil-based alkyds over zinc-rich coatings can also result in saponification, because zinc reacts with moisture to form alkaline zinc hydroxides. The hydroxides (OH^-) cleave (break) the ester linkage in the drying oil to form an organic acid and alcohol.

The bond breaking reduces molecular flexibility, embrittles the film, and ultimately will lead to resin deterioration and the formation of a sticky, soft coating under damp conditions, or a brittle powdery coating when dried. All coating resins containing ester groups are susceptible to such attack. However, some of those resins, such as polyesters and vinyl esters, are much more highly cross linked and formulated with epoxy resins and other materials to sterically hinder the ester group, protecting it from alkali attack. An illustration of alkaline saponification is shown in Fig. 4.

Figure 5 illustrates the vulnerability of various organic linkages to hydrolysis (reaction with water) and saponification (reaction with alkali) (Ref 8).

Acids and alkalis not only cleave covalent bonds of organic resins but may attack acid- or alkaline-susceptible pigments in the paint. Zinc pigments are attacked by both acids and alkalis. Aluminum pigments are susceptible to alkaline attack and have only slightly better acid resistance. Carbonate-containing filler pigments are aggressively attacked by acids. Many color pigments are susceptible to attack by either acids (cadmium red, molybdate orange, zinc yellow, cadmium yellow, ultramarine blue) or alkalis (iron blue, azo red and orange, chrome yellow).

Where there are pinholes and permeability through the coating, chemical species can penetrate, concentrate, and aggressively attack both the pigment and binder. Pigment agglomerations not completely wetted out by the coating resin are susceptible to this, particularly if there are pinholes and voids in the coating. However, ionic permeation is much slower than moisture permeation, and unless the pigment is exposed on the surface (by chalking or surface resin deterioration) or the chemical environment has access through pinholes, voids, or other discontinuities in the paint film, chemical attack of pigments is not usually a major problem.

Table 5 shows the sensitivity of some of the more common pigment types to chemical attack (Ref 8).

Oxygen permeation through a coating at the cathode in a metallic corrosion cell is usually the

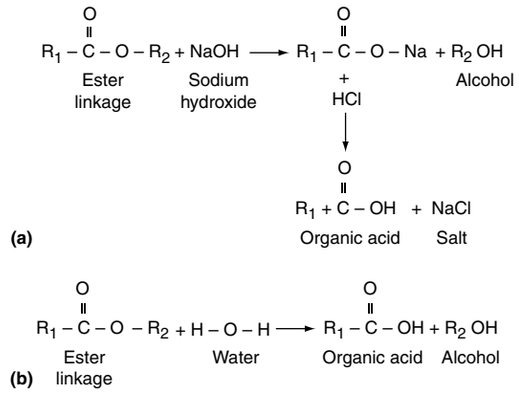

Fig. 4 Ester linkage where R_1 and R_2 are alkyl or aromatic groups. (a) Saponification and (b) hydrolysis of an ester linkage

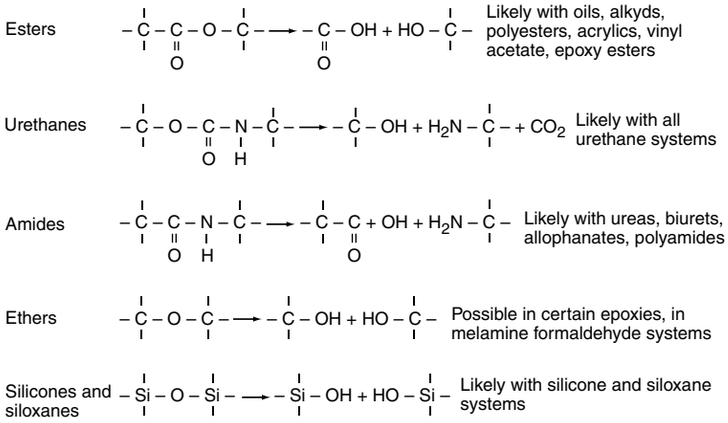

Fig. 5 Hydrolysis reaction of various resins. Source: Ref 8

Table 5 Chemical sensitivity of selected organic and inorganic pigment families

		Sensitivity	
Pigment type	**Examples**	**Alkali**	**Acid**
Inorganic			
Titanium dioxide	...	Excellent	Excellent
Zinc oxide	...	Moderate to good	Poor
Antimony oxide	...	Poor	Poor
Red iron oxide	Synthetic red oxide; Spanish, Indian, or Persian Gulf red	Excellent	Excellent
Cadmium red	...	Excellent	Poor
Molybdate orange	...	Poor to fair	Poor
Lead	Minium, mineral orange	Good	Poor
Yellow iron oxide	Ferrite yellow, sienna, ochre, umber	Excellent	Fair
Chrorme yellow	...	Poor to fair	Fair
Zinc yellow	Zinc potassium chromate	Fair	Poor
Cadmium yellow	...	Excellent	Poor
Nickel titanate yellow	...	Excellent	Excellent
Bismuth vanadate	...	Excellent	Fair
Zinc ferrite	...	Excellent	Good
Chrome green	Brunswick green	Poor	Poor
Chromium green oxide	...	Excellent	Excellent
Iron blue	Prussian blue, Midori blue, Chinese blue, mineral blue	Poor	Very good
Ultramarine blue	...	Very good	Poor
Carbon black	...	Excellent	Excellent
Black iron oxide	...	Excellent	Fair
Micaceous iron oxide	...	Excellent	Excellent
Zinc dust	...	Poor	Poor
Aluminum	...	Poor	Poor
Stainless steel flake	...	Excellent	Very good to Excellent
Organic			
Metallized azo reds	Lithols, permanents, rubines	Poor	Poor
Nonmetallized azo reds	Toluidines, paras, naphthols	Very good	Very good
Azo-based benzimidazolone reds	...	Very good	Very good
Quinacridones	...	Excellent	Excellent
Vat reds	Dibromanthrone, anthraquinone, brominated pyranthrone, perylenes	Excellent	Excellent
Azo-based oranges	Dinitroaniline, pyrazolone, tolyl	Good	Good
	Naphthol orange	Very good	Very good
Azo-based benzimidazolone oranges	...	Very good	Very good
Metallized azo oranges	Clarion red	Poor	Moderate
Monoarylide yellows	Hansa yellows	Very good	Very good
Diarylide yellows	Benzidine yellows	Very good	Very good
Azo-based benzimidazolone yellows	...	Excellent	Excellent
Heterocyclic yellows	Isoindoline, quinophthalone, azomethine, tetrachloroisoindolinone, triazinyl	Excellent	Excellent
Phthalocyanine greens	...	Excellent	Excellent
Phthalocyanine blues	...	Excellent	Excellent
Carbazole violets	...	Very good	Very good

Source: Ref 8

rate-determining factor in the corrosion reaction. The common anodic and cathodic reactions of metallic corrosion are:

Anodic reaction:

$$M \rightarrow M^{n+} + ne^-$$

where M is metal, n is number (of valency electrons), and e is electrons.

Cathodic reactions:

In near-neutral and alkaline environments:

$$^1/_2O_2 + H_2O + 2e^- \rightarrow 2OH^-$$

In acidic environments (in the presence of oxygen):

$$2O_2 + 4H^+ + 8e^- \rightarrow 4OH^-$$

In highly acidic solution and/or with the absence of oxygen:

$$2H^+ + 2e^- \rightarrow H_2 \text{ (gas)}$$

Thus, permeation of molecular oxygen is necessary for metallic corrosion in near-neutral and alkaline environments and, in many instances, determines the rate of corrosion. Corrosion is an expansive process, and undercutting corrosion beneath a well-applied coating system often causes the coating to crack and spall from the substrate, exposing the underlying surface to the environment and further corrosion attack. A means of corrosion protection in the oil industry is to remove oxygen from well injection water. In nuclear and chemical processing and other industries, the vapor space in a tank or vessel is made inert by adding nitrogen, carbon dioxide, combustion gases, or other gases to displace oxygen, thereby reducing or eliminating metallic corrosion.

Oxygen species (nascent atomic elemental oxygen, O; molecular oxygen, O_2; ozone, O_3) are very influential in the degradation of organic materials by UV light and solar radiation. Molecular oxygen absorbs solar radiation in the range of 176 to 210 nm. On absorption of UV radiation, the molecular oxygen is transformed into singlet oxygen, which dissociates, forming two oxygen atoms. The oxygen atoms recombine with molecular oxygen to form ozone. Ozone absorbs UV between 200 and 320 nm and in visible light (420 to 700 nm). In these UV ranges, stratospheric ozone dissipates energy as heat. This is beneficial, because high-energy UV, which is detrimental to life on earth, is absorbed. Ozone in the stratosphere does not influence the formation of ozone near the earth's surface, where ozone is produced by industrial combustion. Ozone is formed indirectly from nitrous oxide, which absorbs UV, forming molecular oxygen, which further reacts with more molecular oxygen to form ozone. Ozone is a strong oxidizer that reacts with most organic materials, including coatings, to form free radicals and ultimately cause photochemical embrittlement degradation.

In most cases, heat or radiation deterioration does not act alone but in conjunction with oxygen. Oxygen is a very reactive molecule, and if a free radical forms in its presence, then the oxygen can combine immediately with it to form a different radical. This radical may then abstract a hydrogen atom and form a hydroperoxide. A hydroperoxide is unstable and will decompose into two radicals. From the initial two radicals, a total of six possible radicals may form. This explains the danger of chain scission in the presence of oxygen, leading to a chain reaction (Ref 9).

The oxygen free radicals thus formed can further react with molecules in a coating or organic material in the same manner as described previously, causing chain scission, depolymerization, and fragmentation of the molecule, reducing its flexibility and resistance to permeation.

Stress Influences

Internal coating stresses build up during drying, curing, and upon aging. Curing stresses are caused by solvent evaporation (volume loss) and polymerization.

Cross-linking shrinkage is considered by some to be a primary cause of premature coating failure. Additionally, external stresses to a coating system are applied by movement of the substrate and by mechanical damage.

Coating Curing and Drying Internal Stresses. Paints and coatings can be formulated to provide specific functions. The fact that a paint can be applied in liquid form gives it the ability to wet, penetrate, seal, cover, and adhere to most substrates, even those with complex shapes. Moreover, application of the liquid by brush, roller, or spray is fast, inexpensive, and relatively convenient. However, the conversion of a paint from liquid to solid provides some inherent stress to the coating and, in extreme conditions or if adhesion is not adequate, may cause failure to the coating.

If a coating is not 100% solids, it contains a volatile material such as water or solvents. Drying of the coating and its conversion from a liquid to a solid results in a volume decrease as the water or solvent evaporates into the atmosphere. Most coating materials will initially gel within seconds to hours after application, because most of the volatiles leave, and the paint dries on the surface. The shrinkage that occurs with the loss of volatile materials will provide some initial stress to the coating and to the coating adhesion. However, this stress is minimal, because the paint has not sufficiently solidified, is still deformable, and can internally dissipate these initial stresses. However, as the paint dries further, and particularly if chemical cross linking occurs, further stresses are applied to the drying coat. Sometimes, low-molecular-weight plasticizers such as pthalates, phosphates, adipates, and chlorinated biphenyls migrate to the surface of the paint and volatilize or at least collect at the surface. When this happens, the molecular volume of the resin decreases. This decrease in volume applies a tensile stress to the cross section of the paint film and, in extreme cases, may result in cracking, peeling, or loss of adhesion. In a similar fashion, progressive cross linking, either by reaction with oxygen from the air (autooxidation) or covalent bonding between reactive moieties of part A and part B components of a coating, provides a further hardening, increasing brittleness, and tensile stress to the coating. In many coatings, these latent cross-linking reactions occur slowly over time, often years, such that the coating slowly hardens and embrittles with age. Where the coating has been applied thickly, the stresses will be greater than in areas where the coating is thin. Variation in thickness will cause an uneven distribution of stress on the coating, further aggravating the potential for cracking or peeling.

Highly cross-linked coatings, particularly 100% solid materials formulated with low-viscosity co-reactants, are particularly susceptible to internal cross-linking stresses. Polyesters, vinyl esters, and other thick-film highly cross-linked coatings must be properly formulated and pigmented to satisfactorily reduce these internal stresses. The low-molecular-weight epoxies, including bisphenol-F and novolac epoxies, must also be properly plasticized and pigmented to dissipate internal curing stresses.

Until recently, the best means of assessing the extent of internal stress/curing stress on a coating would be to apply the coating system to a test panel or a test patch in the area of intended service, wait for curing and drying to occur, and then evaluate the coating over time to see if stress cracking, peeling, disbonding, or other evidence of distress occurred. Recently, tests have been developed (but not yet standardized) whereby a coating material is applied to one side of a thin foil strip that is held in position at one end and allowed to deflect at the other. The amount of deflection at the free end is indicative of the internal shrinkage stress as the coating dries and cures.

External Stress—Vibration, Flexibility, Stress-Strain. External stresses on a coating usually affect an applied coating to a greater extent than internal stresses. One walking across a bridge feels the movement, flexing, and vibration caused by traffic. Changing water level in a water storage tank flexes and bows the side walls and tank bottom. Wind, snow loads, ponding water, and other forces may deflect a metal surface, stressing the coating applied to it. Vehicles and machinery are subject to cyclical stresses, resulting from vibration and flexing, that can be detrimental and can degrade both the metal substrate and any coating applied to that substrate.

Solar heating by day and cooling by night cause expansion and contraction of all materials. Stress resulting from such thermal expansion and contraction can be aggravated under winter conditions in cold weather climates, where a coating becomes somewhat embrittled due to cold temperatures. Relatively rapid heating and cooling during daily temperature fluctuations is often more of a problem in the winter than in the summer. Some accelerated tests done by laboratories have used a freeze-thaw cycle to provide additional stress on a coating to assess its potential for a service environment, even in a warm climate where no freezing is expected. If the coating can survive the freeze-thaw cycling, quite likely it will be able to resist any thermal cycling that may be encountered in actual service. The external stresses resulting from vibration, flexibility, and cyclical stress-strain from thermal expansion and contraction are major detriments to coating systems, particularly those that may have high internal stresses, or for coatings that have been applied to excessive thicknesses.

Impact and Abrasion. While coating curing and drying stresses as well as vibration flexing and stress-strain are relatively slow transient influences, impact and abrasion damage to a coating is usually sudden, localized, and abrupt. Mechanical damage, from dropped tools, stones, or other types of mechanical damage, where the coating surface is impacted either directly or reversely (impacted from either the side the coating is on or from the opposite side), may cause the coating to crack and/or spall. Impact damage is greatest when a coating has high internal stress and is very brittle, or is at or below its T_g.

Abrasion occurs as a result of scraping, scuffing, or erosion due to contact with small moving particulate matter, such as sand or slurries. As a general rule, harder, more brittle coats are more susceptible to abrasion damage than are rubbery, softer coatings. However, specific resistances are dependent on the formulation of the coating, because many hard coatings have abrasion-resistant pigments, such as aluminum oxide, quartz, silica (sand), garnet, and other hard materials, embedded in them to resist abrasion and erosion wear. Rubbery, elastomeric coatings have the ability to deform under abrasion, up to a critical point, after which they recover their original form. Energy transmitted during the abrasion and/or impact is absorbed by the elastomeric resin and dissipated as heat within the flexible molecular structure.

However, hard, brittle coatings and coatings in cold temperatures or below or close to their T_g may not have the flexibility to resist abrasion or erosion wear. In these instances, the coating may tear on the surface or be scraped or ablated away, resulting in a thinning of the coating at the areas of abrasion/erosion.

At areas where abrasion/erosion is expected, natural or synthetic rubbers should be used. Anti-abrasion pigments should be added to the resin or cast and embedded into the top surface of the coating to make it more abrasion resistant. In some cases, a softer, more elastic thick-film coating can also be used to resist scuffing and abrasion.

Biological Influences

Microorganisms are the earliest and most numerous life forms on earth. They are ubiquitous, occurring in virtually all natural environments, including those considered until recently to be inhospitable to life: undersea volcanic vents with high concentrations of sulfur, hot springs, extremely acidic and alkaline chemical environments, anaerobic (no oxygen) environments, and in locations devoid of sunlight. Microorganisms and macroorganisms, such as mildew and marine flora and fauna fouling, can cause considerable damage to coatings and dramatically affect the properties and functions of coating systems, negating their purpose.

Microbiologically Influenced Corrosion. Degradation of coatings can occur from electrochemical and biological processes resulting from the presence of microbes. Microbial adhesion, establishment, and growth into colonies are prerequisites for deterioration of organic materials by microbiologically influenced corrosion (MIC). Much, but not all, microbial growth occurs in a biofilm, which is a gel consisting principally of polysaccharides that protects the microbe and enables it to form an environment that is conducive to its reproduction and colony growth (Ref 10). The process by which a material is decomposed or otherwise altered by a microbe colony results in the formation of degradation products of the polymer, which the microbe uses as a source of energy, notably carbon. This may result in the depolymerization of the organic molecule, breaking it up into smaller units that can be assimilated by the organism.

Most MIC attack on coatings results from acids or enzymes produced by bacteria during metabolism. A MIC attack almost always occurs in immersion or a wet environment. Different bacterial families produce different metabolic products, usually acids of various strengths. Coatings usually specified for immersion or corrosion protection in wet or immersed environments are resistant to the acids and enzymes produced by MIC. However, if resins or pigments used in a coating subject to MIC are not acid resistant, acid attack and deterioration may occur. Deterioration of the coating usually occurs as a result of bacterial access and attack at cracks, pinholes, or voids through the coating, allowing the bacteria and bacterial metabolic byproducts access to the underlying substrate. The deterioration of the substrate at these local areas of attack results in an undermining of the coating and further cracking and bacterial access. Substrate deterioration continues to occur, often in an aggressive fashion. Microbes that may cause damage to a coating may not be implicated in deterioration of a substrate, and conversely, often microbes that will aggressively attack a substrate will not degrade a coating system applied over that substrate.

Mildew. In warm, moist environments, and particularly in the southeastern part of the United States and in tropical countries, the presence of molds and mildews on paint (and, for that matter, many other materials) is of concern. Molds and mildews are forms of fungi whose spores are ubiquitous in the environment. The spores require moisture and heat in order to germinate and grow. Generally, 70% relative humidity with temperatures of 5 to 50 °C (40 to 120 °F) are necessary for mold and mildew growth. Slightly acidic pHs (in the range from 4.5 to 6.5) are preferable. Alkaline conditions above a pH of approximately 8.5 are not conducive to most fungal growth.

In order for fungal growth to occur, the spore must remain in contact with the surface and have moisture and a source of food. Accordingly, a rough-textured surface that collects dirt and holds moisture will provide a good surface for fungal growth. Food sources for the spore can be pollen, organic debris carried in the wind, contamination from intermittent water, or the painted surface itself. Oil-based coatings, alkyds, and polyamide cured epoxies are susceptible to fungal attack due to the fatty acids in the oils or cross-linking copolymer. Phthalate plasticizers may also be a food source for fungi. Latex paint systems, particularly those containing oil or alkyd modifications for adhesion to chalky surfaces, are also very susceptible to mildew or mold growth. The fungal spores can either feed directly on the fatty acid constituents in the paint or secrete enzymes that will break down portions of the paint binder into components that then can be used as food for the fungus.

When a mold or mildew grows on the surface of a paint, the growth can collect more dirt and dust from the atmosphere and hold moisture, perpetuating its growth. As the fungus feeds on the paint, the resinous binder is degraded by scission of ester linkages, oxidation of oil fatty acids, and accumulation of metabolic acidic products. Not only is the paint degraded, but it is covered with an unsightly black growth.

Fungicides formulated into paint reduce or eliminate mildew and mold growth. Basic zinc oxide added to oil-based and latex paints in amounts of 120 to 360 g/L (1 to 3 lb/gal), perhaps in combination with some organic fungicides, substantially reduces or eliminates fungal growth.

Existing molds and mildews can be killed by a dilute hypochlorite solution (bleach). Bleach will kill the fungus turning it white. If dirt is present, it will not be bleached and will remain a dark color. After the fungus, is killed, it should be removed from the paint surface by scraping and/or scrubbing prior to painting. However, if heat, moisture, and a food source are still present after repainting, it is likely that spores may reattach and grow. Mildews and mold are relatively easy to kill by bleaching, but their spores can often survive a bleach treatment and commence growth if conditions are right.

Marine fouling consists of attachment of plant or animal life to an immersed structure. Virtually all underwater surfaces have some type of marine attachment, including ships, piers, and pilings.

Animal fouling species are most commonly barnacles, mussels, and tubeworms. Fouling vegetation are algae or seaweeds (ectocarpus, enteromorpha, or laminaria). Both animal and plant fouling require contact with the substrate for 24 h or more in order to attach. Consequently, if water is fast-moving, over approximately 10 knots (5 m/s, or 17 ft/s), or if the surface is smooth with no fissures or crevices, marine fouling is minimized or eliminated.

Marine foulants generally do not attack paint and degrade it, but by virtue of their adhesion, they roughen the surface to which they are attached, providing considerable friction to the smooth flow of water around the fouled object. If that object is a ship, even minimal marine fouling can reduce its speed and increase its fuel consumption by 10% or more.

Antifouling coatings are used to kill or prevent attachment of marine organisms. Tributyl tin antifoulants were used successfully in the past, but because they accumulate in species used for food and are toxic to most marine life, they have been banned from use on most U.S. flagships. Currently, antifoulants based on copper oxides are most commonly used, but these too are toxins, and there is concern that ultimately these may also be prohibited. Nonstick fluorinated hydrocarbon resins, such as Teflon, and silicone-based binders are being used with only limited success at present. These materials function by providing a surface to which the marine fouling organism cannot tightly attach. When a ship is underway, the friction from flowing water is sufficient to wash growth from the nonstick antifoulant paint surface. Even when marine fouling does attach, it can be more readily removed by scraping or hosing down with high-pressure water washing.

REFERENCES

1. "Corrosion Costs and Prevention Strategies in the United States," FHWA-RD-01-156, U.S. Department of Transportation, Federal Highway Administration, March 2002, p v, C-3
2. "Corrosion Protection of Steel Structures by Protective Paint Systems, Part 2: Classification of Environments," ISO 129444-2, International Organization for Standardization, 1998
3. Systems and Specifications, *SSPC Painting Manual,* Vol 2, 8th ed. SSPC: The Society for Protective Coatings, p 3–7
4. G. Wypch, *Handbook of Weathering,* 3rd ed., ChemTec Publishing, 2003, p 58
5. C.H. Hare, *Protective Coatings,* SSPC 94-17, Technology Publishing Company, 1994, p 464
6. G.P.A. Turner, *Paint Chemistry,* 3rd ed., Chapman and Hall, 1993, p 27
7. M. Hess, H.R. Hamburg, W.M. Morgans, *Hess's Paint Film Defects,* 3rd ed. Chapman and Hall, 1979, p 185

8. C.H. Hare, *Paint Film Degradation,* SSPC: The Society for Protective Coatings, 2001, p 311, 318–319
9. D.P. Garner and G.A. Stahl, Ed., *The Effect of Hostile Environments on Coating and Plastics,* ACS Symposium Series 229, American Chemical Society, 1983, p 15
10. K.B. Tator, Preventing Hydrogen Sulfide and Microbiologically Influenced Corrosion for Wastewater Facilities, *Mater. Perform.,* July 2003, p 33

SELECTED REFERENCES

General

- R. Craft, Light Scattering by Titanium Dioxide Pigment, *Mod. Paint Coat.,* Oct 1989
- Gerteis and Elm, Photochemistry of Titanium Dioxide Pigments and Its Relationship to Chalking, *J. Paint Technol.,* Vol 43 (No. 555) April 1971
- C. Hare, Trouble with Paint, Irreversible Degradation of Paint Films, *J. Prot. Coat. Linings,* Aug 1999
- Pappas, Weathering of Coatings—Formulation and Evaluation, *Prog. Org. Coatings,* Vol 17, 1989, p 107–114
- Sullivan, Weatherability of Titanium Dioxide Containing Paints, *Prog. Org. Coatings,* Vol 1, 1972
- Volz et al., Surface Reactions on Titanium Dioxide Pigments in Paint Films During Weathering, *Prog. Org. Coatings,* Vol 2, 1973–1974, p 223–235

Thermal degradation

- C. Hare, Trouble with Paint, Dehydrochlorination, *J. Prot. Coat. Linings,* Sept 1999
- C. Hare, Trouble with Paint, Thermal Degradation, Part 1, *J. Prot. Coat. Linings,* Sept 1999
- C. Hare, Trouble with Paint, Thermal Degradation, Part 2: Pigments, *J. Prot. Coat. Linings,* Oct 1999

Chemical attack

- C. Hare, Trouble with Paint, Chemically Induced Degradation, *J. Prot. Coat. Linings,* Dec 1999
- Schilling, Caveat Emptor: Understanding Coating Failures in Petrochemical Facilities, *J. Prot. Coat. Linings,* March 1989, p 39–40 (chemical reactivity of red iron oxide pigment)
- Schilling, Understanding Coating Failures: Success Is Rarely an Accident, *J. Prot. Coat. Linings,* March 1990, p 47 (impact of CP), p 49 (chemical reactivity of aluminum pigment)

Radiation effects

- Watson et al., Radiation Effects on Paints, *Mater. Perform.,* Feb 1967

Air pollution

- Campbell et al., Assessing Air Pollution Damage to Coatings, *J. Paint Technol.,* June 1974

Light stabilizer additives

- Callais et al., Synthesis of Acrylic HSC Resins with Peroxides Containing Hindered Amine Light Stabilizers, *Mod. Paint Coat.,* Sept 1988
- Golemba et al., Mechanisms of Ultraviolet Stabilization of Polymer Films, *J. Paint Technol.,* Vol 41, (No. 532), April 1969
- Nielsen and Wicks, Effect of Internal UV Absorbers on Photodegradation of Urethane Coatings, *J. Paint Technol.,* Vol 47 (No. 601), Feb 1975
- Paint Additives, *Raw Materials and Their Usage,* Vol 1, *Surface Coatings,* 3rd ed., Chapman and Hall, 1993

Microbiological degradation

- J.-D. Gu et al., "Microorganisms and Microbial Biofilms in the Degradation of Polymeric Materials," Paper 3570, Corrosion 2003, NACE International
- M. Stranger-Johannessen, *Microbial Deterioration of Corrosion Protective Coatings,* Center of Industrial Research, Oslo, Norway
- Summer, Microbial Degradation of Plastics, *Corros. Technol.,* April 1964

ASM Handbook, Volume 13B: Corrosion: Materials
S.D. Cramer, B.S. Covino, Jr., editors, p600-604
DOI: 10.1361/asmhba0003845

Environmental Performance of Thermosetting Plastics and Resin Matrix Composites

Terry W. Cowley, DuPont

MANY FACTORS contribute to the corrosion-resistant effectiveness of fiberglass-reinforced plastic (FRP) or glass-fiber-reinforced plastic equipment made with thermosetting resins. Simply put, FRP is more than just a plastic and a reinforcing fiber. The thermosetting resin type, the cure system, the degree of cure, the reinforcement types, the design, and the fabricator are all factors to consider. There are a variety of resins available today to handle a wide variety of chemical environments—from organic solvents to 50% caustic solutions to 98% sulfuric acid. However, no single thermosetting resin will handle every environment. More than a basic knowledge of FRP is required in specifying resin and fabrication requirements. Two things that a FRP user or potential user should remember are:

- The best thermosetting resin is no better than the fabrication process and the fabrication standards used.
- Just because a FRP corrosion-resistant liner looks bad does not mean it is not still doing its job.

Fabrication of FRP Equipment

A simplified view of a laminate structure for FRP equipment, such as a tank made with epoxy vinyl-ester and polyester resins, is shown in Fig. 1. The corrosion-resistant liner or corrosion barrier is resin rich, with generally an initial 0.3 to 0.5 mm (10 to 20 mils) thick veil that contains 90 to 95 wt% resin. A veil is a thin surface mat, often composed on glass or organic fibers, intended for increased corrosion resistance due to its higher resin content. The veil is followed by approximately 2 to 2.5 mm (80 to 100 mils) of chopped strand glass mat containing 70 to 80 wt% resin. The structural wall will have an approximate resin content of 30 to 70 wt%, depending on the method of fabrication: hand lay-up, filament winding, or a combination of the two. The resin provides corrosion resistance and holds the shape of the fiberglass. The fiberglass provides strength. Therefore, the most corrosion-resistant portion of FRP equipment is in contact with the corrosive environment. It is recommended that the corrosion-resistant liner be excluded from strength requirements for FRP equipment. By doing this, a 75% loss of corrosion-resistant liner thickness is an acceptable loss before the tank needs to be replaced or relined.

Fiber-reinforced equipment made with epoxy thermosetting resins generally has no corrosion-resistant liner, or a minimal corrosion-resistant liner of one to two veils. Compression-molded parts, such as pipe elbows, fabricated with epoxy vinyl-ester resins do not generally have a corrosion-resistant liner and should not be used in alkaline and strong acid environments. Some smaller FRP equipment is made with an epoxy vinyl-ester resin corrosion-resistant liner and an epoxy resin structural wall. The glass types used in the fabrication of FRP equipment are coated with a sizing material that enables resins to thoroughly wet out the individual glass fibers. Mallinson's book, *Corrosion-Resistant Plastic Composites in Chemical Plant Design,* provides a more detailed description of the various fabrication techniques employed (see Selected References).

Because caustic, sodium hypochlorite, and hydrofluoric acid environments rapidly degrade glass, it is recommended that two layers of synthetic (nonglass) apertured veils, such as a polyester veil, be used for these environments (Ref 1–4). The polyester fibers of an apertured veil are woven in such a manner that a pattern of small squares is formed through the veil. Carbon veil also provides excellent resistance to caustic and hydrofluoric acid environments (Ref 5, 6). Two layers of veils are recommended for concentrated hydrochloric acid environments (Ref 7, 8). It is also appropriate for the end user to specify double the thickness of chopped strand glass mat in the corrosion barrier for many environments, such as caustic, sodium hypochlorite, and concentrated hydrochloric acid solutions (Ref 5, 8–10).

For improved corrosion resistance to all environments, equipment internals should be fabricated with only chopped strand glass mat and specified veil(s). All cut edges exposed to the chemical environment should be covered with the same number and veil type as specified for the corrosion barrier. In doing this, the cut edge becomes similar to the corrosion barrier. All polyester and epoxy vinyl-ester resin laminates exposed to the air (secondary lay-ups) during cure should have a final resin coat containing paraffin to ensure complete resin cure. The final resin coat containing paraffin should be highly catalyzed in order to cure properly.

Types of chopped strand glass mat are manufactured that provide improved resistance to strong acid environments, such as hydrochloric acid. Chopped strand glass mat with improved resistance to caustic environments is currently being developed. The end user should strive to specify glass mat that provides the improved resistance required.

Structural specifications for FRP tanks are provided by codes and standards of the American Society of Mechanical Engineers. Information on these documents, as well as papers describing leak detection systems for FRP equipment, can be found in the Selected References of this article.

Resins and Their Resistance to Various Environments

Corrosion-resistant thermosetting resins can be categorized by families of resins and their associated types, as indicated in Table 1.

The polyester, epoxy, and epoxy vinyl esters are also available halogenated with bromine or chlorine molecules to provide fire-retardant properties. The brominated versions of epoxy

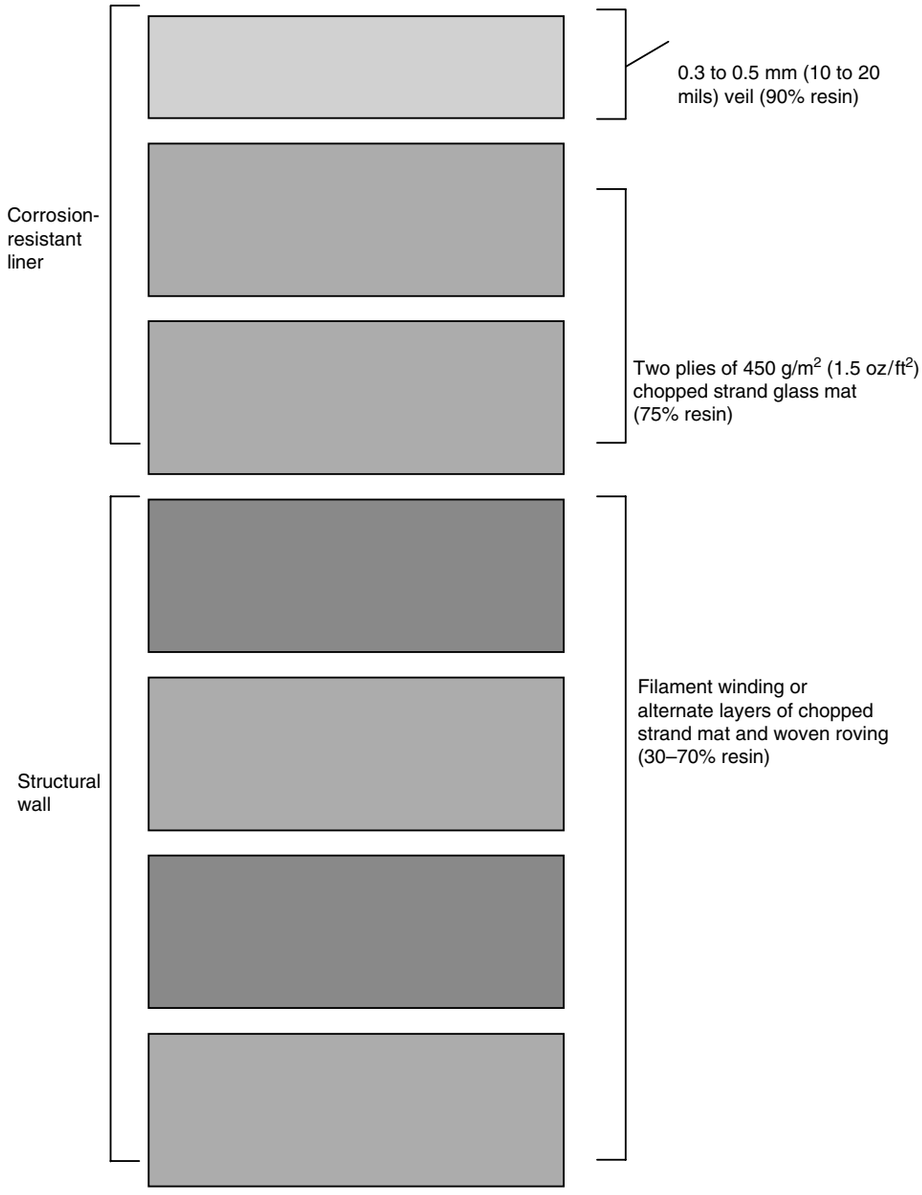

Fig. 1 Typical lay-up sequence for fiberglass-reinforced plastic

Table 1 Corrosion-resistant resins

Family	Types
Polyester	Isophthalic
	Terephthalic
	Bisphenol-A fumarate
	Chlorendic anhydride
Epoxy	Bisphenol-A
	Epoxy novolac
Epoxy vinyl ester	Bisphenol-A
	Epoxy novolac
Furan	No specific types
Phenolic	No specific types

vinyl-ester resins have been shown to provide improved corrosion resistance to sodium hypochlorite, chlorine dioxide, chlorine, and hydrogen peroxide environments (Ref 1, 10–12).

Polyester. The isophthalic and terephthalic resins provide good corrosion resistance to waste-water and weak acid environments but are not recommended for alkaline environments. However, the bisphenol-A fumarate polyester resins were the first resins that provided good corrosion resistance for a wide range and concentration of acids, caustics, and oxidizing environments.

Epoxy resins provide good corrosion resistance against acids, caustics, and solvent environments, although the corrosion resistance is highly dependent on the type of hardener used. One FRP pipe manufacturer uses an epoxy novolac resin with a proprietary hardener to make pipe that will handle 98% sulfuric acid (Ref 13). The same epoxy novolac resin cured with other types of hardeners would not perform as well. Hardeners are discussed in the section "Curing Thermosetting Resin Types" in this article.

Epoxy vinyl-ester resins provide the best overall corrosion resistance to the widest variety of environments, caustics, acids, oxidizing solutions, and solvents. The bisphenol-A and brominated bisphenol-A epoxy vinyl-ester resins provide the best resistance against caustic and alkaline hypochlorite solutions, respectively. The epoxy novolac vinyl-ester resins provide the best resistance to strong acids, such as sulfuric acid, and solvent environments (Ref 1, 5, 7–9, 14).

Furan and phenolic thermosetting resins are known for their solvent resistance as compared to the other resin families (Ref 5, 15, 16). These resins have inherently good fire-retardant properties and produce low levels of smoke, meeting the class 1 flame-spread requirement of ASTM E 84 (Ref 17) without the use of fire-retardant fillers (Ref 15, 16, 18). Halogenated (brominated or chlorinated) thermosetting resins can meet a class 1 flame-spread rating in accordance with ASTM E 84 when antimony trioxide or pentoxide at the level of 3 to 5% is added to the resin. However, the smoke levels are high (Ref 5, 8, 9). The addition of the antimony oxides to a nonhalogenated resin will not make the resin fire retardant. Bromine or chlorine molecules must be present for the antimony oxides to improve resin fire retardancy. Some highly halogenated resins have achieved a class 1 flame-spread rating in accordance with ASTM E 84 without the addition of an antimony oxide (Ref 5, 19). It is recommended that the antimony oxides be added only to the structural portion of FRP equipment, because the addition of a filler may reduce the corrosion resistance of the resin laminate. It is a good practice to use the highest-rated fire-retardant resin without antimony oxide in the corrosion barrier and to use a lower-rated fire-retardant resin with antimony oxide for the structural portion of FRP equipment. Please note that the resins are organic materials, and the fabricated products made with the resins will burn under the right conditions (Ref 8).

Concentration of Chemicals. As a rule, thermosetting resin laminates are degraded more rapidly by more highly concentrated chemical environments. This is certainly true of acid, organic, and solvent environments. Figure 2 shows the degradation of an epoxy vinyl-ester resin laminate in a neutralization tank. Concentrated sulfuric acid had leaked by the inlet valve and, over time, severely damaged the laminate. Notice that the degradation disappears toward the bottom of the figure. This is due to the sulfuric acid being diluted at the aqueous liquid level. Methylene chloride has the same effect on epoxy vinyl-ester resin laminates. When methylene chloride is completely soluble in aqueous solution (< 1.5 wt%), it has virtually no detrimental effect on epoxy vinyl-ester resin laminates. However, if methylene chloride

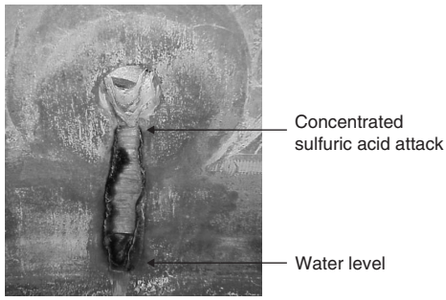

Fig. 2 Concentrated sulfuric acid attack of fiberglass-reinforced plastic tank. Dilution effect shown toward bottom

becomes high enough in concentration to phase out of solution, most epoxy vinyl-ester resins will be destroyed in less than 24 h. An exception to this is laminates made with epoxy novolac vinyl-ester resins with low styrene content, <35 wt%. These laminates may last for several months (Ref 14).

Concentrated hydrochloric acid is known to form blisters in FRP corrosion barriers. For concentrated hydrochloric acid solutions, it is recommended that an epoxy novolac vinyl-ester resin be used with two veils and at least four layers of 450 g/m^2 (1.5 oz/ft^2) hydrochloric-acid-resistant chopped strand glass mat (Ref 8).

Other exceptions to the general rule are alkaline and inorganic salt solutions. Fifty percent sodium hydroxide has no detrimental effect on a thermosetting resin laminate but does become more aggressive at concentrations between 5 and 20%. Saturated brine (sodium chloride) has virtually no effect on thermosetting resin laminates (Ref 2, 20).

Temperature. As the temperature of a chemical environment increases, so does its ability to degrade a resin laminate. Resin manufacturers provide maximum recommended temperatures and concentrations for the resins in specific environments.

Hot distilled and deionized water and steam can cause blisters to form in corrosion-resistant laminates because of osmosis. Water molecules can permeate the resin laminate and form microscopic pools that dissolve any soluble material. This becomes a very concentrated solution because of the small amount of water. Osmosis is driven by concentration. The more dilute solution pumps water to the more concentrated solution to equalize the concentrations of the two solutions. As more water enters the resin laminate, blisters are formed. Blisters can be expected but are not necessarily a cause for concern. They may grow to a certain size and not become any larger (Ref 21–24). The author has observed blisters in vent stacks several feet in size but made no recommendation for repair.

Ultraviolet (UV) light from the sun slowly degrades the resin on the outside surface of FRP equipment, resulting in loose or exposed glass fibers. This is called fiber bloom. This should not be cause for concern, because only 0.3 to 0.5 mm (10 to 20 mils) of the equipment is affected. Although fiber bloom is not aesthetically pleasing, there is no loss of strength in the equipment (Ref 25). Generally, UV inhibitors are used in the outer layer of resin to reduce the degradation, but the inhibitors may be used up over time. It is recommended that a pigmented resin gel coat or coat of pigmented epoxy paint with UV inhibitors be applied to the surface of finished FRP equipment to provide the best resistance to UV light degradation. If FRP equipment is not gel coated or painted, it is recommended that an apertured polyester veil be applied with the last layer of resin to reduce glass fiber bloom. Touching a surface that has fiber bloom can result in cuts from the exposed glass fibers. Using a polyester veil significantly reduces any exposed glass fibers. Particulate erosion may contribute to gel coat degradation as well.

Fillers. It is recommended that no fillers be added to the corrosion barrier, because the filler may be detrimental to the resin laminate corrosion-resistance properties. However, two environments may require the addition of filler to improve the properties of the corrosion barrier:

- Process streams containing solids, where the flow rate may cause abrasion of the laminate (Ref 26, 27)
- Thermal shock

The first response to these two environments should be to choose a resin with the highest percent elongation that will still meet the corrosion-resistance requirements (Ref 26, 28). For abrasion resistance, hard filler, such as silicon carbide and alumina, may be added to the corrosion barrier. Silicon carbide and alumina have a Mohs hardness ranking of 9 (for comparison, diamond is 10) (Ref 26, 27). Synthetic veils, such as apertured polyester, have shown improved abrasion resistance in parallel flows compared to c-glass veil (Ref 4, 29, 30). Erosion can be a problem at sharp turns in FRP pipe if a process stream is flowing at excessive speeds. Abrasion-resistant fillers may be added to the corrosion barrier, or the corrosion barrier may be made thicker (Ref 27).

The second environment that may require a filler in the corrosion barrier is the occurrence of rapid temperature changes. To reduce the effect of severe thermal shock, thermally conductive materials, such as graphite and silicon carbide, may be added to the corrosion barrier. These materials aid the resin laminate in resisting differential thermal expansion damage by rapidly transferring temperature changes throughout the laminate layers (Ref 31, 32). The materials are added in the range of 15 to 30 wt%, based on the resin weight. Also, a thermosetting resin with the highest elongation that will still meet the corrosion-resistance requirements should be used. Many times, a highly flexible resin without thermally conductive fillers is all that is necessary to resist thermal shock (Ref 32, 33).

Graphite, silicon carbide, and alumina are resistant to most chemical environments and thus can be added to corrosion barriers with little to no concern about their effect on the corrosion-resistance properties of corrosion barriers. However, strong sodium hypochlorite bleaching environments will degrade graphite powders.

Graphite may be added to the corrosion barrier to make it electrically conductive (15 to 30 wt%, based on the resin weight). A graphite or carbon veil may be incorporated into the corrosion-resistant barrier to enhance the conductivity of the laminate. This may be desired when the contents of the FRP equipment may cause a static charge to build up on the equipment wall. The conductive corrosion barrier can be attached to ground to dissipate any static charge on the wall (Ref 27, 34–36).

When fillers are added to a resin laminate, the strength of the laminate is affected. This effect is not significant until the filler content exceeds 10 wt% (Ref 27). However, the fillers are to be added to the corrosion barrier only. If, as recommended earlier, the corrosion barrier is not used to contribute to the structural strength, then a loss in physical properties should not be of concern. It is recommended that secondary bonds to the corrosion barrier be doubled in length because of the change in secondary bond strength.

Whenever a filler is added to a resin system, its effect should be tested to ensure that it does not impair the final resin cure.

Food Applications. Several types of thermosetting resins, when properly formulated and cured, comply with the Food and Drug Administration (FDA) regulation 21 CFR 177.2420, allowing their contact with food. Care must be exercised when using the resins for FDA applications, and the end user should work closely with the resin manufacturer and fabricator to assure compliance (Ref 5, 8, 9).

Resin Recommendations. When seeking a corrosion-resistant resin system for specific applications, it is strongly recommended that the end user consult corrosion resistance guides of the various thermosetting resin manufacturers and original equipment manufacturers. If the chemical environment of concern cannot be found, contact the resin manufacturer's technical service group for recommendations. Many times, knowing how different environments affect a resin system will enable the technical representative to make a sound recommendation on an unlisted environment. Also, the manufacturers of epoxy pipe can provide the end user with the best recommendations for their products, because the products have undergone corrosion testing at higher temperatures. Table 2 provides a partial list of North American thermosetting resin manufacturers and the type of resins manufactured.

Curing Thermosetting Resin Types

The great majority of FRP equipment made with polyester and epoxy vinyl-ester resins is

Table 2 Resin manufacturers and resins produced

Manufacturer	Product				
	Polyester	Epoxy	Epoxy vinyl ester	Furan	Phenolic
AOC, Collierville, TN	X	...	X	...	...
Ashland Chemical, Dublin, OH	X	...	X	X	...
Borden Chemical, Naperville, IL	X	...	...	...	X
The Dow Chemical Co., Midland, MI	...	X	...	...	...
Interplastic Corporation, St. Paul, MN	X	...	X	...	...
Penn Specialty, Chemicals, Inc., Memphis, TN	...	...	...	X	...
Reichhold Chemicals, Inc., Research Triangle Park, NC	X	...	X	...	...

cured using methyl ethyl ketone peroxide (the initiator), cobalt naphthenate (the promoter), and in cool/cold weather, N,N-dimethylaniline or N,N-dimethylacetoacetamide (the accelerator). Other liquid peroxides are available that reduce the reaction exothermic temperature as well as reduce foaming. For sodium hypochlorite and hydrogen peroxide applications, the epoxy vinyl-ester resin should be cured with benzoyl peroxide and N,N-dimethylaniline or N,N-diethylaniline. This is because the cobalt decomposes hypochlorite and hydrogen peroxide to produce a by-product that is very aggressive to thermosetting resin laminates and will shorten the service life of the equipment (Ref 1, 3, 12).

Generally, the room-temperature cure of polyester and epoxy vinyl-ester resin laminates is more than sufficient to provide the required corrosion resistance and physical properties for most environments. However, for maximum corrosion resistance and service life in caustic, sodium hypochlorite, hydrogen peroxide, pure water, and steam environments, the corrosion-resistant barrier of the FRP equipment should be postcured at elevated temperatures for specified times. The required temperatures are those of the corrosion-resistant laminate, and time should not start until the laminate reaches the specified temperature. Consult the resin manufacturer's recommendations for postcure temperatures and times.

Because the total curing system for polyester and epoxy vinyl-ester resins is, at the most, 3 wt% of the total resin composition, the corrosion resistance and physical properties of the cured resin laminate are due to the resin properties. However, the choice of hardeners for epoxy resins can have a dramatic effect on resin laminate properties. Epoxy resins can be cured with a wide variety of hardener types, such as aliphatic, cycloaliphatic, and aromatic polyamines; anhydrides; polyamides; and catalytic curing agents. The quantity of hardener used for epoxy resins is much higher than the cure system for polyester and epoxy vinyl-ester resins. The hardener amount can be as high as 1 part resin to 1 part hardener. Because of the high amount of hardener used and the variety of hardeners used to cure epoxy resins, the hardener contributes significantly to the final corrosion resistance and physical properties of the cured epoxy resin. The great majority of FRP equipment made with epoxy resins requires a postcure in order to provide the required corrosion resistance and physical properties. These postcures often require ramped temperatures to prevent damage to the equipment during postcure. Consult the resin manufacturer's recommendations for postcure temperatures and times. Because the cure temperatures for epoxy resins can be significantly higher than for polyester and epoxy vinyl-ester resins, epoxy resin use is most often restricted to smaller parts, such as pipe and relatively small tanks.

Furan and phenolic resins are cured with specific acid initiators. The acid initiators run between 7 and 12%, based on the weight of the resin. Furan and phenolic resin systems must be post-cured to manufacturers' recommendations as well to achieve maximum corrosion resistance and physical properties.

ACKNOWLEDGMENTS

The information in this article is based on the experiences of the author and colleagues associated with the industry, as well as on the references cited. Thanks to Larry Craigie, Don Kelley, and Juan Bustillos, all great teachers and friends.

REFERENCES

1. T.W. Cowley and M.A. Robertson, "The Effect of pH and Temperature on Fiberglass Reinforced Composites in Sodium Hypochlorite Solutions," Paper 305, Corrosion 91, National Association of Corrosion Engineers, March 1991
2. R.C. Allen, "Corrosion Mechanisms in Attack of Resin and Resin-Glass Laminates," 33rd Annual Technical Conference, The Society of the Plastics Industry, Inc., 1978
3. "How to Keep Your FRP Tank from Turning into Modern Art," The Dow Chemical Co., Dec 1994
4. J. Norton, E. Delaby, and R. Moubarac, "ECTFE Veil for Corrosion Resistant FRP Equipment," Paper 01394, Corrosion 2001, National Association of Corrosion Engineers, March 2001
5. *Hetron and Aropol Resin Selection Guide,* 2000 ed., Ashland Chemical Co.
6. "Thermoset Resins Technical Service," Ashland Chemical Co.
7. J.E. Niesse, *Fiber Reinforced Plastic in Hydrochloric Acid Service,* NACE Niagara Frontier Section, Sept 1980, revised Oct 1981
8 *DERAKANE Epoxy Vinyl Ester Resins,* March 1999 ed., The Dow Chemical Company, p 10
9. *Atlac and Dion Corrosion Resin Selection and Design Guide,* Reichhold Chemicals, Inc.
10. L.M. Adkins, D.W. Daniel, and D.A. Rust, "Factors Affecting the Fabrication of Corrosion Barriers for RP Equipment in Bleaching Environments," 49th Annual Conference, Composites Institute, The Society of the Plastics Industry, Inc., Feb 1994
11. T. Bishop and T.W. Cowley, "Corrosion-Resistant Fiberglass Reinforced Plastic Composites for Chlorine Dioxide Environments—Third Report," TAPPI Engineering Conference, 1994
12. M.J. Thompson and T.W. Cowley, "Corrosion-Resistant Fiberglass Reinforced Plastic Composites for Alkaline Peroxide Environments," TAPPI Engineering Conference, 1995
13. "Z-CORE Piping Systems," Bulletin A2115, Smith-Fibercast, Little Rock, AR, and Sand Springs, OK, 1 Nov 2001
14. T.W. Cowley, Evaluation of Fiber Reinforced Plastics for Solvent Resistance and Containment, *Managing Corrosion with Plastics,* National Association of Corrosion Engineers, 1993
15. A. Mekjian, "The Application of Phenolic Resins in FRP Composites," Seventh Western Technical Conference on Corrosion/Construction, The Society of the Plastics Industry, Inc., April 1992
16. "QuaCorr Resin/Catalyst Systems, Media Guide," Penn Specialty Chemicals, Inc.
17 "Test Method for Surface Burning Characteristics of Building Materials," E 84, *Annual Book of ASTM Standards 4.07,* ASTM International, 2004
18. A. Mekjian, "Phenolic RTM—A Boon to Mass Transit," 49th Annual Conference, Composites Institute, The Society of the Plastics Industry, Inc., Feb 1994
19. "Ignition Resistance Test Results of Laminates Made with DERAKANE Resins or DERAKANE Momentum Resins," technical information, The Dow Chemical Company
20. R.F. Regester, Behavior of Fiber Reinforced Plastic Materials in Chemical Service, *Corrosion,* Vol 25 (No. 4), April 1969, p 157–167
21. Osmosis in Resins and Laminates, Chapter 3, *Developments in Reinforced Plastics,* Elsevier Applied Science Publisher, 1984
22. G. Bergman, *Blistering in Process Equipment of Glass-Fiber Reinforced Plastics (FRP)—Damage Mechanisms and*

Influencing Factors Concluded from an Instructive Case, Proc. Eighth Int. Symposium on Corrosion in the Pulp and Paper Industry, Swedish Corrosion Institute, Stockholm, Sweden, May 1995
23. G. Bergman and K. Petersson, "Investigation of Blistering and Delamination Damage in a Flue Gas Scrubber Made of Glass-Fiber Reinforced Ester Plastics (FRP)," Swedish Corrosion Institute, Stockholm, Sweden
24. T. Bishop and T.W. Cowley, "The Corrosion Resistance of Some Fiberglass Reinforced Plastic Laminates in Chlorine Dioxide Solutions and the Part Played by Water," Eighth Symposium on Corrosion in the Pulp and Paper Industry, May 1995 (Stockholm, Sweden)
25. *DERAKANE News,* Vol 2 (No. 3), The Dow Chemical Co., Nov 1983, p 4
26. *Fabricating Tips,* The Dow Chemical Co., Oct 1994, p 37
27. J.H. Mallinson, *Corrosion-Resistant Plastic Composites in Chemical Plant Design,* Marcel Dekker, Inc., 1988, p 417–469
28. M.T. Belford, R. Llewellyn, D. Kumar, and R. Moubarac, "Abrasion and Erosion Resistance of Fiberglass Reinforced Vinyl Ester Composites," Niagara Frontier Section FRP Symposium, (Buffalo, NY), NACE International, 2002.
29. T.O. Bautista, "The Role of Synthetic Veil in the Wear Factor of Corrosion Resistant Laminates," 35th Annual Technical Conference, Reinforced Plastics/Composites Institute, The Society of the Plastics Industry, Inc., 1980
30. D.G. Chandler, G.T. Overholt, and T.F. Anderson, "Synthetic Veil—Why and How to Use It (in Corrosion Resistant Equipment)," 39th Annual Technical Conference, Reinforced Plastics/Composites Institute, The Society of the Plastics Industry, Inc., Jan 1984
31. T.W. Cowley and D. Kelley, "Improvements in Fiberglass Reinforced Plastic Equipment for Power and Recovery Furnaces' Emission Controls," TAPPI Engineering Conference, 1995
32. T.W. Cowley and D. Hatfield, "A Case History of FRP Pipe as an Economical Alternative to Carbon Steel Pipe," Paper 04606, Corrosion 2004, NACE International, March 2004
33. P.A. Blackburn, G.W. Hackworth, R. Mohan, D.A. Rust, and C.J. Spencer, "Factors Affecting Thermal Shock Cracking in RP Corrosion Barriers," 47th Annual Technical Conference, Composites Institute, The Society of the Plastics Industry, Inc., Feb 1992
34. G.A. Van Beek, S.S. Pang, and R.H. Lea, "Development of a New Electrically Conductive Advanced Composite Pipe," ANTEC 1993, Society of Plastics Engineers
35. "Electrical Grounding of FRP Equipment," technical information, The Dow Chemical Co., June 1998
36. "Conductive Lining Systems for FRP Equipment," technical information, The Dow Chemical Co., Dec 1992

SELECTED REFERENCES

- T.F. Anderson, B. Riseborough, R. Moubarac, and R.L. Vockel, "Dual Laminate Tanks with Automated Early Warning of Pre-Leak Detection Changes," Paper 472, Corrosion 98, National Association of Corrosion Engineers
- T.F. Anderson, B. Riseborough, J. Richter, and R.L. Vockel, "Design, Fabrication and Performance of a Pre-Leak Detection Oblation Type FRP Tank with Multi-Conductive Layer Zones," Paper 469, Corrosion 98, National Association of Corrosion Engineers
- G.L. Arthur, "A Guide to the Use of Epoxy, Furan, Polyester and Vinyl Ester Equipment," TAPPI Engineering Conference, Sept 1989
- D.C. Bennett, T.F. Anderson, and S.F. Botten, "Use of Acoustic Emission Inspection to Assess the Condition of Damaged FRP Bleach Towers," TAPPI Engineering Conference, Sept 1994
- G. Bergman, "Corrosion of Glass Fibre-Reinforced Ester Plastics (GRP) Used in Pulp Mill Applications—Effects and Damage Mainly Related to the Influence of Water," Swedish Corrosion Institute, Stockholm, Sweden, 1989
- G. Bergman, *Corrosion of Plastic and Rubber in Process Equipment—Experiences from the Pulp and Paper Industry,* TAPPI Press, 1995
- G. Bergman, "FRP Corrosion," Project Report 66 230 : 6, Swedish Corrosion Institute
- T.W. Cowley, "A Recommended FRP Inspection Procedure for the End-User," Paper 349, Corrosion 1997, National Association of Corrosion Engineers
- T.W. Cowley, Fibreglass Reinforced Plastic Equipment Failure Analyses, *Pulp Paper Can.,* Vol 100 (No. 2), 1999
- *Fiberglass Pipe Handbook,* The Composites Institute of the Society of the Plastics Industry, Inc., 1989
- *Fiber-Reinforced Plastic Pressure Vessels, Section X,* The American Society of Mechanical Engineers
- "Guidelines for Inspecting Used FRP Equipment," TIP 0402-28, TAPPI, 1999
- J.G. Lee, "Leak and Pre-Leak Detection Systems for Dual Laminate Systems—A User's Perspective," Paper 00542, Corrosion 2000, National Association of Corrosion Engineers
- J.H. Mallinson, *Corrosion-Resistant Plastic Composites in Chemical Plant Design,* Marcel Dekker, Inc.
- "Manual for Parabeam 3-D Glass Fabrics in Double Wall Tanks," Parabeam Industries, The Netherlands, www.parabeam3d.com, accessed 2004
- Nonmetallic Piping and Piping Lined with Nonmetals, *Process Piping, ASME Code for Pressure Piping, B31.3,* The American Society of Mechanical Engineers
- "Recommended Practice for Acoustic Emission Testing of Fiberglass Tanks/Vessels," Reinforced Plastics/Composites Institute, The Society of the Plastics Industry, Inc.
- Repair, Alteration and Inspection of Fiber-Reinforced Thermosetting Plastic Pressure Equipment, Appendix 9, *National Board Inspection Code,* The National Board of Boiler and Pressure Vessel Inspectors
- *RTP-1, Reinforced Thermoset Plastic Corrosion Resistant Equipment,* The American Society of Mechanical Engineers, 2000

ASM Handbook, Volume 13B: Corrosion: Materials
S.D. Cramer, B.S. Covino, Jr., editors, p605-607
DOI: 10.1361/asmhba0003847

Environmental Performance of Rubber Linings

Larry DeLashmit, Polycorp, Ltd.

NATURAL AND SYNTHETIC RUBBER LININGS are used extensively in many industries for their corrosion and/or abrasion resistance. These industries include transportation, chemical processing, water treatment, power, mineral processing, and mining. The largest-volume use of rubber linings is in phosphoric acid, hydrochloric acid, and ferric or ferrous chloride manufacture, storage, and transportation.

Unlike many corrosion-resistant linings, rubber linings are applied as sheet materials. The typical thickness is 5 to 6 mm (0.188 to 0.25 in.), with greater thicknesses applied in services requiring high abrasion resistance or higher temperatures. Being elastomers, rubber linings offer good resistance to thermal or mechanical shock and can be formulated for excellent abrasion resistance.

The installation process is very labor-intensive. The sheets are cut and applied by hand to the substrate, and the air is eliminated between the two surfaces with rollers and other specialized tools. Sealing joints requires skill, and careful inspection must follow the installation. The linings are vulcanized or cured with steam after the lining installation is complete. Any air trapped under the lining will result in a blister that will require repair before the equipment can be put into service. Skilled applicators are essential for a lining that will perform as required.

This overview describes the commonly used polymers, lists the advantages and disadvantages of the polymer, and shows service conditions where the lining is frequently used.

Commonly Used Polymers

The article "Rubber Coatings and Linings" in *ASM Handbook,* Volume 13A, 2003, provides physical properties and chemical structures of these materials, as well as details on installation, joints, and inspection.

Rubber is classified as being natural or synthetic. The letter designations for polymers in this article are consistent with ASTM D 1418.

Soft Natural Rubber (NR). Natural rubber is made up of polyisoprene molecules. Rubbers designated NR or isoprene rubber (IR) have similar chemical resistance and physical properties. Natural rubber linings are usually vulcanized using sulfur. Soft rubber refers to linings that are under 75 Shore A durometer hardness. The hardness of soft rubber is adjusted by adding carbon black or other fillers rather than high cross-link density from high levels of sulfur. Pure gum rubber refers to natural rubber linings with little or no fillers and are typically 40 Shore A durometer hardness.

Advantages of soft natural rubber are:

- Excellent abrasion resistance
- Good resistance to many acids and alkalis
- Remains flexible to very low temperatures
- Good resistance to mechanical and thermal shock
- Lower in price than most other linings
- Easy to install and repair

Disadvantages of soft natural rubber are:

- Poor weathering resistance due to sunlight, oxidation, and ozone resistance. (Ingredients can be added to improve these properties.)
- Poor resistance to strong oxidizing acids such as nitric and chromic acid
- Poor resistance to temperatures above 65 °C (150 °F). (Special compounding can raise the upper limit.)
- No resistance to oils or other hydrocarbons
- Hardens with age and temperature in aqueous hydrochloric service

Common uses of soft natural rubber are:

- Hydrochloric acid processing, storage, and transportation equipment. (Pure gum rubber is used for concentrations above 25% HCl.) A minimum of 60 Shore A durometer hardness is preferred for lower concentrations because it has lower water absorption.
- Hydrofluoric acid (HF) storage and transportation for concentrations less than 50% HF
- High-abrasion areas in mining, mineral, and aggregate processing, such as slurry pipes and tanks, screen decks, chutes, and hoppers
- Seawater piping systems

Semihard natural rubber linings are typically 75 to 95 Shore A durometer hardness. The hardness is accomplished with a combination of higher levels of sulfur for a higher cross-link density and filler loading. The higher cross-link density gives higher temperature resistance and lower permeation rates. In general, these linings are not used for acid service because the method of failure is a continued hardening of the lining, ultimately resulting in cracking. The soft natural rubber linings will give longer service life in acid service.

Advantages of semihard natural rubber are:

- Good chemical resistance
- Good heat resistance up to 100 °C (212 °F)
- Low water absorption
- Low permeation rate
- Moderate cost
- Easy to install and repair
- Fair resistance to thermal and mechanical shock

Disadvantages of semihard natural rubber are:

- Poor abrasion resistance
- No oil resistance
- Poor low-temperature properties
- Preference is to autoclave or pressure cure

Common uses of semihard natural rubber are:

- Processes requiring elevated temperatures
- Water treatment tanks
- Metal plating tanks for cadmium, copper, nickel, and zinc. It is not suitable for chrome plating tanks.
- Steel mill pickle tanks. These are normally brick lined over the rubber lining.
- Wet chlorine service. Requires the addition of graphite to the compound

Hard natural rubber is also known as ebonite. The hardness is generally measured on

the Shore D scale and can be harder than 70 Shore D. The hardness is accomplished primarily with very high levels of sulfur (30 to 40 wt%) to get the maximum cross-link density during vulcanization. These are very specialized linings and should be specified only after consulting with the lining manufacturer and the applicator. Hard rubber linings offer resistance to a range of chemicals up to 93 °C (200 °F) and high dielectric strength, but they can fail catastrophically from flexing in the substrate; mechanical shock, such as a sharp blow to the outside of a tank or pipe; or sudden changes in temperature. For these reasons, semihard rubber linings should be the first consideration.

Advantages of hard natural rubber are:

- Excellent chemical resistance
- Good resistance to elevated temperatures up to 121 °C (250 °F)
- Low permeation rate
- Low water absorption
- Good resistance to wet chlorine with the addition of graphite to the compound

Disadvantages of hard natural rubber are:

- Poor resistance to thermal and mechanical shock
- Extremely brittle, so it requires very heavy and stiff substrates to prevent cracking from flexing in the substrate, such as pressure-rated vessels
- Poor low-temperature properties
- Poor abrasion resistance
- Preference is to autoclave or pressure cure

Common uses of hard natural rubber are:

- Wet and dry chlorine service
- High-temperature service

Neoprene or polychloroprene (CR). Neoprene is usually vulcanized using magnesium, zinc, or lead oxides. It does not vulcanize with sulfur. While many think of neoprene as oil resistant, it is only moderately oil resistant and is not suitable for continuous exposure to gasoline or most other petroleum-based products.

Advantages of neoprene are:

- Excellent oxidation, ultraviolet (UV), and ozone resistance
- Moderate oil resistance
- Fire resistant
- Good abrasion resistance
- Good low-temperature properties
- Good resistance to elevated temperatures up to 100 °C (212 °F)

Disadvantages of neoprene are:

- Higher material cost
- Difficult to install. Hot work tables are required to preshrink the lining.

Common uses of neoprene are:

- Seawater piping
- Tumbling barrels
- Services that contain small amounts of oil or other hydrocarbons
- Caustic storage tanks

Chlorobutyl (CIIR) linings are supplied as either unblended or a blend with natural rubber. Sulfur is normally used for vulcanizing. The properties of the unblended and blended linings are roughly the same, but the uses are different. Most, but not all, of these linings are manufactured with a tie gum backing to give a stronger bond to the substrate. The tie gum is a soft natural rubber. The most outstanding properties of chlorobutyl are its low permeation rate, good heat resistance, and resistance to a wide variety of chemicals.

Advantages of chlorobutyl are:

- Excellent oxidation and ozone resistance
- Very low permeation rate
- Low water absorption
- Good resistance to elevated temperatures up to 121 °C (250 °F). Special compounding is required for maximum temperature resistance.
- Good resistance to a wide variety of chemicals

Disadvantages of chlorobutyl are:

- No resistance to oils or hydrocarbons
- Costs more than natural rubber

Common uses of blended chlorobutyl are:

- Phosphoric acid production, storage, and transportation
- Ferric chloride storage and transportation
- Flue gas desulfurization scrubber towers, piping, and limestone slurry tanks
- Sulfuric acid storage up to 50% concentration
- Open-top storage tanks that require good weather resistance
- Aqueous HCl less than 24% concentration

Unblended chlorobutyl is used for:

- Bleach (sodium hypochlorite) production, storage, and transportation
- Hydrofluoric acid (above 50% concentration) storage and transportation
- Aqueous sodium hydroxide

Three-ply linings are specialized linings that usually consist of a soft natural rubber layer for good adhesion; a center layer of semihard or hard

Table 1 Frequently used rubber linings in the chemical process industries

Application	Lining
Hydrochloric acid	
Transportation and storage of 25 to 37% concentration	Pure gum natural rubber
Transportation and storage of lower concentrations, <25%	60 Shore A hardness natural rubber
	Chlorobutyl blends
Storage of acid with trace amounts of organics	Three-ply linings
	Semihard linings
	Chlorinated polyethylene-faced soft natural rubber
Spent hydrochloric acid	Blended chlorobutyl
Phosphoric acid	
Transportation and storage—all concentrations	Blended chlorobutyl
Evaporators	Blended chlorobutyl
	Three-ply linings
Sodium hypochlorite (bleach)	Unblended chlorobutyl
Ferric chloride	Blended chlorobutyl
Hydrofluoric acid	
Concentrations above 50%	Unblended chlorobutyl
Concentrations below 50%	Natural rubber
	Blended chlorobutyl
Hydrofluosilicic acid	Blended chlorobutyl
Sulfuric acid	
Concentrations above 50%	Rubber linings are not generally suitable.
Concentrations below 50%	Blended chlorobutyl
	Hypalon

Table 2 Frequently used rubber linings in other industries

Application	Lining
Power industry	
Scrubber towers	Blended chlorobutyl
Limestone slurry tanks	Blended chlorobutyl
Slurry piping	Blended chlorobutyl
	60 Shore A hardness natural rubber
Seawater cooling water piping	Soft natural rubber
	Neoprene
Metal finishing industry	
Steel mill pickle lines	Semihard natural rubber
	Three-ply linings
Nickel plating	Semihard natural rubber
Chrome plating	Rubber linings are not suitable for the chromic and nitric acids used in this service.
Water treatment industry	
Anion, cation, and mixed-bed vessels	Semihard natural rubber
Chlor-alkali industry	
Chlorine cells	Graphite-filled hard natural rubber

natural rubber for better chemical and permeation resistance; and a top layer that may be a very soft natural rubber, an abrasion-resistant natural rubber, or chlorobutyl. The top layer is designed to tolerate the service conditions. The upper temperature limit is determined by the top layer.

Advantages of three-ply linings are:

- Moderate cost
- Ease of application
- Ease of repair
- Good resistance to permeation

Disadvantages of three-ply linings are:

- No oil resistance
- Only the top layer offers any abrasion resistance
- Generally requires "closed skive" seams

Common uses of three-ply linings are:

- Tanks that require brick lining, such as acid pickling tanks
- Phosphoric acid evaporators
- Hydrochloric acid storage tanks where the solution contains traces of organics. Excessive organics may cause blistering between the hard center layer and the top layer. Maximum concentrations of organics should be less than 50% of the saturation level required to cause free phase formation.

The following linings should be used if the more commonly used linings mentioned previously are not suitable for the service conditions.

Nitrile (NBR) linings are vulcanized using sulfur. Many grades of nitrile are available.

Advantages of nitrile linings include:

- Good resistance to many hydrocarbons

Disadvantages of nitrile linings are:

- High cost
- Difficult to apply
- Difficult to repair
- Poor resistance to UV and ozone exposure

Common uses of nitrile linings include:

- Service where there is exposure to petroleum products

Ethylene propylene with a diene monomer (EPDM) is vulcanized using sulfur for tank linings.

Advantages of EPDM linings are:

- Good resistance to elevated temperatures up to 100 °C (212 °F)
- Good resistance to sunlight and ozone
- Good low-temperature resistance
- Good resistance to aqueous HCl and NaOH

Disadvantages of EPDM linings are:

- Higher cost
- Difficult to apply
- Difficult to repair
- No resistance to hydrocarbons. Aromatic hydrocarbons cause swelling.
- High permeation rate in sulfuric acid

Common uses of EPDM include:

- Sodium hypochlorite

Chlorosulfonated polyethylene (CSM) or trade name Hypalon (duPont). This polymer is generally vulcanized using metal oxides for tank linings.

Advantages of Hypalon linings are:

- Good resistance to sunlight and ozone
- Good resistance to elevated temperatures up to 100 °C (212 °F)
- Good low-temperature resistance
- Good resistance to some hydrocarbons
- Flame resistant
- Resistant to a wide range of sulfuric acid concentrations

Disadvantages of Hypalon linings are:

- Very high cost
- Difficult to apply
- Difficult to repair

Industrial Applications

Combinations of chemicals, or trace amounts of some chemicals, considerably complicate the proper selection of the lining. Always check with the lining supplier for advice on the best lining system for the proposed service conditions. Table 1 indicates the use of specific linings in the chemical process industry, based on pure chemicals.

Rubber linings that are properly selected for the service conditions and correctly installed are a very cost-effective method of protecting equipment from the effects of abrasion and/or corrosion. Always consult with the lining manufacturer or a qualified applicator to determine the suitability of rubber linings for the specific service conditions. Table 2 provides examples of the use of rubber linings in other industries.

SELECTED REFERENCES

- "Practice for Rubber and Rubber Latices—Nomenclature," D 1418, *Annual Book of ASTM Standards,* Vol 9.01, ASTM International
- P.A. Schweitzer, *Corrosion-Resistant Linings and Coatings,* Marcel Dekker, 2001

ASM Handbook, Volume 13B: Corrosion: Materials
S.D. Cramer, B.S. Covino, Jr., editors, p608-617
DOI: 10.1361/asmhba0003848

Environmental Performance of Elastomers

Jim Alexander, Consultant, Pradip Khaladkar, and Bert Moniz, DuPont Company
Bill Stahl and Tommy Taylor, DuPont Performance Elastomers

ELASTOMERS belong to a group of materials known as polymers. Although they exhibit many of the properties of polymers, elastomers also have the property of resiliency. Polymers may be classified as either thermoplastic or thermoset. Once formed thermoplastics can be reshaped. On the other hand, thermosets once formed and cured (vulcanized) cannot be reprocessed or reshaped.

The prime focus of this article is the use of elastomers as seals. Also see the article "Environmental Performance of Rubber Linings" in this Volume.

Thermoplastic materials are long-chain polymers that are not connected by cross links (Fig. 1). Very few elastomers are the thermoplastic type. They acquire their properties and strength from their molecular weight, chain entanglements, and crystalline regions that form when chain segments line up and crystallize. These crystalline regions can deform and/or melt under pressure and heat, causing creep or extrusion of the materials under service conditions. Elastomeric thermoplastic materials share this structure.

Thermoset materials are long-chain polymers that are connected to one another by cross links. Most elastomers are the thermoset type. The Xs in Fig. 2 designates the cross links. The cross links impart a degree of memory, providing resilient recovery characteristics commonly referred to as elasticity. The cross links are stable under certain conditions of temperature and pressure. Excessively high temperatures or pressures can distort, rearrange, and destroy the cross links, leading to a change in seal shape and loss of sealing force.

Sealing is an important application for elastomers, and both thermoset and thermoplastic elastomers have characteristics that are advantageous, as summarized in Table 1. Both classes of materials can exhibit resistance to high temperature and broad chemical compatibility. Thermoset elastomers, however, can show resiliency at both high and low temperatures as well as resistance to creep and retention of sealing force during broad temperature and pressure cycling. Thermoplastic polymers are generally inferior in these characteristics. The mechanical properties of thermoset elastomers decrease rapidly as temperature increases.

Factors Governing the Performance of Elastomers

There are several important technical concepts that define the performance capabilities of an elastomeric part: polymer architecture (molecular building blocks), compounding (the ingredients within the polymer), and vulcanization (cross linking) of the elastomer shape (e.g., sheet or O-ring). Consider these as the dimensions that define a performance volume of the part. In the case of elastomers, once the three dimensions have been accurately defined, the performance capabilities (and limitations) of the elastomeric material used in the part have been established. A fourth dimension (part design), in combination with the above three, fully defines the performance capabilities of an elastomer part in actual service.

Architecture. Consider monomers as building blocks of long polymer chains. The blocks that are selected, how any of each type of block that is incorporated, and their sequence all determine fundamental chemical and thermal capabilities of the polymer.

Molecular weight and molecular weight distribution have a significant effect on both processing and mechanical strength of the final elastomer part. The selection and frequency of atoms and groups attached to the polymer backbone strongly influence chemical and thermal resistance and low-temperature flexibility.

Cross linking (creating the "springy connections" between polymer chains) has a strong influence on the resiliency, a key elastomer property. The stronger the cross links, the greater the chemical and thermal stability of the elastomer. Strong cross links are also important for resistance to compression, deformation, and extrusion.

Six monomer building blocks and special cure monomers may be assembled to create an array

Table 1 Thermoset and thermoplastic elastomer properties

	Elastomers	
Advantageous characteristic	**Thermoset**	**Thermoplastics**
Resistance to high temperature	Yes	Yes
Broad chemical compatibility	Yes	Yes
Resiliency at high temperatures	Yes	No
Resiliency at low temperatures	Yes	No
Resistance to extrusion/creep at high temperatures and pressures	Yes	No
Retention of sealing force during temperature and pressure cycling	Yes	No
High modulus and strength over broad temperature range	No	Yes

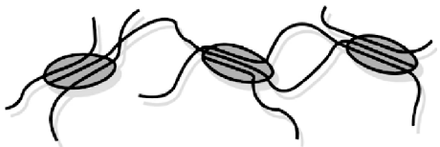

Fig. 1 Thermoplastic elastomers are long-chain polymers that form from regions where polymer chains line up and crystallize.

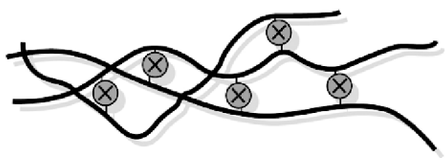

Fig. 2 Thermoset elastomers are long-chain polymers connected by cross links represented by circled Xs.

of elastomer types used for parts (Table 2). Several examples are discussed in the paragraphs that follow.

Natural rubber (NR) is derived from the sap of a number of plants in the form of latex. The typical structure for natural rubber is 100% cis-polyisoprene. This leads to unsaturation in the polymer backbone. This unsaturation and the absence of nonhydrocarbon moieties makes NR very susceptible to attack from oils as well as oxygen, ozone, and other strongly oxidizing agents.

Nitrile rubber (NBR) is composed of two monomers in random sequence, butadiene (BD) and acrylonitrile (ACN). This backbone chain has some unsaturation locations allowing thermal and chemical attack so that elastomers of the NBR type have limited chemical resistance. The performance of NBRs is very dependant on the ACN content of the polymer. For example, as ACN levels increase, low-temperature flexibility decreases and oil resistance increases. Vulcanates of NBR rubber can be compounded to offer very good resistance to extrusion, explosive decompression, and abrasion. Chemical resistance of NBR compounds is considered to be modest. Nitrile rubber seals are generally used below 100 °C (212 °F) in chemical media of low concentrations.

Ethylene propylene rubber (EPR) comprises two monomers in random sequence: ethylene and propylene. Ethylene propylene rubbers have good resistance to water, steam, aqueous acids, and bases at intermediate temperatures.

Ethylene propylene diene rubber (EPDM) polymers have a backbone consisting of repeating methylene units (–CH_2–). The copolymers of ethylene and propylene are referred to as EPM or sometimes EPR, ethylene propylene rubber. The copolymers and terpolymers share the saturated backbone of repeating methylene units. Since the copolymers (EPM) are totally saturated, they can only be cured (cross linked) using peroxides. The EPDM terpolymer contains unsaturation in a side chain by way of the third monomer. This unsaturation makes it possible to sulfur cure EPDM polymers, resulting in flexibility in choice of cure chemistry/chemicals without grossly impacting the stability of the original copolymer. Almost all EPDM polymers use either ethylidene norbornene (ENB) or dicyclopentadiene (DCPD) as the third unconjugated diene monomer.

Chloroprene rubber or neoprene (CR) results from the polymerization of chloroprene (2-chloro-1,3-butadiene). When chloroprene undergoes 1,2 addition, the resulting polymer has some allylic chlorine. The allylic chlorine is labile and is considered to be the cure site, that is, the point of cross linking or vulcanization. Neoprene has a structure very similar to NR with a chlorine (Cl) atom in place of a methyl (–CH_3) group. The presence of chlorine gives neoprene greater resistance to oils and fuels compared with natural rubber. However, similar to natural rubber, neoprene has unsaturation in the polymer backbone and is only modestly more resistant to attack from strong oxidizing agents such as oxygen and ozone.

Silicone rubber (VMQ) contains repeating units of dimethylsiloxane, giving the polymer a backbone of silicone-oxygen linkages (–Si–O–Si–O–). This is in contrast to organic polymers with largely carbon-carbon (–C–C–) linkages in their backbones. The unique chemical structure of silicone rubber affords good temperature stability, but limited chemical resistance and low mechanical properties.

Fluorosilicone rubber (FQMV) has the same backbone structure as silicone rubber. The two differ in the chemical moieties attached to the basic –Si–O–Si–O– backbone. The fluorosilicones have organofluorine atoms attached to the backbone (see Fig. 3) that improve chemical resistance, but significantly reduce the polymers resistance to heat.

Table 2 Six monomer building blocks used to create elastomers

	Identification(a)				
Monomer	**FFKM**	**ETP**	**FKM**	**TFE/P**	**EPR**
Tetra-fluoroethylene	√	√	√	√	…
Perfluoro methyl vinyl ether	√	√	√	…	…
Vinylidene fluoride	…	…	√	…	…
Hexa-fluropropylene	…	…	√	…	…
Propylene	…	…	…	√	√
Ethylene	…	√	…	…	√
Special cure monomers	Yes	No	Yes/No	No	Yes/No
Sequence(b)	R	R	R	A	R

See text for description of elastomers. (a) Per ASTM D 1418. (b) R, random; A, alternating

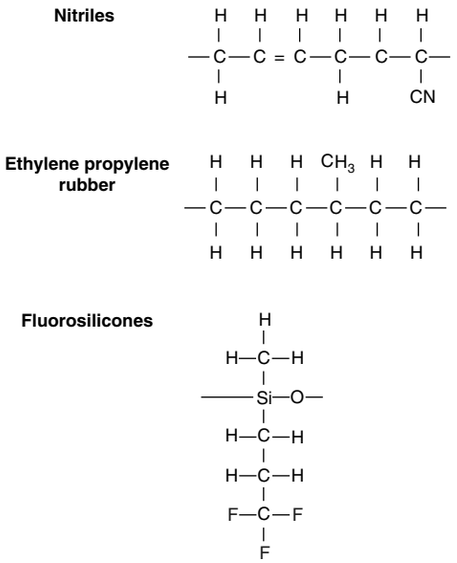

Fig. 3 Elastomer architecture shown by structured chemical formula. Structure has a strong influence on chemical resistance.

Fluoroelastomers (FKM, FFKM) owe their excellent resistance to heat and oil to the high ratio of fluorine to hydrogen, the strength of the carbon-fluorine bond and the absence of unsaturation. The basic building blocks, in the case of FKM dipolymers, are vinylidene fluoride (VF_2) and hexafluoropropylene (HFP). FKM terpolymers make use of tetrafluoroethylene (TFE), perfluoro (methyl vinyl) ether (PMVE), and ethylene as the third monomer. For FFKM, the base monomers are TFE and PMVE, thus leading to a fully fluorinated polymer. The strongest chemical bonds impart the highest performance capabilities. The fluorine-carbon bond is the strongest and most stable bond in organic chemistry. Since strong chemical bonds impart high-performance capabilities, maximizing the fluorine content of the elastomer will maximize resistance to harsh chemicals (see Table 3).

Compounding is the technology of homogeneously mixing other ingredients with raw elastomer gum (polymer) in order to enhance and tailor specific mechanical properties. These may include compression set resistance, tensile strength, modulus, hardness, weatherability, U.S. Food and Drug Administration (FDA) compliance, surface lubricity, colorability, and abrasion resistance.

Compounders design their products by selecting and adding different types of ingredients in varying amounts. The selection, quantity, and quality of each ingredient significantly impact part performance, because the chemical environment to which the part is exposed can extract them. Moreover, wholesale addition of compounding agents can make the elastomer less expensive while also compromising chemical performance. This explains why the performance of two "seemingly identical" elastomer seals with the same generic family name may perform totally differently in the same service. Compounding agents include:

- Various types of elastomers, either of the same class or other families, to create blends
- Fillers such as carbon blacks, or nonblack fillers such as clays and titanium dioxide, to add bulk at low cost
- Metal oxides to promote cure
- Curatives to promote vulcanization
- Extenders, to dilute or soften the elastomer
- Stabilizers to improve ultraviolet, heat, or ozone resistance
- Colorants, for nonblack compounds only
- Process aids, to assist manufacturing of the part

Cure (Vulcanization or Cross Linking). In the process of cure (vulcanization or cross linking), chemistry, heat, and time are harnessed to initiate, complete, and stabilize the cross links ("springs") connecting the polymer chains and providing the elasticity of the part.

During compounding, the elastomer gum (polymer) and all the other ingredients (compounding agents) are homogeneously mixed to form a full compound. The full compound is shaped (molded, extruded, etc.) and heated.

Chemistry of curing begins, and some polymer chains are connected by cross links creating the desired elastomeric properties. Often, with high-performance elastomers, the shaped item is postcured (at longer times and higher temperatures) to complete and stabilize the cross link chemistry. This maximizes and equilibrates the mechanical properties of the part (Fig. 4).

Factors Affecting Chemical Resistance

The aggressiveness of the chemical environment, temperature, and minor constituents in the environment and in the material itself will all affect the chemical resistance of the elastomer.

The temperature capabilities of elastomeric products such as seals, parts, and linings involve:

- The service environment
- Change in mechanical properties over the range of service temperatures—not an aging phenomenon, but rather the effect of temperature on the elasticity of the elastomeric components
- Stability of the architecture of the elastomer to the service environment
- Total part design

Typical published information usually reports only service temperature ranges in dry air, often depicting upper and lower limits of performance, with marginal regions indicated at both extremes. In general, these data do not address the aggressive effects of process media. Such general information should only be used for initial guidance concerning capability (Fig. 5).

Sealing capabilities of elastomers are usually dependent on a variety of factors encountered during service:

- Swell and/or chemical attack can significantly narrow the acceptable temperature range in process media.
- High temperatures significantly reduce the mechanical properties of elastomer seals before any degradation occurs.
- High temperatures also cause degradation of elastomer architecture and cross links.
- Dynamic stresses narrow the performance range compared to static conditions because most elastomers are not robust against dynamic stresses.

Thus, when approaching published limits a conservative approach to performance expectations is recommended.

Table 4 gives the effect of temperature on the initial mechanical properties of a typical elastomeric sealing material, in this case an FKM type. Hardness, elongation, and tensile strength decrease significantly between 23 °C (73 °F) (ambient temperature) and 100 °C (212 °F). Not all elastomers will respond similarly. Additional temperature increases further reduce mechanical properties. These reduced properties significantly influence in-service sealing capabilities (both static and dynamic).

Sealing or property retention at low temperatures (0 to −60 °C, or 32 to −76 °F) presents a different and challenging set of problems. Thermal degradation and chemical attack by aggressive media on the elastomer architecture are greatly diminished. However, at low temperatures, elastomers begin to act like plastics. As the temperature falls and approaches the glass-transition temperature of the elastomer, it becomes hard, rigid, and glasslike. Tensile strength, modulus, and hardness increase, elongation to break decreases, and the seal no longer functions as a resilient elastomer.

At low temperatures, dynamic sealing is more difficult than static sealing. Temperature cycling presents more sealing difficulties than in a constant low-temperature environment. However, sealing system design can compensate and extend low-temperature sealing capabilities.

Chemical Environment. The compatibility of elastomers with process media under service conditions is a very important criterion in guiding specifiers toward the optimum selection in an application. The cause of incompatibility of an elastomeric component in a chemical environment may be simple or complex, based on one phenomenon or based on several simultaneously recurring phenomena. The degree and consequences of these phenomena are dictated by the rules:

- Attack is related to polymer architecture, compounding, and cure (cross linking).
- Attack may be solubility related (reversible) or chemical related (irreversible).
- Attack may cause parts to become soft and weak, or hard and brittle.
- Attack accelerates as temperature increases.
- Attack may be exacerbated by the presence of small concentrations of certain species in the chemical environment.
- Attack may be predicted by accelerated testing techniques.

The following examples illustrate the performance characteristics of selected elastomeric materials after immersion in some aggressive environments. They clearly show that specifiers must be thorough in identifying the complete process medium, including all major and minor components, the normal service temperature range, and expected temperature excursions.

Organic and inorganic solvents and chemicals exhibit a solubility parameter, as does the

Table 3 Fluorine and hydrogen content of elastomers, related to properties

Elastomer family	Fluorine, %	Hydrogen, %	Heat stability, continuous °C	Heat stability, continuous °F	Resistance to chemical attack
High-performance					
FFKM	74	0	315	600	Optimum
FKM-F	70	1.1	200	392	Outstanding
FKM-B	68	1.5	200	392	Excellent
FKM-A	66	1.9	200	392	Very good
TFE/P	55	4.2	180	356	Good
FVMQ	<50	...	200	392	Limited
Mid-performance					
Hydrogenated nitrile	0	...	140	284	Limited
Nitrile	0	...	125	257	Limited
EPR	0	...	120	248	Limited
Neoprene	0	...	100	212	Limited

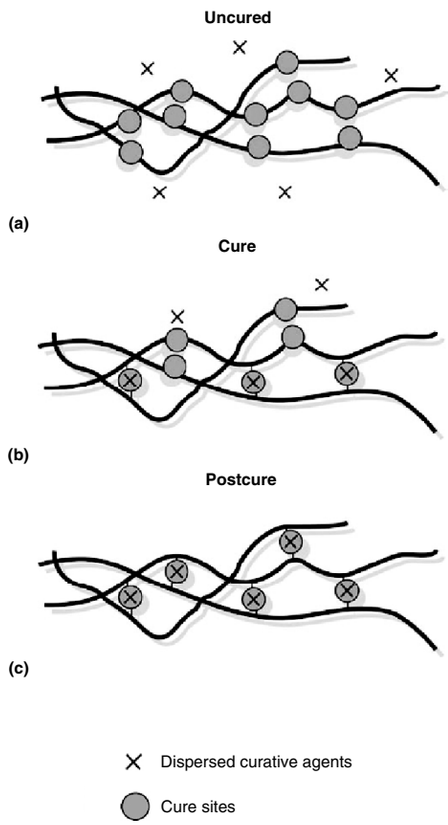

Fig. 4 Elastomers may be cured in one or two stages. The stages proceed from top to bottom. (a) Polymer chains are not connected. (b) Heat drives the chemistry of cure. Many cross links are formed. Some polymer chains are well connected. Elastomeric properties are created. (c) Higher temperature and longer times. Cross-link density is optimized. All polymer chains are highly connected. Elastomeric properties are maximized.

elastomeric seal. The seal absorbs an increasing amount of the solvent as the solubility parameter of the polymeric seal and the process solvent approach one another. In doing so, the seal volume increases, mechanical properties decrease, and the seal softens and become weak. This phenomenon is sometimes called "like likes like."

Swelling from Solvent Uptake. The resistance of several fluoroelastomers in the common polar solvent, methylene chloride at room temperature illustrates important phenomena that are typical for many elastomers. This type of degradation is related to the similarity of the solubility parameters of the elastomer and the solvent. Volume increase occurs rapidly, achieving the equilibrium value and remaining constant at the service temperature. There is no chemical attack on the architecture of the fluoroelastomers, just swelling. If the elastomers are dried out to remove all solvent, their volume reverts back to its original value. This can be repeated again and again (Table 5). The higher the fluorine content of the elastomer, the lower the volume increase in the solvent. However, the consequences of swelling include softening and loss of mechanical strength. As temperature increases, the elastomers equilibrate more quickly and achieve a higher percent volume increase at equilibrium.

Chemical Degradation. The effects of aggressive chemicals on elastomer properties are different from that of solvents. Aggressive chemicals not only swell the elastomer seal, but also chemically attack and degrade the architecture and cross links. This causes progressively greater property changes as time and temperature increase and concentration of the aggressive chemical increases.

For example, consider behavior in 95% sulfuric acid at 100 °C (212 °F) (Fig. 6). Observe the accelerating degradation of FKM-A (66 wt% F) at 70 °C (158 °F) and above. Contrast that with the continuing functional performance of FKM-GF (70 wt% F) at 100 °C (212 °F) and the exceptional resistance of FFKM (~74 wt% F) at 100 °C (212 °F).

At higher temperatures the degradation accelerates. As concentration increases, the rate of degradation increases.

Hydrocarbon Environments. Table 6 summarizes the performance of elastomers in a broad range of hydrocarbon media. Hydrocarbon elastomers (EPR, NBR, TFE/P) are unacceptable because their architecture is similar to that of the hydrocarbon media (the like likes like phenomenon), leading to high-volume swelling. However, some nitrile elastomers (NBR) give acceptable performance in gasoline and diesel fuel environments at ambient temperatures. Standard FKM elastomers perform well up to 100 °C (212 °F) in all hydrocarbon media, but may be affected by additives and/or oxygenates, for which specialty grades are recommended. Only FFKMs perform well in all hydrocarbons, including those containing additives or oxygenates to temperatures of 200 °C (392 °F) and above.

Chemical Combinations and Impurities. Low levels of additives (or impurities in a medium) can have a strong influence on the incompatibility of elastomers. One example is automotive fuel additives, such as the oxygenate methyl tertiary butyl-ether (MTBE). Depending on the region and the season, MTBE may be present in automobile fuels at levels up to 10 wt%. (In manufacture, storage, shipping, and blending, concentrations of MTBE may range from 100 to 10% or less).

Even at the 10 wt% level, manufacturers of gasoline dispensing pumps, meters, and fuel line components have found it necessary to exchange seals based on nitrile elastomers with those of either standard FKM seals (6 wt% F), or higher fluorine containing FKM seals, in order to achieve acceptable levels of seals compatibility and low permeability (Fig. 7).

Effect of Fillers on Chemical Resistance. Although color-coded parts, such as O-rings are commercially available to differentiate the elastomer families, color-coding introduces potentially negative performance issues for elastomers exposed to a range of chemical environments. Nonblack fillers used for color-coded O-rings may be less thermally stable than carbon blacks and may be reactive with many process environments. These reactions can drastically affect the chemical resistance of the seal, retention of its mechanical properties, and sealing reliability.

Carbon blacks impart maximum mechanical reinforcement and are chemically inert to most chemical environments. The Rubber Manufacturers Association (RMA) states, "Black is the preferred color for O-ring materials other than silicones and fluorosilicones" (OR-10,

Table 4 Increasing temperature decreases mechanical properties of an FKM type elastomer

Property	Test temperature 23 °C (73 °F)	Test temperature 100 °C (212 °F)	Decrease in value
Hardness, Shore A	75	65	10 points
Elongation at break, %	180	100	80%
Tensile strength, MPa (psi)	0.44 (3000)	0.07 (500)	0.36 (2500)

Table 5 Swelling is not a sign of chemical attack

Elastomer compound base	Fluorine(a), wt%	Volume increase at 23 °C (73 °F), %
FKM-A	66	25
FKM-GF	70	10
FFKM	74	< 1

(a) Approximate

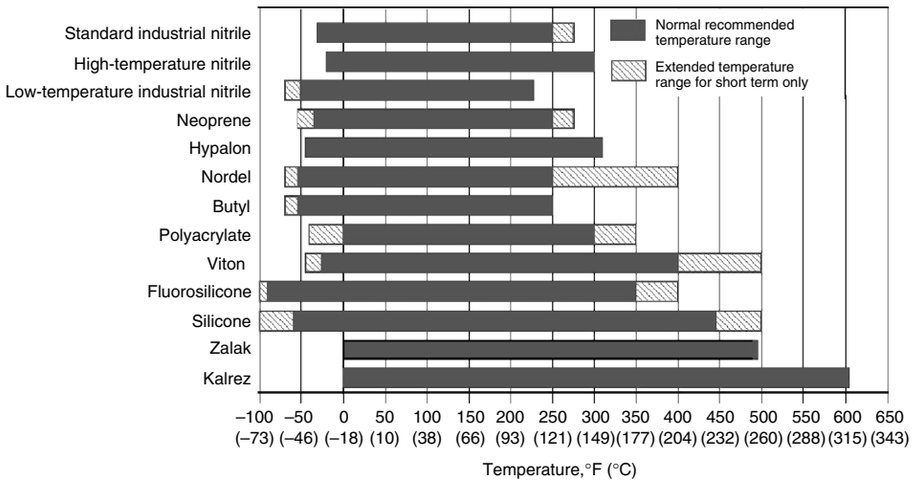

Fig. 5 Typical temperature capability comparison for various elastomers that is valid for dry air. Consult manufacturers for the duration of extended temperature range.

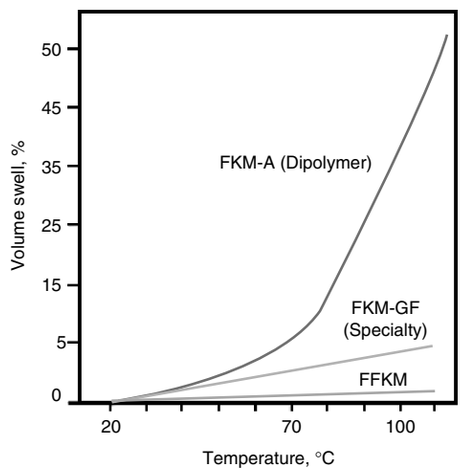

Fig. 6 Chemical resistance of elastomers in 95% sulfuric acid measured by swell, showing influence of temperature during 2 month exposure

1983). However, for typical organic solvents, filler content (carbon black or nonblack) may not affect seal performance.

Since carbon black is the most effective filler material to optimize mechanical and chemical properties, most elastomeric parts are black, creating a serious impediment to positive materials identification.

To avoid product mix-ups or misidentification, the user must manage the supply chain by using the specifications to indicate approved suppliers, the specific elastomer, and the manufacturer's code number. Approved suppliers must verify that their products comply fully with the purchase specification. When the parts arrive at the user's location, they must be stored properly in drawers that clearly and accurately identify the product.

Degradation in Storage. Recommended storage conditions for elastomer parts are:

- Under ambient conditions, low humidity, dark, and ozone and radiation-free environment
- Stored lying flat, without distortion of the original shape

Note that preassembled O-rings, such as in a mechanical seal, will take some compression set during storage. It should be determined by test or inspection whether the incurred compression set is detrimental to the performance of the seal.

Performance Evaluation

Chemical resistance testing of elastomers may be required because a new application is desired, operating conditions have changed, or seals have failed. Tests may consist of simple immersion or a standardized method to evaluate a specific property change.

Samples selected and used for testing should be identical to those purchased and installed. This is usually ensured by citing and ordering products with the same manufacturer's part code used for testing. Samples from specified manufacturers' authorized parts distributors are also acceptable. Otherwise, the test data may not predict performance of a purchased part in service.

The two categories of performance evaluation are basic immersion testing and application specific testing.

Immersion Testing

Immersion testing involves immersing the sample for set periods and measuring change in tensile properties, hardness, and dimensions. This approach is better when there are time constraints or where screening is needed.

Elastomer compound samples from different families (FKM, EPR, NBR, etc.) should not be mixed in the testing container. Product decomposition or compounding ingredients from one elastomer family may chemically attack samples of a second family in the test vessel. The test medium should duplicate that anticipated in the actual operating environment, including trace impurities such as organic solvents.

A minimum of three data points (in addition to a control) should be obtained for any variable. For example:

- Time: 3 days, 14 days, and 56 days
- Temperature: that anticipated in the process or service life, including the possible excursion range
- Pressure: that anticipated in the process or service life, including possible excursions
- Concentration: that anticipated in the process or environment, including possible excursion limits

Adequate preliminary evaluations can be made using Table 7. Observations are dependent on the elastomer compound, process media, and conditions. More than one of the phenomena described may occur simultaneously. The property changes (increase or decrease) typically represent trends for the family of elastomers they are a part of. Some descriptions of the table are:

- Process media absorption leads to increase in volume. Due to the increase in cross section, the tensile strength and modulus may be somewhat reduced. Increase in elongation is usually small. This explanation is strictly for cases where there is only physical absorption without chemical reaction.
- Extraction of elastomer ingredients (leaching) implies removal of the fillers and other additives due to diffusion without chemical degradation. The footprint here is exactly the opposite of that where the fillers are chemically attacked.
- Attack on cross links will revert the structure to nonelastomeric, causing reduction of tensile strength and modulus. Other property changes are slight.
- Attack on polymer backbone is often preceded by attack on cross links. The result is a structure that is both nonelastomeric and nonpolymeric. The most significant changes are reduction in both tensile and elongation. Other changes will be slight.

Interpretation of correctly run elastomer testing data is not always an easy task. No test accurately predicts service life. Various shapes and applications require different combinations of key performance features. For example, an elastomeric compound used as an O-ring, diaphragm, or lining gives the same test results under a given set of test conditions. Yet, those testing data do not necessarily predict actual performance capability or service life for any of the three parts. Actual performance capability is shape and application specific.

Figure 8 illustrates typical data developed by the simple immersion test. The change in properties at different temperatures must also be recognized (Fig. 9). Furthermore, as Fig. 10 demonstrates, short-term data can be misleading.

Application-Specific Testing

Application-specific testing is the optimum approach to evaluating elastomers. Application-specific testing is conducted as indicated by using industry standard tests (Table 8). Standard tests define the test requirements and the type of data to be collected. They sometimes provide pass/fail criteria. Testing for specific application requires knowledge of the test protocol, use of standardized apparatus, and proper interpretation of the results. Critical elastomer applications are dependent on application-specific testing.

Application-specific testing encompasses chemical resistance, permeation, adhesion, tensile, abrasion and compression, and hardness change.

Chemical resistance is determined using the following standards.

ISO 1817, determination of effects of liquids, discusses the most basic and easy-to-perform tests for chemical resistance. It contains information related to total immersion and one-sided exposure of a rubber specimen followed by

Table 6 Relative performance in hydrocarbon products

Hydrocarbon product	FFKM	Specialty FKM	Standard FKM	TFE/P	NBR	EPR
Aromatics	E	E	E	P	F	P
Aliphatics	E	E	E	G	F	P
Oils	E	E	E	G	F	P
Gasoline	E	E	E	P	VG-G	P
Diesel fuel	E	E	E	P	VG-G	P
Jet fuel	E	E	E	P	F	P
Lubricants	E	E	E	F	F	P
Additives	E	VG	F	F	F	P
Oxygenates	E	VG	F	P	F	F

Relative rating: E, excellent; VG, very good; G, good; F, fair; P, poor

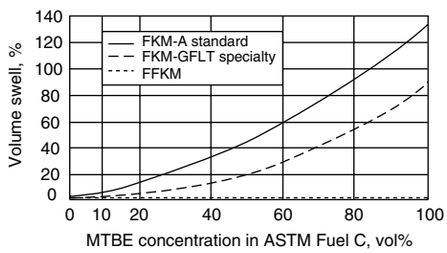

Fig. 7 Relative performance in fuel/oxygenate (MTBE) blends, vol% increase after 1 week at 23 °C (74 °F). MTBE additive, methyl tertiary butyl ether, is normally less than 10% in commercial fuels.

measurements of change in volume, weight, and tensile properties. It can be used for comparative evaluation of various elastomer compounds by using reference fluids or to determine the chemical resistance of a rubber in a chemical of interest. It does not include acceptance criteria, which is usually left to the user. Information regarding specimen dimensions, time for testing, and removal of excessive liquid before testing is provided through reference to other ISO standards. The most important of these are:

- ISO 37 (determination of tensile properties of rubber)
- ISO 48 (determination of hardness)
- ISO 471 (temperatures, humidity, and times for conditioning and testing)
- ISO 4661 (preparation of samples and testpieces)

ASTM D 471, rubber properties—Effect of liquids, is used for comparative evaluation of rubber in reference liquids as well as for evaluating the effect of the liquid of concern. It refers to other ASTM standards. The most important of these are:

- ASTM D 412 (determination of tensile properties)
- ASTM D 1415 (determination of hardness, international)
- ASTM D 2240 (determination of hardness, Durometer)
- ASTM D 3183 (preparation of testpieces from products)

ASTM C 868, determination of effects due to one-sided exposure (atlas cell), is used to determine the effect of one-sided exposure to liquids on an elastomer lining. It simulates the conditions of storage tank or process vessel where the elastomer is used as a lining material bonded to the substrate and includes the temperature differential across it. A description and schematic of the cell are included. Although not explicitly stated, it includes the importance of simulating the volume to surface area ratio. Exposure is followed by a peel pull test to determine retained adhesion and change in hardness, and pinholes are examined after removing excess liquid and drying.

Permeation is assessed by the following standards.

ISO 1399, permeability of gases (constant volume method), is principally used for measuring permeability of gases. The apparatus uses 55 mm (2.17 in.) diam disks of various thicknesses. One side is exposed to pressurized gas; the pressure on the other side is measured versus time to give permeability parameters.

ISO 2782 permeability of gases (constant pressure method), uses an apparatus at constant pressure on one side while measuring the increasing volume on the other side to give permeability parameters.

ISO 2528, vapor permeability, is most useful in determining comparative vapor permeation performance of different elastomer compounds. The elastomer sheet is stretched and sealed over a small dish containing a desiccant. The assembly is placed in a cabinet with controlled temperature and humidity conditions, and the dish is weighed over time to give the permeation (transmission) rate. The test is similar to ASME E 86.

ISO 6179, permeability of liquids, is the most popular method for determining the transmission rate of liquids through polymers. The version used in the United States is the Thwing cup permeation test. It consists of a small cup (60 to 100 cm^3, or 3.7 to 6.1 $in.^3$) partially filled with liquid. An elastomer specimen is stretched over the open end of the cup and clamped securely. The whole assembly is weighed and the cup is inverted. The loss of weight measured over time is used to calculate permeation (transmission) rate.

Materials Technology Institute (MTI) Report R 17, "Guide to Elastomer Testing for Chemical Resistance Applications," is a comprehensive document issued on testing, measuring, and interpreting the chemical resistance of elastomers. It addresses various needs not filled by the above standards. The guide has a section on the theory of permeation, key parameter measurements, test methods currently used, selection methodology, and interpretation of results. Figure 11 illustrates typical permeation data.

Heat aging implies change in properties of an elastomer at elevated temperatures.

Table 7 Evaluating elastomer performance from immersion testing

Property	Cause of property change				
	Process medium absorption	Extraction of elastomer ingredients	Attack on elastomer fillers	Degradation of elastomer cross link or polymer backbone	
Hardness	Decrease	Increase	Usually decreases	Increase (hard/brittle)	Decrease (soft/gummy)
Volume	Increase	Decrease	Increase	Increase	Increase
Tensile strength at break	Decrease	Increase	Decrease	Decrease	Decrease
Modulus	Decrease	Increase	Decrease	Increase	Decrease
Elongation at break	Increase	Decrease	Increase	Decrease	Increase or decrease

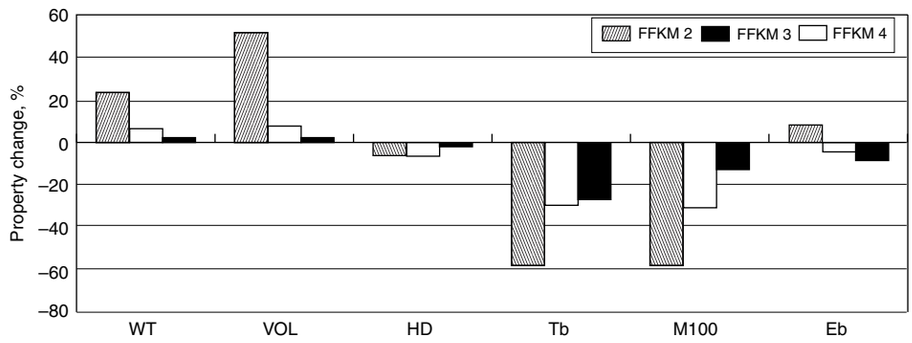

Fig. 8 Property changes of three elastomers in ethylene oxide at 50 °C (122 °F), 672 h test per ASTM D 471 and D 412, WT, weight; VOL, volume; HD, hardness; Tb, tensile strength at break; M100, tensile modulus at 100 s, 20 °C (68 °F); Eb, elongation at break

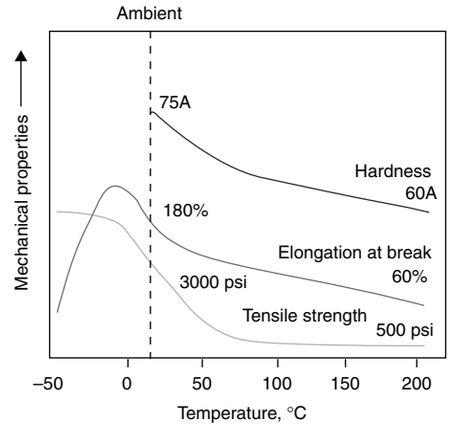

Fig. 9 Effect of temperature on mechanical properties for typical fluorelastomer (FKM) seals

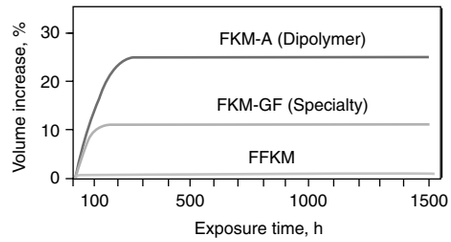

Fig. 10 Resistance to methylene chloride at 23 °C (73 °F) based on volume increase as a function of exposure time

ISO 188, heat aging for high-temperature properties and extrapolation for low-temperature properties, specifies procedures to be carried out either in an air oven or in an oxygen air chamber. Usually one property (such as elongation) is tracked versus time and temperature. The main use of such data is quality control and development of new formulations.

ASTM D 572, deterioration by heat and oxygen, and ASTM D 573, deterioration in an air oven, address the same scope as ISO 188. The ASTM standards separate the environments into air and oxygen.

ASTM D 454, rubber deterioration by heat and air pressure, is similar in approach to the tests mentioned previously, but adds methods for testing under pressure.

Adhesion to Substrate. ASTM D 429, rubber property—adhesion to rigid substrate, describes two approaches to adhesion testing. Method A consists of preparing a sample of rubber between two parallel plates and pulling them apart in tensile shear to determine the force required to separate the plates as well as the method of separation, that is, adhesive or cohesive failure. Method B consists of peeling a rubber liner at a 90° angle from the metal substrate to which it is bonded.

Method A is used to evaluate primers, compare rubber compounds, and study the effect of operating parameters such as temperatures and chemical exposure on the bond. Method B is used to evaluate a specific application such as lining for tanks and piping.

ISO 813 (one plate) and ISO 814 (two plate) combined are similar to ASTM D 429.

Tensile Tests, Percent Modulus, and Elongation at Break. ISO 37, determination of tensile stress strain properties, and ASTM D 412, test methods for vulcanized rubber—tension, are basic standards used for determining these mechanical properties. Although there are some differences, the object is the same, namely, determination of tensile strength, yield strength, and elongation at break.

Abrasion Resistance. There is no abrasion resistance test that measures rate of wear when exposed to slurry. Hence, in slurry abrasion applications, abrader test data combined with chemical resistance data is used to make engineering decisions. These tests are useful by themselves in developing new formulations of rubber in abrasive service.

ISO 4649 and ASTM D 5963, address abrasion resistance by rotary drum device, and include two methods (A and B) measuring weight loss of a rubber test piece on a rotating drum covered with an abrasive sheet. The sample is stationary in test A and rotating in test B. In both cases the weight loss is converted into volume loss and reported as abrasion resistance index.

ASTM D 2228, Pico abrader test, describes a slight variation of the abrader. It includes a pair of blunt tungsten carbide knives, which rub on a rubber specimen on a rotating turntable. Weight loss is reported as an abrasion resistance index. This standard can be used in preference to ISO 4644 and ASTM D 5963 when slurries containing sharp particles are being simulated.

Resistance to Compression. There is no standard test for determining the compression properties of seals and gaskets while exposed to liquid. The approach is to determine the compression properties in air and combine those with the chemical resistance data to make engineering decisions.

ASTM D 395 and ISO 815 describe the apparatus and establish the methods for calculating compression set. Compression set is the residual deformation of a rubber specimen after it has been compressed under a known deflection or force. One test is carried out under constant load, and the other carried out at constant deflection. The constant deflection test is more common and is illustrated in Fig. 12. After the completion of the test, compression set

Table 8 Application-specific tests and standards for evaluating various properties of elastomers

		Applicability						
Property	Standards	Static seal O-ring gaskets	Dynamic seal O-ring gaskets	Diaphragms	Hoses	Linings for vessels, pipe, and accessories	Expansion joints	Lined valves
Chemical resistance	ISO 1817 ASTM D 471	X	...	...	...	...	...	...
	ASTM C 868	...	X	X	X	X	X	X
Permeation	ISO 1399 ISO 2782 ISO 2528 ISO 6179 MTI guide	X	X	X	X	X	X	X
Heat aging (upper use temperature limit)(a)	ISO 188 ASTM D 454 ASTM D 572 ASTM D 573	X	X	X	X	X	X	X
Adhesion to substrate	ISO 814 ISO 813 ASTM D 429(b)	...	...	...	...	X	...	X
Tensile properties	ISO 37 ASTM D 412	X	X	X	X	...	X	X
Abrasion resistance	ISO 4649 ASTM D 2228(c) ASTM D 5963	...	X	X	X	X	X	X
Compression resistance	ASTM D 395 ISO 815	X	X	X	X	...	X	X
Hardness	ASTM D 2240	X	X	...	...	...	...	...

(a) Can be combined with chemical resistance. (b) Used in conjunction with ASTM C 86. (c) Pico abrader

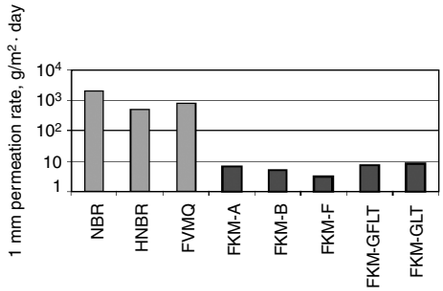

Fig. 11 Permeation rate of elastomers used for handling fuels. Fuel C at 23 °C (73 °F) tested.

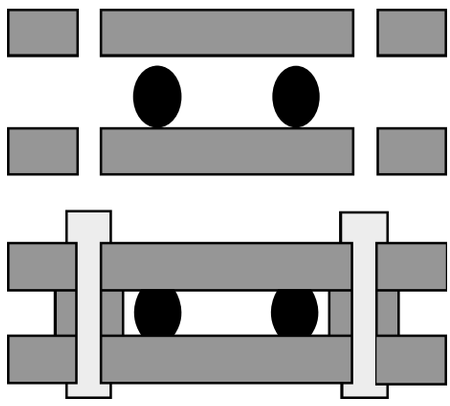

Fig. 12 Compression set is tested by constant deflection by using fixture shown.

is reported as percentage of the original deflection.

Compression set data can be misleading if reported only on the basis of short test exposure of 70 h, as Fig. 13 indicates.

Hardness. ASTM D 2240 and ISO 7619, Durometer hardness is the most commonly used method for measuring hardness of elastomers. An indentor is used to measure the resistance to surface penetration.

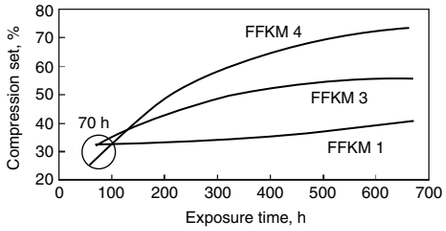

Fig. 13 Compression set determined by testing 672 h at 204 °C (400 °F). ASTM D 395 70 h results are circled.

Failure Analysis

The three elements of failure analysis are: failure modes and effects analysis (FMEA), physical failure analysis, and root cause failure analysis.

Failure modes and effects analysis are used to diagnose the mechanism of failure through experience developed from previous failures. When analyzing a failed part such as an O-ring, care must be taken to consider that the appearance of the part at ambient temperature may not reflect its appearance operating in service. Some FMEA are established to consider all possible failure modes, no matter how unlikely the mode may be. The quality of FMEA depends on the availability of sound historical data. If it cannot provide a reliable answer, or the consequence of the failure requires additional investigation, physical failure analysis should be used.

Physical failure analysis provides a more accurate explanation of the technical cause of a particular failure or loss of performance. This information is essential for understanding the root cause of a problem. If possible, the part should be examined in the condition it is in when removed from the equipment. If chemical decontamination is required, then the chemical used must be specified when submitting the part for analysis. Sometimes the use of a chemical decontaminant can interfere with the analysis. Accurate background information on the failure and the failed part is required. This includes any information concerning temperature excursion beyond the limitations of the part and chemical exposures outside of the norm, such as in cleaning or flushing.

Root cause failure analysis builds on the technical cause and looks deeper into the problem to ensure that the technical fix did not just cure the symptoms. For example, in many sealing failures, the elastomer supply chain is the root cause of the problem because a materials mix-up has occurred. A logic chart of a root cause failure analysis, called a Why Tree (Fig. 14), investigates a corrosion–related system failure.

Elastomer Failure Modes

The following observations are specific to O-rings, but they may be applied to other types of elastomer parts.

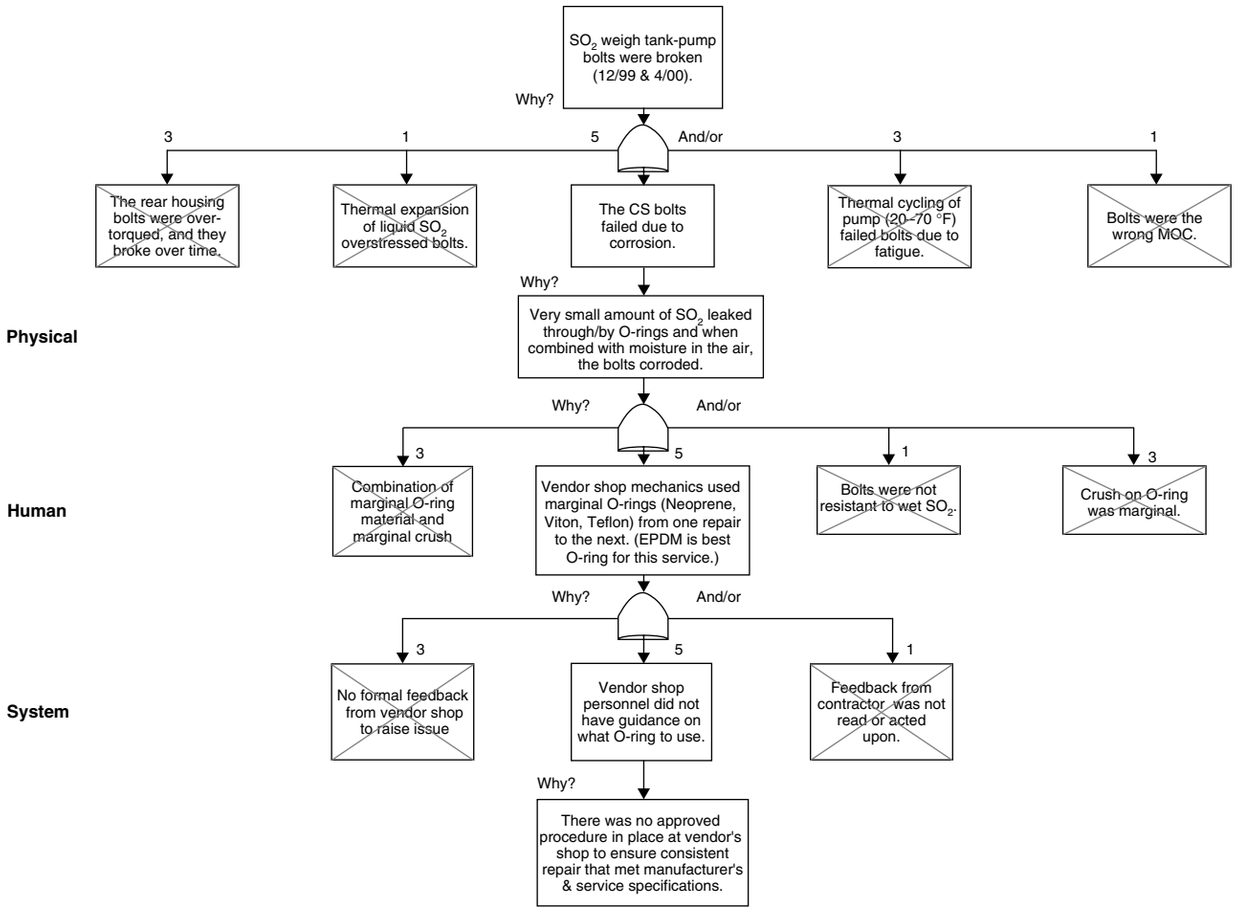

Fig. 14 Root cause failure analysis logic chart called a Why Tree. This failure examines a corrosion-related failure.

Swelling. This is often very obvious when the O-ring is viewed and compared to a "control" O-ring of the same size. This type of attack may be solubility related, or it may be chemical attack. If it is solubility related, then the O-ring will return to normal size after it has been removed from the fluid and has time to dry out. This is because the O-ring absorbs the chemical media, swells to a certain volume, and then does not swell any more. If the event is a chemical attack, then the O-ring will continue to swell while it is exposed to the chemicals, and it will not return to normal size after removal from the media. Chemical attack also often results in the O-ring surface becoming tacky or "gummy." Depending on gland dimensions, the O-ring may extrude in either case. A decision must be made regarding the amount of O-ring swell an application can tolerate.

Hardening/Embrittlement. An O-ring can become hard or embrittled for several reasons. The first possibility is overexposure to high temperatures. Exposing an elastomer to temperatures above its rated service temperature will eventually result in a hardened O-ring. When flexed, the O-ring will typically show cracks on the inside diameter or perhaps break. The O-ring dimensions will not show much of a change. This type of problem can also occur if a chemical solvent extracts oils or plasticizers from the O-ring, resulting in a decrease in part weight and possibly a dimensional change.

Cracks or splits are the result of overstressing the O-ring in localized areas. In the simplest case, an O-ring can be overcompressed and the O-ring will split. This problem can also result if an O-ring is overstressed as the result of thermal expansion. This 'effective' high compression is the result of elevated temperatures. Similarly, if the process chemical causes an O-ring to swell, the combined compressive stress during operation can be great enough to cause splitting. Another problem that can cause splitting is explosive decompression. This problem arises when an elastomer is sealing gases or liquids under high pressure. An example is carbon dioxide. During process operation, carbon dioxide equilibrates in the elastomer seal over time. Since these systems often operate at high pressures (14 MPa, or 2000 psi, For example), the CO_2 in the elastomer is at this condition. If there is a sudden loss of system pressure, the gas inside the O-ring expands rapidly and literally blows the O-ring apart to escape. In less severe cases, the O-ring may blister or have small splits.

Extrusion can be the result of a number of factors. It is easily identifiable as a feathering or "pushing out" of the elastomer into the space it is designed to seal. A small degree of extrusion is typical in all sealing services and helps to create a seal. However, any extrusion that is readily apparent can cause a problem and will result in premature seal failure. One cause of extrusion is the elastomer overfilling the gland. When this occurs, the elastomer will extrude. This scenario may be caused by chemical swell or thermal expansion. The other possibility is extrusion due to a system pressure that is too high when considering the modulus of the elastomer and the gap (space) that needs to be sealed. This second condition can often be solved by using a higher modulus compound, reducing the

Table 9 Elastomer identification techniques

Technique	Acronym	Description	Use	Value
Fourier transform infrared spectroscopy (most commonly used)	FTIR	The interaction of infrared light with a molecule changes the vibration of the molecule. These interactions are unique	Identification of the elastomer	Identifies the elastomer per type; FKM, FFKM, EPDM, etc.
X-ray fluorescence spectroscopy (most commonly used)	XRF	X-rays are bombarded on the sample, and core shell electrons are ejected. The excited atom emits fluorescent radiation.	To perform qualitative and quantitative elemental analysis of the elastomer and identify the specific compound	Identifies a specific compound
Electron spectroscopy for chemical analysis	ESCA	X-rays are focused in the surface of a material and excite the surface atoms. Photoelectrons with energies characteristic of elements on the surface of the sample are ejected and analyzed to obtain information on the surface composition.	To analyze changes in the surface chemistry of an elastomer following exposure to reactants, plasmas, temperature, and specialized chemical environments	Indicates which elements are on the surface of an elastomer; to determine if the surface makeup has changed
Inductively coupled plasma/mass spectroscopy	ICP-MS	The sample is broken down into its ions in an argon plasma, which are separated by their masses, and measured in a mass spectrometer.	To analyze changes in the surface chemistry following exposure to reactants, plasma, temperature, and specialized chemical environments	Indicates the metals extracted from an elastomer by a solvent, for example, when exposed to ultrapure water
Scanning electron microscopy	SEM	Image formed by scattered or secondary electrons from incident beam scanned on specimen.	Evaluation of changes to the microstructure and surface morphology of a sample	Yields a magnified picture of the elastomer surface
Thermogravimetric analysis, infrared	TGA-IR	Volatile compounds formed by temperature programmed pyrolysis are purged through an infrared gas cell while infrared spectra are collected in real time for a given time and temperature.	To develop graphic profiles of off gases versus time and temperature	Indicates temperature at which various components of an elastomer start to break down

Table 10 PDL composite rating system

Weighted value	Weight change(a)	Volume change(a)	Hardness change (units)	Mechanical property retained(b)	Visual observed change(c)	BTT (min)	Permeation rate, ($\mu g/cm^2 \cdot min$)
10	0–0.25	0–2.5	0–2	>= 97	No change	≤1 = 0	≤0.9
9	>0.25–0.5	>2.5–5.0	>2–4	94–<97	...	>1–2 = 2>1≤2	...
8	>0.5–0.75	>5.0–10.0	>4–6	90–<94	...	>2–5 = 3>2≤5	>0.9–9
7	>0.75–1.0	>10.0–20.0	>6–9	85–<90	Slightly discolored, slightly bleached	>5–10 = 4>5≤10	...
6	>1.0–1.5	>20.0–30.0	>8–12	80–<85	Discolored; yellows, slightly flexible	>10–30 = 5>10≤30	>9–90
5	>1.5–2.0	>30.0–40.0	>12–15	75–<80	Possible stress crack agent, flexible, possible oxidizing agent, slightly crazed	>30–120 = 6>30≤120	...
4	>2.0–3.0	>40.0–50.0	>15–18	70–<75	Distorted, warped, softened, slight swelling, blistered, known stress crack agent	>120–240 = 7>120≤240	>90–900
3	>3.0–4.0	>50.0–70.0	>18–21	60–<70	Cracking; crazing; brittle; plasticize, oxidizer; softened; swelling; surface hardened	>240–480 = 9>240≤480	...
2	>4.0–6.0	>60.9–90.0	>21–25	50–<80	Severe distortion; oxidizer and plasticizer, deteriorated	>480–960 = 9>480–≤960	>900–9000
1	>6.0	>90.0	>25	>0–<50	Decomposed	>960 = 10>960	...
...	...	...	...	0	Solvent dissolved, disintegrated	...	>9000

clearance gap by machining the mating parts, or by employing antiextrusion rings.

Polymerization. This problem can occur when a chemical is absorbed into the O-ring and then polymerizes. An example of this is styrene monomer. Styrene monomer is very reactive, and hence, inhibitors must be continuously added to the process stream, otherwise the styrene will polymerize to form polystyrene. Although the exact mechanism is not known for elastomer attack, there is a reasonable hypothesis. Styrene is absorbed into the surface of the O-ring and polymerizes. As it does this, it expands and breaks open new elastomer surface for further styrene absorption, and further polymerization, and so on. The result is an O-ring that has swollen in size and has a hard, friable surface where it was in contact with the liquid. All elastomers appear susceptible to this mode of attack by polymerizing monomers.

Mechanical Damage. A part may be damaged during installation if it has to go over a sharp edge that cuts the part. Another common cause of mechanical damage is a dynamic application that causes abrasion of the elastomer surface.

Elastomer Material Identification

As part of the failure analysis it may be necessary to identify the type of elastomer. Table 9 provides a summary of identification techniques. Several techniques are used to identify elastomers according to their families, but none provide a complete and accurate description of the constituents in the material. The most cost-effective technique/techniques should be used consistent with the value associated with obtaining an accurate identification.

Infrared analysis may be used to determine the elastomer type, that is, EPR, fluoroelastomer, and so forth. This method usually cannot identify the part manufacturer. If, however, a manufacturer produces a part that is fully integrated from the polymer to the finished part, then the manufacturer and product type part may be identifiable.

After an elastomer type is identified, further analysis is required to identify the specific compound. Different ingredients used in the manufacture of a compound can often be identified and that information then used to identify the specific compound. However, this step is difficult and may not be conclusive.

Quantifying Performance

The Plastic Design Library (PDL) has developed a composite interpretation or rating system for elastomers. The percent change in a test parameter is weighted to develop a number from 1 (worst) to 10 (best) for the elastomer under specific exposure conditions. Most of the data supplied to PDL is from suppliers so that the rating is dependent on the quality and accuracy of the information supplied. Factors used to develop the PDL weighting system are:

- Weight change
- Volume change
- Hardness change
- Mechanical property retention
- Appearance change
- Breakthrough time (from initial chemical contact to detection)
- Permeation rate

Table 10 gives the detailed numerical values that determine the rating.

SELECTED REFERENCES

- *Chemical Resistance of Plastics and Elastomers,* 3rd ed., William Andrews Publishing/Plastic Design Library, 2001
- DuPont Dow Elastomers Chemical Resistance Guide, DuPont Dow website, www.dupontdow.com, accessed May 2005
- "Guide to Elastomer Testing for Chemical Resistance Applications," MTI R-17, Materials Technology Institute, 2004

ASM Handbook, Volume 13B: Corrosion: Materials
S.D. Cramer, B.S. Covino, Jr., editors, p621-628
DOI: 10.1361/asmhba0003968

Global Cost of Corrosion—A Historical Review

R. Bhaskaran, N. Palaniswamy, and N.S. Rengaswamy, Central Electrochemical Research Institute
M. Jayachandran, H.H. The Rajah's College

IN 1824, SIR HUMPHRY DAVY demonstrated that coupling of zinc blocks controlled the corrosion of copper sheathing of a ship hull (Ref 1). This shows that even before the mechanism of corrosion was understood, attempts were made to control the cost of corrosion. Considerable efforts have been made since the early 1900s to assess the loss of money due to metallic corrosion. This article analyzes the estimates of the cost of corrosion, made in various countries at various times. These are presented in chronological order by country. The data is extrapolated to a 2004 base and then projected to the global economy.

In the United States (USA) the awareness of the cost of corrosion has been maintained at a high level. Professor Uhlig; the National Bureau of Standards (NBS), now the National Institute of Standards and Technology (NIST); Battelle Columbus Laboratories (BCL); and CC Technologies Laboratories (CC), along with NACE International and the Federal Highway Administration (FHWA), have contributed to the current knowledge on the cost of corrosion. In the United Kingdom (U.K.), the Hoar Committee has played a stellar role in estimating the cost of corrosion. In Japan, three approaches (Uhlig method, Hoar method, and NBS-BCL model) have been used. In India, the Uhlig method was followed in 1958, while the NBS-BCL model was adopted in 1986.

Countries have attempted to relate the cost of corrosion to their gross national product (GNP). However, the present trend seems to lay importance on the gross domestic product (GDP). See the article "Direct Cost of Corrosion in the United States" in *ASM Handbook,* Volume 13A, 2003, for details on the USA studies.

United States of America

The first attempt to evaluate corrosion loss was made in 1916 when the construction industry examined corrosion of steel reinforcements (Ref 2).

Professor Uhlig (Ref 3, 4) paved the way for systematic analysis of the cost of corrosion in the USA. He divided the cost of corrosion into direct losses resulting from the use of special alloys and replacement of corroded equipment, and indirect losses due to shutdown, overdesign, loss of product and efficiency, explosion, and contamination. He showed that the annual direct loss by corrosion, including cost of corrosion control, was $5.5 billion United States dollars (USD), or $35/person per year in the USA. He further predicted that by embarking on a five year research, development, and education program on corrosion and corrosion control, an annual savings of $922 million was possible.

The NACE Technical Committee report in 1959 (Ref 5) projected that nearly $150 million USD was being spent annually to purchase corrosion-resistant materials such as coatings, linings, and corrosion-resistant metals.

The NBS projected that corrosion losses in the USA during 1966 would be $10 billion/year (Ref 6). Reference 7 raised an interesting question in 1974: Which cost more: corrosion, fire, flooding, or earthquake? It showed that the projected cost of corrosion, over $15 billion USD/year, was more than the combined sum of the costs of fires and floods. In fact, corrosion costs may also exceed the sum costs of earthquakes, hurricanes, tornadoes, and landslides.

An investigation of the economic impact of corrosion in the USA was carried out by the NBS in 1978 (Ref 8). The assignment was placed under contract to BCL. A significant feature of the study was that the method employed, input-output analysis, provided a methodological framework that permitted comprehensive treatment of all elements of the costs of corrosion: production costs, capital costs, and changes in useful lives. Using the results obtained in the input-output analysis as a basis, the total cost of corrosion in the USA (1975) was estimated to be $70 billion USD, approximately 4.2% of the GNP. Of this amount, approximately 15% was estimated to be avoidable under the criteria developed in the study. This meant that a significant fraction of the total expended for corrosion control or for replacement or repair of goods because of corrosion, approximately $10 billion USD, could be available for other uses through the economic use of presently available technology.

Reference 9 showed that the indirect losses due to corrosion failures may be put at $50 billion USD, or approximately 2 to 3% of the GNP. It concluded that the total annual expenditure on various corrosion control measures was a huge sum, as high as $9.6 billion USD.

In 1982, an estimate of the cost of corrosion in the USA for energy-related industries (electric power generation, materials protection, personally owned automobiles, and government operations) was projected as $122 billion USD (Ref 10). Of this, $16.9 billion (14%) could be avoided by using the available corrosion prevention and control methods. This was equivalent to an energy savings of approximately 3.3 quads (one quad equals 10^{15} Btu, or approximately 10^{18} J), which would have been approximately 14% of the total energy produced in the USA for that year.

According to Ref 11, the annual cost of corrosion for the USA amounted to approximately $176 billion in 1986 USD. Of this, a minimum $26 billion USD (15%) was avoidable through the use of existing technology.

In 1995, a panel of Battelle scientists updated the data on corrosion cost in the USA by evaluating two decades (1975 to 1995) of corrosion-related changes in scientific knowledge and industrial practices (Ref 12). Accordingly, the total cost of corrosion pertaining to the whole industrial sector was estimated at $296 billion USD. Of this, $104 billion USD (35%) was shown as avoidable cost.

During 1998, a need was felt to carry out a systematic study to estimate the current impact of metallic corrosion on the USA economy. Subsequently, CC Technologies Laboratories conducted this study from 1998 to 2001 in a cooperative agreement with the FHWA and NACE International (Ref 13 and summarized in *ASM Handbook,* Volume 13A, 2003). In this study, the total direct cost of corrosion was determined by analyzing 26 industrial sectors in

which corrosion was known to exist and then extrapolating the results for a nationwide estimate. The total direct cost due to the impact of corrosion for the analyzed sectors was $138 billion USD/year (1.57% of the GDP). Because not all economic sectors were examined, the sum of the estimated costs for the analyzed sectors did not represent the total cost of corrosion for the entire USA economy. By estimating the percentage of USA GDP for the analyzed sectors and by extrapolating the figures to the entire USA economy, a total direct cost of corrosion was estimated as $276 billion USD (3.14% of the nation's GDP). The indirect cost of corrosion was conservatively estimated to be equal to the direct cost, giving a total direct plus indirect cost of $552 billion USD (6% of the GDP).

Attempts have been made to calculate the cost of corrosion in individual industrial sectors from time to time. For example, Table 1 tracks the cost of corrosion for the pipeline industry.

The oil industry has received constant attention from 1952 onward, as seen in Table 2. A modest estimate of the cost of corrosion in the tanker industry was $18 million USD during 1952. The 1998 FHWA report has projected a figure of $1.4 billion USD as the cost of corrosion in oil and gas exploration and production.

Table 3 indicates that automobile industry corrosion costs escalated. The pulp and paper industry has a similar degree of escalation (Table 4). Table 5 indicates estimated savings as well as the cost of corrosion in individual industries.

For the USA, estimates by Uhlig for 1949 showed the direct cost of corrosion as $5.5 billion USD, whereas the 1998 to 2001 estimate using the net present value method showed the direct cost of corrosion as $276 billion USD (3% of the GNP). This is a 50-fold increase in the direct cost of corrosion over a 50 year period.

Table 1 Cost of corrosion in the pipeline industry for the USA economy

Year	Subject	Cost, million USD/yr	Reference
1945	Corrosion in underground pipelines	50	14
1947	Pipeline replacement due to corrosion	200	15
1947	Corrosion of water mains	40	16
1951	Corrosion cost in a large pipeline system prior to installation of sacrificial magnesium anodes	1.5	17
1951	Underground corrosion in American industries	1000	18
1966	Annual savings by application of cathodic protection in pipelines	1.1	19
1998	Corrosion in gas and liquid transmission pipelines	7000	13

USD, United States dollars

United Kingdom

As in the case of the USA, the U.K. construction sector was very much concerned about the huge losses occurring due to the corrosion of metals in concrete. It was therefore not surprising that the Institution of Civil Engineers formed a committee in 1916 to investigate the impact of the deterioration of structures exposed to sea action. At the end of this investigation (Ref 45), it was estimated that the annual world cost of steel and iron wasted by rusting was of the order of £600 million British pounds (GBP). The U.K. was perhaps the pioneering country with regard to assessing the economic loss due to corrosion.

It was estimated in 1936 (Ref 46) that if all the wrought iron and steel produced in Great Britain in that year were given two coats of paint, approximately 32 million gallons would have been required, and the cost of this protection, including the necessary labor, would have been on the order of £40 million GBP. In 1949, the previous estimate was revised to no less than £200 million GBP (Ref 47).

According to Ref 48, the annual cost of corrosion in the U.K. was £200 million GBP during 1954. Of this, at least £5 million was spent toward replacement of corroded buried pipelines.

During 1956, Ref 49 calculated the cost of corrosion for the U.K. by taking into account costs of preventive measures and costs of actual wastage or replacement and arrived at £600 million GBP.

According to a report published in 1967 (Ref 50) and subsequently cited in Ref 51, corrosion control costs £195 million GBP/year. The projection for the entire world was approximately £15 billion GBP/year.

According to Ref 52, the previous estimate of approximately £200 million GBP covered only part of the time-related-cost of corrosion to the British economy. A figure of £400 million GBP/year was stated to represent the time costs more fully in 1969. This represents 1.25% of the British GNP. In other words, the cost of corrosion to the U.K. was the same as one-quarter of the total expenditure on education, or one-fifth of the expenditure on defense, or over one-half of the cost of running the National Health Service. The interesting observation made in Ref 52 was that the indirect costs of corrosion far outweighed the direct costs, and this enormous loss to the economy was surely sufficient reason to make a detailed study of corrosion in all its aspects—chemical, physical, metallurgical, and economic. If the costs of corrosion and corrosion control in the U.K. were reduced by only 5%, it would lead to a savings of at least £20 million GBP/year in addition to increasing human safety and well being.

The Hoar committee on corrosion and protection calculated the annual cost of corrosion in

Table 2 Cost of corrosion in the oil industry for the USA economy

Year	Subject	Cost(a)	Reference
1952	Corrosion in sour oil wells in West Texas, New Mexico, and Kansas	Ranges between $270 and $2000/well per year	20
1952	Corrosion in tanker industry	$18 million	21
1952	Potential savings of Shell Oil Company through the use of corrosion inhibitors	$110,000	22
1953	Condensate well corrosion	$12 million	23
1953	Corrosion in petroleum processing	$0.09/barrel of crude process(b)	24
1957	Repairs to the oil string casing in the petroleum industry	$7.5 million	25
1958	Corrosion in sour oil wells	$32 million	26
1958	Corrosion in refinery equipment	$300 million	27
1959	Damage to refinery equipment through corrosion	$400 million	28
1960	Corrosion in Cleveland Sohio refinery crude units	$0.02/barrel(c)	29
1965	Use of inhibitor for crude oil processing	$300 million	30
1975	Repair cost of corrosion damages at a major refinery in Chicago	$500,000	9
1975	Loss of revenue at Chicago refinery	$5 million	9
1998	Corrosion in oil and gas exploration and production	$1.4 billion	13
2003	Oil spilled due to pipeline corrosion and mechanical damage	$95 million(d)	31

(a) United States dollars. (b) Average cost of crude oil was $2.68/barrel. (c) Average cost of crude oil was $2.88/barrel. (d) 145,000,000 gal spilled; $27.54 cost/barrel (42 gal)

Table 3 Cost of corrosion in the automobile industry for the USA economy

Year	Details	Cost, billion dollars/year	Reference
1960	Corrosion in automobile exhaust systems	0.5	32
1978	Corrosion cost for automobile owners	6–14	33
1991	Corrosion cost for motor vehicle from deicing salts	2.3	34
1998	Corrosion in motor vehicles	23.4	13

Table 4 Cost of corrosion in the paper industry

Year	Details	Cost	Reference
1977	Paper mill corrosion, USA	$8 per metric ton of product (20% of maintenance cost)	35
1977	Global corrosion to the pulp and paper industry	$500 million	36
1998	Corrosion in pulp and paper industrial sector for USA	$6 billion	13

Britain as £1.365 billion GBP (3.5% of the GNP of 1970). Of this, £310 million/year (23%) could be saved by more effective use of existing knowledge (Ref 53).

T.P. Hoar (Ref 54) subsequently revised the figures in 1975 as follows. Total cost of corrosion would be £2.5 billion, of which £500 million (20%) could be considered as avoidable cost. Approximately 25 years subsequent to this estimate, a detailed cost of corrosion survey was undertaken from 1998 to 2001 in five specific industrial sectors by the Paint Research Association of the U.K. (Ref 55). A total cost of corrosion was estimated as £4.645 billion GBP. This estimate approximately doubles the 1975 cost. Approximately £672 million (14.46%) could be saved by the application of better technology.

Whereas in the USA, the estimation of the cost of corrosion in individual sectors as well as the whole economy was being updated at regular intervals, in the U.K. no such attempts for individual sectors appear to have been made. However, as indicated in Table 6, one-time attempts had been made in certain industries, particularly from 1950 to 1970.

Australia

In 1955, the authors of Ref 60 reported a method of determining corrosion cost related to piping (oil, steam, fire, and water pipelines) in a bulk oil terminal and showed that the corrosion cost can be approximately £760 (Australian pounds, or AUP) per annum (10% of installed cost). They further showed that of £760, nearly £40 AUP is the indirect cost of corrosion. Their estimate applied to one oil installation only. However, as reported in Ref 61, Professor Worner of the University of Melbourne, Australia, carried out a detailed analysis on the cost of corrosion to Australia in 1956 and showed that the direct losses ranged from £100 to 120 million AUP ($240 million Australian dollars, or AUD), or £10 to 13 AUP/year for every Australian.

The author of Ref 62 discussed corrosion costs and savings in Australia during the Twelfth Annual Conference of the Australasian Corrosion Association in Melbourne in 1971. He followed the British pattern with regard to the cost of corrosion, and, considering the geographic location of Australia and per capita electricity consumption, he determined a value of $900 million AUD, or 2.67% of the GNP of Australia. In other words, everyone in Australia contributed $15 AUD/year unnecessarily toward corrosion. With regard to savings, he adopted the British pattern of 23% and showed that $200 million AUD/year were avoidable costs.

E.C. Potter (Ref 63) of Commonwealth Scientific and Industrial Research Organization, Sydney, again discussed the cost of corrosion in Australia in 1973 by referring to Worner's 1955 estimate. He converted the 1955 estimate to 1972 conditions by allowing for the change in the value of money and for the increased amount of metal subject to corrosion. The £120 million AUP in 1955 was the monetary equivalent of $385 million AUD in 1972. To account for the increased amount of metal at risk, the latter figure was raised by a factor of 2.4, which represented the ratio of the per capita consumption of electricity for 1972 and 1955. The result was $925 million AUD/year. It was remarkable that the total annual corrosion costs updated from 1955 were virtually the same as the 1970 estimate of $900 million AUD.

In 1973, a detailed estimate on the cost of corrosion in Australia was presented by Revie and Uhlig (Ref 64) at the Fourteenth Annual Conference of the Australasian Corrosion Association. Uhlig's method was followed. The total cost of corrosion was $466.7 million AUD ($550 million USD on the 1973 basis). This represented 1.5% of Australia's GNP for 1973.

According to Ref 65, the avoidable cost of metallic corrosion in Australia at mid-1974 values amounted to $250 million AUD. In 1983, Cherry and Skerry (Ref 66) of Monash University applied the input-output model developed by NBS-BCL of the USA to the Australian economy and showed that the potentially recoverable cost of corrosion to Australia could be of the order of $2 billion AUD at 1982 prices.

In 1995, Cherry (Ref 67) updated the data and showed that for only ten selected industrial sectors in Australia, the potential savings due to application of currently available corrosion knowledge could be approximately $5.7 billion AUD (at 1991 to 1992 values).

Japan

In Japan, a 1956 estimate was made of corrosion losses to underground cables and pipelines based on the number of failures per year caused by chemical and electrolytic corrosion, annual expenditure necessary for replacements and repairs, and average repair expenditure per failure (Ref 68). The annual loss was shown as ¥74 billion (Japanese yen, or JPY) ($0.2 million USD).

A survey made from 1976 to 1977 by a committee on corrosion and protection, under the chairmanship of Professor G. Okamoto, revealed that the annual cost of corrosion to the nation amounted to ¥2500 billion JPY ($9.2 billion USD on a 1974 basis) (Ref 69).

According to Ref 70, the Japan Society of Corrosion Engineering and the Japan Association of Corrosion Control updated the cost of corrosion in Japan. The direct cost of corrosion in 1997 was estimated by the Uhlig, Hoar, and NBS/BCL methods. In accordance with Uhlig's method, the overall cost was ¥3900 billion JPY (0.77% of the GNP of Japan), and Hoar's method resulted in a figure of ¥5200 billion JPY (1.0% of the GNP of Japan). The corrosion cost, using the input-output method (NBS-BCL analysis), was found to be approximately ¥9700 billion JPY (1.9% of the GNP).

Thus, depending on the method of analysis, the cost of corrosion in Japan has a substantial range. Following the Uhlig model in 1976 and 1997 showed an increase from ¥2500 billion to 3900 billion, a 1.5 times increase over a period of 20 years. The other methods would boost the multiplier as much as 2.5 times, depending on the analytical approach.

Canada

Data in Ref 71 showed the annual cost of corrosion in Canada in 1953 to be $300 million Canadian dollars (CAD). The analysis was made on the Uhlig pattern.

Table 5 Cost of corrosion in various industrial sectors for the USA economy

Year	Subject	Cost	Reference
1961	Potential savings by proper painting practices in a chemical industry	26% of painting cost	37
1962	Savings by application of modern concepts of painting in a nickel company	40% of painting cost	38
1963	Corrosion in boilers, direct repair and replacement	$50–100 million/yr	39
1963	Savings by use of plastic materials in chemical process industry	66% of similar metallic installations	40
1975	Corrosion in ammonia unit	Removal of carbon dioxide by this unit cost $550,000/yr	41
1976	Corrosion in aircraft industry	$1.5–2 billion	42
1977	Corrosion in highway bridges	$23 billion	43
1978	Corrosion in electric power industry	$1.1 billion/yr	33
1993	Corrosion in industrial steam generator	>$10 billion/yr	44

Table 6 Cost of corrosion for individual industrial sectors in the U.K. economy

Year	Subject	Cost	Reference
Pipelines			
1952	Corrosion in underground pipelines	£130 million	56
Oil industry			
1960	Direct and indirect cost of corrosion in one major oil company	£1.5 million	57
Automobile industry			
1970	Corrosion cost to Britain's motorists	£250 million	58
1971	Potential savings by application of more suitable materials in automobile industry	£55 million	59

The author of Ref 72 reported that the annual corrosion loss in Canada in 1966 was roughly 3% of the GNP, or $1 billion CAD/year.

It is interesting to note that in Canada, the oil industry and paper industry have received greater attention with regard to corrosion awareness than other industry sectors, as can be seen from Table 7.

Germany

In Germany, the earliest reference to the loss due to corrosion is in 1929 (Ref 77), which reported that only two-thirds of the annual steel and pig iron production was used to increase the amount of metals available in industry, while one-third covered the losses due to corrosion. However, in 1953, it was estimated that 150 million deutsche marks (DM) per year were being spent on rust prevention (Ref 78). German railroads alone spent 72 million DM, the Ruhr coal mines approximately 15 million DM, and the major industries several million each. Of the cost of repainting the German federal railways, 39% was spent on rust removal alone.

Behrens (Ref 79) of DECHEMA reported in 1975 that the corrosion damage incurred by the German economy in one year (on a 1968 to 1969 basis) can be assessed at approximately 19,000 million DM ($6 billion USD, 1969 basis), of which approximately 4300 million DM ($1.5 billion USD, 1969 basis) may be considered as avoidable. Total costs were approximately 3% of the West German GNP for 1969, and avoidable costs were roughly 25% of the total costs.

Poland

The Department of Environment Protection of the Ministry of the Chemical Industry and the Corrosion Control Commission of Poland carried out a corrosion survey and showed that the total sum of direct and indirect losses, as well as corrosion control costs, amounted to 1990 million zlotys (Zl) in 1971, and this increased to 2700 million Zl in 1975 (Ref 80).

During 1977, the economic losses due to corrosion in Poland were approximately 46 billion Zl, and the costs of corrosion prevention were approximately 17 billion Zl (Ref 81). It was 2% of the value of permanent operation materials.

Table 7 Cost of corrosion for individual industrial sectors in the Canadian economy

Year	Subject	Cost, CAD(a)	Reference
Oil industry			
1957	Cost of corrosion to Canadian refineries	$18.5 million	73
1965	Corrosion in a typical refinery	$1.5 million/yr	30
Pulp and paper industry			
1968	Canadian pulp and paper mills corrosion	12% of maintenance costs	74
1974	Estimate of global cost of corrosion in pulp and paper industry	$320 million	75
1976	Replacement of stainless washer drums and molds	$2 million	76
	Repairs in black liquor evaporators	$100,000	...
	Replacement of corroded sewer line	$400,000	...
	Boiler repairs	$1 million	...

(a) Canadian dollars

South Africa

According to a report by the South African Corrosion Council (Ref 82), £20 million GBP was the annual recurring cost toward maintaining structures in South Africa in 1961.

During 1985, corrosion costs in four sectors of the South African economy (mining, power generation, shipping, and transport) were of the order of 1.2 billion rand (ZAR) per year, and by projection, the total cost of corrosion to the whole country was 4 billion ZAR (Ref 83).

Czechoslovakia

Kulis (Ref 84), of the then Czechoslovak Socialist Republic (CSSR), considered the financial effects of the deterioration of construction materials by corrosion and concluded that in Czechoslovakia, the direct corrosion losses in 1975 amounted to 1.7% of the GNP. Kulis, along with Knotkova (Ref 85), carried out a special study on the cost of corrosion in Prague during 1981, with special reference to protection of steel structures exposed to the atmosphere by the application of paints. The study showed that the economic corrosion damage amounted to 488 million koruna. In 1993, two national components, the Czech Republic and Slovakia, were formed.

Belgium

It is well known that Marcel Pourbaix of Brussels was a pioneering corrosion scientist who introduced the concept of the potential-pH diagram in 1945. During 1973, he estimated the direct loss due to corrosion in Belgium as 16 to 25 billion francs/year (Ref 86). He has also given some interesting information on the loss due to corrosion. The quantity of iron destroyed annually by corrosion had been estimated as 25 to 33% of the annual production.

Netherlands

At the Fourth International Congress on Metallic Corrosion held at Amsterdam, Holland, in 1969, the cost of corrosion in Netherlands was projected as 1% of the national income (Ref 87).

Sweden

In Sweden, painting expenditures to combat corrosion were analyzed for the year 1964. These costs were found to be 300 to 400 million krona ($58 to 77 million USD, 1964 basis), of which between 25 and 35% were found to be avoidable (Ref 88).

According to a report published in *Materials Protection* during 1967, the annual cost of corrosion in Sweden was approximately $200 million USD, or $26 USD/person (Ref 89). This estimate referred to corrosion of steel and other metals only. Corrosion of nonmetallic materials, such as wood and concrete, would cost equally as much. The cost of automobile corrosion was estimated as $74 million USD.

Finland

The cost of corrosion for Finland for the year 1965 (Ref 90) was estimated at 150 to 200 million markka ($47 to 62 million USD, 1965 basis).

Union of Soviet Socialist Republics (USSR)

Tomashov (Ref 91) of the USSR had estimated that out of 65 to 70 million tons of steel produced in the USSR during 1965, approximately 6 to 7 million tons would be lost in the same year through corrosion. Assuming a world production of steel of approximately 200 million tons/year, he had projected 20 million tons as a loss to the entire world.

In 1969, losses were stated to be 6 billion rubles ($6.7 billion USD, 1969 basis), or approximately 2% of the GNP for the entire USSR (Ref 92).

In the USSR, the corrosion losses of steel and pig iron during 1976 were estimated to be 30% of the annual production (Ref 93). Since 1991, this economy is divided among 15 independent republics. The largest, Russia, has a GDP estimated as approximately $1.3 trillion USD in 2004. The Ukraine is the second largest economically, with a GDP estimated as equivalent to $260 billion USD in 2004.

Kuwait

In 1987, by using the NBS-BCL model, Ref 94 estimated that the total cost of corrosion for the Kuwait economy was 5.2% of the 1987 GDP ($1 billion USD, 1987 basis). The avoidable cost of corrosion was also estimated as 18% of the total cost ($180 million USD).

India

In India, Rajagopalan of the Central Electrochemical Research Institute (Ref 95) made a pioneering effort in 1958 to estimate the cost of corrosion control in India. He projected a figure of 1540 million rupees for the year 1960 to 1961 ($320 million USD, 1961 basis). He followed the procedure adopted by Uhlig.

During 1986, Rajagopalan (Ref 96) calculated the cost of corrosion in various sectors of the Indian economy by following the model of the NBS-BCL analysis. He showed that for 22 industrial sectors, the direct cost of corrosion totaled 40,800 million rupees (2% of the GNP), out of which 18,000 million rupees were avoidable expenses. After a gap of 15 years, the authors of this article from the Central Electrochemical Research Institute, Karaikudi, embarked on a venture to estimate the updated cost of corrosion for India (Ref 97). They showed that for the year 1996 to 1997, the annual cost of corrosion was approximately 240,000 million rupees (2% of the GNP).

For a developing country like India, it is surprising to find that the direct cost of corrosion had escalated from 1540 million rupees during 1960 to 40,800 million rupees during 1986, which is a 26-fold increase over a period of 26 years, similar to the trend observed in the USA study.

For other countries, the cost of corrosion lies in the range of 1 to 3% of the GNP.

Basque Region

A detailed study of the cost of corrosion in the Basque provinces of Spain, where 60% of the economy is limited to iron and its derivatives, was conducted (Ref 98). The direct cost of corrosion was 75,000 million pesetas by 1988 ($750 million USD). This represented 3% of the total gross Basque product. The cost related to the public buildings and services was estimated at approximately 25,000 million pesetas/year (1988). Indirect costs not taken into account in the responses from industries were estimated at approximately 30,000 million pesetas/year. Thus, the total cost of corrosion in the Basque region was minimum of 130,000 million pesetas/year.

Global Direct Cost of Corrosion

To estimate the direct cost of corrosion at a global level, the available data on the direct cost of corrosion for 17 individual countries were used, as summarized in Table 8. In some cases, data were based on the GDP rather than the GNP. The base year differed for each country, and therefore it was decided to extrapolate the available data from the respective base year to a common year, 2004. The following methodology was adopted.

The exchange rate was used to convert the individual country currency to a common currency, USD. The exchange rates were found from the international financial statistics of the International Monetary Fund and the financial statistics of the Federal Reserve Board of the United States, where the exchange rates were available for 80 countries from 1970 onward.

The cost of corrosion for each country was divided by the respective exchange rate for the particular year to find the value in USD. Data on the inflation rate in the USA economy were used to extrapolate the cost of corrosion from the base year to the common year of 2004. The following inflation factor (F) was used:

$$F = (1 + i)^n$$

where i is the effective inflation rate per year, and n is the number of years between the common year and the base year.

After multiplying the direct cost of corrosion in USD for each country by the inflation factor for the common year of 2004, global direct costs of corrosion for the year 2004 for each country were obtained.

Table 8 indicates that the total direct cost of corrosion in 2004 for 17 countries is approximately $510 billion USD. The maximum contribution (60%) of the total is from the USA. The next largest contributions, in the range of 10%, came from Japan, the USSR, and Germany. The U.K., Australia, and Belgium were in the third category, contributing in the range of just 1.5%. There are approximately 230 countries for which data on the GDP are available for the year 2002. To extrapolate the global cost of corrosion from the data in Table 8, the world GDP as projected for the year 2002 was used, which is $49 trillion USD. Using the USA inflation rate (1.60) for the year 2002, the inflation factor (1.032256) for the year 2004 was estimated, and similarly, the total world GDP for the year 2004 was also estimated as $50.6 trillion USD. This is close to a 2003 estimate that values the global GDP, or gross world output (GWP), as $51.48 trillion USD (Ref 99). The data on the direct cost of corrosion projected in Table 8 were extrapolated to the GWP as $990 billion USD; this is equivalent to 2% of the world GDP.

Figure 1 shows the pattern of percentage contribution by each country to the global direct cost of corrosion as projected for the year 2004. The contribution from the USA is 31%. Japan, the USSR, and Germany contribute in the range of 5 to 6%. The U.K., Australia, and Belgium contribute approximately 1% each. The rest of the world, for which open information on the cost of corrosion is not available, contributes 47%. An international standard for calculating the cost of corrosion would be useful for providing comparative costs for individual countries.

Table 8 Country-specific direct cost of corrosion for the year 2004

Country	Base year	During the base year: Direct cost of corrosion (C), billion	Exchange rate (D) of currency to 1 USD(a)	Direct cost of corrosion (C/D), billion USD	Inflation factor (F)(b)	Direct cost (C/D)F, billion USD
USA	1998	Dollars, 276	1.0000	276.0000	1.1006	303.76
Japan	1997	Yen, 6816.5(c)	129.95	52.4548	1.1252	59.02
USSR	1969	Rubles, 6	0.8955	6.7002	8.2103	55.01
Germany	1969	Deutsche marks, 19	3.1667	6.0000	8.2103	49.26
U.K.	1998	Pounds, 4.645	0.6010	7.7288	1.1006	8.51
Australia	1973	Australian dollars, 0.4667	0.8485	0.5500	13.3154	7.32
Belgium	1973	Francs, 20.5(d)	40.4190	0.5072	13.3154	6.75
India	1986	Rupees, 40.76	13.1220	3.1062	1.2176	3.78
Poland	1998	Zlotys, 11.237(e)	3.5040	3.2069	1.1006	3.53
Canada	1966	Canadian dollars, 1	1.077	0.9282	3.6421	3.38
South Africa	1985	Rand, 4	2.5580	1.5637	2.0312	3.18
Kuwait	1987	Dinars, 0.27	0.2700	1.0000	2.0894	2.09
Basque region	1988	Pesetas, 75	100.00	0.75	1.9977	1.5
Czechoslovakia	1998	Koruna, 31.816(f)	29.8600	1.0655	1.1006	1.17
Netherlands	1969	Guilders, 0.51441	3.6340	0.1416	8.2103	1.16
Sweden	1967	Kroner, 1	5.0000	0.2000	3.0284	0.61
Finland	1965	Markka, 0.175(g)	3.2110	0.0545	2.0995	0.11
Global direct cost of corrosion in 2004						**510.14**

Amounts are in billion USD. (a) USD, United States dollar. (b) $F = (1 + i)^n$, see text. (c) Average of 3938 to 9695 billion yen. (d) Average of 16 to 25 billion francs. (e) 2.03% GDP of 1998. (f) 1.73% GDP of 1998. (g) Average of 150 to 200 million markka

Global Indirect Cost of Corrosion

Even though it has been stated that it is very difficult to assess the indirect cost of corrosion, it

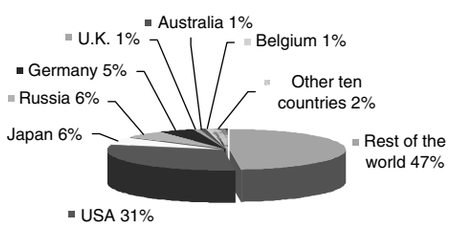

Fig. 1 Pattern of contribution by each country to the global direct cost of corrosion for the year 2004

Table 9 Indirect cost of corrosion for the USA (1998 basis)

Industry sector	Contribution to 1998 GDP, billion USD(a)	Element of indirect cost	Percent of subtotal	Indirect corrosion cost(b), billion USD
Infrastructure				
Highway bridges	674.08	...	...	...
Gas and liquid transmission pipelines	52.47	...	...	...
Waterways and ports	6.96	...	...	...
Hazardous materials storage	111.04	...	...	...
Airports	43.54	...	...	...
Railroads	20.46	...	...	...
Subtotal	**908.55**	Social cost	4.5–5.5	45.42
Utilities				
Gas distribution	52.47	...	...	...
Drinking water and sewer systems	52.47	...	...	...
Electrical utility	52.47	...	...	...
Telecommunications	...	...	...	...
Subtotal	**157.41**	Loss of product	2.0–3.0	3.93
Transportation				
Motor vehicles	186.37	...	...	...
Ships	6.96	...	...	...
Aircraft	43.54	...	...	...
Railroad cars	20.46	...	...	...
Hazardous materials transport	107.99	...	...	...
Subtotal	**365.32**	Loss of efficiency	1.5–2.0	6.39
Production and manufacturing				
Oil and gas exploration and production	76.64	...	...	...
Mining	27.86	...	...	...
Petroleum refining	32.22	...	...	...
Chemical, petrochemical, and pharmaceutical	111.04	...	...	...
Pulp and paper	148.05	...	...	...
Agricultural	126.28	...	...	...
Food processing	123.66	...	...	...
Electronics	...	...	...	...
Home appliances	25.25	...	...	...
Subtotal	**671.00**	Production loss	2.5–5.5	26.84
Government				
Defense	148.05	...	...	...
Nuclear waste storage	148.05	...	...	...
Subtotal	**296.10**	Overdesign	2.5–3.0	8.14
Total annual indirect cost of corrosion				**90.72**

(a) USD, United States dollar. (b) Mean value of percent range is used.

is possible to adopt a rational method and arrive at a figure. Conventionally, there are five elements that contribute toward the indirect cost of corrosion:

- Social cost, otherwise called user cost, incurred due to loss of time and money during the period of repair and rehabilitation
- Loss of product due to spillage or leakage
- Loss of efficiency due to accumulation of corrosion product in the flow stream
- Production loss due to unexpected shutdown
- Cost related to overdesign

The aforementioned five elements are individually related to five major sector categories, as subsequently shown.

The major impact of social cost is felt under the infrastructure sector. It may be in the range of 4.5 to 5.5% of the total productivity of this sector. Loss of product normally occurs under the utilities sector, and this may be approximately 2.0 to 3.0% of the total productivity. Loss of efficiency in the range of 1.5 to 2.0% comes under the transportation sector. Approximately 2.5 to 5.5% is lost under the production and manufacturing sector. The defense and nuclear sector often experience overdesign, which may be approximately 2.5 to 3.0% of their productivity.

Based on this information, the indirect cost of corrosion for the analyzed portion of the USA economy has been projected in Table 9. The indirect cost of corrosion of $91 billion USD represents 1.57% of the GDP. When the nonanalyzed portion of the USA economy is included, it is estimated that this figure doubles to 3.14% of the GDP, or $182 billion USD, 1998 basis.

Using the USA inflation rate (1.61) for the year 1998, the extrapolated indirect cost of corrosion for the USA for 2004 is $200 billion USD. The extrapolated total GDP for the USA for 2004 is $10,730 billion USD. Similarly extrapolated, the GWP for 2004 is $50,600 billion USD. The corresponding global indirect cost of corrosion is $940 billion USD.

Global Cost of Corrosion

Based on the GWP projected for the year 2004, the global direct cost of corrosion is $990 billion USD, and the global indirect cost of corrosion is $940 billion USD; thus, the total global cost of corrosion is $1930 billion USD, or 3.8% of the GWP.

ACKNOWLEDGMENTS

The authors gratefully acknowledge the Senior Research Fellowship awarded to Shri R. Bhaskaran by the Council of Scientific and Industrial Research, EMR Division (New Delhi, India), which allowed them to carry out this work at the Central Electrochemical Research Institute, Karaikudi, India. The authors thank the Director, Central Electrochemical Research Institute, for his kind encouragement in pursuing this study. Also, the authors would like to acknowledge the editorial work done on this article by Stephen D. Cramer and Bernard S. Covino, Jr., of the U.S. Department of Energy Albany Research Center. Without the continuous feedback, encouragement, and thorough review of these people, this study would not contain such enormous data on the cost of corrosion.

REFERENCES

1. H. Davy, *Philos. Trans. R. Soc., (London),* Vol 114, 1824, p 151, 242, 328
2. R.J. Wig and L.R. Fergusion, *Eng. News-Rec.,* Vol 79, 1917, p 689
3. H.H. Uhlig, The Cost of Corrosion to the U.S., *Chem. Eng. News,* Vol 27 (No. 39), 26 Sept 1949, p 2764–2767
4. H.H. Uhlig, The Cost of Corrosion to the United States, *Corrosion,* Vol. 6 (No. 1), 1950, p 29–33
5. Amount of Annual Purchases of Corrosion Resistant Materials by Various Industries—A Report of NACE Technical Unit Committee T-3C, *Corrosion,* Vol 15 (No. 3), March 1959, p 121t–122t
6. S. Lichtenstein, "The Many Faces of Corrosion," STR-3454, U.S. Dept. of Commerce, National Bureau of Standards, Oct 1966
7. J.P. Fraser, Corrosion Economics, *Mater. Perform.,* Vol 13 (No. 4), April 1974, p 15–17
8. L.H. Bennett, K. Kruger, R.I. Parker, E. Passaglia, C. Reimann, A.W. Ruff, H. Yakowitz, and E.B. Berman, "Economic Effects on Metallic Corrosion in United States—A Three Part Study for Congress," Part I: NBS Special Publication 511-1, SD Stock No. SN-003-003-01926-7; Part II: "A Report to NBS by Battelle Columbus Laboratories," NBS Special Publication 511-2, Appendix B, SD Stock No. SN-003-003-01927–5, U.S. Government Printing Office; Part III: "Appendix C, Battelle Columbus Input/Output Tables," NBS

GCR78-122, PB-279 430, National Technical Information Service, 1978
9. R.H. Hausler, Economics of Corrosion Control, *Mater. Perform.,* Vol 17 (No. 6), June 1978, p 9–13
10. E.W. Brooman and J.W. Hurwitch, "Research Needs for Corrosion Control and Prevention in Energy Conservation Systems," File No. DE86003019, National Technical Information Service, Nov 1985
11. E.D. Verink, J. Kolts, J. Rumble, and G.M. Ugiansky, Corrosion Data Program Workshop Summary, *Mater. Perform.,* Vol 26 (No. 4), April 1987, p 55–60
12. "Economic Effects of Metallic Corrosion in the United States—A 1995 Update," Report by Battelle to Specialty Steel Industry of North America, April 1995
13. G.H. Koch, M.P.H. Brongers, N.G. Thompson, Y.P. Virmani, and J.H. Payer, "Corrosion Cost and Preventive Strategies in the United States," FHWA Report RD-01-156, Federal Highway Administration, U.S. Department of Transportation, March 2002, p 1–773
14. J. Campbell Stirling, Economics of Mitigation of External Corrosion on Underground Pipe Lines, *Corrosion,* Vol 1 (No. 1), March 1945, p 17–30
15. H.H. Anderson, Our Billion-Dollar Side Show. . . For Managers Only, *Corrosion,* Vol 3 (No. 6), June 1947, p 2–6
16. H.E. Jordan, Corrosion Costs to the Water Industry, *Corrosion,* Vol 3 (No. 8), Aug 1947, p 367–373
17. E.W. Unruh, *Petrol Eng.,* Vol 23 (No. 8), July 1951, p D-7
18. "Report of Correlating Committee on Cathodic Protection," National Association of Corrosion Engineers, July 1951
19. R.K. Talley, Thirty Years of Proof Corrosion Control Pays Off, *Mater. Prot.,* Vol 5 (No. 2), Feb 1966, p 35–36
20. J.A. Caldwell, Sour Oil Well Corrosion, TP-1D-Sour Oil Well Corrosion, *Corrosion,* Vol 8 (No. 8), Aug 1952, p 292–294
21. J.D. Sudbury, D.A. Shock, and F.W. Mann, A Promising Spray Applied Inhibitor of Internal Corrosion of Oil Tank Ships, *Corrosion,* Vol 10 (No. 8), Aug 1954, p 253–258
22. B.W. Bradley, Pumping Wells Service Costs Cut by Corrosion Control, *World Oil,* Vol 135 (No. 7), Dec 1952, p 214
23. "Condensate Well Corrosion," Natural Gasoline Association of America, 1953
24. What Does Corrosion Cost You?, *Petrol. Process.,* Vol 8 (No. 11), Nov 1953, p 1685–1688
25. J.L. Battle, Casing Corrosion in the Petroleum Industry, *Corrosion,* Vol 13 (No. 2), Feb 1957, p 62–68
26. "Corrosion of Oil and Gas Well Equipment," American Petroleum Institute, 1958
27. A.J. Freedman and A. Dravnieks, Evaluation of Refinery Corrosion Inhibitors, *Corrosion,* Vol 14 (No. 12), Dec 1958, p 567t–570t
28. P.W. Sherwood, Flocculation and Flotation of Aqueous Refinery Wastes, *Werkst. Korros.,* Vol 10 (No. 9), 1959, p 541–544
29. N.J. Landis, Estimating the Cost of Corrosion in Refinery Crude Units, *Corrosion,* Vol 16 (No. 10), Oct 1960, p 479t–486t
30. Tips on How to Reduce Corrosion Costs, *Can. Chem. Process.,* Vol 49 (No. 12), Dec 1965, p 73–75
31. The Cost of Corrosion: U.S. Government Settles Pipeline Spill Case, *Corros. Prev. Control,* Vol 50 (No. 1), March 2003, p 1–2
32. Corrosion Damage of $500 Million Spent for Replacements in 1960, *Corrosion,* Vol 17 (No. 10), Oct 1961, p 18–24, 26–29
33. Corrosion in the United States Costing $70 billion Each Year, *Mater. Perform.,* Vol 17 (No. 4), April 1978, p 53
34. T.R. Menzies, "National Cost of Motor Vehicle Corrosion from Deicing Salts," Corrosion 91/399, NACE, 1991
35. C.C. Nathan and A.J. Piluso, Wet End Corrosion Problems in Paper Mills, *Pulp and Paper Industry Corrosion Problems,* Vol 2, NACE, 1977, p 122–128
36. M. Moskal and K.J. Oswald, International Symposium Finds Corrosion Costs Still on the Rise, *TAPPI,* Vol 60 (No. 7), July 1977, p 38
37. Economics of Chemical Plant Maintenance Painting—A Report of NACE Technical Unit Committee T-6D, *Corrosion,* Vol 12 (No. 12), Dec 1961, p 599t–601t
38. R.K. Swandby, How to Reduce Maintenance Painting Costs, *Chem. Eng.,* Vol 69 (No. 9), 30 April 1962, p 115–120
39. J.I. Bregman, *Corrosion Inhibitors,* The Macmillan Company, 1963, p 19, 128–129
40. W.N. Hall, How One Company Saves Thousands of Dollars by Using Plastic Materials, *Mater. Prot.,* Vol 2 (No. 4), April 1963, p 70–75
41. Carbon Dioxide Removal Cost Cut $550,000/Year, *Oil Gas J.,* Vol 73, 17 March 1975, p 107–110
42. R.W. Staehle, Economics of Corrosion, *The Theory, Significance and Prevention of Corrosion in Aircraft,* Advisory Group for Aerospace Research and Development, Sept 1976, p 3
43. One in Six U.S. Highway Bridges is Deficient, *Eng. News-Rec.,* Vol 198 (No. 10), 10 March 1977, p 18–21
44. O. Jonas, View Point—Reducing Corrosion Costs in U.S. Industrial Steam Generation, *Mater. Perform.,* Vol 32 (No. 2), Feb 1993, p 12–13
45. R. Hadfield, Corrosion of Ferrous Metals, *Minutes Proc. Inst. C.E.,* Vol 214, 1922, p 83
46. J.C. Hudson, *The Corrosion of Iron and Steel,* Chapman & Hall, London, 1940
47. W.H.J. Vernon, *Proceedings of the U.N. Scientific Conference on Conservation and Utilization of Resource Held in 1949*, Vol 2, U.N. Dept. of Economic Affairs, 1951, p 218
48. The Cost of Corrosion, *Corros. Prev. Control,* Vol 1 (No. 1), March 1954, p 9
49. W.H.J. Vernon, *Metallic Corrosion and Conservation: The Conservation of National Resources,* Institution of Civil Engineers, London, 1957, p 105–133
50. Corrosion Control Costs the U.K. £195 Million a Year, *Corros. Prev. Control,* Vol 14 (No. 8), Sept 1967, p 7–9
51. Corrosion Commentary—Corrosion Control in Britain Costs £195 Million a Year, *Anti-Corros. Methods Mater.,* Vol 14 (No. 11), Nov 1967, p 7, 24
52. A. Holme, The Economics of Corrosion and Corrosion Control, *Anti-Corros. Methods Mater.,* Vol 16 (No. 2), Feb 1969, p 12–17
53. T.P. Hoar, "Report of the Committee on Corrosion and Protection—A Survey of Corrosion and Protection in the United Kingdom," Her Majesty's Stationery Office, London, 1971
54. T.P. Hoar, Corrosion of Metals: Its Cost and Control, *Proc. R. Soc. (London) A,* Vol 348 (No. 1652), 10 Feb 1976, p 1–18
55. N. Whitehouse, Paint Research Association, England, personal communication, http://www.pra.org.uk, 2003
56. British Estimate Corrosion Loss in U.K. to Underground Pipe at $130,000,000, *Corrosion,* Vol 8 (No. 3), 1952, p 16–17
57. G.T. Colegate, The Corrosion of Marine Structures and Its Prevention, *Corrosion Problems of the Petroleum Industry,* Society of Chemical Industry, London, and The Macmillan Company, 1960, p 30
58. The Cost of Car Corrosion in Britain, *Corros. Prev. Control,* Vol 17 (No. 6), Dec 1970, p 5–7
59. J. Baggott, Economics and Market Growth, *Anti-Corros. Methods and Mater.,* Vol 18 (No. 8), Aug 1971, p 7–9
60. N.S. Boas and S. Ambrose, *J. Inst. Eng. (Aust.),* Vol 27, 1955, p 109
61. H.K. Worner, The Cost of Corrosion, *Corros. Technol.,* Vol 3 (No. 9), Sept 1956, p 289–292
62. E.C. Potter, The Corrosion Scene in Australia, *Australas. Corros. Eng.,* Vol 16 (No. 3), March 1972, p 27–29
63. E.C. Potter, The Cost of Corrosion, *Electropl. Met. Finish.,* Vol 26 (No. 3), March 1973, p 17–18, 20
64. R.W. Revie and H.H. Uhlig, The Cost of Corrosion to Australia, *J. Inst. Eng. (Austr.),* Vol 46 (No 3–4), March/April 1974, p 3–5, 11
65. E. Potter, The Principles of Corrosion Science, *Australas. Corros. Eng.,* Vol 19 (No. 3), March 1975, p 5–12
66. B.W. Cherry and B.S. Skerry, "Corrosion in Australia—The Report of the Australian National Centre for Corrosion Prevention and Control Feasibility Study," Monash University, Australia, June 1983
67. B.W. Cherry, Cost of Corrosion, *Mater. Forum,* Vol 19, 1995, p 1–7
68. M. Tanaka, An Estimate of Corrosion Losses to Underground Cables and Pipe Lines in

Japan, *Corrosion,* Vol 12 (No. 10), Oct 1956, p 513t–514t
69. Report of the Committee on Corrosion and Protection, *Corros. Eng. (Jpn.),* Vol 26 (No. 7), 1977, p 401–428
70. T. Shibata, Cost of Corrosion in Japan, *Corros. Sci. Technol.,* Vol 31 (No. 2), 2002, p 97–102
71. H.G. Smith, What Corrosion Costs Canada, *Can. Chem. Process.,* Vol 37 (No. 10), Sept 1953, p 10
72. J.D. Palmer, Corrosion: Our $1 Billion Write-Off, *Can. Chem. Process.,* Vol 50 (No. 3), March 1966, p 55–57, 59, 61
73. C.L. Easton, Corrosion Control in Petroleum Refineries Processing Western Canadian Crude Oils, *Corrosion,* Vol 16 (No. 6), June 1960, p 275t–280t
74. F.L. Burns, J.F. Moresby, and P.H. Thorpe, Ed., *Proceedings of the Sixth International Congress on Metallic Corrosion* (Sydney, Australia), Australasian Corrosion Association, Australia, Dec 1975, p 1445
75. M.F. Davy and W.A. Mueller, Pulp and Paper Industry Worldwide Corrosion Costs, *Pulp and Paper Industry Corrosion Problems,* NACE, 1974, p 1–6
76. L. Clay and B.C. Kamloops, Summary of Key Pulp and Paper Industry Corrosion Problems, *Pulp and Paper Industry Corrosion Problems,* NACE, 1976, p 7–8
77. O. Krönke, E. Maass, and W. Beck, *Die Korrosion,* VDI-Buchhandlung, Berlin, 1929
78. A. Pollack, News in the Field of Rust Prevention, *Dtsch. Farben-Z.,* Vol 7, Aug 1953, p 296–300 (in German)
79. D. Behrens, Research and Development Program on Corrosion and Corrosion Protection in the German Federal Republic, *Br. Corros. J.,* Vol 10 (No. 3), 1975, p 122–127
80. T. Pyrzanowski, Economic Consequence of Corrosion in the Polish Chemical Industry Summary, *Korróz. Figy.,* Vol 28 (No. 3), 1978, p 94–97 (in Polish)
81. M. Legowiecki and H. Marczak, Corrosion Prevention to Increase Effectiveness of Raw Materials Use—Present Status and Trends, *Ochr. Przed Koroz.,* Vol 20 (No. 11), Nov 1977, p 279–280
82. Corrosion Cost to S.A., *Corros. Technol.,* Vol 8 (No. 4), April 1961, p 102
83. M.V. Slabbert and F.P.A. Robinson, Economic Effects of Metallic Corrosion in South Africa, *Corros. Coatings, S. A.,* Vol 12 (No. 5), Oct 1985, p 3–8
84. M. Kuliš, Corrosion Losses and Their Share in the Gross National Product of the ČSSR, *Werkst. Korros.,* Vol 27 (No. 12), Dec 1976, p 870–874 (in German)
85. M. Kuliš and D. Knotková, Economic Damage Caused by Corrosion in the Industrial and Ecological Zones of Prague City, *Proceedings of the Symposia on Corrosion Effects of Acid Deposition and Corrosion of Electronic Materials,* F. Mansfeld, V. Kucera, E. Haagenrud, F.H. Haynie, and J.D. Sinclair, Ed., The Electrochemical Society, Inc., 1986
86 M. Pourbaix, *Lectures on Electrochemical Corrosion,* R.W. Staehle and J. Kruger, Ed., Plenum Press, 1973, p 1–5
87. A Report of the Fourth International Congress on Metallic Corrosion, *Anti-Corros. Methods Mater.,* Vol 16 (No. 10), Oct 1969, p 11–12, 14
88. K.F. Trädgåidh, *Tek. Tidskr.,* Vol 95 (No. 43), 1965, p 1191
89. $2 Million Lost Annually to Metal Corrosion in Sweden, *Mater. Prot.,* Vol 6 (No. 2), Feb 1967, p 72
90. V. Vläsaari, *Talouselämä (Economy),* No. 14/15, 1965, p 351
91. N.D. Tomashov, *Theory of Corrosion and Protection of Metals,* B.H. Tytell, I. Geld, and H.S. Preiser, Ed., Macmillan Company, 1967, p 3–6
92. Y. Kolotyrkin, quoted in *Sov. Life*, Vol 9, 1970, p 168
93. V.V. Skorchelletti, *Theory of Metal Corrosion,* D. Slutzkin, Ed., Israel Program for Scientific Translations, Jerusalem, 1976, p 5–8
94. F. Al-Kharafi, A. Al-Hashem, and F. Martrouk, "Economic Effects of Metallic Corrosion in the State of Kuwait," Final Report 4761, KISR Publications, Dec 1995
95. K.S. Rajagopalan, Metallic Corrosion: Cost and Prevention, *J. Sci. Ind. Res.,* Vol 17(A), 1958, p 191–193
96. K.S. Rajagopalan, Application of NBS-BCL Analysis to Cost of Corrosion in Various Sectors of Indian Economy, *Paint India,* Vol 36 (No. 3), March 1986, p 35–40
97. R. Bhaskaran, N.S. Rengaswamy, and N. Palaniswamy, Impact of Metallic Corrosion, Part II: Economic Impact, *Corros. Update,* No. 60, May-June 2001, p 2–4
98. T.F. Otero, A.S. Elola, M.B. Gorrochategui, and I. Cantero, Cost of Corrosion in the Basque Country, *Progress in the Understanding and Prevention of Corrosion,* Vol 1, J.M. Costa and A.D. Mercer, Ed., The Institute of Materials, London, 1993
99. *The World Factbook,* Central Intelligence Agency, accessed at www.cia.gov/cia/publications/factbook/, Jan 2005

SELECTED REFERENCES

- L.H. Bennett, J. Kruger, R.L. Parker, E. Passaglia, C. Reimann, A.W. Ruff, H. Yakowitz, and E.B. Berman, "Economic Effects of Metallic Corrosion in the United States, Part I: A Report to the Congress by the National Bureau of Standards," U.S. Government Printing Office, May 1978
- J.I. Bregman, *Corrosion Inhibitors,* Macmillan Company, 1963, p 177, 179
- Corrosion Costs $10 Billion per Year, *Mater. Prot.,* Vol 6 (No. 4), April 1967, p 29
- S. Linderborg, *Kem. Teollus. (Finland),* Vol 24 (No. 3), 1967, p 234
- R.W. Revie, Ed., *Uhlig's Corrosion Handbook,* 2nd ed., John Wiley & Sons, Inc., 2000, p 8

ASM Handbook, Volume 13B: Corrosion: Materials
S.D. Cramer, B.S. Covino, Jr., editors, p631-646
DOI: 10.1361/asmhba0003969

Gallery of Corrosion Damage

Peter Elliott, Corrosion & Materials Consultancy, Inc.

AS IS APPARENT from Volumes 13A and 13B of the *ASM Handbooks,* all materials will corrode given certain circumstances, conditions, and time. Although much is understood about the mechanisms of corrosion and its control, a high proportion of corrosion damage continues to occur because of misunderstandings, a general lack of awareness, or an absence of effective communication channels; in brief, the "human factor" prevails. Evidence to support this viewpoint is borne out by descriptions of corrosion damage provided in a variety of publications (Ref 1–4).

Pictorial guides (Ref 5–10) to the forms of corrosion are invaluable because they introduce the less aware person to the real-world forms of material degradation, they document specific features of attack that alert operators and inspectors about potential failures, they assist in determining the cause of damage, and they help direct fundamental research activity. Published material is commonly augmented by useful case histories (Ref 11–17).

This gallery of corrosion damage has been selected to draw attention to common pitfalls or situations that have caused premature corrosion—sometimes with expensive consequences. A series of caveats are presented that first outline the background and the type of damage sustained and then provide short summaries of actions to remedy or avoid the problems described. Many of the failures that are here presented were easily avoidable, given that the designer/operator/maintenance engineer had sufficient knowledge and a willingness to take positive action to ensure the safe operation of the plant or equipment. The examples used are not exhaustive; they are presented to highlight the necessity to fully examine materials, conditions, and specific circumstances that together can so easily reduce the anticipated service life of a component or plant.

The examples in this article are categorized according to the type of corrosion following the general order that is adopted in Volume 13A of *ASM Handbook.* Table 1 provides a categorization of the forms of corrosion. As noted in the article "Introduction to Forms of Corrosion" in *ASM Handbook,* Volume 13A, 2003, p 189, various schemes are used for categorizing corrosion in broad and focused manners. Table 1

Table 1 Guide to related articles in *ASM Handbook,* Volume 13A, on forms and mechanisms of corrosion

	Related article in *ASM Handbook*, Volume 13A	
Form or mechanism	**Article title**	**Page**
Uniform corrosion		
Aqueous: waters, chemicals	Aqueous Corrosion	190
Atmospheric: dewpoint, soils	Atmospheric Corrosion	196
Stray current	Stray-Current Corrosion	214
Waterline	Evaluating Uniform Corrosion	543
High-temperature corrosion		
Molten salts; glasses	Molten Salt Corrosion	216
Liquid metals	Liquid Metal Corrosion	220
High-temperature gaseous corrosion	High-Temperature Gaseous Corrosion	228
Oxidation	High-Temperature Gaseous Corrosion (section on High-Temperature Oxidation)	230
Sulfidation	High-Temperature Gaseous Corrosion (section on Sulfidation)	230
Carburization	High-Temperature Gaseous Corrosion (section on Carburization)	231
Localized corrosion		
Pitting	Pitting Corrosion	236
Crevice, underdeposit attack	Crevice Corrosion	242
Filiform	Filiform Corrosion	248
Metallurgically influenced corrosion		
Dealloying	Effects of Metallurgical Variables on Dealloying Corrosion	287
Galvanic	Galvanic Corrosion	210
Weldments	Corrosion of Carbon Steel Weldments	294
	Corrosion of Stainless Steel Weldments	301
Intergranular attack	Effects of Metallurgical Variables on the Corrosion of Stainless Steels	266
	Effects of Metallurgical Variables on the Corrosion of Aluminum Alloys	275
	Effects of Metallurgical Variables on the Corrosion of High-Nickel Alloys	279
End-grain attack	Materials Selection for Corrosion Control	909
Exfoliation	Evaluating Exfoliation Corrosion	572
Mechanically assisted degradation		
Erosion	Forms of Mechanically Assisted Degradation (section on Erosion)	322
Fretting	Forms of Mechanically Assisted Degradation (section on Fretting Corrosion)	324
Cavitation; water drop impingement	Forms of Mechanically Assisted Degradation (section on Cavitation Erosion and Water Drop Impingement)	326
Fatigue	Forms of Mechanically Assisted Degradation (section on Corrosion Fatigue)	328
Environmentally induced cracking		
Stress-corrosion cracking	Stress-Corrosion Cracking	346
Hydrogen damage	Hydrogen Damage	367
Liquid metal embrittlement	Liquid Metal Induced Embrittlement	381
Design related		
Human errors and omissions	Materials Selection for Corrosion Control	909
	Designing to Minimize Corrosion	929

Table 2 Guide to materials addressed in the examples in this article

Material	Corrosion form or mechanism	Figure
Carbon and alloy steel		
Steel	Atmospheric	10
	Aqueous	11
	Localized pitting, microbiologically influenced	27, 28
Carbon steel	Oxidation/overheating	1, 2
	Atmospheric: dewpoint, soils	7, 8, 15
	Fretting	58
	Stray current	19
Carbon steel, lacquer coated	Filiform	47, 48
High-strength low-alloy steel	Apparent galvanic	70
Low-chrome alloy steel	Oxidation	38
Galvanized steel	Atmospheric	17
	Waterline	26
Coated carbon steel	Uniform corrosion	9
	Uniform corrosion, saltwater	3
	Uniform, crevice; underdeposit attack	4
	Atmospheric: dewpoint, soils	16, 18, 22
Iron		
Painted wrought iron	Crevice	21
Painted cast iron	Atmospheric	20
Gray cast iron	Graphitic	49, 50
Stainless steel		
Type 303/304	Pitting	31, 32
Type 304	Metallurgically influenced corrosion	12
	Pitting	23, 24, 37
	Stray current	25
	End-grain attack, intergranular	55
	Stress-corrosion cracking	62, 63, 66
	Crevice, fretting, fatigue	46
Type 316	Uniform	5, 6
Type 316L	Fatigue	60
Type 321	Oxidation	33
Type 321	Pitting	39, 40
Type 420	Uniform	14
Type 20-20 cast	High-temperature sulfidation and carburization	36
Nonferrous alloys		
Copper	Intergranular attack	56, 57
Copper	Stress-corrosion cracking	64, 65
Copper	Localized pitting, formicary	41, 42
Copper	Impingement	59
Copper with elastomeric insulation	Stress-corrosion cracking	67
Nickel, N08330	Sulfidation	34, 35
Ni-Cr-Mo	Crevice	43
Ni-Cu in glass mat	Oxidation	29, 30
Ti-3Al-2.5V	Hydrogen damage	68, 69
Plastics		
Polycarbonate	Stress-corrosion cracking	61
Dissimilar metals		
Carbon steel and aluminum	Atmospheric	13
Carbon steel and stainless steel	Galvanic	44, 45
Carbon steel and stainless steel	Galvanic: weldment intergranular attack	52
Carbon steel and copper	Galvanic: weldment intergranular attack	53, 54
Aluminum and brass	Galvanic	51

Corrosion form and mechanism	Chemical—sulfuric acid, waterline, overheating
Material	Ferrous, carbon steel
Product form	Pipe

Fig. 1 Carbon steel pipe is heat traced to keep concentrated sulfuric acid fluid in cold weather, because concentrated sulfuric acid freezes at ~10 °C (50 °F). During a routine shutdown period, acid remaining in a horizontal pipe was diluted by condensation of the moist atmosphere within the piping system, forming dilute sulfuric acid, which is very corrosive to carbon steel. The plant operators were unaware of the corrosion that had occurred during the maintenance period. One of the heat-tracer retainer clips was inadvertently placed in direct contact with the steel pipe without insulation (Fig. 2). Shortly after the system was back in service, acid leaked out from the area that was locally corroded from the acid side due to waterline attack during the downtime, compounded by local overheating in service caused by metal-to-metal contact between the heat-tracer pipe and the steel tube. An end-on view of the pipe (not shown) showed a water-line effect delineating the level of the diluted acid during shutdown to be approximately one-fourth the height of the pipe.
Control: The acid line should have been properly drained by designing with a sloped pipe or by purging the system with inert gas so that the acid would not dilute and become highly corrosive. The heat-tracer pipe should have been properly positioned, complete with insulation.

also provides a reference to articles or sections of articles in Volume 13A that detail the particular corrosion form or mechanism. The topic coverage is not limited to these articles, but these serve as a gateway. Supportive references for materials in the gallery can be found in this Volume. Table 2 is a guide listing the figures by material. Unless otherwise stated, all of the photographs were supplied by Peter Elliott, the author.

Corrosion form and mechanism	Chemical—sulfuric acid, waterline, overheating
Material	Ferrous, carbon steel
Product form	Pipe

Fig. 2 The area of the same carbon steel pipe system as in Fig. 1 where the heater clips were placed in direct contact with the pipe, without insulation. This caused overheating because the pipe was in direct contact with the steam heater. The combined effect of waterline attack and elevated temperature is the cause of failure.

Corrosion form and mechanism	Uniform corrosion, saltwater
Material	Ferrous metal, coated carbon steel
Product form	4 by 4 vehicle

Fig. 3 The owner complained about the serious rusting and perforation to the rear of his 4 by 4 vehicle after approximately 2 years of use. Subsequent review revealed that the vehicle was used to tow and launch a boat directly into the ocean each weekend during the spring, summer, and fall seasons. The user considered the vehicle to be of rugged construction, and contact with water was to be expected. The vehicle was not intended to be used in this fashion—certainly not without thorough washing of salt and sand after such use. The damage was the result of general corrosion enhanced by chloride-containing deposits, with abrasion of the vehicle coating by sand particles.
Control: The underside and rear of the vehicle should have been vigorously washed free of the salt and sand after each use. Larger drain holes may have been added to improve drainage after use and washing. The owner's manual would caution against such use and would recommend thorough washing after use for preventive maintenance.

Corrosion form and mechanism	Uniform corrosion, crevice corrosion, under-deposit attack
Material	Ferrous metal, coated carbon steel
Product form	Aerosol can

Fig. 4 An aerosol can burst unexpectedly when the owner tried to clean off external rust that had developed over several years' storage inside a bathroom cabinet. The cross section of the joint at the bottom of the can revealed that the product side of the can was not a factor. All the wastage was from the outside of the can. The bottom thin coating had been locally eroded, leaving the can bottom exposed to localized corrosion as moisture and deposits accumulated with time. Attack was enhanced by condensation and evaporation cycles in the bathroom cabinet. The can base was completely penetrated at the time the user attempted to clean away the rust from the can.
Control: The can should have been discarded based on its obvious deteriorated condition.

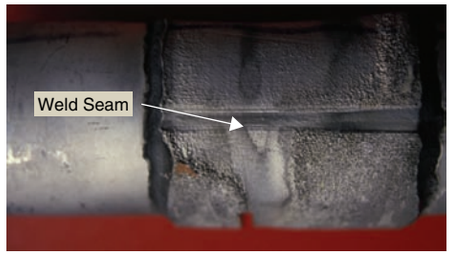

Corrosion form and mechanism	Uniform corrosion, galvanic, weldment intergranular attack
Material	Ferrous metal, type 304 and 316 stainless steel
Product form	Pipe connection sleeve

Fig. 5 A steam-heated stainless steel pipe located along the floor of the cargo hold of a ship was found to be leaking at a connecting sleeve that had been fitted several months earlier during a maintenance repair at a foreign port. The steam pipe was used to keep the cargo, phosphoric acid, above 12 °C (54 °F) and thus prevent it from solidifying during transit. Subsequent investigation showed that the sleeve was made of an improperly heat treated type 304 stainless steel. Further, the sleeve connection was not supposed to be welded.
Control: The repair was considered temporary; maintenance failed to note the change. A better choice of material was needed for the replacement, such as type 316L stainless steel.

Corrosion form and mechanism	Uniform corrosion, galvanic, weldment intergranular attack
Material	Ferrous metal, type 304 and 316 stainless steel
Product form	Pipe connection sleeve

Fig. 6 This cross section of the wall of the pipe and sleeve in Fig. 5 shows general thinning from the outside of the sleeve that was attributed to local overheating. The adjacent areas were insulated by the air gap between the steam tube and the sleeve. OD, outside diameter

Corrosion form and mechanism	General corrosion—dewpoint
Material	Carbon steel
Product form	Filter bag supports

Fig. 7 Flue gases in many processes are passed through filter bags that catch and retain the particulates. This example is from a carbon black plant. Rapid corrosion can occur when metal temperatures fall below the acid dewpoint temperature, which, for sulfuric acid, occurs at ~120 °C (250 °F), dependent on SO_2/SO_3 ratios. Corrosion rate can exceed 1 mm/yr (0.04 in./yr). The carbon steel support on the left has uniformly corroded around the vertical sides where the presence of run-off moisture has sustained the corrosion processes. On the right, a new support is shown for comparison.
Control: Avoiding the dewpoint temperature range, sometimes by eliminating local drafts of cool air, will resolve the problem. Coated steels or corrosion-resistant alloys are recommended.

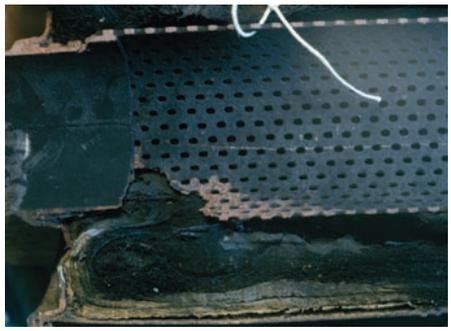

Corrosion form and mechanism	Dewpoint corrosion
Material	Ferrous, carbon steel
Product form	Automotive muffler

Fig. 8 Noisy and odorous exhaust fumes are precursors to muffler corrosion, where the inside steel components are uniformly wasted away over time until the driver is alerted to the situation. Cold-end (dewpoint) corrosion occurs whenever the metal temperature falls below the sulfuric acid dewpoint of the exhaust gas. Typically, the damage occurs in areas that are most prone to condensation and evaporation cycles; insulation once wet can serve to sustain attack.
Control: Automotive exhaust system designs continue to improve as engine sizes and performances improve and emissions are more rigorously controlled. More corrosion- and heat-resistant steels are used to combat the changing systems that include catalytic converters. Aluminized and stainless steels find application in automotive exhaust systems.

Corrosion form and mechanism	Uniform corrosion, atmospheric
Material	Ferrous metal, carbon steel
Product form	Pickle jar lid

Fig. 9 The pickle jar lid fell apart when the homeowner discovered the jar at the back of her pantry. Long-term storage of the opened jar without refrigeration contributed to the general corrosion caused by acidic vapors in the stagnant (closed-space) environment.
Control: The product should have been used in a reasonable time, and once the jar was opened, it should have been refrigerated and then disposed. The jar lid was not designed for multiyear storage and should have been discarded.

Corrosion form and mechanism	Atmospheric, crevice corrosion
Material	Steel
Product form	Nail

Fig. 10 The nail was removed from an outside door frame. Selective crevice-type corrosion was caused by differential aeration where an outer wooden panel was fixed to an inner wooden support. There are possible contributions from the different woods (a softer outer wood nailed to a hardwood base); several woods are acidic in nature. Moisture could have condensed in the space between the wood layers. The nail was probably galvanized when new.
Control: This was an old installation. Coating (painting) will reduce attack.
Source: H.G. Cole, "Corrosion of Metals by Wood," Guide to Practice in Corrosion Control, (No. 2) Her Majesty's Stationery Office, Reprinted 1985

Corrosion form and mechanism	Uniform corrosion, atmospheric
Material	Steel
Product form	Steel column

Fig. 11 Steel support columns were found with significant general corrosion, with easy access to plastic pens that were used as probes to illustrate the problem in the photograph. Some of the steel columns were encased in plaster board that had deteriorated over approximately 20 to 25 years, allowing access of moist vapors from a chemical laboratory. The damage was found around the lowest parts of the columns, the result of gravity runoff of condensing fluids. The failures were revealed from a plant audit as part of a refurbishment exercise.
Control: The corroded sections of the columns were replaced or reinforced. A shorter interval between inspections is warranted, given the severity of the steel corrosion found during this audit. The new construction relied more on coated steel, which was not encased in plaster board and hidden from view.

Corrosion form and mechanism	Metallurgically influenced corrosion
Material	Type 304 stainless steel
Product form	Tank, food reaction vessel

Fig. 12 Rusted areas in a type 304 stainless steel reaction vessel used for processing tomato products were observed after approximately 4 months of operation. The vessel had experienced prior repairs following stress-corrosion cracking. The rusted areas were sourced to carbon steel wire brushing used as part of the pre- and postfabrication work on the vessel.
Control: Carbon steel tools and brushes must be avoided with stainless steel equipment.

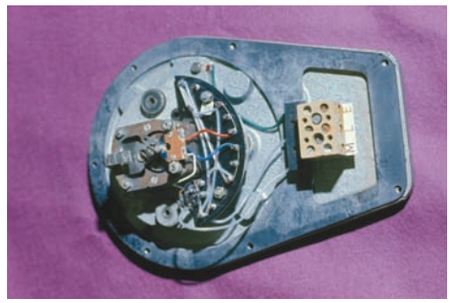

Corrosion form and mechanism	Atmospheric corrosion
Material	Aluminum alloys and carbon steel
Product form	Temperature gauge

Fig. 13 The loss of the recording needle inside the window of the closed instrument casing was at first a mystery to the operators. Subsequent examination revealed that the access way for the electrical wires was not sealed to the elements. In-coming moisture and acid mists corroded the aluminum alloy supports (exfoliation) and allowed rust to form on steel pins and screws.
Control: The access ways for wires in electrical equipment must be properly sealed according to electrical (and other) codes. Lack of attention to details can cause significant (unexpected) failure(s).

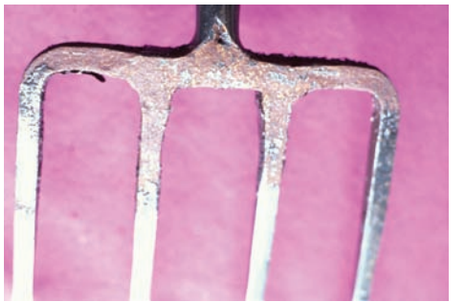

Corrosion form and mechanism	Uniform corrosion, atmospheric, filiform
Material	Type 420 stainless steel
Product form	Pitchfork

Fig. 14 Martensitic stainless steel pitchforks were rusting before they left the storeroom; paint was blistering, and the product was unappealing. The cause was due to incorrect surface preparation compounded by poor storage conditions. The forks were hot forged and quenched to obtain the necessary mechanical properties. Hot forging produces an oxide scale that has to be removed mechanically or chemically, if the stainless steel is to be corrosion resistant (i.e., be passivated). The water in the quench-tempering bath was found to be high in chloride, which was retained within the oxidized layers produced by hot forging. Thus, paint was applied over an oxidized and chloride-rich surface. Once painted and briefly air dried, the garden tools were shrink-wrapped in plastic and placed randomly (usually in front of prior stock) into a storeroom. The plastic wraps created "sweat-box," conditions that worsened the corrosion attack on the steel. The as-forged oxidized stainless steel would not passivate, so corrosion was inevitable.
Control: The forged (oxidized) stainless steel should have been cleaned mechanically or chemically, which would allow the metal to passivate and produce a corrosion-resistant oxide barrier film. The tines of the forks were ground and polished and generally reflective; a lacquer coating was disturbed by filaments of filiform attack. The plastic enclosure, which was moist and contained chlorides, experienced condensation and evaporation cycles that accelerated the corrosion attack. The items were not stored in date order, which contributed further to the extent of failure.

Corrosion form and mechanism	Uniform corrosion, atmospheric
Material	Carbon steel
Product form	Paper staples

Fig. 15 Short-term corrosion resulted in rusted staples in pamphlets advocating corrosion control, which were en route to a corrosion meeting. Poor packaging and contact with water, exacerbated by plastic wrapping, contributed to the damage. The cardboard boxes created "sweat-box," that is, high humidity, conditions, notably in the aircraft cargo hold. Cardboard boxes absorb moisture and may influence attack by releasing active agents from fiberboard and adhesives such as sulfur and chloride.
Control: Better packaging and carriage conditions. Design is usually perfectly adequate.

Corrosion form and mechanism	Atmospheric corrosion, underdeposit attack
Material	Coated carbon steel
Product form	Oil storage tank

Fig. 16 The upper area of an aboveground storage tank displayed local rusting and loss of paint coating, primarily because it could not be drained. The tank was located directly under an apple tree, which contributed to further impacts as fruit fell and was left undisturbed on the coated steel surface. The variations in fluid and debris during the seasons contributed to corrosion processes that included underdeposit attack with differential aeration effects.
Control: The design of the flat steel plate tank and its location contributed to the problem. A tank with a sloped top to allow water and fruit to run off, or a cylindrical tank, which is more common, would improve corrosion resistance.

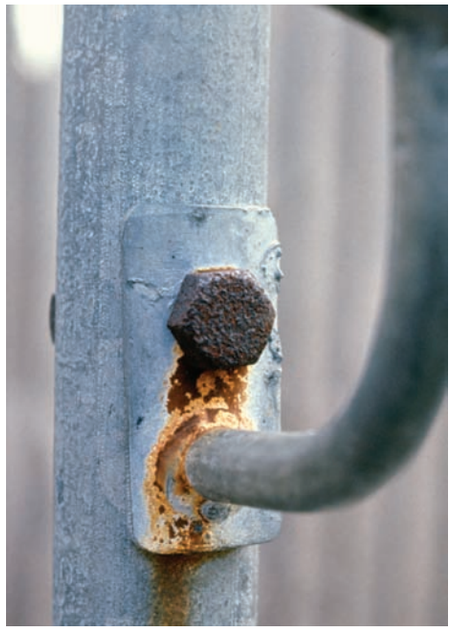

Corrosion form and mechanism	Atmospheric corrosion, materials selection
Material	Galvanized steel
Product form	Bolted support

Fig. 17 The obvious bleed of rust from a carbon steel nut used in an otherwise galvanized steel structure is the result of careless selection by a fitter. The inspector or supervisor missed the error; the rust is not apparent until time (weeks to months) allows the steel to corrode.
Control: Use a galvanized fastener when the system requires it. Improve awareness and inspection.

Corrosion form and mechanism	Atmospheric corrosion
Material	Coated steel
Product form	Surgical instrument

Fig. 18 Rust stains on what should have been a clean surgical chisel prompted an investigation as to the cause. The history of use explains the condition. The instrument was first discarded by a surgeon due to a lack of cutting edge on the tool. Later, small blemishes on the surface alerted the users to concerns about thorough cleaning of a pitted surface that could trap debris and become a site for bacterial activity. The scenario offered as to the cause was that the cutting edge of the tool was dulled from use and was sharpened by grinding. The grinding may have been part of a routine maintenance for these tools. The hard surface coating, probably chromium-plated steel, was lost through overzealous and excessive grinding. The rust patterns seen in the photograph arose from indoor atmospheric corrosion of the exposed steel aggravated by moisture retention following steam sterilization.
Control: Replace rather than reuse worn-out instruments, with better care and attention to maintenance procedures. Create more awareness about corrosion with personnel.

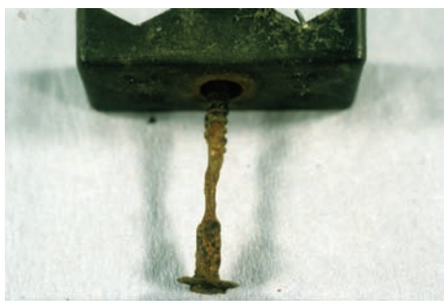

Corrosion form and mechanism	Stray-current corrosion, crevice corrosion
Material	Carbon steel
Product form	Electric cable support

Fig. 19 The electrical cable support became loose following several years of service. The maintenance engineer discovered gross thinning of the carbon steel screw. Other supports were completely detached. The shielded area around the fastener favored crevice corrosion. Stray current from the electric cable accelerated the failure.
Control: Insulated fasteners will preclude crevice and stray-current corrosion.

Corrosion form and mechanism	Atmospheric corrosion, crevice corrosion
Material	Painted cast iron
Product form	Lamp posts

Fig. 20 Several lamp posts along a seaside promenade had rusted because of the severe environment; the posts were immediately adjacent to the beach. The failures were most pronounced around access doors where the fasteners had totally corroded away, primarily from crevice corrosion. Attempts to paint the posts had failed—blistering was very pronounced (see photograph). The wire straps were an attempt to keep the doors in place and restrict access to the internal electrical connections.
Control: The lamp posts are old and should be replaced. This is a further example of the aging infrastructure where local city budgets allow temporary measures, not replacements. Alternative materials are required for a marine environment, including stainless steels or nonmetallic materials.

Corrosion form and mechanism	Crevice and atmospheric corrosion
Material	Painted wrought iron
Product form	Guardrailing

Fig. 21 The guardrail segment was part of a long railing along an esplanade at a popular seaside vacation town. A nearby section of the railing had totally collapsed when a person leaned against it; unfortunately, he died. The subsequent repairs included new guardrails for the part that collapsed; other sections were painted with several thick layers of paint that obscured the bolted connections. A later independent inspection showed that several of the bolted areas were without the through-structure bolt. The thick layers of paint did not improve the inherent weakness of the structure. This is an age-related failure, because the railing was old and had deteriorated beyond its service life due to atmospheric corrosion in a marine environment. The preseason maintenance was more focused on aesthetics than safety; many of the joints had failed through accelerated crevice corrosion, but the onus was to paint over the damage until a future time when budgets became available to replace and/or repair the guardrails.
Control: Improve inspection and maintenance schedules; replace aging structures before they collapse. Assess the risk involved with failure of the part.

Corrosion form and mechanism	Atmospheric corrosion
Material	Coated carbon steel
Product form	Footbridge

Fig. 22 Deterioration of the coated steel along the top of a guardrail had advanced far beyond other sections of the footbridge. The problem was caused by impingement from raindrops falling from a lamp that was positioned directly above the damaged area. Similar damage was found under another lamp.
Control: If the sloping lamps had been positioned 5 to 8 cm (2 to 3 in.) from their actual position, the problem would not have occurred—the run-off water would have missed the guardrail. The immediate solution was to reposition the lamps and box in the top of the railings with wood. The corrosion continued under the wooden covers, which provided shielded areas that supported crevice corrosion attack of the steel. Subsequently, in a few months, the paint deteriorated to expose rusty nails. The bridge was rebuilt approximately 2 years later, using galvanized steel sections.

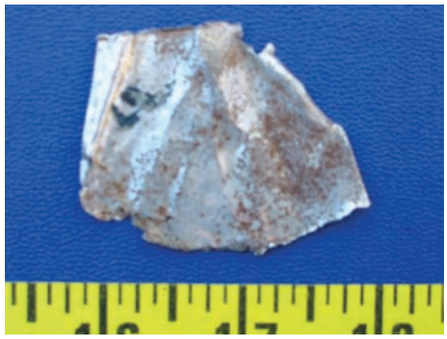

Corrosion form and mechanism	Pitting
Material	Type 304 stainless steel
Product form	Lining—electrostatic precipitator cell

Fig. 23 The carbon steel compartments (cells) in an electrostatic precipitator at a cement works were lined with type 304 stainless steel sheet to prolong service expectations. After approximately one year. The stainless steel lining was perforated by pitting as a result of corrosion by condensed acid that occurred whenever the flue gas cooled below the acid dewpoint temperature. On-site temperature surveys revealed that the cell operated at ~120 °C (250 °F), (acid dewpoint) with cooling periods where the metal reached the water dewpoint temperature, (~45–50 °C or 110–120 °F); corrosion rates increased significantly under such conditions. Pitting in the stainless steel liner resulted from under-deposit attack exacerbated by particulates and pollutants in the flue gas stream, including sulfur and chlorine species.
Control: Eliminate cold-air draughts and maintain temperatures above dewpoint, which for acid gases is typically above ~125–130 °C (257–266 °F). Minimize down time because, during this time, hygroscopic deposits can absorb moisture from the air and set up off-load corrosion attack.
Source: Dewpoint Corrosion, D.R. Holmes, Ed., Ellis Hornwood; D.R. Holmes, "Materials Corrosion Problems and Research," D.B. Meadowcroft & M.I. Manning, (eds) "Corrosion Resistant Materials for Coal Conversion Systems", Applied Science Publishers, distributed by Elsevier Science Publishing Co, (USA), p 3–23, 1983.

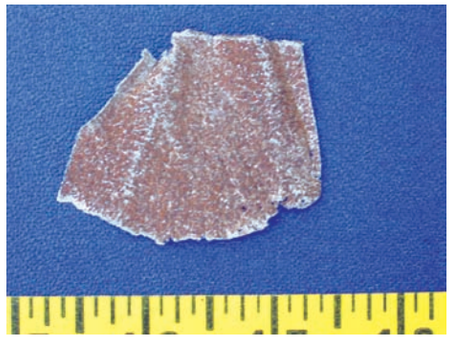

Corrosion form and mechanism	Rust carryover
Material	Type 304 stainless steel
Product form	Lining—electrostatic precipitator cell

Fig. 24 The reverse side of the stainless steel lining shown in Fig. 23 was rusty on the nonprocess side adjacent to the carbon steel cell, (Fig. 24). The carbon steel cell experienced significant dew point corrosion and the inner surface of the stainless steel lining was rust colored—not rusted—because of carryover from the rusting carbon steel vessel.
Control: See Fig. 23

Corrosion form and mechanism	Stray-current corrosion
Material	Type 304 stainless steel
Product form	Flange spacer

Fig. 25 An unexpected leak was discovered on a chemical process line that had operated without event for several years. The chemistries and process conditions showed no historical variations or upsets that could promote such attack in stainless steel. Subsequent investigation revealed repairs to local guard-rails on the plant, at which time the welders had grounded their equipment to the plant, adjacent to the subject flange. The pitting occurred because the spacer became anodic through stray-current effects.
Control: More diligent attention to detail during maintenance would have alerted the welders to the risk of stray-current corrosion. The spacer would have continued to be well suited for its intended purpose.

Corrosion form and mechanism	Underdeposit and waterline attack
Material	Galvanized steel
Product form	Piling for canal bank

Fig. 26 Long-term contact with water (one side) and wet soils (other side) resulted in through-wall attack of the metal piling adjacent to a canal. Loss of galvanized steel occurred over many years (possibly 20 to 25 years), with subsequent perforation along areas where the claylike soil had contacted the piling (differential aeration effects). Waterline attack was noted from the canal side of the piling, with preferential corrosion caused by short diffusion paths where the meniscus zone of the water contacted the metal.
Control: Better coatings and/or cathodic protection are advantageous. The subject piling was relatively old and had served its useful period; replacement was timely and due.

Corrosion form and mechanism	Localized pitting, microbiologically influenced corrosion (MIC)
Material	Steel
Product form	Allen-head bolts

Fig. 27 Deep pitting attack was discovered on steel bolts used to retain parts in a metal-shaping (cutting) machine. The surfaces of the bolts were covered with a black, oily substance, which, on analysis, was found to contain sulfurous species. Other steel parts also failed by pitting attack. Metallurgy revealed deep, rounded pits, reminiscent of microbial corrosion attack, MIC. Subsequent analysis confirmed that sulfate-reducing bacteria, *desulfovibrio*, were present. Apparently, trials on new cutting oils were in progress at the time of the incident. The pH was measured in the range of 4 to 8; the normal pH for the usual cutting oil was 9.
Control: Alternative oils free from the risk of MIC are available, but choice is as much a trial-and-error approach as definitive. Proven oils should be sought from suppliers once they have confirmed the nature and effects of the MIC. Oil and lubricating fluid suppliers should be consulted for MIC-immune product. Higher pH values are usually maintainable for resisting MIC; alternative metals may be considered.

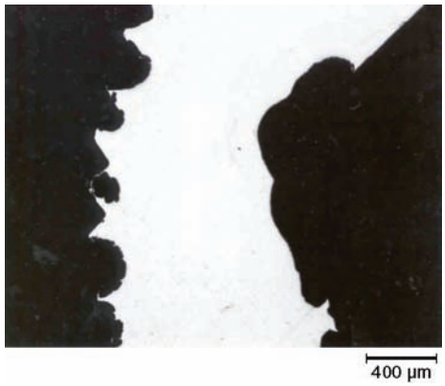

Corrosion form and mechanism	Localized pitting, microbiologically influenced corrosion (MIC)
Material	Steel
Product form	Allen-head bolts

Fig. 28 Photomicrograph of the knurled bolt of Fig. 27. The attack in the central hexagonal section is seen. Original magnification 25×
Control: See Fig. 27

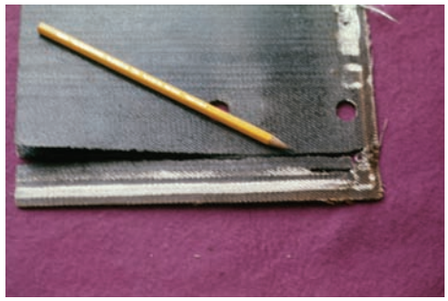

Corrosion form and mechanism	Thermal degradation, oxidation
Material	Nickel-copper alloy/glass fiber mat
Product form	Heating mat

Fig. 29 Heater mats used to stabilize twists in yarn fibers in a textile plant were failing after approximately 1 month. The temperature was measured as 190 °C (375 °F). The mats were composed of nickel-copper corrugated heater elements stitched into fiberglass and encapsulated in resin for rigidity. The charred appearance of the failing mats and the loss of resin to reveal fiberglass (white) are indicative of overheating. Separate tests show that the loss of resin occurred at ~450 °C (840 °F), at which temperature the nickel-copper alloy will oxidize rapidly in air. Sulfur and carbon liberated from the degrading resin will embrittle the nickel-copper alloy. The cause of the failures was primarily incorrect temperature control.
Control: This design was poor. Subsequently, the design was modified to monitor the mat temperature more precisely. The nickel-copper alloy was exchanged for a more heat-resistant nickel-chromium alloy.

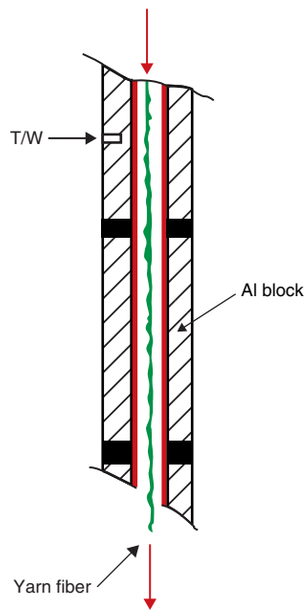

Fig. 30 Schematic of original arrangement of components described in Fig. 29. There was a large temperature gradient between the thermocouple (T/W) in the aluminum block and the interior of the mat beside the yarn. The mat had exceeded 400 to 450 °C (750 to 840 °F), more than double the 190 °C (375 °F) value monitored by the T/W.

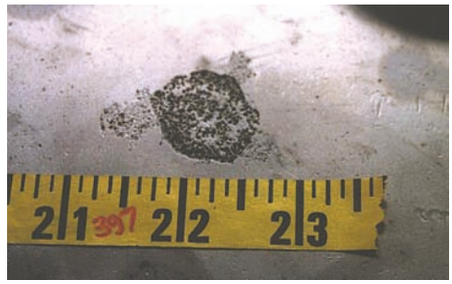

Corrosion form and mechanism	Localized corrosion, pitting
Material	Type 304/303 stainless steel
Product form	Food-processing vessel

Fig. 31 Areas of localized pitting arose in type 304 stainless steel plate material following approximately 18 months service in a food-processing vessel. The damage location was uniquely related to a type 303 stainless steel plug that supported external controls (Fig. 32). The intention was to insert the type 303 stainless steel plug and secure it in place with an overlay of type 304 stainless steel, as indicated. In practice, the type 303 stainless steel weld overlay was lost through excess grinding, which left the end of the type 303 stainless steel plug exposed directly to the food-processing fluids and seasonings. The vessel was also steam cleaned in place. Type 303 stainless steel is not as resistant to corrosion as type 304 stainless steel. The damage comprised a mixture of end-grain attack associated with manganese sulfide stringers and pitting attack of the less corrosion-resistant stainless steel. Pits cannot be allowed, because they can trap and retain food stuffs, which may result in bacteria issues.
Control: Stop using type 303 stainless steel and revert to more resistant type 304/316 stainless steels. Improve the insert geometry and fabrication procedures.

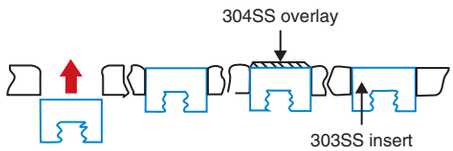

Fig. 32 Arrangement of type 303 stainless steel plugs in the type 304 stainless steel plate shown in Fig. 31. The original design of a type 303 plug with a type 304 stainless steel overlay is shown.

Corrosion form and mechanism	High-temperature corrosion, oxidation, and sulfidation
Material	Type 321 stainless steel
Product form	Gas turbine crossfire tube

Fig. 33 The crossfire tube provides the path for a spark to ignite the gas in a gas turbine. The tube is usually located away from direct heat. In this case, some misalignment occurred, and the tube was exposed directly to flame. It overheated and experienced rapid oxidation, compounded by sulfurous gases in the system. The thick oxide scales and the markedly thin tube section are indicative of gross overheating. Further confirmation of high-temperature oxidation was provided with a magnet; magnetism detected in the thinner sections reflects a local loss of chromium from the steel (in forming oxides), which leaves areas that are magnetic.
Control: Examine the configuration of the component and realign to avoid overheating.

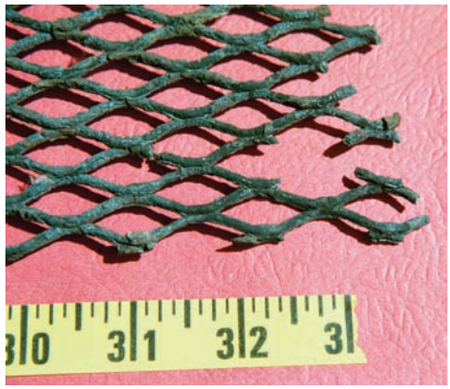

Corrosion form and mechanism	High-temperature corrosion, sulfidation
Material	Nickel alloy N08330
Product form	Mesh support for insulation

Fig. 34 A metal screen used to retain insulation to the inlet box of a gas cooler system in an acid plant disintegrated after a few months' service. The heat-resistant alloy UNS N08330 (Fe-35Ni-19Cr-1.2Si-0.05C) was selected on the basis that the incoming gases (approximately 80% N, 11% O, 9.5% SO_2/SO_3) were to remain oxidizing at all times, with temperatures at 850 to 900 °C (1560 to 1650 °F). Upsets on the acid plant included poor process controls, inadequate air cooling, incomplete combustion, and unstable flames, with very many temperature cycles due to interruptions in power supply. The anticipated oxidizing gases became an alternating sulfidation/oxidation environment, which resulted in gross sulfidation attack with contributions from low-melting phases, such as the Ni-Ni_3S_2 eutectic (melts at 645 °C, or 1195 °F).
Control: Comply with the design requirements that called for oxidizing conditions at all times. Alternative heat- and corrosion-resistant alloys are available if plant conditions cannot be maintained as specified.

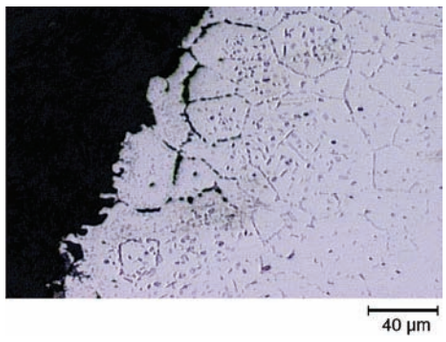

Corrosion form and mechanism	High-temperature corrosion, sulfidation
Material	Nickel alloy N08330
Product form	Mesh support for insulation

Fig. 35 A micrograph of the screen in Fig. 34 shows a zone of intergranular attack with a predominance of sulfides (gray areas) extending deep into metal. Specimen unetched, original 250×.
Control: See Fig. 34

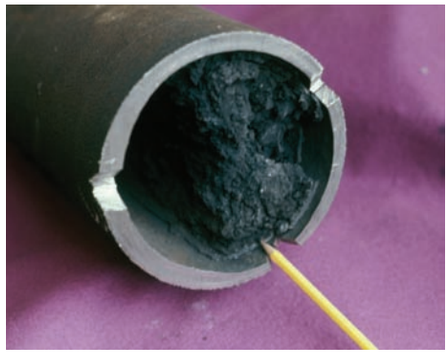

Corrosion form and mechanism	High-temperature corrosion-sulfidation, carburization, flame impingement
Material	Cast stainless steel, cast 20-20-type stainless steel
Product form	Furnace tube—carbon disulfide

Fig. 36 Enhanced metal thinning after approximately 1 to 2 years along one side of an alloy 20-20 (HK 30, UNS J94203) furnace tube was attributed to a combination of local sulfidation attack and external flame impingement. Carbon disulfide is formed by reacting methane with sulfur at approximately 600 to 800 °C (1110 to 1470 °F), with attendant carbonaceous deposits. Chromium-rich carbides were formed in the metal, which effectively left adjacent areas denuded of chromium, where nickel-rich sulfides could form. Sulfur attack was most pronounced above ~635 °C (1175 °F), the melting temperature for Ni-Ni_3S_2 eutectic. The thinned tube was attributed to overheating caused by flame impingement by one of the burner flames.
Control: Alternative alloys should be considered, including the alloy 800 family and other high-temperature nickel alloys. A better alignment of the flames would reduce overheating effects. Replacement furnace tubes were less prone to tube distortion.

Corrosion form and mechanism	High temperature, oxidation, and erosion
Material	Low-chromium steel
Product form	Boiler tube

Fig. 37 Short-term and rapid overheating of a steel boiler tube (reheater, superheater, or similar—source unknown) resulted in a longitudinal "fish-mouth" rupture. The tube had experienced elevated temperatures (455 to >730 °C, or 850 to >1350 °F) where the metal strength is markedly reduced. Rapid heating is indicated by the extensive tube bulging and the thinned edges of the open fracture. Such tube failures are commonly the result of boiler upset conditions, including partial or total tube plugging, insufficient flow of coolant, or excessive fireside conditions (flame impingement and erosion).
Control: Operating procedures and system design are common causes of short-term overheating in boiler tubes. Plant records can help identify the cause, such as new burners with changed firing pattern, prior ineffective cleaning of fouled tubes with scales and debris left in place, recent acid clean treatment, or low water level at startup. Careful monitoring of operation is recommended.

Corrosion form and mechanism	Pitting, underdeposit attack, crevice corrosion
Material	Process pipe connector
Product form	Type 304 stainless steel

Fig. 38 Pits were noticed in the bottom of a type 304 stainless steel three-way flange connector in a food-processing plant when viewed from above. The hot, acidic food (fruit products) passed through this location several times for each production batch. The system was sterilized in place after each processing operation. The blackened area seen on the bottom in the photograph was a stubborn deposit that had formed from the seasoned food products. Pitting was apparent. The cause of the problem was later found to be associated with the shape of the component. The assembly could not be fully drained, which left residual fluid and solids in the vessel that contributed to underdeposit attack.
Control: There is a design deficiency, because as fabricated and installed, the vessel cannot be fully drained.

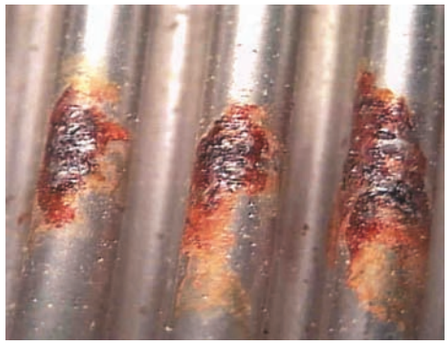

Corrosion form and mechanism	Local corrosion, pitting, crevice
Material	Type 321 stainless steel
Product form	Convoluted bellows-hose system

Fig. 39 A type 321 stainless steel bellows hose jacketed with a type 304 stainless steel braid leaked in 3 months, while other hoses lasted for approximately 1 year. The flexible hose was used to transfer sulfur-containing organic fluids from a tank car. The cause of attack was extreme pitting originating from the inside of the bellows. Analysis showed iron-rich brown products with high chloride and sulfur content. The failures were attributed to pitting corrosion with extreme undercutting, probably resulting from changes in location of the hoses during storage and use. Bleach, used to deodorize the pungent smell of the sulfur compounds being transferred (and presumably left) inside the hoses, contributed to chloride-induced pitting. Remnants of the organic fluid/bleach/water mixture remained stagnant in the valleys of the hose bellows, which experienced condensation/evaporation cycles with intermittent use. The enhanced pitting was exacerbated by the continual supply of chloride as further bleach was added in subsequent deliveries.
Control: Type 300 stainless steels are suitable for the sulfo-organic fluids but not for active chloride ions introduced during attempts to deodorize the product. Alternative materials and/or measures to clean up the residual compounds left on the inside of the hoses warrant consideration.

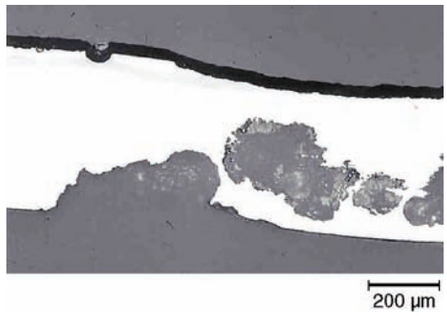

Corrosion form and mechanism	Local corrosion, pitting, crevice
Material	Type 321 stainless steel
Product form	Convoluted bellows-hose system

Fig. 40 Micrograph of a section through the valley of the corrugated bellows in Fig. 39. Pitting exacerbated by chloride bleach is evident. Specimen unetched. Original magnification: 50×

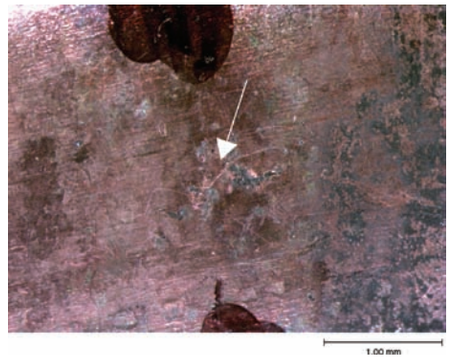

Corrosion form and mechanism	Localized corrosion, pitting, formicary corrosion
Material	Copper
Product form	Evaporator coils; heating, ventilation, and air conditioning

Fig. 41 Formicary (ant-nest) corrosion describes a microtunneling attack of copper (Fig. 42) that typically initiates at minute pinholes on copper tube surfaces, as seen in this figure. The process occurs with the simultaneous presence of air, moisture, and an organic acid of the carboxylic group, for example, acetic and formic acids. Formicary corrosion is considered to be a modified localized corrosion pitting process involving a micro-anode, where dissolved copper ions combine with carboxylic acids to form an unstable cuprous complex that is oxidized to cupric formate, acetate, and cuprous oxide. The process is rapid; total penetration can occur in weeks or months.
Control: Thoroughly clean and dry surfaces are not prone to formicary corrosion. Lubrication or other fluids with <20 ppm carboxylic content are generally considered unlikely to cause attack on copper tubes. Certain coatings are being explored to minimize or eliminate attack. Laboratory testing, typically for times of up to 3 months, using vapors derived from formic and acetic acids or from candidate lubrication fluids is used to determine the propensity for attack, using metallography to substantiate the findings. Original magnification: 32×

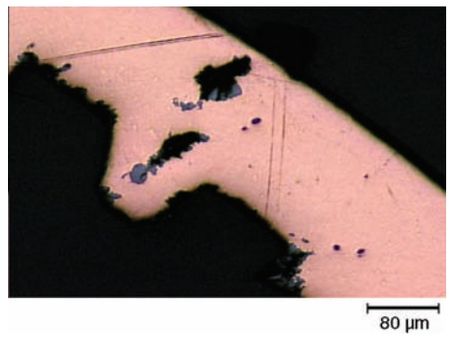

Corrosion form and mechanism	Localized corrosion, pitting, formicary corrosion
Material	Copper
Product form	Evaporator coils; heating, ventilation, and air conditioning

Fig. 42 A cross section of a microtunnel in Fig. 41. Unetched. Original magnification: 125×

Corrosion form and mechanism	Crevice corrosion
Material	Ni-Cr-Mo alloy
Product form	Retainer bolt

Fig. 43 Nickel alloys are generally considered resistant to acids and strong corrodents. Occasionally, the shielded area of an assembly (such as a flange that was retained by the bolt shown here) is too low in oxygen content to permit passivation of the metal. Localized pitting attack resulted from crevice corrosion, and the assembly leaked.
Control: Materials selection for the specific environment has to account for areas where localized attack can occur, such as crevices and underdeposits. Improve alloy selection and/or modify the assembly.

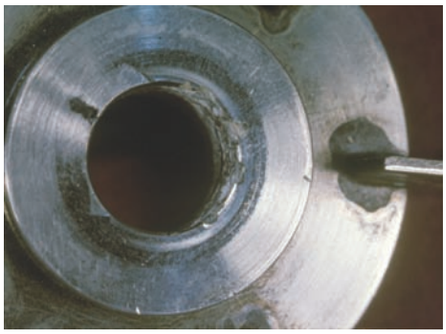

Corrosion form and mechanism	Metallurgically influenced corrosion, galvanic corrosion, crevice corrosion
Material	Stainless steel, carbon steel
Product form	Stirrer

Fig. 44 A stainless steel paddle stirrer was clamped to a stainless steel spindle using a small carbon steel screw (Fig. 45). The fitting worked loose due to localized crevice corrosion exacerbated by galvanic attack. The large cathodic area of the stirrer enhanced the corrosion of the small carbon steel screw (anode).
Control: Select compatible materials; preferably, use the same metals. Avoid large-cathode-to-small-anode areas.

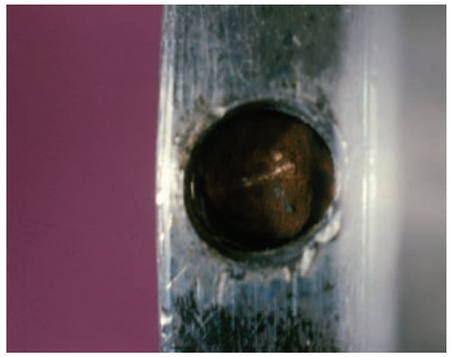

Corrosion form and mechanism	Metallurgically influenced corrosion, galvanic corrosion, crevice corrosion
Material	Stainless steel, carbon steel
Product form	Stirrer

Fig. 45 The small carbon steel machine screw (anode) in the stainless steel stirrer (cathode) shown in Fig. 44

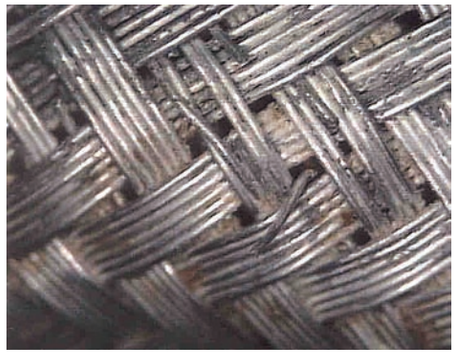

Corrosion form and mechanism	Localized corrosion, crevice corrosion; mechanically assisted corrosion, fretting fatigue
Material	Type 304 stainless steel
Product form	Braided hose sheath

Fig. 46 Braided sheathing is used to contain and support convoluted hoses for many applications. Depending on the particular application, failure modes include crevice corrosion, which can be expected if deposits are able to remain around the wires; fretting damage, if adjacent wires rub against each other during service; and fatigue fractures, if the assembly experiences alternating high stresses. The environment is a key issue in determining the mode of failure. More than one form of corrosion may be involved for the same application.
Control: Handling within design limits of minimum bend radius and tensile load is important to avoid local stress raisers that can influence stress-associated failures. Materials choice should be dictated by the specific environment and from application experience. Outer nonmetallic containment jackets (elastomeric, plastics) provide protection in corrosive applications and underground.

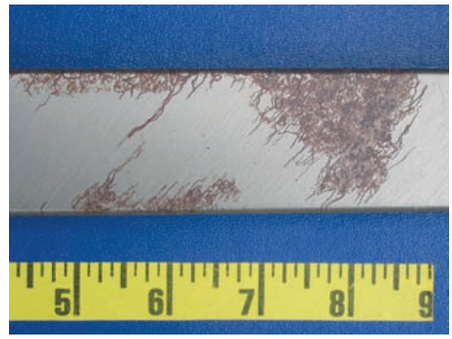

Corrosion form and mechanism	Localized corrosion, filiform corrosion
Material	Carbon steel, lacquer coated
Product form	Indoor furniture panels

Fig. 47 Occasional premature discoloration was noted on polished and coated steel indoor furniture, which worsened over several weeks with threadlike features (filiform corrosion). The polished carbon steel sections were absent of visual blemishes prior to coating with a clear lacquer. The polished steel was not immediately coated; sections were left outdoors unprotected over a weekend before any coating was applied.
Control: Filiform corrosion typically occurs under thin (50 to 100 μm, or 2 to 4 mils, thick) films, such as clear lacquers, and is enhanced by humidity above approximately 65% at approximately ambient temperatures. Sweaty, oily finger contact further contributed to the problem, due to local chloride presence. The steel should be coated as soon as possible after surface preparation, or the surfaces should be kept dry and clean and/or protected from the surrounding atmosphere until coating is possible. Articles should be carefully handled with gloves.

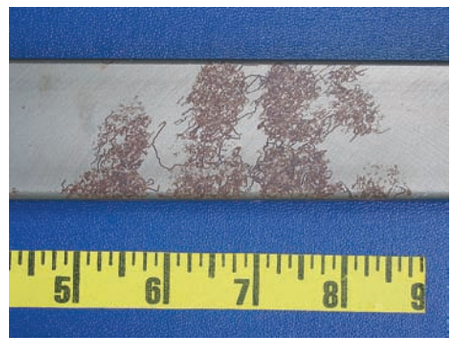

Corrosion form and mechanism	Localized corrosion, filiform corrosion
Material	Carbon steel, lacquer coated
Product form	Indoor furniture panels

Fig. 48 The filiform corrosion problems of Fig. 47 are exacerbated by handling the unlacquered parts without gloves. Fingerprints are obvious in this photograph.

Corrosion form and mechanism	Metallurgically induced corrosion, dealloying graphitic corrosion
Material	Gray cast iron
Product form	Underground mains water pipe

Fig. 49 Over 25 year old gray iron mains water pipe can experience deterioration through selective corrosion, where the iron (anodic) portion of the metal is selectively corroded to form rustlike products that are supported by the unattacked graphite (cathodic) flakes, forming a weakened porous product. The cast iron pipe may appear to have the original dimensions, but darker areas around the pipe can be cut away with a pocket knife. These areas have been selectively corroded by graphitic corrosion. Gray cast iron pipes that experience graphitic corrosion commonly fail unexpectedly from external forces such as impact from a back hoe or excavator, ground movement, or internal forces such as pressure surges.
Control: Planned replacement presents an economic challenge to many national and local authorities as part of an infrastructure crisis relating to aging plants and equipment. Other cast irons (ductile or nodular irons) are not prone to gross selective corrosion.

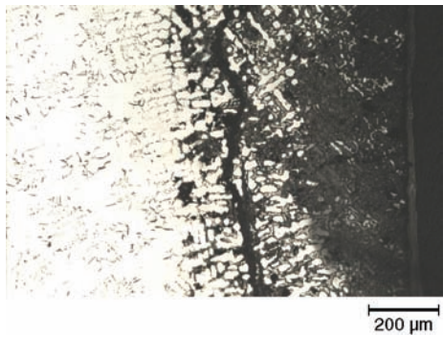

Corrosion form and mechanism	Metallurgically induced corrosion, dealloying graphitic corrosion
Material	Gray cast iron
Product form	Underground mains water pipe

Fig. 50 A micrograph of graphitic corrosion in the wall of the cast iron pipe in Fig. 49. Original magnification: 50×

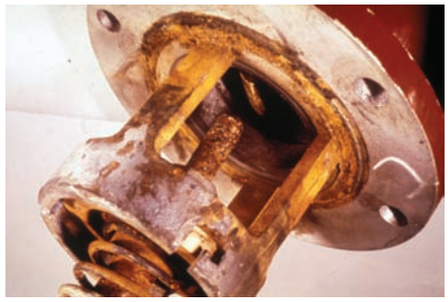

Corrosion form and mechanism	Metallurgically influenced corrosion, galvanic corrosion
Material	Cast aluminum alloy and brass fittings
Product form	Drain valve from road tanker

Fig. 51 The drain valve assembly for a fuel oil road tanker was removed because it had seized. Examination revealed a cast aluminum alloy body and support with a brass spindle and lever retained in place by a steel spring. Local galvanic corrosion associated with the aluminum/copper coupling caused the failure. Other forms of corrosion were apparent from the humid, oily mists that developed within the valve, including pitting of the plated brass spindle, general corrosion of a carbon steel screen (not shown in the photograph), and rusting of the steel spring.
Control: A redesign should eliminate incompatible metals. Nonmetallic materials and coated components warrant consideration.

Corrosion form and mechanism	Aqueous corrosion, crevice corrosion, galvanic corrosion
Material	Carbon steel bolt with stainless steel nut
Product form	Bolted fastener

Fig. 52 The fastener was discovered in a marine estuary. The bolt displayed significant wastage along the shaft and at the end. The attack at the midpoint is considered to be a combination of crevice and abrasion from whatever had been retained by the bolt—possibly a mooring for a boat experiencing the combined effects of a retaining rope, seawater, and sand. The pointed end of the bolt was related to galvanic corrosion effects between the bolt (anode) and the surrounding stainless steel nut (cathode).
Control: The fastener was not designed for the particular purpose, and the dissimilar metals (the bolt and nut) were of no benefit.

Corrosion form and mechanism	Metallurgically influenced corrosion, galvanic
Material	Carbon steel and copper
Product form	Copper water tube

Fig. 53 Human errors or miscalculations cause unexpected failures. Nails inadvertently punched through a copper water pipe hidden by floorboards present such an example, which is found more often than may be expected (two separate examples are noted in Fig. 53 and 54). Water did not escape immediately, because the steel nail effectively plugged the copper tube wall. With time, corrosion processes caused corrosion of the steel nail (small anode) in the copper pipe (large cathode) until the corrosion products were sufficiently formed and were ultimately breached by water under pressure. The corrosion processes were more advanced on the hot water pipe, because temperature influences corrosion rate.
Control: More care (and awareness) by contractors to avoid the metal-to-metal contact. Source: Courtesy of T.K. Ross

Corrosion form and mechanism	Metallurgically influenced corrosion, galvanic
Material	Carbon steel and copper
Product form	Copper water tube

Fig. 54 Location of tubing under a floorboard in a different location from Fig. 53. The corrosion process occurred one time and was not discovered until the ceiling of the lower floor collapsed from the weight of water that had accumulated while the tube was leaking.

Corrosion form and mechanism	Metallurgically influenced corrosion, intergranular (end-grain attack)
Material	Type 304 stainless steel
Product form	Flange

Fig. 55 A general lack of attention to detail in a less accessible part of a process plant allowed the flange to corrode unnoticed until general wastage was considerable. The damage is attributed to end-grain attack caused by condensing acids from the plant.
Control: The flange material should be selected so as to minimize grain-boundary attack. Alternative materials or coatings should be considered. More diligent inspection is warranted.

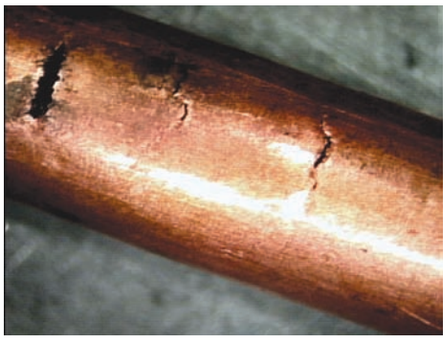

Corrosion form and mechanism	Metallurgically influenced corrosion, intergranular attack
Material	Copper
Product form	Pipe for fuel oil

Fig. 56 A series of lateral cracks occurred within a period of approximately 10 to 15 years' service, resulting in an oil leakage from a 9.5 mm (3/8 in.) diameter copper pipe that supplied No. 2 fuel oil from an underground storage tank.
Control: Intergranular attack (Fig. 57) is not common in copper alloys; only isolated cases are noted under very specific conditions, which are usually not defined in the reference texts. An oily (sulfurous) environment apparently caused this attack. Lateral cracking is commonly associated with poor handling with metal clamps, etc., that leave residual tensile stresses in the metal.

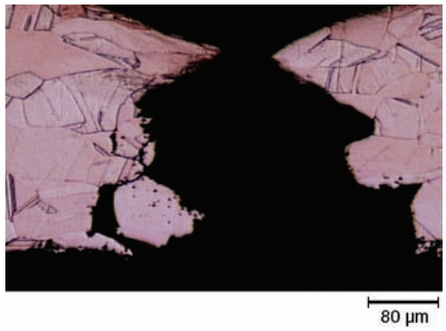

Corrosion form and mechanism	Metallurgically influenced corrosion, intergranular attack
Material	Copper
Product form	Pipe for fuel oil

Fig. 57 The micrograph for a cross section through the copper pipe in Fig. 56 with dichromate etch shows the intergranular attack and includes an area with total grain detachment. Original magnification: 125×

Corrosion form and mechanism	Mechanically assisted degradation, fretting corrosion
Material	Carbon steel
Product form	Automotive muffler pipe

Fig. 58 Metal-to-metal contact was caused by an improperly supported muffler pipe. The repetitive impacting of the metal surfaces under a sustained load, with vehicular movement, had worn away the metal until it was totally perforated. The carbon steel pipe failed because of fretting corrosion, where the oxide coating is constantly removed by the mechanical action.
Control: Proper installation and maintenance, as recommended by the manufacturer, would avoid this failure.

Corrosion form and mechanism	Mechanically assisted degradation, impingement
Material	Copper
Product form	Pipes from chiller unit

Fig. 59 The copper tubes were located low in a lithium bromide chiller unit. Water had filled and overflowed the collector tray under the evaporator coils. The falling droplets impinged directly onto the copper tubes. The areas of perforation were in line of sight of the falling stream of water.
Control: Redesign of the unit ensured proper collection and flow of water away from the copper tubes above the collector trays.

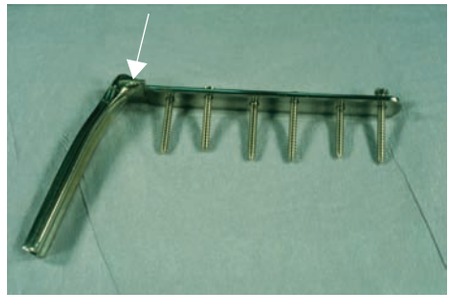

Corrosion form and mechanism	Mechanically assisted degradation, fatigue, galvanic, crevice corrosion
Material	Type 316L stainless steel
Product form	Nail and plate prosthetic device

Fig. 60 A patient complained of pain following implant surgery. The surgeon prescribed pain-killers for arthritis, until an x-ray revealed a fractured device. The implant failed by corrosion fatigue because the patient neglected the advice of the doctors. Prosthetic devices are not designed to support the same load as a healthy bone immediately after surgery. Typically, the device holds the ends of a broken bone in place until healing occurs and the bone becomes one piece again. Although not an issue in this failure, the screws were magnetic, which signifies possible galvanic and/or crevice corrosion under the screwheads where they contact the bone plate.
Control: Better understanding by patients to heed advice. Avoid direct body weight to minimize stresses on the component. For long-term remediation and service, stainless steels are replaced by other more resistant materials, such as titanium alloys (Ti-6Al-4V), cobalt-chromium alloys, or tantalum.

Corrosion form and mechanism	Environmental crazing, stress-corrosion cracking
Material	Polycarbonate
Product form	Window

Fig. 61 Replacement windows manufactured with polycarbonate were cracking, typically after one summer season or less. The manufacturer had made no changes to his product other than to order extruded instead of as-cast polycarbonate panels for the window. Testing showed that the extruded product was extremely sensitive to the environment as compared with the previously used as-cast product. Some chemicals, including alcohol, cracked the extruded product immediately. When it was held under stress, the former as-cast material resisted all identical tests.

Control: The manufactured form of a plastic product is important. In this case, retained stresses from extrusion left the material of the same composition very prone to failure. Environmental testing would resolve the expected service performance. The extruded product required some stress-relieving process for this application.

Corrosion form and mechanism	Environmentally induced cracking, stress-corrosion cracking
Material	Type 304 stainless steel
Product form	Process vessel for food

Fig. 62 Cracks developed in the vicinity of a new flange that had been added to a process vessel a few weeks earlier. The operator at first sent two cut-out rings with the comment that the two were only 5 cm (2 in.) apart, yet one was cracked and the other was not. Once the relative position of the two samples was known, the reason for the failure was clear. The cracked sample was cut from the heat-affected zone associated with the new flange. Residual stresses in this area were sufficiently high as to promote stress-corrosion cracking (SCC). The vessel was part of a food-processing line for tomato products, which were of high chloride content. The failure was the result of chloride-induced SCC.

Control: Better attention to welding with reduced tensile stresses would avoid SCC. Materials that are less prone or immune to SCC should be considered, including ferritic, superferritic and austenitic-ferritic stainless steels and nickel-base alloys.

Corrosion form and mechanism	Environmentally induced cracking, stress-corrosion cracking
Material	Type 304 stainless steel
Product form	Water supply pipe

Fig. 63 The strapped-on plate near the top of the 30 cm (12 in.) diameter pipe was intended to be a short-term palliative measure to contain water/steam that was escaping after a few months' service. The type 304 pipe first supplied water and then air to an adjacent process vessel via a perforated tube. The process fluid was agitated by the air. The vessel and the associated piping were steam cleaned daily. The subject pipe experienced repetitive cycles of cold water/air/steam.

The cause of the leak was chloride-induced stress-corrosion cracking (SCC) resulting from the prior exposure of the new components to marine salts. The stainless steel components had been stored directly adjacent to a marine estuary. Residual tensile stresses were caused by careless fabricators who welded the side pipes to the vessel and did not relieve the stress. The problems were aggravated by the cold water supply from a well with >3000 ppm chloride content.

The combination of tensile stresses from fabrication with the chloride environment in air, from outside unprotected storage, and well water caused SCC.

Control: The new equipment should have been properly stored away from the chloride-rich environment, and the water supply should have been changed or suitably treated. Design and fabrication codes should have been strictly followed to avoid the stresses from welding. An alternative alloy was probably merited, such as a higher-alloyed stainless steel or nickel alloy. The temporary plate caused further potential problems of crevice attack.

Corrosion form and mechanism	Environmentally induced cracking, stress-corrosion cracking
Material	Copper
Product form	Water pipe

Fig. 64 Leaking copper pipes in a recently refurbished bathroom were attributed to stress-corrosion cracking (SCC) caused by tensile stresses arising from improper handling and installation (wrench marks, gouges) and ammonium salts (from leveling compounds in the cement that encased the copper tubing). Longitudinal cracks were revealed by reflection in a mirror.
Control: The fitters were responsible for the applied (tensile) stresses during assembly/installation. The copper pipe was placed in direct contact with wet cement, which is a source of ammonia-leveling compounds. Separate channels to house the copper pipe can avoid the sustained presence of water and contact with soluble compounds that promote SCC.

Corrosion form and mechanism	Environmentally induced cracking, stress-corrosion cracking
Material	Copper
Product form	Water pipe

Fig. 65 Intergranular cracking was observed in cross sections of the pipe in Fig. 64.

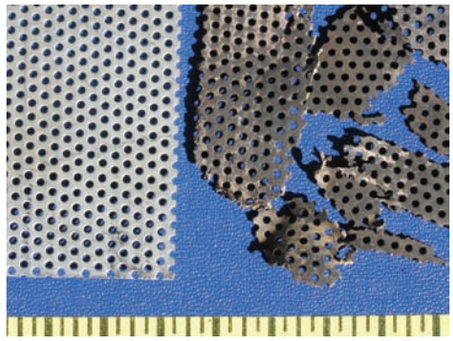

Corrosion form and mechanism	Environmentally induced cracking, stress-corrosion cracking
Material	Type 304 stainless steel
Product form	Perforated screen from solvent recovery plant

Fig. 66 The perforated screen supported a carbon bed through which solvent-laden gases pass. Subsequently, the gas stream switched to steam that strips the solvent from the carbon bed, which can then be used again. The screen failed because of stress-corrosion cracking (SCC) resulting from the simultaneous presence of chloride (derived from steam that was produced from poorly treated well water with high chloride content) and tensile stresses (caused by residual stresses resulting from punching the steel plate to form the screen, without subsequent stress relief). The photograph contrasts new screening with the cracked condition after a few months' service. Note that there can be a strong galvanic corrosion effect from the activated carbon to metallic surfaces in contact with the bed.
Control: The remedy adopted for this case included a change to titanium and a water treatment program to reduce the high chloride level from the steam. Alternative materials include fiber-reinforced plastic construction, nonmetallic linings, and more corrosion-resistant metals such as titanium and Ni-Cr-Mo alloys such as UNS N10276 and N06625, if the cost can be justified.

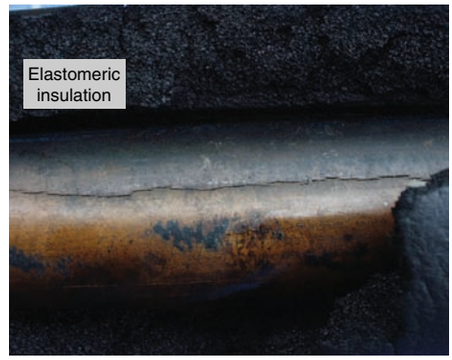

Corrosion form and mechanism	Environmentally induced cracking, stress-corrosion cracking (SCC)
Material	Copper with elastomeric insulation
Product form	Refrigerant pipe

Fig. 67 Longitudinal cracks developed in insulated copper piping used to convey refrigerant to food cabinets in supermarkets. Some pipes leaked within weeks of installation. The cause was attributed to certain formulations of elastomeric insulation that yielded ammonia solutions when the insulation was wet. The copper was in a half-hard condition; additional tensile stresses were sometimes found following incorrect handling during installation. Similar instances of SCC have been reported in high-rise buildings where heating, ventilation, and air conditioning systems are involved. In Germany, in the 1980s to 1990s, more frequent cases of SCC were reported. It was later realized that a corrosion inhibitor, sodium nitrite, was recommended without knowledge that the metal was copper. Subsequent Deutsche Industrie-Normen standards for insulated copper pipe stipulate zero nitrite and $<0.2\%$ ammonia content.
Control: Insulated copper piping should be properly installed, avoiding direct contact with wet soils or moist atmospheres that yield ammonia-containing vapors, for example, liquid smokes. Unknown or new elastomeric insulation materials should be evaluated for possible ammonia, amine, or similar constituents that can contribute to SCC in copper. Copper tube should be used in a manner to avoid unwanted additional tensile stresses from poor handling in fabrication and installation.

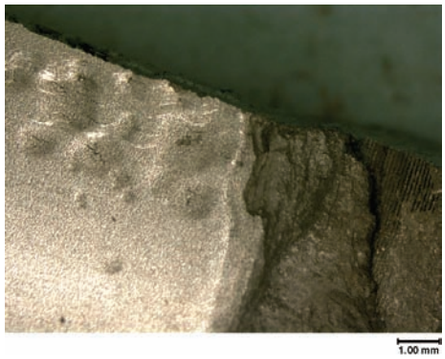

Corrosion form and mechanism	Environmentally assisted degradation, hydrogen damage
Material	Grade 9 titanium alloy, Ti-3Al-2.5V
Product form	Flow monitor

Fig. 68 The flow-monitoring device displayed a blistered surface after approximately 12 to 18 months service, which was determined to be hydrogen blistering. The manufacturer was puzzled because the process fluid was not expected to yield hydrogen. Subsequent investigation revealed that the organic compounds used at an overseas plant (unbeknown to the manufacturers) contained over 300 ppm hydrogen. This figure is near a weld area. Original magnification: 11×
Control: A hydrogen-free environment had been envisioned. Process control and alternative materials were later adopted. Hydrogen embrittlement of titanium can occur from fabrication and metalfinishing processes; iron-contaminated oxide is not good.

Corrosion form and mechanism	Environmentally assisted degradation, hydrogen damage
Material	Grade 9 titanium alloy, Ti-3Al-2.5V
Product form	Flow monitor

Fig. 69 Surface of flow monitor in Fig. 68 with hydrogen blistering. Original magnification: 16×

Corrosion form and mechanism	Apparent galvanic attack
Material	High-strength low-alloy steel
Product form	Pressure vessel

Fig. 70 A surface anomaly approximately 2 cm (0.75 in.) across was discovered on the outside of a pressure vessel by an inspector who thought it may have been caused by galvanic corrosion or some other form of crevice corrosion. The discovery was made during final inspection after the vessel had been pressure tested. It was only after the inside surface was examined that the extent of the lack of quality control was discovered. A large bolt had fallen on to the hot-rolled sheet steel during plate production. This should have been discovered during fabrication of the vessel, and the pressure test was insufficient to detect the flaw at this time. The bolt compromised the pressure vessel integrity, and had it gone undetected it would have been an ideal site for further crevice corrosion.
Control: Careful fabrication and diligent in-process inspection for that which "cannot happen"!

ACKNOWLEDGMENT

The author expresses his sincere thanks to the many people and organizations who have directly, or indirectly, helped instill a sense of urgency to share stories and anecdotes that may assist others to become more aware of corrosion and its enormous toll on industry, the infrastructure, and economies worldwide. It is dangerous to name names, but the author particularly wishes to recognize the following: Pat Burke, Colin Britton, Bob Campbell, Jim Cooper, Rick Corbett, John Dawson, Paul Dillon, David Gearey, Russ Kane, Roger King, Redvers Parkins, Ken Ross, Mervyn Turner, and Graham Wood. His past association with the U.K. Government Department of Energy Corrosion Committee, University of Manchester Institute of Science and Technology Corrosion and Protection Centre, CAPCIS Ltd., Nickel Development Institute, and committees of the Institute of Corrosion and NACE International is also recognized.

REFERENCES

1. C.P. Dillon et al., *Mater. Perform.,* 2000–2004
2. M.E.D. Turner, Corrosion Engineering and Corrosion Science, *Mater. Perform.,* Vol 19 (No. 10), 1980, p 51
3. P. Elliott, Catch-22 and the UCS Factor—Why Must History Repeat Itself? *Mater. Perform.,* Vol 28 (No.7), 1989, p 70; Vol 28 (No. 8), 1989, p 75
4. O.W. Siebert, Classic Blunders in Corrosion Protection, *Mater. Perform.,* Vol 17 (No. 4), 1978, p 33; Vol 22 (No. 10), 1983
5. E.D.D. During, *Corrosion Atlas,* Elsevier Science Publishing Co., Inc., 1988
6. L.M. Wyatt, D.S. Bagley, M.A. Moores, and D.C. Baxter, *An Atlas of Corrosion and Related Failures,* MTI Publication 18, Materials Technology Institute, 1987
7. *Failure Analysis and Prevention,* Vol 11, *ASM Handbook,* ASM International, 2002
8. R.D. Port and H.M. Herro, *Nalco Guide to Boiler Failure Analysis,* McGraw-Hill, Inc., 1991
9. H.M. Herro and R.D. Port, *Nalco Guide to Cooling Water System Failure Analysis,* McGraw-Hill, Inc., 1993
10. R.N. Parkins and K.A. Chandler, *Corrosion Control in Engineering Design,* HMSO, London, 1978
11. C.P. Dillon, Ed., *Forms of Corrosion, Recognition and Prevention,* NACE Handbook No. 1, NACE, 1982
12. P. Elliott, Understanding Corrosion Attack, *Plant Engineering,* 1993, p 68
13. C.P. Dillon, *Unusual Corrosion Problems in the Chemical Industry,* Materials Technology Institute, 2000
14. R.B. Puyear, "Case Histories: Improper Materials, Fabrication and Documentation," MTI Report R-1, Materials Technology Institute, 1996
15. R.B. Puyear, "Corrosion Failure Mechanisms in Process Industries: A Compilation of Experiences," MTI Report R-4, Materials Technology Institute, 1997
16. P. Elliott, *Corrosion Control in Engineering Design,* audio visual, U.K. Government Dept. of Industry, 1981
17. *Corrosion Awareness,* three-part videotape series: *Recognizing Corrosion, Materials Mix-Ups,* and *Non-Destructive Testing,* Materials Technology Institute, 1988–1991

ASM Handbook, Volume 13B: Corrosion: Materials
S.D. Cramer, B.S. Covino, Jr., editors, p430-433
DOI: 10.1361/asmhba0004050

Corrosion of Thermal Spray Coatings at High Temperatures

Tapio Mäntylä, Tampere University of Technology
Mikko Uusitalo, Metso Powdermet Oy

HIGH-TEMPERATURE PROCESSES are an essential and important part of modern industrial activity. They are found in diverse industries and include propulsion units (turbine and rocket), energy production, coal conversion, automotive and chemical industry, waste incineration, and metal, glass, and ceramic processing. The continuous efforts to save energy by improving efficiency while minimizing emissions place heavy demands on materials, because obviously these requirements mean higher operating temperatures and often include exposure to more aggressive environments. Thus, oxidation and hot corrosion have become significant life-limiting material degradation processes that often limit the upper service temperatures and thus have an associated impact on both process efficiency and reliability.

Thermal spray overlay coatings had and still have an essential role in the development of some of these applications, especially gas turbines, since the early 1970s. During this period, thermal spraying as well as coating compositions and structures have undergone huge improvements and now offer tailor-designed coatings with specific structures and composition by well-controlled and repeatable spray processes. In addition to those applications at the leading edge of the development, there is now a wide range of spray shops that have available a variety of spray processes and produce different high-temperature protective coatings for well-established applications.

The successful application of thermal spray coatings requires an understanding of the specific features of each spraying process, the detailed requirements of the application, and the foreseen degradation mechanisms. In the case of environmental protection coatings (EPCs) for high temperatures, several specific features of thermal spray coatings should be considered. All thermal spray coatings contain some open porosity, even coatings sprayed by high-velocity techniques, such as high-velocity oxyfuel (HVOF), and oxides at splat boundaries (Ref 1, 2). Oxidation during spraying can also be controlled by modification of powder composition, such as SiO_2 addition in the case of Ni-20Cr (Ref 3). Recent developments in modified techniques, such as gas-shrouded HVOF, have decreased the oxidation during spraying and improved the protective quality of the coatings (Ref 4). However, such techniques are not yet widely adopted in industrial use. Thermal expansion compatibility between coating and bond coat/substrate is essential in high-temperature applications. The spraying itself may result in compositional changes or create metastable phase structures that may cause problems in further high-temperature use. Certain EPCs may require multilayer structures, bond coat and top coat, complementary sealing treatments (Ref 5) and heat treatments, or remelting such as fusing or sintering (Ref 6, 7).

The oxidation and high-temperature corrosion processes in thermal spray coatings have the same basic mechanisms as these processes, but due to the specific structural details of the coatings, which result from the spraying process, they have their own specific features, which are discussed in detail in the following examples.

Oxidation

In high-temperature oxidation, material reacts with the surrounding gaseous environment and forms reaction products that can be solid scales, liquids, or volatile compounds. Typically, protective scales are stable and dense oxides, such as alumina (Al_2O_3), chromia (Cr_2O_3), or silica (SiO_2). In environments containing other reactive gaseous elements, such as sulfur, scales are also formed, but they are less protective.

Scale (oxide film) will decrease the oxidation rate if it has a combination of the following favorable properties:

- Good adherence, to prevent flaking and spalling
- High melting point
- Low vapor pressure, to resist evaporation
- Oxide film and metal have close to the same coefficients of thermal expansion (CTE)
- Oxide film has high-temperature plasticity, to accommodate differences in specific volumes of oxide and parent metal and differences in CTE
- Oxide film has low electrical conductivity and low diffusion coefficients for metal ions and oxygen

In oxidation-resistant coatings, the protective-scale-forming elements are used as main alloying elements. The growth of the protective scale in alloys depends on the capability for selective oxidation of these elements. There is a minimum concentration of these elements that must be exceeded in order to obtain a continuous protective scale. For nickel-chromium alloys containing more than approximately 10 at.% Cr, a continuous protective chromia layer is formed. A higher chromium level (~25 at.%) is required for cobalt-base alloys, because chromium diffuses more slowly in cobalt and so cannot form a continuous chromia layer at lower concentrations. Chromia scale (Cr_2O_3) can itself oxidize at temperatures higher than approximately 850 °C (1560 °F) to a volatile CrO_3 compound. Because of this, the use of aluminum additions for oxidation resistance is preferred at this temperature and above for key equipment components such as those used in gas turbines (Ref 8). However, for temperatures between 600 and 750 °C (1110 and 1380 °F), where acid fluxing can occur, chromia-forming coatings are preferred (Ref 9).

A broad family of MCrAl*X*-base alloy coatings has been developed for oxidation protection of gas turbines. The early MCrAlY coatings were alloys based on cobalt containing 20 to 40% Cr, 12 to 20% Al, and ~0.5% Y, a typical example being Co-25Cr-14Al-0.5Y. The most recent coatings are more complex, in which M is nickel, cobalt, iron, or a combination of these, and *X* is an oxygen-active element, such as yttrium, silicon, tantalum, or hafnium, or a precious metal, such as platinum, palladium, ruthenium, or rhenium. The composition of the MCrAl part of the

system is selected to give a good balance between corrosion resistance and coating ductility, while the active elements enhance oxide-scale adhesion and decrease oxidation rates. Currently, there is a tendency to combine different active elements to further improve the alloy protective properties. The presence of chromium in these alloys reduces the minimum level of aluminum required to form a protective alumina scale. The presence of as little as 5 to 10% Cr reduces the amount of aluminum necessary from 40 at.% to approximately 10 at.%. Typically, these coatings are applied by electron beam-physical vapor deposition, argon-shrouded plasma spraying, low-pressure or vacuum plasma spraying, HVOF spraying, composite electroplating, or catalytic electroless deposition (Ref 9).

There is also increasing interest in using HVOF-sprayed cemented carbide coatings, such as WC-12Co, WC-17Co, WC-10Co-4Cr, WC-20CrC-7Ni, Cr_3C_2-25NiCr, TiMo(C,N)-29Ni, and TiMo(C,N)-29Co, at high temperatures in oxidizing atmospheres. Typically, these coatings start to oxidize at 350 °C (660 °F). Pronounced oxidation starts at approximately 650 °C (1200 °F). Above this temperature, oxide scale growth differs significantly in different compositions. WC-20CrC-7Ni and Cr_3C_2-NiCr have the highest oxidation resistance, with scale thicknesses less than 10 μm (0.4 mil) after oxidation for 128 h at 800 and 900 °C (1470 and 1650 °F) for the two materials, respectively (Ref 10).

Resistance against corrosion in oxidizing, sulfidizing, and chloridizing environments can be achieved only by formation of a stable, slow-growing, dense oxide layer.

Hot Corrosion

Hot corrosion is a serious problem in power generation equipment, gas turbines, internal combustion engines, fluidized bed combustion, industrial waste incinerators, and paper and pulp industries. Hot corrosion is the accelerated oxidation of a material at elevated temperature induced by a fused (molten) or solid deposit. The most common deposit in combustion processes is Na_2SO_4. The sulfur present in coal or fuel oil yields SO_2 on combustion, which is further partially oxidized to SO_3. Sodium chloride, either as an impurity in fuel or in the air, reacts with SO_3 and water vapor at the combustion temperature and yields Na_2SO_4, which deposits on the metal surfaces either as a solid deposit or, at a sufficiently high temperature (melting temperature is 884 °C, or 1623 °F), as a fused deposit. Other impurities in the fuel, such as vanadium, form highly corrosive molten sulfate-vanadate deposits; the lowest-melting eutectic in the Na_2SO_4-V_2O_5 system is at approximately 500 °C (930 °F). Alkali metal chlorides, such as NaCl and KCl, present in coal and biomass as well as other low-melting metal chlorides, such as $ZnCl_2$ and $PbCl_2$, that often exist in waste incineration induce chloride corrosion.

Corrosion proceeds in two stages. In the incubation period, a protective scale is formed, whereas in the propagation stage, protection is lost due to mechanical rupture of the scale or its dissolution by the molten salt (fluxing). Hot corrosion appears only at intermediate temperatures determined by the melting point and the dewpoint of the salt (Ref 11).

Two forms of hot corrosion are generally recognized in sulfur-containing combustion environments: type I (high temperature) and type II (low temperature).

Type I high-temperature hot corrosion typically occurs between 800 and 950 °C (1470 and 1740 °F), having the maximum rate at approximately 900 °C (1650 °F). In this form, the sulfur from a sulfate deposit (generally Na_2SO_4) is transported across a preformed oxide into the metallic material with the formation of the most stable sulfides. Once stable sulfide formers (e.g., chromium) are fully reacted with the sulfur moving across the scale, then base metal sulfides can form, with catastrophic consequences, because they are molten at temperatures at which type I hot corrosion is observed. Thus, the formation of NiS_2 (molten at 645 °C, or 1195 °F) and Co_xS_y (the lowest liquidus at ~840 °C, or ~1545 °F) can cause degradation levels, which are serious enough to cause major component degradation. The most suitable materials that can resist type I hot corrosion are $PtAl_2$-(Ni-Pt-Al) coatings and MCrAlY coatings up to 25 wt% Cr and 6 wt% Al (Ref 8, 12).

Type II low-temperature hot corrosion typically occurs between 650 and 800 °C (1200 and 1470 °F), with a maximum rate at approximately 700 °C (1290 °F), and involves the formation of base metal (nickel or cobalt) sulfates that require a certain partial pressure of sulfur trioxide for their stabilization. These sulfates react with alkali metal sulfates to form low-melting-point compounds, which prevent a protective oxide formation (Ref 8). Reaction with the material leads to low-melting eutectics (alkali sulfates), resulting in more extensive damage and a more uniform attack, often exhibiting pitting.

Figure 1 illustrates various types of high-temperature corrosion attack as a function of temperature for chromia-forming and alumina-forming alloys. The ideal protective scale would minimize the solubility of fused salt, a property determined by the combustion chemistry and operational environment. In addition to temperature, the degradation modes depend on the nature of contaminants, gas composition, and alloy composition. Alumina-forming materials with low chromium content are very prone to these types of attack. To improve the corrosion resistance of alumina-forming alloys against type I hot corrosion, 15 to 25% Cr is recommended; for type II hot corrosion, approximately 25 to 40% Cr is recommended (Ref 11). The rates of mixed oxidation and chlorination may be greatly increased if molten chlorides are formed, which may cause fluxing of oxide scales.

Corrosion-Resistant Coatings in Boilers

Aggressive environments exist in boilers burning biofuels, especially annual crops and the green parts of the trees, which contain plenty of potassium and chlorine. Besides biofuels, waste-based fuels and high-chlorine coal cause accelerated corrosion due to chlorine. Chlorine may cause corrosion of boiler components in the gas phase, but the most devastating corrosion problems are associated with deposition of alkali chlorides on heat-transfer surfaces. The moisture content and the ash, sulfur, and chlorine content of biofuels, coal, and municipal solid waste (MSW) are given in Table 1 (Ref 13, 14). The chlorine content of coals varies from less than 0.005 to almost 1 wt% (Ref 15). Chlorine in coals is in the form of KCl and NaCl (Ref 16). It has been observed that chlorine increases the release of alkalis (Ref 17).

The composition of MSW-based fuels varies based on the origin of the waste. The MSW typically contains high percentages of chlorine and moisture and has a low heating value. Most of the chlorine present in MSW originates from polyvinyl chloride, bleached paper (Ref 18), and table salt (Ref 19).

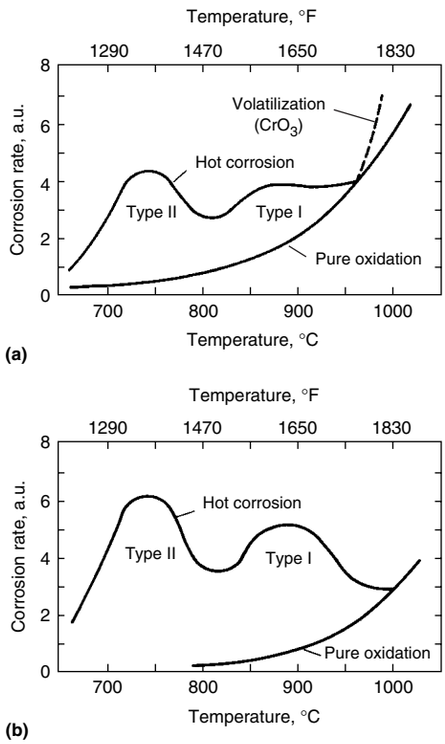

Fig. 1 Various types of high-temperature corrosion attack as a function of temperature for (a) chromia-forming alloys and (b) alumina-forming alloys. Corrosion rates are given in arbitrary units (a.u).

Each 0.1 wt% Cl in biofuels corresponds to approximately 100 ppm (by volume) HCl in flue gases (Ref 13), whereas 0.1 wt% Cl in coal (Ref 17) or MSW (Ref 20) corresponds to approximately 80 ppm HCl in flue gases. Higher HCl content in burning biofuel is due to the higher oxygen content of fuel and thus smaller dilution (Ref 13).

The most severe corrosion in boilers usually takes place in superheater sections where the metal temperatures are highest. The composition of flue gases determines the severity of the gas attack and affects the composition of the deposits that are formed. Recent corrosion tests (Ref 21, 22) with different coatings in oxidizing and reducing chloride-containing atmospheres showed that:

- The corrosion resistance of nickel-base high-chromium coatings, such as Ni49Cr2Si and Ni57CrMoSiB, was good, and they protected the substrate steel in tests performed in gas phase at 550 °C (1020 °F) in the presence of 500 ppm HCl, even in low partial pressures of oxygen.
- In reducing atmospheres, 500 ppm HCl, 600 ppm H_2S, 5% CO, 20% H_2O, and argon in balance at 550 °C (1020 °F), the corrosion resistance increased with increasing chromium content. The coatings having 57% Cr did not suffer corrosion, but the HVOF coatings were penetrated by the corrosive species. The Ni-50Cr coating was covered by oxide and sulfide scale but was not penetrated by corrosive species. This clearly indicates the role of the structure of thermal spray coatings, such as porosity at splat boundaries and oxides formed during spraying, on protective properties.
- In some cases, the corrosive species attacked the substrate through cracks and the interconnected porosity and diluted matrix near oxides at splat boundaries. Even HVOF-sprayed coatings can have some through-coating porosity. Further optimization of spray parameters and strict process control are needed for maximum corrosion resistance.
- Laser remelting of HVOF coatings resulted in fully dense coatings, and there was no corrosion attack in either the Ni49Cr2Si or Ni57CrMoSiB composition.

Hot corrosion below a chloride and sulfate salt mixture (melt proportion 50%) was found to be extremely vigorous in oxidizing atmosphere at 550 °C (1020 °F), even for high-chromium-nickel coatings. The structural details and the homogeneity of the composition, control of splat-boundary oxides, and pore-free structures are essential for good corrosion resistance in this environment. Further development is needed in control or avoidance of splat-boundary oxides and segregation of elements during spraying. Even laser remelting for high-chromium (57%) nickel coatings resulted in dendritic structures in which the chromium-rich dendrites were attacked by chlorine in oxidizing conditions.

In reducing conditions, materials and coatings with high chromium content were able to form a protective layer consisting of chromium, sulfur, and sodium. Corrosion resistance of this layer increased with increasing chromium content. The HVOF Ni-57Cr coating and laser-clad Ni-53Cr coating as well as austenitic steel (Fe27Cr31Ni3.5Mo) and diffusion-chromized coating showed low material loss (Ref 23).

Waste Incinerators

It is generally accepted that the severity of high-temperature corrosion in waste incineration plants is due to gas-phase attack by flue gas containing HCl/Cl_2^- and SO_2/SO_3^-, and liquid-phase attack by molten sulfates, chlorides, and eutectic mixtures of both. This is most pronounced at sites where the liquid can form subsequent to condensation from the gas phase (Ref 24). Table 2 indicates expected components of solid particles in the gas and liquid condensate.

Flame-sprayed, two-layered Al/80Ni-20Cr coatings have a service life of three years or longer in the water wall tubes of waste incineration plants. Recently, HVOF-sprayed, more dense NiCrSiB-alloy coatings have been proposed for these applications (Ref 26). Nickel-base high-chromium alloy coatings, 50Ni-50Cr, have performed well over seven years in the water walls of waste incineration plants (Ref 27). Detonation gun coatings showed the best protective quality, the second best being the HVOF coatings over plasma-sprayed coatings. These 50Ni-50Cr coatings showed better performance than alloy 625 coatings. The HVOF-sprayed 50% Ni alloy 625/50% TiO_2 coatings performed well in secondary superheaters for 6400 h, whereas coatings applied on final superheaters had spalled off after 2000 h exposure (Ref 28).

Table 1 Typical contents of biofuels, coal, and municipal solid waste (MSW) (from a Japanese municipality)

	Content, %			
Fuel	Moisture	Ash	Sulfur(a)	Chlorine(a)
Wood	10–40	1–10	0.03–0.15	0.01–0.04
Salix(b)	40–55	1–2	0.03	0.01
Straw	8–16	3–12	0.05–0.17	0.01–1.5
Bark	45–65	2–10	0.03–0.1	0–0.3
Coal	10	14	<0.5	<0.1
MSW	40–52	7.5–11.5	<0.02	0.14–0.6

(a) Percent in dry solid. (b) Willow tree. Source: Adapted from Ref 13, 14

Table 2 Solid particles in flue gas and vapor condensate deposits on 600 °C (1110 °F) superheater tubes for typical boilers

	Components for fuel and flue gas temperature combinations		
Compounds	MSW at 650 °C (1200 °F)(a)	Coal at 1100 °C (2010 °F)(b)	Black liquor at 1000 °C (1830 °F)
In solid particles			
NaCl	x	...	...
KCl	x	...	...
Na_2SO_4	...	...	x
K_2SO_4	...	...	x
$CaSO_4$	x	x	...
Na_2CO_3	...	...	x
$CaCO_3$	x	...	...
ZnO	x	...	...
Fe_2O_3	...	x	...
As vapor condensate deposits			
NaCl	x	...	x
KCl	x	...	x
Na_2SO_4	...	x	x
K_2SO_4	...	x	...
Na_2CO_3	...	...	x
ZnO	x	...	...

Considering pure solid only. (a) MSW, municipal solid waste. (b) High-chlorine and -sulfur coal. Source: Ref 25

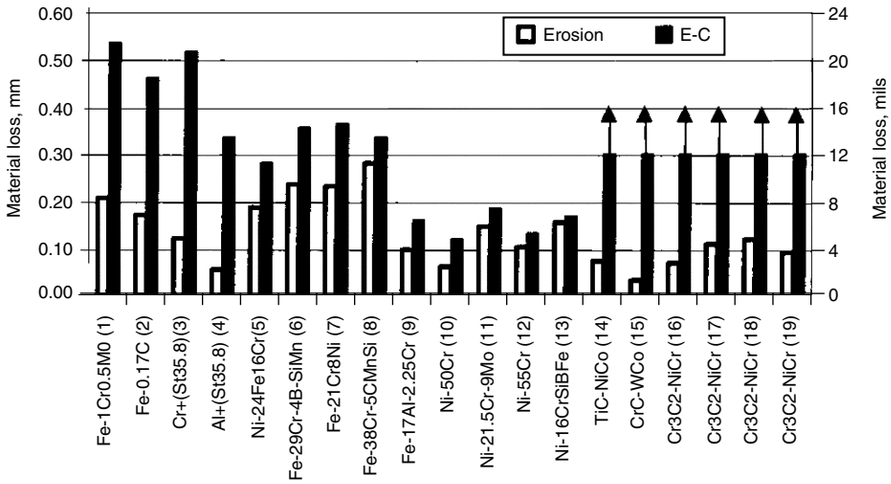

Fig. 2 Material loss in hot erosion and erosion-corrosion tests of 19 materials at 550 °C (1020 °F) by quartz sand/KCl mixture. 1–2, steels; 3–4, diffusion coatings; 5–7, arc-sprayed coatings; 8, combustion arc coating; 9–12, high-velocity oxyfuel (HVOF) coatings; 13, spray and fuse coating; 14, plasma-sprayed coating; 15–19, HVOF coatings. Up arrows indicate material loss greater than 0.30 mm (12 mils) worn through the whole coating thickness. Source: Ref 29

Iron-base Fe-35Cr-5Si coatings have also shown good resistance against high-temperature corrosion resulting from HCl in the flue gas and molten sulfate/chloride mixtures in the deposits on the surface of the tubes. Both HVOF and flame spraying are suitable for producing such coatings. These techniques produce thicker lamellas within the coating and less spraying-produced oxides, so that there is more chromium available for formation of protective oxide scales as compared to plasma-sprayed coatings (Ref 24).

Erosion-Corrosion in Boilers

Chlorine in fuels and particle erosion by bed particles give rise to rapid material wastage by erosion-corrosion in fluidized bed combustion boilers.

The HVOF-sprayed coatings show good hot erosion resistance as compared to low-alloy steels when tested at 550 °C (1020 °F) in an oxidizing atmosphere containing quartz sand particles (Fig. 2.) Even a small amount of KCl significantly accelerates the erosion-corrosion rate at elevated temperatures. The nickel-base HVOF coatings with high chromium content show good resistance against erosion-corrosion at elevated temperature in the presence of chlorine. Carbide-containing HVOF coatings, which show good erosion resistance, cannot resist elevated temperatures and oxygen attack in the presence of chlorine (Ref 29, 30). Erosion-corrosion tests for arc-spray (air and nitrogen as carrier gas), HVOF, and laser-clad coatings were conducted in different biomass and coal power plants. Processes including multibed combustion at 420 °C (790 °F), circulating fluidized bed at 550 °C (1020 °F), and pressurized fluidized bed combustion at 400 °C (750 °F) gave the following results:

- Nickel-base coatings (Ni25Cr8.8Mo1.9-Fe1.9Nb1.0C0.7Si alone or with 15% TiC) have good erosion-corrosion resistance in both biomass- and coal-fired plants.
- Cobalt-base coatings (Stellite 6, Stellite 6+15% TiC, Stellite 21+15% TiC) have good corrosion resistance in power plants fired with coal but are subject to erosion-corrosion in biomass-fired plants.
- Iron-base coatings (Fe12.4Cr0.6Ni0.4Mn0.5Si0.36C) have good corrosion resistance in power plants fired with coal but are subject to corrosion in biomass-fired plants.
- Carbide-containing coatings ($80Cr_3C_2$ 16Ni4Cr, 83WC17Co, 86WC10Co4Cr) are subject to oxidation and a large degree of delamination in all power plants.

REFERENCES

1. V.V. Sobolev and J.M. Guilemany, *Mater. Lett.,* Vol 37, 1998, p 231–235
2. C.-J. Li and W.-Y. Li, *Surf. Coat. Technol.,* Vol 162, 2002, p 31–41
3. W.J. Trompetter, A. Markwitz, and M. Hyland, *Nucl. Instrum. Methods Phys. Res. B,* Vol 190, 2002, p 518–523
4. J. Kawakita, S. Kuroda, T. Fukushima, and T. Kodama, *Sci. Technol. Adv. Mater.,* Vol 4, 2003, p 281–289
5. M. Oksa, E. Turunen, and T. Varis, Sealing of Thermally Sprayed HVOF Coatings for Boiler Applications, Applications VI, *International Thermal Spray Conference ITSC 2004,* Proceedings (Osaka, Japan), German Welding Society, 2004, p 7–12
6. G. Langer, A. Kremsner, and R. Polak, Tero-Composite—Coating Solutions Against High-Temperature Corrosion and Erosion in Boiler Applications, *International Thermal Spray Conference ITSC 2005,* Proceedings (Basel, Switzerland), DVS German Welding Society, 2005, p 67–72
7. J. Tuominen, P. Vuoristo, M. Kylmälahti, T.Mäntylä, J.Vihinen, and P. Andersson, Properties of Nickel Superalloy Coatings As-Sprayed and with Nd-YAG Laser Remelting, *The First International Thermal Spray Conference ITSC 2000,* Proceedings (Montreal, Canada), ASM International, 2000, p 589–596
8. M.J. Pomeroy, *Mater. Des.,* Vol 26, 2005, p 223–231
9. J.R. Nicholls, *MRS Bull.,* Sept 2003, p 659–670
10. L.-M. Berger, R. Zieris, and S. Saaro, Oxidation of HVOF-Sprayed Hardmetal Coatings, *International Thermal Spray Conference ITSC 2005,* Proceedings (Basel, Switzerland), DVS German Welding Society, 2005, p 969–976
11. M.F. Stroosnijder, R. Mevrel, and M.J. Bennett, *Mater. High Temp.,* Vol 12 (No. 1), 1994, p 53–66
12. G.W. Goward, *Surf. Coat. Technol.,* Vol 108–109, 1998, p 73–79
13. K. Salmenoja, "Field and Laboratory Studies on Chlorine-Induced Corrosion in Boilers Fired with Biofuels," Doctoral thesis, Åbo Akademi University, Turku, Finland, 2000
14. N. Otsuka, Y. Nishiyama, and T. Hosoda, Thermodynamic Equilibrium Calculations of Deposits on Superheater Tubes in Waste Incinerators, Paper 229, *Corrosion 2000,* Proceedings (Orlando, FL), National Association of Corrosion Engineers, 2000
15. J.E. Oakey, A.J. Minchener, and N.J. Hodges, *J. Inst. Energy,* Vol 64, 1991, p 3–11
16. L. Tomaczek and H. Palugniok, *Fuel,* Vol 81, 2002, p 1251–1258
17. P.L. Daniel, L.D. Paul, J.M. Tanzosh, and R. Hubinger, *Mater. Perform.,* Vol 27, 1989, p 41–45
18. H.H. Krause, P.L. Daniel, and J.D. Blue, *Mater. Perform.,* Vol 33, 1994, p 63–69
19. S.V. Vassilev, C. Braekman-Danheux, and P. Laurent, *Fuel Process. Technol.,* Vol 59, 1999, p 95–134
20. G. Sorell, *Mater. High Temp.,* Vol 14, 1997, p 207–220
21. M.A. Uusitalo, P.M.J. Vuoristo, and T.A. Mäntylä, *Mater. Sci. Eng.,* Vol 346, 2003, p 168–177
22. M.A. Uusitalo, P.M.J Vuoristo, and T.A. Mäntylä, *Surf. Coat. Technol.,* Vol 161 (No. 2–3), 2002, p 275–285
23. M.A. Uusitalo, P.M.J. Vuoristo, and T.A. Mäntylä, *Corros. Sci.,*Vol 46, 2004, p 1311–1331
24. C. Schroer, M. Spiegel, and H.J. Grabke, Corrosion Resistant Coating Materials for Heat Exchanger Tubes in Waste Incineration Plants, *Materials for Advanced Power Engineering,* Vol 5, Energy Technology, 1998, p 789–798
25. N. Otsuka, *Corros. Sci.,* Vol 44, 2002, p 265–283
26. Y. Kawahara, *Mater. High Temp.,* Vol 14 (No. 3), 1997, p 261–268
27. K. Yamada, Y. Tomono, J. Morimoto, Y. Sasaki, and A. Ohmori, *Vacuum,* Vol 65, 2002, p 533–540
28. Y. Fukuda, K. Kawahara, and T. Hosoda, Application of High Velocity Flame Spraying for Superheater Tubes in Waste Incinerators, Paper 264, *Corrosion 2000,* Proceedings (Orlando, FL), National Association of Corrosion Engineers, 2000
29. M. Uusitalo, P.M.J. Vuoristo, and T.A. Mäntylä, *Wear,* Vol 252, 2002, p 586–594
30. A. Hjörnhede and A. Nylund, Performance of Erosion Resistant Coatings in Different Combustion Environments, *Materials for Advanced Power Engineering 2002,* Proceedings of the Seventh Liège Conference, Forschungszentrum Jülich GmbH, 2002, p 979–988

ASM Handbook, Volume 13B: Corrosion: Materials
S.D. Cramer, B.S. Covino, Jr., editors, p675
DOI: 10.1361/asmhba0003794

Corrosion Rate Conversion

Relationships among some of the units commonly used for corrosion rates

d is metal density in grams per cubic centimeter (g/cm^3)

	Factor for conversion to					
Unit	**mdd**	**$g/m^2/d$**	**μm/yr**	**mm/yr**	**mils/yr**	**in./yr**
Milligrams per square decimeter per day (mdd)	1	0.1	36.5/*d*	0.0365/*d*	1.437/*d*	0.00144/*d*
Grams per square meter per day ($g/m^2/d$)	10	1	365/*d*	0.365/*d*	14.4/*d*	0.0144/*d*
Microns per year (μm/yr)	0.0274*d*	0.00274*d*	1	0.001	0.0394	0.0000394
Millimeters per year (mm/yr)	27.4*d*	2.74*d*	1000	1	39.4	0.0394
Mils per year (mils/yr)	0.696*d*	0.0696*d*	25.4	0.0254	1	0.001
Inches per year (in./yr)	696*d*	69.6*d*	25,400	25.4	1000	1

Adapted from G. Wranglén, *An Introduction to Corrosion and Protection of Metals*, Chapman and Hall, 1985, p 238

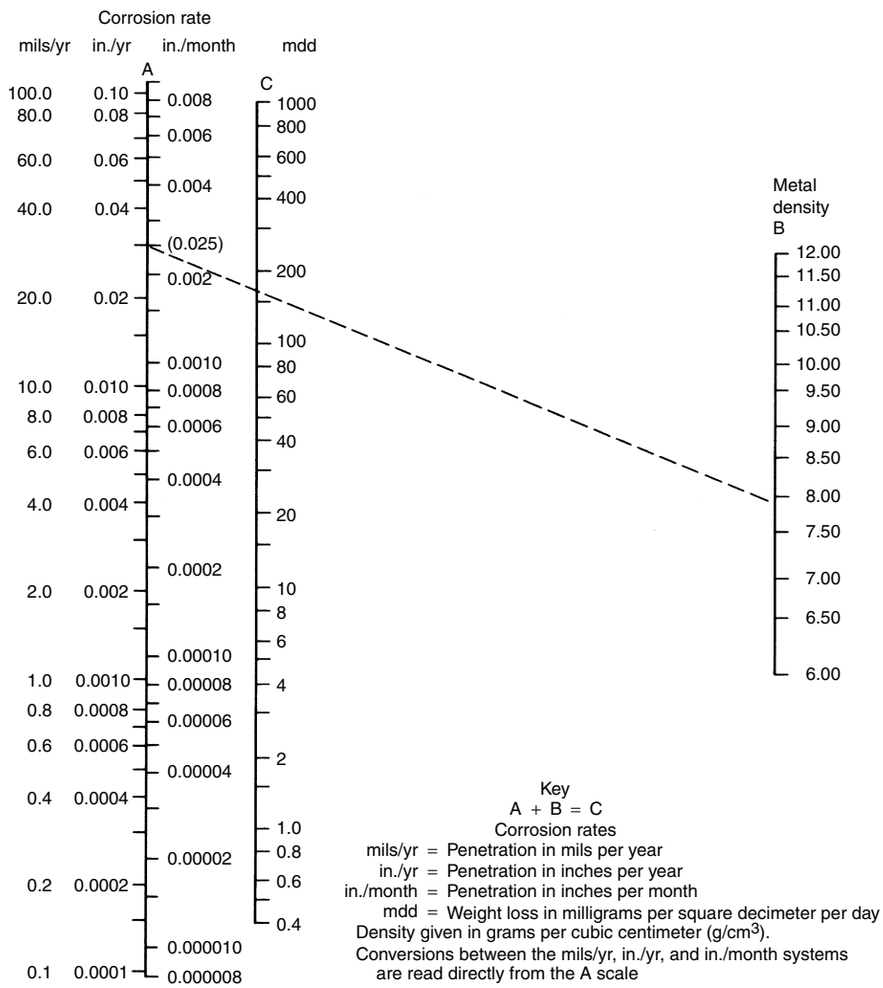

Source: M.G. Fontana, *Corrosion Engineering*, 3rd ed., McGraw-Hill, 1986, p 217

ASM Handbook, Volume 13B: Corrosion: Materials
S.D. Cramer, B.S. Covino, Jr., editors, p672
DOI: 10.1361/asmhba0003796

Galvanic Series of Metals and Alloys in Seawater

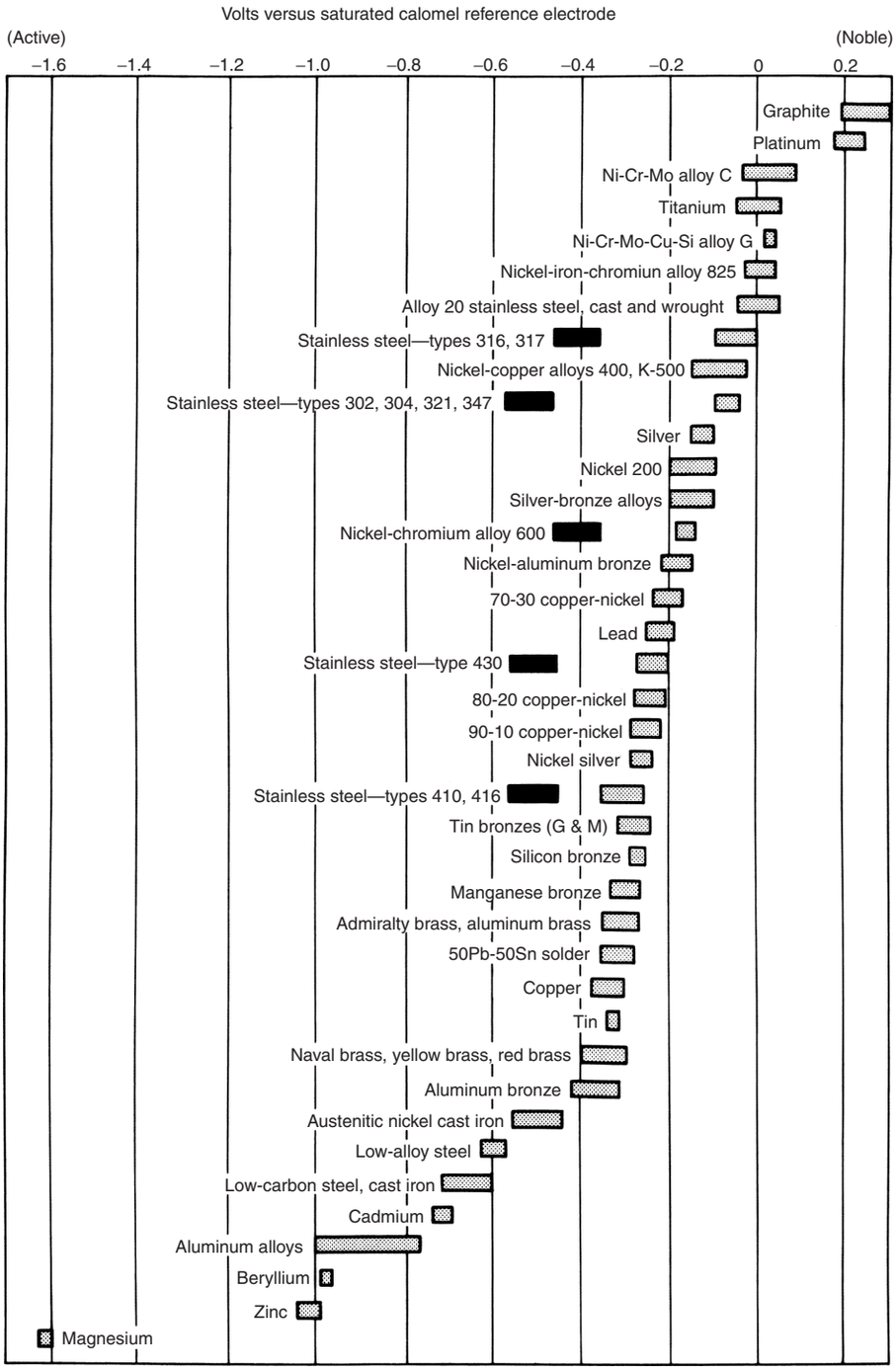

Fig. 1 Galvanic series for seawater. Dark boxes indicate active behavior of active-passive alloys. Applicable to flowing seawater 2.4–4.0 m/s (8–13 ft/s), 10–27 °C (50–80 °F)

Index

A

B

C

D

E

F

G

H

J

K

L

M

N

O

P

Q

R

S

T

U

V

W

X

Y

Z

ASM International is the society for materials engineers and scientists, a worldwide network dedicated to advancing industry, technology, and applications of metals and materials.

ASM International, Materials Park, Ohio, USA
www.asminternational.org

Publication title	Product code
ASM Handbook, Volume 13B, Corrosion: Materials	06508G

To order products from ASM International:

Online Visit www.asminternational.org/bookstore

Telephone 1-800-336-5152 (US) or 1-440-338-5151 (Outside US)

Fax 1-440-338-4634

Mail Customer Service, ASM International
9639 Kinsman Rd, Materials Park, Ohio 44073, USA

Email CustomerService@asminternational.org

In Europe American Technical Publishers Ltd.
27-29 Knowl Piece, Wilbury Way, Hitchin Hertfordshire SG4 0SX, United Kingdom
Telephone: 01462 437933 (account holders), 01462 431525 (credit card)
www.ameritech.co.uk

In Japan Neutrino Inc.
Takahashi Bldg., 44-3 Fuda 1-chome, Chofu-Shi, Tokyo 182 Japan
Telephone: 81 (0) 424 84 5550